PROCEEDINGS OF
THE PHYSICAL SOCIETY

VOL. 72, PART 1 1 July 1958 No. 463

The Fluorescent Decay of CsI(Tl) for Particles of Different Ionization Density

By R. S. STOREY, W. JACK AND A. WARD
The Natural Philosophy Department, The University, Glasgow

MS. received 11*th February* 1958, *and in revised form* 31*st March* 1958

Abstract. New measurements of the decay of the fluorescence produced in CsI(Tl) have been made for different particles. The detailed shape of the decay is found to depend on the average ionization density ρ. The lifetimes τ of the main components are 0·425 ± 0·025 μsec for 4·8 MeV alpha particles, 0·52 ± 0·01 μsec for 2·2 MeV protons, 0·595 ± 0·02 μsec for 8·6 MeV protons and 0·70 ± 0·025 μsec for 0·66 MeV electrons. The variation of τ and ρ is very similar to that observed by others for the variation of τ with temperature for alpha particles, which suggests that the former may be explained in terms of variations in the effective local temperature. It is shown that the differences in τ are sufficient to allow a single crystal detector to be used in experiments where particle type as well as energy determination are required.

§ 1. INTRODUCTION

IN the scintillation counter, the light produced by an ionizing particle in a fluorescent material is converted into an electrical current pulse with the same time variation. It is generally believed that the rate of decay of the main pulse is independent of the type of particle, and that the scintillation counter is only an energy spectrometer. While it is possible to deduce indirectly the type of particle being counted, it would be desirable, from the point of view of achieving a high counting efficiency and simplicity of operation, if the shape of the pulse could be used to identify the particle.

It is therefore of practical, as well as theoretical, interest to consider whether there is any variation for different particles in τ, the mean life of the main pulse in CsI(Tl), a commonly used scintillating material. (Although the fluorescent efficiency of CsI(Tl) is less than that of NaI(Tl), its excellent physical and mechanical properties make it preferable in most applications.)

Van Sciver and Hofstadter (1951), using an RCA 5819 photomultiplier, have found a value for τ of 1·1 ± 0·1 μsec for fast electrons in CsI(Tl), whereas Bonanomi and Rossel (1952), using the same type of photomultiplier, give a value of 0·6 μsec for polonium alpha particles. Knoepfel *et al.* (1956), using an RCA 6655, and also measuring τ for alpha particles obtain a value of 0·55 μsec. Possibly these results have not been interpreted as due to difference in particle, because it is known that other factors can significantly influence the measured lifetime.

Knoepfel *et al.* (1957) have found that τ for alpha particles in CsI(Tl) varies with temperature. Eby and Jentschke (1954) have shown that τ is the same for alphas and electrons in NaI(Tl), but varies with thallium concentration. From these last results, it would be reasonable if the different values of τ measured in CsI(Tl) were at least partly due to a difference in the concentration of thallium in the crystals used. Kallmann and Brucker (1957), using an RCA 5819, have measured τ for fast electrons and alpha particles in a range of organic and inorganic crystals not including CsI(Tl) and find no significant difference.

Summarizing the results of all the above experiments, it can be stated that while different values of τ have been observed for alpha particles and electrons in CsI(Tl), no such effect has been found in the main current pulse of other scintillators, and the measured values of τ may be expected to vary with temperature, concentration of thallium and, possibly, type of photomultiplier.

In the experiments described below, these last three factors were kept constant, and τ has been measured for different energies of alpha particles, protons, and electrons.

§ 2. Experimental Method

The CsI(Tl) crystal was obtained from the Harshaw Chemical Company who stated that the molar concentration of thallium was 0·1%. The dimensions of the crystal were 1·5 cm × 0·9 mm and it was mounted by fine wires on a Du Mont 6292 photomultiplier parallel to the photocathode at a distance of 3·5 cm. A highly reflecting aluminium cylinder, 3·5 cm in diameter by 3·5 cm in length, with a very thin aluminium end window was used as a light reflector. This arrangement has been found to give good pulse height resolution for photomultipliers with photocathodes which are not quite uniformly sensitive.

The current pulses from the photomultiplier were integrated, the leakage time constant being 86 μsec. The integrated current pulses, or voltage pulses, were then fed through a cathode follower and a matched delay line of 1·7 μsec to a Tektronix 517A cathode-ray oscilloscope. Measurements were made on three time scales, 0·2 μsec cm^{-1}, 0·5 μsec cm^{-1} and 2 μsec cm^{-1}. The pulses on the oscilloscope were photographed, projected on a large screen and carefully traced on fine graph paper.

The time base speeds on the Tektronix oscilloscope were compared with the period of a crystal controlled, standard frequency oscillator, Furzehill type G415. This was done by using the crystal controlled oscillator to check the frequency scale of a variable frequency oscillator, type Advance 62. Using convenient frequencies for each time base, the train of sine waves was randomly triggered, photographed and then projected and traced in the same way as the pulses from the CsI(Tl). The probable error in the calibration was ± 1%. The time base speeds indicated on the oscilloscope appeared to be systematically 2% higher than those given by our calibration. Our results have been corrected for this difference.

The electron source was the photopeak and Compton spectrum in the crystal for Cs^{137} gamma rays ($E = 661$ kev). A polonium source (5·3 Mev) was used at different distances from the crystal to give alpha particles of different energies. Higher energy alpha particles were obtained by bombarding boron 10 with 500 kev deuterons. From other experiments with a multichannel pulse height analyser, we have verified that most of the pulses in a limited region of the energy spectrum can be attributed to the reaction $^{10}\mathrm{B}(\mathrm{d}, \alpha)^{8}\mathrm{Be}$ ($Q = 17{\cdot}8$, 14·91 Mev). High energy protons were obtained from the reaction $^{10}\mathrm{B}(\mathrm{d}, \mathrm{p})^{11}\mathrm{B}$ ($Q = 9{\cdot}23$, 7·09, 4·77 Mev).

Five different values of the photomultiplier voltage were used to make the pulse height on the oscilloscope about the same for 1 MeV alpha particles, 4·8 MeV alpha particles, 660 keV electrons, 2 MeV protons and 8·5 MeV protons. The change in photomultiplier gain at these different voltages was later measured using a Hutchinson–Scarrott 100-channel pulse height analyser. Knowing the differences in gain at the five voltages, all of the graphs of the voltage pulses could be normalized to the same gain.

§ 3. RESULTS

When the photographs of the voltage pulses were projected on a large screen, it was immediately obvious that the pulses due to alpha particles were rising more rapidly than those due to electrons, and that the rise time of the proton pulses lay somewhere between the two.

The graphs of the voltage pulses were analysed in two ways. In the first method, voltage pulse heights $V_{1/2}$ and V_4 were measured at 0·5 μsec and 4 μsec. These values were then normalized to allow for the changes in gain of the photomultiplier at the different voltages used in the experiments. When this was done, the values of $V_{1/2}$ were plotted against V_4, and the result is shown in figure 1 in which different symbols are used for points arising from different types of particles. It can be seen that there are three distinct loci for the points, one for each type of particle. The width of the loci can be calculated, if the number of photoelectrons released from the photocathode per unit proton energy is known. From the width of the peaks in the pulse height spectra measured on a multichannel pulse height analyser, we estimate this number to be greater than 5000 per 10 MeV. Choosing

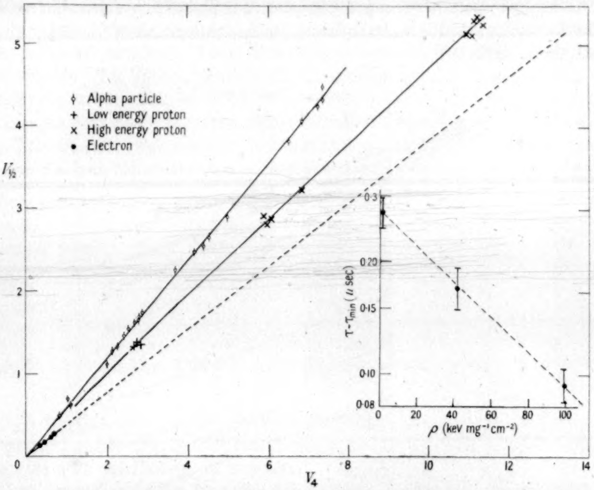

Figure 1. The minimum mass separation using CsI(Tl) as a single crystal detector. $V_{1/2}$ and V_4 are the voltage pulse heights at 0·5 μsec and 4 μsec respectively. Inset: $\tau-\tau_{\min}$ as a function of ρ the average ionization density.

a fixed value of $V_{1/2}$ for 10 Mev protons, the percentage spread in the corresponding value of V_4 is therefore about 1% since $V_{1/2} \simeq \frac{1}{2} V_4$. Only pile up of pulses at very high counting rates can further increase the width of the loci. Figure 1 can be obtained directly using the X and Y plates of an oscilloscope and the mass separation can be further increased by a suitable choice of bandwidths of amplifiers for $V_{1/2}$ and V_4.

In the second method of analysis, the graphs were corrected for the leakage time constant of 86 μsec, and then carefully differentiated to obtain the shape of the current pulses. This was done for electrons of 660 kev, protons of 8·6 and 2·2 Mev and alpha particles of 4·8 Mev, two pulses being analysed in each case. The advantage of measuring the voltage pulse and then differentiating it, rather than measuring the current pulse directly is that it allows a flexible compromise between time resolution and charge fluctuation. When the derivatives of the voltage pulses were plotted, it was found that the current pulses rose with a time constant of 50 ± 10 mμsec, which is attributed to the bandwidth of the delay cable and transit time variations in the Du Mont 6292. The effect of this rise time on the measured values of τ was very small, but the initial decay rates were corrected to allow for its effect. All of the derived current pulses were then normalized to unity at time zero, and the results for the different particles plotted in figure 2. Values have not been plotted for the region 1·6–4 μsec because residual mismatch of the delay line may render them uncertain.

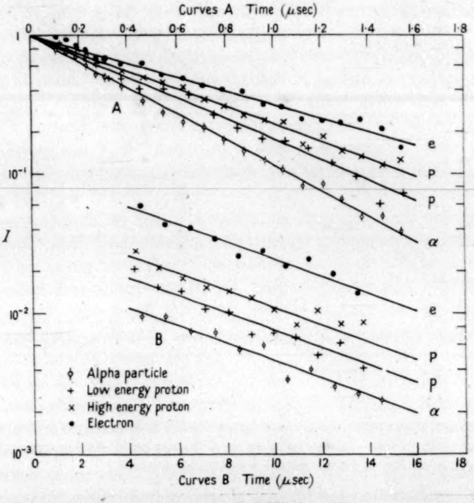

Figure 2. Decay curves in CsI(Tl) for different particles.

It can be seen from figure 2 that the decay of the current pulse can be conveniently described in terms of two components in each case, an initial fast decay and a slow component. If a third component exists with mean life of 2–3 μsec, we estimate that it must contribute less than about 5% to the total voltage pulse at

17 μsec. The subtraction of the common slow component which has a value of $7 \pm 0{\cdot}5$ μsec from the initial decay shown in figure 2, gives the results shown in the table, for the average lifetime τ during the time interval $0{\cdot}1\,\mu$sec–$1{\cdot}6\,\mu$sec. For comparison, the energy of the particles used and the average ionization density ρ defined as the energy divided by the range, are also given in the table. The range for the electron taken from the empirical formula of Katz and Penfold (1952) has been increased by a factor of two to try to allow for electron scattering in the crystal.

The variation of τ with ρ encourages us to believe that τ may be a continuous function of ρ. Consideration of the number and accuracy of the points available does not permit us to derive the function very accurately. However the general behaviour is illustrated by the empirical formula $\tau - \tau_{\mathrm{min}} = (\tau_{\mathrm{max}} - \tau_{\mathrm{min}}) \exp(-\rho/\rho_0)$ which is suggested by the values in the table and also by the loci of figure 1. The inset in figure 1 is a logarithmic plot of $\tau - \tau_{\mathrm{min}}$ against ρ. The value of ρ_0 obtained from this graph is $\rho_0 = 95 \pm 15$ kev mg^{-1} cm^{-2}, if $\tau_{\mathrm{min}} = 0{\cdot}415\,\mu$sec and $\tau_{\mathrm{max}} = 0{\cdot}685\,\mu$sec, our best estimates of τ for alphas and electrons respectively. The values τ_{eqn} in the table are calculated from the empirical formula using the above values.

Since all of our results could be normalized to the same electronic gain, we have been able to estimate the relative voltage pulse height per unit energy (or efficiency) for the different particles. Two efficiencies are given in the table: $\epsilon_{1\cdot5}$ is defined as the efficiency for light emitted in the time range up to $1{\cdot}5\,\mu$sec, and ϵ_∞ is the efficiency for infinite time based on the assumption that there are no contributions from components longer than the common 7 μsec component. Derived values of I_{max}/E, the relative peak currents per unit energy, and of R the ratio of the light output in the long component to the total light output are also given in the table.

	e	p	p	α
Particle	Electron	Proton	Proton	Alpha
Energy E (MEV)	0·66	8·6	2·2	4·8
ρ (kev mg^{-1} cm^{-2})	1·1	42·5	100	680
τ (μsec)	$0{\cdot}70 \pm 0{\cdot}025$	$0{\cdot}60 \pm 0{\cdot}02$	$0{\cdot}52 \pm 0{\cdot}01$	$0{\cdot}425 \pm 0{\cdot}01$
τ_{eqn} (μsec)	0·695	0·60	0·519	0·423
$\epsilon_{1\cdot5}$	$1 \pm 0{\cdot}05$	$1{\cdot}56 \pm 0{\cdot}08$	$1{\cdot}49 \pm 0{\cdot}08$	$0{\cdot}75 \pm 0{\cdot}04$
ϵ_∞	$1 \pm 0{\cdot}05$	$1{\cdot}18 \pm 0{\cdot}05$	$1{\cdot}04 \pm 0{\cdot}05$	$0{\cdot}48 \pm 0{\cdot}03$
I_{max}/E	$1{\cdot}0 \pm 0{\cdot}1$	$1{\cdot}75 \pm 0{\cdot}2$	$1{\cdot}9 \pm 0{\cdot}2$	$1{\cdot}15 \pm 0{\cdot}1$
R	0·50	0·35	0·30	0·25

§ 4. DISCUSSION

Our results show that in CsI(Tl) the efficiency and the decay time of the fluorescence vary with the density of ionization. It might be thought that both effects would be related and arise from the same cause. Kallmann and Brucker (1957) have shown that in a wide variety of scintillators which exhibit effiicency quenching effects which vary with ionization density there is no evidence for any variation in the decay time. Kallmann concludes that the main part of the quenching, at least in the organic scintillators, is finished before any appreciable amount of light is emitted. It might be expected that a similar fast quenching effect occurs to some extent in inorganic scintillators, but that in CsI(Tl) there may also be a slower mechanism for quenching, which competes with the process of emission during the time of emission. Since the efficiency of CsI(Tl) (and also LiI (Eu), Schenck and Neiler 1954) appears to first increase with ionization and then decrease, while the fast quenching mechanisms observed in the organic crystals lead to a monotonic decrease in efficiency, it is necessary to look for a slow quenching mechanism, which will result in the efficiency increasing with increasing ionization density. If the observed variation τ with ionization is attributed to a transport (or recombination) mechanism (Curran 1953), slow quenching occurring during the transport time to the emitting centres would result in a greater decrease in efficiency for smaller ionization densities, which correspond to longer decay times. Thus, qualitatively, this interpretation of our results would explain the observed variations of efficiency and lifetime with ionization density. Such a mechanism, including fast quenching, contains so many adjustable parameters that it is possible that the results for CsI(Tl) could be explained quantitatively, particularly as a transport mechanism would lead to a hyperbolic decay law which would be in rough agreement with our results. However, we have estimated transport or recombination times for CsI(Tl) and these are very much shorter than the observed decay times. Because of this fundamental discrepancy it seems unlikely that our results can be explained in terms of this mechanism.

Since the efficiency variation appears to depend mainly on the fast quenching which is expected to be independent of the emission process, we now go on to consider a possible interpretation of the variation of τ with ρ independently of the variation of efficiency.

The dependence of τ on so many different factors, and the limitations of the present experiments make it necessary to be cautious in comparing the observed variation of τ with ionization density and the results of others in experiments on CsI(T1) crystals. There is, however, a very striking similarity between the variation of τ for alpha particles in CsI (1% Tl) as a function of temperature measured by Knoepfel *et al.* (1957) using an RCA 6655 and our own results for the variation of τ with ionization density at constant temperature. Knoepfel *et al.* find that τ for alpha particles decreases to a limiting value τ_L as the temperature is increased to room temperature. We have plotted the logarithm of $\tau-\tau_L$ as a function of temperature using their results, and find that

$$\tau-\tau_L \propto \exp(-T/T_0)$$

where $T_0 = 13{\cdot}5\,^{\circ}\mathrm{c} \pm 1\,^{\circ}\mathrm{c}$. This empirical expression can be compared with our own results expressed as $\tau-\tau_L \propto \exp(-\rho/\rho_0)$ where $\rho_0 = 95 \pm 15\,\mathrm{kev\,mg^{-1}\,cm^{-2}}$. The similarity of the two expressions, in each of which τ_L is the value found for alpha particles suggests that the effect of changing the particle ionization density is to change the effective local temperature at which the emission takes place. If the change in local temperature is proportional to ρ then it is possible to deduce our results for different particles at the same temperature from those of Knoepfel *et al.* for the same particle at different temperatures.

Our results may be explained in terms of a simple model employing two sets of electron traps at different energy levels. Decay of the trap occurs when it receives enough thermal energy to reach an excited state, decay from which leads to fluorescence. It is supposed that the higher energy trap is responsible for the short lifetimes, while the lower energy trap gives rise to the 7 μsec lifetime. The difference in the two lifetimes is due to the energy difference between the trap and the levels responsible for fluorescence. It would be expected that the trap with the smaller energy difference would be more susceptible to temperature changes than the other one. This would explain the difference in the short lifetimes for different particles if different values of ρ correspond to different effective temperatures in the material surrounding the track, and would also account for the common long lifetime.

In the table R is the ratio of the light emitted due to the long lifetime (7 μsec) to the total light emitted. It is seen that the shorter the initial lifetime, the less there is of the long component. This effect, also seen in figure 2, suggests that the lower energy trap is fed from the higher one in competition with the normal transition to the radiating state. In this case, the lifetime for decay from one trap to another must be of the order of 1 μsec.

This interpretation of our results would lead us to expect a considerably greater change in the values of τ for different particles in CsI(Tl) than are given here if the crystal temperature is lowered below room temperature. This result follows from the behaviour of τ as a function of temperature observed for alpha particles by Knoepfel *et al.* and would result in a considerable increase in the particle separation shown in figure 1.

If this preliminary interpretation of our results is correct, it seems likely that similar effects may occur in other crystals in which non-radiating states are involved. It is possible, however, that it is only in CsI(Tl) that the characteristics of the resonance energy transfer are such as to result in a conveniently large variation in τ as a function of available temperatures, and thus to a useful variation of τ for different particles.

Another quite different interpretation of our results is that the variation in ionization density results in a different distribution in the initial population of radiating states. The observed variation in the value of τ would then reflect the different contributions of many radiating states with different decay times. The simplest and most extreme case would be two radiating states corresponding to the values of τ observed for alpha particles and electrons. It is not possible from our present results to deduce from the straightness of the log plots of the current pulses due to protons whether the values of τ observed for protons are due to a combination of two lifetimes or one single lifetime. However, the order of magnitude of the values of τ observed seems more consistent with those to be expected for traps rather than for radiating states.

A possible interpretation of the results given here could have been that the original decay of the main light pulse from the tracks of the particles is the same but complex. Since the path length of the light passing through the crystal to the photocathode increases in our experiments with increasing ρ, differential absorption of the longer components in the light pulse would tend to a shorter measured decay time for higher values of ρ. However, Wells (private communication) of this department, has found substantially the same values of τ as we have for alpha particles and electrons in a different CsI(0·1%Tl) crystal, obtained from the Harshaw Chemical Company six months later than the one used in the experiments described here. The crystal which Wells used was about three times the thickness of our crystal and was mounted using silicone grease. In both cases we believe that the crystals were cut from the interior of a much larger block of material and therefore that the thallium concentration is uniform throughout our crystals.

It is hoped that further measurements, particularly on the emission spectrum for the different particles, will help to elucidate the mechanism involved. Further experiments will aso be designed from the point of view of improving the mass separation.

ACKNOWLEDGMENTS

One of us (R.S.S.) would like to acknowledge the receipt of an I.C.I. Fellowship, and another (W.J.) wishes to acknowledge the assistance of the Sir James Caird Travelling Scholarships Trust.

REFERENCES

BONANOMI, J., and ROSSEL, J., 1952, *Helv. Phys. Acta*, **25,** 725.

CURRAN, S. C., 1953, *Luminescence and the Scintillation Counter* (London : Butterworths Scientific Publications).

EBY, F. S., and JENTSCHKE, W. K., 1954, *Phys. Rev.*, **96,** 911.

HUTCHINSON, G. W., and SCARROTT, G. G., 1951, *Phil. Mag.*, **42,** 792.

KALLMANN, H., and BRUCKER, G. J., 1957, *Phys. Rev.*, **108,** 1122.

KATZ, L., and PENFOLD, A. S., 1952, *Rev. Mod. Phys.*, **24,** 28.

KNOEPFEL, H., LOEPFE, E., and STOLL, P., 1956, *Helv. Phys. Acta*, **29,** 241; 1957, *Z. Naturf.*, **12a,** 348.

SCHENCK, J., and NEILER, J. H., 1954, *Nucl.*, **12** (3), 28.

VAN SCIVER, W., and HOFSTADTER, R., 1951, *Phys. Rev.*, **84,** 1062.

The Infra-Red Absorption Spectra of α-Quartz between 4 and 15 Microns

By B. D. SAKSENA
National Physical Laboratory of India, New Delhi, India

MS. received 21*st October* 1957, *and in revised form* 21*st February* 1958

Abstract. The infra-red absorption spectra of α-quartz and vitreous quartz between 4 and 15 microns are given and values of the absorption coefficients have been calculated with the help of published reflectance data. Certain results are stated which are not in agreement with the earlier classification of the bands on the basis of point-group D_3.

---

§ 1. INTRODUCTION

The infra-red reflection spectra of α-quartz have been investigated by a number of workers, a bibliography of which has been given by the author (1940). Drummond recorded the absorption spectra from 2 to 7 microns. In the present investigation we have recorded the absorption spectra of α-quartz from 4 to 15 microns.

§ 2. EXPERIMENTAL

The instrument used is a Hilger double beam infra-red spectrometer. Table 1 gives the data about the various plates used which have been named in the text by the numbers given in the first column. We have also investigated the spectra of powdered α-quartz and vitreous quartz in pressed KBr discs.

Table 1. Data about various Crystal Plates

No.	Cut	Thickness (mm)	Polish	Size (cm × cm)	Colour etc.
1.	X	0·089	Uniform and polished	1·2 × 2·2	Shows very feeble colour when placed on white paper.
2.	Plane of plate oblique to optic axis.	0·114	Uniform and polished	1·3 × 2·5	Colourless. Used as a crystal resonator.
3.		0·063	Unpolished in 2 pieces	0·4 × 0·7	Used as a crystal resonator.
4.	Z	0·075	Unpolished	0·6 × 1·0	
5.	Z	0·089	Unpolished	0·8 × 0·7	
6.	Z	0·095	Unpolished	1·0 × 0·4	
7.	Z	0·044	Unpolished	1·0 × 0·7	Shows some colour.
8.	V cut RCA patent	0·031	Uniform and polished	1·3 × 2·5	Shows some colour. Used as a crystal resonator.
9.	Powder specimens: (1) α-quartz (2) vitreous quartz				Worked in pressed KBr discs which were transparent. Specimen of vitreous quartz was taken from fused quartz tube used for arcs.

For the X-cut plate, the electric axis is perpendicular to the plane of the crystal plate. The cut for plate 1 was determined by x-ray methods, (i) by mounting the plate with its plane perpendicular to the axis of rotation on a diffraction unit and taking a rotation photograph and (ii) by recording the Cu K_α

reflection peak on a Bragg spectrometer. For the Z-cut plate, the optic axis is perpendicular to the plane of the crystal plate. For these and for plate 2, the nature of the cut was inferred from the interference figures obtained on a polarising microscope. The thickness of the plates was determined with a screw gauge reading to 0·001 inch.

§ 3. RESULTS

3.1. *Frequencies*

The infra-red spectra are recorded in figures 1 to 5. To avoid the errors arising from electrical disturbances, the spectrum of the same plate was taken several times and also on different dates. This precaution is necessary for weak bands; curves 4, 5, 6 and 7 of figure 1, which refer to different Z-cut plates, are reproduced for this reason.

Region 4 *to* 7 *microns*.

The bands are recorded in figures 1 and 2. The strong bands are the same as those obtained by Drummond, but several weak bands have also been recorded which are seen well resolved in figure 2.

Table 2. Wavelengths of the Bands between 4 and 7 μ

<table>
<tr><th colspan="2">Author
Wavelength (μ)</th><th>Intensity</th><th colspan="2">Drummond (1936)
Wavelength (μ)</th><th>Krishnan
(1945)</th></tr>
<tr><th>X-cut</th><th>Z-cut</th><th></th><th>X-cut</th><th>Z-cut</th><th>Raman freqs.</th></tr>
<tr><td colspan="2">4·31</td><td>v.w.</td><td colspan="2">4·32</td><td></td></tr>
<tr><td colspan="2">4·50</td><td>m.</td><td colspan="2">4·48</td><td>4·45</td></tr>
<tr><td colspan="2">4·70</td><td>w.</td><td colspan="2">4·70</td><td>4·70</td></tr>
<tr><td>5·05</td><td>5·03</td><td>s.</td><td>5·05</td><td>5·03</td><td></td></tr>
<tr><td colspan="2">5·15</td><td>v.w.</td><td></td><td></td><td></td></tr>
<tr><td colspan="2">5·35</td><td>v.s.</td><td colspan="2">5·34</td><td></td></tr>
<tr><td colspan="2">5·58</td><td>v.s.</td><td colspan="2">5·60</td><td></td></tr>
<tr><td>5·76</td><td>5·78</td><td>v.w.</td><td></td><td></td><td></td></tr>
<tr><td>5·82</td><td>5·84</td><td>w.</td><td></td><td></td><td></td></tr>
<tr><td>5·86</td><td>5·90</td><td>w.</td><td></td><td></td><td></td></tr>
<tr><td>5·93</td><td></td><td>w.</td><td></td><td></td><td></td></tr>
<tr><td colspan="2">5·96</td><td>s.</td><td colspan="2">5·96</td><td></td></tr>
<tr><td>6·10</td><td>6·08</td><td>w.</td><td></td><td></td><td></td></tr>
<tr><td>6·24</td><td>6·22</td><td>v.s.</td><td colspan="2">6·24</td><td>6·13</td></tr>
<tr><td>6·47</td><td>6·43</td><td>w.</td><td></td><td></td><td></td></tr>
<tr><td>6·55</td><td>6·58</td><td>m.</td><td>6·58</td><td>6·60</td><td></td></tr>
<tr><td>6·61</td><td>6·63</td><td>w.</td><td></td><td></td><td></td></tr>
<tr><td colspan="2">6·70</td><td>m.</td><td>6·72</td><td>6·70</td><td>6·69</td></tr>
<tr><td>6·75 (m)</td><td>6·79 (w)</td><td>m, w.</td><td></td><td></td><td></td></tr>
<tr><td>6·81</td><td>6·86</td><td>w.</td><td></td><td></td><td></td></tr>
<tr><td></td><td>6·96</td><td>v.w.</td><td></td><td></td><td>6·92</td></tr>
<tr><td></td><td>7·05</td><td>w.</td><td></td><td></td><td></td></tr>
<tr><td>7·15</td><td>7·17</td><td>w.</td><td>7·1</td><td></td><td>7·17</td></tr>
</table>

v.w., very weak; w, weak; m, medium; s, strong; v.s., very strong.

The spectra of plates 2 and 3, whose planes are inclined to the optic axis, are identical with the spectra of plate 1 which is X-cut. But there are slight differences in the spectra of crystals with X- and Z-cuts in the region 6 to 7 μ. Particularly noticeable is the weak intensity of the band at 6·79 μ in the Z-cut specimens (figure 1).

Region 7 *to* 10 *microns.*

From 8 to 9·7 μ the transmission is only 2 to 3%. To bring out the bands in this region we considerably reduce the intensity of the reference beam and take a single beam record with wide slits starting with nearly 90% transmission at 8 μ. The wavelengths of the bands, which may have an error of nearly 1%, are recorded in table 3.

Table 3. Wave Numbers of the Bands between 7 and 10 μ

Infra-red absorption		Intensity	Raman effect	Infra-red reflection	
(μ)	(cm^{-1})		(cm^{-1})	(cm^{-1})	
7·15	1399	v.w.	1394 (K)		
7·3	1370	v.w.			
8·1	1235	v.w.	1228 (Sa)	1250 (SM)	Z, $X_{\parallel}$
8·5	1176	m.	1159 (Sa)	1160 (S)	Z
				1168 (SM)	Z, $X_{\perp}$
9·55	1047	s.	1063 (Sa)	1047 (S)	Z
				1065 (SM)	Z, $X_{\perp}$
				1055 (SM)	$X_{\parallel}$

K, Krishnan 1945; Sa, Saksena 1940; SM, Simon and McMahon 1953; S, Simon 1951; Z, Z-cut; $X_{\parallel}$, $X_{\perp}$, X-cut with electric vector $\parallel$, $\perp$ to optic axis.

Region 10 *to* 15 *microns.*

The bands in this region (see figure 3) are given in table 4.

Table 4. Wave Numbers of the Bands between 10 and 15 μ

Cut	Infra-red absorption		Intensity	Raman effect	Infra-red reflection
	(μ)	(cm^{-1})		(cm^{-1})	(cm^{-1})
—	10·6	943	v.w.	960 (K)	—
—	10·8	926	v.w.	925 (K)	—
V, Z, X,	11·16	890	w.	890 (K)	—
V, Z, X,	11·46	872	w.	864 (K)	—
V, Z,	12·32	812	s.	807795 (Sa)	—
X,	12·5	800	s.	—	802795 (SM) Z, $X_{\perp}$
Z,	12·70	787	s.	—	—
V,	12·75	784	s.	—	—
X,	12·9	775	s.	—	780 (SM) $X_{\parallel}$ 777 (P)
V,	13·0	770	s.	—	—
V, Z,	14·38	695	m.	695 (Sa)	—

K, Krishnan 1945; Sa, Saksena 1940; SM, Simon and McMahon 1953; P, Plyler 1929; Z, Z-cut; V, V-cut; X, X-cut; $X_{\parallel}$, $X_{\perp}$, X-cut with electric vector $\parallel$, $\perp$ to optic axis.

The band at 13·0 μ is not very clearly indicated in figure 3 but can be inferred from the shape of the curve. In figure 4 we reproduce single beam records for this region with plates of different cuts. The interesting point to be noticed is the absence of the band at 14·38 μ (695 cm^{-1}) with the X-cut plate (see curves 1 and 2 of figure 4, curve 2 being the record of the same plate turned through 90°). With all other plates this band is obtained. A double beam record for the region 13 to 15 μ taken with plates 1 and 2 shows the presence of the band at 14·38 μ (695 cm^{-1}) with plate 2 but not with plate 1.

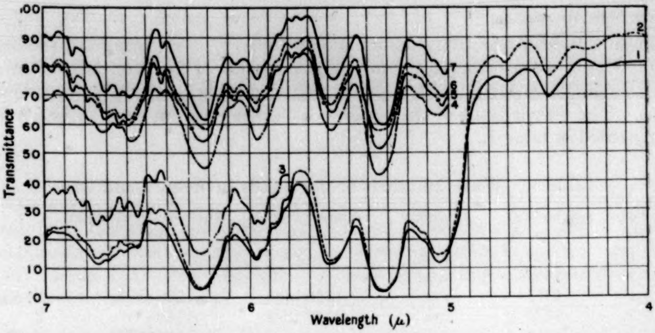

Figure 1. Infra-red spectra between 5 and 7μ. Spectra 1, 2, 3 with plates 2, 1 and 3 (no 1 being X-cut and the other two have their optic axis inclined to the plane of the crystal plate); and spectra 4, 5, 6 and 7 with Z-cut plates 4, 5, and 6. Spectra 3, 4, 5, 6, and 7 have been drawn over spectra 1 and 2 to bring out the common frequencies in the spectra of X- and Z-cut plates and do not represent the transmittance correctly.

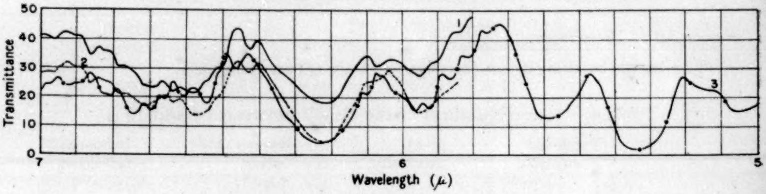

Figure 2. Infra-red absorption spectra between 5 and 7μ, spectrum 3 for X-cut plate, and spectra 1 and 2 for Z-cut plates.

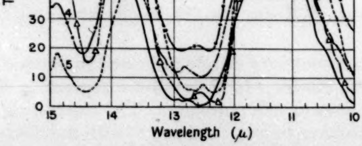

Figure 4. Single beam infra-red absorption spectra from 10–15μ. Spectrum 2 with plate 4 having X-cut; spectrum 1 with the same plate turned through 90° from its first position; spectrum 3 and spectrum 5 with Z-cut plates 4 and 5; and spectrum 1 with plate 3. The incident energy was adjusted to give a large transmittance at 11μ.

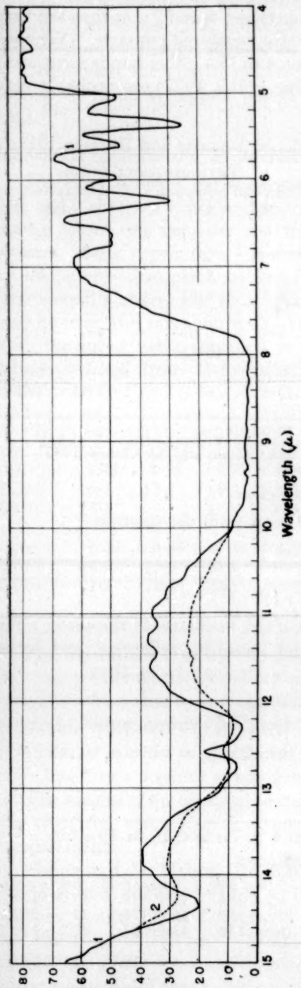

Figure 3. Infra-red absorption spectra—curve 1 between 4 and 15μ with V-cut plate no. 8, and curve 2 between 10 and 15μ with Z-cut plate no. 7.

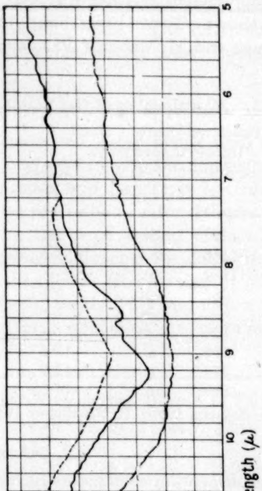

Figure 5. Infra-red absorption spectra in pressed KBr discs of powdered α-quartz (spectrun 1) and of powdered vitreous quartz (spectra 2 and 3).

Spectra of powdered α-quartz and vitreous quartz.

The spectra of powdered α-quartz and of vitreous quartz (see figure 5) are recorded in table 5. No bands are observed between 4 and 7 μ as they are very weak compared to the band at 9·24 μ (1082 cm^{-1}) in powdered α-quartz. Vitreous quartz shows only two broad bands in the region 4 to 15 μ, other bands mentioned by Simon and McMahon (1953) and Reinkobar (1910, 1927) are probably very weak.

Table 5. Wavelengths of the Bands for Powdered α-quartz and Vitreous Quartz

Powdered-quartz			Crystal	Vitreous-quartz		Powder	
Infra-red absorption				Infra-red reflection		Absorption	
Sa			tables 3 & 4	R	SM	Sa	
(μ)	(cm^{-1})	Int.	(μ)	(μ)	(μ)	(μ)	(cm^{-1})
8·0	1250	v.w.	8·1	—	7·41	—	—
8·58	1166	m.s.	8·5	8·3	8·62	—	—
8·76	1142	w.	—	—	—	—	—
9·24	1082	v.s.	9·55	8·9	9·09	9·0	1111
—	—	—	—	—	10·53	—	—
12·12	824	v.w.	—	—	—	—	—
12·56	796	s.	12·5	12·6	—	12·42	805
12·87	777	s.	12·9	—	—	—	—
14·45	690	m.	14·38	14·6 (v.w.)	—	—	—

Sa, Saksena 1940; R, Reinkobar 1910, 1927; SM, Simon and McMahon 1953.

3.2. *Absorption Coefficients*

The absorption coefficients have been obtained from the relations:

$$I/I_0 = e^{-Kd}[(1-r)^2]$$

and

$$r = [(n-1)^2 + k^2]/[(n+1)^2 + k^2]$$

where K is the absorption coefficient ($4\pi k/\lambda$), d the thickness of the plate, r the reflection coefficient, $(1-r)^2$ the correction for losses by reflection, and n the index of refraction. If the transmittance I/I_0 be denoted by m, then

$$K = (1/d) \ln [(1-r)^2/m].$$

A more correct expression has been given by Willmott (1950) which reduces to the expression given when K is small. The absorbance at various wavelengths between 4 and 7 μ for X- and Z-cut plates are given in tables 6 and 7 and refer to the value of d in millimetres.

Table 6. Absorption Coefficients from 4 to 7 μ and 10 to 15 μ for X- and V-cut Specimens

λ (μ)	5·05	5·22	5·36	5·48	5·61	5·76	5·96	6·08	6·25	6·45	6·55
K (X-cut)	20·7	14·9	43·3	14·1	23·3	8·7	21·6	14·7	39·0	13·2	19·0
K (V-cut)	22·4	16·4	43·0	15·3	23·5	10·5	23·0	16·3	38·8	12·9	22·1
K (D) cut ‖ to axis	15·0	11·1	29·4	10·9	16·6	6·9	17·6	11·8	27·3	10·1	17·8
λ (μ)	6·75	6·85	7·0	7·2	7·4	7·6	7·8	8·0	10·0	11·0	12·0
K (X-cut)	21·9	15·8	—	—	—	—	—	—	—	—	—
K (V-cut)	22·3	14·8	15·5	18·3	27·2	42·2	84·5	110·8	67·0	26·1	42·7
K (D) cut ‖ to axis	16·4	11·3	12·0	14·4	21·7	30·8	—	—	—	—	—
λ (μ)	12·3	12·5	12·6	12·75	13·0	13·5	13·8	14·0	14·4	15·0	—
K (V-cut)	92·3	51·2	22·7	54·9	45·2	22·4	22·7	27·6	45·8	7·1	—

(D), Drummond 1936.

Absorption coefficient for X- and V-cut specimens.

The transmittance at 4 μ is 90% which agrees with that recorded by Drummond. The values of K obtained with X-cut and V-cut specimens agree well and are close to, though slightly higher than, the values obtained from the curves of Drummond for quartz specimens cut parallel to axis. The differences are prominent in those regions where the transmittance is very small (nearly 2 to 3%).

Absorption coefficient for Z-cut specimens.

We may compare the absorption coefficients for Z-cut plates from curves 5, 6, and 7 of figure 1. These plates are unpolished and so to account for various energy losses, we consider the transmittance as m/p (where p is considered constant in the region 5 to 7 μ) and determine the value of p for different plates by taking the absorption coefficient at 5·03 μ the same as that obtained from Drummond's curve, i.e. 16·2. The absorption coefficients for different wavelengths from the three curves agree among themselves (the maximum variation from the mean value recorded in table 7 being nearly 5%) and also with the values obtained from Drummond's curve (for a specimen cut perpendicular to the axis).

Table 7. Absorption Coefficient for Z-cut Specimen from 4 to 7·6 μ

λ (μ)	5·03	5·15	5·20	5·35	5·45	5·59	5·70	5·84	5·95	6·10
K (Sa)	16·2	12·1	11·7	25·8	11·1	17·4	8·9	11·4	17·4	14·2
K (D)	16·2	—	11·1	29·7	10·4	17·7	6·6	—	15·9	12·9
λ (μ)	6·26	6·45	6·58	6·70	6·90	7·17	7·20	7·40	7·60	—
K (Sa)	24·6	10·9	21·1	19·8	11·6	15·3	14·4	19·2	27·5	—
K (D)	27·7	8·4	19·1	19·2	10·1	—	13·5	19·9	29·7	—

Sa, Saksena 1940; D, Drummond 1936.

For the region 5 to 8 μ the values of the reflectance r were obtained from the values of the refractive index n and for the region 10 to 15 μ from the reflectance curves for the ordinary and extra-ordinary rays (Wood 1934) and from the (n, λ) curves of Simon and McMahon (1953).

§ 4. DISCUSSION

The results of the absorption studies in the region 12 to 13 μ agree in a general way with the conclusion of Simon and McMahon obtained from reflection measurements:

Simon and McMahon find that a Z-cut specimen shows bands at 795 cm^{-1} (12·58 μ) and 802 cm^{-1} (12·47 μ) but we find that the bands occur at 12·32 μ (812 cm^{-1}) and 12·7 μ (787 cm^{-1}) (see curve 2, figure 3). Further, they state that the band at 780 cm^{-1} (12·82 μ) is not present. We agree with this view because the Z-cut specimen does not show the band at 12·9 μ (775 cm^{-1}) present in the spectrum of the X-cut specimen (curves 2 and 5 of figure 4). It follows therefore that the electric vector is perpendicular to the optic axis for the bands 12·32 and 12·7 μ and parallel to the optic axis for the band 12·9 μ. The band positions are almost the same in the V-cut specimen, i.e. 12·32, 12·75 and 13·0 μ, the difference being not significant on account of the rather large band-width.

For an X-cut specimen Simon and McMahon (1953) record a band at 802 cm^{-1} (12·48 μ) with electric vector perpendicular to optic axis and a band at 780 cm^{-1} (12·82 μ) with electric vector parallel to optic axis. We, too, find that the X-cut specimen shows two bands one at 12·5 μ (800 cm^{-1}) and the other at 12·9 μ (775 cm^{-1}) and there is no band at 12·32 μ (812 cm^{-1}). Since the band at12·9 μ has electric vector parallel to optic axis it is likely that the band at 12·5 μ has electric vector perpendicular to the optic axis and corresponds to the bands at 12·32 and 12·7 μ observed for the Z-cut specimen. We may conclude that *the bands* 12·32 *and* 12·7 μ *are well separated for a Z-cut specimen but merge into a single band at* 12·5 μ *for an X-cut specimen.* This closely follows the earlier remarks of the author (Saksena 1940) from the Raman effect studies "We may here draw attention to a curious feature namely that the frequencies 795 cm^{-1} (12·58 μ) and 807 cm^{-1} (12·39 μ) are sharp and well separated when the optic axis is along the vertical but appear as a broad band of width 13 cm^{-1} with a mean shift of 795 cm^{-1} when the optic axis is along the two perpendicular directions." It may be mentioned here *that the band at* 12·32 μ (812 *cm*$^{-1}$) *is absent in the spectrum of powdered quartz although the bands at* 12·5 μ (800 *cm*$^{-1}$) *and* 12·9 μ (775 *cm*$^{-1}$) *are present* (see figure 5).

Another interesting feature of these studies is the disappearance of the band at 14·38 μ (695 cm^{-1}) with the X-cut specimen. Since the disappearance is maintained when the crystal plate is turned through 90° about the normal to the plate (curves 1 and 2, figure 4) the instrumental polarization is not involved and the band is completely absent. The band is also absent in the double beam record where the instrumental polarization similarly affects both the reference and sample beams. The band is not due to any impurity since it is present in the Raman spectrum.

These results are not explicable on the earlier classification of the author, which has been supported by Simon and McMahon (1953), that these bands can be assigned to degenerate class E of point-group D_3 ($M_z=0$ and $M_x=M_y\neq 0$ where M_z is the change of dipole moment along the optic axis and M_x along the electric axis).

As regards the powder spectrum (figure 5), the frequencies of the observed bands are close to those in the crystal but for some bands, particularly the band at 9·24 μ, the differences are rather marked. Vitreous quartz shows two strong and very broad absorption bands at 1111 cm^{-1} (9·0 μ) and 805 cm^{-1} (12·42 μ) which indicate the presence of an SiO_4 grouping in the glassy state.

REFERENCES

DRUMMOND, D. G., 1936, *Proc. Roy. Soc.* A, **153,** 328.
KRISHNAN, R. S., 1945, *Proc. Ind. Acad. Sci.*, **22A,** 329.
PLYLER, E. K., 1929, *Phys. Rev.*, **33,** 48.
REINKOBAR, O., 1910, *Inaugural Dissertation*, Berlin, p. 39; 1927, *The Properties of Silica*, American Chem. Soc. Monograph (New York: Chemical Catalog Co.), p. 714.
SAKSENA, B. D., 1940, *Proc. Ind. Acad. Sci.*, **12A,** 93.
SIMON, I., 1951, *J. Opt. Soc. Amer.*, **41,** 336.
SIMON, I., and MCMAHON, H. O., 1953, *J. Chem. Phys.*, **21,** 23.
WILLMOTT, J. C., 1950, *Proc. Phys. Soc.* A, **63,** 254.
WOOD, R. W., 1934, *Optics* (New York : MacMillan), 3rd edn, p. 521.

Heat Conduction in Bismuth Telluride†

By H. J. GOLDSMID

Research Laboratories of the General Electric Co. Ltd., Wembley, Middlesex

MS. received 21st January 1958, and in final form 25th March 1958

Abstract. The Lorenz number of the semiconductor Bi_2Te_3 has been evaluated, for the range of partial degeneracy, from data provided by the measurements of electrical conductivity and thermoelectric power. The calculated electronic component of the thermal conductivity, for p-type material, has been found to agree with the experimental results, assuming the lattice thermal conductivity to be independent of the electrical conductivity. Agreement has also been obtained for non-halogen-doped n-type Bi_2Te_3, but not for halogen-doped material. It has been shown that the reason for this is the high effective scattering cross section, for phonons, of the halogen atoms.

The theory of the transport of ionization energy has been found to agree very closely with experiment.

§ 1. Introduction

The measurement of the thermal conductivity of certain semiconductors is of particular interest since, in these materials, the contributions to the transport of heat from the free charge carriers and from the lattice vibrations can be of comparable magnitude. Moreover, there is the possibility of a number of heat conduction effects which are not encountered in metals or dielectric materials. For example, the transfer of the ionization energy of hole–electron pairs has already been observed, and an exciton contribution has been postulated. A summary of the various mechanisms of heat conduction in semiconductors has been given by Joffe and Joffe (1956).

Preliminary accounts of measurements on the thermal conductivity of the semiconductor Bi_2Te_3 have already been given (Goldsmid 1956 a, b) but no allowance was made for the effects of degeneracy, or of the influence of the law governing the scattering of the charge carriers on the Lorenz number, and no distinction was drawn between n-type and p-type material. It is the purpose of the present work to make good this deficiency.

The measurements have all been carried out with the thermal gradient parallel to the cleavage planes using either single crystals or aligned polycrystalline material. The apparatus has already been described briefly in the first of the previous publications. A detailed account of the experimental procedure has been given elsewhere (Goldsmid 1957). A total possible error of 2·5% in the measurements has been estimated.

§ 2. Experimental Results

Before considering the experimental results for the thermal conductivity of Bi_2Te_3, let us see what might be expected for an ideal semiconductor. For such a material it will be supposed that the lattice component of the thermal conductivity is independent of the electrical conductivity. In other words, there is supposed to be no scattering of phonons by electrons or holes, or by the ionized impurities. If the semiconductor obeys classical statistics and simple covalent lattice scattering of the charge carriers predominates, the electronic component of the thermal conductivity κ_e is given by

---

† An account of this work forms part of a Ph.D. thesis submitted to the University of London.

$$\kappa_e = 2\left(\frac{\boldsymbol{k}}{\boldsymbol{e}}\right)^2 \sigma T \qquad \ldots\ldots (1)$$

where σ = electrical conductivity, and
T = absolute temperature.

The total thermal conductivity is then given by

$$\kappa = \kappa_1 + \kappa_e = \kappa_1 + 2\left(\frac{\boldsymbol{k}}{\boldsymbol{e}}\right)^2 \sigma T \qquad \ldots\ldots (2)$$

where κ_1 = lattice component of the thermal conductivity. Thus, for such a material, a plot of the thermal conductivity against the electrical conductivity, for different samples at a given temperature, should be a straight line of slope $2(\boldsymbol{k}/\boldsymbol{e})^2 T$, the intercept on the ordinate axis representing the lattice component.

It would certainly be unexpected if such a simple situation held good for Bi_2Te_3. In the first place, the variation of mobility with temperature indicates that the mean free paths of electrons and holes are not independent of energy (Goldsmid 1958, to be referred to as G). The numerical factor in equation (2) should not therefore be equal to 2, nor should it remain constant, in view of the differing degrees of degeneracy among the samples; thus, a plot of thermal conductivity against electrical conductivity should not be linear. Also, for the purer samples, minority carrier conduction, leading to the transport of ionization energy (Fröhlich and Kittel 1954), should be appreciable, particularly at the higher temperatures. It was, moreover, by no means certain that the lattice

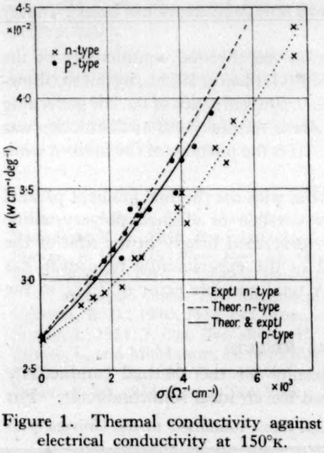

Figure 1. Thermal conductivity against electrical conductivity at 150°K.

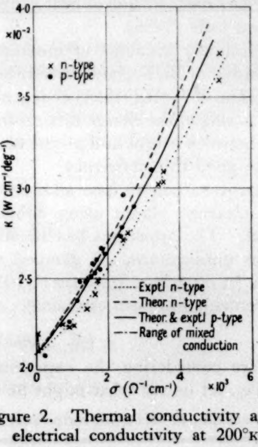

Figure 2. Thermal conductivity against electrical conductivity at 200°K.

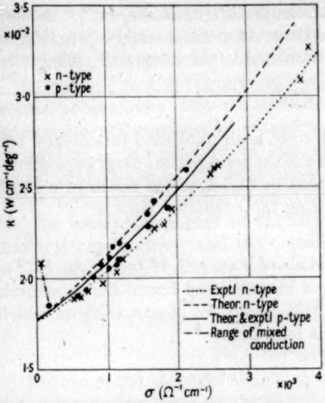

Figure 3. Thermal conductivity against electrical conductivity at 250°K.

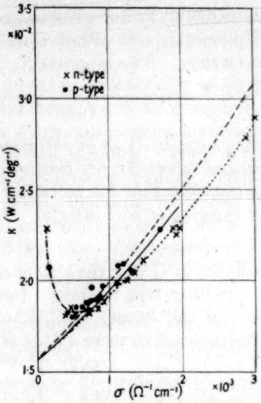

Figure 4. Thermal conductivity against electrical conductivity at 300°K.

thermal conductivity should have remained the same for samples of such widely different carrier concentrations as were encountered.

All these points were borne in mind when the thermal conductivity was plotted against the electrical conductivity, as shown in figures 1, 2, 3 and 4 for 150°K, 200°K, 250°K and 300°K respectively. The results were obtained from p-type samples doped with a number of different impurities, but from n-type ingots doped with iodine and chlorine only. The first feature to be noticed is that, for a given electrical conductivity, the thermal conductivity of p-type Bi_2Te_3 is always higher than for n-type material, though the difference becomes less for extrinsic samples of low electrical conductivity, and the results from both types would indicate the same lattice component when extrapolated to intercept the ordinate axis. For the higher electrical conductivities, particularly for n-type Bi_2Te_3 at low temperatures, for which the widest range of degree of degeneracy has been covered, the predicted curvature may be seen. For samples showing mixed conduction, the thermal conductivity rises sharply as expected.

§ 3. THERMAL CONDUCTIVITY OF EXTRINSIC p-TYPE Bi_2Te_3

The interpretation of the results for p-type Bi_2Te_3 is simpler than for n-type material, so a consideration of the latter will be deferred until the next section.

In order to calculate the electronic component of the thermal conductivity, the Lorenz number L, defined by

$$\kappa_e = L\sigma T, \qquad \ldots\ldots(3)$$

must be related to the Fermi potential. The Lorenz number is given by (Wilson 1953)

$$L \equiv A\left(\frac{\boldsymbol{k}}{\boldsymbol{e}}\right)^2 = \frac{1}{\boldsymbol{e}^2T^2}\left\{\frac{K_3}{K_1} - \left(\frac{K_2}{K_1}\right)^2\right\} \qquad \ldots\ldots(4)$$

where

$$K_n = \frac{16\sqrt{2}\pi m^{*1/2}}{3\boldsymbol{h}^3}\int_0^\infty \tau(E)E^{n+1/2}\frac{\partial f_0(\eta)}{\partial E}\,dE, \qquad \ldots\ldots(5)$$

$f_0=\{1+\exp(x-\eta)\}^{-1}$, E = kinetic energy of charge carriers, $E/\boldsymbol{k}T=x$, η = reduced Fermi potential, m^* = effective mass of charge carriers, τ = relaxation time of charge carriers. The integrals K_n may be related to the integrals F_r where

$$F_r(\eta)=\int_0^\infty x^r f_0\,dx.$$

As pointed out in G these integrals have only been published for integral and half-integral values of r, whereas substitution of the appropriate energy dependence of the relaxation time for holes and electrons in Bi_2Te_3 yields values of r which are not integral or half-integral. Expressing the relaxation time as

$$\tau(E)\propto E^{q/2}, \qquad \ldots\ldots(6)$$

it was shown in G that the appropriate values of q are $-1{\cdot}44$ for n-type Bi_2Te_3 and $-1{\cdot}88$ for p-type material. In terms of the tabulated Fermi-Dirac integrals (McDougall and Stoner 1938, Rhodes 1950) which are closest to those which would correspond to these values of q, it is found that

$$L=\left(\frac{\boldsymbol{k}}{\boldsymbol{e}}\right)^2\left\{3\frac{F_2}{F_0}-4\left(\frac{F_1}{F_0}\right)^2\right\} \quad \text{for } q=-1$$

$$L=\left(\frac{\boldsymbol{k}}{\boldsymbol{e}}\right)^2\left\{5\frac{F_{3/2}}{F_{-1/2}}-9\left(\frac{F_{1/2}}{F_{-1/2}}\right)^2\right\} \text{for } q=-2. \qquad \ldots\ldots(7)$$

In figure 5 the numerical factor A in the Lorenz number has been plotted against the reduced Fermi potential η over the range of partial degeneracy. The top and bottom curves represent the values of A calculated for $q=-1$ and -2 respectively. Now, at the non-degenerate limit the Lorenz number is a linear function of q, while at the degenerate limit it is independent of q. It was, therefore, considered reasonable to use a linear interpolation to determine the Lorenz number in the intermediate range for $q=-1{\cdot}44$ or $q=-1{\cdot}88$, corresponding to n-type and p-type Bi_2Te_3 respectively. The results of the interpolation are represented by the two inner curves of figure 5.

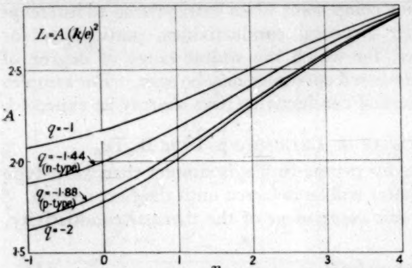

Figure 5. Numerical factor in Lorenz number against reduced Fermi potential.

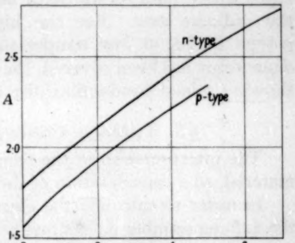

Figure 6. Numerical factor in Lorenz number against electrical conductivity.

The Lorenz number may, therefore, be obtained in terms of the electrical conductivity, using the dependence of the latter on the thermoelectric power as determined experimentally, and using figure 6 of G to relate the thermoelectric power to the reduced Fermi potential. Plots of the numerical factor A plotted against the electrical conductivity for n-type and p-type Bi_2Te_3 are shown in figure 6. This pair of curves covers the complete temperature range since it is found that the dependence of the thermoelectric power on the electrical conductivity hardly changes with temperature.

In figures 1 to 4 the theoretical variation of the electronic component of the thermal conductivity with the electrical conductivity has been compared with the experimental variation for p-type material, on the assumption that the lattice component is independent of the electrical conductivity. The theoretical curves, represented by the solid lines, fit the experimental results very closely, except in the range of mixed conduction. It seems, therefore, for p-type Bi_2Te_3 that the lattice component of the thermal conductivity is independent of the electrical conductivity, and that, qualitatively at least, the assumptions used in G to obtain the scattering law are sound.

§ 4. THERMAL CONDUCTIVITY OF EXTRINSIC n-TYPE Bi_2Te_3

4.1. *Halogen-Doped* Bi_2Te_3

Following the same theoretical procedure as for p-type material, but using the scattering law based on the slightly different temperature dependence of the mobility for electrons as compared with holes, the electronic thermal conductivity for n-type Bi_2Te_3 was also obtained in terms of the electrical conductivity. Using the values of the lattice component which were the best fit for p-type material, and which also corresponded to the limit, $\sigma \to 0$, for extrinsic n-type material, the theoretical dependence of the total thermal conductivity on the electrical conductivity was obtained. This is represented in figures 1 to 4 by the broken lines, the top curve in each case. It is immediately apparent that the experimental results do not fit these curves; at each temperature the experimental curve for n-type Bi_2Te_3 lies below that for the p-type material, whereas theoretically the p-type curve should be lower.

A possible explanation of this discrepancy is that the assumptions upon which the theoretical dependence of the electronic thermal conductivity on the electrical conductivity is based, may be false. For example, it has been assumed in G that the mean free path for carriers of a certain energy is inversely proportional to the absolute temperature. If this is incorrect, a different scattering law would apply. However, in view of the good agreement with theory for p-type Bi_2Te_3, such a gross error in the assumptions, as is needed to explain the experimental results, appears unlikely.

An alternative explanation is that the lattice component of the thermal conductivity may not be independent of the electrical conductivity for n-type Bi_2Te_3. This could arise from electron–phonon interaction or from scattering of phonons by impurities.

Before one or other of the explanations of the discrepancy in the thermal conductivity can be discarded it is essential that the electronic component and the lattice component are separated, preferably by experiment. For metals, such a separation has been carried out by measuring the magneto-resistance and magneto-thermal resistance effects (Makinson 1938), but for Bi_2Te_3 the accuracy of such a method would not be high. The predominance of the lattice component of the thermal conductivity, particularly at low temperatures where the magneto-resistance measurements should be carried out, indicates that the proportional change in the total thermal conductivity under a magnetic field would be small.

Fortunately, another method for separating the components of the thermal conductivity has become available. This method involves measurements on alloys of Bi_2Te_3 and Sb_2Te_3 and will be discussed in detail at a later date.

Briefly, it is found for these alloys that the dependence of thermoelectric power on electrical conductivity is the same as for Bi_2Te_3. However, the lattice thermal conductivity of the alloys is lower than for Bi_2Te_3, so that any extra phonon-scattering processes are of less importance. Thus a comparison of the plots of thermal conductivity against electrical conductivity, for Bi_2Te_3 and a bismuth–antimony telluride alloy, enables any variation of the lattice thermal conductivity with electrical conductivity to be detected. In particular, the fact that such plots, at a given temperature, for p-type material, are parallel to one another confirms that in this case there are no appreciable extra scattering processes. However, for n-type material, the measurements on the alloys have shown that the lattice thermal conductivity is dependent on the electrical conductivity.

The next step is to determine whether the extra scattering of phonons for halogen-doped n-type Bi_2Te_3, is due to collisions with electrons or impurities. Some clue should be given by the temperature dependence of the extra thermal resistivity. If it is assumed that the thermal resistivities, due to different scattering mechanisms, are additive, we may write

$$\frac{1}{\kappa_1(\sigma)} = \frac{1}{\kappa\,(0)} + R \qquad \ldots\ldots (8)$$

where $\kappa_1(\sigma)$ is the lattice thermal conductivity for an electrical conductivity σ and $\kappa_1(0)$ the lattice thermal conductivity for $\sigma = 0$. R = extra-thermal resistivity. Now, assuming the electronic thermal conductivity to be given by the theoretical calculations, as was the case for p-type material, the difference $\{\kappa_1(0) - \kappa_1(\sigma)\}$ is simply the difference between the curves represented by the broken lines and the dotted lines in figures 1 to 4. Thus, knowing $\kappa_1(0)$, it was possible to evaluate the extra-thermal resistivity R at each temperature. Figure 7 shows this extra thermal resistivity, for a fixed carrier concentration, plotted against temperature. ter Haar and Neaves (1956) have shown that for semiconductors, above the Debye temperature, the thermal resistivity should be proportional to $T^{-3/2}$ for phonon–electron scattering, and independent of temperature for phonon–impurity scattering. Stratton (1957) has shown that phonon–electron scattering above the Debye temperature should be negligible. In figure 7 the extra thermal resistivity is only slightly dependent on temperature and it is concluded that it is the result of scattering of phonons by impurity centres.

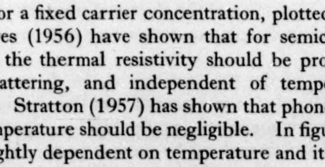

Figure 7. Extra-thermal resistivity against temperature, corresponding to an arbitrary, constant halogen concentration.

4.2. *Non-Halogen-Doped* Bi_2Te_3

All the n-type Bi_2Te_3 which has so far been mentioned has contained either iodine or chlorine as the donor impurity. There was no difference between the thermal conductivity curves for either of these impurities, so, in view of the very different atomic weights of iodine and chlorine, it would appear that it is the position of the impurity in the lattice which is important.

Now there are donor impurities, other than the halogens, which are soluble in Bi_2Te_3, and it would be most unexpected if all these impurities were as effective in scattering phonons as the halogens appear to be. Therefore thermal conductivity measurements have been made on n-type ingots doped with tellurium, lithium and aluminium. The results of these measurements, at 150°K, 200°K, 250°K and 300°K, are shown in figure 8. For each temperature the lower curve (full line) represents the plot of thermal conductivity against electrical conductivity for halogen-doped Bi_2Te_3, while the upper curve (broken line) represents the theoretical variation of the electronic component assuming the lattice component to be constant. The experimental results for the non-halogen-doped ingots lie very close to the upper, theoretical curves, indicating the absence of any appreciable extra thermal resistance. These results confirm the validity of the assumptions used in G in obtaining the scattering law for n-type material.

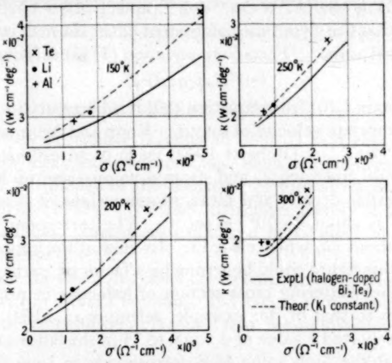

Figure 8. Thermal conductivity of n-type Bi_2Te_3 doped with tellurium, lithium and aluminium.

4.3. *Effective Scattering Cross Section for Halogens*

It is interesting to estimate the effective scattering cross section for halogen, and other impurity atoms in a similar way to that used by Joffe and Joffe (1954) for impurities in germanium and lead telluride. By analogy with the kinetic theory of gases, an effective cross section S for impurities, given by $S=\phi a^2$, is employed, where, for a simple cubic lattice, a is equal to the lattice constant, and thus, a^2 is the physical cross-sectional area of a lattice site. For Bi_2Te_3 it seems reasonable to use a mean interatomic spacing for a, that is about 3 Å. ϕ is a multiplying factor which depends on the position of the impurity in the lattice.

If N_i is the impurity concentration and N_0 the total atomic concentration, N_i being very much less than N_0, a phonon mean free path l_T given by

$$\frac{1}{l_T}=\frac{1}{l_T(0)}+\frac{N_i\phi}{N_0 a} \qquad \ldots\ldots(9)$$

is applicable. $l_T(0)$ is the mean free path in the absence of impurities. Now, the lattice component of the thermal conductivity is given by

$$\kappa_{\phi l} = \tfrac{1}{3} c v l_T \qquad \ldots\ldots(10)$$

where c = specific heat per unit volume and v = velocity of sound. Thus, it is found that

$$\frac{\kappa_l(0)}{\kappa_l} = 1 + \frac{N_1}{N_0} \phi \frac{l_T(0)}{a} \qquad \ldots\ldots(11)$$

For n-type Bi_2Te_3, with an electrical conductivity of 3×10^3 ohm^{-1} cm^{-1} at 300°K, it is estimated that the proportional concentration of halogen, N_1/N_0 is about 0·002. $\kappa_l(0)$ is 0·0157 w cm^{-1} deg^{-1} and $\{\kappa_l(0) - \kappa_l\}$ is 0·0023 w cm^{-1} deg^{-1}, assuming that the electronic component of the thermal conductivity agrees with the theoretical value. Then from equation (11) it is found that

$$0{\cdot}002 l_T \phi / a \simeq 0{\cdot}17.$$

In order to obtain $l_T(0)$ from equation (10) it is necessary to know the specific heat and the appropriate velocity of sound. Kopp and Neumann's modification of Dulong and Petit's law (Roberts 1940) leads to an estimate for the specific heat, c, of 1·2 joule cm^{-3} deg^{-1}, and, from a comparison of Bi_2Te_3 with other compounds of similar density and mean atomic weight, it is estimated that the velocity of sound is about 2×10^5 cm sec^{-1}. The corresponding value of $l_T(0)$ is about 20 Å, or about $7a$, whence $\phi \simeq 13$. In view of the approximations which have been made this figure could be wrong by a factor of, perhaps 2. It is, however, clear that the scattering cross section of halogens in n-type Bi_2Te_3 has a similar high value to that of, for example, selenium in Al Sb or GaSb. Joffe and Joffe (1954) reported a value of ϕ equal to 15 in the latter case. Joffe (1956) has suggested that the high value of ϕ corresponds to impurities entering the lattice interstitially.

If it is supposed that the other impurities have values of ϕ approximately equal to unity, then, even for the most highly doped material, a reduction of less than 1% in the thermal conductivity would be expected; this, being smaller than the experimental error, is, therefore, undetectable.

§ 5. LATTICE COMPONENT OF THE THERMAL CONDUCTIVITY

The close fit of the experimental results, for p-type Bi_2Te_3 and non-halogen-doped n-type Bi_2Te_3, to the theoretical variation of the electronic thermal

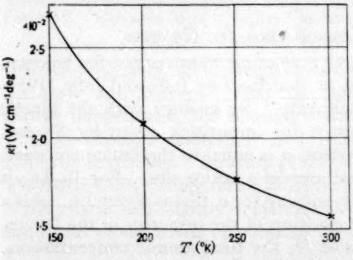

Figure 9. Lattice component of the thermal conductivity of Bi_2Te_3 against temperature.

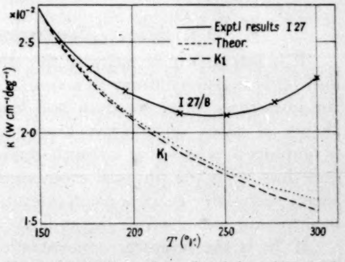

Figure 10. Thermal conductivity of intrinsic Bi_2Te_3. The dotted line shows the theoretical variation assuming normal Lorenz number.

conductivity with the electrical conductivity makes the identification of the lattice component with the thermal conductivity, extrapolated to $\sigma=0$ from the extrinsic range, quite reliable. In figure 9 the lattice thermal conductivity obtained in this way has been plotted against temperature, and may be seen to decrease with rise of T over the range covered by the experiments. However, the rate of decrease of the lattice conductivity with temperature follows neither the inverse temperature law of Peierls (1929), nor an inverse $(T-\theta/3)$ law as suggested by Joffe and Joffe (1956)

The values for the lattice component of the thermal conductivity, shown in figure 9 of 0·0268 and 0·0157 w $\mathrm{cm}^{-1}\,\mathrm{deg}^{-1}$ at 150°K and 300°K respectively, are somewhat lower than the values of 0·034 and 0·017 w $\mathrm{cm}^{-1}\,\mathrm{deg}^{-1}$ reported by Satterthwaite and Ure (1957).

§ 6. INTRINSIC Bi_2Te_3

It has been shown previously (Goldsmid 1956 b) that the rise of thermal conductivity for low electrical conductivities, shown in figures 2 to 4, agrees quantitatively with the theory of the transport of ionization energy by charge carriers given by Price (1955). We shall, therefore, merely show here that the use of the semiconductor parameters calculated in G gives an even closer fit between theory and experiment.

If the expressions for the Soret effect coefficients given in a later paper (Price 1956) are substituted in Price's equation, and taking into account the variation of energy gap ϵ_g with temperature, it is found that, for an intrinsic semiconductor,

$$\left[\frac{\kappa_e}{\kappa_k}\right]_i = 1 + \frac{\mu_n\mu_p}{(\mu_n+\mu_p)(A_n\mu_n+A_p\mu_p)}\left\{\frac{(\epsilon_g)_0}{\boldsymbol{k}T}+A_n+A_p\right\}\left\{\frac{\epsilon_g}{\boldsymbol{k}T}+A_n+A_p\right\} \qquad \ldots\ldots(12)$$

where μ is the carrier mobility and $(\epsilon_g)_0$ is the energy gap at the absolute zero. The subscripts n and p are used to denote electrons and holes respectively. κ_k is the value of the electronic component of the thermal conductivity which would be applicable if the transport of ionization energy could be ignored. Its value, for intrinsic material, is given by

$$(\kappa_k)_i = \frac{A_n\mu_n + A_p\mu_p}{\mu_n+\mu_p}\,\frac{\boldsymbol{k}^2}{\boldsymbol{e}^2}\,\sigma_i T. \qquad \ldots\ldots(13)$$

A comparison of the experimentally determined value of the electronic component of the thermal conductivity at 300°K, for intrinsic Bi_2Te_3, with the value calculated from equation (13), substituting the parameters determined in G, gives

$$\left[\frac{\kappa_e}{\kappa_k}\right]_i = 12{\cdot}8$$

If it is assumed that $(\epsilon_g)_{300}-(\epsilon_g)_0$ is equal to about $-0{\cdot}04$ev in accordance with infra-red transmission measurements (Austin, private communication), and substituting the values of A_n and A_p at the non-degenerate limit as given in figure 6, and the value for the mobility ratio μ_n/μ_p determined in G, it is found that equation (12) is satisfied by putting $(\epsilon_g)_0=0{\cdot}17$ev. This value agrees very closely with that obtained by electrical and optical methods (cf. table 1 of G).

§ 7. CONCLUSIONS

The electronic component of the thermal conductivity in the extrinsic range has been calculated and there has been good agreement between theory and experiment. The lattice component has been found to remain constant, at a given temperature, over the whole range of electrical conductivity, for all the p-type material and for n-type material that was not doped with one of the halogens. However, for halogen-doped n-type Bi_2Te_3, the lattice thermal conductivity has been found to vary with the electrical conductivity and this has been shown to be consistent with a high cross section for scattering of phonons by halogen atoms in Bi_2Te_3. This suggests that they may enter the lattice interstitially.

The lattice thermal conductivity of Bi_2Te_3 decreases with rise of temperature but the decrease does not follow either the traditional $1/T$ law or the $1/(T-\theta/3)$ law of Joffe and Joffe.

Measurements on intrinsic Bi_2Te_3 have shown complete agreement with the theory of transport of ionization energy by charge carriers.

ACKNOWLEDGMENT

The author wishes to express his appreciation to Mr. A. R. Sheard who is responsible for the preparation of bismuth telluride and related compounds and has prepared all the material used in these investigations.

REFERENCES

FRÖHLICH, H., and KITTEL, C., 1954, *Physica*, **20,** 1086.
GOLDSMID, H. J., 1956 a, *Proc. Phys. Soc.* B, **69,** 203; 1956 b, *Report of Rugby Conference on Semiconductors* (London : Physical Society), p. 127; 1957, *Ph.D. Thesis*, University of London; 1958, *Proc. Phys. Soc.*, **71,** 633.
TER HAAR, D., and NEAVES, A., 1956, *Advanc. Phys.*, **5,** 241.
JOFFE, A. F., 1956, *Canad. J. Phys.*, **34,** 1342.
JOFFE, A. V., and JOFFE, A. F., 1954, *Dokl. Akad. Nauk SSSR.*, **98,** 757; 1956, *Izv. Akad. Nauk SSSR, Ser. Fiz.*, **20,** 65.
MAKINSON, R. E. B., 1938, *Proc. Camb. Phil. Soc.*, **34,** 474.
MCDOUGALL, J., and STONER, E. C., 1938, *Phil. Trans. Roy. Soc.*, **237,** 67.
PEIERLS, R., 1929, *Ann. Phys., Lpz.*, **3,** 1055.
PRICE, P. J., 1955, *Phil. Mag.*, **46,** 1252; 1956, *Phys. Rev.*, **102,** 1245.
RHODES, P., 1950, *Proc. Roy. Soc.* A, **204,** 396.
ROBERTS, J. K., 1940, *Heat and Thermodynamics*, 3rd Edn (Glasgow: Blackie), p. 163.
SATTERTHWAITE, S. B., and URE, R. W., Jr., 1957, *Phys. Rev.*, **108,** 1164.
STRATTON, R., 1957, *Phil. Mag.*, **2,** 422.
WILSON, A. H., 1953, *The Theory of Metals*, 2nd Edn (Cambridge: University Press).

Semiconductor Noise as a Queuing Problem

By D. A. BELL

Electrical Engineering Department, University of Birmingham

MS. received 28th December 1956, and in revised form 3rd February 1958

Abstract. The outstanding problem of semiconductor noise is to account for a power spectrum of which the intensity appears to increase without limit as the frequency is decreased. There is no simple explanation in terms of relaxation times for a spectrum which is proportional to a constant power of frequency over many decades and which is found in a wide range of different materials. But it can be explained if the rate at which carriers leave the conduction band is treated as a queuing problem rather than a relaxation problem. The phenomenon in question is related to the presence of current, which implies that the carriers are swept away from the neighbourhood of the centres from which they originated, and the time to recombination is governed by the time taken to find a vacant centre elsewhere, not by the probability of falling back to the originating centre.

---

§ 1. Introduction

Existing theories of the origin of the $1/f$ spectrum of current noise in semiconductors have been based on the hypothetical relaxation times of specific mechanisms, whether diffusion, trapping or any other mechanism. But from an earlier review of the experimental evidence (Bell 1955) it seemed probable that the immediate source of noise is a general random fluctuation in numbers of charge carriers in the conduction band, resulting from the basic generation and re-combination processes. The location of the noise in the bulk conduction, not in contact surfaces, has since been supported by the similarity between conduction noise and Hall effect noise (Brophy and Rostoker 1955) and indirectly by the finding that in compressed graphite powder the interfaces between grains contribute little to the total resistance (Lewis, Orr and Ubbelohde 1957). The widespread occurrence of the typical spectral distribution, namely power spectrum proportional approximately to $1/f$, makes it improbable that specific mechanisms are involved. This view has also been expressed by Blanc-Lapierre and Nifontoff (1956) in the following words: " La forme du spectre est fort probablement beaucoup plus directement liée à des modèles statistiques généraux qu'à un mécanisme physique très particulier ". (It must be remembered, however, that in a simple relaxation model of excitation of charge carriers from a base level to the conduction band and subsequent recapture, the thermodynamic argument that the probability of a carrier being in the conduction band is proportional to exp $(-V/\boldsymbol{k}T)$ where V is the excitation energy, implies that, other things being equal, a long life in the conduction band is associated with a *small* excitation energy. There is thus no energetic difficulty in postulating long lifetimes.) In terms of relaxation times, the $1/f$ spectrum demanded a *uniform* spread of time constants over a greater range than the periods of the highest and lowest observed spectral components. e.g. from 1 μsec to a period greater than 10^3 sec. The mean lifetime should then be of the order of 1000 seconds, and no explanation has been offered of the discrepancy between this value and the value of the order of microseconds which is commonly found for the only directly observable lifetime, namely that of injected carriers. This discrepancy, as well as the ubiquity of the $1/f$ spectrum, is very simply explained by treating the fluctuations in number of carriers in the conduction band in terms of the theory of queues.

§ 2. APPLICATION OF QUEUING THEORY

For the study of problems of congestion and delay, a *queue* is a collection of individuals awaiting service, and arises from a temporary or permanent excess of the rate at which individuals demand service over the rate at which service is available. Some American authors speak of such a collection of individuals being *in a corral*, instead of their constituting a queue, so as to avoid the implication of *sequence* which is sometimes carried by *queue*. But the word *queue* will be used in this paper, whether or not some sequence is preserved amongst the individuals in waiting.

The problem of waiting time in a queue which is served in sequence by a number of outlets has been studied in relation to problems of telephone exchanges and formulae have been published by Erlang (1917) and Fry (1928). More recently, formulae have been deduced for the distribution of waiting times in a random service queue, i.e. a queue in which the sequence in which individuals are served is random and is uncorrelated with the sequence in which they arrived in the queue. Graphs have been published by Riordan† (1953) and Wilkinson (1953) for the expected distribution of delays with random service and mean calling rates less than the mean service rate, and a general formula for the expected delay had previously been given by Pollaczek (1946).

The following postulates of the telephone problem can be taken over into the present problem: (i) members of the queue arrive independently and at random, but with a probability which is uniform in time, (ii) the x available service outlets are indistinguishable from each other, (iii) when a member of the queue finds a vacant outlet, it occupies it for a time which is described statistically as an exponential distribution of holding times:

The semiconductor noise problem is represented as a queuing problem by the following system of equivalences:

(i) The charge carriers in the conduction band constitute the queue.

(ii) The members of the queue join it at random times as a result of excitation from the base levels, this excitation being generally a random process.

(iii) The ' service outlets ' are vacant base levels to which the charge carriers can return (or possibly re-combination centres if there are any restrictions on the method of return of a carrier from the conduction band to a base level).

(iv) The duration of occupation of a service outlet is the interval from the time at which a base level is re-occupied by a carrier to the time at which it becomes vacant again as a result of excitation of the carrier out of that base level into the conduction band again. The duration of this interval is assumed to be described statistically by an exponential distribution with mean value fixed by the excitation energy through the thermodynamic relationship between ' free ' and ' bound ' times. (This relation gives a proportionality only, the actual time depending also on the ' jump frequency ' of the relaxation process.)

† The author is indebted to one of the referees for bringing this work to his notice.

In theories in which the time constants are associated with the relaxation times of specific excitation or trapping processes, the further use of the thermodynamic argument has implied an equilibrium excitation–re-combination system, with either a detailed one-to-one relation between carriers and vacant base levels or a large excess of vacancies so that carriers had a uniform probability of being recaptured. Neither of these hypotheses can be valid. Taking first the suggestion of a liberal supply of vacancies, one has only to remark that in an electrically neutral substance, vacancies are caused by the excitation of carriers into the conduction band; the total number of vacancies is therefore always precisely equal to the *total* number of carriers in the conduction band. But it does not follow that there is a detailed one-to-one correspondence, because in the presence of an applied field (the only condition in which current noise can be observed) a carrier will certainly be removed from the vicinity of the site from which it was excited, and even in the absence of an applied field it is likely to depart by thermal diffusion unless there is some local binding force, and the latter would be contrary to the concept of a conduction band. The model then is that any small region of the semiconductor contains (*a*) the number of vacancies created by those excitations of carriers into the conduction band which occur in that region, and (*b*) a number of carriers governed by the number of excitations which occur in itself and in other adjacent regions. Although the two numbers have equal average values, they will not tally precisely at all times. We thus have precisely the type of situation which has been studied by the telephone engineer: although the number of service outlets matches the number of demands in terms of overall average, there are local variations which can lead to congestion and cause some members of the resulting queue to wait for times which bear no obvious relation to the times of the service processes.

Let the unit of time be the average of the exponential distribution of holding times, x the number of service outlets, i.e. of base-level sites for electrons including those temporarily occupied, and y the rate at which carriers are excited into the conduction band. With our normalized time-unit, x is also the rate at which carriers are withdrawn from the conduction band.

Then queuing theory shows that for any queuing system (regardless of the order of service) the mean waiting time is proportional to $(x-y)^{-1}$ and hence tends to infinity as x approaches y. Thus it follows automatically that if the semiconductor has equal rates of loss from the conduction band and gain into it, the time spent by an individual carrier in the conduction band may have any value up to infinity.

§ 3. THE RANDOM SERVICE QUEUE

If the queue has sequential service and an exponential distribution of times of occupation of the service outlets, it has been shown (Erlang 1917, Fry 1928) that the waiting times in the queue are also distributed exponentially. The probability of a delay in the range $(t, t+dt)$ is found to be

$$P(t, t+dt) = \text{const.}\ (x-y) \exp\left[-(x-y)\,t\right] dt \qquad \ldots\ldots(1)$$

When $x \to y$ the exponential factor in (1) tends to unity, giving equal probabilities for all delays between zero and infinity. The same result may be held to apply even more strongly in a random service queue. Consider a queue which is growing uniformly but receiving no service up to time T when random service commences. Then it is clear that (*a*) those members of the queue which are served have waiting times distributed uniformly over 0 to T, and (*b*) the removal of this uniform sample does not affect the distribution of the remainder at time T.

Now consider a system which has been in equilibrium for a long time under the condition of sequential service described by (1), and suppose that at an arbitrary instant a small part of the service is changed from sequential to random. Then according to (1) with $x = y$ the queue contains a uniform distribution of waiting times from zero to infinity, and extracting a random sample will not alter this distribution. Similarly, changing the remainder of the service from sequential to random will make no difference to the distribution. Hence a random service queue with equal rates of gain and loss contains a uniform spread of waiting times described by

$$P(t, t+dt) = \text{const. } dt. \qquad \ldots\ldots(2)$$

Since the given population has now been spread over an infinite range of the variable, the probability density must tend to zero; and this is indicated by the multiplying factor $x - y$ in (1). At this stage the probability distribution might be regarded as indeterminate, since little can be deduced from the statement that the probability is spread with zero density over an infinite range of the variable. But the important point is that there is now a clear possibility of infinite delays and hence of infinitesimal frequencies in the corresponding spectrum.

§ 4. THE POWER SPECTRUM OF THE PHENOMENON

Pollaczek (1946) has given a formula for the distribution of delay times in a random-service system having a large number of outlets but a mean calling rate less than the mean service rate. In his notation the expectation of a delay at least t is

$$A(t) = -\pi (2b\theta)^{1/2}\{1 + \pi^{1/2} b \exp(-b^2)[1 + \Phi(b)]\}^{-1} \mathrm{H}_1^{(1)}[2i(2b\theta)^{1/2}]\{1 + \mathrm{O}(S^{-1/2})\}. \qquad \ldots\ldots(3)$$

In this formula Φ is the Gaussian integral, $\mathrm{H}_1^{(1)}$ a Hankel function, S the number of service outlets available, η the average calling rate per outlet, $b = (1-\eta)(S/2)^{1/2}$ and $\theta = t(S/2)^{1/2}$. If one regards $A(t)$ as the expectation that a charge carrier which entered the conduction band at $t = 0$ will still be there at time t, the autocorrelation function of the conductivity pulse constituted by that charge carrier will be

$$\psi(\tau) = \int A(t)\, A(t+\tau)\, dt$$

and in principle the corresponding power spectrum is obtainable by evaluating $\psi(\tau)$ as a function of τ and then taking the cosine Fourier transform of this function. The writer is unable to see any practical way of carrying out these analytic operations for the given form of $A(t)$, or even for the simplified form resulting from the following tentative approximation.

Just as there is the physical problem of bounded total energy in admitting the existence of a $1/f^\alpha$ power spectrum, so there is the mathematical dilemma that it appears impossible for a $1/f^\alpha$ spectrum to arise as the transform of a correlation function because its integral would not converge. There are two possible means of escape. One can suppose that $1/f^\alpha$ is not analytically rigorous—the non-integral value of α in some cases tells against a simple analytic basis—and that one is in fact looking at the limiting case of some such function as $(f^{2\alpha} + \beta)^{-1/2}$ with $\beta \to 0$. Alternatively, one can adopt the postulate of van der Ziel (1950) that the observed spectrum is not the transform of the correlation function of a single phenomenon, but of an infinite series of phenomena. It is shown at the end of this section that the queuing analysis lends itself to representation by an infinite series of components.

In the semiconductor problem $S \to \infty$ and $\eta \to 1$. The product $(1-\eta)S$ is the numerical value of the 'spare capacity'. If we suppose that $(1-\eta)S$ remains a finite quantity, Z say, which is characteristic of the mechanism of the semiconductor in question, the limiting form of $A(t)$ will be

$$A(t) \simeq -\pi (Zt)^{1/2} \mathrm{H}_1^{(1)} [2i(Zt)^{1/2}]. \qquad \ldots\ldots(4)$$

The function $\mathrm{H}_1^{(1)}(x)$ is tabulated by Jahnke and Emde (1945) for x up to 16 and for very large values of x one can use the asymptotic approximation (McLachlan and Meyers 1936, Magnus and Oberhettinger 1949)

$$\mathrm{H}_1^{(1)}(ix) \simeq -(2/\pi x)^{1/2} \mathrm{e}^{-x}. \qquad \ldots\ldots(5)$$

Applying this to (4) the limiting approximation for $A(t)$ when Zt is large is

$$A(t) \simeq \pi^{1/2} (Zt)^{1/4} \exp\,[-2(Zt)^{1/2}]. \qquad \ldots\ldots(6)$$

It is obvious that $A(t)$ decreases much more slowly than the customary negative exponential in t, which is consistent with the spectrum varying less rapidly with frequency than the simple relaxation spectrum, i.e. it is qualitatively consistent with a tendency towards $1/f$ rather than $1/f^2$. The low-frequency limit to be expected depends on the value of the time scale-factor Z, the physical significance of which has not yet been identified.

If the form of spectrum corresponding to (3) can be evaluated for η less than 1 this will be useful as providing a direction of approach to the limiting case. There is always the analytic difficulty that queuing formulae are not valid for the calling rate greater than or equal to the service rate, the inequality giving a definitely divergent size of queue and the equality giving an indeterminate size of which infinity is one of the possible values; and the delay times will behave similarly. But one of the difficulties of finding an analytical interpretation of the semiconductor noise spectrum is that it has precisely this characteristic of an indeterminate solution; the fact that no indication of a low-frequency limit has ever been substantiated experimentally, i.e. that the integral of the spectrum is divergent, means that the distribution of lifetimes is also lacking in convergence as it would be in a queue with equal calling and service rates.

The fluctuations involved are, of course, very small compared with the mean conductivity, and the latter is presumed to be constant. Sufficiently large excursions would presumably involve some restoring force which maintains a constant mean; but in the usual practical order of magnitude the $1/f$ spectrum would have to be extended downwards till the period of oscillation was of the order of millions of years in order to get a few per cent change of conductivity. Hence it is reasonable to regard the observed fluctuations extending over periods of hours, days or months as independent of the mechanism which maintains a constant mean.

Failing the evaluation of the spectrum corresponding to (3), one can suggest that the equi-probable distribution of times found as a limit of formula (1) can be regarded as equivalent to the sum of an infinite set of distributions, each of the set being exponentially distributed and the mean lifetimes of the members of the set being uniformly distributed. As is well known (see, for example, van der Ziel 1950) such a uniform distribution of exponential relaxation functions produces in sum a spectrum which approaches $1/f$ when the range of time constants involved is much greater than the range of frequencies over which the spectrum is to be specified. Hitherto this basis for the $1/f$ spectrum has seemed unrealistic, since it has been supposed that there must be a different physical relaxation process corresponding to each member of the infinite set. The infinite range of equivalent relaxation times is now accepted, because in the present context it is seen to be merely a mathematical fiction, a means of approximating analytically a distribution which strictly speaking has no determinate distribution function.

§ 5. THE APPARENT LIFETIME OF A CARRIER

Formula (1) may be regarded as the resultant of a growth process exp yt and a decay process exp $(-xt)$. If a group of carriers is injected into the conduction band by some means which is independent of the equilibrium processes x and y (e.g. hole injection from an electrode, or photo-excitation) this group will, to a first approximation, be subject to the decay process exp $(-xt)$ independently of statistical equilibrium between the normal growth and decay processes. Measurements of the rate of loss from such groups therefore gives a measure of the time constant of the x process, which by itself has no bearing on the spectral distribution of the current noise. But given also the average proportion of carriers which is at any time in the conduction band, the decay rate makes possible a complete analysis of the process, including the determination of the ' jump frequency '.

§ 6. DEPARTURES FROM EXACT $1/f$ LAW

There is some evidence accumulating to show that an exact $1/f$ law holds when the energy of excitation into the conduction band is not too large compared with the thermal energy (metal films, carbon, flicker noise in emission from oxide-coated cathodes) but that a law $1/f^{\alpha}$ with α a little greater than unity tends to occur when the excitation energy is large compared with the thermal energy (germanium, interface noise in thermionic cathodes). It may be that an appropriate physical interpretation of the constants entering into formula (3) will provide an explanation of a relation between the index of f in the spectrum and the excitation energy of the semiconductor.

§ 7. CONCLUSIONS

The queuing concept explains the existence of a wide and uniform range of lifetimes which is independent of the mechanism of excitation of charge carriers into the conduction band and bears no relation to the observable lifetime of injected carriers. The spectrum of a stable random service queue has not yet been evaluated, but it should show a much wider spread of frequencies than results from an exponential relaxation process; the properties of the queue which has equal calling and service rates, and is analytically indeterminate, are consistent with a $1/f$ spectrum.

REFERENCES

BELL, D. A., 1955, *Brit. J. Appl. Phys.*, **6**, 284.

BLANC-LAPIERRE, A., and NIFONTOFF, N., 1956, *J. Phys. et Radium*, **17**, 230.

BROPHY, J., and ROSTOKER, N., 1955, *Phys. Rev.*, **100**, 754.

ERLANG, A. F., 1917, *Post Office Elect. Engr J.*, **10**, 189.

FRY, T. C., 1928, *Probability and its Engineering Uses* (New York : van Nostrand).

JAHNKE, E., and EMDE, F., 1945, *Tables of Functions* (New York: Dover Publications).

LEWIS, F. A., ORR, J., and UBBELOHDE, A. R., 1957, *Proc. Phys. Soc.* B, **70**, 928.

MACLACHLAN, N. W., and MEYERS, A. L., 1936, *Phil. Mag.*, **21**, 425.

MAGNUS, W., and OBERHETTINGER, F., 1949, *Special Functions of Mathematical Physics* (New York: Chelsea Publishing Co.).

POLLACZEK, F., 1946, *C.R. Acad. Sci., Paris*, **222**, 353.

RIORDAN, J., 1953, *Bell Syst. Tech. J.*, **32**, 100.

WILKINSON, R. I., 1953, *Bell Syst. Tech. J.*, **32**, 360.

VAN DER ZIEL, A., 1950, *Physica*, **16**, 359.

Yield Phenomena in Copper–Arsenic Alloys

By K. SCHRÖDER

Division of Tribophysics, Commonwealth Scientific and Industrial Research Organization,
University of Melbourne, Australia

MS. received 25*th February* 1958

Abstract. The occurrence of strain ageing in single crystals of arsenical copper (0·36% As) has been established by simultaneous determinations of stress–strain curves and changes in electrical resistivity. During yielding the electrical resistance increased more rapidly than normally.

The change in resistance during yielding is explained in terms of Cottrell's model of an impurity atmosphere around dislocations.

---

§ 1. INTRODUCTION

MEASUREMENTS of stored energy by Clarebrough, Hargreaves and West (1955) showed that the manner in which the energy stored during deformation was released from copper during annealing varied markedly with the purity of the material. For copper of commercial purity (99·98% Cu) the stored energy was released in a single peak associated with recrystallization and this release of energy was accompanied by a decrease in electrical resistivity. However, for arsenical copper containing 0·35% As a considerable amount of stored energy was released before recrystallization. In addition, the electrical resistivity behaved in an anomalous manner. The first release of energy was accompanied by an increase in resistivity which reached a maximum before recrystallization and then decreased in the normal manner during recrystallization. Further, the resistivity of cold-drawn wires of arsenical copper decreased during resting at room temperature after drawing (Clarebrough and Hargreaves, private communication).

From these results Clarebrough *et al.* suggested that for the conditions of their experiments the arsenical copper was fully strain-aged before the measurements of stored energy were made. Thus the rearrangement of dislocations responsible for the first release of energy involved dislocations breaking away from their atmospheres of arsenic atoms and a consequent increase in electrical resistivity.

Ardley and Cottrell (1953) found that 1% of zinc was necessary to produce a strong yield drop in copper. However, it was likely that a similar yield drop would be produced with less arsenic since Cottrell, Hunter and Nabarro (1953) have shown that the elastic binding energy of an arsenic atom with an edge dislocation in copper is 0·272 ev whilst that for a zinc atom is 0·125 ev.

The objects of the present experiments were to check whether single crystals of arsenical copper of the same composition as that used by Clarebrough *et al.* showed the yield phenomena characteristic of a strain-ageing system and whether any change in electrical resistivity could be detected during yielding.

§ 2. EXPERIMENTAL

2.1. *Preparation of the Specimens*

The alloy used was prepared by melting electrolytic copper (99·98% Cu) with 0·4% by weight of arsenic in an evacuated silica tube in an induction furnace. The tube was quenched after the melting. The ingot so produced was swaged and then drawn to a diameter of about 2 mm. Single crystals were prepared by the method of Andrade and Roscoe (1937), the graphite-coated wires being heated in evacuated silica tubes by a resistance furnace travelling at 4 cm hr^{-1}. Determinations of the arsenic content of various samples by chemical analysis all lay between 0·35 and 0·37%, indicating that no appreciable segregation had taken place. Spectrographic examination provided the following estimates of minor impurities: tin and silver, 0·0002% each; lead and cobalt, 0·0005% each; bismuth, 0·0001%; tellurium, antimony and silicon, 0·001% each; phosphorus, 0·004%; iron and zinc, 0·002% each; beryllium, aluminium, gallium, chromium and nickel, not detected.

The orientations of the crystals are given in figure 1. They were determined by means of X-ray diffraction patterns of rotating crystals. The crystals were cut into specimens 4–5 cm long, all specimens from the same crystal, i.e. of identical orientation, being given the same number. The specimens were fitted with end loops and current and potential leads by silver soldering.

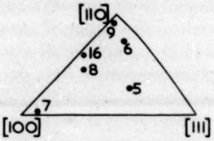

Figure 1. Orientation of specimens.

2.2. *Tensile Tests*

The tensile testing machine was of the Polanyi type, with a hard beam suitable for loads up to 30 kg. The design of the beam was adapted from that devised by Mr. N. A. McKinnon of Aeronautical Research Laboratories, Melbourne. The beam was a cantilever and the load from the specimen was transmitted to it by a rod, yoke and a ball resting in conical seats. The free end of the cantilever was extended beyond the loading point to provide initial mechanical magnification of the movement due to the load. At the free end the usual type of rhomb and mirror fitting was mounted so that optical measurement and photographic recording of the load could be made. The overall magnification was such that 1 mm movement of the light beam at the recorder was equivalent to a change in load of 80 g. A spring was incorporated in the rod connecting the specimen with beam so that a constant pre-load of 200 g could be maintained on the specimen to preserve alignment.

For each specimen the strain rate was kept constant at a value chosen to give an initial rate of shear strain of 4×10^{-5} sec^{-1}. In all tests the temperature was 28·4 ± 0·05°c, but during individual tests the maximum variation was kept to ± 0·02° c, because determinations of electrical resistivity were made simultaneously.

2.3. *Measurements of Electrical Resistivity*

A Kelvin double bridge, similar in principle to that of Lücke (1951), was used to measure the resistance of the specimen R_s. The comparison resistance of the bridge R_c was made of similar material to the specimen and both were submerged, close together, in an oil bath. Thus, a large degree of automatic compensation for changes in temperature was achieved, because the method is essentially a differential one, but only relative values could be found precisely.

The chief modification made to the arrangement of Lücke was in the construction of the comparison resistance which was fitted with a sliding contact so that its resistance could be adjusted equal to that of the specimen before straining. The arms of the Kelvin bridge consisted of four high precision resistances of value 10 ohms and decade boxes variable from 0·1 to 1000 ohms were connected in parallel to two of them so that changes in the resistance of the specimen could be balanced.

The precision of the measurements was affected by changes in temperature of the oil bath, ΔT, because the specimen and comparison resistance differed by 0·04% in arsenic content and because R_s increased during straining. Following Lücke's calculation this difference in composition causes a relative deviation in the measured resistance from the correct value of $\Delta R/R \simeq 10^{-5}$ for $\Delta T = 0{\cdot}02$°c.

The procedure was to make R_s and R_c equal at the start of the test and balance the bridge. During straining no adjustments were made to the bridge, but the deflection of the galvanometer was recorded photographically. The stress was then lowered to the 200 g pre-load and the change in resistance which had occurred was measured by means of the decade box. The specimen was then annealed for 1 hour at 200°c and after cooling to 28·4°c the resistance was measured again and then the value of R_c was adjusted to the new value of R_s. This procedure was repeated several times.

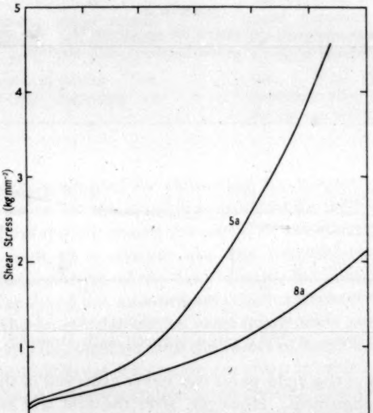

Figure 2. (Shear stress, shear strain) curves for specimens 5a and 8a.

§ 3. RESULTS

3.1. (*Shear Stress, Shear Strain*) *Curves*

The (shear stress, shear strain) curves for the crystals of arsenical copper (figure 2) are similar to those for crystals of pure copper (Diehl 1956) in that they show two distinct linear stages: an easy glide stage followed by a second linear stage of higher rate of hardening.

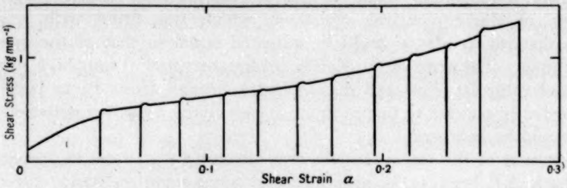

Figure 3. (Shear stress, shear strain) curve for specimen 6. An annealing treatment of 1 hour at 200°c given between each straining.

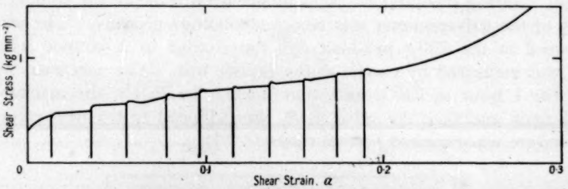

Figure 4. (Shear stress, shear strain) curve for specimen 8b. An annealing treatment of 1 hour at 200°c given between each straining.

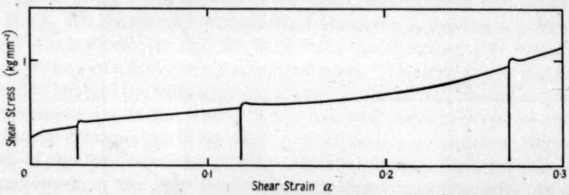

Figure 5. (Shear stress, shear strain) curve for specimen 8c. An annealing treatment of 1 hour at 200°c given between each straining.

A drop in stress at the yield point was never observed in the first test because of imperfect axial alignment. However, after the first test an ageing treatment of one hour at 200°c usually resulted in a yield drop in the second test. Typical (shear stress, shear strain) curves showing yield drops are given in figures 3 to 6. Between each test the crystal was aged for one hour at 200°c. Apart from the initial straining a yield drop was observed in all tests. If a crystal was tested immediately after a yield drop had been observed the yield drop did not appear, but returned again on ageing. An example of this is shown in figure 7.

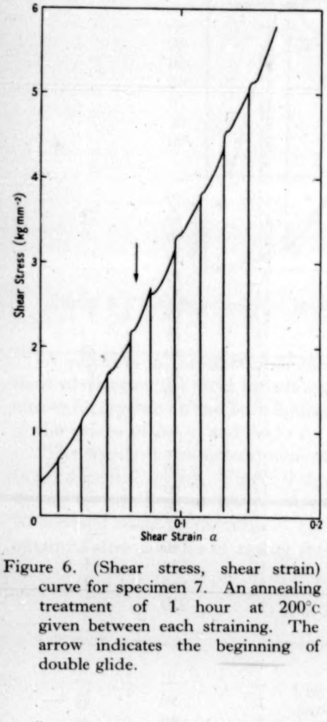

Figure 6. (Shear stress, shear strain) curve for specimen 7. An annealing treatment of 1 hour at 200°c given between each straining. The arrow indicates the beginning of double glide.

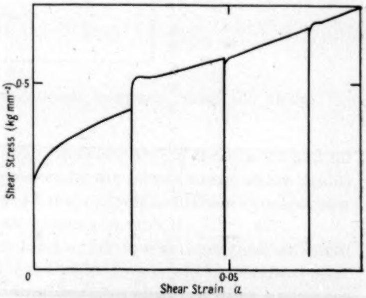

Figure 7. (Shear stress, shear strain) curve for specimen 16. The annealing treatment between the first and second straining was 1 hour at 200°c, and that between the third and fourth straining was 1 hour at 150°c, but the third straining was done immediately after the second straining.

Two methods were adopted for estimating the magnitude of the yield drop. The first of these was to use the actual drop in stress during yielding $\Delta\sigma_1$ (figure 8). The second involved approximating the (shear stress, shear strain) curve beyond the lower yield point by a straight line and extrapolating this back until it intersected the elastic portion of the curve (figure 8). The vertical distance $\Delta\sigma_2$ between this extrapolated line and σ the maximum stress reached was then taken as a measure of the magnitude of the yield drop.

Values of $\Delta\sigma_1$ and $\Delta\sigma_2$ together with the values of $\Delta\sigma_1/\sigma$ and $\Delta\sigma_2/\sigma$ for a number of tests on crystals of different orientation are given in table 1. It can be seen that the variation of $\Delta\sigma_2/\sigma$ with orientation is no greater than the variation obtained in a series of tests on the one crystal. This applies even for orientations which harden very rapidly (figure 6). The arrow in figure 6 indicates the strain at which double glide commenced and the method of von Göler and Sachs (1927)

Table 1

Specimen	Straining	Absolute drop in load		Deviation from linearity		
		$\Delta\sigma_1/\sigma$ (%)	$\Delta\sigma_1$ (g mm^{-2})	$\Delta\sigma_2/\sigma$ (%)	$\Delta\sigma_2$ (g mm^{-2})	$\gamma \times 10^4$
5	1	—	—	—	—	
	2	—	—	2	40	
	3	—	—	3	60	
	4	—	—	3	60	
	5	—	—	3	70	
	6	—	—	2	60	
	7	—	—	3	90	
6	1	—	—	—	—	
	2	—	—	1	10	
	3	2	20	4	40	2¾
	4	¾	10	3	40	—
	5	—	—	2	30	—
	6	—	—	2	30	—
	7	—	—	1¼	20	½
	8	—	—	1	15	1
	9	—	—	1¼	25	½
	10	—	—	2	40	1¾
	11	—	—	¾	20	3
	12	—	—	¾	20	1
7a	1	—	—	—	—	—
	2	—	—	—	—	—
	3	—	—	1⅓	40	—
	4	—	—	1½	60	3
	5	—	—	1½	70	7
	6	—	—	3½	200	8
	7	—	—	2	140	3
	8	—	—	1½	120	4
	9	—	—	1½	140	3
	10	—	—	2	210	3
8b	1	—	—	—	—	—
	2	—	—	—	—	—
	3	—	—	—	—	—
	4	¾	10	3	30	3½
	5	2¼	30	3	40	—
	6	2¼	30	2	25	1½
	7	2¾	40	2½	35	3
	8	1½	20	1½	25	1
	9	1	15	2	30	1
	10	1⅓	20	1⅓	20	2½
	11	2	30	2	30	
8c	1	—	—	—	—	
	2	1	10	1¾	15	
	3	4	50	4	50	
	4	½	10	1¼	20	
9	1	—	—	—	—	
	2	4	60	4	60	

was used to calculate the relation between shear stress and shear strain beyond this point.

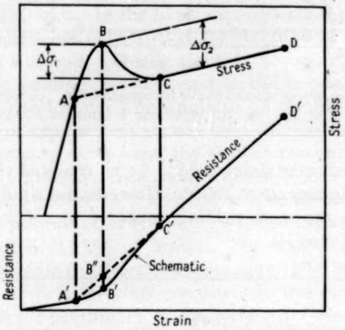

Figure 8. Schematic relation between electrical resistance, stress and strain.

A variation in the amount of shear strain between ageing treatments had no marked effect on the yield behaviour, as shown by the (shear stress, shear strain) curves for crystals 8b and 8c in figures 4 and 5 respectively, and from a comparison of the values of $\Delta\sigma_1/\sigma$ and $\Delta\sigma_2/\sigma$ for these crystals in table 1.

The standard ageing treatment of one hour at 200°c was more than sufficient to produce full ageing. Figure 9 shows that a yield drop could be obtained after ageing for one hour at 100°c. A yield drop was also observed after ageing for 90 hours at room temperature. Table 2 gives the magnitude of the yield drops obtained after a series of ageing treatments for crystal 16.

Table 2. Specimen 16

No. of straining	Annealing before straining	$\Delta\sigma_2/\sigma$ (%)
1	—	—
2	1 hr at 200°c	1
3	immediately after 2nd straining	—
4	1 hr at 150°c	0·7
5	,, 100°c	0·1
6	,, 50°c	—
7	,, 200°c	0·7
8	,, 150°c	0·3
9	,, 100°c	0·2
10	,, 50°c	0·3
11	,, 200°c	0·5
12	,, 150°c	0·15
13	,, 100°c	0·04
14	,, 50°c	—
15	,, 200°c	0·7
16	,, 150°c	0·6
17	,, 100°c	0·17

Straining between annealing is, on average, 0·87%.

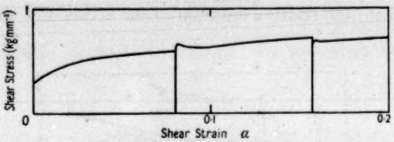

Figure 9. (Shear stress, shear strain) curve for specimen 9. Annealing treatment between first and second straining 1 hour at 200°c.

For single crystals containing 0·35% As no repeated yielding was observed for temperatures of testing up to 200°c. However, for a polycrystalline specimen containing 4·1% As repeated yielding appeared at 156°c and was marked at 178°c as shown in figure 10.

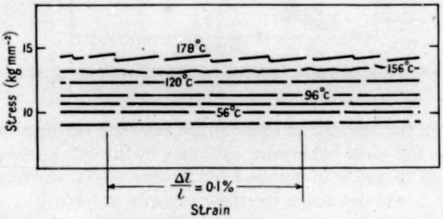

Figure 10. Part of the original photographic stress–strain trace. The straining of a polycrystalline copper wire containing 4·1% arsenic was done in an oil bath, whilst the temperature was gradually increased. The strains at the positions where the temperatures are indicated are as follows:

Temperature (°c)	56	96	120	156	178
Strain (%)	0·9	2·2	2·7	3·5	4·0

3.2. *Resistance Measurements*

The relation between the resistance–strain curve and the stress–strain curve is shown schematically in figure 8. Both curves begin and end with linear stages, but in the range of strain in which yielding occurs the stress and the resistance are not linear functions of the strain. The maximum deviation from linearity in the resistance–strain curve occurs at B′ and B′ corresponds with the maximum stress B within the experimental error $\Delta l/l \simeq 10^{-4}$. Since the maximum deviation from linearity in the resistance–strain curve coincides with the yield point this will be referred to as the 'electrical yield point'. For specifying the magnitude of this electrical yield point the ratio γ of the deviation of resistance from linearity at the yield point (B′B″) to the resistance at the yield point was used. Values of γ for several tests on crystals of different orientation are given in table 1.

No electrical yield point was observed with a crystal of commercially pure copper (99·98% Cu) tested under identical conditions so that the results obtained with the crystals of arsenical copper are not associated with the technique of measurement.

§ 4. DISCUSSION

There is quantitative similarity between the yield phenomena reported here for arsenical copper crystals and those observed by Ardley and Cottrell (1953) in copper containing 1% zinc. In the latter experiments the procedure differed from the present experiments only in that the duration of annealing at 200°C was two hours instead of one. This is unlikely to be important because, in specimen 9 (figure 9), yielding was observed in the present experiments after annealing for one hour at 100°C. The similarity in the magnitude of the yield drop in the two sets of experiments should be attributed to the compensating effects of the larger binding energy and the smaller percentage of solute in the copper–arsenic alloys. Further, Ardley and Cottrell (1953) observed jerky flow in copper specimens containing 10% zinc, but not in those containing 1% and 5% zinc. Jerky flow was not observed in the present experiments for the alloy containing approximately 0·35% of arsenic, but was observed in the alloy containing 4·1% of arsenic in the range of temperature 150–180°C. The behaviour in the two groups of alloys is therefore consistent in this respect also.

Concurrently with the occurrence of the yield drop the electrical resistivity increases at a rate greater than that observed in the slightly later stages of plastic strain; the slope of the curve in figure 8 in the range B′C′ is greater than in the range C′D′. This 'electrical yield point' may be explained in terms of the Cottrell mechanism on the grounds that the sum of the separate contributions to resistivity of a dislocation and its former atmosphere after yielding is greater than the contribution of the combined dislocation and atmosphere before yielding. There may be some dispersion of the atmosphere, in the period of 1–2 minutes during which yielding is observed in the present experiments, if diffusion is accelerated by the movement of vacancies created during the deformation in the manner suggested by Cottrell (1952–53) and Westwood and Broom (1957).

The present experiments establish the occurrence of strain ageing in copper–arsenic alloys, as suggested by Clarebrough *et al.* (1955) and support the explanation advanced by these authors for the behaviour of an alloy of similar composition during recovery.

ACKNOWLEDGMENTS

The author is indebted to Drs. L. M. Clarebrough and M. E. Hargreaves, for outlining the investigation and for their constant help and interest, and to Dr. W. Boas for his encouragement and advice. Thanks are also due to Mr. J. Corbett for chemical analyses of the specimens. Finally, the author wishes to thank the staff of the workshop of the Division and other colleagues for their assistance during the investigation.

REFERENCES

ANDRADE, E. N. DA C., and ROSCOE R., 1937, *Proc. Phys. Soc.*, **49**, 152.

ARDLEY, G. W., and COTTRELL, A. H., 1953, *Proc. Roy. Soc.* A, **219**, 328.

CLAREBROUGH, L. M., HARGREAVES, M. E., and WEST, G. W., 1955, *Proc. Roy. Soc.* A, **232**, 252.

COTTRELL, A. H., 1952–53, *J. Inst. Met.*, **81**, 753.

COTTRELL, A. H., HUNTER, S. C., and NABARRO, F. R. N., 1953, *Phil. Mag.*, **44**, 1064

DIEHL, J., 1956, *Z. Metallk.*, **47**, 331.

VON GÖLER, FRH., and SACHS, G., 1927, *Z. Phys.*, **41**, 103.

LÜCKE, K., 1951, *Z. Metallk.*, **42**, 1.

WESTWOOD, A. R. C., and BROOM, T., 1957, *Acta Met.*, **5**, 249.

Rupture Propagation in Inhomogeneous Solids: An Electron Microscopic Study of Rubber containing Colloidal Carbon Black

By E. H. ANDREWS† and A. WALSH‡

† The British Rubber Producers' Research Association, Welwyn Garden City, Herts.
‡ Northampton College of Advanced Technology, St. John Street, London, E.C.1

MS. received 5th September 1957, *and in revised form* 12*th March* 1958

Abstract. Replica electron microscopy of rupture surfaces has been used to study the rupture process in solid ' two-phase ' systems obtained by dispersing colloidal carbon in rubber. Two parameters are introduced to characterize the surfaces; the total proportion of filler in the surface, and the proportion extracted by the gelatine first-stage replica. The latter quantity provides a measure of carbon-to-rubber adhesion in the rupture surface, whilst values obtained for the former quantity indicate that the rupture deviates strongly from a random plane through the material.

The results, together with a correlation found between adhesion and tearing energy, may be largely explained in terms of the local concentrations of stress which occur at the particles of the dispersed phase.

---

§ 1. Introduction

The propagation of rupture in strained homogeneous solids has been widely studied, and in some cases successfully described in terms of the balance of free energy within the body. (See for example Benbow and Roesler (1957) for brittle materials, and Rivlin and Thomas (1953) for highly elastic materials). In a physically inhomogeneous system, however, the state of strain from point to point fluctuates on the scale of the inhomogeneities and a full account of the rupture process cannot be given solely in terms of the overall energy of the body. A simple case of inhomogeneity arises in a ' two-phase ' system in which particles of one material are distributed uniformly throughout a matrix of the second, and a dispersion of colloidal carbon in rubber approximates to just such a system. This paper describes a direct study of the rupture process in a number of these inhomogeneous materials by the electron microscopy of rupture surfaces.

§ 2. Experimental

2.1. *Materials*

Initially, twelve different rubber–carbon systems were used, representing the twelve combinations of the following variables.

Polymer	Natural rubber; GR-S synthetic rubber.
Cross-linking agent	Sulphur; an organic peroxide.
Type of carbon black	A particle diameter 200–300 Å
	B particle diameter 800–900 Å.
	C particle diameter 3000–3500 Å.

Two further systems incorporating a second carbon black (D) of particle diameter 200–300 Å were used for comparison with type A. In one of these the carbon black had been previously heat treated at 2500°C to modify its surface properties.

The tensile strength, breaking strain and tearing energy T for the different materials are given in the table. The value of T was measured for quasi-static tearing by the method developed for a ' simple extension ' test piece by Rivlin and Thomas (1953).

	Natural Rubber						GR-S Synthetic Rubber					
	Sulphur			Peroxide			Sulphur			Peroxide		
Carbon-black	A	B	C	A	B	C	A	B	C	A	B	C
Tensile strength (kg cm^{-2})	256	207	201	181	176	150	206	165	133	143	104	66
Breaking strain	4·6	5·1	5·8	2·0	2·5	3·2	5·2	6·0	9·0	1·9	4·3	3·0
Tearing energy (erg cm^{-2} $\times 10^{-6}$)	5·8	4·0	5·0	1·2	1·2	1·2	11·6	4·9	8·5	2·4	2·6	0·6

2.2. *Specimen Preparation*

Three strips about 1 inch wide were cut from a $\frac{1}{8}$ inch sheet of each of the rubbers and a small razor cut made normal to one edge. One of the strips was torn across slowly by hand, one was torn as rapidly as possible, and a third, after immersion in liquid oxygen for ten minutes, was fractured under flexure. These three kinds of rupture will be called slow tear, rapid tear, and brittle fracture respectively. Replicas were then taken of the rupture surfaces.

2.3. *Replication, Microscopy and Evaluation*

The replication technique was a two-stage procedure using gelatine as the first and evaporated carbon as the second stage, and is fully described elsewhere (Andrews and Walsh, 1957, 1958). The final replica, which is shadowed lightly, represents carbon particles in three ways. Some of the surface particles are extracted from the rubber by the gelatine and transferred to the carbon film; the remainder are simply replicated and appear as bumps, whilst particles belonging to the opposite surface of the tear show as pits in the final replica. The replicas were photographed, using stereoscopic methods, at instrument magnifications from × 5000 to × 12 500 according to the particle sizes.

The percentage area of the replica occupied by bumps, pits and extracted particles, and that occupied only by the extracted filler, were assessed from the micrographs. When these areas are expressed as the apparent weight percentage of filler in the rubber, they are denoted ' total filler ' and ' extracted filler ' respectively (Andrews and Walsh 1958).

§ 3. RESULTS

3.1. *Surface Roughness*

Figures 1 (*a*) and (*b*) (Plate) show respectively brittle fracture and slow tear surfaces in the GR-S peroxide rubber loaded with black C, and figure 1 (*c*) the surface of slow tear in a rubber containing filler A. An impression of surface roughness can be obtained simply from the micrographs but its qualitative assessment is greatly improved by the use of stereoscopic methods. Different orders of roughness are present. On the smallest scale is that associated with the individual filler particles themselves; this is common to all surfaces, but tends to increase in intensity with increasing ' total filler ' and with decreasing ' extracted filler '. On a larger scale, brittle fractures are smooth in contrast with tear surfaces where the profile is quite ' mountainous ' on the scale of a few microns.

3.2. *Total Filler*

Values of ' total filler ' estimated from the micrographs are given in figure 2. Here the apparent percentage weight of filler in the compounded rubber is plotted as ordinate against the particle diameter, for each mode of rupture in each material. This graphical presentation of results is given for the sake of clarity and does not imply a functional relation between the quantities. In all cases the true loading of filler by weight is approximately 30%.

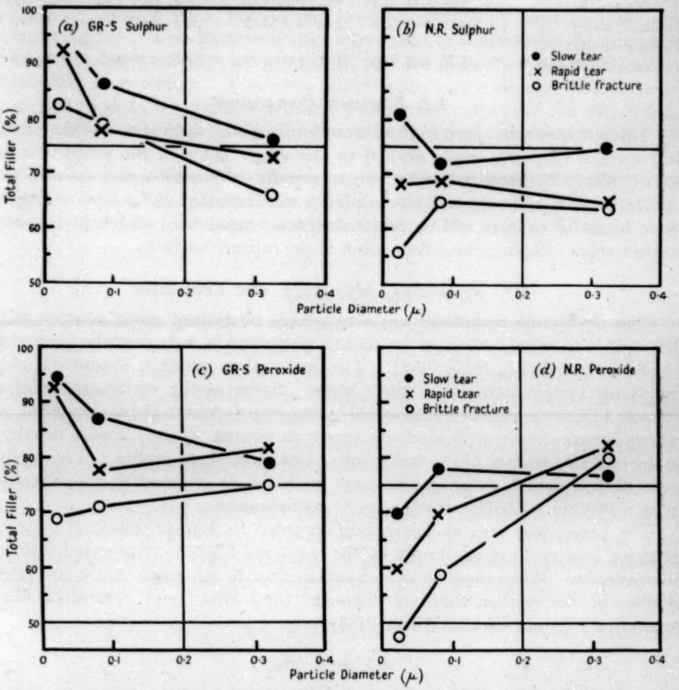

Figure 2. Values of ' total filler ' in the rupture surfaces.

The estimated values of ' total filler ' are always higher than the actual loading. This difference between apparent and actual loading is smallest in brittle fracture and greatest in slow tearing. With the smallest particle size black the value of ' total filler ' is consistently higher in GR-S than in natural rubber, but this difference disappears with the largest particle size. Differences due to the mode of rupture are also least with the latter, and the 'total filler' thus tends to a basic value. This value is different in the sulphur ($\sim 70\%$) and peroxide systems ($\sim 79\%$).

3.3. *Extracted Filler*

Figure 3 gives similar data on the measured values of 'extracted filler' ϵ. These results also show marked dependence on both the mode of rupture and the type of carbon black. 'Extracted filler' is least in brittle fracture and greatest in slow tear. It is also least with the smallest particle sized black and, in general, greatest with the coarse black. The standard sample D (not shown in figure 3) gives twice as much extracted filler as black A, which has a similar particle size, (ϵ for tear in N.R. sulphur $= 17\%$ for D and 8% for A). The heat treated (i.e. surface modified) sample of D is extracted even more readily.

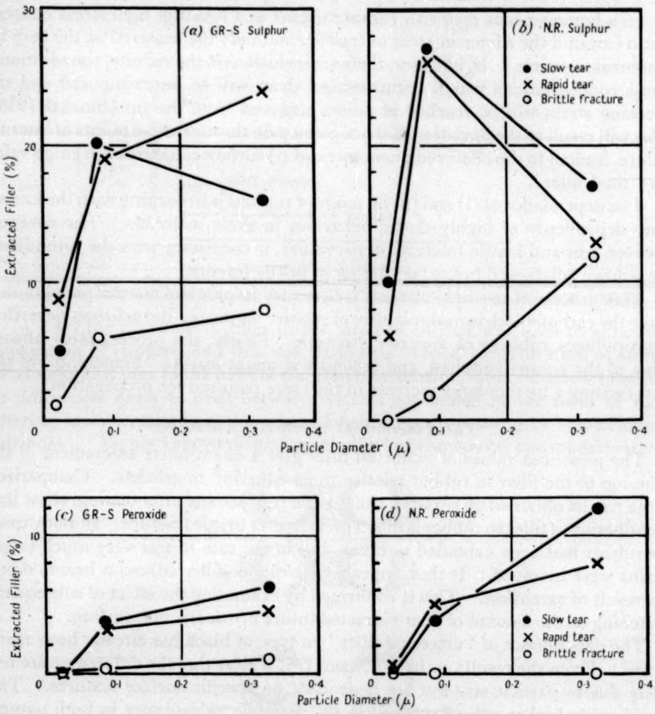

Figure 3. Values of the 'extracted filler'.

The results given in figure 3 also show a pronounced superiority of adhesion (low value of extracted filler) in the peroxide vulcanizates, the value of ϵ here not rising above 12% compared with a maximum of 27% in sulphur cures.

In order to resolve the effect of extension alone upon the value of ϵ, one of the rubbers was subjected to brittle fracture and afterwards extended to a stretch ratio of 2. From a value of 0% for brittle fracture, ϵ increased on stretching to between 2% and 6%. This compared with $\epsilon = 8\%$ to 12% for tear in the same material.

§ 4. DISCUSSION

4.1. *Rupture Surface*

Information about the surface of rupture is obtained from both the surface roughness and the value of the ' total filler '. Both indicate that it is not a simple plane surface through the material, but that the rupture tends to travel from one filler unit to an adjacent one. Since the path followed will be that requiring least energy it appears that filler particles (or groups) or their immediate environment are zones of relative weakness.

In a homogeneous material, rupture occurs as a result of high stress concentration around the advancing tear or fracture and only the material at the very tip is at breaking stress. If, however, there are inclusions in the vicinity, the additional stress concentrations which occur around them will be superimposed and the breaking stress will be reached at points removed from the tip (Smekal 1936). This will result in the deviation of the rupture path through these points of internal failure, leading to the observed phenomena of (i) surface roughness, (ii) high value for ' total filler '.

The dependence of (i) and (ii) on mode of rupture is in keeping with the known time–dependence of highly-elastic behaviour in these materials. The contrast between tear and brittle fracture, in particular, is consistant with the diminished breakdown (discussed below) occurring in brittle fracture.

This process of multiple internal failure may in part explain the paradox that while the carbon black introduces sites of relative weakness, its inclusion nevertheless produces rubbers of superior strength. Firstly, the process must absorb some of the energy supplied, and secondly it might lead to ' branching ' of the tear, causing a further large increase in the force required for propagation.

4.2. *The Adhesion of Carbon-Black to Rubber*

The measured values of extracted filler give a quantitative assessment of the adhesion of the filler to rubber relative to its adhesion to gelatine. Comparison of the results obtained on surfaces after brittle fracture and after tearing, show that the adhesion of filler to rubber is much greater after brittle fracture. In both cases the rubber had been extended to break, but in the case of tear very much larger strains were involved. It thus appears that rubber-filler adhesion breaks down as a result of extension. This is confirmed by examining the effect of subsequent stretching on the amount of filler extracted from a brittle fracture surface.

The dependence of ' extracted filler ' on type of black has already been mentioned. From the results on blacks A and D it is clear that the differences are not solely due to particle size but are dependent on specific surface features. The considerably higher adhesion found in the peroxide vulcanizates in both natural rubber and GR-S also appears to be associated with a specific feature of this type. (In view of the breakdown of adhesion which results from straining it is possible to obtain a false impression of superior adhesion in the less extensible peroxide material. In the present instance however, where the differences in adhesion are equally marked in brittle fracture, there is little doubt that adhesion in the peroxide rubbers is higher than in the sulphur rubbers.)

4.3. *Adhesion and Strength*

Comparison of ' extracted filler ' values for slow rates of tear with the corresponding tearing energies indicate that, within a given vulcanizing system, there exists a correlation between good adhesion and high tear resistance. Figure 4 shows tearing energy T for slow propagation plotted against extracted filler for slow tearing in each of the four kinds of rubber matrix used. As previously noted the peroxide materials are much the weaker, but the general tendency is for T to increase with decreasing extraction (increasing adhesion); the effect is more noticeable in GR-S than in the crystallizing natural rubbers.

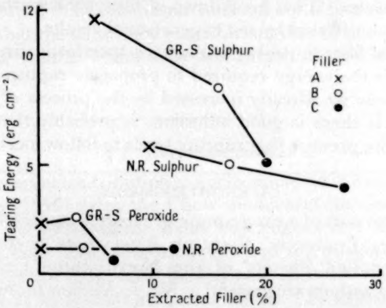

Figure 4. Relation between tearing energy and ' extracted filler ' for slow tearing.

In § 4.1 the presence of filler in the strained rubber was seen to affect the propagation of rupture, and this was attributed to local concentration of stress. Developing this idea in the light of the above correlation, it is of interest to notice the differences likely to exist between systems consisting on one hand of fully adhering inclusions and on the other of holes (approximating to non-adhering inclusions). Figure 5 shows diagrammatically the behaviour of two model systems

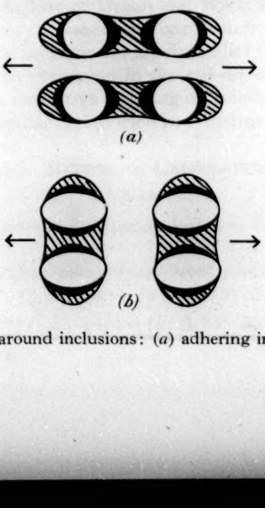
(a)

(b)

Figure 5. Stresses around inclusions: (*a*) adhering inclusions, (*b*) holes.

comprising a sheet of transparent rubber containing either adhering disc or holes. The regions of high stress observed by extending the model systems between crossed nicols are indicated in the figure by shading. For the rubber containing holes the loci of high stress lie in the direction of rupture, whilst for the adhering inclusions they lie normal to this direction. In the latter case the rupture will tend to turn through a right angle and travel along the loci of high stress, greatly increasing the energy required for forward propagation.

§ 5. Conclusion

The deviation of the rupture path in filled rubbers, which is evidenced by surface roughness and excess ' total filler ', may be explained from first principles in terms of multiple internal failure occurring around filler particles just ahead of the advancing rupture. That breakdown of filler-rubber attachment does occur under strain is demonstrated by the experimental results.

The adhesion of filler to rubber is a surface-specific quality, and is related in a positive manner to the energy required to propagate rupture. The mechanism by which tearing energy, already increased by the process of multiple failure, is further enhanced if there is good adhesion, is probably that proposed in § 4.3 which rests upon the premise that rupture tends to follow loci of high stress.

Acknowledgments

This work forms part of a programme of research undertaken by the Board of the British Rubber Producers' Research Association in conjunction with the Department of Applied Physics of the Northampton College of Advanced Technology. The authors are grateful to Mr. L. Mullins for helpful discussion.

References

Andrews, E. H., and Walsh, A., 1957, *Nature, Lond.*, **179,** 729; 1958, *J. Polym. Sci.*, in the press.

Benbow, J. J., and Roesler, F. C., 1957, *Proc. Phys. Soc.* B, **70,** 201.

Rivlin, R. S., and Thomas, A. G., 1953, *J. Polym. Sci.*, **10,** 291.

Smekal, A., 1936, *Ergebn. exakt. Naturw.*, **15,** 106.

Nucleon Magnetic Moment in Cut-off Meson Theory

By S. K. KUNDU

Department of Theoretical Physics, Indian Association for the Cultivation of Science,
Calcutta, India

MS. received 4*th March* 1958

Abstract. The effect of nucleon current contribution to nucleon magnetic moment is considered up to the fourth order of the coupling constant in the cut-off meson theory using the renormalization procedure as developed by Chew. The same parameters as employed to fit the meson–nucleon scattering data have been used here. It is found that the additional contribution due to this effect improves the previous theoretical results where only the mesonic current contribution has been taken into account.

§ 1. INTRODUCTION

THE mesonic current contribution to nucleon magnetic moment was calculated by Friedman (1955) using the Chew model and the nucleon current contribution in the intermediate states was neglected. This results in the equal and opposite value of the anomalous neutron and proton magnetic moment. However, experimentally one finds proton and neutron magnetic moment of value 2·79 and $-1{\cdot}91$ in nuclear magneton units. To explain the difference in the anomalous part of the proton and neutron magnetic moment we consider the effect of the Dirac moment of the proton in the intermediate states and the agreement with the experiment is found better. The present calculation shows that the neglect of the Dirac moment of the proton in the intermediate states is not completely justified and in fact it alters the magnetic moment of the neutron by $-0{\cdot}1462$ nuclear magneton units from that of the neutron as obtained from the mesonic current contribution. Using Chew's cut-off model the present calculation has been carried out up to fourth order in the coupling constant and the usual renormalization procedure of Dyson and Ward as formulated and applied by Chew in the cut-off theory of pseudovector meson fields is used here to achieve this end. The f^4 contribution turns out much smaller than that of the f^2, showing the validity of perturbation expansion in the cut-off model. The Hamiltonian chosen corresponds to the derivative coupling of pseudoscalar meson theory with a fixed extended source, similar to that used by Friedman.

§ 2. METHOD OF CALCULATION

2.1. f^2 *contribution*

The Feynman propagators and vertex operators in the sense of Chew and Wick are as follows:

(*a*) For the emission or absorption of mesons of momentum **k**, we write V_k, V_k^*

where $$V_k = N(f/\mu)\sqrt{(4\pi)}\,\tau_\lambda\,(\boldsymbol{\sigma}\,.\,i\mathbf{k})\,v(k)\,(2\omega_k)^{-1/2}$$

and $$V_k^* = N^*(f/\mu)\sqrt{(4\pi)}\,\tau_\lambda\,(\boldsymbol{\sigma}\,.\,i\mathbf{k})\,v^*(k)\,(2\omega_k)^{-1/2}$$

N being the normalization constant, $v(k)$ is the Fourier transform of the source function $\rho(r)$ and the meson energy $\omega_k=(k^2+\mu^2)^{1/2}$.

(*b*) For the scattering of a nucleon by the electromagnetic field A_μ we write $\psi_{p_2}{}^*\gamma_\mu A_\mu \psi_{p_1}$ (relativistically), where ψ_p's are Dirac spinors. This reduces in non-relativistic limit with which we are interested in the Chew–Low meson theory to

$$u_{p_2}{}^*\left(\frac{p_1+p_2}{2m}\right)u_{p_1}+u_{p_2}{}^*\left\{\frac{ie}{2m}(\boldsymbol{\sigma}\,.\,\mathbf{H})\right\}u_{p_1}$$

where now u_p's denote the non-relativistic two-component spinors of Pauli's wave equation. The contribution to the magnetic moment is obtained from the second term.

(*c*) The propagation of a nucleon with non-relativistic energy E_p is given by $S(E_p-\omega_k)$, i.e. $1/(E_p-\omega_k)$.

The matrix element corresponding to the second order Feynman diagram (cf. figure 1) is given by following the rules (*a*) to (*c*).

$$M_1=\sum_k V_k{}^*\,S(E_{p+p'}-\omega_k)\left\{\frac{ie}{2m}(\boldsymbol{\sigma}\,.\,\mathbf{H})\right\}S(E_p-\omega_k)\,V_k. \qquad \ldots\ldots(1)$$

Now replacing $\sum_k$ by $N^{-2}(2\pi)^{-3}\int d^3k$, we find

$$M_1=\frac{ie}{2m}\,\frac{f^2}{(2\pi)^3}\int d^3k\,v^2(k)\,\frac{(\boldsymbol{\sigma}\,.\,\mathbf{k})(\boldsymbol{\sigma}\,.\,\mathbf{H})(\boldsymbol{\sigma}\,.\,\mathbf{k})}{2\omega_k(E_{p+p'}-\omega_k)(E_p-\omega_k)} \qquad \ldots\ldots(2)$$

where we use $\tau_\lambda{}^2=1$.

The relation (2) in the limit of the approximation of the Chew–Low–Wick theory (Wick 1955) concerned reduces to the following

$$M_1=-\,\frac{ie}{2m}(\boldsymbol{\sigma}\,.\,\mathbf{H})f^2\frac{1}{3\pi}\,\frac{1}{\mu^2}\int_0^\infty\frac{dk\,k^4\,v^2(k)}{(k^2+\mu^2)^{3/2}}. \qquad \ldots\ldots(3)$$

2.2. f^4 *contribution*

The fourth order contributions to the nucleon magnetic moment in the present formalism are achieved with the help of the following diagrams

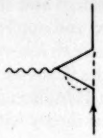
Figure 1 (*a*).

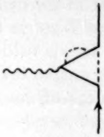
Figure 1 (*b*).

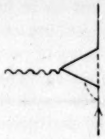
Figure 1 (*c*).

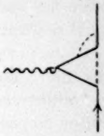
Figure 1 (*d*).

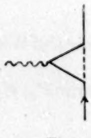
Figure 1.

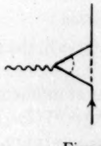
Figure 2.

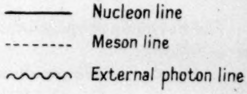

Following Chew (1954) we replace the internal nucleon propagator S_{E} by S_{Er} and the vertex operator V_k by V_{kr}, (the suffix r denotes renormalized) where

$$(S_{\mathrm{Er}})^{-1}=(S_{\mathrm{E}})^{-1}-\sum_l V_l^* V_l\left[\frac{1}{E-\omega_l}+\frac{1}{\omega_l}+\frac{E}{\omega_l^2}\right] \quad \ldots\ldots(4)$$

and $V_{kr}=V_k L_r(E_2,E_1)$ with $L_r(E_2,E_1)=1+\frac{1}{9}\sum_l V_l^* V_l\left[\frac{1}{E_2-\omega_l}\frac{1}{E_1-\omega_l}-\frac{1}{\omega_l^2}\right]$

$$\ldots\ldots(5)$$

E_1, E_2 are the nucleon energies before and after the vertex.

In the present case the expressions given in (4) and (5) reduce to

$$\frac{1}{E_p-\omega_k}+f^2(3/\pi)\frac{1}{\mu^2}\int_0^\infty \frac{dl\, l^4 v^2(l)}{\omega_l^3}\frac{1}{(E_p-\omega_k-\omega_l)} \quad \ldots\ldots(6)$$

and

$$V_k\left\{1+\frac{f^2}{9}\left(\frac{3}{\pi}\right)\frac{1}{\mu^2}\int_0^\infty \frac{dl\, l^4 v^2(l)}{\omega_l}\left[\frac{1}{E_p-\omega_l}\frac{1}{E_p-\omega_k-\omega_l}-\frac{1}{\omega_l^2}\right]\ldots\ldots(7)\right.$$

By the consistent use of the usual renormalization procedure of Dyson and Ward and as followed by Chew, we have the following contribution from the self-energy correction of the nucleon line and from the vertex modification denoted by M_1^{s} and M_1^{v} respectively

$$M_1^{\mathrm{s}}=-\frac{ie}{2m}(\boldsymbol{\sigma}\,.\,\mathbf{H})f^4\frac{1}{\pi^2}\frac{1}{\mu^4}\int_0^\infty\int_0^\infty \frac{dk\,dl\,k^4 v^2(k)\, l^4 v^2(l)}{\omega_k^2\omega_l^3(\omega_k+\omega_l)} \quad \ldots\ldots(8)$$

and

$$M_1^{\mathrm{v}}=\frac{ie}{2m}(\boldsymbol{\sigma}\,.\,\mathbf{H})f^4\frac{1}{9\pi^2}\frac{1}{\mu^4}\int_0^\infty\int_0^\infty \frac{dk\,dl\,k^4 v^2(k)\, l^4 v^2(l)}{\omega_k^3}\left[\frac{1}{\omega_l^3}-\frac{1}{\omega_l^2(\omega_l+\omega_k)}\right]$$

$$=-\frac{1}{9}M_1^{\mathrm{s}}. \quad \ldots\ldots(9)$$

In addition to this we are left with another possible fourth order diagram given by figure 2. This is easily calculated to give the following result

$$M_2=\frac{ie}{2m}(\boldsymbol{\sigma}\,.\,\mathbf{H})f^4\frac{1}{9\pi^2}\frac{1}{\mu^4}\int_0^\infty\int_9^\infty \frac{dk\,dl\,k^4 v^2(k)\, l^4 v^2(l)}{\omega_k^3\omega_l(\omega_k+\omega_l)^2}\,. \quad \ldots\ldots(10)$$

Thus the total contribution to neutron magnetic moment up to fourth order will be $U(N)=U_2(N)+U_4(N)=-0{\cdot}1462$ where $U_2(N)=-0{\cdot}0968$ obtained from (3), and $U_4(N)=2M_1^{\mathrm{s}}+2M_1^{\mathrm{v}}+M_2=-0{\cdot}0494$ obtained from (8), (9) and (10).

In this calculation we use the value of the coupling constant $f^2=0{\cdot}058$ and have taken $v^2(k)$ to be a unit step function with the step at $\omega_{\max}=5{\cdot}6\mu$. It may be remarked that the evaluation of the integrals (8), (9) and (10) has been performed by suitable numerical approximation methods.

§ 3. DISCUSSION

In view of the recent success of Chew's cut-off theory in the analysis of the low energy meson–nucleon processes, we have adopted this theory to explain the anomalous magnetic moments of nucleons. From this standpoint, Friedman has obtained the values of the nucleon magnetic moments, 2·44 for proton and $-1{\cdot}44$ for neutron, taking into account only the effect of mesonic current. In the present treatment we find that there should be an additional contribution of value $-0{\cdot}1462$ to the neutron magnetic moment due to the effect of nucleon current in the intermediate states and subsequently the neutron magnetic moment changes to $-1{\cdot}59$. This improved result gives an anomalous ratio 1·1 against the experimental value 1·06. Of course, we cannot expect exact quantitative agreements because of the uncertainties, in the calculation, of the maximum meson momentum $k_{\max}$, coupling constant and higher order contributions.

REFERENCES

CHEW, G. F., 1954, *Phys. Rev.*, **94**, 1748, 1755.
FRIEDMAN, M. H., 1955, *Phys. Rev.*, **97**, 1123.
WICK, G. C., 1955, *Rev. Mod. Phys.*, **27**, 339.

Energy Transfer in Organic Systems
I: Photofluorescence of Terphenyl-toluene Solutions

By J. B. Birks† and A. J. W. Cameron
Physics Department, Rhodes University, South Africa

MS. received 9th January 1958, *and in final form* 5th *March* 1958

Abstract. The fluorescence quantum intensities of normal and oxygen-free solutions of *para*-terphenyl in toluene have been measured as a function of concentration c and of excitation wavelength λ from 2200 Å to 3300 Å. The absorption spectra of toluene and terphenyl have been observed. The energy transfer coefficient f from excited toluene molecules to terphenyl molecules has thus been obtained.

f is found to depend on λ. For a given c, $f=f_1$ in region 1 ($\lambda=2500$–2650 Å), $f=f_2>f_1$ in region 2 ($\lambda=2200$–2350 Å), and $f_2>f>f_1$ for intermediate λ. Regions 1 and 2 correspond to the first and second excited electronic singlet states of toluene. The solvent–solute energy transfer from the second excited state, which occurs in approximately 10^{-11} sec, competes efficiently with conversion to the 1st excited state of toluene.

---

§ 1. Introduction

The high fluorescence efficiency of certain organic liquid solutions, when excited by ionizing radiations, was observed initially by Ageno, Chiozzoto and Querzoli (1949, 1950), Kallmann (1950), and Reynolds, Harrison, and Salvani (1950). Such solutions are now extensively used for scintillation counting, particularly where a large detection volume and a rapid response time are required.

Kallmann and Furst (1950, 1951) observed that, although the fluorescence is characteristic of the solute, its intensity greatly exceeds that from direct excitation of the solute molecules by the incident ionizing radiation. A transfer of electronic energy from solvent molecules, initially excited, to solute molecules was thus demonstrated. The energy transfer process for a wide range of liquid solutions has been studied by Furst and Kallmann (1952, 1954 a), Reynolds (1952) and others.

The mechanism of the inter-molecular energy transfer in liquids and in related fluorescent organic systems has been a matter of some discussion, and several alternative processes have been proposed. Birks (1953, 1954) has formulated a photon theory of energy transfer. Other observers (e.g. Cohen and Weinreb 1954, 1956, Furst and Kallmann 1952, 1954 a, b, Kallmann and Furst 1950, 1951, Reid 1952, Reynolds 1952, Schmillen 1953, Terenin 1954) consider that such a radiative transfer process is inadequate to account for the magnitude of the energy transfer observed. They propose that the intermolecular energy transfer is primarily non-radiative (Förster 1948, 1949, 1951).

---

† Now at the Physical Laboratories, University of Manchester.

Several non-radiative transfer mechanisms, some of which are equivalent, have been suggested. These include exciton migration, dipole–dipole interaction, quantum-mechanical resonance, or inductive transfer, sensitized fluorescence, collisional transfer and the formation of excited ' double molecules ', or of solvent–solute molecular complexes. While some of these processes are plausible on theoretical grounds, others that have been borrowed by analogy from different physical systems, such as ionic crystals and monatomic gases, are not necessarily applicable to liquid organic solutions.

The use of ionizing radiation for stimulation of the fluorescence complicates the interpretation of the experimental data. The manner of conversion of the primary molecular ionization and excitation energy into lower excited states of the molecules is not yet fully understood. Birks (1953, 1954) has proposed a possible mechanism: a cascade of successive fluorescence and re-absorption transitions from and to higher electronic states, degenerating through vibrational energy dissipation into lower electronic states. The fluorescence from the lowest excited singlet state of the solute ultimately escapes without re-absorption and is observed externally. While many data are consistent with this theory, prior to the present work it lacked any direct verification.

It was therefore considered desirable to study the solvent–solute energy transfer, without the additional effects of primary ionization. Cohen and Weinreb (1954) have shown that such energy transfer occurs in organic liquid solutions, when excited by non-ionizing ultra-violet radiation. Furst and Kallmann (1954 b) have also extended their earlier scintillation studies of various solutions to ultra-violet excitation. However, the latter's use of multi-component solutions complicates the analysis of their results.

In the present work, the fluorescence quantum intensity of a binary solution, *para*-terphenyl in toluene†, has been measured as a function of concentration and of excitation wavelength from 2200 Å to 3300 Å. The absorption spectra of the two components, and other data relevant to a quantitative analysis of the energy transfer, have also been measured.

Since the completion of the experimental work in November 1955, an account of similar studies by Cohen and Weinreb (1956) has been published. Our results, analysis, and conclusions differ from theirs in several important respects.

§ 2. EXPERIMENTAL

2.1. *Absorption Spectra*

High-purity toluene and ' scintillation grade ' *para*-terphenyl were used. The absorption spectra of toluene in ethanol (figure 1, curve A) and of terphenyl in cyclohexane (figure 1, curve B) were measured with a Beckman Model DU spectrophotometer. The absorption spectrum of terphenyl in toluene was measured down to 2950 Å, at which wavelength the toluene starts to absorb, and a similar spectrum to that of the cyclohexane solution was observed. The observed spectra are similar to those reported by Friedel and Orchin (1951).

---

† This solution was chosen because its high scintillation efficiency indicates efficient solvent–solute energy transfer.

The ratio ρ, of the molar extinction coefficients ϵ_y and ϵ_x of terphenyl and toluene respectively, is plotted in figure 1, curve C.

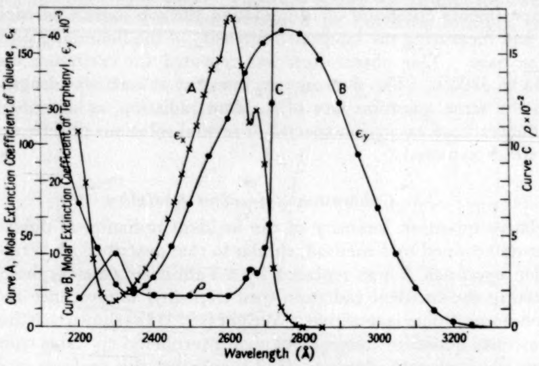

Figure 1. A, absorption spectrum of toluene in ethanol ϵ_x; B, absorption spectrum of *para*-terphenyl in cyclohexane ϵ_y; C, $\rho=\epsilon_y/\epsilon_x$.

2.2. *Fluorescence of Solutions*

The experimental arrangement is shown diagrammatically in figure 2. The solution S was contained in a cylindrical glass vessel, the depth of the solution (1 cm) being the same for all specimens. The fluorescence was excited by illumination with monochromatic radiation from a Beckman Model D U spectrophotometer, the horizontal exit beam M being deflected vertically downwards by a quartz prism Q. The vessel was placed on a Chance OY 10 glass filter F, adjacent to the photo-cathode window of a Du Mont 6291 photomultiplier P mounted vertically.

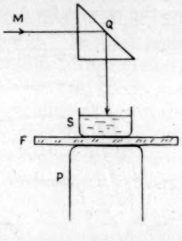

Figure 2. Experimental arrangement. M, exit beam from monochromator; Q, quartz prism; S, solution specimen in glass vessel; F, OY 10 glass filter; P, photomultiplier.

The filter transmits the terphenyl emission efficiently, but it is opaque to shorter wavelength radiation: it thus serves to prevent scattered incident radiation from reaching the photo-cathode. A careful check showed that neither the filter nor the glass vessel were luminescent, an important precaution since fused silica and some glasses luminesce in the near ultra-violet and visible regions. Optical contact between the surfaces was improved by thin films of glycerine.

The experiments consisted of illuminating the top surface of each solution specimen, and measuring the integrated intensity of the fluorescence transmitted through the base. This observation was repeated for excitation wavelengths from 2200 Å to 3300 Å. The fluorescence intensity at each wavelength was normalized to the same quantum flux of incident radiation, as described in § 2.3. Thus the fluorescence excitation spectra of several solutions of different concentrations were determined.

2.3. *Calibration of Incident Radiation*

The relative quantum intensity of the incident radiation at different wavelengths was determined by a method, similar to that described by Wright (1955). The solution specimen S was replaced by a 1 cm cube *para*-terphenyl crystal, thus converting the incident radiation into terphenyl fluorescence radiation to which the photomultiplier is sensitive. Wright (1955) has shown that the technical photofluorescence quantum efficiency of such a terphenyl crystal is constant, and independent of wavelength, down to 2537 Å, and that this uniform response can be assumed to extend down to at least 2200 Å.

The intensity of the integrated fluorescence from the terphenyl crystal was thus taken as directly proportional to the quantum intensity of the incident beam. This calibration was checked down to 2537 Å using the ultra-violet-sensitive phototube, supplied with the spectrophotometer, as detector. The photo-tube response had been previously measured against a Hilger Model F.T. 16 linear vacuum thermopile, fitted with a fluorite window (Wright 1955). Excellent agreement was obtained between the two independent calibrations.

2.4. *Fluorescence Excitation Spectra*

Fluorescence excitation spectra, normalized to a constant flux of incident quanta, were measured from 3300 Å to 2200 Å, for a range of solutions of different concentrations. Figure 3 shows the results for 5 solutions, in normal toluene, of

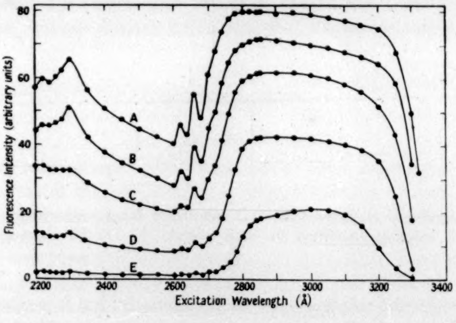

Figure 3. Fluorescence excitation spectra of normal solutions. Concentration: A, 4·15 g l.$^{-1}$; B, 2·07 g l.$^{-1}$; C, 1·04 g l.$^{-1}$; D, 0·415 g l.$^{-1}$; E, 0·091 g l.$^{-1}$.

concentration from 4·15 g l.$^{-1}$ to 0·09 g l.$^{-1}$. These solutions contained dissolved oxygen, which is known to act as a quenching agent, in equilibrium concentration at normal atmospheric pressure. Figure 4 shows the results for two solutions, from which the oxygen had been removed by bubbling nitrogen through the toluene during distillation.

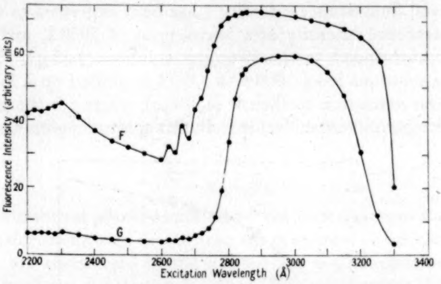

Figure 4. Fluorescence excitation spectra of oxygen-free solutions. Concentration: F, 1·08 g l.$^{-1}$; G, 0·054 g l.$^{-1}$.

§ 3. ANALYSIS OF RESULTS

3.1. *Qualitative Description*

Three distinct regions may be distinguished in the excitation spectra. In the first region (O) from 2800–3300 Å, the toluene is practically transparent, and the terphenyl fluorescence is excited directly by absorption of the incident radiation. This region of direct excitation is bounded at $\lambda \sim 3300$ Å by the terphenyl absorption edge, and at $\lambda \sim 2800$ Å by the onset of the toluene absorption.

In the second and third regions (1 and 2), corresponding to wavelengths below about 2700 Å, the toluene absorption is high, and practically all the incident radiation is absorbed by the solvent. In these regions, the terphenyl fluorescence is mainly excited indirectly by energy transfer from excited toluene molecules.

The fluorescence intensity shows variations, associated with changes in ϵ_X and ϵ_Y with wavelength, and these are allowed for in the subsequent analysis. However it may be noted at this stage, that the fluorescence intensity, which depends on the energy transfer efficiency, is higher at the shorter wavelengths (2200–2350 Å) designated region 2, than at the longer wavelengths (2500–2650 Å), designated region 1.

3.2. *Correction for Excitation Depth*

Before undertaking a quantitative analysis of the results, a correction was made for the variation with wavelength and concentration of the depth of penetration of the incident radiation. This effect was reported by Wright (1955), who studied the fluorescence excitation spectra of organic crystals. These show major variations with excitation wavelength of the transmitted fluorescence intensity, associated with variations in the absorption coefficient.

The effect is clearly seen in the present measurements (figures 3 and 4) for wavelengths from 3000 Å to 3300 Å. In this spectral region the toluene is transparent, all the terphenyl fluorescence is directly excited, and the fluorescence quantum efficiency of terphenyl is constant. Nevertheless, the observed fluorescence intensity decreases with increasing wavelength, due to the decrease in ϵ_y, and the consequent increase in the depth of penetration of the incident radiation.

The observed fluorescence intensity I has been expressed in terms of I_0, the observed fluorescence intensity at a wavelength of 3000 Å, and I/I_0 has been normalized to correspond to the strongest solution (4·15 g l.$^{-1}$) In figure 5, I/I_0 for all the solutions from 3000 Å to 3300 Å is plotted on a logarithmic scale against the molar extinction coefficient $(\epsilon_x + \epsilon_y c)$, where c is the concentration of solute molecules per solvent molecule. In this spectral region $\epsilon_x = 0$.

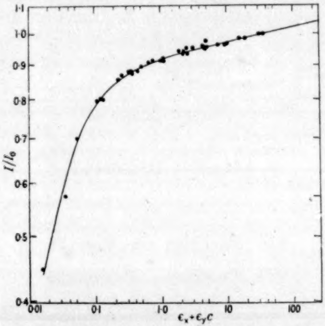

Figure 5. Effect of excitation depth on fluorescence intensity: relative intensity I/I_0 plotted against extinction coefficient $\epsilon_x + \epsilon_y c$.

Within the experimental error, the values of I/I_0 for the different solutions lie on a single smooth curve. For values of $\epsilon_x + \epsilon_y c$ from 1 to 36 the curve is linear, and it is reasonable to extrapolate it linearly to higher values of $\epsilon_x + \epsilon_y c$.

Figure 5 thus shows the change in the observed fluorescence intensity I from the value I_0 that it would have if the molar extinction coefficient $\epsilon_x + \epsilon_y c$ were 36, i.e. if the radiation were absorbed at the same depth as in the strongest solution at $\lambda = 3000$ Å. Figure 5 has therefore been used to correct the observed fluorescence excitation spectra (figures 3 and 4) by normalizing them to the standard excitation depth, corresponding to I_0. This has been done by dividing the observed fluorescence intensity I (figures 3 and 4) by the value of I/I_0 from figure 5, corresponding to the value of $\epsilon_x + \epsilon_y c$, for the particular solution and excitation wavelength.

In the wavelength range 2650–2200 Å, which is analysed below, $\epsilon_x + \epsilon_y c$ varies from 12·4 to 214 over all the solutions, corresponding to correction factors from 0·98 to 1·05. Observations at $\lambda = 2650$–2800 Å are omitted from the subsequent analysis, because of experimental uncertainties in the exact position of the toluene absorption edge, since the absorption spectrum (figure 1, curve A) measured for an ethanol solution, does not correspond exactly to that for pure toluene.

The corrected fluorescence excitation spectra are similar in form to figures 3 and 4, except for uniform plateaux from $\lambda \sim 2900$ Å to 3300 Å.

3.3. *Energy Transfer Coefficient*

We shall now proceed to analyse the corrected excitation spectra, to determine the fraction of quanta transferred from solvent to solute molecules.

For incident photons of wavelength λ, let the fraction absorbed initially by the solvent and solute molecules be n_x and n_y respectively.

$$n_x = \frac{1}{1+\rho c}$$

$$n_y = \frac{\rho c}{1+\rho c} \qquad \ldots\ldots(1)$$

where $\rho = \epsilon_y/\epsilon_x$.

The quantum efficiency q_{fy} of the observed solute fluorescence is

$$q_{fy} = \frac{n_f}{n_y + f n_x} \qquad \ldots\ldots(2)$$

where n_f is the number of photons emitted per incident quantum absorbed, and f is the energy transfer coefficient, i.e. the fraction of quanta, initially absorbed by the solvent, which are transferred to the solute. q_{fy} is characteristic of the solute in the particular solvent at a given value of c. It is independent of λ within the 1st absorption band of the solute (down to 2350 Å in the present case) and, by analogy with other organic fluorescent compounds (Pringsheim 1949, Fuchslocher and Glaser 1954, Wright 1955), it may be expected to remain constant down to at least 2200 Å.

In the spectral region 0, where the solvent is transparent, $n_x = 0$, $n_y = 1$, and

$$q_{fy} = n_{f0} \qquad \ldots\ldots(3)$$

where suffix 0 refers to this spectral region.

An expression for f in terms of experimental parameters is obtained from (1), (2) and (3), namely

$$f = \frac{n_f}{n_{f0}}(1+\rho c) - \rho c. \qquad \ldots\ldots(4)$$

The ratio n_f/n_{f0} is obtained directly from the corrected fluorescence excitation spectra: ρ is obtained from figure 1, curve C.

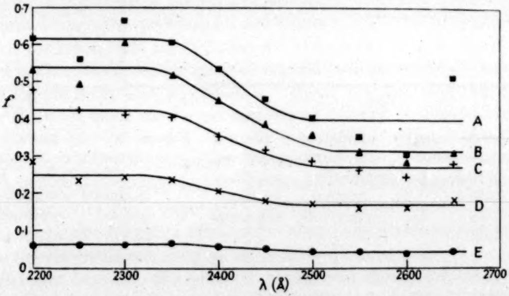

Figure 6. Energy transfer coefficient f plotted against wavelength λ. Normal solutions. Concentration: A, 4·15 g l.$^{-1}$; B, 2·07 g l.$^{-1}$; C, 1·04 g l.$^{-1}$; D, 0·415 g l.$^{-1}$; E, 0·091 g l.$^{-1}$.

The values of f, derived from (4), are plotted against λ in figures 6 and 7. For each solution, it is found that f has two characteristic values: f_1, which is constant within the experimental error, for $\lambda = 2500$–2650 Å (region 1); and f_2, which is similarly constant, but higher, for $\lambda = 2200$–2350 Å (region 2). Between these two spectral regions, f has a value intermediate between f_1 and f_2.

The mean values of f_1 and f_2 are plotted as a function of c in figure 8.

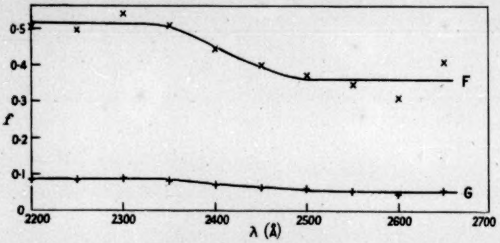

Figure 7. Energy transfer coefficient f plotted against wavelength λ for oxygen-free solutions. Concentration: F, 1·08 g l.$^{-1}$; G, 0·054 g l.$^{-1}$.

3.4. *Energy Transfer and Quenching*

On the photon transfer theory, and some of the alternative non-radiative mechanisms proposed, the probability of solvent–solute transfer is proportional to the concentration c. On an elementary analysis, the probabilities of the various processes competing for the solvent excitation energy may be enumerated as follows: (i) solvent–solute transfer, kc; (ii) quenching by solute, lc; (iii) self-quenching by solvent, s; and (iv) quenching by oxygen, m.

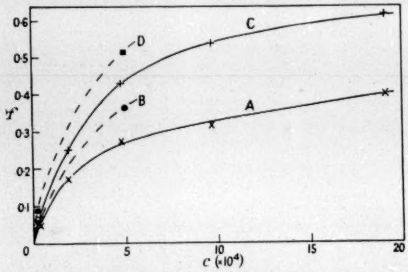

Figure 8. Energy transfer coefficient f plotted against concentration c. A, normal solutions, $\lambda = 2500$–2650 Å; B, oxygen-free solutions $\lambda = 2500$–2650 Å; C, normal solutions $\lambda = 2200$–2350 Å; D, oxygen-free solutions $\lambda = 2200$–2350 Å.

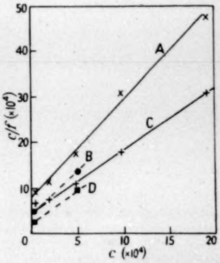

Figure 9. c/f plotted against concentration c. A, normal solutions $\lambda = 2500$–2650 Å; B, oxygen-free solutions $\lambda = 2500$–2650 Å; C, normal solutions $\lambda = 2200$–2350 Å; D, oxygen-free solutions $\lambda = 2200$–2350 Å.

Hence we obtain,

$$f=\frac{kc}{(k+l)c+s+m} \qquad \ldots\ldots(5)$$

$$=\frac{c}{Ac+B} \qquad \ldots\ldots(5a)$$

In figure 9 the experimental values of c/f_1 and c/f_2 are plotted against c for the normal and oxygen-free solutions. Linear relations in agreement with (5*a*) are obtained. From the gradients and intercepts, for the normal solutions $A_1=2\cdot1$, $B_1=8\times10^{-4}$; $A_2=1\cdot4$, $B_2=5\times10^{-4}$; and for the oxygen-free solutions $A_1=2\cdot1$, $B_1=4\times10^{-4}$; $A_2=1\cdot4$, $B_2=2\cdot5\times10^{-4}$, where suffixes 1 and 2 refer to the spectral regions 1 and 2.

It is tempting to evaluate the relative values of k, l, s and m from these data, as has been done by other observers. However, it will be shown by Birks (to be published) that (5) is over-simplified, since the effect of solvent absorption and re-emission (' photon regeneration ', Birks 1953, 1954) has not been allowed for. A fuller theoretical analysis, which leads to a relation similar to (5*a*), is given by Birks (to be published) and A and B are there related to the molecular quantum efficiency of the solvent and the relative solute/solvent absorption coefficient ρ.

§ 4. DISCUSSION

4.1. *Comparison with other Experimental Results*

These results differ in certain important respects from those of Cohen and Weinreb (1956) on similar solutions.

These authors do not refer to the oxygen content of their solutions, which presumably were air-saturated. They reported that the energy transfer coefficient f was independent of λ for wavelengths from 2200–2700 Å. This is in distinct contrast to the present results.

Most of the measurements of Cohen and Weinreb were made using 2537 Å and 3130 Å radiation for excitation, corresponding to our spectral regions 1 and 0. They observed a linear relation between c/f_1 and c as given by (5), but with the parameter $l=0$. Thus they found that f_1 tended towards a limiting value of 1·0, as c increased, rather than to the limits, given by $1/A_1$ and $1/A_2$ of $f_1=0\cdot48$ and $f_2=0\cdot7$ obtained from the present measurements. It may be noted that Cohen and Weinreb assumed $l=0$ in their theoretical analysis, and also that their own measurements on anthracene in anisole, reproduced in figure 2(*b*) of their paper, are not consistent with this hypothesis. Their results, like the present ones, do however show clearly that the probability of solvent–solute transfer is proportional to c.

The other studies of Cohen and Weinreb on the influence of carbon tetrachloride as a quenching agent, and of the dilution of the transferring solvent with cyclohexane, have not been repeated. While there appears to be no reason to question their relative transfer efficiency values, the absolute values are subject to the same degree of uncertainty as the others discussed above.

The difference between the present results and those of Cohen and Weinreb may partly arise from the correction for excitation depth (§ 3.2). While the latter refer to a correction for geometrical and self-absorption effects being applied no details of the correction, which is stated to be generally small, are given.

In the present measurements, covering a similar range of concentrations, the values of $\epsilon_x + \epsilon_y c$ at 2537 Å and 3130 Å (the wavelengths used by these authors) range from 170 down to 0·06, corresponding to values of I/I_0 from 1·04 down to 0·7.

4.2. *Consideration of Assumptions*

Two assumptions made in the analysis and calibration should be noted, since if they were invalid, the results at $\lambda < 2537$ Å might not be reliable. (i) The molecular fluorescence quantum efficiency q_{fy} of terphenyl in solution is constant down to $\lambda = 2200$ Å (§ 3.3.) (ii) The technical fluorescence quantum efficiency of the 1 cm cube terphenyl crystal is constant down to $\lambda = 2200$ Å (§ 2.3). Since crystalline terphenyl is transparent to its own fluorescence emission (Birks and Wright 1954), its technical and molecular fluorescence efficiencies are identical. Hence (i) and (ii) are equivalent assumptions for terphenyl molecules in solution and in the crystalline state.

These assumptions are consistent with all the experimental data on organic fluorescent materials, excited by non-ionizing radiation (Pringsheim 1949, Wright 1955) and there is no reason to doubt their validity. Cohen and Weinreb (1956) also make assumption (i), and a similar assumption to (ii) for the aqueous solution of fluorescein used for calibration.

The choice of terphenyl both as solute and for calibration of the incident radiation flux means that, even if (i) and (ii) are not valid, provided the ratio of the molecular fluorescence efficiencies of terphenyl in solution and in the crystal is constant down to $\lambda = 2200$ Å, the values of f calculated from the observations will be unchanged.

4.3. *Dependence on Wavelength*

The most interesting result is that the energy transfer probability depends on the wavelength of excitation.

The two spectral regions 1 (2500–2650 Å) and 2 (2200–2350 Å) correspond to excitation into the first and second excited electronic singlet states of the toluene molecule. It is found that the energy transfer coefficient from toluene molecules excited initially into the second excited state, is higher than from molecules excited initially into the first excited state.

The lifetimes of the first and second excited states, estimated from the absorption strengths of the electronic transitions, are of the order of 10^{-9} sec and 10^{-11} sec respectively. Cohen and Weinreb (1956) have estimated, by measurements of the effect of carbon tetrachloride on quenching, that energy transfer from the first excited state occurs in the order of 10^{-9} sec. The efficient energy transfer from the second excited state shows that in this case transfer must occur in about 10^{-11} sec or less. The very short lifetime of the second excited state reduces the probability that the energy transfer from this state is collisional in nature, since the average time required by an excited solvent molecule to diffuse into the proximity of a solute molecule is in excess of 10^{-11} sec.

Because of the short lifetime of the second excited state the external quenching will be relatively small. The chief process competing with solvent-solute energy transfer from this state will be conversion into the first excited state of the solvent molecule, either by internal conversion or by solvent–solvent energy transfer. This conversion process is known to be highly efficient and rapid

(Pringsheim 1949). Nevertheless, the results show that the solvent–solute transfer can compete efficiently with such inter-state conversion.

4.4. *Photon Transfer Theory*

The results have been discussed so far without specific reference to any particular mode of energy transfer.

Birks (1954) has suggested fluorescence emission from the second and higher electronic excited states of a fluorescent molecule. The results show that the concept, previously accepted (Pringsheim 1949), that all the excitation energy of such higher electronic states is internally converted into that of the lowest excited state, is invalid. In pure solvents two components, internal conversion and solvent–solvent transfer, combine to give 100% inter-state conversion efficiency; in solutions, solvent–solute transfer is an efficient competitor against solvent–solvent transfer for the excitation energy. The time required for energy transfer is of the order of 10^{-11} and 10^{-9} sec respectively for the second and first excited states. This is about the same as for fluorescence emission from these two states.

Between region 1 and region 2, where all the excited solvent molecules are initially in the first and second excited states respectively, there is a transition region extending from 2350–2500 Å. In this transition region, solvent molecules co-exist initially in either of the two excited states. This region is also that where fluorescence from the second excited state might be expected to occur.

Further information on the energy transfer process is given by the experiments of Cohen and Weinreb (1956), who have shown that the solvent–solute transfer efficiency in region 1 is practically unchanged if the solvent is diluted by a factor of 1000 with an ‘ inert ’ liquid, such as cyclohexane. They have thus demonstrated that solvent-solvent ‘ collisional ’ energy transfer is negligible. It would also appear that any short-range non-radiative solvent–solute transfer processes, which depend on thermal diffusion to bring the excited solvent molecule and the solute molecule into reasonable proximity, are similarly excluded by these observations, since their efficiency would be reduced by an increase in the diffusion time due to dilution. Fluorescence of the solvent, leading to photon transfer, appears the one possible long-range mechanism. The dilutant, cyclohexane, being transparent does not decrease the efficiency of photon transfer.

The fluorescence spectrum of the emission from the first excited state of toluene, observed in dilute alcoholic solution, has vibrational maxima at $\lambda = 2622$, 2646, 2676, 2740, 2808 and 2886 Å (Pringsheim 1949). There is thus a major overlap of the fluorescence and absorption spectrum, and in pure toluene the mean free path of the emitted photons will be only a few microns. The relatively low technical fluorescence efficiency q_t observed with thicker toluene specimens by Kallmann and Furst (1951 b) will be considerably less than the molecular fluorescence efficiency q_0, due to this high self-absorption. Since $q_t = (q_0)^n$, where $1/n$ is the probability of photon escape without absorption (Birks 1954), by taking values of $q_t \sim 0{\cdot}015$ (Kallmann and Furst 1951 b), $n \sim 6$ (estimated from the absorption and emission spectra†) we obtain a rough estimate of $q_0 \sim 0{\cdot}5$. This is in reasonable agreement with the value obtained by a fuller analysis of the results (Birks, to be published).

It is hoped to obtain more direct data on the molecular emission from the first and second excited states (the latter will be even more difficult to observe since it is completely overlapped by the absorption spectrum) by observations on thin films.

---

† $n = 4$–5 for pure anthracene (Birks 1954).

The theory of the scintillation and fluorescence processes in solutions will be developed in more detail by Birks, when experimental data on other liquid and plastic solutions will be considered.

ACKNOWLEDGMENTS

We wish to thank our former colleague, Dr. G. T. Wright, for his suggestion and initial discussion of the experiments. One of us (A.J.W.C.) also wishes to thank Professor J. A. Gledhill for stimulating discussions and encouragement, and to acknowledge the tenure of a bursary and research grant from the South African Council for Scientific and Industrial Research.

REFERENCES

AGENO, M., CHIOZZOTO, M., and QUERZOLI, R., 1949, *R.C. Accad. Lincei*, **6**, 626; 1950, *Phys. Rev.*, **79**, 720.

BIRKS, J. B., 1953, *Scintillation Counters* (London: Pergamon Press; New York: McGraw-Hill); 1954, *Phys. Rev.*, **94**, 1567.

BIRKS, J. B., and WRIGHT, G. T., 1954, *Proc. Phys. Soc.* B, **67**, 657.

COHEN, S., and WEINREB, A., 1954, *Phys. Rev.*, **93**, 1117; 1956, *Proc. Phys. Soc.* B, **69**, 593.

FÖRSTER, TH., 1948, *Ann. Phys., Lpz.*, **2**, 55; 1949, *Z. Naturf.*, **4a**, 321; 1951, *Fluoreszenz organischer Verbindungen* (Göttingen: Vandenhoeck und Ruprecht).

FRIEDEL, R., and ORCHIN, M., 1951, *Ultra-violet Spectra of Aromatic Compounds* (New York: John Wiley; London: Chapman and Hall).

FUCHSLOCHER, G., and GLASER, G., 1954, *Z. Phys.*, **138**, 363.

FURST, M., and KALLMANN, H., 1952, *Phys. Rev.*, **85**, 816; 1954 a, *Ibid.*, **96**, 902; 1954 b, *Ibid.*, **94**, 503; 1955, *Ibid.*, **97**, 583; *J. Chem. Phys.*, **23**, 607.

KALLMANN, H., 1950, *Phys. Rev.*, **78**, 621.

KALLMANN, H., and FURST, M., 1950, *Phys. Rev.*, **79**, 857; 1951 a, *Ibid.*, **81**, 853; 1951 b, *Nucleonics*, **8**, No. 3, 32.

PRINGSHEIM, P., 1949, *Fluorescence and Phosphorescence* (New York and London : Interscience).

REID, C., 1952, *Phys. Rev.*, **88**, 422.

REYNOLDS, G. T., 1952, *Nucleonics*, **10**, No. 7, 46.

REYNOLDS, G. T., HARRISON, F. B., and SALVANI, G., 1950, *Phys. Rev.*, **78**, 488.

SCHMILLEN, A., 1953, *Z. Phys.*, **135**, 294.

TERENIN, A. N., 1954, *Abh. Sowjet. Phys.*, **4**, 240.

WRIGHT, G. T., 1955, *Proc. Phys. Soc.* B, **68**, 701.

Heat Treatment of Polycrystalline Cadmium Oxide

By J. A. BASTIN† and R. W. WRIGHT‡
University College, Ibadan, Nigeria

MS. received 7th January 1958, and in revised form 14th April 1958

Abstract. Measurements have been made of the Hall coefficient and resistivity of a number of specimens of compressed cadmium oxide powder both during and after various heat treatments. The results are explained by assuming that during such heat treatments there may be changes in the intercrystalline resistances and also in the carrier concentration of the microcrystals. In particular it is suggested that the very large change of resistance during sintering is mainly due to a change in intercrystalline resistances. A manner by which the carrier concentration of a specimen may be changed after heavy sintering is described.

§ 1. Introduction

In a previous paper (Wright and Bastin 1958) it was noted that sintered cadmium oxide specimens become electrically unstable above about 550°K. This instability was explained by changes in the effective impurity concentration. Since the impurities (interstitial Cd or O vacancies) are ionized at all temperatures, measurements of the Hall coefficient are very suitable for investigating the kinds of changes which may occur during heating.

Several authors have made investigations of the variation of the electrical properties of cadmium oxide with oxygen pressure. The results are normally applied to a mass action theory which assumes an equilibrium of the type

$$2\mathrm{Cd}^+ + \mathrm{O}_2 + 2e^- \rightleftharpoons 2\mathrm{CdO} \qquad \ldots\ldots (1)$$

In this equation the Cd^+ terms on the left-hand side represent interstitial cadmium ions which give rise to the electrical conductivity of the specimen. The exact variation of the electrical properties with oxygen pressure is unimportant but the theory does imply that for any temperature and oxygen pressure all cadmium oxide specimens should have the same impurity concentration. This is in direct disagreement with previously reported results which show that at temperatures below about 500°K stable specimens may be produced with carrier concentrations which vary for different specimens from $1{\cdot}5 \times 10^{18}\ \mathrm{cm}^{-3}$ to $5 \times 10^{-19}\ \mathrm{cm}^{-3}$. The results may be reconciled with equation (1) by assuming a high activation energy for the movement of cadmium interstitials or oxygen vacancies through the lattice. Below a fairly definite temperature the defect mobility thus becomes very low, and the defects become effectively frozen into the lattice. In the case of cadmium oxide this temperature is about 550°K.

The resistivity of compressed unheated blocks of cadmium oxide powder is of the order of 10^8 ohm cm. After prolonged heating above about 550°K the resistivity drops to about 10^{-1} ohm cm. This heating process, which is known as sintering, will be considered first.

---

† Now at Physics Research Laboratory, University of Reading.

‡ Now at University College, Achimota, Ghana.

§ 2. SINTERING MEASUREMENTS

It is often suggested that the large change of resistance during sintering of metallic oxides is due to an increase in the impurity concentration caused either by a reduction or an oxidation process. Experiments by the authors will now be described which show that in the case of cadmium oxide this is not the most important cause of the increase in conductivity.

Specimens produced by compressing the powdered oxide were sintered at temperatures from 600°K to 1200°K and for times varying from 30 minutes to 180 hours. The Hall coefficient was measured after sintering using a potentiometric method and phosphor-bronze probes. The results for nine typical specimens are shown in table 1. The values of the impurity concentration n (assumed equal to the carrier concentration) are calculated from the Hall coefficient R using the simple relation:—

$$R = 1/n\varepsilon c. \qquad \ldots\ldots(2)$$

Lewis and Sondheimer (1955) have shown that, for all degeneracies of the electron gas in a polar crystal, equation (2) is always approximately true, and never involves errors greater than about 15%. Table 1 shows that there is no obvious simple correlation between the impurity concentration and the length and temperature of sintering. In particular there is no tendency for heavily sintered specimens to have a higher impurity concentration than those that have only been given a light sintering, although this result would clearly be expected if the main electrical characteristic of sintering were a large increase in carrier concentration.

Table 1. Sintering and Hall Coefficient Data for typical Specimens

Specimen Number	Sintering Temp. (°K)	Sintering Time (hr)	Hall Coeff. ($\mathrm{cm}^3\ \mathrm{coul}^{-1}$)	$n(\mathrm{cm}^{-3}) \times 10^{19}$
18	900	0·5	0·17	3·7
5	1200	36·0	0·29	2·3
61	600	12·0	1·0	0·62
4	1220	24·0	1·0	0·62
14	900	0·5	1·4	0·44
24	1200	0·5	1·5	0·41
35	600	180·0	2·0	0·32
28	1250	0·5	2·1	0·30
34	1100	0·5	3·2	0·20

A second set of experiments measured the Hall coefficient as a function of resistance and time during sintering. Several experimental difficulties were encountered. In the first place the Hall effect voltage is small compared with the ohmic voltage across the Hall probes V_0 which is due to the accidental misalignment of the probes with the isopotentials for zero magnetic field.

The changes in resistance of the specimen during sintering will clearly cause large, and at times rapid variations in V_0 so that the actual Hall voltage can only be measured approximately. A second difficulty is caused by the high resistance of the specimen at the beginning of the experiment. The resistance limits the current which may pass through the specimen, so that at the beginning of the experiment the Hall voltages obtained are relatively small. However, successful measurements were made on three specimens. These showed that the Hall coefficient is approximately independent of resistance for changes by a factor of over 10^4 in the latter. The results for a representative specimen are shown in figure 1.

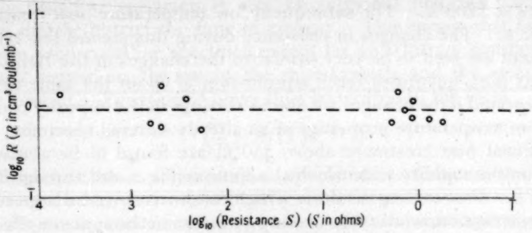

Figure 1. Logarithmic plot of the Hall coefficient R against resistance S for specimen 32 during sintering at 540°K.

Both experiments show that the increase of conductivity during sintering is not primarily due to an increase in carrier concentration. An obvious alternative is to suggest that during sintering the resistances between individual microcrystals are greatly reduced. This might be due to some sort of diffusion process although the exact mechanism is unimportant for the discussion given in the next section. The marked increase of the strength of specimens which always accompanies sintering supports this suggested explanation of the sintering process.

§ 3. Heat Treatment of already Sintered Specimens

Considerable changes of the electrical properties of specimens, which have already been thoroughly sintered, may be produced by an additional, relatively short, heat treatment at temperatures just above 550°K. Marked changes in the Hall coefficient and resistance of such specimens are easily produced. It seems unlikely that the intercrystalline resistances would be further affected by an additional low temperature heat treatment. This is in agreement with the results shown in figure 2. The specimen concerned had previously been sintered

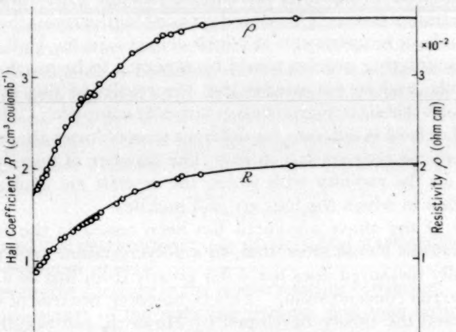

Figure 2. Variation of resistivity and Hall coefficient with time for specimen 35 during heat treatment at 600°K.

for 20 hours at 1200°K. The subsequent low temperature heat treatment took place at 600°K. The changes in resistance during this second low temperature heat treatment are seen to be very similar to the changes in the Hall coefficient. In particular both quantities reach equilibrium at about the same time. This would be expected if the changes are due to a change in the impurity content.

The room temperature properties of an already sintered specimen, subjected to an additional heat treatment above 550°K, are found to be almost entirely dependent on the rapidity with which the specimen is cooled through the region around 550°K. Fast cooling results in a high conductivity and a large conduction electron concentration, whilst slow cooling gives rise to the opposite effects. The same result has been reported for zinc oxide by Harrison (1954). Our results for cadmium oxide are shown in table 2. We feel that these results indicate that above a fixed temperature of about 550°K the defects become mobile. Thus, after a certain time at any fixed temperature, an equilibrium of defects in the lattice is attained (see figure 2). This process, though of necessity included in the initial sintering process, is of negligible effect when compared with the major changes due to the very large decrease in intercrystalline contact resistances.

Table 2. Specimens Sintered at 1200°K with various Rates of Cooling

Specimen Number	24	26	27
Rate of cooling at 600°K (deg sec^{-1})	20	0·05	0·05
Hall coefficient R at 300°K (cm^3 coul^{-1})	1·49	4·2	4·6
$(\partial\rho/\partial T)\times 10^5$ (ohm cm deg^{-1})	2·22	9·30	10·50
$R^{-4/3}(\partial\rho/\partial T)\times 10^5$ (ohm cm^{-3} deg^{-1} coul$^{4/3}$)	1·30	1·37	1·37

If it is assumed that the carrier donors are interstitial cadmium atoms then it is possible to relate the sintering process to the mobility of these donors above 550°K. It is suggested that the bridging of the microcrystalline gaps during sintering is due to mobile cadmium ions. This would account for the result that the sintering process occurs only at temperatures at which changes in the Hall coefficient are observed. This sintering process would be expected to be much more rapid at high temperatures, and so we assume that the results of this section concern specimens in which this sintering process is virtually complete. The equilibrium concentration of defects is different for different temperatures above the temperature region where the ions are frozen in. The number of ions frozen into the lattice depends on the rapidity with which the crystals are cooled through the temperature region in which the ions are still mobile.

The validity of the above argument has been tested in the following way. Simple considerations would show that, in a polycrystalline specimen, the Hall coefficient actually measured does not differ greatly from that of a single crystal with the same carrier concentration. This is, however, not true of the resistivity. For a single crystal the theory developed by Howarth and Sondheimer (1953) shows that the resistivity ρ can be written as

$$\rho=\rho_0+\frac{2\alpha^2\boldsymbol{e}^2m^2}{3^{1/3}a^3M\boldsymbol{kh}}\,\frac{\pi^{4/3}}{T\sinh^2(\Theta/2T)}\,\frac{1}{n^{4/3}} \qquad \ldots\ldots(3)$$

where a is the distance between oppositely charged adjacent lattice ions, $1/M$ is the sum of the reciprocals of the masses of the ions, $\alpha\boldsymbol{e}$ is the ionic charge, $m=m_0G$ is the effective electron mass, and Θ is the characteristic temperature for lattice vibrations. In order to eliminate the residual resistance ρ_0, the temperature coefficient of resistance is measured. Equation (3) gives on differentiation

$$\frac{\partial\rho}{\partial T}=\frac{2\pi^{4/3}\alpha^2\boldsymbol{e}^2m_0{}^2G^2}{3^{1/3}a^3M\boldsymbol{kh}T^2}\,\frac{n^{-4/3}}{\sinh^2(\Theta/2T)}\left\{2\left(\frac{\Theta}{2T}\right)\frac{\cosh(\Theta/2T)}{\sinh(\Theta/2T)}-1\right\} \qquad \ldots\ldots(4)$$

For a polycrystalline specimen it may be supposed that the intercrystalline boundaries merely restrict the flow of current. This means that equation (4) is valid for a polycrystalline specimen except for an arbitrary constant, and this constant will depend on the size of the microcrystals and the areas of microcrystalline contact. Equation (4) may thus be written in the form

$$\frac{\partial\rho}{\partial T}=Af(T)n^{-4/3} \qquad \ldots\ldots(5)$$

which will be true for a polycrystalline specimen. As discussed above, short low temperature heat treatments of heavily sintered specimens would be expected to change the carrier concentration but not to affect the intercrystalline contacts. In terms of equation (5) a second low temperature heat treatment would be expected to change n but not A. Substituting the value of n from equation (2) it follows directly that

$$\frac{\partial\rho}{\partial T}R^{-4/3}=\text{const.} \qquad \ldots\ldots(6)$$

This equation should be true for a heavily sintered specimen when subject to any additional heat treatments. Table 3 shows the results of measurements of the Hall coefficient and temperature coefficient of resistance for specimen 50 both before and after 90 mins heat treatment at 700°K. The results are in surprising agreement with equation (6). Table 2 shows results for three specimens prepared and sintered in exactly the same way but cooled at different rates. These specimens had effectively the same high temperature heat treatment but different subsequent low temperature heat treatments. In terms of equation (5) we should except the same value of A but different values of n. Again the results are in good agreement with equation (6). It seems probable that such good agreement is partly fortuitous. In particular equation (6) assumes that the electron gas is completely degenerate. This is only an approximation in the cases considered, even assuming the low value for the effective electronic mass previously reported for cadmium oxide.

Table 3

	Before	After
Hall coefficient R at 300°K (cm^3 coul^{-1})	2·13	3·58
$(\partial\rho/\partial T)\times10^5$ (ohm cm deg^{-1})	1·71	3·64
$R^{-4/3}(\partial\rho/\partial T)\times10^6$(ohm cm^{-3} deg^{-1} coul$^{4/3}$)	6·3	6·6

§ 4. CONCLUSIONS

It is suggested that two processes may occur in heat treatment of polycrystalline specimens of cadmium oxide:

(i) An irreversible decrease in the intercrystalline resistance. This is thought to form the major part of the sintering process, and may reduce the specimen resistance by a factor of 10^8 or more.

(ii) A reversible change in the equilibrium impurity content of any specimen heated above 550°K. The room temperature conductivity and carrier concentration of a sintered specimen thus depend considerably on the rate of cooling at about 550°K.

REFERENCES

HARRISON, S. E., 1954, *Phys. Rev.*, **93,** 92.
HOWARTH, D., and SONDHEIMER, E., 1953, *Proc. Roy. Soc.* A, **219,** 253.
LEWIS, B., and SONDHEIMER, E., 1955, *Proc. Roy. Soc.* A, **227,** 241.
WRIGHT, R. W., and BASTIN, J. A., 1958, *Proc. Phys. Soc.*, **71,** 109.

The Optical Model at Low Energies and Dispersion Theory

By G. E. BROWN† and C. T. DE DOMINICIS‡

† Department of Mathematical Physics, University of Birmingham
‡ Centre d'Etudes Nucléaires de Saclay

Communicated by R. E. Peierls; MS. received 22nd January 1958, and in final form 19th March 1958

Abstract. Neutron scattering in the low energy region where the compound levels are well separated is considered in detail. It is shown that the average phase can be reproduced by that calculated from a complex potential. The imaginary part of this potential is simply related to the absorption out of the incident beam into compound states. Formulae for the average behaviour of various quantities are derived in a simple and straightforward fashion.

§ 1. Introduction

THE average behaviour of the elastic scattering of low energy neutrons by complex nuclei shows certain characteristics, such as giant resonances in the total cross section, which can be reproduced theoretically by replacing the nucleus by a complex potential (Feshbach, Porter and Weisskopf 1954). This complex potential is supposed to give the average phase of the scattering, determining what is called the 'shape elastic' scattering.

In a previous paper (Brown and De Dominicis 1957 a, to be referred to as I) we have put dispersion theory into a form convenient for discussing this problem, and have shown that the average scattering amplitude can indeed be reproduced by a suitably chosen complex potential. It was also noted that the imaginary part W was simply related to absorption out of the incident beam into compound states. However, as remarked in the note added in proof in I the evaluation of W was carried out erroneously, although the final result was correct.

In this paper we shall consider in detail the low energy region where $\overline{\gamma_{\mathrm{p}}/D} \ll 1$, where γ_{p} is the level width and D is the distance between levels. We shall relate average features of the scattering to the amplitude from the complex well, and shall give a correct and improved derivation of the relation between W and the absorption. Since we are concerned with low energies, we need consider only s-wave scattering.

Much of the development here was given in I and is, therefore, not new. However, several points will be made more precise or corrected.

§ 2. Development

In I we showed that the elastic scattering amplitude for a wave in channel α could be expressed as $\hat{S}_\alpha + s_\alpha{}^{\mathrm{ce}}$ where $\hat{S}_\alpha$ is the amplitude from a complex well $\hat{V}(r)$, and $S_\alpha{}^{\mathrm{ce}}$ is given by

$$S_\alpha{}^{\mathrm{ce}} = -\frac{2M}{\hbar^2 k}\left\{\langle 0\alpha|V-\hat{V}|0\alpha\rangle - \langle 0\alpha|(V-\hat{V})\frac{1}{H-E}(V-\hat{V})|0\alpha\rangle\right\}. \qquad \ldots\ldots(1)$$

---

† Now at the Institute for Theoretical Physics, Copenhagen.

Here V is the actual potential, H the complete Hamiltonian, $|0\alpha\rangle$ is the wave function with the nucleus in the ground state and the incident nucleons in channel α. The notation is explained in detail in I.

A potential $\hat{V}$, which will reproduce the average phase is defined by requiring $\bar{S}_\alpha{}^{\mathrm{ce}}$, the average of $S_\alpha{}^{\mathrm{ce}}$ over an energy interval $\bar{I}$ large compared with the compound-nucleus level width γ_{p}, to be zero. This $\hat{V}$ is defined, then, by requiring the average of the second term in brackets in equation (1) to equal the first term, which varies slowly with energy and need not be averaged. Setting $\hat{V}=-U-iW$ and assuming W to be constant out to some radius R (the generalization to the case of a non-constant W is easy and will be indicated later) we have

$$W=\mathscr{I}\sum_p \overline{\frac{\langle 0\alpha|V-\hat{V}|p\rangle^2}{\langle 0\alpha|0\alpha\rangle(W_p-E)}} \qquad \ldots\ldots(2)$$

where W_p is the energy of the pth compound state $(W_p=\epsilon_p-i\alpha_p/2$ where ϵ_{p} and α_p are real). Equation (2) is obtained from (1) by inserting the unit operator $p\rangle\langle p$ into the second term in braces there.

Of course if one allows the complex potential to vary arbitrarily rapidly with energy and angular momentum l a potential can be found which will reproduce the average phase. If, however, this potential were to vary appreciably over distances of the order of the separation of compound nucleus levels (several electron volts in the energy region we consider here), it would not be a useful quantity for describing the scattering. The usefulness of the $\hat{V}$ which is found empirically to fit the average scattering phase (Feshbach *et al.* 1954) comes from the fact that it varies slowly and regularly with energy and that the same depth and radial dependence can be used for all angular momenta.† In I we demonstrated that $U=-\hat{V}$ to a good accuracy. Hence, U is independent of l, and varies only slowly with energy, this variation resulting from polarization, as discussed in I, and from other velocity dependence coming from nucleon–nucleon exchange forces.

It is not easy to show that W varies slowly with energy. Empirically, in making fits to the experimental data, W is assumed either to be constant, as a function of energy, or to vary only slowly, over distances of the order of the separation of single-particle levels in the well. Our treatment at the present stage is still phenomenological, i.e. we relate W to other quantities, notably the absorption. We have not yet developed the framework for deriving this latter quantity from more fundamental ones. This latter problem seems to be a difficult one; we will return to it briefly at the end of the paper.

The development sketched so far is sufficient to obtain the averages of various important quantities in terms of the parameters of $\hat{V}$, and we will proceed to do this first.

§ 3. VARIOUS AVERAGES

We wish now to obtain the value of the strength function $\overline{\gamma/D}$ in terms of the single-particle parameters. At the same time, we will discuss the behaviour of average cross sections in this low energy region. These averages are related to those calculated by Feshbach, Porter and Weisskopf (1954), who used a single level Breit–Wigner formula with a variable nuclear 'radius' R' to describe the behaviour of the scattering amplitude over one compound resonance. They make the treatment more precise in their Appendix by relating their formulae to the R-matrix theory of Wigner and Eisenbud (1947). These averages have also been carried out by Thomas (1955) in the R-matrix formalism. The development in this section, therefore, does not give new results; it will, however, employ a different formalism, due to Kapur and Peierls, which allows a simple and direct treatment. This formalism has been found previously to be convenient to describe average features of both the elastic and inelastic scattering (Bloch 1957, Brown and De Dominicis 1957 a, b).

---

† Of course, we expect a spin–orbit term to be present also, so that the potential is not strictly independent of l. However, here the l-dependence occurs in a simple way through the $\boldsymbol{\sigma}.\mathbf{L}$ prefixing the radial function, the latter being common to all l.

The complete scattering amplitude can be expressed in the Kapur–Peierls formalism as

$$S_\alpha = \frac{e^{-2ikR}}{2} \sum_p \frac{\gamma_p}{W_p - E} - \sin kR e^{-ikR}. \qquad \ldots\ldots (3)$$

This is an equivalent form to $S_\alpha = \hat{S}_\alpha + S_\alpha{}^{\text{ce}}$ with $S_\alpha{}^{\text{ce}}$ given by (1). One can easily obtain it by replacing $V - \hat{V}$ by $H - \hat{H}$ in (1) and operating on the wave functions. Now the preceding development has shown that $\bar{S}_\alpha$ is equal to $\hat{S}_\alpha$, the scattering by the complex potential $\hat{V}$, if the latter is determined by the procedure described above. This amplitude can be expressed (Brown 1957) in a single particle resonance formalism as

$$\hat{S}_\alpha = \frac{e^{-2ikR}}{2} \sum_m \frac{\Gamma_m}{E_m - E} - \sin kR e^{-ikR} \qquad \ldots\ldots (4)$$

where $E_m = \epsilon_m - \frac{1}{2} i \beta_m - iW$ with ϵ_m, β_m and W real. In this low energy region $\beta_m \simeq \Gamma_m$, $\Gamma_m \ll W$. (It will be assumed that $kR \ll 1$, as in the corresponding part of the article of Feshbach, Porter and Weisskopf 1954.)

We assume $E \simeq \epsilon_n$ since we wish to consider in detail the region of the single particle resonance in this paper, the region between the single particle resonances having been adequately treated in I.

We have shown in I that the contribution from the distant compound levels p lying in the neighbourhood of the mth resonance is well represented by the mth term in (4). Therefore, since $\bar{S}_\alpha = \hat{S}_\alpha$ the following relations must hold for the near compound-nucleus levels

$$P_n(E) + iQ_n(E) \equiv \overline{\sum_p{}' \frac{\gamma_p}{W_p - E}} = \frac{\Gamma_n}{E_n - E} \qquad \ldots\ldots (5)$$

where P and Q are real and the prime on the sum indicates that it is to be carried out only over those compound nucleus levels lying in the region of the nth single particle level. To lowest order in $\overline{\gamma/D}$, $Q_n(E)$ is found by the averaging procedure of Feshbach, Porter and Weisskopf to be equal to $\pi\overline{\gamma/D}$. We cannot express $P_n(E)$ more simply in terms of γ_p. Thus we have

$$\left.\begin{aligned} P_n(E) &= \frac{(\epsilon_n - E)\Gamma_n}{(\epsilon_n - E)^2 + (W + \Gamma_n/2)^2} \\ Q_n(E) = \pi\overline{\gamma/D} &= \frac{\Gamma_n(W + \Gamma_n/2)}{(\epsilon_n - E)^2 + (W + \Gamma_n/2)^2}. \end{aligned}\right\} \qquad \ldots\ldots (5.1)$$

In the following development we will usually neglect the $\Gamma_n/2$ occurring in $W + \Gamma_n/2$; it will be shown that keeping it would give a correction of higher order in kR.

We can now understand the behaviour of average cross sections at low energies. It is shown in Appendix A that on a single particle resonance $\hat{S}_\alpha$ is given well by one term in the sum in (4) for the case treated there, where $\hat{V}$ is a square well of radius R. Thus, for $E \simeq \epsilon_n$,

$$\bar{S}_\alpha \simeq \tfrac{1}{2} e^{-2ikR} \left\{ i\pi \left(\overline{\frac{\gamma}{D}}\right) + P_n(E) \right\} - \sin kR \, e^{-ikR} \simeq i\frac{\pi}{2} \left(\overline{\frac{\gamma}{D}}\right) + (\tfrac{1}{2}P_n - kR). \quad .(5.2)$$

The cross section σ_{se} for shape elastic scattering, defined as

$$\sigma_{\text{se}} = \frac{4\pi}{k^2} |\bar{S}_\alpha|^2 \qquad \ldots\ldots(5.3)$$

is given by

$$\sigma_{\text{se}} = 4\pi R^2 \left\{ \left(\overline{\frac{\pi\gamma}{2kRD}}\right)^2 + \left(1 - \frac{P_n}{2kR}\right)^2 \right\}. \qquad \ldots\ldots(5.4)$$

Now both $\overline{\pi\gamma/2kRD}$ and $P_n/2kR$ are independent of k, since Γ_n contains k as a factor. For a square well of radius R,

$$\Gamma_n = \frac{2k\hbar^2}{MR} = 2kR\left(\frac{\hbar^2}{MR^2}\right). \qquad \ldots\ldots(5.5)$$

We shall use this Γ_n in making rough estimates to give the qualitative behaviour of quantities.

We see from (5.1) that for $\epsilon_n \simeq E$, $\overline{\pi\gamma/2kRD} = (\hbar^2/MR^2)/W$. Now if R is taken as $\frac{1}{2}e^2/mc^2 A^{1/3}$, $\hbar^2/MR^2 \simeq (20/A^{2/3})$ MeV. Remembering that W is of the order of 2 MeV, we see that $\overline{\pi\gamma/2kRD}$ is not always negligible compared with unity on the single-particle resonances. (The estimate of Blatt and Weisskopf 1952, Chap. VIII, would give it as of the order of 10^{-2}.) It should be noted that the expression (5.1) allows one to evaluate this quantity in the neighbourhood of a single particle resonance for a potential $\hat{V}$ of more realistic shape.

For heavy nuclei the term $\overline{\pi\gamma/2kRD}$ can usually be neglected because there $\hbar^2/MR^2$ is small compared with W in which case

$$\sigma_{\text{se}} \simeq 4\pi R'^2 \qquad \ldots\ldots(5.6)$$

with

$$R' = R(1 - P_n/2kR). \qquad \ldots\ldots(5.7)$$

The quantity R' need, of course, never be introduced. For a numerical comparison between theory and experiment it is more straightforward to evaluate $\hat{S}_\alpha$ from a suitable potential. However, R' is often used in the discussion of experiments, especially in connection with the total cross section (see, for example, Hughes 1956), which we shall treat next. As we have indicated, R' does not have the significance of a nuclear radius. Even in the case of strong coupling where W is large, and therefore $R = R'$ since P_n is small, R' is not the nuclear radius since R is only some radius introduced in order to define compound states. The calculation of averages from $\hat{V}$ directly is more satisfactory, in that one need never introduce R or R'.

The average total cross section can easily be found from the relation

$$\sigma_{\text{T}} = \frac{4\pi}{k^2} \mathcal{I} S_\alpha \qquad \ldots\ldots(6)$$

giving

$$\bar{\sigma}_{\text{T}} = \frac{4\pi}{k^2} \mathcal{I} \bar{S}_\alpha = \frac{4\pi}{k^2} \mathcal{I} \hat{S}_\alpha. \qquad \ldots\ldots(6.1)$$

On a single particle resonance, where only one term in the sum in (4) need be used,

$$\bar{\sigma}_{\mathrm{T}} = \frac{2\pi}{k} Q_n(E) + 4\pi R^2 \left\{ \left(1 - \frac{P_n}{2kR}\right)^2 - \left(\frac{P_n}{2kR}\right)^2 \right\} \qquad \ldots\ldots(6.2)$$

where we have kept $Q_n(E)$ rather than replacing it by $\pi\overline{(\gamma/D)}$ since the relation (5.1) between these two quantities is valid only to lowest order in $\overline{\gamma/D}$. The first term on the right-hand side of (6.2) goes as $1/k$ (or $1/v$) for low energies; the second term is constant as a function of k. For heavy nuclei, this term is approximately $4\pi R'^2$, with R' given by (5.7) since there $P_n/2kR$ is small compared with unity. From (5.1) we see that P_n changes sign at $E=\epsilon_n$; thus R' will oscillate about R when plotted as a function of A, being equal to R at the single particle resonances. This is the behaviour observed experimentally (see Hughes 1956). Of course, for a numerical comparison with experiment, one would again calculate $\bar{\sigma}_{\mathrm{T}}$ directly from $\hat{V}$.

It is seen now from equations (5.1) and (5.5) and noting that $\hbar^2/MR^2$ is of the order of W for medium weight nuclei, that the conditions that $\pi\overline{\gamma/D}$ be small compared to unity on a single particle resonance, that $kR \ll 1$ and that $\Gamma \ll W$ are all equivalent.

§ 4. RELATION OF W TO THE ABSORPTION

In I we tried to find the variation of W as a function of energy across a single particle resonance from a relation equivalent to (2). In fact, however, if one evaluates the right-hand side of (2) using the various averages found in the last section, one finds that it is just equal to W. Thus, this only shows consistency in our averaging procedure, and does not allow us to deduce any properties of W. We now sketch briefly how this proceeds, giving in the process the relations which will be necessary for our relation of W to the absorption into compound states. We will carry out the development for the case where the energy is on one of the single particle resonances; the scattering is most sensitive to W at this point.

If the energy is on the nth single particle resonance, we can replace $|0\alpha\rangle$ in (2) by the nth term in the sum,

$$|0\alpha\rangle = \langle 0m|0\alpha\rangle |0m\rangle \qquad \ldots\ldots(7)$$

where $|m\rangle = \hat{\phi}_m(r)$ are the single particle eigenfunctions in the complex well defined in I. Equation (2) becomes then

$$W = \mathscr{I} \sum_p \overline{\frac{\langle 0n|V-\hat{V}|p\rangle^2}{W_p - E}}\,. \qquad \ldots\ldots(8)$$

Now

$$\langle 0n|V-\hat{V}|p\rangle = \langle 0n|H-\hat{H}|p\rangle = (W_p - E_{0n})\langle 0n|p\rangle \quad \ldots\ldots(8.1)$$

giving

$$W = \mathscr{I} \sum_p \overline{\frac{(W_p - E_{0n})^2}{W_p - E}\langle 0n|p\rangle^2}\,. \qquad \ldots\ldots(8.2)$$

Now, the $\langle 0n|p\rangle^2$ occurring on the right are just γ_p/Γ_d and their average value can be obtained from (5.1). After substitution, one finds that the right-hand side of (8.2) is just equal to W. Thus, (8.2) does not give us any information about the energy variation of W; when the various averages are carried out correctly, it is an identity and therefore indicates consistency.

The evaluation of the right-hand side of (8.2) was carried out erroneously in I where only terms for which ϵ_p fell into the interval I were kept. If the evaluation sketched in the preceding paragraph is carried out, it is found that large contributions come from distant terms, in which ϵ_p lies outside I; in fact, from terms over the entire single particle resonance considered. The results of the better treatment sketched here were, however, given in a note added in proof to I.

We can now easily connect W with the absorption into compound states. The cross section for this was evaluated in the Appendix of I under the assumption that cross terms coming from different compound states in the expression for the cross section could be neglected. This is certainly valid at low energies, cross terms being of order γ/D smaller. The result was

$$\sigma_p = 2\pi C |\langle p|V - \hat{V}|0\alpha\rangle|^2 \qquad \ldots\ldots (9)$$

where

$$C = (2l+1)4\pi M/k^3\hbar^2. \qquad \ldots\ldots (9.1)$$

Our $\overline{\sigma_p/D}$ is equivalent to $\bar{\sigma}_c$, the average cross section for compound nucleus formation, of Feshbach, Porter and Weisskopf (1954). We will next evaluate the quantity

$$T(E) = \frac{\pi}{D} \frac{\overline{|\langle_p|V - \hat{V}|0\alpha\rangle|^2}}{\int_0^R ||0\alpha\rangle|^2 \, d\tau}. \qquad \ldots\ldots (10)$$

Assuming once again that the energy is on a single particle resonance and using (7) and (8.1) we find

$$T(E) = \overline{\frac{\pi}{D} |W_p - E_{0n}|^2 |\langle 0n|p\rangle|^2}.$$

Dropping γ_p compared with W and remembering that $\langle 0n|p\rangle$ are real in our approximation, we have

$$T(E) = [(\epsilon_p - \epsilon_{0n})^2 + W^2]\pi \frac{\overline{\langle 0n|p\rangle^2}}{D}. \qquad \ldots\ldots (10.2)$$

Once again, $\langle 0n|p\rangle^2 = \gamma_p/\Gamma_n$ so that, using (5.1), the above becomes

$$T(E) = W. \qquad \ldots\ldots (11)$$

Now, the $\int ||0\alpha\rangle|^2$ in the denominator of (10) can be understood as the probability of the particle in channel α being inside the nucleus. Thus, (10) can be interpreted as saying that W is proportional to the average probability of forming a compound state per unit density of the incident nucleon in the nucleus. One might intuitively expect this quantity to change slowly with incident energy. In the Appendix of I the derivation of equation (10) was carried out in a somewhat different formalism from that used here. In Appendix B of this paper we give, for completeness, a derivation in the present formalism.

The calculation has been carried out for a W that is constant out to the radius R. The generalization to non-constant W is made by replacing W on the left-hand side of (2) by $\langle n|W|n\rangle$. It is inherent in our formalism, starting from equation (1) that we can determine only matrix elements of W, and not W itself. The determination of these matrix elements as a function of angular momentum l of the incident nucleon seems to be equivalent to the determination of W as a function of r, since different regions are important for different angular momenta. This is clearly beyond the scope of the present work, which deals only with s-waves.

§ 5. DISCUSSION

We have shown in the preceding work that the average scattering amplitude can be reproduced by a suitably chosen complex well. The real part of this well was previously shown to be equal to $V(r)$, the value of the actual potential $V(r, \xi)$ averaged over the nuclear ground state. The imaginary part W is shown here to be related to the absorption into compound states by the argument, equations (9)–(11).

Within the context of the present work we cannot obtain the energy variation of W and, in fact, we cannot even show that W is a slowly varying function of energy. It is easily seen (see (5.1)) that W is simply related to the strength function, but we cannot calculate the strength function in our present formalism, which is more of a phenomenological analysis in that it relates various physical quantities with each other. It may prove possible to calculate the strength function using perturbation theory (see Bloch 1957). However, it is by no means clear that the perturbation expansion is valid. It can be seen that perturbation theory will give the average amplitude correctly provided that the average is carried out over a sufficiently large energy interval, as noted by Bloch. However, simple order of magnitude estimates show that this interval may have to be large compared with the width of the single particle resonance, i.e. large compared with W. If this is so, it is then not possible to say anything about the variation of the average amplitude over the single particle resonance from perturbation theory. We are looking into the conditions for validity of perturbation theory at present.

If the strength function is of Lorentz form, then it is clear from (5.1) that W is constant. However, it is not clear that the strength function is of this form and indeed it cannot be so in the wings or it would give an infinite second moment. This is not permissible in our development, which is so far restricted to well-behaved potentials (in particular, we excluded hard core potentials, although the formalism can probably be generalized to handle this case).

Thus it seems to us that—although from our discussion following equation (11) it is most reasonable that W is constant—one should be prepared to consider the consequences of a variation of W with energy;† the precise nature of the variation would depend on that of the departure of the strength function from the Lorentz form. In particular, it is conceivable that W varies non-monotonically across a single particle resonance.

The scattering amplitude for energies off the single particle resonances is insensitive to the value of W, as can be seen by equation (4). It was shown by Brown (1957) that only in exceptional cases is the energy on a single particle resonance, these being very far apart. Thus, it is clear that a variation of the type suggested in W would not affect the theoretical amplitudes over most of the energy range. Such a variation would affect the amplitudes over the region of the single particle resonance, however.

Now the empirical fits to experiment do not seem to us to be sufficiently accurate to rule out such a variation. We can illustrate this in the following way. It is well known that there is a spin–orbit force in the shell model, and this must split the single particle resonances for non-zero angular momenta into two peaks. This effect is certainly as large as any effect from the variation in W would be expected to be. However, this effect has not been exhibited clearly in the experiments, nor is the spin–orbit term included in most of the theoretical analyses applying to the region of separated compound resonances. Thus, we would not expect to see the effect we noted here either in the existing experimental evidence.

---

† We mean here a variation more rapid than the slow and monotonic velocity dependence given by existing optical model fits at various energies.

Although we have not derived the optical model in all detail then, in that we have not either shown that W is constant over a single particle resonance or obtained its energy variation, we have shown that most of the experimental features can be reproduced by the simple model described in I, where only very weak assumptions were employed. It is clear from our development in I and here that any deviation from the simple optical model, in which the parameters vary slowly and regularly with energy, would only be likely to occur for energies which are on a single particle resonance. It is, therefore, also clear that if deviations from the simple optical model occur, they will be found for such energies. This would thus seem to be the region in which to carry out precision experiments.

ACKNOWLEDGMENTS

The authors would like to thank Professor R. E. Peierls for many helpful discussions relating to this work, from which several of the ideas employed here, especially those in Appendix C, arose. They are also grateful to Dr. A. M. Lane for useful suggestions, and to Mr. J. S. Langer for much helpful criticism.

APPENDIX A

It will be shown here that, if the energy E is on a single particle resonance, the $\hat{S}_\alpha$ scattering from a square well is given well by one term in the sum in (4) together with the $\sin kR\mathrm{e}^{-ikR}$ term.

We can easily find the exact expression for $\hat{S}_\alpha$ in terms of the logarithmic derivative f_0 at the edge of the well. This is

$$\begin{aligned}\hat{S} &= \frac{\mathrm{e}^{-2ikR}}{2i}\left\{\frac{f_0+ikR}{f_0-ikR}\right\}-1\\ &= \frac{(1/2i)(\mathrm{e}^{-2ikR}-1)+\frac{1}{2}kRf_0^{-1}(\mathrm{e}^{-2ikR}+1)}{1-ikRf_0^{-1}} \qquad \ldots\ldots(\mathrm{A1})\end{aligned}$$

where

$$f_0=(K+i\kappa)R\tan^{-1}(K+i\kappa)R \qquad \ldots\ldots(\mathrm{A\,1.1})$$

with K and κ the real and imaginary parts of the wave number in the well. Now f_0^{-1} can also be expressed (Thomas 1955) by

$$f_0^{-1}=\sum_m\frac{\hbar^2/MR^2}{E_m'-E-iW}. \qquad \ldots\ldots(\mathrm{A\,2})$$

The energies E_m' are those at which the derivative of the wave function at R is zero; to a very good approximation (Brown 1957) these E_m' are equal to our E_m. Also the absolute value of f_0^{-1} can never become smaller than the order of unity because of the W in the denominator, so we can neglect the $ikRf_0^{-1}$ in the denominator in (A1) to lowest order in kR. Comparing (A1) and (4) and remembering that $\Gamma_m=2k\hbar^2/MR$ we see that the requirement that $\hat{S}_\alpha$ be given well by one term in the sum in (4) is equivalent to that that f_0^{-1} be given well by one term in (A2). It is easy to verify by comparing (A 1.1) and one term of (A2) that f_0^{-1} is given correctly to lowest order in κ/K by the nth term as long as $E-\epsilon_n$ is of the order of W or less. This ratio is small, approximately equal to $W/2U$, which is 0·01–0·04 in the low energy region.

APPENDIX B

Here we shall derive the connection between W and the cross section for compound nucleus formation using the formalism of this paper.

The average cross section for compound nucleus formation can be written

$$\bar{\sigma}_{\mathrm{c}} = \frac{4\pi}{k^2}\{\mathscr{I}\hat{S} - |\hat{S}|^2\}. \qquad \ldots\ldots(\mathrm{B1})$$

Using equation (4) and remembering that Γ_n is of order kR, we obtain to lowest order in kR

$$\bar{\sigma}_{\mathrm{c}} \simeq \frac{4\pi}{k^2}\sum_m \frac{W\Gamma_m/2}{(E-\epsilon_m)^2+W^2}. \qquad \ldots\ldots(\mathrm{B2})$$

We have from equation I (19)

$$|0\alpha\rangle = \left(\frac{\hbar^2 k}{2M}\right)\sum_m \frac{\hat{\phi}_m(R)\hat{\phi}_m(r)}{(E-\epsilon_m)+iW} \qquad \ldots\ldots(\mathrm{B3})$$

to lowest order in kR.

Hence, we see immediately that

$$\frac{\bar{\sigma}_{\mathrm{c}}}{\int_0^R ||0\alpha\rangle|^2\, d\tau} = \frac{8\pi M}{\hbar^2 k^3} W. \qquad \ldots\ldots(\mathrm{B4})$$

It is clear from (B2) that we are keeping only that part of the absorption which relates to inelastic scattering. This is, of course, justifiable, because the compound elastic scattering, which should be included in the absorption, is of order kR smaller than the inelastic scattering at the energies we consider.

APPENDIX C

In I and in Brown (1957) a velocity-dependent potential well $\hat{V}$ was used to describe the average scattering by the nucleus. For completeness, we include here a demonstration that dispersion theory can be used to obtain the scattering amplitude in a velocity-dependent well.

The well used in the optical model can be considered as velocity-dependent in either of two senses. Usually the depth of the well is taken to vary with bombarding energy, i.e. it is taken to be a function of k. This would mean that in dispersion theory the energies of the levels would vary appreciably with energy. (In our theory they unavoidably vary with energy because the boundary condition is dependent on k. However, it was shown by Brown (1957) that this variation was very slight.) In I we implied that the well was velocity-dependent in the other sense, namely, that the depth of the well was different for the different eigen energies at a given k. This was used in showing that the contribution to the scattering amplitude from distant compound-nucleus levels corresponding to a given single particle level was equal to that from the single particle level to within a good approximation. Such a velocity-dependent well $\hat{V}$ can conveniently be discussed by considering it to be a non-local operator $\hat{V}(\mathbf{r}', \mathbf{r})$, which is equivalent to considering a velocity-dependent potential. We will now see what conditions it must satisfy.

We denote the eigenfunctions in this well by $\hat{\phi}_m(\mathbf{r})$, i.e.†

$$T(r')\hat{\phi}_m(\mathbf{r}') + \int \hat{V}(\mathbf{r}', \mathbf{r})\hat{\phi}_m(\mathbf{r})\, d^3r = E_m \hat{\phi}_m(\mathbf{r}'). \qquad \ldots\ldots(\mathrm{C1})$$

Here T is the kinetic energy operator. We multiply on the left by $\hat{\phi}_n(\mathbf{r}')$, integrate and then subtract the corresponding equation obtained by interchanging m and n, obtaining:

$$\int \hat{\phi}_n(\mathbf{r}')\hat{V}(\mathbf{r}', \mathbf{r})\hat{\phi}_m(\mathbf{r})\, d^3r'\, d^3r - \int \hat{\phi}_m(\mathbf{r}')\hat{V}(\mathbf{r}', \mathbf{r})\hat{\phi}_n(\mathbf{r})\, d^3r\, d^3r'$$
$$= (E_m - E_n)\int \hat{\phi}_m(\mathbf{r})\hat{\phi}_n(\mathbf{r})\, d^3r \qquad \ldots\ldots(\mathrm{C2})$$

where we have used the fact that $\hat{\phi}_m$ and $\hat{\phi}_n$ obey the same boundary condition (see Brown 1957, eqn (1.1)). A sufficient condition for orthogonality of the $\hat{\phi}_n$'s is then that $\hat{V}(\mathbf{r}', \mathbf{r}) = \hat{V}(\mathbf{r}, \mathbf{r}')$, i.e. that $\hat{V}$ is symmetrical.

In order to see how this restricts the momentum dependence of $\hat{V}$, we go over to a mixed representation, first introducing the new variables

$$\mathbf{R} = \tfrac{1}{2}(\mathbf{r} + \mathbf{r}'), \qquad \mathbf{x} = \tfrac{1}{2}(\mathbf{r} - \mathbf{r}'). \qquad \ldots\ldots(\mathrm{C3})$$

The symmetry condition is, then, that

$$\hat{V}(\mathbf{R}, \mathbf{x}) = \hat{V}(\mathbf{R}, -\mathbf{x}) \qquad \ldots\ldots(\mathrm{C\,3.1})$$

in terms of the new variables. We expand the $\hat{\phi}$'s in the integrand of the matrix element

$$\hat{V}_{mn} = \int \hat{\phi}_m(\mathbf{R} - \mathbf{x})\hat{V}(\mathbf{R}, \mathbf{x})\hat{\phi}_n(\mathbf{R} + \mathbf{x})\, d^3R\, d^3x \qquad \ldots\ldots(\mathrm{C\,3.2})$$

about $\mathbf{x} = 0$, obtaining

$$\hat{V}_{mn} = \int (\hat{\phi}_m(\mathbf{R}) - i\mathbf{x}\mathbf{p}_R\hat{\phi}_m(\mathbf{R}) + \ldots)\hat{V}(\mathbf{R}, \mathbf{x})(\hat{\phi}_n(\mathbf{R}) + i\mathbf{x}\mathbf{p}_R\hat{\phi}_n(\mathbf{R}))\, d^3R\, d^3x \qquad \ldots\ldots(\mathrm{C\,3.3})$$

where $\mathbf{p}_R = \nabla_R$ and the lower suffix denotes differentiation with respect to the $\mathbf{R}$-coordinate. By partial integration this can be converted into

$$\hat{V}_{mn} = \int \hat{\phi}_m(\mathbf{R})\{V_0 + [\tfrac{1}{2}i\mathbf{p}_R\mathbf{V}_1 + \tfrac{1}{2}i\mathbf{V}_1\mathbf{p}_R] + \ldots\}\hat{\phi}_n(\mathbf{R}) \qquad \ldots\ldots(\mathrm{C4})$$

where

$$V_0 \equiv \int \hat{V}(\mathbf{R}, \mathbf{x})\, d^3x, \qquad \mathbf{V}_1 \equiv \int \hat{V}(\mathbf{R}, \mathbf{x})\mathbf{x}\, d^3x. \qquad \ldots\ldots(\mathrm{C\,4.1})$$

The matrix element $\hat{V}_{nm}$ can be obtained from $\hat{V}_{mn}$ by changing the sign in front of the square brackets and, in general, by changing the sign of all terms odd in $\mathbf{p}_R$. Thus, the above symmetry condition on the $\hat{V}$ is equivalent to the requirement that V depend only on even powers of the momentum.

This will be satisfied by potentials which occur in practice. If they were to contain odd powers of the momentum, they would depend on the direction as well as the magnitude of the momentum. This would be completely unreasonable in infinite nuclear matter, where there is no preferred direction. In the case of the finite nucleus it is true that there is a spin–orbit term proportional to $\boldsymbol{\sigma} . \mathbf{L}$, and this does depend on the direction of the momentum. However, $\hat{\phi}_m$ and $\hat{\phi}_n$ will be eigenfunctions of $\boldsymbol{\sigma} . \mathbf{L}$ and, therefore, this will come out as a factor after operation. It would seem unreasonable for the potential to depend on the direction of the radial velocity, i.e. to be different for particles going inwards and outwards. Furthermore, a term of the type $\mathbf{r} . \mathbf{p}$ would inviolate invariance under time reflection.

---

† We would like $\hat{V}(\mathbf{r}', \mathbf{r})$ to be zero whenever either r' or r is greater than some radius R which is of the order of nuclear dimensions. This puts strong conditions on the velocity dependence of $\hat{V}$. If $\hat{V}$ is to be confined to this region, then Δp, the momentum over which it varies, must be at least as great as $\hbar/R$. Hence, the energy ΔE over which it varies is $\Delta E = p\Delta p/m = v\Delta p \geqslant v\hbar/R$. But this latter quantity is just ΔE_m, the distance between single-particle levels. Thus, our description of $\hat{V}$ as a non-local potential of nuclear dimensions could not be carried through if $\hat{V}$ were to vary rapidly with energy.

Completeness of the eigenfunctions would seem to follow from the proof indicated by Peierls (1947) for the eigenfunctions of the Kapur–Peierls dispersion theory. The essential point for this proof is that the particle behaves as free for sufficiently high energies, and this will be so for any well with a reasonable velocity dependence.

REFERENCES

BLATT, J. M., and WEISSKOPF, V. F., 1952, *Theoretical Nuclear Physics* (New York : John Wiley).
BLOCH, C., 1957, *Nuclear Physics*, **4**, 503.
BROWN, G. E., 1957, *Proc. Phys. Soc.* A, **70**, 681.
BROWN, G. E., and DE DOMINICIS, C. T., 1957 a, *Proc. Phys. Soc.* A, **70**, 668; 1957 b, *Ibid.*, **70**, 681.
BROWN, G. E., and LEVINGER, J. S., 1958, *Proc. Phys. Soc.*, **71**, 733.
FESHBACH, H., PORTER, C. E., and WEISSKOPF, V. F., 1954, *Phys. Rev.*, **96**, 448.
HUGHES, D. J., 1956, *Physica 's Grav.*, **22**, 994.
PEIERLS, R. E., 1947, *Proc. Camb. Phil. Soc.*, **44**, 242.
THOMAS, R. G., 1955, *Phys. Rev.*, **97**, 224.
WIGNER, E. P., and EISENBUD, L., 1947, *Phys. Rev.*, **72**, 29.

A Comparative Study of Ultrasonic Absorption in $MnSO_4$ with $MgSO_4$ Solutions

By G. S. VERMA[†] and S. K. KOR
Department of Physics, University of Allahabad, Allahabad, India

MS. received 10th September 1957, and in revised form 20th January 1958

Abstract. Ultrasonic measurements in $MnSO_4$ in the frequency range 1–6 Mc/s made by the optical method have been compared with those in $MgSO_4$. The concentration behaviour of the absorption and the relaxation frequency, which has been studied in great detail in the range 0·0025 to 1 molar, has been compared with the earlier results in $MgSO_4$. The effect of the dielectric constant and the temperature on the absorption, relaxation frequency and the reaction rate support the dissociation hypothesis.

§ 1. Introduction

Ultrasonic absorption in electrolytes has been studied in great detail by Kurtze and Tamm (1953), Eigen *et al.* (1953), Tamm and Haddenhorst (1954), Tamm *et al.* (1954), and by Wilson (1951). 2–2 valence electrolytes, in general, showed large excess absorption. Tamm investigated the following sulphates, $BeSO_4$, $NiSO_4$, $MgSO_4$, $CoSO_4$, $MnSO_4$, $ZnSO_4$ and $CuSO_4$. Wilson whose results confirm Tamm's, investigated $BeSO_4$, $MgSO_4$ and $ZnSO_4$.

In $MgSO_4$ it was observed that the value α/ν^2 rapidly increases with decreasing frequency at frequencies below 1 Mc/s. It was established from the measurements of absorption in sea water by Liebermann (1948), Leonard (1950), Leonard *et al.* (1949) using spherical resonator methods, that the absorption can be represented by a relaxation curve with a maximum at 130 kc/s.

A chemical relaxation process was assumed to be responsible for the excess sound absorption in $MgSO_4$. Liebermann (1949) proposed that either a unimolecular process or a dissociation type process involving $MgSO_4$ molecules or its ions might be the cause of excess sound absorption. Assuming dissociation process to be responsible for the excess sound absorption, he suggested the absorption to be proportional to the square root of the concentration. But it was shown later by independent measurements of Leonard and Wilson, and Kurtze and Tamm that the absorption is linearly proportional to the concentration. This led to the suggestion that a unimolecular process involving a relaxing transition between two energy states of the ion pairs may be the cause of the excess absorption. But it was pointed out by Barthel (1952) that if the activity coefficients of the ions are taken into account, Wilson's data can be fitted equally well with either the unimolecular or dissociation type process. Bies (1955) considered the variation of the activity coefficients with the passage of the sound wave and derived new equations for the excess sound absorption per wavelength and the relaxation frequency assuming a dissociation process. He found $MgSO_4 \rightleftharpoons Mg^{2+} + SO_4{}^{2-}$ to be responsible for the excess sound absorption. The mechanism is assumed to be pressure dependent and the absorption arises due to its irreversible perturbation by the sound field. He applied these calculations to measurements in $MgSO_4$.

[†] Now at Ultrasonic Research Laboratory, Western Reserve University, Cleveland, Ohio.

However, other dissociation mechanisms have been suggested. According to Barthel, the following reaction may be responsible for the excess sound absorption:

$$Mg^{2+} + H_2O \rightleftharpoons MgOH^+ + H^+.$$

Kurtze and Tamm assume the formation of the complex of MeR, H_2O which represents the normal undissociated state of the electrolyte

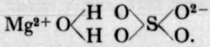

$$Mg^{2+}\,O\begin{smallmatrix}H\\ H\end{smallmatrix}\;\begin{smallmatrix}O\\ O\end{smallmatrix}S\begin{smallmatrix}O^{2-}\\ O.\end{smallmatrix}$$

For this complex two different possibilities of dissociation are assumed.

In one of the possibilities two univalent ions are formed at first,

$$MgSO_4.\ H_2O \rightarrow MgOH^+ + HSO^-_4$$

which each split up in a subsequent step

$$MgOH^+ + HSO_4^- \rightarrow Mg^{2+} + OH^- + H^+ + SO_4^{2-}.$$

The first step is acoustically inefficient. The two dissociation processes in the second step are independent of each other and cause one relaxation mechanism each. The lower maximum at 130 kc/s is ascribed to the dissociation of $MgOH^+$ and the higher one at 200 Mc/s due to the dissociation of HSO_4^-. The second possibility may consist in the separation of either the metal ion or the radical ion from the complex in the form

$$\begin{aligned}(MgSO_4.H_2O) &\rightarrow Mg^{2+} + H_2OSO_4^{2-}\\ &\rightarrow MgH_2O^{2+} + SO_4^{2-}.\end{aligned}$$

The first one with the higher activation energy may correspond to the lower relaxation frequency and the second one with the lower activation energy with the higher relaxation frequency.

$MnSO_4$ has been investigated by Kurtze and Tamm (1953), Carstensen (1954), more recently by Smithson and Litovitz (1956) and by the authors. The relaxation frequency lies near about 3 Mc/s. A secondary relaxation peak has been reported by Smithson and Litovitz near 30 Mc/s. Using heavy water as a solvent they have shown that the decomposition of water or any other reaction involving the hydrogen ion can not be the rate determining step. They rule out further the reaction between two ions of unlike sign as the rate determining step. According to them the experimental results can be explained on the assumption that the reaction is between two dipole molecules. The reaction might be of the type

$$MnSO_4 + H_2O \rightleftharpoons Mn\,.\,H_2O^{2+} + SO_4^{2-}.$$

They consider this reaction to be of the first order because of the excess of the solvent.

§ 2. CONCENTRATION BEHAVIOUR OF THE SOUND ABSORPTION AND RELAXATION FREQUENCY

2.1. *Sound Absorption*

According to Kurtze and Tamm the excess sound absorption in all of the 2–2 valence inorganic electrolytes is approximately linearly dependent upon the concentration. In particular the absorption cross section of $MgSO_4$, $MnSO_4$,

$ZnSO_4$ and $CuSO_4$ is approximately constant over the range 0·001 – 0·1 molar, but slightly diminishes at concentrations above approximately 0·1 molar. Wilson carried out the measurements on the concentration behaviour of excess sound absorption in $MgSO_4$ in somewhat more detail in the concentration range 0·003–0·02 molar. According to him the relationship between the excess sound absorption and the concentration is non-linear, in fact, the absorption cross section tends to zero as the concentration goes to zero.

Smithson and Litovitz (1956) studied the absorption in $MnSO_4$ at four different concentrations, namely 0·05, 0·10, 0·15, and 0·20 molar. In order to determine the exact nature of the concentration behaviour of the ultrasonic absorption in $MnSO_4$, a great detailed study of ultrasonic absorption in $MnSO_4$ at different concentrations varying from 0·0025 to 1 molar has been undertaken. The relationship between the excess sound absorption and concentration is found to be linear from 0·02 to 0·1 molar, but becomes non-linear below and above 0·1 molar (figures 1 and 2). This is in agreement with Wilson's observations in $MgSO_4$ at low concentrations and Kurtze and Tamm's results above 0·1 molar.

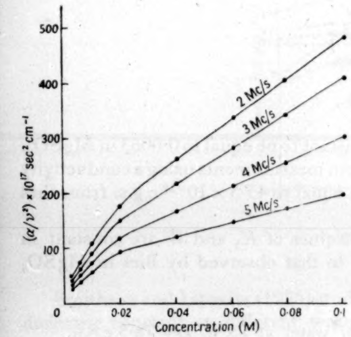

Figure 1.

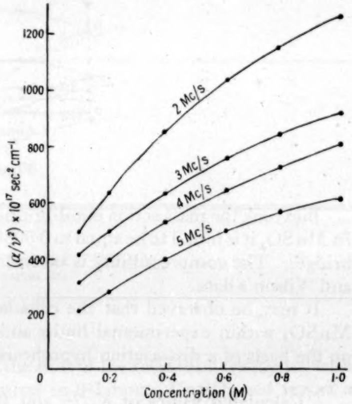

Figure 2.

2.2. *Relaxation Frequency*

According to Wilson's measurements in $MgSO_4$, the relaxation frequency remains approximately constant in the range of concentration 0·003–0·02 molar. Tamm also reports that the relaxation frequency is approximately constant in the range 0·01–0·1 molar.

In $MnSO_4$ Smithson and Litovitz report no effect of the concentration on the secondary relaxation frequency and detect no shift of the primary relaxation frequency with concentration but, according to them, there is indication of small increase beyond 0·1 molar. According to our measurements the relaxation frequency is independent of the concentration in the range 0·02–0·1 molar, but increases with concentration in the range 0·0025–0·02 molar (figure 3). It again varies with concentration above 0·1 molar.

§ 3. CALCULATIONS SIMILAR TO THAT OF BIES IN $MgSO_4$

Utilising equations for the excess sound absorption per wavelength and the relaxation frequency given by D. A. Bies on the assumption that the dissociation process $(AB) \rightleftharpoons (A) + (B)$ is pressure dependent and the absorption arises because of the irreversible perturbation of the dissociation equilibrium, values of the various constants and the reaction rates have been found. His results in $MgSO_4$ are also given for comparison.

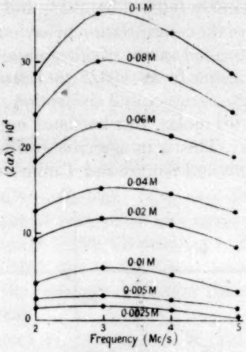

Figure 3.

Bies took the mass action equilibrium constant to be equal to 0·0063 in $MgSO_4$. In $MnSO_4$ it is found to be equal to 0·0050 from measurements using a conductivity bridge. The compressibility is taken to be equal to $45{\cdot}5 \times 10^{-12}$ c.g.s. from Bies and Wilson's data.

It may be observed that the calculated values of K_1 and W are constant in $MnSO_4$ within experimental limits similar to that observed by Bies in $MgSO_4$ on the basis of a dissociation hypothesis.

Calculated values of $K_1/2\pi$ and W for water at 25°c, $D = 78{\cdot}5$ e.s.u.

	$MnSO_4$		$MgSO_4$	
Concentration	$K_1/2\pi$ (Mc/s)	$W \times 10^2$ (cm^6 mole^{-2})	$K_1/2\pi$ (Mc/s)	$W \times 10^3$ (cm^6 mole^{-2})
0·0025	2·1	18·1	114	6·04
0·005	2·2	13·0	112	9·57
0·010	2·2	12·3	101	9·59
0·020	2·2	12·5	116	8·82

§ 4. EFFECT OF THE DIELECTRIC CONSTANT

According to Kurtze and Tamm the electrolytic dissociation is caused by the dipole forces of the molecules of the solute, a measure for which is the dielectric constant of the liquid. With the lowering of the dielectric constant of the solvent medium they expect an increase in the dissociation energy which will result in lowering the relaxation frequency. Shift of the relaxation frequency towards the lower values was experimentally verified by them using water–alcohol mixtures in $MgSO_4$. Bies used water–dioxane mixtures of dielectric constants 67·0 and 56·5 and studied the variation of relaxation frequency with dielectric constant. At a particular concentration the relaxation frequency, according to his measurements, increases at first and then decreases. He finds out the forward reaction rate K_1 from the intercept of the graph of relaxation frequency against concentration. The forward reaction rate K_1, too, first increases and then decreases with the lowering of the dielectric constant. One of the objections put forward by Smithson and Litovitz (1956) against dissociation hypothesis is the lack of any explanation for such anomalous behaviour of the reaction rate K_1. At present there does not seem to be any explanation for it.

But similar calculations performed for the determination of the forward reaction rate K_1, in our measurements for $MnSO_4$ using water–dioxane mixtures for varying the dielectric constant (56·5 and 48·0) show that it continuously increases slightly with the lowering of the dielectric constant [$D = 78{\cdot}5$, $K_1/2\pi\,(\mathrm{Mc/s}) = 2{\cdot}38$; $D = 56{\cdot}5$, $K_1/2\pi = 2{\cdot}90$; $D = 48{\cdot}0$, $K_1/2\pi\,(\mathrm{Mc/s}) = 3{\cdot}00$] (figure 4).

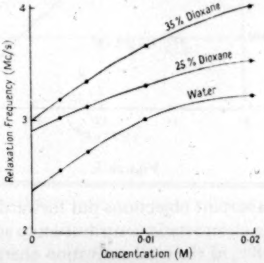

Figure 4.

Smithson and Litovitz (1956) studied the shift of the relaxation frequency with dielectric constant at different temperatures in 0·1 molar $MnSO_4$ and report a slight lowering of the relaxation frequency always with the lowering of the dielectric constant of the solvent. On the other hand, the second relaxation frequency increases with the lowering of the dielectric constant. They, however, question the propriety of arriving at any conclusion on the basis of the effects of dielectric constant about the possibility that the dissociation of an ion pair is the rate determining process in bi-valent salts.

§ 5. Effect of Temperature

The effect of the increase in temperature is to shift the relaxation frequency to higher values with the amount of maximum absorption remaining almost unchanged. A plot of log ν_m/T against $1/T$ yields a straight line as found by Wilson for $MgSO_4$ and by Kurtze and Tamm for $MgSO_4$, $CoSO_4$ and $NiSO_4$. Tamm has reported a detailed series of measurements for 0·05 molar solution of $MgSO_4$ from 11°c to 80°c. The experimental activation energy of the relaxation process can be obtained from the shift of the relaxation frequency with temperature. He obtained about 6·5 kcal mole^{-1} for $MgSO_4$. Wilson gives somewhat higher value for the activation energy.

Smithson and Litovitz from their measurements on $MnSO_4$ at 0·10 molar obtain 8·68 kcal mole^{-1} for the activation energy for the iso-dielectric solution. They studied the temperature shift of the relaxation frequency in the range 5–47°c. Our measurements were performed in the range 20–60°c on 0·1 molar $MnSO_4$. The experimental activation energy comes out to be equal to 0·8 kcal mole^{-1} (figure 5) which is about one tenth of the value obtained by Smithson and Litovitz. One of the important objections put forward by them against dissociation hypothesis is that the electrostatic contribution to activation energy comes out to be equal to just only 8% of the total activation energy where ΔE (total) = ΔE_1 (electrostatic) + ΔE_2 (non-electrostatic). This may suggest that contribution to the activation energy in our case is mostly electrostatic. However, using our own data for $d(K_1)/d(1/D) = -14$ and $d(K_1)/d(1/T) = 3 \times 10^2$ it can be shown, following the method outlined by Amis and Jaffe (1942) that the contribution of electrostatic energy is nearly 50%, which should be the case in a reaction involving two bivalent ions. Moreover $\{d(K_1)/d(1/T)\}/\{d(K_1)/d(1/D)\} < T/D$ which shows further, according to Amis, that the reaction involves ions of the opposite signs. Thus the dissociation hypothesis may still hold good.

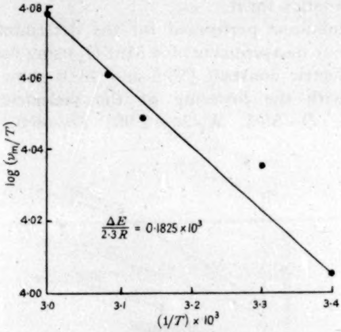

Figure 5.

Acknowledgments

The authors would like to express their grateful thanks to Prof. K. Bannerji for his helpful suggestions and discussions and to the Council of Scientific and Industrial Research for a research grant. One of the authors would like to thank Dr. Ernest Yeager for his valuable discussions.

REFERENCES

AMIS, E. S., and JAFFE, G., 1942, *J. Chem. Phys.*, **10**, 646.

BARTHEL, R., 1952, *J. Acoust. Soc. Amer.*, **24**, 313.

BIES, D. A., 1955, *J. Chem. Phys.*, **23**, 428.

CARSTENSEN, E. L., 1954, *J. Acoust. Soc. Amer.*, **26**, 862.

EIGEN, M., KURTZE, G., and TAMM, K., 1953, *Z. Electrochemie*, **57**, Heft 2, 103.

KURTZE, G., and TAMM, K., 1953, *Acustica*, **3**, 33.

LEONARD, R. W., 1950, *Technical Report* No. I, University of California, Los Angeles.

LEONARD, R. W., COMBS, P. C., SKIDMORE, L. R., 1949, *J. Acoust. Soc. Amer.*, **21**, 63.

LIEBERMANN, L., 1948, *J. Acoust. Soc. Amer.*, **20**, 868; 1949, *Phys. Rev.*, **76**, 1520.

SMITHSON, J. R., and LITOVITZ, T. A., 1956, *J. Acoust. Soc. Amer.*, **28**, 462.

TAMM, K., and HADDENHORST, H. G., 1954, *Acustica*, **4**, 653.

TAMM, K., KURTZE, G., and KAISER, R., 1954, *Acustica* **4**, 380.

WILSON, O. B., Jr., 1951, *Technical Report* No. 4, University of California, Los Angeles.

The Polarization of Protons from the $^{12}C(d, p)^{13}C$ Reaction

By M. S. BOKHARI, J. A. COOKSON, B. HIRD and B. WEESAKUL
Nuclear Physics Research Laboratory, University of Liverpool

Communicated by H. W. B. Skinner; MS. received 23rd December 1957

Abstract. The polarization of the ground state protons emitted when ^{12}C is bombarded with 8·9 MeV deuterons has been measured at several angles. These results have been compared with recent calculations of Newns and Refai. The angular distribution of the polarization was found to have the predicted shape but its sign and magnitude suggest an improbable proton–nucleus interaction.

---

§ 1. INTRODUCTION

CONSIDERABLE experimental work on (d, p) angular distributions has established them as a useful tool in nuclear spectroscopy when analysed by a stripping theory such as that of Butler (1951) or Bhatia *et al.* (1952). For deuterons of several MeV energy and light nuclei, the experimental and theoretical angular distributions are sufficiently close to establish that the stripping mechanism predominates.

Attempts to improve the fit to the experimental curves have been made by several authors (Tobocman and Kalos 1955, Grant 1955, Yoccoz 1954): these take into account some of the various additional interactions which are expected to occur, but which are neglected in the earlier stripping theories. Some improvements to particular cases of the angular distributions have been obtained, but the relative importance of these additional interactions is not clearly established.

More experimental evidence of these interactions can be obtained by measuring the sign and magnitude of the polarization of the emitted protons. The simple stripping theories, since they neglect all interactions of the proton once it is separated from the neutron and all interactions of the deuteron before being stripped, always give zero for the polarization. The measurement of polarization therefore provides a sensitive test of those assumptions.

The polarization to be expected from certain specific interactions has been calculated for particular (d, p) reactions. Newns (1953) assumed the nucleus to be totally absorbing to the outgoing protons while Horowitz and Messiah (1953) and Hittmair (1956) represented the interaction by a scattering potential. Yoccoz (1954) considered the consequence of Coulomb forces on both the deuterons and protons. A more phenomenological picture where the proton-nucleus interaction is represented by a complex potential with a spin–orbit coupling term was used by Cheston (1954). All these various calculations resulted in polarizations which rose to about 30% at certain angles, but they differed in sign. Recently Newns and Refai (private communication, to be published) have calculated the effect, separately and in various combinations of a hard sphere interaction for the incoming deuterons, and a complex potential with and without a spin–orbit term for the outgoing protons. Their results will be discussed in detail later.

Hillman (1956) has experimentally determined the polarization of the ground state protons emitted at 30° from the ^{12}C(d, p)^{13}C reaction using 4·05 MeV deuterons. His value of $-58\% \pm 13\%$ has the same sign but is more than twice as great as that predicted by Cheston.

We have chosen to investigate the same ^{12}C(d, p)^{13}C ground state group because of its good proton yield, and because there is sufficient separation between this and the first excited state group for it to be resolved with our rather poor energy resolution.

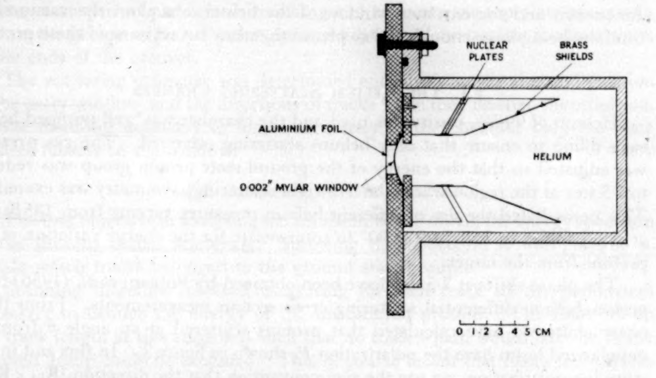

Figure 1.

Nuclear emulsions were used to measure the asymmetry produced when the protons were scattered in helium. The phase shifts for the proton helium elastic scattering process are sufficiently well known for the proton polarization to be calculated from this asymmetry.

§ 2. Experimental Arrangement

About 1 μA of 8·9 MeV deuterons from the Liverpool 37 in. cyclotron were double-focused with a wedge magnet on to a carbon target 6 metres from the cyclotron. The target consisted of a self-supporting strip of pile graphite 0·7 cm × 2·5 cm and 14 mg cm^{-2} thick. The beam, after passing through the target, was stopped and measured on a thick water-cooled gold foil. The protons emitted from the target over a wide range of angles passed out of the chamber through a Mylar window 0·002 in. thick. The angle of the target to the beam was adjusted to minimize the energy spread in the protons at the angle being investigated. To obtain the maximum proton flux the deuteron beam was allowed to fall on the full width of the target which thus defined the size of the source of protons.

The protons from the target chamber passed through a vacuum cell 57 cm long with a Mylar window 0·0005 in. thick at each end, and entered the helium scattering chamber. The side walls of the cell were lined with paraffin so that neutrons from the target would have to pass through almost the whole length of paraffin if they were to reach the nuclear emulsion unscattered. The proton directions entering the helium chamber were defined entirely by the target dimensions and the entrance window of the helium chamber, the vacuum cell windows being large enough and so placed that they cut off none of these protons.

§ 3. THE HELIUM SCATTERING CHAMBER

Helium of 99·5% purity was used and the chamber was well pumped before each filling to ensure that only helium scattering occurred. The gas pressure was adjusted so that the energy of the ground state proton group was reduced to 7·5 MeV at the region where the left–right scattering asymmetry was examined. This necessitated the use of different helium pressures varying from 185 lb in^{-2} at small angles to 75 lb in^{-2} at 90° to compensate for the energy variation of the protons from the target.

The phase shifts at 7·5 MeV have been obtained by Putnam *et al.* (1956) from proton–helium differential scattering cross section measurements. From these phase shifts we have calculated that protons scattered at an angle θ from an unpolarized beam have the polarization P_2 shown in figure 2. In this and in the stripping polarization, we use the sign convention that the direction $[\mathbf{K}_{\text{in}} \times \mathbf{K}_{\text{out}}]$ is positive, where $\mathbf{K}_{\text{in}}$ and $\mathbf{K}_{\text{out}}$ are the wave vectors of the incident and emitted particles respectively.

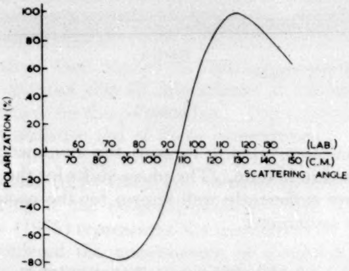

Figure 2. Proton–helium polarization P_2 at 7·5 MeV.

The nuclear plates, 1 in. square, were located vertically on either side at 60° to the direction of the unscattered protons, so that tracks in the emulsion at dip angles between 0° and 30° corresponded to helium scattering angles between 60° and 90° with a slight correction for scattering not in the horizontal plane. Protons scattered at angles of about 100° and larger or from the back of the chamber were screened from the plates by brass covers.

Ilford E1 emulsion of thickness 100 μ was used. This type of emulsion was found to be sufficiently insensitive to γ-rays so that shielding other than the paraffin was unnecessary. To measure the effects of the neutron background an extra plate was placed immediately beneath each of the others so that it was shielded from the helium scattered protons. Because of their close proximity, the two plates on one side recorded equal numbers of knock-on protons from the neutron background. Thus the difference in track counts between them represented the true helium scattering.

The plates were held in accurately cut grooves. A leaf spring served both to keep each pair of plates from touching and to locate the top plate accurately against the groove edges. Further springs kept the plates against accurate stops at the ends of the grooves.

The scattering geometry was determined entirely from the size and position of the entry window, and the directions of tracks when they reached the emulsion. It was therefore necessary to locate accurately in the chamber only the plate holders relative to the window.

§ 4. ANALYSIS OF THE TRACKS

The first objective in analysing the emulsion was to obtain the energy spectrum of the protons before scattering. Knowing this spectrum it was possible to decide which tracks belonged to the ground state group.

Scanning therefore involved measuring for each track all the parameters necessary to deduce the energy of the unscattered protons. The limit set on the track length at this stage was such that no track which would later lie in the selected group could be excluded. This of course meant that many more tracks were recorded than were eventually used.

The criteria adopted were that the track must (i) start on the emulsion surface and be entering not leaving, (ii) be at less than 45° to the horizontal, (iii) have a projected length on the emulsion surface of at least 50 μ, (iv) not dip into the unshrunk emulsion at an angle greater than 30°.

To eliminate the variation of track density over each plate identical areas were scanned on the left and right plates. Personal and microscope variations were minimized by the same scanner, using the same microscope, always scanning corresponding areas on the two top plates. Where a region on one plate was found to be unscannable because of scratching or fogging, the corresponding area was ignored on the other plate. The scanned area in most exposures was the centre 1·5 cm × 1 cm of each plate.

The steps used to obtain the energy spectrum from the track parameters involved calculating in turn for each track, (i) the energy of the proton at the emulsion surface, (ii) the energy loss in the helium between the centre of the scattering volume and the emulsion surface, (iii) the scattering angle, obtained from the dip angle and angle to the horizontal of the track in the emulsion, (iv) the energy before scattering.

As a measure of the personal errors in scanning, the 15° exposure was examined independently by two sets of scanners and their results compared, track for track. In the energy range above 7 MEV it was found that out of 257 tracks on the left plate three had been missed and five tracks were missed out of 317 on the right plate. There were personal tendencies to overestimate or underestimate the dip angles so that a few tracks dipping at nearly 30° did not appear in both scannings. This should not affect the asymmetry if each scanner was consistent. It thus appeared that the scanning was sufficiently reliable for our purpose.

The value of P_2, which represents the efficiency of the helium scattering as a polarization analyser, varies considerably over the range 60° to 90°. Tracks which had been accepted as belonging to the ground state group were therefore sorted into groups according to their scattering angle and angle to the horizontal.

The ratio of tracks on the left plate L to those on the right plate R which have been scattered in the helium at angle θ, for protons emitted to the right from the carbon target, is

$$\frac{L}{R}=\frac{1-P_1P_2\cos\phi}{1+P_1P_2\cos\phi}.$$

Here P_1 is the polarization of the protons produced in the stripping process. ϕ is the angle between the planes of stripping and helium scattering. Both θ and ϕ are calculated from the dip and angle to the horizontal of each track in the emulsion. We wish to determine P_1 and therefore require the mean value of

$$P_1=\frac{R-L}{(R+L)P_2\cos\phi}.$$

Taking the statistical errors on L and R as $\sqrt{L}$ and $\sqrt{R}$, the error in $(R-L)/(R+L)$ is $2(LR)^{1/2}/(R+L)^{3/2}$. Using this error as a measure of the weighting of each group of tracks, the weighted mean of all the groups is

$$\overline{P}_1=\frac{\sum(L-R)P_2\cos\phi(L+R)^2/4LR}{\sum[(L+R)^3/4LR]P_2{}^2\cos^2\phi}$$

and the statistical error of this mean is $[\sum[(L+R)^3/4LR]P_2{}^2\cos^2\phi]^{-1/2}$. In a few of the groups L or R was zero and the formula fails. For these groups we took the error on both L and R to be $[\frac{1}{2}(L+R)]^{1/2}$. This gives them approximately the correct importance in the summations.

§ 5. RESULTS

5.1. *Angles up to* 60°

Figure 3 shows the energy spectrum obtained for protons emitted at 15° from the target. The width of the peak is roughly what is to be expected from the target thickness, track straggling, and accuracy of the track calculation. This energy resolution is sufficient to set 7 MeV as a lower energy cut off above which tracks are certain to belong to the ground state group. The spectra for protons emitted at the larger angles up to 60° showed the same clearly defined peaks.

The underneath plates showed a much smaller number of tracks. When analysed in the same way and with the same cut off as for the upper plates, one track on each side was found in a quarter of the area scanned on the upper plates. The exposure at 50° showed three tracks on each underneath plate on a similar area. As a further check the entire scanning area of the 30° plates was examined. This yielded three tracks on the left plate, and one track on the right.

It seemed from this that the neutron background was small enough to be estimated for the other runs at intermediate angles.

5.2. *The* 90° *Angle*

The energy spectrum here showed a less well defined peak. However, its shape on the left and right plates was so similar that the calculated value of the asymmetry varied very little when different estimates of the energy spread of the ground state group were made.

The background track density from the underneath plate was 16 on the left and 12 on the right from the whole of the scanned area. These larger figures are what might be expected from the angles of the emulsion to the direction of the neutron flux from the cyclotron, and from the longer exposure.

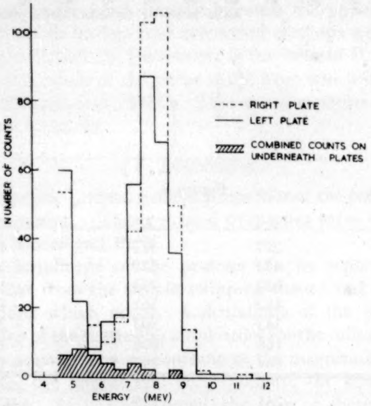

Figure 3.

To reassure ourselves that the sign and magnitude of the asymmetry were produced by the polarization and not by a wrongly loaded plate or misalignment of the helium chamber, a set of plates was examined which had received shorter irradiation at the 90° angle. In between this and the main run the apparatus had been dismantled and reassembled. 32 tracks were found on the left, and 16 on the right in the group, confirming the sign and at least roughly the magnitude. The results are given in the table and graphically in figure 4.

§ 6. ERRORS IN THE POLARIZATION

(i) The track density on each plate is approximately proportional to the inverse of the distance of that plate from the scattering volume. This distance must therefore be made accurately the same on the two sides.

The plate holders were lined up with respect to the entry window of the helium chamber by means of a template with fine lines scribed on it. This adjustment could be made with an estimated accuracy to ± 0·2 mm.

The stops at the ends of the grooves could cause a further misalignment of the plates with respect to the holders of ± 0·1 mm. These two errors together cause about ± 1% uncertainty in the polarization.

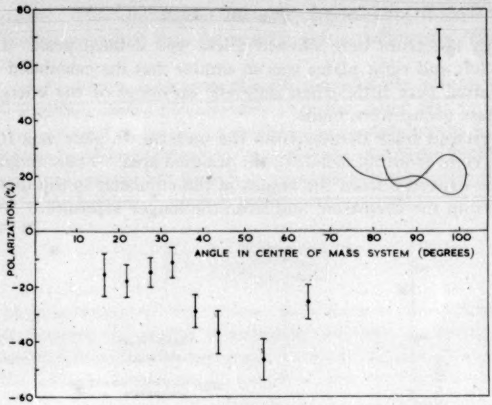

Figure 4.

θ (°)	*L*	*R*	*P* (%)
15±1	257	317	−15·7±7·8
20±1	433	539	−17·9±5·9
25±1	622	735	−14·9±5·3
30±1	482	561	−11·2±5·5
35±1	343	503	−28·9±6·0
40±1	166	268	−36·6±8·0
50±1	164	293	−46·5±7·5
60±1	307	425	−25·5±6·4
90±1	285	133	+62·2±10·1

The polarizations and errors in the table include the effects of geometrical as well as statistical variations. θ, angle of emitted protons (lab. system); *L*, *R*, number of tracks scattered left, right; *P*, polarization (%).

The effects of irregularities in the edges of the plates themselves were eliminated by supporting the plates on the microscope stage in the same way as they were supported in the helium chamber.

(ii) If the angles of the plates are incorrect all the scattering angles will be displaced from the calculated values. Such a displacement alters the plotted energy distribution only slightly in shape, but because the helium scattering differential cross section changes considerably between 60° and 90°, the numbers of tracks recorded will be affected. As with the positioning error it is the difference between the two sides which is important. An optical method was devised to measure this angular difference. The average difference measured in this way was 0·2°, with a spread of ±0·2° when the plates were removed and replaced repeatedly. This is responsible for a 1·5% correction and uncertainty in the polarization results.

(iii) Both the above types of error would also be introduced if the protons did not enter the chamber normal to its front face. The greatest uncertainty here lay in the width of the target and its lack of uniformity, rather than in the accuracy with which the helium chamber could be positioned. This uncertainty in direction provided a further 2% error in the polarization.

(iv) The variation of proton intensity over the solid angle of acceptance of the helium chamber was estimated using the angular distribution curve of Green and Middleton (1956). This resulted in a correction of between 1% and 2% to the polarization. At angles greater than 40° the angular distribution given by Rotblat (1951) suggests that it is nearly isotropic and no correction was made.

Errors which proved to be less important were due to the emulsion surfaces not being exactly vertical and a vertical displacement of one plate with respect to the other. These introduce uncertainties of order 0·1%.

Test runs were made (*a*) with no helium in the chamber and (*b*) with sufficient absorber to stop all protons from the target. Neither of these recorded any significant difference in the track density between the upper and lower plates and they confirm that our background correction methods were justified.

We decided not to include the uncertainty in the value of P_2 in our calculations, since the errors in the values of the phase shifts from which it is derived are not explicitly given by Putnam *et al.* (1956). This omission seems unlikely to increase our estimated errors seriously.

§ 7. DISCUSSION

It is possible to predict certain general properties of the polarization by means of a simple approximation. These general properties seem to be borne out by the calculations of Newns and Refai.

The scattering amplitude of the protons can be separated into the part corresponding to that from the simple stripping theory and contributions from the extra interactions which occur. Calculations of the polarization involve summing the squares of the scattering amplitudes for the different spin directions. If we expand these squared terms according to the magnitude of the amplitudes which they contain, the largest will correspond to the squares of the simple stripping amplitudes. As is well known, the sum of these over the different spin states is zero so that one obtains zero polarization from the simple stripping theory alone.

The next terms in the expansion, and therefore the ones which should be most important in determining the polarization, involve the cross products between the simple stripping amplitudes and the extra interaction amplitudes. Finally, there are the squared and cross product terms from the extra interactions alone. If we suppose that the latter are small then, as Newns and Refai have pointed out, the polarization will have the following properties which can be directly compared with our results: (i) the polarization should change sign at the same angle as the stripping amplitude; (ii) since we are concerned with a product of the simple stripping amplitude with the sum of the amplitudes from the additional interactions, the polarization from all the interactions is, in this approximation, the algebraic sum of the polarizations from each of the interactions considered separately.

We can compare these two predictions with our results. Using a reasonable value for the nuclear radius of ^{12}C of $4{\cdot}1 \times 10^{-13}$ cm, we find that the first sign change in the stripping amplitude occurs at 72°. This is in very good agreement with our measurements. The angular distribution of the polarization also shows a general similarity to the curves of Newns and Refai for the separate deuteron and proton interactions, being small at angles close to the stripping peak and rising to a maximum before changing sign. On the other hand the sign and magnitude are hard to fit. The large negative polarization means that the deuteron interaction must be important, and suggests that the proton interaction is less than the $-(19+0{\cdot}05i)$ MeV potential taken byNewns and Refai. Moreover, the measured polarization rises to more than the theoretical maximum of $33\frac{1}{3}\%$ for purely central forces. Newns and Refai find that the effect of including an additional proton interaction term $-2\mathbf{L}.\mathbf{S}$ MeV is to make the polarization slightly less positive. It may therefore be possible to obtain a fit by including a spin–orbit term of this sign but much larger in magnitude.

The strong deuteron interaction is, of course, to be expected physically. The proposed proton interaction, however, conflicts with the results of proton elastic scattering differential cross section measurements, which suggest that the central part has been underestimated, rather than overestimated, by Newns and Refai. These cross sections are not very sensitive to the amount of spin–orbit coupling, and at these energies, little is known of the magnitude of the latter. It seems unlikely, however, that it should be as large as our results and also the value at 4·05 MeV obtained by Hillman (1956) would require, and the exact explanation of the polarization remains uncertain.

ACKNOWLEDGMENTS

The authors wish to thank Professor H. W. B. Skinner for his support and encouragement, and Dr. H. C. Newns for helpful discussions and the communication of his results before publication. We are also indebted to Miss H. B. Burrows for scanning some of the plates and to Mr. W. H. Ward for running the cyclotron.

REFERENCES

BHATIA, A. B., HUANG, K., HUBY, R., and NEWNS, H. C., 1952, *Phil. Mag.*, **43**, 485.
BUTLER, S. T., 1951, *Proc. Roy. Soc.* A, **208**, 559.
CHESTON, W. B., 1954, *Phys. Rev.*, **96**, 1590.
FRIEDMAN, F. L., and TOBOCMAN, W., 1953, *Phys. Rev.*, **92**, 93.
GRANT, I. P., 1955, *Proc. Phys. Soc.* A, **68**, 244.
GREEN, T. S., and MIDDLETON, R., 1956, *Proc. Phys. Soc.* A, **69**, 28.
HILLMAN, P., 1956, *Phys. Rev.*, **104**, 176.
HITTMAIR, O. H., 1956, *Z. Phys.*, **144**, 449.
HOROWITZ, J., and MESSIAH, A. M. L., 1953, *J. Phys. Radium*, **14**, 731.
NEWNS, H. C., 1953, *Proc. Phys. Soc.* A, **66**, 477.
PUTNAM, R. M., BROLLEY, J. E., and ROSEN, L., 1956, *Phys. Rev.*, **104**, 1303.
ROTBLAT, J., 1951, *Nature, Lond.*, **167**, 1027.
TOBOCMAN, W., and KALOS, M. H., 1955, *Phys. Rev.*, **97**, 132.
YOCCOZ, J., 1954, *Proc. Phys. Soc.* A, **67**, 813.

Time Reversal and the Relation between Angular Distributions of Absorption and Emission Processes

By R. HUBY

University of Liverpool

MS. received 7th February 1958, *and in final form 26th March* 1958

Abstract. A simple rule is given for modifying the formula for the angular distribution of any process, however complicated, which involves absorption of a particle (or radiation) p in the transition stage $p + A \rightarrow B$ so as to yield the angular distribution of the process which differs only in the replacement of the absorption stage by an emission stage $A \rightarrow p + B$. The time-reversal operation is involved, and one is led to the time-reversal of density and efficiency matrices. and of statistical and efficiency tensors.

§ 1. INTRODUCTION

It is well known that the angular distributions of nuclear processes which involve the absorption of particles (or radiation) are closely related to those which involve emission. For example, a nuclear reaction

$$p + A \rightarrow B \rightarrow q + C, \qquad \ldots\ldots(1)$$

where A, B, C are nuclei, and p and q are particles (or radiation), may be compared with a correlation of two emitted cascade radiations:

$$A \rightarrow p + B \quad \text{followed by} \quad B \rightarrow q + C. \qquad \ldots\ldots(2)$$

Obviously, the same symbols in (1) and (2) cannot stand for the same particles throughout, but there is a close *formal* correspondence, as is exemplified by the fact that if all the particles are unpolarized, and if we specialize to the case that p is a nucleon and q is a photon, and only one channel is involved, then the angular distributions of *both* (1) and (2) are given by:

$$W(\theta) \propto (-1)^{I_C - I_A - \frac{1}{2}} \sum_k (j\tfrac{1}{2}, j-\tfrac{1}{2}|k0)(L1, L-1|k0)$$
$$\times W(I_B I_B jj; kI_A) W(I_B I_B LL; kI_C) \mathrm{P}_k(\cos\theta), \qquad \ldots\ldots(3)$$

where k is even; L is the multipole order of q; j is the total angular momentum of p; I_A, I_B and I_C are the spins of A, B and C respectively; and θ is the angle between the directions of p and q. In more complicated problems, the angular distribution of a process which involves the absorption of p in the transition

$$p + A \rightarrow B \qquad \ldots\ldots(4)$$

is not identical with, but is closely related to, the angular distribution of the process in which the stage (4) is replaced by emission

$$A \rightarrow p + B. \qquad \ldots\ldots(5)$$

Particular instances have often been noted, but the general, simple rule for obtaining the correspondence has not apparently been correctly given. This is of interest because, when a formula for the emission (or absorption) problem has been calculated, the rule obviates the need to calculate the other case afresh. Also, in view of the frequent errors in angular distribution formulae existing in the literature, this rule can be used as a check on correctness. A further point is that we are led to the concept of time-reversal of density and efficiency matrices and of statistical and efficiency tensors. The rule extracts an exact statement from the intuition that an emission process is the reverse in time of an absorption.

§ 2. THE RULE

We shall suppose that an angular distribution formula is expressed in terms of reduced matrix elements, and an example will be presented for clarity. The conventions generally will follow those of the review article of Devons and Goldfarb (1957). Eigenstates of angular momentum are supposed to be phased so that the effect of the time-reversal operator K is

$$K|JM\rangle=(-1)^{J-M}|J-M\rangle \qquad \ldots\ldots(6)\dagger$$

(Huby 1954). Our example is again represented by (1) and (2), p being a nucleon and q a photon as in § 1, but now it is supposed that p is initially polarized for the reaction (1), while for the emission (2) p is supposed to be observed by a polarization-sensitive detector, no other polarizations being taken into account. The reaction (1) is described by S-matrix elements which we express in an angular momentum representation, and these lead to reduced matrix elements by the relation

$$\langle I_C M_C, LM_L|S|I_A M_A, jm_j\rangle = \sum_{I_B M_B} (I_A M_A, jm_j|I_B M_B)(I_C M_C, LM_L|I_B M_B) \times \langle I_C, L\|S^{I_B}\|I_A, j\rangle. \qquad \ldots\ldots(7)$$

The cascade decay (2) is described by interaction matrix elements, which are again given in an angular momentum representation, and lead to reduced matrix elements

$$\begin{aligned}\langle I_C M_C, LM_L|H|I_B M_B\rangle\langle I_B M_B, jm_j|H|I_A M_A\rangle &\\ =(I_B M_B, jm_j|I_A M_A)(I_C M_C, LM_L|I_B M_B)&\\ \times \langle I_C, L\|H\|I_B\rangle\langle I_B, j\|H\|I_A\rangle. &\qquad \ldots\ldots(8)\end{aligned}$$

As a general rule, we use 'natural' matrix elements, in which an absorbed particle (or radiation) appears on the ket side and an emitted on the bra side. Also for a consistent mode of forming Clebsch–Gordan coefficients, as in

$$(I_A M_A, jm_j|I_B M_B),$$

we always put the nucleus A before the radiation p. The modifications ensuing

---

† This leaves the state vectors still undetermined to the extent that all the states of any set $|JM\rangle$ ($M=J \ldots\ldots -J$) may be multiplied by a common factor (-1). It would further be possible to use a phase convention alternative to (6), such that

$$K|JM\rangle=(-1)^{J+M}|J-M\rangle,$$

without causing any modification in the general rule.

in the results from the use of different conventions will be mentioned below.† The formula for the angular distribution of the reaction (1), allowing for several channels, is‡

$$
\begin{aligned}
W_{\mathrm{abs}}(\mathbf{k}_1,\mathbf{k}_2,\mathbf{P}) \propto \sum_{\substack{kI_BI_B'\\ jj'll'\\ L\pi L'\pi'}} & (-1)^{I_C-I_A-\frac{1}{2}}\hat{I}_A^{-2}\hat{I}_B^{2}\hat{I}_B'^{2}\hat{j}\hat{j}'\hat{L}\hat{L}' \\
& \times (j\tfrac{1}{2}, j'-\tfrac{1}{2}|k0)(L1, L'-1|k0)W(I_BI_B'jj';kI_A)W(I_BI_B'LL';kI_C) \\
& \times \langle I_C, L(\pi)||S^{I_B}||I_A, j(l)\rangle\langle I_C, L'(\pi')||S^{I'_B}||I_A, j'(l')\rangle^* \\
& \times [\mathrm{P}_k(\cos(\mathbf{k}_1,\mathbf{k}_2)) + if_k(jj',\tfrac{1}{2})(-1)^{l'}\mathrm{P}_k^{1}(\cos(\mathbf{k}_1,\mathbf{k}_2))\mathbf{P}\cdot\mathbf{n}], \qquad \ldots\ldots(9)
\end{aligned}
$$

where l is the orbital angular momentum of p, π is the parity of the photon multipole, k is even or odd according as $l+l'$ is even or odd, $(\mathbf{k}_1,\mathbf{k}_2)$ stands for the angle between the wave vectors $\mathbf{k}_1$ of p and $\mathbf{k}_2$ of q, $\mathbf{P}$ is the initial polarization of p, $\mathbf{n}$ is the unit vector in the direction $\mathbf{k}_1\times\mathbf{k}_2$,

$$\hat{I}_A = (2I_A+1)^{1/2},$$

and

$$f_k(jj',\tfrac{1}{2}) = \frac{(-1)^{j'+\frac{1}{2}}(j\tfrac{1}{2}, j'\tfrac{1}{2}|k1)}{[k(k+1)]^{1/2}(j\tfrac{1}{2}, j'-\tfrac{1}{2}|k0)}. \qquad \ldots\ldots(10)$$

The formula for the angular correlation (2) is‡

$$
\begin{aligned}
W_{\mathrm{em}}(\mathbf{k}_1,\mathbf{k}_2,\mathbf{P}) \propto \sum_{\substack{kI_BI_B'\\ jj'll'\\ L\pi L'\pi'}} & (-1)^{I_C-I_A-\frac{1}{2}+j-j'+I_B-I_B'+k}\hat{I}_B\hat{I}_B'\hat{j}\hat{j}'\hat{L}\hat{L}' \\
& \times (j\tfrac{1}{2}, j'-\tfrac{1}{2}|k0)(L1, L'-1|k0)W(I_BI_B'jj';kI_A)W(I_BI_B'LL';kI_C) \\
& \times \langle I_C, L(\pi)||H||I_B\rangle\langle I_B, j(l)||H||I_A\rangle\langle I_C, L'(\pi')||H||I_B'\rangle^*\langle I_B', j'(l')||H||I_A\rangle^* \\
& \times [\mathrm{P}_k(\cos(\mathbf{k}_1,\mathbf{k}_2)) - if_k(jj',\tfrac{1}{2})(-1)^{l'}\mathrm{P}_k^{1}(\cos(\mathbf{k}_1,\mathbf{k}_2))\mathbf{P}\cdot\mathbf{n}], \qquad \ldots\ldots(11)
\end{aligned}
$$

---

† *Alternative conventions.* There are many different conventions in use for the matrix elements in angular momentum representation and for the reduced matrix elements derived from these. Our reduced matrix element for reactions $\langle I_C, L||S^{I_B}||I_A, j\rangle$ is formed in the same way as Devons and Goldfarb's $\langle I_C\,L\,I_B|\mathcal{O}|I_A jI_B\rangle$ (1957, eqn. 24.1). Our emission reduced matrix element $\langle I_C, L||H||I_B\rangle$ is formed in the same way as Frauenfelder's $(I_C||L||I_B)$ (1955, eqn. 22) or Devons and Goldfarb's $\langle I_C||L||I_B\rangle$ (1957, eqn. 10.8). Our basic procedure of representing the radiation (L, M_L) in the matrix elements by means of bras or kets is equivalent to an alternative method (e.g. Racah 1951), in which the radiation is represented by tensor operators $T^{(L)}_{M_L}$ acting between nuclear states. Thus, if $T^{(L)}_{M_L}$ is a tensor operator which transforms under rotation and time reversal like the ket $|L, M_L\rangle$ and $\overline{T}^{(L)}_{M_L}$ is its Hermitian conjugate, then for photon emission $B\rightarrow q+C$ our matrix element $\langle I_CM_C, LM_L|H|I_BM_B\rangle$ could be replaced by $\langle I_CM_C|\overline{T}^{(L)}_{M_L}|I_BM_B\rangle = \langle I_BM_B|T^{(L)}_{M_L}|I_CM_C\rangle^*$; and for photon absorption $q+B\rightarrow C$, we should have a matrix element $\langle I_CM_C|H|I_BM_B, LM_L\rangle$, which could be replaced by $\langle I_CM_C|T^{(L)}_{M_L}|I_BM_B\rangle$. Racah's convention for obtaining reduced matrix elements for emission $(I_B||T^{(L)}||I_C)$ from the matrix elements of $T^{(L)}_{M_L}$ results in the following correspondence with our reduced matrix elements:—

$$\langle I_C, L||H||I_B\rangle = (2I_B+1)^{-1/2}(I_B||T^{(L)}||I_C)^*.$$

In addition to such differences in procedure for forming matrix elements and reduced matrix elements, it must be remembered that these quantities can differ also as a result of differences in the phasing of the basic states $|I_AM_A\rangle$, $|L, M_L\rangle$ etc. which figure in the matrix elements.

‡ The phase factor in this formula depends on our particular choice of the arbitrary sign of the basic states $|jm_j(l)\rangle$ and $|LM_L(\pi)\rangle$ which is referred to in the footnote following (6). For the nucleon states $|jm_j(l)\rangle$ we have followed the convention of Devons and Goldfarb (1957) § 13, and for the photon states $|LM_L(\pi)\rangle$ we followed § 14, adopting the *lower* of the alternative signs in the formulae there.

where $\mathbf{P}$ is now the measure of the polarization sensitivity of the detector of p (see Devons and Goldfarb 1957, p. 440), but the other symbols have the same meaning as before.

The rule for obtaining the angular distribution formula (such as (11)) when p is emitted in the transition A→p + B, from the formula (such as (9)) when p is absorbed in the transition p + A→B, consists of two parts, as follows (the rule is proved in §3).

(i) The coordinates expressing the state of the absorbed particle are replaced in the formula by the time-reverse of the coordinates expressing the state in which the emitted particle is observed. In our example this means that we make the replacement $\mathbf{k}_1 \to -\mathbf{k}_1$ (and hence $\mathbf{n} \to -\mathbf{n}$) and $\mathbf{P} \to -\mathbf{P}$.

In alternative formulations of the angular distribution, the state of p may sometimes be expressed in terms of, not its dynamical variables (such as $\mathbf{k}$, $\mathbf{P}$, θ), but its density matrix elements of the type $\langle jm_j|\rho|j'm_j'\rangle$ in the case of absorption, or its efficiency matrix elements $\langle jm_j|\epsilon|j'm_j'\rangle$ in the case of emission: a further alternative formulation may be in terms of statistical tensors of the type $\rho_{kx}(jj')$ for absorption, or efficiency tensors $\epsilon_{kx}(jj')$ for emission. The appropriate reformulation of the present rule is then that $\langle jm_j|\rho|j'm_j'\rangle$ in the absorption formula must be replaced by the time-reverse $\langle jm_j|K\epsilon K^{-1}|j'm_j'\rangle$ of $\langle jm_j|\epsilon|j'm_j'\rangle$ for emission, or $\rho_{kx}(jj')$ by the time-reverse $(K\epsilon K^{-1})_{kx}(jj')$ of $\epsilon_{kx}(jj')$, where the formulae for these time-reverses are

$$\langle jm_j|K\epsilon K^{-1}|j'm_j'\rangle = (-1)^{j-m_j+j'-m_j'}\langle j-m_j|\epsilon|j'-m_j'\rangle^*, \qquad \ldots\ldots(12)$$

and

$$(K\epsilon K^{-1})_{kx}(jj') = (-1)^{k+x}\epsilon^*{}_{k-x}(jj'). \qquad \ldots\ldots(13)$$

(ii) The 'natural' matrix element for absorption (such as

$$\langle I_{\mathrm{C}}, L(\pi)||S^{I_{\mathrm{B}}}||I_{\mathrm{A}}, j(l)\rangle)$$

is replaced by that for emission (such as $\langle I_{\mathrm{C}}, L(\pi)||H||I_{\mathrm{B}}\rangle\langle I_{\mathrm{B}}, j(l)||H||I_{\mathrm{A}}\rangle$) multiplied by the factor

$$(-1)^{I_{\mathrm{A}}+j-I_{\mathrm{B}}}\hat{I}_{\mathrm{A}}/\hat{I}_{\mathrm{B}}. \qquad \ldots\ldots(14)$$

It is easily seen that these prescriptions, when applied to the absorption formula (9), lead at once to the emission formula (11).

It is evident how the procedure must be reversed if we wish to obtain an absorption formula from an emission one.

In our example, A, q and C are unpolarized, but the rule would still apply without modification if this restriction were removed, and A, say, were initially polarized. The rule applies generally whenever one particle (or radiation) is taken from the ket (absorption) side to the bra (emission) side, other things being left unaltered.

If conventions different from ours are used for the definition of reduced matrix elements, part (i) of the rule will remain unaltered, but in part (ii) a multiplication factor different from (14) will have to be used. We need not attempt here to cover all possibilities, but it may be remarked that in circumstances in which the reduced matrix elements are treated simply as adjustable parameters, the multiplication factor is of no interest. The use of channel spin instead of total angular momentum j for a nuclear particle p would call for only trivial modifications.

§ 3. PROOF OF RULE

We shall first prove the rule of § 2 in the formulation in which the angular distribution is expressed in terms of density or efficiency matrices. The angular distribution for a process involving the absorption stage p + A→B is

$$W \propto \mathscr{S} \sum_{jj'm_jm_j'} \langle jm_j|\rho|j'm_j'\rangle (I_\mathrm{A}M_\mathrm{A}, jm_j|I_\mathrm{B}M_\mathrm{B})(I_\mathrm{A}'M_\mathrm{A}', j'm_j'|I_\mathrm{B}'M_\mathrm{B}')$$
$$\times \langle I_\mathrm{B}\| \; \|I_\mathrm{A}, j\rangle \langle I_\mathrm{B}'\| \; \|I_\mathrm{A}', j'\rangle^* \ldots\ldots, \qquad \ldots\ldots(15)$$

where $\langle I_\mathrm{B}\| \; \|I_\mathrm{A}, j\rangle$ stands for a 'natural' reduced matrix element for absorption constructed on the lines of (7), the row of dots stands for factors independent of the stage p + A→B, and $\mathscr{S}$ stands for a sum and average over other quantum numbers than j, j', m_j, m_j'. The corresponding formula for the process in which the absorption stage (4) is replaced by the emission stage (5) is

$$W \propto \mathscr{S} \sum_{jj'm_jm_j'} \langle jm_j|\epsilon|j'm_j'\rangle^* (I_\mathrm{B}M_\mathrm{B}, jm_j|I_\mathrm{A}M_\mathrm{A})(I_\mathrm{B}'M_\mathrm{B}', j'm_j'|I_\mathrm{A}'M_\mathrm{A}')$$
$$\times \langle I_\mathrm{B}, j\| \; \|I_\mathrm{A}\rangle \langle I_\mathrm{B}', j'\| \; \|I_\mathrm{A}'\rangle^* \ldots\ldots, \qquad \ldots\ldots(16)$$

where $\langle I_\mathrm{B}, j\| \; \|I_\mathrm{A}\rangle$ stands for a 'natural' reduced matrix element for emission, constructed on the lines of (8). Using well-known transformation properties of Clebsch–Gordan coefficients, we can rewrite (16) as

$$W \propto \mathscr{S} \sum_{jj'm_jm_j'} (-1)^{j-m_j+j'-m_j'} \langle j - m_j|\epsilon|j' - m_j'\rangle^*$$
$$\times (I_\mathrm{A}M_\mathrm{A}, jm_j|I_\mathrm{B}M_\mathrm{B})(I_\mathrm{A}'M_\mathrm{A}', j'm_j'|I_\mathrm{B}'M_\mathrm{B}')$$
$$\times (-1)^{I_\mathrm{A}+j-I_\mathrm{B}} \hat{I}_\mathrm{A} \hat{I}_\mathrm{B}^{-1} \langle I_\mathrm{B}, j\| \; \|I_\mathrm{A}\rangle$$
$$\times (-1)^{I_\mathrm{A}'+j'-I_\mathrm{B}'} \hat{I}_\mathrm{A}' \hat{I}_\mathrm{B}'^{-1} \langle I_\mathrm{B}', j'\| \; \|I_\mathrm{A}'\rangle^* \ldots\ldots\ldots \qquad \ldots\ldots(17)$$

The relation between the absorption formula (15) and the emission formula (17) can be immediately described by the rule of § 2 in one of its formulations there. It remains to demonstrate the equivalence of the various formulations. We first show that the efficiency matrix expression appearing in (17) is related to time-reversal in the way asserted in (12). We can write

$$\langle jm_j|K\epsilon K^{-1}|j'm_j'\rangle = \langle jm_j|\bar{K}^{-1}\bar{K}K\epsilon K^{-1}|j'm_j'\rangle. \qquad \ldots\ldots(18)\dagger$$

By use of the following property of the time-reversal operator K (Wigner 1932)

$$\langle i|\bar{K}K|j\rangle = \langle i|j\rangle^*, \qquad \ldots\ldots(19)$$

we obtain from (18)

$$\langle jm_j|K\epsilon K^{-1}|j'm_j'\rangle = \langle jm_j|\bar{K}^{-1}\epsilon K^{-1}|j'm_j'\rangle^*,$$

and application of the property (6) leads readily to (12). The meaning of the time-reverse $K\epsilon K^{-1}$ of the efficiency operator ϵ is that each state used in specifying the properties of the observing apparatus is to be replaced by the time-reversed state. It follows at once that the formulation in § 2 of the rule in terms of density matrices is equivalent to that in terms of dynamical variables of the particle p.

---

† The operator K is to be understood as acting only on kets, not bras, i.e. to the right only, since it is a non-linear operator. The Hermitian conjugate $\bar{K}$ of K is an operator which acts only on bras, i.e. to the left only, and it is defined by

$$\langle\alpha|\,\bar{K} = \overline{K|\alpha\rangle},$$

where $|\alpha\rangle$ is any ket.

We have finally to show that the formula (12) for time-reversal of the efficiency matrix leads to formula (13) for time-reversal of the efficiency tensors. $\epsilon_{k\chi}$ is defined by

$$\epsilon_{k\chi}(jj')=\sum_{m_j m_j'}(-1)^{j'-m_j'}(jm_j,j'-m_j'|k\chi)\langle jm_j|\epsilon|j'm'\rangle. \qquad \ldots\ldots(20)$$

We have then

$$(K\epsilon K^{-1})_{k\chi}(jj')=\sum_{m_j m_j'}(-1)^{j'-m_j'}(jm_j,j'-m_j'|k\chi)\langle jm_j|K\epsilon K^{-1}|j'm_j'\rangle. \qquad \ldots\ldots(21)$$

Substitution of (12) yields (13) after a little manipulation.

References

Devons, S., and Goldfarb, L. J. B., 1957, *Handbuch der Physik*, **42**, 362 (Berlin: Springer).

Frauenfelder, H., 1955, *Beta- and Gamma-Ray Spectroscopy*, edited by Siegbahn, K. (Amsterdam: North-Holland), p. 531.

Huby, R., 1954, *Proc. Phys. Soc.* A, **67**, 1103.

Racah, G., 1951, *Phys. Rev.*, **84**, 910.

Wigner, E. P., 1932, *Nachr. Ges. Wiss. Göttingen*, **31**, 546.

The Molecular Orbital Theory of the Interaction between an Atom and a Crystal Surface

By T. B. GRIMLEY

Department of Inorganic and Physical Chemistry, University of Liverpool

MS. received 6th February 1958

Abstract. The LCAO method of finding approximate one-electron wave functions is applied to an atom and crystal in mutual interaction. The case of a hydrogen-like atom and a crystal whose valence electrons occupy a band of states derived, in the LCAO approximation, from a single atomic state is discussed with the help of the simplifying assumptions of the tight binding approximation. Formulae are derived for the wave functions and energy levels of this system. If the interaction extends only over a group Ω of crystal atoms near the foreign atom then, depending on the values of the interaction parameters, there may be localized states associated with the foreign atom and the group Ω. The energies of these states lie outside the normal band (including any surface band) of crystal states and their existence allows for the formation of localized bonds between the atom and the crystal.

§ 1. Introduction

One of the standard methods for finding approximate one-electron wave functions for both molecules and crystals is the LCAO (linear combination of atomic orbitals) method. This consists of taking linear combinations of atomic orbitals located on the various atoms and varying the coefficients so as to minimize the mean value of some effective one-electron Hamiltonian operator. In the present paper, this method is applied to a system consisting of an atom (or molecule) and a crystal in mutual interaction. We have, of course, to include as many atomic orbitals on each atom as are required to give an adequate approximation to the electronic structures of the atom and the crystal separately when the interaction between them is neglected. The problem of the electronic structure of the crystal is not, however, presented in its usual form. Normally, if we are interested in this problem we apply periodic boundary conditions so that the crystal functions are eigenfunctions of certain fundamental translation operators. In our crystal problem an essential feature is the existence of a free surface at which interaction with the foreign atom is to take place. This means that part of the translational symmetry of the usual crystal problem has been lost. This complication is not important in the formal development of the theory since we can use the same set of orbitals on the crystal atoms whether periodic boundary conditions are to be applied or not, but the existence of the free crystal surface has to be faced eventually. Some work on this problem using the LCAO approximation has already been published (Goodwin 1939, Artmann 1952, Baldock 1952).

The essential features of our system are exhibited by a one-dimensional model in which the crystal is represented by a straight chain of similar atoms, and the foreign atom is in interaction with one end of this chain. If the electronic structure of the chain consists of just one band, this one-dimensional system is easily treated in the 'tight binding' approximation. This is done in § 2. A more powerful mathematical technique is needed for the corresponding three-dimensional crystal and this, together with the extension to crystals with many bands, and interacting molecules instead of atoms, is given in § 3. The usual assumptions of the 'tight binding' approximation can also be avoided. The mathematical method is that already used by Baldock (1952) and by Koster and Slater (1954) in connection with other problems. Certain numerical calculations by these latter authors are particularly useful in the present work.

§ 2. ONE-DIMENSIONAL CRYSTAL

In this section we take as our model for the crystal a straight chain of similar atoms. The chain is extended in one direction by a foreign atom placed at the end, and we are interested in the one-electron wave functions and energy levels of this system.

With respect to an origin at the end of the chain, let the atoms of the chain be specified by vectors $\mathbf{m} = m\mathbf{a}$, where $|\mathbf{a}|$ is the interatomic distance and m is an integer in the range $0 \leqslant m \leqslant N$. The foreign atom is at the point $\mathbf{m} = \lambda\mathbf{a}$, where λ is negative and non-integral. Associated with each vector $\mathbf{m}$ we introduce an atomic orbital $\phi(\mathbf{r},\mathbf{m})$. These orbitals are divided into two sets. One set $(\mathbf{m}\epsilon A)$ contains only one member which is the orbital on the foreign atom, the other set $(\mathbf{m}\epsilon C)$ consists of the orbitals on the atoms of the crystal. We assume that any wave function, $\psi(\mathbf{r})$, for the system can be expressed in the form

$$\psi(\mathbf{r}) = \sum_{\mathbf{m}} \phi(\mathbf{r},\mathbf{m}) c(\mathbf{m}), \qquad \ldots\ldots(1)$$

and neglecting overlap between the atomic orbitals, we arrive at the usual system of linear equations

$$\sum_{\mathbf{m}} [H(\mathbf{n},\mathbf{m}) - \delta(\mathbf{n},\mathbf{m})E] c(\mathbf{m}) = 0 \qquad \ldots\ldots(2)$$

for the coefficients $c(\mathbf{m})$ and the energy E. In equation (2)

$$H(\mathbf{n},\mathbf{m}) = \int \phi^*(\mathbf{r},\mathbf{n}) \mathscr{H} \phi(\mathbf{r},\mathbf{m})\, d\mathbf{r}, \qquad \ldots\ldots(3)$$

where $\mathscr{H}$ is the effective one-electron Hamiltonian operator for the system. Write

$$H(\mathbf{n},\mathbf{m}) = H^0(\mathbf{n},\mathbf{m}) + V(\mathbf{n},\mathbf{m}), \qquad \ldots\ldots(4)$$

where $H^0(\mathbf{n},\mathbf{m})$ is the Hamiltonian matrix when interactions between the foreign atom and the crystal are neglected, and $V(\mathbf{n},\mathbf{m})$ is the interaction matrix. Now put

$$\left.\begin{aligned} H^0(\mathbf{m},\mathbf{m}) &= \alpha, && m = 1, 2, \ldots N-1, \\ H^0(\mathbf{0},\mathbf{0}) &= \alpha', \\ H^0(\lambda\mathbf{a},\lambda\mathbf{a}) &= \epsilon_A, \\ H^0(\mathbf{m},\mathbf{m} \pm \mathbf{a}) &= \beta, && m = 1, 2, \ldots N-1, \end{aligned}\right\} \qquad \ldots\ldots(5)$$

$$\left.\begin{aligned} V(\mathbf{0},\mathbf{0}) &= V_c, \\ V(\lambda\mathbf{a},\lambda\mathbf{a}) &= V_A, \\ V(\lambda\mathbf{a},\mathbf{0}) &= V(\mathbf{0},\lambda\mathbf{a}) = \beta', \end{aligned}\right\} \qquad \ldots\ldots(6)$$

so that, in the tight binding approximation, equation (2) gives

$$[E-\alpha]c(m) = \beta[c(m+1)+c(m-1)], \quad m=1,2,\ldots N-1, \ldots\ldots(7)$$

with the boundary conditions

$$\left.\begin{aligned} [E-\alpha'-V_c]c(0) &= \beta c(1)+\beta' c(\lambda), \\ [E-\epsilon_A-V_A]c(\lambda) &= \beta' c(0). \end{aligned}\right\} \qquad \ldots\ldots(8)$$

We have still to apply a boundary condition at the end of the chain ($m=N$) remote from the foreign atom. If N is large, this boundary condition cannot affect the conditions near $m=0$ in any important way, and we shall assume that the wave function vanishes at $m=N$. The solution of equations (7) and (8) is now

$$c(m) = \sin(N-m)\theta, \qquad m=0,1,\ldots N. \qquad \ldots\ldots(9)$$

This satisfies the boundary condition at $m=N$. It satisfies equation (7) if

$$E = \alpha + 2\beta\cos\theta, \qquad \ldots\ldots(10)$$

and the boundary conditions (8) if θ is one of the $N+1$ roots of the equation

$$(z+f+\cos\theta+\sin\theta\cot N\theta)(z'+2\cos\theta) = \eta^2. \qquad \ldots\ldots(11)$$

In equation (11),

$$z=(\alpha-\alpha')/\beta, \quad f=-V_c/\beta, \quad z'=(\alpha-\epsilon_A-V_A)/\beta, \quad \eta=\beta'/\beta. \qquad \ldots\ldots(12)$$

Equation (11) has at least $N-1$ real roots. The corresponding wave functions are periodic in the crystal, and their energies lie in the range

$$-1 < E' < 1, \qquad E'=(E-\alpha)/2\beta. \qquad \ldots\ldots(13)$$

These are non-localized states. The remaining two roots may both be real, and in this case they also lie in the band (13) and the system has only non-localized states. On the other hand, one or both of these remaining roots may have values of θ of the form $i\xi$ or $\pi+i\xi$ with ξ real. The corresponding wave functions are damped in the crystal. These are localized states. Their energies lie outside the normal band (13) of crystal states. States with $\theta=i\xi$ have positive values of E' and will be denoted by $\mathscr{P}$; those with $\theta=\pi+i\xi$ have E' negative and will be denoted by $\mathscr{N}$. Since N is large, the eigenvalue condition (11) for $\mathscr{P}$-states is

$$(z+f+\exp\xi)(z'+2\cosh\xi) = \eta^2, \qquad \ldots\ldots(14)$$

and for the wave function and the energy we have

$$c(m) = [c(0)/\sinh N\xi]\sinh(N-m)\xi, \quad E'=\cosh\xi. \qquad \ldots\ldots(15)$$

For $\mathscr{N}$-states

$$(z+f-\exp\xi)(z'-2\cosh\xi) = \eta^2, \qquad \ldots\ldots(16)$$

and

$$c(m) = [c(0)/\sinh N\xi](-1)^m\sinh(N-m)\xi, \quad E'=-\cosh\xi. \qquad \ldots\ldots(17)$$

The values of $z+f$ and z' for which equations (14) and (16) have real roots ξ are determined by the hyperbolae

$$(z+f\pm 1)(z'\pm 2)=\eta^2, \qquad \ldots\ldots (18)$$

and these are plotted in figure 1 for $\eta^2=1$. Localized states occur in the six regions indicated ($\mathscr{N}^2$ means that there are two $\mathscr{N}$-states, $\mathscr{N}\mathscr{P}$ that there is one $\mathscr{N}$-state and one $\mathscr{P}$-state and so forth). An important feature of these results is the existence of a region where localized states are forbidden; in this region the system has only non-localized states. It is easy to show that such a forbidden region exists provided that $\eta^2<2$.

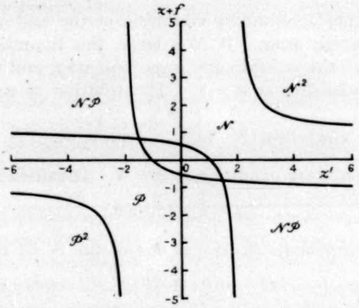

Figure 1. The occurrence of localized states for a foreign atom and a one-dimensional crystal assuming that $\eta^2=1$.

Effective binding between the foreign atom and the chain with the formation of a localized bond is possible if there is a localized state lying below the band (13). If this is an s-band, β is negative, and the required states are $\mathscr{P}$-states. For a p_z-band they would be $\mathscr{N}$-states. In table 1 we give the first few wave function coefficients for a $\mathscr{P}$-state formed when $z+f=0$, $z'=-1{\cdot}5$ and $\eta=1$. Only one $\mathscr{P}$-state exists for these values of the parameters; it has $E'=1{\cdot}083$ and $\xi=0{\cdot}405$.

Table 1. Wave Function Amplitudes for a $\mathscr{P}$-state ($z+f=0$, $z'=-1{\cdot}5$, $\eta=1$)

m	λ	0	1	2	3	4	5	6
$c(m)$	1·500	1·000	0·667	0·444	0·296	0·197	0·132	0·088

The ratio R defined by

$$R=[c(\lambda)]^2\Big/\Big\{[c(\lambda)]^2+\sum_{m=0}^{N}[c(m)]^2\Big\}$$

gives the charge-order of the localized state on the foreign atom. For the above state $R=0{\cdot}556$ so that the electron is concentrated rather more on the foreign atom than the crystal.

If $\eta^2<2$, and both z' and $z+f$ lie in the forbidden region in figure 1, the effect of the foreign atom is to introduce an extra non-localized state into the band (13). No localized states exist, and any binding of the foreign atom to the chain is accomplished without the formation of a localized bond.

§ 3. THREE-DIMENSIONAL CRYSTAL

For a three-dimensional crystal, the difference equation and its boundary conditions corresponding to equations (7) and (8) cannot be solved directly.‡ However, we can obtain the solution (a Green's function solution) by the methods already used by Baldock (1952) in his work on surface states, and by Koster and Slater (1954 a) in treating impurity levels.

3.1. *The Solution of the Difference Equations*

With a straightforward extension of the notation used in § 2, the atoms of the crystal are specified by vectors $\mathbf{m}=m_1\mathbf{a}_1+m_2\mathbf{a}_2+m_3\mathbf{a}_3$, where $\mathbf{a}_1$, $\mathbf{a}_2$ and $\mathbf{a}_3$ are the vectors which map out the unit cell, and m_1, m_2 and m_3 are integers. The foreign atom is on the $\mathbf{a}_3$-axis with position vector $\mathbf{m}=\lambda\mathbf{a}_3$, where λ is negative and non-integral. With this notation, equations (1)–(4) still hold. Substituting (4) into (2), and writing the result in matrix form we have

$$(\mathbf{H}^0-\mathbf{1}E)\mathbf{c}=-\mathbf{V}\mathbf{c}, \qquad \ldots\ldots(19)$$

where $\mathbf{c}$ is a column matrix with elements $c(\mathbf{m})$. Suppose that equation (19) can be solved for $\mathbf{V}=\mathbf{0}$. This means that we can find a unitary matrix $\mathbf{U}$ such that

$$\mathbf{H}^0\mathbf{U}=\mathbf{U}\mathbf{E}^0, \qquad \ldots\ldots(20)$$

where $\mathbf{E}^0$ is a diagonal matrix whose diagonal elements $E^0(\mathbf{k})$ are the energy levels of the unperturbed systems. The corresponding wave functions, $\psi^0(\mathbf{r},\mathbf{k})$, are determined by the elements $U(\mathbf{m},\mathbf{k})$ according to the equation

$$\psi^0(\mathbf{r},\mathbf{k})=\sum_{\mathbf{m}}\phi(\mathbf{r},\mathbf{m})U(\mathbf{m},\mathbf{k}). \qquad \ldots\ldots(21)$$

The indices $\mathbf{k}$ are divided into two sets. One set $(\mathbf{k}\epsilon A)$ contains only one member which identifies the unperturbed state of the foreign atom, the other set $(\mathbf{k}\epsilon C)$ refers to the states of the crystal. We have already introduced a similar division for the indices $\mathbf{m}$, and we note that $U(\mathbf{m},\mathbf{k})=0$ unless both $\mathbf{m}$ and $\mathbf{k}$ belong to the same set. Using equation (20) in equation (19) we have

$$\mathbf{c}=-\mathbf{U}(\mathbf{E}^0-\mathbf{1}E)^{-1}\mathbf{U}^\dagger\mathbf{V}\mathbf{c}, \qquad \ldots\ldots(22)$$

and the $\mathbf{p}$th row of this matrix equation is

$$\left.\begin{aligned} c(\mathbf{p}) &= -\sum_{\mathbf{m}} Z(\mathbf{p},\mathbf{m})c(\mathbf{m}),\\ Z(\mathbf{p},\mathbf{m}) &= \sum_{\mathbf{k},\mathbf{n}} U(\mathbf{p},\mathbf{k})[E^0(\mathbf{k})-E]^{-1}U^*(\mathbf{k},\mathbf{n})V(\mathbf{n},\mathbf{m}). \end{aligned}\right\} \qquad \ldots\ldots(23)$$

This is the Green's function solution.

In the above formulation of our problem we have neglected overlap between the atomic orbitals $\phi(\mathbf{r},\mathbf{m})$. This presents no formal difficulty since we can always take linear combinations of these orbitals to give a new set of orbitals which really are orthogonal. If this is done our formulation above is unchanged. On the other hand we might associate orthogonal atomic orbitals (e.g. Wannier functions) only with the vectors $\mathbf{m}$ in the crystal. There is then an overlapping problem between these orbitals and the orbital on the foreign atom. If we define

$$S(\mathbf{n},\mathbf{m})=\int\phi^*(\mathbf{r},\mathbf{n})\phi(\mathbf{r},\mathbf{m})\,dr, \qquad (\mathbf{n}\epsilon A, \quad \mathbf{m}\epsilon C),$$

---

‡ The solution given by the author in a previous note (Grimley 1957) does not satisfy the boundary conditions.

then this problem is solved by using $V(\mathbf{n},\mathbf{m})-ES(\mathbf{n},\mathbf{m})$ instead of $V(\mathbf{n},\mathbf{m})$ in the definition of $Z(\mathbf{p},\mathbf{m})$ in equation (23).

To use our solution (23) we require the wave functions and energy levels of the unperturbed systems. For the foreign atom we have at once,

$$\left.\begin{aligned} E^0(\mathbf{k})&=\epsilon_A, && (\mathbf{k}\epsilon A), \\ U(\mathbf{m},\mathbf{k})&=1, && (\mathbf{m},\mathbf{k}\epsilon A). \end{aligned}\right\} \qquad \ldots\ldots(24)$$

For the crystal, an essential feature is the existence of a free surface in the XY plane at $m_3=0$. We assume that the crystal orbitals vanish on the plane $m_3=N$ (cf. §2), and in the X and Y directions we apply periodic boundary conditions over the domain $-N<m_1\leqslant N$, $-N<m_2\leqslant N$. With the simple tight binding approximation the crystal states are now easily obtained (see for example Baldock 1952). The normalized wave function coefficients are

$$U(m,k)=2^{-1/2}N^{-3/2}\exp\left[i(m_1\theta_1+m_2\theta_2)\right]\sin(N-m_3)\theta_3, \quad (m,k\epsilon C), \quad \ldots\ldots(25)$$

where θ_1 and θ_2 are integer multiples of π/N, i.e. $\theta_1=k_1\pi/N$, $(-N<k_1\leqslant N)$, and $\theta_2=k_2\pi/N$, $(-N<k_2\leqslant N)$. θ_3 is one of the roots of the equation

$$z\sin N\theta_3+\sin(N+1)\theta_3=0, \qquad \ldots\ldots(26)$$

where z is defined in the same way as in §2, equations (5) and (12). If we write $\theta_3=k_3\pi/N$, the crystal state $\mathbf{k}$ is characterized by the three quantities k_1, k_2 and k_3 but k_3 is non-integral because the crystal has a free surface at $m_3=0$. The energy levels $E^0(\mathbf{k})$ are given by

$$E^0(\mathbf{k})=\alpha+2\beta(\cos\theta_1+\cos\theta_2+\cos\theta_3), \qquad (\mathbf{k}\epsilon C), \quad \ldots\ldots(27)$$

where α and β are again defined in the same way as in §2.

If $|z|>1$, one of the roots of equation (26) is complex, and in addition to the usual band of crystal states there is a band of surface states going with the face $m_3=0$. These states have real values of θ_1 and θ_2 but θ_3 has the form $i\xi$ or $\pi+i\xi$ according as z is negative or positive (Goodwin 1939, Baldock 1952). For these states the normalizing factor in equation (25) is not correct.

3.2. *The Eigenvalue Condition*

In this section we derive the three-dimensional analogue of the eigenvalue condition (11). It will be assumed that the interaction matrix $V(\mathbf{n},\mathbf{m})$ has non-vanishing elements only if the atoms at $\mathbf{n}$ and $\mathbf{m}$ are nearest neighbours. Hence

$$V(00\lambda,00\lambda)=V_A, \qquad V(\mathbf{0},\mathbf{0})=V_c,$$
$$V(00\lambda,\mathbf{0})=V(\mathbf{0},00\lambda)=\beta',$$

and all other elements of $V(\mathbf{n},\mathbf{m})$ are neglected. From equation (23) we now have the eigenvalue condition

$$[1+Z(00\lambda,00\lambda)][1+Z(\mathbf{0},\mathbf{0})]=Z(00\lambda,\mathbf{0})Z(\mathbf{0},00\lambda), \quad \ldots\ldots(28)$$

with

$$Z(00\lambda,00\lambda)=V_A/(\epsilon_A-E), \qquad Z(00\lambda,\mathbf{0})=(\beta'/V_A)Z(00\lambda,00\lambda), \quad \ldots\ldots(29)$$

$$Z(\mathbf{0},\mathbf{0})=V_c\sum_{\mathbf{k}\epsilon c}U(\mathbf{0},\mathbf{k})[E^0(\mathbf{k})-E]^{-1}U^*(\mathbf{k},\mathbf{0}), \qquad Z(\mathbf{0},00\lambda)=(\beta'/V_c)Z(\mathbf{0},\mathbf{0}). \quad \ldots\ldots(30)$$

Suppose first that the unperturbed crystal has no surface states, then $|z| < 1$ and $U(\mathbf{0}, \mathbf{k})$ and $E^0(\mathbf{k})$ in equation (30) are given by equations (25) and (27). The unperturbed energy levels lie in the range

$$-3 < E' < 3, \qquad E' = (E - \alpha)/2\beta. \qquad \ldots\ldots(31)$$

Using equations (25)–(27) we write

$$Z(\mathbf{0}, \mathbf{0}) = fK(z, E'), \qquad \ldots\ldots(32)$$

where $f = -V_c/\beta$, and

$$K(z, E') = \left(\frac{1}{4N^3}\right) \sum_{\theta_1, \theta_2, \theta_3} \frac{\sin^2\theta_3}{(z^2 + 2z\cos\theta_3 + 1)(E' - \cos\theta_1 - \cos\theta_2 - \cos\theta_3)} \qquad \ldots\ldots(33)$$

Making use of equations (29) and (30), equation (28) now becomes

$$[f + K^{-1}(z, E')][z' + 2E'] = \eta^2, \qquad \ldots\ldots(34)$$

where

$$z' = (\alpha - \epsilon_A - V_A)/\beta, \qquad \eta = \beta'/\beta. \qquad \ldots\ldots(35)$$

The real roots E' of equation (34) give the energy levels of our system. If E' lies in the band (31), $K(z, E')$ is a rapidly varying function; it is infinite when E' coincides with one of the levels of the unperturbed crystal, and zero somewhere between successive levels. If E' lies outside the band (31), $K(z, E')$ falls steadily to zero. The roots of equation (34) which lie in the band (31) correspond to non-localized states of our system; those outside the band are localized states associated with the foreign atom and the crystal atom at the origin.

To investigate the occurrence of localized states in detail we note that if $|E'| > 3$, the summations in equation (33) may be converted to integrations. Thus,

$$K(z, E') = \frac{1}{\pi^3}\int_0^\pi\int_0^\pi\int_0^\pi \frac{\sin^2\theta_3\, d\theta_1\, d\theta_2\, d\theta_3}{(z^2 + 2z\cos\theta_3 + 1)(E' - \cos\theta_1 - \cos\theta_2 - \cos\theta_3)}. \qquad \ldots(33')$$

If $E' > 3$, the eigenvalue condition (34) may be written

$$[f + K^{-1}(z, |E'|)][z' + 2|E'|] = \eta^2,$$

and any real roots $|E'|$ of this equation give the states analogous to the $\mathscr{P}$-states of § 2. If $E' < -3$, it is easy to show that equation (34) may be written

$$[f - K^{-1}(-z, |E'|)][z' - 2|E'|] = \eta^2,$$

and its real roots $|E'|$ give the $\mathscr{N}$-states. Now both $K(z, |E'|)$ and $K(-z, |E'|)$ are positive and decrease with increasing $|E'|$ for $|E'| > 3$. Hence, for given z, the values of f and z' for which localized states occur are determined by the hyperbolae

$$[f \pm K^{-1}(\pm z, 3)][z' \pm 6] = \eta^2. \qquad \ldots\ldots(36)$$

These are the three-dimensional analogues of those in equation (18). The essential features of the one-dimensional problem are therefore retained. The maximum number of localized states which can be formed is two, and for certain sets of values of f, z, z' and η^2 there are none.

To plot the hyperbolae (36) we have to evaluate the integrals $K(\pm z, 3)$. For two extreme cases, namely $z = 0$ and $z = 1$, this can be done by the method employed by Koster and Slater (1954 a). We replace

$$(E'-\cos\theta_1-\cos\theta_2-\cos\theta_3)^{-1}$$

in equation (33′) by

$$\int_0^\infty \exp\left[(\cos\theta_1+\cos\theta_2+\cos\theta_3-E')t\right]dt,$$

and in this way obtain

$$\left.\begin{aligned} K(0,|E'|)&=\tfrac{1}{2}\int_0^\infty \exp(-|E'|t)[\mathrm{I}_0(t)]^2[\mathrm{I}_0(t)-\mathrm{I}_2(t)]\,dt,\\ K(\pm1,|E'|)&=\tfrac{1}{2}\int_0^\infty \exp(-|E'|t)[\mathrm{I}_0(t)]^2[\mathrm{I}_0(t)\mp\mathrm{I}_1(t)]\,dt,\end{aligned}\right\} \quad \ldots\ldots(37)$$

where $\mathrm{I}_n(t)$ is the usual Bessel function of imaginary argument. The individual integrals in (37) have been evaluated by Koster and Slater (1954 b) for several values of $|E'|\geqslant 3$. For $|E'|=3$ we find $K(0,3)=0{\cdot}2106$, $K(1,3)=0{\cdot}1666$ and $K(-1,3)=0{\cdot}3324$. Thus the critical hyperbolae (36) are, for $z=0$,

$$(f\pm4{\cdot}749)(z'\pm6)=\eta^2,$$

and for $z=1$,

$$(f+6{\cdot}001)(z'+6)=\eta^2, \qquad (f-3{\cdot}009)(z'-6)=\eta^2.$$

These are plotted in figure 2 for $\eta^2=1$. Comparison with figure 1 shows that, in going to three dimensions, the area of the region where localized states are forbidden is considerably increased. A forbidden region exists if $\eta^2<28{\cdot}5$ for $z=0$, and $\eta^2<27{\cdot}0$ for $z=1$.

So far it has been assumed that $|z|<1$ so that the unperturbed crystal has no surface states. To see how the existence of surface states modifies the results, suppose that $z>1$. There is now a band of surface states (S) with its centre displaced from the centre of the normal band of crystal states. For these states $\theta_3=\pi+i\xi$ in equations (25)–(27) so that

$$U(\mathbf{m},\mathbf{k})=C(1/2N)\exp[i(m_1\theta_1+m_2\theta_2)](-1)^{N-m_3}\sinh(N-\mathbf{m}_3)\xi, \qquad (\mathbf{m}\in C,\ \mathbf{k}\in S),$$

$$E^0(\mathbf{k})=\alpha+2\beta(\cos\theta_1+\cos\theta_2-\cosh\xi), \qquad (\mathbf{k}\in S),$$

and ξ is given by

$$z\sinh N\xi-\sinh(N+1)\xi=0.$$

C is a normalizing constant determined by the equation

$$C^2\sum_{m_3=0}^{N}\sinh^2(N-m_3)\xi=1.$$

The only modification to our theory is that the set of states S must be included in the summation over $\mathbf{k}$ in equation (30). This gives an extra term

$$\tfrac{1}{2}(C/\pi)^2\left(\frac{\sinh^2\xi}{z^2-2z\cosh\xi+1}\right)\int_0^\pi\int_0^\pi\frac{d\theta_1\,d\theta_2}{(E'-\cos\theta_1-\cos\theta_2+\cosh\xi)} \quad \ldots\ldots(38)$$

on the right-hand side of equation (33′), and introduces the additional restriction that a truly localized state must lie outside the surface band as well as outside the main band. Hence, for localized states $|E'|>3$, and $|E'+\cosh\xi|>2$.

If z is large so that the surface band lies well clear of the main band, the integral in equation (33′) is small, and the whole contribution to $K(z, E')$ comes from the expression (38). This occurs because as $z \to \infty$, the amplitudes $U(m_1 m_2 0, \mathbf{k})$ of the normal crystal states on the surface atoms tend to zero. Only the surface states have finite amplitudes on the surface atoms. Consequently, as far as its external interactions are concerned, the crystal behaves like a two-dimensional array of atoms with the surface band playing the part of the main band. This means that the localized states will separate out from the surface band not from the main band. The integral (38) diverges at $|E' + \cosh \xi| = 2$ (this gives the upper and lower limits of the surface band) so that the critical hyperbolae governing the occurrence of localized states are $f(z' \pm 4) = \eta^2$ with $z' = (\alpha' - \epsilon_A - V_A)/\beta$. These hyperbolae do not intersect for any value of η^2, and localized states occur therefore, for all values of z' and f.

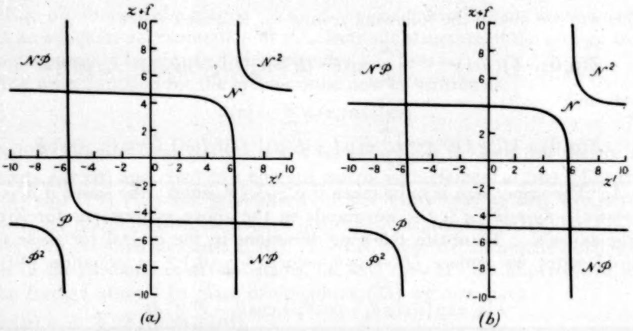

(a) (b)

Figure 2. The occurrence of localized states for a foreign atom and a three-dimensional crystal assuming that $\eta^2 = 1$. Values of z: (*a*) 0, (*b*) 1.

3.3. *The Wave Functions*

From equation (23) the wave function amplitudes $c(\mathbf{p})$ on the crystal atoms $(\mathbf{p} \epsilon C)$ are given by the equation

$$c(\mathbf{p}) = c(\mathbf{0})\{[1 + Z(\mathbf{0}, \mathbf{0})][Z(\mathbf{p}, 00\lambda)/Z(\mathbf{0}, 00\lambda)] - Z(\mathbf{p}, \mathbf{0})\},$$

where

$$\left.\begin{aligned} Z(\mathbf{p}, \mathbf{0}) &= V_c \sum_{\mathbf{k} \epsilon C} U(\mathbf{p}, \mathbf{k})[E^0(\mathbf{k}) - E]^{-1} U^*(\mathbf{k}, \mathbf{0}), \\ Z(\mathbf{p}, 00\lambda) &= (\beta'/V_c) Z(\mathbf{p}, \mathbf{0}). \end{aligned}\right\} \quad \ldots\ldots (39)$$

Thus, for $\mathbf{p} \neq \mathbf{0}$, the ratio $c(\mathbf{p})/c(\mathbf{0})$ is proportional to $Z(\mathbf{p}, \mathbf{0})$. Substituting for $U(\mathbf{p}, \mathbf{k})$ from equation (25), using equations (26) and (27) and converting the summations in equation (39) to integrations we find

$$Z(\mathbf{p}, \mathbf{0}) = (f/\pi^3) \int_0^\pi \int_0^\pi \int_0^\pi \frac{\cos p\theta_1 \cos q\theta_2 \sin \theta_3 [z \sin r\theta_3 + \sin (r+1)\theta_3] \, d\theta_1 \, d\theta_2 \, d\theta_3}{(z^2 + 2z \cos \theta_3 + 1)(E' - \cos \theta_1 - \cos \theta_2 - \cos \theta_3)}, \quad \ldots\ldots (40)$$

where (p, q, r) are the components of $\mathbf{p}$. If $|E'| > 3$, it is clear from the form of the integral in equation (40) that $Z(\mathbf{p}, \mathbf{0})$ is small when either p, q or r is large. Hence, for energies lying outside the band (31), the wave function in the crystal is indeed localized about the origin.

For the extreme cases $z = 0$ and $z = \pm 1$, $Z(\mathbf{p}, \mathbf{0})$ can be reduced to a single integral by following the methods employed by Koster and Slater (1954 a, 1954 b) and Koster (1954). For example, if $E' > 3$, we replace

$$(E' - \cos\theta_1 - \cos\theta_2 - \cos\theta_3)^{-1}$$

in equation (40) by

$$\int_0^\infty \exp\,[(\cos\theta_1 + \cos\theta_2 + \cos\theta_3 - E')t]\,dt.$$

In this way we obtain the following results for localized states:

$$Z(\mathbf{p}, \mathbf{0}) = \tfrac{1}{2} f(\pm 1)^{p+q+r} \int_0^\infty \exp\,(-|E'|t)\mathrm{I}_p(t)\mathrm{I}_q(t)[\mathrm{I}_r(t) - \mathrm{I}_{r+2}(t)]\,dt$$

if $z = 0$, and

$$Z(\mathbf{p}, \mathbf{0}) = \tfrac{1}{2} f(\pm 1)^{p+q+r} \int_0^\infty \exp\,(-|E'|t)\mathrm{I}_p(t)\mathrm{I}_q(t)[\mathrm{I}_r(t) \mp \mathrm{I}_{r+1}(t)]\,dt$$

if $z = 1$. The upper sign is to be taken if $E' > 3$ ($\mathscr{P}$-states), the lower if $E' < -3$ ($\mathscr{N}$-states). For $|E'| < 3$, the integrands in the above expressions for $Z(\mathbf{p}, \mathbf{0})$ diverge as $t \to \infty$. To obtain the wave functions in the crystal for these non-localized states we replace $(E' - \cos\theta_1 - \cos\theta_2 - \cos\theta_3)^{-1}$ in equation (40) by

$$i \int_0^\infty \exp\,[i(\cos\theta_1 + \cos\theta_2 + \cos\theta_3 - E')t]\,dt,$$

then

$$Z(\mathbf{p}, \mathbf{0}) = \tfrac{1}{2} f i^{p+q+r+1} \int_0^\infty \exp\,(-iE't)\mathrm{J}_p(t)\mathrm{J}_q(t)[\mathrm{J}_r(t) + \mathrm{J}_{r+2}(t)]\,dt$$

if $z = 0$, and

$$Z(\mathbf{p}, \mathbf{0}) = \tfrac{1}{2} f i^{p+q+r+1} \int_0^\infty \exp\,(-iE't)\mathrm{J}_p(t)\mathrm{J}_q(t)[\mathrm{J}_r(t) - i\mathrm{J}_{r+1}(t)]\,dt$$

if $z = 1$. In actual fact these last expressions for $Z(\mathbf{p}, \mathbf{0})$ can be used for all values of E' (Koster and Slater 1954 b).

To complete our derivation of the wave function we need $c(00\lambda)$ in terms of $c(\mathbf{0})$. From equation (23) this is given by either of the equivalent expressions

$$c(00\lambda)/c(\mathbf{0}) = -[1 + Z(\mathbf{0}, \mathbf{0})]/Z(\mathbf{0}, 00\lambda) = Z(00\lambda, \mathbf{0})/[1 + Z(00\lambda, 00\lambda)].$$

Equation (40) holds for $|z| \leqslant 1$. If $|z| > 1$, there is a band of surface states which must be included in the summation over $\mathbf{k}$ in equations (39). This gives an extra term in $Z(\mathbf{p}, \mathbf{0})$, namely (cf. eqn (38))

$$\tfrac{1}{2} f(C/\pi)^2(\mp 1)^{r+1} \left\{ \frac{\sinh\xi[z\sinh r\xi \mp \sinh(r+1)\xi]}{z^2 \mp 2z\cosh\xi + 1} \right\} \times \int_0^\pi \int_0^\pi \frac{\cos p\theta_1 \cos q\theta_2\, d\theta_1\, d\theta_2}{E' - \cos\theta_1 - \cos\theta_2 \pm \cosh\xi}, \quad \ldots\ldots (41)$$

where ξ is given by

$$z\sinh N\xi \mp \sinh(N+1)\xi = 0.$$

The upper sign is to be taken if $z > 1$, the lower if $z < -1$. If $|z|$ is large the expression (41) is the dominant term in $Z(\mathbf{p}, \mathbf{0})$, and the wave functions do not penetrate beyond the surface layer of the crystal. This is the situation already mentioned at the end of § 3.2.

3.4. *The Problem of Many Bands*

So far we have assumed that the important electronic structure of the crystal consists of one band derived in the LCAO approximation, from a single atomic state. In general, this is not a realistic picture. The metals, for example, have a complicated system of overlapping bands derived, in the LCAO approximation, from several states. This means that with each vector $\mathbf{m}$ in the crystal we should associate several atomic orbitals $\phi_i(\mathbf{r},\mathbf{m})$, where the index i symbolizes the quantum numbers of the atomic state. A similar generalization may be needed to get an adequate representation of the electronic structure of the foreign atom; it would certainly be required for molecules.

Any wave function for the system must now be written as

$$\psi(\mathbf{r}) = \sum_{i,\mathbf{m}} \phi_i(\mathbf{r},\mathbf{m}) c_i(\mathbf{m}),$$

so that the form (1) can be retained if we regard $\phi(\mathbf{r},\mathbf{m})$ as a row matrix with elements $\phi_i(\mathbf{r},\mathbf{m})$ and $c(\mathbf{m})$ as a column matrix with elements $c_i(\mathbf{m})$. Equations (2)–(4) and (19)–(23) are generalized in the same way so that $V(\mathbf{n},\mathbf{m})$ and $U(\mathbf{m},\mathbf{k})$ are matrices with elements $V_{ij}(\mathbf{n},\mathbf{m})$ and $U_{ij}(\mathbf{m},\mathbf{k})$. $E^0(\mathbf{k})$ is a diagonal matrix with diagonal elements $E_i^0(\mathbf{k})$. For $\mathbf{k} \epsilon C$ these are the unperturbed energy levels in the ith band of crystal states, for $\mathbf{k} \epsilon A$ they are the unperturbed levels of the foreign atom. In place of equations (23) we now have

$$\left.\begin{aligned} c_j(\mathbf{p}) &= -\sum_{i,\mathbf{m}} Z_{ji}(\mathbf{p},\mathbf{m}) c_i(\mathbf{m}), \\ Z_{ji}(\mathbf{p},\mathbf{m}) &= \sum_{s,t,\mathbf{n},\mathbf{k}} U_{js}(\mathbf{p},\mathbf{k})[E_s^0(\mathbf{k}) - E]^{-1} U_{st}^*(\mathbf{k},\mathbf{n}) V_{ti}(\mathbf{n},\mathbf{m}). \end{aligned}\right\} \quad \ldots\ldots (42)$$

These equations give the solution to a very general form of our problem.

The solution can be written in another way which may be more convenient in practice. We note that the coefficients $U_{ij}(\mathbf{m},\mathbf{k})$ determine the wave functions for the unperturbed systems according to the equation

$$\psi_j^0(\mathbf{r},\mathbf{k}) = \sum_{i,\mathbf{m}} \phi_i(\mathbf{r},\mathbf{m}) U_{ij}(\mathbf{m},\mathbf{k}).$$

Now define

$$\chi_j^0(\mathbf{r},\mathbf{k}) = \sum_{\mathbf{m}} \phi_j(\mathbf{r},\mathbf{m}) B_j(\mathbf{m},\mathbf{k}),$$

where the coefficients $B_j(\mathbf{m},\mathbf{k})$ are the elements of the unitary matrix $\mathbf{B}_j$ which diagonalizes the Hamiltonian matrix for the unperturbed systems when expressed in the representation afforded by the functions $\phi_j(\mathbf{r},\mathbf{m})$ for fixed j.‡ Then

$$U_{ij}(\mathbf{m},\mathbf{k}) = B_i(\mathbf{m},\mathbf{k}) W_{ij}(\mathbf{k}),$$

where the quantities $W_{ij}(\mathbf{k})$ are the elements of the unitary matrix $\mathbf{W}(\mathbf{k})$ obtained by solving (for the unperturbed systems) the secular problem between the functions χ_j^0. It is now easy to show that equation (22) is replaced by

$$\mathbf{c} = -\mathbf{B}(\boldsymbol{\mathfrak{C}}^0 - \mathbf{1}E)^{-1}\mathbf{B}^\dagger \mathbf{V}\mathbf{c}, \quad \ldots\ldots (43)$$

---

‡ If we could apply periodic boundary conditions for $\mathbf{k} \epsilon C$, the functions $\chi_j^0(\mathbf{r},\mathbf{k})$ for $\mathbf{k} \epsilon C$ would be the ordinary Bloch functions for the crystal.

where the matrix $\mathfrak{E}^0$ has elements

$$\mathfrak{E}_{ij}^0(\mathbf{k}) = \sum_s W_{is}(\mathbf{k}) E_s^0(\mathbf{k}) W_{sj}^*(\mathbf{k}) = \int \chi_i^{0*}(\mathbf{r},\mathbf{k}) \mathscr{H}^0 \chi_j^0(\mathbf{r},\mathbf{k})\,d\mathbf{r}.$$

Here $\mathscr{H}^0$ is the effective one-electron Hamiltonian operator for the unperturbed systems. Put $\Gamma = (\mathfrak{E}^0 - \mathbf{1}E)^{-1}$, then from equation (43) we have another definition of $Z_{ji}(\mathbf{p},\mathbf{m})$ in equation (42), namely,

$$Z_{ji}(\mathbf{p},\mathbf{m}) = \sum_{s,\mathbf{n},\mathbf{k}} B_j(\mathbf{p},\mathbf{k})\Gamma_{js}(\mathbf{k}) B_s^*(\mathbf{k},\mathbf{n}) V_{si}(\mathbf{n},\mathbf{m}). \qquad \ldots\ldots(44)$$

With this form for $Z_{ji}(\mathbf{p},\mathbf{m})$ we do not have to treat the interacting band system of the unperturbed crystal in detail before going on to the chemisorption problem. Formal simplicity is achieved if we associate Wannier functions with the atoms in the crystal for then the matrix $\Gamma(\mathbf{k})$ in equation (44) is diagonal with diagonal elements $[E_j^0(\mathbf{k}) - E]^{-1}$. The overlapping problem between the orbitals on the atoms in the crystal and those on the foreign atom can, of course, be handled in the manner indicated in §3.1.

From the form of $Z_{ji}(\mathbf{p},\mathbf{m})$ it is clear that, when there is an interacting band problem to be solved for the crystal in the LCAO approximation, any localized states for the whole system must lie outside the resulting set of energy bands. For metals this means that localized states can only occur below the bottom of the valence band; for insulators they can of course lie in the energy gaps in the valence band system.

§ 4. DISCUSSION

In both the one- and three-dimensional models treated in detail in this paper, the maximum number of localized states which can be formed is two. This result depends on our assumptions that only one orbital on the foreign atom and one band of crystal orbitals are in interaction, and that the perturbation of the crystal by the foreign atom extends over only one crystal atom. In general the maximum number of localized states which can be formed is equal to the order of the interaction matrix $V_{ij}(\mathbf{n},\mathbf{m})$. In this way the theory allows for the formation of multiple and multi-centre surface bonds.

Although it is natural to suggest that important binding of the foreign atom to the crystal surface must involve the formation of localized electronic states, we are not yet in a position to comment upon this idea. One reason for this is that the calculations must be made in a self-consistent manner. In a general way we might expect that, if the normally occupied level in the atom lies well below the band of crystal states, no important de-localization of the atomic electron will occur and no strong binding will result. This sort of disposition of the energy levels is found with hydrogen and the alkali metals. The hydrogen level is at -1 Ryd and with sodium, for example, the bottom of the conduction band is at $-0{\cdot}4$ Ryd and the Fermi level at $-0{\cdot}2$ Ryd. In terms of the one-band model treated in §3, z' is large so that the system has at least one localized state which is, however, almost identical with the unperturbed state of the hydrogen atom. With this situation we now expect a further localization of the electrons of the system through electron transfer from the crystal to the hydrogen atom. But if one electron is transferred, the interaction between the two electrons on the atom raises the atomic level to $-0{\cdot}05$ Ryd (the ionization potential of H^-)

and in terms of our model a similar change is to be expected in z'. Because the position of the atomic level (and hence z') varies so much with the amount of charge transferred, a self-consistent calculation is essential. It is the position of the 'self-consistent atomic level' with respect to the crystal band which, together with the interaction parameters, determines whether or not localized states exist.

REFERENCES

ARTMANN, K., 1952, *Z. Phys.*, **131**, 224.
BALDOCK, G. R., 1952, *Proc. Camb. Phil. Soc.*, **48**, 457.
GOODWIN, E. T., 1939, *Proc. Camb. Phil. Soc.*, **35**, 221.
GRIMLEY, T. B., 1957, *Chemisorption*, ed. W. E. Garner (London : Butterworths).
KOSTER, G. F., 1954, *Phys. Rev.*, **95**, 1436.
KOSTER, G. F., and SLATER, J. C., 1954 a, *Phys. Rev.*, **95**, 1167; 1954 b, *Ibid.*, **96**, 1208.

The Scaling Laws for the Stabilized Pinch

By R. J. BICKERTON and H. LONDON
Atomic Energy Research Establishment, Harwell, Berks.

Communicated by D. W. Fry ; *MS. received* 21*st March* 1958

Abstract. The scaling laws for the stabilized pinch are derived. The recent results obtained with such discharges are considered in the light of these relations.

---

§ 1. Introduction

The publication (Thonemann 1958, Ware 1958, Tuck 1958) of results obtained with three stabilized pinched discharges of widely differing dimensions and time scales, Zeta, Sceptre III and Perhapsatron S 3, makes the scaling laws to be applied to such discharges particularly interesting. The stable pinch relies for its stability on the trapping into the plasma of an externally applied axial magnetic field, and the compression of this field as the discharge contracts under the influence of the pinch forces (Shafranov 1956, Tayler 1957, Rosenbluth 1957). The discharge is produced by applying an induced electric field E to a weakly ionized gas contained in a toroidal tube. The life of the discharge may be divided into three phases. When the electric field is first applied, all the processes common in classical gas discharge physics such as ionization, excitation, etc., will occur. As the degree of ionization rises, so the conductivity of the plasma increases, until it is so high that further increases in discharge current flow only on the surface of the discharge. When the self-magnetic field due to the discharge current exceeds the applied axial field the discharge starts to contract away from the walls of the containing vessel. This is the second or contraction phase. The discharge finally settles down at an equilibrium radius, with the axial magnetic field trapped in the highly conducting plasma and the self-magnetic field outside the discharge. This final, or contracted, phase lasts until an appreciable interdiffusion of the axial and azimuthal magnetic fields takes place, after which the discharge is unstable.

Discharges in hydrogen, deuterium or tritium are considered, so that with the removal of one electron ionization is complete, and excitation, ionization etc., may be ignored during the contracting and contracted phases. A discharge is characterized by N, the number of electrons per centimetre length of the tube (line density), and by T_e and T_i, the temperatures of the electrons and ions. The total current I is directly related to these quantities and is independent of the linear dimensions. It will be shown that the time scale has to alter in proportion to the square of the tube radius R. This is true for most of the relevant times: the collision times (which determine reaction rates, internal equilibrium and bremsstrahlung), the times required for the diffusion of magnetic fields (which control stability), and the times for warming up the gas by both Joule heating and adiabatic compression. Consequently, the essential features of the discharge, such as the fraction of ions undergoing nuclear reaction during a pulse, are independent of the tube radius. The only exception is the time required for a sound wave to cross the discharge, which is proportional to R. The line density and the temperature are not so related to the times just mentioned and their increase will make it possible to improve the nuclear yield. Thus we shall consider how the relevant physical quantities scale with R, N, T_e, T_i and I, and the length of the discharge L.

§ 2. THE CLASSICAL DISCHARGE PHASE

Two classical discharges are similar if the ratio E/p is constant (von Engel 1955), where E is the electric field and p is the gas pressure. In terms of N and R this is

$$E \propto N R^{-2} \qquad \ldots\ldots(1)$$

The lateral motion of the electrons in the tube is restricted by the axial magnetic field. There is therefore one further condition, namely that the ratio of the tube radius to the Larmor radius of the electron should be constant. That is

$$B \propto R^{-1} \qquad \ldots\ldots(2)$$

where B is the magnetic field strength.

§ 3. THE CONTRACTING PHASE

The stability theory (Tayler 1957) requires that the axial magnetic field should be trapped in the plasma during the contracting phase. The constriction must therefore take place in a time short compared with that required for the magnetic field to diffuse out of the plasma. This last time t_d is (Spitzer 1956, p. 38)

$$t_d \propto R_p^2 \eta^{-1} \propto R_p^2 T_e^{3/2} \qquad \ldots\ldots(3)$$

where R_p is the radius of the plasma and η the resistivity. For simplicity discharges are considered which collapse to a radius R_p which is a constant fraction of R the tube radius. Define a collapse time t_c, which is a constant small fraction of t_d, then

$$t_c \propto R^2 T_{e_2}^{3/2} \qquad \ldots\ldots(4)$$

where T_{e_2} is a mean value of the electron temperature during this phase. Then for the velocity of collapse v_c,

$$v_c \propto R t_c^{-1} \propto R^{-1} T_{e_2}^{-3/2}. \qquad \ldots\ldots(5)$$

The magnetic fields B, both axial and azimuthal, scale as

$$B \propto I R^{-1}. \qquad \ldots\ldots(6)$$

The sound or Alven speed v_s ($= (B^2/4\pi n M)^{1/2}$) in the plasma then varies as

$$v_s \propto I N^{-1/2}. \qquad \ldots\ldots(7)$$

The ratio of the collapse speed to the sound speed is

$$v_c/v_s \propto R^{-1} I^{-1} T_{e_2}^{-3/2} N^{1/2}. \qquad \ldots\ldots(8)$$

This means that with apparatus of very small dimensions the collapse speed required for field trapping may exceed the sound speed, so that shock wave phenomena occur.

Since the collapse time is of the same order as the rise time of the current, the rate of rise of current dI/dt required for field trapping, scales as

$$\frac{dI}{dt} \propto I R^{-2} T_{e_2}^{-3/2} \qquad \ldots\ldots(9)$$

and hence for the electric field E

$$E \propto I R^{-2} T_{e_2}^{-3/2}. \qquad \ldots\ldots(10)$$

The e.m.f. V around the discharge is therefore given by

$$V \propto I R^{-2} T_{e_3}^{-3/2} L. \qquad \ldots\ldots(11)$$

§ 4. THE CONTRACTED PHASE

The time t_s that the contracted discharge remains stable is determined by the inter-diffusion of the axial and azimuthal magnetic fields.

So from equation (3)

$$t_s \propto R^2 T_{e_3}^{3/2} \qquad \ldots\ldots(12)$$

where T_{e_3} is the electron temperature during this third phase.

The thickness δ of the current sheet as a function of time t can also be deduced from equation (3):

$$\delta \propto t^{1/2} T_{e_3}^{-3/4}. \qquad \ldots\ldots(13)$$

After the time t_s the penetration is, according to (12),

$$\delta_s \propto R; \qquad \ldots\ldots(13a)$$

thus the relative penetration δ_s/R considered as a function of t/t_s, is independent of R, N and T_{e_3}.

The resistivity of a fully ionized plasma is proportional to $T_e^{-3/2}$, thus the resistance Ω per unit length of the discharge has the following variation

$$\Omega \propto R^2 T_{e_3}^{-3/2}. \qquad \ldots\ldots(14)$$

The rate of energy input to unit length of the discharge is $I^2\Omega$, and hence the amount of energy P_j put into unit length of the discharge by Joule heating is

$$P_j = \int_0^{t_s} I^2 \Omega \, dt \propto I^2, \qquad \ldots\ldots(15)$$

i.e. independent of size, line density or electron temperature. A similar dependence applies to the Joule heating during the contracting phase. In the absence of shock phenomena the compression is reversible, so that the energy input through Joule heating in that phase is merely multiplied by a constant proportional to the compression. Therefore under these conditions the electron and ion temperatures at corresponding phases of discharge history are independent of size:

$$T = f(IN). \qquad \ldots\ldots(16)$$

In particular, if losses can be neglected,

$$T \propto I^2 N^{-1}. \qquad \ldots\ldots(17)$$

The number of nuclear reactions per cm^3 per second r_n is (Post 1956)

$$r_n \propto N^2 R^{-4} f(T_{i_3}) \qquad \ldots\ldots(18)$$

where T_{i_3} is the ion temperature during the contracted phase, and $f(T_{i_3})$ represents the variation of the product of the nuclear cross section σ and the ion velocity v, $\overline{\sigma v}$, with temperature. The number of nuclear reactions per second in the whole discharge R_n scales as

$$R_n \propto N^2 L R^{-2} f(T_{i_3}). \qquad \ldots\ldots(19)$$

Finally, the number of reactions in the whole discharge per pulse Y_n (i.e. the neutron yield)

$$Y_n = R_n t_s \propto N^2 L \, T_{e_3}^{3/2} f(T_{i_3}) \qquad \ldots\ldots(20)$$

and the percentage of the nuclear fuel that has been burnt, (B.U.) is

$$(\text{B.U.}) = Y_n/LN \propto N \, T_{e_3}^{3/2} f(T_{i_3}), \qquad \ldots\ldots(21)$$

that is, independent of size.

The product of the ion density n with the time t_s during which these particles are held in the discharge has been shown to be a measure of how nearly a given discharge approaches a self-sustaining thermonuclear reactor (Lawson 1957). For nt_s we obtain

$$nt_s \propto N\,T_{\mathrm{e}_s}{}^{3/2}, \qquad \ldots\ldots(22)$$

independent of size.

An important practical parameter is the heat loading on the wall of the containing vessel. The rate of loss of energy from unit length of the discharge by bremsstrahlung radiation, (BS), is (Spitzer 1956)

$$(\mathrm{BS}) \propto N^2 R^{-2}\, T_{\mathrm{e}_s}{}^{1/2} \qquad \ldots\ldots(23)$$

so that the energy ϵ falling on unit area of the wall per second varies as

$$\epsilon \propto N^2 R^{-3}\, T_{\mathrm{e}_s}{}^{1/2}. \qquad \ldots\ldots(24)$$

The total amount of energy $\epsilon_{\mathrm{T}}\ (=\epsilon t_s)$ falling on unit area of the wall during the lifetime of the discharge is given by

$$\epsilon_{\mathrm{T}} \propto N^2 R^{-1}\, T_{\mathrm{e}_s}{}^{2}. \qquad \ldots\ldots(25)$$

Other sources of heat loading on the wall, such as the diffusion of charged particles and the radiation from excited states, scale in the same way with N and R but have different dependences on the temperature T_{e_s}. It is clear that the problem of the wall material is very much easier the larger the tube radius.

The amount of stored energy (S.E.) required in the condenser bank supplying the discharge is easily scaled, since in the stable pinch the bulk of the energy input goes into the form of magnetic energy. Therefore

$$(\mathrm{S.E.}) \propto I^2 L. \qquad \ldots\ldots(26)$$

The cost of an apparatus is roughly proportional to the stored energy, so for the ratio of neutron yield per pulse Y_{n} to cost we have

$$Y_{\mathrm{n}}/\mathrm{cost} \propto N^2 I^{-2}\, T_{\mathrm{e}_s}{}^{3/2} f(T_{\mathrm{i}_s}) \propto N\, T_{\mathrm{e}_s}{}^{1/2} f(T_{\mathrm{i}_s}), \qquad \ldots\ldots(27)$$

that is, independent of size.

§ 5. Discussion of Recent Results

We now consider the application of these relations to Zeta, Perhapsatron S 3 and Sceptre III. The main parameters and results quoted for the three machines running under optimum conditions are summarized in the table.

Comparison of Discharges

	Zeta	Sceptre	S3
I (kA)	180	160	200
p (microns)	$0\cdot125$	$2\cdot0$	50
R (cm)	50	15	$2\cdot5$
N (ion cm^{-1})	6.10^{16}	8.10^{16}	6.10^{16}
T_{i}(°K)	5.10^{6}	3.10^{6}	$1\rightarrow6.10^{6}$
t_{c} (sec)	10^{-3}	10^{-4}	6.10^{-6}
t_{c}/R^2 (sec cm^{-2})	4.10^{-7}	5.10^{-7}	8.10^{-7}
V (v)	$1\cdot0.10^{3}$	$2\cdot5.10^{3}$	$1\cdot4.10^{4}$
L (cm)	10^{3}	$3\cdot6.10^{2}$	2.10^{2}
VR^2/L (v cm)	$2\cdot5.10^{3}$	$1\cdot6.10^{3}$	5.10^{2}
Y_{n} (neutron pulse^{-1})	10^{6}	10^{5}	2.10^{5}
Y_{n}/L (neutron pulse^{-1}cm^{-1})	10^{3}	3.10^{2}	10^{3}
(nt) (cm^{-3} sec)	10^{11}	10^{11}	10^{11}
E/p (v cm^{-1} mm^{-1})	8.10^{3}	4.10^{3}	$1\cdot4.10^{3}$

It is seen that the line densities and currents used are approximately the same in all three cases. The temperatures achieved are of the same order, in agreement with the idea that temperature is a function of N and I alone. It is interesting to note that on the reduced time scale t_c/R^2, Zeta is the fastest collapsing discharge.

The catastrophic incursion of contaminants from the wall into the discharge in S3, which is not paralleled in Zeta and Sceptre, is illustrative of the scaling laws (24) and (25) for the heat flux to the walls. In terms of their reduced parameters the three discharges are remarkably similar. The product nt achieved in all three discharges is about 10^{11} cm^{-3} sec. Coupled with the achievement of similar temperatures, this implies that these discharges all represent about the same progress towards a thermonuclear reactor.

REFERENCES

von Engel, A., *Ionised Gases* (Oxford : University Press).
Lawson, J. D., 1957, *Proc. Phys. Soc.* B, **70,** 6.
Post, R. F., 1956, *Rev. Mod. Phys.*, **28,** 338.
Rosenbluth, M., 1957, *Proceedings of the Venice Conference.*
Shafranov, V. D., 1956, *Atomnaya Energiya*, **5,** 709.
Spitzer, L., 1956, *Physics of Fully Ionised Gases* (New York : Interscience).
Tayler, R. J., 1957, *Proc. Phys. Soc.* B, **70,** 31.
Thonemann, P. C., 1958, *Nature, Lond.*, **181,** 217 (Thonemann, P. C., *et al.*)
Tuck, J. L., 1958, *Nature, Lond.*, **181,** 231 (Honsaker, J., *et al.*)
Ware, A. A., 1958, *Nature, Lond.*, **181,** 222 (Allen, N. L., *et al.*)

Calculation of the 1s–2s Electron Excitation Cross Section of Hydrogen

By R. MARRIOTT†
Physics Department, University College London

Communicated by H. S. W. Massey; MS. received 20th December 1957

Abstract. The zero order partial cross section for the excitation of hydrogen from the (1s) to the (2s) states by electron collision has been calculated by a numerical method. Full allowance has been made for electron exchange and all direct coupling between the initial and final atomic states has been retained.

The cross sections obtained are compared with those that have been calculated by more approximate methods. In particular, the cross section near the threshold is found to be considerably smaller than that given by Erskine and Massey using the distorted wave approximation.

§ 1. INTRODUCTION

In this paper the cross section for the hydrogen excitation collision process

$$\mathrm{H(1s)} + e^{-} \rightarrow \mathrm{H(2s)} + e^{-} - 10{\cdot}2\ \mathrm{ev}$$

has been calculated.

Several approximations have been employed in previous determinations of this cross section. The results have been tabulated and compared by Massey and Moiseiwitsch (1953) and are reproduced in §4 of this paper. The values differ widely for the cross sections at energies near the threshold, which is the most important region for most applications. It is desirable, therefore, to calculate the cross section more accurately.

In a recent paper on the inelastic collision of electrons with metastable helium (Marriott 1957, to be referred to as I) it has been shown that a better approximation for the treatment of atom–electron collisions may be obtained by use of a numerical method.

As originally developed, the method involved the iterative solution of the appropriate coupled integro-differential equations representing the free electron. However, such a procedure is not particularly suitable for use on an electronic computer, required here in view of the very extensive numerical work involved, because of the amount of memory space necessary for the storage of intermediate solutions. Furthermore, the convergence of the method would probably be poor at the collision energies involved in the present case.

However, recently it has been shown that by a suitable algebraic treatment, it is possible to avoid the need for iteration when solving the integro-differential equations (Percival, private communication). In this paper the method is developed for use with coupled equations and the cross section for the excitation of hydrogen calculated for collision energies ranging from the threshold to 54 ev.

† At present with Canadian Westinghouse, Atomic Energy Division, Hamilton, Ontario.

§ 2. SCATTERING THEORY

Using atomic units throughout, the wave equation for the system hydrogen atom plus colliding electron takes the form

$$\left[\nabla_1^2+\nabla_2^2+2E+\frac{2}{r_1}+\frac{2}{r_2}-\frac{2}{r_{12}}\right]\Psi(12)=0, \qquad \ldots\ldots(1)$$

where the electrons are distinguished by the suffices 1 and 2; their mutual separation by r_{12} and E is the total energy of the system.

In order to describe slow collisions (where the wavelength of the free electron is large compared with the range of the atomic field) in which 1s–2s excitation of the hydrogen atom occurs, it is sufficient (Erskine and Massey 1951) to write the total wave function of the system in the form

$$\Psi(12)=r_2^{-1}\psi_0(r_1)F_0^{\pm}(r_2)\pm r_1^{-1}\psi_0(r_2)F_0^{\pm}(r_1)+r_2^{-1}\psi_1(r_1)F_1^{\pm}(r_2)\pm r_1^{-1}\psi_1(r_2)F_1^{\pm}(r_1), \qquad \ldots\ldots(2)$$

the alternate signs depending on whether the electron spins are antiparallel or parallel respectively. ψ_0, ψ_1 are the wave functions of the 1s and 2s states of hydrogen respectively and $F_0^{\pm}$, $F_1^{\pm}$ are free electron functions, vanishing at $r=0$, which have the asymptotic forms

$$\left.\begin{aligned}F_0^{\pm}(r)&\sim k_0^{-1}\sin k_0r+\alpha^{\pm}\exp ik_0r,\\ F_1^{\pm}(r)&\sim\beta^{\pm}\exp ik_1r,\end{aligned}\right\} \qquad \ldots\ldots(3)$$

where $\frac{1}{2}k_0^2$ is the kinetic energy of the incident electron and $\frac{1}{2}k_1^2$ that of the inelastically scattered electron. The respective zero order partial cross sections for the excitation of the 2s state are given by

$$\sigma_{01}^{\pm}=4\pi\frac{k_1}{k_0}|\beta^{\pm}|^2 \qquad \ldots\ldots(4)$$

and the observed cross section σ_{01} is then the weighted mean

$$\sigma_{01}=\tfrac{3}{4}\sigma_{01}^{-}+\tfrac{1}{4}\sigma_{01}^{+}. \qquad \ldots\ldots(5)$$

By the same procedure as that described by Erskine and Massey, we obtain for $F_0^{\pm}$ and $F_1^{\pm}$ the coupled integro-differential equations

$$\begin{aligned}\left[\frac{d^2}{dr^2}+k_0^2-V_0(r)\right]F_0^{\pm}(r)=V(r)F_1^{\pm}(r)\pm\Big\{&8A(r)\int_0^r r'A(r')F_0^{\pm}(r')\,dr'\\ &+8rA(r)\int_r^\infty A(r')F_0^{\pm}(r')dr'\\ &+\sqrt{8}B(r)\int_0^r r'A(r')F_1^{\pm}(r')\,dr'\\ &+\sqrt{8}rB(r)\int_r^\infty A(r')F_1^{\pm}(r')\,dr'\\ &+8rA(r)(E_0-\tfrac{1}{2}k_0^2)\int_0^\infty r'A(r')F_0^{\pm}(r')\,dr'\\ &+\sqrt{8}rB(r)(E_0-\tfrac{1}{2}k_1^2)\int_0^\infty r'A(r')F_1^{\pm}(r')\,dr'\Big\},\end{aligned} \qquad \ldots\ldots(6)$$

$$\left[\frac{d^2}{dr^2}+k_1^2-V_1(r)\right]F_1^{\pm}(r)=V(r)F_0^{\pm}(r)\pm\left\{\sqrt{8}A(r)\int_0^r r'B(r')F_0^{\pm}(r')\,dr'\right.$$
$$+\sqrt{8}rA(r)\int_r^{\infty}B(r')F_0^{\pm}(r')\,dr'$$
$$+B(r)\int_0^r r'B(r')F_1^{\pm}(r')\,dr'$$
$$+rB(r)\int_r^{\infty}B(r')F_1^{\pm}(r')\,dr'$$
$$+\sqrt{8}rA(r)(E_1-\tfrac{1}{2}k_0^2)\int_0^{\infty}r'B(r')F_0^{\pm}(r')\,dr'$$
$$\left.+rB(r)(E_1-\tfrac{1}{2}k_1^2)\int_0^{\infty}r'B(r')F_1^{\pm}(r')\,dr'\right\}, \qquad \ldots\ldots(7)$$

where the wave functions for the 1s and 2s states of hydrogen are respectively

$$\psi_0(r)=\pi^{-1/2}A(r), \qquad A(r)=\exp(-r),$$
$$\psi_1(r)=(8\pi)^{-1/2}B(r), \qquad B(r)=(1-r/2)\exp(-r/2),$$

and

$$V_0(r)=-2(1+1/r)\exp(-2r),$$
$$V_1(r)=-(4r)^{-1}(r^3+2r^2+6r+8)\exp(-r),$$
$$V(r)=(32/81)^{1/2}(r+2/3)\exp(-3r/2),$$
$$E=E_0+\tfrac{1}{2}k_0^2=E_1+\tfrac{1}{2}k_1^2.$$

§ 3. SOLUTION OF THE COUPLED EQUATIONS AND DERIVATION OF THE CROSS SECTION

Consider a simple equation of the form

$$y''(r)=Q(r)y(r)+\int_0^{\infty}P(r)y(r)\,dr, \qquad \ldots\ldots(8)$$

where $P(r)$ and $Q(r)$ are known functions. This could be solved numerically by an iterative procedure. However, following Percival, if we define $x(r)$, $z(r)$ as solutions of the equations

$$x''(r)=Q(r)x(r), \qquad \ldots\ldots(9)$$
$$z''(r)=Q(r)z(r)+1, \qquad \ldots\ldots(10)$$

then clearly $y(r)=x(r)+az(r)$ is a particular solution of (8) where

$$a=\int_0^{\infty}P(r)x(r)\,dr\Big/\left[1-\int_0^{\infty}P(r)z(r)\,dr\right].$$

Equations of the form (9) and (10) may be solved by non-iterative numerical procedures. Now in a similar way it may be seen that if integrals of the form

$$\int_r^{\infty}\chi(r)\,dr$$

occurring in (6) and (7) are written

$$\int_0^{\infty}\chi(r)\,dr-\int_0^{r}\chi(r)\,dr$$

and the functions

$$\begin{pmatrix} f_0^\pm \\ f_1^\pm \end{pmatrix}, \quad \begin{pmatrix} g_0^\pm \\ g_1^\pm \end{pmatrix}, \quad \begin{pmatrix} h_0^\pm \\ h_1^\pm \end{pmatrix}, \quad \begin{pmatrix} j_0^\pm \\ j_1^\pm \end{pmatrix}$$

are defined as solutions of the coupled equations

$$\left.\begin{array}{ll} \mathcal{D}_0 f_0^\pm = \mathcal{G}(f_0^\pm f_1^\pm) \pm r\,A(r), & \mathcal{D}_0 h_0^\pm = \mathcal{G}(h_0^\pm h_1^\pm) \pm r\,B(r), \\ \mathcal{D}_1 f_1^\pm = \mathcal{H}(f_0^\pm f_1^\pm), & \mathcal{D}_1 h_1^\pm = \mathcal{H}(h_0^\pm h_1^\pm), \\ \mathcal{D}_0 g_0^\pm = \mathcal{G}(g_0^\pm g_1^\pm), & \mathcal{D}_0 j_0^\pm = \mathcal{G}(j_0^\pm j_1^\pm), \\ \mathcal{D}_1 g_1^\pm = \mathcal{H}(g_0^\pm g_1^\pm) \pm r\,A(r), & \mathcal{D}_1 j_1^\pm = \mathcal{H}(j_0^\pm j_1^\pm) \pm r\,B(r), \end{array}\right\} \quad \ldots\ldots(11)$$

where

$$\mathcal{D}_0 = \left(\frac{d^2}{dr^2} + k_0^2 - V_0\right),$$

$$\mathcal{D}_1 = \left(\frac{d^2}{dr^2} + k_1^2 - V_1\right),$$

and

$$\mathcal{G}(f_0^\pm f_1^\pm) = V f_1^\pm \pm \left\{ 8A(r)\int_0^r rA(r) f_0^\pm\,dr - 8rA(r)\int_0^r A(r) f_0^\pm\,dr \right.$$

$$\left. + \sqrt{8}B(r)\int_0^r rA(r) f_1^\pm\,dr - \sqrt{8}rB(r)\int_0^r A(r) f_1^\pm\,dr \right\},$$

$$\mathcal{H}(f_0^\pm f_1^\pm) = V f_0^\pm \pm \left\{ \sqrt{8}A(r)\int_0^r rB(r) f_0^\pm\,dr - \sqrt{8}rA(r)\int_0^r B(r) f_0^\pm\,dr \right.$$

$$\left. + B(r)\int_0^r rB(r) f_1^\pm\,dr - r\,B(r)\int_0^r B(r) f_1^\pm\,dr \right\},$$

then a particular solution of equations (6) and (7) is given by

$$\begin{pmatrix} F_1^\pm \\ F_1^\pm \end{pmatrix} = \begin{pmatrix} f_0^\pm \\ f_1^\pm \end{pmatrix} + u^\pm \begin{pmatrix} g_0^\pm \\ g_1^\pm \end{pmatrix} + v^\pm \begin{pmatrix} h_0^\pm \\ h_1^\pm \end{pmatrix} + w^\pm \begin{pmatrix} j_0^\pm \\ j_1^\pm \end{pmatrix},$$

where $u^\pm$, $v^\pm$ and $w^\pm$ are constants that satisfy the simultaneous equations

$$u^\pm \begin{bmatrix} P_{10}(g^\pm) \\ P_{11}(g^\pm) \\ P_{20}(g^\pm) - 1 \\ P_{21}(g^\pm) \end{bmatrix} + v^\pm \begin{bmatrix} P_{10}(h^\pm) \\ P_{11}(h^\pm) - 1 \\ P_{20}(h^\pm) \\ P_{21}(h^\pm) \end{bmatrix} + w^\pm \begin{bmatrix} P_{10}(j^\pm) \\ P_{11}(j^\pm) \\ P_{20}(j^\pm) \\ P_{21}(j^\pm) - 1 \end{bmatrix} = \begin{bmatrix} 1 - P_{10}(f^\pm) \\ -P_{11}(f^\pm) \\ -P_{20}(f^\pm) \\ -P_{21}(f^\pm) \end{bmatrix}, \quad \ldots\ldots(12)$$

given that

$$P_{10}(g^\pm) = 8\int_0^\infty g_0^\pm A(r)[1 + r(E_0 - \tfrac{1}{2}k_0^2)]\,dr,$$

$$P_{11}(g^\pm) = \sqrt{8}\int_0^\infty g_1^\pm A(r)[1 + r(E_0 - \tfrac{1}{2}k_1^2)]\,dr,$$

$$P_{20}(g^\pm) = \sqrt{8}\int_0^\infty g_0^\pm B(r)[1 + r(E_1 - \tfrac{1}{2}k_0^2)]\,dr,$$

$$P_{21}(g^\pm) = \int_0^\infty g_1^\pm B(r)[1 + r(E_1 - \tfrac{1}{2}k_1^2)]\,dr.$$

For equations (12) to be consistent, it is necessary that the eliminant should be zero. This requirement was satisfied and it was found that the equation based on P_{20} was a simple multiple of that based on P_{11}. The multiplicative factor was $\pm\sqrt{8}$ where the alternate signs have the same meaning as previously. The relation afforded a useful check on the numerical solutions.

A computer was used for the solution of equations (11). The non-iterative numerical method that was employed is described in the Appendix.

It has been shown in I that independent solutions to (6) and (7) may be distinguished by changing the ratio of the slopes of $F_0^\pm$ and $F_1^\pm$ at the origin. In the present case it may be seen that it is necessary to obtain an independent solution for only one of the equations (11) in order that their linear combination should represent an independent solution to (6) and (7).

Denoting the asymptotic forms of the solutions to (11) by

$$\begin{pmatrix} f_0^\pm \\ f_1^\pm \end{pmatrix} \sim \begin{pmatrix} a_{10}^\pm \sin(k_0r+\lambda_{10}^\pm) \\ a_{11}^\pm \sin(k_1r+\lambda_{11}^\pm) \end{pmatrix}, \qquad v^\pm \begin{pmatrix} h_0^\pm \\ h_1^\pm \end{pmatrix} \sim \begin{pmatrix} a_{30}^\pm \sin(k_0r+\lambda_{30}^\pm) \\ a_{31}^\pm \sin(k_1r+\lambda_{31}^\pm) \end{pmatrix}$$

$$u^\pm \begin{pmatrix} g_0^\pm \\ g_1^\pm \end{pmatrix} \sim \begin{pmatrix} a_{20}^\pm \sin(k_0r+\lambda_{20}^\pm) \\ a_{21}^\pm \sin(k_1r+\lambda_{21}^\pm) \end{pmatrix}, \qquad w^\pm \begin{pmatrix} j_0^\pm \\ j_1^\pm \end{pmatrix} \sim \begin{pmatrix} a_{40}^\pm \sin(k_0r+\lambda_{40}^\pm) \\ a_{41}^\pm \sin(k_1r+\lambda_{41}^\pm) \end{pmatrix} \qquad \ldots\ldots(13)$$

and the asymptotic form of a particular solution to (6) and (7) by

$$\begin{pmatrix} F_0^\pm \\ F_1^\pm \end{pmatrix} \sim \begin{pmatrix} a_0^\pm \sin(k_0r+\lambda_0^\pm) \\ a_1^\pm \sin(k_1r+\lambda_1^\pm) \end{pmatrix}, \qquad \ldots\ldots(14)$$

and defining Γ_n and Δ_n by the relations

$$\left.\begin{aligned} \Gamma_n^\pm &= \sum_{m=1}^{4} a_{mn}^\pm \cos\lambda_{mn}^\pm, \\ \Delta_n^\pm &= \sum_{m=1}^{4} a_{mn}^\pm \sin\lambda_{mn}^\pm, \qquad n=0,1, \end{aligned}\right\} \qquad \ldots\ldots(15)$$

then we have for the amplitudes and phases in (14)

$$\left.\begin{aligned} a_n^\pm &= (\Gamma_n^{\pm 2}+\Delta_n^{\pm 2})^{1/2}, \\ \text{and} \quad \tan\lambda_n^\pm &= \Delta_n^\pm/\Gamma_n^\pm, \qquad n=0,1 \end{aligned}\right\}. \qquad \ldots\ldots(16)$$

Similar expressions are obtained for the asymptotic amplitude and phases of the independent solution of (6) and (7) denoted by

$$\begin{pmatrix} G_0^\pm \\ G_1^\pm \end{pmatrix} \sim \begin{pmatrix} b_0^\pm \sin(k_0r+\mu_0^\pm) \\ b_1^\pm \sin(k_1r+\mu_1^\pm) \end{pmatrix},$$

and finally, as shown in I, the inelastic cross sections are given by

$$\sigma_{01}^\pm = 4\pi\frac{k_1}{k_0^3}\,\frac{\sin^2(\lambda_1^\pm-\mu_1^\pm)}{[(a_0^\pm/a_1^\pm)^2+(b_0^\pm/b_1^\pm)^2-2(a_0^\pm b_0^\pm/a_1^\pm b_1^\pm)\cos(\lambda_0^\pm-\lambda_1^\pm-\mu_0^\pm+\mu_1^\pm)]} \qquad \ldots\ldots(17)$$

Thus having solved equations (11) numerically, as shown in the Appendix, the asymptotic amplitudes and phases and the appropriate integrated values of these solutions could be substituted in (12), (15), (16) and (17) and the cross section determined.

§ 4. THE CALCULATED CROSS SECTIONS AND DISCUSSION OF THE RESULTS

The calculated cross sections are given in the table, which also includes for comparison the corresponding results obtained from more approximate methods of calculation.

An indication of the numerical accuracy of the solutions of the coupled equations was afforded by the fact that the detailed balance condition

$$k_1^2\sigma_{10}^{\pm}=k_0^2\sigma_{01}^{\pm}$$

was satisfied to better than ± 2% throughout.

It is apparent that qualitatively the numerical results are more in accord with those of the variational calculations of Massey and Moiseiwitsch than either of the other methods. The poor quantitative agreement is probably a consequence of the use of an over-simplified trial function in the variational calculation.

In the case of the distorted wave calculation of Erskine and Massey, it was to be expected that the calculated values for σ_{01}^{+} were too large near the threshold since for $k_0=1$ the value was as great as 0·7 of the theoretical limit. This approximation is based on the neglect of the terms involving F_1 in equation (6) but the size of the cross section indicates that these coupling terms are, in fact, important.

These considerations would not appear to apply to σ_{01}^{-} for which all approximations are much smaller than the theoretical limit and yet differ very considerably at energies near the threshold. In this case, however, the small values arise from a near cancellation between large amplitudes arising respectively from direct and exchange scattering and neither of the separate amplitudes are given to the necessary accuracy by the approximate methods.

The numerical method as presented here involves the approximation that only coupling between the initial and final atomic states is important and only the zero order partial cross sections are significant. This permits the restriction of the expansion for $\Psi(12)$ given in equation (2) to the four terms shown. However, the approximation is only applicable where the wavelength of the incident electron is large compared with the range of the scattering field (Mott and Massey 1949). The numerical solutions show that the interaction between the electron and the hydrogen atom is still appreciable at separations greater than $10a_0$ and, therefore, the approximation could not be expected to be valid for collision energies above 11 ev.

It is desirable, therefore, that the numerical approach should be extended to include intermediate atomic states and to yield partial cross sections of higher than zero order. In general such a development requires the solution of groups of more than two coupled equations. The number of terms that may be retained in equation (2) for the expansion of $\Psi(12)$ will be limited finally by the capacity of the computers available. Nevertheless, it seems clear that the use of modern computing facilities can lead to a considerable improvement in the calculation of atomic scattering cross sections.

ACKNOWLEDGMENTS

The author wishes to thank Professor H. S. W. Massey for suggesting the problem which formed part of the hydrogen research programme at present being carried out at University College London, on behalf of the Atomic Energy Research Establishment, Harwell.

Cross Sections for the Excitation of the Hydrogen 2s Level Calculated by Different Methods

		σ_{01}^+				σ_{01}^-				$\sigma_{01}=\frac{1}{4}(\sigma_{01}^+ + 3\sigma_{01}^-)$				Theor. max.
k_0	ev	BO	V	DW	N	BO	V	DW	N	BO	V	DW	N	$1/k_0^2$
0·866	10·2	0	0	0	0	0	0	0	0	0	0	0	0	—
0·900	11·0				0·153				0·00054				0·0386	1·235
1·000	13·5	0·287	0·167	0·714	0·288	2·02	0·002	0·036	0·00274	1·59	0·043	0·178	0·0741	1·000
1·100	16·4				0·280				0·00586				0·0745	0·826
1·200	19·4	0·011	0·124	0·344	0·219	0·668	0·004	0·010	0·00814	0·503	0·035	0·094	0·0608	0·694
1·500	30·4	0·014	0·057	0·127	0·0968	0·134	0·007	0·010	0·00974	0·104	0·020	0·035	0·0315	0·444
2·000	54	0·018	0·016	0·025	0·0290	0·020	0·005	0·006	0·00624	0·020	0·008	0·011	0·0119	0·250

BO = Born–Oppenheimer; DW = full distorted wave approximation; V = variational method (see Massey and Moiseiwitsch 1953); N = numerical method. Cross sections in units of πa_0^2.

The author is also indebted to Mr. W. Lawson for considerable assistance given in obtaining the solutions from the electronic computer.

REFERENCES

ERSKINE, G. A., and MASSEY, H. S. W., 1952, *Proc. Roy. Soc.* A, **212,** 521.
MARRIOTT, R., 1957, *Proc. Phys. Soc.* A, **70,** 288.
MASSEY, H. S. W., and MOISEIWITSCH, B. L., 1953, *Proc. Phys. Soc.* A, **65,** 406.
MOTT, N. F., and MASSEY, H. S. W., 1949, *The Theory of Atomic Collisions*, 2nd Edn (Oxford : University Press), Chap. VIII.

APPENDIX

In I an uncoupled equation was solved of the form

$$y''(r) = P(r)y(r) + Q(r),$$

where $P(r)$, $Q(r)$ are known functions.

The integrating routine employed the central difference formula

$$y_n = \frac{\omega^2}{1-\omega^2 P_n/12}\left[\delta^{-2} y_n'' + \frac{1}{12} Q_n\right], \qquad \ldots\ldots(18)$$

where ω is the interval by which r is advanced at each integration cycle.

In the present case we have to solve the coupled equations (11) which may be considered as of the form

$$\left.\begin{aligned} f_0'' &= P_0 f_0 + V f_1 + Q_0(f_0 f_1), \\ f_1'' &= P_1 f_1 + V f_0 + Q_1(f_0 f_1). \end{aligned}\right\} \qquad \ldots\ldots(19)$$

Applying (18) gives at once

$$f_{0n} = \alpha_{0n}\left[\delta^{-2} f_{0n}'' + \frac{1}{12} Q_{0n}(f_0 f_1) + \frac{1}{12} V_n f_{1n}\right], \qquad \ldots\ldots(20)$$

$$f_{1n} = \alpha_{1n}\left[\delta^{-2} f_{1n}'' + \frac{1}{12} Q_{1n}(f_0 f_1) + \frac{1}{12} V_n f_{0n}\right], \qquad \ldots\ldots(21)$$

where

$$\alpha_{mn} = \frac{\omega^2}{1-\omega^2 P_{mn}/12}.$$

If the interval ω is restricted to small values such that $\frac{1}{144} V_n{}^2 \alpha_{0n} \alpha_{1n}$ is zero to the required accuracy (20) and (21) may be combined to give

$$\left.\begin{aligned} f_{0n} &= \alpha_{0n}\left[\delta^{-2} f_{0n}'' + \frac{1}{12} Q_{0n}(f_0 f_1)\right] + \frac{1}{12} V_n \alpha_{0n} \alpha_{1n}\left[\delta^{-2} f_{1n}'' + \frac{1}{12} Q_{1n}(f_0 f_1)\right], \\ f_{1n} &= \alpha_{1n}\left[\delta^{-2} f_{1n}'' + \frac{1}{12} Q_{1n}(f_0 f_1)\right] + \frac{1}{12} V_n \alpha_{0n} \alpha_{1n}\left[\delta^{-2} f_{0n}'' + \frac{1}{12} Q_{0n}(f_0 f_1)\right]. \end{aligned}\right\} \qquad \ldots\ldots(22)$$

This was the integration formula used for the solution of the coupled equations.

Q_0 and Q_1 correspond to the integral terms occurring in $\mathscr{G}$ and $\mathscr{H}$ respectively of equations (11). It may be shown by expansion of these integrals, for example by Simpson's rule, that Q_{0n}, Q_{1n} depend only on the previous $n-1$ values of f_0 and f_1. Thus f_{0n}, f_{1n} as obtained from (22) involve only preceding values of f_0, f_1 and the solutions may be built up step by step.

To commence the integration routine two starting values are required and these may be calculated by means of series expansions at the origin.

Equations (11) mutually differ by the addition of functions $rA(r)$ or $rB(r)$. It may be seen, however, that these functions are equivalent to the addition of a constant to the appropriate integral in $\mathscr{G}$ or $\mathscr{H}$. Thus one programme was sufficient for the solution of equations (11) (a sign change being necessary to give the ± cases), the differences between the equations being introduced by means of different starting values.

In order that the atomic field should be less than 10^{-6} A.U. it was necessary to integrate out to $42a_0$. The interval used was $\omega = 0{\cdot}1a_0$.

The numerical solutions were printed out over the range $42a_0 < r < 43a_0$ and their amplitudes and phases determined and the integrals required for the calculation of P_{10}, P_{11}, P_{20}, P_{21}, in equation (12) were also printed out. The cross sections could then be obtained by numerical substitution in equations (12), (15), (16) and (17).

RESEARCH NOTES

A Semi-empirical Equation for the Initial Susceptibility of Homogeneous Ferromagnetic Alloys

By E. W. LEE and R. C. JACKSON†
Department of Physics, University of Nottingham

Communicated by L. F. Bates; MS. received 15*th January* 1958, *and in revised form* 12*th March* 1958

In weak fields the magnetization of a ferromagnetic substance varies with field according to Rayleigh's law, viz.

$$I=\chi_0 H+bH^2.$$

The constant χ_0 is called the initial susceptibility and is an important characteristic of the material. Experimentally χ_0 is observed to be extremely structure sensitive and invariably decreases with the presence of internal stresses. In strain free material χ_0 can in principle be calculated in terms of the fundamental constants of the material and there have been many attempts to do this, with varying degrees of success. The numerical agreement between theory and experiment depends partly on the model adopted for calculation and it is perhaps unfortunate that most theories produce final formulae containing at least one more or less adjustable constant. All these theories consider only one mechanism providing hindrance to wall movement and in consequence lead to the conclusion that the initial susceptibilities should be infinite if the crystal anisotropy (inclusion theories) or magnetostriction (strain theories) is zero. The single exception is an attempt by Kersten (1953) to combine his own strain and inclusion theories of initial susceptibility (1931 and 1951, respectively). Now the experiments of Bozorth (1953) on Ni–Fe alloys indicate quite clearly that the maximum χ_0 occurs not at the compositions corresponding to zero magnetostriction or zero anisotropy but at some intermediate composition. We suggest therefore that the hindrance to wall movement comes from two independent mechanisms, one depending on magnetostriction and one on crystal anisotropy. The object of this note is to examine briefly the consequences of such an assumption.

The measured initial susceptibility is made up of the rotational and displacement susceptibilities, χ_{R} and χ_{W} respectively. For a polycrystal it is easy to calculate χ_{R} if interactions between crystallites are ignored. Then, for cubic crystals

$$\chi_{\mathrm{R}}=\frac{I_{\mathrm{s}}^2}{3(K_1+\lambda_{\mathrm{s}}\sigma_{\mathrm{i}})} \qquad K_1>0 \qquad \ldots\ldots(1)$$

$$\chi_{\mathrm{R}}=\frac{I_{\mathrm{s}}^2}{2K_1+3K_2/2+3\lambda_{\mathrm{s}}\sigma_{\mathrm{i}}} \qquad K_1<0 \qquad \ldots\ldots(2)$$

---

† Now with the Plessey Co. Ltd., Towcester, Northants.

in which K_1 and K_2 are the first and second anisotropy constants respectively, λ_s is the isotropic magnetostriction constant and σ_i is the internal stress amplitude. In well annealed materials σ_i is of the order of $\lambda_s E$, where E is Young's modulus.

With regard to boundary displacement the situation is by no means as simple. In order to calculate the initial susceptibility due to wall displacements it is necessary to know both the domain wall restoring force per unit area and the mean distance between domain walls. Apart from some calculations by Martin (1957) there is very little information on the latter quantity for random polycrystals. For the former the situation is in some ways worse since it is at present by no means clear what are the factors which determine the restoring force on a domain wall. Possible causes are the presence of non-magnetic inclusions, stresses around dislocations, closure domains and the effects of wall curvature. To make matters worse it is not yet known with certainty what fraction of the initial susceptibility is contributed by 180° walls and what fraction by 90° walls (or similar low angle walls if $K_1 < 0$). Becker and Döring (1939) have given evidence for the view that 90° wall displacements provide almost the sole contribution, and we favour this for the following reason. The experiments of Bozorth on nickel–iron alloys indicate that the initial susceptibility reaches a maximum at the composition at which λ_e rather than K_1 is a minimum. (By λ_e we denote the magnetostriction constant appropriate to the direction of easy magnetization:

$$\lambda_e = \lambda_{100} \text{ if } K_1 > 0; \ \lambda_e = \lambda_{111} \text{ if } K_1 < 0.)$$

Since there is no magnetostriction associated with the movement of a 180° wall it is difficult to see why $\lambda_e = 0$ should be so essential for high initial susceptibility if 180° walls make an appreciable contribution. We shall hereafter assume that only 90° walls need to be taken into account.

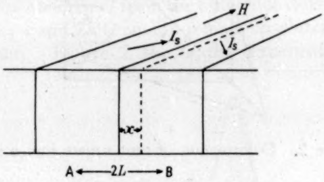

Figure 1. Section through two 90° domains.

To obtain an expression for the initial susceptibility in this case consider a block of material traversed by 90° walls distance $2L$ apart with a field applied parallel to the domain wall (figure 1). If the wall displacements are small it may be assumed that Hooke's law is obeyed and the wall may be characterised by a restoring force per unit area, denoted by α. Then the pressure exerted by the field is $-\sqrt{2}\, H I_s x$ and the restoring force is αx. The displacement of the wall is thus $\sqrt{2} H I_s / \alpha$ and the susceptibility is $\chi_W = 2 I_s^2 / \alpha L$. However, as pointed out by Bozorth, movement of a 90° wall is accompanied by magnetostriction which in this case is a shear strain determined only by λ_e. If the domain wall is prevented from deforming, for example, by neighbouring crystallites, then work is done on the area swept out by the moving wall and its energy is increased. If the angle of shear is θ and G the shear modulus then the energy is $\frac{1}{2} G \theta^2 x$ if the domain is prevented from deforming completely. This, however, cannot be the case. Experimentally, magnetostriction is observed to occur in low fields where boundary movements predominate and so the domain can be only partially prevented from deforming. Detailed calculation would only serve to show how complex the problem of initial susceptibility is for it is intuitively evident that the shear energy will depend amongst other things on the size and shape of the expanding domain and also on the size, shape and orientation of its neighbours. Instead we assume that the shear energy may be expressed by a term of the form $\frac{1}{2}aG\theta^2x.x/L$ where a is a numerical constant probably of the order of unity. The significance of this is that the domain deforms freely for infinitesimal values of the displacement of the wall. As the wall moves further, deformation is resisted by elastic forces. Some evidence that this type of resistance does actually occur may be found in the behaviour of polycrystalline iron where the maximum magnetostrictive elongation very rarely reaches the value of $0{\cdot}55\lambda_{100}$ demanded by elementary theory. The constant a is therefore a measure of the extent to which the domain is allowed to deform, and therefore of the additional restoring force imposed by magnetostriction.

It remains to relate the angle of shear to λ_e. In the area swept out by the moving wall every square is converted to a rhombus with its long diagonal increased by a factor $1+\lambda_e$ and its short diagonal reduced by $1-\lambda_e/2$. Thus from figure 2

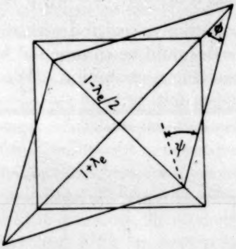

Figure 2. Deformation of unit square into a rhombus.

the angle of shear ψ is $2(\pi/4-\phi)$ and $\tan\phi=(1-\lambda_e/2)/(1+\lambda_e)=1-3\lambda_e/2$. From which, since ψ is a small angle, $\psi=3\lambda_e/2$. The angle $\theta=2\psi$ and so

$$E=9aG\lambda_e^2x^2/2L$$

which we may write

$$E=a'G\lambda_e^2x^2/L \qquad \ldots\ldots(3)$$

in which $a'=9a/2$.

The additional restoring force due to magnetostriction is, from equation (3), $2a'G\lambda_e^2x/L$ from which

$$\chi_W=\frac{2I_s^2}{\alpha L+2a'G\lambda_e^2} \qquad \ldots\ldots(4)$$

We do not know what are the chief contributions to α. However, acting on the supposition that α depends on K_1 there are quite definite limitations to the manner of the dependence of α on K, if equation (4) is to be consistent with the experimental facts. The quantity α appears in the denominator of equation (4) as the product αL. L may be taken roughly as the average domain size. In our view it is extremely probable that for a given material L depends upon the polycrystalline grain size. In the first place the grain diameter must set an upper limit to the maximum domain size. Secondly, Martin's calculations (1957) of the dependence domain size upon crystal size, although derived for isolated single crystals must be qualitatively correct for polycrystalline grains. If α were wholly independent of L and L were roughly proportional to the grain size then equation (4) would indicate that χ_W increased with decreasing grain size. This is never observed in practice; indeed the recent careful measurements of Walters (1955) indicate just the reverse and this is in agreement with the results of a good many other investigators. We suggest that α may depend upon L in such a way that the product αL is reciprocal in L. The simplest assumption is that α is proportional to L^{-2}. Then in order to be dimensionally correct α must be of the form $bK_1\delta/L^2$ where b is a numerical constant and δ has the dimensions of a length. Tentatively identifying δ with the domain wall width, which is $A^{1/2} K_1^{-1/2}$, A being the exchange energy density, we have

$$\alpha = bK_1^{1/2} A^{1/2}/L^2.$$

Substituting this value for α in equation (4),

$$\chi_W = \frac{2I_s^2}{cK_1^{1/2} + 2a'G\lambda_s^2} \qquad \ldots\ldots (5)$$

in which $c = bA^{1/2}/L^2$. The form of this expression, without the magnetostriction term, is almost identical with that recently obtained by Kersten (1956). The total susceptibility $\chi_0 = \chi_R + \chi_W$.

We have attempted to fit Bozorth's data on the initial susceptibilities of iron-nickel alloys to the value of χ_0 calculated from equations (1), (2) and (5) by subtracting the calculated value of χ_R from the measured value of χ_0 and determining the two constants c and $2a'G$ from the difference thus obtained. There is of course no reason why c and $2a'G$ should remain absolutely constant from one composition to another. Figure 3 shows the experimental χ_0-composition curve for the disordered nickel–iron alloys together with the curve calculated from equation (5) using the data given by Bozorth. The constants c and $2a'G$ obtained by fitting the theoretical to the experimental curve at 75% and 80% Ni

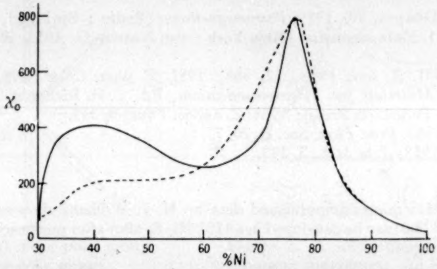

Figure 3. Initial susceptibility of disordered nickel iron alloys. The full curve is calculated from eqn. (5), the broken curve is taken from the experimental data, given by Bozorth (1953). The two curves are coincident in the range 85–100% Ni.

are 78 and 1×10^{13} respectively, from which $a' \simeq 5$, $a \simeq 1$ as anticipated. The agreement between theoretical and experimental curves is good in view of the obvious limitations of the treatment (including the fact that no attempt has been made to find the value of the constants giving the best fit over the entire range of composition) but the theoretical curve is considerably sharper than the experimental one. We think this might be caused by local fluctuations in the composition of the polycrystalline alloys or possibly by localised regions of enhanced crystallographic order. The very small peak† in the initial susceptibility which occurs at 45% is predicted and seems to be attributable to zero λ_e. However at this composition the factor involving K_1 is dominant and the fact that λ_e goes through zero has only a limited effect on the susceptibility. It is interesting to note that for pure nickel, taking the same constants and $I_s = 500$, $\lambda_s = -34 \times 10^{-6}$, $\lambda_e = -24 \times 10^{-6}$, $K_1 = -59 \times 10^3$ erg cm^{-1}. χ_0 is found to be 22, in excellent agreement with experiment.

We should expect the constant c in equation (5) to be strongly dependent on the impurity concentration in the material. If K_1 is large the rotational susceptibility is negligible and the total susceptibility is given by equation (5). In these circumstances the dominating term in the denominator is the first, and so the initial susceptibility is strongly dependent on c, i.e. on the total impurity content. This seems to provide a formal explanation for the fact that in some materials, e.g. iron, very high initial susceptibility may be developed as a result of extreme purification whilst in others, in which the magnetostriction term is presumably important, e.g. nickel, this is not so.

ACKNOWLEDGMENTS

We wish to thank Professor L. F. Bates for his interest in this work and for assistance with the manuscript. We have benefited greatly from a number of discussions with Mr. A. C. Lynch of the Post Office Research Station.

REFERENCES

BECKER, R., and DÖRING, W., 1939, *Ferromagnetismus* (Berlin : Springer).

BOZORTH, R., 1951, *Ferromagnetism* (New York : van Nostrand); 1953, *Rev. Mod. Phys.*, **25,** 42.

KERSTEN, M., 1931, *Z. tech. Phys.*, **12,** 668; 1951, *Z. phys. Chem.*, **198,** 89; 1953, *Soft Magnetic Materials for Telecommunications*, Ed. C. E. Richards and A. C. Lynch (London: Pergamon Press); 1956, *Z. angew. Phys.*, **8,** 313.

MARTIN, D. H., 1957, *Proc. Phys. Soc.* B, **70,** 77.

WALTERS, R. S., 1955, *Acta Met.*, **3,** 293.

---

† Bozorth (1951) quotes unpublished data by H. J. Williams showing that an initial permeability of 15 000 may be developed in a 45% Ni–Fe alloy after purification by prolonged annealing in hydrogen.

An Unconventional Electron Lens

By G. D. ARCHARD
A.E.I. Research Laboratory, Aldermaston, Berks.

MS. received 4th February 1958, and in final form 26th March 1958

An electron lens consisting solely of rotationally symmetrical electrodes is never free from spherical aberration (Scherzer 1936, 1947). In order to remove the aberration it is necessary either to construct the whole lens from non-rotationally symmetrical elements (Burfoot 1953, Whitmer 1956) or to add a correcting system to a conventional lens (Scherzer 1947, Seeliger 1949, 1951). Scherzer's method is flexible, but contains many separate elements and occupies considerable space. Burfoot's method is simple in principle, but the shapes of the electrodes are complicated and their tolerances make practical realization impossible.

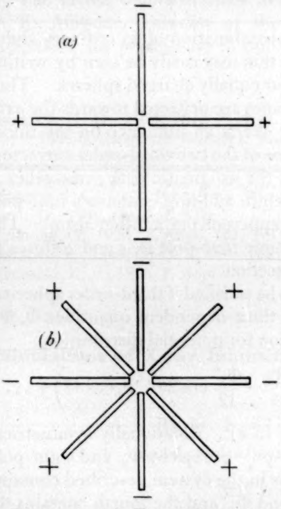

Figure 1. (*a*) Four-pole group; (*b*) eight-pole group.

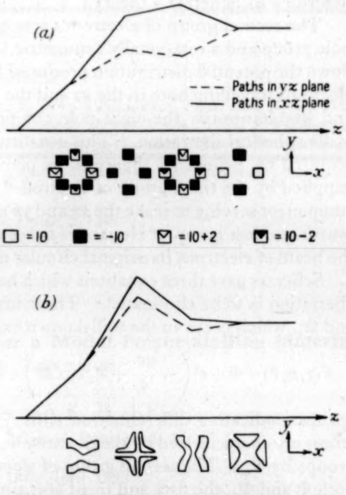

Figure 2. Unconventional lenses: (*a*) present suggestion; (*b*) Burfoot's concept.

Underlying both approaches is the principle of superimposing fields of the 'four-pole' and 'eight-pole' varieties (so-called because they can most simply be produced by symmetrical groups of four and eight electrodes respectively, see figure 1). Scherzer derives these fields from cylindrical lenses and groups of eight laminae of alternate potential distributed symmetrically round the axis (figure 1 (*b*)). Burfoot shapes his electrodes so that individually they give rise to the correct type of field and in combination they assemble these in the required manner. It has been shown mathematically (Scherzer 1947) that three separate fields of the eight-pole form are required and that two of these must be set up in an astigmatic region; actually one of the three can be eliminated (Archard 1954) but not very conveniently.

A distinguishing feature between the two methods is that Scherzer's electrons cross the axis, giving two line foci, whereas Burfoot's electrons do not. Scherzer's system can be simplified (Archard 1955 a) if the cylindrical lenses are replaced by groups of four laminae resembling the stigmator of Rang (1949) (figure 1 (*a*)). It will now be shown that Burfoot's system can be made practicable by analogous means.

Consider, for example, the system of figure 2 (*a*) (Burfoot's system is shown for comparison in figure 2 (*b*): the electrode shapes are only schematic). The first group of electrodes provides superimposed fields of the four- and eight-pole variety. Numbers on an arbitrary scale are affixed in order to show the principle on which the voltages on the various electrodes are made up. The four-pole component deflects electrons travelling in the xz plane outwards and those travelling in the yz plane inwards, thus giving the beam an elliptical cross section. The eight-pole component acts on the third-order spherical aberration in the manner described in Scherzer's theory.

The second group of electrodes acts as the combination of an ordinary eight-pole group and a rotationally symmetric lens; this may easily be seen by writing down the potential distribution produced by four equally charged spheres. Thus electrons travelling both in the xz and the yz planes are deflected towards the axis, and simultaneously the eight-pole component exerts an influence on the third-order spherical aberration. This constitutes one of the two third-order correctors required by Scherzer's theory to be placed in the astigmatic path; the other is supplied by the third group of electrodes, which in addition contains a four-pole component serving to make the xz and yz paths approach one another again. The fourth and last group of electrodes acts as a simple four-pole lens and restores to the beam of electrons its original circular cross section.

Scherzer gave three equations which have to be satisfied if third-order spherical aberration is to be eliminated. These involve the z-dependent quantities Φ, Φ_2, and Φ_4, which occur in the well-known expansion for potential distribution:

$$\phi(r, z, \theta) = \Phi + r^2\left(-\frac{\Phi''}{4} + \Phi_2 \cos 2\theta\right) + r^4\left(\frac{\Phi^{\mathrm{iv}}}{64} - \frac{\Phi_2''}{12}\cos 2\theta + \Phi_4 \cos 4\theta\right) + \dots$$

(primes indicating differentiation with respect to z). Rotationally symmetrical lenses are characterized by the quantity Φ, four-pole groups by Φ_2, and eight-pole groups by Φ_4. The second group of electrodes in the system described contains both Φ and Φ_4, the first and third contain Φ_2 and Φ_4, and the fourth contains Φ_2 only.

Focal length is largely controlled by the Φ component and can be worked out by simple ray tracing. An approximate analytical formula can be obtained for spherical electrodes (Archard 1955 b); this is

$$f/a \simeq (a/\rho)^2 (\Phi_A/\Phi_S)^2$$

where a = distance of centres of spheres from axis, ρ = radius of spheres, Φ_S = voltage on spheres, Φ_A = accelerating voltage. With typical values $a = 4\rho = 0{\cdot}2$ cm,

$\Phi_S = \Phi_A$, this gives $f \sim 3$ cm. Spherical electrodes would never be used in practice, and in fact the laminar electrodes proposed would give considerably lower values of focal length (Archard 1956).

It is elementary but cumbersome to substitute into Scherzer's equations the potential distributions of the several electrode groups and to deduce the voltage requirements in any particular case. Typical values would be of the order of a few kilovolts positive or negative. On the assumption that small fine adjustments (of the order of 1%) could if necessary be made to the voltages, typical positioning tolerances would be of the order of 10 microns. This estimate is based on calculations made earlier for a lens of shorter focus (Archard 1954), but is believed to be reasonably correct. The system described thus compares favourably with Burfoot's original system as regards tolerances, while it is simpler than Scherzer's in that (i) it contains no conventional high-voltage rotationally symmetrical lens and (ii) there are only four stages of deflection instead of seven. It is therefore felt that a useful lens, internally corrected for spherical aberration, could be constructed on the general principle of the system described.

ACKNOWLEDGMENTS

The author wishes to thank Mr. D. P. R. Petrie for helpful comment and Dr. T. E. Allibone, Director of the Research Laboratory, Associated Electrical Industries, for permission to publish this note.

REFERENCES

ARCHARD, G. D., 1954, *Brit. J. Appl. Phys.*, **5**, 294; 1955 a, *Proc. Phys. Soc.* B, **68**, 156; 1955 b, *Associated Electrical Industries Research Report* A 424; 1956, *Proceedings of* 1954 *International Conference on Electron Microscopy* (London : Royal Microscopical Society), p. 97.

BURFOOT, J. C., 1953, *Proc. Phys. Soc.* B, **66**, 775.

RANG, O., 1949, *Optik*, **5**, 518.

SCHERZER, O., 1936, *Z. Phys.*, **101**, 593; 1947, *Optik*, **2**, 114.

SEELIGER, R., 1949, *Optik*, **5**, 490; 1951, *Ibid.*, **8**, 311.

WHITMER, R. F., 1956, *J. Appl. Phys.*, **27**, 808.

Calculations of X-ray Intensities for a Model Polycrystalline Material in Simple Extension

BY M. F. CULPIN AND K. W. KEMP
British Nylon Spinners Limited, Pontypool, Mon.

MS. received 14*th April* 1958

THE distribution of intensity in the X-ray diffraction pattern of a model polycrystalline fibre undergoing a simple extension has been discussed (Culpin and Kemp 1956). It has been shown that in the case of the model described there, the intensity of the diffracted radiation at a point P on the Debye–Scherrer circle is proportional to $f(\lambda, \psi)$, where

$$f(\lambda, \psi) = \frac{\lambda^3 E[\{2b/(b+1)\}^{1/2}, \tfrac{1}{2}\pi]}{\pi^2(1-b)\{a^3(1+b)\}^{1/2}}, \qquad \ldots\ldots(1)$$

λ = extension ratio, ψ = angular distance of P from *equator* of Debye–Scherrer circle, $a = 1 + \frac{1}{2}(\lambda^3 - 1)(1 + m)$, $b = \frac{1}{2}a^{-1}(\lambda^3 - 1)(1 - m)$, $m = \cos^2\theta \sin^2\psi$, θ = Bragg angle and

$$E(k, \Phi) = \int_0^{\Phi} (1 - k^2 \sin^2 \phi)^{1/2}\, d\phi.$$

From these expressions it can be seen that the value of $f(\lambda, \psi)$ is determined by the values of λ and m. For a given value of θ the value of ψ associated with an intensity of $f(\lambda, \psi)$ can be determined from the equation

$$\psi = \sin^{-1}(m^{1/2}/\cos\theta). \qquad \ldots\ldots(2)$$

Thus, from one table of values of $f(\lambda, \psi)$ computed for different values of λ and m it is possible, with sufficient accuracy for practical purposes, to obtain by graphical methods values for the intensity of radiation round the Debye–Scherrer ring for a variety of values of θ. Table 1 can be used in this way. Values of ψ corresponding to the values of m shown in the table are given at the end of the table for θ having the particular values $\theta = 10°$ and $\theta = 20°$.

Table 1. Values of $f(\lambda, \psi)$ for different λ and m

						ψ	
m	$\lambda = 2$	$\lambda = 3$	$\lambda = 4$	$\lambda = 5$	$\lambda = 6$	$\theta = 10°$	$\theta = 20°$
0·0000	0·3222	0·5497	0·8288	1·1473	1·5029	0	0·0
0·0074	0·3086	0·4660	0·5741	0·6054	0·5869	5	5·3
0·0292	0·2722	0·3216	0·3014	0·2615	0·2121	10	10·3
0·1135	0·1908	0·1520	0·1120	0·0843	0·0657	20	21·0
0·2425	0·1342	0·0883	0·0608	0·0441	0·0339	30	31·6
0·4007	0·1007	0·0605	0·0384	0·0291	0·0223	40	42·4
0·5691	0·0814	0·0462	0·0294	0·0220	0·0169	50	53·4
0·7274	0·0695	0·0386	0·0250	0·0180	0·0138	60	65·2
0·8564	0·0624	0·0343	0·0224	0·0161	0·0121	70	80·0
0·9406	0·0586	0·0321	0·0211	0·0148	0·0115	80	—
0·9699	0·0574	0·0311	0·0198	0·0146	0·0110	90	—

We have determined the values of m for which $f(\lambda, \psi)$ takes values which are 70%, 50% and 30% of the maximum height above the background level. These values, denoted by $m(70\%)$, $m(50\%)$ and $m(30\%)$, are given in Table 2.

Table 2. Values of $m(70\%)$, $m(50\%)$ and $m(30\%)$ for different λ

λ	$m(70\%)$	$m(50\%)$	$m(30\%)$
2·0	0·0529	0·1135	0·2352
3·0	0·0144	0·0392	0·0867
4·0	0·0068	0·0161	0·0386
5·0	0·0027	0·0080	0·0179
6·0	0·0019	0·0047	0·0106

Curves of the peak widths denoted by $W(70\%)$, $W(50\%)$ and $W(30\%)$ expressed in terms of ψ for the particular values $\theta = 10°$ and $\theta = 20°$ are shown in figures 1 and 2. By use of these curves any experimental determinations of $f(\lambda, \psi)$ can be compared immediately by means of peak widths with the distribution of intensity for our model fibre if a Bragg angle of 10° or 20° is involved. The curve for $\theta = 5°$ does not differ appreciably from the one for $\theta = 10°$. These curves can therefore be usefully compared with experimental results when the Bragg angle

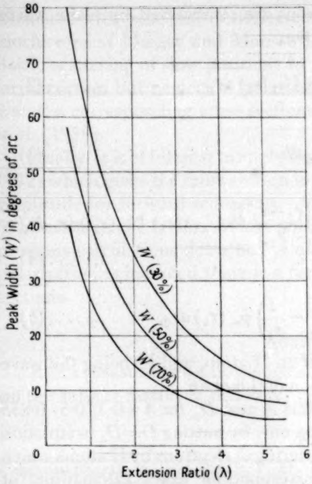

Figure 1. Relationship of peak width to extension ratio for a Bragg angle of 10°.

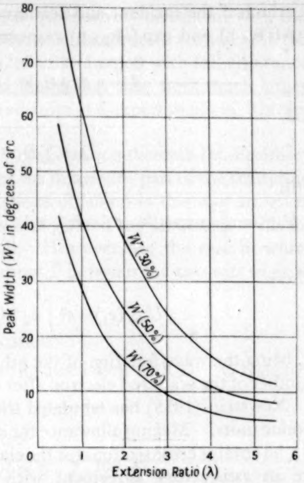

Figure 2. Relationship of peak width to extension ratio for a Bragg angle of 20°.

lies between 5° and 20°. For other values of θ, peak widths can be determined with use of table 2 and equation (2).

ACKNOWLEDGMENT

We wish to thank the directors of British Nylon Spinners Limited for permission to publish this note.

REFERENCE

CULPIN, M. K., and KEMP, K. W., 1956, *Proc. Phys. Soc.* B, **69**, 1301.

Elastic Scattering of Slow Positrons by Hydrogen Atoms

BY B. L. MOISEIWITSCH
Department of Applied Mathematics, The Queen's University of Belfast

Communicated by D. R. Bates; MS. received 8th April 1958

By applying the Schwinger variational method to the elastic scattering of slow electrons by hydrogen atoms it may be shown (cf. Newstein 1955) that if exchange is ignored the scattering amplitude f can be expressed in the form

$$f=-\frac{1}{4\pi}\frac{A^2}{A-D} \qquad \ldots\ldots(1)$$

in which if the incident and scattered electrons are represented by plane waves $\exp(i\mathbf{k}\cdot\mathbf{r})$ and $\exp(i\mathbf{k}_1\cdot\mathbf{r})$ respectively, then

$$A=\int \exp\{i(\mathbf{k}-\mathbf{k}_1)\cdot\mathbf{r}_1\}\,U_{11}(r_1)\,d\mathbf{r}_1 \qquad \ldots\ldots(2)$$

and

$$D=\sum_{n=1}^{\infty}D_n+\int_0^{\infty}D_k\,dk \qquad \ldots\ldots(3)$$

with

$$D_n=-\iint \exp\{i(\mathbf{k}\cdot\mathbf{r}_1'-\mathbf{k}_1\cdot\mathbf{r}_1)\}\frac{\exp\{ik_n|\mathbf{r}_1-\mathbf{r}_1'|\}}{4\pi|\mathbf{r}_1-\mathbf{r}_1'|}\,U_{n1}^*(r_1)\,U_{n1}(r_1')\,d\mathbf{r}_1\,d\mathbf{r}_1' \qquad \ldots\ldots(4)$$

where

$$U_{nm}(r_1)=e^2\int \phi_n^*(r_2)\left(\frac{1}{r_{12}}-\frac{1}{r_1}\right)\phi_m(\mathbf{r}_2)\,d\mathbf{r}_2, \qquad \ldots\ldots(5)$$

ϕ_n being the wave function of the nth state of an H atom, and k_n being the wave number of the scattered electron after excitation of this state.

Newstein (1955) has tabulated the integrals A and D_n for $k=0{\cdot}3$, $0{\cdot}5$, $0{\cdot}835$ atomic units. Making allowance for distortion only by putting $D=D_1$ in equation (1), he obtains cross sections for the elastic scattering of electrons by H atoms which are in satisfactory agreement with the corresponding exact calculations of Chandrasekhar and Breen (1946).

In the case of the elastic scattering of positrons by H atoms we may use the expression

$$f=\frac{1}{4\pi}\frac{A^2}{A+D} \qquad \ldots\ldots(6)$$

for the scattering amplitude, which follows directly from (1) be replacing A by $-A$ due to the change in sign of the charge of the incident particle.

If only distortion effects are considered so that polarization is neglected in the first instance, comparison can be made with the corresponding exact calculations of Massey and Moussa (1958) for the elastic scattering of positrons with zero angular momentum by H atoms. In the table their cross sections are compared with those obtained by using expression (6) with $D=D_1$. There is satisfactory agreement between the two sets of calculations.

Wave number k (in A.U.)	Cross sections (in units of πa_0^2)				
	Polarization neglected			Polarization included	
	Exact	Variational		Variational	
0·2	1·30				
0·3		1·16	(1·21)†	0·41	(0·25)†
0·5	1·09	1·00	(1·13)†	0·42	(0·22)†
0·835		0·81	(0·95)†	0·30	(0·13)†
1·0	0·67				

† The cross sections in brackets are those given by Feenberg's cross section theorem.

This suggests that if the complex expression (3) for D is used in (6) so that account is taken of polarization effects, the values of the resulting cross sections should be fairly reliable. The last column of the table gives the values of the cross sections computed in this way. They are smaller than the cross sections calculated with polarization neglected. This is qualitatively consistent with the conclusions of Massey and Moussa (1958) who calculated cross sections for the elastic scattering of slow positions by helium, neon and argon with full allowance for distortion but neglect of polarization and found that they were much larger than the corresponding cross sections obtained from the experiments of Marder *et al.* (1956).

Finally, it is of interest to apply Feenberg's cross section theorem (cf. Feenberg 1932) which gives the cross section in terms of the imaginary part of the scattering amplitude for forward scattering. Cross sections obtained in this way are given in brackets in the table. When polarization is neglected the agreement with the previous calculations described is quite good. However, for the case in which polarization is included there is a factor of about 2 between the two sets of cross sections.

ACKNOWLEDGMENT

It is a pleasure to acknowledge a stimulating discussion with Dr. A. Dalgarno on the subject matter of this note.

REFERENCES

CHANDRASEKHAR, S., and BREEN, F. H., 1946, *Astrophys. J.*, **103**, 41.
FEENBERG, E., 1932, *Phys. Rev.*, **40**, 40.
MARDER, S., HUGHES, V. W., WU, C. S., and BENNETT, W., 1956, *Phys. Rev.*, **103**, 1258.
MASSEY, H. S. W., and MOUSSA, A. H. A., 1958, *Proc. Phys. Soc.*, **71**, 38.
NEWSTEIN, M. C., 1955, *Technical Report* No. 4, Massachusetts Institute of Technology.

On the $(2p)^2\,{}^1S$ State Solution of the Non-relativistic Schrödinger Helium Equation

BY E. HOLØIEN
Institute of Theoretical Physics, University of Oslo, Norway

MS. received 17th February 1958, and in revised form 14th April 1958

§ 1. INTRODUCTION

In a previous paper (Holøien 1958, to be referred to as Paper I) an approach, based on the application of the Ritz variational principle in the method of configurational interaction, was given to the non-relativistic Schrödinger equation for helium and the negative hydrogen ion in the $(2s)^2\,{}^1S$ state. The present paper deals in like manner with the $(2p)^2\,{}^1S$ state solution of the helium equation. The success of the previous work suggested the desirability of determining more accurately the term value of this important energy state of doubly excited helium. Since no essentially new features were developed for the present investigation, any description of the procedure will be omitted because this is fully described in Paper I.

§ 2. RESULTS AND DISCUSSION

The results concerning the numerical solution of helium (20-parameter approximation) are condensed in table 1.

Table 1. The Eigenvector (given by the coefficients $c(m, n, q \mid \eta)$, see I, (11), (12)) and the Eigenvalue (Ryd)

Eigenvector	The order of configuration: $(2p)^2$, $(1s)^2$, 1s2s, $(2s)^2$, 1s3s, 1s4s, 2s3s, $(3s)^2$, 2p3p, $(3p)^2$, $(3d)^2$, 2s4s, 3s4s, $(4s)^2$, 2p4p, 3p4p, $(4p)^2$, 3d4d, $(4d)^2$ and $(4f)^2$. +0·77511, +0·17169, −0·33313, +0·33906, +0·120835, −0·08215, −0·09980, −0·09667, −0·11438, −0·14398, −0·18110, +0.08694, −0·00343, −0·00166, +0·15989, −0·00101, −0·00429, −0·06673, −0·02771, −0·03072.		
Eigenvalue	Input $\eta=0{\cdot}8125$ $-E=1{\cdot}237794$	$L=1{\cdot}8641273$ $L'=0{\cdot}6787679$ $M=1{\cdot}87821225$ $N=1{\cdot}00000$	From (I, 6) $\eta=0{\cdot}8118$ $-E=1{\cdot}237795$
Contributions from different configura-ations to the eigenvalue	$E=-1{\cdot}225098+0{\cdot}014393+0{\cdot}017215+0{\cdot}158222+0{\cdot}004472$ $-0{\cdot}000045+0{\cdot}000065-0{\cdot}012459-0{\cdot}001726-0{\cdot}021492$ $-0{\cdot}088769-0{\cdot}045823-0{\cdot}000010-0{\cdot}000002-0{\cdot}027904$ $-0{\cdot}000000-0{\cdot}000055-0{\cdot}004685-0{\cdot}002044-0{\cdot}002049$ $=\underline{-1{\cdot}237794}$		

As it is emphasized in I, the solution obtained for the doubly excited states are not rigorously orthogonal to all the infinitely many lower *lsns* ^1S states. This lack of orthogonality implies that the solutions include a small admixture of some of the lower energy state functions, and thus lead to a spurious lowering of the eigenvalue. The previous work (Paper I) has shown, however, that the eigenvalue is rather insensitive to this defect, and can thus be considered approximately as the upper limit to the true energy. In spite of this fact there still remains a considerable uncertainty in the results obtained until the infinite matrix problem can be solved numerically.

Nevertheless, we can draw some interesting conclusions from the results reported in table 1. In the last section of the table we have quoted the contributions to the eigenvalue from different configurations in the 20-parameter approximation. As can be seen the automatic orthogonality to the first members of the configurational series *lsns* and the lower $(2s)^2$-term, leads to a raising of the eigenvalue, whereas the higher configurations of the series seem only to lower it analogous to what was found in the $(2s)^{2\,1}S$ state solution (14-parameter approximation, I, table 1). We are greatly surprised at seeing the considerable raising of the eigenvalue brought about by the orthogonality to the lower $(2s)\,^{21}S$ level. At first it also came as a surprise to us that the 2s3s term raises the eigenvalue. The contrary was expected since we first believed that the 2s3s level lay higher, but, however, figure 2 shows that it is likely that this level is lower since the approximation used in the figure is very bad for the 2s3s ^1S state.

To be sure of operating with the correct root of the secular equation (I, 3), we have tabulated all the nodes of the 4 × 4 matrix problem as well as the 10 × 10 matrix problem for adjusted values of the scale parameter. The nodes which are most interesting, are shown in the figures 1 and 2. The sensitiveness to the scale parameter is also illustrated in figure 1.

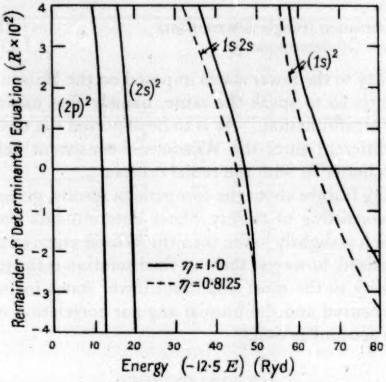

Figure 1. The nodes of the 4-parameter approximation (4 × 4 matrix).

As table 1 shows, the substitution of L, L', M and N in (I, 6) gives a satisfactory check of the minimum point on the energy curve $E(\eta)$, namely to better than 1 part in 10^6 for E and 7 parts in 10^4 for η.

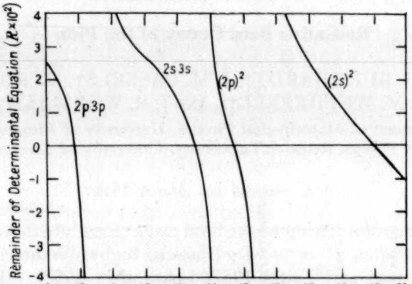

Figure 2. Some of the most important nodes from the 10-parameter approximation (10 × 10 matrix) $\eta=1{\cdot}0$.

Finally, it is of considerable interest to compare the results with those obtained by Wilson (1935) using as one-electron orbitals in a single Slater determinant the 2p orbital of the self-consistent field approximation. This comparison is made in table 2.

Table 2. Comparison with Previous Results

Functions	Total Energy (Ryd)
Wilson function (Single determinant)	−1·2323
Our solution :	
First approximation (Single determinant)	−1·2268
Final solution (20 determinants)	−1·2378

The orthogonality to the lower states imposed on the Wilson function and our first approximation is so to speak the same, namely that arising from the pure angular part of the eigenfunction. As is to be expected the eigenvalues obtained by either set are different since the Wilson self-consistent field approximation usually gives much better fit with the radial orbitals.

The most striking feature about the comparison results, given in table 2, is that the final solution consisting of twenty Slater determinants gives an eigenvalue (−1·2378 Ryd) which is slightly lower than the Wilson eigenvalue (−1·2323 Ryd) It should be emphasized, however, that our final solution is the most reliable since rigorous orthogonality to the most important lower states including the $(2s)^{2\,1}S$ state especially is ensured and the mutual angular correlation of the electrons is properly taken into account as well.

Acknowledgment

The author is much indebted for the grant from the Norwegian Research Council for Science and Humanities, Oslo, by which this further investigation has been supported.

References

Holøien, E., 1958, *Proc. Phys. Soc.*, **71**, 357.
Wilson, W. S., 1935, *Phys. Rev.*, **48**, 536.

Radiative Beta Decay of the Pion

By G. H. BURKHARDT†, J. M. CASSELS‡, M. RIGBY‡,
A. M. WETHERELL‡§, and J. R. WORMALD‡
† Department of Mathematical Physics, University of Birmingham.
‡ Nuclear Physics Research Laboratory, University of Liverpool.

MS. received 6th March 1958

Three unsuccessful attempts have been made recently to detect radiative beta decay of the pion, $\pi^+ \rightarrow e^+ + \nu + \gamma$ (Cassels, Rigby, Wetherell and Wormald 1957, Anderson and Lattes 1957, Lokanathan 1958). The purpose of this note is to review the theoretical situation and to report the negative result of further experimental work.

The existence of T interaction in nuclear beta decay was thought to be an established fact, but very recent experiments indicate that the interaction may be a V, A rather than an S, T mixture. Radiative beta decay of the pion would also be produced by either V or A interaction, and the corresponding decay rates have therefore been calculated, together with the e–γ angular correlation and various spectral shapes.

---

§ Now at the California Institute of Technology, Pasadena, California.

The results are presented in the table. Row 1 lists the three nuclear beta

1. Nuclear beta decay interaction	Tensor (T)	Vector (V)	Axial Vector (A)
2. Pion radiative beta decay rate (sec^{-1})	$\frac{\mu}{768\pi^5}\alpha G^2(g_T\mu^2)^2$ $\sim 5\times 10^3$	$\frac{\mu}{15\,360\pi^5}\alpha G^2(g_V\mu^2)^2\left(\frac{\mu}{M}\right)^2$ ~ 5	$\frac{\mu}{138\,240\pi^5}\alpha G^2(g_A\mu^2)^2\left(\frac{\mu}{M}\right)^2$ $\sim \frac{1}{2}$
3. Branching ratio ρ	10^{-4}	10^{-7}	10^{-8}
4. Matrix element	$k(1-\cos\theta)(1-\cos\phi)$	$k(1-\cos\theta\cos\phi)$	
5. Overall electron energy spectrum	$96E^2(1-2E)$	$40E^2(3-12E+14E^2)$	
6. Overall photon energy spectrum	$64k^3$	$320k^3(1-2k)$	
7. Photon–electron angular correlation	$16(1-u)^{-5}\{2(1-u)(26+29u+5u^2)$ $+3(1+u)(25+14u+u^2)\ln\frac{1}{2}(1+u)\}$	$15(1-u)^{-6}\{(1-u)(427+687u+297u^2+29u^3)$ $+8(1+u)(77+81u+21u^2+u^3)\ln\frac{1}{2}(1+u)\}$	
8. Electron energy spectrum ($\theta=\pi$)	$24E^2$	$\delta(E-\frac{1}{2})$	
9. Photon energy spectrum ($\theta=\pi$)	$\delta(k-\frac{1}{2})$	$64k^3$	
10. Experimental ρ	$(1{\cdot}4\pm 1{\cdot}8)\times 10^{-6}$	$(2{\cdot}1\pm 2{\cdot}7)\times 10^{-6}$	
11. Experimental upper limits to ρ (99% confidence)	$5{\cdot}5\times 10^{-6}$	$8{\cdot}3\times 10^{-6}$	

decay interactions of interest†, and row 2 gives the theoretical decay rate. The result given for the T rate corrects an error of a factor 8 in the formula quoted by Cassels *et al.* (1957); it differs trivially from that of Kawaguchi and Nishijima (1957) because of a different definition of g_T. The V result agrees precisely with that of Kawaguchi and Nishijima. Row 3 shows the ratio ρ of the calculated rates to the *experimental* rate for $\pi^+ \rightarrow \mu^+ + \nu$.

Row 4 shows that the V and A matrix elements have the same form, but both differ from the T matrix element. Rows 5 and 6 give the overall electron and photon spectra, and row 7 the e–γ angular distribution. Rows 8 and 9 show the spectra of electrons and photons emitted in opposite directions ($\theta = \pi$). All these distributions are normalized to give unity when integrated over the variable concerned.

Many previous theoretical treatments of this problem, approached from somewhat varying points of view, have been published (Kawaguchi and Nishijima 1957, Taylor 1957, Treiman and Wyld 1956, Bludman and Ruderman 1956, Eguchi 1956, Miyazawa and Oehme 1955, Iwata *et al.* 1955, Ruderman 1952, Ruderman and Finkelstein 1949).

The present calculation assumes the decay to take place through a virtual nucleon pair, and uses perturbation theory to the lowest order in all coupling constants. The results for V and A are convergent, while for T a cut-off Λ has been applied so that $\log(\Lambda/M) = 1$. Terms of order m_e/μ or μ/M smaller than the leading terms have been neglected.

For the A interaction, where the non-radiative decay is allowed, the infra-red divergent terms arising from inner bremsstrahlung are proportional to m_e/μ and are omitted. It is consistent to drop these terms because they arise as a small correction to the so far unobserved non-radiative decay. The P interaction has not been considered for the same reason. These terms would, in any case, yield soft γ-rays to which the experimental apparatus is insensitive; the non-locality of the equivalent direct decay interaction is essential for the production of energetic γ-rays, which arise from the virtual nucleon current in this picture.

Apart from the normal reservations to be felt about the use of perturbation theory, Taylor's (1957) suggestion of a change in the form of the pion–nucleon interaction increases caution about these results. Finally, there is the possibility of a partial cancellation caused by hyperon virtual states. However, it may be remarked that the V interaction, so far as the nucleons are concerned, is exactly analogous to the decay of the π^0 where the perturbation calculation does not greatly overestimate the decay rate (Orear 1957). Gauge invariance does not seem to impose any further restriction on the π^0 decay.

Row 10 shows the experimental values of ρ as now established at Liverpool. The apparatus was improved in two respects since the earlier results were reported. Counter 3 was replaced by a pair of counters in coincidence, and an electronic 'rationing' device was included to space out in time the pions accepted by the apparatus. This reduced greatly the number of random coincidences arising from $\pi - \mu - e$ events. The efficiency of the apparatus for detecting V or A types of decay was about 2/3 the efficiency for T type decay, as a result of the differences in the $e-\gamma$ angular distribution and the correlated spectra. Finally, row 11 gives the experimental upper limits to ρ, fixed at the 99% confidence level. These upper limits are consistent with, but lower than, those established in the other experiments already cited.

---

† See Cassels *et al.* (1957) for notation. The coupling constants are defined by
$H_{\text{int}} = (8\pi)^{1/2} \, G\phi_{\pi+}(\bar{\psi}_P \gamma^5 \psi_N)$ for the pion–nucleon interaction ($G^2 = 15$),
and $H_{\text{int}} = \frac{1}{2} g_T(\bar{\psi}_N \, \sigma_{\mu\nu} \, \psi_P)(\bar{\psi}_e \sigma_{\mu\nu} \, \psi_\nu) + \text{c.c.}$, $g_V(\bar{\psi}_N \gamma_\mu \, \psi_P)(\bar{\psi} \;\; \gamma^\mu \, \psi \;) + \text{c.c.}$,
and $g_A(\bar{\psi}_N \gamma^5 \gamma_\mu \psi_P)(\bar{\psi}_e \gamma^5 \gamma_\mu \psi_\nu) + \text{c.c.}$ for the beta interactions ($g_{T,V,A}\mu^2 = 2 \times 10^{-7}$).

It is clear that the experimental results are entirely consistent with expectation unless nuclear beta decay proves to have a T component. More interest now centres on the direct decay, $\pi^+ \rightarrow e^+ + \nu$ which has been shown (Lokanathan and Steinberger 1955, Anderson and Lattes 1957) to have a branching ratio less than 2×10^{-5}. The direct decay is allowed by the A interaction and, according to recent ideas about nuclear beta decay, should have shown up by now. It is hoped to investigate this problem further at Liverpool in the near future.

ACKNOWLEDGMENTS

We wish to thank Professor R. H. Dalitz for his continued interest and encouragement in this work. We are also grateful to Mr. Halliday and the crew of the Liverpool cyclotron for their co-operation, and to Mr. T. W. O'Keeffe for help in taking the data.

REFERENCES

ANDERSON, H. L., and LATTES, C. M. G., 1957, *Nuovo Cim.*, **6,** 1356.
BLUDMAN, S. A., and RUDERMAN, M. A., 1956, *Phys. Rev.*, **101,** 910.
CASSELS, J. M., RIGBY, M., WETHERELL, A. M., and WORMALD, J. R., 1957, *Proc. Phys. Soc.* A, **70,** 729.
EGUCHI, T., 1956, *Phys. Rev.*, **102,** 879.
IWATA, K., OGAWA, S., OKONOGI, H., SAKITA B., and ONEDA, S., 1955, *Progr. Theor. Phys.*, **13,** 330.
KAWAGUCHI, M., and NISHIJIMA, K., 1957, *Phys. Rev.*, **108,** 905.
LOKANATHAN, S., 1958, *Phys. Rev.*, in the press.
LOKANATHAN, S., and STEINBERGER, J., 1955, *Nuovo Cim., Suppl.* **2,** 151.
MIYAZAWA, H., and OEHME, R., 1955, *Phys. Rev.*, **99,** 315.
OREAR, J., HARRIS, G., and TAYLOR, S., 1957, *Phys. Rev.*, **106,** 327.
RUDERMAN, M., 1952, *Phys. Rev.*, **85,** 157.
RUDERMAN, M., and FINKELSTEIN, R., 1949, *Phys. Rev.*, **76,** 1458.
TAYLOR, J. C., 1957, *Nuovo Cim.*, **6,** 1226.
TREIMAN, S. B., and WYLD, H. W., 1956, *Phys. Rev.*, **101,** 1552.

LETTERS TO THE EDITOR

A Re-measurement of two Gamma Ray Lines from ^{152}Eu and ^{154}Eu

A new measurement (see Andersson 1956) of the 0·122 MeV and 0·123 MeV gamma-ray lines has been made with our curved crystal gamma-ray spectrometer at the Physical Department of AB. Atomenergi, Stockholm. The line profiles have been studied on both sides of the zero point of the spectrometer (four measurements on each side).

Isotope	Present Measurement	
	Wavelength (mÅ)	Energy (MeV)
^{152}Eu	101·72 ± 0·05	0·12187 ± 0·00006
^{154}Eu	100·61 ± 0·03	0·12321 ± 0·00004

Department of Physics,
Chalmers University of Technology,
Gothenburg, Sweden.
21st April 1958.

B. ANDERSSON.

ANDERSSON, B., 1956, *Proc. Phys. Soc.* A, **69**, 415.

REVIEWS OF BOOKS

Handbuch der Physik, Vol. XLII, *Nuclear Reactions* III, edited by S. FLÜGGE. Pp. xii + 626. (Berlin: Springer.) DM 135.

This book is one of three in the Encyclopaedia on the subject of nuclear reactions. The other two, volumes 40 and 41, are devoted to general surveys. The present one contains articles on specific topics which are not covered adequately in the surveys. These topics have little in common apart from being connected with nuclear reactions. In the case of the article on the transuranic elements, the emphasis on chemistry means that even this contact hardly exists.

The general standard of the articles is high. Many physicists will wish to have copies of one or more of them, although few will have need of the entire set because of their diversity.

Nuclear Isomerism, by D. E. Alburger, pp. 108.

The main feature of this article is a set of level diagrams of decay schemes involving radiative transitions with lifetimes greater than 10^{-6} sec. With accompanying references, it is the most complete collection available of the data on isomeric transition phenomena. The absence of mention of the extraordinary isomer of ^{235}U must be attributed to its discovery coming after the submission date. Transitions of lifetimes shorter than 10^{-6} sec, including those whose lifetimes are deduced indirectly from the method of Coulomb excitation, are listed in a useful table. The rest of the article is divided between a careful survey of experimental techniques and discussion of theoretical interpretations. The latter is generally adequate but has minor omissions such as the absence of estimates for lifetimes of E0 transitions.

Alpha Radioactivity, by I. Perlman and J. O. Rasmussen, pp. 96.

This article is a well-written account of the interpretation and theory of alpha decay in terms of current views on nuclear structure. It is authoritative as one might expect from authors who have recently made several important contributions to the subject. There is no discussion of experimental techniques, but all available experimental data are included in the form of tables. Decay rates and other data are analysed to yield values for nuclear matrix elements and ' hindrance factors ', rather than the old-fashioned ' effective radii '. Especially interesting is a theory of decay from spheroidal nuclei but, oddly, the effect of spheroidicity on penetration factors is not revealed explicitly. No application of this theory to recent results on directional emission from aligned nuclei is included, but one may assume that such will appear in computational results that are promised for the future.

The Transuranic Elements, by E. K. Hyde and G. T. Seaborg, pp. 104.

The majority of this article is concerned with chemistry, and its inclusion in an encyclopaedia of physics, especially in a volume on nuclear reactions, is disconcerting to a physicist, in particular to the present reviewer. Little allowance is made in presentation for possible weakness of readers backgrounds in chemistry and terms unfamiliar to the physicist abound. However this barrier is easily surmounted by consultation of standard texts. The article opens with arguments to justify the label ' actinide ' for the transuranic elements. Then follows an account of the chemistry of these elements, and finally a short survey of their physics such as evidence of a shell-closure at $N=152$, energy systematics, alpha decay and fission.

Nuclear Photoeffect, by G. R. Bishop and R. Wilson, pp. 55.

Following a short introduction on sources of gamma rays, about a third of this article is devoted to photodisintegration of the deuteron. This is a significant phenomenon, but its description at such length would seem to be more appropriate in the article on the two-nucleon problem in volume 39. After this detailed exposition, admirable in itself, the remainder of the article, which surveys the photoeffect in heavier nuclei, seems bare and abrupt. All work on collective models of the photo effect is summarized in less than a page. There is no mention of some recent theories of photo-fission, and no consideration of inelastic photon scattering. The absence of the last subject is hard to understand especially as it is mentioned even in the general surveys of reactions in volume 40.

Angular Correlations, by S. Devons and L. J. B. Goldfarb, pp. 193.

This article is exhaustive and, if one tried to read it through, quite exhausting. This is not a criticism, although it is true that the style of writing does not exactly electrify the reader. Rather, it is a natural result of the subject matter, and the extreme thoroughness of its treatment. Essentially all questions on angular correlations are answered, except those involving transitions in which parity is not conserved, and those involving oriented nuclei (see below). There is mention of correlation in ' direct ' nuclear reactions like Coulomb excitation and stripping, in internal conversion and in meson processes. This and other special features, such as numerical examples, establish this article as the most useful one available. Correlations in external fields are also discussed.

Nuclear Orientation, by R. J. Blin-Stoyle and M. A. Grace, pp. 56.

This article deals with the angular correlation problems not covered explicitly by the previous one, namely those involving oriented nuclei. Such nuclei may decay spontaneously, or they may be polarized particles in a bombardment. Both kinds of situation are discussed. In each case, there is a theoretical introduction followed by a description of experimental techniques, and some examples of the applications of the theory. The only problems not treated are those involving parity non-conservation, a circumstance which arises from the submission date preceding the discovery of the phenomenon. There is even mention of the recent work on directional emission in alpha decay from polarized nuclei.

A. M. LANE.

Numerical Methods, by R. A. BUCKINGHAM. Pp. xii + 597. (London : Pitman, 1957.) 70*s*.

Ten years ago Whittaker and Robinson's *Calculus of Observations* was almost the only guide to computing; now there are a score of books, all, like the present one, primarily concerned with manual computing. The basic knowledge of numerical analysis is common to manual and automatic computing; manual methods are better for isolated calculations and are a valuable preliminary to extensive automatic computations. For all these reasons books like the present one, which is based on a wide range of practical experience, are a welcome aid to the growing number of scientists who make substantial calculations.

Rather than a science, numerical analysis is an art, not unlike the culinary art; accordingly, one values a book for its recipes, their clear description and accessibility, as well as for some connoisseurs' notes to guide the discerning in their choice, on grounds of flavour and of labour, between the multifarious delicacies described. Dr. Buckingham does all this well; his advice is almost invariably irreproachable although there are rare occasions when one regrets that the learner is not told why he should select one method and avoid another. On the other hand, the last thing one welcomes in a book of recipes is a long theoretical introduction; to my taste the present book, like most of its competitors, devotes excessive space to the derivation of polynomial interpolation formulae and employs some superfluous notation, such as forward and backward differences and sums. In regard to sums this superfluity is illustrated humorously enough: central sums are defined on page 51, but integration formulae on page 133 are quoted without reference to them; they are first used in Chapter 8 (on differential equations), by which time a new notation has been adopted! More explicit help might have been given with the normalization of these sums, which beginners always find difficult.

A discussion of mechanical aids concludes the first chapter, which must have been written some years before publication and which, like all other such chapters I have ever seen, fails to give adequate guidance to the user on his choice between available machines and, *a fortiori*, to the makers on the lines for future development.

The next five chapters cover interpolation, differentiation and integration. On the whole the treatment is both sound and clear but one may make several minor criticisms. The discussion of interpolation throw-back is weak; simultaneous throw-back is not mentioned, nor are economized polynomials. The discussion of mixed differences might have been clearer without being longer. The comparison of Stirling's with other central difference formulae is vague and partly inaccurate and the reader is referred to Whittaker and Robinson, who on this point are definitely wrong.

Chapters 7 and 8, which treat ordinary differential equations, include brief but clear outlines of topics often left to mathematical texts, e.g. Fuchsian theory and the method of perturbations. In view of the latter it is curious that Lagrange's method of variation of parameters is not described. On the whole, however, the treatment of differential equations is extremely sound without being unduly selective.

Chapters 9 to 11 cover algebraic equations, least squares and simultaneous linear equations; in Chapter 12 matrix methods are introduced; Chapter 13 describes relaxation and other methods for linear equations. In Chapter 14 a return is made to differential equations, but now with two-point boundary conditions. Chapter 15 discusses interpolation and integration in two variables, perhaps with overmuch formality and with insufficient emphasis on throw-back. This leads to a final chapter on partial differential equations. Each chapter is followed by a set of exercises.

Appendices include useful collections of formulae, which would be even better if they were more comprehensive. The index needs some slight revision: e.g. there is no entry under 'throw-back', and those under 'Chebyshev' and 'Tchebycheff' refer one to pages 120 and 312 respectively.

Despite these minor criticisms, this is a scholarly and well documented work. If it is neither as well adapted to cursory consultation (nor as well printed) as Hartree's, nor yet in some particulars as stimulating to a numerical analyst as Kopal's, still, for the physicist to whom the results of computations are of serious importance, it is, in my view, by a large margin the best single textbook available.

J. C. E. JENNINGS.

Tablitsy Interpoljatsionnykh Koèffitsientov, by L. N. Karmazina and L. V. Kurochkina. Pp. 365 + 5 nomograms. (Moscow: Izdatel'stvo Akademii Nauk SSSR, 1956.) 37*r.* 65*k.*

The tables give interpolation coefficients to ten decimals. The Bessel coefficients B_2 to B_7 are tabulated at an interval of 0·0001; the even coefficients are those for mean differences, i.e. they are twice as great as those given in *Interpolation and Allied Tables.*

All the remaining tables are at interval 0·001, viz. Newton-Gregory, Stirling and Everett, all as far as the coefficient of the seventh difference; Lagrange coefficients are given for 3, 4, 5, 6, 7 and 8-point interpolation. The Lagrange coefficients, except for part of the range of those for 8 points, have been taken from the U.S. Bureau of Standards tables (1944).

J. C. E. JENNINGS.

Problems in Nuclear Engineering, Vols. I and II, by D. J. Hughes, S. McLain and C. Williams. Pp. ix + 365 and vii + 278. (London: Pergamon Press, 1957.) £6 each.

These volumes contain papers from the Nuclear Engineering and Science Congress held in Cleveland, December 1955. The Congress presented to American Scientists and Engineers information released at the Geneva Conference together with some additional material. The editors of these two volumes, in selecting and arranging less than a quarter of the 358 miscellaneous papers given at the Congress, have done a commendable job in producing good overall coverage with a logical sequence. They have devoted Volume I to materials for reactors and to the design, safety and heat transfer problems of reactors. Volume II covers the recovery of irradiated fuels and the handling of plant effluents. In addition this volume includes miscellaneous items such as reactor physics experimentation, and the control with instrumentation of nuclear reactors.

In the first Section of Volume I the editors have selected papers which give in sequence a general survey of reactor types, the engineering details of some of these reactors and the principles of site selection and safe reactor operation. Noteworthy gaps, admitted by the editors, include the design and construction of the last line of defence (the container) and the hazards associated with the chemical fires of reactor materials. The next section reviews the materials available as nuclear fuels, fuel cans and structural metals, including papers on the oxides, hydrides and alloys of uranium. Section III includes a rather miscellaneous collection of papers on reactor components, on the design of three reactor types, together with two useful bibliographies on nuclear engineering literature. One of the latter papers comments on the difficulty in distinguishing useful and reliable references from those that are based on incomplete investigation, are speculative or purely descriptive—a very pertinent comment in view of the tremendous bulk of reports now available. The final section in this volume covers heat transfer from liquid metals and water and discusses various problems on reactor stability.

Volume II is devoted mainly to waste disposal and fuel processing. The waste disposal section includes present day methods of waste treatment together with development work which is in progress on methods of ultimate disposal of fission products. Pertinent literature on radiation hazards and protective measures is summarized in one paper. The large section on chemical processing covers the dissolution of solid fuel elements, the chemical engineering of the aqueous processing of fuel and blanket materials, the processing of fuel from the Homogeneous Aqueous Reactor and the Liquid Metal Fuel Reactor, and descriptions of possible methods involving pyrochemical processes or fluoride volatility differences. Papers representative of the types of research now prevalent in reactor physics are collected in Section III. Exponential and critical assembly methods of studying nuclear reactor parameters are described. The final section is a very miscellaneous assembly of papers of general interest to those working in the field of the instrumentation and control of nuclear reactors.

In view of the time taken to produce these volumes it is fortunate that most of the papers of the Congress have already been published in the regular engineering journals. However, these two volumes represent a worthwhile logical collection of papers on the wide subject of nuclear engineering. I. WELLS.

The Physics of Clouds, by B. J. MASON. Pp. xx + 481. (Oxford: University Press, 1957.) 70*s*.

The investigation of the physics of clouds and the mechanism of rainfall has advanced very considerably during the last two decades. There are several reasons for this—a new economic incentive arising from the discovery that some clouds may be made to precipitate or to dissipate by injecting substances such as solid carbon dioxide or silver iodide particles into them; a considerable increase in flying through clouds with greater hazards due to icing, turbulence and impact with the larger cloud particles; and also the use of powerful new tools for cloud investigations such as radar and well instrumented aircraft. In addition, however, the study of cloud physics has the advantage not shared with some of the other branches of meteorology that many aspects of it can to a large extent be studied in miniature in the laboratory and hence it has attracted University workers who may not have the expensive facilities required for field studies. As a result the literature on the subject is now very large and rather widely dispersed and the need for a comprehensive account of modern theoretical and experimental researches was very apparent. Dr. Mason has admirably met this requirement in *The Physics of Clouds*, the first of a series of Oxford Monographs on Meteorology under the editorship of Professor P. A. Sheppard, Department of Meteorology, Imperial College of Science and Technology. The subjects covered are condensation of water vapour in clear air and on nuclei, the growth of cloud droplets, ice-forming nuclei and the formation of ice crystals, the physics of natural precipitation together with a critical appraisal of the possibilities of its artificial stimulation, radar studies of clouds and the electrification of clouds. In each case the status of the subject at about the beginning of 1957 is established and the great majority of important contributions described in some detail. Coupled with the use of an extensive bibliography, which is appended, research workers and physicists getting to know this field will find this an extremely useful reference book. The student, however, may sometimes find himself not quite so well placed without further study as, in some sections, the discussion hinges on the conclusion of an investigation or a result well known only to those in this field rather than starting from a more elementary stage. The meteorologist will become more conscious also that the understanding of the microphysics of clouds is now ahead of the understanding of the macrophysics—the dynamic framework in which the microphysical processes operate—and will look forward to the appearance one day of a book of comparable calibre on this other aspect of the problem. R. J. MURGATROYD.

Light Scattering by Small Particles, by H. C. van de Hulst. Pp. xiv + 470. (New York: John Wiley; London: Chapman and Hall, 1957.) 96*s*.

This book provides a full exposition, analysis, and discussion of the mathematical theory of light scattering by particles sufficiently far apart for co-operative effects to be ignored. Problems of multiple scattering and radiative transfer are not dealt with. There are three parts.

The first introductory part (56 pages) outlines the propagation of light *in vacuo* and in scattering media in a generalized manner, and introduces the functions and quantities which will be used in the rest of the book. Relations are derived which do not employ detailed knowledge of the shape and size of scatterers. The treatment is most interesting and novel, particularly in regard to the pioneer work of Fresnel, Huygens and Young. Apart from a rather difficult final chapter in which relations between the polarization of the radiation and the symmetry of the particles are discussed this part will repay study by teachers of physical optics at undergraduate level.

The second part (317 pages) starts with three chapters in which those problems are solved which can be treated without formal solution of Maxwell's equations. If $x = ka$, where k is wave number $2\pi/\lambda$ and a is a length of the order of the particle size, these problems lie in the domains of (*a*) small x, (*b*) small relative refractive index, (*c*) small product of x and relative index, and (*d*) very large x. The treatment is not *ab initio* and does not claim to repeat the details found in text-books; but suitable books and articles are listed at the end of the chapter.

Next come nine chapters based on solution of Maxwell's equations. Headings are: Spheres of arbitrary size, Non-absorbing raindrops, Absorbing spheres, Circular cylinders, Other forms, and Edge phenomena and surface waves. Specialists on the mathematical theory will be glad to have all this material collected together, but in addition experimentalists will find that they are carefully catered for. The author provides very wise guidance as to the use of approximations in the various domains. As regards the computations from rigorous theory there is, on p. 167, a list of 35 references to these. Users are, however, warned that in some domains the functions oscillate rapidly with changing angle, x, or relative index, and the computations may not have been made at sufficiently small intervals of variable to reproduce the oscillations. Another warning refers to experimental situations in which a *range* of variables is presented, distribution of particle size for example. Experimenters are recommended to reduce the width of the range as much as possible before using computations valid for one value of the variable. But in domains of rapid oscillation sufficient reduction of the range may not be possible. There still seems a need for someone to point out measurements which will yield particle size unambiguously in domains where oscillations of the functions cannot be followed experimentally.

The third part (63 pages) is a review of light scattering as a tool in chemistry, meteorology, and astronomy. It should serve as an introduction for new experimenters, and the usual full list of references at the end of the chapters tell where details may be found.

The general impression of the book is one of originality, which might be expected since so much of it is based on the author's own contributions, in particular on the well-known Utrecht thesis. Mathematical physicists should note that the book is much more than a compilation; there are entirely new derivations and computations throughout the book, too numerous to be listed here. Furthermore, the references at the end of chapters are accompanied by comments when the author considers that errors have been made. Much of the mathematics of the subject is shared by parts of quantum mechanics, and specialists in the latter field should be aware of this book. Other potential readers to whom the book is recommended are teachers of physical optics. The apparent specialist title should not be allowed to hide the presence of much illuminating insight into optics as such.

Experimenters will find that the book will oblige them to deepen their knowledge of the subject; it is really planned to be read as a whole, though the author suggests that Part III might be read first.

Layout and printing are very good, with lavish provision of curves and tables. A slight blemish is the absence of numbering of equations except in one chapter. S. P. F. HUMPHREYS-OWEN.

Optics, by B. Rossi. Pp. xii + 510. (Reading, Mass.: Addison-Wesley, 1957.) $8.50.

This book purports to " acquaint the reader with the most significant facts concerning light phenomena, and with the basic physical concepts that underlie their interpretation ". In the reviewer's opinion, it is a pity that the author has adhered to his purpose with such singleness of mind.

The book is arranged in a somewhat original manner. The text is largely devoted to theoretical matters, and a collection of problems is given at the end of each chapter. These include not only the usual numerical examples based on the foregoing text, but also a considerable amount of descriptive matter covering practical applications of the theory. To take two examples, the Michelson stellar interferometer and radio astronomy are both introduced in this manner. About two-thirds of the book is devoted to geometrical and wave optics and the rest to the electromagnetic theory of light and to certain quantum considerations.

It is evident that the author regards optics as primarily an intellectual exercise. Description of experimental arrangements is almost non-existent, and figure 3-11, illustrating the arrangement of the Fresnel double-mirror experiment, might be positively misleading to the student. A few photographs, chiefly of interference and diffraction patterns, are given and most are quite good; hence, it is a pity that figure 4-50 is a transparent fake.

It is a curious feature of this book that certain topics, such as Huygen's principle, are treated at considerable length and in a rather novel manner, whereas other almost equally important matters, such as the modern theory of partial coherence, are completely ignored. Practical aspects of optics are treated very lightly; thus, the whole art and mystery of ruling diffraction gratings is dismissed in the sentence " Gratings of higher quality are made of glass plates on which fine grooves have been machine ruled ". The theory of concave gratings is covered in two sentences, and the question of the division of light between orders, which one might think very suitable for a book of this nature, is not mentioned.

In spite of the above criticisms, this book can be read with enjoyment for its novel method of treatment of familiar problems. It is well printed and produced, and the standard of the diagrams is high; but it does not seem likely that the student will acquire any great interest in optics from this book. J. DYSON.

Handbuch der Physik, Vol. XXVIII, *Spectroscopy* II, edited by S. FLÜGGE Pp. vi + 448. (Berlin: Springer, 1957.) DM. 72.40.

This volume contains five articles: Microwave spectroscopy by W. Gordy (78 pp., in English), Continuous spectra by W. Finkelnberg and T. Peters (126 pp., in German), Crystal spectra by E. Fick and G. Joos (91 pp., in German), The Zeeman effect by J. C. van den Bosch (36 pp., in English) and Optical activity by J. P. Mathieu (100 pp., in French). There is a table of contents, a double index, German–English and English–German, covering the first four articles, and a separate index in French for the article by Mathieu.

These are accounts written by experts in which the emphasis lies rather on theoretical exposition than on practice and application. They vary somewhat in their degree of completeness. For example, in the article on the Zeeman effect there is in fact treated only the Zeeman effect in atomic spectra: the quadratic Zeeman effect is not considered at all, and there is no mention (except through the index) of the Zeeman effect in molecules which is discussed in the article on microwave spectroscopy. Neither article refers to the review by F. H. Crawford (*Reports on Progress in Physics*, 1939, **6**, 155). This instance, and others—for example, some aspects of crystal spectra discussed by Gordy are also considered by Fick and Joos—suggest that no very serious effort has been made to provide cross references, either within the volume, or to other volumes of the *Handbuch*. However, it is easy to criticize features of this kind, for the co-ordination of treatments by individual specialists of different subjects, many of which are in rapid development, raises insuperable problems, and the book is to be judged, not as a unified text but as a symposium. At this level, it is admirable. The articles are both authoritative and interesting, and the standard of production and illustration is such as to tempt the reader who consults the book for the answer to a specific problem to read on and on. There are available elsewhere excellent, but longer and more detailed, accounts of some of the subjects treated in this volume: however, the articles on crystal spectra and on optical activity would alone suffice to render it a most desirable acquisition for any serious library.

R. F. BARROW.

Piezoelectricity, selected engineering reports of the Post Office Research Station. Pp. x + 369. (London: H.M. Stationery Office, 1957). 75*s*.

Although there are as many as ten contributors to this collection of reports by members of the Post Office Research Station, excellent editing has turned the eleven papers into a story easy to read from beginning to end with enjoyment unmarred by gaps; the treatment appears to have been inspired by R. Bechmann and has the thoroughness and elegance we are accustomed to expect from him.

Report 1, not so broad as its title (Fundamental properties) implies, gives the relations between moduli of crystals and formulae for their transformation under axial rotation. Report 2 gives the derivation of the equations of motion of plates in thickness and contour vibration, an account to a large extent based on Bechmann's earlier work. The next two papers discuss the equivalent electric circuit and the prediction of cuts with small thermal coefficients of frequency; the next on determination of equivalent circuits describes methods undoubtedly good, but useful when vibrators are tested in large numbers rather than singly. All who want to grow crystals will welcome the account (Report 6) of the careful work done by the Post Office on the subject. Likewise the description of measurement of orientation by X-rays and the accompanying Bragg angle charts (Report 7), although too long and elaborate for the reader whose only interest is to know the principle of the method, will be welcomed by specialists; that, however, this subject is one to be mastered by practice as much as by reading, and to be adapted to circumstances, is evident from the author's own conclusion that although all orientations can be covered with the equipment described, a different technique would be preferable for production. On the other hand the description of the wet string method of cutting crystals gives the production engineer in a simple easy manner the benefit of experience acquired by patient and skilful work.

The needs of multichannel telephony no doubt inspired the search for crystals suitable for channel filters; it would be interesting to know whether ethylenediamine tartrate and potassium tartrate which the report (No. 8) suggests as rivals to quartz for that purpose, are being used and are proving satisfactory. A theoretical study amply confirmed by experiment is devoted to electrodes covering a part only of the vibrator faces; it is shown that the rate of the dynamic to the dielectric capacitance, which for many purposes is a figure of merit of the vibrator, can be raised some 30% by that means. Finally, every worker on piezoelectricity will be grateful for the tables of electric, dielectric and piezoelectric constants and of other properties of over thirty crystals.

Although the title ' Piezoelectricity ' which alone appears on the binding and the dust cover is too broad for this collection, the book, well produced and bound, is a worthy addition to Cady's great work of the same name. P. VIGOUREUX.

The Detection and Measurement of Infra-Red Radiation, by R. A. SMITH, F. E. JONES and R. P. CHASMAR. Pp. xiii + 458. (Oxford: University Press, 1957.) 70*s*.

In their preface the authors state that their aim has been to present an account of modern practice in infra-red techniques. Let it be said at once that they have done an excellent job. This book has a good plan and is so well written that it is easy and indeed a pleasure to find one's way about in the traditional ' mine of information ' which it contains. The appearance of such a book is most timely because of the many and important advances in infra-red techniques which have been made in the past twenty years and the increasing number of applications of infra-red techniques to pure and applied science.

Starting with a brief survey of the history of infra-red detectors, the authors go on to outline the physical principles governing the absorption and emission of radiation. The main characteristics of all present-day detectors are next presented, but before discussing their ultimate sensitivity, a full account is given of the fundamental limitations on infra-red detection which are set by random fluctuations in all the elements of any detector system and also in the radiation field. This enables the authors to give a clear derivation of the minimum detectable power for each type of detector. There follow chapters on sources of infra-red radiation, optical materials and components, infra-red spectrometers, amplifiers and the transmission of infra-red radiation through the earth's atmosphere.

It would be impossible to cover such a wide field without making a few slips and omissions, but those this reviewer has noticed are relatively unimportant. For instance, it is surely an oversight that the pioneer work of the Admiralty group (Sosnowski, Starkiewicz and Simpson) during the war on lead sulphide detectors is not referred to in Chapter I. The statement that photoconductive detectors enable one " to record spectra in a fraction of a second which a few years ago took hours to obtain " requires some modification. Pure rotation spectra in the far infra-red do not always consist of regularly spaced ' lines ' (cf. water vapour). In a few instances some of the more up-to-date figures are not quoted (especially in infra-red spectrometry).

The most valuable part of this book is undoubtedly that which deals with the ultimate sensitivity of detectors. To have all this material woven together in a logical and systematic manner is a real contribution to the physics of infra-red detection. A good deal of the other material is reasonably accessible of review articles and (unless new editions are frequent) will tend to date slightly. However, it is extremely convenient to have everything important in the current situation between the same two covers. G. B. B. M. SUTHERLAND.

Intermediate Physics, by C. J. SMITH, 4th Edn. Pp. xiii + 1322. (London: Arnold, 1957). 45*s*.

Dr. Smith's well-known textbook, which first appeared in 1932, will be familiar to many scientists who, sometime during the past quarter of a century, learned physics in the sixth form with the help of this excellent work. A considerable extension and revision has been undertaken in this latest edition which covers the syllabuses in physics for Intermediate B.Sc., Advanced Level G.C.E., Scholarship examinations of the various universities, and Part I of the London B.Sc. (General) Degree.

Perhaps the outstanding merit of this work is the clear, simple style in which it is written; it is difficult to find anywhere in the text an ambiguous statement or sentence. This has been accomplished by the use of short sentences, careful attention to correct grammar, and the avoidance of the colloquial expressions which are too frequently found in modern textbooks, especially those on electricity and electronics. A second factor which has contributed to its success is the emphasis on experimental work: in almost all cases, relevant experiments with simple apparatus are described to accompany the enunciation or deduction of important laws in physics. Thirdly, careful attention has been given to the correct statement of these laws, the most important and fundamental of which are invariably printed in bold type. Fourthly, the standard of the mathematical treatment—with the calculus used where appropriate—is well suited to the type of student concerned and is such that, in a sixth form course, his knowledge of physics will advance in sympathy with his knowledge of mathematics. Fifthly, ample attention is paid to the question of units and the correct working of numerical examples.

In almost all sections, extensions of the text have been made in the new edition in order to explain in more detail the elementary parts of the subject and to discuss at length the more difficult concepts, particularly those necessary to the scholarship candidate. Extensive additions have been made, in particular, to the accounts of acoustics, electricity and magnetism, and the physics of the atom. Furthermore, the number of examples given at the ends of the chapters has been greatly increased.

In view of the general excellence of this work, can it be said to be unkind to remark, nevertheless, that the approach is too old-fashioned in a number of instances? Perhaps two examples will serve to illustrate this criticism. Firstly, the mercury vapour pump described on p. 100 (due to Waran 1923) is not the usual modern type and, being a single-stage model, would hardly produce an 'x-ray vacuum' (why not give the appropriate pressure?) when backed by a filter pump. Secondly, the introductory accounts of electrostatics and magnetism follow the conventional practice (admittedly partly due to Dr. Smith in his earlier editions) of discussing such topics as the lodestone, the breaking of magnets, the use of pith-balls, proof-planes and the gold-leaf electroscope. Whilst the discussion of such topics is very necessary and, furthermore, can be readily and simply illustrated by experiments and demonstrations, is there not virtue in the modern approach whereby much of this data is coordinated by a greater use of the concepts of the atom and the electron?

With regard to m.k.s. units—which Dr. Smith refuses even to mention by name—he states in his preface : " In recent years there has been a tendency to use a system of units which, it is claimed, would make the path of knowledge easier to follow. The author has always maintained, and here he is not alone, that such a system is useless for teaching purposes and gradually the weaknesses of the new system are revealing themselves to its one-time adherents ."

It is refreshing in these days of controversy on this matter to read such an uncompromising statement from such an experienced writer and lecturer as Dr. Smith, but is he justified in ignoring with such fine scorn all the recent efforts to change (improve?) the teaching of electricity? The reviewer is not an ardent devotee of the new system and is by no means persuaded that the m.k.s. *vs.* c.g.s. controversy is vitally important. Nevertheless, it is felt that some aspects of the teaching of electricity and magnetism have been refreshingly revised in recent texts. Thus, an introductory explanation of magnetic induction preferably utilizes the concept of the Rowland ring rather than the idea of a small cavity in a magnetized specimen. Again, in describing the Bainbridge mass spectrograph (and why not mention the pioneer Dempster instrument, which is just as easy to understand?) and other examples, though m.k.s. units may not be an advantage, is it not preferable to avoid the confusion of using mixed units and hence the occurrence of **c**, the velocity of light in free space, in the equations?

Despite these criticisms, this is a first-class textbook. It has for long been a standard work, and, in its new edition, will surely remain as highly regarded as hitherto. J. YARWOOD.

The Galactic Novae, by C. PAYNE-GAPOSCHKIN. Pp. x + 336. (Amsterdam: North-Holland, 1957.) 30.5 guilder, 61*s*.

This book, the first volume of a *Series in Astrophysics* under the editorship of J. H. Oort, M. G. J. Minnaert, and H. C. van de Hulst, is written by Mrs. Payne-Gaposchkin, the well-known Professor of Astronomy at Harvard. The book has been written from the point of view that little is known about novae except the observational facts. The aim of the book is to summarize the known data in order to provide a basis for interpretation of the nova process. " The problem ", writes the author in the preface, " can be reduced to three questions. What is a nova outburst? How does it proceed? What causes it? The first can be answered confidently, if vaguely: the nova phenonen in an explosion. The answer to the third is clearly multiple, and is merely touched upon in the final chapter. Most of the book is concerned with the facts that bear on the second ". The value of the book clearly lies in the thoroughness and authority with which the observational data, hitherto scattered throughout the literature, is collected, assessed and discussed. The original sources are given in extensive bibliographies at the end of each chapter and the location of the references for a given chapter is printed at the top of each double page of text, thereby enabling the reader to go straight to the list of references without resorting to the usual method of trial and error. There are no less than 900 references in the book to original papers on the subject, a thoroughness which stands in marked contrast to the inadequate documentation exhibited in some other books on astrophysics.

The book begins somewhat abruptly with a chapter on Statistics of Galactic Novae in which a census of the 150 known galactic novae is followed by a detailed analysis of the characteristics of the light variation and spectral changes of typical galactic novae. Chapter 2 deals with the space distribution of novae in the galaxy using data in Chapter 1 for about a hundred well-observed novae. Chapter 3 grapples with the complex spectral development shown by novae, leading to a geometrical reconstruction of a nova outburst, and a stimulating discussion of the largely untouched theoretical problems in the spectra of novae. In the following three chapters, the salient data for galactic novae are presented and discussed. Of the 150 known galactic novae, the data for only seventeen are considered as first class, forty-six as second class, and for the remainder the data are fragmentary. These data are very thoroughly discussed in Chapters 4, 5 and 6 respectively, with the assistance of plates and well-drawn diagrams. Chapters 7 and 8 deal with some related groups of variable stars which are brought into the discussion on the reasonable ground that contrasting the similarities and differences between the groups might lead to some further elucidation of the nova phenomenon. Chapter 9 is devoted to supernovae of which some fifty cases, both galactic and extragalactic, are known at the present time. Of the three supernovae which have definitely appeared in our galaxy, the most famous is the supernova of 1054 with its conspicuous remnant, the Crab Nebula, which is a powerful radio source. Recent work on the polarization of the light from the Crab Nebula is described and discussed.

Chapter 10 gives a comparative study of spectral development in novae which might have been expected to follow Chapter 3, but for reasons best known to the author appears as the penultimate chapter of the book. The concluding chapter is a stimulating account of evolutionary and theoretical problems of novae and supernovae. An account is given of attempts to explain the exponential decline in the light curve of several supernovae in terms of a source of energy in the envelope which decays exponentially with time with a half-life of 55 days. Three possible energy sources are considered, the most energetic nucleus with the required half-life being ^{254}Cf which undergoes spontaneous fission with an energy release per radioactive nucleus about 200 times the energy released by processes involving simple β decay. Clearly the author has spared no effort to keep the book up to date in these interesting though speculative suggestions. The chapters on supernovae and theoretical problems were, in fact, largely re-written while the book was in proof.

As a result of Mrs. Payne-Gaposchkin's diligence and scholarship, we have this informative and stimulating book which brings together all the relevant observational facts and carries out a synthesis to the point where, to quote the author, " it seems that we are approaching a reasonably clear idea of the origin and course of the nova process, and of the stage of the stellar life history at which it can occur ". Physicists and astronomers will, no doubt, extend a warm welcome to this first volume of the new *Series in Astrophysics*.

The book is thoughtfully dedicated to Dr. H. W. Wright, a former Director of the Lick Observatory of the University of California, whose name figures prominently in the earlier literature on novae. D. W. N. STIBBS.

The Fundamental Principles of Transistors, by J. EVANS. Pp. xii + 255. (London: Heywood, 1957.) 45*s*.

This book is an introduction to the basic concepts of semiconductors and is not, as its title might suggest, a highly involved treatise on the subject. As such, it is ideally suitable for background reading by circuit engineers who are using transistors and can be used as a simple textbook for students. The subject matter is set out in a logical manner, starting with the basic principles of semiconductors and proceeding to the theory of p–n junctions and junction transistors. Since the book covers a wide field of topics, the semiconductor theory is only given briefly. There is no attempt to develop the mathematical theory; instead the author has concentrated on the physical aspects of the subject, giving only the necessary formulae.

In addition to the theory, the measurement of the parameters of semiconductors and transistors is described. The outlines of the test methods are given without going into the details which are beyond the scope of this book. In the final chapters the reader is introduced to the new types of transistor, that are at present being developed, and to the properties of silicon and other transistor materials.

This is a useful book written in a style that is easily read and is suitable for readers who do not require a detailed knowledge of the subject.

R. A. HILBOURNE.

Electromagnetism and Relativity, by E. G. CULLWICK. Pp. xxiii + 299. (London: Longmans, Green, 1957.) 63*s*.

In Part I, the author seeks to develop a first order theory of the electromagnetism of moving bodies at a level which " can be taught to undergraduate students of physics and electrical engineering ". In later sections he deals with more intricate problems including higher order effects. The concepts of magnetic pole and components of field are stressed—in opposition to the usual electron theory of electromagnetism in which electric charge is the fundamental concept.

The author believes that in this way he is able to reveal physical principles which are implicit in the standard mathematical treatments, though he agrees that the standard methods give correct results. The author has given considerable thought to a difficult subject and some of his ideas deserve consideration. I think, however, that physicists will prefer themore usual methods of dealing with electromagnetism.

The book includes a considerable section on the 'clock paradox'. The author supports the view put forward by Professor Dingle. I doubt whether even the small minority of physicists who agree with the conclusion will be able to accept the author's arguments which seem to me to reveal serious misunderstanding of Einstein's theory. R. W. D.

Handbuch der Physik, Vol. XV, *Low Temperature Physics II*, edited by S. FLÜGGE. Pp. vii + 477. (Berlin: Springer, 1956.) DM. 112.

This volume of the *Handbuch der Physik* is concerned with the classical problems of work at extreme low temperatures, liquid helium, superconductivity, and adiabatic demagnetization. All the articles are in English. It opens with a short review by Dr. J. van den Handel of low temperature magnetism. This is much less specialized than the others in the volume, but gives a useful introductory summary. It is followed by an encyclopedic article by Dr. D. de Klerk on adiabatic demagnetization. This is far the most comprehensive account of this subject available today, and is especially valuable for its detailed description of the phenomena observed near the maximum of susceptibility which all the salts display at sufficiently low temperatures. Superconductivity receives two articles, one on experimental work by Dr. B. Serin and another on the theory by Dr. J. Bardeen. This last is a long and authoritative work, even though the author had to conclude that " We still do not have a good mathematical theory, or even a good physical picture of the difference between the normal and superconducting states ". The volume closes with an article by Dr. K. Mendelssohn on liquid helium. A particularly valuable feature of this article is the extensive historical survey, ranging from the first liquefaction by Kamerlingh Onnes to the latest experiments on nuclear alignment in liquid ^{3}He.

This is the second volume of the *Handbuch* to be devoted to low temperature physics. The first was concerned with cryogenic technique, thermal and electrical conductivities, and specific heats. Taken together, they form a convenient and authoritative summary of the present position in low temperature physics, though the reader must be cautioned that the articles differ considerably in their manner of approach, some containing long introductory sections suitable for a student, while others are addressed directly to workers active in the particular fields discussed. A. H. COOKE.

Ferroelectricity in Crystals, by H. D. MEGAW. Pp. ix + 220. (London: Methuen, 1957.) 27*s*. 6*d*.

In this, the first collected and separate book intended as an introduction to the subject of ferroelectricity, the authoress has taken full advantage of her specialised knowledge of crystallography and has performed excellently the useful task of collecting together, classifying and briefly describing the widely scattered references on the subject, The emphasis is on discussion and description of structures. Of the 220 pages, 112 are crystallographic in their subject matter and 49 pages are devoted to the theories so that subtracting 23 index and references pages it would appear that the title might have been a little more specific, for example " The Structure (and Introduction to Theory) of Ferroelectrics ".

The book is divided into ten chapters. After the introduction there is a chapter each on rochelle salt and the phosphates, followed by three chapters on barium titanate and the perovskite family, a chapter on miscellaneous ferroelectric structures and the last three are a description of the theories. Each chapter has its own extensive reference list totalling 250 in all and, apart from those not mentioned in the text, includes 21 for 1955 and 4 for 1956 which makes the book very useful for references purposes as well as comprising an introduction to those having little previous knowledge of the subject.

All practical aspects of ferroelectricity, crystal and ceramic preparation, measurements, and applications in the field of dielectrics and acoustics are omitted; domains and their mechanisms are only briefly referred to.

The production is good and contains adequate illustrative diagrams and tables. The text is well documented. The price of 27*s*. 6*d*. is reasonable. H. F. KAY.

New Intermediate Physics, by G. R. NOAKES, Pp. viii + 961. (London: Macmillan; New York: St. Martins, 1957.) 30*s*. net.

There can be few teachers of Sixth Form Physics in this country who are not familiar with the four textbooks on general physics, heat, light and electricity and magnetism written by Mr. Noakes and published during the last two decades. The clarity of expression, methodical treatment and, above all, the excellence of production and presentation have made them deservedly popular to teacher and student alike.

The purpose of a textbook is to provide a background to the lessons in the lecture room or laboratory, so that the student can read for himself fuller details of what has been presented to him orally or in concise notes. The physics textbook should also give the reader a logical development from fundamental principles; it should stimulate him to know more by experiment and, if necessary, delve into the original records. The winning of the principles in Natural Philosophy has been one of mankind's greatest achievements and no true student should be left in doubt as to the debt we owe to the pioneers of the scientific method.

The present volume follows the suggestion that by judicious pruning the four textbooks could be incorporated. At the same time new methods of approach could be adopted to bring the treatment into line with the latest recommendations of such bodies as the Science Masters' Association.

The first half of the book consists of the two volumes of general physics and heat, but opportunity has been taken to give a wider treatment of sound while reducing the more advanced sections on the propagation of heat. In light the elementary formulae for reflection and refraction at plane and curved surfaces are developed from the wave theory, a policy strongly advocated fifty years ago by the late Professor Silvanus P. Thompson. Mr. Noakes's logical work here is admirable and will stimulate mathematical and non-mathematical students equally. Following the *Report of the Physical Society's Committee on the Teaching of Geometrical Optics*, the sign convention of all real distances positive and virtual distances negative is chosen, but, at the same time, for the more mathematically minded student a solution following Cartesian coordinates is found adjacent. Physical optics receives generous space, so do the subjects of photometry, spectra, colour, optical instruments and the defects of curved mirrors and lenses. Two minor criticisms can be offered: first the error in the impure spectrum (p. 241) and corrected subsequently (fig. 555). Secondly, the future biologist who may drop the formal study of physics after Advanced Level should be acquainted with the theory of the oil immersion microscope and its dependence on aplanatic points.

By far the greatest change has been made in the subjects of electricity and magnetism in the second half of the book. The general line recommended in the Science Masters' Association Report on the *Teaching of Electricity* has been followed, though it is obvious that Mr. Noakes has read widely all that has been said about the m.k.s. system. In the first few pages of the book both c.g.s. and m.k.s. units are introduced as well as the practical ones. The reader returns to the problem after a rapid qualitative survey of electrostatics, the effects of current electricity, elementary magnetism, Ohm's law, energy and power, variable currents. Beginning with current and the associated magnetic field the ampere becomes an additional fundamental unit defining it through the forces involved in current-carrying conductors. By the introduction of μ_0, the magnetic permeability of free space—i.e. the space constant equal to $4\pi \times 10^{-7}$ m.k.s. units—a quantitative development of electromagnetism follows and only one system of units is necessary, an obvious advantage. For those teachers holding to the c.g.s. electrostatic, electromagnetic and practical electrical units, and anxious to retain this historical approach, the change may appear an additional load for the already overburdened student. However, the m.k.s. is a logical system used by electrical engineers, starting from their practical units—amperes, volts, ohms, watts and henries. Hitherto, the majority of English textbooks, both elementary and advanced, have used the c.g.s. system only. To the reviewer it seems obvious that the serious student will have to know and use m.k.s. and c.g.s., especially as physicists and engineers increasingly share in the solution of research problems.

A very adequate mathematical treatment is given of electrostatics, electromagnetism, electrochemistry and the electrical nature of matter. Formal magnetism is obviously somewhat compressed, but the essential facts are there neatly dovetailed in the chapter on the electrical and magnetic properties of solids. All chapters are followed by a wide range of questions, and there is a good index.

In a work of this kind it is always difficult to know what to include and what to omit. Thus atomic physics has been treated almost too briefly, but this is largely unavoidable, if the book is to be kept at its present length.

One does not get quite the emphasis on the historical development that the reviewer would like, but Mr. Noakes has done a fine job of work. The publishers, too, are to be congratulated on a clear format, neat diagrams, and an effective type script. In the ever-increasing demand for a modern presentation of physics for good Advanced Level by students in VI Forms, or Higher National Certificate, or the university first year, the book will be welcome and widely used.

F. OLDHAM.

Passive Network Synthesis, by JAMES E. STORER. Pp. x + 319. (London, New York : McGraw-Hill, 1957.) 64*s*.

Network synthesis is an art rapidly descending from the clouds of abstruse mathematical theory into the arena of practical engineering action. There are now convincing theories of system design which yield in their conclusion the requirement of a network function, specified as a rational function, which has to be realized by means of physical elements. It is to be expected that interest in the subject will be more widespread than among the small circle of enthusiasts who have so single-mindedly devoted themselves to this field in the past ; it is to be feared that we shall have a spate of books of the genre ' cook-book ' in sympathy with this broader appeal of the subject.

The present author has clearly rejected the temptation to descend to the handbook level but he has, in wishing to produce a concise text, been in some difficulty in presenting his topics. He has tried hard with fair success to give us a modern review of the field in sufficient detail for the informed reader to follow the logical pattern of development and has prefaced this (Part 1 and 2) by a plausible summary of the older methods with references to the original papers. In this connection it is alarming to find, if we are to believe the author, that no contributions to this subject have come from anywhere in the world except his own countrymen since Cauer (1927). This subject has benefited more than most from a truly international interest and the peculiar bias given to this book by referring only to part of these contributions is a serious weakness.

Within these limitations the author has set himself he does a business-like job. Part 1 is largely introductory on the classical impedance synthesis—Foster, Brune, Darlington. Part 2 concerns the image parameter method, still the most widely used for filters and the easiest to apply ; it could hardly be omitted on practical grounds. Part 3 outlines the insertion loss method and modern lattice procedures and also gives a good treatment of 2-element synthesis with accent on the RC types. In spite of the title of the book, active elements figure here as they must in any sensible treatment. The final part deals with the all-important approximation problem ; probably the least well-developed aspect of the field at the present time. This part is excellent, if terse, although one regrets the omissions through insufficiently wide reading.

The author might have been better advised to reduce the space devoted to review of early work in order to gain sufficient space to give the modern methods more thorough treatment, but the temptation of somehow achieving a comprehensive text is understandable. J. H. WESTCOTT.

Two-point Boundary Problems (*in Ordinary Differential Equations*), by L. FOX. Pp. xi + 371. (Oxford: Clarendon Press, 1957.) 60*s*.

This is an excellent book by an acknowledged authority on the subject. Linear differential equations often arise in physics and engineering (e.g. in the theory of elasticity applied to stresses in straight beams), and this book is primarily concerned with obtaining numerical solutions to such equations in which the boundary conditions are specified at two points in the range of integration. The methods described essentially amount to replacing the differential coefficients by finite differences and solving the resulting algebraic equations (linear, if the differential equation is linear) by ' relaxation ' or some direct method. The book is a result of the author's work in this field over the last ten years at the National Physical Laboratory.

The author's main contribution to this subject has been the so called ' difference-correction ' method which enables one to reduce the truncation errors in the finite difference approximations without having to decrease the finite difference interval. Briefly, this amounts to taking account of higher terms in the difference expansions for the differential coefficients, but these corrections are introduced in such a way as not to complicate the algebraic structure of the simultaneous equations which have to be solved. This is done by first obtaining a solution using only crude approximations to the differential coefficients involved (e.g. $y'' \simeq y_{n+1} - 2y_n + y_{n-1}$) and then differencing this solution to obtain numerical estimates of the higher differences. These are then incorporated into the right-hand sides of the linear equations which are solved to obtain a better solution, and so on. The method has been strikingly successful as is illustrated by the numerous examples given.

The first chapter is a basic account of finite differences, and although the author does not go very deeply into the analytic basis of this topic, it is nevertheless an extremely good account from a computer's point of view and enables him to recognize such phenomena as divergence of differences in the neighbourhood of a singularity. The next chapter is an account of the solution of linear algebraic equations by the relaxation method and by direct methods. Here again the author has made notable contributions in developing the method of triangular resolution. The next part of the book gets on to differential equations proper and although the author confines himself mainly to linear equations of second, third and fourth orders, these are dealt with very thoroughly indeed. There is also an interesting account of the solution of first order equations (which by their nature are initial value problems) by the methods developed for boundary value problems, which in many cases involve less labour than a step-by-step method. Eigenvalue problems come next and for this purpose the properties of latent roots and vectors of matrixes are discussed. There is a chapter on the use of initial value techniques for boundary-value problems; these amount to generating two independent solutions starting from arbitrary initial conditions and then combining them to satisfy the required terminal conditions. The accuracy and precision of all the methods described is treated at some length in a separate chapter. Finally, there is a chapter on such miscellaneous topics as the 'deferred approach to the limit', and semi-analytic methods, such as the method of least squares, which make no use of finite differences.

R. A. BROOKER.

L'Automatique des Informations (Évolution des Sciences No. 9), by F. H. Raymond. Pp. 188. (Paris: Masson et Cie, 1957.) 1600 *fr*.

The expressed object of the present work is to produce an account of automatic data processing in a form which is intelligible to non-specialists. From the fact that the reviewer found no difficulty in following the text, although written in a foreign language, it may be assumed that the author has succeeded.

There are eight chapters, the first defines 'information' and discusses methods of handling it and leads to a short history of digital calculators and of the punched card. Then follow two chapters on analogue and digital representation and the rôle of feedback.

The remainder of the book is concerned with digital machines and discusses coding systems, Boolean algebra, the definition of a Universal machine, the structure of machines and programming. A short concluding chapter discusses the question of the relation between machines and intelligent behaviour.

A. D. BOOTH.

Technische Kunstgriffe bei physikalischen Untersuchungen, edited by E. VON ANGERER and H. EBERT. Pp. vii + 369. (Brunswick: Vieweg, 1957.) DM 18.80.

Structure Reports for 1940–1941. Volume 8, edited by A. J. C. WILSON. Pp. vii + 384. (Utrecht: Oosthoek, 1956).

Instrumentation in Testing Aircraft, by C. N. JACQUES. Pp. xi + 291. (London: Chapman and Hall, 1957.) 45*s*.

Five Mathematical Structural Models in Natural Philosophy with Technical Physical Quaternions, by O. F. FISCHER. Pp. vi + 412. (Stockholm: Axion Institute, 1957.) $10.

Der Ultraschall: Nachtrag zum Literaturverzeichnis der 1954 *erschienenen*. 6. Auflage. By L. BERGMAN. Pp. 66. (Stuttgart: Verlag, 1957.)

Handbuch der Physik, Ed. by S. FLÜGGE. Band XXIV. *Grundlagen der Optik*. Pp. viii + 656. (Berlin, Göttingen, Heidelberg: Springer-Verlag, 1956.) DM. 105.60.

Science and Information Theory, by L. BRILLOUIN. Pp. xvii + 320. (New York: Academic Press; London: Academic Books, 1956).

Geometric Integration Theory, by H. WHITNEY. Pp. xv + 387. (Princeton: University Press; London: Oxford University Press, 1957.) 68*s*.

Cloud Study, by F. H. LUDLAM and R. S. SCORER. Pp. 80. (London: John Murray, 1957.) 12*s*. 6*d*.

Order–Disorder Phenomena, by E. W. ELCOCK. Pp. ix + 166. (London: Methuen; New York: Wiley, 1956.) 11*s*. 6*d*.

Elements of Heat Transfer, 3rd edn., by M. JAKOB and G. A. HAWKINS. Pp. xxv + 317. (New York: Wiley; London: Chapman and Hall, 1957.) 54*s*.

Proceedings of the Joint Conference on Combustion, Boston and London, 1955. Pp. viii + 457. (London: Institution of Mechanical Engineers.)

Constantes sélectionnées: Diamagnétisme et paramagnétisme, by G. FOËX; *Relaxation paramagnétique*, by C.-J. GORTER and L.-J. SMITS. Pp. 317. (Paris: Masson, 1957.) 8.800 *fr*.

PARIS: PUBLICATIONS SCIENTIFIQUES ET TECHNIQUES DU MINISTÈRE DE L'AIR.

Conductibilité électrique aux très basses températures des métaux de très haute pureté et application aux phénomènes de recristallisation, par M. CARON, Pp. 58. No. 328, 1957. 1100 *fr*.

Étude de quelques problèmes sur les ondes liquides de gravité, par G. Brillouet. Pp. 145. No. 329, 1957. 1700 *fr.*

Photoélasticité tridimensionelle: *aspects théoriques et expérimentaux*, by C. L. Gaudfernau. Pp. 86. No. 330, 1957. 1200 *fr.*

Méthodes d'exploration dynamique et thermique et étude de la couche-limite laminaire compressible de la plaque plane, par M. Plan. Pp. v + 123. No. 331, 1957. 1500 *fr.*

Contribution a l'étude de la convection forcée de la chaleur sur des parois rugueuses, par G. Brunello. Pp. 75. No. 332, 1957, 1350 *fr.*

Recherches théoriques et expérimentales sur les mouvements des liquides pesants avec surface libre, by A. S. Apté. Pp. 115. No. 333, 1957. 1450 *fr.*

Les séries chronologiques et la théorie de hasard, par M. Kivelovitch et J. Vialar. Pp. 129. No. N.T. 65, 1957. 1650 *fr.*

Les méthodes scientifiques dans les techniques modernes: quelques écueils, by P. Vernotte. Pp. 61. No. 70, 1957. 700 *fr.*

Recherches sur quelques propriétés de certains hypergols, by Jacques Françon. Pp. 46. No. N.T. 66, 1957.

Contribution à la mesure des chaleurs spécifiques des gaz et des vapeurs, by N. Huetz-Aubert. Pp. 182. No. N.T. 68, 1957.

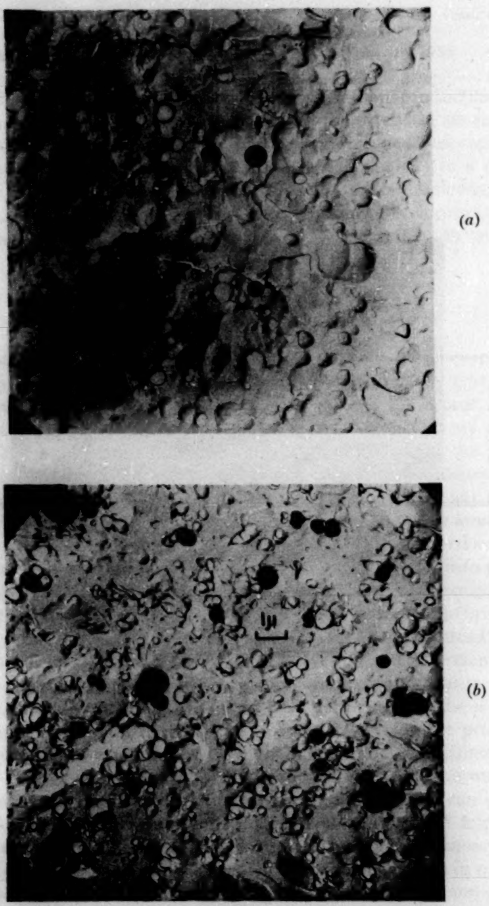

Figure 1. (*a*) Brittle fracture and (*b*) slow tear, in GR-S peroxide filled with black C.

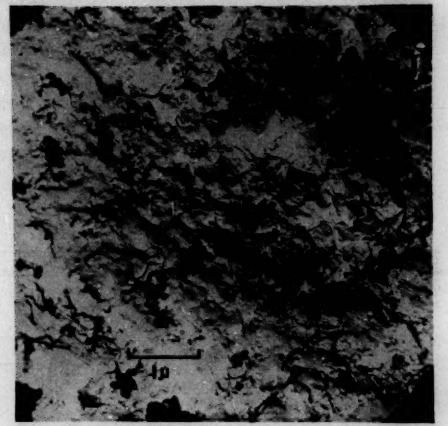

(*c*)

Figure 1. (*c*) Slow tear in a rubber containing black A.

Distribution of K-Mesons Produced in High Energy Nuclear Interactions

By S. N. BISWAS

Department of Mathematical Physics, University of Adelaide, South Australia

MS. received 30th July 1957, and in revised form 17th February 1958

Abstract. As an example of the application of the K-meson production cross section we have considered the K-meson component in the extensive air-showers. A cascade theory of the cosmic-ray shower has been developed embracing the fact that the heavy mesons and hyperons cascade in the nucleus in a manner analogous to the pions and nucleons. Numerical results for the nucleons, pions, hyperons and the K-meson components in the longitudinal development of the cosmic-ray air shower have been presented and compared with available experimental data.

---

§ 1. Introduction

A VARIETY of new particles has been observed in cosmic-ray events. Of these the heavy mesons and hyperons play an interesting part in the development of cosmic-ray showers which is very important at high altitudes. The usual cascade theories for the description of cosmic-ray showers neglect the role of heavy mesons and hyperons and are based on the picture, that the primary radiation incident on the top of the atmosphere consists mainly of high energy protons (with a percentage of α-particles and other heavy nuclei); a nucleon cascade develops from collisions with nuclei in the upper atmosphere and also mesons are produced in such nuclear interactions. The charged π-mesons decay into penetrating μ-mesons while the neutral π-mesons decay into photons which initiate electron–photon (soft) component. The muons contribute only in a minor way by their decay to electrons. The object of this paper is to investigate the contributions of K-mesons (heavy mesons), and hyperons produced in high energy nuclear interactions, in the longitudinal development of extensive air showers. The K-mesons are produced in nucleon–nucleon and also in meson–nucleon collisions, and, by their further decay may contribute to the μ-mesons and soft component showers. Originally the cascade theory for the production of meson and proton shower particles in high energy nucleon disintegration was proposed by Heitler and Jánossy (1950) who assumed that the nucleus is transparent to the mesons emitted in the individual nucleon–nucleon collision and no account is taken of the production of heavy mesons and hyperons.† Later Messel, Potts and McCusker (1952) modified the Heitler–Jánossy model by assuming that very high energy mesons cascade within a nucleus in a manner entirely analogous to that for nucleons: for high energies, each meson–nucleon collision gives rise to two mesons and one nucleon, thus

A: meson + nucleon→meson + meson + nucleon;

B: nucleon + nucleon→nucleon + nucleon + meson,

and the cross sections for processes A and B are equal. In our model we would make the following assumption in addition to those made in the Messel, Potts and McCusker model. We assume that the shower particles consist not only of pions and nucleons but also of heavy mesons and hyperons, and the heavy mesons and hyperons cascade in the nucleus like the nucleons and mesons. For this purpose we will set up a system of master diffusion equations for the mixed nucleon–meson–heavy meson–hyperon cascades in the nucleus. As is well known, to carry out this process we need to know the production cross sections of K-meson and hyperons in the nucleon–nucleon and meson–nucleon interactions. We will calculate this production cross section from pseudoscalar meson field theory and the K-mesons will be considered as the excited bound states of two pions. In an earlier work (Biswas 1958) a detailed theory of heavy mesons as composite particles has been given. Since the heavy mesons are produced in association with hyperons (or other heavy mesons) we would assume the hyperon is also a composite particle formed from a meson and a nucleon. For the cross sections of the processes mentioned in A and B we will take the results of the earlier authors, i.e. of Messel *et al.* (1952). According to Messel (1951) in a nucleon–nucleon collision a primary nucleon of energy E_0 should give rise to secondary and recoil nucleons of energies E_1 and E_2 (and an energy loss E_m due to production of meson or mesons); the cross section should be symmetrical in the variables E_1 and E_2 since it is impossible to distinguish between the recoil and secondary nucleons after the collisions. The cross section for the process should be taken the same as that of A. This assumption is probably an oversimplification but it may be justified empirically (see Messel *et al.* 1952). In the mixed nucleon–meson–heavy meson–hyperon cascades we assume that some of the heavy mesons and hyperons produced by the nuclear interaction may further interact with the nucleons. Hence, we should also determine the scattering cross sections of the heavy mesons and hyperons by the nucleons. The cross section can be obtained from the observed isotropic symmetry of the scattered heavy mesons in the centre-of-mass system and from relativistic considerations.

---

† For detailed account see Messel (1954).

We will first determine the average number of nucleons, mesons and heavy mesons and hyperons as a function of the depth in homogeneous nuclear matter for the model mentioned before. Assuming that nuclei are spherical in shape, it is necessary to average the results over all possible path lengths through a nucleus. Next we will proceed to solve the diffusion equations describing the longitudinal behaviour of an extensive air shower consisting of nucleons, hyperons and heavy mesons. We do not consider here the muons, electrons and photon components in the air shower. Apart from consideration of the longitudinal development in a cosmic-ray shower, we can also find the distribution of the K-mesons and hyperons produced in the nuclear interaction in the absorber of a high energy accelerator machine. The modifications necessary to determine this distribution from that of the air shower will be pointed out in § 3.

In § 4 we will present some numerical results for the average number of particles (nucleons, pions, hyperons and heavy mesons) in the different components of the cosmic radiation in the atmosphere. It is found that pions, hyperons and heavy mesons have a maximum at a depth of 75 g cm^{-2}. Pions like the nucleons decrease quickly with energy and depth. The number of hyperons and heavy mesons at energy 3 GeV are almost the same, which seems plausible because of their associated production. The size of the nucleon component is almost a hundred times larger than that of the hyperons and the heavy mesons. The ratios of the K-particles and pions as well as Y-particles and pions have also been determined; this ratio has the value of the order of 0·09, whereas the experimental finding of Perkins (1953) is approximately 0·13 ± 0·05; our value is within this limit. The number of K-particles is appreciable compared to pions at mountain altitudes ($x=10$ in units of $75\,\mathrm{g\,cm^{-2}}$) and above.

§ 2. MIXED NUCLEON–PION–HYPERON–K-MESON CASCADES IN THE NUCLEUS

We now give a set of diffusion equations for the average number of nucleons, π-mesons and hyperons and K-mesons at a depth x collision units (in $\mathrm{g\,cm^{-2}}$) in homogeneous nuclear matter, for the most general scheme of shower production where we assume that pions, hyperons and K-mesons cascade in the nucleus in an exactly analogous manner to the nucleons. The problem of mixed pion–nucleon cascades has been discussed and tabulated by Messel *et al.* (1952). In the following we will give the general solution for meson, nucleon, hyperon and heavy mesons but we will restrict ourselves, for the present, to deducing the explicit result for the distribution functions for the scheme of shower production mentioned in the introduction. Let $\omega_i^{(j)}(E,x)$ be the differential number of particles of the ith kind at a depth of x collision units emitted in the energy range E, $E+dE$ from a nucleus due to a collision by a primary particle of the jth kind. $i=1, 2, 3, 4$ and $j=1, 2, 3, 4$ for nucleon, pion, K-meson and hyperon respectively. Further we define $F_{ki}(E|E')$ to be the collision cross section of the kth particle in interaction with the nucleon to produce the ith type of particle. ($k=1, 2, 3, 4$ denoting nucleon, pion, heavy meson and hyperon respectively.) We normalize all the collision cross sections by dividing them by the total n–n cross section. We write in the matrix form the integro-differential equations for the various $\omega_i^{(j)}$'s in the following way:

$$\left(\frac{\partial}{\partial x}+q_i\right)\omega_i^{(j)}(E,x)=\sum_{k=1}^{4}\int_E^{\infty}\omega_k^{(j)}(E',x)F_{ki}(E|E')\,dE'/E' \qquad \ldots\ldots(2.1)$$

where

$$\left.q_i=\begin{cases}1 \text{ for } i=1,2\\ q \text{ for } i=3,4\end{cases} \quad\text{and}\quad q=\int_E^{\infty}F_k{}^s(E|E')\,dE'/E'.\right\} \qquad \ldots\ldots(2.2)$$

The matrix F_{ki} can be written as

$$(F_{ki})=\left\{\begin{matrix}\overline{F}(E|E') & k(E|E') & F_k{}^s(E|E') & F_k{}^s(E|E')\\ l(E|E') & \tfrac{1}{2}\overline{F}(E|E') & F_k{}^s(E|E') & F_k{}^{\mathrm{I}}(E|E')\\ F_k(E|E') & F_k(E|E') & F_k{}^s(E|E') & F_k{}^s(E|E')\\ F_k(E|E') & F_k(E|E') & F_k{}^{\mathrm{I}}(E|E') & F_k{}^s(E|E')\end{matrix}\right]. \qquad \ldots\ldots(2.3)$$

We give here the meaning of the various matrix elements F_{ki} of the matrix (F_{ki})

$$\overline{F}(\eta_1)=\int_0^1\{F(\eta_1,\eta_2)+F(\eta_2,\eta_1)\}\,d\eta_2 \qquad \ldots\ldots(2.4)$$

where $F(\eta_1,\eta_2)$ denotes the cross section for meson production in nucleon–nucleon collisions; η's denote the ratios of the secondary to primary particle energy. The explicit form of the cross section $F(\eta_1\eta_2)=120\eta_1\eta_2(1-\eta_1-\eta_2)$, for the inelastic nucleon–nucleon collisions is taken from the work of Messel (1951), and $k(E/E') = \frac{1}{2}\bar{F}(E/E')$; $l(E/E') = \bar{F}(E/E')$.

From the field-theoretic calculation of the last section the production cross section of heavy mesons and hyperons in n–n and n–π collisions divided by the total n–n collision cross section, which is 42 mbn at 2·6 GeV and remains fairly constant at higher energies, is given by

$$F_k(\eta) = \sigma\left\{\frac{4}{3}\eta^4 - \frac{5}{2}\eta^3 + \frac{25}{16}\eta^2\right\}. \qquad \ldots\ldots(2.5)$$

σ = const, where η is the ratio of the secondary to primary energy of the process. The production cross section of the hyperon in n–n and π–n interaction can also be taken from the same calculation of $F_k(\eta)$ where now η will be the ratio of the emergent hyperon energy to incident particle energy. As for the interaction of $\mathrm{K}+\mathrm{N} \rightarrow \begin{cases}\mathrm{Y}+\pi \\ \mathrm{K}+\mathrm{N}\end{cases}$ we have either the production of hyperons or a simple scattering process. The cross section for this reaction has been taken as $F_k{}^s(\eta)$. We determine the K-meson nucleon scattering cross section from relativistic considerations and the observed fact of the isotropic emission of the K-mesons in the centre-of-mass system; it is given by $F_k{}^s(\eta) = \text{constant} = 0{\cdot}025$ where we have assumed the total scattering cross section of K's to be of the order of 1 mbn and n–n cross section of the order of 42 mbn. For the interaction of a Y-hyperon with the nucleon we notice that there may be direct scattering which is denoted by $F_k{}^s(\eta)$ and the other possible inelastic processes namely $\mathrm{Y}+\mathrm{N} \rightarrow \begin{cases}\mathrm{Y}+\mathrm{N}+\pi \\ \mathrm{N}+\mathrm{N}+\mathrm{K}\end{cases}$; we have designated this interaction by $F_k{}^{\mathrm{I}}(\eta)$.

We now write down the general solution of (2.1) by introducing the Laplace transform of the variable x and the Mellin transform of the variable E,

$$\omega_i^{(j)}(s, \lambda) = \int_0^\infty \int_0^\infty \omega_i^{(j)}(E, x) E^{s-1} e^{-\lambda x}\, dE\, dx \qquad \ldots\ldots(2.6)$$

with the initial condition that $\omega_i^{(j)}(\eta, 0) = \delta(1-\eta)$ where η is the ratio of the final to initial energy of the process.

The solution can be easily written down as

$$\omega_i^{(j)}(E, x) = \frac{1}{(2\pi i)^2} \int_{c_0 - i\infty}^{c_0 + i\infty} \int_{s_0 - i\infty}^{s_0 + i\infty} g_{ki}(s, \lambda) \Delta^{-1}(s, \lambda) e^{-\lambda x} E^s\, ds\, d\lambda \quad \ldots\ldots(2.7)$$

where g_{ki} is the co-factor of the matrix G_{ki} obtained from the matrix F_{ki} by subtracting the terms $q_i + \lambda$ from the diagonal elements, F_{ii} of F_{ki} and $\Delta(s, \lambda)$ is $\det G_{ki}$. The evaluation of (2.7) is straightforward by finding the zeros of the $\det \Delta$ and applying the Cauchy integral.

In the following we will state the results of integration of (2.7) to obtain the various distribution functions, $\omega_i^{(j)}(E, x)$ for the scheme of shower production considering the existence of hyperons and heavy mesons. We have discussed this scheme in the introduction of our paper. Finally, averaging over all possible path lengths through the nucleus, i.e. using the operator

$$N(D_{\mathrm{A}}) = \int_0^{D_{\mathrm{A}}} 2x\, dx / D_{\mathrm{A}}{}^2$$

where D_{A} is the average number of collisions which a particle suffers on making a diametrical passage through a nucleus of atomic weight A, we give below in the matrix form the values of $\omega_i^{(j)}$ where $j=1, 2$ and $i=1, 2, 3, 4$; $j=1$ denotes nucleon, $j=2$ for pions, $i=1$ for nucleons, 2 for pions, 3 for heavy mesons and 4 for hyperons.

For such a simple model the equations for the nucleon and pion components denoted by $\omega_1^{(j)}$ and $\omega_2^{(j)}$ can be easily solved. In solving the equations for heavy mesons and hyperons we have assumed the production cross sections for both of them to be the same. In fact both types of particles are produced in the strong interactions with equal numbers. Another assumption has been made that both the elastic and inelastic collision cross section of $\mathrm{K}+\mathrm{N}\rightarrow\mathrm{K}+\mathrm{N}$ and $\mathrm{K}+\mathrm{N}\rightarrow\mathrm{Y}+n\pi$ are the same; similar assumptions can be made for the Y-particles because of their equal and opposite strangeness number. This seems to be the best choice at present in view of the unavailability of experimental findings. Under these assumptions the diffusion equations satisfied by the K-meson and Y-hyperon are the same. The solutions of the various $\omega_i^{(j)}$'s are given by the following:

$$\begin{bmatrix} \omega_1^{(1)} & \omega_1^{(2)} \\ \omega_2^{(1)} & \omega_2^{(2)} \\ \omega_3^{(1)} & \omega_3^{(2)} \\ \omega_4^{(1)} & \omega_4^{(2)} \end{bmatrix} = I_1\{\lambda_1(s)-\lambda_2(s)\} \begin{bmatrix} V_1W(0_1s) & -V_1W(0_1s) \\ -V_1W(0_1s) & V_1W(0_1s) \\ V_2(5W(0_1s)-1) & 2V_2W(0_1s) \\ V_2(5W(0_1s)-1) & 2V_2W(0_1s) \end{bmatrix} \quad \ldots\ldots(2.8)$$

where

$$V_1 = V[D_\mathrm{A}\lambda_1(s)],$$

$$V_2 = \frac{V[D_\mathrm{A}q(s)] - V[D_\mathrm{A}\{q(s)-\lambda_2(s)\}]}{\lambda_2(s)}\,\beta(s),$$

$$I_1 = \frac{1}{2\pi i}\int_{s_0-i\infty}^{s_0+i\infty} (E_0/E)^{s+1}\,ds,$$

$$\lambda_1(s) = 1-W(0,s), \qquad \lambda_2(s) = 1-3W(0,s),$$

$$W(0,s) = 120\{(s+2)(s+3)(s+4)(s+5)\}^{-1},$$

$$V(\lambda) = 2[1-(1+\lambda)e^{-\lambda}]/\lambda^2,$$

$$\beta(s) = \int_0^1 F_k(\eta)\eta^s\,d\eta; \qquad q(s) = q-\tfrac{1}{2}\int_0^1 F_k{}^s(\eta)\eta^s\,d\eta.$$

Taking the radius of the nucleus to be $1{\cdot}37\times10^{-3}A^{1/3}$ cm we have $D_\mathrm{A} = 1{\cdot}5A^{1/3}(R_k/1{\cdot}37\times10^{-13})^2$; R_k is the range of the nuclear forces. $D_\mathrm{A} = 3{\cdot}7$ for air, 6·8 for bromine and silver.

In the next section we will develop the longitudinal development of nucleon, meson and heavy meson components in the atmospheric air shower.

§ 3. LONGITUDINAL DEVELOPMENT OF AIR SHOWERS

One important problem in cosmic-ray physics is the consideration of the development of cosmic-ray showers in the atmosphere. A complete mathematical theory was previously impossible as the details of the interaction of pions and nucleons with nuclei were not fully known. Recently a good deal of experimental information has made clear the mode of formation of various new particles other than pions and nucleons; the role of these new particles in the formation of the longitudinal development of the cosmic-ray showers is the subject matter of this section.

We first write down the diffusion equations describing the longitudinal behaviour of an extensive air shower consisting of nucleons, pions, heavy mesons and hyperons. We will not consider the productions of muons, photons and electrons at present. Let $q^{(j)}(E_0, E, x)\,dE$ be the differential average number of nucleons, charged pions, heavy mesons (charged and neutral) and hyperons (charged and neutral) with energy in the range $E, E+dE$ at a depth $x\,\mathrm{g\,cm^{-2}}$, due to a single primary proton of energy E_0 for $j=1, 2, 3$ and 4 respectively. The corresponding average number of particles with energies greater than E will be denoted by

$$Q^{(j)} = \int_E^\infty q^{(j)}(E_0, E_1)\,dE_1.$$

Neutral pions are ignored because they decay (lifetime $< 5\times 10^{-15}$ sec) in the moment they are produced and contribute to the soft component which we are not going to study.

The diffusion equations can be put in the following matrix equation

$$\left\{ l^{(j)}\frac{\partial}{\partial x} - \beta^{(j)}\frac{\partial}{\partial E} - \frac{c\alpha^{(j)}}{Ex'(t)} + c^{(j)} \right\} q^{(j)}(E_0, E, x)$$
$$= \sum_{k=1}^{4} a_{jk}\int_E^\infty q^{(k)}(E_0, E_1, x)\,\omega_j^{(k)}(E_1, E)\,dE_1, \qquad \ldots\ldots (3.1)$$
$$j = 1, 2, 3, 4.$$

where $\omega_j^{(k)}(E_1, E)$ are already defined in § 2 and they are given by the equation (2.7). $l^{(j)}$ denotes the interaction mean-free-paths for the jth particle measured in $\mathrm{g\,cm^{-2}}$; $\beta^{(j)}$ denotes the energy losses by ionization in Mev per $\mathrm{g\,cm^{-2}}$ by the jth particle; $\alpha^{(j)}$ denotes the ratio of the mass and mean lifetime in seconds in centre-of-mass system of the jth kind of particle. However $\alpha_j = 0$ when $j=1$. $c_j = 1$ for $j=1$ and 2 and it is equal to a constant for $j=3$ and 4; this constant is effectively the ratio of the production cross sections of K and Y particles with the n–n total collision cross section. Furthermore $a_{jk} = l^{(j)}/l^{(k)}$, $l^{(j)}$'s are already defined; c is the velocity of light. Finally $x'(t) = dx(t)/dt$ where $x(t)$ defines the depth in the absorber in $\mathrm{g\,cm^{-2}}$ expressed as a function of the height t.

The exact solutions of these systems of integro-differential equations can be obtained by using the Mellin transform of the energy variable and the Laplace transform to the variable x. In treating these equations we should assume that the various $\omega_j^{(k)}$'s are homogeneous functions of the primary and secondary energies only. Another point we must observe is that the Mellin transform of the energy variable will lead to a difference equation owing to the absence of a factor E in $\beta^j\,d/dE$ and the presence of E in the denominator of the decay term α^j in the left-hand side of the equation (3.1). To avoid such a difficulty we replace $\beta^j\,d/dE$ by $\beta^j E_{\mathrm{av}}{}^{-1} E\,d/dE$ and E in the decay term by E_{av}. Since the average energy, E_{av}, depends on the density of the medium, we may take

$$E_{\mathrm{av}}x'(t) = \text{constant} = d \qquad \text{(say)}.$$

In obtaining the exact solutions we need further to know the energy spectrum of the primary particles on the top of the atmosphere. The primary particles are protons and we consider a power law spectrum of protons of the form

$$n(E) = \begin{cases} \gamma E_c{}^\gamma / E^{\gamma+1}; & E > E_c \\ 0 & E < E_c \end{cases} \qquad \ldots\ldots (3.2)$$

where E_c is the latitude cut-off energy and γ is some numerical constant.

Introducing the Mellin and Laplace transform to $q^{(j)}$'s we have

$$\mathbf{q}^{(j)}(s,\lambda)=\int_0^\infty\int_0^\infty \exp\left[-(\lambda x)/l^{(j)}\right]E^{s-1}q^{(j)}(E_0,E,x)\,dx\,dE$$

and for (3.1), the following system of algebraic equations

$$\begin{aligned}(\lambda-\beta^{(j)}E_{\text{av}}-k^{(j)})\mathbf{q}^{(j)}(s,\lambda)+\mathbf{q}^{(j)}(0) &= \sum_k a_{kj}\mathbf{q}^{(k)}(s,\lambda)\boldsymbol{\omega}_j^{(k)}(s)\\ &= \sum_k A_{kj}\mathbf{q}^{(k)}(s,\lambda) \qquad \ldots\ldots(3.3)\end{aligned}$$

where $A_{kj}=a_{kj}\omega_j^{(k)}$, $k^{(j)}=d^{(j)}c/d-c^{(j)}$; $\boldsymbol{\omega}_j^{k}(s)$ is the Mellin transform of $\omega_j^{(k)}(E/E_1)$ and

$$\mathbf{q}^{(j)}(0)=\int_0^\infty q^{(j)}(E_0,E,x=0)E^{s-1}\,dE; \qquad q^{(j)}(E_0,E,x=0)$$

can be taken as $n(E)$ given in (3.2).

Equation (3.3) can be easily solved and taking the inverse of the Mellin–Laplace transform of $\mathbf{q}^{(j)}(s,\lambda)$ we can get the required functions $q^{(j)}$. The solution $q^{(j)}(E,x)$ is

$$q^{(j)}(E,x)=\frac{1}{(2\pi i)^2}\int_{c_0-i\infty}^{c_0+i\infty}\int_{s_0-i\infty}^{s_0+i}\mathbf{q}^{(j)}(0)\frac{b_{kj}(s,\lambda)}{D(s,\lambda)}\exp\left[(\lambda x)/l^{(j)}\right]E^{-s}\,ds\,d\lambda \quad \ldots\ldots(3.4)$$

where b_{kj} is the co-factor of the element B_{kj} in the determinant $|B_{kj}|$ where $((B_{kj}))$ matrix is obtained from the matrix A_{kj} by subtracting the expression $(\lambda-\beta^{(j)}E_{\text{av}}-k^{(j)})$ from the diagonal elements A_{jj} of $((A_{kj}))$; $D(s,\lambda)=\det B_{kj}$. In the following we will give detailed solutions of the $q^{(j)}$ for the scheme of shower production mentioned in the introduction. Messel and Potts (1953) considered a model in which they neglected the interactions of the charged pions with nuclei; it was assumed that most of them would decay before further interaction. According to their conclusion such an assumption must be abandoned and in fact a large proportion of pions do interact again with nuclei. In our scheme we would take this interaction into consideration and also consider the behaviour of the heavy mesons and hyperons.

Neglecting the energy losses due to ionization by protons and charged mesons and thus confining to the high energy regions we get the following equations from (3.1):

$$\left.\begin{aligned}\left(l^{(1)}\frac{\partial}{\partial x}+1\right)q^{(1)} &= \int_E^\infty q^{(1)}(E_0,E_1,x)\omega_1^{(1)}(E_1,E_0)\,dE_1+l^{(1)}/l^{(2)}\\ &\quad\times\int_E^\infty q^{(2)}(E_0,Ex)\omega_1^{(2)}(E_1,E)\,dE_1\\ \left(l^{(2)}\frac{\partial}{\partial x}-d^{(2)}\frac{c}{d}+1\right)q^{(2)} &= \frac{l^{(2)}}{l^{(1)}}\int_E^\infty q^{(1)}(E_0,E_1,x)\omega_2^{(1)}(E_1,E)\,dE_1\\ &\quad+\int_E^\infty q^{(2)}(E_0,E_1,x)\omega_2^{(2)}(E_1,E)\,dE_1\end{aligned}\right\}\ldots\ldots(3.5)$$

$$\left.\begin{aligned}&\left\{l^{(3,4)}\frac{\partial}{\partial x}-l^{(3,4)}\beta_i^{(3,4)}\frac{\partial}{\partial E}-\alpha^{(3,4)}\frac{c}{Ex'(t)}+c_i\right\}q_i^{(3,4)}\\ &\qquad=\frac{l^{(3,4)}}{l^{(1)}}\int_E^\infty q^{(1)}(E_0,E_1,x)\omega_{3,4}^{(1)}(E_1,E)\,dE_1\\ &\qquad+\frac{l^{(3,4)}}{l^{(2)}}\int_E^\infty q^{(2)}(E_0,E_1,x)\omega_{3,4}^{(2)}(E_1,E)\,dE_1\end{aligned}\right\}\ldots\ldots(3.6)$$

where the indices (3, 4) in the third equation denote the heavy meson and hyperon respectively, and the suffix i has been introduced in the same equation only to distinguish the charged and neutral heavy mesons or hyperons.

Following the general method described at the beginning of this section for the solution of (3.1) we can at once write down the solutions of the first pair of the above system of equations. We give here the result for the average number of particles denoted by $Q^{(j)}$ with energy greater than E by the following:

$$Q^{(1)}(E_c, E, x) = \left(\frac{E_0}{E}\right)^{\gamma} \exp\left\{-x\frac{a+b}{2l^{(1)}}\right\} \cosh\mu\left\{\frac{x}{l^{(1)}} + \frac{a-b}{2\mu}\sinh\mu\frac{x}{l^{(1)}}\right\} \quad \ldots\ldots (3.7)$$

$$Q^{(2)}(E_c, E, x) = \left(\frac{E_c}{E}\right)^{\gamma} \exp\left\{-x\frac{a+b}{2l^{(2)}}\right\} \left\{\frac{l^{(2)}}{l^{(1)}}\frac{\alpha_2(\gamma+1)}{\mu}\sinh\mu\frac{x}{l^{(2)}}\right\} \quad \ldots\ldots (3.8)$$

where

$$a+b = 1+K-\alpha_4(\gamma+1)-\alpha_1(\gamma+1)$$

$$a-b = K-1+\alpha_1(\gamma+1)-\alpha_4(\gamma+1)$$

$$\mu = \{\alpha_2(\gamma+1)\alpha_3(\gamma+1)+\tfrac{1}{4}(a-b)^2\}^{1/2}$$

$$\begin{pmatrix}\alpha_1(\gamma+1) & \alpha_3(\gamma+1)\\ \alpha_2(\gamma+1) & \alpha_4(\gamma+1)\end{pmatrix} = V[D_A\lambda_1(\gamma)]\begin{pmatrix}-1 & 1\\ 1 & -1\end{pmatrix} + V[D_A\lambda_2(\gamma)]\begin{pmatrix}1 & 1\\ 1 & 1\end{pmatrix}$$

and $K = (1-\alpha^{(2)}c/d)$.

For the solution of the last equation of the above system we notice it to be a partial differential equation and the solution is

$$q_i^{(3)}(E_0, E, x) = \exp\{-c_i x/l^{(3)}\}\left(\frac{E}{x}\right)^{u}\int_0^x R(E_0, E+\beta_i^{(3)}(x-z), z)$$
$$\times\left\{\frac{E+\beta_i^{(3)}(x-z)}{z}\right\}^{u}\exp\{c_i x/l^{(3)}\}\,dz \quad \ldots\ldots (3.9)$$

where

$$R(E_0, E, x) = \frac{1}{l^{(3)}}\int_E^\infty q^{(1)}(E_0, E, x)\omega_3^{(1)}(E_1, E)\,dE_1 + \frac{1}{l^{(3)}}\int_E^\infty q^{(2)}(E_0, E_1, x)\omega_3^{(2)}(E_1, E)\,dE_1$$

and $u = l_1/(E+\beta_i^{(3)}x)$.

We have also considered the atmosphere as an example of an absorber whose density is not constant and take it to be isothermal, $x'(t) = -g(\delta_0/p_0)x(t)$ and p_0, δ_0 and g are surface pressure, surface air density and acceleration due to gravity.

In substituting the values of the expressions for q's from (3.8) and (3.9) we notice that the cosh and sinh terms may well be approximated by $\exp x$. To determine the average number of K-mesons and hyperons with energies greater than E, we have $Q_i^{(3,4)}(E_c, E, x) = \int_E^\infty q_i^{(3,4)}(E_c, E, x)\,dE$. The result of this integration gives the following:

For small values of x we have for Q_i

$$Q_i^{(3,4)}(E_c, E, x) \simeq \exp\left\{-\frac{c_i x}{l^{(1)}}\right\}\sum_{n=0}^{\infty}\sum_{j=1}^{2}\gamma\left(\frac{E_c}{l_1}\right)^{\gamma}\left\{\frac{a_j}{b_j l^{(1)}}\right\}\frac{(xb_j)^{n+1}}{n!}f(\gamma, n) \quad \ldots\ldots (3.10)$$

and for large values of x we have

$$Q_i^{(3,4)}(E_c, E, x) \simeq \exp\left(-c_i\frac{x}{l^{(3)}}\right)\sum_{j=1}^{2}\gamma\left(\frac{E_c}{l^{(1)}}\right)^{\gamma}\left\{\frac{a_j}{b_j l^{(1)}}\right\}g(\gamma) \quad \ldots\ldots (3.11)$$

where

$$f(\gamma,n)=I(\gamma-1,n+1)+\left(\frac{\beta^{(3,4)}x}{l_1}\right)[I(\gamma)+(\gamma+1)I(\gamma,n+2)-(n+2)I(\gamma,n+2)]$$

$$\begin{aligned}g(\gamma)=I(\gamma-1)-(c_{\mathrm{E}}-\log xb_j)I(\gamma)-\exp(-b_jx)I(\gamma-1)\\ -\frac{(\beta^{(3,4)}x)}{l_1}\exp(-b_jx)I(\gamma)+\left(\frac{\beta^{(3,4)}x}{l_1}\right)\\ \times[(\gamma+1)I(\gamma)+\{(\gamma+2)-(\gamma+1)(c_{\mathrm{E}}-\log xb_j)\}I(\gamma+1)]\end{aligned}$$

$$l_1=l_{(3,4)}=\frac{m^{(3,4)}cp_0}{\tau^{(3,4)}g\delta_0}, \qquad c_{\mathrm{E}}=\text{Euler's constant}=0\cdot577\ldots$$

$$\begin{aligned}I(\gamma-1,n)=2\left[\left(\frac{l_1}{E}\right)^{1/2}-n\tan^{-1}\left(\frac{l_1}{n^2E}\right)^{1/2}\right]+2\left(\frac{\beta_k{}^ix}{l_1}\right)\\ \times\left[\frac{1}{5}\left(\frac{l_1}{E}\right)^{5/2}+\frac{n}{3}\left(\frac{l_1}{E}\right)^{3/2}+n^2\left(\frac{l_1}{E}\right)^{1/2}-n^3\tan^{-1}\left(\frac{l_1}{n^2E}\right)^{1/2}\right]\end{aligned}$$

$$I(\gamma,n)=\frac{2}{3}\left(\frac{l_1}{E}\right)^{3/2}-\frac{2}{7}\left(\frac{l_1}{E}\right)^{7/2}\left(\frac{\beta_k{}^ix}{l_1}\right)-nI(\gamma-1,n)$$

$$I(\gamma)=\frac{1}{\gamma+1}\left(\frac{l_1}{E}\right)^{\gamma+1}-\left(\frac{\beta_k{}^ix}{l_1}\right)\frac{1}{\gamma+3}\left(\frac{l_1}{E}\right)^{\gamma+3}$$

and further

$$a_1=\omega_{(3,4)}{}^{(1)}(\gamma)\left\{\frac{1}{2}+\frac{a-b}{2\mu}\right\}; \qquad a_2=\omega_{(3,4)}{}^{2}(\gamma)\left\{\frac{l^{(2)}l^{(1)}\alpha_2(\gamma+1)}{2\mu}\right\}$$

$$b_1=\frac{a+b}{2l^{(1)}}-\frac{\mu}{l^{(1)}}-\frac{c_i}{l^{(1)}}; \qquad b_2=\frac{a+b}{2l^{(2)}}-\frac{\mu}{l^{(2)}}-\frac{c_i}{l^{(3,4)}}.$$

$\omega_{(3,4)}{}^{(1)}(\gamma)$ and $\omega_{(3,4)}{}^{(2)}(\gamma)$ are obtained from (2.8) by omitting the inverse Mellin transform operator I_1 from the right-hand side and replacing s by γ throughout. The second term in the expression of $f(\gamma,n)$ and terms multiplied by $\beta^{(3,4)}$ in the result of $g(\gamma)$ may be treated as corrections due to ionization loss. The relevant formula for determining the rate of energy loss per g cm^{-2} due to ionization is given by Rossi and Greisen (1941). It is found that in air for heavy mesons it is 2 MEV per g cm^{-2} for primary energy 10 GEV of the heavy meson, and it remains fairly constant for higher energies.

§ 4. NUMERICAL RESULTS

In this section we will present some numerical calculations of the results (3.7), (3.8), (3.10) and (3.11) denoting the average number of particles at certain depths and energies based on the model of the plural production of mesons and showing that the mesons do interact with the nuclei; in addition we have taken into consideration the heavy mesons and hyperons produced in the high energy nuclear disintegration in the atmosphere. Only the high energy is considered here so that the energy loss by ionization can be neglected for nucleons and pions. It has already been mentioned that primary radiation consisting of protons obeys a power law spectrum with the exponent $\gamma=1\cdot5$. The incidences of heavy nuclei and α-particles are negligibly small, again their mean free path being 30 g cm^{-2} compared with 75 g cm^{-2} for protons. It may be noticed that the average number Q for different particles depends on the latitude cut-off energy, E_c, through $(E_c)^\gamma$, hence the latitude effect should be the same for all components. Hence, following Messel and Potts (1953), we evaluate $G^{(1)}(E,x)$ defined by

$$G^{(1)}(E,x) = \left(\frac{180}{E_0}\right)^{1\cdot5} Q^{(1)}(E,x).$$

That is, the nucleon primary integral spectrum is $(180/E_0)^{1\cdot5}$ where E_0 is the primary energy of the nucleon and $l = 180$ GeV. We tabulate $G^{(1)}$ for $l/E = 60$, 18, 9, 3 giving $E = 3$, 10, 20, 60 GeV at different depths $x = 0$, 1, 3, 10, 13·3 in units of 75 g cm^{-2}.

(*a*) *Nucleons.* From equation (3.5) we obtain table 1.

Table 1. Average Number of Nucleons with energy greater than E GeV at depth x in units of 75 g cm^{-2} in the atmosphere assuming a nucleon primary energy spectrum $(180/E_c)^{1\cdot5}$

x / E	0	1	3	10	13·3
3	465·76	186·28	23·285	0·06664	0·00401
10	76·40	30·24	3·820	0·01110	0·000729
20	27·00	10·96	1·350	0·00405	0·000236
60	5·200	2·07	0·2600	0·00078	0·0000469

(*b*) *Charged pions.* From (3.7), the average number of charged pions with energy greater than $E > E_c$ GeV at depth x measured in units of $l^{(2)}$(75 g cm^{-2}) obeying the same primary energy spectrum $(180/E_c)^{1\cdot5}$ is given in table 2. We have assumed the interaction mean free path of pions is the same as that of nucleons.

Table 2. Average Number of Charged Pions, $G^{(2)}(E,\,x) = \left(\frac{180}{E_0}\right)^{1\cdot5} Q^{(2)}(E,\,x)$ with energy greater than E GeV at depth x in units of 75 g cm^{-2}

x / E	0	1	3	10	13·3
3	0	18·628	6·9855	0·04664	0·003408
10	0	3·024	1·1460	0·00781	0·0006196
20	0	1·096	0·4050	0·00283	0·0002086
60	0	0·207	0·0780	0·000546	0·0000469

(*c*) *Heavy mesons.* As in the cases of nucleons and pions we give our results of the average number of heavy mesons, independent of the cut-off energy by computing the functions $G_i^{(3,\,4)}(E,x)$ instead of $Q_i^{(3,\,4)}(E,\,x)$ where

$$G_i^{(3,\,4)}(E,x) = \left(\frac{l}{E_c}\right)^{1\cdot5} Q_i^{(3,\,4)}(E,x).$$

We will confine ourselves to the low-energy region (in 3 GeV region). In this energy range we may neglect the energy loss due to ionization. With this approximation we may reduce our results for $Q_i^{(3,\,4)}$ by the following

$$Q^{(3,\,4)} = \sum_{j=1}^{2} a_j\gamma \left(\frac{E_c}{l_1}\right)^{\gamma} \exp\left(-c_i\frac{x}{l^{(3,\,4)}}\right)\frac{x}{l^{(3,\,4)}}\int_0^{l_1/E} u^{1/2}\,du \int_0^1 t^u \exp\,(-b_jxt)\,dt$$

with $l_1 = l_{(3,4)}$ given in the earlier section. Using the numerical values of a_j, b_j, γ and $l^{(3)}$ we write down $G_i^{(3)}(E, x)$ defined above, as

$$G_i^{(3)} = \begin{cases} 0{\cdot}15442x \exp(-0{\cdot}05x) \displaystyle\int_0^{625/E} u^{1/2}\,du \int_0^1 t^u \exp(-0{\cdot}84xt)\,dt \\ 0{\cdot}15442x \displaystyle\int_0^{625/E} u^{1/2}\,du \int_0^1 t^u \exp(-0{\cdot}79xt)\,dt \end{cases}$$

where x is in units of 75 g cm^{-2}. The first formula is used when we consider the interaction of the K-particles with the nucleons and the second formula when we neglect this interaction. Considering the former possibility we tabulate the numerical results for $G_i^{(3)}$ (table 3). We give in table 4 another set of numerical results at high energies computed directly from (3.10), neglecting energy loss by ionization and taking interaction of K-particles with the nucleons at small depths of the atmosphere.

Table 3. Average Number of Heavy Mesons of energy 3 GeV at depths x (in units of 75 g cm^{-2}) obeying the primary proton power law spectrum. $x = 10$ corresponds to the mountain altitude. The interaction mean free path is assumed to be the same as that for pions

x	0	1	3	10
E				
3 GeV	0	1·7568	0·65775	0·00175
K/π		0·0943	0·0940	0·038

Table 4. Average Number of Heavy Mesons at depth x (in units of 75 g cm^{-2}) of energy greater than E GeV assuming nucleon primary energy spectrum $(180/E_c)$

x	0	1	3
E			
10 GeV	0	0·1504	0·0162
20 GeV	0	0·1032	0·0108
60 GeV	0	0·0544	0·0047

(*d*) *Y particles.* We give in table 5 the average number of hyperons of energy 3 GeV at depths x in units of 75 g cm^{-2}. We assume here that the interaction mean free path of hyperons is the same as that for heavy mesons. Assuming the mass of a hyperon to be approximately 2182 times electron mass and the lifetime approximately 10^{-8} sec, we compute $G_i^{(4)}(E, x)$ neglecting as before the energy loss by ionization. The function $G_i^{(4)}(E, x)$ is obtained from $G_i^{(3)}$ simply by replacing the value of $l_{(3)}$ by $l_{(4)}$.

Table 5. Average Number of Hyperons of energy 3 GeV at depth x assuming the nuclear primary energy spectrum $(180/E_c)^\gamma$

x	0	1	3	10
E				
3 GeV	0	1·254	0·4626	0·00125
K/π		0·0674	0·0671	0·0272

It appears from table 4 that the particles do not decrease rapidly with the high decrease of the primary energy. This may be attributed to neglect of the energy losses of the particles due to collision and radiation processes. The detailed theory has been given from which detailed numerical results for very high energies can be obtained.

In this connection we should also point out how one can apply our results in a finite absorber, as for example, to find the distributions of the K-mesons in a high energy accelerator in the laboratory. For this purpose we might neglect the ionization losses as well as decay in flight of these particles from the equation (3.7). We state here the result without giving any numerical results. For absorbers of constant density $x'(t) = -\delta$, where δ is the density of absorber measured in $\mathrm{g\,cm^{-2}}$ we have

$$q_i(E_0, E, x) = \exp(-c_i x/l^{(3)}) \int_0^x R(E_0, E, z) \exp(c_i z/l^{(3)})\, dz$$

where $R(E_0, E, x)$ is given in (3.9).

From tables 1, 3 and 5 we notice that at an energy 3 GeV the number of nucleons is a few hundred times the number of heavy mesons and hyperons at nearly all depths; and at higher energies the ratio remains fairly constant. From table 2 we compare the charged pions with the nucleons. The results of the nucleon components show that the assumed primary law spectrum persists at all depths. The number of nucleons decreases with energy and depth. The pion components have a maximum at a depth of $75\,\mathrm{g\,cm^{-2}}$ and then decrease with decrease in the nucleonic components. This fact was not disclosed by the earlier work of Messel and Potts (1953) due to the neglect of the interactions of pions with nucleons.

The relative number of K-particles among the secondaries of penetrating showers has been the subject of some speculation (Perkins 1953). Recently Duller and Walker (1954) have set up an upper limit on the fraction of K's. Their experimental result was based on some information obtained by Bridge *et al.* (1953). Assuming the lifetime of $\mathrm{K} \sim 10^{-8}$ sec or more, they set 0·05 as the upper limit of the fraction of K's among the secondaries. Perkins (1953) presented the ratio $R = (\text{number of K}/\text{number of } \pi)$ for energy range $1{\cdot}5\,\mathrm{GeV} < E < 8\,\mathrm{GeV}$ to have the value $0{\cdot}13 \pm 0{\cdot}05$. We have presented the numerical values of R, in the third line of the tables 3 and 5, of K/π and Y/π. Our value is in reasonable agreement with his experimental results. The theoretical result of the ratio R shows that it is fairly constant at high altitudes but the fractions of K's are much smaller than the pions at the mountain altitudes. Another interesting result comes out when we consider the variations of the pion–nucleon components with depth. Although direct experimental data on the high energy region of extensive air showers which have been considered and tabulated in tables 1 and 2 are scanty, one, however, may make a comparison of the variation with altitude of the rate of very large 'bursts' associated with extensive air showers (Stinchcomb 1951, Schein and Gill 1939, Lapp 1946). Stinchcomb has suggested that the large bursts are not due to the soft component, but are mainly due to the penetrating component of extensive air showers. This has been confirmed by Bridge and Rediker (1952). From Stinchcomb's experiment, one finds 'burst' rate due to nucleons and pions as a function of height. The experimental results show that the 'burst' rate due to the pion–nucleon component differs by a factor of about 14 between mountain altitudes and sea level, and practically all the large 'bursts' are produced by this component. In our calculation we observe that the nucleon component varies by a factor of about 16 between $x = 10$ and $13{\cdot}3$ corresponding to the mountain altitude and sea level respectively, while the pion component varies over the same altitude by about 13. In the work of Messel and Potts (1953) a too rapid increase in the number of nucleons and a too slow increase in the number of pions with altitude could be attributed to their assumption that the pions do not interact with the nuclei. In the present work this fact has been taken into consideration; the results thus obtained are in very reasonable agreement with the experimental data.

From the ionization chamber measurements, Bridge and Rediker (1952) have given the intensity of the charged 'burst' producing N-rays incident from the atmosphere at sea level and at mountain altitude: their result shows that intensity of the N-component varies over the same range of heights by a factor of 16, which is in agreement with our finding. It is now known that high energy charged pions should give rise to 'bursts' so that our result is in good agreement with the experimental results.

Acknowledgments

The author is grateful to Professor H. S. Green for suggesting the problem and for his continued help and guidance throughout the investigation of the problem. Sincere thanks are also due to Drs. C. A. Hurst and R. B. Potts for many helpful discussions.

References

Biswas, S. N., 1958, *Nuovo Cim.*, **7**, 577.

Bridge, H. S., Peyron, C., Rossi, B., and Safford, R., 1953, *Phys. Rev.*, **90**, 921.

Bridge, H. S., and Rediker, R. H., 1952, *Phys. Rev.*, **88**, 206.

Duller, N. M., and Walker, W. D., 1954, *Phys. Rev.*, **93**, 215.

Heitler, W., and Jánossy, L., 1949, *Proc. Phys. Soc.* A, **62**, 374; 1950, *Helv. Phys. Acta*, **23**, 417.

Lapp, R. E., 1946, *Phys. Rev.*, **69**, 321.

Messel, H., 1951, *Proc. Phys. Soc.* A, **64**, 726; 1954, *Prog. of Cosmic Ray Physics*, Vol. II, Chap. IV (Amsterdam: North Holland).

Messel, H., and Potts, R. B., 1953, *Nuovo Cim.*, **10**, 754.

Messel, H., Potts, R. B., and McCusker, C. B. A., 1952, *Phil. Mag.*, **43**, 889.

Perkins, D. H., 1953, *Proceedings of Third Annual Rochester Conference* (New York: Interscience), pp. 43–46.

Rossi, B., and Greisen, K., 1941, *Rev. Mod. Phys.*, **13**, 240.

Schein, M., and Gill, P. S., 1939, *Rev. Mod. Phys.*, **11**, 267.

Stinchcomb, T. G., 1951, *Phys. Rev.*, **83**, 422.

Variational Methods based on the Density Matrix

By N. H. MARCH and W. H. YOUNG
Department of Physics, The University, Sheffield

MS. received 27th February 1958, *and in final form* 1st *May* 1958

Abstract. A method of setting up variational density matrices which satisfy the necessary subsidiary conditions is discussed, and some explicit variational forms are presented. Each variational matrix is defined essentially in terms of the density matrix for a known problem, for example a system of free particles in a box, using either stationary wave or progressive wave solutions. The latter form is shown, by suitable transformation along lines suggested by earlier work of Macke, to lead very directly to a method intimately connected with that proposed by von Weizsäcker, and a completely quantum-mechanical variational basis for this method is thereby provided. One- and three-dimensional cases for particles moving in a common potential are considered explicitly, and ways of achieving greater accuracy than is possible with von Weizsäcker's scheme are clear, especially in the three-dimensional case. A simple example is worked out in order to compare the results obtained from the various approximate variational forms with the exact density matrix for a linear harmonic oscillator potential, and the results are encouraging.

§ 1. Introduction

Only recently has much attention been given to the use of the density matrix in discussing many-particle problems, but it seems clear already that such a procedure has a number of advantages over the more conventional approaches based on approximations to the many-body wave function. However, much of the work done so far has been of a rather formal kind (see, for example, Löwdin 1955 a, b, c, Chirgwin 1957), although some authors (for example McWeeny 1956) have also attempted to develop the method from a more practical point of view. The present investigation represents an attempt to approximate to the density matrix in many-particle problems by setting up some restricted variational schemes based on explicit functional forms for the density matrix. The most widely useful forms from a practical point of view are closely related to the usual statistical theories, and indeed the present approach has stemmed directly from recent developments in the fundamental theory underlying the use of these methods (see especially Macke 1955 a, b, March 1957 a, b). We believe that the work we report here opens up more general possibilities but, at very least, it indicates how the statistical methods may be extended and improved and, for the first time, puts von Weizsäcker's method† on a completely proper wave-mechanical footing with all traces of semi-classical arguments removed from the foundations.

We think it may be useful, in considering possible variational methods based on the density matrix, to distinguish between two types of approach. The first and obvious class is that in which all subsidiary conditions are exactly satisfied at

† Strictly a very closely related method derived in §§ 2 and 4.

the outset. The second class is one in which no attempt is made originally to satisfy the subsidiary conditions exactly, but in which some further iterative scheme might then be contemplated in order to improve the accuracy with which the subsidiary conditions are satisfied, perhaps along lines such as those suggested by McWeeny (1956, see especially Appendix 2). This kind of procedure may well have advantages from a practical point of view, since the most awkward condition to fulfil in setting up variational density matrices of any generality is that of idempotency (see, for example, equation (3) below). With reference to the statistical theories, we show in this work that the extended method of von Weizsäcker belongs, essentially, to the first class, in contrast to the original Thomas–Fermi theory which it seems may usefully be viewed as belonging to the second class (see March 1957 b). We shall restrict our considerations in the present work to density matrices which exactly satisfy the subsidiary conditions, although we hope to return to a discussion of the possibilities of the alternative approach later.

§ 2. VARIATIONAL METHODS IN ONE-DIMENSIONAL PROBLEMS

We set ourselves originally the task of approximating by a variational approach to the density matrix for N particles obeying the exclusion principle and filling the lowest levels singly for a given potential $V(x)$. Then we may approximate to the sum of the eigenvalues by

$$\mathscr{E} = -\frac{\hbar^2}{2m}\int\left[\frac{\partial^2\rho(x', x)}{\partial x^2}\right]_{x'=x} dx + \int\rho(x, x)\, V dx \qquad \ldots\ldots (1)$$

(see, for example, March 1957 b), and dealing with the subsidiary conditions exactly we require further that

$$\int\rho(x, x)\, dx = N \qquad \ldots\ldots (2)$$

and

$$\int\rho(x', x'')\,\rho(x'', x)\, dx'' = \rho(x', x), \qquad \ldots\ldots (3)$$

equation (2) representing the normalization condition on the diagonal element (particle density), while equation (3) is an expression of the condition that the density matrix ρ shall be idempotent.

We follow the general ideas of the method proposed by Macke in setting up variational density matrices although we should emphasize that he did not make use of the density matrix at all in his work. Macke started from a known system of orthogonal wave functions, and transformed them into a new orthogonal system in what amounted essentially to a different space. Thinking in density matrix terms, we shall therefore begin with the exact density matrix $\rho_0(x', x)$ for a known problem and transform this as follows:

$$\rho(x', x) = (y_1' y_1)^{1/2} \rho_0(y', y) \qquad \ldots\ldots (4)$$

where $y(x)$ is the actual variational function, $y' \equiv y(x')$, and y_1 is written for dy/dx. It is easily shown that (4) then satisfies the requirements (2) and (3), and we emphasize at this stage that the advantage of our method is that one-particle functions are never explicitly introduced for the actual potential $V(x)$ in which we are interested. We believe this to be highly desirable because such one-particle functions are not uniquely defined, any unitary transformation of the one-particle forms leaving the density matrix invariant. We shall often use one-particle functions to construct ρ_0, but we must emphasize that this is purely a matter of practical convenience and indeed such one-particle functions need have no direct physical significance (see for example case (*b*) below). Any comparisons with exact results, such as we make in § 3 for the linear harmonic oscillator, are therefore carried out in terms of the unambiguous density matrices. Considering still the case of a general ρ_0, we find that the sum of the eigenvalues is then given by

$$\mathscr{E} = -\frac{\hbar^2}{2m}\int dx\left[\left(\frac{1}{2}y_3-\frac{1}{4}\frac{y_2^2}{y_1}\right)\rho_0+2y_1y_2\frac{\partial\rho_0}{\partial y}+y_1^3\frac{\partial^2\rho_0}{\partial y^2}\right]_{x'=x}+\int\rho(x,x)\,V(x)\,dx. \qquad \ldots\ldots(5)$$

While it is possible in principle to write down an Euler equation for $y(x)$ by minimizing (5) subject to the normalization condition (2), it turns out to be desirable to focus attention on some special forms of ρ_0, and we now consider three different possibilities. We should emphasize that, in principle, a wide variety of choice in ρ_0 exists, but for practical reasons certain forms seem to have great merits over any others. Clearly, however, choice of a model having a close physical resemblance to the given problem is sufficient to ensure that the method leads to results of high accuracy, but we do not believe this is always necessary.

(*a*) *'Particle in box' density matrix.*

Although this method has been discussed fully in one dimension by March (1957 a), it will be convenient here to write it in the density matrix form, which was not used previously. Then, in terms of the function χ_N introduced in the earlier work, and given by

$$\chi_N(x) = N+\tfrac{1}{2}-\frac{\sin\{\pi(2N+1)x\}}{2\sin\pi x} \qquad \ldots\ldots(6)$$

the density matrix ρ_0 may be written

$$\rho_0(x',x) = \chi_N\left(\frac{x'+x}{2}\right)-\chi_N\left(\frac{x'-x}{2}\right) \qquad \ldots\ldots(7)$$

as is easily shown by generalization of results previously given. We then obtain the results reported by March (1957 a) when we minimize (5) with ρ_0 given by (7), and further discussion of this case will be limited to a practical remark in § 3.

(*b*) *Free particle functions of progressive wave type.*

It occurred to us that a more practicable method of the present kind might result from the use of plane waves in calculating ρ_0, the orthogonality properties being suitably introduced as indicated below. This choice seems to have less physical significance perhaps at first sight than (*a*), but we have already warned against the dangers of attaching too much significance to the one-particle functions from which a density matrix is formed. Any choice of N orthonormal one-particle wave functions will lead to a density matrix satisfying the condition that it be idempotent, which is the only important consideration from the present point of view.

We then form the density matrices given below, the cases N odd and N even being treated separately, although the final result for the density matrix is the same. Other choices are possible, but turn out to provide less favourable schemes from the standpoint of the variational theorem. For N odd and writing therefore $N=2m+1$ with m an integer, we choose

$$\begin{aligned}\rho_0(x',x) &= \sum_{-m}^{m}\exp(-2\pi irx')\exp(2\pi irx)\\ &= 1+\sum_{1}^{m}(2^{1/2}\sin 2\pi rx'\times 2^{1/2}\sin 2\pi rx+2^{1/2}\cos 2\pi rx'\times 2^{1/2}\cos 2\pi rx)\end{aligned}$$

and for N even, and writing $N=2m$ therefore,

$$\begin{aligned}\rho_0(x',x) &= \sum_{-(m-1)}^{m} \exp\{-\pi i(2r-1)x'\}\exp\{\pi i(2r-1)x\}\\ &= \sum_{1}^{m}\{2^{1/2}\sin(2r-1)\pi x' \times 2^{1/2}\sin(2r-1)\pi x\\ &\qquad\qquad + 2^{1/2}\cos(2r-1)\pi x' \times 2^{1/2}\cos(2r-1)\pi x\}.\end{aligned}$$

We have written the density matrix in terms of plane waves and sine and cosine functions to give a clear cut illustration of the non-uniqueness of the one-particle functions in such cases. The final result for all N is the same, as we have already remarked, and may be written

$$\rho_0(x',x) = \frac{\sin N\pi(x'-x)}{\sin\pi(x'-x)}. \qquad \ldots\ldots(8)$$

Using (4), (5) and (8) the sum of the eigenvalues may then be written as

$$\mathscr{E} = \frac{\hbar^2\pi^2}{6m}N(N^2-1)\int y_1{}^3\,dx + \frac{\hbar^2}{8m}N\int\frac{(y_2)^2}{y_1}\,dx + \int\rho(x,x)\,V\,dx \qquad \ldots\ldots(9)$$

and the Euler equation is, putting $\rho(x,x)=n(x)=Ny_1$ from (4) and (8),

$$\frac{\mathrm{h}^2}{8m}\frac{(N^2-1)}{N^2}n^2 - \frac{\hbar^2}{4m}\frac{n''}{n} + \frac{\hbar^2}{8m}\frac{n'^2}{n^2} + V = E'. \qquad \ldots\ldots(10)$$

We see that the present treatment leads to a method which differs only from that of von Weizsäcker in that the coefficient of the 'Fermi energy' is multiplied by $(N^2-1)/N^2$, which tends rapidly to unity as N increases.[†] In the case $N=1$, it will be noted that (10) leads to the exact solution, whereas the ordinary von Weizsäcker method does not. We see, furthermore, that the energy derived from the original von Weizsäcker method will always be higher than that derived from our method, proving that von Weizsäcker's method always leads to an upper bound to the eigenvalue sum. Clearly, it will almost always be worth including the simple factor $(N^2-1)/N^2$ in the final evaluation of the eigenvalue sum, if not actually in the calculation of the particle density. Thus a proper foundation is provided for von Weizsäcker's scheme on the wave-mechanical variational principle, the connection demonstrated here with the plane wave density matrix being, as seems intuitively reasonable,[‡] much closer than with the sine wave case discussed previously. Whether method (*a*) or method (*b*) will be more accurate in any given problem is a question we are not able to answer convincingly, but we feel it will often be desirable on purely practical grounds to use method (*b*) rather than (*a*).

(*c*) *Linear harmonic oscillator density matrix.*

Methods (*a*) and (*b*) seem on the whole to be much the most likely to be widely useful of all the possible schemes, but as a third example which we shall use later in

---

[†] von Weizsäcker's equation results if we take, for example, the density matrix $\rho(x',x)=(y_1{}'\,y_1)^{\frac{1}{2}}\sin N\pi(y'-y)/[\pi(y'-y)]$ (cf. equation (13) below). This does not satisfy condition (3) and may not be unique.

Note added in proof. The complex Hermitian density matrix

$$\rho(x',x) = \exp\left\{\frac{-i\pi}{\sqrt{3}}(x'-x)\right\}\frac{\sin N\pi(x'-x)}{\sin\pi(x'-x)}$$

satisfies (2) and (3) exactly and leads directly to the original von Weizsäcker equation.

[‡] See, for example, the discussion given by Berg and Wilets (1955) of the von Weizsäcker method.

another connection we consider the density matrix for the linear harmonic oscillator. This has been considered by Husimi (1940), who obtained the result, in closed form, that

$$\rho_0(x',x) = -\tfrac{1}{2}\psi_N(x')\psi_N(x) + \frac{1}{2(x'-x)}\begin{vmatrix}\psi_N(x') & \psi_N(x)\\ \psi_N'(x') & \psi_N'(x)\end{vmatrix} \quad \ldots\ldots(11)$$

where $\psi_N(x)$ is the usual normalized Hermite function. In principle, use of (4), (5) and (11) would lead to a new Euler equation, but we think that only in very obvious cases where the actual problem bears some simple physical resemblance to the linear harmonic oscillator problem would numerical use of such a scheme be worth contemplating.

§ 3. COMPARISON OF VARIOUS APPROXIMATE DENSITY MATRICES FOR AN OSCILLATOR POTENTIAL

In order to illustrate the kind of results which the present methods yield, we have considered the case of the linear harmonic oscillator with the first ten levels singly occupied. This example has been used previously, and in particular the particle density given by von Weizsäcker's method has been obtained (Ballinger and March 1954). Since our method (*b*) differs only from the von Weizsäcker equation by a factor 0·99 multiplying the first term in the equation, we have contented ourselves with the von Weizsäcker density, rather than the optimum density given by our method (*b*), since for the present purpose the differences are completely unimportant.

We note first that whereas previously only the diagonal element of the density matrix has been obtained by the von Weizsäcker method, we are now in a position in principle to compare the entire density matrix given by (4) and (8) with the exact form obtained from (11). Since it is difficult to make a useful comparison directly with functions of two variables, contours of equal ρ giving no very critical means of comparison, we have chosen to expand the density matrix around the point $x' = x$, and to write

$$\rho(x',x) = n\left(\frac{x'+x}{2}\right) - c_2\left(\frac{x'+x}{2}\right)(x'-x)^2 + \ldots\ldots \quad \ldots\ldots(12)$$

We restrict our comparison to the two terms given in (12), and of these the particle density given by von Weizsäcker's method is already known to give a good average account of the exact wave-mechanical density, although not yielding the oscillations (see Figure of Ballinger and March 1954). With the available results for the particle density we have prepared our figure, the broken curve giving the result of our method (*b*) with the von Weizsäcker density inserted, while the full curve shows the exact result which follows from expansion of (11). We thought it also of interest to show in the figure the result obtained using the Thomas–Fermi density matrix in the form given by March (1957 b); that is

$$\rho(x',x) = \frac{1}{\pi(x-x')}\sin\left[\pi(x-x')n\left(\frac{x+x'}{2}\right)\right], \quad \ldots\ldots(13)$$

and following the point of view proposed there, we restrict $n(x)$ to be a well-behaved density in the wave-mechanical sense. Since therefore, the von Weizsäcker and Thomas–Fermi densities are known to be very similar except near the classical turning point, where the unmodified Thomas–Fermi density is not well behaved, the von Weizsäcker density was inserted in (13) for the present purposes, and the result is shown in the dotted curve of the figure. The agreement in each case is seen to be very gratifying. We should remark, however, that the second term in (12) is, essentially, the kinetic energy integrand, and we would expect for higher terms in (12) that the agreement will be less good. For numerous purposes, however, the first two terms seem to be much the most important.

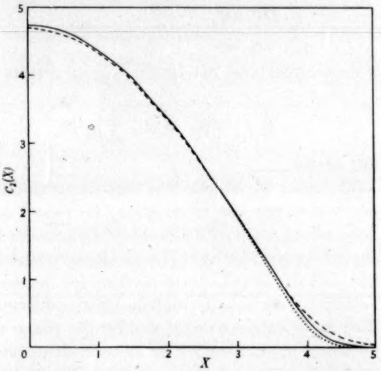

Coefficient $c_2\left(\frac{x'+x}{2}\right)$ of term in $(x'-x)^2$ for linear harmonic oscillator density matrix (cf. equation (12)). Full curve, exact wave-mechanical result, given by

$$c_2(X)=\tfrac{1}{12}\left[10(41-2X^2)\psi_{10}{}^2-\sqrt{20}X\,(40-2X^2)\,\psi_9\psi_{10}+10\,(39-2X^2)\,\psi_9{}^2\right],$$

with $X=\frac{1}{2}(x'+x)$. Broken curve, modified von Weizsäcker result, given by

$$c_2=\left[\frac{\pi^2}{6}\frac{(N^2-1)}{N^2}\,n^3+\frac{1}{8}\frac{n'^2}{n}-\frac{n''}{8}\right],$$

with $N=10$. Dotted curve, Thomas–Fermi result, given by $c_2=\frac{1}{6}\pi^2\,n^3$.

§ 4. Density Matrices in Three-Dimensional Problems

Having dealt fully with the one-dimensional case, we now turn to a discussion of the physically more important three-dimensional case. We might mention however, that should the two-dimensional results eventually be required, they can easily be obtained using the methods we shall now describe.

The appropriate generalization of equation (1) to three dimensions is readily shown to be

$$\mathscr{E}=-\frac{\hbar^2}{2m}\int[\nabla_{\mathbf{r}}{}^2\rho\,(\mathbf{r}',\mathbf{r})]_{\mathbf{r}'=\mathbf{r}}d\tau+\int\rho\,(\mathbf{r},\mathbf{r})\,V(\mathbf{r})\,d\tau, \qquad \ldots\ldots(14)$$

while the normalization and idempotency conditions are obvious generalizations of (2) and (3). Assuming for convenience one particle per level as before, we attempt to form our variational density matrices from a known matrix ρ_0 using a generalized transformation $\mathbf{R}\,(\mathbf{r})$, with components $X_1(\mathbf{r})$, $X_2(\mathbf{r})$ and $X_3(\mathbf{r})$. Thus we write as the generalization of (4)

$$\rho\,(\mathbf{r}',\mathbf{r})=[J(\mathbf{r}')J(\mathbf{r})]^{1/2}\rho_0\,(\mathbf{R}',\mathbf{R}) \qquad \ldots\ldots(15)$$

where J is the Jacobian of the transformation and $\mathbf{R}' \equiv \mathbf{R}(\mathbf{r}')$. Then the appropriate generalization of (5) is

$$\mathscr{E} = -\frac{\hbar^2}{2m}\int d\tau \left[\left(\tfrac{1}{2}\nabla^2 J - \tfrac{1}{4}\frac{(\nabla J)^2}{J}\right)\rho_0 + \nabla J \,.\, \nabla \rho_0 + J\nabla^2\rho_0\right]_{\mathbf{r}'=\mathbf{r}} + \int \rho(\mathbf{r},\mathbf{r})\, V(\mathbf{r})\, d\tau. \qquad \ldots\ldots(16)$$

In the following, we will consider only orthogonal transformations specified by the equations

$$\sum_{l=1}^{3} \frac{\partial X_i}{\partial x_l}\frac{\partial X_j}{\partial x_l} = f_i^2 \delta_{ij} \quad (f_i > 0). \qquad \ldots\ldots(17)$$

As a consequence of these equations, two further useful results which we shall need later are

$$J = \prod_{i=1}^{3} f_i; \quad (\nabla \boldsymbol{\mu} \,.\, \mathbf{R})^2 = \sum_{i=1}^{3} \mu_i^2 f_i^2, \qquad \ldots\ldots(18)$$

where $\boldsymbol{\mu}$ is a constant vector.

The case discussed earlier by Macke was that using sine wave functions, and there, in order to carry through the calculation, he found it necessary to make certain approximations which we wish to avoid in the present framework. Thus, we feel that from the standpoint of a rigorous variation method, the sine wave case is not very practicable, and the simplicity of method (*b*) in one dimension suggests that we again focus attention on density matrices derived from plane waves. We set up below therefore two matrices suggested by the plane wave case; the first being a somewhat intuitive generalization of the one-dimensional case, while the second is less transparent but more accurate in general, and amounts essentially to a direct attempt to generalize method (*b*) of § 2 to three dimensions. We shall see that in certain special cases the two density matrices thus obtained lead to the same results.

4.1. *Intuitive Generalization of Density Matrix for One-Dimensional Progressive Wave Case*

The simple expression for ρ_0 given in equation (8) suggests that we form the generalized density matrix

$$\rho_0(\mathbf{r}', \mathbf{r}) = \frac{\sin K_1\pi(x_1' - x_1)}{\sin \pi(x_1' - x_1)} \frac{\sin K_2\pi(x_2' - x_2)}{\sin \pi(x_2' - x_2)} \frac{\sin K_3\pi(x_3' - x_3)}{\sin \pi(x_3' - x_3)} \qquad \ldots\ldots(19)$$

where K_1, K_2 and K_3 are integers, and it is then easily shown that (17) satisfies the normalization and idempotency conditions when the product $K_1K_2K_3$ is chosen equal to N. Using (15)–(19) we obtain

$$\begin{aligned}
&[\rho_0]_{\mathbf{r}'=\mathbf{r}} = N,\\
&[\nabla\rho_0]_{\mathbf{r}'=\mathbf{r}} = 0,\\
&[\nabla^2\rho_0]_{\mathbf{r}'=\mathbf{r}} = -\tfrac{1}{3}N\pi^2[(K_1^2-1)f_1^2 + (K_2^2-1)f_2^2 + (K_3^2-1)f_3^2]
\end{aligned} \qquad \ldots(20)$$

and thus, in the case $f_1 = f_2 = f_3 = f$ we have

$$n = Nf^3, \; [\nabla^2\rho_0]_{\mathbf{r}'=\mathbf{r}} = -\tfrac{1}{3}N\pi^2 f^2 (K_1^2 + K_2^2 + K_3^2 - 3). \qquad \ldots\ldots(21)$$

The kinetic energy T then becomes

$$\begin{aligned}
T &= -\frac{\hbar^2}{2m}\int d\tau \left[\tfrac{1}{2}\nabla^2 n - \tfrac{1}{4}\frac{(\nabla n)^2}{n} - \tfrac{1}{3}n\pi^2 (K_1^2 + K_2^2 + K_3^2 - 3)\left(\frac{n}{N}\right)^{2/3}\right]\\
&= \frac{\hbar^2}{2m}\left[\frac{K_1^2 + K_2^2 + K_3^2}{3} - 1\right]\frac{\pi^2}{N^{2/3}}\int n^{5/3} d\tau + \frac{\hbar^2}{8m}\int \frac{(\nabla n)^2}{n}\, d\tau.
\end{aligned} \qquad \ldots\ldots(22)$$

In the case when N is the cube of an integer, we may take $K_1 = K_2 = K_3 = N^{1/3}$ and then we have

$$T = \frac{\hbar^2\pi^2}{2m}\frac{(N^{2/3}-1)}{N^{2/3}}\int n^{5/3}d\tau + \frac{\hbar^2}{8m}\int\frac{(\nabla n)^2}{n}d\tau. \qquad \ldots\ldots(23)$$

We see that as $N \rightarrow \infty$ we obtain for the first term in the kinetic energy

$$\frac{\hbar^2\pi^2}{2m}\int n^{5/3}d\tau \qquad \ldots\ldots(24)$$

whereas the usual statistical kinetic energy term is this quantity multiplied by $\frac{3}{5}(6/\pi)^{2/3} \simeq 0{\cdot}924$. Thus, for large N which are perfect cubes, this method does not quite tend to the correct limit. For small N however, it is possible to obtain a lower energy than with the customary von Weizsäcker method.

4.2. *Extension of Method (b) of § 2 to Three Dimensions*

The considerations of § 2 suggested to us that we should take the set of plane waves

$$\phi_{\mathbf{k}_i} = \exp\{2\pi i(\mathbf{k}_i - \mathbf{G}).\mathbf{r}\}, \qquad \ldots\ldots(25)$$

where the $\mathbf{k}_i$ are distinct vectors whose coordinates are integers, and $\mathbf{G}$ is a constant vector (coordinates not necessarily integers), as an appropriate starting point. Then we may write the particle density $\rho(\mathbf{r}, \mathbf{r})$ as

$$\rho(\mathbf{r}, \mathbf{r}) \equiv n(\mathbf{r}) = NJ(\mathbf{r}) \qquad \ldots\ldots(26)$$

and furthermore the kinetic energy, after some manipulation, may be expressed in the form

$$T = \frac{2\pi^2\hbar^2}{m}\int d\tau \sum J[\nabla(\mathbf{k}_i - \mathbf{G}).\mathbf{R}]^2 + \frac{\hbar^2}{8m}N\int\frac{(\nabla J)^2}{J}d\tau. \qquad \ldots\ldots(27)$$

Considering only orthogonal transformations, equations (17) and (18) may be applied, and hence we find

$$T = \frac{2\pi^2\hbar^2}{m}\int d\tau \prod f_i \sum_{\mathbf{k}_i}\sum_{\alpha}(\mathbf{k}_i - \mathbf{G})_\alpha^{\,2} f_\alpha^{\,2} + \frac{\hbar^2}{8m}N\int\frac{(\nabla\prod f_i)^2}{\prod f_i}d\tau. \ldots\ldots(28)$$

Conformal case.

We shall refer to the special case $f_1 = f_2 = f_3$ as the conformal case (see for example Phillips 1939), and then we see that equation (28) may be written

$$T = \frac{2\pi^2\hbar^2}{m}\frac{\sum(\mathbf{k}_i - \mathbf{G})^2}{N^{5/3}}\int n^{5/3}d\tau + \frac{\hbar^2}{8m}\int\frac{(\nabla n)^2}{n}d\tau. \qquad \ldots\ldots(29)$$

To obtain the best method of the present type, we wish therefore to minimize $\Sigma(\mathbf{k}_i - \mathbf{G})^2/N^{5/3}$ by suitable choice of $\mathbf{G}$. Writing

$$\sum(\mathbf{k}_i - \mathbf{G})^2 = \sum\mathbf{k}_i^{\,2} - \frac{1}{N}(\sum\mathbf{k}_i)^2 + N\left(\mathbf{G} - \frac{\sum\mathbf{k}_i}{N}\right)^2, \qquad \ldots\ldots(30)$$

we see that the minimum occurs when

$$\mathbf{G} = \frac{1}{N}\sum\mathbf{k}_i, \qquad \ldots\ldots(31)$$

and we might mention here that it is from considerations such as this in one dimension that it was possible to remark in § 2, method (*b*), that we had made the most favourable choice from the standpoint of the variational theorem. In the present three-dimensional case, the minimum value of $\Sigma(\mathbf{k}_i-\mathbf{G})^2/N^{5/3}$ is given by

$$c_N=\frac{\sum \mathbf{k}_i^2-(\sum \mathbf{k}_i)^2/N}{N^{5/3}}. \qquad \ldots\ldots(32)$$

The method of obtaining the sets of $\mathbf{k}_i$'s which lead to the lowest c_N's seems difficult to systematize completely, and in general we feel it best to proceed by inspection. The unmodified von Weizsäcker method would yield a value of c_N given by $(3/20)(6/\pi)^{2/3}\simeq 0{\cdot}2309$ and it will be seen from results collected in the table that some considerable improvement may, on occasions, be achieved over this value. Again, it will always be worth using the modified coefficient in the final calculation of $\mathscr{E}$, even if it proves practically desirable to use existing densities derived from the unmodified von Weizsäcker method.

Minimum Values of c_N from equation (32)

N	$\mathbf{k}_N$ †	$\frac{1}{N}\sum_1^N \mathbf{k}_n$	$\frac{1}{N}\left(\sum_1^N \mathbf{k}_n\right)^2$	$\sum_1^N \mathbf{k}_n^2$	c_N
1	(0, 0, 0)	(0, 0, 0)	0	0	0
2	(1, 0, 0)	$(\frac{1}{2}, 0, 0)$	1/2	1	0·1575
3	(0, 1, 0)	$(\frac{1}{3}, \frac{1}{3}, 0)$	2/3	2	0·2137
4	(1, 1, 0)	$(\frac{1}{2}, \frac{1}{2}, 0)$	2	4	0·1984
5	(0, 0, 1)	$(\frac{2}{5}, \frac{2}{5}, \frac{1}{5})$	9/5	5	0·2189
6	(1, 0, 1)	$(\frac{1}{2}, \frac{1}{3}, \frac{1}{3})$	17/6	7	0·2103
7	(0, 1, 1)	$(\frac{3}{7}, \frac{3}{7}, \frac{3}{7})$	27/7	9	0·2008
8	(1, 1, 1)	$(\frac{1}{2}, \frac{1}{2}, \frac{1}{2})$	6	12	0·1875
9	(−1, 0, 0)	$(\frac{1}{3}, \frac{4}{9}, \frac{4}{9})$	41/9	13	0·2169
10	(−1, 1, 0)	$(\frac{1}{5}, \frac{1}{2}, \frac{2}{5})$	9/2	15	0·2262
⋮					
27		(0, 0, 0)	0	54	0·2222
⋮					
88					0·2309
89					0·2314

† $\mathbf{k}_N$ is to be added to the $(N-1)$th set of vectors to give the Nth set $(1\leqslant N\leqslant 10)$.

With regard to the present theory, we should remark that the three-dimensional unmodified von Weizsäcker equation has not been proved to give an upper bound to the energy in every case, unlike the one-dimensional form. For in order to prove this, it would be necessary to show that c_N of equation (32) is always less than the usual coefficient of the von Weizsäcker method, and while from the table this is seen to almost always be true, for $N=89$ we have been unable to make a choice leading to a value of c_N as low as the usual von Weizsäcker result. However, it is possible to show quite rigorously that c_N tends to the usual result as N tends to infinity. We might remark at this point that the somewhat irregular variation of c_N shown in the table seems to be a rather artificial consequence of the present variational method. For central-field problems, for example, we feel it should be possible in principle to find an improved method based on a density matrix expressed directly in spherical polar coordinates, but so far we have not seen how to construct a useful variation function. Also, it might be mentioned here that the simple density matrices of § 4.1 yield the same results as the present method for certain cases, for example, $N=1, 2, 4, 8$ and 27. In general, however, the method just described is of course to be used in preference to the treatment given in § 4.1.

General orthogonal case.

In the general case we may write

$$\mathcal{E}=\frac{2\pi^2\hbar^2}{m}\sum_{\mathbf{k}_i}\sum_{\alpha}(\mathbf{k}_i-\mathbf{G})_\alpha{}^2\int d\tau f_\alpha{}^2\prod f_i+\frac{\hbar^2}{8m}N\int\frac{(\nabla\prod f_i)^2}{\prod f_i}d\tau$$
$$+N\int\prod f_i V\,d\tau, \qquad \ldots\ldots(33)$$

and the choice of the $\mathbf{k}_i$'s is not as clear as in the conformal case. However, making the same choice as in that case will ensure that at least as good an energy is obtained. After therefore making some choice of these vectors, let us suppose that we have

$$2\pi^2\sum_{\mathbf{k}_i}(\mathbf{k}_i-\mathbf{G})_\alpha{}^2=\lambda_\alpha \qquad \ldots\ldots(34)$$

Then

$$\begin{aligned}\delta\mathcal{E}=&\frac{\hbar^2}{m}\lambda_1\int(3f_1{}^2f_2f_3\delta f_1+f_1{}^3f_3\delta f_2+f_1{}^3f_2\delta f_3)d\tau\\&+\frac{\hbar^2}{m}\lambda_2\int(f_2{}^3f_3\delta f_1+3f_2{}^2f_3f_1\delta f_2+f_2{}^3f_1\delta f_3)d\tau\\&+\frac{\hbar^2}{m}\lambda_3\int(f_3{}^3f_2\delta f_1+f_3{}^3f_1\delta f_2+3f_3{}^2f_1f_2\delta f_3)d\tau\\&+\frac{\hbar^2}{8m}N\int\left\{\frac{(\nabla f_1f_2f_3)^2}{(f_1f_2f_3)^2}-\frac{2\nabla^2f_1f_2f_3}{f_1f_2f_3}\right\}\delta(f_1f_2f_3)d\tau+N\int V\delta(f_1f_2f_3)d\tau,\end{aligned}$$
$$\ldots\ldots(35)$$

and hence the Euler equations are

$$\left.\begin{aligned}&\frac{\hbar^2}{m}\left(3\lambda_1f_1{}^2+\lambda_2f_2{}^2+\lambda_3f_3{}^2+\frac{N}{8}\phi\right)+NV=\mathcal{E}'\\&\frac{\hbar^2}{m}\left(\lambda_1f_1{}^2+3\lambda_2f_2{}^2+\lambda_3f_3{}^2+\frac{N}{8}\phi\right)+NV=\mathcal{E}'\\&\frac{\hbar^2}{m}\left(\lambda_1f_1{}^2+\lambda_2f_2{}^2+3\lambda_3f_3{}^2+\frac{N}{8}\phi\right)+NV=\mathcal{E}'\end{aligned}\right\} \qquad \ldots\ldots(36)$$

where

$$\phi=\frac{(\nabla f_1f_2f_3)^2}{(f_1f_2f_3)^2}-\frac{2\nabla^2f_1f_2f_3}{f_1f_2f_3},$$

and $\mathcal{E}'$ is a constant to be determined by normalization requirements as usual.

We feel that in certain cases where the potential field is highly anisotropic, as in some molecules for example, such a method would perhaps lead to significantly better results than the conformal case. However, from a practical point of view it will be seen that the difficulties of solving the coupled equations (36) for f_1, f_2 and f_3 are very great, and it is likely to be some time, even with modern electronic computing techniques, before such a project could successfully be undertaken.

§ 5. Conclusions

We see then that some definite progress can be made in such a variational approach to the solution of eigenvalue problems by means of the density matrix, and that a proper basis is thereby provided for von Weizsäcker's method on the wave-mechanical variational principle. Our work completes the von Weizsäcker scheme, or strictly a very closely related one, by supplying the complete density matrix from which it can be derived, although in general we should point out that to obtain the explicit form will require the additional integration of equations (17). For many purposes, however, this will not be necessary. We think that this work points the way to further progress in density matrix methods, and we are now continuing to examine how the present results might be profitably used as the starting point of an iterative scheme to approximate more closely to the true density matrix.

Acknowledgments

One of us (W. H. Y.) wishes to acknowledge the award of a Town Trustees Fellowship by the University of Sheffield.

References

Ballinger, R. A., and March, N. H., 1954, *Proc. Phys. Soc.* A, **67,** 378.

Berg, R., and Wilets, L., 1955, *Proc. Phys. Soc.* A, **68,** 229.

Chirgwin, B. H., 1957, *Phys. Rev.*, **107,** 1013.

Husimi, K., 1940, *Proc. Phys.-Math. Soc. Japan*, **22,** 264.

Löwdin, P. O., 1955 a, *Phys. Rev.*, **97,** 1474; 1955 b, *Ibid.*, **97,** 1490; 1955 c, *Ibid.*, **97,** 1509.

Macke, W., 1955 a, *Phys. Rev.*, **100,** 992; 1955 b, *Ann. Phys., Lpz.*, **17,** 1.

McWeeny, R., 1956, *Proc. Roy. Soc.* A, **235,** 496.

March, N. H., 1957 a, *Proc. Phys. Soc.* A, **70,** 169; 1957 b, *Ibid.*, **70,** 839.

Phillips, E. G., 1939, *A Course of Analysis* (Cambridge: University Press), p. 299.

The Electrical Conductivity and Hall Effect of Silicon

By E. H. PUTLEY and W. H. MITCHELL
Royal Radar Establishment, Malvern, Worcs.

MS. received 27*th February* 1958, *and in final form* 18*th April* 1958

Abstract. The electrical conductivity and Hall effect have been measured over the temperature range 20°K to 500°K on single crystals of silicon with extrinsic carrier concentrations between 2 and 5×10^{12} cm^{-3}. The Hall mobility for electrons and holes can be represented between 100° and 300°K by the expression $1{\cdot}2 \times 10^8 T^{-2}$ and $2{\cdot}9 \times 10^9 T^{-2{\cdot}7}$ respectively. Both these results indicate a higher Hall mobility than has been previously reported, and the result for holes is greater than values reported for the drift mobility. From the results between 350° and 500°K the expression $n_i = 3{\cdot}10 \times 10^{16} T^{3/2} \exp -0{\cdot}603/\boldsymbol{k}T$ was obtained for the intrinsic concentration. Attempts were made to estimate the total impurity concentration in these specimens. The variation of extrinsic carrier concentration with temperature and the effect of impurity scattering at 20°K both indicate that the total concentration of impurities is less than 10^{14} cm^{-3}.

§ 1. INTRODUCTION

RECENT improvements in the techniques for preparing silicon (Wilson 1957) have made it possible to extend measurements on the intrinsic conductivity to a lower temperature than has been previously reported (Morin and Maita 1954). In addition, measurements have been made down to 20°K in order to estimate the purity of the material and to study the behaviour of the Hall mobility. Mobilities of both electrons and holes are found to be greater than previously observed. In particular, on comparing the Hall mobility of holes with recent measurements of drift mobility (Ludwig and Watters 1956, Cronemeyer 1957), it is found that the ratio of Hall to drift mobility is not less than unity and is practically independent of temperature. The impurity in the p-type specimens used is believed to be boron, and in the n-type specimen phosphorus.

§ 2. EXPERIMENTAL DETAILS

Samples of the shape shown in figure 1 and about 1 mm thick were cut from plates of silicon using an ultrasonic drill. The material had been prepared in single crystal form as described elsewhere (Wilson 1957). Contacts were made to them by fusing spots of aluminium to the p-type specimens and antimony–gold alloy to the n-type specimen. The samples were mounted in a cryostat for measurements below room temperature and in an oil bath for measurements up to 500°K. Measurements were made using either an Applied Physics Corporation vibrating reed electrometer, or, where the resistance was sufficiently low, a potentiometer and galvanometer. The electric fields used were not allowed to exceed 1 v cm^{-1} because it was found that some departure from Ohm's law could be observed for fields between 1 and 10 v cm^{-1} both at 20°K and room temperature. A magnetic induction of 2300 gauss was used except where stated.

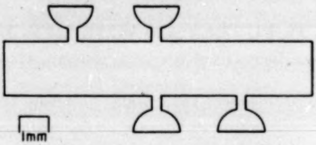

Figure 1. Plan of specimen.

It was found that with both the p-type specimens the nature of the surface was important. If an etched surface were used, then surface conductance appeared to be present above 300°K, causing a rapid rise in the conductance of the specimen before the intrinsic range was entered and causing the Hall coefficient to change sign at a lower temperature than would be expected. These effects disappeared if the surface of the specimen were lightly sandblasted. Between 20°K and 300°K the results were independent of the nature of the surface. In figure 2 the results obtained with an etched and a sandblasted surface are compared. These effects were not found in n-type specimens.

The accuracy of the results is estimated to be to between 5 and 10%. For the conductivity measurements this is determined by the accuracy with which the dimensions of the samples could be determined. For Hall effect measurements the largest source of error was measuring the Hall voltage.

§ 3. RESULTS BELOW ROOM TEMPERATURE

Figure 3 shows a plot of log σ and log R against $1/T$ down to 20°K for two p- and one n-type specimen. Between 50° and 20°K the plots are approximately straight lines. If it is assumed that both donor and acceptor levels are present in all specimens, then the variation of the electron concentration n in an n-type specimen is given by:

$$\frac{n(N_A+n)}{(N_D-N_A-n)}=\frac{(2\pi m^* \boldsymbol{k}T)^{3/2}}{h^3}\exp\left(-\frac{E_D}{\boldsymbol{k}T}\right). \qquad \ldots\ldots(1)$$

In deriving this expression it is assumed that each impurity level can accommodate one electron of either spin (Wilson 1953).

At low enough temperatures, $n \ll N_A$ and N_D-N_A, so that the expression becomes

$$n=\frac{N_D-N_A}{N_A}\frac{(2\pi m \boldsymbol{k}T)^{3/2}}{h^3}\left(\frac{m^*}{m}\right)^{3/2}\exp\left(-\frac{E_D}{\boldsymbol{k}T}\right) \qquad \ldots\ldots(2)$$

and a similar expression can be written down for p the hole concentration in a p-type specimen.

To fit (2) to the experimental results, n was obtained from the Hall coefficient:

$$R=-\frac{3\pi}{8}\left(\frac{1}{ne}\right). \qquad \ldots\ldots(3)$$

The value for N_D-N_A was found from the Hall coefficient in the exhaustion region. Then from the slope of the plot of log $(nT^{-3/2})$ against $1/T$ the value of E_D was found while the intercept of this plot gave the quantity $(m^*/m)^{3/2}/N_A$. In some cases it is possible to determine N_A and m^*/m independently by fitting the results to equation (1), but in this case the behaviour was so insensitive to the value of m^*/m that the calculation was not practicable. A similar difficulty was found when the method of analysis described by Lee (1957) was applied. Thus, in order to obtain a value for N_A (or, for the p-type specimen, N_D) an assumption has to be made of the value m^*/m. According to the results given by Lax and Mavroides (1955) and assuming the six ellipsoid model for the conduction band, probable values for the density-of-states effective masses are:

$$\frac{m^*}{m} = 1{\cdot}0 \text{ (electrons)}; \quad \frac{m^*}{m} = 0{\cdot}6 \text{ (holes)}.$$

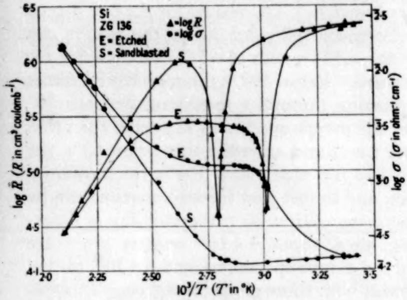

Figure 2. Influence of surface on behaviour above room temperature.

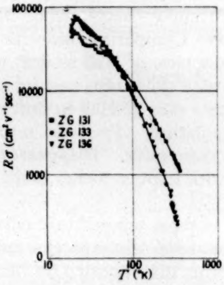

Figure 4. Hall mobility.

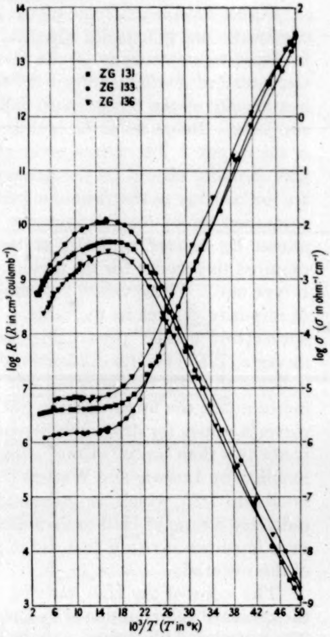

Figure 3. Behaviour of R and σ: 20°K upwards.

Using these values, N_A and N_D were calculated. The results obtained and the values found for E_D or E_A are given in the table. This table also gives N_I the concentration of impurity scattering centres required to account for the mobility at 20°K (see next section).

(1)	(2)	(3)	(4)	(5)	(6)	(7)
ZG 131	n	0·045	$2{\cdot}12 \times 10^{12}$	$1{\cdot}8 \times 10^{13}$	2×10^{13}	6×10^{13}
ZG 136	p	0·043	$1{\cdot}31 \times 10^{12}$	$3{\cdot}5 \times 10^{13}$	$3{\cdot}3 \times 10^{13}$	4×10^{13}
ZG 133	p	0·043	$5{\cdot}84 \times 10^{12}$	$5{\cdot}3 \times 10^{13}$	$4{\cdot}7 \times 10^{13}$	

(1) specimen; (2) sign of excess carriers; (3) E_D or E_A (ev); (4) N_A–N_D or N_D–N_A (cm⁻³); (5) N_A (cm⁻³); (6) N_D (cm⁻³); (7) N_I (cm⁻³).

The values found for E_A and E_D are in satisfactory agreement with those found by other workers for boron and phosphorus levels respectively. There was some difficulty in assigning a value for $N_A - N_D$ for ZG 136 because just below room temperature R started to fall as the temperature rose, suggesting the presence of a deeper acceptor level. The value used was found by estimating from the results at 150°K for the value which would have been found at room temperature in the absence of the deeper level.

§ 4. HALL MOBILITY

Figure 4 is a logarithmic plot of $R\sigma$ against T. The results for the two p-type specimens are practically identical. Between 100° and 300°K the results can be fitted to expressions of the form $R\sigma = AT^{-\alpha}$ with $A = 1{\cdot}2 \times 10^8$, $\alpha = 2{\cdot}0$ for electrons and $A = 2{\cdot}9 \times 10^9$, $\alpha = 2{\cdot}7$ for holes. Below 100°K the mobility increases less rapidly as the temperature falls, passing through a maximum between 20° and 30°K. Below 60°K the mobility of the p-type specimens is greater than that of the n-type. The values given above for A and α predict that below 63°K the hole mobility should be the greater. The fact that below 100°K the mobilities are not as large as the formulae predict, and in fact pass through maxima can be accounted for by ionized impurity scattering. If at 20°K the mobility is determined by ionized impurity scattering, then about 4×10^{13} centres cm^{-3} are required to account for the mobility of the p-type specimens, and 6×10^{13} for the n-type one. These values are comparable with those given for the concentration of impurity centres in the table. The Hall mobility obtained here for holes is appreciably greater than values reported previously. Thus at 298°K Cronemeyer's (1957) results obtained on material of less than 1000 ohm cm resistivity indicate that $R\sigma$ is flattening out at about 410 cm^2 v^{-1} sec^{-1}, while our data indicate that the upper limit is not less than 500. Comparing this with Cronemeyer's values for drift mobility suggests that the ratio of Hall to drift mobility is not less than unity. Comparing our results with those obtained for the drift mobility by Ludwig and Watters (1956) indicates a ratio of Hall to drift mobility of about 1·26 which is independent of temperature. Previous results had indicated a ratio of Hall to drift mobility of less than unity. It appears that this ratio in silicon is rising as it did in germanium with improvements in the quality of the material.

The value of the Hall mobility of electrons at room temperature falls within the spread of values obtained by Cronemeyer for material of comparable resistivity. The variation with temperature ($\alpha T^{-2{\cdot}0}$) differs from that reported by Morin and Maita (1954) ($\alpha T^{-2{\cdot}5}$). It is seen (figure 3) that at temperatures where the variation of electron concentration is a constant, the conductivity shows a similar variation with temperature to that of the Hall mobility. Since the conductivity variation is determined by that of the drift mobility, the ratio of Hall to drift mobility must be independent of temperature. Hence the difference between the rate of variation of Hall mobility found here and the previously reported values for it and for the rate of variation of drift mobility with temperature (Ludwig and Watters 1956), cannot be accounted for by supposing that in our case the ratio of Hall to drift mobility is varying with temperature. It is possible that the rate of variation of the electron mobility given by Morin and Maita may be too high because their value was obtained after making a correction for impurity scattering. Between 200 and 300°K the uncorrected Hall mobility of their purest specimen varies as more like $T^{-2\cdot0}$ and their values are only about 15% smaller than those found in this material. For an estimated concentration of scattering centres of about 6×10^{13} impurity scattering in the material used here will be negligible above 200°K. An overestimate by Morin and Maita of the effect of impurity scattering in their material may account for this discrepancy between the rates of variation of the electron mobility.

§ 5. RESULTS IN THE INTRINSIC RANGE

Figures 5 and 6 show the behaviour of the conductivity and Hall coefficient from room temperature up to above 500°K. It is seen that the intrinsic properties become dominant above about 370°K. The p-type specimens were examined

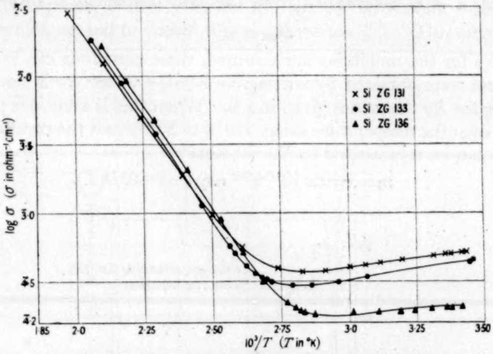

Figure 5. Conductivity above room temperature.

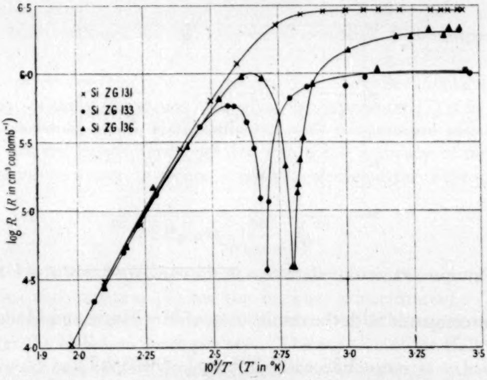

Figure 6. Hall coefficient above room temperature.

carefully near the temperatures at which the Hall coefficients change sign to see if the presence of light holes could be detected, as has been found in germanium (Willardson *et al.* 1954), but the Hall coefficient appeared independent of induction over the range 1000 to 10 000 gauss. The measurements of the conductivity of the n-type specimen were considered the most reliable of these results (accuracy to ± 5%). The conductivity can be written

$$\sigma = ne\mu_n + pe\mu_p \qquad \ldots\ldots (4)$$

where n and p are the concentration of electrons and holes and will be related to each other by

$$np = n_i^2, \quad n - p = m \qquad \ldots\ldots (5)$$

where n_i is the intrinsic carrier concentration and m the electron concentration, when all the impurity levels are ionized. μ_n and μ_p are the conductivity mobilities.

Hence, if m is determined from the Hall coefficient at room temperature,

$$R_{ex} = -3\pi/8em \qquad \ldots\ldots (6)$$

and values for the mobilities are assumed, these equations can be solved for n_i. The values were obtained by writing $\mu = 8R\sigma/3\pi$ where $R\sigma$ is the Hall mobility and using for $R\sigma$ the values given in § 4. When this is done it is possible to calculate n_i over the temperature range 370°K to 500°K and the results obtained (see figure 7) can be represented by the formula

$$n_i = 3{\cdot}10 \times 10^{16}\, T^{3/2} \exp(-0{\cdot}603/\boldsymbol{k}T). \qquad \ldots\ldots (7)$$

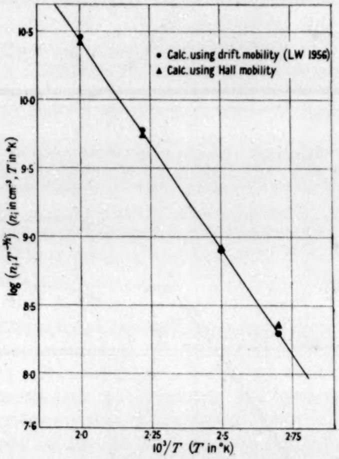

Figure 7. Intrinsic carrier concentration in silicon (LW = Ludwig and Watters 1956).

This can be compared with the results obtained by Morin and Maita, valid above 450°K

$$n_i = 3{\cdot}88 \times 10^{16}\, T^{3/2} \exp(-0{\cdot}605/\boldsymbol{k}T). \qquad \ldots\ldots (8)$$

It is seen that the rates of variation with temperature are almost identical. The values obtained here are about 25% smaller than those of Morin and Maita. This difference is somewhat larger than the probable error of the calculation. Our values for the intrinsic conductivity are in very close agreement with Morin and Maita's values, and therefore the lower values we obtain for n_i are accounted for by the higher values we have used for the mobility.

Our results depend on the somewhat arbitrary assumption that the ratio of Hall to conductivity mobility is a constant, $3\pi/8$. As has already been pointed out, comparison of the Hall mobility with the conductivity in the exhaustion range leads to the conclusion that the ratio of the two mobilities is independent of the temperature. Comparison of our values for the Hall mobility of holes with recent measurements of drift mobility (Ludwig and Watters 1956) suggest that $3\pi/8$ is not an unreasonable value to take for the ratio, but a similar comparison for electrons leads to no definite conclusion. An alternative calculation of n_i was made using Ludwig and Watter's results in place of our mobility data. This led to results which agreed to within 5% of expression (7). This suggests that our assumptions do not lead to errors greater than the experimental error in the available data. Taking the values of n_i given by expression (7) it is possible to calculate the variation of the Hall coefficient with temperature and to obtain a curve which fits the experimental results within the accuracy of measurement (10%). The curve drawn in figure 8 is that calculated for ZG136 using the expression

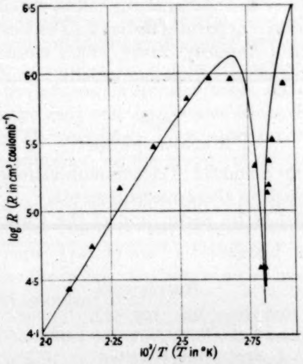

Figure 8. Hall coefficient for ZG 136—curve calculated, points experimental.

$$R = -\frac{3\pi}{8\mathbf{e}}\frac{nc^2 - p}{(nc+p)^2}$$

with $p - n = 1{\cdot}4 \times 10^{12}$ and $np = n_i^2$; c and n_i are taken from the expression for the Hall mobilities and equation (7) for the intrinsic concentration. The points plotted are the measured ones. It is seen that above 400°K the agreement is good, but the fit near the Hall zero is not perfect. The position of the Hall zero agrees with what would be expected from the hole concentration at exhaustion (see table) and the mobility ratio calculated from the expressions for the electron and hole mobilities. The measured Hall maximum is smaller than the calculated one and below the Hall zero temperature the Hall coefficient starts to fall at a much lower temperature than would be expected, but at a slower rate.

These discrepancies may be accounted for by the presence of deeper acceptor levels (as already suggested) or of light holes.

§ 6. CONCLUSION

Silicon can now be prepared in which the total concentration of impurities is less than 10^{14} cm^{-3}. In this material the Hall mobility of both holes and electrons is greater than the values found in less pure material. It now appears that the ratio of Hall to drift mobilities for holes is greater than unity.

The intrinsic carrier concentration has been calculated down to 370°K. The results are in good agreement with those found by Morin and Maita above 450°K.

One surprising feature of these results is that the calculations in § 3 indicate a high degree of compensation. If this is so it is difficult to explain the high values obtained for the mobilities and the uniform values obtained for the conductivity from samples cut from different parts of the crystals unless there is some interaction between the two types of impurity centre which eliminates the point-to-point fluctuation in the degree of compensation usually found in highly compensated material.

ACKNOWLEDGMENTS

We are indebted to Standard Telecommunications Laboratories Ltd. for supplying the silicon used for these measurements.

This paper is published by permission of the Controller, H.M. Stationery Office.

REFERENCES

CRONEMEYER, D. C., 1957, *Phys. Rev.*, **105,** 522.
LAX, B., and MAVROIDES, J. G., 1955, *Phys. Rev.*, **100,** 1650.
LEE, P. A., 1957, *Brit. J. Appl. Phys.*, **8,** 340.
LUDWIG, G. W., and WATTERS, R. L., 1956, *Phys. Rev.*, **101,** 1699.
MORIN, F. J., and MAITA, J. F., 1954, *Phys. Rev.*, **96,** 28.
WILLARDSON, R. K., HARMAN, T. C., and BEER, A. C., 1954, *Phys. Rev.*, **96,** 1512.
WILSON, A. H., 1953, *Theory of Metals*, p. 115 (Cambridge: University Press).
WILSON, J. M., 1957, *Research*, **10,** 166.

Note added in proof. Recent studies of the nature of impurity levels in silicon (see Kohn, 1957, *Solid State Physics*, **5,** 257, Academic Press Inc., New York) indicate that equation (1) should be modified to take into account the four-fold degeneracy of the acceptor ground state and the proximity of excited states close to the ground state of the donor impurities. These modifications reduce the number of impurity centres given in the table to about half for the p-type specimens and to about 65% for the n-type specimen.

A Second Order Calculation of the Energy of Interaction between Two Normal Helium Atoms

By N. LYNN

Department of Applied Mathematics, The Queen's University of Belfast

Communicated by D. R. Bates; MS. received 27th March 1958

Abstract. The energy of interaction between two normal helium atoms is calculated to the second order using a perturbation method which employs properly symmetrized unperturbed wave functions. The results obtained are in good agreement with experimentally derived interaction energies for both large and small internuclear separations.

---

§ 1. Introduction

Dalgarno and Lynn (1956, to be referred to as I) have discussed a simple perturbation procedure for calculating the energies of states of homonuclear molecules at large internuclear separations R and have suggested a semi-empirical modification designed to overcome the inherent inaccuracy of the perturbation method for smaller separations. The method, which carries calculations to the second order and takes account of exchange, was applied with success to the $1s\sigma_g$ and $2p\sigma_u$ states of the H_2^+ ion and also to the $^1\Sigma_g$ and $^3\Sigma_u$ states of the H_2 molecule. This paper is concerned with its further application to the determination of the energy of the ground state of the He_2 molecule.

The only previous second order calculation in the literature of the interaction between two normal helium atoms is that of Margenau (1939) who employed a variational method (cf. paper I) and took for his second order exchange term that which he had obtained for the interaction between two hydrogen atoms but with a different scale for the internuclear distance.

§ 2. Theory and Method

Consider a system which, in its unperturbed state, consists of two normal helium atoms with nuclei A and B separated by an infinite distance and let the numerals 1, 2, 3 and 4 specify the four electrons. If spin–orbit interactions are ignored the wave function $\psi_A(1,2)$ of the normal atom with nucleus A and electrons 1 and 2 may be written

$$\psi_A(1,2)=a(1,2)\{\alpha(1)\beta(2)-\alpha(2)\beta(1)\}/\sqrt{2} \qquad \ldots\ldots(1)$$

where $a(1,2)$ is the symmetrical space wave function for the normal helium atom and α and β are spin functions. It may be shown that for the unperturbed system of two normal helium atoms there is only one combination of products of the atomic wave functions which is antisymmetrical in all four electrons. It may be written

$$\Psi_0(1,2,3,4)=\frac{1}{N}\{\mathscr{I}+P_{13}P_{24}-P_{23}-P_{14}-P_{24}-P_{13}\}\psi_A(1,2)\psi_B(3,4) \qquad \ldots\ldots(2)$$

where P_{mn} is a permutation operator which interchanges both space and spin coordinates of electrons m and n, $\mathscr{I}$ is the identity operator and N is the normalization factor (cf. Buckingham and Dalgarno 1952).

The Hamiltonian of the unperturbed system is simply the sum of the Hamiltonians $\mathscr{H}_A(1,2)$ and $\mathscr{H}_B(3,4)$ of the separate atomic systems. In what follows length is measured in units of a_0 ($a_0 = 5{\cdot}29 \times 10^{-9}$ cm) and energy in rydbergs. The Hamiltonian $\mathscr{H}_A(1,2)$ is given by

$$\mathscr{H}_A(1,2) = -\nabla_1^2 - \nabla_2^2 + \frac{2}{r_{12}} - 4\left(\frac{1}{r_{a1}} + \frac{1}{r_{a2}}\right) \qquad \ldots\ldots(3)$$

where r_{a1} and r_{a2} are the distances from the nucleus A to the electrons 1 and 2 respectively and r_{12} is the distance between the two electrons. $\mathscr{H}_B(3,4)$ is given by a similar expression. When the system is perturbed so that the two nuclei are separated by a finite distance R the total Hamiltonian may conveniently be written

$$\mathscr{H} = \mathscr{H}_A(1,2) + \mathscr{H}_B(3,4) + V_{AB}(12,34) \qquad \ldots\ldots(4)$$

where $V_{AB}(12,34)$, which may be regarded as an interaction potential, is given by

$$V_{AB}(12,34) = 2\left(\frac{1}{r_{13}} + \frac{1}{r_{14}} + \frac{1}{r_{23}} + \frac{1}{r_{24}}\right) - 4\left(\frac{1}{r_{a3}} + \frac{1}{r_{a4}} + \frac{1}{r_{b1}} + \frac{1}{r_{b2}}\right) + 8/R. \qquad \ldots\ldots(5)$$

The procedure consists of developing a second order perturbation method using as a basis a set of unperturbed wave functions properly symmetrized to take account of the Pauli principle. When this is done, and the well-known Unsöld approximation is made, there results the expression

$$E = \int \Psi_0 \mathscr{H} \Psi_0 d\tau + \frac{1}{\epsilon}\left\{\int \Psi_0 \mathscr{H}^2 \Psi_0 d\tau - \left(\int \Psi_0 \mathscr{H} \Psi_0 d\tau\right)^2\right\} \qquad \ldots\ldots(6)$$

for the perturbed system energy E where $\mathscr{H}$ is the complete Hamiltonian of the system, ϵ is Unsöld's constant and Ψ_0 is a properly symmetrized wave function for the unperturbed system which, in the case under consideration, is given by equation (2).

The first term occurring on the right-hand side of equation (6) is the familiar expression for the sum of the valence energy and the energy of the unperturbed system E_0. Margenau and Rosen (1953) have discussed its evaluation in the case of helium and have pointed out that two basically different procedures have been used in the literature, depending on whether the assumption of exactness of the atomic wave functions is, or is not, made. The two methods will not in general give the same result except in the case of hydrogen where exact atomic wave functions are available. The earlier calculations by Slater (1928), Gentile (1930) and N. Rosen (1931) all assume exact wave functions. However, it is clearly preferable, as Margenau and Rosen emphasise, not to make such an assumption and the more recent calculations of P. Rosen (1950) and Griffing and Wehner (1955) in fact do not. Margenau and Rosen also point out that even when the latter procedure is followed the result is still quite sensitive to the approximate atomic wave function adopted (see also Dalgarno and McDowell 1956). Griffing and Wehner in their calculation used the simple single-parameter function defined by

$$a(1,2) = \frac{Z^3}{\pi} \exp[-Z(r_{a1} + r_{a2})] \qquad \ldots\ldots(7)$$

where $Z = 27/16$, while P. Rosen adopted the more accurate two-parameter Eckart (1930) wave function defined by

$$a(1,2) = \left(\frac{Z_1^3}{\pi}\right)^{1/2} \left(\frac{Z_2^3}{\pi}\right)^{1/2} (2 + 2t_0^2)^{-1/2} [\exp(-Z_1 r_{a1} - Z_2 r_{a2}) + \exp(-Z_1 r_{a2} - Z_2 r_{a1})] \qquad \ldots\ldots(8)$$

where t_0 is a normalization constant, $Z_1 = 2{\cdot}15$ and $Z_2 = 1{\cdot}19$. Rosen's calculations appear to be the best available over a suitable range of internuclear separations and are adopted in the present work.

In the evaluation of the second-order term in equation (6) the single parameter wave function (7) has been used and the assumption of exact wave functions has been made. These simplifications are considered justifiable because of the manner in which ϵ is chosen and because of the necessity to approximate to part of the exchange contribution. By applying two theorems due to Buckingham and Dalgarno (1952) involving the permutation operators, integrating over the spin coordinates and assuming exact wave functions, we obtain

$$\int \Psi_0 \mathscr{H}^2 \Psi_0 d\tau - \left(\int \Psi_0 \mathscr{H} \Psi_0 d\tau\right)^2 = \frac{M}{\Delta} - \left(\frac{L}{\Delta}\right)^2 \qquad \ldots\ldots(9)$$

where

$$\Delta = \int \{a(1,2)b(3,4)\}\{\mathscr{I} + p_{13}p_{24} - 2p_{13}\}\{a(1,2)b(3,4)\}d\tau, \qquad \ldots\ldots(10)$$

$$L = \int \{a(1,2)b(3,4)\}V_{\mathrm{AB}}(12,34)\{\mathscr{I} + p_{13}p_{24} - 2p_{13}\}\{a(1,2)b(3,4)\}d\tau, \qquad \ldots\ldots(11)$$

and

$$M = \int \{a(1,2)b(3,4)\}V_{\mathrm{AB}}(12,34)\{\mathscr{I} + p_{13}p_{24} - 2p_{13}\}V_{\mathrm{AB}}(12,34)\{a(1,2)b(3,4)\}d\tau \qquad \ldots\ldots(12)$$

the permutation operator p_{mn} being such as to interchange the position coordinates of electrons m and n and $b(3,4)$ being defined analogously to $a(1,2)$. The integrals Δ and L are readily expressed in terms of basic two-centre integrals all of which are tabulated over a convenient range of R by Hirschfelder and Linnett† (1950). M is evaluated in two parts M_1 and M_2 given by

$$M_1 = \int \{a(1,2)b(3,4)\}V_{\mathrm{AB}}^2(12,34)\{a(1,2)b(3,4)\}d\tau \qquad \ldots\ldots(13)$$

and

$$M_2 = \int \{a(1,2)b(3,4)\}V_{\mathrm{AB}}(12,34)\{p_{13}p_{24} - 2p_{13}\}V_{\mathrm{AB}}(12,34)\{a(1,2)b(3,4)\}d\tau \qquad \ldots\ldots(14)$$

M_1 is readily reduced to basic molecular integrals, those that are not tabulated by Hirschfelder and Linnett having been evaluated analytically by Howell (1954). The exact evaluation of M_2 would be a formidable computational task and an approximation equivalent to that used in the case of hydrogen (cf. paper I) is adopted. It is assumed that

$$M_2 \simeq \frac{\int \{a(1,2)b(3,4)\}V_{\mathrm{AB}}^*(12,34)\{p_{13}p_{24} - 2p_{13}\}V_{\mathrm{AB}}(12,34)\{a(1,2)b(3,4)\}d\tau}{\int \{a(1,2)b(3,4)\}V_{\mathrm{AB}}^*(12,34)\{p_{13}p_{24} - 2p_{13}\}\{a(1,2)b(3,4)\}d\tau} \times$$

$$\int \{a(1,2)b(3,4)\}V_{\mathrm{AB}}(12,34)\{p_{13}p_{24} - 2p_{13}\}\{a(1,2)b(3,4)\}d\tau \qquad \ldots\ldots(15)$$

† There is a misprint in the definition of one of the integrals tabulated in this paper. Equation (44) should read

$$L_{08,\,08} = \iint a_0(1)b_8(1)a_8(2)b_0(2)\cos(\phi_2 - \phi_1)/r_{12}.$$

where V_{AB}^{*} (12,34) is the first term in the expansion of the interaction potential $V_{AB}(12,34)$ in inverse powers of R. The three integrals occurring in (15) can be expressed in terms of simple integrals all of which are tabulated in the literature (cf. Hirschfelder and Linnett 1950, Roothaan 1955, Preuss 1956).

§ 3. RESULTS AND DISCUSSION

If ϵ in equation (6) is chosen so that the asymptotic form of (6) for large R is identical with the accurate result

$$E-E_0 \sim -3{\cdot}001/R^6 \qquad \ldots\ldots (16)$$

obtained by Dalgarno and Lynn (1957), we get the interaction energies displayed in column (1) of the table. These may be improved by following the suggestion in paper I which requires an accurate experimental or theoretical knowledge of the interaction energy at some relatively small internuclear distance. Buckingham (1958) has obtained an analytical expression for the energy of interaction, arrived at by fitting experimental data, which is given by

Energy of Interaction between Two Normal Helium Atoms $E-E_0$(Ryd)

$R(a_0)$	(1)	(2)	(3)
1·778	0·1446	0·2283	0·2283
2·370	0·0813	0·0862	0·0861
2·963	0·0238	0·0241	0·0261
3·556	0·00605	0·00607	0·00642
4·148	0·001341	0·001342	0·001190
4·741	0·0001976	0·0001977	0·0000845
5·926	−0·0000510	−0·0000510	—
7·111	−0·0000252	−0·0000252	—
8·296	−0·00001029	−0·00001029	—
9·482	−0·00000453	−0·00000453	—
10·667	−0·00000219	−0·00000219	—
11·852	−0·000001149	−0·000001149	—

(1) ϵ constant; (2) ϵ varied; (3) Buckingham's empirical expression.

$$E-E_0 = \frac{8}{R}\left\{1+0{\cdot}265R-2{\cdot}419R^2+2{\cdot}616R^3-0{\cdot}436R^4\right\}\exp(-2{\cdot}48R). \qquad \ldots\ldots (17)$$

This expression, besides behaving correctly in the limit as R tends to zero, represents quite well the interactions derived from two sets of scattering experiments by Amdur (1949) for $1<R<2$ and Amdur and Harkness (1954) for $2{\cdot}5<R<3$, while the position of its zero is in fair agreement with values derived from analyses of equilibrium and transport properties of gaseous helium. Consequently, the expression (17) can be taken to be a reasonable representation of the experimental results for the repulsive field for values of R up to about 5 and values of the interaction energy computed using it are given in column (3) of the table. If ϵ is now assumed to vary as

$$\epsilon(R)=\epsilon(\infty)+C(1-\Delta) \qquad \ldots\ldots (18)$$

(cf. paper I) and the constant C determined from the value of ϵ required in (6) to give the same interaction as (17) at $R=1{\cdot}778$, we obtain the results in column (2) of the table.

The interaction energies obtained with ϵ constant are in good agreement with the experimental fit at small R and, when ϵ is allowed to vary, agreement is improved considerably for very small R but remains effectively unchanged for values of R greater than about 3.

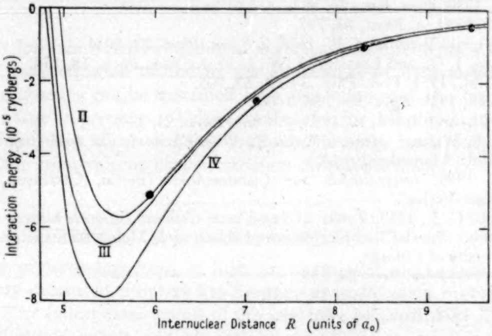

Energy of interaction $E-E_0$ between two normal helium atoms. Interactions II, III and IV are reproduced from Massey and Burhop (1952). Plotted points are interaction energies obtained here.

The properties of helium at low temperatures are determined mainly by the attractive part of the interaction and are very insensitive to the detailed form of the repulsion. Buckingham, Hamilton and Massey (1941) have considered several analytical expressions for the attractive field, and have compared the values of the viscosities, thermal conductivities and second virial coefficients computed, using them with experimental data. A discussion of this investigation is given by Massey and Burhop (1952) whose curves II, III and IV are reproduced in the figure along with values obtained in the present investigation. It was found that interaction III was that in best agreement with thermal conductivity measurements while interactions III and IV were those in best agreement with virial coefficient data but these results were not consistent with viscosity measurements. Massey and Burhop conclude nevertheless that an interaction between II and IV is the most likely and it is encouraging to find that the interaction energies obtained here do in fact lie within this range in the attractive region besides being in good agreement as has already been seen, with Buckingham's experimental fit in the region of the repulsive field.

ACKNOWLEDGMENT

It is a pleasure to thank Dr. A. Dalgarno for many helpful suggestions and for his continued interest and encouragement throughout the course of this investigation.

REFERENCES

AMDUR, I., 1949, *J. Chem. Phys.*, **17,** 844.

AMDUR, I., and HARKNESS, A. L., 1954, *J. Chem. Phys.*, **22,** 664.

BUCKINGHAM, R. A., 1958, *Trans. Faraday Soc.*, in the press.

BUCKINGHAM, R. A., and DALGARNO, A., 1952, *Proc. Roy. Soc.* A, **213,** 327.

BUCKINGHAM, R. A., HAMILTON, J., and MASSEY, H. S. W., 1941, *Proc. Roy. Soc.* A, **179,** 103.

DALGARNO, A., and LYNN, N., 1956, *Proc. Phys. Soc.* A, **69,** 821; 1957, *Ibid.*, **70,** 802.

DALGARNO, A., and McDOWELL, M. R. C., 1956, *Proc. Phys. Soc.* A, **69,** 615.

ECKART, C., 1930, *Phys. Rev.*, **36,** 883.

GENTILE, G., 1930, *Z. Phys.*, **63,** 795.

GRIFFING, V., and WEHNER, J. F., 1955, *J. Chem. Phys.*, **23,** 1024.

HIRSCHFELDER, J. O., and LINNETT, J. W., 1950, *J. Chem. Phys.*, **18,** 130.

HOWELL, K. M., 1954, *Proc. Phys. Soc.* A, **67,** 705.

MARGENAU, H., 1939, *Phys. Rev.*, **56,** 1000.

MARGENAU, H., and ROSEN, P., 1953, *J. Chem. Phys.*, **21,** 394.

MASSEY, H. S. W., and BURHOP, E. H. S., 1952, *Electronic and Ionic Impact Phenomena* (Oxford: Clarendon Press).

PREUSS, H., 1956, *Integraltafeln zur Quantenchemie* (Berlin, Göttingen, Heidelberg: Springer-Verlag).

ROOTHAAN, C. C. J., 1955, *Tables of Two-Center Coulomb Integrals between* 1s, 2s *and* 2p *Orbitals*. Special Technical Report, Laboratory of Molecular Structure and Spectra, University of Chicago.

ROSEN, N., 1931, *Phys. Rev.*, **38,** 255.

ROSEN, P., 1950, *J. Chem. Phys.*, **18,** 1182.

SLATER, J. C., 1928, *Phys. Rev.*, **32,** 349.

The Pressure Dependence of the Ferromagnetic Anisotropy Energy

By D. GUGAN† and G. ROWLANDS†‡
Division of Pure Physics, National Research Council, Ottawa, Canada

MS. received 10*th March* 1958

Abstract. A formula is derived and used to analyse measurements of the change of technical magnetization caused by the application of hydrostatic pressure. Some of the changes can be described by a dependence of the ferromagnetic anisotropy energy on pressure. Values are obtained for this pressure dependence in certain nickel–iron alloys and they are found to agree moderately well with estimates made from volume magnetostriction measurements.

---

§ 1. Introduction

In studies of ferromagnetism at high pressures, the most easily and most frequently measured property has been the magnetization in low magnetic fields. The fullest experiments of this sort have been made by Yeh (1925) on iron, nickel and cobalt, and by Steinberger (1933) on iron, nickel and a series of their alloys. Their results are in general agreement, those of Steinberger however, revealing several details not found by Yeh. Steinberger found that only in certain cases did the magnetization vary linearly with pressure. In many other cases the variation was non-linear, exhibited hysteresis (a true pressure effect, not to be confused with magnetic field hysteresis), and changed irreversibly on initial application of hydrostatic pressure.

In the course of work on the change of spontaneous magnetization with hydrostatic pressure (Gugan 1956) some measurements were also made at low fields. The results of these experiments were in general agreement with the findings of Steinberger. The irreversible changes of magnetization with pressure have been interpreted there as evidence for a non-uniform change of internal strain under the action of a uniform external pressure. It is the purpose of this paper to discuss the reversible changes of magnetization with pressure; these are in many cases the largest changes observed.

A new method of analysing these results is discussed below: the pressure coefficient of magnetization, $(\partial I/\partial p)_H/I$, and the relative differential susceptibility, $(\partial I/\partial H)_p/I$, are correlated in terms of a parameter d'' which can in certain cases be identified with the pressure coefficient of the first magnetocrystalline anisotropy constant, $(dK/dp)/K$. The essential step in the derivation is the replacement of the temperature T by the pressure p in certain magnetothermal relationships.

Before discussing this new method, we first discuss a treatment given by Becker (1934). His treatment enables values of dK/dP to be obtained from experimental measurements of the changes of volume of ferromagnetic materials in low fields.

† National Research Laboratories Postdoctorate Fellow.

‡ Now at Atomic Energy Research Establishment, Harwell, Didcot, Berks.

§ 2. BECKER'S METHOD

Several different processes can contribute to the change caused by pressure in the magnetization in low magnetic fields. These include change of domain volume, change of demagnetizing field, rotation of domain magnetization vectors, and change of spontaneous magnetization with pressure. This last process is relatively small in the technical magnetization region, especially for materials with a high incremental permeability; however, there are some cases where it can be the dominant effect: examples are the invar alloys. Of the other three processes, the only one which has been treated theoretically is the rotation of domain magnetization with pressure. The effect is obviously equivalent to a pressure dependence of anisotropy energy; Becker (1934) postulated such a pressure dependence in order to account for the volume magnetostriction associated with rotation of domain vectors, termed by him the ' crystal effect '. For a cubic material with only the first anisotropy coefficient significant, Becker was able to derive an expression for the crystal effect in polycrystals with *randomly oriented* grains:

$$\omega_K = \frac{K}{5}\left(\frac{1}{K}\frac{dK}{dp} - \beta\right); \qquad K \text{ positive} \qquad \ldots\ldots(1)$$

$$\omega_K = -\frac{2K}{15}\left(\frac{1}{K}\frac{dK}{dp} - \beta\right); \qquad K \text{ negative} \qquad \ldots\ldots(2)$$

ω_K is the relative change of volume caused by the rotation of domain vectors from their initial directions of easy magnetization into the direction of the external field, K is the first anisotropy constant, and β the volume compressibility.

These are useful expressions for giving the order of magnitude of the pressure coefficient of anisotropy energy ($\sim 1\%/10^3$ atm), but when precise results are needed they have several disadvantages which we mention briefly. In obtaining the above equations it has been assumed that the individual grains comprising the crystal are randomly orientated, which unfortunately in practice is the exception rather than the rule. Also, no account has been taken of changes of volume arising from sources other than the rotation of domain vectors: the experimental results presented later will show that this can be a serious objection to the use of Becker's equations. The other main difficulties in applying Becker's equations are experimental ones. Firstly, the crystal effect is small and not at all easy to measure. Secondly, the anisotropy constant, K, must be known for the sample whose crystal effect is being measured before values of $(dK/dp)/K$ can be obtained (cf. eqns (1) and (2)).

The general method of analysis which we give below is free from the deficiencies of Becker's analysis; moreover, the quantities which enter the analysis are relatively easy to obtain experimentally.

§ 3. GENERAL METHOD

Stoner and Rhodes (1949), and more recently Teale and Rowlands (1957), have shown how it is possible to determine from an analysis of certain magnetothermal effects, the extent and character of the various elementary processes occurring over certain parts of the magnetization curve. The experimental results, namely the *reversible* changes in the net magnetization I with changes in the temperature T and the field H, are analysed in terms of a quantity b'', defined by

$$b'' = -\left\{\frac{T(\partial I/\partial T)_H + a[I + H(\partial I/\partial H)_T]}{H(\partial I/\partial H)_T}\right\} \qquad \ldots\ldots(3)$$

where $a = -(T/I_0)(dI_0/dT)_H$, I_0 being the spontaneous magnetization.

If the changes in magnetization are due only to changes in the spontaneous magnetization and to rotations of the magnetization vectors against the magnetocrystalline anisotropy forces, then it is shown in the above-mentioned papers that

$$b'' = \frac{TdK}{KdT} = b \qquad \ldots\ldots(4)$$

where K is the first anisotropy constant. Under these conditions the coefficient b'' is thus independent of the field; in general, however, b'' will vary with field.

From an analysis of experimental results it is found that in the high field region b'' is sensibly constant and of order b (cf. Tebble and Teale 1957; reference to earlier work is given in this paper), and from this it may be concluded that the changes in magnetization mentioned above indeed predominate in this region. Further, it is found from an analysis of the *total* change in I due to changes in H and T (i.e. irreversible as well as reversible changes of I) that the value of b'' obtained by using (2) is still sensibly constant over a range of fields in the high field region (cf. Stoner and Rhodes 1949). This means that the predominant changes in this region are not only due to the changes in magnetization considered above, but are also reversible.

It is shown in the paper by Teale and Rowlands (1957) that when the changes in magnetization are due only to changes in the spontaneous magnetization and to rotation of the magnetization vectors against anisotropy forces, the magnetization curve may be written in the parametric form

$$\frac{I}{I_0} = f(h); \qquad h = \frac{HI_0}{K} \qquad \ldots\ldots(5)$$

where f is some function, generally unknown, of the reduced variable h. It is readily shown by combining the values for $(\partial I/\partial T)_H$ and $(\partial I/\partial H)_T$ obtained from (5), that the value of b'' as defined by (3) is equal to b. A similar analysis can be carried out if the pressure p is substituted for the temperature T, and a quantity d'' analogous to b'' can be defined:

$$d'' = -\left\{\frac{p(\partial I/\partial p)_H + a'[I + H(\partial I/\partial H)_p]}{H(\partial I/\partial H)_p}\right\} \qquad \ldots\ldots(6)$$

where $a' = -(p/I_0)(\partial I_0/\partial p)_H$. The quantity d'' is now to be considered as determinable experimentally from measurements made under isothermal conditions. It is to be expected that the value of d'' will tend to a constant value of $(p/K)(dK/dp)$ in the high field region, but deviations will be expected in the lower field region. This thus gives a method of determining a value for $(dK/dp)/K$ from values of $(\partial I/\partial H)_p$ and $(\partial I/\partial p)_H$.

§ 4. EXPERIMENTAL

To use equation (6) we need to know $(\partial I/\partial H)_p/I$ and $(\partial I/\partial p)_H/I$ as p tends to zero; calculated values of d'' are then plotted against H in order to find the limiting value of this coefficient in the rotational region. Values of a' can be found from experiments on the change of spontaneous magnetization with pressure (Gugan 1956).

To reduce the labour involved in these experiments it is usual to derive values of $(\partial I/\partial p)_H/I$ from complete magnetization curves measured at two different pressures. The pressure coefficient thus found is an average one which may, because of hysteresis and non-linearity in the pressure effect, be quite different from the coefficient as p tends to zero. This point is well illustrated by Steinberger's results for 30% nickel–iron where a separate (I, p) run shows a very strong curvature. Another disadvantage of using this method to find pressure coefficients is that where the pressure coefficient becomes small, as it usually does in the rotation region, small errors in the magnetization curves measured at the two pressures can have an enormous effect on the apparent pressure coefficient. The reversal of the pressure coefficient of Steinberger's 60% nickel–iron alloy is almost certainly due to this source of error, and it is possible that this also accounts for several others of his apparent reversals of the pressure effect in high fields.

In the present experiments† precise measurements of magnetization curves were made at three pressures, approximately 0, 2500 and 5000 atmospheres. These results showed that for the substances investigated, nickel and 48% nickel–iron, the change of magnetization was nearly proportional to the pressure. Curvature in the (I, p) relation has been allowed for to a first approximation by evaluating the coefficents $(\partial I/\partial p)_H/I$, $(\partial I/\partial H)_p/I$ at a pressure which is the mean of those from which the average pressure coefficients are found,

$$\text{i.e.}\ \frac{1}{I}\left(\frac{\partial I}{\partial H}\right)_p = \frac{1}{I_{2500}}\left(\frac{\partial I_{2500}}{\partial H}\right)_p; \quad \frac{1}{I}\left(\frac{\partial I}{\partial p}\right)_H = \frac{1}{I_{2500}}\left(\frac{I_{5000}-I_0}{\Delta p}\right)_H.$$

(The subscripts to I here all refer to the pressure at which the magnetization was measured). Substituting these values in equation (6) then gives a value of d'' appropriate to this mean pressure, about 2500 atmospheres. However, this value of d'' should not be much different from the value at 1 atmosphere.

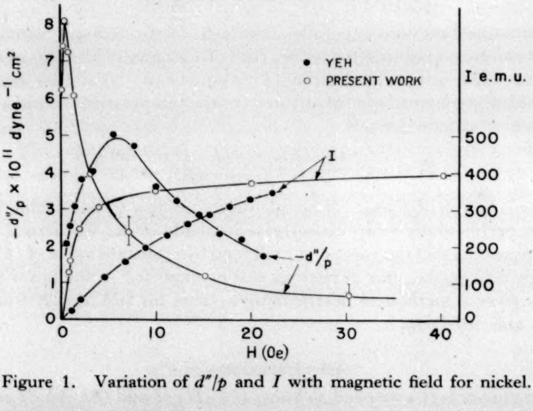

Figure 1. Variation of d''/p and I with magnetic field for nickel.

Values of d''/p calculated by using equation (6) are plotted against H in figures 1 and 2. The (I, H) curves for the specimens are also plotted in these figures.

---

† Details of the measurements are given by Gugan (1956); it suffices here to say that the magnetization curves were measured by a ring ballistic method.

The limiting values of d''/p are for nickel, -6×10^{-12} dyn^{-1} cm^2, and for 48% nickel–iron, 2×10^{-11} dyn^{-1}cm^2. These should be compared with values of $(dK/dp)/K$ deduced from Becker's equations (1) and (2), -10×10^{-12} and 3×10^{-11} dyn^{-1}cm^2 respectively.

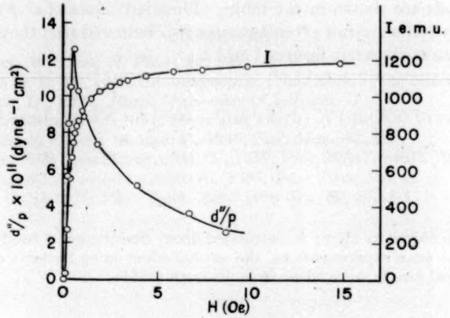

Figure 2. Variation of d''/p and I with magnetic field for 48% nickel–iron.

The numerical values substituted in equations (1) and (2) were taken from Bozorth (1951), except for the value chosen for the anisotropy energy of the 48% nickel–iron alloy, $3{\cdot}3\times10^{-4}$ erg cm^{-3}. This value is considerably higher than the most recent values ($\sim1\times10^{-4}$ erg cm^{-3}) but it was a typical value for this alloy when the magnetostriction measurements were made.

§ 5. DISCUSSION

Considering the inadequacies of the experimental results, the test of equation (6) is encouraging. The figures show that the calculated values of d''/p do indeed tend to a constant value in the region of domain vector rotations. Also, the values of $(dK/dp)/K$ agree reasonably well with values calculated from Becker's equations. Of course, Becker's equations do not take account of any possible volume changes due to processes other than rotation of domain magnetization vectors, and for this reason any agreement between the present values of $(dK/dp)/K$ and values deduced using equations (1) and (2) must be suspect. However, details of the experiments on the ' crystal effect ' are very vague, and it is probable that the measurements were made not from the demagnetized state to saturation, but from the remanent point to saturation; if this were the case then the conditions assumed in equations (1) and (2) would apply much more closely.

The only other experimenal results which appear suitable for comparison with the present measurements are those obtained by Yeh for nickel; they are compared with the present measurements in figure 1. It may be seen that the calculated values of d''/p agree reasonably well for similar values of magnetization I. Steinberger gives results for nickel and for 50% nickel–iron; unfortunately both these materials show apparent reversals of the pressure coefficient in the higher field range and, as explained earlier, it is doubtful whether these results represent the true behaviour of these substances. We have calculated values of d''/p from

Steinberger's results for several nickel–iron alloys and in some cases they show a region where this coefficient is fairly constant. If this constant value is identified with $(dK/dp)/K$ we find a qualitative agreement between these calculated values and values of $(dK/dp)/K$ derived from using Becker's formulae (1) and (2) to analyse measurements of the crystal effect. Values of $(dK/dp)/K$ calculated by the two methods are shown in the table. Detailed values of d''/p calculated from Steinberger's results are not given because it is believed that they are less typical than are the results shown in figures 1 and 2.

Values of $(dK/dp)/K$ (dyn^{-1} cm^2 × 10^{11}) for Nickel–Iron Alloys

a	0	20	40	50	60	70	80	90	100
b	—	0·5	5	3·5	10	—	1·5	0	—
c	−0·5	1·5	8	3	6	6	4	1	−1

a, percentage nickel in alloy; *b*, calculated from Steinberger's results using equation (6); *c*, calculated from experiments on the crystal effect using Becker's equations (1) and (2): the numerical results were taken from Bozorth (1951).

As is shown in figures 1 and 2, the variation of d''/p with H is large, much larger than the variation of the corresponding coefficient b'' in the magnetothermal case. It must be emphasized once more that the partial derivatives used in (6) should be those applying to reversible processes. While it is believed that this is true for the values of $(\partial I/\partial p)_H/I$, a comparison of the measured values of $(\partial I/\partial H)_p$ with values of κ_{rev} obtained by Tebble and Teale (1957) shows that only in the rotation region does the coefficient used here apply to reversible processes. The values of $(dK/dp)/K$ calculated from the limiting value of d''/p are thus believed to be reasonably reliable, but it is clear that substitution of $(1/I)(\partial I/\partial H)_{p,\text{rev}}$ in (6) would produce a much stronger variation of d''/p with H. The maximum value of d''/p for nickel would be about ten times larger than that shown in figure 1. This conclusion certainly needs further test, but if it is true it might indicate that the demagnetization field or the domain wall energy, or both, depend very critically upon volume. A detailed consideration has been made by Teale and Rowlands (1957) of the effects of these two factors on the low-field magnetothermal behaviour; they find that the coefficient b'' has different values for different magnetic processes. The same considerations may be applied to the pressure effects, and they lead to the conclusion that it is unlikely that the coefficient describing the low-field pressure effects should be much greater than that describing the effect of pressure on domain rotations $(dK/dp)/K$. A more careful study of the pressure effect is obviously needed.

The present status of equation (6) is somewhat similar to that of the Stoner and Rhodes magnetothermal equation when it was first propounded. More detailed work needs to be done to test the equation in the low field region, but already it appears that this is a useful method of finding the volume dependence of the ferromagnetic anisotropy constants. The method is probably somewhat simpler than more direct methods of finding this volume dependence, but it must be emphasized that considerable care is necessary in order to obtain accurate results because in the rotation region the difference between $(\partial I/\partial p)_H/I$ and $(dI_0/dp)I_0$ is very small.

ACKNOWLEDGMENTS

We would like to thank the National Research Council of Canada for the award of Postdoctorate Fellowships during the tenure of which much of this work was done. We would also like to thank several of our colleagues for their comments on this paper.

REFERENCES

BECKER, R., 1934, *Z. Phys.*, **87**, 547.
BOZORTH, R. M., 1951, *Ferromagnetism*, (New York : Van Nostrand).
GUGAN, D., 1956, *Thesis*, University of London.
STEINBERGER, R. L., 1933, *Physics*, **4**, 153.
STONER, E. C., and RHODES, P., 1949, *Phil. Mag.*, **40**, 481.
TEALE, R. W., and ROWLANDS, G., 1957, *Proc. Phys. Soc.* B, **70**, 1123.
TEBBLE, R. S., and TEALE, R. W., 1957, *Proc. Phys. Soc.* B, **70**, 51.
YEH, C. S., 1925, *Proc. Amer. Acad. Arts Sci.*, **60**, 503.

Solid Solution in $A^{III}B^{V}$ Compounds

By J. C. WOOLLEY and B. A. SMITH
Department of Physics, University of Nottingham

Communicated by L. F. Bates ; MS. received 19th March 1958

Abstract. Ranges of solid solution have been investigated in systems composed of two $A^{III}B^{V}$ compounds, particularly GaSb–InSb, GaAs–InAs and InAs–InSb. It is found that in practically all cases considered complete solid solution throughout the whole range of composition can be obtained, but that this equilibrium condition can only be reached under special conditions of temperature and time of annealing. The work includes the investigation of solidus curves and the possible presence of low temperature miscibility gaps.

In all cases, it is found that if normal annealing methods are used, equilibrium can be attained with a reasonable length of time of anneal only in the case of compressed powder specimens. Consideration is given to the methods available for producing alloys in equilibrium in the solid form.

§ 1. INTRODUCTION

INTEREST has increased recently in the semiconducting materials which are obtained when solid solution occurs between two compounds of the type $A^{III}B^{V}$, e.g. InSb, GaAs, etc. These have been termed alloy semiconductors and the work up to the present has been reviewed by Herman, Glicksman and Parmenter (1957).

The initial work of this type, but on elements rather than compounds, was that of Stöhr and Klemm (1939), who established that single phase solid solution occurred at all compositions in the binary system Ge–Si. Because of the importance of the possible increase in the range of available semiconducting materials, this work has been followed up by various workers. Measurements have been made on the variation of the optical energy gap (Levitas, Wang and Alexander 1954), and of the Hall mobility (Glicksman 1956), with composition, and these results have received qualitative treatment in terms of the band theory (Herman 1954, Herman, Glicksman and Parmenter 1957). On the theoretical side, alloy semiconductors are of interest because, in certain cases, the detailed band structures of the components are known (Herman 1955) and the analysis of a representative case of a disordered crystal has been attempted by the application of virtual crystal methods (Parmenter 1955 a, b, 1956).

In the case of the alloy $A^{III}B^{V}$ materials, this work has not progressed so far and is limited in many cases to investigations of the range of solid solution in various materials. Shih and Peretti (1953) investigated the system InAs–InSb and obtained a degenerate eutectic diagram, the maximum extent of terminal solid solution being 2%. Köster and Thoma (1955) investigated the systems GaSb–InSb, AlSb–InSb and AlSb–GaSb. In each case, they reported degenerate eutectic diagrams without appreciable terminal solid solution. However, Folberth (1955) investigated the systems InAs–InP and GaAs–GaP and for each found solid solutions throughout the whole of the composition range. Folberth gave the variation of energy gap with composition for each system, and the variation of Hall mobility with composition for the InAs–InP system.

Recent Russian work throws some doubt on the results of Köster and Thoma. Thus Goryunova and Fedorova (1955) investigated two alloys in each of the systems GaSb–InSb and GaAs–InAs. In the latter system, they did not obtain single phase alloys with the time of anneal used, but they noticed some change in the form of the X-ray diffraction photographs for the alloys as annealing proceeded. In the case of GaSb–InSb, in contrast to the results of Köster and Thoma, Goryunova and Fedorova found that the two alloys investigated became single phase after a considerable time of anneal at high temperatures.

Goryunova and Fedorova (1955) also reported investigations of the system InAs–InSb which were in reasonable agreement with the results of Shih and Peretti, reporting immiscibility over a large range of composition, with a maximum range of terminal solid solution of some 3%.

In later work Woolley, Smith and Lees (1956), and Woolley and Smith (1957), hereafter referred to as I and II respectively, showed that complete solid solution can be obtained in both the systems GaSb–InSb and GaAs–InAs, provided that the alloys are annealed for a sufficiently long time at the correct temperature. The discrepancies in previous work appear probably to be due to different annealing times used by the various workers. Thus Blakemore (1957) reported measurements of various properties of a single 50 : 50 alloy in the GaSb–InSb system, but it appears probable from the data given and from a consideration of the results given here that his alloy was not in the equilibrium condition. Thus, the results quoted give little indication of the properties of an equilibrium alloy. Further, Kolm, Kubin and Averbach (1957) published results on the GaSb–InSb system, where solid solution is reported to be limited to approximately 10% at each end of the diagram. No details of the heat treatment of the specimens are given, but again consideration of the data available indicates that probably a final equilibrium condition had not been reached. This is particularly the case if solid specimens were used, for, as indicated in I, these require times of annealing very much longer than the corresponding times for powders. Once again, therefore, the value of the results quoted is rather limited.

In view of the above discrepancies it was decided to re-investigate the $A^{III}B^{V}$ type alloy systems as the initial step in a programme of work on the physical properties of these alloys, and the results of the investigation of solid solution in these alloy systems are reported here.

§ 2. METHOD

The alloys used in all the investigations were made up by sealing the required quantities of the appropriate compounds in evacuated quartz tubes (except in the case of the AlSb alloys when an internal graphite crucible was used), heating to a temperature above the melting point of the higher melting point compound, and quenching in water. In the case of the compounds themselves, the antimonides were made in a similar way, using in each case elements of purity greater than 99·9%, which is considered sufficient for crystallographic work. The arsenides were kindly provided by the Services Electronics Research Laboratory, Baldock.

Each alloy was powdered and x-rayed and then compressed and resealed *in vacuo* and annealed initially at a temperature corresponding to the melting point of the lower melting point component. After a suitable time of anneal the alloy was cooled, re-powdered, and x-rayed. It was then annealed at a progressively higher temperature until equilibrium was reached, the approach to the equilibrium condition being followed by x-ray methods. This procedure is that used by Stöhr and Klemm in their work on the Ge–Si system. The period of annealing and the increase in temperature in each case was determined by the progress to equilibrium shown by the x-ray photographs, all of which were taken with a 9 cm powder camera using Cu Kα radiation.

The main problem in all the alloy systems investigated was the exceedingly slow diffusion rates in the materials and the resulting long times of annealing required before equilibrium was reached. Thus, although in some cases equilibrium was obtained by annealing specimens at a suitable temperature for one or two weeks, other materials required months of annealing before showing any appreciable movement towards an equilibrium condition. This is for specimens in a compressed powder form; solid specimens were found to take very much longer times to reach equilibrium than powders. Thus, in the case of GaSb–InSb alloys, while compressed powders required some eight weeks to reach single phase condition, solids of the same composition were relatively unchanged after annealing for some nine months at the same temperature. The problem is further complicated by the fact that, even when annealings are carried out for this period, it is necessary that the annealing temperature be close to the solidus temperature if equilibrium is to be obtained. At lower temperatures, the diffusion rates are so small that conclusive results cannot be obtained. Since the solidus curve cannot be determined until alloys in equilibrium are available, the problem can only be solved by a tedious continuous approximation method.

To determine the solidus curve by standard methods, it is necessary to make heating curve measurements on specimens already in equilibrium in the solid form, the equilibrium condition being lost during the measurement. The problems involved in such determinations in the system GaSb–InSb are discussed elsewhere (Woolley and Lees, to be published). It was decided that, with the particular substances being investigated, it would be useful to use x-ray methods to determine the solidus curve and also, if possible, the other solid–solid phase boundaries. The solidus determination involved holding a suitable specimen at a temperature in its liquidus–solidus range until equilibrium was reached, and then quenching in the phases obtained. In this range, equilibrium is attained much more rapidly than in the case of completely solid material. The composition of the solid component of the quenched material was then found by determining its lattice parameter by x-ray powder photographs, and comparing this value with the graph of variation of lattice parameter with composition for single phase alloys already obtained. Choice of suitable temperature was simplified in those cases in which the liquidus had been determined by other workers; it was also much simplified, in the absence of the liquidus data, when one or two points on the solidus had been determined.

The method is not normally a satisfactory one as it is usually impossible to quench in the equilibrium solid phase without some change in composition. But the exceedingly slow diffusion rates in the solid form of these materials (Eisin and Birchenall 1957) would appear to favour it. To check the method, the results in the case of the GaSb–InSb system were compared with the solidus curve obtained by normal heating curve methods (Woolley and Lees, to be published elsewhere). Although the X-ray method gives only the solidus curve, the liquidus curve can more easily be determined by standard thermal methods. Moreover, in work on the preparation of these alloys, both in normal annealing and in zone melting work, it is the solidus curve which is important.

§ 3. RESULTS OF SOLID SOLUTION INVESTIGATIONS

3.1. *GaSb–InSb system*

The initial results on this system have already been published (I). It was found that solid solution was obtained at all compositions throughout the alloy range; the alloys having the usual zinc blende structure. Within the limits of experimental error, the variation of lattice parameter with composition (figure 1) is linear, i.e. Vegard's law is obeyed. With this system, and also that of GaAs–InAs discussed later, a sufficient degree of equilibrium was reached that the measured parameters are estimated to be accurate to approximately ± 0·002Å. Also shown in I is the variation of the profile of a typical line in the powder photograph as a function of time of annealing. It began as a wide banded form, showing two peaks corresponding to a GaSb rich and an InSb rich component, but with annealing slowly narrowed down to a single line characteristic of a single phase material. Annealing for some eight weeks in the temperature range 510°–540°C was necessary before good equilibrium was obtained for alloys in the compressed powder form.

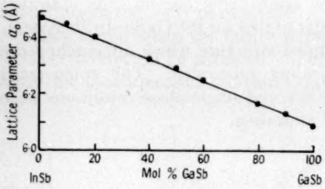

Figure 1. Variation of lattice parameter a_0 as a function of composition in the GaSb–InSb system.

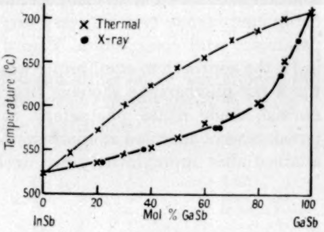

Figure 2. Equilibrium diagram of GaSb–InSb system. Thermal, determined by standard thermal methods, (see Woolley and Lees, to be published); X-ray, determined by X-ray investigation.

The lattice parameter–composition curve being known for all compositions, the solidus curve for the system was obtained as described in § 2. The results obtained in this way are shown in figure 2, together with the results obtained by the heating curve method. The accuracy of the temperatures given is estimated in each case to be ± 5°C. The reasonable agreement between the two sets of results was taken to justify the use of the X-ray method for these materials.

Another factor investigated was whether in the liquidus–solidus region the diagram may be treated as quasi-binary, i.e. with the tie lines lying in the GaSb–InSb plane. To check this, alloys of various compositions were heated to equilibrium at the same temperature and then quenched, and the lattice parameter of the solid phase measured for each. The lattice parameter was found constant for a given temperature, indicating quasi-binary behaviour. This investigation was considered necessary as sections consisting of similar materials have been found not to show quasi-binary behaviour. (It is hoped to publish details of these at a later date.)

An attempt was also made to see whether a closed miscibility gap occurs in the equilibrium diagram. Alloys of various compositions across the diagram were first annealed to single phase equilibrium and then left to anneal at 450°c for several months. X-ray measurements showed no change from the single phase condition and this result indicates that no miscibility gap occurs at temperatures of 450°c or above. The difficulty here, however, is that the diffusion rates at 450°c are probably so slow that, even if at any composition the equilibrium condition were two-phase, movement towards this condition would not be observed. This effect will be discussed in more detail when the InAs–InSb system is considered. In no case after the long periods of annealing was any indication observed of ordering of the Ga and In atoms on the appropriate sublattice.

3.2. *GaAs–InAs System*

The preliminary results on this system have also been published (II). Solid solution is obtained at all compositions throughout the alloy range, the structure being zinc blende type in every case. Figure 3 shows the variation of lattice parameter with composition, Vegard's law again being obeyed. As indicated in II, the approach to equilibrium was similar to that for the GaSb–InSb system, the x-ray photographs showing first a banded structure which approached the normal single phase photograph as annealing proceeded. The compressed powders were annealed at approximately 900°c and single phase conditions were attained after approximately two weeks of annealing.

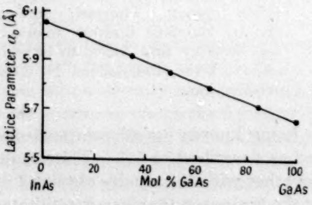

Figure 3. Variation of lattice parameter a_0 as a function of composition in the GaAs–InAs system.

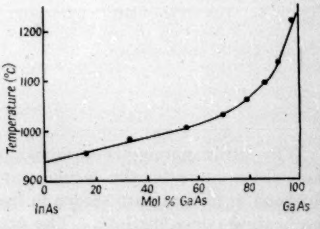

Figure 4. Solidus curve for GaAs–InAs system.

The solidus curve was obtained by the X-ray method, and the results are shown in figure 4, the estimated accuracy again being ± 5°C. Measurements using specimens of different compositions again showed the system to be quasi-binary. Annealing single phase alloys at temperatures lower than 900°C showed no sign of a two phase region, but as indicated above, this result is not conclusive. Again, in no case was any indication observed of ordering of the Ga and In atoms on their sublattice.

3.3. *InAs–InSb System*

Here, in contradiction to previous results in this system, solid solution was obtained throughout the whole range of composition. These final results were, however, much more difficult to obtain than in the case of the previous two systems. Representative alloys were first annealed at 525°C. After some three months at this temperature, alloys over a considerable range of composition were approaching a single phase state, but alloys in the approximate range of 90–40 mol % InAs showed an apparent equilibrium two phase condition when investigated by X-ray methods. When these alloys were annealed at 600°C and above, they were found to split up into a different two-phase combination, apparently showing that they were now being annealed above the solidus temperature. Finally, by careful annealing for several weeks at temperatures between 525°C and 600°C (e.g. 570°C in the case of 70 mol % InAs alloy) conditions approaching single phase were obtained at all compositions. Even under these conditions, good single phase equilibrium was not reached, the higher order lines in the X-ray photograph being broad and blurred. The approach to the single phase state, however, was sufficiently clear to show that this was the equilibrium condition and to enable the appropriate lattice parameter to be determined. The variation of lattice parameter with composition is shown in figure 5, the spread indicated on each determination being that corresponding to the total width of the high order lines in the X-ray photograph.

Once again, when the lattice parameter–composition curve was known, the solidus curve could be obtained. The results in this case are shown in figure 6. Again the measurements indicate a quasi-binary behaviour.

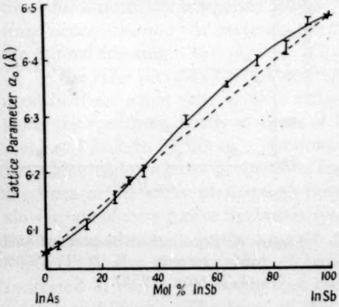

Figure 5. Variation of lattice parameter a_0 as a function of composition in the InAs–InSb system.

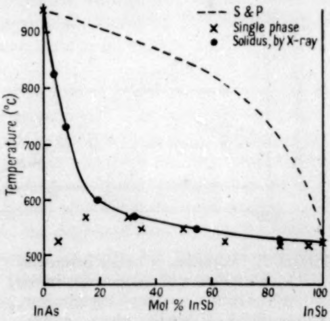

Figure 6. Equilibrium diagram of the InAs–InSb system. S & P, Shih and Peretti (1953).

It is seen from figure 5 that in this system Vegard's law is not satisfied, the maximum departure from this being 0·030Å in a cell parameter of 6·330Å, and that the experimental curve crosses the Vegard line at approximately 67 mol % InAs. From alloy theory considerations (Aptekar and Finkelstein 1951), this can be taken to indicate a tendency for the system to show either a closed miscibility gap or else ordering, centred on this composition. In order to investigate these possibilities, it is necessary to determine the equilibrium condition at lower temperatures for alloys around this composition. An attempt was made to do so at 525°c (only 40–50°c below the solidus). Even at this temperature, however, the equilibrium conditions could not be determined unambiguously. As already indicated, alloys annealed from the quenched state appeared to reach a two-phase equilibrium at 525°c. When alloys of the same composition, first annealed to single phase at 550°c were annealed at 525°c for approximately three months no indication of any splitting into a two-phase condition could be observed by x-ray investigation. It would thus appear that at these compositions the diffusion rates in the solid are so slow that even at temperatures only some 50°c below the solidus, equilibrium cannot be attained under normal practical conditions, and the form of the equilibrium diagram at temperatures below 550°c cannot be determined.

3.4. *AlSb–InSb System*

This system presented problems very similar to those described in § 3.3 with the additional difficulties usually met with in dealing with AlSb. Representative alloys were first annealed at approximately 525°c for three months. After this time the results were comparable with those for InAs–InSb, i.e. a range of solid solution at each end of the diagram, with a central region in which equilibrium appeared to be two phase. It was at first assumed that this was the true

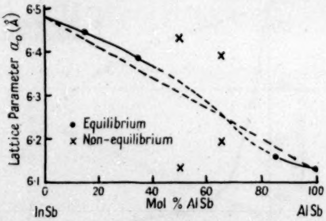

Figure 7. Variation of lattice parameter a_0 as a function of composition in the AlSb–InSb system. Equilibrium, equilibrium single phase points; non-equilibrium, non-equilibrium apparent two-phase points.

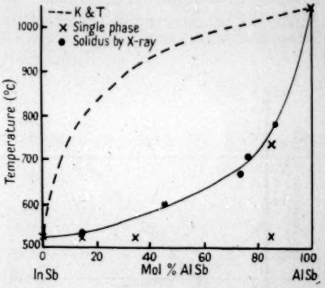

Figure 8. Equilibrium diagram of AlSb–InSb system. K & T, Köster and Thoma (1955).

equilibrium condition and measurements were then made to determine the solidus curve. Comparison of all the results with those for the InAs–InSb system, however, seems to indicate that the probable true equilibrium condition is single phase through the whole diagram. Figure 7 shows the experimental results obtained, together with a roughly estimated section where equilibrium has not been reached. Figure 8 is the solidus curve for the system obtained by using the curve of figure 7 and the methods of § 2. It is hoped to extend this work later.

3.5. *AlSb–GaSb System*

Only preliminary measurements have been carried out in this system, but they are very similar to those for the system AlSb–InSb at a comparable stage. It is probable therefore that the comments on the AlSb–InSb system apply similarly to the AlSb–GaSb system. Further work on this system has not been done, however, as the close similarity of the lattice parameters of AlSb and GaSb make x-ray work difficult, especially when non-equilibrium conditions have to be interpreted.

3.6. *GaAs–GaSb System*

Only preliminary measurements have been made on this system, but the results appear similar to those for the InAs–InSb system, so that it appears probable that solid solution occurs throughout the whole alloy range. (It is hoped to publish further details of this system later.)

§ 4. FURTHER INVESTIGATION OF METHODS OF PREPARING ALLOYS

All the investigations of solid equilibrium described above have been made with powdered specimens, because the approach to equilibrium was very much slower with a solid ingot. For physical measurements however a solid ingot is usually required, and therefore it was necessary to investigate possible methods of accelerating the approach to equilibrium for solid specimens.

Investigations were carried out on specimens from the GaSb–InSb system. The initial rate of cooling from the melt made very little difference to the condition of the material, the rates of cooling being varied from chill casting into a copper mould to a rate of cooling of approximately 40°C per day through the liquidus–solidus interval. In both cases the x-ray results were practically identical with those for a normally quenched alloy. It appeared, therefore, that other methods were necessary, and the methods tried were slow zone recrystallization and slow directional freezing.

In the zone recrystallization an ingot of 50 mol % GaSb 50 mol % InSb was used in the normal type of zone refining apparatus. The zone was swept once along the specimen, firstly at a rate of 1 inch in ten hours, and in a second experiment at 1 inch in 24 hours. Sections were then cut from the ingot and x-rayed. In neither experiment was complete equilibrium attained at any point in the ingot, the lines of the x-ray photograph being broad and diffuse at high angles. The slower rate of sweep gave the better results, the degree of equilibrium corresponding to that obtained in the case of powders by some six weeks of annealing. Figure 9 shows the variation of lattice parameter along the ingot, the spread indicated at each point being that corresponding to the total width of the high order x-ray lines. The form of the curve shows that probably the conditions were not sufficiently steady, either from the point of view of zone temperature or mechanical stability. It would appear however that this method might give solid specimens in equilibrium condition if a still slower rate of sweep were used and sufficiently steady conditions of temperature and mechanical stability obtained. The composition of the material varies with position along the ingot, but it is possible to determine the composition from the lattice parameter.

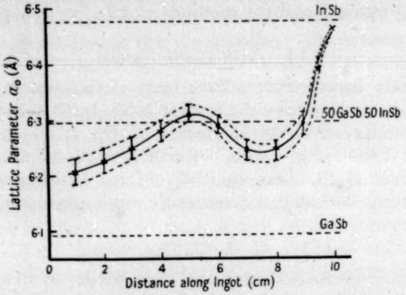

Figure 9. Variation of lattice parameter a_0 with position along a zone recrystallized ingot of mean composition 50 mol% GaSb 50 mol% InSb.

In order to carry out the slow directional freezing, a furnace was wound with an asymmetrical winding so that in the temperature range 500–700°C there was a temperature gradient along its axis of approximately 12°C cm^{-1} over some 25 cm. An ingot of the 50 mol % GaSb 50 mol % InSb some 14 cm long was sealed in quartz and placed in the furnace. The furnace conditions were adjusted so that the low temperature end of the ingot was at 700°C. The temperature of the whole furnace was then slowly reduced by 30° per day until the high temperature end of the ingot was at 500°C, the whole process taking 14 days. The ingot was then removed from the furnace and sections taken at several points along its length were x-rayed. Figure 10 shows the values of lattice parameter as a function of position in the ingot, the spread indicating, as before, the total width

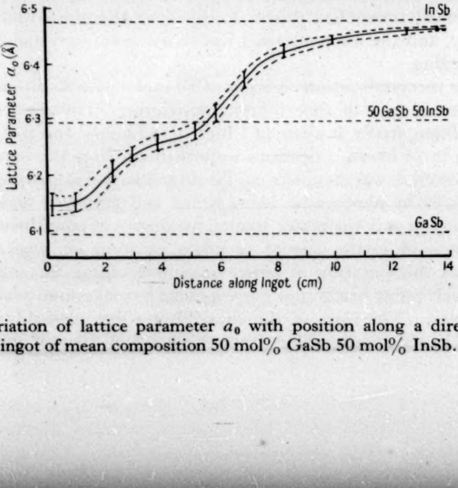

Figure 10. Variation of lattice parameter a_0 with position along a directionally frozen ingot of mean composition 50 mol% GaSb 50 mol% InSb.

of the high order x-ray lines. It is seen that the degree of homogeneity is very similar to that for the slow zone melting case. A slower reduction of the temperature, i.e. a slower movement of the point of solidification along the ingot, should give sections nearer to equilibrium. While there seems little to choose between the two methods for the GaSb–InSb system, the directional freezing method will probably be more convenient for systems involving higher melting point components and especially when one component contains a volatile constituent.

§ 5. CONCLUSIONS

Taking the above results in conjunction with those of Folberth (1955), it appears probable that in all systems composed of two $A^{III}B^{V}$ compounds, a large range of solid solution will occur, and that in many, if not all, cases there will be complete solid solution throughout the whole range of composition. The conflicting results of previous work appears to be due to non-attainment of equilibrium because of insufficient time, and possibly too low a temperature, of annealing. While powders can be brought to equilibrium under favourable conditions by annealing for times of the order of three months or less, it would appear that solid ingots require considerably longer times if normal annealing methods are used. Thus the production of solid specimens in equilibrium condition would seem to require techniques such as the slow zone recrystallization or the slow directional freezing methods described above.

ACKNOWLEDGMENTS

The authors are indebted to Professor L. F. Bates for the facilities of his laboratory. The work described forms part of an investigation carried out for the Admiralty, and acknowledgment is made to Dr. O. Simpson and Mr. J. T. Edmond of the Services Electronics Research Laboratory, Baldock, for helpful discussions, for the provision of the GaAs and InAs used in the work and for permission to publish this work.

REFERENCES

APTEKAR, A. I., and FINKELSTEIN, B. N., 1951, *J. Exp Theor. Phys.*, **21,** (8), 900.
BLAKEMORE, J. S., 1957, *Canad. J. Phys.*, **35,** 91.
EISIN, F. H., and BIRCHENALL, C. E., 1957, *Acta Met.*, **5,** 265.
FOLBERTH, O. G., 1955, *Z. Naturf.*, **10a,** 502.
GLICKSMAN, M., 1956, *Phys. Rev.*, **102,** 1496.
GORYUNOVA, N. A., and FEDOROVA, N. N., 1955, *J. Tech. Phys., Moscow*, **24,** 1339.
HERMAN, F., 1954, *Phys. Rev.*, **95,** 847; 1955, *Proc. Inst. Radio Engrs*, **43,** 1703.
HERMAN, F., GLICKSMAN, M., and PARMENTER, R. H., 1957, *Progress in Semiconductors*, **2** (London : Heywood), 1.
KOLM, C., KULIN, S. A., and AVERBACH, B. L., 1957, *Phys. Rev.*, **108,** 965.
KÖSTER, W., and THOMA, B., 1955, *Z. Metallk.*, **46,** 293.
LEVITAS, A., WANG, C. C., and ALEXANDER, B. H., 1954, *Phys. Rev.*, **95,** 846.
PARMENTER, R. H., 1955 a, *Phys. Rev.*, **97,** 587 ; 1955 b, *Ibid.*, **99,** 1759 ; 1956, *Ibid.*, **104,** 22.
SHIH, C., and PERETTI, E. A., 1953, *J. Amer. Chem. Soc.*, **74,** 608.
STÖHR, C., and KLEMM, W., 1939, *Z. anorg. Chem.*, **241,** 305.
WOOLLEY, J. C., and SMITH, B. A., 1957, *Proc. Phys. Soc.* B, **70,** 153.
WOOLLEY, J. C., SMITH, B. A., and LEES, D. G., 1956, *Proc. Phys. Soc.* B, **69,** 1339.

Magnetization Processes in a Polycrystalline Manganese Zinc Ferrite

By L. F. BATES, H. CLOW, D. J. CRAIK† and P. M. GRIFFITHS
Department of Physics, University of Nottingham

MS. received 13*th March* 1958, *and in final form* 5*th May* 1958

Abstract. A description is given of Bitter figure, magneto-thermal and Barkhausen studies of the behaviour of a polycrystalline manganese zinc ferrite during magnetization, from which it is concluded that the processes of magnetization are entirely rotational.

---

§ 1. Introduction

Work has recently been done (Bates, Christoffel, Clow and Davis 1957) on the magnetization of soft ferromagnetic metals in order to correlate magnetization changes with changes in the domain configurations observed in Bitter figure experiments. In single crystal ferromagnetic specimens, magnetization in low fields occurs mainly by domain wall motion, and in high fields by rotation of the magnetic vectors from a direction of easy magnetization. Corresponding effects are found in polycrystalline metal specimens. Wall motion was observed by Galt (1954) in a single crystal specimen of nickel ferrite cut as a picture frame with sides parallel to the [111] easy direction, and the wall position corresponded to the intensity of magnetization of the specimen. Work has also been done on the magnetization of polycrystalline ferrites, but no direct investigations of their domain structures have been published. In this paper are given the results of an examination of the behaviour of a manganese zinc ferrite, by Bitter figure and magneto-thermal methods, which suggest that the magnetization processes for this specimen are entirely rotational.

§ 2. Powder Pattern Observations

Several specimens of zinc substituted manganese ferrite of the composition of $Mn_{0\cdot7}Zn_{0\cdot3}Fe_2O_4$ were kindly prepared by Dr. A. J. E. Welch, Imperial College of Science. They were in the form of cylinders, approximately 0·7 cm diameter and 2 cm long. Their density was 4·1g cm^{-3}, corresponding to an 86% x-ray density. A flat surface was ground parallel to the long axis of one of them, and the polishing was finished with 0000 emery. This produced a glass-like surface with occasional pits left by the removal of whole crystallites during the initial grinding. The best surface was obtained when as much as possible of the abrasion was done with the fine grade emery paper. A film of magnetite colloid in ' Celacol ' was dried on the surface and observed both by optical and electron microscopy, as described by Craik and Griffiths (1958).

The pattern seen in figure 1 (Plate I) consists of an array of curved domain walls shown inside the circle which extend over each individual grain, the walls being usually perpendicular to the grinding direction. Grain boundaries are located, in part, by colloid deposits caused by divergence of the magnetic field between neighbouring crystallites the outlines of whose boundaries are shown by broken lines. When a small normal magnetic field was applied to the specimen three types of pattern were observed. The first, figure 2 (*a*) and (*b*) (Plate I), was a series of heavy band deposits, formed over alternate domains bordered by the domain walls previously observed in the absence of the field. In figure 2 (*b*) is reproduced the electron micrograph of a region similar to that encircled in figure 2 (*a*); the arrow shows the direction of polishing. The heavy deposits could be shifted to alternate domains by field reversal. The band patterns, figure 2 (*a*) and (*b*), could be altered by a magnetic field applied parallel to the long axis of the specimen, and when a sufficiently high field was applied the rod saturated and the surface configuration disappeared.

---

† Now at Boots Pure Drug Co. Ltd., Beeston, Notts.

The second type consisted of a roughly parallel array of zig-zag lines, spaced 1μ apart, as in figure 3 (Plate I), the patterns being perpendicular to the grinding scratches. In the third type, the pattern was not coherent and irregular colloid deposits due to scratches were formed (see left-hand side of figure 2 (*b*)).

Since it was considered that the patterns were caused by strain effects in a surface layer, an attempt was made to obtain a strain-free surface by alternately etching and polishing with the finest metallurgical cream. The specimen was etched in boiling concentrated HCl, which served to reveal the grain size. After etching for two minutes in the HCl, little of the original surface was left.

When the specimen was etched for 100 sec and very lightly polished, a fourth type of pattern was observed (figure 4, Plate II); it consisted of fine irregular lines on certain grains only, and it appeared to have no connection with the direction of the final polish. Since the material has a very low crystal anisotropy, stated below to be about -15×10^3 erg cm^{-3}, the lines might still have been due to polishing strain. Consequently, the surface was re-etched for another 100 sec without further polishing. No structure was observed with or without applied vertical or horizontal magnetic field.

§ 3. ANALYSIS OF POWDER PATTERN OBSERVATIONS

All the types of pattern described above are clearly due to strain, and are purely surface effects. Even the lightest polish produced such effects. The complete absence of structure found on the well-etched surface, which may reasonably be assumed to be strain free, can have one of two possible explanations. Either there is no domain structure, which means that the crystals are below the critical size for single domain particles, or a domain structure exists which present techniques are not adequate to manifest.

The observation of powder patterns depends on the saturation magnetization I_0 of the specimen and on the domain wall thickness. The latter is governed by the crystal anisotropy K_1 and is inversely proportional to $\sqrt{K_1}$. Since this manganese zinc ferrite is magnetically soft, $I_0 = 340$ gauss and K_1 is estimated to be -15×10^3 erg cm^{-3} (from Bozorth, Tilden and Williams 1955), some difficulty must be expected in the observation of powder patterns. However, we have observed patterns on the (110) surface of a single crystal specimen of manganese ferrite which had a crystal anisotropy $K_1 = -30 \times 10^3$ erg cm^{-3}. Its surface had been similarly prepared by etching and polishing. The observed patterns resembled some obtained on the (110) surface of a single crystal of nickel (Stephan 1955, Yamamoto and Iwata 1953). They were well defined and easily seen with the dried film technique. The effects of polishing strain were very like those found for the polycrystalline specimen. Figure 5 (Plate II) shows 'wriggly' boundaries, observed after etching and a final light polish of the single crystal surface, which resemble the patterns observed on the polycrystalline specimen after similar treatment. Figure 6 (Plate II) shows some tree patterns, typical of a surface having a slight misorientation from the true crystallographic (110) plane, obtained when the surface was well etched and not subsequently polished. Figure 7 (Plate II) shows an electron micrograph of a 'stepped' wall formed by 109° and 180° domain boundaries.

The approximate wall widths may be measured directly from the electron micrographs, figure 4 and figure 7, for the strained polycrystalline $Mn_{0.7}Zn_{0.3}Fe_2O_4$ and the single crystal $MnFe_2O_4$ specimens, respectively, assuming that the finest continuous line of colloid particles gives a true representation of the domain wall section above which they lie.

Using the formula $\delta = 7(A/K_1)^{1/2}$ given by Smit and Wijn (1954), where δ is the wall width and A the exchange coupling energy (cf. Bates 1951), the anisotropy constant K_1 may be calculated. From the photographic measurements with the polycrystalline specimen of the manganese zinc ferrite, K_1 is found to be -12×10^4 erg cm^{-3}; from those with a single crystal of manganese ferrite ($MnFe_2O_4$), K_1 is -3×10^4 erg cm^{-3}, using Smit and Wijn's value for $A = 10^{-6}$ erg cm^{-1}. The latter value agrees very closely with that found by torque magnetometer and resonance methods (Bozorth, Tilden and Williams 1955). The former value, however, is greater by almost a factor of ten than the estimated value -15×10^3 erg cm^{-3} for this manganese zinc ferrite.

The large difference between the measured and calculated values of K_1 for the polycrystalline material suggests that a large stress component, due to the final light polish, was present in the specimen surface. The structure shown in figure 4 must therefore belong to a strained surface.

Since the wall thickness of $MnFe_2O_4$ differs from that of the manganese zinc ferrite only by a factor of $\sqrt{2}$, and the values of I_0 are comparable, any method which reveals walls on the one ought to reveal them on the other. Remembering that the surface preparation was the same in both cases, we conclude from the absence of patterns on the polycrystalline manganese zinc ferrite that no domain structure exists in it.

The measured grain size of the specimen was between 50 and 100μ; the estimated grain size for single domain particles is about 1μ or less. This is, however, smaller than the calculated wall thickness and hence the generally accepted formulae are inapplicable.

§ 4. THERMAL MEASUREMENTS

Another method of investigating the nature of the magnetic processes is to measure the temperature changes which take place as a specimen is taken step by step around a magnetization cycle. By comparing the observed thermal changes with those calculated for various mechanisms, the actual method of magnetization of the specimen may be deduced.

Stoner and Rhodes (1949) showed that the reversible component of a thermal change ΔQ_R for a field change from H_1 to H is given by

$$\left[\Delta Q_R\right]_{H_1}^{H} = a\int_{H_1}^{H} d(HI) + b\int_{H_1}^{H} H dI_R \qquad \ldots\ldots(1)$$

where I is the intensity of magnetization and dI_R a reversible increment of I.

The first term on the right-hand side represents the thermal change due to the intrinsic or Weiss and Forrer magneto-caloric effects, and $a = -(T/I_0)(\partial I_0/\partial T)$, where I_0 is the intensity of intrinsic magnetization. The second term represents the thermal change due to reversible rotation processes such as are found in the region between remanence and saturation and $b = (T/K_1)(\partial K_1/\partial T)$, where K_1 is the first order anisotropy constant.

Teale and Rowlands (1957) showed that

$$\Big[\Delta Q_{\mathrm{R}}\Big]_{H_1}^{H} = a\Big[HI - H_1 I_1\Big] + c\int_{H1}^{H} H dI_{\mathrm{R}}. \qquad \ldots\ldots (2)$$

The first term now applies both to reversible and irreversible magnetic changes, but the second term still holds for reversible changes only. The constant a remains the same as before, but the constant b is now replaced by a more general constant c, which has different values for different magnetic processes. If the free energy can be expressed in the form $F = Af(I/I_0)$, where A is a constant for the material and is a function of T, $c = (T/A)(\partial A/\partial T)$. Thus, for rotation processes, $F = K_1 f(I/I_0)$ and $c = (T/K_1)(\partial K_1/\partial T) = b$; in other words we have equation (1).

The second term in equation (2) includes $\int H dI_{\mathrm{R}}$, and can therefore be applied only to *one* magnetization process at a time.

Consequently, to analyse the experimental curve we calculate the heating due to the intrinsic or magneto-caloric effect using the first term of equation (2) and subtract it from the experimentally observed heating Q_{R}'. We then define

$$Q_{\mathrm{R}}'' = Q_{\mathrm{R}}' - a\int_{H1}^{H} d(HI)$$

so that an experimental value of c known as c'' may be calculated from the relation

$$c'' = Q_{\mathrm{R}}'' \Big/ \int_{H_1}^{H} H dI_{\mathrm{R}}.$$

This calculated value of c'' can then be compared with the theoretical values to be expected for c when different magnetization processes are envisaged; c'' is equivalent to b'' when rotation processes alone are present.

§ 5. RESULTS OF THERMAL MEASUREMENTS

The thermal changes were measured by the method frequently used in Nottingham (Bates and Sherry 1955, Bates and Christoffel 1957) in which the specimen under investigation is ideally a rod some 30 cm long and 3 or 4 mm in diameter. It is mounted vertically in a solenoid which supplies the magnetizing field. The required temperature changes were measured by ten differential copper–constantan thermocouples connected as described in the above references. Stout leads carried the thermocouple currents to separate windings on a mumetal core or transformer. The transformer output was fed to a galvanometer amplifier with pen recorder. The recorder showed the general trends of any thermal drifts, so that allowance could be made for them. In this way the accuracy of the apparatus was much improved. The specimen used here was made by carefully cementing together ten pieces of the ferrite, end to end, to form a composite rod some 17 cm long and 0·6 cm in diameter. This had a demagnetizing factor of 0·018 (Bozorth and Chapin 1942).

The apparatus is usually calibrated by producing an adiabatic cooling of the specimen by suddenly hanging a weight on it, but the present specimen was too fragile. Calibration by electrical heating was also out of the question, owing to the composite nature of the specimen. A calibration based on the Warburg heating (total hysteresis loss) was also impossible as it was too small (100 erg cm^{-3} per cycle). The only calibration, therefore, was made by equating the heating of the specimen from -800 Oe to -600 Oe with that calculated for the intrinsic or magneto-caloric effect. This rough calibration was used to obtain a value of b'', so that the heating due to rotation could be calculated. This was added to the magneto-caloric effect for the field change from -800 Oe to -600 Oe, and a more accurate calibration, $188 \pm 3{\cdot}0$ erg mm^{-1} on the recorder, was obtained. The value of the constant a used in this calibration was obtained by measuring the variation of I_0 with temperature, using an apparatus like that used by Weiss and Forrer; at 20°c a was found to be $-0{\cdot}88 \pm 0{\cdot}01$.

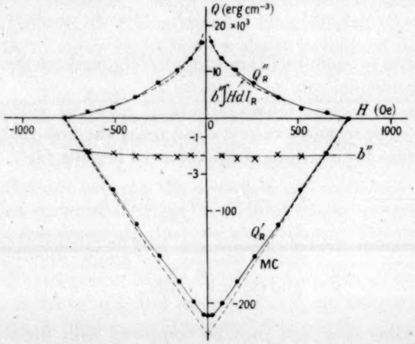

Figure 8. Curve of thermal changes over whole range of field. Q_R', experimental values of reversible heat changes, MC, magneto-caloric effect (Weiss and Forrer), Q_R'' obtained by subtracting MC curve from Q_R', b'', calculated from $Q_R''/\int HdI_R$.

The experimental results, shown in figure 8, represent one half of the magnetization cycle, starting at -800 Oe and ending at $+800$ Oe. The curve Q_R' shows the reversible thermal changes which occur as the specimen is taken round the cycle using the method of backward steps (Bates and Sherry 1955). No difference could be observed between the 'total' and the 'reversible' thermal curves for this specimen. The heating due to the magneto-caloric effect is shown by the broken curve MC, and the difference between the latter and Q_R' is plotted as Q_R''. This is compared with $-2\int HdI_R$, (since b was found to be equal to -2 for all except very small fields); the constancy of b'' with field is shown.

In order that the low field region might be studied more carefully, the sensitivity of the apparatus was increased by a factor of 10 to 18·8 erg mm^{-1} on the recorder while field changes between -20 Oe and $+20$ Oe were being investigated.

§ 6. Analysis of the Results

The value of $b=(T/K_1)(\partial K_1/\partial T)$ is required before a thermal curve can be analysed. The value of K_1 was found using the relation given by Hoselitz for negative values of K_1, viz

$$\int_{H=0}^{H=\infty} H\,dI = -\frac{2}{15}K_1. \qquad \ldots\ldots(3)$$

It is assumed that at remanence the magnetization vectors lie along the nearest easy direction to the field, and so that the magneto-crystalline energy is $K_0+\frac{1}{3}K_1$, while at saturation the vectors lie along the field direction and the magneto-crystalline energy is $K_0+\frac{1}{5}K_1$. The difference between these energies must be equal to the change in magnetic energy between saturation and remanence if vector rotations alone take place, and we then have equation (3).

In the ferrite under discussion it is obvious from the magnetization curve, figure 9, that at remanence the vectors have turned much further than is envisaged above, and the value of I which would exist when the vectors have just reached the nearest easy direction to the field has been calculated by Gans (1932) to be $0{\cdot}866I_0$.

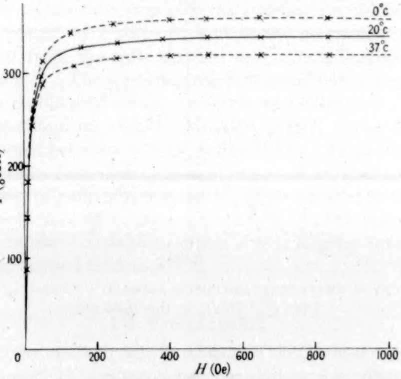

Figure 9. Magnetization curve, showing one half cycle.

Hence, when $I=0{\cdot}866I_0$ it has the correct value for the magnetization vectors to lie in the nearest easy direction to the field, i.e. for rotations to have ended. They will not have ended in practice, as the different magnetic processes overlap, but as this value of I lies on the knee of the magnetization curve, it has been assumed that to a first approximation rotations occur only in higher fields, and that the remaining processes take place in lower fields. A small overlapping of the low field processes and the high field rotations will not appreciably affect the thermal analysis. In this way $\int H dI_R$ can be split up into two parts, one due to rotations and the remainder due to special low field processes, and an estimate of the value of the constant c'' for the latter can be made.

The field for which $I=0{\cdot}866I_0$ is 53 Oe for the 20° magnetization curve, and $\int HdI$ from saturation to 53 Oe was used to calculate K_1 from equation (3) giving the remarkably low value $-1{\cdot}3 \pm 0{\cdot}5 \times 10^3$ erg cm^{-3}, but as equation (3) is not rigorous there is little point in pursuing this matter. The above analysis, however, should lead to reasonable results when used to calculate $(T/K_1)(\partial K_1/T)$, as the numerical value of K_1 cancels out. Magnetization curves were measured at 0, 20 and 37°C, and b was found in this way to be $-2{\cdot}0 \pm 0{\cdot}3$, which is in agreement with the experimental constant b''. The slight decrease in b'' in high fields, shown in figure 8, may be due to the effect of the second anisotropy constant K_2. Thus it is seen that above 53 Oe exact agreement between experiment and the Stoner and Rhodes theory is obtained.

Between fields of -53 and $+53$ Oe a different magnetization process must take place, and it is assumed that the effect of this is very much greater than that of any slight rotation which might occur in this region. Values of $\int H dI_R$ from -53 to $+53$ Oe were compared with the changes in Q_R'' in this field range to obtain experimental values of the constant c'' (as opposed to the theoretical values c). The best value for c'' was $-1{\cdot}6$, and a graph of $-1{\cdot}6\int H dI_R$ is compared with Q_R'' in figure 10; the experimental values of c'' are also given in this figure.

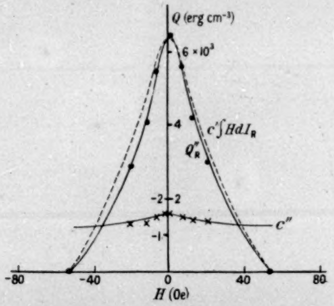

Figure 10. Analysis of thermomagnetic curves between -53 and $+53$ Oe. c'' calculated from $Q_R''/\int H dI_R$ in this field range.

Teale and Rowlands (1957) considered the problem of the rotation of the magnetization vector in a particle without domains. If the main energy change is due to the change in magnetostatic energy of its surface magnetization, the value of c is $(2T/I_0)(\partial I_0/\partial T)$, with a numerical value $-1{\cdot}76 \pm 0{\cdot}02$. This is in very good agreement with $-1{\cdot}6$ obtained for c'' and indicates that in low fields the magnetization changes by unusual rotations in which the magnetostatic energy rather than the magnetocrystalline energy is changed. This implies that the rotations take place by jumps from one easy direction to another.

The table gives in a convenient form the theoretical expressions for c and their corresponding numerical values, together with the values found for b'' and c'' for the ferrite under discussion. The quantity $(T/\lambda_s)(\partial\lambda_s/\partial T)$, where λ_s is the saturation magnetostriction, was measured by an optical lever method, but the value of $+2$ obtained must be regarded as an order of magnitude only.

It can be seen that the values of c for the domain wall theories cannot be made to fit c'' in spite of the uncertainty in $(T/\lambda_s)(\partial\lambda_s/\partial T)$, and that wall movement would have given a 'dip' in the thermal curve.

Table of Values of the Constant c

	(1)	(2)	(3)	(4)	(5)
c (theor)	$\frac{T}{K_1}\frac{\partial K_1}{\partial T}=b$	$\frac{2T}{I_0}\frac{\partial I_0}{\partial T}$	$\frac{T}{\gamma}\frac{\partial \gamma}{\partial T}$	$\frac{T}{I_0}\frac{\partial I_0}{\partial T}+\frac{T}{2\lambda_s}\frac{\partial \lambda_s}{\partial T}$	$\frac{2T}{\lambda_s}\frac{\partial \lambda_s}{\partial T}-\frac{T}{K_1}\frac{\partial K_1}{\partial T}$
c (num)	$-2{\cdot}0\pm0{\cdot}3$	$-1{\cdot}76\pm0{\cdot}02$	$-0{\cdot}95\pm0{\cdot}2$	$+0{\cdot}12$	$+6$

Nature of magnetic process: (1) rotation against crystalline anisotropy; (2) rotation against magnetostatic energy; (3) wall formation; (4) wall movement using strain theory; (5) wall movement using disperse-field theory. $b''=-2{\cdot}0$, $c''=-1{\cdot}6$, γ = wall energy. c (theor) = theoretical expression for c, c (num) = numerical value of c.

§ 7. BARKHAUSEN EFFECTS

Since both the preceding sets of measurements indicated that the magnetization occurred by rotation processes, it remained to investigate their nature, as these could be either continuous or discontinuous; i.e. the magnetic vectors could either sweep gradually between the easy directions under the influence of an applied field or they could switch almost instantaneously. Observations were therefore made of the Barkhausen effects in the composite specimen used for the thermal measurements. Two coils each of 10 000 turns were wound in series opposition on a glass tube in which the specimen could be placed. The whole system was placed in a solenoid and as the magnetic field was slowly changed, the output from the coils was fed into an oscilloscope which had a sensitivity of 1 mv cm^{-1}. The apparatus was first tested with a large single crystal of iron with which Barkhausen effects were observed with ease.

Barkhausen discontinuities with the $Mn_{0{\cdot}7}Zn_{0{\cdot}3}Fe_2O_4$ were observed to occur with small field changes between -35 Oe and $+35$ Oe. From the magnetization curve, rotation between easy directions was expected to continue up to 53 Oe. At 35 Oe the intensity of magnetization is 93% of its value at 53 Oe, so that 93% of the rotations should have taken place when a field of 35 Oe was reached. The apparatus was not sensitive enough to detect any remaining rotations occurring with increase in the applied field to 53 Oe.

§ 8. CONCLUSIONS

We have shown that no bulk domain walls can be detected on the specimen of manganese zinc ferrite by the Bitter figure techniques which gave domain structures on a large crystal of an essentially similar material. The thermal measurements suggest that the magnetization of the specimen occurs by normal rotation of the magnetic vectors away from the easy direction nearest to the applied magnetic field in high field regions; in low field regions, magnetization changes occur by unusual rotations between the easy directions themselves. Barkhausen observations show that the low field rotations are discontinuous. In the latter region the rotations can take place either by reversals in one easy direction or by rotation in two or three steps between adjacent easy directions.

ACKNOWLEDGMENTS

D. J. C. wishes to thank Mr. W. J. Randall for his interest and encouragement. H. C. and P. M. G. wish to thank the Department of Scientific and Industrial Research for maintenance allowances.

References

Bates, L. F., 1951, *Modern Magnetism* (Cambridge: University Press), p. 446.

Bates, L. F., and Christoffel, D. A., 1957, *Proc. Instn Elect. Engrs*, B, **104**, 231.

Bates, L. F., Christoffel, D. A., Clow, H., and Davis, P. F., 1957, *Proc. Roy. Soc.* A, **243**, 160.

Bates, L. F., and Sherry, N. P. R., 1955, *Proc. Phys. Soc.* B, **68**, 304, 642.

Bozorth, R. M., and Chapin, D. M., 1942, *J. Appl. Phys.*, **13**, 320.

Bozorth, R. M., Tilden, E. F., and Williams, A. J., 1955, *Phys. Rev.*, **99**, 1788.

Craik, D. J., and Griffiths, P. M., 1958, *Brit. J. Appl. Phys.*, in the press.

Galt, J. K., 1954, *Bell Syst. Tech. J.*, **33**, 1023.

Gans, R., 1932, *Ann. Phys., Lpz.*, **15**, 28.

Hoselitz, K., 1952, *Ferromagnetic Properties of Metals and Alloys* (Oxford: Clarendon Press), p. 65.

Smit, J., and Wijn, H. P. J., 1954, *Advances in Electronics and Electron Physics*, Vol. VI, Editor: L. Marton (New York: Academic Press).

Stephan, W., 1955, *Exp. Tech. Phys.*, **1**, 1.

Stoner, E. C., and Rhodes, P., 1949, *Phil. Mag.*, **40**, 481.

Teale, R. W., and Rowlands, G. R., 1957, *Proc. Phys. Soc.* B, **70**, 1123.

Yamamoto, M., and Iwata, T., 1953, *Sci. Rep. Res. Insts. Tôhoku Univ.*, A-Vol. 5, No. 5.

The Use of the Kerr Effect for Studying the Magnetization of a Reflecting Surface

By E. W. LEE,† D. R. CALLABY† and A. C. LYNCH‡

† Department of Physics, University of Nottingham
‡ Post Office Research Station, Dollis Hill, London, N.W.2

Communicated by L. F. Bates ; MS. received 10th March 1958

Abstract. If a moving domain wall crosses a small illuminated area, the reflection coefficient may change and the plane of polarization of the reflected light may be rotated. If the wall moves in an alternating field, the change can be detected by collecting the light on a photomultiplier cell and amplifying the alternating component of its output signal.

Using a specimen of a magnetically annealed Perminvar-type alloy, the variation of the output signal and of the signal-to-noise ratio with the angle of polarization has been shown to agree closely with that predicted by theory, both for longitudinal and transverse magnetizations. It is unnecessary to use both a polarizer and an analyser; indeed, an effect is observable with neither.

---

§ 1. Introduction

Since the pioneer investigations of Bitter (1931) and Elmore (1938) the experimental study of domains in ferromagnetic crystals by the powder pattern technique has been both extensive and fruitful. As a result of such studies we now have a fairly clear picture of the nature of ferromagnetic domains and of the process of magnetization (see for example Bates 1954, 1957, Williams, Bozorth and Shockley 1949). At the same time there has been a growing realization of the limitations of the powder pattern technique, the most notable of which are: (i) it cannot easily be used at any other than room temperature, although the experiments of Andrä and Schwabe (1956) with dry Fe_3O_4 powder go some way to removing this restriction, (ii) it cannot be used to study domain walls in rapid motion, i.e. under dynamic conditions, and (iii) it can only be used with materials possessing large anisotropy and, thereby, narrow domain walls. The latter is a consequence of the fact that the powder patterns require the existence of local surface fields for their formation and these are small in soft magnetic materials having low anisotropy. Various other techniques have been suggested for investigating domains, notably electron scattering and similar methods (Germer 1942, Blackman and Grünbaum 1956) and the Permalloy probe method of Kaczer (1955). Some of these certainly possess certain advantages over the powder pattern method.

A more promising approach appears to be to make use of the magnetic Kerr effect. This method, first employed by Williams, Foster and Wood (1951) was later developed by Fowler and Fryer (1952, 1954 a) to a high degree of sensitivity and precision. If the surface of a ferromagnetic crystal is illuminated by plane polarized light and the reflected light is viewed through a Nicol or similar polarizing element in the nearly crossed position the domains appear as alternate bright and dark bands which may be photographed. Direct visual observation is possible but the lack of contrast often makes it difficult to see the domains clearly and almost impossible to investigate the finer details of their structure. The undoubted success of Fowler and Fryer seems to have been achieved only as a result of considerable skill, ingenuity and long experience; and they had to develop special photographic techniques to distinguish the domain pattern from the background due to surface imperfections (Fowler and Fryer 1954 b). In view of this we have examined in detail another way whereby the Kerr effect may be used to study domains.

Consider a small area of the specimen illuminated with plane polarized light, and reflecting it through a nearly crossed analyser. If a domain wall moves across this area, the intensity of the light leaving the analyser will change. If this movement is made periodic by the application of a small alternating field to the specimen the intensity of the emergent light will be modulated. This light, when received on the photocathode of a photomultiplier, will give rise to a small alternating current which can be amplified independently of the larger steady current on which it is superposed. In this way the presence of a signal having the same frequency as the applied field may be taken as evidence of a domain wall moving across or within the area of illumination.

In practice we have found this method to be entirely feasible and the object of this paper is to present results of a systematic investigation into the application of the Kerr effect. Since the nature of the effect itself does not appear to be well known we have thought it worth while to give a brief description of it first. More details are given in the review articles by von Laue (1928) and Schütz (1936), but the most complete account remains that of Voigt (1908) who was primarily responsible for the elucidation of the effect.

§ 2. THE KERR EFFECT

If a beam of plane polarized light illuminates a metallic surface the reflected light will in general be elliptically polarized. If, however, the plane of polarization of the incident light (here defined as the plane containing the electric vector) is either parallel or perpendicular to the plane of incidence then the reflected light is also plane polarized. That this is so is in no way due to any peculiarities of metallic reflection but follows straightway from the fact that the plane of incidence is a plane of symmetry for the system. Incident light polarized parallel or perpendicular to this plane is therefore always reflected as plane polarized light. This symmetry is destroyed by the presence of a magnetic field, for although a uniform magnetic field possesses a plane of symmetry perpendicular to the direction of the field its sign is associated with an unsymmetrical rotation about this direction. Consequently, if the reflecting surface is magnetized the reflected light will in general be elliptically polarized even if the incident light is polarized parallel or perpendicular to the plane of incidence. This phenomenon is known as the Kerr effect. The degree of ellipticity imparted to the reflected beam is small and the effect can be regarded as a rotation of the plane of polarization of the light on reflection. The effect is greatest in the ferromagnetic metals, is smaller in ferrites and barely observable in paramagnetic metals.

There are three different dispositions of the magnetic field with respect to the plane of incidence and these give rise to three different effects each governed by slightly different laws. These are:

(*a*) *Polar effect* (figure 1 (*a*)), i.e. magnetization normal to the reflecting surface. The effect is largest in this case and it is the only situation in which an effect exists with light incident normally on the surface.

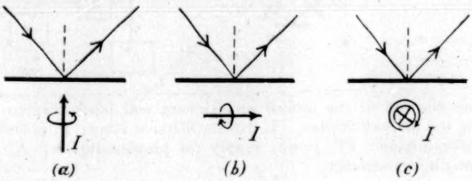

Figure 1. Diagram illustrating the disposition of the magnetization vector *I* with respect to the plane of incidence of the light beam. The arrow indicates the sense of the rotation associated with the magnetization vector. (*a*) polar effect, (*b*) longitudinal effect, (*c*) transverse effect.

(*b*) *Longitudinal effect* (figure 1 (*b*)), i.e. magnetization in the plane of the reflecting surface parallel to the plane of incidence. This is often referred to as the meridional effect. The rotation is smaller than for the polar effect, usually by a factor of 3 or 4.

(*c*) *Transverse effect* (figure 1 (*c*)), i.e. magnetization in the plane of the reflecting surface and perpendicular to the plane of incidence. This is sometimes referred to as the equatorial effect. Any other situation can easily be seen to be a combination of two or more of these.

In this paper are recorded systematic observations on the longitudinal and transverse Kerr effects only, the polar effect being of little use except for materials having large uniaxial anisotropy.

§ 3. APPARATUS

The optical side of the apparatus is very similar to that used by Fowler and Fryer (1952) and is shown in figure 2. It consists essentially of two identica polarizing microscope barrels each mounted so that they may be rotated about a horizontal axis perpendicular to the plane of the diagram. These barrel mounts are themselves mounted on a lathe bed by means of a set of traverses which allows movement of each barrel in three perpendicular directions. By this means accurate alignment of the optical system and also variation of the angle of incidence is made possible. The specimen under investigation is placed on a horizontal platform fitted with micrometer movements in two horizontal directions at right angles to each other. The light source is a 6 volt 100 watt ribbon filament lamp, run from batteries. The light from this passes through a slit of variable width and is focused by the first microscope on to the surface of the specimen in the form of a narrow rectangle of light. This will be referred to as the light probe. The reflected light is received by the second microscope, and then falls upon the cathode of a photomultiplier which takes the place of the usual eyepiece. Polarizers and analysers are inserted as required.

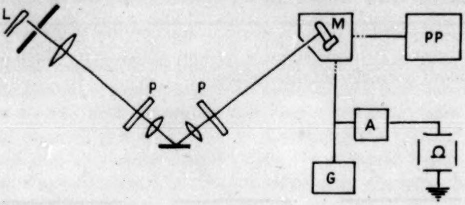

Figure 2. Line diagram of the optical arrangement and block diagram of the stages following the photomultiplier. L, ribbon filament lamp; P, polarizing elements; M, photomultiplier; PP, power supply for photomultiplier; A, amplifier; G, monitoring microammeter.

The principle of operation has been outlined in § 1 wherein it was stated that when a domain wall is made to vibrate across or within the light probe the output from the photomultiplier consists of a steady component and a small alternating one. The latter can be amplified and displayed on an oscilloscope screen. It was found convenient to monitor the system by measuring the steady current from the photomultiplier with a sensitive galvanometer. This provides a useful check on the degree of alignment of the optical system and also serves as a check to avoid saturation of the photomultiplier.

§ 4. SPECIMENS AND MATERIALS

The material used for the investigation was a Perminvar-type alloy (45% Ni, 25% Co, 30% Fe), made by powder metallurgy. It was in the form of stamped rings, magnetically annealed and possessing a rectangular hysteresis loop. This material is very convenient for this purpose because (i) it saturates easily and so stray fields from the toroidal magnetizing windings, which might affect the photomultiplier, are kept small, (ii) magnetization is believed to take place by radial movement of circular walls separating antiparallel domains. The specimens were not polished in any way and were used as received.

A 50 c/s magnetic field was applied to such a specimen and the position of the light probe was altered until a signal was observed from the photomultiplier. This was taken as evidence of the movement of a 180° domain boundary across the light probe.

§ 5. PERFORMANCE OF THE APPARATUS

Under the conditions of operation outlined in the previous sections the signal obtained from the photomultiplier was of the form of an approximately square wave. To secure optimum performance several factors were investigated and these are discussed separately.

5.1. *Signal to Noise Ratio*

The light intensity incident upon the photocathode of the photomultiplier consists essentially of very lightly modulated steady illumination. The percentage modulation depends on the specimen and the geometrical disposition of the incident light with respect to the reflecting surface. The output current from the photomultiplier therefore also consists of a large steady component and a small alternating one. The former is useful for monitoring the alignment of the apparatus and the latter is the signal proper. Unfortunately, this signal is accompanied by a good deal of random noise. This noise seems to be wholly attributable to random fluctuations in the electron emission from the photocathode and dynodes (shot noise). Under these circumstances the mean square noise voltage output is proportional to the steady output current (figure 3). Thus, since the signal voltage is proportional to the light intensity and the noise voltage to the square root of this, it follows that the signal-to-noise ratio is proportional to the square root of the light intensity incident on the photocathode (figure 4). Thus there is some advantage to be gained by using a specimen with a highly polished surface to reflect as much as possible of the incident light, whose intensity is necessarily limited in practice. Secondly, it follows that since the noise is produced as a result of the inherent randomness of the physical nature of photoelectric and secondary emission no particular type of photomultiplier is to be preferred for this purpose.

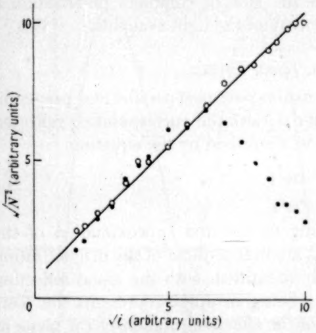

Figure 3. Root-mean-square noise voltage as a function of the square root of the steady output current. The solid circles show the reduction in noise voltage produced by the space charge obtained by using too low a voltage on the final dynode.

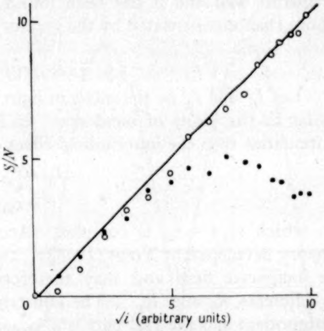

Figure 4. Signal-to-noise ratio as a function of the square root of the steady output current. The solid circles show the reduction in signal-to-noise ratio produced by allowing space-charge effects to occur.

5.2. *Space Charge Effects in the Photomultiplier*

One of the consequences of using a photomultiplier under the conditions of large steady illumination is the possibility of building up a space charge on the last stage of the photomultiplier. This can occur if the voltage applied to the final stage is very low compared with the total applied voltage. This effect was investigated by measuring the noise voltage N and the steady current i as the intensity of illumination of the photocathode was varied. The effect is clearly shown in the right-hand part of figure 3. The noise falls below its normal level, but the amplification of the system becomes non-linear and the signal, if greater than the noise, is reduced in an even greater ratio. Thus the signal-to-noise ratio is decreased by the effect of the space charge, as shown in figure 4.

In all subsequent investigations checks were made to see that space charge effects did not occur.

5.3. *Polarizing Elements*

Originally, double-layer polaroids were used in both the incident and reflected beams. These produce a very high degree of polarization but transmit little light. Single-layer polaroids whilst producing a smaller degree of polarization transmit well and it has been found that the lack of complete polarization is more than compensated by the greater intensity of the light available.

§ 6. LONGITUDINAL KERR EFFECT

Let $I_{\parallel}^{\rm i}$ and $I_{\perp}^{\rm i}$ be the incident light intensities polarized parallel and perpendicular to the plane of incidence. If $I_{\parallel}^{\rm r}$ and $I_{\perp}^{\rm r}$ are the corresponding reflected intensities then the longitudinal effect can be described by the equation

$$I_{\parallel}^{\rm r} = r_{11} I_{\parallel}^{\rm i} + r_{12} I_{\perp}^{\rm i}$$
$$I^{\rm r} = r_{21} I_{\parallel}^{\rm i} + r_{22} I_{\perp}^{\rm i}$$

in which $r_{12} = -r_{21}$ is complex. According to the first approximation of the theory developed by Voigt (1908) r_{11} and r_{22} are independent of the magnetization or magnetic field and may therefore be identified with the usual reflection coefficients $R_{\parallel}$ and $R_{\perp}$. The constant r_{12} being complex represents the Kerr component and the real part is a measure of the effective rotation of the plane of polarization on reflection. According to Voigt r_{12} is proportional to a certain complex quantity Q which involves the magnetic field or magnetization in the first degree. Reversing the direction of the magnetization therefore reverses the sign of r_{12}. The effect is known to depend upon the angle of incidence reaching a broad maximum at about 60°. This angle was kept fixed at 50° in the experiments described below.

Suppose there is no polarizing element in the incident beam and that an analyser is placed in the reflected beam only. Then the intensity of light incident upon the photocathode is

$$I_{\theta} = c_1 R_{\parallel} \cos^2\theta + c_2 R_{\perp} \sin^2\theta$$

where θ is the angle between the plane of polarization of the analyser and the plane of incidence. If the incident light were completely unpolarized c_1 and c_2 would be equal but this is not likely to occur because of polarization in the optical system and because the light is emitted obliquely from the ribbon filament. We suppose that the effect of the Kerr rotation is to change θ to $\theta \pm \theta'$ for the first term and to $\theta \pm \theta''$ for the second. The fact that $\theta' \neq \theta''$ is in agreement with previous observations and arises from second-order effects. The signal is then

$$S_{\theta} = \tfrac{1}{2} c_1 R_{\parallel} \{\cos^2(\theta+\theta') - \cos^2(\theta-\theta')\} + \tfrac{1}{2} c_2 R_{\perp} \{\sin^2(\theta-\theta'') - \sin^2(\theta+\theta'')\}$$

and the mean light intensity

$$I_{\theta} = \tfrac{1}{2} c_1 R_{\parallel} \{\cos^2(\theta+\theta') + \cos^2(\theta-\theta')\} + \tfrac{1}{2} c_2 R_{\perp} \{\sin^2(\theta-\theta'') + \sin^2(\theta+\theta'')\}$$

from which the ratio

$$\frac{S_{\theta}}{I_{\theta}} = -\frac{2\sin 2\theta\ (\theta' + P\theta'')}{1 + P + (1-P)\cos 2\theta} \qquad \ldots\ldots(1)$$

where $P=c_2R_\perp/c_1R_\parallel$. In this equation and in equations (2)—(4) below θ' and θ'' are small angles and the approximations $\sin\theta'=\theta'$, $\sin\theta''=\theta''$, $\cos\theta'=\cos\theta''=1$ have been made throughout. By direct measurement of the reflected intensities P was found to equal 1·6.

Figure 5 shows the observed ratio S_θ/I_θ using a polarizer only and using an analyser only. The experimental points are to be compared with the curve calculated from equation (1) with $P=1{\cdot}6$, $\theta'=6'$, $\theta''=7\tfrac{1}{2}'$.

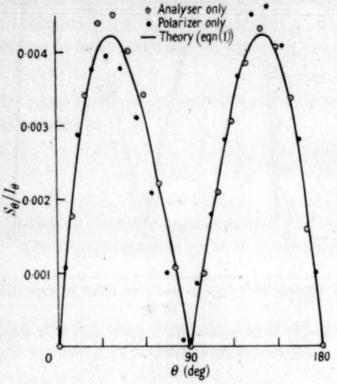

Figure 5. S_θ/I_θ as function of θ.

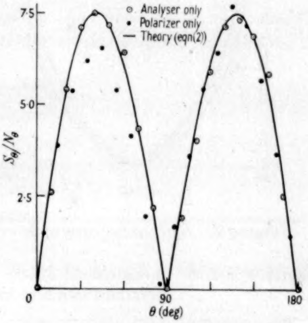

Figure 6. Signal-to-noise ratio as function of θ.

Figures 5 and 6. Longitudinal effect: single polarizing element. E vector in plane of incidence at $\theta=0$ and 180°.

The signal-to-noise ratio is

$$\frac{S_\theta}{N_\theta}\propto\frac{S_\theta}{I_\theta^{1/2}}\propto\frac{2\sin2\theta\,(\theta'+P\theta'')}{\{1+P+(1-P)\cos2\theta\}^{1/2}}. \qquad \ldots\ldots(2)$$

Figure 6 shows the measured signal-to-noise ratio with analyser only and with polarizer only. The calculated curve was obtained from equation (2) using the same value for the constants as before.

The effect of using a polarizing element in both incident and reflected beams was also investigated. In this case, suppose the angle between the plane of polarization of the two elements be θ, then the light intensity on the photocathode is $I_\theta=I_0\cos^2\theta$. Proceeding exactly as before one finds

$$\frac{S_\theta}{I_\theta}=-\frac{2\theta'\sin2\theta}{1+\cos2\theta} \qquad \ldots\ldots(3)$$

if the plane of polarization of the incident beam is parallel to the plane of incidence, with a similar formula involving θ'' for the other case. The comparison with experiment for the two cases is shown in figure 7 using the same values for θ' and θ'' as before. The agreement is quite good except near $\theta=\pm90°$. It will be noticed from equation (3) that the ratio S_θ/I_θ is unity when $\theta=90°+\theta'$. In practice $\theta=\pm90°+\theta'$ corresponds to positions where the polarizing elements are nearly crossed. In the experimental arrangement used single-layer polaroids were used for reasons previously stated. These transmit a good deal of light when crossed and so the ratio S_θ/I_θ falls below the theoretical value of unity.

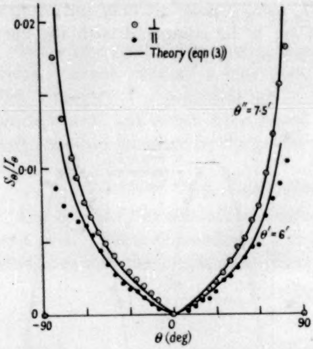

Figure 7. S_θ/I_θ as function of θ.

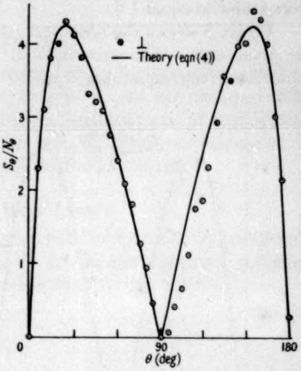

Figure 8. Signal-to-noise ratio as function of θ.

Figures 7 and 8. Longitudinal effect: polarizer and analyser. ⊥, ∥, incident light polarized with E vector ⊥, ∥ to plane of incidence.

The signal-to-noise ratio is

$$\frac{S_\theta}{N_\theta} \propto \frac{2\theta' \sin 2\theta}{\{1+\delta+\cos 2\theta\}^{1/2}} \qquad \ldots\ldots(4)$$

in which a small quantity δ has been included to take into account the finite transmission through the polaroids at $\theta = 90°$. Figure 8 shows the observed signal-to-noise ratio with the incident light polarized at right angles to the plane of incidence and with $\delta = 0{\cdot}08$. The effect of the finite transmission is to shift the position of maximum signal-to-noise ratio to $\theta = 65°$.

In this case the maximum signal-to-noise ratio is inferior to that obtained using only a single polarizing element. This is caused by a reduction in the light intensity reaching the photocathode due to the additional absorption of light by the extra element.

§ 7. TRANSVERSE KERR EFFECT

The symmetry of this arrangement precludes the possibility of a rotation of the plane of polarization and in this case the effect is wholly ascribable to a change in reflection coefficient. By symmetry the reflection coefficient $R_\perp$ for incident light polarized at right angles to the plane of incidence must be unaltered and so only $R_\parallel$ is affected by the magnetization. The theory of the effect given by Voigt shows that

$$R_\parallel = CR_\perp \frac{A \pm \alpha Q}{B \pm \alpha Q}$$

where Q has the same significance as before. Since αQ is much smaller than A or B this may be written

$$R_\parallel = C' R_\perp (1 \pm 2\alpha' Q)$$

where $C' = CA/B$ and $\alpha' = \alpha/AB$. This shows that reversal of the direction of the magnetization will produce a change in the reflection coefficient $R_{\parallel}$.

For the first experiments an analyser only was used. The reflected light intensity incident on the photocathode is therefore

$$I_\theta = c_1(R_{\parallel} \pm r)\cos^2\theta + c_2 R_{\perp}\sin^2\theta$$

where θ is the angle between the plane of polarization of the analyser and the plane of incidence. If the incident light were completely unpolarized c_1 and c_2 would be equal but this was not so because of polarization in the optical system and because the light is emitted obliquely from the ribbon filament. The change in light intensity incident on the photocathode is

$$S_\theta = 2c_1 r\cos^2\theta.$$

The ratio $S_\theta/2I_\theta$ represents the signal expressed as a fraction of the mean total d.c. output and is

$$\frac{S_\theta}{I_\theta} = \frac{(r/R_{\parallel})\cos^2\theta}{P-(P-1)\cos^2\theta} \qquad \ldots\ldots(5)$$

where $P = c_2R_{\perp}/c_1R_{\parallel}$ as before. Equation (5), with $r/R_{\parallel} = 1{\cdot}17 \times 10^{-2}$, $P = 1{\cdot}6$ is shown in figure 9 together with the experimental points.

The signal-to-noise ratio is proportional to $S_\theta/I_\theta^{1/2}$, i.e.

$$\frac{S_\theta}{N_\theta} = \text{const.}\,\frac{\cos^2\theta}{\{P-(P-1)\cos^2\theta\}^{1/2}}. \qquad \ldots\ldots(6)$$

With $P = 1{\cdot}6$ as before the constant was found to be $9{\cdot}5$. The comparison with experiment is shown in figure 10.

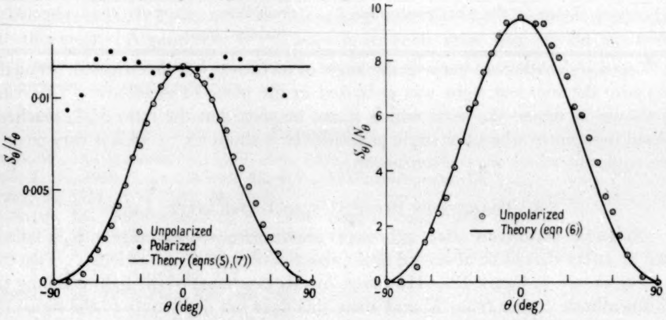

Figure 9. S_θ/I_θ as function of θ.

Figure 10. Signal-to-noise ratio as function of θ.

Figures 9 and 10. Transverse effect: analyser in reflected beam. E vector of analyser in plane of incidence at $\theta = 0$. Polarized—incident light polarized in plane of incidence.

It is evident that the light intensity represented by $c_2R_{\perp}\sin^2\theta$ is contributing to the noise and not to the signal. Therefore for any angle θ other than zero the signal-to-noise ratio should be improved by using incident light polarized in the plane of incidence. Under these circumstances equations (4) and (5) become

$$S_\theta/I_\theta = r/R_{\parallel} \qquad \ldots\ldots(7)$$

and

$$S_\theta/N_\theta = \text{const.}\cos\theta \qquad \ldots\ldots(8)$$

θ now being the angle between the planes of polarizer and analyser. Experimental results are shown in figures 9 and 11. It is evident that the maximum signal-to-noise ratio is actually decreased. This is due to the extra absorption by the additional polaroid as in the longitudinal effect.

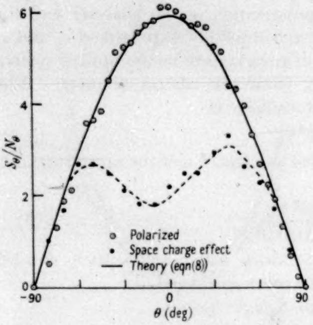

Figure 11. Transverse effect: analyser in reflected beam; incident light polarized in the plane of incidence. Signal-to-noise ratio. The two sets of points illustrated the deleterious effects of space charge in the photomultiplier.

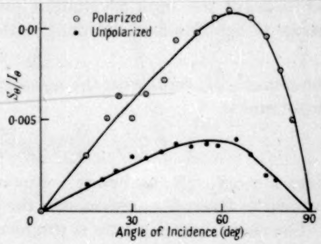

Figure 12. Transverse effect: without analyser. S_θ/I_θ as a function of angle of incidence. Polarized—incident light polarized with E-vector in plane of incidence. Note the complete absence of polarizing elements for unpolarized incident light.

Finally the effect of varying the angle of incidence was investigated. For this purpose the incident light was polarized in the plane of incidence. The result is shown in figure 12, from which it can be seen that the ratio S_θ/I_θ reaches a broad maximum when the angle of incidence is about 65°. This is very close to the angle for which $R_\parallel$ is a minimum.

§ 8. TRANSVERSE EFFECT USING UNPOLARIZED LIGHT

Since the transverse effect is brought about merely by a change in $R_\parallel$ it follows that an effect should be observed in the absence of polarizing elements. That this is so is shown in figure 12. However, in this case most of the light reaching the photocathode comes from $R_\perp$ and since this does not contribute to the signal the ratio S_θ/I_θ is much smaller.

§ 9. CONCLUSIONS

The results given in previous sections indicate that it should be possible to observe moving domain walls using the Kerr technique. It would appear that either the longitudinal or the transverse effects may be used. In the former, the best signal-to-noise ratio is obtained with a single polarizing element in either the incident or reflected beam. The element should possess good transmitting power and be set so that its plane of polarization is at roughly 45° to the plane of incidence. This angle will vary somewhat from one material to another, owing to variations in the Kerr rotation and the reflection coefficients, and is best determined separately for each material used. The optimum angle of incidence is about 60°.

Using the transverse effect the best signal-to-noise ratio is obtained using again a high-transmission polarizing element in either incident or reflected beam, but this time with its plane of polarization in the plane of incidence. The optimum angle of incidence is about 65°. Which of the two effects gives the better signal-to-noise ratio will, of course, depend on the relative magnitudes of the two effects and will vary from one material to another.

It will have been noted that in § 5 it was stated that an approximately square-wave output was obtained. This indicates that the domain wall was passing right across the width of the light probe. An alternative technique for mapping domains is to apply a very small alternating field to the specimen so that the wall moves always within the area of the light probe. This method requires a much greater sensitivity than the previous method and can only be obtained at the expense of a much reduced bandwidth in the amplifiers following the photomultiplier.

The method described here seems to have several advantages not possessed by other techniques. In the first place it does not rely on stray surface fields and can therefore be used, in principle, on all materials. Secondly, it requires no special preparation of the surface since imperfections such as scratches and rolling marks merely contribute to a steady signal which is removed. The main disadvantages are that owing to the finite size of the light probe, the method is limited to the investigation of relatively coarse domain structure and that it cannot distinguish between a domain wall at rest and absence of a domain wall.

ACKNOWLEDGMENTS

We wish to thank Professor L. F. Bates for his interest and advice in connection with this work. A good deal of the work in its early stage was carried out with equipment kindly lent by Professor W. D. Evans of the Department of Geology to whom we are very grateful.

REFERENCES

ANDRÄ, W., and SCHWABE, E., 1956, *Ann. Phys., Lpz.*, **17**, 55.
BATES, L. F., 1954, *J. Inst. Metals*, **82**, 417 ; 1957, *Endeavour*, **16**, 151.
BITTER, F., 1931, *Phys. Rev.*, **38**, 1903.
BLACKMAN, M., and GRÜNBAUM, E., 1956, *Nature, Lond.*, **178**, 584.
ELMORE, W. C., 1938, *Phys. Rev.*, **54**, 1092.
FOWLER, C. A., and FRYER, E. M., 1952, *Phys. Rev.*, **86**, 426; 1954 a, *Ibid.*, **94**, 52 ; 1954 b, *J. Opt. Soc. Amer.*, **44**, 256.
GERMER, L. H., 1942, *Phys. Rev.*, **62**, 295.
KACZER, J., 1955, *Czech. J. Phys.*, **5**, 239.
VON LAUE, M., 1928, *Handbuch der Experimentalphysik* (Leipzig: Akad. Verlag), **18**, 185.
SCHÜTZ, W., 1936, *Handbuch der Experimentalphysik* (Leipzig : Akad. Verlag), **16**, 319.
VOIGT, W., 1908, *Magneto-und-Elektro-Optik* (Leipzig : Teubner).
WILLIAMS, H. J., BOZORTH, R. M., and SHOCKLEY, W., 1949, *Phys. Rev.*, **75**, 155.
WILLIAMS, H. J., FOSTER, F. G., and WOOD, E. A., 1951, *Phys. Rev.*, **82**, 119.

Hysteresis Loops associated with a Simple Domain Structure

By A. HART
Post Office Research Station, Dollis Hill, London, N.W.2

MS. received 7th March 1958

Abstract. The complex domain structures existing in most ferromagnetic specimens prevent precise information about individual domain processes from being obtained from technical magnetization curves. Experiments on ring specimens of a magnetically annealed Perminvar-type alloy show that reversal of magnetization in such specimens involves only one 180° domain wall. Rings of varying external to internal diameter ratio were used, and the hysteresis loops of all specimens could be explained using a simple theoretical model. All specimens except those whose hysteresis loops were controlled by nucleation processes had the same coercive field, 0·09 oersted. This field gave a direct measure of the impedance to motion of an isolated 180° wall.

The experiments also show that the use of a specimen with large external to internal diameter ratio effectively reduces the slope of the sides of the measured (B, H) loop; a close approach to a rectangular loop is possible only in specimens with small radial width. The effects of nucleation are evident in all of the loops, and in the case of the specimens with the smallest radial width, the loop shapes are controlled entirely by nucleation.

§ 1. INTRODUCTION

THE specimens normally used for measuring the (B, H) characteristics of magnetic materials contain many domains, with their directions of magnetization more or less randomly oriented with respect to the direction of the measuring field. The (B, H) relation observed thus represents a summation of individual domain processes over many domains and over all orientations of the field relative to the domain magnetizations. Information about individual domain processes characteristic solely of the material can only be obtained by using specimens with specially simple domain structures (Williams and Shockley 1949).

Experiments were made on magnetically annealed rings of a Perminvar-type alloy. The field-induced uniaxial anisotropy overrides the crystal anisotropy, and thus the easy direction may be made everywhere parallel to the measuring field (directed circumferentially). The demagnetizing factor of the ring in the direction of the magnetizing field is zero; consequently the minimum energy state of the specimen is the one in which it is magnetized to saturation in one or other of the antiparallel easy directions. Application of a field in a direction to reverse the magnetization may then affect the reversal by the movement of a single 180° domain wall across the width of the ring, and in this case the magnetization curve of the specimen can be calculated in terms of the field required to move a single 180° wall. This calculation is made, and measurements on rings with varying inner diameters serve to clarify further the domain processes occurring during a cycle of magnetization.

§ 2. Theory

Consider a model consisting of a section of 180° wall entirely separated from other domain walls, in a material having uniaxial magnetic anisotropy. The variation in energy of this section of wall with position in the material is such that there exist elastic forces which require a field H_c parallel to the wall to cause irreversible wall movement. This is a familiar model, and leads to an ideally rectangular hysteresis loop with sides at $\pm H_c$, $\pm B_s$ where B_s is the saturation induction. Consider an annular specimen of this material, with inner and outer radii a, b, and let the easy direction be everywhere parallel to the circumference of the annulus. If the specimen is magnetized to saturation in one direction, and an increasing field is then applied in the opposite sense, reversal of the magnetization will be initiated by the formation of a 180° wall at the inner edge of the annulus. Nucleation problems will be ignored. Since the applied field falls off inversely as the radius, this wall will not move outwards until the applied field is increased. If the theoretical (B, H) loop is plotted in terms of the field at the arithmetic mean radius r_n of the ring, then in the field range over which the reversal occurs the side of the loop has a constant slope, corresponding to a differential permeability μ_n. The field, measured at r_n, at which the reversal begins is given by $H_i = aH_c/r_n$. Reversal is complete at $H_0 = bH_c/r_n$. Writing $x = b/a$, then $H_0/H_i = x$, and $H_0 - H_i = 2H_c(x-1)/(x+1)$. Hence $\mu_n = B_s(x+1)/H_c(x-1)$.

Values of x and $2(x-1)/(x+1)$ calculated from the dimensions of the specimens used are shown in columns (2) and (3) of the table.

(1)	(2)	(3)	(4)	(5)	(6)	(7)	(8)	(9)
7/8	1·15	0·07	0·106†	0·90	2900	16	1·1	0·085
11/16	1·45	0·37	0·092	0·92	2000	6·7	1·4	0·34
5/16	3·23	1·05	0·094	0·95	800	2·2	3·5	1·27
3/16	5·32	1·37	0·094	0·95	800	1·8	4·9	1·64

(1) Internal diameter (in.); (2) external diameter/internal diameter $(= x)$; (3) $2(x-1)/(x+1)$; (4) H_c; (5) B_r/B_m; (6) μ_r; (7) $\mu_n \times 10^{-5}$; (8) H_0/H_i; (9) $(H_0 - H_i)/H_c$. All rings have external diameter 1 in. † Measurement with nucleating field.

The value of μ_n depends markedly on the specimen dimensions, and is reduced more and more from its infinite ' intrinsic ' value, as the annulus becomes wider. The rectangular loop becomes a parallelogram loop, but the measured value of coercivity H_c remains unchanged.

During a cycle of magnetization the only hysteresis loss arises from the expenditure of energy required to move the wall against the constant impeding force. This loss, represented by the area enclosed by the (B, H) loop, $B_s H_c/\pi$, is obviously constant for all specimens, being characteristic of the material. Loops for specimens of different annular widths are all parallelograms, and since B_s is constant, so is H_c.‡

As the wall traverses the specimen, its length increases, and there exists an effective field $H_T = \sigma/2I_s r$ (σ is the wall energy per unit area, I_s the saturation magnetization) tending to reduce the wall radius. The first measurements of

---

‡ The viewpoint used in this paragraph was suggested to the author by a referee.

H_c showed that for the specimens used $H_c \simeq 200 H_T$ and consequently H_T has been ignored in the above calculations. It has already been suggested that a direct measure of wall energy could be obtained from a specimen for which $H_T \simeq H_c$ (Williams and Goertz 1952). In the present case, a specimen of radius of the order of 0·005 cm would be required. It is interesting to note that if $H_T > H_c$ there is no stable position for a wall in the specimen, and an ideally rectangular loop is obtained.

§ 3. EXPERIMENTAL

The material used was an alloy of composition Ni 45%, Fe 30%, Co 25% made by powder metallurgy and rolled into strip $1\frac{1}{8}$ in. wide, 160 microns thick. Ring specimens were punched from the strip. All rings had an outer diameter of 1 in., and the inner diameters were $\frac{3}{16}$ in., $\frac{5}{16}$ in., $\frac{11}{16}$ in. and $\frac{7}{8}$ in. The different rings will be denoted by referring to their inner diameters. The specimens were annealed for three hours at 1050°c in dry hydrogen, and then magnetically annealed by cooling from 650°c to 400°c in a field of 9·5 oersteds. This field was provided by a coil wound on a refractory former containing the specimens.

The rings were transferred to polystyrene formers, which were then wound with two coils, one for the magnetizing current and the other for measuring the flux changes. The (B, H) loops of the specimens were measured by a ballistic method, using a sensitive long-period galvanometer. Three specimens of each size were measured individually. Values of induction B were plotted against corresponding values of field H_n measured at the arithmetic mean radius r_n. The maximum value of H_n was 11·5 oersteds for all specimens.

§ 4. RESULTS

The figure shows the (B, H) loop for one of the $\frac{5}{16}$ in. rings. This loop will be considered in detail, and results for all other rings will then be related to this first loop. It extends to field strengths of only twice the coercive field, and on this scale the portions KL, ST of the loop appear to be parallel to the H axis. In fact, the slopes of the sections near to the remanence points L, T,

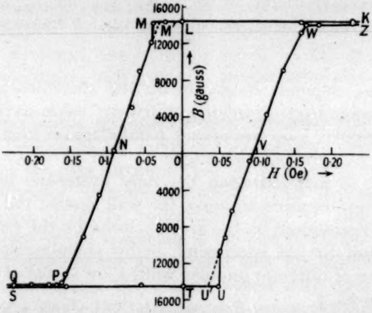

Hysteresis loop for ring with O.D. 1 in., I.D. $\frac{5}{16}$ in.

correspond to differential permeabilities of approximately 800. In a field of about five oersteds this permeability is reduced to 30. The ascending and descending branches of the loop coincide at all fields greater than 1 oersted.

The remanence values at L and T differ by about 2%, as do the values of H_c deduced from the intersections at N, V. The sides MP, UW of the loop are approximately straight and parallel over a large fraction of their length. The individual points on these sides were never exactly reproducible, and this applied particularly to the corners at M, U. The corner at M′, obtained by producing the straight portion of the line PNM until it meets the line KLM, occurs at a field value agreeing closely with that obtained at *U′* by a similar construction; but the excess field M′M differs markedly from the corresponding excess field U′U.

Two other $\frac{5}{16}$ in. rings gave loops with the same features. The B_r/B_m ratios for all three rings were contained in the range 0·94 to 0·96, while the H_c values were between 0·092 and 0·096 oersted. The largest 'excess' field, M′M, was 0·06 oersted.

Loops for $\frac{3}{16}$ in. and $\frac{11}{16}$ in. rings gave B_r/B_m and H_c values close to those for the $\frac{5}{16}$ in. rings. The differential permeability as measured at several fields along the section KL was considerably greater for the $\frac{11}{16}$ in. ring than for the wider rings. Its value at L, for example, was 2000. The major difference between the loops for the different ring sizes is in the slope of the parallel sides M′P, U′W. These sides become progressively steeper as the ring width becomes less. Immediately after their heat treatment all specimens were in the remanent condition. None was 'unmagnetized'.

Columns (4) and (5) of the table give values of H_c and B_r/B_m for different sizes of ring. Column (6) gives the differential permeability at remanence, and in column (7) are the differential permeabilities μ_n calculated from the observed flux changes between M′ and P, U′ and W. These permeabilities are approximately constant over the whole of the sections involved. For comparison with the second and third columns of the table, columns (8) and (9) give measured values of H_0/H_1 and $(H_0 - H_1)/H_c$.

Figures for $\frac{7}{8}$ in. rings are included in the table. The loops for these rings were distinctive in two ways. First, the two B_r/B_m ratios for a specimen differed by as much as 8%. Secondly, the sides of the loop were vertical, and no matter how fine the field control, points on the loop sides could not be obtained. In a typical case, a reversal of magnetization could sometimes be obtained using fields as low as 0·128 oersted, while in other cycles of magnetization failure to reverse was recorded on the *same* side of the loop in fields of 0·15 oersted. The fields required to obtain the two sides of the loop are in a ratio of up to 1·2 : 1; the higher field value always occurred in the same quadrant of the cycle as the higher B_r/B_m ratio.

It was deduced that the steep loop sides were due to a nucleation process which delayed the formation of the main wall until such a high field was reached that the wall, once formed, swept right across the ring. To cause the wall to start moving in the smallest possible field, a magnetic-recording erasing head was used to provide a local nucleating field. This field was increased until a loop with a side which sloped over its whole length (as MP) was obtained. Side UW was still vertical. By reversing the nucleating field, and adjusting its value, the sloping and vertical sides were interchanged. Under these conditions, the values of coercive field obtained from the two sloping sides were equal. The values of H_c, H_0/H_1 and $(H_0-H_1)/H_c$ for the $\frac{7}{8}$ in. rings, incorporated in the table, were obtained in this manner.

§ 5. CONCLUSIONS

Agreement between columns (3) and (9) and columns (2) and (8) of the table, and the constant H_c value observed for the different specimen sizes, shows that the reversal of magnetization takes place by 180° wall movement, the wall being nucleated at the inner edge of the specimen. The H_c value of 0·09 oersted is thus a direct measure of the impedance to motion of an isolated 180° domain wall.

The change in slope of the loop sides in going from a $\frac{3}{16}$ in. to a $\frac{7}{8}$ in. ring is very marked. For a given material, the specimen with smallest radial width, i.e. the one which has the closest approach to a uniform field, will always exhibit the highest differential permeability. For square loop materials the requirement of uniform field is even more necessary, since the magnetization process takes place only in a very limited field range (at only one field value, H_c, in the case considered). In practical applications of square loop materials, every effort should be made to reduce radial width to a minimum (Roberts and Van Nice 1955).

The (B, H) loops were not closed until fields of about one oersted were applied, and the differential permeabilities on the branches KL, ST of the loops were quite large. In association with B_r/B_m ratios of 0·92–0·96, these figures suggest the presence of regions of reverse magnetization separated from the bulk of the specimen by 180° walls. These walls can contribute to the permeability of the specimens outside the limited field range over which the main 180° wall exists. They are also important since nucleation of the main wall probably requires the growth and merging of two or more such reverse regions. It is to be noted that nucleation effects were observed in all specimens and, in the case of the $\frac{7}{8}$ in. rings, entirely controlled the loop shape. For the $\frac{7}{8}$ in. rings, the quoted value of H_c is some 10% greater than that for the wider rings. In view of this discrepancy, other $\frac{7}{8}$ in. rings were tested. Values of H_c for these rings were in the range $0{\cdot}1-0{\cdot}14$ oersted, none being as low as 0·095 oersted. These results imply a larger hysteresis loss $(=B_sH_c/\pi)$ for the $\frac{7}{8}$ in. rings than for the wider rings. It is suggested that this anomalous result is due to the relatively large regions of reverse magnetization which are required for nucleation. The presence of these regions, and their associated walls, vitiates the assumptions of the single-wall model, and the hysteresis loss is no longer exactly calculable.

ACKNOWLEDGMENTS

Acknowledgment is made to the Engineer-in-Chief of the Post Office and to the Controller of H.M. Stationery Office for permission to publish this paper. The author records his thanks to Mr. A. C. Lynch for his interest in the work and useful comment during the preparation of the manuscript. He is also indebted to Dr. E. W. Lee for many interesting and helpful discussions.

REFERENCES

ROBERTS, R. W., and VAN NICE, R. I., 1955, *Trans. Amer. Inst. Elect. Engrs*, I, **74**, 599.
WILLIAMS, H. J., and GOERTZ, M., 1952, *J. Appl. Phys.*, **23**, 316.
WILLIAMS, H. J., and SHOCKLEY, W., 1949, *Phys. Rev.*, **75**, 178.

Magnetostriction Curves of Polycrystalline Ferromagnetics

By E. W. LEE

Department of Physics, University of Nottingham

Communicated by L. F. Bates; MS. received 10*th March* 1958

Abstract. An approximate method is given for calculating the magnetostriction of a random polycrystal as a function of the magnetization in the range over which magnetization occurs by rotation of the domain magnetization vectors. Calculations valid for the cases of cubic and hexagonal symmetry (these only for the case in which the easy axis is the hexagonal axis) are given in parametric form. Using these calculations and earlier calculations of Brown for the range of magnetization where boundary displacements occur it is possible to calculate the magnetostriction as a function of magnetization over the entire range from zero to saturation.

---

§ 1. INTRODUCTION

QUITE generally the term magnetostriction refers to any mechanical effect produced by magnetization. The usual restricted use of the term signifies the change in length of a ferromagnetic body when magnetized (Joule effect). The form of the magnetostriction–field curve is often complicated but is always one of four basic types (Bozorth, Tilden and Williams 1955).

The accepted explanation of the magnetostriction effect is that every region in which the magnetization is constant in magnitude and direction, i.e. every domain, is spontaneously strained by the presence of the spontaneous magnetization. This strain varies with the direction of the spontaneous magnetization within the crystal lattice. Since the exact form of this variation is not known the assumption is made that the strain may be characterized by a strain tensor whose components may be expanded in a power series in $\alpha_i (i = 1, 2 \text{ or } 3)$, the direction cosines of the spontaneous magnetization vector with respect to the crystal axes, the only restrictions on the coefficients being those imposed by the requirements of crystal symmetry and the degree of approximation required. It may be shown that for cubic crystals the magnetostriction of a single domain must have the following form

$$\lambda = \tfrac{3}{2}\lambda_{100}(\alpha_1^2\beta_1^2 + \alpha_2^2\beta_2^2 + \alpha_3^2\beta_3^2 - \tfrac{1}{3}) + 3\lambda_{111}(\alpha_1\alpha_2\beta_1\beta_2 + \alpha_2\alpha_3\beta_2\beta_3 + \alpha_3\alpha_1\beta_3\beta_1) \qquad \ldots\ldots (1)$$

in which the β_i are the direction cosines of the direction of measurement referred to the crystal axes. For crystals of lower symmetry equations involving more than two constants are needed to describe the behaviour. If in equation (1) $\lambda_{100} = \lambda_{111} = \lambda_s$, then

$$\lambda = \tfrac{3}{2}\lambda_s(\cos^2\theta - \tfrac{1}{3}) \qquad \ldots\ldots (2)$$

where $\cos\theta = \Sigma\alpha_i\beta_i$. This is the isotropic form of (1).

In order to calculate magnetostriction curves it is necessary to remember that equation (1) refers to a single domain only. To calculate the magnetostriction of an assembly of domains such as exists in most ferromagnetic materials, this equation must be averaged; it is necessary, in principle, to know the number, size and shape of each domain as well as the direction of its magnetization vector. This information is usually lacking, and instead it is invariably assumed that the number of domains is so great that the material may be regarded as being in a state of uniform stress, in which case the mean strain is simply the volume average of the individual strains. Only the distribution of the direction of the domain vectors need then be known. If this may be characterized by a distribution function F, then the mean magnetostriction

$$\frac{dl}{l}=\frac{\int F\lambda d\omega}{\int F d\omega} \qquad \ldots\ldots(3)$$

where $d\omega$ is an elementary solid angle. In single crystals F may, in principle, be determined from Bitter figure studies or, in the region where magnetization occurs by rotation of the domain magnetization vectors, from considerations of symmetry. In all other cases dl/l can be calculated only by assigning a certain form to the distribution function F. This has been done by Brown (1938), who assumes that when magnetization takes place by displacement of domain boundaries the distribution function F is of the Boltzmann type. The main object of the present paper is to supplement Brown's calculations for polycrystals by calculations relevant to the situation in higher fields where rotation of the domain magnetization vectors is the dominant process, thereby obtaining magnetostriction curves over the whole range of magnetization to saturation.

§ 2. CALCULATION OF MAGNETOSTRICTION CURVES

By magnetostriction curve we mean the dependence of mean magnetostriction dl/l on either magnetic field strength H or mean intensity of magnetization I. The $(dl/l, I)$ curves are more fundamental and these are the ones presented here. If experimental or theoretical (I, H) curves are available it is of course possible to convert the $(dl/l, I)$ curves to $(dl/l, H)$ curves. The calculations have been carried out for four different cases given below.

2.1. *Isotropic Magnetostriction*

This is the simplest case, which occurs when equation (2) is an adequate representation of experimental results. The magnetostriction is given by combining equations (2) and (3) and the reduced magnetization $\eta = I/I_S$ is

$$\eta=\langle\cos\theta\rangle_{\text{av}}=\frac{\int F\cos\theta\, d\omega}{\int F d\omega}. \qquad \ldots\ldots(4)$$

Elimination of F from (3) and (4) gives the required $(dl/l, \eta)$ curve. Brown assumes a statistical distribution function of the form

$$F=A\exp LHI. \qquad \ldots\ldots(5)$$

This expression appears to have no theoretical basis and consequently no physical significance can be attached to L, which is best regarded simply as an undetermined multiplier. The quantity L thus appears as a parameter in the expressions for dl/l and η. In the absence of any further information equation (5) seems much the most reasonable form of distribution function to take. The resulting equations for dl/l and η are, however, quite complicated.

A simple form of distribution function which, although less plausible than equation (5), does lead to a much simpler result is

$$\begin{aligned} F(\theta)&=\text{const.} \qquad 0<\theta<\theta_m \\ F(\theta)&=0 \qquad \theta_m<\theta<\pi. \end{aligned} \qquad \ldots\ldots(6)$$

Physically this means that at any stage of magnetization all the domain magnetization vectors are distributed uniformly in a cone of semi-angle θ_m. The same distribution function has been used by Bozorth (1947) in an attempt to explain low remanence values in certain alloys. Under the conditions imposed by equation (6), equations (3) and (4) are, respectively,

$$\frac{dl}{l}=\frac{\int_0^{\theta_m}\sin\theta\cos^2\theta\,d\theta}{\int_0^{\theta_m}\sin\theta\,d\theta}$$

$$\eta=\frac{\int_0^{\theta_m}\sin\theta\cos\theta\,d\theta}{\int_0^{\theta_m}\sin\theta\,d\theta}$$

from which one obtains

$$dl/l=\lambda_s\eta(2\eta-1). \qquad \ldots\ldots(7)$$

This expression is shown in figure 1 together with the curve calculated by Brown using equation (5). An excellent test of the two calculations is provided by measurements on heavily cold-worked nickel obtained by a method described previously (Lee 1952). In this material the easy directions are believed to be determined by local stress anisotropy which varies in direction from place to place inside the material. Under these conditions the magnetostriction must be isotropic and equation (2) a good approximation. Moreover, the situation corresponds more closely to Brown's idea of isotropic domains than is likely to exist

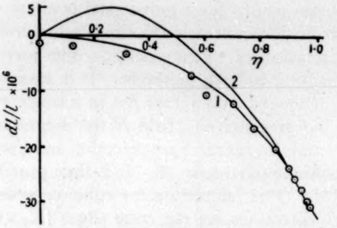

Figure 1. Magnetostriction of cold-worked nickel. Curve 1 is calculated from Brown's results, curve 2 from eqn (7) using $\lambda_s=32{\cdot}9\times10^{-6}$. Apart from the fact that the experimental points have all been shifted downwards to account for non-randomness in the demagnetized state, there are no disposable constants in the calculated curves since the value of λ_s is obtained using the values of λ_{100} and λ_{111} obtained by Bozorth and Hamming (1953) from measurements on a single crystal.

in any other material. The experimental points are shown in figure 1. It can be seen that equation (7) fails completely for η less than 0·5 since it predicts values of dl/l negative with respect to λ_s. Such negative values are often observed during a hysteresis cycle between remanence and the coercive force and were at one time the subject of much controversy. The assumptions leading to equation (7) provide a formal physical explanation for these negative values. Brown's curve and that of equation (7) are not greatly different in the range $0{\cdot}8 < \eta < 1$ but elsewhere the superiority of the former is in no doubt and in fact predicts the observed dependence of dl/l on η with remarkable accuracy.

2.2. *Anisotropic Magnetostriction*

The remarkable agreement between Brown's statistical treatment and experiment lends support to the view that when boundary movements are the dominant magnetic process, a similar statistical approach is equally valid. The usual view is that in a polycrystal boundary movements take place until all the magnetization vectors in each grain lie in that easy direction which is nearest the field direction. Thereafter magnetization proceeds by rotation of the magnetization vectors towards the field direction. The problem of calculating the magnetostriction in this situation is simply that of calculating the distribution function F. In principle this can be done by writing the total energy of the system, viz.

$$E = -I_s H \cos\theta + K_1(\alpha_1{}^2\alpha_2{}^2 + \alpha_2{}^2\alpha_3{}^2 + \alpha_3{}^2\alpha_1{}^2)$$

comprising field and anisotropy energy respectively, and applying the condition that E should be a minimum. However, the resulting equations cannot be solved explicitly for α_i. In order to obtain α_i at all it is necessary either to use series approximations valid for small or large values of H or to be content with numerical solutions. In the first case, which is that used by Gans (1932) for magnetization curves, the validity of the solution is limited and in the second, since the averaging process required to obtain results for a polycrystal involves a double integration which must necessarily be done numerically, the labour involved is not commensurate with the interest attached to the results. The method adopted here is essentially an approximation to both methods. It is assumed, as is customary, that in zero field each magnetization vector lies in a single easy direction. It is then assumed that in the presence of a field H the magnetization vector always lies on a line joining H and the nearest easy direction and that its position may be specified in terms of a single parameter A. It is then possible to calculate both dl/l and η in terms of A. The calculation for cubic crystals depends somewhat upon whether the easy directions are the cube edges ($K_1 > 0$) or body diagonals ($K_1 < 0$).

(*a*) $K_1 > 0$.

The geometry for the case $K_1 > 0$ is shown in figure 2, which shows the intersection of the vectors I_s and H on the unit sphere. If the coordinates of H are θ and ϕ and those of I_s are θ_0 and ϕ_0 then by virtue of the above assumptions

$$\theta_0 = A\theta, \quad \phi_0 = \phi \qquad \ldots\ldots(8)$$

where A is a numerical constant such that $A = 0$ when $H = 0$, and $A = 1$ corresponds to saturation. The mean magnetization is

$$\eta = \langle\cos(\theta - \theta_0)\rangle_{\text{av}} = \langle\cos(1 - A)\theta\rangle_{\text{av}}.$$

This is obtained by averaging over that part of the unit sphere enclosed by the thick lines on figure 2. Thus

$$\eta = \frac{12}{\pi}\int_0^{\pi/4}\int_0^{\psi} \sin\theta \cos(1-A)\theta \, d\theta \, d\phi$$

where ψ is given by $\tan\psi = \sec\phi$. This reduces to

$$\eta = \frac{3}{A(2-A)} - \frac{6}{\pi(2-A)}\int_0^{\pi/4} \cos(2-A)\psi \, d\phi - \frac{6}{\pi A}\int_0^{\pi/4} \cos A\psi \, d\phi. \quad \ldots\ldots(9)$$

This was integrated numerically for fixed values of A.

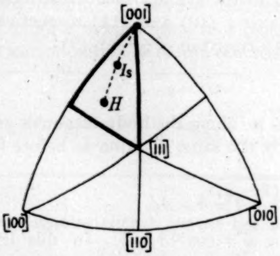

Figure 2. Magnetization vector geometry for the case in which $K_1 > 0$ and for hexagonal crystals if the hexagonal axis is taken to coincide with the [001] direction.

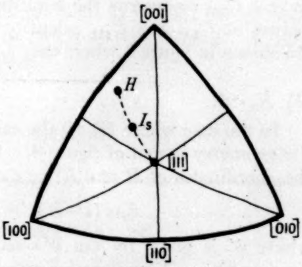

Figure 4. Magnetization vector geometry for the case in which $K_1 < 0$.

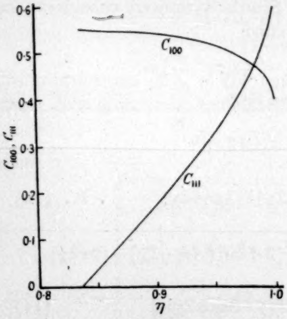

Figure 3. Variation of C_{100} and C_{111} with reduced magnetization for the case in which $K_1 > 0$.

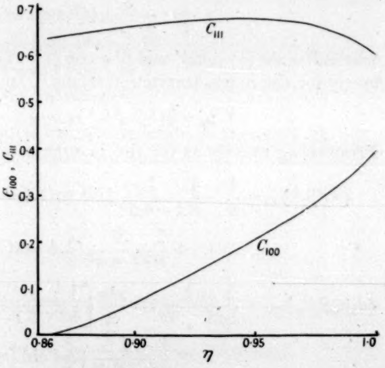

Figure 5. Variation of C_{100} and C_{111} with reduced magnetization for the case in which $K_1 < 0$.

For the magnetostriction, expressing α_i and β_i in terms of θ_0, ϕ_0 and θ, ϕ, respectively, one obtains from equations (1) and (8)

$$\sum \alpha_i^2\beta_i^2 = \sin^2 A\theta \sin^2\theta\,(1+\cos^4\phi+\sin^4\phi)+\cos^2\theta-\sin^2 A\theta \qquad \ldots\ldots(10)$$

$$\sum_{i>j} \alpha_i\alpha_j\beta_i\beta_j = \sin\theta\sin A\theta\cos\theta\cos A\theta+\sin^2\theta\sin^2 A\theta\sin^2\phi\cos^2\phi. \qquad \ldots\ldots(11)$$

Both these expressions were averaged using the same method as for η. The integration over θ is elementary but laborious and except for a few terms the ϕ integration was carried out numerically. It is convenient to express the resulting magnetostriction of a random assembly of domains in the form

$$dl/l = C_{100}\lambda_{100}+C_{111}\lambda_{111}$$

so that C_{100} represents the contribution of λ_{100} to the average magnetostriction. Values of C_{100} and C_{111} calculated from equations (10) and (11) respectively are shown in figure 3 where they are plotted as a function of η (eqn (9)).

(*b*) $K_1 < 0$.

In the case where $K_1 < 0$ the easy directions lie along the body diagonals and the geometry is that of figure 4. Using exactly the same notation as before for the coordinates of H and I_s we have

$$\theta_0 = (1-A)\psi' + A\theta, \quad \phi_0 = (1-A)\pi/4 + A\phi$$

where ψ' is given by $\tan\psi' = \sec\pi/4$. Thus $\psi' = \cos^{-1} 1/\sqrt{3}$. In this case $\eta = \langle\cos\theta\rangle_{\mathrm{av}}$. Now $\cos\theta = \Sigma\alpha_i\beta_i$ and by symmetry

$$\langle\alpha_1\beta_1\rangle_{\mathrm{av}} = \langle\alpha_2\beta_2\rangle_{\mathrm{av}} = \langle\alpha_3\beta_3\rangle_{\mathrm{av}}.$$

Therefore

$$\langle\cos\theta\rangle_{\mathrm{av}} = 3\langle\alpha_3\beta_3\rangle_{\mathrm{av}} = \frac{6}{\pi}\int_0^{\pi/2}\int_0^{\pi/2}\sin\theta\cos\theta\cos\theta_0\,d\theta\,d\phi$$

from which one obtains

$$\eta = \frac{3}{4-A^2}\{Q\cos\tfrac{1}{2}A\pi + Q - P\sin\tfrac{1}{2}A\pi\} \qquad \ldots\ldots(12)$$

where $P = \sin(1-A)\psi'$ and $Q = \cos(1-A)\psi'$. Similar symmetry considerations apply for the magnetostriction terms. In particular

$$C_{100} = \tfrac{3}{2}(3\langle\alpha_3^2\beta_3^2\rangle_{\mathrm{av}} - \tfrac{1}{3}), \quad C_{111} = 9\langle\alpha_1\alpha_2\beta_1\beta_2\rangle_{\mathrm{av}}.$$

Proceeding exactly as for the magnetization one finds

$$\begin{aligned}\langle\alpha_3^2\beta_3^2\rangle_{\mathrm{av}} = \frac{1}{6} - \frac{1}{8}\frac{1}{1-4A^2}\{2A\sin(A\pi+2\chi)-\cos 2\chi\}\\ + \frac{1}{8}\frac{1}{9-4A^2}\{2A\sin(A\pi+2\chi)+3\cos 2\chi\}\end{aligned} \qquad \ldots\ldots(13)$$

$$\begin{aligned}\langle\alpha_1\alpha_2\beta_1\beta_2\rangle_{\mathrm{av}} = \frac{1}{2\pi}\frac{1}{1-A^2}\cos\frac{A\pi}{2}\Big[\frac{1}{3} + \frac{3}{8}\frac{1}{1-4A^2}\{2A\sin(A\pi+2\chi)-\cos 2\chi\}\\ + \frac{1}{8}\frac{1}{9-4A^2}\{2A\sin(A\pi+2\chi)+3\cos 2\chi\}\Big]\end{aligned} \qquad \ldots\ldots(14)$$

in which $\chi = (1-A)\psi'$. Values of C_{100} and C_{111} calculated from equations (13) and (14) are shown in figure 5 as a function of η (eqn (12)).

These results confirm that above the knee of the magnetization curve both λ_{100} and λ_{111} contribute to the magnetostriction. This is contrary to the statement sometimes made (implicitly by Yamamoto and Miyasawa (1952) for instance) that for domain vector rotations only the magnetostriction in the difficult direction of magnetization contributes to the observed magnetostriction. The statement is, however, much more nearly true for the case in which $K_1 < 0$ than for that in which $K_1 > 0$.

2.3. *Hexagonal Crystals*

For the case of hexagonal crystals we treat only the case of cylindrical symmetry where the easy direction is parallel to the cylinder axis. If we take this to be the z axis in figure 2, then the calculation is exactly the same as in § 2.1 except that the range of integration is now from 0 to $\pi/2$ for θ and from 0 to 2π for ϕ. Using the same notation as before one has $\theta_0 = A\theta$, $\phi_0 = \phi$,

$$\begin{aligned}\eta &= \langle \cos(1-A)\theta \rangle_{\mathrm{av}} \\ &= \frac{1}{2\pi}\int_0^{2\pi}\int_0^{\pi/2} \sin\theta \cos(1-A)\theta \, d\theta \, d\phi \\ &= \frac{1}{A(2-A)}\left\{1-(1-A)\cos\frac{A\pi}{2}\right\}. \qquad \ldots\ldots(15)\end{aligned}$$

For magnetostriction we use the formula of Mason (1954), viz.

$$\begin{aligned}\lambda = {} & \lambda_1\{(\alpha_1\beta_1+\alpha_2\beta_2)^2-(\alpha_1\beta_1+\alpha_2\beta_2)\alpha_3\beta_3\} \\ & +\lambda_2\{(1-\alpha_3{}^2)(1-\beta_3{}^2)-(\alpha_1\beta_1+\alpha_2\beta_2)^2\} \\ & +\lambda_3\{(1-\alpha_3{}^2)\beta_3{}^2-(\alpha_1\beta_1+\alpha_2\beta_2)\alpha_3\beta_3\} \\ & +4\lambda_4(\alpha_1\beta_1+\alpha_2\beta_2)\alpha_3\beta_3 \qquad \ldots\ldots(16)\end{aligned}$$

in which the cylindrical axis (hexagonal c axis) is taken as the z axis ($i=3$). Expressing α_i and β_i in terms of θ and ϕ as before we find

$$\begin{aligned}(\alpha_1\beta_1+\alpha_2\beta_2)^2 &= \sin^2\theta\sin^2 A\theta \\ (\alpha_1\beta_1+\alpha_2\beta_2)\alpha_3\beta_3 &= \tfrac{1}{4}\sin 2\theta \sin 2A\theta \\ (1-\alpha_3{}^2)(1-\beta_3{}^2) &= \sin^2\theta\sin^2 A\theta \\ (1-\alpha_3{}^2)\beta_3{}^2 &= \sin^2 A\theta\cos^2\theta.\end{aligned}$$

The contribution of λ_2 to the longitudinal magnetostriction is therefore always zero. Averaging these four quantities as before we find

$$dl/l = (X-Y)\lambda_1 + (Z-Y)\lambda_3 + 4Y\lambda_4 \qquad \ldots\ldots(17)$$

where

$$\begin{aligned}X &= \frac{1}{3} - \frac{3}{8}\frac{1}{1-4A^2}\{1-2A\sin A\pi\} + \frac{1}{8}\frac{1}{9-4A^2}\{3+2A\sin A\pi\} \\ Y &= \frac{1}{8}\frac{1}{1-4A^2}\{\sin A\pi - 2A\} + \frac{1}{8}\frac{1}{9-4A^2}\{2A+3\sin A\pi\} \\ Z &= \frac{1}{6} - \frac{1}{8}\frac{1}{1-4A^2}\{1-2A\sin A\pi\} - \frac{1}{8}\frac{1}{9-4A^2}\{3+2A\sin A\pi\}.\end{aligned}$$

No account has been taken of the fact that ordinarily cobalt in hexagonal form contains many stacking faults and may be regarded as a mixture of face-centred cubic and hexagonal close-packed structures since the same situation presumably exists in both single crystal and polycrystalline forms. No experimental $(dl/l, \eta)$ curves are available for comparison.

If we express equation (17) in the form

$$dl/l = C_1\lambda_1 + C_3\lambda_3 + C_4\lambda_4$$

the values of the constants C_1, C_3 and C_4 are shown in figure 6 as a function of η (eqn (15)). It is interesting to note that the experimental results of Bozorth (1954) show all constants in equation (16) to be negative except λ_3. However, C_3 is always zero and so (16) might well be rewritten with the terms inside the braces interchanged.

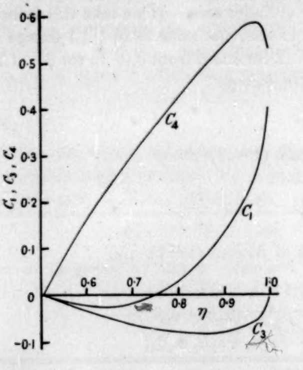

Figure 6. Variation of C_1, C_3 and C_4 with reduced magnetization for hexagonal crystals (cylindrical symmetry) having the easy axis along the hexagonal axis.

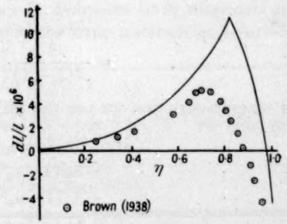

Figure 7. Calculated magnetostriction of polycrystalline iron and experimental results due to Brown (1938).

§ 3. MAGNETOSTRICTION CURVES FOR IRON, NICKEL AND COBALT

It is now possible to calculate magnetostriction curves for the three ferromagnetic elements using Brown's calculations for the boundary movements and the present results for rotations. It was originally intended to compare the calculated and experimental curves. However, it was surprising to find a great dearth of suitable experimental data. In no case in which $(dl/l, \eta)$ curves were measured was it also established that no preferred grain or domain orientation exists. Consequently, there exists a wide variety of $(dl/l, \eta)$ curves and by suitable selection it would no doubt be possible to find one which fitted the calculated curves well. Such a procedure would be quite valueless and we merely draw attention to some general features which emerge from a study of experimental $(dl/l, \eta)$ curves.

For iron the calculated curve is shown in figure 7 using $\lambda_{100} = 20{\cdot}7 \times 10^{-6}$, $\lambda_{111} = -21{\cdot}2 \times 10^{-6}$ (Carr and Smoluchowski 1951). Most of the experimental curves have a maximum at $\eta = 0{\cdot}7$ or thereabouts, rather than at the value of 0·83 required by the present treatment. A typical set of experimental points due to Brown (1938) is shown for comparison. It is evident that no amount of curve-fitting can put all the points on the curve. It is suggested that the difference between experimental and theoretical behaviour is significant and that the mechanism of magnetization upon which the theoretical curve is based cannot be true for iron. An alternative suggestion is discussed in § 4. Nickel is not a very good substance for comparison since its magnetostriction is nearly isotropic and any monotonic curve is bound to fit the experimental results to a certain extent. The curve of figure 8 calculated using $\lambda_{100} = -45{\cdot}9 \times 10^{-6}$, $\lambda_{111} = -24{\cdot}3 \times 10^{-6}$ (Bozorth and Hamming 1953) fits the experimental results of Schulze (1928) and of the present author rather well over the entire range. The calculated $(dl/l, \eta)$ curve for cobalt is shown in figure 9 using the constants given by Bozorth (1954).

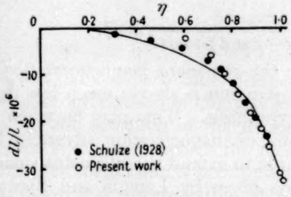

Figure 8. Calculated magnetostriction of polycrystalline nickel and experimental results due to Schulze (1928) and to the present author.

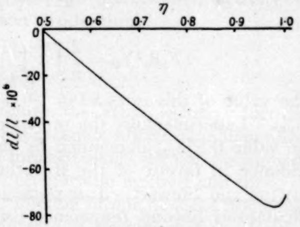

Figure 9. Magnetostriction of polycrystalline cobalt. No experimental data appear to exist.

§ 4. DISCUSSION

The high field calculations presented here are all based on the hypothesis, first advanced by Gans (1932), that boundary movements occur until all the magnetic domain vectors lie in that easy direction nearest the field. This is the conventional picture of remanence and it means that in each crystal grain the magnetization lies in a single easy direction. It is difficult to see how this can be correct since the normal components of I cannot be continuous across a grain boundary, and thus give rise to internal demagnetizing fields. In any case the work of Néel (1944) and Lawton and Stewart (1948) showed that in isolated crystals the single vector state is not reached until very near saturation. It is not easy to see why the situation is so very different in a crystal grain in a polycrystal. Lawton and Stewart (1950) give a method of calculating magnetization curves in the rotation region given by using their previous calculations for a long single crystal rod. These calculations apply only when $K_1 > 0$. In this approximation the mean magnetization of each grain is assumed to be the same throughout the polycrystal and at remanence all the domain magnetization vectors lie in the three easy directions lying nearest the field direction (five in the special case in which this coincides with an easy direction), the distribution being such that the component of magnetization perpendicular to the axis of the rod is zero. In this case the distribution function is known (Becker and Döring 1939) and is

$$F_i = \frac{\beta_i}{\beta_1 + \beta_2 + \beta_3}$$

where the β_i are the direction cosines of the rod's axis, here taken to be coincident with that of the field referred to the crystal axes. The reduced remanent magnetization is $\eta_R = 1/\sqrt{3}$. The magnetostriction at remanence may be calculated as follows. Since each domain vector lies in an easy direction two of the α_i are zero for each domain. Therefore for each crystal grain

$$\begin{aligned}\lambda &= F_1\{\tfrac{3}{2}\lambda_{100}(\beta_1^2 - \tfrac{1}{3})\} + F_2\{\tfrac{3}{2}\lambda_{100}(\beta_2^2 - \tfrac{1}{3})\} + F_3\{\tfrac{3}{2}\lambda_{100}(\beta_3^2 - \tfrac{1}{3})\} \\ &= \tfrac{3}{2}\lambda_{100}\{F_1\beta_1^2 + F_2\beta_2^2 + F_3\beta_3^2 - \tfrac{1}{3}\}\end{aligned}$$

since $\Sigma F_i = 1$. By symmetry

$$\langle F_1\beta_1^2\rangle_{\text{av}} = \langle F_2\beta_2^2\rangle_{\text{av}} = \langle F_3\beta_3^2\rangle_{\text{av}}.$$

Hence the mean magnetostriction may be taken as

$$dl/l = \tfrac{3}{2}\lambda_{100}\{3\langle F_3\beta_3^2\rangle_{\text{av}} - \tfrac{1}{3}\}$$

with

$$\langle F_3\beta_3^2\rangle_{\text{av}} = \frac{2}{\pi}\int_0^{\pi/2}\int_0^{\pi/2} \frac{\sin\theta\cos^3\theta}{\sin\theta(\sin\phi + \cos\phi) + \cos\theta}\, d\theta d\phi.$$

The value of this integral is 1/6 from which the remanent magnetostriction is $\frac{1}{4}\lambda_{100}$. Experimentally the remanent magnetostriction is always much less than the value $0{\cdot}55\lambda_{100}$ demanded by the Gans hypothesis. This may be taken as evidence in favour of the hypothesis of uniform magnetization advanced by Lawton and Stewart. It is possible in principle to extend the magnetostriction calculations beyond remanence using the data given by Lawton and Stewart but the labour involved appears prohibitive. In any case it is doubtful whether a typical polycrystalline ferromagnetic substance exists. So much appears to depend on factors such as domain size, grain size and surface effects which cannot be taken into account, that it may be that no useful purpose would be served by such a calculation. It is of course obvious that the magnetization curve calculations of Gans and of Lawton and Stewart are simply extreme cases valid for very high and very low crystal anisotropy respectively. A careful investigation of the magnitudes of the magnetization and magnetostriction at remanence would be of considerable value in indicating the range of validity of each approximation.

ACKNOWLEDGMENT

The author would like to express his thanks to Professor L. F. Bates for much useful advice in connection with this work and for providing facilities for most of the computational work.

REFERENCES

BECKER, R., and DÖRING, W., 1939, *Ferromagnetismus* (Berlin: Springer) (1943 Photolithoprint reproduction, Ann Arbor, Michigan: Edwards Brothers).
BOZORTH, R. M., 1947, *Z. Phys.*, **124,** 519; 1954, *Phys. Rev.*, **96,** 311.
BOZORTH, R. M., and HAMMING, R. W., 1953, *Phys. Rev.*, **89,** 865.
BOZORTH, R. M., TILDEN, E. F., and WILLIAMS, A. J., 1955, *Phys. Rev.*, **99,** 1788.
BROWN, W. F., 1938, *Phys. Rev.*, **53,** 482.
CARR, W. J., and SMOLUCHOWSKI, R., 1951, *Phys. Rev.*, **83,** 1236.
GANS, R., 1932, *Ann. Phys., Lpz.*, **15,** 28.
LAWTON, H., and STEWART, K. H., 1948, *Proc. Roy. Soc.* A, **193,** 72; 1950, *Proc. Phys. Soc.* A, **63,** 848.
LEE, E. W., 1952, *J. Iron and Steel Inst.*, **171,** 160.
MASON, W. P., 1954, *Phys. Rev.*, **96,** 302.
NÉEL, L., 1944, *J. Phys. Radium*, **5,** 241.
SCHULZE, A., 1928, *Z. Phys.*, **50,** 448.
YAMAMOTO, M., and MIYASAWA, R., 1952, *Sci. Rep. Res. Insts Tôhoku Univ.*, **5,** 113.

Photoproduction of π – Mesons from Boron

By I. S. HUGHES† and P. V. MARCH

Natural Philosophy Department, University of Glasgow

MS. received 14*th May* 1958

Abstract. The reaction $^{11}B(\gamma\pi^-)^{11}C$ has been studied using bremsstrahlung having peak energies from 70 MeV to 320 MeV, by measuring the activity of the ^{11}C product of the reaction. The cross section for the reaction is in agreement with theoretical values for surface production. An unexplained activity is detected below the energy threshold for meson production.

§ 1. INTRODUCTION

PREVIOUS experiments designed to measure the cross sections for the photoproduction of charged π mesons from complex nuclei have depended on the detection of the mesons. Such measurements do not distinguish between reactions in which the meson is the only particle emitted and those in which meson emission is accompanied by the emission of one or more nucleons. The theoretical interpretation of meson production is simplified if the former type of reaction can be distinguished from the many other possible reactions in which a meson is produced. A reaction in which only the meson is emitted may be investigated if the residual nucleus can be identified by some characteristic activity. The most readily studied of such reactions is $^{11}B(\gamma\pi^-)^{11}C$ where the residual nucleus ^{11}C is identified by observing its positron activity which has a half-life of 20 minutes. The cross section of this reaction has been studied as a function of photon energy up to 320 MeV.

§ 2. EXPERIMENTAL PROCEDURE

Natural boron (81·2% ^{11}B, 18·8% ^{10}B) of purity 99·5% in the form of an amorphous powder was exposed to the uncollimated bremsstrahlung of the Glasgow 330 MeV synchrotron. The powder was packed uniformly into thin walled copper boxes of dimensions 1 in. × 1 in. × $\frac{1}{4}$ in. and exposed simultaneously with a 1 in. × 1 in. × $\frac{1}{8}$ in. piece of distrene (C_8H_8). The distrene acts as a monitor because the predominant reaction occurring in it is $^{12}C(\gamma, n)^{11}C$ which results in the same residual nucleus as the reaction $^{11}B(\gamma\pi^-)^{11}C$. Thus fluctuations in the intensity of the beam during the exposure are allowed for automatically by measuring the ratio of the activity produced in the boron sample to that produced in the distrene sample.

After exposure the boron powder was transferred to another copper box with walls thick enough to absorb the 0·96 MeV positrons from ^{11}C. This box was placed between two $1\frac{1}{2}$ in. × 2 in. sodium iodide scintillators mounted on E.M.I. photomultipliers and the 0·51 MeV photons resulting from the annihilation of the positrons were counted in coincidence. This method is preferable to counting the positrons directly since it permits the use of thick samples and also reduces the background counting rates.

---

† Now at Department of Physics, Duke University, U.S.A.

The pulses from one photomultiplier were used to gate the pulse from the other and the coincident pulses were counted either with a scaler or with a 100 channel kicksorter.

The half-life of the positron activity produced in the boron was found to be $20{\cdot}8 \pm 0{\cdot}6$ minutes and that in the distrene to be $20{\cdot}7 \pm 0{\cdot}7$ minutes. These values are in good agreement with the value of $20{\cdot}3 \pm 0{\cdot}1$ minutes obtained by Barber *et al.* (1955) for the positron activity of ^{11}C.

§ 3. RESULTS

The ratio R of the positron activity per gramme of the boron sample to the positron activity per gramme of the distrene sample was measured as a function of the maximum energy $E_{\gamma\max}$ of the bremsstrahlung spectrum. The results are shown in the figure.

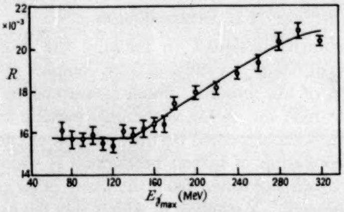

The ratio R of the β^+ activity per gramme of boron to the β^+ activity per gramme of distrene as a function of the peak energy of the bremsstrahlung, $E_{\gamma\max}$.

If all the positron activity produced in the boron sample were due to the reaction $^{11}\mathrm{B}(\gamma\pi^-)^{11}\mathrm{C}$ then R should be zero when $E_{\gamma\max}$ was below the threshold energy for meson production in boron (~ 140 MEV). However, R has a constant value of $1{\cdot}58 \times 10^{-2}$ for values of $E_{\gamma\max}$ between 140 MEV and 70 MEV the lowest energy at which significant counting statistics could be obtained. Above 140 MEV R increases to reach a value of $2{\cdot}08 \times 10^{-2}$ at 320 MEV.

The fact that R is constant at low energies and that the increase in R at high energies begins at meson threshold suggests that the increase is due to meson production. Hence it is reasonable to subtract the constant value of R found at low energies from the values found above 140 MEV and to assume that the difference is due to the reaction $^{11}\mathrm{B}(\gamma\pi^-)^{11}\mathrm{C}$. The cross section for this reaction can then be obtained using the results of Barber *et al.* (1955) for the cross section of the reaction $^{12}\mathrm{C}(\gamma\mathrm{n})^{11}\mathrm{C}$. The cross section may also be determined by exposing the distrene sample in the collimated beam of the synchrotron and using a Cornell chamber as a monitor. Using these two methods the values obtained for the cross section for the reaction $^{11}\mathrm{B}(\gamma\pi^-)^{11}\mathrm{C}$ averaged over the photon energy range $E_\gamma = 140$ to 320 MEV are $(2{\cdot}6 \pm 0{\cdot}2) \times 10^{-29}$ and $(2{\cdot}9 \pm 0{\cdot}2) \times 10^{-29}$ cm^2 respectively. The mean value given by these two methods was used to obtain the cross sections. The bremsstrahlung spectrum used in obtaining these cross sections was that for a tungsten target of 0·020 in. effective thickness. The effective thickness was determined by a measurement of the angular distribution of the photon beam and is in agreement with measurements of the spectrum made with a pair spectrometer.

The cross section as a function of photon energy is given in the table where it is compared with the theoretical values calculated by Laing and Moorhouse (1957). These authors assume a simple independent particle model for the nucleus in which interparticle forces and spin–orbit coupling are neglected. The primary photoproduction process is assumed to occur at a single nucleon which goes into a discrete bound state. They calculate the cross sections σ_s for photoproduction at the nuclear surface only, and σ_V, for photoproduction throughout the nuclear volume. The experimental values are in good agreement with the theoretical values for surface production.

Photon energy (Mev)	140–170	170–200	200–230	230–260	260–290	290–320
Calculated σ_V (10^{-29} cm^2)	17·3	21·5	19·0	15·2	12·0	9·6
Calculated σ_S (10^{-29} cm^2)	2·7	3·8	3·2	2·5	2·1	1·8
Measured σ (10^{-29} cm^2) (errors ±20%)	2·8	3·0	3·1	3·1	2·8	1·9

The constant non-zero value of R below the meson threshold has not been explained. The activity is certainly a positron activity with a half-life of 20 minutes. The following investigations of possible sources of this activity have been made:

(1) *Impurities in the boron sample.*

It is clear that an impurity of about 1·5% of carbon in the boron sample would be sufficient to produce the activity observed. However, the carbon content of the boron is quoted by the manufacturers as less than 0·1% and an independent analysis of the boron made after the experimental runs gave a value of less than 0·3% for the carbon content.

The manufacturers' analysis quotes impurities of about 0·1% magnesium, aluminium, manganese, iron and oxygen. All these elements have been irradiated and the positron activity produced in these compared with that produced in distrene. The results show that impurities of at least 30% of any of these elements would be necessary to produce the activity found in the boron at low energies. Thus it seems improbable that impurities are the cause of this activity.

(2) *The reaction* ^{11}B(pn)^{11}C.

Another possibility is the production of ^{11}C by the interaction with boron of secondary particles generated by the bremsstrahlung. The only reactions possible are ^{11}B(pn)^{11}C and ^{10}B(pγ)^{11}C. It was found that R was unchanged when the boron sample was shielded by various thicknesses of lead and copper and when the material used for the container was changed. R was also unchanged when the irradiation was made behind a scrubbing magnet. Thus protons originating outside the sample are not responsible.

For photoprotons produced in the boron sample itself and having a range greater than the thickness of the sample, the number of ^{11}C nuclei produced by the two stage process ^{11}B(γp)^{10}Be then ^{11}B(pn)^{11}C should vary approximately as the square of the sample thickness. For a single reaction such as ^{11}B($\gamma\pi^-$)^{11}C the variation should be linear with thickness. Experimentally the variation with sample thickness was found to be linear for all thicknesses used (1 cm to 0·1 cm). If the range of the photoprotons were less than 0·1 cm in the boron sample (density 0·6), then their energy would be less than 6 Mev and the cross sections for the (γp) and (pn) reactions in boron would be much too small to produce the activity observed.

Thus the obvious sources of the positron activity at low energies cannot account for the magnitude of the effect observed.

A reaction of the type $^{11}B(\gamma e^-)^{11}C$ would lead to the effect observed, but such a reaction has not been reported and would not be expected to have a large cross section. The cross section required would be of the order of 10^{-28} cm^2. Further investigations of this activity are in progress.

ACKNOWLEDGMENTS

The authors are grateful for the interest and encouragement of Professor P. I. Dee. They wish to thank Dr. E. W. Laing, Dr. R. G. Moorhouse, Dr. H. Muirhead and Dr. J. G. Rutherglen for valuable discussions, Dr. W. McFarlane and the synchrotron crew for their assistance and cooperation during the irradiations, Mr. G. Walker for assistance with some of the runs, and Dr. R. I. Reed of the Chemistry Department for analysing the boron samples. One of us (I.S.H.) wishes to acknowledge the award of a fellowship by the Department of Scientific and Industrial Research.

REFERENCES

BARBER, W. C., GEORGE, W. D., and REAGAN, D. D., 1955, *Phys. Rev.*, **98,** 73.
LAING, E. W., and MOORHOUSE, R. G., 1957, *Proc. Phys. Soc.* B, **70,** 629.

RESEARCH NOTES

An Anisotropic Cosmological Solution in General Relativity

By AMALKUMAR RAYCHAUDHURI

Theoretical Physics Department, Indian Association for the Cultivation of Science,
Jadavpur, Calcutta, India

MS. received 18*th February* 1958, *and in final form* 3*rd April* 1958

In the field of cosmology, it is usual to take spatial isotropy as a basic postulate. Here we present a solution of the Einstein gravitational equations which is cosmologic in the sense that it extends through all space and the world lines of matter form a coherent pencil of geodesics. The solution is, however, not spatially isotropic although the distribution of matter is uniform. It is not our purpose to suggest that this solution is in any way a better representation of the actual universe than the isotropic models. However, we think that the solution is of some interest especially in view of the fact that there is remarkably little discussion of anisotropic solutions in the literature.

We suppose that the space-time admits an Abelian G_3 of motions with space-like generators. Then choosing the time axis orthogonal to the invariant varieties, we may write the line element in the form

$$ds^2 = dt^2 - h_{ik}dx^i dx^k. \qquad \ldots\ldots(1)$$

Further, the x^i axes being chosen to be the paths of the translations, the h_{ik}'s are functions of t alone. Now writing (Taub 1951)

$$K_j^{\ i} = \tfrac{1}{2}h^{ik}\frac{dh_{kj}}{dt} \qquad \ldots\ldots(2)$$

the field equations give

$$8\pi\rho = -\tfrac{1}{2}K_j^{\ i}K_i^{\ j} + \tfrac{1}{2}(K_l^{\ l})^2 \qquad \ldots\ldots(3)$$

$$0 = \frac{dK_j^{\ i}}{dt} + K_l^{\ l}K_j^{\ i} - \left\{\frac{dK_l^{\ l}}{dt} + \tfrac{1}{2}K_m^{\ l}K_l^{\ m} + \tfrac{1}{2}(K_l^{\ l})^2\right\}\delta_j^{\ i} \qquad \ldots\ldots(4)$$

where we have taken $T_4^{\ 4} = \rho$ and all other components of $T_\nu^{\ \mu}$ vanish.

Equation (4) on integration gives

$$K_j^{\ i} = c_j^{\ i}/h^{1/2} + \frac{dh/dt}{6h}\delta_j^{\ i} \qquad \ldots\ldots(5)$$

and

$$h \equiv \det|h_{ik}|,\ c_i^{\ i} = 0,\ h_{ik}c_j^{\ i} = h_{ij}c^i_{\ k}. \qquad \ldots\ldots(6)$$

Substituting from (5) in (4), we get,

$$\frac{d^2h}{dt^2} - \frac{3}{4}\frac{(dh/dt)^2}{h} + \frac{3}{2}c_j^{\ i}c_i^{\ j} = 0 \qquad \ldots\ldots(7)$$

which on integration gives

$$h^{1/2} = a(t^2 - \mu^2 a^{-2}) \qquad \ldots\ldots(8)$$

where

$$\mu^2 \equiv \tfrac{3}{8}c_j^{\ i}c_i^{\ j} \qquad \ldots\ldots(9)$$

and a is an arbitrary constant.

Further, we note that if the matrix $c_j{}^i$ be diagonal, then $K_j{}^i$ would also be diagonal and it is easy to see from equation (2) that h_{ik} would also be diagonal. We then have

$$\frac{dh_{ii}}{dt} = 2h_{ii}K_i{}^i \quad (i \text{ not summed}). \qquad \ldots\ldots (10)$$

Using (5) and (8) in (10) we get on integration

$$h_{ii} = a^{2/3}(t^2 - \mu^2 a^{-2})^{2/3} \left\{ \frac{t - \mu a^{-1}}{t + \mu a^{-1}} \right\}^{c_i{}^i \mu^{-1}} \quad (\text{no summation over } i). \qquad \ldots\ldots (11)$$

If $c_j{}^i$ were not diagonal, we should have in general

$$\frac{dh_{ik}}{dt} = 2h_{il}c_k{}^l h^{-1/2} + \frac{dh/dt}{3h} h_{ik}. \qquad \ldots\ldots (12)$$

This equation system may be integrated without much difficulty. One obtains

$$h_{ik} = a^{2/3}(t^2 - \mu^2 a^{-2})^{2/3} \left[a_{ik} \left(\frac{t - \mu a^{-1}}{t + \mu a^{-1}} \right)^{\lambda_1 \mu^{-1}} + b_{ik} \left(\frac{t - \mu a^{-1}}{t + \mu a^{-1}} \right)^{\lambda_2 \mu^{-1}} + c_{ik} \left(\frac{t - \mu a^{-1}}{t + \mu a^{-1}} \right)^{\lambda_3 \mu^{-1}} \right] \qquad \ldots\ldots (13)$$

where the λ's are the latent roots of the $c_j{}^i$ matrix and are therefore connected by the relation $\lambda_1 + \lambda_2 + \lambda_3 = 0$. The eighteen constants a_{ik}, b_{ik} and c_{ik} are, however, not independent of each other.

In any case we have in general from (5), (8) and (3)

$$6\pi\rho(t^2 - \mu^2 a^{-2}) = 1. \qquad \ldots\ldots (14)$$

Thus in general we have a contracting space for $-\infty < t < -\mu a^{-1}$ and an expanding space for $+\mu a^{-1} < t < +\infty$. The solutions, although in general anisotropic, tend towards isotropy as $|t| \to \infty$.

REFERENCE

TAUB, A. H., 1951, *Ann. Math.*, **53**, 472.

Temperature Dependence of Point Contact Injection Ratio in Germanium

BY D. GERLICH

Department of Physics, The Hebrew University, Jerusalem, Israel

MS. received 10*th December* 1957, *and in revised form* 20*th March* 1958

MEASUREMENTS of point contact injection ratio in germanium have been reported by various authors (Shockley, Pearson and Haynes 1949, Banbury 1953, Hogarth 1953, Banbury and Houghton 1954, 1955, Low 1955 b). The present communication describes a method for the measuring of the point contact injection ratio γ (the composition ratio, $I_{\text{minority}}/I_{\text{total}}$, of the current entering the bulk via the point contact) by direct compensation, as well as results obtained for n- and p-type material over an extended range of temperatures. In particular the range is extended below room temperatures.

The filament is inserted into one arm of a bridge circuit (Many 1954) and a point contact is applied approximately at its middle. This is connected via a variable resistor to the forward-biased soldered contact, which is rendered non-injecting. Square-wave pulses of low repetition rate (50 c/s) are applied to the bridge. The emitter current I flowing into the filament through the point contact injects holes into it, modulating its conductivity by an amount $\Delta G(t)$. The latter decays exponentially with time and, as has been shown previously (Many 1954, Low 1955 a), there exists the relation

$$\frac{\Delta G(t)}{G_0}=\frac{(\mu_n+\mu_p)(\gamma-\gamma_0)I\tau}{\boldsymbol{e}(\mu_n n_0+\mu_p p_0)u}\,[1-\exp(-t/\tau)] \qquad \ldots\ldots(1)$$

where G_0 is the equilibrium conductivity of the filament, μ_n and μ_p are the electron and hole mobilities respectively, τ is the lifetime of the filament, $\boldsymbol{e}$ is the electronic charge, n_0 and p_0 are the electron and hole equilibrium concentrations respectively, u is the volume of the filament and γ_0 is the value of γ under equilibrium, namely $\mu_p p_0/(\mu_n n_0+\mu_p p_0)$. (In the extrinsic range $\gamma \gg \gamma_0$, so that here γ_0 can be neglected.) This change in filament conductance is simulated by the compensating RC circuit in the bridge, thus permitting the direct determination of γ and τ simultaneously. It should be noted that the product $\mu_p\tau$, and hence the value of γ, is not affected by trapping (Lawrence, Gibson and Granville 1954).

Measurements were carried out on etched (CP4) n- and p-type filaments in a vacuum of 10^{-5} mm Hg and γ was measured as a function of I for a series of temperatures in the range 150°K to 350°K. It has been found in n-type samples that γ decreases monotonically with increasing I. In p-type samples, however, γ increases with increasing I in the region of low currents, reaches a maximum, and then decreases as I is increased further. This behaviour, also observed by Low (1955 b), is contrary to theoretical predictions (Bardeen and Brattain 1949). As yet no interpretation is available. A notable characteristic of the curves for the n-type samples and the descending part of those for the p-type samples is that the average slope decreases with decreasing temperature.

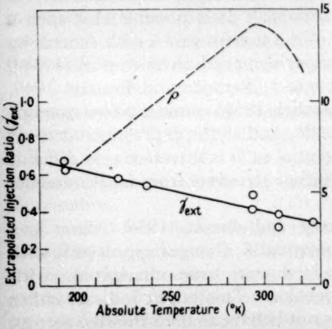

Figure 1. The injection ratio extrapolated to zero emitter current as a function of temperature for an n-type filament, resistivity 14 ohm cm.

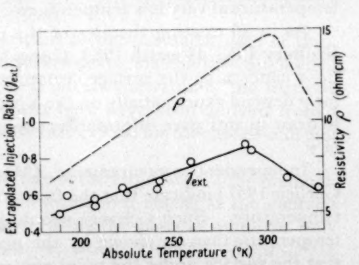

Figure 2. The injection ratio extrapolated to zero emitter current as a function of temperature for an n-type filament, resistivity 14 ohm cm.

The full line curves of figures 1 and 2 are plots of γ extrapolated to zero emitter current as a function of the absolute temperature for n-type filaments, each of 14 ohm cm resistivity. The broken curves show the resistivity of these filaments as a function of the temperature. It is noteworthy that although both samples were cut from the same ingot and received identical surface treatment, and although the measurements were carried out under similar conditions, the curves are different in character. The full line curve in figure 3 is the maximum value of γ plotted against the absolute temperature for a p-type filament of 6·8 ohm cm resistivity. It is interesting to note that this maximum is effectively constant over the entire range of temperatures covered.

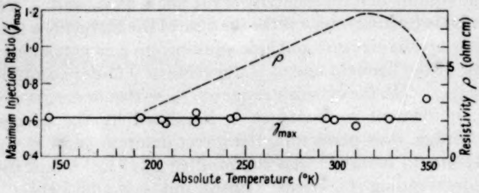

Figure 3. The maximum value of the injection ratio as a function of temperature for a p-type filament, resistivity 6·8 ohm cm.

The results presented above show γ to be extremely sensitive to the surface structure. Although the surfaces of all the filaments investigated were given the same treatment, the behaviour of γ as a function of temperature differs completely in character, even for the two similar n-type samples. The completely different character of the (γ, I) and the (γ, T) curves for n- and p-type samples suggests that there exists an inherent difference between them, due to a variation in either the surface conditions or the process of injection, or both.

As can be seen from the results presented here, the assumption that γ is constant with temperature is not always justifiable. It is possible that such a variation in γ caused the anomalous decrease of the current gain α with decreasing temperature at very low temperatures in the experiment of Lawrence *et al.* (1954).

As in all existing theories of the point contact (Bardeen and Brattain 1949, Banbury 1953, Hogarth 1953, Gunn 1954, Gerlich 1956), some *a priori* assumptions concerning the surface structure are made; and as the expressions derived for γ depend exponentially on the surface potential ϕ_s, it is therefore very difficult to draw quantitative information about the surface structure from measurements of γ.

Independent measurements (Montgomery and Brown 1956, Many and Gerlich 1957) indicate that the free surface potential ϕ_s changes appreciably with temperature. Such a change should have caused much larger changes in γ with temperature than are shown by the present results. This might indicate either that the surface under the point contact does not behave as does the free germanium surface, that the point contact causes some constriction to the surface beneath it, or that the assumptions made in developing the theories are too stringent and are not realized in practice.

REFERENCES

BANBURY, P. C., 1953, *Proc. Phys. Soc.* B, **66,** 833.

BANBURY, P. C., and HOUGHTON, J., 1954, *Physica*, **20,** 1050; 1955, *Proc. Phys. Soc.* B, **68,** 17.

BARDEEN, J., and BRATTAIN, W. H., 1949, *Phys. Rev.*, **75,** 1208.

GERLICH, D., 1956, *Proc. Phys. Soc.* B, **69,** 1350.

GUNN, J. B., 1954, *Proc. Phys Soc.* B, **67,** 575.

HOGARTH, C. A., 1953, *Proc. Phys. Soc.* B, **66,** 845.

LAWRENCE, R., GIBSON, A. F., and GRANVILLE, J. W., 1954, *Proc. Phys. Soc.* B, **67,** 625.

LOW, G. G. E., 1955 a, *Proc. Phys. Soc.* B, **68,** 310; 1955 b, *Ibid.*, **68,** 447.

MANY, A., 1954, *Proc. Phys. Soc.* B, **67,** 9.

MANY, A., and GERLICH, D., 1957, *Phys. Rev.*, **107,** 404.

MONTGOMERY, H. C., and BROWN, W. L., 1956, *Phys. Rev.*, **103,** 865.

SHOCKLEY, W., PEARSON, G. L., and HAYNES, J. R., 1949, *Bell Syst. Tech. J.*, **28,** 344.

Sweep-out Effects in the Phase Shift Method of Carrier Lifetime Measurements

BY N. B. GROVER† AND E. HARNIK

Department of Physics, The Hebrew University, Jerusalem, Israel

MS. received 3rd April 1958

WHEN carriers are injected into a semiconductor by periodically modulated illumination, the associated photoconductance signal lags in phase as a result of the finite lifetime of the excess carriers. The relation between the phase lag of the photoconductance signal ϕ, the bulk lifetime τ_0 and the surface recombination velocity s has been investigated by several authors (Schultz 1955, Ridout 1956, Engler and Kevane 1957, van der Pauw 1957). In all these treatments, the sweeping electric field has been assumed small enough for its effect on the measured value of the phase angle (i.e. sweep-out effects at the contacts) to be neglected. As, however, the sensitivity of the measurements increases with the applied field, it was thought desirable to extend the available treatments with a view to determining an upper limit for the value of the applied field consistent with negligible sweep-out effects.

In this note the discussion will be restricted to the particular case of thin, rectangular filaments with ohmic contacts and low-level, sinusoidally modulated illumination. Trapping, except in so far as it affects the value of the lifetime, will not be considered. The results presented here have been derived from a treatment analogous to the one described by Rittner (1956) for the case of constant illumination.

Consider first the case where the whole of one of the large faces of the filament, including the contacts, is illuminated. When sweep-out effects at the contacts are neglected, the photocurrent can be derived on the basis of uniform bulk generation and an effective filament lifetime τ, where $1/\tau = 1/\tau_0 + 2s/d + s^2/D$, provided that the filament thickness d is small compared with L_0 sech a, where sinh $2a = \omega\tau_0$, $L_0 = (D\tau_0)^{1/2}$ is a diffusion length, ω is the angular frequency of the injecting light signal and D is the ambipolar diffusion constant. The phase shift ϕ between the photoconductance and the injecting light signals is, under these conditions, given by $\tan^{-1}\omega\tau$. It should be noted that for well-etched surfaces, the last term in the expression for τ may be neglected.

---

† Canadian Hadassah Research Fellow 1955–1958.

When sweep-out effects are taken into account, the model of uniform bulk generation can be retained only when d is small compared with $bL_0 \operatorname{sech} a$, where $b^{-2}=1+(w_0/2L_0)^2+(\pi L_0/2l)^2$, $w_0=\mu_0 E\tau_0$ is a drift length, $2l$ is the filament length, μ_0 is the ambipolar mobility and E is the measuring electric field. Under these conditions the photoconductance signal is proportional to

$$\frac{E\tau\exp(j\omega t)}{1+j\omega\tau}\left\{1-\frac{(k_1-k_2)\sinh(k_1 l)\sinh(k_2 l)}{k_1 k_2 l\sinh(k_1-k_2)l}\right\} \qquad \ldots\ldots (1)$$

where $k_{1,2}=-w/2L^2\pm\{(w/2L^2)^2+(1+j\omega\tau)/L^2\}^{1/2}$. Here $\exp(j\omega t)$ represents the time dependence of the injecting light signal, $L=(D\tau)^{1/2}$ and $w=\mu_0 E\tau$ are the effective diffusion length and effective drift length respectively. To represent the effects of sweep-out at the contacts on the measured phase angle ϕ, a correction factor $1-f$ can be defined such that $\tan\phi=\omega\tau(1-f)$.

It follows from equation (1) that for f to be small the filament length $2l$ must be large compared with both the effective diffusion length L and the effective drift length w. In practice for thin, well-etched filaments L is of the order of 1 mm or less and so is small compared with the values of l generally encountered. Thus the factor of interest affecting f is usually w. From equation (1) f can then be calculated as a function of $|w/2L|$ for various values of the parameters l/L and $\omega\tau$. These results are shown in figure 1. It can be seen that, for $|w/2L|\lesssim 1$, f remains small and fairly constant, whereas for higher values it begins to rise rapidly. The curves also show that f is not sensitive to $\omega\tau$. It should be pointed out that for the range of parameters considered, f does not reach zero even for $w/2L=0$.

Thus added sensitivity consistent with a negligible increase in sweep-out effects can be obtained by raising w (i.e. by raising E) until $\tan\phi$ begins to decrease

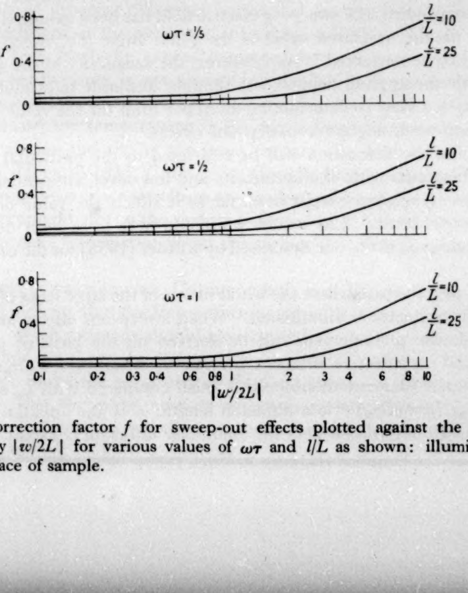

Figure 1. Correction factor f for sweep-out effects plotted against the dimensionless quantity $|w/2L|$ for various values of $\omega\tau$ and l/L as shown: illumination of one entire face of sample.

rapidly. The value of f is then read off the appropriate curve and τ corrected for where necessary. Values of τ obtained in this way compare well with those measured on the same samples by the Many bridge method (Many 1954).

Smaller sweep-out effects are to be expected if the filament is illuminated in but a narrow band far from the contacts. It can be shown that in this case the photocurrent for an n-type sample of length $l_1 + l_2$ is proportional to

$$\frac{E\tau \exp(j\omega t)}{1+j\omega\tau}\left\{1+\frac{L^2k_1\sinh(k_2\delta)\exp(k_2l_2)}{\delta(1+j\omega\tau)}\right\}\frac{2\delta}{l_1+l_2} \qquad \ldots\ldots (2)$$

provided that $|k_1l_1| \gg 1$, a condition easily fulfilled in practice. Here 2δ is the width of the illuminated band and l_2 is the distance between the mid-point of this band and the end of the filament measured in the direction of the drift of the minority carriers. Completely analogous results are obtained for p-type material. Sample curves, applicable to either n- or p-type filaments, are shown in figure 2 where f is plotted as a function of $|w/2L|$ for various values of l_2/L with $\omega\tau = \frac{1}{2}$ and $\delta/L = 2{\cdot}5$. These curves indicate that here f may become practically zero for values of $|w/2L|$ which are far from negligible and which increase with the filament length. Thus the loss in sensitivity caused by partial illumination may be more than compensated for by the higher values of the applied field now permissible.

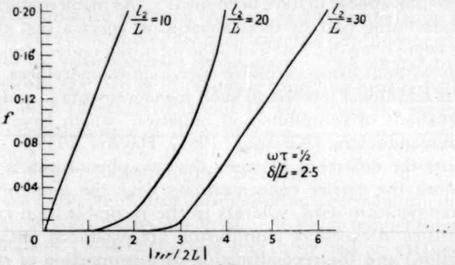

Figure 2. Correction factor f for sweep-out effects plotted against the dimensionless quantity $|w/2L|$ for various values of l_2/L as shown with $\omega\tau = \frac{1}{2}$ and $\delta/L = 2{\cdot}5$: illumination in a narrow band on surface.

REFERENCES

ENGLER, A. R., and KEVANE, C. J., 1957, *Rev. Sci. Instrum.*, **28**, 548.
MANY, A., 1954, *Proc. Phys. Soc.* B, **67**, 9.
VAN DER PAUW, L. J., 1957, *Philips Res. Rep.*, **12**, 364.
RIDOUT, M. S., 1956, *Halbleiter und Phosphore* (Braunschweig: Vieweg).
RITTNER, E. S., 1956, *Photoconductivity Conference*, ed. R. G. Breckenbridge *et al.* (New York: John Wiley).
SCHULTZ, B. H., 1955, *Philips Res. Rep.*, **10**, 337.

The Infra-Red Emissivities of Indium Antimonide and Germanium

BY T. S. MOSS AND T. D. H. HAWKINS
Radio Department, R.A.E., Farnborough, Hants.

MS. received 17*th March* 1958, *and in final form* 25*th April* 1958

§ 1. INTRODUCTION

ALTHOUGH a great deal of work has been carried out on optical absorption in semiconductors, no corresponding measurements of emission of thermal radiation appear to have been made. As many important semiconductors have the interesting part of their absorption spectra (i.e. the long wavelength absorption edge) lying quite well into the infra-red region, emission measurements are possible without using excessive specimen temperatures.

There is additional interest in such measurements in order to compare them with observations of recombination radiation, which have now been made on several semiconductors (Newman 1953, Haynes 1955). From the physical point of view the difference between the two phenomena is that in the thermal emission work the carrier concentrations have the equilibrium values for the specimen temperature used, whereas in the recombination radiation experiment carrier densities in excess of equilibrium are produced (either photoelectrically or by injection) and the recombination of a proportion of these excess carriers produces radiation.

§ 2. THEORY

Consider a unit solid block of material of refractive index n and absorption constant K. Now the number of possible frequencies in a frequency interval $d\nu$ is $8\pi\nu^2 d\nu v^{-3}$ where $v = c/n$ is the velocity of propagation of the radiation. The number of photons per unit volume is thus

$$q\,d\nu = \frac{8\pi\nu^2 d\nu}{v^3\{\exp(\boldsymbol{h}\nu/\boldsymbol{k}T)-1\}} \qquad \ldots\ldots(1)$$

The absorption in distance dx is $qK\,dx$, and in time dt is $qvK\,dt$. Now this must equal the photon generation rate $r_\nu\,d\nu\,dt$, so that

$$r_\nu\,d\nu = \frac{8\pi K\nu^2 d\nu}{v^2\{\exp(\boldsymbol{h}\nu/\boldsymbol{k}T)-1\}} \qquad \ldots\ldots(2)$$

or

$$-r_\nu\,d\nu \equiv r\,d\lambda = \frac{8\pi Kcn^2\lambda^{-4}d\lambda}{\exp(\boldsymbol{h}\nu/\boldsymbol{k}T)-1} \qquad \ldots\ldots(3)$$

where λ is the wavelength *in vacuo*.

This radiation is generated in a solid angle 4π, so that the volume rate of photon generation for unit waveband in a small solid angle $d\omega$ is

$$r\,d\omega = n^2KQ\,d\omega/\pi \qquad \ldots\ldots(4)$$

where

$$Q = 2\pi c\lambda^{-4}/\{\exp(\boldsymbol{h}\nu/\boldsymbol{k}T)-1\} \qquad \ldots\ldots(5)$$

is the tabulated Planck function.

By summing multiple reflections in a parallel sided slab of material it is found that the normal emission per unit area of surface (of reflectance R) is

$$\frac{Q}{\pi}\frac{(1-R)(1-T)}{1-RT}\,d\Omega$$

where T is the true transmittance of the slab and $d\Omega = n^2 d\omega$ is the solid angle into which the radiation is refracted. Now the normal photon emission of a black body is simply $(Q/\pi)\,d\Omega$, so that the emissivity ϵ of the material is given by

$$\epsilon = (1-R)(1-T)/(1-RT). \qquad \ldots\ldots(6)$$

It should be noted that this expression is independent of n (except through R), and it is a bulk effect and not merely a surface one. It will be seen that if the slab is highly absorbing, with $T=0$, then $\epsilon = 1-R$. On the other hand, if $T\to 1$, $\epsilon \to 0$. The emissivity of a semiconductor should therefore be fairly high at short wavelengths and should decrease sharply at the absorption edge.

There is a close resemblance between thermal and recombination radiation. For example, equation (4) above shows the same spectral dependence as equation (1) of Moss (1957) for the *same specimen temperature*. The outstanding experimental difference between the two is in response time, the heat radiation being governed by thermal time constants of about 10 sec, while the recombination radiation will have a relaxation time of 10^{-8}–10^{-4} sec.

§ 3. Experimental Details

Measurements were made on indium antimonide and germanium, in the form of single crystal slices of high purity material. At room temperature the germanium was near intrinsic ($\sim 40\,\Omega$ cm) and the InSb had an extrinsic carrier concentration only of the order of 10% of intrinsic. The thickness of the Ge was 0·22 mm, and of the InSb, 45μ.

In order to measure the emission from the semiconductor only, it is essential to avoid both reflections from the specimen surface and transmission through the material. Both these difficulties were overcome by having the specimens in the open and heating them electrically. Measurement of the resistance of the specimens provided an effective way of determining their temperature. An actual resistance–temperature calibration was made for each specimen using a liquid bath and low measuring currents.

All measurements were made using a Leiss double monochromator. For the InSb work, rock salt prisms and a thermopile detector with 5 c/s amplifier were used. With a spectral resolution of approximately $0{\cdot}15\,\mu$ it was possible to operate at specimen temperatures as low as 35°c.

For the germanium work, silica prisms were used. In order to cover all the region of changing emissivity it was necessary to measure down to about $1{\cdot}5\,\mu$, where, at the lowest temperatures used, black-body radiation is only about 10^{-5} that of the peak radiation, so that the best possible detector was required. This was a liquid-air cooled PbS cell, operated at 800 c/s. The spectral bandwidth was $0{\cdot}09\,\mu$ at $2\,\mu$. In the experiments records were taken alternately of the emission from the specimen and from a comparison black body.

For the InSb, an absolute measurement of the emissivity was made in the short wavelength, high emissivity region, using a P.E.M. type InSb detector. The spectral response of this detector is fairly flat up to $6{\cdot}0\,\mu$ and is low beyond $7\,\mu$, so that it detects almost all of the radiation emitted below the absorption edge but is insensitive to the emission beyond the absorption edge. With this detector, and no monochromator, signal levels were sufficiently high to eliminate the necessity for optical systems, so that a direct comparison could be made with a black-body source using the inverse square law. The width of the specimen was measured carefully at various points, and the length of specimen radiating was defined by an aperture which screened off radiation from the ends.

§ 4. EXPERIMENTAL RESULTS

Plots of the relative emissivity of InSb at various temperatures are shown in figure 1. The behaviour is as expected theoretically, with high emissivity at wavelengths below the edge, and relatively low emissivity at long wavelengths. The minimum observed emissivity is 28% of the maximum. Thus from equation (6), $(1-T)/(1-RT)=0{\cdot}28$, giving $T=0{\cdot}81$ and $K=55$ cm^{-1}. This is in reasonable agreement with measured absorption coefficients at elevated temperatures (Avery *et al.* 1954).

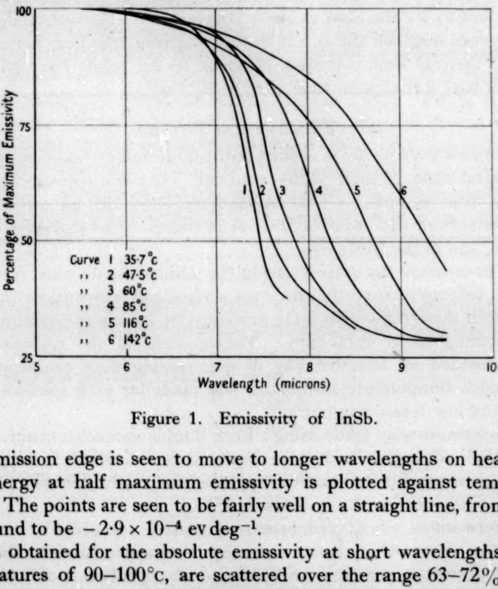

Figure 1. Emissivity of InSb.

The emission edge is seen to move to longer wavelengths on heating. The photon energy at half maximum emissivity is plotted against temperature in figure 2. The points are seen to be fairly well on a straight line, from which the shift is found to be $-2{\cdot}9\times10^{-4}$ ev deg^{-1}.

Values obtained for the absolute emissivity at short wavelengths, measured at temperatures of 90–100°c, are scattered over the range 63–72%. For this spectral region $n=4{\cdot}02$ and $k<0{\cdot}1$ (Moss *et al.* 1957), giving $R=36\%$ and an expected emissivity of 64%. The measured values are thus in reasonable accord with expectations.

The relative emissivity of germanium is plotted in figure 3. For this material the long wavelength emissivity is only of the order of 5% at the lower temperatures, with a significant increase above 200°c. At 235°c the emissivity is 0·12 of maximum, which from equation (6) is equivalent to $K=4$ cm^{-1}. Again the edge moves to longer wavelengths at higher temperatures, the shift being nearly -5×10^{-4}ev deg^{-1} (figure 2).

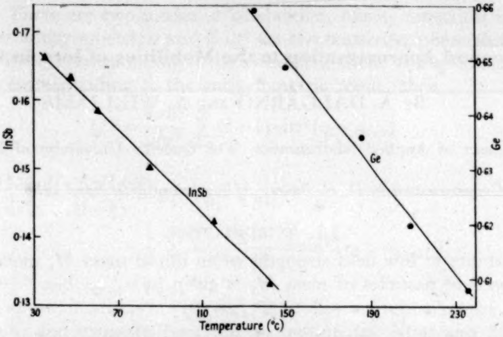

Figure 2. Temperature dependence of photon energy (ev) at half maximum emissivity for InSb and Ge.

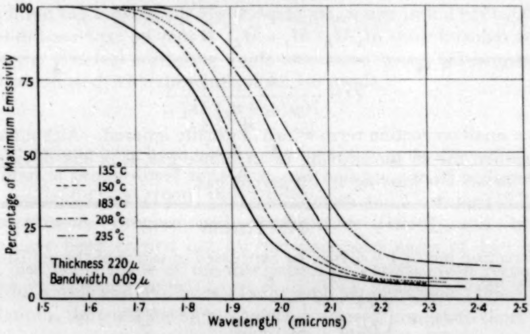

Figure 3. Emissivity of germanium.

§ 5. Conclusions

The infra-red emissivities of InSb and Ge vary markedly in the region of the absorption edges, as expected from the theory given. The shifts of these edges are found to be approximately -3×10^{-4} ev deg^{-1} for InSb and -5×10^{-4} ev deg^{-1} for Ge. The absolute emissivity of InSb is in accord with calculations from the optical constants.

Acknowledgments

Thanks are due to Dr. K. W. Taylor for preparing InSb specimens, and Miss D. Webber for help in analysing the results.

References

Avery, D. G., Goodwin, D. W., Lawson, W. D., and Moss, T. S., 1954, *Proc. Phys. Soc.* B, **67,** 761.
Haynes, J. R., 1955, *Phys. Rev.*, **98,** 1866.
Moss, T. S., 1957, *Proc. Phys. Soc.* B, **70,** 247.
Moss, T. S., Smith, S. D., and Hawkins, T. D. F., 1957, *Proc. Phys. Soc.* B, **70,** 776.
Newman, R., 1953, *Phys. Rev.*, **91,** 1313.

The Second Approximation to the Mobilities of Ions in Gases

By A. DALGARNO and A. WILLIAMS

Department of Applied Mathematics, The Queen's University of Belfast

Communicated by D. R. Bates; *MS. received* 28*th April* 1958

§ 1. INTRODUCTION

The mobility at low field strengths of an ion of mass M_1 moving in a gas composed of particles of mass M_2 is given by

$$K = eD/\boldsymbol{k}T \qquad \ldots\ldots (1)$$

where D is the diffusion coefficient and e the charge of the ion, $\boldsymbol{k}$ is Boltzmann's constant and T is the absolute temperature (cf. Massey and Burhop 1952). According to the Chapman–Enskog theory (cf. Chapman and Cowling 1939, Kihara 1953, 1954), if n_1 and n_2 are respectively the ion and gas number densities and μ is the reduced mass $M_1M_2/(M_1+M_2)$, D may be expressed in terms of the collision integral $\Omega_{(1,1)}$ as

$$D = \frac{3\boldsymbol{k}T}{16\mu(n_1+n_2)}\,\frac{1+\epsilon_0}{\Omega_{(1,1)}} \qquad \ldots\ldots (2)$$

where ϵ_0 is a small correction term which is usually ignored. Although its neglect is easily justified for an ion moving in an unlike gas, it is less obvious that this is the case for an ion moving in its parent gas.

§ 2. THEORY

The correction factor $1+\epsilon_0$ may be expressed in terms of the collision integrals $\Omega_{(l,s)}$ defined by

$$\Omega_{(l,s)} = \left(\frac{\boldsymbol{k}T}{2\pi\mu}\right)^{1/2} \int_0^\infty \exp(-\gamma^2)\gamma^{2s+3}Q^{(l)}(v)\,d\gamma \qquad \ldots\ldots (3)$$

where γ is related to the relative velocity v by $2\boldsymbol{k}T\gamma^2 = \mu v^2$ and $Q^{(l)}(v)$ is an elastic collision cross section

$$Q(v)^{(l)} = 2\pi \int_0^\infty (1-\cos^l\chi)b\,db, \qquad \ldots\ldots (4)$$

b being the impact parameter and $\chi(b)$ the corresponding scattering angle (cf. Hirschfelder, Curtiss and Bird 1954). According to the Chapman–Cowling method (see also Furry and Pitkanen 1951)

$$\epsilon_0 = 5(C-1)^2\{5-4B+6(M_1/M_2)^2+8A(M_1/M_2)\}^{-1} \qquad \ldots\ldots (5)$$

and according to the Kihara method

$$\epsilon_0 = 5(C-1)^2\{2+6(M_1/M_2)^2+8A(M_1/M_2)\}^{-1} \qquad \ldots\ldots (6)$$

where

$$A = \Omega_{(2,2)}/5\Omega_{(1,1)}, \qquad \ldots\ldots (7)$$

$$B = \{5\Omega_{(1,2)} - \Omega_{(1,3)}\}/5\Omega_{(1,1)}, \qquad \ldots\ldots (8)$$

$$C = 2\Omega_{(1,2)}/5\Omega_{(1,1)}. \qquad \ldots\ldots (9)$$

Expression (4) for the cross section cannot be used for an ion moving in its parent gas for quantal symmetry modifications (Massey and Mohr 1934) are important. There are two modes of interaction, one symmetrical in the nuclei and the other antisymmetrical and if η_l^+ are the scattering phase shifts (cf. Mott and Massey 1949) corresponding to the symmetric mode and η_l^- are the scattering phase shifts corresponding to the antisymmetric mode, then

$$Q^{(1)}=\frac{4\pi\hbar^2}{\mu^2v^2}\sum_{l=0}^{\infty}(l+1)\sin^2(\eta_l-\eta_{l+1}) \qquad \ldots\ldots(10)$$

and

$$Q^{(2)}=\frac{4\pi\hbar^2}{\mu^2v^2}\left\{\frac{1}{2}\sum_{l=0}^{\infty}\frac{(l+1)(l+2)}{(l+\frac{3}{2})}\sin^2(\eta_l^+-\eta_{l+2}^+)\right. \\ \left.+\frac{1}{2}\sum_{l=0}^{\infty}\frac{(l+1)(l+2)}{(l+\frac{3}{2})}\sin^2(\eta_l^--\eta_{l+2}^-)\right\}. \qquad \ldots\ldots(11)$$

where $\eta_{2r}=\eta_{2r}^{\pm}$ and $\eta_{2r+1}=\eta_{2r+1}^{\mp}$.

Classical approximations to (10) and (11) follow on replacing the summations by integrations and using Jeffreys' approximation (cf. Mott and Massey 1949) to calculate the phase shifts (de Boer and Bird 1954). The formula for $Q^{(1)}$ has been given by Dalgarno (1958), that for $Q^{(2)}$ is

$$Q^{(2)}=\pi\int_0^{\infty}\{\sin^2\chi^+ +\sin^2\chi^-\}b\,db \qquad \ldots\ldots(12)$$

where χ^+ is the classical scattering angle associated with the symmetric mode and χ^- that associated with the antisymmetric mode.

§ 3. RESULTS

Exact calculations have been carried out for the general case when the interaction potential is proportional to $\pm R^{-n}$, use being made of collision integrals given by Hasse and Cook (1929, 1931), Chapman and Cowling (1939), Kotani (1942) and Eliason, Stogryn and Hirschfelder (1956), and approximate calculations have been carried out for the particular cases of Li^+ in He and He^+ in He, use being made of the interaction potentials given respectively by Dalgarno, McDowell and Williams (1958) and Moiseiwitsch (1956). For the latter calculations, the methods employed were entirely similar to those described by Dalgarno *et al.* except that the collision integrals were also computed using a technique due to Burnett (1937); for He^+ in He a check was provided by substituting into (10) and (11) the phase shifts computed by Lynn and Moiseiwitsch (1957).

Table 1. The correction term ϵ_0 for $V=d/R^n$

	$d>0$				$d<0$			
n	$M_1 \ll M_2$		$M_1=M_2$ †		$M_1 \ll M_2$		$M_1=M_2$ †	
	Eqn (5)	Eqn (6)	Eqn (5)	Eqn (6)	Eqn (5)	Eqn (6)	Eqn (5)	Eqn (6)
2	0·111	0·100	0·017	0·016	0·111	0·100	0·019	0·019
3	0·012	0·011	0·002	0·002	0·012	0·011	0·002	0·002
4	0·000	0·000	0·000‡	0·000	0·000	0·000	0·000	0·000
6	0·010	0·010	0·002	0·002	0·010	0·011	0·002	0·002
8	0·022	0·025	0·004‡	0·004				
10	0·031	0·036	0·006	0·006				
12	0·038	0·044	0·007	0·008				
∞	0·077	0·100	0·017‡	0·018				

† For $M_1 \gg M_2$, $\epsilon_0=0$.

‡ These values have been given previously by Chapman and Cowling (1939).

Table 2. The correction term ϵ_0 for Li^+ in He and for He^+ in He

Li⁺ in He		He⁺ in He		
T(°K)	Eqn (5) or (6)	T(°K)	Eqn (5)	Eqn (6)
0	0·0000	0	0·0000	0·0000
195	0·0009	100	0·0057	0·0059
291	0·0017	200	0·0067	0·0069
389	0·0012	300	0·0074	0·0077
483	0·0005	400	0·0081	0·0085
600	0·0002	500	0·0088	0·0092

The correction terms are shown in tables 1 and 2. When the interaction potential is proportional to R^{-n} the correction term is independent of temperature and only for the case of a light ion in a heavy gas with a very long range interaction does it become greater than 10%. For Li^+ in He the term is less than 0·2% for temperatures below 600°K though it probably increases to about 1% at very high temperatures. The corrections are of the same general order of magnitude as those obtaining for the diffusion coefficients of neutral atoms (for references see Mason 1957). Although the quantum modifications increase the magnitude of ϵ_0 for He^+ in He it remains small and even at very high temperatures is probably less than the rigid sphere value of 1·7%. At temperatures for which measurements are available, ϵ_0 is less than the experimental error.

ACKNOWLEDGMENTS

One of us (A. W.) wishes to thank the Colonial Welfare and Development Fund for a grant.

REFERENCES

BURNETT, D., 1937, *Proc. Camb. Phil. Soc.*, **37,** 359.

CHAPMAN, S., and COWLING, T. G., 1939, *The Mathematical Theory of Non-Uniform Gases* (Cambridge: University Press).

DALGARNO, A., 1958, *Phil. Trans. Roy. Soc.* A, **250,** 426.

DALGARNO, A., MCDOWELL, M. R. C., and WILLIAMS, A., 1958, *Phil. Trans. Roy. Soc. A*, **250,** 411.

DE BOER, J., and BIRD, R. B., 1954, *Physica*, **20,** 185.

ELIASON, M. A., STOGRYN, D. E., and HIRSCHFELDER, J. O., 1956, *Proc. Nat. Acad. Sci.*, **42,** 546.

FURRY, W. H., and PITKANEN, P. H., 1951, *J. Chem. Phys.*, **19,** 729.

HASSE, H. R., and COOK, W. R., 1929, *Proc. Roy. Soc.* A, **125,** 196; 1931, *Phil. Mag.*, **12,** 544.

HIRSCHFELDER, J. O., CURTISS, C. F., and BIRD, R. B., 1954, *Molecular Theory of Gases and Liquids* (New York: Wiley).

KIHARA, T., 1953, *Rev. Mod. Phys.*, **25,** 844; 1954, *Imperfect Gases* (Technical report: U.S.A. Air Force).

KOTANI, M., 1942, *Proc. Phys.-Math. Soc. Japan*, **24,** 76.

LYNN, N., and MOISEIWITSCH, B. L., 1957, *Proc. Phys. Soc.* A, **70,** 474.

MASON, E. A., 1957, *J. Chem. Phys.*, **27,** 75 and 782.

MASSEY, H. S. W., and BURHOP, E. H. S., 1952, *Electronic and Ionic Impact Phenomena* (Oxford: Clarendon Press).

MASSEY, H. S. W., and MOHR, C. B. O., 1934, *Proc. Roy. Soc.* A, **144,** 188.

MOISEIWITSCH, B. L., 1956, *Proc. Phys. Soc.* A, **69,** 653.

MOTT, N. F., and MASSEY, H. S. W., 1949, *Theory of Atomic Collisions* (Oxford: Clarendon Press), 2nd Edn.

The Absorptivity of Anisotropic Metals

By R. ENGLMAN

H. H. Wills Physical Laboratory, University of Bristol

MS. received 21*st April* 1958

One of the impressions gained at the recent Physical Society Conference on Band Theory of Metals and the Structure of the Fermi Surface was that in some favourable cases it is now possible to piece together the Fermi surface of metals. The accounts of the thoroughgoing and laborious experiments with the de Haas–van Alphen effect (the reference is to papers read by D. Shoenberg and A. Gold) and the microwave experiment of the anomalous skin effect (described by A. B. Pippard) certainly represent a departure from, and an advance over, previous attempts to reconstruct the Fermi surface in terms of some particular model with adjustable parameters. On the other hand, there is no doubt that simple models are simple, and this truism has been exploited by the earlier work of Fawcett (1955) on tin. His experiments in the microwave region (36 Gc/s) suggested a tentative identification of the Fermi surface with three ellipsoids. The relevant formulae for the surface resistance were essentially those due to Sondheimer (1954), who first utilized the ellipsoidal model in this context.

In this note I want to point out that expressions can be found for the optical absorptivity of metals in terms of the ellipsoidal model. It seems that these expressions may be rather useful for the purpose of developing further models or checking existing ones in the light of experiments in the *optical* range of frequencies. The reader is referred to the quoted papers and to those by Reuter and Sondheimer (1948) and Dingle (1953) for the formulation of the problem and to a thesis (Englman 1957) for details of the solution.

A single crystal metal is considered, whose plane boundary surface is illuminated normally and where the principal crystal axis makes an angle ψ with the normal to the plane. The Fermi surface is made up of a number of ellipsoids; the ith ellipsoid is represented by the surface in k space

$$E=\frac{\hbar^2}{2m_i}[k_1{}^2+(1+c_i)k_2{}^2+(1+a_i)k_3{}^2].$$

For many purposes it is sufficient to consider k_2 to lie in a plane parallel to the boundary, while k_3 is along the principal axis of the crystal. In this case the results for the leading terms of the two principal absorptivities $\mathscr{A}_1$ and $\mathscr{A}_2$ (these are defined analogously to the two principal surface resistances) are as follows:

$$\mathscr{A}_1=\frac{3}{4c}\,\frac{\Sigma[\sigma_i l_i(1+a_i+2a_i\sin^2\psi\cos^2\psi)/\tau_i{}^2(1+a_i\cos^2\psi)^{1/2}]-8\sin^2\psi\cos^2\psi K(\psi)}{\Sigma[\sigma_i(1+a_i\sin^2\psi)/\tau_i]-\sin^2\psi\cos^2\psi(\Sigma\sigma_i a_i/\tau_i)^2[\Sigma\sigma_i(1+a_i\cos^2\psi)/\tau_i]^{-1}},$$

where

$$K(\psi)=\frac{1}{\pi}\int_0^\infty\left\{\frac{2}{3}\,\frac{(\Sigma\sigma_i a_i/\tau_i)^2}{\Sigma\sigma_i(1+a_i\cos^2\psi)/\tau_i}-\frac{[\Sigma(\sigma_i a_i/\tau_i)I(sL_i/\tau_i)]^2}{[\{\sigma_i(1+a_i\cos^2\psi)/\tau_i\}I(sL_i/\tau_i)]}\right\}\frac{ds}{s^2}$$

and

$$I(u)=2u^{-3}[u-\tan^{-1}u];$$

$$\mathscr{A}_2=\frac{3}{4c}\,\frac{\Sigma\sigma_i l_i(1+c_i)(1+a_i\cos^2\psi)^{1/2}/\tau_i{}^2}{\Sigma\sigma_i(1+c_i)/\tau_i}.$$

The summation is in every case over all ellipsoids.

The symbols in the above, rather lengthy, expressions are defined in such a way that (with $\zeta =$ Fermi energy) for each surface

$$L = l(1 + a\cos^2\psi)^{1/2}, \qquad l = \tau\zeta^{1/2}m^{-1/2},$$

$$\sigma = \frac{16\pi \boldsymbol{e}^2\zeta^{3/2}\tau(2m)^{1/2}}{3\boldsymbol{h}^3(1+c)^{1/2}(1+a)^{1/2}}.$$

Also, in terms of the bulk conductivities $\sigma_{\parallel}$ and $\sigma_{\perp}$ parallel and perpendicular to the principal axis, $\sigma_{\perp} = \Sigma\sigma_i$, $\sigma_{\perp} = \Sigma\sigma_i(1+c_i)$, $\sigma_{\parallel} = \Sigma\sigma_i(1+a_i)$.

If we substitute the parameters which give the best fit for Fawcett's results in the microwave region, we can predict for the relative absorptivities of tin as functions of ψ the two curves shown (figures 1 and 2).

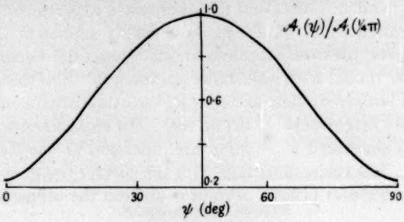

Figure 1.

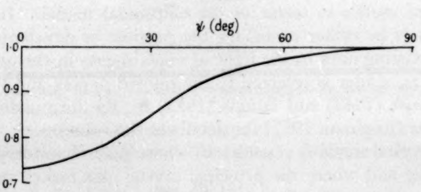

Figure 2.

The most striking feature of the results is the very strong anisotropy exhibited by $\mathscr{A}_1$. The shape of the curve is similar to the one obtained for the surface resistance, but the relative variation in $\mathscr{A}_1$ is greater by a factor 2. This is not what one would expect from general considerations (since it is in the microwave case that the contribution to the current is confined to a small portion of the Fermi surface); it is due to the particular combination in which σ, l, τ enter the expressions.

The curve for $\mathscr{A}_2$ possesses (like the analogous surface resistance of the same model) only a moderate degree of anisotropy.

I feel obliged to Dr. E. H. Sondheimer for stimulating this work.

REFERENCES

DINGLE, R. B., 1953, *Physica, s' Grav.*, **19**, 729.
ENGLMAN, R., 1957, *Ph.D.Thesis*, University of London.
FAWCETT, E., 1955, *Proc. Roy. Soc.* A, **232**, 519.
REUTER, G. E. H., and SONDHEIMER, E. H., 1948, *Proc. Roy. Soc.* A, **195**, 336.
SONDHEIMER, E. H., 1954, *Proc. Roy. Soc.* A, **224**, 260.

Pressure Shift and Broadening in the Resonance Line of Calcium

By W. R. HINDMARSH
University Observatory, Oxford

Communicated by H. H. Plaskett ; MS. received 14th May 1958

According to the theories of Lindholm (1945) and of Foley (1946), a spectral line is in general shifted as well as broadened as a result of the collisions between the radiating atom and its neighbours. In the low pressure approximation, where statistical effects are negligible, the line is symmetrically broadened, and, if the potential energy of the interaction between the two colliding atoms varies as the inverse sixth power of the distance between them (r^{-6} interaction), the ratio of the half intensity width to the shift is 2·8. Much of the previous experimental work on pressure broadening has been carried out at pressures so high that the low pressure approximation is invalid, and the lines must have been asymmetrical. The Lindholm–Foley theory has been tested at sufficiently low pressures for the case of the sodium D lines broadened by argon by Kleman and Lindholm (1945), and the ratio of width to shift was found to be about 4·0 at the lowest pressure. As a further contribution to the testing of the theory, the shift and broadening of the resonance line of calcium, λ4227 Å, produced by helium at about 1 atmosphere pressure, have been measured.

The calcium and helium were contained in a steel absorption tube 6 in. long and $\frac{3}{4}$ in. in diameter, which was heated to a temperature of about 600°c by means of an electric furnace. At this temperature the vapour pressure of the calcium was sufficiently high to give an absorption line of fairly small but easily measurable central intensity. The ends of the tube were cooled by means of water jackets, and apiezon wax was used to attach glass windows. The tube was connected to a mercury manometer and to a cylinder containing helium through a liquid oxygen cooled charcoal trap.

A tungsten strip filament lamp provided a source of continuous radiation. The light passed through the absorption tube in a collimated beam, then through a suitable combination of colour filters to isolate the spectral region required, and finally an image of the strip was formed on the slit of a plane grating Littrow spectrograph of 12 metres focal length. The grating was ruled by H. W. Babcock. It has 600 lines per millimetre and an aperture of 20 cm. It was used in the sixth order, where the blaze was effective, and the dispersion produced was about 7 mm per Å. A similar grating has been found by Pierce (1957) to have a resolving power of $6{\cdot}6 \times 10^5$ in the sixth order. The spectrograph slit was covered with a diaphragm which divided the slit length into four sections each of which could be opened or closed by means of a shutter. On the lower two of these divisions fell the image of the strip filament, while on the upper pair light from a G.E.C. cadmium lamp could be directed with the use of a right angled prism. The cadmium green line λ5086 Å in the fifth order fell about 5 cm from the calcium line λ4227 Å in the sixth order, and the long-wavelength, hyperfine-structure component of this cadmium line was used as a reference line to evaluate spurious shifts due to changing atmospheric pressure and other causes. The experimental procedure was as follows. Helium at a pressure of 6 cm Hg was admitted to the absorption tube, which was at a temperature of about 600°c. The continuous spectrum of the strip filament lamp was then exposed simultaneously with the cadmium green line, each through one of the four divisions of the slit length. Then the shutters were moved to open the other two divisions, the helium pressure increased to 75 cm Hg and a similar exposure taken. With Ilford Zenith plates a time of two hours was required for each of the two exposures. Intensity marks were also photographed on each plate with the use of a calibrated rhodium step filter.

To evaluate the shift caused by increasing the helium pressure from 6 to 75 cm Hg, the positions of the calcium and cadmium lines were measured on a microscope whose plate-holder could be moved in two mutually perpendicular directions, and the measuring procedure was such as to eliminate any errors caused by inaccurate alignment of the plate or curvature of the carriage ways.

The calcium line produced with a helium pressure of 75 cm Hg was measured with the use of a Moll-type microphotometer, and the photographic density reduced to intensity of light in the usual way. It was assumed that the intensity emerging at wave number ν from the absorption tube was given by an expression of the form $I(\nu)=I_0 e^{-\alpha(\nu)}$ where $\alpha(\nu)$ is the volume absorption coefficient of the calcium vapour multiplied by the effective length of the absorption path. $\alpha(\nu)$ was computed from the measured $I(\nu)$, and the resulting curve fitted to a Voigt profile, with the use of the tables given by van de Hulst and Reesinck (1947). The half-intensity width of the damping contribution to $\alpha(\nu)$, and therefore to the absorption coefficient itself, was thus obtained. It was estimated that any contribution to the damping width due to the finite resolving power of the spectrograph was negligible, as was the natural damping width of the line, so that the measured damping width was due to the pressure effect alone. The Gaussian contribution to the Voigt profile was also evaluated, and this could be accounted for by components due to the Doppler width of the line, and the finite resolving power of the spectrograph. The fit to the Voigt profile was in all cases better than 3% of the maximum value of $\alpha(\nu)$, and the observed profile of $\alpha(\nu)$ was in all cases symmetrical.

The results of the measurements are as follows. The errors quoted are standard deviations of the mean.

Shift between lines at He pressures 6 and 75 cm Hg (average of 5 plates)	$+0{\cdot}0062 \pm 0{\cdot}0017\ \mathrm{cm}^{-1}$
Half-intensity pressure width of absorption coefficient at He pressure 75 cm Hg (average of three measurements, two being from different parts of 1 plate)	$0{\cdot}224 \pm 0{\cdot}011\ \mathrm{cm}^{-1}$

The shift is barely significant, but the broadening is appreciable. The measurements are therefore in marked disagreement with the theory, which, for the measured width, predicts a shift of 0·074 cm^{-1}, and for a resonance line the shift would be expected to be towards lower rather than higher wave number. One possible explanation of the discrepancy is that the interaction is not an r^{-6} interaction, but varies in some more complicated way with the distance between the colliding atoms. 'Self-broadening' must be negligible at the low vapour pressure of calcium in this experiment, and calculation of the r^{-6} interaction, with the use of calculated f values, indicates an expected broadening of 0·27 cm^{-1} in the conditions of this experiment. The agreement of this with the measured value is some indication that the interaction may vary as r^{-8}, though this cannot be regarded as conclusive. The other possible explanation of the discrepancy is that the Lindholm–Foley theory is incorrect in its treatment of the distant collisions which give rise to the shift.

A more detailed account of these and further measurements will be published in due course.

REFERENCES

FOLEY, H. M., 1946, *Phys. Rev.*, **69**, 616.
VAN DE HULST, H. C., and REESINCK, J. J. M., 1947, *Astrophys. J.*, **106**, 121.
KLEMAN, B., and LINDHOLM, E., 1945, *Ark. f. Mat. Astron. Fys.*, **32 B**, No. 10.
LINDHOLM, E., 1945, *Ark. f. Mat. Astron. Fys.*, **32 A**, No. 17.
PIERCE, A. K., 1957, *J. Opt. Soc. Amer.*, **47**, 9.

A Note on the Cellular Method for Energy Bands in Solids

BY L. PINCHERLE
Bedford College, University of London

MS. received 8th May 1958

ALTMANN (1958) has modified recently Schiff's (1955) method for extracting the best value of the energy out of a point matching procedure: a number of points are chosen where one satisfies the boundary conditions for ψ and $\partial\psi/\partial n$, obtaining p equations. The number of coefficients α_r in the expansion of ψ is $n<p$. One has then p equations

$$\sum_{r=1}^{n} a_{sr}\alpha_r = 0$$

between the n unknown quantities α_r, the coefficients α_{sr} being determined by the wave vector **k** and by the values of the basic functions (assumed to be normalized), and their normal derivatives, at the chosen points. These functions are calculated for trial values E_t of the energy. It is then suggested to minimize the quantity

$$S^2 = \sum_{s=1}^{p}\left(\sum_{r=1}^{n} a_{sr}\alpha_r\right)^2$$

subject to the condition $\sum_{r=1}^{n}\alpha_r = 1$.

If A is the rectangular matrix of the coefficients a_{sr}, and $B=\tilde{A}A$, differentiation with respect to the α_r leads to the secular equation

$$\begin{vmatrix} b_{11}-\lambda & b_{12} & \text{—} & \text{—} & \text{—} \\ b_{21} & b_{22}-\lambda & \text{—} & \text{—} & \text{—} \\ \text{—}\;\text{—} & \text{—}\;\text{—} & \text{—} & \text{—} & \text{—} \end{vmatrix} = 0. \qquad \ldots\ldots (1)$$

Altmann then goes on to find the n eigenvectors of B and to obtain the n corresponding values of S^2. He then chooses the eigenvector that gives the smallest of these residuals S_0 and finds for which value of E_t S_0 is minimum. This value of E_t is taken to approximate the correct eigenvalue.

The purpose of this note is first to point out that it is not necessary to find the eigenvectors of (1), since by a general property of these variational procedures the value of S^2 is equal to the corresponding eigenvalue λ of (1), and thus it is only necessary to determine the smallest of these eigenvalues.

Secondly, the new conditions have been applied to the empty lattice test (Shockley 1937) and compared with other available methods of matching the wave functions in different cells. The level chosen was the second Γ_s level of a simple cubic lattice (for notation, see for instance Bell 1954). Let the side of the cube be 2, then the lattice distance in the reciprocal lattice is π and the exact energy of the state in question is π^2.

The philosophy of the cellular method must be that of obtaining the best value of the energy with as few terms as possible in the development of ψ: thus the test should be applied with an imperfect trial function. Take then only two terms in the expansion of ψ:

$$\psi = \alpha_1 \mathrm{j}_0(\gamma r) + \alpha_2 \left(\frac{x^4 + y^4 + z^4}{r^4} - \frac{3}{5} \right) \mathrm{j}_4(\gamma r),$$

where $\gamma = \sqrt{E}$, and j_0, j_4 are spherical Bessel functions, e.g. $\mathrm{j}_0(x) = (\sin x)/x$. It is only necessary to consider one eighth of one of the faces of the cube, and for Γ_s the boundary conditions are simply that $\partial\psi/\partial n$ should vanish at all points of this surface.

The following methods were tested: (*a*) matching at a number of points; (*b*) point matching and minimizing residuals according to Schiff (1955); (*c*) point matching and minimizing residuals according to Altmann (1958); (*d*) Legendre matching (Bell *et al.* 1953), that is in this case expanding $\partial\psi/\partial n$ on the surface of the cube in terms of Legendre functions and equating to zero the lowest coefficients; (*e*) Fourier matching (Bell *et al.* 1953): the same, but expanding in terms of sines and cosines; (*f*) Kohn's (1952) variational procedure, by both methods discussed by Jenkins and Pincherle (1954); (*g*) least squares method (Bell *et al.* 1953): in this case minimizing $\int (\partial\psi/\partial n)^2 \, d\sigma$ over the surface of the cell, subject to the condition $\alpha_1^2 + \alpha_2^2 = 1$.

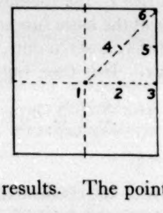

The table summarizes the results. The points considered in (*a*), (*b*), (*c*) are shown in the figure.

Table

(*a*) Point matching

Matching at	1–2	1–3	1–4	1–5	1–6	2–3	2–4	2–5
γ	3·20	3·34	3·16	3·19	3·00	3·34	3·08	3·19

Matching at	2–6	3–4	3–5	3–6	4–5	4–6	5–6
γ	3·02	3·31	—†	—†	3·18	3·04	—†

† No root within 0·2 of π.

(*b*) Point matching and minimizing residuals according to Schiff

Coefficient determined at point	1	2	3	4	5	6
γ	3·155	~3·3	3·145	3·174	~3·0	3·164

(*c*) Point matching and minimizing residuals according to Altmann	$\gamma=$	3·130
(*d*) Legendre matching		3·178
(*e*) Fourier matching		3·165
(*f*) Variational procedure.		
Minimizing only with respect to coefficients		3·138
Minimizing also with respect to E_t		3·149
(*g*) Least squares		3·140

It is clear that to reach definite conclusions from (*a*) and (*b*) one has to reject some of the combinations: in practice one would use more terms in the expansion of ψ. But with the other methods the approximation would in practice be sufficient; with (*c*), (*f*), (*g*) one meets the practical difficulty that the small eigenvalue appears as the difference of much larger quantities.

REFERENCES

ALTMANN, S. L., 1958, *Proc. Roy. Soc.* A, **244,** 141, 153.
BELL, D. G., 1954, *Rev. Mod. Phys.*, **26,** 311.
BELL, D. G., HUM, D. M., PINCHERLE, L., SCIAMA, D. W., and WOODWARD, P. M., 1953, *Proc. Roy. Soc.* A, **217,** 71.
JENKINS, D. P., and PINCHERLE, L., 1954, *Phil. Mag.*, **45,** 93.
KOHN, W., 1952, *Phys. Rev.*, **87,** 472.
SCHIFF, B., 1955, *Proc. Phys. Soc.* A, **68,** 686.
SHOCKLEY, W., 1937, *Phys. Rev.*, **52,** 866.

Theoretical and Experimental Relaxation Times of Solutions

BY R. J. MEAKINS
National Standards Laboratory, Commonwealth Scientific and Industrial Research Organisation, Sydney, Australia

MS. received 9th April 1958, *and in final form 21st May* 1958

IN an attempt to calculate the dielectric relaxation time τ of a polar liquid, Debye (1929) proposed the equation

$$\tau=\frac{4\pi\eta a^3}{\boldsymbol{k}T} \qquad \ldots\ldots(1)$$

in which the molecules are treated as spheres of radius a moving in a medium of viscosity η; $\boldsymbol{k}$ is Boltzmann's constant and T is the absolute temperature.

Recent measurements (Meakins 1958) have shown that this equation applies to dilute solutions in which the solute molecules are considerably larger than those of the solvent. When the solute and solvent molecules are more equal in size, however, there are large discrepancies (Jackson and Powles 1946, Whiffen and Thompson 1946) between the experimental relaxation times and the values calculated according to equation (1). In such systems it is apparent that the macroscopic viscosity is not a true representation of the resistance to the rotation of the individual solute molecules and it is necessary to consider the solute–solvent interaction in more detail.

A useful approach to this problem has recently been made by Hill (1954) using Andrade's model for the viscosity of a liquid. In this work it is considered that the interaction between a moving solute molecule and its surroundings can be represented by a mutual viscosity parameter η_{AB} defined by the equation

$$\eta_{\mathrm{m}}\sigma_{\mathrm{m}} = f_{\mathrm{A}}^2\eta_{\mathrm{A}}\sigma_{\mathrm{A}} + f_{\mathrm{B}}^2\eta_{\mathrm{B}}\sigma_{\mathrm{B}} + 2f_{\mathrm{A}}f_{\mathrm{B}}\eta_{\mathrm{AB}}\sigma_{\mathrm{AB}} \qquad \ldots\ldots (2)$$

where η_{m}, η_{A} and η_{B} are the viscosities of the mixture, the solvent and the solute, respectively, f_{A} and f_{B} are the mole fractions of the solvent and solute, $\sigma_{\mathrm{A}} = (M_{\mathrm{A}}/\boldsymbol{N}\rho_{\mathrm{A}})^{1/3}$ and σ_{B} is similarly defined (Hill, private communication), $\sigma_{\mathrm{m}} = \{(f_{\mathrm{A}}M_{\mathrm{A}} + f_{\mathrm{B}}M_{\mathrm{B}})/\boldsymbol{N}\rho_{\mathrm{m}}\}^{1/3}$, M_{A} and M_{B} are the molecular weights of solvent and solute, $\boldsymbol{N}$ is Avogadro's number, ρ_{A}, ρ_{B} and ρ_{m} are the densities of the solvent, solute and the mixture, respectively.

The model then leads to a discussion of the retarding effects of molecular collisions on rotating solute molecules and this introduces a factor involving the moments of inertia and masses of the molecules, giving the following equation for the relaxation time:

$$\tau = \frac{3}{\boldsymbol{k}T}\frac{I_{\mathrm{AB}}I_{\mathrm{B}}}{I_{\mathrm{AB}}+I_{\mathrm{B}}}\frac{m_{\mathrm{A}}+m_{\mathrm{B}}}{m_{\mathrm{A}}m_{\mathrm{B}}}\eta_{\mathrm{AB}}\sigma_{\mathrm{AB}} \qquad \ldots\ldots (3)$$

where I_{B} is the moment of inertia of the polar molecule, I_{AB} is the moment of inertia of the solvent molecule about the centre of mass of the solute molecule at the moment of collision, and m_{A} and m_{B} are the masses of the solvent and solute molecules.

In the present paper Hill's equations are used to calculate the relaxation times of solutions of a number of polar solutes in benzene and decalin solvents and the results are compared with the experimental values and also with those obtained from Debye's equation. In calculating the term I_{AB} reference was made to scale molecular models (Courtauld) to determine the distance of closest approach.

The preparation and properties of the compounds and the methods of measurement are mentioned elsewhere (Davies and Meakins 1957, Meakins 1958).

The solvents benzene and decalin (decahydronaphthalene) are cyclic structures and the molecules should be sufficiently rigid to approximate to the requirements of the theory, in this regard. The solute molecules are also mostly rigid. With pentachloroethane the rotation around the C–C bond would be considerably hindered by the large chlorine atoms. In tricyclohexylcarbinol the results refer only to the rotation of the molecule as a rigid structure and not to the separate absorption due to independent orientation of the hydroxyl group (Davies and Meakins 1957). The nonpolar side-chain in cholestenone is probably too small to have much effect on the results.

The concentrations of the polar solutes were chosen for convenience in the electrical measurements. In calculating the mutual viscosities, however, it was found that some of the solutions gave very small values for the expression

$$\eta_{\mathrm{m}}\sigma_{\mathrm{m}} - f_{\mathrm{A}}^2\eta_{\mathrm{A}}\sigma_{\mathrm{A}} - f_{\mathrm{B}}^2\eta_{\mathrm{B}}\sigma_{\mathrm{B}}$$

in equation (2) and, in order to obtain better accuracy, further measurements of viscosity were made with more concentrated solutions. The values of τ_{calc}

(Hill 1954) shown in table 1 for trichloroethylene, o-dichlorobenzene and 1 : 2 : 4-trichlorobenzene refer to these more concentrated solutions ($f_A : f_B = 70 : 30$). With the trichlorobenzene solute, several different concentrations were tested and were found to give approximately the same value in each case.

A further difficulty in calculating the mutual viscosities is encountered with solid solutes, where the factor η_B possesses no physical significance. However, it was considered that with the comparatively dilute solutions used in the present work, collisions between solute molecules would be sufficiently infrequent for their effect to be neglected, so that the term $f_B{}^2\eta_B\sigma_B$ could be omitted. This procedure was checked with two of the solutes for which calculations were also made by eliminating η_B from the equations for two different concentrations. This gave almost the same result as the simplified method mentioned above.

Table 1. Comparison of Calculated and Experimental Relaxation Times at 20°C

(1)	(2)	(3)	(4)	(5)	(6)	(7)	(8)
Solutions in Benzene							
Benzene	84	0·879	0·647				
Gammexane, 0·15 M	196	0·898	0·682	138	47	2·9	2·1
Cholestenone, 0·05 M	406	0·880	0·672	337	233	1·4	0·9
Solutions in Decalin							
Decalin	154	0·880	2·66				
Chloroform, 0·7 M	75	0·913	2·26	13·5	6·6	2·0	19
Trichloroethylene, 0·5 M	81	0·911	2·30	9·1	9·3	1·0	15
Cyclohexanone, 0·2 M	100	0·884	2·61	48	9·9	4·8	20
o-Dichlorobenzene, 0·2 M	116	0·890	2·57	44	15·3	2·9	14
Pentachloroethane, 1·0 M	124	0·977	2·55	87	13·3	6·5	18
1 : 2 : 4-Trichlorobenzene, 0·7 M	133	0·934	2·39	62	29	2·1	8
1 : 2 : 3 : 4-Tetrachlorobenzene, 0·5 M	149	0·932	2·65	118	34	3·5	9
Pentachlorobenzene, 0·5 M	165	0·946	2·75	173	35	4·9	10
Gammexane, 0·15 M	196	0·899	2·67	169	79	2·1	5
Tricyclohexylcarbinol, 0·36 M	298	0·885	2·84	375	185	2·0	3·4
Chloestenone, 0·1 M	406	0·886	2·97	1370	690	2·0	1·3

(1) Solution; (2) molecular volume (cubic Å); (3) specific gravity of solution; (4) viscosity (cP); (5) relaxation time $\tau_{\text{calc}}(10^{-12}$ sec) (Hill); (6) $\tau_{\text{exp}}(10^{-12}$ sec); (7) $\tau_{\text{calc}}(\text{Hill})/\tau_{\text{exp}}$; (8) $\tau_{\text{calc}}(\text{Debye})/\tau_{\text{exp}}$.

The results given in table 1 show that in most cases, and particularly with the smaller solute molecules, the agreement between theory and experiment is much better with Hill's equations than with Debye's equation. In most cases the largest improvement is associated with the difference in the constant factor which, in Hill's equation, is only about one quarter of that in Debye's equation. The introduction of the mutual viscosity parameter $\eta_{AB}\sigma_{AB}$ in place of η_A gives a further significant improvement in some cases, but the presence of the factor

$$\frac{I_{AB}I_B}{I_{AB}+I_B}\,\frac{m_A+m_B}{m_Am_B}$$

in place of a^2 gives a comparatively small difference. The corresponding factors are compared in table 2.

Table 2. Comparison of Corresponding Parameters in the Equations of Debye and Hill for Dielectric Relaxation Time

(1)	(2)	(3)	(4)	(5)
Solutions in Benzene				
Gammexane	17	13	11	2·5
Cholestenone	28	21	16	3·1
Solutions in Decalin				
Chloroform	5	7	4	6
Trichloroethylene	5	7	2·4	6
Cyclohexanone	5	8	12	8
o-Dichlorobenzene	8	9	8	8
Pentachloroethane	8	10	14	8
1:2:4-Trichlorobenzene	8	10	10	8
1:2:3:4-Tetrachlorobenzene	11	11	17	9
Pentachlorobenzene	14	12	21	9
Gammexane	14	13	18	10
Tricyclohexylcarbinol	17	17	30	12
Cholestenone	23	21	80	12

(1) Solution; (2) Hill: $\frac{I_{AB}I_B}{I_{AB}+I_B}\frac{m_A+m_B}{m_Am_B}$ (10^{-16} cm^2); (3) Debye a^2 (10^{-16} cm^2); (4) Hill $\eta_{AB}\sigma_{AB}$ (10^{-10} poise cm); (5) Debye ηa (10^{-10} poise cm).

The remaining discrepancies between theory (Hill 1954) and experiment seem most likely to be chiefly associated with the mutual viscosity parameter $\eta_{AB}\sigma_{AB}$ which would be considerably affected by the values used for the intermolecular distance in equation (2). The method described for determining these values undoubtedly represents a considerable simplification of the true position, since the colliding molecules could come together with various mutual orientations. However, it would be difficult to take account of this and the method used is probably the best possible approximation.

REFERENCES

Davies, M., and Meakins, R. J., 1957, *J. Chem. Phys.*, **26**, 1584.
Debye, P., 1929, *Polar Molecules* (New York: Chemical Catalog Co.).
Hill, N., 1954, *Proc. Phys. Soc.* B, **67**, 149.
Jackson, W., and Powles, J. G., 1946, *Trans. Faraday Soc.*, **42a**, 101.
Meakins, R. J., 1958, *Trans. Faraday Soc.*, **54**, 1160.
Whiffen, D. H., and Thompson, H. W., 1946, *Trans. Faraday Soc.*, **42a**, 114.

Some Electron Collision Cross Sections for Nitrogen and Oxygen

By D. T. STEWART[†] and E. GABATHULER[†]
Physics Department, Queen's University, Belfast

Communicated by K. G. Emeléus; MS. received 3rd April 1958

In a previous communication (Stewart 1956) an optical method for measuring the inelastic electron collision cross sections of atmospheric gases was described and some results were given for the first negative system of N_2^+ $(\mathrm{B}^2\Sigma_u^+ - \mathrm{X}^2\Sigma_g^+)$. In this a photoelectric spectrophotometer was used to measure the intensities in absolute units of bands produced in a controlled electron beam source. The present note describes similar measurements for the second positive bands of N_2 $(\mathrm{C}^3\Pi_u - \mathrm{B}^3\Pi_g)$, the first negative bands of O_2^+ $(^4\Sigma_g^- - {}^4\Pi_u)$ and for the second negative bands of O_2^+ $(\mathrm{A}^2\Pi_u - \mathrm{X}^2\Pi_g)$. The apparatus was adapted for recording in the ultra-violet region by replacing the glass spectrometer with a Hilger quartz monochromator. The spectrophotometer was standardized for absolute intensities by tungsten filament lamps calibrated by the National Physical Laboratory and by a Philips tungsten ribbon lamp with a quartz window of known transmission (De Vos 1954).

It was found that the intensities of all observed bands (see table 1) of the second positive system of N_2 were directly proportional both to beam current up to 1×10^{-3} A, and to gas pressure up to 2×10^{-2} mm Hg, indicating that under our experimental conditions the $\mathrm{C}^3\Pi_u$ level was being populated by direct electron excitation from the $\mathrm{X}^1\Sigma_g^+$ ground state. The relative excitation function of the (0, 0) band is shown in the figure. The curve rises to a sharp maximum at 17 v, close to the appearance potential at 13 v, followed by a rapid decrease with increasing electron energy. This result further confirms the above evidence

Table 1. Cross sections $Q_{v'v''}$ for excitation of the second positive bands of N_2 at 35 v and cross sections $Q_{v'}$ of the vibrational levels of the $\mathrm{C}^3\Pi_u$ state derived from these measurements

Band (v', v'')	$Q_{v'v''} \times 10^{-18}$ cm²	$Q_{v'} \times 10^{-18}$ cm²
(0, 0)	2·96	6·2
(0, 2)	0·858	6·3
(0, 3)	0·269	6·8
(1, 2)	0·635	4·6
(1, 3)	0·71	4·8
(2, 0)	0·71	1·9
(2, 4)	0·22	2·3
(3, 3)	0·084	1·7
(3, 5)	0·05	1·7
(4, 4)	0·038	0·16

[†] Now at Department of Natural Philosophy, University of Glasgow

for direct excitation of the $c^3\Pi_u$ level, as this type of excitation function is characteristic of a transition involving a spin change where electron exchange is the predominant mechanism of excitation (Massey and Burhop 1952).

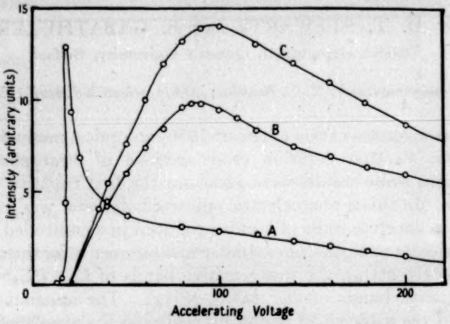

Relative excitation functions of: A, the (0, 0) band of the second positive system of N_2; B, the (2, 1) band of the first negative system of O_2^+; C, the (2, 5) band of the second negative system of O_2^+.

The cross sections, $Q_{v'v''}$, for excitation of the bands at 35 v are shown in table 1. Values of the cross section $Q_{v'}$ for the vibrational levels of the $c^3\Pi_u$ state, derived from these measurements using tables of the relative transition probabilities $A_{v'v''}/A_{v'}$ of the bands calculated by Bates (1949), Jarmain, Fraser and Nicholls (1953) and Pillow (1951) are also shown. It can be seen that despite the difficulty of determining the total absolute intensities of bands which extend over a wavelength range from 4500 Å to 3000 Å there is good agreement between values of a given $Q_{v'}$ calculated from different band measurements.

Investigation of the O_2^+ bands proved to be less satisfactory. Instead of an indirectly heated cathode a platinum filament coated with barium and strontium oxides (Hagstrum 1951) had to be used as a source of electrons. This reduced the efficiency of the electron gun and it was difficult to obtain a well-collimated electron beam at accelerating voltages less than 30 v. Moreover, it was not possible to isolate an individual band of the complex first negative system and as the bands of the second negative system are doublets, the two heads being separated by 200 cm^{-1}, absolute measurements of the band intensity are altogether less reliable than in the case of the second positive system of N_2.

The intensities of bands of both systems were found to be directly proportional to beam current up to $1{\cdot}0 \times 10^{-3}$ A but not to gas pressure above 8×10^{-3} mm Hg, varying in a way that suggested that some secondary process involving depopulation of the $^4\Sigma_g^-$ and $A^2\Pi_u$ levels becomes important as the pressure is increased above this value. This effect was more pronounced for the first negative system than for the second negative system. The relative excitation functions of the two systems (see figure) are similar. There is a sharp rise from an onset potential occurring at 20 v approximately to a broad maximum at 85 v for the first negative system and 100 v for the second negative system, followed by a gradual fall off with increasing electron energy. These curves are characteristic of excitation of levels involving ionization.

Some results for the cross sections $Q_{v'v''}$ of those second negative bands which could be completely isolated are given in table 2, but we were unable to study a sufficient number of bands in each progression to derive values of $Q_{v'}$.

Table 2. Cross sections $Q_{v'v''}$ for excitation of the second negative bands of O_2^+ at 100 v

Band (v', v'')	$Q_{v'v''} \times 10^{-20}$ cm^2
(2, 4)	3·75
(2, 5)	5·9
(3, 3)	1·65
(4, 3)	1·2
(5, 2)	0·33
(5, 3)	0·1

ACKNOWLEDGMENTS

It is a pleasure to acknowledge the advice and encouragement given by Professor K. G. Emeléus in the course of this investigation.

REFERENCES

BATES, D. R., 1949, *Proc. Roy. Soc.* A, **196,** 217.
DE VOS, J. C., 1954, *Thesis*, Amsterdam.
HAGSTRUM, H. D., 1951, *Rev. Mod. Phys.*, **23,** 185.
JARMAIN, W. R., FRASER, P. A., and NICHOLLS, R. W., 1953, *Astrophys. J.*, **118,** 228.
MASSEY, H. S. W., and BURHOP, E. H. S., 1952, *Electronic and Ionic Impact Phenomena* (Oxford: Clarendon Press).
PILLOW, M. E., 1951, *Proc. Phys. Soc.* A, **64,** 772.
STEWART, D. T., 1956, *Proc. Phys. Soc.* A, **69,** 437.

A Measurement of the Spin Correlation Coefficient C_{nn} in p–p Scattering at 382 MeV, for 90° Centre of Mass Scattering Angle

A. ASHMORE, A. N. DIDDENS, G. B. HUXTABLE, AND K. SKARSVÅG †
Nuclear Physics Research Laboratory, University of Liverpool

MS. received 6*th May* 1958

THE coefficient C_{nn} in p–p scattering is a measure of the correlation between the components of the spins of the two protons normal to the scattering plane. It is the expectation value $\langle \boldsymbol{\sigma}_1 . \mathbf{n}\ \boldsymbol{\sigma}_2 . \mathbf{n} \rangle$ where $\boldsymbol{\sigma}_1$ and $\boldsymbol{\sigma}_2$ are the spins of the incident and target protons and $\mathbf{n}$ is unit vector normal to the scattering plane. For scattering at 90° in the centre-of-mass system

$$C_{nn} = (\sigma_t - \sigma_s)/(\sigma_t + \sigma_s) \qquad \ldots\ldots (1)$$

where σ_t and σ_s are the triplet and singlet cross sections (Stapp 1955). As suggested by Chamberlain *et al.* (1957) experimental measurements of spin correlation should be valuable in the phase shift analysis of high energy p–p scattering. They may help to decide between the five sets of phase shifts consistent with the single, double, and triple scattering measurements in p–p scattering at 310 MeV (Stapp, Ypsilantis and Metropolis 1957).

---

† Now at the Joint Establishment for Nuclear Energy Research, Kjeller, Norway.

Spin correlation can be measured by a second scattering of both protons from a complex nucleus such as carbon, with analysis in coincidence. For a measurement of C_{nn} the second scattering must be to the left or right in the same plane as the first scattering. The asymmetry e in such a measurement is defined by the formula

$$e=\frac{RR+LL-LR-RL}{RR+LL+LR+RL} \qquad \ldots\ldots(2)$$

where RR is the number of coincidence counts with both second scatterings to the right, LL with both to the left, etc. C_{nn} is related to the asymmetry by the formula

$$C_{\mathrm{nn}}=e/P_1P_2 \qquad \ldots\ldots(3)$$

where P_1 and P_2 are the analysing powers in the second scattering for the two protons.

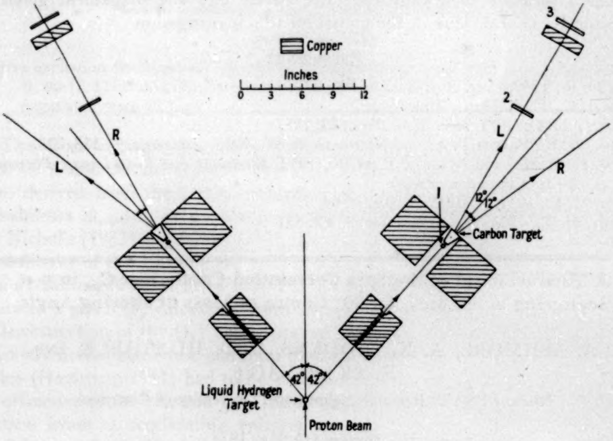

Figure 1. Plan of the experimental arrangement.

A plan of the experimental arrangement is shown in figure 1. The unpolarized 382 Mev extracted proton beam was incident on a liquid hydrogen target, consisting of a vertical cylinder of ½ in. diameter made from mylar 0·001 in. thick. At the target the beam spot was about ¾ in. wide and 1¼ in. high. The solid angle for the first scattering was defined by the scintillators in the counters 1, which were ⅜ in. wide and 2 in. high. These were made narrow in order to give good energy resolution, which was 4·5 Mev (standard deviation). The angular resolution was 0·5° (standard deviation).

Carbon was chosen for the second target since it has a high analysing power, and being a light element gives relatively little multiple scattering; also the first few excited states are well separated from the ground state. The geometry of the second scattering was chosen on the basis of the experimental data from

Uppsala (Alphonce, Johannson and Tibell 1957, Tyren, Hillman and Johannson 1957 and private communication) and from Rochester (Chesnut, Hafner and Roberts 1956). A mean scattering angle of 12° was chosen, and the solid angle made as large as was consistent with keeping the analysing power reasonably high. From this point of view a larger angular spread was permissible in the vertical than in the horizontal direction. The solid angle was defined by the scintillators in the counters 3 which were 3 in. wide and 8 in. high, giving an angular resolution of 3·3° (standard deviation). Changing of the counters 2 and 3 between the left and right positions was done by means of a rotation of the supporting arm about the axis defined by the first scattering. The thickness of the copper absorbers between the counters 2 and 3 was set just above the knee of the range curve, three times the standard deviation ($1{\cdot}5\ \mathrm{g\ cm}^{-2}$) below the mean range of the elastically scattered protons. Thus, the contribution due to protons inelastically scattered in the second target was kept small and could easily be estimated with sufficient accuracy.

All the counters consisted of plastic scintillators viewed by R.C.A. 6342 photomultipliers. Triple coincidences between the counters 1, 2 and 3 on each side were fed into two fast coincidence circuits, with a resolving time $2\tau = 10$ mμsec (Skarsvåg 1957). The outputs from these two circuits were fed into a rather slower coincidence circuit with a resolving time $2\tau = 50$ mμsec (Collinge, Eccleshall and Merrison 1956). The proton beam was monitored by passing it through an argon-filled ionization chamber connected to a beam integrator. As a check on variations due to bubbles in the hydrogen target and to movements of the beam across the target, a double coincidence counter telescope was arranged below the beam level to count scattered protons from the target.

The analysing powers of the second scatterings were measured in a double scattering experiment with a carbon first target. A polyethylene absorber was placed in the proton beam so that the energy of the protons incident on the second target was the same as in the actual measurement of C_{nn}. The polarization in the first scattering was calculated from the experimental data from Uppsala. The values obtained for the analysing powers were

$$P_1 = 0{\cdot}663 \pm 0{\cdot}024, \quad P_2 = 0{\cdot}673 \pm 0{\cdot}025.$$

The measurement of C_{nn} was made in two runs of 64 and 74 hours duration. The beam intensity was adjusted to about $1{\cdot}4 \times 10^9$ protons sec^{-1} intercepting the target, at which level the random coincidence rate was still relatively small. This rate was estimated from the measured single, double and triple counting rates on the two sides of the apparatus. The most important contribution was from p–p scattering events causing the operation of all three counters on one side but only the first counter on the other side, the remaining two counters being operated by a background proton or by a random coincidence. A total of 1305 counts were obtained of which 208 were estimated to be random counts. For a scattering angle of 90° in the centre of mass it should be found that $RR = LL$ and $LR = RL$. The values given in table 1 show that these equalities are satisfied within the experimental error. They give a value for the asymmetry $e = +0{\cdot}192 \pm 0{\cdot}035$.

Table 1. Number of Coincidence Counts for the Four Positions

LL	325 ± 21	*LR*	207 ± 17
RR	329 ± 21	*RL*	236 ± 20

A contribution to the asymmetry can arise in the geometry of the first scattering (Chamberlain, private communication). Depending on the point in the hydrogen target where the scattering takes place there will be a tendency for the two protons to go either to the same side or to the opposite sides of the second targets. The extent to which these effects will cancel out depends on the geometry. An estimate for the geometry used showed that the observed asymmetry should be reduced by 0·007. Then from formula (3), using the measured values of P_1 and P_2, $C_{nn} = +0{\cdot}416 \pm 0{\cdot}084$. Substitution of this value in formula (1) shows that 70·8 ± 4·2% of the scattering is in triplet states, and 29·2 ± 4·2% in singlet states. This clearly indicates the importance of spin dependent forces since for central forces only singlet states contribute to the scattering at 90° in the centre-of-mass system.

Table 2. Values of C_{nn} calculated from the Berkeley Sets of Phase Shifts

Set No.	1	2	3	4	6
C_{nn}	$+0{\cdot}351 \pm 0{\cdot}084$	$+0{\cdot}711 \pm 0{\cdot}054$	$+0{\cdot}300 \pm 0{\cdot}084$	$+0{\cdot}490 \pm 0{\cdot}064$	$+0{\cdot}425 \pm 0{\cdot}080$

The values of C_{nn} calculated from the Berkeley sets of phase shifts at 310 Mev (Stapp, Ypsilantis and Metropolis 1957) are given in table 2. The experimental value is in the region predicted by these sets. An estimate was made of the variation with energy of C_{nn} using the potential model of Gammel and Thaler (1957, referred to hereafter as GT) taking the singlet phase shifts from Table IV (*a*) and the triplet phase shifts from Table IV (*c*) of their paper. The results of this calculation are given in figure 2. Values of C_{nn} were also calculated with the potential model of Signell and Marshak (1958) at 100, 150 and 300 Mev where sets of phase shifts were available. These values are plotted in figure 2 and are seen to be similar to the values calculated from GT. Since the experimental value of C_{nn} disagrees with the predictions of GT, the variation of C_{nn} with

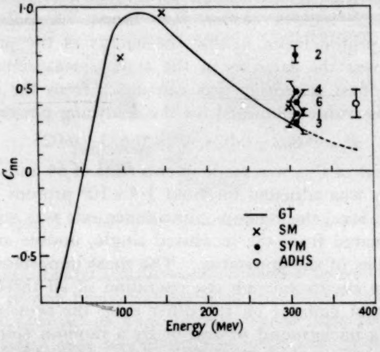

Figure 2. Variation of C_{nn} with proton energy. Curve is calculated from Gammel and Thaler (1957), SM calculated from Signell and Marshak (1958), SYM calculated from phase shifts of Stapp, Ypsilantis and Metropolis (1957), ADHS value from present measurements.

energy remains uncertain and so none of the Berkeley sets of phase shifts can be ruled out. A measurement of C_{kp}, the correlation coefficient in the plane of scattering, will help to settle the matter particularly as set 6 gives a negative value and all the others give positive values. Modifications are being made to the apparatus for this measurement.

ACKNOWLEDGMENTS

The authors are indebted to Professor H. W. B. Skinner and Professor J. M. Cassels for their help and encouragement, to Mr. A. Amery for the detailed design of the scattering table, and to the cyclotron crew for their co-operation. A.N.D. is indebted to CERN, G.B.H. to the Department of Scientific and Industrial Research, and K.S. to the Royal Norwegian Council for Scientific and Industrial Research for the provision of fellowships. K.S. is also indebted to the Joint Establishment for Nuclear Energy Research for leave of absence.

REFERENCES

ALPHONCE, R., JOHANSSON, A., and TIBELL, G., 1957, *Nuclear Physics*, **3**, 185.

CHAMBERLAIN, O., SEGRÈ, E., TRIPP, R. D., WIEGAND, C., and YPSILANTIS, T. J., 1957, *Phys. Rev.*, **105**, 288.

CHESNUT, W. G., HAFNER, E. M., and ROBERTS, A., 1956, *Phys. Rev.*, **104**, 449.

COLLINGE, B., ECCLESHALL, D., and MERRISON, A. W., 1956, *J. Sci. Instrum.*, **33**, 72.

GAMMEL, J. L., and THALER, R. M., 1957, *Phys. Rev.*, **107**, 291.

SIGNELL, P. S., and MARSHAK, R. E., 1958, *Phys. Rev.*, **109**, 1229.

SKARSVÅG, K., 1957, *Ph.D. Thesis*, University of Liverpool.

STAPP, H. P., 1955, U.C.R.L. 3098.

STAPP, H. P., YPSILANTIS, T. J., and METROPOLIS, N., 1957, *Phys. Rev.*, **105**, 302.

TYREN, H., HILLMAN, P., and JOHANSSON, A., 1957, *Nuclear Physics*, **3**, 336.

Mass Dependence of Inelastic Atomic Collisions

BY H. B. GILBODY AND J. B. HASTED
University College, London

MS. received 10*th February* 1958, *and in revised form* 28*th April* 1958

THERE is evidence (Gilbody and Hasted 1956) that cross sections for inelastic ion–atom collisions of the charge transfer type may be interpreted in terms of the extent to which the process approximates to adiabatic conditions (Massey 1949). It is found that the cross section may be expected to reach a maximum value at an incident ion energy V_{m} electron volts, where the adiabatic parameter $\Delta E\sqrt{m_1}$ is proportional to $\sqrt{V_{\mathrm{m}}}$, assuming the range of interaction to be roughly constant. ΔE is the energy defect of the process and m_1 the mass of the incident ion. However in certain collisions the initial and final potential energy curves of the system virtually cross over each other and the minimum energy separation $\Delta U_{R_{\mathrm{m}}}$ between them at an internuclear separation R_{m} may be small (Bates and Massey 1954). Uncertainties in the value of $\Delta U_{R_{\mathrm{m}}}$ make predictions of the variation of cross section with energy difficult, although success has been achieved in the calculation of partial charge transfer cross sections.

It has become obvious that there are types of inelastic collision which do not conform to adiabatic theory in that their cross sections are not small when $\Delta E\sqrt{m_1}$ is large, nor is their energy dependence typical. They include cases for which potential energy curve-crossing is unlikely to occur. In the absence of quantum theory calculations, it seems worth while examining such reactions to see whether the cross sections can be interpreted along simple lines.

The reactions include:

detachment of electrons from negative ions: $X^- + Y \rightarrow X + e + Y - \Delta E$,
ionization by positive ions: $X^+ + Y \rightarrow X^+ + Y^+ + e - \Delta E$,
electron loss: $X + Y \rightarrow X^+ + Y + e - \Delta E$.

The detachment cross sections rise to a flat maximum at an energy often within the adiabatic region. For the detachment cross sections of Bydin and Dukelskii (1957) F^-, Cl^-, Br^- and I^- in H_2, He, Ne, A, Kr and Xe, the maximum is at 1800 ev, but Hasted (1952) observed a rather lower energy.

Analysis shows that for all heavy incident ion detachment cross sections at present known, the maximum value is proportional to $m_2/(m_1+m_2)$, where m_2 is the mass of the bombarded ion. We shall call this ratio ρ, and in figure 1 the maximum cross sections Q_m are plotted against ρ for the detachment collisions listed above. A linear dependence is obtained for collisions involving the same incident ion, the slopes of the straight lines being proportional to m_1, as in figure 2. Thus a plot of Q_m against reduced mass μ would also be linear.

It seems that the maximum cross section is proportional to the maximum kinetic energy of motion available for internal excitation, which on classical grounds would be expected to be $\frac{1}{2}\mu v^2 = Tm_2/(m_1+m_2)$ where T is the kinetic energy $\frac{1}{2}mv^2$ of the incident ion.

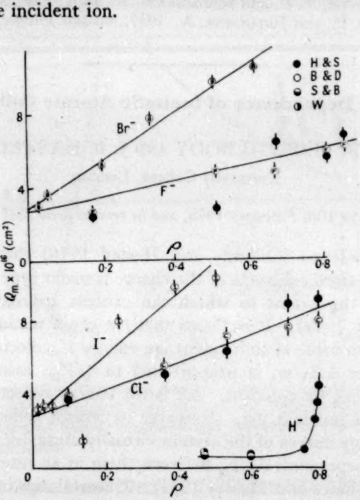

Figure 1. Dependence of Q_m on ρ for negative ion detachment collisions. H & S, Hasted and Stedeford ; B & D, Bydin and Dukelskii ; S & B, Stier and Barnett ; W, Whittier.

Similar analysis could be applied to the heavy incident ion ionization cross sections due to Gilbody and Hasted (1957) for Ne^+, A^+ in H_2, He, Ne, A and A^+ also in N_2, Kr; but in the energy range below 40 kev a maximum has not yet been reached. It is possible that this is due to the importance of multiple ionization, hitherto neglected in all methods not employing mass-spectrometric secondary ion analysis. Fedorenko (1957) has shown that in the case of He^+ in A, multiple ionization is significant at energies of tens of kilovolts, and his data show flat maxima at energies lower than would appear from measurements of total ionization cross section.

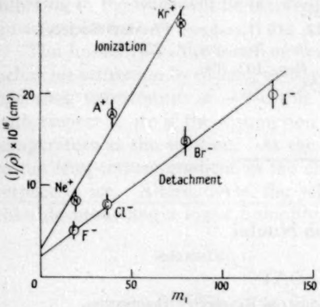

Figure 2. Dependence of slopes of (Q_m, ρ) curves upon m_1 for detachment and ionization collisions, Kr^+ deduced indirectly.

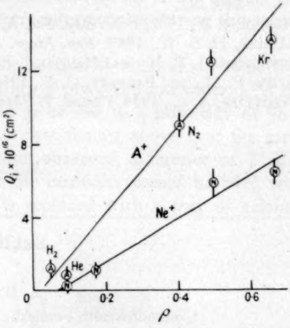

Figure 3. Dependence of Q_i upon ρ for ionization collisions.

In the absence of large numbers of maximum single ionization cross sections, it is of interest to apply a very crude approximation, and analyse the total cross sections Q_t at a low arbitrary energy, 10 kev. From figures 3 and 1 it will be seen that these behave in the same way as the maximum detachment cross section: $Q_t = cpm_1$, where c is a constant for the process.

Where the incident ion is light ($m_1 \leqslant 4$) the maximum cross section is no longer linearly proportional to incident ion mass; the maximum kinetic energy available for conversion to internal kinetic energy does not directly determine the maximum value of the cross section reached. A typical plot of Q_m against ρ for H^- detachment in He, Ne, A, Kr and Xe (Stedeford and Hasted 1955), including the data of Whittier (1954) for H^- in H_2 and Stier and Barnett (1956) for H^- in He, is shown in figure 1. Similar behaviour is observed for the electron loss cross sections measured by Stier and Barnett for H atoms in H_2, He, N_2, O_2, Ne and A, and for the total ionization cross sections H^+, $H_2{}^+$ and He^+ in H_2, He, Ne and A measured by Gilbody and Hasted. It is of interest to note that in these reactions $Q_m = cfm_1/(1-\rho)$, the form of $f(m_1)$ being such that it decreases rapidly as m_1 increases, and the hydrogen molecule appearing as exceptional throughout.

It does appear, however, that where the incident ion is heavy an 'available kinetic energy' rule may be applied to predict roughly the magnitudes of certain inelastic collision cross sections, and it will be of interest to see how far measurements at present in the course of being made conform to these ideas.

REFERENCES

BATES, D. R., and MASSEY, H. S. W., 1954, *Phil. Mag.*, **45**, 111.

BYDIN, I. F., and DUKELSKII, V. M., 1957, *J.E.T.P.*, **31**, 474.

FEDORENKO, N. V., 1957, *Societa Italiana di Fisica, Terzo Congresso Internazionale Sui fenomeni d'ionizzazione nei gas.* Milano, 1957, p. 295.

GILBODY, H. B., and HASTED, J. B., 1956, *Proc. Roy. Soc.* A, **238**, 334 ; 1957, *Ibid.*, **240**, 382.

HASTED, J. B., 1952, *Proc. Roy. Soc.* A, **212**, 235.

MASSEY, H. S. W., 1949, *Rep. Progr. Phys.*, **12**, 249 (London : Physical Society).

STEDEFORD, J. B. H., and HASTED, J. B., 1955, *Proc. Roy. Soc.* A, **227**, 466.

STIER, P. M., and BARNETT, C. F., 1956, *Phys. Rev.*, **103**, 896.

WHITTIER, A. C., 1954, *Canad. J. Phys.*, **32**, 275.

Sublimation Nuclei

By G. A. DAY

Commonwealth Scientific and Industrial Research Organisation,
Radiophysics Laboratory, Sydney, Australia

MS. received 1st *April* 1958

§ 1. INTRODUCTION

It has been reported (Fournier d'Albe 1949, Mossop 1956) that various substances can act as sublimation nuclei after once having an ice crystal formed on them at some low temperature. Iceland spar is given as one of these substances and the explanation suggested is that on warming the ice crystal in an unsaturated atmosphere only partial evaporation of the ice takes place and that a microscopic film of ice is retained on the nucleus which permits subsequent ice crystal growth direct from the vapour stage.

Mossop states that on warming ice crystals formed on iceland spar from −41 °c, the threshold temperature for the spontaneous nucleation of supercooled water drops, between 1 and 5% of the particles acted as sublimation nuclei until a temperature of −3·7 °c was reached. This limiting temperature is much warmer than that at which iceland spar operates as a normal freezing nucleus (according to Mossop 0·1% are effective at −38 °c and 0·01% at −32 °c) and higher than that at which any known substance is capable of promoting ice formation.

This phenomenon has an important bearing on nucleation processes in supercooled clouds and in view of this a series of experiments was made to determine whether these 'sublimation nuclei' particles would retain this singular property after prolonged drying and then be capable of regrowing ice crystals at these warm temperatures.

§ 2. Description and Operation of Equipment

The equipment, a freezing chamber maintained at −9°c, is shown in section in figure 1. It consists of two large concentric cylinders together with a detachable smaller cylinder known as the gun. The gun is sealed at one end with a rubber disc and may be pressurized through a valve at the other. The rubber disc is chosen so that an adiabatic expansion from bursting pressure to atmospheric pressure cools the air within the gun by at least 70°c. This cooling is so rapid that the smallest mote will be involved in condensation and so large that the minute water drops formed will become frozen. Thus, when a particular substance is to be activated, a small quantity, ground to a fine powder, is placed in the gun prior to the expansion. It is almost certain that all of the powder not adhering to the walls will be involved in the freezing process during the subsequent explosion.

The humidity in the outer or evaporation section is maintained somewhat below ice saturation by placing therein a solution of glycerine and water. At the operating temperature of −9°c this solution gives rise to a humidity of 98% with respect to ice if the assumption is made that the air above is at the same temperature as the solution. At the maximum observed difference of 2° due to the temperature gradient in the chamber the humidity would be 84% with respect to ice. Alternatively, the solution is replaced with a tray of calcium chloride producing a lower humidity.

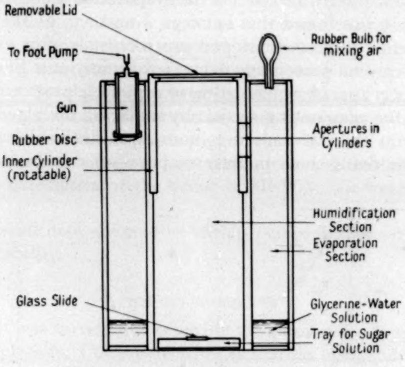

Figure 1. Section of freezing chamber.

By rotating the inner or humidifying cylinder, an aperture in its wall can be made to align with a similar aperture in the evaporating section and in this position the air, ice crystals, motes etc., can be pumped from the evaporating to the humidifying section. At the bottom of the humidifying section a tray containing a solution of sugar and water, which at the operating temperature is supercooled, catches any crystals falling into it, where they grow and are counted. A glass slide placed over a portion of this tray permits the number of particles falling on to it to be counted with the aid of a microscope and thus the ratio of ice crystals to particles determined.

Before each test a number of explosions are made without placing any substance in the gun. Thousands of ice crystals form on the particles present in the air and if these are immediately pumped into the humidified inner section, they can be seen to grow in the sugar solution. However, a delay of a few seconds in the evaporation section reduces the number of crystals to zero suggesting that no naturally occurring particles having a long after-activity time are usually present although the air is rich with condensation nuclei.

§ 3. PRESENT WORK

A quantity of iceland spar was ground in a ball mill and the powder separated by elutriation. Particles from 1 to 15μ diameter were used with large numbers in the range from 1 to 3μ whose fall-out time would be long compared with the duration of each test. For each test a small quantity was placed in the gun and the gun exploded. The crystals so formed by the explosion were left to evaporate for periods of up to ten minutes before the inner section of the chamber was humidified; the air therein permitted to take up the temperature of the walls, and the ice crystals and motes pumped from the outer to the inner section. Here the crystals that grew in the sugar solution and the particles that fell on the slide were counted.

Results of these tests with iceland spar are shown in figure 2 in which the number of ice crystals per 10^6 particles pumped from the evaporation section are plotted as a function of the time spent in the evaporation section over the glycerine–water solution. It was found that between 1 and 5% of the particles pumped from the evaporation section developed as ice crystals after evaporation for one minute. However, this percentage decreased rapidly as a function of time and after five minutes evaporation had fallen to negligible proportions. Decrease of humidity within the evaporating section by replacing the glycerine solution with the tray of calcium chloride caused a more rapid decline in the number of ice crystals, none surviving one minute evaporation. Iceland spar which had

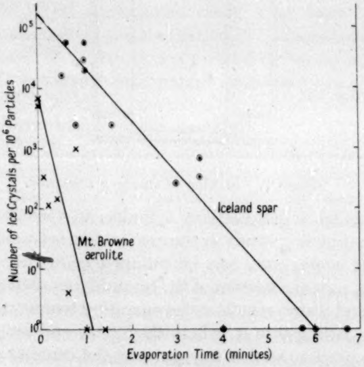

Figure 2. Number of ice crystals which grew after evaporation over glycerine–water solution.

been freshly ground in order that the surfaces of the particles would not be contaminated by exposure to the atmosphere gave similar results.

Primarily to ensure the method of introducing the substance as particles into the equipment did not impair their nucleating properties, silver iodide (the most active freezing nucleus known) was tested by dusting a small quantity as a powder into the top of the humidified section. It immediately became apparent that silver iodide was active as a freezing nucleus when used in this manner and it was necessary to warm the chamber to -6°c, the known temperature at which AgI is active as a freezing nucleus, to determine the onset of crystal growth. However, when silver iodide was cooled by expansion in the gun and then de-humidified it was not found to promote ice crystal growth at a warmer temperature than -6°c.

A number of substances which might be expected to be present in the atmosphere were subjected to experiments similar to the iceland spar. These included meteorites, volcanic rock, quartz, mica, clay and gypsum. The meteorites consisted of aerolites, identified by location of fall as Mount Browne, Binda, Barratta and Gilgoin. The results of the Mount Browne which was typical of all four aerolites and similar to the other substances tested are also shown in figure 2.

§ 4. CONCLUSION

The suggestion (Mossop 1956) that this phenomenon might enable ice particles from cirrus clouds to persist under conditions where they would normally disappear by sublimation, then grow again on entering air saturated with respect to ice, could be taken to imply that it operates independently of environment and time. Unfortunately, these tests do not substantiate such an implication. There appears little doubt of the ability of iceland spar to retain its nucleating properties for a greater time than the naturally occurring particles in the atmosphere and the other substances tested but these results suggest that retention of any film of ice on the surface is limited to rather special circumstances and that after exposure for several minutes to humidities of the order of 80–90% the evaporation appears complete.

Although this result does not conflict with previous findings it does emphasize their limited applicability.

ACKNOWLEDGMENTS

This experiment was carried out as part of the cloud physics programme of the Division of Radiophysics, Commonwealth Scientific and Industrial Research Organisation, and was suggested by Dr. E. K. Bigg under whose supervision the work was carried out. The sample of aerolites were kindly supplied by Mr. Chalmers of the Australian Museum, Sydney.

REFERENCES

FOURNIER D'ALBE, E. M., 1949, *Quart. J. R. Met. Soc.*, **75**, 1.
MOSSOP, S. C., 1956, *Proc. Phys. Soc.* B, **69**, 161.

The Branching Ratio of Thorium C

By P. RICE EVANS and N. J. FREEMAN
Bedford College, University of London

Communicated by H. O. W. Richardson; *MS. received 27th March* 1958

Thorium C (^{212}Bi) is known to decay by α emission to ThC″ and by β^- emission to ThC′, and the latter then by α emission to ThD.

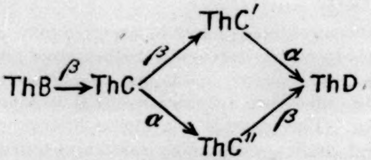

Early measurements of the branching ratio $\alpha/(\alpha+\beta)$ of ^{212}Bi are shown in the table. Recently Senftle, Farley and Lazar (1956), using a 2π proportional counter, have redetermined the branching ratio and have obtained a value 0·362 which is 7·4% higher than the value obtained by Kovarich and Adams (1938).

Author	Method used	$\alpha/(\alpha+\beta)$
Marsden & Barratt (1911)	Counting of scintillations	$0{\cdot}35 \pm 0{\cdot}02$
Meitner & Freitrag (1926)	Cloud chamber	$0{\cdot}343 \pm 0{\cdot}0018$
Kovarich & Adams (1938)	Ionization chamber	$0{\cdot}337 \pm 0{\cdot}01$
Senftle, Farley & Lazar (1956)	2π proportional counter	$0{\cdot}362 \pm 0{\cdot}006$

In the present work the branching ratio was determined from the intensities of the two α particle groups studied with a scintillation counter. The α particles were detected in a KI (thallium activated) crystal, which is convenient because of its non-deliquescent nature.

Franzen, Peelle and Sherr (1950) have shown that the ratio of the conversion efficiencies of the KI(Tl) crystal for α and β particles is about unity. The α particle peaks are thus well resolved from the β continuum in view of their greater energies.

Factors which often preclude the use of this phosphor for β and γ ray spectroscopy, for example the natural ^{40}K radioactivity and the emission of delayed phosphorescent pulses, do not arise here because of the high level of discrimination. Silicone fluid was used to couple the crystal optically to the photocathode of the Dumont 6260 photomultiplier.

Sources of ThB were electrodeposited from thoron on a polished brass surface, 1 mm in diameter, and were mounted 1 cm above an aperture of the same diameter in a mica disc covering the crystal. The spectrum in the figure was measured with a single-channel analyser with a channel width of 0·5 volt. A resolution to 5% was obtained.

To obtain the branching ratio the analyser was used as an integral discriminator with the bias adjusted to count the number of particles, first in the high energy peak and then in both peaks. Thirty-four counts totalling 120000 particles were made at equal intervals of 2 minutes, readjusting the bias between successive counts so that the effect of decay was averaged out. The branching ratio was found to be $\alpha/(\alpha+\beta)=0{\cdot}359\pm0{\cdot}002$ which is in agreement with the recent value of Senftle *et al.* (1956).

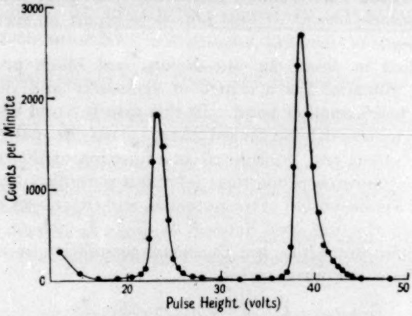

The α particle spectrum of Th(C+C′) taken with a channel width of 0·5 volt. The lower peak corresponds to the 6·2 Mev α group from ThC and the other to the 8·9 kev α group from ThC′.

ACKNOWLEDGMENTS

We wish to express our appreciation for the guidance and encouragement of Professor H. O. W. Richardson. We are indebted to Dr. D. K. Butt for the loan of the crystal and to Bedford College for financial support during the course of this work.

REFERENCES

FRANZEN, W., PEELLE, R. W., and SHERR, R., 1950, *Phys. Rev.*, **79**, 742.
KOVARICK, A. F., and ADAMS, N. I., 1938, *Phys. Rev.*, **54**, 420.
MARSDEN, E., and BARRATT, T., 1911, *Proc. Phys. Soc.*, **24**, 50.
MEITNER, L., and FREITAG, K., 1926, *Z. Physik*, **37**, 481.
SENFTLE, F. E., FARLEY, T. A., and LAZAR, N., 1956, *Phys. Rev.*, **104**, 1629.

Properties of Wannier Functions

BY W. KOHN[†] AND S. MICHAELSON
Imperial College of Science and Technology, London

Communicated by H. Jones; *MS. received 3rd June 1958*

THE Wannier function (Wannier 1937) $a(\mathbf{r})$ corresponding to a simple energy band is defined as follows. Let $\phi_{\mathbf{k}}(\mathbf{r})$ be normalized Bloch waves corresponding to this band. Then

$$a(\mathbf{r})=\Omega^{-1/2}\int_{\Omega} d\mathbf{k}\,\phi_{\mathbf{k}}(\mathbf{r}) \qquad \ldots\ldots (1)$$

[†] Senior Post Doctoral Fellow of the United States National Science Foundation, on leave of absence from Carnegie Institute of Technology, Pittsburgh, U.S.A.

where Ω is the volume of the fundamental Brillouin zone. Since the phase of $\phi_{\mathbf{k}}$ is not defined, the function $a(\mathbf{r})$ is not uniquely determined by (1). It appears to be generally believed that Wannier functions, while somewhat localized, fall off slowly with distance, like r^{-1}. This note is to report on some results which bear on this question.

We have studied in detail the one-dimensional Bloch problem. It was assumed that the potential has a centre of symmetry and that the band in question does not touch another band. In this case it could be shown that the phases of the Bloch waves can be so chosen that $\phi_k(x)$ may be analytically continued into the complex k-plane and, considered as a function of the complex variable $k=k_1+ik_2$, has the following properties: (i) it is a periodic function of k_1, with period $2\pi/b$, where b is the period of the potential, and (ii) it is an analytic function in a strip enclosing the real axis defined by $|k_2|<k_0$, where k_0 is a positive number. From these properties and the quasi-periodicity in x, it follows that $\phi_k(x)$ can be written as a Fourier series

$$\phi_k(x)=\left(\frac{b}{2\pi}\right)^{1/2}\sum_n A_n(x)\exp(inkb) \qquad \ldots\ldots(2)$$

where the $A_n(x)$ satisfy the following relations:

$$A_n(x+b)=A_{n-1}(x), \qquad \ldots\ldots(3)$$

and

$$|A_n(x)|\leqslant M(x)\exp(-|n|k_0b) \qquad \ldots\ldots(4)$$

where $M(x)$ is some non-negative bounded function of x. Use of (2) and (3) in the equation (1) defining the Wannier function gives

$$\begin{aligned} a(x+mb) &= \left(\frac{b}{2\pi}\right)\int dk\sum_n A_n(x+mb)\exp(inkb) \\ &= A_0(x+mb)=A_{-m}(x). \qquad \ldots\ldots(5)\end{aligned}$$

Therefore, by (4), we have the estimate

$$|a(x+mb)|\leqslant M(x)\exp(-|m|k_0b), \qquad \ldots\ldots(6)$$

showing that this Wannier function decreases exponentially.

The magnitude of the largest possible k_0 for which (6) holds can be determined by a simple procedure. Loosely speaking it is the larger the more separated the band in question is from its neighbours.

A mathematically rigorous discussion of three-dimensional Wannier functions is very much more complex, but there can be little doubt that they also fall off exponentially.

Another simple property, which holds in any number of dimensions, might be mentioned. If the potential has a centre of inversion, there exists for each simple band one and only one Wannier function which is real and symmetric (or antisymmetric) under inversion.

A more detailed account will be published elsewhere. One of us (W. K.) wishes to express his appreciation to the Imperial College of Science and Technology and in particular to Professor H. Jones for the hospitality which has been extended to him.

REFERENCE

WANNIER, G., 1937, *Phys. Rev.*, **52**, 191.

‘ Virtual ’ Fresnel Diffraction Patterns

By R. M. SILLITTO and M. D. WILSON
Department of Natural Philosophy, University of Edinburgh

Communicated by G. R. Evans; MS. received 8th April 1958

A FEW years ago, while developing an Honours laboratory experiment on the use of Zernike's ‘coherent background’ in diffraction studies, we came across an aspect of Fresnel diffraction which does not seem to be widely known, although it can be predicted by a simple extension of the ordinary elementary textbook treatment of diffraction.

We may consider as an example the Fresnel diffraction pattern of a straight edge, produced when light diverging from a line source at L is diffracted by the

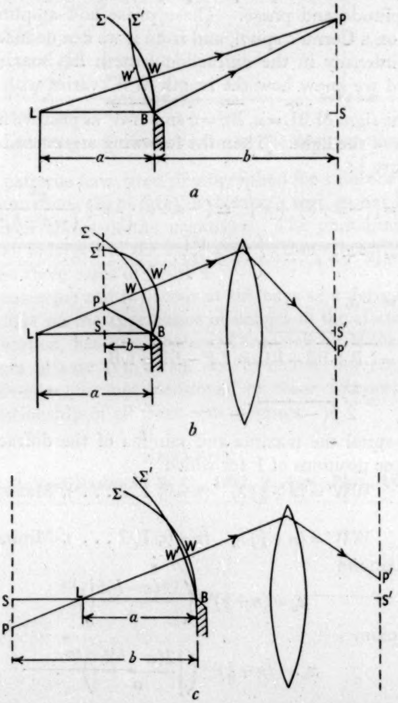

Figure 1. Geometrical arrangement for formation of Fresnel diffraction pattern using line source L and straight edge B. In (*a*) ‘ real ’ fringes are seen in the plane SP; in (*b*) and (*c*) ‘ virtual ’ fringes in the plane SP are imaged by the lens on the plane S′P′.

edge B of a plate (figure 1 (*a*)). The pattern may be observed on a screen to the right of the diffracting object, say at SP, (figure 1 (*a*)) or photographed by means of a camera whose lens forms on the photographic plate a real image of a plane such as SP. We found that when a camera is focused on a plane between L and B, as in figure 1 (*b*), or even on a plane to the left of L as in figure 1 (*c*), a diffraction pattern is recorded which is similar to the one observed with the conventional arrangement of figure 1 (*a*), although in the case of figure 1 (*c*) the diffraction pattern is laterally inverted.

These findings may be understood as follows: In figure 1 Σ represents a cylindrical wave front spreading out from L and meeting the diffracting edge B, while Σ' represents a cylindrical surface through B whose centre is at P. Then the effect at P in the diffraction pattern, or at P′ in the image plane, is the summation of the effects of those secondary wavelets from Σ whose envelope is Σ', which is not a surface of constant phase; hence as the position of P is varied in PS the summation of the amplitude vectors over Σ' gives a resultant at P or P′ of varying amplitude and phase. These phase and amplitude variations can be represented on a Cornu's spiral, and from it we can deduce the positions of P for which the intensity in the diffraction pattern has maximum or minimum values, provided we know how the length WW′ varies with the position of P.

We define the signs of $\overrightarrow{\mathrm{BL}} = a$, $\overrightarrow{\mathrm{BS}} = b$ and $\overrightarrow{\mathrm{WW'}}$ as positive if they are measured in the direction of the light. Then the following argument is valid for all three diagrams in figure 1:

$$\overrightarrow{\mathrm{LP}} = \{(-a+b)^2 + x^2\}^{1/2} \simeq (-a+b)\left\{1 + \tfrac{1}{2}\frac{x^2}{(-a+b)^2}\right\},$$

$$\overrightarrow{\mathrm{BP}} = \{b^2 + x^2\}^{1/2} \simeq b\left\{1 + \tfrac{1}{2}\frac{x^2}{b^2}\right\},$$

$$\overrightarrow{\mathrm{LB}} = -a.$$

Now

$$\left.\begin{aligned}\overrightarrow{\mathrm{WW'}} &= \overrightarrow{\mathrm{LP}} + \overrightarrow{\mathrm{PB}} + \overrightarrow{\mathrm{BL}} = \overrightarrow{\mathrm{LP}} - \overrightarrow{\mathrm{BP}} - \overrightarrow{\mathrm{LB}} \\ &\simeq \frac{x^2}{2}\,\frac{a}{b(-a+b)}.\end{aligned}\right\} \quad \ldots\ldots(1)$$

From Cornu's spiral the maxima and minima of the diffraction pattern occur very near to those positions of P for which

$$\mathrm{WW'} = (n+\tfrac{3}{8})\,\lambda, \quad (n = 0, 1, 2\ldots), \text{ Maxima}$$

and

$$\mathrm{WW'} = (n+\tfrac{7}{8})\,\lambda, \quad (n = 0, 1, 2\ldots), \text{ Minima.}$$

Thus for a maximum

$$x_n = (n+\tfrac{3}{8})^{1/2}\left(\left|\frac{2(a-b)b}{a}\right|\right)^{1/2} \quad \ldots\ldots(2)$$

and for a minimum

$$x_{n'} = (n+\tfrac{7}{8})^{1/2}\left(\left|\frac{2(a-b)b}{a}\right|\right)^{1/2}. \quad \ldots\ldots(3)$$

Inspection of the figures shows that in (*a*) and (*b*) the illuminated region of the plane SP is that in which x is positive, while in (*c*) x is negative in the illuminated region. It follows that in the third case the diffraction pattern appears to be inverted.

Figure 2 shows, for a number of values of *n*, the variation of x_n with *b*, i.e. the positions of the maxima on a 'screen' which is moved continuously from a position to the right of B to a position to the left of L.

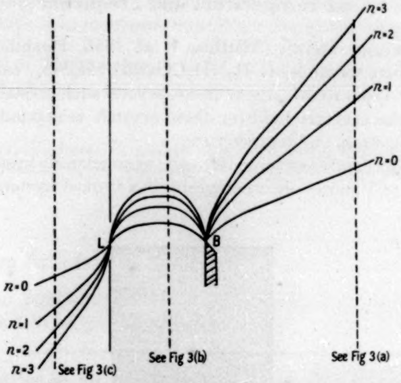

Figure 2. Loci of bright fringes of constant order for the three arrangements of figure 1.

The diffraction patterns have been photographed for a number of values of *b*, and the validity of equations (2) and (3) in the three regions has been confirmed from microphotometer traces of the negatives. The photographs in figure 3 (Plate), which are all enlarged to the same degree, show the diffraction patterns corresponding to the three cases of figure 1.

The fringes of cases (*a*) and (*b*) occur at the edge of a defocused image of a knife-edge; their effect on the appearance of images in the electron microscope, with parallel illumination, has been discussed in detail by Hillier and Ramberg (1947). The fringes of case (*c*), which are, of course, far removed from the vicinity of the knife-edge, are not mentioned by these authors; our treatment shows the close relationship of all three sets of fringes.

REFERENCE

HILLIER, J., and RAMBERG, E. G., 1947, *J. Appl. Phys.*, **18**, 48.

LETTERS TO THE EDITOR

The Dependence of the Coercive Field of Tri-Glycine Sulphate on Temperature and Frequency

It recently became known (Matthias *et al.* 1956, Hoshino *et al.* 1957) that tri-glycine sulphate crystals $(CH_2NH_2COOH)_3.H_2SO_4$ exhibit ferroelectric properties and, in order to investigate these, several such crystals were grown. It was found that the coercive field for these crystals is dependent on frequency, maximum electric stress and temperature.

At room temperature rectangular and symmetrical hysteresis loops were observed. Figure 1 shows an oscillogram of a typical hysteresis loop for these crystals at 50 c/s.

Figure 1. Dielectric hysteresis loop for tri-glycine sulphate at room temperature (freq. 50 c/s, $E_{max} = 1400$ v cm^{-1}).

The coercive field, E_c at room temperature, was found to be of the order of 430 v cm^{-1} when an electric stress of 1500 v cm^{-1} (50 c/s) was applied. Figure 2 shows the coercive field as a function of temperature at constant electric stress. As can be seen, the 50 c/s coercive field strength remains reasonably constant in the vicinity of room temperature, but begins to increase rapidly at around -30°c.

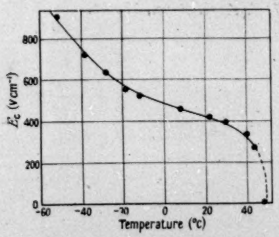

Figure 2. Coercive field strength E_c as a function of temperature for tri-glycine sulphate.

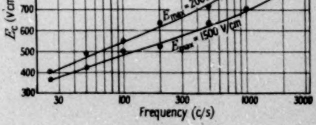

Figure 3. Coercive field strength as a function of frequency for tri-glycine sulphate.

Of course, such an increase of E_c is common behaviour for many ferroelectric substances. This increase of E_c at lower temperatures for these crystals seems to be caused by a freezing-in of the dipoles, but more investigation is required to confirm this assumption.

The frequency dependence of coercive field for these crystals is shown in figure 3. The coercive field increases with frequency in the range investigated.

Battersea College of Technology,
London, S.W.11.
28th April 1958.

S. Domanski.

Hoshino, S., Mitsui, T., Jona, F., and Pepinsky, R., 1957, *Phys. Rev.*, **107**, 1255.
Matthias, B. T., Miller, C. F., and Remeika, J. P., 1956, *Phys. Rev.*, **104**, 899.

The Polarization Reversal Process in Ferroelectric Single Crystals

The peak current flowing through a single crystal due to a pulse switching field E has been found to be given empirically by

$$i = F(P) \exp(-\alpha/E)$$

for all the ferroelectrics so far investigated (Merz 1950, Mitsui and Furuichi 1953, Wieder 1956, Prutton 1957). The parameter α is a temperature dependent 'activation field' and $F(P)$ is a function of the polarization P which changes slowly compared with the exponential term. Merz (1954) has suggested that in the case of barium titanate this behaviour of the switching current arises because the polarization reversal is governed by the nucleation of new domains of reversed polarization which are subsequently able to grow at the expense of unfavourably orientated regions in the crystal. Such a nucleation would occur at a rate

$$\frac{dn}{dt} \propto \exp\left(-\frac{U_0}{\boldsymbol{k}T}\right) \qquad \ldots\ldots(1)$$

where U_0 is the energy required to form a nucleus, $\boldsymbol{k}$ is Boltzmann's constant and T is the absolute temperature. Landauer (1957) has calculated values of U_0 in barium titanate single crystals by assuming that the energy available for the growth of a nucleus is that remaining after the energy required by the domain wall and the depolarizing field of the new domain have been deducted from the energy supplied to the crystal by the applied field. These values of U_0 are of the order of $10^8 \boldsymbol{k}T$ so that the rate of nucleation of domains described by (1) must be entirely negligible. Furthermore, the sizes of domains which are able to grow as predicted by Landauer are much too large. The author has obtained similar results for the ferroelectrics rochelle salt, potassium dihydrogen phosphate and guanidine aluminium sulphate hexahydrate (GASH).

Landauer assumes that the wall energy density is independent of the orientation of the domain wall with respect to the crystal axes. By assuming that the ferroelectric domain wall is similar to the Bloch wall of ferromagnetics the author has removed this limitation from Landauer's theory but values of U_0 and the minimum domain size are still much too large for thermal generation of nuclei to be feasible.

The existence of surface layers in ferroelectric single crystals was first postulated by Känzig (1955) and then demonstrated by Merz (1955) and Chynoweth (1956) for $BaTiO_3$ and Wieder (1957) for GASH. These surface layers may provide nuclei for the start of the reversal of the polarization. Electronic and ionic conductors may be expected to show a surface region where a high field prevails because of the existence of Tamm energy levels or Schottky or Frenkel lattice defects respectively. These regions generally have thicknesses of the order of 10^{-6} cm and field strengths of the order of 10^5 volt cm^{-1}.

If these mechanisms operate in ferroelectric crystals then the fields in the surface layers must induce saturation polarization and from considerations of symmetry the surface layers must be polarized in opposite directions. If each layer is of uniform thickness its depolarizing field strength is high and the energy of the system could be reduced if each layer is non-uniform, perhaps as is indicated in the figure. Such a configuration could provide very small nuclei of reversed polarization permanently situated at each surface perpendicular to the ferroelectric axis, which may form a basis for the commencement of the reversal of the polarization of the bulk of the crystal. It may also provide an explanation for the permanent bias observed in the hysteresis loops of some GASH crystals. No observations of the surface domain structure of ferroelectric crystals have yet been reported.

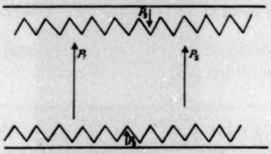

Surface layers (not to scale).

Department of Numerical Automation,
Birkbeck College,
Malet Street,
London W.C.1.

M. Prutton.

2nd May 1958.

Chynoweth, C. G., 1956, *Phys. Rev.*, **104**, 2.
Känzig, W., 1955, *Phys. Rev.*, **98**, 549.
Landauer, R., 1957, *J. Appl. Phys.*, **28**, 227.
Merz, W. J., 1950, *Phys. Rev.*, **78**, 92; 1954, *Ibid.*, **95**, 690; 1955, *Ibid.*, **98**, 409.
Mitsui, T., and Furuichi, J., 1953, *Phys. Rev.*, **90**, 193.
Prutton, M., 1957, *Proc. Phys. Soc.* B, **70**, 1064.
Wieder, H. H., 1956, *Bull. Amer. Phys. Soc.*, **1**, 254; 1957, *Proc. Inst. Radio Engrs*, **45**, 1094.

CORRIGENDUM

A New Formulation of Scalar Diffraction Theory for Restricted Aperture, by J. M. COWLEY and A. F. MOODIE (*Proc. Phys. Soc.*, 1958, **71**, 533).

In equation (3.4), Q_1 should not be separated from its argument $\left(-\frac{k}{R_n}x\right)$ by a multiplication sign.

The equation in the middle of p. 542 *should read*

$$\psi(x)\psi^*(x)=K_2K_2^*\,.\,q\left(-\frac{R_{n-1}}{R_n}x\right).\,q^*\left(-\frac{R_{n-1}}{R_n}x\right)$$

and the equation at the top of p. 543 *should read*

$$\psi(x)\psi^*(x)$$
$$=K_2K_2^*\left[q\left(-\frac{R_{n-1}}{R_n}x\right)q^*\left(-\frac{R_{n-1}}{R_n}x\right)\star H\left(-\frac{k}{R_n}x\right).\,H^*\left(-\frac{k}{R_n}x\right)\right].$$

REVIEWS OF BOOKS

Neutron Cross Sections, by D. J. HUGHES. International Series of Monographs on Nuclear Energy, Division II, Nuclear Physics, Vol I. Pp. x + 182. (London : Pergamon Press, 1957.) 30*s*.

To the nuclear engineer, tables and graphs of neutron cross sections are as important as steam tables, but less intelligible unless he has been trained as a nuclear physicist. During the past decade the staff of Brookhaven National Laboratory have done a magnificent job in collecting from all over the world a growing wealth of precise information about neutron cross sections which they have issued in their famous Barn Book and its supplements. Dr. Hughes, who has played such a large part in this work, has now provided what amounts to an explanatory commentary upon the Barn Book. He discusses the theory of cross sections and the principles of their measurement, and is at pains to point out not only their significance from the point of view of the nucleus but their practical application to reactor theory. He addresses himself to those many individuals who must make practical application of the Barn Book without prior training in nuclear physics. Faced with such a task it is not surprising that he sometimes falls between two stools. Simplification has in places led to errors of interpretation, yet in spite of the simple style there are whole passages which still must surely be unintelligible without some background of training in quantum theory. In reading a book of this kind one must be prepared to take a great deal on trust; yet the author has sometimes preferred to give a too condensed explanation which raises more questions than it resolves. Notation is usually straightforward; however, the author has chosen to use the Greek ν for velocity as well as for the number of neutrons per fission (albeit in different fount), except when he forgets his perverse convention and uses Latin v instead. In spite of these criticisms, it would be surprising if this book did not find its rightful place on the shelves of all concerned with the practical application of neutron physics. One of an important series of monographs it is, like the others, beautifully printed, with many clear diagrams and illustrations, and reasonably priced.

B. H. FLOWERS.

Geometrical and Physical Optics, by R. S. LONGHURST. Pp. xvi + 534. (London: Longmans, Green, 1957.) 60*s*.

The author of this book set himself the difficult task of writing a textbook for Honours Physics students which would be suitable for those reading for a Pass Degree, and of use to post-graduate students of optics. He has succeeded well in the case of undergraduates but his book is less likely to attract the more specialised undergraduate worker. It ranges from a discussion of levelling the prism of a spectrometer to Kirchhoff's formulation of Huygens' principle and electromagnetic theory. Some elementary topics might have been omitted, but some, like the very neat chapter on the simple determination of the paraxial constants of optical systems, are useful. The book is a reasonable mixture of mathematical analysis of the subject and less advanced treatment for the weaker student.

Rigid division of the subject into geometrical and physical optics has been avoided, as, for example, when two chapters on the occurrence and control of aberrations, follow ones on Fresnel and Fraunhofer diffraction and the physical theory of image formation. There are chapters on visual optics, photometry, dispersion, and optical activity, and sections on most topics which an Honours student is likely to encounter. As is usual nowadays in books of this kind, spectroscopy is omitted entirely except for some elementary consideration of spectrographic equipment.

In a textbook covering such a wide field it is impossible to include enough information to satisfy the more advanced student. Nevertheless, references to original papers have been omitted (" an undergraduate is always desperately short of time "), and replaced by a short appendix listing standard texts suitable for further reading. This list is useful but it is probable that to follow an enquiry through these is unlikely to take less time, and may be less useful, than an immediate reference to an original paper. Recent work has been described in some places, as, for example, in the chapter on the velocity of light where recent microwave and band spectra experiments are mentioned, and in the chapter on the theory of image formation where the method of image formation by means of reconstructed wave fronts is described.

The notation used in the elementary discussion of geometrical optics does, as the author points out, appear cumbersome, and one feels that the procedure adopted in deriving formulae may lead a student into difficulties. This procedure is " to ignore completely all signs and deduce an equation relating the quantities concerned from the geometry of a figure illustrating any special case. When the final equation is obtained, it is necessary to change the sign in front of all quantities that are negative (according to the sign convention) in the figure ".

The book is well produced with a large number of clear diagrams, and a few excellent plates of interference and diffraction effects. The index and list of contents are very full and helpful. W. J. BATES.

Thermodynamics (3rd Edn), by E. A. GUGGENHEIM. Pp. xxiii + 476. (Amsterdam: North-Holland Publishing Company, 1957.) 69*s*.

This is a very well-known textbook brought up-to-date with the inclusion, since the 1950 edition, of a short chapter on Onsager's relations, and incorporating some changes of arrangement in the discussion on mixtures. It is extremely comprehensive and deals with almost every possible type of thermodynamic system under almost every possible set of conditions. It will disappoint anyone who thinks thermodynamics is about cycles (there is no reference to engines or refrigerators), and it is too formidable for undergraduate teaching. As a compendium for advanced students and practising physicists and chemists it is, however, admirable and has the advantage that on points of controversy it is usually right. G. O. J.

Interpolation and Allied Tables, prepared by H.M. Nautical Almanac Office. Pp. 80. (London: H.M.S.O., 1956.) 5*s*.

The first edition of these tables, edited by the late Dr. L. J. Comrie, F.R.S., has long been valued by computers, but has for some years been out of print. The new edition, a joint effort with the Mathematics Division, N.P.L., offers, at five times the original price, most of the original and some new material, together with a largely expanded and clarified explanatory section, which constitutes an excellent summary outline of the numerical calculus.

The notation has been changed rather radically, for reasons which, one suspects, seem more cogent at Teddington than at Herstmonceux; some, at least, of the changes appear gratuitous in a practical manual. The chief changes in the major tables are: (1) the old critical table of Bessel interpolation coefficients is replaced by one of B_2, E_2 and F_2, i.e. B_3 has been suppressed and Everett coefficients added. This seems to be highly disadvantageous for inverse interpolation. (2) The Everett interpolation table is at steps of 0·001 instead of 0·01, a great improvement; it also includes coefficients for a generalized simultaneous throw-back of Everett type; (3) the table of Stirling differentiation coefficients (Table XXVIII) has been suppressed, I think, unwisely; but the Bessel table remains; (4) a new table of integration coefficients (Bessel type only) is given at a tabular interval of 0·01. One of Comrie's rare errors of judgment, the truncation of B_4 to 4 decimals, has been carried over into the new table 7 from the old table XXV, thereby restricting its usefulness.

The tables are indispensable to those whose computations much exceed slide-rule accuracy. J. C. E. JENNINGS.

Experimental Crystal Physics, by W. A. WOOSTER. Pp. viii + 115. (Oxford: Clarendon Press, 1957). 18*s*.

Physicists may feel that a more appropriate title for this book might be *Experimental Techniques of Physical Crystallography*. When discussing the magnetic properties of crystals, for example, the author is concerned not with the origin of these properties but with the indications of crystal symmetry provided by the anisotropy of the susceptibility. Whatever the reason for making measurements on crystals, however, the techniques used by a student of solid-state physics in making them are the same as those used by the mineralogy students for whom the experiments described in this book were developed; and it may prove a useful guide to those seeking some elementary experiments in solid-state physics for the teaching laboratories of physics departments. A number of simple experiments (taking two to three hours to carry out) on the optical, magnetic, thermal, plastic, piezoelectric, pyroelectric, and elastic properties of crystals are described in detail. The principles involved in the experiments are discussed in rather elementary (in some places, very elementary) terms, and although tensor notation is introduced only simple coefficients are used in the examples. The price seems unnecessarily high. B. R. COLES.

Basic Physics, by A. R. MEETHAM. Pp. xi + 144. (London, New York: Pergamon Press, 1957.) 21*s*.

The aim of this book, as set forth in the preface, appears to be to supplement the traditional Advanced-level physics course by offering pupils an " extra discipline of pure physics ", which " will provide a foundation, more resistant to the passage of time, on which they may build later in life ". The recipe for its compilation reads very much like Gilbert's well-known formula for heavy dragoons. Take, says Dr. Meetham, any complete set of Advanced-level physics textbooks; eliminate everything that is human, historical, or experimental; set it out formally in any order that you like; and the residuum is what may be called pure or basic in physics as it is now taught in schools and in preliminary courses at universities. This concentrated distillate's strength ought to be as the strength of ten, because its heart is pure; unfortunately it would be better described as decinormal. It is a disappointing book.

It is necessarily condensed in treatment, but not correspondingly terse in style; and the impression it conveys in the first place is of superficiality rather than discipline. This is reinforced by the use of inverted commas for technical terms, and of parentheses for important defining or qualifying statements. Some of the chapters, including one on optics and three on heat and temperature, into which experimental results are allowed to intrude, are to that extent a good deal better than the rest. But in too many places assertions are offered without explanation, and mathematical formulae (which are not always accurate) are given to be taken on trust. For example, all that pure physics has to offer on the detection of infra-red radiation is the following one sentence: " Thermal radiation is obvious enough when the body is red hot; at lower temperatures it can be detected when the body is enclosed in a very cold shield ". Again, the water triple-point cell " could also be used as a standard of pressure ". I began to lose contact with the book at the author's treatment of Newton's laws of motion, and became more confident as I went on that it has nothing whatever to add as supplement or embellishment to any sound conventional teaching course. G. R. NOAKES.

Microwave Measurements, by E. L. GINTZON. Pp. xvii + 515. (New York: McGraw-Hill, 1957.) 90*s*.

This book was planned in collaboration with the late Dr. W. W. Hansen, one of the pioneers in the subject of microwaves, and has now been written by the Director of the Microwave Section of the Hansen Laboratories at Stanford University. The emphasis is on basic measurement problems and these are covered in a most comprehensive manner.

A first impression of the volume is that it is more than a book on measurements and that it provides a reasonably complete account of the problems of microwave generation, transmission and reception. The treatment of this background material is, however, directed towards providing an appreciation of the problems which arise in measurements. The topics covered in this section include klystrons, travelling wave tubes, harmonic generators, noise generators, crystal rectifiers (including a useful account of the mechanism of rectification), bolometers, thermistors, etc. All of this material is treated at a level, well within the reach of the graduate engineer or physicist approaching the subject for the first time, and ample references are provided to the literature to lead the inquisitive reader to more advanced discussions.

The basic microwave measurements are those of power, impedance, wavelength, frequency, attenuation and the properties of resonant cavities, one or more chapters being devoted to each. In each case, the theoretical background is either given in detail or adequately summarised, and particular attention is given to points of principle such as the meaning of impedance in a waveguide. The section on the determination of the equivalent circuits of microwave junctions is particularly valuable, giving as it does a comprehensive account of the many sophisticated techniques which have been developed in recent years.

The layout of the text and the quality of the many diagrams are well up to the usual standard to be expected from this publisher. Misprints are few and not likely to cause serious trouble : the most unfortunate is in the Appendix on physical constants, where the charge/mass ratio of an electron is quoted as 1·7578 coulomb/kg !

Specialized measurements such as those of receiver and transmitter performance, aerials, and the properties of materials, and those arising in such fields as microwave spectroscopy are not specificially discussed. Since many of these measurements are basically modifications of the fundamental techniques which are examined, this is perhaps not such a serious limitation as might as first be supposed.

The stated objective of this book, the provision of a text for a first-year postgraduate course in microwave measurements, is admirably achieved. It can also be strongly recommended as a reference book for those research workers who have occasion to make detailed measurements in the microwave field. J. BROWN.

Fundamentals of Optics (3rd Edn), by F. A. JENKINS and H. E. WHITE. Pp. vii + 637. (New York, Toronto, London: McGraw-Hill.) 64*s*.

The third edition of this well-known textbook on Optics shows no increase in size over the second edition. It is, however, by no means a mere reprint with minor alterations. While many chapters have remained substantially the same, a number of topics have been given less space and new developments have been included. Typical examples are the Lummer plate and the transmission echelon which have become practically obsolete and are now only briefly mentioned while the echelle is described in some detail. Also the mathematical treatment has been improved in many ways; for example, the use of complex amplitudes in interferences has been introduced. The chapters on reflection and double refraction have been interchanged and some other minor rearrangements made.

Most of the important new developments have received some attention, but the authors have, with evident intention, kept the treatment elementary throughout and have omitted topics requiring more advanced methods. It is presumably for this reason that the treatment of the phase contrast microscope has even been shortened. In this and in other similar cases, references to fuller treatments are given.

Every writer of a textbook on optics must be tempted to drift into fields which are connected with optics but for which one would normally look in another kind of book. The authors have wisely resisted this temptation: the section on light sources and spectra has been kept short, and also photoelectricity, newly introduced in this edition, has been restricted to the essentials.

The book still consists mainly of two parts: I, Geometrical Optics, and II, Physical Optics, while the section on Quantum Optics, forming part III, is more in the nature of an appendix. Part I includes a number of new developments in geometrical optics and provides a useful, elementary introduction to the subject. The predominant use of rays is justified in an elementary book of this kind, but the primary importance of the concept of the wave surface and the merely formal, secondary nature of the ray concept might have been stressed more. The main value of the book lies in the part on Physical Optics which also occupies by far the greatest portion. The thorough understanding of the physics is always kept in the foreground, and mathematical detail takes a second, very minor place. Numerous excellent illustrations contribute to this general note of reality. The student, after having read the book, should be able to carry out actual experiments, not only to solve some numerical questions.

In the paragraphs on diffraction, the authors might have stressed that the diffraction pattern due to a single aperture is always of the Fraunhofer type when it is not observed in the image plane, not only when the light is parallel. This would have helped the student in the subsequent application to the resolving power of the microscope. There are only very few points of stress and detail where the reviewer hopes for still further improvement in a future fourth edition, and they do not affect his opinion of the book as a whole, both with regard to the choice of material and the treatment, that this is essentially the right way of teaching optics in an Honours course of Physics. This third edition, so well brought up to date and improved in many details, should retain for the book its leading place among University textbooks on optics. H. G. K.

Electricity and Magnetism, by B. I. BLEANEY and B. BLEANEY. Pp. xiv + 676. (Oxford: University Press, 1957.) 63*s*.

The authors have undertaken the formidable task of writing a new textbook on electricity and magnetism, suitable for honours undergraduate and also postgraduate students, which should not only cover the phenomenological, classical and the atomic, quantum theory of the electromagnetic phenomena but also give a fairly detailed and up-to-date account of experimental methods and techniques, their applications and results. They have, on the whole, succeeded to a remarkable degree. The text is written lucidly and in excellent scientific language, the mathematical arguments are presented concisely and are easy to follow, and there is a great number of clear diagrams and tables. The book is beautifully printed.

The first part of the book deals with classical electromagnetic theory on more or less traditional lines, but also contains very useful modern chapters on filters, transmission lines and wave-guides. The second part is mainly of an experimental nature, dealing with electromagnetic machinery, radio and methods of measurement. The third part is devoted to atomic theory of electromagnetic phenomena and contains chapters on fluctuations, theory of dielectrics, conduction in solids, magnetism and magnetic resonance.

The m.k.s. system is used throughout but not adhered to pedantically, and for the benefit of those readers who prefer the traditional systems of units a final chapter is added in which the translations of the equations from the m.k.s. into the c.g.s. system can be found.

A particularly valuable feature of the book is the large collection of 'problems' which not only gives the student the opportunity to apply the general theory to special, useful examples, but also makes it possible to deal with a considerable amount of detail without overburdening the text.

No more than elementary knowledge of quantum theory is demanded from the reader although extensive use of quantum-mechanical considerations is made in part 3 of the book, the necessary information being given here and there, whenever it is just required. This does not seem to be a very good procedure, and it would probably be better to devote a special short chapter to the elements of quantum theory to which reference could be made.

It is, of course, only right that the newest and most reliable experimental methods should always be described. But this ought not to prevent the authors from at least mentioning the pioneer work of previous investigators with reference to their original publications. I could, by the way, not find any reference to the fundamental work on resonance phenomena by B. Bleaney himself and his collaborators. A separate name index would be a useful addition.

A book of this type can naturally not cover all aspects of the field but the authors may consider whether it would not be possible to incorporate some of the following items in a future edition without unduly increasing its size. Theoretical subjects: The notion of electromagnetic momentum and Maxwell stresses; the Lorentz–Maxwell equations, their invariance against Lorentz transformations, and the derivation of the phenomenological Maxwell equations from them; the notion of 'Brillouin zones', the thermomagnetic effect in paramagnetic substances. Experimental subjects: The measurement of dielectric constants of electrolytes, accumulators, metal rectifiers, electrostatic generators.

R. FÜRTH.

Annual Review of Nuclear Science, Vol. 7, 1957, edited by J. G. BECKERLEY. Pp. v + 496. (Palo Alto, Calif.: Annual Review Inc. 1957.) $7.50.

The seventh volume of this Annual Review follows the usual, rather odd, pattern. It consists of twelve articles, about half of which are highbrow reviews of current advances in nuclear physics, some involving considerable knowledge of theoretical physics. The other half of the articles are on radiochemistry and radiobiology. It is rather difficult to see how the two halves can both appeal to the same reader. At any rate, I myself am not able to judge the biological articles.

But, having said this, I hasten to add that the physics articles are excellent. The preface says " The present volume begins with mesons and ends with mesons ". The ' beginning ' is an article by J. Rainwater on ' Mu-meson Physics '. This is a useful compilation of the known properties of these particles, including a discussion of Alvarez's mu-induced fission, of parity non-conservation in π–μ–e decay, of mu-mesonic atoms, etc. There is nothing fundamentally new to help us to understand the mu-meson problem. The ' end ' is an extremely comprehensive article by Gell-Mann and Rosenfeld entitled ' Hyperons and Heavy Mesons (systematics and decay) '. This builds up, as far as it is possible at present, a coherent description of the known properties of particles, including not only strange particles, but also pions and muons. For instance the π–μ–e decay problem is considered in more detail than in the Rainwater article. The methods used for ordinary mesons are then extended to the strange particles. This is certainly a very important article for anyone working in meson or strange particle physics.

In between the meson articles, there is a comprehensive account by Hofstadter on his very beautiful experiments using high energy electron beams to explore the structures of nuclei. There are also articles by Villars on ' The Collective Model of Nuclei ', by Lindenbaum on ' Collision of $\leqslant 1$ GEV Particles (Excluding Electrons and Photons) with Nuclei ', a rather clumsily worded title for a very useful article, and by Nierenberg on ' The measurement of Nuclear Spins and Static Moments of Radioactive Isotopes ', as well as the non-physics articles.

H. W. B. SKINNER.

Zirconium (*Metallurgy of the Rarer Metals*, 2) 2nd. edn., by G. L. MILLER. Pp. xxi + 548. (London: Butterworths Scientific Publications, 1957.) 70*s*.

With the rapid development in metallurgy there is a continuing need for authoritative reference books giving up-to-date information. The study of the rarer metals is being served in this respect by a series of monographs, which includes the volume under review. This is a second edition of Dr. Miller's monograph on zirconium following only three years after the first. Contributing significantly to the flow of published information on zirconium during this period has been much which at the time of writing of the first edition was classified, but has since become available for general reference. Dr. Miller points out that he has been able, in this second edition " to replace, in many instances, doubtful information by well authenticated results ", and recent developments in zirconium technology are also described.

The monograph covers the whole field of zirconium metallurgy from the occurrence and extraction of the metal to the physical metallurgy and fabrication technology. The latter two aspects together occupy the major portion of the volume.

In the first part of the book there are chapters dealing with such subjects as the occurrence of zirconium, the uses of the metal and its alloys and compounds, extraction from the ore, the separation of zirconium and hafnium, commercial production of zirconium and production development.

The section devoted to physical metallurgy has been expanded considerably as compared with the first edition. There is a comprehensive survey of the literature on the physical and structural properties of zirconium, and the available information on the mechanical properties of zirconium and its alloys is fully reviewed. Studies of the reactions with the common gases, and with various corrosive media are of great practical importance and these are described in considerable detail, including much recently published information, e.g. on ' breakaway ' corrosion and corrosion by liquid metals. The alloying behaviour of zirconium is discussed from theoretical considerations, and the binary phase diagrams which have so far been determined are presented and described.

There follow chapters on fabrication technology in which melting practices and mechanical working, joining, and powder metallurgy processes are described. Much valuable practical information is given. In particular, the subject of melting practice is considered in detail, with new information made available since the first edition. The concluding chapter deals with the production and properties of some special zirconium compounds, namely, the nitride, carbide, boride and silicides. There is an appendix describing metallographic procedures for zirconium and its alloys.

Throughout the monograph the information is presented with the aid of tables and diagrams, and each chapter has a full bibliography : a general subject index is also provided.

The monograph will be of great value to all who are especially concerned with zirconium metallurgy, and will also prove of general interest to a wider circle of readers. D. R. F. WEST.

Molecular Physics, edited by H. C. LONGUET-HIGGINS, Vol. 1, No. 1, Jan. 1958. Pp. 98. (London : Taylor and Francis, 1958.) 25*s*. (£4 15*s*. per volume of four issues.)

This is a new journal, under the editorship of Professor H. C. Longuet-Higgins of Cambridge, and concerned with all aspects of molecular physics. A first question is whether any new journal is needed : but a glance at the present issue, containing research papers in molecular structure and dipole moments, nuclear magnetic resonance, pressure-induced rotational absorption in H_2, irreversible processes in quantum mechanics, and the statistical thermodynamics of mixtures and energy transport, is sufficient to show how wide is this field ; further, there is no recognized journal where all this material would naturally appear together except the American *Journal of Chemical Physics*. It has long been felt that a preponderantly European parallel to this latter journal would serve a useful purpose. Professor Longuet-Higgins and his associate editor Dr. J. H. van der Waals of Amsterdam are to be congratulated on an excellent start. C. A. COULSON.

On Nuclear Energy: Its Potential for Peacetime Uses, by D. J. HUGHES. Pp. xi + 263. (Harvard : University Press ; London : Oxford University Press, 1958.) 30*s*.

Dr. Hughes has given us a comprehensive survey of the whole problem of nuclear energy. From the basic nuclear physics and its use in the development of power stations, both fission and fusion, he takes us via the uses of radio-isotopes in research, industry and medicine, and the genetic effects of radiation, to the rights of individuals, the safety of nations, and international control and co-operation. In all these fields, and many more, he writes with supreme confidence. He is at pains to explain to the more thoughtful American layman that, in spite of the notable achievements of other nations, the United States remains sufficiently in the lead to justify the huge sums spent on the taxpayers' behalf by the U.S.A.E.C. There is actually a vast amount of easily digestible information here for the layman. It is only a pity that it must have been written in such a hurry, with so much enthusiastic repetition, and often with too hasty judgments on the programmes of other nations, based on incomplete information gleaned in fleeting visits rather than from documentary information available at the time of writing. For example, one learns that the whole British nuclear power programme is being carried through—in contrast to the United States programme—by nationalized industry, whereas in fact a large part is now being borne by private industry. No attempt is made to relate national effort to national income. We learn that the British go-it-alone policy may have arisen from national pride : no mention here that the fruitful wartime partnership between the United States and the Commonwealth was abruptly terminated at the end of the war. On the other hand, powerful arguments are presented for the need of continual declassification and increased freedom of communication between the scientists of all nations. Particularly telling is the argument that at Geneva the Russians lagged most in the fields which only they had continued to hold classified. In the fields in which he is an acknowledged expert, Dr. Hughes has given us a book containing many good things. In the fields in which he is not perhaps so expert, we find a greater naïvety than the Foreword by Admiral Strauss would lead us to expect. B. H. FLOWERS.

Nuclear Masses and their Determination, edited by H. HINTENBERGER. Pp. ix + 267. (London: Pergamon Press, 1957). 84*s*.

The proceedings of the conference on the determination of atomic nuclear masses held in July 1956 at the Max-Planck Institute for Chemistry in Mainz have been published as a book edited by Professor Hintenberger. The data which are presented were determined by mass spectrometry, by microwave spectroscopy, by the measurement of *Q*-values (i.e. the energies released in nuclear reactions) or from disintegration energies as measured by beta- and gamma-ray spectra. By discussing the discrepancies between the results of these four methods, the conference aimed to speed the day when the physicist will have at his disposal " a table of masses which will have the stability of, say, the table of the general physical constants, and the accuracy required for its use in many fields ". (The quotation is from K. T. Bainbridge's introductory paper.)

Although this book consists of a series of papers by experts for experts, the non-expert will not be discouraged if he starts by reading Professor Bainbridge's introduction and follows this with Professor W. W. Beuchner's article ' The Determination of Nuclear *Q*-values '. The section on instruments should be digested by all designers, constructors and users of mass spectrometers.

The book is very well produced and the diagrams reach a high standard of clarity. At a price of four guineas, it should appeal to the well-to-do physicist.

A. H. TURNBULL.

Zum Weltbild der Physik, 7th Edn, by C. F. VON WEIZSÄCKER. Pp. 378. (Stuttgart: S. Hirzel Verlag, 1958.) DM. 14.70.

It has been very noticeable since the war that philosophy is a totally different subject in Great Britain and on the Continent, and this book serves to underline this. Ostwald said " The name Natural Philosophy, with which I have endeavoured to designate the content of our present talks, has a very bad reputation". He goes on to quote Liebig as saying " I, too, have lived through this period, so rich in words and ideas and so poor in true knowledge and proper studies; it has cost me two valuable years of my life; I cannot describe the shock and the horror, when I awoke to consciousness from this trance ". Such is the effect of this book, at least on the reviewer. There are chapters on the foundations of quantum mechanics from a philosophical point of view which do not seem very closely related to quantum mechanics as understood in the laboratory. There is a chapter on the infinite nature of the world, relating the geometrical infinity to the difficulties in the foundations of mathematics—not in a very convincing manner; but the sort of essay which leaves one most surprised is that which relates quantum mechanics to Kant, and even more that which relates theoretical physics to Heidegger's thoughts. It will, perhaps, serve to give an idea of the book if we quote from an introduction which appears at the end. We are told that modern physics concerns itself not only with space, time and causality, but also with the sense of the word ' being ', and so in analysing quantum mechanics we are dealing already with an ontological problem.

C. W. KILMISTER.

Handbuch der Physik, Vol. L, *Astrophysics I*, edited by S. Flügge. Pp. vii + 458. (Berlin: Springer, 1958.) 98 DM.

The 50th volume of the well-known *Handbuch der Physik*, just off the press, has been set apart by its editors for an outline of the astrophysics of stellar surface phenomena and double-star astronomy. The contents of the major part of this volume, dedicated to stellar atmospheres and semi-transparent layers, consist of seven separate contributions presenting a comprehensive and up-to-date account of such topics as stellar classification (Fehrenbach and Keenan), molecular spectra in the stars (Swings), the spectra of white dwarfs (Greenstein), of planetary nebulae (Wurm), together with an outline of the general theory of the physical processes operative in stellar atmospheres by D. Barbier. All these contributions are well written as well as illustrated, and their high standard bespeaks the wisdom of the editors in the choice of their collaborators.

The contributions dealing with the double stars have, alas, not fared equally well. The chapter on visual binaries by P. v. d. Kamp is clear and concise, but errs on the side of brevity; that on spectroscopic binaries (Struve and Huang) is eclectic and rather speculative—features which might be commendable in an original publication, but are perhaps not quite fair to the reader of a survey presentation. The section on eclipsing binaries from the pen of S. Gaposchkin of Harvard is, unfortunately, sufficient to mar the level of the whole volume. Suffice it to say that the surrealist illustrations with which the reader is served on pp. 238 or 241 are (in the best of surrealist tradition) the outgrowth of the author's pure imagination untarnished with any touch of reality; and the material of Table 1 (pp. 228–232), claimed to be based largely on Gaposchkin's own work, looks it.

Apart from this single real and hardly excusable blemish, the volume under review represents without doubt a worth-while addition to the current astronomical literature. The external appearance of the volume is up to the well-known high standards of all Springer publications, its only defect being a relatively high price.

Z. KOPAL.

White Dwarfs, by E. Schatzman. Pp. 180. (Amsterdam: North-Holland Publishing Company, 1958.) 19 guilders.

The present monograph on the physics of degenerate-gas configurations and its application to the stars in the white-dwarf stage, which appeared as the second volume of a new Series in Astrophysics inaugurated recently by the North-Holland Publishing Company in Amsterdam, represents indeed a welcome addition to the current astronomical literature. The physics of white dwarfs—those shadowy degenerate denizens of the stellar graveyard deep below the Main Sequence—have kept intriguing astronomers and physicists alike since the discovery of the first such object in 1910; yet in spite of a widespread interest in their study, their field has not so far received monographic treatment in any language.

The present book by Evry Schatzman of the University of Paris meets this need in a very satisfactory manner: in 180 pages of his text the author surveys all salient features of the observational evidence pertaining to white dwarfs and fully develops the theoretical aspects of their significance. Of particular interest is the author's account of the vibrational stability of white dwarfs which, it is to be hoped, may soon be extended to cover the stability criteria—not only with respect to radial pulsations, but to non-radial oscillations as well. The presentation throughout is comprehensive and easy to follow; every student of its subject should find it an invaluable help.

The volume is attractively published and reasonably priced. Both its author and the publishers deserve our appreciation for providing us with this timely and useful contribution to the existing astronomical literature. Z. KOPAL.

Elements of Pulse Circuits, by F. J. M. FARLEY. Pp. viii + 143. (London : Methuen, 1956.) 8*s.* 6*d.*

This is a Methuen Monograph; it contains seven chapters, entitled : Basic Concepts, Fundamental Valve Circuits, Square Wave Generators, Trigger Circuits, Time Bases, Pulse Amplifiers, and Applications.

The first deals with concepts particularly important in the field of pulse circuits, such as differentiation, integration and output impedance. The treatment is without use of Laplace transforms; in the reviewer's opinion this is an advantage. There is a separate section entitled " current flows *through* a condenser ". This is a courageous step; there are many who do not fully understand the fact! It is presumably due to the usual introduction to the concept of condensers in the teaching of electrostatics. In the section on Thévenin's theorem, a statement appears that output impedance is usually resistive; the reviewer feels this might mislead.

The choice of circuits whose operation is explained in the following chapters is very good. In the confined space available almost all the important valve circuits, which form the bricks of which pulse circuits are built, are explained. The descriptions are very lucid, well illustrated by circuit diagrams and wave-forms, and there are no complicated mathematical analyses. Regrettably there is no mention of transmission lines as pulse-forming networks; it is to be hoped that this may be included in future editions.

A very useful section on the limitations of linear equivalent circuits, where finite amplitudes are handled, appears in the chapter on amplifiers.

This monograph should be a useful addition to the library of the physicist who handles or designs pulse circuits. A. FOLKIERSKI.

Figure 1.

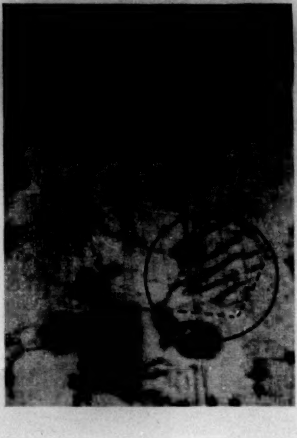

Figure 2 (*a*).

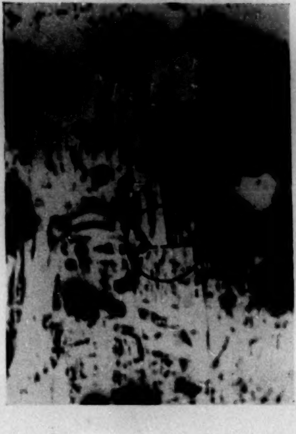

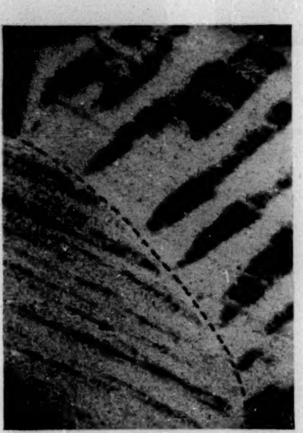

Figure 2 (*b*).

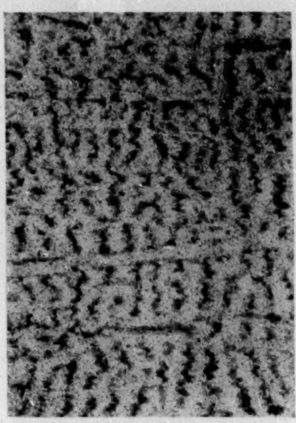

Figure 3.

Figure 1. Optical examination of manganese zinc ferrite, polished with 0000 emery. Domain walls across a crystallite (encircled); note that grain boundaries are denoted by colloid where the magnetic divergence is greatest and outlined by broken lines elsewhere. (× 375).

Figure 2. (*a*) Optical examination of manganese zinc ferrite polished with 0000 emery, small normal field applied. Domain bands lying across several crystallites, outlined by broken lines, mainly perpendicular to grinding direction (× 375). (*b*) Electron micrograph of similar region to encircled portion of (*a*); small normal field. Right-hand side shows heavy band deposits; on the left-hand crystallite only scratches are seen. Arrow indicates direction of polishing (× 2700).

Figure 3. Electron micrograph of second type of pattern on a manganese zinc ferrite. Fine system of zigzag domains perpendicular to grinding direction. Small normal field (× 4125).

Plate I

Figure 4.

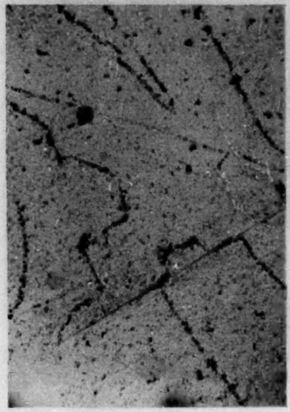

Figure 5.

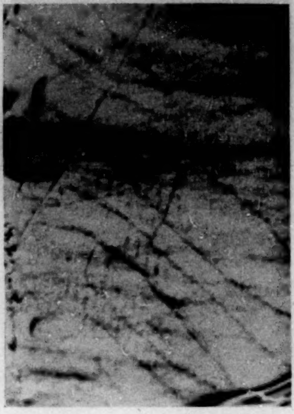

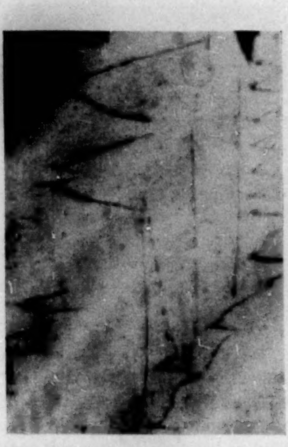

Figure 6.

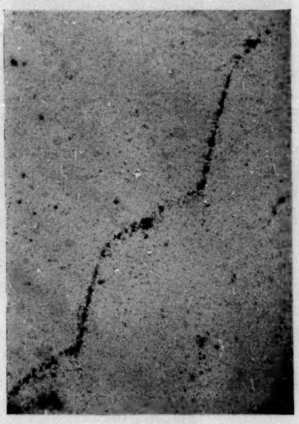

Figure 7.

Figure 4. Electron micrograph of lightly etched surface of manganese zinc ferrite showing wriggly boundaries, small normal field (× 3375).

Figure 5. Optical examination of manganese ferrite single crystal lightly etched surface showing wriggly boundaries, small normal field (× 375).

Figure 6. Optical examination of manganese ferrite single crystal, well etched surface, 180° domain wall running from bottom right to top left. Note tree patterns, small normal field (× 375).

Figure 7. Electron micrograph of manganese ferrite single crystal. Stepped domain wall consisting of 180° and 109° walls. Small normal field (× 2625).

Plate II

Figure 3. Photographs of the ' real ' and ' virtual ' fringes for the three arrangements of figure 1. (*a*) ' real '; $a=-9{\cdot}85$ cm, $b=6{\cdot}2$ cm. (*b*) ' virtual '; $a=-6{\cdot}4$ cm, $b=-4{\cdot}9$ cm. (*c*) ' virtual ' ; $a=-6{\cdot}9$ cm, $b=-9{\cdot}4$ cm. In all cases $\lambda=5461$ Å.

The Photodisintegration of Potassium by ^{7}Li(p, γ) Radiation

By T. R. OPHEL

Research School of Physical Sciences, Australian National University, Canberra

Communicated by Professor E. W. Titterton; MS. received 19th March 1958

Abstract. The proton spectrum of the reaction ^{39}K(γ, p) has been obtained at 17·6 MeV. Transitions to known levels in ^{38}A at 2·16 and 3·75 MeV were identified and proton groups of energies as low as 2 MeV were resolved, corresponding to levels in ^{38}A at 4·3, 5·0, 5·4, 6·3, 6·6, 7·3 and 7·85 MeV.

The total (γ, p) cross section for the reaction at 17·6 MeV is found to be in excess of 11 mbn.

§ 1. INTRODUCTION

PHOTOPROTON spectra arising from the photodisintegration by bremsstrahlung radiation of a number of the middle-weight nuclei have been obtained (reviewed by Titterton 1955), but only three (γ, p) reactions in this region, viz. ^{40}A(γ, p) (Wilkinson and Carver 1951), Cu(γ, p) (Chastel 1956) and ^{127}I(γ, p) (Ophel and Wright 1958, to be referred to as I), have been observed using monochromatic radiation. Measurements made with monochromatic gamma rays provide information concerning photonuclear reactions which is not easily obtainable with bremsstrahlung, but the irradiation of thin foil targets, the technique most commonly employed with bremsstrahlung, is not normally practicable since only low intensity gamma-ray fluxes are attainable from particle reactions.

The present work investigates, at a gamma-ray energy of 17·6 MeV, the reaction ^{39}K(γ, p) in thallium-activated potassium iodide using the technique employed by Ophel and Wright (I) whereby the phosphor detects photoprotons produced within its volume.

§ 2. EXPERIMENTAL METHOD

The apparatus and experimental procedure were essentially the same as those described in I. Gamma rays from the ^{7}Li(p, γ) reaction, produced at a proton bombarding energy of 500 keV with a thick lithium metal target, were used for the experiment, the radiation being monitored with a thick-walled brass Geiger counter (Barnes *et al.* 1952).

A small thin potassium iodide crystal was mounted on a Perspex disc with Ciba Araldite and covered with aluminium foil (1·5 mg cm^{-2}) to improve light collection at the photocathode. Pulses from the photomultiplier (EMI type 6097B) and the associated cathode follower were amplified with a linear amplifier and analysed with a Hutchinson–Scarrott type multichannel analyser. As before, a constant check on the stability of the total gain of the system was maintained with a (ThC + ThC′) alpha-particle source mounted behind a polythene shutter.

Polythene, of a sufficient thickness to stop protons of energy less than 10 Mev, surrounded the crystal, so that protons produced externally would not be detected. No high-energy protons can be produced in the polythene since the threshold of the $^{12}C(\gamma, p)$ reaction is 15·95 Mev.

Protons from the $^{10}B(d, p)$ reaction were used to calibrate the spectrometer, the number of proton energies which served as calibration points being increased by means of aluminium absorber foils of thicknesses 5·5, 20·0, 48·4 and 91·3 mg cm^{-2} which were interposed between the boron target and the crystal. The calibration chamber and procedure have been fully described in I.

§ 3. Results

The spectra (each representing a summation of a number of individual runs of approximately 30 minutes duration) listed in table 1 were recorded with resonance radiation.

Table 1

Fig. No.	Crystal dimensions	Energy region examined
1	¼″ × ¼″ × 0·030″	3·5– 12 Mev
2	¼″ × ¼″ × 0·030″	5·0–8·5 Mev
3	¼″ × ¼″ × 0·030″	2·5– 12 Mev

The energy calibration of the spectra in figures 1 and 2 was obtained from two calibration runs, one of which is shown in figure 3. The energies of the groups as determined from the two calibrations are listed in table 2, the experimental error being estimated at less than ±0·1 Mev between 3 and 8·8 Mev. The calibration of the spectra in figures 1 and 2 was made by assuming a linear relationship between energy and channel number and using the measured energies of the appropriate groups (in the region 3–8·8 Mev) to fix the straight line.

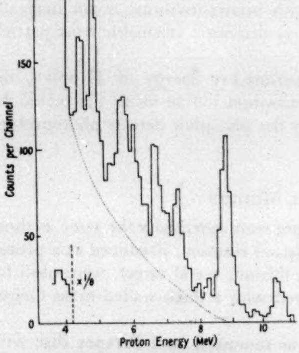

Figure 1. Spectrum for crystal ¼ in. × ¼ in. × 0·030 in.

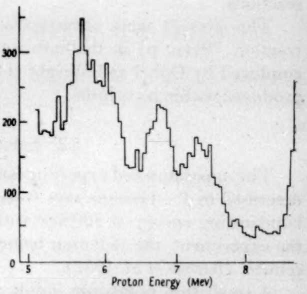

Figure 2. Spectrum showing detail between 5 and 8 Mev.

All of the groups listed in table 2 are clearly identifiable with the exception of the group at 6·06 Mev (figures 1 and 3), but the expanded spectrum of figure 2 supports the existence of a group at this energy.

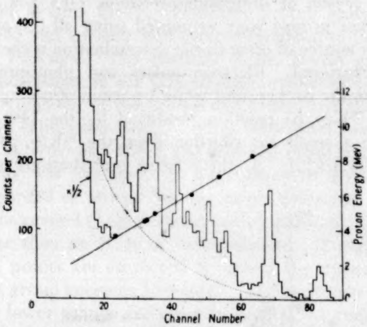

Figure 3. ^{39}K(γ, p) spectrum and proton calibration curve.

Some spectra (not given) were recorded with crystals of dimensions $\frac{1}{16}$ in. × $\frac{1}{16}$ in. × 0·010 in. and $\frac{1}{8}$ in. × $\frac{1}{8}$ in. × 0·010 in. and though interpretation of these spectra is doubtful because of the poor statistics and the large escape losses from the highest energy groups, they tend to confirm the possible group at 2·5 Mev which appears as a shoulder on the electron edge in figure 3 and indicate further proton groups down to and even below 2 Mev.

Table 2†

Group energy	10·5	8·81	7·33	6·75	6·06	5·70	4·78	4·55	3·8	3·3
Excitation of ^{38}A	0	2·16	3·75	4·3	5·0	5·4	6·3	6·6	7·3	7·85
Cross section (mbn)	0·9	2·4	1·0	1·4	2·4		1·2	0·5	1·3	0·3

† The group at 2·5 Mev (see text) corresponding to a level at 8·6 Mev is not included in table 2.

The spectra listed in table 1 will contain photoprotons from both the narrow 17·6 Mev line and the broad 14·8 Mev line of the ^{7}Li(p, γ) radiation. Thus the observed sharp groups can be attributed to either absorption of the 17·6 Mev line or selective absorption of the broad 14·8 Mev component into narrow levels of ^{39}K.

In order to allow identification of the proton groups, a spectrum was obtained with non-resonant ^{7}Li(p, γ) radiation at a proton bombarding energy of 760 kev with a target 150 kev thick (I). The non-resonance spectrum, along with a resonance spectrum produced under identical geometrical conditions with a total gamma ray flux approximately 1·6 times as great, is given in figure 4. So far as the low energy groups may be identified, each displays an upward energy displacement relative to the corresponding group of the resonance spectrum and there is no indication of an increase in magnitude of any one of the groups.

Consequently, all groups are attributed to transitions induced by 17·6 MeV radiation. The corresponding excitation energies of the residual ^{38}A nucleus for these transitions are listed in table 2 (see § 4).

The cross section of the 8·8 MeV group was established with a well-defined geometry using a crystal of dimensions 0·516 in. × 0·531 in. × 0·048 in. Cross sections for the other groups were estimated using all the appropriate spectra available. A major source of error in the determination is the uncertainty of the nature of the background. Electron pulses and photoprotons from iodine contribute in part to the background while a portion of it could comprise photoprotons from the ^{39}K(γ, p) reaction produced by the 14·8 MeV gamma rays. There will also be a small contribution from the ^{41}K(γ, p) reaction (relative abundance of ^{41}K is 6·5%). As the relative contributions of the four sources are unknown, a smooth background was assumed (see figures 1 and 3) and, as a result, the estimated cross sections may be considerably in error. Loss corrections were made assuming isotropic angular distributions and using proton ranges in potassium iodide of 0·036 in. ($E_p = 10{\cdot}8$ MeV), 0·026 in. (8·8), 0·019 in. (7·3), 0·017 in. (6·7), 0·013 in. (5·7), 0·010 in. (4·78), 0·009 in. (4·55) and 0·006 in. (3·8). A correction was also made for the isotopic composition of natural potassium iodide (White, Collins and Rourke 1956). The error in determining the cross section of the 8·8 MeV group is estimated at ± 20% giving a result of 2·4 ± 0·5 mbn.

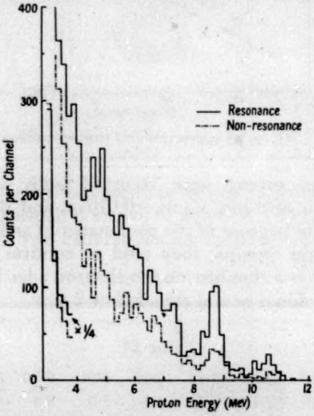

Figure 4. Spectra obtained with resonance and non-resonance radiation (without normalization to the same gamma-ray flux; see text). Crystal size ¼ in. × ¼ in. × 0·030 in. and non-resonance running time 9·5 hours.

The gamma-ray flux was measured with a thick-walled brass Geiger counter of the type described by Barnes *et al.* (1952) using the reported sensitivity of 2·66 counts/quantum/cm^2 for 17·6 MeV gamma rays and 2·1 counts/quantum/cm^2 for 14·8 MeV gamma rays and a relative gamma-ray intensity of 1·7 for resonance radiation (Stearns and McDaniel 1951).

§ 4. DISCUSSION

Endt and Braams (1957) give a Q value of $-6{\cdot}389$ MeV for the ^{39}K(γ, p) reaction on the basis of the observed ^{39}K(γ, n)^{38}K threshold and the energy release in ^{38}K(β^+)^{38}A. Excited states in ^{38}A have been established at 2·16 and 3·75 MeV (Endt and Braams 1957). Therefore proton groups would be anticipated at 10·95, 8·85 and 7·3 MeV, and these correspond to the observed groups at 10·5, 8·81 and 7·33 MeV. The energies of the lowest groups are in good agreement; the discrepancy in the ground-state transition energy may arise as a result of the extrapolation of the proton calibration line almost 2 MeV beyond the highest energy calibration point. When this work was carried out, the Q value was taken as $-6{\cdot}5$ MeV (Endt and Kluyver 1954) so that the anticipated ground state energy was 10·8 MeV. A discrepancy of 0·3 MeV in this energy region was not regarded as serious but the larger difference of 0·45 MeV which arises from using the revised Q value would seem to indicate a non-linearity of the energy scale rather than an error of extrapolation. If only the four highest energy calibration points are employed to define the upper scale, the energy of the ground state group becomes 10·9 MeV. The excitation levels in ^{38}A which correspond to the lower groups are given in table 2. Levels at approximately 5·0 and 6·7 MeV have been reported by Towle, Berenbaum and Matthews (1957). They obtained gamma-ray spectra of the ^{37}Cl(p, γ) reaction at the 1070, 1135, 1533 and 1725 kev resonances, and identified gamma-ray transitions corresponding to levels at 5·0 and 6·7 MeV. These two levels are presumably the levels at 5·0 and 6·6 MeV established by the present experiment.

The total (γ, p) cross section for the ^{39}K(γ, p) reaction at 17·6 MeV is larger than 11 mbn, whereas the ^{39}K(γ, n) cross section at 17·6 MeV has been measured as 5·4 ± 1·4 mbn (Wäffler and Hirzel 1948) and 9 mbn (McDaniel, Walker and Stearns 1950), but the larger proton yield is possible without assuming some direct interaction since the proton threshold is 7 MeV lower than the neutron threshold.

ACKNOWLEDGMENTS

Thanks are due to Mr. N. F. Bowkett for operation and maintenance of the accelerator and to Mr. H. Owen for construction of apparatus.

REFERENCES

BARNES, C. A., CARVER, J. H., STAFFORD, G. H., and WILKINSON, D. H., 1952, *Phys. Rev.*, **86,** 359.
CHASTEL, R., 1956, *J. Phys. Radium*, **17,** 518.
ENDT, P. M., and BRAAMS, C. M., 1957, *Rev. Mod. Phys.*, **29,** 683.
ENDT, P. M., and KLUYVER, J. C., 1954, *Rev. Mod. Phys.*, **26,** 95.
MCDANIEL, B. D., WALKER, R. L., and STEARNS, M. B., 1950, *Phys. Rev.*, **80,** 807.
OPHEL, T. R., and WRIGHT, I. F., 1958, *Proc. Phys. Soc.*, **71,** 389.
STEARNS, M. B., and MCDANIEL, B. D., 1951, *Phys. Rev.*, **82,** 450.
TITTERTON, E. W., 1955, *Progress in Nuclear Physics*, **4,** 1.
TOWLE, J. H., BERENBAUM, R., and MATTHEWS, J. H., 1957, *Proc. Phys. Soc.*, **70,** 84.
WÄFFLER, H., and HIRZEL, O., 1948, *Helv. Phys. Acta*, **21,** 200.
WHITE, F. A., COLLINS, T. L., and ROURKE, F. M., 1956, *Phys. Rev.*, **101,** 1786.
WILKINSON, D. H., and CARVER, J. H., 1951, *Phys. Rev.*, **83,** 466 (L).

Some Consequences of the Compound Ion Model

By E. BARANGER and E. GERJUOY†

University of Pittsburgh and Westinghouse Research Laboratory, Pittsburgh, Pennsylvania

MS. received 14*th April* 1958

Abstract. Cross sections for excitation of atomic levels by electrons often vary sharply with energy near threshold, as if resonating with a state of the compound ion. Some consequences of this 'compound ion model' of excitation are explored. In particular it is shown that information bearing on the validity of the model can be obtained from measurements of the angular distribution and polarization of the light emitted following excitation to radiating states. Possible applications to mercury and to helium are discussed.

§ 1. Introduction

Cross sections for excitation of atomic levels by electrons often vary sharply with energy near threshold, as if passing through one or more resonances (Meier-Leibnitz 1935, Dorrestein 1942, Smit and Jongerius 1955, Jongerius, Van Egmond and Smit 1956, Schulz and Fox 1957). The similar energy dependence of nuclear excitation cross sections is customarily regarded as evidence favouring the 'compound nucleus model'. In fact the cross section (Schulz and Fox 1957) for electron excitation of the $2^3S_1(1s, 2s)$ metastable level of atomic He can be fitted (Baranger and Gerjuoy 1957) by the one-level Breit–Wigner formula, with the peak at about 0·6 ev above threshold supposedly resulting from resonance with a compound $^2S_{1/2}$ state of He^-.

Such resonating states of the compound ion temporarily capture and emit electrons by radiationless processes akin to autoionization; autoionization lifetimes (Burhop 1952) in neutral atoms suggest that the ionic level widths are not likely to be much smaller than the level spacing. We anticipate therefore that only under specially favourable circumstances will atomic excitation functions show pronounced resonant structure and be well represented by one-level or two-level Breit–Wigner expressions, because at most energies more than one or two levels of the compound ion will make appreciable contributions to the excitation cross section. On the other hand we recognize that the one-level Breit–Wigner formula (and certainly the two-level formula) contains a number of parameters which can be adjusted to yield approximate fits to a wide variety of curves. For these reasons, despite the result (Baranger and Gerjuoy 1957) for the He $^3S_1$ metastable, we are far from convinced that a 'compound ion model' of electron excitation has any basis in reality, nor would we be convinced by similar results, using one-level or two-level Breit–Wigner formulae, for other levels of He and for other atoms. Belief in the compound model for nuclear reactions is not based solely on our ability to fit individual peaks in excitation functions with the Breit–Wigner formula. Our confidence in the compound nucleus model stems instead from the many instances wherein resonances and angular distributions in a number of nuclear reactions, involving a variety of bombarding particles and final end products, are accounted for by the economical postulate of a single intermediate compound level.

---

† Now at John Jay Hopkins Laboratory for Pure and Applied Science, General Atomic Division of General Dynamics Corporation, San Diego, California.

Confirmation of the validity or approximate validity of the compound model near excitation thresholds would have considerable import for our general understanding of electron collision processes; stimulation of experimental interest in testing the model is the primary intent of this paper. Unfortunately, the experimental possibilities for demonstrating resonances in several reactions at energies corresponding to the same intermediate compound level seem more restricted in the atomic than in the nuclear case, because (i) only a pair of bombarding particles† is available for reaching states of the compound ion X^-, namely electrons incident on the normal or excited neutral atom X; and (ii) the atomic excitation curves show structure near threshold only, which empirical fact further limits the number of useful reactions. In He for example, where apparently (Schulz and Fox 1957, Frost and Phelps 1957) there is structure in the $2\,{}^1S_0(1s, 2s)$ metastable excitation function as well as in the $2\,{}^3S_1$ metastable excitation function: (i) the data are not good enough to decide whether or not the $2\,{}^3S_1$ cross section shows structure at the $2\,{}^1S_0$ excitation function maximum; (ii) the incident electron energy required for ionization of normal helium, or of helium metastable atoms, is too high to correspond to these excitation peaks; (iii) excitation, elastic scattering and de-excitation of He metastable atoms must be measured at very low incident electron energies, in order that such measurements bear on the compound ion explanation of the curves for electron excitation of normal He. Moreover, while corresponding structure in different reactions is strong evidence for the reality of compound resonances, failure to observe such structure is less conclusive. In He the reported elastic cross section is structureless (Massey and Burhop 1952), a result which is understandable in view of the poor energy resolution of the measurements, but which also is explicable by a small partial width (Baranger and Gerjuoy 1957) for breakup (of the hypothesized ${}^2S_{1/2}$ compound state of He^-) into an electron and a neutral He atom in its ground ${}^1S_0$ state.

Searching for corresponding structure in different reactions is not the only way to test the compound model. To illustrate alternative means of drawing inferences concerning the validity of the model, we have computed, for a number of special cases, the expected relative populations in magnetic sublevels of radiating states following electron excitation; the experiments we envisage are measurements of the angular distributions and polarizations of the radiated light, with apparatus resembling those used by Skinner and Appleyard (1927) and by Smit (1935). Since the inelastically scattered electrons are very slow at the excitation peaks near threshold, it is pointless to measure their angular distribution, which will be isotropic on any model. These computations, and the predicted angular distributions and polarizations in the special cases examined, are described in the next (final) section, which embodies a discussion of the contrasting physical assumptions implicit in the compound ion model and in the more customary 'direct interaction model'. Near threshold the measured polarization (Lamb 1957, Lamb and Maiman 1957) of the He $3^3P \to 2^3S$(3889 Å) radiation does not agree with computations based on the direct model; explanations of these data, as well as of polarization measurements (Skinner and Appleyard 1927) in Hg, are suggested by the compound ion model. The point to be noted is that such explanations are consistent with the direct model, but do not readily come to mind in conventional calculations of excitation cross sections. We realize that the good energy resolution required to resolve the excitation function peaks implies low intensities, and therefore that accurate determinations of the populations in different magnetic sub-levels may demand more refined techniques than those we have subsumed, but we emphasize that the data would have to be improved, and the validity of the compound model better established, before we should take these suggested explanations seriously.

---

† For completeness we mention also photodetachment (the inverse of radiative capture) in which the bombarding particles are photons incident on stable states of the negative ion X^-.

§ 2. RELATIVE POPULATION OF SUB-LEVELS

We denote by j, m respectively the angular momentum and magnetic quantum number of the isolated atom, by μ the z component of the electron spin; α stands for all the quantum numbers, in addition to j, m, necessary to specify completely the state of the isolated atom; the initial and final states are indexed by subscripts i and f. The excitation cross section $\sigma(\mu_i m_i j_i \to \mu_f m_f j_f)$ is proportional to the square of the reaction amplitude $A(\mu_i m_i j_i \to \mu_f m_f j_f)$ which near threshold has the general form

$$A(\mu_i m_i j_i \to \mu_f m_f j_f) = -\tfrac{1}{2} \sum_{l, C, J} i^l (2l+1)^{1/2}$$

$$\times (j_i \tfrac{1}{2} m_i \mu_i | j_i \tfrac{1}{2} C M)(l C 0 M | l C J M)(j_f \tfrac{1}{2} m_f \mu_f | j_f \tfrac{1}{2} J M) S^J (l C j_i \alpha_i \to j_f \alpha_f). \qquad \ldots\ldots(1)$$

Equation (1) follows from Blatt and Biedenharn (1952). The quantities $S^J(lCj_i\alpha_i \to j_f\alpha_f)$ are elements of the scattering matrix connecting initial and final states of total angular momentum J and total $J_z = M$; S^J is independent of M, and the interaction cannot connect states of different J, M. The physically furnished initial states are specified by the values of l, μ_i, m_i, j_i and α_i, where l is the incident orbital angular momentum. Through the Clebsch–Gordan coefficients (Condon and Shortley 1935) $(j_i \frac{1}{2} m_i \mu_i | j_i \frac{1}{2} C M)$ and $(lC0M|lCJM)$ these physically furnished states are projected on a complete set of initial states specified by J, M, l, C, j_i, α_i, where the channel spin $\mathbf{C} = \mathbf{j}_i + \frac{1}{2}$, and $\mathbf{J} = \mathbf{l} + \mathbf{C}$. Since we confine our attention to reactions near threshold, the outgoing electrons are slow and have orbital angular momentum zero. Therefore the only possible values of J in the final states are $J = j_f \pm \frac{1}{2}$; a single Clebsch–Gordan coefficient $(j_f \frac{1}{2} m_f \mu_f | j_f \frac{1}{2} J M)$ suffices to project the physical final states on a complete set of final states J, M; and $A(\mathrm{i} \to \mathrm{f})$ in equation (1) does not depend on the direction into which the outgoing electron is scattered. The right side of equation (1) is summed coherently over all C, l, J; of course $\mu_i + m_i = M = \mu_f + m_f$, which fixes $\mu_f = \mu_i + m_i - m_f$. The cross section $\sigma(j_i \to j_f m_f)$ is

$$\sigma(j_i \to j_f m_f) = \frac{4\pi}{k^2} \frac{(2j_i+1)^{-1}}{2} \sum_{\mu_i m_i} |A(\mu_i m_i j_i \to \mu_f m_f j_f)|^2 \qquad \ldots\ldots(2)$$

summed over all μ_i, mi. With unpolarized electrons and atoms (which we assume) initial states labelled by C and M are incoherent and equations (1) and (2) can be replaced by the usually more convenient

$$\sigma(j_i \to j_f m_f) = \frac{2\pi}{k^2}(2j_i+1)^{-1} \sum_{M,C} |A(MC \to \mu_f m_f j_f)|^2 \quad \ldots\ldots (3)$$

$$A(MC \to \mu_f m_f j_f) = -\tfrac{1}{2} \sum_{l,J} i^l(2l+1)^{1/2}$$
$$\times (lC0M|lCJM)(j_f\tfrac{1}{2}m_f\mu_f|j_f\tfrac{1}{2}JM)S^J(lCj_i\alpha_i \to j_f\alpha_f). \quad \ldots\ldots (4)$$

In equation (3) $\mu_f = M - m_f$, and the sum extends from $M = -C$ to C for each value $C = j_i \pm \frac{1}{2}$.

The above equations possess the significant feature that, except for the factor k^{-2}, the cross sections $\sigma(j_i \to j_f m_f)$ depend on the incident energy $E = (2m)^{-1}\hbar^2 k^2$ only through the quantities $S^J(lCj_i\alpha_i \to j_f\alpha_f)$. The compound ion model asserts that the rapid energy variation of the observed cross section results from resonances with quasi-bound states of the compound ion. A compound state of total angular momentum J contributes only to those S^J belonging to the same value of J; in the neighbourhood of a resonance *each* $S^J(lCj_i\alpha_i \to j_f\alpha_f)$ is approximated by (Blatt and Biedenharn 1952)

$$S^J(lCj_i\alpha_i \to j_f\alpha_f) = \frac{e^{i\delta}(\Gamma_{ilC}\Gamma_f)^{1/2}}{E - E_r + \frac{1}{2}i\Gamma} \quad \ldots\ldots (5)$$

where $\delta(l, C, j_i, \alpha_i, j_f, \alpha_f)$ is slowly dependent on the energy E; E_r is the energy of the compound state; Γ is the total width of the level; Γ_{ilC} is the partial width for disintegration of the compound state into the initial state indexed by J, l, C, j_i, α_i; and Γ_f is the partial width for disintegration into the final state J, j_f, α_f. If several compound levels of different J have about the same energy, one simply replaces each S^J in equation (4) by the approximate expression (5). It is implicit however that compound states of the same J are well separated, i.e.

$$E_{1r} - E_{2r} \gg \tfrac{1}{2}(\Gamma_1 + \Gamma_2),$$

where 1 and 2 refer to two adjacent levels of equal J; otherwise equation (5) is incorrect, while the correct formula (Wigner 1946) is too complicated to be of much use.

2.1. *Heavy Elements*

Equation (4) is always summed over the two values of $J = j_f \pm \frac{1}{2}$. We exclude the trivial cases $j_f = 0$ and $j_f = \frac{1}{2}$, for which the populations of the final magnetic sub-levels $m_f = 0$ and $m_f = \pm\frac{1}{2}$ obviously do not depend on m_f, so that the emitted radiation must be isotropic and unpolarized. For the moment let us confine our attention to heavy atoms with large spin–orbit splitting, e.g. Hg; lighter atoms, e.g. He, are discussed later. For these heavy atoms we may adopt the working hypothesis that each peak in an observed excitation function results from resonance with a single compound state of $J = j_f \pm \frac{1}{2}$. In effect we are assuming that the breakdown of Russell–Saunders coupling means there is no reason for compound levels of different J to overlap, unless of course the level widths are so large that many compound levels of the same J are overlapping; In these unfavourable circumstances pronounced resonant structure is less likely and the compound ion model will not be useful anyway. In heavy atoms therefore, the total excitation function in the vicinity of an isolated peak should be represented by the one-level formula (Blatt and Biedenharn 1952)

$$\sigma(j_i \to j_f) = \sum_{m_f} \sigma(j_i \to j_f m_f) = \frac{\pi}{2k^2}\frac{(2J+1)}{(2j_i+1)} \sum_{C,l} \frac{\Gamma_{ilC}\Gamma_f}{(E-E_r)^2 + (\frac{1}{2}\Gamma)^2}. \quad \ldots\ldots (6)$$

At energies well removed from any peaks equations (1)–(4) remain valid, but there is no justification for introducing the simplifying compound model approximation (5). As a measure of the validity of our working hypothesis we remark that in Hg the 6^3P_1 excitation function (Jongerius, Van Egmond and Smit 1956) near threshold shows two distinct peaks in an energy interval no larger than the total spin–orbit splitting $^3P_2$–$^3P_0$ of the first excited $6p^3P$ atomic levels.

Use of equation (6) to fit an atomic excitation function has been described previously (Baranger and Gerjuoy 1957). As we have explained in § 1, at our present stage of understanding there is little to be gained from a similar analysis of the observations in Hg (Jongerius, Van Egmond and Smit 1956). Valuable supplemental information can be obtained from measurements of the relative populations in the final magnetic sublevels m_f. Measuring these populations in effect amounts to measuring several excitation functions, whose relative intensities and energy dependence must be consistent with the Breit–Wigner analysis of their sum, the total excitation function. Because the Clebsch–Gordan coefficients in equation (4) depend on J, our interpretation of the excitation peaks as resonances associated with a single value of J means that the relative populations in the final sublevels should vary sharply as the incident electron energy sweeps through a peak. Near each peak, $A(MC \to \mu_f m_f j_f)$ is dominated† by one of the two sets S^J, $J = j_f \pm \frac{1}{2}$, whereas at energies well removed from any peaks there is no justification for expecting either value of J to dominate in equation (4), and the relative populations, like the total excitation function, should vary slowly with energy.

In general, even when the value of J associated with the resonance is specified it is not possible to predict the relative m_f populations independently of assumptions about the quantities $S^J(lC)$, which in essence are arbitrary parameters depending on the detailed properties of the compound state. Whenever $j_i = 0$ however (the most common case in practice), $C = \frac{1}{2}$ only, and but one value of l is allowed for each J; we recollect that $l + P_i + P_f$ must equal an even integer, where the atomic states have parity $(-)^P$. Thus when $j_i = 0$ there is no sum over l in equation (4), and at each peak the population ratios depend only on the J associated with that peak. Using the special properties of the Clebsch–Gordan coefficients (Condon and Shortley 1935) $(j_i \frac{1}{2} m_1 m_2 | j_i \frac{1}{2} J M)$ we find for $j_i = 0$

$$\sigma(j_i \to j_f m_f) = \frac{\pi}{4k^2} \frac{2J+1}{2j_f+1} |S^J|^2 c(J, m_f) \qquad \ldots\ldots (7)$$

where $c(J, 0) = 2J + 1$; $c(j_f + \frac{1}{2}, 1) = j_f$; $c(j_f - \frac{1}{2}, 1) = j_f + 1$; $c(J, -1) = c(J, 1)$; and the only magnetic sub-levels occupied are $m_f = 0, \pm 1$.

The angular distribution $R(\theta)$ and polarization $\Pi(\theta) = (I_\parallel - I_\perp)/(I_\parallel + I_\perp)$, of the radiation emitted in an arbitrary electric dipole transition are

$$R(\theta) = 1 + \frac{q-p}{q+p} \cos^2\theta \qquad \ldots\ldots (8)$$

$$\Pi(\theta) = \frac{p-q}{p+q} \sin^2\theta \times \left(1 + \frac{q-p}{q+p} \cos^2\theta\right)^{-1} \qquad \ldots\ldots (9)$$

with θ the angle between the incident electron (z axis) and the direction at which the radiation is observed, and $I_\parallel(\theta)$, $I_\perp(\theta)$ the intensities respectively of the parallel and perpendicularly polarized components at angle θ. For the transition $j_f \to j'$ from the 'final' state j_f to some lower lying atomic level whose angular momentum is j', the quantities p and q are calculated from the relative populations $a(m_f)$ of the radiating sublevels m_f employing

---

† We note the unlikely possibility that the relative populations in the final sub-levels are accidentally insensitive to the relative amplitudes of the two allowed sets S^J, suppressing the energy dependence of the m_f population ratios.

$$\left.\begin{aligned} p &= \sum_{m_f} (j_f 1 m_f 0 | j_f 1 j' m_f)^2 a(m_f) \\ q &= \sum_{m_f} (j_f 1 m_f 1 | j_f 1 j' m_f+1)^2 a(m_f) \end{aligned}\right\} \quad \ldots\ldots (10)$$

In equations (8)–(10) we have used $a(-m_f) = a(m_f)$, valid for unpolarized incident electrons and atoms; except for this restriction the relative populations $a(m_f)$ are arbitrary. For radiation following excitation near threshold from an arbitrary initial j_i, sublevels $|m_f| \leqslant j_i + 1$ are populated. Kraus *et al.* (1956) have published expressions for $R(\theta)$ applicable to a wider class of reactions than those we are considering.

As can be seen from equations (8)–(10), our working hypothesis that excitation peaks in heavy atoms are resonances associated with a single value of J implies angular distributions and polarizations of radiations $j_f \to j'$ should vary sharply as the incident energy sweeps through a peak, except for unlikely accidental insensitivity† to the relative amplitudes S^J; at energies well removed from any peaks the angular distributions and polarizations should vary slowly with energy. The table lists the predicted relative m_f populations, $R(\theta)$ and $\Pi(\theta)$, in each of the two possible cases $J = j_f \pm \frac{1}{2}$, computed from equations (7) to (10) for several typical cases of excitation $j_i = 0 \to j_f$ followed by radiation $j_f \to j'$. The predictions for $J = \frac{1}{2}$ are trivial since they merely illustrate the general theorem that, irrespective of assumptions about j_i or the angular momentum of the outgoing electron, reactions proceeding via a compound state

Predicted angular distributions and polarizations of radiation following electron excitation, where excitation has proceeded through a single compound state with total angular momentum J. $\mu = \cos\theta$.

j_i	j_f	J	m_f	$a(m_f)$	j'	$R(\theta)$	$\Pi(90°)$
0	1	$\frac{1}{2}$				1	0
		$\frac{3}{2}$	1	1			
			0	4	0	$1 - 3\mu^2/5$	$\frac{3}{5}$
					1	$1 + 3\mu^2/7$	$-\frac{3}{7}$
					2	$1 - 3\mu^2/41$	$\frac{3}{41}$
0	2	$\frac{3}{2}$	1	3			
			0	4	1	$1 - 21\mu^2/47$	$\frac{21}{47}$
		$\frac{5}{2}$	1	1			
			0	3	1	$1 - \mu^2/2$	$\frac{1}{2}$

---

† See footnote on previous page

of $J=0$ or $\frac{1}{2}$ populate the final sublevels equally. The transitions $j_f=1\rightarrow j'=0$ and $j_f=1\rightarrow j'=1$ following excitation from the ground $j_i=0$ to the radiating $j_f=1$ state correspond to excitation of the $7s^3S_1$ level of Hg, followed by the respective radiations $7s^3S_1\rightarrow 6p^3P_0$ (4047Å) and $7s^3S_1\rightarrow 6p^3P_1$ (4358Å). Observed polarizations (Skinner and Appleyard 1927) for these lines vary with energy near threshold in a fashion which can be termed consistent with the table, choosing $J=\frac{3}{2}$. Thus it is suggested that the larger peak near threshold in the Hg $7s^3S_1$ excitation function (Jongerius, Von Egmond and Smit 1956) proceeds via a compound $J=\frac{3}{2}$ state of Hg^-; the polarization data (Skinner and Appleyard 1927) are too poor to warrant any stronger assertion or any further discussion. We add that the excitation functions in Hg (and in He) indicate level widths which are not much smaller than their spacings, so that it is not justified to neglect wholly one of the two sets S^J in equation (4); consequently we must expect qualitative rather than quantitative agreement with the predictions of the table.

The foregoing discussion has ignored the effects of nuclear spin, discussed by Penney (1932) (there are some numerical errors in Penney's work) and by Seaton (1958), i.e. we have been assuming the nuclear spin I is zero. Actually, because the hyperfine states (for most atoms) are separated in energy by an amount larger than their natural widths, states of different $\mathbf{F}=\mathbf{j}+\mathbf{I}$ radiate incoherently. Thus $R(\theta)$ and $\Pi(\theta)$ do depend on I, even though the nuclear spin does not flip in the original electron excitation process, nor in the subsequent electric dipole radiation from $j_f\rightarrow j'$. Assuming the hyperfine structure of the radiating line $j_f\rightarrow j'$ is not resolved, p and q of equations (8) and (9) now are calculated from

$$\left.\begin{aligned} p &= \sum_{F_f M_f} a(F_f, M_f) \sum_{\beta} (j_f I \beta M_f-\beta | j_f I F_f M_f)^2 (j_f 1 \beta 0 | j_f 1 j' \beta)^2 \\ q &= \sum_{F_f M_f} a(F_f, M_f) \sum_{\beta} (j_f I \beta M_f-\beta | j_f I F_f M_f)^2 (j_f 1 \beta 1 | j_f 1 j' \beta+1)^2 \end{aligned}\right\} \quad \ldots\ldots (11)$$

where $a(F_f, M_f)$ denotes the population in the 'final' radiating state labelled by F_f and total magnetic quantum number M_f; the magnetic quantum number β runs from $-j_f$ to j_f; and we have used $a(F_f, M_f)=a(F_f, -M_f)$. With the further assumption that the initially incident atomic hyperfine states F_i, M_i are equally populated, the relative populations $a(F_f, M_f)$ are given by

$$a(F_f, M_f)=\frac{1}{2I+1}\sum_{m_f}(j_f I m_f M_f-m_f | j_f I F_f M_f)^2 a(m_f) \quad \ldots\ldots (12)$$

wherein $a(m_f)$ are the relative populations employed previously in equation (10). In other words $a(m_f)$ are the populations of the excited radiating sublevels m_f for the case $I=0$. As previously, recalling equation (7), in the vicinity of an excitation function peak $a(F_f, M_f)$, $R(\theta)$ and $\Pi(\theta)$ depend only on the value of $J=j_f\pm\frac{1}{2}$ in the resonating compound state. For Hg the hyperfine structure of the odd isotopes produces a small but not negligible correction to the $j_f=1\rightarrow j'=0$ and $j_f=1\rightarrow j'=1$ predictions of the table, corresponding respectively to the 4047Å and 4358Å lines.

2.2. *Light Elements*

In light elements, where the spin–orbit interaction is very small, at first sight it seems reasonable to assume that total orbital angular momentum L and total spin angular momentum S are conserved during the excitation $j_i\rightarrow j_f$. In this event the scattering matrix is diagonal not only in the J, M representation but also in the L, S, M_L, M_S representation, and equation (1) can be replaced by

$$A(\mu_i m_i j_i \rightarrow \mu_f m_f j_f) = \sum (l_i s_i \beta_i \gamma_i | l_i s_i j_i m_i)(l_f s_f \beta_f \gamma_f | l_f s_f j_f m_f) \times A(\mu_i \beta_i \gamma_i l_i s_i \rightarrow \mu_f \beta_f \gamma_f l_f s_f) \qquad \ldots\ldots (13)$$

$$A(\mu_i \beta_i \gamma_i l_i s_i \rightarrow \mu_f \beta_f \gamma_f l_f s_f) = -\tfrac{1}{2} \sum_{l, S} i^l (2l+1)^{1/2} \; (l_i l \beta_i 0 | l_i l L M_L) \times (s_i \tfrac{1}{2} \gamma_i \mu_i | s_i \tfrac{1}{2} S M_S)(s_f \tfrac{1}{2} \gamma_f \mu_f | s_f \tfrac{1}{2} S M_S) S^{LS}(l l_i s_i \alpha_i \rightarrow l_f s_f \alpha_f). \qquad \ldots\ldots (14)$$

Here l_i, s_i are respectively the orbital and spin angular momentum of the initial atomic state, $\mathbf{j}_i = \mathbf{l}_i + \mathbf{s}_i$; similarly $\mathbf{j}_f = \mathbf{l}_f + \mathbf{s}_f$. Equation (13) is summed over $\beta_i = -l_i$ to l_i, $\gamma_i = -s_i$ to s_i, $\beta_f = -l_f$ to l_f, $\gamma_f = -s_f$ to s_f. The quantities $S^{LS}(l l_i s_i \alpha_i \rightarrow l_f s_f \alpha_f)$ (not to be confused with total spin S) are elements of the scattering matrix connecting initial states of total L, S specified by l, l_i, s_i, α_i with final states of the same total L, S specified by l_f, s_f, α_f; S^{LS} is independent of total orbital magnetic quantum number M_L and total spin magnetic quantum number M_S. Because the orbital angular momentum of the outgoing electron is zero near threshold, $L = l_f$ in equation (14); similarly $s_i \pm \frac{1}{2} = S = s_f \pm \frac{1}{2}$. Thus equation (14) is summed over all values of incident plane wave orbital angular momentum l subject to parity conservation and to the condition $\mathbf{l}_i + \mathbf{l} = \mathbf{l}_f$; over at most two values of $S = s_i \pm \frac{1}{2}$; and need not be summed over L. Moreover, in equation (14) $\beta_i = M_L = \beta_f, \gamma_i + \mu_i = M_S = \gamma_f + \mu_f$. Since we are interested mainly in He, and also for simplicity, the nuclear spin I has been equated to zero.

If $s_i = s_f$, two value of $S = s_i \pm \frac{1}{2}$ are allowed in equation (14) and the relative populations $a(m_f)$ computed from equations (13) and (14) generally depend on the ratios of $|S^{LS}(l)|^2$, even when the selection rules determine l. In the special case that $l_i = 0$ however, whether or not $s_i = s_f$, substituting $A(\mu_i m_i j_i \rightarrow \mu_f m_f j_f)$ from equation s(13) and (14) in equation (2), it can be seen that

$$\sigma(j_i \rightarrow j_f m_f) = \frac{\pi}{2k^2} \frac{(2l_f + 1)}{(2j_i + 1)(2s_f + 1)} (l_f s_f 0 m_f | l_f s_f j_f m_f)^2 \times \sum_S (2S+1)|S^{LS}|^2. \qquad \ldots\ldots (15)$$

As Lamb (1957) remarks, equation (15)—which is essentially the same as Lamb's equation (20)—implies that the relative populations $a(m_f)$ are model independent, i.e. do not depend on the magnitudes of the scattering matrix elements S^{LS}. In other words when $l_i = 0$ the angular distribution and polarization near threshold of any subsequent radiation $j_f \rightarrow j'$ can be predicted solely in terms of Clebsch–Gordan coefficients. Nonetheless, the measured polarization of the He 3889Å line following excitation from the ground $^1S_0$ state of He does not agree with this prediction. This experimental result, if correct, can be understood only by abandoning the fundamental assumption leading to equation (15), namely the assumption that L and S are conserved during the excitation $j_i \rightarrow j_f$.

With exact wave functions Ψ the matrix elements $\psi_f^* V_f \Psi_i^{(+)} = \Psi_f^{(-)*} V_i \psi_i$ yield the excitation cross section exactly. Here the incident wave function $\psi_i = u_i \exp(i\mathbf{k}_i \cdot \mathbf{r})$, u_i the product of the incident electron spin function and the wave function of the atom in its initial state; $\Psi_i^{(+)}$ is the solution to the Schrödinger equation $(H-E)\Psi = 0$ for the total Hamiltonian H, satisfying the boundary condition that $\Psi_i^{(+)} - \psi_i$ is 'everywhere outgoing'; the final wave function ψ_f and the corresponding solution $\Psi_f^{(-)}$ to Schrödinger's equation are defined similarly; V_i is the 'prior' interaction, V_f the 'post' interaction. Conventional means of computing the excitation cross section attempt to estimate these matrix elements; this approach we term the 'direct interaction model'. Physically the direct interaction model assumes the excitation results from direct interaction of the electron and atom in their initial (and final) channels, during which process the functions $\Psi_i^{(+)}$ (and $\Psi_f^{(-)*}$) presumably do not differ too greatly from their asymptotic forms in these channels. Thus in Born approximation $\Psi_i^{(+)}$ is replaced by $\psi_i, \Psi_f^{(-)*}$ by ψ_f^*; in distorted wave approximation $\Psi_i^{(+)}$ is replaced by $\chi_i^{(+)}=u_i F_i(\mathbf{r})$, F_i the wave function of an electron incident along $\mathbf{k}_i$ and scattered by the average potential of the atom in its initial state. Clearly on the direct model it is almost incredible that L and S should not be conserved during the excitation, since the L, S conserving Coulomb interactions between the incident electron and the atom are very much larger than the spin–orbit interaction terms in the Hamiltonian, and since moreover the amount of spin–orbit admixture in the initial and final atomic states j_i and j_f is extremely small.

On the compound ion model non-conservation of L and S during the excitation is more believable. The compound model assumes that in the region of interaction the total wave function is best approximated by a linear combination of quasi-bound eigenstates of the total Hamiltonian H. These quasi-bound ionic states are very different from simple combinations of atomic bound states and incident plane or distorted waves. In particular the fact that there is little spin–orbit admixture between the very widely spaced (compared to their natural widths) levels of the atom does not mean there must be equally small admixture between the broad compound ion states, whose properties are so different from the atomic states. Moreover the extremely large observed cross sections (Frost and Phelps 1957) for the spin non-conserving excitation transfer

$$\mathrm{He}(n^1\mathrm{P})+\mathrm{He}(1^1\mathrm{S})\rightarrow\mathrm{He}(1^1\mathrm{S})+\mathrm{He}(n^3\mathrm{D}) \qquad \ldots\ldots(16)$$

demonstrate empirically that neglecting the small spin–orbit interaction can be completely wrong for some collisions.

Equations (1)–(5) are valid for light atoms as well as heavy. In equation (1), had we been so inclined, we could have projected the physically furnished states on complete sets specified respectively by J, M, L_i, S_i, l, l_i, s_i, α_i and J, M, L_f, S_f, l_f, s_f, α_f, in which circumstances $A(\mu_i m_i j_i \rightarrow \mu_f m_f j_f)$ of equation (1) would have been expressed in terms of scattering matrix elements $S^J(L_i S_i l l_i s_i \alpha_i \rightarrow L_f S_f l_f s_f \alpha_f)$. These matrix elements $S^J(L_i S_i \rightarrow L_f S_f)$ are linear combinations of $S^J(lCj_i\alpha_i \rightarrow j_f \alpha_f)$, and, with appropriate re-indexing of the widths, are approximated by the Breit–Wigner formula (5) in the neighbourhood of a resonance. So far this matrix is perfectly general. The assumptions of equations (13) and (14) imply $S^J(L_i S_i \rightarrow L_f S_f)$ conserves L and S and, for fixed l, l_i, s_i, α_i and l_f, s_f, α_f, is independent of the values of $J=|L-S|$ to $|L+S|$ specifying the initial and final states in the J, M representation. In light elements therefore, if equations (13) and (14) hold, our working hypothesis is that each peak in the excitation function results from resonance with a single compound state of definite L and S. Since all the $(2L+1)$ $(2S+1)$ degenerate levels of the 'single' compound state have the same partial widths, each peak can be thought to result from resonance with a set of exactly overlapping compound levels, whose values of J run from $|L-S|$ to $|L+S|$, and whose partial widths for disintegration into final states indexed by L, S, l_f, s_f, α_f are independent of J. Of course the partial widths for breakup into final states indexed as in equations (1) to (5) by j_f, α_f are not independent of J; near threshold J cannot disintegrate into j_f, α_f unless $J = j_f \pm \frac{1}{2}$.

The considerations of the preceding paragraph bear on the possibility of understanding the measured polarization of the He 3889Å line. If for any reason the levels $J = |L-S|$ to $|L+S|$ are not completely overlapping at a resonance, or have properties not in agreement with expectation from L, S conservation, then it must be true that the scattering matrix is not diagonal in the L, S, M_L, M_S representation. Consequently, equations (13) and (14) must be incorrect, and it is necessary to return to our original equation (1). In this event, as we have illustrated in the table, the relative populations $a(m_f)$ will not be model independent, but will depend on the ratios of $|S^J(lC)|^2$ for $J = j_f \pm \frac{1}{2}$, which ratios essentially are model dependent and unpredictable, except apparently in special cases, e.g. $l_i = 0$ and the scattering matrix diagonal in L, S. Actually, the properties of the $^4\mathrm{P}(1s, 2s, 2p)$ states of He$^-$ are quite different from expectation based on L, S conservation. If these states were pure $^4\mathrm{P}$, autoionization would be forbidden by selection rules (Holøien and Midtdal 1955), and each of the $^4\mathrm{P}_{5/2}$, $^4\mathrm{P}_{3/2}$, $^4\mathrm{P}_{1/2}$ levels would have a long life and small width. However, the $^4\mathrm{P}_{3/2}$ and $^4\mathrm{P}_{1/2}$ levels can mix respectively with the broad autoionizing $^2\mathrm{P}_{3/2}$ and $^2\mathrm{P}_{1/2}$ levels of the same configuration; the $^4\mathrm{P}_{5/2}$ level has no autoionizing level with which to mix. Hence the relatively small spin–orbit interaction very greatly modifies the properties of the $^4\mathrm{P}$ levels, since it makes the $^4\mathrm{P}_{3/2}$ and $^4\mathrm{P}_{1/2}$ levels comparatively short-lived and broad, whereas the $^4\mathrm{P}_{5/2}$ level remains very narrow. It is not improbable that similar P states of He$^-$ play a role in the excitation of the He $3^3\mathrm{P}$ 3889Å radiating level. We observe that if equation (15) fails near threshold, it is just as likely to fail off resonance as at an excitation peak.

In conclusion we stress that there is no unambiguous distinction nor inconsistency between the direct and compound models, though there are differences in interpretation and interpretability. With exact wave functions Ψ the direct matrix elements $\psi_f{}^* V_f \Psi_i{}^{(+)} = \Psi_f{}^{(-)*} V_i \psi_i$ must duplicate whatever resonant structure actually occurs. Even when the Born or distorted wave approximations are quite good however, the direct interaction model has the defect that it conceals the significant parameters on which the cross sections depend. Conversely equation (1) also is exact, and with a sufficient number of intermediate compound states it should be possible to reproduce the characteristically non-resonant predictions of the direct interaction model. On the other hand, at energies where the excitation happens to proceed via only one or two intermediate states, the compound model enables us to express all the scattering amplitudes $A(\mathrm{i}\to\mathrm{f})$ in terms of a limited number of readily interpretable (though not necessarily easily predictable) parameters.

ACKNOWLEDGMENTS

The authors thank Dr. Michel Baranger for many valuable discussions, and acknowledge assistance by the joint programme of the Office of Naval Research and the U.S. Atomic Energy Commission, through the Sarah Mellon Scaife Radiation Laboratory.

References

Baranger, E., and **Gerjuoy, E.**, 1957, *Phys. Rev.*, **106**, 1182.

Blatt, J. M., and **Biedenhahn, L. C.**, 1952, *Rev. Mod. Phys.*, **24**, 258.

Burhop, E. H. S., 1952, *The Auger Effect and other Radiationless Transitions* (Cambridge: University Press), esp. p. 173.

Condon, E. U., and **Shortley, G. H.**, 1935, *Theory of Atomic Spectra* (Cambridge: University Press).

Dorrestein, R., 1942, *Physica*, **9**, 447.

Frost, L. S., and **Phelps, A. V.**, 1957, *Excitation Functions and Rates for the Principal Levels in Helium* (Westinghouse Research Laboratories Research Report 6-94439-6-R3).

Holøien, E., and **Midtdal, J.**, 1955, *Proc. Phys. Soc.* A, **68**, 815.

Jongerius, H. M., **Van Egmond, W.**, and **Smit, J. A.**, 1956, *Physica*, **22**, 845.

Kraus, A. A., Jr., **Schiffer, J. P.**, **Prosser, F. W.**, Jr., and **Biedenharn, L. C.**, 1956, *Phys. Rev.*, **104**, 1667.

Lamb, W. E., Jr., 1957, *Phys. Rev.*, **105**, 559.

Lamb, W. E., Jr., and **Maiman, T. H.**, 1957, *Phys. Rev.*, **105**, 573.

Massey, H. S. W., and **Burhop, E. H. S.**, 1952, *Electronic and Ionic Impact Phenomena* (Oxford: Clarendon Press), Chaps. I–IV, esp. p. 10.

Meier-Leibnitz, H., 1935, *Z. Phys.*, **95**, 499.

Penney, W. G., 1932, *Proc. Nat. Acad. Sci., Wash.*, **18**, 231.

Schulz, G. J., and **Fox, R. E.**, 1957, *Phys. Rev.*, **106**, 1179.

Seaton, M. J., 1958, *Report at the Conference on Physics of Electronic and Atomic Collisions* (New York University).

Skinner, H. W. B., and **Appleyard, E. T. S.**, 1927, *Proc. Roy. Soc.* A, **117**, 224.

Smit, J. A., 1935, *Physica*, **2**, 104.

Smit, J. A., and **Jongerius, H. M.**, 1955, *Appl. Sci. Res., Hague*, B **5**, 59.

Wigner, E. P., 1946, *Phys. Rev.*, **70**, 606.

The Resonant Absorption of γ-Rays in ^{14}N

By G. M. GRIFFITHS†
Cavendish Laboratory, Cambridge

Communicated by D. H. Wilkinson; MS. received 28th February 1958

Abstract. Using a nitrogen filled proportional counter the resonant absorption of γ-rays to the 8·06 MeV level in ^{14}N has been observed by means of the ^{14}N(γ, p)^{13}C reaction. The inverse reaction ^{13}C(p, γ)^{14}N at the 554 kev resonance was used as the source of γ-rays. The γ-ray flux was accurately measured with a scintillation counter and from the results the width of the 8·06 MeV level for ground state γ-ray transitions was found to be $10{\cdot}5 \pm 0{\cdot}6$ ev. This is in good agreement with the value obtained from the results of Seagrave on the inverse reaction ^{13}C(p, γ)^{14}N. Since the γ-ray energy is a function of angle due to a Doppler shift the resonant character of the absorption has been shown by varying the angle of the proportional counter with respect to the proton beam direction and noting the change in proton yield.

§ 1. INTRODUCTION

THE resonant reaction ^{14}N(γ, p)^{13}C has been observed by means of the discrete proton groups produced in ^{14}N by the continuous gamma-ray spectrum from the Glasgow betatron (Wright *et al.* 1956). In the present work we have studied this reaction in more detail at one resonance only, using the inverse reaction ^{13}C(p, γ)^{14}N as a source of gamma rays and observing the reaction in a nitrogen filled proportional counter. Experiments of this type are in general difficult due to Doppler shifts and recoil losses of the γ-ray energy (Moon 1951). The possibility of observing the reaction at the 8·06 MeV level in ^{14}N is suggested by two facts: first the large proton width of the level, $32{\cdot}5 \pm 1$ kev (Seagrave 1952), means that Doppler and recoil shifts are not serious (thermal broadening effects are negligible) and second, at the appropriate forward angle of observation the recoil losses occurring both on emission and absorption by ^{14}N nuclei are just compensated for by the Doppler shift resulting from the forward motion of the ^{14}N nuclei in the ^{13}C target. Also the change in energy of the emitted γ-rays with angle due to the Doppler shift allows one to demonstrate the resonant character of the ^{14}N(γ, p)^{13}C reaction.

In this experiment a thick carbon target containing 65% ^{13}C was bombarded with protons with an energy well above the 554 kev resonance (670 kev). In slowing down in the target the protons pass through the 554 kev resonance region giving a γ-ray yield characterized by the full integral over the resonance. 89% of the transitions from the 8·06 MeV level, excited in ^{14}N by the ^{13}C(p, γ)^{14}N reaction, go by electric dipole radiation to the ground state and 11% cascade through the 3·95 MeV level. Only the ground state γ-rays are of interest here as they are the only ones that can excite ^{14}N from its ground state to produce the inverse photodisintegration. The intensity of these γ-rays was measured with a calibrated scintillation counter and the photodisintegration was observed by counting proton pulses in a nitrogen filled proportional counter placed close to the target. In order to obtain a γ-ray width for the ground state transition from the 8·06 MeV level from the results it is necessary to integrate the γ-ray flux over the counter volume taking into account the 32 keV width of the γ-ray spectrum and the fact that the mean energy of this spectrum is a function of recoil shifts and of angle through the Doppler shift. If reciprocity applies to the reaction then the γ-ray width so obtained should be the same as that obtained for the inverse reaction $^{13}C(p, \gamma)^{14}N$ (Woodbury *et al.* 1953) after taking into account the branching ratio for γ-ray decays of the 8·06 MeV state. A preliminary report of the experimental method has been presented previously (Griffiths 1956).

---

† Now at the Physics Department, University of British Columbia, Canada.

§ 2. THE ^{14}N PROPORTIONAL COUNTER

The counter consisted of a Pyrex tube 4·07 ± 0·05 cm inside diameter and 45 cm long with an active length of 26·8 cm defined by glass guard rings as shown in figure 1.

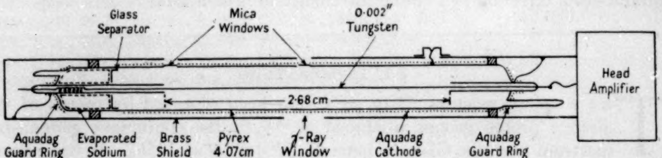

Figure 1. The ^{14}N proportional counter.

Before filling a small piece of sodium metal was evaporated over the inside of one end of the counter to give continuous gas purification. The glass separator shown in the figure prevented sodium from entering the active counter volume. In operation this separator rested in the opposite end of the counter which was operated in a vertical position. The counter was provided with two 13 mm air equivalent mica windows to admit alpha particles for testing and calibration. The cathode was a layer of Aquadag painted on the outside of the Pyrex tube. Only for γ-ray fluxes or gas amplifications much higher than used in the present experiments could any effects of polarization of the glass be noted.

After thorough outgassing the counter was filled with nitrogen to a pressure of 72·40 cm of mercury at 21·3°C. The nitrogen was purified by passing it through hot copper turnings and then through a liquid air trap. Operated at 2800 volts the counter gave a gas amplification of 14 with differentiating and integrating time constants set at 2 microseconds. The amplifier output was fed to a Wilkinson 100 channel kicksorter (Wilkinson 1950).

The energy scale of the counter was obtained by putting Po alpha particles into the counter through the side windows of known thickness and also by surrounding the counter with wax and placing a Po–Be neutron source beside it and observing the $^{14}N(n, p)^{14}C$ protons. Results of these calibration runs are shown in figure 2.

The width of the alpha curve is due to straggling which is also shown by the characteristic asymmetry. The $^{14}N(n,p)^{14}C$ reaction has a measured Q of 0·627 MeV thus producing protons of 0·585 MeV. The peak shown in figure 2 has an energy of 0·63 MeV from comparison with several different alpha particle curves. With estimated errors of about 25 keV, this suggests that the recoiling ^{14}C contributes most of its energy to the ionization produced in the gas.

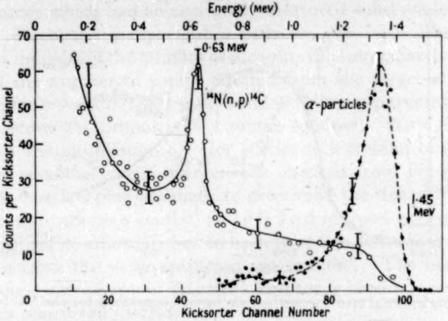

Figure 2. Energy calibration of the proportional counter.

§ 3. The ^{13}C Target and γ-ray Spectrum

The targets used were 65% ^{13}C plus ^{12}C separated in the Harwell diffusion column in gaseous form and then thermally cracked on to platinum or copper foils. These foils were soldered to a water cooled copper plate shown in figure 3. The beam current had to be limited to 100 microamperes spread over an area 1·5 cm by 2·3 cm to limit sputtering.

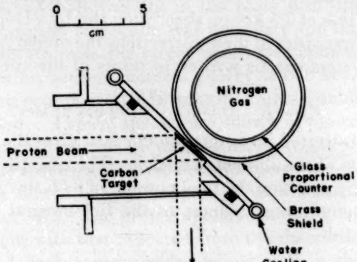
0
5
cm
Nitrogen Gas
Proton Beam
Carbon Target
Glass Proportional Counter
Brass Shield
Water Cooling
γ-Rays to Scintillation Counter

Figure 3. The target arrangement.

An excitation function for a typical target is shown in figure 4 together with theoretical curves for targets of various thicknesses. The tail on the high energy side of the experimental curve is due to non-uniform target thickness and due to a contribution from the wide level at 1·25 Mev. A detailed analysis shows that if the target is bombarded with 670 kev protons, they leave the target at about 445 kev and consequently the 8·06 Mev γ-ray spectrum from the 554 kev resonance should be characterized by a Breit–Wigner shape with a width of 32·5 kev. Thus

$$N_\gamma(E_\gamma)=N_1A_\gamma\frac{\Gamma_p\Gamma_\gamma}{(E_\gamma-E_{\gamma r})^2+(\frac{1}{2}\Gamma)^2} \qquad \ldots\ldots(1)$$

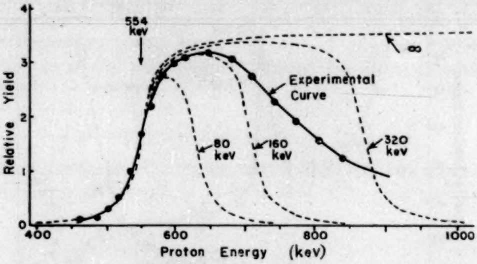

Figure 4. Experimental and theoretical excitation functions for the ^{13}C (p, γ)^{14}N reaction.

where $N\gamma(E\gamma)$ represents the number of γ-rays per unit energy range about E_γ, N_1 represents the number of incident protons, A_γ contains statistical factors, proton wavelength and the number of ^{13}C nuclei seen by the incident protons per unit energy range, Γ_p is the proton width of the level which can be taken as the observed laboratory width and Γ_γ is the width for ground state γ-ray transitions and $E_{\gamma r}$ is the resonance γ-ray energy calculated from the Q of the reaction.

However this is not the spectrum seen in the centre of mass of the absorbing nuclei. First the spectrum will be modified by a recoil loss of 2·5 kev on emission and a second recoil loss of 2·5 kev on absorption and by a Doppler shift depending on angle so that to first order in these corrections the excitation energy E_e available in the absorbing system can be written in terms of the energy release E_γ in the emitting system as

$$E_e=(E_\gamma-0{\cdot}005+0{\cdot}0199\cos\theta)\ \text{Mev}. \qquad \ldots\ldots(2)$$

This expression substituted into equation (1) then gives the γ-ray spectrum seen in the centre of mass of the absorbing nuclei. The quantity N_1A_γ was evaluated in this experiment by equating the total number of 8·06 Mev γ-rays independently measured with a scintillation counter to the full integral over expression (1). This leads to the result

$$N_1A_\gamma=\frac{N_\gamma}{\Gamma_p\Gamma_\gamma}\,\frac{\Gamma/2}{3{\cdot}112}. \qquad \ldots\ldots(3)$$

§ 4. Scintillation Counter Efficiency

The counter used to determine the γ-ray flux was a sodium iodide crystal 6·48 cm long by 4·38 cm in diameter mounted on an E.M.I. 6262 photomultiplier. The spectra were analysed with a Hutchinson and Scarrott (1951) 60-channel kicksorter.

An absolute measure of the number of γ-rays from the $^{13}C(p, \gamma)^{14}N$ reaction required a knowledge of the absolute efficiency of the counter. This was obtained by making an absolute measurement at 6·14 Mev as described below and extrapolating to 8·06 Mev using theoretical γ-ray absorption coefficients.

The method used for 6·14 Mev γ-rays is essentially that suggested by Van Allen and Smith (1941). A target of CaF_2 was bombarded with 340 kev protons and the α-particles were counted in a thin window (6·1 mm air equivalent mica) proportional counter which had an accurately measured solid angle with respect to the target. Since the γ-rays and α-particles are both isotropic at the resonance used, a measure of the number of α-counts can immediately be converted to a measure of the number of γ-rays emitted from the target after making a 2·5% correction for 6·9 and 7·1 Mev γ-rays which follow α-particles insufficiently energetic to penetrate the proportional counter window. With this accurately known γ-ray flux the scintillation counter efficiency was determined as follows. The linearity of response of the counter was checked from 0·5 Mev to 12 Mev and an inverse square law plot was made to determine the distance from the end of the crystal to the 'effective centre' ($2{\cdot}2 \pm 0{\cdot}2$ cm in good agreement with the theoretical value). The efficiency has to be referred to some bias energy below which no pulses from the γ-ray spectrum are counted. The bias energy was chosen at half the γ-ray energy in this work and for 6·14 Mev γ-rays the experimental efficiency was $0{\cdot}428 \pm 0{\cdot}008$.

To find the efficiency for the 8·06 Mev $^{13}C(p, \gamma)^{14}N$ γ-rays it was assumed that the ratio of the efficiencies at 6·14 and 8·06 Mev was equal to the ratio of the theoretical total absorption cross sections for these γ-rays in the given crystal. This gives the 8·06 Mev efficiency as 0·495 for a bias set at pulses corresponding to half the γ-ray energy.

§ 5. EXPERIMENTAL RESULTS

The proportional counter was mounted next to the target in a vertical position as shown in figure 3. A hole was cut in the brass wall opposite to the target so that no γ-ray absorption correction was necessary for this wall. The γ-ray counter was placed 65 cm from the target which was bombarded with 50 to 75 microamperes of protons with an incident energy of 670 kev. In about 8 hours running 2×10^6 γ-ray counts and 1650 proton counts (small backgrounds subtracted) were recorded. Typical spectra are shown in figures 5 and 6.

Due to the presence of a small ^{19}F contamination in the thick target used, the lower part of the γ-ray spectrum down to the bias energy of 4·03 Mev was corrected to that shown by the dotted line by comparison with a smaller ^{13}C target which appeared to be free of ^{19}F. The proton spectra showed a tail on the low energy side in good agreement with that expected from the theoretical wall effect. This tail was extrapolated back to zero pulse height with a shape and magnitude predicted theoretically and the total number of protons was calculated to be 15% greater than the number in the main peak from 0·45 Mev to 0·65 Mev. It was confirmed that the peak at 550 kev was really due to the resonant reaction by subjecting the counter to 6, 12 and 17 Mev γ-rays and noting that no peaks occurred in the spectrum. The secondary electron suppression from the target was not good so that no use has been made of the yield in terms of the number of incident protons. What has been measured is the ratio of the number of protons released in the proportional counter N_p to the number of γ-rays emitted by the target. Results of four different runs are given in table 1.

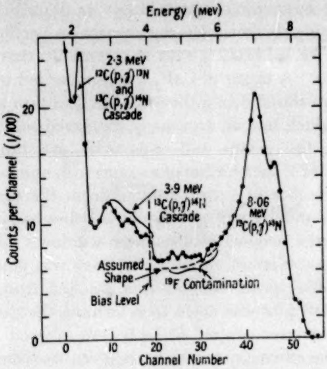

Figure 5. $^{13}C(p, \gamma)^{14}N$ gamma-ray spectrum.

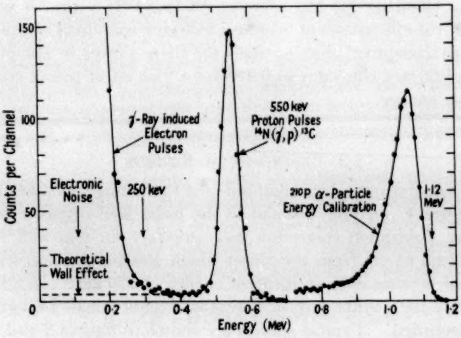

Figure 6. ^{14}N proportional counter spectra showing the test α-particles on the right and the proton spectrum from the $^{14}N(\gamma, p)^{13}C$ reaction in the middle.

Table 1. Experimental Results for the Proton to γ-ray Ratio at 45°

Run	$N_\gamma \times 10^{-8}$	N_p	$(N_p/N_\gamma) \times 10^8$
1	7·53	98	13·0
2	23·3	285	12·2
3	94·6	1110	11·8
4	24·9	289	11·6
		Weighted Average	$11{\cdot}80 \times 10^{-8}$ protons per γ-ray.

In order to check the resonant nature of the absorption a run was taken with the proton counter axis at 0° to the beam and another with the axis at 90° to the beam, these positions being possible with the target shown in figure 3 with some increase in mean target to counter distance. The results are discussed below.

§ 6. DISCUSSION

To relate the above experimental ratio to the γ-ray width Γ_γ of the ground state transitions from the 8·06 MeV level we write the following expression for the proton yield N_p from the nitrogen filled proportional counter:

$$N_\mathrm{p}=N_\mathrm{n}\int_{C}\frac{A_s}{4\pi r_s{}^2}\left[\int_{E_\mathrm{e}}N_\gamma(E_\gamma)\,.\,\tfrac{1}{2}\pi\lambda\!\!\!^{-}_\gamma{}^2\frac{\Gamma_\mathrm{p}\Gamma_\gamma}{(E_\mathrm{e}-E_{\gamma\mathrm{r}})^2+(\frac{1}{2}\Gamma)^2}\,dE_\mathrm{e}\right]dv_s \qquad \ldots\ldots(4)$$

where

$$N_\gamma(E_\gamma)=\frac{N_\gamma}{\Gamma_\mathrm{p}\Gamma_\gamma}\,\frac{\frac{1}{2}\Gamma}{3{\cdot}112}\,\frac{\Gamma_\mathrm{p}\Gamma_\gamma}{(E_\mathrm{e}+0{\cdot}005-0{\cdot}0199\cos\theta_s-E_{\gamma\mathrm{r}})^2+(\frac{1}{2}\Gamma)^2}$$

obtained by combining equations (1), (2) and (3); N_n is the number of nitrogen nuclei per cubic centimetre in the proportional counter, A_s the absorption factor for the target backing and the glass walls of the proportional counter; this depends on the particular counter section s being considered; r_s is the distance from the target to the element of counter volume dv_s and $\lambda\!\!\!^{-}_\gamma$ the γ-ray wavelength divided by 2π.

The first integral is taken over the counter volume, the second over the Breit–Wigner resonance for γ-ray absorption and proton emission. It is important to note that the factor $\cos\theta_s$ in the γ-ray spectrum depends on the particular counter volume element s. The integral over the energy can be analytically integrated assuming $\lambda\!\!\!^{-}_\gamma$ and Γ_p are independent of energy over the resonance, but because of the factors A_s and $\cos\theta_s$ the integral over the counter volume was evaluated numerically for the counter placed at 45° to the incident beam direction, as shown in figure 3. For this evaluation half the counter only was considered since the top and bottom are symmetrical with respect to γ-rays from the target. This half was divided into 70 volume elements with a volume which increased with the distance of the section from the target so that the contribution to the yield and also the errors in this contribution were roughly constant for all sections. This computation leads to the result

$$\frac{N_\mathrm{p}}{N_\gamma}=N_\mathrm{n}\lambda\!\!\!^{-}_\gamma{}^2\frac{\Gamma_\mathrm{p}\Gamma_\gamma}{\Gamma^2}\times1{\cdot}26=N_\mathrm{n}\lambda\!\!\!^{-}_\gamma{}^2\frac{\Gamma_\gamma}{\Gamma}\times1{\cdot}26$$

assuming that $\Gamma_\mathrm{p}\simeq\Gamma$ as has been assumed throughout the calculation. Putting in the experimental values for N_p/N_γ, N_n, $\lambda\!\!\!^{-}_\gamma{}^2$ and $\Gamma=\Gamma_\mathrm{p}=32{\cdot}5$ kev we get $\Gamma_\gamma=10{\cdot}5\pm0{\cdot}6$ ev for the γ-ray width for ground state transitions from the 8·06 MeV level in ^{14}N. The stated error is based on estimated errors of 3% in the γ-ray flux, 2·5% due to counting statistics and 4% in the integration over the counter volume.

The γ-ray width for ground state transitions from this level can also be deduced from the data of Seagrave (1952) who studied the inverse reaction ^{13}C(p, γ)^{14}N. From his results we conclude that $\Gamma_\gamma=10{\cdot}2$ ev in excellent agreement with the above value.

As a final check on the resonant character of the absorption, measurements were made with the counter at 0° and at 90° to the proton beam. This modifies the mean energy of the γ-rays in the proton counter due to the Doppler shift. The ratio of N_p/N_γ normalized to 1·0 at 45° is shown in table 2 for both experimental and theoretical cases.

Table 2. Experimental and Theoretical Proton to γ-ray Ratios at Different Angles Normalized to 1·0 at 45°

Angle (deg)	Ratio Theory	Ratio Experiment
0	0·75	$0{\cdot}7 \pm 0{\cdot}15$
45	1·0	1·0
90	1·0	$0{\cdot}9 \pm 0{\cdot}15$

The reasonable agreement again supports the assumptions used.

ACKNOWLEDGMENTS

I would like to thank Professor D. H. Wilkinson who suggested this experiment to me and who helped to make my stay at Cambridge a pleasant one. The writer is also indebted to Dr. M. L. Smith of the Atomic Energy Research Establishment at Harwell for his careful preparation of the ^{13}C targets used, to Mr. D. D. Stewart for operating the Cavendish high tension set and to Mrs. Griffiths for doing the numerical integrations. The writer gratefully acknowledges receipt of a Rutherford Memorial Fellowship from the Royal Society of Canada and the National Research Council of Canada.

REFERENCES

GRIFFITHS, G. M., 1956, *Canad. J. Phys.*, **34**, 339.
HUTCHINSON, G., and SCARROTT, G., 1951, *Phil. Mag.*, **42**, 792.
MOON, P. B., 1951, *Proc. Phys. Soc.* A, **64**, 76.
SEAGRAVE, J. D., 1952, *Phys. Rev.*, **85**, 197.
VAN ALLEN, J., and SMITH, N., 1941, *Phys. Rev.*, **59**, 618.
WILKINSON, D. H., 1950, *Proc. Camb. Phil. Soc.*, **46**, 508.
WOODBURY, H., DAY, R., and TOLLESTRUP, A., 1953, *Phys. Rev.*, **92**, 1199.
WRIGHT, I., MORRISON, D., REID, J., and ATKINSON, J., 1956, *Proc. Phys. Soc.* A, **69**, 77.

The Magnetic Susceptibilities of Alloys of Cerium with Thorium

By L. F. BATES and M. M. NEWMANN
Department of Physics, University of Nottingham

MS. received 8th April 1958

Abstract. The paramagnetic susceptibilities of 90, 71, 60, 42, 20, 10 and 5 atomic per cent cerium in thorium alloys have been measured over the temperature range 90°K to 700°K. The temperature dependence of the resistivity of 90, 60, 40, 20 and 5 atomic per cent cerium–thorium alloys has been investigated over the range 90°K to 293°K. The thermal expansion of the 60% alloy has also been measured over this temperature range. All the alloys exhibit a sharp decrease in susceptibility at low temperatures. This has been attributed to the excitation of some of the 4f electrons of the cerium atoms into the conduction band at these temperatures, and the resistivity and expansion results support this hypothesis. Above room temperature the susceptibilities of all the alloys obey a Curie–Weiss law, $\chi = C/(T-\theta)$, over at least part of the temperature range. The effective magnetic moments per cerium atom calculated from the Curie constants C increased with decreasing cerium content. A model has been proposed in which coupling between the cerium f electron and the conduction electrons causes polarization of the latter in the neighbourhood of the cerium atoms. The apparent increase in p_{eff} is attributed to this induced moment.

§ 1. INTRODUCTION

THE phase diagram and lattice parameters of the cerium–thorium alloy system have been investigated by Weiner, Freeth and Raynor (1957, to be referred to as WFR)† and by Van Vucht (1957). They found that intersolubility of the component metals exists over the complete range of composition at room temperature, all the alloys having a face-centred cubic structure. Thorium has the electron configuration ... $6s^2 6p^6 6d^2 7s^2$ and an atomic radius of 1·80Å as calculated from the closest distance of approach of the atoms in its face-centred cubic structure. Cerium has the configuration ... $4d^{10} 4f^1 5s^2 5p^6 5d^1 6s^2$ and an atomic radius of 1·82Å in the face-centred cubic structure at room temperature. WFR found that the lattice parameter of the alloys does not increase linearly with increase of cerium content but actually decreases from the value for thorium upon first adding cerium to it and then remains constant up to 33% cerium, after which it increases linearly up to the value for cerium. Van Vucht did not observe the initial decrease in lattice parameter but his results are otherwise the same. It is known that the cerium atom contracts upon losing its 4f electron so WFR suggested that the anomalous variation of lattice parameter was due to the creation of a Ce^{4+} ion on adding cerium (Ce^{3+} ions) to the thorium, the 4f electron going into the conduction band. The present work was undertaken to throw further light on this problem.

Cerium has a large paramagnetism, almost entirely due to its one 4f electron. At 293°K the mass susceptibility is $17{\cdot}4 \pm 0{\cdot}2 \times 10^{-6}$ e.m.u. g^{-1}. The susceptibility follows a Curie–Weiss law, $\chi = C/(T-\theta)$, over the temperature range 20°K to 350°K (Bates, Leach and Loasby 1955, La Blanchetais 1954, Lock 1957). The susceptibility of thorium is $0{\cdot}422 \pm 0{\cdot}003 \times 10^{-6}$ e.m.u. g^{-1} at room temperature and is practically temperature independent (Leach 1955). Hence, even small quantities of cerium dissolved in thorium should have a marked effect upon the latter's magnetic properties. If, however, the cerium atoms have lost their 4f electrons to the conduction band, as postulated by WFR, it is likely that they will not appreciably affect the susceptibility of the thorium. Thus measurements of the temperature dependence of the susceptibilities of the alloys might enable the number of cerium atoms retaining a 4f electron in each alloy to be estimated. In view of the magnetic data it was decided to measure the resistivity of some of the alloys and also the fractional change in length of one of them over the temperature range 90°K to 293°K. One of the alloys was also investigated by means of neutron diffraction at low temperatures at Harwell.

---

† The authors are indebted to the Atomic Energy Research Establishment, Harwell, for a report on this work prior to publication.

§ 2. EXPERIMENTAL DETAILS

2.1. *Magnetic Measurements*

The temperature dependence of the susceptibilities of seven alloys of the cerium–thorium system was investigated over the range 90°K to 700°K. The alloys had the compositions 90, 71, 60, 42, 20, 10 and 5 atomic per cent of cerium in thorium (hereafter termed the 90%, 71% etc. alloys, respectively.) The specimens, in the form of small beads, were prepared in an argon arc furnace by the Metallurgy Division of the Atomic Energy Research Establishment, Harwell. The cerium used, obtained from Johnson, Matthey and Co. Ltd., was of purity greater than 99·9%. No other rare earths were detected, the only metallic impurities present being lithium (0·05%) and iron (0·002%). The thorium, provided by the Atomic Energy Research Establishment, Harwell, contained thorium oxide as the principal impurity which may have been present up to 1%. The change of weight upon preparing the alloys was negligible, so that their composition was determined from the weights of the metals used.

Each alloy was wrapped in tantalum foil, sealed in an evacuated quartz tube and given a three-week homogenizing anneal at 575°C. This temperature was chosen because it is approximately the maximum temperature at which no volatilization of the cerium takes place. A trial experiment with the 60% alloy showed that a further three-week anneal had no effect upon the susceptibility. Hence, it was assumed that the alloys were homogeneous. All the specimens were tested for the presence of ferromagnetic impurity at 293°K and 90°K using fields up to 4500 Oe and their susceptibilities were independent of field.

The temperature variation of susceptibility was measured for each alloy using an apparatus designed for the measurement of the susceptibilities of small irregularly shaped specimens over the temperature range 90°K to 700°K (Leach 1955, Newmann 1958). The apparatus was calibrated using pure tantalum as a standard (Hoare and Walling 1951).

2.2. *Resistance Measurements*

The temperature variation of resistivity of five cerium–thorium alloys was investigated over the range 90°K to 293°K. The alloys had the compositions 90, 60, 40, 20 and 5 atomic per cent cerium in thorium. The specimens, prepared in an argon arc furnace by the Atomic Energy Research Establishment, Harwell, were given a homogenizing anneal at 575°C. They were then machined into cyilndrical rods 4 cm long × 4 mm diameter.

The potential differences across the specimen and across a standard resistance in series with it were measured on a potentiometer (Loasby 1957), the specimen holder being designed to allow for the large contraction of some of the alloys upon cooling.

2.3. *Expansion Measurements*

The thermal expansion of the 60% alloy was investigated over the range 90°K to 293°K using a simple extensometer, the specimen being the 4 cm rod used in the resistivity measurements.

§ 3. EXPERIMENTAL RESULTS

3.1. *Paramagnetic Susceptibility Measurements*

In order to obtain the effective moment of the cerium atoms in the alloys the results are analysed on the assumption that the atomic susceptibility of the thorium in the alloy is the same as in the pure metal. The contribution of the cerium atoms to the susceptibility is then estimated. Figure 1 shows values of $1/\chi$ for the alloys plotted against absolute temperature, T, where the susceptibility per gramme of cerium is given by $\chi = [\chi_a - (1-y)\chi_T]/y$. Here χ_T is the susceptibility per gramme of thorium and χ_a the observed susceptibility per gramme of an alloy containing a fraction y by weight of cerium.

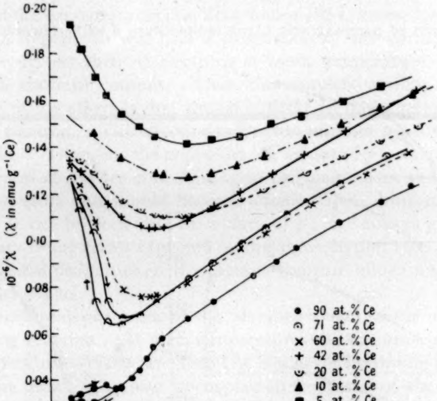

Figure 1. Temperature variation of $1/\chi$ for cerium–thorium alloys.

All the $(1/\chi, T)$ curves are of the same general shape, being characterized by a well-defined minimum in the low temperature region. Thus, as the temperature is decreased the susceptibility at first increases, and then shows a more marked decrease which persists to the lowest recorded temperature. The position of susceptibility maximum T_m moves to successively higher temperatures as the percentage of cerium in the alloys is decreased. The 90% and 71% alloys

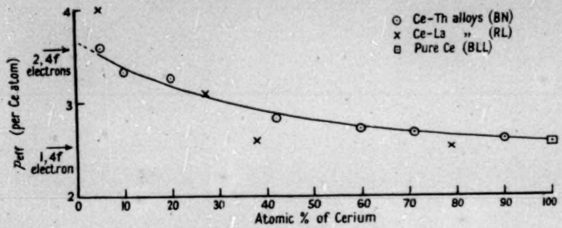

Figure 2. Variation of effective moment per Ce atom with concentration of cerium. BN, present authors; RL, Roberts and Lock 1957; BLL, Bates, Leach and Loasby 1955.

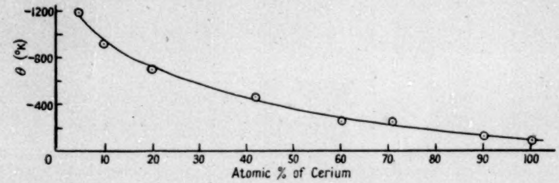

Figure 3. Variation of paramagnetic Curie temperature θ with concentration of cerium.

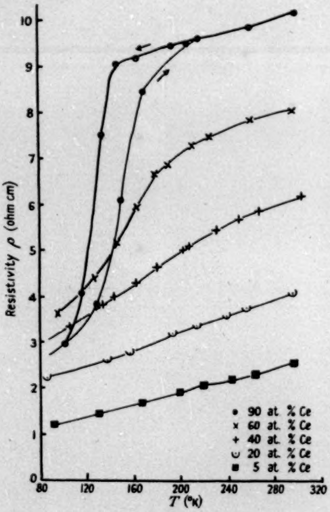

Figure 4. Temperature variation of resistivity for cerium–thorium alloys.

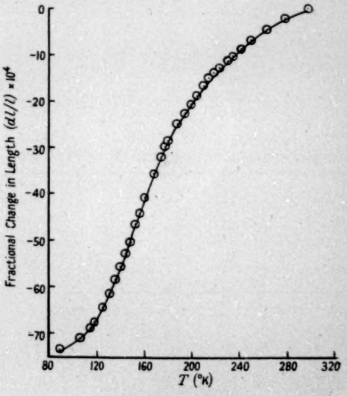

Figure 5. Thermal expansion of 60 at. % Ce alloy.

show a temperature hysteresis associated with this anomalous decrease in susceptibility. Above room temperature a Curie–Weiss law, $\chi = C/(T-\theta)$, is obeyed over at least part of the temperature range giving values for the effective moment per cerium atom, calculated using the formula $p_{\text{eff}} = 2{\cdot}839\sqrt{C}$ (Bates 1951), and the paramagnetic Curie temperature θ which increase with decreasing cerium content. The values of p_{eff} and θ are plotted against composition in figures 2 and 3 respectively.

3.2. *Resistance Measurements*

Figure 4 shows the resistivities of the alloys plotted against temperature. With decrease in temperature all the alloys investigated show a sharp fall in resistance near T_{m}, the temperature at which the susceptibility maximum occurs. The 90% alloy exhibits a temperature hysteresis over the temperature range 90°K to 170°K.

3.3. *Expansion Measurements*

The fractional change in length of the 60% alloy plotted against temperature is shown in figure 5. There is a large increase in the rate of contraction below T_{m}.

§ 4. DISCUSSION

It is well known that the magnetic properties of metallic cerium can be explained on the assumption that all the paramagnetism arises from the one electron in the 4f shell of the cerium atoms (La Blanchetais 1954, Bates, Leach and Loasby 1955). WFR's hypothesis was that a proportion of the cerium atoms in the alloys have already lost their 4f electrons at room temperature, this proportion increasing with thorium content. Then the simplest assumption is that the paramagnetism of the alloys is due almost entirely to those cerium atoms which retain their 4f electron. The effective magneton number p_{eff} for one 4f electron per atom is 2·54. Thus, on the above model, values of p_{eff} calculated assuming that all the cerium atoms are contributing to the magnetism should be less than 2·54 per cerium atom and should become smaller upon dilution of the cerium. From figure 2 it can be seen that the values of p_{eff} are always greater than 2·54 which is contrary to the result expected on the above hypotheses, and an explanation of the physical properties of the cerium–thorium alloys must be sought in terms of another model.

The temperature dependence of the paramagnetism of the alloys shows two other interesting features. At high temperatures the cerium-rich alloys show a departure from a Curie–Weiss law, the $(1/\chi, T)$ curves becoming concave towards the temperature axis. This can be explained in terms of thermal population of an excited state of the cerium atom. For example, in metallic cerium the ground state is $^2F_{5/2}$ and the first excited level is $^2F_{7/2}$, giving the values 2·54 and 4·54 respectively for p_{eff}, therefore population of the $^2F_{7/2}$ state will increase the susceptibility (Bates, Leach and Loasby 1955).

At low temperatures the susceptibility shows a sudden decrease. There are two possible explanations for this effect. Either antiferromagnetic ordering of the magnetic atoms is taking place or some of the 4f electrons are being promoted into the conduction band. Neutron diffraction measurements on the 42% alloy by the Metallurgy Division, Atomic Energy Research Establishment, Harwell, showed that no antiferromagnetic structure exists in the temperature range investigated in this work.

It is well known that when face-centred cubic γ-phase cerium is cooled to liquid oxygen temperatures an appreciable amount of face-centred cubic α-phase is produced. The transition from γ- to α-phase is accompanied by a contraction in atomic volume of 16·5% (Schuch and Sturdivant 1950). Measurements of many physical properties of cerium indicated that this transformation is associated with the transference of the 4f electron to the conduction band. Leach (1955) showed that the transition is dependent upon strains produced by impurities in the cerium. The high pressure experiments of Lawson and Tang (1949) indicate that the strains should be compressive. It is now suggested that the cerium–thorium alloys show a similar effect, the thorium atoms producing strains in the cerium atoms so that at low temperatures their electrons are ejected from the 4f shell. This would explain the drop in susceptibility at these temperatures. Measurement of the expansion of the 60% alloy over the range 90°K to 293°K (figure 5) showed that, on lowering the temperature, there was a large increase in the rate of contraction near T_m, the temperature at which the maximum in susceptibility occurs. This is to be expected if Ce^{4+} ions are being formed. The sharp fall in resistance below T_m observed for all the alloys (figure 4) is in accordance with the idea that extra electrons are contributing towards the conduction or that spin-dependent scattering disappears. Finally, the (susceptibility, temperature) curves of the 90% and 71% alloys show a temperature hysteresis similar to that obtained in impure cerium at the γ- to α-phase transition. Hence, all the evidence indicates that the decrease in susceptibility at low temperatures is due to promotion of electrons from the 4f shell of the cerium atoms into the conduction band of the alloys. It is interesting that the cerium–lanthanum alloys do not show this effect at low temperatures (Roberts and Lock 1957). This is probably because the cerium–lanthanum alloys are close-packed hexagonal, while the cerium–thorium are face-centred cubic. Schuch and Sturdivant (1950) have shown that the α-phase is only formed from face-centred cubic γ-phase cerium and not from the close-packed hexagonal β-phase. Another possible explanation is that the lanthanum atoms, being larger than the cerium atoms, do not produce the necessary compressive strains when cerium is introduced into their lattice, whereas the thorium atoms, being smaller than the cerium, are able to do so.

Figure 2 shows that as the concentration of cerium decreases the value of p_{eff} rises from 2·57 for pure cerium to 3·65 per cerium atom when extrapolated to infinite dilution. Roberts and Lock (1957) investigated the magnetic properties of solid solutions of cerium in lanthanum and likewise found that the effective moment per cerium atom increased upon dilution. Their results are also shown in figure 2. They suggested in explanation that the cerium atoms in the dilute cerium–lanthanum alloys gained one or even two extra electrons in the 4f shell. An atom with two 4f electrons has a p_{eff} of 3·58. This value is close to the maximum p_{eff} obtained for the cerium–thorium alloys. Hence the results of the magnetic measurements upon both cerium–lanthanum and cerium–thorium alloys might seem to indicate that as cerium is diluted, an increasing proportion of the cerium atoms gain an extra 4f electron, until at infinite dilution all the cerium atoms have at least two electrons in the 4f shell.

However, the above hypothesis raises certain difficulties. On this model the magnetism of the alloys arises from atoms of two kinds, those having one 4f electron and those having two 4f electrons. It is rather surprising that the susceptibility of such a system should obey a Curie–Weiss law. In order to explain the observed variation of lattice parameter with composition of the cerium–thorium alloys it is necessary to assume that the cerium atom contracts upon gaining an extra 4f electron. This seems unlikely, as the atom also contracts upon losing its 4f electron to form Ce^{4+} ions as in α-phase cerium. Again, as indicated above, the most probable explanation for the anomalous decrease in susceptibility at low temperatures is formation of Ce^{4+} ions. It appears improbable that some of the cerium atoms should possess an extra 4f electron only to lose both at a lower temperature. It is apparent that the theory outlined above is unsatisfactory as it introduces more difficulties than it explains and another explanation will be considered below.

Investigation of the Hall effect for thorium indicates that conduction is due to about 1·6 electrons per atom (Bodine 1956). This suggests that the two 7s electrons form a conduction band, while the two 6d electrons are either localized or are in a very narrow band. Whatever the band structure there must be, on average, four electrons in a unit cell round each thorium ion core. The charge distribution in a metal may be considered to be the sum of two distributions, one with positive spin and one with negative. In thorium metal these will be identical and the resultant moment, which is the difference between the two, will be zero. If a cerium atom is introduced into the thorium lattice the charge distribution will be altered in the neighbourhood of the impurity (cerium) site. The cerium atom has three electrons outside a filled 5p shell and in order to maintain electrical neutrality, even if these electrons enter the thorium conduction band, there will be on average three electrons round the cerium core. It is suggested that exchange coupling occurs between the localized electron in the cerium 4f shell and these outer electrons in the cerium–thorium alloys. Then it is probable that the charge distribution will no longer be the same for positive and negative spins, thus giving rise to a resultant moment of the conduction electrons. Following Yosida (1957), it might be expected that this polarization of the conduction electrons would be concentrated near the cerium atoms. Thus, apart from the usual 4f moment, there would be a resultant moment, not necessarily integral, associated with each cerium atom. As the concentration of cerium in the alloys is increased this polarization will tend to be ‘ smoothed out ’ and the f–s interactions will be manifest as indirect coupling of the f electrons rather than as extra moments in the alloy. This is probably the reason why the susceptibility of cerium obeys a Curie–Weiss law and not a Curie law at low temperatures.

On this model, WFR’s explanation of the variation of lattice parameter still applies. It may be supposed that a certain proportion of the cerium atoms have lost their 4f electron thus causing an anomalous shrinkage of the alloy. The rest, with their associated conduction electron moment, can still give rise to an apparent p_{eff} larger than 2·54. It is perhaps physically more probable that, instead of the cerium atoms either possessing or being completely without a 4f electron, there is a dynamic arrangement such that an electron spends part of the time in the cerium 4f shell and part outside in, say, the 5d shell. This idea might also explain the large magnitude of the f–s coupling in the thorium-rich alloys, as the longer the electron spends outside the f shell the more chance it has to interact with the conduction electrons. At low temperatures the electron is completely removed from the 4f shell and the coupling is destroyed. There is no guarantee that this model would give rise to a Curie–Weiss law for the alloys, or that it would predict values of θ as large as those found experimentally. However, the concepts of θ and p_{eff} are the consequences of the method of analysis and this may not have been justified.

§ 5. CONCLUSION

A model has been proposed to explain the variation of lattice parameter with composition and the temperature dependence of the susceptibility of alloys of the cerium–thorium system. It is supposed that the cerium ions in the alloy are resonating between Ce^{3+} and Ce^{4+} states, so that, on average, a certain proportion of the atoms may be considered to be without 4f electrons, thus causing an anomalous shrinkage of the lattice. It is further proposed that the f electrons are coupled to the conduction electrons so causing polarization of the latter in the vicinity of the cerium atoms, the apparent increase in p_{eff} being attributed to this induced moment. The decrease in susceptibility at low temperatures can be explained by assuming the complete removal of some of the 4f electrons into the conduction band at these temperatures.

ACKNOWLEDGMENTS

The authors are particularly indebted to Dr. P. C. L. Pfeil, Atomic Energy Research Establishment, Harwell, for his interest in the topic and for arranging the neutron diffraction measurements, and to Miss J. R. Murray, also of Atomic Energy Research Establishment, who prepared the specimens. They also thank Dr. K. W. H. Stevens for the suggested explanation and Dr. S. J. Leach for helpful discussions. M.M.N. is grateful to the Department of Scientific and Industrial Research for a maintenance grant which made the work possible.

REFERENCES

BATES, L. F., 1951, *Modern Magnetism* (Cambridge: University Press).
BATES, L. F., LEACH, S. J., and LOASBY, R. G., 1955, *Proc. Phys. Soc.* B, **68,** 859.
BODINE, J. H., 1956, *Phys. Rev.*, **102,** 1459.
HOARE, F. E., and WALLING, J. C., 1951, *Proc. Phys. Soc.* B, **64,** 337.
LA BLANCHETAIS, H., 1954, *J. Rech.*, **29,** 103.
LAWSON, A. W., and TANG, T. Y., 1949, *Phys. Rev.*, **76,** 301.
LEACH, S. J., 1955, *Thesis*, University of Nottingham.
LOASBY, R. G., 1957, *Thesis*, University of Nottingham.
LOCK, J. M., 1957, *Proc. Phys. Soc.* B, **70,** 566.
NEWMANN, M. M., 1958, *Thesis*, University of Nottingham.
ROBERTS, L. M., and LOCK, J. M., 1957, *Phil. Mag.*, **2,** 811.
SCHUCH, A. F., and STURDIVANT, J. H., 1950, *J. Chem. Phys.*, **18,** 145.
VAN VUCHT, J. H. N., 1957, *Philips Res. Rep.*, **12,** 351.
WEINER, R. T., FREETH, W. E., and RAYNOR, G. V., 1957, *J. Inst. Metals*, **86,** 185.
YOSIDA, K., 1957, *Phys. Rev.*, **106,** 893.

Thermal Diffusion in Ionized Gases

By SYDNEY CHAPMAN

Geophysical Institute, University of Alaska and High Altitude Observatory†, Boulder, Colorado

MS. received 17*th March* 1958, *and in final form* 28*th May* 1958

Abstract. Thermal diffusion in mixed gases depends on a ' thermal diffusion factor ' α, which is less than unity in all known *neutral* gas mixtures (in which the particles have no electric charge).

In simple *ionized* gases α exceeds unity, being of order $Z+1$, where Ze is the charge on the ions. However, in the steady state of such a gas, at non-uniform temperature, thermal diffusion does not produce a concentration gradient of the electrons relative to the ions; instead it sets up an electric field, which keeps the gas electrically neutral almost everywhere. In an ionized atmosphere subject to gravity, in which the temperature increases upwards, this electric field opposes and reduces the electric field that keeps the electrons and ions together, despite the great difference between their masses. The thermal diffusion factor seems to be greatest for the ions of different kinds in a mixed ionized gas, composed mainly of electrons and light ions of small charge Ze, with a small admixture of heavy ions of greater charge $Z'e$. In this case α is of order $2{\cdot}5\,(Z'/Z)^2$, and can amount to several hundred. In such a gas, at non-uniform temperature, thermal diffusion can much increase the (still small) proportion of the heavy multiple ions in the hotter regions. The electric field that keeps the electrons with the ions, so that the gas is neutral, reinforces this tendency of the multiple ions, in the cases here considered.

This tendency may have some importance in the solar corona, if turbulence is not too great and temperature inequalities persist long enough.

It seems likely also that thermal diffusion will influence the distribution of the multiple ions present in the ZETA nuclear fusion apparatus.

§ 1. Introduction

In a mixed gas four different kinds of diffusion can occur: they are (*a*) forced diffusion, produced by external forces that differently accelerate the particles of different kinds, and (*b*), (*c*), (*d*) ordinary, pressure, and thermal diffusion, produced respectively by gradients of concentration, pressure and temperature.

Thermal diffusion, discovered theoretically by Enskog (1911, 1912, 1917) and myself (1916) independently, was first experimentally verified in 1916 (Chapman and Dootson 1917). Two books (Chapman and Cowling 1939, 1952, Grew and Ibbs 1952), here for brevity indicated by the initials CC and GI, give general accounts of the subject. Thermal diffusion has much scientific interest, and also practical importance, as shown by the use of the thermal diffusion column (Clusius and Dickel 1938) for isotope separation, in nuclear research establishments and elsewhere. In Nature, however, thermal diffusion

---

† The portion of this work done at High Altitude Observatory was supported by the National Bureau of Standards and the Air Force Cambridge Research Center.

has hitherto seemed to be of only minor interest as, for example, in the earth's atmosphere (Chapman 1955) and in stars (Chapman 1917 a, b, 1922).

However, in June 1957 I found that in multiply ionized gases thermal diffusion can be powerful (Chapman 1958). It may be important in the solar corona. This and other astronomical cases will be discussed elsewhere (Aller and Chapman 1958, Chapman and Tandberg-Hanssen 1958). The phenomenon may also be of interest in connection with apparatus for producing nuclear power from hydrogen.

Here I give a general account of thermal diffusion in ionized gases, using only the formulae appropriate to a binary mixture. These seem to suffice to treat approximately some important cases of multiple mixtures. A fuller treatment of the latter will be given elsewhere, in conjunction with E. Tandberg-Hanssen.

§ 2. BINARY DIFFUSION

The equation of diffusion in a binary mixed gas (CC p. 244) may be written

$$\overline{\mathbf{C}}_1 - \overline{\mathbf{C}}_2 = -D_{12}\left\{\frac{\operatorname{grad} c_1}{c_1 c_2} - \frac{m_1 - m_2}{m}\operatorname{grad}\ln p + \alpha_{12}\operatorname{grad}\ln T - \frac{m_1 m_2}{kmT}\left(\frac{\mathbf{F}_1}{m_1} - \frac{\mathbf{F}_2}{m_2}\right)\right\}. \qquad \ldots\ldots(1)$$

The notation here used is the same as that used in CC and GI, except that c_1 and c_2 here replace n_{10} and n_{20} (or n_1/n and n_2/n) for the relative concentrations of the particles of the two kinds 1, 2, and m signifies the mean mass

$$m = c_1 m_1 + c_2 m_2\,; \qquad \ldots\ldots(2)$$

also $\mathbf{F}_1$ and $\mathbf{F}_2$ signify the external *forces* on the particles, instead of the corresponding *accelerations* (as in CC p. 47). The equation (1) expresses the diffusion velocity (on the left) as the sum of four parts, the velocities of ordinary, pressure, thermal and forced diffusion.

The factor α_{12} in (1) is called the thermal diffusion factor (Furry, Clark Jones and Onsager 1939); it is related to the thermal diffusion ratio k_T (CC p. 144), used in CC p. 244, as follows:

$$k_T = c_1 c_2 \alpha_{12} = -c_1 c_2 \alpha_{21}. \qquad \ldots\ldots(3)$$

When the particles 1 or 2 are electrons, protons or ions (of other kinds), the suffixes e or p or i may when convenient be used instead of 1 or 2. The kinetic theory evaluates α_{12} in the form of an infinite series; in general the terms are complicated. Fortunately even the first term is a fair approximation. In CC and GI this approximation is denoted by $[\alpha_{12}]_1$, but here the bracket symbol will be omitted. That is, here α_{12} will generally signify the first approximation. The true value in the cases of interest in this paper will, however, be rather greater than the first approximation. For a Lorentzian ionized gas the increase needed is about 30% (that is, the increase is by a factor 1/0·77; see CC p. 196, Table 7, last column, row 1). Such an increase will apply also approximately to the case of thermal diffusion between protons and multiply charged ions that are many times heavier than the protons (see CC p. 187, 10.5, condition (*b*)); this corresponds to the problem considered in § 7.

As in CC p. 253 and GI p. 27,

$$\alpha_{12} = 5(C-1)\,\frac{c_1 S_1 - c_2 S_2}{c_1^2 Q_1 + c_1 c_2 Q_{12} + c_2^2 Q_2}. \qquad \ldots\ldots(4)$$

§ 3. The Thermal Diffusion Factor for a Fully Ionized Gas

In a fully ionized gas the forces between the particles, with charges e_1, e_2, at distance r apart, are

$$e_1{}^2/r^2,\ e_2{}^2/r^2 \text{ and } e_1e_2/r^2,$$

all varying as the inverse square. In this case (CC pp. 172, 179)

$$5(C-1) = -3, \qquad \ldots\ldots (5)$$

and other magnitudes involved in the expressions for the S's and Q's in (4) have the special values:

$$\left.\begin{aligned} A &= \frac{2}{5}\left\{1 - \frac{x^2}{(1+x^2)\ln(1+x^2)}\right\}, \quad B = \tfrac{3}{5}, \\ E_1 &= \left(\frac{2}{M_2}\right)^{1/2}\left(\frac{e_1}{e_2}\right)^2, \quad E_2 = \left(\frac{2}{M_1}\right)^{1/2}\left(\frac{e_2}{e_1}\right)^2 \end{aligned}\right\}. \qquad \ldots\ldots (6)$$

Here E_1 and E_2 are the magnitudes so denoted in GI p. 26, which in CC are denoted by $M_1E/[\mu_1]_1$ and $M_2E/[\mu_2]_1$; and

$$x^2 = (4dkT/e_1e_2)^2, \qquad \ldots\ldots (7)$$

where d denotes a ' cut-off ' length, the upper limit for certain definite integrals. The length d has been variously estimated; one estimate (Chapman 1922), which may be denoted by d_C, is given by

$$d_C = 1/n^{1/3}; \qquad \ldots\ldots (8)$$

another, d_D, based on Debye's theory of charge shielding (Persico 1926), is given (Landau 1936, Bohm and Aller 1947, Cohen, Spitzer and Routly 1950) by

$$d_D{}^2 = kT/4\pi ne^2. \qquad \ldots\ldots (9)$$

In each case n signifies the number of particles per cm³. The two estimates may differ considerably. For example, if T is 10^6 deg K, and n is $2 \times 10^9\,\text{cm}^{-3}$ (these values may be appropriate for the solar corona at the level of average maximum T), d_C is 8×10^{-4} and d_D is 0·15 cm. The corresponding values of x^2 are given by

$$Z_1{}^2Z_2{}^2x_C{}^2 = 3{\cdot}6 \times 10^{12}, \quad Z_1{}^2Z_2{}^2x_D{}^2 = 1{\cdot}3 \times 10^{17}. \qquad \ldots\ldots (10)$$

Here Z_1 and Z_2 denote the charge numbers, such that

$$e_1 = Z_1\boldsymbol{e}, \quad e_2 = Z_2\boldsymbol{e},$$

where $\boldsymbol{e}$ signifies the unitary charge $4{\cdot}802 \times 10^{-10}$ e.s.u.

Despite the great difference between the two values in (10), the corresponding values of A differ little; for example, if both Z's are unity, A_C is 0·386 and A_D is 0·390. The greater the values of d and x, the more nearly does A approach its upper limit 0·4. The following table gives some values of A for a range of values of x^2.

Table 1

$x^2 = 10^s$

s	1	2	3	4	5	6	7	8	9	10
A	0·248	0·314	0·342	0·356	0·365	0·371	0·375	0·378	0·381	0·383

In the present case, of inverse square forces, the magnitudes S, Q in (4) are given by

$$S_1 = M_1(2M_2)^{1/2}(Z_1/Z_2)^2A - 4AM_1M_2 + 3M_2(M_1 - M_2) \qquad \ldots\ldots (11)$$

$$Q_1 = (2M_2)^{1/2}(Z_1/Z_2)^2A(6M_2{}^2 + 2{\cdot}6M_1{}^2 + 8AM_1M_2) \qquad \ldots\ldots (12)$$

$$Q_{12} = 4(M_1M_2)^{1/2}A^2 + 7{\cdot}8(M_1 - M_2)^2 + 34{\cdot}4AM_1M_2, \qquad \ldots\ldots (13)$$

and similarly, by interchange of the suffixes 1, 2, for S_2 and Q_2. Here

$$M_1 = m_1/(m_1+m_2), \quad M_2 = m_2/(m_1+m_2) = 1 - M_1, \qquad \ldots\ldots(14)$$

where m_1 and m_2 denote the masses of the particles of kinds 1, 2.

Thus α_{12} is a function of c_1, M_1, Z_1/Z_2, and also, to a less extent, through A, of n and T.

It would be of value to study the dependence of α_{12} on the variables c_1, M_1 and Z_1/Z_2 for one or two values of A, such as 0·4 and 0·375, perhaps on the lines of my earlier discussion of the characteristics of thermal diffusion in neutral gases (Chapman 1940). As a first step toward such a study, some interesting special cases will here be considered.

§ 4. AN IONIZED GAS: ELECTRONS AND IONS, OR POSITIVE AND NEGATIVE IONS

As an ionized gas must be neutral to a high degree of approximation,

$$c_1e_1 + c_2e_2 = 0, \quad c_1Z_1 + c_2Z_2 = 0, \quad \frac{e_1}{m_1} - \frac{e_2}{m_2} = \frac{m(e_1-e_2)}{m_1m_2}. \qquad \ldots\ldots(15)$$

If the negative charges (2) are electrons, M_2 is very small. The limiting value of α_{12} in this case, for which Z_2 is -1, is given by

$$\lim_{M_2\to 0} \alpha_{12} = \frac{-3(Z_1+1)}{2{\cdot}6 + 2\sqrt{2A/Z_1}} = \lim \alpha_{1e}. \qquad \ldots\ldots(16)$$

The minus sign in (16) implies that the ions tend towards the hotter regions.

The following table gives values of $-\lim \alpha_{1e}$ for a few values of Z_1, and for two values of A.

Table 2

Z_1		1	2	3	4	5	6	7	8	9	10
α_{1e}	$A=0{\cdot}4$	1·61	2·85	4·03	5·21	6·4	7·5	8·7	9·9	11·0	12·2
	$A=0{\cdot}3$	1·74	2·97	4·17	5·35	6·5	7·7	8·8	10·0	11·2	12·3

All these values of $\lim \alpha_{1e}$ numerically exceed the greatest known value of α_{12} for gas mixtures of neutral particles; the greatest observed value, for a helium–radon mixture, is 0·64. Thus thermal diffusion is more powerful in an ionized gas consisting of electrons and ions, than in neutral gases, and the more so, the higher the charge number of the ions.

The values of $\lim \alpha_{1e}$ may be supposed to refer to electrons and infinitely massive ions. But the value of α_{1e} for electrons and ions of finite mass—even the smallest, namely when the ions are protons—is scarcely different. The next approximation to α_{1e}, for finite but small M_2, is given by multiplying the expression in (16) by

$$(a - M_2)/(a - bM_2), \qquad \ldots\ldots(17)$$

where

$$a = 1 + (3/AZ_1)(\tfrac{1}{2}M_2)^{1/2}, \quad b = (5{\cdot}2 - 8A - \sqrt{2A/Z_1})/(2{\cdot}6 - 2\sqrt{2A/Z_1}). \qquad \ldots\ldots(18)$$

The new factor in (17) is greatest for the case $Z_1 = 1$, and for the lightest ions, protons, for which M is 1/1838. For $A = 0{\cdot}4$, the factor is then 0·9997. Thus it appears that in all cases (16) is a valid approximation to α_{1e}.

Another case, of less physical interest, is that of a gas composed entirely of positive and negative ions, formed by ionizing dissociation of molecules, or by attachment of electrons originally formed. If the charges are of equal magnitude ($Z_1 = -Z_2$), and the masses also are equal, then $M_1 = M_2 = \frac{1}{2}$; in this case α_{12} is zero. If the charges are equal and opposite, but the masses are unequal, the heavier ions will tend to the hotter regions. The greater the mass ratio, the greater is α_{12}, and as M_2 tends to zero α_{12} tends to the value given by (16). The following table shows how $-\alpha_{12}$ varies with M_2 for equally charged positive and negative ions, when A is 0·4.

Table 3

Values of $-\alpha_{12}$ when $Z_1 = -Z_2$, $A = 0{\cdot}4$; $c_1 = c_2 = \frac{1}{2}$

m_1/m_2	∞	16	4			
M_2	0	0·059	0·2	0·35	0·45	0·5
$-\alpha_{12}$	1·61	1·55	1·29	0·76	0·26	0
Example:		O^-, H^+	He^+, H^-			

§ 5. THE BINARY ION–ION THERMAL DIFFUSION FACTOR: SPECIAL CASE

Next consider a triple mixture consisting of two sorts of ions, one (1) much more abundant than the other (2), together with electrons (3), so that the gas is neutral. The condition of neutrality is

$$c_1 Z_1 + c_2 Z_2 = c_3.$$

The discussion of diffusion in a triple mixture involves very complicated equations, but in the present case it is of interest to calculate the binary thermal diffusion factor for the two kinds of ion, ignoring the presence of the electrons. The general formula (4), when c_2 is very small, tends to the limiting form:

$$\lim_{c_2 \to 0} \alpha_{12} = 5(C-1) S_1/Q_1 = -3 S_1/Q_1. \qquad \ldots\ldots (19)$$

Taking A to be 0·4, this can be expressed thus:

$$\lim_{c_1 \to 0} \alpha_{12} = -3 \frac{1 - M_2 - 5\sqrt{2}(Z_2/Z_1)^2 (1{\cdot}1 M_2^{5/2} - 0{\cdot}35 M_2^{3/2})}{2{\cdot}6 - 2M_2 + 5{\cdot}4 M_2^2}. \qquad \ldots\ldots (20)$$

Here α_{12} is expressed as a function of only two parameters, M_2 and $(Z_2/Z_1)^2$.

One special case is when M_2 tends to zero; then

$$\alpha_{12} \to -1{\cdot}13 \quad (c_2 \to 0,\ M_2 \to 0). \qquad \ldots\ldots (21)$$

Another special case is when M_2 tends to 1, or M_1 tends to zero : then

$$\alpha_{12} \to 2{\cdot}65 (Z_2/Z_1)^2 \quad (c_2 \to 0,\ M_1 \to 0); \qquad \ldots\ldots (22)$$

the factor 2·65 represents $15/4\sqrt{2}$.

It may also be noted that when $M_1 = M_2 = \frac{1}{2}$, the formula for α_{12}, whatever the value of c_2, contains the factor $Z_1^2 - Z_2^2$, so that if the charges are equal there is no thermal diffusion between the ions; this is natural, because their masses and fields of force are then equal, except for the signs of the forces, which do not affect α_{12}. For any value of Z_1/Z_2 there is a certain range of M_1 (or M_2) for which α_{12} changes sign as c_1 increases from 0 to 1.

The case of greatest interest above is (22), because when the rare ions are much more highly charged than the abundant ions, so that Z_2/Z_1 is large, α_{12} can take very large values. An example, relevant to the solar corona, is that of a mixture of rare heavy multiple ions such as Ni XVI in an excess of ionized atomic hydrogen. In this case Z_2/Z_1 is 15, and M_1 is 1/59·2. The limiting value of (22) for $M_2 = 0$ and $Z_2/Z_1 = 15$ is 596, almost a thousand times the greatest known value of α_{12} for neutral particles (0·64; cf. §4). This limiting value needs correction for the finite value of M_1, by the factor, applicable to (22),

$$1-2{\cdot}567M_1+(2\sqrt{2}/15)(Z_1/Z_2)^2M_1. \qquad \ldots\ldots(23)$$

In the case of the hydrogen–Ni XVI mixture, this reduces α_{12} by 4·34% to 570.

The signs of α_{12} in (21) and (22) differ because the heavier particles are of kind 1 in (21) and of kind 2 in (22); in both cases the heavier particles tend towards the hotter regions.

§ 6. THERMAL DIFFUSION IN A BINARY IONIZED GAS

In a mixed gas at constant pressure, whose particles are subject to no external forces, a temperature gradient will tend to set up a steady state, in which there is a gradient of concentration, from c_1 at one end of the vessel, where the temperature is T, to c_1' at the other end, where the temperature is T', so that the ordinary and thermal diffusion velocities balance one another. This requires that

$$\operatorname{grad} c_1 = -k_T \operatorname{grad} \ln T, \quad \text{or} \operatorname{grad} \ln c_1 = \alpha_{12} \operatorname{grad} \ln T. \qquad \ldots\ldots(24)$$

If the actual and proportionate changes of c_1 from one end of the vessel to the other are small enough to permit k_T to be treated as constant along the vessel, an approximate solution of (24) is

$$c_1 - c_1' = k_T \ln (T'/T). \qquad \ldots\ldots(25)$$

But if c_1 is small, and its proportionate change along the vessel is not small, a more accurate approximation to the solution of (24) is

$$c_1'/c_1 = (T/T')^{\alpha_{12}}. \qquad \ldots\ldots(26)$$

This is valid only so long as both c_1 and c_1' are small. When α_{12} is very large, as in the case cited at the end of the last section, a very small gradient of T can produce a large proportionate change of c_1—for example from $c_1 = 10^{-6}$ to $c_1 = 10^{-2}$.

But such large values of α_{12} only arise in connection with ionized gases, and in their case any tendency to modify c_1 from the value given by the neutrality condition (15) will set up an electric field. This is so whether the diffusion tendency is due to a gradient of T or of the pressure p. A very minute electric field suffices to keep the gas neutral to a very high degree of approximation. This subject is well discussed by Eddington (1926) in connection with stellar gases.

Consider first a binary ionized gas, consisting of only one kind of positive particles and one of negative. If the gas is subject to gravity $\mathbf{g}$ as well as to the electric field set up as stated, we have:

$$\mathbf{F}_1 = m_1\mathbf{g} + \mathbf{E}e_1 = m_1\mathbf{g} + Z_1\mathbf{E}e, \quad \mathbf{F}_2 = m_2\mathbf{g} + Z_2\mathbf{E}e. \qquad \ldots\ldots(27)$$

Hence

$$\frac{\mathbf{F}_1}{m_1} - \frac{\mathbf{F}_2}{m_2} = \left(\frac{Z_1}{m_1} - \frac{Z_2}{m_2}\right)\mathbf{E}e = \frac{m(Z_1 - Z_2)\mathbf{E}e}{m_1 m_2}, \qquad \ldots\ldots(28)$$

using (15). Gravity does not appear in (28), but it determines the pressure gradient, according to the statical equation

$$\operatorname{grad} p = nm\mathbf{g} \qquad \ldots\ldots(29)$$

or

$$\operatorname{grad} \ln p = m\mathbf{g}/kT. \qquad \ldots\ldots(30)$$

The electric field does not appear in (29, 30) because the charge density is effectively zero.

Hence when the steady state of no diffusion is reached, (1) gives the electric field $\mathbf{E}$ that is set up to maintain the neutrality:

$$(Z_1 - Z_2)e\mathbf{E} = (m_2 - m_1)\mathbf{g} - k\alpha_{12}\,\mathrm{grad}\,T. \qquad \ldots\ldots (31)$$

Thus $\mathbf{E}$ has two parts, determined by the directions of $\mathbf{g}$ and of grad T. The electric component perpendicular to $\mathbf{g}$ is determined by grad T alone.

In §4 it has been shown that for a gas consisting of electrons and ions of one kind only, α_{1e} is practically independent of the ionic mass, the electronic mass being in any case so small in proportion. In such a gas Z_2 is -1, and the part $\mathbf{E}_{\mathrm{T}}$ of $\mathbf{E}$ due to the temperature gradient is given by

$$\mathbf{E}_{\mathrm{T}} = (k\alpha_{1e}\,\mathrm{grad}\,T)/(Z_1 + 1)e = -(3k\,\mathrm{grad}\,T)/(2{\cdot}6 + 2\sqrt{2A/Z_1})e, \quad \ldots (32)$$

using (16).

It is of interest to estimate the order of magnitude of this electric field in an 'ionosphere' composed of oxygen ions O^+ and electrons, with an upward gradient of T of amount 5 deg km^{-1}; in this case Z_1 is 1, and the electric force on an electron is $-e\mathbf{E}_T$, which, taking A to be 0·4, is $5{\cdot}5 \times 10^{-21}$ dyn upwards; if the field of gravity is taken to be 950 cm sec^{-2}, the part of the electric force on an electron due to the gravitational part of $\mathbf{E}$ is $-12{\cdot}6 \times 10^{-21}$ dyn downwards; thus thermal diffusion, which makes the electrons tend towards the cooler regions, that is, to move downwards, partly annuls the electric field arising from their tendency to rise above the heavier ions. The thermal part of $\mathbf{E}$ is almost independent of the ionic mass, unlike the gravitational part; in an ionosphere composed of *protons* and electrons—as in the outermost part of the earth's atmosphere—the downward gravitationally produced electric force on the electrons would be much exceeded by the upward electric force on them, due to the temperature gradient, if this were as much as 5 deg km^{-1}; however, in that part of the earth's atmosphere grad T will be smaller than 5 deg km^{-1}, and the net force on the electrons will, of course, be downward.

In a singly ionized gas whose negative particles are electrons, the electric field produced by a temperature gradient is practically the same, whatever the ionic mass; the latter, however, does determine the pressure and density gradient, in accordance with (30).

§ 7. HORIZONTAL THERMAL DIFFUSION IN A SPECIAL TYPE OF IONIZED MIXED GAS

The equation (1) of binary diffusion will next be applied to determine the equilibrium state in a special type of triple mixture, in the presence of a temperature gradient; for simplicity this will be supposed horizontal, so that gravity need not be considered, nor the pressure gradient in (1).

The special mixture consists of electrons together with ions of two kinds, kind 1 being light and abundant, kind 2 being heavy, highly charged, and rare. Such a gas is a simplified version of the solar coronal gas, in which the ions are mainly protons (with about 10% of alpha particles, He^{2+}); but there are also rare ions of argon, calcium, iron and nickel (such as Ni XVI, as mentioned already in § 5).

Diffusion in triple mixtures must in general be treated by a set of three simultaneous equations. But in the present special case it seems possible to obtain an approximate solution by means of equations of binary diffusion.

In a gas consisting solely of electrons and ions of kind 1, the temperature gradient will set up a horizontal electric field E_{1e}; this is given by (32) if the suffixes 1, 2 there are replaced by 1, e. The same equation, with the suffixes 1, 2 replaced by 2, e, will give the electric field E_{2e} set up by the temperature gradient in a gas consisting solely of electrons and ions of the kind 2. The ratio E_{2e}/E_{1e} is $(2{\cdot}6+2\sqrt{2A/Z_1})/(2{\cdot}6+2\sqrt{2A/Z_2})$. If Z_1 is 1 and Z_2 is 15, as when the ions 2 are Ni XVI, this ratio is 1·4; if instead Z_1 is 2 (e.g. for alpha particles) the ratio is 1·18. In the triple gas here considered, it seems reasonable to infer that the actual electric field will deviate very little from E_{1e}, being slightly increased by the presence of the ions of kind 2. Hence in considering the equation (1), the electric field will be taken to be E_{1e}.

The temperature gradient will also affect the distribution of the ions. Thermal diffusive action between them will make the ions of kind 2 tend towards the hotter regions, as indicated in § 5. This tendency will slightly affect the electric field, but will not be nullified by the field, as is the thermal diffusive tendency in a mixture of electrons and ions of only one kind. The electric field in the triple mixture will cause the electrons easily and quickly to adjust their distribution so as to preserve the neutrality of the gas, despite a gradient of relative concentration of the ions 1, 2. The change in the electric field on this account will be small, and in (1) the field will be taken to be E_{1e}. The term $(\operatorname{grad} c_1)/c_1c_2$ will be changed to the equal term $(-\operatorname{grad} c_2)/c_1c_2$, or, taking c_1 to be effectively unity, to $-\operatorname{grad}\ln c_2$. Also m in the last term of (1) is replaced by m_1, as the ions 2 are rare. In this last term it is not possible to use equations (15) and (28), which depend on the neutrality condition in a binary ionized gas; here there is no fixed relation between c_1/c_2 and Z_1/Z_2, and in fact the former is supposed large and the latter a moderate fraction. Thus (1) leads to the approximate steady state relation

$$\operatorname{grad}\ln c_2 = (\alpha_{12}-\alpha_{12e})\operatorname{grad}\ln T \qquad \ldots\ldots(33)$$

where α_{12} is given by (22), to a first approximation, and

$$\alpha_{12e} = 3(m_2Z_1/m_1 - Z_2)/(2{\cdot}6+2\sqrt{2A/Z_1}). \qquad \ldots\ldots(34)$$

A better approximation to α_{12} is given by inserting the factor (23) into (22).

If the rare ions are Ni XVI, and the main ions are protons, so that Z_1 is 1 and Z_2 is 15, and m_2/m_1 is 59·2, α_{12e} is 35·5. As α_{12}, from (22) corrected by (23), is in this case 570, the factor of $\operatorname{grad}\ln T$ in (33) is 605. Hence $\operatorname{grad}\ln c_2$ is in this case 605 $\operatorname{grad}\ln T$. Corresponding to (26) we have

$$c_2'/c_2 = (T/T')^{\alpha_{21}} = (T'/T)^{\alpha_{12}}. \qquad \ldots\ldots(35)$$

If T' exceeds T, c_2' will exceed c_2 because α_{12} is positive; that is, the Ni ions will be more abundant in the hotter than in the colder regions; (35) is valid only so long as both c_2 and c_2' are small.

In conclusion it may be indicated why in this example the electric field caused by the thermal diffusive action between the electrons and ions enhances the thermal diffusive action between the ions themselves. The field set up by the former action resists the tendency of the ions to seek the hotter region; hence the force it exerts on the ions is towards the colder region. The force is greater on the ions 2 than on the less highly charged ions 1; but the accelerative action on the ions 1 is the greater, because m_2 exceeds m_1 more than Z_2 exceeds Z_1.

Hence the field E_{1e} tends to concentrate the ions 1 towards the colder region, and enhances the tendency of the ions 2 to seek the hotter region.

§ 8. APPLICATION TO THE ZETA NUCLEAR FUSION APPARATUS

In the ZETA nuclear fusion apparatus (Thonemann *et al.* 1958) a gas consisting largely of deuterium, though containing minor amounts of other gases, is raised to a high temperature by the passage through it of a strong electric current. The number density of the gas is of order 10^{13} to 10^{14}. A magnetic field of order 160 gauss (Thonemann *et al.* 1958, Figs. 2, 3) is applied along the direction of the current; the lines of magnetic force of the combined external field and the field of the current are helices round the direction of the current. The temperatures attained are estimated in more than one way—by calculation from the observed neutron yield, and from the Doppler width of certain lines of multiply charged ions, such as N IV and O V, seen in the spectrum of the discharge. The values are of order 2 to 5 million degrees; the estimates from the Doppler widths are mainly less than those calculated from the neutron yield (Thonemann *et al.* 1958, Fig. 6). The deuterium will be completely ionized.

It seems of interest to consider whether thermal diffusion can operate to any material extent in this apparatus, so as to concentrate the multiply charged ions towards the axis of the current, where T will be greatest. The case is to some degree similar to that considered in § 7, though here Z_2 is 3 or 4 instead of 15; as there, Z_1 for the deuterium ions is 1. The important question is whether the duration of the current—estimated as of the order of milliseconds—suffices to allow a significant degree of such concentration of the multiple ions to occur.

In a binary gas in which c_2 is small and initially equal to $C_2 \exp(-x/L)$, the time of relaxation, in the absence of maintaining causes, is L^2/D_{12}. The present case is more complicated. The thermal gradient generates diffusion with speed $-\alpha_{12}D_{12}\operatorname{grad}\ln T$, which tends to set up a concentration gradient. But a concentration gradient generates an opposing diffusion with speed $-D_{12}\operatorname{grad}\ln c_2$ (when c_2 is small and c_1 practically unity). The steady state is given by (26), but there appears to be no simple exponential mode of approach with a definite relaxation time. However, we may as before adopt L^2/D_{12} as giving the order of magnitude of the time required.

The first approximation to D_{12} is given by CC p. 179 as

$$\frac{3(2kT)^{5/2}}{16n(\pi m_1 M_2)^2 Z_1^2 Z_2^2 e^4 A_1(2)},$$

where, cf. (7), $A_1(2) = \ln(1+x^2)$. In the present case $A_1(2)$ will be about 20. For deuterium, m_1 is $3{\cdot}3 \times 10^{-24}$, and here M_2 is 8/9. Taking T to be 2×10^6, the value found for D_{12} is 8×10^8; but this is less than the true value by a factor approximately equal to 3·4 (CC p. 196, Table 6, last row and column), giving $2{\cdot}7 \times 10^9$.

However, in an ionized gas D_{12} is reduced by the presence of a magnetic field transverse to the direction of diffusion. The reduction factor (CC p. 335) is approximately

$$1/(1+\omega^2\tau^2)$$

where (now using electromagnetic units of charge)

$$\omega = \frac{H(n_2 e_1 m_2/m_1 + n_1 e_2 m_1/m_2)}{n_1 m_1 + n_2 m_2} \quad \text{and} \quad \tau = \frac{m_1 m_2 n D_{12}}{kT(n_1 m_1 + n_2 m_2)}.$$

As n_1/n_2 is supposed large, these formulae approximate to

$$\omega = e_2H/m_2, \quad \tau = m_2D_{12}/kT, \quad \omega\tau = e_2HD_{12}/kT.$$

For a mixture D II, O V, with H equal to 160 gauss, these formulae give $\omega\tau$ as about 100; at the centre of the Zeta tube H may be as much as 1000 gauss, making $\omega\tau$ about 600. Thus the reduced values of D_{12} will be about 3×10^5 or 10^4.

Taking the length L to be 15 cm (as the current diameter is given as from 20 to 40 cm) the time L^2/D_{12} is found to be about 0·8 millisecond in the weaker part of the magnetic field (160 gauss); for the stronger part (1000 gauss) the value of L to be taken will be smaller, say 5 cm; in this case L^2/D_{12} is of order 2·5 msec. Thus there seems a likelihood that thermal diffusion may appreciably affect the distribution of the heavier ions in the tube, so that the Doppler widths shown by the spectrum would correspond to the greater temperatures in the gas. This calculation is very rough and is perhaps worth elaborating and refining.

ACKNOWLEDGMENTS

It is a pleasure to acknowledge the assistance, in the preparation of this paper, of Dr. E. Tandberg-Hanssen, of the High Altitude Observatory, Boulder, Colorado. The part of this work that was done at the Observatory was supported by the National Bureau of Standards and the Air Force Cambridge Research Center.

REFERENCES

ALLER, L. H., and CHAPMAN, S., 1958, *Astrophys. J.*, **127**, 797.

BOHM, D., and ALLER, L. H., 1947, *Astrophys. J.*, **105**, 131.

CHAPMAN, S., 1916, *Proc. Roy. Soc.* A, **93**, 1; 1917 a, *Mon. Not. R. Astron. Soc.*, **77**, 539; 1917 b, *Ibid.*, **77**, 540; 1922, *Ibid.*, **82**, 292; 1940, *Proc. Roy. Soc.* A, **177**, 38; 1955, *J. Met.*, **12**, 11; 1958, *Transport Phenomena in Gases*, (ed. A. B. Cambel and J. B. Fenn), (Evanston, Illinois: Northwestern University Press), p. 149.

CHAPMAN, S., and COWLING, T. G., 1939, 1952, *The Mathematical Theory of Non-Uniform Gases* (Cambridge: University Press).

CHAPMAN, S., and DOOTSON, F. W., 1917, *Phil. Mag.*, (6), **33**, 248.

CHAPMAN, S., and TANDBERG-HANSSEN, E., 1958, *Extremely High Temperatures*, (ed. H. Fischer and L. C. Mansur), (Boston, Mass.: John Wiley), p. 139.

CLUSIUS, K., and DICKEL, G., 1938, *Naturwissenschaften*, **26**, 546.

COHEN, R. S., SPITZER, L., JR., and ROUTLY, P. M., 1950, *Phys. Rev.*, **80**, 230.

EDDINGTON, A. S., 1926, *The Internal Constitution of the Stars* (Cambridge: University Press).

ENSKOG, D., 1911, *Phys. Z.*, **12**, 533; 1912, *Ann. Phys., Lpz.*, **38**, 731; 1917, *Dissertation*, Upsala.

FURRY, W. H., CLARK JONES, R., and ONSAGER, L., 1939, *Phys. Rev.*, **55**, 1083.

GREW, K. E., and IBBS, T. L., 1952, *Thermal Diffusion in Gases* (Cambridge: University Press).

LANDAU, L., 1936, *Phys. Z. Sowjet*, **10**, 154.

PERSICO, E., 1926, *Mon. Not. R. Astron. Soc.*, **86**, 93.

THONEMANN, P. C., *et al.*, 1958, *Nature, Lond.*, **181**, 217.

The Experimental Determination of the Primary Ionization Coefficients at Low Gas Pressures

By EIFIONYDD JONES and F. LLEWELLYN JONES
Department of Physics, University College of Swansea

MS. received 12*th March* 1958, *and in final form* 23*rd April* 1958

Abstract. An assessment of the method used to measure values of the Townsend primary coefficient of ionization at low pressures is given. This shows that the secondary processes of ionization must, in general, be taken into consideration in the analysis of the data, especially at pressures of the order of a few millimetres of mercury, in order to obtain accurate values of α/p_0.

§ 1. INTRODUCTION

In recent studies of the temporal growth of ionization currents (Morgan 1956) in hydrogen in uniform fields carried out at Swansea, application of the rigorous theory of the growth to the calculation of the current in specific cases requires a knowledge of accurate values of the Townsend primary coefficient of ionization α and of the generalized secondary coefficient ω/α. Experiments have accordingly been carried out to determine these coefficients for hydrogen over a wide range of the parameter E/p, where E is the electric intensity and p the gas pressure. The usual method of measuring these coefficients for a constant uniform field is based on the measurement of spatial growth of the steady state current I between parallel plates; indeed the coefficient α was originally defined in relation to just such conditions. From the definition of the coefficients it then follows that the steady current between electrodes distance d apart is given by the well-known equation

$$I=\frac{I_0\exp\{\alpha(d-d_0)\}}{1-(\omega/\alpha)[\exp\{\alpha(d-d_0)\}-1]} \quad \ldots\ldots (1)$$

where d_0 is a certain minimum distance which is usually small compared with d and in many cases is negligible. This distance d_0 is related to the minimum distance d_0' required by the electron stream to attain a mean energy corresponding to the value of E/p applied to the gap. Clearly d_0 cannot be sharply defined, because the electron energies increase through the distance d_0' from the energy of emission from the cathode to the equilibrium energy distribution determined by the value of E/p in the gap. The amplification of current due to direct electron collision in this small region d_0' is given by

$$\exp\left(\int_0^{d_0'}\alpha_x dx\right)$$

where α_x is the value of α at a distance x from the cathode and d_0' is the distance at which α_x is equal to the equilibrium value of α. For large values of x, greater than d_0', this factor can be expressed as $\exp\{\alpha(x-d_0)\}$, and d_0 is in general of the order of, but not equal to, d_0'. Provided the secondary coefficient ω/α is independent of x in this small layer of thickness d_0, then equation (1) correctly describes the growth due to primary and secondary processes. In hydrogen, ω/α can be expressed as $\gamma+\delta/\alpha$, and the relative influence of these two effects depends upon E/p and the pressure; at low pressures and high values of E/p the contribution due to positive ions predominates. When this is the case, ω/α would be constant throughout the thin lamina of thickness d_0; on the other hand, at high gas pressures when photoelectric action might predominate, then d_0 is in any case negligible, so that equation (1) can be regarded as giving the current amplification with sufficient accuracy.

Clearly, if ω/α is small compared with α, the factor $(\omega/\alpha)\exp\{\alpha(d-d_0)\}$ is negligible compared with unity when d is sufficiently small; further, under usual conditions (when the gap distance is much greater than the mean free path) d_0 is negligible compared with d, and equation (1) reduces to the simple form

$$I = I_0 \exp \alpha d. \qquad \ldots\ldots(2)$$

This relation has usually formed the basis of the experimental determination of α, which is then equal to the slope of the $(\log I, d)$ graph, when d is small. Under certain conditions this procedure is satisfactory. For example, in air at high pressures when $E/p \sim 40\,\mathrm{v\,cm^{-1}\,(mm\,Hg)^{-1}}$, d about 1 cm and $d_0 \sim 10^{-4}$, the experimental $(\log I, d)$ graph is satisfactorily linear in its early stages (Llewellyn Jones 1957) because $\omega/\alpha \sim 3\times10^{-5}$.

However, this method in all conditions is not satisfactory, and in particular in those cases where ω/α is comparable with, say, $\alpha/10$. The $(\log I, d)$ graph is then never linear and it is not possible to determine α merely by considering the slope of the graph. At the lower gas pressures, with higher values of E/p, ω/α is sufficiently great to make the non-linearity of the $(\log I, d)$ curve serious; this is also the case in many other gases and the problem is accentuated in the monatomic gases where ω/α can be as high (Llewellyn Jones 1957) as 0·1. Precision methods of analysis of the experimental data (Crompton *et al.* 1956) for the determination of α have been developed in this laboratory which take into account the non-linearity of the curve and employ a measure of the initial current I_0; in that work the initial current density was also estimated.

It is essential that the electron mean energy should remain at a constant value for all gap separations d greater than this d_0 during an experimental investigation of current growth. It is only if this condition is satisfied that the application of equations (1) and (2) has any meaning, and in order to obtain experimentally an accurate value of α, the gap distance d must be sufficiently greater than d_0. As indicated above, $d_0/d \sim 10^{-4}$ at high gas pressures so that d_0 can be neglected, and a linear $(\log I, d)$ curve is obtained (Llewellyn Jones 1957) for quite conveniently small values of d. On the other hand, at low gas pressures d_0 may not be negligibly small and can, in fact, be comparable with the gap separation at high values of $E/p(>350\,\mathrm{v\,cm^{-1}(mm\,Hg)^{-1}})$. Reference to the Paschen curve shows that this region corresponds to the conditions where $pd < pd_{\min}$.

Bearing in mind that the coefficient α is a statistical concept in that the number of ionizations in an infinite plane lamina of thickness dx is $n\alpha dx$, where n is the (large) number of electrons in the lamina, it follows that the smallest gap separation in an experimental measurement of current I must be greater than d_0, but not necessarily very much greater.

It is now important to consider how d_0 enters into calculation of α when using the precision analysis. Reference to the original paper (Crompton *et al.* 1956) shows that currents must be measured at three different separations d_1, d_2, d_3. An accurate value of α may then be obtained from the expression

$$(1-K_2)\exp\{-\alpha(d_3-d_1)\}-(1-K_3)\exp\{-\alpha(d_2-d_1)\}=K_3-K_2 \quad \ldots\ldots(3)$$

where $K_2=R_1/R_2$, $K_3=R_1/R_3$, $R_1=I_1/I_0$, $R_2=I_2/I_0$, $R_3=I_3/I_0$. I_1, I_2 and I_3 are the currents flowing at the three gap separations d_1, d_2, d_3.

The secondary coefficient ω/α may be obtained from

$$\frac{\omega}{\alpha}\frac{I}{I_0}=\frac{he^{\alpha d}}{1-he^{\alpha d}} \quad \ldots\ldots(4)$$

where
$$h=\frac{K_2\exp(-\alpha d_1)-\exp(-\alpha d_2)}{K_2-1}=\frac{(\omega/\alpha)\exp(-\alpha d_0)}{1+\omega/\alpha}. \quad \ldots\ldots(5)$$

Examination of these expressions shows that α, ω/α and d_0 may be calculated by simply measuring the ionization currents at three gap separations $d_3>d_2>d_1$ where $d_1>d_0$.

It is now interesting to examine experimental data in the light of these considerations for the case of hydrogen at pressures of a few millimetres of mercury. Under these conditions the minimum gap separation d_1 at which the current I_1 was measured is greater than approximately $10d_0$. Finally, it must be shown that the α and ω/α thus calculated when inserted in equation (1) fit the whole experimental curve.

§ 2. EXPERIMENTAL PROCEDURE

The ionization chamber consisted of plane parallel silver discs 3 cm in diameter, and bevelled at the edges. One of the electrodes was movable axially, its support moving in a V-slot so as to maintain the electrodes parallel at all separations. The centre of the anode was perforated with 10 holes of 0·5 mm diameter, covering a disc of 0·5 cm diameter, through which ultra-violet light from a stabilized mercury arc passed to irradiate the cathode. The electrode system was mounted in a hard glass envelope, and the whole could be outgassed by heating. The gap separation was measured with a travelling microscope, and the separation was altered by turning a screw by means of a magnet external to the envelope.

The ionization currents were measured with the aid of an electrometer valve and a series of high resistors ranging from 10^7 ohms to 10^{12} ohms. This method is similar to that used by Crompton *et al.* (1956).

Care was taken in the purification of the hydrogen. The gas was prepared by the electrolysis of pure barium hydroxide, and dried by storage over phosphorous pentoxide. It was then diffused through the wall of a heated palladium tube and afterwards stored in traps at liquid air temperature. The gas was then passed over activated uranium, and the hydride thus formed was used as a reservoir of hydrogen for use in the ionization chamber. On heating, the uranium hydride gave off pure hydrogen, which was passed through another system of liquid air traps before entering the ionization chamber; the liquid air trap at the entrance of the ionization chamber was cooled throughout the duration of each experiment.

Measurements were carried out over a range of E/p_0 from 40 to 350 v cm^{-1}(mm Hg)$^{-1}$ where p_0 is the pressure at 0°c. The experimental data were analysed by the method previously described bearing in mind the considerations of the previous section, and the values of α/p_0 as a function of E/p_0 are given by the black triangles in figure 1. These values represent the mean of three separate determinations using completely different samples of hydrogen from the uranium hydride reservoir. The results were reproducible to within the experimental error of $\pm 5\%$. This error of $\pm 5\%$ is approaching the limit of experimental accuracy to which α may be determined under these conditions at the lower gas pressures. This is because the accuracy of the measurement of the ionization currents depends upon the accuracy to which the high resistors (10^{12} ohms to 10^7 ohms) and the gap separations (d_1, d_2, d_3) may be measured. The experimental error in the values of the resistors amounts to $\pm 1\%$. The values of the gap separations cannot be determined to better than $\pm 3\%$ with a travelling microscope because for high values of E/p with pressures of about a few millimetres of mercury the gap separations are of the order of millimetres. Consideration of these errors shows that the total error in the determination of α amounts to $\pm 5\%$. The maximum spread of the results is illustrated by the fact that ten different samples of hydrogen for the value $E/p = 100$ v cm^{-1}(mm Hg)$^{-1}$ at 20°c gave values of α/p which fell between 1·26 and 1·30, i.e. within $\pm 2\%$ of the mean value.

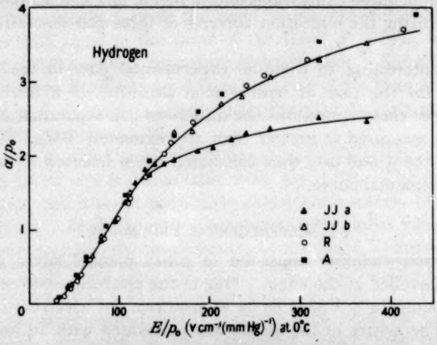

Figure 1. α/p_0 plotted against E/p_0 (v cm^{-1} (mm Hg)$^{-1}$) at 0°c.

JJ a E. Jones and F. Llewellyn Jones calculated from $\dfrac{I_0\, e^{\alpha d}}{1-(\omega/\alpha)(e^{\alpha d}-1)}$

JJ b E. Jones and F. Llewellyn Jones calculated from $I_0\, e^{\alpha d}$

R D. J. Rose

A T. L. R. Ayres

It now remains to consider whether the values of α and ω/α, calculated by the method discussed above, when inserted in equation (1), give values of current which are in agreement with the experimentally measured ionization currents over the full range of the gap separation for the particular value of E/p. Since it is only at high values of E/p that the effect of neglecting ω/α becomes particularly important, a ($\log I, d$) curve at $E/p = 350$ v cm^{-1}(mm Hg)$^{-1}$ at 20°c will now be considered. For this value of E/p the current measurements for three gap separations d_1, d_2, d_3 with the analysis described above yielded a value of $\alpha = 6{\cdot}10$ and $\omega/\alpha = 0{\cdot}22$. Substitution in expression (1) together with the measured I/I_0 for the smallest gap separation ($d = 0{\cdot}025$ cm) consistent with reasonably accurate measurement yielded a value of d_0 which is less than 0·002 cm, and this is so small that it has a negligible effect at larger separations. With $E = 896$ v cm^{-1} (corresponding to $E/p = 350$) the energy acquired by electrons in traversing a distance $d_0 \sim 0{\cdot}002$ is about 2 ev so that the fact that d_0 is negligible is to be expected because the energy gained in a mean free path ($l \sim 2 \times 10^{-2}$ cm under these conditions) is of the order of 18 ev.

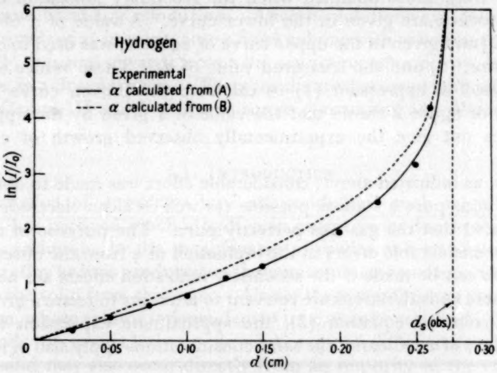

Figure 2. ln (I/I_0) plotted against d (cm) in hydrogen.
$p = 2{\cdot}56$ mm Hg at 20°c. $E/p = 350$ v cm^{-1} (mm Hg)$^{-1}$ at 20°c.

$\alpha = 6{\cdot}10$, $\omega/\alpha = 0{\cdot}22$, calculated from equation $I = I_0 \dfrac{e^{\alpha d}}{1 - (\omega/\alpha)(e^{\alpha d} - 1)}$ . . (A)

$\alpha = 8{\cdot}84$, $\omega/\alpha = 0{\cdot}096$, calculated from d_s (measured) $= 0{\cdot}275$ and $I = I_0\, e^{\alpha d}$ . . . (B)

The full theoretical curve represented by equation (1) corresponding to $E/p = 350$ v cm^{-1}(mm Hg)$^{-1}$ can now be drawn and this is given by the full line curve in figure 2. The experimental observations of current for all other values of d are given by the dots. The measured distance $d_s = 0{\cdot}275$ cm corresponding to the observed sparking potential for $E/p = 350$ v cm^{-1} (mm Hg)$^{-1}$ is indicated by the dotted line. The value of d_s calculated from the relation

$$1 - (\omega/\alpha)\{\exp(\alpha d_s) - 1\} = 0 \qquad \ldots\ldots (6)$$

is 0·273 cm, and this is consistent with the fact that the relation (6) is the criterion which sets the sparking potential.

§ 3. DISCUSSION

The results given by the black triangles in figure 1 represent the values of α/p_0 deduced from the experiments described above on the correct assumption that no part of the experimental $(\log I, d)$ curve is, in fact, linear, although by inspection the curve might appear to be so. It is now interesting to consider what happens when the curve is assumed to be linear in the early stages for the smaller values of d, and α is calculated using the relation (2). These results are also plotted in the diagram and are marked by the white triangles. It is seen at once that while for the lower values of E/p_0, less than about 130 v cm^{-1}(mm Hg)$^{-1}$, the two sets of values of α are identical, there is a marked divergence for higher values of E/p_0. The top curve also contains values of α/p_0 given by previous observers for hydrogen at low pressure (Rose 1956, Ayres 1923). It is seen that these values are in agreement over the whole range of E/p_0 with those deduced from our data on the assumption that the effects of the secondary coefficient are negligible at the smaller gap separations; on the other hand, at the high values of E/p_0, the values of α/p_0 obtained by the other observers differ considerably from those obtained when the secondary ionization is taken into account and which are given in the lower curve. A value of α obtained from expression (2) and given in the upper curve of figure 1, was used to calculate ω/α from expression (6) and the measured value of d_s. These values of α and ω/α were then used in expression (1) to calculate the broken curve in figure 2. Examination of figure 2 shows that the value of α given by the upper curve in figure 1 does not give the experimentally observed growth of current with distance.

Although, as indicated above, considerable effort was made to obtain samples of hydrogen in as pure a state as possible (as well as clean electrode surfaces) it is not suggested that the gas was perfectly pure. The purpose of this paper is to show that considerable errors in the evaluation of α from the observed current measurements can be made if the secondary ionization effects are not taken into account. These considerations are relevant to attempts to relate a given observed ionization current to equation (2), the approximate expression for I, using published values of α. Clearly, the same considerations apply also in non-uniform fields.

ACKNOWLEDGMENTS

Thanks are due to the University College of Swansea for a scholarship (1954–57) to one of us (E. J.), and also to The Electricity Supply Research Council for a Research Fellowship during 1957–58; a grant for apparatus from the Research Council is also gratefully acknowledged.

REFERENCES

AYRES, T. L. R., 1923, *Phil. Mag.*, **45**, 13.
CROMPTON, R. W., DUTTON, J., and HAYDON, S. C., 1956, *Proc. Phys. Soc.* B, **69**, 1.
LLEWELLYN JONES, F., 1957, *Ionization and Breakdown in Gases* (London: Methuen), chap. 4.
MORGAN, C. G., 1956, *Phys. Rev.*, **104**, 566.
ROSE, D. J., 1956, *Phys. Rev.*, **104**, 273.

Diffusion across a Semiconductor–Vapour Interface

By R. BULLOUGH, R. C. NEWMAN and J. WAKEFIELD
Research Laboratory, Associated Electrical Industries, Aldermaston, Berks.

MS. received 26*th March* 1958, *and in final form* 16*th May* 1958

Abstract. General boundary conditions associated with diffusion across a solid–vapour interface are considered in detail and the diffusion equation is solved subject to these boundary conditions. Analytic solutions are derived for: (*a*) diffusion outwards of an impurity into a finite volume with or without simultaneous pumping; (*b*) diffusion inwards from a limited source of impurity, initially in the vapour phase, in a closed system. These results are discussed with reference to the diffusion of Group III and V elements across germanium and silicon surfaces.

---

§ 1. Introduction

The diffusion of impurities into semiconductors such as germanium and silicon has received much attention in recent years due to the importance of this technique in the manufacture of diodes and transistors. Usually a chemical or alloy layer is produced on the semiconductor surface and the impurity diffuses into the solid from this layer. Under these conditions a constant surface concentration, whose value is independent of time, may be assumed; this boundary condition leads to a particularly simple solution of the diffusion equation. Diffusion into a solid may also occur directly from an impurity in the vapour phase: alternatively, impurities in the solid may diffuse out during heat treatment with the resultant build-up of an impurity vapour pressure externally, unless the system is pumped continuously at a very high rate. In these cases the impurity surface concentration in the solid varies with time and more complex solutions of the diffusion equation are to be expected. So far no comprehensive analyses of these systems have been given, although Torrey and Whitmer (1948) give the solution when the semiconductor is bounded by a perfect vacuum (see also Zagrubskiĭ 1939). Smits and Miller (1956) also derive an approximate solution for the case of a solid heated in a finite volume pumped at a finite rate, provided this rate is sufficiently large; the validity of this solution is discussed in § 3.

In the present work a detailed analysis is given for this last case without any restrictions being placed on the value of the pumping rate. In § 2 the boundary conditions are derived from fundamental considerations and then in § 3 Fick's diffusion equation is solved subject to these conditions. It is shown how the general solution is modified for (*a*) zero pumping speed, i.e. diffusion outwards into a finite sealed volume, and (*b*) infinite pumping speed, i.e. the vacuum ambient case given by Torrey and Whitmer (1948). It will also be shown that the boundary conditions for diffusion into the solid from a limited quantity of impurity initially in the vapour phase are similar to case (*a*) above, and hence the form of the solution is similar. Finally, in § 4 the results obtained are discussed in relation to previous work including the experiments of Miller and Smits (1957) and Lehovec *et al.* (1956).

§ 2. Boundary Conditions

In order to derive a continuity equation at the surface of the semiconductor, it is necessary to introduce a model of energy levels for impurity atoms in different positions. The model used throughout this analysis is shown in figure 1. A substitutional impurity atom inside the solid must overcome a barrier of height E_D, the activation energy for diffusion, to move from one lattice site to the next. On reaching the surface, an atom can escape from the solid only if it acquires an energy equal to or greater than E_1; the value of E_1 is expected to be similar to E_D. An atom in the external gaseous phase must possess a thermal energy greater than E_3 before it can penetrate into the solid by direct impact. Atoms from the vapour phase may also become adsorbed on the surface and then enter the solid by a diffusion mechanism; this requires an activation energy of E_2. The diffusion flow to or from the surface in the solid will be given by the net rate of transport of atoms across the surface by the mechanisms described above. This continuity condition is now derived analytically.

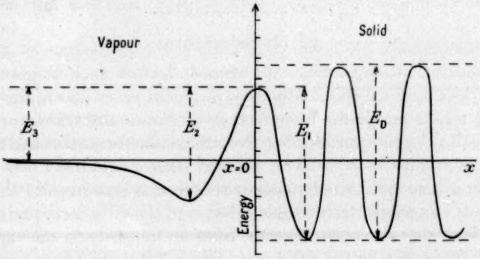

Figure 1. Energy level model ; $x=0$ is the semiconductor surface.

The number of atoms leaving the semiconductor per unit time is

$$Aac(0,t)\,\nu_1\,\alpha_1 \exp[-E_1/\boldsymbol{k}T] \qquad \ldots\ldots(1)$$

where A is the surface area of the semiconductor, a is the interatomic spacing in a direction normal to the surface, $c(0, t)$ is the concentration of atoms in the surface layer at time t, ν_1 is a parameter which includes the frequency of atomic vibrations and the relevant entropy factor, α_1 is a geometric factor giving the probability of an impurity atom making a jump in the negative x-direction, that is into the vapour phase, T is the absolute temperature and $\boldsymbol{k}$ is the Boltzmann constant. The number of atoms entering the solid per unit time by a direct transition from the gaseous phase is

$$AC_g(t)\bar{v}\beta_0 \exp(-E_3/\boldsymbol{k}T) \qquad \ldots\ldots(2)$$

where $C_g(t)$ is the concentration of impurity atoms in the gaseous phase at time t, $\bar{v}$ is the mean velocity of the atoms, and β_0 is a constant which allows for the direction of impinging atoms and the absolute sticking probability. The number of adsorbed atoms entering the solid per unit time is

$$AQ_A(t)\,\nu_2\,\alpha_2 \exp(-E_2/\boldsymbol{k}T) \qquad \ldots\ldots(3)$$

where $Q_A(t)$ is the number of adsorbed atoms per unit area on the surface and the other constants are defined similarly to those in (1). For small vapour pressures,

Q_A should be proportional to C_g, and it is convenient to introduce a parameter ϕ defined by

$$Q_A = a\phi C_g. \qquad \ldots\ldots(4)$$

The net rate of flow of impurities out of the solid is thus (1) minus the sum of (2) and (3), and must equal the diffusion flow to the surface. The continuity equation at the surface is therefore:

$$D\frac{\partial c(0,t)}{\partial x} = K[c(0,t) - k_g C_g(t)] \qquad \ldots\ldots(5)$$

where

$$K = a\alpha_1\nu_1 \exp(-E_1/\boldsymbol{k}T) \qquad \ldots\ldots(6)$$

and

$$k_g = K^{-1}\{\bar{v}\beta_0 \exp(-E_3/\boldsymbol{k}T) + a\phi\alpha_2\nu_2 \exp(-E_2/\boldsymbol{k}T)\}. \qquad \ldots\ldots(7)$$

2.1. *The Boundary Conditions for Diffusion outwards*

The semiconductor of surface area A and initially containing a uniform impurity concentration c_0 is heated in a volume V which is pumped continuously at a rate L. It is assumed that the specimen is sufficiently thick for it to be represented by a semi-infinite model. In order to find $C_g(t)$, it is necessary to examine the rate of change of the number of atoms in the gaseous phase; this is equal to the rate of out-flow from the solid minus the rate of back-flow, minus the rate of removal of atoms by the pump. Hence we may write:

$$V'\frac{dC_g(t)}{dt} = AKc(0,t) - AKk_g C_g(t) - LC_g(t) \qquad \ldots\ldots(8)$$

where V' is defined as

$$V' = V + a\phi A \qquad \ldots\ldots(9)$$

and thus allows for the presence of adsorbed atoms on the surface.

Combining equations (8) and (5) we obtain, after integration,

$$C_g(t) = \frac{AD}{V'}\exp(-Lt/V')\int_0^t \frac{\partial c(0,t)}{\partial x}\exp(Lt/V')\,dt. \qquad \ldots\ldots(10)$$

The relevant boundary condition is thus, from (5) and (10)

$$D\frac{\partial c(0,t)}{\partial x} = K\left\{c(0,t) - k_g\frac{AD}{V'}\exp(-Lt/V')\int_0^t \frac{\partial c(0,t)}{\partial x}\exp(Lt/V')dt\right\} \qquad \ldots\ldots(11)$$

together with the initial condition $c = c_0$. When $L = 0$, (11) reduces to

$$D\frac{\partial c(0,t)}{\partial x} = K\left\{c(0,t) - k_g\frac{AD}{V'}\int_0^t \frac{\partial c(0,t)\,dt}{\partial x}\right\} \qquad \ldots\ldots(12)$$

which further reduces to

$$D\frac{\partial c(0,t)}{\partial x} = Kc(0,t) \qquad \ldots\ldots(13)$$

when V' tends to infinity.

2.2. *The Boundary Conditions for Diffusion inwards*

A semiconductor with zero initial impurity concentration is heated in a volume V initially containing a gaseous impurity concentration $C_g(0)$. This is the general case of diffusion inwards from a limited quantity of diffusant.

The rate of change of the number of atoms in the vapour phase must equal the net rate of flow across the surface; that is

$$V'\frac{dC_g(t)}{dt}=AD\frac{\partial c(0,t)}{\partial x} \qquad \ldots\ldots(14)$$

which gives on integration

$$C_g(t)=C_g(0)+\frac{AD}{V'}\int_0^t \frac{\partial c(0,t)}{\partial x}\,dt. \qquad \ldots\ldots(15)$$

The complete boundary condition is thus

$$D\frac{\partial c(0,t)}{\partial x}=K\left\{c(0,t)-k_g\left[C_g(0)+\frac{AD}{V'}\int_0^t \frac{\partial c(0,t)}{\partial x}\,dt\right]\right\} \qquad \ldots\ldots(16)$$

with $c=0$ at $t=0$. When C_g is a constant and independent of time (16) reduces to

$$D\frac{\partial c(0,t)}{\partial x}=K\{c(0,t)-k_gC_g\}. \qquad \ldots\ldots(17)$$

§ 3. SOLUTIONS OF FICK'S EQUATION

A detailed derivation of the solution of Fick's equation

$$D\frac{\partial^2 c(x,t)}{\partial x^2}=\frac{\partial c(x,t)}{\partial t}, \qquad \ldots\ldots(18)$$

subject to the very general boundary conditions (11) for diffusion outwards, will be given, from which the solutions appropriate to the less restricted boundary conditions (12) and (13) can be directly obtained. Because of the similarity of the derivation the corresponding solutions for diffusion inwards will only be quoted. We therefore require a solution $c(x, t)$ of (18) subject to the boundary condition (11) and the initial condition

$$c(x,0)=c_0 \qquad \ldots\ldots(19)$$

where c_0 is a constant. Proceeding by the standard method of Laplace transforms, we multiply both sides of (11) by $\exp\{-t(p-L/V')\}$ and integrate each term from $t=0$ to $t=\infty$; we obtain

$$D\frac{d\bar{c}(0,p')}{dx}=K\left[\bar{c}(0,p')-\frac{k_gAD}{V'}\left(\frac{1}{p}\right)\frac{d\bar{c}(0,p')}{dx}\right] \qquad \ldots\ldots(20)$$

where

$$p'=p-L/V' \qquad \ldots\ldots(21)$$

and

$$\bar{c}(x,p')=\int_0^\infty c(x,t)\exp(-p't)\,dt. \qquad \ldots\ldots(22)$$

The partial differential equation (18) may be similarly transformed into the ordinary differential equation

$$D\frac{d^2\bar{c}(x,p')}{dx^2}=-c_0+p'\,\bar{c}(x,p') \qquad \ldots\ldots(23)$$

of which the required solution is

$$\bar{c}(x,p')=R(p')\exp\{-x(p'/D)^{1/2}\}+c_0/p' \qquad \ldots\ldots(24)$$

and where $R(p')$ is to be determined with the aid of (20); the substitution of $d\bar{c}(0,p')/dx$ and $\bar{c}(0,p')$ from (24) into (20) yields

$$R(q)=-c_0\alpha(q^2+\beta)/Dq^2\{q^3+\alpha q^2+(\beta+\alpha\gamma)q+\alpha\beta\} \qquad \ldots\ldots(25)$$

where $\alpha = K/D$, $\beta = L/V'D$ and $\gamma = k_g A/V'$ are constants and

$$p' = Dq^2. \qquad \ldots\ldots(26)$$

If we split (25) into partial fractions, $c(x, t)$ can be obtained either by simple integration by parts or from published tables of Laplace transforms (Carslaw and Jaeger 1947); that is

$$c(x,t)/c_0 = \operatorname{erf}\frac{x}{2(Dt)^{1/2}} - \sum_{\substack{i=1\\ i\neq j\neq k}}^{3}\left[\frac{\alpha h_i^2+\alpha\beta}{h_i(h_j-h_i)(h_k-h_i)}\exp\left(-h_i x + Dth_i^2\right)\right.$$
$$\left.\times\operatorname{erfc}\left\{\frac{x}{2(Dt)^{1/2}} - h_i\,(Dt)^{1/2}\right\}\right] \qquad \ldots\ldots(27)$$

where $j, k = 1, 2$ or 3, and h_1, h_2, h_3 are the roots of the cubic

$$z^3+\alpha z^2+(\beta+\alpha\gamma)z+\alpha\beta=0. \qquad \ldots\ldots(28)$$

(27) is therefore the required solution appropriate to diffusion outwards into a finite, but continuously pumped, volume. A useful approximate solution, valid only for large pumping rates L, may easily be obtained by expanding $R(q)$, given by (25), as a power series in β^{-1}, and, on transforming the resulting $\bar{c}(x,p')$ given by (24), we obtain

$$c(x,t)/c_0 \simeq \operatorname{erf}\frac{x}{2(Dt)^{1/2}} + \exp\left(\alpha' x + Dt\alpha'^2\right)\operatorname{erfc}\left[\frac{x}{2(Dt)^{1/2}} + \alpha'(Dt)^{1/2}\right]$$
$$+\beta^{-1}c_1(x,t) + \mathrm{O}(\beta^{-2}) \qquad \ldots\ldots(29)$$

where

$$c_1(x,t) = \frac{\alpha'(\alpha'-\alpha)}{\alpha D}\left[\left\{\left(\frac{D}{\pi t}\right)^{1/2} + 2\alpha'^2\left(\frac{D^3 t}{\pi}\right)^{1/2}\right\}\exp\left(-x^2/4Dt\right)\right.$$
$$\left.-\alpha' D\left(2+\alpha' x + 2\alpha'^2 Dt\right)\exp\left(\alpha' x + Dt\alpha'^2\right)\operatorname{erfc}\left(\frac{x}{2(Dt)^{1/2}} + \alpha'(Dt)^{1/2}\right)\right] \qquad \ldots\ldots(30)$$

and

$$\alpha' = \alpha\beta/(\beta+\alpha\gamma) = K'/D. \qquad \ldots\ldots(31)$$

Substituting the values of α, β and γ into (31) we find

$$K' = KL/(L+k_g KA). \qquad \ldots\ldots(32)$$

In the expression of $R(q)$, α' arises because we do not neglect γ in comparison with β. We do this simply because it is not a practical proposition, with a given large pumping rate, to increase this pumping rate further without simultaneously decreasing the volume V. Thus, any rise in $\beta = L/V'D$, due to an increase in L, is assumed to lead to an increase (though of necessity a smaller increase) in $\gamma = k_g A/V'$; the term $\beta+\alpha\gamma$ is therefore conserved in the expansion. The zero-order solution, that is the first two terms in (29), is of precisely the same form as the solution (41) appropriate to diffusion outwards into a high vacuum ambient, the only difference being the replacement of α in (41) by α'. This zero order solution has been obtained by Smits and Miller (1956) by a somewhat involved argument. The analysis above clearly indicates that it is only a valid solution when the pumping rate is large; otherwise either the first order term (30) should be included or the exact solution (27) used.

The idea of having a continuously pumped system is due to Smits *et al.* (1956) and was devised solely as a means of estimating k_g by fitting the zero order solution in (29) to give K' and then using (32) with known values of K, L and A. Unfortunately, Smits had to use a rather low pumping rate for his estimation of K' and for this reason the validity of using the zero order approximate solution is somewhat doubtful. However, rather than criticize Smits' approach, we would like to suggest what we consider a simpler and more accurate method of measuring k_g, that is by removing the pump altogether and considering the diffusion outwards into a closed volume system. The appropriate boundary condition is (12) and the required solution can be obtained immediately by setting $L=0$ ($\beta=0$) in the general solution (27); thus

$$c(x,t)/c_0 = 1 - \frac{\alpha}{(h_1-h_2)}\left[\exp(-h_1x+Dth_1^2)\,\mathrm{erfc}\left\{\frac{x}{2(Dt)^{1/2}} - h_1(Dt)^{1/2}\right\}\right.$$
$$\left. - \exp(-h_2x+Dth_2^2)\,\mathrm{erfc}\left\{\frac{x}{2(Dt)^{1/2}} - h_2(Dt)^{1/2}\right\}\right] \qquad \ldots\ldots(33)$$

where h_1, h_2 are the roots of the quadratic

$$z^2+\alpha z+\alpha\gamma=0. \qquad \ldots\ldots(34)$$

If the roots of the quadratic are equal, that is $h_1=h_2=-\frac{1}{2}\alpha$, then by expanding the numerator of (33) for small h_1-h_2, we obtain

$$c(x,t)/c_0 = 1-\alpha\left[2\left\{\frac{Dt}{\pi}\right\}^{1/2}\exp(-x^2/4Dt)-(x+\alpha Dt)\exp\{(\alpha x/2)+\alpha^2Dt/4\}\right.$$
$$\left.\times\,\mathrm{erfc}\left\{\frac{x}{2(Dt)^{1/2}}+\frac{\alpha}{2}(Dt)^{1/2}\right\}\right]. \qquad \ldots\ldots(35)$$

(33) is valid, of course, for real ($\alpha>4\gamma$), equal ($\alpha=4\gamma$) or complex conjugate ($\alpha<4\gamma$), h_1, h_2. In the last case, the solution may be written in the real form

$$c(x,t)/c_0 = 1-\frac{\alpha}{b}\left[\exp\{(\alpha x/2)+Dt(\alpha^2/4-b^2)\}\sin b(x+\alpha Dt)\,\mathrm{erfc}\left\{\frac{x}{2(Dt)^{1/2}}\right.\right.$$
$$\left.+\frac{\alpha}{2}(Dt)^{1/2}\right\}+2\left\{\frac{Dt}{\pi}\right\}^{1/2}\exp(-x^2/4Dt)\int_0^b\exp\{-Dt(y^2-2by)\}$$
$$\left.\times\cos y(x+\alpha Dt)\,dy\right] \qquad \ldots\ldots(36)$$

where $b=\frac{1}{2}\alpha\,[4(\gamma/\alpha)-1]^{1/2}$. By using the asymptotic expansion for the error functions in (33), we see that after some time the surface concentration $c(0,t)$ is given by

$$c(0,t)/c_0 \simeq 1-\frac{V'}{k_gA}[\pi Dt]^{-1/2}. \qquad \ldots\ldots(37)$$

This result is, of course, valid for real or complex h_1, h_2, and therefore can also be directly derived from either (35) or (36). The variation of $c(0,t)$ with t is shown in figure 2 for the case of equal roots; that is when $V'/A=4k_gD/K$. We see that this curve becomes coincident with the asymptotic form (37) for $K^2t/4D \gtrsim 10$, and with the somewhat small value of K found by Smits for the diffusion outwards of antimony in germanium, the inequality indicates that t should be $\gtrsim 10$ hr. It follows that (37) may be used to deduce the value of k_g as long as the time is sufficiently large.

V.
19

The gaseous concentration $C_g(t)$ is given by either

$$C_g(t) = \frac{A}{V'}\int_0^\infty \{c_0 - c(x,t)\}\,dx \qquad \dots\dots (38)$$

or

$$C_g(t) = \frac{DA}{V'}\int_0^t \left[\frac{\partial c}{\partial x}\right]_{x=0} dt. \qquad \dots\dots (39)$$

In either case with $c(x,t)$ given by (33) we obtain

$$\frac{k_g C_g(t)}{c_0} = 1 - \frac{h_2\exp(Dh_1{}^2t)\operatorname{erfc}[-h_1(Dt)^{1/2}] - h_1\exp(Dh_2{}^2t)\operatorname{erfc}[-h_2(Dt)^{1/2}]}{h_2 - h_1} \qquad \dots\dots (40)$$

where again h_1 and h_2 are the roots of the quadratic (34). $k_gC_g(t)/c_0$ is shown in figure 3 for three different values of V'/A. Curve A is for $V'/A = 8k_gD/K$ and h_1, h_2 are real roots; curve B is for $V'/A = 4k_gD/K$ and $h_1 = h_2$; curve C is for $V'/A = 2k_gD/K$ and h_1, h_2 are complex conjugate roots. These curves are instructive for two reasons. Firstly, they indicate a continuous transition in the form of $C_g(t)$ when the roots h_1, h_2 become complex†, and secondly that the larger

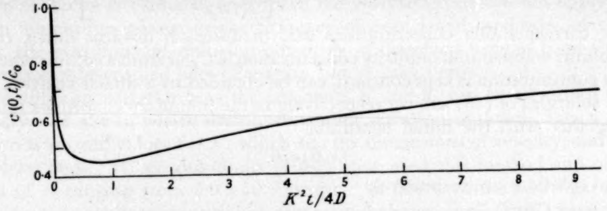

Figure 2. The variation of the surface concentration when the roots of the quadratic are equal ; that is when $V'/A = 4k_g\,D/K$.

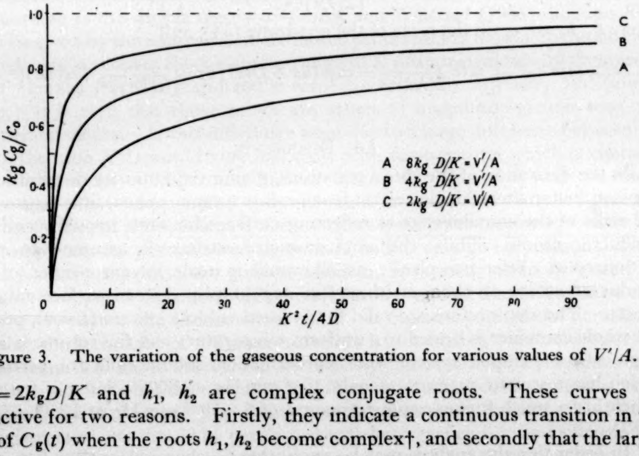

Figure 3. The variation of the gaseous concentration for various values of V'/A.

---

† The analytic form of $C_g(t)$ when h_1, h_2 become complex undergoes a change similar to that of $c(x,t)$ (eqns. (33) to (36)), yet there is little change in the graphical form of these equations (figure 3).

the value of K the quicker will the concentration in the gas rise to its final equilibrium value c_0/k_g. Furthermore, it is interesting to note that when t is sufficiently large for the asymptotic approximation (37) to be valid, the validity of a similar asymptotic form of (40) is assured and $k_g C_g(t) \simeq c(0,t)$.

The solution for diffusion outwards into a perfect vacuum, boundary condition (13), can be obtained directly from (33) by letting V tend to ∞, that is γ tend to 0:

$$c(x,t)/c_0 = \operatorname{erf}\frac{x}{2(Dt)^{1/2}} + \exp(\alpha x + \alpha^2 Dt)\operatorname{erfc}\left[\frac{x}{2(Dt)^{1/2}} + \alpha(Dt)^{1/2}\right]. \qquad \ldots\ldots(41)$$

This can also be obtained by letting the pumping rate L in the general solution (27) tend to infinity. Finally, since the value of α is expected to be large (see §4), a pertinent solution is when $\alpha \to \infty$. This limit is most easily taken in (33):

$$c(x,t)/c_0 = 1 - \exp(\gamma x + \gamma^2 Dt)\operatorname{erfc}\left[\frac{x}{2(Dt)^{1/2}} + \gamma(Dt)^{1/2}\right]. \qquad \ldots\ldots(42)$$

The corresponding concentrations due to diffusion inwards either from a finite volume whose initial impurity concentration is C_g or from a volume where the gaseous concentration is kept constant, can be obtained by a similar analysis. We require solutions of (18) subject respectively to the boundary conditions (16) and (17) together with the initial condition

$$c(x,0) = 0. \qquad \ldots\ldots(43)$$

The two solutions are respectively

$$c(x,t) = \frac{\alpha k_g C_g}{h_1 - h_2}\left[\exp(-h_1 x + Dth_1^2)\operatorname{erfc}\left\{\frac{x}{2(Dt)^{1/2}} - h_1(Dt)^{1/2}\right\} - \exp(-h_2 x + Dth_2^2)\operatorname{erfc}\left\{\frac{x}{2(Dt)^{1/2}} - h_2(Dt)^{1/2}\right\}\right] \qquad \ldots\ldots(44)$$

where h_1, h_2 are again the roots of the quadratic (34), and

$$c(x,t) = k_g C_g\left[\operatorname{erfc}\frac{x}{2(Dt)^{1/2}} - \exp(\alpha x + Dt\alpha^2)\operatorname{erfc}\left\{\frac{x}{2(Dt)^{1/2}} + \alpha(Dt)^{1/2}\right\}\right]. \qquad \ldots\ldots(45)$$

§ 4. Discussion

In the derivation of the above equations, giving the impurity distribution in a semiconductor after diffusion either from or into a vapour phase, it is assumed that the walls of the container act as reflecting surfaces for both impurity and semiconductor atoms. Thus, the semiconductor surface is assumed to remain stationary as a reference plane; no allowance is made for evaporation of semiconductor atoms or changes in surface topography due to surface migration effects. The assumptions are valid for a closed volume system ($L=0$), provided the whole container is heated to a uniform temperature and the volume is not too large. In a pumped system, the approximation should hold for germanium which has a vapour pressure of only 10^{-8} mm Hg at 800°c, but not for silicon which has a much higher vapour pressure of 5×10^{-5} mm Hg at 1250°c (Honig 1957).

In order that the analysis may be applicable no chemical or alloy layers must be formed during the high-temperature treatments used in the diffusion process, i.e. a true semiconductor vapour interface must be preserved. This is not a serious limitation with germanium. We have found, however, that a layer of silicon carbide is formed on silicon surfaces heated to temperatures greater than about 1000°c in a sealed quartz tube (Newman and Wakefield, paper read at International Solid State Conference at Brussels 1958), whether or not impurity atoms of Group III or V are present. Some of this carbide formation could result from the diffusion outwards of carbon initially introduced into the silicon during the growth of the ingots (Papazian and Wolsky 1956). Since this growth is in the form of discrete crystallites ranging from 50 to 500 Å in diameter, as revealed by electron microscopy, its presence may not affect the boundary conditions significantly. The above analysis may thus be applicable to the systems boron–silicon and antimony–silicon. Electron diffraction evidence suggests that an amorphous oxide layer forms at a silicon surface during diffusion of aluminium either inwards or outwards, carried out in an evacuated sealed-off silica tube. It has been shown by Frosch and Derick (1957) that the boundary conditions are altered when the surface of silicon is oxidized, and hence the analysis given will not apply to the system aluminium–silicon in the presence of even small quantities of oxygen. Again, the possibility of diffusion outwards of dissolved oxygen from the bulk silicon cannot be ignored here (Papazian and Wolsky 1956).

We will now consider how the constants K and k_g can be measured experimentally. If the impurity distribution after diffusion outwards into a perfect vacuum is known, values for K, which has the dimensions of velocity, and D may be determined. Miller and Smits (1957) have used this method and obtained values of K ranging from $3{\cdot}9 \times 10^{-7}\,\mathrm{cm\,sec^{-1}}$ at 900°c to $6{\cdot}6 \times 10^{-8}\,\mathrm{cm\,sec^{-1}}$ at 800°c for the antimony–germanium system. Lehovec *et al.* (1957) have used an indirect electrical method to determine K for this system, and they give a value of $3 \times 10^{-8}\,\mathrm{cm\,sec^{-1}}$ at 700°c. Smits *et al.* (1956) have also reported a value of K greater than $6 \times 10^{-6}\,\mathrm{cm\,sec^{-1}}$ for the system aluminium–silicon at 1250°c.

According to the simple theory of Torrey and Whitmer (1948) the ratio K/D should be given by the reciprocal of the lattice plane spacing normal to the surface. If this spacing is taken as 3 Å, we obtain values of K of approximately $10^{-2}\,\mathrm{cm\,sec^{-1}}$ and $10^{-3}\,\mathrm{cm\,sec^{-1}}$ at 900°c and 800°c respectively for the antimony–germanium system. It is seen that these values are orders of magnitude greater than the experimental values. If this difference were due to a large difference between E_D and E_1, the ratio K/D would vary markedly with temperature, which is contrary to the observations of Miller and Smits. Thus, the value of ν_1 must be much smaller than the corresponding ν in the bulk crystal. This implies that the diffusion coefficient is also lowered in the surface layer by the factor ν_1/ν, since the same jump frequency is involved in both K and D at a given position; if the impurity atom jumps into the gaseous ambient, K is used, while D is used for jumps in the opposite direction. Thus, it is further implied that D is a function of position very near to the surface of the solid. It must be pointed out here, however, that the technique of diffusion outwards is not entirely satisfactory for the measurement of K due to the relative insensitivity of the method; a very small shift in the impurity distribution measured by Miller and Smits would change the value of K from $2{\cdot}4 \times 10^{-7}\,\mathrm{cm\,sec^{-1}}$ to infinity. It therefore seems desirable that further detailed experiments should be performed with both germanium and silicon and a range of impurity elements to determine the constant K for these systems.

Our analysis shows that k_g can be determined from experiments on diffusion outwards in the closed volume system (eqn. (37)) by a measurement of the surface concentration after a sufficiently long time. The validity of this approximation has already been discussed in § 3. k_g can also be determined from experiments on diffusion inwards where C_g is held constant at a low value. The value of the surface concentration $c(0,t)$ is here given by $k_g C_g$, provided again that t is sufficiently large. The value of C_g may be controlled experimentally by the use of a tube with two temperature zones: the hotter zone contains the semiconductor, while the vapour pressure of the desired impurity is controlled by the temperature of the second cooler zone. These techniques appear to be simpler than the pumped systems used by Miller and Smits (1957), who first had to find a value of K before k_g could be found. Now according to the definition of k_g (eqn. (7)) we have

$$k_g = \frac{\beta_0 \bar{v}}{\alpha_1 \nu_1} \frac{1}{a} \exp\left(\frac{E_1 - E_3}{\boldsymbol{k}T}\right) + \phi \exp\left(\frac{E_1 - E_2}{\boldsymbol{k}T}\right)$$

where we have assumed $\alpha_1 = \alpha_2$ and $\nu_1 = \nu_2$. Theoretically, both these terms will contribute to k_g, but in practice one term may be much greater than the other. Miller and Smits find that k_g may be represented by $k_g = k_{g0} \exp \Delta E/\boldsymbol{k}T$ where $k_{g0} = 6{\cdot}7$ and $\Delta E = 1{\cdot}2$ ev, and they associate these values with the first term only. This seems reasonable in this case, since the numerical value computed for $(\beta_0 \bar{v}/\alpha_1 \nu_1)(1/a)$ is close to that of k_{g0}. It is interesting, however, to see the implication of neglecting the first term completely. We would then have ϕ and $E_1 - E_2$ equal to 6·7 and 1·2 ev respectively. This reduces the height of the barrier (Miller and Smits 1957, fig. 7) and increases the binding energy by an amount equal to $E_2 - E_3$ which is the energy of adsorption. According to Burton *et al.* (1951), this will be given by $H/20$, where H is the latent heat of evaporation of the crystal substrate. This would give $E_2 - E_3$ equal to approximately 0·15 ev for silicon using the value of H given by Kubaschewski and Evans (1956).

We will now interpret the value of ϕ by considering a diffusion inwards experiment with the antimony–germanium system at a temperature of 850°c, where $k_g = 10^6$ as given by Miller and Smits. If we take the concentration of antimony atoms in the vapour phase as 10^{12} atoms cm^{-3}, the surface concentration of antimony in the germanium will approach 10^{18} atoms cm^{-3} after a certain time. A value of $\phi = 6{\cdot}7$ gives a value of Q the number of adsorbed atoms per unit area equal to $1{\cdot}4 \times 10^5$ atoms cm^{-2} if the lattice parameter a is taken as 2 Å. This is only 10^{-10} of a monolayer and obviously would not be detectable by even the radiotracer technique (see Smits *et al.* 1956). It would therefore be somewhat dangerous to state that the monolayer mechanism for entry of impurities into the lattice is unimportant compared with the direct mechanism. In fact, we have obtained values of k_g greater than 10^{15} for the system boron–silicon, assuming the value of the vapour pressure of boron given by Honig (1957). It must be assumed that the adsorption mechanism is dominant here to explain this very high value.

Finally, the value of the impurity distribution derived above is discussed in relation to practical techniques, although obviously values of K and k_g must be obtained before explicit distributions can be given. During the diffusion inwards into a doped crystal, there will inevitably be some simultaneous and independent diffusion outwards of this dope which will affect both the position and gradient of the resulting p–n junction. This effect will be particularly marked for aluminium-doped silicon. Furthermore, it is obvious that limited quantities of unwanted impurities will be present in the container. Due allowance for any diffusion inwards of these impurities can now be made (eqn. (44)).

ACKNOWLEDGMENT

Thanks are due to Dr. T. E. Allibone, Director of the Research Laboratory, Associated Electrical Industries, and to the Admiralty, for permission to publish this paper.

REFERENCES

BURTON, W. K., CABRERA, N., and FRANK, F. C., 1951, *Phil. Trans.* A, **243,** 299.
CARSLAW, H. S., and JAEGER, J. C., 1947, *Conduction of Heat in Solids*, Appendix V (Oxford : Clarendon Press).
FROSCH, C. J., and DERICK, L., 1957, *J. Electrochem. Soc.*, **104,** 547.
HONIG, R. E., 1957, *R.C.A. Review*, **18,** 195.
LEHOVEC, K., SCHOENI, K., and ZULEEG, R., 1957, *J. Appl. Phys.*, **28,** 420.
KUBASCHEWSKI, O., and EVANS, E. Ll., 1956, *Metallurgical Thermochemistry*, 2nd edition (London : Pergamon Press).
MILLER, R. C., and SMITS, F. M., 1957, *Phys. Rev.*, **107,** 65.
PAPAZIAN, H. A., and WOLSKY, S. P., 1956, *J. Appl. Phys.*, **27,** 1561.
SMITS, F. M., and MILLER, R. C., 1956, *Phys. Rev.*, **104,** 1242.
SMITS, F. M., MILLER, R. C., and BATDORF, R. L., 1956, *International Colloquium on Semiconductors and Phosphors, Garmisch-Partenkirchen, Germany*. (Brunswick Vieweg).
TORREY, H. C., and WHITMER, C. A., 1948, *Crystal Rectifiers*, p. 93 (New York : McGraw-Hill).
ZAGRUBSKIĬ, A. M., 1939, *J. tech. Phys., Moscow*, **9,** 1767.

Galvanomagnetic Effects in p-Type Bismuth Telluride

By J. R. DRABBLE
Research Laboratories of the General Electric Company Limited, Wembley, Middx.

MS. received 3rd April 1958

Abstract. The resistivity components, Hall coefficients and low field magnetoresistance coefficients have been measured on a number of single crystal specimens of p-type bismuth telluride at 77°K. The results are shown to be consistent with a many-valley form of the valence band for which the energy extrema are on the reflection planes in momentum space. The parameters associated with the model are evaluated and are used to obtain the relations between the Hall coefficients and the density of carriers. The results are used to discuss the variation of the resistivities and the Hall coefficients with temperature over the range 77°K to 290°K and, in particular, to obtain the conductivity mobility for holes for current flow parallel to the cleavage planes. This mobility varies as $T^{-1.98}$ and, for one specimen, has a value of 515 cm^2 volt^{-1} sec^{-1} at 290°K.

---

§ 1. Introduction

In a previous paper (Drabble, Groves and Wolfe 1958, to be referred to as I) it has been suggested that the analysis of measurements of the resistivity and Hall coefficients of bismuth telluride is complicated by the anisotropy of the crystal structure, which belongs to the class R$\bar{3}$m. In particular, some modifications to the relations connecting the Hall coefficient to the density of carriers which hold for a cubic crystal are certainly necessary since there are two resistivities and two Hall coefficients to deal with, and it is not immediately obvious how to combine these in such a way as to relate the result to the fundamental properties of the material.

The simplest model which provides a satisfactory explanation of the anisotropy of the galvanomagnetic effects in bismuth telluride is one in which the band associated with the transport properties is of the many-valley type, where, of course, the distribution of the valleys in momentum space conforms to the crystal symmetry. A model of this type appropriate to bismuth telluride was discussed by Drabble and Wolfe (1956) with the assumption that the scattering processes could be described in terms of a relaxation time. A more general treatment has been given by Keyes (1956) for any semiconductor with an axis of symmetry, with the same assumption about the scattering law.

In I it was shown that such a model in which the valleys are centred on reflection planes in momentum space was consistent with measurements of the galvanomagnetic effects on n-type bismuth telluride at 77°K. Similar, though more extensive, measurements have now been made on single crystal specimens of p-type bismuth telluride and these are discussed in this paper. It is shown that these results are also consistent with a many-valley form of the valence band for which the energy maxima are on the reflection planes. The parameters associated with the proposed form of the valence band have been evaluated and expressions have been derived for the density of states effective mass and the density of carriers. The variation of the resistivities and Hall coefficients with temperature over the range 77°K to 290°K are discussed in terms of the proposed model.

§ 2. Experimental Procedure and Results

The experimental techniques used in this investigation were similar to those used in the work on n-type material which are described in I, and it is only necessary to discuss those which involve a significant departure from the previous case.

2.1. *Preparation of Specimens*

The specimens of p-type bismuth telluride which have been investigated were obtained from two single-crystal ingots prepared by A. R. Sheard and numbered 19 and 23. Ingot 23 was prepared from zone-refined bismuth and tellurium with no additional impurities. For ingot 19, a small amount of iodine was added to the charge to compensate partly the p-type properties of the undoped material. Both ingots showed an almost uniform value of thermoelectric power along their lengths.

In contrast to the work on n-type material, these ingots yielded specimens of such a length and quality that measurements could be made with the current flowing in a direction perpendicular to the cleavage planes, i.e. parallel to the three-fold axis of rotation. Such measurements provide an important check on the subsequent analysis of the experimental results. It will be convenient to call these 'parallel' specimens to distinguish them from 'perpendicular' specimens for which measurements were made with the current flowing in a direction perpendicular to the rotation axis. For each ingot, both types of specimen were taken as close together as possible so as to minimize the effect of possible inhomogeneities in the ingot. A check on the magnitude of such effects is provided by the experimental measurements discussed below.

2.2. *The Galvanomagnetic Coefficients at Liquid Nitrogen Temperature*

The galvanomagnetic components are defined up to and including quadratic terms by the expression

$$E_i = \rho_{ij} J_j - \rho_{ijk} J_j B_k + \rho_{ijkl} J_j B_k B_l$$

which uses the summation convention to relate the components of the electric field **E** to the components of the current density **J** and of the magnetic induction **B**. As discussed in I, for bismuth telluride there are two independent components of the resistivity tensor ρ_{ij}, two of the Hall tensor ρ_{ijk} and eight of the magnetoresistivity tensor ρ_{ijkl}. These twelve components were measured for a particular ingot using three experimental arrangements, in each of which the magnetic field was horizontal and could be rotated about a vertical axis. In the first and second arrangements a 'perpendicular' specimen was mounted with the rotation axis vertical and horizontal respectively and in the third arrangement a 'parallel' specimen was mounted with the rotation axis horizontal. These arrangements are illustrated in figure 1.

The components of the electric field in the crystal could be measured in three directions in each of the first two arrangements but it was only necessary to measure them in two directions in the third arrangement. These components were: E_J parallel to the current, $E_{\parallel}$ parallel to the rotation axis and $E_{\perp}$ perpendicular to the rotation axis and to the current.

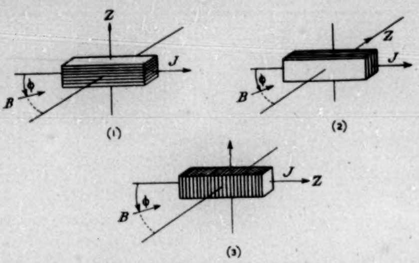

Figure 1. Experimental arrangements. The rotation axis is in the direction indicated by z.

For the third arrangement E_J and $E_{\parallel}$ coincide. If ϕ is the angle between the magnetic field and the current, the following expressions may be obtained for these components:

Arrangement 1

$$\left.\begin{aligned}E_J &= \rho_{11}J + JB^2(\rho_{1111}\cos^2\phi + \rho_{1122}\sin^2\phi)\\ E_{\parallel} &= -\rho_{312}JB\sin\phi + JB^2\rho_{3111}\cos(3\theta+2\phi)\\ E_{\perp} &= JB^2\sin\phi\cos\phi(\rho_{1111}-\rho_{1122})\end{aligned}\right\}\quad\ldots\ldots(1)$$

Arrangement 2

$$\left.\begin{aligned}E_J &= \rho_{11}J + JB^2(\rho_{1111}\cos^2\phi + \rho_{1133}\sin^2\phi + \rho_{1131}\cos 3\theta\sin 2\phi)\\ E_{\parallel} &= JB^2(\rho_{3111}\cos 3\theta\cos^2\phi + \rho_{3113}\sin 2\phi)\\ E_{\perp} &= \rho_{123}JB\sin\phi - JB^2\rho_{1131}\sin 3\theta\sin 2\phi\end{aligned}\right\}\quad\ldots\ldots(2)$$

Arrangement 3

$$\left.\begin{aligned}E_J &= \rho_{33}J + JB^2(\rho_{3333}\cos^2\phi + \rho_{3311}\sin^2\phi)\\ E_{\perp} &= \rho_{312}JB\sin\phi - JB^2\rho_{3111}\cos 3\chi\sin 2\phi\end{aligned}\right\}\quad\ldots\ldots(3)$$

In these expressions, the galvanomagnetic coefficients are referred to crystal axes in which the z axis is parallel to the axis of rotation and the xz plane is one of the three equivalent reflection planes. The angle θ is the angle between the direction of current flow and a plane of reflection in the first two arrangements and χ is the angle between the direction of measurement of $E_{\perp}$ and a reflection plane in the third arrangement.

The procedure used to determine the galvanomagnetic coefficients was as follows. In each arrangement, the voltages associated with the components of the electric field were measured for a number of values of ϕ. For each such value, the magnetic field was reversed through 180° and the contributions to the voltage which were even in the magnetic field and those which were odd were thus obtained separately. Various corrections had to be applied for out of balance voltages. The direction of the magnetic field corresponding to $\phi = 0$ was determined in each arrangement by the vanishing of the corresponding Hall voltage and could be obtained to better than half a degree.

In this way, the experimental variations with ϕ were compared with the corresponding variations predicted by the phenomenological equations (1)–(3). A least squares method was applied to the experimental readings to obtain the best fit to the predicted form. The parameters determined in this way were used in conjunction with measurements of the current density, the dimensions of the specimen and the absolute value of the magnetic field to obtain the associated galvanomagnetic coefficients.

The comparison of the observed angular variation with the predicted form provides a method of determining the errors introduced by a number of factors. Among these, the principal ones are instability of the magnetic field, distortion of the current flow from the ideal due to local inhomogeneity and spurious voltages associated with stray thermal gradients. The observed variation should be independent of other factors such as the dimensions of the specimen and the absolute value of the magnetic field, which however have to be introduced in order to obtain the absolute value of the galvanomagnetic coefficients.

No appreciable variation of the coefficients with magnetic field was found for fields up to 8000 oersteds, and consequently all the results to be described were obtained using a magnetic field strength of about 7600 oersteds.

In each arrangement and for each ingot it was found that the variation with ϕ of the voltage associated with E_J agreed with the predicted variation very closely, the maximum departure being about 3%. The Hall voltages showed equally good agreement with the expected sinusoidal variation. From the discussion given above, it follows that the principal errors in deducing the absolute values of the associated galvanomagnetic coefficients arise from errors in the absolute value of the magnetic field and of the specimen dimensions. It is worth noting that certain ratios of the galvanomagnetic coefficients, notably ρ_{1122}/ρ_{1111}, ρ_{1133}/ρ_{1111} and ρ_{3311}/ρ_{3333} are independent of these errors and should therefore be accurate to better than 3%.

It is also important to note that the Hall coefficient ρ_{312} was measured twice for a given ingot, once on a ' perpendicular ' specimen in arrangement 1 and again on a ' parallel ' specimen in arrangement 3. For each ingot, the two values of ρ_{312} agreed to within 3%, and this fact provides justification for assuming that the two specimens from a given ingot did not differ appreciably in their physical composition.

Thus, the galvanomagnetic coefficients obtained from the above measurements may be regarded as reasonably reliable. In contrast, the remaining coefficients ρ_{3111}, ρ_{1131} and ρ_{3113} are subject to a considerable uncertainty. The voltages associated with these terms varied with ϕ in ways which differed appreciably from those predicted by equations (1)–(3), although in some cases, the general predictions regarding the position of zero signal etc were obeyed reasonably well. It seems likely that there are two reasons for this. In the first place, the voltages were very much smaller than those associated with E_J and the Hall voltage, so that the relative experimental accuracy was low. Secondly, the voltages arise from contributions to the electric field which are particularly sensitive to the direction of current flow relative to the crystal axes. This may be seen from equations (1)–(3) from which it is evident that variations in the angles θ and χ do not produce any effect on the principal terms of E_J or on the Hall terms, but may have a large effect on the remaining components of the electric field. Thus, any deviations in the direction of the current flow down the specimen would produce a large effect on the angular variation of the latter as compared with the effect on the former components.

The values of these ' cross ' terms are therefore uncertain to an unknown extent. However, it has been thought worth while to include some estimates of them in the sets of galvanomagnetic coefficients for both ingots, which are given in the table in a form suitable for comparison with the analysis of the band structure, which is discussed in a subsequent section.

Experimental and Calculated Values of the Galvanomagnetic Coefficients for Ingots 19 and 23 at 77°K
All quantities in m.k.s. units

	Ingot 19		Ingot 23	
	Expt	Calc †	Expt	Calc ‡
ρ_{11}	$4{\cdot}23\times10^{-6}$		$1{\cdot}395\times10^{-6}$	
ρ_{33}/ρ_{11}	2·96	2·81	3·14	3·16
ρ_{123}	$1{\cdot}06\times10^{-6}$		$0{\cdot}240\times10^{-6}$	
ρ_{312}/ρ_{123}	2·04	2·08	2·38	2·53
$\rho_{11}\rho_{1111}/\rho_{123}^2$	0·472	0·495	1·029	0·979
ρ_{1122}/ρ_{1111}	1·32	1·32	1·20	1·20
ρ_{1133}/ρ_{1111}	2·74	2·74	2·03	2·03
$\rho_{11}\rho_{3333}/\rho_{123}^2$	0·674	0·642	3·23	3·35
ρ_{3311}/ρ_{3333}	0·900	0·896	0·372	0·344
ρ_{1113}/ρ_{1111}	0·376	—	0·151	
ρ_{3111}/ρ_{1111}	0·174	—		

† $u=6{\cdot}254$, $v=1{\cdot}252$, $w=1{\cdot}134$, $\beta=0{\cdot}8939$.
‡ $u=8{\cdot}416$, $v=1{\cdot}492$, $w=0{\cdot}962$, $\beta=0{\cdot}8813$. (β is defined in the Appendix.)

2.3. *Resistivity and Hall Coefficients in the range* 77°–290°K

The two resistivity components and the two Hall coefficients were measured on specimens from both ingots over the temperature range 77–290°K. These components are: $\rho_{11}(\rho_{33})$ resistivity with the current flowing perpendicular (parallel) to the rotation axis, $\rho_{312}(\rho_{123})$ Hall coefficient with the magnetic field perpendicular (parallel) to the rotation axis. The Hall coefficient ρ_{312} can be measured on both parallel and perpendicular specimens. The values obtained from two such specimens from the same ingot were found to agree within experimental error over the whole of the temperature range investigated.

The results are illustrated in figures 2, 3 and 4.

§ 3. DISCUSSION

3.1. *The Band Structure of p-type Bismuth Telluride*

The galvanomagnetic coefficients can be used to test proposed models of the band structure of p-type bismuth telluride if some assumption about the form of the scattering mechanism is made. The simplest hypothesis is to assume that the scattering can be described by a relaxation time of the form $\tau=aE^{\lambda}$, where E is the energy of the charge carriers. With this assumption, an analysis of the galvanomagnetic coefficients has shown that these are consistent with a many-valley form of the band structure in which the surfaces of constant energy are sets of ellipsoids, centred on the reflection planes in momentum space. This result is similar to that obtained from an analysis of the galvanomagnetic coefficients on n-type bismuth telluride, given in I.

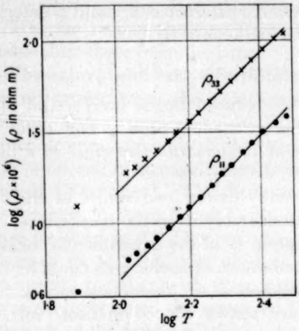

Figure 2. Variation of resistivities with temperature for ingot 19.

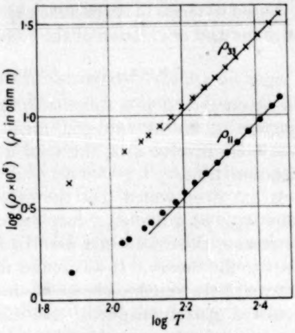

Figure 3. Variation of resistivities with temperature for ingot 23.

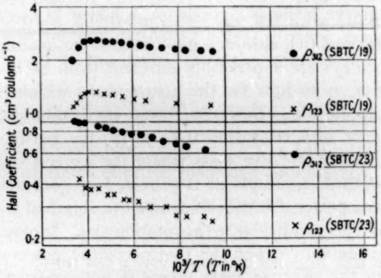

Figure 4. Hall coefficients plotted against temperature.

In the proposed model, the relation between the energy and wave vector of charge carriers occupying states in the valley centred on the reflection plane which forms the (x, z) plane of the crystal axis system is taken as

$$E = E_0 - \frac{h^2}{2m_0}(\alpha_{11}k_1{}^2 + \alpha_{22}k_2{}^2 + \alpha_{33}k_3{}^2 + 2\alpha_{13}k_1k_3) \qquad \ldots\ldots (4)$$

where E_0 is the maximum energy in the valley, m_0 is the free electron mass and the components of the wave vector **k** are measured from the position of maximum energy. The remaining cross terms are zero from symmetry considerations. The corresponding relations for the other valleys can be obtained by applying the symmetry operations of three-fold rotation about the z axis and inversion through the origin.

Expressions for the resistivity, Hall coefficient and magnetoresistance components can be obtained from the method given by Drabble and Wolfe (1956) specifically for this model or from the more general method given by Keyes (1956) for any semiconductor with an axis of rotation. For ease of reference, these expressions are given in an Appendix. The twelve coefficients can all be expressed in terms of six parameters. The three parameters u, v and w determine the shape and orientation of the valleys and are defined by

$$u=\alpha_{22}/\alpha_{11}, \quad v=\alpha_{33}/\alpha_{11}, \quad w=(\alpha_{11}\alpha_{33}-\alpha_{13}^2)/\alpha_{11}^2. \qquad \ldots\ldots(5)$$

The parameter β is a function only of the reduced Fermi level η and of the exponent λ in the assumed form of the relaxation time. The other two parameters involve η, λ, the total density of carriers and the value of a in the relaxation time.

It has been stated that the experimentally determined values of the cross terms ρ_{1131}, ρ_{3111} and ρ_{3113} may deviate considerably from the true values. For this reason, these were not used in attempting to fit the experimental measurements to the theory. It was found that the remaining coefficients could be fitted very well by a suitable choice of the parameters of the theoretical model. The calculated galvanomagnetic coefficients are shown for comparison with the experimental values in the table. In this form only the four parameters u, v, w and β are involved and the remaining two are left undetermined. The values used in the theory were

(i) $u=6{\cdot}254$, $v=1{\cdot}252$, $w=1{\cdot}134$, $\beta=0{\cdot}8939$ for the results on specimens from ingot 19 and (ii) $u=8{\cdot}416$, $v=1{\cdot}492$, $w=0{\cdot}962$, $\beta=0{\cdot}8813$ for ingot 23.

The two sets (i) and (ii), although giving the same qualitative features about the shape of the valleys are appreciably different from each other. This raises the general question as to how far the assumptions which have been made in the analysis are applicable. Basically, three such assumptions are involved, viz, (*a*) the existence of a relaxation time τ, (*b*) the particular form of τ and (*c*) the use of a constant effective mass tensor for a given valley.

Some check on these assumptions is provided by considering the anisotropy of the thermoelectric power, i.e. the relative values obtained with the temperature gradient parallel and perpendicular to the rotation axis. It may be shown that with the assumptions made above, then the thermoelectric power would be isotropic. If, however, either the effective mass tensor is not constant, in the sense that the coefficients α vary with $\mathbf{k}$, or a relaxation time exists but is not just a function of the energy, then the theory would predict that in general, the thermoelectric power would be anisotropic. It has been observed experimentally by Goldsmid (1957) that in p-type bismuth telluride the thermoelectric power is isotropic with an accuracy to 1% over the temperature range 150–300°K, and this therefore provides considerable support for the assumptions of a constant effective mass tensor and of a relaxation time which is a function of energy only.

The particular form of the relaxation time is, however, open to some objections, although it has been shown to be consistent with the temperature dependence of the conductivity, thermoelectric power and electronic thermal conductivity (Goldsmid 1957) over the temperature range 150°K to 300°K. At lower temperatures, however, it seems likely that impurity scattering may be important and give a more complex dependence of τ on energy than that assumed above. It is believed that the large differences observed for example in the ratios of the principal magnetoresistance components of ingot 19 and 23 are associated with such an effect since it is well known that the galvanomagnetic coefficients are very sensitive to even small amounts of impurity scattering. If this is the correct explanation, then, since a comparison of the relative Hall mobilities (defined as ρ_{123}/ρ_{11}) shows that the specimens from ingot 19 have a Hall mobility greater than that of specimens from ingot 23 by a factor of 1·45 at 77°K, the results obtained from the analysis on the former ingot are more reliable than those from the latter.

The subsequent analysis will therefore be restricted to results on ingot 19. The reasonable fit of the experimental results to the proposed form of band structure and scattering law provides a justification for extending the analysis to include measurements of the thermoelectric power. A measurement of this at 77°K on one of the specimens from ingot 19 (made by P. A. Walker) gave a value of $120\mu\text{v deg}^{-1}$. The theoretical expression for the thermoelectric power is a function of the reduced Fermi level and of λ, i.e. the same two parameters as are involved in β. Thus an estimate of η and λ separately can be made and, for ingot 19 at 77°K, this gives $\eta=+1{\cdot}8$, $\lambda=-0{\cdot}5$. A knowledge of these parameters, together with those previously determined can be used to obtain the relations between the measured Hall coefficients and the density of carriers. These are of the form

$$\rho_{123}=\frac{1}{pe}\times\frac{4u}{(1+u)^2} \quad \ldots\ldots(6a) \qquad \rho_{312}=\frac{r}{pe}\times\frac{(w+uv)}{v(1+u)} \quad \ldots\ldots(6b)$$

where r is a function of η and λ, involving the usual averages over the carrier distribution, and p is the total density of holes. For the values of η and λ given above, r has the value 1·08 and hence, using the values of u, v and w for ingot 19

$$\rho_{123}=\frac{1}{pe}\times 0{\cdot}514; \quad \rho_{312}=\frac{1}{pe}\times 1{\cdot}06.$$

Thus, the estimated density of carriers at 77°K is $3{\cdot}03\times10^{18}\ \text{cm}^{-3}$. From this result, the density of states effective mass can be obtained. This is given by

$$m^*/m_0=(3N)^{2/3}\Delta^{-1/3} \quad \ldots\ldots(7)$$

where $3N$ is the number of valleys and Δ is the determinant of the α coefficients in the relation (4). From the above results it is found that $m^*=0{\cdot}511m_0$. For the case $N=2$, this leads to the values.

$$\alpha_{11}=3{\cdot}26,\ \alpha_{22}=19{\cdot}8,\ \alpha_{33}=4{\cdot}12,\ \alpha_{11}\alpha_{33}-\alpha_{13}{}^2=12{\cdot}4.$$

Thus, the value of α_{13} is very small in comparison with the other values and it follows that the principal axes of the valley almost coincide with the chosen crystal axes. The effective mass in the y direction is small, being one-twentieth of the free electron mass if $N=2$, and the other two principal effective masses are about four and eight times larger.

3.2 *The Variation of Resistivity and Hall Coefficients with Temperature*

The variation with temperature of the resistivity components ρ_{11} and ρ_{33} is shown in figures 2 and 3 for specimens from ingots 19 and 23 respectively. The

Hall coefficients ρ_{123} and ρ_{312} on the same specimens are plotted logarithmically against $1/T$ in figure 4. In this form, the Hall coefficients as functions of temperature may be compared directly with the results of Satterthwaite and Ure (1957). In figure 7 of their paper these authors show the variation of the coefficient ρ_{123} with temperature for three p-type samples and the general form of their curves is very similar to the corresponding curves in our figure 4.

On the basis of the model discussed in the last section the ratios ρ_{33}/ρ_{11} and ρ_{312}/ρ_{123} are functions only of the parameters describing the band structure and it is therefore of interest to examine these ratios as functions of temperature. For both ingots, there appears to be a slight change in the ratio ρ_{33}/ρ_{11} as the temperature increases from 77°K. This ratio is 2·97 at 77°K for ingot 19 and decreases to 2·85 at 224°K. It does not seem to be legitimate to discuss the ratio at higher temperatures for this ingot since, from the variation of the Hall coefficients, the specimen appears to be entering the intrinsic region. For ingot 23, the ratio ρ_{33}/ρ_{11} varies from 3·10 at 77°K through 2·88 at 222°K to 2·85 at 292°K.

There is no significant variation in the ratio of the Hall coefficients with temperature in either ingot over the whole of the temperature range investigated. This result is in agreement with that of Satterthwaite and Ure who found no variation in the ratio ρ_{312}/ρ_{123} for a p-type specimen over the temperature range 77° to 200°K. It should be noted however that these authors found a value of 1·4 for this ratio in contrast to the values of greater than two which have been observed in the present work.

From these observations, it may be concluded that any changes in the band structure over the temperature range investigated are small and do not contribute to the changes of the resistivity and Hall coefficients with temperature.

A noticeable feature of the variation of the Hall coefficients with temperature is the tendency to increase as the temperature increases from 77°K. In ingot 23 this trend continues up to 290°K, but in ingot 19 the coefficients show a maximum at about 225°K and thereafter decrease sharply with increasing temperature, presumably due to the onset of intrinsic behaviour.

There seems to be no satisfactory explanation of these observations. The general trend is consistent with the changing degree of degeneracy of the specimens with temperature but the magnitudes of the changes appear to be too large to be accounted for in this way. Neither the sign nor the magnitude of the changes is consistent with a change in the density of the carriers. Further, it has been shown (Goldsmid 1957) that the thermoelectric power and resistivity variations with temperature of similar p-type samples are consistent with the assumption that the density of carriers is constant.

Thus there seems little point in plotting a ' Hall mobility ' as a function of temperature as was done, for example, by Satterthwaite and Ure, who plotted the expression ρ_{123}/ρ_{11} as a function of temperature for a number of p-type specimens. The effect of the scattering processes is more correctly described by assuming the density of carriers to be constant in the temperature range over which the Hall coefficients are increasing with temperature, and regarding the variation of the conductivity as determining the variation of a conductivity mobility, defined for example by $1/\rho_{11} = pe\mu_{\mathrm{p}}$ where μ_{p} is the conductivity mobility for current flow perpendicular to the rotation axis and p is the density of holes.

The temperature variation of μ_p for the two ingots may be obtained from figures 2 and 3. For ingot 19, it is to be expected that the argument is only valid up to temperatures of about 225°K since, above this temperature, the specimens are becoming intrinsic. From figure 2, the value of μ_p for ingot 19 as defined by the above equation varies with temperature as $T^{-1\cdot 98}$ over the range 150° to 240°K. Below 150° the variation does not follow a simple power law and the deviations are consistent with the increasing degree of degeneracy. The variation with temperature of μ_p for ingot 23 is of the form which would be expected from the results on 19 allowing for the increased density of carriers. For example, there is no evidence of intrinsic behaviour and the departure from the $T^{-1\cdot 98}$ law occurs at a higher temperature.

Extrapolating the straight line portion of figure 2 to room temperature and using the value for the density of carriers in ingot 19 determined in the last section, gives a value of μ_p at 290°K of 515 cm^2 v^{-1} sec^{-1}.

The value of μ_p determined in this way cannot be compared directly with the values of Hall mobility which have been obtained by other workers, and which are summarized in the paper by Satterthwaite and Ure. The value of the Hall mobility in ingot 23 at 290°K was 420 cm^2 v^{-1} sec^{-1}. This is in good agreement with the value given by Satterthwaite and Ure for their zone-refined sample which had a similar value of the Hall coefficient ρ_{123}.

APPENDIX

For convenience, and as an indication of the method of analysis of the results, expressions for the twelve galvanomagnetic coefficients for the proposed band structure and scattering mechanism are given. These coefficients are defined with respect to a set of axes in which the z axis is parallel to the three-fold axis of rotation of bismuth telluride and the xz plane is parallel to one of the three equivalent reflection planes.

Assuming one valley to be centred on the plane and that the relation between energy and wave vector **k** for this valley has the form

$$E = E_0 - \frac{h^2}{2m}\left(\alpha_{11}k_1{}^2 + \alpha_{22}k_2{}^2 + \alpha_{33}k_3{}^2 + 2\alpha_{13}k_1k_3\right) \qquad \ldots\ldots\text{(A1)}$$

(see eqn (4)), then the total number of valleys will be $3N$, where $N=1$ if the maximum energy E_0 occurs at the edge of the Brillouin zone and $N=2$ otherwise. Then

$$\rho_{11} = \frac{1}{\alpha_{11}I_0}\,\frac{2}{3N(1+u)}, \quad \rho_{33} = \rho_{11}\,\frac{(1+u)}{2v}$$

$$\rho_{123} = \frac{I_1}{I_0{}^2}\,\frac{4u}{3N(1+u)^2}, \quad \rho_{312} = \rho_{123} \times (w+uv)\,\frac{(1+u)}{4uv}$$

$$\rho_{1111} = \frac{I_2\alpha_{11}}{I_0{}^2}\,\frac{(w-5uw+3uv+u^2v)}{6N(1+u)^2} = b\,\frac{(w-5uw+3uv+u^2v)(1+u)}{16\beta u^2}$$

where $\quad b = \rho_{123}{}^2/\rho_{11}, \; \beta = I_1{}^2/I_0I_2$

$$\rho_{1122} = b\left\{\left[\frac{(3w+uw+uv+3u^2v)(1+u)}{16\beta u^2}\right] - \left[\frac{2v}{a^2(1+u)}\right]\right\}$$

where $a = \rho_{123}/\rho_{312}$

$$\rho_{1133} = b\left(\frac{(1+u)^2}{4u\beta} - 1\right) \qquad \rho_{3333} = b\,\frac{(1+u)^3(v-w)}{8\beta u v^2}$$

$$\rho_{3311} = b\left(\frac{(1+u)^3(w+uv)}{16\beta u^2 v} - \frac{1}{a^2}\right) \qquad \rho_{1131} = b\,\frac{(u^2-1)(v-w)^{1/2}}{8\beta u}$$

$$\rho_{3111} = b\,\frac{(u+1)^2(uv-w)(v-w)^{1/2}}{16\beta u^2 v} \qquad \rho_{3113} + \rho_{3131} = b\left(\frac{-(u+1)^2}{4u\beta} + \frac{1}{a}\right).$$

In these equations, u, v and w are defined by

$$u = \alpha_{22}/\alpha_{11}, \quad v = \alpha_{33}/\alpha_{11}, \quad w = (\alpha_{11}\alpha_{33} - \alpha_{13}{}^2)/\alpha_{11}{}^2.$$

The integrals I_n are defined by

$$I_n = -\left(\frac{e}{m}\right)^n \frac{e^2}{3\pi^2 m}\left(\frac{2m}{h^2}\right)^{3/2} \frac{1}{\Delta^{1/2}} \int \tau^{n+1} E^{3/2} \frac{\delta f_0}{\delta E}\, dE$$

where m is the free electron mass, Δ is the determinant of the tensor α_{ij}, and the integrals are taken over the energy states associated with a single valley. These integrals correspond to the ξ_n defined by Keyes (1956) apart from the factor $\Delta^{1/2}$, which it is thought has been omitted in error by Keyes.

The value of $I_1/I_0{}^2$ is related to the density of carriers in one valley, which is given by

$$p_v = \frac{1}{2\pi^2}\left(\frac{2mkT}{h^2 \Delta^{1/3}}\right)^{3/2} F_{1/2}(\eta)$$

where $F_{1/2}(\eta)$ is the Fermi–Dirac integral of order $\frac{1}{2}$ and η is the reduced Fermi level.

REFERENCES

Drabble, J. R., Groves, R. D., and Wolfe, R., 1958, *Proc. Phys. Soc.*, **71**, 430.

Drabble, J. R., and Wolfe, R., 1956, *Proc. Phys. Soc.* B, **69**, 1101.

Goldsmid, H. J., 1957, *Ph.D. Thesis*, University of London.

Keyes, R. W., 1956, *J. Electronics*, **2**, 279.

Satterthwaite, C. B., and Ure, R. W., 1957, *Phys. Rev.*, **108**, 1164.

The Transport Theory of Temperature Waves in Insulators

By R. ENGLMAN
H. H. Wills Physics Laboratory, University of Bristol

MS. received 19*th May* 1958

Abstract. Heating the surface of an insulator by a rapidly fluctuating source results in a temperature distribution in the solid, which is usually described as an attenuated wave. For high frequency fluctuations, when this description may not be valid, the temperature is found as a solution of the Boltzmann equation. Expressions are derived for various related quantities in terms of the phonon source, its frequency and the coefficient of reflection of the phonons at the boundary.

---

§ 1. Introduction

THE following problem is considered:

A solid is heated from a periodically varying source, what is the temperature distribution in the solid? We specify the geometry of the problem by taking the solid to be of semi-infinite extent, with a plane surface which is uniformly heated by the source. For simplicity we consider insulators, that is such substances in which the transport of heat is exclusively or predominantly due to the vibrations of the lattice (phonon-transport). We do not, however, specify as yet in what manner the vibrations are set up at the boundary plane, that is, how the phonon-packets are introduced across the surface. In the detailed consideration of special cases two simplifications are made. One is to assume the existence of times of relaxation for the various scattering processes to which the phonons are subject in the solid and, secondly, to take a single (some sort of average) value u_0 for the velocity of sound for oscillations of both longitudinal and transverse type.

Under these conditions the transport equation (the Boltzmann equation) is solved in § 2. This equation contains the temperature as an unknown function of the space variables, and it will be our business to set up and solve an equation for this function. For low frequency variations of the heat source a solution, based on a simple phenomenological description, may be given in terms of temperature waves, which attenuate exponentially with a penetration depth of $(2\kappa/\omega C)^{1/2}$ and which are propagated with a phase velocity $(2\kappa\omega/C)^{1/2}$. Here κ denotes the thermal conductivity, C the specific heat per unit volume of the solid and ω the angular frequency of the source. The validity of this solution is limited by the fact, which was pointed out by Howling, Mendoza and Zimmermann (1955), that the velocity of the waves cannot be arbitrarily increased with increasing frequency beyond the velocity of the carriers of heat in the solid. Instead, for high frequencies and at low temperatures, a rigorous solution of the Boltzmann equation is required, leading to an integral equation to determine the resultant temperature function. In essence, the integral equation takes account of the fact that the number of phonons reaching a point from some other point will depend on the temperature at the point of their origin. Whereas for the low frequency case the temperature could be taken as a quasi-constant, slowly decreasing exponential, such assumption is clearly not legitimate as soon as the free-path of the phonons exceeds the penetration-depth of the temperature waves. With high-frequency *electric* waves a similar situation is known to give rise to the anomalous skin effect (Pippard 1947, Reuter and Sondheimer 1948). Putting this in a quantitative way, we may say that the phenomenological description is quite in order some distance away from the boundary (it will never be quite valid close to the boundary) and for such conditions that $\omega\tau \ll 1$ where τ is the time of relaxation of the scattering. Conversely, a less restricted situation requires a more searching investigation of the transport process and this is presented here. Many important questions, such as the scattering of phonons in the bulk and at boundaries and the detailed mechanism of phonon transfer are dismissed all too lightly; they do, however, fall outside the intended scope of this work.

Essentially, the emphasis is on very high frequency temperature waves, such, that is, that $\omega\tau \gg 1$ and, apart from giving correction terms for low frequencies, we mainly derive limiting expressions valid in that extreme. Now, with a characteristic velocity of sound in insulators of the order of 10^5 cm sec^{-1} and a mean free path of order 1 cm, this means that we are talking about frequencies of 10^{-5} sec^{-1}, higher than those in use at present—nevertheless, within reach of practical possibilities.

§ 2. THE TRANSPORT EQUATION

2.1. We now set up the Boltzmann equation for the distribution of the energy in the solid, assuming that the statistical equilibrium is maintained by collisions of the lattice waves. These may be of the kind due to anharmonicities or else collisions either with irregularities of the lattice or at the boundaries.

We consider a semi-infinite solid whose surface is the plane $x=0$, and in which a temperature gradient is produced in the x direction. With the lattice wave number $\mathbf{q}$ and velocity of sound u_i ($i=1$ for vibrations of the longitudinal type, $i=2, 3$ for those of the transverse type), the velocity of waves is $u_i\mathbf{q}/q$ so that the equation for $E(\mathbf{q}, x, t)$, the energy per unit volume per interval $d\mathbf{q}$ due to phonons in the interval between $\mathbf{q}+d\mathbf{q}$ and q and at the point x, is

$$u_i \frac{q_1}{q}\frac{\partial E}{\partial x} + \frac{\partial E}{\partial t} = \left[\frac{\partial E}{\partial t}\right]_{\text{coll}}, \qquad \ldots\ldots(1)$$

where q_1 denotes the component of $\mathbf{q}$ in the x direction.

As usual we assume that, compared to the steady temperature T_0 of the surroundings, the fluctuating temperature and the temperature gradient are small. We also assume sinusoidal oscillation with angular frequency ω. Then writing $T=T_0+T_1(x)\mathrm{e}^{i\omega t}$, only terms linear in $T_1(x)$ or $dT_1(x)/dx$ are considered. Consequently $E(\mathbf{q}, x, t)$ may be written in this approximation as $E_0+E_1\mathrm{e}^{i\omega t}$, where

$$E_0 = \frac{h\nu}{\exp(h\nu/kT)-1} \qquad \ldots\ldots(2)$$

is the equilibrium value for the energy density due to lattice vibrations of frequency ν, T being given as above.

The collision term on the right-hand side of (1) is an integral involving E_1 whose exact form will depend on the type of collision considered. For our purposes and to the approximation linear in $T_1(x)$, it may be taken to be

$$\left[\frac{\partial E}{\partial t}\right]_{\text{coll}} = \int V(\mathbf{q}, \mathbf{q}')\{E_1(\mathbf{q}') - E_1(\mathbf{q})\}d\mathbf{q}'$$

where

$$V(\mathbf{q}, \mathbf{q}') = V(\mathbf{q}', \mathbf{q}).$$

The more complicated form of Peierls (1955, p. 49) that holds for collisions due to anharmonicities leads to the same conclusions.

Equation (1) will then be written

$$u_0 \frac{q_1}{q} \frac{\partial E_1}{\partial t} + i\omega E_1 - \frac{i\omega\eta}{T_0} \frac{\partial E_0}{\partial \eta} T_1(x) - u_0 \frac{q_1}{q} \frac{\eta}{T_0} \frac{\partial E_0}{\partial \eta} \frac{\partial T_1(x)}{\partial x} = \int V(\mathbf{q}, \mathbf{q}')\{E_1(\mathbf{q}') - E_1(\mathbf{q})\}d\mathbf{q}', \qquad \ldots\ldots(3)$$

where $\eta = h\nu/kT$.

2.2. The solution for low frequencies may be easily obtained as follows: As a first approximation to the solution of (3) terms with $i\omega$, the second and third on the left-hand side, can be neglected, as can also be the first term. For the right-hand member it is sufficient to assume that the effect of the various collisions may be represented by the appropriate free paths.

Thus

$$\left[\frac{\partial E}{\partial t}\right]_{\text{coll}} = -\frac{E_1}{L(\mathbf{q}, T_0)} u_0. \qquad \ldots\ldots(4)$$

For the simplest case of anharmonic scattering L may be taken to be independent of $\mathbf{q}$.

From (3) we have then

$$E_1 = \frac{Lq_1}{q} \frac{\eta}{T_0} \frac{\partial E_0}{\partial \eta} \frac{\partial T_1}{\partial x}.$$

To solve for the hitherto unknown function $T_1(x)$, E_1 is substituted back into the full equation (3). We integrate over the whole $\mathbf{q}$-space and, noting that E_1 is odd in $\mathbf{q}$, we find that all but the first and third terms vanish, so that we are left with

$$u_0 L \frac{\partial^2 T_1}{\partial x^2} \int \frac{\eta}{T_0} \frac{q_1^2}{q^2} \frac{\partial E_0}{\partial \eta} d\mathbf{q} - i\omega T_1 \int \frac{\eta}{T_0} \frac{\partial E_0}{\partial \eta} d\mathbf{q} = 0 \qquad \ldots\ldots(5)$$

or

$$\frac{\partial^2 T_1}{\partial x^2} = \frac{3i\omega}{u_0 L} T_1. \qquad \ldots\ldots(5a)$$

This has the exponential solution

$$T_1(x) \propto \exp\left[-(1+i)\left(\frac{3\omega}{2u_0 L}\right)^{1/2} x\right]. \qquad \ldots\ldots(6)$$

It will be seen that equation (5) is equivalent to the equation of conservation of energy

$$\operatorname{div} \mathbf{w} + \partial U/\partial t = 0, \qquad \ldots\ldots(7)$$

with $\mathbf{w}$ the thermal current density and U the heat content per unit volume of the solid, as it must be, since the last equation is merely one of the integrated forms of the Boltzmann equation and a direct consequence of it (see, for example, Chapman and Cowling 1939, p. 50).

The solution (6) is identical with that of Howling, Mendoza and Zimmermann if we put for κ the lattice thermal conductivity value $\kappa = \frac{1}{3} C u_0 L$ (Wilson 1953, p. 294).

2.3. For the more general problem considered in the introduction, the integro-differential equation for E_1 must be solved without neglecting any of the terms in (3), and $T_1(x)$ determined as the temperature corresponding to equilibrium.

From the statistical definition of the local temperature,

$$\int E_0(T)d\mathbf{q} = \int E(\mathbf{q}, x, t)d\mathbf{q}$$

we immediately find

$$\int E_1 d\mathbf{q} = 0. \qquad \ldots\ldots (8)$$

This equation contains the temperature implicitly, and the object of the following paragraphs, the determination of the temperature function, will be achieved by consideration of this equation.

If the assumption of a mean free path for the scattering processes is retained, then (3) is soluble and

$$\begin{aligned} E_1 = & -\frac{\eta}{T_0}\frac{\partial E_0}{\partial \eta}\int_{-\infty}^{x} \exp\left\{(x'-x)\frac{q(1+i\omega\tau)}{Lq_1}\right\}\left[\frac{\partial T_1}{\partial x'} + \frac{i\omega\tau}{L}\frac{q}{q_1}T_1\right]dx' \\ & + \frac{\eta}{T_0}\frac{\partial E_0}{\partial \eta}Q(\mathbf{q})\exp\left\{-x\frac{q}{Lq_1}(1+i\omega\tau)\right\}, \qquad q_1 > 0 \\ = & \frac{\eta}{T_0}\frac{\partial E_0}{\partial \eta}\int_{x}^{\infty} \exp\left\{(x'-x)\frac{q}{Lq_1}(1+i\omega\tau)\right\}\left[\frac{\partial T_1}{\partial x'} + \frac{i\omega\tau}{L}\frac{q}{q_1}T_1\right]dx', \quad q_1 < 0 \end{aligned}$$

where we have written τ for L/u_0.

For q_1 less than zero the constant of integration has been taken to be such that $E_1 \to 0$ as $x \to \infty$. The number of phonons, in excess of the number present in the equilibrium distribution, which travel from the boundary inwards ($q_1 > 0$), is considered to be the sum of the number injected by the source and that reflected back specularly from the surface. If for the latter we assume that a single number p suffices to describe that proportion of phonons which is reflected on reaching the surface (a fraction $1-p$ of these phonons then leaves the solid), then we should define in the first expression above

$$T_1(x) = pT_1(-x) \text{ for } x < 0.$$

The second term in the same expression is the source term.

$$\mathscr{R}\frac{\partial E_0}{\partial \eta}\frac{u_0}{kT_0}\frac{q_1}{q}Q(\mathbf{q})e^{i\omega t}$$

is the number of phonons of wave vector $\mathbf{q}$ injected per unit area per unit time. The appropriate form of Q will be specified by the mode of introduction of phonons into the solids.

From the solution of the Boltzmann equation we next calculate

$$\begin{aligned} \int E_1 d\mathbf{q} = & -\int \frac{\eta}{T_0}\frac{\partial E_0}{\partial \eta}q^2 dq\int_0^{2\pi} d\phi\left\{\int_0^{\pi/2}\sin\theta d\theta\int_{-\infty}^{x}\left[\frac{\partial T_1}{\partial x'}\right.\right. \\ & \left. + \frac{i\omega}{u_0\cos\theta}T_1\right]\exp\left[\frac{x'-x}{L\cos\theta}(1+i\omega\tau)\right]dx' \\ & - \int_{\pi/2}^{\pi}\sin\theta d\theta\int_x^{\infty}\left[\frac{\partial T_1}{\partial x'} + \frac{i\omega}{u_0\cos\theta}T_1\right]\exp\left[\frac{x'-x}{L\cos\theta}(1+i\omega\tau)\right]dx' \\ & \left. - \int_0^{\pi/2}\sin\theta d\theta Q(\mathbf{q})\exp\left[-\frac{x}{L\cos\theta}(1+i\omega\tau)\right]\right\}, \end{aligned}$$

where polar coordinates ($\mathbf{q}$, θ, ϕ) are used on the right-hand side to carry out the integration in $\mathbf{q}$-space. $\eta = h\nu/kT$ is now supposed to depend on $|\mathbf{q}|$ only, while L is regarded as either independent of $\mathbf{q}$, or representing some mean value when integrated over $\mathbf{q}$.

§ 3. THE TEMPERATURE DISTRIBUTION

3.1. We use now equation (8) and arrive after some reduction at the following equation

$$2T_1(x) = (1-p)T_1(0)\mathrm{Ei}_2\left(\frac{xa}{L}\right) + \frac{1}{L}\int_{-\infty}^{\infty} d\xi\, T_1(\xi)\mathrm{Ei}_1\left[\frac{|x-\xi|a}{L}\right] + \int_1^{\infty} \frac{ds}{s^2} Q(s)\mathrm{e}^{-sxa/L} \qquad \ldots\ldots (9)$$

where $\mathrm{Ei}_n(t)$ is the nth exponential integral $= \int_1^{\infty} ds\, s^{-n}\mathrm{e}^{-st}$.

$Q(\sec\theta)$ is the result of integration of $Q(\mathbf{q})$ over q and ϕ, and $T_1(\xi)$ is defined for negative arguments as above. We have written $a = 1 + i\omega\tau$ for brevity.

This is the integral equation to be solved for $T_1(x)$, depending essentially on the adjustable parameters $\omega\tau$ or a. While a detailed solution for T_1 will not be given except in some cases when p and $Q(\mathbf{q})$ are specified, certain statements about the behaviour of the solutions may already be made with p and Q left quite general, though the point of these statements may only emerge after some simple special models have been considered. This will be done in the following paragraph.

3.2. We first consider some limiting cases and focus our attention on the asymptotic behaviour of $T_1(x)$ for large x. (In the following qualitative statements lengths are always compared to the free path L.)

For low frequencies ($\omega\tau$ small) it is found, after repeated integration by parts of the second terms in the right-hand member of (9), that well inside the material, i.e. where $\mathrm{e}^{-xa/L} \sim 0$,

$$i\omega\tau T_1(x) = \tfrac{1}{3}L^2 T_1''(x).$$

This has the exponential solution (6).

In the opposite extreme of large $\varpi\tau$ a solution by integration may be obtained. In the first approximation

$$2T_1(x) = \frac{1-p}{1+p}\mathrm{Ei}_2(xa/L)\int_1^{\infty} ds\, s^{-2}Q(s) + \int_1^{\infty} ds\, s^{-2}Q(s)\mathrm{e}^{-sxa/L},$$

with the value

$$T_1(0) = [T_1(x)]_{x\to 0+} = \frac{1}{1+p}\int_1^{\infty} ds\, s^{-2}Q(s).$$

Further approximations arise from the repeated substitutions for $T_1(x)$ in the right-hand side of (9), with the consistency of the solution at $x = 0$ always checked as for example, in the first approximation.

3.3. The general character of the temperature function may now be seen to be as follows.

Near the surface the injected phonons make a direct contribution to the temperature by an amount depending on the form of $Q(s)$. In addition, inside the solid the scattering mechanism establishes a temperature wave of an exponential type, namely one varying as $\exp[-x(A+iB)]$ (A and B may be read off from figure 1 as functions of $\omega\tau$). This exponential wave will asymptotically dominate the behaviour of the temperature function as long as $\omega\tau < 0{\cdot}8$. Turning to the expression for E_1, we see that for all such $\omega\tau$ the excess phonons will be asymptotically isotropically distributed, while for $\omega\tau > 0{\cdot}8$ the phonons moving along the normal to the boundary will be dominant asymptotically. For such high frequencies that $\omega\tau > 1{\cdot}31$ we have the notable result, that the exponential-type temperature waves will be altogether absent. This situation may be loosely but suggestively described in a borrowed idiom by saying that when the raw phonons arrive too fast, the digesting mechanism is unable to turn them into exponential waves.

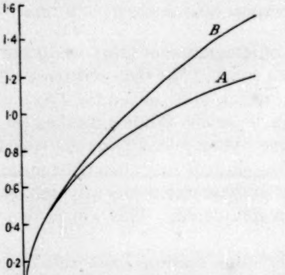

Figure 1. $A = \mathscr{R}u(1+i\omega\tau)$; $B = \mathscr{I}u(1+i\omega\tau)$. (See figure 2.)

For the detailed solution of equation (9) we shall consider two simple extreme characterizations for the injection of phonons at the surface. In the one case phonons are regarded as entering the solid isotropically distributed, in the other extreme all phonons are supposed to move in a definite direction. The first case seems to be approximated in practice when the solid is heated by a gas, for the second case (called the albedo problem) a particular instance is that when a source sheet is embedded between two media and the phonons enter the solid normally. In so far as the isotropic or random injection of phonons can be regarded as a superposition of unidirectional phonon-injections (and so can, indeed, any arbitrary distribution of phonons) the second case is evidently the more fundamental. Nevertheless, since different physical situations correspond to the two cases, they will be considered under separate headings. In each case some assumption about the internal reflection at the boundary must also be made and here we have been forced to adopt the gross simplification of assuming either total specular reflection ($p = 1$) or no reflection at all ($p = 0$).

Subject to these idealizations we shall give explicit solutions for $T_1(x)$. In addition, we calculate two quantities that may be related to experimental verification of our results: the flux across the surface and the temperature at the surface.

§ 4. Random Distribution of Phonons

4.1. When the distribution of the injected phonons is random $Q(s)=Q$, a constant. For specular reflection we write now equation (9) as

$p=1.$

$$2T_1(x) = \int_{-\infty}^{\infty} T_1(\xi)\mathrm{Ei}_1\left(\frac{|x-\xi|\,a}{L}\right)d\xi + Q\mathrm{Ei}_2(xa/L)$$

and $T_1(x)$ is now even.

The solution of this equation is best effected by means of complex Fourier transforms. The definition of these is

$$F(u)=\int_{-\infty}^{\infty} T_1(\xi L)e^{\xi u}d\xi. \qquad \ldots\ldots(10)$$

On taking the transform of equation (9) and applying the faltung theorem, we find easily that

$$F(u)=-Q\frac{1}{u'}\,\frac{\log(1-u'^2)}{2au'-\log\{(1+u')/(1-u')\}}$$

where $u' \equiv u/a \equiv u/(1+i\omega\tau)$.

The roots u_1 of $\log\{(1+u)/(1-u)\}=2au$ are evidently of interest. These occur in pairs $(u_1, -u_1)$, real and imaginary parts of one branch are shown in figure 2. It is shown in the appendix that no roots exist for $\omega\tau > 1{\cdot}31$. Similarly, it may be proved quite simply, or read off from the graph of figure 2, that no root whatsoever lies in the sector bounded in the finite part of the u plane by the imaginary axis and the line at an angle $-\tan^{-1}\omega\tau$ to it.

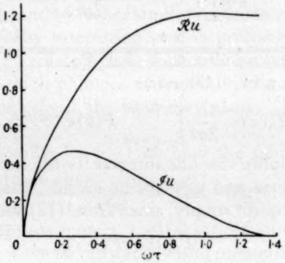

Figure 2. Roots of $\log\dfrac{1+u}{1-u}=2u(1+i\omega\tau)$.

From the inversion formula we obtain the temperature as

$$T_1(x)=Q\frac{a}{2\pi i}\int_{-i\infty}^{i\infty}\frac{\log(1-u'^2)}{2au'-\log\{(1+u')/(1-u')\}}\exp(-u'xa/L)\frac{du'}{u'}$$

where in changing the variable of integration from u to u' the statement about the location of the roots has been used.

After a simple contour integration we find that

$$T_1(x)=Qa\frac{\log(1-u_1^2)}{2u_1[(1-u_1^2)^{-1}-a]}\exp(-u_1xa/L) + 2Qa\int_1^{\infty}\frac{ds}{s}\,e^{-sxa/L}\,\frac{as-\log(1+s)}{[2a^2-\log\{(1+s)/(s-1)\}]^2+\pi^2}. \qquad \ldots\ldots(11)$$

It is readily seen that limiting cases of § 3.2 for $\omega\tau \ll 1$ (when

$$u_1 \sim (3i\omega\tau)^{1/2} - \tfrac{3}{10}(3i\omega\tau)^{3/2})$$

and for $\omega\tau \gg 1$ are regained from (11).

4.2. $p=0$.

The equation of § 3.1 now becomes

$$T_1(x) = \tfrac{1}{2}\int_0^\infty T_1(\xi)\mathrm{Ei}_1\left(\frac{|x-\xi|a}{L}\right)d\xi + \tfrac{1}{2}(T_1(0)+Q)\mathrm{Ei}_2(xa/L).$$

This equation differs from the inhomogeneous integral equations encountered in neutron transport theory only by the complex argument of the exponential integral. Like those, it may be solved by an extension of the method originally due to Hopf and Wiener. The details of the solution will be dispensed with and only the result in terms of the one-sided Fourier transform of the temperature function will be given. Substitution of the solution in the equation, and, possibly, reference to a textbook, such as Paley and Wiener (1934), should establish the correctness of our solution.

Defining, as above,

$$\begin{aligned} F(u) &= \int_0^\infty T_1(zL)\,\mathrm{e}^{zu}\,dz \\ &= -\frac{T_1(0)+Q}{2a}\,\frac{1}{2\pi i}\int_{c-i\infty}^{c+i\infty}\frac{ds}{s-u}\,\frac{\log(1-s^2)}{s^2} \\ &\quad \times \exp\left\{\frac{1}{2\pi i}\int_{-c-i\infty}^{-c+i\infty}\log\left[1-\frac{\log\{(1+v)/(1-v)\}}{2av}\right]dv\left[\frac{1}{v-s}+\frac{1}{v+u}\right]\right\} \end{aligned} \qquad \ldots\ldots(12)$$

where c is a positive real number such that $\mathscr{R}u > c$.

The temperature is now obtained as

$$T_1(x) = \frac{1}{2\pi i}\int_{-c'-i\infty}^{-c'+i\infty}F(u)\,\mathrm{e}^{-ux/L}du.$$

It is possible to simplify this line integral for the limiting cases as before, but this is somewhat involved and will not be given. Instead, we calculate $T_1(0)$. This may be obtained quite simply, since from (12) we find that

$$T_1(0) = sF(-s)_{s\to\infty},$$

so that

$$T_1(0) = \frac{QR}{1-R},$$

where

$$R = \tfrac{1}{2}\int_1^\infty ds\, s^{-2}\exp\left\{\frac{1}{2\pi i}\int_{-i\infty}^{i\infty}\frac{du}{u-s}\log\left[1-\frac{\log\{(1+u)/(1-u)\}}{2au}\right]\right\}. \qquad \ldots\ldots(13)$$

Leading terms for R may be obtained for large $\omega\tau$.

$$R \sim \tfrac{1}{2} + \frac{1}{4a}\int_1^\infty ds\, s^{-3}\log(1+s).$$

Thus $T_1(0) \sim Q[1+0{\cdot}494a^{-1}]$. [For $p=1$ the corresponding value is exactly half of this: $T_1(0) \sim \tfrac{1}{2}Q(1+0{\cdot}494a^{-1})$.] For small values of $\omega\tau$, R has to be computed numerically.

4.3. We ask now, what is the net rate of energy flow across unit surface of the solid? For $p=1$ this is clearly the heat current density of the phonons injected, but for $p \neq 1$ phonons escape from the solid in the outward direction. We will therefore integrate equation (7) over the whole volume of the solid. Application of Gauss' theorem gives at once for the normal heat flow across the boundary plane the equation,

$$w_x(0) = -\frac{\partial}{\partial t}\int_{-\infty}^{\infty} dx\,U(T) = -iwC\int_{-\infty}^{\infty} dx\,T_1(x),$$

the specific heat C being defined as $C = \partial U/\partial T$. In the special case considered above, when $p=0$, we find that

$$\begin{aligned} w_x(0) &= -i\omega CLF(0) \\ &= -\frac{i\omega CL}{2a}\,(T_1(0)+Q)\int_1^{\infty}\frac{ds}{s^3}\exp\left\{\frac{1}{2\pi i}\int_{-c-i\infty}^{-c+i\infty}\log\left[1-\frac{\log\{(1+t)/(1-t)\}}{2at}\right]\right. \\ &\quad \left.\times\left[\frac{1}{t-s}+\frac{1}{t}\right]dt\right\}. \end{aligned}$$

For sufficiently high frequencies this reduces to

$$w_x(0) \sim -\frac{i\omega CLQ}{2a}\,[1+1{\cdot}04a^{-1}].$$

§ 5. THE 'ALBEDO' PROBLEM

If all phonons enter the solid moving at an angle $\cos^{-1}\rho$ to the normal, then the source function $Q(\mathbf{q})$ may be written as the delta function $Q(q,\phi)\delta(\cos\theta-\rho)$.

In this problem equation (9) is again soluble for the cases that yielded solution in the previous paragraph, and by rather similar methods. There is this difference, however, that the physically interesting case is probably that of total specular reflection, since, as noted earlier, a plane source of heat inserted in the solid will establish a situation in which phonons enter the medium presumably normally and which is symmetrical about the boundary plane. In this case, then, $p=1$ and $\rho=1$.

Somewhat more generally, for $p=1$ we have the solution

$$T_1(x) = \frac{Q\rho^3 a}{\pi i}\int_{-i\infty}^{i\infty}\frac{du\,u\exp(-uxa)}{1-u^2\rho^2}\,[2au-\log\{(1+u)/(1-u)\}]^{-1}.$$

In particular, we have approximately $T_1(0) \sim \frac{1}{2}Q\rho^2[1+a^{-1}\rho\log(1+\rho^{-1})]$.

In the contrary case, when all outward bound phonons escape at the boundary ($p=0$), the solution is rather similar in form to that given by equation (12). Corresponding expressions may be found for $T_1(0)$. In fact $T_1(0) = QS/(1-R)$ where R is given by (13), and

$$S = \tfrac{1}{2}\rho^2\exp\left\{\frac{1}{2\pi i}\int_{-c-i\infty}^{-c+i\infty}\frac{dz}{z-\rho^{-1}}\log\left[1-\frac{\log\{(1+z)/(1-z)\}}{2az}\right]\right\}.$$

In the high frequency limit this can be expanded in inverse powers of a:

$$S \sim \tfrac{1}{2}\rho^2[1+\tfrac{1}{2}a^{-1}\rho\log(1+\rho^{-1})].$$

Likewise, the energy flux may be approximated by the expression

$$w_x(0) = -\frac{i\omega CLQ}{4a}\{1+2\rho+a^{-1}[1{\cdot}04+\rho+\tfrac{1}{2}(1+2\rho)\log(1+\rho^{-1})]\}.$$

It has already been remarked, that the results of this paragraph enable us to find, quite generally, the appropriate results for any known form of $Q(\mathbf{q})$ by suitable superposition of the albedo problem.

Our final remark concerns temperature waves in metals. Here the situation is complicated by the presence of an electric field, which is induced so as to preclude any charge flow. In addition, on account of the much higher velocity of electrons as compared to vibrations, $(\omega\tau)_{\mathrm{el}}$ is considerably lower than the corresponding quantity for insulators, so that to reach the region $\omega\tau > 1$ very high frequencies indeed would be necessary.

ACKNOWLEDGMENTS

My best thanks are due to Professor M. H. L. Pryce and to Dr. E. H. Sondheimer of Queen Mary College, London, for discussions and advice and to Dr. E. Mendoza for suggesting the problem. I am indebted to Miss M. J. Littleton for calculating the roots of $\log\{(1+u)/(1-u)\} = 2u(1+i\omega\tau)$.

APPENDIX

The roots of $\log \dfrac{1+u}{1-u} - 2(1+i\omega\tau)u$.

Let $W = \log\{(1+u)/(1-u)\}/2u$ and map on to the complex W plane the contour in the u plane, consisting of the real axis and an infinitely large semicircle in the upper half plane (figure 3).

Then $W-(1+i\omega\tau)$ will have a root in the upper half-plane of u if, and only if, the contour of W encloses the point $1+i\omega\tau$. It is easy to show that the highest value of $\omega\tau$ that satisfies this condition is $\omega\tau = 1{\cdot}31$.

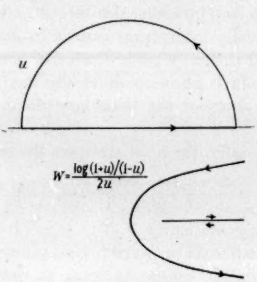

Figure 3.

REFERENCES

CHAPMAN, S., and COWLING, T. G., 1939, *The Mathematical Theory of Non-Uniform Gases* (Cambridge : University Press).

HOWLING, D. H., MENDOZA, E., and ZIMMERMANN, J. E., 1955, *Proc. Roy. Soc.* A, **229,** 86.

PALEY, R. E. A. C., and WIENER, N., 1934, *Fourier Transforms in the Complex Domain* (New York : Amer. Math. Soc.).

PEIERLS, R., 1955, *Quantum Theory of Solids* (Oxford : University Press).

PIPPARD, A. B., 1947, *Proc. Roy. Soc.* A, **191,** 385.

REUTER, G. E. H., and SONDHEIMER, E. H., 1948, *Proc. Roy. Soc.* A, **195,** 336.

WILSON, A. H., 1953, *The Theory of Metals*, 2nd Edn (Cambridge : University Press).

Magnetothermal Resistance and Magnetothermoelectric Effects in Bismuth Telluride

By A. E. BOWLEY, R. DELVES and H. J. GOLDSMID
Research Laboratories of The General Electric Company Limited, Wembley, Middlesex

MS. received 21*st April* 1958

Abstract. The magnetothermal resistance and magnetothermoelectric effects have been measured for samples of p-type and n-type Bi_2Te_3 at 77°K. Scattering laws for the charge carriers have been derived from the magnetothermoelectric effect and also from the magnetothermal resistance effect for p-type material. It has, however, not been possible to fit a simple scattering law to the results from the magnetothermal resistance effect in n-type material.

§ 1. Introduction

The change in thermal resistance on the application of a magnetic field has been studied for a number of metals, e.g. bismuth (Reddemann 1934) and beryllium (Grüneisen and Erfling 1940). A comparison of this change with the corresponding change in the electrical resistance can, in principle, enable any contribution to the transfer of heat by lattice conduction to be distinguished from the electronic contribution. The total heat conductivity κ may be written as

$$\kappa = \kappa_l + \kappa_e = \kappa_l + A\left(\frac{\boldsymbol{k}}{\boldsymbol{e}}\right)^2 \sigma T \qquad \ldots\ldots(1)$$

where κ_l and κ_e are the lattice and electronic components respectively, σ is the electrical conductivity and A is a multiplying factor which is theoretically $\pi^2/3$ for a completely degenerate conductor (Sommerfeld 1928). If it is assumed that the lattice component is not affected by a magnetic field

$$\kappa_H = \kappa_l + \kappa_{eH} = \kappa_l + A_H\left(\frac{\boldsymbol{k}}{\boldsymbol{e}}\right)^2 \sigma_H T \qquad \ldots\ldots(2)$$

the subscript H referring to properties with a magnetic field H applied. If it could also be assumed that A_H is independent of the field, i.e. $A_H = A$, then a measurement of κ_H and σ_H would enable the Lorenz number $A(\boldsymbol{k}/\boldsymbol{e})^2$ to be calculated.

This method was applied to tungsten by de Haas and de Nobel (1938), but later de Nobel (1949) showed that the Lorenz number obtained in this way was not independent of the magnetic field. However, even if measurements of the magnetothermal resistance and magnetoresistance effects do not yield the Lorenz number directly, they should certainly throw some light on the scattering law for the charge carriers and, thus, enable a reasonable estimate of the electronic component of the thermal conductivity to be made.

In semiconductors the lattice component of the thermal conductivity is generally so much greater than the electronic component that the change of thermal resistance on the application of a magnetic field is negligible. Steele (1957) showed that there was no measurable magnetothermal resistance effect for germanium. He did, however, demonstrate an appreciable magnetothermoelectric effect and pointed out that this, also, is related to the scattering process for the charge carriers.

The electronic component of the thermal conductivity in the semiconductor bismuth telluride is comparable with the lattice component and it therefore seemed that, for this material, it might be possible to observe a magnetothermal resistance effect as well as a magnetothermoelectric effect. Since the thermomagnetic and galvanomagnetic effects increase with the carrier mobility and this, in turn, increases as the temperature is reduced, all the measurements were carried out at 77°K, the temperature of liquid nitrogen.

§ 2. Experimental Procedure

The electrical conductivity, Hall coefficient and magnetoresistance coefficient were measured as described by Drabble *et al.* (1958). The specimens were cut from single crystals so that the current flow, with no magnetic field, was perpendicular to the *c* crystal axis. Magnetic fields parallel to the *c* axis were invariably employed.

The samples for the thermomagnetic and galvanomagnetic measurements came from adjacent portions of the same crystals. As pointed out by Drabble and Wolfe (1957), geometric effects in magnetoresistance measurements can be avoided if the potential probes are suitably placed on samples with a length-to-width ratio substantially greater than 2 : 1. However, other considerations made the use of such samples undesirable for experiments on the magnetothermal resistance effect, so for the thermomagnetic measurements length-to-width ratios of 2 : 1 and 1 : 1 were employed. It was intended to calculate the geometric correction, due to the Righi–Leduc effect, from the difference between the changes of thermal resistivity on the application of a magnetic field for two adjacent samples of different length. In fact, in no case was such a difference observed. However, the measurements on two samples from each crystal did enable the thermal resistance of the contacts to be calculated.

The measurement of thermal conductivity consists, in principle, of supplying heat at a known rate to one end of a test sample and passing it into a sink at the other end. A knowledge of the temperature difference over the sample and its dimensions enables the thermal conductivity to be calculated. The apparatus which was employed in the measurements to be described here is shown in figure 1.

The heat sink was a copper cylinder connected to a vacuum system at one end, and with a removable copper cap at the other end. Inside the cylinder was soldered a narrow copper tube through which passed the electrical leads. The latter were cemented in place at the lower end with 'Araldite' synthetic resin which had been loaded with magnesia powder. All the leads to the heater were of known length so the heat losses, other than through the specimen, could be calculated. At the temperature of the experiment the losses from the heater by radiation were negligible.

The source of heat was a hollow copper block with an internal constantan heating coil embedded in 'Araldite' synthetic resin. Its thermal capacity was made as small as possible so that thermal equilibrium could be reached rapidly.

The copper current leads were joined to the heater winding internally. One potential lead was joined to the appropriate current lead where it entered the heater, while the other junction between potential and current leads was made at the sink. This eliminated any errors due to Joule heating in the current leads. The temperature difference was measured using copper–constantan thermocouples soldered into holes drilled in the source and the sink.

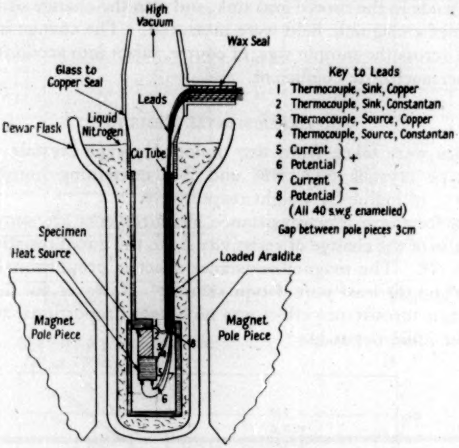
High Vacuum
Wax Seal
Glass to Copper Seal
Leads
Liquid Nitrogen
Dewar Flask
Cu Tube
Key to Leads
1 Thermocouple, Sink, Copper
2 Thermocouple, Sink, Constantan
3 Thermocouple, Source, Copper
4 Thermocouple, Source, Constantan
5 Current
6 Potential
+
7 Current
8 Potential
–
(All 40 s.w.g. enamelled)
Gap between pole pieces 3cm
Specimen
Heat Source
Loaded Araldite
Magnet Pole Piece
Magnet Pole Piece
2
3
4
5
6
7
8

Figure 1. Apparatus for measurement of magnetothermal resistance and magnetothermoelectric effects.

Each specimen was soldered in place after its ends had been rhodium-plated and its dimensions measured. The various stages of the assembly of the apparatus were carried out using a range of solders having different melting points.

The apparatus was evacuated and immersed in liquid nitrogen which held it at a perfectly steady temperature. The difference between the thermocouple voltages for zero heater current was found and then a steady current was passed through the heater. After equilibrium had been reached and the thermocouple voltages observed, the magnetic field was switched on. Magnetic fields of up to 10 kilo-oersteds were employed. The equilibrium thermocouple voltages were measured with the field in each direction. Then the field was switched off and the steady thermocouple voltages were observed once more. This procedure was carried out twice at each field strength.

The change in the difference between the thermocouple readings after the application of a magnetic field amounted to between 1 and 5 μv. Since the potentiometer which was available only recorded steps of 1 μv some means had to be adopted to increase the sensitivity. This was achieved by noting the changes in the deflection of the galvanometer spot for fixed positions of the potentiometer dials. The galvanometer sensitivity with each of the thermocouples was measured in a previous experiment.

The mean temperature for a thermal conductivity measurement was, of course, slightly higher than that of liquid nitrogen. It was therefore necessary to make measurements for a number of heater currents, i.e. for a number of mean temperatures. The thermal resistance and magnetothermal resistance coefficient of the sample at 77°K were then obtained by extrapolation.

The magnetothermoelectric effect was observed at the same time as the magnetothermal resistance effect. The Seebeck voltage between the copper thermocouple leads to the source and sink, and also the change of this voltage on the application of a magnetic field were measured. The change in the temperature difference across the sample was, of course, taken into account in calculating the magnetothermoelectric coefficient.

§ 3. Experimental Results

The samples were taken from two undoped p-type crystals S22 and S24, and three n-type crystals S17, S15 and S11 containing nominally 0·055%, 0·09% and 0·4% of iodine by weight respectively.

The results for the magnetoresistance measurements are shown in figure 2 in which the ratio of the change of resistivity $\Delta\rho$ to the initial resistivity ρ has been plotted against H^2. The magnetoresistance effect is proportional to H^2 for the p-type samples and the least pure n-type sample. However, for the purer n-type samples the magnetoresistance effect was no longer proportional to H^2 for fields exceeding about 7 kilo-oersteds.

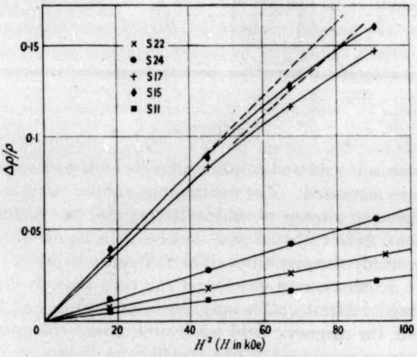

Figure 2. $\Delta\rho/\rho$ plotted against H^2 at 77°K.

The change in the thermal resistance of a given sample for a fixed magnetic field was found to vary only very slightly with temperature, at least for the range of mean temperatures 77°K to 90°K covered by the experiment. This is because the increase in the lattice thermal conductivity as the temperature is lowered compensates for the increase of mobility.

In figure 3 the ratio of the change in the thermal resistivity $\Delta(\kappa^{-1})$ to the electrical resistivity change $\Delta\rho$ has been plotted against H^2. Even for the purer n-type sampes $\Delta(\kappa^{-1})/\Delta\rho$ is independent of the magnetic field. Similarly, as shown in figure 4, the ratio of the change in the thermoelectric power $\Delta\alpha$ to the resistivity change $\Delta\rho$ is independent of the field strength.

The complete experimental data at 77°K are given in table 1.

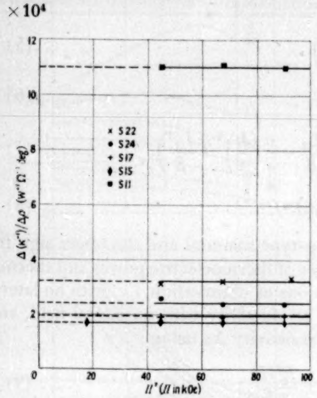

Figure 3. $\Delta(\kappa^{-1})/\Delta\rho$ plotted against H^2 at 77°K.

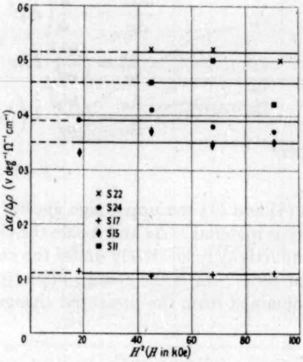

Figure 4. $\Delta\alpha/\Delta\rho$ plotted against H^2 at 77°K.

Table 1. Experimental Data at 77°K

Specimen	S22	S24	S17	S15	S11
Condition	Undoped, p	Undoped, p	0·055% I†, n	0·09% I†, n	0·4% I†, n
$(\Omega^{-1}\,cm^{-1})$	$6{\cdot}9 \times 10^3$	$5{\cdot}85 \times 10^3$	$1{\cdot}71 \times 10^3$	$6{\cdot}3 \times 10^3$	$1{\cdot}52 \times 10^4$
$R(cm^3\,coul^{-1})$	$1{\cdot}92 \times 10^{-1}$	$3{\cdot}13 \times 10^{-1}$	$-4{\cdot}27$	$-5{\cdot}38 \times 10^{-1}$	$-4{\cdot}44 \times 10^{-2}$
$R\sigma\,|\,(cm^2\,v^{-1}\,sec^{-1})$	$1{\cdot}33 \times 10^3$	$1{\cdot}83 \times 10^3$	$7{\cdot}3 \times 10^3$	$3{\cdot}4 \times 10^3$	$6{\cdot}8 \times 10^2$
$(w\,cm^{-1}\,deg^{-1})$	$7{\cdot}2 \times 10^{-2}$	$7{\cdot}2 \times 10^{-2}$	$5{\cdot}8 \times 10^{-2}$	$6{\cdot}6 \times 10^{-2}$	$7{\cdot}6 \times 10^{-2}$
$\Delta(\kappa^{-1})/\Delta\rho(w^{-1}\Omega^{-1}\,deg)$	$3{\cdot}2 \times 10^4$	$2{\cdot}4 \times 10^4$	$1{\cdot}95 \times 10^4$	$1{\cdot}7 \times 10^4$	$1{\cdot}1 \times 10^5$
$(v\,deg^{-1})$	$6{\cdot}1 \times 10^{-5}$	$6{\cdot}8 \times 10^{-5}$	$-1{\cdot}39 \times 10^{-4}$	$-7{\cdot}3 \times 10^{-5}$	$-2{\cdot}2 \times 10^{-5}$
$\Delta\alpha/\Delta\rho(v\,deg^{-1}\Omega^{-1}\,cm^{-1})$	$5{\cdot}1 \times 10^{-1}$	$3{\cdot}9 \times 10^{-1}$	$-1{\cdot}1 \times 10^{-1}$	$-3{\cdot}5 \times 10^{-1}$	$-4{\cdot}6 \times 10^{-1}$

† These iodine concentrations are the percentages by weight added to the melt. It is estimated hat the iodine concentrations in the crystals are two-thirds of these values.

§ 4. Theory

It will be assumed that the relaxation time τ for charge carriers is a function of the energy E only, and may be expressed as

$$\tau \propto E^{\lambda} \qquad \ldots\ldots(3)$$

where λ is a constant. It will also be assumed that there are one or more energy minima such that, around each minimum, the energy is proportional to $|\mathbf{K}^2|$ multiplied by a factor which depends only on direction in momentum space,

$\hbar\mathbf{K}$ being the crystal momentum. Then the solution of the Boltzmann equation in the presence of weak magnetic fields gives (Wilson 1953, chap. 8)

$$\alpha = \pm \frac{\mathbf{k}}{\mathbf{e}} K_1 \qquad \ldots\ldots(4)$$

$$\frac{\sigma\Delta\alpha}{\Delta\sigma} = \mp \frac{\mathbf{k}}{\mathbf{e}}\left(K_2 - \frac{K_3}{\beta}\right) \qquad \ldots\ldots(5)$$

$$\frac{\kappa_{\mathrm{e}}}{\sigma} = \left(\frac{\mathbf{k}}{\mathbf{e}}\right)^2 T L_1 \qquad \ldots\ldots(6)$$

$$\frac{\Delta\kappa}{\Delta\sigma} = \left(\frac{\mathbf{k}}{\mathbf{e}}\right)^2 T\left(L_2 - \frac{L_3}{\beta} - \frac{\sigma}{\kappa}\left(\frac{\mathbf{k}}{\mathbf{e}}\right)^2 T\frac{L_4{}^2}{\beta}\right), \qquad \ldots\ldots(7)$$

where

$$\beta = 1 + \rho\Delta\rho/R^2H^2. \qquad \ldots\ldots(8)$$

In (4) and (5) the upper sign applies for p-type material and the lower sign for n-type material. $\Delta\alpha$ and $\Delta\kappa$ are the changes of thermoelectric power and thermal conductivity respectively under the conditions of observation, i.e. with no lateral heat flow. $\Delta\sigma$ is the change of electrical conductivity with no lateral field, and is obtained from the measured change of resistivity $\Delta\rho$ using

$$-\frac{\Delta\sigma}{\sigma} = \frac{\Delta\rho}{\rho} + \frac{R^2H^2}{\rho^2}; \qquad \ldots\ldots(9)$$

R is the Hall coefficient in the appropriate units.

The K_n and L_n are functions only of η, the reduced Fermi potential, and λ; these functions are given in the Appendix. The terms containing K_3 and L_3 arise because of a potential difference across the sample due to the Ettingshausen–Nernst effect and the term containing L_4 arises because of the Righi–Leduc effect.

Equations (4) to (7) may be expressed more simply when classical statistics are applicable. Then

$$\alpha = \pm \frac{\mathbf{k}}{\mathbf{e}}(\lambda + \tfrac{5}{2} - \eta) \qquad \ldots\ldots(4a)$$

$$\frac{\sigma\Delta\alpha}{\Delta\sigma} = \pm \frac{\mathbf{k}}{\mathbf{e}}\left(2 - \frac{1}{\beta}\right)\lambda \qquad \ldots\ldots(5a)$$

$$\frac{\kappa_{\mathrm{e}}}{\sigma} = \left(\frac{\mathbf{k}}{\mathbf{e}}\right)^2 T(\lambda + \tfrac{5}{2}) \qquad \ldots\ldots(6a)$$

$$\frac{\Delta\kappa}{\Delta\sigma} = \left(\frac{\mathbf{k}}{\mathbf{e}}\right)^2 T\left\{(4\lambda^2 + 3\lambda + \tfrac{5}{2}) - \frac{\lambda^2}{\beta} - \frac{\sigma}{\kappa}\left(\frac{\mathbf{k}}{\mathbf{e}}\right)^2 T\frac{(\lambda^2 + 2\lambda + \tfrac{5}{2})^2}{\beta}\right\}. \qquad \ldots\ldots(7a)$$

It may be seen that $\Delta\alpha$ has the same sign as α if λ is negative and the opposite sign if λ is positive. The terms containing β in equation (7*a*) are generally only minor factors for this material so that $\Delta\kappa/\Delta\sigma$ is approximately equal to $\kappa_{\mathrm{e}}/\sigma$ when $\lambda = -\frac{1}{2}$ or 0. However, in the general case, the Lorenz number changes upon the application of a magnetic field.

At 77°K none of the samples upon which measurements were made could be considered to be non-degenerate so that expressions (4*a*) to (7*a*) were inapplicable. It was necessary to calculate the K_n and L_n in (4) to (7) using Fermi–Dirac statistics. These calculations were carried out for η between 0 and 4 and for λ between $-0{\cdot}7$ and 0. The values of K_1, K_2, L_1 and L_2 are given in figures 5 and 6. The terms involving β in equations (5) and (7) were comparatively small and the values of K_3, L_3 and L_4 were calculated separately for each sample.

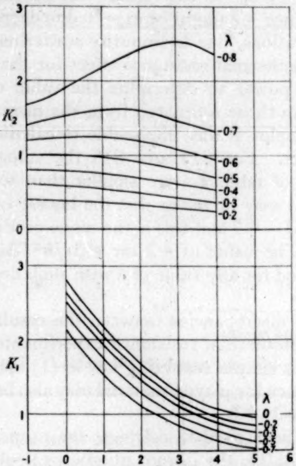

Figure 5. K_1 and K_2 plotted against reduced Fermi potential.

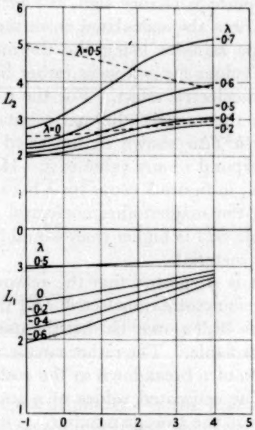

Figure 6. L_1 and L_2 plotted against reduced Fermi potential.

§ 5. DISCUSSION

The reduced Fermi potential η and the exponent in the scattering law λ may be calculated from the measured thermoelectric power and its change with magnetic field using expressions (4) and (5). For every sample the sign of $\Delta\alpha$ was the same as the sign of α indicating that λ is negative in all cases. The values of η and λ calculated from the experimental results are given in table 2. For sample S11 the degenerate approximations to equations (4) and (5) were used:

$$\alpha = \pm \frac{\pi^2}{3}\frac{\boldsymbol{k}}{\boldsymbol{e}}\frac{\lambda+\frac{3}{2}}{\eta} \quad \ldots\ldots(4b) \qquad \frac{\sigma\Delta\alpha}{\Delta\sigma} = \pm\frac{2\pi^2}{3}\frac{\boldsymbol{k}}{\boldsymbol{e}}\frac{\lambda}{\eta}\left(1-\frac{1}{\beta}\right). \quad \ldots\ldots(5b)$$

Table 2. Calculation of η and λ

	Experimental Quantities				M.T.E.†		M.T.R.†	
	$\frac{\boldsymbol{e}\alpha}{\boldsymbol{k}}$	$-\frac{\boldsymbol{e}}{\boldsymbol{k}}\frac{\sigma\Delta\alpha}{\Delta\sigma}$	$\frac{\boldsymbol{e}^2}{\boldsymbol{k}^2T}\frac{\Delta\kappa}{\Delta\sigma}$	β	η	λ	η	λ
S22	0·71	0·67	4·7	4·6	4·4	−0·55	3·7	−0·65
S24	0·78	0·57	4·7	3·9	4·1	−0·5	3·3	−0·65
S17	−1·61	−0·32	1·5	1·8	1·8	−0·25		
S15	−0·84	−0·44	2·2	3·8	4·0	−0·4		
S11	−0·25	−0·31	4·2	9·2	11·5	−0·6		

† Calculated from the magnetothermoelectric and magnetothermal resistance effects respectively.

The values of λ calculated for the two p-type samples were both close to $-0{\cdot}5$, the theoretical value for covalent type lattice scattering. For n-type Bi_2Te_3 the values ranged from $-0{\cdot}25$ to $-0{\cdot}6$, $-\lambda$ increasing with the carrier concentration. This is rather surprising since $-\lambda$ might be expected to decrease, and perhaps change sign, at high concentrations, due to impurity scattering.

λ was also calculated from the magnetothermal resistance effect for the two p-type samples using the thermoelectric power to determine the value of η. The values for $-\lambda$ were rather higher than those estimated from the magneto-thermoelectric effect. For the n-type samples it was impossible to calculate λ from the magnetothermal resistance effect. For S17 and S15 the values of $\boldsymbol{e}^2\Delta\kappa/\boldsymbol{k}^2T\Delta\sigma$ shown in the third column of table 2 were smaller than would correspond to any value of λ. However, it may be noted that the lowest values for K_2 in figure 5 occur for λ between 0 and $-0{\cdot}5$ and this is the range predicted from the magnetothermoelectric effect. The value of 4·2 for $\boldsymbol{e}^2\Delta\kappa/\boldsymbol{k}^2T\Delta\sigma$ for sample S11 is higher than would be expected for any value of λ with such degenerate material.

It is suggested that the reason for the discrepancies between the results of the magnetothermoelectric and the magnetothermal resistance experiments for n-type Bi_2Te_3 may be that the use of such a simple scattering law as (1) may be unjustifiable. The rather smaller discrepancy for p-type material may also be the results of a breakdown in the scattering law.

The estimated values of η and λ have been used to calculate the numerical factor in the Lorenz number. For p-type Bi_2Te_3 the Lorenz numbers calculated from the magnetothermoelectric and the magnetothermal resistance effects do not differ greatly and it is, therefore, thought that the estimations of the electronic thermal conductivity shown in table 3 should be quite accurate. The electronic component must be small for sample S17 so that in this case the value of κ_l, the lattice component, should be accurate. It will be seen that κ_l for this sample is rather lower than the values calculated from S22 and S24. If the Lorenz numbers estimated from the magnetothermoelectric effect are used to determine κ_e for S15 and S11 the corresponding values of κ_l are again less than for the undoped p-type material. In order to bring all the values of κ_l equal it would be necessary to use Lorenz numbers of about $4{\cdot}8(\boldsymbol{k}/\boldsymbol{e})^2$ for the p-type material and $2{\cdot}4(\boldsymbol{k}/\boldsymbol{e})^2$ for the highly doped n-type sample S11. The use of such Lorenz numbers seems unrealistic and it seems reasonable to suppose that the lattice thermal conductivity of Bi_2Te_3 decreases with increasing iodine concentration as shown in figure 7. This is in agreement with the results of measurements at higher temperatures which have been reported previously (Goldsmid 1958).

Table 3. Estimation of κ_e and κ_l

	$\boldsymbol{e}^2\kappa_e/\boldsymbol{k}^2T\sigma$		κ_e	κ_l
	M.T.E.†	M.T.R.†	(w cm^{-1} deg^{-1})	(w cm^{-1} deg^{-1})
S22	2·9	2·7	$1{\cdot}1\times10^{-2}$	$6{\cdot}1\times10^{-2}$
S24	2·9	2·6	$0{\cdot}9\times10^{-2}$	$6{\cdot}3\times10^{-2}$
S17	2·6		$0{\cdot}3\times10^{-2}$	$5{\cdot}5\times10^{-2}$
S15	2·9		$1{\cdot}1\times10^{-2}$	$5{\cdot}5\times10^{-2}$
S11	3·3		$2{\cdot}9\times10^{-2}$	$4{\cdot}7\times10^{-2}$

† Calculated from magnetothermoelectric and magnetothermal resistance effects respectively.

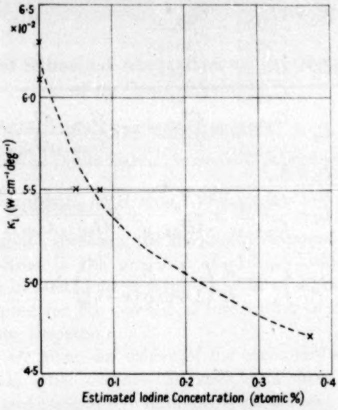

Figure 7. Lattice thermal conductivity plotted against estimated iodine concentration.

§ 6. Conclusions

It has been possible to calculate the value of the exponent λ in the scattering law for p-type Bi_2Te_3 from the magnetothermoelectric effect and also from the magnetothermal resistance effect. The results in the two cases have shown fair agreement. It has, therefore, been possible to estimate the Lorenz number and, thus, the electronic thermal conductivity. For n-type material it has only been possible to derive λ from the magnetothermoelectric effect but, unless the errors in such a derivation are very considerable, it appears that marked scattering of phonons by iodine atoms must take place.

References

Drabble, J. R., Groves, R. D., and Wolfe, R., 1958, *Proc. Phys. Soc.*, **71**, 430.
Drabble, J. R., and Wolfe, R., 1957, *J. Electronics and Control*, **3**, 259.
Goldsmid, H. J., 1958, *Proc. Phys. Soc.*, **72**, 17.
Grüneisen, E., and Erfling, H. D., 1940, *Ann. Phys., Lpz.*, **38**, 399.
de Haas, W. J., and de Nobel, J., 1938, *Physica*, **5**, 449.
de Nobel, J., 1949, *Physica*, **15**, 532.
Reddemann, H., 1934, *Ann. Phys., Lpz.*, **20**, 441.
Sommerfeld, A., 1928, *Z. Phys.*, **47**, 1.
Steele, M. C., 1957, *Phys. Rev.*, **107**, 81.
Wilson, A. H., 1953, *The Theory of Metals*, 2nd Edn (Cambridge : University Press).

APPENDIX

Expressions for $K_n(\eta, \lambda)$ and $L_n(\eta, \lambda)$.

$$K_1 = \frac{G_{5/2+\lambda}}{G_{3/2+\lambda}} - \eta \qquad \ldots\ldots (A1)$$

$$K_2 = \frac{G_{5/2+\lambda}}{G_{3/2+\lambda}} - \frac{G_{5/2+3\lambda}}{G_{3/2+3\lambda}} \qquad \ldots\ldots (A2)$$

$$K_3 = \frac{G_{5/2+\lambda}}{G_{3/2+\lambda}} - \frac{G_{5/2+2\lambda}}{G_{3/2+2\lambda}} \qquad \ldots\ldots\text{(A3)}$$

$$L_1 = \frac{G_{7/2+\lambda}}{G_{3/2+\lambda}} - \frac{G^2{}_{5/2+\lambda}}{G^2{}_{3/2+\lambda}} \qquad \ldots\ldots\text{(A4)}$$

$$L_2 = \frac{G_{7/2+3\lambda}}{G_{3/2+3\lambda}} + \frac{G^2{}_{5/2+\lambda}}{G^2{}_{3/2+\lambda}} - 2\frac{G_{5/2+3\lambda}G_{5/2+\lambda}}{G_{3/2+3\lambda}G_{3/2+\lambda}} \qquad \ldots\ldots\text{(A5)}$$

$$L_3 = K_3{}^2 \qquad \ldots\ldots\text{(A6)}$$

$$L_4 = \frac{G_{7/2+2\lambda}}{G_{3/2+2\lambda}} + \frac{G^2{}_{5/2+\lambda}}{G^2{}_{3/2+\lambda}} - 2\frac{G_{5/2+2\lambda}G_{5/2+\lambda}}{G_{3/2+2\lambda}G_{3/2+\lambda}} \qquad \ldots\ldots\text{(A7)}$$

where

$$G_n = \int_0^\infty x^n \frac{d}{dx}\left(\frac{1}{1+\exp\,(x-\eta)}\right) dx. \qquad \ldots\ldots\text{(A8)}$$

The Influence of Spherical Aberration on the Response Function of an Optical System

By A. M. GOODBODY
Technical Optics Section, Imperial College, London

Communicated by H. H. Hopkins ; *MS. received* 13*th May* 1958

Abstract. The integral expressing the frequency response of an optical system in different focal planes in the presence of primary and secondary spherical aberration has been evaluated for a large number of cases employing a Deuce computer, programmed for the numerical integration of double integrals by a method described by Hopkins.

Detailed results are given for values of the secondary spherical (wave front) aberration $w_{60} = -4\lambda$, -6λ, -9λ, -12λ, each with three different amounts of primary aberration and each in five different focal planes; and curves are given showing the frequency response that can be obtained when the performance is optimized for low frequencies according to Hopkins' criterion, where a low frequency is one for which the response is greater than or equal to 0·8. For these low frequencies it is confirmed that an under-corrected marginal ray gives the best image quality. For frequencies greater than that for which the response is approximately 0·6, an over-corrected margin is to be preferred.

It is found that, in agreement with the prediction of geometrical optics, the values of the response, $D(s, \psi)$, plotted as functions of the product sw_{60} (or sw_{40}, for the case $w_{60} = 0$), where s is the reduced spatial frequency, lie closely on a single curve, when $sw_{60} \leqslant 1{\cdot}2$ (or $sw_{40} \leqslant 0{\cdot}3$, for $w_{60} = 0$).

§ 1. Introduction

The methods of frequency response for specifying optical image quality are becoming well established and attention has accordingly been directed to the numerical evaluation of the frequency response itself in terms of the image forming properties of the optical system. The modulus of the frequency response is defined to be the ratio of the contrast in the image of a sinusoidal intensity distribution to the contrast in the object itself, and is independent of the absolute value of the intensity. The use of frequency response methods presupposes that the condition known as isoplanatism is fulfilled. That is to say the intensity distribution in the image of an incoherent line source does not vary appreciably for short line sources imaged geometrically within the region where the image of a single line source has significant intensity. In practice, of course, non-isoplanatic systems have aberrations too great for them to be of great practical use for image formation. The influence of image formation on a sinusoidal intensity distribution of incoherent light is not always merely to reduce the contrast, but also to shift the resulting sinusoidal distribution laterally in the image plane relative to the geometrical image. It is convenient to express this as a phase shift which then appears as the argument of the complex number representing the frequency response. The imaginary part of the frequency response is zero for aberrations other than those of the coma type, so that the response is either positive or negative, the latter denoting a reversal of contrast. This is so for spherical aberration with a circular aperture, which is the case to be considered here.

The analytical expression for frequency response for monochromatic light may be written in the form

$$D(s,\psi)=\frac{1}{A}\iint_S \exp\left\{\frac{2\pi i}{\lambda}sV(x,y;s)\right\}dx\,dy \qquad \ldots\ldots(1)$$

in which

$$sV(x,y;s)=W(x+\tfrac{1}{2}s,y)-W(x-\tfrac{1}{2}s,y)\dagger \qquad \ldots\ldots(2)$$

A is the area of the pupil, $W(x,y)$ is the aberration function of the system referred to coordinate axes (x,y) in the pupil, the y axis being parallel to the direction of the 'lines' of the sinusoidal grating of reduced spatial frequency s, and S is the area common to two pupil areas centred on the points $(\pm\tfrac{1}{2}s,0)$. ψ is the angle of the line structure to the meridian plane of the optical system. Because of symmetry the response is independent of ψ for our case: it is retained here merely for consistency in notation. If R' is the number of 'lines' per unit length in the image,

$$s=\frac{\lambda}{n'\sin\alpha'}R'$$

is used to define the reduced spatial frequency, λ is the wavelength of the light and $n'\sin\alpha'$ the numerical aperture of the image forming cone.

The integral for $D(s,\psi)$ has been evaluated analytically for a defocused optical system (Hopkins 1955) and for a system suffering from astigmatism (De 1955). Hopkins (1957 a) has also shown that a system of tolerances applicable to systems with large aberrations may be based on this formula. Comparable formulae have also been studied by Steel (1956). These treatments show that for any given higher order aberration type and a chosen spatial frequency s, the optimum form of correction with primary aberrations and the best choice of focal plane may be determined. The tolerance criterion is expressed in terms of the relative frequency response of an optical system defined to be (Hopkins 1956)

$$M(s,\psi)\exp\{i\theta(s,\psi)\}=D(s,\psi)/D_0(s,\psi) \qquad \ldots\ldots(3)$$

where $D_0(s,\psi)$ is the frequency response for the same system in the absence of aberration. It has been found convenient to take as this criterion of image quality the condition that $M(s,\psi)\geqslant 0{\cdot}80$. This means that aberration is not permitted to cause the contrast for a given frequency to fall below 80% of that obtained in the absence of aberrations. With this criterion, it is a relatively simple matter to find for a system with a given form of aberration and focal plane the largest permissible values of the aberration.

The tolerance theory of Hopkins gives a satisfactory account of image quality provided $M(s,\psi)$ is greater than about 0·7. It is, however, frequently necessary to know the form of the frequency response curve for the whole frequency band for which significant response is obtained. Black and Linfoot (1957) have studied the effects of primary spherical aberration on the response function using Simpson's rule to evaluate the integral. This work showed the value to be derived from a detailed study of the frequency response curves in different planes of focus.

---

† In earlier papers of Hopkins, $V(x,y;\,s)$ has been denoted by $W(x,y\,;s)$. The notation is changed here to avoid confusion with the aberration function $W(x,y)$.

If the effects of secondary spherical aberration are included, it is necessary to study the optimum balance of primary and secondary aberration as well as the best choice of focal plane. Such a programme of work necessarily involves rather extensive computation. This was carried out on a Deuce electronic computer, using a method of numerical integration described by Hopkins (1957 b).

§ 2. METHOD OF COMPUTATION

The difficulty of obtaining numerical values of frequency response for systems with aberrations other than defect of focus and astigmatism lies mainly in the fact that the argument of the exponential function in the integrand contains powers of the variables (x, y) greater than unity. A further difficulty arises because the region of integration is often not of simple analytical form. These circumstances account for the intractability of the integral (1) to analytical treatment.

In the method of numerical integration mentioned above, the (x, y) plane is divided into a rectangular mesh, each rectangle having sides of length $2\epsilon_x$, $2\epsilon_y$ respectively. The argument of the integrand is expanded in a Taylor series about point (x_p, y_q), where $x_p = (2p-1)\epsilon_x$, $y_q = (2q-1)\epsilon_y$ are the coordinates of the centre of a typical rectangle. The first two terms of the Taylor series are retained and integration is effected over this rectangle, which is bounded by the lines $x = x_p \pm \epsilon_x$, $y = y_q \pm \epsilon_y$. The contributions from all rectangles whose centres lie within the region of integration are then summed. This leads to the formula

$$D(s, \psi) = \frac{1}{N_A} \sum_p \sum_q \cos Z \frac{\sin X}{X} \frac{\sin Y}{Y} \qquad \ldots\ldots (4)$$

where

$$\left.\begin{aligned} Z &= V(x_p, y_q; s) \\ X &= \epsilon_x V'_x(x_p, y_q; s) \\ Y &= \epsilon_y V'_x(x_p, y_q; s) \end{aligned}\right\} \qquad \ldots\ldots (5)$$

and N_A is the number of rectangles whose centres lie in the pupil area A. To obtain the relative response (3), the number N_A is merely replaced by N_S, the number of rectangles with centres within the region S. In both cases the summation over (p, q) is confined to the rectangles N_S. The above computational procedure was programmed for the English Electric Deuce Computer.

The case of spherical aberration including both primary and secondary terms, has a wave front aberration of the form

$$W(x, y) = w_{20}(x^2 + y^2) + w_{40}(x^2 + y^2)^2 + w_{60}(x^2 + y^2)^3 \qquad \ldots\ldots (6)$$

where w_{20}, w_{40}, w_{60} measure defect of focus from the paraxial image plane, primary spherical aberration and secondary spherical aberration respectively. In the integral (1) the argument then has

$$V(x, y; s) = W_x'(x, y) + \frac{1}{3!} (\tfrac{1}{2}s)^2 W_x'''(x, y) + \frac{1}{5!} (\tfrac{1}{2}s)^4 W_x^{\mathrm{v}}(x, y). \qquad \ldots\ldots (7)$$

If the pupil is taken to be circular and of radius $(x^2 + y^2)^{1/2} = 1$, both the pupil A and the region S are symmetrical with respect to the coordinate axes. In consequence the symbols A and S in (1) may be taken to denote merely those parts of these domains lying in the first quadrant. Similarly, the summation in (4) extends only over one quadrant and the numbers N_A, N_S accordingly also refer only to rectangles within one quadrant.

The problem as stated above is not in its most suitable form for numerical computation on a digital computer. To minimize the amount of programming necessary for the solution of any given problem, the calculation must as far as possible be reduced to a series of standard operations for which subroutines already exist. For this reason, the aberration function which can be written in general terms as

$$W(x,y)=\sum_{m}\sum_{n} w_{m,n}\,(x^2+y^2)^{m/2}(x\sin\psi+y\cos\psi)^n \qquad \ldots\ldots(8)$$

is first converted into a power series of the form

$$W(x,y)=\sum_{m}\sum_{n} a_{m,n}x^m y^n. \qquad \ldots\ldots(9)$$

The differentiation of this series and the summations of the derived series may then be more readily carried out on the computer and the same programme can be used for aberrations other than spherical aberration.

The stages in the programme are briefly as follows: The coefficients $a_{m,n}$ in the power series (9) for the aberration function $W(x,y)$ and those in the series for its derivatives are formed and stored on tracks of the magnetic drum. These coefficients enable the numerical values of $W(x,y)$ and its derivatives to be calculated at the centre of every rectangle lying in one quadrant of the pupil area.

The initial value of s is then introduced in order to compute $V(x,y;s)$, $V_x'(x,y;s)$, $V_y'(x,y;s)$ and hence the product $\cos Z(\sin X/X)\,(\sin Y/Y)$ as shown in equations (5) and (7). This is done at the centre of every rectangle included in the region S. $D(s)$ is then found as a summation of the products as shown in (4).

It is important to establish the largest mesh size which will give sufficient accuracy. The accuracy achieved will clearly depend on the number of rectangles included in the region of integration and this number is dependent upon both ϵ and s; for any given mesh size 2ϵ, the accuracy will diminish as s becomes larger. For this reason it would seem desirable to decrease ϵ as s increases in such a way as to keep approximately the same number of rectangles included in the region of integration. This, however, would both greatly increase the amount of computation and the length and complexity of the programme. The value of s is restricted to the range $0\leqslant s\leqslant 2$, but for most practical purposes only smaller values of s, less than about 0·5, will be of interest and the accuracy will not be expected to vary greatly over such a range. A preliminary survey was therefore carried out to examine empirically the effect of the mesh size on accuracy.

For this purpose, response curves were computed for several sizes of mesh and the calculated values of $M(s)$ plotted as a function of ϵ for suitable spaced values of s. In the case of typically good response it was found that the value of $M(s)$ followed a smooth curve increasing monotonically with decreasing ϵ towards a limiting value. In the case of a typically poor response, the curve of $M(s)$ against ϵ showed oscillations but still tended towards a definite limit with decreasing ϵ.

The error in the method of integration used arises from two causes. Firstly, there is the approximation involved in neglecting all but the first two terms of the Taylor series of the argument of the integrand in (1), and secondly that involved in replacing the circular boundary of the region of integratiom by the zigzag contour of the rectangular mesh. It is possible to obtain an expression for the error due to the rejection of the higher terms of the Taylor series as follows.

The contribution to the integral (1) from the rectangle with centre (x_p, y_q) is

$$J_{p,q} = \frac{1}{4\epsilon_x\epsilon_y}\int_{x_p-\epsilon_x}^{x_p+\epsilon_x}\int_{y_q-\epsilon_y}^{y_q+\epsilon_y} \exp if(x,y)\,dx\,dy \qquad \ldots\ldots(10)$$

where

$$f(x,y) = \frac{2\pi s}{\lambda}V(x,y;s).$$

Let the variables u, v be defined by the relations

$$u\epsilon_x = x - x_p; \quad v\epsilon_y = y - y_q \qquad \ldots\ldots(11)$$

then

$$J_{p,q} = \tfrac{1}{4}\int_{-1}^{+1}\int_{-1}^{+1}\exp\left\{i\sum_{n=0}^{\infty}\frac{1}{n!}\left(u\epsilon_x\frac{\partial}{\partial x} + v\epsilon_y\frac{\partial}{\partial y}\right)^n f(x_p, y_q)\right\}du\,dv. \qquad \ldots\ldots(12)$$

The terms $n=0$ and $n=1$ may be written as separate factors, and then, expanding the remaining exponential term in the integral of (12), we obtain

$$J_{p,q} = \exp iZ\sum_{m=0}^{\infty}\frac{i^m}{m!}\int_{-1}^{+1}\int_{-1}^{+1}\left\{\sum_{n=2}^{\infty}\frac{1}{n!}\left(u\epsilon_x\frac{\partial}{\partial x} + V\epsilon_y\frac{\partial}{\partial y}\right)^n f(x_p, y_q)\right\}^m \times \exp i(Xu + Yv)\,du\,dv \qquad \ldots\ldots(13)$$

where

$$\left.\begin{aligned} Z &= f(x_p, y_q) \\ X &= \epsilon_x\frac{\partial}{\partial x}f(x_p, y_q) \\ Y &= \epsilon_y\frac{\partial}{\partial y}f(x_p, y_q) \end{aligned}\right\} \qquad \ldots\ldots(14)$$

Apart from the factor $(\exp iZ)i^m$, which is equal to $\exp i(Z + \frac{1}{2}m\pi)$, (13) is real. Hence we may write

$$J_{p,q} = \exp iZ\frac{\sin X}{X}\frac{\sin Y}{Y} + \sum_{m=1}^{\infty}\sum_{n=2}^{\infty}\exp i(Z + \tfrac{1}{2}m\pi)K_{m,n} \qquad \ldots\ldots(15)$$

where

$$K_{m,n} = \int_{-1}^{+1}\int_{-1}^{+1}\frac{1}{m!\,n!}\left\{\left(u\epsilon_x\frac{\partial}{\partial x} + v\epsilon_y\frac{\partial}{\partial y}\right)^n f(x_p, y_q)\right\}^m \cos(Xu + Yv)\,du\,dv. \qquad \ldots\ldots(16)$$

$K_{m,n}$ is a term arising from the inclusion of the mth term of the exponential series and the nth term of the Taylor series and can be expressed in terms of the function $\psi_p(X)$, where

$$\psi_p(X) = \tfrac{1}{2}i^p\int_{-1}^{+1}u^p \exp iXu\,du \qquad \ldots\ldots(17)$$

$$= \frac{\partial^p}{\partial X^p}\left\{\frac{\sin X}{X}\right\} = \frac{\partial^p}{\partial X^p}\left\{\sqrt{\frac{\pi}{2X}}\,\mathrm{J}_{1/2}(X)\right\} \qquad \ldots\ldots(18)$$

$\mathrm{J}_{1/2}(X)$ being a Bessel function of order one half (Watson 1942).

For the case of spherical aberration for which the imaginary part of $D(s,\psi)$ vanishes identically, we are only interested in the real part of (15) which is given by

$$\mathscr{R}[J_{p,q}] = \cos Z\frac{\sin X}{X}\frac{\sin Y}{Y} + \sum_{m=1}^{\infty}\sum_{n=2}^{\infty}\cos(Z + \tfrac{1}{2}m\pi)K_{m,n}. \qquad \ldots\ldots(19)$$

The relative response $M(s)$ and the correction factors depending on the terms $K_{1,2}$, $K_{2,2}$ were calculated for the case $w_{20} = -9\lambda$, $w_{40} = +19\lambda$, $w_{60} = -11\lambda$ using a mesh size of $2\epsilon_x = 2\epsilon_y = 0{\cdot}10$. For comparison, $M(s)$ was calculated on the computer for six other mesh sizes in the range from $2\epsilon = 1/24$ to $2\epsilon = 0\cdot 16$. A comparison of the results obtained for three values of s with $2\epsilon = 1/24$ and $2\epsilon = 0\cdot 10$ are shown in table 1.

Table 1

s	$M(s)(2\epsilon=\frac{1}{24})$	$M(s)(2\epsilon=0\cdot 1)$	$\delta_{1,2}$	$\delta_{2,2}$
0·06	0·8128	0·7922	0·0054	−0·0009
0·12	0·4664	0·4382	0·0202	−0·0006
0·24	0·0453	0·0281	0·0056	+0·0035

$\delta_{1,2}$ is the correction produced by the term in $K_{1,2}$ and $\delta_{2,2}$ is that associated with $K_{2,2}$. It will be seen that these two correction terms only partially account for the discrepancy between the values of $M(s)$ calculated on the basis of the two different mesh sizes. The subsequent correction terms would be numerically smaller than $\delta_{1,2}$, $\delta_{2,2}$. It would appear probable, therefore, that the difference arises from the closer approximation to the true region of integration obtained with a smaller mesh size. The total of the results obtained suggests that errors significantly greater than 0·02 will only rarely occur with a mesh size of $2\epsilon = 0\cdot 10$.

§ 3. RESULTS

A number of calculations for cases of primary aberration were first carried out in order to compare the results with those of Black and Linfoot (1957), additional details of which were kindly provided by those authors. For a mesh size $2\epsilon = 1/30$, the agreement was found to be within less than 0·005 for values of s less than or equal to 1·8.

The values of the primary aberration w_{40} used were 1, 2, 3, 4, and 8λ, in various planes of focus on either side of the best focus.

For convenience in considering results of calculations taking into account secondary as well as primary spherical aberration we shall put

$$w_{20}/w_{60} = \beta_2; \quad w_{40}/w_{60} = \beta_4.$$

The values of these quantities which optimize the response according to the tolerance theory of Hopkins (1957 a), will be denoted by β_2' and β_4' respectively.

In the diagrams of figures 1–4, those labelled (*b*) in each case represent the optimum correction for higher order aberration. Thus figure 1 (*b*) shows frequency response curves calculated for the case of higher order aberration $w_{60} = -4\lambda$, together with the optimum amount of primary aberration. The five curves shown correspond to the five focal planes denoted by

$$\beta_2 = \beta_2', \ \beta_2' \pm 0\cdot 25, \ \beta_2' \pm 0\cdot 5.$$

The upper diagram compares the profile of the wave front in the best focal plane with that at the paraxial focus. Figures 1 (*a*) and 1 (*c*) show similar curves but with amounts of primary aberration given by $\beta_4' - 0\cdot 5$ and $\beta_4' + 0\cdot 5$ respectively. In each case the new best focal plane has been calculated and two others taken either side as before. Figures 2–4 repeat the curves of figure 1 but with −6, −9,

Figures 1–4. Frequency response in the presence of primary and secondary spherical aberration in various focal planes. In the upper diagrams in each case are compared the shape of the wave front in the best focal plane for low frequencies and that at the paraxial focus. r is a polar coordinate in the aperture, which latter is taken to be of unit radius.

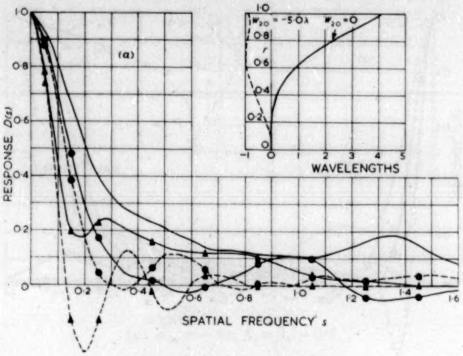

(*a*) $w_{60} = -4\lambda$, $\beta_4 = \beta_4' - 0{\cdot}5$.

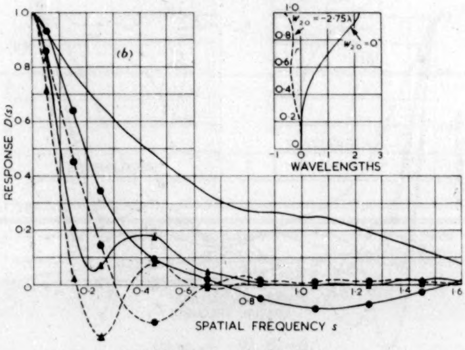

(*b*) $w_{60} = -4\lambda$, $\beta_4 = \beta_4'$.

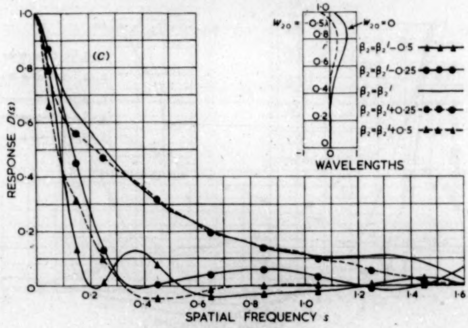

(*c*) $w_{60} = -4\lambda$, $\beta = \beta_4' + 0{\cdot}5$

Figure 1.

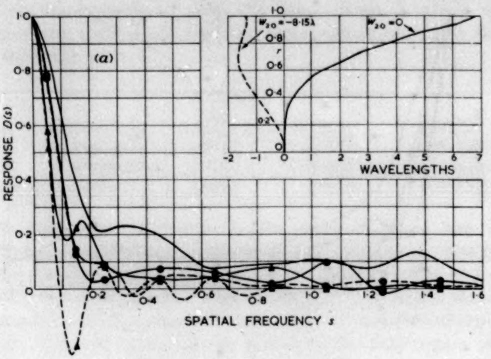

(*a*) $w_{60}=-6\lambda,\ \beta_4=\beta_4'-0\cdot5$.

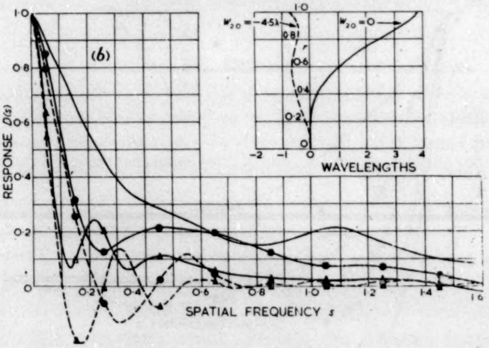

(*b*) $w_{60}=-6\lambda,\ \beta_4=\beta_4'$.

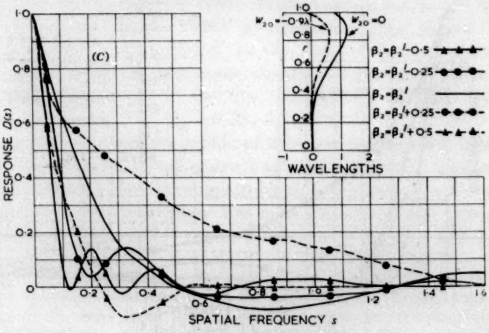

(*c*) $w_{60}=-6\lambda,\ \beta_4=\beta_4'+0\cdot5$.

Figure 2.

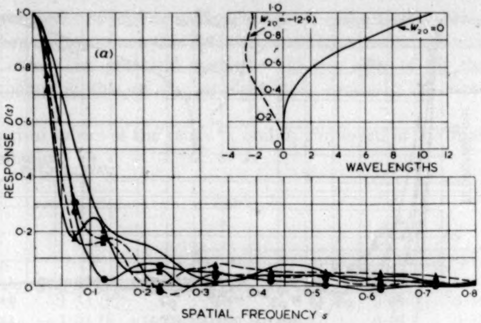

(*a*) $w_{60} = -9\lambda$, $\beta_4 = \beta_4' - 0{\cdot}5$.

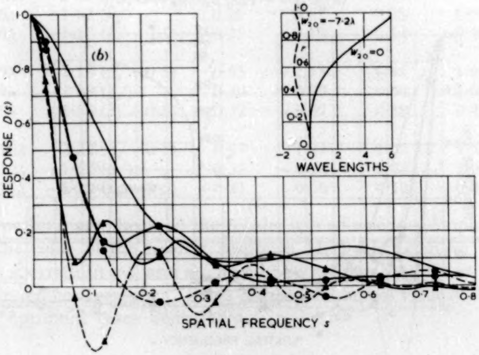

(*b*) $w_{60} = -9\lambda$, $\beta_4 = \beta_4'$.

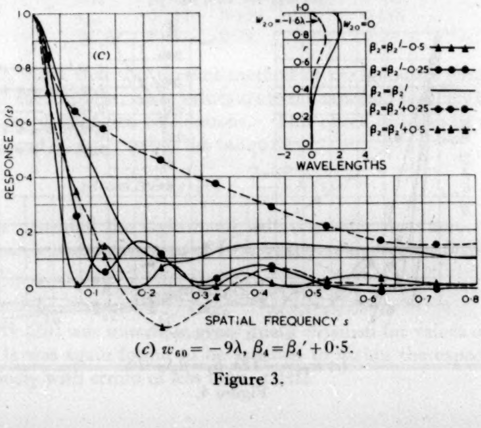

(*c*) $w_{60} = -9\lambda$, $\beta_4 = \beta_4' + 0{\cdot}5$.

Figure 3.

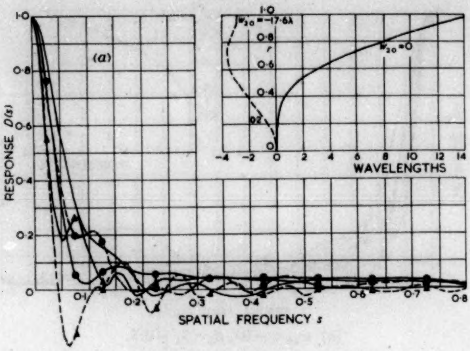

(*a*) $w_{60} = -12\lambda,\ \beta_4 = \beta_4' - 0{\cdot}5$.

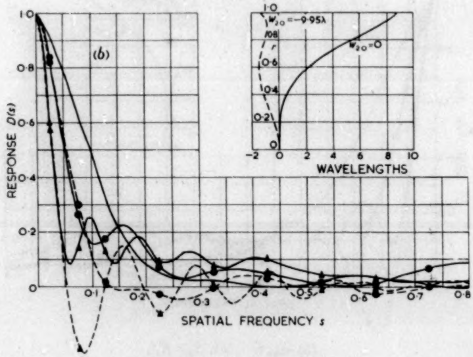

(*b*) $w_{60} = -12\lambda,\ \beta_4 = \beta_4'$.

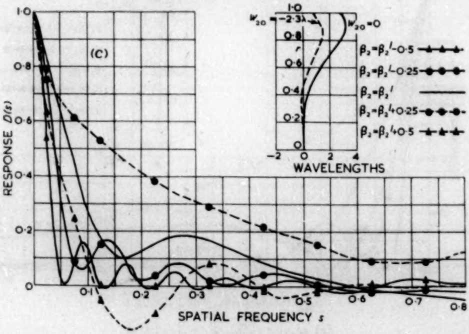

(*c*) $w_{60} = -12\lambda,\ \beta_4 = \beta_4' + 0{\cdot}5$.

Figure 4.

and −12 wavelengths of higher order aberration respectively. Negative values of w_{60} have been chosen, since this is the sign of higher order spherical aberration that usually occurs in practical systems. If the sign of all the aberration coefficients, including that of w_{20}, are changed, precisely the same curves are obtained.

The numerical values of the ratios β_2 and β_4 employed in the final calculations are shown in table 2

Table 2

			β_2				
Figure	w_{60}	β_4	$\beta_2'-0{\cdot}5$	$\beta_2'-0{\cdot}25$	β_2'	$\beta_2'+0{\cdot}25$	$\beta_2'+0{\cdot}5$
1 (*a*)	-4λ	$-2{\cdot}03\ (\beta_4'-0{\cdot}5)$	0·75	1·00	1·25	1·50	1·75
1 (*b*)	-4λ	$-1{\cdot}53\ (\beta_4')$	0·19	0·44	0·69	0·94	1·19
1 (*c*)	-4λ	$-1{\cdot}03\ (\beta_4'+0{\cdot}5)$	−0·37	−0·12	0·13	0·38	0·63
2 (*a*)	-6λ	$-2{\cdot}13\ (\beta_4'-0{\cdot}5)$	0·86	1·11	1·36	1·61	1·86
2 (*b*)	-6λ	$-1{\cdot}63\ (\beta_4')$	0.26	0·51	0·76	1·01	1·26
2 (*c*)	-6λ	$-1{\cdot}13\ (\beta_4'+0{\cdot}5)$	−0·35	−0·10	0·15	0·40	0·65
3 (*a*)	-9λ	$-2{\cdot}19\ (\beta_4'-0{\cdot}5)$	0·93	1·18	1·43	1·68	1·93
3 (*b*)	-9λ	$-1{\cdot}69\ (\beta_4')$	0·30	0·55	0·80	1·05	1·30
3 (*c*)	-9λ	$-1{\cdot}19\ (\beta_4'+0{\cdot}5)$	−0·32	−0·07	0·18	0·43	0·68
4 (*a*)	-12λ	$-2{\cdot}22\ (\beta_4'-0{\cdot}5)$	0·97	1·22	1·47	1·72	1·97
4 (*b*)	-12λ	$-1{\cdot}72\ (\beta_4')$	0·33	0·58	0·83	1·08	1·33
4 (*c*)	-12λ	$-1{\cdot}22\ (\beta_4'+0{\cdot}5)$	−0·31	−0·06	0·19	0·44	0·69

A useful preliminary check on the results was afforded by Hopkins' tolerance formula. The value of the relative response $M(s)$ calculated for the optimum values of the aberrations w_{20} and w_{40} should be not less than 0·8 at the value of s given by the tolerance formula. Table 3 shows the actual value of $M(s)$ obtained for the four optimum cases considered.

Table 3

w_{60}	-4λ	-6λ	-9λ	-12λ
s_{tol}	0·232	0·129	0·077	0·055
$M(s)$	0·81	0·79	0·79	0·79

Bearing in mind that the present method of computation tends slightly to underestimate the response, these values are to the expected accuracy in accordance with the results of tolerance calculations. This check can also be applied even when $\beta_2 \neq \beta_2'$ and $\beta_4 \neq \beta_4'$, using the inequality

$$M(s) \geqslant 1 - \frac{2\pi^2 s^2}{\lambda^2} K(s) \qquad \ldots\ldots(20)$$

which is true provided the right-hand side is greater than zero. $K(s)$ is the minimum mean squared deviation of $V(x, y; s)$ over the region S and is given by

$$K(s) = \iint_S V^2 dS - \left\{\iint_S V dS\right\}^2,$$

The inequality (20) was tested for every curve obtained for values of s for which $D(s) \simeq 0{\cdot}8$. It was again found to be satisfied to within the expected limits of accuracy, namely with errors of less than $<0{\cdot}02$.

An instructive way of presenting some of the information in these curves is to plot the response as a function of the position of the focal plane. The resulting curves confirm that the optimum values of β_2 and of β_4 are given correctly by the tolerance theory of Hopkins, provided the response so obtained is not less than 0·8. What is more, the results of this treatment appear from the curves of the figures labelled (*a*) and (*b*) respectively in figures 1–4 to be an adequate guide to the performance of the system for all spatial frequencies of practical interest when the marginal ray is under-corrected ($\beta_4 < -1{\cdot}5$). On the other hand the curves labelled (*c*) relate to cases where the marginal ray is over-corrected ($\beta_4 > -1{\cdot}5$). Here the best focal plane for values of s having $D(s)$ equal to

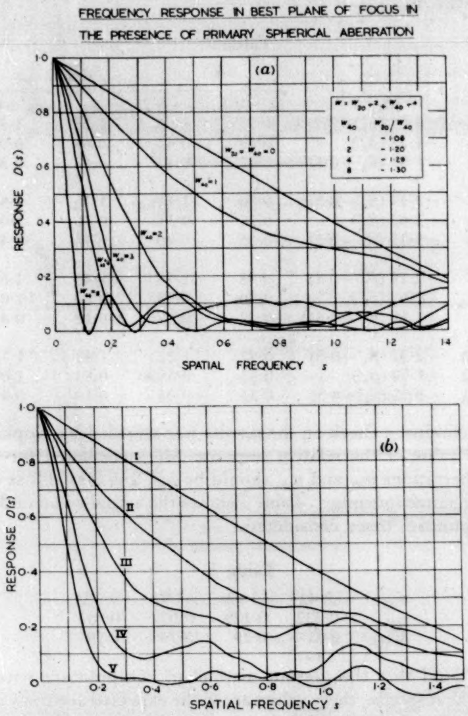

Figure 5 (*a*) Frequency response in the best low frequency plane of focus in the presence of primary spherical aberration. (*b*) Frequency response in the presence of primary and secondary spherical aberration with optimum correction and in the best plane of focus for low frequencies.

I. $w_{60} = w_{40} = w_{20} = 0$; II. $w_{60} = -4$, $w_{40} = 6{\cdot}13$, $w_{20} = -2{\cdot}75$;
III. $w_{60} = -6$, $w_{40} = 9{\cdot}78$, $w_{20} = -4{\cdot}53$; IV. $w_{60} = -9$, $w_{40} = 15{\cdot}24$, $w_{20} = -7{\cdot}24$;
V. $w_{60} = -12$, $w_{40} = 20{\cdot}66$, $w_{20} = -9{\cdot}95$.

0·4, say, is appreciably inside the best focal plane (that is when $\beta_2 > \beta_2'$) for values of s for which $D(s) \geqslant 0{\cdot}8$. Thus, for a system having an over-corrected marginal ray the tolerance theory of Hopkins is not an adequate guide to the performance of the system when frequencies for which $D(s)$ is less than 0·8 have to be taken into account. In particular, for $w_{60} = -6\lambda$, -9λ, and -12λ for example, the curves corresponding to $\beta_4 = \beta_4' + 0{\cdot}5$, $\beta_2 = \beta_2' + 0{\cdot}25$ show a markedly better response than those for $\beta_4 = \beta_4'$, $\beta_2 = \beta_2'$ when s exceeds the value for which $D(s) \simeq 0{\cdot}6$.

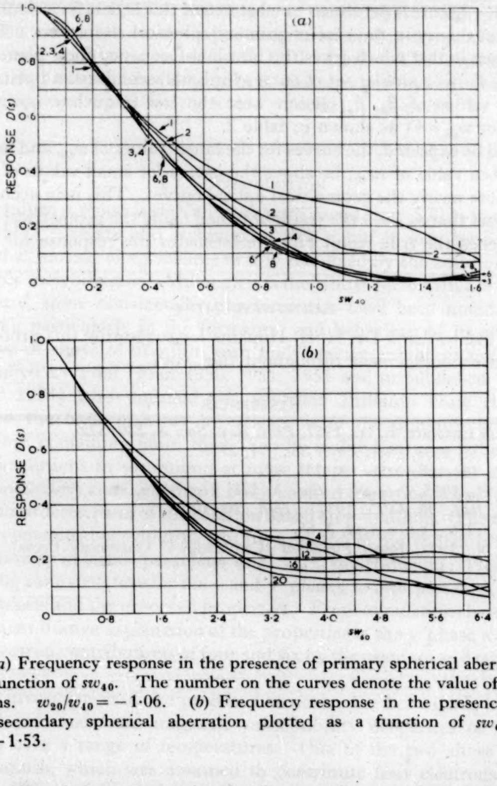

Figure 6. (*a*) Frequency response in the presence of primary spherical aberration plotted as a function of sw_{40}. The number on the curves denote the value of w_{20} in wavelengths. $w_{20}/w_{40} = -1{\cdot}06$. (*b*) Frequency response in the presence of primary and secondary spherical aberration plotted as a function of sw_{60}. $\beta_2 = 0{\cdot}69$, $\beta_4 = -1{\cdot}53$.

On the other hand the converse is true (in accordance with the tolerance treatment) for values of s for which $D(s) \geqslant 0{\cdot}8$. Consequently for use with low-pass detectors such as television systems the correction $\beta_4 = \beta_4'$, giving slight under-correction, will be appropriate; when detectors such as photographic emulsions are used, however, a form of correction $\beta_4 = \beta_4' + 0{\cdot}5$ corresponding to over-correction would give better limiting resolution. This latter is of course, in accordance with results in practice.

If the performance of the system is to be optimized for the low-frequency range, in accordance with Hopkins' tolerance theory, it is useful to know the form of the optimum frequency response curve for given amounts of aberration. These curves are shown in figure 5 (*a*), for primary spherical aberration alone and in figure 5 (*b*) for different amounts of secondary spherical aberration.

Bromilow (1958) has given some results based on the geometrical optical approximation in which, for given values of β_2 and β_4, the response is a function of sw_{60}. When $w_{60}=0$, the response is a function of sw_{40}, when the ratio w_{20}/w_{40} is kept fixed. Figure 6 (*a*) shows to what extent this is true for calculations based on diffraction theory in the case of primary spherical aberration. The value of w_{20}/w_{40} chosen is that which gives the best low-frequency focal plane for $w_{40}=1$. Figure 6 (*b*) shows a similar set of curves for both secondary and primary aberration. The values of β_2, β_4 chosen were the low-frequency optimum values calculated for $w_{60}=4\lambda$ as shown in table 2.

As would be expected, the curves for the larger values of w_{40}, and hence smaller s for any given value of sw_{40}, lie above the others for small values of sw_{40} and so approach more nearly the geometrical optical curve. This is in accordance with the known fact that as $s\to 0$ the result obtained using the geometrical approximation approaches the true result but overestimates the response for small finite values of s.

ACKNOWLEDGMENT

I would like to thank Dr. H. H. Hopkins for suggesting this problem and for his help and encouragement throughout this work.

REFERENCES

BLACK, G., and LINFOOT, E. H., 1957, *Proc. Roy. Soc.* A, **239**, 522.
BROMILOW, N. S., 1958, *Proc. Phys. Soc.*, **71**, 231.
DE, M., 1955, *Proc. Roy. Soc.* A, **233**, 91.
HOPKINS, H. H., 1955, *Proc. Roy. Soc.* A, **231**, 91 ; 1956, *Proc. Phys. Soc.* B, **69**, 562 ; 1957 a, *Ibid.*, **70**, 449 ; 1957 b, *Ibid.*, **70**, 1002.
STEEL, W. H., 1956, *Optica Acta*, **3**, 65.
WATSON, G. N., 1942, *Bessel Functions* (Cambridge : University Press).

The γ Phase in Uranium Alloys

By R. G. LOASBY†
Department of Physics, University of Nottingham

Communicated by L. F. Bates; MS. received 2nd May 1958, *and in final form 17th June* 1958

Abstract. Electrical resistivity and magnetic susceptibility properties of two alloys based on γ-uranium are described and interpreted in terms of a theoretical structure derived from x-ray work by P. C. L. Pfeil. The implication of the earlier work, that uranium in the γ form is characterized by only four electrons per atom (as opposed to six for the α and β forms) is supported by the present results.

§ 1. INTRODUCTION

THE uranium γ phase is stable in the pure metal from 770°C to the melting point 1133°C (Katz and Rabinowitz 1951), but it may be conveniently studied at normal temperatures as it is stabilized by the addition of several metals, notably molybdenum. Although it is metallic in form with a body-centred cubic structure, some non-metallic characteristics have been noted (Pfeil and Browne 1954), particularly in the formation and behaviour of its alloys.

The group of alloys of uranium with molybdenum, niobium and zirconium has been studied by Pfeil (Pfeil 1950, 1951, 1955 and unpublished work, Pfeil and Browne 1954) who outlined the probable Brillouin zone structure of γ-uranium on the basis of x-ray investigations of the uranium molybdenum system. Alloys containing more than 10 at.% molybdenum may be quenched to form solid solutions in γ-uranium at room temperature, but the equilibrium structure produced by annealing has a body-centred tetragonal form (denoted by γ') which is an ordered form of the solution based on γ-uranium. The alloy in this form shows anomalous behaviour in that the addition of molybdenum results in a sharp discontinuity in lattice parameter at 31 at.% molybdenum; Pfeil proposed an overlapping zone structure for the γ and γ' phases to interpret both the formation of the γ' phase and the observed properties. From calculations based on x-ray data, a semi-quantitative explanation of the properties of the γ' phase was made on the basis of electron contributions of four and six by the uranium and molybdenum respectively.

A further investigation of the proposed structure has been made by studying the electrical resistance and magnetic susceptibility properties of two alloys of γ-uranium over a range of temperatures. One of the two alloys contained 70 at.% zirconium, which was assumed to contribute four electrons per atom to the alloy. The structure of this alloy is given by Mueller (1955) as body-centred cubic, being based on γ-uranium. A second alloy containing 25 at.% molybdenum (assumed contribution six electrons per atom) was examined both in the initial quenched condition, when it consisted of γ-uranium with the molybdenum in solid solution, and in two annealed conditions when it contained different proportions of the γ' phase.

---

† Now at United Kingdom Atomic Energy Authority, Aldermaston, Berks.

§ 2. RESULTS

The alloys were prepared from high purity components (>99·9%) in an argon arc furnace. Both alloys were subjected to a homogenizing anneal at 1000°c for 150 hours, and the zirconium alloy was further annealed for 800 hours at 580°c to produce the body-centred cubic structure. The apparatus for both susceptibility and resistance measurements was similar to that described in a previous paper (Bates and Loasby, to be published). The absolute susceptibility values are quoted in terms of tantalum (Hoare, Kouvelites, Matthews and Preston 1954) and without correction for the diamagnetism of the atomic core.

Uranium 70 *at.% zirconium*

The volume susceptibility at 20°c was $15{\cdot}7 \times 10^{-6}$ e.m.u. cm^{-3} which, with the density value $9{\cdot}97\ \mathrm{g\,cm}^{-3}$, gives a mass susceptibility of $1{\cdot}57 \pm 0{\cdot}01 \times 10^{-6}$ e.m.u. g^{-1}. No ferromagnetic impurity was found at room temperature. The temperature variation of susceptibility is shown in figure 1.

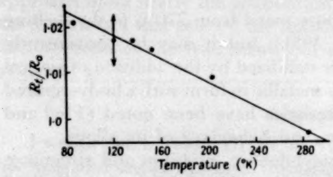

Figure 2

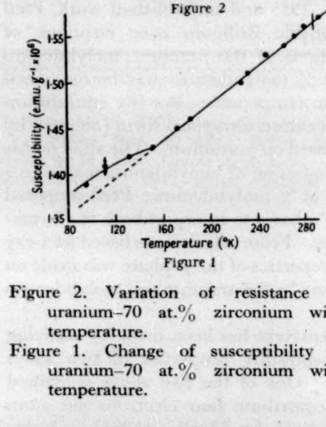

Figure 1

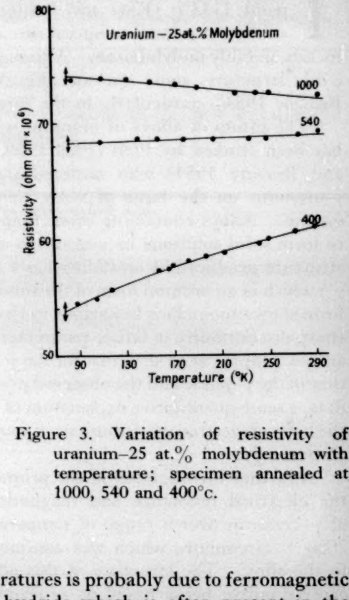

Figure 2. Variation of resistance of uranium–70 at.% zirconium with temperature.

Figure 1. Change of susceptibility of uranium–70 at.% zirconium with temperature.

Figure 3. Variation of resistivity of uranium–25 at.% molybdenum with temperature; specimen annealed at 1000, 540 and 400°c.

The deviation from linearity at low temperatures is probably due to ferromagnetic impurity; this is likely to be uranium hydride which is often present in the alloys. No ferromagnetic impurity measurements were carried out at low temperatures as the available magnetic fields were too low. The electrical resistivity values, uncorrected for thermal expansion, are shown in figure 2. The resistivity has the value $184 \pm 2 \times 10^{-6}$ ohm cm at 0°c and the temperature coefficient over the range 90°K to 300°K the value $-1{\cdot}1 \times 10^{-4}\ \mathrm{deg}^{-1}$.

Uranium 25 *at.*% *molybdenum*

The magnetic susceptibility of the alloy in the initial quenched condition was $1{\cdot}82 \pm 0{\cdot}02 \times 10^{-6}$ e.m.u. g^{-1} at 20°c the density being $16{\cdot}9 \pm 0{\cdot}1$ g cm^{-3}. After correction for ferromagnetic impurity at low temperatures, the paramagnetism was independent of temperature over the range 90°K to 300°K. Further measurements, after annealing the specimen at 540°c for 400 hours, showed no alteration in the properties within the accuracy of the apparatus. A second anneal of 400 hours at 400°c resulted in a decrease in susceptibility to $1{\cdot}72 \times 10^{-6}$ e.m.u. g^{-1}, the temperature independence of the susceptibility being retained. The electrical resistivity curves for the alloys after annealing at 1000°c, 540°c and 400°c are shown in figure 3, the values at 0°c being 72·4, 68·8 and $60{\cdot}6 \pm 0{\cdot}3 \times 10^{-6}$ ohm cm respectively. No correction was made to the curves for thermal expansion, no values being available, but on the basis of the pure metal values, an error of not more than 2% is likely from lack of this correction.

§ 3. DISCUSSION

The zirconium alloy with the ordered body-centred cubic structure and the molybdenum alloy in the initial quenched condition both retain the structural form of the γ phase of uranium. The resistance properties of the two alloys are similar, both having higher resistivities than the pure metal, and negative temperature coefficients of approximately the same magnitude. The negative sign of the coefficients is in qualitative agreement with the proposition of an electron overlap condition in the γ phase, more energy states becoming available for conduction electrons as the temperature, and the population of a second zone, is increased.

The lower anneal temperature for the molybdenum alloy is in a two-phase $(\alpha + \gamma')$ region and some α phase will be present after the heat treatment. There is conflicting evidence on this portion of the phase diagram (see Bostrom and Halteman 1957) concerning the α phase content which, if large, could explain the resistivity observations of the alloy annealed at 400°c but metallographic studies (Pfeil 1951, Pfeil and Browne 1954) show the amount to be small, and this is supported by the temperature independence of the magnetic susceptibility of the alloy: α-uranium has a positive coefficient (Bates and Loasby, to be published). It is assumed, therefore, that the effects produced by annealing are primarily due to the presence of the γ' phase.

The decreases in resistivity found in the successively annealed alloy may be correlated with the presence of the ordered γ' phase and the changes are consistent with the presence of a higher degree of order at the lower temperatures. The changes in the temperature coefficient of resistivity, from a negative value for the γ solution to a small positive value for the γ' phase indicate a progressive change from the overlapping zone condition and imply that the new zone, characteristic of the γ' phase, can just accommodate the number of electrons present. The susceptibility value, which decreases with annealing, may be taken as supporting this interpretation, a lower density of states following from a nearly full zone structure. On the basis of an electron concentration of 4·5 electrons per atom in the alloy, good agreement is shown with the calculated zone volume of 4·57 electrons per atom.

Summarizing the results, the resistance and susceptibility properties of the two alloys show fair agreement with the proposed structure based on a contribution of four electrons per atom by uranium in the γ and γ' modifications.

ACKNOWLEDGMENTS

The author is indebted to Professor L. F. Bates for valuable discussion and for supervision of the work, to Miss J. R. Murray of Atomic Energy Research Establishment, Harwell, for the provision of the alloys, to the Metallurgy Division of Atomic Energy Research Establishment, Harwell, for a maintenance grant covering the period of research and to the Director for permission to publish.

REFERENCES

BOSTROM, N. A., and HALTEMAN, E. K., 1957, *2nd Nuclear Engineering and Science Conference*, paper 57, N.E.S.C. 12 (*Philadelphia*).

HOARE, F. E., KOUVELITES, J. S., MATTHEWS, J. C., and PRESTON, J., 1954, *Proc. Phys. Soc.* B, **67**, 728.

KATZ, J. J., and ROBINOWITZ, E., 1951, *The Chemistry of Uranium*, National Nuclear Energy Series, Division VIII, Vol. 5, Part 1 (New York: McGraw-Hill).

MUELLER, M. H., 1955, *Acta Cryst., Camb.*, **8**, 849.

PFEIL, P. C. L., 1950, *J. Inst. Metals*, **77**, 553; 1951, *Ibid.*, **78**, 760; 1955, *Geneva Conference on the Peaceful Uses of Atomic Energy*, Vol. IX, p. 117.

PFEIL, P. C. L., and BROWNE, J., 1954, *A.E.R.E. Report* M.R. 1333.

Conservation of Parity in a Nuclear Interaction at 350 MeV

By D. P. JONES, P. G. MURPHY AND P. L. O'NEILL
Nuclear Physics Research Laboratory, University of Liverpool

MS. received 30*th May* 1958

Abstract. If parity is conserved, neutrons produced in the interaction of unpolarized protons with an unpolarized target should have zero longitudinal component of polarization. An experiment is described in which the longitudinal polarization of the 350 MeV neutron beam emerging from an internal beryllium target in a synchrocyclotron is measured. The result is that, if the reaction matrix describing the neutron production process contains a term $F(\boldsymbol{\sigma} \,.\, \mathbf{P}/P)$, where $\boldsymbol{\sigma}$, $\mathbf{P}$ are the neutron spin and momentum, then $|F|^2 \leqslant 3{\cdot}6 \times 10^{-6}$ with 95% confidence.

---

§ 1. Introduction

Several experiments to test the conservation of parity in nuclear interactions have recently been reported (Wilkinson 1958, Tanner 1957, Segel, Kane and Wilkinson 1958). They show that the intensity of the part of the wave function which violates parity is at most of the order of $|F|^2$, where $|F|^2$ has values from 1×10^{-4} to 3×10^{-8} in various nuclear interactions. In all these experiments low energy beams of particles have been used. It is of interest to investigate the situation at higher energies; the present experiment tests parity conservation in the production of neutrons by 380 MeV protons, the neutrons emerging with minimum kinetic energy of 340 MeV.

If parity is conserved the reaction matrix, which describes neutron production at an angle θ to an unpolarized proton beam striking an unpolarized target, is (cf. Soloviev 1958)

$$R = g(\theta)I + h(\theta)\boldsymbol{\sigma} \,.\, \mathbf{P}_{\mathrm{n}} \times \mathbf{P}_{\mathrm{p}}$$

where $\mathbf{P}_{\mathrm{n}}$ = neutron momentum, $\mathbf{P}_{\mathrm{p}}$ = proton momentum. In this experiment $\mathbf{P}_{\mathrm{n}}$ is parallel to $\mathbf{P}_{\mathrm{p}}$: $\theta = 0$. If parity conservation is not assumed then the reaction matrix for neutron production in the forward direction has the form

$$R = g\left\{I + F\frac{\boldsymbol{\sigma} \,.\, \mathbf{P}_{\mathrm{n}}}{P_n}\right\}.$$

The neutrons would have a longitudinal polarization of magnitude $2|F|$.

In order to detect longitudinal polarization a transverse magnetic field must be applied to the neutrons to make their spins precess through 90°. The resultant transverse polarization can then be detected by measuring the asymmetry in scattering from the hydrogen in a polyethylene target. The experimental arrangement is shown in the figure (not to scale).

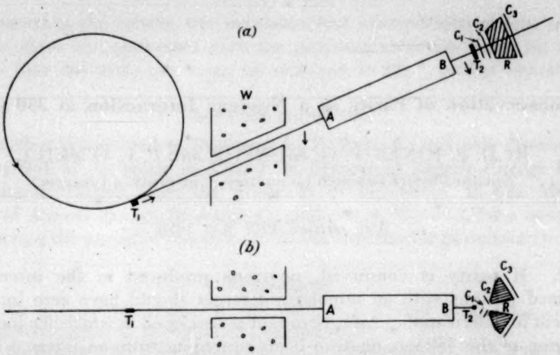

(*a*) Plan. (*b*) Elevation of experimental layout. T_1 internal beryllium target; T_2 carbon or CH_2 target; AB magnet; W concrete wall; C_1, C_2, C_3 telescope of three scintillation counters; R copper absorber. The arrows show the orientations of the neutron polarization.

§ 2. EXPERIMENTAL METHOD

The line integral $\int H\,dl$ of the transverse magnetic field along the neutron trajectory from the target to a point outside the cyclotron field was measured with a long flip coil. It was found that the neutron spin must precess through +120° in the fringing field, where by convention a positive rotation is clockwise when viewed from above.

The magnet AB was 12 feet long with a gap $\frac{3}{8}$ in. × $2\frac{1}{2}$ in.; the direction of the field was opposite to that of the cyclotron field. The field in the magnet could be adjusted to give precession angles of −30° or −210°, making total precession angles of ±90°. The corresponding fields in the long magnet were 1600 gauss and 11 200 gauss. T_2 was 14 feet from B.

Any transverse polarization of the neutron beam can, combined with errors in the magnetic field or misalignment of the apparatus, give an observable effect on changing the magnetic field. This was minimized by ensuring that the neutron beam was as near as possible tangential to the proton orbit at the internal target. The orientation of the proton orbit was investigated by measuring the distribution of activity in copper targets placed in different positions around the orbit. It was found that the neutron beam was tangential to the proton orbit within 12 minutes of arc in the vertical plane. Any instrumental effect must come from a combination of at least two misalignments and must therefore be at worst a second-order effect.

The neutron beam, collimated by the gap in the long magnet, was scattered by a target of either polyethylene (0·55 in. × 0·84 in. × $4\frac{3}{4}$ in.) or carbon (0·56 in. × 0·56 in. × $4\frac{3}{4}$ in.). A pair of scintillation counter telescopes, each covering scattering angles between $12\frac{1}{2}$° and $47\frac{1}{2}$° and azimuthal angles between ±30°, simultaneously counted protons scattered up and down. Copper absorbers between the scintillators ensured that only protons with enough energy to come from elastic scattering events were counted. The thickness of the absorbers was such that the neutrons had to have at least 340 MeV.

No attempt was made to eliminate instrumental asymmetry completely. The effect sought in the experiment was a change in asymmetry on changing the precession angle from +90° to −90°. The precession angle was reversed at intervals of about 15 minutes.

A change in the asymmetry in the background (no second target) was detected on reversing the precession angle. This was attributed to charged particles produced by reaction of the neutrons with the iron of the long magnet; these particles would be affected by the magnetic field. Background runs were therefore made and an appropriate correction applied to the asymmetries with target in place. The background counting rate was about 3% of the target-in counting rate.

The neutron beam was monitored by counting the number of charged particles which were scattered from the long magnet into a counter telescope. Because these charged particles were deflected in the magnetic field, the monitor efficiency was different for the two different magnetic fields used.

§ 3. RESULTS

The results for carbon and polyethylene targets, with background subtracted, are shown in the first four rows of the table. The last two rows give the numbers of counts from the hydrogen in the polyethylene, obtained by subtracting the results for the carbon target multiplied by the appropriate factor. The last column gives the asymmetries.

Target	Precession angle	Monitor counts	Down counts	Up counts	Asymmetry $\times 10^4$
CH_2	+90°	1928544	35094632	35310437	30·6
	−90°	1134084	34768685	34999141	33·0
C	+90°	1254472	15667791	16307550	20·0
	−90°	728404	15451119	16078801	19·9
H	+90°	1928544	21321617	20941142	90·0
(by subtraction)	−90°	1134084	21072006	20698622	89·4

The asymmetry in scattering from hydrogen changes by $0{\cdot}6 \times 10^{-4}$ on reversing the direction of transverse polarization. The standard deviation in this quantity is $3{\cdot}25 \times 10^{-4}$. It is therefore 95% certain that the asymmetry change is less than $7{\cdot}1 \times 10^{-4}$.

§ 4. DISCUSSION OF RESULTS

From the experiments of Siegel, Hartzler and Love (1956) it can be seen that a 16% polarized neutron beam would give 3% asymmetry change in this experiment. It follows that the upper limit for the amount of longitudinal polarization of the neutron beam is $3{\cdot}8 \times 10^{-3}$. Since $|F|$ is numerically equal to half the polarization, as mentioned in the Introduction, the result is that $|F|^2 \leqslant 3{\cdot}6 \times 10^{-6}$ with 95% confidence. To this order of accuracy parity is conserved in the production of 350 MeV neutrons in the forward direction from a beryllium target.

ACKNOWLEDGMENTS

We are grateful to Professor J. M. Cassels for suggesting this experiment and also for designing the long magnet. We would also like to thank Dr. J. R. Wormald for much helpful advice and criticism, and the cyclotron crew for their co-operation in running the experiment. Two of us (D. P. J. and P. L. O'N.) are grateful to the Department of Scientific and Industrial Research for maintenance grants and one (P. G. M.) is grateful to I.C.I., Ltd., for a Fellowship.

REFERENCES

SEGEL, R. E., KANE, J. V., and WILKINSON, D. H., 1958, *Phil. Mag.*, **3**, 204.
SIEGEL, R. T., HARTZLER, A. J., and LOVE, W. A., 1956, *Phys. Rev.*, **101**, 838.
SOLOVIEV, V. G., 1958, *Nuclear Physics*, **6**, 618.
TANNER, N., 1957, *Phys. Rev.*, **107**, 1203.
WILKINSON, D. H., 1958, *Phys. Rev.*, **109**, 1603, 1610, 1614.

The Polarization of Neutrons emitted from Nuclei by Protons

By E. J. SQUIRES
U.K.A.E.A. Research Group, Atomic Energy Research Establishment, Harwell, Didcot, Berks.

Communicated by B. H. Flowers; MS. received 29th April 1958, *and in final form* 16*th June* 1958

Abstract. A discussion is given of the effects of the nuclear potential, and of multiple scattering, on the polarization of neutrons produced when nuclei are bombarded by high energy protons. The results indicate that, in order to explain the observed polarization at large angles, in particular its sign, multiple scattering must play an important part in the process.

---

§ 1. INTRODUCTION

It has been shown by Stafford, Tornabene and Whitehead (1957) that the neutrons in the energy range 65–100 MeV emitted at 55° from nuclei bombarded by 165 MeV protons, are polarized in the opposite direction to that which would be obtained by considering the events as free p–n collisions. The magnitude of the polarization is around 20% for heavy elements and 30% for Be and C whereas the simple model would predict about minus 30%. Confirmation of these results is available from the work of Roberts, Tinlot and Hafner (1954), who find polarizations of about 15% when using 230 MeV protons.

The purpose of this note is to report the results of calculations in which the explanation of this discrepancy was sought in two modifications of the simple model: (i) the effect of the nuclear potential, i.e. coherent scattering by the rest of the nucleus, and (ii) the effect of double scattering inside the nucleus.

§ 2. THE EFFECT OF THE NUCLEAR POTENTIAL

To estimate the effect of the nuclear potential V the plane waves of the incident proton and emerging neutron were replaced by 'outgoing' and 'incoming' scattering solutions, respectively, of the potential V. The W.K.B. approximation was used and the spin–orbit part of V, denoted by V_{so} was treated in first order. V_{so} was assumed to have the form of the derivative of the central potential, which was taken as Gaussian. The magnitude of V_{so} was calculated, at both incident and emerging energy, from the work of Levintov (1956) by assuming reasonable values for the central part of the potential. The t-matrix for the p–n interaction was assumed to vary little in the region of momenta associated with neutron production at a given energy and angle. The differential cross section and polarization obtained can be written in the form:

$$\frac{d^2\sigma}{dE\,d\Omega} = (A + [B_{\mathrm{p}} + B_{\mathrm{n}}]P_{\mathrm{pn}})\sigma_{\mathrm{pn}}$$

and

$$P\frac{d^2\sigma}{dE\,d\Omega} = -(AP_{\mathrm{pn}} + B_{\mathrm{p}}D_{\mathrm{pn}}[PN] + B_{\mathrm{n}})\sigma_{\mathrm{pn}},$$

where $\sigma_{\rm pn}$, $P_{\rm pn}$ and $D_{\rm pn}[PN]$ are the free p–n differential cross section, polarization and depolarization, as defined by Stapp (1955), all taken at an angle equal to the mean free scattering angle associated with the neutron production considered, and where A, $B_{\rm p}$ and $B_{\rm n}$ are complicated integrals containing the nuclear potential parameters. A is independent of $V_{\rm so}$, while $B_{\rm p}$ and $B_{\rm n}$ contain $V_{\rm so}$ as a factor, and give the effect of $V_{\rm so}$ on the incident proton and emitted neutron respectively. The quantity A is always positive.

An estimate of the mean free scattering angle to be used can be obtained by taking the neutron to be initially at rest. From the known energies, outside the nucleus, of the incident proton and emitted neutron it follows that the scattering angle is about 90° in the centre-of-mass system of the two nucleons. The values of the free scattering parameters are thus taken at this angle. The energy used is the incident energy, 165 Mev, together with a contribution of 15 Mev from the nuclear potential.

The numerical calculations have been performed approximately for certain cases. When only the real spin–orbit part of the nuclear potential is taken into account, $B_{\rm p}$ and $B_{\rm n}$ are both positive and approximately equal to one-third of A. Thus taking $P_{\rm pn} \simeq \frac{1}{3}$, we have $P \simeq -(2+D_{\rm pn}[PN])/3{\cdot}7$. Since $D_{\rm pn}[PN]$ is limited by the relation $-1+2P_{\rm pn} \leqslant D_{\rm pn}[PN] \leqslant 1$ it follows that the effect of this potential makes the discrepancy between theory and experiment rather worse.

When an imaginary central part is included in V, the cross term of its contribution to the scattering amplitude with the contribution of $V_{\rm so}$ gives rise to a polarization opposite to the above. However, since the absorbed part of the incident wave must be less than the total, one would not expect this to change the sign of the polarization. Calculations show that the value of A is reduced to approximately one-tenth of its previous value and that $B_{\rm p}$ and $B_{\rm n}$ are reduced still further, to about one-seventh of A, but remain the same sign, in agreement with the above qualitative argument.

The reason why the reduction in the cross section due to the absorption is so large is that it causes an increase in the relative contributions of the nuclear density, as one goes further from the centre of the nucleus. This effectively makes the nucleus larger and so reduces the production of neutrons in the energy and angular region considered (as the radius of the nucleus is increased the energy distribution for neutron production at a given angle becomes more sharply peaked about a value corresponding to that of free scattering, which is below the energy cut-off used for the experiment considered).

One can see why the suggestion (Stafford, Tornabene and Whitehead 1957), made on the basis of elastic polarization results, that the effect of the nuclear potential in neutron production would be in the right direction to explain the experiments, has not been confirmed by these calculations. In elastic scattering the main contribution comes from the cross terms between the effects of the imaginary central and real spin–orbit parts of V, whereas in the case of neutron production one must consider also the cross term between the unperturbed plane waves and the real spin–orbit part of V. The latter is likely to be larger and to have opposite sign since the imaginary central part of V produces a wave which cancels some part of the original plane wave. Thus the polarization produced will be in the opposite direction in the two cases.

The effect of real central and imaginary spin–orbit potentials has not been considered in detail. The latter is known to be such as to increase the polarization in elastic scattering (Heckrotte 1956) and so, since it does not give rise to any cross terms with the unperturbed wave, its presence is likely to give rise to a positive contribution to P. However there is reason (Bethe 1958) to believe that it is very much smaller than the real spin–orbit part† and so its effect is unlikely to be large.

The above numerical estimates depend upon the use of the expression of Levintov (1956) for $|V_{\text{so}}|$. That this over-estimates $|V_{\text{so}}|$ by a factor of almost three at 300 MeV has been shown by Bethe (1958), and so it seems reasonable that the effects of V_{so} considered above have all been similarly over-estimated in magnitude. It seems reasonable to conclude, therefore, that the effect of the nuclear potential cannot give rise to the observed polarization.

§ 3. THE EFFECT OF DOUBLE SCATTERING

There are four types of double scattering possible according to whether the collisions are pp and pn, pn and nn, pn and pn with neutron common to both or pn and pn with proton common to both. In estimating their effect the following approximations have been made: (i) energy is conserved between collisions, (ii) interference between different types can be ignored, and (iii) the t matrix factors can be taken out of the integrals over momenta and given suitable average values. The first two of these approximations are reasonable because kR is large, where R is the nuclear radius. The third is justified by the fact that the maximum phase space of the two unobserved final states occurs when the two scattering angles are approximately equal. Thus in each collision we consider the particle which leaves at an angle of about 27½° to the incident direction. The polarization can then be written in the form

$$\begin{aligned}P=\{&+Z(-P'_{\text{pn}}-P'_{\text{pp}}D'_{\text{pn}}[PN])\sigma'_{\text{pn}}\sigma'_{\text{pp}}+Z(P''_{\text{pn}}-P'_{\text{pn}}D''_{\text{pn}}[P,P])\sigma''_{\text{pn}}\sigma'_{\text{pn}}\\&+(N-1)(-P'_{\text{pn}}+P''_{\text{pn}}D'_{\text{pn}}[PN])\sigma'_{\text{pn}}\sigma''_{\text{pn}}\\&+(N-1)(P''_{\text{pp}}-P'_{\text{pn}}D''_{\text{pp}})\sigma''_{\text{pp}}\sigma'_{\text{pn}}\}\\&\div\{Z(1+P'_{\text{pn}}P'_{\text{pp}})\sigma'_{\text{pn}}\sigma'_{\text{pp}}+Z(1-P''_{\text{pn}}P'_{\text{pn}})\sigma''_{\text{pn}}\sigma'_{\text{pn}}\\&\qquad+(N-1)(1-P'_{\text{pn}}P''_{\text{pn}})\sigma'_{\text{pn}}\sigma''_{\text{pn}}+(N-1)(1+P'_{\text{pp}}P'_{\text{pn}})\sigma'_{\text{pp}}\sigma'_{\text{pn}}\},\end{aligned}$$

where Z, N are the numbers of protons and neutrons in the nucleus and where σ', P', D' refer to scattering through 125° and σ'', P'', D'' refer to scattering through 55°, in the centre-of-mass system of the two nucleons. The suffixes indicate whether a p–p or p–n collision is considered and the notation used for the depolarization functions is that of Stapp (1955). Charge independence is assumed. Although not explicitly indicated in the above formula, one should really take the parameters of the second collision at a rather lower energy.

Using the experimental values for the cross sections and polarizations and using the limiting values of the depolarization functions, one finds, for the ^{9}Be nucleus, that the polarization of the double scattering contribution lies between 8% and 44%. No measurements are available for the p–n depolarization function so it is not possible to determine the value of P precisely. However, since it is unlikely that all the depolarization functions will take their limiting values over the angular regions of interest, and since some cancellation of the effects of the D's is possible, the result is likely to be around the mean of the above figures, i.e. 25%. This is in the right direction and has the right order of magnitude to explain the experimental result.

---

† At energies below about 100 MeV this seems necessary in order to explain the observed reduction in polarization at these energies.

Numerical calculations have been performed to estimate the double scattering cross section for the process under consideration. The results indicate that, when the nuclear potential is ignored in both cases, the double and single scattering contributions to the process considered are about equal. Since, as seen in § 2, the single scattering contribution is reduced by multiple collisions (i.e. absorption) by a factor of one-tenth it seems plausible that the multiple scattering contribution, which will be mainly double scattering in light nuclei, predominates over the single. It is worth noting also that any contributions of triple and higher order scatterings to this process will have the same sign of polarization as the double scattering contribution. This is because the scatterings involved will be through rather smaller angles than in the double scattering case, and the free polarization functions remain of the same sign when the angles are altered in this way.

§ 4. CONCLUSIONS

It is concluded that the effect of the nuclear potential on the polarization of emitted neutrons is small in the situation considered, and that it cannot give rise to the observed sign of the polarization when only single scattering contributions are taken into account. The observed polarization must therefore be due to neutrons emerging after multiple collisions have taken place in the nucleus. The results of § 3 show that double scattering does indeed give a contribution to the polarization which has the right sign and order of magnitude, and, though exact calculations would be very difficult, it is made plausible that such a contribution would dominate over that from single scattering.

Support for the above conclusion is available from the experiments of Donaldson and Bradner (1955) showing that, if the neutrons are counted only when a proton, with energy greater than seven-tenths of that to be expected in a free collision and in approximately the right direction, is seen in coincidence, then the observed polarization is reversed and agrees with that to be expected in a free collision.

When these calculations were commenced it was hoped to be able to predict, theoretically, the optimum angles and energies for producing neutron beams of maximum polarization for use in other experiments. The complexity of the considerations involved however make this quite impracticable.

ACKNOWLEDGMENTS

I wish to thank Dr. T. H. R. Skyrme, G. H. Stafford and S. Tornabene for discussions on this problem.

REFERENCES

BETHE, H. A., 1958, *Ann. Phys.*, **3**, 190.
DONALDSON, R. E., and BRADNER, H., 1955, *Phys. Rev.* **99**, 892.
HECKROTTE, W., 1956, *Phys. Rev.* **101**, 1406.
LEVINTOV, I. I., 1956, *Dokl. Akad. Nauk, U.S.S.R.*, **107**, 240.
ROBERTS, A., TINLOT, J., and HAFNER, E. M., 1954, *Phys. Rev.*, **95**, 1099.
STAFFORD, G. H., TORNABENE, S., and WHITEHEAD, C., 1957, *Phys. Rev.* **106**, 831.
STAPP, H. P., 1955, *University of California Radiation Laboratory Report*, U.C.R.L./3098.

The L/K-Capture Ratio in ^{126}I

By J. SCOBIE† and E. GABATHULER
Department of Natural Philosophy, University of Glasgow

MS. received 13*th May* 1958, *and in final form* 11*th June* 1958

Abstract. A direct measurement has been made of the relative intensities of the L and K x-radiations emitted in the electron capture decay of ^{126}I. The source was distributed throughout the central portion of the NaI crystal in which the x-radiations were measured, and coincidences were taken with the gamma rays from the excited states.

The L/K-capture ratio was observed to be $0{\cdot}142^{+0{\cdot}005}_{-0{\cdot}018}$, which is close to the theoretical value of 0·126.

---

§ 1. Introduction

Extensive use has been made of theoretical results on orbital electron capture to deduce transition energies and L-fluorescence yields from measured values of the L/K-capture ratio and of the ratio of L x-ray intensity to K x-ray intensity. This work has been reviewed by Robinson and Fink (1955). However, evidence as to the validity of the theory can only be obtained from a comparison of the experimental and theoretical values of the L/K ratio for transitions in which the decay energies are accurately known, and few such cases have been investigated. Relatively good agreement with theory is obtained for the two cases in which a direct measurement has been made, namely ^{37}A (Langevin and Radvanyi 1955) and ^{71}Ge (Drever and Moljk 1957), but in the latter case the experimental L/K ratio of $0{\cdot}128^{+0{\cdot}005}_{-0{\cdot}003}$ is significantly higher than the theoretical value of 0·106. The very large discrepancies observed for several transitions could be due to uncertainties in the decay schemes or to the use of inaccurate values of the K-fluorescence yields in the calculation of the experimental results from the measured data (Robinson and Fink 1955). More accurate experimental data are required, particularly for the heavier elements, before the theoretical results on orbital capture transition probabilities can be used with complete confidence.

The decay scheme of ^{126}I is shown in figure 1 (Koerts *et al.* 1955, Perlman and Welker 1954). In the present work the L/K-capture ratio has been obtained for the ($\Delta I = 0$, yes) transitions to the excited states of tellurium-126, by measuring the relative intensities of the L and K x-radiations of tellurium in coincidence with the gamma rays from the excited states. The source was distributed throughout the central portion of the NaI crystal in which the x-radiations were measured, and corrections for geometry, absorption and scattering, and for L and K-fluorescence yields are negligible. By taking coincidences the pulses due to K and L x-radiations are isolated from those due to the emitted particles and, in addition, the photomultiplier thermal noise contribution is very considerably reduced. The latter advantage is of critical importance in the measurement of the 4·9 kev L x-radiations.

† Now at Chemistry Department, University of Arkansas.

§ 2. Experimental Procedure

A NaI crystal 1 in. long and 1½ in. in diameter was irradiated in the photon beam from the Glasgow 350 MeV electron synchrotron for a period of about two days. At the position, close to the collimator, in which the crystal was situated the beam is about ¼ in. in diameter, and it is assumed that the activity resulting from the reaction $^{127}\mathrm{I}(\gamma, \mathrm{n})^{126}\mathrm{I}$ is concentrated in a cylinder of about ¼ in. diameter along the axis of the crystal. This assumption is not critical.

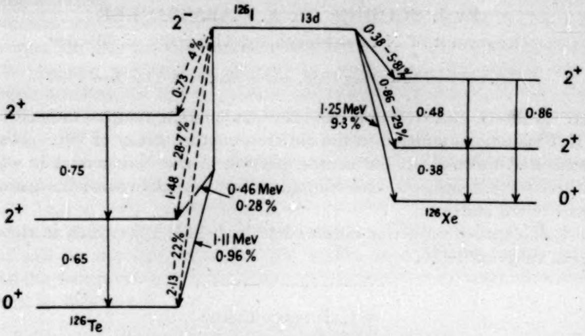

Figure 1. The decay scheme of ^{126}I.

The source crystal was mounted on a photomultiplier (Dumont 6292) which had been selected for its low thermal noise. Another NaI crystal 2 in. long and 1¾ in. in diameter was mounted on a photomultiplier and was placed close to the source crystal. A coincidence unit with a resolving time of 1 μsec controlling a linear coincidence gate unit with a gate length of 10 μsec was used to select those pulses from the source crystal which were in coincidence with pulses from the other crystal corresponding to energies greater than 550 kev. This section of the apparatus was calibrated with annihilation radiation from ^{22}Na and with the 661 kev gamma rays from ^{137}Cs.

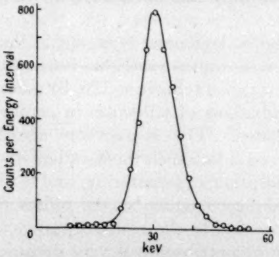

Figure 2. Part of the ^{126}I coincidence pulse spectrum from the source crystal showing the K-capture peak.

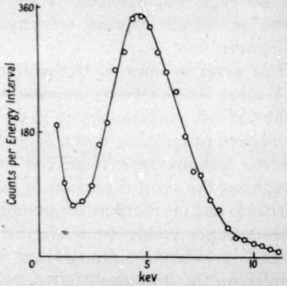

Figure 3. Part of the ^{126}I coincidence pulse spectrum from the source crystal showing the L-capture peak.

The low energy end of the pulse spectrum passing through the gate was analysed with a Hutchinson–Scarrott multichannel kicksorter, and a prominent peak was observed (figure 2), whose energy, by comparison with the 46·5 kev calibration peak from a RaD source, was found to be 32 kev, corresponding to the K absorption energy of tellurium. The amplifier gain was increased by a factor of six and the pulse spectrum analysed as before. Another peak was observed (figure 3) at 4·9 kev, corresponding to the L absorption energy of tellurium. It was not possible to analyse the two peaks simultaneously, but a check was made on the stability of the electronics by counting the total number of pulses above 12 kev in each run and ascertaining that this number remained constant.

The intensity of ^{126}I gamma rays detected in the large crystal was about one-half that of the natural background, and an approximate measurement of the accidental coincidence spectrum in the source crystal was obtained by separating the two counters. This spectrum was of negligible intensity except in the region of thermal noise, where the intensity due to this cause was not appreciably reduced by separating the crystals. In the spectra shown this has not been subtracted.

The gamma-ray spectrum from the large crystal in coincidence with x-radiations in the source crystal was examined with the multichannel kicksorter. No peaks were observed with a relative intensity of more than 3% other than those expected from the decay scheme of figure 1. Some 60-day ^{125}I is formed in the crystal due to the reaction $^{127}\mathrm{I}(\gamma, 2\mathrm{n})^{125}\mathrm{I}$, but the electron capture decay of this isotope is not followed by a high energy gamma ray and therefore would not contribute to the observed peaks.

§ 3. RESULTS

The ratio of counts in the L-peak to counts in the K-peak was observed to be $0{\cdot}144^{+0{\cdot}005}_{-0{\cdot}018}$, the mean of several measurements. The position of the bottom of the L-peak was estimated by assuming a Poisson distribution for the pulse heights, but the lower limit allows for the possibility of this procedure being in error.

A K-capture event in which a Kα x-ray escapes from the source crystal gives rise to the detection of an L x-ray which does not correspond to L-capture, and accordingly a small correction has to be applied to take account of this effect. It is assumed that escape occurs mainly from the ends of the crystal, and an approximate calculation (Glasstone 1956) leads to the result that 0·2% of the K x-radiations are not absorbed. This assumption is not critical since in the extreme case of the source being distributed uniformly throughout the crystal the correction to the K x-radiation intensity would still be only 0·9% (Hammersley 1951). The above fraction of K-capture events then gives rise to an increase of 1·4% in the number of counts in the L-peak. The corrected value for the L/K-capture ratio is $0{\cdot}142^{+0.005}_{-0.018}$.

§ 4. DISCUSSION

Transition probabilities for electron capture from the L and K shells can be calculated using the equations and wave function ratios given by Brysk and Rose (1955). For a first forbidden ($\Delta I=0$, yes) transition, where several different nuclear matrix elements are involved, the theoretical L/K ratio is a complicated function of these matrix elements, of the components of the Dirac radial wave functions for L and K electrons, and of the momenta of the neutrinos emitted in L- and K-capture. However, provided that the transition energy is much greater than the K-shell binding energy, the L/K-capture ratio associated with each matrix element has the same value as the theoretical allowed L/K ratio within a few per cent (for ^{126}I about 2%), as a consequence of the equality of the ratios of the 'large' and 'small' components of the Dirac wave functions, and the actual magnitudes of the nuclear matrix elements have little effect on the total L/K ratio.

The decay energies of the transitions studied here are given by Koerts *et al.* (1955) as 1·48 MEV and 0·73 MEV, in the intensity ratio of seven to one. The L/K-capture ratios for these transitions are calculated to be 0·125 and 0·129 respectively. The theoretical ratio for the sum of these transitions is then 0·126, which is just within the experimental limits on the observed value. However, on the basis of the Poisson fit which was made to the measured L-peak it appears to be more likely that the experimental ratio is slightly larger than the theoretical value.

ACKNOWLEDGMENTS

We would like to thank Professor P. I. Dee for his interest and encouragement, and Dr. G. M. Lewis for his supervision and advice. We are also grateful to Dr. W. McFarlane and the synchrotron crew for their co-operation. We are indebted for the award of research scholarships to the University of Glasgow (J. S.) and the Government of Northern Ireland (E. G.).

REFERENCES

BRYSK, H., and ROSE, M. E., 1955, *Oak Ridge National Laboratory Report*, 1830.
DREVER, R. W. P., and MOLJK, A., 1957, *Phil. Mag.*, **2**, 427.
GLASSTONE, S., 1956, *Principles of Nuclear Reactor Engineering* (London : Macmillan), p. 629.
HAMMERSLEY, J. M., 1951, *Proc. Roy. Soc.* A, **210**, 98.
KOERTS, L., MACKLIN, P., FARRELLY, B., VAN LIESHOUT, R., and WU, C. S., 1955, *Phys. Rev.*, **98**, 1230.
LANGEVIN, M., and RADVANYI, P., 1955, *C. R. Acad. Sci., Paris*, **241**, 33.
PERLMAN, M. L., and WELKER, J. P., 1954, *Phys. Rev.*, **95**, 133.
ROBINSON, B. L., and FINK, R. W., 1955, *Rev. Mod. Phys.*, **27**, 424.

The Measurement at Low Frequencies of the Dielectric Constant of Conducting Liquids

BY V. I. LITTLE

Department of Physics, Bedford College, London

MS. received 20*th May* 1958, *and in final form* 21*st June* 1958

Abstract. The dielectric constants of aqueous solutions of the chlorides of Li, Na, K, Rb and Cs have been measured over the concentration range 10^{-4} to 10^{-2} normal at 25°C, using a novel form of electrometer. An accuracy to $\pm\frac{1}{2}\%$ is claimed, and the results indicate that the fall in dielectric constant at concentrations below 10^{-3} normal is proportional to the square root of the concentration.

---

§ 1. INTRODUCTION

An instrument is described in which a null balance is achieved between two couples which act together momentarily on an electrode which is free to turn in the liquid. One couple is produced by electric forces which are dependent upon the dielectric constant of the liquid, and the other by magnetic forces produced by electric currents flowing in coils. The latter currents at a balance constitute a measure of the dielectric constant of the liquid at the frequency of the source—in the present case 2000 c/s.

Results are quoted for solutions of the chlorides of Li, Na, K, Rb and Cs.

§ 2. THEORY OF THE INSTRUMENT

Consider figure 1. Let A and A′ represent two fixed platinum plates, and let B and B′ be two similar but smaller plates rigidly connected together by a conducting rod CC′. Let Y be a small coil of insulated wire, fixed to the centre of CC′ but insulated from it electrically. The system BCB′ is suspended from the mid-point O so that it can swing in a horizontal plane. Coils X form a

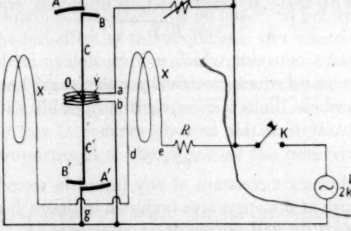

Figure 1. Circuit diagram of experimental arrangement. The letters of figure 2 correspond.

Helmholtz pair with coil Y at their mid-point. When the key K is closed, two couples act on BCB′, one due to the currents flowing in coils X and Y, and the other due to the electric fields between A and B and A′ and B′. When the connections to the coils are correctly arranged, these couples are in opposition and when equal may be represented by:

$$\tfrac{1}{2}\epsilon V^2 \frac{\partial C_0}{\partial \theta} = i_X i_Y \cos\phi \frac{\partial M}{\partial \theta} \qquad \ldots\ldots(1)$$

in which ϵ is the dielectric constant of the surrounding medium, V the r.m.s. value of the source of e.m.f. in figure 1, C_0 the capacity *in vacuo* between plates A and A′, M the mutual inductance between coils X and Y, and ϕ is the phase angle between the currents which flow in X and Y, the r.m.s. values of which are i_X and i_Y respectively. If L_X and L_Y are the self-inductances of coils X and Y respectively, and R and S in figure 1 include the resistances of these coils, then we may write

$$i_X = V/(R^2 + L_X{}^2\omega^2)^{1/2}, \qquad \ldots\ldots(2)$$

$$i_Y = V/(S^2 + L_Y{}^2\omega^2)^{1/2}. \qquad \ldots\ldots(3)$$

In practice $L_Y\omega$ can be made small compared with S so that equation (1) may be written

$$\tfrac{1}{2}\epsilon V^2 \frac{\partial C_0}{\partial \theta} = \frac{V^2 \cos\phi\,(\partial M/\partial\theta)}{S(R^2 + L_X{}^2\omega^2)^{1/2}}. \qquad \ldots\ldots(4)$$

In this expression $\cos\phi = (SR + L_X L_Y \omega^2)/\{(S^2 + L^2{}_Y\omega^2)(R^2 + L^2{}_X\omega^2)\}^{1/2}$ which can be made almost independent of the value of S provided S is large enough. Hence if R, L_X, L_Y and ω are constants, equation (4) reduces to

$$\epsilon = \frac{D\,\partial M/\partial\theta}{S\,\partial C_0/\partial\theta} \qquad \ldots\ldots(5)$$

where D is an apparatus function which is sensibly independent of variations in S.

If the zero position of the beam BCB′ is such that the axis of Y is perpendicular to the field produced by X, then the value of $\partial M/\partial\theta$ is a maximum and is sensibly constant for small variations in θ on either side of the zero position. Furthermore, if the electrodes are suitably shaped, $\partial C_0/\partial\theta$ may also be made independent of θ. With these structural details observed, equation (5) becomes

$$\epsilon = T/S \qquad \ldots\ldots(6)$$

where T is an apparatus constant which can be determined by measuring the dielectric constant of a liquid whose electrical properties are known. A preliminary experiment on water whose dielectric constant is ϵ_0 yields a value of S for water given by S_w. Substitution of this into (6) gives

$$\epsilon = \epsilon_0 S_w/S \qquad \ldots\ldots(7)$$

which expresses the dielectric constant of any liquid in terms of the value of S.

A simplified diagram of the apparatus is shown in figure 2, and a more detailed account of the construction will appear later elsewhere.

§ 3. FACTORS AFFECTING PERFORMANCE AND ACCURACY

3.1. *The effect of lateral sway.* This produces only a very small effect because the net capacity between A and A′ for a given orientation of BB′ is independent of the nearness of B′ to A′, or A to B. Hence any change ensuing will be due to changes in the fringing fields only.

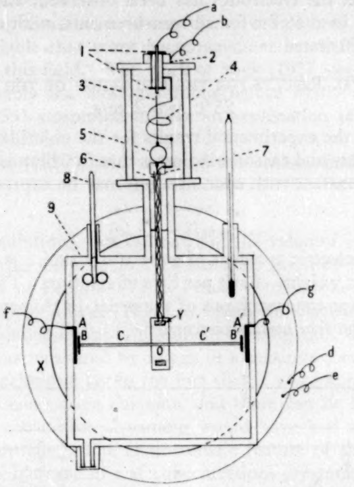

Figure 2. Front elevation of apparatus with one coil of Helmholtz pair removed. 1, Insulating washers; 2, brass tube with flange; 3, phosphor bronze galvanometer strip; 4, phosphor bronze return lead; 5, concave mirror; 6, glass tube; 7, polythene bush; 8, glass stirrer; 9, Perspex box $15 \times 15 \times 2\frac{1}{2}$ cm.

Coils X and Y are shown twice normal size with respect to the rest of the apparatus for purpose of clarity.

3.2. *The effect of local heating.* This effect imposes an upper limit to the solution conductivity which can be accommodated in this kind of apparatus. The intense local heating gives rise to convection currents, which in turn produce violent agitation of the suspended electrode. Fortunately, the null character of the instrument enables the balance to be observed before convection streaming can take place; the full effect of this requires about a second to develop, whereas the motion of the beam is instantaneous under the influence of excess electric or magnetic couples. Nevertheless, as the conductivity increases, so the impedance of the instrument to the source of alternating e.m.f. decreases. This is a serious matter unless very low impedance sources are available, because the sensitivity of the device is proportional to the square of the potential difference appearing between A and A′.

3.3. *The effect of frequency drift.* In the present design, a 5% frequency change produces a 1% change in balance, thus a frequency stability to 0·1% is desirable. This frequency sensitivity, however, is dependent on the reactances in the system. In practice, there is no reason why these reactances should not be tuned out, though in the present instance it was not considered worth while.

3.4. *The effect of electrolysis.* Gassing at the electrode surfaces and edges does occur at frequencies below 1500 c/s in saline solution. At 2000 c/s and over no gassing at the electrodes has been observed, and in this instrument 2000 c/s has been used so far for all measurements, with a maximum available power of about 100 watts.

§ 4. EXPERIMENTAL RESULTS FOR THE CHLORIDES OF THE ALKALI METALS AT 25°C AND 2 kc/s

An analysis of the experimental results for the chlorides of lithium, sodium, potassium, rubidium and caesium indicates that for dilute solutions the variation of the dielectric constant with concentration may be expressed by the empirical formula

$$\epsilon = \epsilon_0 (1 - K\sqrt{c}) \qquad \ldots\ldots (8)$$

where ϵ_0 is the dielectric constant of pure water and c is the concentration in gramme equivalent weights of salt per litre of solution. The experimental value of K is about 1·4 for concentrations of the order 10^{-3} normal and below, and is the same for all the five metals concerned.

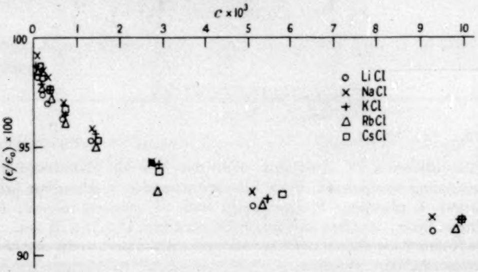

Figure 3. Dielectric constant of solution as a percentage of that of pure water plotted against concentration. Results for chlorides of Li, Na, K, Rb and Cs.

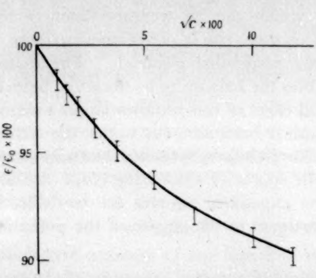

Figure 4. Dielectric constant of solution as a percentage of that of pure water plotted against the square root of the concentration.

In figure 3 the results are plotted for each metal against concentration c, and in figure 4 points representing the mean values of ϵ for all the salts are plotted against c. The scatter between the points of figure 3 may be accounted for in terms of an experimental error of about ½% in any given null point.

§ 5. COMMENT AND CONCLUSION

In the past the experimental evidence of the variation of ϵ with c has been so meagre and unreliable that scant encouragement has been forthcoming for theoretical studies in this field. The work of Sack (1927, see also Debye 1929, pp. 114 ff.) was probably the most ambitious before 1930. At a very simple level, the author (1955) attempted to give an explanation of the experimental results of Pechhold (1927).

Sack's calculations (1927), and those of the author, both led to formulae of the form

$$\epsilon = \epsilon_0(1-\gamma c) \qquad \ldots\ldots(9)$$

at sufficiently dilute solutions, but estimates of the value of γ vary very widely. A good summary of this work up to 1928 has been given by Debye (1929). In this respect, the work of Pechhold (1927) must be mentioned. Pechhold used an apparatus designed by Fürth (1924) in which the electric couple acting on a small ellipsoid suspended in the liquid under investigation, due to the presence of an electric field, was measured by means of a sensitive torsion balance. The great defect of this technique lay in the fact that it was impossible to eliminate the effect of thermal convection currents, and there can be little doubt that at high concentrations convection streaming would have had a marked effect on the equilibrium conditions. The characteristic feature of the results obtained by Pechhold was the increase in ϵ at concentrations greater than 0·008 normal. The present results do not show this effect, but indicate a fall in the value of ϵ at a rate which diminishes as the concentration increases. This fall is still in progress at 0·015 normal, a concentration at which Pechhold found that the value of ϵ was greater than that for pure water.

In order to check that the results obtained in the present work were not excessively perturbed by convection currents, the moving vanes were given a slight twist so that convection streaming would aid the electric couple in one set of experiments and oppose it in another set. In both cases, the experimental points lay within the normal scatter. This was because convection streaming took longer to develop than the 0·1 second or so required to test the state of the balance.

An explanation of equation (8) still needs to be sought, and requires a formal treatment of the dielectric constant of ionic solutions. This could conceivably be drawn from a combination of the Debye–Hückel (1923) theory of electrolytes, and Kirkwood's theory (Kirkwood 1939, see also Kirkwood and Oster 1943) of the dielectric structure of water. It would seem to be fairly conclusive from the present work that the large initial slope of the curve in figure 3 implies a wide spread structure breaking effect in addition to local electrical saturation effects in the vicinity of an ion.

A point of great significance is that the size of a positive monovalent ion has little effect upon the dielectric constant, for all sizes of ion between lithium and caesium. It will also be noted that the concept of dielectric decrement γ, which follows from equation (9), can now no longer have any meaning if the empirical equation (8) is valid at concentrations below 10^{-4} normal. If equation (8) is indeed valid at very low concentrations, then it must follow that water has a very extensive structure. Such a structure should be temperature sensitive, and, to test this possibility, work is at present in hand to determine the dependence of K in equation (8) on both temperature and valency.

ACKNOWLEDGMENTS

The author wishes to express his sincere thanks to Professor E. E. Turner for his most valuable help and advice on the preparation of materials. In addition, his thanks are also due to Miss J. Bond and Miss M. Mills for their enthusiastic help in the early stages of the development of the apparatus.

REFERENCES

DEBYE, P., 1929, *Polar Molecules* (New York: Chemical Catalog Co.).
DEBYE, P., and HÜCKEL, E. A., 1923, *Phys. Z.*, **24**, 305.
FÜRTH, R., 1924, *Phys. Z.*, **25**, 676.
KIRKWOOD, J., 1939, *J. Chem. Phys.*, **6**, 666.
KIRKWOOD, J., and OSTER, G., *J. Chem. Phys.*, 1943, **11**, 175.
LITTLE, V. I., 1955, *Proc. Phys. Soc.* B, **68**, 357.
PECHHOLD, R., 1927, *Ann. Phys. Lpz.*, **83**, 427.
SACK, H., 1927, *Phys. Z.*, **28**, 199.

Fractures Produced by Stress Pulses in Glass-like Solids

By H. KOLSKY and Y. Y. SHI
Brown University, Providence, Rhode Island, U.S.A.

MS. received 10*th March* 1958, *and in revised form* 16*th May* 1958

Abstract. Measurements have been made of the amplitudes of the maximum tensile stress pulses which could propagate along rods of glass and of two glass-like plastics (polystyrene and polymethylmethacrylate) without producing fracture. Small quantities of explosive were detonated at one end of the rod so that a compression pulse travelled down the rod and on reflection at the opposite end returned as a tension pulse. The displacement–time curve of the free end was recorded with a condenser-microphone arrangement and the stress was obtained by differentiating this curve numerically. The maximum amplitudes were compared with the tensile strength of the specimen as measured in a standard tensile testing machine. Since the loading time with the stress pulses was only a few microseconds, the ratio of loading rates between the 'static' and dynamic tests was of the order of 10^6. For all three materials the dynamic value was about twice the static. In the two plastics, it was found possible to produce purely internal cracks which resulted from the slightly higher tensile stress in the interior of the rod. With glass no such internal cracks were observed. These results indicate that the strength of the plastics will not depend markedly on the surface condition of the specimen.

§ 1. Introduction

The fractures produced when compression pulses are reflected at the free boundaries of a specimen were first described by Hopkinson (1912), and have more recently been studied by a number of other workers (Kolsky and Shearman 1949, Rinehart 1951, Evans 1952, Kolsky 1953, 1955, Rinehart and Pearson 1954).

The value of such investigations in the study of fracture is twofold. First, they enable the strength of materials to be measured for loading times as short as one or two microseconds; secondly, by this means it is possible to set up stress distributions which could not be produced in any other way. For example, under stress-wave loading the interior of a specimen may be under tension while all the surfaces of the specimen are stress-free.

The tensile strength of glass has been found to depend very markedly both on the time of application of tensile stresses and on the condition of the surfaces of the specimen, and it was considered of interest to determine the magnitude of the maximum tensile stress pulse which glass and some glass-like plastics could transmit without fracturing.

The specimens used in the experiments described in this paper were in the form of rods. A small explosive charge was detonated at one end of the rod so that a sharp compression pulse was produced. This travelled the length of the rod and, on being reflected at the opposite end, set up tensile stresses. The stress distribution when a plane compression pulse is reflected at the free end of a rod is shown diagrammatically in figure 1. The reflected pulse is one of tension, and the resultant stress obtained by summing the stresses due to the incident and reflected pulses is denoted by the thickest lines in the figure. The exact point which is first subjected to this maximum tension depends on the shape of the incident pulse. For a steep-fronted pulse it is exactly half the pulse length; for a symmetrical pulse it is one quarter of the pulse length.

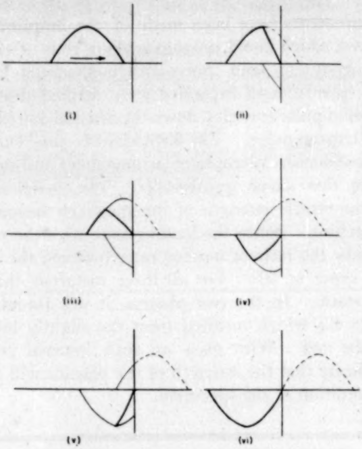
(i)
(ii)
(iii)
(iv)
(v)
(vi)

Figure 1. Reflection of a pulse at a free boundary.

§ 2. Experimental Arrangements

The experimental arrangements are shown schematically in figure 2 and are similar to those described in earlier work (Kolsky 1956). The electrical circuits were similar to those described by Davies (1948) and by Kolsky (1949, 1954).

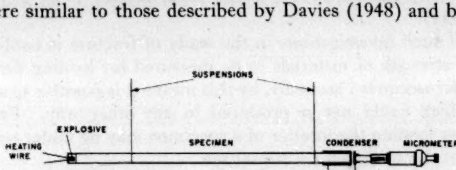
SUSPENSIONS
EXPLOSIVE
HEATING WIRE
SPECIMEN
CONDENSER
MICROMETER HEAD
PHOTOCELL
CATHODE RAY OSCILLOGRAPH
AMPLIFIER
FEED UNIT
OSCILLATOR

Figure 2. Experimental arrangement.

The vertical displacement of the oscillograph spot was proportional to the longitudinal displacement of the detector end u (so long as u was small compared with the gap in the condenser unit). Thus, the oscillograph trace gives a displacement–time curve of the end of the rod. For a non-dispersive medium u is related to the stress σ in the incident pulse by the relation (Kolsky 1953, p.91).

$$\sigma = \tfrac{1}{2}\rho c \frac{du}{dt} \qquad \ldots\ldots (1)$$

where ρ is the density of the specimen and c is the velocity of extensional waves in it; $c = (E/\rho)^{1/2}$, where E is Young's modulus.

In the present experiments, rods of glass, polymethylmethacrylate and polystyrene of $\tfrac{1}{4}$ in. and $\tfrac{1}{2}$ in. diameter were employed. The size of the charge and the lengths of the rods were varied in order to determine the critical amplitude of stress pulse at which a Hopkinson fracture was first formed at the detector end of the rod.

It may be seen from equation (1) that for a non-dispersive medium the shape of the stress–time curve may be determined by differentiating the displacement–time curve given by the oscillograph record. The absolute values of u and hence of σ can be calculated if the sensitivity of the condenser unit and the electronic equipment is known accurately (see Davies 1948). A more direct method is to measure the momentum of the pulse M produced by a given weight of explosive. This was done by using one of the rods as a ballistic pendulum. Thus

$$M = A\int \sigma dt \qquad \ldots\ldots (2)$$

where A is the cross sectional area of the rod and substitution from equation (1) leads to

$$M = \tfrac{1}{2}A\rho c\bar{u} \qquad \ldots\ldots (3)$$

where $\bar{u}$ is the maximum displacement of the end of the rod. From equation (3) the absolute value of the maximum displacement can be found, and hence the scale of the displacement–time curve can be determined. The velocity c was obtained from an oscillograph record which gave the intervals between successive reflections of the pulse as it travelled back and forth along the rod (cf. Kolsky 1956).

For comparison, the tensile strength of the rods under static loading was measured. A standard testing machine was used for the plastics, extending them at constant rate of strain up to fracture. The strain rates employed were between 0·04 and 0·4 per minute. The tensile strength of the glass rods was measured in bending.

§ 3. EXPERIMENTAL RESULTS

Since the internal friction for soda-glass and polystyrene is small, the stress amplitude of the pulse does not decay rapidly with distance. The main cause of dispersion with these materials was the lateral inertia of the bar. This resulted in an attenuation of the pulse until it was several diameters of the bar in length, after which the change in length and amplitude was slow (cf. Kolsky 1956). With polymethylmethacrylate the viscoelastic behaviour of the material results in a continuous attenuation with distance and, in order to obtain fractures in this material, short rods had to be employed.

Polystyrene

The maximum tensile stress amplitude which could be transmitted through rods of this material without fracture occurring was found to be about

10 500 lb in^{-2}. This stress was set up, for example near the detector end of a rod of polystyrene 10 in. in length and $\frac{1}{2}$ in. in diameter, when a 0·16 g lead azide charge was detonated at the opposite end. The stress–time curve for the pulse was obtained by the numerical differentiation of the oscillograph record and this showed that the pulse was rounded, about 25 microseconds in duration, and roughly symmetrical.

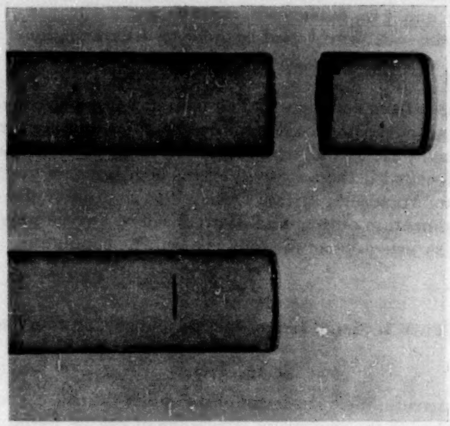

Figure 3. Hopkinson fractures in polystyrene rods $\frac{1}{2}$ in. diameter.

If slightly heavier charges were used with this length of rod, fracture always took place, and figure 3 is a photograph of two such fractures in rods of this length. In the upper rod the fracture was complete and the small cylinder separated from the rest of the rod and flew off with the momentum trapped in it like the end-piece of a Hopkinson pressure bar (Hopkinson 1914). In the lower rod the charge was a little smaller and produced the beginnings of a fracture in the interior of the rod which did not spread to the surface. The reason that the fracture started at the centre is probably the slightly higher tensile stress in this region, resulting from the effect of lateral inertia; this shows that surface flaws do not play a large part in determining the strength of this material. It may be seen that in both rods the fractures occurred about $\frac{1}{2}$ in. from the end of the rod. The velocity of the pulse was found to be about 6000 ft sec^{-1}, so that the pulse length is about 2 in.; thus, fracture has taken place a quarter of the pulse length away from the end of the bar. As mentioned earlier, for a symmetrical pulse this is the point on the bar which is first subjected to the maximum tensile stress.

It may be shown from the exact theory of wave propagation in cylindrical bars, originally formulated by Pochhammer (1876), that the stress distribution produced by an extensional wave travelling in a rod of finite diameter is not uniform. Davies (1948) has carried out the analysis for sinusoidal waves for a bar of material of Poisson's ratio 0·29. He has shown that, in this case, if the wavelength is about five times the radius of the bar, the stress component along the direction of the bar is about 30% greater at the axis of the bar than it is at the surface of the bar.

In order to find the corresponding difference for a pulse, it would be necessary to consider the distribution for each of its Fourier components and then integrate. Qualitatively, it is to be expected, however, that for the pulses in the polystyrene rods whose length was about eight times the radius of the rod, the difference will be of the same order as, but somewhat smaller than, that calculated by Davies. Any high frequency components of wavelength considerably shorter than five times the radius would travel with lower group velocities and consequently would not contribute much to the peak pressure.

For a fixed weight of charge, using rods of different lengths, it was found that the attenuation of the pulse produced by internal friction and lateral inertia resulted in a critical length for fracture. Thus, with a 0·16 g charge, fractures were never produced for rods 11 in. long, but were always produced in rods 9 in. long.

When larger explosive charges were employed, multiple fractures could be produced; thus, with a rod 6 in. in length and a 0·2 g charge, three parallel fracture surfaces were produced. This effect results from the reflection of the tail of the pulse at the new surface produced by the fracture, and is discussed by Rinehart and Pearson (1954).

The maximum tensile stress which the polystyrene rods were able to withstand in the tensile testing machine was found to be about 5500 lb in^{-2}, which is about half the amplitude of the maximum tensile stress pulse which could be transmitted through them. The higher dynamic value may be associated with the viscoelastic properties of polystyrene which result in an increase of modulus with increased rate of loading (Lethersich 1950). Alternatively, it may be analogous to the fracture delay effects observed in glass, which are not associated with viscoelastic behaviour but are due to the slow growth of flaws under the effect of applied tensile stresses.

Polymethylmethacrylate

The larger internal friction of this material resulted in Hopkinson fractures being produced in only fairly short rods. The reason for this is that the compression pulse, as it travels down the rod, sets up complementary hoop tensions, which can produce radial fractures, and this places an upper limit to the amplitude of the maximum compression pulse which can be introduced at the firing end of the rod.

The maximum tensile stress amplitude which did not produce fracture in this material was found to be about 16 000 lb in^{-2}. With a 0·15 g lead azide charge this was set up at the detector end of a rod 3 in. in length and $\frac{1}{2}$ in. in diameter. When a shorter rod was used with this weight of charge, or a larger charge was used with a 3 in. rod, fractures similar to those shown in figure 3 were formed. The fractures were again found to be about $\frac{1}{2}$ in. from the end of the rod. The duration of the pulse for a 3 in. rod was found to be about 20 microseconds and the velocity of the pulse was about 6500 ft sec^{-1} so that, as in the polystyrene experiments, the distance of the fracture from the end corresponded to a quarter of the pulse length. It should be noted that the measured stress is somewhat in excess of that which produced the fracture, since the reflected pulse has to travel an additional half inch through the material after reaching the detector end. Earlier work (Kolsky 1956) shows that the amplitude of a pulse of this duration would not be reduced by more than a few per cent in traversing this extra distance.

The mean 'static' tensile strength of the material obtained on the testing machine was found to be about 6200 lb in^{-2}, which is considerably less than half the dynamic value as measured by stress pulses.

Glass

The internal friction of glass is an order lower than that of the plastics, and the only observable change in pulse shape is that produced by lateral inertia effects. Hopkinson fractures could consequently be produced in rods of this material 6 ft or more in length. The maximum tensile stress amplitude which could be transmitted through the glass rods used in the present experiments without fracture occurring was found to be about 25 000 lb in^{-2}. This was the maximum tensile stress set up at the detector end by a 0·02 g lead azide charge on a glass bar 0·25 in. in diameter and 1 ft long. The effective duration of the pulse was about 6 microseconds.

In the absence of internal friction in this material, the lateral inertia effects resulted in the main pulse being followed by a *coda* of high frequency oscillations (cf. Davies 1948, Hsieh and Kolsky 1958.) These were of much smaller amplitude than the main pulse, and consequently, were not important in the fracture phenomena.

With slightly larger charges, fractures were produced about 0·25 in. from the end of the rod. The velocity of propagation of the pulses was found to be about 16 500 ft sec^{-1} so that once again the fracture was about a quarter of a pulse length from the end of the rod.

With glass specimens, it was not found possible to produce partial fractures like the one shown in figure 3. After the experiments, either the glass rods were unharmed or an end piece had broken off completely

The mean tensile strength measured by resting the glass rods horizontally on two cylindrical supports and loading the middle of the rod was found to be 11 500 lb in^{-2} so that here again the dynamic tensile strength was more than twice that measured statically.

§ 4. CONCLUSIONS

It has been shown that for loading times of the order of a few microseconds the tensile strength of the three materials investigated was about twice that observed under loading time of the order of a second. The sensitivity of tensile strength of glass to time of loading was first investigated by Grenet (1899), who found that for loading times of 40 hours the strength was about one half that for a loading time of 1 second. It is perhaps worth noting that the ratio of loading times between the dynamic and static experiments described here is of the same order as that quoted by Grenet, and that a factor of about two is once again observed.

With regard to the influence of surface flaws on the strength of these materials, it seems clear that for the two plastics investigated, viz. polystyrene and polymethylmethacrylate, they do not play an important role in determining the tensile strength, since internal fractures can be produced at stresses not much in excess of those which start at the surface. For glass this does not appear to be so and the surface condition is known to play a very large part in determining the strength.

ACKNOWLEDGMENT

The work described in this paper was carried out under Contract Nonr 562(14) between the Office of Naval Research and Brown University.

REFERENCES

DAVIES, R. M., 1948, *Phil. Trans. Roy. Soc.* A, **240**, 375.
EVANS, W. M., 1952, *Research, Lond.*, **5**, 502.
GRENET, L., 1899, *Bull. Soc. Encouragement*, **4**, 839.
HOPKINSON, B., 1912, *Collected Scientific Papers*, (Cambridge : University Press), p. 423 ; 1914, *Phil. Trans.* A, **213**, 437.
HSIEH, D. Y., and KOLSKY, H., 1958, *Proc. Phys. Soc.*, **71**, 608.
KOLSKY, H., 1949, *Proc. Phys. Soc.* B, **62** 676 ; 1953, *Stress Waves in Solids* (Oxford : Clarendon Press) ; 1954, *Phil. Mag.*, **45**, 712 ; 1955, *J. Soc. Glass Tech.*, **39**, 394T ; 1956, *Phil. Mag.*, **1**, 693.
KOLSKY, H., and SHEARMAN, A. C., 1949, *Research, Lond.*, **2**, 384.
LETHERSICH, W., 1950, *Brit. J. Appl. Phys.*, **1**, 294.
POCHHAMMER, L., 1876, *J. reine angew Math.*, **81**, 324.
RINEHART, J. S., 1951, *J. Appl. Phys.*, **22**, 1178.
RINEHART, J. S., and PEARSON, J., 1954, *Behavior of Metals under Impulsive Loads* (Cleveland : American Society for Metals).

RESEARCH NOTES

The Viscosity and Density of Benzene near its Freezing Point

By P. M. HU and R. W. PARSONS

Physics Department, University of Hong Kong

MS. received 4*th March* 1958, *and in revised form* 9*th May* 1958

§ 1. Introduction

It has been reported by Dodd and Hu (1949) that for two organic liquids, phenyl ether and m-chlor-nitrobenzene, the equation $\eta = a \exp(c/T)$ (de Guzman 1913, Frenkel 1926, Andrade 1934, Eyring 1936) cannot be used to represent the relation between the viscosity η and the absolute temperature T over a range including both the normal and supercooled states. They found that, in each case, the graph of $(\log \eta, 1/T)$ showed a discontinuous change of slope at the freezing point, the value of c for the supercooled state being significantly greater than that for the normal state, and this was attributed to a change of structure of the liquid. Their results have been queried by Moore, Burkardt and McEwan (1956), although a similar effect was found for other liquids by Greenwood and Martin (1952).

This behaviour has been observed only in liquids which are either polar or ionic. However, Greenwood and Martin point out that when the results of Meyer and Mylius (1920) for the viscosity of benzene are plotted, the only point in the supercooled region is significantly off the extrapolated line which passes through the points in the normal region. The object of the present work was to determine whether benzene also shows this discontinuous behaviour.

§ 2. Experimental Procedure

The kinematic viscosity γ was measured with a suspended level viscometer at intervals of approximately 1°c between $-7{\cdot}5$°c and 26°c, the lowest temperature being 13° below the freezing point, 5·5°c. The viscometer was mounted in a double-walled tank. This was contained in a refrigerated vessel, and its temperature was controlled to within $\pm 0{\cdot}005$°c with a thermostat using a resistance thermometer and a galvanometer–photocell amplifier as developed by Hu and Parsons (1957).

The time of flow t, which varied from 250 to 420 seconds, was measured by a photoelectric method somewhat similar to that used by Dodd and Hu, a dekatron scaling unit and 1000 c/s tuning-fork-controlled oscillator being used instead of an electric clock.

The kinematic viscosity γ was found from the equation $\gamma = At - B/t$. The values of A and B were found by calibrating with distilled water at 20°c and 40°c, the kinematic viscosity at these temperatures being taken as 1·0038 and 0·6582 cs respectively (Swindells, Coe and Godfrey 1952, Hardy and Cottington 1949).

Since surface tension can significantly affect the time of flow in a suspended level viscometer (Barr 1946), the measurements were repeated at 5° intervals with a U-tube viscometer in which the reservoir and timing bulbs were, as nearly as possible, identical. The quantity of liquid was adjusted so that, when the upper meniscus was at the entrance to the timing bulb the lower meniscus was at the entrance to the reservoir. In these circumstances surface tension effects should, to a first approximation, be eliminated.

The density was measured with a Pyrex dilatometer at intervals of approximately 2° between $-7{\cdot}5\,^\circ\mathrm{C}$ and $30\,^\circ\mathrm{C}$. A mercury slug in the capillary, separated from the benzene by an air space of approximately 1 cm, was used to prevent loss by evaporation.

§ 3. RESULTS

3.1. *Density*

The density depends linearly on the temperature over the entire range. Two sets of measurements were made, using different samples of benzene, and the straight line which fitted the results best was found by the method of least squares to be

$$\rho = 0{\cdot}9002 - 0{\cdot}001066\,\theta \pm 0{\cdot}0001$$

where ρ is the density in g cm^{-3} at temperature $\theta\,^\circ\mathrm{C}$. This gives $\rho = 0{\cdot}8789$ g cm^{-3} when $\theta = 20\,^\circ\mathrm{C}$; by comparison, Meyer and Mylius give 0·8791, while the value quoted in the tables of Kaye and Laby (1955) is 0·8790.

3.2. *Viscosity*

The results of the measurements made with the suspended level viscometer are shown in figure 1, η being the dynamic viscosity $\gamma\rho$ in centipoise and T the absolute temperature. The straight line $\log_{10}\eta = \alpha + \beta/T$ which fits the points best is also shown, the coefficients α and β being determined by the method of least squares. The deviations of the experimental points from the straight line are shown in figure 2. This is a very smooth curve and there is no sign of any discontinuous behaviour. It can be represented well by a quadratic equation of the form

$$\delta = p\left(\frac{1}{T} - q\right)^2 + r$$

where p, q and r are suitably chosen constants and $\delta = \log_{10}\eta - (\alpha + \beta/T)$.

From this it follows that

$$\begin{aligned}\log_{10}\eta &= \alpha + \beta/T + \delta\\ &= -1{\cdot}08648 - \frac{32{\cdot}657}{T} + \frac{8{\cdot}71\times10^4}{T^2}.\end{aligned} \qquad \ldots\ldots(1)$$

Viscosities calculated from this equation agreed well with the measured values, the r.m.s. error being 0·0002, and the deviations being quite random.

According to the suspended level viscometer, the viscosity of benzene at 20 °C is 0·654 cP, while the result obtained with the U-tube instrument was 0·6507 cP. This difference is presumably due to surface tension, and since the U-tube instrument was designed to reduce the effect of surface tension on the flow time, the value obtained with it seems more reliable. Values of the viscosity at 20 °C, and also of η_0/η_{20} are given in the table, η_0 being the viscosity at 0 °C; the results of other observers, which are tabulated by Meyer and Mylius, are included for comparison.

	η_{20}(cP)	η_0/η_{20}
Hu and Parsons, U-tube	0·6507	1·398
Hu and Parsons, suspended level	0·6541	1·398
Meyer and Mylius	0·6519	1·401
Thorpe and Rodger	0·6540	1·385
Bingham and Harrison	0·6489	1·391

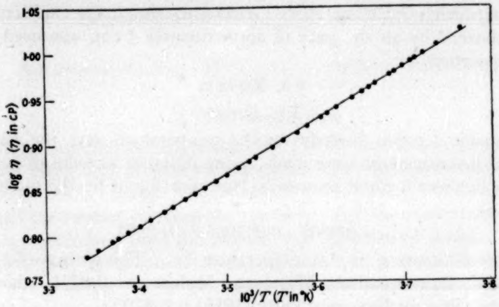

Figure 1.

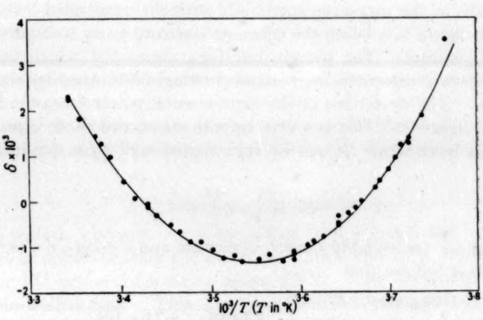

Figure 2.

For relative measurements the agreement between the two instruments was good, but over the whole temperature range the values of the viscosity obtained with the U-tube viscometer were smaller by a factor of 0·9947 ± 0·0003 than the values obtained with the suspended level instrument. Equation (1) can be modified, by the addition of log 0·9947 to the right-hand side, to represent the results obtained with the U-tube viscometer. It then becomes

$$\log \eta = -1{\cdot}08879 - \frac{32{\cdot}657}{T} + \frac{8{\cdot}71 \times 10^4}{T^2}$$

and it seems reasonable to take this as the most reliable result.

§ 4. CONCLUSION

The object of the work was to determine whether there is any discontinuous behaviour at the freezing point. None was observed. This supports the suggestion of Greenwood and Martin that the effect in polar liquids may be due to association of molecules into small aggregates. The simple exponential relation is only an approximation, and the term c is not strictly constant but is temperature dependent. This might be interpreted in terms of the temperature dependence of the average intermolecular separation, since benzene has a large coefficient of expansion, and so the modified relation due to Andrade (1934) $\eta v^{1/3} = a \exp (c/vt)$ where v is the specific volume, should be a better approximation. To check this, log $\eta v^{1/3}$ was plotted against $1/vT$, but the resulting graph was still curved and did not differ greatly in curvature from figure 1.

ACKNOWLEDGEMENT

The authors are indebted to Mr. E. R. Sutton of the Ho Tung Workshop for his assistance with the construction of the apparatus.

REFERENCES

ANDRADE, E. N. DA C., 1934, *Phil. Mag.*, **17,** 698.

BARR, G., 1946, *Proc. Phys. Soc.*, **58,** 575.

DODD, C., and HU, P. M., 1949, *Proc. Phys. Soc.* B, **62,** 454.

EYRING, H., 1936, *J. Chem. Phys.*, **4,** 283.

FRENKEL, J., 1926, *Z. Phys.*, **35,** 652.

GREENWOOD, N. N., and MARTIN, R. L., 1952, *Proc. Roy. Soc.* A, **215,** 46.

DE GUZMAN, J., 1913, *Anales de la Sociedad Espanola de Fisica y Quimica*, **11,** 353.

HARDY, R. C., and COTTINGTON, R. L., 1949, *J. Res. Nat. Bur. Stand.*, **42,** 573.

HU, P. M., and PARSONS, R. W., 1957, *J. Sci. Instrum.*, **34,** 283.

KAYE, G. W. C., and LABY, T. H., 1955, *Tables of Physical and Chemical Constants* (London: Longmans Green).

MEYER, J., and MYLIUS, B., 1920, *Z. Phys. Chem.*, **95,** 349.

MOORE, D. W., BURKARDT, L. A., and MCEWAN, W. S., 1956, *J. Chem. Phys.*, **25,** 1235.

SWINDELLS, J. F., COE, J. R., and GODFREY, T. B., 1952, *J. Res. Nat. Bur. Stand.*, **48,** 1.

The Stripping Mechanism in the Reaction ^{9}Be(α, n)^{12}C

BY N. W. TANNER[†]
Cavendish Laboratory, Cambridge

Communicated by E. S. Shire ; MS. received 27th May 1958

§ 1. INTRODUCTION

MADANSKY AND OWEN (1955) have suggested that the reaction ^{9}Be(α, n)^{12}C might show stripping characteristics similar to deuteron reactions. If the deuteron in conventional stripping theory is replaced with the ^{9}Be nucleus (regarded as ^{8}Be + n), then the neutron angular distribution is predicted to be peaked in the direction of the ^{9}Be momentum. Angular distribution measurements at α-particle energies near 1 MeV (James, Jones and Wilkinson 1956) and from 2 to 5 MeV (Risser, Price and Class 1957) are not favourable to the stripping interpretation, but it should be noted that a very moderate contribution from resonant processes could produce confusing interference terms. In general such interference effects cannot be readily calculated, at least for the broad and overlapping resonances apparently effective in this reaction. This paper deals with a singular case in which the interference terms reduce to a simple form, which allows a much more sensitive test for the stripping mechanism.

[†] Now at the Kellogg Radiation Laboratory, California Institute of Technology, Pasadena, California.

§ 2. THE n–γ ANGULAR CORRELATION

The correlation theory for deuteron stripping (Satchelor and Spiers 1952) can be readily adapted to the $^9\mathrm{Be}(\alpha, \mathrm{n})^{12}\mathrm{C}^*(\gamma)^{12}\mathrm{C}$ reaction. In the approximation that ^{9}Be can be described as a ^{8}Be (ground state) core and a neutron in a single particle state of angular momentum l, the n–γ correlation is the same as the angular distribution of γ-radiation following a $^8\mathrm{Be}+\alpha$ capture reaction along an axis $\mathbf{k}=\mathbf{k}_9-\frac{1}{3}\mathbf{k}_\mathrm{n}$; $\mathbf{k}_9$ and $\mathbf{k}_\mathrm{n}$ are the wave vectors for ^{9}Be and the neutron relative to ^{4}He and ^{12}C respectively. As ^{8}Be and the α-particle both have zero spin, the only magnetic substate M of the $^{12}\mathrm{C}^*$ state J that can be excited is $M=0$. For the excited state of ^{12}C with $J=2$ which radiates to the $J=0$ ground state, the angular correlation is then $\sin^2(2\theta_\gamma)$, with θ_γ measured with respect to the quantization axis $\mathbf{k}$.

If neutrons are observed in the direction of the stripping peak, $\mathbf{k}$ is parallel to the α-particle beam. With this axis of quantization, a resonant process excites the various substates M of $^{12}\mathrm{C}^*$ incoherently. As stripping populates only the substate $M=0$, the only stripping-resonant interference term that can occur is that for $M=0$. This is sufficient to determine the form of the interference term as $\sin^2(2\theta_\gamma)$, and is independent of the resonant process.

This physical argument has been verified by writing out the amplitudes for stripping and resonant processes in full (Tanner 1956).

§ 3. EXPERIMENTAL n–γ CORRELATION

A ^{9}Be target of 60 kev thickness for 1 MeV α-particles was bombarded with a He$^+$ beam of energy 1·15 MeV and 2·8 MeV. Neutrons were detected by a liquid scintillator and the 4·43 MeV γ-rays from the first excited state of ^{12}C by a NaI crystal, coincidences being recorded with a resolving time of 0·3 μsec. Random coincidences were monitored by the usual method of inserting a delay (in this case 1 μsec) in one of the coincidence channels.

The desired geometry of $\mathbf{k}_\mathrm{n}$ parallel to $\mathbf{k}_9$ was approximated by placing the neutron counter at the most backward angle possible (relative to the He$^+$ beam) consistent with a reasonable counting rate. In centre-of-mass coordinates, the mean angle between the neutron counter and the ^{9}Be momentum was about 14°, with the counter subtending an angle of ±6° at the target. The γ-counter subtended an angle of ±10°.

Counts were taken at 5 angles at 1·15 MeV and 3 angles at 2·8 MeV, in each case the maxima and zeroes of the function $\sin^2(2\theta_\gamma)$ being selected. Within the errors of 10% (mainly due to the counting statistics) no departure from isotropy was established and a limit of 20% could be put on such a departure.

§ 4. Discussion

The measurements of the n–γ correlation show no evidence for the form $\sin^2(2\theta_\gamma)$ expected from stripping or stripping-resonance interference and suggest that stripping makes no important contribution to the reaction at bombarding energies near 1 MEV or 3 MEV. In setting a limit on the stripping contribution recognition must be made of the conditions favourable to stripping:

(i) The stripping-resonance interference term is proportional to the amplitude for stripping.

(ii) The neutrons were observed in the direction of the hypothetical stripping maximum.

(iii) The bombarding energies chosen were remote from the apparent resonances in ^{9}Be(α, n)^{12}C (Bonner *et al.* 1956).

(iv) It is likely that a resonant process would give rise to a n–γ correlation approximately isotropic compared with the extreme form $\sin^2(2\theta_\gamma)$ predicted by stripping.

In view of these considerations it seems likely that an amplitude for stripping of 10 or 20% relative to resonant processes would have shown up in the measurements as a marked departure from isotropy.

References

Bonner, T. W., Kraus, A. A., Marion, J. B., and Schiffer, J. P., 1956, *Phys. Rev.*, **102,** 1348.

James, D. B., Jones, G. A., and Wilkinson, D. H., 1956, *Phil. Mag.* (8), **1,** 949.

Madansky, M. L., and Owen, G. E., 1955, *Phys. Rev.*, **99,** 1608.

Risser, J. R., Price, J. E., and Class, C. M., 1957, *Phys. Rev.*, **105,** 1288.

Satchelor, G. R., and Spiers, J. A., 1952, *Proc. Phys. Soc.* A, **65,** 980.

Tanner, N. W., 1956, *Ph.D. Thesis*, University of Cambridge.

The Growth of an Orientated Monolayer of Lead on a Silver Single-Crystal Substrate

By E. GRÜNBAUM†

Physics Department, Imperial College, London

Communicated by M. Blackman; MS. received 28th May 1958

§ 1. Introduction

Interesting results about the initial stages of growth of several metals evaporated in a vacuum on to a smooth (111) surface of a silver single crystal at room temperature were obtained by Newman (1957). From a study by means of electron diffraction using the reflection technique he concluded that a lead deposit when first detected formed a monatomic layer on the silver substrate. This layer was not continuous, but consisted of islands. It had a close-packed arrangement of atoms, orientated parallel with respect to the (111) plane of the silver surface. Its lattice spacing was only 2% smaller than that of bulk lead, whilst the corresponding spacing of the silver substrate was 19% smaller.

† Now at Laboratorio de Cristalografia, Universidad de Chile, Casilla 147, Santiago, Chile.

Newman's conclusion that the lead formed a monolayer was based mainly on the observation in the electron diffraction patterns of streaks in a direction perpendicular to the silver surface without periodic variations of intensity. This characteristic of the streaks did not change with the angle of incidence of the electron beam.

The knowledge of the formation of an orientated monolayer in the first stage of growth is of considerable interest for any theory of orientated overgrowth. It was therefore considered useful to obtain further evidence for the formation of an orientated monolayer in the case of lead. For this purpose, in the present work, the gradual change in the electron diffraction patterns observed when the lead deposit was increased, was studied in more detail using very slow rates of deposition. This change was compared with that to be expected theoretically from the building up of successive layers in a cubic close-packed arrangement, starting from a monolayer.

§ 2. Experimental Techniques

The experimental techniques were the same as those used by Newman (1957), and are summarized below. The atomically smooth silver single crystal substrates with a (111) surface were prepared by vacuum evaporation of a film of silver, about 1500 Å thick, on to the cleavage face of mica heated to about 270°c (Newman and Pashley 1955). The lead deposits were formed by evaporation of lead from a heated molybdenum wire spiral *in situ* in an electron diffraction camera. The electron diffraction patterns were obtained by the reflection technique. The changes produced in these patterns as the deposit was built up could be continuously recorded on a photographic film (Kehoe, Newman and Pashley 1954).

The mean thickness of the lead deposits was estimated by the following method. Lead was simultaneously deposited on to the cleavage face of a rock-salt single crystal mounted next to the silver single crystal. At regular intervals the primary electron beam was shifted to be incident on the rock-salt crystal and the electron diffraction pattern was recorded. The moment of the first appearance of a lead deposit on the rock-salt could thus be determined from the diffraction patterns. The mean thickness corresponding to this deposit was estimated as about 0·5 Å from the previous results of the study of deposits of radioactive copper on the same surface (Newman 1955). The rate of deposition of lead on the silver substrate could then be calculated if two assumptions were made. Firstly, that the rate of evaporation of lead from the heated wire spiral was uniform in time, which was justified by the previous measurements on the radioactive copper deposits. Secondly, it was assumed that the same fraction of the incident lead beam adhered to the silver and to the rock-salt surfaces, which was more doubtful in view of the fact that only a relatively small fraction adhered to the surfaces.

The rate of deposition of lead used in the present experiments was 0·1 to 0·2 Å min^{-1}, which was 50 to 100 times slower than that used by Newman. A trap cooled by liquid air, attached to the electron diffraction camera, prevented the disturbing effects observed by Newman when he used rates of 1 Å min^{-1}, and which were possibly due to oxidation of the lead or attack by the residual water vapour.

§ 3. Results and Comments

The electron diffraction patterns obtained in the present study showed that the growth in the first stages had the same general characteristics as those found by

Newman (see § 1). The estimated values of the mean thickness of the deposits at the various stages were, however, different. (The mean thickness is the thickness which the deposit would have if it was uniformly distributed over the surface.) The first signs of a lead deposit appeared at a mean thickness of 0·1 to 0·2 Å as faint streaks (figure 1 (for figures 1–4 see Plate)). These streaks were situated parallel to and inside the streaked spots due to the silver substrate, and did not show any maxima of intensity. (A diffraction pattern from a typical silver specimen has already been published: see Newman and Pashley 1955.) This was the case for low and high angles of incidence of the electron beam. As the thickness of the deposit increased the streaks became gradually more intense, but did not show periodic variations of intensity (figure 2).

At 1·9 Å of deposit, maxima of intensity became visible on the streaks (figure 3). At 3·4 Å of deposit, the maxima showed a dip of intensity in their middle (figure 4). With further increase of the thickness of the deposit, this dip of intensity developed gradually into a pair of sharp spots. This was the case for an angle of incidence of 2·5°. For an angle of incidence of 1°, pairs of spots on top of the maxima of intensity were already visible at 2·0 Å of deposit.

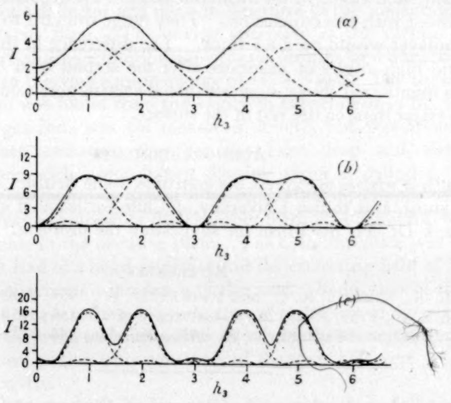

Figure 5. Theoretical intensity distribution in the electron diffraction patterns, on the first two streaks on either side of the central line, for an increasing number of close-packed layers : (*a*) two layers, (*b*) three layers, (*c*) four layers. Dotted lines : separate intensity distributions for the two possible orientations ; full lines : resultant intensity distribution, assuming equal probability for the two orientations.

These patterns were compared with those to be expected theoretically from the building up of successive close-packed layers in a cubic close-packed arrangement, starting from a monolayer. The relevant feature of these patterns is the distribution of the intensity I in the direction h_3 in reciprocal space, perpendicular to the substrate surface. Only the intensity distribution of the first two streaks on either side of the central line is of interest, and will be discussed here. On the central line the intensity distributions due to the lead and silver are superimposed, and do not give useful information. For a monolayer the intensity distribution should show no periodic variation in a direction perpendicular to the substrate surface, because no interference can take place in this direction. This is seen to be the case for figures 1 and 2. For N close-packed layers the intensity distribution is given by the formula

$$I=\frac{\sin^2\{N\pi(h_3\pm 1)/3\}}{\sin^2\{\pi(h_3\pm 1)/3\}}.$$

The atomic form factor has been neglected here, because it only introduces a gradual change of intensity from the central spot outwards. This formula has been represented in figure 5 by dotted lines for two, three and four layers. The ± sign in the formula, and the two dotted curves, arise from the fact that the second layer can grow on the first one in two possible positions, rotated by 180° about an axis perpendicular to the surface. The full lines of figure 5 represent the resultant intensity distribution, assuming an equal probability for the two orientations. Comparing figures 3 and 4 with figures 5 (*a*) and 5 (*b*), it can be seen that the first set corresponds to a deposit consisting of two layers and the second to three layers. The preceding analysis, which shows that the lead deposit is gradually built up as successive close-packed layers, gives thus further support to Newman's conclusion that in the first stage of growth monolayer islands are present.

The estimated values of the mean thickness of the deposits of the first stage are also consistent with this conclusion. They range from 0·1 to 1·6 Å ,whilst a complete monolayer would be 2·8 Å thick. The difference in the patterns observed for low and high angles of incidence after the second layer has started forming, which was mentioned above, suggests that at certain points on the surface the lead builds up faster than on the rest of the surface.

ACKNOWLEDGMENTS

The author wishes to express his gratitude to the British Council for a scholarship and grant, and to the University of Chile for leave of absence. He would like to thank Dr. M. Blackman for suggesting the problem.

REFERENCES

KEHOE, R. B., NEWMAN, R. C., and PASHLEY, D. W., 1954, *J. Sci. Instrum.*, **31**, 399.
NEWMAN, R. C., 1955, *Ph.D. Thesis*, University of London ; 1957, *Phil. Mag.*, **2**, 750.
NEWMAN, R. C., and PASHLEY, D. W., 1955, *Phil. Mag.*, **46**, 927.

The Ionization produced by Beams of Carbon and Nitrogen Ions

BY W. E. BURCHAM† AND M. A. F. ALVES‡
†Department of Physics, University of Birmingham
‡University of Coimbra, Portugal

§ 1. INTRODUCTION

THE rate of loss of energy of heavy charged particles passing through matter may be written in the form

$$-\frac{dE}{dx}=Z_e^2F(v) \qquad \ldots\ldots(1)$$

where Z_e is the effective ionic charge for a velocity v and $F(v)$ is a function of v and of the ionization potential of the absorbing medium. The effective ionic charge is usually taken to be the average charge per ion of an ion beam of given velocity passing through matter. Although it is not certain that the average charge defined in this way can be used to predict effects depending on the square of the actual charge, an expression of the form (1) has been used successfully by Livesey (1956) to calculate the range–energy curves for heavy ions in air and in nuclear emulsion. Part of the energy loss is due to ionization and this should also depend on the quantity $Z_e{}^2F(v)$. If Z_e is known it may therefore be possible to predict the variation of ionization along the path of a heavy ion from the known specific ionization due to protons of the same velocity. In the present note the ionization produced by carbon ions, calculated in this way, is compared with that observed for both carbon and nitrogen ions of energies up to about 80 MeV passing through argon.

§ 2. Experimental Method

Carbon and nitrogen ions were accelerated in the Nuffield cyclotron of the University of Birmingham to an energy of about 9 MeV per nucleon. A small beam of ions was extracted electrostatically and deflected magnetically into an ionization chamber about 20 feet from the cyclotron. The accelerating mechanism did not provide a mono-energetic beam but the combination of the electrostatic extractor, the magnetic deflector and the ¼ in. aperture of the ionization chamber formed a crude velocity filter. The energy spectrum of the carbon ion beam was determined by recording a distribution of track lengths in a nuclear emulsion and is shown in figure 1, giving a mean energy of 113 ± 3 MeV. The angular spread of the incident beam was found from the emulsion experiment to be $\pm 2°$. The energy of the nitrogen ions was not measured directly but was about 130 MeV.

The parallel-plate ionization chamber was 1 cm deep and was filled to atmospheric pressure with argon taken directly from a cylinder. Charged particles from the cyclotron first passed through a 0·001 in. copper window and then entered the effective volume of the chamber through a 5 micron aluminium foil closing a ¼ in. hole in the negative plate. The collector plate was connected directly to the input lead of a head amplifier and the collecting field of $300\,\mathrm{v\,cm^{-1}}$ was parallel to the direction of incidence of the ions. Reduction of the field by a factor of 3 resulted in a less than 5% reduction of pulse size and it was assumed that the chamber was giving electron pulses of nearly the saturation value. The differentiation and integration time constants of the amplifier were set at $10\,\mu$sec and $0{\cdot}8\,\mu$sec respectively.

The beam energy was reduced by interposing aluminium foils in the path of the ions before the ionization chamber, and for each foil the distribution of pulse sizes obtained from the ionization chamber and amplifier was displayed on an oscilloscope and recorded photographically. The linearity of the system was checked using a signal generator and calibrated attenuator. Relative mean pulse heights for each beam energy and for both carbon and nitrogen ions were obtained from histograms plotted from the photographic records. An approximate calibration of the pulse height scale was obtained by observing the pulse size for alpha particles from polonium and also from thorium C + C′ near the end of their range in the ionization chamber.

§ 3. Results and Discussion

The observed relative ionization by the beam in 1 cm of argon at atmospheric pressure is plotted in figure 2 (*a*) and (*b*) as a function of the total absorber (in mg cm^{-2} of aluminium equivalent) in the path of the heavy ions before the ionization chamber. The difference in range and in maximum ionization between the carbon and nitrogen ions is clear.

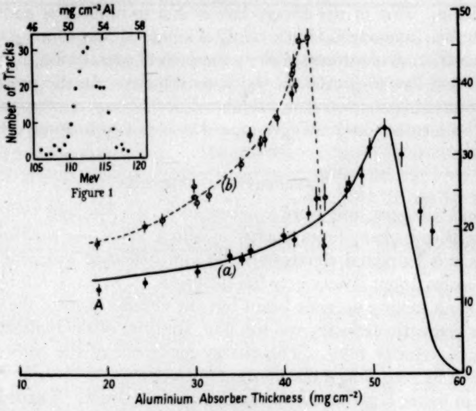

Figure 2.

Figure 1 (inset). Energy distribution in carbon ion beam.

Figure 2. (*a*) Observed relative ionization in argon due to a beam of 113 Mev ^{12}C ions. The full line is a curve calculated as described in the text.
(*b*) Observed relative ionization in argon due to a beam of 130 Mev ^{14}N ions.

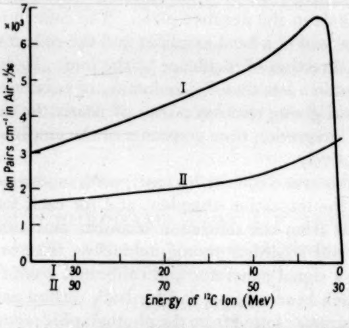

Figure 3. Specific ionization curve for ^{12}C ion in air (15°c and 760 mm Hg) calculated from proton ionization.

In order to compare these results with theoretical prediction, use was made of the curves for the specific ionization of protons in air given by Jentschke (1940) and of alpha particles in air given by Holloway and Livingston (1938). At the highest energies used in this experiment (point A in figure 2) the carbon ions were nearly fully charged ($Z_e = 0{\cdot}97$). The carbon ion energy at this point, from the range–energy curve found in an earlier experiment (Burcham 1957) was about 85 MeV, and the energy of a proton of the same velocity is 7·08 MeV. The ionization (in air) due to such a proton is 1850 ion pairs cm^{-1} and the expected ionization for the carbon ion is then $6{\cdot}3 \times 10^4$ ion pairs cm^{-1}. The observed pulse size, converted to equivalent ionization in air by use of the polonium and thorium calibration, was $7{\cdot}0 \pm 0{\cdot}5 \times 10^4$ ion pairs cm^{-1} of air, showing that ionizations of the expected order of magnitude were being measured. In this calculation no correction has been made for possible energy dependence of the ratio of specific ionization in air to that in argon.

A curve (figure 3) was then constructed showing the specific ionization in air expected from a carbon ion as a function of energy. This is essentially the proton ionization curve of Jentschke multiplied at each point by Z_e^2 where Z_e is the effective charge of the carbon ion obtained from the semi-empirical curve given by Papineau (1956); a few of the low energy points were corrected for the effective charge of the proton in air using information collected by Evans (1955, p. 636). It is not certain that the effective charge Z_e for an ion of given velocity is independent of the nature of the stopping medium, but the agreement between the charges of heavy ions observed in nickel, aluminium, formvar, nitrogen and argon, and compared by Papineau (1956), suggests that this is a reasonable assumption.

The proton ionization curve of Jentschke indicates a maximum ionization of 2750 ion pairs mm^{-1} at a residual range of 1·7 mm in air. This disagrees with a direct observation of 0·8 mm for single proton tracks in an expansion chamber (Bower 1938, see also Feather 1941) and in deriving the curve of figure 3 the position of maximum ionization for a proton has been set at 1 mm range. This is in accord with observations of the energy loss for slow protons in air given by Reynolds, Dunbar, Wenzel and Whaling (1953), converted to range using the graph given by Bethe and Ashkin (1953, p. 182). This range–energy relation was also used in converting the air ranges given by Jentschke to energy. As a check on the whole procedure the specific ionization curve for a single alpha particle was calculated from the proton ionization curve using values of effective charge plotted by Evans (1955, p. 636). This was found to be in reasonable agreement with the observations of Holloway and Livingston (1938).

The curve of figure 3 was assumed also to give the form of the specific ionization curve for a carbon ion passing through argon. This will be so if the ratio of the specific ionizations of the ion in air and in argon is independent of velocity. Although this has not been verified for the whole range of velocities corresponding to figure 3, the energy loss calculations of Aron, Hoffman and Williams (1949) and the figures for energy expenditure per ion pair given by Bethe and Ashkin (1953, p. 233) suggest that the assumption is true to better than 10% over the energy range 5–85 MeV for a carbon-12 ion. The observed ionization curve for argon (figure 2 (*a*)) then differs in form from the curve of figure 3, expressed in terms of residual range, because of range straggling, of chamber depth, and of beam energy distribution. The range straggling was estimated from the formula given by Bethe and Ashkin (1953, p. 248) and also by numerical integration of the expression for the standard deviation σ of the range distribution (see, for example, Evans 1955, p. 662). A value of σ of 0·4% of the mean range was found for 113 MeV carbon ions. Such straggling effects may in this case be neglected in comparison with the beam energy spread of ±2%

shown in figure 1. Nuclear stopping effects (Evans 1955, p. 669) were estimated to be less than 5% of the energy loss to electrons even for singly charged carbon ions, and were also neglected. The abscissa scale of figure 3 was converted to residual range in aluminium by using a range–energy curve based on direct observation (Burcham 1957) and on scaling of the range–energy curves for ^{12}C in emulsion (Papineau 1956) and for ^{13}C in air (Lillie 1952); corrections for the velocity variation of the stopping power of emulsion relative to that of aluminium were made where necessary using data collected by Bethe and Ashkin (1953, p. 201) for alpha particles. The resulting ionization–range curve was then averaged for chamber depth (1·5 mg cm^{-2}) and for the beam energy distribution. The final curve predicted for ^{12}C is plotted as a full line in figure 2 (*a*), with fitting to the experimental points at the peak.

The predicted and observed curves for ^{12}C are in reasonable agreement. This suggests that calculations based on the semi-empirical effective charge are probably valid, although the necessity in this experiment for averaging over a wide energy distribution inevitably obscures details of the basic specific ionization curve such as the displacement of the ionization maximum from the end of the range. The shape of the ionization curve on the high energy side of the maximum is however less affected by energy spread, and more directly determined by the single particle ionization curve.

ACKNOWLEDGMENTS

We are grateful to Mrs. J. I. Kellett for scanning the nuclear emulsions and films used in this work. One of us (M. A. F. A.) is indebted to the Instituto de Alta Cultura of Portugal for a scholarship.

REFERENCES

ARON, W. A., HOFFMAN, B. G., and WILLIAMS, F. C., 1949, *U.S. Atomic Energy Commission* Report No. 663.

BETHE, H. A., and ASHKIN, J., 1953, in *Experimental Nuclear Physics*, Vol. 1, Ed. E. Segrè (New York: John Wiley).

BOWER, J. C., 1938, *Proc. Camb. Phil. Soc.*, **34,** 450.

BURCHAM, W. E., 1957, *Proc. Phys. Soc.* A, **70,** 309.

EVANS, R. D., 1955, *The Atomic Nucleus* (New York: McGraw-Hill).

FEATHER, N., 1941, *Nature, Lond.*, **147,** 510.

HOLLOWAY, M. G., and LIVINGSTON, M. S., 1938, *Phys. Rev.*, **54,** 18.

JENTSCHKE, W. K., 1940, *Phys. Z.*, **41,** 524.

LILLIE, A. B., 1952, *Phys. Rev.*, **87,** 716.

LIVESEY, D. L., 1956, *Canad. J. Phys.*, **34,** 203.

PAPINEAU, A., 1956, *C. R. Acad. Sci., Paris*, **242,** 2933.

REYNOLDS, H. K., DUNBAR, D. N. F., WENZEL, W. A., and WHALING, W., 1953, *Phys. Rev.*, **92,** 742.

Note added in proof.—Since this note was prepared the authors have seen a paper by Teplova, Nikolayev, Dmitriev, and Fateyeva (*J. Exp. Theor. Phys.*, 1958, **34,** 559) in which extensive work on the range and specific ionization for heavy ions of energies up to about 10 MeV is reported.

Positive Ion Emission from Metal Surfaces caused by Ion Bombardment

By A. RIDDOCH and J. H. LECK
Department of Electrical Engineering, University of Liverpool

MS. received 14*th April* 1958, *and in final form* 20*th May* 1958

§ 1. Summary

The phenomenon reported in this paper was first observed during an investigation into the adsorption of gas on to metal surfaces. When tungsten targets were bombarded with positive ions of the noble gases, and subsequently degassed by heating, a positive ion emission was often observed in addition to a desorption of gas from the target. These ions have been analysed with a mass spectrometer and shown to be sodium, potassium, rubidium and caesium. This is reasonable, as these elements form significant impurities in tungsten and may, because of their low ionization potential, be expected to desorb mainly as ions. This result is interesting in view of some recently published work of Bills (1957) who observed similar ion currents after bombardment with both electrons and ions. In view of the results reported here it is almost certain that these ions also originate from impurities already present in the target before the bombardment took place, rather than directly from the adsorbed ions.

§ 2. Experimental Procedure and Results

In the investigation of argon adsorption metal target surfaces were bombarded by argon ions of a known energy for a given time. To determine the adsorption which had taken place during this bombardment the target was subsequently heated to a high temperature (by passing an electric current through it) and the quantity of desorbed gas measured. The quantity desorbed was found to increase approximately linearly with both the number of bombarding ions and their energy. In addition to the gas desorption a positive ion emission was found to occur dependent in a similar way upon the previous bombardment. The curves in figure 1 plotted from a typical set of results show the pressure and ion current transients on the same time scale. Simple observation with various retarding electrodes verified that the ions came from the target surface and had thermal energies.

In order to determine the nature of these charged particles simple modifications to the ion source of a conventional 'Nier' type 90° deflection mass spectrometer were undertaken. The general arrangement of new electrode system is shown in the schematic diagram, figure 2. A tungsten ribbon target 0·030 in. × 0·001 in. section 1 in. long was mounted above the first slit of the ion gun assembly, taking the place of the electron beam in the normal source. Two thermionic filaments were mounted at right angles to and a little above the target and a grid G was placed between the target and the filaments.

After the assembly had been completed and a reasonably good vacuum had been achieved—better than 10^{-6} mm Hg, as measured by an ionization gauge—the target was slowly heated to about 1600°c. During this heating positive ion emission, which started at about 500°c, increased rapidly with increasing temperature. By keeping the grid G and the first slit A of the ion gun at the same potential a significant fraction of these ions passed through A and were analysed by the mass spectrometer in the normal way. They were, in fact, the alkali metal impurities in the tungsten which, because of their low ionization potentials (which are considerably less than the work function of tungsten), must be desorbed almost entirely as positive ions. Potassium was the most abundant ion followed by sodium with but small amounts of rubidium and caesium. After having been heated for two hours the intensity of the ion beams had fallen considerably, to the point where none could be detected below a temperature of 1000°c. (The sodium beam fell much more quickly than the potassium.)

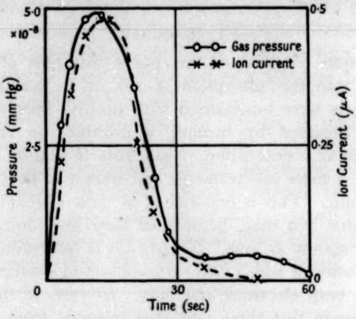

Figure 1. The ion current and argon desorption transients occurring when a tungsten ribbon is heated to 500°c after being bombarded with a 1 μA argon ion current for 140 minutes. (Effective gas conductance for argon at the target was 1 l. sec^{-1}.)

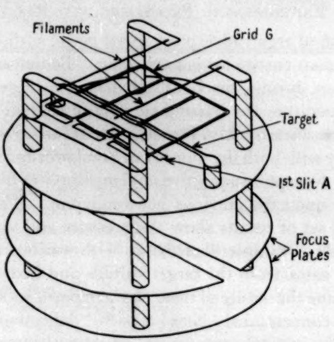

Figure 2. Schematic diagram of the modified mass spectrometer source.

At this stage bombarding and subsequent degassing cycles were started. First argon was introduced to the source at a pressure of 10^{-5} mm Hg (the vacuum and gas handling plant was virtually the same as that described by Brown and Leck (1955)) and an electron current of the order of 1 to 10 mA passed between the filaments and the grid (figure 2). The target was made to collect a significant fraction of the argon ions produced in the electron stream by making its potential negative V_0 volts with respect to the grid. After a measured interval during which the current to the target was held at 0·1 μA (by adjusting the electron current) the argon was pumped from the system and the discharge switched off. To complete the experiment the target was slowly heated to 1000°c. At a temperature of about 500°c in every case the target emitted a burst of ions having an amplitude and duration dependent upon the rate of rise of temperature. The mass spectrometer analysis showed these ions to be largely potassium with a very small fraction of sodium.

This procedure of bombardment followed by desorption was carried out many times and always produced the same pattern for the potassium ion desorption. But after the first five or so experiments with a 'new' target the sodium emission had fallen to an insignificant value. The pattern was always the same when other gases such as neon or nitrogen was used instead of argon. Although careful observations were made no ions of the bombarding gases were ever detected in the emission from the target and in fact in no experiment were ions other than those of the alkali metals ever detected. The dependence of the number of desorbed ions upon the previous bombardment is illustrated by figure 3.

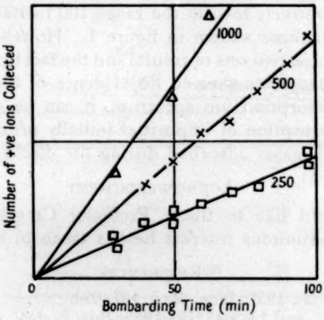

Figure 3. The number of positive ions of potassium reaching the mass spectrometer collector (the scale is expressed in arbitrary units) shown as a function of the number of argon ions striking the collector in the previous bombardment. The target potential with respect to the filament (V_0 volts) during the bombardment is marked on each curve.

Here the total charge of potassium ions reaching the mass spectrometer collector is shown as a function of the number of bombarding ions for various values of V_0. (The mean energy of the argon ions incident on the target is clearly proportional to V_0 the potential between target and grid.)

§ 3. DISCUSSION

The mass spectrometer analysis carried out in this work shows conclusively that the burst of positive ions occurring after a bombardment arises from an impurity of potassium in the tungsten target. The total quantity of potassium desorbed can be accounted for by only a minute impurity in the tungsten target.

(Because the total impurity is small and quickly removed, the sodium transients can be neglected in comparison with potassium.) For example, in the experiment shown in figure 1, approximately 10^{14} ions were desorbed corresponding to a mass of 10^{-8} g or only 10^{-5} % of the total weight of the target. This is small compared with the total impurity of potassium in commercial tungsten, which is of the order of 0·01%. It is in all probability the change in the surface condition brought about by the high-voltage discharge which allows the further release of the impurities; sputtering, for example, must be sufficiently intense to remove a significant fraction of the top surface atoms. This is consistent with the fact that the potassium released increases both with duration and energy of the bombardment. Further, this explanation is rather analogous to the observations of positive ion desorption made by Richardson (1913). He noted that the transient emission of potassium obtained on heating a new sample of platinum wire could be revived by heating the wire in air or in a bunsen flame or by subjecting it to a small mechanical strain, i.e. in each case by changing the surface.

It is interesting to compare the results obtained in the above experiments with the recently reported work by Bills (1957). In his experiments Bills subjected tungsten targets to bombardment by both positive ions and electrons. In either case he observed a transient ion emission current on subsequent heating, for which no simple explanation could be offered. The energies of the bombarding particles were comparatively low, in the range 100 to 160 ev, and the desorption currents smaller than those shown in figure 1. However from the qualitative agreement between these two sets of results and the fact that in the work described above the mass spectrometer showed no evidence of the bombarding particles in the subsequent desorption ion spectrum, it can be assumed that Bills was also observing the desorption of impurities initially present in the target rather than, as he suggested, gases adsorbed during the discharge.

ACKNOWLEDGMENT

The authors would like to thank Professor Craggs of the University of Liverpool for the continuous interest he has taken in this work.

REFERENCES

BILLS, D. G., 1957, *Phys. Rev.*, **107**, 994.
BROWN, E., and LECK, J. H., 1955, *Brit. J. Appl. Phys.*, **6**, 161.
RICHARDSON, O. W., 1913, *Proc. Roy. Soc.*, **89**, 507.

Gold–Manganese Alloys; Some Preliminary Studies by Neutron Diffraction

BY G. E. BACON† AND R. STREET‡
† Atomic Energy Research Establishment, Harwell
‡ Department of Physics, University of Sheffield

MS. received 23rd *May* 1958 *and in final form* 10*th June* 1958

SEVERAL papers have appeared in the literature during the past few years concerning the magnetic properties of gold–manganese alloys. For example Meyer and Taglang (1956) showed that the alloy Au_2Mn, which is antiferromagnetic in zero and weak magnetic fields, becomes ferromagnetic when a magnetic field above a certain threshold value is applied. The saturation magnetization corresponds to a moment of $3{\cdot}49\,\mu_B$ per manganese atom. Meyer (1956) has described a ferromagnetic form of $MnAu_4$ bearing a magnetic moment of $4{\cdot}15\,\mu_B$ per manganese atom, suggesting that the manganese is in an ionic form. Giansoldati (1955) has shown that the composition AuMn has a peaked magnetic susceptibility curve characteristic of an antiferromagnetic with a Néel temperature of about 230°c.

We have been using neutron diffraction techniques to study the gold–manganese system, not only to elucidate further the magnetic properties deduced from the researches quoted above but also as a development of our own earlier study (Bacon *et al.* 1957) of the copper–manganese system. The present note gives a preliminary account of our results. At the manganese-rich end of the Au–Mn system there is at least a qualitative similarity to Cu–Mn and the diffraction pattern suggests that the same face-centred antiferromagnetic structure exists. However, the shape of the (magnetic alignment, temperature) curve deduced experimentally seems to be more close to a true Brillouin curve, without the rapid disordering as the Néel temperature is approached which was observed for the copper alloys.

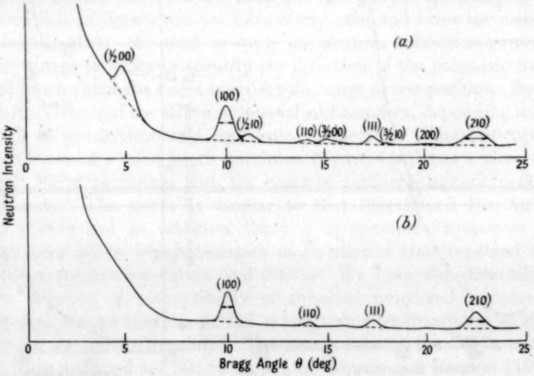

Figure 1. Neutron diffraction pattern of polycrystalline AuMn, (*a*) at room temperature showing, in particular, the ($\frac{1}{2}$, 0, 0) magnetic reflection; (*b*) at 260°c in the paramagnetic region.

A detailed study is being carried out in the neighbourhood of the composition AuMn. The crystal structure in this region is tetragonal with c/a only slightly different from unity. The structure seems to be completely ordered under all conditions of heat treatment, with the manganese and gold atoms occupying the corners and body centres, respectively, of the unit cell. The unit cell may therefore be regarded as effectively simple cubic, rather than body-centred. We have studied the neutron diffraction pattern of such alloys, in the form of solid polycrystalline blocks, over a range of a few atomic per cent on each side of the 50:50 composition. The most interesting characteristic of the pattern is the appearance of the intense extra line which is indexed as ($\frac{1}{2}$, 0, 0) in figure 1 (*a*) and which does not appear in X-ray diffraction patterns. There are also less

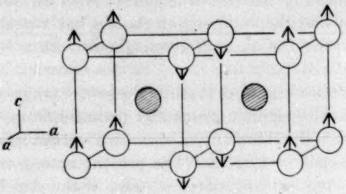

Figure 2. The magnetic structure of AuMn at room temperature. The plain circles represent manganese atoms; the shaded ones gold. The arrows represent the directions of the magnetic spins.

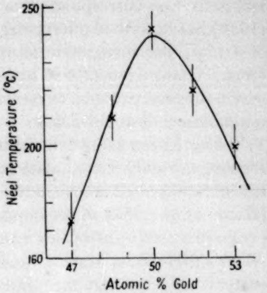

Figure 3. Variation of Néel temperature with atomic percentage of gold.

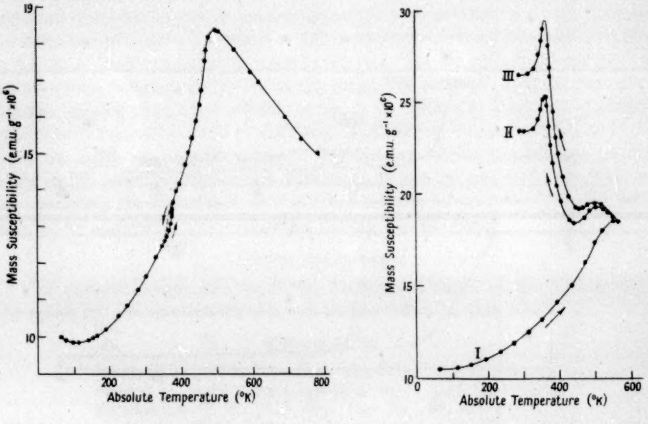

(*a*) (*b*)

Figure 4. Temperature variation of magnetic susceptibility of alloys containing 48·5 atomic % of gold. (*a*) For a block specimen. In the hysteresis region near 365°K the direction of temperature change is indicated by the arrows. (*b*) For a powdered specimen: curves I, II and III were obtained as described in the text.

obvious lines of weaker intensity which correspond to the reflections $(\frac{1}{2}, 1, 0)$ and $(\frac{3}{2}, 0, 0)$. The appearance of these lines, which are deduced to be magnetic in origin, is readily explained by assuming that the magnetic structure of the alloy is that shown in figure 2. The arrangement is a simple packing of ferromagnetic sheets, for which the magnetic moments lie in the plane of the sheets, arranged with the magnetic spins directed alternately upwards and downwards. From the intensities of the magnetic lines (which are mutually consistent) it is estimated that the magnetic moment on the manganese atoms is about $3{\cdot}5\,\mu_B$, on the assumption that there is no moment on the gold atoms. The diffraction pattern shown in figure 1 (*b*) was obtained at 260°C; here the magnetic order has disappeared and the magnetic lines, mentioned above, are no longer present. It may also be noted that the widths of the (100), (210) nuclear lines are reduced, because the symmetry has changed from tetragonal to cubic.

We have determined the Néel temperature for the antiferromagnetic→paramagnetic transition for these alloys by observing the temperature dependence of the magnetic reflections in the neutron diffraction pattern. The results are shown in figure 3 from which it is seen that the Néel temperature reaches a maximum at the composition AuMn. There is no significant difference between the Néel temperatures of slow-cooled and quenched specimens. X-ray examination of the same samples has shown that there is a transition from tetragonal to cubic symmetry on heating through the Néel temperature. For alloys containing 47 and 50 atomic per cent of gold the ratio of c/a is about 1·04 at room temperature: with 53% of gold the ratio is 0·95. There does not appear to be any alloy composition which gives cubic symmetry at room temperature and this is consistent with the essentially anisotropic magnetic structure of figure 2.

Although we believe that the above description of these alloys is largely correct there are a number of details not yet fully interpreted and some inconsistencies to be examined further. We wish to study the neutron diffraction pattern with improved resolution in order to identify the direction of the magnetic moments unequivocally with either the c or a axes over the range of composition. Secondly, the magnetic behaviour of the alloys is unusual and complex, depending markedly on their state of subdivision and mechanical treatment. The (susceptibility, temperature) curve of a solid block specimen (figure 4 (*a*)) has a characteristic peak at about 500°K consistent with the onset of antiferromagnetic ordering at this temperature. The curve is similar to that determined for AuMn by Giansoldati (1955) but in addition there is temperature hysteresis of the susceptibility near 365°K which becomes more marked after repeated thermal cycling between room temperature and 800°K. We have also determined the temperature variation of susceptibility of annealed powdered samples. The curves have pronounced maxima at 365°K and a smaller maximum at the Néel temperature of the particular alloy. The occurrence of the 365°K maximum has already been reported for 50:50 AuMn by Morris and Preston (1956) but the mass susceptibilities which they give are approximately eight times greater than ours. The marked influence of cold working is shown in figure 4 (*b*). The lower curve I shows the results obtained using a powdered specimen which had not been annealed after crushing. During the measurements the temperature was raised to slightly higher than the Néel temperature and observations were made during cooling (curve II). The development of a maximum at 365°K is obvious. The temperature of the specimen was then maintained at about the Néel temperature for five hours and the results plotted on curve III were obtained during cooling. Measurements made during subsequent heating and cooling cycles differed very little from those shown on curve III.

In spite of the marked differences between the curves in figures 4 (*a*) and 4 (*b*) we have not been able to confirm by neutron or X-ray diffraction techniques the apparent differences between block and powder specimens of AuMn alloys. It is evident that further detailed examination of these materials concurrently by different techniques is essential.

REFERENCES

BACON, G. E., DUNMUR, I. W., SMITH, J. H., and STREET, R., 1957, *Proc. Roy. Soc.* A, **241,** 223.

GIANSOLDATI, A., 1955, *J. Phys. Radium,* **16,** 342.

MEYER, A. J. P., 1956, *C.R. Acad. Sci., Paris,* **242,** 2315.

MEYER, A. J. P., and TAGLANG, P., 1956, *J. Phys. Radium,* **17,** 457.

MORRIS, D. P., and PRESTON, R. P., 1956, *Proc. Phys. Soc.* B, **69,** 849.

REVIEWS OF BOOKS

Theorie schallnaher Strömungen (Theory of Transonic Flow), by K. G. GUDERLEY. Pp. xv + 376. (Berlin, Göttingen, Heidelburg: Springer-Verlag, 1957.) DM. 42.

This book provides impressive testimony to the development and expansion of the subject of high speed flow of gases; the whole volume is concerned with the flow of an inviscid perfect gas at speeds in the neighbourhood of the sonic speed. This may look like extreme specialization, but for those interested in fluid mechanics it reflects only the fact that transonic flow is a many-sided problem, full of subtleties arising from the near equality of the velocity of the fluid and the velocity with which small pressure changes are propagated. Dr. Guderley is known for his notable contributions to the study of transonic flow, and he has now provided a connected and complete account of the whole subject. The emphasis is on the theoretical side, as might have been expected with this very mathematical subject, but the mathematics is well organized and is not allowed to get out of hand. So far as I can tell, with an imperfect command of the language and the subject, the material is well chosen and clearly described.

G. K. BATCHELOR.

An Introduction to Chemical Thermodynamics, by E. F. CALDIN. Pp. xiv + 424. (Oxford: University Press, 1958.) 50*s*.

This book is exactly described by its title and is directed mainly to undergraduate students of physical chemistry. Physicists will find in the second half of the book a very clear and readable account of the third law of thermodynamics, chemical equilibria and solutions. In giving this the author has achieved the difficult task of combining a sound theoretical attack with plenty of experimental results and adequate references to recent literature. In contrast to this agreeable and instructive material, the introductory part of the book is dangerously bad. The chemical potential is introduced (p. 29) by means of the equation $dE = đq - đw + \mu\, dn$ applied to *open* systems—for which $đq$ and $đw$ are not defined; on p. 30 the author states a convention for positive work which contradicts his algebra and—perhaps because of this—his table of elementary work expressions (p. 31) has incorrect signs; finally, his statement of the second law (p. 131) is wrong, or, at best, incomplete. The statement in question is: " The direction of spontaneous change in an inanimate system is such that the system can be made to do work on its surroundings." Ignore the word ' inanimate ' (which has unpleasant, vitalistic overtones) and agree to interpret ' spontaneous change ' as meaning one which takes place in an isolated system (a point not made clear by the author). It is still necessary to add the phrase " with the help of heat drawn from a given external reservoir ", or something equivalent, in order to get a meaningful and true statement of the second law. These serious blemishes seem to make this book, in spite of its considerable merits, unsuitable as a teaching manual.

R. O. DAVIES.

Programming for an Automatic Digital Computer, by K. H. V. Booth. Pp. vii + 238. (London: Butterworths Scientific Publications, 1958.) 42*s*.

It is necessary to indicate the limitations as well as the achievements of this volume by Dr. Kathleen Booth. First, it is an exposition of programming for an actual computer, the APEXC at Birkbeck College, using a 1 + 1 address system of instructions with only 15 basic function codes (including however a slightly unusual facility known as ' vector ' recording). The programmes described in detail are partly elementary in purpose, e.g. division, square root, simple matrix processes, and partly specialized, e.g. routines arising in problems of mechanical translation, which forms the subject of a companion volume to this.

It might appear that only those directly interested in the above machine would benefit, but though this is partially true, the author also has chapters describing the use of interpretive routines and pseudo-codes (with applications to floating-point arithmetic), and a short section on methods of programme checking. There is also a welcome insistence on three levels of programming, represented by a flow diagram, a schematic programme using a form of symbolic addresses, and a detailed programme using real addresses. These features, and the methods used, may well interest a much wider class of reader, and in addition there are the linguistic problems which to many are likely to be entirely novel.

R. A. BUCKINGHAM.

Electron Impact Phenomena and the Properties of Gaseous Ions, by F. H. Field and J. L. Franklin. Pp. ix + 348. (New York: Academic Press; London: Academic Books, 1957.) $ 8.50.

This is the first volume of a new series of monographs and textbooks on pure and applied physics. It is excellently produced and authoritatively written. (The reviewer noticed only two printing errors on pages 167 and 232). The authors who are in the refining research and development division of the Houston Oil and Refining Company, Texas, have been actively engaged in research in the field and have here produced a very comprehensive and well documented monograph on an extensive but clearly limited area of research.

To be comprehensive in a field so vast as that implied by the title, especially by the short title—' Electron Impact Phenomena '—would, of course, require several volumes, and it would not have been surprising if the remainder of the title had been given as an alternative ' *or* The Properties of Gaseous Ions '. As it is, however, even this title would have been far too wide, for the book turns out to be concerned almost entirely with the mass spectrometry of organic compounds, in spite of the remark in the preface " we have tabulated and, where possible, interpreted all available energetic data pertaining to electron impact phenomena ". The boundaries of physics with mathematics, chemistry and biology, are rightly vague and the term is evidently interpreted broadly in this series of monographs (*Irreducible Tensorial Sets* is the next volume) but *Electron Impact Phenomena* is in reality a book for the physical chemist. However, when the chemist or physicist has recovered from his initial pleasure or disappointment at the misleading title, he will find he has in his hands a very careful and critical work. There are over 500 references to original papers and in many cases the results are presented with the conclusions both of the authors of the papers and of the authors of the book, the reasons for these conclusions being carefully weighed and clearly given.

The authors are primarily concerned with energetics and although the initial measurements always concern ions the energetics of non-ionic reactions are frequently elucidated. The seventy-eight page appendix is devoted solely to ions, their heats of formation being given in kcal mol^{-1} (this unit is used almost to the exclusion of electron volts in the text) and the appearance or ionization potential in electron volts. The chapters on Apparatus and Methods and on Theory are adequate in view of the highly specialized nature of the work, though both could have benefited by more diagrams.

Amongst the methods of studying electron impact phenomena which are not considered are the use of crossed beams, of swarms and of electric discharges, but in view of the relatively small contribution these methods have so far made in the limited field under consideration, this omission is not serious. The indexes of References, Authors and Subjects are good and the value of this volume as a work of reference for the physical chemist and mass analyst will find it a useful place in many a library. R. L. F. BOYD.

Pressure Measurement in Vacuum Systems, by J. H. LECK. Pp. viii + 132. (London : Chapman & Hall for the Institute of Physics, 1957.) 30*s*.

This book is intended to give a detailed account of the measurement of pressure in vacuum systems. In fact it achieves the slightly different objective of giving a detailed account of the various types of gauge employed for this purpose.

The first four chapters cover respectively mechanical manometers, thermal conductivity types, ionization gauges and Knudsen type gauges. These chapters give a detailed account of present knowledge of the various gauges ; the large amount of work in which Mr. Leck must have been involved in such a thorough coverage of the relevant literature would be very evident even without the excellent bibliography which is provided. Some omissions, such as that of the mechanical manometer of Opstelten *et al.*, are to be expected in a book of this size, but the section on ionization gauges for use at very low pressures could well have referred to the work of Metson, particularly as the suppressor principle used by him is useful in other applications.

Chapter 5 gives as complete an account of surface reaction techniques for low pressure measurement as could be expected in the compass of six pages. Again a useful bibliography is provided.

The final chapter deals with gauge calibration, and deals with it inadequately. The important effects of ' beaming ' or incomplete diffusion of admitted gas, and the directional effects of different gauge connections, first reported by Dayton, are not mentioned. The fallacy that adequate trapping of mercury vapour is possible with a solid carbon dioxide cooled trap is also perpetuated. It is to be hoped that in future editions the chapter will be expanded to the extent required by the importance of its subject. The opportunity might well be taken to add some discussion of the choice and positioning of gauges in typical laboratory and industrial systems.

Such additions would add to the already considerable usefulness of the book and provide more justification for its place in the *Physics in Industry* series, and for its price. The latter, for a book of this size and specialization, may well deter the student, to whom the book in its present form could be more useful than to the industrial physicist. J. POLLARD.

Servomechanismes, Théorie et Technologie, by M. BONAMY. Pp. 284. (Paris : Masson, 1957.) 4200 *fr*.

In various countries engineering literature tends to have its special style and flavour. The many books now appearing in divers tongues on the Theory of Control Systems often cover similar ground and present similar facts, but with forms of presentation and variations in detail that make them of interest outside their countries of origin. This could be said of Professor Bonamy's book, in French. It is limited to a presentation of Control Theory in 170 pages, followed by 100 pages of descriptive notes on a wide range of transducer and circuit elements. Nevertheless, it reflects the French leaning towards fully logical analysis and has the distinction of apt and occasionally unusual invocation of the mathematics of circuit theory.

Thus as a book for instructing engineers in the possibilities of control systems it would be well suited to those who, like its author, are already well versed in circuit analysis and operational methods. An excellent but rather compressed exposition is given of the application of these methods to general feedback systems, in the course of which the relationships usually associated with the names of Carson, Mellin, Laplace, Fourier and Heaviside all appear, and in which the relationship between them is illuminated.

Just because of this commendable combination of logic and brevity the book would scarcely be suitable for readers not so prepared. The approach is mathematical and, as in most books of this kind, the author tends unduly to presume that the various parameters such as inertias and time constants are merely ' given ', whereas the engineer's job is often to contrive constructions in which they are absent or different.

Nevertheless, this is an excellent book of its kind and is a noteworthy addition to the literature on control systems in the French language. A. TUSTIN.

Solid State Physics, Vol. 4, edited by F. SEITZ and D. TURNBULL. Pp. xiv + 540. (London : Academic Books, 1957.) $12.00.

The high standard of review articles in earlier volumes of this series is maintained in the present one. A comprehensive article on ' Ferroelectrics and Antiferroelectrics ' by W. Kanzig takes up the first third of the book. Experimental properties of the large number of compounds now known to be ferro- or antiferro-electric are summarized, including a discussion of domain structures. The various dielectric, piezoelectric and thermal properties are correlated by thermodynamic theories based on the fact that ferroelectrics are generally slightly distorted nonpolar structures. These thermodynamic concepts have been successfully extended in a phenomenological way to antiferroelectrics. One is struck by how little is understood from basic molecular theory. Most success has been obtained with Slater's model for KH_2PO_4, since verified by neutron diffraction experiments, which involves an ordering of hydrogens about the PO_4 groups.

F. J. Blatt's article on 'Theory of Mobility of Electrons in Solids' is more comprehensive than the title indicates because it includes a review of solutions of the Boltzmann equation for the usual transport phenomena in addition to discussions of scattering mechanisms in metals and semiconductors. Much of the recent theoretical and experimental work on germanium and silicon, including solutions for non-spherical energy surfaces, ionized impurity scattering, phonon drag and the 'hot electron' problem is covered. There is no discussion of motion of electrons in ionic crystals and the 'polaron' problem.

The article of T. O. Woodruff on 'The Orthogonalized Plane-Wave Method' should be of interest to the general reader who would like to see how calculations of band structure are actually carried out by this method, as well as to one starting work in this area. There is a very clear, straightforward discussion of procedures used, followed by an application to the band structure of silicon. A 'Bibliography of Atomic Wave Functions' by R. S. Knox lists the many atoms and ions for which Hartree or Hartree–Fock wave functions are available.

The final article by W. G. Pfann discusses zone melting techniques which he developed for purification and growth of crystals. These methods have proved to be extremely valuable for the preparation of the near perfect crystals required for the study and control of what used to be called 'structure sensitive' properties.

From the long list of 'Articles Planned for Future Volumes' we are assured of many more volumes of this useful and important series. J. BARDEEN.

Handbuch der Physik, Vol. V, Part I : *Principles of Quantum Mechanics*, I, edited by S. FLÜGGE. Pp. iv + 376. (Berlin : Springer-Verlag, 1958.) DM90.

This volume contains two excellent contributions (both in German). Professor Pauli's article on quantum theory, first published in the original Handbuch in 1933, has been reprinted except for a few minor changes and corrections. It continues to be one of the most enlightening accounts of this subject.

The last 28 pages of Pauli's original article have been replaced by a 200-page article by Dr. Källén on quantum electrodynamics, virtually a new subject since the first Handbuch appeared. Dr. Källén gives a very readable systematic account, the emphasis being on the abstract side as one might expect from this author. However, the interaction picture is eventually introduced (although perturbation theory is first developed in the Heisenberg picture) and an almost comprehensive selection of 'elementary' problems is discussed in detail. There follows a very lucid perturbation-theoretic treatment of renormalization and radiative corrections including applications to the electron's anomalous magnetic moment, electron scattering in an external field, hyperfine structure, the Lamb shift, etc. A few points, usually left obscure in the literature, would have benefited from further elucidation. For example, in the analysis of the Lamb shift on page 319 the omission of longitudinal and scalar photons is justified by the far from obvious statement that the electrostatic self-energy of a free and a bound electron are the same. In the same calculation, the reason given for neglecting retardation (page 320, following equation (37.25)) seems misleading (cf. Bethe and Salpeter, *Encyclopedia of Physics*, vol. XXXV, section 19 (γ)). Dr. Källén concludes with a discussion of general renormalization theory. It seems unfortunate that he only mentions but does not discuss the analysis of the Lee model, to which he has himself made important contributions and which at any rate suggests the sort of inconsistencies one might meet in quantum electrodynamics. But these are minor criticisms of an otherwise excellent article. F. Mandl.

Advances in Nuclear Engineering, Vols. I and II, edited by J. R. Dunning and B. R. Prentice. (Proceedings of the Second Nuclear Engineering and Science Congress held at Philadelphia, 1957.) Pp. vii + 523 and vii + 581. (London: Pergamon Press, 1957.) £7 7*s.* per volume.

Volume I.

This part of the proceedings contains the papers on manufacture, production, recovery, processing, plant containment concepts and design, plant components, waste disposal, protection and safety measures and radiation processing. The papers dealing with the chemistry of fuel cycling are in general rather short and somewhat lacking in detail, but nevertheless they are valuable in their demonstration of how processing can be complicated by the requirements of reactor design. A more detailed and useful paper by Benedict and Pigford deals with the calculation of single region thermal reactor performance using programmed refuelling and including both ^{238}U and ^{232}Th fertile materials. Other papers on economics deal with cost estimates for processing irradiated natural uranium and fabrication of fuel elements form the plutonium and depleted uranium so obtained and also the economics of ceramic fuel elements.

In the section dealing with plant containment a most informative paper by Heineman and Fromm deals with the design of containment shell for the E.B.W.R. reactor at the Argonne National Laboratory. After some opening remarks on the philosophy of containment of reactors there follows a detailed description of the containing vessel, the design criteria on which it was based, and the methods of construction and testing which were developed specially for it. Some other papers on containment deal generally with the type of incidents which must be considered and the determination of their effects on the gas-tight containing vessel.

The section on plant components deals with the design of electromagnetic and mechanical pumps, the fabrication of pressure ducts, the problems of designing adequate steel valves for use in reactor plants and finally the performance of pressurisers for pressurised water systems. There are eight most useful papers devoted to these topics.

This volume of the proceedings contains a total of sixty two papers and mention has been made only of what are considered to be the most informative ones.

Volume II.

The papers in this volume perhaps cover an even wider field than those in Volume I. Subjects dealt with are reactor core design, heat transfer, operation and instrumentation of reactors, maintenance of reactors, metallurgy, educational uses of reactors and standardization in the nuclear field.

An interesting paper by Hammitt and Ohlgren deals with the possible use of the gas turbine cycle with various types of nuclear reactor and draws the conclusions that steam cycle efficiences are likely to be slightly higher up to 1500°F coolant outlet temperatures, that the steam plant will be rather less costly up to these temperatures and that the weights of the two types of plant are likely to be roughly comparable.

Papers dealing with specific reactor designs are given on the Engineering Test Reactor, the E.B.R. II control system and two low powered reactors, the Argonaut (10 kw) and the so called Laboratory Reactor constructed by Atomics International. These descriptions are considerably detailed and in the latter two cases proposals for their use in the education field are set out.

In the heat transfer section a very interesting review of organic coolants is given by Shinarzaki and Anderson. Such coolants are discussed from the point of view of stability, corrosion and obtainable heat transfer rates, with predictions of critical heat flux. The paper dealing with gas cooling, however, is only very general and presents very little new information. The final paper in this section deals with the heat transfer correlations with liquid metal cooling, particularly in non-circular ducts. The information is new and valuable.

Two papers on transient thermodynamic effects are of interest. One deals generally with the calculation of transient temperatures in reactors under variable load, while the second paper develops a method for the calculation of transient thermal stresses in cylindrical fuel elements.

The volume contains some sixty papers, most of which would be of interest to reactor designers. A few of the papers are rather specialized but the volume represents a good summary of the modern problems in reactor construction and operation. D. V. WORDSWORTH.

A History of Mathematics from Antiquity to the Beginning of the Nineteenth Century, by J. F. Scott. Pp. x + 266. (London : Taylor & Francis, 1958.) 63*s*.

This book will be useful to general readers and as a text-book for students, as well as to scholars who are already familiar with the subject. It gives the main lines of development of mathematical knowledge from the earliest times, and goes into some, but not too much, detail. Dr. Scott, who is well versed in the history, has quoted extensively from the original works of mathematicians in bygone days, illustrated by a frontispiece and six plates which are aptly chosen and add vividness and interest to the book : a facsimile of a fragment of the Rhind Papyrus represents the earliest period, prior to Greek mathematics, which is carefully treated.

Physicists will find that the developments in applied mathematics are clearly set out, from ancient times, through that of Archimedes, to the mechanics of the sixteenth century when interest was revived. Significant advances made by Stevin, Galileo, Descartes, Huygens and others are stressed, and help the reader to appreciate what Newton achieved.

There are useful appendices giving brief biographical notes upon persons mentioned in the story, and brief notes on mathematical topics and terminology, followed by a bibliography. H. W. TURNBULL.

Physique Electronique des Gaz et des Solides, by M. BAYET. Pp. 246. (Paris: Masson, 1958.) Fr. 4900.

The subject matter of this book represents the content of an advanced course of lectures for a certificate in electronics at Toulouse University, and covers the essentials of the physics of transport phenomena in gases and metals. In eight chapters it deals at a somewhat elementary level with statistical physics, the kinetic theory of transport processes in gases, the non-degenerate ' Lorentz gas ', electromagnetic properties of plasmas, basic phenomena in ionized gases, the principles of the electrical discharge, and electrons in metals, solids and semiconductors. At every stage of the account, the reader is referred to various specialist textbooks whenever possible, for fuller or more rigorous treatment.

It is clear that within the scope of 250 pages some of the subjects in this very wide field can only be treated somewhat cursorily, and this is particularly the case with the accounts of ionization phenomena and electrical discharges. In dealing with solids, crystalline structure, mechanical properties and magnetic phenomena are omitted. On the other hand, the subject here presents a certain unity, as it is sometimes forgotten that the investigation of the electrical properties of gases is generally carried out when the gas is itself in contact with metals.

F. Ll. J.

Mechanical Resolution of Linguistic Problems, by A. D. BOOTH, L. BRANDWOOD and J. P. CLEAVE. Pp. vii + 306. (London: Butterworths Scientific Publications, 1958.) 50*s*.

One of the aims of linguistic analysis is to describe, unambiguously, various object-languages in the formal linguists' ' meta-language '. If this can be done, then the linguist has, simultaneously, specified a (conceptual) machine for doing the same thing. But human languages are ' open systems ' not obeying rigid, unbreakable rules, and so we must expect to find that translating-machines can deal effectively only with scientific texts and the like, possessing the formulated rules of ' language-systems '. Such translation is more aptly termed ' syntactic transcription ', since only syntax is involved, but no semantic associations.

The practical work of Booth and his colleagues has shown that pure syntactic transcription, aided by human pre- and post-editors, can lead to remarkable success.

The book opens with some historical notes and proceeds to explain the principles of digital computors, illustrating their use for statistical analysis (e.g. word counts) of texts and for analysis of grammatical structures. The results of such analysis have been used for identifying unknown authors of classical texts. The techniques of coding dictionaries for rapid machine searching are described and the whole scheme for transcribing into Braille explained. Chapters are included which concern analysis and machine translation of texts in French (14 pages), Russian (4 pages) and German (160 pages—half the book; a silent comment upon the syntax of that remarkable language !).

COLIN CHERRY.

The Cosmic Radiation, by J. E. HOOPER and M. SCHARFF. Methuen Monograph. Pp. 172. (London: Methuen, 1958.) 12*s*. 6*d*.

Any account of the cosmic radiation in a book of this size must be selective and so is likely to reflect the interests and activities of the authors. Its success must stem from the combination of this proper emphasis with a sufficiently sympathetic review of the remainder of the subject. By these standards, the present authors have certainly succeeded, and this book must rank as the most effective short survey at present available.

The development of secondary cosmic radiation, in particular as this falls within the scope of the emulsion technique, receives the most detailed attention and, notably, the early electromagnetic interactions are treated in addition to those of nuclei. In rather less detail, but nevertheless adequately, other chapters cover the primary radiation, the strange particles, the atmospheric distribution and the sea level and underground observations including time variations. A chapter on experimental techniques is perhaps the least successful. These are not as unusual as they once were, and this chapter falls between the levels of general information and useful instruction.

This is altogether a most welcome book and a worthy addition to the 'Monograph' series. JOHN G. WILSON.

Electrical Discharges in Gases, by F. M. PENNING. Pp. viii + 78. (London: Cleaver-Hume Press, 1957.) 15*s*.

The name of the author of this book, Dr. Frans Michel Penning, is well-known and distinguished in the subject of electrical discharges. Dr. Penning commenced his investigations in this field in 1924 in the Research Laboratory of the Philips' Company at Eindhoven. His death in 1953 was a great loss to physics. In 1955 his book, *Electrische gasontladingen*, was published, and with a view to making it available to a wider public, the publishers have issued editions in English, French and German in addition to the original Dutch edition, as it was felt that the book could profitably be used by engineers concerned in this field as a basis for further study. The English edition was translated by A. F. Monypenny.

This book consists of ten short chapters (some only 2–3 pages long), a short bibliography, and a list of about 50 papers referred to in the text. The following are the chapter headings: Gas discharges, natural and man-made; The conduction of electricity in metals and gases; Non self-sustaining discharges; The movement of electron and ions through a gas; The non self-sustaining arc discharge; The Townsend discharge and breakdown; Sparks and lightning; The glow discharge; The self-sustaining arc discharge; The positive column. It must be clear from the size of the book that some of these subjects can only be barely touched upon. For example, sparks and lightning are dealt with in less than five pages devoted mainly to a qualitative account of the propagation of an avalanche, both in the spark gap and in the lightning flash. The level at which the material is treated varies considerably from chapter to chapter. The accounts of the arc discharge (Chapters V and IX), for instance, are treated at a standard approximating to that of the 'A' level of the G.C.E. school examination, while other chapters are even more elementary. There is no account nor assessment of modern post-war developments in the subject; this applies especially to the treatment of sparks and the development of breakdown with time. On the other hand, the account of the positive column (Chapter X) is an excellent survey which is much nearer university degree level.

Thus it is very difficult to see for whom this book is really meant as the scope and treatment are so variable, and it is a pity that more indication of the actual standard of treatment is not given on the dustcover or inside. If its purpose is to interest those engineers having little physical background in the field of the conduction of electricity in gases and the dynamical theory of transport phenomena, then it can be regarded as serving its purpose. F.Ll.J.

The Exploration of Space by Radio, by R. Hanbury Brown and A. C. B. Lovell. Pp. xii + 207. (London: Chapman and Hall, 1957.) 35*s*.

This book is a short account of all the aspects of radio and radar astronomy, by two of the most eminent practitioners of the art. Following a summary account of the basic ideas of present-day astronomy and of the relevant radio techniques, the authors explain the application of the radio techniques to the study of galactic and extragalactic radio sources, interstellar hydrogen, the scintillation of radio sources, the solar corona, meteors, the aurora borealis and the moon and planets.

The book is attractively produced; the information given is up to date (even the word ' maser ' is mentioned), and the errors are few—this reviewer noticed only two, an amusing sideways slip of the pen in Figure 33 and a discrepancy between Figure 83 and its caption. The emphasis is on the astronomical results, but enough is written about the techniques to make the nature of the observations, and their various limitations, quite clear to the reader.

This book can be warmly recommended to all physicists who wish to know something about the subject (and they will find it easy reading); on the other hand, only elementary mathematics is used, and used sparingly, so that the book should also appeal to a much wider audience. P. A. G. SCHEUER.

Combination of Observations, by W. M. Smart. Pp. xiv + 253. (Cambridge: University Press, 1958.) 35*s*.

One of the basic concepts in statistical theory is that of the probability distribution or population underlying the observations to be analysed. The appropriate distribution is commonly one of a family, specified by one or more numerical parameters, and one of the principal problems in statistical inference is to estimate these unknown constants from the data. It is fundamental that an estimate of a parameter is logically distinct from the parameter itself: the one is an observed value of a random variable, and is, therefore, subject to fluctuations in repetitions of the observing process, while the other is a fixed (even if unknown) constant.

In an exposition of the analysis of observations, therefore, it would be natural to expect an account of some at least of the more useful distributions, with a discussion of their principal properties and the circumstances in which it is appropriate to use one rather than another. Secondly, one looks for instruction in methods of choosing suitable combinations of observations to be used as estimates of the parameters of the relevant distribution, and an account of their properties: in particular, one needs some method of specifying the reliability of the estimated value. Related to this is the desirability of providing significance tests, which are procedures for deciding whether observed discrepancies are small enough to be attributable to chance fluctuations or whether they are so improbably large as to cast doubt on the underlying assumptions. The book under review cannot be said to satisfy these requirements.

The catalogue of available distributions is seriously deficient. No discrete distributions are mentioned and the only continuous ones are the Normal and the Pearson family. The tabulation of the Normal integral in the ' erf ' form and the retention of the *probable error* (" favoured in English-speaking countries ") have perhaps a certain old-world charm but little else to recommend them.

In the greater part of the book, there is no clear distinction between population and sample and, therefore, there is a confusion of population parameters and the sample statistics used to estimate them, the idea of standard error being particularly ambiguous. The concept of significance tests is almost entirely lacking: in one typical case the assessment of agreement between two sets of figures is an entirely subjective judgment that " agreement is remarkably close on the whole". This apparent mistrust of objective probabilistic assessment is perhaps related to the astonishing idea that " frequency is not strictly related to probability when the number of measures is small". The one occasion where ' significance ' in the technical sense is invoked is where a computed correlation coefficient r "may be regarded as *significant* if $|r|$ is not less than 0·5, and as highly significant if $|r|$ is 0·8". In fact, of course, a statement of the alleged significance of a correlation coefficient which does not specify the number of observations involved is meaningless.

As always with this Press, the standard of typography is very high.

E. H. LLOYD.

The Elements of Classical Thermodynamics, by A. B. PIPPARD. Pp. vii + 165. (Cambridge: University Press, 1957.) 15*s*.

Although there is little that is essentially new in this book it has a freshness, brevity and elegance which will delight the physicist who is (or who is prepared to become) enthusiastic about thermodynamics. It concentrates on fundamentals and is designed for final-year undergraduate students who nowadays have little time to spare for a second course on the subject. Special features which this reviewer found appealing include a modest and yet rigorous approach to the work of magnetization, emphasizing the way in which the differential element appearing (e.g. HdI) depends on a (conventional) choice of surroundings; a justification for neglecting ' mechanical work ' in many magnetic arguments; a debunking of the often-repeated shibboleth which says that the second law is true only ' on the average '; some nice modern instances such as the phase diagram of ^{3}He and an application of Kirchhoff's law of radiation to radio observations of the sun. Students should be warned that there is a fallacious ' proof ' of the existence of adiabatic surfaces on p. 38. Suitably patched up, the line of reasoning here does lead from the Kelvin–Planck statement of the second law to the basic axiom of Carathéodory's theory—and this is of course worth doing since the axiom is not otherwise very ' intuitive '. The author does not prove Carathéodory's theorem, although he gives a plausible geometrical argument in favour of it.

The Cambridge University Press are to be congratulated on bringing out a paper-covered edition of this book for 15*s*. One had feared that this sort of thing was—at least in physics—being left to the Americans. R. O. DAVIES.

Currents, Fields and Particles, by FRANCIS BITTER. Pp. xiv + 599. (New York: John Wiley; London: Chapman and Hall, 1956.) 68*s*.

This is an unorthodox textbook. The author states in the preface that it is the result of efforts to base the second year of a two-year physics course on atomic physics.

The list of chapter headings is as follows: The Basic Electrical Quantities and their Measurement; Electric Fields; The Electrical Properties of Matter; Applied Electricity; Magnetic Fields; Induced Electromotive Force and Inductance; Electromagnetic Oscillations; The Poynting Vector and Electromagnetic Waves; Optics: Reflection and Refraction; Optics: Interference and Diffraction; The Experimental Basis of Atomic Physics; Wave Mechanics; Atoms and Electrons; Atomic Nuclei and Radiations.

Thus there are eight chapters which by custom would be found in a textbook on electricity, and there are two chapters on optics and four on atomic and nuclear physics, which is a formidable list of contents for a book of 600 pages. The treatment is very lucid. First, the principal concepts are introduced, then they are illustrated by simple applications. Then, and this is the novelty of the book, they are semi-quantitatively explained in terms of atomic concepts. Lastly, almost as an appendix to each chapter, the more tedious calculations and illustrations follow.

The development of the subject matter can be clearly seen in the chapter on the electrical properties of matter. This starts with sections on protons, electrons and the nuclear model of the atom (including the Rutherford scattering law). Next comes a section on excitation, ionization and conduction in gases. Then the conductivity of metals and semi-conductors is discussed, and a section on resistance in series and in parallel is interpolated. The next topic tackled is polarization, and an estimate is made of the dipole moment per unit volume on the basis of the size of the atom and the charge of the nucleus. Now follow the definitions of susceptibility, permittivity and the dielectric coefficient. These are again evaluated in terms of atomic constants and concepts. Then condensers, displacement currents, boundary conditions on dielectric surfaces and the energy in polarized dielectrics are discussed.

The book is very carefully edited, and very adequately illustrated with diagrams. A concise summary is provided at the end of each chapter. The reviewer has found only a few misprints, which are quite trivial.

It is difficult to see the place of this textbook in relation to the usual methods of teaching physics in the universities of this country. The amount of detail in any one chapter is not sufficient for the requirements of an honours degree. As an introduction to the subjects covered the book is too long. In fact it must be quite hard to read, unless one is fairly familiar with the subject matter; otherwise the rate of introduction of new concepts would be prohibitive. Thus the text is not really suited to the requirements of undergraduate students, but it might very well be the teacher's book. It contains a lot of worked-out ideas on correlating various fields of physics which are usually taught as separate entities. The author evidently considers this separation inadvisable and most teachers of physics would agree on this. The book is a courageous and interesting attempt at unification.

A. FOLKIERSKI.

Review of Magneto-Hydrodynamics (*A Symposium*), edited by ROLF K. LANDSHOFF. Pp. viii + 115. (Oxford: University Press, 1957.) 32*s*.

Although, in general, symposia are less satisfactory than monographs, they have some advantages in the rapidly developing field of magneto-hydrodynamics. The relations between physical system and mathematical description, and between experiment and theory, are still obscure enough to make a collection of brief sketches from several viewpoints a useful work.

This book contains twelve papers, some extremely short, and all rather sketchy, which describe both theoretical and experimental aspects of the flow of conducting fluids in magnetic fields. Kantrowitz and Petshek discuss the physical processes dominating the behaviour of conducting media in varying ranges of temperature and density in an attempt to define the applicability of magneto-hydrodynamics. Elsasser and Hoyle, very briefly, consider the consequence of the 'frozen-in field ', while Burgess discusses magneto-hydrodynamic shocks and considers the passage of a weak shock through an inhomogeneous magnetic field. Finally, Rosenbluth indicates the limitations of magneto-hydrodynamics in his analysis of the constricted discharge.

Among the experimental papers three describe the production of very strong shocks by magnetically driving an ionized gas, while one describes the interaction of a shock in ionized gas with a steady magnetic field. One experiment is undoubtedly magneto-hydrodynamics; Colgate's study of the instability of a magnetically driven column of liquid sodium. The final paper describes a projected experimental study of Alfvén waves.

Perhaps it is inevitable that such a work should suffer simultaneously from repetitions and abruptness, but in a field so ill provided with books this one is welcome, although no substitute for a thorough monograph. W. B. THOMPSON.

X-ray Crystal Structure, by DAN MCLACHLAN, JR. Pp. xiii + 416. (New York, Toronto, London : McGraw-Hill, 1957.) £5 16*s*. 6*d*.

This is a general book on the diffraction of X-rays by single crystals. It deals with symmetry and space-group theory; X-rays and their scattering by crystals; Fourier series; the phase problem (that is, the problem of finding the relative phases of the waves scattered by a crystal); computing aids; and examples of crystal-structure determination. Such a book could be valuable for students, but the present one fails because of its extremely uneven standard; apparently those topics that appeal to the author—for example, group theory of symmetry—are treated at great length, while others are dismissed quite cursorily.

There are some sad mistakes in physics. For example, on p. 178, an electromagnetic wave is shown with E and H in phase and on p. 286, a grating of three units is said to give discrete orders of diffraction. Mistakes such as these are particularly deplorable in a book which claims to expound physical principles.

Many of the diagrams are poor, having apparently been drawn with insufficient attention to detail. On p. 17, for example, ellipses are drawn as two circular arcs intersecting in points. Elsewhere, crystal drawings are not always clear and are not correlated with the symmetry representations alongside.

To summarize, the book gives the impression—supported by the ill-chosen title—that it consists of selected lecture notes hastily strung together with inadequate connecting matter. Knowing the author, one can say that it does not do him justice. H. LIPSON.

Advances in Electronics and Electron Physics, Vol. IX, edited by L. MARTON. Pp. x + 347. (London: Academic Books; New York: Academic Press, 1957.) $9.00.

This volume, the ninth of a series, is a departure from the form of the previous volumes, in that it is a devoted to a single main theme. This theme is geophysical and was suggested by the International Geophysical Year. The volume contains seven review articles on different geophysical subjects. The aim is stated to be two-fold; first to acquaint geophysicists with some modern electronic techniques, and secondly to acquaint workers in electronics with interesting problems posed by geophysics.

It is doubtful whether the first aim will be achieved. Most of the reviews are written by geophysicists, and the emphasis is on the physics rather than the techniques. In general, the methods of measurement are described only in brief outline, and sometimes not at all. It is very doubtful whether any geophysicist will find here any new technique of the existence of which he was unaware. The second aim, however, should be achieved, for the various reviews are well presented and written by experts. Workers in electronics should find here much that is interesting and they may be able to suggest new techniques for use in geophycics.

The first review on the aurora borealis, by C. T. Elvey, is a useful survey of the known facts about the aurora obtained by many methods including radio echo observations, spectroscopy, and rocket observations. The second chapter is by L. M. Branscomb on negative ions. Experimental methods are not described, but the main facts about atomic and molecular negative ions are surveyed. The role of negative ions in the upper atmosphere is discussed. There follows a very useful survey of radio methods of observing meteors by J. G. Davies. This includes a discussion of the use of meteors in giving information about atmospheric scale heights and atmospheric winds. Then there is a chapter by D. C. Rose on intensity variations of cosmic rays. The emphasis here is on the relevance of the intensity variations to theories of the origin of cosmic rays. The next review is on radio wave propagation by R. L. Smith-Rose. This is a large subject and only certain aspects are discussed; these are the velocity of radio waves, low frequency ground wave propagation, the absorption and angle of arrival of ionospherically reflected waves, and the back scattering of waves from the ground. Finally, there are chapters on electronics in oceanography by J. B. Hersey, and contributions of electronics to seismology and geomagnetism by B. S. Meltone. The latter includes a brief description of the nuclear precession magnetometer.

The book is very well produced, and each chapter ends with an extensive bibliography. B. H. BRIGGS.

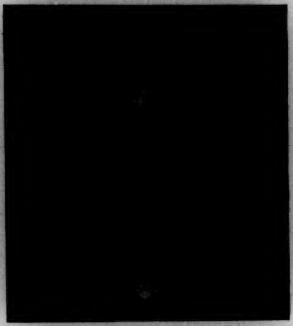

Figure 1. 0·2 Å of lead : faint streaks without maxima of intensity appear.

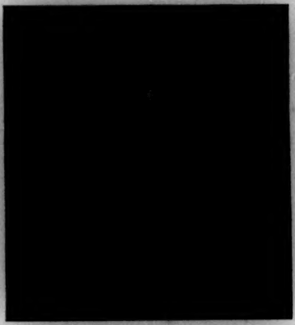

Figure 2. 0·8 Å of lead : the streaks without maxima of intensity become stronger.

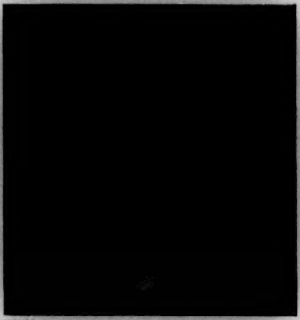

Figure 3. 1·9 Å of lead : maxima of intensity appear on the streaks.

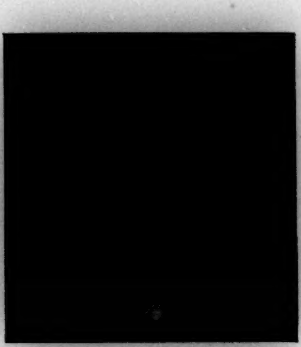

Figure 4. 3·4 Å of lead : the maxima show a dip of intensity in their middle.

Figures 1–4. Deposits of increasing thickness of lead evaporated on to a smooth silver single-crystal substrate, (111) face, $[1\bar{1}0]$ azimuth, angle of incidence of electron beam 2·5°.

Measurement of Polarizations in Stripping Reactions

By B. HIRD, J. A. COOKSON and M. S. BOKHARI
Nuclear Physics Research Laboratory, University of Liverpool

Communicated by H. W. B. Skinner; *MS. received* 13*th May* 1958

Abstract. The polarization of the protons from the reaction $^{12}C(d, p)^{13}C$ at 6·9 MeV bombarding energy, and from the reactions $^{9}Be(d, p)^{10}Be$, $^{10}B(d, p)^{11}B$ and $^{40}Ca(d, p)^{41}Ca$ at 8·9 MeV bombarding energy has been measured at certain angles of emission. The sign of the polarization was found to be positive when $j_n = l_n + \frac{1}{2}$ and negative when $j_n = l_n - \frac{1}{2}$ except for the reaction $^{40}Ca(d, p)^{41}Ca$. The results of the $^{12}C(d, p)^{13}C$ measurements suggest that the polarization does not vary rapidly with bombarding energy.

---

§ 1. INTRODUCTION

In a previous paper (Bokhari, Cookson, Hird and Weesakul 1958) we described a measurement of the angular distribution of the polarization in the ground state group from the $^{12}C(d, p)^{13}C$ reaction using 8·9 MeV deuterons. This was compared with the predictions of Newns and Refai (1958) who considered the effects of relaxing the assumptions of stripping theory by including a hard sphere interaction of the incoming deuterons with the target nucleus, and a complex potential with a spin–orbit term as the interaction of the emitted protons with the final nucleus. The experimental angular distribution was similar in shape to these predictions, particularly in the angle at which the polarization passes through zero. However, the experimental sign of the polarization was opposite to that predicted theoretically.

We have investigated further general properties which the polarization should show if it is produced by these types of interactions:

(*a*) There should be no rapid variation in the polarization with bombarding energy. There is some indication that this occurs at low energies. Hillman (1956) obtained a polarization of $-58 \pm 13\%$ for the $^{12}C(d, p)^{13}C$ ground state group near the stripping peak, using a bombarding energy of 4·05 MeV, whereas at 11·9 MeV (Juveland and Jentschke 1956) and at 8·9 MeV the polarization is in the region of -10% to -20%. If confirmed, this large difference may be due to the presence of some resonance effect at the lower energy, or to a steady variation of the interaction parameters with energy. We have therefore made further measurements on the same reaction at an intermediate energy of 6·9 MeV.

(*b*) The polarization should differ in sign for reactions where $j_n = l_n + \frac{1}{2}$ and where $j_n = l_n - \frac{1}{2}$ for the captured neutron. This, of course, assumes that the deuteron and proton interaction potentials are the same for the two cases. We have measured the polarization of the ground state proton groups of the reactions $^{9}Be(d, p)^{10}Be$ and $^{10}B(d, p)^{11}B$, which have $l_n = 1$ but differ from the $^{12}C(d, p)^{13}C$ reaction in that $j_n = l_n + \frac{1}{2}$, and also $^{40}Ca(d, p)^{41}Ca$ where $l_n = 3$ and j_n is probably 7/2.

The experimental arrangement and the method of calculating the polarization from the track parameters were substantially the same as described in our previous paper.

§ 2. TARGET PREPARATION AND EXPERIMENTAL DETAILS

$^{12}C(d, p)^{13}C$.

The beam energy from the cyclotron was reduced to 6·9 MEV by placing a tantalum foil of thickness 52 mg cm^{-2} in the beam 20 cm from the target. This distance represents a compromise between loss of beam intensity, and uncertainty in the beam direction, due to multiple scattering in the foil. Anti-scattering slits between the foil and the target prevented deuterons from striking the walls and the window of the target chamber. Because of the reduced energy of the emitted protons, it was necessary to use a lower helium pressure of 75 lb in^{-2} in the scattering chamber in order to obtain adequate track lengths in the emulsion.

$^{9}Be(d, p)^{10}Be$.

The target consisted of a foil of 99·8% pure beryllium metal, 0·001 in. thick. Because of the large energy separation of the ground state group and its high Q-value, we were able to use a pressure of 400 lb in^{-2} in the helium chamber, the Mylar entry window being increased to a thickness of 0·015 in. to sustain this pressure.

$^{10}B(d, p)^{11}B$.

The isotope target, consisting of a 2·2 mg cm^{-2} deposit on thick gold, was inclined at about 15° to the deuteron beam direction. A single measurement was made on the protons emitted from the front of the target at an angle of 25° to the deuteron direction.

$^{40}Ca(d, p)^{41}Ca$.

Targets were prepared by hammering flakes of the natural calcium metal until they had a mean thickness of about 10 mg cm^{-2}. The presence of oxidized surface layers on these targets was unimportant since protons from the oxygen had insufficient energy to reach the emulsions. In order to resolve the ground state group we found it necessary to limit the helium pressure to 200 lb in^{-2}. At higher pressures the energy loss of the protons in passing through the scattering volume resulted in a significant loss of resolution in the calculated energy distribution.

The energy of the protons entering the scattering chamber was reduced to about 9·5 MEV in the $^{9}Be(d, p)^{10}Be$, $^{40}Ca(d, p)^{41}Ca$, and $^{10}B(d, p)^{11}B$ reactions, by means of aluminium foils. These foils were placed mid-way between the target and scattering chamber to minimize the uncertainty in proton direction caused by multiple scattering.

§ 3. RESULTS

The energy spectra of the protons before the scattering in helium, were calculated from the lengths and directions of the proton tracks in the emulsions. These are shown in the figure. In each case the protons of energy greater than that indicated by the arrow were selected and regrouped according to dip and angle to the horizontal for the calculation of the polarization. The polarization

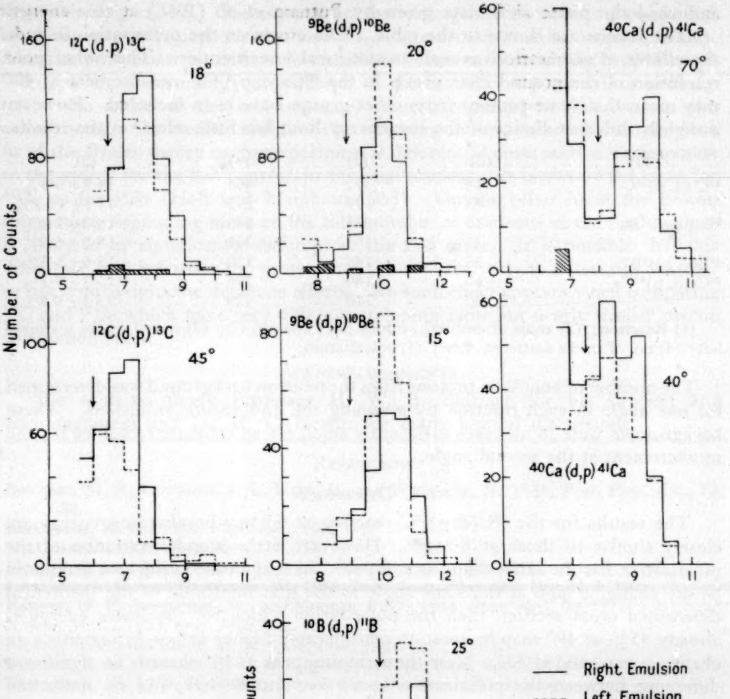

in the proton–helium scattering was obtained from the phase shifts at 7·5 Mev proton energy, as given by Putnam, Brolley and Rosen (1956) and used in these calculations for the $^{12}C(d, p)^{13}C$ measurement at 18°. At 45° the proton energy from this reaction was somewhat lower and values of the phase shifts at 7·0 Mev were obtained by interpolation between the 7·5 Mev data and those at lower energy (Kreger, Jentschke and Kruger 1954). A possible $d_{5/2}$ resonance in the proton–helium scattering between 10 Mev and 17·5 Mev (Brockman 1956) makes a similar interpolation in the phase shifts in the latter energy region unreliable.

We therefore reduced the proton energy in the other reactions to about 9·5 Mev and used the phase shift data given by Putnam *et al.* (1956) at this energy.

The results are shown in the table. The errors on the polarization include the effects of geometrical as well as statistical uncertainties. The rather poor resolution of the ground state group in the ^{40}Ca(d, p)^{41}Ca measurement at 40° may mean that some protons from other groups have been included. However a slightly different choice of the low energy limit has little effect on the results.

(1)	(2)	(3)	(4)	(5)
^{12}C (d, p)^{13}C	18	372	464	$-14{\cdot}8 \pm 6{\cdot}4\%$
	45	199	292	$-43{\cdot}5 \pm 10{\cdot}2\%$
^{9}Be(d, p)^{10}Be	15	235	186	$+18{\cdot}3 \pm 7{\cdot}0\%$
	20	363	321	$+\ 8{\cdot}2 \pm 6{\cdot}0\%$
^{10}B(d, p)^{11}B	25	146	120	$+15{\cdot}6 \pm 8{\cdot}9\%$
^{40}Ca(d, p)^{41}Ca	40	180	226	$-16{\cdot}3 \pm 9{\cdot}3\%$
	70	110	129	$-15{\cdot}1 \pm 9{\cdot}8\%$

(1) Reaction; (2) angle of emitted protons (lab. system) (°); (3) no. of tracks scattered left; (4) no. of tracks scattered right; (5) polarization.

The number of knock-on protons from the neutron background was determined for one angle in each reaction by scanning the underneath emulsions. These backgrounds were in all cases sufficiently small for an estimate to suffice for the measurement at the second angle.

§ 4. Discussion

The results for the ^{12}C(d, p)^{13}C reaction at 6·9 Mev bombarding energy are closely similar to those at 8·9 Mev. However, if the angular variation of the polarization has the same shape as at 8·9 Mev, its magnitude rising to a maximum before changing sign at the same angle as the first minimum of the theoretical differential cross section, then the polarization which for the lower energy is already 43% at 40° may increase to considerably higher values before this sign change is expected at 83°. Near the stripping peak at 18° there is no significant difference between the polarization at 6·9 Mev and 8·9 Mev, and no indication of a rise to the -58% found by Hillman at 4·05 Mev.

In the ^{9}Be(d, p)^{10}Be, and ^{10}B(d, p)^{11}B reactions $j_n = l_n + \frac{1}{2}$, and, as predicted, we obtain the sign of polarization opposite to that from the ^{12}C(d, p)^{13}C reaction.

Recently Weidenmüller (private communication) has made a calculation of the polarization in ^{12}C(d, p)^{13}C at 11·9 Mev bombarding energy, similar to that made by Newns and Refai at 3·21 Mev. Both calculations confirm the classical arguments (Newns 1953, Tobocman 1956) that at angles near the peak in the differential cross section, the deuteron interaction produces negative polarization and the proton interaction positive polarization. However, there is an essential difference between the two calculations as to the relative magnitude of these opposing effects and hence in the resultant sign of the polarization. Weidenmüller, in spite of using a larger proton well depth than Newns and Refai, finds that the deuteron interaction effect predominates and he therefore predicts a negative sign for the reaction ^{12}C(d, p)^{13}C. All the signs are interchanged in a reaction where $j_n = l_n + \frac{1}{2}$, and the polarization would presumably be positive. These are the signs we find in our measurements on ^{12}C(d, p)^{13}C, ^{9}Be(d, p)^{10}Be and ^{10}B(d, p)^{11}B. It is not clear whether the differences of sign in the two calculations are due to their being done at very different bombarding energies.

The negative sign of the ^{40}Ca(d, p)^{41}Ca polarization does not agree with the theory since $j_n = l_n + \frac{1}{2}$. One expects the classical arguments, which are confirmed by quantum mechanical calculations for $l_n = 1$, to remain true for larger l_n values. Also the proton energy is here intermediate between those of ^{9}Be(d, p)^{10}Be and ^{10}B(d, p)^{11}B, so an energy dependence of the interaction potentials is unlikely to be the cause of the inconsistency. Another parameter involved in the calculations is the nuclear radius. The stripping radius, deduced from the best fit of the Butler theory to the experimental differential cross section corresponds to the radius for the last neutron in the final nucleus. It is almost the same for ^{41}Ca as for ^{10}Be (Holt and Marsham 1953). On the other hand the proton interaction, depending more on the total number of nucleons in the final nucleus is likely to be significantly different in the two cases. It is possible that this difference may influence the proton interaction sufficiently to determine whether or not it outweighs the deuteron effects. No such effect appears when comparing ^{13}C and ^{10}Be which have very different stripping radii but nearly similar proton interaction radii.

ACKNOWLEDGMENTS

We wish to thank Professor H. W. B. Skinner for his support and encouragement and Dr. H. C. Newns for many helpful discussions.

REFERENCES

BOKHARI, M. S., COOKSON, J. A., HIRD, B., and WEESAKUL, B., 1958, *Proc. Phys. Soc.*, **72,** 88.

BROCKMAN, K. W., 1956, *Phys. Rev.*, **102,** 391.

HILLMAN, P., 1956, *Phys. Rev.*, **104,** 176.

HOLT, J. R., and MARSHAM, T. N., 1953, *Proc. Phys. Soc.*, **66,** 1032.

JUVELAND, A. C., and JENTSCHKE, W., 1956, *Bull. Amer. Phys. Soc.* Ser. II, **1,** 193.

KREGER, W. E., JENTSCHKE, W., and KRUGER, P. G., 1954, *Phys. Rev.*, **93,** 837.

NEWNS, H. C., 1953, *Proc. Phys. Soc.* A, **66,** 477.

NEWNS, H. C., and REFAI, M. Y., 1958, *Proc. Phys. Soc.*, **71,** 627.

PUTNAM, T. M., BROLLEY, J. E., and ROSEN, L., 1956, *Phys. Rev.*, **104,** 1303.

TOBOCMAN, W., 1956, *Tech. Rep.*, No. 29, Case Institute of Technology.

Capture Rates for Negative Muons in Various Elements

By A. ASTBURY, M. A. R. KEMP, N. H. LIPMAN, H. MUIRHEAD,
R. G. P. VOSS, C. ZANGGER† AND A. KIRK‡
Nuclear Physics Research Laboratory, University of Liverpool

MS. received 21*st May* 1958

Abstract. An experiment is described in which the capture rates of negative muons were measured for selected elements. A comparison between the experimental results and the theoretical predictions of Tolkoek and Luyten suggests that tensor and/or axial vector couplings are favoured in the interaction.

---

§ 1. Introduction

Recently a great deal of interest has centred on the weak interactions. The strengths of the coupling in β-decay, muon decay, and muon capture are approximately equal (Puppi 1948, Tiomno and Wheeler 1949). It now appears that it may be possible to describe each of these interactions in terms of V and A couplings, though as yet little is known of the coupling responsible for muon capture. (In this paper the symbols S, V, T, A and P refer to scalar, vector, tensor, axial vector and pseudoscalar couplings respectively). This has led to the suggestion (Marshak and Sudarshan, unpublished, Feynman and Gell-Mann 1958) that weak interactions can be described by a universal Fermi interaction. For this hypothesis to hold, it is necessary to show that muon capture can also be characterized by a mixture of V and A couplings.

The present experiment is an attempt to obtain information about the coupling operative in muon capture by measuring the capture rates of negative muons in various elements.

Tolhoek and Luyten (1957) have calculated the capture rates for muons in nuclei with almost closed shells, using a simple form of the shell model to describe the initial and final nuclear states involved. They find two values for the capture rate λ_c for each element considered: one for Gamow–Teller coupling (T and A), and another for Fermi coupling (S and V). The values of λ_c given by the calculations for various naturally occurring isotopic mixtures are shown in table 1. It will be seen that in the case of calcium the Gamow–Teller coupling gives exactly three times the capture rate predicted by Fermi coupling. It is convenient to

Table 1. Predicted Muon Capture Rates for Fermi Coupling, $\lambda_c(S, V)$, and Gamow–Teller Coupling, λ_c (T, A)

Element	Ca	Sc	Ti	V	Cr	Mn	Fe	Co	Ni
$\frac{1}{3}\lambda_c(T, A)/10^{101}$ (g^2)	145	136	147	150	185	207	246	268	320
$\lambda_c(S, V)/10^{101}$ (g^2)	145	130	128	111	130	137	157	165	194

---

† Now at Atomelectra Ltd., Zurich.

‡ Department of Applied Mathematics, University of Liverpool.

express the capture rates for the various elements as ratios to the calcium rates. If the coupling actually responsible for muon capture is a mixture of Gamow–Teller and Fermi interactions, the capture rate will be given by

$$\lambda_c = |C_S + C_V|^2 \lambda_c(\mathrm{S, V}) + |C_A + C_T|^2 \lambda_c(\mathrm{T, A}) \qquad \ldots\ldots(1)$$

where $\lambda_c(\mathrm{S, V})$ and $\lambda_c(\mathrm{T, A})$ are the capture rates due to pure Fermi and Gamow–Teller interactions respectively.

A simpler theory has been derived by Primakoff (reported by Sens, Swanson, Telegdi and Yovanovitch 1957) which predicts the muon capture rates in elements throughout the periodic table. This theory is insensitive to the type of coupling that prevails in the interaction, and gives the capture rate

$$\lambda_c(A, Z) = \lambda_c(1, 1)\gamma Z_{\mathrm{eff}}^4 \left(1 - \delta \frac{A - Z}{2A}\right) \qquad \ldots\ldots(2)$$

where $\lambda_c(1, 1) = 220$/sec is obtained from β-decay results, and γ and δ are calculated constants having the values of 0·73 and 3 respectively.

Sens *et al.* (1957) have measured muon capture rates for a large number of elements. The results are in good agreement with the predictions of Primakoff, and also with those of Tolhoek and Luyten if the interaction is assumed to be of pure Gamow–Teller type. If the interaction is of Fermi type, which leads to more rigid selection rules, then Tolhoek and Luyten predict that in particular elements the capture rate will fluctuate widely from the smooth behaviour described by equation (2). Sens *et al.* found that these variations did not appear, and the present more accurate experiment confirms this conclusion.

§ 2. EXPERIMENTAL METHOD

The external negative pion beam of the Liverpool synchrocyclotron was used for the experiment. This beam comprises approximately 86% negative pions, 11% electrons and 3% negative muons. The experimental arrangement is shown in the figure. The beam passed through a sheet of lead 1·3 cm thick before entering the bending magnet. The lead sheet caused most of the electrons to radiate energy, and they were then bent out of the beam by the magnet. The field of the magnet was adjusted to select muons of the appropriate momentum, and these were brought to rest in the target by means of the absorber shown. Since the range of pions is less than that of muons of the same energy, the absorber prevented any pions from reaching counter 2.

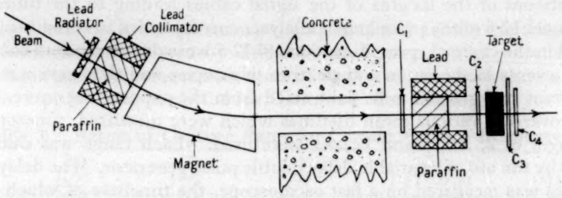

The arrival of a muon in the target was indicated by a coincidence between counters 1 and 2, with counter 3 in anticoincidence. This will be referred to as a $12\bar{3}$ event. In the same notation, a decay electron from a muon in the target produces a $\bar{2}34$ event. An electronic analyser (referred to hereafter as a timesorter) then generated a pulse whose height was proportional to the time interval between the two signals, and the output was registered on a 72-channel pulse height analyser. The resulting display on the pulse height analyser represented a decay curve of the form

$$N=N_0\exp(-\lambda_L\, t)+\text{background}$$

where λ_L is the muon disappearance rate.

If the muon capture rate is λ_c and the free muon decay rate λ_d then the disappearance rate is given by $\lambda_L=\lambda_c+\lambda_d$. The value of λ_d was taken to be $4{\cdot}5\times10^5$/sec (Bell and Hincks 1951). It should be noted that when a muon decays in close proximity to a nucleus, the decay process will be perturbed by the presence of the electric field surrounding the nucleus (Porter and Primakoff 1951, Muto, Tanifuji, Inoue and Inoue 1952). Consequently it may be necessary to use a modified value of λ_d. Although there is this uncertainty in the value of λ_d, since λ_d is much smaller than λ_c, an error in it will have a relatively small effect on the value of λ_c.

The authors are at present engaged in an experiment in which it is hoped to measure the change in λ_d due to the presence of the Coulomb field of the nucleus.

§ 3. ELECTRONIC TECHNIQUE

The muon mean lifetimes in the elements considered ranged from 150 to 1500 mμsec. In order to achieve adequate stability it was therefore necessary that the uncertainties in rise times within the electronic system should be small compared with a time of 150 mμsec. By removing the target and disconnecting the anticoincidence channels $\bar{2}$ and $\bar{3}$, it was possible to obtain coincidences between the muon and electron telescopes for the same particles passing through each. In this way it was possible to define a channel on the pulse height analyser corresponding to 'zero time'; periodic measurements showed that the overall instability was less than 10 mμsec.

The electron pulse ($\bar{2}34$) was delayed with respect to the muon pulse ($12\bar{3}$) by adjustment of the lengths of the signal cables leading to the timesorter, so that channel 12·5 of the pulse height analyser corresponded to zero time. Counts obtained in the channels preceding channel 12·5 were due to random coincidences between events in the muon and electron telescopes, and thus gave a measure of the constant background to be subtracted from the exponential curve.

To cover the various mean lifetimes which were measured, timesorter timebase ranges of 2, 3·5, 5 and 12 μsec were used. Each range was calibrated at intervals by the use of a variable delay double pulse generator. The delay between the pulses was measured on a fast oscilloscope, the timebase of which was calibrated accurately against a standard frequency waveform. It was estimated that the overall accuracy of calibration was 0·5%; the difference between separate calibrations during the complete experiment was never greater than 1%.

It should be noted that the slight shift in zero time mentioned above could introduce no error into the measured lifetimes.

§ 4. RESULTS

The pattern obtained on the pulse height analyser represented a curve of the form

$$y=A\exp(-\lambda_L t)+B\exp(-{}^*\lambda t)+C$$

where λ_L is the muon disappearance rate in the target material, C is the constant background due to random coincidences, and λ^* is the muon disappearance rate in carbon. Two factors give rise to the term $B \exp(-\lambda^* t)$. Firstly, some muons came to rest in counter 3 without giving a pulse large enough from that counter to prevent the event being recorded as a 123 event. Since the material of the scintillator was predominantly carbon, these muons then disappeared at the rate λ^*. Secondly, some of the target materials were contained in thin plastic boxes, and muons stopping in the walls of these boxes also disappeared at the rate λ^*.

The constant background obtained from the early channels in the pulse height analyser was subtracted, and the two exponentials were separated by means of a weighted least squares fit made with the Manchester electronic computer.

Values for muon capture rates were obtained for calcium, manganese, vanadium, nickel, cobalt, copper, aluminium and fluorine. In table 2 a comparison is made between the capture rates obtained in the present experiment, the results of Sens *et al.* (1957) and the calculated values of Primakoff. A better fit to the data can be obtained from Primakoff's theory by using modified values of the parameters $\gamma\lambda_c(1,1)$ and δ, viz. $\gamma\lambda_c(1,1) = 141/\text{sec}$ and $\delta = 2{\cdot}85$. The figures so obtained are given in parentheses in column (2).

Table 2. Muon Capture Rates

(1)	(2)	(3)	(4)
F	1·68 (1·75)	2·72 ± 0·2	2·54 ± 0·22
Al	6·60 (6·61)	6·90 ± 0·18	7·85 ± 0·44
Ca	27·8 (28·0)	26·8 ± 0·4	25·1 ± 0·9
V	29·2 (33·2)	31·3 ± 0·7	33·4 ± 0·8
Mn	37·4 (39·9)	40·4 ± 0·8	37·3 ± 1·2
Co	46·3 (49·8)	50·6 ± 0·9	—
Ni	58·6 (61·0)	61·6 ± 1·2	58·8 ± 1·9
Cu	54·5 (58·5)	60·0 ± 0·8	67·9 ± 2·2

(1) Element; (2) predictions of Primakoff ($\times 10^5$/sec); (3) present experiment ($\times 10^5$/sec); (4) experiment of Sens *et al.* ($\times 10^5$/sec).

In table 3 the ratios λ_c (element)/λ_c(Ca) obtained in the experiment are compared with those calculated by Tolhoek and Luyten. The present results are seen to be in good agreement with those of Sens *et al.*, and both show a preference for the capture rates predicted for Gamow–Teller coupling.

Table 3. Ratios of Capture Rates for Certain Pairs of Elements

(1)	(2)	(3)	(4)	(5)	(6)
V/Ca	0·77	1·03	0·97	1·17 ± 0·03	1·33 ± 0·10
Mn/Ca	0·95	1·43	1·31	1·51 ± 0·04	1·48 ± 0·08
Co/Ca	1·14	1·85	1·67	1·89 ± 0·05	—
Ni/Ca	1·34	2·21	1·99	2·29 ± 0·06	2·34 ± 0·12

(1) Elements compared; (2), (3), (4) ratios predicted by Tolhoek and Luyten: (2) S, V coupling, (3) T, A coupling, (4) equal amounts of S, V and T, A coupling; (5) present experiment; (6) experiment of Sens *et al.*

The ratios given above for pure Gamow–Teller and Fermi couplings are slightly misleading if in fact a mixture of the two interactions is present. This is due to the fact that $\lambda_c($ (T, A) is appreciably larger than λ_c (S, V), and so weights the ratio towards that of pure Gamow–Teller interactions. To illustrate this a column is included in table 3 giving the ratios $\lambda_c(\text{element})/\lambda_c(\text{Ca})$ for equal amounts of Gamow–Teller and Fermi interactions.

§ 5. CONCLUSION

It is clear from table 3 that the experimental results agree both with the simple theory of Primakoff, which avoids detail, and with the theory of Tolhoek and Luyten if pure Gamow–Teller interaction is assumed. One of two conclusions can be drawn from this: either Tolhoek and Luyten's calculations are based on an oversimplified picture of the nucleus, or the universal Fermi interaction must be abandoned.

An experiment is in progress in which the authors hope to measure the asymmetry of the neutrons produced in the capture of polarized negative muons. If a sufficiently high accuracy can be obtained, it should be possible to decide whether the coupling is pure Fermi, pure Gamow–Teller, or a mixture of the two.

ACKNOWLEDGMENTS

The authors wish to thank Professor H. W. B. Skinner for his interest and encouragement and Professor J. M. Cassels for many stimulating discussions. They also wish to thank Dr. B. Collinge for his work in the design of the time-sorter, and Mr. K. Aitcheson for his ready response to calls for assistance at unusual hours when troubles developed in the pulse height analyser. The authors are indebted to Messrs. T. Edge and W. Smithers of the United Kingdom Atomic Energy Authority and to Mr. W. Steven of the Mond Nickel Company for the loan of the target materials.

Lastly, thanks are due to Mr. B. Halliday and the cyclotron crew for their co-operation during the course of the experiment.

Three of us (A. A., M. A. R. K. and N. H. L.) acknowledge the receipt of grants from the Department of Scientific and Industrial Research. One of us (C. Z.) was supported by a CERN Fellowship.

REFERENCES

BELL, W. E., and HINCKS, E. P., 1951, *Phys. Rev.*, **84,** 1243.
FEYNMAN, R. P., and GELL-MANN, M., 1958, *Phys. Rev.*, **109,** 193.
MUTO, T., TANIFUJI, M., INOUE, K., and INOUE, T., 1952, *Progr. Theor. Phys.*, **8,** 13.
PORTER, C. E., and PRIMAKOFF, H., 1951, *Phys. Rev.*, **83,** 849.
PUPPI, G., 1948, *Nuovo Cim.*, **5,** 587.
SENS, J. C., SWANSON, R. A., TELEGDI, V. L., and YOVANOVITCH, D. D., 1957, *Phys. Rev.*, **107,** 1464.
TIOMNO, J., and WHEELER, J. A., 1949, *Rev. Mod. Phys.*, **21,** 144.
TOLHOEK, H. A., and LUYTEN, J. R., 1957, *Nucl. Phys.*, **3,** 679.

On the Binding Energy of the ^{16}O Nucleus
II. Higher Clusters

By J. DABROWSKI†

Department of Mathematical Physics, University of Birmingham

Communicated by R. E. Peierls; MS. received 13th June 1958

Abstract. The paper contains a calculation of the higher cluster terms neglected in the variational calculation of the binding energy of the ^{16}O nucleus given in an earlier paper. All the different contributions to the next term in the Ursell–Jastrow cluster development are calculated with help of an approximation based on the short range of the correlations. The wave function found in the earlier paper is used. The numerical results show that with the higher cluster terms both binding and density of the ^{16}O nucleus are still reproduced by the two-body interaction with the repulsive core radius between 0·2 and 0·6 fermi. The higher cluster terms are found to be of importance in any attempt at quantitative results.

§ 1. Introduction

A variational calculation of the binding energy of the ^{16}O nucleus was presented in an earlier paper (Dabrowski 1958, to be referred to as I). The two-body central Yukawa interaction $V(ij)$ with the hard core of radius a, and with Serber exchange, equations (I, 4–5), was assumed and the parameters adjusted to fit the low energy data, table I, 1. Applying the Jastrow (1955) method a trial function Ψ in the form of a product of the Slater function Φ, and the factorized correlation function Πf, equations (I, 1–2) was assumed and the cluster development of the expectation value of the energy was applied. For the function Φ we used the shell model wave function for the configuration $(1s^2)_N(1p^6)_N(1s^2)_P(1p^6)_P$ with the harmonic oscillator radial functions with the parameter ν, equations (I, 11–13). For the correlation function f we used the function varying monotonically from zero at $r=a$ to unity at large r containing one parameter β, equation (I, 17). In the cluster development of the energy E we restricted ourselves to the first term $\mathscr{E}$, equations (I, 7–10), which was analytically expressed with the help of the two parameters ν, β, equations (I, 14–16). By numerical calculation the values of ν and β minimizing $\mathscr{E}$ were found. A repulsive core radius $a=0{\cdot}2$ f and 0·6 f was assumed. The results given in figure I, 1 and in table I, 2 showed that the assumed two-body interaction V was capable of reproducing the saturation of both binding and density of the ^{16}O nucleus.

The aim of the present paper is to evaluate the contribution of the higher cluster terms to the energy E. In the cluster development we have

$$E=\langle\Psi|H|\Psi\rangle/\langle\Psi|\Psi\rangle=\mathscr{E}+O(\Omega_c/\Omega), \qquad \ldots\ldots(1)$$

where the higher cluster terms contained in $O(\Omega_c/\Omega)$ are of the order Ω_c/Ω compared with $\mathscr{E}$ ($\Omega=$ the volume of the nucleus, $\Omega_c=$ the total volume within which the correlations are strong). The Ω_c/Ω was estimated to be equal to about 5% for $a=0{\cdot}2\,\mathrm{f}$ and to 16% for $a=0{\cdot}6\,\mathrm{f}$. Although the corrections of these orders of magnitude to $\mathscr{E}$ would not change the conclusions of I, the situation was not quite satisfactory, since $\mathscr{E}$ calculated in I was the difference between two large quantities, the potential and kinetic parts. To clarify this point and so to remove the main uncertainty of the results obtained in I we calculate in this paper all the terms of the order Ω_c/Ω in O for the values of ν, β minimizing $\mathscr{E}$. After introducing some reasonable approximations the calculation of the terms of the order Ω_c/Ω is essentially simple, although the analytical expressions obtained are far from being short. For this reason, we restrict ourselves in the numerical calculation of those terms to the case $a=0{\cdot}6\,\mathrm{f}$ only. We chose this case, because as we shall see, these terms give an additional binding. The critical question is if this additional binding in the case of $a=0{\cdot}6\,\mathrm{f}$ can give a resultant total binding, greater than the experimental value E_{exp}, whereas an additional binding in the case $a=0{\cdot}2\,\mathrm{f}$ has no influence on the conclusion of I about the saturation of the binding and size of the ^{16}O nucleus. Furthermore the greater value of Ω_c/Ω in the case $a=0{\cdot}6\,\mathrm{f}$ makes it especially desirable to know the value of the higher cluster contribution in this case.

---

† On leave of absence from the Institute of Theoretical Physics, Warsaw, Poland.

§ 2. CALCULATION OF THE CONTRIBUTION TO THE BINDING ENERGY OF ORDER Ω_c/Ω

A systematic derivation of the cluster development was given recently by Iwamoto and Yamada (1957 a). All the terms of order 1 and Ω_c/Ω are given in the equations (31)–(32) of their paper. These equations contain several summations over the occupied states of the system with the restriction that no two of the summation indices are equal to each other. This restriction is automatically fulfilled in almost all the terms due to the antisymmetrization. The only exceptions are the last term of equation (31) and the last term of equation (32). We introduce this restriction explicitly into the above terms. Further, we introduce into equation (32) the contribution of the term ΣX_{ij}^2 of equation (28), neglected by Iwamoto and Yamada. Then with the help of simple manipulations we may rewrite all the Ω_c/Ω terms, denoted hereafter by Δ, in the following shorter form:

$$\Delta=\Delta_0+\Delta_1+\Delta_2+\Delta_3, \qquad \ldots\ldots(2)$$

where

$$\left.\begin{aligned}
\Delta_0 &= \sum_{ij}\sum_{\mathrm{P}_2}\epsilon_{\mathrm{P}_2}\Big[\langle\phi_{\mathrm{P}i}(1)\phi_{\mathrm{P}j}(2)|h(12)T(1)|\phi_i(1)\phi_j(2)\rangle \\
&\quad -\sum_k\langle\phi_{\mathrm{P}i}(1)\phi_{\mathrm{P}j}(2)|h(12)|\phi_k(1)\phi_j(2)\rangle\langle\phi_k(1)|T(1)|\phi_i(1)\rangle\Big], \\
\Delta_1 &= \frac{1}{4}\sum_{ijkl}\sum_{\mathrm{P}_4}{}'\epsilon_{\mathrm{P}_4}\langle\phi_{\mathrm{P}i}(1)\phi_{\mathrm{P}j}(2)\phi_{\mathrm{P}k}(3)\phi_{\mathrm{P}l}(4)|h(34)\mathscr{W}(12)|\phi_i(1)\phi_j(2)\phi_k(3)\phi_l(4)\rangle, \\
\Delta_2 &= \frac{1}{2}\sum_{ijk}\sum_{\mathrm{P}_3}\epsilon_{\mathrm{P}_3}\langle\phi_{\mathrm{P}i}(1)\phi_{\mathrm{P}j}(2)\phi_{\mathrm{P}k}(3)|[1+f^2(13)]h(23)\mathscr{W}(12)|\phi_i(1)\phi_j(2)\phi_k(3)\rangle, \\
\Delta_3 &= -\frac{1}{8}\frac{\hbar^2}{m}\sum_{ijk}\sum_{\mathrm{P}_3}\epsilon_{\mathrm{P}_3}\langle\phi_{\mathrm{P}i}(1)\phi_{\mathrm{P}j}(2)\phi_{\mathrm{P}k}(3)|f^2(31)\nabla_2 h(12) \\
&\qquad\qquad\cdot\nabla_2 h(23)|\phi_i(1)\phi_j(2)\phi_k(3)\rangle.
\end{aligned}\right\} \qquad \ldots\ldots(3)$$

In (3) we used the notation of I, i.e. $T(k)$ is the operator of the kinetic energy of the k-th particle and $\phi_i(k)$ are the functions of the Slater determinant, the detailed form of which is defined in equations (I, 11–13). The new notations are:

$$h(12) = h(r_{12}) = f^2(12) - 1 = f^2(r_{12}) - 1, \qquad \ldots\ldots(4)$$

$$\mathscr{W}(12) = -\frac{\hbar^2}{m} f(12) \sum_{i=1}^{2} [\tfrac{1}{2}\Delta_i f(12) + \nabla_i f(12) \cdot \nabla_i] + f^2(12) V(12). \qquad \ldots\ldots(5)$$

$V(12)$ is the nuclear interaction, equations (I, 4–5); the Coulomb interaction is neglected in the present calculation, since its contribution to Δ is negligibly small. The summations over P_2, P_3 and P_4 are to be performed over all permutations of the indices

$$\begin{pmatrix} \mathrm{p}i & \mathrm{p}j \\ i & j \end{pmatrix}, \quad \begin{pmatrix} \mathrm{p}i & \mathrm{p}j & \mathrm{p}k \\ i & j & k \end{pmatrix} \text{ and } \begin{pmatrix} \mathrm{p}i & \mathrm{p}j & \mathrm{p}k & \mathrm{p}l \\ i & j & k & l \end{pmatrix} \text{ with}$$

the proper signs ϵ_{P_2}, ϵ_{P_3} and ϵ_{P_4} respectively. The prime in $\sum'_{P_4}$ means that the cyclic permutations 1, (ij), (kl), $(ij)(kl)$ are excluded from the summation. In the expressions (3) the indices i, j, k, l run now independently over all occupied states of the system without any of the restrictions mentioned above.

The origin of the different terms in (3) is evident. One part of them has its origin in the orthonormalization (Δ_1 and the second part of Δ_0). This involves calculating the normalization denominator and the integrals over the coordinates of the remaining particles 2, 3, ..., A or 3, 4, ..., A while calculating $\langle T(1) \rangle$ or $\langle \mathscr{W}(1,2) \rangle$. We do not get unity or zero in the sub-integrations because of the correlations among the remaining particles. The correlations between one of the remaining particles and the particle 1 or 2 is the origin of Δ_2 and the first part of Δ_0. The term Δ_3 arises from the coupling of the kinetic energies due to the term $\nabla f . \nabla f$.

It is to be mentioned that $\langle \mathscr{W}(12) \rangle$ without coupling with the remaining particles, may be transformed by integration by parts into $\langle \mathscr{V}(12) \rangle$, where $\mathscr{V}(12)$ is the effective potential of equation (I, 9). This was done in I while calculating $\mathscr{E}$. In the terms appearing in Δ this transformation is not possible in general.

With our form of the Slater functions $\phi_i(j)$, equations (I, 11–13), and of the correlation function f, equation (I, 17), we can obtain exact analytical expressions for Δ_0 and Δ_1, applying the technique of the oscillator wave functions (Talmi 1952, Thieberger 1956/7, Tauber and Wu 1957). The calculation of Δ_2 is much more difficult, since it contains three-body integrals. We solve this difficulty reducing these three-body integrals to the two-body integrals by applying an approximation based on the following observation. The function $h(r_{23})$ in Δ_2 equals -1 inside the small region $r_{23} < a$ and outside this region approaches zero very rapidly. All the other functions are slowly varying functions of r_{23}. This observation leads to the following approximation:

$$h(r_{23}) \simeq -\tfrac{4}{3}\pi r_c^3 \delta(\mathbf{r}_{23}), \qquad \ldots\ldots(6)$$

where the radius of the correlation region r_c is defined by

$$-\tfrac{4}{3}\pi r_c^3 = 4\pi \int_0^\infty dr\, r^2 \exp(-\tfrac{1}{2}\nu r^2) h(r). \qquad \ldots\ldots(6.1)$$

The tactor $\exp(-\frac{1}{2}\nu r^2)$ in (6.1) is used for the following reason. In the case of a short-range function like $h(r)$ the decisive contribution to the integral comes from the S part of the relative motion, and $\exp(-\frac{1}{2}\nu r^2)$ is just the square of the radial function of the relative coordinate in the S state for our oscillator wave functions.

To check the approximation (6) a part of Δ_1 corresponding to $l=j$ was calculated exactly. The approximate calculation with the help of (6) gave a result differing from the exact one by 4·4%. Since such an accuracy is quite sufficient for our purpose, we used the approximation (6) for the h functions in Δ_0 and Δ_1 too, simplifying the calculations essentially. For Δ_0 we get

$$\Delta_0 = -\frac{93}{4(2\pi)^{1/2}} r_c{}^3 \nu^{3/2} \frac{\hbar^2}{m} \nu. \qquad \ldots\ldots(7)$$

In the case of Δ_1, Δ_2 one introduces the variables $\mathbf{r}_{12}=\mathbf{r}_2-\mathbf{r}_1$ and $\mathbf{R}_1=\frac{1}{2}(\mathbf{r}_1+\mathbf{r}_2)$, $\mathbf{R}_2=\frac{1}{3}(\mathbf{r}_1+2\mathbf{r}_2)$ respectively. The integration over $\mathbf{R}_1$ and $\mathbf{R}_2$ can be easily performed and the problem is reduced to the calculation of integrals similar to the I_l's and J_l's of equations (I, 15–16). The calculation of the last integrals with our form of f is an elementary task.

Δ_3 is also awkward for exact calculation as it also contains three-body integrals. But since under the integrals occurs the cosine of the angle between $\mathbf{r}_{21}$ and $\mathbf{r}_{23}$, resulting from the scalar product of the gradients of the two short-range functions $h(21)$, $h(23)$, it is evident that Δ_3 is a small term. So we may calculate it in an approximate way. We notice that the factors $\nabla_2 h(12)$ and $\nabla_2 h(23)$ are essentially different from zero only for $r_{12}\cong a$ and $r_{23}\cong a$ respectively. Since on the other hand the functions $\phi_l(k)$ are varying smoothly we put

$$\mathbf{r}_1=\mathbf{r}_2,\ \mathbf{r}_3=\mathbf{r}_2 \text{ in the arguments of the functions } \phi_l. \qquad \ldots\ldots(8)$$

With the help of the approximation (8), one can perform most of the integrations and obtain

$$\Delta_3 = -\frac{764}{9\sqrt{3}} \pi \frac{\hbar^2}{m} \nu^3 \int_a^\infty dr_{12} \frac{dh(r_{12})}{dr_{12}} \int_a^\infty dr_{23} \frac{dh(r_{23})}{dr_{23}}$$
$$\times \int_{|r_{23}-r_{12}|}^{r_{23}+r_{12}} dr_{13}\, r_{13} f^2(r_{13}) (r_{23}{}^2 + r_{12}{}^2 - r_{13}{}^2). \qquad \ldots\ldots(9)$$

The integrations in (9) with our form of f are elementary.†

The numerical results for the case $a=0·6$ f ($\beta=2$, $\nu^{1/2}=0·55\ \mathrm{f}^{-1}$) are given in the table.

Values in MEV for the different parts of the Ω_c/Ω contribution to the binding energy of the ^{16}O nucleus for a repulsive core radius $a=0·6$ f.

	Δ_0	Δ_1	Δ_2	Δ_3	Δ
Kinetic part	−9	100	−90	5	6
Potential part	—	−195	164	—	−31
Total	−9	−95	74	5	−25

§ 3. DISCUSSION

The first term in the cluster development, $\mathscr{E}$, was calculated in I to be equal to −65 MEV for $a=0·6$ f. If we add to it the value −25 MEV of Δ we get $\mathscr{E}+\Delta=-90$ MEV. This is still greater than the experimental value $E_{\mathrm{exp}}=-127·56$ MEV, the difference being −30 MEV.

---

† One could calculate Δ_2 and Δ_3 exactly expanding the respective integrals in the spirit of the usual Slater method (J. Snowball, private communication). But such a calculation seems to us unneccessarily onerous for our purpose.

It is difficult to compare the separate terms in $\mathscr{E}$ with the corresponding terms in Δ since the division of $\Delta_1+\Delta_2$ into Δ_1 and Δ_2 is essentially arbitrary. In any case all the terms in the table are smaller (at least three times) than the corresponding terms of $\mathscr{E}$ in table I, 2, as it should be since the cluster expansion is convergent. Since the difference of 30 Mev between $\mathscr{E}+\Delta$ and E_{exp} is still greater than Δ, there is good reason to assume that the terms of order higher than Ω_c/Ω will not change the inequality $\langle\Psi|H|\Psi\rangle/\langle\Psi|\Psi\rangle > E_{\text{exp}}$.

The values of ν and β minimizing $\mathscr{E}+\Delta$ are slightly different from those minimizing $\mathscr{E}$ alone. The difference should not be too large since Δ, as giving an additional binding, is expected to have a behaviour as a function of ν and β similar to $\mathscr{E}$. Since the nuclear radius calculated in I for $a=0{\cdot}6$ f was about 17% greater than the experimental value, there is no doubt that, even after taking into account Δ, the calculated radius is still greater than the experimental one.

On the other hand, as was mentioned in the Introduction, taking into account Δ in the case $a=0{\cdot}2$ f would not change any of the conclusions reached in I. It is obvious without any calculation that for a sufficiently small a the binding increases and the size decreases rapidly since the Serber force without the repulsive core does not satisfy the saturation conditions.

So the second term in the cluster development Δ and, with all probability, the higher terms, do not change our main qualitative conclusion that a two-body potential fitted to the scattering data with a repulsive core of the radius somewhere between 0·2 f and 0·6 f is capable of reproducing both binding and density of the ^{16}O nucleus.

On the other hand the quantitative side of the problem is far from being satisfactory. We mention the following points.

The large value of Δ makes it clear that in any attempt at quantitative results one has to consider in the variational treatment at least the cluster terms of order Ω_c/Ω together with the two-body term $\mathscr{E}$. A similar difficulty is to be mentioned in the Brueckner theory. Omitted terms of the second and higher order in the transition matrix have been discussed by Hugenholtz and Van Hove (1958), Thouless (1958), and Brueckner (1958) and shown to be non-negligible so far as they contribute to the single particle energy which appears in the theory. It is not yet definitely settled how the omitted terms change the results for the binding energy of nucleus, although Thouless' (1958) estimate that the effective mass may be increased to $0{\cdot}9m$ suggests that the change may be appreciable, perhaps more than 25%.

Since the binding energy is a small difference between large potential and kinetic parts, the resulting binding is sensitive to the details of the two-body potential (e.g. the interaction in the P state), although they are of small relative importance for the potential part alone. Similar sensitivity was observed in the calculations with the Brueckner method (Gammel, private communication).

An open question which should be mentioned is the shape of the correlation function f. It is well known that a variational method can give good value for the energy with a poor approximation to the wave function. Nevertheless it would be desirable to introduce one parameter more into f, to allow for attractive correlations. In this case, however, one must consider both terms, $\mathscr{E}$ and Δ, together since the normalization correction in Δ are then essential as was shown by Emery (1958). Support for our form of f comes from the results obtained by Gomes, Walecka and Weisskopf (1958) which in the frame of the Brueckner theory give correlations which are essentially repulsive.

An interesting question is how the finite size of the nucleus influences the correlations. Here it would be desirable to compare our results with similar results in the case of infinite nuclear matter. A comparison with the result of Iwamoto and Yamada (1957 b) for nuclear matter would be difficult, since they use a different two-body potential and their approximation for the Ω_c/Ω terms introduces a large uncertainty in their values for these terms.

ACKNOWLEDGMENTS

The author expresses his deep gratitude to Professor R. E. Peierls for his kind hospitality and his encouragement during the course of this work. Sincere thanks are expressed to the author's colleagues at the Universities of Birmingham and Cambridge for many helpful discussions. The author is very grateful to Dr. J. L. Gammel for his enlightening comments about the present state of the Brueckner theory.

A grant from the Polish Academy of Sciences is also acknowledged.

REFERENCES

BRUECKNER, K. A., 1958, *Phys. Rev.*, **110,** 597.
DABROWSKI, J., 1958, *Proc. Phys. Soc.*, **71,** 658.
EMERY, V. J., 1958, *Nuclear Physics*, **6,** 585.
GOMES, L. C., WALECKA, J. D., and WEISSKOPF, V. F., 1958, *Annals of Physics*, **3,** 241.
HUGENHOLTZ, N. M., and VAN HOVE, L., 1958, *Physica*, **24,** 363.
IWAMOTO, F., and YAMADA, M., 1957 a, *Progr. Theor. Phys., Japan*, **17,** 543; 1957 b, *Ibid.*, **18,** 345.
JASTROW, R., 1955, *Phys. Rev.*, **98,** 1479.
TALMI, J., 1952, *Helv. Phys. Acta*, **25,** 185.
TAUBER, G. E., and WU, T. Y., 1957, *Phys. Rev.*, **105,** 1772.
THIEBERGER, R., 1956/57, *Nuclear Physics*, **2,** 533.
THOULESS, D. J., 1958, *Phys. Rev.*, in the press.

Radiative Capture Cross Sections for 14·5 MeV Neutrons

By J. L. PERKIN, L. P. O'CONNOR and R. F. COLEMAN
Atomic Weapons Research Establishment, Aldermaston, Berks.

Communicated by K. W. Allen ; MS. received 17th March 1958, and in revised form 27th May 1958

Abstract. The radiative capture cross sections for 14·5 MeV neutrons have been measured for some 30 nuclides selected over a wide range of the periodic table. Chemical procedures were found essential to separate and identify the residual activities arising from capture reactions from the activities caused by the many other competing reactions possible at this neutron energy. Errors due to capture reactions caused by the small percentage of low energy neutrons, which were unavoidably present during the irradiations, were taken into account.

The cross sections found were of the order of 5 mbn for all except the lightest of the nuclides examined. A plot of these cross sections with respect to neutron number indicates relatively low values for the cross section near magic neutron numbers. These depressions are not so marked as those observed in experiments with fission neutrons. The general level of 5 mbn found for radiative capture cross sections for 14·5 MeV neutrons is much higher than the value predicted from some considerations of the theory of the compound nucleus. The consequences of this disagreement are discussed.

---

§ 1. Introduction

This survey of radiative capture cross sections for 14·5 MeV neutrons was undertaken as part of a more general investigation of the interaction of neutrons of this energy with various nuclides. In addition it was hoped that the results obtained would give some indication of the density of the excited states of the compound nuclei produced by capture.

There is very little published data concerning capture cross sections for fast neutrons. Hughes, Garth and Levin (1953) using unmoderated fission neutrons, measured the capture cross sections for a wide range of nuclides by activation techniques. Holmes, McVicar, Rose, Smith and Shepherd (1955) made a similar survey using the softer degraded fission spectrum obtained at the centre of the fast reactor ' Zephyr '. Apart from these two surveys, only a few capture cross sections have been measured for neutrons of energy above thermal and less than 5 MeV (Hughes and Harvey 1955).

The effective energy of unmoderated fission neutrons for the (n, γ) reaction is about 1 MeV. For many nuclides, the principal alternative to the capture of a neutron of this energy is the re-emission of a neutron of the same energy. The probability for the re-emission of a neutron of reduced energy is fairly small due to the scarcity of low lying levels in the target nucleus. Under these conditions the theory developed by Feshbach, Peaslee and Weisskopf (1947) leads to a simple relation between the capture cross section, the product of the average radiative width of the levels excited by capture, and the density of these levels. The plot of the cross sections obtained by Hughes, Garth and Levin against the neutron number of the target nuclide shows an initial sharp rise followed by values of the order of 150 mbn for all heavy nuclides except those near closed neutron shells where the cross sections are relatively low. As it has been found that the average radiative width for a given excitation energy does not vary greatly with neutron number, the initial sharp rise in the values for the capture cross section must be due to the expected increase in the level density. Similarly, the low values observed near the magic neutron numbers are due to the relatively low level densities of nuclides having a closed neutron shell structure.

In the present experiments with 14·5 Mev neutrons, this picture of the capture process is complicated by the competition of (n, n′), (n, 2n), (n, 3n), (n, p) (n, α) and (n, f) processes. The extension of the theory already mentioned to account for this competition predicts radiative capture cross sections very much smaller than those actually found. The consequences of this disagreement are discussed later in § 4.

§ 2. GENERAL METHOD

2.1. *Neutron Irradiation*

Fast neutrons were obtained by bombarding a tritiated zirconium target with 440 kev deuterons. Neutron emission from the target was maintained at about 5×10^9 to 10^{10} per second during the course of the experiments. Even with this high output it was necessary to place materials for irradiation close to the back of the tritium target in order that sufficient activity from (n, γ) reactions could be observed.

The ^{27}Al (n, α) ^{24}Na reaction was used to monitor the neutron flux in this close position. A thin layer of each sample was placed between two thin aluminium discs. After irradiation the activity of the discs was measured with an end-window Geiger counter.

In order to calibrate this activity in terms of neutron flux, a separate experiment was carried out in which the neutron output from the target was found by counting the associated α particles from the (D, T) reaction in a known geometry and at an angle of 135° to the beam. Two aluminium discs were placed symmetrically around the tritium target in a position of known geometry with respect to the target. After irradiation they were counted in the same way as the discs sandwiching samples.

Errors incurred in calculating the known geometry due to the finite size of the tritium target were greatly reduced by this method of using two discs and taking a mean of the activity produced in each.

Taking into account other errors involved in the counting statistics, it is concluded that the neutron flux through the samples as calculated is accurate to ± 3%. The probable error was higher than this in experiments for which the period of irradiation was less than 5 minutes.

2.2. *Chemical Separations and the Choice of Target Elements*

The choice of capture reactions which could be examined without too much difficulty was very restricted.

The target element had to be available in a suitable chemical and physical form of reasonable purity. In the present experiments only about 100 mg of sample were irradiated and it was thus practicable to use mainly spectroscopically pure chemicals. This eliminated much of the uncertainty associated with activities due to impurities of high cross section. In the few cases where analytical grade chemicals had to be used, chemical separations eliminated impurities after the irradiation. Only target nuclides of reasonable abundance which, on capturing a neutron, gave rise to residual nuclei with convenient half lives (i.e. between three minutes and one week) were examined.

The main restriction in this work with 14·5 MeV neutrons was the conflicting and obscuring effect of the activities produced by the many other reactions taking place. No (n, γ) cross section could be measured easily for an isotope where the residual nucleus formed by capture could also be formed by an (n, 2n) or (n, 3n) reaction with another isotope of the same element. The activities produced by (n, 2n) reactions in these other isotopes quite often swamped the activity produced by the (n, γ) reaction being considered even when the respective half lives were quite different.

Obscuring the conflicting activities from (n, α) and (n, p) reactions also made the measurement of (n, γ) cross sections difficult unless the end products could be removed chemically in a time comparable with the half life of the residual nucleus resulting from capture.

The separations performed on the individual target elements examined are shown in the table. Purification schemes based generally on ion exchange, solvent extraction, and precipitation reactions were devised to free the target element of (n, p) and (n, α) products. In the case of thorium and uranium, the separation of fission products and natural radioactive daughters to a very high degree of decontamination was found essential.

In a few cases, the residual nucleus formed by the decay of the (n, γ) product was itself radioactive. It was then possible to separate this activity chemically from all other induced activities.

Another method of separating the activity required from obscuring activities, especially those resulting from (n, 2n) reactions, was to use elements enriched in the isotope examined. This is generally only useful when the relative abundance of the particular isotope concerned can be increased to practically 100%. In the present experiments this method was used to find the capture cross sections for the two isotopes of copper.

The contamination of the target elements by recoil nuclei from (n, p) and (n, α) reactions in the aluminium discs used to monitor the neutron flux was observed during the course of the present experiments. Chemical separations were performed to confirm the origin of this unexpected activity, and thin layers of tape were used to prevent the penetration of the recoil nuclei in subsequent irradiations.

The very important part played by chemical techniques in all the present work cannot be over-emphasized.

2.3. *Counting Techniques*

After irradiation and chemical treatment, most of the samples were counted with a two inch diameter end-window Geiger counter. Uniform and reproducible sources were prepared by passing an alcohol slurry of the final precipitate through a demountable filter.

In the majority of cases the Geiger counter was calibrated directly for the activity observed. Special sources for this purpose were prepared from material of high specific activity obtained by an irradiation in a high thermal neutron flux. The samples of high specific activity were calibrated by absolute beta counting. This method enabled the efficiency of the Geiger counter to be calculated irrespective of the complexity of the decay scheme of the (n, γ) product and the particular geometry used.

About one milligramme of the target element was used for the high thermal flux irradiation. This was dissolved in a suitable solvent and a known fraction of the solution was counted for several half lives in a 4π beta counter in order to standardize the solution and to check the purity of the particular nuclide formed.

A second fraction was mixed with a solution containing the same weight of the inactive element as that originally counted in the 14·5 MeV neutron experiment. The element was precipitated, mounted, and counted exactly as in the original experiment. All the supernates and washings from the active material were combined and counted in a liquid Geiger counter which was calibrated with a third fraction of the standardized solution.

When the half-life of a particular nuclide made this procedure inconvenient, an unirradiated target element sample of the same weight as that used was impregnated with beta emitters of various energies and the efficiency of the counter was found for each. The efficiency for counting the particular (n, γ) product in the sample was then found by interpolation.

In those cases for which it was possible to extract the radioactive daughter of the (n, γ) residual nucleus, the former was mounted on a thin ($20\,\mu$g cm^{-2}) foil and counted directly in a 4π beta counter.

When the combination of relatively long chemical treatment and short half-life made the usual method of mounting unsuitable, the sample was counted in a glass walled liquid Geiger counter which had been calibrated with beta emitters of various energies.

§ 3. CORRECTIONS FOR LOW ENERGY NEUTRONS

3.1. *General*

In addition to the neutrons from the (D, T) reaction, the target elements were irradiated with neutrons from the following sources: (*a*) thermal and epithermal neutrons diffusing back from the walls of the laboratory and other large masses; (*b*) (D, T) neutrons scattered inelastically from material in the immediate vicinity of the neutron source: the majority of these had energies of the order of 1 MeV; (*c*) (D, D) neutrons produced by deuteron bombardment of deuterium which was gradually absorbed into the tritium target with use: those going though the target element (i.e. in the forward direction) would have energies of about 3 MeV.

The use of mercury vapour pumps minimized the accumulation of carbon on the tritium targets, and there was no visible deposit even after many hours of bombardment. Errors due to low energy neutrons from the ^{12}C (d, n) reaction could therefore be neglected.

The presence of low energy neutrons during the irradiation, even in comparatively low intensities, could cause quite serious errors due to the increase in the radiative capture cross section at low energies.

Thus the activity corresponding to a given (n, γ) reaction is given by

$$N\,(n_{14}\,\sigma_{14}+n_E\,\sigma_E)$$

where N is the number of target nuclei, n_{14} and n_E are the neutron fluxes, and σ_{14} and σ_E are the (n, γ) cross sections corresponding to neutrons of 14 MeV and a lower energy E.

It follows that $\sigma_{14} = \sigma_{14}(\mathrm{obs}) - n_E \sigma_E / n_{14}$ where σ_{14} (obs) is the value of the cross section calculated from the observed activity which is assumed to be due solely to 14 MeV neutrons. Thus the values found for σ_{14} will be too high by $100\, \sigma_E n_E / \sigma(\mathrm{obs})\, n_{14}\%$.

An estimate of this error for the three different sources of low energy neutrons is given in the following sections.

3.2. *Thermal and Epithermal Neutrons*

An activation experiment was carried out to find the intensity of the thermal and epithermal neutron flux near the target. Holmium with its high thermal cross section of 64 barns and its many resonances of greater than 1000 barns in the region 1 to 100 ev, was chosen as a detector. Two simultaneous irradiations were made, one in the usual close position and the other 10 cm from the source without cadmium shielding. The very low activity observed with this second sample was almost entirely accounted for by the low 14 MeV neutron flux at the remote position. As the slow neutron flux would not vary significantly over a distance of 10 cm around the neutron source, it was possible from this experiment to fix an upper limit of 3×10^{-7} for the ratio of thermal to 14 MeV neutron fluxes at the normal position of irradiation close to the neutron source. This meant that none of the radiative capture cross sections found were subject to appreciable error due to thermal or epithermal activation. The particularly low thermal neutron background found was to be expected as the laboratory in which the irradiations were performed was designed so as to give a scatter-free space within five metres in any direction from the fast neutron source.

3.3. *Inelastic Neutrons*

Inelastic scattering of the (D, T) neutrons took place mainly in the cadmium shield around the target element. An estimate of the ratio n_E/n_{14} can be made using the value of 1·95 barns found by Graves and Davis (1955) for the total inelastic cross section in this element for 14 MeV neutrons. With the geometrical arrangement used for irradiation, this ratio was approximately 5×10^{-3}. Calculated values for the cross sections will therefore be too high by $0{\cdot}5\, \sigma_1/\sigma_{14}(\mathrm{obs})\%$.

3.4. (*D*, *D*) *Neutrons*

The magnitude of the (D, D) neutron component was found by counting the associated protons and comparing these with the α particles from the (D, T) reaction. None of the tritium targets was used in the present experiments for longer than 250 microampere hours. The ratio of (D, D) to (D, T) neutrons for a target of this age was found to be about 5×10^{-3}, which is in good agreement with the more comprehensive work of Coon, Graves, Battat and Davis (1955).

Thus the values of the calculated cross sections will be too high by up to $0{\cdot}5 \times \sigma_3/\sigma_{14}(\mathrm{obs})\%$ according to the age of the tritium target used. The radiative capture cross section has been found to decrease with neutron energy in all cases where it has been measured in the energy region 1 to 3 MeV. The correction can be expressed therefore as up to $0{\cdot}5 \times \sigma_1/\sigma_{14}(\mathrm{obs})\%$.

Values for these corrections corresponding to individual target elements are shown in the table in all cases where this correction is not negligible. The values of σ_1 used were taken either directly or by interpolation from the work of Hughes and Harvey (1955).

§ 4. RESULTS AND DISCUSSIONS

4.1. *Experimental Values for* σ(n, γ) *for* 14·5 MEV *Neutrons*

The results obtained are presented in Table 1 and in the figure. A comparison of these results for 14·5 MEV neutrons with those of Hughes, Garth and Levin (1953) for fission neutrons, shows that the radiative capture cross sections for heavy elements have fallen from about 150 mbn to about 5 mbn. On the other hand the cross sections for the light elements and those nuclei with neutron numbers close to the magic neutron numbers have remained fairly constant.

Table 1

(1)	(2)	(3)	(4)	(5)	(6)	(7)
^{23}Na	12	0·33	10	0·8	—	None
^{26}Mg	14	0·2	25	3·0	—	(n, α) and (n, p) products
^{27}Al	14	0·53	25	0·7	—	(n, p) products
^{30}Si	16	0·49	10	2·25	—	None
^{41}K	22	3·5	20	0·8	—	None
^{50}Ti	28	3·5	30	($\sim$1)	—	None
^{55}Mn	30	0·76	10	5·0	—	None
^{63}Cu	34	2·56	15	4·4	—	(isotopically enriched)
^{65}Cu	36	6·3	30	1·0	—	(,, ,,)
^{71}Ga	40	1·9	10	($\sim$10)	5	(n, α) and (n, p) products
^{82}Se	48	0·65	30	—	—	Extract ^{83}Br (^{83}Kr)
^{81}Br	46	3·5	25	4·8	—	(n, α) and (n, p) products
^{89}Y	50	2·9	10	2·4	—	,, ,, ,,
^{96}Zr	56	$\leqslant$4 ‖	—	—	—	Extract ^{97}Nb
^{104}Ru	60	13.6	20	2·3	—	(n, α) and (n, p) products
^{110}Pd	64	2·0	20	($\sim$30)	15	Extract ^{111}Ag
^{127}I	74	2·5	20	35	18	(n, α) and (n, p) products
^{138}Ba	82	1·3	30	1·8	—	,, ,, ,,
^{139}La	82	1·48	10	3·4	—	,, ,, ,,
^{142}Ce	84	$\leqslant$7·5 ‖	—	—	—	,, ,, ,,
^{141}Pr	82	3·33	10	3·3	—	None
^{160}Gd	96	18·5	30	($\sim$5)	—	None
^{165}Ho	98	$\geqslant$9·45 ¶	—	—	—	None
^{186}W	112	4·0	20	17	9	(n, α) and (n, p) products
^{198}Pt	120	1·7	20	32	11	Extract ^{199}Au
^{205}Tl	124	2·0	20	—	—	(n, α) and (n, p) products
^{208}Pb	126	3·05	15	0·7	—	,, ,, ,,
^{209}Bi	126	1·45	12	2·4	—	,, ,, ,,
^{232}Th	142	5·2	15	17	9	(n, α) (n, p) (n, f) and nat. daughters
^{238}U	146	3·3	15	35	28	,, ,, ,,

(1) Target nuclide ; (2) neutron number ; (3) σ(n, γ) (mbn) † ; (4) standard deviation (%) ; (5) σ_1/σ_{14} (obs) ‡ ; (6) low energy neutron correction (%) § ; (7) chemical separation.

† The figures in this column have been corrected for the low energy neutron error.

‡ Values in brackets in this column were obtained using interpolated values for σ_1.

§ Errors not quoted are all small compared with the standard deviation error of the cross section.

‖ Upper limit only due to insufficient yield.

¶ Lower limit only as ^{166}Ho$^{\mathrm{m}}$($>$30y) was not observed.

The well marked dips in the general level of cross sections near magic neutron numbers observed for fission neutrons are not so marked for neutrons of 14·5 MEV.

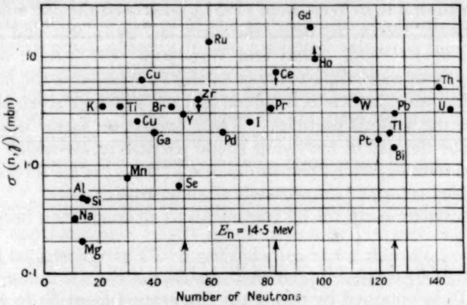

Radiative capture cross sections for 14·5 MEV neutrons. The target nuclide symbols with arrows indicate upper and lower limits ; the positions of closed neutron shells are shown along the neutron number axis.

4.2. *Theoretical Prediction of* σ (n, γ) *for* 14·5 MEV *Neutrons*

As there appear to be no published data concerning capture cross sections for neutrons of energy greater than 5 MEV, it is of interest to try and predict the magnitude of capture cross sections for 14·5 MEV neutrons, using the theory developed by Blatt and Weisskopf (1952).

The radiative capture cross section can be expressed in the form

$$\sigma(\mathrm{n},\gamma)=\sigma(\mathrm{c})\,\alpha\Gamma_\gamma/\Gamma\sim\sigma(\mathrm{c})\,\alpha\Gamma_\gamma/\Gamma_\mathrm{n}$$

where $\sigma(\mathrm{c})$ is the cross section for the formation of the compound nucleus and Γ_γ and Γ_n are the average values of the radiative and neutron widths. Γ is the average total width of the excited levels of the compound nucleus formed.

In these experiments the compound nucleus is excited to about 21 MEV and the predominant mode of disintegration will be neutron emission, so that $\Gamma\sim\Gamma_\mathrm{n}$. α is that fraction of primary γ rays leading to levels below the region of the neutron binding energy of the compound nucleus. Only these γ rays will result in a radiative capture process as the probability of neutron emission from all other higher levels is so high.

(*a*) *Estimation of* Γ_n.

The neutron width is given by the expression,

$$\Gamma_\mathrm{n}=\frac{1}{\pi^2\rho_\mathrm{c}(W)}\int_0^{E\,\mathrm{max}}\frac{mE_\mathrm{n}}{\hbar^2}\,\sigma(E_\mathrm{n})\,\rho_\mathrm{R}(E_\mathrm{max}-E_\mathrm{n})\,dE_\mathrm{n}$$

where $\rho_\mathrm{c}(W)$ is the density of levels of the compound nucleus for an excitation energy W, $\rho_\mathrm{R}(E_\mathrm{max}-E_\mathrm{n})$ is the density of levels of the residual nucleus after emission of a neutron energy E_n (maximum energy E_max), m is the mass of the neutron and $\sigma(E_\mathrm{n})$ is the cross section for the production of a neutron of energy E_n.

Blatt and Weisskopf (1952) have calculated this function using the statistical model of the nucleus. The density of levels in this model is given by the expression $\rho(W)=c\exp\sqrt{(aW)}$ in which c and a are constants which vary only with atomic weight.

(*b*) *Estimation of* Γ_γ.

The radiative width for an E1 transition between two levels is given by the following expression due to Weisskopf (1951), who used the extreme one particle model, $\Gamma_\gamma = 0{\cdot}047\,E_\gamma^3 R^2$ ev, E_γ being the γ-ray energy in Mev and R the nuclear radius in units of 10^{-13} cm. Blatt and Weisskopf (1952) have shown that at excitation energies of more than 1 Mev or so this expression is too large. This is because more than one particle is involved and the width as given above must be shared amongst the various particles. Their correction factor is $\rho(0)/\rho(W_{\max})$ where $\rho(0)$ is the density of low-lying single particle levels which can combine with the ground state to give E1 transitions and $\rho(W_{\max})$ is the level density of the compound nucleus as formed immediately after neutron capture.

The total radiative width for E1 transitions to all levels then becomes

$$\Gamma_\gamma = \left(\frac{R}{\hbar c}\right)^2 \frac{1}{137[1.3.\ldots(2l+1)]^2}\,\frac{\rho(0)}{\rho(W_{\max})}\int_0^{W_{\max}} E_\gamma^3\,\rho(W_{\max}-E_\gamma)\,dE_\gamma.$$

The product $\alpha\Gamma_\gamma$ is obtained by taking the integration from E_B to $W_{\max}$ instead of from zero to $W_{\max}$, where E_B is the binding energy of the neutron.

(*c*) *Estimation of* $\sigma(\mathrm{n},\gamma)$.

This estimation will be restricted to heavy elements in the region $A \sim 160$ and to incident neutron energies of 1 Mev and 14·5 Mev.

In order to evaluate Γ_n, Γ_γ and α, values for the constants in the level density formula are required. Blatt and Weisskopf have estimated these from various measurements of level spacings. In particular it is known from thermal neutron capture experiments that $\rho(W) \sim 10^5$ Mev^{-1} for $W \sim 6{\cdot}5$ Mev.

In the expression for Γ_γ a value of the order of 7×10^{-3} Mev^{-1} has been taken for the quantity $\rho(0)$. This is the value found necessary to obtain agreement between the work of Levin and Hughes (1956) and Kinsey and Bartholomew (1954) on thermal neutron capture γ-ray widths and the expression above for Γ_γ. It is, however, an order of magnitude smaller than that expected for a single particle in a nuclear well.

The magnitude of the remaining factor in the expression for $\sigma(\mathrm{n},\gamma)$, namely $\sigma(\mathrm{c})$, is of the order of 10^{-24} cm^2 for neutrons both of 1 Mev and 14·5 Mev.

The results of these calculations are summarized in the following table.

Table 2

	$E_\mathrm{n} = 1$ Mev	$E_\mathrm{n} = 14{\cdot}5$ Mev
Γ_n (ev)	5	50×10^3
Γ_γ (ev)	0·15	1·5
α	0·95	$2{\cdot}5 \times 10^{-3}$
$\sigma(\mathrm{n}\gamma)$ (mbn)	~ 30	$\sim 10^{-4}$

From the work of Levin and Hughes it can be seen that the cross section for 1 Mev neutrons for elements in the region $A \sim 160$ is about 150 mbn. At this energy the re-emission of a neutron will leave a residual nucleus with an excitation energy of less than 1 Mev. Only a few levels will be excited and the statistical theory will not be strictly valid. For this reason the agreement between the approximate estimate in table 2 and experimentally observed values for the capture cross section for 1 Mev neutrons can be considered satisfactory.

On the other hand the values found in the present experiments for the capture cross section at 14·5 MeV are four orders of magnitude greater than the value predicted in the table.

Drastic changes in the values of the constants in the level density formula result in relatively small changes in the predicted value for the total radiative width. On the other hand the value of α is quite sensitive to these changes. The transit time of a 14·5 MeV neutron across a heavy nucleus corresponds to a width of the order of 500 kev. Thus, the estimate for the total neutron width of 50 kev given in the table appears reasonable and the discrepancy between the observed and predicted values of the radiative cross section must be due to an incorrect assessment of Γ_γ.

It is of interest to note that the extreme one particle formula predicts a total γ-ray width of approximately 3·5 kev for excitation by 14·5 MeV neutrons. Using this value and taking the value of α quoted already for this energy, the predicted value for the radiative cross section amounts to approximately 0·5 mbn, which is the right order of magnitude.

If in fact radiative capture processes do derive from transitions by one or two nucleons which take up most of the energy of the incident neutron, something akin to a direct interaction mechanism is taking place.

Lane and Lynn (to be published) have recently developed a theory of direct radiative capture involving radiation from the incident neutron going into a bound orbit before the formation of a compound nucleus. This theory predicts radiative capture cross sections for 14·5 MeV neutrons in substantial agreement with those found.

More experimental evidence is required before the capture mechanism is really understood. Especially useful would be the capture γ-ray spectrum and the variation of the capture cross section with neutron energy for neutrons of between 10 and 20 MeV.

ACKNOWLEDGMENTS

The authors would like to take this opportunity of thanking Dr. K. W. Allen, Dr. B. B. Kinsey, Dr. A. M. Lane and Mr. J. E. Lynn for many useful comments concerning the theoretical implications of this work, and Mr. J. Prosser for his assistance in the preparation and irradiation of the samples.

REFERENCES

BLATT, J. M., and WEISSKOPF, V. F., 1952, *Theoretical Nuclear Physics* (New York : Wiley), p. 373.

COON, J. H., GRAVES, E. R., BATTAT, M. E., and DAVIS, R. W., 1955, quoted in a paper by Bonner, T. W., *Proc. Int. Conf. on Peaceful Uses of Atom. En. Geneva*, Vol. 4, p. 92.

FESHBACH, H., PEASLEE, D. C., and WEISSKOPF, V. F., 1947, *Phys. Rev.*, **71,** 145.

GRAVES, E. R., and DAVIS, R. W., 1955, *Phys. Rev.*, **97,** 1205.

HOLMES, J. E. R., MCVICAR, D. D., ROSE, H., SMITH, R. D., SHEPHERD, L. R., 1955, *Proc. Int. Conf. on Peaceful Uses of Atom. En. Geneva*, Vol. 5, p. 331.

HUGHES, D. J., GARTH, R. C., and LEVIN, J. S., 1953, *Phys. Rev.*, **91,** 1423 (see also Hughes, D. J., Spatz W. D. B., and Goldstein, N., 1949, *Phys. Rev.*, **75,** 1781, and Hughes, D. J., and Sherman, D., 1950, *Phys. Rev.*, **78,** 632).

HUGHES, D. J., and HARVEY, J. A., 1955, *U.S. Atomic Energy Commission Report* BNL 325 and BNL 325 Supplement No. 1.

KINSEY, B. B., and BARTHOLOMEW, G. A., 1954, *Phys. Rev.*, **93,** 1260.

LEVIN, J. S., and HUGHES, D. J., 1956, *Phys. Rev.*, **101,** 1328.

WEISSKOPF., V. F., 1951, *Phys. Rev.*, **83,** 1073.

Observation by Cyclotron Resonance of the Effect of Strain on Germanium and Silicon

By A. C. ROSE-INNES

Services Electronics Research Laboratory, Baldock, Herts.

MS. received 26*th February* 1958, *and in final form* 14*th May* 1958

Abstract. Cyclotron resonance at microwave frequencies is used to observe the changes in the band structure of germanium and silicon caused by a non-isotropic elastic strain. It is shown that an elongation of the crystal in a given direction raises the energy of those minima of the conduction band which lie on the corresponding direction in momentum space and, conversely, a contraction lowers the energy. A non-isotropic strain decreases the intensities of the hole resonances but this effect has not been studied in detail. The results are consistent with conclusions drawn from piezo-resistance measurements.

---

§ 1. Introduction

The nature of the band edges in semiconductors depends on the symmetry of the crystal lattice, and if the crystal is distorted by a non-isotropic strain, such as that produced by a uniaxial tension, the form of these surfaces will be altered. The effect of this has been observed in piezo-resistance measurements on germanium and silicon (Smith 1954) and has been discussed by Herring (1955) and Adams (1954). Cyclotron resonance at low temperatures enables us to observe directly electrons and holes lying close to the band edges, and so it is to be expected that a strain will have an effect on the cyclotron resonance spectrum of a semiconductor. I have observed such an effect on the microwave cyclotron resonance spectrum of electrons and holes in both germanium and silicon at liquid helium temperatures.

Let us first consider electrons. In germanium the minima of the conduction band lie on the [111] directions in momentum space, and in silicon along the [100] directions. Piezo-resistance measurements indicate that, if a tension is applied to a crystal producing an elongation in a certain direction relative to the crystal axes, those minima which lie in a corresponding direction in momentum space have their energy raised and, conversely, a compression lowers the energy. Those minima which are raised relative to others will become less populated by an amount depending on the energy difference (figure 1). Electrons on minima lying in different directions in momentum space give rise to separate lines in the cyclotron resonance spectrum and so, if the crystal is in a state of strain, those minima which have been lowered should give rise to stronger lines because they contain more electrons.

A different situation occurs for holes. In germanium and silicon the edge of the valence band has the form of a 'warped sphere' with cubic symmetry, and the maximum lies at the origin in momentum space. The band is doubly degenerate at the edge giving rise to light and heavy holes. Since there is only one maximum the mechanism described above for electrons cannot operate.

It appears that a non-isotropic strain may remove the degeneracy, separating the light and heavy hole bands, and will also increase the warping of the energy surfaces. The first effect would alter the relative intensities of the light and heavy hole resonances. The second effect would alter the shape of the resonance.

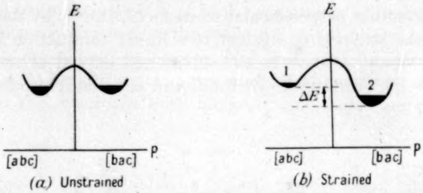

Figure 1. The effect of strain on the conduction band.

§ 2. EXPERIMENTAL

The cyclotron resonance spectra were recorded at a wavelength of about 3·2 cm with the frequency-modulated microwave spectrometer described elsewhere (Rose-Innes 1957). Measurements, unless otherwise stated, were made at 4·2°K and the electron and holes were created by means of white light from an electric bulb, a quartz light guide being used to carry the light down into the resonant cavity.

In these experiments it is important to keep the microwave power in the cavity low. Too much power has the effect of broadening the resonance lines and altering their relative intensities. This is particularly noticeable in specimens which are strained. The microwave power was kept below about 10 μW, at which level it was found that these troublesome effects do not occur. The relative intensities of the various peaks of the spectra seemed to be independent of the intensity of the light (i.e. of the number of carriers) over a range from dull red to brilliant white heat of the filament.

The specimens of germanium and silicon were rectangular slabs about 8 mm × 4 mm × 0·4 mm. The surfaces were etched, about 0·05 mm being removed from each surface. The resistivities of the germanium specimens were between 20 and 40 ohm cm at room temperature and those of the silicon specimens were between 400 and 1000 ohm cm.

In order to produce strains in the specimens, the difference in thermal expansion of the semiconductor and of silica was used. Figure 2 (*a*) shows the specimen holder for producing a tension. A silica rod of 4 mm diameter has slots cut into it as shown and has a slotted cap of equal diameter. The narrow slots s are filled with tap grease and the specimen is put into the holder with the ends of the specimen in these narrow slots, as shown diagrammatically in figure 2 (*b*). Below room temperature tap grease hardens to a cement gripping the ends of the specimen firmly. On cooling down to liquid helium temperatures the semiconductor shrinks much more than the silica which has only a small coefficient of expansion (Keesom and Doborzynski 1934, McSkimin 1953). Since the silica specimen holder is thick compared to the specimen, the specimen is under tension in a vertical direction. We shall refer to this as the 'tension' method. Figure 2 (*c*) shows another way of distorting the specimen. A segment q is cut from a silica rod and the thin specimen is stuck on to the plane face p with a film of tap grease, q is then stuck on to the other face of the specimen with tap grease, so the final assembly is as shown in figure 2 (*d*). When the holder is cooled to liquid helium temperatures the semiconductor would contract but the plane faces are prevented from doing so by the adhesion to the silica. The specimen can, however, still freely contract in the direction perpendicular to its faces, shown by the arrow. In this case, therefore, the strain is equivalent to a linear contraction in the horizontal direction of the arrow, relative to the unstrained crystal at room temperature. We shall call this the 'sandwich' method, and say that it produces an 'effective contraction'.

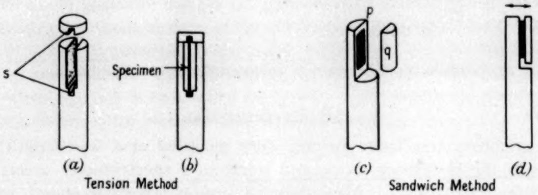

Figure 2. Specimen holders for producing strain.

Unfortunately, it has not been possible to measure experimentally the magnitude of strain produced in the specimens. We can, however, make a rough estimate. The thermal expansion of germanium has been measured down to liquid oxygen temperatures (MacNair, see McSkimin 1953): at 100°K the change in length relative to the length at 273°K is

$$\frac{[l(100^\circ)-l(273^\circ)]}{l(273^\circ)}=-85\times10^{-5}.$$

It seems that in most materials the contraction at 100°K is about 90% of the final contraction at very low temperatures (see, for example, Bijl and Pullan 1955) and so we may estimate that at liquid helium temperatures the contraction of germanium is about

$$\frac{l(4{\cdot}2^\circ)-l(273^\circ)}{l(273^\circ)}\simeq-10^{-3}. \qquad \ldots\ldots(1)$$

The thermal expansion of fused silica has been measured down to very low temperatures (Laquer, Los Alamos Scientific Laboratory Report AECD 3706) and is $+10^{-4}$ at 4·2°K, negligible with respect to germanium. Hence we can take (1) as the strain in our germanium specimen at liquid helium temperatures. Fine (1955) has measured the elastic constants of germanium down to 1·7°K and gives Young's modulus in the [100] direction as $10{\cdot}4\times10^{11}\,\mathrm{dyn\,cm^{-2}}$. Our stresses therefore correspond to about $10^{9}\,\mathrm{dyn\,cm^{-2}}$. The strain produced on cooling down is not necessarily equivalent to the complete difference in the thermal contractions between the silica and the semiconductor, because there is some slip between the surface of the specimen and that of the silica holder. This slip is greater in the case of a specimen in the 'tension' holder, because only a small part of the surface is being gripped. It is found that the sandwich method produces a strain equivalent to at least twice that of the tension method.

§ 3. RESULTS FOR GERMANIUM AND SILICON

The cyclotron resonance spectra of both germanium and silicon were affected while the crystals were strained in the ways described above. Typical spectra obtained at 4·2°K are shown in figures 3 (*c*) and 3 (*e*) for germanium, and in figures 4 (*a*) and 4 (*b*) for silicon. In our method of creating carriers by shining white light on to the specimen both electrons and holes are present, and the

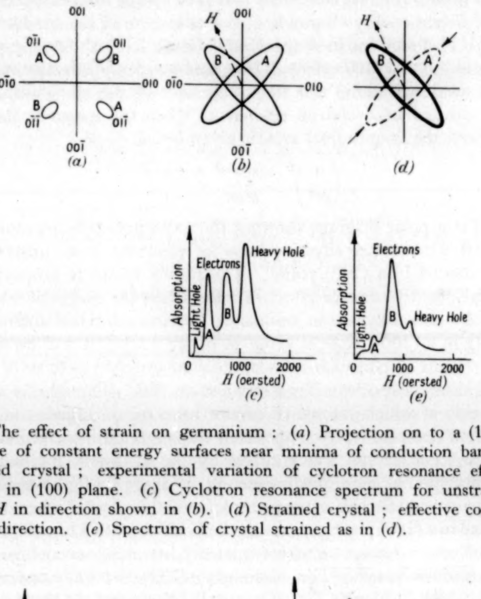

Figure 3. The effect of strain on germanium : (*a*) Projection on to a (100) plane in *k*-space of constant energy surfaces near minima of conduction band. (*b*) Unstrained crystal ; experimental variation of cyclotron resonance effective mass for *H* in (100) plane. (*c*) Cyclotron resonance spectrum for unstrained crystal with *H* in direction shown in (*b*). (*d*) Strained crystal ; effective compression in [011] direction. (*e*) Spectrum of crystal strained as in (*d*).

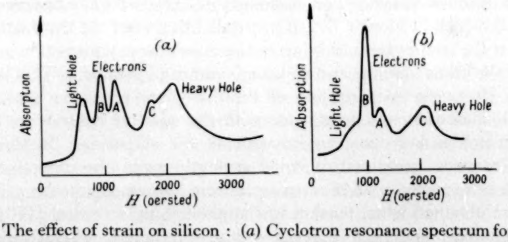

Figure 4. The effect of strain on silicon : (*a*) Cyclotron resonance spectrum for unstrained crystal with *H* in a (100) plane at about 35° from a [001] direction. (*b*) Spectrum of strained crystal with *H* in same direction as 4 (*a*), but with effective contraction in an [001] direction.

spectra contain peaks from all of these. The peaks were identified by use of the cyclotron resonance results of Dresselhaus, Kip and Kittel (1955) and of Dexter, Zeiger and Lax (1956). To confirm that the changes in the spectra were due to elastic strain of the lattice and not due to the creation of permanent lattice defects by the stress, crystals which had been measured under strain were measured again in an unstrained condition. In all cases the latter spectra, both for holes and electrons, corresponded to those of an unstrained crystal. This shows that the effects are the result of reversible elastic strain.

3.1. *Electrons*

We shall first discuss the results for electrons. Results obtained for germanium at 4·2°K with the magnetic field in a (100) plane are illustrated in figure 3. The eight constant energy ellipsoids of the minimum of the conduction band lie along the [111] directions in k-space, and figure 3 (*a*) shows the projection of these ellipsoids on to a (100) plane. If m_l and m_t are the effective masses corresponding to the longitudinal and transverse axes of the ellipsoids, the effective mass m^* measured by cyclotron resonance, when the magnetic field H makes an angle θ with the longitudinal axis, is given by

$$\left(\frac{1}{m^*}\right)^2 = \frac{\sin^2\theta}{m_l m_t} + \frac{\cos^2\theta}{m_t^2}.$$

Figure 3 (*b*) is a polar diagram showing the experimentally measured variation of the cyclotron resonance effective mass for electrons in an unstrained crystal when H is rotated in a (100) plane. The radius vector is proportional to the measured cyclotron resonance effective mass when the magnetic field is in that direction. An actual cyclotron resonance spectrum for the unstrained crystal with H lying in a (100) plane is given in figure 3 (*c*). It will be seen that the peaks for electrons on ellipsoids A are of the same intensity as those of ellipsoids B. Figure 3 (*e*) shows a spectrum for a strained crystal. Though the values of the magnetic fields at which resonance occurs have not changed, the intensity of resonance from electrons lying on one set of ellipsoids has increased at the expense of the other. The crystal was strained by the sandwich method to give an effective contraction along a [110] direction. Figure 3 (*d*) shows the measured cyclotron resonance effective mass pattern from this crystal when the magnetic field is rotated in a (100) plane containing the [110] direction of contraction. The dark line indicates a resonance whose intensity has increased and the broken line one which has decreased. The resonance which has increased is that from ellipsoids B, which lie along a direction parallel to that of the contraction. This implies that the energy minima lying in the direction of contraction are lowered relative to the other minima, and so become more populated. This is in agreement with Herring's interpretation of Smith's piezo-resistance measurements. As a check, measurements were made with the effective contraction in a [001] direction which makes equal angles with all the ellipsoids. In this case the electron resonances remained of equal strength, as in the unstrained crystal, which is to be expected if all minima are lowered an equal amount. Consistent results were obtained when tension was applied along a vertical [110] direction and cyclotron resonance was observed with H in a horizontal (110) plane.

Similar experiments were carried out with silicon, which has six minima of the conduction band lying along the [100] directions. Results consistent with the above interpretation for germanium were obtained both with a tension in the [110] direction and with effective contraction by the sandwich method in the (100) plane. As in germanium, those minima lying in a direction of contraction were lowered while those in a direction of extension were raised. (In the spectrum of the unstrained crystal the peak C from the electrons on the ellipsoid whose axis is perpendicular to the plane in which H lies seems to be weaker than the other two (figure 4 (*b*)) but it is not properly resolved from the heavy hole resonance.)

If the change in the intensities of the electron resonances in a strained crystal is a result of a difference in the populations of the valleys, the relative intensities should vary with temperature. Let n_1 and n_2 be the equilibrium numbers of electrons in the lower and higher valleys. Electrons are raised from the valence band up into the conduction band at a constant rate by the white light, and fall into the valleys at a rate dn/dt. Each valley loses electrons both by recombination into the valence band and by scattering into the other valley. Let τ_r and τ_{12}, τ_{21} be the relaxation times for the recombination and intervalley scattering: then in equilibrium

$$\frac{dn_1}{dt}=\frac{dn}{dt}+\frac{1}{\tau_{21}}n_2-\frac{1}{\tau_{12}}n_1-\frac{1}{\tau_r}n_1=0$$

and

$$\frac{dn_2}{dt}=\frac{dn}{dt}+\frac{1}{\tau_{12}}n_1-\frac{1}{\tau_{21}}n_2-\frac{1}{\tau_r}n_2=0$$

where

$$\tau_{12}/\tau_{21}=\exp(\Delta E/kT)$$

and ΔE is the amount by which the energy of valley 2 is above that of valley 1. These equations give

$$\frac{n_1}{n_2}=\frac{2+\tau_{21}/\tau_r}{\tau_{21}/\tau_r+2\exp(-\Delta E/kT)}. \qquad \ldots\ldots(2)$$

The approximation has been made that the relaxation times are independent of temperature over the range considered. If the intervalley scattering time is short compared to the recombination time ($\tau_{21}/\tau_r \ll 1$), equation (2) reduces to a simple Boltzmann distribution, $n_1/n_2=\exp(\Delta E/kT)$. If the intervalley scattering time is very long compared to the recombination time ($\tau_{21}/\tau_r \gg 1$), $n_1 \simeq n_2$ for all temperatures. In figure 5 are plotted curves, obtained from equation (2), of $\ln(n_1/n_2)$ against $\Delta E/kT$ for various values of τ_{21}/τ_r.

An experiment was performed on a germanium specimen under tension in a [110] direction. The areas under the resonance curves of electrons belonging to minima shifted by the strain were measured over the temperature range 4·2 to 1·7°K. These areas will be proportional to the number of electrons in the minima. The results are plotted in figure 5, the value of $\Delta E/kT$ for the point obtained at 4·2°K being adjusted so that the points lie on one of the calculated curves. Though there is some scatter among the points, they fit fairly well on the curve with $\tau_{21}/\tau_r=0{\cdot}16$. For this specimen τ_{21}/τ_r must be less than about 0·22, because the curve corresponding to this value rises asymptotically to a value less than the highest experimental point. The experimental points would not fit well on a curve corresponding to τ_{21}/τ_r less than about 0·10.

Taking the component of strain along the [111] directions where the minima lie, I find for this germanium specimen $\Delta E \simeq 7\times10^{-4}$ ev, giving a value of about +2 ev per unit strain for the shift in the conduction band edge. Smith (1954) has deduced a value of the order of several electron volts from piezo-resistance measurements on n-type silicon and Brooks (1955) calculates values of +2·3 or −5·8 ev per unit dilation for the conduction band edge in germanium at liquid nitrogen temperatures. The present results show that the value must be positive.

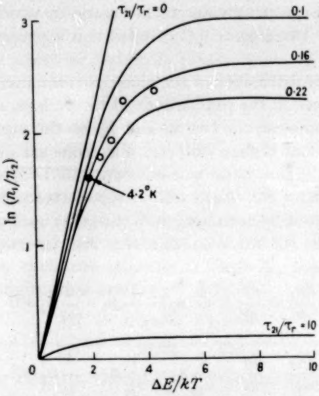

Figure 5. Variation with temperature of relative populations of two minima.

3.2. *Holes*

It is found that the hole resonances, both in germanium and silicon, are reduced when the specimens are strained, and that the light hole is reduced relative to the heavy hole (see figures 3 and 4). This must be the result of a different mechanism from that operating on electrons, because the valence band has only one maximum, situated at the origin in momentum-space. The constant energy surfaces of an unstrained crystal are not ellipsoidal but have a 'warped sphere' form, which can be written

$$E = \frac{p^2}{2m}[1 + g(\mathbf{p}/p)],$$

where m is the average effective mass and $g(\mathbf{p}/p)$ is a small non-spherical term depending only on angle (Zeiger, Lax and Dexter 1957). Because the surfaces are not ellipsoids there is not a unique value of the cyclotron resonance effective mass, but a distribution of values. As a result the breadth and intensity of a hole resonance vary with the direction of the magnetic field. Another effect of the fluted nature of the surfaces is to give resonance absorption at harmonics of the fundamental cyclotron frequency (Zeiger, Lax and Dexter 1957). The intensities of these harmonics are very dependent on the direction of the magnetic field.

Unfortunately, because of the variation of the shapes and intensities of the hole resonances with the direction of the magnetic field, and the presence of electron resonances which overlap those of the holes, it has not been possible to make a complete study of the hole resonances. Furthermore, in a strained crystal the light hole resonance may be so reduced that it is often impossible to measure its intensity. In an unstrained crystal of silicon the ratio of the integrated intensity of the light hole resonance relative to that of the heavy hole was about 1 : 5, which agrees with the ratios of the effective masses. When the same crystal was under tension in a [110] direction, the ratio was decreased to about 1 : 10. This ratio did not appear to change as the temperature was lowered from 4·2 to 2°K.

The piezo-resistance of p-type germanium and silicon has been interpreted (Adams 1954, Morin, Geballe and Herring 1957) as being the result of the strain splitting the degeneracy at the band edge and increasing the warping of the energy surfaces. The decrease of the light hole resonance relative to that of the heavy hole is consistent with the strain lowering the light hole band below that of the heavy hole, thus decreasing the relative population.

No change due to strain was observed in the anisotropy of the measured effective mass of the heavy hole. This means that any such change was less than about 10%. I have not been able to find a satisfactory explanation in terms of distortion of the band structure for the decrease in the strength of the heavy hole resonance in a strained crystal. If strain produces a small increase in the warping of the heavy hole band we might expect that the intensity of the harmonics of the heavy hole resonance would increase relative to the fundamental, but it was not possible to measure the intensities of the harmonics because of the presence of electron resonances. It should, however, be possible to perform such measurements using shorter wavelengths (say 8 mm) on p-type material, where only holes would be excited by the microwaves.

§ 4. CONCLUSIONS

The cyclotron resonance experiments have shown directly the effect of a non-isotropic strain on the conduction band edges in germanium and silicon. Those minima of the conduction band which lie on a direction in momentum space parallel to an extension in the crystal are raised in energy, while those in a direction of contraction are lowered.

A non-isotropic strain decreases the intensities of the hole resonances, and the decrease of the light hole peak relative to that of the heavy hole is consistent with the strain removing the degeneracy at $k=0$. It has not been possible to explain the decrease in the heavy hole resonance by a distortion of the valence band edge.

ACKNOWLEDGMENTS

My thanks are due to Drs. R. Barrie, G. Rickayzen, E. H. Rhoderick and O. Simpson for much helpful discussion and advice. Dr. A. F. Gibson of the Royal Radar Establishment, Malvern, kindly gave me a piece of 1000 ohm cm silicon, and I am indebted to Dr. D. M. S. Bagguley for making some cyclotron resonance measurements for me at the Clarendon Laboratory, Oxford. Acknowledgment is made to the Admiralty for permission to publish this paper.

REFERENCES

ADAMS, E. N., 1954, *Phys. Rev.*, **96,** 803.
BIJL, D., and PULLAN, H., 1955, *Physica*, **21,** 285.
BROOKS, H., 1955, *Advanc. Electron.*, **7,** 85.
DEXTER, R. N., ZEIGER, H. J., and LAX, B., 1956, *Phys. Rev.*, **104,** 637.

Dresselhaus, G., **Kip**, A. F., and **Kittel**, C., 1955, *Phys. Rev.*, **98**, 368.
Fine, M. E., 1955, *J. Appl. Phys.*, **26**, 862.
Herring, C., 1955, *Bell Syst. Tech. J.*, **34**, 251.
Keesom, W. H., and **Doborzynski**, D. W., 1934, *Physica*, **1**, 1085.
McSkimin, H. J., 1953, *J. Appl. Phys.*, **24**, 988.
Morin, F. J., **Geballe**, T. H., and **Herring**, C., 1957, *Phys. Rev.*, **105**, 525.
Rose-Innes, A. C., 1957, *J. Sci. Instrum.*, **34**, 276.
Smith, C. S., 1954, *Phys. Rev.*, **94**, 42.
Zeiger, H. J., **Lax**, B., and **Dexter**, R. N., 1957, *Phys. Rev.*, **105**, 495.

Electron Excitation of Atomic Hydrogen in the 2s State

By T. J. M. BOYD†

Department of Applied Mathematics, The Queen's University of Belfast

Communicated by D. R. Bates; *MS. received 9th May* 1958

Abstract. Using an interpolation procedure the Born approximation to the cross sections for the excitation of hydrogen atoms from the 2s state to the eighth and higher levels has been obtained from computed cross sections for transitions to the lower discrete levels and to the continuum. An incident energy range of from 5 ev to 120 ev is covered.

§ 1. Introduction

The determination of excitation cross sections when the higher discrete levels of an atom are concerned, is rendered difficult by the algebraic complexity of the expressions involved, becoming progressively more tedious with increase of the principal quantum number n of the level into which the electron is excited. Accordingly, it is desirable to have available an alternative to the direct computation of these cross sections. An interpolation method using excitation cross sections calculated for $n \leqslant 7$ and differential ionization cross sections near to the ionization threshold has been adopted to determine excitation cross sections for hydrogen when $n \geqslant 8$. Such a method was found by McCarroll (1957) to be sufficiently accurate in the case of excitation from the ground state.

Many theoretical studies of the excitation of hydrogen atoms under electron impact have been made (Elsasser 1927, Bethe 1930, Massey and Mohr 1931, Goldstein 1933, McCarroll 1957). However, in all cases, with the exception of the work of Goldstein, the atoms have been initially in the ground state. Bethe derived an expression for the cross section for excitation to any discrete level having principal quantum number n, while Massey and Mohr found the cross section corresponding to the excitation of the atom to the (n, l, m) state. Goldstein, in an exhaustive study, calculated the integrals occurring in the expressions for the matrix elements for transitions from *any* initial state (n, l) to *any* final state (n', l').

Several authors (Goldstein 1933, Burhop 1940, Yavorsky 1945, Mandl 1952, Swan 1955) have considered the ionization of hydrogen atoms from excited states. For his study of ionization Goldstein used not the customary Sommerfeld wave function, but a function due to Gordon. It is scarcely feasible to derive explicit forms for the cross sections since this would require the evaluation of the integrals occurring in terms of infinite series which do not necessarily have a large radius of convergence. In an investigation of the inner shell ionization of atoms under electron impact Burhop gave expressions for the differential ionization cross sections from the K- and L-shells. Yavorsky studied the 'stepped ionization' of hydrogen by electron impact and computed ionization cross sections for the second and third levels; his analysis refers to hydrogen atoms initially in S-states. Mandl derived expressions for the cross section for ionization of hydrogen atoms in the 2s and 2p states by electron impact but carried out a numerical computation only for the 2p ($m=\pm 1$) case, since his expressions do not lend themselves readily to numerical work. It may be shown after considerable algebraic manipulation that in the 2s case (the only one considered in the present work), the expression given by Mandl for the ionization cross section reduces to that found by Burhop. Swan has published cross sections for the ionization by electrons of hydrogen atoms in the 2s and 2p states.

---

† Now at Department of Electron Physics, University of Birmingham.

In the present work general expressions have been obtained for the excitation cross section from the 2s state to any discrete state characterized by quantum numbers n, l, m and for the cross section for excitation from the same initial state to all discrete states having principal quantum number n.

§ 2. THEORY

The method used has been described by McCarroll (1957) and is based on the fact that $\frac{1}{2}n^3Q_{2s,\,n}$, in which n is the principal quantum number of the level excited and $Q_{2s,\,n}$ the total cross section for the excitation of that level from the 2s state, regarded as a function of E_n, the energy of the nth level, is a continuous function with $Q_\epsilon^{\,1}$ the cross section for the ejection of the atomic electron into the continuum with energy in the range ϵ, $\epsilon+d\epsilon$ regarded as a function of ϵ so that

$$\lim_{n\to\infty} \tfrac{1}{2}n^3Q_{2s,\,n}=Q_0^{\,1}. \qquad \ldots\ldots(1)$$

Provided $Q_{2s,\,n}$ is determined for a few of the lower values of n and $Q_\epsilon^{\,1}$ for some small values of ϵ, the cross sections for the excitation of the higher discrete levels may be determined sufficiently accurately by interpolation.

2.1. *Excitation Cross Sections*

The total cross section for the excitation of all discrete levels of principal quantum number n from the 2s state is

$$Q_{2s,\,n}=\frac{2n^2}{(ka_0)^2}\int_{\zeta\min}^{\zeta\max}\frac{1}{\zeta^3}\sum_{l=0}^{n-1}|\epsilon_{2s;\,n,\,l}(\zeta)|^2\,d\zeta\,\pi a_0^{\,2}, \qquad \ldots\ldots(2)$$

with

$$\zeta=\tfrac{1}{2}nKa_0$$

$$\epsilon_{2s;\,n,\,l}(\zeta)=\int \mathrm{e}^{iKr\cos\theta}\psi_{2,\,0}(\mathbf{r})\psi^*_{n,\,l}(\mathbf{r})\,d\mathbf{r} \qquad \ldots\ldots(3)$$

in which K is the magnitude of the change in momentum suffered by the scattered electron (cf. Mott and Massey 1949). The value of (3) may be calculated for all n, l to yield

$$\epsilon_{2s;\,n,\,l}(\zeta)=\frac{i^l\pi}{2K^{1/2}}\left(\frac{1}{a_0}\right)^{3/2}N_{n,\,l}\left(\frac{na_0}{2}\right)^{l+5/2}I_{n,\,l}(\zeta), \qquad \ldots\ldots(4)$$

in which

$$\begin{aligned} I_{n,l}(\zeta) = D(n+l)!\,[(n+2)C^{l+2}_{n-l-1}(x)\gamma^{n-l-1} - 2nC^{l+2}_{n-l-2}(x)\gamma^{n-l-2} \\ + (n-2)C^{l+2}_{n-l-3}(x)\gamma^{n-l-3}] \\ + \frac{Dn(n+l)!}{(n+2)^2+16\zeta^2}\{[(2l+3)(2-n)^2 - 16\zeta^2]C^{l+3}_{n-l-5}(x)\gamma^{n-l-5} \\ + 4[(2l+3)n(2-n)+16\zeta^2]C^{l+3}_{n-l-4}(x)\gamma^{n-l-4} \\ + 2[(2l+3)(3n^2-4)-48\zeta^2]C^{l+3}_{n-l-3}(x)\gamma^{n-l-3} \\ - 4[(2l+3)n(n+2)-16\zeta^2]C^{l+3}_{n-l-2}(x)\gamma^{n-l-2} \\ + [(2l+3)(n+2)^2-16\zeta^2]C^{l+3}_{n-l-1}(x)\gamma^{n-l-1}\} \end{aligned} \qquad \ldots\ldots(5)$$

with

$$\left.\begin{aligned} D &= \frac{2^{3l+13/2}\zeta^{l+1/2}\Gamma(2l+3)}{\Gamma(l+\frac{3}{2})[(n+2)^2+16\zeta^2]^{l+2}} \\ x &= \frac{n^2-4+16\zeta^2}{\{(n+2)^2+16\zeta^2\}^{1/2}\{(n-2)^2+16\zeta^2\}^{1/2}} \\ \gamma^2 &= \{(n-2)^2+16\zeta^2\}/\{(n+2)^2+16\zeta^2\} \\ N_{n,l}{}^2 &= \frac{2^{2l}}{n\pi}(2l+1)\frac{(n-l-1)!}{\{(n+l)!\}^3}\left(\frac{1}{na_0}\right)^{2l+3} \end{aligned}\right\} \qquad \ldots\ldots(6)$$

and $C^\nu_s(x)$ are the Gegenbauer polynomials defined by the generating function

$$(1-2tx+t^2)^{-\nu} = \sum_{s=0}^{\infty} C^\nu_s(x)t^s. \qquad \ldots\ldots(7)$$

On substituting (4) with $I_{n,l}(\zeta)$ given by (5) into (2) (and ignoring the summation sign), one can determine the cross section for excitation from the 2s state to the n, l state. If this is repeated for each value of l corresponding to the value of n under consideration, one may then sum over the azimuthal quantum number to obtain an expression for

$$\sum_{l=0}^{n-1}|\epsilon_{2s;\,n,l}(\zeta)|^2.$$

This method was used for $n=3$ but involves so much tedious algebra that an alternative method was sought for higher values of n. To evaluate

$$\sum_{l=0}^{n-1}|\epsilon_{2s;\,n,l}(\zeta)|^2$$

directly is an exceedingly difficult task whenever $\epsilon_{2s;\,n,l}(\zeta)$ is expressed in terms of Gegenbauer polynomials as in (5). However, the problem becomes tractable if one evaluates the matrix element using parabolic coordinates, as was done by Bethe (1930) for the ground state case.

The eigenfunction representing the nth level in terms of parabolic coordinates (ξ, η, ϕ) is given by

$$\psi_n = \frac{1}{\sqrt{(\pi n)}n_1!\,n_2!}\left(\frac{1}{na_0}\right)^{3/2}\exp\left(-\frac{\xi+\eta}{2na_0}\right)L_{n_1}\left(\frac{\xi}{na_0}\right)L_{n_2}\left(\frac{\eta}{na_0}\right) \qquad \ldots\ldots(8)$$

in which n_1, n_2 are parabolic quantum numbers and $n=n_1+n_2+1$ (Sommerfeld 1931). The matrix element $\epsilon_{2s;\,n_1,n_2}(y)$ now becomes

$$\begin{aligned}\epsilon_{2s;\,n_1,\,n_2}(y) = &-2^{7/2}n^2\frac{(n-2-2iny)^{n_1}(n-2+2iny)^{n_2}}{(n+2-2iny)^{n\ +1}(n+2+2iny)^{n_2+1}}\times \\ &\times[(n+2)^2+4n^2y^2]^{-2}[(n-2)^2+4n^2y^2]^{-2} \\ &\times[\{-32n^2y^2(9n^4-16n^3-8n^2+16-32n^2n_1n_2) \\ &\qquad\qquad+16^2n^4y^4(3n^2-4)-8^3n^6y^6\} \\ &+32iny(n_1-n_2)\{(n-4)^2-8(3n^2-4)n^2y^2+16n^4y^4\}] \qquad \ldots\ldots(9)\end{aligned}$$

in which

$$y = Ka_0.$$

Multiplying (9) by its complex conjugate and summing over all possible values of $n_1-n_2=-n+1,\ -n+3,\ \ldots,\ n-3,\ n-1$, one finds

$$\begin{aligned}|\epsilon_{2,\,n}(y)|^2 = &\frac{2^{17}n^7y^2}{15}\frac{[(n-2)^2+4n^2y^2]^{n-5}}{[(n+2)^2+4n^2y^2]^{n+5}} \\ &\times\{B^2[15n^2y^2+5(n^2-1)]+80n^4(n^2-4)By^2+64n^6(n^2-4)(3n^2-8)y^2\} \\ = &\sum_{l=0}^{n-1}|\epsilon_{2s;\,n,\,l}(y)|^2, \qquad \ldots\ldots(10)\end{aligned}$$

in which

$$B=\{(n^2-4)^2-8n^2(3n^2-4)y^2+16n^4y^4\}. \qquad \ldots\ldots(11)$$

Substituting (10) in (2) gives an expression for the cross section for excitation to the *n*th level. If one denotes

$$\sum_{l=0}^{n-1}|\epsilon_{2s;\,n,\,l}(\zeta)|^2$$

by $\mathscr{I}(2s;n;\zeta)$ then

$$\left.\begin{aligned}\mathscr{I}(2s;3;\zeta) &= \frac{3^4\,.\,2^{21}\zeta^2}{(25+16\zeta^2)^8}\{3\,.\,2^8\zeta^6-250\,.\,2^4\zeta^4+4771\zeta^2+1250\} \\ \mathscr{I}(2s;4;\zeta) &= \frac{2^{17}\zeta^2}{(9+4\zeta^2)^9}\{2^8\zeta^8-40\,.\,2^6\zeta^6+386\,.\,2^4\zeta^4+320\,.\,2^2\zeta^2+405\} \\ \mathscr{I}(2s;5;\zeta) &= \frac{2^{19}\,.\,5^5\zeta^2}{(49+16\zeta^2)^{10}}\{256\,.\,2^{10}\zeta^{10}-16128\,.\,2^8\zeta^8+236128\,.\,2^6\zeta^6 \\ &\qquad+602512\,.\,2^4\zeta^4+1173473\,.\,2^2\zeta^2+1555848\} \\ \mathscr{I}(2s;6;\zeta) &= \frac{3^4\zeta^2(1+\zeta^2)}{2^8(4+\zeta^2)^{11}}\{3\,.\,2^{10}\zeta^{10}-277\,.\,2^8\zeta^8+6008\,.\,2^6\zeta^6+19248\,.\,2^4\zeta^4 \\ &\qquad+60416\,.\,2^2\zeta^2+143360\} \\ \mathscr{I}(2s;7;\zeta) &= \frac{2^{19}\,.\,7^5\zeta^2(25+16\zeta^2)^2}{(81+16\zeta^2)^{12}}\{256\,.\,2^{10}\zeta^{10}-32512\,.\,2^8\zeta^8+975968\,.\,2^6\zeta^6 \\ &\qquad+3889936\,.\,2^4\zeta^4+17861313\,.\,2^2\zeta^2+65610000\}.\end{aligned}\right\} \qquad \ldots\ldots(12)$$

Writing

$$F_{9s,\,n}(\zeta)=\frac{2n^2}{(ka_0)^2}\int\frac{1}{\zeta^3}\mathscr{I}(2s;n;\zeta)\,d\zeta,$$

one has

$$Q_{2s,\,n}=[F_{2s,\,n}(\zeta\text{max})-F_{2s,\,n}(\zeta\text{min})]\pi a_0{}^2, \qquad \ldots\ldots(13)$$

where

$$\left.\begin{aligned}
F_{2s,\,3}(\zeta) &= \frac{2^{22}\,.\,3^{6}}{5^{12}(ka_0)^2}\Bigg[-\frac{15}{32}P_3{}^5(\zeta)+\frac{25}{12}P_3{}^6(\zeta)-\frac{403}{175}P_3{}^7(\zeta)\\
&\qquad +\ln\left(\frac{16\zeta^2}{25}P_3(\zeta)\right)+\sum_{s=1}^{7}\frac{1}{s}P_3{}^s(\zeta)\Bigg]\\
F_{2s,\,4}(\zeta) &= \frac{2^{21}}{3^{14}(ka_0)^2}\Bigg[-\frac{81}{5}P_4{}^5(\zeta)+\frac{201}{2}P_4{}^6(\zeta)-\frac{1349}{7}P_4{}^7(\zeta)+\frac{7123}{72}P_4{}^8(\zeta)\\
&\qquad +5\left\{\ln\left(\frac{4\zeta^2}{9}P_4(\zeta)\right)+\sum_{s=1}^{8}\frac{1}{s}P_4{}^s(\zeta)\right\}\Bigg]\\
F_{2s,\,5}(\zeta) &= \frac{2^{22}\,.\,5^{7}}{7^{16}(ka_0)^2}\Bigg[-\frac{117649}{160}P_5{}^5(\zeta)+\frac{16807}{3}P_5{}^6(\zeta)-14483P_5{}^7(\zeta)\\
&\qquad +\frac{111919}{8}P_5{}^8(\zeta)-\frac{32063}{7}P_5{}^9(\zeta)\\
&\qquad +81\left\{\ln\left(\frac{16\zeta^2}{49}P_5(\zeta)\right)+\sum_{s=1}^{9}\frac{1}{s}P_5{}^s(\zeta)\right\}\Bigg]\\
F_{2s,\,6}(\zeta) &= \frac{3^{6}}{2^{16}(ka_0)^2}\Bigg[-\frac{3072}{5}P_6{}^5(\zeta)+\frac{16160}{3}P_6{}^6(\zeta)-16880P_6{}^7(\zeta)\\
&\qquad +\frac{45115}{2}P_6{}^8(\zeta)-\frac{122507}{9}P_6{}^9(\zeta)+\frac{30583}{10}P_6{}^{10}(\zeta)\\
&\qquad +35\left\{\ln\left(\frac{\zeta^2}{4}P_6(\zeta)\right)+\sum_{s=1}^{10}\frac{1}{s}P_6{}^s(\zeta)\right\}\Bigg]\\
F_{2s,\,7}(\zeta) &= \frac{2^{17}\,.\,7^{7}}{3^{40}(ka_0)^2}\Bigg[-\frac{3486784401}{5}P_7{}^5(\zeta)+6772684104P_7{}^6(\zeta)\\
&\qquad -\frac{170129144448}{7}P_7{}^7(\zeta)+39947934456P_7{}^8(\zeta)\\
&\qquad -33389798976P_7{}^9(\zeta)+\frac{69379703776}{5}P_7{}^{10}(\zeta)\\
&\qquad -\frac{679176548032}{297}P_7{}^{11}(\zeta)\\
&\qquad +25\,.\,10^6\left\{\ln\left(\frac{16\zeta^2}{81}P_7(\zeta)\right)+\sum_{s=1}^{11}\frac{1}{s}P_7{}^s(\zeta)\right\}\Bigg]
\end{aligned}\right\} \qquad \ldots\ldots(14)$$

in which

$$P_j{}^k(\zeta)=\left\{\frac{(j+2)^2}{16\zeta^2+(j+2)^2}\right\}^k.$$

It is clear that

$$\zeta_{\min}=\tfrac{1}{2}nK_{\max}=\tfrac{1}{2}n(k+k'),$$
$$\zeta_{\min}=\tfrac{1}{2}nK_{\min}=\tfrac{1}{2}n(k-k'),$$

k' being the magnitude of the momentum of the scattered electron which is determined by the energy conservation relation

$$k^2-\tfrac{1}{4}=k'^2-\frac{1}{n^2}.$$

2.2. *Ionization Cross Section*

The differential ionization cross section $I(K,\kappa)$ for the ejection of an electron having momentum in the range $\kappa\hbar$ and $(\kappa+d\kappa)\hbar$ and with a change in the magnitude of the momentum of the incident electron between $K\hbar$ and $(K+dK)\hbar$ has been given by Burhop (1940) as

$$I(K,\kappa)=\frac{2^8\kappa}{15k^2K}\frac{1}{(1-\mathrm{e}^{-2\pi/\kappa})}\times\exp\left\{-\frac{2}{\kappa}\tan^{-1}\frac{2\mu_L\kappa}{K^2-\kappa^2+\mu_L^2}\right\}$$
$$\times\{\mu_L^4+2(K^2+\kappa^2)\mu_L^2+(K^2-\kappa^2)^2\}^{-5}A \qquad \ldots\ldots(15)$$

in which (for the 2s case)

$$A=\{20\mu_L^{10}+\mu_L^8(85\kappa^2+47K^2)+\mu_L^6(140\kappa^4+100K^4)$$
$$+\mu_L^4(110\kappa^6-82\kappa^4K^2-310\kappa^2K^4+410K^6)$$
$$+40\mu_L^2(\kappa^2-K^2)^2(\kappa^4+\kappa^2K^2-4K^4)+5(\kappa^2-K^2)^4(\kappa^2+3K^2)\} \ldots(16)$$

and $\mu_L=1/2a_0$. The expression (16) may be derived following the method used by Massey and Mohr (1933) for the ground state case. Alternatively, it may be evaluated as in the discrete case, by making use of parabolic coordinates and the method of contour integration in the analysis. The total ionization cross section is given by

$$Q_1^{\text{tot}}=\int_{\kappa=0}^{\kappa=\kappa\text{max}}\int_{K=k-k'}^{K=k+k'} I(K,\kappa)\,dK\,d\kappa \qquad \ldots\ldots(17)$$

in which $\kappa_{\max}=(k^2-0{\cdot}25)^{1/2}$. It may be remarked that the formula given by Swan (1955) for $I(K,\kappa)$ is incorrect.

The functional forms of the cross section for excitation of the discrete states and for ionization (given by equations (10) and (13), and (15) and (17) respectively) are quite dissimilar. However, they may be correlated on making the energy identification

$$\kappa^2=-\frac{1}{n^2} \qquad \ldots\ldots(18)$$

and it may be shown that $\frac{1}{2}n^3Q_{2s,n}$ transforms to $Q_\epsilon^{\,i}$ where $Q_\epsilon^{\,i}$ is such that the total ionization cross section Q_1^{tot} is given by

$$Q_1^{\text{tot}}=\int_0^{\kappa\text{max}}\frac{2\kappa Q_\epsilon^{\,i}(\kappa)\,d\kappa}{[1-\exp(-4\pi\mu_L/\kappa)]}. \qquad \ldots\ldots(19)$$

Both the excitation and the ionization cross section formulae may be divided essentially into three parts; each part may then be correlated individually. The major algebraic task is to show that A in (16) transforms according to

$$A\to2^{-8}n^{-10}\{B^2[15n^2y^2+5(n^2-1)]+80n^4(n^2-4)By^2+64n^6(n^2-4)(3n^2-8)y^2\} \qquad \ldots\ldots(20)$$

with B defined by (11). The transformation

$$[\mu_L^4+2(K^2+\kappa^2)\mu_L^2+(K^2-\kappa^2)^2]^{-5}\to2^{20}n^{20}\frac{[(n-2)^2+4n^2K^2a_0^2]^{-5}}{[(n+2)^2+4n^2K^2a_0^2]^5} \qquad \ldots\ldots(21)$$

follows immediately, as does

$$\exp\left\{-\frac{2}{\kappa}\tan^{-1}\frac{2\mu_L\kappa}{K^2-\kappa^2+\mu_L^2}\right\}\to\left\{\frac{(n-2)^2+4n^2K^2a_0^2}{(n+2)^2+4n^2K^2a_0^2}\right\}^n, \qquad \ldots\ldots(22)$$

on making use of the relation

$$\tan^{-1} iy = \frac{i}{2} \ln \frac{1+y}{1-y} + 2p\pi.$$

On multiplying these three components together and allowing for the appropriate numerical factor one finds that

$$Q_\epsilon^{\,1}(\kappa) \rightarrow \tfrac{1}{2} n^3 Q_{2s,\,n}. \qquad \ldots\ldots (23)$$

§ 3. CALCULATIONS AND RESULTS

Cross sections for the excitation of the third, fourth, fifth, sixth and seventh levels of atomic hydrogen were computed from the formulae (13) and (14) for a range of values of the incident electron energy from 0·36 to 9 rydbergs. Values of $Q_\epsilon^{\,1}(\kappa)$ were determined for a few values of κ in the neighbourhood of the ionization threshold ($\kappa = 0, 0{\cdot}1, 0{\cdot}2, 0{\cdot}3$). For each energy of impact a graph was plotted of $\tfrac{1}{2} n^3 Q_{2s,\,n}$ and $Q_\epsilon^{\,1}$ against the energy of the excited state and the energy of the ejected electron respectively. A representative selection of these curves is shown in the figure. From these cross section against energy curves one may readily interpolate in the energy region $-1/49 < E_n < 0$ and so determine values for the excitation cross sections for $n \geqslant 8$. McCarroll (1957) has found

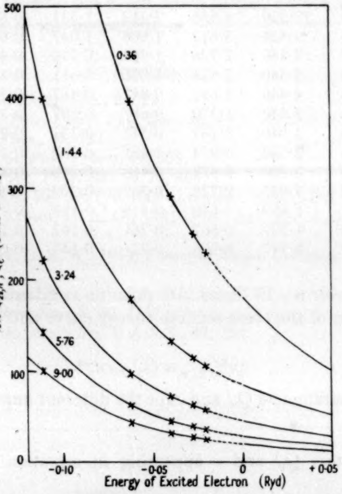

Illustration of the continuity of $\tfrac{1}{2} n^3 Q_{2s,\,n}$ (as a function of E_n) with $Q_\epsilon^{\,1}$ (as a function of ϵ). The numbers on the graphs refer to the energy of impact of the incident electron in rydbergs. Positive energies of the excited electron correspond to the ejection of the electron into the continuum and negative energies to the excitation of a discrete level. The interpolated (broken) sections of the curves for which $-1/49 < E_n < 0$ yield information on the cross sections for the excitation of the 8th and higher levels.

that this was a satisfactory method in the case of excitation from the ground state, the maximum error arising from interpolation being nowhere greater than 0·2%. To confirm that the method provides equally satisfactory results in the present case the following simple test was applied. Cross section against energy curves were drawn from the computed data, excluding the values corresponding to $n=7$. Values for $Q_{2s,7}$ were found by interpolation for each value of k, the incident electron momentum, and these were then compared with the computed values of this cross section. In no case was the discrepancy between the computed and interpolated values greater than 0·4%. Accordingly, one would expect that the percentage error in the excitation cross sections interpolated from the present data should be much less than 0·4 and is probably no greater than 0·2.

Values for the excitation cross sections $Q_{2s,n}$, $n=8$, 9, 10 obtained by interpolation are displayed in table 1 as are the cross sections computed for $n=3$, 4, 5, 6, 7. Whenever $n>10$ linear interpolation is adequate; a straight line is fitted to this section of the cross section–energy curve and $Q_{2s,n}$ ($n>10$) is given by

$$\tfrac{1}{2}n^3 Q_{2s,n} = Q_0^1 + cn^{-2}. \qquad \ldots\ldots(24)$$

The values of the parameters Q_0^1 and c for the different impact energies are given in table 2.

Table 1. Total Cross Sections for the Excitation of Discrete Levels of Hydrogen from the 2s State (units of πa_0^2)

Impact energy (Ryd)	$Q_{2s,3}$	$Q_{2s,4}$	$Q_{2s,5}$	$Q_{2s,6}$	$Q_{2s,7}$	$Q_{2s,8}$	$Q_{2s,9}$	$Q_{2s,10}$
0·36	65·019	12·330	4·658	2·312	1·331	0·843	0·569	0·404
0·64	49·441	9·454	3·612	1·808	1·047	0·664	0·450	0·320
1·00	37·667	7·150	2·726	1·364	0·790	0·499	0·339	0·241
1·44	29·488	5·560	2·114	1·056	0·611	0·390	0·264	0·188
1·96	23·703	4·446	1·687	0·842	0·487	0·309	0·209	0·149
2·56	19·488	3·640	1·379	0·687	0·397	0·252	0·170	0·121
3·24	16·326	3·040	1·149	0·572	0·331	0·210	0·142	0·101
4·00	13·895	2·580	0·974	0·485	0·280	0·179	0·121	0·086
4·84	11·984	2·200	0·837	0·416	0·240	0·153	0·103	0·073
5·76	10·452	1·933	0·728	0·362	0·209	0·133	0·090	0·064
6·76	9·206	1·699	0·640	0·318	0·183	0·116	0·079	0·056
7·84	8·176	1·507	0·567	0·281	0·162	0·103	0·070	0·050
9·00	7·317	1·347	0·506	0·251	0·145	0·091	0·062	0·044

Table 2. Parameters Q_0^1 and c appearing in equation (24) (units of πa_0^2)

Impact energy (Ryd)	Q_0^1	c	Impact energy (Ryd)	Q_0^1	c
0·36	179·9	$21{\cdot}7\times10^2$	4·00	38·4	$4{\cdot}2\times10^2$
0·64	144·6	15·0	4·84	32·9	3·7
1·00	109·0	11·4	5·76	28·5	3·2
1·44	84·2	9·2	6·76	25·0	2·8
1·96	67·0	7·0	7·84	22·2	2·5
2·56	54·5	5·8	9·00	19·8	2·2
3·24	45·4	5·0			

The values obtained for the excitation cross sections are very much larger than the excitation cross sections from the ground state. This is in agreement with expectation and with the trend found in ionization cross sections by Yavorsky, Mandl and Swan. On the basis of the present computations it was possible to estimate the total cross section for ionization for any particular value of incident electron energy. While this involves a considerable extrapolation over the range of κ, the momentum of the ejected electron, it should, nonetheless, be accurate to within perhaps 20%. The values thus obtained for Q_1^{tot} for a few chosen values of the impact energy differed markedly from those of Swan, being smaller by a factor of about 2. It is to be noted that the cross sections calculated by Yavorsky also differ substantially from those given by Swan; for example Yavorsky finds the maximum ionization cross section to be about $18\pi a_0^2$ whereas Swan finds it to be about $36\pi a_0^2$.

ACKNOWLEDGMENTS

This work was carried out under contract for the United Kingdom Atomic Energy Authority. Thanks are due to the Director of the Atomic Energy Research Establishment, Harwell, for permission to publish the results and to Professor D. R. Bates who has given much helpful advice and encouragement throughout the course of the investigation.

REFERENCES

BETHE, H. A., 1930, *Ann. Phys., Lpz.*, **5,** 325.
BURHOP, E. H. S., 1940, *Proc. Camb. Phil. Soc.*, **36,** 43.
ELSASSER, W., 1927, *Z. Phys.*, **45,** 522.
GOLDSTEIN, L., 1933, *Ann. Phys., Paris*, **19,** 305.
MCCARROLL, R., 1957, *Proc. Phys. Soc.* A, **70,** 460.
MANDL, F., 1952, A.E.R.E. Report T/R 1006 (London: H.M.S.O.).
MASSEY, H. S. W., and MOHR, C. B. O., 1931, *Proc. Roy. Soc.* A, **132,** 605; 1933, *Ibid.*, **140**, 613.
MOTT, N. F., and MASSEY, H. S. W., 1949, *Theory of Atomic Collisions* (Oxford: Clarendon Press)
SOMMERFELD A., 1931, *Ann Phys., Lpz.*, **9,** 257.
SWAN, P., 1955, *Proc. Phys. Soc.* A. **68,** 1157.
YAVORSKY, B., 1945, *C. R. Acad. Sci. U.R.S.S.*, **49,** 250.

The Application of Onsager's Theory to Dielectric Dispersion

By N. E. HILL

Department of Physics, Bedford College, London

MS. received 26*th March* 1958

Abstract. It is shown that previous applications of Onsager's theory to dielectric dispersion have contained an incorrect assumption about the behaviour of the reaction field when the applied field is varying. An equation for the complex dielectric constant is derived, using Onsager's model and taking proper account of the reaction field. An approximate method of solving the equation is developed and it is shown that the equation approximates closely to the simple Debye equation

$$\epsilon-\epsilon_\infty=(\epsilon_0-\epsilon_\infty)/(1+j\omega\tau)$$

the microscopic and macroscopic relaxation times being almost identical.

---

§ 1. Introduction

Experimental measurements of the dielectric constant and loss in liquids at frequencies at which dielectric dispersion occurs are usually interpreted in terms of the equation

$$\epsilon=\epsilon_\infty+\frac{\epsilon_0-\epsilon_\infty}{1+j\omega\tau'} \qquad \ldots\ldots(1)$$

where ϵ_0 is the static dielectric constant, ϵ_∞ is the dielectric constant in the high-frequency limit when the orientation polarization has fallen to zero, τ' is a characteristic (macroscopic) relaxation time and ϵ is the complex dielectric constant at frequency ω.

This equation represents the experimental results very well in the case of liquids having a simple rigid molecular structure (e.g. Poley 1955). For more complex molecules, particularly where there is a possibility of intramolecular rotation, the equation may be generalized (Cole and Cole 1941) to

$$\epsilon=\epsilon_\infty+\frac{\epsilon_0-\epsilon_\infty}{1+(j\omega\tau')^{1-\alpha}}. \qquad \ldots\ldots(2)$$

In the interpretation of the experimental results in terms of molecular properties one uses the microscopic relaxation time τ. In terms of this relaxation time Debye (1929) found that the average moment parallel to an alternating field $F=F_0e^{j\omega t}$ of a molecule of moment μ is

$$\overline{m}=\frac{\mu^2F}{3kT}\frac{1}{1+j\omega\tau}. \qquad \ldots\ldots(3)$$

It is possible to predict the value of the microscopic relaxation time in terms of molecular properties, but in order to compare the predicted values with the experimental results it is necessary to know the relation between τ and τ'. Any theory of dielectric polarization will give an equation relating ϵ to ϵ_0, ϵ_∞ and τ. In general it will not be possible to express this in the form (1) so as to get an explicit equation for τ' in the form $\tau/\tau'=f(\epsilon_0, \epsilon_\infty)$ although the experimental results lead one to expect that this should be possible for a successful theory, at least to a first approximation.

A number of attempts to solve this problem have been made. The success of Onsager's theory (1936) in accounting for the static dielectric properties of liquids makes the application of the same model to the case of a high-frequency field of great interest. This generalization has been carried out by a number of authors (Cole 1938, Fuoss and Kirkwood 1941, Bolton 1948) on the assumption that the only effect of the varying field is to multiply the term giving the orientation polarization by a factor $1/(1+j\omega\tau)$, thus giving

$$\frac{(\epsilon-\epsilon_\infty)(2\epsilon+\epsilon_\infty)}{\epsilon(\epsilon_\infty+2)^2}=\frac{4\pi N_1}{9kT}\frac{\mu^2}{1+j\omega\tau} \qquad \ldots\ldots(4)$$

or

$$\frac{(\epsilon-\epsilon_\infty)(2\epsilon+\epsilon_\infty)}{\epsilon}=\frac{(\epsilon_0-\epsilon_\infty)(2\epsilon_0+\epsilon_\infty)}{\epsilon_0}\frac{1}{1+j\omega\tau} \qquad \ldots\ldots(5)$$

(N_1 is the number of molecules per unit volume).

This generalization is not quite correct however, because it contains the assumption that the reaction field, due to the polarization by any chosen molecule of its surroundings, falls off as the frequency of the applied field is increased. This would only be true if the moment of the molecule varied with the same frequency as the field. In fact this is only so for the part of the moment induced by the field. Most of the variation which the reaction field has to follow is the thermal motion of the molecule, and is the same at high frequency as in the static case. Whether the reaction field is in fact able to follow this thermal motion, that is, whether it is correct to use the static dielectric constant in calculating the reaction field, as is assumed in Onsager's theory, is arguable; but if the assumption is valid in the static case it is valid in the high-frequency case also.

The purpose of the present paper is to generalize Onsager's equation to the high-frequency case, taking proper account of the reaction field.

§ 2. ONSAGER'S MODEL IN AN ALTERNATING FIELD

Onsager's model consists of a spherical molecule of radius a, polarizability γ and permanent moment $\boldsymbol{\mu}_0$, in a cavity of radius a in a continuum having the macroscopic properties of the material. When a steady electric field $\mathbf{E}_0$ is applied, the field $\mathbf{F}_0$ acting on the molecule is

$$\mathbf{F}_0=\mathbf{G}_0+\mathbf{R}_0=g_0\mathbf{E}_0+r_0\mathbf{m}/a^3 \qquad \ldots\ldots(6)$$

where $g_0=3\epsilon_0/(2\epsilon_0+1)$ and $r_0=2(\epsilon_0-1)/(2\epsilon_0+1)$. $\mathbf{G}_0$ is the cavity field and $\mathbf{R}_0$ the reaction field due to the polarization of the surroundings by the total moment, permanent and induced, $\mathbf{m}$, of the dipole. $\mathbf{R}_0$ is parallel to the total moment and plays no part in orienting the molecule. Its only effect is to alter the value of the total moment. The couple acting to turn the molecule parallel to the applied field is $\mathbf{m}\times\mathbf{G}_0$, and is dependent on $\mathbf{R}_0$ through the influence of $\mathbf{R}_0$ on $\mathbf{m}$.

If now we replace $\mathbf{E}_0$ by an alternating field $\mathbf{E}_0 e^{j\omega t}$, the cavity field becomes

$$\mathbf{G}=g\mathbf{E}=\frac{3\epsilon}{2\epsilon+1}\mathbf{E}. \qquad \ldots\ldots(7)$$

It is no longer in phase with the applied field, but this is taken into account by the fact that ϵ is now complex, and there is no need to take it into account separately as was done by Mandel (1951).

For the reaction field we must write

$$\mathbf{R}=r_0\frac{\boldsymbol{\mu}_0}{a^3}+r\frac{\gamma}{a^3}\mathbf{E} \qquad \ldots\ldots(8)$$

where $r=2(\epsilon-1)/(2\epsilon+1)$ since the static dielectric constant is appropriate to account for the response of the material to the slow variations of $\boldsymbol{\mu}_0$, but the dielectric constant corresponding to the frequency ω must be used in dealing with the response to the varying induced polarization. Provided the field due to the dipole is not sufficient to saturate the surrounding material, these two effects superpose linearly. The assumption that no saturation occurs is present in the Onsager theory in the static case. It is unlikely to be valid for liquids of high dielectric constant, and this limitation must be borne in mind.

Substituting these values of $\mathbf{G}$ and $\mathbf{R}$ we find for $\mathbf{F}$

$$\mathbf{F}\left(1-\frac{\gamma}{a^3}r\right)=g\mathbf{E}+\frac{r_0}{a^3}\boldsymbol{\mu}_0 \qquad \ldots\ldots(9)$$

hence

$$\mathbf{m}=\boldsymbol{\mu}_0+\gamma\mathbf{F}=\boldsymbol{\mu}_0\left(1+\frac{r_0\gamma/a^3}{1-r\gamma/a^3}\right)+\frac{\gamma g}{1-r\gamma/a^3}\mathbf{E}. \qquad \ldots\ldots(10)$$

Since $\mathbf{R}$ is always parallel to $\mathbf{m}$, the couple tending to turn the molecule is

$$\mathbf{m}\times\mathbf{G}=\boldsymbol{\mu}_0\left(1+\frac{r_0\gamma/a^3}{1-r\gamma/a^3}\right)\times g\mathbf{E}. \qquad \ldots\ldots(11)$$

Then following Debye's calculation (1929) for the mean cosine of the angle between the permanent dipole moment and an alternating applied field, we find

$$\overline{\cos\theta}=\frac{1+(r_0-r)\gamma/a^3}{1-r\gamma/a^3}\,g\,\frac{\mu_0E}{3kT}\,\frac{1}{1+j\omega\tau} \qquad \ldots\ldots(12)$$

and the mean polarization in the direction of the field is

$$\mathbf{P}=\frac{\epsilon-1}{4\pi}\mathbf{E}=\frac{N}{V}\left\{\frac{\gamma g}{1-r\gamma/a^3}+\left[\frac{1+(r_0-r)\gamma/a^3}{1-r\gamma/a^3}\right]^2 g\,\frac{\mu_0{}^2}{3kT}\,\frac{1}{1+j\omega\tau}\right\}\mathbf{E} \qquad \ldots\ldots(13)$$

where N is Avogadro's number and V is the molar volume.

Substituting the values for g and r, and using, as in Onsager's calculation, $4\pi N\gamma/V=3\gamma/a^3=3(\epsilon_\infty-1)/(\epsilon_\infty+2)$, we find after some reduction

$$\frac{(\epsilon-\epsilon_\infty)(2\epsilon+\epsilon_\infty)}{\epsilon(\epsilon_\infty+2)^2}=\frac{4\pi N}{3V}\,\frac{\mu_0{}^2}{3kT}\,\frac{[1+(r_0-r)(\epsilon_\infty-1)/(\epsilon_\infty+2)]^2}{1+j\omega\tau}. \qquad \ldots\ldots(14)$$

If the difference between r_0 and r is neglected, this reduces to the equation (5) used by Cole, Fuoss and Kirkwood and Bolton. At low frequency it reduces, as it should, to Onsager's equation. Replacing $\mu_0{}^2/3kT$ in terms of the static dielectric constant and using $r_0-r=6(\epsilon_0-\epsilon)/(2\epsilon_0+1)(2\epsilon+1)$ we have finally

$$\frac{(\epsilon-\epsilon_\infty)(2\epsilon+\epsilon_\infty)}{\epsilon}=\frac{(\epsilon_0-\epsilon_\infty)(2\epsilon_0+\epsilon_\infty)}{\epsilon_0}\left[1+\frac{6(\epsilon_\infty-1)}{(\epsilon_\infty+2)(2\epsilon_0+1)}\,\frac{\epsilon_0-\epsilon}{2\epsilon+1}\right]^2\Big/(1+j\omega\tau) \qquad \ldots\ldots(15)$$

as the correct equation for a substance to which Onsager's model is applicable, in the region of dielectric dispersion.

§ 3. THE APPROXIMATE SOLUTION OF THE EQUATION

The relation of this equation to the equations (1) and (6) is not immediately obvious, and its exact solution for ϵ in terms of $\omega\tau$ is complicated. An approximate solution may be obtained by writing the equation

$$\epsilon - \epsilon_\infty = \frac{\epsilon_0 - \epsilon_\infty}{1 + j\omega\tau} C_1 C_2$$

where $C_1 = \epsilon(2\epsilon_0 + \epsilon_\infty)/\epsilon_0(2\epsilon + \epsilon_\infty)$ and may be considered as a correction term converting equation (1) (with τ' put equal to τ) to equation (5), and

$$C_2 = \left[1 + \frac{6(\epsilon_\infty - 1)}{(\epsilon_\infty + 2)(2\epsilon_0 + 1)} \frac{\epsilon_0 - \epsilon}{2\epsilon + 1}\right]^2. \qquad \ldots\ldots(16)$$

C_2 is a second correction factor which takes into account the changed effect of the reaction field. In these correction factors ϵ may be replaced by

$$\epsilon_0 = \epsilon_\infty + \frac{\epsilon_0 - \epsilon_\infty}{1 + j\omega\tau} \qquad \ldots\ldots(17)$$

and then equation (15) may be solved for ϵ.

This procedure is carried out below, applying first C_1 only, and then C_1 and C_2 together When only C_1 is used the result is very similar to that obtained by Bolton (1948) and Poley (1955) by exact calculation from equation (5).

Making the substitution (17) the correction terms become

$$C_1 = \left\{1 + \frac{3\epsilon_\infty{}^2 x^2}{\epsilon_0(2\epsilon_0 + \epsilon_\infty)} - jx \frac{\epsilon_\infty(\epsilon_0 - \epsilon_\infty)}{\epsilon_0(2\epsilon_0 + \epsilon_\infty)}\right\} \Big/ \left\{1 + \frac{9\epsilon_\infty{}^2 x^2}{(2\epsilon_0 + \epsilon_\infty)^2}\right\}$$

$$C_2 = \left[1 + \frac{6(\epsilon_\infty - 1)(\epsilon_0 - \epsilon_\infty)}{(\epsilon_\infty + 2)(2\epsilon_0 + 1)^2} \left(\frac{2\epsilon_\infty + 1}{2\epsilon_0 + 1} x^2 + jx\right) \Big/ \left\{1 + \left(\frac{2\epsilon_\infty + 1}{2\epsilon_0 + 1}\right)^2 x^2\right\}\right]^2$$

$(x = \omega\tau)$.

x	C_1	C_2	ϵ_1	ϵ_2	ϵ (Debye)
0·0	1·000 − 0·0000j	1·000 + 0·0000j	12·50 − 0·00j	12·50 − 0·00j	12·50 − 0·00j
0·2	0·999 − 0·0145j	1·000 + 0·0118j	12·11 − 2·06j	12·14 − 1·95j	12·11 − 1·92j
0·4	0·997 − 0·0288j	1·002 + 0·0235j	10·99 − 3·69j	11·10 − 3·49j	11·12 − 3·45j
0·6	0·993 − 0·0425j	1·004 + 0·0349j	9·61 − 4·69j	9·81 − 4·47j	9·85 − 4·41j
0·8	0·988 − 0·0555j	1·008 + 0·0460j	8·05 − 5·18j	8·54 − 4·96j	8·60 − 4·90j
1·0	0·982 − 0·0677j	1·012 + 0·0565j	7·07 − 5·25j	7·42 − 5·05j	7·60 − 5·00j
1·2	0·974 − 0·0788j	1·017 + 0·0665j	6·11 − 5·10j	6·51 − 4·95j	6·60 − 4·91j
1·5	0·962 − 0·0935j	1·026 + 0·0804j	5·03 − 4·73j	5·47 − 4·65j	5·58 − 4·62j
2·0	0·939 − 0·1121j	1·043 + 0·0998j	3·93 − 3·98j	4·39 − 4·01j	4·50 − 4·00j
3·0	0·893 − 0·1307j	1·081 + 0·1250j	3·00 − 2·81j	3·39 − 2·98j	3·50 − 3·00j
5·0	0·823 − 0·1271j	1·147 + 0·1362j	2·57 − 1·64j	2·81 − 1·87j	2·89 − 1·92j
∞	0·733 − 0·0000j	1·280 + 0·0000j	2·50 − 0·00j	2·50 − 0·00j	2·50 − 0·00j

Values of C_1 and C_2 and the values of ϵ (denoted respectively by ϵ_1 and ϵ_2) obtained by applying C_1 only and C_1 and C_2 together are shown in the table, for various values of x, in the particular case $\epsilon_\infty = 2{\cdot}5$, $\epsilon_0 = 12{\cdot}5$. These values of ϵ_∞ and ϵ_0 were chosen so that the result may be compared with Poley's calculation (1955) from equation (5). The last column of the table shows the value of ϵ from the simple equation (17).

It will be seen from this table that the correction C_1 is largely compensated by the correction C_2, so that the values of ϵ calculated from equation (15) differ from those calculated from the simple equation (17) by little more than 1%

in most cases. The use of (17) in calculating C_1 and C_2 is therefore justified.

The fact that equation (15) approximates closely to equation (17) means, comparing equations (17) and (1). that the microscopic and macroscopic relaxation times are almost identical.

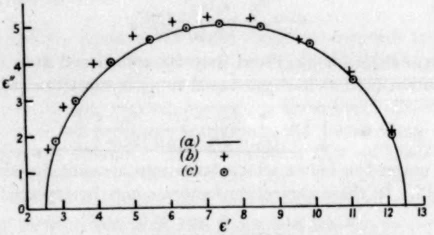

Arc plot showing ϵ'' as a function of ϵ' for (*a*) the simple Debye equation, (*b*) Cole's development of Onsager's equation, (*c*) the present development of Onsager's equation.

In the figure the values of ϵ obtained from equations (17), (5) and (15) are shown on an arc plot. It will be seen that equation (15) gives a curve which is almost indistinguishable from a semi–circle. This is consistent with the experimental results of Poley (1955).

§ 5. CONCLUSION

It has been shown that if Onsager's theory is extended to the case of an alternating field, and the reaction field is properly included, the equation obtained for the complex dielectric constant at circular frequency ω, namely

$$\frac{(\epsilon-\epsilon_\infty)(2\epsilon+\epsilon_\infty)}{\epsilon}=\frac{(\epsilon_0-\epsilon_\infty)(2\epsilon_0+\epsilon_\infty)}{\epsilon_0}\left[1+\frac{6(\epsilon_\infty-1)}{(\epsilon_\infty+2)(\epsilon_0+1)}\frac{\epsilon_0-\epsilon}{2\epsilon+1}\right]^2\Bigg/(1+j\omega\tau)$$

gives results which differ very little from those obtained using the simple equation

$$\epsilon_0=\epsilon_\infty+\frac{\epsilon_0-\epsilon_\infty}{1+j\omega\tau}$$

so that a plot of ϵ'' against ϵ' $(\epsilon=\epsilon'-j\epsilon'')$ approximates to a semi-circle, and the macroscopic relaxation time is almost identical with the microscopic relaxation time.

REFERENCES

BOLTON, H. C., 1948, *J. Chem. Phys.*, **16**, 486.
COLE, K. S., and COLE, R. H., 1941, *J. Chem. Phys.*, **9**, 341.
COLE, R. H., 1938, *J. Chem. Phys.*, **6**, 385.
DEBYE, P., 1929, *Polar Molecules* (New York: Chemical Catalog Co.).
FUOSS, R. M., and KIRKWOOD, J. G., 1941, *J. Amer. Chem. Soc.*, **63**, 385.
MANDEL, M., 1951, *Physica, 's Grav.*, **17**, 799.
ONSAGER, L., 1936, *J. Amer. Chem. Soc.*, **58**, 1486.
POLEY, J. Ph., 1955, *Appl. Sci. Res.*, **4**, 337.

Criteria determining the Design and Performance of a Source-modulated Microwave Cavity Spectrometer

By R. W. R. HOISINGTON†, L. KELLNER and M. J. PENTZ
Imperial College of Science and Technology, London

MS. received 16*th September* 1957, *and in revised form* 18*th April* 1958

Abstract. An analysis is given of the radio- and audio-frequency modulation method employed in microwave spectroscopy. The results of the theory are compared with measurements taken on a 8 mm microwave spectrometer and are found to be in close agreement. The calculations are extended to include the case where an absorbing gas is enclosed in a resonant cavity.

§ 1. Introduction

In the course of developing a millimetre-wave Zeeman spectrometer (Hoisington, Kellner and Pentz 1956) the authors found it necessary to look into the factors upon which the spectrometer sensitivity depends. There are a number of passing references and partial analyses in the literature, but, as far as could be seen, no detailed treatment directly applicable to the practical problem of getting a source-modulated cavity spectrometer to work properly. As the analysis in the following sections shows, there are several critical parameters which must all be correctly adjusted if an optimum signal, or indeed any signal in some cases, is to be observed.

§ 2. Source Modulation

2.1. *Introduction*

It is well known that frequency modulation of the klystron source of a microwave spectrometer will lead to an improvement of the signal to noise ratio (Gordy 1948). The performance of such a spectrometer depends critically on the modulating voltage in the case of sinusoidal modulation.

Hershberger (1948) has derived a formula for the sinusoidal Stark modulation of a gas absorption line while Karplus (1948) has developed a general theory for the case when a frequency modulated electromagnetic field passes through an absorbing gas. In addition to this, Jen (1948) has pointed out that a certain relationship between all the available parameters is required to ensure a good representation of the gas absorption line on the oscilloscope screen.

However, some difficulties were experienced by the authors of the present paper in choosing the right parameters for a proper performance, and it was therefore decided to carry out a new calculation. The analysis includes the effects of radio- and audio-frequency modulation on the amplitude and shape of the signal obtained on the oscilloscope screen. Furthermore, the case is discussed in which several components of a line are observed against the background of a cavity resonance as in the Zeeman effect of a gas contained in a resonant cavity. The theory is supported by a series of measurements taken on the spectrometer.

---

† Now at University College, Ibadan, Nigeria.

In the instrument under investigation a sinusoidal radio-frequency voltage, produced by a signal generator, was applied to the reflector of the klystron source in addition to the saw-tooth audio-frequency modulation. The doubly-modulated microwave energy passes through the absorbing gas and is detected by a silicon crystal. A tuned receiver connected to the crystal selects the appropriate component from the crystal current, and its output is applied after suitable radio-frequency amplification, detection and audio-frequency amplification, to the Y plates of an oscilloscope. The modulating audio frequency, on the other hand, provides the time-base for the X plates. If the klystron is tuned to the absorption frequency of the gas in the waveguide or cavity, the very narrow gas resonance acts as a discriminator transforming the frequency modulation into an amplitude modulation. The amplitude of the crystal current can be represented as a Fourier series in terms of the modulating frequency from which the receiver selects the component of that harmonic to which it is tuned. In fact, it performs the function of a Fourier analyser. As will be shown, the shape of the trace on the screen depends on the receiver frequency.

2.2. *Theory*

The klystron which is tuned to the resonant frequency of the gas absorption line is doubly modulated: firstly, by a saw-tooth voltage of low (audio) frequency $\omega_a = 2\pi\nu_a$ and secondly by a radio frequency $\omega_r = 2\pi\nu_r$. It will be seen later that ω_a must not exceed a certain upper limit to produce a good representation of the line on the oscilloscope screen.

The saw-tooth modulation can be represented in the following way: for $0 \leqslant t \leqslant 1/\nu_a$, $V = \nu_a V_a t$ where t is the time and V_a the peak voltage of the modulation; when $t = 1/\nu_a$, $V = 0$. The corresponding modulation of the klystron frequency is then given by $\alpha V_a \nu_a t$ where α = rate of modulation of the klystron. The radio-frequency modulation is produced by application of the voltage $V_r \cos \omega_r t$. The total frequency of the klystron at any instant is then $\omega = \omega_0 + \alpha V_a \nu_a t + \alpha V_r \cos \omega_r t$.

If the voltage incident on the gas is $V_0 \cos \omega t$, α_c the absorption coefficient in the walls of the waveguide cell of length l, and α_g the absorption coefficient of the gas, the voltage V after passage through the guide will be $V_0 \exp\{-(\alpha_g + \alpha_c)l\} \cos \omega t$ where $\alpha_g = \alpha_0[1 + (\omega^2 - \omega_0^2)^2/\omega^2 \Delta\omega_0^2]^{-1}$. α_0 denotes the peak absorption at the resonance frequency ω_0 and $\Delta\omega_0$ the width of the line at half power points. For the very narrow lines under investigation, $\omega \simeq \omega_0$ and α_g reduces to

$$\alpha_g = \alpha_0[1 + 4(\omega - \omega_0)^2/\Delta\omega_0^2]^{-1}. \qquad \ldots\ldots(1)$$

The current produced in the crystal is in our case proportional to the square of the incident voltage so that the fractional change $\Delta i/i_0$ of the crystal current as a result of the gas absorption will be:

$$\frac{\Delta i}{i_0} = \frac{\alpha_0\{1 + \cos 2(\omega_0 t + p\Delta\omega_0 + m \sin \omega_r t)\}}{1 + 4(p + s \cos \omega_r t)^2}$$

where $m = \alpha V_r/\nu_r$; $\Delta\nu_0$ is of course a function of the gas pressure; $p = \alpha V_a \nu_a t/\Delta\nu_0$ and $s = \alpha V_r/\Delta\nu_0$; m denotes the modulation index. The function $\Delta i/i_0$ must now be expressed as a Fourier series of the modulating frequency ω_r:

$$\begin{aligned}\frac{\Delta i}{i_0} = \sum_1^\infty a_n \cos n\omega_r t + \cos 2\omega_0 t \Big\{ & J_0(2m) \sum_1^\infty a_n \cos n\omega_r t \\ & + \sum_n \sum_k J_{2k}(2m)(a_{2k+n} + a_{2k-n}) \cos n\omega_r t \Big\} \\ & - \sin 2\omega_0 t \Big\{ \sum_n \sum_k J_{2k-1}(2m)(a_{2k-n-1} - a_{2k+n-1}) \cos n\omega_r t \Big\}\end{aligned}$$

with

$$a_n = \frac{\alpha_0}{\pi} \int_0^{2\pi} \frac{\cos nx\, dx}{1 + 4(p + s\cos x)^2},$$

where $x = \omega_r t$ and the $J_k(2m)$ denote the Bessel functions of order k and argument $2m$. The integration leads to the following results

$$a_0 = 0,$$

$$a_n = -(-1)^n \alpha_0 \frac{\rho^n}{(2s)^n r^{1/2}} \left\{ \sum_0^n (-1)^l l! \left(\frac{r^{1/2}}{\rho} \right)^l \sin \left[\frac{(n-l)\psi + \frac{1}{2}(l-1)\Phi}{l!\,(n-l)!} \right] \right\}.$$

Here

$$r = [(4p^2 - 4s^2 - 1) + 16p^2]^{1/2}, \qquad \rho = (4p^2 + 1)^{1/2},$$

$$\psi = \tan^{-1}(1/2p) \quad \text{and} \quad \Phi = \tan^{-1}\{4p/(4p^2 - 4s^2 - 1)\}.$$

If the receiver is tuned to ω_r, the Fourier component a_1 passed by the receiver will be $a_1 = \alpha_0 \rho \sin(\psi - \frac{1}{2}\Phi)/2sr^{1/2}$ (in agreement with Hershberger 1948). a_1 will reach an extreme value if $p = \pm \frac{1}{6}\sqrt{3[1 - 2(1 + 3s^2)^{1/2}]}$, leading to

$$(a_1)_{\max} = \alpha_0 \sqrt{3[1 - (1 + 3s^2)^{1/2}]}/4s[2(1 + 3s^2)^{1/2} - 1]^{1/2}; \qquad \ldots\ldots (2)$$

the optimum value of $(a_1)_{\max}$ with respect to s is $(a_1)_{\text{opt}} = \pm \frac{1}{4}\alpha_0$ and $p_{\text{opt}} = \mp \frac{1}{2}\sqrt{3}$, $s = 1$.

The signal has maximum amplitude if $\alpha V_r = \Delta\nu_0$; thus the optimum modulation voltage depends upon the gas pressure. It will be seen that $da_1/dp \to -4sp\alpha_0/(4p^2 + 1)^2$ for $s^2 \ll 1$ which term, apart from a numerical factor, has the form of the differential coefficient of (1). For that reason, the curve produced by source modulation is often referred to as the differential representation of the original shape of the absorption line. If the receiver is tuned to the second harmonic $2\omega_r$ of the modulating frequency, the trace on the oscilloscope screen should show the form of a_2:

$$a_2 = -\alpha_0 \{ r^{1/2} \sin \tfrac{1}{2}\Phi - 2\rho \sin\psi + \rho^2 \sin(2\psi - \tfrac{1}{2}\Phi)/r^{1/2} \}/4s^2.$$

Calculation shows that a_2 has a maximum if $s = 1{\cdot}5$. In figures 1 and 2, a_1 and a_2 have been plotted as functions of p; it will be seen that a_2 has a maximum at $p = 0$ and that the curve is symmetrical about the ordinate axis. It does not, however, faithfully reproduce the shape of the absorption line since it exhibits two additional, secondary maxima. The amplitude of the signal reaches a maximum and then decreases again as V_r is increased while the width of the trace increases monotonically. To gain in resolving power, it is therefore advisable to keep the radio-frequency voltage below the optimum value if the sensitivity of the spectrometer will permit it. The appearance of the calculated curves of figures 1 and 2 may be compared with figures 3 and 4 (Plate) which are photographs of the trace on the oscilloscope screen, obtained with the 35 791 Mc/s line of ethylene oxide under optimum conditions. The spread of a_1 from maximum to minimum is $\sqrt{3}\Delta\nu_0$ for $s = 1$, and for a_2, a halfwidth of $1{\cdot}9\Delta\nu_0$ is obtained for $s = 1{\cdot}5$.

The amplitude of the trace as a function of V_r was observed for the ethylene oxide line at 35 791 Mc/s. The measured values are plotted in figure 5: the points represent the experimental data while the full line was calculated from equation (2).

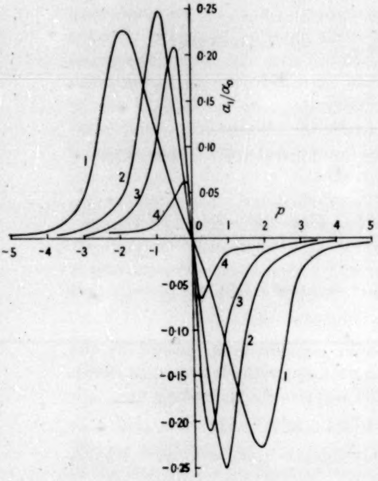

Figure 1. First harmonic component of receiver radio-frequency output plotted against klystron frequency.

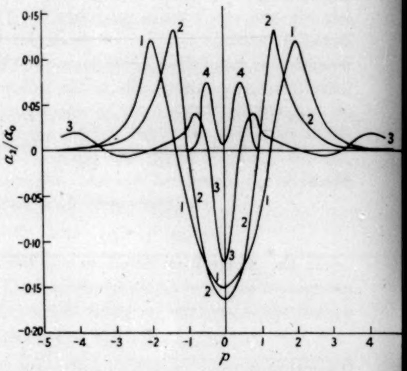

Figure 2. Second harmonic component of receive radio-frequency output plotted against klystron frequency.

Curve 1, $s=2$; curve 2, $s=1$; curve 3, $s=0{\cdot}5$; curve 4, $s=0{\cdot}1$.

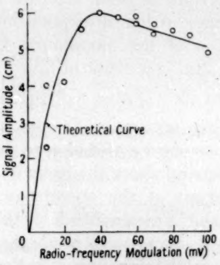

Figure 5. Dependence of sensitivity upon radio-frequency modulation.

2.3. *Audio-frequency Modulation and Representation*

The terms called here a_n are those Fourier components of the crystal current which can be passed by the receiver tuned to the frequency $n\nu_r$; they are still audio-frequency modulated, and the true representation of these terms a_n depends on the band-width of the receiver, the audio-frequency and the other parameters mentioned above. As Jen (1948) has pointed out, if n Fourier components must be passed by the receiver to give a faithful representation of the input current, the band-width Δf of the receiver and the audio frequency ν_a applied to the klystron must be chosen in such a manner that

$$\nu_{\mathrm{a}} = \Delta f \Delta \nu_0 / n \alpha V_{\mathrm{a}}.$$

In the following paragraphs an attempt has been made to study in detail how many Fourier components are needed to provide a recognizable signal and also the connection between the radio-frequency and audio-frequency voltages and the other parameters.

The analysis is based on the well-known expression for the passage of a pulse through an amplifier: if n is the number of Fourier components of the pulse, necessary to give a faithful reproduction, then $n = t_2 \Delta f$ where Δf = amplifier band-width, t_2 = the duration of the pulse.

In the present case, the pulse is represented by a_1 (a function of $\alpha V_{\mathrm{a}} \nu_{\mathrm{a}} t / \Delta \nu_0$) which can be expressed as a Fourier series of ν_{a}. The duration of the pulse t_2 is determined by the width Δp of the signal a_1, and Δf is the receiver band-width. To facilitate the Fourier analysis of a_1 in terms of ν_{a}, a_1 has been approximated by three straight lines cutting off the wings of a_1. t_2 is a function of s, i.e. the radio-frequency voltage; the optimum value $s = 1$ has been chosen. Then

$$a_1 = \frac{\alpha_0 \left\{ \sum_n [\sin n\pi q - (t_2/t_1) \sin n\pi q t_1/t_2] \sin 2n\pi q t/t_2 \right\}}{2\pi^2 q n^2 (1 - t_1/t_2)} \qquad \ldots\ldots(3)$$

with $t_1 = \sqrt{3}\Delta \nu_0 / \alpha V_{\mathrm{a}} \nu_{\mathrm{a}}$, $q = \nu_{\mathrm{a}} t_2$, $t_2 = l \Delta \nu_0 / \alpha V_{\mathrm{a}} \nu_{\mathrm{a}}$ where l is a number determining the width of the pulse to be passed by the receiver ($l \Delta \nu_0 = \Delta p$). l is found to be 4·3. For the series in (3) to be rapidly convergent $1/\nu_{\mathrm{a}} \geqslant t_2$, i.e. $q \leqslant 1$. A numerical calculation of (3) has been carried out for various values of the parameter q summing in every case over four and eight Fourier terms. The results are summarized in the table. It will be seen that the representation of the signal in shape and amplitude will be an optimum for $q = 1$ and that about eight Fourier components will be needed.

Fourier Series of a_1 for Summation over 4 and 8 Components

	Over 4 components		Over 8 components	
q	(1)	(2)	(1)	(2)
0·25	43	Distorted.	15	Satisfactory.
0·75	13	Flattened at top.	7	Satisfactory.
1·0	8	Good.	5	Good.
1·25	14	Slight distortion.	14	Slight distortion.
4·5	93	Distorted wave.	92	Distorted wave.

(1) Reduction in amplitude (%); (2) shape of signal.

Optimum conditions will therefore obtain if $\alpha V_{\mathrm{r}} = \Delta \nu_0$, i.e. $s = 1$; $\nu_{\mathrm{a}} = \Delta f / n$, i.e. $q = 1$. For $q \neq 1$ $\nu_{\mathrm{a}} = l \Delta f \Delta \nu_0 / \alpha V_{\mathrm{a}} n$, for $q = 1$ $V_{\mathrm{a}} = l V_{\mathrm{r}}$; this formula agrees with that given by Jen (1948) for $l = 1$. The choice of the audio frequency ν_{a} is determined by the receiver band-width Δf (which should be kept as small as possible to ensure a high spectrometer sensitivity) and n, the number of Fourier components to be passed (at least eight) together with the line width $\Delta\nu_0$ and the peak voltage V_a of the saw-tooth voltage. A low value of V_a (corresponding to a narrow slit-width in an optical spectrometer) improves the representation of the signal shape if the other parameters are kept constant.

It may be noted here that the audio-frequency modulation contributes to the reduction of the signal amplitude if the radio-frequency voltage is increased beyond the optimum value. As mentioned above, the width of the component a_1 (or a_2) and therefore l increases with increasing radio-frequency voltage. Since the other parameters (V_a, ν_a, $\Delta\nu_0$, Δf) are kept constant, the receiver will pass a smaller number of Fourier components which means an additional reduction in signal amplitude as can be seen from the table.

To sum up, the radio-frequency voltage must be adjusted for optimum signal amplitude, i.e. $\alpha V_r = \Delta\nu_0$. This means for a modulating rate α of the klystron of, for example, 1·5 Mc/s per volt, the gas pressure should be of the order of 5–10 μ Hg and the radio frequency peak voltage V_r will then lie between 30 and 60 mv r.m.s. The audio frequency is then determined by the band-width of the receiver and the audio-frequency voltage; the sweep voltage V_a depends also on the half-width.

2.4. *Representation of the Signal produced by a Gas-filled Cavity*

The adjustments of the spectrometer used in this investigation allowed us to observe the power absorbed in the gas-filled cavity. The absorption coefficient Γ_g of the cavity becomes then

$$\Gamma_g = 1/[1 + Q\epsilon'' + 2j(\omega - \omega_0)Q/\omega_0]$$

(Townes and Schawlow 1955) where it is assumed that the coupling into the cavity obtains under optimum conditions. Here Q is the Q-factor of the cavity $= 1/\delta$, $\epsilon'' = \alpha_g\lambda/2\pi$, λ is the free-space wavelength and ω_0 the resonance frequency of the cavity. If the gas possesses several resonance frequencies (as in the case of the Zeeman splitting of a single line)

$$\alpha_g = \sum_{i=1}^{N} \alpha_{0i}/[1 + 4(\omega - \omega_i)^2/\Delta\omega_i^2]$$

where the α_{0i} denote the individual peak absorption coefficients of the lines of resonance frequencies ω_i and half-widths $\Delta\omega_i$. The electric field incident upon the gas-filled cavity is diminished by an amount Γ_g; this behaviour can be described by an equivalent circuit consisting of a resonant LC circuit in which the condenser is filled with a lossy dielectric. In such a circuit, a resistance R, an inductance L and a condenser C filled with a dielectric of dielectric constant $\epsilon' - j\epsilon''$ are connected in series. Its impedance Z is then given by

$$Z = R\{1 + \epsilon'' Q + 2jQ(\omega - \omega_0)/\omega_0\}$$

if $\omega \simeq \omega_0$, $\epsilon' \simeq 1$, $\epsilon'' \ll \epsilon'$. $Q = \omega_0 L/R$ as usually defined. If a voltage V is applied, a current $i = V/Z$ will flow in the circuit. Now in our case,

$$V = V_0 \exp\{j(\omega t + m\cos\omega_r t)\}$$

where $\omega = \omega_0 + \alpha V_a \nu_a t$ as before. V can be expanded in terms of Bessel functions of the first kind:

$$V = V_0 \sum_{=-\infty}^{\infty} \mathrm{J}_l(m)\exp\{j(\omega + l\omega_r)t\}.$$

The current i can then be represented in the form

$$i = \sum_{k=-\infty}^{\infty} \mathrm{J}_k(m)[\exp\{j(\omega + k\omega_r)t\}]/Z_k$$

with

$$Z_k = R\left\{1 + \frac{cQ}{\omega_0}\sum_{i=1}^{N}\frac{\alpha_{0i}}{1+4(\omega-\omega_i+k\omega_r)^2/\Delta\omega_i^2} + \frac{2jQ}{\omega_0}(\omega-\omega_0+k\omega_r)\right\}.$$

Writing $Z_k = R_k + jX_k$, the power absorbed in the circuit P_a becomes

$$P_a = \tfrac{1}{2}V_0^2 \sum_{l=-\infty}^{\infty}\sum_{k=-\infty}^{\infty} \mathrm{J}_l(m)\mathrm{J}_k(m)\{\cos[(2\omega + k\omega_r + l\omega_r)t - \phi_k] \\ + \cos[(k-l)\omega_r t - \phi_k]\}/Z_k$$

with $\cos\phi_k = R_k/|Z_k|$. The crystal current is proportional to P_a; the component of the current fluctuating with $n\omega_r$ is obtained by setting $k-l=\pm n$. Therefore, we find finally that the output from the receiver tuned to the harmonic $n\omega_r$ is proportional to a quantity A_n where

$$A_n = \sum_{k=-\infty}^{\infty} |Z_k|^{-2}\{\mathrm{J}_k(m)\cos n\omega_r t R_k(\mathrm{J}_{k+n} + \mathrm{J}_{k-n}) - \mathrm{J}_k(m)\sin n\omega_r t X_k(\mathrm{J}_{k+n} - \mathrm{J}_{k-n})\} \qquad \ldots\ldots(4)$$

where

$$X_k = 2R(p + ks/m)$$

$$R_k = R\left\{1 + \frac{cQ}{\omega_0}\sum_{i=1}^{N}\alpha_{0i}\Big/\left[1 + 4\Delta\omega_0^2\left(p + \frac{\omega_0-\omega_i}{\Delta\omega_0} + \frac{ks}{m}\right)^2\Big/\Delta\omega_i^2\right]\right\}$$

and $|Z_k|^2 = R_k^2 + X_k^2$. The terms p and s have the same meaning as in § 2.2. Formula (4) passes into the formula given by Karplus (1948) for $n=1$ and $\alpha_{0i}=0$.

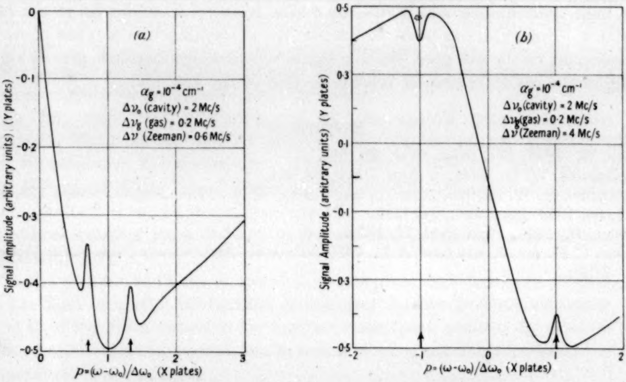

Figure 6. Presentation of a doublet in cavity resonance.
(*a*) Theoretical curve for $\nu_1 - \nu_2 = 0{\cdot}6$ Mc/s.
(*b*) Theoretical curve for $\nu_1 - \nu_2 = 4$ Mc/s.

In figure 6 (*a*), (*b*) graphs have been plotted of A_1 as a function of p. The curves are plotted for the case $N=2$, $\alpha_{01}=\alpha_{02}=10^{-4}$ cm^{-1}, $\Delta\omega_0 = 2$ Mc/s and $\Delta\omega_0/\Delta\omega_i = 10$. (*a*) represents the case where $\nu_1-\nu_2 = 0{\cdot}6$ Mc/s and (*b*) obtains when $\omega_1 - \omega_2 = 2\Delta\omega_0$. It will be seen from (*a*) that two lines of equal intensity will be represented by signals of unequal intensity owing to the slope of the background against which they appear. Figure 6 (*b*) shows that the same line will appear as a peak if the background signal (here the cavity resonance) is concave with respect to the abscissa and as a trough if the background signal is convex towards the abscissa. Formula (4) also describes the appearance of a gas absorption line if sharp reflections are present. The radio-frequency voltage in all these cases must be adjusted to match the half-width of the absorption line of the gas and not that of the cavity resonance or sharp reflections so that the background is to some extent reduced while the amplitude of the line to be investigated becomes enhanced as much as possible.

The theoretical curves of figure 6 may be compared with the photograph of the Zeeman effect of $^{14}NH_3$ ($J, K = 13, 13$) shown in figure 7 (Plate).

§ 3. CONCLUSIONS

The results of the investigations presented above may be summed up as follows. The output from the radio-frequency receiver reaches a maximum when the frequency range through which the klystron is swept, equals the half-width of the gas absorption line to be observed. It may be mentioned here that the width of these lines is of the order of 20 Mc/s per mm Hg pressure. To ensure after adjustment of the radio-frequency voltage that a faithful representation of the signal is obtained on the screen of the oscilloscope, the audio frequency which determines the repetition rate of the time-base must be made equal to the ratio of the receiver band-width to the number of Fourier components to be passed by the receiver. Since this number is found to be at least eight, and since the band-width should be kept at the order of 200–300 c/s for a high spectrometer sensitivity, the audio frequency should lie in the range 20–40 c/s. Finally, it has been shown that the absorption line of a gas contained in a resonant cavity will give rise to a signal whose shape depends greatly on the tuning of the cavity resonance relative to that of the gas line.

REFERENCES

GORDY, W., 1948, *Rev. Mod. Phys.*, **20,** 668.
HERSHBERGER, W. D., 1948, *J. Appl. Phys.*, **19,** 411.
HOISINGTON, R. W. R., KELLNER, L., and PENTZ, M. J., 1956, *Nature, Lond.*, **178,** 1111.
JEN, J. K., 1948, *Phys. Rev.*, **74,** 1396.
KARPLUS, R., 1948, *Phys. Rev.*, **73,** 1026.
TOWNES, C. H., and SCHAWLOW, A. L., 1955, *Microwave Spectroscopy* (New York: McGraw-Hill).

The Optical Properties of Bismuth Telluride

By I. G. AUSTIN

Research Laboratories of The General Electric Company Limited, Wembley, Middx.

MS. received 13th June 1958, and in final form 15th July 1958

Abstract. The shape of the absorption edge in the semiconductor Bi_2Te_3 has been determined from transmission measurements on cleavage sections. The edge is of the form expected for indirect transitions, but an interpretation in terms of phonons characterized by a single energy is not applicable. A brief study of anisotropy effects is included.

The energy gap at room temperature is close to 0·13 ev with a temperature coefficient of $-0{\cdot}95 \times 10^{-4}$ ev deg^{-1}. The refractive index, determined from interference fringes, is 9·2 in the region 8–14μ.

In degenerate samples the absorption edge is displaced towards higher energies. A simple quantitative discussion of this effect is given.

§ 1. INTRODUCTION

A number of workers have recently reported detailed studies of the electrical and thermal properties of the semiconductor Bi_2Te_3 (Konorov 1956, Goldsmid 1956, 1958, Black *et al.* 1957, Harman *et al.* 1957). These investigations have been stimulated by the possibility of using this material for thermoelectric cooling and generation (Wright 1958). Many of the properties are anisotropic, since Bi_2Te_3 crystallizes in the class R$\bar{3}$m. Drabble and Wolfe (1956) have made use of the anisotropy of the resistivity and Hall effect to deduce possible models for the energy band structure.

So far, very few measurements of the optical properties have been reported. Black *et al.* (1957) deduced an optical energy gap of 0·15 ev from transmission measurements. The present author has reported a similar value (Wright 1956). These estimates contrast with the value of approximately 0·3 ev obtained from photoconductivity effects in thin films by Gibson (1950), and values ranging from 0·16 ev to 0·3 ev from electrical measurements (see Goldsmid 1958).

In the present work the shape of the absorption edge has been studied, since this can lead to useful information concerning the energy band structure. The shape is of the form expected for indirect transitions, assisted by phonon interaction, but a simple interpretation in terms of phonons characterized by a single temperature is not possible.

An interesting feature of this material is the unusually high refractive index (9·2).

In some of the samples we have studied, the absorption edge is displaced towards higher energies. This appears to be a consequence of degeneracy and is similar to the effects described by Burstein (1954) and Moss (1954) for n-type InSb.

§ 2. EXPERIMENTAL METHOD

The single crystals used in this work were prepared by Mr. A. R. Sheard, using a zone melting process. The ingots obtained from stoichiometric quantities of the elements were always p-type. Intrinsic and n-type material was produced by adding iodine.

Single crystals of Bi_2Te_3 show an excellent cleavage parallel to the (0001) plane and sections of thickness from about 5 microns upwards were readily obtained. The uniformity of thin samples was judged from the regularity of the transmission interference fringes (see § 4.4). In the absence of fringes, visual examination of the surfaces was used. The specimen thickness was calculated from the weight and area, assuming a value of 7·86 for the density (Goldsmid, private communication).

Transmission measurements were made using a Hilger H.800 double beam prism spectrometer, with a rock salt prism. Low temperature measurements were carried out in a vacuum cryostat fitted with KBr windows. The specimens were clamped between well-greased brass plates. In order to reduce temperature gradients, the surface area exposed to the incident radiation was reduced to a minimum, consistent with utilizing the full aperture of the spectrometer slits.

§ 3. ABSORPTION MEASUREMENTS

Transmission measurements, in the temperature range $-155°$c to $20°$c, were made on the crystals listed in the table. All measurements, except those in §4.3, refer to cleavage specimens in which the incident radiation was directed along the principal axis of the crystal.

As it was difficult to measure the absolute transmission of samples, the following procedure was adopted. Graphs of the ratio of the log (transmission) to thickness plotted against wave number were prepared for samples of different thickness. These could be fitted together to form a continuous absorption edge, with reasonable agreement in the region of overlap, by suitable displacement of the vertical scales.

No. of ingot		SBT/6	SBT/16	SBT/27	SBT/19	SBT/14
Type of ingot		n	n	n	p	p
Reduced Fermi levels η	20°c	0·1	~ -2	$\sim$mid†	~ -1	0·1
	$-155°$c	3·1	0·4	$-0·5$	0·6	2·8

† $\sim$middle of forbidden gap.

The Fermi levels are measured in kT with respect to the appropriate band edges and were obtained from thermoelectric data. Negative values indicate Fermi levels within the forbidden gap.

This method assumes that the transmitted intensity is simply proportional to $\exp(-Kt)$, where K is the absorption coefficient and t the thickness, and ignores effects arising from internal reflections. This assumption is valid when $\exp(-Kt) \ll 1$, and care was taken to select only those transmission measurements which were thought to satisfy this condition.

The absorption arising from free carriers was found to increase smoothly with increasing wavelength. This component was extrapolated beyond the absorption edge, and subtracted. On cooling to $-155°$c, a large decrease in the free carrier absorption occurred in both n- and p-type material. This is presumably due to the increase in carrier mobility, since it is known from electrical measurements (Goldsmid 1958) that the carrier concentration remains constant in all the samples, except SBT/27.

Measurements on the samples listed in the table indicated a variation in the position of the absorption edge from one sample to another. This variation was attributed to degeneracy and is discussed in § 5. The results on a nearly intrinsic specimen (SBT/27) are discussed first, since these should not be complicated by degeneracy.

§ 4. ABSORPTION EDGE IN INTRINSIC MATERIAL

4.1. *Theory*

The form of the absorption edge in semiconductors has been discussed by a number of authors (see Fan 1956 for a review). In general, the absorption is proportional to $(h\nu - E_G)^n$, where $n = \frac{1}{2}$ or $\frac{3}{2}$ for direct transitions, and $n = 2$ or 3 for indirect transitions. E_G is closely related to the minimum band gap.

Macfarlane and Roberts (1955) have proposed the expression,

$$K = A\left[\frac{(h\nu - E_G - k\theta)^2}{1 - e^{-\theta/T}} + \frac{(h\nu - E_G + k\theta)^2}{e^{+\theta/T} - 1}\right] \qquad \ldots\ldots(1)$$

for indirect transitions assisted by phonon interaction, which takes into account the energy $k\theta$ of the phonon required to conserve momentum. The first term corresponds to the emission of a phonon and the second to absorption.

4.2. *Results*

In figure 1 the absorption edge for SBT/27 has been plotted as the square root of the absorption coefficient against wave number, at three different temperatures. In each case, the absorption edge appears to break into two straight line sections.

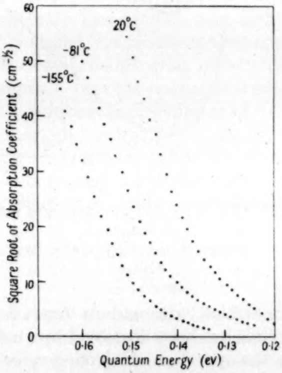

Figure 1. Absorption edge data for SBT/27, plotted as the square root of the absorption coefficient against quantum energy.

Although the general behaviour predicted by equation (1) is followed a good quantitative fit cannot be obtained. The measured ratios of the slopes of the straight line portions are roughly three times greater than the ratios calculated from the intercepts on the frequency axis.

A plausible explanation is that the absorption edge consists of several components, similar to equation (1), each being characterized by a different phonon energy. In support of this, some of the low temperature records indicate discontinuities in the slope of the edge, but measurements with better resolution are required for a more detailed analysis.

4.3. *Polarized Light Measurements*

Since Bi_2Te_3 is rhombohedral we expect the optical properties to be anisotropic. Transmission measurements, using polarized light, were made on thin sections in which faces perpendicular to the cleavage planes were produced by grinding and polishing. Owing to the soft nature and easy cleavage of the material, only a few suitable specimens were obtained. Six sheets of silver chloride, set at the Brewster angle, were used to polarize the light.

Figure 2 shows some results on SBT/27. The free carrier absorption differs appreciably for the two directions of polarization, and is greatest when the electric vector is parallel to the cleavage planes. The position of the absorption edge, on the other hand, is only slightly dependent on the polarization direction.

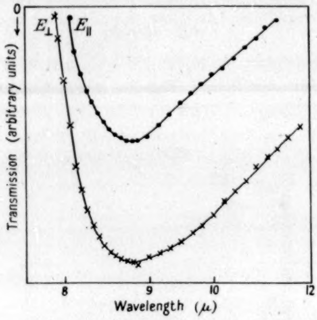

Figure 2. Transmission of SBT/27 at -155°c, using light polarized in the two principal directions.
$E_\parallel$ electric vector parallel to cleavage planes; $E_\perp$ electric vector perpendicular to cleavage planes.

The shape of the absorption edge and its dependence on the polarization vector in anisotropic crystals has been discussed by Dresselhaus (1957). In the case of direct transitions, the operation of selection rules may give rise to a change in shape of the absorption edge with direction of polarization and hence to a large apparent displacement (cf. the work on Te by Loferski 1954). The shift for indirect transitions is expected to be small, as the only variation with polarization is in the constant of proportionality (A in equation (1)). The present measurements are consistent with the assumption of indirect transitions.

4.4. *Refractive Index*

Many specimens showed well-defined transmission interference fringes and and these were used to calculate the refractive index n, using the relation, $2nt = N\lambda$ where t is the sample thickness and N the fringe number. Approximate values of the refractive index were obtained from the fringe spacing, and used to identify the fringe numbers in a thin sample. The fringe numbers were then used to calculate a more accurate dispersion curve, in the manner described by Moss *et al.* (1957).

Figure 3 shows the results on SBT/27 at −155°c.

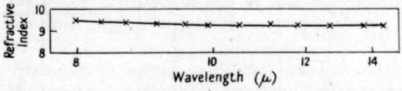

Figure 3. Refractive index of SBT/27 at −155°c.

4.5. *Discussion*

Drabble *et al.* (1956, 1958) have proposed energy band models of the many-valley type for Bi_2Te_3, on the basis of resistivity, Hall effect and magnetoresistance measurements. It was suggested that, in both n- and p-type material, six equivalent energy extrema are situated on reflection planes in **k** space.

In such a scheme we may envisage indirect transitions from each valley in the valence band to all six conduction band minima. Because of the symmetry, these transitions would be characterized by four different momentum changes. Further complications may arise from the multiplicity of branches in the elastic spectrum of the solid, as in the case of Ge (Macfarlane *et al.* 1957). Corresponding to a given momentum, there will exist in different branches, phonons with appreciably different energies. The present data, although consistent with the general predictions of this model, are clearly inadequate to offer a sensitive test. It is hoped to extend the measurements using higher resolution.

We may infer from figure 1 that the optical energy gap at room temperature is close to 0·13 ev, with a temperature coefficient of $-0{\cdot}95 \times 10^{-4}$ ev deg^{-1}.

The unusually high refractive index, 9·2, of Bi_2Te_3 implies a large dielectric constant (~85). This may be linked with the absence of ionized impurity scattering in samples containing relatively high impurity concentrations ($\sim 10^{20}\,\mathrm{cm}^{-3}$), noted by Black *et al.* (1957) and Goldsmid (1958).

§ 5. DEGENERACY EFFECTS

5.1. *Results*

The absorption edges for all the samples listed in the table were obtained at 20°c and −155°c. The results for n-type specimens are shown in figure 4 (crosses and dots) and for p-type in figure 5 (crosses and squares). Owing to the pronounced wavelength dependence of the free carrier absorption in samples 6 and 14, extrapolation beyond the absorption edge was less reliable. Also shown in the table are the Fermi levels, estimated from thermoelectric measurements on adjacent specimens (Goldsmid, private communication). Most of the samples are at least partially degenerate.

It is clear from figures 4 and 5 that, compared with intrinsic material (SBT/27), the absorption edges are displaced towards higher energies with increasing degeneracy. These effects are most pronounced at low temperatures.

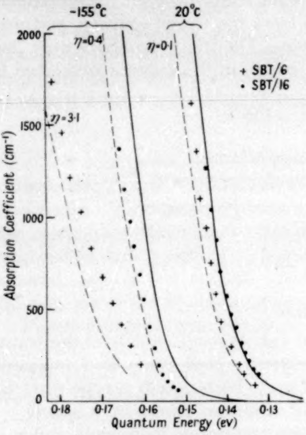

Figure 4.

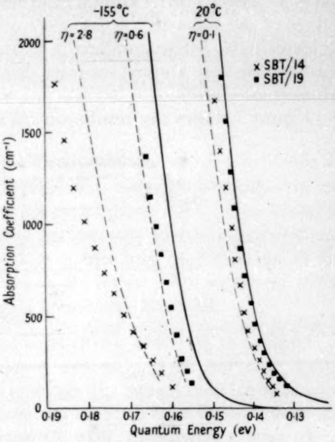

Figure 5.

Figure 4. A comparison between the measured and calculated absorption edges in two n-type samples, showing the effects of degeneracy at 20°c and −155°c.

The full lines show the absorption edges for the intrinsic sample SBT/27. The broken lines are the calculated edges. Crosses and dots correspond to measurements.

Figure 5. Similar to figure 4, but for p-type material.

The displacement of the absorption edge with increasing degeneracy is similar to that observed by Burstein (1954) and Moss (1954) for n-type InSb, and follows from the increasing occupation of states near the band edges.

5.2. *Calculated Effect of Degeneracy*

A simple modification (see Appendix) of Macfarlane and Roberts' expression (eqn. (1)), taking into account degeneracy, leads to

$$K \propto (h\nu - E_G - k\theta)^2[1+\exp(\eta - A/2kT)]^{-1} \qquad \ldots\ldots(2)$$

for the phonon emission component, where $A=(h\nu - E_G - k\theta)$; η is the reduced Fermi level; the approximation is valid when $A \lesssim kT$.

When components corresponding to phonons of different energies are present, the absorption is given by a summation of terms similar to equation (2). However, if the phonon energies are small compared with kT, the factors containing the Fermi level may be removed from within the summation sign and replaced by an average factor outside. This simplification is assumed to apply here. Thus the effect of degeneracy is to reduce the absorption coefficient, at a frequency ν, by the factor $[1+\exp(\eta - A/2kT)]^{-1}$ where A now contains an average θ value. Similar considerations apply to the phonon absorption components.

The positions of the absorption edge corresponding to the Fermi levels in the table were estimated, taking as data for an intrinsic specimen the measurements on SBT/27. According to the table, this specimen is weakly degenerate at −155°C, but a rough calculation suggests that the effect on the absorption edge is sufficiently small to be neglected in the present discussion.

The low temperature calculations were simplified by subtracting the phonon absorption contribution. The broken curves in figures 4 and 5 show the results.

5.3. *Discussion*

All the calculated displacements are somewhat larger than the observed variations, except for SBT/14. Also, in this sample which is highly degenerate at −155°C, the calculated edge is appreciably steeper than the measurements indicate.

However, the Fermi levels in the table are based on the use of a simple relaxation time of the form $\tau \propto v^r$, for the scattering of change carriers, where v is the velocity. A value of $r = -1$ was assumed, but a value between -1 and -2 would bring the calculated and measured absorption edges into better agreement. In view of the approximations involved in the above calculations, and the uncertainty regarding the scattering law, the present discrepancy is not unreasonable.

Although degeneracy effects appear to offer a plausible explanation for the displacement of the edge, a contributory factor should be mentioned. X-ray measurements show that the introduction of iodine leads to a slight increase in the c parameter of the unit cell (Francombe, private communication). The difference between SBT/14 and SBT/16 amounts to 0·03%. An approximate calculation of the corresponding decrease in energy gap using $\delta E/\delta T$ from optical data and $\delta c/\delta T$ from X-ray data suggests that the decrease arising from lattice expansion is considerably smaller than the observed variation.

Finally, it should be noted that all the measurements reported here have been made on compensated samples. The evidence from electrical data, by Black *et al.* (1957) and Goldsmid (1958), indicates that the impurity levels have merged with the band edges in these samples, corresponding to an overlapping impurity band. We have assumed in our discussion that the density of states near the band edge is proportional to the square root of the energy. The impurity levels may cause the density of states to depart from this simple law. Such a deviation would presumably be reflected as a change in the slope of the absorption edge, with varying impurity content.

§ 6. CONCLUSIONS

Although a complete analysis of the absorption edge has not been possible, the present data lend some support to current models for the energy band structure. A more reliable estimate than hitherto of the optical energy gap and its temperature variation has been made.

The refractive index of this material is higher than any value previously reported for a semiconductor. A knowledge of this quantity may prove useful in understanding certain aspects of the electrical behaviour.

The calculated effects of degeneracy on the absorption edge are in substantial agreement with the observations. Although better agreement would be obtained with the assumption of a slightly different scattering law for charge carriers, some of the discrepancy may be due to the presence of impurity levels which perturb the density of states near the band edge.

APPENDIX

The probability per unit time of an electron being raised from a state i in the valence band to a state near f in the conduction band, by the absorption of a photon, accompanied by phonon emission is (see Fan 1956)

$$P_{\mathrm{if}} \propto \frac{M_1^2 M_2^2}{(E_{\mathrm{n}}-E_{\mathrm{i}})^2}\rho_{\mathrm{f}}(E) \qquad \ldots\ldots\text{(A1)}$$

$\rho_{\mathrm{f}}(E)$ is the density of states at f, M_1 and M_2 are matrix elements for photon and phonon interaction. E_{n} is an intermediate energy state.

The absorption coefficient, for a frequency ν, is obtained by integrating over all possible values of i in the valence band, thus

$$K \propto \int_0^{h\nu - E_{\mathrm{G}} - k\theta} P_{\mathrm{if}}\rho_{\mathrm{i}}(E_{\mathrm{i}})\,d(E_{\mathrm{V}}-E_{\mathrm{i}}) \qquad \ldots\ldots\text{(A2)}$$

E_{G} is the energy gap and E_{V} the energy at the top of the valence band.

If the Fermi energy E_η is close to the conduction band edge E_{C}

$$\rho_{\mathrm{f}} \propto (E_{\mathrm{f}}-E_{\mathrm{C}})^{1/2}[1+\exp{(E_\eta - E_{\mathrm{f}})}/kT]^{-1} \qquad \ldots\ldots\text{(A3)}$$

$$\rho_{\mathrm{i}} \propto (E_{\mathrm{V}}-E_{\mathrm{i}})^{1/2}.$$

Integration of (A2) without the Fermi factor in (A3), and assuming that M_1, M_2 and $E_\eta - E_{\mathrm{i}}$ are essentially independent of frequency, leads to equation (1) in the text.

When the Fermi factor is included, explicit evaluation is difficult. If the Fermi factor varies slowly across the range of integration, i.e. $h\nu - E_{\mathrm{G}} - k\theta \lesssim kT$, it may be replaced by a mean value. This approximation leads to equation (2) in the text.

REFERENCES

Black, J., Conwell, E. M., Seigle, L., and Spencer, C. W., 1957, *J. Phys. Chem. Solids*, **2**, 240.

Burstein, E., 1954, *Phys. Rev.*, **93**, 632.

Drabble, J. R., 1958, *Proc. Phys. Soc.*, **72**, 380.

Drabble, J. R., Groves, R., and Wolfe, R., 1958, *Proc. Phys. Soc.*, **71**, 430.

Drabble, J. R., and Wolfe, R., 1956, *Proc. Phys. Soc.* B, **69**, 1101.

Dresselhaus, G., 1957, *Phys. Rev.*, **105**, 135.

Fan, H. Y., 1956, *Rep. Progr. Phys.*, **19**, 107 (London : Physical Society).

Gibson, A. F., 1950, *Proc. Phys. Soc.* A, **63**, 176.

Goldsmid, H. J., 1956, *Proc. Phys. Soc.* B, **69**, 203; 1958, *Ibid.*, **71**, 633,

Harman, T. C., Paris, B., Miller, S. E., and Goering, H. L., 1957, *J. Phys. Chem. Solids*, **2**, 181.

Konorov, P. P., 1956, *J. Tech. Phys., Moscow*, **26**, 1400.

Loferski, J. J., 1954, *Phys. Rev.*, **93**, 707.

Macfarlane, G. G., McLean, T. P., Quarrington, J. E., and Roberts, V., 1957, *Phys. Rev.*, **108**, 1377.

Macfarlane, G. G., and Roberts, V., 1955, *Phys. Rev.*, **97**, 1714.

Moss, T. S., 1954, *Proc. Phys. Soc.* B, **67**, 775.

Moss, T. S., Smith, S. D., and Hawkins, T. D. F., 1957, *Proc. Phys. Soc.* B, **70**, 776.

Wright, D. A., 1956, *Proceedings of the Garmisch Conference. Halbleiter-Probleme*, **4**; 1958, *Nature, Lond.*, **181**, 834.

Theory of the Effect of a Magnetic Field on the Absorption Edge in Semiconductors

By R. J. ELLIOTT†, T. P. McLEAN‡ and G. G. MACFARLANE‡
† Clarendon Laboratory, Oxford
‡ Royal Radar Establishment, Malvern, Worcs.

MS. received 12th May 1958, and in final form 26th June 1958

Abstract. A magnetic field splits up electron energy bands in a solid into a series of sub-bands. The absorption edge which arises from transitions between two such bands across an energy gap then shows a structure from transitions between the various sub-bands. The shape of this structure is considered for direct transitions between simple spherical bands, spheroidal bands and degenerate bands. This often takes the form of a series of peaks from which the effective masses of the bands can be determined, but there are cases in which the effect of the field is less dramatic and forms a series of steps. Absorption from indirect transitions involving phonons also forms a series of steps.

---

§ 1. Introduction

The electronic properties of semiconductors are largely determined by the properties of those one-electron energy states which lie just above and below the forbidden energy gap. A considerable amount of information about these states has recently been obtained by a detailed study of the optical absorption in semiconductors—particularly the main absorption edge and its associated structure (Macfarlane and Roberts 1955 a, b, Macfarlane, McLean *et al.* 1957, Roberts and Quarrington 1955, Blount *et al.* 1956, Potter 1956, Dumke 1957, Choyke and Patrick 1957 a, b). Cyclotron resonance (Dresselhaus *et al.* 1955, Lax *et al.* 1956) has been used to make a direct determination of the effective masses at the band edges. This is essentially a measure of the optical absorption between states of the same band in the presence of a strong magnetic field and is made at microwave or far infra-red frequencies. Recently, the first measurements have been made of the effect of magnetic fields on the absorption in the edge between states on opposite sides of the gap. This effect which is analogous to the Zeeman effect in atomic spectra has been observed in direct transitions in InSb by Burstein and Picus (1957), Zwerdling and Lax (1957) and by Zwerdling, Lax and Roth (1957) in Ge, InSb and InAs. In those substances the absorption edge is split up into a series of peaks from the spacing of which the effective masses in the bands may be determined. No attempt has apparently been made so far to study the detailed shape of this absorption. With such a study in mind we present here a theoretical discussion of shape of the absorption edge which may be expected from both direct and indirect transitions. This is found to take different forms under various conditions and will not always be peaked in the fashion already observed.

§ 2. WAVE FUNCTIONS AND ENERGY LEVELS IN A MAGNETIC FIELD

2.1. *General Theory*

The one-electron wave functions in a uniform magnetic field defined by a vector potential $\mathbf{A}=(-\frac{1}{2}Hy, \frac{1}{2}Hx, 0)$ in a solid are the solutions of

$$\left[\frac{1}{2m}\left(\mathbf{p}+\frac{e\mathbf{A}}{c}\right)^2+V(\mathbf{r})\right]\Psi=E\Psi \qquad \ldots\ldots (2.1)$$

where m is the free electron mass and $V(\mathbf{r})$ the periodic potential. When $\mathbf{A}=0$ the solutions of (2.1) are of course the Bloch functions $u_{\alpha\mathbf{k}}(\mathbf{r})\exp(i\mathbf{k}.\mathbf{r})$, where α specifies the band. The solutions of (2.1) close to a band edge may be found in terms of the band edge wave functions by a perturbation method usually called the effective mass approximation which has been extensively developed by Luttinger and Kohn (1955). An expansion in terms of the original Bloch states may be made in the form

$$\Psi_\alpha(\mathbf{r})=\sum_{\alpha'}\int d\mathbf{k}A_{\alpha\alpha'}(\mathbf{k})u_{\alpha'0}(\mathbf{r})e^{i\mathbf{k}.\mathbf{r}} \qquad \ldots\ldots (2.2)$$

where $u_{\alpha'0}(\mathbf{r})$ is the Bloch function at the band edge which has been chosen for convenience at $\mathbf{k}=0$. The $A_{\alpha\alpha'}(\mathbf{k})$ are related to matrix elements between Bloch states in different bands which are proportional to either $\mathbf{k}$ or $eH/\hbar c$. In either case these are small because k^{-1} and $L=\sqrt{(\hbar c/eH)}$ are much larger than the interatomic spacing when $k\sim 0$ close to the band edge and $H\sim 10^4$–10^5 oersteds.

By making a suitable transformation A can be made diagonal to first order in k and L^{-1} and the cross terms neglected. This transformation is given by

$$A_{\alpha\alpha'}(\mathbf{k})=\sum_{\gamma}\int d\mathbf{k}'\exp[\langle\alpha',\mathbf{k}|S|\gamma,\mathbf{k}'\rangle]B_{\gamma\alpha}(\mathbf{k}') \qquad \ldots\ldots (2.3)$$

where

$$\left.\begin{array}{rll}\langle\alpha',\mathbf{k}|S|\gamma,\mathbf{k}'\rangle = & -\dfrac{\hbar}{m(\epsilon_{\alpha'}(0)-\epsilon_\gamma(0))} & \\ & \times\left\{\mathbf{k}.\mathbf{p}_{\alpha\gamma}(0)-\dfrac{eH}{2\hbar c}(\mathbf{p}_{\alpha\gamma}(0)\times\nabla_{k'})_z\right\}\delta(\mathbf{k}'-\mathbf{k}) & \\ & & \epsilon_{\alpha'}(0)\neq\epsilon_\gamma(0) \\ =0, & & \epsilon_{\alpha'}(0)=\epsilon_\gamma(0)\end{array}\right\} \qquad \ldots\ldots (2.4)$$

and one works to first order in S. $\epsilon_\alpha(\mathbf{k})$ is the energy of an electron in band α with wave-vector $\mathbf{k}$ and $\mathbf{p}_{\alpha\gamma}(\mathbf{k})$ is the momentum matrix element,

$$\mathbf{p}_{\alpha\gamma}(\mathbf{k})=-i\hbar[(2\pi)^3/\Omega]\int_{\text{unit cell}} d\mathbf{r}u_{\alpha\mathbf{k}}{}^*(\mathbf{r})\nabla u_{\gamma\mathbf{k}}(\mathbf{r}) \qquad \ldots\ldots (2.5)$$

where Ω is the volume of the unit cell. Transforming back to coordinate space

$$F_\alpha(\mathbf{r})=\int d\mathbf{k}B_{\alpha\alpha}(\mathbf{k})e^{i\mathbf{k}.\mathbf{r}} \qquad \ldots\ldots (2.6)$$

describes the overall motion of the particle which is modulated around the lattice points like $u_{\alpha0}(\mathbf{r})$. $F(\mathbf{r})$ may then be shown to be the solution of a differential equation.

The most general case of interest arises when the band edge is degenerate with Bloch functions $u_{\alpha 0}$, $u_{\beta 0}$, ... etc. In the absence of a magnetic field the energy levels for small $\mathbf{k}$ may be determined as above by second-order perturbation theory (Shockley 1950). The zero-order wave functions are

$$\sum_{\alpha} a_{\alpha} u_{\alpha 0}(\mathbf{r}) e^{i\mathbf{k}.\mathbf{r}} \qquad \ldots\ldots (2.7)$$

where the a_{α} are constants determined from the matrix equation

$$\sum_{\beta} (D_{\alpha\beta}(\mathbf{k}) - E\delta_{\alpha\beta}) a_{\beta} = 0 \qquad \ldots\ldots (2.8)$$

the sums in (2.7) and (2.8) being over the degenerate set of states.

$D_{\alpha\beta}(\mathbf{k})$ is a quadratic function of $\mathbf{k}$

$$D_{\alpha\beta}(\mathbf{k}) = \frac{\hbar^2 k^2}{2m} \delta_{\alpha\beta} + \frac{\hbar^2}{m^2} \sum_{\gamma} \frac{\mathbf{k}.\mathbf{p}_{\alpha\gamma}(0)\mathbf{k}.\mathbf{p}_{\gamma\beta}(0)}{\epsilon_{\alpha}(0) - \epsilon_{\gamma}(0)} \qquad \ldots\ldots (2.9)$$

where the sum is over all bands excluding the degenerate set u_{α}, u_{β} etc. With the perturbing magnetic field present the zero-order functions are

$$\sum_{\alpha} F_{\alpha}(\mathbf{r}) u_{\alpha 0}(\mathbf{r}) \qquad \ldots\ldots (2.10)$$

the sum being taken over degenerate states and F_{α} are the solutions of

$$\sum_{\beta} \left[D_{\alpha\beta}\left(-i\nabla + \frac{e\mathbf{A}}{\hbar c} \right) - E\delta_{\alpha\beta} \right] F_{\beta}(\mathbf{r}) = 0. \qquad \ldots\ldots (2.11)$$

2.2. *Spherical Band*

The simplest case arises for a simple band with a spherical energy surface defined by effective mass m_{α}

$$\epsilon_{\alpha}(\mathbf{k}) = \epsilon_{\alpha}(0) + \hbar^2 k^2 / 2m_{\alpha} \qquad \ldots\ldots (2.12)$$

and only spin degeneracy, when equation (2.11) becomes the Schrödinger equation of an electron mass m_{α} in a magnetic field:

$$\left[-\frac{\hbar^2}{2m_{\alpha}} \nabla^2 - \frac{ie\hbar H}{2m_{\alpha} c} \left(x \frac{\partial}{\partial y} - y \frac{\partial}{\partial x} \right) + \frac{e^2 H^2}{8 m_{\alpha} c^2} (x^2 + y^2) \right] F(\mathbf{r}) = EF(\mathbf{r}). \qquad \ldots\ldots (2.13)$$

The solution of this was first given by Landau (1930) in cartesian coordinates

$$F_{\alpha, n, x_0, k_z}(\mathbf{r}) = (L_z L_y)^{-1/2} \exp(ik_z z) \exp[ieH(x - 2x_0)y / 2\hbar c] H_{\mathrm{n}}(x - x_0 / R_0) \qquad \ldots\ldots (2.14)$$

where H_{n} is the normalized wave function of a harmonic oscillator of frequency

$$\omega = eH/mc \qquad \ldots\ldots (2.15)$$

so that its characteristic length $R_0 = \sqrt{(\hbar / m\omega)}$. L_y and L_z are the dimensions of the specimen in the y and z directions and $n = 0, 1, 2 \ldots$. Dingle (1952) has found a solution of (2.13) in cylindrical polar coordinates (ρ, ϕ, z) which is sometimes more convenient to use:

$$F_{\alpha,n,l,k}(\mathbf{r}) = \left(\frac{eHn!}{hcL_z(n+l)!^3}\right)^{1/2} \exp(ik_z z)\exp(-il\phi)\eta^{l/2}\exp(-\eta/2)L^l_{n+l}(\eta) \qquad \ldots\ldots(2.1)$$

where $\eta = eH\rho^2/2\hbar c$ and $L^l{}_{n+l}(\eta)$ is the associated Laguerre polynomial of degree $(n+l)$ and order l. Again $n = 0, 1, 2\ldots$ and the component of angular momentum l can take values $0, 1, 2 \ldots eHA/hc$ where A is the cross-sectional area of the specimen perpendicular to z.

The energy eigenvalues of (2.13) are degenerate. In (2.14), this degeneracy arises from the many values of x_0 which allow periodic boundary conditions on the y-dependent part of the function and, since x_0 determines the centre point of the oscillator functions, it is restricted to lie within the crystal boundaries. Thus the number of degenerate states for each energy is eHA/hc. The degeneracy in (2.16) arises from the eHA/hc possible values which the angular momentum can assume. The degenerate energy levels are

$$E_{\alpha n}(k_z) = \epsilon_\alpha(0) + \frac{\hbar^2 k_z{}^2}{2m_\alpha} + (2n+1)\frac{e\hbar H}{2m_\alpha c} \pm \beta H \qquad \ldots\ldots(2.17)$$

where $\beta = e\hbar/2mc$. The last term arises from the interaction of the field with the electron spin and is included for completeness although the spin terms have been omitted from (2.13). If the doubly degenerate band in question arises because of a spin–orbit splitting, Luttinger (1956) has pointed out that (2.11) gives in addition to (2.17) a term which gives a splitting of the double degeneracy

$$\pm \tfrac{1}{2}g^*\beta H = \pm \frac{\beta H}{m}\sum_\gamma \frac{p^x_{\alpha\gamma}(0)p^y_{\gamma\alpha}(0) - p^y_{\alpha\gamma}(0)p^x_{\gamma\alpha}(0)}{\epsilon_\alpha(0) - \epsilon_\gamma(0)}. \qquad \ldots\ldots(2.18)$$

The spin term will also give rise to an effect different from that of (2.17), namely $\pm\frac{1}{2}g_s\beta H$ the splitting caused by $2\beta\mathbf{s}.\mathbf{H}$ of the Bloch functions $u_{\alpha 0}(\mathbf{r})$, giving

$$\pm \tfrac{1}{2}(g^* + g_s)\beta H \qquad \ldots\ldots(2.19)$$

in all. The two terms represent the contributions of orbital and spin angular momentum to the magnetic moment. The former is of order $\beta m/m^*$.

2.3. *Spheroidal Band*

In an anisotropic crystal, the most general band form is ellipsoidal in the absence of degeneracy. This case is quite complicated to deal with and, since many crystals have at least an axis of symmetry, we consider instead a spheroidal band

$$\epsilon_\alpha(\mathbf{k}) = \epsilon_\alpha(0) + \frac{\hbar^2}{2m_t}(k_1{}^2 + k_2{}^2) + \frac{\hbar^2}{2m_l}k_3{}^2 \qquad \ldots\ldots(2.20)$$

where 1, 2, 3 define three mutually perpendicular axes. $\mathbf{H}$ will in general not lie in one of these directions but may be taken to be in the (2, 3) plane making an angle θ with 3. Defining the direction of $\mathbf{H}$ as z, as before, and x as the direction 1, the wave function F in the magnetic field may be written as

$$F(\mathbf{R}) \qquad \ldots\ldots(2.21)$$

where F is the function given in (2.14) or (2.16) and the vector $\mathbf{R}$ has components (X, Y, z) where

$$\left.\begin{aligned} X &= \sqrt{\frac{m_t}{m}}\left[x + \frac{2\hbar c s' c'(m_l - m_t)}{eH(m_l c'^2 + m_t s'^2)}k_z\right] \\ \text{and}\qquad Y &= \left(\frac{m_l m_t}{m(m_l c'^2 + m_t s'^2)}\right)^{1/2} y \end{aligned}\right\} \qquad \ldots\ldots(2.22)$$

with s' and c' being $\sin\theta$ and $\cos\theta$ respectively and, in F, H is replaced by

$$H' = \frac{m}{m_t}\left(\frac{m_l c'^2 + m_t s'^2}{m_l}\right)^{1/2} H. \qquad \ldots\ldots(2.23)$$

The energy levels for such a band are

$$E_{\alpha n}(k_z) = \epsilon_\alpha(0) + \frac{\hbar^2 k_z^{\ 2}}{2(m_l c'^2 + m_t s'^2)} + (2n+1)\frac{e\hbar H'}{2mc}. \qquad \ldots\ldots(2.24)$$

2.4. *Degenerate Bands*

The case where the band edge has additional degeneracy is of considerable practical importance since Ge, Si, InSb and other substances all show this in their valence bands. The solution of (2.11) is, however, extremely difficult and we shall confine ourselves to a special case which has been solved in detail by Luttinger (1956) and is a good approximation in Ge. This assumes that the two energy surfaces, degenerate at $\mathbf{k}=0$, are both spherical and takes $k_z=0$. The effects of finite k_z and the actual fluting of these surfaces may be treated by perturbation theory, but the essential features of the magneto-band absorption are given in the simplified model. The wave functions of the levels in the presence of a magnetic field are

$$\left.\begin{aligned} a_1^{\pm}F_{n-2,l+2,0}(\mathbf{r})u_{3/2} + a_2^{\pm}F_{n,l,0}(\mathbf{r})u_{-1/2} \\ b_1^{\pm}F_{n-2,l+2,0}(\mathbf{r})u_{1/2} + b_2^{\pm}F_{n,l,0}(\mathbf{r})u_{-3/2} \end{aligned}\right\} \qquad \ldots\ldots(2.25)$$

where the F's are given by (2.16) and the u's are the four degenerate Bloch functions at $\mathbf{k}=0$. The coefficients $a(n)$ are shown by Luttinger to be given by

$$\left.\begin{aligned} [(\gamma_1+\bar{\gamma})(n-\tfrac{3}{2})+\tfrac{3}{2}\kappa]a_1^{\pm}(n) - \bar{\gamma}[3n(n-1)]^{1/2}a_2^{\pm}(n) &= \epsilon_1^{\pm}(n)a_1^{\pm}(n) \\ -\bar{\gamma}[3n(n-1)]^{1/2}a_1^{\pm}(n) + [(\gamma_1-\bar{\gamma})(n+\tfrac{1}{2})-\tfrac{1}{2}\kappa]a_2^{\pm}(n) &= \epsilon_1^{\pm}(n)a_2^{\pm}(n) \end{aligned}\right\} \qquad \ldots\ldots(2.26)$$

in his notation where the energy levels

$$\epsilon_1^{\pm}(n) = \gamma_1 n - (\tfrac{1}{2}\gamma_1 + \bar{\gamma} - \tfrac{1}{2}\kappa) \pm \{[\bar{\gamma}n - (\gamma_1 + \tfrac{1}{2}\bar{\gamma} - \kappa)]^2 + 3\bar{\gamma}^2 n(n-1)\}^{1/2}. \qquad \ldots\ldots(2.27)$$

The coefficients b are solutions of equations obtained from (2.26) by replacing $\bar{\gamma}$ by $-\bar{\gamma}$ and putting b_1 for a_1 and $-b_2$ for a_2, and the energies $\epsilon_2^{\pm}(n)$ of the second kind of level are obtained from the $\epsilon_1^{\pm}(n)$ by putting $\bar{\gamma}\to-\bar{\gamma}$ and reducing the values by κ. For $n=0$, 1 only ϵ_1^{+} and ϵ_2^{+} are defined. For large values of n, the energy levels become equally spaced and are given by (2.17) with the two values m_α of the energy surfaces and anomalous g-factors as in (2.19). In this notation

$$\hbar^2\frac{m}{m_\alpha} = (\gamma_1 \pm 2\bar{\gamma}). \qquad \ldots\ldots(2.28)$$

The dependence of energy on k_z is quadratic near $k_z=0$ and may therefore be defined by an effective mass parameter m_l. This depends on n and may be obtained by second-order perturbation theory as

$$\left.\begin{aligned}
\frac{m}{m_1{}^+} &= [|a_1{}^+(n)|^2(\gamma_1-2\bar{\gamma})+|a_2{}^+(n)|^2(\gamma_1+2\bar{\gamma})] \\
&\quad+\frac{12\bar{\gamma}^2\sum_{\pm}|b_1{}^{\pm *}(n+1)a_1{}^+(n)\sqrt{(n-1)}-b_2{}^{\pm *}(n+1)a_2{}^+(n)\sqrt{(n+1)}|^2}{[\epsilon_1{}^+(n)-\epsilon_2{}^{\pm}(n+1)]} \\
\frac{m}{m_2{}^+} &= [|b_1{}^+(n)|^2(\gamma_1+2\bar{\gamma})+|b_2{}^+(n)|^2(\gamma_1-2\bar{\gamma})] \\
&\quad+\frac{12\bar{\gamma}^2\sum_{\pm}|a_1{}^{\pm *}(n-1)b_1{}^+(n)\sqrt{(n-2)}-a_2{}^{\pm *}(n-1)b_2{}^+(n)\sqrt{n}|^2}{[\epsilon_2{}^+(n)-\epsilon_1{}^{\pm}(n+1)]}
\end{aligned}\right\} \quad \ldots\ldots (2.29)$$

with similar expressions for $m_1{}^-$ and $m_2{}^-$. For small n the dependence only remains quadratic when this energy is much smaller than the energy denominators in (2.29) but at large n these become appreciable and the effective masses become the same as those in (2.28) which determine the level spacing.

§ 3. DIRECT TRANSITIONS

3.1. *Matrix Elements*

The probability of transitions between states i, f because of the interaction of the electron with the electromagnetic field is proportional to the square of the matrix element

$$\langle \mathrm{f}|\boldsymbol{\alpha}\,.\,\mathbf{p}|\mathrm{i}\rangle = -i\hbar\int \Psi_{\mathrm{f}}{}^*(\mathbf{r})\boldsymbol{\alpha}\,.\,\nabla\Psi_{\mathrm{i}}(\mathbf{r})\,d\mathbf{r} \quad \ldots\ldots (3.1)$$

when the wavelength of the radiation is much longer than a lattice spacing in the solid. $\boldsymbol{\alpha}$ is the polarization vector of the radiation. The wave functions may be written in terms of Bloch functions (2.2) and expanding in powers of k and $eH/\hbar c$ as far as the first, (3.1) may be transformed by means of (2.3), (2.4) and (2.6) and written in terms of the F. Between a state in the valence band and a state in the conduction band when neither band edge is degenerate (except for spin) (3.1) may be written

$$\begin{aligned}
\langle \mathrm{c}|\boldsymbol{\alpha}\,.\,\mathbf{p}|\mathrm{v}\rangle &= \boldsymbol{\alpha}\,.\,\mathbf{P}_{\mathrm{cv}}(0)\int F_{\mathrm{c}}{}^*(\mathbf{r})F_{\mathrm{v}}(\mathbf{r})\,d\mathbf{r} - i\hbar\mathbf{M}_{\mathrm{cv}}(0)\,.\int F_{\mathrm{c}}{}^*(\mathbf{r})\nabla F_{\mathrm{v}}(\mathbf{r})\,d\mathbf{r} \\
&\quad -\frac{eH}{2c}\left[\mathbf{M}_{\mathrm{cv}}(0)\times\int F_{\mathrm{c}}{}^*(\mathbf{r})\mathbf{r}F_{\mathrm{v}}(\mathbf{r})\,d\mathbf{r}\right]_z
\end{aligned} \quad \ldots\ldots (3.2)$$

where $\mathbf{P}_{\mathrm{cv}}(0)$, $\mathbf{M}_{\mathrm{cv}}(0)$ are defined by

$$\boldsymbol{\alpha}\,.\,\mathbf{P}_{\mathrm{cv}}(0) = \boldsymbol{\alpha}\,.\,\mathbf{p}_{\mathrm{cv}}(0) + \frac{ie\hbar H}{2mc}[\boldsymbol{\alpha}\times\mathbf{p}_{\mathrm{cv}}(0)]_z/[\epsilon_{\mathrm{c}}(0)-\epsilon_{\mathrm{v}}(0)] \quad \ldots\ldots (3.3)$$

$$\begin{aligned}
\mathbf{M}_{\mathrm{cv}}(0) &= \frac{1}{m}\sum_{\alpha}\left[\frac{\mathbf{p}_{\mathrm{c}\alpha}(0)\,(\boldsymbol{\alpha}\,.\,\mathbf{p}_{\alpha\mathrm{v}}(0))}{\epsilon_{\mathrm{c}}(0)-\epsilon_{\alpha}(0)} - \frac{(\boldsymbol{\alpha}\,.\,\mathbf{p}_{\mathrm{c}\alpha}(0))\,\mathbf{p}_{\alpha\mathrm{v}}(0)}{\epsilon_{\alpha}(0)-\epsilon_{\mathrm{c}}(0)}\right] \\
&= \frac{1}{\hbar}[\nabla_k(\boldsymbol{\alpha}\,.\,\mathbf{p}_{\mathrm{cv}}(\mathbf{k}))]_{k=0}
\end{aligned} \quad \ldots\ldots (3.4)$$

using the sum rules developed by Luttinger and Kohn (1955).

3.2. *Spherical Bands*

For non-degenerate spherical bands F is given by (2.16) for both bands. The matrix element between states characterized by (v, n, l, k_z), $(\mathrm{c}, n', l', k_z')$ becomes

$$\langle \mathrm{c}|\boldsymbol{\alpha}\,.\,\mathbf{p}|\mathrm{v}\rangle = [\boldsymbol{\alpha}\,.\,\mathbf{P}_{\mathrm{cv}}(0) + \hbar k_z M_{\mathrm{cv}}{}^{z}(0)]\delta(k_z' - k_z)\delta_{ll'}\delta_{nn'}$$
$$+ i\sqrt{\left(\frac{e\hbar H}{2c}\right)}[M_{\mathrm{cv}}{}^{-}(0)\sqrt{(n+1)}\delta_{l-1,l'}\delta_{n+1,n'}$$
$$- M_{\mathrm{cv}}{}^{+}(0)\sqrt{n}\delta_{l+1,l'}\delta_{n-1,n'}]\delta(k_z' - k_z) \qquad \ldots\ldots(3.5)$$

where $M^{\pm} = M_x \pm iM_y$.

When no magnetic field is present F has the form of $e^{i\mathbf{k}\cdot\mathbf{r}}$ and

$$\langle \mathrm{c}|\boldsymbol{\alpha}\,.\,\mathbf{p}|\mathrm{v}\rangle = [\boldsymbol{\alpha}\,.\,\mathbf{p}_{\mathrm{cv}}(0) + \hbar\mathbf{k}\,.\,\mathbf{M}_{\mathrm{cv}}(0)]\delta(\mathbf{k}' - \mathbf{k}). \qquad \ldots\ldots(3.6)$$

The absorption coefficient is obtained by summing the square of the matrix element over all states arising from both bands. For a frequency ω

$$K(\omega, H) = \frac{Ze^2}{\nu A m^2 c^2 \hbar\omega}\sum_{nn'}\sum_{ll'}\int dk_z\, dk_z' |\langle \mathrm{c}|\boldsymbol{\alpha}\,.\,\mathbf{p}|\mathrm{v}\rangle|^2 \delta(E_{\mathrm{c}n'}(k_z') - E_{\mathrm{v}n}(k_z) - \hbar\omega) \qquad \ldots\ldots(3.7)$$

where ν is the refractive index of the solid.

There are two distinct cases which are called allowed and forbidden according as $p_{\mathrm{cv}}(0) \neq 0$ or $= 0$. For allowed transitions all the terms in (3.2) and (3.6) are negligible compared with the first and

$$K(\omega, 0) = \frac{\gamma}{\omega}|\boldsymbol{\alpha}\,.\,\mathbf{p}_{\mathrm{cv}}(0)|^2(\hbar\omega - E_{\mathrm{G}})^{1/2} \qquad \ldots\ldots(3.8)$$

$$K(\omega, H) = \frac{\gamma}{2\omega}|\boldsymbol{\alpha}\,.\,\mathbf{p}_{\mathrm{cv}}(0)|^2 \frac{e\hbar H}{2m^* c}\sum_{n=0}^{\infty}\left[\hbar\omega - E_{\mathrm{G}} - (2n+1)\frac{e\hbar H}{2m^* c}\right]^{-1/2} \qquad \ldots\ldots(3.9)$$

where

$$\gamma = 2e^2(2m^*)^{3/2}/\pi\nu m^2 c\hbar^3 \qquad \ldots\ldots(3.9\,a)$$

$$m^* = m_{\mathrm{C}} m_{\mathrm{V}}/(m_{\mathrm{C}} + m_{\mathrm{V}}) \qquad \ldots\ldots(3.9\,b)$$

and E_{G} is the energy gap between valence and conduction bands at $\mathbf{k} = 0$.

For forbidden transitions (3.6) gives

$$K(\omega, 0) = \frac{2m^*\gamma}{3\omega\hbar^2}|\mathbf{M}_{\mathrm{cv}}(0)|^2(\hbar\omega - E_{\mathrm{G}})^{3/2}. \qquad \ldots\ldots(3.10)$$

In the presence of a magnetic field the form of K depends on the polarization of the incident radiation. In this isotropic case, $\mathbf{M}$ is parallel to $\boldsymbol{\alpha}$ (3.4). Thus for light with its $\mathbf{E}$ vector parallel to $\mathbf{H}$

$$K(\omega, H) = \frac{m^*\gamma}{\omega\hbar^2}\left(\frac{e\hbar H}{2m^* c}\right)\sum_{n=0}^{\infty}\left(\hbar\omega - E_{\mathrm{G}} - (2n+1)\frac{e\hbar H}{2m^* c}\right)^{1/2}|M_{\mathrm{cv}}{}^{z}(0)|^2 \qquad \ldots\ldots(3.11)$$

while for **E** perpendicular to **H**

$$K(\omega, H)=\frac{m^*\gamma}{2\omega\hbar^2}\left(\frac{e\hbar H}{2m^*c}\right)^2 \times \sum_{n=0}^{\infty}\left\{(n+1)|M_{\mathrm{cv}}{}^{-}(0)|^2\left[\hbar\omega-E_{\mathrm{G}}-\frac{e\hbar H}{2c}\left(\frac{2n+1}{m^*}+\frac{2}{m_{\mathrm{c}}}\right)\right]^{-1/2} + n|M_{\mathrm{cv}}{}^{+}(0)|^2\left[\hbar\omega-E_{\mathrm{G}}-\frac{e\hbar H}{2c}\left(\frac{2n+1}{m^*}+\frac{2}{m_{\mathrm{v}}}\right)\right]^{-1/2}\right\}. \quad \ldots\ldots(3.12)$$

The number of terms contributing to the summations in (3.9), (3.11) and (3.12) is increased when spin effects are taken into account especially if one or both band edges have been considerably affected by spin–orbit coupling so that the g-factors, as in (2.19) are different from 2. For incident radiation polarized parallel to the magnetic field, each term in (3.9) and (3.11) becomes two with $\pm\frac{1}{2}(g_{\mathrm{c}}-g_{\mathrm{v}})\beta H$ included in each bracket. For perpendicular polarization, $\pm\frac{1}{2}(g_{\mathrm{c}}+g_{\mathrm{v}})\beta H$ must be included in (3.9) but for forbidden transitions it is again $\pm\frac{1}{2}(g_{\mathrm{c}}-g_{\mathrm{v}})\beta H$ in (3.12).

Thus, for allowed transitions between bands of this type, the effect of the magnetic field is to break the absorption curve into four series of peaks. In each series the intensity of the peaks is proportional to H and to the sum of the inverses of the effective masses in each band. The spacing is the same in each series as given by (3.9) and the relative positions of the four series are $\pm\frac{1}{2}(g_{\mathrm{c}}-g_{\mathrm{v}})\beta H$, $\pm\frac{1}{2}(g_{\mathrm{c}}+g_{\mathrm{v}})\beta H$. The first two are observed with that component of the radiation which has **E** parallel to **H** and the second two with that which has **E** perpendicular to **H**. The peaks in both series have equal intensity but those at higher n are superimposed on the $(\Delta E)^{-1/2}$ tails of the lower n peaks. Peaked absorption of this kind has been observed but, because of the line width, the shape has not been studied experimentally.

In the case of forbidden transitions, peaks are also predicted when the radiation is polarized with **E** perpendicular to the applied field. Neglecting spin effects for the moment, we see from (3.12) that there are two series of peaks. In each series, the peak intensity increases with n and, while the peaks in each series are separated by $2\beta mH/m^*$, the two series are separated by $2\beta mH(1/m_{\mathrm{c}}-1/m_{\mathrm{v}})$ so that in this case both effective masses may be determined. If the band edges are affected by spin–orbit coupling, each series will be split into two separated by $(g_{\mathrm{c}}-g_{\mathrm{v}})\beta H$. If **E** is parallel to the applied field, the peaks disappear and the edge has the form of a series of steps shaped like $(\Delta E)^{1/2}$ of equal intensity beginning at intervals of $2\beta mH/m^*$. Again, when spin–orbit coupling is of importance, each of these steps becomes two separated by $(g_{\mathrm{c}}-g_{\mathrm{v}})\beta H$.

The average value of K is independent of H in all the expressions (3.9), (3.11) and (3.12) provided this average is taken over an energy interval large compared to the splitting caused by the magnetic field. The expressions (3.8) and (3.10) for $K(\omega, 0)$ are well known, having been first determined by Hall, Bardeen and Blatt (1954, 1956).

3.3. *Spheroidal Bands*

In order to obtain the intensities and selection rules for this case it is necessary to calculate the integrals of (3.2) with wave functions (2.21). Since the variables X, Y depend on the effective masses they are different in the two bands, so that these integrals become very complicated, e.g.

$$\int F_{c,n,X_0,k_z}(\mathbf{R})F_{v,n',X_0',k_z'}(\mathbf{R}')\,d\mathbf{r}$$
$$= \frac{1}{L_zL_y}\delta(k_z-k_z')\delta\left[s'c'k_z\left\{\frac{m_t-m_t}{m_tc'^2+m_ts'^2}-\frac{m_t'-m_t'}{m_t'c'^2+m_t's'^2}\right\}\right.$$
$$\left.-\frac{eH}{\hbar c}\left\{\sqrt{\left(\frac{m}{m_t}\right)}X_0-\sqrt{\left(\frac{m}{m_t'}\right)}X_0'\right\}\right]\int H_n(X-X_0/R_0)H_{n'}(X'-X_0'/R_0')\,dx. \qquad \ldots\ldots(3.13)$$

Thus for allowed transitions there is a selection rule $k_z = k_z'$, and another restricting X_0, X_0' to specific pairs as given by the δ-function, but there is no restriction on n and n', and the transition probabilities will be dependent on k_z. There will thus be many more peaks than in the isotropic case, and although they will have the form $(\Delta E)^{-1/2}$ at the beginning, this law will not hold over a very wide range.

Dresselhaus (1957) has shown that the absorption in such a crystal is likely to depend strongly on the polarization of the light relative to the crystal axes, and usually transitions will be allowed only for the E vector parallel (or in some cases perpendicular) to the crystal axis. The absorption determined above is therefore only likely to dominate if $\boldsymbol{\alpha}$ has a component along 3. When $\boldsymbol{\alpha}$ is perpendicular to this direction the other integrals in (3.2) are required, and these also show a lack of a selection rule in n.

In special cases, the absorption spectrum will simplify; notably when $\mathbf{H}$ is along the 3-axis. Then for $\mathbf{E}$ parallel to $\mathbf{H}$ the spectrum is that given by (3.9) while for $\mathbf{E}$ perpendicular to $\mathbf{H}$ it is given by (3.12) with the masses in these expressions defined in terms of the transverse masses of the bands inside the summation and in terms of the longitudinal masses elsewhere. If $\mathbf{H}$ is parallel to 2, the integral (3.13) simplifies in that $\sqrt{(m/m_t)}X_0 = \sqrt{(m/m_t')}X_0'$ and the harmonic oscillator functions are centred at the same point but still have different characteristic lengths if m_l/m_t differs in the two bands. This means that for transitions which are allowed when $\mathbf{E}$ is parallel to 3, there is a selection rule Δn even and the peaks have the $-\frac{1}{2}$ power law. If $\mathbf{E}$ is parallel to 2, Δn is odd and the peaks again have the $-\frac{1}{2}$ power law but, if $\mathbf{E}$ is parallel to 1, Δn is even and the $\frac{1}{2}$ power law again holds.

3.4. *Degenerate Bands*

In the case of Ge discussed in § 2.4 the lowest energy direct transitions occur between the degenerate valence band and the conduction band which transforms at $\mathbf{k} = 0$ like Γ_2^- and is built predominantly from s atomic functions. The transitions are therefore allowed and the absorption arises predominantly from the first term in (3.2). Using the wave functions (2.25) the matrix elements of $\mathbf{p}$ between the four u_{v} degenerate states and two $u_{\mathrm{c}}^{\pm}$ (corresponding to the two spin orientations) are dependent on direction. Only

$$\langle u_{\mathrm{c}}^{\pm}|p_z|u_{\pm 1/2}\rangle = p_{\mathrm{cv}}$$

and

$$\left.\begin{aligned}\langle u_{\mathrm{c}}^{\pm}|p_x|u_{\pm 3/2}\rangle &= \mp\langle u_{\mathrm{c}}^{\pm}|ip_y|u_{\pm 3/2}\rangle = \pm\tfrac{1}{2}\sqrt{3}p_{\mathrm{cv}}\\ \langle u_{\mathrm{c}}^{\pm}|p_x|u_{\mp 1/2}\rangle &= \pm\langle u_{\mathrm{c}}^{\pm}|ip_y|u_{\mp 1/2}\rangle = \pm\tfrac{1}{2}p_{\mathrm{cv}}\end{aligned}\right\} \qquad \ldots\ldots(3.14)$$

are not zero.

In the valence bands there are four sub-bands of levels with each n which are labelled by Luttinger (1956) $1^{\pm}$, $2^{\pm}$ and have minimum energies $\epsilon_{1,2}{}^{\pm}(n)$. In the conduction band there are two sets of sub-bands corresponding to spin components of $\pm\frac{1}{2}$. Transitions are allowed between sub-bands as follows:

	$w(n)$	$E(n)$
E||H.		
$1^{\pm}(n)\rightarrow c^{-}(n)$	$\|a_2{}^{\pm}(n)\|^2$	$\epsilon_1{}^{\pm}(n)+\dfrac{e\hbar H}{m_c c}(2n+1)-\beta H$
$2^{\pm}(n)\rightarrow c^{+}(n-2)$	$\|b_1{}^{\pm}(n)\|^2$	$\epsilon_2{}^{\pm}(n)+\dfrac{e\hbar H}{m_c c}(2n-3)+\beta H$
E⊥H.		
$1^{\pm}(n)\rightarrow c^{+}(n)$	$\frac{1}{4}\|a_2{}^{\pm}(n)\|^2$	$\epsilon_1{}^{\pm}(n)+\dfrac{e\hbar H}{m_c c}(2n+1)+\beta H$
$1^{\pm}(n)\rightarrow c^{+}(n-2)$	$\frac{3}{4}\|a_1{}^{\pm}(n)\|^2$	$\epsilon_1{}^{\pm}(n)+\dfrac{e\hbar H}{m_c c}(2n-3)+\beta H$
$2^{\pm}(n)\rightarrow c^{-}(n)$	$\frac{3}{4}\|b_2{}^{\pm}(n)\|^2$	$\epsilon_2{}^{\pm}(n)+\dfrac{e\hbar H}{m_c c}(2n+1)-\beta H$
$2^{\pm}(n)\rightarrow c^{-}(n-2)$	$\frac{1}{4}\|b_1{}^{\pm}(n)\|^2$	$\epsilon_2{}^{\pm}(n)+\dfrac{e\hbar H}{m_c c}(2n-3)-\beta H$

The second column gives the relative weight of each transition, and the third the energy of the transition $k_z=0$ in addition to E_G.

At small k_z the kinetic energy was shown in (2.29) to be quadratic with an effective mass appropriate to each sub-band. Thus each of the transitions listed above is the beginning of a continuous absorption which has the form

$$K(\omega,H)=\frac{e^3H(2m_z{}^*(n))^{1/2}}{\pi v m^2c^2\hbar^2\omega}\,w(n)|\boldsymbol{\alpha}\,.\,\mathbf{p}_{cv}|^2(\hbar\omega-E_G-E(n))^{-1/2}\quad\ldots\ldots(3.15)$$

where $m_z{}^*(n)=m_c m_l(n)/[m_c+m_l(n)]$ and $m_l(n)$ has the value given in (2.29) appropriate to the valence sub-band involved.

The $-\frac{1}{2}$ power law will hold only where the expressions (2.29) for m_l are valid. For low n values this means that the shape may vary appreciably in between the peaks. At high n, however, this variation is only appreciable in the tails where it is obscured by other peaks.

§ 4. INDIRECT TRANSITIONS

The extrema in the valence and conduction bands need not in general occur at the same value of $\mathbf{k}$. The transitions of lowest energy take place between these extrema and are termed indirect transitions since they are forbidden because of the law of momentum conservation. They do exist in higher order processes in which momentum is conserved by the simultaneous absorption or emission of a phonon and give a weak absorption which begins below the main direct edge.† The effect of a magnetic field on this absorption will now be studied.

As a typical case we shall consider transitions between a valence band with maximum at $\mathbf{k}=0$ and a conduction band with N_c minima at $\mathbf{k}=\mathbf{k}_c$ and equivalent points in the zone. In Si and Ge where the band structure is similar to this these minima are spheroidal with principal axis parallel to $\mathbf{k}_{\mathrm{c}}$ which are (100) and (111) axes respectively. In a magnetic field of arbitrary orientation the wave functions of the conduction band states have the form

---

† The most detailed observations yet made are reported by Macfarlane *et al.* (1957).

$$F_{\mathrm{c},n,X_0,k_z-k_{\mathrm{c}z}}(\mathbf{R})u_{\mathrm{c}\mathbf{k}_{\mathrm{c}}}(\mathbf{r})\exp(i\mathbf{k}_{\mathrm{c}}\,.\,\mathbf{r}) \qquad \ldots\ldots(4.1)$$

where F is a function of the form (2.14) when k_z is measured relative to $\mathbf{k}_{\mathrm{c}}$ and $\mathbf{R}=(X,Y,z)$ as given by (2.22).

The indirect transitions are second order and require a sum over intermediate states.† The matrix element involving phonons of wave vector $\mathbf{q}$ has the form

$$\begin{aligned}\sum_{i,t''} & \langle \mathrm{v},t,n_{\mathbf{q}}|\boldsymbol{\alpha}\,.\,\mathbf{p}|i,t'',n_{\mathbf{q}}\rangle\langle i,t'',n_{\mathbf{q}}|\mathscr{H}_{\mathrm{p}}|\mathrm{c},t',n_{\mathbf{q}}\pm 1\rangle/[E_i(t'')-E_{\mathrm{c}}(t')\mp\hbar\omega_{\mathbf{q}}]\\ & +\langle \mathrm{v},t,n_{\mathbf{q}}|\mathscr{H}_{\mathrm{p}}|i,t'',n_{\mathbf{q}}\pm 1\rangle\langle i,t'',n_{\mathbf{q}}\pm 1|\boldsymbol{\alpha}\,.\,\mathbf{p}|\mathrm{c},t',n_{\mathbf{q}}\pm 1\rangle/[E_i(t'')-E_{\mathrm{v}}(t)\pm\hbar\omega_{\mathbf{q}}]\end{aligned} \qquad \ldots\ldots(4.2)$$

where t, t', t'' specify the sets of three quantum numbers n, l or X_0, and k_z defining the magnetic states. $\mathscr{H}_{\mathrm{p}}$ is the electron–phonon interaction, and $n_{\mathbf{q}}$ the number of phonons of wave vector $\mathbf{q}$ with energy $\hbar\omega_{\mathbf{q}}$

$$n_q=[\exp(\hbar\omega_{\mathbf{q}}/kT)-1]^{-1}. \qquad \ldots\ldots(4.3)$$

Writing the wave functions in terms of their Fourier transforms (2.6)

$$\left.\begin{aligned}F_{\mathrm{v},t}(\mathbf{r}) &= \int B_{\mathrm{v},t}(\mathbf{k})\exp(i\mathbf{k}\,.\,\mathbf{r})\,d\mathbf{k}\\ F_{\mathrm{c},t'}(\mathbf{r}) &= \int B_{\mathrm{c},t'}(\mathbf{k}-\mathbf{k}_{\mathrm{c}})\exp\{i(\mathbf{k}-\mathbf{k}_{\mathrm{c}})\,.\,\mathbf{r}\}\,d\mathbf{k}.\end{aligned}\right\} \qquad \ldots\ldots(4.4)$$

For small values of n, k_z which give the absorption close to the edge $B(\mathbf{k})$ is only appreciable over a small range of $\mathbf{k}$ space about the origin. In the sum over intermediate states it can be shown that the variation of the energy denominators with t is small and will be neglected. It is then possible to choose an alternative basis of unperturbed Bloch states for the intermediate states. For a particular state $|i,\mathbf{k}\rangle$ the first and last matrix elements in (4.2) may be written

$$\boldsymbol{\alpha}\,.\,\mathbf{p}_{\mathrm{vi}}(0)B_{\mathrm{v},t}{}^*(\mathbf{k}) \quad \text{and} \quad \boldsymbol{\alpha}\,.\,\mathbf{p}_{\mathrm{ci}}(\mathbf{k}_{\mathrm{c}})B_{\mathrm{c},t'}(\mathbf{k}-\mathbf{k}_{\mathrm{c}}) \qquad \ldots\ldots(4.5)$$

for those bands i which have allowed transitions to the valence band near $\mathbf{k}=0$ and the conduction band near $\mathbf{k}_{\mathrm{c}}$. Since $B(\mathbf{k})$ is restricted to a small range the variation of $p(\mathbf{k})$ is neglected. The matrix elements of H_{p} may be written

$$Q_{\mathrm{ci}}(\mathbf{q})(n_{\mathbf{q}}+\tfrac{1}{2}\pm\tfrac{1}{2})^{1/2}B_{\mathrm{c},t'}(\mathbf{k}+\mathbf{q}-\mathbf{k}_{\mathrm{c}}) \quad \text{and} \quad Q_{\mathrm{vi}}(\mathbf{q})(n_{\mathbf{q}}+\tfrac{1}{2}\pm\tfrac{1}{2})^{1/2}B_{\mathrm{v},t}{}^*(\mathbf{k}-\mathbf{q}) \qquad \ldots\ldots(4.6)$$

where Q is a measure of the electron–phonon interaction between Bloch states in the two bands. Again, since $B(\mathbf{k})$ is only appreciable near $\mathbf{k}=0$ the $\mathbf{q}$ values must be close to $\mathbf{k}_{\mathrm{c}}$ for both (4.5) and (4.6) to be appreciable. (4.2) becomes

$$\begin{aligned}(n_{\mathbf{q}}+\tfrac{1}{2}\pm\tfrac{1}{2})^{1/2}\sum_i\Bigg\{ & \boldsymbol{\alpha}\,.\,\mathbf{p}_{\mathrm{vi}}(0)Q_{\mathrm{ci}}(\mathbf{q})\int\frac{B_{\mathrm{v},t}{}^*(\mathbf{k})B_{\mathrm{c},t'}(\mathbf{k}+\mathbf{q}-\mathbf{k}_{\mathrm{c}})\,d\mathbf{k}}{(\epsilon_{\mathrm{i}}(0)-\epsilon_{\mathrm{c}}(\mathbf{k}_{\mathrm{c}})\mp\hbar\omega_{\mathbf{q}})}\\ & +\boldsymbol{\alpha}\,.\,\mathbf{p}_{\mathrm{ci}}(\mathbf{k}_{\mathrm{c}})Q_{\mathrm{vi}}(\mathbf{q})\int\frac{B_{\mathrm{v},t}{}^*(\mathbf{k}-\mathbf{k}_{\mathrm{c}})B_{\mathrm{c},t'}(\mathbf{k}-\mathbf{q})\,d\mathbf{k}}{(\epsilon_{\mathrm{i}}(\mathbf{k}_{\mathrm{c}})-\epsilon_{\mathrm{v}}(0)\pm\hbar\omega_{\mathbf{q}})}.\end{aligned} \qquad \ldots\ldots(4.7)$$

---

† For theory between band states see Hall *et al.* (1954, 1956). A calculation using the same method for exciton effects has been given by Elliott (1957).

In the case of $\mathbf{H}=0$ when the initial and final states are defined by $\mathbf{k}_1$ and $\mathbf{k}_2$ the matrix element is the same with the integrals replaced by $\delta(\mathbf{k}_1+\mathbf{q}-\mathbf{k}_2)$. In that case a summation over all $\mathbf{k}_1$, $\mathbf{k}_2$ and $\mathbf{q}$ shows that the transition probability between any pair of states is roughly constant so that

$$K(\omega,0)=K_+(\omega,0)+K_-(\omega,0) \qquad \ldots\ldots(4.8)$$

where

$$K_\pm(\omega,0)=N_\mathrm{c}D\omega^{-1}(n_{\mathbf{k}_\mathrm{c}}+\tfrac{1}{2}\pm\tfrac{1}{2})\int d\mathbf{k}_1\,d\mathbf{k}_2\,\delta[\epsilon_\mathrm{c}(\mathbf{k}_2)-\epsilon_\mathrm{v}(\mathbf{k}_1)-\hbar\omega\mp\hbar\omega_{\mathbf{k}_\mathrm{c}}]. \qquad \ldots\ldots(4.9)$$

The constant D depends on the sum of matrix elements in (4.7) with $\mathbf{q}$ replaced by $\mathbf{k}_\mathrm{c}$. On integrating this gives the well-known result

$$K_\pm(\omega,0)=N_\mathrm{c}D'\omega^{-1}(n_{\mathbf{k}_\mathrm{c}}+\tfrac{1}{2}\pm\tfrac{1}{2})(\hbar\omega-E_\mathrm{G}\mp\hbar\omega_{\mathbf{k}_\mathrm{c}})^2. \qquad \ldots\ldots(4.10)$$

If in (4.7) the weak dependence on $\mathbf{q}$ is ignored the matrix elements connecting states t, t' do not depend upon k_z, k_z' and $K_\pm$ are changed in shape solely by the change which takes place in the density of states. Then

$$K_\pm(\omega,H)=\sum_{N_\mathrm{c}}D\omega^{-1}W_{tt'}(n_{\mathbf{k}_\mathrm{c}}+\tfrac{1}{2}\pm\tfrac{1}{2})\int dk_{1z}\,dk_{2z}\,\delta(E_\mathrm{c}(t)-E_\mathrm{v}(t')-\hbar\omega\mp\hbar\omega_{\mathbf{k}_\mathrm{c}}) \qquad \ldots\ldots(4.11)$$

where

$$W_{tt'}=\left|\int B_{\mathrm{v},t'}{}^*(\mathbf{k})B_{\mathrm{c},t}(\mathbf{k}+\mathbf{q}-\mathbf{k}_\mathrm{c})\,d\mathbf{k}\right|^2\sim\left|\int F_{\mathrm{v},t'}(\mathbf{r})F_{\mathrm{c},t}(\mathbf{r})\,d\mathbf{r}\right|^2.$$

On integrating this gives

$$K_\pm(\omega,H)\sim\sum_{N_\mathrm{c}}D'\omega^{-1}W_{nn'}(n_{\mathbf{k}_\mathrm{c}}+\tfrac{1}{2}\pm\tfrac{1}{2})\left(\frac{e\hbar H}{2mc}\right)^2\sum_{nn'}S(\hbar\omega-E_\mathrm{G}\mp\hbar\omega_{\mathbf{k}_\mathrm{c}}-E_{\mathrm{c},n}-E_{\mathrm{v},n'}) \qquad \ldots\ldots(4.13)$$

where $S(x)$ is a step function defined by

$$S(x)=0,\quad x<0;\qquad S(x)=1,\quad x>0$$

and $E_{\mathrm{c},n}$ and $E_{\mathrm{c},n'}$ are the minimum energies in the sub-bands relative to the band edge; they can be obtained from (2.17), (2.24) or (2.27) according to the type of band. The summation is over the conduction band minima which, in view of the anisotropy, may each give different $E_{\mathrm{c},n}$ etc. The step functions will in fact be modified by the dependence of (4.7) on $\mathbf{q}$ and of $W_{tt'}$ on k_z but each contribution will begin in roughly this fashion. The splitting of each sub-band because of the two spin orientations introduces a further splitting up of the step functions if one or both bands show appreciable spin–orbit effects.

Thus we see that the indirect absorption which rises like $(\Delta E)^2$ from a threshold when no magnetic field is present is broken up into a series of steps when a magnetic field is applied. Between each step the absorption will be roughly constant and proportional to H^2. There is a step corresponding to each pair of sub-bands—in the conduction and valence bands. The intensity in each step is dependent on the form of the wave functions (4.12) and is difficult to interpret, but a measurement of the energy of the steps should give useful information about the effective masses, their anisotropy and spin–orbit effects in the bands. As in the case of direct transitions, the average value of K is independent of H provided the average is taken over an energy interval large compared with the splitting caused by the magnetic field. The various branches of the phonon spectrum give separate contributions to (4.13) as to (4.10) (see discussion in Macfarlane *et al.* (1957)), but the relative positions, temperature dependence and magnitude of these contributions are unaffected by the field.

§ 5. CONCLUSION

The effects predicted in this paper have been observed under favourable conditions by Zwerdling *et al.* (1957) and Burstein and Picus (1957). The separation of the peaks or other features in the spectra is of order $\beta Hm/m^*$, i.e. about $10^{-4}(m/m^*)\,\mathrm{cm}^{-1}\,\mathrm{gauss}^{-1}$, so that high magnetic fields and high resolution are always required and the cases with small effective mass particularly favourable. The intensity of the peaks in the direct allowed cases is large but depends on the magnitude of the field and the width of the energy levels due to thermal broadening. K might well be of the order of $10^4\,\mathrm{cm}^{-1}$ in a typical case so that thin samples are necessary. The first peaks in the forbidden case should be weaker by a factor (radius of magnetic orbit/atomic radius)^2. In the indirect case the absorption is typically found at low K levels of 1–$10^3\,\mathrm{cm}^{-1}$ (cf. Macfarlane *et al.* 1957).

ACKNOWLEDGMENTS

This work was begun in the summer of 1956 when one of us (R. J. E.) was a Vacation Consultant at the Royal Radar Establishment, and has recently been revised and extended because of a growing interest in these effects. He (R. J. E.) would like to thank the staff of the Physics Division at the Royal Radar Establishment for a most pleasant and stimulating time.

REFERENCES

BLOUNT, E., CALLAWAY, J., COHEN, M., DUMKE, W. P., and PHILLIPS, J., 1956, *Phys. Rev.*, **101,** 563.

BURSTEIN, E., and PICUS, G. S., 1957, *Phys. Rev.*, **105,** 1123.

CHOYKE, W. J., and PATRICK, L., 1957 a, *Phys. Rev.*, **105,** 1721; 1957 b, *Ibid.*, **108,** 25.

DINGLE, R. B., 1952, *Proc. Roy. Soc.* A, **211,** 500.

DRESSELHAUS, G., 1957, *Phys. Rev.*, **105,** 135.

DRESSELHAUS, G., KIP, A. F., and KITTEL, C., 1955, *Phys. Rev.*, **98,** 368.

DUMKE, W. P., 1957, *Phys. Rev.*, **108,** 1419.

ELLIOTT, R. J., 1957, *Phys. Rev.*, **108,** 1384.

HALL, L. H., BARDEEN, J., and BLATT, F. J., 1954, *Phys. Rev.*, **95,** 559; 1956, *Proceedings of the Conference on Photoconductivity*, Atlantic City, 1954 (New York: Wiley).

LANDAU, L., 1930, *Z. Phys.*, **64,** 629.

LAX, B., DEXTER, R. N., and ZEIGER, H. J., 1956, *Phys. Rev.*, **104,** 637.

LUTTINGER, J. M., 1956, *Phys. Rev.*, **102,** 1030.

LUTTINGER, J. M., and KOHN, W., 1955, *Phys. Rev.*, **97,** 869.

MACFARLANE, G. G., MCLEAN, T. P., QUARRINGTON, J. E., and ROBERTS, V., 1957, *Phys. Rev.*, **108,** 1377.

MACFARLANE, G. G., and ROBERTS, V., 1955 a, *Phys. Rev.*, **97,** 1714; 1955 b, *Ibid.*, **98,** 1865.

POTTER, R. F., 1956, *Phys. Rev.*, **103,** 861.

ROBERTS, V., and QUARRINGTON, J. E., 1955, *J. Electronics*, **1,** 152.

SHOCKLEY, W., 1950, *Phys. Rev.*, **78,** 173.

ZWERDLING, S., and LAX, B., 1957, *Phys. Rev.*, **106,** 51.

ZWERDLING, S., LAX, B., and ROTH, L. M., 1957, *Phys. Rev.*, **108,** 1402.

Elastic Constants of Calcium Fluoride

By R. SRINIVASAN

Physics Department, Indian Institute of Science, Bangalore

MS. received 27th March 1958, *and in revised form* 23*rd May* 1958

Abstract. Employing Born's theory of crystal lattices, the elastic constants of fluorspar have been evaluated theoretically. Besides the coulomb forces, repulsive forces between nearest neighbour calcium and fluorine atoms and fluorine–fluorine atoms have been assumed and the constants of the repulsive energy were evaluated from the equilibrium condition, the experimentally determined compressibility and the principal Raman frequency of fluorspar. The experimental values of c_{11}, c_{12} and c_{44} are in fair agreement with the theoretically calculated values. Born's theory gives the sign of $c_{12}-c_{44}$ for fluorspar correctly but the theoretically calculated value of $c_{12}-c_{44}$ is only about half the experimentally observed value.

---

§ 1. Introduction

The purpose of the present investigation is to apply the theory of crystal lattices developed by Born to the calculation of the elastic constants of fluorspar. Such a calculation has already been carried out for crystals belonging to the NaCl and CsCl type of lattices (Kellermann 1940, Krishnan and Roy 1951, 1952). But in such lattices every atom is at a position of centre of symmetry. On the assumption of central forces, Born's theory predicts that $c_{12}=c_{44}$ in such cases. On the contrary, fluorspar is an ionic crystal, in which the fluorine atoms do not occupy positions of centre of symmetry and Born's theory actually predicts a difference between c_{12} and c_{44} in this case. Hence an application of Born's theory to calculate the elastic constants of fluorspar would be of interest to find whether the experimentally observed difference between c_{12} and c_{44} agrees in sign and magnitude with that calculated theoretically.

§ 2. Coupling Coefficients of Fluorspar

The first step in the evaluation of the elastic constants is to derive expressions for the coupling coefficients $\left[\begin{smallmatrix}K & K'\\ x & y\end{smallmatrix}\right]$ defined as

$$\left[\begin{smallmatrix}K & K'\\ x & y\end{smallmatrix}\right]=S_l(\phi^l_{K'K})_{xy}\exp\{2\pi i(\mathbf{k}\,.\,\mathbf{r}^l_{K'K})\} \qquad \ldots\ldots(1)$$

in the usual notation. K and K' represent the basis indices; l, the cell index; $\mathbf{k}$ the wave vector whose magnitude is $1/\lambda$ and whose direction is the direction of propagation of the wave with wavelength λ; $\phi^l_{K'K}$ the potential energy of interaction of the particle K' in cell l with particle K in the basis cell $\mathbf{r}^l_{K'K}$ is the vector distance from the particle K in the basis cell to the particle K' in the lth cell. S_l represents a summation over the cell index l.

$$(\phi^l_{K'K})_{xy}=\left[\frac{\partial^2}{\partial x\partial y}\,(\phi^l_{K'K})\right]_{\mathbf{r}^l_{K'K}}.$$

As usual, we assume that the potential energy of interaction $\phi^{l}_{K'K}$ can be split up into a coulomb and non-coulomb part

$$\phi^{l}_{K'K} = {}^{\mathrm{C}}\phi^{l}_{K'K} + {}^{\mathrm{R}}\phi^{l}_{K'K}. \qquad \ldots\ldots(2)$$

Correspondingly we can write the coupling coefficients as

$$\left[\begin{smallmatrix} KK' \\ x\,y \end{smallmatrix}\right] = {}^{\mathrm{C}}\!\left[\begin{smallmatrix} KK' \\ x\,y \end{smallmatrix}\right] + {}^{\mathrm{R}}\!\left[\begin{smallmatrix} KK' \\ x\,y \end{smallmatrix}\right]. \qquad \ldots\ldots(3)$$

We have to evaluate the two parts separately.

2.1. *Coulomb Part of the Coupling Coefficients*

Kellermann (1940) gives the following expressions for the coulomb parts of the coupling coefficients.

$$\begin{aligned} {}^{\mathrm{C}}\!\left[\begin{smallmatrix} KK' \\ x\,y \end{smallmatrix}\right] = e_K e_{K'} \Bigg\{ & -\frac{4\pi}{v_a} \sum_h \frac{(b_{h_x}+k_x)(b_{h_y}+k_y)}{(\mathbf{b}_h+\mathbf{k})^2} \\ & \times \exp\{-(\pi^2/E^2)(\mathbf{b}_h+\mathbf{k})^2 - 2\pi i(\mathbf{b}_h \cdot \mathbf{r}_{K'K})\} \\ & + E^2 \sum_l \Bigg[\psi'(E|r^l_{K'K}|)\, \frac{\delta_{xy}}{|r^l_{K'K}|} + \Bigg(E\psi''(E|r^l_{K'K}|) \\ & - \frac{\psi'(E|r^l_{K'K}|)}{|r^l_{K'K}|} \Bigg) \frac{x^l_{K'K}\, y^l_{K'K}}{|r^l_{K'K}|^2} \Bigg] \\ & \times \exp\{2\pi i(\mathbf{k} \cdot \mathbf{r}^l_{K'K})\} \Bigg\} \end{aligned} \qquad \ldots\ldots(4a)$$

$$\begin{aligned} {}^{\mathrm{C}}\!\left[\begin{smallmatrix} K\,K \\ x\,y \end{smallmatrix}\right] = e_K^2 \Bigg\{ & -\frac{4\pi}{v_a} \sum_h \frac{(b_{h_x}+k_x)(b_{h_y}+k_y)}{(\mathbf{b}_h+\mathbf{k})^2} \exp\left(-\frac{\pi^2}{E^2}(\mathbf{b}_h+\mathbf{k})^2\right) \\ & + \frac{4E^3}{3\pi^{1/2}}\delta_{xy} + E^2 \sum_e \Bigg[\psi'(E|a^l|)\, \frac{\delta_{xy}}{|a^l|} \\ & + \left(E\psi''(E|a^l|) - \frac{\psi'(E|a^l|)}{|a^l|} \right) \frac{a_x{}^l a_y{}^l}{|a^l|^2} \Bigg] \exp\{2\pi i(\mathbf{k} \cdot \mathbf{a}^l)\} \Bigg\}. \end{aligned} \qquad \ldots\ldots(4b)$$

Here E is an arbitrarily chosen quantity to ensure rapid convergence of the sums,

$$\psi(x) = \frac{H(x)}{x}, \qquad H(x) = 1 - \frac{2}{\sqrt{\pi}} \int_0^x \exp(-x^2)\, dx,$$

$$\psi'(x) = \frac{d}{dx}\psi(x), \quad \psi''(x) = \frac{d^2}{dx^2}\psi(x),$$

e_K is the charge on the Kth atom, v_a the volume of the unit cell, $\mathbf{b}_h$ a vector in the reciprocal lattice with components b_{h_x}, b_{h_y}, b_{h_z}, and $\mathbf{a}^l$ a lattice vector with components $a^l{}_x$, $a^l{}_y$ and $a^l{}_z$.

The above equations hold for $\mathbf{k} \neq 0$. When $\mathbf{k} = 0$, Kellermann (1940) gives

$$\left.\begin{aligned} & {}^{\mathrm{C}}\!\left[\begin{smallmatrix} KK' \\ x\,x \end{smallmatrix}\right]_{\mathbf{k}=0} = {}^{\mathrm{C}}\!\left[\begin{smallmatrix} KK' \\ y\,y \end{smallmatrix}\right]_{\mathbf{k}=0} = {}^{\mathrm{C}}\!\left[\begin{smallmatrix} KK' \\ z\,z \end{smallmatrix}\right]_{\mathbf{k}=0} = \frac{4\pi}{3v_a} e_K e_{K'} \\ & {}^{\mathrm{C}}\!\left[\begin{smallmatrix} KK \\ x\,x \end{smallmatrix}\right]_{\mathbf{k}=0} = {}^{\mathrm{C}}\!\left[\begin{smallmatrix} KK \\ y\,y \end{smallmatrix}\right]_{\mathbf{k}=0} = {}^{\mathrm{C}}\!\left[\begin{smallmatrix} KK \\ z\,z \end{smallmatrix}\right]_{\mathbf{k}=0} = \frac{4\pi}{3v_a} e_K{}^2 \\ \text{and} \quad & {}^{\mathrm{C}}\!\left[\begin{smallmatrix} KK \\ x\,y \end{smallmatrix}\right]_{\mathbf{k}=0} = {}^{\mathrm{C}}\!\left[\begin{smallmatrix} KK' \\ x\,y \end{smallmatrix}\right]_{\mathbf{k}=0} = 0 \text{ if } x \neq y. \end{aligned}\right\} \qquad \ldots\ldots(5)$$

The fluorspar lattice is a 'diagonal' lattice. The unit cell can be chosen as a rhombohedron of volume $v_a = 2r_0^3$ bounded by the edges $\mathbf{a}_1 = r_0(011)$; $\mathbf{a}_2 = r_0(101)$; $\mathbf{a}_3 = r_0(110)$ where r_0 is half the lattice constant. The position of the particles in the unit cell are specified by the vectors $\mathbf{r}_k = \frac{1}{2}r_0(K-1)$ (111) where $K=1$ denotes the calcium atom, $K=2$ the fluorine atom F^1 and $K=4$ the fluorine atom F^2. Therefore

$$\mathbf{r}_{21} = -\mathbf{r}_{12} = \tfrac{1}{2}\mathbf{r}_0(111);\ \mathbf{r}_{41} = -\mathbf{r}_{14} = \tfrac{3}{2}r_0\,(111);\ \mathbf{r}_{42} = -\mathbf{r}_{24} = r_0(111).$$

The lattice vector

$$\mathbf{a}^l = l_1\mathbf{a}_1 + l_2\mathbf{a}_2 + l_3\mathbf{a}_3 = r_0(l_x, l_y, l_z)$$

where $\Sigma_x l_x$ is even. The vectors

$$\begin{aligned}
\mathbf{r}^l_{21} &= r_0(n_x, n_y, n_z);\ n_x = l_x + \tfrac{1}{2};\ n_y = l_y + \tfrac{1}{2};\ n_z = l_z + \tfrac{1}{2}\\
\mathbf{r}^l_{41} &= r_0(p_x, p_y, p_z);\ p_x = l_x + \tfrac{3}{2};\ p_y = l_y + \tfrac{3}{2};\ p_z = l_z + \tfrac{3}{2}\\
\mathbf{r}^l_{42} &= r_0(m_x, m_y, m_z);\ \Sigma_x m_x \text{ is odd}
\end{aligned}$$

and the m_x are integers. Corresponding to a vector $\mathbf{r}^l_{21} = r_0(n_x, n_y, n_z)$ there is always a vector $\mathbf{r}^l_{41} = r_0(-n_x, -n_y, -n_z)$. The reciprocal lattice basis vectors are

$$\mathbf{b}_1 = \frac{1}{2r_0}(-1, 1, 1);\ \mathbf{b}_2 = \frac{1}{2r_0}(1, -1, 1);\ \mathbf{b}_3 = \frac{1}{2r_0}(1, 1, -1),$$

and any reciprocal lattice vector

$$\mathbf{b}_h = \frac{1}{2r_0}(h_x, h_y, h_z)$$

where h_x, h_y, h_z are all even or all odd. The vector $\mathbf{k} = (2r_0)^{-1}\ (q_x, q_y, q_z)$ where the q's are fractional.

Using these relations and choosing $E = \epsilon/r_0$ where ϵ is an arbitrary number, we obtain from (5)

$$\left.\begin{aligned}
\frac{v_a}{e_K{}^2}\,\mathrm{C}\!\left[\begin{smallmatrix}K&K\\x&y\end{smallmatrix}\right] &= -G^{KK}_{xy} + \underset{(l)}{H_{xy}} + \frac{8}{3}\frac{\epsilon^3}{\pi^{1/2}}\delta_{xy}\\
\frac{v_a}{e_1e_2}\,\mathrm{C}\!\left[\begin{smallmatrix}1&2\\x&y\end{smallmatrix}\right] &= -G^{1\,2}_{x\,y} + \underset{(n)}{H_{xy}}\\
\frac{v_a}{e_2e_4}\,\mathrm{C}\!\left[\begin{smallmatrix}2&4\\x&y\end{smallmatrix}\right] &= -G^{2\,4}_{x\,y} + \underset{(m)}{H_{xy}}
\end{aligned}\right\}\quad\ldots\ldots(6)$$

where

$$\left.\begin{aligned}
G^{KK}_{xy} &= 4\pi\sum_h \frac{(h_x+q_x)(h_y+q_y)}{(\mathbf{h}+\mathbf{q})^2}\exp\left(-\frac{\pi^2}{4\epsilon^2}(\mathbf{h}+\mathbf{q})^2\right)\\
G^{2\,4}_{x\,y} &= 4\pi\sum_h \frac{(h_x+q_x)(h_y+q_y)}{(\mathbf{h}+\mathbf{q})^2}\exp\left(-\frac{\pi^2}{4\epsilon^2}(\mathbf{h}+\mathbf{q})^2\right)\\
&\qquad\times\cos\pi(h_x+h_y+h_z)\\
G^{1\,2}_{x\,y} &= 4\pi\sum_h \frac{(h_x+q_x)(h_y+q_y)}{(\mathbf{h}+\mathbf{q})^2}\exp\left(-\frac{\pi^2}{4\epsilon^2}(\mathbf{h}+\mathbf{q})^2\right)\\
&\qquad\times\exp\{-\tfrac{1}{2}i\pi(h_x+h_y+h_z)\}\\
\underset{(l)}{H_{xy}} &= 2\sum_l\left[-f(l)\delta_{xy} + g(l)\frac{l_xl_y}{l^2}\right]\cos\pi(\mathbf{q}\,.\,\mathbf{l})\\
\underset{(m)}{H_{xy}} &= 2\sum_m\left[-f(m)\delta_{xy} + g(m)\frac{m_xm_y}{m^2}\right]\cos\pi(\mathbf{q}\cdot\mathbf{m})\\
\underset{(n)}{H_{xy}} &= 2\sum_n\left[-f(n)\delta_{xy} + g(n)\frac{n_xn_y}{n^2}\right]\exp\{i\pi(\mathbf{q}\cdot\mathbf{n})\}.
\end{aligned}\right\}\quad\ldots\ldots(7)$$

Here

$$f(l)=\frac{2}{\sqrt{\pi}}\frac{\epsilon}{|l|^2}\exp(-\epsilon^2|l|^2)+\frac{H(\epsilon|l|)}{|l|^3}\ ;\ H(x)=1-\frac{2}{\sqrt{\pi}}\int_0^x\exp(-x^2)\,dx.$$

$$g(l)=3f(l)+\frac{4}{\sqrt{\pi}}\epsilon^3\exp(-\epsilon^2|l|^2).$$

Since $G^{1\,2}_{x\,y}$ and $\underset{(n)}{H_{xy}}$ are complex quantities ${}^{\mathrm{C}}\left[\begin{smallmatrix}1&2\\x&y\end{smallmatrix}\right]$ is complex.

We have also the following additional relations

and

$$\left.\begin{aligned}{}^{\mathrm{C}}\left[\begin{smallmatrix}KK'\\x\,y\end{smallmatrix}\right]&={}^{\mathrm{C}}\left[\begin{smallmatrix}KK'\\y\,x\end{smallmatrix}\right]={}^{\mathrm{C}}\left[\begin{smallmatrix}K'K\\x\,y\end{smallmatrix}\right]^*\\{}^{\mathrm{C}}\left[\begin{smallmatrix}1&4\\x&y\end{smallmatrix}\right]&={}^{\mathrm{C}}\left[\begin{smallmatrix}1&2\\x&y\end{smallmatrix}\right]^*\end{aligned}\right\}\qquad\ldots\ldots(8)$$

since for any vector $\mathbf{r}^l_{21}$ there is a vector $\mathbf{r}^l_{41}=-\mathbf{r}^l_{21}$.

2.2. *Repulsive Part of the Coupling Coefficients*

We assume that there exists a potential $\phi_1(r)$ between the calcium and fluorine atoms (nearest neighbour atoms) and a potential $\phi_2(r_0)$ between the nearest neighbour fluorine atoms of type 1 and type 2. For every calcium atom there are four nearest neighbour fluorine atoms of type 1 at

$$\tfrac{1}{2}r_0(111);\ \tfrac{1}{2}r_0(1,-1,-1);\ \tfrac{1}{2}r_0(-1,1,-1);\ \tfrac{1}{2}r_0(-1,-1,1)$$

and four nearest neighbour fluorine atoms of type 2 at

$$\tfrac{1}{2}r_0(-1,-1,-1);\ \tfrac{1}{2}r_0(-1,1,1);\ \tfrac{1}{2}r_0(1,-1,1);\ \tfrac{1}{2}r_0(1,1,-1).$$

For any fluorine atom there are six neighbouring fluorine atoms of the other type at $r_0(\pm1,0,0)$; $r_0(0,\pm1,0)$; $r_0(0,0,\pm1)$.

The potential energy of a unit cell can be written as

$$\tfrac{1}{2}\Phi_0=-\frac{\alpha e^2}{r_0}+8\phi_1(r)+6\phi_2(r_0)$$

where α is the Madelung constant $=5{\cdot}818$ and $r=(\sqrt{3}/2)\,r_0$. For equilibrium

$$\frac{d}{dr_0}\left(\frac{1}{2}\Phi_0\right)=0$$

$$\frac{\alpha e^2}{r_0^{\,2}}+4\sqrt{3}\,A_1+6A_2=0.\qquad\ldots\ldots(9)$$

The bulk modulus K of the crystal is given by

$$K=\frac{1}{18r_0}\frac{d^2}{dr_0^{\,2}}\left(\frac{1}{2}\Phi_0\right)=\frac{1}{18r_0}\left[-\frac{2\alpha e^2}{r_0^{\,3}}+6B_1+6B_2\right].\qquad\ldots\ldots(10)$$

In these equations

$$A_1=\frac{d}{dr}\phi_1(r)\qquad\qquad A_2=\frac{d}{dr_0}\phi_2(r_0)$$

$$B_1=\frac{d^2}{dr^2}\phi_1(r)\qquad\qquad B_2=\frac{d^2}{dr_0^{\,2}}\phi_2(r_0).$$

The repulsive part of the coupling coefficient $\left[\begin{smallmatrix}1&2\\x&y\end{smallmatrix}\right]$ is

$${}^{\mathrm{R}}\left[\begin{smallmatrix}1&2\\x&y\end{smallmatrix}\right]=S_l(\phi_1(r))_{xy}\exp\{2\pi i(\mathbf{k}\,.\,\mathbf{r}^l_{21})\}$$

where the summation has to be extended over the four nearest neighbour fluorine atoms of type 1.

Substituting in the above expression we obtain

$$\left.\begin{aligned}
{}^{\mathrm{R}}\left[\begin{smallmatrix}1&2\\x&x\end{smallmatrix}\right] &= \frac{4}{3}\left[\frac{2A_1}{r}+B_1\right]\Big[\cos\frac{\pi}{2}q_x\cos\frac{\pi}{2}q_y\cos\frac{\pi}{2}q_z\\
&\qquad\qquad -i\sin\frac{\pi}{2}q_x\sin\frac{\pi}{2}q_y\sin\frac{\pi}{2}q_z\Big]\\
{}^{\mathrm{R}}\left[\begin{smallmatrix}1&2\\x&y\end{smallmatrix}\right] &= \frac{4}{3}\left[B_1-\frac{A_1}{r}\right]\Big[-\sin\frac{\pi}{2}q_x\sin\frac{\pi}{2}q_y\cos\frac{\pi}{2}q_z\\
&\qquad\qquad +i\cos\frac{\pi}{2}q_x\cos\frac{\pi}{2}q_y\sin\frac{\pi}{2}q_z\Big].\\
\text{Similarly}\quad {}^{\mathrm{R}}\left[\begin{smallmatrix}2&4\\x&x\end{smallmatrix}\right] &= 2B_2\cos\pi q_x+\frac{2A_2}{r_0}[\cos\pi q_y+\cos\pi q_z]\\
{}^{\mathrm{R}}\left[\begin{smallmatrix}2&4\\x&y\end{smallmatrix}\right] &= 0 \text{ when } x\neq y.\\
\text{Also}\quad {}^{\mathrm{R}}\left[\begin{smallmatrix}1&4\\x&y\end{smallmatrix}\right] &= {}^{\mathrm{R}}\left[\begin{smallmatrix}1&2\\x&y\end{smallmatrix}\right]^{*}.
\end{aligned}\right\}\quad\ldots\ldots(11)$$

From these coefficients we can evaluate coefficients of the type ${}^{\mathrm{R}}\left[\begin{smallmatrix}KK\\x\,y\end{smallmatrix}\right]$

$${}^{\mathrm{R}}\left[\begin{smallmatrix}KK\\x\,y\end{smallmatrix}\right]_{\mathbf{k}\neq0}={}^{\mathrm{R}}\left[\begin{smallmatrix}KK\\x\,y\end{smallmatrix}\right]_{\mathbf{k}=0}$$

since $K=K'$ and the cell index $l=0$ for this case.

Also $\sum_{K'}{}^{\mathrm{R}}\left[\begin{smallmatrix}KK'\\x\,y\end{smallmatrix}\right]_{\mathbf{k}=0}=0.$

$$\left.\begin{aligned}
\text{Therefore}\quad {}^{\mathrm{R}}\left[\begin{smallmatrix}K\,K\\x\,y\end{smallmatrix}\right] &= -\sum_{K'\neq K}{}^{\mathrm{R}}\left[\begin{smallmatrix}KK'\\x\,y\end{smallmatrix}\right]_{\mathbf{k}=0}\\
{}^{\mathrm{R}}\left[\begin{smallmatrix}1\,1\\x\,x\end{smallmatrix}\right] &= -\frac{8}{3}\left(\frac{2A_1}{r}+B_1\right)\\
{}^{\mathrm{R}}\left[\begin{smallmatrix}2\,2\\x\,x\end{smallmatrix}\right]={}^{\mathrm{R}}\left[\begin{smallmatrix}4\,4\\x\,x\end{smallmatrix}\right] &= -\frac{4}{3}\left(\frac{2A_1}{r}+B_1\right)-2\left(B_2+\frac{2A_2}{r_0}\right)\\
{}^{\mathrm{R}}\left[\begin{smallmatrix}K\,K\\x\,y\end{smallmatrix}\right] &= 0 \text{ when } x\neq y.
\end{aligned}\right\}\quad\ldots\ldots(12)$$

§ 3. ELASTIC CONSTANTS OF FLUORSPAR

For fluorspar, Born has given the expressions† for the elastic constants Born (1923). The expressions are

$$\left.\begin{aligned}
&\left.\begin{aligned}c_{11}&=A=[xxxx]\\ c_{12}&=B=[xxyy]\end{aligned}\right\}\ [x\bar{x}y\bar{y}]=\frac{1}{2v_a}\sum_{KK'}S_l(\phi^{l}_{K'K})_{xy}\bar{x}^{l}_{K'K}\bar{y}^{l}_{K'K}\\
&c_{44}=B-\frac{2C^2}{D}\\
&C=\left[\begin{smallmatrix}2\\xyz\end{smallmatrix}\right]\ ;\ \left[\begin{smallmatrix}K\\xyz\end{smallmatrix}\right]=\frac{1}{v_a}\sum_{K'}S_l(\phi^{l}_{K'K})_{xy}z^{l}_{K'K}\\
&D=\frac{1}{v_a}\left[\begin{smallmatrix}1&2\\x&x\end{smallmatrix}\right]_{\mathbf{k}=0}.
\end{aligned}\right\}\quad\ldots\ldots(13)$$

From equations (1) and (13) we get

$$\left.\begin{aligned}
&i\sum_{\bar{x}}\left[\begin{smallmatrix}K\\xy\bar{x}\end{smallmatrix}\right]S_{\bar{x}}=\frac{1}{v_a}\left[\frac{\partial}{\partial\tau}\sum_{K'}\left[\begin{smallmatrix}KK'\\x\,y\end{smallmatrix}\right]\right]_{\tau=0}\\
\text{and}\quad &-\sum_{\bar{x}}\sum_{\bar{y}}S_{\bar{x}}S_{\bar{y}}[x\bar{x}y\bar{y}]=\frac{1}{2v_a}\left[\frac{\partial^2}{\partial\tau^2}\sum_{KK'}\left[\begin{smallmatrix}KK'\\x\,y\end{smallmatrix}\right]\right]_{\tau=0}.
\end{aligned}\right\}\quad\ldots\ldots(14)$$

---

† The bracket symbol $[x\bar{x}, y\bar{y}]$ is wrongly denoted by $[xy,]$ in Born's book and Kellermann's paper 1940.

Here $\tau\mathbf{S}=2\pi\mathbf{k}$; $\mathbf{S}$ is a unit vector in the direction of propagation of the wave and $\tau=2\pi/\lambda$. We can calculate the coulomb contributions to the elastic constants by performing the differentiation with respect to τ of the coulomb part of the corresponding coupling coefficients. The value of $[xxxx]$ is derived from $\left[\frac{\partial^2}{\partial\tau^2}\sum_{KK'}\left[{KK' \atop x\,x}\right]\right]_{\tau=0}$ and the value of $[xx, yy]$ from $\left[\frac{\partial^2}{\partial\tau^2}\sum_{KK'}\left[{KK' \atop x\,y}\right]\right]_{\tau=0}$.
Performing the differentiation we obtain

$$\left[\frac{\partial^2}{\partial\tau^2}\sum_{KK'}{}^{\mathrm{C}}\!\left[{KK' \atop x\,x}\right]\right]_{\tau=0}=-\frac{2e^2}{v_a}\times 2r_0^2\left\{\left[\frac{2}{\sqrt{\pi}}\chi_x(h)+3\underset{(l)}{\xi_x}+\underset{(m)}{\xi_x}-4\underset{(n)}{\xi_x}\right]S_x^2\right.$$
$$+\left[\frac{2}{\sqrt{\pi}}\chi_y(h)+3\underset{(l)}{\xi_y}+\underset{(m)}{\xi_y}-4\underset{(n)}{\xi_y}\right]S_y^2$$
$$\left.+\left[\frac{2}{\sqrt{\pi}}\chi_z(h)+3\underset{(l)}{\xi_z}+\underset{(m)}{\xi_z}-4\underset{(n)}{\xi_z}\right]S_z^2\right\}\qquad\ldots\ldots(15\,a)$$

and $$\left[\frac{\partial^2}{\partial\tau^2}\sum_{KK'}{}^{\mathrm{C}}\!\left[{KK' \atop x\,y}\right]\right]_{\tau=0}=-\frac{8e^2r_0^2}{v_a}\left[\frac{1}{\sqrt{\pi}}\rho(h)+3\underset{(l)}{\xi'}+\underset{(m)}{\xi'}-4\underset{(n)}{\xi'}\right]S_xS_y.\qquad\ldots\ldots(15\,b)$$

From equations (15 *a*), (15 *b*) and (14) we obtain

$$\begin{aligned}
{}^{\mathrm{C}}[xxxx]={}^{\mathrm{C}}c_{11}&=\frac{e^2}{2r_0^4}\left\{\frac{2}{\sqrt{\pi}}\chi_x(h)+3\underset{(l)}{\xi_x}+\underset{(m)}{\xi_x}-4\underset{(n)}{\xi_x}\right\}\\
{}^{\mathrm{C}}[xxyy]={}^{\mathrm{C}}c_{12}&=\frac{e^2}{2r_0^4}\left\{\frac{1}{\sqrt{\pi}}\rho(h)+\underset{(l)}{3\xi'}+\underset{(m)}{\xi'}-\underset{(n)}{4\xi'}\right\}\\
{}^{\mathrm{C}}[xyxy]&=\frac{e^2}{2r_0^4}\left\{\frac{2}{\sqrt{\pi}}\chi_y(h)+3\underset{(l)}{\xi_y}+\underset{(m)}{\xi_y}-4\underset{(n)}{\xi_y}\right\}
\end{aligned}\qquad\ldots\ldots(16)$$

where

$$\left.\begin{aligned}
\chi_y(h)&=\sum_h\frac{2}{\pi^{1/2}}\frac{\exp\{(-\pi^2/4\epsilon^2)|h|^2\}}{|h|^2}\left[4\frac{h_x^2h_y^2}{h^4}-\frac{h_x^2}{h^2}+\frac{\pi^4}{\epsilon^2}\left(\frac{h_x^2h_y^2}{h^2}-\frac{h_x^2}{4}\right)\right.\\
&\quad\left.+\frac{\pi^4}{\epsilon^4}\frac{h_x^2h_y^2}{8}+\delta xy\left(1-4\frac{h_x^2}{h^2}-\frac{\pi^2}{\epsilon^2}h_x^2\right)\right]\\
&\quad\times\left[3+\cos\pi\sum_x h_x-4\cos\frac{\pi}{2}\sum_x h_x\right]\\
\underset{(l)}{\xi_y}&=\sum_l\left[-f(l)+g(l)\frac{l_x^2}{l^2}\right]l_y^2\\
\rho(h)&=\sum_h\frac{2}{\pi^{1/2}}\frac{\exp\{(-\pi^2/4\epsilon^2)|h|^2\}}{|h|^2}\left[1-2\frac{(h_x^2+h_y^2)}{h^2}+8\frac{h_x^2h_y^2}{h^4}\right.\\
&\quad\left.+2\frac{\pi^2}{\epsilon^2}\left(\frac{h_x^2h_y^2}{h^2}-\frac{1}{4}(h_x^2+h_y^2)\right)+\frac{\pi^4}{\epsilon^4}\frac{h_x^2h_y^2}{4}\right]\\
&\quad\times\left[3+\cos\pi\sum_x h_x-4\cos\frac{\pi}{2}\sum_x h_x\right]\\
\underset{(l)}{\xi'}&=\sum_l g(l)\frac{l_x^2l_y^2}{l^2}.
\end{aligned}\right\}\ldots(17)$$

In a similar manner we obtain

$$ {}^{\mathrm{C}}\!\left[{2 \atop xyz}\right] = -4r_0 \frac{e^2}{{v_a}^2}\left[4\eta_h + \zeta_n\right] $$

where

$$ \left.\begin{aligned} \eta_h &= \left[1+\frac{\pi^2}{4\epsilon^2}\right]\sum_h \exp\left(-\frac{\pi^2}{4\epsilon^2}|h|^2\right)\frac{h_x h_y h_z}{h^2}\sin\frac{\pi}{2}\sum_x h_x \\ &\text{and} \\ \zeta_n &= \sum_n g(n)\frac{n_x n_y n_z}{n^2}. \end{aligned}\right\} \quad \ldots\ldots(18) $$

The various lattice sums $\chi_x(h)$, $\chi_y(h)$, $\rho(h)$, $\underset{(l)}{\xi_x}$, $\underset{(l)}{\xi_y}$, $\underset{(l)}{\xi'}$, $\underset{(m)}{\xi_x}$, $\underset{(m)}{\xi_y}$, $\underset{(m)}{\xi'}$, $\underset{(n)}{\xi_x}$, $\underset{(n)}{\xi_y}$, $\underset{(n)}{\xi'}$, η_h and ζ_n have been evaluated and found to be

$$ \left.\begin{array}{ll} \chi_x(h) = 0{\cdot}006999; & \chi_y(h) = 0{\cdot}048279 \\ \underset{(l)}{\xi_x} = 2{\cdot}181517; & \rho(h) = 0{\cdot}079791 \\ \underset{(m)}{\xi_x} = 4{\cdot}738457; & \underset{(l)}{\xi_y} = 0{\cdot}447359 \\ \underset{(n)}{\xi_x} = 2{\cdot}003683; & \underset{(m)}{\xi_y} = -0{\cdot}781322 \\ \underset{(l)}{\xi'} = 1{\cdot}259515; & \underset{(n)}{\xi_y} = 0{\cdot}535531 \\ \underset{(m)}{\xi'} = 0{\cdot}601221; & \eta_h = -0{\cdot}005662 \\ \underset{(n)}{\xi'} = 1{\cdot}971532; & \zeta_n = -2{\cdot}496657 \end{array}\right\} \quad \ldots\ldots(19) $$

We calculate the repulsive parts of the elastic constants in a similar way and obtain

$$ \left.\begin{aligned} {}^{\mathrm{R}}[xxxx] = {}^{\mathrm{R}}c_{11} &= \frac{1}{4r_0}\left[\frac{4}{3}\left(\frac{2A_1}{r}+B_1\right)+2B_2\right] \\ {}^{\mathrm{R}}[xxyy] = {}^{\mathrm{R}}c_{12} &= \frac{1}{3r_0}\left[B_1-\frac{A_1}{r}\right] \\ {}^{\mathrm{R}}[xyxy] &= \frac{1}{4r_0}\left[\frac{4}{3}\left(\frac{2A_1}{r}+B_1\right)+\frac{2A_2}{r_0}\right] \\ &\text{and} \\ {}^{\mathrm{R}}\!\left[{2 \atop xyz}\right] = {}^{\mathrm{R}}c &= -1/3{r_0}^2\left[B_1-\frac{A_1}{r}\right]. \end{aligned}\right\} \quad \ldots\ldots(20) $$

Substituting the lattice sums evaluated in (19) and (18) we get

$$ \left.\begin{aligned} [xxxx] = c_{11} = {}^{\mathrm{C}}c_{11} + {}^{\mathrm{R}}c_{11} &= \frac{3{\cdot}276e^2}{2{r_0}^4} + \frac{1}{4r_0}\left[\frac{4}{3}\left(\frac{2A_1}{r}+B_1\right)+2B_2\right] \\ [xxyy] = c_{12} = {}^{\mathrm{C}}c_{12} + {}^{\mathrm{R}}c_{12} &= -\frac{3{\cdot}461e^2}{2{r_0}^4} + \frac{1}{3r_0}\left[B_1-\frac{A_1}{r}\right] \\ [xyxy] = {}^{\mathrm{C}}[xyxy] + {}^{\mathrm{R}}[xyxy] &= -\frac{1{\cdot}527e^2}{2{r_0}^4} + \frac{1}{4r_0}\left[\frac{4}{3}\left(\frac{2A_1}{r}+B_1\right)+\frac{2A_2}{r_0}\right] \\ c_{12} - c_{44} &= \frac{2C^2}{D} \\ C = {}^{\mathrm{C}}\!\left[{2 \atop xyz}\right] + {}^{\mathrm{R}}\!\left[{2 \atop xyz}\right] &= 2{\cdot}519\frac{e^2}{{r_0}^5} - \frac{1}{3{r_0}^2}\left[B_1-\frac{A_1}{r}\right] \\ D = \frac{1}{v_a}\left\{{}^{\mathrm{C}}\!\left[{12 \atop xx}\right]_{\mathbf{k}=0} + {}^{\mathrm{R}}\!\left[{12 \atop xx}\right]_{\mathbf{k}=0}\right\} &= -\frac{2\pi}{3}\frac{e^2}{{r_0}^6} + \frac{2\pi}{3{r_0}^3}\left[\frac{2A_1}{r}+B_1\right]. \end{aligned}\right\} \quad ..(21) $$

A check on the evaluation of the lattice sums could be made in the following way. The value of $-3[{}^{C}c_{11}+2{}^{C}c_{12}]r_0^4/e^2$ must be nearly equal to the Madelung constant α. Using the values for ${}^{C}c_{11}$ and ${}^{C}c_{12}$ from (20) we obtain

$$-3[{}^{C}c_{11}+2{}^{C}c_{12}]r_0^4/e^2=\tfrac{3}{2}\times 3{\cdot}646=5{\cdot}469$$

which is nearly equal to the Madelung constant $\alpha=5{\cdot}818$ for fluorspar.

Theory requires that

$$[xyxy]=[xxyy] \qquad \ldots\ldots(22)$$

though the coulomb and repulsive contributions to these bracket symbols need not be equal individually. This relation can be used as a check on the calculations when the repulsive contributions have been evaluated. From relation (22) it follows that

$$\begin{aligned} c_{12} &= -3{\cdot}461\,\frac{e^2}{2r_0^{\,4}}+\frac{1}{3r_0}\left[B_1-\frac{A_1}{r}\right] \\ &= -1{\cdot}527\,\frac{e^2}{2r_0^{\,4}}+\frac{1}{4r_0}\left[\frac{4}{3}\left(\frac{2A_1}{r}+B_1\right)+\frac{2A_2}{r_0}\right]. \qquad \ldots\ldots(23) \end{aligned}$$

3.1. *Evaluation of the Quantities A_1, B_1, A_2 and B_2*

Employing the second of the relations (23) for c_{12} we note that

$$c_{11}-c_{12}=4{\cdot}803\,\frac{e^2}{2r_0^{\,4}}+\frac{2}{4r_0}\left[B_2-\frac{A_2}{r_0}\right].$$

From the experimentally observed values of the elastic constants (Bhagavantam 1955), we find $c_{11}-c_{12}=11{\cdot}4\times 10^{11}$ dyn cm^{-2}. The contribution of the first term on the right hand side amounts to $10{\cdot}1\times 10^{11}$ dyn cm^{-2} taking $r_0=2{\cdot}725$ Å from Landolt–Bornstein Tables. The second term involves only the fluorine–fluorine repulsion and this term amounts to only 10% of the value $c_{11}-c_{12}$. Hence fluorine–fluorine repulsive energy can be safely approximated by an expression of the type A_{24}/r_0^{10} the exponent 10 being nearly the value given by Lennard-Jones and Dent (1926) for the repulsive potential energy between ions of the neon configuration. Then

$$A_2=\frac{d}{dr_0}\,\phi_2(r_0)=-10\,\frac{A_{24}}{r_0^{\,11}},\quad B_2=\frac{d^2}{dr_0^{\,2}}\,\phi_2(r_0)=110\,\frac{A_{24}}{r_0^{\,12}}.$$

We have three quantities A_1, B_1 and A_{24} to be evaluated. We have already two equations for this purpose—the equilibrium equation (9), and the compressibility equation (10). We want one more relation between the three unknowns before we can solve for them. The principal Raman frequency of fluorspar is $321{\cdot}5$ cm^{-1} and corresponds to the oscillation of one fluorine lattice against another. The expression for this frequency is

$$\begin{aligned} \omega^2=4\pi^2\nu^2 &= -\frac{\left\{\left[{22 \atop xx}\right]_{\mathbf{k}=0}-\left[{24 \atop xx}\right]_{\mathbf{k}=0}\right\}}{m_{\mathrm{F}}} \\ &= \frac{1}{m_{\mathrm{F}}}\left\{\frac{4}{3}\left[\frac{2A_1}{r}+B_1\right]+360\,\frac{A_{24}}{r_0^{\,12}}\right\}. \qquad \ldots\ldots(24) \end{aligned}$$

Using the three equations (9), (10) and (24) and the measured value of the bulk modulus K (Bhagavantam 1955) the following values were obtained: $A_1=-2{\cdot}662\times 10^{-4}$, $B_1=8{\cdot}63\times 10^{4}$, $A_{24}=1{\cdot}488\times 10^{-89}$.

3.2. *Numerical Values for the Elastic Constants*

Using these values for A_1, B_1 and A_{24} the elastic constants come out as

$$[xxxx]=c_{11}={}^{\mathrm{C}}c_{11}+{}^{\mathrm{R}}c_{11}=(6{\cdot}85+9{\cdot}95)10^{11}=16{\cdot}8\times10^{11}\,\mathrm{dyn\,cm^{-2}}$$

$$[xxyy]=c_{12}={}^{\mathrm{C}}c_{12}+{}^{\mathrm{R}}c_{12}=(-7{\cdot}24\times11{\cdot}99)10^{11}=4{\cdot}75\times10^{11}\,\mathrm{dyn\,cm^{-2}}$$

$$[xyxy]={}^{\mathrm{C}}[xyxy]+{}^{\mathrm{R}}[xyxy]=(-3{\cdot}19+8{\cdot}00)10^{11}=4{\cdot}81\times10^{11}\,\mathrm{dyn\,cm^{-2}}$$

$$C={}^{\mathrm{C}}\left[{2 \atop xyz}\right]+{}^{\mathrm{R}}\left[{2 \atop xyz}\right]=(3{\cdot}868-4{\cdot}482)10^{19}=-0{\cdot}614\times10^{19}$$

$$D=\frac{1}{v_a}\left\{{}^{\mathrm{C}}\left[{12 \atop xx}\right]_{\mathbf{k}=0}+{}^{\mathrm{R}}\left[{12 \atop xx}\right]_{\mathbf{k}=0}\right\}=(-1{\cdot}180+2{\cdot}200)10^{27}=1{\cdot}020\times10^{27}.$$

Hence $c_{12}-c_{44}=\dfrac{2C^2}{D}=0{\cdot}74\times10^{11}\,\mathrm{dyn\,cm^{-2}}$.

So $\qquad c_{44}=4{\cdot}0\times10^{11}\,\mathrm{dyn\,cm^{-2}}$.

We find that the value of $[xxyy]$ equals the value of $[xyxy]$ as required by theory.

In the following table, the calculated values of the elastic constants are compared with the experimentally observed values at room temperature (~30°c) (Bhagavantam 1955).

Comparison of Theoretical and Experimental Values of the Elastic Constants of Calcium Fluoride

The values of the elastic constants are in units of $10^{11}\,\mathrm{dyn\,cm^{-2}}$.

Constant	Observed	Calculated
c_{11}	16·4	16·8
c_{12}	5·0	4·8
c_{44}	3·47	4·0
K	8·8	—

The agreement is very good for c_{11} and c_{12} which is not surprising as the parameters have been evaluated from two experimentally determined quantities (bulk modulus, and the principal Raman frequency). The theory yields a value for $c_{12}-c_{44}$ which is nearly half the experimentally observed one. This difference $c_{12}-c_{44}$ depends on the quantities C and D; and as these quantities are obtained as differences, the margin of error in the estimation of $c_{12}-c_{44}$ will be considerably larger than in the estimation of the quantities c_{11} and c_{12}. Also the assumption of central forces is only an approximation. When many body forces are considered (Lundqvist 1952, Herpin 1953) they yield a contribution to $c_{12}-c_{44}$ in the case of the alkali halides whereas the assumption of central forces leads to $c_{12}=c_{44}$ in these crystals. It is possible that many body forces may yield a similar contribution to $c_{12}-c_{44}$ in calcium fluoride. The main features of the calculation are (i) Born's theory gives correctly the sign and order of magnitude of $c_{12}-c_{44}$ in calcium fluoride, (ii) the fluorine–fluorine interaction is small as is evidenced by its contribution to $c_{11}-c_{12}$ of this crystal, and (iii) the repulsive contribution to $c_{12}-c_{44}$ arises entirely from the calcium–fluorine interaction in the approximation employed here.

ACKNOWLEDGMENTS

The author wishes to express his thanks to Professor R. S. Krishnan for his keen interest and guidance; he is also grateful to referees of the paper for their helpful criticisms and suggestions.

References

Bhagavantam, S., 1955, *Proc. Indian Acad. Sci.* A, **41,** 72.
Born, M., 1923, *Atomtheorie des festen Zustandes.*
Herpin, A., 1953, *J. Phys. Radium*, **14,** 611.
Kellermann, E. W., 1940, *Phil. Trans. Roy. Soc.* A, **238,** 513.
Krishnan, K. S., and **Roy**, S. K., 1951, *Nature, Lond.*, **168,** 869 ; 1952, *Proc. Roy. Soc.* A, **210,** 481.
Lennard-Jones, J. E., and **Dent**, B. M., 1926, *Proc. Roy. Soc.* A, **112,** 230.
Lundqvist, S. O., 1952, *Ark. Fys.*, **6,** 25.

Viscosity Determination by the Oscillating Vessel Method
I: Theoretical Considerations

By R. ROSCOE
Physics Department, King's College, Newcastle upon Tyne

MS. received 5th May 1958, and in final form 30th June 1958

Abstract. When a liquid is placed in a vessel held by a torsional suspension and the whole is set in rotation about a vertical axis, the viscosity of the liquid may be deduced from observations of the time period and decrement of the oscillations. This method of measuring viscosity has many practical advantages, but there are mathematical difficulties in making the calculations. The cases of spherical and cylindrical vessels are considered in detail and formulae are obtained for the calculation of the viscosity which are very accurate and easier to use than those previously proposed. The case of an axially symmetrical vessel which departs slightly from the spherical form is also considered, and formulae (valid only when the frequency of oscillation is high) are obtained for an axially symmetrical vessel of any shape. Corrections for the effect of external air resistance are also discussed.

§ 1. INTRODUCTION

A VERY simple viscometer consists of a containing vessel held by a torsional suspension. When the vessel is set in oscillation about a vertical axis, the resulting motion is damped on account of the viscosity of the liquid η, and the latter can be calculated from measurements of the decrement and frequency of the oscillations. Until recently, however, the method has been used but little because of mathematical difficulties in carrying out the calculations.

The practical advantages of the method are considerable. The decrement and frequency of the oscillations can easily be measured to a high degree of accuracy, and temperature control is simple because the liquid is confined to a volume of small dimensions. Also, since a closed vessel can be used, the method is applicable to molten metals and other liquids which must be kept out of contact with air. For these reasons it has been revived by a number of authors such as Andrade and Chiong (1936) who used a spherical vessel, and Hopkins and Toye (1950) who used a cylindrical vessel.

It is fairly easy, as these authors have shown, to derive an equation of motion for the vessel if it is of a simple and axially symmetrical form. From this equation exact formulae can be obtained from which, in principle, the viscosity can be calculated but which are too complicated to be of practical use. Both Andrade and Chiong and Hopkins and Toye simplified these formulae by making a number of approximations, but their method of calculating η involves a cumbersome process of working by successive approximations between several equations, and it is difficult to see how much the approximations made in the formulae affect the accuracy of the final result.

In Part I of the present work, formulae are deduced from the equation of motion, both for the sphere and the cylinder, making only one approximation (which leads to very small errors in the calculation of η). That calculation can be made from a single equation by successive approximations. Consideration is also given to vessels of other axially symmetrical forms, and a method is given for the calculation of the effect of external air resistance. The use of these results is illustrated in Part II (Roscoe and Bainbridge 1958) which describes an accurate determination of the viscosity of water.

§ 2. THE SPHERICAL VESSEL

It is unnecessary to repeat the derivation of the equation of motion which has been given by Andrade and Chiong. They solve the Navier–Stokes equations for the motion of the liquid within the vessel (neglecting the non-linear terms) when the angular deflection of the vessel θ varies with time t in proportion to $e_{\alpha t}$, α being a constant. It may then be shown that the drag of the liquid produces a restoring torque G on the vessel given by

$$G = L\,d\theta/dt \qquad \ldots\ldots(1)$$

where

$$L = \frac{8}{3}\pi\eta R^3 \frac{(bR)^2 - 3bR\coth bR + 3}{bR\coth bR - 1}. \qquad \ldots\ldots(2)$$

Here R is the radius of the sphere, η the viscosity of the liquid, ρ its density and $b = \sqrt{(\alpha/\nu)}$ where ν is the 'kinematic viscosity' η/ρ. The equation of motion of the vessel is thus

$$I\frac{d^2\theta}{dt^2} + L\frac{d\theta}{dt} + f\theta = 0 \qquad \ldots\ldots(3)$$

where I is its moment of inertia and f is the torsional constant of the suspension; so the possible values for α are given by

$$I\alpha^2 + L\alpha + f = 0 \qquad \ldots\ldots(4)$$

where L is given by (2) and hence is a function of α. Now a solution of the form

$$\alpha = -\beta + i\gamma \qquad \ldots.(5)$$

corresponds to oscillatory motion with period T and logarithmic decrement $2\pi\Delta$ (between successive swings in the same sense) where

$$T = 2\pi/\gamma, \quad \Delta = \beta/\gamma \qquad \ldots\ldots(6)$$

Two formulae are obtained by inserting (5) in (4) and separating real and imaginary parts:

$$-2I\beta\gamma - \beta N + \gamma M = 0 \qquad \ldots\ldots(7)$$

$$I(\beta^2 - \gamma^2) - \beta M - \gamma N + f = 0 \qquad \ldots\ldots(8)$$

where M and N are respectively the real and imaginary parts of L. Now it is possible in principle to calculate η from the observed values of β and γ using either of these formulae, but since L is a function of the complex quantity bR where

$$b = \left(\frac{\alpha}{\nu}\right)^{1/2} = \left(\frac{-\beta + i\gamma}{\nu}\right)^{1/2} \qquad \ldots\ldots(9)$$

the formulae are very difficult to handle. Andrade and Chiong simplify matters by effectively setting coth bR equal to unity in (2) so as to give

$$L = \frac{8}{3}\pi\eta R^3\{bR - 2 + 1/(bR - 1)\} \qquad \ldots\ldots(10)$$

This approximation may be justified as follows: If A denotes the real part of bR, it is easily shown that the real part of coth bR lies between the bounds coth A and tanh A, and the imaginary part between $\pm i(\coth A - \tanh A)/2$. Now for accurate measurement of the decrement, conditions must be such that a large number of oscillations can be observed; that is to say β must be much less than γ. Thus it appears from (6) and (9) that A will be approximately equal to $(\pi/\nu T)^{1/2}R$ which is usually a large quantity. For example when $R = 3$ cm, $\nu = 1$ centistoke and $T = 10$ sec, it has the value 16·8 so that coth A exceeds unity by only $5{\cdot}1 \times 10^{-15}$. Hence the real part of coth bR can only differ from unity by this amount, and the imaginary part can only differ from zero by $5{\cdot}1 \times 10^{-15}i$.

At this point we cease to follow Andrade and Chiong, as they make further approximations before arriving at working formulae. Now it can be seen from (10) that L can be expressed as a series of descending powers of bR which is convergent as long as $|bR|$ is greater than unity. After some algebraic manipulation this allows (7) to be put in the form

$$I\Delta = \frac{2}{3} R^4 (\pi\eta\rho T)^{1/2} \left\{ a_0 - \frac{2}{p} + \frac{a_2}{2p^2} + 0 - \frac{a_4}{4p^4} - \frac{a_5}{4p^5} \dots \right\} \qquad \dots\dots (11)$$

where $p = (\pi/\nu T)^{1/2}R$, $2\pi\Delta$ is the logarithmic decrement between consecutive swings in the same sense and the coefficients a_n (which are all close to unity) have the values

$$\left.\begin{aligned} a_0 &= (1-\Delta)\left\{\frac{\sqrt{(1+\Delta^2)}+1}{2}\right\}^{1/2} - (1+\Delta)\left\{\frac{\sqrt{(1+\Delta^2)}-1}{2}\right\}^{1/2} \\ &= 1 - {}_2\Delta - \tfrac{3}{8}\Delta^2 - \tfrac{1}{16}\Delta^3 \dots \\ a_2 &= \left\{\frac{\sqrt{(1+\Delta^2)}+1}{2}\right\}^{1/2} + \left\{\frac{\sqrt{(1+\Delta^2)}-1}{2}\right\}^{1/2} \\ &= 1 + \tfrac{1}{2}\Delta + \tfrac{1}{8}\Delta^2 - \tfrac{1}{16}\Delta^3 \dots \\ a_4 &= a_2/(1+\Delta^2)^{1/2} = 1 + \tfrac{1}{2}\Delta - \tfrac{3}{8}\Delta^2 - \tfrac{5}{16}\Delta^3 \dots \\ a_5 &= (1+\Delta^2)^{-1} = 1 - \Delta^2 + \Delta^4 \dots \end{aligned}\right\} \quad (12)$$

Similarly (8) may be written as

$$\begin{aligned} & I\{T^2/T_0^2 - (1-\Delta^2)\} \\ &\quad = \frac{4}{3} R^4 (\pi\eta\rho T)^{1/2} \left\{ b_0 - \frac{2\Delta}{p} - \frac{b_2}{2p^2} - \frac{1}{2p^3} - \frac{b_4}{4p^4} + \frac{b_5\Delta}{p^5} \dots \right\} \qquad \dots (13) \end{aligned}$$

where $T_0 = 2\pi(I/f)^{1/2}$ is the time period that the system would have in the absence of viscous damping, and the coefficients b_n are given by a similar set of expressions to the a_n coefficients. The expanded forms for these may be obtained by substituting $-\Delta$ for Δ in the corresponding expansions for a_n.

It is a simple matter to calculate η from (11) by successive approximations. Equation (13) can also be used to calculate η, but the accuracy of the result is relatively low because the bracket term on the left is the difference of two quantities obtained from measurements, both of which are close to unity. Equation (11) also possesses an advantage over (13) in that it does not involve T_0. That quantity is not simply equal to the time period when the bulb is empty, because the torsional constant f always depends to a certain extent upon the weight of the suspended part, and hence special methods have to be used for its determination.

The only approximation made in deriving these equations from the equation of motion consists in the replacement of coth bR by unity in (2) so as to obtain (10). The maximum errors which can arise on this account in the value of η calculated from (11) are as follows for various values of $p=(\pi/\nu T)^{1/2}R$:

p	5	10	15	20
Fractional error	5×10^{-4}	2×10^{-8}	7×10^{-13}	3×10^{-17}.

It must be remembered, however, that the equation of motion itself involves an approximation since the non-linear 'inertia' terms in the hydrodynamic equations have been neglected: a point which is obscured in Andrade and Chiong's paper by their failure to quote the equations for all three possible components of the velocity. It is difficult to take account of these non-linear terms theoretically, but they must have the effect of making the decrement depend on the amplitude of the oscillations when the latter is large. Such a dependence must always be looked for when measurements are made; and if it appears perceptibly, lower amplitudes must be used.

Finally, it should be noted that a very general treatment of the type of problem considered here has been given by Havelock (1921) from which it is to be concluded that equations such as (4) above have an infinite number of roots. According to the conditions existing, all the roots are real and negative, or there is a pair of conjugate complex roots $\alpha=-\beta\pm i\gamma$ together with an infinite number of real negative roots all greater in magnitude than β. Now a real negative root corresponds to a state of motion in which the vessel returns continuously towards its equilibrium orientation. We are therefore only interested in the second case where oscillatory motion can occur, and here it must not be forgotten that non-oscillatory types of motion will also be present, their relative proportions depending on the manner in which the motion is started. These die out more rapidly than the oscillatory motion, but their presence can cause asymmetry of the oscillations during the early stages. This, of course, applied to vessels of all shapes.

§ 3. THE CYLINDRICAL VESSEL

Hopkins and Toye have dealt with the case of a cylinder having its lower end closed, the upper surface of the liquid being free. (The similar problem of a cylinder closed at upper and lower ends has been treated by Okaya and Hasegawa (1933) and Okaya (1936), but somewhat less accurately.) The treatment follows the same lines as that of Andrade and Chiong for the sphere, equations (1) to (8) applying as before, with the exception of (2) which is replaced by a different expression for L. In considering the latter we shall alter Hopkins and Toye's notation so as to bring it into line with that of the other authors. Thus we write R for the radius of the cylinder and H for the height of liquid within it, and b for the quantity defined by (9).

In following through the treatment given by these authors, one notes a Bessel function of order zero occurs in their equation (8), which should be of the second order. This is evidently an error in transcription as the correction leads to their final result. Also, they define the quantity l_n^2 occurring in that equation as $m^2-k_n^2$ while it is actually $k_n^2-m^2$ if the equation is to be correct. With the altered notation, their expression for L becomes

$$L=2\pi\eta\left\{bR^3H\frac{\mathrm{J}_2(ibR)}{i\mathrm{J}_1(ibR)}+2b^4R^7\sum_{n=1}^{\infty}\frac{\tanh[(j_n^{\,2}+b^2R^2)^{1/2}H/R]}{j_n^{\,2}(j_n^{\,2}+b^2R^2)^{3/2}}\right\} \quad \ldots\ldots (14)$$

where $J_1(z)$ and $J_2(z)$ are respectively Bessel functions of the first kind of order one and two, and j_1, j_2, j_3 etc. are the positive roots of $J_1(z)=0$ in ascending order of magnitude.

Hopkins and Toye approximate at this stage by effectively neglecting β in equation (9) for b. This is a rather serious approximation as it gives fractional errors in the calculated value of η of the order of 3Δ, where $2\pi\Delta$ is the logarithmic decrement. They also replace the Bessel functions by the first two terms of asymptotic expansions valid for large values of the variable, and this introduces fractional errors in of the order of p^{-2}, where $p=(\pi/\nu T)^{1/2}R$. Their final calculations are made by a method of successive approximations. They suggest no simplification of the series term, however, and since b is complex the labour of computing and re-computing must be enormous if any degree of accuracy is to be obtained. We shall therefore proceed differently and show that both parts of L can be expressed as a series of descending powers of bR so that the subsequent treatment can follow the lines given above for the spherical vessel.

Now the asymptotic expansion for $J_1(z)$ valid for large $|z|$ and $\arg z<\pi$ (Watson 1944, p. 199) may be expressed as the sum of two series of inverse powers of z, multiplied respectively by

$$(2/\pi z)^{1/2}\sin(z-\tfrac{1}{4}\pi) \qquad \text{and} \qquad (2/\pi z)^{1/2}\cos(z-\tfrac{1}{4}\pi)$$

and the same applies to $J_2(z)$. Also, when $|z|$ is very large and $0<\arg z<\pi$ then $\sin(z-\frac{1}{4}\pi)$ is closely equal to $i\cos(z-\frac{1}{4}\pi)$, so $J_2(z)/J_1(z)$ can be obtained by division as a series of descending powers of z. Writing $z=iy$ in this series, one obtains

$$\frac{J_2(iy)}{iJ_1(iy)} \sim 1-\frac{3}{2y}+\frac{3}{8y^2}+\frac{3}{8y^3}+\frac{63}{128y^4}+\dots \qquad \dots\dots(15)$$

which is valid for large $|y|$ with $-\frac{1}{2}\pi<\arg y<\frac{1}{2}\pi$. Setting y equal to bR gives the required expansion for the first term in (14) as the above conditions apply to bR. The approximation involved may be shown to be equivalent to setting $\coth A=1$ where A is the real part of bR which is approximately equal to $(\pi/\nu T)^{1/2}R$ and it is thus exactly the same as that made in obtaining (10) from (8) in the case of the spherical vessel.

A simplification can be made in the series term of (14) by setting each of the hyperbolic tangents equal to unity, since the real part of $(j_n^2+b^2R^2)^{1/2}H/R$ is always large. It can be shown that, as H is of the same order as R, the consequent errors are of the same order as those introduced by the use of (15) for the first term. In order to reduce the resulting series

$$\sum_{n=1}^{\infty}\frac{1}{j_n^2(j_n^2+b^2R^2)^{3/2}}$$

to a series of descending powers of bR, it is necessary to use the following contour integration. We consider the function $f(z)$ of the complex variable z given by

$$f(z)=\frac{1}{z(z^2+1)^{3/2}}\frac{J_2(mz)}{mzJ_1(mz)} \qquad \dots\dots(16)$$

where m is a complex quantity. This function has poles wherever $mz=\pm j_n$ and a pole at $z=0$, and the sum of all the residues is

$$\frac{1}{4}-2\sum_{n=1}^{\infty}\frac{m^3}{j_n^2(j_n^2+m^2)^{3/2}}.$$

Now $f(z)$ has essential singularities extending along the imaginary axis from i to $i\infty$ and from $-i$ to $-i\infty$. A path for contour integration is therefore chosen as in figure 1. Now $J_2(mz)/J_1(mz)$ is bounded (Watson 1944, p. 498), so when the radius of the large circle is taken as being indefinitely great, the only contribution to the contour integral arises from the paths round the two cuts such as ABCD. Along AB and CD, z can be set equal to iy, and $f(z)$ takes respectively the values

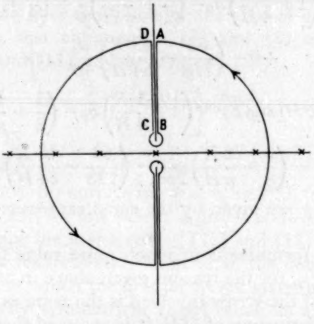

Figure 1.

$$\pm \frac{1}{my^2(y^2-1)^{3/2}} \cdot \frac{J_2(imy)}{iJ_1(imy)}$$

and when m is large and $-\tfrac{1}{2}\pi < \arg m < \tfrac{1}{2}\pi$ the expansion (15) can be used for the second part of this expression. The whole can thus be represented as a series of terms each consisting of a real function of the real variable y multiplied by a complex coefficient, so the integration with respect to $dz = i\,dy$ (from $y = 1 + r$ to ∞, where r is the radius of the small circle) can be carried out term by term by elementary methods. Each term gives one part independent of r and another proportional to $r^{-1/2}$. The latter parts can be collected together by means of (15) to give finally

$$\int_{AB} f(z)dz = \int_{CD} f(z)dz$$

$$= \frac{i}{m}\left(2 - \frac{9\pi}{8m} + \frac{1}{m^2} + \frac{45\pi}{128m^3} + \frac{63}{40m^4} + \dots\right) - \frac{1}{\sqrt{(2r)}m}\frac{J_2(im)}{J_1(im)}. \quad \dots\dots(17)$$

The integration round the small circle is performed by setting $z = i + r \exp i\theta$ and gives $\sqrt{2}/m\sqrt{r}.J_2(im)/J_1(im)$. Thus the complete contour integral is simply four times the first term in (17), and since it is also $2\pi i$ times the sum of the residues we have

$$\sum_{n=1}^{\infty} \frac{m^3}{j_n^2(j_n^2+m^2)^{3/2}} = \left\{\frac{1}{8} - \frac{2}{\pi m} + \frac{9}{8m^2} - \frac{1}{\pi m^3} - \frac{45}{128m^4} - \frac{63}{40\pi m^5} - \dots\right\} \quad \dots\dots(18)$$

As bR complies with the restrictions on m given above, this expansion can be used for the series in (14), and so with the help of (15) the whole expression for

L can be obtained as a series of descending powers of bR. The real and imaginary parts of αL are worked out from this series, and insertion in (7) and (8) gives the working formulae

$$I\Delta = \frac{R^3H}{2}(\pi\eta\rho T)^{1/2}\left\{\left(1+\frac{1}{4}\frac{R}{H}\right)a_0 - \left(\frac{3}{2}+\frac{4}{\pi}\frac{R}{H}\right)\frac{1}{p} + \left(\frac{3}{8}+\frac{9}{4}\frac{R}{H}\right)\frac{a_2}{2p^2}\right.$$
$$\left. + 0 - \left(\frac{63}{128}-\frac{45}{64}\frac{R}{H}\right)\frac{a_4}{4p^4}\cdots\right\} \qquad \text{......(19)}$$

$$I\left\{\frac{T^2}{T_0^2}-(1-\Delta^2)\right\} = R^3H(\pi\eta\rho T)^{1/2}\left\{\left(1+\frac{1}{4}\frac{R}{H}\right)b_0 - \left(\frac{3}{2}+\frac{4}{\pi}\frac{R}{H}\right)\frac{\Delta}{p}\right.$$
$$\left. - \left(\frac{3}{8}+\frac{9}{4}\frac{R}{H}\right)\frac{b_2}{2p^2} - \left(\frac{3}{8}-\frac{2}{\pi}\frac{R}{H}\right)\frac{1}{2p^3} - \left(\frac{63}{128}-\frac{45}{64}\frac{R}{H}\right)\frac{b_4}{4p^4}\cdots\right\} \qquad \text{......(20)}$$

where T_0, a_n, b_n and p are given by the same expressions as in the case of the sphere.

The first of these formulae is of much more value than the second for the purpose of calculating η, for the reasons given above in considering the spherical vessel, and the order of the errors involved is the same as in that case. It should be noted that, in the derivation of (14), it is assumed that the free surface of the liquid remains plane during the motion, and as this is not strictly correct a small correction may be necessary on that account. No such difficulty arises in the case of a cylindrical vessel with both ends closed by plane surfaces and completely filled with liquid. For such a vessel (height $2H$), formulae (19) and (20) have to be modified by simply multiplying each right hand side by a factor of 2.

§ 4. Vessels of General Form

If the frequency of oscillation is very high, the solution of the problem can be obtained very simply for any vessel whose form is a surface of revolution about a vertical axis. We first consider the case of a fluid bounded by a plane wall which moves in its own plane with a velocity in the $x+$direction given by $ae^{\alpha t}$ where a is a constant and α is a complex quantity. This problem has been treated by Lamb (1953, p. 619), and it can readily be shown that the velocity of the fluid parallel to the wall at a distance y away from it is

$$u = a\exp(\alpha t \pm by) \qquad \text{......(21)}$$

where $b=(\alpha/\nu)^{1/2}$, and the shear stress on the wall is therefore $\eta b u_0$ where u_0 is the wall velocity. Here we are interested in the case in which the fluid is at rest at great distances from the wall, so the lower sign is taken. Now if the motion is of the damped oscillatory type, b is given by (9), and if the damping is small the real part of b is approximately equal to $(\pi/\nu T)^{1/2}$ where T is the period of the oscillations. Thus the motion of the fluid is only appreciable within a layer against the wall of thickness of the order $(\nu T/\pi)^{1/2}$, which becomes very thin at high frequencies. This theory applies to the rectilinear motion of a plane wall; but any small part of the wall of a rotating, axially symmetrical vessel can be treated as plane and in rectilinear motion, provided that the thickness of the layer of moving liquid is small compared with the radius of curvature R'' of the stream-lines near the wall. Thus the stress on an element of the wall may be set equal to $\eta b u_0$ provided that the quantity $(\pi/\nu T)^{1/2}R''$ is large. But u_0 can be written as $r d\theta/dt$ where r is the distance of the element from the axis of rotation and symmetry, so the total torque exerted by the liquid on the vessel can be written as $Ld\theta/dt$ where

$$L = \eta b \int_S r^2 dS \qquad \ldots\ldots(22)$$

the integration extending over the whole of the area of contact S of the liquid with the wall. Using this equation in (7) and (8) one obtains equations corresponding to (11) and (13), and to (19) and (20):

$$I\Delta = \frac{1}{4\pi}\int_S r^2 dS\,(\pi\eta\rho T)^{1/2} a_0 \qquad \ldots\ldots(23)$$

$$I\left\{\frac{T^2}{T_0^{\,2}} - (1-\Delta^2)\right\} = \frac{1}{2\pi}\int_S r^2 dS\,(\pi\eta\rho T)^{1/2} b_0. \qquad \ldots\ldots(24)$$

For a spherical surface, the surface integral is $8\pi R^4/3$, for a cylindrical surface (height H) it is $2\pi R^3 H$, and for one side of a disc it is $\frac{1}{2}\pi R^4$. With these results, (23) and (24) give at once the first terms of (11) and (13) and (19) and (20) for the sphere and cylinder respectively. In general, the complete relations would be in the form of series of which the first terms are given by (23) and (24).

The case of an axially symmetrical vessel (such as a carefully blown glass bulb) which departs but little from the spherical form is of special importance. The first term in the expression for $I\Delta$ is given by (23), so comparison with (11) gives for the effective radius of the vessel $\bar{R}$

$$\frac{8}{3}\pi\bar{R}^4 = \int_S r^2 dS. \qquad \ldots\ldots(25)$$

Now the further terms are small, and since the vessel is nearly spherical they may be replaced by the corresponding terms of (11) with R replaced by $\bar{R}$. Thus the complete expression (11), and similarly (13), may be used with this effective radius which may be determined as follows. An origin of coordinates is chosen on the axis of symmetry, half-way between the poles which are supposed to be separated by a distance $2R_0$; and spherical coordinates Ψ and $R_0+\delta R$ are used. δR is thus a small distance representing the local departure from spherical form, so by neglecting the square of the differential of δR with respect to Ψ, the area dS of an annulus of the surface can be written as $2\pi r(R_0+\delta R)d\Psi$. But $r=(R_0+\delta R)\sin\Psi$, so from (25)

$$\frac{8}{3}\pi\bar{R}^4 = 2\pi\int_0^\pi (R_0+\delta R)^4 \sin^3\Psi\, d\Psi = \frac{8}{3}\pi R_0^{\,4}\left\{1+3\int_0^\pi \frac{\delta R}{R_0}\sin^3\Psi\, d\Psi\right\}$$

and since δR is much less than R_0 this gives

$$\bar{R} = R_0\left\{1+\frac{3}{4}\int_0^\pi \frac{\delta R}{R_0}\sin^3\Psi\, d\Psi\right\}. \qquad \ldots\ldots(26)$$

Now the moment of inertia of a solid of unit density which would fill the vessel may be written down as the moment of inertia of a sphere of radius R_0 plus the excess due to the extra volume $\delta R dS$ added on to each annulus. It is therefore

$$\frac{8}{15}\pi R_0^{\,5} + 2\pi R_0^{\,4}\int_0^\pi \delta R \sin^3\Psi\, d\Psi$$
$$= \frac{8}{15}\pi R_0^{\,5}\left\{1+\frac{15}{4}\int_0^\pi \frac{\delta R}{R_0}\sin^3\Psi\, d\Psi\right\} = \frac{8}{15}\pi\bar{R}^5$$

by (26), since δR is much less than R_0. Hence $\bar{R}$ is the effective radius of a solid filling the vessel calculated from its moment of inertia and assuming it to be truly spherical. This suggests a direct experimental method of determining $\overline{R}$. It also gives the following useful formula for the calculation of $\overline{R}$ from an internal survey of the bulb:

$$\frac{8}{15}\pi\overline{R}^5=\frac{\pi}{2}\int_{-R_0}^{R_0} r^4 dz \qquad \ldots\ldots(27)$$

where z represents distance measured along the axis of symmetry.

§ 5. The Correction for Air Resistance

If there is air outside the vessel, it produces a small torque on the system. The effect of this is to add a term to the expression for L, and this results in additive corrections on the right-hand side of formulae (11), (13), (19) and (20). In the case of a spherical vessel, the corrections may be shown to have the same form as the existing expressions on the right-hand side of (11) and (13), except that the signs of alternate terms in the series are reversed. Here, of course, R must be replaced by R' the external radius, and η, ρ and p must be replaced by values appropriate to air (η', ρ', p'). In general, the corrections to be added to the expressions for $I\Delta$ and $I\{T^2/T_0^2-(1-\Delta^2)\}$ have respectively the forms

$$\frac{1}{4\pi}\int_{S'} r'^2 dS'(\pi\eta'\rho' T)^{1/2}\left\{a_0+\frac{k_1}{p'}+\frac{k_2a_2}{p'^2}+0-\frac{k_4a_4}{p'^4}\ldots\right\}$$

and

$$\frac{1}{2\pi}\int_{S'} r'^2 dS'(\pi\eta'\rho' T)^{1/2}\left\{b_0+\frac{k_1\Delta}{p'}-\frac{k_2b_2}{p'^2}+\frac{k_3}{p'^3}-\frac{k_4b_4}{p'^4}\ldots\right\}$$

where k_1, $k_2\ldots$ are constants depending on the external form of the vessel, and p' is defined as $(\pi/\nu' T)^{1/2}R'$ where R' is now some arbitrarily chosen dimension of the apparatus. The integral, which is calculated over S' (the external surface of the vessel and any other parts of the suspended system), is easy to compute. On the other hand, exact expressions for k_1, $k_2\ldots$ cannot be obtained easily except when the external surface is spherical, but the terms in which they occur are small under normal working conditions. Approximate corrections for the effect of air resistance can therefore be calculated from the above expressions by neglecting all except the first term in each series. For accurate work, however, the effect of air resistance must be determined by special experiments such as those described in the relevant section of Part II. The theoretical expressions are then useful for calculating the variation of the effect with small changes in the values of η', ρ' and T.

References

Andrade, E. N. da C., and Chiong, Y. S., 1936, *Proc. Phys. Soc.*, **48**, 247.
Havelock, T. H., 1921, *Phil. Mag.*, **42**, 628.
Hopkins, M. R., and Toye, T. C., 1950, *Proc. Phys. Soc.* B, **63**, 773.
Lamb, H., 1953, *Hydrodynamics*, 6th Edn (Cambridge: University Press).
Okaya, T., and Hasegawa, M., 1933, *Jap. J. Phys.*, **11**, 23.
Okaya, T., 1936, *Proc. Phys.-Math. Soc. Japan*, **18**, 268.
Roscoe, R., and Bainbridge, W., 1958, *Proc. Phys. Soc.*, **72**, 585.
Watson, G. N., 1944, *A Treatise on the Theory of Bessel Functions*, 2nd Edn (Cambridge: University Press).

Viscosity Determination by the Oscillating Vessel Method
II: The Viscosity of Water at 20°C.

By R. ROSCOE and W. BAINBRIDGE
Physics Department, King's College, Newcastle upon Tyne

MS. received 5*th May* 1958, *and in final form* 30*th June* 1958

Abstract. The practical possibilities of the oscillating vessel method for accurate absolute measurements have been investigated. An improvement in Andrade and Chiong's apparatus was effected by using a capillary tube for the stem of the spherical bulb so that the liquid acted as its own thermometer. Abnormally large logarithmic decrements were found to occur with large amplitudes of rotation, and attention has been given to the best statistical method of calculating the decrement while avoiding this effect. A value of $1{\cdot}0025 \pm 0{\cdot}0005$ cP was obtained for the viscosity of water at 20°C, but an analysis of the sources of error indicates that the accuracy could be increased by further improvements well beyond that of the best capillary tube determination ($1{\cdot}0019 \pm 0{\cdot}0003$ cP). These improvements would include the replacement of the spherical bulb by a cylindrical vessel.

---

§ 1. Introduction

An investigation of the use of the oscillating vessel method for accurate viscosity determination was made by Andrade and Chiong (1936). Since then the method has been used in a number of measurements such as those of Hopkins and Toye (1950) and Andrade and Dobbs (1952), usually on liquid metals. The present work, on the other hand, is a continuation of Andrade and Chiong's investigation of the possibilities of the method for precise measurement, and an accuracy has been attained which is ten times greater than theirs. At the same time, confirmation has been obtained of the only accurate determination of the viscosity of water at 20°C hitherto made.

A spherical vessel was used, and the design of the apparatus followed that of Andrade and Chiong in most respects. The suspended part was not enclosed in a vacuum, however, as it was thought to be better to make an accurate determination of the air resistance correction than to complicate the construction of the apparatus. Also, as the water temperature had to be measured accurately, the stem of the bulb was constructed of capillary tubing so that the vessel acted as its own thermometer. The water used was triply distilled in Pyrex glass vessels.

The calculation was based on a formula derived in the new presentation of the theory given in Part I of this work (Roscoe 1958). This may be written in the form

$$I\Delta = \tfrac{2}{3}R^4(\pi\eta\rho T)^{1/2}F(\Delta, p) \qquad \ldots\ldots(1)$$

where I is the moment of inertia of the suspended part and T its time period, $2\pi\Delta$ is the logarithmic decrement of the oscillations Λ, R is the radius of the bulb, η is the viscosity of the liquid and ρ its density. The symbol p stands for

$(\pi\rho/\eta T)^{1/2}R$, and the function F (which approaches unity as Δ becomes very small and p very great) is given in series form in equation (11) of Part I.

The formulae used by Andrade and Chiong involve the torsional constant of the suspension, and for the determination of that quantity it is necessary that the suspended part should include two symmetrical placed moveable masses. These are required for the purpose of varying the moment of inertia without affecting the total weight (on which the torsional constant of a bifilar suspension depends). Since (1) does not involve the torsional constant, in the present work the moveable masses were replaced by an inertia ring. Two sets of decrement measurements were made, one with the ring and one without, and from the ratio of the two values of Δ the value of the moment of inertia of the suspended part I_0 alone could be calculated from the known moment of inertia of the ring I_1. The value of I_1 was accurately known, and thus the much smaller value of I_0 was determined with reasonable precision. The sum I_0+I_1 was therefore known to a high percentage accuracy, so that values of the decrement obtained with the combination were used in the actual calculation of the viscosity.

The following values of physical quantities at 20°c and 76 cm Hg were used in the calculations:

Water:	Density	$0{\cdot}998\,20$ g cm^{-3}
	Temperature coefficient of density	$-0{\cdot}000\,20$ g cm^{-3} deg^{-1}
	Temperature coefficient of viscosity	$-2{\cdot}485\times10^{-4}$ P deg^{-1}
	Compressibility	5×10^{-5} bar^{-1}
Dry air:	Density	$0{\cdot}001\,205$ g cm^{-3}
	Viscosity	$1{\cdot}820\times10^{-4}$ P
	Temperature coefficient of viscosity	$0{\cdot}005\times10^{-4}$ P deg^{-1}
Brass:	Coefficient of linear expansion	$2{\cdot}1\times10^{-5}$ deg^{-1}
Pyrex:	Coefficient of linear expansion	$0{\cdot}3\times10^{-5}$ deg^{-1}

The absolute value of the viscosity of air was only required for a correction to the air resistance corrections which were determined empirically, and an error of one part in a thousand in the assumed value would only lead to an error of one part in 300 000 in the final result. In addition to these figures, a value of $\eta=1{\cdot}0020$ cP for water at 20°c was used in calculating small terms in obtaining the moment of inertia of the system. An error of one part in a thousand here would lead to an error of only one part in 100 000 in the final result. This same value was used as a starting point for the final calculation of the viscosity of water at 20°c by successive approximations.

§ 2. APPARATUS

The rotatable suspension head was similar to that used by Andrade and Chiong, but modifications were made to the suspended part (figure 1). The bifilar suspension S consisted of a loop of tungsten wire of diameter 0·014 cm, and the distance from the suspension head to the wheel W was 68 cm. The frame F holding this wheel and the mirror M, the disc D supporting the inertia rings R, and the threaded tube T all formed one unit which was carefully machined to secure alignment. The thread on the brass collar C fixed to the stem of the bulb fitted loosely into the threaded tube, so constant alignment of the bulb was secured by contact between the horizontal surfaces of the base of the tube and the projection below the threaded part of the collar. The suspension wire was cemented on to the frame above the wheel after the water-filled bulb had been screwed into position, as in Andrade and Chiong's apparatus.

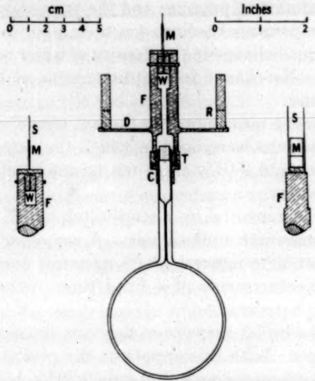

Figure 1. Section of suspended part of the apparatus, with side views of frame holding mirror and wheel.

The two inertia rings *R* were machined from the same piece of brass, one twice the height of the other. As they were always used together in the measurements, they are referred to elsewhere as 'the ring'. Care was taken to avoid strain when the rings were parted and the ends turned. Measurements on the internal and external diameters were made at 20°c with instruments checked with standard gauges. These were repeated after one month and again after the observations had been completed, in order to check that no afterworking had occurred. A range of variation of diameter with orientation of 0·001 cm was found with both rings, and a range of variation with height of 0·004 cm. A full survey of each ring was therefore made, and the mean internal and external diameters were determined graphically with an accuracy of ± 0·0002 cm. The masses of the rings were measured and the moment of inertia of the combination was calculated for the temperature at which the important measurements were made as $I_1 = 2992{\cdot}51 \pm 0{\cdot}13$ g cm^{-2} at 19·75°c.

The rotation of the bulb was observed by means of the image of a fine thread formed by a lens and reflected by the plane mirror M on to a suitably curved scale 300 cm away. The amplitude of oscillation was measured by eye to the nearest millimetre on this scale. The suspended part was shielded from draughts by means of a box provided with holes to admit the suspension and the light beam.

The Pyrex vessel was made by Messrs. James A. Jobling and Co. Ltd. Graduations were etched on the stem, and the water thermometer so formed had a sensitivity of 0·05° per millimetre at 20°c. It was calibrated over the length of the scale in a thermostatically controlled water bath against three standard thermometers with N.P.L. certificates. The smoothed calibration curve was accurate to ± 0·002°c, and individual measurements with the bulb showed a standard deviation from this curve of ± 0·005°c. Although the bulb was loosely stoppered with a rubber bung, evaporation occurred during the experiments. It was therefore weighed at intervals against a fixed set of weights on a balance with which masses could be estimated to 0·02 mg, allowance being made for changing barometric pressure and the temperature being kept at 20°c. A correction to the temperature readings was then made to allow for this evaporation and also for the small change in the density of water occurring with changing barometric pressure. No change in the dimensions of the bulb was found to occur while it was in use.

During the decrement measurements the air temperature was controlled to ±0·05°c. Only those runs were used in which the extreme variation in water temperature did not exceed 0·01°c from ten minutes before the measurements until after their completion.

Time intervals were measured by a stop-watch which was calibrated against a chronometer and Greenwich time signals. A smoothed calibration curve was plotted of error against time interval (2–60 minutes) correct to about 0·01 sec, although individual measurements of a fixed time interval showed a standard deviation of 0·1 sec.

The time period of a bifilar suspension depends appreciably on the amplitude when the latter is large. With this apparatus the period was 0·2% high when the amplitude was 100 cm on the scale, but only 0·002% high when the amplitude was 10 cm.

§ 3. THE EFFECTIVE RADIUS OF THE BULB

The bulb possessed a high degree of axial symmetry, the extreme values of the external width measured in different directions differing by only 0·001 cm. The mean value of this width was found to be 6·5328 cm with a standard error of measurement of ±0·0007 cm. In order to determine the internal width, the apparent thickness of the glass in the equatorial region was measured with a travelling microscope in sodium light and found to be $0{\cdot}0834_5 \pm 0{\cdot}0003$ cm. The true thickness was calculated from the expression $\mu d/\{1-(\mu-1)d/R'\}$ where μ is the refractive index of the glass, d its apparent thickness and R' the external radius of the bulb. μ was determined by immersing the bulb in benzene and adding paraffin oil until the surface of the bulb most nearly disappeared when viewed in sodium light, and then measuring the refractive index of the liquid (1·476). The true thickness of the glass was thus obtained as 0·1217 ± 0·0004 cm, giving the internal width of the bulb as 6·2894 ± 0·0011 cm.

The vessel had been made from a round bottom Pyrex flask. The wide neck had been drawn down so as to make a joint with the capillary tubing, using a glass lathe to secure alignment. Consequently, there was a roughly cylindrical space of about 0·30 cm in height and 0·27 cm in radius between the bulb proper and the capillary tubing. In the decrement experiments the damping effect of the water in this space and in the capillary tubing was altogether negligible compared with that of the water in the bulb proper, so the space was neglected in calculating the effective radius of the bulb $\bar{R}$.

The total volume up to one of the capillary tube divisions was obtained by subtracting the empty weight from an accurate measurement of the water-filled weight made during the temperature calibration. As this figure included the volume of occupied capillary and of the cylindrical space, it was necessary to determine the volume of the latter. For this purpose photographs were made of the bulb filled and surrounded with the benzene–paraffin mixture. It is not possible to make absolute measurements of the main dimensions of the bulb from these, because very small departures of the refractive index of the liquid from that of the glass cause appreciable changes in the observed wall thickness with oblique viewing. The small cylindrical volume could, however, be measured with sufficient accuracy from the photographs; and by subtracting this result and the volume of occupied capillary from the total volume, the volume of the bulb proper was obtained as $129{\cdot}653 \pm 0{\cdot}005$ cm^3.

The inside of the bulb was surveyed by admitting different volumes of liquid and measuring the corresponding heights x to which they stood in the bulb. Ether was used for this purpose rather than water, as slight traces of grease on the glass may seriously affect the volume of water drawn up at the edge of the meniscus. A needle, passing down through the capillary tube and carried by a vernier scale accurate to 0·0005 cm, was used to measure the values of x. The volume of ether was determined by weighing the bulb before and after each height determination. In addition to the buoyancy correction, allowance had to be made for the density of the ether vapour which saturated the air space above the liquid. The measurements were made at 20°c and a pressure of 76 cm Hg.

The volume V beneath a plane horizontal surface at a height x in the bulb was obtained by subtracting the calculated volume of liquid drawn up at the edges of the meniscus from the measured volume. In calculating the former quantity, it is permissible to assume that the bulb is spherical and the surface is plane at its centre. The volume drawn up is then $2\pi T'x'/\rho' g$ where T' is the surface tension of the liquid and ρ' its density, and x' is the height of the edge of the meniscus above the bottom of the bulb. For a sphere of 3·14 cm radius and over the range of measured values of x (0·5–5·9 cm), it was found by calculation to be sufficiently accurate to take x' as $x + 0{\cdot}13$ cm when using ether.

Analysis of the results showed that the bulb was nearly spheroidal, but possessed a slight asymmetry about the equatorial plane. It was therefore tentatively assumed that the inner surface was represented by the equation

$$r^2 = \frac{b^2}{a^2}(2a - x)x\left(1 - \frac{a - x}{c}\right) \qquad \ldots\ldots (2)$$

where r is the distance from the axis to the surface. This form approaches a spheroid as c becomes very great, the second term in the last bracket representing the departure from symmetry about the equatorial plane. The height of the bulb is $2a$ and its volume $4\pi ab^2/3$.

A simple expression for the volume V filling the bulb to a height x is obtained by integrating (2). This contains the three parameters a, b, c which can be varied independently in order to fit this expression to the observations. The total volume, however, was determined with a much greater accuracy than was possible with the other values of V, and its value fixes ab^2. There thus remain only two independent parameters a or b, and c. Numerical calculation was used to find the values of a and c which minimalise the mean square deviation of the observations from the formula values. With ab^2 as $30{\cdot}9524 \pm 0{\cdot}0011$ cm, this gave

$$a = 3{\cdot}1321 \pm 0{\cdot}0014, \quad c = 50 \pm 5, \quad \bar{R} = 3{\cdot}141\,65 \pm 0{\cdot}000\,28 \text{ cm}.$$

The standard errors for a and c were calculated as the changes in those quantities which increase the square of the standard deviation of the volumes from the formula by a fraction equal to the reciprocal of the number of observations. The value of $\bar{R}$ was obtained from the formula

$$\bar{R}^5 = ab^4(1 + a^2/7c^2) \qquad \ldots\ldots (3)$$

which is valid when b is close to a and a/c is small. It is derived by inserting the expression for r^2 given by (2) in equation (27) of Part I which is valid for a nearly spherical surface.

The deviations of the measured volumes from the formula with the above values of the parameters are shown plotted against x in figure 2. A comparison of this graph with plots of random numbers drawn from a normal distribution with the same standard deviation suggests that the departures from the formula are not entirely random. This view is supported by the fact that the standard deviation of 0·08 cm³ is appreciably greater than the standard deviation of repeated measurements of 0·03 cm³. (In both cases the deviations are in part due to errors in x.) A better value of $\bar{R}$ is therefore obtainable by treating the deviations shown in figure 2 as real. The addition to $\bar{R}$ was calculated numerically by means of equation (27) of Part I and found to be only 0·000 05 cm. Taking the standard error of the result to correspond to the actual errors of measurement rather than the deviations shown in figure 2, this gives $\bar{R} = 3{\cdot}141\,70 \pm 0{\cdot}000\,10$ cm.

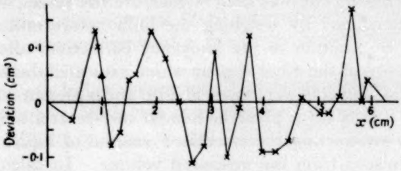

Figure 2. Deviations of the volume filling the bulb to a height x from the calculated value, using $a = 3{\cdot}1321$, $b = 3{\cdot}1436$, $c = 50$ cm.

A second value of $\bar{R}$ was obtained by a method independent of the ether survey. Use was made of the value of ab^2 given by the total volume, and of the maximum internal width of the bulb. The latter is given by (2) as $2b(1 + \frac{1}{8}a^2/c^2)$ when a/c is small. The ratio a/c was obtained from measurements on the photographs which were sufficiently accurate for this purpose. The results gave

$$a = 3{\cdot}1333 \pm 0{\cdot}0010,\ c = 47 \pm 5,\ \bar{R} = 3{\cdot}141\,45 \pm 0{\cdot}000\,20 \text{ cm}.$$

The weighted mean of this and the previous result is $\bar{R} = 3{\cdot}141\,65 \pm 0{\cdot}000\,09$ cm.

§ 4. THE DECREMENT MEASUREMENTS

In orber to set the bulb oscillating, the torsion head was rapidly turned through 90°. There was then an interval of about 10 minutes before the amplitude had fallen to less than 50 cm on the scale. This gave ample time for the non-oscillatory part of the motion (see Part I) to decay to negligible proportions in relation to the oscillatory part before measurement was started. In each run with the ring in position, 64 successive observations were made of the maximum deflections on each side of the zero, which ranged from about 45 cm to 1·4 cm. Pairs of left and right deflections were averaged, each average being denoted by the symbol θ_n where n ranges from 0 to 63, and 9 runs were made.

If non-linear effects due to the neglected inertia terms in the hydrodynamic equations were appreciable, the calculation of the viscosity η from the logarithmic decrement Λ would be vitiated. In such a case, or if some unsuspected disturbance were present, the value of Λ would not be constant. It was therefore essential to check whether the observations were, within the errors of measurement, consistent with a constant decrement. For this purpose it was easiest to use mean values of θ_n obtained by averaging corresponding values in all 9 runs. As the range of temperature (19·67–19·83 °C) and atmospheric pressure (73·1–73·9 cm Hg) was small throughout the series of runs, it was legitimate to treat these mean values as corresponding to an actual run carried out at the mean temperature and pressure of all nine, but having much reduced errors of observation. The actual scale readings are subject to an error uniformly distributed between $\pm 0{\cdot}05$ cm, since each reading was made to the nearest millimetre mark, so that the root mean square error was $0{\cdot}05/\sqrt{3}$ cm. Since each value of θ_n was the average of left and right readings, each mean of nine such values was subject to a root mean square error of $0{\cdot}05/\sqrt{54}$ cm or 0·0068 cm with a practically normal distribution.

With a constant decrement and errors ϵ_n which are distributed independently of the magnitude of θ_n, each of the mean values can be represented by the expression

$$\theta_n = A\,\mathrm{e}^{-n\Lambda} + \epsilon_n \qquad \ldots\ldots(4)$$

and the best pair of values for A and Λ which can be extracted from the results are given by the condition that the sum of all the $\epsilon_n{}^2$ shall be a minimum. This gives the relations

$$\frac{\Sigma\theta_n\,\mathrm{e}^{-n\Lambda}}{\Sigma\,\mathrm{e}^{-2n\Lambda}} = A = \frac{\Sigma n\theta_n\,\mathrm{e}^{-n\Lambda}}{\Sigma n\,\mathrm{e}^{-2n\Lambda}} \qquad \ldots\ldots(5)$$

where n is taken from 0 to one less than the number of values of θ_n. In order to solve these equations, an approximate value for Λ (calculated from a pair of values of θ_n) is at first assumed, and values of A are calculated from the left- and right-hand quotients in (5). In general these two differ, so the calculation is repeated with another value of Λ differing only slightly from the first, and the value of Λ which makes the two values of A equal is found by linear interpolation or extrapolation.

This calculation with the 64 figures gave the result $A = 44{\cdot}9708$ cm and $\Lambda = 0{\cdot}0553154$. The standard deviation of the values of θ_n from the exponential formula, calculated as the square root of $\Sigma\epsilon_n{}^2$ divided by the number of values less one, was found to be 0·0085 cm. As this is significantly greater than the value 0·0068 cm calculated from the inherent inaccuracy in the scale readings, it is clear that other random errors were present or that the decrement was not constant. The calculation was therefore repeated using only the last 54 figures. This gave $A = 25{\cdot}8531$ cm and $\Lambda = 0{\cdot}055\,280\,2$, and the standard deviation of the last 54 figures from the formula was 0·0074 cm. Further calculations in which more of the earlier figures were omitted gave standard deviations which were practically constant at this value, indicating that the decrement is constant after the first ten values, and the random deviations from the formula are then almost entirely due to the errors of scale measurement. The values of ϵ_n are shown plotted against n in figure 3, which makes it clear that the earlier readings are subject to an abnormally large decrement, probably on account of the neglected inertia effect. The standard error in the value of Λ found by this method is readily shown to be $\sigma/A(\Sigma n^2 e^{-n\Lambda})^{1/2}$ where σ is the standard deviation of the observations from the formula. The sum extends from $n=0$ up to one less than the number of figures, that is to say up to 53 in the present case. This gives the standard error in Λ as 0·000 007 7.

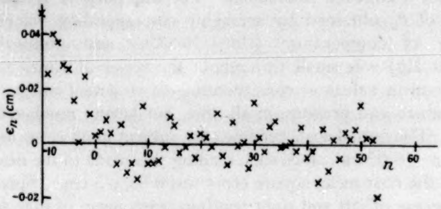

Figure 3. Deviations of θ_n from $Ae^{-n\Lambda}$ with $A=25{\cdot}8531$ cm and $\Lambda=0{\cdot}0552802$.

The decrement was also measured without the inertia ring. Here a lower degree of accuracy was permissible, so only six runs with left- and right-hand readings were made. The same method of analysis was used and it was found necessary to exclude all results until the deflection had fallen to 14 cm. The value of σ had then fallen to 0·0091 cm compared with the value 0·0083 cm calculated from the scale reading error, and it could not be reduced further by eliminating more of the early figures. With n running from 0 to 12, A was obtained as 14·0415 cm and Λ as 0·248 71 with a standard error of 0·000 17. Other decrement measurements were made, for the determination of air damping, with the bulb empty and also filled with a gelatine jelly. All these are collected in table 1.

Table 1. Values of $\Lambda=2\pi\Delta$

	Mean Λ	T (sec)	Temp. (°c)	Press. (cm Hg)
Water, ring	0·055 280 ± 0·000 008	9·0200	19·750	73·48
Water, no ring	0·248 71 ± 0·000 17	5·1149	20·091	72·99
Air, ring	0·001 826 ± 0·000 007	10·0636	21·5	76·4
Air, no ring	0·005 59 ± 0·000 02	6·3055	19·6	76·4
Gelatine, ring	0·001 381 ± 0·000 006	9·5230	20·0	76·6

§ 5. THE AIR RESISTANCE CORRECTION

As air resistance contributed nearly 3% to the damping in the measurements made with the ring (which were to be used for the actual calculation of the viscosity) it was necessary to determine the appropriate correction to a fairly high accuracy. For this purpose a value for the moment of inertia of the suspended part without the inertia ring I_0 was required. In the absence of air damping this could be calculated from the known moment of inertia of the ring I_1 by means of the formula

$$\frac{I_0}{I_0+I_1}=\frac{\Lambda_2}{\Lambda_1}\left(\frac{\eta_1\rho_1T_1}{\eta_2\rho_2T_2}\right)^{1/2}\frac{F(\Delta_1,p_1)}{F(\Delta_2,p_2)} \qquad \ldots\ldots(6)$$

which follows from (1). Here quantities with the suffix 1 refer to measurements without the ring and those with suffix 2 to measurements with it. In both experiments, however, air damping gave an addition to the right-hand side of (1) which must be approximately equal to the value of $I\Delta$ in the corresponding measurements without water. Thus the air resistance was allowed for by subtracting the corresponding decrements obtained with the empty bulb from Λ_2 and Λ_1 and using the ratio of these figures instead of Λ_2/Λ_1 in (6). This gave the result $I_0 = 574$ g cm^2. Actually, the air damping depends somewhat on the time period T which is not quite the same in corresponding measurements with and without water. For this reason, and because in the latter case there was air inside the bulb as well as outside, this value of I_0 is only approximate, although sufficiently accurate for the calculation of the air resistance corrections.

The moments of inertia being known, the values of $I\Delta$ were calculated for the two measurements with the empty bulb. This quantity is equal to the expression on the right-hand side of (1) with η and ρ replaced by the values η' and ρ' referring to air (representing the resistance of the air inside the bulb) together with another term representing the resistance of the air outside. The latter was found by subtracting the calculated value of the former from $I\Delta$, and the results with and without the ring are shown in the second column of table 2, together with a second result with the ring obtained from the measurement made when the bulb was filled with a jelly containing 0·25 g of gelatine per cm^3. In the latter case I was obtained by adding the calculated moment of inertia of the jelly (555·1 g cm^2) on to $I_0 + I_1$.

These air resistance effects were also estimated theoretically by means of the expression derived in Part I:

$$\frac{1}{4\pi}\int_{S'} r^2 dS' \,(\pi\eta'\rho' T)^{1/2}\left\{a_0 + \frac{k_1}{p'} + \frac{k_2 a_2}{p'^2} + 0 - \ldots\right\}$$

where a_0, a_2..... are known functions of Δ. In the integral, dS' represents an element of area of the outer surface and r' its distance from the axis of symmetry. The integral was found to be 1652 cm^4 without the ring and 2998 cm^4 with the ring. Only part of the outer surface was spherical, but for the purpose of this estimation k_1, k_2,..... were given the values 2, 1/2..... appropriate to a sphere, the values of p' being taken as $(\pi\rho'/\eta' T)^{1/2} R'$ where R' is the external radius of the bulb. The results are shown in the first column of table 2.

Table 2. Addition to $I\Delta$ due to external air resistance

	Theoretical	Observed	With water (calc.)
Air, no ring	0·371	0·421 ± 0·002	0·345 ± 0·002
Air, ring	0·912	0·937 ± 0·004	0·852 ± 0·004
Gelatine, ring	0·879	0·906 ± 0·004	0·854 ± 0·004

The difference between the observed and theoretical values must be in some part due to the use of the values of k_1, k_2..... appropriate to a spherical surface, although it should be noted that the terms involving these quantities only make up 25–30 per cent of the whole effect. Furthermore, the effects of any hysteresis in the suspension would increase the observed values. Whatever the cause of the differences, they are so small that it is legitimate to use the variation of the air resistance effect with η', ρ' and T given by the above expression (with k_1, k_2..... having the values for a sphere) in calculating the air resistance effects for the water-filled bulb from the figures given in the second column. These calculated values are shown in the last column of table 2.

§ 6. CALCULATION OF THE VISCOSITY OF WATER

A really accurate value for the total moment of inertia of the system with the ring was required for the calculation of η. The value of I_0 was therefore recalculated using the value 0·345 g cm² for the air resistance correction without the ring, and a mean value of 0·853 g cm² for that quantity with the ring. This gave $I_0 = 573{\cdot}5 \pm 0{\cdot}4$ g cm² so that the value taken for I was $I_0 + I_1 = 3566{\cdot}0$ g cm² at 19·75 °C.

The value of $I\Delta$ with the ring and with water in the bulb was thus 31·3741 ± 0·0045 g cm². The air resistance correction of 0·853 ± 0·003 g cm² was subtracted from this figure before it was used in (1) for the calculation of η. That quantity appears as $\eta^{1/2}$ on the right-hand side of (1), and also in the small terms involving inverse powers of p in $F(\Delta, p)$. Successive approximations were therefore used, the value $\eta = 1{\cdot}0082$ cP at 19·750 °C being initially assumed so as to calculate $F(\Delta, p)$. At the second calculation it was found that $\eta = 1{\cdot}008\,69$ cP and further recalculation would not have altered this result. The temperature coefficient of viscosity between 19·75 and 20 °C obtained from the interpolation formulae given by Kampmeyer (1952) and Weber (1955) is $-0{\cdot}024\,85 \pm 0{\cdot}000\,05$ cP deg^{-1}, so that $\eta = 1{\cdot}0025 \pm 0{\cdot}0005$ cP at 20 °C. The standard error of 0·0005 cP is made up as shown in table 3.

Table 3

Source of error	Error in η (10^{-4} cP)
Λ (with ring)	± 3·3
$\bar{R}$	± 2·5
I_0	± 2·5
Air damping correction	± 2·2
I_1	± 0·8
Temperature	± 0·7
T	± 0·4

§ 7. CONCLUSIONS

The only published result of greater accuracy than the above is the figure $\eta = 1{\cdot}0019 \pm 0{\cdot}0003$ cP at 20 °C given by Swindells, Coe and Godfrey (1952) who used the capillary tube method. The principal errors in both cases are believed to be statistical rather than systematic, and the figures shown are standard errors. The agreement between the two is therefore satisfactory.

The inaccuracy in the capillary tube determination arises chiefly in the determination of end-corrections, and it is hard to see how it could be reduced further. On the other hand, the greater part of the inaccuracy in the present work arises in the determination of logarithmic decrements, and it has been shown that the error here is due to the inaccuracy of the scale measurements. It should be possible to reduce this considerably by using photographic or photoelectric techniques, and such a reduction would affect the first, third and fourth sources of error shown in table 3.

The remaining large source of error is the determination of $\bar{R}$. This would be very much reduced if a cylindrical vessel were used instead of a sphere. The calculation in the former case is no more difficult than in the latter when the formulae given in Part I are used. It should be possible to construct a cylindrical vessel with much greater accuracy than a spherical one, and the determination of its height and mean radius would be much simpler than the determination of $\bar{R}$ for a sphere. With all these improvements it should be possible to reduce each of the constituent errors in table 3 to about $0{\cdot}5 \times 10^{-4}$ cP so that the standard error of the result would not be much in excess of 10^{-4}cP.

It is probably better to follow Andrade and Chiong in enclosing the apparatus in a vacuum than to allow for a large air resistance correction as in the present work. The simplicity of the apparatus without the vacuum is offset by the extra labour in calculation. It must be remembered, however, that decrement measurements have to be made with the bulb empty even when a vacuum enclosure is employed, in order to allow for the effects of residual air and hysteresis in the suspension. The use of a vacuum should facilitate the attainment of temperature equilibrium by the liquid in the vessel.

ACKNOWLEDGMENTS

The authors wish to thank Mr. W. Ingo of the Physics Department, who made the inertia ring and other parts of the apparatus. They are also indebted to the Director of the Northern Coke Research Laboratory for the use of a constant-temperature water bath and a standard thermometer, and to the Director of the Stevenson Engineering Laboratories of King's College for the use of measuring equipment and gauges.

REFERENCES

ANDRADE, E. N. DA C., and CHIONG, Y. S., 1936, *Proc. Phys. Soc.*, **48,** 247.
ANDRADE, E. N. DA C., and DOBBS, E. R., 1952, *Proc. Roy. Soc.* A, **211,** 12.
HOPKINS, M. R., and TOYE, T. C., 1950, *Proc. Phys. Soc.* B, **63,** 773.
KAMPMEYER, P. M., 1952, *J. Appl. Phys.*, **23,** 99.
ROSCOE, R., 1958, *Proc. Phys. Soc.*, **72,** 576.
SWINDELLS, J. F., COE, J. R., and GODFREY, T. B., 1952, *J. Res. Nat. Bur. Stand.*, **48,** 1.
WEBER, W., 1955, *Z. angew. Phys.*, **7,** 96.

Reversible Permeability and Losses in Magnetically annealed Perminvar

By E. W. LEE and A. G. H. TROUGHTON[†]
Department of Physics, University of Nottingham

Communicated by L. F. Bates; *MS. received 5th June* 1958, *and in final form 27th June* 1958

Abstract. Measurements are reported of reversible permeability and associated losses for a specimen of magnetically annealed Perminvar possessing a rectangular *B–H* loop. Measurements were recorded both as the hysteresis cycle was traversed and when a circular domain was nucleated and pushed into the centre of the specimen using a small pulsed field. Under these conditions the observed eddy current losses were twelve times those calculated from a uniform permeability model. A tentative explanation of the nature of the restoring force on the circular wall is given.

§ 1. INTRODUCTION

In this paper the term reversible permeability is taken to mean the quantity defined by

$$\mu_{\mathrm{r},0} = \lim_{\Delta H \to 0} \frac{\Delta B}{\Delta H}$$

in which ΔH is the amplitude of an alternating field and ΔB the corresponding measured induction amplitude. The significance of μ_r depends rather on what provides the dominant magnetization process at any stage of magnetization. Where boundary movements predominate, it is a measure of the ease with which a domain boundary can be reversibly displaced from its equilibrium position in a magnetic field. When rotations occur, it is a measure of the ease of reversible rotation of a domain magnetization vector about its position of equilibrium. In either case, measurements of μ_r can give valuable information about the ratio of reversible to irreversible changes if such measurements are coupled with static *B–H* loop determinations (Tebble *et al.* 1951). It is not proposed to discuss further the significance or interpretation of μ_r since this has been comprehensively done by Tebble and Corner (1950) whose paper should be consulted for further details.

Although many observations of μ_r have been carried out for many different materials we are unaware of any investigation into the reversible permeability of materials possessing markedly rectangular *B–H* loops. Many materials of this kind possess rectangular *B–H* loops because of their very simple domain structure. Examples are single crystals cut with the long axis along a direction of easy magnetization (Williams and Shockley 1949), heavily stressed materials and those in which a uniaxial anisotropy has been induced by annealing in a magnetic field. Perminvar (45% Ni, 30% Fe, 25% Co) is an example of the latter and powder pattern investigations by Williams and Goertz (1952) showed that a ring of Perminvar, after a magnetic anneal, possessed a simple domain structure of two or more circular domains running right round the specimen, magnetized in opposite directions and separated by one or more 180° boundaries. This type of domain structure is essentially the same as that obtained by Williams and Shockley in a 'picture frame' single crystal of 3·5% SiFe. Magnetization takes place in Perminvar by radial movement of the domain boundary and the *B–H* loop is rectangular because the field necessary to nucleate a circumferential wall is greater than that required to make it expand irreversibly. Consequently the boundary, once formed, is unstable and moves across the specimen without further change in field. If the field is removed before the domain boundary has had time to complete its journey it is halted and comes to rest in a position of equilibrium.

[†] Now at Services Electronics Research Laboratory, Baldock, Herts.

The purpose of this paper is to describe measurements of the reversible permeability and the associated eddy-current losses in magnetically annealed Perminvar. The investigation was carried out with two main objectives. The first of these was to investigate the nature and magnitude of the restoring force on a circular domain boundary by observing its contribution to the overall reversible permeability. The second is of a different nature. It has been shown by Williams, Shockley and Kittel (1950) that the eddy-current losses arising from the motion of a single domain wall should be very much greater than those which would arise if the substance could be characterized by a uniform scalar permeability. It is becoming increasingly clear that the well known eddy-current anomaly encountered by electrical engineers is explicable in terms of the domain-and-wall structure possessed by real ferromagnetic materials (Aspden 1956, Lee 1958). It is of interest and importance therefore to see to what extent the observed eddy-current losses in materials possessing simple domain structure, can be ascribed to the movement of domain boundaries.

§ 2. EXPERIMENTAL METHOD

The reversible permeability was measured using an a.c. mutual inductance bridge designed by A. C. Lynch. This is a modified Maxwell bridge using the device first employed by Wilde (1952) enabling one side of the input and output leads to be at earth potential. In this method the permeability is determined from measurements of mutual inductance in terms of capacity, and the associated losses in terms of an equivalent parallel resistance. Specimens were in the form of stamped rings of 1 in. external, and 11/16 in. internal diameter, having a nominal thickness of 100 microns. These were placed in special bakelite holders whose thickness was reduced to 0·75 mm in order to keep air-flux corrections as low as possible. 200 turns of well twinned 36 s.w.g. Lewmex wire were wound on these holders, serving as primary and secondary windings of the mutual inductance. Polarizing fields were provided by an additional winding of 20 turns of 22 s.w.g. Lewmex. Mutual inductances thus formed were kept in constant temperature enclosures some distance from the bridge to which they were connected through switches via coaxial cable. Measurements were carried out at 0°c and at −183°c by placing the specimens in liquid oxygen. Intermediate temperatures were obtained using cooled methylated spirit as a result of which temperatures between −183° and −120°c were not available. Measurements were also taken up to 100°c by placing the specimens in a water bath. The same set of windings served as magnetizing and pick-up coils for induction measurements and the *B–H* loops were obtained in the usual manner using a ballistic galvanometer. No compensation for air-flux was made during these measurements as the necessary correction was found to be only 1% over the field range used. Reversible permeability and *B–H* loops were measured alternately by switching the mutual inductances first to the bridge and then to the ballistic galvanometer circuits. No interaction between the two circuits could be observed so that no spurious effects were thereby introduced.

The specimens were made by powder metallurgy and so are essentially high precision alloys containing a minimum of impurities (Richards, Walker and Lynch 1957). Complete fabrication, including magnetic annealing, was carried out at the Post Office Research Station.

§ 3. EXPERIMENTAL RESULTS

Preliminary measurements were carried out using a stack of 1 in. rings, as received. Having established that the sensitivities of the apparatus were sufficient the specimens were investigated one by one. Small variations in magnetic behaviour were found from one specimen to another but their gross properties were essentially the same. A single specimen was selected for detailed measurements, namely the one having the largest 'as received' permeability. This selection was made, not because it was thought to indicate the presence of any special properties but from considerations of bridge sensitivity. The results presented below refer to this single specimen. At room temperature its magnetic properties were reasonably stable, and the remanent state was characterized by a reversible permeability constant to 1%. The low temperature measurements were likewise easy to obtain, both with the bridge and the *B–H* tester but at 100°c measurements were more difficult owing to instability in magnetic behaviour. Reversible permeability measurements were in all cases carried out for a number of different values of the exciting field. In most cases the reversible permeability was observed to obey a relation of the form $\mu_{r,0}=\mu_{r,H}+bH$, and the required value of $\mu_{r,0}$ was obtained by extrapolation to zero exciting field. The fields used were the smallest allowing a useful measurement to be made and varied from 10 to 60 milli-oersteds.

Figures 1 (*a*) to (*c*) show the observed *B–H* loops and figures 1 (*d*) to (*f*) the corresponding reversible permeability curves obtained at −183°, 0° and 100°c. The *B–H* loops are rectangular, giving support to the view that the domain structure is simple. The corners of the loops are rounded at 0° and 100° indicating a finite range of field over which wall nucleation took place. At −183°c the corners are remarkably sharp and if the correct reverse field was applied the flux change took place in several distinct steps with a pause of about 1 second between each. This suggests wall movement assisted by thermal activation in the manner suggested by Street and Woolley (1949). The reversible permeability curves follow the same form as that observed in ordinary materials and the actual values of μ_r, though small in comparison with the differential permeability, are, in fact, of the same order as those observed by Tebble *et al.* for annealed nickel. During measurements in the intermediate range −183°–0°c large changes in μ_r were sometimes observed. Their cause was eventually traced and attributed to the effects of stress caused by traces of water or methylated spirit trapped in the specimen holder, which froze at the low temperatures and strained the specimen. Such effects were deliberately introduced and we obtained the surprising result that at −183°c μ_r at remanence was increased by 500%.

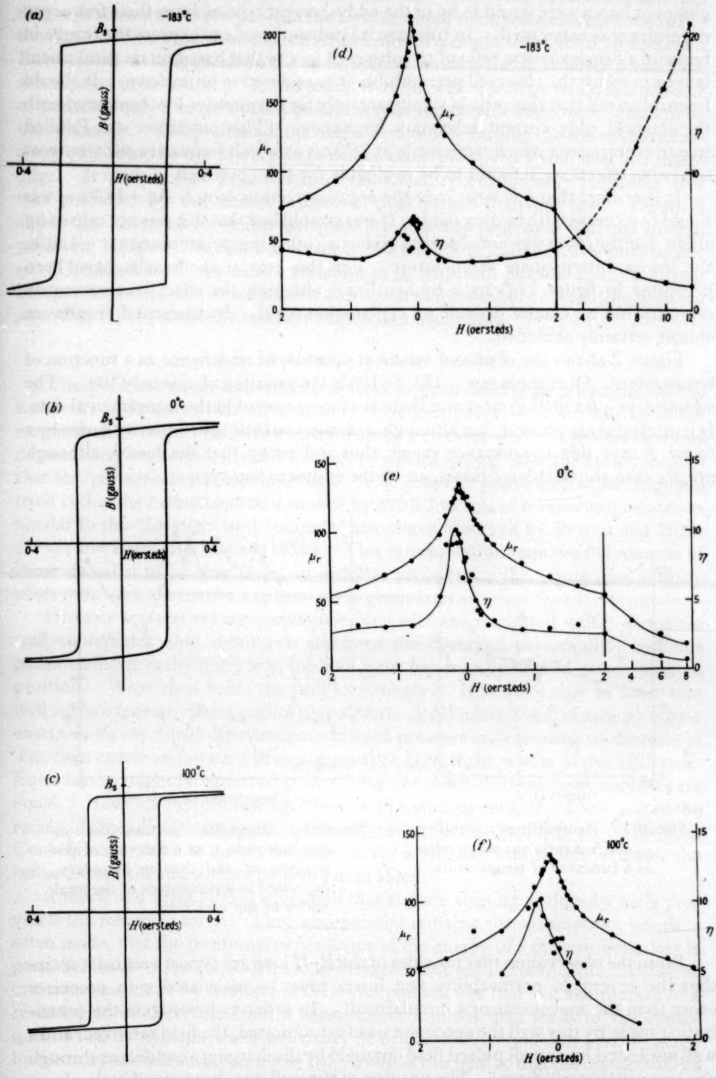

Figure 1. *B–H* loops : reversible permeability μ_r and loss ratio η as a function of field strength for a single ring of Perminvar at three different temperatures.

Also plotted in figures 1 (*d*) to (*f*) are the loss ratios, denoted here by η. The observed losses were found to be of the eddy-current type as far as their frequency dependence is concerned. In this case it is advantageous to express the results in terms of a dimensionless ratio of the observed loss to that based on classical calculations in which the observed permeability is considered to be uniform. It should be emphasized that this ratio is significant only for frequencies low compared with the classical eddy-current relaxation frequency. (This condition was fulfilled in our experiments which were made at 2·7 kc/s at which frequency eddy-current screening effects were found to be negligible for this specimen.)

It is evident that η is large over the entire hysteresis loop. At − 183 °C η was found to increase with biasing field. It was established that this was not caused by strain, but the effect was not observed at the two other temperatures nor at − 120 °C, the lowest intermediate temperature. For this reason the results have been presented in figure 1 (*d*) by a broken line; although the effect was accurately reproducible we cannot provide an explanation for it. Instrumental origins are almost certainly excluded.

Figure 2 shows the observed values of μ_r and η at remanence as a function of temperature. Over the range − 183° to 100 °C the variation of μ_r is only 10%. The variation in η is a little greater and there is a larger spread in the experimental data. It is interesting to observe that although η changes so little the resistivity varies by a factor 3 over this temperature range, thus indicating that the losses, although greater than the calculated losses, are of the eddy-current type.

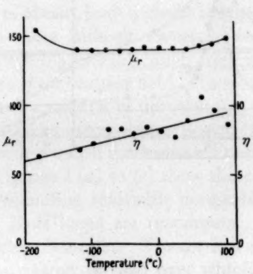

Figure 2. Reversible permeability μ_r and loss ratio η at remanence as a function of temperature.

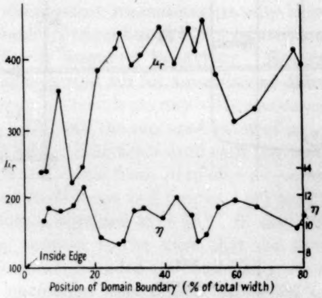

Figure 3. Reversible permeability μ_r and loss ratio η as a function of the position of the domain boundary, expressed as a percentage of the total width of the specimen.

From the observation that the sides of the *B–H* loop are almost vertical it seems that the reversible permeability and losses must be associated with processes other than the movement of a circular wall. In order to investigate the contribution made by this wall the specimen was first saturated, the field removed, and a wall nucleated by a small pulsed field obtained by discharging a condenser through the magnetizing windings. The position of the wall was determined by applying a saturating field in the opposite sense to the original one and comparing the deflection obtained on a ballistic galvanometer with that obtained when the magnetization was reversed. (At the time at which the measurements were made the fact that this procedure nucleated and moved a single wall had to be assumed. Subsequent investigations on the same specimen using the Kerr effect proved the assumption to be sound.) It was found that the wall would go to a small number of positions only; in particular, positions near the outside edge were found to be unobtainable. The position of the wall was varied by varying the size of the nucleating pulse but the use of very large pulses often produced a wall near the inside edge. It is likely that the discharge was oscillatory and for large pulses the wall was produced by the second (negative) peak rather than the first. Figure 3 shows the observed reversible permeability and loss ratio as a function of wall position. It is evident that the presence of a nucleated wall increases both μ_r and η. There is a small systematic variation of μ_r with wall position but η is almost independent of it. Closer inspection shows that there is a slight correlation between μ_r and η in that η is usually smallest when μ_r is a maximum.

§ 4. INTERPRETATION OF RESULTS

The presence of an appreciable reversible permeability at all points on the hysteresis cycle shows that there must be magnetic processes contributing to the magnetization other than radial movement of a circular wall. The fact that this permeability is associated with a loss ratio η significantly greater than unity implies that the permeability is non-uniform. The simplest possibility which suggests itself is that the magnetization is caused by small domains of reverse magnetization similar to the ‘lozenge’ and ‘tadpole’ structures observed by Paxton and Nilan (1955) and Bates and Davies (1956). This interpretation requires the number of these domains to be very large, in order to account for the values of η actually observed. An alternative explanation is given later.

Of more interest are the results obtained with the nucleated wall. Since the wall contributes only about two thirds of the observed permeability and this permeability is really quite low, the wall must be strongly held in its equilibrium position. What then holds the wall so strongly? It is quite easy to show that wall surface tension effects cannot play a part. A cylindrical wall of radius r whose energy is σ_w cm^{-2} will experience an inward pressure σ_w/r tending to decrease r. The field exerts an outward pressure equal to $2HI_s$ if the wall is of the 180° type. Equilibrium might be expected at that value of r at which these two quantities are equal. However in a circular specimen with a circular wall, $H=2Ni/r$ and so the radius of the wall does not appear in the expression for the condition of equilibrium. Consequently there is no stable position for a circular wall if this is under the influence of field and surface tension forces alone.

Rodbell and Bean (1956) suggested that surface pinning of domain walls provided the restoring force. They also pointed out that the assumption, which is often made, that the positional dependence of the energy of a domain boundary is periodic, leads to results which are in disagreement with experiment. A similar criticism was made by Stewart (1951) who pointed out that the assumption of a restoring force derivable from a conservative internal field leads to the consequence that in principle a substance may be magnetized without any loss of energy by the external field since one needs only to adjust this field so that the instantaneous rate of magnetization is zero. In order to account for the essentially dissipative nature of hysteresis some mechanism for the restoring force in a domain wall has to be invoked which cannot be described by a conservative internal field. Shockley (discussion following paper by Stewart 1951) pointed out that the Neel spikes arising from inhomogeneities in the material, which attach themselves to a plane domain wall and are dragged out by it provide a non-linear type of restoring force necessary to account for hysteresis effects.

Bearing in mind these factors we tentatively advance the following interpretation. Close examination of the powder patterns obtained by Williams and Goertz shows that the walls in Perminvar are not true circles but consist of a number of short straight segments. It is now known (Taniguchi 1955, Chikazumi 1956) that the effect of a magnetic anneal is to induce uniaxial anisotropy with an energy minimum which lies between the one of the symmetry axes of the crystal and the direction of the field during annealing. Consequently within a crystal grain the domain boundary must be straight. The domain boundary traverses the grain boundaries, changing direction as it does so to comply with the requirements of the induced anisotropy. On this picture it seems highly probable that there will exist a large but finite number of stable wall positions between which the wall is not free to be situated. Thus the positional free energy of the wall is not of the conservative type. Moreover one would expect that the wall would as a whole strongly resist deformation by an external field since this would imply rotation of the magnetization vector against the induced anisotropy in certain crystal grains. This model would also explain the observed variation of μ_r with field strength since the magnetization in each grain will not in general coincide with the field direction. The observed permeability is then due to rotations. However since the direction of the induced anisotropy varies in direction from grain to grain this rotational permeability is sufficiently non-uniform to account for the high loss ratios observed.

Finally, we would like to point out that the losses we observed, although high, are not nearly as high as would be expected if the permeability were caused solely by an oscillating circular wall. In this case it may be shown (Lee, unpublished) that $\eta \simeq 3L/pd$ where $2L$ is the width of the specimen, d its thickness and p the number of walls. In our specimen $L = 0{\cdot}2$ cm, $d = 0{\cdot}01$ cm and so $\eta \simeq 60$ if $p = 1$. This is to be compared with the observed average value of about 12. This result is not sufficient to confirm the results of eddy-current calculations using the domain-and-wall model. It merely confirms the conclusions already reached, that in Perminvar the contribution of the circular wall to reversible magnetic phenomena is somewhat masked by effects occurring elsewhere.

ACKNOWLEDGMENTS

We wish to record our sincere thanks to Professor L. F. Bates for his interest in this work and for placing every facility at our disposal. The Perminvar was made at the Post Office Research Station, Dollis Hill, London, and we are indebted to Mr. A. C. Lynch and Dr. A. Hart both for supplying the specimens and for many enlightening discussions.

REFERENCES

ASPDEN, H., 1956, *Proc. Instn Elect. Engrs, Monograph No.* 164M (103 C, 272).
BATES, L. F., and DAVIS, P. F., 1956, *Proc. Phys. Soc.* B, **69,** 1109.
CHIKAZUMI, S., 1956, *J. Phys. Soc. Japan,* **11,** 551.
LEE, E. W., 1958, *Proc. Instn Elect. Engrs, Monograph No.* 284M.

PAXTON, W. S., and NILAN, T. G., 1955, *J. Appl. Phys.*, **26,** 994.
RICHARDS, C. E., WALKER, E. V., and LYNCH, A. C., 1957, *Proc. Instn Elect. Engrs*, **104,** B, 343.
RODBELL, D. S., and BEAN, C. P., 1956, *Phys. Rev.*, **103,** 886.
STEWART, K. H., 1951, *J. Phys. Radium*, **27,** 177 (Grenoble Conference 1950).
STREET, R., and WOOLLEY, J. C., 1949, *Proc. Phys. Soc.* A, **62,** 743.
TANIGUCHI, S., 1955, *Sci. Rep. Res. Insts Tôhoku Univ.*, A, **7,** 269.
TEBBLE, R. S., and CORNER, W. D., 1950, *Proc. Phys. Soc.* B, **63,** 1005.
TEBBLE, R. S., CORNER, W. D., and WOOD, J. E., 1951, *Proc. Phys. Soc.* B, **64,** 753.
WILDE, H., 1952, *Arch. Elektr. Übertr.*, **6,** 354.
WILLIAMS, H. J., and GOERTZ, M., 1952, *J. Appl. Phys.*, **23,** 316.
WILLIAMS, H. J., and SHOCKLEY, W., 1949, *Phys. Rev.*, **75,** 178.
WILLIAMS, H. J., SHOCKLEY, W., and KITTEL, C., 1950, *Phys. Rev.*, **80,** 1093.

The Interpretation of Magnetic Susceptibility and the ΔE Effect in Terms of Domain Processes

By B. LEWIS† and R. STREET‡
† Department of Physics, University of Nottingham
‡ Department of Physics, University of Sheffield

MS. received 20*th May* 1958

Abstract. General formulae applicable to any model or any domain process are derived for the magnetic susceptibility χ and the magnetically dependent part of Young's modulus ΔE. From these formulae expressions are obtained for χ and ΔE in the initial magnetization regions for domain assemblies where magnetization proceeds by (*a*) rotation of domain magnetization vectors against internal strain anisotropy, (*b*) rotation against magnetocrystalline anisotropy characterized by one, three or four preferred axes and (*c*) simple movement of 90° and 180° boundary walls. It is then shown how the types and relative importance of the domain processes operative in the initial magnetization region may be determined from measurements of χ and ΔE. Examples of this procedure are given and include the case of annealed cobalt for which the ΔE effect is due entirely to rotations against uniaxial magnetocrystalline anisotropy energy, while the susceptibility arises mainly from 180° boundary wall movement. For annealed nickel, experimental values of ΔE and χ obtained by a number of workers vary widely and this is shown to be due to (i) differences in the relative proportions of 90° and 180° boundaries and (ii) the influence of the annealing process on the ease of boundary wall movement.

§ 1. INTRODUCTION

A MAGNETIC field applied to a ferromagnetic specimen brings about a change in magnetization and a magnetostrictive deformation. Both these observed changes are due to rearrangement of the spontaneously magnetized and deformed domains which the specimen contains.

A linear stress also induces domain changes giving a magnetostrictive deformation, except when all the domain vectors are aligned by a strong magnetic field and the intensity of magnetization has its saturation value. Thus a strain of magnetic origin is added to the normal elastic strain and Young's modulus E for the states of zero and intermediate magnetization is less than that for the saturation state. The change of Young's modulus with magnetization is called the ΔE effect. The object of this paper is to examine the ΔE effect and magnetic susceptibility in terms of more recent and more exact knowledge of domain structures.

One of the major difficulties of any theory of domain phenomena lies in the description of the domain structure, or domain vector distribution. The assumption of a statistical distribution among the alternative preferred directions has proved moderately successful when applied to calculations of magnetization and magnetostriction curves and has been used for the ΔE effect by Akulov (1933), by Brown (1936, 1937) and by Takagi (1939). In these theories no account is taken of the ways in which the structure changes from one state to another.

---

† Now at the Research Laboratories of The General Electric Company Ltd., Wembley.

In previous theoretical treatments calculations have been made of the ΔE effect and initial susceptibility for one domain process controlled by a particular postulated mechanism. For example Kersten (1931, 1932, 1933) deals with the rotation of domain magnetization vectors against internal strain anisotropy, Becker and Döring (1939) with boundary movement controlled by inhomogeneous internal strain and Kersten (1956) with the bulging of 90° walls between points at which they are anchored by inclusions.

The basis of the approach adopted here is that all types of domain process which can occur in any given case make their individual contributions to the observed effects, which, therefore, represent summations of components from each process. General equations applicable to any domain process are derived and then used to obtain relations for each process. These relations are applied to interpret experimental observations of the ΔE effect and magnetic susceptibility. Apart from the case of rotations against magnetocrystalline anisotropy energy the question of the mechanism by which a particular domain process is controlled is not considered.

§ 2. GENERAL THEORY OF REVERSIBLE DOMAIN PROCESSES

The analysis is confined to reversible domain processes. The independent variables to be considered are the magnetic field H and the applied stress Z. The dependent variables are I and λ which are respectively the components of the intensity of magnetization and the magnetostrictive deformation resolved along the measuring direction which is the common direction of the field and stress. I and λ may be expressed in terms of the spontaneous intensity of magnetization I_s and a magnetostrictive coefficient λ_c:

$$I = I_s \phi (M) \qquad \ldots\ldots (1)$$

$$\lambda = \lambda_c \psi (M). \qquad \ldots\ldots (2)$$

The functions ϕ and ψ defined by these equations depend on a parameter M which is characteristic of the domain process considered. For example if rotation of a domain magnetization vector occurs during magnetization then M is the angle of rotation; when domain boundary movements are involved, M is the positional coordinate of the boundary.

The magnetostatic energy density $f_1(M)$ for an applied field H, parallel to I, is

$$f_1(M) = -HI = -HI_s \phi (M). \qquad \ldots\ldots (3)$$

The strain energy density $f_2(M)$ for an applied stress Z, parallel to λ is

$$f_2(M) = -Z \int_0^M d\lambda = -Z\lambda_c \int_0^M \psi' (M)\, dM \qquad \ldots\ldots (4)$$

or

$$f_2'(M) = -Z\lambda_c \psi'(M) \qquad \ldots\ldots (4a)$$

where the prime denotes differentiation with respect to M.

In addition to the magnetostatic and strain energies given by equations (3) and (4), the energy of an assembly of domains will have contributions arising from magnetocrystalline and internal strain anisotropy energies, boundary wall energy etc. The sum of these contributions, depending on the parameter M and not involving H and Z explicitly, will be represented by $f_A(M)$. Thus the total free energy of the domain assembly is $f_1+f_2+f_A$ per unit volume.

For reversible changes, the equilibrium value of M for fixed values of H and Z will be given by

$$f_1'+f_2'+f_A' = -HI_s\phi'(M) - Z\lambda_c\psi'(M) + f_A'(M) = 0. \qquad \ldots\ldots(5)$$

Equation (5) is an implicit relation between H, Z and M from which the rate of change of M with respect to H and Z may be derived. For changes in H when Z is constant

$$I_s\phi'(M) = \frac{\partial M}{\partial H}F''(M) \qquad \ldots\ldots(6)$$

where

$$F''(M) = -HI_s\phi''(M) - Z\lambda_c\psi''(M) + f_A''(M).$$

Thus

$$\frac{\partial M}{\partial H} = \frac{I_s\phi'(M)}{F''(M)}. \qquad \ldots\ldots(7)$$

Similarly

$$\frac{\partial M}{\partial Z} = \frac{\lambda_c\psi'(M)}{F''(M)}. \qquad \ldots\ldots(8)$$

Combining equations (7) and (8) with dI/dM and $d\lambda/dM$ from (1) and (2) gives

$$\frac{\partial I}{\partial Z} = \frac{\partial M}{\partial Z}\frac{dI}{dM} = \frac{I_s\phi'(M)\lambda_c\psi'(M)}{F''(M)} \qquad \ldots\ldots(9)$$

$$\frac{\partial I}{\partial H} = \frac{\partial M}{\partial H}\frac{dI}{dM} = \frac{[I_s\phi'(M)]^2}{F''(M)} \qquad \ldots\ldots(10)$$

$$\frac{\partial \lambda}{\partial Z} = \frac{\partial M}{\partial Z}\frac{d\lambda}{dM} = \frac{[\lambda_c\psi'(M)]^2}{F''(M)} \qquad \ldots\ldots(11)$$

$$\frac{\partial \lambda}{\partial H} = \frac{\partial M}{\partial H}\frac{d\lambda}{dM} = \frac{I_s\phi'(M)\lambda_c\psi'(M)}{F''(M)}. \qquad \ldots\ldots(12)$$

Equation (9) gives the reversible rate of change of intensity of magnetization with respect to stress under constant field conditions. The well known equality $\partial\lambda/\partial H = \partial I/\partial Z$ follows from a comparison of equations (9) and (12). $\partial\lambda/\partial Z$ given by equation (11) has the dimensions of compliance (inverse modulus of elasticity) and is the contribution to the total compliance of the material due to the influence of stress on the magnetic domain structure. The application of stress produces no change in the domain structure when the material is magnetically saturated, i.e. $\partial\lambda/\partial Z = 0$ and the compliance may be written $1/E_s$. In any magnetically non-saturated state the total compliance $1/E$ is thus the sum of $1/E_s$ and $\partial\lambda/\partial Z$. Hence

$$\frac{\partial\lambda}{\partial z} = \frac{1}{E} - \frac{1}{E_s} = \Delta\frac{1}{E}. \qquad \ldots\ldots(13)$$

Equations (9)–(12) may thus be written

$$\frac{\partial\lambda}{\partial H} = \frac{\partial I}{\partial Z} = I_s\lambda_c\frac{\phi'(M)\psi'(M)}{F''(M)} \qquad \ldots\ldots(9\,a),\ (12\,a)$$

$$\chi = I_s^2\frac{[\phi'(M)]^2}{F''(M)} \qquad \ldots\ldots(10\,a)$$

$$\Delta\frac{1}{E} = \lambda_c^2\frac{[\psi'(M)]^2}{F''(M)}. \qquad \ldots\ldots(11\,a)$$

In order to apply these results to specific cases it is necessary to evaluate the functions $\phi'(M)$, $\psi'(M)$ and $F''(M)$ for the domain processes involved and then average the expressions to take account of the domain distribution. It has been assumed that the stress is uniform throughout the specimen; the consequences of the alternative assumption of uniform strain have been fully discussed by Becker and Döring (1939) who have also derived a correction factor for the value of $\Delta(1/E)$ in elastically anisotropic materials.

The following two sections are concerned with the substitutions into the general equations which are required to derive values of χ and $\Delta(1/E)$ for particular domain processes.

§ 3. ROTATIONAL PROCESSES

For processes involving the rotation of magnetization vectors the parameter M of the general equations is the angle θ between a domain vector and the common axis of applied field, stress and measurement.

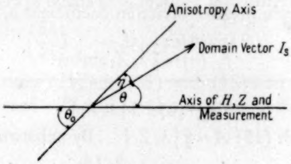

Figure 1.

If, as shown in figure 1, a domain vector has been displaced through an angle η from an anisotropy axis which makes an angle θ_0 with the measuring direction, then $\theta = \theta_0 - \eta$ and $d\theta = -d\eta$. Equation (1) becomes $I = I_s \cos\theta$ and hence

$$\phi'(\theta) = \frac{1}{I_s}\frac{dI}{d\theta} = -\sin\theta.$$

If the magnetostriction can be expressed in terms of a single magnetostrictive coefficient λ_c equation (2) becomes $\lambda = \frac{3}{2}\lambda_c(\cos^2\theta - \frac{1}{3})$ and hence

$$\psi'(\theta) = \frac{1}{\lambda_c}\frac{d\lambda}{d\theta} = -3\sin\theta\cos\theta. \qquad \ldots\ldots(14)$$

It is convenient to proceed to equations characterizing the rotational process, without specifying the origin of the anisotropy energy involved, by writing

$$f_A''(\eta = 0) = 2A. \qquad \ldots\ldots(15)$$

This corresponds to uniaxial anisotropy of the form $f_A(\eta) = A\sin^2\eta$. The equations for special cases can then be conveniently obtained by comparison of the appropriate values of $f_A''(\eta = 0)$ with equation (15).

Considering only the unmagnetized and remanent states for which $H \to 0$, $\theta \to \theta_0$ and $\eta \to 0$ equations (10 *a*) and (11 *a*) give

$$\chi_{H\to 0, Z=0} = I_s^2\frac{[\phi'(0)]^2}{f_A''(0)} = \frac{I_s^2\sin^2\theta_0}{2A} \qquad \ldots\ldots(16)$$

$$\left(\Delta\frac{1}{E}\right)_{H=0, Z\to 0} = \lambda_c^2\frac{[\psi'(0)]^2}{f_A''(0)} = \frac{9\lambda_c^2\sin^2\theta_0\cos^2\theta_0}{2A}. \qquad \ldots\ldots(17)$$

For an assembly of domains it is necessary to average the trigonometrical terms to take account of the distribution of preferred axes of the magnetization vectors. In a polycrystalline specimen having no preferred crystallographic orientation of the crystallites, θ_0 is uniformly distributed over a complete sphere when the specimen is unmagnetized, whereas at remanence the distribution is over a hemisphere. The mean values of $\sin^2\theta_0$ and $\sin^2\theta_0\cos^2\theta_0$ for these two cases are given in the Appendix. Distinguishing values in the unmagnetized and remanent states by 0 and R and substituting into (16) and (17):

$$\chi_0=\chi_R=\frac{I_s^2}{3A} \qquad \ldots\ldots(18)$$

$$\left(\Delta\frac{1}{E}\right)_0=\left(\Delta\frac{1}{E}\right)_R=\frac{3\lambda_c^2}{5A}. \qquad \ldots\ldots(19)$$

The ratio $\chi_0/[\Delta(1/E)]_0$ is thus independent of the anisotropy coefficient.

3.1. *Rotations against Anisotropy due to High Internal Stress*

Kersten (1931) showed that under high internal stress the strain energy density, for material with isotropic magnetostriction coefficient λ_s and internal stress Z_i is given by

$$f_{Z_i}(\eta)=\tfrac{3}{2}\lambda_s Z_i\sin^2\eta.$$

Hence

$$f_{Z_i}''(0)=3\,|\lambda_s Z_i|$$

and by comparison with (15) $A=\frac{3}{2}|\lambda_s Z_i|$. By substitution into (18) and (19)

$$\chi_0=\chi_R=\frac{2}{9}\frac{I_s^2}{\lambda_s Z_i} \qquad \ldots\ldots(20)$$

$$\left(\Delta\frac{1}{E}\right)_0=\left(\Delta\frac{1}{E}\right)_R=\frac{2}{5}\frac{\lambda_s}{Z_i} \qquad \ldots\ldots(21)$$

which are the equations derived by Kersten. The essential feature of the model is that a type of anisotropy exists, *postulated* to be due to high internal stress, which does not permit movement of domain boundary walls but does permit rotation of domain magnetization vectors.

3.2. *Rotations against Magnetocrystalline Anisotropy*

Magnetocrystalline anisotropy energy may result in: (*a*) a single preferred axis as in cobalt; (*b*) three preferred [100]-type axes, as in iron; (*c*) four preferred [111] axes, as in nickel.

For each case $f''(\eta)$ and $\psi'(\theta_0-\eta)$ are evaluated below; η is the polar angle between a preferred axis and the domain magnetization vector, θ_0 is the angle between the preferred axis and the direction of measurement.

(*a*) *Uniaxial magnetocrystalline anisotropy*.

In this case the anisotropy energy density can be written

$$f_u(\eta)=K_1\sin^2\eta+\text{higher order terms}$$

(Becker and Döring 1939), and K_1 replaces A in equations (15)–(19).

If the magnetostriction can be represented by a single constant formula $\lambda=\frac{3}{2}\lambda_c[\cos^2(\theta_0-\eta)-\frac{1}{3}]$ and

$$\left(\frac{\partial\lambda}{\partial\eta}\right)_{\eta=0}=3\lambda_c\sin\theta_0\cos\theta_0 \qquad \ldots\ldots(22)$$

and the magnetostriction coefficient in equations (15)–(19) remains λ_c.

Mason (1954) has derived an equation for the magnetostriction of uniaxial crystals in terms of four coefficients λ_A, λ_B, λ_C and λ_D. This equation may be expressed in terms of the angles η and θ_0, defined above, and by differentiation it is found that

$$\left(\frac{\partial\lambda}{\partial\eta}\right)_{\eta=0} = (4\lambda_D - \lambda_A - \lambda_C)\sin\theta_0\cos\theta_0 . \qquad \ldots\ldots(23)$$

Comparison of equations (22) and (23) leads to $\lambda_c = \frac{1}{3}(4\lambda_D - \lambda_A - \lambda_C)$.

(*b*) *Positive cubic magnetocrystalline anisotropy.*

Kittel (1949) has derived an expression for the anisotropy energy in terms of the polar angle η and an azimuthal angle ξ, both referred to the preferred [100]-type directions

$$f_{c+}(\eta) = K_1(\sin^2\eta - \tfrac{7}{8}\sin^4\eta - \tfrac{1}{8}\sin^4\eta\cos^4\eta\cos 4\xi)$$

giving

$$f_{c+}''(\eta=0) = 2K_1 . \qquad \ldots\ldots(24)$$

Writing the two-constant equation for the magnetostriction of cubic crystals (Becker and Döring 1939) in terms of θ_0, η and ξ and differentiating

$$\left(\frac{\partial\lambda}{\partial\eta}\right)_{\eta=0} = 3\lambda_{111}\sin\theta_0\cos\theta_0 . \qquad \ldots\ldots(25)$$

Comparison of equations (24) and (25) with (15) and (14) respectively shows that for this particular case $A = K_1$ and $\lambda_c = \lambda_{111}$ are the coefficients to be substituted into equations (16)–(19).

(*c*) *Negative cubic magnetocrystalline anisotropy.*

When K_1 is negative the cube diagonal, [111] direction, is the preferred axis from which the angles η and θ_0 are measured. The azimuthal angle ξ is again referred to a cube edge.

The anisotropy energy, given by Kittel (1949), is

$$f_{c-}(\eta) = K_1\left(\tfrac{1}{3}\cos^4\eta + \tfrac{1}{4}\sin^4\eta - \frac{\sqrt{2}}{3}\cos\eta\sin^3\eta\cos 3\xi\right)$$

giving

$$f_{c-}''(\eta=0) = -\tfrac{4}{3}K_1. \qquad \ldots\ldots(26)$$

The two-constant magnetostriction equation in this case gives

$$\left(\frac{\partial\lambda}{\partial\eta}\right)_{\eta=0} = (2\lambda_{100} + \lambda_{111})\sin\theta_0\cos\theta_0 + \frac{1}{\sqrt{2}}(\lambda_{100} - \lambda_{111})\sin^2\theta_0\cos 3\xi . \qquad \ldots\ldots(27)$$

Equation (27) contains an additional term in $\sin^2\theta_0$ and therefore the direct comparison with (14) adopted in (*a*) and (*b*) above is not possible. For this case it is necessary to return to the general equations (9 *a*)–(12 *a*) and substitute the values of $\phi'(\eta)$, $\psi'(\eta)$ and $F''(\eta)$. Hence it is found that χ is given by (16) and (18) with $A = -\frac{2}{3}K_1$ and the values of $\Delta(1/E)$ by (17) and (19) with $A = -\frac{2}{3}K_1$ and $\lambda_c = \frac{1}{3}[(2\lambda_{100} + \lambda_{111})^2 + (\lambda_{100} - \lambda_{111})^2]^{1/2}$.

§ 4. BOUNDARY MOVEMENT PROCESSES

4.1. *Stability of Domain Boundaries*

The equilibrium position and stability of a boundary wall separating domains magnetized along different crystallographic axes depend on a number of factors. The positional energy of a domain boundary wall cannot be calculated except in simple, rather idealized cases. For the present purposes the positional energy will be written as $f(x)$ without specifying its origin.

For a material characterized by high uniaxial magnetocrystalline anisotropy there are only 180° boundaries. Powder pattern studies of cobalt show that even in the fine structure associated with free surfaces the volume occupied by 90° domains is vanishingly small. Iron, with [100]-type preferred axes, has 180° and 90° boundaries. The ratio of the areas of the two types of walls depends on the sizes and shapes of the crystals, on internal strain and structural inhomogeneity. If the magnetocrystalline anisotropy energy has minimum values along [111] axes, as in nickel, 180°, 109° and 71° boundary walls exist.

The contributions of the different types of boundary wall movement to the ΔE effect and susceptibility are now examined.

4.2. 180° *Boundary Movement*

Consider two domains magnetized in antiparallel directions, with their magnetization vectors inclined at angles θ and $\theta-\pi$ to the direction of applied field, stress and measurement (figure 2).

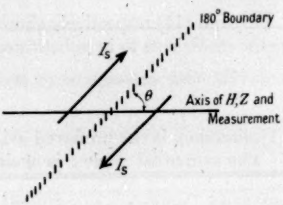

Figure 2.

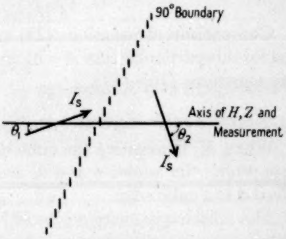

Figure 3.

The change of magnetization resolved along the measuring direction dI for a displacement dx of the boundary wall perpendicular to its plane is

$$dI = 2I_s \cos\theta\, S_{180}\, dx$$

and

$$\phi'(x) = \frac{1}{I_s}\frac{dI}{dx} = 2\cos\theta\, S_{180} \qquad \ldots\ldots(28)$$

where S_{180} denotes the area of 180° boundary wall per unit volume.

Magnetostriction depends only on domain orientation and is independent of sense. Hence

$$\psi'(x) = \frac{1}{\lambda_c}\frac{d\lambda}{dx} = 0 \quad \text{and} \quad \left(\Delta\frac{1}{E}\right)_{180} = 0.$$

The second derivative of the positional energy of a 180° wall may be written as $f_{180}''(x)$ and substitution into equation (10) gives χ in terms of θ. When $H=Z=0$ both vectors lie along the direction of the common anisotropy axis and $\theta=\theta_0$. Thus

$$\chi_0 = \frac{4I_s^2\cos^2\theta_0 S_{180}^2}{f_{180}''(0)}. \qquad \ldots\ldots(29)$$

For a random distribution of preferred axes $\cos^2\theta_0$ is $\frac{1}{3}$ (see Appendix) and hence for a polycrystalline material with no crystallographic texture

$$\chi_0 = \frac{4I_s^2 S_{180}^2}{3f_{180}''(0)}. \qquad \ldots\ldots(30)$$

4.3. 90° *Boundary Movement*

Magnetostatic and magnetostrictive strain energies are minimized if the geometry of 90° boundaries is such that the normal component of magnetization and the tangential component of magnetostrictive deformation are continuous through the boundary. Both these conditions are satisfied in the domain geometry indicated in figure 3. For materials in which the preferred directions are [111] axes 180°, 109° and 71° boundary walls occur. It will be assumed that the behaviour of an assembly of domains with 71° and 109° boundaries is similar to one having an equal area of 90° boundaries.

Let the direction cosines of the magnetization vectors of a pair of domains, referred to the direction of measurement, be γ_1 and γ_2 respectively. Then a normal displacement dx of the plane boundary wall between the domains will result in a change of magnetization dI along the measuring direction where

$$dI = I_s\gamma_1 S_{90}\,dx - I_s\gamma_2 S_{90}\,dx$$

therefore

$$\phi'(x) = \frac{1}{I_s}\frac{dI}{dx} = S_{90}(\gamma_1 - \gamma_2) \qquad \ldots\ldots(31)$$

where S_{90} is the area of 90° boundary per unit volume of material.

The two-constant equation for the magnetostriction of cubic crystals, for the case when the domain vector is confined to a preferred direction, reduces to $\lambda = \frac{3}{2}\lambda_p(\gamma^2 - \frac{1}{3})$ where λ is the magnetostrictive deformation along the measuring axis and $\lambda_p = \lambda_{100}$ or λ_{111} for preferred axes in [100]-type and [111] directions respectively.

The change of magnetostrictive deformation of a domain resulting from a normal displacement dx of a plane boundary is

$$\begin{aligned} d\lambda &= \lambda \times \text{(fractional change in length of domain)} \\ &= \lambda \times \text{(fractional change in volume of domain)} \\ &= \lambda \,.\, S_{90}dx. \end{aligned}$$

For a pair of domains having magnetization vectors with direction cosines γ_1 and γ_2 with respect to the direction of measurement the change of magnetostrictive deformation will be $S_{90}\,dx(\lambda_1 - \lambda_2)$ and hence

$$\psi'(x) = \frac{1}{\lambda_p}\frac{d\lambda}{dx} = \frac{3}{2}(\gamma_1^2 - \gamma_2^2)S_{90}. \qquad \ldots\ldots(32)$$

The second derivative of the positional energy of the 90° boundary wall is written as $f_{90}''(x)$ and substitution in equations (10 *a*) and (11 *a*) gives

$$\chi_{H\to 0} = \frac{I_s^2 S_{90}^2}{f_{90}''(0)}(\gamma_1 - \gamma_2)^2 \qquad \ldots\ldots(33)$$

$$\left(\Delta\frac{1}{E}\right)_{H=0} = \frac{9\lambda_p^2 S_{90}^2}{4f_{90}''(0)}(\gamma_1^2 - \gamma_2^2)^2. \qquad \ldots\ldots(34)$$

Average values of the trigonometrical functions in the unmagnetized state have been calculated by Becker and Döring (1939) for particular crystal orientations and for polycrystalline materials. When the preferred axes are [100]-type

$$\chi_{100}=\chi_{110}=\chi_{111}=\chi_0=\frac{2I_s^2S_{90}^2}{3f_{90}''(0)} \qquad \text{......(35)}$$

$$\left.\begin{aligned} \left(\Delta\frac{1}{E}\right)_{100} &= \frac{3\lambda_{100}^2S_{90}^2}{2f_{90}''(0)} \\ \left(\Delta\frac{1}{E}\right)_{110} &= \frac{3\lambda_{100}^2S_{90}^2}{8f_{90}''(0)} \\ \left(\Delta\frac{1}{E}\right)_{111} &= 0. \end{aligned}\right\} \qquad \text{......(36)}$$

For a polycrystalline specimen $[\Delta(1/E)]_0$ may be obtained by averaging equation (36) assuming a random distribution of crystallographic axes. Hence

$$\left(\Delta\frac{1}{E}\right)_0 = \frac{3\lambda_{100}^2S_{90}^2}{5f_{90}''(0)}. \qquad \text{......(37)}$$

For a material characterized by [111] preferred axes

$$\left(\Delta\frac{1}{E}\right)_0 = \frac{8\lambda_{111}^2S_{90}^2}{15f_{90}''(0)}. \qquad \text{......(38)}$$

In both cases the ratio $\chi_0/[\Delta(1/E)]_0$ is independent of S_{90} and $f_{90}''(0)$. This ratio together with equations (36), (37) and (38) may have to be corrected for elastic anisotropy as indicated in § 2.

§ 5. ANALYSIS OF EXPERIMENTAL DATA

For convenience in their application to experimental data the relevant functions and results discussed in preceding sections are summarized in table 1. The suffixes used below to characterize the various types of magnetization processes are also given in this table.

When a magnetic field or an external stress is applied to a ferromagnetic material several domain processes may occur. The experimentally observed effects are summations of several contributing processes and the object of the analyses given below is to break down the observed effects into their several components. As examples, we consider first the experimental data for annealed cobalt (§ 6). Cobalt in the hexagonal phase is characterized by high uniaxial magnetocrystalline anisotropy and magnetization proceeds by 180° boundary movement and rotation of domain magnetization vectors away from the anisotropy axis. The ΔE effect arises entirely from rotation processes.

In cubic materials, with magnetocrystalline anisotropy energy greater than internal strain energy, 180° and 90° boundary movement and rotation of domain magnetization vectors all occur. By considering each component in turn and calculating the magnitude of their effects from the formulae in table 1 the relative importance of the three magnetization processes may be estimated. As a second example of the application of the results established above we analyse the experimental results for annealed nickel (§ 7).

Table 1. Formulae for Susceptibility and $\Delta(1/E)$ for Unmagnetized State

Process	Text Ref. and Suffix		Orientation θ_0		Isotropic Distribution		
			χ_0	$[\Delta(1/E)]_0$	χ_0	$[\Delta(1/E)]_0$	$\dfrac{\chi_0}{[\Delta(1/E)]_0}$
Rotations against							
Uniaxial Strain Anisotropy	§ 3·1	rz	$\dfrac{I_S^2 s^2}{3\lambda_S Z_1}$	$\dfrac{3\lambda_S s^2 c^2}{Z_1}$	$\dfrac{2I_S^2}{9\lambda_S Z_1}$	$\dfrac{2\lambda_S}{5Z_1}$	$\dfrac{5I_S^2}{9\lambda_S^2}$
Uniaxial Magnetocrystalline Anisotropy	§ 3·2 (*a*)	ru	$\dfrac{I_S^2 s^2}{2K}$	$\dfrac{9\lambda_C^2 s^2 c^2}{2K}$	$\dfrac{I_S^2}{3K}$	$\dfrac{3\lambda_C^2}{5K}$	$\dfrac{5I_S^2}{9\lambda_C^2}$
Positive Cubic Anisotropy	§ 3·2 (*b*)	rc+	$\dfrac{I_S^2 s^2}{2K_1}$	$\dfrac{9\lambda_{111}^2 s^2 c^2}{2K_1}$	$\dfrac{I_S^2}{3K_1}$	$\dfrac{3\lambda_{111}^2}{5K_1}$	$\dfrac{5I_S^2}{9\lambda_{111}^2}$
Negative Cubic Anisotropy	§ 3·2 (*c*)	rc−	$\dfrac{3I_S^2 s^2}{4\|K_1\|}$	$\dfrac{27\lambda_C^2 s^2 c^2}{4\|K_1\|}$	$\dfrac{I_S^2}{2\|K_1\|}$	$\dfrac{9\lambda_C^2}{10\|K_1\|}$	$\dfrac{5I_S^2}{9\lambda_C^2}$
Boundary Wall Movement							
180° Boundaries	§ 4·2	180	$\dfrac{4I_S^2 S_{180}^2 c^2}{f_{180}''(0)}$	0	$\dfrac{4I_S^2 S_{180}^2}{3f_{180}''(0)}$	0	—
90° Boundaries	§ 4·3	90	$\dfrac{I_S^2 S_{90}^2(\gamma_1-\gamma_2)^2}{f_{90}''(0)}$	$\dfrac{9\lambda_{100}^2 S_{90}^2(\gamma_1^2-\gamma_2^2)^2}{4f_{90}''(0)}$	$\dfrac{2I_S^2 S_{90}^2}{3f_{90}''(0)}$	$\dfrac{3\lambda_{100}^2 S_{90}^2}{5f_{90}''(0)}$	$\dfrac{10I_S^2}{9\lambda_{100}^2}$
71° and 109° Boundaries	§ 4·3	90	$\dfrac{Is^2 S_{90}^2(\gamma_1-\gamma_2)^2}{f_{90}''(0)}$	$\dfrac{9\lambda_{111}^2 S_{90}^2(\gamma_1^2-\gamma_2^2)^2}{4f_{90}''(0)}$	$\dfrac{2I_S^2 S_{90}^2}{3f_{90}''(0)}$	$\dfrac{8\lambda_{111}^2 S_{90}^2}{15f_{90}''(0)}$	$\dfrac{5I_S^2}{4\lambda_{111}^2}$

Notes on Table.

θ_0 = angle between the preferred axis and the axis of measurement. $s = \sin\theta_0$, $c = \cos\theta_0$. γ_1, γ_2—direction cosines defined in § 4.3.

λ_S = isotropic magnetostriction coefficient (§ 3.1). λ_{100}, λ_{111}—magnetostriction coefficients for cubic crystals.

$\lambda_C = \frac{1}{3}(4\lambda_D - \lambda_A - \lambda_C)$ for uniaxial crystals (§ 3.2 (*a*)).

$= \frac{1}{3}[(2\lambda_{100}+\lambda_{111})^2 + (\lambda_{100}-\lambda_{111})^2]^{1/2}$ for cubic crystals with negative anisotropy coefficient (§ 3.2 (*c*)).

S = areas of boundary wall per unit volume. K – anisotropy coefficients. I_S – spontaneous intensity of magnetization.

$f''(0)$ are functions defined in the text.

§ 6. MAGNETOELASTIC PROPERTIES OF ANNEALED COBALT

Street (1948) and Lee (1952) have measured the ΔE effect, magnetostriction and magnetization curves of a specimen of cobalt, annealed at 700°c for 1 hour *in vacuo*. The intensity of magnetization initially increases relatively rapidly with applied field up to about one third of saturation, but the corresponding changes of Young's modulus and magnetostriction are only about 5% of their maximum values. In this region magnetization is almost entirely due to 180° boundary wall movement.

The main contribution to the initial susceptibility is χ_{180}, from 180° boundary movement. There will also be contributions to the susceptibility and to the ΔE effect due to rotation against magnetocrystalline anisotropy forces; these may be calculated using the formulae of table 1. With $K_1 = 4 \times 10^6 \,\mathrm{erg\,cm^{-3}}$ and $I_s = 1430$ c.g.s. units and assuming a random distribution of preferred axes $\chi_{\mathrm{ru}} = I_s^2/3K_1 = 0{\cdot}2$. The observed value of susceptibility is 6·5 and hence $\chi_{180} = \chi_{\mathrm{obs}} - \chi_{\mathrm{ru}} = 6{\cdot}3$. It is not possible to calculate this value directly since both S_{180} and $f_{180}''(0)$ are unknown.

The ΔE effect in cobalt must be entirely due to rotation of domain magnetization vectors for which $[\Delta(1/E)]_{\mathrm{ru}} = 3\lambda_c^2/5K_1$. The observed value of $[\Delta(1/E)]_0 = 35 \times 10^{-16} \,\mathrm{cm^2\,dyn^{-1}}$ and by substitution it follows that the magnetostrictive coefficient $\lambda_c = \pm 150 \times 10^{-6}$. In § 3.2 it is shown that

$$\lambda_c = \tfrac{1}{3}(4\lambda_D - \lambda_A - \lambda_C)$$

and substituting values determined by Bozorth (1954): $\lambda_A = -45 \times 10^{-6}$, $\lambda_C = 110 \times 10^{-6}$ and $\lambda_D = -100 \times 10^{-6}$ we find $\lambda_c = -155 \times 10^{-6}$ in excellent agreement with the value deduced from the ΔE effect data.

§ 7. MAGNETOELASTIC PROPERTIES OF ANNEALED NICKEL

The ΔE effect and initial susceptibility of nickel have been measured many times and the recorded values vary over wide ranges, even for specimens subjected to similar heat treatment. It is a well established fact that the structure dependent magnetic properties of annealed nickel particularly are extremely sensitive to mechanical treatment but the reasons for this have not been fully considered. The order of magnitude of internal strain energy density is given by $\lambda_s Z_i$. For annealed nickel the internal stress may be about $1 \,\mathrm{kg\,mm^{-2}}$ which gives an internal strain energy of approximately $4 \times 10^3 \,\mathrm{erg\,cm^{-3}}$, a value which is about one tenth of the magnetocrystalline anisotropy energy density at room temperature. It is therefore likely that in annealed nickel the preferred directions of magnetization are not significantly affected by internal stress. In any case variation of internal stress from one specimen to another cannot directly account for the observed variations in $\Delta E/E_0$ and χ_0. For example, Siegel and Quimby (1936) found $\Delta E/E_0 = 6{\cdot}7\%$ for annealed nickel with $\chi_0 = 24$ whereas Köster (1943) gives $\Delta E/E_0 = 20{\cdot}2\%$ and $\chi_0 = 15{\cdot}6$.

Analysis of the experimental values of $[\Delta(1/E)]_0$ and χ_0 makes it possible to determine the relative importance of the various types of domain process occurring in the initial stage of magnetization. The experimental data for annealed nickel are given in table 2 together with an analysis of the initial susceptibility into the three components $\chi_{\mathrm{rc}-}$, χ_{90} and χ_{180}. (As explained in § 4.3 it is assumed that the behaviour of an assembly of domains having 71° and 109° boundary walls is the same as one having an equal area of 90° boundary walls.) The first step in the analysis is the calculation of χ_{rc-}, $[\Delta(1/E)]_{rc-}$ and the ratio $\chi_{90}/[\Delta(1/E)]_{90}$, using the constants: $I_s = 490$ c.g.s. units, $K_1 = -59 \times 10^3\,\mathrm{erg\,cm^{-3}}$ (Bozorth and Walker 1953), $\lambda_{111} = -26 \times 10^{-6}$, $\lambda_{100} = -45 \times 10^{-6}$ (Bozorth and Hamming 1953) and hence $|\lambda_c| = \frac{1}{3}[(2\lambda_{100}+\lambda_{111})^2 + (\lambda_{100}-\lambda_{111})^2]^{1/2} = 39 \times 10^{-6}$. From the formulae in table 1, $\chi_{rc-} = 2$, $[\Delta(1/E)]_{rc-} = 230 \times 10^{-16}\,\mathrm{cm^2\,dyn^{-1}}$ and using a correction factor for elastic anisotropy of 1·8 (calculated from data given by Bozorth, Mason and McSkimin 1951) $\chi_{90} = 0{\cdot}025[\Delta(1/E)]_{90}$.

Table. 2. Magnetic and Magnetoelastic Properties of Annealed Nickel

Specimen Reference	Treatment	$[\Delta(1/E)]_{obs}$	$[\Delta(1/E)]_{90}$	χ_{obs}	χ_{rc-}	χ_{90}	χ_{180}
		($\mathrm{cm^2dyn^{-1}} \times 10^{-16}$)					
1	Slow Cool	760	530	20	2	13	5
2	Anneal in Hydrogen at 1100°c	300	70	24	2	2	20
3	700°c Anneal	300	70	6·5	2	2	2·5
4	700°c Anneal	410	180	6	2	4·5	0
5	900°c Anneal	600	370	8·2	2	9	0
6	1100°c Anneal	735	505	11·2	2	12	0
7	1300°c Anneal	880	650	15·6	2	16	0
8	1050°c Anneal	950	720	27	2	18	6

References. 1. Nakamura (1935). 2. Siegel and Quimby (1936), Kirkham (1937). 3. Engler (1938). 4–7. Köster (1943). 8. Bozorth, Mason and McSkimin (1951).

The methods of calculation are given in the text.

It will be noted that the observed values of $\Delta(1/E)$ given in table 2 are in each case greater than $230 \times 10^{-16}\,\mathrm{cm^2\,dyn^{-1}}$. Since only rotational processes and 90° wall movement contribute to the ΔE effect it follows that for each specimen

$$\left(\Delta\frac{1}{E}\right)_{90} = \left(\Delta\frac{1}{E}\right)_{obs} - \left(\Delta\frac{1}{E}\right)_{rc-}.$$

The values of $[\Delta(1/E)]_{90}$ so derived are given in table 2 and from them are calculated χ_{90}. Finally, $\chi_{180} = \chi_{obs} - \chi_{90} - \chi_{rc-}$.

The most significant feature of the analysis is that the ratio of the areas of the 90° and 180° boundary walls, as indicated by χ_{90}/χ_{180}, varies considerably. Specimens 4–7 contain very few 180° boundaries and it appears that the effect of progressively higher annealing temperatures eases 90° boundary wall movement, presumably by internal strain relief. Specimens 1 and 8 have a higher proportion of 180° boundaries and specimen 2, which is recorded as having a grain size of approximately 400μ, has a preponderance of 180° boundaries. The high value of initial susceptibility of these three specimens show that boundary wall movement is unrestricted suggesting that the heat treatment has assisted the growth of large homogeneous crystallites free from strain and impurities. A simple primary domain structure has been established which, as predicted by Néel (1944), contains mainly 180° boundaries. We believe that the more irregular domain structure containing many 71° and 109° boundaries which is characteristictic of the other specimens is due to the presence of impurity and strain centres.

The lack of uniform correlation between the observed values of χ_0 and $[\Delta(1/E)]_0$ is thus due to differences in the domain structure of the various specimens in the demagnetized state. The actual domain structure obtained depends critically on the preparation and heat treatment of the specimen.

Siegel and Quimby (1936), Kirkham (1937) and Köster (1943) have all measured the ΔE effect and initial susceptibility of annealed nickel specimens over a wide temperature range. Values of I_s, K_1 and λ_s as functions of temperature are also available but the single crystal magnetostrictive coefficients have only been measured at room temperature. A complete analysis of the ΔE effect data cannot therefore be attempted but it is possible to discuss the influence of temperature on magnetization processes in general terms; details, particularly of the relative importance of 90° and 180° boundary wall movements, are necessarily lacking.

At temperatures above about 200°c the magnetocrystalline anisotropy energy of nickel is very low and the observed values of $[\Delta(1/E)]_0$ and χ_0 are less than the calculated values of $[\Delta(1/E)]_{\mathrm{rc}}$ and χ_{rc}. This shows that for these temperatures the magnetocrystalline energy is smaller than the internal strain energy and that χ and $\Delta(1/E)$ are both due to rotation of domain magnetization vectors against internal strain energy. The internal stress Z_i calculated from $[\Delta(1/E)]_{\mathrm{rz}}$ is found to be independent of temperature.

As already discussed, at room temperature $[\Delta(1/E)]_{\mathrm{obs}} > [\Delta(1/E)]_{\mathrm{rc}-}$ which shows that boundary movements occur and magnetocrystalline anisotropy energy now outweighs internal strain energy. Below room temperature K_1 increases still further $[\Delta(1/E)]_{\mathrm{rc}-}$ is reduced and $\chi_{\mathrm{rc}-}$ becomes negligibly small.

For a given specimen the magnetocrystalline and internal strain anisotropy energies will be equal at a temperature T_0 lying between 200°c and room temperature. At temperatures below T_0 initial magnetization will proceed mainly by boundary wall movement, above T_0 rotations against internal strain anisotropy will be dominant. Köster's results (1943) show, as is to be expected, that the transition temperature depends on the preparation and heat treatment of the specimen.

§ 8. Reversible Domain Processes at Non-zero magnetization

It would be of obvious value if the type of analysis illustrated above for the unmagnetized state could be carried out at other states of magnetization. Although there is no difficulty in measuring χ and E as functions of magnetization, difficulties do arise in the interpretation of the results:

(*a*) Due to eddy current shielding, the modulus of an electrically conducting specimen, measured by the usual dynamic methods, is no longer that appropriate to constant H conditions but approximates more closely to constant B conditions. Correction of the measured value to constant H is possible in principle but may be inaccurate.

(*b*) $f_{\mathrm{A}}''(\eta)$ for magnetocrystalline anisotropy can readily be evaluated for $H=0$ and $\eta=0$ but the corresponding term $f_{\mathrm{A}}''(\eta)-H\phi''(\eta)$ for $H\neq 0$ can only be determined if η is known; η in turn depends on the orientation of the domain.

(*c*) The greatest difficulty arises at that stage of the calculation where expressions for χ and $\Delta(1/E)$ for domains of a particular orientation must be averaged to take account of all domains. Unless some assumption is made about the domain distribution no calculation is possible. Moreover, agreement of calculated and observed values is of little significance since different assumed distributions or domain mechanisms may lead to similar results.

ACKNOWLEDGMENTS

The majority of the work reported here was carried out when the authors were members of the Department of Physics, University of Nottingham. Their thanks are due to Professor L. F. Bates for his encouragement and the provision of laboratory facilities.

APPENDIX

The average value of a function $f(\theta)$, where θ is a polar angle with respect to a given axis, for a uniform distribution of vectors within a solid angle limited by $\theta = \theta_m$ is given by

$$\overline{f(\theta)} = \frac{2\pi \int_0^{\theta_m} f(\theta) \sin\theta \, d\theta}{2\pi \int_0^{\theta_m} \sin\theta \, d\theta}.$$

For convenience the values of $\overline{f(\theta)}$ for the functions involved in the text are given below in terms of $s = \sin\theta_m$ and $c = \cos\theta_m$.

		Values of $\overline{f(\theta)}$ for θ_m		
$f(\theta)$	$\overline{f(\theta)}$	$=0$	$=\pi/2$	$=\pi$†
$\cos^2\theta$	$\frac{1}{3}(1+c+c^2)$	1	1/3	1/3
$\sin^2\theta$	$\frac{1}{3}(2-c^2-c^3)$	0	2/3	2/3
$\sin^2\theta\cos^2\theta$	$\frac{1}{15}\,\frac{2-2c^3-3s^2c^3}{1-c}$	0	2/15	2/15
$\sin^4\theta$	$\frac{1}{15}\,\frac{8-c(3s^4+4s^2-8)}{1-c}$	0	8/15	8/15

† $\theta_m = \pi$ corresponds to the case of an isotropic distribution of vectors.

REFERENCES

AKULOV, N., 1933, *Z. Phys.*, **85**, 661.
BECKER, R., and DÖRING, W., 1939, *Ferromagnetismus* (Berlin : Springer).
BOZORTH, R. M., 1954, *Phys. Rev.*, **96**, 311.
BOZORTH, R. M., and HAMMING, R. W., 1953, *Phys. Rev.*, **89**, 865.
BOZORTH, R. M., MASON, W. P., and MCSKIMIN, H. J., 1951, *Bell Syst. Tech. J.*, **30**, 970.
BOZORTH, R. M., and WALKER, J. G., 1953, *Phys. Rev.*, **89**, 624.
BROWN, W. F., 1936, *Phys. Rev.*, **50**, 1165 ; 1937, *Ibid.*, **52**, 325.
ENGLER, O., 1938, *Ann. Phys., Lpz.*, **31**, 145.
KERSTEN, M., 1931, *Z. Tech. Phys.*, **12**, 665 ; 1932, *Z. Phys.*, **76**, 505 ; 1933, *Z. Phys.*, **82**, 723 ; 1956, *Z. angew. Phys.*, **8**, 313.
KIRKHAM, D., 1937, *Phys. Rev.*, **52**, 1162.
KITTEL, C., 1949, *Rev. Mod. Phys.*, **21**, 541.
KÖSTER, W., 1943, *Z. Metallk.*, **35**, 57, 68, 194, 246.
LEE, E. W., 1952, *Thesis*, University of Nottingham.
MASON, W. P., 1954, *Phys. Rev.*, **96**, 302.
NAKAMURA, K., 1935, *Z. Phys.*, **94**, 707.
NÉEL, L., 1944, *J. Phys. Radium*, **5**, 241.
SIEGEL, S., and QUIMBY, S. L., 1936, *Phys. Rev.*, **49**, 663.
STREET, R., 1948, *Proc. Phys. Soc.*, **61**, 391.
TAKAGI, M., 1939, *Sci. Rep. Tohoku Univ.*, **28**, 20.

The Amplification of a Magnetic Field by a High Current Discharge

By R. J. BICKERTON

Atomic Energy Research Establishment, Harwell, Berks.

Communicated by P. C. Thonemann; *MS. received* 9*th May* 1958

Abstract. A discharge in a longitudinal magnetic field in which the plasma pressure is balanced by electrodynamic forces is considered. It is shown that the resulting current flow is helical about the axis of the discharge. The direction of the helix is such that the initial longitudinal field is amplified inside the discharge channel. Some experimental evidence supporting the theory is presented.

§ 1. INTRODUCTION

THE behaviour of a high current gas discharge in an axial magnetic field is of interest because of the possibilities of producing very high plasma temperatures using such a system (Ware 1958, Tuck 1958, Thonemann 1958). The externally applied magnetic field is used to stabilize the discharge. The highly conducting plasma traps and compresses the axial field as it contracts under the influence of the self-magnetic field (Tayler 1957). Because of the finite conductivity of the plasma, such trapping and the resultant stability are essentially transient phenomena. In time the trapped magnetic field diffuses out of the plasma (Bickerton and London 1958). In this paper the final steady state distributions of magnetic field and current are calculated. The question of discharge stability is ignored.

§ 2. THEORY

A cylindrically symmetric discharge is considered in which all parameters are functions only of the distance r from the axis. It is supposed that the plasma is fully ionized and that recombination in the volume is negligible. An electric field Z is applied parallel to the axis of the discharge. The resistance to the motion of electrons is due entirely to Coulomb scattering by the positive ions. The transport coefficients for such a fully ionized gas in a magnetic field have been calculated (Landshoff 1949). The magnetic field lines resulting from the combination of the self-magnetic field and the externally applied axial field are helical about the axis of symmetry. Let the field B at the surface r make an angle θ with the z (axial) direction. Then, by summing the drift velocities due to the concentration gradient, electric fields and the temperature gradient, the three components of electron current density, j_ϕ, j_r and j_z, are obtained:

$$j_r = \frac{\boldsymbol{neD}}{\boldsymbol{c}}\left[\alpha_1\left(\frac{\boldsymbol{Re}}{\boldsymbol{k}T_e} + \frac{1}{n}\frac{dn}{dr}\right) + \alpha_2\frac{1}{T_e}\frac{dT_e}{dr} + \beta_1\frac{\boldsymbol{Ze}}{\boldsymbol{k}T_e}\sin\theta\right], \quad \ldots\ldots (1)$$

$$j_\phi = \frac{\boldsymbol{neD}}{\boldsymbol{c}}\left[-\alpha_1\frac{\boldsymbol{Ze}}{\boldsymbol{k}T_e}\sin\theta\cos\theta + 2\frac{\boldsymbol{Ze}}{\boldsymbol{k}T_e}\sin\theta\cos\theta + \beta_1\left(\frac{\boldsymbol{Re}}{\boldsymbol{k}T_e} + \frac{1}{n}\frac{dn}{dr}\right)\right.$$
$$\left. + \beta_2\frac{1}{T_e}\frac{dT_e}{dr}\cos\theta\right], \quad \ldots\ldots (2)$$

$$j_z = \frac{\boldsymbol{ne}D}{\boldsymbol{c}}\left[-\beta_1\left(\frac{R\boldsymbol{e}}{\boldsymbol{k}T_e}+\frac{1}{n}\frac{dn}{dr}\right)\sin\theta-\beta_2\frac{1}{T_e}\frac{dT_e}{dr}\sin\theta+\alpha_1\frac{Z\boldsymbol{e}}{\boldsymbol{k}T_e}\sin^2\theta\right.$$
$$\left.+2\frac{Z\boldsymbol{e}}{\boldsymbol{k}T_e}\cos^2\theta\right]. \qquad \ldots\ldots(3)$$

Here, n is the electron density, D is the electron diffusion coefficient ($=\tau\boldsymbol{k}T_e/\boldsymbol{m}$), τ is the mean electron–ion collision time, T_e is the electron temperature and the α's and β's are the coefficients calculated by Landshoff. R is the radial electric field, the result of charge separation. It is through this field that the pinch forces which act on the current-carrying electron gas are transferred to the heavy positive ions. We now assume that in the steady state $j_r=0$ and that $\omega\tau \gg 1$, where ω is the Larmor frequency of the electrons ($=\boldsymbol{e}B/\boldsymbol{mc}$). In the plasma where the magnetic forces are balanced by the plasma pressure, the first assumption is true in the sense that the radial drift current is at least one order of magnitude less than any of the single drifts summed in equation (1). The second assumption is valid in most experimental situations. When $\omega\tau \gg 1$ the Landshoff coefficients reduce to the following simple forms:

$$\alpha_1=\frac{1}{\omega^2\tau^2},\quad \alpha_2=-\frac{1}{2\omega^2\tau^2},\quad \beta_1=\frac{1}{\omega\tau},\quad \beta_2=\frac{1}{\omega\tau}. \qquad \ldots\ldots(4)$$

Substituting for these in equations (2) and (3) and eliminating R and dn/dr, we obtain the following:

$$j_\phi=\frac{\boldsymbol{ne}D}{\boldsymbol{c}}\left[\frac{Z\boldsymbol{e}}{\boldsymbol{k}T_e}\sin\theta\cos\theta+\frac{3\cos\theta}{2\omega\tau}\frac{1}{T_e}\frac{dT_e}{dr}\right], \qquad \ldots\ldots(5)$$

$$j_z=\frac{\boldsymbol{ne}D}{\boldsymbol{c}}\left[\frac{Z\boldsymbol{e}}{\boldsymbol{k}T_e}(1+\cos^2\theta)-\frac{3\cos\theta}{2\omega\tau}\frac{1}{T_e}\frac{dT_e}{dr}\right]. \qquad \ldots\ldots(6)$$

A positive value for j_ϕ indicates a paramagnetic effect, that is a rotational current in such a direction as to increase the axial component of magnetic field. A qualitative discussion of this effect has been given previously (Bezbachenko *et al.* 1956). It is now assumed that the thermal gradient terms are negligible, i.e. the plasma is isothermal to the extent that

$$\frac{1}{T_e}\frac{dT_e}{dr}<\frac{2}{3}\omega\tau\sin\theta\frac{Z\boldsymbol{e}}{\boldsymbol{k}T_e}. \qquad \ldots\ldots(7)$$

By substituting the components of the magnetic field B_0 and B_z for the trigonometric functions, the following is obtained:

$$j_z=\frac{\boldsymbol{ne}D}{\boldsymbol{c}}\frac{Z\boldsymbol{e}}{\boldsymbol{k}T_e}\left[1+\frac{B_z^2}{B_\phi^2+B_z^2}\right], \qquad \ldots\ldots(8)$$

$$j_\phi=\frac{\boldsymbol{ne}D}{\boldsymbol{c}}\frac{Z\boldsymbol{e}}{\boldsymbol{k}T_e}\left[\frac{B_\phi B_z}{B_\phi^2+B_z^2}\right]. \qquad \ldots\ldots(9)$$

From equation (8) it can be seen that when the current flow is entirely parallel to the magnetic field ($B_\phi=0$) the electrical conductivity of the plasma is $2\boldsymbol{ne}^2D/\boldsymbol{ck}T_e$; when it is entirely perpendicular to the field ($B_z=0$) the conductivity is $\boldsymbol{ne}^2D/\boldsymbol{ck}T_e$, i.e. half the previous value. This result has been obtained previously by a different method (Spitzer 1956).

In equilibrium the plasma pressure is balanced by the electrodynamic forces, so that

$$-\frac{d}{dr}n\boldsymbol{k}(T_{\rm e}+T_{\rm i})=j_zB_\phi-j_\phi B_z, \qquad \ldots\ldots(10)$$

where $T_{\rm i}$ is the temperature of the ions. Substitution for j_ϕ and j_z leads to

$$-\frac{d}{dr}n\boldsymbol{k}(T_{\rm e}+T_{\rm i})=\frac{n\boldsymbol{e}^2D}{\boldsymbol{ck}T_{\rm e}}ZB_\phi. \qquad \ldots\ldots(11)$$

The term $Zn\boldsymbol{e}^2D/\boldsymbol{ck}T_{\rm e}$, which is the axial current density when $B_z=0$, is less than the actual current density when $B_z\neq 0$ (see equation (8)). This is because some of the inward pinch forces due to the axial current are then taken up in opposing the radial gradient of B_z.

The equations (8) and (9) for the current densities may be supplemented by Maxwell's equations. With cylindrical symmetry

$$j_z=\frac{1}{4\pi}\left[\frac{dB_\phi}{dr}+\frac{B_\phi}{r}\right], \qquad \ldots\ldots(12)$$

$$j_\phi=-\frac{1}{4\pi}\frac{dB_z}{dr}. \qquad \ldots\ldots(13)$$

Eliminating the current densities from (8), (9), (12), and (13) and putting into dimensionless form, we obtain two differential equations:

$$\frac{d\xi}{d\eta}=\frac{2\zeta^2+\xi^2}{\zeta^2+\xi^2}-\frac{\xi}{\eta} \qquad \ldots\ldots(14)$$

$$\frac{d\zeta}{d\eta}=-\frac{\zeta\xi}{\zeta^2+\xi^2} \qquad \ldots\ldots(15)$$

where $\xi=B_\phi/B_0$, $\zeta=B_z/B_0$ and the dimensionless radius

$$\eta=\frac{4\pi n\boldsymbol{e}^2DZr}{\boldsymbol{ck}T_{\rm e}B_0}=4\pi\sigma\frac{Zr}{B_0}$$

where σ is the conductivity of the plasma perpendicular to the magnetic field. B_0 is the value of the axial magnetic field on the axis of symmetry ($r=0$). These two equations have been solved numerically and the results are shown in figure 1. The parameter B_z/B_0 approaches zero as η goes to infinity. The paramagnetic effect is therefore not self-generating, i.e. an axial magnetic field cannot be generated spontaneously without the presence of a small 'seed' field $B_{\rm e}$ external to the plasma. For example if the boundary of the plasma is represented by the dotted line in figure 1, then the 'seed' field $B_{\rm e}$ is amplified by the paramagnetic current flow to the value B_0 on the axis. When $B_\phi>B_{\rm e}$ at the boundary, the amplification factor A is given by

$$A=B_0/B_{\rm e}\simeq 1{\cdot}36(B_\phi/B_{\rm e})^{2/3}. \qquad \ldots\ldots(16)$$

In many experiments, for reasons of stability, high current discharges are produced inside conducting metal tubes (Tayler 1957). The thickness and conductivity of the tube wall is such that for the duration of the discharge pulse the total axial magnetic flux inside the tube is constant. As the helical current flow increases the axial field inside the discharge so the field external to the discharge is decreased by currents induced in the conducting wall. Let ϕ_0 be

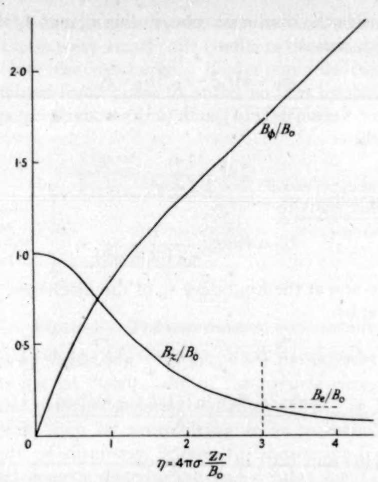

Figure 1. The magnetic field distributions for an isothermal plasma in a steady state.

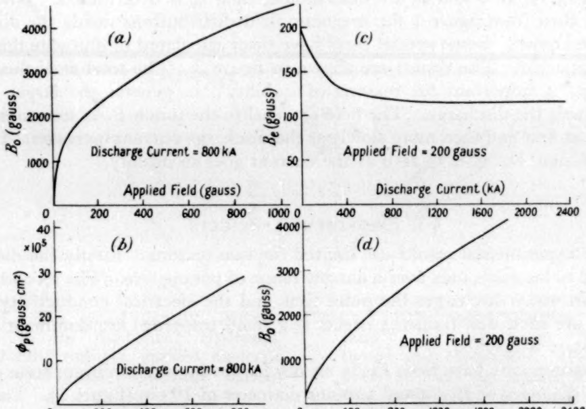

Figure 2. The steady state in an infinitely conducting tube. Tube radius $r_0 = 50$ cm. Discharge radius $r_p = 25$ cm. (*a*) The z component of magnetic field on the axis of the discharge B_0 plotted against the initial applied magnetic field. (*b*) The total axial flux in the discharge ϕ_p plotted against initial applied magnetic field. (*c*) The z component of magnetic field outside the discharge B_e plotted against discharge current. (*d*) The z component of magnetic field on the axis of the discharge B_0 plotted against discharge current.

the total axial flux inside the discharge tube, radius r_0, and ϕ_p the axial flux within the discharge plasma, radius r_p; then

$$\phi_p + \pi(r_0^2 - r_p^2)B_e = \phi_0. \qquad \ldots\ldots(17)$$

An approximate solution of (14) and (15) obtained by curve fitting, which is valid when $B_\phi > B_z$, is

$$\zeta = \frac{1{\cdot}6}{1{\cdot}2 + \eta^2}. \qquad \ldots\ldots(18)$$

Substituting for ζ this leads to

$$B_e = 4\pi\sigma r_p \frac{1{\cdot}6}{\eta_0(1{\cdot}2 + \eta_0^2)} \qquad \ldots\ldots(19)$$

where η_0 is the value of η at the boundary r_p of the discharge. The flux through the pinch ϕ_p is given by

$$\left.\begin{aligned} \phi_p &= 2\pi \int_0^{r_p} B_z r\, dr = 8\pi^2\sigma Z r_p^3 \int_0^{\eta_0} \eta\zeta\, d\eta; \\ \text{or} \qquad \phi_p &= \frac{8\pi^2\sigma Z r_p^3 0{\cdot}8 \ln\{(1{\cdot}2 + \eta_0^2)/1{\cdot}6\}}{\eta_0^3}. \end{aligned}\right\} \qquad \ldots\ldots(20)$$

Substituting from (19) and (20) in (17) gives

$$\frac{0{\cdot}8 \ln\{(1{\cdot}2 + \eta_0^2)/1{\cdot}6\}}{\eta_0^3} = \frac{\phi_0}{8\pi^2\sigma Z r_p^3} - \frac{(r_0^2 - r_p^2)}{r_p^2} \frac{0{\cdot}8}{\eta_0(1{\cdot}2 + \eta_0^3)}. \qquad \ldots\ldots(21)$$

Thus if r_0, r_p, Z, σ and ϕ_0 are determined, then η_0 is determined. When η_0 is known, then from figure 1 the magnetic field distributions inside the discharge tube are known. Some special cases have been calculated to illustrate the effects to be expected. The results are shown in figure 2. The total axial flux in the pinch ϕ_p is important for reasons of stability; in general the larger ϕ_p the more stable the discharge. The field external to the pinch B_e is seen to decrease rapidly at first and then more slowly as the discharge current increases. It never reverses sign, but goes to zero as the current goes to infinity.

§ 3. EXPERIMENTAL RESULTS

The experimental results are limited for two reasons. Firstly the discharge is found to be stable only over a narrow range of parameters. The second reason is that in many discharges the pulse time and the electrical conductivity of the plasma are such that transient effects (e.g. field trapping) are dominant and no steady state is reached.

Measurements have been made on discharges in an aluminium torus having a major diameter of 30 cm and a minor diameter of 10 cm (figure 3). The torus had two gaps to prevent a short circuit, and was linked by an iron core carrying the primary winding. The discharge was in effect the single turn secondary of a pulse transformer. A condenser bank of 12 μF at 25 kv was discharged through a triggered spark-gap into the primary winding. Discharge currents of up to 50 000 A were produced in hydrogen gas. The starting gas pressure was of order 10^{-3} mm Hg, and the axial magnetic field was variable up to 2000 gauss. The duration of the discharge was between 200 μsec and 2 msec depending on conditions.

The magnetic field distribution in the current channel was measured using magnetic probes. These were small coils (~ 8 mm diameter) sheathed in quartz tubes and inserted into the discharge. Under suitable conditions repeatable results could be obtained from pulse to pulse, so that by successive positioning of the probe the spatial distributions of B_ϕ and B_z were found. From these distributions and using equations (12) and (13) the current densities j_ϕ and j_z were deduced. The spatial distribution of the particle energy density can then be obtained from the pressure balance equation (10). If $T_\mathrm{i} + T_\mathrm{e}$ is assumed independent of radius, then by normalizing so as to include all the electrons per centimetre length of discharge known to be present (i.e. assuming 100% ionization) the radial density distribution and a value for $T_\mathrm{i} + T_\mathrm{e}$ are obtained.

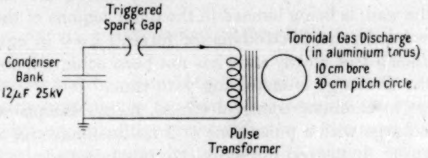

Figure 3. The experimental arrangement.

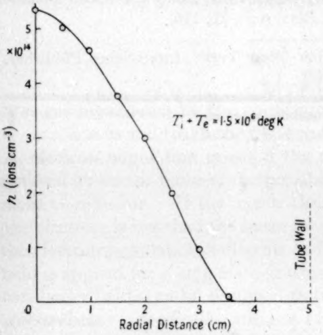

Figure 4. The radial density distribution in the discharge. Hydrogen, $p = 2 \times 10^{-3}$ mm Hg, applied magnetic field 1400 gauss; discharge current 25 kA.

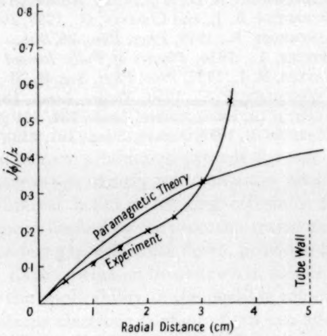

Figure 5. The radial variation of the ratio j_ϕ/j_z, comparison between theory and experiment. Hydrogen, $p = 2 \times 10^{-3}$ mm Hg; applied magnetic field 1400 gauss; discharge current 25 kA.

The results for a 25 000 ampere discharge in an applied field of 1400 gauss are shown in figure 4. The value for $T_\mathrm{i} + T_\mathrm{e}$ in this case is $1{\cdot}5 \times 10^6$ deg K. The measured values of the electric field and the current density on the axis, combined with the resistivity equation for a fully ionized gas (Spitzer 1956), lead to a value for T_e of only 5×10^5 deg K. The ions would not be expected to be hotter than the electrons, so that there is an apparent discrepancy between these results. This remains unexplained.

The ratio j_ϕ/j_z measured in this discharge is shown in figure 5 compared with the ratio predicted by the paramagnetic theory. In the core of the discharge the agreement is satisfactory; near the walls the rotational j_ϕ currents are higher than the theory predicts. In fact the current in this region is flowing along the magnetic field lines (i.e. a force-free configuration). One possible explanation is that neutral gas outside the pinch, left behind during the initial collapse or liberated from the wall, is being ionized in the outer regions of the discharge and then carried inwards by the electrodynamic forces ($j_r \neq 0$ in equation (1)). If this is the case then a true steady state has not been achieved, since the number of particles in the discharge is increasing with time.

In an attempt to eliminate transient effects, measurements were made on a 1500 ampere discharge with a pulse time of 3 milliseconds and an applied axial field of 1000 gauss. It proved impossible to obtain an accurate measurement of the radial distribution of B_z because the changes in the axial field due to the current flow were only of the order of 1 or 2 gauss. However, on the tube axis, where the interference from the B_ϕ field was a minimum, the axial field was shown to increase by $2 \pm 0{\cdot}5$ gauss. This increase persisted for the whole duration of the pulse. The theory predicts an increase of 1·8 gauss under the conditions of this experiment.

REFERENCES

BEZBACHENKO, A. L., *et al.*, 1956, *Atomnaya Energiya*, **1,** No. 5, 26.

BICKERTON, R. J., and LONDON, H., 1958, *Proc. Phys. Soc.*, **71,** 116.

LANDSHOFF, R., 1949, *Phys. Rev.*, **76,** 904.

SPITZER, L., 1956, *Physics of Fully Ionised Gases* (New York: Interscience Publishers).

TAYLER, R. J., 1957, *Proc. Phys. Soc.* B, **70.** 1049.

THONEMANN, P. C., 1958, *Nature, Lond.*, **181,** 217 (Thonemann, P. C., *et al.*).

TUCK, J. L., 1958, *Nature, Lond.*, **181,** 231 (Honsaker, J., *et al.*).

WARE, A. A., 1958, *Nature, Lond.*, **181,** 223 (Allen, N. L., *et al.*).

Ultra-High-Frequency Gas Breakdown between Rogowski Electrodes

By W. A. PROWSE and J. L. CLARK
Department of Physics, University of Durham

MS. received 6th June 1958

Abstract. Electrons may be removed from the gas between a pair of plane parallel electrodes by being swept out by the field, by recombination, by attachment or by diffusion. At high enough frequencies diffusion is the most likely mechanism. This can be tested quantitatively by plotting the relation between $E\Lambda$ and $p\Lambda$ (E = electric field required to produce breakdown, p = gas pressure, Λ = ' diffusion length ' for the gap). It can also be tested qualitatively by observing the decrease of E with increasing gap width d. The electrodes must be properly profiled to avoid breakdown beginning at the edges.

The necessary observations of breakdown voltage, electrode spacing, electrode size and gas pressure are made for air, hydrogen, nitrogen and neon, at 9·5 Mc/s. The ($E\Lambda$, $p\Lambda$) plot gives a single line for ultra-high-frequency breakdown, and E decreases with increasing d in accordance with diffusion theory. Values of the ionizing efficiency η are calculated.

§ 1. Introduction

In gas breakdown by the application of ultra-high-frequency fields, electrons oscillate to and fro in the test gap without being swept to the electrodes: the electron population grows if the rate of new production exceeds the rate of removal by one or more of the possible processes, namely recombination, attachment or diffusion. If the mean time interval between ionizing collisions, for one electron, is less than the mean life-time as limited by the processes mentioned, the electron population will grow and the test gap will break down, provided the field is applied for a long enough time. Experiments on breakdown in sustained oscillatory fields can be designed to test the applicability of the possible removal mechanisms: specifically, the use of various electrode configurations can affect electron removal by diffusion processes without affecting recombination or attachment.

A large body of experimental work now exists on breakdown in sustained oscillatory fields. The results on hydrogen are of special interest, as molecular hydrogen is a non-attaching gas, and the data have been assembled by Brown (1955) who has shown that practically all of them can be represented on a single three-dimensional graph, which accords with the assumption that in the ultra-high-frequency region diffusion is the removal process.

It is evident that if this is the mechanism, then in a given experiment on breakdown between plane parallel electrodes the breakdown stress should increase as the electrodes approach one another because the rate of removal of electrons will be accelerated thereby. Experiments of this simple type have been made (Pim 1949, Prowse and Lane 1955, Fucks *et al.* 1956) and some of these have supported the existence of a constant breakdown stress, independent of gap width, rather than the variation required by the diffusion theory. In some of these experiments considerable weight was attached to the fact that the discharges took place in the central region between the electrodes: this is not now regarded as sufficient evidence that the discharges actually began there. There is at least a possibility that incipient discharges in strong edge fields may have transferred to the centre region, by irradiation and diffusion processes, and there have become visible crossing the gap. Thus a number of the existing measurements may not properly refer to uniform-field breakdown.

The conditions to be satisfied in a uniform-field measurement are (i) there should be a uniform-field region in the centre of the space between the electrodes, (ii) this field should continue uniform up to the electrode surfaces in the central region, (iii) beyond the central region the field strength should fall off continuously along any equipotential surface, including the surface of the electrode, (iv) the walls of the discharge chamber should be remote enough not to take part in the process.

These conditions are familiar in the study of breakdown in unidirectional fields where the first three can be satisfied by suitable design of the electrodes. In microwave work they may be satisfied in a different way. Labrum (1947) has measured breakdown stresses in air and in neon confined in a rectangular wave guide: here the stress is uniform across the gap between the broad faces of the guide and falls off steadily from the centre of the guide towards the narrow faces where it vanishes. Brown and others (MacDonald and Brown 1949, Reder and Brown 1954) have measured breakdown in cylindrical resonators, where the field, in the mode employed, is uniform across the gap between opposite plane faces and falls off steadily to zero at the curved boundary walls.

The present paper is concerned with measurements of breakdown stresses in various gases, at frequencies in the 10 Mc/s range, using electrodes of Rogowski profile, which satisfy the conditions enumerated. It is possible to state quantitatively the effect of changes in gap configuration on the mean life-time of an electron if diffusion is the removal process, but the sensitivity of breakdown stress to such changes will depend on how rapidly collision ionization varies with the applied stress. A sudden onset of collision ionization at a particular field strength would result in apparent constancy of breakdown stress.

§ 2. REMOVAL OF ELECTRONS BY DIFFUSION : EXPERIMENTAL CRITERIA

Qualitatively, the measurements of greatest importance are those of breakdown stresses between large plane electrodes when the gap width d is varied. If the diffusion theory applies, the breakdown stress will decrease with increasing gap width. The magnitude of the change is not directly susceptible of calculation unless the relation between the rate of ionization by collision and the applied field is known.

For a numerical statement of the properties of a given gap geometry, the most convenient quantity is the ‘ diffusion length ’ Λ, which for a cylinder of length d and radius r is given by

$$\frac{1}{\Lambda^2}=\left(\frac{\pi}{d}\right)^2+\left(\frac{2{\cdot}405}{r}\right)^2. \qquad \ldots\ldots(1)$$

The diffusion length is related to the mean life-time of an electron t_d and the coefficient of diffusion D for electrons by the relation

$$t_d = \Lambda^2/D. \qquad \ldots\ldots(2)$$

Breakdown will eventually occur if at least one ionizing collision is made per electron in the time t_d. The number of ionizing collisions made per electron per second is αW, where α is Townsend's first coefficient and W is the drift velocity of the electron in the field E. Thus the limiting condition for breakdown is

$$\alpha W t_d = 1. \qquad \ldots\ldots(3)$$

According to Townsend (1947), D is related to W and the random electron velocity V by

$$D = \left(\frac{\boldsymbol{m}}{3\boldsymbol{e}}\right)\left(\frac{V^2W}{E}\right)$$

where $\boldsymbol{e}/\boldsymbol{m}$ is the specific charge of the electron. Combining this with (2) and (3) we have

$$\alpha W = \frac{1}{\Lambda^2 Ep}\frac{\boldsymbol{m}}{3\boldsymbol{e}}pV^2W$$

or

$$\frac{\alpha}{p} = \frac{1}{E\Lambda\,.\,p\Lambda}\frac{\boldsymbol{m}}{3\boldsymbol{e}}V^2. \qquad \ldots\ldots(4)$$

But

$$\frac{\alpha}{p} = f\left(\frac{E}{p}\right) = f\left(\frac{E\Lambda}{p\Lambda}\right) \quad \text{and} \quad V^2 = F\left(\frac{E}{p}\right) = F\left(\frac{E\Lambda}{p\Lambda}\right)$$

where f and F are functions depending on the nature of the gas. Thus (4) may be written

$$f\left(\frac{E\Lambda}{p\Lambda}\right) = \frac{\boldsymbol{m}}{3\boldsymbol{e}}\frac{1}{E\Lambda\,.\,p\Lambda}F\left(\frac{E\Lambda}{p\Lambda}\right)$$

showing that the relation between $E\Lambda$ and $p\Lambda$ depends only on the nature of the gas. Thus if diffusion is the removal mechanism the curve relating $E\Lambda$ and $p\Lambda$ will be unique for any one gas. This may be contrasted with the familiar Paschen condition for breakdown in unidirectional fields, that the (Ed, pd) plot is unique for any one gas. The comparison of these two types of display affords a stringent test of the applicability of diffusion theory. MacDonald and Brown (1949) have applied dimensional analysis to show that $E\Lambda$ and $p\Lambda$ are suitable variables for discussing ultra-high-frequency breakdown.

It is evident from (1) that for large electrodes, i.e. when $r/d \gg 1$, d is sensibly equal to $\pi\Lambda$ and the curves relating $E\Lambda$ with $p\Lambda$ will differ only by the factor π from the Paschen curves relating Ed with pd. In this region the qualitative test first referred to is the most useful. The ($E\Lambda, p\Lambda$) plot becomes sensitive where r is comparable with d; if it reconciles results for different electrode sizes as well as for changes in spacing and pressure it establishes diffusion as the removal mechanism.

§ 3. EXPERIMENTAL ARRANGEMENTS

Four sets of brass electrodes of Rogowski profile were prepared according to methods given by Jones (1956) (table 1). In this profile the flat centre region of the electrodes is continued outwards by surfaces of gradually increasing curvature, and it is the radius of the centre region—about two-thirds of the overall radius—

which is given in the table. The boundary of the uniform-field region between the electrodes is a waisted figure rather than a true cylinder so that the proper value of r is a matter of some doubt, but the waisting is probably to some extent compensated by the regions near the electrodes where the field falls off only slowly as the centre region is left.

Table 1

r (cm)		1·85	1·58	0·79	0·32
$\pi\Lambda$ (cm)	$d=0{\cdot}76$ cm	0·68	0·64	0·46	0·23
	$d=1{\cdot}02$ cm	0·88	0·81	0·51	0·24

Radii r of flat centre portions of the electrodes. Values of $\pi\Lambda$ are also given for two gap widths d. For infinitely large plane electrodes $\pi\Lambda=d$.

The electrodes were mounted in a cylindrical glass enclosure of diameter 9·5 cm and length 15 cm using bellows seals. Provision was made to irradiate the gas in mid-gap with radiation from a short spark in the gas being examined. Mercury vapour was excluded from the system and pressures were measured by means of differential gauges. Spectroscopically pure gases were used, but no additional purification was attempted. When air was employed it was filtered and dried. A cold trap was inserted between the discharge vessel and the rest of the gas-control apparatus.

In a given measurement, the system was first pumped down and cleaned by Tesla discharges, then flushed several times with the gas to be used and finally filled to the required pressure. Pulses were then applied to the irradiating spark gap at the rate of some hundreds per second while the ultra-high-frequency voltage on the electrodes was increased in steps until discharge occurred. This was then repeated using smaller and smaller steps until the breakdown voltage had been established, usually to the precision of the measuring instruments. Diode rectifiers and electrostatic voltmeters were used for the voltage determinations.

After each discharge a period of waiting, up to some minutes, was necessary for the gap to recover: if the field was re-applied too quickly the observed breakdown stress was a funcion of the time elapsing between switching off and re-application. Appreciable statistical lags were encountered, less in hydrogen than in other gases, in agreement with other work. Checks were made from time to time by refilling with fresh gas. The new measurements invariably agreed with the old.

Most of the measurements were made at a frequency of 9·5 Mc/s, but some were taken at 5·5 Mc/s. Except that true ultra-high-frequency conditions persisted to a narrower gap width at the higher frequency there was no significant difference, and all the results given below relate to the higher frequency. Also, unless otherwise stated, the results refer to the largest pair of electrodes.

§ 4. EXPERIMENTAL RESULTS

4.1. *Influence of Gap Width on Ultra-high-frequency Breakdown Stress*

Typical results for hydrogen, nitrogen and air are shown in figure 1. These represent only a few of the many series of measurements recorded, but are sufficient for illustration. Each curve is taken at constant pressure and it will be seen that, starting from a very short gap, the breakdown stress shows a rapid decrease with increasing gap width, followed by a flattening after a fairly sharp transition. For the shorter gaps, electrons are trapped by the electrodes and only the flatter portion of the curve refers to true ultra-high-frequency breakdown. This is confirmed by calculations based on published values of electron drift velocity.

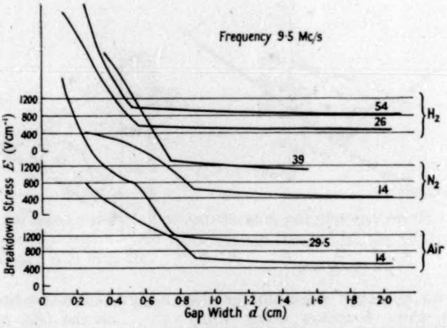

Figure 1. Breakdown stress as a function of gap width for hydrogen, nitrogen and air. The steeper parts of the curves occur when electrons are trapped by the electrodes. The less steep parts refer to true ultra-high-frequency breakdown. Each gas is given its own set of ordinates, for clarity. Gas pressures in mm Hg are shown on the curves.

The ultra-high-frequency breakdown stress shows a definite decrease with increasing gap width. In the figure, in the ultra-high-frequency region all of the experimental points fall within the thickness of the line, and so the slope is clearly established in every set of observations, in firm support of the view that diffusion is the electron removal mechanism.

The different shapes of the left-hand branches of the curves are not without significance. In this region there may be time for one or more electron transits per half cycle; the variations associated with the number of transits have been discussed by Pim (1949) and more fully by Fucks *et al.* (1956).

Similar observations to those on hydrogen, nitrogen and air were made for neon. In this gas the change in ultra-high-frequency breakdown stress with gap width is more pronounced, but, as observed by Gill and von Engel (1948, 1949), the transition to ultra-high-frequency conditions is much less marked than in the polyatomic gases. The results are displayed in a different way in figure 4 (*b*), where the transition is readily identifiable by the fusion of the separate curves with the common line.

4.2. *Breakdown Stress and Diffusion Length for one Pair of Electrodes*

In hydrogen, experimental results for varying gap width at four different values of the pressure, and for varying pressure using three fixed gaps are all shown in figure 2 on a logarithmic scale as a relation between $E\Lambda$ and $p\Lambda$. The points representing ultra-high-frequency breakdown lie on a single line, in accordance with diffusion theory. Branches occur for conditions such that the electron ambit exceeds the gap width. To complete this evidence, it is desirable to show that the results are not equally consistent with other possible views. Figure 3 shows the customary Paschen curves (*Ed*, *pd*) for the higher pressure results; it seems clear that in the ultra-high-frequency region there is not a unique (*Ed*, *pd*) curve for hydrogen, but there is a unique ($E\Lambda$, $p\Lambda$) curve.

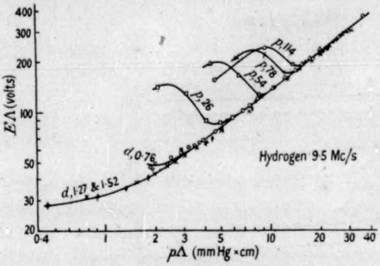

Figure 2. Data for hydrogen assembled on the ($E\Lambda$, $p\Lambda$) plot. Branches occur when electrons are trapped by the electrodes. The common lower curve is for ultra-high-frequency breakdown. Experiments at fixed pressure and at fixed gap width are both represented and the figures on the curves give p in mm Hg or d in cm.

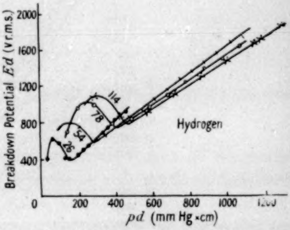

Figure 3. Data for hydrogen assembled on the (*Ed*, *pd*) plot (Paschen curve). The straight portions represent ultra-high-frequency breakdown. p in mm Hg is marked on the transition region of each curve. There is no common curve for ultra-high-frequency breakdown.

At lower pressures the distinction between the (*Ed*, *pd*) curves on the one hand and the ($E\Lambda$, $p\Lambda$) curves on the other is less marked, but in this region the decrease of E with increasing d at constant pressure is very noticeable and this again supports the diffusion theory (table 2).

Table 2. Peak Values of Ultra-high-frequency Breakdown Stress E_s in Hydrogen, for various gap widths, to show the decrease of E_s with increasing d

p (mm Hg)	10	13	16
d (cm)			
0·76	$3\cdot2\times10^2$	$3\cdot7\times10^2$	$4\cdot2\times10^2$
1·27	$2\cdot6\times10^2$	$3\cdot0\times10^2$	$3\cdot5\times10^2$
1·52	$2\cdot3\times10^2$	$2\cdot6\times10^2$	$3\cdot2\times10^2$

E_s in v cm^{-1}.

Observations were also made on nitrogen and on air covering the same general range as that for hydrogen, though not quite so completely. They show the same features, especially that the ($E\Lambda$, $p\Lambda$) plot is a better representation of the results than the (*Ed*, *pd*) plot: the ultra-high-frequency breakdown line is unique on the ($E\Lambda$, $p\Lambda$) plot.

Similar observations were also made for neon and these are illustrated in figures 4 (*a*) and (*b*). In this gas the transition to ultra-high-frequency conditions is much less marked than in the polyatomic gases studied (figure 1), i.e. the variation of ultra-high-frequency breakdown stress with gap width is itself so marked that no noticeable levelling-off occurs where the electron ambit is less than the gap width. The Paschen curves (*Ed*, *pd*) for three different pressures are quite separate from one another, whereas the ($E\Lambda$, $p\Lambda$) curves fuse into a single curve for ultra-high-frequency conditions, the branches beginning where the electron ambit becomes comparable with the gap width.

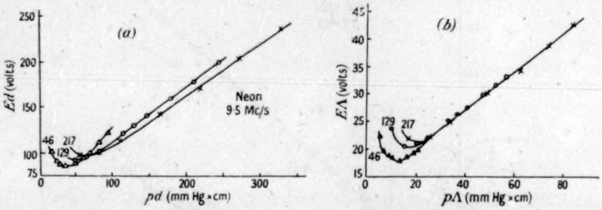

Figure 4. Data for neon assembled on (*a*) the (*Ed*, *pd*) plot and on (*b*) the ($E\Lambda$, $p\Lambda$) plot. Branching in (*b*) occurs when electrons are trapped by the electrodes. Figures on the curves give p in mm Hg.

4.3. *Breakdown Stress and Electrode Diameter* (*Hydrogen*, 9·5 *Mc/s*)

Breakdown voltage was measured as a function of pressure for two values of gap width, $d = 0{\cdot}762$ cm and 1·016 cm for each of the four pairs of electrodes of table 1. The stress required to break down a gap of given spacing at a given pressure increases progressively with decreasing electrode diameter. An electron diffusing laterally out of the strong field region for small electrodes would still have been in the strong field region had larger electrodes been used. Thus diffusion acts more effectively in removing electrons the smaller the electrodes, and the results are in qualitative conformity with the diffusion theory. Figure 5 shows the results for $d = 0{\cdot}76$ cm plotted as the ($E\Lambda$, $p\Lambda$) relation with (inset) the (*Ed*, *pd*) curves for comparison. It is clear that the results for the four sets of electrodes are reconciled on the ($E\Lambda$, $p\Lambda$) plot, i.e. that the diffusion length Λ again correctly describes the nature of the gap so far as electron removal processes are concerned.

Field distortion has a quite different effect on breakdown stress. The number of equipotential surfaces crossed in going from one electrode to the other is the same, for a given steady applied voltage, whatever the shape of the electrodes. Thus the weakening of the field at the centre which could arise with small electrodes is compensated by a strengthening near the electrodes. When a unidirectional field is used the number of electrons reaching the anode for each electron starting from the cathode is

$$\exp \int_0^d \alpha \, dx$$

where α is Townsend's first coefficient and x is distance measured towards the anode. For the gases, and over the pressure range used,

$$\int_0^d (\alpha \, dx) > \alpha d$$

so that the field distortion increases the ionizing efficiency of the electron. This is borne out by the published values of sphere-gap breakdown potentials in air, which show that for a given gap width the breakdown potential increases slightly when the electrode size is increased, i.e. when field distortion is reduced (Meek and Craggs 1953). This is in the opposite sense to the ultra-high-frequency results for hydrogen.

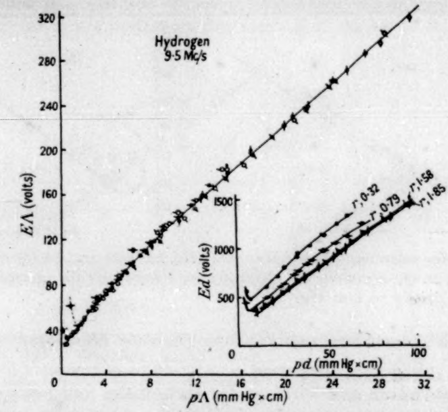

Figure 5. Showing the ($E\Lambda$, $p\Lambda$) and the (Ed, pd) (inset) curves for four electrode sizes, at one gap width (0·76 cm). Hydrogen, 9·5 Mc/s. Open circles on the ($E\Lambda$, $p\Lambda$) plot refer to a gap width of 1·02 cm ; otherwise the experimental points are marked in the same way on the main diagram and on the inset.

§ 5. Discussion

The form of the relation between $E\Lambda$ and $p\Lambda$, particularly when electrodes of various sizes are considered, requires that diffusion should be at least the predominant removal mechanism for electrons. Provided suitable data on diffusion as a function of E/p are available, it now becomes possible to calculate values of α/p from the breakdown data. Measurements on the diffusion of a swarm of electrons have been made by Townsend and his school, who express the results in terms of a quantity k which is the ratio of the energy of random movement of the average electron to the energy of random movement of the average molecule.

From (2) and (3), at breakdown $D/\Lambda^2 = \alpha W$. Also (Townsend 1947, Huxley and Zaazou 1949) $D = Wk/40{\cdot}3E$ so that

$$\frac{40{\cdot}3E}{p}(p\Lambda)^2 = \frac{k}{\alpha/p}\,; \qquad \ldots\ldots(5)$$

a somewhat similar expresson has been given by Holstein (1946).

It is often more convenient to use the ionizing efficiency η (the number of ionizing collisions per volt) than α/p. Thus

$$\eta = \frac{\alpha/p}{E/p} = \frac{k}{40{\cdot}3E^2\Lambda^2}. \qquad \ldots\ldots(6)$$

Values of η calculated from this relation, using k for hydrogen and nitrogen as given by Townsend, and using Huxley and Zaazou's values of k for air, are shown in figure 6, together with values of η calculated from recent direct measurements of α/p. Allowing for the considerable uncertainty in the values of k and possibly of the measured values of α/p at the lower end of the range of E/p the agreement is quite satisfactory. In particular it indicates that it is not necessary to look beyond single-stage collision ionization on the one hand, and electron diffusion on the other, to explain all of the cases of breakdown recorded here.

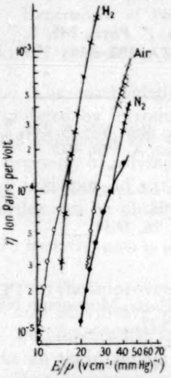

Figure 6. Ionizing efficiency η of electrons in hydrogen, air and nitrogen. Open and closed circles, present measurements. Crosses: air, Llewellyn Jones and Parker (1952); nitrogen, Dutton, Haydon and Llewellyn Jones (1952); hydrogen, Hopwood, Peacock and Wilkes (1956).

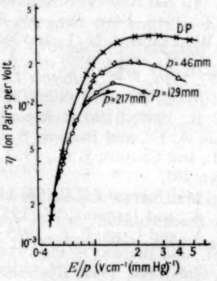

Figure 7. Ionizing efficiency of electrons in neon. DP, Druyvesteyn and Penning's values of η for Ne + 10^{-4}A. The present results (circles and triangles) depart from a common curve when electrons are trapped by the electrodes.

A similar plot for neon is shown in figure 7 but the comparison is somewhat less direct. The curve marked DP refers to Druyvesteyn and Penning's (1940) measurements on neon containing 1 part in 10^4 of argon. No values of k for pure neon were available for use in equation (6), so Bailey's (1924) data for neon contaminated with 1% of helium were used. Since the ionization and excitation potentials of helium are slightly higher than the corresponding potentials for neon, the probability of inelastic collisions is not increased by the helium content. Most of the electron collisions at these values of E/p are elastic so that the helium content is not likely materially to affect the electron temperature in relation to that of the gas atoms. It will be noticed that the curves for $p = 217$ mm and $p = 129$ mm break away when conditions for true ultra-high-frequency breakdown no longer hold. On the whole these results for neon support the same conclusions as those drawn for the polyatomic gases.

ACKNOWLEDGMENTS

The authors wish to acknowledge their indebtedness to the British Electrical and Allied Industries Association for generous financial help, including a maintenance grant to one of them (J. L. C.), and to the Director of that Association for permission to publish this paper.

REFERENCES

ALLIS, W. P., and BROWN, S. C., 1952, *Phys. Rev.*, **87**, 419.

BAILEY, V. A., 1924, *Phil. Mag.*, **47**, 379.

BROWN, S. C., 1955, *App. Sci. Res.* B, **5**, 97.

DRUYVESTEYN, M. J., and PENNING, F. M., 1940, *Rev. Mod. Phys.*, **12**, 87.

DUTTON, J., HAYDON, S. C., and LLEWELLYN JONES, F., 1952, *Proc. Roy. Soc.* A, **213**, 203.

FUCKS, W., GRAF, L., MUES, G., and MÜLLER, H. G., 1956, *Z. Phys.*, **145**, 1.

GILL, E. W. B., and VON ENGEL, A., 1948, *Proc. Roy. Soc.* A, **192**, 446; 1949, *Ibid.*, **197**, 107.

HERLIN, M. A., and BROWN, S. C., 1948, *Phys. Rev.*, **74**, 291, 1650.

HOLSTEIN, T., 1946, *Phys. Rev.*, **69**, 50.

HOPWOOD, W., PEACOCK, N. J., and WILKES, A., 1956, *Proc. Roy. Soc.* A, **235**, 334.

HUXLEY, L. G. H., and ZAAZOU, A. A., 1949, *Proc. Roy. Soc.* A, **196**, 402.

JONES, C. V., 1956, *E.R.A. Report L/T* 334.

LLEWELLYN JONES, F., and PARKER, A. B., 1952, *Proc. Roy. Soc.* A, **213**, 185.

LABRUM, N. R., 1947, *C.S.I.R. Report, Australia* ; *R.P.R.*, **85**.

MACDONALD, A. D., and BROWN, S. C., 1949, *Phys. Rev.*, **76**, 1634.

MEEK, J. M., and CRAGGS, J. D., 1953, *Electrical Breakdown of Gases* (Oxford : University Press), 305.

PIM, J. A., 1949, *Journal I.E.E.*, **96**, 117.

PROWSE, W. A., and JASINSKI, W., 1952, *Proc. Instn Elect. Engrs*, Monograph No. 32.

PROWSE, W. A., and LANE, P. E., 1955, *App. Sci. Res.* B, **5**, 127.

REDER, F. H., and BROWN, S. C., 1954, *Phys. Rev.*, **95**, 885.

TOWNSEND, SIR JOHN, 1947, *Electrons in Gases* (London : Hutchinson).

Energy Levels of Polyatomic Molecules

By S. DATTA MAJUMDAR

Department of Physics, University College of Science, Calcutta

MS. received 1st *January* 1958, *and in revised form* 2nd *June* 1958

Abstract. The mathematical theory of semi-rigid asymmetric top molecules is re-formulated by introducing a new set of operators for angular momentum. All matrix equations are thereby replaced by ordinary differential equations, and the necessity of solving a formidable secular equation for the determination of energy is dispensed with. An analytic expression for energy correct to the second order can be obtained by the methods delineated here.

§ 1. INTRODUCTION

WITH the improvement of experimental technique in the field of infra-red and microwave spectroscopy accuracy in the measurement of spectral frequencies has reached such a stage that a complete explanation of the spectra in all their details is no longer possible without incorporating in the Hamiltonian terms representing centrifugal stretching and the various interactions between rotation and vibration. The correct quantum-mechanical Hamiltonian for calculating these finer interactions was given by Wilson and Howard (1936) over twenty years ago. Although a considerable amount of work has been done on the subject since then, one serious computational difficulty does not seem to have been removed. In evaluating the matrix elements for the individual terms of the Hamiltonian, integration over the vibrational coordinates can be carried out quite easily, but, for high *j*-values, trouble arises from the rotational part, because the basic rotational functions, the wave functions of the asymmetrical top, are known only in the form of lengthy and complicated series expansions. The object of the present paper is to remove this difficulty by replacing these complicated functions by simpler functions of one variable which satisfy an ordinary differential equation of a very convenient type. The problem will thus be solved completely if the series expansions can be avoided and the solution of this equation written in a compact form which makes analytical integration possible.

In the previous work on triatomic molecules (Majumdar 1954, to be referred to as I) an effective step towards this was taken by removing two of the Eulerian angles (χ, θ, ϕ) from the quantum-mechanical Hamiltonian by a simple artifice. The Eulerian angle χ was removed by taking the angular momentum along a space-fixed z axis to be zero, and θ was removed by considering the behaviour of the wave function only for the particular value $\pi/2$ of θ. (Detailed arguments in support of the second step are given in I and the notation of I is used as far as possible in the present paper.) As a result, P_x^2, P_y^2, P_z^2, $P_xP_y+P_yP_x$ and the purely rotational part of the Hamiltonian were found to be second-order operators involving the single variable ϕ, the angle of rotation about the body-fixed z axis. This was a great simplification of the mathematical problem because a perturbation calculation yielding the corrections to energy due to interaction between rotation and vibration could be carried out by evaluating integrals over the eigenfunctions of an ordinary differential equation of manageable form. The previous algebraic method of evaluating a secular determinant whose size and complexity increase with the value of j could thus be replaced by a simple analytical method, in which j occurs merely as a parameter and causes no more trouble for high than for low values. In spite of this, however, the meaning of the rather accidental reduction obtained in I, and the algebraic origin of the new operators for P_x^2 etc. (I, § 2) were not understood, and a generalization to polyatomic molecules could not be made. These defects are removed and the goal aimed at in I is reached in the present paper by an entirely different approach. The awkward Euler angles are discarded from the very beginning, and with the commutation relations as the starting point suitable one-variable operators are constructed not merely for P_x^2 etc., as was done in I, but for the components[†] P_x, P_y, P_z themselves and, therefore, for any combination of them. The difficulty in the generalization to polyatomic molecules is thus removed. Further investigation shows that the problem of reduction to a single variable admits of two independent solutions only one of which was accidentally arrived at in I. The second reduction, which leads to an equally powerful method of calculating the vibration rotation energies of polyatomic molecules, is discussed briefly in § 7.

The method is applicable whenever the Hamiltonian is free from functions of angular variables and contains, in addition to other variables, only components of angular momentum, spin or orbital. It is therefore particularly suitable for handling molecular spectra. In the case of atomic spectra, however, it does not seem to possess any advantage over the existing methods, for the simple reason that the perturbation terms often involve functions of angular variables. In § 9 the correctness of the entire procedure is tested by deriving the Clebsch–Gordan coefficients by this method, which has the advantage of removing all irrational factors from the calculations.

§ 2. ANALYTICAL OPERATORS FOR ANGULAR MOMENTUM

If $\hbar M_x$, $\hbar M_y$, $\hbar M_z$ are the components of angular momentum about space-fixed axes, the commutation relations and the matrix elements are

$$[M_x, M_y] = iM_z \text{ etc.}, \quad (M_z)_{mm} = m$$

$$(M_x + iM_y)_{m+1,m} = [(j-m)(j+m+1)]^{1/2} = [f(m)]^{1/2} = (M_x - iM_y)_{m,m+1}.$$

Let $[\alpha]_{(p)}$ denote a diagonal matrix with α as the first p diagonal elements and unity as the remaining ones, and let us subject the matrices to the transformation $[\alpha^{-1}]_{(p)}M[\alpha]_{(p)}$, where M stands for any one of the matrices $M_x \pm iM_y$, M_z. From the form of the matrices M it is clear that the result of such a transformation will be simply to multiply the element $(M_x + iM_y)_{p+1,p}$ by α and the element $(M_x - iM_y)_{p,p+1}$ by α^{-1}.

Next, let

$$\alpha = -f(m)^{1/2}, \quad p = j+m+1, \qquad \text{when } j-m \text{ is even,}$$

$$\alpha = f(m)^{-1/2}, \quad p = j+m+1, \qquad \text{when } j-m \text{ is odd.}$$

[†] It is interesting to note that given P_z and any one of the operators P_x^2, P_y^2, P_xP_y, P_yP_x the remaining three can be deduced. But it is impossible to construct from them P_x and P_y. If, for instance, we write $P_x^2 = -\sin^2\phi\,(F+D^2) - \frac{1}{2}\sin 2\phi\, D = (\lambda + \mu D)^2$ (where $D = d/d\phi$) then by comparing coefficients we have $\lambda = 0$.

After one such transformation all the matrix elements remain unaltered with the exception of $(M_x+iM_y)_{m+1,m}$ and $(M_x-iM_y)_{m,m+1}$. These two elements become respectively $-f(m)$, -1 if $j-m$ is even, and $1, f(m)$ if $j-m$ is odd. As m takes on the values $-j, -j+1, \ldots, j-1$, we get $2j$ successive transformations of this type, which, taken together, give rise to the transformation

$$\prod_{i=1}^{j} [f(j-2i+1)^{1/2}]_{(2j-2i+2)}[-f(j-2i)^{-1/2}]_{(2j-2i+1)}M$$
$$\times \prod_{i=1}^{j} [f(j-2i+1)^{-1/2}]_{(2j-2i+2)}[-f(j-2i)^{1/2}]_{(2j-2i+1)} \qquad \ldots\ldots (1)$$

where Π denotes a matrix product. The resulting new forms of the matrices M are

$$M_x+iM_y=\begin{bmatrix} \cdot & & & \\ -f(-j) & \cdot & & \\ & 1 & \cdot & \\ & & -f(-j+2) & \cdot \end{bmatrix}$$

$$M_x-iM_y=\begin{bmatrix} \cdot & -1 & & \\ & \cdot & f(-j+1) & \\ & & \cdot & -1 \\ & & & \cdot \end{bmatrix}$$

$$M_z=\begin{bmatrix} -j & & & \\ & -j+1 & & \\ & & -j+2 & \\ & & & \cdot \end{bmatrix}$$

It will be seen later that this transformed matrix is necessary if the problem of pure rotation is to lead to Lamé's equation. Other transformations are possible, but they lead to more complicated equations.

If we take the functions $e^{im\phi}$ $(m=-j$ to $+j)$ to form the basis of a $(2j+1)$ dimensional function space V_{2j+1}, these matrices can be generated by analytical operators which, because of the peculiar transformation adopted here, assume two different forms for the two types of functions

$$u^{+}=\sum_{p} a_{j-2p}e^{i(j-2p)\phi}, \qquad u^{-}=\sum_{p} a_{j-2p-1}e^{i(j-2p-1)\phi}.$$

We call u^{+} a function of the first class and u^{-} a function of the second class.

For functions of the first class

$$\begin{aligned}(M_x+iM_y)^{+}&=-e^{i\phi}(F+D^2+iD),\\ (M_x-iM_y)^{+}&=e^{-i\phi}(F+D^2-iD)\end{aligned} \qquad \text{......} (2a)$$

where $F\equiv j(j+1)$, $D\equiv d/d\phi$ and for functions of the second class

$$(M_x+iM_y)^{-}=e^{i\phi}, \qquad (M_x-iM_y)^{-}=-e^{-i\phi}. \qquad \text{......} (2b)$$

For M_z, however, no discrimination is necessary and the operator has the same form for both classes of functions:

$$(M_z)^{+}=(M_z)^{-}=-iD. \qquad \text{......} (2c)$$

For integral values of j, $e^{ij\phi}$ and $e^{-ij\phi}$ are both of the first class, and therefore

$$(M_x+iM_y)^{+}e^{ij\phi}=-e^{i(j+1)\phi}f(j)=0, \qquad (M_x-iM_y)^{+}e^{-ij\phi}=e^{-i(j+1)\phi}f(-j-1)=0.$$

Thus the operators are closed with respect to the $2j+1$ dimensional function space. But for half-integral values of j, if $e^{ij\phi}$ is a function of the first class, then $e^{-ij\phi}$ belongs to the second class, and

$$(M_x-iM_y)^{-}e^{-ij\phi}=-e^{-i(j+1)\phi}\neq 0.$$

Since the operations are not closed, the method breaks down for half-integral values of j. An alternative method will be developed in § 7 to include both spin and orbital angular momentum in the same scheme.

For a particular value of j, integral or half-integral, the angular momentum matrices break up in a suitable representation into three blocks, of which the central one alone is of physical interest. Since the matrices are replaced here by analytical operators the entry of the infinite irreducible blocks† into the present treatment cannot be prevented. For instance, the differential equation (2) of I has an infinite number of eigenvalues in addition to the $2j+1$ in common with the asymmetrical top. This unlimited number of non-physical eigenvalues is connected with the infinite blocks. For these infinite blocks however, the roles of the operators M_x^{+}, M_y^{+} and M_x^{-}, M_y^{-} are interchanged, so that M_x^{+} operates on a second class u and M_x^{-} on a first class u.

From (2) we can construct the following operators for $(M_x^2)^{+}$, $(M_x^2)^{-}$ etc.:

$$\left.\begin{aligned}(M_x^2)^{+}&=\sin^2\phi(F+D^2)+\tfrac{1}{2}\sin 2\phi D=F+D^2-(M_y^2)^{+}\\ (M_xM_y)^{+}&=-\tfrac{1}{2}\sin 2\phi(F+D^2)+\sin^2\phi D=(M_yM_x)^{+}+D\\ (M_x^2)^{-}&=\sin^2\phi(F+D^2)+\tfrac{3}{2}\sin 2\phi D+\cos 2\phi=F+D^2-(M_y^2)^{-}\\ (M_xM_y)^{-}&=-\tfrac{1}{2}\sin 2\phi(F+D^2)+\tfrac{1}{2}(1-3\cos 2\phi)D+\sin 2\phi=(M_yM_x)^{-}+D.\end{aligned}\right\} \qquad \text{......} (3)$$

It is to be noted that $(M_x^2)^{+}$, $(M_y^2)^{+}$, $(M_xM_y+M_yM_x)^{+}$ are adjoint to the corresponding operators for second-class functions, while $(M_xM_y)^{+}$, $(M_yM_x)^{+}$ are adjoint respectively to $(M_xM_y)^{-}-D$, $(M_yM_x)^{-}+D$.

The operators for $(M_x^2)^{+}$, $(M_y^2)^{+}$, $(M_xM_y+M_yM_x)^{+}$ in (3) are identical with those given in § 2 of I but for a difference in sign. This arises from the different meaning of P_x, P_y, P_z which are $i/\hbar$ times the components of angular momentum about axes rotating with the molecule. It is well known that the latter satisfy the same commutation relations as M_x, M_y, M_z but with the sign reversed, so that, instead of $[M_x, M_y] = iM_z$ etc., we have $[P_x, P_y] = P_z$ etc. We can therefore write

---

† These can be obtained from the commutation relations by allowing $|m|$ to take values greater than j. The two infinite blocks correspond to $m<-j$ and $m>+j$.

$$P_x, P_y, P_z = -iM_x, -iM_y, -iM_z.$$

But the operators $(P_xP_y + P_yP_x)^+$ and P_z still have the opposite sign. To explain this we observe that, when ϕ is changed to $-\phi$, the commutation relations and the operators P_x^2, P_y^2, P_z^2 remain unchanged while P_xP_y, P_yP_x and P_z undergo a change of sign. By changing ϕ to $-\phi$ we therefore get another possible representation of the matrices as one-variable operators which are also closed with respect to V_{2j+1}. The significance of the operators used in I is thus fully understood.

§ 3. THE REDUCED EQUATION FOR THE ASYMMETRICAL TOP

The wave equation

$$(aP_x^2 + bP_y^2 + cP_z^2 + E)u = 0 \qquad \ldots\ldots(4)$$

for the asymmetrical top with moments of inertia $A = \hbar^2/2a$, $B = \hbar^2/2b$, $C = \hbar^2/2c$ thus reduces to the following two adjoint differential equations for the two classes of functions:

$$(L + \mu)u^+ \equiv [g(F + D^2) + \tfrac{1}{2}g'D + \mu]u^+ = 0 \qquad \ldots\ldots(5\,a)$$

$$(L^* + \mu)u^- \equiv [g(F + D^2) + \tfrac{3}{2}g'D - 2g + 2 + \mu]u^- = 0 \qquad \ldots\ldots(5\,b)$$

where $g = 1 - k\cos 2\phi$, $k = (b-a)/(2c-a-b)$, $\mu = (E - cF)/\{c - \tfrac{1}{2}(a+b)\}$. The recurrence relations for the Fourier coefficients of a solution are

$$a_{r-2}\tfrac{1}{2}kf(r-2) + a_r(r^2 - F - \mu) + a_{r+2}\tfrac{1}{2}kf(r+1) = 0 \qquad \ldots\ldots(6\,a)$$

$$a_{r-2}\tfrac{1}{2}kf(r-1) + a_r(r^2 - F - \mu) + a_{r+2}\tfrac{1}{2}kf(r) = 0 \qquad \ldots\ldots(6\,b)$$

respectively. The matrix of the coefficients of a_r can be brought into the self-adjoint form of Wang

$$E_{rr} = r^2 - F - \mu, \qquad E_{r,r+2} = E_{r+2,r} = \tfrac{1}{2}k[f(r)f(r+1)]^{1/2}$$

by the transformation inverse to (1).

If we denote the eigenfunctions of equation (5 *a*) by v and those of equation (5 *b*) by w, then it is evident from the recurrence relations (6 *a*) and (6 *b*) that equation (5 *a*) has exactly $j+1$ eigenfunctions of the first class, but none of the second class, lying in V_{2j+1}. Similarly, equation (5 *b*) has j eigenfunctions of the second class, but none of the first class, lying in V_{2j+1}. In addition to these, both the equations have an infinite number of eigenfunctions v^{out} and w^{out} which, as stated before, are connected with the infinite matrices for angular momentum.

It is important to note that the eigenfunctions v and w are connected by the simple relation

$$v = g^{1/2}w \qquad \ldots\ldots(7)$$

whence

$$g^{-1/2}Lg^{1/2} = L^*. \qquad \ldots\ldots(8)$$

Since the eigenfunctions of equation (5 *a*) are orthogonal with the weight factor $g^{-1/4}$, we have

$$\int g^{-1/2}v^{+}(g^{1/2}w^{+\mathrm{out}}) = \int v^{+}w^{+\mathrm{out}} = 0$$

and

$$\int g^{-1/2}(g^{1/2}w^{-})v^{-\mathrm{out}} = \int w^{-}v^{-\mathrm{out}} = 0.$$

The eigenfunctions $v^{-\mathrm{out}}$ and $w^{+\mathrm{out}}$, therefore, lie entirely outside V_{2j+1}.

The determination of the Fourier coefficients from equations (6 *a*) and (6 *b*) presents as much difficulty as is usually encountered in evaluating the coefficients of the symmetric rotor-functions in the expansion of the wave function for the asymmetrical top. Moreover, a perturbation calculation based on these series expansions is also equally difficult to carry out in practice. So, one might think that very little has been gained by subjecting the matrices to a rather complicated transformation and then replacing them by certain operators of a very unusual type. This is, however, not the case. It was shown in I that even for moderately high *j*-values the differential equation (5 *a*) can be solved with a high degree of accuracy by less laborious methods, and the solution written in a compact analytic form.

Since the wave function for the asymmetrical top can be written (Kramers and Ittmann 1929 a, b, 1930) as a product of Lamé functions in elliptic coordinates, it is natural to expect that some connection exists between equation (5) and Lamé's equation

$$\left[4\Delta\xi\frac{d}{d\xi}\left(\Delta\xi\frac{d}{d\xi}\right)-j(j+1)-B\right]u(\xi)=0 \qquad \ldots\ldots(9)$$

where $\Delta\xi=[(\xi-e_1)(\xi-e_2)(\xi-e_3)]^{1/2}$, $e_1+e_2+e_3=0$, $e_1>e_2>e_3$. In fact, it is easily verified that the substitution

$$\xi=e_3+(e_2-e_3)\cos^2\phi \qquad \ldots\ldots(10)$$

transforms Lamé's equation into equation (5) with

$$\mu=-\frac{2}{3e_1}(B+e_1F), \qquad k=(e_2-e_3)/(3e_1).$$

While Lamé functions are usually expressed as doubly periodic functions, they appear here as functions possessing a single period 2π. Incidentally, we have also obtained generalized Lamé functions which are connected with the eigenfunctions of equations (5 *a*) and (5 *b*) outside V_{2j+1}. The doubly periodic form was used by Kramers and Ittmann (1929 a, b, 1930) in their pioneer work on the asymmetric rotor problem. This form is obtained by the substitution

$$\begin{aligned}\xi=\mathscr{P}(u;e_1,e_2,e_3)&=e_3+(e_1-e_3)\mathrm{ns}^2\{u(e_1-e_3)^{1/2}\}\\&=e_3+(e_1-e_3)\mathrm{ns}^2(\alpha-iK')=e_3+(e_2-e_3)\mathrm{sn}^2\alpha \qquad \ldots\ldots(11)\end{aligned}$$

(in the standard notation) where the modulus of the Jacobian elliptic functions is $\{(e_2-e_3)/(e_1-e_3)\}^{1/2}$. Comparing (10) and (11) we have $\mathrm{sn}^2\alpha=\cos^2\phi$. The transformation (10) or (11) makes it easier to solve the equation by approximate methods, the eigenfunctions being determined by the simple periodicity condition.

§ 4. PERTURBATION THEORY

The Hamiltonian of a polyatomic molecule, as given by Wilson and Howard (1936), is

$$H=\tfrac{1}{2}\mu^{1/2}\sum_{\alpha,\beta}(i\hbar P_\alpha+p_\alpha)\mu_{\alpha\beta}\mu^{-1/2}(i\hbar P_\beta+p_\beta)+\tfrac{1}{2}\mu^{1/2}\sum_k p_k\mu^{-1/2}p_k+V \quad \ldots\ldots(12)$$

where $\alpha, \beta=x, y, z$, $\mu_{\alpha\beta}$ are functions of normal coordinates, p_x, p_y, p_z are vibrational angular momenta, p_k are momenta conjugate to the normal coordinates and μ is the determinant of $\mu_{\alpha\beta}$. In the lowest approximation, when all small effects are neglected, H splits up into a vibrational and a rotational part, the latter being identical with the Hamiltonian of the asymmetrical top. The zero order wave functions are therefore $\psi_V{}^0\psi_R{}^0$ where $\psi_V{}^0$ is a product of oscillator functions corresponding to the normal modes of vibration of the molecule and $\psi_R{}^0$ is an eigenfunction of equation (5 *a*) or (5 *b*) belonging to V_{2j+1}. To calculate the corrections to energy arising from centrifugal stretching and the coupling of rotation and vibration by a perturbation procedure one must evaluate the matrix elements of H on the basis of the functions $\psi_V{}^0\psi_R{}^0$ which form a linearly independent but non-orthogonal set. In the present case, however, non-orthogonality of the basic functions causes no trouble, and the matrix elements can be calculated quite easily in the manner shown below. Since the Hamiltonian operator is closed with respect to the function space V_{2j+1}, consistent solutions will be obtained by considering functions in V_{2j+1} only, and these are the only solutions of physical interest.

An arbitrary function in V_{2j+1} can be expanded in a series of the form

$$f=\sum_i a_i v_i{}^+ + \sum_\mu a_\mu w_\mu{}^-$$

where Roman indices are used for first class functions and Greek indices for second class functions and $\int v_i w_j=\delta_{ij}$. Let M be a simple product of the type $P_iP_jP_k\ldots$ It is obvious that if M converts a u^+ into a u^- then it will simultaneously convert a u^- into a u^+. On the other hand, if M converts a u^+ into a u^+, it will at the same time convert a u^- into a u^-. In the first case,

$$f=\sum a_i v_i{}^+ + \sum a_\mu w_\mu{}^-, \qquad Mf=\sum b_i v_i{}^+ + \sum b_\mu w_\mu{}^-$$

and, we have

$$b_i=\int g^{-1/2}v_i{}^+Mf=\sum a_\mu\int g^{-1/2}v_i{}^+Mw_\mu{}^-, \qquad b_\mu=\sum a_i\int g^{1/2}w_\mu{}^-Mv_i{}^+.$$

Therefore,

$$M_{i\mu}=\int w_i{}^+Mw_\mu{}^- \text{ and } M_{\mu i}=\int v_\mu{}^-Mv_i{}^+.$$

In the second case,

$$M_{ij}=\int w_i{}^+Mv_j{}^+, \qquad M_{\mu\nu}=\int v_\mu{}^-Mw_\nu{}^-.$$

If $M_{ij}\neq 0$ then $M_{i\mu}=M_{\mu i}=0$, and if $M_{i\mu}\neq 0$ then $M_{ij}=M_{\mu\nu}=0$. The matrices, therefore, break up into two blocks either along the principal diagonal or along the second diagonal. The following argument, however, shows that they actually break up into four blocks symmetrically arranged with respect to the principal diagonal. First, we note that the eigenfunctions of equation (5 *a*) belong to four different types, $u^{+\text{even}}$, $u^{+\text{odd}}$, $u^{-\text{even}}$, $u^{-\text{odd}}$. The effect of an operator P_i

on any one of these functions is shown diagrammatically in the figure. Starting from a function represented by a vertex of the tetrahedron we proceed along a side to get the function into which it is converted by the corresponding operator. The diagram makes it clear that the situation is perfectly symmetrical with respect to P_x, P_y, P_z and further shows that P_iP_j, P_jP_i and P_k (for i, j, k all different) convert a function of the same initial type into a function of the same final type. This immediately leads to the above conclusion. In the case of P_x, P_y, P_z none of the blocks lies on the principal diagonal, while, for $P_x{}^2$, $P_y{}^2$, $P_z{}^2$ they all lie along the principal diagonal and the representation is completely reduced. The factorization of Wang's secular equation is a consequence of this.

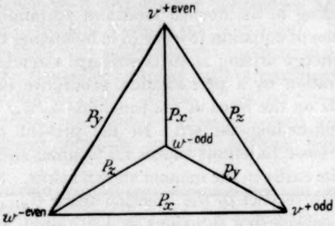

For evaluating the matrix elements the only thing necessary now is to obtain the solution of equation (5 *a*) or (5 *b*) in a compact form suitable for numerical work. Both the equations have the same normal form (equation (6) of I),

$$\left[D^2 + \frac{3k^2}{4g^2}\sin^2 2\phi + 1 + F + \frac{\mu-1}{g}\right]U = 0 \qquad \ldots\ldots(13)$$

where $U = g^{1/4}v = g^{3/4}w$. In the case of the highest and the lowest energy levels (for a given j), which are essentially degenerate, very satisfactory results can be obtained by using the first approximation of the BWK solution (equation (7) of I),

$$U = \left(1 + \frac{\mu-1}{(1+F)g}\right)^{-1/4} \begin{matrix}\cos\\ \sin\end{matrix} \int_0^{\phi}\left(1 + F + \frac{\mu-1}{g}\right)^{1/2} d\phi.$$

§ 5. SECOND ORDER CORRECTIONS TO ENERGY

To obtain the corrections to energy up to the second order Wilson and Howard (1936) remove the non-diagonal terms in V of the first order by a unitary transformation, so that the Hamiltonian matrix, evaluated on the basis of the symmetric rotor functions, factorizes into rotational blocks $\mathscr{H}$, one for each vibrational state. If $E_{VR}{}^0 - \mathrm{E}_{V''R''}{}^0$ is replaced by $E_V{}^0 - E_{V''}{}^0$, $\mathscr{H}$ takes the form

$$\mathscr{H}_{RR'} = H_{VR,\,VR'} + \frac{\sum\limits_{V'',R''}^{V''\neq V} H_{VR,\,V''R''}H_{V''R'',VR'}}{E_V{}^0 - E_{V''}{}^0}\,. \qquad \ldots\ldots(14)$$

If we sum over the index R'' the matrix $\mathscr{H}$ is clearly seen to be a polynomial of the fourth degree in the matrices P_i with constant coefficients which are formed from integrals over the vibrational functions. An examination of these integrals further shows that the coefficients of the linear and cubic terms in the P_i all vanish, and therefore,[†]

$$\mathscr{H}=E_V-\sigma_{ij}P_iP_j+\tau_{ijkl}P_iP_jP_kP_l \qquad \sigma_{ij}=\sigma_{ji}. \qquad \ldots\ldots(15)$$

The eigenvalues of this matrix are to be determined by directly solving the secular equation, which is, in general, a very laborious task. These heavy calculations can now be avoided by replacing the matrices P_i by the analytical operators of § 2, setting up a fourth order differential equation, and then trying to solve it by more convenient methods. As in I, § 3, this alternative procedure gives us greater freedom in solving the eigenvalue problem, and does not restrict us to the customary perturbation technique.

A straightforward application of the perturbation theory leads to the following formula for energy correct to the second order:

$$E_{VR}=H_{VR,VR}+\frac{\sum\limits_{V'',R''}^{V''R''\neq VR} H_{VR,V''R''}H_{V''R'',VR}}{E_{VR}{}^0-E_{V''R''}{}^0}. \qquad \ldots\ldots(16)$$

Terms in which $V''R''=VR$ are omitted in the summation, and $E_{VR}{}^0-E_{V''R''}{}^0$ is replaced by $E_V{}^0-E_{V''}{}^0$ in the denominator when $V''\neq V$. This formula differs from equation (14) also in that the basic rotational functions, labelled by the index R, are the solutions of the zero order rotational problem. For $V''\neq V$ the series in equations (14) and (16) become identical if R' is replaced by R. For $V''=V$, $R''\neq R$ the matrix elements $H_{VR,VR''}$ and $H_{VR'',VR}$ all vanish in the first order, if the basic rotational functions are taken to be the eigenfunctions of an operator of the type $-\sigma_{ij}P_iP_j$ the coefficients σ_{ij} being the same as $\frac{1}{2}\hbar^2(\mu_{ij})_{VV}$ but for differences of the second order. Such terms, therefore, need not be considered in obtaining the energy correct to the second order. On summing over the index R'' equation (16) now reduces to the average value equation

$$E_{VR}=E_V-\sigma_{ij}\langle P_iP_j\rangle+\tau_{ijkl}\langle P_iP_jP_kP_l\rangle \qquad \ldots\ldots(17)$$

where $\langle\ \rangle$ denotes averages over the eigenfunctions of the equation

$$(\sigma_{ij}P_iP_j+E)u=0. \qquad \ldots\ldots(18)$$

The results of a second-order treatment of the Hamiltonian (12) therefore agree with those of a first-order calculation based on equation (15).

Equation (18) can be brought into the form

$$(aP_x{}^{*2}+bP_y{}^{*2}+cP_z{}^{*2}+E)v=0$$

by an orthogonal transformation of the matrix vector (P_x, P_y, P_z) the transformation coefficients being ordinary numbers. Let A be a non-singular matrix, and let B be an antisymmetrical matrix. Then,

$$\sum_k B_k[P_i{}^*, P_j{}^*]=B_{pq}A_{pm}A_{qn}P_mP_n=\sum_{\gamma,k}B_\gamma DA_{k\gamma}{}^{-1}[P_i, P_j]$$

where i, j, k are cyclic permutations of 1, 2, 3, $B_{ij}=B_k$, $D=$ determinant of A. The commutation relations therefore remain unchanged if, and only if, A is a pure rotation matrix. For a rotation combined with a reflection they change sign. To determine a, b, c we write the general rotation matrix in the form

$$A=1-\Omega\sin\theta+\Omega^2(1-\cos\theta)$$

where Ω is antisymmetrical, and then use the perturbation technique, which is valid because of the smallness of the coefficients σ_{ij} for $i\neq j$.

[†] The coefficients σ, τ here are numerical multiples of those of Wilson and Howard (1936, eqn (49)).

§ 6. CALCULATION OF AVERAGE VALUES

From the discussions of § 5 we see that the determination of the energy levels up to the second order by a perturbation procedure reduces to the calculation of average values of products of angular momentum operators over an eigenfunction of equation (5 *a*). In order that an average may have a non-zero value it should be possible to return to the starting point after making a complete detour along the sides of the tetrahedron of the figure. We thus get the following non-vanishing averages: (i) $\langle P_i P_j \rangle$ for $i=j$, (ii) $\langle P_i P_j P_k \rangle$ for i, j, k all different, (iii) $\langle P_i P_j P_k P_l \rangle$ for i, j, k, l equal in pairs. For such combinations of angular momenta the matrices are completely reduced to the block form.

Next, let A or B denote one of the operators 1, P_i^2, $P_x P_y + P_y P_x$. Then A^+ is adjoint to A^-, $(AB)^+ = A^+B^+$, $(AB)^- = A^-B^-$. For symmetrized products of the type $M = AB + BA$, we have

$$M_{ij} = \int g^{-1/2} v_i^+ M^+ v_j^+, \qquad M_{\mu\nu} = \int v_\mu^- M^- w_\nu^- = \int g^{-1/2} v_\nu^- M^+ v_\mu^-.$$

For all eigenfunctions the average value $\langle M \rangle$ has therefore the same analytic form $\langle M \rangle = \int g^{-1/2} v M^+ v$. For unsymmetrized products of the type AB, we have

$$(AB)_{ij} = \int g^{-1/2} v_i^+ (AB)^+ v_j^+, \qquad (AB)_{\mu\nu} = \int v_\mu^- (AB)^- w_\nu^- = \int g^{-1/2} v_\nu^- (BA)^+ v_\mu^-.$$

$\langle AB \rangle^+$, $\langle BA \rangle^-$, and in particular $\langle A \rangle^+$ and $\langle A \rangle^-$, have therefore the same analytic form. Also

$$\langle L^{*n} \rangle = \int v^- L^{*n} w^- = \int g^{-1/2} v^- L^n v^-.$$

Next we establish the important result that $\langle P_i^2 \rangle$, $\langle P_i^2 P_j^2 \rangle$ can all be expressed in terms μ, $d\mu/dk$ and $\langle P_z^4 \rangle$. Using the same symbol Λ for both L and L^* we have

$$\tfrac{1}{2}(2c-a-b)\Lambda = aP_x^2 + bP_y^2 + c(F+P_z^2).$$

The eigenvalue μ and the eigenfunction u of Λ depend on a single parameter k and not on a, b, c separately. Keeping k fixed we subtract b from a, b, c obtaining a relation between P_x^2 and P_z^2,

$$\left.\begin{aligned} \Lambda = \frac{2}{2c-a-b}[(a-b)P_x^2 + (c-b)(F+P_z^2)] &= -2kP_x^2 + (1-k)(F+P_z^2) \\ &= 2kP_y^2 + (1+k)(F+P_z^2) = -\mu, \\ \Lambda^2 = 4k^2P_y^4 + (1+k)^2(F+P_z^2)^2 + 2k(1+k)[2FP_y^2 + P_y^2P_z^2 + P_z^2P_y^2] &= \mu^2. \end{aligned}\right\} \qquad \ldots\ldots(19)$$

Now, if M is an operator with eigenfunction u, then it is easily seen that $\partial\langle M \rangle/\partial\alpha = \langle \partial M/\partial\alpha \rangle$ where α is any parameter occurring in M. The most important operator of this type is $M = \sum a_n \Lambda^n$. Using this interesting result we have

$$-\frac{d\mu}{dk} = 2\langle P_y^2 \rangle + F + \langle P_z^2 \rangle, \qquad \langle P_z^2 \rangle = -\mu + k\frac{d\mu}{dk} - F. \qquad \ldots\ldots(20)$$

Differentiating (19) with respect to k and combining the independent relation so obtained with (19) we have

$$k\langle P_y^2P_z^2 + P_z^2P_y^2 \rangle = \left(\mu - k\frac{d\mu}{dk} + F\right)[\mu + (1+k)F] - (1+k)\langle P_z^4 \rangle.$$

It is thus shown that the perturbed energies of a polyatomic molecule can be obtained in terms of a single parameter k without introducing the moments of inertia at any stage of the calculation.

For the evaluation of $\langle P_z^4 \rangle$ a straightforward integration over the wave function seems to be unavoidable. By the use of equation (5 *a*) or (5 *b*), which enables one to replace all higher derivatives by the first derivative, and a subsequent integration by parts, the integral for any average value can be brought into the form $\int \lambda(\phi) U^2$, where U is an eigenfunction of equation (13). Although the exact expression for $\lambda(\phi)$ is usually long and complicated, most of the terms can be neglected without appreciably affecting the result.

§ 7. AN ALTERNATIVE REDUCTION OF THE PROBLEM

It was mentioned in the Introduction that the problem of reduction to a single variable admits of two independent solutions, of which one was chosen for a detailed study in the preceding articles. The reason for this is that the basic differential equation to which it leads is directly *related to Lamé's equation*, which has been thoroughly studied by mathematicians, and is comparatively easy to solve by approximate methods. Secondly, it is a natural extension of the author's previous work and most of the work done on the problem by others. But the alternative reduction of this Section also has its advantages, although the connection with Lamé's equation is not clear, and is quite suitable for application to spectroscopic problems. To obtain this second reduction we subject the matrices to the transformation

$$\prod_{p=1}^{2j} [(2j+1-p)^{-1/2} p^{1/2}]_{(p)} (\;) \prod_{p=1}^{2j} [(2j+1-p)^{1/2} p^{-1/2}]_{(p)}. \qquad \ldots\ldots(21)$$

After the transformation the matrices assume the forms

$$(M_x + iM_y)_{m+1,m} = j - m, \qquad (M_x - iM_y)_{m,m+1} = j + m + 1, \qquad (M_z)_{mm} = m$$

which can be generated by the operators

$$\left.\begin{aligned} M_x \pm iM_y = \mathrm{e}^{\pm i\phi}(j \pm iD), \qquad M_z = -iD \\ M_x = j\cos\phi - \sin\phi D, \qquad M_y = j\sin\phi + \cos\phi D, \qquad M_z = -iD\;. \end{aligned}\right\} \qquad \ldots\ldots(22)$$

The restriction that these operators are defined only for one value of j can be removed by replacing any such operator M by $\mathrm{e}^{i(1+F)\phi} M \mathrm{e}^{-i(1+F)\phi}$. The function spaces on which they operate then get separated from one another.

These operators obey the usual commutation rules, and, since they are closed with respect to V_{2j+1} both for integral and half-integral values of j, permit spin to be treated on the same footing as orbital angular momentum. We have, therefore, the spin functions $\mathrm{e}^{-i\phi/2}$, $\mathrm{e}^{i\phi/2}$ and the spin operators $\sigma_x = \cos\phi - 2\sin\phi D$, $\sigma_y = \sin\phi + 2\cos\phi D$, $\sigma_z = -2iD$ in place of the Pauli matrices.

The equation for the asymmetrical top now takes the form

$$[g(F + D^2) - \tfrac{1}{2}g'(2j-1)D + 2j^2(1-g) + \mu]u = 0. \qquad \ldots\ldots(23)$$

This equation has no direct connection with Lamé's equation or equation (5 *a*) and seems to be new, although the eigenvalues are, of course, the same. The recurrence relations for the Fourier coefficients of a solution are

$$a_{r-2}\tfrac{1}{2}k(j-r+1)(j-r+2) + a_r(F + \mu - r^2) + a_{r+2}\tfrac{1}{2}k(j+r+1)(j+r+2) = 0$$

which show that the $2j+1$ eigenfunctions of physical interest all lie in V_{2j+1}, unlike those of equations (5*a*) and (5*b*). By a similarity transformation the matrix of the coefficients of a_r can be brought into Wang's self-adjoint form, with changed signs for the diagonal elements. As the determinant is clearly an even function of k this change of sign has no effect on the eigenvalues.

To show that the non-physical eigenvalues corresponding to the infinite irreducible blocks are also contained in (23) we bring the matrices into the forms

$$(M_x+iM_y)_{m+1,m}=j+m+1, \qquad (M_x-iM_y)_{m,m+1}=j-m$$

by a suitable transformation. The corresponding operators

$$M_x+iM_y=(j-iD)\mathrm{e}^{i\phi}, \qquad M_x-iM_y=(j+iD)\mathrm{e}^{-i\varphi}$$

are adjoint to the operators (22). For the asymmetrical top we, therefore, get the adjoint equation

$$[g(F+D^2)+\tfrac{1}{2}g'(2j+3)D+2(j+1)^2(1-g)+\mu]v=0$$

which has the same set of eigenvalues as (23).

§ 8. Passage to the Original Basis

In this Section we show how to go back to the basis of spherical harmonics (in the case of atomic spectra) or symmetric rotor functions (in the case of molecular spectra) after carrying out calculations in either of the above schemes (§§ 2 and 7).

Let the transformations (1) and (21) be $A^{-1}(\ )A$. If, at the end of the calculations, we get a function $f(\phi)$ then the Fourier expansion of $f(\phi)$ will terminate and will be

$$f(\phi)=\sum_{m=-j}^{+j} a_m\mathrm{e}^{im\phi}=\sum_{m=-j}^{+j} A_{mm}a_m(\mathrm{e}^{im\phi}/A_{mm}).$$

To get the expansions in terms of spherical harmonics $\mathrm{Y}_j^m(\theta,\phi)$ or symmetric rotor functions $u_{mk}^j(\chi,\theta,\phi)$ we need only replace $\mathrm{e}^{im\phi}/A_{mm}$ in this equation by Y_j^m or u_{mk}^j so that

$$F(\theta,\phi)=\sum_{m=-j}^{+j} A_{mm}a_m\mathrm{Y}_j^m(\theta,\phi), \qquad G_m(\chi,\theta,\phi)=\sum_{k=-j}^{+j} A_{kk}a_ku_{mk}^j(\chi,\theta,\phi)$$

where θ,ϕ in $F(\theta,\phi)$ are the polar and azimuthal angles, and χ,θ,ϕ in $G_m(\chi,\theta,\phi)$ are the Euler angles.

It is known from group theory that the wave function for the asymmetrical top admits of an expansion of the form

$$G_m(\chi,\theta,\phi)=\sum_{k=-j}^{+j} D^j(\chi,\theta,\phi)_{mk}{}^*B_k{}^j$$

where the coefficients $B_k{}^j$ are independent of m (the angular momentum about a space-fixed z axis), and $D^j(\chi,\theta,\phi)_{mk}$ are the matrix elements of the $(2j+1)$-dimensional representation of the rotation group. The expression for $D^j(\chi,\theta,\phi)_{mk}{}^*$ is

$$\begin{aligned} u_{mk}{}^j &= D^j(\chi,\theta,\phi)_{mk}{}^* \\ &= \sum_p (-1)^p \frac{[(j-k)!\,(j+k)!\,(j-m)!\,(j+m)!]^{1/2}}{(j+m-p)!\,(j-k-p)!\,p!\,(p-m+k)!}\,\mathrm{e}^{im\chi+ik\phi} \\ &\quad \times(\cos\tfrac{1}{2}\theta)^{2j}(\tan\tfrac{1}{2}\theta)^{2p-m+k} \qquad \ldots\ldots(24) \end{aligned}$$

where p takes all integral values consistent with the factorial notation, the factorial of a negative number being meaningless. To verify that the matrices of § 2 are generated by these functions we operate on them by the operators

$$P_x \pm iP_y = \mathrm{e}^{\mp i\phi}[\pm iD_\theta - \operatorname{cosec}\theta D_\chi + \cot\theta D_\phi], \qquad P_z = D_\phi$$

for angular momentum about body-fixed axes, and the operators

$$M_x \pm iM_y = \mathrm{e}^{\pm i\chi}[-iD_\theta \mp \operatorname{cosec}\theta D_\phi \pm \cot\theta D_\chi], \qquad M_z = -iD_\chi$$

for angular momentum about space-fixed axes. The results show that the representation of §2 is obtained on changing k to $-k$ on the right-hand side of (24) and multiplying by appropriate normalization factors.

Finally, for the transformation (21) the value of A_{mm} is found to be $A_{mm} = [(j-m)!\,(j+m)!]^{1/2}$ if an unimportant factor involving j is omitted, while, for the transformation (1)

$$A_{mm} = (-1)^{-m/2} \frac{\{\tfrac{1}{2}(j-m)\}!\,\{\tfrac{1}{2}(j+m)\}!}{[(j-m)!\,(j+m)!]^{1/2}},$$

if $j-m$ is even and

$$A_{mm} = (-1)^{-(m+1)/2} \times \tfrac{1}{2} \frac{\{\tfrac{1}{2}(j-m-1)\}!\,\{\tfrac{1}{2}(j+m-1)\}!}{[(j-m)!\,(j+m)!]^{1/2}},$$

if $j-m$ is odd.

§ 9. The Product Space and the Clebsch–Gordan Coefficents

For a dynamical system with two angular momenta M_1 and M_2 the eigenfunction Ψ_{jm} of $M^2 = (M_1 + M_2)^2$ is a linear combination of the products of eigenfunctions of $(M_1)^2$ and $(M_2)^2$

$$\Psi_{jm} = \sum_{m_1 m_2} \{m_1 m_2 | jm\} \mathrm{Y}_{j_1}{}^{m_1}(\theta_1, \phi_1) \mathrm{Y}_{j_2}{}^{m_2}(\theta_2, \phi_2).$$

The coefficients $\{m_1 m_2 | jm\}$ of this linear combination are called the Clebsch–Gordan coefficients which play a very important role in the theory of complex spectra. Wigner was the first to obtain a closed expression for these coefficients by group theoretical methods. Both the formula and its mode of derivation were subsequently improved by Racah (1942) and brought into a useful form by using elementary algebra. Further simplification is, however, expected to result from the use of the transformation (21) of §7. We therefore replace the usual angular momentum operators by the one-variable operators (22) of §7 and the normalized spherical harmonics $\mathrm{Y}_{j_1}{}^{m_1}(\theta_1, \phi_1)$, $\mathrm{Y}_{j_2}{}^{m_2}(\theta_2, \phi_2)$ by $\exp(im_1\phi_1)$, $\exp(im_2\phi_2)$, obtaining the double Fourier series

$$\Phi_{jm} = \sum_{m_1 m_2} (m_1 m_2 | jm) \exp(im_1\phi_1 + im_2\phi_2).$$

The coefficients $(m_1 m_2 | jm)$ of this series may be called the 'modified Clebsch–Gordan coefficients'. Considerations of §8 show that the connection between the modified and the actual Clebsch–Gordan coefficients is

$$\{m_1 m_2 | jm\} = (m_1 m_2 | jm) \left[\frac{(j_1 - m_1)!\,(j_1 + m_1)!\,(j_2 - m_2)!\,(j_2 + m_2)!}{(j-m)!\,(j+m)!}\right]^{1/2}. \quad \ldots\ldots (25)$$

On introducing the variables $\xi = \phi_1$, $\eta = \phi_1 - \phi_2$ the eigenfunction

$$\Phi_{jm} = \sum_{m_2} (m_1 m_2 | jm) \exp(im\xi - im_2\eta)$$

is found to satisfy the ordinary differential equation†

$$[M^2-F]\Phi_{jm}=[e^{i\eta}(j_1-m+iD_\eta)(j_2+iD_\eta)+e^{-i\eta}(j_1+m-iD_\eta)(j_2-iD_\eta)$$
$$+2(im+D_\eta)D_\eta+F_1+F_2-F]\Phi_{jm}=0 \qquad \ldots\ldots(26)$$

where $F_1=j_1(j_1+1)$, $F_2=j_2(j_2+1)$, $m=m_1+m_2$. A glance at this differential equation or the equation in ϕ_1, ϕ_2 reveals some of the symmetry properties of the Clebsch–Gordan coefficients. The orthogonality relation

$$\sum_{m_2}\{m_1m_2|jm\}\{m_1m_2|j'm'\}=C_{jm}\delta_{jj'}\delta_{mm'}$$

also follows immediately. The recurrence relations for the Fourier coefficients $(m_1m_2|jm)$ of Φ_{jm} are

$$(m_1+1,m_2-1|jm)(j_1+m_1+1)(j_2-m_2+1)+(m_1m_2|jm)(F_1+F_2-F+2m_1m_2)$$
$$+(m_1-1,m_2+1|jm)(j_1-m_1+1)(j_2+m_2+1)=0. \qquad \ldots\ldots(27)$$

The calculation of the Clebsch–Gordan coefficients from these relations is possible, in principle, but is a formidable undertaking when one considers the difficulty of solving the simultaneous equations and normalizing the complicated series for Ψ_{jm} so obtained. The calculation is, however, much simplified if one starts from the following two recurrence relations:

$$(j-m)(m_1m_2+1|jm+1)=(m_1-1,m_2+1|jm)(j_1-m_1+1)$$
$$+(m_1m_2|jm)(j_2-m_2), \qquad \ldots\ldots(28)$$

$$(j+m)(m_1m_2-1|jm-1)=(m_1+1,m_2-1|jm)(j_1+m_1+1)$$
$$+(m_1m_2|jm)(j_2+m_2). \qquad \ldots\ldots(29)$$

These relations are obtained by applying the operators $M_x \pm iM_y$ to the function Φ_{jm}. It is easily verified that they lead to the relation (27) obtained independently from equation (26).

To calculate the coefficients we follow Racah in putting $m=j$ in equation (28). This gives

$$(m_1m_2|jj)=(-1)^{j_1-m_1}\frac{(j_1+j_2-j)!(j_1,j-j_1|jj)}{(j_1-m_1)!(j_2-m_2)!}=(-1)^{j_2-m_2}\frac{(j_1+j_2-j)!(j-j_2,j_2|jj)}{(j_1-m_1)!(j_2-m_2)!}.$$

Writing B_j for $(j_1+j_2-j)!(j_1,j-j_1|jj)$ and substituting this expression for $(m_1m_2|jj)$ in the right-hand side of (29) we get $(m_1m_2|j,j-1)$. Proceeding in this way we get the general formula

$$(m_1m_2|jm)=\frac{B_j(-1)^{j_1-m_1}(j-m)!(j+m)!}{(2j)!(j_1+m_1)!(j_2+m_2)!}$$
$$\times\sum_t(-1)^t\frac{(j_1+m_1+t)!(j_2+j-m_1-t)!}{t!(j-m-t)!(j_1-m_1-t)!(j_2-j+m_1+t)!}.$$

The relation between B_j and Racah's A_j is $B_j=(2j)!A_j$. This is as far as we can go by the present method.

REFERENCES

KRAMERS, H. A., and ITTMANN, G. P., 1929 a, *Z. Phys.*, **53,** 553; 1929 b, *Ibid.*, **58,** 217; 1930, *Ibid.*, **60,** 663.

MAJUMDAR, S. D., 1954, *Proc. Phys. Soc.* A, **67,** 351.

RACAH, G., 1942, *Phys. Rev.*, **62,** 438.

WILSON, E. B., and HOWARD, J. B., 1936, *J. Chem. Phys.* **4,** 260.

---

† $M^2=(M_1)^2+(M_2)^2+2\sum_{i=x,y,z}M_{i1}M_{i2}=F_1+F_2+\exp\{i(\phi_1-\phi_2)\}(j_1+iD_1)(j_2-iD_2)$
$+\exp\{-i(\phi_1-\phi_2)\}(j_1-iD_1)(j_2+iD_2)-2D_1D_2=$ a function of η, D_ξ, D_η.
Notice that D_ξ commutes with M^2.

Dilution Effects in Regular Assemblies

By G. M. BELL

Mathematics Department, The Manchester College of Science and Technology

MS. received 25th February 1958, *and in revised form 23rd May* 1958

Abstract. A study is made of the thermal behaviour of solid mixtures, containing a component A with molecules having several orientation states whose co-operative interaction leads, in pure A, to a second-order transition with a discontinuity in the specific heat and a diluting component B with molecules of the same size. Regular models are used and it can be shown from previous work on ternary assemblies that if A has two equivalent orientation states and complete equilibrium is attained, then the curve of critical temperature against the mole fraction x_A of A passes through the origin. It is shown here that if A–B diffusion is forbidden in the temperature range concerned so that the distribution of A and B is fixed, though A molecules can change their orientation, then the specific heat is continuous below a critical value of x_A. This effect depends on short-range ordering and a first-order quasi-chemical approximation is used. Similar results are obtained when A has three available orientation states. A short investigation is also made of results when the interaction with B removes the equivalence between the two states of A. The effects here do not depend on short-range ordering, a random statistical approximation is used and it is found that even the smallest proportion of B renders the specific heat continuous with a maximum replacing the discontinuity. Finally, these various types of behaviour are briefly compared with some observed dilution effects.

§ 1. INTRODUCTION

SECOND-ORDER transitions or λ-points with discontinuities in the specific heat but not in the energy or entropy occur in many solids and the effects of alteration in the thermodynamic variables are of considerable interest. This paper deals theoretically with the dilution of a component A which displays a second-order transition by a component B which does not. The models used are of the regular type with N_A molecules of A and N_B of B, assumed to be of the same size, distributed on $N = N_A + N_B$ lattice sites, each of the latter having z other sites as nearest neighbours. The mole fractions x_A and x_B of A and B respectively are given by

$$x_A = N_A/N, \qquad x_B = 1 - x_A = N_B/N. \qquad \ldots\ldots(1)$$

The molecules of A have several possible orientations relative to the lattice and the transition is a co-operative effect of the interactions between them. Below the critical temperature where the transition occurs there is long-range order among the orientations of A. Except in § 6 the interaction energy of a B with an A molecule is independent of the orientation states of the latter. If these are two in number the assembly is then a mixture of an 'Ising model' component (see, for instance, Temperley 1956) with an 'inert' component.

Two processes can be distinguished in the attainment of minimum free energy by an A–B mixture after a change of temperature. The first is the re-orientation of molecules of A and the second is the migration of A and B molecules to new sites. The second process is inhibited if the activation energy for an exchange of A and B molecules between neighbouring sites is large compared with $\boldsymbol{k}T$, where $\boldsymbol{k}$ is Boltzmann's constant and T the absolute temperature. If A has two available orientation states and if A–B diffusion can occur freely then the theory of this binary (two-component) model is closely related to that of a ternary (three-component) model considered by the author in a previous paper (Bell 1953). As the connection with the binary model was only briefly mentioned there relevant results will be summarized here at the end of § 2. Since cases where the temperature is low enough for migration to be prohibited are of considerable interest, the consequences of this will be considered fully here, it being supposed that the A and B molecules remain fixed in position on the lattice and that the free energy takes up the lowest value consistent with this requirement. In the random (zero-order or Bragg–Williams) approximation the numbers of nearest neighbour pairs of each type are equal to those found in a random distribution so that it is necessary, in estimating the effect of a fixed A–B distribution, to use at least the first-order statistical approximation. This will be applied below to models where the numbers of possible orientations of an A molecule are two and three respectively. In § 6, with a two-orientation model for A, the consequences of removing the condition that the interaction with B is independent of the state of A will be examined. In conclusion, the applicability of the theory to observations on ammonium–rubidium chloride, solid ortho-para hydrogen and methane–krypton mixtures will be discussed.

§ 2. Free Energy and Complete Equilibrium

In a regular model the configurational energy E_c, entropy S_c and Helmholtz free energy F_c are given by

$$F_c = E_c - TS_c = \sum_{i,j} e_{ij} N_{ij} - \boldsymbol{k}T \ln g(N_i, N_{ij}). \qquad \ldots\ldots(2)$$

Here $g(N_i, N_{ij})$ is the number of arrangements of N_i molecules of each species i which give N_{ij} nearest neighbour pairs of each type i–j and e_{ij} is the interaction energy of one nearest neighbour i–j pair. The numbers N_{ij} are not independent since there exists for each species i the relation

$$zN_i = 2N_{ii} + \sum_{j \neq i} N_{ij}, \qquad \ldots\ldots(3)$$

where z is the number of nearest neighbours of each lattice site and the total number N of sites is large enough for boundary effects to be negligible. The quasi-chemical first-order approximation is introduced by assuming (Guggenheim and McGlashan 1951)

$$\begin{aligned}\ln g = &-(z-1)\Big(N \ln N - \sum_i N_i \ln N_i\Big) \\ &+ \tfrac{1}{2}zN \ln\left(\tfrac{1}{2}zN\right) - \sum_i N_{ii} \ln N_{ii} - \sum_{i<j} N_{ij} \ln\left(\tfrac{1}{2}N_{ij}\right). \qquad \ldots\ldots(4)\end{aligned}$$

If the molecules of A can take up two orientations then, in these orientation states, they will be labelled as species 1 and 2 respectively. For second-order transitions to occur in pure A or A–B mixtures these two species must have equivalent properties and the interaction energies take the form

$$e_{11} = e_{22} = e_{AA} - \tfrac{1}{2}w, \quad e_{12} = e_{AA} + \tfrac{1}{2}w, \quad e_{1B} = e_{2B} = e_{AB}, \qquad \ldots\ldots(5)$$

where w will be assumed positive. From (2), (4) and (5) the free energy F_c is symmetrical with respect to species 1 and 2 so that its value is unchanged if each molecule of species 1 is replaced by a 2 and each 2 by a 1. The case where there is free site to site movement of A and B molecules, so that complete equilibrium can be attained, will now be considered. If species 1 and 2 are regarded as separate components but the interactions still have the form given by (5), then the resulting three-component (ternary) mixture is of the type discussed previously by the author. The free energy F_c is the same function of N_1, N_2 and N_B in both models and the condition giving the composition of conjugate phases symmetrical with respect to components 1 and 2 in the ternary mixture (Bell 1953, eqn 2.10) also gives the proportions of species 1 and 2 in an ordered phase of the binary mixture at the same temperature. The temperature at which these conjugate phases first appear in the ternary mixture is thus equal to the critical or λ-point temperature in the binary mixture below which a majority of the A molecules are either in state 1 or state 2 (long-range order). Although it has been supposed for definiteness that w is positive it can be shown (Bell 1953, § 6) that the equilibrium equations also apply where w is negative. In this case the numbers of 1 and 2 remain equal below the transition point but they form superlattices, giving another type of long-range order.

If critical temperature is plotted against x_A the curve always passes through the origin so that a transition occurs in any mixture of constant composition, however small the mole fraction of A. Before the temperature can reach zero, however, separation occurs into an A-rich and a B-rich phase and the proportion of A in the latter decreases to zero so rapidly that a transition to an ordered state is impossible. If T_c is the critical temperature for a mixture with a given mole fraction x_A of A and T_1 that for pure A then, with a zero-order or random approximation, T_c/T_1 is equal to x_A. If the first-order approximation, which takes account to some extent of short-range order effects, is used the ratio T_c/T_1 is found to be larger than x_A for positive values of $e_{AB}-\frac{1}{2}e_{AA}-\frac{1}{2}e_{BB}$. This is due to the fact that A–B repulsion causes clustering so that the fraction of A molecules among the nearest neighbours of a given A molecule will be rather larger than x_A. (For critical temperature curves see figures 4 and 5 and, for the tendency to phase separation, figure 1 of Bell (1953). The symbols x_3 and w' are equivalent to x_B and $e_{AB}-\frac{1}{2}(e_{AA}+e_{BB})+\frac{1}{4}w$ respectively of the present paper.) The case where there is a strong attractive interaction between A and B molecules, tending to A–B superlattice formation, will not be considered here.

§ 3. EQUILIBRIUM EQUATIONS WITH FIXED COMPONENT DISTRIBUTION

The free energy defined by (2) and (4) will be minimized with the distribution of A and B molecules on the lattice 'frozen'. In this section the A molecules are supposed to have three available orientation states, labelled 1, 2 and 3, so that

$$N_A = N_1 + N_2 + N_3. \qquad \ldots\ldots(6)$$

Results for the simpler model where A molecules have only two orientation states will be considered in § 4 but the relations for this case can easily be obtained from those derived here by putting N_3 and the pair numbers with an index 3 equal to zero. Since N_A is a constant (6) will be regarded as expressing N_1 in terms of the independent variables N_2 and N_3. The N_B molecules of component B form only one species so that there are four relations of type (3) between N_1,

N_2, N_3 and N_B and the ten species pair numbers N_{ij} $(=N_{ji})$ which result from letting the suffixes i and j run through 1, 2, 3 and B. Of the three component pair numbers N_{AA}, N_{BB} and N_{AB} the last is also a species pair number while the first two are given by

$$N_{AA}=N_{11}+N_{22}+N_{33}+N_{12}+N_{13}+N_{23}, \quad N_{AB}=N_{1B}+N_{2B}+N_{3B}. \quad \ldots\ldots(7)$$

It may be shown from (3), (6) and (7) that, as would be expected,

$$zN_A=2N_{AA}+N_{AB}, \quad zN_B=2N_{BB}+N_{AB}, \quad \ldots\ldots(8)$$

so that fixing one of the three component pair numbers automatically fixes the other two. With the lattice positions of A and B fixed N_{BB} is constant and there remain nine variable species pair numbers which satisfy the four relations of type (3) so that only five of them are independent. These are chosen to be N_{12}, N_{13}, N_{23}, N_{2B} and N_{3B} and from (3), (6), (7) and (8) the others are given by

$$\left.\begin{aligned} N_{11}&=N_{AA}-\tfrac{1}{2}zN_2-\tfrac{1}{2}zN_3-\tfrac{1}{2}N_{12}-\tfrac{1}{2}N_{13}+\tfrac{1}{2}N_{2B}+\tfrac{1}{2}N_{3B},\\ N_{22}&=\tfrac{1}{2}zN_2-\tfrac{1}{2}N_{12}-\tfrac{1}{2}N_{23}-\tfrac{1}{2}N_{2B},\\ N_{33}&=\tfrac{1}{2}zN_3-\tfrac{1}{2}N_{13}-\tfrac{1}{2}N_{23}-\tfrac{1}{2}N_{3B}, \qquad N_{1B}=N_{AB}-N_{2B}-N_{3B}. \end{aligned}\right\} \ldots\ldots(9)$$

The interaction energies not involving state 3 of A are given by (5). If the free energy is to remain symmetrical with respect to states 1 and 2 of A, where a third state exists, e_{13} must be equal to e_{23}. It will be assumed that

$$e_{13}=e_{23}=e_{33}=e_{AA}, \quad e_{3B}=e_{AB} \quad \ldots\ldots(10)$$

so that component B has the same interaction with all three states of A. The configurational energy is now given by

$$\begin{aligned} E_c=(e_{AA}-\tfrac{1}{2}w)N_{AA}+e_{AB}N_{AB}+e_{BB}N_{BB}\\ +\tfrac{1}{4}zwN_3+wN_{12}+\tfrac{1}{4}w(N_{13}+N_{23})-\tfrac{1}{4}wN_{3B}. \end{aligned} \quad \ldots\ldots(11)$$

Certain variables, in terms of which it is convenient to express the relations arising from the minimization of the free energy, will now be defined by

$$\left.\begin{aligned} \eta=\exp(-w/\boldsymbol{k}T), \qquad \zeta=\eta^{1/4}=\exp(-\tfrac{1}{4}w/\boldsymbol{k}T),\\ t^2=\frac{N_{22}}{N_{11}}, \qquad u^2=\frac{N_{33}}{N_{11}}, \qquad v=\frac{\tfrac{1}{2}N_{1B}}{N_{11}}. \end{aligned}\right\} \ldots\ldots(12)$$

If the derivatives of F_c with respect to the five independent species pair numbers are equated to zero the following relations can be obtained:

$$\left.\begin{aligned} N_{12}=2\eta tN_{11}, \quad N_{2B}=2vtN_{11}, \quad N_{3B}=2\zeta^{-1}uvN_{11},\\ N_{13}=2\zeta uN_{11}, \quad N_{23}=2\zeta utN_{11}. \end{aligned}\right\} \ldots\ldots(13)$$

It is useful to express the degree of local order among the molecules of components A and B by a constant, κ, where

$$\kappa=\tfrac{1}{2}N_{AB}/N_{AA}. \quad \ldots\ldots(14)$$

The variable v can be expressed in terms of the other quantities defined in (12) and of the constant κ by substitution of (7) and (13) into (14) and rearrangement to give

$$v=\frac{\kappa(1+t^2+u^2+2\eta t+2\zeta u+2\zeta ut)}{1+t+\zeta^{-1}u} \quad \ldots\ldots(15)$$

If the mixture has been brought down from a temperature where mixing is random without sufficient time being given for A–B diffusion to occur then

$$\kappa = (1 - x_A)/x_A = x_B/(1 - x_B). \qquad \ldots\ldots(16)$$

By writing out equations of type (3) for N_1, N_2 and N_3, dividing and substituting it can be proved that

$$\frac{N_2}{N_1} = \frac{t\phi}{\theta}, \qquad \frac{N_3}{N_1} = \frac{u\psi}{\theta} \qquad \ldots\ldots(17)$$

where

$$\theta = 1 + \eta t + \zeta u + v, \qquad \phi = t + \eta + \zeta u + v, \qquad \psi = u + \zeta + \zeta t + \zeta^{-1} v. \qquad \ldots\ldots(18)$$

From the relations derived above for N_i and N_{ij} the free energy F_c may be expressed in terms of constant quantities, the temperature and the variables t and u, which are themselves given implicitly in terms of N_2 and N_3 by (17). The equilibrium values of N_2 and N_3 are obtained by equating to zero the partial derivatives of F_c with respect to N_2 and N_3. With the help of (6) and (9) this yields the relations

$$\frac{1}{\boldsymbol{k}T}\frac{\partial F_c}{\partial N_2} = -(z-1)\ln\frac{N_2}{N_1} + \tfrac{1}{2}z\ln\frac{N_{22}}{N_{11}} = \ln\left\{t\left(\frac{\theta}{\phi}\right)^{z-1}\right\} = 0, \qquad \ldots\ldots(19)$$

$$\frac{1}{\boldsymbol{k}T}\frac{\partial F_c}{\partial N_3} = -(z-1)\ln\frac{N_3}{N_1} + \tfrac{1}{2}z\ln\frac{N_{33}}{N_{11}} = \ln\left\{u\left(\frac{\theta}{\psi}\right)^{z-1}\zeta^{-z}\right\} = 0. \qquad \ldots\ldots(20)$$

This pair of equations may be solved for the equilibrium values of t and u. It can be proved that if the values t_0 and u_0 satisfy (19) and (20) then so do t_0^{-1} and $t_0^{-1}u_0$. This second solution interchanges the values of N_2 and N_1 while leaving E_c and S_c unaltered. Thus, to each equilibrium state where $N_1 \neq N_2$ there corresponds another equilibrium state in which these values of N_1 and N_2 are interchanged.

§ 4. TWO-ORIENTATION MODEL

It will now be supposed that the A–B distribution is fixed and the A molecules have two available orientation states. The equilibrium equations can be obtained from those given in the previous section by putting N_3, the pair numbers with an index 3 and the variable u equal to zero. The interaction energies are given by (5) and from (11) the variable part of the configurational energy is now simply wN_{12}. The independent species pair numbers are N_{12} and N_{2B}, and equating the corresponding derivatives of F_c to zero gives the first two relations of (13). From (17)

$$\frac{N_2}{N_1} = \frac{t(t + \eta + v)}{1 + \eta t + v} \qquad \ldots\ldots(21)$$

where v is expressed as a function of t by (15), with u put equal to zero. Since N_3 and N_{33} are zero equation (20) has no significance but equation (19), the result of equating $\partial F/\partial N_2$ to zero, takes the form

$$f(t) = \frac{t(1 + \eta t + v)^{z-1}}{(\eta + t + v)^{z-1}} = 1. \qquad \ldots\ldots(22)$$

From this equation the values of t and, hence, of the configurational thermodynamic functions can be calculated at any temperature. If $x_A = 1$ so that $v = 0$ then (21) and (22) become equivalent to equations (12) and (13 A) respectively of Bethe (1935).

For all values of η and hence of the temperature (22) is satisfied by $t=1$ which, from (21), gives $N_1=N_2=\frac{1}{2}N_A$. It may be shown that if $t=t_0$, where $t_0 \neq 1$, is also a solution of (22) then so is $t=t_0^{-1}$. From (21) this means that if there exists a solution of (22) giving $N_1 \neq N_2$ then there is another solution in which these values of N_1 and N_2 are interchanged. For high values of the temperature the function $f(t)$ increases steadily from $t=0$ to $t=\infty$ so that $t=1$ is the only solution of (22) and, as would be expected, long-range order is absent. For the lower values of κ, df/dt at $t=1$ is negative below a certain temperature and, since t is an increasing function of N_2, this means that F_c plotted against N_2 has negative curvature at $N_2=\frac{1}{2}N_A$, making the solution unstable. It can be proved that there is then a unique pair of reciprocal values of t satisfying (22) and for these values df/dt is positive so that the solutions are thermodynamically stable. The temperature defined by the equation

$$(df/dt)_{t=1}=0 \qquad \ldots\ldots(23)$$

is thus a critical one above which $N_1=N_2$ in the state of minimum free energy and below which $N_1 \neq N_2$ so that there is long-range order in the orientations of A.

From (23) it is easy to show that the critical temperature T_c obeys the relation

$$\eta_c=\exp(-w/\mathbf{k}T_c)=(z-2-\kappa)/(z+\kappa). \qquad \ldots\ldots(24)$$

Thus η_c depends on the mole fraction x_A only through κ and T_c decreases steadily as κ increases. When $\kappa=z-2$, $T_c=0$ and for higher values of κ there is no critical temperature and no development of long-range order. This disappearance of critical phenomena is obtained without the introduction of any interaction energy parameter except w, which determines the critical temperature in pure A. The quantity κ (which for complete equilibrium would be a function of the state) may here be looked on as a new parameter but if the 'frozen' A–B distribution is taken to be a random one then κ is given in terms of x_A by (16). With this assumption T_c/T_1 is plotted against x_A for $z=6$, 8 and 12 in figure 1. It is to be expected that the value of x_A at which $T_c=0$ should decrease with increasing

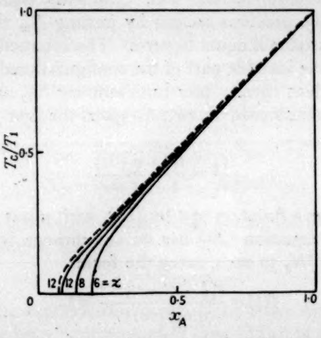

Figure 1. Critical temperature ratio plotted against mole fraction of A component. (T_1 is critical temperature at $x_A=1$.) Broken curve: three-orientation states for component A; $z=12$. Full curves: Two-orientation states for component A; $z=12$, 8, 6.

z since as $z \to \infty$ the properties of a regular mixture approach those of random arrangement of orientations on the lattice in which the T_c, x_A curve is a line through the origin. The absence of a transition temperature below a critical value of x_A is thus an effect of short-range order among the orientations of A. In those two-species models where the results of approximations of order higher than the first are available it is found that first-order quasi-chemical results lie between these and those of the random approximation (Rushbrooke 1949, Guggenheim 1952). Thus, as would be expected, the first-order approximation underestimates the effect of short-range ordering and it is likely that if exact statistical solutions could be obtained for the models treated here the transition points would disappear at higher values of x_A than those derived from $\kappa = z - 2$.

The configurational specific heat is given by the relation

$$C_c = \frac{dE_c}{dT} = w\frac{dN_{12}}{dT} = \boldsymbol{k}(\ln\eta)^2\eta\frac{dN_{12}}{d\eta}. \qquad \ldots\ldots(25)$$

Where $t = 1$ and $dt/d\eta = 0$ (i.e. above the transition point where $\kappa < z - 2$ and for all values of T where $\kappa > z - 2$) the specific heat is given by

$$C_c = C^*(\eta) = \tfrac{1}{2}\boldsymbol{k}zN_A(1+\kappa)^{-1}(\ln\eta)^2\eta(1+\eta)^{-2}. \qquad \ldots\ldots(26)$$

It can be shown that the specific heat discontinuity at T_c satisfies the relation

$$\Delta C_c = \boldsymbol{k}N_A(\ln\eta_c)^2\tfrac{3}{8}z(z-2-\kappa)^2(z+\kappa)^2(z-1)^{-1}(1+\kappa)^{-2}\{z(z-2)+3\kappa(z-1)\}^{-1} \qquad \ldots\ldots(27)$$

which reduces, for $\kappa = 0$, to equation (1319, 16) of Fowler and Guggenheim (1939). However, though this magnitude is useful in computing the specific heat curve, no great significance should be attached to it. In the two-dimensional regular assemblies whose exact thermodynamic functions have been found (Onsager 1944, Onsager and Kaufman 1949) the specific heat discontinuities are, in fact, infinite though approximate methods make them finite and it is quite possible that this happens in the models treated here. Some results for $z = 12$ are presented in figure 2 where the full curve is $C_c/\boldsymbol{k}N_A$ plotted against T/T_c for $\kappa = 5$. Above $T/T_c = 1$, $C_c = C^*(\eta)$ while below C_c is calculated from (25) and (22). Below $T/T_c = 1$ $C^*(\eta)/\boldsymbol{k}N_A$ is shown as a dotted curve; the complete curve of $C^*(\eta)$, multiplied by a scale factor $6/(\kappa+1)$, gives the specific heat for $\kappa > 10$. For comparison with $\kappa = 5$ the dashed curve gives $0{\cdot}41337C_c/\boldsymbol{k}N_A$ for

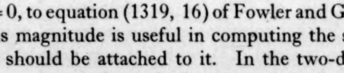

Figure 2. Configurational specific heat plotted against temperature.

the case $\kappa=0$, $x_A=1$. The factor 0·41337 makes the two curves coincide at the top of the discontinuity and the difference in shape can thus be clearly seen. The curve for $\kappa=5$ is less sharp than that for the pure A component, the ratio of specific heat just after the transition to that just before being much greater.

§ 5. THREE-ORIENTATION MODEL

It will now be supposed that the A–B distribution is fixed but that the molecules of component A can take up three orientations relative to the lattice so that the equilibrium equations derived in § 3 are applicable in their complete form. Changing the number of orientation states of A from two to three greatly increases the complexity of the analysis but it will be possible to derive a (T_c, x_A) curve where the additional interaction energies have the simple form given by (10). The A component is now an extension of the Ising model, bearing the same relation to an assembly of systems with spin quantum number 1 as the latter does to those of quantum number $\frac{1}{2}$ (Van Vleck 1945) so that the transition temperatures of pure A are of some interest and will be considered as a particular case. If u is regarded as a function of t given by (20) then (19), which can be put into the form

$$f(t)=t\{\theta(t)/\phi(t)\}^{z-1}=1, \qquad \ldots\ldots(28)$$

gives values of t for a free energy minimum. It can be seen at once from (18) that $t=1$ is a solution of (28) for all temperatures. From the symmetry considerations of § 3 other solutions exist in reciprocal pairs of type t_0, t_0^{-1} and the critical condition is again (23), with $f(t)$ now defined by (28). This critical condition can easily be expressed in the simple form

$$v+\zeta u=z-2-z\eta \qquad \ldots\ldots(29)$$

where u and v are evaluated at $t=1$.

If $x_A=1$ so that κ and v are zero then on substituting the expression for u given by (29) into (20) it is found that the critical temperature T_1 satisfies the relation

$$\zeta_1^{-2}(z-2-z\eta_1)\{(z-1)(1-\eta_1)/(z-2-z\eta_1+2\zeta_1^2)\}^{z-1}=1, \qquad \ldots\ldots(30)$$

where $\eta_1=\exp(-w/\boldsymbol{k}T_1)$ and $\zeta_1=\exp(-\frac{1}{2}w/\boldsymbol{k}T_1)$. Values of η_1 have been obtained for $z=4$, $z=6$ and $z=12$ and are shown in the table compared with the corresponding values of η_1 for the two-orientation model, given by the well-known expression $(z-2)/z$.

	$z=4$	$z=6$	$z=12$
$\eta_1(3)$	0·3797	0·5590	0·7652
$\eta_1(2)$	0·5000	0·6667	0·8333
$T_1(3)/T_1(2)$	0·7158	0·6972	0·6816

For given z and w $(=e_{12}-\frac{1}{2}e_{11}-\frac{1}{2}e_{22})$ the ratio $T_1(3)/T_1(2)$ of the critical temperature in the three-orientation model to that in the two-orientation model is considerably less than 1 and decreases as z increases. It can easily be shown in the random approximation, which corresponds to $z=\infty$, the ratio is 2/3.

The ratio T_c/T_1 for the three-orientation A–B mixture with $z=12$ is plotted against x_A in figure 1 (dashed curve). It is assumed that the 'frozen' A–B distribution is a random one so that κ is given by (16). The procedure adopted was to substitute (29) into (20) obtaining, with $t=1$, the relation

$$u\left\{\frac{(z-1)(1-\eta)}{z-2-z\eta+2\zeta^2}\right\}^{z-1}=\zeta. \qquad \ldots\ldots(31)$$

If a value of the critical temperature, and hence of η and of ζ is assumed, then the critical value of u is given immediately by (31). By substitution in (29) and (15) the associated values of v and κ are found and then, by (16), the mole fraction x_A. It can be seen from figure 1 that the critical temperature curve is very close to that of the two-orientation model with the same value of z.

§ 6. TWO-ORIENTATION MODEL WITH SYMMETRY-DESTROYING SOLUTE

It will now be supposed that the molecules of A have two orientation states but the condition that the interaction with B is independent of the state of A no longer applies. For e_{11}, e_{22} and e_{12} (5) still holds but the A–B interactions are now given by

$$e_{1B}=e_{AB}, \qquad e_{2B}=e_{AB}-w_0, \qquad \ldots\ldots(32)$$

where w_0 is positive. Second and higher order transitions frequently occur because some internal parameter of the system able to vary continuously at lower temperatures reaches a limit at some finite temperature beyond which it must remain constant. In the models considered up to this point this parameter is provided by the difference N_2-N_1. Because of the equivalence of states 1 and 2 and the resulting symmetry of F_c with respect to these states N_2-N_1 is zero above a transition temperature but below this can assume equal and opposite non-zero values. In the present model even the smallest portion of B removes the equivalence of states 1 and 2 which, because of the relation $e_{11}=e_{22}$, exists in pure A. It will be found that N_2-N_1 varies continuously over the whole temperature range and there is no specific heat discontinuity in any A–B mixture. This result is similar to that of the application of a magnetic field to an Ising model (Domb 1949). Since the effect can be seen even in the random approximation this will be used here and the pair numbers N_{ij} will be given the random distribution values zN_iN_j $(i\neq j)$, $\frac{1}{2}zN_i^2$.

It is useful to define a 'magnetization' m by

$$m=(N_2-N_1)/N_A. \qquad \ldots\ldots(33)$$

If F_c is expressed in terms of m and the derivative dF_c/dm is equated to zero there results the relation

$$\tfrac{1}{2}\ln(1+m)/(1-m)-\beta(m+c)=0. \qquad \ldots\ldots(34)$$

Here $c=x_Bw_0/x_Aw$ and $\beta=x_AT_1/T$ where $T_1=\frac{1}{2}zw/k$ is the transition temperature at $x_A=1$. If x_B, and hence c, are zero the only solution of (34) for $T>T_1$ is $m=0$ while for $T<T_1$ this solution is unstable but there are a pair of values of m, equal in magnitude but opposite in sign, giving stable solutions (i.e. $d^2F_c/dm^2>0$, see Fowler and Guggenheim (1939), § 1315). These give equal values of F_c so that either can correspond to an equilibrium state. For non-zero values of c, however small, the situation is quite different since $m=0$ satisfies (34) only at $T=\infty$ and for large finite T the only solution is a small positive m. As T decreases this solution of (34) may cease to be unique but it continues to give the lowest value of F_c and thus to correspond with the equilibrium state.

The configurational specific heat C_c is given by

$$C_c = dE_c/dT = x_A \boldsymbol{k} N \beta^2 (m+c)^2 / \{(1-m^2)^{-1} - \beta\}. \qquad \ldots\ldots (35)$$

For calculation w_0 is put equal to w and in figure 3 curves of $C_c/\boldsymbol{k}N_A$ are plotted against $T/x_A T_1$ for $x_A = 1$, $x_A = 100/101$ and $x_A = 10/11$ giving $c=0$, $c=0{\cdot}01$ and $c=0{\cdot}1$ respectively. In the well-known curve for $c=0$ the specific heat is zero above T_1 and undergoes at T_1 a discontinuity below which it decreases steadily with T but for a small non-zero value of c the specific heat is continuous with a maximum near $x_A T_1$. The maximum becomes sharper as c approaches zero and the discontinuity is obtained as a limiting case.

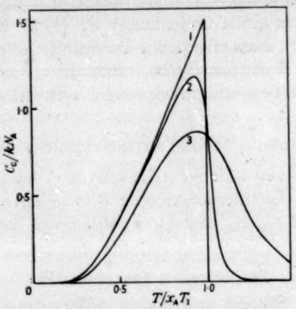

Figure 3. Configurational specific heat plotted against temperature (for case where component B removes equivalence of orientation states of component A). 1, $c=0$ (pure A component); 2, $c=0{\cdot}01$ (slight admixture of second component); 3, $c=0{\cdot}1$ (larger admixture of second component). With the energy parameters w and w_0 assumed equal $c=(1-x_A)/x_A$.

§ 7. CONCLUSION

From the work presented here three types of behaviour can be distinguished. If A and B molecules can migrate freely from site to site on the lattice the (T_c, x_A) curve passes through the origin though phase separation prevents the realization of the lower part of the curve. In the metastable equilibrium states where the A–B distribution is ‘frozen’ it appears from §§ 4 and 5 that with both the two-orientation model and the three-orientation model introduced here for A the specific heat is continuous when the mole fraction x_A is less than a critical value. This is an effect of the reduction in the free energy F_c due to short-range ordering among the orientations of A. When the addition of B affects the symmetry of F_c with respect to the states of A even the smallest proportion of B makes the specific heat continuous. This occurs in § 6 where it is supposed that A has two orientation states with unequal interactions with B. These dilution effects will now be briefly compared with observations on certain systems where the diluting molecules are spherically symmetrical and of nearly the same size as those they replace.

The transition in solid ammonium chloride at 242·3°K is probably due to co-operative orientation among the ammonium ions (see Staveley 1949, Stephenson, Blue and Stout 1952, Temperley 1956). The ammonium ions can be replaced by up to about 20% of rubidium before phase separation takes place and Smith and Spice (1958, private communication) found that with 6% and 13% of rubidium chloride the critical temperatures are respectively 2·1% and 5·0% lower than in the pure ammonium salt. Since phase separation occurs there is free exchange of sites and an effective repulsion between the two types of cation so that it is in accordance with § 2 that $1-x_A$ should be larger than $(T_1-T_c)/T_1$. Since co-operative effects among the cations are responsible for the transition the number of nearest neighbour cations to a given cation corresponds to z, so that $z=6$. With $e_{AB}-\frac{1}{2}(e_{AA}+e_{BB})$ given the rather large value of $4{\cdot}25w$ it has been calculated that 12·8% dilution gives a critical temperature decrease of 5·0% though only 3·5% dilution gives a critical temperature decrease of 2·1%. One of the basic assumptions of the regular mixture method is that the interactions e_{ij} are independent of the temperature and distribution and it should be noted that this is applied here to a system at constant pressure.

In solid ortho–para hydrogen mixtures there are λ-point transitions from an ortho mole fraction of about 60% to the maximum, 75%, but below 60% the specific heat is continuous (Hill and Ricketson 1954, Hill, Ricketson and Simon 1955). The entropy change over the transition range is $\boldsymbol{k}\ln 3$ for each ortho molecule and these authors conclude that there is no site to site movement of molecules, in agreement with the deduction of Hatton and Rollin (1949) from nuclear magnetic resonance measurements. Since the ortho–para site distribution is fixed and nearly all the ortho-molecules will be in the rotational state $J=1$, giving three values of the axial quantum number, comparison with the three-orientation model of § 5 is of interest. There is a critical mole fraction in both cases but the theoretical value of 8% is small compared with the observed 60% and the observed transition temperature does not tend to zero as the ortho mole fraction approaches its critical value so that the lower part of the curve of figure 1 is missing experimentally. Furthermore, the entropy change of $\boldsymbol{k}\ln 3$ for each ortho-molecule implies complete orientational order at 0°K in spite of the fixed site distribution. It thus seems that an improved regular model for this system must be more elaborate than that of § 5 and should probably include a preferential interaction of B with state 3 of A. Solid hydrogen mixtures were considered theoretically by Tomita (1955). It was assumed that, with a lattice coordination number z_0 and an ortho mole fraction x, all ortho-molecules had the same number xz_0 of ortho nearest neighbours and the system was then treated as an assembly of ortho-molecules alone on a lattice of coordination number xz_0.

Solid methane has a λ-point transition at 20·4°K but, from the curves given by Eucken and Veith (1936), it appears that a small admixture of krypton makes the specific heat curves continuous, the discontinuity being replaced by a maximum. This very marked dilution effect is of the third type mentioned above and was obtained with the model of § 6. It is possible that the Ising model 'orientation' terminology is inapplicable here and that the A molecules should be regarded as capable of assuming different rotational states (Franck and Clusius 1937, Ruhemann 1937, Part II, Temperley 1956, Ubbelohde 1957).

ACKNOWLEDGMENTS

I would like to thank Dr. R. W. Hill (Clarendon Laboratory, Oxford) for drawing my attention to the solid hydrogen problem and for several helpful letters and discussions, Dr. J. E. Spice (Inorganic and Physical Chemistry Department, University of Liverpool) for unpublished measurements on ammonium–rubidium chloride, Professor K. Clusius (Physikalisch-Chemisches Institut, Zürich) for references and reprints, Dr. J. Standring (Modern Languages Department, Manchester College of Science and Technology) for assistance with translation and Miss Swallow for typing the script.

REFERENCES

BELL, G. M., 1953, *Trans. Faraday Soc.*, **49**, 122.

BETHE, H. A., 1935, *Proc. Roy. Soc.* A, **150**, 552.

DOMB, C., 1949, *Proc. Roy. Soc.* A, **199**, 199.

EUCKEN, A., and VEITH, H., 1936, *Z. Phys. Chem.*, **34**, 275.

FOWLER, R., and GUGGENHEIM, E. A., 1939, *Statistical Thermodynamics* (Cambridge: University Press).

FRANCK, A., and CLUSIUS, K., 1937, *Z. Phys. Chem.*, **36**, 291.

GUGGENHEIM, E. A., 1952, *Mixtures* (Oxford: University Press), Tables 4.1–4.8. pp. 59–62.

GUGGENHEIM, E. A., and MCGLASHAN, M. C., 1951, *Proc. Roy. Soc.* A, **206**, 335.

HATTON, J., and ROLLIN, B. V., 1949, *Proc. Roy. Soc.* A, **199**, 222.

HILL, R. W., and RICKETSON, B. W. A., 1954, *Phil. Mag.*, **45**, 277.

HILL, R. W., RICKETSON, B. W. A., and SIMON, F., 1955, *Conférence de Physique des Basses Températures, Paris* (Paris: Institut du Froid), p. 317.

ONSAGER, L., 1944, *Phys. Rev.*, **65**, 117.

ONSAGER, L., and KAUFMAN, B., 1949, *Phys. Rev.*, **76**, 1232, 1244.

RUHEMANN, M., 1937, *Low Temperature Physics* (Cambridge: University Press).

RUSHBROOKE, S., 1949, *Statistical Mechanics* (Oxford: University Press).

STAVELY, L. A. K., 1949, *Quart. Rev. Chem. Soc.*, **3**, 65.

STEPHENSON, C. C., BLUE, R. W., and STOUT, J. W., 1952, *J. Chem. Phys.*, **20**, 1046.

TEMPERLEY, H. N. V., 1956, *Change of State* (London: Cleaver Hulme).

TOMITA, K., 1955, *Proc. Phys. Soc.* A, **68**, 214.

UBBELOHDE, A. R., 1957, *Quart. Rev. Chem. Soc.*, **11**, 246.

VAN VLECK, J. H., 1945, *Rev. Mod. Phys.*, **17**, 27.

Determination of the Fourier Spectra of Photographic Images

BY J. CH. VIÉNOT[†]
Department of Physics, Imperial College, London

MS. received 17*th March* 1958 *and in final form* 13*th June* 1958

Abstract. The determination of the spatial frequency density in the image recorded by a film or a photographic plate is shown to be possible by the measure of the total flux transmitted when the film or plate is illuminated by a sinusoidal distribution of light superposed on the transparency. The sinusoidal light distribution is produced in the form of two-beam interference fringes. In the present instrument fringes of good contrast are obtainable at frequencies greater than 20 per millimetre. The apparatus has been used to determine the frequency spectra of slits, a line-grating and of different scenes taken by air photography.

§ 1. INTRODUCTION

INVESTIGATIONS into the assessment of the optical performance of photographic systems have been concerned until recently mainly with the determination of the limit of resolution of objectives and sensitive materials.

The objective yields an aerial image; then the film or the photographic plate records the final image. The fact that these elements are not perfect and consequently act to degrade the output of the system leads to a loss of information. If, in the language of information theory, the input is assumed to contain both the original message and noise, it has been shown that the system objective–emulsion may be considered as a low-pass spatial frequency filter. It is, therefore, of fundamental importance to determine which spatial frequencies have been recorded in an image, their relative amplitudes, and also the form of the frequency spectrum of any given object.

The method presented here has the following aims in view: (i) the study of object statistics; (ii) investigations concerning degraded images and the influence of the frequency spectrum on recognizability; (iii) the measurement of the frequency response of emulsions by analysing the contact image of a fine slit; (iv) the indirect measurement of the frequency response of lenses by analysing the photograph of a slit imaged by a lens; (v) the study of the frequency response of the combination of lens and photographic emulsion.

It is pertinent to enquire what the criteria of a good image are, from the user's point of view, so that it seems useful to discuss briefly what the observer requires when interpreting a picture. The main qualities demanded are expressed qualitatively by the term image sharpness, by the ability to distinguish an isolated piece of detail and by the resolution of fine structures. All these factors are limited not only by the transmission properties of the objective but also by the effects of the structure of the emulsion, and this has led to a definition of the overall quality of the system in terms of the number of elements which can be resolved per unit area in the final photographic image. More usually the resolving power is expressed in numbers of lines per millimetre; or, in air photography, in terms of ground resolution. The performance of lenses and the properties of photographic emulsions do not often appear to have been studied separately, at least when given lenses and emulsions have to be used together for a given purpose. On the other hand, the resolution in a photographic image depends upon many factors arising from the conditions of photography and processing; these factors have been the subject of much study. The experiments have been generally carried out in order to determine the optimum working conditions, and different tests have been proposed (Foucault line gratings, Cobb charts, high contrast and variable contrast test charts, sector and annular types of test objects). Frieser (1938) has established theoretically a relation between the contrast of the test object and the resolving power of the emulsion.

[†] On leave of absence from the Laboratoire de Physique, Université de Besançon, France.

The orders of magnitude of the limiting resolving powers, in lines per millimetre, are about 100 for those used in cinematography, 200 for 'microfile', and between 600 and 1000 for special photographic materials; the resolving power of Aero Super XX employed in air photography, measured at high contrast, is greater than 100, but, in practice, the resolving power is of the order of 30 if the relative contrast in the image is as low as 0·2, which is that which is usually obtained in aerial photography (see for example Fish 1951). The above figures give only the limiting resolving power of these emulsions: they do not specify the contrast with which resolved structures appear, nor do they include the influence of the contrast in the test object. Selwyn (1948) has extended the method of Frieser to give the expected limit of resolution for any given combination of lens and emulsion. Nevertheless, recent work has shown the need to study the reproduction of spatial frequencies for the whole frequency range. Such studies call for the measurement of the frequency density characteristics of photographs and it is in this context that the present instrument has been developed.

§ 2. Determination of the Spectrum

2.1. *Previous Work*

Using as test object several series of periodic targets of the same structure, but of smaller and smaller period, Duffieux (1940, 1942) applied the methods of harmonic analysis to establish the existence of a frequency limit, defined as a reciprocal spacing beyond which periodic structure vanishes in the image. He also determined the Fourier spectrum corresponding to the final image as a function of the aerial image, the image being further degraded when taking the photograph. These results were later used by Mlle Gaultier du Marache (1952) and Croce (1956). The former study, on photographic images, consists of a comparison between the distributions of light in the Fraunhofer diffraction pattern of an amplitude grating and that of its photographic contact image. Experiments with a grating are easier than with a single slit because the light lies along a series of lines and the peaks are better defined, so, apart from a constant factor, each term of the spectrum is equivalent to the term of the same frequency in the slit spectrum. Using microphotometry, the decrease of contrast in the images of test charts was measured by scanning the image with a narrow slit, a slit-width correction being applied in the calculation of the spectrum. O'Neill (1954) made a study of the auto-correlation function evaluated by cascading two identical transparencies of the photograph and measuring the resultant transmission of the system as a function of the shift of one transparency with respect to the second. The power spectrum of the image is then given by the inverse Fourier transform of the auto-correlation function measured. A similar technique has been used by Kubota and Ohzu (1957) to measure the response function of an objective by means of random charts.

In these methods, there are difficulties because of errors arising in the photographic copying. The amplitude, for example, should be proportional to the opacity of the original image, which in practice implies working inside a small tolerance of γ; the two duplicates must moreover be identical. Even then information is obtained only about the modulus of the spectrum and even if it may be assumed that the localized phase changes between two adjacent strips are random fluctuations, the general phase shift cannot be detected directly.

Particular methods have been used to estimate the quality of optical systems (Sayanagi and Ito 1956) and also to measure granularity (Frieser 1935, Selwyn 1948, Shade 1951). In much of the recent work particular attention has been paid to the study of the spectrum or frequency response of emulsions which now appears as a necessary step in the evaluation of the overall optical system (Frieser 1955, 1956 a, b, Sayanagi 1957, Ingelstam and Djurle 1957).

2.2. *Formulation of the Problem*

A cosinusoidal distribution of light, conveniently produced by means of two-beam interference fringes, will have the form

$$P(\xi)=\alpha+\beta\cos 2\pi R\xi, \qquad \ldots\ldots (2.1)$$

where $R=1/p$ is the spatial frequency (i.e. the number of fringes per millimetre, p being the spacing of the fringes in millimetres) and the ξ axis is perpendicular to the fringes. α is the mean intensity of the fringes and $\alpha+\beta$ is the maximum intensity, so that the ratio β/α represents the visibility of the fringes according to the definition

$$V=\frac{I_{\max}-I_{\min}}{I_{\max}+I_{\min}}.$$

In the arrangement used β/α contains the product of three factors which diminish the visibility. These are the spatial coherence, the chromatic coherence, and a factor arising from inequality of amplitude between the two beams in the interferometer.

The interference fringes are made to fall on the plate or photographic film to be measured. Let the transparency† of this latter be $B(\xi,\eta)$, and let this transparency be defined to be zero outside the region illuminated by the fringes. $B(\xi,\eta)$, then represents a filter for the fringe distribution $P(\xi)$, and the total light flux transmitted by the plate will be

$$E(\xi_0)=\iint_{-\infty}^{+\infty} B(\xi,\eta)\,[\alpha+\beta\cos 2\pi R(\xi+\xi_0)]\,d\xi\,d\eta, \qquad \ldots\ldots (2.2)$$

where $-\xi_0$ is the displacement along the ξ axis of the fringe system from its initial position. It will be convenient to use $B(\xi)$, defined by

$$B(\xi)=\int_{-\infty}^{+\infty} B(\xi,\eta)\,d\eta,$$

to represent the integrated transparency along $\xi=$ constant.

---

† By transparency is meant here the ratio of the transmitted to the incident intensity.

If the above expression for $E(\xi_0)$ is written in the form

$$E(\xi_0)=\alpha\int_{-\infty}^{+\infty}B(\xi)\,d\xi+\beta\left\{\cos 2\pi R\xi_0\int_{-\infty}^{+\infty}B(\xi)\cos 2\pi R\xi\,d\xi\right.$$
$$\left.-\sin 2\pi R\xi_0\int_{-\infty}^{+\infty}B(\xi)\sin 2\pi R\xi\,d\xi\right\} \qquad \ldots\ldots(2.3)$$

we may easily write the various integrals in terms of the inverse Fourier transform of $B(\xi)$. Thus the Fourier spectrum of $B(\xi)$ is

$$b(R)=\int_{-\infty}^{+\infty}B(\xi)\exp\{-i2\pi R\xi\}\,d\xi, \qquad \ldots\ldots(2.4)$$

or

$$b(R)=C(R)-iS(R)$$

where

$$C(R)=\int_{-\infty}^{+\infty}B(\xi)\cos 2\pi R\xi\,d\xi,\quad S(R)=\int_{-\infty}^{+\infty}B(\xi)\sin 2\pi R\xi\,d\xi,$$

are the magnitude of the real and imaginary parts of the Fourier spectrum $b(R)$. The modulus of the Fourier spectrum is the frequency density and will be denoted by $\rho(R)=\{|C(R)|^2+|S(R)|^2\}^{1/2}$ and we shall put $\phi(R)=\tan^{-1}[S(R)/C(R)]$, subject to the restriction $0\leqslant\phi(R)\leqslant\pi$, for the argument of $b(R)$. Using these definitions in the relation (2.3), we obtain

$$E(\xi_0)=\alpha\rho(0)+\beta\rho(R)\cos[2\pi R\xi_0-\phi(R)].$$

It is convenient to use a reduced frequency density, defined by $T(R)=\rho(R)/\rho(0)$. Then the total flux transmitted by the transparency $B(\xi,\eta)$ may be written, apart from the constant factor $\rho(0)$,

$$E(\xi_0)=\alpha+\beta T(R)\cos[2\pi R\xi_0-\phi(R)]. \qquad \ldots\ldots(2.5)$$

As ξ_0 varies, the total flux then has a zero frequency component of amplitude α, and a component of frequency R of amplitude $\beta T(R)$ and phase $\phi(R)$. Hence by measurement of $E(\xi_0)$ for varying ξ_0, the Fourier spectrum $T(R)\exp\{i\phi(R)\}$ may be found. If only the frequency density $T(R)$ is needed the phase $\phi(R)$ need not be measured. This is the procedure adopted in the initial experiments to be described here. The precautions necessary for accurate measurement of $E(\xi_0)$ require (*a*) that all the light passing through the illuminated region of the plate D, is gathered by the photocathode of the receptor. This region is therefore imaged by an objective Ob such that the image of D lies well inside the useful area of the photomultiplier entrance window; and (*b*) that the angle α_L subtended by the objective is large enough according to the condition $\lambda R/\sin\alpha_L\leqslant 1$, to avoid loss of light by diffraction outside the acceptance angle of the objective. For the lens used, this condition would impose an upper limit of the order of 400 mm^{-1} on R. It should be noted that the Fourier spectrum of the local form of the transparency is measured, because only a finite region of the plate is illuminated. Account has been taken of this by defining $B(\xi,\eta)$ to be zero outside the region D. To obtain meaningful results it is only necessary to ensure that D is large compared with the largest fringe spacing $1/R_{\min}$ which has to be measured.

§ 3. EXPERIMENTAL PROCEDURE

The relation (2.5) indicates how the experiments have to be carried out. The maxima and minima or the total flux transmitted through the transparency for a given spatial frequency R are measured by moving the plate or film along the ξ_0 axis or by displacing the fringe distribution $P(\xi)$ relatively to the photograph, so that

$$2\alpha = E(\xi_0)_{\max} + E(\xi_0)_{\min}, \quad 2\beta T(R_i) = E(\xi_0)_{\max} - E(\xi_0)_{\min}.$$

From the ratio of these two quantities, we get $(\beta/\alpha)\,T(R_i)$. Then R is changed by changing the period of the fringes, and the measurements repeated. The results so obtained represent the form of $T(R)$, provided β/α keeps a constant value; as will be seen, the variations of this coefficient is minimized in the apparatus used; and, in any case, the curve $\beta/\alpha = f(R)$ is easily found by measurement in our range of frequencies.

§ 4. APPARATUS

4.1. *Experimental Arrangement*

A schematic view of the optical system is shown in figure 1.

The interferometer. A sinusoidal intensity distribution in the fringe pattern being required in front of the transparency, a two-beam interferometer has been designed, with independent adjustments, which allows a wide field to be used, and has a good contrast in the fringes over a wide range of fringe spacings. Mechanical stability is obtained by using cushions of latex foam rubber alternating with aluminium plates between the base casting and a solid wooden table. In fact, an important part of the vibrations transmitted by the floor is reduced by damping in the table. The components are mounted on a thick iron casting. Two practically identical $1\frac{1}{2}$ in. by $2\frac{1}{2}$ in. glass plates are used as beam-splitter and compensator; their surfaces are bloomed with magnesium fluoride films to reduce stray light and gain contrast. The semi-reflecting surface of the beam-splitter is a multilayer dielectric reflector. The mirrors M_1 and M_2 are similarly mounted in frames with conventional screw and spring adjustments. The adjustment for equality of paths for the two beams is effected by means of a ball-bearing kinematic slide seated on ground rods, the slide carrying the mirror M_1. This slide is moved by means of a screw micrometer. Initially the mirror M_2 was tilted around a vertical axis by means of a long lever actuated by a screw micrometer. The fringes due to the

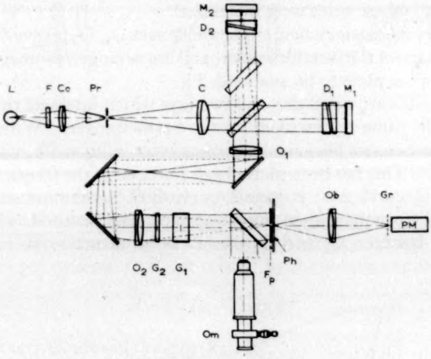

Figure 1. Schematic diagram of the apparatus.

effective air wedge introduced remain vertical only provided the axis of rotation is exactly vertical. Although this arrangement worked reasonably satisfactorily for a long time, an obvious disadvantage was the need to reset the fine adjustment of the interferometer to maintain the fringes vertical before readings. For this reason an alternative method was introduced and successfully used.

The illuminating system. The incident beam is collimated by a F/15 lens C from a symmetrically opening Hilger slit. A medium pressure mercury lamp L was used as the light source, a Wratten filter No. 77 A being used to isolate the green line (5461 Å). Instability of the supply voltage was minimized by using a 168 volt battery supply, the fluctuations due to the output of the light source being less than 1%. This was determined by recording separately the fluctuations of light intensity along each of the two arms of the interferometer for an output signal from the photomultiplier and amplifier of the order of 13 μA. However, the illumination of the image on the collimator slit, formed by the condenser C_0, varies because of the unsteady position of the light column in the lamp. This may be corrected by enlarging the column image, but the luminance of the source is then not sufficient, it being necessary to retain the maximum amount of light. A wedge prism Pr was therefore used as a light funnel; the luminance at its exit end was then found to remain constant. It was found necessary for the condenser to image the lamp inside the prism, whose sides were metallized.

The auxiliary telescopic system. The two lenses O_1, O_2 form a telescopic system in the fringe-space of the interferometer, and are arranged to image the mirror M_2 at the photographic plate to be analysed, Ph.

In this way, it is arranged that any two rays which intersect the plane Ph have derived from the same ray incident on the beam-splitter. Without this system there is loss of coherence between the beams interfering at Ph, with a consequent loss of contrast. This has been plotted as a function of the frequency in the fringe pattern (figure 2, curve A). Figure 2, curve B shows the measured variation of β/α with spatial frequency when the telescopic system is used. The three plane mirrors placed between O_1 and O_2 merely serve to make the instrument more compact.

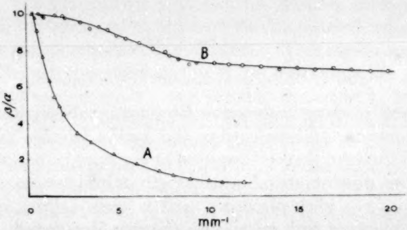

Figure 2. Visibility of the fringes with and without the telescopic system.

The fringe displacement ξ_0. As indicated in § 3, the measurement of the maxima and minima of the flux for a given frequency calls for the shifting of the fringe pattern along the ξ-axis. This is effected by means of two parallel plates G_1, G_2 of thicknesses in the ratio 1 : 10, each rotatable about a vertical axis and providing fast and slow motions respectively. The limits of this rotation were set at ± 10°.

Diasporameters†. A disadvantage of tilting the mirror M_2 to vary the frequency R is that the precision demanded of the mechanical axis is very difficult to achieve in practice. Errors in this mechanical axis cause the direction of the fringes to rotate out of the vertical. A new method was therefore used. The system to be described was arranged to be mechanically independent of the interferometer proper. It is mounted on a separate bridge structure, which also carries all components other than the beam-splitter, compensator and the plane mirrors M_1, M_2.

The schematic diagram (figure 3) shows the optical elements of the interferometer with one pair of exactly matched small angle prisms in each arm. If the two prisms of each pair rotate simultaneously, but in opposite directions, around the optical axis at the same speed, the effect on the transmitted light beams is equivalent to that of variable angle glass prisms. By using a symmetrical arrangement, the optical paths in air and glass along the two arms of the interferometer remain constant.

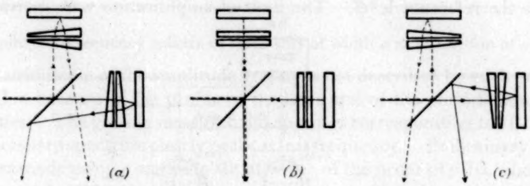

Figure 3. Successive positions of the diasporameters in each arm of the interferometer.

The successive positions of these diasporameters are indicated in figures 3 (*a*), (*b*) and (*c*). When the interferometer is in position (*b*) there is no deviation produced by them. After a rotation θ of all prisms, the angle α of each prism and the number of fringes per millimetre R, are related by the simple expression

$$R = 8\frac{\alpha}{\lambda}(n-1)\sin\theta$$

where n is the refractive index of the glass.

Backlash in the driving mechanism is eliminated by the use of gear-wheels made of two halves slightly unkeyed one with respect to the other and sprung apart. The shaft from which the prisms are driven may be rotated continuously. The angle of each prism is 1°, and this means that the arrangement will cover the range of frequencies from zero up to 134 mm^{-1}.

Plate holder and microscope. To scan a photograph element by element along the two coordinate axes ξ and η a double slide is used. The small domain to be analysed is limited by means of an adjustable slit F_p. A beam-splitter similar to that of the interferometer provides a fringe pattern at the plane conjugate to F_p, which is also the object plane of a long working distance microscope objective. The spacing of the fringes is measured by means of a × 10 micrometer eyepiece measuring 0·01 mm in the primary image.

---

† This term is commonly employed in France to denote a pair of identical prisms capable of rotation in opposite senses.

4.2. *Integration of the Light Flux*

The region of the photographic image of which the spectrum is to be determined is imaged on the sensitive surface of a photomultiplier PM by means of the objective Ob. The light flux in the image is evenly distributed over the surface of the photocathode by using a transparent plastic grating in the manner described by Baker (1955). This type of diffuser has a very small light loss. The optimum distance of the grating from the photocathode was determined by experiment. The photomultiplier is an eleven stage EMI type, fed by a highly stabilized power supply. Its dark current and noise are low and in normal use the output current is measured directly by a sensitive galvanometer, with which 1 mm on the scale represents $0{\cdot}92 \times 10^{-8}$ A at the highest sensitivity. The short period fluctuations were damped by increasing the time response, using capacitors of a few microfarads. When the opacity of the photograph was too great, a d.c. amplifier was employed. It is a balanced circuit (figure 4) whose main feature is the use of two electrometer pentodes providing a large range of gain determined by the load resistor R, and adjusted by R_K and the grid voltage supply of the second valve which is taken as the reference level. The limit of amplification with increasing R is determined by overloading. The only difficulty of such a circuit is to stabilize it. Shielding and high stability resistors were used, the gain being kept below its maximum level. Consistent results were obtained with an amplification close to 1000. The linearity of the photomultiplier and amplifier response was checked using as the input signal a light beam passing through two sheets of polaroid. The resulting graph of galvanometer deflection against the square of the cosine of the angle between the principal axis of two polariods was linear to within 2% of the maximum deflection. A current gain of 994 was used in these measurements.

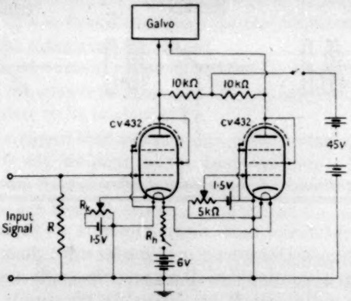

Figure 4. Electric equipment.

§ 5. Results and Discussion

A few preliminary results of measurements with the apparatus have been briefly presented elsewhere (Viénot 1957). The curves of the frequency spectra of three slits of widths 130 μ, 84 μ, 56 μ (figure 5) and of an amplitude grating (figure 6) are reproduced here in more detail. The frequency spectrum of a slit of width a has a modulus of the form

$$T(R) = \left| \frac{\sin \pi a R}{\pi a R} \right|.$$

The modulus $T(R)$, giving the frequency density, is shown in figure 5 as a function of aR. For comparison the three sets of experimental points are also plotted against aR.

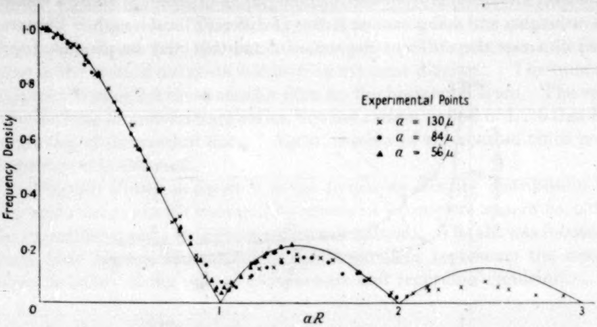

Figure 5. Frequency spectra of three slits of width a as a function of aR.

The transmission of the amplitude grating is not described by such an elementary function because of the profile of the lines and of the periodic and random irregularities. The grating measured has spacings corresponding to 10 lines/mm, and the measured spectrum clearly peaks at this frequency. Preliminary measurements were made using a scanning slit of width of the order of $p/10$, where p is the length of period. This served to determine the ratio β/α, which gives the contrast in the fringes. To measure the spectrum, a larger slit is used. The spectrum so determined is the spectrum of the function defined to be equal to $B(\xi)$ within the slit domain D and zero outside it. If the transparency contains an obvious periodicity the slit width is usefully made to include several periods. It is in any case an advantage to use as large an area of the plate as is permitted by the uniformity of contrast in the fringes, since the greater this area the greater both the total light flux and its amplitude of variation with ξ_0. The error tends therefore to be minimized by using many fringes.

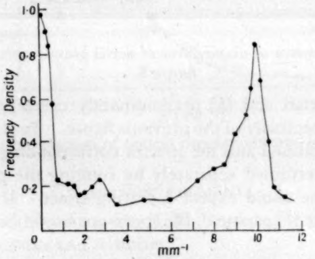

Figure 6. Frequency spectrum of an amplitude grating.

The reproducibility of measurement was to an accuracy of a few per cent. In practice, three or four sets of readings were usually taken on different days, going from the low up to high frequencies and conversely.

Experimental curves are shown in figure 7, in which the frequency densities are plotted against the spatial frequency. These curves are the spectra of the diapositives of the corresponding photographs shown in figure 8 (plate). These photographs are sections from aerial photographs of different scenes, taken from different heights and using camera lenses of different focal length. Figures 8 (*a*) and (*b*) illustrate the different degrees of detail that may be present, (*a*) being predominantly fine detail and (*b*) predominantly coarse, and correspond to the curves (*a*) and (*b*) respectively of the previous figure. In (*c*) is the roof of a building. This has been scanned and the spectra corresponding to the horizontal and vertical directions determined separately by rotating the photograph through a right angle. Here one could expect a grating effect. If N is the number of elements of the grating of spacing d, the spectrum would be expected to be of the form

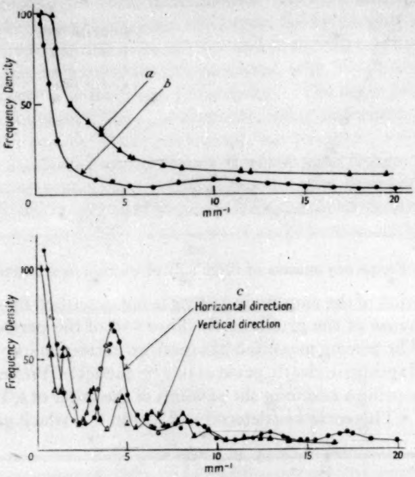

Figure 7. Frequency spectra of diapositives of aerial photographs of the scenes shown in figure 8.

$$G(R) = A_0 \frac{\sin N\pi Rd}{\sin \pi Rd}\, g(R),$$

where $g(R)$ is a slowly varying factor; it represents the spectrum of a single slit, here the gap between two adjacent tiles. Over a small region of the spectrum considered as a function of R the factor $g(R)$ will be almost constant. In the neighbourhood of a principal maximum, $\sin \pi Rd \sim \pi Rd$. Thus, apart from this constant factor, the spectrum in the neighbourhood of the principal maxima will be of the form

$$G(R) = A_0 N\left(\frac{\sin N\pi Rd}{N\pi Rd}\right),$$

which is simply the spectrum that would be given by a single aperture of the same width, equal to Nd, as the domain D. This indicates why these maxima are not sharp. Moreover, the secondary maxima will also be broadened because of the small number of pseudo-periods enclosed in D. For this reason, they do not appear in the full curve of figure 7. The mean spacing of the elements in the horizontal direction corresponds to a fundamental frequency $R_0 = 4{\cdot}3\ \mathrm{mm}^{-1}$ in the actual diapositive. This is in good agreement with the positions of the maxima in the figure 7 (*c*) (horizontal scanning). The spectrum obtained by scanning in the vertical direction is shown on the same diagram. The fundamental frequency here is 2·6 times smaller than for the horizontal scan. The spacing between the long horizontal lines varies, but has a mean period of 1/2·6 that for the mean spacing of the vertical lines. Again, in view of the aperiodicities present, good agreement is obtained.

The diagram shown in figure 9 is the frequency density distribution in the photographic image of a slit enlarged by means of a complete apparatus, comprising the camera lens and a long focus collimator system. The slit was focused with a minus blue filter. The spectrum measured here represents the combined response function of the optical components and recording emulsion.

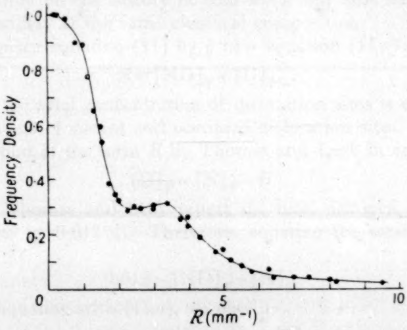

Figure 9. Response function of optical components and emulsion combined.

Acknowledgments

I wish to express my thanks to Dr. H. H. Hopkins for suggesting this problem, and for helpful discussions and criticism.

References

Baker, L. R., 1955, *J. Sci. Instrum.*, **32,** 418.

Croce, P., 1956, *Thesis*, Paris.

Duffieux, P. M., 1940, *Ann. Phys.*, Paris, **14,** 302 ; 1942, *Sci. et Industr. Photog.*, **13,** 103.

Fish, R. W., 1951, *R.A.E. Techn. Note Ph.* 455.

Frieser, H., 1935, *Kinotechnik*, **17,** 167 ; 1935, *Sci. et Industr. Photog.*, **6,** 342 ; 1938, *Z. Wiss. Phot.*, **37,** 251 ; 1955, *Photog. Korresp.*, **91,** 69 ; 1956 *a*, *Ibid.*, **92,** 51 ; 1956 *b*, *Ibid.*, **92,** 183.

Gaultier du Marache, J., 1952, *Thesis*, Paris.

Ingelstam, E., and Djurle, 1957, *J. Opt. Soc. Amer.*, **47,** 567.

Kubota, H., and Ohzu, H., 1957, *J. Opt. Soc. Amer.*, **47,** 7, 666.

O'Neill, E. L., 1954, *Tech. Note* 110, Boston University.

SAYANAGI, K., 1957, *J. Opt. Soc. Amer.*, **47**, 566.
SAYANAGI, K., and ITO, H., 1956, *J. Appl. Phys. Japan*, **25**.
SELWYN, E. W. H., 1948, *Phot. J.*, **88** B, 6, 46.
SHADE, O. H., 1951, *Optical Image Evaluation, Nat. Bur. Stand.*, **526**, 231.
VIÉNOT, J. CH., 1957, *Int. Symposium Phys. Prob. of Col. Television, Paris, Acta Elect.*, **2**, 279.

LETTERS TO THE EDITOR

The Binding Energy of Nitrogen in a Dislocation

We wish to call attention to the fact that the value for 'binding energy' reported by Thomas and Leak (1955) results from an incorrect mathematical treatment of their data.

The principal error in their analysis occurs in equation (11)

$$A=[\mathrm{ND}]_T+[\mathrm{N}]_T \qquad \ldots\ldots(11)$$

which asserts that the total concentration of dislocation sites is equal to the total concentration of nitrogen distributed between regular lattice sites and dislocation sites. Equation (11) is not generally correct since the concentration of dislocation sites depends mainly on the history of cold work and heat treatment and this could be varied widely at the same chemical composition.

We would replace equation (11) by a new equation (11 *a*):

$$A=[\mathrm{ND}]_T+[\mathrm{D}]_T. \qquad \ldots\ldots(11\,a)$$

This means that the total concentration of dislocation sites is equal to the sum of the concentrations of vacant and occupied dislocation sites.

The introduction of the term B by Thomas and Leak in equation (13)

$$[\mathrm{D}]_T=[\mathrm{N}]_T-B \qquad \ldots\ldots(13)$$

is unnecessary. Thomas and Leak report the total nitrogen concentration in their specimens to be 0·012%. Therefore, equating the total nitrogen to the sum of its parts,

$$0{\cdot}012=[\mathrm{ND}]_T+[\mathrm{N}]_T.$$

Combining this equation with (11 *a*), we obtain

$$[\mathrm{D}]_T=[\mathrm{N}]_T+A-0{\cdot}012.$$

It is now possible to replace equation (14) by substituting the correct expressions for $[\mathrm{ND}]_T$ and $[\mathrm{D}]_T$ in equation (9)

$$K=\frac{[\mathrm{N}][\mathrm{D}]}{[\mathrm{ND}]}. \qquad \ldots\ldots(9)$$

Thus,

$$K(T)=\frac{[\mathrm{N}]_T\{A+[\mathrm{N}]_T-0{\cdot}012\}}{0{\cdot}012-[\mathrm{N}]_T}. \qquad \ldots\ldots(14\,a)$$

Because of the incorrect mathematical treatment, it became necessary for Thomas and Leak to obtain A, the concentration of dislocation sites, by estimation. When the correct mathematical treatment is used, A may be obtained, in principle, from the experimental data alone. By a procedure similar to that which Thomas and Leak employed to obtain B, one should be able to select a value of A, from among a set of test values, by the criterion of linearity in a $(\log K(T), 1/T)$ plot.

The figure shows the experimental data calculated according to equation (14 *a*) with two test values of A. Unfortunately, the scatter in these experimental data precludes the selection of A by the criterion of linearity. Moreover, the plot shows the sensitivity of slope to the value chosen for A. Since ΔH, the heat of the reaction $N + D = ND$, is directly proportional to the slope, the weakness inherent in obtaining ΔH by using an estimate of A is evident. The value of ΔH ('binding energy') reported by Thomas and Leak is, therefore, much less reliable than their error limits suggest.

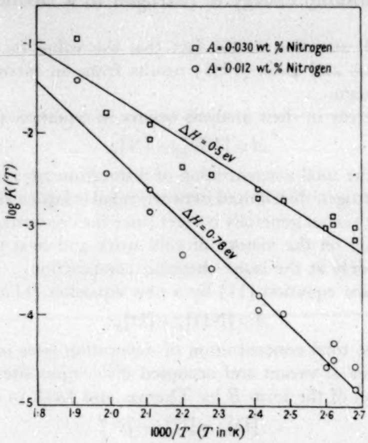

While it is feasible to determine A and ΔH by this experimental method, greatly increased accuracy in measuring $[N]_T$ is necessary.

Edgar C. Bain Laboratory for Fundamental Research, United States Steel Corporation Research Center, Monroeville, Pennsylvania.
H. A. Wriedt.
J. C. Swartz.

30th December 1957.

Thomas, W. R., and Leak, G. M., 1955, *Proc. Phys. Soc.* B, **68**, 1001.

The criticism by Dr. Wriedt and Dr. Swartz that equation (11) of our paper is wrongly defined is undoubtedly correct. The value for A, correctly defined on p. 1005, has subsequently been taken as equal to the maximum amount of nitrogen which could be absorbed by the maximum possible dislocation density, i.e. 0·03 wt % nitrogen. Equation (11) must be written

$$[ND]_T = A' - [N]_T$$

where A' is defined as the maximum possible value for [ND] for the material concerned, i.e. 0·012 wt % nitrogen. Then equation (14) follows correctly.

The constant B replaces the term $(0{\cdot}012 - A)$ used by Wriedt and Swartz (note that their A is no longer equivalent to the A' of Thomas and Leak but is the total concentration of dislocation sites).

A (defined by Wriedt and Swartz) $= [\mathrm{D}]_T + [\mathrm{ND}]_T$

$$0{\cdot}012 = [\mathrm{N}]_T + [\mathrm{ND}]_T$$

so that

$$[\mathrm{N}]_T - [\mathrm{D}]_T = 0{\cdot}012 - A.$$

At the arbitrary temperature T_0

$$B = [\mathrm{N}]_{T_0} - [\mathrm{D}]_{T_0} = 0{\cdot}012 - A.$$

Hence equations (14*a*) and (14) (corrected) are identical.

The final criticism is that Thomas and Leak's results contain too great a scatter to give a reliable value for V, the binding energy. The requirement is to adjust the constant B (or the value $[\mathrm{D}]_{T_0}$) in equation (14) or the value for A in equation (14*a*), to give linearity in a plot of log K against $1/T$. Figures 3 and 4 in the paper by Thomas and Leak show points taken from the line drawn through the experimental points of figure 2 (note that the relevant curve of figure 2 is not a straight line). Using this procedure and selecting arbitrary values for $[\mathrm{D}]_{105}$ of 10^{-5}, 10^{-4} and 10^{-3} wt % nitrogen one can easily show graphically that the resulting curves of (log K, $1/T$) are of the form shown in figure 3. The slope of the straight line portion is again about 0·8 ev per atom. The curve becomes linear for some value of $[\mathrm{D}]_{105}$ near to 10^{-4} wt % nitrogen. As Wriedt and Swartz point out, in view of the scatter of the present results it is not worth while estimating the precise value for $[\mathrm{D}]_{105}$, nor the precise value for A, the dislocation density as defined by Wriedt and Swartz. The curves as drawn by them fail to show this trend due to their somewhat arbitrary choice of a straight line for each set of points, whilst Thomas and Leak have drawn curves which follow more closely the trends of the points.

In conclusion, the authors are grateful to Dr. Wriedt and Dr. Swartz for pointing out the error in their calculation. When the analysis is corrected the results yield a value for the binding energy which is about 0·8 ev per nitrogen atom. This value does not appear to depend markedly on the dislocation density.

Department of Mines and Technical Surveys,
Atomic Energy Project,
Chalk River, Ontario, Canada.
W. R. Thomas.

British Iron and Steel Research Association,
Metallurgy Division,
Sheffield.
G. M. Leak.

CORRIGENDA

The Branching Ratios of ^{86}*Rb and* ^{42}*K*, by E. W. Emery and N. Veall (*Proc. Phys. Soc.* A, 1955, **68,** 346).

Lines 13 and 14 of page 347 *should read* . . . . . in 8·5 ± 0·5% of disintegrations of ^{86}Rb, and in 17·8 ± 0·9% of disintegrations of ^{42}K.

Thermal Diffusion in Ionized Gases, by Sydney Chapman (*Proc. Phys. Soc.*, 1958, **72,** 353).

The formula for D_{12} on p. 361 *should read*

$$\frac{3(2kT)^{5/2}}{16n(\pi m_1 M_2)^{1/2} Z_1{}^2 Z_2{}^2 e^4 A_1(2)} \quad \text{i.e. } (\pi m_1 M_2)^{1/2} \text{ not } (\pi m_1 M_2)^2$$

REVIEWS OF BOOKS

Rheology: Theory and Applications, Vol. 2, edited by F. R. Eirich. Pp. xiii + 591. (New York: Academic Press; London: Academic Books, 1958.) $18.00.

In this volume on Rheology—the second of a series of three—the general pattern is similar to that of Volume 1. The separate contributions, covering a wide range of subjects, are essentially independent expositions with comparatively little explicit relationship to one another. In this method of presentation, as the editor points out, a certain amount of overlapping may be inevitable; on the other hand the expression of various points of view on subjects which are still at the stage of rapid development may be a positive advantage.

In the present volume the emphasis is very largely on polymers. It opens with a general treatment of visco-elastic phenomena from the mathematical standpoint by H. Leaderman, followed by a study of stress–relaxation effects, rather more specificially related to particular materials, by A. V. Tobosky. This is followed by a chapter on the ‘ relaxation theory ’ of transport phenomena (including Non-Newtonian flow and diffusion) by Taikyue Rhee and H. Eyring. Organic glasses are discussed by R. Buchdahl, and the rheological properties of raw elastomers (mainly rubber) by M. Mooney. The next four chapters are concerned respectively with cellulose derivatives (E. B. Atkinson), fibres (R. Meredith), gelatin (A. G. Ward and P. R. Saunders) and asphalts (R. N. J. Saal and J. W. A. Labout). A chapter on the rheology of the interior of the earth (B. Gutenberg) forms an independent essay. This is followed by a discussion of general experimental methods for the study of visco-elastic phenomena in chapters by J. D. Ferry and by B. A. Toms, respectively. The final chapter, by A. Jobling and J. E. Roberts, is entitled ‘ Goniometry of flow and rupture ’.

From the physicist's standpoint it is clear that the subject of rheology is still far from achieving a unifying philosophy, and the contributions to the volume under review are by no means equally satisfying scientifically. However, in bringing together these various points of view on a range of subjects which includes the whole field, the Editor has performed a valuable service not only to physicists who are concerned with understanding the properties of materials, but also to chemists, who may be required to provide them. L. R. G. TRELOAR.

Physik im Wandel meiner Zeit, by Max Born. Pp. vii + 252. (Braunschweig: Vieweg, 1957.)

Professor Born has selected some twenty of the articles of a non-technical and epistemological character which he has written on various occasions in the course of the last thirty years, and published them in two parallel editions, an English and a German one; the latter is here under review. In this collection, the pupils and friends of the great master will find all the pithy and inspiring essays which they read with such pleasure as they came out; but the real importance of this publication does not lie in its value as a memorial of one of the most momentous epochs in the history of science. Born's thought has such an originality and vigour, and it is expressed with such freshness and directness, that his message should appeal to the coming generation of physicists as much as it did to our own. In fact, it conveys more truly the real spirit of science, with its liberal implications, than similar writings of other great men (like Planck or Eddington) who were stifled by the atmosphere of social and clerical reaction in which they lived. Born is one of the very few among the founders of modern science who were able to uphold the liberal ideal of free and fearless thinking, and to give expression to its noblest and purest aspirations. To this ideal and no other the young generation of scientists must return if it wants to save the scientific tradition from the decay which threatens it in the very countries in which it grew up. This unpretentious, but weighty little book will give them the right inspiration.

L. ROSENFELD.

The Principles of Quantum Mechanics, 4th edition, by P. A. M. DIRAC. Pp. xii + 312. (Clarendon Press ; Oxford University Press, 1958.) 35*s*.

It is always a pleasure to dip into a well-known and much beloved classic. The appearance of the 4th Edition of this great work enables one to savour again a clarity of writing and of thought that is far from common in scientific textbooks. This edition differs essentially from the earlier one only in that the last chapter on quantum electrodynamics has been reformulated. However, the final paragraph ends on the same sombre note presaging a drastic change in the whole theory, and there is only a passing hint of the remarkable progress that has been made in deriving useful results from modern field theory in spite of its logical difficulties. Although the whole book is mainly preoccupied with the logical foundations of quantum mechanics, one nevertheless feels that it is a superb exposition of how the theory has been made to be useful. In comparison with the rest of the book, the final chapter therefore seems a little out of tune.

B. H. FLOWERS

Mécanique Statistique des Fluides—Fluctuations et Propriétés Locales, by D. MASSIGNON. Pp. xiv + 263. (Paris : Dunod, 1957.) 3900 *fr*.

There are powerful general methods in classical statistical physics for discussing a quantity A which can be expressed as a function of the $6N$ coordinates and momenta of an N-particle system. The average of A over phase space (weighted by the phase space probability function f_N appropriate to the statistical state of the system) gives the expectation value $\bar{A}$ of a measurement of A. Moreover, given the Hamiltonian, one can at once equate $d\bar{A}/dt$ to a function of the coordinates and momenta, and this function can generally be interpreted as a linear combination of familiar physical quantities. It follows that $d\bar{A}/dt$ is equal to the same linear combination of the expectation values of these physical quantities. If A is a hydrodynamic quantity one expects that this straightforward procedure, which does not require a knowledge of f_N, will yield a transport equation.

However, to express a typical hydrodynamic quantity, such as density *at a point*, in terms of the $6N$ coordinates and momenta requires the use of δ-functions, and statistical hydrodynamics has usually been approached in other ways. The present work exploits the fact that the δ-function can now be regarded as an example of the generalized functions (distributions) of Schwartz and the above procedure for deriving transport equations is carried through in a systematic way. In Schwartz's theory his generalized functions can be differentiated arbitrarily often and so are amenable to many of the ordinary processes of analysis. Professor Temple's article 'The Theory of Generalized Functions' (*Proc. Roy. Soc.* A, 1955, **228**, 175) gives sufficient background for following most of the argument and may be found a useful supplement to Massignon's references.

Fluctuation and correlation problems figure prominently in the book. The fluctuations (higher moments) of a hydrodynamic quantity *at a point* cannot be found because powers of the generalized functions of Schwartz are not defined: this is regarded as giving the root of difficulties in kinetic theory discussions of hydrodynamic fluctuations. The difficulty is circumvented by defining quantities in which the δ-functions are replaced by sharply peaked ordinary functions, for which the difficulty does not arise. These quantities correspond to physically measured quantities, which never relate to one point.

An advantage of the procedures presented is that the transition to a quantum basis is easy. Prescriptions are given for going over to density matrix, Wigner distribution or second quantization formulations, all of which are neatly discussed.

Little space is devoted to applications. Where the methods of the book yield results which appear to go beyond those of Yvon, Kirkwood, Born and Green and others (as in the generalization of the Langevin Brownian motion equation) the discussion is hardly pushed far enough to show how useful the results are. Nevertheless, the book can be commended to those interested in theoretical problems in statistical hydrodynamics. In addition to presenting clearly and convincingly the author's own approach, it includes interesting accounts of many of the fundamental ideas of the subject. C. W. M^cCOMBIE.

Dislocations and Mechanical Properties of Crystals, edited by J. C. FISHER, W. G. JOHNSTON, R. THOMSON and T. VREELAND, JR. Pp. xiv + 634. (New York : Wiley ; London : Chapman and Hall, 1958.) 120*s*.

This book is the report of a small informal conference on dislocations and mechanical properties of crystals, held at Lake Placid from September 6th–8th 1956. The conference was sponsored by the U.S. Air Force Office of Scientific Research and the General Electric Research Laboratory, and was attended by 41 leading experts in the field of crystal plasticity. The report contains a full record of the proceedings of the conference dealing with the most recent developments in this field, together with interesting and stimulating discussion, and will be of great value to both experimentalists and theoreticians working in this field. The editors and publishers are to be congratulated on the very fine book which they have produced.

The report is divided into eight parts. The first deals with direct methods of observing dislocations. Techniques are described by which dislocations can be made visible by decoration, by etching, or by transmission electron microscopy of thin metal foils. On reading this section it is quite clear that dislocation arrangements in crystals, which were so much a matter for theoretical speculation a few years ago, are rapidly becoming the subject of experimental observation. These methods have helped to put dislocation theory on a firm foundation.

The second part deals with work on the deformation of pure single crystals, and some important results on twinning and low temperature deformation of copper crystals are reported by Blewitt, Coltman and Redman. The next part, on recovery and work hardening, contains a comprehensive review by

Seeger on the present state of theories of work hardening in hexagonal and face-centred cubic metals. After reading this, one is left with the feeling that whereas the properties of individual dislocations are fairly well understood, the collective behaviour of dislocations still needs further experimental investigation, particularly by direct methods of observation, in order to test the proposed theories. A paper by Boas on stored energy and electrical resistivity measurements in metals emphasises the discrepancies between dislocation densities determined by these methods. These are attributed by Seeger to resistivity effects associated with stacking faults of extended dislocations. Further theoretical calculations on this last point would be welcome.

A section on alloys includes a theoretical paper by H. Suzuki on the yield strength of binary alloys, as well as a number of experimental papers. Next there is a review of internal friction phenomena by Lücke and Granato, followed by two papers on fatigue. The short section on dislocation theory includes a paper by Leibfried on the thermal motion of dislocations. Finally, there are some papers on whiskers followed by a section on radiation damage. The detailed interpretation of the complicated annealing characteristics and the precise nature of the damage are far from clear.

The theme of this conference report illustrates the present trend in dislocation physics. In this subject experimental methods are becoming increasingly important in suggesting new lines for theoretical studies. The only disappointing feature about this book is its price. M. J. WHELAN.

Atomic Physics, by MAX BORN. Sixth Edition. Pp. xiv + 445. (Glasgow: Blackie, 1957.) 40*s*.

This is a book which is so widely known among scientists as to render unnecessary any general remarks on its content. The topics chosen for discussion in the original edition have proved surprisingly stable in a world of scientific change, and were treated with a thoroughness very characteristic of the author.

Subsequent editions over the past twenty years have differed mainly by the addition of new material as discovered, and by the gradual refinement of explanation as that, too, became more certain and precise. The continuing popularity of the book over such a long time is an indication of its value as a text.

In this last edition, revised in collaboration with Dr. R. J. Blin-Stoyle, opportunity has once again been taken to make a few carefully chosen additions. These include a discussion on the shell and collective nuclear models and sections on high energy machines, the fundamental particles, and the various resonance methods for the determination of magnetic and quadrupole moments. In keeping with the style of the book the additions have been written with care so as to be intelligible to the non-specialist. R. LATHAM.

Theoretical Physics—Thermodynamics, Electromagnetism, Waves and Particles, by F. WOODBRIDGE CONSTANT. Pp. xiii + 364. (Massachusetts: Addison-Wesley, 1958.) 64*s*.

This book consists of a notably clear presentation of the basic elementary theory of electromagnetism (150 pages) ' topped up ' with some *very* elementary thermodynamics, statistical mechanics, physical optics, special relativity and wave mechanics, all treated (if you please) in a further 200 pages. Needless to say this is not really theoretical physics, but parts of the book may be found useful by undergraduates during their first two years. R. O. DAVIES.

Thermodynamics of One-component Systems, by WILLIAM N. LACEY and BRUCE H. SAGE. Pp. xii + 376. (New York: Academic Press, 1957.) $8.00.

Physicists should not be misled by the title of this text: it is firmly within the tradition of engineering thermodynamics and it is not for them. Half the book is on ' fundamentals '. Here important matters are skimped and unimportant questions treated in remarkable detail. The other half gives a nice, simple account of the principles of steady flow processes, turbines, engines, compressors, refrigerators and liquefiers. This would be pleasant reading, if it were not for the horrible engineering units used. It is not that one is bigoted enough to insist on a c.g.s.-centigrade system but rather that the authors use ' lb ' to denote *both* a mass and a force, e.g. specific energy is reckoned in terms of ft. lb. per lb. Unless engineers are prepared to use—say—' lbf ' for the unit of force they cannot expect reasonable scientists to follow them.

R. O. DAVIES.

Progress in Nuclear Physics, Volume 6, edited by O. R. FRISCH. Pp. vii + 300. (London, New York, Paris: Pergamon Press, 1957.) 84*s*.

The annual series of which the volume under review is the latest member plays an important part in the documentation of nuclear physics. Its function is to provide expert reviews of limited fields of research in which current developments are of particular interest. The articles in the present volume, as in its predecessors, are written primarily for the non-specialist and attempt to relate the field under consideration to a wider background whenever possible. Such articles are of especial value to the degree student and the Editor is to be congratulated on having once more made available reports on a wide range of interesting topics.

Several of the chapters are concerned directly or indirectly with atomic masses. The accuracy of mass measurements both from nuclear reaction cycles and from mass spectroscopy is now extremely high and a detailed comparison and combination of results obtained by the two methods leads firstly to ' best ' values and secondly to knowledge of the fine structure of the mass surface. The careful survey, ' Masses of Atoms of $A < 40$ ', given by J. Mattauch and F. Everling, perhaps takes the matter further than the general reader will wish, but well exhibits the detail now available and comments on small residual discrepancies between the nuclear-reaction and mass-spectroscopic values. For heavier atoms the time is not yet ripe for such refined analysis and the article ' Masses of Atoms of $A > 40$ ', by H. E. Duckworth, concentrates on a survey of existing results, including some very recent ones, and on the setting up of heavy standards of mass. There is a general discussion of shell effects and a useful table of masses.

The evolution of mass spectrographs into isotope separators has now made available at least milligramme quantities of practically every known stable isotope. In a review of the subject of ' Electromagnetic Enrichment of Stable Isotopes ' M. L. Smith outlines the wartime development of large scale electromagnetic methods and gives details of existing facilities together with an interesting summary of the numerous applications of separated material. Although single stage separation by this method is generally applicable other procedures are more economical in special cases. Both large scale and laboratory methods of separation based on such processes as electrolysis, distillation, diffusion and chemical exchange are discussed by T. F. Johns (Isotope Separation by Multistage Methods).

One of the features of modern nuclear physics is the proliferation of nuclear models. R. J. Eden, in a clear and authoritative article on this subject, shows how many of these models are defined, extended and inter-related and how they are connected with the basic nuclear many-body problem. The determination of nuclear moments is, of course, of prime importance for model testing and many readers will be grateful to K. F. Smith for a well arranged account (Nuclear Moments and Spins) of the numerous accurate methods now available in this field. There is a comprehensive table of magnetic dipole and electric quadrupole moments.

In her article ' The Spectroscopy of Mesonic Atoms ' Mrs. Stearns contributes a striking account of this relatively simple but powerful method of studying nuclear properties. The accurate determination of meson masses by the critical absorption technique is an achievement of remarkable elegance. Fission is always topical and in a stimulating chapter of unusual interest (Fission Recoil and its Effects) G. N. Walton examines the physical and chemical phenomena observed in the slowing down of heavy highly charged ions. Experimental results are related to the Bohr theory of stopping power.

O. R. Frisch and T. H. R. Skyrme have been able, through fortunate timing, to publish in the final chapter of this book the first review of a major development in physics, under the title ' Parity Non-Conservation in Weak Interactions '. This is a straightforward introduction to the language now being employed; inevitably much more must now be added and it is to be hoped that future volumes will provide the necessary supplement. W. E. BURCHAM.

Structure Reports, volume 15, edited by A. J. C. WILSON. Pp. viii + 588. (Netherlands: N. V. van de Garde and Co.'s Drukkerij, Zaltbommel, 1957.) £10 10*s*.

During the past three years the *Structure Reports* for the war and immediate post-war years have been completed and volume 15 takes up again the annual series. This volume covers work published in 1951.

Le Dépôt Électrolytique des Métaux, by A. T. VAGRAMYAN and Z. A. SOLOVIEVA, translated by C. R. MONNEY. Pp. x + 220. (Paris: Dunod, 1958.) 2.450 *fr*.

The gap between the practising electrodepositor and the electrochemist or metal physicist remains wide. This book lies in that gap but cannot be said to fill it. Since there is virtually no discussion of the theory of the deposition process itself, the approach is mainly from the practical side. The authors give full descriptions of techniques developed in their own laboratory for the study of the properties of metal deposits such as brightness, durability, internal stress, adherence and amount of occluded hydrogen. They discuss empirically the effect of surface-active agents, current distribution, alternating current and ultra-sound on these properties as well as methods of depositing alloys. It is unfortunate that the effect of surface active agents in retarding the rate of electrodeposition is described as ' passivation ' and that this term is retained by the translator.

In the measurement of the polarization properties of electrodes great stress is rightly given to the importance of the variation with time which was pointed out by Roiter and by Vagramyan. However, the techniques described here are adequate only for processes having a duration of about 10 seconds. No mention is made of the more modern use of relaxation techniques applicable to times down to a fraction of a millisecond which are essential for the study of fast reactions such as electrodeposition.

The translation appears to be accurate and complete with one important exception: all the references to the original papers have been omitted. Many of the illustrations are better reproduced in the translation than in the original and the binding is also improved. R. PARSONS.

Proceedings of the Sixth International Conference on Spectroscopy, by W. VAN TONGEREN and F. FREESE. Pp. vii + 663. (London, New York, Paris, Los Angeles: Pergamon Press, 1957.) £8 8*s*.

The Latin title *Colloquium Spectroscopicum Internationale VI* reflects the truly international character of this tri-lingual conference, held in Amsterdam in May 1956, with contributions from all parts of the world, including near and far East. These Proceedings are published as a supplement to the *Spectrochimica Acta*. Spectrochemical analysis in emission formed the main theme, but work on absorption spectra and molecular structure has been included. The range of subjects may be judged from the chapter headings: I. Flame Spectroscopy, II. Emission Spectrometry. III. Arc Emission. IV. Spark Emission. V. Emission (General). VI. Instrumentation (Emission). VII. Instrumentation of Absorption Methods. VIII. Ultraviolet Absorptiometry. IX. Infra-red Spectroscopy.

Of the 108 articles, some are concerned with mainly technical points and are addressed to the specialist only, but others deal with topics of more general interest to physicists. A few of the latter may be mentioned in the following: Mutual influence of two elements, simultaneously present in the flame, on the intensity of their spectra. Temperature and concentration of ions and electrons in arcs, and intensity of the continuous background due to bremsstrahlung (free–free transitions) and recombination. Relative intensities of lines of the same element. The mechanism of the spark formation based on high speed photographs by Schlieren and interference methods. The use of sliding sparks *in vacuo*. Continuous atomic and molecular spectra of mercury. Spectra of Au_2, CuAg and AuAg. Hg and He lamps for Raman excitation. Effects of environment on electronic spectra of molecules. Exciton spectra in CdS crystals. Infra-red spectra of organic molecules in relation to their structure. Infra-red spectra of phthalocyanines with different metal atoms.

In spite of the essentially specialist nature of the conference many physicists not specializing in this field will find useful material in this volume.

H. G. KUHN.

The Ionosphere, by KARL RAWER. Pp. 202. (London: Crosby Lockwood and Son, 1958.) 42*s*.

Amongst the few books on the ionosphere the one written in German, in 1952, by Dr. K. Rawer, is probably the best modern introduction. It is therefore fortunate that its appeal has now been widened by the appearance of an English translation.

It starts by describing the observation of the ionosphere by radio, spectroscopic, magnetic, and other methods. The results are summarised and an account is given of some of the current theories. The development of the subject has been so rapid since 1952 that parts of this theoretical section are a little out of date. A final section is devoted to describing how the ionosphere influences the propagation of radio waves, and how the propagation conditions can be predicted. The book provides a valuable introduction both for the student of ionospheric physics and for the engineer concerned with radio propagation.

Although, for an Englishman, the German of the original book was unusually easy to read, unfortunately the English of the translation is particularly awkward and unidiomatic. It is difficult to concentrate on the scientific content of a book which repeatedly uses expressions like " Consequently it has been tried to follow at least the intensity variation of the strongest line by photo electric means ", or " One has succeeded to demonstrate echo phenomena which belong to a layer beneath the E-layer with extremely long waves ".

J. A. RATCLIFFE

Semiconductor Thermoelements and Thermoelectric Cooling, by A. F. IOFFE. Pp. 184. (London: Infosearch, 1957) 42*s.*

Thermoelectric refrigeration and generation have become important subjects in recent years, and research on them has now become widespread. Research on the utilization of semiconductors for these applications became active in 1950 in Ioffe's Institute in Leningrad, so that his book on the subject is fully authoritative. The reviewer has been closely concerned for several years with work on these problems, mainly concentrated however on bismuth telluride, so that he is very appreciative of the Russian contribution and the stimulating effect of Ioffe's thought on the subject.

The book suffers somewhat from the fact that it is based on two separate books published in Russian in 1956. In consequence some of the sections are repetitive and the lay-out fails to give a logical development of the subject. The subject matter is however comprehensive, and includes the basic theory, the requirements for good thermoelectric performance, the physical measurements and the applications. Thermoelectric generation and refrigeration are both discussed. Little information is given however on the preparation of the materials used, and the problems encountered in the assembly of cooling or generating units are not discussed in any detail.

The book is well written and translated.

D. A. WRIGHT.

Proceedings of the International Conference on Fatigue of Metals 1956. Pp. v + 961. (London : Institution of Mechanical Engineers.) £4 10*s.*

Sixth Symposium (*International*) *on Combustion* 1956. Pp. xxi + 943. (For the Combustion Institute—New York : Reinhold Publishing Corporation, London : Chapman and Hall.) £11 4*s.*

The Physics of Fluids, Vol. 1, No. 1, edited by F. N. Frenkiel. Jan.–Feb. 1958. Pp. ii + 72. (New York : American Institute of Physics.) Subscription price U.S. and Canada $10.00, elsewhere $11.00.

PARIS : PUBLICATIONS SCIENTIFIQUES ET TECHNIQUES DU MINISTÈRE DE L'AIR :

Etude expérimentale de l'écoulement turbulent dans un divergent bidimensionnel parcouru par de l'air, par J. P. MILLIAT. Pp. 134. No. 335. 1957. 2000 *fr*.

Nouvelle méthode approchée de calcul des couches limites laminaire et turbulente en écoulement compressible, par A. WALZ. Pp. 48. No. 336. 1957. 900 *fr*.

Contribution à l'étude de l'interféromètre différential à biprisme de Wollaston, par G. GONTIER. Pp. 110. No. 338. 1957. 1200 *fr*.

Méthodes théoriques d'étude des écoulements supersoniques, par P. CARRIÈRE. Pp. 234. No. 339. 1957. 3000 *fr*.

Résolution de problèmes d'infiltrations à surface libre au moyen d'analogies électriques, par P. HUARD DE LA MARRE. Pp. 154. No. 340. 1958. 2540 *fr*.

Applications des constantes et données thermodynamiques des mélanges gazeux aux températures élevées, par G. RIBAUD et N. MANSON. Pp. 191. No. 341. 1958. 2700 *fr*.

Etude critique de certains prolongements de la mécanique rationnelle : Thermodynamique et viscosité, par H. DU BOSCQ DE BEAUMONT. Pp. 47. No. N.T. 72. 1957. 1000 *fr*.

Séminaire d'aérothermique de la Faculté des Sciences de Paris, Année 1956–1957. Pp. 192. No. N.T. 73. 1958. 2730 *fr*.

Optique de la photographie sous-marine, par C. MAUREAU. Pp. 104. No. N.T. 74. 1958. 1800 *fr*.

Stabilisation des transports d'énergie à longue distance, par R. PERRET. Pp. 171. No. N.T. 75. 1958. 3300 *fr*.

Limites d'applications de la théorie de la ligne portante au calcul d'ailes d'avions munies de spoïlers, par A. FAUQUET. Pp. 73. No. B.S.T. 120. 1957. 1500 *fr*.

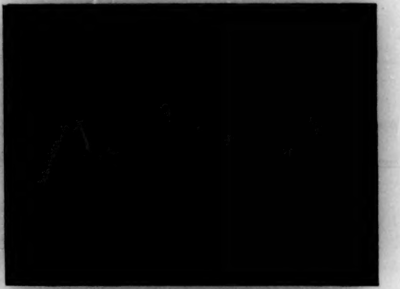

Figure 3. Ethylene oxide transition at 35 791 Mc/s in cavity resonance. Receiver tuned to first harmonic of ν_r.

Figure 4. Ethylene oxide transition at 34 150 Mc/s in cavity resonance. Receiver tuned to second harmonic of ν_r.

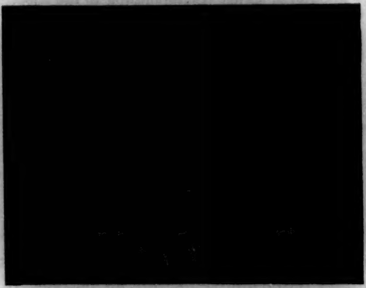

Figure 7. Zeeman doublet of $^{14}NH_3$ ($J,K = 13,13$) in cavity resonance.

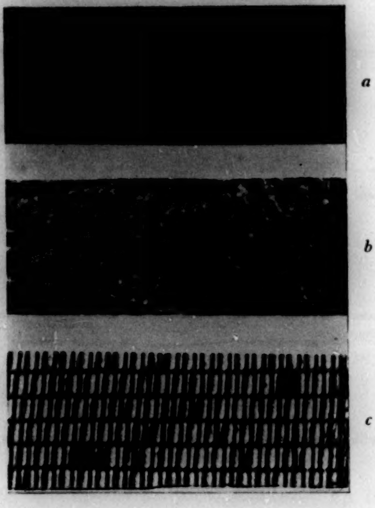

Figure 8. Aerial scenes corresponding to the spectra of figure 7.

The Collective Treatment of a Fermi Gas: I

By S. F. EDWARDS†

Department of Mathematical Physics, University of Birmingham

Communicated by R. E. Peierls; MS. received 2nd June 1958, *and in final form* 11*th July* 1958

Abstract. The collective approach to a Fermi gas is discussed by considering the wave functions of non-interacting Fermi gases in one and three dimensions, and of the interacting Fermi gas. It is shown how to write the one-dimensional case exactly in terms of collective coordinates, and how these have a well defined existence for long wavelengths even without interaction. This is extended as far as possible to three dimensions, and it is shown how the statistics affect the collective motion in the presence of interaction. A brief discussion is given of how calculations may be performed when redundant sets of coordinates are used.

§ 1. INTRODUCTION

This paper is concerned with the correlations of the particles of a Fermi gas which appear as collective fluctuations of its density. It is well known that these are of great importance when long range forces are present as in the Coulomb plasma problem, and also possibly in certain collective nuclear motions. The aim of this paper is to express the well established ideas (Tomonaga 1950, Bohm and Pines 1953), in a rather more explicit form than is usual, and thus avoid various steps in the usual treatment whose errors are not clearly defined, and in this way set up a calculation of, say, the ground state of an interacting Fermi gas in a form which can be improved by higher order calculations in a straightforward way. The paper will proceed thus: firstly, a non-interacting Fermi gas in one dimension will be discussed in terms of collective oscillations by writing the well-known determinantal wave function in terms of the Fourier components of the density. It will be shown that even without interaction the long-wave fluctuations of density are good coordinates for the system, and, for example, have a well defined kinetic energy. This will suggest extensions to three dimensions, and the differences are then discussed. It is then shown how interactions modify the non-interacting case, in particular how the statistics affect the frequency of the fluctuations. This is set up without the use of subsidiary conditions, and it is shown how integrals using overlapping sets of degrees of freedom can be evaluated.

Detailed variational calculations of the ground state energy are deferred to a subsequent paper.

§ 2. THE ONE DIMENSIONAL FERMI GAS

For fermions on a line of length 2π, with periodic boundary conditions, the solution to Schrödinger's equation for the antisymmetrized ground state is the determinant of plane waves, taking for convenience $N+1$ particles,

---

† Now at Atomic Energy Research Establishment, Harwell, Didcot, Berks.

$$\Psi = \begin{vmatrix} \exp(\tfrac{1}{2}Nix_1) & \exp(\tfrac{1}{2}Nix_2) & \cdot & \cdot \\ \exp\{(\tfrac{1}{2}N-1)\,ix_1\} & \cdot & \cdot & \cdot \\ \cdot & & & \\ \cdot & & & \\ \cdot & & & \\ \exp(-\tfrac{1}{2}Nix_1) & \cdot & \cdot & \cdot \end{vmatrix} \qquad \ldots\ldots(1)$$

This determinant can be evaluated in the form of a product by writing $\exp(ix_k) = \xi_k$ which gives

$$\Psi = \exp(-\tfrac{1}{2}Ni\textstyle\sum x_k) \begin{vmatrix} \xi_1{}^N & \xi_2{}^N & \cdot\ \cdot\ \cdot & \xi_{N+1}{}^N \\ \cdot & & & \cdot \\ \cdot & & & \cdot \\ \cdot & & & \cdot \\ \cdot & & & \cdot \\ 1 & 1 & \cdot\ \cdot\ \cdot & 1 \end{vmatrix} \qquad \ldots\ldots(2)$$

the latter being Van der Monde's determinant, clearly vanishing when $\xi_\alpha = \xi_\beta$ and equals

$$\Psi = \exp(-\tfrac{1}{2}iN\textstyle\sum x_k) \, . \displaystyle\prod_{\alpha>\beta} (\xi_\alpha - \xi_\beta). \qquad \ldots\ldots(3)$$

But $\quad \xi_\alpha - \xi_\beta = \exp\{\tfrac{1}{2}i(x_\alpha + x_\beta)\}[\exp\{\tfrac{1}{2}i(x_\alpha - x_\beta)\} - \exp\{-\tfrac{1}{2}i(x_\alpha - x_\beta)\}]$

$$= 2i\exp\{\tfrac{1}{2}i(x_\alpha - x_\beta)\}\sin[\tfrac{1}{2}(x_\alpha - x_\beta)]. \qquad \ldots\ldots(4)$$

So $\quad \Psi = \prod 2i \sin[\tfrac{1}{2}(x_\alpha - x_\beta)] \qquad \ldots\ldots(5)$

$$= \prod_{\alpha>\beta} \sin[\tfrac{1}{2}(x_\alpha - x_\beta)](2i)^{N(N+1)/2}. \qquad \ldots\ldots(6)$$

Some further understanding of Ψ can be obtained by considering it as a function of x_1 when all the other x_k's are fixed. More simply, consider $\prod(\xi_\alpha - \xi_\beta)$ for α greater than β as a function of ξ_1, when all the other ξ_k's are fixed. This product represents a polynomial in ξ_1, of order N which vanishes at the N points $\xi_1 = \xi_k$ which are in fact $x_1 = x_k$. As a function of ξ_1 Ψ is of the general shape shown in the figure; it has no other roots than the ξ_k's and for example if the ξ_k's were equidistant, Ψ would be a Tschebyscheff polynomial, which has this property of equally spaced roots.

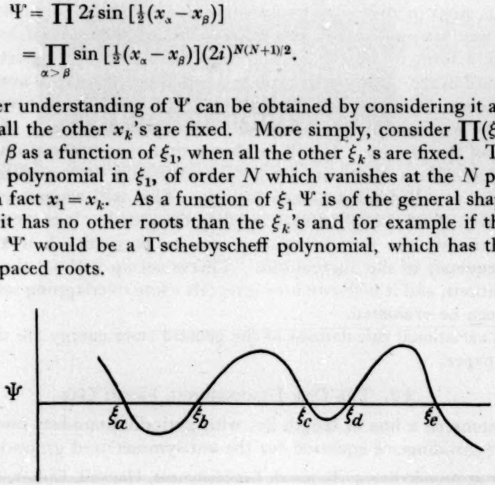

Now consider Ψ in terms of the collective coordinates ρ_k. To write it in terms of them, use (dropping the $(i)^{N(N-1)/2}$ since this factor will not affect our discussion)

$$\begin{aligned}\Psi &= 2^{N(N+1)/2}\prod_{\alpha>\beta}\theta(x_\alpha-x_\beta)|\sin[\tfrac{1}{2}(x_\alpha-x_\beta)]| \\ &= 2^{N(N+1)/2}\prod_{\alpha>\beta}\theta(x_\alpha-x_\beta)\,[\sin^2\{\tfrac{1}{2}(x_\alpha-x_\beta)\}]^{1/2} \\ &= \prod_{\alpha>\beta}\theta(x_\alpha-x_\beta)[1-\exp\{\tfrac{1}{2}i(x_\alpha-x_\beta)\}]^{1/2}[1-\exp\{-\tfrac{1}{2}i(x_\alpha-x_\beta)\}]^{1/2} \\ &= \prod_{\alpha>\beta}\theta(x_\alpha-x_\beta)\exp\Big[-\tfrac{1}{2}\sum_{\alpha>\beta}\sum_n\frac{1}{n}\exp\{\tfrac{1}{2}in(x_\alpha-x_\beta)\} \\ &\qquad -\tfrac{1}{2}\sum_{\alpha>\beta}\sum_n\frac{1}{n}\exp\{-\tfrac{1}{2}in(x_\alpha-x_\beta)\}\Big] \qquad \ldots\ldots(8)\end{aligned}$$

where the exponents are the series expansion of the logarithms of

$$1-\exp[\tfrac{1}{2}i(x_\alpha-x_\beta)] \quad \text{and} \quad 1-\exp[-\tfrac{1}{2}i(x_\alpha-x_\beta)], \quad \text{and}$$
$$\theta(x)=1,\quad x>0;\quad \theta(x)=-1,\quad x<0.$$

Thus

$$\Psi=\prod_{\alpha>\beta}\theta(x_\alpha-x_\beta)\exp\Big[-\tfrac{1}{2}\sum_1^\infty\frac{1}{k}\{\rho_k\rho_k{}^*-N-1\}\Big] \qquad \ldots\ldots(9)$$

where $\rho_k=\Sigma_\alpha\exp(ikx_\alpha)$. This series in the ρ's is on the limit of convergence of the expansion of the logarithm, and, if used up to ρ_∞, is clearly very dangerous. But a certain number, M say, of the ρ's may be kept in the exponent, whilst the remainder are taken back into the infinite product. So if $\phi(x_\alpha-x_\beta)$ is defined by

$$\log|\phi|=\tfrac{1}{2}\sum_{M+1}^\infty\{\rho_k\rho_k{}^*-N-1\}/k, \qquad \ldots\ldots(10)$$
$$\phi(x)=-\phi(-x), \qquad \ldots\ldots(11)$$

then

$$\Psi=\prod_{\alpha>\beta}\phi(x_\alpha-x_\beta)\exp\Big[-\tfrac{1}{2}\sum_1^M\frac{1}{k}(\rho_k\rho_k{}^*-N-1)\Big]. \qquad \ldots\ldots(12)$$

In this way the function Ψ has been separated into two parts. Considered as a function of x_1, say, the first part is approximately equal to $\prod\theta(x_\alpha-x_\beta)$ and equal to ± 1 except when x_1 approaches an x_α; there it changes sign over a distance of order 2π times length of the enclosure divided by the maximum wave number M. If, for example, M were of the order of the total number of fermions, the changeover would take place in the order of an interparticle distance. The rest of Ψ consists of a term which is the ground state wave functions of harmonic oscillations of the variables $\rho_k, \rho_k{}^*$ the oscillator frequency being inversely proportional to the wave number.

So far the discussion is exact. Now consider taking a number of the ρ_k's as basic coordinates. The assumption that for small k's, the ρ_k behave as independent useful coordinates can be checked in this simple one-dimensional case since all calculation can in fact be carried out exactly. For example, if we wish to evaluate an integral like $\int\rho_n\rho_n{}^*\Psi^*\Psi\prod dx$ and treat the ρ's as independent, then since the Jacobian from x to ρ is $\exp[-\Sigma\rho_n\rho_n{}^*/N+1]$ (Bohm and Pines 1953) one has (dropping the 1 from $N+1$ for convenience)

$$\int\rho_n\rho_n{}^*\exp[-\rho_n\rho_n{}^*(N^{-1}+n^{-1})]\,d\rho_n d\rho_n{}^*\Big/\int\exp[-\rho_n\rho_n{}^*(N^{-1}+n^{-1})]d\rho_n d\rho_n{}^*$$
$$=(N^{-1}+n^{-1})^{-1}=n(1+nN^{-1})^{-1}. \qquad \ldots\ldots(13)$$

Now if $\int \Psi^* \Psi \prod dx = \nu$ one has exactly

$$\begin{aligned}\nu^{-1} \int \rho_n \rho_n{}^* \Psi^* \Psi \prod dx &= \nu^{-1} \sum_{\alpha>\beta} \int \exp\{in/(x_\alpha - x_\beta)\} \epsilon_{\alpha_1\alpha_2} \epsilon_{\alpha_1'\alpha_2'} \cdots \\ &\qquad \times \exp\{i \sum (\alpha_k - \alpha_k')x_k\} \prod dx \\ = (\delta_{\alpha_1\alpha_1'}\delta_{\alpha_2\alpha_2'} - \delta_{\alpha_1\alpha_2'}\delta_{\alpha_2\alpha_1'}) & \{N\delta_{\alpha_1\alpha_1'}\delta_{\alpha_2\alpha_2'} \\ &\qquad + \delta(\alpha_1 - \alpha_1' + n)\delta(\alpha_2 - \alpha_2' - n)\} \qquad \ldots\ldots(14) \\ &= N - \sum_{\frac{1}{2}N}^{\frac{1}{2}N-n} 1 = N - (N-n) = n. \qquad \ldots\ldots(15)\end{aligned}$$

A comparison shows that the error is $nN^{-1}(1+nN^{-1})^{-1}$ and is negligible until $n \sim N$. In the same way the value $\langle \rho_n \rho_m{}^* \rangle$ is readily shown to be zero.

Similarly, one can ask how much of the kinetic energy of the Fermi gas can be associated with one of the ρ's and how good is the picture of kinetic energy being associated with a ρ, i.e. how important is the cross term between the harmonic oscillation of a ρ and the short-range part of Ψ.

The Schrödinger equation can be treated directly, or one could attempt to write it in terms of the ρ's via

$$\begin{aligned}-\sum \nabla_\alpha{}^2 &\equiv \sum nm\rho_{n+m}\rho_n\rho_m \frac{\partial^2}{\partial\rho_n\partial\rho_m} + \sum n^2\rho_n \frac{\partial}{\partial\rho_n} \\ &\sim n^2 N \rho_n \rho_n{}^* \frac{\partial^2}{\partial\rho_n \partial\rho_n{}^*} \qquad \ldots\ldots(16)\end{aligned}$$

since in the sum $\rho_0 = N$ predominates. One would then, however, still have to check on the magnitude of the carrier, and it is therefore preferable to use the exact method directly.

We now write $$\Psi = (\Psi e^S)e^{-S} \qquad \ldots\ldots(17)$$

where $$S = \rho_n \rho_n{}^*/2n. \qquad \ldots\ldots(18)$$

Then $$\int \Psi^* \nabla^2 \Psi \prod dx = -\frac{2m}{\hbar^2} \int \Psi^* E \Psi \prod dx \qquad \ldots\ldots(19)$$

giving

$$E = \frac{\hbar^2}{2m} \left(\int \Psi^* \Psi \prod dx \right)^{-1} \left[\int \Psi^* (A+B+C) \prod dx \right] \qquad \ldots\ldots(20)$$

where

$$A = \nabla^2 \Psi + (S_\mu{}^2 + S_{\mu\mu})\Psi + 2S_\mu \Psi_\mu \qquad \ldots\ldots(21)$$

$$B = -2S_\mu(S_\mu \Psi + \Psi_\mu) \qquad \ldots\ldots(22)$$

$$C = (S_\mu{}^2 - S_{\mu\mu})\Psi. \qquad \ldots\ldots(23)$$

C represents the kinetic energy associated with the ρ_n, A the residual kinetic energy and B the cross term, which should approximately vanish if the ρ's give a good picture.

A detailed calculation now yields the values

$$A = -\sum_{-N/2}^{N/2} k^2 + \tfrac{1}{2}Nn, \quad B = +n^2, \quad C = -\tfrac{1}{2}Nn - n^2. \qquad \ldots\ldots(24)$$

By comparing B with C we confirm that the ρ_n's are sensible coordinates provided that $n < N$. It is not practicable, however, to attempt to use (16) to obtain the entire kinetic energy via the ρ's since the expression for Ψ entirely in terms of ρ's is on the circle of convergence, and the differentiations in the Schrödinger equation go across the circle of convergence and rather artificial summations of divergent series are needed to obtain the correct answer. This is, however, no drawback to extracting a few of the ρ's if required and treating them as above.

As a final comment on the one-dimensional case consider the excitations of the Fermi gas. These are easily understood in the original determinantal expression. Take the lowest excitation in which the top electron goes up one level. In terms of the ξ's the row with $\xi_k{}^N$ becomes $\xi_k{}^{N+1}$. But Ψ clearly still vanishes for $\xi_\alpha = \xi_\beta$ and thus retains the original $\prod(\xi_\alpha - \xi_\beta)$ term for α greater than β, the total power in ξ having increased, however, by 1. Therefore

$$\Psi_1 = \Psi\chi \qquad \ldots\ldots(25)$$

where χ is linear in the ξ's, and symmetric. χ must therefore be $\Sigma\xi_k = \rho_1$ and the coefficient is also correct:

$$\Psi_1 = \rho_1 \Psi. \qquad \ldots\ldots(26)$$

In the ρ picture this is the first excited state of the harmonic oscillation of ρ_1. Similarly, when the excitation results in a change in the power in ξ of Ψ the appropriate χ can be written as a symmetric function of the ξ's, hence can be written as functions of $\Sigma_k \xi_k{}^l$, $\Sigma_k \xi_k{}^{-i}$ i.e. ρ_l, $\rho_l{}^*$ and the excited Ψ can be written as a sum of products of hermite polynomials in the ρ's times the ground state function. This picture will have less and less usefulness as the wave number of the ρ and the order of the hermite polynomial increase, but for low excitations and low wave numbers clearly *all* excitations can be written in terms of the ρ's. So in one dimension all excitations in which particles are not lifted too far above the top of the Fermi sea can be regarded as harmonic excitations of the fourier components of the density.

It is perhaps worth mentioning that the manipulation of this section can also be performed when box boundary conditions rather than periodic boundary conditions are imposed, i.e. when sines rather than exponentials appear in the determinant, and that analogues of (12) exist for this case, but are rather more complicated.

§ 3. THE THREE DIMENSIONAL FERMI GAS

One cannot get as far in the three-dimensional case as in the one-dimensional, but one can still take the theory as far as in practice it will be required. Consider firstly why there is trouble in the three-dimensional case.

The ξ variable is replaced by

$$\xi_k = \exp(ix_k), \quad \eta_k = \exp(iy_k), \quad \zeta_k = \exp(iz_k) \qquad \ldots\ldots(27)$$

and now consider Ψ in a simple case. To avoid unnecessary complication consider two dimensions first. Say there are five particles and

$$\Psi = \begin{vmatrix} \exp(-iy_1) & . & . & . & . & . & . & . \\ \exp(-ix_1) & . & . & . & . & . & . & . \\ 1 & . & . & . & . & . & . & . \\ \exp(ix_1) & . & . & . & . & . & . & . \\ \exp(iy_1) & . & . & . & . & . & . & . \end{vmatrix} \qquad \ldots\ldots(28)$$

or

$$\Psi = \exp\{-i\sum(x_k + y_k)\} \begin{vmatrix} \exp(iy_1) & . & . & . & . & . & . & . \\ \exp(ix_1) & . & . & . & . & . & . & . \\ \exp\{i(x_1+y_1)\} & . & . & . & . & . & . \\ \exp(2ix_1) & . & . & . & . & . & . & . \\ \exp(2iy_1) & . & . & . & . & . & . & . \end{vmatrix} \qquad \ldots\ldots(29)$$

$$= \exp\{-i\textstyle\sum(x_k+y_k)\}\begin{vmatrix} \eta_1^2 & \cdot & \cdot & \cdot & \cdot & \cdot & \cdot & \cdot \\ \xi_1^2 & \cdot & \cdot & \cdot & \cdot & \cdot & \cdot & \cdot \\ \xi_1\eta_1 & \cdot & \cdot & \cdot & \cdot & \cdot & \cdot & \cdot \\ \eta_1 & \cdot & \cdot & \cdot & \cdot & \cdot & \cdot & \cdot \\ \xi_1 & \cdot & \cdot & \cdot & \cdot & \cdot & \cdot & \cdot \end{vmatrix} \qquad \ldots\ldots(30)$$

If the other four ξ's are considered fixed, this determinant in the ξ_1, η_1 represents a conic through the origin, and the points ξ_α, η_α. $\Psi(\xi_1, \eta_1)=0$ is a locus, and not as in one dimension a series of points. This result is quite general; and in three dimensions with N particles $\Psi=0$ represents a surface which will pass through all the other points, and be of the degree prescribed by the form of the determinant (there are, of course, increasingly many degenerate levels to be chosen from as the radius of the Fermi sphere increases). However, the proximity of ξ, η, ζ to this surface in no way implies their proximity to any other of the ξ, η, ζ's. For the $\rho_{\mathbf{k}}$ with low wave number $|\mathbf{k}|$ the picture of harmonic vibrations of density is still very plausible, and one can still try to force the answer by applying the check calculation of (15). Assume then that Ψ will have a dependence upon the $\rho_{\mathbf{k}}$ for small $\mathbf{k}$ like

$$\exp\left[\textstyle\sum b(\mathbf{k})\rho_{\mathbf{k}}\rho_{\mathbf{k}}^*\right].$$

Then it ought to follow that

$$\int\rho_{\mathbf{j}}\rho_{\mathbf{l}}^*\exp\left[-\sum_k\left(2b(k)+\frac{1}{N}\right)\rho_{\mathbf{k}}\rho_{\mathbf{k}}^*\right]d\rho_{\mathbf{k}}\Big/\int\exp\left[-\sum_{\mathbf{k}}\left(2b+\frac{1}{N}\right)\rho_{\mathbf{k}}\rho_{\mathbf{k}}^*\right]d\rho_{\mathbf{k}}$$

$$=\left((2b(j)+\frac{1}{N}\right)^{-1}. \qquad \ldots\ldots(31)$$

Actually this integral when performed exactly gives an answer which is the volume traced out by a vector $\mathbf{j}$ either end of which lies on the Fermi surface whilst none of the vector ever gets outside it. This is approximately $2\pi K^2|\mathbf{j}|$ where K is the Fermi radius $4\pi K^3=3N$. With $|\mathbf{j}|^3 \ll N$ then,

$$\frac{1}{2b(j)} \simeq 2\pi K^2|\mathbf{j}|$$

$$b(j)\simeq 1/4\pi K^2 j. \qquad \ldots\ldots(32)$$

That this assignment is reasonable can readily be checked by performing other integrals similar to (31) by the exact and approximate methods and showing that they agree to the accuracy with which the approximation is being made.

§ 4. THE INTERACTING FERMI GAS

As an illustration of the further development of the ideas of the last section, consider the problem of fermions interacting with a long-range two-body potential. In general one can split up any potential into a long- and short-range part, the long-range part being such that only a certain number of Fourier components come in

$$\sum V_{ij}=\sum v_{ij}+\sum_{|\mathbf{k}|<K_1} v(k)\rho_{\mathbf{k}}\rho_{\mathbf{k}}^*. \qquad \ldots\ldots(33)$$

Now consider the solution of the Schrödinger equation

$$\left(\frac{\hbar^2}{2m}\sum\nabla^2+E-\sum v(k)\rho_{\mathbf{k}}\rho_{\mathbf{k}}^*-\sum u_{ij}\right)\Psi=0. \qquad \ldots\ldots(34)$$

The idea is that ψ can be split into three parts, the first being the determinant of plane waves, the second takes account of the long-range effects and the third the short-range effects and the inadequacies in the long-range treatment. This latter part is essentially to be treated by perturbation theory, so let us consider at first the solution of

$$\left(\frac{\hbar^2}{2m}\sum\nabla^2+E-\sum v\rho_{\mathbf{k}}\rho_{\mathbf{k}}{}^*\right)\Phi=0. \qquad \ldots\ldots(35)$$

Look for a solution in the form

$$\Phi=\Psi\exp\left[-\sum c(h)\rho_{\mathbf{k}}\rho_{\mathbf{k}}{}^*\right] \qquad \ldots\ldots(36)$$

where Ψ is the determinant of plane waves and the $c(k)$ are to be determined. Then one obtains

$$\frac{\hbar^2}{2m}\left[-\sum\mathbf{k}\,.\,\mathbf{j}\rho_{\mathbf{k}+\mathbf{j}}\rho_{\mathbf{k}}\rho_{\mathbf{j}}c(k)c(j)-2\sum k^2\rho_{\mathbf{k}}\rho_{\mathbf{k}}{}^*c(k)+\text{c.c.}+2N\sum k^2c(k)\right]$$
$$-E+\sum v(k)\rho_{\mathbf{k}}\rho_{\mathbf{k}}{}^*+\frac{2i\hbar^2}{2m}\sum\Psi_{\mu}k_{\mu}\Psi^{-1}c(k)\exp(ikx_{\alpha})=0. \qquad \ldots\ldots(37)$$

Now, as far as long range effects are concerned, we can treat Ψ as represented by $\exp[-\sum\rho_{\mathbf{k}}\rho_{\mathbf{k}}{}^*b(k)]$ and hence, separating the term in $\mathbf{k}+\mathbf{j}=0$ in the first sum,

$$\frac{\hbar^2}{2m}\sum\rho_{\mathbf{k}}\rho_{\mathbf{k}}{}^*\left[k^2c^2(k)N-k^2c(k)+2k^2Nc(k)b(k)-\frac{2m}{\hbar^2}v(k)\right]$$
$$-E+N\sum k^2c(k)+\sum_{k\neq j}\rho_{\mathbf{k}+\mathbf{j}}\rho_{\mathbf{k}}\rho_{\mathbf{j}}c(k)c(j)$$
$$+2\sum(\Psi_{\mu}k_{\mu}\Psi^{-1}\exp(ikx_{\alpha})-Nk^2c(k)b(k)=0. \qquad \ldots\ldots(38)$$

The last two terms have expectation value zero with the approximate wave function, and are to be treated as a perturbation with the short range potential. The rest of the expression vanishes provided that

$$k^2Nc^2(k)-k^2c(k)+2Nk^2c(k)b(k)=\frac{2mv(k)}{\hbar^2} \qquad \ldots\ldots(39)$$

and contributes $2N\Sigma k^2c(k)$ to the energy of the system. The separation of the $\mathbf{k}+\mathbf{j}=0$ term is the random phase approximation, which though clearly very plausible is to be justified by the evaluation of the higher order contributions. Looking at (39) we see that the second term, which appeared with $N\Sigma k^2c(k)$ in the calculation, is very small, and is indeed of the same character as those terms neglected by the random phase approximation; only its simpler structure means that it can be left in here if required. Ignoring it one is left with two terms, the first being present even if the statistics were ignored, whilst the last is the cross term between the random Fermi gas motion (albeit collective) and the addition to the wave function. If this latter term is ignored one has

$$c(k)=(2mv/k^2N\hbar^2)^{1/2}, \qquad \ldots\ldots(40)$$

$$E=N\sum k^2c(k)=N\sum k(2mv/N\hbar^2)^{1/2} \qquad \ldots\ldots(41)$$

For a Coulomb potential $v=e^2/2\pi^2k^2$ and

$$E=\sum(4\pi e^2n/m)^{1/2}\tfrac{1}{2}\hbar \qquad \ldots\ldots(42)$$

where n is the density of fermions.

The zero point energies of a set of degenerate oscillators having the well-known plasma frequency. There is no need of course to ignore the cross term and one can use the general solution

$$c(k)=k^{-2}N^{-1}[-k^2(2Nb-1)+\{k^4(2Nb-1)^2+8k^2Nmv/\hbar^2\}^{1/2}]. \qquad \ldots\ldots(43)$$

This formula expresses the effect of the statistics on the amplitude of the collective oscillation.

The effect of the cross term is comparable to the main term if

$$c(k)\sim 2b(k)=(2\pi K^2k)^{-1} \quad (k^2<K^2) \qquad \ldots\ldots(44)$$

and if $c(k)$ reaches this value the simple picture of collective oscillations cannot be maintained. It implies that

$$k^2>K^2\ \frac{\text{interparticle distance}}{\text{Bohr radius}} \qquad \ldots\ldots(45)$$

and this is never approached in the usual cases of electrons in metals.

An evaluation of the short range and neglected terms is now required to complete the calculation, which so far has not required any evaluating of integrals. This paper will conclude by pointing out how integrals with the basic trial function can be carried out.

§ 5. The Evaluation of Mixed Integrals

It will be seen that so far the Schrödinger equation has been solved by exact manipulations, the left-over terms of which are reserved for a higher accuracy calculation. To show the feasibility of this we must be able to perform integrals involving both the ρ's and the x's, a simple example of which is say

$$\int \rho_j\rho_j^*\Psi^*\Psi\exp[-\textstyle\sum\rho_k\rho_k^*c(k)]\prod dx. \qquad \ldots\ldots(46)$$

The crudest approach is to hope that the ρ's do not interfere much with the x's and ignore the presence of the $\Psi^*\Psi$ or more formally to say that a subsidiary condition applies connecting them. However, it is not easy to apply such subsidiary conditions in practice, and it is much better to be able to evaluate these integrals explicitly. Consider firstly how this would go if the short range effects were dropped and the integral converted to one over ρ, ρ^*. Neglecting the Jacobian $\exp[-\sum\rho\rho^*/N]$ one has

$$\Psi\Psi^*\sim\exp[-\textstyle\sum\rho_k\rho_k^*b(k)],$$

$$\int\rho_j\rho_j^*\exp[-\textstyle\sum(d(k)+b(k))\rho_k\rho_k^*]\prod d\rho_k\Big/\int\exp[\ldots]\prod d\rho_k$$

$$=(c(j)+b(j))^{-1}. \qquad \ldots\ldots(47)$$

Now imagine for the moment that c is small and expansion can take place in c/b:

$$=b^{-1}-cb^{-2}+c^2b^{-3}-\ldots. \qquad \ldots\ldots(48)$$

This form can be obtained directly, however, from

$$\frac{\int\rho_j\rho_j^*\{\sum_m(-[\sum c(k)\rho_k\rho_k^*]m/m!)\}\exp(-\sum\rho_k\rho_k^*b(k))\prod d\rho_k}{\int\{2\sum_m(-[\sum c(k)\rho_k\rho_k^*]m/m!)\}\exp(-\sum\rho_k\rho_k^*b(k))\prod d\rho_k}$$

In this form the taking of the ρ's as basic coordinates can be dispensed with and the original employed. So

$$\int \rho_{\mathbf{j}}\rho_{\mathbf{j}}^* \exp\left[-\sum c(k)\rho_{\mathbf{k}}\rho_{\mathbf{k}}^*\right]\Psi^*\Psi\prod d\rho \Big/ \int \exp\left[-\sum c(k)\rho_{\mathbf{k}}\rho_{\mathbf{k}}^*\right]\Psi^*\Psi\prod d\rho$$

$$= \int \rho_{\mathbf{j}}\rho_{\mathbf{j}}^* \left[\sum_m \frac{(-\sum c(k)\rho_{\mathbf{k}}\rho_{\mathbf{k}}^*)^m}{m!}\right]\Psi^*\Psi\prod d\rho \Big/ \int [\ldots]\Psi^*\Psi\prod d\rho. \quad \ldots\ldots(50)$$

The important point is to realise that this series is geometric, and can be formally summed even if it is not convergent, giving

$$(b + a_0 + a_1 + \ldots)^{-1} \quad \ldots\ldots(51)$$

where

$$\frac{a_0}{b^2} = \left\{\int \rho_{\mathbf{j}}\rho_{\mathbf{j}}^* \sum c(k)\rho_{\mathbf{k}}\rho_{\mathbf{k}}^*\Psi^*\Psi\prod d\rho \int \Psi^*\Psi\prod d\rho - \int \rho_{\mathbf{j}}\rho_{\mathbf{j}}^*\Psi^*\Psi\prod d\rho \int \sum c(k)\rho_{\mathbf{k}}\rho_{\mathbf{k}}^*\Psi^*\Psi\prod d\rho\right\} \times \left\{\int \Psi^*\Psi\prod d\rho\right\}^{-2} \quad \ldots\ldots(52)$$

and so on.

The a_0 of course checks exactly to order $1/N$, but the subsequent terms, $a_1, a_2, \ldots$ do not. The series $\sum a_j$, however, converges very rapidly and evaluates this integral to within any accuracy which is consistent with the rest of the calculation. Other integrals can be handled in a similar way, and this technique removes the awkwardness of subsidiary conditions.

It is planned to give a detailed account of these ideas in a variational calculation of the ground state energy of a Fermi gas with long-range interaction in a subsequent paper.

ACKNOWLEDGMENTS

The author would like to thank Professor R. E. Peierls and members of this department for helpful discussions, and Mr. R. C. L. Jenkins for checking and discussing the equations in the paper.

REFERENCES

BOHM, D., and PINES, D., 1953, *Phys. Rev.*, **92**, 22.
TOMONAGA, S., 1950, *Prog. Theor. Phys.*, **5**, 544.

Charge Transfer of Protons in Excited Atomic Hydrogen

By T. J. M. BOYD† and A. DALGARNO
Department of Applied Mathematics, The Queen's University of Belfast

Communicated by D. R. Bates; MS. received 7th July 1958

Abstract. Resonance charge transfer cross sections are calculated for protons in atomic hydrogen in the ground and first two excited states. The cross sections for an excited atom are nearly an order of magnitude larger than those for the ground state.

§ 1. INTRODUCTION

APART from the work of Buckingham and Dalgarno (1952) on excitation transfer and diffusion of metastable helium atoms in normal helium, there appear to be no calculations of elastic collision cross sections of processes involving excited atoms. The neglect of these cross sections, which are important parameters in theories of flame propagation, shock wave structure and other high temperature phenomena, stems largely from the lack of information on the interaction energies of the colliding species. However, for the important case of protons in excited hydrogen (and equivalently of deuterons in excited deuterium), there are available the calculations of Bates, Ledsham and Stewart (1953), and of Wallis and Hulburt (1954) of the energy levels of the hydrogen molecular ion.

§ 2. COLLISION THEORY

Improved methods for the theoretical discussion of slow heavy particle collisions have been described recently by Bates (1957, 1958) and by Bates and McCarroll (1958), and these suggest that the original perturbed stationary state method (Massey and Smith 1933, Bates, Massey and Stewart 1953) leads to a satisfactory expression for the cross sections for symmetrical resonance collisions. In the perturbed stationary state method, the entire system is taken to be in equilibrium and the relative motion is introduced as a perturbation. Omitting certain small terms, the Schrödinger wave equation for an electron of mass m in the field of two nuclei A and B of charges Z_{A} and Z_{B} respectively and of reduced mass M is

$$\left\{\frac{\hbar^2}{2m}\nabla^2\rho_{\mathrm{a}} + \frac{\hbar^2}{2M}\nabla_R{}^2 + E - V(\boldsymbol{\rho}_{\mathrm{a}}, \mathbf{R}) - \frac{Z_{\mathrm{A}}Z_{\mathrm{B}}}{R}\right\}\Psi = 0 \qquad \ldots\ldots(1)$$

where $\boldsymbol{\rho}_{\mathrm{a}}$ is the position vector of the electron referred to the origin A, $\mathbf{R}$ is the vector joining the nuclei, V is the complete electrostatic interaction potential and E is the total energy. In the case when $Z_{\mathrm{A}} = Z_{\mathrm{B}} = Z$, say, Ψ may be expanded according to

$$\Psi = \sum_n F_n{}^+(\mathbf{R})\chi_n{}^+(\boldsymbol{\rho}_{\mathrm{a}}, \mathbf{R}) + \sum F_n{}^-(\mathbf{R})\chi_n{}^-(\boldsymbol{\rho}_{\mathrm{a}}, \mathbf{R}) \qquad \ldots\ldots(2)$$

---

† Now at Department of Electron Physics, The University of Birmingham.

where χ_n^+ and χ_n^- are molecular wave functions satisfying the equation

$$\left\{\frac{\hbar^2}{2m}\nabla^2\rho_{\mathrm{a}} - V(\boldsymbol{\rho}_{\mathrm{a}}, \mathbf{R})\right\}\chi_n^{\pm} = -\epsilon_n^{\pm}\chi_n^{\pm} \qquad \ldots\ldots(3)$$

where $\epsilon_n^{\pm}(R)$ is the eigenvalue and $\chi_n^{+}(\boldsymbol{\rho}_{\mathrm{a}}, \mathbf{R})$ is symmetric and $\chi_n^{-}(\boldsymbol{\rho}_{\mathrm{a}}, \mathbf{R})$ antisymmetric with respect to interchange of A and B. Following the usual procedure (cf. Bates, Massey and Stewart 1953), we obtain the set of coupled differential equations

$$\begin{aligned}\left\{\frac{\hbar^2}{2M}\nabla_R^{\,2} + E - \epsilon_p^{\pm}(R) - \frac{Z^2}{R}\right\}F_p^{\pm}(\mathbf{R}) \\ = -\frac{\hbar^2}{2M}\left\{\sum_m F_m^{\pm}(\mathbf{R})\int \chi_p^{\pm *}\nabla_R^{\,2}\chi_m^{\pm}\, d\boldsymbol{\rho}_{\mathrm{a}}\right. \\ \left. + 2\sum_m \nabla_R F_m^{\mp}(\mathbf{R}) . \int \chi_p^{\pm *}\,\nabla_R\chi_m^{\mp} d\boldsymbol{\rho}_{\mathrm{a}}\right\}. \qquad \ldots\ldots(4)\end{aligned}$$

Provided the coupling with states $m \neq p$ is small, (4) may be replaced by the pair of equations

$$\begin{aligned}\left\{\frac{\hbar^2}{2M}\nabla_R^{\,2} + E - \epsilon_p^{\pm}(R) - \frac{Z^2}{R}\right\}F_p^{\pm}(\mathbf{R}) \\ = -\frac{\hbar^2}{2M}\left\{F_p^{\pm}(\mathbf{R})\int \chi_p^{\pm *}\nabla_R^{\,2}\chi_p^{\pm} d\boldsymbol{\rho}_{\mathrm{a}}\right. \\ \left. + 2\nabla_R F_p^{\mp}(\mathbf{R}) . \int \chi_p^{\pm *}\nabla_R\chi_p^{\mp} d\boldsymbol{\rho}_{\mathrm{a}}\right\}, \qquad \ldots\ldots(5)\end{aligned}$$

both terms on the right-hand side of which may be neglected (Bates and McCarroll 1958) so that (5) simplifies to the pair of uncoupled equations

$$\left\{\frac{\hbar^2}{2M}\nabla_R^{\,2} + E - \epsilon_p^{\pm}(R) - \frac{Z^2}{R}\right\}F_p^{\pm}(\mathbf{R}) = 0. \qquad \ldots\ldots(6)$$

Solutions of (6) may be obtained by the conventional phase shift analysis. Thus expanding $F_p^{\pm}(\mathbf{R})$ according to

$$F_p^{\pm}(\mathbf{R}) = R^{-1}\sum_{l=0}^{\infty} g_l^{\pm}(R)\mathrm{P}_l(\cos\theta) \qquad \ldots\ldots(7)$$

where (R, θ, ϕ) are the spherical polar coordinates of the point with position vector $\mathbf{R}$, it may be shown that

$$\frac{d^2 g_l^{\pm}}{dR^2} + \left\{k^2 - u_p^{\pm} - \frac{l(l+1)}{R^2}\right\}g_l^{\pm} = 0 \qquad \ldots\ldots(8)$$

where

$$k^2 = \frac{2M}{\hbar^2}(E - E_p) \qquad \ldots\ldots(9)$$

$$u_p^{\pm}(R) = \frac{2M}{\hbar^2}\left(\frac{Z^2}{R} + \epsilon_p^{\pm}(R) - E_p\right), \qquad \ldots\ldots(10)$$

E_p being the common limiting value of $\epsilon_p^{\pm}(R)$ as R tends to infinity. If we now prescribe that asymptotically

$$F_p^{\pm}(\mathbf{R}) \sim \frac{1}{\sqrt{2}}\{\exp(ik\mathbf{n}.\mathbf{R}) + R^{-1}f_p^{\pm}(\theta)\exp(ikR)\}, \qquad \ldots\ldots(11)$$

then

$$f_p^{\pm}(\theta) = \frac{1}{2ik}\sum_{l=0}^{\infty}(2l+1)\{\exp(2i\eta_l^{\pm}) - 1\}\mathrm{P}_l(\cos\theta) \qquad \ldots\ldots(12)$$

where the phase shifts $\eta_l^\pm$ are such that the regular solutions of (8) behave asymptotically as

$$g_l^\pm \sim k^{-1} \sin (kR - \tfrac{1}{2} l\pi + \eta_l^\pm). \qquad \ldots\ldots(13)$$

The eigenvalues $\epsilon_p^\pm(R)$ corresponding to the approach of a proton and a hydrogen atom in the ground and first two excited states have been tabulated over a wide range of separations R by Bates, Ledsham and Stewart (1953), and by Wallis and Hulburt (1954). For the ground state case, ϵ_0^+ and χ_0^+ are associated with the $1s\sigma_g$ orbital and ϵ_0^- and χ_0^- with the $2p\sigma_u$ orbital, their asymptotic forms as R tends to infinity being given by

$$\chi_0^\pm \sim \frac{1}{\sqrt{2}}\{\psi(\mathbf{r}_a|1s) \pm \psi(\mathbf{r}_b|1s)\} \qquad \ldots\ldots(14)$$

$$\epsilon_0^\pm \sim E(1s) - 9/2R^4 \qquad \ldots\ldots(15)$$

where $\psi\ (\mathbf{r}_a|1s)$ is the wave function of the 1s state of a hydrogen atom with nucleus A, $E(1s)$ is its energy and all energies are now measured in rydbergs.

If the electron is initially bound to nucleus A, the incident wave is represented at large R by

$$\Psi \sim \exp (ik\mathbf{n} . \mathbf{R})\psi(\mathbf{r}_a|1s) \qquad \ldots\ldots(16)$$

which may be written

$$\Psi \sim \frac{\exp (ik\mathbf{n} . \mathbf{R})}{\sqrt{2}}\{\chi_0^+ + \chi_0^-\}. \qquad \ldots\ldots(17)$$

By taking a suitable combination of (11) it follows that the cross section for scattering with charge transfer is

$$^0Q_t = \tfrac{1}{4} \iint |f_0^+ - f_0^-|^2 \sin\theta\, d\theta\, d\phi \qquad \ldots\ldots(18)$$

$$= \frac{\pi}{k^2} \sum_{l=0}^{\infty} (2l+1) \sin^2 ({}^0\eta_l^+ - {}^0\eta_l^-) \qquad \ldots\ldots(19)$$

when we make use of (12).

The $n=2$ excited state case is complicated by sp degeneracies and there are six possible orbitals which occur in pairs ($2s\sigma_g$, $3p\sigma_u$), ($3d\sigma_g$, $4f\sigma_u$) and ($2p\pi_u$, $3d\pi_g$) such that respectively

$$\chi_1^\pm \sim \tfrac{1}{2}\{[\psi(\mathbf{r}_a|2s) + \psi(\mathbf{r}_a|2p_0)] \pm [\psi(\mathbf{r}_b|2s) + \psi(\mathbf{r}_b|2p_0]\} \qquad \ldots\ldots(20)$$

$$\chi_2^\pm \sim \tfrac{1}{2}\{[\psi(\mathbf{r}_a|2s) - \psi(\mathbf{r}_a|2p_0)] \pm [\psi(\mathbf{r}_b|2s) - \psi(\mathbf{r}_b|2p_0)]\} \qquad \ldots\ldots(21)$$

$$\chi_3^\pm \sim \frac{1}{\sqrt{2}}\{\psi(\mathbf{r}_a|2p_1) \pm \psi(\mathbf{r}_b|2p_1)\} \qquad \ldots\ldots(22)$$

and

$$\epsilon_1^\pm \sim E(2s, 2p_0) + 6/R^2 \qquad \ldots\ldots(23)$$

$$\epsilon_2^\pm \sim E(2s, 2p_0) - 6/R^2 \qquad \ldots\ldots(24)$$

$$\epsilon_3^\pm \sim E(2p_1) + 12/R^3 \qquad \ldots\ldots(25)$$

where $\psi(\mathbf{r}_a|2s)$ is the wave function of the 2s state of the hydrogen atom with nucleus A, $\psi(\mathbf{r}_a|2p_0)$ and $\psi(\mathbf{r}_a|2p_1)$ are the wave functions of the 2p state with magnetic quantum number zero and unity respectively and

$$E(2s) = E(2p_0) = E(2p_1)$$

is their common eigenvalue.

The case when the electron is in the $2p_1$ state of a hydrogen atom with nucleus A is similar to that of the ground state and the cross section is given by (19), the phase shifts being determined from the eigenvalues $\epsilon_3{}^{\pm}(R)$ of the $2p\pi_u$ and $3d\pi_g$ orbitals, but when the electron is in the 2s state, the incident wave must be represented at large R by

$$\Psi \sim \exp(ik\mathbf{n}.\mathbf{R})\psi(\mathbf{r}_a|2s) \qquad \ldots\ldots(26)$$

which may be written

$$\Psi \sim \tfrac{1}{2}\exp(ik\mathbf{n}.\mathbf{R})\{\chi_1{}^+ + \chi_2{}^+ + \chi_1{}^- + \chi_2{}^-\} \qquad \ldots\ldots(27)$$

and when the electron is in the $2p_0$ state by

$$\Psi \sim \exp(ik\mathbf{n}.\mathbf{R})\psi(\mathbf{r}_a|2p_0) \qquad \ldots\ldots(28)$$

which may be written

$$\Psi \sim \tfrac{1}{2}\exp(ik\mathbf{n}.\mathbf{R})\{\chi_1{}^+ - \chi_2{}^+ + \chi_1{}^- - \chi_2{}^-\}. \qquad \ldots\ldots(29)$$

By suitably combining (11) it follows that the cross sections for the charge transfer processes

$$\psi(\mathbf{r}_a|2s) \to \frac{1}{\sqrt{2}}\{\psi(\mathbf{r}_b|2s) + \psi(\mathbf{r}_b|2p_0)\}$$

and

$$\psi(\mathbf{r}_a|2p_0) \to \frac{1}{\sqrt{2}}\{\psi(\mathbf{r}_b|2s) + \psi(\mathbf{r}_b|2p_0)\}$$

are both given by

$${}^1Q_t = \tfrac{1}{8}\iint |f_1{}^+ - f_1{}^-|^2 \sin\theta\, d\theta\, d\phi \qquad \ldots\ldots(30)$$

and the cross sections for the charge transfer processes

$$\psi(\mathbf{r}_a|2s) \to \frac{1}{\sqrt{2}}\{\psi(\mathbf{r}_b|2s) - \psi(\mathbf{r}_b|2p_0)\}$$

and

$$\psi(\mathbf{r}_a|2p_0) \to \frac{1}{\sqrt{2}}\{\psi(\mathbf{r}_b|2s) - \psi(\mathbf{r}_b|2p_0)\}$$

are both given by

$${}^2Q_t = \tfrac{1}{8}\iint |f_2{}^+ - f_2{}^-|^2 \sin\theta\, d\theta\, d\phi. \qquad \ldots\ldots(31)$$

If ${}^1\eta_l{}^{\pm}$ and ${}^2\eta_l{}^{\pm}$ are the phase shifts corresponding to $\epsilon_1{}^{\pm}$ and $\epsilon_2{}^{\pm}$ respectively, (30) and (31) become

$${}^1Q_t = \frac{\pi}{2k^2}\sum_{l=0}^{\infty}(2l+1)\sin^2({}^1\eta_l{}^+ - {}^1\eta_l{}^-) \qquad \ldots\ldots(32)$$

and

$${}^2Q_t = \frac{\pi}{2k^2}\sum_{l=0}^{\infty}(2l+1)\sin^2({}^2\eta_l{}^+ - {}^2\eta_l{}^-). \qquad \ldots\ldots(33)$$

If ${}^3Q_t$ is the charge transfer process for the $2p_1$ case, we have finally that the effective charge transfer cross section for a proton and an excited hydrogen atom in a state of principal quantum number 2 is

$$\overline{Q}_t = \tfrac{1}{2}({}^1Q_t + {}^2Q_t + {}^3Q_t). \qquad \ldots\ldots(34)$$

Except at very low temperatures where it is necessary to take account of the differing nuclear statistics, identical formulae apply in the cases of protons in atomic deuterium, of deuterons in atomic hydrogen and of deuterons in atomic deuterium provided only that the appropriate reduced mass is used.

§ 3. APPROXIMATE FORMULAE

By using Jeffreys' approximation, Bates *et al.* show that (19) can be written as

$$Q_t = 2\pi \int_0^\infty p \sin^2 \zeta(p)\,dp \qquad \ldots\ldots(35)$$

where

$$\zeta(p) = \frac{1}{\hbar}\int_{R_c}^\infty \frac{\Delta E(R)}{v(R)}\left\{1-\frac{v^2}{[v(R)]^2}\frac{p^2}{R^2}\right\}^{-1/2} dR \qquad \ldots\ldots(36)$$

in which

$$\Delta E(R) = \epsilon^+(R) - \epsilon^-(R), \qquad \ldots\ldots(37)$$

$v(R)$ is the velocity of relative motion when the nuclei are a distance R apart, $v = v(\infty)$ and R_c is the outermost root of the integrand. It is usually possible to replace $v(R)$ by v without serious loss of accuracy (Jackson 1954) so that (36) simplifies to

$$\zeta(p) = \frac{1}{\hbar v}\int_p^\infty \frac{R\Delta E(R)}{(R^2-p^2)^{1/2}}\,dR. \qquad \ldots\ldots(38)$$

Jeffreys' approximation to the phase shifts (cf. Mott and Massey 1949) is

$$\eta_l = \int_{R_0}^\infty \left\{k^2 - u(R) - \frac{l(l+1)}{R^2}\right\}^{1/2} dR - \int_{R_0'}^\infty \left\{k^2 - \frac{l(l+1)}{R^2}\right\}^{1/2} dR \qquad \ldots\ldots(39)$$

where R_0 and R_0' are the outermost zero of the respective integrands, and Massey and Mohr (1934) have shown that for large l, (39) can be further approximated by

$$\eta_l = -\tfrac{1}{2}\int_{R_0'}^\infty \frac{u(R)}{\{k^2 - l(l+1)/R^2\}^{1/2}}\,dR. \qquad \ldots\ldots(40)$$

Then if we modify (19) by replacing the summation over l by an integration over $p = k^{-1}\{l(l+1)\}^{1/2}$ and by using (40) for the phase shifts, it follows that

$$\eta_l^+ - \eta_l^- = \zeta(p) \qquad \ldots\ldots(41)$$

and (19) becomes identical to (35).

Dalgarno and McDowell (1956) have suggested that since the major contribution to $\zeta(p)$ comes from values of R in the neighbourhood of p it is convenient to evaluate (38) by fitting $\Delta E(R)$ in the region of p by functions of the form $A \exp(-\gamma R)$, A and γ being functions of p. Then (38) may be evaluated analytically (Dalgarno and McDowell 1956, Dalgarno 1958) in terms of modified Bessel functions $K_0(\gamma p)$ and $K_1(\gamma p)$ of the second kind (cf. Watson 1944) of which adequate tables are available (Bickley 1950, 1952). It may be computationally simpler to avoid the dependence of A and γ on p by fitting $\Delta E(R)$ at all values of R with more complex functions of the form

$$\sum_n A_n R^n \exp(-\gamma_n R) \qquad \ldots\ldots(42)$$

where A_n and γ_n are constants independent of p. The integrals (38) can still be evaluated in terms of K_0 and K_1, and a list of the more useful formulae is given in the Appendix.

The evaluation of the integral (35) may be accomplished by observing that for small values of p (for which the Massey–Mohr approximation is inadequate), $\sin \zeta(p)$ oscillates rapidly so that $\sin^2 \zeta(p)$ may be replaced by its average value of $\frac{1}{2}$. Then if the integral (35) is broken into two parts at $p=p^*$ where p^* is some value of p in the oscillating region

$$Q_t = \tfrac{1}{2}\pi p^{*2} + \int_{p^*}^{\infty} p \sin^2 \zeta(p)\,dp\,; \qquad \ldots\ldots(43)$$

the integration from p^* to ∞ must in general be carried out numerically. For the method to be useful, (43) must be independent of p^* and it is found in practice that it is an oscillatory function of p^* with an amplitude equal to only a small fraction of the mean value. No significant loss of accuracy results from taking Q_t as the average value of (43) over any one complete oscillation.

§ 4. RESULTS AND DISCUSSION

The calculation of Q_t according to (35) proceeds in a straightforward way once $\Delta E(R)$ has been fitted by a function of the form (42) and values of ${}^0Q_t$, ${}^1Q_t$, ${}^2Q_t$, ${}^3Q_t$ and $\overline{Q}_t$ are shown in the figure for protons with impact energies ϵ up to 100 ev in atomic hydrogen. The cross sections for H$^+$ in H, H$^+$ in D, D$^+$ in H and D$^+$ in D are equal at any particular relative velocity so that cross sections for the last three cases may be obtained from the figure by simple changes in the energy scale. A check on the accuracy of the methods employed is provided by the calculations of ${}^0Q_t$ by Dalgarno and Yadav (1953) who followed the more accurate procedure of substituting phase shifts computed from Jeffreys' approximation (39) into the quantal summation (19) and their results are given by the points in the figure. The slight discrepancies arise largely from the different averaging procedures employed and because of this the values obtained here are probably to be preferred.

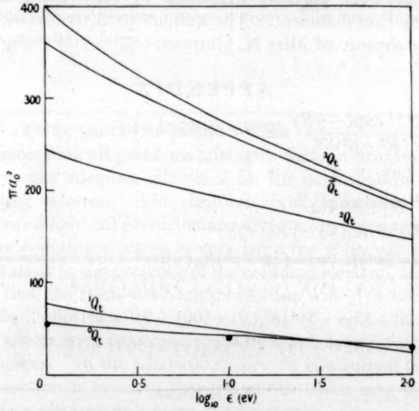

Charge transfer cross sections ${}^0Q_t$, ${}^1Q_t$, ${}^2Q_t$, ${}^3Q_t$ and $\overline{Q}_t$. The points refer to calculations of ${}^0Q_t$ by Dalgarno and Yadav (1953).

The curves may be extrapolated to energies up to 10 kev without much loss of computational accuracy by fitting them by functions of the form

$$a + b(\log \epsilon) + c(\log \epsilon)^2,$$

a, *b* and *c* being constants, but because the theory ignores the momentum of the transferred electron, the values so derived will tend to be too large. It is not easy to estimate above what energy the theory is no longer adequate. For the ground state case, the perturbed stationary state method appears to give satisfactory results for proton impact energies up to several kev (Bates and Dalgarno 1952, Dalgarno and Yadav 1953), but for the excited states the theory may fail at much lower energies. The neglect of coupling in the solving of (4) may be a more serious limitation but for the energy range covered by the figure, the cross sections are probably correct. The curves illustrate the differences which are to be expected generally between cross sections for elastic collisions involving normal and excited atoms, the increased magnitude for excited atoms arising primarily from the much longer range of the interaction potentials.

ACKNOWLEDGMENTS

This work has been partially supported by the United Kingdom Atomic Energy Research Establishment. The authors wish to acknowledge the skilled computational assistance of Miss N. Gorman.

APPENDIX

If $I_n = \int_p^\infty \frac{R^{n+1}\exp(-\gamma R)}{(R^2-p^2)^{1/2}}\,dR$, we obtain on writing $\gamma p = y$,

$$I_0 = pK_1(y)$$
$$I_1 = p\{K_1(y) + yK_0(y)\}/\gamma$$
$$I_2 = p\{(2+y^2)K_1(y) + yK_0(y)\}/\gamma^2$$
$$I_3 = p\{(6+2y^2)K_1(y) + (3y+y^3)K_0(y)\}/\gamma^3$$
$$I_4 = p\{(24+7y^2+y^4)K_1(y) + (12y+2y^3)K_0(y)\}/\gamma^4$$
$$I_5 = p\{(120+33y^2+3y^4)K_1(y) + (60y+9y^3+y^5)K_0(y)\}/\gamma^5$$
$$I_8 = p\{(720+192y^2+15y^4+y^6)K_1(y) + (360y+51y^3+3y^5)K_0(y)\}/\gamma^6.$$

REFERENCES

BATES, D. R., 1957, *Proc. Roy. Soc.* A, **240,** 437 ; 1958, *Ibid.*, **243,** 15.
BATES, D. R., and DALGARNO, A., 1952, *Proc. Phys. Soc.* A, **65,** 919.
BATES, D. R., LEDSHAM, K., and STEWART, A. L., 1953, *Phil. Trans. Roy. Soc.* A, **246,** 215.
BATES, D. R., MASSEY, H. S. W., and STEWART, A. L., 1953, *Proc. Roy. Soc.* A, **216,** 437.
BATES, D. R., and MCCARROLL, R., 1958, *Proc. Roy. Soc.* A, **245,** 175.
BICKLEY, W. G. (Ed.), 1950, *B.A. Tables of Bessel Functions*, Pt. I. (Cambridge : University Press) ; 1952, *Ibid.*, Pt. II.
BUCKINGHAM, R. A., and DALGARNO, A., 1952, *Proc. Roy. Soc.* A, **213**, 327 and 506.
DALGARNO, A., 1958, *Phil. Trans. Roy. Soc. A*, **250,** 426.
DALGARNO, A., and MCDOWELL, M. R. C., 1956, *Proc. Phys. Soc.* A, **69,** 615.
DALGARNO, A., and YADAV, H. N., 1953, *Proc. Phys. Soc.* A, **66,** 173.
JACKSON, J. D., 1954, *Canad. J. Phys.*, **32,** 60.
MASSEY, H. S. W., and MOHR, C. B. O., 1934, *Proc. Roy. Soc.* A, **144,** 188.
MASSEY, H. S. W., and SMITH, R. A., 1933, *Proc. Roy. Soc.* A, **142,** 142.
MOTT, N. F., and MASSEY, H. S. W., 1949, *The Theory of Atomic Collisions* (Oxford : Clarendon Press).
WALLIS, R. F., and HULBURT, H. M., 1954, *J. Chem. Phys.*, **22,** 774.
WATSON, G. N., 1944, *Theory of Bessel Functions* (Cambridge : University Press), 2nd Edn.

On the Use of the Adiabatic Theory in Electron–Atom Collision Calculations

By V. M. MARTIN, M. J. SEATON and J. B. G. WALLACE
Department of Physics, University College London

MS. received 16th June 1958, and in final form 24th July 1958

Abstract. The adiabatic theory allows for perturbation of the atom by treating the colliding electron as a fixed point charge. The form of the wave functions obtained may be shown to be correct in the limit of large separations. Numerical results are discussed for the s- and p-phases in electron–hydrogen collisions. It is considered that the adiabatic theory over-estimates the effect of perturbations of the atom for separations of order 1 atomic unit. The error introduced for the s-wave may be particularly large.

§ 1. Introduction

One of the most difficult problems arising in electron–atom collision calculations is to make adequate allowance for the perturbation of the atom by the colliding electron. The simplest of all approximations treats the atom as a static central field, all perturbations of the atom being neglected. When the velocity of the colliding electron is very large the atom will have little time in which to adjust itself to the presence of the colliding electron, and it may therefore be expected that the static-field approximation will give reasonable results in the limit of large velocities.

Perturbation effects may be expected to be most important in the limit of small impact velocities. In the adiabatic theory[†] it is assumed that the velocity of the colliding electron is so small that the perturbation may be calculated on treating the colliding electron as a point charge at rest.

It may be shown that the adiabatic theory is correct in the limit of large separations and for incident electron energies which are too small for inelastic collisions to occur. The main effect at large separations is that a dipole moment is induced in the atom and that the colliding electron moves in the induced-dipole potential $V_{\mathrm{p}} \sim -\alpha/2r^4$, α being the atom polarizability.

Even if the incident electron has a very low velocity at large separations it will have a much greater velocity at small separations due to the attractive field of the atom. Since the atomic electron will then have insufficient time to adjust itself to the presence of the fast electron the perturbation calculated using adiabatic theory would be expected to be too large. A further effect must also be considered. When the colliding electron is relatively close to the nucleus the atomic electron will be edged out to highly excited states. In this situation capture of the colliding electron and ejection of the atomic electron will readily occur. Therefore, part of the perturbation allowed for in the adiabatic theory may already have been taken into account if allowance has been made for the possibility of electron exchange.

[†] The adiabatic theory has been employed in a number of electron–atom collision calculations ; see, for example, Staver (1951) and Bransden, Dalgarno, John and Seaton (1958).

In this paper we present results of calculations for electron–hydrogen collisions which appear to confirm that the adiabatic theory over-estimates the effect of shorter range perturbations.

§ 2. FORMULATION OF THE COLLISION PROBLEM

2.1. *General Formulation*

The Schrödinger equation for the electron–hydrogen atom system is $[H-E]\Psi=0$ where

$$H(\mathbf{r}_1,\mathbf{r}_2)=-\frac{1}{2}\nabla_1{}^2-\frac{1}{2}\nabla_2{}^2-\frac{1}{r_1}-\frac{1}{r_2}+\frac{1}{r_{12}} \qquad \ldots\ldots(1)$$

atomic units being used. The atomic wave functions will be denoted by $\psi_\gamma(\mathbf{r})$ and the atomic energy levels by E_γ. For the 1s ground state we put $\gamma=1$. We shall consider only the case for which the total energy E is such that inelastic collisions are energetically impossible. Putting $E=E_\gamma+\frac{1}{2}k_\gamma{}^2$ we then have

$$k_1{}^2>0, \quad k_\gamma{}^2<0(\gamma\neq 1)\,; \qquad \ldots\ldots(2)$$

$k_1{}^2$ is numerically equal to the electron kinetic energy in units of 13·60 ev.

The complete wave function may be represented by the symmetrized expansion

$$\Psi=\frac{1}{\sqrt{2}}\sum_\gamma\{\psi_\gamma(\mathbf{r}_1)\chi_\gamma(\mathbf{r}_2)\pm\psi_\gamma(\mathbf{r}_2)\chi_\gamma(\mathbf{r}_1)\} \qquad \ldots\ldots(3)$$

where the plus sign goes with the singlet spin interaction and the minus sign with the triplet interaction. For the l-partial wave we impose the boundary condition

$$\chi_1(\mathbf{r})\sim Y_{lm}(\hat{\mathbf{r}})\frac{1}{k_1 r}\{\sin(k_1 r-\tfrac{1}{2}l\pi)+a_l{}^{\pm}\cos(k_1 r-\tfrac{1}{2}l\pi)\} \qquad \ldots\ldots(4)$$

where $Y_{lm}(\hat{\mathbf{r}})$ is a normalized spherical harmonic. Putting $\eta_l{}^{\pm}=\arctan a_l{}^{\pm}$ the elastic cross section is

$$Q(k_1{}^2)=\frac{\pi\mathbf{a}_0{}^2}{k_1{}^2}\sum_l(2l+1)\{\sin^2\eta_l{}^{+}+3\sin^2\eta_l{}^{-}\}. \qquad \ldots\ldots(5)$$

Castillejo, Percival and Seaton (to be published) show that, when the conditions (2) are satisfied,

$$\chi_\gamma(\mathbf{r})\sim-\frac{V_{\gamma 1}(\mathbf{r})\chi_1(\mathbf{r})}{(E_\gamma-E_1)}\ (\gamma\neq 1) \qquad \ldots\ldots(6)$$

where

$$V_{\gamma\gamma'}(\mathbf{r})=\int\psi_\gamma{}^*(\mathbf{r}')\frac{1}{|\mathbf{r}-\mathbf{r}'|}\psi_{\gamma'}(\mathbf{r}')d\mathbf{r}' \qquad \ldots\ldots(7)$$

and that the equation satisfied by $\chi_1(\mathbf{r})$ in the limit of large r is

$$\left[\nabla^2+\frac{\alpha}{r^4}+k_1{}^2\right]\chi_1=0 \qquad \ldots\ldots(8)$$

where the polarizability α is defined by

$$\alpha=\frac{2}{3}\sum_{\gamma\neq 1}\frac{|(1|\mathbf{r}|\gamma)|^2}{(E_\gamma-E_1)}. \qquad \ldots\ldots(9)$$

For hydrogen $\alpha = 4{\cdot}5$ atomic units. Since $V_{\gamma 1}(\mathbf{r})$ goes to zero at least as fast as $1/r^2$ the functions χ_γ for $\gamma \neq 1$ do not contribute to the asymptotic flux.

2.2. *Variational Methods*

In seeking approximate solutions of $[H-E]\Psi = 0$ we shall make use of variational methods. For small variations about the exact function

$$\delta\left\{\int \Psi^*[H-E]\Psi d\tau - \frac{a_l^{\pm}}{2k_1}\right\} = 0 \qquad \ldots\ldots(10)$$

(Hulthén 1944, Kohn 1948). The condition (10) will be used in two different ways: (i) if restrictions are placed on the functional form of Ψ, equation (6) may be imposed for all variations consistent with these restrictions, and (ii) with a given function Ψ^t having phase parameter $a_l^{\pm(t)}$ an improved estimate for $a_l^{\pm}$ will be given by

$$a_l^{\pm(K)} = a_l^{\pm(t)} - 2k_1 \int \Psi^{t*}[H-E]\Psi^t d\tau, \qquad \ldots\ldots(11)$$

the error in $a_l^{\pm(K)}$ being proportional to

$$\int \Delta\Psi^{t*}[H-E]\Delta\Psi^t d\tau$$

where $\Delta\Psi^t$ is the error in Ψ^t (Kohn 1948).

2.3. *The Exchange Approximation*

Putting $\chi_\gamma = 0$ for $\gamma \neq 1$ we obtain the approximate wave function

$$\Psi = \frac{1}{\sqrt{2}}\{\psi_1(\mathbf{r}_1)\chi_1(\mathbf{r}_2) \pm \psi_1(\mathbf{r}_2)\chi_1(\mathbf{r}_1)\}. \qquad \ldots\ldots(12)$$

This approximation allows for the possibility of electron exchange but otherwise neglects distortion of the atom by the colliding electron. Adopting (12) and imposing the condition (10) for variation of χ_1, we obtain the exchange equations

$$\left[\nabla^2 + \frac{2}{r} + k_1^2\right]\chi_1 = 2[V_{11} \pm W_{11}]\chi_1 \qquad \ldots\ldots(13)$$

where $V_{\gamma\gamma'}$ is defined by (7) and where $W_{\gamma\gamma'}$ is the exchange operator defined by

$$W_{\gamma\gamma'}\chi_{\gamma'}(\mathbf{r}) = \int \psi_\gamma^*(\mathbf{r}')[H(\mathbf{r},\mathbf{r}') - E]\chi_{\gamma'}(\mathbf{r}')d\mathbf{r}'\psi_\gamma(\mathbf{r}). \quad \ldots\ldots(14)$$

Substituting solutions of (13) in (12) one obtains

$$\int \Psi^*[H-E]\Psi d\tau = 0 \text{ and hence } a_l^{\pm(K)} = a_l^{\pm(t)} \text{ in (11).}$$

We shall refer to (12) and (13) as the *exchange approximation.*

Since W_{11} and $(V_{11} - 1/r)$ go to zero exponentially for large r the exchange function χ_1 does not satisfy equation (8) in the limit of large r.

2.4. *Behaviour of Phases at Low Energies*

Bransden, Dalgarno, John and Seaton (1958) have shown that the exact phases $\eta_l(k_1)$ for $l > 0$ vary as k_1^2 when k_1 is small. In the exchange approximation, however, the phases $\eta_l(k_1)$ for $l > 0$ vary as k_1^{2l+1} for k_1 small; the effect of polarization, neglected in the exchange approximation, is the dominant effect determining the phases when k_1 is sufficiently small and $l > 0$.

In all cases the s-wave phases $\eta_0^\pm(k_1)$ vary as k_1 for k_1 small. The *scattering length* $A_0^\pm$ is defined by

$$A_0^\pm = \lim_{k_1\to 0}\left\{\frac{\tan\eta_0^\pm(k_1)}{k_1}\right\}. \qquad \ldots\ldots(15)$$

The zero-energy limit of the cross section is

$$Q(0)=\pi\mathbf{a}_0^2\{(A_0^+)^2+3(A_0^-)^2\}. \qquad \ldots\ldots(16)$$

2.5. *The Exchange–Correlation Approximation*

In the attempt to improve on the exchange approximation one may consider wave functions of the type

$$\Psi=\frac{1}{\sqrt{2}}\{\psi_1(\mathbf{r}_1)\chi_1(\mathbf{r}_2)\pm\psi_1(\mathbf{r}_2)\chi_1(\mathbf{r}_1)\}+\Phi(\mathbf{r}_1,\mathbf{r}_2). \qquad \ldots\ldots(17)$$

With some convenient analytic expression chosen for Φ the function (17) may be determined using the variational principle. To be consistent with (6) the function Φ should go to zero as r_1^{-3} or r_2^{-3} for r_1 large or r_2 large. In practice functions Φ have been chosen which go to zero exponentially for r_1 or r_2 large. The use of such functions, which allow for short-range electron correlation effects but not for long-range polarization, will be termed the *exchange–correlation* approximation.

§ 3. THE ADIABATIC THEORY

The fundamental assumption of the adiabatic theory is that the perturbation of the atom may be considered to be due to a fixed point charge.

3.1. *Use of Second-order Perturbation Theory*

In applying the adiabatic theory we make the further assumption that the perturbation may be calculated using second-order perturbation theory. In place of $\psi_1(\mathbf{r}_1)$ one obtains the perturbed atomic wave function

$$\psi'(\mathbf{r}_1;\mathbf{r}_2)=\psi_1(\mathbf{r}_1)-\sum_{\gamma\neq 1}\frac{V_{\gamma 1}(\mathbf{r}_2)\psi_\gamma(\mathbf{r}_1)}{(E_\gamma-E_1)}. \qquad \ldots\ldots(18)$$

The contribution to the potential due to this perturbation is

$$V_{\mathrm{P}}(r)=-\sum_{\gamma\neq 1}\frac{|V_{\gamma 1}(\mathbf{r})|^2}{(E_\gamma-E_1)}. \qquad \ldots\ldots(19)$$

This function has been calculated numerically by Dalgarno and Lynn (1957).

3.2. *The Exchange–Adiabatic Approximation*

In this approximation one considers the equations

$$[\nabla^2+\frac{2}{r}+k_1^2]\chi_1=2[V_{11}+V_{\mathrm{P}}\pm W_{11}]\chi_1. \qquad \ldots\ldots(20)$$

It should be emphasized that, unlike the exchange equations (13), the equation (20) cannot be derived from a consistent variational argument.

Let $a_l^{\pm(\mathrm{EA})}$ be the phase parameter obtained from (20) and let $\chi_1^\pm$ be a solution of the exchange equation with phase parameter $a_l^{\pm(\mathrm{E})}$. By the Kohn variational method we obtain the approximation

$$a_l^{\pm(\mathrm{EA})}=a_l^{\pm(\mathrm{E})}+k_1P \qquad \ldots\ldots(21)$$

where

$$P=-2\int\chi_1^{\pm *}(\mathbf{r})V_{\mathrm{P}}(\mathbf{r})\chi_1^\pm(\mathbf{r})d\mathbf{r}. \qquad \ldots\ldots(22)$$

3.3. *Behaviour of the Polarization Potential*

In the limit of large r the polarization potential behaves as

$$V_{\mathrm{p}}(r) \sim -\tfrac{1}{3}\sum_{\gamma\neq 1}\frac{|(1|\mathbf{r}|\gamma)|^2}{(E_\gamma - E_1)}\ (r\to\infty) \qquad \ldots\ldots(23)$$

and in the limit of small r as

$$V_{\mathrm{p}}(r) \simeq -\frac{r^2}{3}\sum_{\gamma\neq 1}\frac{|(1|\mathbf{r}/r^3|\gamma)|^2}{(E_\gamma - E_1)}\ (r\to 0). \qquad \ldots\ldots(24)$$

From (23) we have $V_{\mathrm{p}} \sim -\alpha/2r^4$. The equation (20) of the exchange–adiabatic approximation therefore has the correct asymptotic form (eqn (8)).

From the usual relation between the dipole length and dipole acceleration matrix elements

$$\left(1\left|\frac{\mathbf{r}}{r^3}\right|\gamma\right) = -(E_\gamma - E_1)^2(1|\mathbf{r}|\gamma). \qquad \ldots\ldots(25)$$

The expansion (24) for r small may therefore be written

$$V_{\mathrm{p}}(r) \simeq -\tfrac{1}{3}r^2\sum_{\gamma\neq 1}(E_\gamma - E_1)^3|(1|\mathbf{r}|\gamma)|^2, \quad (r\to 0). \qquad \ldots\ldots(26)$$

Comparison of the expansions (23), (26) shows that the contribution from highly excited states will be more important for small r than for large r.

The contribution to V_{p} from the 2p states is

$$V_{(2\mathrm{p})}(r) = -\sum_m \frac{|V_{2pm,\,1}(\mathbf{r})|^2}{(E_2 - E_1)}. \qquad \ldots\ldots(27)$$

In figure 1 we give graphs of $-2r^4V_{\mathrm{p}}/\alpha$ which tends to unity for large r and of $-2r^4V_{(2\mathrm{p})}/\alpha$ which tends to 0·6577 for large r. The 2p states are seen to contribute 65·77% of the sum (19) in the limit of large r but a much smaller percentage for smaller values of r.

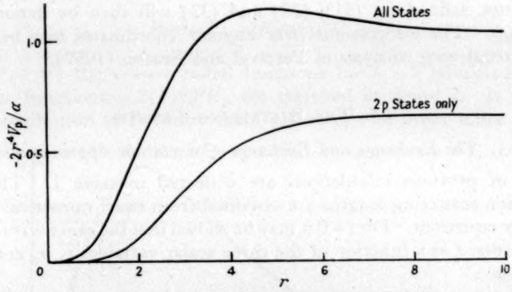

Figure 1. The adiabatic potential V_{p}. The curves show $-2r^4V_{\mathrm{p}}/\alpha$ calculated with all states and with 2p states only.

3.4. *Discussion of the Adiabatic Theory*

If one substitutes the perturbed function $\psi'(\mathbf{r}_1;\mathbf{r}_2)$ in place of $\psi_1(\mathbf{r}_1)$ in the exchange function (12) one obtains an expansion of type (3) with

$$\chi_\gamma = -\frac{V_{\gamma 1}\chi_1}{(E_\gamma - E_1)}\ (\gamma\neq 1). \qquad \ldots\ldots(28)$$

According to (6) such functions have the correct asymptotic form.

We consider that the adiabatic theory provides us with an approximate wave function which may be substituted in the Kohn variational expression (11). This gives

$$a_l^{\pm} = a_l^{\pm(E)} + k_1[P+R+S] \qquad \ldots\ldots(29)$$

where

$$a_l^{\pm(E)} = a_l^{\pm(t)} + k_1 \int \chi_1^* \left\{ \left[\nabla^2 + \frac{2}{r} + k_1^2 \right] - 2[V_{11} \pm W_{11}] \right\} \chi_1 d\mathbf{r} \qquad \ldots\ldots(30)$$

$$P = -2 \int \chi_1^* \sum_{\gamma' \neq 1} V_{1\gamma'} \chi_{\gamma'} d\mathbf{r} = -2 \int \chi_1^* V_{\mathrm{P}} \chi_1 d\mathbf{r} \qquad \ldots\ldots(31)$$

$$R = -2 \int \chi_1^* \sum_{\gamma' \neq 1} W_{1\gamma'} \chi_{\gamma'} d\mathbf{r} \qquad \ldots\ldots(32)$$

$$S = \sum_{\gamma \neq 1} \int \chi_\gamma^* \left\{ [\nabla^2 + \frac{2}{r} + k_\gamma^2] \chi_\gamma - 2 \sum_{\gamma'} [V_{\gamma\gamma'} \pm W_{\gamma\gamma'}] \chi_{\gamma'} \right\} d\mathbf{r}. \qquad \ldots\ldots(33)$$

We suppose that χ_1 has asymptotic form (4) with phase parameter $a_l^{\pm(t)}$ and that χ_γ is given by (28) for $\gamma \neq 1$. For the scattering length the expression corresponding to (29) is

$$A_0^{\pm} = A_0^{\pm(E)} + P + R + S \qquad \ldots\ldots(34)$$

where P, R and S are calculated in the limit of $k_1 \to 0$.

The various contributions to (29) may be interpreted as follows: $a_l^{\pm(E)}$ is the value of $a_l^{\pm}$ which would be obtained in the exchange approximation; P is a correction for the polarization potential V_{P}; R is an exchange analogue of P; S provides a correction for the fact that the adiabatic theory is exact only in the limit of large r. The use of (29) or (34) will be referred to as the *Kohn–exchange–adiabatic* approximation.

For practical calculations we use (28) for the 2_{p} states only and put $\chi_\gamma = 0$ for all other excited states. We thus allow for 65·77% of the long-range polarization. The quantities defined by (31), (32) and (33) will then be denoted by $P_{(2\mathrm{p})}$, $R_{(2\mathrm{p})}$ and $S_{(2\mathrm{p})}$. The integrations over angular coordinates may be carried out using the partial wave analysis of Percival and Seaton (1957).

§ 4. THE SCATTERING LENGTH

4.1. *The Exchange and Exchange–Correlation Approximation*

Results of previous calculations are collected in table 1. The exchange approximation scattering lengths are obtained from exact numerical solutions of the exchange equations. For $l = 0$ it may be shown that the exact wave functions Ψ may be expressed as a function of the three scalar variables r_1, r_2 and r_{12}.

Table 1. The Exchange and Exchange–Correlation Approximations for the Scattering Length

Approximation	Reference	A_0^+	A_0^-
Exchange	Seaton (1957)	−8·058	−2·347
Exchange–correlation	Massey & Moiseiwitsch (1951)	−7·4	−2·33
	Seaton (1957)	−7·01	—
	Borowitz & Greenberg (1957)	−7·746	—
	Ohmura, Hara & Yamanouchi (1958)	−7·03	−2·346

Functions Φ (eqn (17)) depending explicitly on r_{12} have been used in all the exchange-correlation calculations listed in table 1 but in all cases the functions chosen go to zero exponentially for r_1 or r_2 large. The anti-symmetric function Ψ vanishes identically for $r_1 = r_2$ and electron–correlation effects are therefore small for A_0^-.

4.2. *The Exchange–Adiabatic Approximation*

Approximate solutions of (20) have been obtained by Staver (1951) using variational methods. As a check on Staver's numerical results we have calculated

$$A_0^{\pm(\mathrm{EA})} = A_0^{\pm(\mathrm{E})} + P \qquad \ldots\ldots(35)$$

using exact solutions of the exchange equations for the calculation of P. It is seen (table 2) that both calculations give values for $A_0^{+(\mathrm{EA})}$ which are about one-half of the values of A_0^+ obtained in the exchange–correlation approximations. The exchange–adiabatic and exchange–correlation methods therefore give very different results for the zero-energy cross section.

Table 2. The Exchange–Adiabatic Approximation for the Scattering Length

		+ case	− case
Staver (1951)	$A_0^{\pm(\mathrm{EA})}$	−3·47	−1·82
Equation (35)	$A_0^{\pm(\mathrm{E})}$	−8·06	−2·35
	P	+4·37	+1·02
	$A_0^{\pm(\mathrm{EA})}$	−3·69	−1·33

The integral for P in (35) may be written

$$P = -2\int_0^\infty [F_0^{\pm}(r)]^2 V_{\mathrm{p}}\, dr \qquad \ldots\ldots(36)$$

where the $F_0^{\pm}$ are the s-wave radial functions for $k_1 = 0$ tabulated by Seaton (1957). The functions $-2(F_0^{\pm})^2 V_{\mathrm{p}}$ are sketched in figure 2. It is seen that the main contribution to P comes from values of r of order unity rather than

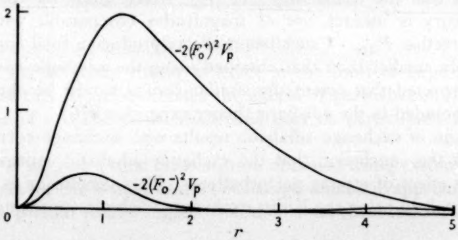

Figure 2. The integrands $-2(F_0^{\pm})^2 V_{\mathrm{p}}$ occurring in equation (36).

from larger values of r where long-range polarization effects, neglected in the exchange–correlation calculations, will be important. For $r \simeq 1$ there is probably no large error in the exchange–correlation wave functions but the validity of the adiabatic theory is uncertain. We therefore conclude that the exchange-correlation results are more reliable than the exchange–adiabatic results and that the exchange–adiabatic approximation considerably over-estimates the effect of atomic perturbations for $r \simeq 1$.

4.3. *The Kohn–Exchange–Adiabatic Approximation*

The integrals occurring in (31), (32) and (33) have been evaluated numerically for the 2p states using for χ_1 the exact exchange functions for $l=0$, $k_1=0$. The results obtained are shown in table 3 (*a*). Values of the integrals occurring in $S_{(2p)}$ are shown separately in table 3 (*b*) in order to indicate which terms are predominant and the extent to which there is chance cancellation.

Table 3(*a*). The Kohn–Exchange–Adiabatic Approximation for the Scattering Length

	+ case	− case
$A_0^{\pm(E)}$	−8·058	−2·347
$P_{(2p)}$	+0·908	+0·423
$R_{(2p)}$	+0·975	−0·045
$S_{(2p)}$	−0·197	−0·024
$A_0^{\pm}$	−6·372	−1·993

Table 3 (*b*). The Integrals forming $S_{(2p)}$ of Table 3 (*a*)

	+ case	− case
$\int \chi_2^*(\nabla^2 + k_2^2)\chi_2 d\mathbf{r}$	−1·912	−0·598
$-2\int \chi_2^* V_{21}\chi_1 d\mathbf{r}$	+0·908	+0·423
$-(\pm)2\int \chi_2^* W_{21}\chi_1 d\mathbf{r}$	+0·975	−0·045
$-2\int \chi_2^* \left(V_{22} - \frac{1}{r}\right)\chi_2 d\mathbf{r}$	+0·470	+0·038
$-(\pm)2\int \chi_2^* W_{22}\chi_2 d\mathbf{r}$	−0·638	+0·158
$S_{(2p)}$	−0·197	−0·024

It is seen that the terms $R_{(2p)}$ and $S_{(2p)}$, which allow for the fact that the adiabatic theory is inexact, are of magnitudes comparable with that of the adiabatic correction $P_{(2p)}$. Cancellation effects produce a total correction which is considerably smaller than that obtained using the adiabatic correction alone. It may be expected that essentially similar results would be obtained if more states were included in the adiabatic theory expansion (18).

Comparison of exchange–adiabatic results with exchange–correlation results (§ 4.2) led to the conclusion that the exchange–adiabatic approximation over-estimates the effect of atomic perturbations. This conclusion is confirmed by the results obtained using the Kohn–exchange–adiabatic approximation.

§ 5. CALCULATIONS FOR THE p-WAVE

Bransden, Dalgarno, John and Seaton (1958) have calculated the phases $\eta_1^{\pm}$ in the exchange–adiabatic approximation using for χ_1 the Born function

$$\chi_1 = Y_{1m}(\hat{\mathbf{r}})(\tfrac{1}{2}\pi)^{1/2} J_{3/2}(kr) \qquad \ldots\ldots (37)$$

and also using variational solutions of the exchange equations. Results for $k_1 = 0{\cdot}5$ are given in table 4.

Kohn–exchange–adiabatic calculations have been made for $k_1 = 0{\cdot}5$ (2p states only) using for χ_1 the Born function (37). The results obtained are given in table 5. As in the s-wave case the correction to be applied when $P_{(2p)}$, $R_{(2p)}$ and $S_{(2p)}$ are all included is smaller than that which would be obtained with $P_{(2p)}$ alone. It seems probable that the p-wave phases are somewhat over-estimated in the exchange adiabatic approximation of Bransden *et al.*, but the error in the exchange–adiabatic approximation for the p-wave will be a good deal less than that for the s-wave since the p-wave radial functions are small for small values of r.

Table 4. Exchange–Adiabatic Results for the p-wave ($k_1 = 0{\cdot}5$)

Approximation for χ_1		+ case	− case
Born	$a_1{}^{\pm(E)}$	−0·077	+0·124
	$6\,k_1P$	+0·126	+0·126
	$a_1{}^{\pm(EA)}$	+0·049	+0·250
Exchange	$a_1{}^{\pm(E)}$	−0·071	+0·170
	k_1P	+0·107	+0·205
	$a_1{}^{\pm(EA)}$	+0·036	+0·375

Table 5. Kohn–Exchange–Adiabatic Results for the p-wave (2p states only, $k_1 = 0{\cdot}5$, the Born function (37) for χ_1)

	+ case	− case
$a_1{}^{\pm(E)}$	−0·0774	+0·1237
$k_1P_{(2p)}$	+0·0491	+0·0491
$k_1R_{(2p)}$	+0·0079	−0·0079
$k_1S_{(2p)}$	−0·0183	−0·0111
$a_1{}^{\pm}$	−0·0387	+0·1538

§6. CONCLUSIONS

Although the adiabatic theory is exact in the limit of large r, our present results suggest that it over-estimates the effects of perturbation of the atom for smaller values of r. The error introduced may be particularly serious for the s-wave.

Bransden *et al.* give a total cross section obtained using exchange–correlation approximations for the s-wave and an exchange–adiabatic approximation for the p-wave. The present results suggest that their total cross section may be slightly too large.

ACKNOWLEDGMENT

One of us (V. M. M.) wishes to acknowledge financial support provided by the Atomic Energy Research Establishment.

REFERENCES

BOROWITZ, S., and GREENBERG, H., 1957, *Phys. Rev.*, **108,** 716.

BRANSDEN, B. H., DALGARNO, A., JOHN, T. L., and SEATON, M. J., 1958, *Proc. Phys. Soc.*, **71,** 877.

DALGARNO, A., and LYNN, N., 1957, *Proc. Phys. Soc.* A, **70,** 223.

HULTHÉN, L., 1944, *K. fysiogr. Sällsk. Lund. Förh.*, **14,** No. 21.

KOHN, W., 1948, *Phys. Rev.*, **74,** 1763.

MASSEY, H. S. W., and MOISEIWITSCH, B. L., 1951, *Proc. Roy. Soc.* A, **205,** 483.

OHMURA, T., HARA, Y., and YAMANOUCHI, T., 1958, *Progr. Theor. Phys.*, **20,** 82.

PERCIVAL, I. C., and SEATON, M. J., 1957, *Proc. Camb. Phil. Soc.*, **53,** 654.

SEATON, M. J., 1957, *Proc. Roy. Soc.* A, **241,** 522.

STAVER, T. B., 1951, *Arch. Math. Naturv.* B, **51,** 29.

Flow Anisotropy in the Theory of Liquids

By J. V. CHAMPION
Sir John Cass College, London

Communicated by R. H. Humphry ; MS. received 4th November 1957, and in revised form 4th June 1958

Abstract. From the theory of Eisenschitz (1949) on the steady non-uniform state of a liquid, a magnitude has been calculated for the anisotropy of flow in a liquid due to a distortion of the radial distribution function by a shearing force. The optical anisotropy has been obtained by using the Bragg (1924) method of calculating double refraction from the variation of the polarization due to the distorted distribution function. The value $\Delta n = 7{\cdot}1 \times 10^{-8}$ (calculated for chloroform, for which the distribution function is known and of which the polarizability does not differ greatly from that of carbon tetrachloride) shows that the effect may be detected experimentally in a liquid normally isotropic.

The calculation also shows that the main contribution to the anisotropy arises from small values of the range r, and the magnitude of the anisotropy is independent of the precise way in which the distortion decreases at large distances. This implies that the 'strong' condition of Eisenschitz cannot be supported by an appeal to the isotropy of flow.

§ 1. INTRODUCTION

SEVERAL attempts have been made in recent years (Kirkwood 1946, Born and Green 1947, Eisenschitz 1949) to treat a non-uniform liquid by the method of kinetic theory and permit the transport coefficients to be calculated. In this connection the existence or otherwise of flow anisotropy has been used in support of some assumptions made.

Eisenschitz (1949) described the liquid state in the terms of the relative coordinates (r, θ, ϕ) of two representative molecules, inserting in the Smoluchowski equation a term to account for a non-uniform velocity. In a steady non-uniform state the distribution function $g(r)$ becomes distorted, i.e.

$$g(r) = g_0(r)\,(1+\omega)$$

where g_0 is the equilibrium distribution given by

$$g_0(r) = \frac{N}{V} \exp\left(\frac{-\Phi}{kT}\right)$$

where N is the number of molecules in a volume V and $\omega = u(r)\sin^2\theta \sin\phi \cos\phi$. The change of sign of ω which occurs at $\phi = 0, \pi/2, \pi, 3\pi/2$ indicates an anisotropic distribution of molecules in a flowing liquid.

$u(r)$ satisfies the equation

$$\frac{d^2u}{dr^2} + \left[\frac{2}{r} - \frac{1}{kT}\frac{d\Phi}{dr}\right]\frac{du}{dr} - \frac{6u}{r^2} = -\frac{a\beta m}{(kT)^2}\, r\, \frac{d\Phi}{dr}$$

where $a/2$ is the rate of shear and β the friction constant.

On integration of the differential equation the constants of integration are evaluated by substitution of the necessary boundary conditions. One of these constants is arranged such that $u(r)$ vanishes at infinity, while alternative assumptions usually referrred to as (*a*) the strong condition and (*b*) the weak condition, can be made regarding the second.

The strong condition assumes that $u(r)\ r^3 \to 0$ as $r \to \infty$ which requires terms of order r^{-3} or higher in $u(r)$ to be neglected, thus making the integral of the distribution function convergent. This implies, in the view of Eisenschitz, that there is no appreciable anisotropy in a flowing liquid in which a uniform velocity gradient exists. It follows from this condition that $u(r)$ becomes infinite at $r=0$, a result which appears physically unreasonable.

The weak condition assumes that $u(r) \to 0$ as $r \to 0$. This overcomes the difficulty of an infinity at the origin, but is not consistent with the requirement of no appreciable anisotropy in a flowing liquid.

However, the well-known temperature dependence of viscosity follows, without further assumption, from the strong condition, which has been further supported by Suddaby (1954) in his treatment of the Smoluchowski equation by an expansion to a higher degree of approximation. This showed that the assumption of no appreciable anisotropy need not be invoked, although it would have been consistent with the other experimental results of the theory.

§ 2. CALCULATION OF THE MAGNITUDE OF THE ANISOTROPY

Since the anisotropy gives rise to double refraction in the liquid, its magnitude may be calculated by evaluating the distortion function and using the Bragg (1924) method of calculating double refraction. This is done by considering the effect of one induced dipole on a neighbouring atom or molecule which is dependent upon the configuration of the molecules in various directions of the applied field (the electric vector of the light passed through the liquid).

If a distorted distribution function is taken for a simple liquid, the distortion in this case being due to a shearing force, then the total variation of the field (i.e. the magnitude of the polarization) at the origin, can be found. The polarization of a representative molecule will vary with the direction of the applied electric field relative to the coordinates of the distorted distribution function.

2.1. *Variation of the Electric Field*

If the molecular polarizability is assumed to be isotropic and the applied field to be parallel to the xy plane, the field strength $E_\parallel$ at the origin, due to an induced dipole of moment μ at P (figure 1) is given by

$$E_\parallel = \mu\,(3\cos^2 A - 1)\,r^{-3}.$$

It is further found from simple geometry that

$$\cos A = \sin\theta\cos(\phi - \psi)$$

where the meaning of the symbols is evident from the figure.

The distorted distribution function has the form

$$g(r) = g_0(r)\,[1 + u(r)\sin^2\theta\sin\phi\cos\phi]$$

where $g_0(r) = (N/V)\exp(-\Phi/\boldsymbol{k}T)$ and Φ is the mean intermolecular potential. Considering the contribution from the anisotropic part only, the variation ΔE

of the electric field at the origin is given by

$$\Delta E=\mu\int_0^{2\pi}\int_0^{\pi}\int_r^R \frac{3\cos^2 A-1}{r^3}\,g_0(r)\,u(r)\sin^3\theta\sin\phi\cos\phi\,4\pi r^2\,dr\,d\theta\,d\phi,$$

where the range $r\to R$ is taken as the region from which the main contribution to the anisotropy comes. Substituting for A in terms of θ, ϕ and ψ and integrating with respect to θ and ϕ,

$$\Delta E=\frac{32\pi^2}{5}\sin\psi\cos\psi\frac{N}{V}\mu\int_r^R\exp\left(-\Phi/\boldsymbol{k}T\right)\frac{u(r)}{r}\,dr.$$

Thus, if $u(r)$ and $\Phi(r)$ are known for a given liquid, ΔE may be calculated from this expression.

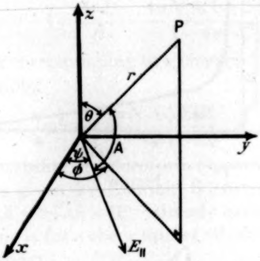

Figure 1.

2.2. *Calculation of* ΔE *for Chloroform*

The solution of the differential equation for $u(r)$ has been obtained by Cole (1952) for chloroform and thus the calculations have been made for this liquid. Although chloroform is anisotropic, its maximum polarizability (along two axes) is of the same order as that of carbon tetrachloride, which has no orientation axis and may be taken to have the same kind of potential function. The results are shown graphically, figure 2 giving the mean potential curve for chloroform.

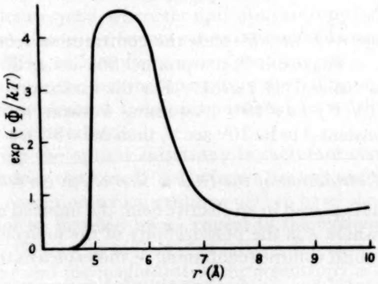

Figure 2.

The small molecular asymmetry being neglected as a first approximation, the intermolecular field has been assumed central with a superposed dipole field. Figure 3 shows the curve for $u(r)/r$ which was derived from the Smoluchowski equation assuming the strong boundary condition. Figure 4 shows the curve for the function $\exp(-\Phi/\boldsymbol{k}T)\{u(r)/r\}$. In all the graphs r is in ångströms, and the values of the ordinates involving $u(r)$ are, for convenience of comparison, those obtained by multiplying $u(r)$ by α, where $\alpha = a\beta m/\boldsymbol{k}T$.

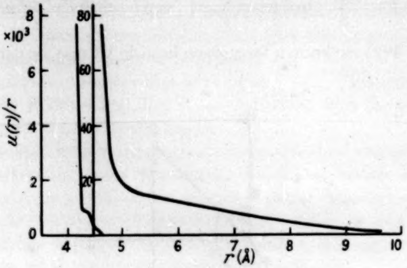

Figure 3.

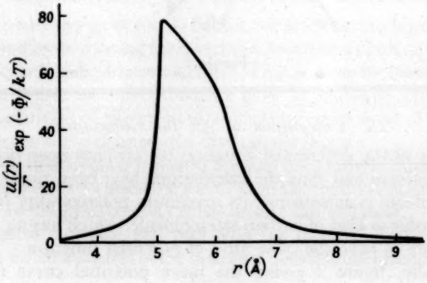

Figure 4.

Taking the range $r \to R$ as 3 Å→10 Å, the contribution from the integral gives 96α, providing α is in ångström^{-2}, the product 96α being dimensionless. Then $\Delta E = (32\pi^2/5) \sin\psi \cos\psi \,(N/V)\, \mu 96\alpha$. For the maximum value (0·5) of $\sin\psi \cos\psi$, $\Delta E = 2{\cdot}04\ (N/V)\ \mu\alpha \times 10^3$. Assuming a shear rate of 50 000 sec^{-1}†, and the friction constant β to be 10^{11} sec^{-1}, then $\Delta E = 8{\cdot}7\ \mu \times 10^{-8}$ Å^{-3}.

2.3. *Calculation of the Double Refraction Δn from ΔE*

When a molecule is placed in an electric field, the induced dipole has a moment μ given by $\mu = \lambda\mathscr{E}$ where λ is the polarizability of the molecule and $\mathscr{E}$ is the field. The polarization per unit volume (containing N_1 molecules) is then $P = N_1\mu = N_1\lambda\mathscr{E}$.

† This rate of shear has been used as apparatus is being constructed in which this can be attained.

Using the standard method of treatment for an isotropic dielectric, the field experienced by the molecule at the centre of a small spherical cavity in the medium is $E+4\pi P/3$ where E is the applied field. This value of the field follows from the assumption that the molecular dipoles within the cavity are randomly distributed and it leads to the relations

$$K-1=n^2-1=\frac{4\pi P}{E}=\frac{4\pi N_1\lambda}{1-4\pi N_1\lambda/3} \qquad \ldots\ldots(1)$$

where K is the dielectric constant and n is the refractive index.

If, however, following the argument of Bragg (1924), the dipoles within the cavity have a non-uniform distribution, giving the additional field ΔE, already calculated in § 2.2, the field which the molecule experiences will be $E+4\pi P/3+\Delta E$ and then

$$(n+\Delta n)^2-1=\frac{4\pi P}{E}=\frac{4\pi N_1\lambda(1+\Delta E/E)}{1-4\pi N_1\lambda/3} \qquad \ldots\ldots(2)$$

where Δn is the change in n corresponding to a change ΔE in E. Hence from (1) and (2), $(\Delta n)^2$ being negligible,

$$2n\,\Delta n=\frac{4\pi N_1\lambda\,\Delta E/E}{1-4N_1\pi\lambda/3}. \qquad \ldots\ldots(3)$$

If we take the average polarizability of chloroform ($\lambda_{\mathrm{av}}=82{\cdot}3\times10^{-25}\,\mathrm{cm}^3=8{\cdot}23\,\text{Å}^3$) calculated from the values given by Landolt–Börnstein (1951), together with $n=1{\cdot}45$ and the value of $\Delta E=8{\cdot}7\lambda E\times10^{-8}$ already calculated, equation (3) gives $\Delta n=7{\cdot}1\times10^{-8}$. This value is for a shear rate of 50 000 sec^{-1}†, Δn being directly proportional to the rate of shear.

The value also depends upon the validity of the numerical evaluation of the distorted distribution function $u(r)$. A similar type of calculation on the effect of an electric field on liquid viscosity by Eisenschitz and Cole (1954) gave a result within 15% of experimental values and appears to justify the evaluation. In the case of carbon tetrachloride, which is closely related to chloroform, the polarizability is $105\times10^{-25}\,\mathrm{cm}^3$ and the potential function will not differ greatly from that of chloroform; thus the double refraction will be of the same magnitude.

§ 3. DISCUSSION

(*a*) The main contribution to the optical anisotropy of a flowing liquid, due to the effect discussed, comes from a range $4\,\text{Å}<r<8\,\text{Å}$ as seen from figure 4.

In the case of a calcite crystal, where the optical anisotropy is readily measurable, the main contribution also arises from a range immediately near the central atom ($2\,\text{Å}<r<6\,\text{Å}$, Bragg 1924), and implies a convergent integral.

This situation is due to the fact that apart from the falling off of the distribution function, there is an additional factor proportional to r^{-3} in the effect of the induced dipoles on the central atom.

The integral giving the optical anisotropy is therefore convergent providing $u(r)$ has, at large distances, the form $\mathrm{O}(r^{-\epsilon})$ where ϵ has any positive value. Hence Eisenschitz's strong condition which requires $u(r)$ to have the form $\mathrm{O}(r^{-(3+\epsilon)})$ at large distances cannot be justified by an appeal to the existence or otherwise of optical anisotropy. So long as $u(r)\leqslant r^{-\epsilon}$ at large r, the main contribution arises from small values of r and the magnitude of the anisotropy is independent of the precise way in which $u(r)$ decreases at large distances. This means that the strong condition can still be valid, but appeal to the isotropy of flow cannot be used to support it.

---

† See footnote on p. 714.

(*b*) The magnitude of the anisotropy calculated indicates that the effect may be detectable.

Anisotropy of flow in a pure liquid has been normally associated with an orientation or distortion of the molecule itself. Both of these effects produce a double refraction considerably larger than that due to the distortion of the distribution function, for the same rate of shear, by a factor of twenty or more, according to the magnitude of the anisotropic shape of the molecule. In this paper the birefringence due to the distortion of the distribution function has been calculated for an anisotropic molecule (chloroform) for which the distribution function is known. The magnitude of this birefringence would not differ greatly from that arising from the same cause in a related molecule, viz. carbon tetrachloride, which would show no orientation or distortion anisotropy. Thus if such a tetrahedral molecule were subjected to a sufficiently large rate of shear, while retaining laminar flow in the liquid, the effect of the distorted distribution function might be measured, a birefringence Δn of magnitude 7×10^{-8} being expected for a rate of shear of 50 000 $\sec^{-1}$. The same order of birefringence might be expected for a spherically symmetrical molecule.

Acknowledgments

The author is indebted to Professor Eisenschitz for his interest in the work and wishes to thank Dr. A. Suddaby and Dr. G. H. A. Cole for many helpful discussions.

References

Born, M., and Green, H. S., 1947, *Proc. Roy. Soc.* A, **190,** 455.
Bragg, W. L., 1924, *Proc. Roy, Soc.* A, **105,** 370.
Cole, G. H. A., 1952, *Ph.D. Thesis* (University of London).
Eisenschitz, R., 1949, *Proc. Phys. Soc.* A, **62,** 41.
Eisenschitz, R., and Cole, G. H. A., 1954, *Phil. Mag.*, **45,** 394.
Kirkwood, J. G., 1946, *J. Chem. Phys.*, **14,** 180.
Landolt–Börnstein, 1951, *Zahlenwerte und Functionen,* **1,** Part 1, 510.
Suddaby, A., 1954, *Ph.D. Thesis* (University of London).

The Probability of Multiple Emissions of Secondary Electrons

By R. E. BARRINGTON† and J. M. ANDERSON
Department of Physics, University of Toronto, Canada

MS. received 15*th April* 1958, *and in revised form* 14*th July* 1958

Abstract. Probabilities P_n have been determined for the emission of electrons in groups of n numbering from zero to eight occurring as a result of a single primary. Beryllium copper surfaces under different activation conditions have been studied for primary energies between 100 and 300 ev, P_0, having values between 0·5 and 0·2 falling to a minimum at intermediate energies, and P_1 with values 0·3 to 0·4 rising to a maximum at intermediate energies remain larger than any other probability. Probabilities above P_1 for constant primary energy fall off with number in two distinct curves, that for even numbers lying above and falling less steeply than that for odd numbers. Separation of these curves depends on surface treatment. For activated surfaces probabilities P_1 to P_6 show evidence of maxima in the energy range covered; P_7 and P_8 are still rising at the end of the range. For unactivated surfaces only P's for odd numbers of electrons show a clear decrease at higher energies; P's for even numbers of electrons, with the possible exception of P_2, are still rising at the end of the range.

---

§ 1. INTRODUCTION

PREVIOUS measurements on secondary electron emission have been confined to determination of average behaviour over very large numbers of events each due to the arrival of a single primary particle. No information as to the probability of emission of a particular number of electrons in a single event has been available except for contradictory estimates by Allen (1947) and Cowan (1950, 1954) of the probability of no electron being emitted. The results of Hayner and Kurrelmeyer (1937) from noise measurements show that an appreciable probability must exist in some cases of four or more electrons being emitted in a single event. In the work described below the individual probabilities of events, in which zero up to and including eight electrons are emitted as a result of a single primary, have been determined for beryllium–copper alloy surfaces.

Having defined P_n as the probability of emission of n electrons in a single event due to a single primary, one can easily show that

$$\sum_{n=0}^{n=\infty} P_n = 1\,; \qquad \sum_{n=0}^{n=\infty} nP_n = \delta\,; \qquad \sum_{n=0}^{n=\infty} n^2P_n = r\,; \qquad \ldots\ldots(1)$$

where δ is the secondary emission coefficient or average number of electrons emitted per incident primary and r is the ratio of the shot noise in a current due to secondary emission to the noise in the thermionic emission current causing it. Wipler (1937) has shown directly that thermionic emission currents involve only emission of single electrons. These equations would permit unique solution for not more than three specific n's and more are known to exist. In the experiments described below the ratios P_n/P_{n+1} for n from one to seven have been determined and the results combined with equations (1) to find the probabilities individually.

---

† Now at Defence Research Telecommunications Establishment, Ottawa.

§ 2. Apparatus

To distinguish between events in which different numbers of electrons are emitted, it was necessary to develop a counter, giving a measurable pulse whose height is proportional to the number of secondary electrons in a single event, and which will ignore the incident primary electron. This counter, shown in figure 1, consists of two stainless steel cones C with a common axis and with a distance of about 2 mm between their flattened peaks. Primary electrons are shot in along the axis with known energy from the electron gun FGM mounted inside the cone to the left in figure 1. The surface whose secondary emission is to be studied is a small circular plate B, mounted perpendicular to the axis in front of the other cone. For reasons given below, arrangements H are provided for heating this surface. The gun and bombarded surface were separately supported by heat resisting 'Teflon' plastic supports T. A coaxial ring A, two centimetres in diameter, is mounted as shown with the lead brought out through the enclosing metal walls by a glass metal seal S. The whole unit is suspended from a kovar ring in a glass vacuum jacket. To avoid adding extra capacity the electrical lead from the collector ring is brought out through a separate seal in the walls of this vessel. To avoid glow discharge breakdown between the leads, each is enclosed in a conducting shield spaced from it a distance less than the dark space.

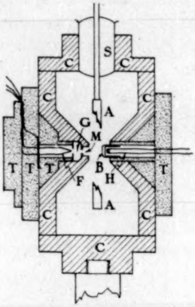

Figure 1. Electron proportional counter.

The collector ring is nearly at ground potential with all other elements maintained at steady high negative values. A beam of electrons of controlled energy and number is directed from the gun on the secondary emission target. Because the enclosing metal walls are maintained negative with respect to the target, secondary electrons emitted from it will be deflected away from them toward the collector ring. Since the walls could not be made more negative than the cathode of the gun in this system, a secondary reflected exactly back along the axis with the full primary energy could re-enter the gun and be lost. Because of the very small apertures used and the small chance of exact return along the axis with the full energy this process is extremely improbable. A steady magnetic field is maintained along the axis of the counter, of such value that the vacuum magnetron cut-off field is greatly exceeded for electrons emitted near the axis from the target and proceeding toward the collector ring as anode. Thus in a perfect vacuum no electron current can reach the ring.

Argon at a pressure of approximately $1{\cdot}5 \times 10^{-2}$ mm Hg, admitted to the counter, as counting gas, still allows primary electrons to reach the target with negligible chance of ionizing collisions because their path in the counter (unaffected by the axial field) is very much less than the mean free path. Secondary electrons, with the negligible exception noted above, acquire a radial velocity and under the influence of the high radial field perform cycloidal orbits until collision with a gas molecule occurs. Because of the energy gained in the high radial field many of these collisions will ionize the argon atoms. From the site of such a collision two electrons start on new cycloidal orbits. Because kinetic energy is given up in each ionizing collision, return to the axis cannot occur and all electrons must migrate outward to be collected by the ring. The heavy positive ions are relatively unaffected by the magnetic field and migrate to the walls of the counter. Such wall collisions may cause a secondary electron to be emitted which could suffer multiplication in the gas and add to the total charge collected at the ring. Positive ion bombardment of the target itself is negligible.

The number of electrons collected at the ring following a secondary emission event at the target will be strictly proportional to the number of electrons emitted in that event so long as the total ion population in the vessel does not rise so high as to change appreciably the probability of ionization occurring in a collision. In practice this limiting level was never reached and secondary emission pulses always fell into groups whose heights were in integral ratios.

Counter voltage was set at approximately 950 volts and maintained constant by electronic regulation. After allowing time for temperature equilibrium to be obtained at a slightly lower field, the magnetic field was adjusted for best pulse height multiplication to a value in the neighbourhood of 400 oersteds and maintained constant by use of a storage battery as current source. These numerical values are extremely sensitive to the exact geometry.

The resolving power of the counter was tested by heating the target until thermionic electrons were emitted. The results confirmed Wipler's (1937) conclusion that thermionic electrons are emitted singly. Pulse heights in this case clustered about a single value with a spread only very slightly larger than that resulting from amplifier noise and the statistical variation expected from the large but finite number of ionizing events in each multiplication process.

Multiplication ratios giving 2000 to 5000 collected electrons for each emitted electron could easily be obtained. Special amplifiers were constructed and the band width adjusted for best signal to noise ratio using methods outlined by Gillespie (1953). The final noise was equivalent to pulses of 200 electrons. The pulses were displayed on the screen of a Tektronix 511AD oscilloscope, modified for increased gain, and with its time base disconnected. The time base gating of the beam brightness was used to avoid halation at the base line, the gate being set to open only on the largest noise pulses. Pulses were photographed on a moving film with a modified Cossor camera at a rate of between five and twenty per second the rate being adjusted by setting the temperature of the gun filament or of the target depending on whether secondary emission electrons or thermionic electrons were being studied.

§ 3. METHOD

Slow drifts in counter conditions caused a noticeable variation in multiplication ratio in periods of the order of half an hour. The effect was negligible during the two minutes taken to expose the six-foot sections of film used because the thermionic peak width was found to be accounted for by amplifier noise and statistical fluctuations of the counter process.

Images of the developed films together with the image of a scale at the focal plane of the projector were projected on a six foot square screen. Pulse heights occurring in each scale division were recorded as the film was moved one frame at a time. A histogram of this number of pulses in each height division was then drawn as in figure 2. In every case secondary electron pulses clustered around pulse heights in integral ratio, while direct thermionic emission showed only a single narrow peak.

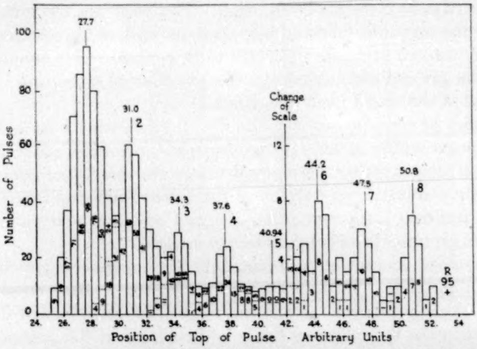

Figure 2. Example of histogram of pulse heights obtained from a single film.

Because the peaks as shown in figure 2 overlap to some extent, assumptions are necessary to determine the total area to be assigned to each peak. It was assumed in this work that each bar of the histogram contained pulses from only two adjacent peaks and in the overlapping region the bar was divided between the peaks with the parts in the ratio of the size of the peaks. It was assumed that the peaks were symmetrical for lack of information to the contrary. From histograms for each film the number of pulses in each peak was determined as well as the total number of pulses whose height exceeded the highest resolved peak. These large pulses R were not divided among separated peaks because the small number occurring on any one film made the statistical accuracy of such determinations very poor especially where the total number of pulses on a film was rather small. In most cases all pulses greater in height than the eighth peak and in the remaining cases all greater than the sixth peak were assigned to a remainder and given a probability designation P_r. This number is so large that it cannot in all cases be neglected. The number of pulses in each peak and the total number of pulses recorded were evaluated for each film. A weighted average, for all films taken under given conditions, of the ratio of the number of pulses in a given peak to the total number recorded was found. Ratios of these values are the ratios of the probabilities necessary for complete solution using in addition relations (1). Ratios of the numbers of pulses in a given peak to the total number recorded are not themselves probabilities because this procedure takes no account of events in which no secondary occurs.

To find absolute values of the probabilities for emission of numbers of electrons equal to or greater than one, the ratios determined as described above must be combined with the second of equations (1). P_0 can then be found from the first of equations (1). Thus δ the secondary emission coefficient of the surface must be found. This quantity could not be determined with the target in position in the counter described above because the very high voltages (for above normal operation) necessary to collect all secondaries at the ring would defocus the primary beam so that only a part of it strikes the target. Tests showed that, for the beryllium–copper alloy used, the secondary emission properties of a surface could be reproduced provided the temperature used in the sensitizing process was the same. Within rather wide limits the secondary emission yields were found to be independent of the time of the conditioning process.

Accordingly δ was determined in a special triode with a beryllium–copper anode using the method of Bruining (1954). Three surface conditions were studied. In the first case, A, the surface was polished with emery and rouge and carefully washed. A target for the counter and an anode for the triode were made from parts of the same sheet, mounted, connected to the same pumps so that pressure and ambient gas would be the same at all times, and exhausted without heat treatment for a long period until the pressure was less than 10^{-5} mm. Secondary emission coefficient measurements were made with results as in curve A of figure 3 and probability ratios were determined for the target in the counter at various energies of the incident electrons.

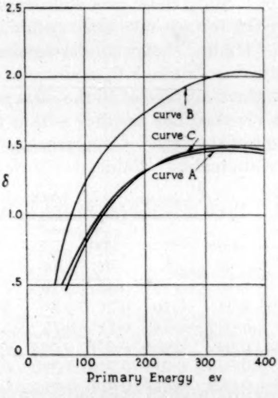

Figure 3. Variation of δ with V_p.

To prepare the second surface, type B, air was admitted to the system to provide oxygen for activation. The system was pumped down to 10^{-1} mm pressure and the plate of the secondary emission triode heated by an induction heater until thermionic emission from the plate to the other electrodes could just be measured with a sensitive galvanometer. After a set conditioning time (15 min) the chamber was re-exhausted and secondary emission measurements taken, curve B of figure 3. The target of the counter was sensitized in a similar manner for the same time, the temperature being raised until thermionic emission from the target was just detectable. Since thermionic emission is such a steeply varying function of temperature and secondary emission properties are found to change very little for moderate changes of conditioning temperature in this region the two surfaces were considered to have received the same treatment. Ratios of secondary emission probabilities were determined for this sensitized target as described above.

In preparing the third surface condition, the apparatus was exhausted and maintained at a high vacuum for eight hours with both the triode plate and counter target maintained at the previous conditioning temperature. Secondary emission coefficients, as in curve C of figure 3, were obtained. These are considered to be the same as in curve A within the limits of error. Since, as will be shown below, the probabilities for the unheated surface and those for the surface heated for a long period in a vacuum are found to be the same within the limits of error, it is considered that these two surfaces are actually identical and in the final curves data for these two surfaces are combined. It seems likely that the sensitized surface found to be so stable by previous workers as well as in this work is due to an oxidized layer which sublimes off at high temperature in high vacuum.

§ 4. RESULTS

The probabilities of emission of different numbers of electrons from a beryllium–copper surface for primary energies between 100 and 300 volts, found as described above are shown in tables 1 and 2.

Table 1 shows the probabilities for surface A unheated and for surface C heated in vacuum for eight hours. Since these probabilities were found to be the same within the limits of error the results have been combined to give a single result for unactivated surfaces. Table 2 shows similar results for the surface activated by heating in air at low pressure, surface B, as described above. In these tables each probability is the weighted average of all the films measured for a given set of conditions. These films checked one another within the limits to be expected from the statistical accuracy of the data. Comparison of values for surfaces A and C illustrates the accuracy attainable. Values for surface C were obtained from

Table 1. Probabilities for Surfaces A and C

V_p	100			150	200			250	300		
	A	C	Av	C	A	C	Av	C	A	C	Av
P_0	0·50	0·48	0·50	0·49	0·37	0·45	0·39	0·40	0·45	0·43	0·45
P_1	0·33	0·34	0·33	0·31	0·30	0·27	0·29	0·30	0·27	0·29	0·27
P_2	0·086	0·084	0·086	0·089	0·14	0·12	0·13	0·11	0·11	0·11	0·11
P_3	0·041	0·044	0·041	0·049	0·066	0·058	0·064	0·054	0·028	0·026	0·028
P_4	0·020	0·017	0·020	0·026	0·043	0·040	0·042	0·047	0·057	0·054	0·057
P_5	0·0075	0·006	0·0074	0·009	0·017	0·011	0·015	0·014	0·010	0·012	0·010
P_6	0·007	0·007	0·007	0·010	0·028	0·027	0·028	0·025	0·032	0·029	0·032
P_7	—	—	—	—	—	—	—	0·005	0·006	0·005	0·006
P_8	—	—	—	—	—	—	—	0·010	0·017	0·015	0·017
P_r	0·010	0·012	0·010	0·020	0·025	0·027	0·025	0·028	0·022	0·026	0·022
δ	0·86	0·83		1·17	1·38	1·40		1·44	1·44	1·48	

Table 2. Probabilities for Surface B

V_p	100	150	200	250	300
P_0	0·37	0·21	0·22	0·29	0·36
P_1	0·38	0·45	0·38	0·30	0·25
P_2	0·15	0·17	0·16	0·18	0·16
P_3	0·047	0·069	0·094	0·062	0·083
P_4	0·034	0·047	0·049	0·068	0·045
P_5	0·020	0·028	0·031	0·028	0·021
P_6	0·017	0·013	0·023	0·021	0·020
P_7	—	—	0·010	0·014	0·014
P_8	—	—	0·007	0·011	0·015
P_r	0·013	0·019	0·016	0·033	0·049
δ	1·19	1·57	1·75	1·90	1·99

single two minute exposures. The percentage accuracy decreases for the larger values of n because of the relatively small numbers of events of this nature found on the films.

In figures 4 and 5 log P_n is plotted against n for different primary energies for the unactivated and activated surfaces respectively. It may be noted that P_0 and P_1 do not lie on the same smooth curves as the probabilities for higher numbers. This is not unexpected since the peak for single secondaries includes reflections without loss of energy as well as the contribution to this peak of secondaries emerging with only a few volts energy. Since the processes involved are probably quite different some discrepancy is to be expected.

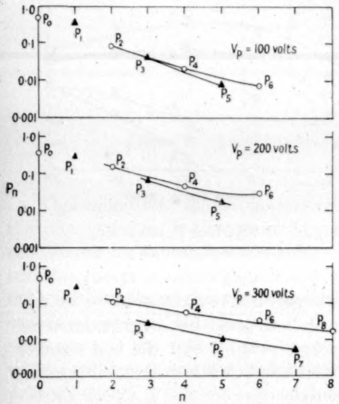

Figure 4. Surface A, unactivated, variation of P_n with n.

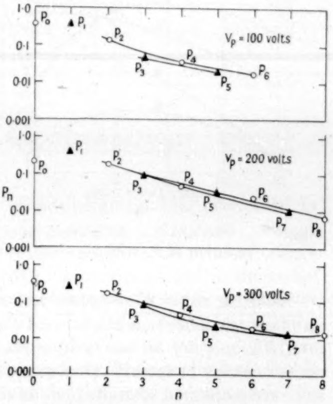

Figure 5. Surface B, activated, variation of P_n with n.

The probabilities of higher order than P_1 lie on two distinct curves in every case. The curve for even number emissions lies higher than that for odd numbers and slopes downward less steeply as n increases. This effect is more prominent in the results with the unactivated surface than for the activated surface though qualitatively of the same nature.

In figures 6 and 7 a plot of P_n against incident energy for different values of n is shown. For surface B, figure 7, P_0 varies between 0·2 and 0·4 in the energy region studied falling to its minimum value at 170 volts. This is considerably below the voltage at which δ reaches its maximum. These values are consistent with the estimate of Cowan (1954) that P_0 is less than 0·4 and not extremely small. They contradict the estimate of Allen (1947) that P_0 is negligibly small. Apart from P_0 the probabilities appear to rise to maximum and fall off again as primary voltage is increased, maxima for higher n tending to be at higher incident energies. In the range up to 300 volts as used here the probabilities P_7 and P_8 are still rising. For the unactivated surfaces A and C only P's for odd numbers and possibly P_2 show maxima in figure 6 in the voltage range covered.

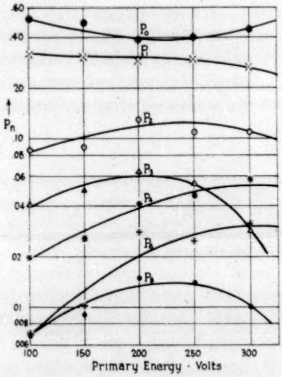

Figure 6. Surfaces A and C, unactivated, variation of P_n with V_p.

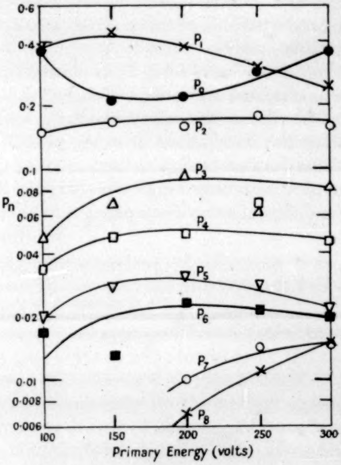

Figure 7. Surface B, activated, variation of P_n with V_p.

Since the rise in δ on surface activation is largely due to increase in P's for odd numbers and since maxima for odd P's occur in both cases, but are prominent for even P's only for an activated surface, it seems possible that the odd number emissions may be largely associated with surface effects while even number emissions are associated with the body of the material.

Using the values of the probabilities listed in tables 1 and 2 and assigning an average number ten to the probability P_r for events giving numbers greater than eight secondaries, we can evaluate for each primary voltage the shot noise ratio r from the third of equations (1). A plot of this ratio against primary energy shows an approximately linear relation in agreement with the work of Hayner and Kurrelmeyer (1937) for nickel.

As pointed out above the spread of the peak heights about a mean value for thermionic electrons is accounted for by amplifier noise and the expected statistical variation in the number of ionizing events in the counter. Because of the greater number of electrons collected in each pulse in the peaks due to multiple emissions of secondaries it might be expected that the peak width would increase with *n* and the resolution of the counter correspondingly decrease as the number associated with the peak rises. Precisely the contrary trend is found in practice, with the effect being more marked at the lower numbers. Figure 8 shows the shape of the peak due to emission of single electrons for thermionic emission and for secondary emission at different primary voltages. All peaks have been normalized to a single height. High accuracy for the shape of the peaks cannot be claimed but the difference between peak width for thermionic electrons and for the single secondaries at different primary energies is quite evident.

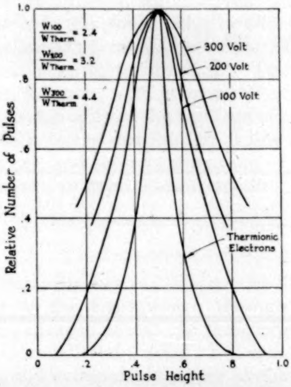

Figure 8. Comparison of *W*, the peak width at half height.

Thermionic electrons all possess very low initial energies and the peak width in this case is practically all explained by statistical and noise considerations. Single secondaries are known to occur at least in some cases with the full primary energy and this energy is not negligible compared with the energy gained in the radial field. It is believed that the large initial energy of some of the single secondaries causes an appreciable difference in the radius at which the first ionizing collision takes place in the counter and hence alters the multiplication ratio. The peak width continues to increase with primary voltage and sets the upper limit of useable primary energy in this work, since the lower number peaks are no longer resolved at higher energies. The peak width due to this effect is so large that widths due to statistical fluctuations and noise are negligible for secondary emission peaks. This would seem to indicate that the spread in initial conditions between a number of electrons emitted in a single event is much less than the spread between the same number emitted as single secondaries due to different primaries, or in other words that multiple emissions occur with a relatively uniform velocity for the whole group.

ACKNOWLEDGMENTS

The authors wish to acknowledge a grant (DRB9512–23) to one of us (J. M. A.) by the Defence Research Board, Canada. This allowed purchase of necessary equipment. The assistance of the Canadian Kodak Co. by the award of the Kodak Scholarship to one of us (R. E. B.) permitted the work to be carried to completion.

REFERENCES

ALLEN, J. S., 1947, *Rev. Sci. Instrum.*, **18**, 739.
BRUINING, H., 1954, *Secondary Electron Emission* (New York : McGraw-Hill).
COWAN, J. A., 1950, *Ph.D. Thesis*, University of Toronto; 1954, *Canad. J. Phys.*, **32**, 101.
GILLESPIE, A. B., 1953, *Signal, Noise and Resolution in Nuclear Counter Amplifiers* (London : Pergamon Press).
HAYNER, L. J., and KURRELMEYER, B., 1937, *Phys. Rev.*, **52**, 952.
WIPLER, E. H., 1937, *Z. Phys.*, **107**, 37.

The Transmission of Electrons through Metallic Foils

By B. N. C. AGU, T. A. BURDETT and E. MATSUKAWA
Department of Physics, University of Leicester

MS. received 25th March 1958, and in revised form 13th June 1958

Abstract. Electron transmission measurements, using a collecting cup and galvanometers, have been made for homogeneous energy beams in the range 0·25–0·75 Mev in foils of Be, Al, Cu, Ag and Au. The discrepancy between the present measurement of extrapolated range in aluminium and the generally accepted range–energy relationship cannot be simply explained in terms of low energy secondary emission or geometrical effects. Transmission measurements through silver foils agree, however, with other published results. The angular distribution of electrons emerging from the exit side of a foil has been examined. This appears to approach a cosine distribution at low transmissions. Further information on range values, and some confirmation of voltage calibration have been obtained from ionization in depth measurements.

§ 1. Introduction

In a previous paper (Agu, Burdett and Matsukawa 1958), we have described some measurements of the transmission through aluminium foils of an initially homogeneous electron beam. In these experiments the transmitted electron current was measured directly, using a collecting cup and galvanometers. The transmission curves and extrapolated ranges so obtained differed from those of other investigators using ionization chamber detection or Geiger counters. In view of this discrepancy in the extrapolated range values, a more detailed examination of the aluminium transmission characteristics has been made in order to determine the influence of secondary emission and collector geometry upon range values.

Energy measurement in the present work depends ultimately on sphere spark gap calibration, and the possibility must be borne in mind that the presently available figures are, in fact, not reliable. It was therefore desirable to obtain a set of experimental range values which could be compared directly with values obtained by other investigators using the same method. Measurements were made using a shallow ionization chamber similar to those described by Trump, Van de Graaff and Cloud (1940), Trump, Wright and Clarke (1950) and Frantz (see Spencer 1955), to obtain ionization in depth curves. Measurements of this type have been made primarily to determine ionization distributions for biological purposes, but consistent range values may also be obtained by extrapolating the linear section of the ionization curve.

Information on the transmission of monoenergetic beams through foils other than aluminium is rather scarce. Transmission measurements and some ionization in depth measurements have therefore been carried out to cover a range of atomic number, using foils of Be, Cu, Ag and Au.

§ 2. EXPERIMENTAL DETAILS

2.1. *Apparatus*

For the transmission measurements, an electron beam of 5–20 μA, derived from an electrostatic generator, was directed onto the foil and collector assembly described previously. The geometry of collection could be varied systematically by inserting cylindrical spacers below the foil in the foil clamp. The maximum collecting angle θ_m was varied between 86° (the upper limit with zero thickness spacer) and 41° representing collection efficiencies of 93% down to 20% of 2π.

For the ionization in depth measurements, the beam was reduced to about 1 μA and brought out from vacuum through a thin (15 mg cm^{-2}) Be window. A correction was made for the electron energy loss in passing through the window, and a further 1 cm of air, before striking the experimental foil (e.g. 27 kv at 0·5 Mev). The experimental foil formed the upper collecting electrode of a shallow parallel plate ion chamber. An 'infinitely thick' plane h.t. electrode of the same material as the foil was separated from the foil by a Distrene spacer 1·5 mm thick with a circular aperture 2·25 cm in diameter. This chamber saturated at about 400 volts h.t. Readings were taken with and without chamber h.t. so that ion current could be differentiated from primary electron current.

The accuracy of the present results depends largely upon the accuracy of voltage measurement. The overall sensitivity of the generating voltmeter could be measured before each transmission run and allowance made for any change in sensitivity from that obtained during a previous spark gap calibration. With this procedure it was found that transmission measurements taken several months apart were reproducible to within 2%.

2.2. *Correction for Collector Backscattering*

It will be seen in the next section that the geometry of the present arrangement is not significantly different from 2π, and that the change in angular distribution of transmitted electrons is relatively small over the complete foil thickness range examined. A constant percentage correction to the apparent transmission to compensate for collector backscattering is therefore justified, and the extrapolated range values will therefore be independent of this correction. The measured backscattering, using a dummy foil containing a 1·0 cm hole at 100 v positive bias, was 4% of the beam incident upon the collector and independent of energy. The ratio of true to apparent transmission was therefore taken as 1·04, this value being also consistent with the shape of the transmission curves at small thicknesses when 100% transmission is not exceeded with a biased foil (see curves in figure 3).

§ 3. EFFECT OF VARIATION OF COLLECTOR GEOMETRY

Discrepancies in the published range values for aluminium are often attributed to the different geometrical conditions of the measurements. An examination was therefore made of the variation in shape of the transmission curve as the maximum angle of acceptance of electrons from the foil was reduced. The typical dependence of transmission upon geometry is shown in figure 1 for various angles and foil thicknesses; the curves have been normalized to the value 100 at 100% geometry. (The collection efficiency $\xi = \omega/2\pi$ where ω is the solid angle of

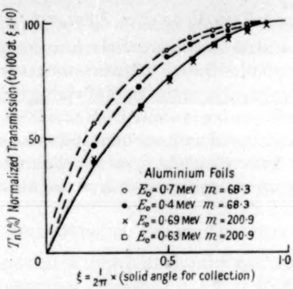

Figure 1. Variation of angular distribution of transmitted electrons with transmission value.

acceptance.) We may describe the angular distribution of the transmitted electrons by the function $B(\theta)$, defined by the equation

$$T(\xi) = 2\pi \int_0^{\theta_m} B(\theta) \sin\theta d\theta,$$

where $T(\xi)$ is the transmission measured when the maximum acceptance angle from the foil is θ_m, corresponding to a collection efficiency $\xi = 1 - \cos\theta_m$. For the present calculations it is considered sufficiently accurate to neglect the finite width of the incident beam.

The solid curve in figure 1 corresponds to $B(\theta) \propto \cos\theta$. This cosine distribution appears to be the limiting distribution for transmissions (into 2π solid angle) less than about 20%. Higher transmissions can be fitted by the angular distribution function $B(\theta) \propto \cos\theta(a + b\cos\theta)$. Actually the upper dotted curve in figure 1, representing a transmission of 90% at $\xi = 1{\cdot}0$, corresponds to a $\cos^2\theta$ angular distribution. It may be noted that if an elementary diffusion theory became applicable to the emerging electrons at small transmissions, then the experimentally found intermediate distribution $\cos\theta(a + b\cos\theta)$ would be obtained. As stated above, the distribution at low transmissions actually becomes close to a cosine distribution with a most probable emergent angle of 45°.

For a cosine distribution, the difference in tranmissions between 100% and 90% collection efficiency is only 1% and this difference will be rather less for higher transmissions. Thus the present results may justifiably be compared with others obtained with full 2π collection.

The effect of increasingly poor geometry of collection upon extrapolated range values may be estimated here. A single result for poor geometry measurement was quoted in the previous paper, where it was found that a geometry somewhat poorer than 2π resulted in a slightly increased range value. This now appears to be a false conclusion, and was probably due to the method then employed to change the geometry (the whole foil assembly was spaced away from the collecting cup by glass insulators). From a large number of measurements with the present arrangement it is found that extrapolation of the still significantly linear section of poor geometry transmission curves results in range values which decrease systematically with ξ. The decrease ΔR_p is, of course, very small for ξ between 1·0 and 0·9, but it is possible to describe the magnitude of the effect by the approximate equation $\Delta R_p \simeq 0{\cdot}1(1 - \xi)R_p$, for ξ between 0·9 and about 0·2.

§ 4. Effect of Bias Voltages Applied to the Foil

It was found by experiment that most of the low energy secondaries from the foil have energy less than about 15 ev. Measurements were therefore taken at a fixed positive bias of 100 volts, where the rate of change of transmission with bias has become very small. From an examination of a large number of aluminium transmission curves taken with and without bias, it was found that the transmission change ΔT produced by 100 volts bias was approximately proportional to the apparent transmission T_a up to transmissions of the order 70%.

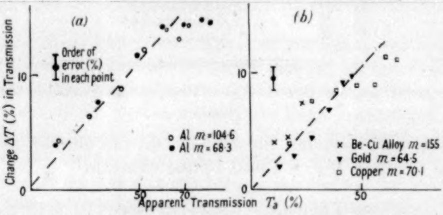

Figure 2. Effect of +100 volts bias on the foil on apparent transmission values.

This result is shown in figure 2 (*a*), where for simplicity, only two different foil thicknesses have been used in plotting. The fact that ΔT is proportional to T_a over the linear portion of a transmission curve implies that the extrapolated range values from measurements at 100 volts bias will be the same as those obtained at zero bias.

The approximately constant value $\Delta T/T_a \simeq 0{\cdot}105$ obtained for aluminium was also found to apply to other metal foils, including copper, gold, and a copper–beryllium alloy, as shown in figure 2 (*b*). The low energy secondary emission of a foil in the present experiments was therefore probably determined by a surface layer of contamination, for example, vacuum pump oil, common to all the foils.

§ 5. Transmission Measurements

A set of universal collector cup transmission curves obtained with 100 volts foil bias, and corrected for collector backscattering, is given in figure 3 for a

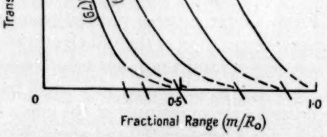

Figure 3. Universal transmission curves for metals.

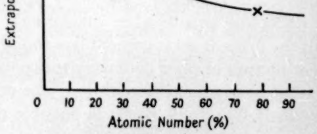

Figure 4. Ratio R_p/R_0 as a function of atomic number.

range of metals. The existence of a linear section is evident for all the metals, except gold, for which an extrapolation procedure is somewhat dubious. The ratio of extrapolated range to true range (Spencer 1955) is shown as a function of atomic number in figure 4. The silver curve agrees, within experimental error, with that obtained by Seliger (1955) using a 2π counter, this being the only available comparison curve, other than for aluminium, taken with good geometry. There is also close agreement of the gold curve with Seliger's curve for lead, suggesting good agreement for large atomic numbers generally.

§ 6. Ionization in Depth Measurements

The variation of ionization in depth in aluminium, measured using the shallow ionization chamber arrangement described in § 2, is shown in figure 5 (*a*). Here the ratio of ion current to primary beam current has been plotted as a function of the ratio of foil thickness m to true range R_0 (fractional range). Curves for 0·3 MeV up to 0·7 MeV are shown; these normalize to a single curve like the transmission curves if normalized in height over their evident linear sections. The curves show a broad maximum at $m/R_0 \sim 0{\cdot}2$, while the extrapolation to zero output yields $m/R_0 = 0{\cdot}755$. This is actually in very good agreement with results incorporated in the Katz and Penfold (1952) relationship. Ionization in depth results, using a silver foil and silver reflector are shown in figure 5 (*b*).

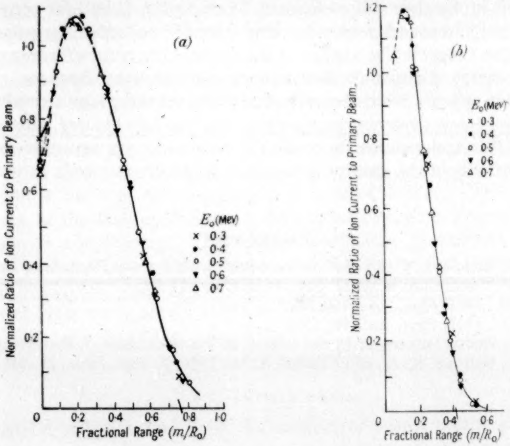

Figure 5. Ionization in depth curve (*a*) for aluminium, (*b*) for silver.

§ 7. Discussion

The results presented in this paper indicate that the discrepancy between range measured by collector cup and the Katz and Penfold range is not simply explicable in terms of low energy secondary emission or geometrical effects. Some independent confirmation of voltage measurement is obtained in the fact that the present ion chamber results for aluminium show excellent agreement in extrapolation intercept, and good agreement in shape, with the results of Frantz at 0·5 MeV. Further, this extrapolation intercept is in agreement with the Katz and Penfold relationship which, in turn, incorporates results of Trump, Wright and Clarke taken by a similar method. These measurements were, however, taken at 2·0 and 3·0 MeV. Similar measurements of Trump, Van de Graaff and Cloud in the range 0·5–1·5 MeV appear to yield the extrapolation intercept 0·77, showing fair agreement with the Katz and Penfold relationship. However, detailed comparison in this case is not justified since a steel h.t. electrode was used throughout the latter work.

The lower range from collector cup measurement, compared with that from shallow ionization chamber measurement, is again found in the present work in the case of silver, where the difference is about 10%. This type of result is further supported by comparison of the present collector cup range values with the shallow ion chamber range values of Trump *et al.* (1940) for copper, and of Frantz for beryllium and gold. In each case, the collector cup measurements yield a shorter range. The shapes of the curves obtained by Frantz agree with theoretical energy dissipation distributions calculated by Spencer.

Finally, it appears from the reproducibility, of the present results and the demonstrated insensitivity to geometry which can be obtained, that foil transmission measurement could be made into a simple, yet sensitive method for energy calibration of the electron beam from an accelerator such as was used for this work.

REFERENCES

AGU, B. N. C., BURDETT, T. A., and MATSUKAWA, E., 1958, *Proc. Phys. Soc.*, **71,** 201.
KATZ, L., and PENFOLD, A. S., 1952, *Rev. Mod. Phys.*, **24,** 28.
SELIGER, H. H., 1955, *Phys. Rev.*, **100,** 1029.
SPENCER, L. V., 1955, *Phys. Rev.*, **98,** 1597.
TRUMP, J. G., VAN DE GRAAFF, R. J., and CLOUD, R. W., 1940, *Amer. J. Roentgenol.*, **43,** 728.
TRUMP, J. G., WRIGHT, K. A., and CLARKE, A. M., 1950, *J. Appl. Phys.*, **21,** 345.

The Electrical Properties of Bismuth Telluride

By R. MANSFIELD and W. WILLIAMS
Physics Department, Bedford College, London

MS. received 2nd June 1958

Abstract. Measurements of the electrical conductivity, Hall coefficient, thermoelectric power and Nernst coefficient on specimens cut from zone melted Bi_2Te_3 and on a single crystal are described. The current flow was parallel to the cleavage planes and the galvanomagnetic effects of the single crystal were measured with the magnetic field perpendicular and parallel to the cleavage planes. For the other specimens the Hall and Nernst coefficients were measured with the magnetic field perpendicular to the cleavage planes. The temperature range was 100°K to 600°K and specimens with a wide variation of impurity content were used. Analysis of the thermoelectric power and conductivity in the extrinsic range indicated that the specimens were partially degenerate, and when allowance is made for this, the temperature dependence of mobility is $T^{-1\cdot63}$ for electrons and $T^{-1\cdot91}$ for holes. In the high temperature range the conductivity measurements yield a value of the energy gap at 0°K of 0·21 ev. The temperature dependence of the Hall coefficient in the extrinsic range is anomalous and the explanation is not known. The Nernst coefficient Q exhibits the general behaviour expected for a semiconductor, and it is shown that it obeys a relation which can be derived from Moreau's relation, Q being proportional to $TR\sigma d^2E/dT^2$ (thermoelectric power $= dE/dT$, Hall coefficient $= R$, conductivity $= \sigma$).

---

§ 1. Introduction

Bismuth telluride has been the subject of many recent papers. It is a semiconductor and impurities can be introduced so as to produce both n- and p-type material. Because of its small energy gap the transition from extrinsic to intrinsic conduction can be studied readily and the phenomena associated with ambipolar diffusion of electrons and holes can be examined. It has interesting thermoelectric properties and has been used in thermoelectric devices. The present paper describes measurements of the electrical conductivity, Hall coefficient, Nernst coefficient and thermoelectric power over the temperature range 100°K to 600°K on specimens having widely differing impurity content.

§ 2. Experimental Procedure

With the exception of R8, the specimens were cut from suitably doped zone melted ingots of Bi_2Te_3. Goldsmid (1958) has reported that such ingots are usually polycrystalline with, however, the *c* axis of the individual crystals perpendicular to the direction of zone refining; he also reports that no difference between the properties of single crystals and of the zone refined material has been found. Specimen R8 was cut from a single p-type crystal of doped Bi_2Te_3.

All measurements were made with the current flow parallel to the cleavage plane. Initial experiments were made to investigate the uniformity of the specimens by determining the potential gradient down the length of the specimen with a constant current flowing. Only those results obtained with specimens having a uniform potential gradient or constant conductivity down their length are reported here.

Difficulty was experienced in making good current contacts to the specimens. Because of the high temperature readings soldered contacts were not possible and pressure contacts had to be used. These were spring loaded and the contacts were of silver or platinum. The potential probes were in the form of thermocouples, which were required for the measurement of the thermoelectric power and Nernst coefficient. They were made by silver soldering 40 s.w.g. T_1T_2 alloys. The junctions were made as small as possible and were pressed against the side of the specimen. When the electrical contact so formed was improved by a condenser discharge, a satisfactory probe was produced which was suitable over the whole temperature range studied. A saturated vapour pressure thermometer was used to calibrate the thermocouples below room temperature, and above room temperature the standard calibration was checked and found to be satisfactory. The Hall probes were of T_1 alloy, also spot-welded to the specimen. The magnetic field was usually perpendicular to the cleavage plane, except in the case of R8 for which measurements were made of the galvanomagnetic effects with the field both perpendicular and parallel to the cleavage plane. The magnetic field was determined using the Hall effect of a specimen of InSb which had been calibrated over a range of magnetic fields using a proton resonance method.

The conventional d.c. method was used for the measurement of conductivity and Hall coefficient. The thermoelectric power and Nernst effect were determined by having a small temperature gradient down the specimen produced by a heater placed at one end. The temperature difference between the two thermocouples was determined and the e.m.f. between the T_1 arms of the thermocouples was measured. Hence the thermoelectric power of Bi_2Te_3 relative to T_1 alloy was calculated. This result was then corrected to give the thermoelectric power of Bi_2Te_3 relative to lead, using the previously determined thermoelectric power of T_1 relative to lead. A check was made by repeating some of the readings using the T_2 alloy and correcting in the same manner. The results obtained were independent of the intermediate metal used, and both thermoelectric power and Nernst effect appeared independent of the temperature gradient over the range 5° to 40° per centimetre. The galvanomagnetic effects were determined under approximately adiabatic conditions.

It is difficult to assess the accuracy of the measurements. As is usual when measuring the bulk electrical properties of solids, the accuracy with which one can measure the change of the electrical properties with temperature appears much greater than the measurement of the absolute quantities, which depend on the determination of the dimensions of the specimen, the distance between the probes and the crystalline state of the specimen. However, in the case of Bi_2Te_3, because of the large thermoelectric power, the use of a d.c. method introduces additional errors, the importance of which are difficult to estimate. The influence of the Peltier effect on the conductivity can be reduced by measurements on the centre portion of a long specimen. This was possible for R5 and R8. In each case the conductivity was determined by measuring the change of potential between the probes on reversing the current as quickly as possible.

Preliminary experiments showed that irreversible effects were produced on heating if copper was in contact with the specimen; such an effect has been reported by Goldsmid (1958). With the contacts used subsequently, the readings of the conductivity, Hall coefficient and Nernst coefficient were reproducible. However, in the case of the thermoelectric power, the value obtained was dependent on the surface conditions. For specimen R8 the room temperature value of the thermoelectric power was reduced by 10%, after heating the specimen to 620°K. After cleaning the surface the original value and variation with temperature could be obtained, although values of the thermoelectric power at room temperature differing by 20% were obtained when the thermocouples were in contact with different parts of the specimen.

§ 3. Results and Discussion

The temperature variation of the various electrical properties are illustrated in figures 1 to 4.

In many respects the results are in agreement with the results obtained with other semiconductors and the properties can be explained in general terms by the usual theory. However, Drabble, Groves and Wolfe (1958) have pointed out that the anisotropic structure of bismuth telluride appreciably affects the derivation from the experimental results of the various parameters such as mobility and concentration of charge carriers. Furthermore, the values of the thermoelectric power indicate that there is a transition from non-degenerate to degenerate statistics over the extrinsic range. Consequently, only a qualitative discussion of the results can be given at this stage.

The temperature dependence of the Hall coefficient is anomalous and for this reason it is more useful to consider the conductivity mobility (Drabble *et al.* 1958) rather than the Hall mobility. Consequently, in figure 1 the conductivity has been plotted on a double logarithmic scale. The shape of the curve indicates that below 300°K the specimens are extrinsic, and if it is assumed that the concentration of charge carriers is constant in this region, then this figure gives the temperature dependence of the conductivity mobility. The n-type specimens R7 and R3·21 have widely differing impurity content, and it is seen that the temperature dependence of mobility is different for these specimens. R7 behaves like a metal with mobility proportional to T^{-1}, whereas R3·21 has the temperature dependence of a semiconductor, $T^{-1\cdot 5}$. This difference is what would be expected if there is a transition from degenerate to non-degenerate statistics.

In order to discuss the effect of degeneracy it is necessary to know the Fermi level. This can be calculated directly from the thermoelectric power provided the energy dependence of the relaxation time is a simple power law $\tau \sim \epsilon^r$. The value of r which is most consistent with the observations is that given by scattering of the charge carriers by acoustical modes $(r = -\frac{1}{2})$. It might be considered that for a compound semiconductor scattering by optical modes should be important, however it is likely that the Debye temperature is low for Bi_2Te_3 and consequently the high temperature approximation would be applicable. In this case $r = \frac{1}{2}$ and the temperature variation of mobility would be much less rapid than that observed.

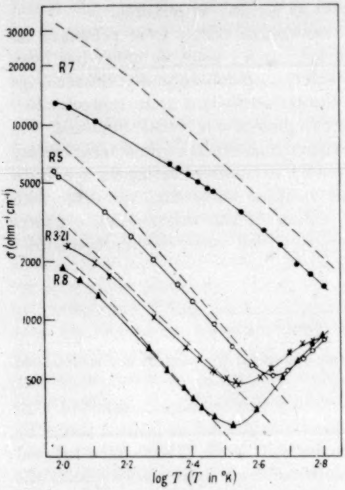

Figure 1. Electrical conductivity of Bi_2Te_3.

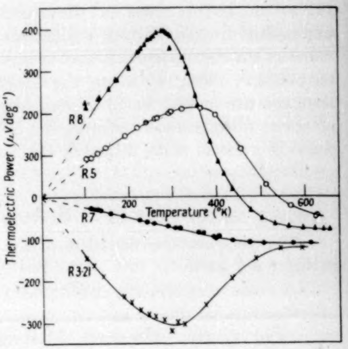

Figure 2. Thermoelectric power of Bi_2Te_3.

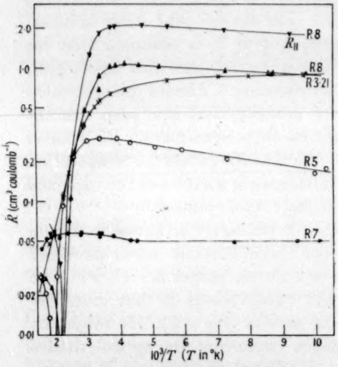

Figure 3. Hall coefficient of Bi_2Te_3. $R_{\|}$ obtained with field parallel to cleavage plane; other results obtained with field perpendicular to the cleavage plane.

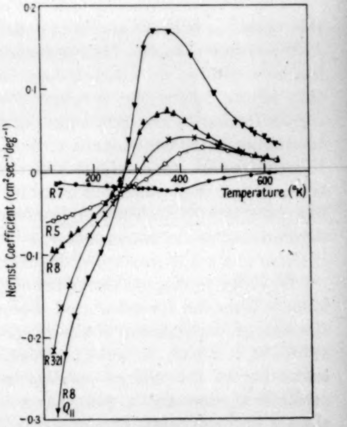

Figure 4. Nernst Coefficient. $Q_{\|}$ obtained with field parallel to cleavage plane; other results obtained with field perpendicular to cleavage plane.

Assuming therefore a scattering mechanism giving $r = -\frac{1}{2}$, the reduced Fermi level η^* was determined from the thermoelectric power, using the equation

$$\frac{dE}{dT} = -\frac{\boldsymbol{k}}{\boldsymbol{e}}\left(\frac{2F_1(\eta^*)}{F_0(\eta^*)} - \eta^*\right), \qquad F_m(\eta^*) = \int_0^\infty \frac{\eta^m \, d\eta}{1 + \exp(\eta - \eta^*)}$$

and the conductivity σ_0 which would be obtained if there were no degeneracy was calculated from the measured conductivity σ, using the expression

$$\sigma_0 = \sigma \frac{2F_{1/2}(\eta^*)}{\sqrt{\pi} F_0(\eta^*)}.$$

The derived curves in figure 1 show the values of σ_0. It is seen that for the two n-type specimens the mobility varies as $T^{-1\cdot63}$. The temperature dependence of the two p-type specimens differs slightly, being $T^{-2\cdot12}$ for R5 and $T^{-1\cdot94}$ for R8. The latter value, obtained on a single crystal, is probably more reliable.

The energy gap between valence and conduction bands can be calculated from the high temperature conductivity measurements, provided that the contribution to the conductivity due to extrinsic carriers is small in this range. Black *et al.* (1957) obtained a value of the energy gap at the absolute zero of temperature $E_G = 0\cdot16$ ev from the slope of $\log \sigma$ against $1/T$. Goldsmid (1958), taking into account the departure of the mobility from the expected $T^{-1\cdot5}$ dependence, also obtained a value of 0·16 ev. However, Satterthwaite and Ure (1957) and Shigetomi and Mori (1956) obtained a value of 0·2 ev by calculating np/T^3 from conductivity and Hall coefficient measurements. This method might be criticized because of its dependence on the relation $R = 3\pi/8n\boldsymbol{e}$. However, it is possible to obtain the temperature dependence of np/T^3 from the conductivity without using the Hall coefficient as follows. For material which is p-type in the extrinsic range

$$\sigma = n\boldsymbol{e}u_n + p\boldsymbol{e}u_p, \qquad n = p - p_s$$

hence

$$np = (p - p_s)p$$

and

$$\frac{np}{T^3} = \frac{1}{\boldsymbol{e}^2(u_n + u_p)^2 T^3}(\sigma - \sigma_s)(\sigma + b\sigma_s) = N_c N_v \exp(-E_G/\boldsymbol{k}T)$$

where $\sigma_s = p_s \boldsymbol{e} u_p$ is the extrapolated extrinsic conductivity, N_c and N_v are the density of states in the conduction and valence bands, and b is the ratio of the mobilities u_n and u_p of electrons and holes. A similar expression is obtained for n-type extrinsic material with $1/b$ substituted for b. Specimen R8, the specimen with the least concentration of extrinsic carriers, was analysed using this equation. It was assumed that u_n was proportional to $T^{-1\cdot63}$ and u_p to $T^{-1\cdot94}$. The ratio of mobilities was considered to be close to unity and was determined by assuming $b = 1$ at 380°K. The reason for this assumption is that a sign reversal of the Hall effect is observed in the p-type specimens shown in figure 3, and has also been observed by Shigetomi and Mori (1956), indicating that $b > 1$ above 430°K, whereas Satterthwaite and Ure, using n-type specimens with low impurity content, find a reversal in the Hall coefficient, indicating that $b < 1$ below 320°K. The value of the energy gap obtained by this method was 0·21 ev. It is probable that the lower value obtained by authors using the $(\log \sigma, 1/T)$ plot was because the condition $\sigma \gg \sigma_s$ was not satisfied. Thus in the case of R8, figure 5 shows the measured conductivity σ at high temperatures. Also shown are the extrapolated extrinsic conductivity obtained from figure 1 and the calculated intrinsic conductivity σ_i obtained from the equation $\sigma_i = (\sigma - \sigma_s)(\sigma + b\sigma_s)$. It is seen that the graph of the measured conductivity appears linear and this linear portion gives $E_G = 0{\cdot}16$ ev (when $\log \sigma T^{0{\cdot}33}$ is plotted against $1/T$, $E_G = 0{\cdot}19$ ev), in agreement with other authors who used this method. However, in the case of specimen R8, the condition $\sigma \gg \sigma_s$, which is required to estimate the energy from conductivity measurements directly, was not satisfied.

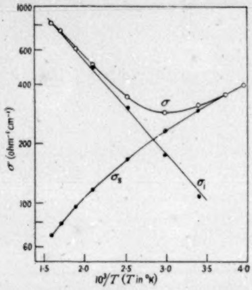

Figure 5. High temperature conductivity of R8 (single crystal).

On the assumption of a constant concentration of carriers in the extrinsic range, the isothermal Hall coefficient should be almost independent of temperature up to 300°K. Figure 3 shows, however, that for the p-type specimens there is a decrease in R and for R3·21 an increase as temperature decreases. There should be a slight change due to the effect of degeneracy which can be calculated using the expression (assuming $r = -\frac{1}{2}$)

$$R = \frac{x}{ne} \ldots, \qquad x = \frac{3}{4} \frac{F_{1/2}(\eta^*) F_{-1/2}(\eta^*)}{\{F_0(\eta^*)\}^2}.$$

The effect is a small decrease in the Hall coefficient, which in the case of R5 is 8% as the temperature changes from 300°K to 100°K and does not explain the observed decrease.

Now the Hall coefficient was measured under conditions which approximate to adiabatic rather than isothermal conditions, and because of the large thermoelectric power it is possible that there will be an appreciable difference between the adiabatic and isothermal coefficients. The difference arises from a transverse temperature gradient due to the Ettingshausen effect which, together with the thermoelectric effect, gives rise to a voltage which is combined with the Hall voltage. On applying the magnetic field the transverse voltage should change as the temperature gradient is established. Experiments to observe such a change were unsuccessful and any effect must have occurred during the interval when the field was established or removed (2 seconds). Because of the simple thermodynamic relation between the Ettingshausen and the Nernst coefficients, $P = QT/K$ where K is the thermal conductivity, when $Q = 0$ the two Hall coefficients R_a and R_i will be identical, and this condition is satisfied at approximately 300°K. At lower temperatures the Ettingshausen effect should be negative and consequently for both n- and p-type material $R_a > R_i$. The anomalous decrease in the Hall coefficient of p-type material as the temperature is decreased from 300°K to 100°K cannot therefore be explained by this effect. In fact, the anomaly becomes even larger if there is a difference between the two coefficients. Experiments were carried out to test whether this anomaly could be due to a dependence of R on magnetic field. At room temperature, however, the Hall coefficient of R5 was independent of magnetic field up to 14000 gauss. Finally, Drabble, Groves and Wolfe (1958) have shown that an anisotropic factor has to be introduced into the equation for the Hall coefficient and there is a possibility of a degeneracy or temperature dependence of this factor.

The temperature variation of the Nernst coefficient shown in figure 4 is in rough agreement with theory. In the extrinsic range the Nernst coefficient is negative and increases as the temperature decreases. For a semiconductor in the extrinsic range the Nernst coefficient should be negative if r is negative ($\tau \sim \epsilon^r$) and should be proportional to the mobility. It is found, however, that the Nernst coefficient does not vary so rapidly with the temperature as the mobility, and this is to be expected if the specimens become degenerate.

A comparison of figures 2 and 4 is of interest. For the specimens which show mixed conduction it is found that the temperature for which $Q=0$ coincides with the maximum of the thermoelectric power, and that the temperature for which the Nernst coefficient is a maximum coincides with the point of inflexion of the thermoelectric power. This would suggest a simple relation between Q and d^2E/dT^2. Now Moreau proposed a relation between the Nernst coefficient, Thomson coefficient μ, Hall coefficient and electrical conductivity which is as follows (Bridgman 1924: a negative sign has been introduced because of the different sign convention of the thermoelectric effects):

$$Q_0 = -\mu R\sigma = -T\frac{d^2E}{dT^2}R\sigma$$

since $\mu = T\,d^2E/dT^2$.

In the table are compared the values of Q_0 deduced from the above formula with the experimental values Q_E and shows that over a wide variation of Q_E the ratio Q_E/Q_0 is constant. The actual value of the constant depends on the measurements of the absolute values of the various electrical properties and the cumulative error involved will be large. However, there is an indication that the constant increases with impurity content. This relation is not obeyed in the intrinsic range.

Measurements of R and Q with the magnetic field parallel to the cleavage plane were made on specimen R8 and are shown in figures 3 and 4. The ratio of the Hall coefficient for the two orientations of the field is $2{\cdot}0 \pm 0{\cdot}1$ and is independent of temperature. A similar result is obtained for the Nernst coefficient with the ratio $2{\cdot}4 \pm 0{\cdot}1$. Measurement of the ratio of the electrical conductivity with current flow parallel and perpendicular to the cleavage plane was made on n-type material. The ratio is 3·9. Similar results have been obtained by Drabble *et al.* (1958) for the Hall coefficient and conductivity.

§ 4. CONCLUSIONS

The results obtained for the conductivity, Hall coefficient and thermoelectric power confirm those obtained by other authors. The variation of the Hall coefficient with temperature in the extrinsic range is anomalous and the explanation

Specimen	R 3·21			R 5			R 7			R 8		
T (°K)	Q_0	Q_E	Q_E/Q_0	Q_0	Q_E	Q_E/Q_0	Q_0	Q_E	Q_E/Q_0	Q_0	Q_E	Q_E/Q_0
120	−0·281	−0·169	0·60	−0·096	−0·056	0·58	−0·016	−0·014	0·88	−0·228	−0·090	0·39
160	−0·189	−0·110	0·58	−0·070	−0·049	0·70	−0·016	−0·015	0·94	−0·202	−0·071	0·35
240	−0·073	−0·040	0·55	−0·052	−0·033	0·63	−0·017	−0·017	1·00	−0·124	−0·029	0·23
320				−0·017	−0·010	0·59	−0·017	−0·020	1·17	+0·166	+0·055	0·33
400	+0·038	+0·040	1·05	+0·030	+0·021	0·70	−0·016	−0·022	1·37	+0·036	+0·065	1·80
480	+0·015	+0·033	2·2	+0·016	+0·028	1·7	−0·003	−0·010	3·3	0	+0·038	—

is not known. The Nernst coefficient agrees qualitatively with theory and there appears to be an interesting relation between the various electrical properties except at high temperatures.

Further measurements on the isothermal rather than adiabatic effects would be of interest. The use of an a.c. method for measuring the Nernst coefficient would be difficult since a large alternating magnetic field would be required. A simple arrangement would be to use probes of the same material as the specimen.

ACKNOWLEDGMENTS

The authors are grateful to the General Electric Company and the Associated Electrical Companies for supplying the specimens of Bi_2Te_3 used in this investigation. This work was aided by a grant from the research fund of the University of London.

REFERENCES

BLACK, J., CONWELL, E. M., SEIGLE, L., and SPENCER, C. W., 1957, *J. Phys. Chem. Solids*, **2**, 240.
BRIDGMAN, P. W., 1924, *Phys. Rev.*, **24**, 644.
DRABBLE, J. R., GROVES, R. D., and WOLFE, R., 1958, *Proc. Phys. Soc.*, **71**, 430.
GOLDSMID, H. J., 1958, *Proc. Phys. Soc.*, **71**, 633.
SATTERTHWAITE, C. B., and URE, R. W., 1957, *Phys. Rev.*, **108**, 1164.
SHIGETOMI, S., and MORI, S., 1956, *J. Phys. Soc. Japan*, **11**, 915.

The Colour of Thin Oxide Films on Metals

By A. M. MacSWAN
Caswell Research Laboratories, The Plessey Co. Ltd., Caswell, Towcester, Northants.

Communicated by F. Llewellyn Jones; *MS. received 27th February* 1958, *and in revised form* 14*th July* 1958

Abstract. The colours observed when white light is reflected from metals covered with a thin oxide film are considered, and a theory of selective transmission of light into the metal is developed. The Smith Chart is used to calculate the variation of the composition of the reflected light with the thickness of the oxide film.

§ 1. Introduction

Oxide films may be formed on the surface of many metals by either thermal or electrolytic treatment. When viewed in white light, the reflected light may be coloured; with some metals, e.g. tantalum and iron, the colours may be quite pronounced whereas with others such as aluminium the colours are barely visible. Spectrophotometric analysis of the reflected light shows that certain colours are missing or depleted.

V.
19

§ 2. Previous Explanation of Colour Formation

A theory of the origin of these colours has been given by Charlesby and Polling (1955). This theory considers the interference between the ray reflected at the front surface and those which emerge from the oxide layer after multiple reflection between the oxide–metal and oxide–air interfaces; the layer is assumed to be transparent and the metal a perfect reflector. They conclude that the production of the colours depends chiefly upon the reflectivity of the air–oxide interface. No account is taken of the phase difference introduced in the traversal of the oxide film and this leads to an incorrect value for the sum of the emergent energy. Since no mechanism by which energy may be absorbed is postulated, this theory involves the 'destruction of energy' by interference, which is physically impossible. The correct application of the multiple reflection theory to a transparent layer on a perfect reflector gives complete reflection for all values of the film thickness.

§ 3. Selective Transmission

In order to account for the colour of the film it is necessary to know where the missing energy has gone.

Since the metal is not a perfect reflector, energy will be transmitted into it; the actual amount depending upon the optical constants of the film and metal and on the thickness of the oxide film.

It is shown in § 7.2.1 that if a layer of refractive index n' and thickness d is deposited on a metal of constants (n, k) perfect matching (i.e. no reflected power) will occur when

$$n' = \frac{[(n+n')^2+k^2]^{1/2}+[(n-n')^2+k^2]^{1/2}}{[(n+n')^2+k^2]^{1/2}-[(n-n')^2+k^2]^{1/2}} \qquad \ldots\ldots(1)$$

and

$$n'd = \frac{\lambda}{4}\left(2f+\frac{1}{\pi}\tan^{-1}\frac{2kn'}{n'^2-n^2-k^2}\right) \qquad \ldots\ldots(2)$$

where $f=0, 1, 2, 3, \ldots$.

When equation (1) is not obeyed, there will be no wavelength at which the reflection coefficient is zero. There will, however, still be wavelengths, given by equation (2), at which the reflection coefficient is a minimum. The value of the power reflection coefficient at the minimum is given by equation (9) of § 7.2.2.

Usually the incident radiation will consist of white light and thus the reflected light will comprise the incident light less the matched components. This is the explanation of the dark bands observed in the spectrophotometric analyses; it is also the explanation of the colour of the oxide films.

For tantalum at $0{\cdot}58\,\mu$, $n=2{\cdot}05$ and $k=1{\cdot}13$ and $n'=2{\cdot}5$ (Hodgman 1957) giving $|\overline{R}|^2=0{\cdot}028$. For aluminium at $0{\cdot}59\,\mu$, $n=1{\cdot}44$, $k=3{\cdot}70$ and $n'=1{\cdot}8$ leading to $|\overline{R}|^2=0{\cdot}95$. Thus, for tantalum the colours should be pronounced, whereas for aluminium they should be very faint. This is in accordance with observation.

§ 4. THE FORMATION OF THE FILM COLOURS

In order to give a systematic account of the sequence of colours that is observed with increasing thickness of oxide film, the power reflection coefficient has been calculated as a function of wavelength, in the visible region, for various thicknesses of oxide film. This has been done for a metal with refractive index 3·0 and absorption index 1·41 coated with an oxide film which has a refractive index 2·0; these constants give exact matching. The reflection coefficients have been evaluated by means of the Smith chart technique as described in §7.1. The graphs of power reflection coefficient versus wavelength are shown in figure 1, (*a*) and (*b*).

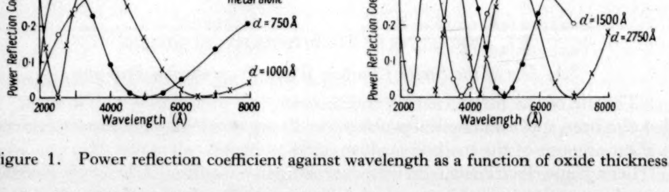

Figure 1. Power reflection coefficient against wavelength as a function of oxide thickness.

For the thinnest film considered, 250 Å, the only effect is a slight diminution in the violet–blue end of the spectrum leading to the reflected light having a faint straw colour. At 400 Å, the trough 1 has moved into the visible region and the reflected light should be purple in colour. At 1000 Å, the trough 1 is at the red end and so the light will be blue. Further increase in thickness will result in a further blue colour until at about 1500 Å the reflected light should be nearly clear.

As the peak A moves through the visible towards the red, the trough 2 moves through the visible and the straw, brown and mauve will be repeated. A further series of colours is caused by a sharper peak B moving through the visible; these colours are purer than those of the previous series. Prediction of colour from the graph becomes more complicated when the film thickness is greater than about 3000 Å. At great thicknesses, the number of peaks and troughs in the visible region is very large and the resulting film should have no pronounced colour.

§ 5. Oxide Film with Thin Reflecting Coating

It is of interest to discuss one further phenomenon which has a resemblance to the previous problem.

It has been noticed that with metals which show faint colours, the colour of the reflected light can be made more brilliant if the surface of the oxide film is coated with a thin, semi-transparent layer of a highly reflecting metal such as gold, silver or aluminium. This effect is the optical analogue of a phenomenon well known at microwave frequencies, namely that if a thin conducting film is placed one quarter (or an odd number of quarter) wavelengths in front of a highly reflecting surface, if the thickness and conductivity of the film are correct, the incident radiation will be absorbed (Ramo and Whinnery 1953). In the optical case, the radiation consists of white light and so the reflected light will have a coloured appearance.

In this case the energy is not transmitted into the base metal but it is absorbed in the thin conducting film which is placed in a region of high electrical field (Wood 1934, p. 207).

§ 6. Reduction of Reflection at a Metal Surface

While the discussion has, so far, been confined to the colours of oxide films, it is obvious that the present theory may be applied to the 'blooming' of light sensitive devices such as photocells, when it is desirable to reduce the amount of light reflected. Some indication of the additional quantity of light which can be introduced may be obtained from figure 1.

§ 7. Derivation of Conditions for Blooming

7.1. *Use of the Smith Chart in Wave Transmission Problems*

The use of the Smith chart in transmission line problems is well known. It has also been applied to optical problems by Leurgans (1951), but for convenience a short account of the method is given here.

Let a plane electromagnetic wave travelling in a medium of dielectric constant ϵ_1, and magnetic permeability μ_1, be incident normally upon another medium with constants (ϵ_2, μ_2).

Let the amplitude of the electric vector of the incident wave just before it reaches the interface be 1, and that of the reflected wave at the same point R. Then, if a and c are the amplitudes of the incident and reflected waves just inside

(ϵ_2, μ_2), the conditions for continuity of the electric and magnetic fields at the interface are

$$1+R=a+c\,; \quad \left(\frac{\epsilon_1}{\mu_1}\right)^{1/2}(1-R)=\left(\frac{\epsilon_2}{\mu_2}\right)^{1/2}(a-c).$$

whence

$$\frac{1+R}{1-R}=\frac{(\epsilon_1/\mu_1)^{1/2}}{(\epsilon_2/\mu_2)^{1/2}}\frac{a+c}{a-c}=\frac{Z_2}{Z_1}\frac{a+c}{a-c}$$

where $(\mu_r/\epsilon_r)^{1/2}=Z_r=$ characteristic impedance of medium r.

The quantity (sum of electric fields)/(difference of electric fields) is called the impedance and it is seen that the product of impedance and characteristic impedance is a constant at an interface.

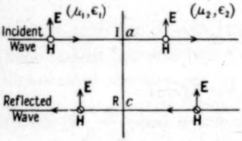

Figure 2. Reflection at an interface.

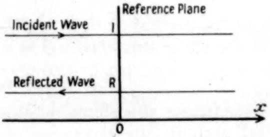

Figure 3. Propagation through medium (n, k).

Consider now an incident and a reflected wave travelling in a medium of refractive index n, absorption coefficient k, where $(\mu\epsilon)^{1/2}=n-ik$. It is necessary to know the rule for determining the impedance $Z(x+d)$ at $x+d$ from its value $Z(x)$ at x.

The value of the incident wave at any x will be

$$\mathscr{I}\exp\left\{iw\left(t-\frac{n-ik}{c}x\right)\right\}$$

and of the reflected wave

$$\mathscr{R}\exp\left\{iw\left(t+\frac{n-ik}{c}x\right)\right\}$$

where $\mathscr{I}$ and $\mathscr{R}$ are the amplitudes of the waves at the origin. The impedances at x and $x+d$ will be

$$Z(x)=\frac{\mathscr{I}+\mathscr{R}\exp(\alpha x)}{\mathscr{I}-\mathscr{R}\exp(\alpha x)}, \quad Z\,(x+d)=\frac{\mathscr{I}+\mathscr{R}\exp(\alpha x)\exp(\alpha d)}{\mathscr{I}-\mathscr{R}\exp(\alpha x)\exp(\alpha d)}.$$

where α has been written for $2w(k+in)/c$.

Since $Z(x)=(1+R)/(1-R)$ where $R=$reflection coefficient at x, it is seen that the reflection coefficient at $x+d$ may be formed from that at x by multiplying it by $\exp(\alpha d)$ when the direction of transformation is in the direction of the incident wave, d is positive and when with the reflected wave, negative. The impedance is found in the usual way.

The quantity R is a complex number which may have any modulus between 0 and 1. The Smith chart consists of a polar plot of $R=|R|\exp(+i\theta)$, $0\leqslant|R|\leqslant 1$, and within this circle, the values of $Z=Z_r+iZ_i$ where Z_r and Z_i are the real and imaginary parts of Z. A sketch of the chart is given in figure 4.

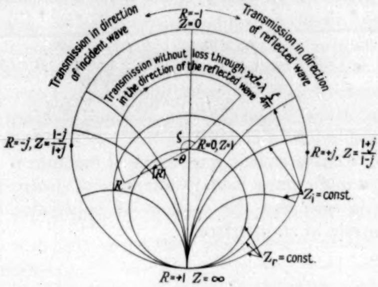
Transmission in direction of incident wave
R=-1
Z=0
Transmission in direction of reflected wave
Transmission without loss through λ=2πx in the direction of the reflected wave
$\frac{\zeta}{4\pi}$
$R=-j, Z=\frac{1-j}{1+j}$
ζ
R=0, Z=1
$-\theta$
|R|
R
$R=+j, Z=\frac{1+j}{1-j}$
Z_i=const.
Z_r=const.
R=+1 Z=∞

Figure 4. The Smith chart.

7.2. *Blooming of a Non-perfect Metal*

Consider an absorbing medium (n, k) which has a layer $(n', 0)$ directly in contact with it, the thickness of the lossless layer being d; electromagnetic radiation of wavelength λ is incident upon this system.

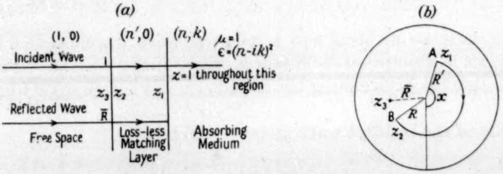
(a)
(1, 0)
(n′,0)
(n,k)
$\mu=1$
$\epsilon=(n-ik)^2$
Incident Wave
z=1 throughout this region
z_3
z_2
z_1
Reflected Wave
$\bar{R}$
Free Space
Loss-less Matching Layer
Absorbing Medium
(b)
A z_1
R'
$\bar{R}$
x
z_3
B
R
z_2

Figure 5. (*a*) Dielectric system. (*b*) Representation of dielectric system on Smith chart.

The problem will be treated here by the Smith chart technique. Transformation from medium (n, k) to $(n', 0)$ gives an impedance $z_1 = n'/(n-ik)$ and the associated reflection coefficient $R' = (z_1-1)/(z_1+1)$.

Since $(n', 0)$ is lossless, transmission through it is represented by the circular arc AB and the impedance z_2 just inside $(n', 0)$ is $z_2 = (1+R)/(1-R)$ where $|R'| = |R|$.

On emerging into free space, the impedance is z_3 where $z_3 = z_2/n'$ and the reflection coefficient of the system is

$$\bar{R} = \frac{z_3-1}{z_3+1} = \frac{1+R-n'(1-R)}{1+R+n'(1-R)}$$

which since $R = R_r + iR_i$ reduces to

$$\bar{R} = \frac{1-n'+R_r(1+n')+iR_i(1+n')}{1+n'+R_r(1-n')+iR_i(1-n')}. \qquad \ldots\ldots(3)$$

The power reflection coefficient of the system is

$$|\bar{R}|^2 = \frac{(1-n')^2+(1+n')^2|R|^2+2R_i(1-n'^2)}{(1+n')^2+(1-n')^2|R|^2+2R_i(1-n'^2)}.$$

7.2.1. *Perfect matching.*

For perfect matching to occur, it is necessary that $\overline{R} \equiv 0$. It is evident that for perfect matching, the impedance just outside the front face must be unity and therefore the impedance just inside the oxide n', and it must lie on the same circle as the point corresponding to $n'/(n-ik)$. The angular distance in a clockwise direction between these points gives the thickness of the oxide film.

Equation of the real and imaginary parts of (3) to zero gives

$$R_i = 0; \; R_r = \frac{n'-1}{n'+1} \text{ or } R_r = \frac{n'+1}{n'-1}$$

and since R_r is less than unity, the two conditions are

$$R_i = 0; \; R_r = \frac{n'-1}{n'+1}.$$

Thus $R = R_r = |R'|$ or $R = |R'| \exp(-i2\pi f)$ where $f = 0, 1, 2, 3, \ldots$

These conditions will be expressed in terms of the constants of the materials, the thickness of the lossless layer and the wavelength of the incident radiation.

$$R' = \frac{z_1-1}{z_1+1} = \frac{n'-n+ik}{n'+n-ik} = \left[\frac{(n-n')^2+k^2}{(n+n')^2+k^2}\right]^{1/2} \exp\left\{i\left(\tan^{-1}\frac{k}{n'-n} + \tan^{-1}\frac{k}{n'+1}\right)\right\}$$
$$= |R'| \exp(i \tan^{-1} x)$$

whence

$$R = |R'| \exp(i \tan^{-1} x) \exp\{-i(\tan^{-1} x + 2\pi f)\}. \qquad \ldots\ldots(4)$$

This angle $\tan^{-1} x + 2\pi f$ represents transmission through $(n', 0)$ in the direction of the reflected radiation. Since one half wavelength in the material corresponds to 2π then

$$n'd = \frac{\lambda}{4}\left(2f + \frac{1}{\pi}\tan^{-1}\frac{2kn'}{n'^2 - n^2 - k^2}\right), \qquad \ldots\ldots(5)$$

which is equation (2).

In all cases $\tan^{-1} x$ must be an angle between 0 and π, so that for the first order of matching, $n'd$ will be less than a quarter wave. (The only materials here considered have $\mu \equiv 1$ which is true for almost all materials at optical frequencies.)

The value of n' for perfect matching is found from $|R| = (n'-1)/(n'+1)$

$$\text{i.e. } n' = \frac{[(n'+n)^2+k^2]^{1/2} + [(n-n')^2+k^2]^{1/2}}{[(n'+n)^2+k^2]^{1/2} - [(n-n')^2+k^2]^{1/2}} \qquad \ldots\ldots(6)$$

which is equation (1).

7.2.2. *General case.*

Usually the oxide layer on a metal will not have the correct refractive index for perfect matching. In this case, it is necessary to consider the turning values of $|\overline{R}|^2$ subject to the condition that $R_r{}^2 + R_i{}^2 - |R|^2 = 0 = \phi(R_r, R_i)$.

These values are given by

$$d|\overline{R}|^2 + \eta \, d\phi = 0$$

$$\text{i.e. } \frac{\partial |\overline{R}|^2}{\partial R_i} + \eta \frac{\partial \phi}{\partial R_i} = 0 \quad \text{and} \quad \frac{\partial |\overline{R}|^2}{\partial R_r} + \eta \frac{\partial \phi}{\partial R_r} = 0. \qquad \ldots\ldots(7)$$

The first of equations (7) gives

$$R_i = 0$$

and the second

$$|\bar{R}|^2=\frac{(1-n')^2+(1+n')^2|R|^2+2|R|(1-n'^2)}{(1+n')^2+(1-n')^2|R|^2+2|R|(1-n'^2)}. \qquad \ldots\ldots(8)$$

Inserting the value of $|R|$ given by (4) in (8)

$$|\bar{R}|^2=\frac{(1-n')^2N_1+(1+n')^2N_2+2(1-n'^2)(N_1N_2)^{1/2}}{(1+n')^2N_1+(1-n')^2N_2+2(1-n'^2)(N_1N_2)^{1/2}} \qquad \ldots\ldots(9)$$

where N_1 has been written for $(n+n')^2+k^2$ and N_2 for $(n-n')^2+k^2$.

Since R_1 is still zero in this case, the condition for matching is given by (5) and the value of the power reflection coefficient by (9).

It is of interest to note that the condition $R_i=0$ is satisfied not only when $R_r=|R|$, but also when $R_r=-|R|$. This condition obviously corresponds to a maximum value of the reflection coefficient and will occur at a thickness one quarter of a wavelength (in the material) greater than that for extinction or a minimum. The maximum value of the reflection coefficient is

$$|\bar{R}|^2=\frac{(1-n')^2+(1+n')^2|R|^2-2|R|(1-n'^2)}{(1+n')^2+(1-n')^2|R|^2-2|R|(1-n'^2)}$$

and the thickness at which it occurs

$$n'd=\frac{\lambda}{4}\left(2f+1+\frac{1}{\pi}\tan^{-1}\frac{2kn'}{n'^2-n^2-k^2}\right)$$

where $f=0, 1, 2, \ldots$

§ 8. CONCLUSIONS

The origin of the colours observed when certain metals are covered with a thin oxide film has been considered, and it is suggested that the colours are due to selective transmission into the medium. This transmission depends on the optical properties of both the oxide film and the underlying metal and also on the thickness of the film. The results show that the effect is much more pronounced with certain metals than others.

ACKNOWLEDGMENTS

I wish to thank Professor R. W. Ditchburn for helpful discussion and I am indebted to the Plessey Company Limited, in whose laboratories the investigations were carried out, for permission to publish this paper.

REFERENCES

CHARLESBY, A., and POLLING, J. J., 1955, *Proc. Roy. Soc.* A, **227,** 434.
HODGMAN, C. D., 1957, *Handbook of Chemistry and Physics*, 38th edn (Cleveland, Ohio : Chemical Rubber Publishing Co.).
LEURGANS, P. J., 1951, *J. Opt. Soc. Amer.*, **41,** 714.
RAMO, S., and WHINNERY, J. R., 1953, *Fields and Waves in Modern Radio* (London: Chapman and Hall).
WOOD, R. W., 1934, *Physical Optics*, 3rd edn (London : Macmillan).

Apodization and Frequency Response with Incoherent Light

By J. A. MACDONALD

Department of Physics, Imperial College, London†

MS. received 14*th November* 1957, *and in revised form* 21*st May* 1958

Abstract. A study is made of the possibility of increasing the response of an optical system to a given spatial frequency by means of apodization, when the wave front aberrations and defocusing are supposed to be known.

By the usual methods of the calculus of variations, the condition for maximization of frequency response for variation of transparency is expressed as a functional equation, which may be approximated to by a linear second-order eigenvalue problem, for the transparency. Some examples are discussed.

§ 1. Introduction

Various authors (Straubel 1931, Dossier 1953) have shown that if the exit pupil of a perfect optical system is illuminated non-uniformly, by insertion of a suitable screen or otherwise, then the brightness of the outer Airy rings in the image of a point can be made less than with uniform illumination; this process is called apodization. A similar process is well known in radio antenna theory (Spencer 1955) where variation of illumination across an aperture is used to reduce side lobe power.

The frequency-response criterion for image assessment is a comparatively recent development in optics; it is therefore of interest to study apodization with the aim of maximizing the normalized frequency-response function. The paper deals with apodization from this point of view, and the calculations have been made on the supposition that a known amount of aberration and defocusing error is present. The notation is based on that of Hopkins (1955, 1957).

§ 2. Formulation of Problem

We consider the intensity distribution in the object plane to be resolved by Fourier analysis into component line structures of different azimuths and spatial frequencies; for a representative component, ψ specifies the azimuth and s the reduced spatial frequency, defined by $s=R\lambda/(n\sin\alpha)$, where R is the number of cycles per unit length measured across the component, λ the vacuum wavelength of the light, n the refractive index in the object space, and α the angle between the incident reference ray and the axis of the optical system.

The frequency response function is given by

$$D(s\cos\psi,\, s\sin\psi)=g(s\cos\psi,\, s\sin\psi)/g(0,0) \qquad \ldots\ldots(2.1)$$

$$g(s\cos\psi,\, s\sin\psi)=\int f(x+\tfrac{1}{2}s\cos\psi,\, y+\tfrac{1}{2}s\sin\psi)\times f^*(x-\tfrac{1}{2}s\cos\psi,\, y-\tfrac{1}{2}s\sin\psi)\,dS, \qquad \ldots\ldots(2.2)$$

---

† Now at Defence Standards Laboratories, Department of Supply, Australia.

where $f(x, y)$ denotes the pupil function, $f^*(x, y)$ its complex conjugate, and the integration may be regarded as being taken over the whole pupil plane. In addition,

$$f(x, y) = \tau(x, y) \exp\{ikW(x, y)\}, \qquad \ldots\ldots(2.3)$$

where $\tau(x, y)$ is the pupil transparency function (non-negative inside the pupil on its boundary, and zero outside) and $W(x, y)$ the wave aberration function.

We now assume that the system is axially symmetric, and write

$$x = r\cos(\phi+\psi), \quad y = r\sin(\phi+\psi), \quad \tau(x, y) = t(r), \qquad \ldots\ldots(2.4)$$

the pupil being bounded by $r = 1$; further, we confine ourselves to considering the mean value $\bar{D}(s)$ of the frequency response function as ψ (the angle of orientation of the structure) varies from $-\pi$ to π. Since the integrand of (2.2) is replaced by its complex conjugate when ψ is replaced by $\psi \pm \pi$, or when s is replaced by $-s$, it follows that $\bar{D}(s)$ is real and even in s; we therefore assume that $s \geqslant 0$.

Using substitutions from (2.3), (2.4) into (2.2), we find that

$$\begin{aligned} \bar{D}(s) &= \int_{-\pi}^{\pi} g(s\cos\psi, s\sin\psi)\, d\psi / 2\pi g(0, 0) \\ &= \int t(q)t(p)\Omega\, dS \Big/ \int \{t(r)\}^2 dS, \qquad \ldots\ldots(2.5) \end{aligned}$$

where $\qquad q = (r^2 + \tfrac{1}{4}s^2 + sr\cos\phi)^{1/2}, \quad p = (r^2 + \tfrac{1}{4}s^2 - sr\cos\phi)^{1/2}$,

and Ω is a function of position on the pupil, depending also on s and the functional form of the aberration; explicitly,

$$\begin{aligned} \Omega = \frac{1}{2\pi}\int_{-\pi}^{\pi} \cos\,[&kW\{r\cos(\phi+\psi) + \tfrac{1}{2}s\cos\psi, r\sin(\phi+\psi) + \tfrac{1}{2}s\sin\psi\} \\ &- kW\{r\cos(\phi+\psi) - \tfrac{1}{2}s\cos\psi, r\sin(\phi+\psi) - \tfrac{1}{2}s\sin\psi\}]\, d\psi. \qquad \ldots\ldots(2.6) \end{aligned}$$

If the wave front error is entirely due to defocusing and spherical aberration, then $W(x, y)$, $f(x, y)$, $f^*(x, y)$ are functions of r only and by (2.2) $g(s\cos\psi, s\sin\psi)$ is independent of ψ; it follows that in this case $\bar{D}(s) = D(s, 0)$.

Our aim is to maximize $\bar{D}(s)$ for variation of $t(r)$ as a function of r, when s and $W(x, y)$ are given. The condition that Ω shall be non-negative at all points of the pupil including the boundary is sufficient to ensure that $\bar{D}(s)$ will be maximized by a finite non-negative $t(r)$, as required in practice (for if $t(r)$ were not one-signed, then a larger value of $\bar{D}(s)$ would be obtained by replacing $t(r)$ by $|t(r)|$); since $W(x, y)$ is given, this condition implies that s must be less than some limiting value depending on $W(x, y)$.

§ 3. APPLICATION OF VARIATIONAL METHOD

In (2.5) we may change the variables of integration to p, q and obtain

$$\bar{D}(s) = \int t(q)t(p)\Omega J\, d\Sigma \int\Big/ \{t(p)\}^2 J\, d\Sigma, \qquad \ldots\ldots(3.1)$$

where we have used a shift of (x, y) origin in the denominator, and denoted the relevant Jacobian by J; the region Σ of integration consists of the region $p + q \geqslant s$, $|p - q| \leqslant s$ taken twice because to each pair of values p, q correspond two pairs of values x, $\pm y$.

We now replace $t(r)$ by $t(r) + \delta\{t(r)\}$, where $\delta\{t(r)\}$ is a permissible small change in $t(r)$; $\delta\{t(r)\}$ must vanish for $r > 1$, because of the condition that $t(r) = 0$ for $r > 1$.

The effect of this change is to replace $\bar{D}(s)$ by $\bar{D}(s)+\delta\{\bar{D}(s)\}$, where

$$\frac{\delta\{\bar{D}(s)\}}{\bar{D}(s)} \simeq \frac{2\int t(q)\delta\{t(p)\}\Omega J\,d\Sigma}{\int t(q)t(p)\Omega J\,d\Sigma} - \frac{2\int t(p)\delta\{t(p)\}J\,d\Sigma}{\int\{t(p)\}^2 J\,d\Sigma}. \quad \ldots\ldots(3.2)$$

In the first numerator on the right we have used the fact that Ω may be expressed as a symmetric function of p, q (for interchange of p, q is equivalent to changing the sign of s, and by (2.6) this leaves Ω unaltered). From (2.1), (2.2), $\bar{D}(s)$ is stationary ($\delta\{\bar{D}(s)\}\simeq 0$) for all permissible small changes $\delta\{t(r)\}$, provided that

$$\int t(q)\Omega J\,dq = \bar{D}(s)\int t(p)J\,dq, \quad \ldots\ldots(3.3)$$

where the range of integration with respect to q is determined by the above-mentioned region Σ. Since all permissible small changes vanish when the argument of the function is greater than 1, it follows that (3.3) (like similar subsequent equations) holds only when $p\leqslant 1$.

It is convenient at this stage to introduce an angular coordinate χ corresponding to p, such that $r\cos\phi = p\cos\chi+\frac{1}{2}s$, $r\sin\phi = p\sin\chi$. Then q, Ω, and the element of area in the (x, y) plane are respectively given by

$$q=(p^2+s^2+2sp\cos\chi)^{1/2}, \quad \ldots\ldots(3.4)$$

$$\Omega=\frac{1}{2\pi}\int_{-\pi}^{\pi}\cos\,[kW\{p\cos(\chi+\psi)+s\cos\psi,\, p\sin(\chi+\psi)+s\sin\psi\}$$
$$-kW\{p\cos(\chi+\psi),\, p\sin(\chi+\psi)\}]\,d\psi, \quad \ldots\ldots(3.5)$$

$$J\,d(p, q)=p\,d(p, \chi); \quad \ldots\ldots(3.6)$$

hence, from (3.6), for constant p,

$$J\,dq=p\,d\chi. \quad \ldots\ldots(3.7)$$

Substituting from (3.7) into (3.3) and cancelling p, we get

$$\int_{-\pi}^{\pi} t(q)\Omega\,d\chi=2\pi\bar{D}(s)t(p), \quad \ldots\ldots(3.8)$$

where $p\leqslant 1$ and q, Ω are given by (3.4), (3.5) respectively; if $p>1-s$, then, for some values of χ, $q>1$ and therefore $t(q)=0$.

As it stands, (3.8) seems insufficient to determine the two unknown functions $\bar{D}$, t; but, because s is fixed, we may express $\bar{D}(s)$ in terms of t by substituting any convenient special value for p in (3.8). If we substitute $p=0$, then we get

$$\int_{-\pi}^{\pi} t(s)\Omega_0\,d\chi=2\pi\bar{D}(s)t(0), \quad \ldots\ldots(3.9)$$

where

$$\Omega_0=\frac{1}{2\pi}\int_{-\pi}^{\pi}\cos\,\{kW(s\cos\psi,\, s\sin\psi)\}\,d\psi, \quad \ldots\ldots(3.10)$$

and we have followed the convention of fixing the zero of phase in such a way that $W(0, 0)=0$. From (3.9),

$$\bar{D}(s)=\Omega_0 t(s)/t(0); \quad \ldots\ldots(3.11)$$

substitution from (3.11) into (3.8) gives

$$\int_{-\pi}^{\pi} t(q)\Omega\,d\chi=2\pi\Omega_0 t(s)t(p)/t(0), \quad \ldots\ldots(3.12)$$

a functional equation for t, which holds provided that the arguments are not greater than 1. Exact solution of the non-linear functional equation (3.12) appears to be impossible in general, although numerical solution may be feasible in particular cases; we therefore proceed to show how (3.12) may be approximately replaced in a linear eigenvalue problem.

§ 4. APPROXIMATE EIGENVALUE PROBLEM

The method of approximation is particularly appropriate for small values of the argument; it consists in determining one boundary condition by putting $p=1$ in (3.12) and taking the limit as $s\rightarrow 0$, and determining the other boundary condition and the differential equation by differentiating (3.12) twice with respect to p and taking the respective limits as $p\rightarrow 0$.

For the first boundary condition, we observe that $\Omega\rightarrow 1$, $\Omega_0\rightarrow 1$ as $s\rightarrow 0$; if $p=1$, then as $s\rightarrow 0$, $t(q)\rightarrow 0$ for $|\chi|\leqslant \frac{1}{2}\pi$, $t(q)\rightarrow t(1)$ for $\frac{1}{2}\pi<|\chi|\leqslant\pi$ (the edge of the pupil is approached from the outside and from the inside in the respective cases). Substitution in (3.12) leads to the boundary condition

$$t(1)=0; \qquad \ldots\ldots(4.1)$$

if this is satisfied, then there is no discontinuity in the transparency at the edge of the pupil.

For the second boundary condition, we differentiate (3.12) with respect to p, obtaining

$$\int_{-\pi}^{\pi}\left\{t'(q)\frac{\partial q}{\partial p}\,\Omega+t(q)\frac{\partial\Omega}{\partial p}\right\}d\chi=\frac{2\pi\Omega_0 t(s)t'(p)}{t(0)}. \qquad \ldots\ldots(4.2)$$

As $p\rightarrow 0$ we have $q\rightarrow s$, $\partial q/\partial p\rightarrow\cos\chi$, and $\partial\Omega/\partial p\rightarrow A\cos\chi+B\sin\chi$, where A, B are independent of χ; hence the left-hand member of (4.2) tends to 0, and we obtain the boundary condition

$$t'(0)=0. \qquad \ldots\ldots(4.3)$$

For the differential equation we differentiate (4.2) with respect to p, obtaining

$$\int_{-\pi}^{\pi}\left\{t''(q)\left(\frac{\partial q}{\partial p}\right)^2\Omega+t'(q)\frac{\partial^2 q}{\partial p^2}\,\Omega+2t'(q)\frac{\partial q}{\partial p}\frac{\partial\Omega}{\partial p}+t(q)\frac{\partial^2\Omega}{\partial p^2}\right\}d\chi=2\pi\Omega_0\frac{t(s)t''(p)}{t(0)}. \qquad \ldots\ldots(4.4)$$

By taking the limit as $p\rightarrow 0$ and dividing by π we have $\partial^2 q/\partial p^2\rightarrow s^{-1}\sin^2\chi$, and thence we obtain the differential equation

$$\Omega_0 t''(s)+\left\{\frac{\Omega_0}{s}+\frac{2}{\pi}\int_{-\pi}^{\pi}\left(\frac{\partial\Omega}{\partial p}\right)_0\cos\chi\,d\chi\right\}t'(s)+\left\{\frac{1}{\pi}\int_{-\pi}^{\pi}\left(\frac{\partial^2\Omega}{\partial p^2}\right)_0 d\chi-\frac{2t''(0)\Omega_0}{t(0)}\right\}t(s)=0, \qquad \ldots\ldots(4.5)$$

where a subscript 0 on a derivative of Ω, like a subscript on Ω itself, indicates a particular value obtained by taking the limit as $p\rightarrow 0$.

In (4.5), s is regarded as the independent variable, whereas strictly it is a fixed parameter, so we should express any resulting solution in terms of r as independent variable (as is done in (5.4) below, for example); this solution should then be satisfactory for all sufficiently small values of s.

The differential equation (4.5) and the boundary conditions (4.1), (4.3) together form the linear eigenvalue problem referred to above.

§ 5. SPHERICAL ABERRATION CASE

If the only wave front error is due to spherical aberration, without defocusing, then the eigenvalue problem can be solved exactly.

In this case (and when defocusing is present also) $W(x, y)$ is a function of r only, so that the integrand in (2.6) is independent of ψ, and

$$\Omega = \cos\{kW(q, 0) - kW(p, 0)\}; \qquad \ldots\ldots(5.1)$$

similarly from (3.10)

$$\Omega_0 = \cos\{kW(s, 0)\}. \qquad \ldots\ldots(5.2)$$

On substituting in (4.5) we find that if the first two derivatives of $W(s, 0)$ with respect to s tend to 0 as $s \to 0$ (that is, if defocusing is absent), then

$$\left(\frac{\partial\Omega}{\partial p}\right)_0 = \frac{\partial\Omega_0}{\partial s}\cos\chi, \left(\frac{\partial^2\Omega}{\partial p^2}\right)_0 = \frac{\partial^2\Omega_0}{\partial s^2}\cos^2\chi + \frac{1}{s}\frac{\partial\Omega_0}{\partial s}\sin^2\chi,$$

so that (4.5) becomes

$$\frac{\partial^2}{\partial s^2}\{\Omega_0 t(s)\} + \frac{1}{s}\frac{\partial}{\partial s}\{\Omega_0 t(s)\} - \frac{2t''(0)}{t(0)}\Omega_0 t(s) = 0. \qquad \ldots\ldots(5.3)$$

The Bessel differential equation (5.3) is consistent with the boundary conditions (4.1), (4.3), if and only if $2t''(0)/t(0) = -\mathrm{j}_n{}^2$, where j_n is a zero of the zero-order Bessel function $\mathrm{J}_0(z)$; the relevant solution of (5.3) is then

$$\Omega_0 t(s) = t(0)\mathrm{J}_0(\mathrm{j}_n s).$$

To ensure that the transparency function is everywhere finite and non-negative, it is sufficient to assume that the wave aberration is less than a quarter wavelength (so that $0 < \Omega_0 \leqslant 1$, by (5.2)) at all points of the pupil, and to choose the first zero j_1 of $\mathrm{J}_0(z)$; then

$$t(r) = t(0)\mathrm{J}_0(\mathrm{j}_1 r)\sec\{kW(r, 0)\}. \qquad \ldots\ldots(5.4)$$

From (3.11) and (5.4) $\bar{D}(s) = \mathrm{J}_0(\mathrm{j}_1 s)$; as this does not involve the wave aberration function, we may state that if a known amount of spherical aberration, less than a quarter wavelength at all points of the pupil, is the only wave front error present, then it is possible to determine an apodizing screen by means of which the low-frequency response may be made nearly equal to that of a perfect system.

§ 6. SERIES-EXPANSION METHOD

If we initially assume s small (and non-negative, as above), then we may expand $\bar{D}(s)$ in powers of s, and choose the transparency function so as to maximize the quadratic approximation to $\bar{D}(s)$; a similar procedure has been adopted by Lohmann (private communication).

With the assumptions (2.4) we obtain

$$\bar{D}(s) = 1 - \frac{\{t(1)\}^2}{\pi\int_0^1 \{t(r)\}^2 r\,dr}s - \frac{\int_0^1 t(r)\{k^2U^2t(r) - t''(r) - r^{-1}t'(r)\}r\,dr}{4\int_0^1 \{t(r)\}^2 r\,dr}s^2 - \ldots, \qquad \ldots\ldots(6.1)$$

where

$$U^2 = \frac{1}{2\pi}\int_{-\pi}^{\pi}\left\{\left(\frac{\partial W}{\partial r}\right)^2 + \frac{1}{r^2}\left(\frac{\partial W}{\partial\phi}\right)^2\right\}d\phi$$

W being used as an abbreviation for $W\{r\cos(\phi+\psi), r\sin(\phi+\psi)\}$. In obtaining (6.1) it is necessary to allow for the fact that the region in which the integrand of (2.2) is non-zero depends on s.

We impose the condition (4.1) in order to maximize the coefficient of s on the right of (6.1); in this case the coefficient is zero, but otherwise it would be negative. Then

$$\bar{D}(s)=1-\frac{\int_0^1 [\{t'(r)\}^2+k^2U^2\{t(r)\}^2]r\,dr}{4\int_0^1 \{t(r)\}^2 r\,dr}\,s^2-\dots, \qquad \dots\dots(6.2)$$

where we have performed a partial integration in the numerator of the fraction on the right. By applying the variational method as in § 3, we find that the coefficient of s^2 on the right of (6.2) is maximized if

$$\frac{d}{dr}\{rt'(r)\}+(\mu-k^2U^2)rt(r)=0, \qquad \dots\dots(6.3)$$

where μ is an appropriate eigenvalue, and that in this case

$$\bar{D}(s)=1-\tfrac{1}{4}\mu s^2-\dots. \qquad \dots\dots(6.4)$$

Instead of the subsidiary condition (4.3) there is a regularity condition at $r=0$; but in other respects this eigenvalue problem resembles that of § 4, and may be regarded as an approximation to it.

We may express $\bar{D}(s)$ in terms of the intensity-distribution function $G(u, v)$ for a point-source image by making the substitution

$$g(s\cos\psi,\ s\sin\psi)=\iint_{-\infty}^{\infty} G(u, v)\exp\{-2\pi is(u\cos\psi+v\sin\psi)\}du\,dv$$

in (2.1); we then obtain

$$\bar{D}(s)=\iint_{-\infty}^{\infty} G(u, v)\mathrm{J}_0\{2\pi s(u^2+v^2)^{1/2}\}du\,dv \Big/ \iint_{-\infty}^{\infty} G(u, v)\,du\,dv. \qquad \dots\dots(6.5)$$

Expansion of the Bessel function in (6.5) suggests that the coefficient of s^2 in the expansion of $\bar{D}(s)$ may be equal to $-\pi^2$ times the squared radius of gyration of the point-source image about an axis perpendicular to those of u and v; but in general this assertion is not true, because discontinuity in transparency at the edge of the pupil entails an infinite radius of gyration of the point-source image. The last result is due to Duffieux, who showed in the same paper (Duffieux 1952) that there is a finite difference between the values of squared radius of gyration for perfect and imperfect optical systems of the same transparency. In our treatment, Duffieux's results may be obtained by observing that if s is permitted to take either sign, than the second term on the right of (6.1) involves $|s|$ instead of s, and therefore gives an infinite contribution to $\bar{D}''(0)$ in general; but, as this contribution depends only on the transparency, $\bar{D}_0''(0)-\bar{D}''(0)$ is finite (where $\bar{D}_0(s)$ is obtained from $\bar{D}(s)$ by putting $W=0$). In any case this series-expansion procedure, which approximately maximizes the low-frequency response, also minimizes the squared radius of gyration of the point-source image.

§ 7. ADDITIONAL REMARKS

(*a*) *Defocusing case.* If defocusing alone is present ($W=w_{20}r^2$) then (6.3) becomes

$$rt''(r)+t'(r)+(\mu-4k^2w_{20}{}^2r^2)t(r)=0; \qquad \dots\dots(7.1)$$

the appropriate solution is

$$t(r)=t(0)\exp(-k|w_{20}|r^2)\,{}_1F_1\left(\tfrac{1}{2}-\frac{\mu}{8k|w_{20}|}\ ;\ 1;\ 2k|w_{20}|r^2\right), \qquad \dots\dots(7.2)$$

where μ is determined by (4.1) and the condition $t(r)\geqslant 0$ for $0\leqslant r<1$.

If $k|w_{20}|$ is comparatively large, then the exponential factor on the right of (7.2) is small except when r is small; in the latter case the confluent hypergeometric function is nearly equal to 1. This suggests the approximation of omitting the last factor on the right of (7.2), so that $\mu \simeq 4k|w_{20}|$ and the eigenfunctions of (7.1) are approximately Laguerre functions of $2k|w_{20}|r^2$. Hence if the screen required for maximum frequency response has a proportional transmission

$$2\{t(0)\}^{-2}\int_0^\infty \{t(r)\}^2 r\,dr \simeq (2k|w_{20}|)^{-1}$$

which is too small for practical requirements, then it may be possible to determine a screen which simultaneously gives satisfactory frequency response and satisfactory transmission by expressing the transparency of the screen as the sum of a suitable Laguerre function series.

The above-mentioned approximation is equivalent to replacing (4.1) by the condition $t(\infty)=0$; in this form, it may be used whenever there are large aberrations of any kind. The reason for this statement is that, if the aberrations are large and $r>1$, then Ω in (2.5) oscillates rapidly, thereby reducing the error committed by permitting $t(r)$ to be non-zero.

(*b*) *Perfect 'one-dimensional' system.* We proceed to discuss an analogous special case in which the corresponding functional equation can be solved exactly.

If all the optical properties of the system can be expressed in terms of one normalized transverse Cartesian coordinate x, then by analogy with (2.1), (2.2), (2.3) we obtain

$$D(s)=g(s)/g(0),$$
$$g(s)=\int_{-\infty}^{\infty}\tau(x+\tfrac{1}{2}s)\tau(x-\tfrac{1}{2}s)\exp\{ikW(x+\tfrac{1}{2}s)-ikW(x-\tfrac{1}{2}s)\}dx,$$

where $\tau(x)=0$ for $|x|>1$. If the system is perfect, then $W=0$, and (6.3), (6.4) give

$$D_0(s)=\int_{-\infty}^{\infty}\tau(x+\tfrac{1}{2}s)\tau(x-\tfrac{1}{2}s)dx\Big/\int_{-\infty}^{\infty}\{\tau(x)\}^2dx,$$

where (as in § 5) the subscript 0 indicates that the system is perfect; thus $D_0(s)$ is the autocorrelation function of $\tau(x)$. In the same way as in § 2, we find that $D_0(s)$ is stationary, provided that

$$\tau(x+s)+\tau(x-s)=2D_0(s)\tau(x). \qquad \ldots\ldots(7.3)$$

The recurrence relation (7.3), together with the conditions $\tau(x)\geqslant 0$ for $|x|\leqslant 1$, $\tau(x)=0$ for $|x|>1$, can be solved exactly; assuming that $s>0$, we obtain

$$\left.\begin{array}{l}\tau(x)=C(x+\tfrac{1}{2}ms-ns)\sin\{(n+1)\pi/(m+2)\} \text{ for}\\ \qquad -1+ns\leqslant x\leqslant -1+(n+1)s\\ \text{where } m \text{ is the integral part of } 2/s \text{ and}\\ \quad C(x) \text{ is an arbitrary positive function for } |x|\leqslant 1-\tfrac{1}{2}ms\\ \quad C(x)=0 \text{ for } 1-\tfrac{1}{2}ms<|x|\leqslant \tfrac{1}{2}s;\end{array}\right\} \qquad \ldots\ldots(7.4)$$

further,

$$D_0(s)=\cos\{\pi/(m+2)\}. \qquad \ldots\ldots(7.5)$$

The screen which gives maximum frequency response therefore consists of m opaque bands of width $(m+1)s-2$ separating $m+1$ transparent strips of width $2-ms$, where the transparency varies in the same way across the respective strips, and the transparency of the nth strip from either end is proportional to $\sin \{n\pi\}/(m+2)\}$.

If in (7.4) and (7.5) we consider a reduced spatial frequency s such that $1 < s \leqslant 2$ (so that $m=1$) and take $C(x)$ constant for $|x| \leqslant 1-\frac{1}{2}s$, then we find that the frequency response function attains its maximum value $\frac{1}{2}$ with a screen which is equivalent to Young's two-slit arrangement. With this screen, the frequency response function $D_0(s')$ for any other reduced spatial frequency s' within the limit of resolution is given by

$$D_0(s') = \begin{cases} 1-\frac{1}{2}s'(2-s) & \text{for } 0 \leqslant s' \leqslant 2-s \\ \frac{1}{2} & \text{for } 2-s \leqslant s' \leqslant s \\ \frac{1}{2}(2-s')/(2-s) & \text{for } s \leqslant s' \leqslant 2. \end{cases}$$

The second of these equations implies that the same screen maximizes the frequency response function for all spatial frequencies such that $1 < s' \leqslant s$; on the other hand its proportional transmission $2-s$ is not the largest possible unless $s' = s$.

As in § 4 or § 6 we may approximate to the exact solution (7.4) by converting (7.3) into a differential equation of the form

$$\tau''(x) + \mu\tau(x) = 0;$$

the boundary conditions become

$$\tau(1) = 0, \quad \tau(-1) = 0.$$

The appropriate solution of this eigenvalue problem is

$$\tau(x) = \cos \tfrac{1}{2}\pi x, \qquad \ldots\ldots (7.6)$$

$$D_0(s) = (1-\tfrac{1}{2}s)\cos \tfrac{1}{2}\pi s + \pi^{-1} \sin \tfrac{1}{2}\pi s; \qquad \ldots\ldots (7.7)$$

comparing the solution (7.6), (7.7) with the exact solution (7.4), (7.5), we see that for small s the approximation to the maximum frequency response is very close, and that the proportional transmission is larger because there is no 'fine structure' involving opaque bands.

ACKNOWLEDGMENTS

The author wishes to express his thanks to the Chief Scientist, Department of Supply, Australia, for enabling him to study in England, and to Dr. H. H. Hopkins for suggesting this investigation, and for useful discussion.

REFERENCES

DOSSIER, B., 1953, *Thesis*, University of Paris.
DUFFIEUX, P. M., 1952, *Rev. Opt.*, **31**, 265.
HOPKINS, H. H., 1955, *Proc. Roy. Soc.* A, **231**, 91 ; 1957, *Proc. Phys. Soc.* B, **70**, 449.
SPENCER, R. C., 1955, *Astronomical Optics Symposium* (Amsterdam : North-Holland Publishing Co.), p. 130.
STRAUBEL, R., 1931, *Eighth International Congress on Photography* (Leipzig : Barth), p. 353.

Magnetic Susceptibility and Electrical Resistance Properties of some Uranium Alloys

By L. F. BATES and R. G. LOASBY†
Department of Physics, University of Nottingham

MS. received 10*th February* 1958, *and in revised form* 17*th June* 1958

Abstract. The magnetic susceptibilities and electrical properties of a series of quenched alloys of uranium with zirconium, niobium and molybdenum, metals which have four, five and six outer electrons respectively, were measured over the temperature range 90 to 300°K. The general features of the three systems are the same, with anomalies at about 0·5 and 2·0 atomic per cent of the solute. The first anomaly is of unknown origin, and the second suggests that alloys containing up to about 2 atomic per cent of the solute may be obtained in the α-form by quenching them from the γ-phase field, and that within this composition range the behaviour is consistent with the full Brillouin zone structure that has been proposed for α-uranium.

§ 1. Introduction

The corrugated layer structure of α-uranium (orthorhombic) and the physical properties of the phase distinguish it from the Group VI elements chromium, molybdenum and tungsten which have a body-centred cubic structure. Experimental investigations are made difficult by the nature of α-uranium which, even in a relatively pure condition, may contain considerable strain which gives rise to a wide variation in properties. The solid solubility of other metals in the α-phase is restricted, being normally less than 0·5 at.%; but by quenching solutions in γ-uranium which are stable above 800°C, metastable alloys consisting primarily of solutions in α-uranium may be formed. X-ray and metallographic work shows that almost pure single phase alloys containing up to 6 at.% of solute may be obtained by this method but that, generally, the nature of the phase changes within the solubility range. Evidence of a similar structure to the α-phase, but with different lattice parameters, has been found but it is not clear whether this arises as a separate phase or is merely due to distortion introduced by supersaturation.

Besides these changes, which may be caused by strain processes, other marked changes may be obtained in a particular alloy by varying the heat treatment. Slow cooling, which results in equilibrium conditions, in general produces two phase alloys, the second phase being usually of quite different structure from the α-phase. Intermediate cooling rates introduce complications due to the growth of other phases to an extent controlled by diffusion rates, and can lead to complex structures, especially in alloys passing through mixed phase regions on cooling.

The alloys of zirconium, niobium and molybdenum with uranium have been previously studied by Pfeil (1950) who has discussed the possible Brillouin zone structure of the α-phase on the basis of X-ray investigations of the uranium–molybdenum system. The analysis, taken with the properties of α-uranium which suggested that it may be characterized by a zone which is nearly full, led him to identify the zone as that containing a possible 4·09 electrons per atom. Later work on the other phases of uranium and their alloys emphasized the full zone characteristics of the α-phase but suggested that the zone more probably was one containing six electrons per atom. Mallard (1952) also pointed out that the characteristic zone could, with little distortion, contain either four or six electrons per atom.

---

† Now at United Kingdom Atomic Energy Authority, Aldermaston, Berks.

The present work constitutes a systematic investigation of the effects of varying the electron concentration in the α-phase. Three series of alloys with zirconium, niobium and molybdenum, metals which have four, five and six outer electrons respectively, as solutes, were investigated, and the magnetic susceptibility and electrical resistance properties were measured over the range 90°K to 300°K. To increase the range of investigation and to obtain data on the phase boundaries, the alloys were studied in the quenched condition. This condition reduces the importance of the absolute values, which will vary with quenching temperature, cooling rate, etc., but care was taken to standardize the heat treatment, and on this basis comparison between the alloys is made.

§ 2. EXPERIMENTAL PROCEDURE

For the measurement of magnetic susceptibilities an apparatus based on the Gouy method was used, employing a Sucksmith ring balance for the measurement of force (Bates 1951). The specimens were 4 cm long and 4 mm in diameter and were suspended in a platinum cage from a Pyrex fibre. The fields used varied between 4 kOe and 16 kOe and were sufficiently large throughout the specimen length to saturate any ferromagnetic impurity likely to be present. While the presence of iron in any form could not be discounted, the reproducibility of the properties on inversion of the specimen and the linearity of the ferromagnetic impurity test curves suggest that it is unlikely. The reproducibility on inversion is also a simple test that the specimen is homogeneous. Tests for ferromagnetism were made at 90°K and 293°K for all the specimens. The absolute susceptibilities are quoted in terms of a tantalum standard (Hoare, Kouvelites, Matthews and Preston 1954) and without correction for diamagnetism of the atomic core.

The apparatus for the measurement of absolute and that for relative susceptibilities were essentially similar, the latter being mounted within a vacuum chamber with the usual accessories for the measurement of temperature variation of susceptibility over the range 90°K to 300°K.

The electrical resistances were measured by a potentiometer method, the same specimens being used. Absolute values were obtained by comparison with the potential across a standard 5 milliohm resistance. No correction was made to the resistance values for thermal expansion as no values are available for uranium alloys, but on the basis of the values for the pure metal, an error of some 2% is likely from lack of this correction.

The alloys were prepared from materials of purity of the order 99·95%, the principal impurities being carbon, silicon and oxygen. All the alloys were prepared by direct melting of the components in an argon arc furnace; pick-up of carbon and copper was negligible. After preparation, the specimens with the exception of those specifically mentioned as having further treatment to test homogeneity, were annealed at 1000°C for three days to homogenize them and were afterwards quenched in water. Before investigation, the alloys were further annealed at 900°C for several hours and after water quenching, cleaned in nitric acid and distilled water, washed in alcohol and dried. Chemical analyses were made on some specimens but were found inaccurate at the low concentrations. Since no losses occurred during preparation, the compositions were taken from the components as correct. The standardized method of preparation was based on homogeneity tests during metallography work on specimens in this composition range, but no systematic tests were made on the actual specimens except the simple magnetic one described above.

§ 3. RESULTS

The properties and characteristics of the alloy systems are first outlined separately and then discussed as a group in the next section.

3.1. *Uranium–Molybdenum Alloys*

Eight alloys in the range 0–5 at.% Mo were studied. The variation of absolute susceptibility with addition of molybdenum is shown in the top graph of figure 1. The value for pure uranium was $31{\cdot}8\times10^{-6}$ e.m.u. cm^{-3} which, taking the measured value of the density $19{\cdot}0$ g cm^{-3}, gives a mass susceptibility $1{\cdot}67\pm0{\cdot}02\times10^{-6}$ e.m.u. g^{-1} at 21°C. A sharp drop of some 5% to $1{\cdot}61\times10^{-6}$ e.m.u. g^{-1} on initial addition of 0·5 at.% Mo and a break in the curve in the region of 2 at.% is to be noted. Further addition of molybdenum produces an increase in susceptibility, and above 2 at.% the susceptibility increases approximately linearly to $1{\cdot}73\times10^{-6}$ e.m.u. g^{-1} at 4·9 at.% molybdenum. No

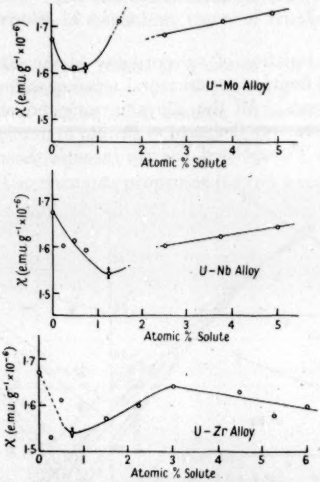

Figure 1. Quenched alloys 293°K.

discontinuity was found in the corresponding density values, a linear decrease to 18·48 ± 0·05 g cm^{-3} for the 4·9 at.% alloy being found. No ferromagnetic impurity was found at room temperature.

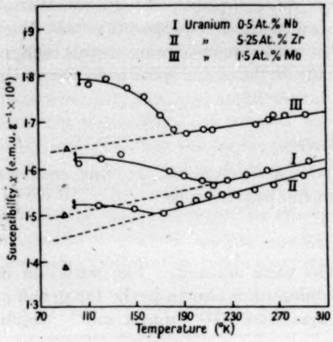

Figure 2.

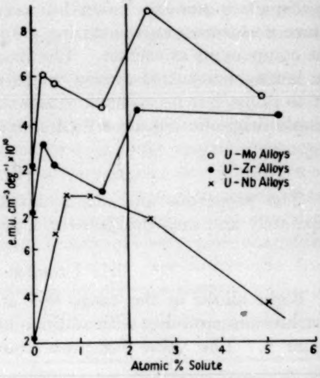

Figure 3. (Curves displaced for clarity.)

The temperature variation of susceptibility in the alloys was of the form shown in figure 2, the limits of experimental accuracy at low temperatures being indicated by the arrows. All the alloys investigated showed ferromagnetic impurity at low temperatures (believed to be due to uranium hydride), and the graphs are tentatively extrapolated linearly through the corrected points (see

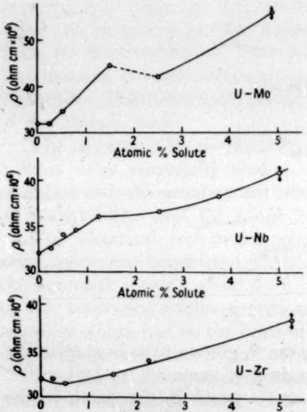

Figure 4. Quenched alloys 293°K.

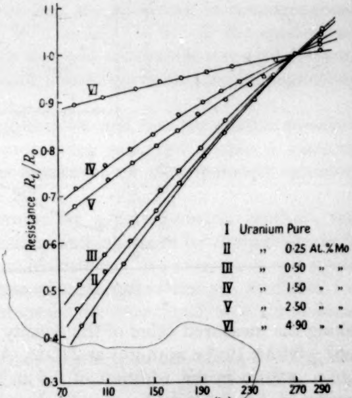

Figure 5. Uranium–molybdenum alloys quenched.

the original work of Kriessman and McGuire (1952) on pure uranium). The collected data on the variation of the temperature coefficient of susceptibility dk/dT with solute content are shown in figure 3. Discontinuities are again shown in the region of 0·5 at.% and 2·0 at.% solute content.

The variation of electrical resistivity with molybdenum content is shown in figure 4 and the temperature variation of resistance for each of the alloys, in reduced values, in figure 5. Discontinuities are again shown in the regions 0·5 at.% and 2 at.%.

In view of the persistent anomalies found in the region of 2% molybdenum content the alloys containing 2·5 and 4·9 at.% were again heat treated in case the initial treatment had been inadequate to give homogeneity. They were subjected to a further 50 hours at 900°C before quenching in water as before. In each case, however, the first results were reproduced.

3.2. *Uranium–Niobium Alloys*

Little work has been done on uranium–niobium alloys and information is restricted to an incomplete phase diagram (Waldron 1952†). In this work seven alloys containing between 0·25 at.% and 5 at.% Nb were investigated. X-ray investigations of alloys in this range showed that, within the limits of detection, up to 5 at.% niobium may be retained in solid solution by quenching (Pfeil, private communication). The alloys used were therefore assumed to be mainly single phase solid solutions in α-uranium, traces of retained γ-phase also being present.

Addition of niobium again results in a decrease in absolute susceptibility (figure 1) the value falling from $1{\cdot}67 \times 10^{-6}$ e.m.u. g^{-1} for pure uranium to $1{\cdot}54 \times 10^{-6}$ e.m.u. g^{-1} at 1·25 at.% Nb content. The temperature variation of susceptibility (figures 2 and 3) shows the same form as the molybdenum alloys but the onset of ferromagnetism in the region of 220°K is less well defined than in the other series. The resistance properties (figures 4 and 6) also show a break

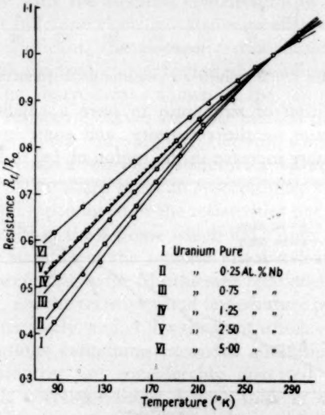

Figure 6. Uranium–niobium alloys quenched.

---

† Inter-Service Metallurgical Research Council Report, ISMET 1048, B.P. 169.

in the region 1·25 at.% and further show that niobium has a smaller effect on the resistivity of α-uranium than molybdenum, the values for alloys containing 5% of these solutes being $25{\cdot}4\times10^{-6}$ ohm cm and $50{\cdot}2\times10^{-6}$ ohm cm respectively at 90°K.

3.3. *Uranium–Zirconium Alloys*

Although there is considerable scatter of experimental points, the susceptibility behaviour appears to resemble that of the molybdenum alloys with the difference that above 3 at.% zirconium the susceptibility decreases, having the value $1{\cdot}60\times10^{-6}$ e.m.u. g^{-1} at 6 at.% Zr content. The temperature–susceptibility behaviour is also similar and is shown in figures 1 and 3.

The addition of up to 1·5 at.% zirconium to α-uranium results in little increase in the resistivity (figure 4), some evidence even being found for a decrease in the region of 0·5 at.% Zr. Figure 7, giving the temperature variation of reduced resistivity, shows addition of zirconium to have a smaller effect than either niobium or molybdenum on the resistivity, and some evidence is seen of a discontinuity in resistivity increase in the region of 1·0 to 2·0 at.% Zr.

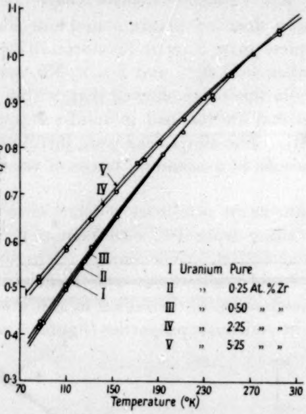

Figure 7. Uranium–zirconium alloys quenched.

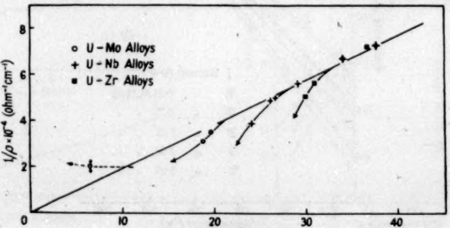

Figure 8. Matthiessen plot.

The combined resistivity–temperature values for the three alloy systems are shown in figure 8 where the inverse resistivity $1/\rho$ is plotted against α, the temperature coefficient, to give a ' Matthiessen plot ' of the equation $\rho\alpha = \text{constant}$, the values at 90°K being taken.

§ 4. DISCUSSION

The general features of the three systems are the same and it is probable that the characteristics shown have a common explanation. An anomaly occurs in each system at solute concentrations of between 0·5 at.% and 1·5 at.% and a further discontinuity in the observed properties occurs in the region of 2%. The change in properties at the higher concentration is most marked in the molybdenum alloys but is barely discernible in the niobium alloys.

No clear explanation of the minimum in the region of 0·5 at.% is apparent. It is possible that it is associated with the solubility limits for these solutes which are in the region of 0·9 at.% but, if this is so, it is difficult to understand why the resistivity and susceptibility of the alloys should decrease with solute content up to this limit. The concentration at which the minimum occurs varies between the systems but bears no obvious relationship to the solute elements, coming at a maximum concentration of 1·25 at.% in the niobium alloys. Some comparison with the X-ray evidence of a definite change in structure may be made, the present results supporting the suggestion of a deviation from the normal α-phase structure. The narrow range over which the anomaly occurs and the fact that it persists in the alloys when annealed, suggest that it is not directly connected with the supersaturation process, but the former point hardly supports a change in structure. Metallographical examination might give further evidence on this point, but it is doubtful whether slight deviations in phase structure could be distinguished, especially when the second phase may be present in small quantities.

The discontinuity in the region of 2 at.% solute may be due to the breakdown of the single phase condition. The resistivity values in the three alloy systems show a rapid increase with the electron contribution of the solute and if the α-phase has an almost full zone electronic structure effects of the type discussed by Jones might be significant, the electronic contribution to the free energy increasing sharply with electron concentration and leading to the appearance of two-phase alloys. The sharp breaks shown in the (dk/dT, % solute) curves (figure 3) and in the resistance curves are most marked in the uranium–molybdenum alloys which, having the highest electron concentration, would be expected to break down into a two-phase structure at lower solute concentrations than the other alloys. The sharp break in susceptibility values in the uranium–zirconium system is not reproduced in the resistivities but it is possible that it is obscured by the presence of the δ-phase which has a high resistance.

The extent of the stability of the α-phase may be clearly shown by plotting the resistivity results according to the Matthiessen relationship $\rho_T\alpha_T = A$ (Hibbard 1954) where ρ_T and α_T are the resistivity and temperature coefficient of resistance at temperature T, respectively, and A is a constant which varies with the solvent. Metastable solid solutions containing excessive quantities of solute quenched in from high temperatures are considerably distorted structurally, and the electrical resistance is correspondingly higher than in equilibrium solutions. Thus ρ_T will increase more rapidly with solute addition above the normal solubility limit than below it. As long as the alloy remains single phase, however, the graph should remain continuous but deviate from the theoretical curve. Figure 8 shows these values plotted for the three alloy systems. Deviations from linearity occur for each alloy series and the direction of the deviation is consistent with the presence of strain in the alloys. The shape of the molybdenum alloy curve, which recrosses the theoretical line, suggests that the second phase is of the γ-form, which has a lower resistivity than the α-phase. Metallographic examinations of alloys in these systems are extensive, but since evidence so obtained is equally dependent on specimen treatment, no direct comparison may be made with this work.

Summarizing the results, there is an indication that a maximum of about 2 at.% of the solute may be quenched into solution in α-uranium and within this range the behaviour is consistent with the proposed full zone structure for the phase. Such a structure would account for the non-metallic form of both the physical and metallurgical properties of α-uranium. In general, a complex crystal structure may be correlated with an almost full zone structure, resulting from the necessity of forming a zone which will accommodate the number of electrons present. The high resistance, positive Hall coefficient and low thermal conductivity could result from a full zone condition and the restricted formation of alloys may also be explained. There is some further evidence of a change in the structure of the α-phase in the 0·1 at.% solute range.

ACKNOWLEDGMENTS

We are indebted to Dr. P. C. L. Pfeil and Miss J. R. Murray of the Metallurgy Division, Atomic Energy Research Establishment, Harwell, for much discussion and for the provision of the alloys for this work; we have also had the benefit of helpful discussions with Dr. K. W. H. Stevens. One of us (R. G. L.) thanks A.E.R.E. for the provision of a maintenance grant throughout the period of this study, and our warm thanks are due to the Director, A.E.R.E., for permission to publish the results.

REFERENCES

BATES, L. F., 1951, *Modern Magnetism* (Cambridge : University Press), p. 115.

HIBBARD, W., 1954, *Trans. Amer. Inst. Min.* (*Metall.*), **200,** 594.

HOARE, F. E., KOUVELITES, J. S., MATTHEWS, J. C., and PRESTON, P., 1954, *Proc. Phys. Soc.* B, **67,** 728.

KRIESSMAN, C. J., JR., and MCGUIRE, T. R., 1952, *Phys. Rev.*, **85,** 71.

MALLARD, J. R., 1952, *Thesis*, University of Nottingham.

PFEIL, P. C. L., 1950, *J. Inst. Metals*, **77,** 553.

The Demagnetizing Energy and Domain Structure of a Uniaxial Single Crystal†

By M. FOX‡ and R. S. TEBBLE§
Department of Physics, University of Leeds

MS. received 4th June 1958

Abstract. The conditions under which a reduction in the demagnetizing energy in a uniaxial crystal can be brought about by rotation of the magnetization vectors (μ^* effect) is examined and an expression for the energy reduction is obtained for materials with high anisotropy ($K > 2\pi I_0^2$). The closure domain structure of cobalt has been examined by Bitter pattern technique on the curved surface of a disc, and the results give the conditions under which domains of reverse magnetization are preferred. Suggestions for future development are made.

§ 1. Introduction

The energy associated with the domain structure of a ferro-magnetic material is controlled to a considerable extent by the nature of the domain configuration near the surface of the crystal at which 'free pole' is produced by the discontinuity in the component of the magnetization normal to the surface. The energy due to this 'free pole' distribution is generally quite large and it is usual for some modification of the domain structure to take place which results in a reduction of the energy of the system. In materials with three easy directions of magnetization such as iron, closure domains are usually formed as in figure 1 (*a*).

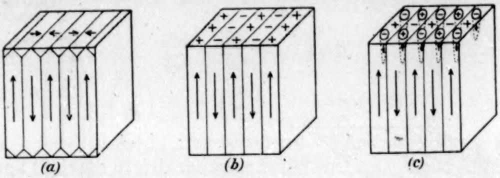

Figure 1. Domain structures: (*a*) with closure domains as in iron, (*b*) without closure domains as in cobalt, (*c*) with domains of reverse magnetization. In each case the directions of magnetization are parallel to the easy directions.

In a material such as cobalt with one single easy direction of magnetization (parallel to the hexagonal axis), the energy cannot be reduced in this manner because of the large energy which would be involved in rotating the magnetization vector through 90° against the high magneto-crystalline anisotropic forces, and instead a Kittel type of structure is to be expected (figure 1 (*b*)). The energy can then be reduced either by (*a*) a reversal of magnetization over small regions to produce domains of reverse magnetization ('spikes') as in the figure, or by (*b*) the rotation of the magnetic vector through a relatively small angle so that any increase in energy due to anisotropy would be compensated for by the change in the energy due to the reduction in the free pole density on the surface. For materials with low anisotropy the mechanism (*b*) would be energetically more favourable whilst a high anisotropy would favour (*a*). Cobalt is of considerable interest, because, although the anisotropy is high it is not sufficiently high to ensure in every case the formation of spikes, and the purpose of the present paper is to examine the conditions under which one or other of these processes predominate. In the first part an original expression is derived for the reduction in energy associated with a rotation of the magnetization vector (the μ^* effect) and in the second part, a description is given of an experimental investigation into the nature of the closure domain formed, for a range of surface orientations.

---

† The experimental part of this paper was described in a paper presented at the Canadian Metal Physics Conference, Kingston, Ontario, September 1957.

‡ Now at the University of Ottawa.

§ Now at the University of Sheffield.

§ 2. THEORETICAL : REDUCTION IN THE DEMAGNETIZATION ENERGY DUE TO THE μ^* EFFECT

In the Kittel type structure of figure 1 (*b*), it is supposed that near the surface, which is in the basal plane, the magnetization vectors rotate with a permeability at right angles to the easy direction given by $\mu^* = 1 + 2\pi I_0^2/K$ (Kittel 1949); it is assumed that the permeability parallel to the easy direction is unity since the magnetization in that direction cannot be changed appreciably. The permeability tensor with respect to the crystal axes $(x_1 x_2 x_3)$ (figure 2) is then

$$\mu_{ij} = \begin{pmatrix} \mu^* & & \\ & \mu^* & \\ & & 1 \end{pmatrix}. \qquad \ldots\ldots(1)$$

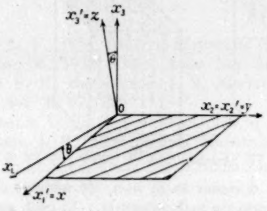

Figure 2. Surface orientation: Ox_3 is the easy direction of magnetization.

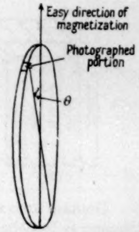

Figure 4. Orientation of disc.

Consider now the effect of cutting a surface in the specimen with the plane of the surface $(x_1' x_2')$ making an angle θ with the basal plane $(x_1 x_2)$. The easy direction of magnetization is Ox_3. The boundaries of figure 1 (*b*) are parallel to the $(x_1 x_3)$ and $(x_1' x_3')$ planes and are taken to extend to infinity so that the magnetic field, induction B and surface 'free pole' density σ, do not change with x_1 or x_1' $(\partial/\partial x_1' \equiv 0)$.

The permeability tensor with respect to the axes $(x_1' x_2' x_3')$ is now, transforming from (1),

$$\mu_{ij}' = \begin{pmatrix} 1+(\mu^*-1)\cos^2\theta & 0 & \sin\theta\cos\theta \\ 0 & \mu^* & 0 \\ \sin\theta\cos\theta & 0 & 1+(\mu^*-1)\sin^2\theta \end{pmatrix}. \quad \ldots\ldots(2)$$

The required potential $\psi(x_1' x_2' x_3')$ is obtained by applying the conditions (*a*) $\nabla \cdot B = 0$ except on the surface, (*b*) at the surface the normal component of B changes by $4\pi\sigma(x_1' x_2' 0)$ i.e. $\sigma(x_1' x_2' 0) = I_0 \cos\theta$, (*c*) the angle of rotation from the easy direction is small. Then

$$\frac{\partial^2\psi}{\partial x_i' \partial x_i'} = 0, \quad z > 0 \quad \ldots\ldots(3)$$

$$\mu_{ij}' \left(\frac{\partial^2\psi}{\partial x_i' \partial x_j'}\right) = 0, \quad z < 0 \quad \ldots\ldots(4)$$

$$\mu_{3j}' \left(\frac{\partial\psi}{\partial x_j'}\right)_{x_3'=0-} - \left(\frac{\partial\psi}{\partial x_j'}\right)_{x_3'=0+} = 4\pi\sigma(x_1' x_2' 0). \quad \ldots\ldots(5)$$

Writing for simplicity of symbols, $x_1' = x$, $x_2' = y$, $x_3' = z$, and $k^* = \mu^* - 1$, and remembering that $\partial/\partial x \equiv 0$,

$$\frac{\partial^2\psi}{\partial y^2} + \frac{\partial^2\psi}{\partial z^2} = 0 \quad z > 0 \quad \ldots\ldots(6)$$

$$(1+k^*)\frac{\partial^2\psi}{\partial y^2} + (1+k^*\sin^2\theta)\frac{\partial^2\psi}{\partial z^2} = 0 \quad z < 0 \quad \ldots\ldots(7)$$

$$(1+k^*\sin^2\theta)\left(\frac{\partial\psi}{\partial z}\right)_{z=0-} - \left(\frac{\partial\psi}{\partial z}\right)_{z=0+} = 4\pi\sigma(y,0). \quad \ldots\ldots(8)$$

Following Kittel (1949), a solution of the following form is postulated

$$\psi(y,z) = A\phi(y,\alpha z), \quad z > 0 \quad \ldots\ldots(9)$$

$$\psi(y,z) = A\phi(y,\beta z), \quad z < 0 \quad \ldots\ldots(10)$$

where ϕ is the potential satisfying the equations when $\mu^* = 1$ (infinite anisotropy), i.e.

$$\frac{\partial^2\phi}{\partial y^2} + \frac{\partial^2\phi}{\partial z^2} = 0, \quad z \neq 0 \quad \ldots\ldots(11)$$

$$\left(\frac{\partial\phi}{\partial z}\right)_{z=0-} - \left(\frac{\partial\phi}{\partial z}\right)_{z=0+} = 4\pi\sigma(y,0) \quad \ldots\ldots(12)$$

and $(\partial\phi/\partial z)_{z=0-} = -(\partial\phi/\partial z)_{z=0+}$, by symmetry. Then substituting (9) and (10) in (6), (7) and (8), with $\sigma(y,0)$ the same for $k^* = \mu^* - 1 = 0$ and $k^* = \mu^* - 1$ finite (condition (*c*)) we have,

$$\alpha = 1, \beta = \left(\frac{1+k^*}{1+k^*\sin^2\theta}\right)^{1/2} \quad \text{and} \quad A = 2/[1+(1+k^*)^{1/2}(1+k^*\sin^2\theta)^{1/2}]. \ (13)$$

Now the demagnetizing energy is given by

$$\begin{aligned} F_{\mathrm{m}} &= \frac{1}{2}\iint \sigma(x,y,0)\psi(x,y,0)\,dx\,dy \\ &= \frac{1}{2}\iint \frac{2\sigma(y,0)\phi(y,0)\,dx\,dy}{1+(1+k^*)^{1/2}(1+k^*\sin^2\theta)^{1/2}} \\ &= \left[\frac{2}{1+(1+k^*)^{1/2}(1+k^*\sin^2\theta)^{1/2}}\right]\left(\frac{1}{2}\iint I_0\cos\theta\,.\,\phi_0\cos\theta\,dx\,dy\right) \quad \ldots\ldots(14) \end{aligned}$$

where $\phi = \phi_0$ for $\theta = 0$.

The factor in square brackets is the demagnetizing energy of a Kittel-block structure with infinite anisotropy so that the energy in a material with finite anisotropy is reduced by a factor

$$\lambda(\theta) = \frac{2}{1+(1+k^*)^{1/2}(1+k^*\sin^2\theta)^{1/2}}. \qquad \ldots\ldots(15)$$

For cobalt the values of I_0 and K at 20°c are 1430 e.m.u. and $4{\cdot}3 \times 10^6$ erg cm^{-3} respectively, giving, very conveniently, $k^* = 3{\cdot}0$ and $\mu^* = 4{\cdot}0$. The condition (*c*) that rotations from the easy direction should be small is however only satisfied, in general, if $K > 2\pi I_0^2$ i.e. if $k^* < 1$. Even though the anisotropy coefficient of cobalt is the highest of any material that can be conveniently obtained, except for MnBi, this condition is not satisfied. Nevertheless, the results of the experiment described in the following section are still of interest. A curve showing the variation of $\lambda(\theta)$ with θ is shown in figure 3 for $\mu^* = 4{\cdot}0$, giving $\lambda = 2/3$ for $\theta = 0$ and $\lambda = 2/5$ for $\theta = 90°$.

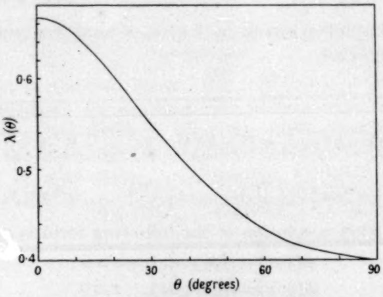

Figure 3. Variation of $\lambda(\theta)$ with θ.

§ 3. EXPERIMENTAL: THE EFFECT OF SURFACE ORIENTATION ON THE SUPERFICIAL DOMAIN STRUCTURE

An examination was carried out of the Bitter patterns produced on the curved surface of a disc, cut from a single crystal of cobalt with the hexagonal axis in the plane of the disc so that, in effect, a small region of the curved surface under observation could be treated as a plane cut at an angle θ with the basal plane (figure 4). This angle was measured with a simple goniometer attached to the crystal. Photographs of the main features of the pattern are shown in figure 5 (Plate). At $\theta = 90°$, (figure 5 (*a*)) with the surface parallel to the hexagonal axis, the pattern was composed of parallel, almost straight lines; these were similar to those on the face of the disc but with a somewhat different spacing. As the disc was rotated the pattern was modified giving the appearance of strands of wicker work (figure 5 (*b*)). At $\theta = 57°$ a transition took place and a chain pattern was produced with the sides of the chain parallel to the plane of the disc. Finally as rotation proceeded this pattern merged into the usual lace pattern. Clearly at $\theta = 57°$ a transition takes place between processes involving a reduction in energy by rotation and those involving the production of reverse spikes, with the chain (and also the lace) pattern representing sections through the 'spikes' (these patterns are discussed in detail by Goodenough (1956) and Kittel (1949)). For $\theta=57^\circ$ $\lambda=0{\cdot}44$ compared with a value of $0{\cdot}40$ for $\theta=90^\circ$, so that with a rotation of only 33° and a correspondingly small increase in λ, the formation of reverse domains becomes energetically more favourable.

Similar results have been obtained by Hall (1957) with patterns obtained on selected crystal faces of a polycrystalline ingot, when it was found that the transition from a chain to a wickerwork pattern took place between $\theta=54^\circ$ and $\theta=62^\circ$.

§ 4. CONCLUSION

It has been shown that a reduction in the demagnetizing energy associated with the Kittel type of domain structure in a uniaxial crystal can be brought about by the rotation of the magnetization vectors near the surface; an expression for the reduction in the energy has been obtained for materials with relatively high magnetocrystalline anisotropy ($K>2\pi I_0^2$). Under the most favourable circumstances, with the surface parallel to the easy direction ($\theta=90^\circ$) this effect cannot reduce the energy by a factor λ of more than $0{\cdot}40$ in cobalt and for $\theta=0$ the value of λ is only $0{\cdot}67$. The conditions under which the formation of domains of reverse magnetization might result in a greater reduction in energy have been investigated experimentally from an examination of the Bitter pattern produced on the surface of a single crystal of cobalt, for which K is large but less than $2\pi I_0^2$. It is found that reverse domains are formed when the angle between the surface and the easy direction is 33° or greater, i.e. when $\theta\leqslant 57^\circ$ and $\lambda\geqslant 0{\cdot}44$; when the angle with the easy direction is small ($<33^\circ$) there is no closure domain structure and any reduction in demagnetizing energy can only be brought about by rotation of the magnetization vectors.

Further development of this work may take the form of an extension of the theoretical treatment to produce a manageable expression for the energy appropriate to materials with low magnetic anisotropy; alternatively it may be possible to produce single crystals of materials, in a suitable form, with relatively high anisotropy.

ACKNOWLEDGMENTS

Thanks are due to Professor E. C. Stoner for his helpful advice and encouragement, and to the Department of Scientific and Industrial Research for a maintenance grant (to M.F.).

REFERENCES

GOODENOUGH, J. B., 1956, *Phys. Rev.*, **102**, 356.
HALL, E. O., 1957, *Proc. Phys. Soc.* B, **70**, 254.
KITTEL, C., 1949, *Rev. Mod. Phys.*, **21**, 541.

The Elastic Scattering of Protons by Tritons and ^{3}He

By B. H. BRANSDEN† and H. H. ROBERTSON‡

† Department of Natural Philosophy, The University of Glasgow
‡ The National Physical Laboratory, Teddington, Middlesex

MS. received 21*st April* 1958, *and in revised form* 16*th June* 1958

Abstract. This paper describes the extension of earlier work on the elastic scattering of neutrons by tritons and ^{3}He to proton scattering over the energy range 1 to 14 MeV. Cross sections and phase shifts are calculated assuming central two body interactions, of various exchange types and of Gaussian radial form.

Comparison with experiment favours the Serber rather than the symmetrical type of exchange interaction. Detailed agreement between the calculated and experimental cross sections is however lacking at the lowest energies.

§ 1. Introduction

A theoretical discussion of the elastic scattering of neutrons, having energies up to 14 MeV, by tritons and ^{3}He has been given in a previous paper (Bransden, Robertson and Swan 1956, to be referred to as I). The calculations assumed a two-body interaction of the form

$$\mathscr{V}(ij)=(w+mM+hH+bMH)V(ij)+\epsilon_{ij}V_{\mathrm{C}}(ij)$$
$$\text{where } V(r)=V_0\exp(-\mu r^2)$$
$$\text{and } V_0=-45\,\text{MeV},\ \mu=0{\cdot}2669\times10^{26}\,\text{cm}^{-2}; \qquad \ldots\ldots(1)$$

M and H are the Majorana and Heisenberg exchange operators and w, m, b, h are constants depending on the exchange nature of the interaction. V_{C} is the Coulomb potential and $\epsilon_{ij}=1$ if i, j are both protons and zero otherwise.

Although it is known that the nuclear interaction contains non-central components of the tensor and spin–orbit types, low energy scattering phenomena are generally well described in terms of an equivalent central potential such as (1). There is, however, some difficulty in determining the best equivalent central potential for a many-body problem, but as de Borde and Massey (1955) have pointed out, it is reasonable to suppose that the best equivalent central potential for the n-body scattering problem is that which gives the n-body binding energy correctly. The potential (1) is consistent with the binding energy of the deuteron and of the alpha particle, but is of rather longer range than is indicated by the two body scattering data.

The wave functions were of resonating group form using triton and ^{3}He ground state wave functions given by

$$\psi_{\mathrm{T}}=N_{\mathrm{T}}\exp\left(-\tfrac{1}{2}\lambda\sum_{ij}r_{ij}^2\right)$$
$$\psi_{\mathrm{H}}=N_{\mathrm{H}}\exp\left(-\tfrac{1}{2}\mu\sum_{ij}r_{ij}^2\right) \qquad \ldots\ldots(2)$$

the constants λ, μ being determined to give the best binding energies by the variational method. With these assumptions, integro-differential equations were derived, from which the scattering phase shifts were determined for the Serber and symmetrical interactions by an exact numerical solution with the help of the pilot ACE electronic computer of the National Physical Laboratory.

The calculated cross sections of paper I depended sensitively on the assumed exchange property of the two body interaction. This encouraged the hope that a comparison with experiment would enable the exchange property of the interaction to be identified, but the only available measurements of angular distributions were for neutron–triton scattering at 14 MeV (Coon, Bockelman and Barschall 1951) at angles greater than 80° where the Serber and symmetrical interaction gave similar results. However, measurements of the total cross section for neutron–triton and ^{3}He scattering by Cranberg† (1955) which are illustrated below (figure 7) show good agreement with the calculated total elastic cross sections for a Serber interaction. On the other hand the calculated cross sections using the symmetrical interaction are in definite disagreement with the observed total cross sections. Below 4 MeV, the charge exchange processes $n + {}^3He \rightarrow p + T$ contributes appreciably to the total cross section for $n + {}^3He$ scattering, so that agreement is not expected in this region.

As both the proton–triton and the proton–^{3}He differential cross sections have been measured at various energies below 11 MeV, the previous calculations have been extended to cover these collisions. In this paper the results of the new calculations are reported, cross sections and phase shifts having been obtained for proton–triton and proton–^{3}He scattering with interactons of the Serber and symmetrical type, and in addition, for proton–triton scattering, calculations have been made with ordinary and Majorana–Heisenberg exchange forces. Some results obtained using the formulation of Swan (1953) are also discussed.

§ 2. THEORY

Using the methods and notation of paper I, the integro differential equations that describe the scattering may be written in the form

$$\left(\frac{d^2}{dr^2} + k^2 - \frac{n(n+1)}{r^2}\right) f_n(r) = V(r) f_n(r) + \int_0^\infty k_n(r, r') f_n(r') dr' \qquad \ldots\ldots (3)$$

where $$V(r) = \alpha U(r) + ZC(r)$$

and

$$k_n = \beta(q_n + s_n) + \gamma t_n + \delta r_n + \eta \left\{\left(\frac{E_n}{E_T} + 1\right) n_n + p_n\right\} + \chi h_n + \omega g_n. \qquad \ldots\ldots (4)$$

The potential function $U(r)$ and the kernels $q_n \ldots\ldots p_n$ are the same as those that occur in the corresponding n–T and n–^{3}He scattering problems and detailed formulae have been given in paper I. $C(r)$ h_n, g_n are similar potential and kernel functions arising from the Coulomb potential

---

† We are indebted to Professor J. D. Seagrave for informing us of Dr. Cranberg's measurements and also of measurements of angular distributions now in progress by Dr. Cranberg and himself.

$$C(r)=\left(\frac{9}{8}\right)^3\frac{m}{\hbar^2}\iint d\mathbf{R}d\mathbf{r}'\{\psi(123)\}^2\,V_{\mathrm{c}}(14)$$

$$\left.\begin{matrix}h_n(r,r')\\ g_n(r,r')\end{matrix}\right\}=(rr')\int_{-1}^{+1}d\cos\Theta\ \mathrm{P}_n(\cos\Theta)\left(\frac{9}{8}\right)^3\frac{m}{\hbar^2}\int d\mathbf{R}\psi(123)\psi(124)$$

$$\times\left\{\begin{matrix}V_{\mathrm{c}}(34)\\ V_{\mathrm{c}}(14)+V_{\mathrm{c}}(13)\end{matrix}\right.$$

where $$rr'\cos\Theta=\mathbf{r}\,.\,\mathbf{r}' \qquad \ldots\ldots(5)$$

$\alpha, \beta, \gamma \ldots \omega$ are constants depending on the total spin of the system and on the values of w, m, b and h.

Solutions of (3) are required subject to the boundary conditions

$$f_n(0)=0\,;\ f_n(r)\sim k^{-1}\sin(kr-\tfrac{1}{2}n\pi-\alpha\log 2kr+\sigma_n+\delta_n) \qquad \ldots\ldots(6)$$

where
$$\alpha=\left(\frac{8M^2e^2}{9\hbar^2k}\right)\text{ and }\sigma_n=\arg\Gamma(1+i\alpha+n).$$

The singlet and triplet scattering amplitudes ${}^{1,3}g(\theta)$ can then be expressed in terms of the phase shifts ${}^{3,1}\delta_n$, so that

$${}^{3,1}g(\theta)=f_{\mathrm{c}}(\theta)+\frac{1}{2ik}\sum_n\exp(2i\sigma_n)(\exp(2i\,{}^{3,1}\delta_n)-1)(2n+1)\mathrm{P}_n(\cos\theta) \qquad \ldots\ldots(7)$$

where $f_{\mathrm{c}}(\theta)$ is the amplitude for Rutherford scattering

$$f_{\mathrm{c}}(\theta)=\frac{16e^2M^2}{27k^2}\operatorname{cosec}^2\tfrac{1}{2}\theta\exp(-i\alpha\log\sin^2\tfrac{1}{2}\theta+2i\sigma_0+i\pi)$$

and finally, the differential cross section $I(\theta)$ is

$$I(\theta)=\tfrac{3}{4}|{}^3g(\theta)|^2+\tfrac{1}{4}|{}^1g(\theta)|^2. \qquad \ldots\ldots(8)$$

§ 3. NUMERICAL CALCULATION

Accurate solutions of equations (3) with boundary conditions (6) have been obtained with the pilot ACE electronic computer of the National Physical Laboratory using a programme constructed by one of us (H. H. R) and described elsewhere (Robertson 1956). The phases for singlet and triplet scattering, ${}^1\delta_n$, ${}^3\delta_n$, have been found for all significant n (up to $n=4$) for incident proton energies of $E_{\mathrm{lab}}=1{\cdot}0$, $2{\cdot}5$, $5{\cdot}0$, $8{\cdot}0$ and $14{\cdot}0$ MeV, and using both the Serber and symmetrical forms of interaction

Serber $m=w=\tfrac{1}{4}(1+x)$; $h=b=\tfrac{1}{2}(1-x)$

Symmetrical $m=2b=\tfrac{1}{3}(1+3x)$; $h=2w=\tfrac{1}{3}(1-3x)$

where x is the ratio of the singlet and triplet neutron–proton interactions in an even state.

Although theoretical work on neutron–deuteron scattering (de Borde and Massey 1955) appears to rule out the neutral and Majorana–Heisenberg forms of the interaction, it is interesting to determine the cross section for these interactions as they are the extreme cases of (*a*) no exchange and (*b*) all exchange force

Neutral $m=h=0$; $w=\tfrac{1}{2}(1+x)$, $b=\tfrac{1}{2}(1-x)$

Majorana–Heisenberg $w=b=0$; $m=\tfrac{1}{2}(1+x)$, $b=\tfrac{1}{2}(1-x)$

so that, for proton–triton scattering only, calculations with these interactions have been performed in addition.

Calculated Phases

Phases are given in degrees and decimals and normalized so that $\delta \pm \pi$ is recorded if $|\delta|$ exceeds $\frac{1}{2}\pi$. The energy is in MEV (lab).

1. Proton–Triton Collisions

$n=$	0	1	2	3	4
(*a*) *Serber interaction—total spin* 1.					
1·0	−21·048	+ 5·738	−0·017	0	0
2·5	−38·061	+28·982	−0·157	+0·010	0
5·0	−55·817	+59·212	−0·646	+0·092	0
8·0	−70·284	+66·709	−1·311	+0·366	−0·003
14·0	−89·374	+63·347	−1·668	+1·504	−0·012
(*b*) *Serber interaction—total spin* 0.					
1·0	− 6·910	− 0·538	+ 0·049	0	0
2·5	−14·957	− 1·703	+ 0·513	−1·163	0
5·0	−26·114	− 1·995	+ 2·630	−0·017	+0·004
8·0	−37·385	+ 1·857	+ 7·106	−0·030	+0·024
14·0	−55·295	+20·845	+18·440	+0·211	+0·191
(*c*) *Symmetrical interaction—total spin* 1.					
1·0	−22·439	+ 0·415	−0·027	0	0
2·5	−40·657	+10·328	−0·263	+0·007	0
5·0	−59·967	+23·022	−1·188	+0·060	−0·002
8·0	−76·086	+30·170	−2·807	+0·220	+0·014
14·0	+81·772	+30·912	−6·163	+0·757	−0·086
(*d*) *Symmetrical interaction—total spin* 0.					
1·0	−11·415	− 1·076	+ 0·038	0	0
2·5	−22·201	− 4·054	+ 0·388	−0·005	0
5·0	−35·292	− 8·929	+ 1·903	−0·039	+0·003
8·0	−47·653	−13·112	+ 4·867	−0·129	+0·018
14·0	−66·755	−15·596	+11·601	−0·301	+0·138
(*e*) *Symmetrical interaction* (*Swan formulation*)*—total spin* 1.					
1·0	−20·095	+4·089	−0·012	0	0
2·5	−32·350	−3·558	+0·126	−0·009	0
5·0	−49·705	−6·817	+0·412	−0·077	+0·003
8·0	−65·427	−7·500	+0·475	−0·277	+0·018
14·0	−89·001	+0·262	−1·268	−0·878	+0·107
(*f*) *Symmetrical interaction* (*Swan formulation*)*—total spin* 0.					
1·0	−17·229	− 1·003	+0·015	0	0
2·5	−35·969	+17·109	−0·162	+0·009	0
5·0	−51·784	+32·739	−0·588	+0·081	−0·002
8·0	−63·806	+36·422	−0·895	+0·297	−0·012
14·0	−78·393	+30·573	+0·821	+1·014	−0·056
(*g*) *Neutral interaction—total spin* 1.					
1·0	−14·525	− 5·303	− 0·638	+0·001	0
2·5	−25·390	−15·584	+ 0·154	+0·016	0
5·0	−34·679	−28·522	+ 1·134	+0·162	+0·002
8·0	−40·072	−38·180	+ 4·361	+0·692	−0·012
14·0	−44·883	−52·602	+20·276	+3·308	+0·137
(*h*) *Neutral interaction—total spin* 0.					
1·0	+ 6·394	+ 5·551	+ 0·067	0	0
2·5	+ 3·774	+67·635	+ 0·732	0	0
5·0	− 5·494	−58·109	+ 4·018	+0·013	+0·005
8·0	−16·387	−58·584	+11·812	+0·111	+0·032
14·0	−34·030	−68·288	+33·842	+0·977	+0·264

(*i*) *Majorana–Heisenberg exchange interaction—total spin* 1.

n =	0	1	2	3	4
1·0	−23·289	+ 1·321	−0·034	0	0
2·5	−42·224	+ 5·178	−0·336	+0·004	0
5·0	−62·435	+10·717	−1·551	+0·035	−0·003
8·0	−79·491	+13·407	−3·766	+0·109	−0·019
14·0	+76·663	+11·643	−8·842	+0·209	−0·145

(*j*) *Majorana–Heisenberg exchange interaction—total spin* 0.

1·0	−12·332	− 1·176	+ 0·035	0	0
2·5	−23·720	− 4·460	+ 0·357	−0·005	0
5·0	−37·295	−10·007	+ 1·728	−0·045	+0·003
8·0	−49·968	−15·195	+ 4·349	−0·156	+0·016
14·0	−69·438	−20·317	−15·782	−0·437	+0·123

2. Proton–^{3}He Collisions

(*a*) *Serber interaction—total spin* 1.

n =	0	1	2	3	4
1·0	−15·292	+ 2·994	−0·014	0	0
2·5	−33·308	+17·927	−0·156	+0·008	0
5·0	−52·588	+44·694	−0·714	+0·085	+0·894
8·0	−68·334	+55·570	−1·558	+0·345	−0·006
14·0	−89·058	+54·906	−2·365	+1·427	−0·031

(*b*) *Serber interaction—total spin* 0.

1·0	−16·044	+ 2·496	−0·017	0	0
2·5	−34·876	+13·915	−0·193	+0·008	0
5·0	−55·086	+33·759	−0·904	+0·086	+0·894
8·0	−71·686	+42·781	−2·040	+0·347	−0·009
14·0	+86·318	+41·871	−3·526	+1·376	−0·057

(*c*) *Symmetrical interaction—total spin* 1.

1·0	−15·931	+ 1·876	−0·018	0	0
2·5	−34·694	+10·122	−0·211	+0·008	0
5·0	−54·941	+25·242	−1·023	+0·067	+0·894
8·0	−71·731	+33·974	−2·458	+0·259	−0·011
14·0	+85·560	+34·941	−5·216	+0·970	−0·076

(*d*) *Symmetrical interaction—total spin* 0.

1·0	−17·049	+ 1·138	−0·025	0	0
2·5	−37·040	+ 5·507	−0·297	+0·005	0
5·0	−58·745	+12·292	−1·477	+0·050	+0·893
8·0	−76·964	+15·297	−3·666	+0·177	−0·019
14·0	+77·901	+12·166	−8·526	+0·489	−0·149

§ 4. The Results

At the highest incident energy, 14 Mev, comparison of the present results with those of paper I indicates that the phase shifts for proton–triton scattering are close to those for neutron–^{3}He scattering. At lower incident energies the Coulomb interaction has the effect of reducing the phase shifts for proton scattering below those for neutron scattering. A similar result holds for the proton–^{3}He, neutron–triton systems.

Qualitatively, the proton scattering phases behave in the same way as those for neutron scattering. The phase shifts for proton–^{3}He scattering are nearly independent of the total spin of the system and the zero order phases are also insensitive to the exchange nature of the interaction. The higher order phases are, on the other hand, considerably larger for the Serber than for the symmetrical interaction.

The proton–triton phases are, as expected, both spin and interaction depent dent (there being a bound four-body state of the system when $S=0$† but nowhen $S=1$). The neutral and Serber interaction generally produce the largest phase shifts and cross sections, the Majorana–Heisenberg and symmetrical interactions produce the smallest. This is because the potential part of equation (3) $U(r)$ is more effective in producing large phase shifts than the kernel $k_n(r, r^1)$, and the importance of $U(r)$ is enhanced for the neutral and Serber and decreased for the Majorana–Heisenberg and symmetrical exchange interactions.

From the table it is seen that, with the exception of the zero order phase shift, phase shifts for the symmetrical interaction calculated using the Swan (1953 a, b) formulation are smaller and of opposite sign to those found from equation (3). This confirms the belief, expressed in paper I, that the differences between the present work and that of Swan are due to the different forms of kernel employed and not to the variational method used in the latter.

§ 5. Comparison with Experiment

5.1. *Proton–^{3}He Collisions*

Angular distributions for proton–^{3}He elastic scattering have been measured at incident proton energies in the laboratory system of 1·01 to 3·52 Mev (Famularo Brown, Holmgren and Stratten 1954), at 5·0 Mev and 8·6 Mev (Sweetman 1955, who measured the scattering of ^{3}He from protons) and at 9·75 Mev (Lovberg 1956).

Famularo *et al.* state that the cross section for 0·01 Mev protons has a constant value of 12×10^{-26} cm^2 at centre-of-mass scattering angles greater than 90°, and at angles less than this approaches the values expected from pure Coulomb scattering. At proton energies of 1·60, 2·25 and 3·52 Mev the measured angular distributions have broad minima around 90° of magnitude 11, 9, 8×10^{-26} cm^2 respectively, while the cross section at 169° increases from 11×10^{-26} cm^2 at 0·4 Mev to 27×10^{-26} cm^2 at 3·5 Mev. Reference to figures 1 and 2 shows that this description fits the calculated cross sections qualitatively, but that for both interactions considered, the theoretical cross sections are, in general, too large.

The measurements of Sweetman (1955) at a proton laboratory energy of 5·0 Mev are included in figure 3. The experimental and both the calculated cross sections show a minimum at 90°, of magnitude 6×10^{-26} cm^2. The rapid rise of the experimental cross sections at large scattering angles agrees qualitatively with the calculated cross section for the Serber interaction, but is in disagreement with that for the symmetrical interaction. At angles less than 90° the only two experimental measurements, at 43° and 69°, fall below both the calculated results. Preliminary measurements by Sweetman at a proton laboratory energy of 8·6 Mev, show that the minimum in the cross section has moved to 104°, which is in harmony with the theoretical results.

---

† It is interesting to note that a calculation of the binding energy of the alpha particle from equation (3) imposing boundary conditions $f_0(0)=0, f_0(r) \sim 0$ yields a binding energy of -26 Mev for both Serber and symmetrical interactions. This suggests that (1) is indeed a suitable equivalent central interaction for use with the resonating group method in the four body problem.

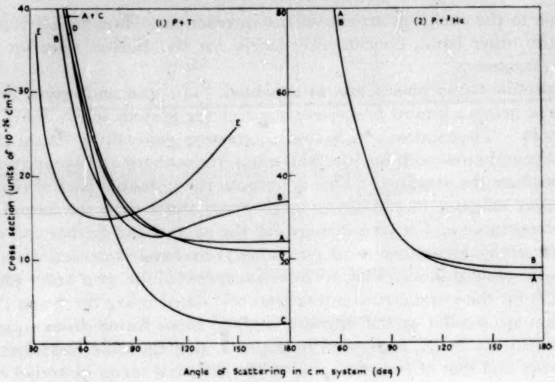

Figure 1.

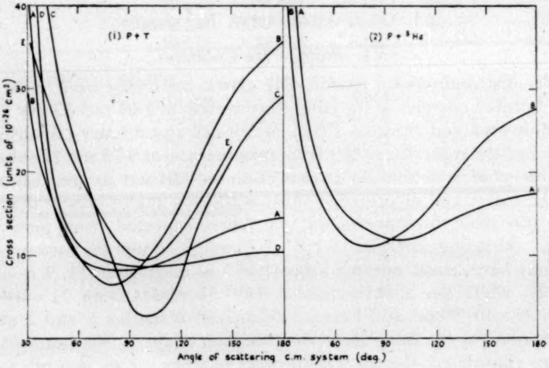

Figure 2.

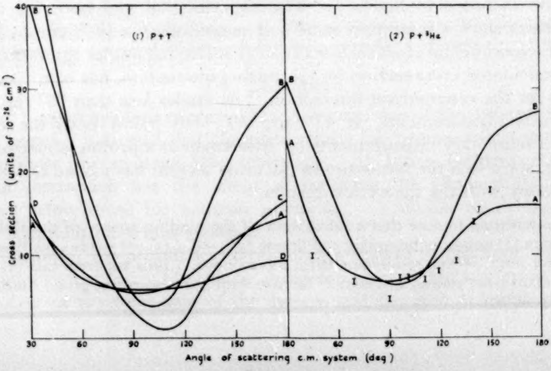

Figure 3.

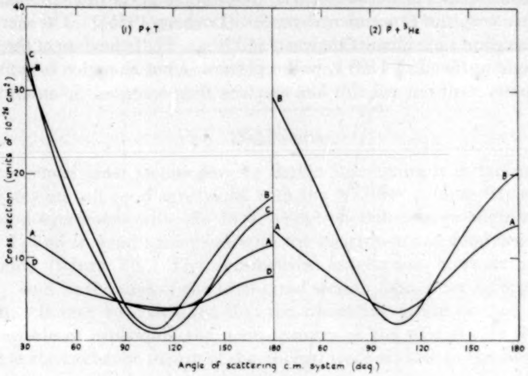

Figure 4.

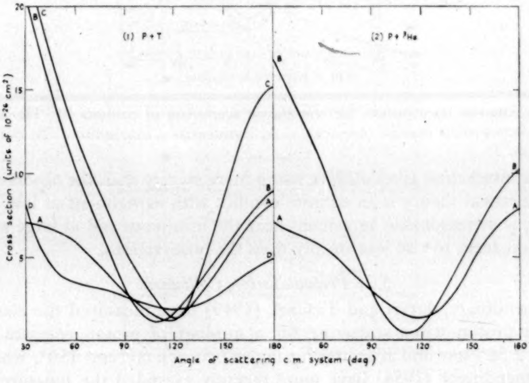

Figure 5.

Figures 1 to 5. Angular distributions for the elastic scattering of protons by ^{3}He and tritons at incident proton energies of 1·0, 2·5, 5·0, 8·0, 14·0 MEV respectively.
A, Symmetrical interaction. B, Serber interaction. C, Neutral interaction. D, Majorana–Heisenberg interaction. E, Experimental cross section (Ennis and Hemmendinger 1954). I, Experimental measurements of Sweetman (1955) at 5·0 MEV.

At 9·75 MeV (figure 6) we have interpolated in the calculated values of the angular distributions to an estimated accuracy of 0·2 in the units plotted to obtain comparison with the experimental results (Lovberg 1956). The Serber interaction gives good agreement at angles up to 130°. The behaviour at the minimum in the neighbourhood of 110° is well represented but at angles larger than 130° the Serber interaction gives a curve rising more steeply than the observed values. The symmetrical theory is in definite conflict with experiment at low angles of scattering, is in reasonable agreement near the minimum and at large angles the curve would seem to rise less steeply than the observations.

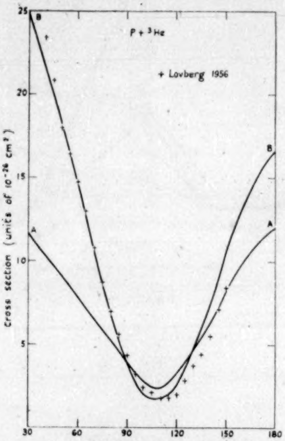

Figure 6. Angular distribution for the elastic scattering of protons by ^{3}He at 9·75 MeV incident proton energy (see text). A, Symmetrical interaction. B, Serber interaction.

5.2. *Proton–Triton Collisions*

Hemmendinger, Jarvis and Taschek (1949) have measured the elastic cross section for proton–triton scattering for a number of proton energies between 0·990 and 2·548 MeV and at scattering angles between 60° and 150°, while Ennis and Hemmendinger (1954) have more recently extended the measurements to cover the angular range 20° to 150° at the same energies. From 2·5 to 3·5 MeV and from 55° to 169° the cross section has been measured by Claassen, Brown, Freier and Stratton (1951) and at 2·5 MeV, where comparison is possible, these measurements are in reasonable agreement with those of Hemmendinger *et al.* In figures 1 and 2 curves representing the experimental results at 0·99 and 2·54 MeV are included. At the lower energy the experimental cross section is comparable with the theoretical cross section for the Serber and neutral interactions although quantitative agreement is not obtained. The predictions of the Majorana–Heisenberg and symmetrical exchange interactions are, however, definitely at variance with the experiments.

Various authors (McIntosh, Gluckstern and Sack 1952, Lowen 1954, Frank and Gammel 1955) have made phase shift analyses of the 1 to 3·5 Mev proton–triton and the 1 to 5 Mev proton–^{3}He scattering data. The agreement of the calculated and experimental cross sections is not sufficiently close at these energies for a meaningful comparison to be made between the calculated phases and the various solutions of the phase shift analyses and this has not been attempted.

§ 6. Discussion

The theoretical cross section for the Serber interaction is in fair agreement with the 5 Mev and in good agreement with the 9·75 Mev proton–^{3}He scattering data, in good agreement with the 14 Mev neutron–triton large angle scattering (see paper I) and in good agreement with the neutron–triton total cross section measurements (figure 7). The symmetrical interaction however gives less satisfactory, and in the case of the total cross section data, poor agreement with experiment. It may be concluded that the resonating group method of calculation is capable of explaining the main features of the proton–^{3}He interaction and also that the exchange nature of the nuclear force is close to the Serber type.

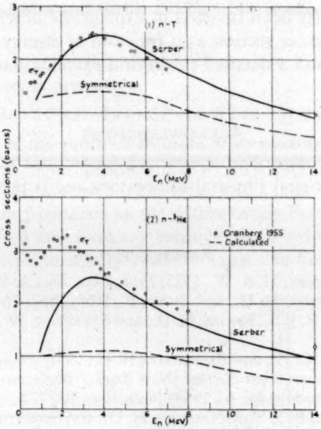

Figure 7. Calculated and experimental total neutron–triton and neutron–^{3}He cross sections.

These conclusions are in harmony with the results of theoretical studies of neutron–deuteron and neutron–alpha particle scattering. The neutron–deuteron scattering cross section is not so sensitive to the exchange nature of the interaction as is that for n–^{3}He and n–T scattering, and while it has been shown that an interaction of the exchange type is required, it has not been possible to decide between the merits of different exchange potentials (de Borde and Massey 1955). For neutron–alpha particle scattering it is again found that exchange rather than ordinary forces are required to explain the observed cross sections and that the

Serber interaction gives better agreement than the symmetrical (Hochberg, Massey, Robertson and Underhill 1955).

Below 2 MeV the neutron–triton and proton–^{3}He cross sections are both greater than those calculated, and this is presumably due to the neglect of polarization of the target nuclei in the wave functions used. At the higher energies, where polarization is not expected to be of any importance much better agreement could probably be obtained by the use of better triton and ^{3}He wave functions. The approximate wave functions (2) certainly lead to kernels of too short a range, but improvement in this direction is difficult, for the use of wave functions of a different form would involve a prohibitive amount of machine calculation.

The proton–triton and neutron–^{3}He scattering is clearly not so well described by the theory. The total elastic neutron–^{3}He cross section is in fair agreement with experiment above 3 MeV (figure 7)—again the symmetrical theory is in definite disagreement at all energies—while the proton–triton scattering data are in disagreement with the theory at 1 MeV and in only fair accord at 2·5 MeV. That the present theory fails to describe the proton–triton system so well as the proton–^{3}He may be attributed to the coupling between p + T and n + ^{3}He states by the reaction

$$\mathrm{p} + \mathrm{T} \rightleftharpoons \mathrm{n} + {}^3\mathrm{He}.$$

This mechanism has been invoked to explain the observed minimum in the proton–triton elastic cross section as a function of energy near the T(p, n)^{3}He threshold at 1·1 MeV, and a detailed theoretical examination of this effect is at an advanced stage.

ACKNOWLEDGMENT

Some of the work described above was carried out as part of the research programme of the National Physical Laboratory and is published by permission of the Director.

REFERENCES

DE BORDE, A. H., and MASSEY, H. S. W., 1955, *Proc. Phys. Soc.* A, **68,** 769.

BRANSDEN, B. H., ROBERTSON, H. H., and SWAN, P., 1956, *Proc. Phys. Soc.* A, **69,** 877.

CLAASSEN, R. S., BROWN, R. J. S., FREIER, G. D., and STRATTON, W. R., 1951, *Phys. Rev.*, **82,** 589.

COON, J. H., BOCKELMAN, C. K., and BARSCHALL, H. H., 1951, *Phys. Rev.*, **81,** 33.

CRANBERG, L., 1955, *Neutron Cross Section* (New York : McGraw-Hill).

ENNIS, M. E., and HEMMENDINGER, A., 1954, *Phys. Rev.*, **95,** 772.

FAMULARO, K. F., BROWN, R. J. S., HOLMGREN, H. D., and STRATTON, F., 1954, *Phys. Rev.*, **93,** 928.

FRANK, R. M., and GAMMEL, J. L., 1955, *Phys. Rev.*, **99,** 1406.

HEMMENDINGER, A., JARVIS, G. A., and TASCHEK, R. F., 1949, *Phys. Rev.*, **76,** 1137.

HOCHBERG, S., MASSEY, H. S. W., ROBERTSON, H., and UNDERHILL, L. H., 1955, *Proc. Phys. Soc.* A, **68,** 746.

MCINTOSH, J. S., GLUCKSTERN, R. L., and SACK, S., 1952, *Phys. Rev.*, **88,** 752.

LOVBERG, R. H., 1956, *Phys. Rev.*, **103,** 1393.

LOWEN, R. W., 1954, *Phys. Rev.*, **96,** 826.

ROBERTSON, H. H., 1956, *Proc. Camb. Phil. Soc.*, **52,** 538.

SWAN, P., 1953 a, *Proc. Phys. Soc.* A, **66,** 238; 1953 b, *Ibid.*, **66,** 740.

SWEETMAN, D. R., 1955, *Phil. Mag.*, [7], **46,** 358.

Energy Dependence of the Spatial Asymmetry in Polarized Muon Decay

By J. M. CASSELS, T. W. O'KEEFFE, M. RIGBY and J. R. WORMALD
Nuclear Physics Research Laboratory, University of Liverpool

MS. received 16th June 1958

Abstract. The spatial asymmetry of the positrons from polarized muon decay has been measured, with and without discrimination in favour of high energies. The high energy positrons were found to be more asymmetric than the average, and the effect is quantitatively consistent with the two-component neutrino theory.

---

§ 1. Introduction

The two-component neutrino theory makes rather definite predictions about the energy and angular distribution of the electrons emitted in muon decay (Lee and Yang 1957, Salam 1957, Landau 1957, Bouchiat and Michel 1957, Kinoshita and Sirlin 1957). For positive muons decaying by the process

$$\mu^+ \rightarrow e^+ + \nu + \tilde{\nu} \qquad \ldots\ldots(1)$$

the positron distribution is given by

$$d^3N(x, \theta, t) = \tfrac{1}{4}\lambda e^{-\lambda t} x^2\{(3-2x) + \xi P \cos\theta(2x-1)\} \sin\theta d\theta dx dt \quad \ldots\ldots(2)$$

where x is the energy of the positron in units of its maximum possible energy, θ is the angle of emission of the positron relative to a suitable reference direction for the polarization of the muons, t is the time, and λ is the decay constant of the muon. The parameter ξ depends on the nature of the Fermi interaction responsible for the decay, and it may have any value between -1 and $+1$; the polarization P of the muons experimentally available must also lie between -1 and $+1$.

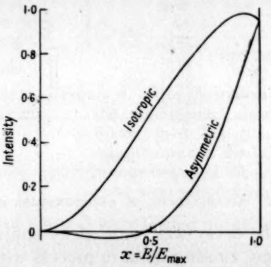

Figure 1. Energy spectra for the isotropic and asymmetric components, according to the two-component theory. The symmetric spectrum should be multiplied by $\xi P \cos\theta$ to get the actual distribution.

In this paper no special assumptions will be made about the product ξP; it is in fact large and negative for muons from the Liverpool cyclotron stopped in carbon, if the direction of motion of the beam before stopping is used as the reference for P (Cassels, O'Keeffe, Rigby, Wetherell and Wormald 1957).

The energy distributions of the isotropic and asymmetric parts of the spectrum are shown in figure 1; radiative corrections (Kinoshita and Sirlin 1957) have been included, although they make a negligible difference to the conclusions of this paper.

The isotropic spectrum has often been studied experimentally, and the latest work shows a close if not exact correspondence with the two-component prediction (Rosenson 1958). The experiment reported here was designed to study the ratio of the asymmetric part of the spectrum to the isotropic part, as a function of positron energy. The spatial asymmetry of the positrons was in fact studied in two conditions: (*a*) with no energy discrimination, when equation (2) integrated over x predicts that the positron distribution should be proportional to $1+\frac{1}{3}\xi P\cos\theta$; (*b*) with selection of the highest energy positrons: ideally equation (2) with $x=1$ predicts a distribution proportional to $1+\xi P\cos\theta$, so that the asymmetry coefficient should be a factor 3 bigger than in condition (*a*). In practice the energy resolution of the experiment was not perfect, and a rather smaller increase in the asymmetry is to be expected (§ 3).

§ 2. APPARATUS

The layout of the experimental apparatus is shown in figure 2. A 110 MeV longitudinally polarized muon beam from the Liverpool cyclotron was slowed down in a polyethylene absorber. Some of the muons stopped in the carbon target, their arrival being signalled by a $12\overline{3}$ coincidence–anticoincidence event in the first three counters. Forward decays of these muons were signalled by a later $34\overline{2}$ event. Counters 1–4 were made of scintillating plastic, and their pulses were mixed with resolving times of the order of 10^{-8} second. For part (*b*) of the experiment, when energy discrimination was required, a sodium iodide crystal 6 in. long and 5 in. in diameter was set up behind counter 4. The linear pulse from this crystal could be used to gate the $34\overline{2}$ events.

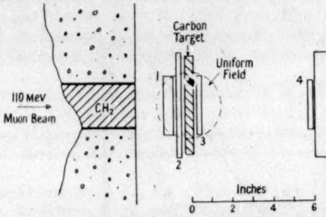

Figure 2. Arrangement of experimental apparatus.

The asymmetry of the decay was revealed by applying a uniform magnetic field to the stopped muons, causing them to precess with the frequency

$$\omega = geH/2m_{\mu}c,$$

where H is the magnetic field and the other symbols have their usual meanings. Because of the precession θ in equation (1) must be replaced by $\theta+\omega t$, so that for forward decays

$$e^{\lambda t}d^3N(x,0,t)=\tfrac{1}{4}\lambda x^2\{(3-2x)+\xi P\cos(\omega t)(2x-1)\}\sin\theta\, d\theta\, dx\, dt. \quad \ldots\ldots(3)$$

The positron intensity, multiplied by $e^{\lambda t}$, reveals the spatial asymmetry in the form of a simple harmonic time modulation. The depth of this modulation was a measure of the amount of asymmetry; no corrections for finite geometry or time resolution were required, because the distributions in both parts (*a*) and (*b*) of the experiment were affected in the same way.

The time distribution of the delays between the $12\bar{3}$ and $34\bar{2}$ events was turned into a pulse height distribution by an electronic timesorter, and the results were recorded on a pulse height analyser. A delay of $\frac{1}{2}$ μsec was introduced into the $34\bar{2}$ line, so that time intervals from $-\frac{1}{2}$ μsec to $+3\frac{1}{2}$ μsec between the two events were displayed; the events with negative delay were caused by random correlations between the two kinds of event, and the counts in this range were used as measures of the backgrounds.

§ 3. ENERGY RESOLUTION

The energy resolution (figure 3) of the sodium iodide crystal was measured with the help of a positron beam of variable energy, set up in the manner described by Cassels, Fidecaro, Wetherell and Wormald (1957). For geometrical reasons the positron beam itself had some energy spread, but at 50 MeV ($x=1$) this was just equivalent to the spread introduced by the finite thickness of the target in the main experiment.

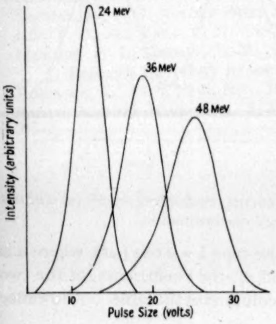

Figure 3. Experimental energy resolution of the sodium iodide crystal.

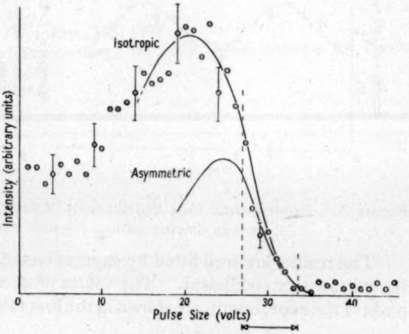

Figure 4. The theoretical spectra of figure 1, with the experimental energy resolution of figure 2 folded in. The points are an experimental measurement of the isotropic component. The broken lines and the arrows indicate the range of pulse sizes selected in part (*b*) of the experiment.

The resolution curves of figure 3 were folded numerically into the theoretical spectra of figure 1, the result (figure 4) being the expected pulse height distribution from the crystal for the isotropic and asymmetric parts of the positron distribution. The experimental points in figure 4 show the pulse height distribution actually found when positive pions were stopped in the apparatus. The decay in the target of the pions produced an unpolarized source of muons, since no particular direction of muon emission was favoured, and so the points should follow the isotropic curve. The result of this test is considered satisfactory.

The vertical broken lines in figure 4 show the upper and lower limits of pulse height which operated the selection gate for part (*b*) of the experiment. By integrating numerically the area between the broken lines and under the two curves it was found that the positron distribution in part (*b*) of the experiment should theoretically be proportional to $1+(0{\cdot}775 \pm 0{\cdot}020)\xi P\cos\theta$. The loss of low energy positrons caused by the finite thickness of the target ($1{\cdot}6\ \mathrm{g\ cm^{-2}}$) and counter 3 ($0{\cdot}7\ \mathrm{g\ cm^{-2}}$) should not have significantly affected the asymmetry coefficient in part (*a*) of the experiment. Thus the asymmetry coefficient was expected to increase by a factor $(0{\cdot}775 \pm 0{\cdot}020)/\tfrac{1}{3} = 2{\cdot}32 \pm 0{\cdot}06$ in going from part (*a*) to part (*b*) of the experiment.

§ 4. EXPERIMENTAL RESULTS

The time distribution of the real decay events, multiplied by $e^{\lambda t}$, are shown in figures 5 (*a*) and 5 (*b*). In part (*a*) of the experiment the subtracted background was equal to 9·8% of the isotropic contribution at $t=0$, and in part (*b*) it was 7·3%. Real decays were observed at the total rate of about 6 per minute in part (*a*), and about 2/3 per minute in part (*b*).

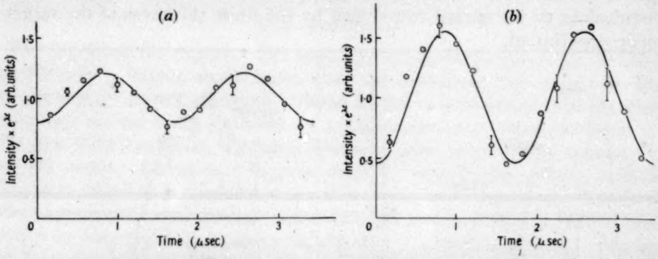

Figure 5. Experimental time distributions of decay events, multiplied by $e^{\lambda t}$ (*a*) without energy discrimination, (*b*) with energy discrimination.

The results are well fitted by expressions of the type $1+a\cos(\omega t)$, where a is the asymmetry coefficient. The values of a_a and a_b, the coefficients for the two parts of the experiment, are shown in the first two columns of the table. Allowance is made both for statistical and for possible systematic errors, for example in estimating the backgrounds. The third column shows the experimental ratio of the asymmetry coefficients, and the fourth column notes again the theoretical ratio according to the two-component theory.

Experimental and Theoretical Asymmetry Coefficients

a_a (exp.)	a_b (exp.)	a_b/a_a (exp.)	a_b/a_a (theor.)
$-0{\cdot}197 \pm 0{\cdot}021$	$-0{\cdot}539 \pm 0{\cdot}034$	$2{\cdot}73 \pm 0{\cdot}33$	$2{\cdot}32 = 0{\cdot}06$

§ 5. CONCLUSION

It is clear that the result of the experiment is consistent with the two-component prediction, although the experimental a_b/a_a is actually larger than the theoretical one by 1·1 times the combined standard deviation. Other experimenters, who have examined the high energy electron asymmetry by range methods, have also found agreement with the two-component theory (Berley, Coffin, Garwin, Lederman and Weinrich 1957, Mukhin, Ozerov and Pontecorvo 1958).

Finally, it is well to point out that there are versions of the four-component neutrino theory, not reducible to the two-component theory, which give the same phenomenological distribution (2). The agreement found here and elsewhere with this formula does not prove that the two-component theory is correct; it merely allows it to be correct.

ACKNOWLEDGMENTS

We should like to thank Mr. Halliday and the cyclotron crew for running this experiment, Dr. Collinge for providing important parts of the electronic equipment, and Dr. Murphy and Messrs. Jones and O'Neill for help in recording the data. One of us (T. W. O'K.) is indebted to the Department of Scientific and Industrial Research for a maintenance grant.

REFERENCES

BERLEY, D., COFFIN, T., GARWIN, R. L., LEDERMAN, L. M., and WEINRICH, M., 1957, *Phys. Rev.*, **106**, 835.
BOUCHIAT, C., and MICHEL, L., 1957, *Phys. Rev.*, **106**, 170.
CASSELS, J. M., O'KEEFFE, T. W., RIGBY, M., WETHERELL, A. M., and WORMALD, J. R., 1957, *Proc. Phys. Soc.* A, **70**, 543.
KINOSHITA, T., and SIRLIN, A., 1957, *Phys. Rev.*, **107**, 593.
LANDAU, L., 1957, *Nuclear Phys.*, **3**, 127.
LEE, T. D., and YANG, C. N., 1957, *Phys. Rev.*, **105**, 1671.
MUKHIN, A. I., OZEROV, E. B., and PONTECORVO, B., 1958, Joint Institute for Nuclear Research (Moscow) Report P-159.
ROSENSON, L., 1958, *Phys. Rev.*, **109**, 958.
SALAM, A., 1957, *Nuovo Cim.*, **5**, 299.

The Excitation of Helium by Electrons of Low Energy

By S. J. B. CORRIGAN and A. von ENGEL
Clarendon Laboratory, Oxford

MS. received 14*th July* 1958

Abstract. An analysis has been made of the main excitation processes caused by an electron swarm passing through helium. Recent experimental studies of energy losses of monoenergetic electron beams in helium together with published theoretical excitation functions have been used to obtain approximate cross sections for the principal transitions leading to metastable and resonance states.

The energy balance for an electron swarm in helium is derived and compared with that found previously for molecular hydrogen.

---

§ 1. Introduction

The excitation of helium atoms by electrons of uniform energy has been studied experimentally by many workers (Massey 1956). The methods employed depend either on observing the electron energy loss, the production of photons or detection of metastable atoms. Very few experiments have yielded absolute values for transition probabilities from the ground state to the various excited levels largely on account of difficulties of calibration of the detector, difficult geometry or the use of excessively large currents. In the case of optical excitations most workers have measured only visible radiation which arises from transitions between excited states.

An important study of the total inelastic cross section in helium has been made by Maier-Leibnitz (1935) who measured the energy distribution of electrons diffusing through the gas to a collector. His results have been used by Smit (1936) to calculate the electron energy distribution for a swarm. This distribution function gave the right values of the ionization coefficient, a convincing proof of its correctness (for further work see Abdelnabi and Massey 1953).

The rate of excitation by an electron swarm can be expressed by a coefficient ϵ_k, giving the number of excitations of type k per electron per centimetre of drift in the field direction. In the case of helium it is appropriate to consider the coefficients ϵ_{met} and ϵ_{rad} giving the rate of production of metastable atoms and ultraviolet quanta respectively. It will be shown here that sufficient information on the various cross sections exists to enable these cross sections to be calculated. Considerations of the energy balance for the swarm provide a test that no important excitation coefficients have been neglected. The authors have recently (1958) made an experimental study of the competing excitation processes in molecular hydrogen; the same approach could in principle be used for helium. However, experimental difficulties seemed formidable and newly published work with electron beams appeared to have made it unnecessary.

§ 2. Excitation Cross Sections

Recently Schulz and Fox (1957) measured the total excitation cross section in helium up to 22 v. They used an apparatus giving much improved energy resolution as a result of which they found two well defined peaks within this energy range. Their absolute cross sections agree with those of Maier-Leibnitz to within 25%. Thus it seems that the best approximation to the total excitation function may be obtained by scaling the low energy curve of Schulz and Fox to join the curve of Maier-Leibnitz at about 22 v.

In figure 1, curve A shows the total cross section of Maier-Leibnitz obtained with an electron energy spread of half width about 0·5 v. This spread masks any detail of the excitation curve extending over an energy range of the same order of magnitude and explains the absence of pronounced peaks in curve A which are found in A′, the excitation function of Schulz and Fox (for an earlier experiment with a narrow energy spread see Löhner 1935).

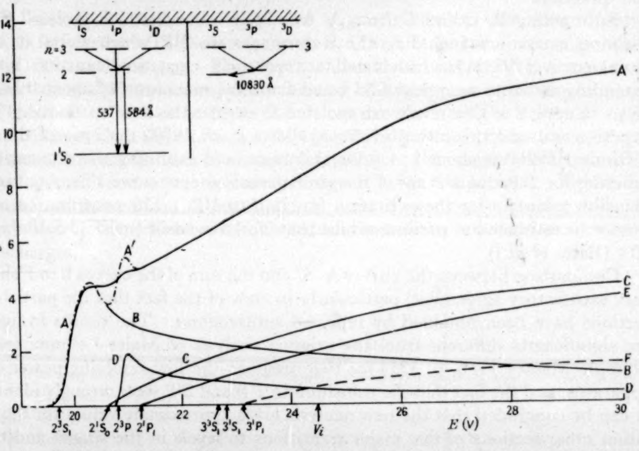

Figure 1. Excitation cross sections q as a function of the electron energy E. A, total excitation cross section (low energy resolution); A′, total excitation cross section (high energy resolution); B, excitation cross section to 2^3S; C to 2^1S; D to 2^3P; E to 2^1P; F to 3^1P. Inset: simplified level diagram of helium.

The first transition 1^1S_0–2^3S_1 starting at 19·8 v produces metastable atoms. The next critical potential is at 20·6 v for the transition 2^1S_0, therefore the part of curve A′ below 20·6 v is simply the excitation function for 2^3S. In order to find a plausible shape for the continuation of this function beyond 20·6 v where other excitation contributes to curve A′, use is made of a theoretical curve computed by Massey and Moiseiwitsch (1954). Their theoretical approach is most likely to be in error for energies close to the onset potential; however at higher energies their various approximations converge to a smoothly decaying curve. Since for energies up to 20·6 v the only excitation is to 2^3S, the first peak in A′ must give the actual peak in the triplet excitation function. Beyond 20·6 v the curve is extrapolated by joining it to the tail of the Massey and Moiseiwitsch average curve multiplied by a scaling factor to give a smooth connection. This gives curve B in figure 1. Massey and Moiseiwitsch have also computed the excitation function for the state 2^1S down to an energy of 1·5 v above the onset. As is expected for a singlet–singlet transition this curve rises gradually to a broad maximum at about 14 v above onset. Curve C is their excitation function extrapolated down to the onset at 20·6 v.

At 20·9 v the transition 1^1S_0–2^3P sets in after which the next critical potential is for 2^1P at 21·2 v. Subtracting B and C from A the remaining part of the total excitation cross section is found to have a peak (the second peak in A′) between 20·9 and 21·2 v which must therefore be identified with a maximum in the triplet excitation function to 2^3P. The part of (A′–B–C) up to 20·2 v gives the initial part of curve D, the excitation function for 2^3P. The curve is extended to higher energies by assuming that its tail has the same form as B. Excitation to 2^3P results in a transition to the metastable state 2^3S with emission of an infra-red quantum.

Subtracting B, C and D from A′ we obtain a curve which gives all the remaining excitations including the resonance state 2^1P which starts at 21·2 v. Rothenstein (1954) has calculated a theoretical excitation function for 2^1P extending down to energies of 33 v and finds the maximum of about $0{\cdot}1\pi a_0^2$ at 65 v. Curve E is this result extrapolated to zero at the onset potential. From experimental and theoretical evidence (Bates *et al.* 1950) the ratio of the cross sections $3^1P/2^1P$ is about 1 : 4. On this basis, and assuming that the excitation function for 2^1P and 3^1P are of the same general shape, curve F is obtained as a plausible estimate for the excitation function to 3^1P. The contribution of 3^3S cannot be estimated at present, whilst that of 3^1S is small (max $\simeq 3{\cdot}5.10^{-3}\pi a_0^2$ at 60 v (Bates *et al.*)).

Comparison between the curves A–A′ and the sum of the curves B to F shows a very satisfactory agreement, particularly in view of the fact that the partial cross sections have been obtained by repeated subtractions. The results in figure 1 are significantly different from the original analysis of Maier-Leibnitz (see for example Massey 1956, p. 335) for two reasons: the low resolving power of his apparatus, and the fact that the transition to 2^1S and 2^3P were wrongly identified. It can be concluded that the new analysis gives approximate values for the excitation cross sections of five major transitions to levels in the singlet and triplet systems of helium. In addition it is shown that for electrons of low energy the overwhelming number of inelastic collisions produce metastable atoms, whereas only a small fraction results in the emission of quanta in the far u.v. At higher electron energies the position is probably reversed.

§ 3. EXCITATION COEFFICIENTS AND ENERGY BALANCE FOR ELECTRON SWARMS

By analogy with the ionization coefficients α we define ϵ_k as the number of atoms which have been raised to the kth state per electron per centimetre of path in the field direction. In general the coefficients ϵ are functions of X/p, the electric field reduced to unit pressure, provided only single collisions occur. This is the case when the current density is sufficiently low.

Using the cross sections given in figure 1 together with Smit's energy distribution, it is now possible to evaluate the coefficients ϵ_{met} and ϵ_{rad} corresponding to transitions to metastable and radiating levels respectively. If the electron energy distribution is $f(E)dE$ and the electron velocity v, the cross section for excitation to the kth level q_k with an onset at E_k, the drift velocity of electrons v_{d} and $N_1 = 3{\cdot}6 \times 10^{16}$ atoms/cm³ at $p = 1$ mm, then the excitation coefficient

$$\frac{\epsilon_k}{p} = \frac{N_1}{v_{\mathrm{d}}} \int_{E_k}^{\infty} q_k v f(E) dE \qquad \ldots\ldots(1)$$

Smit's electron energy distribution is based on curve A for the total inelastic losses. Hence the total excitation coefficient $\epsilon_0 = \epsilon_{\text{met}} + \epsilon_{\text{rad}}$ is fixed by energy balance considerations. One electron in travelling unit distance in the field direction gains X ev and in the steady state must lose an equal amount in elastic, exciting and ionizing collisions. The elastic loss can easily be computed and the ionizing loss is given by αV_i, hence ϵ_e can be found. The ratio of the

$$\frac{\epsilon_{\text{rad}}}{\epsilon_{\text{met}}} = \frac{\int_0^\infty q_{\text{rad}} f(E) dE}{\int_0^\infty q_{\text{met}} f(E) dE} \qquad \ldots\ldots (2)$$

partial excitation coefficients ϵ_{met} and ϵ_{rad} is given by assuming constant collision frequency. The sum of curves B, C and D is taken for q_{met}, whilst A′–B–C–D is used for q_{rad}. This approach has the advantage of giving $\epsilon_{\text{rad}}/\epsilon_{\text{met}}$ without using drift velocities, the values of which appear uncertain.

The results are given in figure 2. It can be seen that the values of ϵ_{met}/p are much larger than those of ϵ_{rad}/p showing that the rate of production of metastable atoms far exceeds that of ultra-violet quanta in the range considered. The ionization coefficient α/p is included in figure 2 for comparison. Figure 3 is derived from figure 2 and shows Z_e/Z_i, the ratio of exciting to ionizing collisions as a function of X/p, which is useful for calculations of secondary electron emission in discharges.

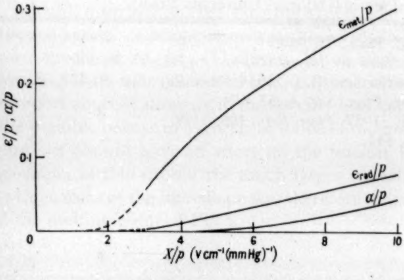

Figure 2. Ionization coefficient α/p, excitation coefficient to the metastable levels ϵ_{met}/p and excitation coefficient to ultra-violet radiating levels ϵ_{rad}/p as a function of the electric field X at $p = 1$ mm Hg.

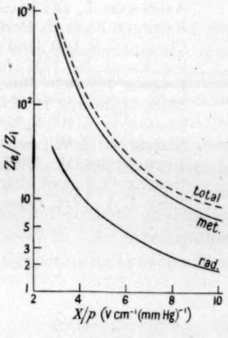

Figure 3. Ratio of the number of excitations and ionizations Z_e/Z_i as a function of the electric field X at $p = 1$ mm Hg. Z_e refers to the total number of excitations, to excitations to metastable levels and to radiating levels respectively.

The energy balance for the losses of an electron swarm in helium is derived from the results in figure 2 and is given in the table for two values of the reduced field. The balance for molecular hydrogen is also shown for comparison (Corrigan and von Engel 1958). In both cases the fraction of the total energy spent on quantum production increases as X/p is raised. However, the surprising result emerges that the ratio of energy spent producing ultra-violet quanta to that forming one ion pair is of the same order of magnitude in helium as in molecular hydrogen. It is also interesting to note that the fraction of total energy used to produce metastable atoms in helium seems to be approximately the same as that to produce dissociation in hydrogen.

Approximate Losses in vcm^{-1} for Helium and for Molecular Hydrogen in Comparison (X/p in vcm^{-1} (mm Hg)$^{-1}$)

X/p	elastic	vibr.	rad.	met.	diss.	ioniz.
			Helium			
4	1·2	—	0·25	2·4	—	0·03
10	1·1	—	1·5	6·2	—	1·1
			Hydrogen			
40	0·5	2	10	—	27	2·5
100	1	2	22	—	66	21

It has long been known that the drift velocity of an electron swarm in helium (von Engel 1955) begins to depart from the values predicted by considering elastic losses only for X/p greater than 2. From figure 2 it is seen that even at such low values of the reduced field inelastic losses become important.

REFERENCES

ABDELNABI, I., and MASSEY, H. S. W., 1953, *Proc. Phys. Soc.* A, **66,** 288.
BATES, D. R., *et al.*, 1951, *Phil. Trans. Roy. Soc.* A, **243,** 93.
CORRIGAN, S. J. B., and VON ENGEL, A., 1958, *Proc. Roy. Soc.* A, **245,** 335.
VON ENGEL, A., 1955, *Ionized Gases* (Oxford: University Press).
LÖHNER, H., 1935, *Ann. Phys., Lpz.*, **22,** 81.
MAIER-LEIBNITZ, H., 1935, *Z. Phys.*, **95,** 489.
MASSEY, H. S. W., 1956, *Handbuch der Physik* (Berlin: Springer) **36,** 306.
MASSEY, H. S. W., and MOISEIWITSCH, B. L., 1954, *Proc. Roy. Soc.* A, **227,** 38.
ROTHENSTEIN, W., 1954, *Proc. Phys. Soc.* A, **67,** 673.
SCHULZ, G. J., and FOX, R. E., 1957, *Phys. Rev.*, **106,** 1179.
SMIT, J. A., 1936, *Physica*, **3,** 543.

Nuclear Magnetic Resonance in Solid *Cyclo*pentene

By I. J. LAWRENSON and F. A. RUSHWORTH

Department of Natural Philosophy, St. Salvator's College, University of St. Andrews, Scotland

Communicated by J. F. Allen; *MS. received 8th July* 1958

Abstract. The variation of the nuclear magnetic resonance absorption line of *cyclo*pentene has been measured from 20°K to the melting point at 138°K. Below the specific heat transition temperature of 87°K the lattice is effectively rigid and there is no evidence corresponding to a reported specific heat anomaly at 54°K. Above 87°K the second moment of the absorption line is reduced and this is interpreted in terms of molecular motion about an axis perpendicular to the plane of the four co-planar carbon atoms of the molecule. Above 124°K a further reduction in the second moment is thought to be due to self-diffusion of the molecules through the crystal lattice. Information is also obtained which confirms the nonplanar structure of the *cyclo*pentene molecule.

§ 1. Introduction

In certain cases information obtained from an analysis of the variation of the nuclear magnetic resonance absorption line-shape with temperature can give valuable information regarding both molecular structure and molecular motion in the solid state. *Cyclo*pentene was chosen for such an investigation because of its known specific heat data (Huffman, Eaton and Oliver 1948). These authors report a specific heat transition at 87°K, the melting point being 138°K, and they also report another anomaly in the specific heat curve at 54°K which they attribute to the possible release of a frozen-in mode of motion. Provided this motion is fast enough, it should have an effect on the nuclear magnetic resonance absorption line-shape, as also should the much larger transition at 87°K. An investigation into the nature of the line-shape was therefore made at temperatures between 20°K and the melting point of 138°K.

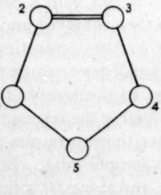

Figure 1. Carbon ring structure of *cyclo*-pentene molecule.

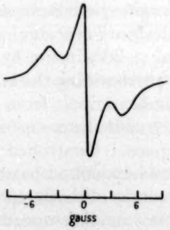

Figure 2. Line-shape derivative curve at 124°K.

It was also hoped that information might be obtained regarding the molecular structure of *cyclo*pentene. Beckett, Freeman and Pitzer (1948) studied the thermodynamic properties of *cyclo*pentene and considered two possible molecular models. The first model, where the carbon ring structure indicated in figure 1 was taken as planar, was not thought to be likely because it would involve opposed configurations of the hydrogen atoms attached to carbon atom 5 relative to the hydrogen atoms attached to carbon atoms 1 and 4. They considered that the torsional forces about the double bond were strong enough to ensure that carbon atoms 1, 2, 3 and 4 were coplanar, but that the repulsions between the hydrogen atoms already mentioned would force carbon atom 5 out of this plane. Calculation of the strain energy of the puckered model showed that this atom could be out of the plane of the other four by an amount up to 0·3 Å without appreciably affecting this energy. The second molecular model used is therefore one in which carbon atom 5 is taken as being 0·3 Å distant from the plane of the other four carbon atoms.

§ 2. EXPERIMENTAL DETAILS

The sample of *cyclo*pentene was obtained from the Chemical Research Laboratory, Teddington, and had a mole per cent purity of 99·97 ± 0·02 as determined from freezing point measurements. The sample was transferred under vacuum from the standard ampoule in which it was supplied to a thin-walled Pyrex tube specially made to fit the nuclear resonance coil.

The nuclear magnetic resonance absorption line was detected by a bridge method, using a twin-T bridge followed by a radio-frequency amplifier and a commercial receiver. Since the lines were all relatively broad, the final detection was carried out using a phase-sensitive detector feeding a recording microammeter. The traces on this recorder gave the first derivative of the true absorption line-shape, since the technique adopted was to use a modulating field with a peak to peak value about one-third of the line-width and to sweep through the line at a constant rate using an automatic field control. The second moments were calculated from these derivative curves using the trapezium rule and applying a correction for the finite modulating field (Andrew 1953). The magnetic field of 5260 oersteds was supplied by a permanent magnet having pole faces 20 cm in diameter and a gap of 5·5 cm (Andrew and Rushworth 1955).

The sample could be kept at any temperature from 20°K upwards by means of a specially designed cryostat. For the lower range of temperature the coil assembly was cooled to 20°K using hydrogen gas as thermal contact with a bath of liquid hydrogen surrounding the assembly. The gas was then removed and the system virtually isolated apart from the small heat leaks down the connecting wires and tubes which could be compensated for by allowing a small gas pressure to remain in the interspace. Controlled heat could be supplied to the sample through two non-inductively wound heaters, one above and one below the resonance coil, and the temperature of the sample was determined by two thermocouples placed so as to detect any small temperature gradient along the sample tube. For temperatures above 62°K liquid nitrogen was used as coolant, and above 90°K liquid oxygen was used as coolant. Once an equilibrium temperature had been reached it could easily be kept constant for the time needed to take several derivative curves.

§ 3. Results and Discussion

The variations with temperature of the width and the second moment of the absorption line are shown in figure 3. The line-width is defined as the interval in gauss between points of maximum and minimum slope. Because of the nature of the resonance line at the higher temperatures, two line-widths have been plotted, the shape of the derivative curve at 124°K being shown in figure 2.

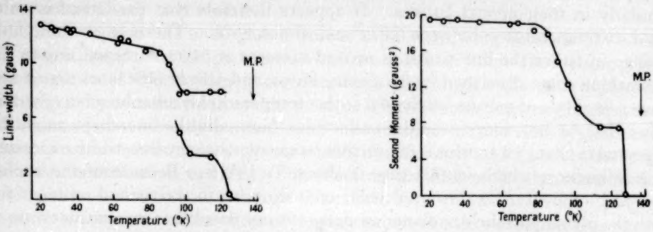

(*a*) (*b*)

Figure 3. Variation of (*a*) line-width and (*b*) second moment with temperature.

Between 20°K and 85°K the line-width and second moment are effectively constant, apart from a small gradual change attributable to thermal expansion of the lattice. The mean experimental second moment at 20°K is $19{\cdot}6 \pm 0{\cdot}25$ gauss² and this has to be compared with the theoretical value of the second moment calculated according to the two molecular models mentioned in § 1. Following the theory first given by Van Vleck (1948) and using the known values of the relevant physical constants it can be shown that the second moment S of a polycrystalline material with only one species of magnetic nucleus is given by

$$S = 7{\cdot}159 \times 10^{-46} N^{-1} \sum_{j>k} r_{jk}^{-6},$$

where N is the number of nuclei considered and r_{jk} the internuclear distance between nuclei j and k (see for example Andrew and Eades 1953). This calculation can conveniently be split into two parts, the intramolecular contribution due to interactions between nuclei in the same molecule, and the intermolecular contribution due to interactions between nuclei in different molecules. The first part can be calculated reasonably accurately for any given molecular structure but an accurate evaluation of the second part necessitates a knowledge of the dispositions of the molecules in the lattice and therefore can only be approximately estimated when the complete crystal structure is not known. For both molecular models the C–C bond was taken as 1·54 Å, the C=C bond as 1·34 Å and the two possible C–H bonds as 1·10 Å and 1·07 Å depending on whether or not it was adjacent to a C–C or a C=C bond. Tetrahedral angles were taken where applicable and reasonable values used for the other angles.

The intramolecular second moment of *cyclo*pentene calculated on this basis is 12·9 gauss² for the planar model and 13·0 gauss² for the non-planar model. In each case about 60% is contributed by the sum of the mutual interactions between the two protons of each methylene group. This leaves about 6·6 gauss² for the intermolecular contribution. This cannot be calculated since the crystal structure of *cyclo*pentene is not known, but an estimate can be made by comparison with values estimated and calculated for other hydrocarbons. These usually lie in the range 4 to 10 gauss^2; for example the estimated value for *cyclo*hexane was 10 gauss^2 (Andrew and Eades 1953). The ratio of the numbers of protons in the two molecules is about the same as the ratio of their intermolecular contributions to the second moments and although this may be fortuitous, it does suggest that the value of 6·6 gauss^2 for the intermolecular contribution to the second moment of *cyclo*pentene is reasonable, and that probably the two molecules are packed similarly in their crystal lattices. It appears therefore that the lattice is quite rigid at temperatures between 20°K and about 85°K. There is no noticeable change in either the line-width or second moment at 54°K corresponding to the anomalous effect described by Huffman, Eaton and Oliver (1948) so that if any frozen-in mode of motion is released at that temperature it must be relatively slow otherwise the line-shape would be affected. Normally the line-shape might be expected to change if motion is of a greater frequency than the line-width expressed as a frequency, which in this case is about 5×10^4 c/s. Because of the almost identical values for the intramolecular contributions to the second moment for both the planar and the nonplanar models, it is not possible from consideration of the rigid lattice second moments alone to distinguish between these models.

At about 87°K, corresponding to the large specific heat transition, the absorption line starts to narrow, and the second moment drops to $7{\cdot}6 \pm 0{\cdot}2$ gauss^2 at 110°K, while the actual shape of the line begins to show fine structure. This narrowing may be explained on the basis of molecular motion. The most likely motion is that about an axis perpendicular to the plane of the five carbon atoms in the planar model or to the plane of the four coplanar carbon atoms in the nonplanar model. In this type of motion protons from adjacent molecules approach each other less closely than in the case of rotation about other axes. The effect of this motion was calculated using the method first suggested by Gutowsky and Pake (1950). In the planar case the intramolecular contribution is only reduced from 12·9 gauss^2 to 9·4 gauss^2 since the dominant contribution comes from the individual methylene groups and as these interproton vectors are parallel to the axis of rotation there is no reduction in their contribution to the second moment. In the nonplanar case, however, the reduction is greater since these interproton vectors are no longer parallel to the axis of rotation. The reduced intramolecular contribution in this case is calculated to be 6·7 gauss^2. For the intermolecular contribution to the second moment comparison must again be made with similar molecules. In the case of *cyclo*hexane, Andrew and Eades (1953) show that rotation about the corresponding axis reduces the intermolecular contribution by a factor 0·24. Because of the possibility of similar packing mentioned previously we might expect the intermolecular contribution to the second moment of *cyclo*pentene to be reduced by approximately the same factor. This gives a value of 1·6 gauss^2 with a large uncertainty. The total second moment in the rotating case is therefore approximately 8·3 gauss^2 compared with the experimental value of $7{\cdot}6 \pm 0{\cdot}2$ gauss^2, which, considering the assumptions which have to be made because of the lack of knowledge of the crystal structure, must be considered as satisfactory agreement. Because of the lack of symmetry in the nonplanar model there might well be a slight rocking motion associated with the rotation which would reduce the calculated value by a small amount. The planar model is quite unable to explain this reduced second moment, since the reduced intramolecular contribution alone is greater than the total experimental second moment. We can therefore distinguish between the two models in favour of the non-planar model, a distinction which could not be drawn from analysis of the rigid lattice values of the second moments.

The only other motion which might be considered is about an axis in the plane of the carbon atoms passing through the centre of the double bond 2=3 and at right angles to it. In the case of the planar model this would be a diad axis. Calculation shows that for neither model would the reduction in second moment be sufficient to account for the experimental value and so this type of motion must be considered very improbable.

The absorption line undergoes a further rapid narrowing between 124°K and 128°K such that at these temperatures, which are about 10° below the melting point, the experimental second moment is reduced to a value smaller than that of the field inhomogeneity over the volume of the sample. This reduction can only be explained by motion of a more random nature than the rotational motion already described. Free spherical rotation of the molecule would, if sufficiently rapid, reduce the intramolecular contribution to zero. The effect on the intermolecular contribution would not be so drastic and, although this cannot be calculated accurately, judging by previous estimates of the effect of this motion we should not expect this part of the second moment to be reduced to a value smaller than 1 gauss^2 (see for example Andrew and Eades 1953, Rushworth 1954). This type of motion is therefore insufficient to account for the very small value of the second moment. We have thus used up all the rotational degrees of freedom and are left with translational degrees of freedom. Self-diffusion of the molecules through the lattice has been reported in several hydrocarbons (Andrew 1954) and reduces the time-averaged intermolecular field to zero provided it is sufficiently rapid. If this diffusion process is occurring, therefore, we must have the mean frequency of motion greater than the line-width, and so in this case we must postulate at least 10^4 random jumps per second in order to affect the line-width.

The considerable motion which must be taking place in the solid immediately below the melting point is not reflected in the heat of melting, since this is about seven times as large as the heat of transition.

We must now explain the fine structure of the absorption line. The protons in the *cyclo*pentene molecule may be divided into two classes, those lying in pairs in the methylene groups and the two protons adjacent to the double bond which are relatively remote from their nearest neighbours. The absorption line might therefore be a superposition of the curves for a single proton and for a proton pair. The proton pair in a polycrystalline material should give an absorption curve with two peaks separated by $3\mu/d^3$ where μ is the magnetic moment of the proton and d the interproton distance. For the rigid lattice, however, the overall interactions between protons in different methylene groups are large and obscure the curve obtained from a single pair. When the molecule starts to rotate about an axis perpendicular to the plane of the carbon atoms, the interactions between protons in different groups are considerably reduced whereas the mutual interactions between the protons in each individual group are affected less since these interproton vectors are more nearly parallel to the axis of rotation. Of the reduced intramolecular second moment of 6·7 gauss^2 the sum of the contributions of the individual methylene groups is 5·9 gauss^2. In these circumstances we might expect the curve for the proton pair to become more dominant, and this accounts for the line-shape indicated by the derivative curve in figure 2. Using the bond lengths already given, and assuming a tetrahedral angle between the

CH bonds in each CH_2 group, the interproton separation is 1·796 Å and this should correspond to a separation between the peaks of the proton pair absorption curve of 7·3 gauss. While it is difficult to measure this separation from the combined curve, it can be seen from figure 2 that the separation is approximately this value.

REFERENCES

ANDREW, E. R., 1953, *Phys. Rev.*, **91,** 425; 1954, *Report of the Conference on Defects in Crystalline Solids* (London: Physical Society).

ANDREW, E. R., and EADES, R. G., 1953, *Proc. Roy. Soc.* A, **216,** 398.

ANDREW, E. R., and RUSHWORTH, F. A., 1955, *Elect. J.*, **155,** 1344.

BECKETT, C. W., FREEMAN, N. K., and PITZER, K. S., 1948, *J. Amer. Chem. Soc.*, **70,** 4227.

GUTOWSKY, H. S., and PAKE, G. E., 1950, *J. Chem. Phys.*, **18,** 162.

HUFFMAN, H. M., EATON, M., and OLIVER, C. D., 1948, *J. Amer. Chem. Soc.*, **70,** 2911.

RUSHWORTH, F. A., 1954, *Proc. Roy. Soc.* A, **222,** 526.

VAN VLECK, J. H., 1948, *Phys. Rev.*, **74,** 1168.

Copper Nuclear Magnetic Resonance in Cu–Ni and Cu–Mn Alloys

By A. C. CHAPMAN and E. F. W. SEYMOUR
Department of Physics, University of Leeds

MS. received 24th June 1958

Abstract. The ^{63}Cu resonance has been observed in copper–nickel alloys containing up to 9·2% Ni, at 3 Mc/s and 7 Mc/s in the temperature range 20°K to 290°K. The resonance shows a reduction in intensity and a shift to lower frequencies which are larger at the lower frequency and substantially independent of temperature. The line width is not much greater than in pure copper. These effects are interpreted as due to an interaction between the electric quadrupole moment of the ^{63}Cu nucleus and electric field gradients resulting from the difference in size between copper and nickel ions. Any magnetic effect of nickel ions is negligible. The resonance in copper–manganese alloys containing up to 6·1% Mn at the same frequencies and temperatures has a width proportional to the applied field and inversely proportional to the absolute temperature. The direct magnetic interaction with manganese ions is insufficient to account for the broadening. If the results are interpreted in terms of an indirect interaction through the conduction electrons, of the form proposed by Behringer and Yosida, an s–d exchange constant six times the Mn free atom value must be assumed. A large decrease in width on heat treatment is tentatively attributed to clustering of Mn ions.

§ 1. INTRODUCTION

An experimental investigation has been made of the nuclear magnetic resonance of ^{63}Cu in alloys of copper with small amounts of nickel and manganese with a view to obtaining information about the internal electric and magnetic fields in these alloys. Local deviations from cubic symmetry in the lattice, caused by solute ions, will give rise to inhomogeneous electric fields which may be expected to affect the resonance through an interaction with the electric quadrupole moments of the copper nuclei. In addition there is the possibility of detecting the presence of solute ions having resultant magnetic moments through the local magnetic fields they produce; this possibility was the main reason for the present investigation.

The theory of electric quadrupolar interaction is well established (see, for instance, Pound 1950). The gradient of an electric field of axial symmetry is completely specified by the quantity $\partial^2 V/\partial z'^2$, often written $\boldsymbol{e}q$, where V is the electrostatic potential and z' denotes the symmetry axis; in such a field the resonance of nuclei of spin I and electric quadrupole moment $\boldsymbol{e}Q$ is split into $2I+1$ components. For odd half-integral spin there is a central component, undisplaced to a first order in $\boldsymbol{e}^2Qq/\boldsymbol{h}\nu$, where ν is the frequency of resonance. The intensity of the central component is a fraction $3(I+\frac{1}{2})^2/2I(I+1)(2I+1)$ of that of the line in the absence of a quadrupolar interaction; this fraction is 2/5 for ^{63}Cu. The remaining $2I$ components are spread over a range of frequencies of the order of $\boldsymbol{e}^2Qq/\boldsymbol{h}$, and hence may be unobservable in a polycrystalline material.

In a second order of approximation the central component is also shifted (and hence may appear broadened in polycrystalline material) by an amount inversely proportional to the resonance frequency. The magnitude of a quadrupolar interaction would not be expected to depend markedly on temperature except in cases where the atoms are capable of rapid relative motion such as diffusion.

Localized magnetic moments may be expected to affect the resonance in the following way. The direction of such a moment will be continually changing due to spin–lattice, spin–spin and, possibly, exchange interactions. If the changes are very rapid compared with the spin–spin relaxation rate of the nuclei, the nuclei will experience an effective local magnetic field of the order of $\bar{\mu}/r^3$, where $\bar{\mu}$ is the time-averaged ionic moment and r is the distance of a nucleus from the ion. The resonance will thus be broadened by an amount proportional to $\bar{\mu}$; if Curie's law is obeyed, the broadening may be expected to be proportional to H/T, where H is the magnetic field in which the resonance is observed and T is the absolute temperature. Thus the two interactions may be distinguished from one another by their frequency and temperature dependence.

§ 2. EXPERIMENTAL

A series of copper–nickel alloys was prepared from copper of purity 99·99% and spectrographically standardized nickel. The metals were melted in an induction furnace *in vacuo*; argon was then admitted to reduce evaporation and resulting ionization troubles, and the alloys chill-cast in a copper mould. The alloys were given an homogenizing anneal at 950°C for 24 hours, and the homogeneity confirmed by metallographic examination. The copper–manganese alloys had already been prepared in this laboratory for another investigation (Booth 1956, unpublished) using spectrographically standardized materials. The face-centred cubic γ-phase had been retained by quenching from a high temperature at which this phase is stable. Although quenching is not necessary for manganese contents of less than about 20% since the γ-phase is stable at room temperature, alloys with concentrations in this range had been quenched from 700°C to ensure uniformity of treatment. The compositions of all alloys were determined by chemical analysis.

Powder samples were prepared by filing; only those particles which passed through a 300-mesh sieve were retained. The maximum particle size was then approximately 30 microns and corrections (Chapman, Rhodes and Seymour 1957) for eddy current distortion of the resonances were negligible except for pure copper at the lowest temperatures reached. Ferromagnetic contamination from the files was removed by boiling the powder in N/5 hydrochloric acid for three quarters of an hour. The particles were insulated from one another by a thick lubricating oil.

Resonances were observed by means of a marginal oscillator fitted with a 'calibrator' to facilitate comparison of signal intensities (Pound 1952). The method of recording the resonances has already been described (Chapman, Rhodes and Seymour 1957).

§ 3. THE COPPER–NICKEL SYSTEM

3.1. *Experimental Results*

The ^{63}Cu resonance was observed in alloys containing $1{\cdot}0_2$, $1{\cdot}9_3$, $5{\cdot}0_4$ and $9{\cdot}2_1$ atomic % nickel. For nearly all alloys resonances were observable

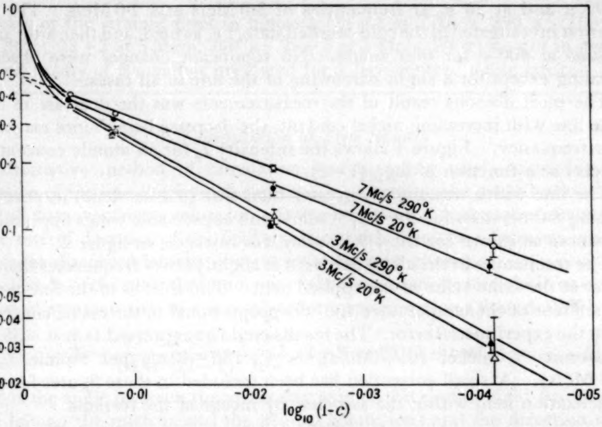

Figure 1. The maximum intensity of the ^{63}Cu resonance in Cu–Ni alloys as a function of nickel content. I_c/I_0 is the intensity as a fraction of that in pure annealed copper.

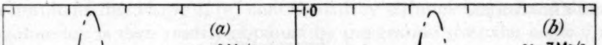

Figure 2. The observed (full lines) and computed (broken lines) derivatives of the ^{63}Cu resonance in a Cu–$1{\cdot}9_3$% Ni alloy at (*a*) 3 Mc/s, (*b*) 7 Mc/s. δH is the value of the applied field measured from the centre of the resonance in pure copper at the same frequency. The chain lines show the observed derivatives in pure cold-worked copper.

at 290°K and at 20°K, at frequencies of 3·0 Mc/s and 7·0 Mc/s. The samples were first investigated in the cold-worked state, i.e. as filed, and then after annealing *in vacuo* at 400°C for four hours. No significant changes were observed on annealing except for a slight narrowing of the line in all cases.

The most obvious result of the measurements was the decrease in intensity of the line with increasing nickel content, the decrease being more marked at the lower frequency. Figure 1 shows the intensity I_c for an atomic concentration c of nickel as a function of $\log_{10}(1-c)$.

The line width was slightly greater than that (6·4 oersteds) in pure copper, reaching 8·0 oersteds for the $9{\cdot}2_1\%$ alloy, and appreciable wings appeared on the resonances as shown for the $1{\cdot}9_3\%$ alloy, for instance, in figure 2.

The resonances in the alloys occurred at slightly lower frequencies than in pure copper at the same value of the applied field. The shift $\delta\nu$ of the line centre was independent of the temperature and was proportional to the nickel concentration within the experimental error. The results could be expressed as $\delta\nu = -35 \pm 20$ c/s per atomic % nickel ($\nu = 7$ Mc/s), $\delta\nu = -130 \pm 40$ c/s per atomic % nickel ($\nu = 3$ Mc/s). A small correction has been included in these figures for the bulk magnetization field within the samples, by means of the formula

$$H_1 = H\{1 + (4\pi/3 - D)\kappa\} \qquad \ldots\ldots(3.1)$$

where H_1 is the field within the material, H is the external field, κ is the mean volume susceptibility of the sample and $D = 1{\cdot}7\pi$ is a demagnetizing factor arrived at by approximating the sample by a homogeneous ellipsoid of the same extreme dimensions.

3.2. *Interpretation*

The fact that the shift and the intensity decrease were larger at the lower frequency indicated that a second-order quadrupolar interaction might be responsible, in which case the rapid intensity decrease at low concentrations would be attributable to the first-order effect. Bloembergen and Rowland (1953) have observed a similar decrease of the ^{63}Cu resonance intensity in Cu–Zn alloys but with no shift or broadening. They developed the following particularly simple interpretation: the first-order effect of electric field gradients due to the solute ions is large enough to make the satellites due to all copper nuclei unobservable; further, when a solute ion occupies one of the n lattice sites within a critical distance from a copper nucleus the second-order shift of the central component is so large that this nucleus does not contribute to the observed line; if a nucleus does not have a solute ion as close as this the central component is unaffected. For a face-centred cubic lattice the number n may be expected to have one of the values 12, 18, 42,... corresponding to the numbers of nearest neighbours, first and second nearest neighbours, and so on. They showed that this model leads to the relation

$$\log(I_c/0{\cdot}4I_0) = n\log(1-c) \qquad \ldots\ldots(3.2)$$

where I_0, I_c are the intensities in the pure solvent and at solute concentration c respectively. The intensity of the central component in the pure solvent is $0{\cdot}4I_0$ (for nuclear spin 3/2).

Although the intensity decrease observed here (figure 1) fits this equation very well, the model cannot be considered entirely satisfactory in this case since it does not account for the observed line shifts and shape changes. Furthermore, the slopes n of the straight lines in figure 1 (18 ± 1 at 7 Mc/s, 290°K; 21 ± 1 at 7 Mc/s, 20°K; 28 ± 2 at 3 Mc/s, 290°K; 29 ± 2 at 3 Mc/s, 20°K) do not in general correspond to any of the values predicted for a face-centred cubic lattice.

3.3. *Computation of Line Shapes*

An alternative method of calculation was therefore used, consisting of a computation of the line shape to be expected by summing the contributions from nuclei at all distances from a solute ion. It was necessary to make some assumption as to the rate of decrease of the field gradient with distance r from an ion; for reasons to be discussed later an inverse cube law was chosen.

The shift $\Delta\nu$ of the central component of the resonance of a nucleus in an electric field of axial symmetry is, in a second-order approximation (Pound 1950),

$$\Delta\nu = \frac{9}{64}\frac{2I+3}{4I^2(2I-1)}\frac{e^4Q^2q^2}{h^2\nu}(1-9\cos^2\theta)(1-\cos^2\theta) \quad \ldots\ldots (3.3)$$

where θ is the angle between the symmetry axis of the electric field (in this case the line joining the nucleus and the nearest solute ion) and the direction of the magnetic field. Thus the shift falls off as r^{-6}, and at the concentrations used, only the nearest solute ion need be considered. The assumption of axial symmetry is approximately justified since there is effectively only one solute ion near to the nucleus. For ^{63}Cu, $Q = 0{\cdot}156 \times 10^{-24}$ cm^2.

The resultant line shape $I_r'(\nu)$ contributed by all nuclei at a fixed distance r from a solute ion is then readily obtained by integration over the angle θ using

$$I_r'(\nu)\,d\nu \propto \sin\theta \frac{d\theta}{d\nu}\,d\nu \quad \ldots\ldots (3.4)$$

with $\nu = \nu_0 + \Delta\nu(r)$, where ν_0 is the undisplaced resonance frequency. This relation follows since in polycrystalline material all directions in space of the symmetry axis are equally likely, so that the probability that an angle θ will occur is proportional to $\sin\theta$.

For the summation over values of r a random distribution of nickel ions was assumed and the probabilities of the possible configurations of copper and nickel ions around a chosen nucleus were evaluated. The probability that a nucleus has no solute ion among the u neighbours in the first m 'shells' surrounding it, but at least one solute ion among the v neighbours in the $(m+1)$th shell is $P_r = f^u(1-f^v)$ where $f = 1-c$ is the atomic concentration of copper. P_r was evaluated for $u = 0, 12, 18 \ldots$, with $v = 12, 6, 24 \ldots$, respectively, corresponding to the numbers of neighbours in the shells of a face-centred cubic lattice. Since the effects of solute ions other than the nearest may be neglected, and since the occurrence of more than one solute ion in any one shell is rare at small concentrations, the contributions $I_r'(\nu)$ may be taken as occurring with the probabilities P_r, and a weighted sum $I'(\nu)$ calculated.

Finally, this line shape $I'(\nu)$ was broadened to allow for nuclear dipole–dipole interactions using

$$I(\nu) = \int_{-\infty}^{\infty} I'(\nu-\nu')g(\nu')\,d\nu' \quad \ldots\ldots (3.5)$$

where $g(\nu')$ is the experimental line shape for pure copper.

3.4. *Comparison with Experiment*

By a process of trial it was found that best agreement between the computed curves $I(\nu)$ and the measured line shapes and intensities was obtained using for second nearest neighbours $eq = 8{\cdot}4 \times 10^{13}$ c.g.s. e.s.u. It may readily be checked that the first order splitting resulting from gradients calculated from this value with an inverse cube law is sufficient to make the satellite resonances due to almost all nuclei unobservable even in the most dilute alloy, in agreement with observation. As an example of the results, the calculated derivatives (broken lines) dI/dH for the $1{\cdot}9_3\%$ alloy are compared with the experimental curves (full lines) in figures 2 (*a*) and 2 (*b*), for $\nu = 3$ Mc/s and 7 Mc/s respectively. The origins of abscissae represent the centres of the lines in pure copper at the same frequencies; the ordinates are measured in terms of the maximum values of the derivatives in pure cold-worked copper at the same frequencies. The feature of the experimental results which is least well reproduced is the shift of the line centre; the shifts of the computed curves are in the observed direction but are too large in magnitude. The calculated values are $\delta\nu = -200$ c/s per atomic % nickel ($\nu = 7$ Mc/s), $\delta\nu = -300$ c/s per atomic % nickel ($\nu = 3$ Mc/s). This leaves a shift, apparently independent of frequency, of about $+170$ c/s per atomic % nickel, unaccounted for. This may be due to the approximations in the method of calculation; any increase in the conduction electron shift would be expected to be proportional to the frequency.

The rates of intensity decrease at 20°K are rather larger than at 290°K. Now it is often found that quadrupole coupling constants increase by a few per cent as the temperature is decreased to a low value, but this cannot be the complete explanation since the increase in the rate is apparently greater at 7 Mc/s than at 3 Mc/s. It is possible that a magnetic interaction proportional to the time-averaged magnetic moments of nickel ions may be having an observable effect at 20°K. An approximate estimate based on the known magnetic susceptibilities of these alloys indicates that such effects might just be observable. The question can probably be resolved by extending the measurements to lower temperatures.

3.5. *Origin of the Field Gradients*

The origin of electric field gradients in alloys has been discussed by Bloembergen (1955). Any extra charge on a solute ion of valency different from that of the solvent is so heavily screened by the conduction electrons that it produces only a very small gradient even at near neighbours. The differing sizes of solute and solvent ions can, however, produce a local distortion from cubic symmetry and an appreciable gradient. It is reasonable to suppose that the gradients produced by different solute ions in the same solvent would be proportional to $(a_1 - a_0)/a_0$, where a_1, a_0 are the radii of solute and solvent ions. (The inverse cube dependence of gradient on distance assumed earlier was chosen as a reasonable approximation since the strain due to a spherical inclusion in a homogeneous medium falls off in this manner.) Now a comparison of the present experimental results for Cu–Ni with those of Bloembergen and Rowland for Cu–Zn shows the gradients at corresponding lattice points to be closely similar in the two systems. However, the values of ionic sizes in the pure metals, deduced from the lattice parameters (Smithells 1955) in the way used by Raynor (1949), lead to $|(a_{\mathrm{Zn}} - a_{\mathrm{Cu}})/(a_{\mathrm{Ni}} - a_{\mathrm{Cu}})| = 1{\cdot}7$, rather than unity. Further the gross distortion of the copper lattice as measured by the initial change in lattice constant per unit solute concentration is greater for zinc as solute than for nickel as solute by a factor 2 (Pearson 1957). Rowland (1955) from a similar investigation of Al–Mg and Al–Zn has found a similar lack of agreement. It is concluded that while the quadrupolar interaction associated with solute ions in alloys may have its origin in the difference in size between solute and solvent ions, the magnitude of the interaction is not simply proportional to size difference.

§ 4. THE COPPER–MANGANESE SYSTEM

4.1. *Experimental Results*

Measurements of the ^{63}Cu resonance were made at 20°K, 77°K and 290°K, at frequencies 3·0 Mc/s and 7·0 Mc/s, in alloys containing 0·5, 1·2, 2·4 and 6·1 atomic % manganese. Some features of the resonances were widely different depending on whether the samples consisted of powder as filed, or of powder which had been annealed *in vacuo* at 400°C for four hours or more. The two cases will be treated separately.

For the unannealed powder samples the resonance width was markedly increased and the intensity correspondingly decreased by an amount which was larger the higher the frequency and manganese content and the lower the temperature. The broadening was so severe that the resonance was observed at 20°K only in the 0·5% alloy, and that in the 6·1% alloy only at 290°K at 3 Mc/s. The widths h_1 between extremes of the derivative curves are given in the table.

Width h_1 (Oe) and Fractional Shift $\delta\nu/\nu$ in Resonance Frequency of the ^{63}Cu Resonance in Unannealed Cu–Mn Alloys

	h_1			
	293°K		77°K	
At. % Mn	3 Mc/s	7 Mc/s	3 Mc/s	7 Mc/s
0	6·1 ± 0·2	6·5 ± 0·3	6·0 ± 0·3	6·5 ± 0·2
0·5	7·0 0·4	8·3 0·3	10·6 0·4	13·3 0·8
1·2	7·7 0·5	13·4 0·7	13·4 0·9	13·6 0·8
2·4	10·0 0·9	13 2		
6·1	27 4			

	h_1		$10^6\ \delta\nu/\nu$	
	20°K		293°K	20°K
	3 Mc/s	7 Mc/s	7 Mc/s	7 Mc/s
0				
0·5	5·6 ± 0·3	6·2 ± 0·3	0	0
1·2	19·4 0·6	48	−35 ± 35	−270 ± 80
2·4			+165 ± 35	
6·1			+200 ± 55	

The shifts $\delta\nu/\nu$ of the line centres relative to that in pure metallic copper at the same applied field were small and did not vary in a simple way with concentration. Values are given in the table.

While this work was in progress the results of a similar investigation by Owen, Browne, Knight and Kittel (1956) on an unannealed alloy containing 0·029 atomic % manganese became known. In order to make a quantitative comparison between the two sets of results we make use of a parameter h_5 used by them to describe the relative intensity of the wings of the resonance, and defined as half the separation of the points at which the derivative falls to one-fifth of its maximum value. The increase in h_5 over its value in pure copper, per unit concentration of manganese, is plotted in figure 3 as a function of H/T, the ratio of applied field at resonance to absolute temperature. The straight line represents the results of Owen *et al.* The combined results show that the broadening is approximately proportional to concentration up to a few per cent manganese.

Brief reports of two other observations of the ^{63}Cu resonance in dilute Cu–Mn alloys ($c < 0{\cdot}1\%$) have recently been published (van der Lugt, Poulis, Hardeman and Hass 1957, Sugawara 1957). The results appear to be qualitatively similar to the present ones.

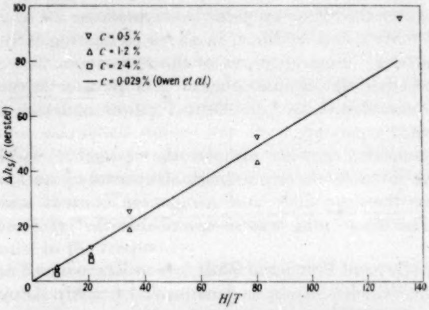

Figure 3. Observed widths of the ^{63}Cu resonance in unannealed Cu–Mn alloys showing dependence on concentration, field and temperature.

In contrast with the very large broadening in the unannealed alloys, the widths h_1 in samples which had been annealed at 400°C for four hours were not more than 2 oersteds greater than in pure copper. Wings appeared on the resonances at small values of H/T ($H/T \lesssim 30$ Oe deg^{-1}), but did not become more pronounced for larger values of this ratio; indeed in some cases the width h_5 passed through a broad maximum as the temperature was reduced.

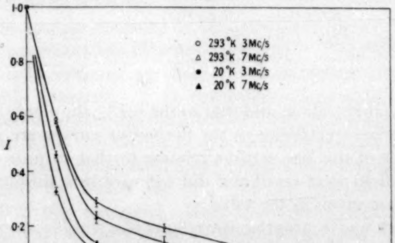

Figure 4. The intensity of the ^{63}Cu resonance in annealed Cu–Mn alloys as a function of manganese content.

The intensities of the resonances were much greater than in the unannealed samples, so that resonances could be observed at 20°K for the 2·4% alloy. The maximum value of the absorption, expressed as a fraction of that in pure annealed copper at the same frequency and temperature, is shown as a function of concentration in figure 4 for 293°K and 20°K. The values for 77°K lie between the curves for 293°K and 20°K and are omitted for clarity.

The shifts $\delta\nu/\nu$ (relative to pure copper) were in all cases smaller than in the unannealed powders, being less than the experimental error of 20×10^{-6} at 293°K, and increasing with concentration at $-(70 \pm 20) \times 10^{-6}$ per atomic % manganese at 20°K.

A second anneal at 400°C had no further effect on the resonances.

4.2. *Interpretation of the Results for Unannealed Alloys*

The proportionality of Δh_5 with H/T is a strong indication that a magnetic interaction with Mn ions is responsible for the broadening. Unlike the case of the Cu–Ni system this interaction is apparently large enough to obscure any quadrupole effects, a result qualitatively reasonable in view of the larger magnetic susceptibilities of the Cu–Mn system. However, as will be shown, the spread in local field produced directly by the Mn magnetic dipoles is insufficient to account for the broadening. Behringer (1957) has found the same of the results of Owen *et al.* on the 0·029% alloy. Neither was the non-uniformity in demagnetizing field (eqn (3.1)) within the powder particles sufficient.

Owen *et al.* (1956), Pratt (1957), Yosida (1957 a) and Behringer (1957) have considered that the Mn ions and the copper nuclei are indirectly coupled by the conduction electrons through an exchange interaction between the ions and the conduction electrons, and the hyperfine interaction between the nuclei and the conduction electrons. Owen *et al.* and Pratt make use of the concept of an effective molecular field, the magnitude of which at a nucleus is independent of its distance from near solute ions. Their treatments thus predict a shift of the whole resonance, and do not account for the broadening. The treatments of Yosida and Behringer (see also Hart 1957), on the other hand, involve a variation of the effective field with distance from an ion, and hence predict a variety of shifts with a resultant line broadening.

Line shapes resulting from combined direct and indirect magnetic interactions were computed in a manner somewhat similar to that of § 3.3, and compared with experiment. The local z component of magnetic field at a nucleus due to the direct dipolar effect of a Mn ion is

$$\Delta h_1 = g\beta\bar{S}_z \frac{3\cos^2\theta - 1}{r^3}, \qquad \ldots\ldots(4.1)$$

and that due to the indirect interaction is (Yosida 1957 a)

$$\Delta h_2 = -\frac{|\bar{S}_z|}{g_N\beta_N}\left(\frac{3n}{N}\right)^2 \frac{2\pi}{E_f} AJ \left\{\frac{2k_{\mathrm{m}}r\cos(2k_{\mathrm{m}}r) - \sin(2k_{\mathrm{m}}r)}{(2k_{\mathrm{m}}r)^4}\right\} \qquad \ldots\ldots(4.2)$$

where r, θ are the coordinates of the nucleus with the Mn ion as origin and the direction of the applied field as the polar (z) axis, $g\beta S$, $g_N\beta_N I$ are the magnetic moments of the ion and nucleus, respectively, $2n$, N are the numbers of conduction electrons and lattice points in unit volume, respectively, k_{m}, E_{f} are the wave number and energy of a conduction electron at the Fermi surface, J is the exchange energy of a conduction electron with a Mn ion and A is the hyperfine energy of a conduction electron with a copper nucleus.

The contribution to the resonance from nuclei having a Mn ion at a given distance has a shape governed by the θ-dependence of Δh_1 and evaluated using equation (3.4). The whole contribution is shifted an amount Δh_2 (Δh_2 being independent of θ). As far as Δh_1 is concerned only the nearest Mn ion need be considered. However, Δh_2 does not decrease monotonically with r, so that configurations in which there are two near neighbours were counted explicitly by adding the shifts Δh_2 due to each separately. More than two near neighbours rarely occur.

The probabilities of the possible configurations of Cu and Mn ions round a chosen nucleus were evaluated by a straightforward extension of the method of § 3.3, and the weighted summation for values of r continued until the splittings were small compared with the nuclear dipolar width.

4.3. *Comparison with Experiment*: *Unannealed Alloys*

The following values of the quantities occurring in equations (4.1) and (4.2) were used: $\bar{\mu} = g\beta\bar{S}_z$ from a Curie law with $S = 5/2$ and $g = 2$ corresponding to Mn^{2+} ions in a ${}^6S_{5/2}$ state; $k_{\mathrm{m}} = 1{\cdot}36 \times 10^8\,\mathrm{cm}^{-1}$ from the Fermi energy $E_{\mathrm{f}} = 1{\cdot}1 \times 10^{-11}$ erg for copper, using a free electron approximation $A = \boldsymbol{h}\xi\nu_{\mathrm{a}}/(I + \frac{1}{2})$ where $\nu_{\mathrm{a}} = 0{\cdot}190\,\mathrm{cm}^{-1}$ is the observed hyperfine splitting in a free copper atom and $\xi = 0{\cdot}53$ (Knight 1956) is the ratio of the average probability density of a valence electron at the nucleus in the metal to that in the free atom. J was treated as an adjustable parameter. Best agreement with experiment was obtained using $J = 4{\cdot}2 \times 10^{-12}$ erg. Figures 5 (*a*) and 5 (*b*) show computed and observed line shapes for the 0·5% alloy at 20°K, at 3 Mc/s and 7 Mc/s respectively, using this value of J. The smooth curves represent the experimental results and the histograms the computed line shapes, the vertical scales of the former being chosen to make the areas enclosed equal. (Intensity measurements were uncertain because of saturation difficulties, but observed intensities agreed with computed values within the rather large experimental uncertainty.) For comparison figures 5 (*c*) and 5 (*d*) show the corresponding line shapes computed from the direct magnetic dipolar interaction alone, plotted on the same scale.

It is difficult to estimate the shifts of the line centres, as given by the zeros of the derivatives, from the irregular histograms of figures 5 (*a*) and 5 (*b*). However, the centres of gravity of the lines are shifted to higher applied fields by about +5 parts in 10^4, compared with the corresponding experimental value of $+2{\cdot}7 \pm 0{\cdot}8$ parts in 10^4. The shifts in the 1·2% and 2·4% alloys at room temperature, in contrast, are in the opposite sense and cannot be explained in this way. It can be said, however, that the large shifts predicted by Owen *et al.* do not occur, and that the results are much more nearly in agreement with the theoretical expressions given by Yosida and Behringer.

The value of J required to explain the results is six times the free atom value J_{a}. This is to be compared with a value $1{\cdot}7J_{\mathrm{a}}$ found by Yosida (1957 b) from an analysis of the electrical resistivity, and with a value two to three times J_{a} deduced by Behringer from the nuclear resonance results of Owen *et al.*

Presumably the value of about $J_a/5$ found by Owen *et al.* from magnetic susceptibility and electron resonance experiments using a molecular field treatment is to be increased if the effects of the s–d interaction have not the long range originally supposed, but are given instead by an equation of the the form (4.2). The disagreement between the two figures deduced from nuclear resonance experiments is due to the fact that different methods of computing were used. Behringer calculated the effect of a central manganese ion on the contributions of the $1/c$ nuclei in a sphere surrounding it, where c is the concentration of manganese, and then summed these contributions. This method is best suited to the case of an

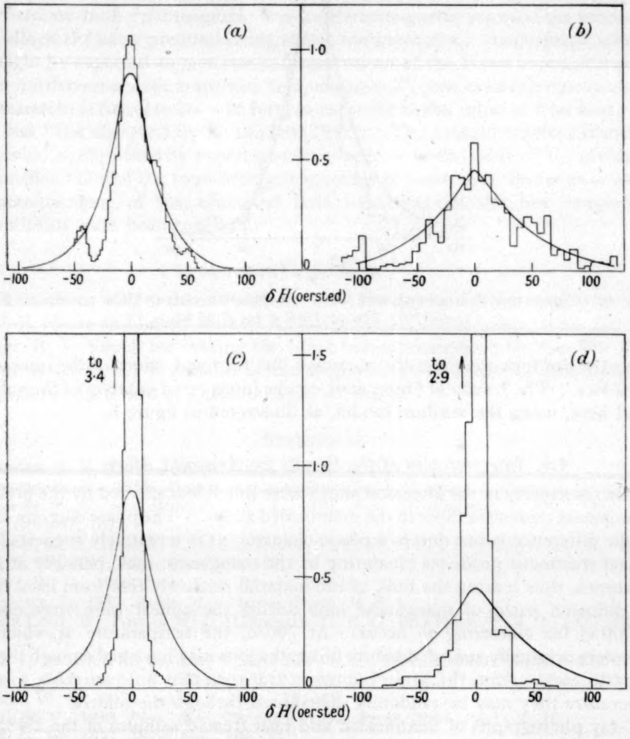

Figure 5. Computed and observed ^{63}Cu resonance lines in unannealed Cu–0·5% Mn at 20°K for : (*a*) and (*c*) 3 Mc/s, (*b*) and (*d*) 7 Mc/s. The smooth curves represent the experimental results. δH is the value of the applied field measured from the centre of the resonance in pure copper. The ordinate scale is arbitrary. The computed histograms allow for : (*a*) and (*b*) : direct and indirect magnetic interactions with Mn ions, with $J = 4{\cdot}2 \times 10^{-12}$ erg, using a random model ; (*c*) and (*d*): direct interactions only.

ordered arrangement of ions, for which there appears to be no evidence, and it is felt that our method based on a random arrangement is preferable. Of the two models the random one gives the narrower line for fixed values of the interaction parameters. The results of Owen *et al.* can be interpreted in terms of the value of J used here, using the random model, as illustrated in figure 6.

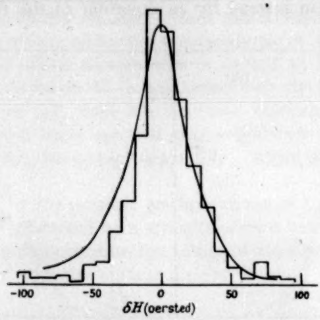

Figure 6. Computed (histogram) and observed (smooth curve) ^{63}Cu resonance line in Cu–0·029% Mn at 1·65°K for 5·98 Mc/s.

4.4. *Interpretation of the Results for Annealed Alloys*

The resonances in the annealed alloys were much less affected by the presence of manganese than were those in the unannealed alloys. The phase diagram shows that the difference is not due to a phase change. It is tentatively suggested that the heat treatment produces clustering of the manganese ions, possibly at grain boundaries, thus leaving the bulk of the material relatively free from local fields. The diffusion paths of manganese ions during the anneal were large enough (~5000 Å) for clustering to occur. At 700°C, the temperature at which the alloys were originally annealed before filing, the ions may have had enough thermal energy to escape from the grain boundary traps, so that on quenching to room temperature they may be randomly distributed through the matrix.

X-ray photographs of unannealed and heat treated samples of the 2·4% and 6·1% alloys were taken, and no difference could be detected between the two patterns for either alloy. However, it is possible that the formation of clusters of the size required to explain the present results might escape detection by this means.

The fact that the resonance intensity decreased as H/T increased indicated that the predominant effect was still a magnetic one, although the initial rapid intensity decrease to about 0·4 of the intensity in pure copper might well be a first order quadrupole effect. To provide a rough check on the cluster hypothesis line shapes were computed for the 1·2% alloy assuming the same magnetic interaction parameters as before but with the arbitrary assumption of clusters of 13 ions, i.e. central ions with the 12 nearest neighbour sites also filled by manganese ions.

Quite close agreement with experimental line shapes and intensities was obtained for temperatures of 293°K and 77°K but the histograms computed for a temperature of 20°K were far too broad, and the maximum intensities far too small. This result is not unreasonable if the interactions between Mn ions within a cluster are enhanced on account of the smaller separation compared with a random distribution. It is known from the work of Owen, Browne, Arp and Kip (1957) that there are both ferromagnetic and antiferromagnetic interactions present in these alloys, the latter predominating at low temperatures. Accordingly, clustering might be expected to give rise to larger values of the Weiss constant θ and to higher antiferromagnetic transition temperatures T_N just as an increase in overall concentration is found to do. In fact, an increase in the value of θ on heat treatment has been observed by Kronquist (1947). The present results obtained at 20°K could be explained by a corresponding increase in the value of T_N, giving rise to a smaller value of the time-averaged moment of a cluster. So far as is known no measurements of the effects of heat treatment on the low temperature susceptibility have been reported.

ACKNOWLEDGMENTS

The authors wish to thank Professor E. C. Stoner for his interest in this work, Dr. F. E. Hoare and his co-workers for the provision of low temperature facilities, and Dr. R. F. Youell for making the X-ray measurements on the Cu–Mn alloys. One of us (A. C. C.) is grateful to the Department of Scientific and Industrial Research for the award of a maintenance allowance.

REFERENCES

BEHRINGER, R. E., 1957, *J. Phys. Chem. Solids*, **2**, 209.
BLOEMBERGEN, N., 1955, *Defects in Crystalline Solids* (London : Physical Society).
BLOEMBERGEN, N., and ROWLAND, T. J., 1953, *Acta Metallurgica*, **1**, 731 ; 1955, *Phys. Rev.*, **97**, 1679.
CHAPMAN, A. C., RHODES, P., and SEYMOUR, E. F. W., 1957, *Proc. Phys. Soc.* B, **70**, 345.
HART, E. W., 1957, *Phys. Rev.*, **106**, 467.
KNIGHT, W. D., 1956, *Solid State Physics*, **2**, 124.
KRONQUIST, E., 1947, *Arkiv Mat. Astron. Fysik*, **34** B, 1.
VAN DER LUGT, W., POULIS, N. J., HARDEMAN, G. E. G., and HASS, W. P. A., 1957, *Physica*, **23**, 797.
OWEN, J., BROWNE, M. E., ARP, V., and KIP, A. F., 1957, *J. Phys. Chem. Solids*, **2**, 85.
OWEN, J., BROWNE, M. E., KNIGHT, W. D., and KITTEL, C., 1956, *Phys. Rev.*, **102**, 1501.
PEARSON, W. B., 1957, *Canad. J. Phys.*, **35**, 358.
POUND, R. V., 1950, *Phys. Rev.*, **79**, 685 ; 1952, *Progr. Nucl. Phys.*, **2**, 21.
PRATT, G. W., 1957, *Phys. Rev.*, **106**, 53.
RAYNOR, G. V., 1949, *Trans. Faraday Soc.*, **45**, 698.
ROWLAND, T. J., 1955, *Acta Metallurgica*, **3**, 74.
SMITHELLS, C. J., 1955, *Metals Reference Book* (London : Butterworths Scientific Publications).
SUGAWARA, T., 1957, *J. Phys. Soc., Japan*, **12**, 309.
YOSIDA, K., 1957 a, *Phys. Rev.*, **106**, 893 ; 1957 b, *Ibid.*, **107**, 396.

Theory of Phase Transformations in Alkali Metals

By M. A. E. NUTKINS

Northern Polytechnic, London

Communicated by H. Jones; *MS. received* 29*th May* 1958

Abstract. A theory is suggested to account for the phase changes which have been observed by Barrett in lithium and sodium. The elastic constants for the face-centred and body-centred cubic structures have been calculated and from them the free energies determined. An interesting conclusion is that the electrostatic and ionic terms alone are not sufficient to account for the phase change. The Fermi energy of the conduction electrons is affected by shear, and hence this part of the total energy gives rise to a contribution to the elastic shear constants. The difference in this contribution between the two cubic structures was found to be adequate to account for the observed phase change. An estimation of the transition temperature indicated that it lies in the range 40°–100°K.

§ 1. Introduction

In a recent paper, Barrett (1956) describes experimental results which show that sodium partially transforms on cooling below 36°K, or on deforming below 51°K, from a body-centred cubic structure to a close-packed hexagonal structure with stacking faults. Reversion to the cubic structure starts on heating to 60°–75°K and is completed at 100°–110°K or at lower temperatures if there is no cold work. The purpose of the present calculation is to give a possible theoretical explanation of these results.

For such a phase change to occur, the curves of the free energy as a function of temperature for the two structures must cross at the transition temperature and the free energy of the close-packed hexagonal structure must be below that of the body-centred cubic structure for temperatures below the transition point. This is illustrated by the sketch in figure 1.

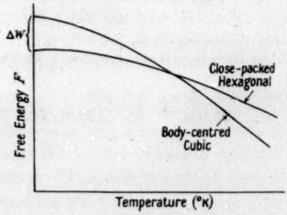

Figure 1. The free energies of the close-packed hexagonal and body-centred cubic structures plotted against temperature. (Schematic.)

The only term in the free energy which changes appreciably with temperature, is the free energy due to the lattice vibrations. This may be calculated from the elastic constants of the structure.

The axial ratio c/a for the close-packed hexagonal sodium is given by Barrett as 1·634, which corresponds almost exactly to the ideal case of close-packing, $c/a=(8/3)^{1/2}$. The twelve nearest neighbours to an atom of an ideal close-packed hexagonal lattice are exactly at the same distance from the atom considered as the twelve nearest neighbours in a face-centred cubic lattice having the same atomic volume. The magnitude of the forces between the atoms of these two lattices must therefore be very similar and hence it is reasonable to suppose that the free energies are approximately the same. This is borne out by the presence of stacking faults in the close-packed hexagonal structure. In order to simplify the calculation, a phase change from body-centred cubic to face-centred cubic has therefore been considered instead of the phase change from body-centred cubic to close-packed hexagonal. In lithium the transition to face-centred cubic does actually occur (Barrett 1947, 1948, 1956, Barrett and Trautz 1948).

In the following sections the elastic constants of the face-centred cubic and body-centred cubic structures are calculated by taking into account the electrostatic, ionic, Fermi energy and Brillouin zone boundary effects. From these constants the free energies as functions of temperature are determined for the two structures. In addition the difference in the internal energy at absolute zero temperature due to these effects is calculated and hence the transition temperature determined.

§ 2. CALCULATION OF THE FREE ENERGY OF THE LATTICE VIBRATIONS FROM THE ELASTIC CONSTANTS

The temperature dependent free energy per atom $F(T)$ due to the lattice vibrations is given by

$$F(T)=kT\int_0^\infty g(\nu)\log\left[1-\exp\left(-h\nu/kT\right)\right]d\nu, \qquad \ldots\ldots(1)$$

where $g(\nu)$ is the frequency distribution of the vibrations which must satisfy the condition

$$\int_0^\infty g(\nu)d\nu=3. \qquad \ldots\ldots(2)$$

In order to obtain $g(\nu)$ for a particular lattice, using the method given by Fuchs (1936 b), the wave velocity c must first be calculated in terms of the elastic constants c_{11}, c_{12}, c_{44}. In the direction (l, m, n) there are three values of c given by the roots of the equation

$$x^3-x^2(B+C-A)+4x(B-A)(C+B)(l^2m^2+m^2n^2+n^2l^2)$$
$$+(3C+A)(B-A)^2l^2m^2n^2=0, \qquad \ldots\ldots(3)$$

where $x=\rho c^2-c_{44}$, $A=c_{44}$, $B=\frac{1}{2}(c_{11}-c_{12})$ and $C=\frac{1}{3}(c_{11}+2c_{12})$, ρ being the density. The three roots of this equation give three values of c which may be denoted by c_i $(i=1,2,3)$.

The frequency distribution $g(\nu)$ is therefore given by

$$g(\nu)=\Omega\nu^2\sum_{i=1}^{3}\int\frac{1}{c_i^3}\,d\omega, \qquad \ldots\ldots(4)$$

where Ω is the atomic volume, $d\omega$ is the element of solid angle and the integration is taken over the region $c_i \geqslant \lambda_m \nu$, where $\lambda_m = (4\pi\Omega/3)^{1/3}$.

From equations (1) and (4), the temperature dependent free energy $F(T)$ is given by

$$F(T) = kT\Omega \int_0^\infty \nu^2 \sum_{i=1}^{3} \int\int \frac{1}{c_i^3} \log\left[1 - \exp\left(-h\nu/kT\right)\right] d\omega \, d\nu. \quad \ldots\ldots(5)$$

This may be rewritten as

$$F(T) = kT\Omega \int_0^{2\pi} \int_0^{\pi} \sum_{i=1}^{3} \int_0^{c_i/\lambda_m} \frac{\nu^2}{c_i^3} \log\left[1 - \exp\left(-h\nu/kT\right)\right] d\nu \sin\theta \, d\theta \, d\phi, \quad \ldots\ldots(6)$$

where θ and ϕ are the usual spherical polar coordinates. We write

$$\int_0^{c_i/\lambda_m} \nu^2 \log\left[1 - \exp\left(-h\nu/kT\right)\right] d\nu = 2\eta(y) - \frac{\pi^4}{45}, \quad \ldots\ldots(7)$$

where

$$\eta(y) = -\tfrac{1}{2} \int_y^\infty x^2 \log\left[1 - \exp(-x)\right] dx \text{ and } y = hc_i/\lambda_m kT.$$

$\eta(y)$ may be tabulated by using tables of the incomplete gamma function.

The temperature dependent free energy is therefore given by

$$F(T) = \frac{2k^4T^4\Omega}{h^3} \sum_{i=1}^{3} \int_0^{2\pi} \int_0^{\pi} \left[\frac{\pi^4}{90} - \eta(y)\right] \frac{1}{c_i^3} \sin\theta \, d\theta \, d\phi. \quad \ldots\ldots(8)$$

$F(T)$ can be obtained numerically as a function of temperature from equations (3) and (8), when the values of the elastic constants are known. The numerical work presents two main problems: first, the solution of equation (3) for at least seventy different values of (l, m, n), secondly, the numerical double integration of equation (8) for a number of temperatures. To reduce the numerical work the following approximations are made. At low temperatures, since $\eta(y) \to 0$ as $T \to 0$, (8) may be written as

$$F(T) = \frac{-16\Omega\pi^4k^4T^4}{45h^3} I, \quad \ldots\ldots(9)$$

where

$$I = \frac{1}{16} \sum_{i=1}^{3} \int_0^{2\pi} \int_0^{\pi} \frac{1}{c_i^3} \sin\theta \, d\theta \, d\phi. \quad \ldots\ldots(10)$$

The Debye theory in the same limit gives

$$F(T) = \frac{-\pi^4kT^4}{5\theta_D^3} \quad \ldots\ldots(11)$$

where θ_D is the characteristic temperature. Hence, by comparing equations (9) and (11), we obtain

$$\theta_D = \frac{h}{k}\left(\frac{16}{9}\Omega I\right)^{-1/3}. \quad \ldots\ldots(12)$$

At higher temperatures, according to the Debye theory

$$F(T) = \frac{-18kT^4}{\theta_D^3}\left[\frac{\pi^4}{90} - \eta\left(\frac{\theta_D}{T}\right)\right], \quad \ldots\ldots(13)$$

and therefore in this range an approximation for $F(T)$ is

$$F(T)=\frac{-32k^4T^4I\Omega}{h^3}\left[\frac{\pi^4}{90}-\eta\left(\frac{\theta_D}{T}\right)\right]. \qquad \ldots\ldots(14)$$

Hence, if the integral I can be found, the free energy may be obtained from equations (12) and (14).

In order to find an approximation to the integral I, the values of the wave velocities have been found for the directions (l, m, n) for which equation (3) factorizes. The directions and the values obtained are shown in table 1.

Table 1

Direction (l, m, n)	ρc_1^2	ρc_2^2	ρc_3^2
$(1, 0, 0)$	A	A	$C+\frac{4B}{3}$
$\left(\frac{1}{\sqrt{2}}, \frac{1}{\sqrt{2}}, 0\right)$	B	A	$C+\frac{B}{3}+A$
$\left(\frac{1}{\sqrt{3}}, \frac{1}{\sqrt{3}}, \frac{1}{\sqrt{3}}\right)$	$\frac{2B}{3}+\frac{A}{3}$	$\frac{2B}{3}+\frac{A}{3}$	$C+\frac{4A}{3}$

The value of $\sum_{i=1}^{3}\frac{1}{c_i^3}$ in the (l, m, n) direction may be denoted by

$$\left(\sum_{i=1}^{3}\frac{1}{c_i^3}\right)_{(l,m,n)}.$$

For two given sets of values of the elastic constants equation (3) was solved for seventy different values of (l, m, n). The integral I is one sixteenth of the area of the surface formed by plotting $\sum_{i=1}^{3}\frac{1}{c_i^3}$ as the spherical polar coordinate r, the θ and ϕ coordinates being easily obtained from (l, m, n). If the whole surface is considered, there are six axes of symmetry similar to the (1, 0, 0) axis, twelve similar to the (1, 1, 0) axis and eight similar to the (1, 1, 1) axis. Detailed calculations show that the integral I may be approximated to by giving the value

$$\left(\sum_{i=1}^{3}\frac{1}{c_i^3}\right)_{(1,0,0)}$$

to all the radii r lying within a solid angle $4\pi/21$ surrounding the (1, 0, 0) axis, the value

$$\left(\sum_{i=1}^{3}\frac{1}{c_i^3}\right)_{\left(\frac{1}{\sqrt{2}},\frac{1}{\sqrt{2}},0\right)}$$

to all the radii r lying within a solid angle $\pi/21$ surrounding the (1, 1, 0) axis and the value

$$\left(\sum_{i=1}^{3}\frac{1}{c_i^3}\right)_{\left(\frac{1}{\sqrt{3}},\frac{1}{\sqrt{3}},\frac{1}{\sqrt{3}}\right)}$$

to all the radii r lying within the solid angle $2\pi/7$ surrounding the (1, 1, 1) axis.

An approximate value of the integral I has therefore been taken as

$$I=\frac{\pi}{28}\left\{2\left(\sum_{i=1}^{3}\frac{1}{c_i^3}\right)_{(1,0,0)}+\left(\sum_{i=1}^{3}\frac{1}{c_i^3}\right)_{\left(\frac{1}{\sqrt{2}},\frac{1}{\sqrt{2}},0\right)}+4\left(\sum_{i=1}^{3}\frac{1}{c_i^3}\right)_{\left(\frac{1}{\sqrt{3}},\frac{1}{\sqrt{3}},\frac{1}{\sqrt{3}}\right)}\right\}. \qquad \ldots\ldots(15)$$

The surface is illustrated by the two sections given in figure 2 and the above value for I is only appropriate to surfaces which are very nearly of the same shape. The value in the (1, 1, 0) direction is the greatest and the reason for its comparatively light weighting is apparent from the figure.

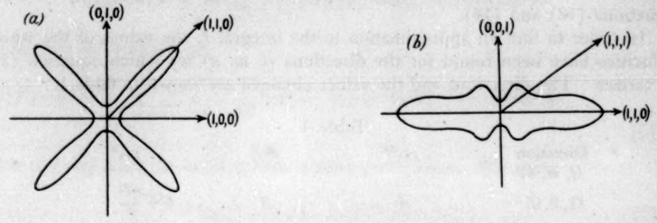

Figure 2. Sections of the surface formed by plotting $\left(\sum_{i=1}^{3}\frac{1}{c_i^3}\right)$ as the spherical polar coordinate r: (a) intersection with the plane $z=0$, (b) intersection with the plane $x=y$.

§ 3. EVALUATION OF THE ELASTIC CONSTANTS

Three different energies which contribute to the elastic constants are considered: (i) the electrostatic energy terms which arise from the electrostatic interaction of the valence electrons and the ions, (ii) the ionic terms, which arise from the interaction between the closed ionic shells, (iii) the terms due to the depression of the Fermi energy caused by the Brillouin zone structure.

The electrostatic terms and the ionic terms have been calculated by the method given by Fuchs (1936 a). The lattice constant for body-centred cubic sodium is taken to be the experimental value given by Barrett (1956), i.e. $4{\cdot}225\times10^{-8}$ cm, and the atomic volume is assumed to be the same for both phases. The values obtained are given in table 2.

Table 2

	Face-centred cubic		Body-centred cubic	
	$\frac{1}{2}(c_{11}-c_{12})$	c_{44}	$\frac{1}{2}(c_{11}-c_{12})$	c_{44}
Electrostatic terms	0·06074	0·54445	0·07215	0·53718
Ionic terms	0·01129	0·04088	−0·00103	0·04907
Total	0·07203	0·58533	0·07112	0·58625

All the terms in the table above should be multiplied by 10^{11} dyn cm^{-2}.

The electrostatic terms alone are not sufficient to explain the phase change. It can easily be seen from equation (14) that in order that the free energy curves may cross in the manner sketched in figure 1, the integral I must be greater for the body-centred cubic lattice than for the face-centred cubic lattice. From tables 1 and 2 and equation (15), it can be seen that the greatest contribution to the integral I is given by the value of B [$=\frac{1}{2}(c_{11}-c_{12})$], and therefore, since B occurs as $B^{-3/2}$ in the expression for the integral I, the condition for the curves to cross is that $\frac{1}{2}(c_{11}-c_{12})$ must be smaller for the body-centred cubic lattice than for the face-centred cubic lattice. Table 2 shows that if the electrostatic terms alone are considered, this is not the case and consequently a phase change from face-centred cubic to body-centred cubic would be impossible. This result is independent of the lattice constant.

If the totals of the electrostatic and ionic terms are examined, it can be seen that the total differences between the values of the elastic constants for the two structures are extremely small. The corresponding differences in the temperature dependent free energy, for temperatures in the range 0°–120°K, are found to be far too small to explain the phase change which occurs.

In order to calculate the ionic terms, the mutual potential energy W_{I} of two ions at a distance r apart, has been taken to be given by the empirical formula

$$W_{\mathrm{I}} = A_0 \exp\left(\frac{r_s - r}{\rho}\right), \qquad \ldots\ldots (16)$$

where for sodium, $\rho = 0{\cdot}345 \times 10^{-8}$cm, $r_s = 0{\cdot}875 \times 10^{-8}$ cm and $A_0 = 1{\cdot}25 \times 10^{-12}$ ergs. This formula was obtained from the heats of vaporization and the compressibilities of the alkali halides, by Born and Mayer (1932), Mayer and Helmholtz (1932) and Huggins and Mayer (1933). An investigation was made to discover whether small alterations in ρ or r_s would produce contributions to the elastic constants which would be large enough to account for the phase change. It was found that it is not possible to obtain a satisfactory result by altering ρ and the only possibility is to change the ionic radius r_s to at least $1{\cdot}065 \times 10^{-8}$ cm. This change is equivalent to tripling the ionic terms and in view of the experimental results this does not seem reasonable. Alterations in A_0 are not possible since the value chosen is implicit in the model used.

The third contribution to the elastic constants is from the effect on the Fermi energy of the shear of the Brillouin zones. These contributions may be calculated by the method given by Jones (1952) for a body-centred cubic lattice.

In the following work, the energies are measured in rydberg units and the lengths are measured in units of the first Bohr hydrogen orbit.

If a denotes the lattice constant, the planes which form the boundaries of the Brillouin zones of a cubic lattice are given by

$$\mathbf{n} \cdot \mathbf{k} = (\pi/a)\mathbf{n}^2, \qquad \ldots\ldots (17)$$

where $\mathbf{k}$ is the wave vector and $\mathbf{n}$ has integer components (n_1, n_2, n_3). The first Brillouin zone of the body-centred cubic lattice is formed by the set of twelve {1, 1, 0} planes and the first Brillouin zone of the face-centred cubic lattice is formed by the set of eight {1, 1, 1} planes and the set of six {2, 0, 0} planes.

The values of the perpendicular distance p from the origin of $\mathbf{k}$ space on to the appropriate Brillouin zone planes are:

$p = \sqrt{2}\pi/a$ for the {1, 1, 0} planes,
$p = \sqrt{3}\pi/a$ for the {1, 1, 1} planes,
$p = 2\pi/a$ for the {2, 0, 0} planes.

The lattice constant a is different for the two structures, but if the atomic volume is assumed to be the same for both,

$$(a)_{\mathrm{fcc}} = 2^{1/3}(a)_{\mathrm{bcc}}. \qquad \ldots\ldots (18)$$

The contributions to the shear elastic constants calculated by the method given by Jones are shown in table 3.

Table 3

	Set of Planes	$\{1, 1, 1\}$	$\{2, 0, 0\}$
F.C.C.	$\frac{1}{2}(c_{11}-c_{12})_F$	$\frac{4}{3}p\frac{dW_F}{dp}$	$\frac{1}{2}p^2\frac{d^2W_F}{dp^2}+\frac{1}{2}p\frac{dW_F}{dp}$
	$(c_{44})_F$	$\frac{4}{9}p^2\frac{d^2W_F}{dp^2}+\frac{8}{9}p\frac{dW_F}{dp}$	$p\frac{dW_F}{dp}$
	Set of Planes	$\{1, 1, 0\}$	
B.C.C.	$\frac{1}{2}(c_{11}-c_{12})_F$	$\frac{1}{4}p^2\frac{d^2W_F}{dp^2}+\frac{7}{4}p\frac{dW_F}{dp}$	
	$(c_{44})_F$	$\frac{1}{2}p^2\frac{d^2W_F}{dp^2}+\frac{3}{2}p\frac{dW_F}{dp}$	

In order to evaluate $(c_{44})_F$ and $\frac{1}{2}(c_{11}-c_{12})_F$, the terms dW_F/dp and d^2W_F/dp^2 must be calculated. The effect on the Fermi energy of a single pair of planes $(\pm\mathbf{n})$ may be found by assuming that the energy at any point $\mathbf{k}=(k_x, k_y, k_z)$ is given by

$$E=k_x^2+k_y^2+p^2f(k_z/p), \qquad \ldots\ldots(19)$$

where the axes in $\mathbf{k}$ space have been chosen so that k_z coincides with the normal to the two planes $(\pm\mathbf{n})$. When the energy has this form, the density of states function $N(E)$ can be evaluated immediately and is given by

$$N(E)=\frac{1}{4\pi^3}\int\frac{1}{|\text{grad }\mathbf{E}|}dS=\frac{1}{2\pi^2}k_z\text{ (max)}, \qquad \ldots\ldots(20)$$

where k_z(max) is the greatest value of k_z on the energy surface E.

From equation (19), if $k_z(\text{max})/p=z$, then

$$E=p^2f(z), \qquad \ldots\ldots(21)$$

and since from equation (20)

$$N(E)=pz/2\pi^2, \qquad \ldots\ldots(22)$$

the inversion of (21) gives

$$N(E)=\sqrt{E}\psi(E/p^2), \qquad \ldots\ldots(23)$$

where $\psi(x)$ is the inverse function of $f(x)$.

If n_0 is the number of atoms per unit volume and ζ is the value of E at the Fermi surface, then,

$$n_0=\int_0^\zeta N(E)dE, \qquad \ldots\ldots(24)$$

hence,

$$n_0=p^3\int_0^\xi x^{1/2}\psi(x)dx, \qquad \ldots\ldots(25)$$

where $x=E/p^2$ and $\xi=\zeta/p$

Similarly, if W_F is the Fermi energy per unit volume,

$$W_F = \int_0^{\zeta} EN(E)dE, \qquad \ldots\ldots (26)$$

hence

$$W_F = p^5 \int_0^{\xi} x^{3/2}\psi(x)dx. \qquad \ldots\ldots (27)$$

If equations (25) and (27) are differentiated with respect to p we have

$$\frac{d}{dp}\left(\frac{W_F}{p^5}\right) = \xi^{3/2}\psi(\xi)\frac{d\xi}{dp}, \qquad \ldots\ldots (28)$$

and

$$0 = \frac{3n_0}{p^4} + \xi^{1/2}\psi(\xi)\frac{d\xi}{dp}, \qquad \ldots\ldots (29)$$

since n_0 is a constant. Eliminating $d\xi/dp$ between equations (28) and (29) we obtain

$$p\frac{dW_F}{dp} = 5W_F - 3n\zeta. \qquad \ldots\ldots (30)$$

$p^2\, d^2W_F/dp^2$ may be obtained in a similar manner by differentiating equation (30) and using equation (29) to eliminate $d\xi/dp$. The expression obtained is

$$p^2\frac{d^2W_F}{dp^2} = 20W_F - 18n\zeta + \frac{9n^2}{N(\zeta)}. \qquad \ldots\ldots (31)$$

Equations (30) and (31) are not exact since the integration should be taken over the region of the actual Brillouin zone, but the evaluation of W_F by the method given by Jones (1937) shows that the error involved is small.

If Ω is the atomic volume and z_0 is given by $\xi = f(z_0)$, equations (21), (22) and (25) give

$$\frac{1}{\Omega} = \frac{p^3}{2\pi^2}\int_0^{z_0}\frac{\partial f}{\partial z}z\,dz, \qquad \ldots\ldots (32)$$

and therefore ξ and hence ζ may obtained. Similarly, W_F per unit volume is given by

$$W_F = \frac{p^5}{2\pi^2}\int_0^{z_0}\frac{\partial f}{\partial z}zf(z)\,dz. \qquad \ldots\ldots (33)$$

All the terms in equations (30) and (31) may then be found if a specific form is assumed for $f(z)$.

For free electrons, $E = k^2$, and hence for this model $f(z) = z^2$. In this case it can easily be seen from equations (35) and (36) that both derivatives dW_F/dp and d^2W_F/dp^2 vanish. Any contributions to these terms therefore come from the deviation from the form z^2 below the Fermi surface. If the Brillouin zone structure is considered it may be assumed that for small z the energy is the same as it is for free electrons. $f(z)$ must therefore satisfy the following condition,

$$f(z) \to z^2 \text{ as } z \to 0. \qquad \ldots\ldots (34)$$

The energy is known to be discontinuous on crossing the Brillouin zone boundary and hence it is reasonable to suppose that

$$f(1) = 1 - \lambda, \qquad \ldots\ldots (35)$$

where λp^2 is half the energy gap across the boundary. In addition, the energy surface is known to be normal to the Brillouin zone boundary at the points of intersection and therefore the further condition

$$f'(1)=0, \qquad \ldots\ldots(36)$$

must also be satisfied.

As the function $f(z)$ is not known over the whole range from $z=0$ to $z=1$, three possible forms of $f(z)$ were considered. The only model suitable for the present calculation was that given by Leigh (1951). The function is

$$f(z)=z^2-z^{2/\lambda}, \qquad \ldots\ldots(37)$$

which obviously satisfies all the conditions (34), (35) and (36). In order to simplify the algebra it is convenient to use $\alpha(=2/\lambda)$ instead of λ.

z_0 may be found by successive approximation to the solution of equation (37). A first approximation y_0 may be found by taking $f(z)=z^2$; this gives

$$y_0=(3\pi^2/\Omega p^3)^{1/3}. \qquad \ldots\ldots(38)$$

Substituting for Ω and p we have $y_0=0{\cdot}8775$ for the {1, 1, 0} planes of the body-centred cubic lattice, $y_0=0{\cdot}9025$ for the {1, 1, 1} planes of the face-centred cubic lattice, $y_0=0{\cdot}7816$ for the {2, 0, 0} planes of the face-centred cubic lattice. Two further successive approximations give the expansion of z_0 in powers of y_0 as far as the term in $y_0^{2\alpha-1}$, the higher powers of y_0 being negligible for appropriate values of α. The approximation to z_0 is

$$z_0=y_0+\frac{1}{(\alpha+1)}y_0^{\alpha-1}+\frac{\alpha}{(\alpha+1)^2}y_0^{2\alpha-1}. \qquad \ldots\ldots(39)$$

All the terms in equations (30) and (31) may now be found in terms of y_0, the results correct to the term $y_0^{2\alpha-1}$ being

$$p\frac{dW_{\mathrm{F}}}{dp}=\frac{2p^5}{\pi^2}y_0^{\alpha+3}\frac{\alpha-2}{\alpha+1}\left\{\frac{1}{\alpha(\alpha+3)}+\frac{1}{(2\alpha+1)(\alpha+1)}y_0^{\alpha-2}\right\}\times 6{\cdot}1008\times10^{-28}\ \mathrm{dyn\ cm^{-2}}, \qquad \ldots\ldots(40)$$

and

$$p^2\frac{d^2W_{\mathrm{F}}}{dp^2}=\frac{2p^5}{\pi^2}y_0^{\alpha+3}\frac{\alpha-2}{\alpha+1}\left\{\frac{-(\alpha-1)}{\alpha+3}+\frac{3-2\alpha}{(2\alpha+1)(\alpha+1)}y_0^{\alpha-2}\right\}\times 6{\cdot}1008\times10^{-28}\ \mathrm{dyn\ cm^{-2}}; \qquad \ldots\ldots(41)$$

p is expressed in c.g.s. units.

The values of $\frac{1}{2}(c_{11}-c_{12})_{\mathrm{F}}$ and $(c_{44})_{\mathrm{F}}$ can be obtained for various values of α by using equations (40) and (41) in conjunction with table 3. The appropriate values of y_0 and p are substituted in each case.

The same value of α (i.e. the same energy gap as a function of the free electron energy at the Brillouin zone boundary) has been assumed for both structures and for both sets of planes for the face-centred cubic lattice. The values taken are $\alpha=20$, 16, 14, 12 and 10, corresponding to energy gaps of 0·062, 0·077, 0·088, 0·103 and 0·124 Ryd at the {1, 1, 0} boundary for the body-centred cubic lattice. The energy gap found by Howarth and Jones (1952) corresponds to $\alpha=26$.

The numerical values obtained for sodium are given in table 4 together with the total contributions from the electrostatic terms, the ionic terms and the Fermi energy terms.

Table 4

α		Face-centred cubic		Body-centred cubic	
		$\frac{1}{2}(c_{11}-c_{12})$	c_{44}	$\frac{1}{2}(c_{11}-c_{12})$	c_{44}
20	Fermi energy term	0·00185	−0·02136	−0·00596	−0·01499
	Total	0·07368	0·56397	0·06516	0·57126
16	Fermi energy term	0·00294	−0·03825	−0·00887	−0·02552
	Total	0·07497	0·54708	0·06225	0·56073
14	Fermi energy term	0·00335	−0·04956	−0·01125	−0·03520
	Total	0·07538	0·53577	0·05987	0·55105
12	Fermi energy term	0·00378	−0·06667	−0·01438	−0·04968
	Total	0·07581	0·51866	0·05674	0·53675
10	Fermi energy term	0·00428	−0·08678	−0·01956	−0·07212
	Total	0·07631	0·49855	0·05156	0·51413

All the values in the above table should be multiplied by 10^{11} dyn cm^{-2}.

The value of $\frac{1}{3}(c_{11}+2c_{12})$ has been calculated by the method due to Fröhlich (1937). This term has been taken as the same for both structures because it can easily be seen that the effect of the difference on the final calculation will be negligible. The numerical value found for sodium is

$$C=\tfrac{1}{3}(c_{11}+2c_{12})=0{\cdot}81544\times10^{11}\ \text{dyn cm}^{-2}.$$

4. The Difference Between the Free Energies of the Two Lattices at Absolute Zero Temperature

At absolute zero temperature the free energy equals the internal energy W and four terms which contribute to the difference in W for the two structures have been considered. These are the electrostatic terms, the ionic terms, the Fermi energy terms and the difference between the energies found when the term $\frac{1}{2}h\nu$, which is the zero point energy of the lattice vibrations, is integrated over the frequency distribution of ν.

The difference in the energies of the electrostatic terms has been evaluated by Fuchs (1935) and the numerical value obtained for sodium is

$$(W_{\mathrm{E}})_{\mathrm{bcc}}-(W_{\mathrm{E}})_{\mathrm{fcc}}=-2{\cdot}06\times10^{7}\ \text{erg cm}^{-3},$$

where W_{E} is the electrostatic energy.

The contribution to the difference from the ionic terms may be found directly from equation (16). Taking into account both nearest neighbours and next nearest neighbours in both lattices the value obtained for sodium is

$$(W_{\mathrm{I}})_{\mathrm{bcc}}-(W_{\mathrm{I}})_{\mathrm{fcc}}=1{\cdot}48\times10^{7}\ \text{erg cm}^{-3}.$$

The difference between the Fermi energy terms for the two lattices may be calculated by using a similar method to that used for calculating the elastic constants. Equations (33) and (37) give W_F for a pair of planes as

$$W_F = \frac{p^5}{\pi^2}\left\{\frac{z_0^5}{5} - \frac{(2+\alpha)}{\alpha(\alpha+3)} z_0^{\alpha+3} + \frac{2}{\alpha(2+\alpha)} z_0^{2\alpha+1}\right\} \qquad \ldots\ldots(42)$$

in rydberg units.

For free electrons,

$$W_F = \frac{p^5 y_0^5}{5\pi^2}, \qquad \ldots\ldots(43)$$

where y_0 is given the appropriate value. The difference between the values for W_F obtained from equations (42) and (43) is denoted by δW_F and may be expressed as

$$\delta W_F = \frac{-p^5}{\pi^2(1+\alpha)} y_0^{\alpha+3}\left\{\frac{2}{\alpha(\alpha+3)} + \frac{1}{(1+\alpha)(2+\alpha)} y_0^{\alpha-2}\right\}$$
$$\times 6{\cdot}1008 \times 10^{-28} \text{ erg cm}^{-3}, \qquad \ldots\ldots(44)$$

correct to the power $2\alpha+1$ of y_0; p is expressed in c.g.s. units.

The total difference from the free electron value for the body-centred cubic lattice is $6(\delta W_F)_{(1,1,0)}$, and for the face-centred cubic lattice is

$$4(\delta W_F)_{(1,1,1)} + 3(\delta W_F)_{(2,0,0)},$$

where $(\delta W_F)_{(1,1,0)}$ denotes the term given by (44) for the {1, 1, 0} planes etc. Figure 3 shows the results for values of $\alpha = 30$, 25, 20, 16, 12 and 10 plotted as a function of the energy gap across the {1, 1, 0} planes. The dotted line shows the result if the {1, 1, 1} planes alone are considered for the face-centred cubic lattice. It can be seen that for larger values of λ it is essential to consider the {2, 0, 0} planes as well in order to obtain a result giving the energy of the face-centred cubic lattice lower than that of the body-centred cubic lattice.

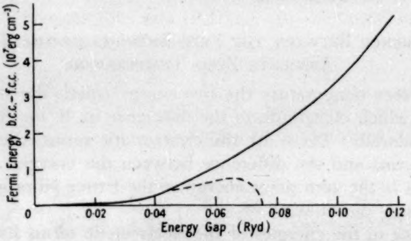

Figure 3. The difference between the Fermi energies of the body-centred and face-centred cubic lattices plotted against the energy gap across the first Brillouin zone boundary of the body-centred cubic lattice. The broken line shows the difference if only the {1, 1, 1} planes are considered for the face-centred cubic lattice.

The difference in the internal energy of the two structures at absolute zero temperature, due to the zero point energy $\frac{1}{2}h\nu$ of the oscillations, may be calculated by considering, for each structure, the total energy per atom from this source which is given by

$$\int_0^{\nu_m} \tfrac{1}{2}h\nu g(\nu)\,d\nu, \qquad \ldots\ldots(45)$$

where ν_m is the maximum frequency.

W_0, the total energy per unit volume derived from the zero point energy, is then given by

$$W_0 = \frac{3h}{2\pi}\left(\frac{3}{4\pi\Omega^4}\right)^{1/3} J, \qquad \ldots\ldots(46)$$

where

$$J = \frac{1}{16}\sum_{i=1}^{3}\int_0^{2\pi}\int_0^{\pi} c_i \sin\theta \, d\theta d\phi. \qquad \ldots\ldots(47)$$

An approximate value of J is obtained by finding the average of the three values of $\sum_{i=1}^{3} c_i$ obtained from table 1 and multiplying this result by $\pi/4$. More accurate calculations for two sets of elastic constants show that this gives a reasonable approximation to the integral. The resulting difference $(W_0)_{\text{bcc}} - (W_0)_{\text{fcc}}$ together with the totals obtained by adding to it the contributions from the ionic terms, the electrostatic terms and the Fermi energy terms are given in table 5.

Table 5

α	20	16	14	12	10
Term from $\frac{1}{2}h\nu$	0·06	−0·07	−0·21	−0·50	−1·17
Total	0·42	1·06	1·53	2·29	4·03

All the terms in the above table must be multiplied by 10^7 erg cm^{-3}.

§ 5. DISCUSSION OF THE NUMERICAL RESULTS

The free energy curves obtained for both lattices for values of $\alpha = 20$, 16, 14, 12 and 10 have been plotted and it is found that the free energies of the two lattices are very close to one another over a considerable range of temperature on either side of the transition point given by the intersection of the two curves. This is in agreement with the experimental results because it indicates that both forms may exist simultaneously over a large range of temperature. The transition temperatures have been found by interpolation since it is impossible to obtain a sharp point of intersection graphically. These temperatures are plotted in figure 4 as a function of the energy gap across the face of the first Brillouin zone boundary of the body-centred cubic lattice. The actual numerical values of

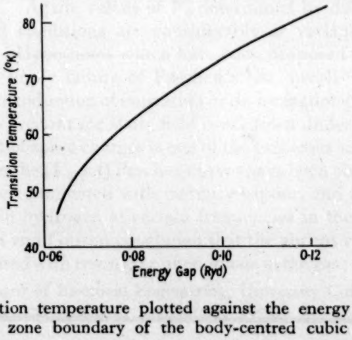

Figure 4. The transition temperature plotted against the energy gap across the first Brillouin zone boundary of the body-centred cubic lattice.

the temperature cannot be regarded as significant because of the various approximations used. They do, however, indicate that the actual transition temperature is in the range 40°–100°K.

The difference between the free energies of the two lattices is most pronounced, and a clearer transition point is given when the highest value of the energy gap is taken. This is in general agreement with the experimental results since, in the case of lithium which has a higher energy gap, the final transition to a face-centred cubic lattice does take place. Detailed calculations for lithium cannot be made by the present method because of the deviation from the free electron model is much greater and in consequence the approximations no longer hold.

ACKNOWLEDGMENT

The author wishes to express her sincere gratitude to Professor H. Jones, Head of the Department of Mathematics, Imperial College, for his advice and assistance in this work.

REFERENCES

BARRETT, C. S., 1947, *Phys. Rev.*, **72,** 245; 1948, *Amer. Min.*, **33,** 749; 1956, *Acta Cryst.*, *Camb.*, **9,** 671.
BARRETT, C. S., and TRAUTZ, O. R., 1948, *Trans. Amer. Inst. Min.* (*Metall.*) *Engrs*, **175,** 579.
BORN, M., and MAYER, J. E., 1932, *Z. Phys.*, **75,** 1.
FUCHS, K., 1935, *Proc. Roy. Soc.* A, **151,** 585; 1936 a, *Ibid.*, **153,** 622; 1936 b, *Ibid.*, **157,** 444.
FRÖHLICH, H., 1937, *Proc. Roy. Soc.* A, **158,** 97.
HOWARTH, D. J., and JONES, H., 1952, *Proc. Phys. Soc.* A, **65,** 385.
HUGGINS, M. L., and MAYER, J. E., 1933, *J. Chem. Phys.*, **1,** 643.
JONES, H., 1937, *Proc. Phys. Soc.*, **49,** 250; 1952, *Phil. Mag.*, [7], **43,** 105.
LEIGH, E. S., 1951, *Phil. Mag.*, [7], **42,** 139.
MAYER, J. E., and HELMHOLTZ, L., 1932, *Z. Phys.*, **75,** 19.

The Electrical Breakdown of Gases in Uniform High Frequency Fields at Low Pressure

By W. G. TOWNSEND† and G. C. WILLIAMS‡
Department of Physics, University College of Swansea

Communicated by F. Llewellyn Jones ; MS. received 18*th June* 1958, *and in final form* 21*st July* 1958

Abstract. Electrical breakdown in air and in hydrogen for uniform high frequency and static fields was investigated using a pair of geometrically similar electrode systems. Static breakdown potentials for values of $pd \leqslant 15$ mm Hg cm were measured and high frequency data obtained over a range of frequencies f from 5 Mc/s to 70 Mc/s. The results support the view that there is only one mode of breakdown, contrary to the views proposed by many previous workers. The similarity relationship was found to be satisfied for certain pairs of frequencies provided that the discharge was confined to the regions of uniform field between the electrodes, and that the electrode surfaces were clean. On the other hand, when the electrodes were covered with oxide layers, the similarity theorem did not apply. This result indicates that at least one process of electron generation or loss was not a function of E/p; the most probable process, cold emission, was identified by correlating the results with those obtained under similar conditions with static fields.

§ 1. Introduction

Some published papers on high frequency breakdown between parallel plate electrodes have revealed anomalous features for which no adequate or consistent explanation has been proposed.

According to Thomson (1937) the breakdown potential V_s at low pressures in hydrogen does not appear to vary in a regular manner with *pd* for frequencies in the range 1—100 Mc/s, and Paschen curves for these frequencies sometimes contain two minima. Again, values of V_s determined by different observers for similar experimental conditions are considerably at variance with each other (see Githens 1940). Hypotheses which have been proposed to account for these observations, which imply failure of Paschen's law, involve complex modes of breakdown and the introduction of ionization or de-ionization processes in addition to those necessary to account for static field breakdown under similar conditions; the effect of the onset of space charges is one of the processes suggested.

Double minima in the (V_s, pd) Paschen curves have been observed by Thomson (1934) in hydrogen contaminated with mercury vapour, and recorded by Gutton and Gutton (1928) in hydrogen at certain frequencies in the range from 50 kc/s to 99 Mc/s. Gutton and Gutton concluded that the abrupt variations of V_s with pressure were associated with resonance phenomena in the gas; Gill and Donaldson

---

† Now at Department of Electrical Engineering, University College of Swansea.

‡ Now at the Electrical Research Laboratory, Joseph Lucas (Electrical) Limited, Birmingham.

(1931), however, showed that this view was not tenable, and that the observations were simply due to wall effects.

Breakdown in uniform fields in hydrogen for frequencies from 5 to 11 Mc/s and for values of *pd* from 0·2 to 30 mm Hg cm was studied by Githens (1940), who attempted to correlate the appearance of the minima of the (V_s, *pd*) curves with the position of the walls of the discharge tube relative to the electrodes. Githens concluded that the initiation of the high frequency discharge occurred through three different processes which he denoted by modes *a*, *b* and *c*, each of which gave rise to a minimum in the (V_s, *pd*) curve. In mode *a*, V_s was independent of frequency, and breakdown was attributed to the oscillatory motion of charged particles and the build up of space charges between the electrodes; in mode *b*, the space charge accumulated was considered to be insufficient to initiate mode *a* breakdown, and for mode *c* the discharge did not occur between the electrodes but took a longer path in the space between the electrodes and the walls of the discharge tube. In this latter case abnormally low values of V_s were observed and these were attributed to the accumulation of space charge on the non-conducting walls of the discharge tube. The transition of the breakdown mechanism from one mode to another as the pressure was reduced was considered by Githens to account for the occurrence of more than one minimum in the (V_s, *pd*) curve.

Breakdown potentials for air in uniform fields have been measured by Pim (1949) using steel electrodes with a maximum separation of 0·10 cm at frequencies ranging from 100 to 300 Mc/s and pressures from 50 to 1000 mm Hg. The experimental results were considered to support the view that breakdown is the result of the formation of a critical concentration of positive ions in the gap producing enhanced values of the coefficient α as suggested by Reukema (1928). It was concluded that Paschen's law did not hold, and that breakdown was initiated in one of three different modes, each mode being represented by a curve that separately obeyed Paschen's law. In discussing this work Prowse (1950) concluded that if breakdown for frequencies in the range considered by Pim (1949) is not initiated in the uniform field region then it cannot be initiated elsewhere. Further, breakdown for $f \leqslant 10$ Mc/s has been studied by Bright (1950) using spherical electrodes. Below a critical electrode separation *d* the Paschen curves for air, oxygen and nitrogen at 50 c/s coincide with those at higher frequencies, but for values greater than *d*, curves for frequencies from 1·4 to 8·0 Mc/s were lower than the curve for 50 c/s. From this departure it was concluded that space charges play an important part in the high frequency breakdown mechanism by distorting the electric field. Both Pim and Bright, however, neglected the important parameter f/p in their consideration of this problem. It is not surprising therefore that they observed an apparent failure of Paschen's law, since the similarity theorem was incorrectly applied. The neglect of either of the parameters *pd* and f/p will consequently give rise to non-similarity, as the discharge paths in the two systems will not be homologous.

Experiments by Fatehchand (1951) and Dalton (1953) in which an ionized air stream was directed across the gap between two parallel plate electrodes showed that when a high frequency potential was applied to the plates a large positive ion current was collected just prior to breakdown by a probe placed in the path of the emerging air. They concluded that a large space charge concentration accumulated in the gap prior to breakdown, a factor which also accounted for the lower values of V_s obtained with high frequency oscillatory fields than with 50 c/s fields.

From the above account it can be seen that considerable data, accumulated in recent years, have not been adequately explained. It would appear that no consistent theory involving a single mode of breakdown has been put forward to account for the properties reported over a large range of pressure and frequency; also, the precise role played by space charges is little understood. Consequently, there is a need for a systematic experimental investigation of the electrical breakdown of gases in uniform high frequency fields and the object of the present paper is to investigate the fundamental discharge processes which are involved in uniform field breakdown and to find the range within which they apply. In particular, the phenomena leading to two minima in the Paschen curve under certain conditions of pressure and frequency require investigation in view of the role attributed to impurities in the gas.

This paper describes an experimental investigation of electrical breakdown of air and hydrogen in uniform high frequency fields of frequency in the range 5–70 Mc/s for values of the parameter pd between 0·01 and 20 mm Hg cm, where p is the gas pressure in mm Hg and d the electrode separation in centimetres.

§ 2. EXPERIMENTAL PROCEDURE

The basic techniques used in our investigations were similar to those described in previous papers (Llewellyn Jones and Morgan 1951, Llewellyn Jones and Williams 1953), which also described the form of the breakdown and the precise experimental method by which it was measured both in high frequency and d.c. discharges. Important information can be obtained by studying the conditions under which the similarity relationship applies, and, in particular, the general nature of the ionization and de-ionization processes operative under different conditions may be identified. Two geometrically similar discharge systems D and E were used to examine the influence of the nature of the electrode surfaces on breakdown in air and hydrogen under uniform static and high frequency fields; careful observation was made of the paths of the discharges from one electrode to the other.

The electrode systems D and E consisted of copper discs 2·5 cm and 5 cm in diameter maintained parallel at distances d apart of 0·5 cm and 1·0 cm respectively by means of hard glass frames. The electrodes were rigidly mounted in two large glass envelopes jointed to the vacuum line and mercury free gas system. Care was taken in the preparation of the electrodes to avoid small imperfections on the surface that are known to cause local intensification of the electric field; the edges were bevelled and the flat portions polished with fine grades of emery paper and finally with rouge, washed in distilled water and dried. The electrodes and the glass envelopes were initially heated to temperatures from 300–400°c for several days while being continuously evacuated to remove occluded impurities. The air and hydrogen used were dried over phosphorous pentoxide before passing through a train of liquid air traps. Hydrogen was generated by the electrolysis of a hot solution of barium hydroxide and diffused through the walls of a heated palladium thimble. Mercury was completely excluded from the vacuum system. The pressure was measured with an Apiezon oil manometer, the oil being freed from dissolved gases. An oil diffusion pump, isolated with liquid air traps, was used for evacuating the system.

Measurements of V_s were first made in air for frequencies within the range 10 Mc/s to 70 Mc/s, and pressures from 0·01 mm Hg to 30 mm Hg. Paschen curves for tubes D and E were obtained for each frequency separately; at least one minute was allowed to elapse between consecutive readings. Before measurements of V_s in hydrogen were made, the tubes were alternately filled with hydrogen and evacuated a number of times before finally filling the system with gas to the maximum pressure used (about 30 mm Hg). The preliminary work in hydrogen was undertaken over the same range of pressure and frequency as in air; the electrodes were covered with thin oxide layers formed during long exposure to the atmosphere.

§ 3. Experimental Results

3.1. *Air*

Typical (V_s, pd) curves for air for tubes D and E are given in figures 1 (*a*) and 1 (*b*). For tube D, where the electrode separation d was 0·5 cm, V_s showed a minimum at two values of p for all the frequencies investigated. As the frequency was decreased, the two minima became more pronounced. The values of V_s and p at which the first minimum occurs were not very sensitive to frequency, but the second minimum moved to higher values of V_s and p as the frequency was decreased. For values of p greater than those indicated by the dotted curve in figures 1 (*a*) and 1 (*b*), the discharge occurred in the uniform field between the electrodes; for lower values of p, however, the discharge occurred in the region between the electrode edges and the glass envelopes, and thus followed a path greater than the electrode separation.

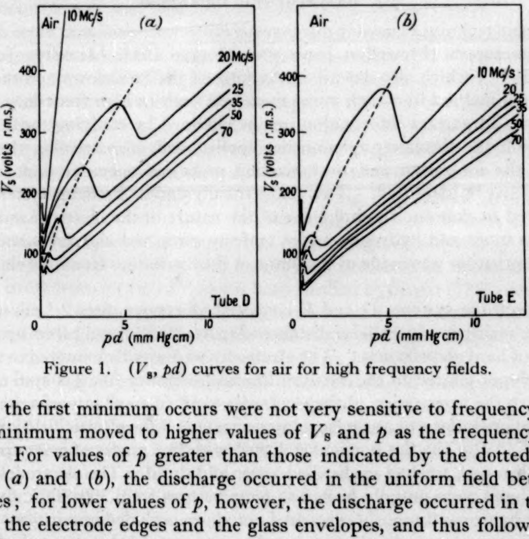

Figure 1. (V_s, pd) curves for air for high frequency fields.

The (V_s, pd) curves for tube E (which had an electrode separation equal to twice that for tube D) were of the same form as the Paschen curves for static fields when the frequency was greater than 35 Mc/s as shown in figure 1 (*b*). When the frequency was decreased below this value, however, two minima in the (V_s, pd) curves were obtained, as with tube D. The discharge occurred in the region between the edges of the electrodes and the glass envelope when pd had values lower than those indicated by the dotted curve (figure 1 (*b*)).

The values of V_s obtained for tube D at various frequencies f and pressures p were compared with those obtained for tube E at frequencies $f/2$ and pressures $p/2$ in order to test whether the similarity relation for high frequency oscillatory fields (Llewellyn Jones and Morgan 1951)

$$V_s = \phi(pd, f/p) \qquad \ldots\ldots(1)$$

applied to these tubes. A typical set of results for air is given in figure 2 where the values of V_s for tube D are indicated by full curves and those for tube E by the circles and dots. Within the limits of the experimental error the results show that for the pairs of frequencies 70 and 35 Mc/s, 50 and 25 Mc/s the similarity relation was obeyed provided the discharge took place in the uniform field between the electrode faces.

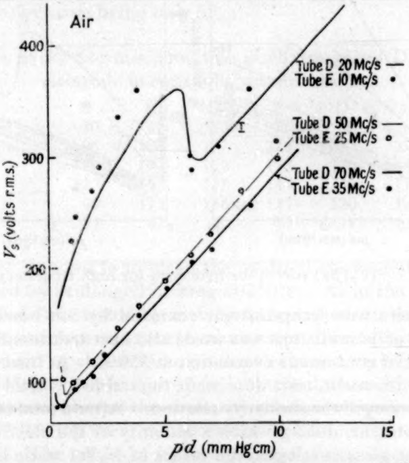

Figure 2. Similarity principle at high frequency for air.

3.2. *Hydrogen*

The form of the (V_s, pd) curves obtained with hydrogen using oxidized electrodes, was the same as that found for air. Two minima were obtained in the (V_s, pd) curve for tube D with all values of frequency exceeding 5 Mc/s (figure 3 (*a*)), but for tube E (figure 3 (*b*)) two sharp minima were only obtained for frequencies lower than 35 Mc/s. The dotted lines in figures 3 (*a*) and (*b*) again indicate the minimum values of pd at which the discharge occurred in the uniform field between the electrodes.

At frequencies greater than 30 Mc/s the (V_s, pd) data in hydrogen for tube D could be reproduced to within the limits of the experimental error. However, at lower frequencies the values of V_s could not be reproduced after passing a discharge; this appeared to support the view that the electrodes played some part in the discharge mechanism.

The values of (V_s, pd) shown in figures 3 (*a*) and (*b*) for hydrogen were used to test the similarity relation (1). Under these conditions, when the electrodes were oxidized the relation was not obeyed for any pair of frequencies. To test the influence of the cathode on V_s the electrodes were used in different conditions varying from heavily oxidized surfaces to clean surfaces.

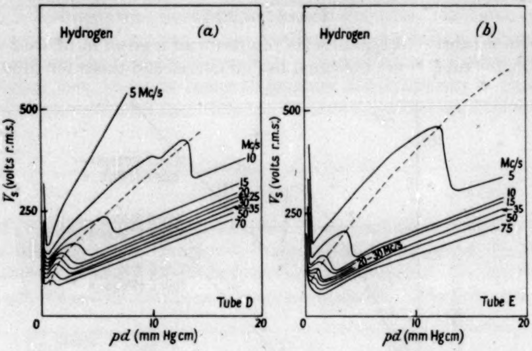

Figure 3. (V_s, pd) curves for hydrogen for high frequency fields.

The oxide layers were progressively removed by ion bombardment (a d.c. discharge current of 10 milliamps was used) and heat treatment in hydrogen followed by a period of continuous evacuation at 350°c. At intervals of about five hours during this treatment, tests were made to establish whether the values of V_s under static fields obeyed the similarity relation. After a total of about 100 hours of this severe treatment, during which a quantity of the electrode material was sputtered on to the glass envelopes, the values of V_s for static fields satisfied the similarity relation when the clean electrode was cathode (figure 4 (*a*), but the relation was not satisfied when the other electrode which had not been so treated was the cathode (figure 4 (*b*)). Immediately after these measurements, determinations of V_s with high frequency fields were made and the values were used to

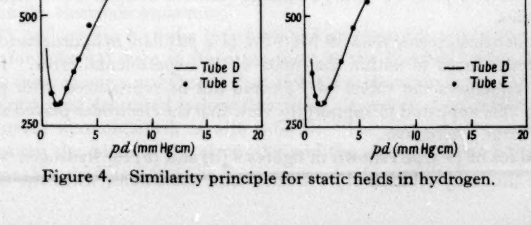

Figure 4. Similarity principle for static fields in hydrogen.

test the similarity relation (table 1). At 70 Mc/s for tube D and 35 Mc/s for tube E the breakdown potentials for both tubes were about 27 v lower than those obtained previously when both electrodes were oxidized. Even when one of the electrodes was in a de-oxidized condition the values of V_s did not satisfy the similarity relation (1). For example, when the value of *pd* was 10 mm Hg cm (see table 1) the difference in the values of V_s for tubes D and E was 22 v giving a difference of 13% which was considerably larger than the experimental error. The agreement between the values of V_s at 30 and 15 Mc/s and 20 and 10 Mc/s (table 1) at the same value of *pd* was better, the deviation being only 5%.

Table 1. Values of V_s (v r.m.s.) for two discharge tubes D and E when one electrode in each tube was de-oxidized

Tube	D	E	D	E	D	E	D	E
Frequency (Mc/s)	70	35	50	25	30	15	20	10
pd = 15	196	223	217	228	232	238	241	247
10	149	170	162	173	176	182	188	190
7·5	127	145	135	144	149	154	159	163
5	99	115	116	117	120	126	134	138
2·5	72	82	80	83	111	105	—	—

Attempts were then made to clean the oxidized electrode by glow discharge treatment followed by prolonged heating at 350°C. As in the previous case, the state of the electrode was tested by making it the cathode in determination of V_s under static fields, and then using these values to test the similarity relation. After a period of treatment of about 50 hours the electrodes were in such a condition that the values of V_s (as given in figure 4 (*a*)), obtained when either of the electrodes was made the cathode, obeyed the similarity relation within experimental error.

Immediately following these measurements breakdown potentials in h.f. fields were determined. The values of V_s for the range of frequencies from 30 Mc/s to 10 Mc/s now obeyed the similarity relation provided the parameter *pd* was not too low, as is indicated by the departure of the dotted lines from the full curves in figure 5. This result indicates that when the discharge occurred in the region of

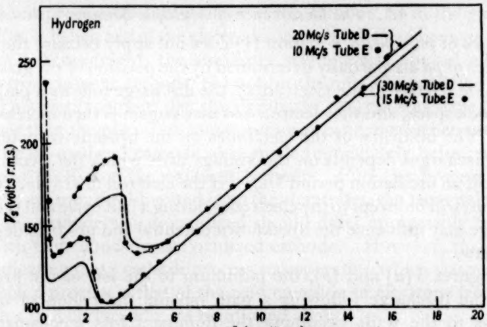

Figure 5. Similarity principle satisfied for frequency range 10–30 Mc/s ; both electrode surfaces de-oxidized in each tube.

uniform field between the electrode faces and the electrode separation d was the actual length of the discharge path, all the significant discharge processes were functions of the parameter E/p. Thus the process or processes which gave rise to dissimilarity did not play a significant part in the discharge mechanism when both electrodes were smooth and clean.

For the pairs of frequencies 70, 35 and 50, 25 Mc/s, the values of V_s are not in accordance with the similarity relation. This result is illustrated in table 2 where the values of V_s for tube D at 70 Mc/s and 50 Mc/s are compared with the values obtained for tube E at 35 and 25 Mc/s for different values of pd.

Table 2. Values of V_s (v r.m.s.) for two discharge tubes D and E after all electrodes had been de-oxidized

Frequency (Mc/s)	70	35	50	25
$pd=15$	200	224	213	231
10	149	170	160	173
7·5	117	142	134	144
5	99	115	107	116
2·5	73	81	81	85

§ 4.1 DISCUSSION

The above experimental results may be readily interpreted by considering the similarity relationship. For electrical breakdown under static field conditions drift of ions and electrons to the electrodes and losses to the walls by diffusion are balanced by primary ionization in the gas column and by secondary ionization due to processes such as the impact of positive ions, the photoelectric effect, or field emission acting at the cathode. For h.f. breakdown involving the gas only, e.g. an electrodeless discharge, on the other hand, losses through lateral diffusion are balanced by primary ionization by electron collision and no secondary ionization is necessary for discharge maintenance. The similarity relation for high frequency breakdown differs from that for static fields only because it is necessary to consider the parameter f/p in addition to pd (eqn. (1)). Consider now the occurrence of two minima in the observed Paschen curves for high frequency fields.

4.1. *The Occurrence of Multiple Minima*

For values of $pd < pd_{\min}$ equation (1) does not apply because the values of V_s for low values of pd are partially determined by the position of the glass walls of the discharge tube relative to the electrodes; the discharge follows a path outside the inter-electrode space, and the electron loss mechanism is then increased by loss to the walls. The influence of the electrodes on the breakdown potential in high frequency discharges depends on the average drift which the electron cloud can make in a half an oscillation period $1/2f$. If the electron drift velocity $W \to 2fd$ the electron cloud will be swept to the electrodes during a half cycle and the consequent loss of charge may influence the breakdown potential and produce departure from Paschen's law.

In the figures 3 (*a*) and (*b*), the minimum to the left of the broken lines is caused by the discharge following a path outside the region of uniform field, electron loss to the walls becoming the dominant loss mechanism. For the range of pd when $d < W_{-}\tau/2 < \frac{1}{2}D$ (D is the discharge tube diameter), the loss mechanisms to the tube walls and the electrodes are inefficient, giving rise to values of V_s for $pd < pd_{\min}$ lower than those obtained for the Paschen minimum itself. The occurrence of multiple minima in the Paschen (V_s, pd) curves for uniform high frequency fields, may therefore be simply interpreted on the basis of a single breakdown mechanism involving electron generation by collision with gas molecules, and loss by diffusion and drift to the electrodes and to the walls of the discharge tube. There is no evidence that the multiple minima, and the departures from the similarity relation at low values of pd are the results of different modes of breakdown, or due to gas impurities (mercury vapour for example).

4.2. *Application of the Similarity Relation*

With cold, clean, smooth electrode surfaces, when all the processes of electron and ion generation and loss are functions of E/p, the breakdown potential V_s for static fields may be expressed as simply $f(pd)$, provided the systems are geometrically similar and the electron current paths in both cases lie within the region of uniform field between the electrodes. When, however, V_s depends on secondary ionization processes which are not a function of E/p, e.g. field-dependent surface emission, which is some function of E only, V_s is then dependent on the condition of the surface (Llewellyn Jones and Perrelle 1953). Thus when the surfaces are active, as for example when a field-dependent electron emitting process occurs from an oxidized surface, the similarity relationship does not apply.

Brown (1955) has shown that equation (1) applies over a wide range of values of p and f with the exception of those results obtained in uniform high frequency fields at values of $pd < pd_{\min}$. It has also been shown (Llewellyn Jones and Morgan 1951) that the similarity relation applies in non-uniform static fields with clean electrodes, and again in pure gases in non-uniform high frequency fields when the electrodes play little part in the discharge mechanism. On the other hand, in the present work it would appear that the role played by the electrode surfaces is of paramount importance in determining V_s because of the way in which the electrodes could affect similarity.

In the present work the effect of the electrode surfaces was investigated by making measurements of V_s in static fields under the same discharge conditions as were used for the high frequency measurements. In hydrogen for static fields the similarity relation was not satisfied when the electrodes were oxidized, indicating that a significant process operative either at the cathode, or in the gas, was not a function of E/p. When one of the electrodes in each tube had been de-oxidized by hydrogen ion bombardment, the similarity relation was obeyed when the de-oxidized electrode was the cathode, but not for the opposite polarity (figures 4 (*a*) and (*b*)). This result showed that the significant process was dependent on the cathode rather than the gas. This conclusion was confirmed when measurements of V_s with the de-oxidized cathode were made immediately before and after the determinations of V_s for the oxidised cathode. Had the process been a gas process, due to an impurity liberated from the electrodes, the second determination of V_s when the cathode was de-oxidized should differ appreciably from the first and agree with that found for the oxidized cathode. However, this was not the case, thus indicating that a cathode process was operating which was not dependent on E/p. Such a process is that of the cold emission of electrons from electrodes covered with a thin surface film, as mentioned above.

The macroscopic field in the high frequency experiments was of the order of 500 v cm^{-1}, a value too low by many orders of magnitude to give rise to Fowler–Nordheim cold emission from clean, smooth nickel. The work of Llewellyn

Jones and Morgan (1953), however, has shown that a layer of positive ions near or on an oxide film can give rise to an intense field, very much greater than the macroscopic applied field, across the layer which may lead to the field-dependent emission of a copious supply of electrons. This condition probably also obtains under high-frequency fields when the electrodes are covered with an oxide film. Under these conditions the similarity relation is not obeyed, as shown by experiment (table 1).

When, however, all the electrodes had been de-oxidized the similarity relation was obeyed for static and high frequency fields for tube D at 30 and 20 Mc/s and tube E at 15 and 10 Mc/s. Under these conditions the discharge paths in the two systems were similar and all the significant discharge processes functions of the parameter E/p. This implies that for values of $f < 35$ Mc/s space charge distortion of the field, giving rise to some ambiguous form of electron generation, played no significant part in the discharge mechanism. Even when the conditions are such that the similarity relation does not apply for these frequencies, it is far more probable that cold emission of electrons is the operative process and not space charge distortion; it is difficult to establish how the latter process would be influenced in any way by the cleaning of the electrodes.

It may be concluded therefore that the occurrence of multiple minima and the deviations from Paschen's law may be adequately explained by consideration of the effects of changes in the electrode surfaces and the geometry of the discharge path.

ACKNOWLEDGMENTS

We are grateful to Professor Llewellyn Jones, in whose laboratory this work was carried out, for his help and encouragement throughout the investigation. We also wish to thank the Council of the University of Wales for the award of a Post-graduate Studentship to one of us (W.G.T.) to undertake this work.

REFERENCES

BRIGHT, A. W., 1950, *Nature, Lond.*, **165**, 811.
BROWN, S. C., 1955, *Appl. Sci. Rev.* B, **5**, 97.
DALTON, D. C., 1953, *Nature, Lond.*, **172**, 798.
FATEHCHAND, R., 1951, *Nature, Lond.*, **167**, 566.
GILL, E. W. B., and DONALDSON, R. H., 1931, *Phil. Mag.*, **13**, 719.
GITHENS, S., 1940, *Phys. Rev.*, **57**, 822.
GUTTON, C., and GUTTON, H., 1928, *C. R. Acad. Sci., Paris*, **186**, 303.
LLEWELLYN JONES, F., and MORGAN, C. G., 1953, *Proc. Roy. Soc.* A, **218**, 88.
LLEWELLYN JONES, F., and MORGAN, G. D., 1951, *Proc. Phys. Soc.* B, **64**, 560.
LLEWELLYN JONES, F., and DE LA PERRELLE, E. T., 1953, *Proc. Roy. Soc.* A, **216**, 267.
LLEWELLYN JONES, F., and WILLIAMS, G. C., 1953, *Proc. Phys. Soc.* B, **66**, 17, 345.
PIM, J. A., 1949, *Proc. Instn Elect. Engrs*, Pt. III, **96**, 117.
PROWSE, W. A., 1950, *Proc. Instn Elect. Engrs*, Pt. III, **96**, 253.
REUKEMA, L. E., 1928, *Trans. Amer. Inst. Elect. Engrs*, **47**, 38.
THOMSON, J., 1934, *Phil. Mag.*, **18**, 696 ; 1937, *Ibid.*, **23**, 1.

The Propagation of Ultrasonics in Suspensions of Liquid Globules in Another Liquid

BY P. A. ALLINSON AND E. G. RICHARDSON
King's College, Newcastle upon Tyne

MS. received 20th February 1958, and in revised form 19th June 1958

Abstract. In continuation of earlier work, measurements have been made of the attenuation of ultrasonics in a liquid containing globules of another liquid in suspension, viz. an emulsion. The effect of the viscosity of the continuous liquid and of the mean size of the globules of the other liquid on the attenuation is investigated and tested against a theoretical formula.

It is shown that besides viscous loss relevant factors are (*a*) scattering of the radiation out of the direct beam, (*b*) pulsation of the globules.

---

§ 1. INTRODUCTION

In a previous paper (Busby and Richardson 1956, to be referred to as I) measurements of the attenuation of ultrasonics in suspensions of solid particles in a liquid were described. The present report covers an extension of this investigation to suspensions of liquid globules, such as are found in emulsions.

The formulae given in I are relevant to this case also, though possible differences may arise due to: (*a*) compression of the globules, (*b*) internal circulation of the fluid in the globules, (*c*) deformation and subsequent pulsation of the globules.

From the data presented it appears that the pairs of liquid media chosen have compressibilities and densities so close in value that (though there is some difference in acoustic impedance) changes of *size* of the globules produced by the passage of the sound waves cannot be important.

While in theory the viscosity of such a suspension is affected by the circulations that may be set up in the globules by shearing actions with the matrix medium, Bond and Newton (1928) have shown that the rate of fall of a liquid sphere through another liquid is the same as that of a rigid sphere of the same size provided $(\rho-\rho')d^2g/\sigma<5$ where $\rho-\rho'$ is the density difference, d the globule size and σ the interfacial tension. The parameter, insofar as it is relevant, was of order 0·0001 in our experiments.

That a globule in motion through another fluid may be deformed into an ellipsoid and thereafter may oscillate about the equilibrium figure has been shown by Tyler and Watkin (1932). In doing so it can absorb energy—in this case acoustic energy—and increase the attenuation of the sound wave. This effect is evident in some of our results.

§ 2. PREPARATION OF THE SUSPENSIONS

There are several ways of dispersing one liquid as globules in another. In this case violent mixing was employed in an instrument called a 'dispersator'.

It consists of a hollow cylinder into which a liquid is sucked at the base. Internal baffles cause the liquid to rotate with the cylinder and eject it by centrifugal force from slits at the side in a finely divided form. Thus by directing oil into the base of the cylinder, it can be dispersed into water or into a solution.

It is necessary to add a stabilizing agent to the continuous medium to prevent coagulation. The function of the agent is to lower the interfacial tension. To stabilize emulsions of the oil-in-water type, a one per cent solution of sodium oleate was added to the water. The same agent at a lower concentration served also when the continuous medium contained glycerine.

§ 3. MEASUREMENT OF PARTICLE SIZE

For the measurement of particle size a photographic method was used, a drop of the emulsion being hung from beneath a cover slip which in turn was placed above a recess in a glass slide. This was mounted under a vertical photomicroscope, with a magnification of 100 to 500, and a photograph taken in green light. Comparison photographs of a slide carrying a graticule were also taken. The size of individual globules, a sample of about 300 in each case, was measured with vernier callipers. A typical size–frequency curve is shown in figure 1. The mean particle diameter of globules produced by the dispersator lay between 1 and 5 microns, and the mass median (size of particle having the greatest volume) between 6·5 and 10 microns.

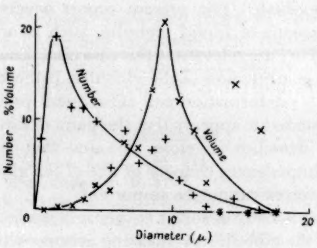

Figure 1. Globule size distribution.

Coarser suspensions produced by ejection of the one liquid into the other had mean diameters up to 55 microns, mass median up to 160 microns.

§ 4. MEASUREMENT OF VISCOSITY

A concentric cylinder viscometer was used. The diameters of the cylinders were 1 in. and 2 in., the suspension filling the interspace. The outer was rotated at constant speed, and the deflection of the inner noted through the usual mirror on the wire suspending the inner cylinder and a lamp and scale. The instrument was calibrated with sucrose solutions for which the viscosities have been published (Hatschek 1928).

As disperse systems are non-Newtonian in flow, it was necessary to fix on a certain (low) rate of shear up to which, according to the experiments of Richardson (1950 a, b), the relation between angular velocity of the outer cylinder and deflection of inner is nearly linear. In our viscometer, the standard rotation was taken as 0·3 rev sec^{-1}. Over the range of mass median particle diameter attained (7 to 160 microns) no change of viscosity with globule size could be established. Figure 2 shows the variation of (apparent) kinematic viscosity with concentration for benzene dispersed in a glycerine–water mixture at 20°c. The densities were measured by hydrometer.

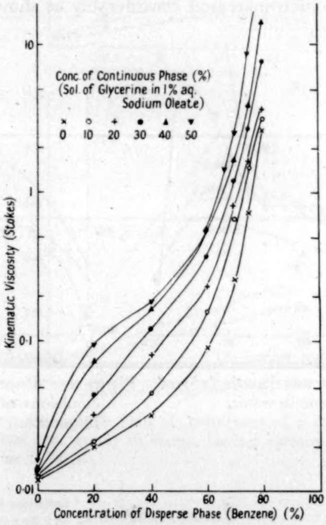

Figure 2. Kinematic viscosity of emulsions of benzene in glycerine–water mixtures.

§ 5. ULTRASONIC ATTENUATION

A pulse system having two transducers, one to emit and one to receive, similar to that described in I, was used. It was first tested on the homogeneous phases, water, benzene and carbon tetrachloride and results in satisfactory agreement with those reported by others obtained. In the first of these, with an attenuation of 0·25 dB cm^{-1}, coefficients to a standard deviation of 10% were attained; in the latter, with about 1 dB cm^{-1}, a standard deviation of 2% and in a dispersion of high concentration giving 12 dB cm^{-1}, a standard deviation was attained.

The only previously reported measurements of attenuation were those of Urick and Ament (1949) at one frequency (15 Mc/s) using bromoform dispersed in water and mercury dispersed in water. They found agreement with the theory (for rigid spheres) up to concentrations of 20% by volume.

We used benzene in water, water in benzene, benzene in glycerine–water mixtures (to vary the viscosity of the continuous phase), a mixture of benzene and carbon tetrachloride (of specific gravity unity) in water, the first type at 2, 3, 4, 6 and 10 Mc/s, the second at 2, 4 and 6 Mc/s and the last two at 2 and 6 Mc/s.

Figure 3 shows the absorption per wavelength $\alpha\lambda$ in suspensions of benzene in water; figure 4 shows that for reversed phases, at 95% benzene in water, the system is quasi-solid. Above 40% water in benzene, the system breaks down.

When the viscosity of the continuous phase was varied by diluting glycerine with water, the attenuation increased considerably as shown in figure 5.

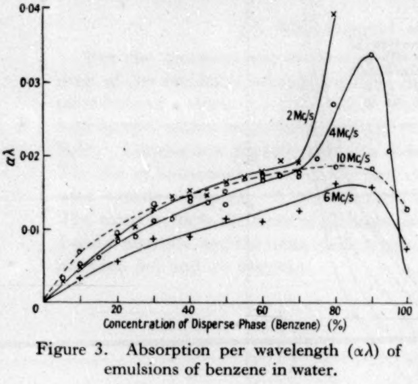

Figure 3. Absorption per wavelength ($\alpha\lambda$) of emulsions of benzene in water.

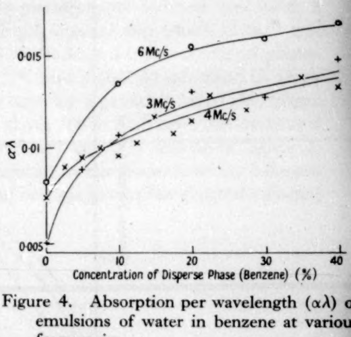

Figure 4. Absorption per wavelength ($\alpha\lambda$) of emulsions of water in benzene at various frequencies.

V.
19

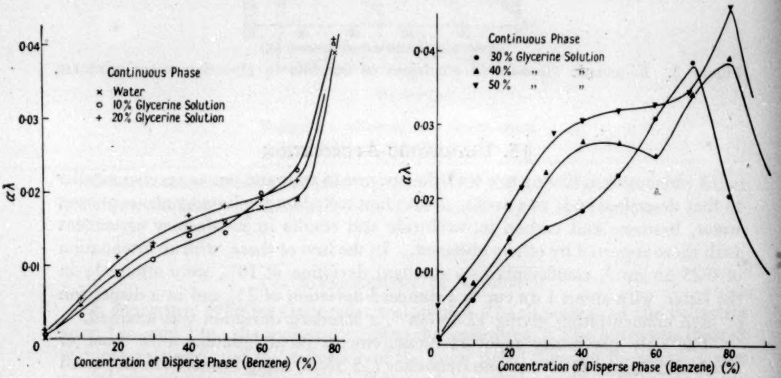

(a) (b)

Figure 5 (a), (b). Absorption per wavelength ($\alpha\lambda$) of emulsions of benzene in glycerine–water mixtures at 2 Mc/s.

When the mean particle size was changed there was an increase in $\alpha\lambda$ nearly linear with concentration of disperse phase. In figure 6 are given results for a mixture of benzene and carbon tetrachloride to give the same density as the water in which it was dispersed. (This adjustment was necessary to prevent creaming.)

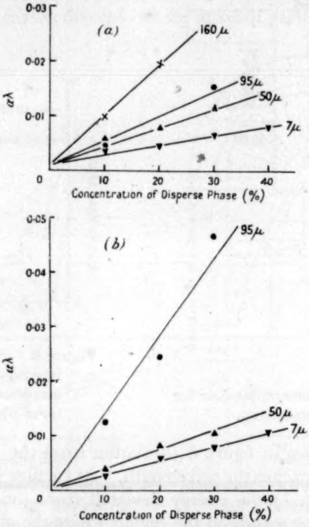

Figure 6. Absorption per wavelength ($\alpha\lambda$) of emulsions of a mixture of carbon tetrachloride and benzene (sp. gr. 1) in water, having various (volume) globule sizes, (*a*) at 2 Mc/s, (*b*) at 6 Mc/s.

§ 6. SCATTERING

The formula (1) of I contains two terms, one expressing the scattering of the sound waves by a sphere of small dimensions and, like Rayleigh's well-known optical formula, involving the fourth power of the wavelength and the square of the volume, the other expressing the effect of viscosity and giving an absorption inversely proportional to the wavelength (hence the introduction of $\alpha\lambda$ in some of the graphs).

To investigate the extent of such scattering it was necessary (*a*) to mask the receiver crystal so that it received energy into a small aperture (about $\frac{1}{8}$ in. diameter for 2 Mc/s and $\frac{3}{8}$ in. diameter for 6 Mc/s), (*b*) to scan the receiver over an area in the liquid, with the transmitter as centre. The arrangement for doing this is shown in figure 7.

A plate is fastened to the main frame of the apparatus and to it the lower crystal holder is attached by a bracket which can be rotated about an axis through the centre of the lower face of the top crystal, the position of which can be adjusted by spring-loaded adjustment nuts and bolts. The bracket also carries a pointer which moves over a circular scale. By this simple modification a useful tool is provided with which the nature of the sound field around the transmitting crystal can be investigated. The signal amplitude is obtained from its relative height read against the graticule on the face of a cathode-ray oscilloscope.

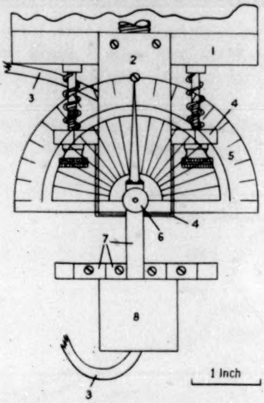

Figure 7. Attachment of detector for measuring scattering.

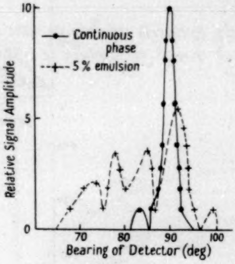

Figure 8. Signal at various bearings to emitter in emulsion and in continuous phase at 6 Mc/s.

The scattering shown in figure 8 (deviation from the main beam) increases as the particle size approaches the wavelength. At smaller values of the scattering parameter ($\gamma=\pi d/\lambda$, cf. I) the energy deviated from the main beam is small. We were in fact working mainly in the region where the absorption is viscous in origin and $\alpha\lambda$ is the relevant parameter rather than $\alpha\lambda^4$.

§ 7. COMPARISON OF EXPERIMENT AND THEORY

Calculations from the formula have been made (for a number of frequencies) of the absorption per unit concentration by globules of diameter 1 and 10 microns respectively in benzene and water emulsions as this size range includes most of the particles in the experimental emulsions, and the mass median, used in the calculation. lies close to the latter diameter. These values are given in the table.

Frequency (Mc/s)	Attenuation per unit concentration Calc. for 1 μ	Calc. for 10 μ	Exptl
2	0·0012	0·0026	0·0054
3	—	—	0·0067
4	0·0025	0·0011	0·0120
5	0·0028	0·0040	0·0128
8	0·0049	0·0200	—
10	0·0049	0·0273	0·0352

The trend of the actual results bears comparison with those calculated for 10 microns but the overall values are higher (cf. figure 9). The same is true of emulsions in glycerine when the viscosity of the continuous phase is varied.

When the mass median was varied over the range 7 to 160 microns at constant frequency, there was less variation in the observed attenuation coefficient than theory would indicate. The formula predicts a sharper fall of absorption for the finer dispersions than is observed in practice (see figure 10). We see from this figure that as particle size increases the experimental and calculated curves tend in the same way (the absorption for 160 μ diameter at 6 Mc/s was too high to measure, but would be of the same order as the calculated value), but the experimental and calculated curves diverge rapidly at small particle sizes.

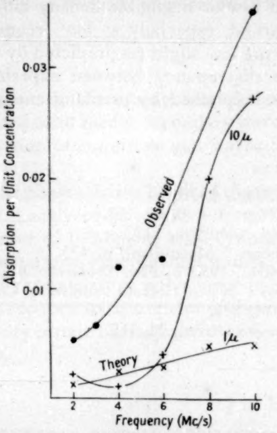

Figure 9. Calculated and experimental values of absorption per unit concentration.

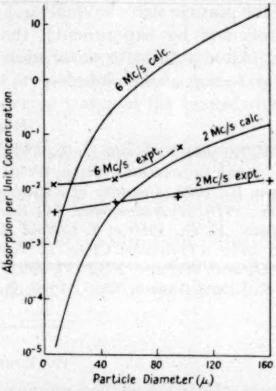

Figure 10. Values of absorption per unit concentration in emulsions at various frequencies.

However, in the calculations one source of energy dissipation has not yet been invoked and this may account for the discrepancy. This is the pulsation of the globules as they become disturbed from the spherical shape, a feature which may be distinguished in the photographs made by Tyler and Watkin of a jet of organic liquid squirted into water and breaking up by friction with its surroundings. Lamb (1916) has a formula for the natural circular frequency ω of such pulsations when, as in the present instances, the media have nearly unit density, i.e. $\omega^2 = 8n(n^2-1)(n+2)\sigma/d^3$ (n is an integer). We have calculated the first five partial values of ω for globules of 7 μ and 50 μ respectively. These are

Size	n 2	3	4	5	6	
7 μ	0·66	1·2	2·0	2·6	4·5	Mc/s
50 μ	22	36	60	78	135	kc/s

It appears that at frequencies of the order of Mc/s only high and unlikely partial pulsations of a 50 μ globule could be excited, but that a 7 μ globule might readily be excited in resonance and produce additional dissipation at such frequencies. Thus as the particle size decreases, and the absorption calculated from the expression (1) tends to zero, dissipation due to pulsations of the globules at the frequencies employed would ensue, and could account for the measured absorption.

Conclusion

From the above and other results (Busby and Richardson, Urick, etc.) of sound loss in hydrosols, it is apparent that the expression obtained by Lamb and modified by Urick and Ament agrees well with measurements obtained on suspensions having components of large density difference, and/or at high frequencies.

In the present work where hydrosols of low or negligible density difference were employed agreement was not so marked, especially at low frequencies. Where the particle size was small and scattering loss slight (as predicted by theory and confirmed by experiment), the large discrepancy between experimental and calculated values for absorption is best explained by invoking energy loss due to pulsation of the globules.

References

Bond, W. N., and Newton, D. A., 1928, *Phil. Mag.*, **4**, 704.

Busby, J., and Richardson, E. G., 1956, *Proc. Phys. Soc.* B, **69**, 193.

Hatschek, E., 1928, *Viscosity of Liquids* (London : Bell), p. 112.

Lamb, H., 1916, *Hydrodynamics*, 6th Edn. (London : Macmillan), p. 475.

Richardson, E. G., 1950 a, *J. Colloid Sci.*, **5**, 404 ; 1950 b, *Flow Properties of Disperse Systems.* Hermans, Chap. II (Amsterdam : North Holland Publishing Co.).

Tyler, E., and Watkin, F., 1932, *Phil. Mag.*, **14**, 849.

Urick, R. J., and Ament, W. S., 1949, *J. Acoust. Soc. Amer.*, **21**, 115.

The Generation of Secondary Signals in the Propagation of Ultrasonic Waves in Bounded Solids

By M. REDWOOD

Electrical Engineering Department, Imperial College, London

Communicated by J. Lamb; *MS. received* 22*nd April* 1958, *and in revised form* 1*st July* 1958

Abstract. In the propagation of short duration trains of compressional waves in bounded solid media, secondary wave trains are generated as a result of the partial conversion of compressional waves to transverse waves at the boundaries of the media.

The phase relation between these secondary signals and the main compressional signal is analysed here, with reference to the propagation of waves of frequency of the order of 10 Mc/s in solid cylindrical specimens. The theoretical analysis is compared with experimental results.

The results are of importance in applications of the ultrasonic pulse technique to the accurate measurement of the velocity and absorption in solids, and also help to clarify certain characteristics of the propagation of continuous waves in bounded media.

§ 1. INTRODUCTION

THE main purpose of this paper is to examine further the results reported in two other papers, both of which deal with the propagation of compressional waves of frequencies of 10 Mc/s and above in a cylindrical specimen of an isotropic solid. The first of these papers (Redwood and Lamb 1957) contains a theoretical analysis of the propagation of continuous waves in such a cylinder, while the second (Redwood 1957 a) describes a theoretical and experimental study of the propagation of trains of waves of a few microseconds duration.

One important feature of the ‘ pulse technique ’ using these short wave trains is the formation of ‘ secondary signals ’ resulting from the conversion of part of the energy of the compressional waves into transverse waves at the boundaries of the specimen. Certain aspects of the generation of these secondary signals have already been discussed (McSkimin 1956, Redwood 1957 a, b); an extension of the discussion is presented here.

§ 2. THE GENERATION OF SECONDARY SIGNALS

The most important features of the previous analyses of this problem will be summarized in this section.

The specimen is in the form of a cylinder of circular cross section, with the transducer completely covering one end face. The ‘ pulse ’ applied to the transmitting transducer consists of a train of electrical waves of a few microseconds duration (1–20 μsec) of the desired frequency (10–500 Mc/s) and of constant amplitude.

The electrical output from the receiving transducer, resulting from the successive reflections of the pulse between the ends of the specimen, is amplified and demodulated before display. Each train of waves contains a large number of cycles of the high-frequency oscillation, and the uniform-amplitude portion of the demodulated signal is used in measurements. It may be assumed that propagation takes place at a single frequency only, since the main components of the signal lie within an extremely narrow frequency band.

Initially, it is assumed that the medium behaves as a fluid. It may be shown that several modes of propagation are excited, each with a different phase velocity, and their relative amplitudes may be calculated: the effects of phase interference between the signals propagating in these different modes are, however, small, since the signal in what will be termed the ' first-order ' mode (that with phase velocity closest to the velocity of compressional waves in an unbounded medium c_d) is of very much larger amplitude than the signals in other modes.

The characteristic pressure distribution across a diameter associated with each mode in a cylindrical guide is a Bessel function, and such a pressure distribution may be synthesised from a set of intersecting plane waves, each propagating with a velocity c_d, and reflected back and forth between the boundaries in a zigzag path. Two of these waves are illustrated in figure 1 (*a*). An infinite number of such waves are necessary to represent the Bessel function. (For a wave guided by a pair of parallel surfaces (the ' slab ' waveguide) the set would be composed of two plane waves, and the distribution of pressure between the surfaces would be sinusoidal.) The angle of incidence a_d of each plane wave on the wall of the guide is given by :

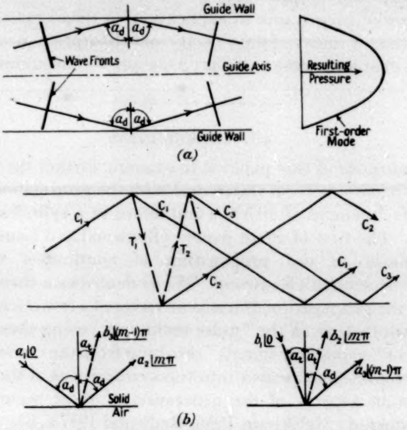

Figure 1. Representation of a mode of propagation by a set of plane waves : (*a*) fluid guide, (*b*) solid guide.

cylinder : $\cos a_d = (j_{0n}/a)(c_d/\omega)$ ..... (1)

slab : $\cos a_d = (n\pi/2b)(c_d/\omega)$. ..... (2)

For both the cylinder and slab, the phase velocity of propagation

$$c_p = c_d/\sin a_d . \qquad \text{.....} (3)$$

In these equations $\omega = 2\pi f$ where f is the frequency, $2a$ is the diameter of the cylinder, $2b$ is the thickness of the slab, c_d is the velocity of compressional (dilatational) waves in an unbounded medium, j_{0n} is any root of the Bessel function $J_0(x) = 0$; $n = 1, 2, 3$ etc. Axial symmetry is assumed, and the boundary conditions are taken to be that the pressure be zero at the radial wall. These conditions are used in order to maintain the analogy to the solid guide later.

The discussion may be extended to include the solid waveguide by considering the reflection of the plane waves at the walls of the guide. In the case of the fluid guide the incident plane compressional wave is reflected as a pure compressional wave, without loss of amplitude (figure 1 (*a*)) but in the solid guide (figure 1 (*b*)) the incident compressional wave C_1 is partially converted to a transverse wave T_1 which is reflected at an angle a_t where

$$\sin a_d / \sin a_t = c_d / c_t \qquad \ldots\ldots (4)$$

c_t being the velocity of transverse waves in an unbounded medium. The angle a_d is governed in this case of a guided wave by frequency, guide dimensions and mode number, through equation (1) or (2).

This conversion gives rise to a series of secondary signals in the following manner. The energy that is converted to a transverse wave travels across the guide with velocity c_t, which is usually about $\frac{1}{2}c_d$, the wave front making a much smaller angle with the axis of the guide than in the case of the compressional wave. When this transverse wave strikes the opposite wall of the guide it is partially reconverted to a compressional wave C_2 which travels in exactly the same manner as C_1, and partly reflected as a transverse wave T_2 which gives rise to another compressional wave C_3 and so on.

For guides of radius of about 1 cm and wave trains of duration of about 5 microseconds, the secondary signal C_2 reaches the receiving transducer some time after the main signal C_1, as a result of the time delay introduced when T_1 traverses the guide. The resulting effect on the decay pattern of successive reflections is shown in figure 2 (*a*).†

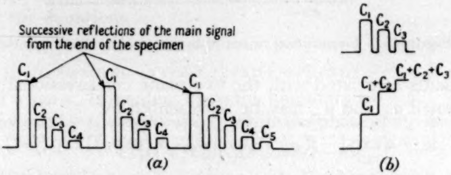
Successive reflections of the main signal from the end of the specimen
C1
C2
C3
C4
C1
C2
C3
C4
C1
C2
C3
C4
C5
(a)
C1
C2
C3
C1+C2+C3
C1+C2
C1
(b)

Figure 2. The effect of secondary signals on the decay pattern of successive reflections (after demodulation).

The relations between the phases of the various components of reflection are of most importance here, and are shown in figure 1 (*b*). These are most conveniently described by introducing a factor m, where m is an odd integer except for materials of Poisson ratio less than 0·26, when over a certain range of angles of incidence it may become an even integer (Arenberg 1948). The reflected and incident waves, of all types, are therefore either in phase or 180° out of phase with each other.

---

† A perfect reflection, without conversion, at the end of the specimen, is assumed. The plane compressional waves representing the mode strike the end walls at an angle which is generally within a few degrees of normal incidence at frequencies above about 10 Mc/s, and the energy converted to transverse waves is negligibly small. The transverse waves generated at the side walls are incident on the end walls at an angle greater than critical, and are reflected without loss.

§ 3. THE PHASES OF THE MAIN AND SECONDARY SIGNALS

3.1. *Phase Relations between the Various Wave Fronts*

In the present work the phase relation between the signals C_1, C_2, C_3, etc., was examined. Both these compressional signals and the transverse signals from which they are generated may easily be shown to be propagating with the same phase velocities, and at first sight it might appear that these signals will therefore be in phase at all frequencies, but a more thorough analysis shows that this conclusion is incorrect.

In the first part of the analysis which follows, it will be assumed that propagation takes place in a single mode only, the first-order mode. The effects of other modes will be considered later.

In order to present a simpler picture of the physical mechanisms involved in the generation of secondary signals, and of the phase relations between the main and secondary signals, it is convenient to start by considering the ' slab ' waveguide, i.e. a waveguide bounded by two parallel surfaces. Consider the slab illustrated in figure 3, infinite in the y direction, semi-infinite in the z direction.

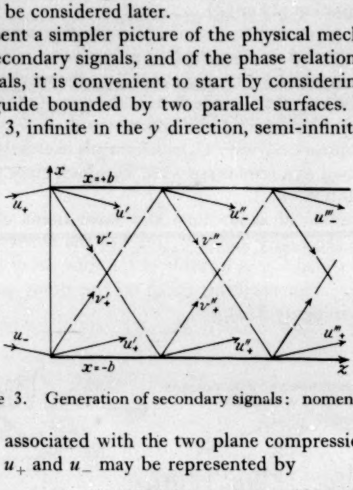

Figure 3. Generation of secondary signals: nomenclature.

The displacements associated with the two plane compressional waves shown at the source, termed u_+ and u_- may be represented by

$$u_+ = a \exp[-j(\omega/c_d)(z \sin a_d + x \cos a_d)] \exp(j\omega t) \quad \ldots\ldots (5\,a)$$

$$u_- = a \exp[-j(\omega/c_d)(z \sin a_d - x \cos a_d)] \exp(j\omega t) \quad \ldots\ldots (5\,b)$$

and the z component of the resultant of these two waves will be

$$u_z = (u_+ + u_-) \sin a_d = 2a \sin a_d \cos[(\omega/c_d) x \cos a_d] \exp[-j(\omega/c_d) z \sin a_d] \exp(j\omega t). \quad \ldots\ldots (5\,c)$$

Consider now the pair of plane compressional waves u_+' and u_-' generated when the original pair of waves u_+ and u_- strikes the boundaries at $x = \pm b$.

$$u_+' = a' \exp[-j(\omega/c_d)(z \sin a_d + x \cos a_d)] \exp(j\omega t) \exp(-j\Delta_{CC1}) \quad \ldots\ldots (6\,a)$$

$$u_-' = a' \exp[-j(\omega/c_d)(z \sin a_d - x \cos a_d)] \exp(j\omega t) \exp(-j\Delta_{CC2}) \quad \ldots\ldots (6\,b)$$

where Δ_{CC1} and Δ_{CC2} are constants to allow for the phase shift which occurs when u_+' is generated by u_- at $x=-b$, and when u_-' is generated by u_+ at $x=+b$. (The suffix CC refers to the generation of a compressional wave by a compressional wave). In order to determine Δ_{CC1} it is necessary to consider the phases of u_- and u_+' at $-b$, and to set the difference between them equal to $m\pi$, (where m is any integer, as described in § 2.3). z and t may be put equal to zero for the purpose of these calculations, since the variation of phase with z and t will not affect the analysis.

The phase of u_- at $-b$ is given by the term $\exp[-j(\omega/c_{\mathrm{d}})(b\cos a_{\mathrm{d}})]$, while the phase of u_+' at $-b$ is given by $\exp[+j(\omega/c_{\mathrm{d}})(b\cos a_{\mathrm{d}})-j\Delta_{\mathrm{CC1}}]$, hence

$$(\omega/c_{\mathrm{d}})(b\cos a_{\mathrm{d}})=-(\omega/c_{\mathrm{d}})(b\cos a_{\mathrm{d}})+\Delta_{\mathrm{CC1}}+m\pi \qquad \ldots\ldots(7)$$

$$\Delta_{\mathrm{CC1}}=2(\omega/c_{\mathrm{d}})(b\cos a_{\mathrm{d}})-m\pi. \qquad \ldots\ldots(8\,a)$$

The statement that the phase difference between the two waves at the boundary must equal $m\pi$ radians, while away from the boundary it may have some other value, may at first appear to be contradictory. Since z and t have been taken to be equal for both incident and reflected waves, the statement is equivalent to saying that when a wave front is incident at an angle on a surface from which it is reflected with a phase change of $m\pi$ radians, then at some point away from the surface the phase difference between the wave that arrives at that point directly and the wave that arrives by reflection is not necessarily $m\pi$. In general this is possible (although in the propagation of a true waveguide mode it is not). A similar examination of the generation of u_-' from u_+ at $x=+b$ shows that

$$\Delta_{\mathrm{CC2}}=\Delta_{\mathrm{CC1}}=\Delta_{\mathrm{CC}},\ \text{say}. \qquad \ldots\ldots(8\,b)$$

The resultant wave front is

$$u_z'=2a'\sin a_{\mathrm{d}}\cos[(\omega/c_{\mathrm{d}})x\cos a_{\mathrm{d}}]\exp[-j(\omega/c_{\mathrm{d}})z\sin a_{\mathrm{d}}]\exp(-j\Delta_{\mathrm{CC}})\exp(j\omega t). \qquad \ldots\ldots(9)$$

u_z' propagates with the same phase velocity as u_z, and the displacement distribution across the guide is of the same form, but it is out of phase with u_z by an angle Δ_{CC}.

A similar analysis gives the phases of the transverse waves; v_+' and v_-' may be represented by the equations

$$v_+'=b'\exp[-j(\omega/c_{\mathrm{t}})(z\sin a_{\mathrm{t}}+x\cos a_{\mathrm{t}})]\exp(j\omega t)\exp(-j\Delta_{\mathrm{CT1}}). \qquad \ldots\ldots(10\,a)$$

$$v_-'=b'\exp[-j(\omega/c_{\mathrm{t}})(z\sin a_{\mathrm{t}}-x\cos a_{\mathrm{t}})]\exp(j\omega t)\exp(-j\Delta_{\mathrm{CT2}}). \qquad \ldots\ldots(10\,b)$$

v_+' is generated when u_- is incident upon the boundary $x=-b$. The phase of u_- at $-b$ is given by $\exp[-j(\omega/c_{\mathrm{d}})b\cos a_{\mathrm{d}}]$, while the phase of v_+' is

$$\exp[+j(\omega/c_{\mathrm{t}})(b\cos a_{\mathrm{t}})-j\Delta_{\mathrm{CT1}}].$$

The phase difference between these two waves is $(m-1)\pi$, hence

$$\Delta_{\mathrm{CT1}}=(\omega/c_{\mathrm{d}})b\cos a_{\mathrm{d}}+(\omega/c_{\mathrm{t}})b\cos a_{\mathrm{t}}-(m-1)\pi. \qquad \ldots\ldots(11)$$

By considering the reflection of u_+ at $+b$, and the generation of v_-' there, it may be shown that

$$\Delta_{\mathrm{CT1}}=\Delta_{\mathrm{CT2}}=\Delta_{\mathrm{CT}},\ \text{say}. \qquad \ldots\ldots(12)$$

The resultant displacement in the z direction due to the combination of the transverse waves v_+' and v_-' will be of the form

$$v_z'=2b'\cos a_{\mathrm{t}}\cos[(\omega/c_{\mathrm{t}})x\cos a_{\mathrm{t}}]\exp[-j(\omega/c_{\mathrm{t}})z\sin a_{\mathrm{t}}]\exp(-j\Delta_{\mathrm{CT}})\exp(j\omega t) \qquad \ldots\ldots(13)$$

The phase velocity of this wave front is given by the term in z, and is $c_t/\sin a_t$. Since the law of reflection at a solid–air interface gives $c_t/\sin a_t = c_d/\sin a_d$, the phase velocity of the transverse wave front v_z' (eqn (13)) is identical with that of the compressional wave fronts u_z and u_z' (eqns (5c) and (9)). There is however a phase difference between the transverse wave front and the original compressional wave front, given by the term Δ_{CT}.

The secondary compressional signal, represented by the pair of plane waves u_-'' and u_+'', is generated from the pair of transverse waves v_+' and v_-', incident at $x=+b$ and $-b$ respectively. Letting the phase change on generation of the compressional wave from the transverse wave be Δ_{TC}, and using the phase relation between v_+' and u_-'' to find Δ_{TC} as before, gives

$$\Delta_{TC} = (\omega/c_t)b\cos a_t + (\omega/c_d)b\cos a_d - (m-1)\pi \qquad \ldots\ldots(14)$$

i.e. $\Delta_{TC} = \Delta_{CT}$.

Note that the phase of the wave front v_+', v_-' with respect to the original compressional wave u_+, u_- is Δ_{CT}, and that the phase of the wave front u_+'', u_-'' is therefore $\Delta_{CT}+\Delta_{TC}=2\Delta_{CT}$. This is the phase difference between the main and secondary compressional signals.

For completeness it is desirable to determine the phase change Δ_{TT} which occurs on the generation of the pair of transverse waves v_+'', v_-'' from the pair of transverse waves v_-' v_+', and this may be shown to be (cf. eqn (8))

$$\Delta_{TT} = 2(\omega/c_t)\,b\cos a_t - m\pi. \qquad \ldots\ldots(15)$$

It is now necessary to take into account the fact that, in waveguide propagation, several of the wave fronts so far considered separately are in fact superimposed, which imposes certain restrictions in the permitted values of a_d and a_t.

3.2. *Phase Relation between Main and Secondary Compressional Signals*

The main signal is composed of the superimposed signals, u_+, u_-; u_+', u_-'; etc. All these wave fronts have the same phase velocity and they must also have the same phase, since it is necessary that they shall reinforce if the total signal resulting from them is to propagate along the waveguide with this phase velocity. For this $\Delta_{CC}=0$ and

$$2(\omega/c_d)\,b\cos a_d = m\pi. \qquad \ldots\ldots(16)$$

This is the expression previously quoted (eqn (2)) which may be arrived at in a rigorous fashion by deducing the allowed phase velocities for individual modes from the solution of the wave equation for a fluid, subject to the appropriate boundary conditions.

Interest here centres on the phase difference between the main compressional wave front u_+, u_- (or u_+' u_-', which is in phase with it by virtue of the relation above) and the secondary wave front u_+'', u_-''. This phase difference will be

$$\Delta_{CT}+\Delta_{TC} = 2(\omega/c_d)b\cos a_d + 2(\omega/c_t)b\cos a_t - 2(m-1)\pi$$

and, from equation (16),

$$\Delta_{CT}+\Delta_{TC} = 2(\omega/c_t)b\cos a_t - m\pi + 2\pi. \qquad \ldots\ldots(17)$$

It is important to note that the restriction placed upon the various components of the main signal is not placed upon the relation between the main and secondary signals simply because they are normally separated in time and do not interfere (see also § 5). The 'in-phase' frequencies $f_0(=\omega_0/2\pi)$, at which the main signal and the first secondary signal are $2n\pi$ radians out of phase (n an integer) will be given by

$$\Delta_{\mathrm{CT}}+\Delta_{\mathrm{TC}}=2n\pi=2(\omega_0/c_{\mathrm{t}})b\cos a_{\mathrm{t}}-m\pi+2\pi \quad (n=0, 1, 2 \text{ etc.}). \qquad \ldots\ldots(18)$$

The 'out-of-phase' frequencies f_π $(=\omega_\pi/2\pi)$ will be given by

$$\Delta_{\mathrm{CT}}+\Delta_{\mathrm{TC}}=(2n-1)\pi=2(\omega_\pi/c_{\mathrm{t}})\,b\cos a_{\mathrm{t}}-m\pi+2\pi. \qquad \ldots\ldots(19)$$

For a material for which m is an odd integer, $\omega_0=\omega_0'$, say, and is given by $2(\omega_0'/c_{\mathrm{t}})\,b\cos a_{\mathrm{t}}=\pi, 3\pi, 5\pi$ etc. and this may conveniently be written as

$$\cos[(\omega_0'/c_{\mathrm{t}})\,b\cos a_{\mathrm{t}})]=0. \qquad \ldots\ldots(20)$$

The out-of-phase frequencies are given by

$$\sin[(\omega_\pi'/c_{\mathrm{t}})\,b\cos a_{\mathrm{t}}]=0. \qquad \ldots\ldots(21)$$

For a material for which m is sometimes an even integer, $\omega_0=\omega_0''$, say, when m is even, and $2(\omega_0''/c_{\mathrm{t}})\,b\cos a_{\mathrm{t}}=0, 2\pi, 4\pi$, etc.,

$$\sin[(\omega_0''/c_{\mathrm{t}})\,b\cos a_{\mathrm{t}}]=0 \quad \ldots\ldots(22) \qquad \cos[(\omega_\pi''/c_{\mathrm{t}})\,b\cos a_{\mathrm{t}}]=0\ \ldots\ldots(23)$$

This analysis gives the phase relation between the main signal and the first secondary signal; a simple extension permits the phase relation between the main signal and any of the other secondary signals to be obtained.

3.3. *Extension to the Cylindrical Guide*

A close analogy holds between the slab and cylinder, and can be seen from the brief comparison drawn here. Further details of the relation may be found elsewhere (Redwood 1957 b, Holden 1951). Equations (20) to (23) refer to the slab, and the analogous equations in the case of the cylinder of radius a are

$$\mathrm{J}_0[(\omega_0'/c_{\mathrm{t}})a\cos a_{\mathrm{t}}]=0 \quad \ldots\ldots(20\,a) \qquad \mathrm{J}_1[(\omega_\pi'/c_{\mathrm{t}})a\cos a_{\mathrm{t}}]=0 \quad \ldots\ldots(21\,a)$$

$$\mathrm{J}_1[(\omega_0''/c_{\mathrm{t}})a\cos a_{\mathrm{t}}]=0 \quad \ldots\ldots(22\,a) \qquad \mathrm{J}_0[(\omega_\pi''/c_{\mathrm{t}})a\cos a_{\mathrm{t}}]=0 \quad \ldots\ldots(23\,a)$$

where $c_{\mathrm{p}}=c_{\mathrm{d}}/\sin a_{\mathrm{d}}=c_{\mathrm{t}}/\sin a_{\mathrm{t}}$, as for the slab, while $\cos a_{\mathrm{d}}=(\mathrm{j}_{0n}/a)(c_{\mathrm{d}}/\omega)$(eqn (1)). The term $(\omega/c_{\mathrm{t}})\,a\cos a_{\mathrm{t}}$ which appears in equations (20 a) to (23 a) may therefore be rewritten as $a\omega\,[(1/c_{\mathrm{t}})^2-(1/c_{\mathrm{p}})^2]^{1/2}$, and setting

$$\omega\,[(1/c_{\mathrm{t}})^2-(1/c_{\mathrm{p}})^2]^{1/2}=\beta \qquad \ldots\ldots(24)$$

equations (20a) to (23a) become

$$\mathrm{J}_0(\beta_0'a)=0 \quad \ldots\ldots(20\,b) \qquad \mathrm{J}_1(\beta_\pi'a)=0 \quad \ldots\ldots(21\,b)$$

$$\mathrm{J}_1(\beta_0''a)=0 \quad \ldots\ldots(22\,b) \qquad \mathrm{J}_0(\beta_\pi''a)=0 \quad \ldots\ldots(23\,b)$$

§ 4. EXPERIMENTAL

4.1. *In-phase and Out-of-phase Frequencies*

In order to check the theory outlined in the previous section, some measurements of the difference in phase between the main signal and the first secondary signal were made, using part of an apparatus developed for the accurate measurement of phase velocity (Williams and Lamb 1958). Three specimens of fused silica (Herasil I) were used, of diameters 14·02 mm, 7·06 mm and 4·95 mm, and each 60·31 mm in length. The ends of each specimen were parallel to within about 0·5 minutes of arc: the diameters of the two larger specimens were constant to within ±0·005 mm, the smallest to within ±0·02 mm. All surfaces were polished. Two transducers were placed on each specimen, these transducers being of 10 Mc/s resonant frequency, and of diameter equal to that of the specimen.

By increasing the duration of the wave train applied to the transmitting transducer it was possible to 'overlap' the first main signal arriving at the receiving transducer with the first secondary signal (cf. figure 2). The frequency of the signal was then varied between 9 and 11 Mc/s and measurements were made of the 'in-phase' frequencies at which constructive interference was a maximum (the amplitude of the combined signal a maximum) and the 'anti-phase' frequencies at which destructive interference was a maximum (the amplitude of the combined signal a minimum). The wave train applied to the transducer was derived (via a gating circuit) from a c.w. oscillator, and by use of a digital frequency meter to measure the frequency of this oscillator, the 'out-of-phase' frequencies could be located to within about 10 kc/s.

The in-phase frequencies f_0 and anti-phase frequencies f_π are listed in the table and the theoretical values of f_0 and f_π, calculated from equations (20 *b*)—(23 *b*) are also given.

In order to calculate the theoretical values of f_0 and f_π it was necessary to know, accurately, the velocities of compressional and transverse waves in these specimens, and attempts were made to measure them by the method described by Williams and Lamb (1958). Using compressional waves, reproducible results were obtained for $c_d(5{\cdot}961 \times 10^5\,\mathrm{cm\,sec^{-1}})$, but in the case of transverse waves the difficulties of making a successful bond between the transducers and the specimen prevented reproducible results and the average value of c_t for Herasil I given by Pennell (1952) $(3{\cdot}77 \times 10^5\,\mathrm{cm\,sec^{-1}})$ was used. Some approximations may be made which simplify calculations. In the expression for β (eqn (24)) c_t is a constant, but c_p is a function of frequency. For each of the three specimens, however, it is possible to assume that c_p is a constant over the frequency range of interest (9–11 Mc/s), and has a value of $c_d/\sin a_d$, where $\cos a_d = (j_{0n}/a)(c_d/\omega)$, ω being set equal to its mean value, $2\pi \times 10$ Mc/s and $j_{0n} = j_{01}$ (since it is also assumed that only the first-order mode of propagation is excited). Substitution of the three values of the radius a gives three values for $\cos a_d$, and hence c_p for each of the three specimens. The values of f_0 and f_π may then be obtained rapidly by substituting β (which with this approximation is simply proportional to the frequency) into equations (20 *b*) and (21 *b*), or (22 *b*) and (23 *b*). The approximation leads to an error of less than $0{\cdot}1\%$ in the calculated values of f_0 and f_π.

In order to determine whether the pair of equations (20 *b*) and (21 *b*) or the pair (22 *b*) and (23 *b*) are to be used it is necessary to find whether the factor m is even or odd for the angles of incidence a_d at various frequencies. For fused silica (Poisson ratio $= 0{\cdot}17$) m is an odd integer except for angles of incidence a_d between 45° and 87°. Equation (1) shows that for the largest specimen a_d is greater than 87° at all frequencies between 9 and 11 Mc/s, while for the other two specimens a_d is less than 87° at these frequencies. m is therefore odd in the case of the largest specimen, and equations (20 *b*) and (21 *b*) are appropriate, but equations (22 *b*) and (23 *b*) must be used for the other specimens.

Figures are also given in the table for the average interval between adjacent in-phase frequencies, or adjacent anti-phase frequencies. βa has large values in these experiments, being near 90 for the largest specimen, 30 for the smallest and 45 for the intermediate size, and in these ranges the difference between the successive roots of the Bessel functions $J_0(\beta a)$ and $J_1(\beta a)$ is very nearly constant. It is therefore possible to calculate, from theory, the interval between adajacent values of f_0, or of f_π, and this interval changes negligibly between 9 and 11 Mc/s.

The interval quoted in the experimental results has been calculated by averaging the observed intervals. It is important to note that the intervals will only be evenly spaced if the frequency at which the integer *m* changes from odd to even does not fall in the frequency range considered. If this change does take place (i.e. if a_d passes through 45° or 87°), theory predicts that between one pair of in-phase frequencies the interval will be only one-half of its normal values. Such a change is not expected in the present work, but might be of importance with specimens of other diameters, or at other frequencies.†

Theoretical and Experimental In-phase and Anti-phase Frequencies

Experimental		Theoretical	
f_0(Mc/s)	f_π(Mc/s)	f_0(Mc/s)	f_π(Mc/s)
Specimen 1. (Diameter = 14·02 mm)			
9·04		8·94	
	9·21		9·11
9·39		9·29	
	9·54		9·46
9·72		9·63	
	9·89		9·80
10·07		9·97	
	10·25		10·15
10·42		10·32	
	10·60		10·50
10·76		10·67	
	10·93		10·85
11·10		11·01	
Average interval = 0·34$_6$ Mc/s.		Average interval = 0·34$_7$ Mc/s.	
Specimen 2. (Diameter = 7·06 mm)			
	9·26		9·49
9·61		9·83	
	9·92		10·17
10·21		10·51	
	10·62		10·86
10·93		11·20	
Average interval = 0·69 Mc/s.		Average interval = 0·69 Mc/s.	
Specimen 3. (Diameter = 4·95 mm)			
	9·40		9·58
‡		10·06	
	10·36		10·56
Average interval = 0·96 Mc/s.		Average interval = 0·98 Mc/s.	

‡ Not determined.

The angle of incidence of the plane waves representing the first-order mode vary for specimen 1 from 87° 55′ at 9 Mc/s to 88° 20′ at 11 Mc/s, for specimen 2 from 85° 50′ to 86° 35′ and for specimen 3 from 84° 5′ to 85° 10′. The angles of reflection of the generated transverse waves are over this range always within about 15′ of 39° 10′. The time delays between the main signal and the first secondary signal, due to the passage of the transverse wave across the specimen, are approximately 2·8 μsec, 1·4 μsec, and 1·0 μsec for specimens 1, 2 and 3.

---

† The effect will be complicated, however, by the presence of other modes of propagation, and by the change in form of the displacement distribution which accompanies the change in *m*.

It can be seen from the table that there is a very close agreement between the theoretical and experimental determinations of the frequency separation between successive in-phase (or anti-phase) conditions, for each of the three specimens.

The agreement between the actual frequencies at which in-phase conditions hold is not close, however, the difference between the calculated and measured values of f_0 being about 0·1 Mc/s for specimen 1, 0·3 Mc/s for specimen 2 and 0·2 Mc/s for specimen 3. It is possible that this might be caused by an error in the value assumed for c_t, or by uncertainties in the figures for the diameters of the specimens, but it seems most likely that the effect is due to the presence of other modes of propagation in the specimen, and this will now be discussed.

4.2. *The Effects of Higher Order Modes of Propagation*

The signal present in the secondary compressional wave has been assumed in the preceding analysis to result entirely from, and to be interfering with, a main signal propagating in the first mode. In practice many modes are excited. With the ' piston ' source, the output signal (in the absence of any conversion to transverse waves) would consist of 1 part of the first order mode, 0·19 part of the second, 0·077 part of the third, etc. and these modes have different phase velocities. The secondary signal, however, will not be composed of the same proportions of these modes, for, as shown elsewhere (Redwood 1957*a*), the conversion of each mode into transverse waves takes place at a different rate, this being a consequence of the variation of the relative amplitudes of incident and reflected waves with angle of incidence, for this angle is different for each mode. There will therefore be a phase difference between the secondary signal and the main signal due to the presence of more than one mode of propagation, and this will be additional to that phase difference due to the method of generation of the secondary signal (described in § 3). This additional phase difference will obviously affect the frequencies at which the main and secondary signals are in and out of phase.

For the purposes of discussing the effect it is convenient to assume the propagation of two modes only, and a much more radical change in the proportions of the components in the main and secondary signals than will normally occur in practice. Suppose that the main signal is composed entirely of a signal propagating in the first-order mode, while the secondary signal is composed entirely of a signal propagating in the second mode (i.e. assume that by the time the original signal reaches the receiving transducer the whole of the component representing the second mode has been converted to transverse waves, and hence to a secondary compressional signal, while the whole of the component representing the first mode remains unchanged—this is, of course, not strictly possible in practice, though it may be realized approximately). For a specimen of diameter 1·4 cm, at a frequency of 10 Mc/s, it is possible for there to be a phase difference of π radians between the main and secondary signals, due solely to their different phase velocities, after a time of travel of the main signal from the source of only 23 microseconds. Under these conditions, the frequencies determined by the analysis of § 3 to be in-phase frequencies would now appear in practice as anti-phase frequencies, due to the relative phase shift of π radians resulting from the presence of more than one mode. It is not surprising, therefore, even though in practice conditions are not as extreme as those assumed, that the anti-phase frequencies predicted by a theory which is based on the assumption that a single mode was propagated do not agree with the results of experiments in which several modes were excited.

The effect of higher-order modes on the frequency *interval* will, however, be small. With the assumptions just made, the predicted phase difference of 180° at 10 Mc/s will fall to about 160° at 11 Mc/s, and rise to 200° at 9 Mc/s. The true frequency separation between anti-phase frequencies is 0·34 Mc/s so that the additional phase difference over the frequency interval due to the presence of more than one mode will be only about 6°. This will cause the frequency interval to change by less than 2%. At a receiving transducer placed further from the source a greater change might be experienced, but in present work observations were confined to the first signals to arrive at the receiving transducer, and these have travelled only 6 cm ($=10\,\mu$sec).

§ 5. THE SIGNIFICANCE OF SECONDARY SIGNALS IN THE PROPAGATION OF CONTINUOUS WAVES

The manner in which the phase difference between the main and secondary signals varies with frequency is related to certain aspects of the frequency variation of the phase velocity of *continuous waves* propagating in a bounded medium. Figure 4 shows the variation of phase velocity c_{p} over a limited frequency range near 10 Mc/s, computed for those modes of propagation in a solid cylinder for which c_{p} is nearest c_{d} (the velocity of compressional waves in an unbounded medium) (Redwood and Lamb 1957). The main feature of interest is the rapid change of phase velocity which occurs in the region of curves $J_1(\beta a)=0$. These regions, here termed ‘ steps ’, are joined by ‘ plateaux ’, over which the phase velocity changes only slightly with frequency. Curves of similar form also describe the propagation of continuous waves in a solid ‘ slab ’ wave guide (Tolstoy

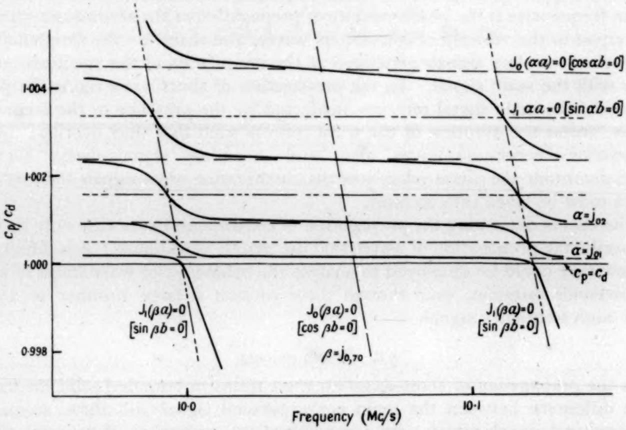

Figure 4. Phase velocity of continuous compressional waves in a solid cylinder at high frequencies. Poisson ratio = 1/3. Radius of cylinder = 1 cm. $c_{\mathrm{d}}=5\times10^5$ cm sec^{-1}. The labelling in brackets refers to the analogous slab waveguide.

and Usdin 1957) and in layered fluids (Tolstoy 1956). The phenomenon would appear to be characteristic at high frequencies whenever two velocities of propagation are possible, and when energy may be transferred from that part of the signal which travels with one velocity into the part which travels with the other velocity, as happens at a boundary.

Figure 4 also shows the curves $J_0(\alpha a)=0$; $J_1(\alpha a)=0$; $J_0(\beta a)=0$, $J_1(\beta a)=0$ where β is defined by equation (24) and $\alpha=\omega\,[(1/c_d)^2-(1/c_p)^2]^{1/2}$; the sets $J_0(\alpha a)=0$, $J_1(\alpha a)=0$ would describe the modes of propagation of waves of velocity c_d in a fluid guide, the sets $J_0(\beta a)=0$ the propagation of waves of velocity c_t. In the case of the slab, the equivalent curves are $\cos\alpha b=0$, $\sin\alpha b=0$; $\cos\beta b=0$, $\sin\beta b=0$, as indicated in brackets in figure 4.

The points near which the phase velocity changes rapidly, and where $J_1(\beta a)=0$ correspond to those frequencies at which the main signal is in anti-phase with the first secondary signal in the case of the propagation of short wave trains (cf. eqn (21 *b*)), and the centres of the plateaux correspond to the frequencies at which the main and secondary signals are in phase (eqn (20 *b*)).

There is a marked difference between the propagation of short-duration wave trains and the propagation of continuous waves in solid waveguides, since the phase velocity of the main signal in the propagation of short wave trains is described by the curves $J_0(\alpha a)=0$. It is necessary to employ two distinctly different lines of approach to predict the phase velocities of propagation in the two cases: only at certain frequencies is the phase velocity of propagation of the short duration wave train equal to the velocity of continuous waves, and these are the frequencies at which the secondary signals generated at the boundaries of the specimen are in phase with the main signal. In the propagation of short wave trains the phase velocity of the main signal remains unaffected by the presence of the secondary signals, unless the duration of the wave train is such that they overlap; in the propagation of continuous waves ' main ' and ' secondary ' signals always ' overlap' and to determine the phase velocity of the combination of all signals their relative phases must be taken into account.

The curves describing the propagation of continuous waves may only be used to describe the propagation of waves that are *strictly* continuous: it is difficult to see how they could be employed to analyse the behaviour of wave trains of a few microseconds duration, even though these contain a large number of cycles of the high frequency signal.

§ 6. CONCLUSIONS

In the propagation of short-duration wave trains in bounded solid media the phase difference between the main compressional signal and those secondary compressional signals which arise as a result of the conversion of the main signal to transverse waves is a function of frequency, even though for each mode all the individual wave fronts travelling along the axis of the specimen have the same phase velocity. Experimental results confirm the theoretical analysis which leads to these conclusions.

The results of the analysis which has been presented here have important consequences in the accurate measurement of the absorption and velocity in solids, for frequently the wave trains in use are sufficiently long for main and secondary signals to interfere. Since the phase and amplitude of the combined signal is then very dependent on frequency, considerable errors of measurement may arise.

The discussion is also relevant to other problems concerning waveguides in which two velocities of propagation are possible, as for example in the propagation of seismic waves in layered fluid and solid media (Ewing, Jardetsky and Press 1957).

ACKNOWLEDGMENTS

The author is grateful to Mr. J. R. Williams for allowing the use of an apparatus developed by him, and to Dr. J. Lamb for his encouragement in this work. The receipt of a Research Fellowship from the Department of Scientific and Industrial Research is also acknowledged.

REFERENCES

ARENBERG, D. L., 1948, *J. Acoust. Soc. Amer.*, **20**, 1.
EWING, W. M., JARDETSKY, W. S., and PRESS, F., 1957, *Elastic Waves in Layered Media* (New York : McGraw-Hill).
HOLDEN, A. N., 1951, *Bell Syst. Tech. J.*, **30**, 956.
MCSKIMIN, H. J., 1956, *J. Acoust. Soc. Amer.*, **28**, 484.
PENNELL, E. S., 1952, *Elect. Engng, N.Y.*, **71**, 817.
REDWOOD, M., 1957 a, *Proc. Phys. Soc.* B, **70**, 721; 1957 b, *Ph.D. Thesis*, University of London.
REDWOOD, M., and LAMB, J., 1957, *Proc. Phys. Soc.* B, **70**, 136.
TOLSTOY, I., 1956, *J. Acoust. Soc. Amer.*, **28**, 1182.
TOLSTOY, I., and USDIN, U., 1957, *J. Acoust. Soc. Amer.*, **29**, 37.
WILLIAMS, J. R., and LAMB, J., 1958, *J. Acoust. Soc. Amer.*, **30**, 308.

The Surface Tensions of Liquid Argon and Nitrogen

By D. STANSFIELD†

H. H. Wills Physical Laboratory, University of Bristol

MS. received 8th April 1958, *and in final form 14th July* 1958

Abstract. The surface tensions of liquid argon and nitrogen have been measured over their complete liquid ranges, from triple point to critical point, using a capillary rise method. The experimental results are given and compared with values obtained theoretically. Agreement between theory and experiment is not good for temperatures near the critical point.

§ 1. Introduction

The variation with temperature of the surface tensions of liquids composed of simple molecules may generally be described fairly accurately by the equation proposed by Ferguson and Kennedy (1936),

$$\gamma = \gamma_0 (1 - T/T_c)^p \qquad \ldots\ldots (1)$$

where γ is the surface tension, T the absolute temperature, T_c the critical temperature and γ_0 and p constants. Ferguson showed that, for many pure unassociated organic liquids, the index p has a value of about 1·2; γ_0 takes values characteristic of the particular liquids. Guggenheim (1945) has approached the problem from the standpoint of the principle of corresponding states, and has found $p = 11/9$. He has also obtained another universal constant C, related to γ_0 by the equation

$$C = \gamma_0 V_c^{2/3} T_c^{-1} \qquad \ldots\ldots (2)$$

where V_c is the molar critical volume. The difference between the co-existent liquid and vapour densities ρ_l and ρ_g obeys a similar relation

$$\rho_l - \rho_g = \rho_0 (1 - T/T_c)^n \qquad \ldots\ldots (3)$$

in which n is usually near to 1/3 for simple liquids.

It is of interest to see if these relations apply reasonably well over extended temperature ranges to liquids composed of monatomic molecules and for which quantum effects are unimportant, i.e. to the inert gases except helium and neon. For this work we therefore chose argon, which has a liquid phase extending over a convenient temperature range, high enough for quantum effects to be relatively unimportant, and which is readily obtainable in a pure state. The surface tension was measured over almost the complete liquid range, from triple point to near the critical point, but no particular effort was made to investigate the relationship between γ and $\rho_l - \rho_g$ very near to T_c. Measurements were also made on liquid nitrogen, as an example of a fluid composed of molecules slightly more complex than those of argon. Both sets of measurements are described in §§ 2 and 3.

---

† Now at H.M. Underwater Detection Establishment, Portland, Dorset.

In addition to these somewhat empirical relations between γ and other macroscopic quantities, there exist many attempts to relate surface tension to the molecular properties of the fluids. These attempts are all applicable most readily to spherically symmetrical molecules such as those of argon, and § 4 presents some comparisons between experimental and theoretical values.

§ 2. APPARATUS AND PROCEDURES

2.1. *The Gases*

The argon used for these measurements was of 'lead seal' quality, for which the suppliers (British Oxygen Co. Ltd.) quoted a typical analysis as follows: argon 99·93%, nitrogen 0·07%, oxygen about 2 volumes per million, hydrogen usually <3 volumes per million, carbon dioxide <3 volumes per million, other carbon compounds <2 volumes per million, water vapour usually $<0{\cdot}02$ g m^{-3}.

Preliminary measurements were made on argon of 99·8% purity, the main impurity again being nitrogen.

The results on nitrogen were obtained using 'oxygen-free' nitrogen, which had a typical analysis of: nitrogen 99·9%, oxygen <10 volumes per million, carbon dioxide <20 volumes per million, other carbon compounds <5 volumes per million, neon $<0{\cdot}1$%, helium $<0{\cdot}03$%, argon <50 volumes per million. Each gas was supplied in cylinders at 120 atmospheres.

2.2. *Measurement of Surface Tension*

Of the many methods available for the measurement of surface tension, that using capillary tubes seemed most suitable for the present purpose, in view of the necessity for the apparatus to be capable of withstanding pressures up to the critical pressure of argon (48 atmospheres.) We therefore chose a method proposed by Sugden (1921), in which the vertical distance between the free liquid surfaces in two tubes of different bore is measured; a third tube was added as a check.

The main disadvantages inherent in any capillary rise method of measuring surface tension have been listed by Dorsey (1926). They are: (i) The contact angle between the liquid and the wall of the tube must be known. (ii) There is difficulty in accurately measuring the bores of the tubes. (iii) As the liquid surface is small, a small impurity content may have a disproportionately large effect. (iv) The cleaning of small tubes is not easy. (v) The difference between the densities of the liquid and vapour must be known.

We assumed the contact angle to be zero, an assumption supported by visual observation. This also seems reasonable for a liquid composed of spherical molecules in contact with glass, particularly when, as in this case, the liquid can be made to run down the walls in order to wet them thoroughly. The accurate measurement of the bores of the narrow tubes was difficult, and this introduced an important limitation to the absolute accuracy of the surface tension values. It does not, however, appreciably affect the measured dependence of the surface tension on temperature.

The nominal inside diameters of the capillary tubes were 0·2, 0·4 and 2·0 mm, giving a maximum difference in meniscus levels of about 2 cm; the outside diameters were 5 mm. The tubes were made of 'Veridia' precision bore tubing, manufactured to be of uniform cross section, the bore being advertised as within

0·01 mm of the nominal diameter. The use of this tube eliminated the tedious search for a tube of uniform and circular bore which would have been necessary with hand-drawn tubes. To eliminate contamination of the tubes, the bores were not measured until after the experiments; the tubes were then broken at several places and the cross sections measured under a microscope with an accuracy closer than 1%. None of the tubes showed any indication of ellipticity greater than 3%, and the mean bore along each tube showed only slight and fairly smooth variation over the working length of about 3 cm. The measured diameters were within 2% of the nominal bores. The errors introduced by the thermal expansion of the tubes, by ellipticity of the bores, and by non-uniformity of the walls of the tubes and surrounding vessels, were small compared with those involved in the actual measurement of capillary rise.

The capillary tubes were cleaned before use with hot chromic acid, water, and alcohol, and were then heated, to decompose any grease left on the walls. Occasionally during use, they were also heated to 250°C and evacuated to about 5×10^{-3} mm Hg to pump off any grease which might subsequently have condensed on the inner walls. It was found necessary to bend the narrow tubes into the widest one as shown in figure 1, in order to eliminate bubbles and condensed liquid, which tended to block the narrow tubes and give unsteady levels. An easily demountable glass–metal joint (similar to one described by Newitt (1940)) was used between the glass tubes and the remainder of the argon system outside the cryostat, and the whole system was pressure tested to 90 atmospheres. Gauges were fitted between the tubes and the supply cylinder, to measure the argon

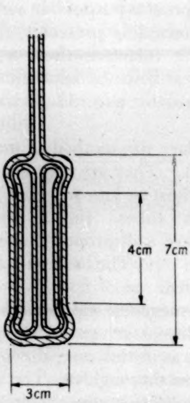

Figure 1. The capillary tubes.

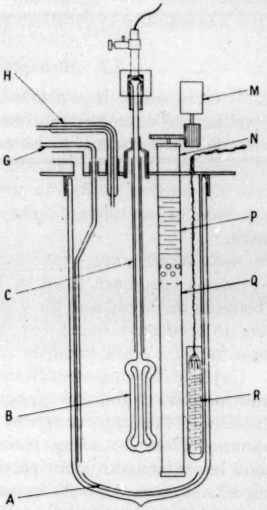

Figure 2. The cryostat.

vapour pressure, but the dead space between the capillary tubes and the main shut-off tap was kept small, in order to minimize the effect of ambient temperature fluctuations.

Scales were marked along the capillary tubes by means of a fine-pointed writing diamond, and these were then calibrated with a Cambridge measuring instrument. The height of the meniscus in a tube could thus be measured approximately by direct use of a cathetometer, and more accurately by interpolation between the scale marks, using a scale in the eyepiece of the cathetometer. In this way, errors due to optical irregularities in the walls of the surrounding vessels were minimized. Slits were left in the silvering of the cryostat Dewar vessel, to enable the argon tubes to be illuminated from behind, but it was at first found difficult to see the menisci in the two narrow tubes clearly, particularly at the higher temperatures. This was due primarily to the astigmatism introduced by the cylindrical walls of the tubes and Dewar. Best visibility was obtained by using a narrow horizontal slit aperture at the cathetometer objective, and a horizontal opaque screen which could be moved up and down between the Dewar and the illuminating light until its upper edge cast a shadow just below the level of the meniscus. This arrangement largely eliminated the light, collected in the vertical plane, which reduced the contrast of the narrow dark region caused by the scattering of light by the meniscus.

2.3. *Temperature Control and Measurement*

In order to cover the liquid ranges of both argon and nitrogen, temperatures within the range from 63° to 150°K were required. Baths of the three liquids listed in table 1, boiling at or below atmospheric pressure, were used in the cryostat. The methane and ethylene were liquefied by passing the gas under pressure through copper coils immersed in liquid oxygen.

Table 1

Liquid	Triple point Temp. (°K)	Triple point Pressure (mm Hg)	Boiling point Temp. (°K)
Oxygen	54·8	2·0	90·2
Methane	90·1	70	111·8
Ethylene	104·2	<4	169·5

The cryostat itself is shown diagrammatically in figure 2. The stirrer was of the lift-pump type, the motor M driving a fan at the bottom of the tube Q so as to expel liquid through holes at the top of the tube. An insert P of slotted German silver tube was necessary to prevent freezing of the gland in its casing N. Liquid coolant could be siphoned into or out of the cryostat through the tubes H and G, and shield A was inserted to protect the glass Dewar vessel in the event of a breakage of the argon tubes B. The thin copper shield C eliminated condensation in the stem of the capillary tubes due to temperature gradients near the surface of the cryostat liquid.

The temperature of the enclosure was kept constant by maintaining a constant pressure over the liquid bath, using a glass Cartesian manostat (Gilmont 1951) which could maintain a temperature constant to about 0·005°C. A platinum resistance thermometer R, suspended by the side of the capillary tubes B, was used to measure the temperature of the liquid bath. For the measurements on liquid argon, a thermometer of rather impure platinum was used, but this was later compared with a more satisfactory thermometer, which was also used during the experiments on nitrogen. These thermometers were calibrated at the ice, oxygen, steam, and mercury points, the accuracy of the corrected temperature measurements being of the order of 0·05 °c.

2.4. *Experimental Procedure*

Before every run the whole gas system was evacuated and flushed several times with the gas to be used. The required temperature was obtained by control of the pressure over the cryostat liquid, and a suitable volume of argon introduced into the capillary tubes. The temperature was then kept constant to within about ± 0·005 °c for 20 minutes or more before any measurements were attempted. Small changes in the temperature of the tubes, resulting mainly from evaporation of the bath liquid, caused the meniscus levels to show a gradual drift, particularly when the argon vapour density was high. The meniscus heights were therefore measured in each tube in turn, over an interval of about 30 minutes, and the differences in level were obtained by interpolation.

The temperature in the cryostat could then be raised, more argon introduced, and another set of measurements made at this higher temperature. The highest temperature at which satisfactory results were obtained was limited by the unsteadiness of the liquid levels caused by the slight temperature fluctuations, and by the difficulty of seeing the menisci sufficiently clearly.

§ 3. RESULTS

We denote by H_{13} the difference in height between the lowest points of the menisci in the tubes of bore 0·2 mm and 2·0 mm: and by H_{23} that for the tubes of bore 0·4 mm and 2·0 mm. Each value below is the mean value obtained, for the particular temperature, from measurements (usually about eight for each tube) made as described in the preceding section. At the lower temperatures the standard deviation of the actual measurements about each mean value was about ± 0·02 mm, and at temperatures near the critical point it increased to about ± 0·04 mm. We used Sugden's tables (1921) for the calculation of the meniscus corrections, thus obtaining values of a_{13}^2 and a_{23}^2 from the measurements of H_{13} and H_{23} respectively. Here a_{13} and a_{23} are the experimental values of a parameter defined (suppressing suffices) by

$$a^2 = 2\gamma / g(\rho_l - \rho_g) \qquad \ldots\ldots (4)$$

where g is the acceleration due to gravity. A knowledge of $\rho_l - \rho_g$ at the appropriate temperatures was then necessary for values of surface tension to be calculated.

3.1. *Argon*

The results for argon both of 99·8% and of 99·93% purity are given in table 2. Agreement between corresponding values of a_{13}^2 and a_{23}^2 is satisfactory. The blank spaces usually indicate occasions when bubbles or condensed liquid caused large and obvious errors in the meniscus levels; they are more frequent for the first set of results, for which an earlier design for the capillary tubes was used. Figure 3 shows values of log a_{13}^2 plotted against log $(T_c - T)$, using for argon the critical temperature $T_c = 150{\cdot}7\,^\circ$K given by Mathias, Onnes and Crommelin (1912).

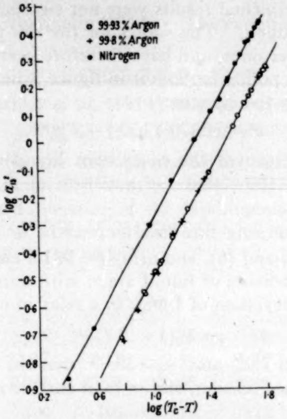

Figure 3. log a_{13}^2 plotted against log (T_c-T) for argon and nitrogen.

Table 2

	Temp. (°K)	H_{13} (mm)	H_{23} (mm)	a_{13}^2 (mm^2)	a_{23}^2 (mm^2)
99·8% Argon					
	84·51	17·13	8·00	1·876	1·909
	87·61	16·34	7·74	1·811	1·841
	90·25	15·72	7·49	1·742	1·787
	90·47	—	7·24	—	1·731
	126·77	6·76	3·32	0·737	0·778
	129·28	6·10	—	0·661	—
	134·31	4·74	—	0·512	—
	136·61	4·29	—	0·463	—
	139·54	—	1·45	—	0·330
	139·98	3·10	—	0·333	—
	140·65	3·09	—	0·331	—
	142·90	2·30	1·22	0·244	0·275
	144·51	1·78	—	0·189	—
99·93% Argon					
	84·22	17·24	7·88	1·884	1·891
	86·32	16·66	7·75	1·830	1·855
	90·39	15·75	7·35	1·745	1·749
	97·96	14·01	6·49	1·544	1·549
	100·37	13·42	6·20	1·475	1·468
	104·00	12·68	5·82	1·388	1·385
	108·82	11·35	5·26	1·251	1·246
	111·97	10·38	—	1·140	—
	125·47	7·10	—	0·775	—
	132·59	5·29	2·52	0·570	0·581
	136·65	4·17	1·95	0·449	0·450
	139·16	3·47	—	0·371	—
	139·37	3·38	1·53	0·359	0·344
	140·42	3·18	1·51	0·338	0·347
	141·90	2·64	1·16	0·281	0·264
	142·01	2·68	1·18	0·286	0·266
	144·69	1·84	—	0·195	—

It is clear that the experimental results were not significantly affected by the increase in purity of the argon. The values for the less pure gas, however, were less reliable than the later ones, and have therefore been omitted for the results below. The remaining points for argon in figure 3 lie with good accuracy on the straight line given by the equation

$$a^2 = 0{\cdot}03707(150{\cdot}7 - T)^{0{\cdot}940}. \qquad \ldots\ldots(5)$$

Mathias *et al.* (1912) measured the co-existent liquid and vapour densities of argon, and their values show that the variation of $\rho_l - \rho_g$ may be described adequately by

$$\rho_l - \rho_g = 0{\cdot}3392(150{\cdot}7 - T)^{0{\cdot}341}. \qquad \ldots\ldots(6)$$

Combining equations (5) and (6), and using $g = 981{\cdot}2$ cm sec^{-2}, we find that the variation of the surface tension of liquid argon with temperature may be represented, with a standard deviation of 1·6%, by a relation of the usual type

$$\gamma = \gamma_0(1 - T/T_c)^p \qquad \ldots\ldots(1)$$

with $p = 1{\cdot}281$, $T_c = 150{\cdot}7$°K, and $\gamma_0 = 38{\cdot}07$ dyn cm^{-1}. Table 3 contains smoothed values of surface tension, and of total surface energy E, defined in the usual way:

$$E = \gamma - T d\gamma/dT. \qquad \ldots\ldots(7)$$

Table 3

Temperature (°K)	85	90	95	100	105	110	115
γ (dyn cm^{-1})	13·12	11·86	10·63	9·42	8·24	7·10	6·01
E (erg cm^{-2})	34·90	34·42	33·88	33·25	32·53	31·73	30·82

Temperature (°K)	120	125	130	135	140	145	150·7
γ (dyn cm^{-1})	4·95	3·94	2·99	2·10	1·28	0·57	0
E (erg cm^{-2})	29·77	28·53	27·06	25·22	22·81	19·24	0

3.2. *Nitrogen*

The results for nitrogen are given in table 4. Values of log a_{13}^2 for nitrogen are plotted against log $(T_c - T)$ in figure 3, using the value $T_c = 126{\cdot}0$°K given

Table 4

Temp. (°K)	H_{13} (mm)	H_{23} (mm)	a_{13}^2 (mm^2)	a_{23}^2 (mm^2)
65·44	25·34	11·38	2·759	2·748
65·89	25·01	11·28	2·723	2·720
68·65	23·80	10·81	2·622	2·600
72·01	22·52	10·32	2·499	2·475
72·10	22·49	10·28	2·454	2·478
75·43	21·50	9·66	2·334	2·330
77·10	20·92	9·39	2·317	2·249
81·35	19·00	8·64	2·088	2·076
84·98	17·50	7·88	1·928	1·890
90·13	15·38	7·08	1·704	1·684
90·64	15·18	—	1·669	—
95·19	13·55	5·94	1·429	1·414
99·60	11·82	—	1·302	—
105·60	9·32	4·19	1·017	0·992
112·04	6·49	3·01	0·723	0·707
116·41	4·62	2·09	0·495	0·477
122·26	1·98	0·87	0·210	0·195
123·54	1·30	0·50	0·138	0·112

by Mathias, Onnes and Crommelin (1914). The variation of a_{13}^2 with temperature is described by

$$a^2 = 0{\cdot}06084(126{\cdot}0 - T)^{0{\cdot}930}. \qquad \ldots\ldots(8)$$

The density data of Mathias *et al.* (1914) may be summarized by the equation

$$\rho_l - \rho_g = 0{\cdot}2341(126{\cdot}0 - T)^{0{\cdot}317} \qquad \ldots\ldots(9)$$

which, with (8), gives for the dependence of the surface tension of nitrogen on temperature the equation (1), with $p = 1{\cdot}247$, $T_c = 126{\cdot}0$°K, and $\gamma_0 = 29{\cdot}09$ dyn cm^{-1}. The standard deviation of the experimental values from this curve is again 1·6%. Values of surface tension and total surface energy calculated from this equation are shown in table 5.

Table 5

Temperature (°K)	65	70	75	80		90	95
γ (dyn cm^{-1})	11·77	10·58	9·41	8·28	7·16	6·10	5·06
E (erg cm^{-2})	27·41	27·08	26·68	26·24	25·71	25·10	24·39
Temperature (°K)	100	105	110	115	120	126	
γ (dyn cm^{-1})	4·06	3·11	2·22	1·39	0·65	0	
E (erg cm^{-2})	23·54	22·50	21·21	19·48	16·89	0	

§ 4. DISCUSSION

The experimental results show that the surface tensions of liquid argon and nitrogen may be described by Ferguson's relation (1), in which the index $p = 1{\cdot}281$ for argon, and $p = 1{\cdot}247$ for nitrogen. These values are a little higher than that suggested by Ferguson himself (1936) (who gave $p = 1{\cdot}210$ as the mean for about forty organic liquids) and than the value $p = 11/9$ proposed by Guggenheim (1945). Jones and Bowden (1946) found $p = 1{\cdot}244$, which is in better agreement with our results. The probable errors in our values of p are about 0·01, so that the difference between the indices for the two liquids appears to be significant (and is almost equal to that between the indices in equations (6) and (9) for $\rho_l - \rho_g$).

The law of corresponding states leads to the conclusion that γ_0 is such that

$$\gamma_0 V_c^{2/3} T_c^{-1} = C \qquad \ldots\ldots(2)$$

is a universal constant (Guggenheim 1945). Using $V_c = 75{\cdot}3$ cm^3 mole^{-1} for argon and $V_c = 90{\cdot}2$ cm^3 mole^{-1} for nitrogen, we find $C = 4{\cdot}50$ erg deg^{-1} mole$^{-2/3}$ for argon, and $C = 4{\cdot}66$ erg deg^{-1} mole$^{-2/3}$ for nitrogen, in reasonable agreement with the values given by Guggenheim.

Measurements of the surface tensions of argon and nitrogen at temperatures up to 90°K have previously been made by Baly and Donnan (1902) (values corrected by Rudorf (1909)). Our results over this temperature range agree with theirs to nearer than 1%. Their measurements of liquid densities also agree to within 1% with those of Mathias, Onnes and Crommelin (1912, 1914), who claimed that the impurity content of the argon used by them was less than 0·1%, and that the nitrogen was 'very pure'.

The index q in Macleod's equation (Macleod 1923)

$$\gamma(\rho_l - \rho_g)^{-q} = \text{constant} \qquad \ldots\ldots(10)$$

has the value 3·76 for argon and 3·94 for nitrogen, in agreement with the usual result that q is a little less than 4·0. There is no evidence to support the prediction (for example, Yvon, 1948) that q should tend to the value 3 near the critical point, but it should be remembered that no special efforts were made to investigate this region.

§ 5. THEORETICAL RESULTS

In this section we present some calculations based on results derived from a general statistical mechanical theory of monatomic liquids. One such theory of surface tension has been given by Kirkwood and Buff (1949), and a comparison of the numerical results of this theory with experimental values for argon should afford a useful measure of the accuracy of the approximations involved in the calculations.

In their treatment Kirkwood and Buff recognized the existence of a transition zone between liquid and vapour, and used the concept of surface tension as the stress across a plane surface extending across the transition layer. Using a rectangular coordinate system, with the (x,y) axes in an arbitrary Gibbs surface in a plane transition zone, and with the z axis normal to it and directed from phase α to phase β, they define an excess singlet density $\rho_s^{(1)}$ such that

$$\rho_s^{(1)}(z)=\rho^{(1)}(z)-\rho_{\alpha\beta}^{(1)} \qquad \ldots\ldots(11)$$

where $\rho^{(1)}(z)$ specifies the average number of molecules, $\rho^{(1)}(z)dv$, in the volume element dv at a point given by the coordinate z, and where

$$\begin{aligned}\rho_{\alpha\beta}^{(1)}&=\rho_\alpha^{(1)} \text{ for } z<0\\ &=\rho_\beta^{(1)} \text{ for } z\geqslant 0.\end{aligned} \qquad \ldots\ldots(12)$$

Similarly, they define the excess pair density

$$\rho_s^{(2)}(z_1,\mathbf{R}_{12})=\rho^{(2)}(z_1,\mathbf{R}_{12})-\rho_{\alpha\beta}^{(2)} \qquad \ldots\ldots(13)$$

in which $\rho^{(2)}(z_1,\mathbf{R}_{12})$ is the pair density specifying the average number of molecular pairs, $\rho^{(2)}(z_1,\mathbf{R}_{12})dv_1dv_2$ one member of which is in dv_1 at z_1, and the other in dv_2 at $\mathbf{R}_{12}$ relative to the first molecule of the pair. Again,

$$\begin{aligned}\rho_{\alpha\beta}^{(2)}&=\rho_\alpha^{(2)} \text{ for } z_1<0\\ &=\rho_\beta^{(2)} \text{ for } z_1\geqslant 0.\end{aligned} \qquad \ldots\ldots(14)$$

Kirkwood and Buff thus arrive at the general expression for the surface tension of the fluid,

$$\gamma=-\Gamma_s^{(1)}kT+\tfrac{1}{2}\int\frac{x_{12}^2}{R_{12}}\frac{dV}{dR_{12}}\Gamma_s^{(2)}(\mathbf{R}_{12})dv_{12}. \qquad \ldots\ldots(15)$$

Here $V(R_{12})$ is the interatomic potential, assumed to depend only on the magnitude of R_{12} and

$$\Gamma_s^{(1)}=\int_{-\infty}^{+\infty}\rho_s^{(1)}(z)dz \qquad \ldots\ldots(16)$$

$$\Gamma_s^{(2)}=\int_{-\infty}^{+\infty}\rho_s^{(2)}(z,\mathbf{R}_{12})dz. \qquad \ldots\ldots(17)$$

By making a suitable choice for the dividing surface, $\Gamma_s^{(1)}$ may be made to vanish, and the general expression then becomes

$$\gamma=\tfrac{1}{2}\int\frac{x_{12}^2}{R_{12}}\frac{dV}{dR_{12}}\Gamma_s^{(2)}(\mathbf{R}_{12})dv_{12}. \qquad \ldots\ldots(18)$$

The calculation of γ thus necessitates a knowledge of the behaviour of $\rho^{(2)}$ in the surface region. As there was no accurate and explicit theory for this behaviour, Kirkwood and Buff considered an approximation in which the transition zone was shrunk to a mathematical dividing surface, and used

$$\rho^{(2)}(z_1,\mathbf{R}_{12})=\rho^{(1)}(z_1)\rho^{(1)}(z_1+z_{12})g^{(2)}(z_1,\mathbf{R}_{12}) \qquad \ldots\ldots(19)$$

where $g^{(2)}(z_1,\mathbf{R}_{12})$ is the pair distribution function often encountered in the theory of liquids. Then, neglecting the effect of the vapour, they let

$$\begin{aligned} \rho^{(1)}(z) &= \rho_\alpha^{(1)} \quad \text{for } z \leqslant 0 \\ &= 0 \quad \text{for } z > 0 \qquad \ldots\ldots(20) \\ g^{(2)}(z_1,\mathbf{R}_{12}) &= g_\alpha^{(2)}(R_{12}) \text{ for } z_1 \leqslant 0. \qquad \ldots\ldots(21) \end{aligned}$$

Equation (18) then becomes

$$\gamma=\frac{\pi\rho_\alpha^{(1)2}}{8}\int_0^\infty R^4\frac{dV}{dR}g_\alpha^{(2)}(R)dR. \qquad \ldots\ldots(22)$$

Similarly, the total surface energy (with the same approximations, and using the same choice for the dividing surface) may be shown to be

$$E=-\frac{\pi\rho_\alpha^{(1)2}}{2}\int_0^\infty R^3V(R)g_\alpha^{(2)}(R)dR. \qquad \ldots\ldots(23)$$

Equation (22) has also been obtained by MacLellan (1952), using a different treatment.

In evaluating γ from equation (22), Kirkwood and Buff used an analytical approximation to the first peak of the radial distribution function $g_\alpha^{(2)}(R)$ determined experimentally by Eisenstein and Gingrich (1942). We use here the radial distribution functions $g_L(R)$ given by Zwanzig, Kirkwood, Stripp and Oppenheim (1953) for fluids having a Lennard-Jones type of interatomic potential,

$$V(R)=4\epsilon\{(a/R)^{12}-(a/R)^6\}. \qquad \ldots\ldots(24)$$

The values of the parameters ϵ and a for argon are those given by Michels, Wijker and Wijker (1949): $\epsilon=1{\cdot}653\times10^{-14}$ erg, $a=3{\cdot}405\times10^{-8}$ cm.

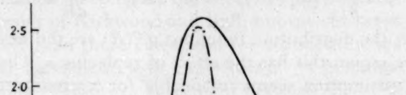

Figure 4. $g^{(2)}(R)$ for argon at 90°K.

The function $g_L(R)$ given by Zwanzig *et al.* for liquid argon at 90°K, and that used by Kirkwood and Buff, are compared in figure 4 with the experimental function of Eisenstein and Gingrich. Zwanzig *et al.* introduced also a function $g_L(cR)$ in which c was an arbitrary correcting factor inserted into the calculated functions to give better agreement with any one experimental thermodynamic quantity.

In the computation of γ and E, the Lennard-Jones potential (24) was assumed, and the radial distribution function was approximated by the function

$$\begin{aligned} g_\alpha^{(2)}(R) &= g_L(R) \qquad \text{for } 0<R<2{\cdot}5a \\ &=1 \qquad \text{for } R \geqslant 2{\cdot}5a. \end{aligned} \qquad \ldots\ldots(25)$$

This approximation takes account of the first two maxima in $g_L(R)$, and the errors introduced by putting $g^{(2)}(R)=1$ beyond $R=2{\cdot}5a$ are only small. γ and E were also evaluated (to give values $\gamma(c)$ and $E(c)$) using the functions $g_L(cR)$ instead of $g_L(R)$ in (22) and (23), the values of c being those given by Zwanzig *et al.* to agree with equation of state data. The results are given in table 6 for the three temperatures to which the calculations of Zwanzig *et al.* may readily be applied.

Table 6

Temp.	γ (dyn cm^{-1})			E (erg cm^{-2})			c
(°K)	γ_{theor}	$\gamma(c)$	γ_{exp}	E_{theor}	$E(c)$	E_{exp}	
90·0	20·47	14·05	11·86	27·92	26·89	34·39	1·026
123·0	12·97	10·62	4·35	18·56	18·19	29·02	1·014
149·0	5·28	4·85	0·16	7·87	7·64	13·80	1·0066

Kirkwood and Buff's calculated values for argon at 90°K were $\gamma=14{\cdot}9$ dyn cm^{-1}, and $E=27{\cdot}2$ erg cm^{-2}.

In proposing an improvement to the theory for temperatures near T_c, by taking account of the effect of the vapour phase, MacLellan (1952) suggested the equation

$$\gamma = \frac{\pi}{8}\int_0^\infty [\{\rho_\alpha^{(2)}(R)\}^{1/2} - \{\rho_\beta^{(2)}(R)\}^{1/2}]^2 \frac{dV}{dR} R^4 dR. \qquad \ldots\ldots(26)$$

If we assume that the distribution functions $g^{(2)}(R)$ are the same for both phases and in the surface region this has the effect of replacing $\rho_\alpha^{(1)}$ by $\rho_\alpha^{(1)}-\rho_\beta^{(1)}$ in (22) and (23). This assumption seems reasonable for temperatures near T_c, where the effect of the vapour is most important. Values of $\gamma(c)'$ and $E(c)'$ are given in table 7, calculated from the equations,

$$\gamma(c)' = \frac{\pi}{8}(\rho_\alpha^{(1)}-\rho_\beta^{(1)})^2 \int_0^\infty R^4 \frac{dV}{dR} g^{(2)}(cR) dR \qquad \ldots\ldots(27)$$

$$E(c)' = -\frac{\pi}{2}(\rho_\alpha^{(1)}-\rho_\beta^{(1)})^2 \int_0^\infty R^3 V(R) g^{(2)}(cR) dR. \qquad \ldots\ldots(28)$$

Table 7

Temperature (°K)	90·0	123·0	149·0
$\gamma(c)'$ (dyn cm^{-1})	14·00	9·23	1·52
$E(c)'$ (erg cm^{-2})	26·81	15·78	2·39

These results for $\gamma(c)'$ are in better agreement with experiment than are those for $\gamma(c)$ given above, but the calculated value at 149°K is still too large by a factor of nearly ten. The values for $E(c)'$ show poorer agreement with experiment than do those for $E(c)$.

§ 6. COMPARISON OF THEORETICAL AND EXPERIMENTAL RESULTS

Agreement between the theoretical and experimental values of surface tension is reasonably good for the lower temperatures, but becomes much poorer as the temperature approaches T_c. In seeking the reasons for this poor agreement, we consider in this section the approximations which seem likely to introduce the largest errors into the calculations.

The errors due to the use by Zwanzig *et al.* of the 'superposition approximation' in the calculations of $g_L(R)$ have been discussed by Rushbrooke and Scoins (1951). They are difficult to estimate, but should be least for fluids of low density (i.e. at the higher temperatures). The use of the Lennard-Jones potential function (24) has been largely justified by its success in many studies of the monatomic liquids. Several authors (for example, Jansen and Dawson 1955) have pointed out that it is not entirely satisfactory, but there is as yet little support for any more acceptable alternative. The errors are again difficult to estimate, but it seems unlikely that either these or those due to the superposition approximation can account for the increasing discrepancy as the temperature increases.

Thirdly, we must consider the assumption of a sharp dividing surface between liquid and vapour, and of a distribution function $g^{(2)}(R)$ which is the same in both phases and near the surface. The approximation of a discontinuous change between phases may be acceptable at 90°K, but clearly becomes less accurate as the temperature approaches the critical point. Kirkwood and Buff (1949) took no account of the vapour phase in their computations, and the inclusion of a term for the effect of the vapour in calculating $\gamma(c)'$ still ignores the surface transition region. We believe that this neglect of the transition zone is probably the main reason for the poor agreement between theory and experiment at the higher temperatures. The assumption that $g^{(2)}(R)$ is uniform throughout the system should be more satisfactory for those temperatures approaching T_c where the effect of the vapour phase becomes most important.

Attempts were made to compute the effect of an exponential type of transition zone, using the theory of Kirkwood and Buff, but the corrected values for surface tension were higher than those calculated for a discontinuous change, and thus resulted in poorer agreement with experiment. A comment should be made concerning attempts to improve agreement between theory and experiment for both γ and E. In our calculations we have found $\gamma_{\text{theor}} > \gamma_{\text{exp}}$ and $E_{\text{theor}} < E_{\text{exp}}$ at all three temperatures. If agreement between γ_{theor} and γ_{exp} is improved, then the value of $d\gamma_{\text{theor}}/dT$ must be increased in order that γ_{theor} should still vanish at T_c. It follows that, if E_{theor} obeys relation (7), values of E_{theor} must be decreased, and agreement with experiment for E is thus worsened. A possible reason for this discrepancy would appear to be the assumption in calculating E_{theor} that the dividing surface may be chosen so as to make $\Gamma_s^{(1)}$ vanish, and more reliable values should result from the use of relation (7) in deriving E_{theor}.

§ 7. CONCLUSION

Phenomenological relations such as Ferguson's equation (1) can describe well the variation with temperature of the surface tensions of liquid argon and nitrogen. The position with regard to theoretical computations of surface tension is, however, not so satisfactory; agreement with experiment is reasonably good at low temperatures, but becomes much worse at temperatures approaching T_c.

It appears likely that this poor agreement arises mainly from inadequacies in our knowledge of the surface transition zone.

ACKNOWLEDGMENTS

It is a pleasure to acknowledge the help and encouragement given by Dr. E. B. Mendoza, Dr. L. C. Jackson, and other members of the laboratory during this work, which was supported by the award of a maintenance grant from the Department of Scientific and Industrial Research.

REFERENCES

BALY, E. C. C., and DONNAN, F. G., 1902, *J. Chem. Soc.*, **81**, 907.
DORSEY, N. E., 1926, *Sci. Pap. Nat. Bur. Stand., Wash.*, **21**, **563**.
EISENSTEIN, A., and GINGRICH, N. H., 1942, *Phys. Rev.*, **62**, 261.
FERGUSON, A., and KENNEDY, S. J., 1936, *Trans. Faraday Soc.*, **32**, 1474.
GILMONT, R., 1951, *Analyt. Chem.*, **23**, 157.
GUGGENHEIM, E. A., 1945, *J. Chem. Phys.*, **13**, 253.
JANSEN, J., and DAWSON, L. M., 1955, *J. Chem. Phys.*, **23**, 482.
JONES, W. J., and BOWDEN, S. T., 1946, *Phil. Mag.*, **37**, 480.
KIRKWOOD, J. G., and BUFF, F. P., 1949, *J. Chem. Phys.*, **17**, 338.
MACLELLAN, A. G., 1952, *Proc. Roy. Soc.* A, **213**, 274.
MACLEOD, D. L. B., 1923, *Trans. Faraday Soc.*, **19**, 38.
MATHIAS, E., ONNES, H. K., and CROMMELIN, C. A., 1912, *Leiden Comm.* 131 (a) ; 1914, *Leiden Comm.* 145 (c).
MICHELS, A., WIJKER, HUB, and WIJKER, H. K., 1949, *Physica*, **15**, 627.
NEWITT, D. M., 1940, *Design of High Pressure Plant* (Oxford : University Press), p. 92.
RUDORF, G., 1909, *Ann. Phys., Lpz.* (4), **29**, 751.
RUSHBROOKE, G. S., and SCOINS, H. I., 1951, *Phil. Mag.*, **42**, 582.
SUGDEN, S., 1921, *J. Chem. Soc.*, **119**, 1483.
YVON, J., 1948, *Colloque de Thermodynamique*, Bruxelles.
ZWANZIG, R. W., KIRKWOOD, J. G., STRIPP, K. F., and OPPENHEIM, I., 1953, *J. Chem. Phys.*, **21**, 1268.

Solid Solution in Zinc Blende Type $A_2^{III}B_3^{VI}$ Compounds

By J. C. WOOLLEY and B. A. SMITH
Department of Physics, University of Nottingham

Communicated by L. F. Bates; MS. received 2nd June 1958, *and in final form* 1*st August* 1958.

Abstract. Ranges of solid solution have been investigated in systems composed of either two $A_2^{III}B_3^{VI}$ compounds or one $A^{III}B^{V}$ and one $A_2^{III}B_3^{VI}$ compound. It is found that in practically all cases considered complete solid solution throughout the whole range of composition can be obtained, but that in some cases this equilibrium condition can only be reached under special conditions of temperature and time of annealing. The possibility of ordering and of the occurrence of low temperature miscibility gaps is investigated.

---

§ 1. INTRODUCTION

THE work on zinc blende type semiconducting compounds has been concerned mainly with the $A^{III}B^{V}$ and the $A^{II}B^{VI}$ compounds. Another group of compounds possessing zinc blende structure on which much less work has been done is the $A_2^{III}B_3^{VI}$ group. Compounds of this composition which take the zinc blende structure do so by leaving vacant every third site on the A sublattice (Hahn and Klingler 1949). Under normal conditions of preparation the vacancies are distributed at random throughout the A sublattice. It has been shown by various workers that it is possible in certain cases to cause the vacancies to order on the lattice. This can be achieved in the case of Ga_2Se_3, Ga_2Te_3 and In_2Te_3 by normal annealing of the solid (Hahn 1952), but only after very long periods of annealing. But Inuzuka and Sugaike (1954) have shown that in the case of In_2Te_3 the use of the Stockbarger double furnace technique produces crystals which have the vacancies ordered, giving a superlattice which remains cubic but with a three-fold increase in lattice parameter compared with the disordered structure.

The measurements of the electrical properties of these compounds are very limited. Appel (1954) and Sugaike (1957) investigated In_2Te_3 and showed that the resistivity is very high at room temperature, and has a negative temperature coefficient, from which Sugaike calculated an energy gap of 1·15 ev. Data on electrical properties of the other compounds do not seem to have been obtained.

As has been indicated in the case of $A^{III}B^{V}$ compounds (Woolley and Smith 1958, to be referred to as I) the occurrence of solid solution between various compounds is of interest both from the academic and also from the technological point of view in that it appears probable that a range of physical properties intermediate between those of the compounds can be obtained. Although the $A_2^{III}B_3^{VI}$ compounds have not as yet been investigated to any great extent, ranges of solid solution in this type of compound are of interest if the variation of physical properties with solid solution in semiconducting compounds is to be investigated.

Data on solid solution in zinc blende type $A_2^{III}B_3^{VI}$ compounds at present published appears to be limited to the papers by Goryunova (1955) and Goryunova and Grigor'eva (1957). In the first, it is indicated that a considerable range of solid solution occurs in the systems Ga_2Te_3–In_2Te_3, GaAs–Ga_2Se_3, ZnSe–Ga_2Se_3 and ZnTe–Ga_2Te_3, although no further details are given. In the second paper, some details of the system GaAs–Ga_2Se_3 are given. Solid solution is obtained over a wide range of composition at each end of the diagram, but there is a range of some 20% around the composition 2GaAs.3Ga_2Se_3 where the structure seems uncertain, and the x-ray photograph shows extra lines in addition to those of the zinc blende structure. The variation of electrical conductivity with composition is found, however, to show a smooth monotonic curve throughout the whole range of composition.

Some further data on possible solid solution in these compounds is given by the work of Busch, Mooser and Pearson (1956) on compounds of the form $ZnIn_2Te_4$ etc. It is stated that the compounds are not limited to the stoichiometric composition and this variation represents a range of solid solution in the systems ZnTe–In_2Te_3 etc.

In the present paper, work is described investigating the range of solid solution which can be obtained in systems formed between two zinc blende type $A_2^{III}B_3^{VI}$ compounds and also in mixed systems between these compounds and $A^{III}B^{V}$ compounds.

§ 2. METHOD

The method used was that used by the authors in investigating $A^{III}B^{V}$ alloys (I). The alloys were made by sealing the required quantities of the appropriate compounds in evacuated quartz tubes, heating to a temperature above the melting point of the higher melting point compound and quenching in water. In the case of the compounds themselves, the antimonides, tellurides and selenides were made in a similar way, while the arsenides were kindly provided by the Services Electronics Research Laboratory, Baldock.

Each alloy was powdered and x-rayed and then compressed, resealed *in vacuo*, annealed at a temperature somewhat lower than the melting point of the lower melting point compound for approximately a week and then x-rayed again. The results of the x-ray photographs then determined the further treatment of the alloy. In some systems, where one component was an $A^{III}B^{V}$ compound, the diffusion rates were again very low and long annealing at progressively higher temperatures was necessary to attain equilibrium, as has been described for the $A^{III}B^{V}$ systems (I). In other cases, however, the presence of the $A_2^{III}B_3^{VI}$ compound, with its vacant lattice sites, produced very much higher diffusion rates and the quenched alloy was found to be very close to an equilibrium condition. In all cases, the equilibrium conditions were determined by means of x-ray photographs taken with a 9 cm powder camera using Cu Kα radiation.

Owing to the problems involved in analysis of these materials, analysis of the specimens after annealing was not carried out, and the quoted compositions are the initial amounts of component used in each case. This necessitated care to prevent loss of components in the various processes involved; for example the specimens were always sealed under vacuum in relatively small quartz containers, and heated only under these conditions. The relative agreement of the various results for a given system despite the differences in composition, in times and temperatures of annealing and in the total weight of the various specimens, the constancy of parameter with further annealing once equilibrium was reached, and the absence of extra lines on the X-ray photograph could all be used as a check on the problem of possible loss of components.

It would appear that the method used to determine the solidus curve by X-ray means in the case of $A^{III}B^{V}$ alloys (I) cannot be used in many of the $A_2^{III}B_3^{VI}$ systems because of the much greater diffusion rates. A more fundamental objection to the method however became clear when it was found, as will be described later, that in several cases the systems concerned could not be treated as quasi-binary sections of the complete ternary system. Therefore, no such solidus determinations have been made for these materials.

When complete solid solution occurred in a system the possible existence of closed miscibility gaps was also investigated. This was done by bringing the specimen to a single phase equilibrium and then annealing for a suitable time at an appropriate lower temperature. Any break up of the single phase condition was taken to indicate the presence of a closed miscibility gap.

§ 3. Results

3.1. *Ga_2Te_3–In_2Te_3 System*

In this system, equilibrium was attained rapidly, the quenched alloys having a single phase appearance, although further annealing at 600°C for a week was carried out. Solid solution was obtained at all compositions throughout the alloy range, the alloys having the usual zinc blende structure. The variation of the lattice parameter with composition is shown in figure 1, the accuracy of the lattice parameter values being estimated to be to ± 0·002 Å. It is seen that although the graph is linear over a large range of composition, the lattice parameter in this range is some 0·01 Å greater than the Vegard value (i.e. that obtained by drawing a straight line between the parameter values for the two compounds concerned).

From the point of view of lattice parameter, the Ga_2Te_3–In_2Te_3 system seemed to be nearest to ideal solid solution of all the systems investigated here. However, thermal measurements (Woolley and Lees, to be published elsewhere), show that the solidus has a form which rules out the possibility of this diagram being treated as a quasi-binary section of the Ga–In–Te diagram.

No sign of a miscibility gap was observed at temperatures down to 500°C, nor was any sign of ordering observed in the system.

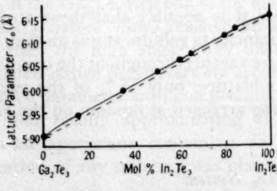

Figure 1. Variation of lattice parameter a_0 as a function of composition in the Ga_2Te_3–In_2Te_3 system.

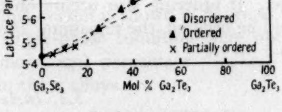

Figure 2. Variation of lattice parameter a_0 as a function of composition in the Ga_2Se_3–Ga_2Te_3 system.

3.2. *Ga_2Se_3–Ga_2Te_3 System*

The alloys were prepared as indicated previously, powdered and x-rayed, annealed for a short time at 775°c and x-rayed again. In the range of compositio 40–100 mol percentage Ga_2Te_3, the equilibrium condition was obtained o quenching, showing a single phase zinc blende structure. The alloys containing a high percentage of Ga_2Se_3, however, gave more complicated results. Alloys containing 5, 10, 15, 25 and 35 mol percentage Ga_2Te_3 respectively were investigated and, on quenching, all showed in x-ray photographs the broad lines apparently characteristic of a non-equilibrium condition. These therefore were further annealed at 775°c. In the case of the 25 and 35 mol percentage Ga_2Te_3 alloys, after further annealing for approximately four weeks, the x-ray photograph showed extra lines in addition to the normal zinc blende lines indicating the occurrence of ordering in these alloys. Analysis of these results indicated a tetragonal unit cell of approximate dimensions $a_0 \times a_0 \times 2a_0$, where a_0 is the cell parameter of the corresponding zinc blende lattice. In an attempt to estimate the ratio c/a for the 35% alloy, a value of 1·98 was obtained, but in neither of the alloys investigated could sufficiently sharp x-ray lines be obtained to enable an accurate determination to be made.

In the case of the 5, 10 and 15 mol percentage Ga_2Te_3 specimens, after two weeks annealing the x-ray photographs showed some sharp lines with others remaining very broad and diffuse. A further four weeks annealing made no difference to this condition. The blurring of the lines in this case was different from the effect described in the case of the InAs–In_2Te_3 alloys (described below), where splitting into two phases of very similar lattice parameter caused blurring of only the high Bragg angle lines. In the present case, the blurred lines occurred at all ranges of Bragg angle, i.e. in the typical zinc blende type photograph, the 111, 311, 331, 511 and 531 lines were blurred while the 220, 400, 422 and 440 lines were quite sharp. From this it appears that partial ordering is occurring in these alloys, this being the equilibrium condition. For further annealing at 775°c or at 700°c made no change in the x-ray photographs.

For all alloys a value of lattice parameter a_0 was calculated (in the case of the ordered alloys as defined above) and figure 2 shows the variation of this parameter with composition. It is seen that the graph is not linear, but intersects the Vegard line at 25 mol percentage Ga_2Te_3. This would appear to be the optimum composition for ordering to occur (Aptekar and Finkelstein 1951). Qualitative consideration of intensities indicated that the ordering was probably the same as that shown by chalcopyrite. This would require the ordering of one position in four on the sublattice A or B. The ratio of Te to Se at the 25 percentage composition satisfies this requirement, and it is possible that these atoms are concerned in the ordering. The ratio of vacancies to gallium atoms on the gallium sublattice remains at 1 : 2 (i.e. one site in three vacant) throughout the composition range. If ordering also occurs on this sublattice, only 75% of the vacancies would be ordered, the remaining 25% being arranged at random on the gallium sites.

3.3. *InAs–In_2Te_3 System*

The alloys were prepared as previously described, x-rayed, annealed for 1 week at 600°c and x-rayed again. It was found that, although all of the alloys appeared single phase on quenching, after annealing at 600°c, those alloys containing 50, 60 and 65 mol percentage In_2Te_3[†] gave x-ray photographs showing a small splitting of the high angle lines. In contrast to the effects observed with the Ga_2Se_3–Ga_2Te_3 alloys described above, in this case the splitting occurred in the high Bragg angle lines only, thus indicating the occurrence of two zinc blende type phases of slightly different lattice parameter. These alloys were therefore annealed at 680°c for a week and were found to have regained the single-phase condition. Thus again solid solution throughout the whole composition range is obtained. Figure 3 shows the variation of lattice parameter with composition.

The effect observed by annealing at 600°c indicates that a closed miscibility gap occurs in this case. To investigate it, all alloys were annealed at 520°c for approximately three weeks. Splitting of the x-ray lines was observed on the alloys containing 50, 60 and 65 mol percentage In_2Te_3 but not in those containing 15, 35 or 85 mol percentage In_2Te_3, so giving a rough indication of the range of the miscibility gap at 520°c. It was not possible, however, to determine the range of the miscibility gap by normal extrapolation methods, as the splitting was small, the high angle x-ray lines being blurred rather than completely split, and moreover the splitting appears to be different in the three alloys concerned. This indicates that the tie-lines in this field do not coincide with the plane of the section, and hence as in the case of Ga_2Te_3–In_2Te_3, this diagram cannot be treated as quasi-binary.

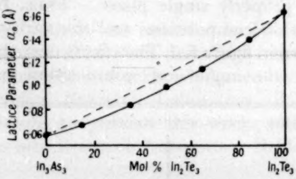

Figure 3. Variation of lattice parameter a_0 as a function of composition in the $InAs$–In_2Te_3 system.

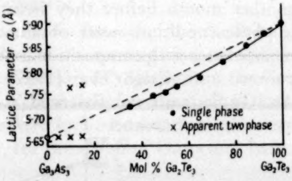

Figure 4. Variation of lattice parameter a_0 as a function of composition in the $GaAs$–Ga_2Te_3 system.

3.4. *GaAs–Ga_2Te_3 System*

In this system, all alloys investigated appeared to have very low diffusion rates, and the process of long anneal at progressively higher temperatures had to be used. This was particularly the case at the GaAs rich end of the diagram. Even at the Ga_2Te_3 rich end of the diagram, annealing for at least two months was necessary before alloys reached an approximately single-phase condition, and even then the high angle x-ray lines were still broad and diffuse. Thus the calculated lattice parameters are accurate only to some ± 0·004 Å. The variation of lattice parameter with composition for this system is shown in figure 4. It is seen that results approximating to the single-phase condition were obtained with all specimens containing 35 or more mol percentage Ga_2Te_3. No indication of any ordering was observed in these alloys.

[†] In calculating mol percentage in all systems composed of one $A^{III}B^{V}$ compound and one $A_2^{III}B_3^{VI}$ compound, the molecules have been taken as $A_3^{III}B_3^{V}$ and $A_2^{III}B_3^{VI}$, i.e. the percentage is strictly the percentage of B^{V} and B^{VI} on the B sublattice.

Specimens containing 5, 10 and 15 mol percentage Ga_2Te_3 respectively were not, however, brought to the single phase state. Progressive annealing left these alloys in an apparent two phase condition even when the annealing temperature was raised to 1000°c. The lattice parameters corresponding to these phases are shown in figure 4. Since this condition did not seem to change with annealing at different temperatures, it is possible that this represents a miscibility gap in the system. Bearing in mind, however, the difficulties in the case of $A^{III}B^{V}$ compounds described previously (I), it is possible that this two phase condition is due only to the fact that the diffusion rates were insufficient to attain equilibrium at the temperatures used. The spread in the lattice parameters of the two phases compared with those of the single phase alloys nearer the centre of the composition range show that if this is indeed equilibrium two phase behaviour, once again this section cannot be treated as quasi-binary. Thus, the range of composition of a miscibility gap cannot be determined by the normal extrapolation methods.

3.5. *GaAs–Ga_2Se_3 System*

The rate of approach to equilibrium in this case was not as slow as in the previous system, but considerably slower than for the other systems considered here. All of the alloys after quenching were annealed at 900°c. After annealing for one month, the alloys at the Ga_2Se_3 rich end of the diagram had reached a single phase condition, but the GaAs rich alloys required annealing at 900°c for another month before they became properly single phase. Thus, finally, single phase conditions were obtained at all compositions and the variation of lattice parameter with composition is shown in figure 5. The effects described by Goryunova and Grigor'eva (1957) in the region of composition around $2GaAs.3Ga_2Se_3$ were not observed.

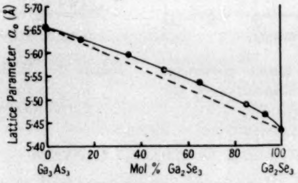

Figure 5. Variation of lattice parameter a_0 as a function of composition in the GaAs–Ga_2Se_3 system.

The graph shows considerable deviation from the Vegard line at the Ga_2Se_3 rich end of the diagram. With this type of curve, the occurrence of a closed miscibility gap was possible, but although alloys were annealed for six weeks at 800°c and at 725°c in neither case was any deviation from the single phase condition observed. Once again, this result cannot be considered conclusive because of the low diffusion rates occurring in these alloys. Again no indication of ordering was observed in any of the alloys.

3.6. *InSb–In_2Te_3, GaSb–Ga_2Te_3 and GaSb–Ga_2Se_3 Systems*

In each of these systems only the 50:50 alloy was investigated. In each case, when the molten alloy had been quenched and x-rayed, the photograph obtained was very complex, having a large number of lines. It appears that in alloys containing antimony the zinc blende structure is lost and other, more complex, structures are formed. These systems have not therefore been investigated further.

§ 4. CONCLUSIONS

The results are very similar to those obtained for the $A^{III}B^{V}$ systems, in that in many cases a large range of solid solution occurs, in some cases there being complete solid solution throughout the whole range of composition. Solid solution between $A^{III}B^{V}$ and $A_2^{III}B_3^{VI}$ compounds appears to take place when the $A^{III}B^{V}$ compound is an arsenide but not in the case of antimonides when other structures are formed. In many cases, it appears that the section cannot be treated as quasi-binary.

These ranges of solid solution should provide useful sources of experimental data when theories of semiconducting alloys are being considered and it is hoped to investigate the variation of such parameters as energy gap, conductivity etc. as a function of composition in various systems. An additional factor of interest in the $A_2^{III}B_3^{VI}$ compounds is the presence of lattice vacancies and their resulting effects. These can be systematically filled by alloying with $A^{III}B^{V}$ compounds, and can also be ordered, possibly in more than one way, if suitable alloys are chosen.

ACKNOWLEDGMENTS

The authors are indebted to Professor L. F. Bates for the facilities of his laboratory. The work described forms part of an investigation carried out for the Admiralty and acknowledgment is made to Dr. O. Simpson of the Services Electronics Research Laboratory, Baldock, for helpful discussions, and for permission to publish this work, and to Mr. J. T. Edmond of the Services Electronics Research Laboratory, Baldock, for provision of GaAs and InAs.

REFERENCES

APPEL, J., 1954, *Z. Naturf.*, **99**, 265.
APTEKAR, A. I., and FINKELSTEIN, B. N., 1951, *J. Exp. Theor. Phys.*, **21** (8), 900.
BUSCH, G., MOOSER, E., and PEARSON, W. B., 1956, *Helv. Phys. Acta*, **29**, 192.
GORYUNOVA, N. A., 1955, *Problems in the Theory, Investigation and Metallurgy of Semiconductors* (*Izv. Akad. Nauk SSSR, Moscow*).
GORYUNOVA, N. A., and GRIGOR'EVA, V. S., 1957, *Sov. Phys. Tech. Phys.*, **1**, 2094.
HAHN, H., 1952, *Angew. Chem.*, **64**, 203.
HAHN, H., and KLINGER, W., 1949, *Z. anorg. Chem.*, **260**, 97.
INUZUKA, H., and SUGAIKE, S., 1954, *Proc. Imp. Acad. Japan*, **30**, 383.
SUGAIKE, S., 1957, *Mineral J.* (*Japan*), **2**, 63.
WOOLLEY, J. C., and SMITH, B. A., 1958, *Proc. Phys. Soc.*, **72**, 214.

Eigenphaseshifts in terms of Wigner's Nuclear Reaction Theory

BY L. C. BIEDENHARN[†] AND H. B. WILLARD[‡]
† University of Manchester
‡ Oak Ridge National Laboratory

MS. received 14*th August* 1958

Abstract. Eigenphaseshifts and eigenvectors of the nuclear scattering are constructed from the Wigner many level approximation, after separation of the potential scattering. The two level case is discussed in detail, and a simple approximation based upon the eigenphaseshift formalism is suggested.

THERE are two quite different ways in which one may give a general description or more accurately, a parametrization, of nuclear reactions; one method is to utilize the parameters of Wigner's nuclear reaction theory (references to the extensive literature on this theory may be found in a recent review by Lane and Thomas (1958)), the partial reduced widths $\gamma_{\lambda c}$ and the energy levels E_λ; the other method employs the parametrization of the scattering matrix in terms of its eigenphaseshifts and (real) eigenvectors[§] (Blatt and Biedenhарn 1952). This latter procedure is a natural extension of the phase-shift description in spinless particle elastic scattering, and is particularly suited to a discussion of the angular distributions.

It is of interest to enquire how these two parametrizations are related. Except for the elastic scattering of spinless particles (where the relation is trivial), the question is, however, rather too broad to admit of a practical answer, for the potential scattering greatly complicates the problem. One can avoid this difficulty by explicitly separating the nuclear and potential parts of the scattering matrix: that is, following the notation of Lane and Thomas (1958),

$$1-\mathbf{S}=(1-\boldsymbol{\Omega}^2)+\boldsymbol{\Omega}\mathbf{P}^{1/2}[1-(1-\mathbf{RL})^{-1}(1-\mathbf{RL}^*)]\mathbf{P}^{-1/2}\boldsymbol{\Omega} \quad \ldots\ldots(1\,a)$$

$$\equiv(1-\mathbf{S}_{\text{pot}})+\boldsymbol{\Omega}(1-\mathbf{S}_{\text{nuclear}})\boldsymbol{\Omega}, \quad \ldots\ldots(1\,b)$$

where the latter equation constitutes a definition of the potential and nuclear contributions. The nuclear part of the scattering $\mathbf{S}_{\text{nuclear}}$ is now seen to admit of the same parametrization as the scattering matrix itself, that is,

$$\mathbf{S}_{\text{nuclear}}=\tilde{\mathbf{u}}(\exp 2i\boldsymbol{\delta})\mathbf{u}, \quad \ldots\ldots(2)$$

where $\mathbf{u}$ is real and orthogonal (the eigenvector matrix) and $\boldsymbol{\delta}$ is real and diagonal (the eigenphaseshift matrix). The differential cross sections that result from this formulation are readily found using the methods of Blatt and Biedenharn (1952), and need not be given[‖] here. The problem of obtaining these nuclear scattering quantities in terms of the Wigner theory can now be solved explicitly in terms of the Wigner many-level expansion (Wigner 1946); the object of the present note is to detail this solution.

[†] Fulbright Fellow 1958, on sabbatical leave from The Rice Institute, Houston, Texas.

[§] We shall assume here that the scattering matrix is unitary and symmetric. Both features may be lost if time-reversal invariance does not hold; see e.g. Phillips (1958) and references quoted there.

[‖] Formulae for neutron induced processes are given in detail by Fowler and Marion (1959, chap. V).

The Wigner n-level expansion approximates the complete $\mathbf{R}$ matrix by†:

$$\mathbf{R} \simeq \mathbf{R}_n \equiv \sum_{\lambda=1}^{n} \frac{\boldsymbol{\gamma}_\lambda \times \boldsymbol{\gamma}_\lambda}{E_\lambda - E}. \qquad \ldots\ldots(3)$$

The determinant of $\mathbf{R}_n$ vanishes if $n < N$ (the number of channels) or if the number of linearly independent $\boldsymbol{\gamma}_\lambda$ is less than N, as can be seen directly from the special form of the $\mathbf{R}$ matrix. In practice, n is generally chosen less than the number of channels; moreover, we shall assume all the $\boldsymbol{\gamma}_\lambda$ to be linearly independent. It follows from (2), and the definition of $\mathbf{S}_{\text{nuclear}}$ (eqn. (1*b*)), that $N-n$ of the eigenphaseshifts are zero. (If some of the $\boldsymbol{\gamma}_\lambda$ are linearly dependent the number of zero eigenphaseshifts is correspondingly greater.) As a result only n eigenvectors have any effect in the nuclear scattering.

The n-level expansion obtains a solution to the inversion $(1-\mathbf{RL})^{-1}\mathbf{R}$ in the form

$$(1-\mathbf{RL})^{-1}\mathbf{R} = \sum_{i,\,j=1}^{n} \boldsymbol{\gamma}_i \times \boldsymbol{\gamma}_j A_{ij}, \qquad \ldots\ldots(4\,a)$$

where

$$\mathbf{A}^{-1} = \overline{\mathbf{E}} - E\mathbf{1} + \xi \qquad \ldots\ldots(4b)$$

$$\xi_{ij} = \xi_{ji} \equiv \boldsymbol{\gamma}_i \,.\, \mathbf{L} \,.\, \boldsymbol{\gamma}_j = -\tfrac{1}{2} i\Gamma_{ij} + \Delta_{ij} \qquad \ldots\ldots(4\,c)$$

$$\overline{E}_{ij} = \delta_{ij} E_i. \qquad \ldots\ldots(4\,d)$$

(The matrices in equations (4 *b*, *c*, *d*) are $n \times n$.)

Using equations (1*b*), (2) and (4), one finds that

$$\sum_{ij} (\mathbf{P}^{1/2}\boldsymbol{\gamma}_i) \times (\mathbf{P}^{1/2}\boldsymbol{\gamma}_j) A_{ij} = \tilde{\mathbf{u}}(\exp i\boldsymbol{\delta} \sin \boldsymbol{\delta})\mathbf{u}. \qquad \ldots\ldots(5)$$

The vectors, $\mathbf{P}^{1/2}\boldsymbol{\gamma}_i \equiv \mathbf{v}_i$, may be expressed in terms of the eigenvectors $\mathbf{u}^{(k)}$ (which are orthonormal, i.e.

$$\mathbf{u}^{(k)} \,.\, \mathbf{u}^{(k')} = \sum_c u_c^{(k)} u_c^{(k')} = \delta_{kk'}).$$

Thus we may write

$$\mathbf{v}_i = \mathbf{P}^{1/2}\boldsymbol{\gamma}_i = \sum_k w_{ik} \mathbf{u}^{(k)}. \qquad \ldots\ldots(6)$$

(Note that the w_{ik} are not square but rectangular matrices—since i runs over the n levels ($n < N$) whereas k runs over the N channels.) Introducing this into equation (5) we find

$$\sum_{\substack{kk'\\ ij}} \mathbf{u}^{(k)} \times \mathbf{u}^{(k')} w_{ik} A_{ij} w_{jk'} = \tilde{\mathbf{u}}(\exp i\boldsymbol{\delta} \sin \boldsymbol{\delta})\mathbf{u}$$

$$= \sum_k \mathbf{u}^{(k)} \times \mathbf{u}^{(k)} \exp i\boldsymbol{\delta}^{(k)} \sin \boldsymbol{\delta}^{(k)}, \qquad \ldots\ldots(7)$$

and thus,

$$\sum_{ij} w_{ik} A_{ij} w_{jk'} = \delta_{kk'} \exp i\boldsymbol{\delta}^{(k)} \sin \boldsymbol{\delta}^{(k)}. \qquad \ldots\ldots(8)$$

A solution to these equations can be obtained by noting that $w_{ik} = 0$ (and $\delta^{(k)} = 0$) for k not in the set $1, \ldots, n$. We restrict attention only to this range of values, and for this range the w_{ik} are now *square* matrices. The problem to be solved is then the $n \times n$ matrix problem:

---

† More generally one adds an energy-independent background $\mathbf{R}$ matrix, $\mathbf{R}^{(\infty)}$, to the right-hand side of (3). The changes caused by non-zero $\mathbf{R}^{(\infty)}$ (cf. Lane and Thomas 1958) affect the present work only in details for the usual case where $\mathbf{R}^{(\infty)}$ is assumed diagonal.

$$\tilde{\mathbf{w}}\mathbf{A}\mathbf{w} = \exp i\boldsymbol{\delta} \sin \boldsymbol{\delta}. \qquad \ldots\ldots (9)$$

Introducing the definition of $\mathbf{A}$ (eqn. (4*b*)), and taking the real and imaginary parts separately one finds

$$\bar{\mathbf{E}} + \Delta - E\mathbf{1} = \mathbf{w}(\cot \boldsymbol{\delta})\tilde{\mathbf{w}} \qquad \ldots\ldots (10a)$$

$$\tfrac{1}{2}\boldsymbol{\Gamma} = \mathbf{w}\tilde{\mathbf{w}}. \qquad \ldots\ldots (10b)$$

Since both $\bar{\mathbf{E}} + \Delta$ and $\boldsymbol{\Gamma}$ are symmetrical and real we may write them in the form:

$$\bar{\mathbf{E}} + \Delta = \mathbf{U}\boldsymbol{\epsilon}\tilde{\mathbf{U}} \qquad \ldots\ldots (11a)$$

$$\tfrac{1}{2}\boldsymbol{\Gamma} = \mathbf{V}\mathbf{g}^2\tilde{\mathbf{V}}, \qquad \ldots\ldots (11b)$$

where $\mathbf{U}$, $\mathbf{V}$ are real and orthogonal and $\boldsymbol{\epsilon}$ and $\mathbf{g}^2$ are real and diagonal. (The diagonal values of $\mathbf{g}^2$ are positive from the Schwarz inequality.)

The general solution for $\mathbf{w}$ is then

$$\mathbf{w} = \mathbf{V}\mathbf{g}\mathbf{W}, \qquad \ldots\ldots (12)$$

with $\mathbf{W}$ real and orthogonal. The final result is then

$$\mathbf{g}^{-1}\tilde{\mathbf{V}}\mathbf{U}(\boldsymbol{\epsilon} - E\mathbf{1})\mathbf{U}\mathbf{V}\mathbf{g}^{-1} = \tilde{\mathbf{W}}(\cot \boldsymbol{\delta})\tilde{\mathbf{W}}. \qquad \ldots\ldots (13)$$

Equation (13) *is the desired matrix formulation for the spectral parameters of the scattering.* One notes that all the matrices on the left are known while those on the right are to be determined. Since the left side is real and symmetric, the problem is once again a diagonalization just as in the determination of $\mathbf{U}$ and $\mathbf{V}$ in equation (11).

Before we discuss some examples of the above procedure, it is of interest to note that this result is useful in discussing the question of what constitutes a resonance. There are at least two different definitions in the literature, each with advantages and disadvantages. The most natural definition would seem to be that a resonance energy is defined as that energy for which an eigenphaseshift has the value $\pi/2 + k\pi$. This is a generalization of the familiar spinless-particle elastic-scattering result. Although this definition seems reasonable enough, it suffers from the fact that the potential scattering phase shifts make any determination of the eigenphaseshifts in terms of the Wigner parameters a difficult task, as mentioned earlier. Consequently, a different definition of a resonance level has been introduced: a resonance energy is defined as that energy for which the eigenphaseshifts assume the value $\pi/2 + k\pi$, *with the potential scattering set equal to zero*. (These phaseshifts are just those obtained in equation (13) above.) The advantage of this definition is that these resonance energies are directly related to the poles of the $\mathbf{R}$ matrix.†

The disadvantage of this definition is that the resonance so defined may not appear as maxima in the cross sections, the point at issue being that the split into potential and resonance scattering is not well defined physically. Nevertheless, this definition is in common usage; in the one-level expansion it agrees with the usual resonance energy of the Breit–Wigner dispersion shape. In order to apply this latter definition to the Wigner n-level expansion it is necessary to put the nuclear scattering into the spectral form. The results obtained above show that *the resonance energies are just the zeros of the determinant of* $(\overline{\mathbf{E}} - E\mathbf{1} + \Delta)$.

---

† At least for the one-dimensional case, where a proof has been given by Thomas (Lane and Thomas 1958), that the resonance energies are in a one-to-one correspondence with the poles of the derivative **R** function.

The one-level approximation is the simplest example for applying equation (13), and all of the matrix manipulations are unnecessary. The eigenphaseshift is just

$$\cot \delta_1 = 2(E_1 + \Delta - E)\Gamma^{-1}, \qquad \ldots\ldots (14\,a)$$

while the eigenvector $\mathbf{u}^{(1)}$ is given by

$$\mathbf{u}^{(1)} = (2/\Gamma)^{1/2}\boldsymbol{\gamma}. \qquad \ldots\ldots (14\,b)$$

The two-level approximation is not so straightforward. The diagonalization of the $\frac{1}{2}\boldsymbol{\Gamma}$ and $\overline{\mathbf{E}} + \Delta$ matrices leads to

$$\mathbf{U} = \begin{pmatrix} \cos\phi & -\sin\phi \\ \sin\phi & \cos\phi \end{pmatrix} \qquad \tan 2\phi = \frac{2\Delta_{12}}{\Delta_{11} - \Delta_{12}} \qquad \ldots\ldots (15\,a)$$

$$\mathbf{V} = \begin{pmatrix} \cos\theta & -\sin\theta \\ \sin\theta & \cos\theta \end{pmatrix} \qquad \tan 2\theta = \frac{2\Gamma_{12}}{\Gamma_{11} - \Gamma_{22}} \qquad \ldots\ldots (15\,b)$$

$$\mathbf{g} = \begin{pmatrix} g_{\mathrm{a}} & 0 \\ 0 & g_{\mathrm{b}} \end{pmatrix},\ g_{\mathrm{a},\,\mathrm{b}}^{2} = \tfrac{1}{4}[\Gamma_{11} + \Gamma_{22} \pm \sqrt{\{(\Gamma_{11} - \Gamma_{22})^2 + 4\Gamma_{12}^{2}\}}] \equiv \tfrac{1}{2}\Gamma_{\mathrm{a},\,\mathrm{b}} \qquad \ldots\ldots (15\,c)$$

$$\boldsymbol{\epsilon} = \begin{pmatrix} \epsilon_{\mathrm{a}} & 0 \\ 0 & \epsilon_{\mathrm{b}} \end{pmatrix},\ \epsilon_{\mathrm{a},\,\mathrm{b}} = \tfrac{1}{2}[E_{11} + \Delta_{11} + E_{22} + \Delta_{22} \pm \sqrt{\{(E_{11} + \Delta_{11} - E_{22} - \Delta_{22})^2 + 4\Delta_{12}^{2}\}}]. \qquad \ldots\ldots (15\,d)$$

One notes the tendency of both the diagonal widths and energy values to be 'pushed apart' by the coupling through Γ_{12} and Δ_{12}. This is, in fact, just the example for the resonance energies given by Wigner (Proceedings of the International Conference on Neutron Interactions with the Nucleus, Columbia Univ., September (1957), reported in TID–7574, p. 49) in discussing neutron resonance level spacings.

The solution for the two eigenphaseshifts is rather complicated:

$$\begin{aligned}\cot\delta_{\mathrm{a},\,\mathrm{b}} = \tfrac{1}{2}\Bigg[&\left(\frac{1}{\Gamma_{\mathrm{a}}} + \frac{1}{\Gamma_{\mathrm{b}}}\right)(\epsilon_{\mathrm{a}} + \epsilon_{\mathrm{b}} - 2E) + \left(\frac{1}{\Gamma_{\mathrm{a}}} - \frac{1}{\Gamma_{\mathrm{b}}}\right)(\epsilon_{\mathrm{a}} - \epsilon_{\mathrm{b}})\cos 2(\phi - \theta) \\ &\pm\left\{\left[\left(\frac{1}{\Gamma_{\mathrm{a}}} + \frac{1}{\Gamma_{\mathrm{b}}}\right)(\epsilon_{\mathrm{a}} + \epsilon_{\mathrm{b}} - 2E) + \left(\frac{1}{\Gamma_{\mathrm{a}}} - \frac{1}{\Gamma_{\mathrm{b}}}\right)(\epsilon_{\mathrm{a}} - \epsilon_{\mathrm{b}})\cos 2(\phi - \theta)\right]^2 \right. \\ &\left. - 4\,\frac{(\epsilon_{\mathrm{a}} - E)\,(\epsilon_{\mathrm{b}} - E)}{\Gamma_{\mathrm{a}}\Gamma_{\mathrm{b}}}\right\}^{1/2}\Bigg] \qquad \ldots\ldots (16\,a)\end{aligned}$$

$$\tan 2\chi = \frac{(\epsilon_{\mathrm{a}} - \epsilon_{\mathrm{b}})\,2\sin^2(\phi - \theta)}{(\Gamma_{\mathrm{a}}^{-1} - \Gamma_{\mathrm{b}}^{-1})(\epsilon_{\mathrm{a}} + \epsilon_{\mathrm{b}} - 2E) + (\Gamma_{\mathrm{a}}^{-1} + \Gamma_{\mathrm{b}}^{-1})(\epsilon_{\mathrm{a}} - \epsilon_{\mathrm{b}})\cos 2(\phi - \theta)} \qquad \ldots\ldots (16\,b)$$

where

$$\mathbf{W} = \begin{pmatrix} \cos\chi & -\sin\chi \\ \sin\chi & \cos\chi \end{pmatrix}.$$

The general behaviour of these results is that the cotangent of each eigenphase has but a single zero ('resonance'), and is constrained such that $\cos\delta_{\mathrm{a}} \neq \cot\delta_{\mathrm{b}}$ anywhere. The mixing accomplished by $\mathbf{W}$ has a single pole for $\tan 2\chi$. Although the energy derivative of the two eigenphases is always positive (neglecting the energy variation of the external parameters), the complicated form of equation (16 *a*) seems to indicate that $\tan\delta_{\mathrm{a},\,\mathrm{b}}$ does not have the form of a Wigner *R*-function.

The results for the two-level case are so complicated as to seem rather impracticable of application. There is a possibility of remedying this for it will be noted that if $\phi=\theta$ then $\mathbf{W}=1$ and $\cos\delta_{\mathrm{a}}=2(\epsilon_{\mathrm{a}}-E)/\Gamma_{\mathrm{a}}$, and similarly for $\cot\delta_{\mathrm{b}}$ with a$\longleftrightarrow$b. This simple case occurs naturally if Γ is diagonal and the boundary condition matrix, **b**, is set equal to $\mathscr{S}$ (the shift function matrix) so that $\Delta=0$. The boundary condition matrix, **b**, is however, at our disposal and it is advantageous so to choose the values of its elements b_c that we *require* $\phi=\theta$ at some energy, i.e. the condition is that

$$\frac{\Gamma_{12}}{\Gamma_{11}-\Gamma_{22}}=\frac{\Delta_{12}}{E_{11}+\Delta_{11}-E_{22}-\Delta_{22}}\,. \qquad \ldots\ldots(17)$$

(It is advantageous to choose the energy at which equation (17) is imposed so that when first-order effects are included, the pole in $\tan 2\chi$ is eliminated, i.e. $E_0=(\Gamma_{\mathrm{a}}E_{\mathrm{b}}-\Gamma_{\mathrm{b}}E_{\mathrm{a}})/(\Gamma_{\mathrm{b}}-\Gamma_{\mathrm{a}})$.

Although the b_c are indeed free parameters it must be remembered that the γ_λ, and E_λ, are implicit functions of b_c (Teichman and Wigner 1952). This dependence cannot be specified in any detailed way, but it would be most unlikely that one could not manage to fit equation (13) with the number of b_c available (at least 2).

More serious is this point†. If the energy shifts required by equation (13) are so large that the observed levels ϵ_{a}, ϵ_{b} are far from the levels E_{11}, E_{22} then we may have to reconsider the validity of the approximation (3). In practice, however, this difficulty should not arise, since the b_c required by equation (13) are of the order

$$b_c-\mathscr{S}_c\sim\frac{\epsilon_{\mathrm{a}}-\epsilon_{\mathrm{b}}}{\Gamma_{\mathrm{a}}-\Gamma_{\mathrm{b}}}\sim\frac{\Delta E}{\Gamma}$$

and this quantity must be of order unity or less in order that the levels interfere strongly. The non-interfering levels must then be at an energy separation from either ϵ_{a} or ϵ_{b} large compared with ΔE, which is not a stringent requirement, and means only that the two levels considered lie unusually close compared with the average level separation D.

The advantages of this choice of **b** are clear: the eigenphaseshifts are decoupled by this procedure, aside from a slight coupling through the energy dependence of the external functions. The mixing of the vectors $\mathbf{P}^{1/2}\boldsymbol{\gamma}_i$ to form the eigenvectors $\mathbf{u}_i$ is in the same approximation independent of energy. (The next approximation is straightforward to carry through.) *The general two-level case becomes then no more difficult to apply than two one-level cases having different values of* $J\pi$ but shows now coherent mixing in the total cross section.

One may view this result in an alternative, and more practical way. The end result of the Wigner theory is to establish the form, using the notation of Bloch (1957),

$$S=\mathrm{e}^{i\xi}\Big[1-i\sum_{s,t}\Big\langle s\Big|\frac{1}{\epsilon-E-\Delta+i\Gamma/2}\Big|t\Big\rangle\mathbf{G}_s\times\mathbf{G}_t\Big]\mathrm{e}^{i\xi} \qquad \ldots\ldots(18)$$

where all the parameters are real. In applications it is tempting simply to neglect the off-diagonal terms and use the 'many-level' formula

$$S=\mathrm{e}^{i\xi}\left[1-i\sum_s\frac{\mathbf{G}_s\times\mathbf{G}_s}{\epsilon-E_s-\Delta_s+i\Gamma_s/2}\right]\mathrm{e}^{i\xi}$$

which has no valid basis, and may lead to considerable error (Wigner 1946). Now one may diagonalize the result in equation (18) by a complex orthogonal transformation (Lane and Thomas 1958). This leads to

$$S=\mathrm{e}^{i\xi}\left[1-i\sum_s\frac{\overline{\mathbf{G}}_s\times\overline{\mathbf{G}}_s}{\epsilon-\bar{\epsilon}_s+i\Gamma_s/2}\right]\mathrm{e}^{i\xi}; \qquad \ldots\ldots(19)$$

---

† This question was raised by Dr. A. M. Lane.

where $\overline{\mathbf{G}}_s$ and $\overline{\epsilon}_s$ are now, unlike the Wigner result, both complex and energy dependent in a complicated way. The Kapur–Peierls (1938) treatment leads directly to the form of equation (19). For application to the case of separated resonances, and particularly so for angular distributions, the fact that the parameters of equation (19) are both complex and energy dependent is a handicap, at least comparable with the difficulties in applying equation (18). The results obtained above suggest that the eigenphaseshift formulation itself be considered as a basis for approximations to the nuclear scattering from interfering levels. In particular, for the two-level case, the resulting approximation is equivalent to the usual Wigner two-level case, and combines in effect the advantages associated with both equations (18) and (19).

Note added in proof. Scattering and reaction theory in terms of eigenphaseshifts and eigenvectors has recently been discussed, from a different point of view, by Y. Yamaguchi, to appear in *Supplement to Progress of Theoretical Physics (Japan)*.

ACKNOWLEDGMENT

The authors would like to thank Dr. A. M. Lane for his help and interest, and Dr. E. Vogt for his remarks on the manuscript.

REFERENCES

BLATT, J. M., and BIEDENHARN, L. C., 1952, *Rev. Mod. Phys.*, **24**, 258.
BLOCH, C., 1957, *Nucl. Phys.*, **4**, 503.
FOWLER, J. L., and MARION, J. B., Editors, 1959, *Fast Neutron Physics* (New York: Academic Press).
KAPUR, P. L., and PEIERLS, R. E., 1938, *Proc. Roy. Soc.* A, **166**, 277.
LANE, A. M., and THOMAS, R. G., 1958, *Rev. Mod. Phys.*, **30**, 257.
PHILLIPS, R. J. N., 1958, *Nuovo Cim.*, **8**, 265.
TEICHMAN, T., and WIGNER, E. P., 1952, *Phys. Rev.*, **87**, 123.
WIGNER, E. P., 1946, *Phys. Rev.*, **70**, 606.

The Photoproduction of π^0 Mesons at Helium

By P. PALIT and E. H. BELLAMY
Department of Natural Philosophy, University of Glasgow

MS. received 21st July 1958, and in final form 15th August 1958

Abstract. The elastic photoproduction of neutral mesons from helium has been studied at centre-of-mass angles of 70°, 90°, 115° and 135° for the meson in the photon energy range 220–320 Mev. The reaction has been identified by detecting the recoiling ^{4}He particles in a pair of gridded ionization chambers which discriminated against other particles by dE/dx and E measurements. The measured cross sections are compared with the predictions of an impulse approximation calculation with which they are in qualitative agreement. They are smaller by an order of magnitude than some of the previous measurements of this reaction.

§ 1. Introduction

Measurements of the elastic photoproduction of π^0 mesons at deuterium (Wolfe, Silverman and De Wire 1955, Davies and Corson 1955, Rosengren and Baron 1955) are consistent with the predictions of charge independence (Kemmer 1938) and the application of the impulse approximation (Chappelear 1955). Knowledge of the elastic photoproduction of mesons at helium, i.e. the reaction $\gamma + {}^4\text{He} \rightarrow \pi^0 + {}^4\text{He}$ in principle allows a test of the validity of applying the impulse approximation to a more tightly bound nucleus.

Earlier measurements on π^0 production at helium have been made by Goldwasser and Koester (1956) who measured the total π^0 production at 90° as a function of the maximum energy of the bremsstrahlung beam, and by de Saussure and Osborne (1955) who detected the recoil α-particles with photographic plates. The first of these methods measures the total elastic and inelastic production except at threshold where the inelastic production is zero and the elastic production alone may be measured. The second method did not distinguish between ^{3}He and ^{4}He particles, and while the ^{3}He particles arising from photodisintegration may be subtracted by a run with the maximum photon energy below 150 Mev, ^{3}He particles accompanying the production of negative and neutral pions cannot be subtracted. The measured cross sections are very much larger than those obtained by Goldwasser and Koester particularly for photon energies below 200 Mev. At higher photon energies, around 250 Mev, one would expect the inelastic production at 90° to predominate over the elastic production. There would thus appear to be a large discrepancy between the measurements made hitherto.

The present experiment detects the α-particle recoils in two gridded ionization chambers, and since the ^{3}He and ^{4}He particles are separated, these subtraction difficulties are eliminated.

§ 2. Apparatus

The apparatus is illustrated in figure 1. The photon beam passes through the helium gas at a pressure from 2 to 5 atmospheres, the recoil particles being detected by the gridded ionization chambers CD and GH in coincidence. The particles were recorded as spots on a cathode ray screen with the pulse heights from the ionization counters as cartesian coordinates. The positions of the spots were compared with calculated loci to give the mass and energy spectra of the particles. Polonium α-sources situated as shown were used to calibrate the counters. The effective target thickness and solid angle were obtained by numerical integration of $dt\,d\Omega$, where dt and $d\Omega$ are elements of target thickness and solid angle respectively, and were measured on a scale diagram of the apparatus. A detailed description of the apparatus and the analysis procedure is given by McWhirter, Palit and Bellamy (1958).

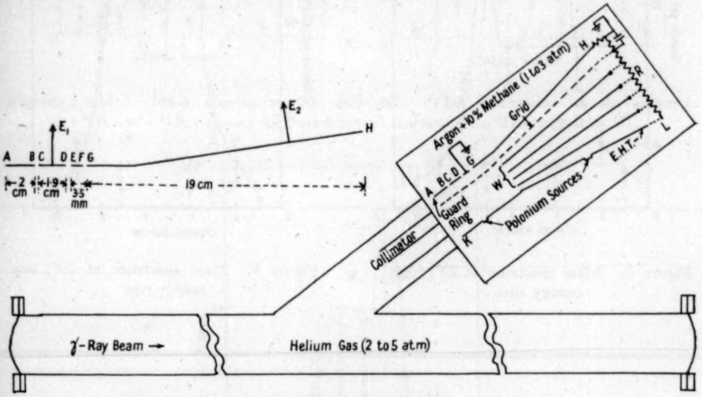

Figure 1. General layout of the apparatus (not to scale).

§ 3. EXPERIMENTAL DATA

Measurements were made of the yield of helium particles at laboratory angles of 20°, 30°, 40°, 50° and 90° to the beam, the pressures of the helium target and ionization chamber gas being varied between 2 and 5 atmospheres and 1 and 3 atmospheres respectively in order to measure α-particles of the desired energy at each angle. These energies varied from 10 to 35 MEV at creation, corresponding to elastic production by γ-rays of energy 220 to 325 MEV. The mass distributions obtained are shown in figures 2–7. ^{3}H and other singly charged particles are not recorded. From these distributions it is seen that the ^{3}He and ^{4}He particles are sufficiently separated for the yield of ^{4}He particles to be measured. The kinematics of the reaction

$$\gamma + {}^4\text{He} \rightarrow \pi^0 + {}^4\text{He} \qquad \ldots\ldots(1)$$

are such that there is no yield of ^{4}He particles at 90° to the beam. As is seen from figure 5, only ^{3}He particles are detected at this angle and the agreement between the experimental and calculated loci at this angle is verified.

The ^{3}He particles can arise from the reactions:

$$\gamma + {}^4\text{He} \rightarrow {}^3\text{He} + \text{n} \qquad \ldots\ldots(2)$$

$$\left.\begin{array}{r} \gamma + {}^4\text{He} \rightarrow \pi^- + \text{p} \\ \pi^0 + \text{n} \end{array}\right\} + {}^3\text{He}. \qquad \ldots\ldots(3)$$

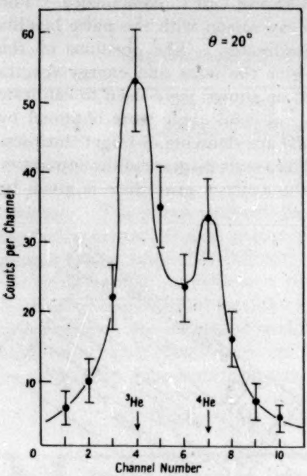

Figure 2. Mass spectrum at 20°, high energy run.

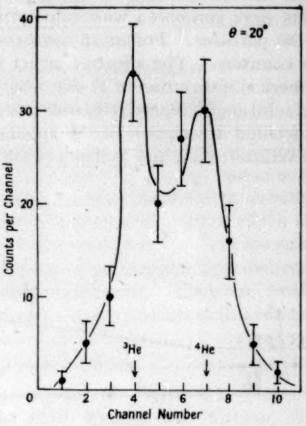

Figure 3. Mass spectrum at 20°, low energy run.

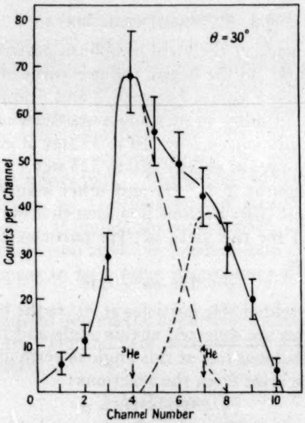

Figure 4. Mass spectrum at 30°.

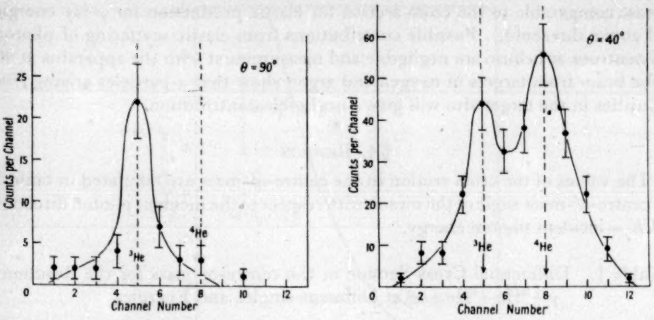

Figures 5 and 6. Mass spectra at 90° and 40°. The kinematics of the process $\gamma + {}^4\text{He} \rightarrow \pi^0 + {}^4\text{He}$ rule out the possibility of emission of a ⁴He particle at 90°.

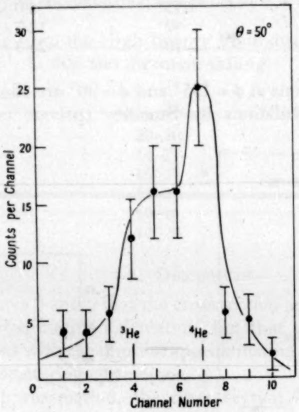

Figure 7. Mass spectrum at 50°.

It is possible to subtract the contribution from reaction (2) since the ³He particles having energies and angles of emission with respect to the incident photon direction such that they are recorded under the experimental conditions used are all produced below meson threshold. A separate run at lower maximum beam energy can thus be used to determine their contribution. This was not done with the present apparatus since the separation of the two types of particle enabled them to be eliminated.

No precise predictions can be made about the contributions from reaction (3), although plausible arguments can be advanced to suggest that ³He particles of such high energies will have a small probability of being produced in these reactions, even though the cross section for the reactions would be expected to be at least comparable to the cross section for elastic production for γ-ray energies well above threshold. Possible contributions from elastic scattering of photons and neutrons at helium are negligible and measurement with the apparatus at 90° to the beam from targets of oxygen and argon show that α-particles arising from impurities in the target also will give a negligible contribution.

§ 4. RESULTS

The values of the cross section in the centre-of-mass are tabulated in table 1: ϕ = centre-of-mass angle of the meson with respect to the incident photon direction, and E_γ = incident photon energy.

Table 1. Differential Cross Section in the centre-of-mass for the Reaction $\gamma + {}^4\text{He} \rightarrow {}^4\text{He} + \pi^0$ at Different Angles and Energies

E_γ (MeV)	ϕ	$\frac{d\sigma}{d\Omega}$ (μbn sterad^{-1})
256–306	135°	$3{\cdot}5 \pm 0{\cdot}5$
223–260	135°	$10{\cdot}7 \pm 1{\cdot}4$
254–313	115°	$4{\cdot}0 \pm 0{\cdot}9$
263–315	92°	$12{\cdot}7 \pm 1{\cdot}0$
280–325	70°	$24{\cdot}3 \pm 5{\cdot}3$

The excitation functions at $\phi = 135°$ and $\phi = 90°$ are shown in figures 8 and 9, and compared with calculations by Stoodley (private communication, to be published) using an impulse approximation. At $\phi = 90°$, the lower curve shows the effects of a calculation allowing for multiple scattering. The variation of cross section with angle is shown in figure 10.

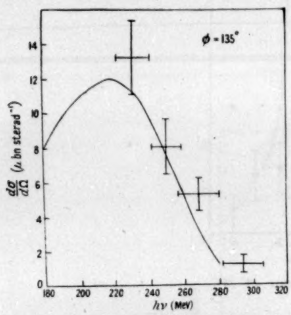

Figure 8. Excitation function for the reaction $\gamma + {}^4\text{He} \rightarrow \pi^0 + {}^4\text{He}$ at a c.m. angle of 135° for the π^0. The curve has been calculated on the impulse approximation (Stoodley).

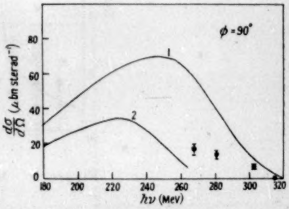

Figure 9. Excitation function for the reaction $\gamma + {}^4\text{He} \rightarrow \pi^0 + {}^4\text{He}$ at a c.m. angle of 90°. The upper curve is based on the impulse approximation. The lower one includes multiple scattering correction.

The yields of ^{3}He particles at each angle in units of yield MeV^{-1} Q^{-1} sterad^{-1} are given in table 2; θ is the laboratory angle.

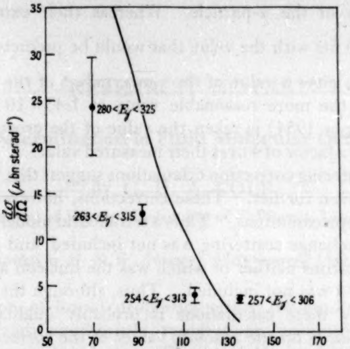

Figure 10. Angular distribution for the process $\gamma + {}^4\text{He} \rightarrow \pi^0 + {}^4\text{He}$. The curve is based on impulse approximation and refers to $E_\gamma = 290$ MEV.

Table 2. Yield of ^{3}He from the High Energy Photodisintegration of Helium by 325 MEV Bremsstrahlung

θ	$\Delta E_{^3\text{He}}$ (MEV)	Yield (10^{-31} cm^2 MEV^{-1} Q^{-1} sterad^{-1})
20°	20–30	$3 \cdot 6 \pm 0 \cdot 4$
	14–21	$8 \cdot 1 \pm 1 \cdot 0$
30°	16–27	$3 \cdot 8 \pm 0 \cdot 6$
40°	12–21	$5 \cdot 5 \pm 0 \cdot 5$
50	10–16	$7 \cdot 4 \pm 2 \cdot 4$
90°	12–20	$5 \cdot 5 \pm 1 \cdot 0$

§ 5. DISCUSSION

It is seen from figures 8 and 9 that the cross section at $\phi = 135°$ is in agreement with the impulse approximation calculation, but that at $\phi = 90°$, the results lie between the calculations with the impulse approximation and the impulse approximation with multiple scattering corrections.

In the impulse approximation, the cross section for reaction (1) may be expressed as:

$$\left(\frac{d\sigma}{d\Omega}\right)_{\text{He}} = 16 f_{\text{He}}(q, \phi) \times |\text{L}_0|^2 |F|^2. \qquad \ldots\ldots (4)$$

The corresponding cross section for production at hydrogen is:

$$\left(\frac{d\sigma}{d\Omega}\right)_{\text{H}} = f_{\text{H}}(q, \phi)\{|\text{K}_0|^2 + |\text{L}_0|^2\}. \qquad \ldots\ldots (5)$$

$|\text{K}_0|$ and $|\text{L}_0|$ are the spin flip and non spin flip parts of the matrix element for photoproduction at a single nucleon.

$|\text{L}_0| \propto \sin\phi$ and from the angular variation of the cross section (4) due to the form factor F, a value of the mean radius of the α-particle may be derived. The value of $\left(\frac{d\sigma}{d\Omega}\right) \Big/ \sin^2\phi$ as $\phi \rightarrow 0$ is determined independent of this radius, since $F \simeq 1$ at forward angles. De Saussure and Osborne analysed their results to obtain a value of the radius of the α-particle. Whereas their extrapolated value of $\left(\frac{d\sigma}{d\Omega}\right)\Big/\sin^2\phi$ as $\phi\to 0$ fits with the value that would be predicted by equation (4), the angular variation gives a value of the r.m.s. radius of the α-particle equal to $0{\cdot}93\times 10^{-13}$cm. If the more reasonable value of $1{\cdot}43\times 10^{-13}$cm (Hofstadter, McAllister and Weiner 1954) is taken the value of the cross section at $\phi=90°$ would be reduced by a factor of 4 over their measured value.

The multiple scattering correction calculations suggest that these cross sections should be reduced even further. These corrections, however, have been made using a number of approximations. Thus a tetrahedral model of the ^{4}He nucleus was taken, charge exchange scattering was not included, and multiple scattering between pairs of nucleons neither of which was the nucleon at which the meson was initially produced was not included. Thus, although the reduction in cross section predicted by these calculations is probably qualitatively correct, no reliance should be placed on the absolute values of the correction.

Goldwasser and Koester (1956) who essentially measured the total π^0 production at 90° found that the cross section per nucleon from ^{4}He was about equal to the production from hydrogen at photon energies near threshold, but was rather lower at photon energies near 300 MeV. At photon energies of about 200MeV, these cross sections are also very much lower than these of de Saussure and Osborne. At higher photon energies ~280 MeV, their cross section which includes the inelastic production is comparable to the cross section for elastic production found by de Saussure and Osborne. At this energy it would be expected that the inelastic production would predominate over the elastic production.

An impulse approximation calculation by Yamaguchi (1955) at 200 MeV is in rough agreement with the measurements of Goldwasser and Koester.

§ 6. CONCLUSION

Although these results differ considerably from the measurements already quoted, there is some confirmation of their validity both from the measurements of the total π^0 yield and their broad agreement with the calculations using the impulse approximation. A more detailed comparison with calculated values requires a more rigorous derivation of the effects of multiple scattering.

ACKNOWLEDGMENTS

We wish to thank Dr. W. McFarlane and the synchrotron crew for running the machine, Professor P. I. Dee for his encouragement throughout and Dr. K. D. C. Stoodley for communicating the results of his calculations before publication. Mr. R. W. P. McWhirter collaborated in the work in the early stages.

REFERENCES

CHAPPELEAR, J., 1955, *Phys. Rev.*, **99**, 254.

DAVIES, H. L., and CORSON, D. R., 1955, *Phys. Rev.*, **99**, 273.

GOLDWASSER, E. L., and KOESTER, L. J., Jr., 1956, *Nuovo Cim. Suppl.*, **4**, 950.

HOFSTADTER, R., MCALLISTER, R., and WEINER, E., 1954, *Phys. Rev.*, **96**, 854.

KEMMER, N., 1938, *Proc. Camb. Phil. Soc.*, **34**, 354.

MCWHIRTER, R. W. P., PALIT, P., and BELLAMY, E. H., 1958, *Nuclear Instrum.*, **3**, 80.

ROSENGREN, J. W., and BARON, N., 1955, *Phys. Rev.*, **101**, 410.

DE SAUSSURE, G., and OSBORNE, L. S., 1955, *Phys. Rev.*, **99**, 843.

WOLFE, B., SILVERMAN, A., and DE WIRE, J. W., 1955, *Phys. Rev.*, **99**, 268.

YAMAGUCHI, Y., 1955, *Progr. Theor. Phys., Japan*, **13**, 459.

RESEARCH NOTES

Determination of Fluid Molecular Order

By G. H. A. COLE
Department of Physics, University of California, Los Angeles

Communicated by H. S. W. Massey; *MS. received* 15*th May* 1958

THE calculation of liquid properties either for equilibrium or for small deviations from equilibrium requires an accurate knowledge of the equilibrium pair distribution (Born and Green 1949, Eisenschitz 1949, Kirkwood *et al.* 1952). It is a notoriously difficult task to obtain this information in general: in the present note a simple method is suggested for obtaining it from less accurate data (e.g. experimental curves) which may be of value in certain circumstances. Values calculated in this way may possibly be sufficient in themselves, or alternatively may form a suitable starting point for solving the second-order differential equation recently proposed by Cole (1958) as an alternative to the first-order integro-differential equations previously given, for example, independently by Born and Green (1949) and Kirkwood and Boggs (1942). As for the method involving the differential equations, so also in the present method it is necessary to invoke the superposition approximation. It will be seen that the approach is essentially an extension of that used earlier by Eisenschitz and Cole (1954) to derive the perturbing effect of a steady electric field on the liquid equilibrium pair distribution, either due to the presence of liquid molecular dipoles or to molecular polarizability.

Representing the liquid by N identical particles contained in a volume V, and interacting mutually with the actual total potential energy, written $\Psi_A(\mathbf{r}_1, \mathbf{r}_2, \ldots \mathbf{r}_N)$, the pair distribution, $n^{(2)}(\mathbf{r}_1, \mathbf{r}_2)$, is defined by the expression

$$Zn^2 n^{(2)}(\mathbf{r}_1, \mathbf{r}_2) = \frac{1}{(N-2)!}\int \ldots \int \exp\{-X_A\}\, d\mathbf{r}_3 \ldots d\mathbf{r}_N \quad \ldots\ldots (1)$$

where $kTX_A = \Psi_A$, $N = Vn$, and $\mathbf{r}_i$ is the position of the ith particle. In equation (1), Z is as usual the configurational partition function. Suppose some known (e.g. experimentally determined), although not exact, pair distribution is written $n_0^{(2)}(\mathbf{r}_1, \mathbf{r}_2)$, then if $n_0^{(2)}$ differs from $n^{(2)}$ not too drastically, it can be expected that some virtual total interaction energy, $\Psi_0(\mathbf{r}_1, \mathbf{r}_2, \ldots \mathbf{r}_N)$, exists such that

$$Zn^2 n_0^{(2)}(\mathbf{r}_1, \mathbf{r}_2) = \frac{1}{(N-2)!}\int \ldots \int \exp\{-X_0\}\, d\mathbf{r}_3 \ldots d\mathbf{r}_N \quad \ldots\ldots (2)$$

where $kTX_0 = \Psi_0$. The difference between X_0 and X_A is a measure of the difference between the already known function $n_0^{(2)}$ and the required (i.e. more exact) function $n^{(2)}$. If this difference is not large it is physically reasonable to assume the function X_1 defined by

$$X_1 = X_A - X_0 \quad \ldots\ldots (3)$$

to be a small quantity. If it is of the first order of small quantities, the function $\exp\{-\mathrm{X}_{\mathrm{A}}\}$ can be written in terms of $\exp\{-\mathrm{X}_0\}$ according to

$$\exp\{-\mathrm{X}_{\mathrm{A}}\}=\exp\{-\mathrm{X}_0\}(1-\mathrm{X}_1+\mathrm{O}(\mathrm{X}_1)^2). \qquad \ldots\ldots(4)$$

The insertion of (4) into (1) provides a relation between $n^{(2)}$ and $n_0^{(2)}$:

$$n^2 n^{(2)}(\mathbf{r}_1,\mathbf{r}_2)=n^2 n_0^{(2)}(\mathbf{r}_1,\mathbf{r}_2)-\frac{1/Z}{(N-2)!}\int\ldots\int \mathrm{X}_1\exp\{-\mathrm{X}_0\}\,d\mathbf{r}_3\ldots d\mathbf{r}_N \quad \ldots\ldots(5)$$

involving the two unknown functions X_1 and X_0. The integral in (5) can, however, be replaced by four terms involving $n_0^{(2)}$, $n_0^{(3)}$, $n_0^{(4)}$, the last two distribution functions being obtained by equating h in (6) successively to 3 and 4:

$$Zn^h n^{(h)}(\mathbf{r}_1,\mathbf{r}_2,\ldots\mathbf{r}_h)=\frac{1}{(N-h)!}\int\ldots\int\exp\{-\mathrm{X}_0\}\,d\mathbf{r}_{h+1}\ldots d\mathbf{r}_N. \quad \ldots\ldots(6)$$

For, differentiating (2) with respect to temperature, and rearranging the resulting expression, there follows the relation

$$\begin{aligned}&-\frac{1}{(N-2)!}\int\ldots\int \mathrm{X}_1\exp\{-\mathrm{X}_0\}\,d\mathbf{r}_3\ldots d\mathbf{r}_N\\ &=n^2T\left.\frac{\partial n_0^{(2)}(\mathbf{r}_1,\mathbf{r}_2)}{\partial T}\right|_T-\frac{1}{(N-2)!}\int\ldots\int \mathrm{X}_{\mathrm{A}}\exp\{-\mathrm{X}_0\}\,d\mathbf{r}_3\ldots d\mathbf{r}_N \quad \ldots\ldots(7)\end{aligned}$$

applying at the temperature T only.

For simple liquids the total potential of interaction can be written as the sum of the separate pair interactions, i.e.

$$\mathrm{X}(\mathbf{r}_1,\mathbf{r}_2,\ldots\mathbf{r}_N)=\sum_{i=1}^{N}\sum_{j>i}^{N}\chi(\mathbf{r}_i,\mathbf{r}_j) \qquad \ldots\ldots(8)$$

where $kT\chi(\mathbf{r}_i,\mathbf{r}_j)=\psi(\mathbf{r}_i,\mathbf{r}_j)$, and ψ is the mutual pair potential between particles i and j. Using (7), and (8) applied to X_{A}, in (5), together with (2) and (6), there results the relation

$$\begin{aligned}n^{(2)}(\mathbf{r}_1,\mathbf{r}_2)=n_0^{(2)}(\mathbf{r}_1,\mathbf{r}_2)[1-\chi_{\mathrm{A}}(\mathbf{r}_1,\mathbf{r}_2)]&+T\left.\frac{\partial n_0^{(2)}(\mathbf{r}_1,\mathbf{r}_2)}{\partial T}\right|_T\\ &-2n\int\chi_{\mathrm{A}}(\mathbf{r}_1,\mathbf{r}_3)n_0^{(3)}(\mathbf{r}_1,\mathbf{r}_2,\mathbf{r}_3)\,d\mathbf{r}_3\\ &-n^2\int\chi_{\mathrm{A}}(\mathbf{r}_3,\mathbf{r}_4)n_0^{(4)}(\mathbf{r}_1,\mathbf{r}_2,\mathbf{r}_3,\mathbf{r}_4)\,d\mathbf{r}_3\,d\mathbf{r}_4. \quad \ldots\ldots(9)\end{aligned}$$

In order to evaluate the right-hand side of (9) it is necessary to express $n_0^{(3)}$ and $n_0^{(4)}$ in terms of $n_0^{(2)}$: at the present time this must involve the superposition approximation applied to triplet and quadruplet particle groupings

$$\left.\begin{aligned}n_0^{(3)}(\mathbf{r}_1,\mathbf{r}_2,\mathbf{r}_3)&=n_0^{(2)}(\mathbf{r}_1,\mathbf{r}_2)n_0^{(2)}(\mathbf{r}_1,\mathbf{r}_3)n_0^{(2)}(\mathbf{r}_2,\mathbf{r}_3)\\ n_0^{(4)}(\mathbf{r}_1,\mathbf{r}_2,\mathbf{r}_3,\mathbf{r}_4)&=n_0^{(3)}(\mathbf{r}_1,\mathbf{r}_2,\mathbf{r}_3)n_0^{(2)}(\mathbf{r}_1,\mathbf{r}_4)n_0^{(2)}(\mathbf{r}_2,\mathbf{r}_4)n_0^{(2)}(\mathbf{r}_3,\mathbf{r}_4)\cdot\end{aligned}\right\}\ldots\ldots(10)$$

By using (10), (9) then involves $n_0^{(2)}$ only, and can be used to determine $n^{(2)}$ if χ_{A} and the temperature dependence of $n_0^{(2)}$ for temperature T are known. It should be noted that (9) refers to the single temperature T, and $\partial n_0^{(2)}/\partial T|_T$ is the limit of the temperature change about T. By finding $n^{(2)}$ for a small temperature range about T it can be expected that (9) will yield some further improved accuracy for $n^{(2)}$ by an iteration centred around the second (temperature) term on the right-hand side.

The method outlined here is useful when the expansion (4) is valid, the rigorous inclusion of small quantities of higher order than the first seeming not to be possible: in physical terms this restricts the argument to those cases where $n_0^{(2)}$ is already a good first approximation. The method would seem perhaps to be of some value for the correction of certain (as yet) not fully accurate experimental liquid measurements: alternatively it is likely to have wider scope in connection with dense gases.

REFERENCES

BORN, M., and GREEN, H. S., 1949, *A General Kinetic Theory of Liquids* (Cambridge: University Press).
COLE, G. H. A., 1958, *J. Chem. Phys.*, **28**, 912.
EISENSCHITZ, R., 1949, *Proc. Phys. Soc.* A, **52**, 41.
EISENSCHITZ, R., and COLE, G. H. A., 1954, *Phil. Mag.*, **45**, 394.
KIRKWOOD, J. G., and BOGGS, E. M., 1942, *J. Chem. Phys.*, **10**, 394.
KIRKWOOD, J. G., LEWINSON, V. A., and ALDER, B., 1952, *J. Chem. Phys.*, **20**, 929.

The Polarization of Helium-like Atoms

BY A. DALGARNO
Department of Applied Mathematics, The Queen's University of Belfast

Communicated by D. R. Bates; MS. received 25th July 1958

THE polarization of an atom by a charged particle has been discussed in the past by expanding the interaction potential in inverse powers of the distance *r* between the atom and the charged particle, a procedure which results in an expression for the perturbed energy which is a power series in r^{-1}; attention has generally been restricted to the coefficients of the first one or two non-vanishing terms. Quite apart from the convergence difficulties that arise, the assumption has been implicitly made in the calculation of the coefficients that *r* is infinite and the range of *r* for which the results are applicable may thus be severely limited.

Only cases involving a single-electron atom are exactly soluble, but by adopting an approximation due to Sternheimer (1954) representative data can be obtained for the helium iso-electronic sequence, which at least for the higher members should be essentially exact.

Sternheimer (1954) has calculated the first and second terms of the power series representations for members of the helium iso-electronic sequence by writing their electron orbitals in the form suggested by Löwdin (1953)

$$\psi_0(\mathbf{r}') = c_1 \exp(-Z_1 r') + c_2 \exp(-Z_2 r') \qquad \ldots\ldots (1)$$

and assuming that the solutions of the appropriate first-order perturbed equations are simply the sums of the solutions corresponding to the individual terms $c_1 \exp(-Z_1 r')$ and $c_2 \exp(-Z_2 r')$. These individual terms represent orbitals describing the 1s electron of a hydrogen-like atom of nuclear charge Z_1 and Z_2, for which the calculation of the first two terms (which are proportional to the dipole and quadrupole polarizabilities) is easily carried out. A comparison of the results of this procedure with those of more accurate treatments of Sternheimer (1957), Wikner and Das (1957), Das and Bersohn (1956) and Dalgarno and Stewart

(1958), is made in table 1 from which it is clear that Sternheimer's approximate procedure introduces only a small error.

Table 1. Dipole (α_d) and Quadrupole (α_q) Polarizabilities

Atom	†He	Li$^+$	Be^{2+}
$\alpha_d(\text{Å}^3)$			
Sternheimer (1954)	0·236	0·0316	0·0083
Sternheimer (1957)	0·224	0·0307	0·00825
Wikner and Das (1957)	0·218	0·0305	0·00813
Dalgarno and Stewart (1958)	0·206	0·0299	0·00806
$\alpha_q(\text{Å}^5)$			
Sternheimer (1954)	0·101	0·00477	0·000640
Sternheimer (1957)	0·0993	0·00473	0·000637
Das and Bersohn (1956)	0·0949	0·00471	0·000633

†The experimental value of α_d for He is 0·206 (Essen 1953).

Recently Dalgarno and Lynn (1957) have solved exactly the first-order perturbed equation for a 1s-electron atom of arbitrary nuclear charge ζ without expanding the interaction potential. Denoting their solution by $\phi(\mathbf{r}';\zeta)$ the interaction energy is assumed to be

$$V(r)=2\int \psi_0(\mathbf{r}')\left\{\frac{2}{r}-\frac{2}{|\mathbf{r}-\mathbf{r}'|}\right\}\{c_1\phi(\mathbf{r}';Z_1)+c_2\phi(\mathbf{r}';Z_2)\}\,d\mathbf{r}', \qquad \ldots\ldots(2)$$

measured in rydbergs. The analytical evaluation of (2) is very lengthy and only the numerical results will be presented. They are given in table 2 for He, Li$^+$ and Be^{2+} in the form of the ratio of the actual polarization energy $V(r)$ to its asymptotic value $-\alpha/r^4$, α being the dipole polarizability. Within the limits of Sternheimer's approximation scheme, they are correct at all values of r.

Table 2. $V(r)/(-\alpha/r^4)$

r	He	Li$^+$	Be^{2+}
0	$0{\cdot}00_0$	$0{\cdot}00_0$	$0{\cdot}00_0$
1	$0{\cdot}26_4$	$0{\cdot}72_2$	$1{\cdot}03_9$
2	$0{\cdot}99_3$	$1{\cdot}12_7$	$1{\cdot}15_0$
3	$1{\cdot}11_9$	$1{\cdot}09_6$	$1{\cdot}02_6$
4	$1{\cdot}11_2$	$1{\cdot}02_7$	$1{\cdot}01_0$
5	$1{\cdot}08_8$	$1{\cdot}01_4$	$1{\cdot}00_3$
6	$1{\cdot}04_2$	$1{\cdot}00_9$	$1{\cdot}00_1$
7	$1{\cdot}02_8$	$1{\cdot}00_6$	$1{\cdot}00_0$
8	$1{\cdot}02_0$	$1{\cdot}00_4$	$1{\cdot}00_0$
9	$1{\cdot}01_4$	$1{\cdot}00_2$	$1{\cdot}00_0$
10	$1{\cdot}01_0$	$1{\cdot}00_1$	$1{\cdot}00_0$

The results show that the dipole approximation leads to an error never greater than say 15% except at such small values of r that effects other than polarization will usually be more significant.

ACKNOWLEDGMENTS

This work is partially supported by the Atomic Energy Research Establishment, Harwell. Computational assistance has been provided by Mrs. N. Scott.

REFERENCES

DALGARNO, A., and LYNN, N., 1957, *Proc. Phys. Soc.* A, **70,** 223.
DALGARNO, A., and STEWART, A. L., 1958, *Proc. Roy. Soc.* A, in the press.
DAS, T. P., and BERSOHN, R., 1956, *Phys. Rev.*, **102,** 733.
ESSEN, L., 1953, *Proc. Phys. Soc.* B, **66,** 189.
LÖWDIN, P. O., 1953, *Phys. Rev.*, **90,** 120.
STERNHEIMER, R. M., 1954, *Phys. Rev.*, **96,** 951; 1957, *Ibid.*, **107,** 1564.
WIKNER, E. G., and DAS, T. P., 1957, *Phys. Rev.*, **107,** 497.

Proposed Method for Direct Measurement of the *g*-Factor of Free Electrons

BY P. S. FARAGO

Department of Natural Philosophy, University of Edinburgh

Communicated by N. Feather; MS. received 16*th June* 1958

§ 1. INTRODUCTION

ACCORDING to quantum electrodynamics, and confirmed by measurements on electrons bound in atoms, the magnetic moment μ of the electron deviates from the Bohr magneton μ_0:

$$\mu=\mu_0\left(1+\frac{\alpha}{2\pi}+\text{terms of higher order in }\alpha\right)$$

where $\alpha \sim 1/137$ is the fine-structure constant.

All suggestions for the measurement of μ, or rather $g=2\mu/\mu_0$ are based on the possibility of a direct comparison of the Larmor precessional frequency ω_{L} of the electron spin in a magnetic field with the 'cyclotron' frequency ω of orbital motion in the same field, the two quantities being related to one another by the equation $\omega_{\mathrm{L}}=g\omega/2$. High precision comparison of ω_{L} and ω can be carried out by either of the two following methods: (i) the frequency of the radio-frequency field producing 'cyclotron' resonance is compared with the resonance frequency for spin re-orientation, both phenomena being observed in the same external magnetic field (Bloch 1953, Frisch 1955, private communication, Farago 1957); (ii) the change of angle between the directions of the orbital and spin momenta of electrons moving in a magnetic field is observed (Tolhoek and de Groot 1951, Crane, Pidd and Louisell 1953). To date no satisfactory experimental results have been reported by either method.

The basic idea of the experiment proposed below is essentially the same as that suggested by Crane, Pidd and Louisell (1953). If electrons are moving in a homogeneous magnetic field in a plane perpendicular to the field, with their spins in the plane of their orbits, the angle between the orbital momentum and that of the spin will slowly change, because $\omega_{\mathrm{L}}-\omega\neq 0$. Crane proposed the use of a pulsed beam of polarized electrons, which should be trapped for a large number of orbital revolutions. By observing the azimuthal asymmetry of the Coulomb scattering from a thin target of a heavy element as a function of the number of orbital revolutions one should obtain a periodic curve revealing the progressive change of the angle between orbital and spin momenta. The number k of orbital revolutions would be determined from the time which the electron spent in the magnetic field before scattering. If the experiment showed that it took

k_0 orbital revolutions to achieve a complete period of variation of the asymmetry of scattering, then $\frac{1}{2}g-1 \sim 1/k_0$, i.e. k_0 would measure the anomaly of the g-factor. If k_0 were determined with an accuracy to, say, 1% the accuracy of g would be to about 1 part in 100 000.

The difficulty of the experiment outlined above is related to the problem of injecting the electrons into the trapping field and ejecting them later on to the target at a prescribed instant. However, the attractive feature of high precision can be kept and the technical difficulties can be considerably reduced if a β-active sample is used as a source of polarized electrons, and the electron motion and spin precession is observed in crossed homogeneous electric and magnetic fields.

§ 2. OUTLINE OF EXPERIMENTAL METHOD

The sample S, situated in the crossed homogeneous electric and magnetic fields $\mathbf{E}=(0, E, 0)$ and $\mathbf{H}=(0, 0, H)$ respectively, should emit electrons of velocity u only in one hemisphere (see figure). It is easy to show that, if $(cE/uH)^2 \ll 1$, then the electron orbits can be considered as circles of radius $\rho=u/\omega=cmu/eH$ drifting with a velocity cE/H in the direction of the x axis, the drift per orbital revolution being $d \sim 2\pi c^2 mE/eH^2$. In this case the number of orbital revolutions necessary to bring the electrons from the source to a target T at a distance $L \sim 2\rho$ is $k=L/d=\beta H/\pi E$ (where $\beta=u/c$). To take a numerical example, consider electrons of 128 kev energy ($\beta \sim 0{\cdot}6$) in a field $H=260$ oersteds with $E=15$ v cm^{-1}. We find $\rho \sim 5$ cm, $d \sim 0{\cdot}01$ cm and $k \sim 1000$. By varying E a wide range of values of k can be covered.

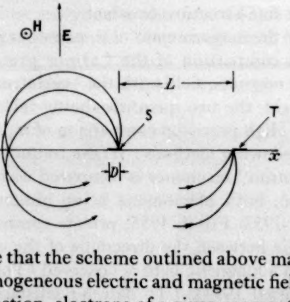

It is important to note that the scheme outlined above makes use of the imaging properties of crossed homogeneous electric and magnetic fields. It is known that, whatever their initial direction, electrons of a given momentum emitted by a point source are focused in one point again after any complete number of orbital revolutions. Consequently, if a point source is located on the x axis, all electrons will reach a target on the same axis after the same number of orbital revolutions. The actual source is, of course, of finite width D, but its ' effective ' width corresponds to the region from which electrons, when emitted, will be able to pass by the edge of the source holder after having completed the first orbit and is equal to the width of the image and to the distance by which the image is shifted after one orbital revolution. Thus the uncertainty of the number of orbital revolutions is $\delta k=1$, assuming that the electrons can cross the target surface only once. It is rather improbable that multiple crossing could take place without the electron being scattered out of the beam or being depolarized. The uncertainty in k due to the spread of the momenta of electrons can be kept within a few per cent with the aid of a suitably situated baffle without limiting the solid angle considerably.

The polarization of the electrons reaching the target is detected by observing the azimuthal asymmetry of Coulomb scattering with the aid of two scintillation counters situated opposite one another in a line perpendicular to the plane of the orbital rotation of the electrons. The greatest difficulty of the experiment is to achieve counting rates high enough for an accurate determination of the asymmetry as a function of the number of orbital revolutions. The reason for this is obviously the large total length of the electron trajectories yielding a very small solid angle, even if the angular aperture of the beam in the plane of the orbital motion can be fairly large (~30°). It was found that with reasonable geometrical arrangement and dimensions of source, target, counters, etc. and a source activity of 1 mc mm^{-2} an average counting rate of about 200 hour^{-1} can be obtained at the maximum number of orbital revolutions, i.e. under the most difficult experimental conditions.

§ 3. SPIN PRECESSION IN CROSSED HOMOGENEOUS ELECTRIC AND MAGNETIC FIELDS

Before the observed experimental results can be evaluated, the following doubts have to be resolved: (i) at relativistic velocities the magnetic field as seen by the electrons is different from that measured in the laboratory system; (ii) the superposition of an electric field may modify the spin precession by spin–orbit coupling.

In relation to (i), for motion in a magnetic field only, Mendlowitz and Case (1955) and Carrassi (1958), by quantum mechanical considerations, showed that

$$\omega_{\mathrm{L}} = \omega[1 + (1-\beta^2)^{-1/2}(\tfrac{1}{2}g - 1)]. \qquad \ldots\ldots(1)$$

Concerning (ii), only the effects of longitudinal and transverse electric fields have so far been studied (Tolhoek and de Groot 1951). Obviously neither of these conditions obtains in the present scheme; the electrons see a rotating electric field. However, the validity of equation (1) can be easily generalized so that it should give an answer to our problem.

First of all it should be realized that our experiment measures directly the 'relative' spin precession rate $(\omega_{\mathrm{L}} - \omega)/\omega$. This quantity can be considered as the ratio of two clock readings: one of the clocks is defined by the rate of change of the angle between the spin and orbital momentum, and the other by the angular velocity of the orbital motion. The two clocks are at rest relative to one another and therefore both are equally affected by any Lorentz transformation. Consequently, if the equation

$$(\omega'_{\mathrm{L}} - \omega')/\omega' = (1-\beta'^2)^{-1/2}(\tfrac{1}{2}g - 1) \qquad \ldots\ldots(2)$$

is valid in a reference frame S′ in which $E' = 0$, then the same will be valid in any reference frame S moving uniformly relative to S′ ; note that $\beta' = u'/c$, where u' is the velocity of the electron in S′ in which $E' = 0$.

Now, if the fields in the laboratory system S are $\mathbf{H} = (0, 0, H)$ and $\mathbf{E} = (0, E, 0)$, $(E < H)$ as chosen in our experimental arrangement, then one can always define a reference frame S′ moving with a velocity $\mathbf{v} = (v, 0, 0)$ in which the electric field E' will vanish. From the relativistic transformation equations of electromagnetic fields the condition for this is $v/c = E/H$.

This equation enables us to express β' in terms of β. If in the laboratory system S the electron velocity is $\mathbf{u}=(u\cos\phi, u\sin\phi, 0)$, u' can be found by a straightforward Lorentz transformation, and we get

$$(1-\beta'^2)^{-1/2}=\left(1-\frac{E}{H}\beta\cos\phi\right)\left(1-\frac{E^2}{H^2}\right)^{-1/2}(1-\beta^2)^{-1/2}.$$

Substituting this expression into (2), we get for the relative precession rate in the laboratory system

$$\frac{\omega_{\mathrm{L}}-\omega}{\omega}=\left(1-\frac{E}{H}\beta\cos\phi\right)\left(1-\frac{E^2}{H^2}\right)^{-1/2}(1-\beta^2)(\tfrac{1}{2}g-1). \quad\ldots\ldots(3)$$

In practice it is advantageous to choose $\cos\phi=E/\beta H$, yielding

$$\frac{\omega_{\mathrm{L}}-\omega}{\omega}=\left(1-\frac{E^2}{H^2}\right)^{1/2}(1-\beta^2)^{-1/2}(\tfrac{1}{2}g-1). \quad\ldots\ldots(4)$$

Equation (3) shows that the contribution of the electric field to the relative spin precession is proportional to the g-factor anomaly $\frac{1}{2}g-1$, and not to the g-factor itself, and this effect is negligible if $E/H \ll 1$.

It is interesting to note that the result (2) and therefore also (3) can be obtained by semi-classical considerations of the motion of a point particle with spin. The spin precession frequency is calculated in the instantaneous rest frame of the electron and it is compared with the angular velocity of the orbital motion, taking proper account of the ' Thomas precession '. The success of the semi-classical calculation is not surprising, since in the problem the fields concerned are constant over a region of dimensions of the de Broglie wavelength.

§ 4. CONCLUSIONS

By comparing the spin precession frequency ω_{L} and the angular velocity ω of orbital motion of polarized electrons emitted by a β-active source in crossed homogeneous electric and magnetic fields the g-factor of the electrons can be determined with an accuracy to about $1:10^5$. Therefore the results should give a significant evidence of the magnetic moment anomaly of free electrons.

It was shown that the effect of the electric field is negligible in the circumstances of the experiment.

The method is equally suitable for the direct measurement of the g-factor of positrons. The only modification necessary is a change in the method of detection of the polarization of the beam. That means that when studying positrons Møller scattering should be applied instead of Coulomb scattering.

Experiments based on the principles described above are in preparation.

ACKNOWLEDGMENT

The author is indebted to Dr. D. L. Pursey for many fruitful discussions on various aspects of spin kinematics.

REFERENCES

BLOCH, F., 1953, *Physica*, **19**, 821.
CARRASSI, L. M., 1958, *Nuovo Cim.*, **7**, 524.
CRANE, H. R., PIDD., R.W., and LOUISELL, W. M., 1953, *Phys. Rev.*, **91**, 475 (A).
FARAGO, P. S., 1957, *Arch. des Sci.*, **10**, 88.
MENDLOWITZ, H., and CASE, K. M., 1955, *Phys. Rev.*, **97**, 33.
TOLHOEK, H. A., and DE GROOT, S. R., 1951, *Physica*, **17**, 17.

The Photoproduction of Charged Pions from Deuterium

By W. R. HOGG and E. H. BELLAMY
Department of Natural Philosophy, University of Glasgow

MS. received 7th July 1958

THE relative yields of π^- and π^+ mesons from deuterium have been measured at 75° to a photon beam of maximum energy of 235 ± 5 MeV. Three energy ranges of pions were detected simultaneously, viz. 11–15 MeV, 24–30 MeV and 44–51 MeV. The pions were produced in a liquid deuterium target and a double focusing magnetic spectrometer was used as the detector. After selection by charge and momentum, the pions were detected in telescopes of proportional counters.

The main interest of this work is at pion threshold, and this is two-fold : firstly there is a theoretical prediction of 1·4 (see for example Chew *et al.* 1957) for the π^-/π^+ ratio at threshold :

$$R_0 = \frac{\sigma(\gamma + \mathrm{n} \to \pi^- + \mathrm{p})}{\sigma(\gamma + \mathrm{p} \to \pi^+ + \mathrm{n})}$$

and secondly there is a relationship between R_0, the Panofsky ratio P, and the difference of the s-wave scattering lengths for the $\frac{3}{2}$ and the $\frac{1}{2}$ isotopic spin states of the (π^-, p) system ($\lambda_3 - \lambda_1$) (Anderson and Fermi 1952).

Recent results of measured π^-/π^+ ratios from deuterium have indicated a value greater than unity at low pion energies. In particular, two groups have published important work in this field ; the California Institute of Technology (Sands, Teasdale and Walker 1954, and Watson *et al.* 1956) found a value of R_0 consistent with the above theoretical prediction. The Rome–Illinois group (Beneventano *et al.* 1956) based their analysis on measurements of the ratio at a centre-of-mass angle of 90°, and on a semi-phenomenological basis they extrapolated their results to a ratio R_0 of 1·87. It has been since pointed out by Moravcsik (1958) that this analysis was not unambiguous in its prediction of the threshold value of the ratio. As an illustration, Beneventano's extrapolated curve (dotted) and one obtained from equation (3.9) of Moravcsik's paper (dashed), are shown in figure 1 with the more recent experimental data. It is to be noted that the dashed curve was obtained from Beneventano's by applying small justifiable corrections to parameters in the original analysis. Explicitly, the modified curve shown assumes $\lambda/\sqrt{a_0} = 0{\cdot}05$, in the notation of Moravcsik, and is drawn for $R_0 = 1{\cdot}60$. From this, it is concluded that Beneventano's extrapolation showed too great an energy dependence at threshold, supporting Moravcsik's view. This is further borne out by the additional ratios obtained in the present work. Due to the lack of accurate ratios in the interesting low energy region, it was thought that the best curve fitted to the nine experimental points was just as significant as the above analysis. This is shown in figure 2 where the best curve gives a value of $R_0 = 1{\cdot}65$. It must not be overlooked that the rise in the extrapolated curve near pion threshold is fitted solely to two observed ratios at pion energies less than 20 MeV where it is more difficult to obtain accurate results. If any emphasis is to be placed on the extrapolated results, more accurate determinations of the ratio in this energy range must be made. The present work is being continued, both by the described technique and by a scintillation counter telescope system, and will be reported in full later.

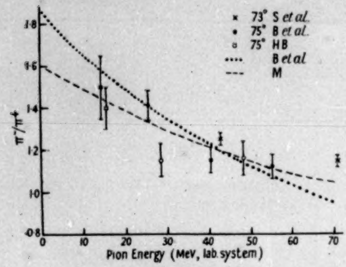

Figure 1.

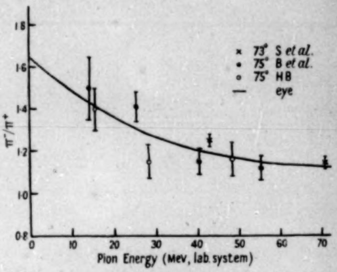

Figure 2.

π^-/π^+ ratio from deuterium as a function of pion energy, angles measured in the laboratory system.

S *et al.*, Sands *et al.* (1954) ; B *et al.*, Beneventano *et al.* (1956) ; HB, present work ; M, Moravcsik (1958) ; eye, curve fitted by eye.

To obtain the threshold π^-/π^+ ratio from free nucleons, a Coulomb correction must be applied to the measured ratios from deuterium. This correction is more important at lower pion energies. (For a discussion of this and other corrections see Moravcsik 1957.) If a 10% reduction is therefore applied to the measured ratios at the lowest pion energy (see figure 2), then the extrapolated ratio at pion threshold would be about 1·4, which is compatible with the field theory value. This conclusion is in agreement with Baldin (1958). A Coulomb correction of this magnitude and sign was estimated by Baldin (1958) who deduced that the π^-/π^+ ratio from free nucleons was constant in the photon energy range of 153 to 193 Mev. In Baldin's calculation of the Coulomb correction he made use of the results of Adamovich *et al.* (1956) who measured the cross section of the photoproduction of π^- mesons from deuterium.

The second important feature of this work concerns the s-wave pion–nucleon interaction, giving rise to the relationship between R_0, P and $\lambda_3 - \lambda_1$ (see for example Fischer, March and Marshall 1958). If the following experimental data are used

$$\lambda_3 - \lambda_1 = 0{\cdot}27 \pm 0{\cdot}02 \text{ (Orear 1956),}$$

$$\sigma_{\mathrm{T}}{}^{+} = (1{\cdot}43 \pm 0{\cdot}02) \times 10^{-28}\eta \text{ (Beneventano } et\ al. \text{ 1956),}$$

$$v_0 = 0{\cdot}20 \pm 0{\cdot}01 \text{ (Chinowsky and Steinberger 1954),}$$

where $\sigma_{\mathrm{T}}{}^{+}$ is the measured π^+ photoproduction cross section for the process $\gamma + \mathrm{p} \rightarrow \pi^+ + \mathrm{n}$, where η is the centre-of-mass momentum of the pion in units of μc where μ is the pion mass, and where v_0 is the centre-of-mass velocity of the π^0 meson in charge exchange scattering

$$\pi^- + \mathrm{p} \rightarrow \pi^0 + \mathrm{n}$$

and if it is assumed that the theoretical value of R_0 is correct, then the indirect calculation of the value of the Panofsky ratio is

$$P = 2{\cdot}4 \pm 0{\cdot}4.$$

This is to be compared with the observed measurements of P : 0·94 ± 0·20 Panofsky, Aamodt and Hadley (1951); 1·50 ± 0·15 Cassels *et al.* (1957); 1·60 ± 0·17 Kuehner, Merrison and Tornabene (to be published, reported by Cassels *et al.* 1957); 1·87 ± 0·10 Fischer, March and Marshall (1958). Hence from this there exists a discrepancy between the negative energy result of the Panofsky ratio measured from capture data, and that predicted from positive energy results of pion scattering and photoproduction. If one, however, considers the experimental determinations of P, it is manifest that this value is far from being firmly established.

There are at least two alternative explanations of this discrepancy: either the solution lies in the inaccuracy of the experimental data and in the neglect of possible corrections which should be used in deriving the relationship between them (e.g. the Noyes (1956) correction), or else there is a flaw in the basic physics of the problem. This latter view was adopted by Baldin (1958) who looked on the disparity in the value of P as evidence for thinking in terms of the two-component π^0 meson field hypothesis.

When one considers, however, the statistical errors of each of the experimental data involved in the scheme linking pion scattering and photoproduction, as well as overall uncertainties (e.g. the value of the s-wave total cross section of π^+ production is subject to beam calibration measurements), it is apparent that the problem may still be solved by making more accurate experimental measurements in all branches of this field. There are also some doubtful theoretical assumptions included in the above scheme which require further study. In particular, the Noyes (1956) correction, which accounts for the failure in isotopic spin conservation in the $(\pi^- + p \rightarrow \pi^0 + n)$ system, was estimated at 10% (whereby causing a corresponding decrease in the predicted value of P) when the analysis was adjusted using the early value of the Panofsky ratio of 0·94.

It is concluded that the present experimental situation is such that a solution of the above problem should first be sought in obtaining more reliable experimental data and by examining critically all possible theoretical corrections to the relationship between $\lambda_3 - \lambda_1$, P and R_0.

Note added in proof. Further measurements have yielded values of the π^-/π^+ ratio of 1·34 ± 0·08 for pions in the energy range 18–23 MEV, and 1·29 ± 0·07 for 36–44 MEV. These results add further weight to the argument given in the text.

ACKNOWLEDGMENTS

The authors wish to acknowledge the assistance given by Mr. H. C. Evans and Mr. D. B. Miller in the collection of data. We are grateful to Dr. W. McFarlane and his associates of the Synchrotron group for their co-operation during this experiment. We are indebted to Professor P. I. Dee and Professor J. C. Gunn for their encouragement and interest in this work.

REFERENCES

ADAMOVICH, M. I., VEKSLER, V. I., KUZMICHEVA, G. V., LARIONOVA, V. G., and KHARLAMOV, S. P., 1956, *Proceedings of CERN Symposium*, Geneva, 1956.
ANDERSON, H. L., and FERMI, E., 1952, *Phys. Rev.*, **86**, 794.
BALDIN, A. M., 1958, *Nuovo Cim.*, **8**, 569.

Beneventano, M., Bernardini, G., Carlson-Lee, D., Stoppini, G., and Tau, L., 1956, *Nuovo Cim.*, **4,** 323.
Cassels, J. M., Fidecaro, G., Wetherell, A. M., and Wormald, J. R., 1957, *Proc. Phys. Soc.* A, **70,** 405.
Chew, G. F., Goldberger, M. L., Low, F. E., and Nambu, Y., 1957, *Phys. Rev.*, **106,** 1345.
Chinowsky, W., and Steinberger, J., 1954, *Phys. Rev.*, **93,** 586.
Fischer, J., March, R., and Marshall, L., 1958, *Phys. Rev.*, **109,** 533.
Moravcsik, M. J., 1957, *Phys. Rev.*, **105,** 267 ; 1958, *Nuovo Cim.*, **7,** 442.
Noyes, H. P., 1956, *Phys. Rev.*, **101,** 320.
Orear, J., 1956, *Nuovo Cim.*, **4,** 856.
Panofsky, W. K. H., Aamodt, R. L., and Hadley, J., 1951, *Phys. Rev.*, **81,** 565.
Sands, M., Teasdale, J. G., and Walker, R. L., 1954, *Phys. Rev.*, **95,** 592.
Watson, K. M., Keck, J. C., Tollestrup, A. V., and Walker, R. L., 1956, *Phys. Rev.* **101,** 1159.

The Absolute Scale of Thermoelectric Power at High Temperature

By N. CUSACK and P. KENDALL
Department of Physics, Birkbeck College, London

MS. received 7th July 1958

The absolute thermoelectric power, S, of a conductor at absolute temperature T is defined by

$$S=\int_0^T \frac{\sigma_T}{T}\,dT \qquad \ldots\ldots(1)$$

where σ_T is the Thomson coefficient. The thermoelectric power of a couple made of conductors A and B is, with the usual sign convention,

$$P_{AB}=S_B-S_A. \qquad \ldots\ldots(2)$$

The problem of determining S was first solved by Borelius *et al.* (1932) by measuring P at temperatures for which one member of the couple was superconducting and therefore had $S=0$. The subject has recently been re-opened by Pearson and Templeton and they have used a superconductor of high transition temperature to re-establish the scale of thermoelectric power more firmly (Pearson and Templeton 1955, Christian *et al.* 1958).

The objects of the present note are to point out that a combination of measurements now available in the literature enables the absolute thermoelectric power scale to be extended to high temperatures, and to provide tables of S for each of several high melting point metals. These values are largely independent of one another and any, or all, of the metals might be used, where chemically suitable, for measuring the absolute thermoelectric power of an unknown material up to about 2000°K.

The main measurements drawn upon are: the recently published absolute scale for Pb up to 293°K; the extensive measurements of Borelius and co-workers; the measurements of the Thomson coefficients of Cu, Ag, Au, Pt, Pd, Mo, W from 400°K upwards by Lander (1948). The general method of calculation, subject to variation mentioned below, was to take Borelius's values of the thermoelectric power of a pure metal, M, versus Pb, in the region 100–300°K and to calculate S_M at, say, 200°K, from equation (2), using the S_{Pb} given by Pearson and Templeton. The values of σ_T measured by Borelius up to 300°K, were then joined smoothly on to those of Lander which start at 400°K, using independent intermediate values where possible. The (σ_T, T) curve was then used to calculate

S_M to high temperatures using equation (1). Since the new and old S_{Pb} scales differ by only 0·03 μv deg^{-1} at 20°K, any S_M computed from Borelius's P_{MPb} and the new scale will disagree by only this amount with the value used up till now.

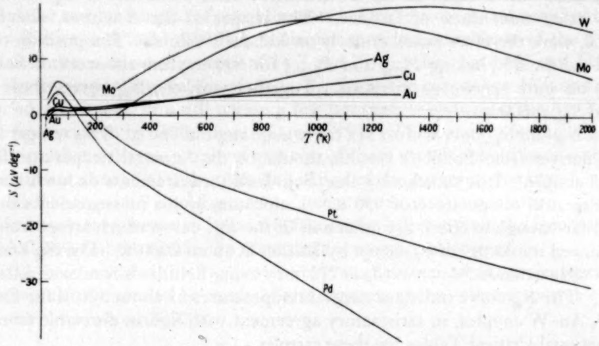

Cu, *Ag*, *Au*: for these metals smooth curves through Borelius's values of σ_T were joined to Lander's at 500°K. Lander's results are least accurate at the low temperature extreme of his measurements and, in the interest of smooth interpolation, the curves were allowed to depart from his 400°K observation by about 5%.

Pt: Lander's and Borelius's values of σ_T agree less well for Pt and, if appropriately extrapolated, give values at 250°K which differ by several μv deg^{-1}. Fortunately, Berg's measurements (1910) span the temperature gap and give values which lie numerically between those of Borelius and Lander. The extreme ends of the latter workers' measurement ranges were therefore discounted, and a curve drawn to join Borelius's values smoothly at 150°K, Lander's at 600°K, and to include Berg's in between. This curve and equation (1) were used to extend S_{Pt} from 273°K to high temperatures. To fix the values up to and including 273°K, the measurements of P_{PtPb} by Borelius were used together with the new S_{Pb} scale. P_{PtPb} measured by Bridgman and others and quoted in International Critical Tables would give values of S_{Pt} about 4% higher.

Pd: a disagreement between Lander's and Borelius's extrapolated values of σ_T makes another procedure desirable for Pd. Agreement between thermoelectric power measurements is more to be expected than between different determinations of σ_T. Probably the discrepancy here is in part due to the thermoelectric variability of Pd recently commented on by Barber and Pemberton (1955).

The latter workers investigated Pd–Ag couples and have given an e.m.f.–temperature curve from 200 to 600°C. S_{Pd} at 800°K was obtained from this, using equation (2) and the previously computed curve of S_{Ag}. This fixes the position of the S_{Pd} curve; its shape was obtained from Lander's results and equation (1). It is in fact a straight line. Agreement is good between this line and other values of S_{Pd} calculated from Barber and Pemberton's curve. Extrapolated back to 273°K, the line agrees well with Borelius's values corrected to the new S_{Pb} scale although there is a noticeable change of slope from low to high temperatures, not unlike that in S_{Pt}. Holborn and Day (1899) discuss two Pd specimens whose powers against Pt differ by several per cent. The average P_{PdPt} of these two is higher than the value of $S_{Pt} - S_{Pd}$, taken from the present curves, by 3% at 273°K and 9% at 1400°K.

W, *Mo*: there seem to be no extensive measurements of σ_T for these metals other than those of Lander. The shapes of the S curves, which are unusual, were therefore based entirely on Lander's values. The position of the curves was fixed by taking P_{PtW} and P_{PtMo}, for 600°K, from the work of Schulze (1932) on pure specimens *in vacuo*. Together with the S_{Pt} curve, these give S_W and S_{Mo} at 600°K.

The S_W and S_{Mo} curves cross at a fairly large angle at 960°K. This temperature, which derives from Lander's results, should be the 'neutral temperature' of a W–Mo couple. It is satisfactory that Schulze's measurements on such couples gave a neutral temperature of 950°K. Unfortunately his measurements do not extend far enough to check the inflection in the S_{Mo} curve which arises from the pronounced minimum of σ_T shown by Lander at about 2000°K. The S_W and S_{Mo} curves were extended downwards to 273°K by using Schulze's results and the S_{Pt} curve. The S_W curve indicates neutral temperatures of about 320°K for Cu–W, Ag–W, Au–W couples, in satisfactory agreement with figures derivable from the International Critical Tables for these couples.

Absolute Thermoelectric Powers (μv deg^{-1})

Metal T(°K)	Cu	Ag	Au	Pt	Pd	W	Mo
100	1·19	0·73	0·82	4·29	2·00	—	—
150	1·12	0·85	1·02	1·32	−1·63	—	—
200	1·29	1·05	1·34	−1·27	−4·85	—	—
273	1·70	1·38	1·79	−4·45	−9·00	0·13	4·71
300	1·83	1·51	1·94	−5·28	−9·99	1·07	5·57
400	2·34	2·08	2·46	−7·83	−13·00	4·44	8·52
500	2·83	2·82	2·86	−9·89	−16·03	7·53	11·12
600	3·33	3·72	3·18	−11·66	−19·06	10·29	13·27
700	3·83	4·72	3·43	−13·31	−22·09	12·66	14·94
800	4·34	5·77	3·63	−14·88	−25·12	14·65	16·13
900	4·85	6·85	3·77	−16·39	−28·15	16·28	16·86
1000	5·36	7·95	3·85	−17·86	−31·18	17·57	17·16
1100	5·88	9·06	3·88	−19·29	−34·21	18·53	17·08
1200	6·40	10·15	3·86	−20·69	−37·24	19·18	16·65
1300	6·91		3·78	−22·06	−40·27	19·53	15·92
1400				−23·41	−43·30	19·60	14·94
1600				−26·06	−49·36	18·97	12·42
1800				−28·66	−55·42	17·41	9·52
2000				−31·23	−61·48	15·05	6·67
2200						12·01	4·30
2400						8·39	2·87

The values of S are tabulated to 0·01 μv deg^{-1} but this does not indicate the absolute accuracy. The latter is rather difficult to estimate. At 18°K, the value of S_{Pb}, according to the recent measurement, is $-0{\cdot}78 \pm 0{\cdot}015$ μv deg^{-1}. At higher temperatures, S values still rely to some extent on the measurements by Borelius of the Thomson coefficient of his silver normal alloy, and his own estimate of error in S was $\pm 0{\cdot}1$ μv deg^{-1} at room temperature. The small value of σ_T for Au at high temperatures means that S_{Au} is not sensitive to large percentage errors in Lander's results; but this is less applicable to the other metals. An overall inaccuracy of about 5%, increasing near the high temperature cut-off of each curve, seems a reasonable estimate.

Apart from those already mentioned, further checks on the mutual compatibility of the S curves can be obtained from the e.m.f.–temperature curves in the literature for various couples of pure elements. One or two more examples will be given. Roeser and Dahl (1938) in their extensive measurements of the Pt–Cu couple find thermoelectric powers of 14·7 and 27·3 μv deg^{-1} at 600° and 1200°K, while the corresponding values of $S_{\mathrm{Cu}} - S_{\mathrm{Pt}}$ from the curves are 15·0 and 27·1. Less good agreement, but still within a few per cent, is shown by the Ag–Pt and Au–Pt figures given by Holborn and Day (1899). The S curves for Ag, Cu, and Au indicate that a thermocouple of any two of these metals should have a neutral temperature at about 500°K, but the disposition of the curves in this region is such that a small change in S would greatly influence the neutral temperature. In fact, neutral temperatures between 300 and 800°K can be inferred from the International Critical Tables but the data in the literature are not very consistent.

It may be concluded that the present curves allow several almost independent experimental estimates to be made of the absolute thermoelectric power of any conductor up to about 2000°K.

ACKNOWLEDGMENTS

The authors are indebted to Dr. W. B. Pearson for a copy of the absolute scale for Pb in advance of publication and to Dr. C. Barber for information about Pd.

REFERENCES

BARBER, C. R., and PEMBERTON, L. H., 1955, *J. Sci. Instrum.*, **32**, 486.

BERG, O., 1910, *Ann. Phys., Lpz.*, **32**, 447.

BORELIUS, G., KEESOM, W. H., JOHANSSON, C. H., and LINDE, J. O., 1932, *Proc. Acad. Sci., Amst.*, **35**, 10.

CHRISTIAN, J. W., JAN., J. P., PEARSON, W. B., and TEMPLETON, I. M., 1958, *Proc. Roy. Soc.* A, **245**, 213.

HOLBORN, L., and DAY, A., 1899, *Amer. J. Sci.* (Ser. 4), **8**, 308.

LANDER, J. J., 1948, *Phys. Rev.*, **74**, 479.

PEARSON, W. B., and TEMPLETON, I. M., 1955, *Proc. Roy. Soc.* A, **231**, 534.

ROESER, W., and DAHL, A., 1938, *J. Res. Nat. Bur. Stand.*, **20**, 342.

SCHULZE, A., 1932, *Z. Metallk.*, **24**, 206.

Diffraction by an Opaque Strip

BY R. S. LONGHURST

Physics Department, Chelsea College of Science and Technology, London

MS. received 3rd June 1958.

§ 1. EFFECT OF SOURCE WIDTH

In a two-beam interference experiment the visibility of the fringes is dependent upon the degree of coherence between the superposed disturbances. For example, in the arrangement shown in figure 1, S_1 and S_2 are equal very small apertures receiving light from the aperture S behind which there is an extended source. If S is of finite size the disturbances emerging from S_1 and S_2 are partially coherent and the visibility of the fringes in a plane such as AB is reduced below unity. It follows from the theory of partial coherence (Hopkins 1951) that for certain dimensions of S the degree of coherence is negative (i.e. has an argument of π). This means that the disturbances from S_1 and S_2 are effectively out of phase by π and that the fringes across AB are displaced relative to those formed with a very small primary slit S, the positions of the bright and dark fringes being interchanged.

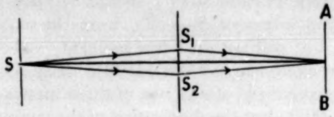

Figure 1. Light from two apertures.

Thompson (1958) has described an experiment employing circular apertures which confirms the existence of this effective phase change. It is, perhaps, worth noting that an experiment described in an earlier paper by Marković (1957) also confirms the existence of this phase change although this was not pointed out at the time. It is well known that if an opaque strip or wire is illuminated by light from a narrow slit source which is parallel to the strip (figure 2), the disturbances within the region of the geometrical shadow approximate closely to cylindrical wave envelopes diverging from the edges P_1 and P_2 of the obstacle and that the fringes that can be observed within the shadow can be looked upon as resulting from the interference between those two cylindrical wave envelopes. The arrangement is a useful one since it avoids the necessity of using two slits having very small and equal widths. Marković has discussed from first principles the effect of increasing the width of the source slit S.

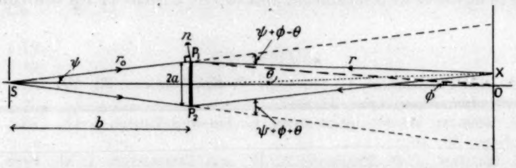

Figure 2. The opaque strip.

Now the complex degree of coherence between two points P_1 and P_2 in a plane illuminated by a uniform incoherent source of finite size is equal to the complex amplitude at one of the points P_1 in the diffraction pattern formed by a uniform wave emerging from an aperture whose boundaries are those of the source, the wave being focused on the other point P_2, and the pattern normalized in the usual manner.

In the present example the distance b from the slit to the obstacle is much larger than the width of the obstacle $2a$ and, since one may reduce the problem to one in two dimensions, the complex degree of coherence between P_1 and P_2 is effectively given by the familiar single slit expression $(\sin\alpha)/\alpha$ where in this case $\alpha = \pi s \, . \, 2a/b\lambda$, s being the width of the slit S. This may now be used to give the degree of coherence between the edge waves from P_1 and P_2 and to find the visibility of the fringes observed within the shadow. It will be seen that the degree of coherence, and hence the visibility of the fringes, falls to zero when $\alpha = p\pi$ (p integral), i.e. when $s = p\,(b/2a)\,\lambda$. This agrees exactly with the result obtained by Marković.

The expression $(\sin\alpha)/\alpha$ reaches extreme values, i.e. the fringes have maximum visibility, when $p = 0,\ 1{\cdot}4303,\ 2{\cdot}4590,\ 3{\cdot}4707\ldots$; $(\sin\alpha)/\alpha$ assumes negative values between alternative pairs of zeros and for the corresponding slit widths the disturbances from P_1 and P_2 are effectively out of phase by π; the central fringes are dark instead of bright. This occurs for values of p between 1 and 2, 3 and 4, 5 and 6, and so on, and is confirmed by the experimental results given by Marković.

§ 2. Variation of Visibility across the Pattern

As shown above, the edge waves are partially coherent when the source slit has finite width. The edge waves are also non-uniform in amplitude and, in consequence, the visibility of the fringes varies across the region of geometrical shadow. The form of this variation will be the same for all source slit widths; for a given width the partial coherence of the edge waves simply causes the visibility in every part of the pattern to be multiplied by γ_{12}.

Rubinowicz (1917) has transformed the Kirchhoff diffraction integral into a line integral along the edge of the diffracting screen and has derived an obliquity factor for the edge waves. It will be seen below that this leads to a simple expression for the fringe visibility across the shadow of an opaque strip. Sommerfeld (1896, 1949) has given a rigorous solution for the diffraction of a linearly polarized plane electromagnetic wave by a perfectly conducting infinite half-plane and has shown that except near the boundary of the geometrical shadow the disturbance within the shadow is of the form of an edge wave resembling that given by Rubinowicz.

As one moves away from the centre of the pattern the amplitude of one edge wave increases whilst that of the other decreases. Hence the variation in fringe visibility is very sensitive to errors in the obliquity factor for the edge waves. In what follows the fringe visibility derived from the Rubinowicz obliquity factor is compared with that derived from the exact Sommerfeld solution and with the experimental results given by Marković.

Rubinowicz discussed the problem of diffraction of light from a point source by a thin opaque screen and gave, for the disturbance at the point X within the region of geometrical shadow,

$$u = \frac{1}{4\pi}\int_l \frac{\exp(-ikr_0)}{r_0}\,\frac{\exp(-ikr)}{r}\,\frac{\cos(n,r)}{1+\cos(r,r_0)}\sin(r_0,dl)\,dl$$

where dl is an element of the diffracting edge, r_0 is the radius vector from the source to dl, r is the radius vector from X to dl, and n is the normal at dl to the cone defined by rays from the source to points on the diffracting edge.

Referring to figure 2, the opaque strip subtends angles 2ψ at the source and 2ϕ at the centre of the pattern. The position of the off-axis point X in the pattern is defined by the angle θ subtended at the centre of the strip. It will be assumed that all these angles are small so that $\angle P_1XP_2 \simeq 2\phi$ and $\angle XP_1O \simeq \angle XP_2O \simeq \theta$. It then follows from the diagram that for the element at P_1

$$\cos(n,r) = \sin(\psi+\phi-\theta), \quad \cos(r,r_0) = -\cos(\psi+\phi-\theta), \quad \sin(r_0,dl) = 1.$$

That is, one may write

$$\cos(n,r) = (\psi+\phi-\theta), \quad 1+\cos(r,r_0) = \tfrac{1}{2}(\psi+\phi-\theta)^2.$$

For the edge P_2 one has

$$\cos(n, r) = (\psi + \phi + \theta), \quad 1 + \cos(r, r_0) = \tfrac{1}{2}(\psi + \phi + \theta)^2, \quad \sin(r_0, dl) = 1.$$

One may, as usual, reduce the problem to the two-dimensional one illustrated in figure 2 and, since one need discuss only relative amplitudes, one can write, for the amplitudes at X due to the edge waves from P_1 and P_2,

$$I_1^{1/2} = \frac{2}{\psi + \phi - \theta}, \quad I_2^{1/2} = \frac{2}{\psi + \phi + \theta}$$

I_1 and I_2 being the relative intensities. The fringe visibility is then given by

$$V = \frac{2(I_1 I_2)^{1/2}}{I_1 + I_2} |\gamma_{12}| = \frac{(\psi + \phi)^2 - \theta^2}{(\psi + \phi)^2 + \theta^2} |\gamma_{12}|$$

or

$$V = \frac{1 - R^2}{1 + R^2} |\gamma_{12}| \qquad \ldots\ldots(1)$$

where $R = \theta/(\psi + \phi)$ and $|\gamma_{12}| = 1$ for a slit of infinitesimal width. For a plane incident wave one simply has $\psi = 0$ and $R = \theta/\phi$.

The form of the function (1) is shown by the broken curve in figure 3. It will be seen that V falls to zero when $R = 1$, i.e. when X is on the boundary of the geometrical shadow. It is to be expected that the formula will give this result and will cease to hold in this region since on the shadow boundary the Rubinowicz formula yields an infinite amplitude for the wave from the edge that casts the shadow.

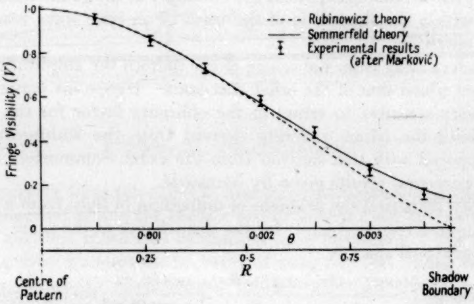

Figure 3. Variation of fringe visibility in the shadow of an opaque strip.

Sommerfeld has discussed the diffraction by a thin, perfectly conducting, infinite half-plane, of a plane wave linearly polarized with the electric vector parallel to the diffracting edge. His solution does not break down in the region of the shadow boundary and gives, for the amplitude u within the shadow,

$$\left|\frac{u}{u_0}\right| = \frac{1}{\sqrt{2}} |F(\infty) - F(\rho)|,$$

u_0 being the undisturbed amplitude, and $F(\rho)$ the Fresnel integral

$$\int_0^\rho \exp(i\tfrac{1}{2}\pi\tau^2)\, d\tau.$$

ρ is defined by $\rho = 2(kr/\pi)^{1/2}\sin\frac{1}{2}\delta$ where $k = 2\pi/\lambda$ and δ is the angle of diffraction. In figure 2 δ takes the values $\psi + \phi - \theta$ and $\psi + \phi + \theta$ at P_1 and P_2 respectively, i.e. $\phi - \theta$ and $\phi + \theta$ respectively for a plane incident wave.

Since one need discuss only relative intensities one may write, for the intensity within the shadow,

$$I = [\tfrac{1}{2} - C(\rho)]^2 + [\tfrac{1}{2} - S(\rho)]^2 \qquad \ldots\ldots(2)$$

where

$$C(\rho) = \int_0^\rho \cos\tfrac{1}{2}\pi\tau^2\,d\tau \quad \text{and} \quad S(\rho) = \int_0^\rho \sin\tfrac{1}{2}\pi\tau^2\,d\tau \quad \text{and} \quad C(\infty) = S(\infty) = \tfrac{1}{2}.$$

The fringe visibilities within the geometrical shadow of an opaque strip have been calculated by applying equation (2) to each diffracting edge. As a typical example, r was taken as 20 cm and the width of the strip was taken as 0·15 cm, giving $\phi = 0{\cdot}00375$. It would seem that these proportions are similar to those employed experimentally by Marković.

Except near the shadow boundaries, the values of $C(\rho)$ and $S(\rho)$ have been taken from Pearcey's tables (1956). Near the shadow boundaries the largest values of ρ lie beyond the range of the tables and the smallest values lie in a region in which interpolation is difficult. For these values of ρ, C and S have been computed from the usual series or asymptotic expressions. The resulting values of the fringe visibilities are shown in figure 3 by the unbroken curve. It is interesting to notice that the results derived from the Rubinowicz obliquity factor agree with those derived from the more rigorous theory of Sommerfeld for points that are not close to the shadow boundary. The disagreement is less than 10% over nearly three-quarters of the pattern.

Marković has recorded the intensity distribution across the fringes but does not give full details of the dimensions involved in his experimental arrangement. However, since the Rubinowicz theory applies to all source and screen distances, it is interesting to compare the results. Fringe visibilities have been estimated from the published curves of Marković and are indicated by the points on figure 3. The accuracy with which these calculations can be made is rather low and an estimate of the accuracy is indicated on the figure. It will be seen that the experimental results tend to follow the curve deduced from Sommerfeld's theory even though the latter applies strictly to a plane incident wave; they certainly show up the failure of the Rubinowicz formula near the shadow boundary.

REFERENCES

HOPKINS, H. H., 1951, *Proc. Roy. Soc.* A, **208,** 263.

MARKOVIC, B., 1957, *J. Opt. Soc. Amer.*, **47,** 1074.

PEARCEY, T., 1956, *Table of the Fresnel Integral* (Cambridge : University Press).

RUBINOWICZ, A., 1917, *Ann. Phys., Lpz.*, **53,** 257.

SOMMERFELD, A., 1896, *Math. Ann.*, **47,** 317; 1949, *Optics* (English translation 1954, New York : Academic Press).

THOMPSON, B. J., 1958, *J. Opt. Soc. Amer.*, **48,** 95.

Refractive Index of Non-Uniform Films

By O. S. HEAVENS† and J. C. KELLY‡

† Department of Physics, Royal Holloway College, University of London
‡ Physics Research Laboratories, University of Reading

MS. received 27th May 1958

§ 1. Introduction

The refractive index of a uniform film on a smooth substrate is conveniently measured by the Brewster angle method (Abelès 1949). Using light polarized with the electric vector parallel to the plane of incidence, the angle of incidence ϕ is measured at which the filmed and unfilmed surfaces have equal reflectance. The film index is given simply by $n=\tan\phi$. The equal reflectance condition is independent of film thickness although for certain thicknesses the discrimination around the Brewster angle is poor.

If a film is formed under changing external conditions, there arises the possibility that the refractive index throughout the film is not constant. The Brewster angle method of index measurement will give a result, even if the index of the film varies in a direction normal to the plane of the film. Further observations are, however, needed to distinguish uniform from non-uniform films. Such inhomogeneity could be detected by a detailed study of the state of polarization of light reflected by the surface but this calls for greater complexity of apparatus and considerable labour in calculating the results. It is of interest to examine whether simple reflectance measurements made at angles near to the Brewster angle can serve to indicate the presence of gradients in refractive index. The case dealt with below is that of a non-absorbing film on an absorbing substrate. The simplification to the case of a transparent substrate is trivial.

§ 2. Theory

Explicit expressions for the reflectance of a filmed, absorbing substrate are unrewardingly cumbersome. Calculation is conveniently done stepwise from the expression (1) giving the (amplitude) reflectance of the filmed surface in terms of the Fresnel coefficients r_1 and r_2:

$$R_f=\frac{r_1\,e^{i\delta}+r_2\,e^{-i\delta}}{e^{i\delta}+r_1r_2\,e^{-i\delta}} \qquad \ldots\ldots(1)$$

where, for the p-component,

$$r_1=\frac{n_0\cos\phi_1-n_1\cos\phi_0}{n_0\cos\phi_1+n_1\cos\phi_0} \qquad \ldots\ldots(2)$$

$$r_2=\frac{n_1\cos\Phi_s-(n_s-ik_s)\cos\phi_1}{n_1\cos\Phi_s+(n_s-ik_s)\cos\phi_1}. \qquad \ldots\ldots(3)$$

The light is incident at angle ϕ_0 in medium of refractive index n_0. n_1 is the film index and n_s-ik_s the substrate index.

$$n_0\sin\phi_0=n_1\sin\phi_1=(n_s-ik_s)\sin\Phi_s \qquad \ldots\ldots(4)$$

and δ is given by the path integral

$$\delta=\frac{2\pi}{\lambda}\int_0^d n_1\cos\phi_1\,dx \qquad \ldots\ldots(5)$$

where x is measured normal to the plane of the film of thickness d. For a uniform film δ reduces to the usual expression $(2\pi/\lambda)\, n_1 d \cos \phi_1$.

The value of δ depends on the form of the dependence of n_1 on x. For a film in which the refractive index changes linearly from n_1 to n_2 in a distance d, δ may be easily calculated.

$$\delta = \frac{\pi d}{\lambda(n_2 - n_1)} \left\{ n_2(n_2{}^2 - b^2)^{1/2} - n_1(n_1{}^2 - b^2)^{1/2} - b^2 \ln \left[\frac{n_2 + (n_2{}^2 - b^2)^{1/2}}{n_1 + (n_1{}^2 - b^2)^{1/2}} \right] \right\} \quad \ldots\ldots(6)$$

where $b = n_0 \sin \phi_0$.

The amplitude reflectance (p-component) of the uncoated substrate is given by

$$R_{\mathrm{p}} = \frac{n_0 \cos \Phi_{\mathrm{s}} - (n_{\mathrm{s}} - ik_{\mathrm{s}}) \cos \phi_0}{n_0 \cos \Phi_{\mathrm{s}} + (n_{\mathrm{s}} - ik_{\mathrm{s}}) \cos \phi_0}. \quad \ldots\ldots(7)$$

The real and imaginary parts of Φ_{s} are readily found from equation (4).

§ 3. ANALYSIS OF EXPERIMENTAL RESULTS

Reflectance measurements are made for the p-component of light incident on both coated and uncoated parts of the substrate for angles a few degrees either side of the Brewster angle for the film. On account of the variability shown in reported values of optical constants of metals, it is necessary to determine those for the surface under examination. This is done by fitting a reflectance-angle-of-incidence curve by trial-and-error. With reflectance measurements reliable to ± 0·5%, values of n_{s} and k_{s} in the neighbourhood of 2 can be determined to within ± 1–2%. From the intersection of the reflectance curves for the bare and coated substrates, the Brewster angle is found. Uniformity of the film index is checked by calculating the reflectance–angle-of-incidence curve for an assumed uniform film and comparing with the experimentally observed curve. In the results obtained for tantalum films, formed by evaporation and anodized in $N/10$ sodium sulphate electrolyte, the curves shown in the figure were obtained. The experimental points are seen to agree very closely with the curve calculated

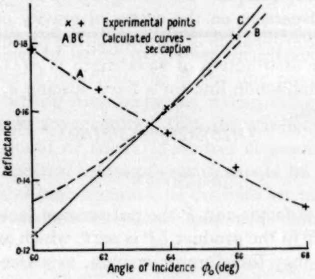

Reflectance–angle-of-incidence curves for anodic tantalum oxide film near the Brewster angle for the oxide.

A, uncoated metal with $n_{\mathrm{s}} = 2{\cdot}40$, $k_{\mathrm{s}} = 2{\cdot}09$; B, uniform oxide, $n = 2{\cdot}00$; C, oxide film with linear index gradient from 1·95 to 2·15.

for a non-uniform film in which the refractive index varies linearly from 1·95 to 2·15. It is of interest to note that the index obtained for such a film by the Brewster angle method lies significantly below the mean index of the film.

ACKNOWLEDGMENT

One of the authors (J. C. K.) is indebted to the Director of the Atomic Energy Research Establishment, Harwell, for financial support during the course of this work.

REFERENCE

ABELÈS, F., 1949, *C. R. Acad. Sci., Paris*, **228**, 553.

Effect of Lorentz Factor and Dispersion on Measurement of Lattice Parameters with Powder Cameras

BY E. R. PIKE AND A. J. C. WILSON
Viriamu Jones Laboratory, University College, Cardiff

MS. received 13*th June* 1958

THE widths of diffraction lines at high values of 2θ are largely due to the finite spread of wavelength in the characteristic radiation. In a recent paper Pike (1958, compare also Lang 1956) has given the effect of the Lorentz factor and dispersion on the centre of gravity of a diffraction line, in connection with the determination of accurate lattice parameters with the counter diffractometer. If the distribution of wavelength is $F(\lambda)$, then the distribution of intensity across a diffraction line for a fixed spacing d, say $Q(2\theta)$, is derived from the two equations,

$$Q(2\theta)\delta(2\theta)=LPF(\lambda)\delta\lambda \qquad \ldots\ldots (1)$$

and

$$\lambda=2d\sin\theta \qquad \ldots\ldots (2)$$

where L is the Lorentz factor and P the polarization factor. The only rapidly varying term at high 2θ in the product LP is $\sec\theta$, which arises from the Lorentz factor. Equation (1) may therefore be written, to a close approximation,

$$Q(2\theta)\delta(2\theta) \propto \sec\theta F(\lambda)\delta\lambda.$$

Since d is constant for a given line this may be expressed in the form

$$Q(2\theta)\delta(2\theta) \propto \sec\theta F(\lambda)\left[\frac{\partial\lambda}{\partial(2\theta)}\right]_d \delta(2\theta),$$

i.e.

$$Q(2\theta)\delta(2\theta) \propto \sec\theta F(\lambda)\cos\theta\,\delta(2\theta),$$

giving

$$Q(2\theta) \propto F(\lambda)=F(2d\sin\theta).$$

The profile can be thought of as 'stretched' at the high-angle end by the dispersion, and the drop in the ordinates, which would be expected if the integrated intensity were to be conserved, is made up exactly by the increase in intensity due to the Lorentz factor. Thus the Lorentz factor and the dispersion together cause no shift of the peak of a diffraction line but the centre of gravity is shifted to higher Bragg angles. There is an interesting difference between this effect and the normal geometrical aberrations, since the latter, as shown by Wilson (1950), cause identical shifts of centre of gravity and peak, to the first order of approximation, for lines in the back-reflection region.

It is generally appreciated that when the powder camera is used for accurate lattice-parameter determination, care must be taken to allow for subjective error in estimating the 'centres' of the diffraction profiles. Ekstein and Siegel (1949) have shown that one observer may choose consistently a different point from a second observer and that, in general, the standard deviation of a set of readings of the position of a given line is much smaller for a single observer than for a group of observers. Bradley and Jay (1932) state "... it is most natural to choose a point somewhere near the centre of the line, but where the line is not symmetrical there is a bias towards the blacker side. As a convenient approximation, we may suppose that measurement is made to the centre of gravity of blackening of the line ... [partial resolution of the α doublet] gives rise to an optical illusion. The α doublets appear to be further apart than is actually the case. ... This is a phenomenon which we have observed many times ...". Such considerations lead to the conclusion that it is not really known what particular characteristic of a line profile is singled out by any particular observer, but that for unresolved and well-resolved doublets it is probable that many observers will choose points nearer the centre of blackening or centre of gravity than to the point of maximum intensity. For partially resolved doublets the bias may be the other way.

In conjunction with the normal geometrical aberrations, such subjective errors will lead to values of lattice parameter on extrapolation which contain not only random errors of measurement of the line positions, but also errors, which may be larger, arising from using the wrong value of wavelength in the Bragg equation. If peaks are measured, then the wavelength of the peak of the spectral distribution should be used; if centres of gravity are measured then the wavelength of the spectral centre of gravity should be used. The difference is appreciable for work of high accuracy, as the lines are naturally asymmetrical. The extrapolation procedure in either case will eliminate the important geometrical aberrations.

In the case of the distortion of the line profiles by the dispersion and Lorentz factors, however, not only is the shift of centre of gravity different from that of the peak, but the error does not extrapolate to zero at 180° 2θ. The shift of centre of gravity is given by

$$\underset{(\text{c.g., rad})}{\Delta 2\theta} = c\frac{\beta^2}{\lambda^2}\tan^3\theta$$

(slightly modified from Pike 1958) where β is the spectral-line half-width and c is a constant depending on the line profile and on the amount of the line on either side of its 'centre' taken into account in the visual estimation of the centre of blackening. For a Cauchy profile c is of the order of 2 or 3. For the line used for illustration by Ekstein and Siegel (Zn 213, Cu$K\alpha$, at $\theta = 87{\cdot}5°$) the shift of centre of gravity amounts to 0·2 to 0·3° 2θ, or an error in lattice parameter of the order of 1 part in 10^4. This error is additional to any introduced by natural asymmetry of the line.

This line, of course, is unusually high, and also a typical subjective measurement will lie between the peak and centre of gravity, and hence will have an appropriately smaller error.

It is hoped that future work with the counter diffractometer with which accurate line profiles can be generated directly, will be of superior accuracy to present camera techniques, because of the elimination of subjective effects and also the effects of film graininess. Film graininess sets a limit to the accuracy obtainable with a camera, of the same nature as the limit set by statistical fluctuations in measurements with a counter diffractometer. The latter, however, may in principle be reduced to any desired extent by increasing the time of counting. Such counter data, when available, will be of great interest in shedding more light on the problem of subjective errors in film measurement, and hence of the ultimate accuracy of the powder camera.

REFERENCES

BRADLEY, A. J., and JAY, A. H., 1932, *Proc. Phys. Soc.*, **44**, 563.
EKSTEIN, H., and SIEGEL, S., 1949, *Acta Cryst., Camb.*, **2**, 99.
LANG, A. R., 1956, *J. Appl. Phys.*, **27**, 485.
PIKE, E. R., 1958, *Acta Cryst., Camb.*, in the press.
WILSON, A. J. C., 1950, *J. Sci. Instrum.*, **27**, 321.

A Method of Studying Surface Barrier Height Changes on Transistors

BY J. R. A. BEALE, D. E. THOMAS AND T. B. WATKINS
Mullard Research Laboratories, Salfords, Redhill, Surrey

MS. received 20th June 1958

§ 1. INTRODUCTION

A NUMBER of transistor parameters depend upon the properties of the surface of the base material surrounding the emitter and collector junctions and in recent years the knowledge of these properties particularly with regard to germanium has considerably increased (Kingston 1956). It is known that changes of transistor parameters can occur with time and with changes of ambient atmosphere and temperature. These changes are evidently associated with variations in the properties of the surface, but so far the known methods of investigating surfaces have not been applied to the working surfaces of a transistor.

Two of the most useful methods of studying surfaces are that of the field effect and the Bardeen–Brattain ambient cycle (1953). In these, a transverse field is produced at the surface and the induced charge changes the surface barrier height. This causes the surface conductance to vary and also the surface recombination velocity s.

In a transistor the main effects of barrier height changes are variations in s and possible channel formation around the collector junction. This paper deals with the first of these two effects.

§ 2. THE VARIATION OF α' WITH BARRIER HEIGHT

One of the most sensitive of transistor parameters to changes of surface condition is α', the collector to base current gain which may be expressed as $\alpha' = \alpha/(1-\alpha)$ where α is the emitter to collector current gain.

Assuming an emitter efficiency of unity $1-\alpha$ becomes that fraction of the emitter current that is lost by recombination in the base. For a p–n–p alloy junction structure neglecting bulk recombination, this may be written as

$$I_{\mathrm{e}}(1-\alpha)=Ase(p_{\mathrm{e}}-p_{\mathrm{n}}) \qquad \ldots\ldots(1)$$

where A is the effective recombination area around the emitter, e the electronic charge, p_{e} the hole concentration at emitter, and p_{n} the equilibrium hole concentration.

We therefore have approximately

$$\alpha'=1/ks \qquad \ldots\ldots(2)$$

where k is a constant for a fixed emitter current. Changes in A with s are neglected as the transverse diffusion length in the base is largely controlled by the reverse biased collector junction.

Variations in s can occur in two ways, firstly by a change in the barrier height, and secondly by a change in the number or energy level of the recombination centres. The variation of s with barrier height has been studied by Stevenson and Keyes (1954) and it as been shown by Many and Gerlich (1957) that small changes in the recombination centres occur with alterations in the ambient atmosphere. The barrier height can be altered by the Bardeen–Brattain ambient cycle and to a smaller extent by the application of a transverse field to the surface. Neglecting the small changes in the recombination centres a variation of α' with barrier height should be observed which is the inverse of the usual curve s of plotted against barrier height.

It should also be pointed out that the collector reverse current (with zero emitter current) is a function of the barrier height of the surface around the emitter junction and, provided channel effects around the collector are prevented, curves of s against barrier height may also be observed in a similar manner to that of Thomas and Rediker (1956).

§ 3. METHOD

3.1. *General*

Equation (2) shows that α' varies inversely with s and therefore the effects of changes in s in the transistor can readily be seen by using the simplified expression

$$I_{\mathrm{c}}=I_{\mathrm{b}}\alpha' \qquad \ldots\ldots(3)$$

which by partial differentiation gives

$$\delta I_{\mathrm{c}}=I_{\mathrm{b}}\delta\alpha'+\alpha'\delta I_{\mathrm{b}}. \qquad \ldots\ldots(4)$$

By differentiating (2) and substituting for $\delta\alpha'$ in (4)

$$\delta I_{\mathrm{c}}=-I_{\mathrm{b}}\alpha'\frac{\delta s}{s}+\alpha'\delta I_{\mathrm{b}}. \qquad \ldots\ldots(5)$$

By maintaining a constant base current the second term can be made zero. Therefore changes in barrier height can be seen as changes in collector current whether they are induced by alteration of the ambient or by the field effect.

When using the field effect it is necessary to use an alternating voltage of a sufficiently high frequency to prevent the slow states from reaching equilibrium. The voltage can also be readily applied to the X plates of an oscilloscope, the collector voltage being applied to the Y plates. Since s is a function of the barrier height ϕ_s of the form shown in the figure, it is evident from equation (5) that the oscilloscope trace will be roughly similar to this curve. It will not be exactly similar because the barrier height is not linearly related to the field. It will therefore indicate the sign and relative magnitude of ϕ_s in different ambients, the curvature of the trace being valuable in differentiating between parts of the curve at which the tangents are parallel.

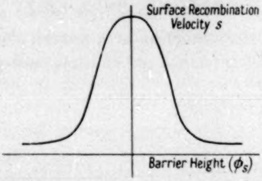

Surface recombination velocity s as a function of barrier height ϕ_s.

3.2. *Discussion of Assumptions and Simplifications*

3.2.1. *Effect of using a small probe.*

It is impossible to apply the field effect quite uniformly to the base region, and in fact in our experiments there was no attempt to do so, a probe being used. The general effects of this can readily be seen by splitting the right-hand side of equation (1) into two terms, which leads to

$$I_e(1-\alpha)=I_b=(A_1s_1+A_2s_2)e(p_e-p_n) \qquad \ldots\ldots(1\,a)$$

and hence to

$$\alpha'=\frac{1}{k_1s_1+k_2s_2} \qquad \ldots\ldots(2\,a)$$

where the parameters have the same meanings as in equations (1) and (2), but the suffix 1 indicates the region under the probe and suffix 2 the region outside the probe.

If, in a given ambient, the mean value of s_1 equals s_2, small changes in s_1 can readily be shown to give changes in α' such that

$$\frac{\delta\alpha'}{\alpha'}=-\frac{\delta s_1}{s_1}\left(\frac{k_1}{k_1+k_2}\right). \qquad \ldots\ldots(6)$$

This expression is identical with that obtained by differentiation of (2) except for a constant factor which is simply the ratio of the effective area under the probe to the total effective area. Therefore the significance of the observations is the same whether a small probe or a complete ring is used.

3.2.2. *Variation of signal with I_b.*

Equation (3) gives a simplified expression for I_c. A much more accurate expression for I_c in the working range is

$$I_c=(I_b+I_{co})\alpha'+I_{co}-c_1 \qquad \ldots\ldots(3\,a)$$

where I_{co} is the collector saturation current and c_1 is an arbitrary constant to allow for transistor non-linearity at low currents. If I_{co} is due to carriers generated at the surface it may be written as c_2/α' and equation (5) becomes

$$\delta I_c=-(I_b\alpha'-I_{co})\frac{\delta s}{s}+\alpha'\delta I_b. \qquad \ldots\ldots(5\,a)$$

Therefore, if $I_{co} \ll I_b\alpha'$, changes in I_c with changing values of s will be very nearly proportional to I_b.

3.2.3. *Frequency dependence of signal.*

Although the current reaching the base terminal can be maintained constant by feeding the base from a high resistance source, the value of I_b which must be used in all these equations is the sum of the base current and the capacitive charging current to the probe. Therefore δI_b in equation (5 *a*) will not be zero but will be approximately proportional to frequency, and will give rise to changes in I_c which are 90° out of phase with the required signal. If the frequency is too high the oscilloscope trace will start to become elliptical and the shape will become difficult to interpret. Since the minimum operating frequency is limited by the slow states it is important to arrange that most of the area of the probe is effective in changing α' and not merely in inducing capacitive currents.

3.2.4. *Operation in grounded base.*

Similar equations can readily be written down for operation in grounded base, and from these it is evident that in this configuration the signal is less by a factor of approximately $1+\alpha'$. They also show that changes in temperature are relatively as important as in grounded emitter, but the well-known positive feedback, due to I_{co}, between dissipation and temperature is reduced. Changes in collector current due to capacitive currents will also be relatively smaller, so grounded base may be better in certain cases in spite of the reduced sensitivity.

§ 4. APPARATUS

The transistor was connected in the grounded emitter configuration, the base being current fed from a high impedance source. A probe was placed perpendicular on to the base material adjacent to the emitter pellet. The transistor and probe were enclosed in a temperature controlled gas chamber, the d.c. supplies and a.c. signal being connected externally.

The signal appearing at the collector, due to the field effect should either be in phase with the signal on the probe, or 180° out of phase according to whether the surface is n- or p-type.

§ 5. RESULTS

A p–n–p alloyed junction transistor was used in the Bardeen–Brattain ambient cycle between the extremes of ozone to wet nitrogen. The resulting patterns on the oscilloscope when joined together gave a curve that is the inverse of that shown in the figure. The wet ambient drives the surface n-type, while the ozone drives the surface p-type. It was noticed that at any particular part of the curve, the slope was proportional to the base current as was expected from equation (5 *a*). The frequency of the alternating field used in these experiments was 30 c/s. With the size of probe used, the frequency range 20–80 c/s could be used without capacitive current tending to make the curve elliptical or the slow states coming into equilibrium, causing the amplitude to be decreased.

It has been observed that the addition of certain impurities to the encapsulant increases α', e.g. the addition of a small amount of water. It was decided to observe what change in barrier height and α' occurred when the dry ambient surrounding the transistor was replaced by one having a 10% relative humidity. The results of this experiment are set out in the table. The introduction of moisture on to the transistor surface has increased the barrier height on the n-type side, so reducing the surface recombination velocity and increasing the α' of the transistor.

Time and Ambient	α'	Oscilloscope Trace	Slope
Start of cycle. Dry oxygen	29·5		1·07
10 min. after changing to wet oxygen	40		1·43
3 hrs. after changing to wet oxygen	41		1·14
10 min. after changing back to dry oxygen	30		1·11
3 hrs. after changing back to dry oxygen	29·5		1·07

§ 6. CONCLUSION

A method has been developed for studying the causes of the variation in transistor parameters with changing ambient conditions. The technique may be readily applied to all transistors, and should give valuable information on problems of stability and ageing.

REFERENCES

BARDEEN, J., and BRATTAIN, W. H., 1953, *Bell Teleph. Syst. Tech. Publ.*, **82,** 1.

KINGSTON, R. H., 1956, *J. Appl. Phys.*, **27,** 101.

MANY, A., and GERLICH, D., 1957, *Phys. Rev.*, **107,** 404.

STEVENSON, D. T., and KEYES, R. J., 1954, *Proc. International Conference on Semiconductors*, Amsterdam, p. 1041.

THOMAS, J. E., and REDIKER, R. H., 1956, *Phys. Rev.*, **101,** 984.

The Vibrational Spectrum and Specific Heat of Germanium

BY F. A. JOHNSON AND J. M. LOCK

Royal Radar Establishment, Great Malvern, Worcs.

MS. received 14*th July* 1958, *and in final form* 7*th August* 1958

THE lattice–vibration spectrum of germanium has recently been investigated by Brockhouse and Iyengar (1958 a, b) using the technique of neutron spectrometry. This note describes the results of correlating these measurements with the experimentally determined specific heat of germanium at low temperatures (Hill and Parkinson 1952, Estermann and Weertman 1952, Keesom and Pearlman 1952, 1953).

The atomic heat of a crystal can be expressed as

$$C_\nu = -\frac{1}{r}\int_0^\infty n(\nu)\,\frac{\partial^2}{\partial\nu\partial T}E(\nu, T)\,d\nu \qquad \ldots\ldots(1)$$

where $E(\nu, T) = \boldsymbol{h}\nu/\{\exp(\boldsymbol{h}\nu/\boldsymbol{k}T) - 1\}$, r is the number of atoms per unit cell (2 for germanium), and where $n(\nu)$ is the integrated distribution function of the modes of vibration given by

$$n(\nu) = \int_0^\nu \rho(\nu)\,d\nu \qquad \ldots\ldots(2)$$

where $\rho(\nu)$ is the number of modes per unit range of frequency (ν) for N unit cells. $n(\nu)$ increases monotonically from 0 at $\nu=0$ to $3rN$ for frequencies greater than or equal to the maximum vibrational frequency. The double derivative can be calculated exactly, so that a knowledge of $n(\nu)$ suffices to calculate the specific heat.

Brockhouse and Iyengar (1958b) give the complete frequency–wavenumber (k) relations for germanium for vibrations in the 100 and 111 directions, and in addition a few results in other directions. A fact of the greatest importance which emerges from their work is the extraordinarily low frequency of the transverse acoustic branch of the spectrum at the reduced-zone edge compared with the frequencies at the edge of all other branches. Excitation of this branch is therefore the dominant factor in the specific heat of germanium over the most interesting temperature range, 0°K to about 50°K.

In calculating $n(\nu)$ we have adopted the following simple, though necessarily rough, procedure. $n(\nu)$ is proportional to the volume enclosed by the surface of constant frequency ν in wavenumber space. Accurate construction of these surfaces is not possible with the available data, but an approximation has been made (for the transverse acoustic branch) by taking three spheres, one of radius k_{100}, another of radius k_{111}, and a third of radius k_{110}, where k_{100}, k_{111} and k_{110} are the wavenumbers of the modes of frequency ν propagated along the 100, 111 and 110 axes respectively. A mean volume has been calculated by weighting the volumes of these spheres in proportion to the number of directions in k-space appropriate to each axis, namely 6 for the 100, 8 for the 111 and 12 for the 110 axis. To make up for the lack of detailed information about the (ν, k) relation along the 110 axis a smooth curve has been drawn for this direction joining the measured point at the zone edge to the mean slope at the origin calculated from the elastic constants.† The weighted mean volume obtained in this way for frequencies up to the maximum of the transverse acoustic branch is within 2% of the total volume of the reduced Brillouin zone. The calculated values have therefore been scaled by this small amount to give the correct total volume. For the longitudinal acoustic and the longitudinal and transverse optical branches we have less detailed information, since the frequencies at the zone edge in the 110 direction were not measured. We have therefore taken two spheres only, and the weighted mean volume in this case requires a larger scaling correction of about 17% to give the correct volume. (For the optical branches it is the difference between the volume enclosed by the constant energy surface and that of the complete zone which gives their contribution to $n(\nu)$.) These branches are, however, much less important in the calculation of the specific heat, and errors in their contribution to $n(\nu)$ are unlikely to be serious.

The complete $n(\nu)$ curve is shown in figure 1. The ordinate gives the number of modes of vibration per unit cell of 2 atoms. Each transverse branch contributes 2 and each longitudinal branch 1, thus making up the total of 6 per unit cell when the Raman frequency 9×10^{12} c/s is reached. The three pronounced steps at frequencies of 1·96, 2·46 and $3{\cdot}54\times10^{12}$ c/s represent the rapid expansion of the constant frequency surface as it nears the zone edge in the 111, 100 and 110 directions respectively. The third of these steps brings the value of $n(\nu)$ up to 2·07, so that at this point the contribution of the longitudinal acoustic branch is only 3½% that of the transverse. At frequencies less than 10^{12} c/s ν is proportional to k, and $n(\nu)$ is therefore proportional to ν^3.

† There are, of course, two distinct transverse acoustic branches in the 110 direction having a common point at the edge of the zone. We have, for the purpose of the calculation, assumed a mean curve for the two branches in this direction.

Using these values of $n(\nu)$ the integrand of equation (1) has been plotted as a function of ν at various temperatures, and by numerical integration corresponding values of the atomic heat have been obtained. These are represented in figure 2 by the customary plot of Θ_D against T, and are compared with the experimental values of various workers.

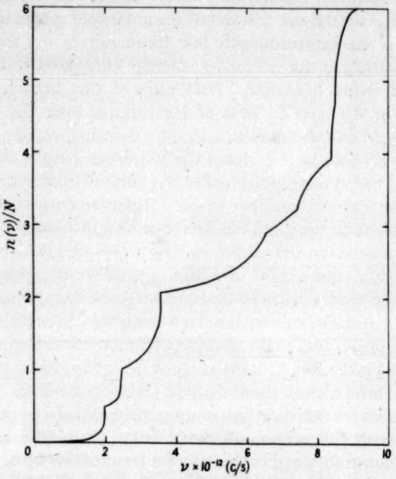

Figure 1. The integrated distribution function for germanium.

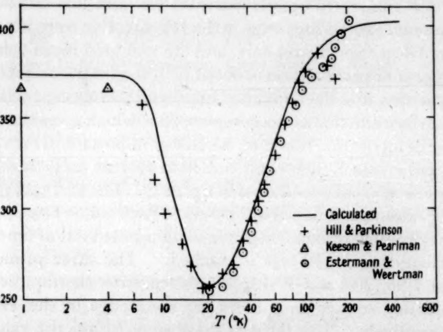

Figure 2. Variation of Θ_D with temperature for germanium.

The excellent agreement with the measured specific heat does not imply that the calculated $n(\nu)$ curve is accurate in detail, particularly for large ν for which the specific heat is comparatively insensitive to the exact values of $n(\nu)$. It is improbable, however, that the remarkable dip in Θ_D from about 370°K at 5°K to 256°K at

20°K can be accounted for other than by the rapid rise in $n(\nu)$ up to about 0·5 per unit cell at $1{\cdot}96 \times 10^{12}$ c/s, thus providing confirmation of the unusually low frequency at the zone edge of the transverse acoustic branch in germanium. The true $n(\nu)$ relation is unlikely to show the sharp changes of gradient seen in figure 1, but a slight smoothing of the curve does not greatly affect the agreement with the specific heat, and indeed a less sharp fall of $n(\nu)$ below $1{\cdot}96 \times 10^{12}$ c/s has the effect of increasing the specific heat just below 20°K, thus lowering Θ_D in even better agreement with the experimental values.

We thus see that the (ν, k) relation for germanium obtained by neutron spectrometry is consistent with the observed low temperature specific heat. While this was to be expected, it provides for the first time an interesting direct confirmation in the case of germanium of the correctness of lattice vibration theory in its application to the calculation of specific heats.

ACKNOWLEDGMENTS

We are most grateful to Drs. Brockhouse and Iyengar for permission to make use of their results prior to publication.

This paper is published by permission of the Controller, H.M. Stationery Office.

REFERENCES

BROCKHOUSE, B. N., and IYENGAR, P. K., 1958 a, *Bull. Amer. Phys. Soc.*, **3,** 192; 1958 b, *Phys. Rev.*, in the press.

ESTERMANN, I., and WEERTMAN, J. R., 1952, *J. Chem. Phys.*, **20,** 972.

HILL, R. W., and PARKINSON, D. H., 1952, *Phil. Mag.*, **43,** 309.

KEESOM, P. H., and PEARLMAN, N., 1952, *Phys. Rev.*, **85,** 730; 1953, *Ibid.*, **91,** 1347.

The Temperature Variation of the Concentration of Impurity Carriers in Silicon

BY E. H. PUTLEY
Royal Radar Establishment, Great Malvern, Worcs.

MS. received 30*th July* 1958

DISCUSSION of the variation of the electron concentration with temperature in semiconductors has frequently been based upon the expression

$$\frac{n(N_A+n)}{N_D-N_A-n} = \left(\frac{2\pi m^* \boldsymbol{k} T}{h^2}\right)^{3/2} \exp\left(\frac{E}{\boldsymbol{k}T}\right) \qquad \ldots\ldots(1)$$

(Wilson 1953). A corresponding expression can be written for holes. This assumes that only one group of impurity levels of energy E (zero energy at bottom of conduction band) need be considered and that each level can accommodate one electron which may have either spin. n is the concentration of conduction electrons, m^* is the density of states effective mass, N_D is the concentration of donor levels of energy E and N_A is the concentration of deep acceptor levels. A more general case, taking into account the excited states of the impurity centre, has been considered by Shifrin (1944), Landsberg (1956) and Conwell (1955). A more general form of (1) can be written

$$\frac{n(N_A+n)}{N_D-N_A-n} = \frac{N_c}{F} = \Phi \qquad \ldots\ldots (2)$$

where

$$N_c = 2\left(\frac{2\pi m^* kT}{h^2}\right)^{3/2}$$

and

$$F = \sum_i g_i \exp\frac{-E_i}{kT}$$

where g_i is the degeneracy of the ith level energy E_i. Putting $g_1 = 2$, $E_1 = E$ and neglecting the excited states (2) reduces to (1).

To compare the results obtained from (2) with those from (1) it is convenient to re-write (2)

$$\frac{n(N_A+n)}{N_D-N_A-n} = \frac{2}{g_1}\left(\frac{2\pi m^* kT}{h^2}\right)^{3/2} \exp\frac{E_1}{kT}\left\{1+\sum_2^\infty \frac{g_i}{g_1}\exp\frac{E_1-E_i}{kT}\right\}^{-1}. \qquad \ldots\ldots (3)$$

A corresponding expression can be written for holes. With the detailed information now available on the groups III and V impurity centres in silicon, it is possible to apply (3) to the analysis of the temperature variation of the impurity concentration.

To consider specific examples, figure (1) shows energy level schemes for boron and phosphorus impurities in silicon based on theoretical studies by Kohn (1957) and optical data of Hrostowski and Kaiser (1958) and of Picus, Burstein and Henvis (1956). In a recent paper (Putley and Mitchell 1958) the properties of silicon containing these impurities has been discussed, making use of equation (1). It will therefore be of interest to consider the extent to which the conclusions reached are modified by employing (3) together with the energy level scheme shown in the figure.

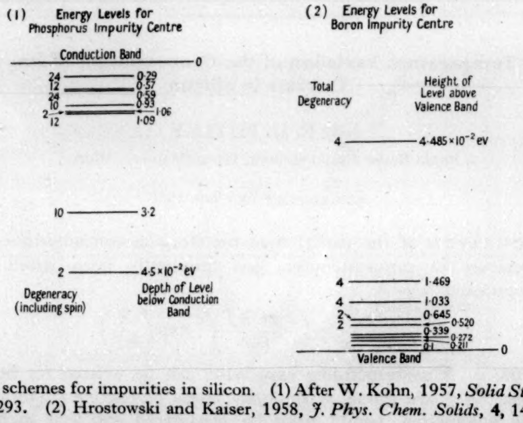
(1) Energy Levels for Phosphorus Impurity Centre
Conduction Band
0
24
12
24
10
2
12
0·29
0·57
0·59
0·93
1·06
1·09
10
3·2
2
4·5×10⁻²eV
Degeneracy (including spin)
Depth of Level below Conduction Band
(2) Energy Levels for Boron Impurity Centre
Total Degeneracy
Height of Level above Valence Band
4
4·485×10⁻²eV
4
1·469
4
1·033
2
2
0·645
0·520
0·339
0·272
0·211
0·1
0
Valence Band

Energy level schemes for impurities in silicon. (1) After W. Kohn, 1957, *Solid State Physics*, **5**, 293. (2) Hrostowski and Kaiser, 1958, *J. Phys. Chem. Solids*, **4**, 148.

First, at temperatures between 20° and 50°K, the electron or hole concentration varies exponentially with reciprocal temperature. Considering the values of the term

$$\left\{1+\sum_{2}^{\infty}\frac{g_i}{g_1}\exp\frac{E_1-E_i}{kT}\right\}$$

in (3) shows that over the temperature range used for determining the thermal energy level, the correction introduced in the case of boron will be less than 1%, which is smaller than the experimental error. For phosphorus, there will be a small correction from the first term of the summation, but the higher terms may be neglected. This correction arises from the splitting of the degenerate ground state into two groups of states with a relatively small energy separation. If Kohn's value for the separation between the lower 1S states and the higher 1S states is used, then the correction increases the distance of the thermal energy level below the conduction band from 0·045 to 0·046 ev.

In employing (2) to determine the concentration of impurity centres it is convenient to solve it for n, writing the solution

$$n=\tfrac{1}{2}(\Phi+N_A)\left\{\left[1+\frac{4(N_D-N_A)\Phi}{(\Phi+N_A)^2}\right]^{1/2}-1\right\}; \qquad \ldots\ldots (4)$$

if

$$\frac{4(N_D-N_A)\Phi}{(\Phi+N_A)^2}\ll 1$$

the solution becomes

$$n=\frac{(N_D-N_A)\Phi}{\Phi+N_A}. \qquad \ldots\ldots (5)$$

Two cases are important. First, at low temperature $\Phi \ll N_A$, then

$$n=\frac{N_D-N_A}{N_A}\Phi. \qquad \ldots\ldots (6)$$

This case leads to the exponential variation of n with $1/T$. Secondly, at high temperature $\Phi \gg N_A$. Then

$$n=N_D-N_A \qquad \ldots\ldots (7)$$

Thus n is independent of temperature. This is the so-called 'exhaustion range' when all the electrons are excited into the conduction band. Between these two limiting cases it will usually be necessary to calculate n using the complete expression (4). In highly compensated material it may be permissible to use (5) instead of (4) everywhere, for it is easily seen that $4(N_D-N_A)\Phi/(\Phi+N_A)^2$ has a maximum value of $(N_D-N_A)/N_A$ when $\Phi=N_A$ and if, as may happen, $(N_D-N_A)/N_A \ll 1$, the approximation leading to (5) will be valid at all temperatures. The temperature at which $\Phi=N_A$ corresponds to the intersection of the two limiting expressions (6) and (7) and this fact may be used as a means of determining N_A. Lee (1957) has proposed a method which depends upon measuring the difference between the exhaustion concentration N_D-N_A and the value of n at the temperature at which $\Phi=N_A$. This method has the advantage that the explicit value of Φ is not required but it has the disadvantage that in some cases the difference required is small and cannot be determined reliably from experimental results. In order to get over this difficulty it is necessary to assume a value for Φ. This implies assuming values for the energy levels, the degree of degeneracy and the density of states effective mass. The majority of energy levels can be determined from experimental data, but at present it is necessary to rely on theoretical estimates to determine the splitting between the donor 1S levels. The degeneracy must be determined from theoretical considerations based upon knowledge of the band structure and the characteristics of the impurity levels (Kohn, 1957) and the effective mass from a combination of knowledge of the band structure and data from experiments such as cyclotron resonance (Lax and Mavroides 1955). For silicon and germanium there seems to be sufficient detailed knowledge to justify the calculation of Φ for use in the determination of impurity level concentrations. The procedure is then to measure n at temperatures where the limiting cases (6) and (7) are valid and, assuming Φ, to solve for N_A and N_D.

The procedure used by Putley and Mitchell (1958) was of this type, but the data presented in that paper have been recalculated to take into account the first state above the ground state for phosphorus impurities. For boron only the ground state need be included in (3) but Kohn considers that the degeneracy factor should be 4 not 2, as has been previously assumed by many workers. In the table the results previously obtained, using equation (1), are compared with those now obtained employing (3) and the more detailed information now available on the properties of the impurity levels.

Comparison of Results calculated from equation (1) with those obtained using equation (3)

Specimen No.	Dominant impurity	Eqn.	Thermal ionization energy (ev)	N_A (cm^{-3})	N_D (cm^{-3})
ZG 131	P	(1)	0·045	$1{\cdot}8\times10^{13}$	$2{\cdot}0\times10^{13}$
		(3)	0·046	$1{\cdot}1\times10^{13}$	$1{\cdot}3\times10^{13}$
ZG 133	B	(1)	0·043	$5{\cdot}3\times10^{13}$	$4{\cdot}7\times10^{13}$
		(3)	0·043	$2{\cdot}9\times10^{13}$	$2{\cdot}3\times10^{13}$
ZG 136	B	(1)	0·043	$3{\cdot}5\times10^{13}$	$3{\cdot}3\times10^{13}$
		(3)	0·043	$1{\cdot}8\times10^{13}$	$1{\cdot}6\times10^{13}$

In these calculations the following values were used for the density-of-states effective masses: electrons $m^*/m = 1{\cdot}0$, holes $m^*/m = 0{\cdot}6$.

The data presented in the table show that the results of analyses of carrier concentration data based on the use of equation (1) may be considerably modified when detailed knowledge of the various impurity centres becomes available.

ACKNOWLEDGMENTS

The author would like to thank Dr. T. P. McLean for helpful discussions. This note is published by permission of the controller, H.M. Stationery Office.

REFERENCES

CONWELL, E. M., 1955, *Phys. Rev.*, **99**, 1195.
HROSTOWSKI, H. J., and KAISER, R. H., 1958, *J. Phys. Chem. Solids*, **4**, 148.
LANDSBERG, P. T., 1956, *Proc. Phys. Soc.* B, **69**, 1056
KOHN, W., 1957, *Solid State Physics*, **5** (New York : Academic Press Inc.), p. 257.
LAX, B., and MAVROIDES, J. G., 1955, *Phys. Rev.*, **100**, 1650.
LEE, P. A., 1957, *Brit. J. Appl. Phys.*, **8**, 340.
PICUS, G. S., BURSTEIN, E., and HENVIS, B., 1956, *J. Phys. Chem. Solids*, **1**, 75.
PUTLEY, E. H., and MITCHELL, W. H., 1958, *Proc. Phys. Soc.*, **72**, 193.
SHIFRIN, K. S., 1944, *J. Tech. Phys., Moscow*, **14**, 43.
WILSON, A. H., 1953, *Theory of Metals* (Cambridge : University Press), p. 115.

Experimental Determination of Electron Temperature in High Electric Fields applied to Germanium

By E. G. S. PAIGE

Royal Radar Establishment, Great Malvern, Worcs.

MS. received 5th August 1958

STRATTON (1957) has pointed out that above a critical electron density interelectronic collisions ensure that the distribution function for electrons remains Maxwellian in the presence of high electric fields. Accordingly, above this critical density the electron distribution can be described by an electron temperature, T_e. Sufficiently high electric fields can increase T_e considerably above the temperature of the lattice, T_L. In this note a method of determining the electron temperature is described and some preliminary results are presented.

The electron temperature is deduced from the piezoresistance effect first observed for germanium by Smith (1954). For a strain, u, and electric field, E, in the ⟨110⟩ direction the elastoresistance coefficient (cf. Morin, Geballe and Herring 1957, where $T_e = T_L$) is given by

$$\frac{\Delta\rho}{\rho u} = m_{44} = \frac{1}{3}\frac{\Xi^{\mathrm{u}}}{\boldsymbol{k}T_e}\frac{(\mu_{\parallel}-\mu_{\perp})}{(\mu_{\parallel}+2\mu_{\perp})}. \qquad \ldots\ldots(1)$$

Here $\Delta\rho/\rho$ is the fractional change in resistivity, Ξ_u is the deformation potential for uniaxial shear, and $\mu_{\parallel}$ and $\mu_{\perp}$ are the mobilities parallel and perpendicular to the symmetry axis of a single valley. Herring and Vogt (1956) have shown that for scattering by acoustical modes the relaxation time is isotropic within a valley, hence $u_{\parallel} \ll \mu_{\perp}$. There is experimental evidence (Morin, Geballe and Herring 1957) that this condition is fulfilled also when there is a large amount of impurity scattering. Equation (1) may, therefore, be written in the form

$$\frac{\Delta\rho}{\rho u} = \left[1 - \frac{(v/E)_0}{(v/E)_s}\right]\frac{1}{u} = -\frac{\Xi_{\mathrm{u}}}{6\boldsymbol{k}T_e}, \qquad \ldots\ldots(2)$$

where $(v/E)_0$ and $(v/E)_s$ are the drift velocity per unit field in the absence and presence of strain respectively for the same T_e. Thus by observing the field dependence of drift velocity for an n-type germanium specimen in a strained and unstrained state the electron temperature can be deduced.

A dumb-bell shaped specimen was cut with the filament in the ⟨110⟩ direction from n-type germanium containing $2{\cdot}5 \times 10^{15}$ free electrons cm^{-3}, a high enough concentration to satisfy the interelectronic collision condition. End injection effects were avoided by using NN+ alloy contacts and by the dumb-bell shape of the specimen. Probes to measure the field were alloyed to the filament. The current through the sample was determined from the voltage drop across a resistor in series with it. Voltage pulses of $\frac{1}{2}$ μsec in duration and of repetition frequency 30 sec^{-1} were used. A tension of 5 kg mm^{-2} was applied to strain the specimen which was cooled to 77°K to enhance the piezoresistance effect.

Figure 1 shows a pair of velocity field curves obtained with and without the stress applied. To deduce an electron temperature at a field E_1 from equation (2) a pair of points, $(v_1/E_1)_0$ and $(v/\mathrm{E})_s$, must be considered which have the same T_e.

The condition for T_e to be the same is simply that the power dissipated, proportional to vE, should be equal for the pair. In figure 2 the dependence of electron temperature on the electric field is shown. The experimental error in T_e is estimated to be less than $\pm 20\%$ while the error in a given point on the velocity field curve is $\pm 4\%$. Corrections to T_e have been applied which are necessary because of the deviation from equation (1) observed by Morin, Geballe and Herring (1957) and attributed to intervalley scattering and because equation (1) is not strictly valid for the large strain induced in the crystal. Changes in the relative population of valleys due to the electric field (Sasaki, Shibuya and Mizuguchi 1958) are expected to be negligible due to the interelectronic collisions equalizing the electron temperature in all valleys.

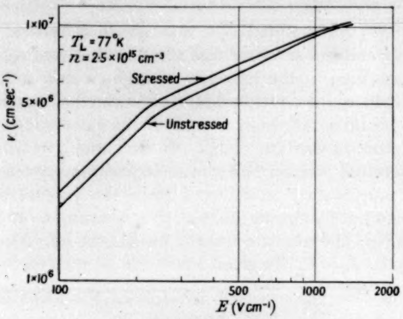

Figure 1. The variation of electron drift velocity with electric field with and without stress (5 kg mm^{-2}) applied.

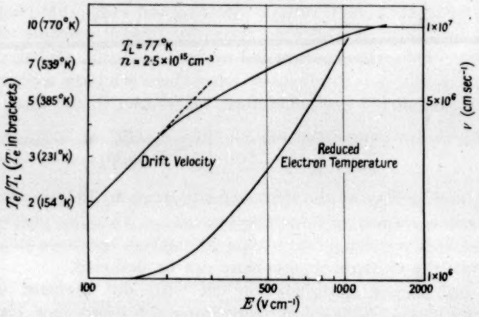

Figure 2. The variation of electron temperature and drift velocity with electric field.

It is possible to reconstruct the velocity field curve by calculating the mobility at a given electron temperature and using the observed field dependence of the electron temperature. The success of such a self-consistent approach would imply that (i) the correct electron temperature was observed and (ii) the relaxation times of the appropriate scattering mechanisms were not significantly in error.

The relaxation time at a given electron temperature was determined from constants deduced by assuming that the $T^{-1\cdot 66}$ law for lattice mobility of electrons in germanium is due to both optical and acoustical mode scattering (Harrison 1956). Taking the equivalent temperature of the optical modes as 400°K (Brockhouse and Iyenger 1958), the ratio of coupling constants, as defined by Herring's (1955) expression for relaxation time, is $w_2/w_1 = 0\cdot 14$, where w_2 refers to the optical mode and w_1 to the acoustical mode. The impurity scattering formula of Brooks (1955) and Herring was used, choosing the concentration of ionized impurities to fit the observed mobility at 77°K. Integration over the summed reciprocal relaxation times was performed graphically. Though the observed and calculated velocity field curves did not agree within experimental error, the calculated values of v/E being too high, replacement of the impurity scattering formula by the impurity scattering deduced from the observed conductivity as a function of lattice temperature did produce agreement within the experimental error of less than $\pm\frac{1}{2}(20)\%$.

Work is in progress to modify the method of measurement of T_e which will produce a significant increase in accuracy.

ACKNOWLEDGMENTS

The author is indebted to his colleagues at Royal Radar Establishment for advice and assistance. This note is published by permission of the Controller, H.M. Stationery Office.

REFERENCES

BROCKHOUSE, B. N., and IYENGER, P. K., 1958, *Bull. Amer. Phys. Soc.*, **3,** 192.

BROOKS, H., 1955, *Advances in Electronics and Electron Physics*, Vol. 7 (New York : Academic Press), p. 157.

HARRISON, W. A., 1956, *Phys. Rev.*, **104,** 1281.

HERRING, C., 1955, *Bell Syst. Tech. J.*, **34,** 237.

HERRING, C., and VOGT, E., 1956, *Phys. Rev.*, **101,** 944.

MORIN, F. J., GEBALLE, T. H., and HERRING, C., 1957, *Phys. Rev.*, **105,** 525.

SASAKI, W., SHIBUYA, M., and MIZUGUCHI, K., 1958, *J. Phys. Soc. Japan*, **13,** 456.

SMITH, C. S., 1954, *Phys. Rev.*, **94,** 42.

STRATTON, R., 1957, *Proc. Roy. Soc.* A, **245,** 355.

LETTERS TO THE EDITOR

Effect of Absorption on Mean Wavelength of X-ray Emission Lines

Methods of lattice-parameter measurement based on the centres of gravity of diffractometer line profiles (Ladell, Parrish and Taylor, 1957, Pike, Hughes and Wilson 1957) that seem likely to lead to reproducibility better than 1 in 10^5 are being developed. The absolute accuracy is limited by uncertainties in the mean wavelength of the x-ray emission lines. The purpose of this note is to draw attention to a probable variation of mean wavelength with the amount of absorption in the tube target and window, the beta filter (if used), the window of the detector, and possibly in the specimen itself.

Consider for simplicity the beta filter. This reduces the intensity of the transmitted x-ray beam by a factor $\exp(-\mu t)$, where t is the thickness and μ is the linear absorption coefficient of the facter. The absorption coefficient is a function of the wavelength of the x-rays, being approximately proportional to λ^3 between absorption edges. If $I(\lambda)d\lambda$ is the wavelength distribution of the intensity of the incident beam, the distribution in the transmitted beam will be $I(\lambda)\exp(-\mu t)\,d\lambda$. The mean incident wavelength is then

$$\langle\lambda\rangle = \frac{\int_\lambda \lambda I(\lambda)\,d\lambda}{\int_\lambda I(\lambda)\,d\lambda} = \lambda_0, \text{ say,} \qquad \ldots\ldots(1)$$

where the integration is over the range of wavelengths to be used in determining the centre of gravity. The mean wavelength of the transmitted radiation is, however,

$$\langle\lambda\rangle = \frac{\int_\lambda \lambda I(\lambda)\exp(-\mu t)\,d\lambda}{\int_\lambda I(\lambda)\exp(-\mu t)\,d\lambda} \qquad \ldots\ldots(2)$$

$$= \lambda_0 + \frac{\int_\lambda (\lambda-\lambda_0)\,I(\lambda)\exp(-\mu t)\,d\lambda}{\int_\lambda I(\lambda)\exp(-\mu t)\,d\lambda}. \qquad \ldots\ldots(3)$$

Over the small range of wavelengths involved we may put

$$\mu = \mu_0 + (\lambda-\lambda_0)\frac{\partial\mu}{\partial\lambda} + \ldots, \qquad \ldots\ldots(4)$$

where μ_0 and $\partial\mu/\partial\lambda$ are the absorption coefficient and its derivative for $\lambda=\lambda_0$, provided that no absorption edge is close. Equation (3) may therefore be written

$$\begin{aligned}\langle\lambda\rangle &= \lambda_0 + \frac{\int_\lambda (\lambda-\lambda_0)[1-(\lambda-\lambda_0)\,t\,(\partial\mu/\partial\lambda)+\ldots]\,I(\lambda)\,d\lambda}{\int_\lambda [1-(\lambda-\lambda_0)t\,(\partial\mu/\partial\lambda)+\ldots]\,I(\lambda)\,d\lambda} \\ &= \lambda_0 + \frac{0 - Vt\,(\partial\mu/\partial\lambda)+\ldots}{1-0+\ldots} \\ &= \lambda_0 - Vt\frac{\partial\mu}{\partial\lambda} + \ldots, \qquad \ldots\ldots(5)\end{aligned}$$

where V is the variance of the line profile about its centre of gravity λ_0.

The importance of the correction term in (5) will depend on the value of $\partial\mu/\partial\lambda$. If $\mu=\mu_0\lambda^3/\lambda_0^3$ the correction term is $-3V\mu t/\lambda$. Ordinary filters reduce the intensity by a factor of two or three, so μt is of the order of unity. The variance of an alpha doublet is about $\frac{1}{3}(\Delta\lambda)^2$, where $\Delta\lambda$ is the doublet separation, so the fractional decrease in wavelength through filtration is of the order of $(\Delta\lambda/\lambda)^2$. For copper radiation this amounts to 6 parts in 10^6, and for molybdenum radiation to 3·5 parts in 10^5. Absorption in tube and detector windows will increase these amounts slightly, so the correction may be important for the shorter-wavelength radiations, and worth making even for Cu Kα.

Peaks also are displaced by approximately $3\mu tI_0/\lambda I_0''$, where I_0 is the peak intensity and I_0'' the second derivative of the intensity at the peak.

Absorption in the target will produçe a similar change, as most of the X-rays come from slightly below the target surface. The effect is complicated, since the thickness of target traversed is proportional to the cosecant of the take-off angle, and thus varies with position on the specimen. The effective depth of production of the X-rays will increase with the potential difference applied to the tube, so the change in mean wavelength will be a complex function of the experimental conditions. The effect of absorption in the specimen is not clear; it may be zero for μ proportional to λ^3.

Similar considerations would apply to photographic methods, but the reproducibility is not ordinarily good enough to warrant any correction.

University College,
Cardiff.
A. J. C. Wilson.

22nd July 1958.

Ladell, J., Parrish, W., and Taylor, J., 1957, Philips Technical Report No. 122; abstract in *Acta Cryst., Copenhagen.*, **10,** 741.

Pike, E. R., Hughes, J. W., and Wilson, A. J. C., 1957, *Acta Cryst., Copenhagen*, **10,** 852.

The Nature of Binding in Cadmium Telluride

Cadmium telluride is an important member of the II–VI group of semiconductors and one which also shows luminescence emission in the infra-red region. We have made extensive studies of the latter which suggest that no appreciable Franck–Condon shifts exist between excitation and emission bands. Such behaviour is characteristic of a solid with homopolar rather than ionic or mixed ionic–homopolar binding. In a previous publication Goodman (1955) suggested a fair degree of ionic behaviour in this compound but his conclusions were based on the use of a limited approach which ignored the electronegativity difference between the constituent atoms in energy estimates. It appeared therefore to be useful to look for other and independent evidence for homopolar binding. The simplest measurements to make appeared to be those of the optical refractive index and of the dielectric constant at low frequencies. It has been established by de Nobel and Hofman (1956) that the latter is 11·0 ± 0·3 for cadmium telluride in single crystal form. We have now measured the refractive index of a similar single crystal at wavelengths beyond the absorption edge of the crystal (880 mμ at 290°K) using interference filters to provide 903 mμ

or 1100 mμ monochromatic radiation and a microscope provided with a 17 kv vacuum tube image converter for the near infra-red region. The crystal (which was n type and indium doped) was provided by the Services Electronics Research Laboratory, Baldock, and a disc of about 5 mm in diameter and 1 mm thick was prepared with polished faces. The 'real over apparent depth' method was employed and the results are as follows.

No. of independent measurements	25	25
Wavelength (mμ)	903	1100
Refractive index (n)	$3{\cdot}47 \pm 0{\cdot}05$	$3{\cdot}13 \pm 0{\cdot}04$
n^2	12·0	9·8

The results for 903 mμ are probably affected by the proximity of this wavelength to the absorption edge. However, it is clear from the results that there is reasonable agreement between the dielectric constant at low frequencies and the square of the optical refractive index. We conclude therefore that in cadmium telluride the lattice binding is predominantly homopolar in character (Mott and Gurney 1946, Garlick 1956). This conclusion is also supported by other facts, e.g. the relatively high carrier mobilities in cadmium telluride compared with those of zinc sulphide, cadmium sulphide and cadmium selenide, and the agreement between the optical (van Doorn and de Nobel 1956) and thermal values (Appel and Lautz 1954) for the energy band gap of cadmium telluride.

Department of Physics,
University of Hull.
21st August 1958.

G. F. J. Garlick.
J. M. Hough.
R. A. Fatehally.

References

Appel, J., and Lautz, G., 1954, *Physica*, **20,** 1110.
van Doorn, C. Z., and de Nobel, D., 1956, *Physica*, **22,** 338.
Garlick, G. F. J., 1956, *Photoconductivity: Handbuch der Physik*, Vol. 19 (Berlin: Springer).
Goodman, C. H. L., 1955, *J. Electronics*, **1,** 115.
Mott, N. F., and Gurney, R. W., 1946, *Electronic Processes in Ionic Crystals* (Oxford: University Press).
de Nobel, D., and Hofman, D., 1956, *Physica*, **22,** 252.

REVIEWS OF BOOKS

Surface Chemistry—Theory and Applications, 2nd Edn., by J. J. BIKERMAN. Pp. x + 501. (New York: Academic Press Inc., 1958.) $15.00.

The author aims to serve the needs of industrial laboratories, and now also those of university scientists and students. The subject, which is a rather specialized and scattered field of physical chemistry, certainly covers much that concerns physics and physicists, both pure and applied. It is necessarily treated here rather concisely, leading to some abruptness in style, but the book contains a large amount of information and helpful discussion.

The contents are grouped into six large chapters: I Liquid–Gas, II Liquid–Liquid, III Solid–Gas, IV Solid–Liquid, V Solid–Liquid–Gas and Solid–Liquid–Liquid, VI Electric Surface Phenomena. Much space is given to surface and interfacial tension, drops, bubbles, foams, fogs, aerosols, dusts, emulsions, adsorption and the electric double layer and electrokinetic phenomena.

Even allowing for the limited space available, rather less than justice is done to such important and by now extensively developed subjects as the corrosion of solids by gases and liquids, the nature and properties of vacuum-condensed metal films, epitaxial crystal growth, and friction, wear and lubrication. At least some references to the excellent recent reviews available would have been expected.
H. WILMAN.

Static Electrification, by LEONARD B. LOEB. Pp. xii + 240. (Berlin, Göttingen, Heidelberg: Springer-Verlag, 1958.) DM. 48.

In this book, Professor Loeb extends the title of static electrification beyond the usual meaning of solid–solid contacts and includes, among other processes, electrolytic effects, spray charging and gaseous electronic effects. He is concerned particularly with those aspects of the subject in which important work has been done by students working under his direction and in which emphasis has been laid on the fundamental physical principles involved; he has, therefore, perhaps neglected some of the pioneer work in which the conditions were not sufficiently controlled and of which the results no longer appear significant.

It is unfortunate that this work and the review article by Harper (*Phil. Mag. Suppl.* 1957, **6**, 365–417) were written at about the same time, so that neither contains comments on the other, comments which would have been valuable since on a number of points they do not agree with one another.

While Professor Loeb does not attempt to solve the technical industrial problems of static electrification, he expresses the hope, which appears justified, that his analysis of the fundamental phenomena must form a basis for those concerned with these problems.

The book is a ' must ' for those directly concerned with the subject, but is probably too detailed to be easy reading for those whose interest is less close and one would like to see a shorter summary by Professor Loeb, giving the conclusions without such detailed experimental results. The book is well produced, with clear diagrams and a very adequate bibliography.
J. A. C.

Angular Momentum in Quantum Mechanics, by A. R. EDMONDS. Pp. 146. (Oxford: University Press, 1957.) $3.75.

Elementary Theory of Angular Momentum, by M. E. ROSE. Pp. x+248. (London: Chapman and Hall, 1957.) 80*s*.

The conservation of angular momentum plays an important part in many dynamical systems, but in nuclear physics it takes on a special significance since it largely determines the fashion in which nuclear radiations are emitted. The measurement of angular distributions of reaction products, or of angular correlations between successive quanta, is common enough; and yet the analysis of such measurements to give spins and parities of nuclear levels and multipolarities of radiations, is fraught with endless pitfalls. The theory of angular momentum in quantum mechanics is simple in essence : unfortunately it has been brought to a state verging on chaos by the number of confused and incomplete expositions to which the luckless student has been subjected—a regular swamp of lush notations and tangled phrases in which even the most experienced explorer can readily sink. In these two books we have at last some clarity of presentation and precision of definition. The student will find Dr. Rose's book the easier to read and probably the more informative : it is more physical in its approach, contains many examples and applications, and does not attempt to go to the very ends of complication. Thus, there are chapters on multipole fields, oriented nuclei and angular correlations, and on angular distributions in nuclear reactions; but the 9j-symbol (or X-coefficient) which concerns the successive coupling of four angular momenta is barely introduced in spite of its importance in angular correlation theory. For the more advanced, however, Dr. Edmonds' book will be found invaluable. It contains in the most concise fashion most of the mathematical results and derivations one could ever want, including a thorough treatment of the 9j-symbol and its evaluation, and even some mention of the two 12j-symbols; and it ends with some very useful tables. It is a pity that in such a work of reference and concise exposition a few errors of phase and of convention should have crept in, although they are all of the kind that can easily be expunged from the second edition. The worst, of which the reader should beware, is that the Euler angles of the rotation matrices have been incorrectly defined. Some applications are given, but these are not the main purpose of the book. However, it does seem a pity that the theory of angular correlations, which contains so many special formulae, and uses the whole apparatus of the theory, should not have been included in what is otherwise so complete a work. In both books the publishers have maintained high standards of printing, and there appear to be surprisingly few misprints. It is too much to expect that the two authors should have used entirely the same notations and conventions; but the similarities are sufficient to introduce a marked degree of clarity if only future writers will follow their lead.

B. H. FLOWERS.

Physics, Volume II—Electricity and Magnetism, by L. S. POWELL. Pp. xv+543. (London: Sir Isaac Pitman and Sons, 1958.) 30*s*.

Mr. Powell's volume on *Electricity and Magnetism*, the second of a series written for National Certificate students, is timely, and will be widely welcomed. Timely, because the scheme in Applied Physics, during some eight years or so,

V. 19

has established its own distinctive character which few existing books matched both in outlook and in standard; and welcomed because of its excellence for the purpose. It covers the three years' work for the Ordinary certificate, going slowly and steadily in the earlier chapters on simple d.c. circuits and measurements; expanding in the treatment of electromagnetism (with m.k.s. units and a *Teaching of Electricity* approach) and its applications; and finally taking more difficult circuits, alternating current, and electronics to a very good standard for the S 3 year, using mathematics appropriate to the student's development at each stage. Practical instructions are given for a good selection of experiments, some of them of the simple and really fundamental type—for example the measurement of a potential difference in terms of joules per coulomb, the demonstration that a capacitor really *does* possess a constant capacitance, and finding the results of putting an ordinary sort of voltmeter across part of a high-resistance circuit. You can tell people these things, but they never believe them, let alone understand them, until they have seen what happens practically; Mr. Powell has this situation well in hand.

The book is well and carefully written, and only two minor points—the treatment of the fuel cell on page 99 and a paragraph on X-rays on page 462—are suggested for reconsideration in a future edition. G. R. NOAKES.

Leybold Vakuum-Taschenbuch, edited by K. DIELS and R. JAECKEL. Pp. viii + 270. (Berlin, Göttingen, Heidelberg: Springer-Verlag, 1958.) DM. 39.

This book is difficult to assess and, in some ways, peculiar. In the main it contains an enormous amount of technical data, referring to gas content of metals, diffusion of gases, operation of getters, vacuum drying, motion of vapour jets etc., all of which would lead one to imagine it to be purely a technical book. However, there is much information, such as reference to diffusion of He through a variety of glasses, and an account of Wagener's measurements of the effect of getters, which make the book at least an introduction to ultra-high vacuum.

In my opinion it is an essential book for technical vacuum workers, but also useful for most physicists using high vacuum. It has much less padding than most books. C. S. BULL.

Physique et Technique des Tubes Electroniques, Tome 1—*Eléments de Technique du Vide*, by R. CHAMPEIX. Pp. xiv + 214. (Paris: Dunod, 1958.) 2900 *fr.*

With a view to training engineers for the valve industry Dr. R. Champeix initiated ten years ago a course on the physics and construction of electronic tubes which is now regularly given at the Ecole Française de Radioélectricité. The present volume, together with one to follow dealing with the design and technology of valves, contains the substance of these courses.

The first volume is a well-written introduction to high vacuum technique. It begins with a review of the relevant parts of physics in general, such as thermometry and the laws of the gaseous state which, on account of its brevity and lucidity is more stimulating than oppressive. It then deals successively with the physics and chemistry of low pressures, with design of pumps, vacuum gauges, the lay-out of vacuum units and applications.

In spite of its simplicity the book is densely packed with data and information. It covers recent developments such as Roots, ionization and titanium evaporation pumps, the Bayard and Alpert ionization gauge and the alphatron. Most relevant formulae are given and are derived in a simple and elegant manner, although in a few cases the process of simplification has been carried too far. There are many useful tables and diagrams.

The book contains easily as much as a physicist or technician using, but not specializing in, vacuum technique needs to know. It makes very pleasant reading and may be recommended not only to beginners but also to those who want to brush up their vacuum together with their French. W. EHRENBERG.

Proceedings of the Rehovoth Conference on Nuclear Structure, edited by H. J. LIPKIN. Pp. xvi + 614. (Amsterdam: North-Holland Publishing Company, 1958.) 45 guilders.

The Rehovoth Conference on Nuclear Structure was held at the Weizmann Institute of Science, Rehovoth, Israel, September 8th–14th, 1957. It was one of a quasi-regular series of international nuclear structure conferences, coming between that held in Amsterdam in 1956 and that to be held in Paris in 1958. It was well organized, pleasant and profitable.

The most important effect of such conferences is that one finds out how one's colleagues think as well as how they write. They also, for the fortunate few who can attend them all, obviate the necessity of reading. For the rest, the next best thing is a rapidly published account such as this one, which not only gives all the papers, but also the greater part of the spontaneous discussions which take place from the floor after the various formal contributions.

The organization of this conference followed the now normal pattern of a few lengthy review papers and a number of shorter individual communications on various general topics. The successive sessions dealt with shell model evidence, the unified model, group theoretical methods in nuclear spectroscopy, electromagnetic transitions and heavy nuclei, effects of the finite size of the nucleus, β-decay and parity, extra-nuclear effects on angular correlation, instruments of nuclear spectroscopy and the measurement of very short nuclear life-times. The (low energy) parity session was particularly timely and the summary of it in the present volume is probably the most interesting and complete account available in print at the moment. Apart from this however, the general atmosphere of the conference was one of the development and consolidation of established ideas and methods, and nothing very novel or surprising was introduced from either the experimental or the theoretical sides. This is not to say that the conference was without interest: very far from it, but rather that it was chiefly concerned for example with the techniques for the application of the shell and collective models and the derivation of the foundation of those two models rather than with the sort of empirical justification for their utility with which previous conferences have been concerned.

The reviewer has noticed the omission of the author's name from reference 11 on page 600. It is O. D. Suess. He has also noticed that the legend of the interesting group photograph which forms the frontispiece of this report has not been correctly anti-symmetrized with respect to Pauli. Apart from this there are few misprints and the standards of editing and publishing alike are most excellent. D. H. WILKINSON.

Handbuch der Physik, Vol. XLV, *Nuclear Instrumentation* II, edited by E. CREUTZ. Pp. vii + 544. (Berlin: Springer, 1958.) DM. 128.

The great series of volumes of which this is one has, so far as the numbers on nuclear physics go, sprawled unorganized across its subject and has exhibited extensive and undisciplined overlapping between the various articles. The volume now under review escapes this censure and is divided neatly into a number of individually self-contained and mutually complementary pamphlets. The topics and authors are: Ionization Chambers in Nuclear Physics, by H. W. Fulbright; Geiger Counters, by S. A. Korff; Scintillation and Čerenkov Counters, by W. E. Mott and R. B. Sutton; The Proportional Counter as Detector and Spectrometer, by S. C. Curran; The Coincidence Method, by S. de Bendetti and R. W. Findley; Cloud Chambers, by C. M. York; The Bubble Chamber, by D. A. Glaser; Nuclear Emulsions, by M. M. Shapiro; Detection of Neutrons, by H. H. Barschall; High Energy Neutron Detectors, by R. T. Segel. With the exception of the second of these articles which is so uncritical and innocent of references as to be almost anecdotal, these reviews are extremely competent and valuable. They summarize a great many useful data and one can feel confidence in the author's choice and presentation of the most reliable parameters. They will help the user to exploit the various techniques to the full. The excellent accounts by Mott and Sutton, and by Shapiro will be particularly valuable as works of reference. Those of Fulbright and Curran are most welcome as guides by experienced masters to the ways of sensitive but sometimes capricious handmaidens. The juxtaposition of the articles by York and by Glaser is a most interesting one. The former is an account of what is probably the summit of a mature technique while the second is an almost dramatic report on the first few years of the lusty young infant who has already almost taken over the business from his sexagenarian predecessor. Be it said, however, that Glaser attempts no floccinaucinihilipilification of the senior partner.

As are all members of this series, the present volume is most beautifully printed, sumptuously produced and impossibly priced; like them it also has a disturbingly large number of misprints. Some of the detailed editing is annoyingly eccentric. Why, for example, is the reader continually referred in footnotes to other footnotes on the very same page, thereby wasting both his time and his money ? And why does footnote 1 on p. 443 do no more than refer us to footnote 1 on p. 442 which itself does no more than refer us to footnote 1 on p. 441 ? D. H. WILKINSON.

Physics of Nuclear Fission, translated from the Russian by J. E. S. BRADLEY. Pp. vi + 182. (London, Paris, New York, Los Angeles: Pergamon Press, 1958.) 60*s*.

This book is a translation of Supplement No. 1 to the Soviet journal *Atomnaya Energiya*, containing twelve papers by Russian authors on various aspects of nuclear fission. The supplement was published in 1957 as the proceedings of a conference held in January 1956. It thus deals with material available up to that date, and no attempt has been made to include later results.

The titles and authors of the twelve chapters are: (1) Nuclear Fission Theory, by B. T. Geilikman; (2) Fast Neutron Fission Cross Sections, by Iu. S.

Zamiatnin; (3) Charge and Mass Distributions of Fission Products, by A. N. Murin; (4) Theory of Fission of Heavy Nuclei near Threshold, by V. G. Nosov; (5) Anisotropy in Fission Processes, by I. M. Frank; (6) Fission Neutrons, by B. G. Erozolimskii; (7) Some Features of Nuclear Fission at High and Low Excitation Energies, by N. A. Perfilov; (8) High-Energy Proton Fission Cross Sections for Uranium, and an Analysis of the Light Charged Particles Emitted, by N. S. Ivanova; (9) Determination of Emissive Fission Thresholds by the Thick-layer Photographic Plate Methods, by V. P. Shamov; (10) Spontaneous Fission of Heavy Nuclei, by K. A. Petrzhak; (11) Some Aspects of Spontaneous Fission in Heavy Nuclei, by V. N. Mekhedov; (12) Photofission, by L. E. Lazcreva and N. V. Nikitina. Chapters 1–3, 5–7, 10 and 12 are review articles, Chapter 4 is a brief presentation of Nosov's theory of asymmetric fission, Chapters 8 and 9 are collected presentations of the work done with the Moscow synchro-cyclotron on high-energy proton fission, and Chapter 11 is a short discussion on the relative probabilities of spontaneous fission and α-decay.

From the title, the reader might expect a comprehensive and logically developed treatment of the experimental and theoretical aspects of nuclear fission, and if so he would be disappointed. Each article has evidently been written as a separate contribution, and often without much reference to the other articles. There is a good deal of repetition; for example, three chapters contain discussions of asymmetric fission, the conclusion, however, in each case being that considerable work remains to be done. On the other hand, a number of important topics are dealt with only briefly, for example, the angular distribution of fission neutrons and the kinetic energy of the fragments.

The main value of the book is that it brings together in a concise form, and in English, the results of the large amount of work on fission which has been done in the Soviet Union, much of which is unpublished, or has been published in reports not readily available in English translation. Although the articles include the results of foreign investigators, the emphasis is on the Russian work.

Probably the most interesting chapters are those dealing with the research on high-energy proton fission carried out at Moscow. These contributions contain a fairly complete presentation and discussion of the data obtained on cross sections and the evaporation of charged particles prior to fission.

The reviewer cannot vouch for the accuracy of the translation, but the English style is clear and readable, and the text and diagrams are well presented and accurate. This book should be read by every serious student of nuclear fission, but its value as a reference book is limited. There is no index, and the references are given separately for each chapter in numerical order. It does not fulfil the pressing need for a really complete book on nuclear fission, which may well have to wait till the theory is in a more satisfactory state. G. N. HARDING.

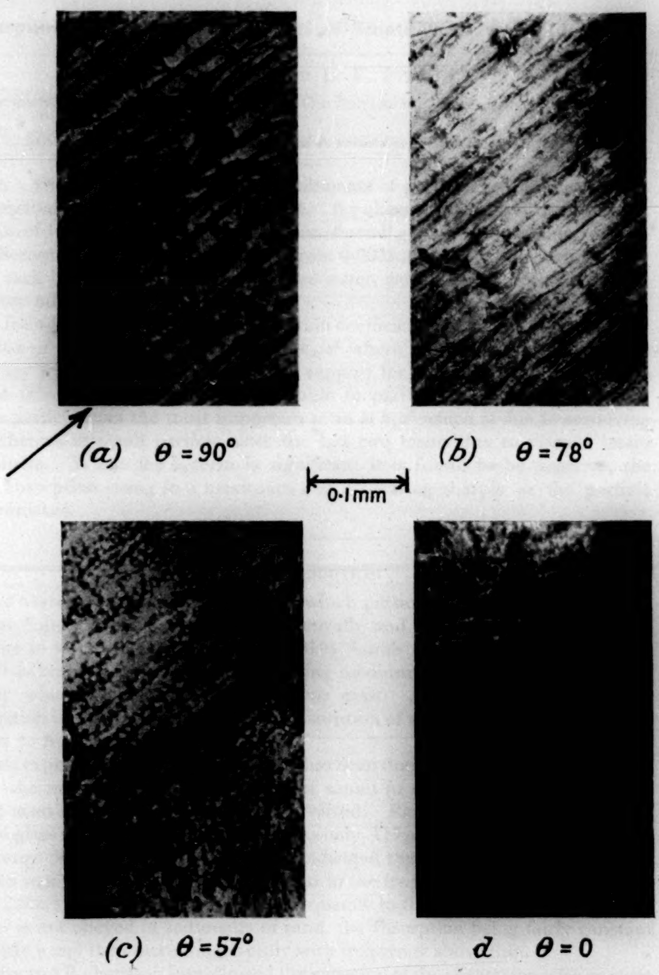
(a) θ = 90°
(b) θ = 78°
0·1mm
(c) θ = 57°
d θ = 0

Figure 5. Powder patterns on the curved surface of a single crystal disc of cobalt. (Arrow in (*a*) shows direction of hexagonal axis.)

Absorption of Sound in Sediments of Small Particles in Liquids

By K. BARRON[†] and L. E. LAWLEY[‡]

Department of Mathematics and Physics, The Polytechnic, Regent Street, London

MS. received 2nd January 1958, and in revised form 6th August 1958

Abstract. The absorption of sound in sediments of particles in different liquids is investigated as the particle size is varied. A pulse method is used at a constant frequency of 1 Mc/s. The sediments consist of small glass spheres of uniform size, eight different particle sizes in the range from 0·0035 cm to 0·016 cm radius being used in each liquid. The liquids used are water, carbon tetrachloride, benzene and castor oil.

It is found that in all cases the absorption coefficient can be represented by an expression of the form $2\alpha = k_1a^3 + k_2/a + k_3/a^2$ where k_1, k_2 and k_3 are constants which vary with the liquid used. Some support for an equation of this form is obtained from Sewell's equation applicable to particles suspended in a fluid. At large particle sizes the most important term is k_1a^3 which is due to scattering losses whereas at small particle sizes the last two terms due to viscous losses predominate. Where the k_3 term is significant it is found to be negative, the viscous absorption rising to a maximum and decreasing sharply as the particle size diminishes.

§ 1. Introduction

The absorption of sound in fluids in which particles are suspended has been previously investigated both theoretically and experimentally. Theories due to Rayleigh (1878), Sewell (1910), Lamb (1932) and Epstein (1941) for various types of particle and suspending medium have been verified experimentally when the appropriate conditions exist. A logical step for further investigation is the consideration of the absorption of sound in sediments of small particles in liquids.

Some experimental work on this topic has been done by Busby and Richardson (1956) who investigated the absorption of sound in sediments of glass spheres and also sand in water as the frequency is varied. Results were obtained in sediments of glass spheres, with one particle size only, 117 μ, at six different frequencies in the range 500 kc/s to 3 Mc/s. These indicated that the absorption coefficient increased in a manner directly proportional to the frequency for low frequencies, (below 2 Mc/s), and proportional to the frequency to the fourth power above this. The law is not obeyed in sediments of sand, the absorption being fairly constant up to 1 Mc/s and then increasing rapidly with frequency above this.

Busby and Richardson investigated the variation of the absorption with particle size in the case of sand, but the particles were not spherical or of uniform size and the results showed only that there was a general increase of absorption with particle size.

[†] Now at Mining Research Establishment, National Coal Board, Isleworth, Middlesex.

[‡] Now Head of Physics and Mathematics Department, Kingston Technical College.

The work here described is an investigation of the absorption of sound in sediments of small particles of uniform size. The particle size and the permeating liquid are varied but the frequency is kept constant.

§ 2. THEORETICAL ASPECTS

The absorption mechanism in the case of sediments is complicated and, as yet, no theory has been developed. The theoretical work of Sewell on particles in suspension is, however, relevant. He considered the case of rigid spheres fixed in position in a viscous medium, assuming that the radius a of the particles was small compared with the wavelength of the sound and that the volume occupied by the particles was only a small fraction of the total volume of the medium. The absorption was found to be due to two main causes: (i) absorption due to viscous effects in the medium, and (ii) absorption due to scattering of energy by the spheres from the primary beam (Rayleigh scattering).

For N particles in suspension Sewell obtained the amplitude coefficient of absorption α as:—

$$2\alpha = N\pi a^2 \left\{\frac{7}{9}\frac{\omega^4 a^4}{c^4} + 3\sqrt{2}\,\frac{\omega^{1/2}\nu^{1/2}}{c} + \frac{6\nu}{ca}\right\} \qquad \ldots\ldots (1)$$

where a = particle radius, ν = kinematic viscosity, c = velocity of sound in the medium and $\omega = 2\pi \times$ frequency. The first term of this expression represents the proportion of incident energy lost by scattering to a distance and the other terms that lost by friction. If C is the concentration by volume of the spheres then $C = 4\pi N a^3/3$ and Sewell's equation may be written as

$$2\alpha = \tfrac{3}{4}\,C\left\{\frac{7}{9}\frac{\omega^4}{c^4}a^3 + 3\sqrt{2}\,\frac{\omega^{1/2}\nu^{1/2}}{ca} + \frac{6\nu}{ca^2}\right\}. \qquad \ldots\ldots (2)$$

In the case of glass spheres forming a sediment, the spheres are assumed to pack together in the most compact manner which gives a constant concentration by volume of 74% for all particle sizes. Thus Sewell's assumption that the volume occupied by the spheres is small compared with the total volume is no longer valid in this case. This means that the absorption due to N particles may no longer be considered to be N times that due to a single particle owing to interparticle effects. The other assumptions of Sewell's theory are valid in the case of sediments; the particles are rigid and fixed in position and their diameter is much less than the wavelength of the sound used. Thus although the same physical phenomena of scattering and viscous energy losses may make up the absorption in sediments their magnitude will be different from that given by Sewell's theory.

Consider first absorption due to scattering. In the case of a sediment of uniform particle size, owing to the proximity of the spheres, multiple scattering will take place and some of the energy scattered from the beam by one particle may be returned to it by another. Each individual scatter will, however, be governed by the single scatter law. Thus with a constant concentration of particles, the loss of energy from the sound beam due to multiple scattering should be proportional to a^3 as in equation (2), although the multiplying constant will be different. If this is the case then the absorption coefficient due to scattering, $2\alpha_S = k_1 a^3$ where k_1 is a constant. (One would expect that

$$k_1 \ll \frac{7}{9}\frac{\omega^4}{c^4}\frac{3}{4}C$$

which occurs in equation (2) as energy is scattered back into the beam.)

The viscous effects due to a streamline flow round a single particle depend on the relative motion of the particle and the fluid. In sediments the particles are fixed in position and do not move with the sound field. As the radius diminishes the surface area presented by the particles in a sediment of constant concentration increases and thus the viscous absorption will increase. Also, owing to the proximity of the spheres there will be a viscous loss due to the movement of the liquid between the small spaces between the spheres, this loss may be high as these spaces are small. The magnitude of these effects is difficult to estimate but if we represent the viscous absorption by terms of the same form as Sewell's equation we have:— the viscous absorption, $2\alpha_V = k_2/a + k_3/a^2$ where k_2 and k_3 are unknown constants.

Thus if the absorption of sound in sediments is due to the energy losses caused by scattering and viscous effects the amplitude absorption coefficient, α, may be represented by the following equation:

$$2\alpha = k_1 a^3 + k_2/a + k_3/a^2. \qquad \ldots\ldots (3)$$

The absorption will be mainly due to viscosity when the particles are small and to scattering when they are large. Hence a position of minimum absorption will usually occur at some interim particle size. Experimental investigation of the variation of absorption with particle size (all other parameters being kept constant), should reveal whether such a minimum occurs and also if it is explained by an expression of the form of equation (3).

§ 3. APPARATUS

Experimental measurements were made by means of a pulse method. A 1 Mc/s r.f. pulse from a pulse generator excites a barium titanate transducer and the sound wave emitted from it passes through the medium to an identical receiving transducer. It is then passed through a calibrated attenuator, amplified and displayed on an oscilloscope. A direct pulse from the generator triggers the time base of the oscilloscope.

Figure 1 shows a diagram of the liquid container which is a glass tube A of internal diameter 4 in. and length 12 in. This tube is clamped vertically by means

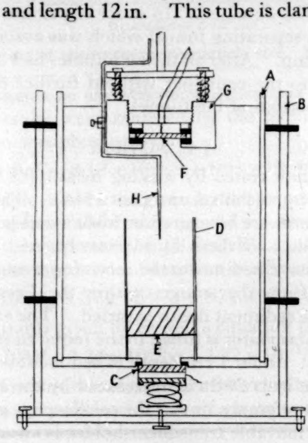

Figure 1.

of supports B which are fixed to a base plate which may be levelled by means of three screws placed symmetrically round its edge. The top of the tube is open to the air whilst the lower end is sealed into an aluminium disc. The transmitting transducer C is mounted in the centre of this disc with its radiating face exposed to the liquid in the container.

In order to reduce the volume of sediment required and to prevent damping of the transducer by sediment resting directly on it, an additional container D is placed in the large tube. This consists of two glass tubes of equal diameter, slightly larger than the transducer, which are cemented together with a thin sheet of mica E between them. This tube fits rigidly into a recess at the bottom of the large container, directly over the transducer.

The receiving transducer F is mounted in a holder G which may be moved towards or away from the transmitter through accurately known distances by means of a stage adapted from a travelling microscope. The holder may be adjusted by means of three spring loaded screws so that the transducers may be set parallel. A needle H is attached to the holder to facilitate the measurement of sediment depth. This needle may be swung in or out of the acoustic path.

Angular alignment of the transducers is carried out by means of the screws at the base of the container and the spring loaded screws of the transducer holder. In order to align the transducers axially the container was rested on a base which could be moved in two directions at right angles. Thus the transmitting transducer C could be accurately centred under the receiver F.

The sediments used in the experiments consisted of small glass spheres of a uniform size which were obtained commercially. When viewed under a microscope these particles were seen to be almost perfectly spherical. A determination of the most probable diameter was made by measuring a large number of particles under a microscope and plotting a frequency distribution curve of particle size. The spread of particle sizes within each sample was found to be small, e.g. when the mean particle size was 0·032 cm diameter the standard deviation was 0·0048 cm.

It is essential that no bubbles of air are trapped in the sediment otherwise high absorption readings will be obtained. In order to prevent this the particles were placed in the liquid in a separating funnel which was evacuated for several hours by means of a filter pump. After all the air bubbles had been removed the sediment was introduced into the container without further contact with the air by opening the tap at the bottom of the funnel.

§ 4. METHOD

The apparatus was first tested by making measurements in pure liquids by the standard pulse technique (Pellam and Galt 1946). The absorption of carbon tetrachloride and benzene were measured at 5 Mc/s and good agreement (within 2%) with the accepted values for these liquids was obtained.

For the measurements in sediments the receiving transducer is kept at a constant known distance from the source, within the Fresnel diffraction region (Pinkerton 1949) and the sediment depth is varied. The experimental procedure is as follows; the pulsed oscillator is tuned to the required frequency (1 Mc/s) and the transducers aligned. About 1 cm depth of sediment is placed in the acoustic path, an attenuation of at least 20 dB is introduced by the attenuator and the first received pulse is set on a reference line of the oscilloscope graticule. The needle which is attached to the movable transducer holder is swung into the beam and lowered until it touches the top of the sediment. A reading corresponding to the level of the top of the sediment is obtained from the vernier scale of the microscope stage. The receiver is then moved back to its original position, and the needle swung out of the beam. Attenuation of 1 dB is then removed and the pulse height rises. Sediment is slowly introduced into the tube until the pulse regains its original height. The needle is again swung into the beam, lowered to touch the top of the sediment and a vernier reading corresponding to the new sediment level is obtained. The difference in these vernier readings, say x cm, gives the increase in sediment depth. The acoustic path has therefore been changed by an increase of x cm of sediment and a corresponding decrease of pure liquid causing an attenuation of 1 dB. (The absorption due to the removal of x cm of pure liquid at this frequency is negligible for all liquids except castor oil.) Repetition of this procedure enables a graph of attenuation against increase of sediment depth to be plotted. Hence the attenuation α' in dB cm^{-1} and thus the amplitude absorption coefficient α at this frequency may be calculated. Results were obtained for sediments of eight different particle sizes in water, benzene, carbon tetrachloride and castor oil.

§ 5. RESULTS

The points on figure 2 show the experimental variation of α' with particle radius in the case of water. It may be seen from this that a point of minimum absorption occurs and it now remains to investigate whether this curve is of the form of equation (3). The results were analysed by the method of least squares and the following equation was obtained:

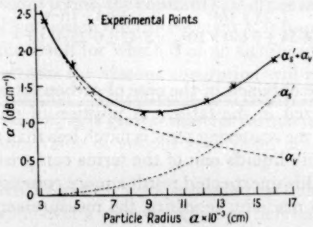

Figure 2. Variation of absorption with particle size. Sediments in water.

$$\alpha' = \alpha_s' + \alpha_v' = 3\cdot18 \times 10^5 a^3 + [8\cdot12 \times 10^{-3}/a + 1\cdot03 \times 10^{-6}/a^2]\ \text{dB cm}^{-1}. \quad \ldots\ldots (4)$$

The full line of the graph shows α' as given by this expression; the contributions of the scattering and viscous absorption α_s' and α_v' are also shown individually. In order to compare this expression with Sewell's equation (2), equation (4) is written in terms of α the amplitude absorption coefficient

$$2\alpha = 7\cdot34 \times 10^4 a^3 + 1\cdot87 \times 10^{-3}/a + 2\cdot38 \times 10^{-7}/a^2\ \text{cm}^{-1}. \quad \ldots\ldots (5)$$

Evaluation of the constants given by Sewell's equation (2) gives

$$2\alpha_{\text{Sewell}} = 1\cdot33 \times 10^6 a^3 + 1\cdot24 \times 10^{-3}/a + 2\cdot22 \times 10^{-7}/a^2\ \text{cm}^{-1}. \quad \ldots\ldots (6)$$

(Note. It is assumed in this calculation that the velocity of sound in the sediment was the same as that in the pure liquid. A rough experimental check showed that it did not differ by more than 2%.)

It may be seen by comparison of equations (5) and (6) that the scattering term (first term) is much less experimentally than that given by equation (2). This is expected as Sewell's equation does not take into account energy returned to the beam by multiple scattering. The viscous terms are of the same order as indicated by equation (2) but as may be seen from the table the accuracy of the last term is very low and the value stated has no significance. In the case of water the contribution to the total absorption made by this term is negligible even for the smallest particles.

Liquid	k_1	k_2	k_3
Water			
Sewell	$1{\cdot}33 \times 10^6$	$1{\cdot}23 \times 10^{-3}$	$2{\cdot}22 \times 10^{-7}$
Experimental	$(7{\cdot}34 \pm 0{\cdot}58) \times 10^4$	$(1{\cdot}87 \pm 0{\cdot}21) \times 10^{-3}$	$(2 \pm 9) \times 10^{-7}$
Carbon tetrachloride			
Sewell	$2{\cdot}16 \times 10^6$	$4{\cdot}95 \times 10^{-3}$	$2{\cdot}18 \times 10^{-7}$
Experimental	$(2{\cdot}36 \pm 0{\cdot}09) \times 10^5$	$(4{\cdot}24 \pm 0{\cdot}32) \times 10^{-3}$	$-(9{\cdot}4 \pm 0{\cdot}41) \times 10^{-6}$
Benzene			
Sewell	$2{\cdot}35 \times 10^6$	$4{\cdot}38 \times 10^{-3}$	$2{\cdot}38 \times 10^{-7}$
Experimental	$(6{\cdot}6 \pm 0{\cdot}48) \times 10^4$	$(3{\cdot}43 \pm 0{\cdot}17) \times 10^{-3}$	$-(5{\cdot}18 \pm 0{\cdot}76) \times 10^{-6}$
Castor oil			
Sewell	$1{\cdot}33 \times 10^6$	$3{\cdot}98 \times 10^{-2}$	$2{\cdot}27 \times 10^{-5}$
Experimental	$(4{\cdot}34 \pm 0{\cdot}69) \times 10^5$	$(5{\cdot}47 \pm 0{\cdot}25) \times 10^{-2}$	$-(1{\cdot}43 \pm 0{\cdot}11) \times 10^{-4}$

Similar results were obtained in the case of carbon tetrachloride and benzene and they are summarized in the table. A position of minimum absorption is observed and as before the scattering term is much less than that given by Sewell's equation. In both these liquids one of the terms comprising the viscous loss is negative. In view of this unexpected result a more complete investigation of the viscous absorption was made by repeating the measurements using castor oil.

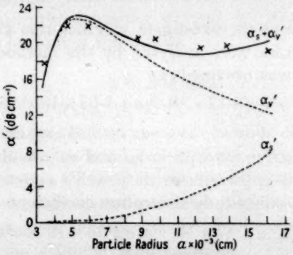

Figure 3. Variation of absorption with particle size. Sediments in castor oil.

Figure 3 shows the results in sediments in castor oil. The points on the graph are those obtained experimentally and the full lines are derived from an expression having the form of equation (3) by the method of least squares. The accuracy of these results is not so high as in the other liquids, this is mainly due to temperature variations between experiments affecting the viscosity of castor oil. The errors occurring in these and the other experiments are not more than 5% of the minimum absorption value.

The results using castor oil show a sudden drop in the absorption for the smallest particles. An expression of the form of equation (3) still fits the experimental results but the negative term in the viscous expression becomes large at these small particles sizes and hence the overall viscous absorption is greatly diminished. The results are summarized in the table.

§ 6. CONCLUSIONS

The table gives a comparison of the terms in the equation $2\alpha = k_1a^3 + k_2/a + k_3/a^2$ obtained experimentally in different liquids with corresponding terms calculated from Sewell's equation (2).

It may be concluded that an expression of this form accurately accounts for the absorption in sediments of spherical particles.

In each case the scattering term is considerably less than the normal Rayleigh scattering predicted by Sewell's theory. This is due to multiple scattering effects which causes energy previously scattered to be returned to the beam. This multiple scattering effect is least for castor oil where the high viscous absorption reduces the proportion of scattered energy returned to the beam.

Considering the viscous terms, the constant k_2 is of the same order of magnitude as that given by Sewell's equation but the constant k_3 is found to be negative for all liquids except water, the result for which is of no significance. This implies that as the particle size decreases the viscous absorption will rise to a maximum and then begin to decrease sharply. This effect is seen clearly for the smallest particles in castor oil where the ratio k_3/k_2 is greater than for carbon tetrachloride or benzene and hence the maximum value of viscous absorption occurs at a larger particle size.

It is felt that further theoretical work is needed on this problem and also that more experimental results over a wider range of particle size and frequency would be useful.

REFERENCES

BUSBY, J., 1954, *Ph. D. Thesis*, University of Durham.

BUSBY, J., and RICHARDSON, E. G., 1956, *Proc. Phys. Soc.* B, **69**, 193.

EPSTEIN, P. S., 1941, *Theodore von Kármán Anniv. Vol.*, Cal. Tech., 162.

LAMB, H., 1932, *Hydrodynamics*, 6th Edn (Cambridge : University Press), p. 657.

PELLAM, J. R., and GALT, J. K., 1946, *J. Chem. Phys.*, **14**, 608.

PINKERTON, J. M. M., 1949, *Proc. Phys. Soc.* B, **62**, 286.

RAYLEIGH, LORD, 1878, *Theory of Sound*, **II** (London : Macmillan).

SEWELL, C. J. T., 1910, *Phil. Trans. Roy. Soc.* A, **210**, 239.

Vibrational Relaxation Times of a Number of Polyatomic Gases Derived from Measurements of Acoustic Absorption

By P. D. EDMONDS† and J. LAMB
Electrical Engineering Department, Imperial College, London

MS. received 27*th May* 1958, *and in revised form* 8*th August* 1958

Abstract. The authors have described in a previous paper a method for deriving the acoustic absorption coefficient of gases from measurements of the decay time of a cylindrical resonator containing the gas in question. This technique has been applied to determine the relaxational contribution to the absorption at frequencies well below the dispersion region for a number of gases. The information is then used to evaluate the relaxation times for deactivation of the vibrational energy and results are given for boron trifluoride, cyclopropane, methane, methyl chloride, carbon tetrafluoride, ethylene, acetylene, 1,3- butadiene and 1,2- dichlorotetrafluoroethane. Agreement is found with relaxation times evaluated from ultrasonic velocity measurements in cases where comparison can be made.

§ 1. Introduction

A method for deriving the acoustic absorption coefficient of gases from measurements of the decay time of a cylindrical resonator was described in a previous paper (Edmonds and Lamb 1958). Knowledge of the acoustic absorption in a gas at values of frequency divided by pressure (f/p_0) which are well below the relaxation region enables the relaxation time for deactivation of the vibrational energy to be estimated, whereas this information cannot be obtained solely from measurement of the velocity of sound under similar conditions. To recapitulate briefly, a volume of the gas to be investigated is contained in a glass cylinder and is excited intermittently at one of its resonant frequencies; the decay time of the acoustic field is recorded during the periods when the source is quiescent. The total acoustic power loss resulting from the various absorption mechanisms is obtained from the measured decay time corresponding to a known resonant condition. The power losses attributed to the thermal and viscous boundary layers at the walls of the resonator and the power loss in the 'body' of the gas due to the 'classical' processes of shear viscosity and thermal conduction are each calculated for the resonance in question and subtracted from the measured value. The remaining difference, expressed as a value of $p_0\alpha^{(r)}/f^2$, is accounted for by a relaxational contribution $\alpha^{(r)}$ to the acoustic absorption, which, for the gases in question, is associated with relaxation of the vibrational specific heat. Here p_0 is the static pressure and f the acoustic frequency which in these experiments ranged from 0·1 to 1 atm and from 1 to 10 kc/s, respectively.

In calculating the relaxation time for deactivation of the vibrational energy, it is assumed that the measured value of $p_0\alpha^{(r)}/f^2$ relates to the relaxation of the

---

† Now with Imperial Chemical Industries Limited, Akers Research Laboratories, Welwyn, Herts.

total vibrational specific heat. This has been shown to be the condition most frequently satisfied; the only exceptions, to date, being methylene chloride (Sette, Busala and Hubbard 1955, Andreae 1957) and sulphur dioxide (Dickens and Linnett 1957, Lambert and Salter 1957, Bass and Lamb 1957), both of which exhibit double dispersion. It is assumed, in addition, that relaxation of the rotational specific heat of the molecules is associated with such a small relaxation time that the resulting contribution to the absorption can be sensibly neglected in the range of f/p_0 covered in the experiments.

§ 2 is concerned with the calculation of the vibrational relaxation time from the value of $p_0\alpha^{(\tau)}/f^2$ measured at frequencies well below the relaxation region. The results of such measurements on a number of polyatomic gases and vapours at 25°C are given in table 3. Comparisons are made with the relaxation times of a number of gases as derived from measurements of the velocity dispersion; these include cyclopropane, methane, methyl chloride, carbon tetrafluoride and ethylene. New information is given for the vibrational relaxation times of boron trifluoride, acetylene and 1, 2-dichlorotetrafluoroethane.

§ 2. DERIVATION OF THE RELAXATION TIME

For the case of a 'thermal' relaxation of the vibrational specific heat the relaxation time at constant temperature τ_T is independent of other thermodynamic constraints. It is related to the relaxation time at constant pressure and entropy τ_{pS} by (Davies and Lamb 1956):

$$\tau_T \text{ (thermal process)} \equiv \tau_{pT} \equiv \tau_{VT} = \left(\frac{\bar{C}_p}{C_p}\right) \tau_{pS}\,. \qquad \ldots\ldots(1)$$

Here C_p represents the 'instantaneous' specific heat at constant pressure and $\bar{C}_p$ the equilibrium value. The relaxational contribution to the absorption is expressed in terms of the relaxation strength, $r = 1 - \bar{C}_p C_V / \bar{C}_V C_p$, by

$$p_0\alpha^{(\tau)}/f^2 = \frac{A}{1 + [(f/p_0)/(f/p_0)_c]^2} = \frac{A}{1 + (\omega\tau_m)^2}\,, \qquad \ldots\ldots(2)$$

where

$$(f/p_0)_c = (p_0 \,.\, 2\pi\tau_m)^{-1}, \qquad \ldots\ldots(3)$$

and

$$A = [p_0\alpha^{(\tau)}/f^2]_{(\omega\tau_m \ll 1)} = \pi r (1 - r)^{-1/4} / \bar{v} (f/p_0)_c \qquad \ldots\ldots(4)$$

$\bar{v}$ is the velocity of sound at low frequencies ($\omega\tau_m \ll 1$) and the 'measured' relaxation time τ_m is related to τ_T and τ_{pS} by

$$\tau_m = \tau_{pS}(1 - r)^{1/4} = \tau_{pS}[\bar{C}_p C_V / \bar{C}_V C_p]^{1/4} = \tau_T [C_p/\bar{C}_p]^{3/4} [C_V/\bar{C}_V]^{1/4}. \quad \ldots\ldots(5)$$

The above equations are approximate but can be used in practice for $r < 0{\cdot}4$; their derivation can be followed from the workings of Davies and Lamb (1957) and Bass and Lamb (1957, 1958).

The basis of the present work is that $\bar{v}$ and A are measured directly; r is evaluated from the vibrational specific heat and thus $(f/p_0)_c$ is calculated from equation (4), giving τ_T from equation (5).

It is usual for experimental workers who study velocity dispersion to express their results in terms of a relaxation time, β, which appears in the expression for the velocity dispersion due to Kneser (1931).

$$(v/\bar{v})^2 = (\bar{C}_V/C_p)\left\{1 + R\,\frac{\bar{C}_V + \omega^2\beta^2 C_V}{\bar{C}_V{}^2 + \omega^2\beta^2 C_V{}^2}\right\}. \qquad \ldots\ldots(6)$$

The present results will be expressed in terms of β since this quantity is frequently used in the literature concerned with relaxation in gases. It should be realized, however, that 'thermodynamic' relaxation times, such as τ_{pS} and τ_T are the quantities of fundamental significance; these are related to β by

$$\beta = \tau_{pS}\left[\frac{\bar{C}_p\bar{C}_V}{C_p C_V}\right]^{1/2} = \tau_T\left[\frac{C_p\bar{C}_V}{\bar{C}_p C_V}\right]^{1/2}. \qquad \ldots\ldots(7)$$

In practice, owing to limitations of experimental accuracy, it is often unnecessary to distinguish between the various relaxation times particularly in cases where the relaxation strength is sufficiently small ($r \ll 1$).

§ 3. EXPERIMENTAL

The resonant conditions which have been employed result from sound propagation in the plane longitudinal mode ($m=0$, $n=0$, in the previous paper), now denoted by L, in the first radial mode ($m=1$, $n=0$) and the second radial mode ($m=2$, $n=0$), denoted by R_1 and R_2 respectively. A summary is given in table 1 of the outstanding features of the measurements, which were made in the manner previously described (Edmonds and Lamb 1958).

One feature of the experiments which was not significant in the work already reported is that measurements made at the lower end of the frequency range tended to give an effective value for $p_0\alpha^{(r)}/f^2$ which depended upon pressure. The divergence from the usual behaviour, where $p_0\alpha^{(r)}/f^2$ is independent of pressure, became greater at the higher pressures approaching 1 atm. This is compatible with a loss of energy from the acoustic field by coupling to the walls of the resonator. It is presumed that this effect was associated with favourable conditions for the excitation of vibrations of the resonator shell, the frequencies of which would not be affected by changing the gas within. Difficulties of this nature were only encountered when measurements were made at the lower end of the frequency range (approaching 1 kc/s) for gases with comparatively low values for the velocity of sound, and then only for relatively high gas pressures in the region of 1 atm.

In the present work sufficient experimental data was available for the readings at the higher pressures to be excluded in cases where an excess loss of this type occurred. The experimental results for such gases are based on measurements made at low pressures, where the coupling of energy to the wall of the resonator was minimized; in addition, preference was given to results obtained from the second radial mode, the resonant conditions of which occurred at the higher end of the frequency range, above those of the longitudinal or first radial modes.

§ 4. NOTES ON THE EVALUATION OF THE RESULTS

(i) Values of the physical constants which were used to calculate the boundary layer losses are given in table 2. In almost all cases it was necessary to interpolate from the published data in order to obtain values at 25 °c and at atmospheric pressure.

(ii) Sutherland's equation was employed when extrapolation from experimental results was necessary, even though in some cases the critical temperature

Table 1. Details of Measurements

Substance	Supplier and Purity	Additional Purification	Resonant modes employed	Min. press (atm (Max. = 1 atm)
Boron trifluoride	Imperial Smelting Corporation 99·8%	None	$R_1(l=5$ to $13)$ $R_2(l=5$ to $14)$	0·3 0·3
Cyclopropane	B.O.C. B.P. anaesthetic grade 99·8%	Dried over KOH. Twice distilled.	$L(l=5$ to $7)$ $R_1(l=5$ to $14)$ $R_2(l=5$ to $12)$	0·15 0·15 0·46
Methane	National Coal Board 98·5%	Bubbled through KOH solution to remove CO_2. Dried over KOH. Distilled three times with intermediate solidification.	$L(l=3$ to $7)$ $R_1(l=5$ to $12)$	0·35 0·35
Methyl chloride	I.C.I. 99% (1% dimethyl ether)	Distilled.	$R_1(l=5$ to $14)$ $R_2(l=5$ to $16)$	0·15 0·4
Carbon tetrafluoride	I.C.I. 99%	Bubbled through KOH solution. Dried over KOH. Twice distilled.	$R_1(l=5$ to $11)$ $R_2(l=5$ to $8)$	0·3 0·8
Ethylene	B.O.C. 98·2%	Bubbled through KOH solution. Dried over KOH. Solidified and twice distilled.	$R_1(l=5$ to $7)$ $R_2(l=5$ to $11)$	0·1 0·1
Acetylene	B.O.C. 99·2% Dissolved in acetone	Passed through cooling trap to remove acetone.	$R_1(l=5$ to $14)$ $R_2(l=5$ to $15)$	0·4 0·4
1,3- Butadiene	Private supply	Dried over KOH. Twice distilled.	$R_1(l=5$ to $13)$ $R_2(l=5$ to $16)$	0·15 0·15
1,2- dichlorotetrafluoroethane	I.C.I. 95% (5% CF_3CFCl_2)	Bubbled through KOH solution. Dried over KOH and P_2O_5. Twice distilled.	$R_1(l=5$ to $14)$ $R_2(l=5$ to $15)$	0·2 0·2

Table 2. Physical Constants at 25°C and 1 atm

(1)	(2)	(3)	(4)	(5)	(6)	(7)	(8)	(9)	(10)
BF_3	169(6)	44·0(7)	2·81(8)	0·179(4,9)	1·20	208	194·6(6)	260·8(3)	49·2(3)
Cyclo-C_3H_6	89·8(11)	42·1(11)	1·744(12)	0·320(4,13)	1·18	262	267(25)	397·8(10)	54·2(10)
CH_4	111(1,2)	78·1(1)	0·657(12)	0·533(5)	1·30	448	164(1)	191(10)	45·8(10)
CH_3Cl	108(1,2)	24·8(2,14)	2·125(12)	0·197(4,15)	1·26	246	454(1)	416·2(12)	65·9(12)
CF_4	172(11,17)	40·2(11)	3·61(8,18)	0·168(4,15)	1·16	180	166(25)	227·5(17)	36·9(17)
$CH_2{\cdot}CH_2$	102·3(1,11)	54·5(11)	1·157(12)	0·371(9,19,20)	1·25	330	241(1)	282·8(10)	50·7(10)
$CH{\vdots}CH$	103·8(1,27)	45·0(2)	1·081(12)	0·394(4)	1·24	341	215(1)	308·5(12)	61·7(12)
$CH_2{:}CH.CH{:}CH_2$	87(11)	42·9(11)	2·31(26)	0·357(22)	1·13	223	303(16)	435(10)	42·6(10)
$ClF_2C.CF_2Cl$	115·3(23)	25·5(21,24)	7·34(24)	0·159(23,24)	1·089(23)	122·5	103(16)	419(23)	32·2(23)

(1) Substance; (2) viscosity $\eta \times 10^6$ (poise); (3) thermal conductivity $\kappa \times 10^6$ (cal cm^{-1} sec^{-1} deg^{-1}); (4) density $\rho \times 10^3$ (g cm^{-3}); (5) specific heat $\overline{C}_p$(cal g^{-1} deg^{-1}); (6) ratio of specific heats $\bar{\gamma}$; (7) velocity of sound $v \times 10^{-2}$(cm sec^{-1}); (8) Sutherland's constant C; (9) (10) critical constants: (9) T_c(°K), (10) p_c (atm).

References.
1. Partington (1949), 2. Int. Crit. Tab. (1929), 3. Booth and Carter (1932), 4. Calculated from spectroscopic data (see 5), 5. Herzberg (1945), 6. Cooke and Mackenzie (1951), 7. Mackenzie and Raw (1953), 8. Amer. Inst. Phys. Hdbk. (1957), 9. Farkas (1953), 10. Stull (1943), 11. Lambert *et al.* (1955), 12. Timmermans (1950), 13. Correction to value given in Edmonds and Lamb (1958), 14. Vines and Bennett (1954), 15. Gelles and Pitzer (1953), 16. Estimated from viscosity data, 17. I.C.I. data on Arcton ' O ', 18. Ruff and Keim (1930), 19. Burcik, Eyster and Yost (1941), 20. Arnett and Crawford (1950), 21. Keyes (1954), 22. Aston *et al.* (1944), 23. Benning and McHarness (1944), 24. I.C.I. data on Arcton ' 33 ', 25. McCoubrey and Singh (1957), 26. Calculated, assuming Berthelot's equation, 27. Doss (1943).

Table 3. Experimental Results at 25 °c and 1 atm

(1)	(2)	(3)	(4)	(5)	(6)	(7)
BF_3	83	56·5	3·0	0·90	None	0·85
Cyclo— C_3H_6	102	151	1·07	2·9	3·07 Corran *et al.* (1958) 3·15 Maccoll (private communication).	2·7
CH_4	44	170	0·094	18·6	16·8 Cottrell and Martin (1957)—at 30°c	18·4
CH_3Cl	102	85	0·96	2·16	2·0 Lambert (private communication) 1·85 Sette, Busala and Hubbard (1955) 1·9 Rossing and Legvold (1955)—at 27°c	2·1
CF_4	44	593	0·38	8·8	8·2 Corran *et al.* (1958) 7·5 Rossing and Legvold (1955)—at 27°c 7·8 Byers (1943)—at 22°c	8·2
$CH_2{:}CH_2$	53	64	1·1	1·9	2·15 Nomoto (1952)—at 27°c 3·75 Corran *et al.* (1958)	1·8
$CH{:}CH$	69	39·6	1·9	1·2	None	1·1
$CH_2{:}CH.CH{:}CH_2$	141	8·1	34	0·13	less than 0·13 Griffith (1950)—at 21°c	0·12
$ClF_2C.CF_2Cl$	34	41·7	10 14	0·56† 0·46‡	None	0·50 0·41

†Internal rotation fully active at 25°c.
‡Internal rotation inactive at 25°c.

(1) Substance; (2) number of recordings; (3) $A \times 10^{13}$ (sec^2 cm^{-1} atm); (4) $(f/p_0)_c$ (Mc/s atm^{-1}); (5) $\beta \times 10^7$(sec); (6) $\beta \times 10^7$(sec)—other workers; (7) $\tau_T \times 10^7$(sec).

T_c was greater than 25°C. The measurements of Ziebland and Burton (1958) indicate that regular behaviour of the coefficient of thermal conductivity can be expected down to $T/T_c \sim 0{\cdot}6$ at 1 atm ($\ll p_c$).

(iii) Berthelot's equation of state was assumed to apply to all the gases and the deviation from ideal gas behaviour at 1 atm was evaluated from the critical constants (table 2). Greater reliance was placed on measured values of viscosity and thermal conductivity and on values of specific heats calculated from spectroscopic data by the Einstein formula.

(iv) Values of the ratio of specific heats $\bar{\gamma}$ were deduced from the calculated specific heats.

(v) Values of the velocity of sound were calculated from the measured resonant frequencies.

(vi) The specific heat of dichlorotetrafluoroethane was derived from the empirical equation of Benning and McHarness (1944);

$$C_p = 0{\cdot}1482 + 0{\cdot}000134t \text{ B.T.U. lb}^{-1}(\text{deg F})^{-1} \text{ [or cal g}^{-1}(\text{deg C})^{-1}],$$

where t is the temperature in °F.

A summary of the experimental results is given in table 3.

§ 5. DISCUSSION

Agreement with acceptable values of β reported by other workers is obtained within ±10% for cyclopropane, methane, methyl chloride and carbon tetrafluoride. The result for methyl chloride is in disagreement with the measurements reported by Corran *et al.* (1958) who gave evidence for the existence of a peak in the curve of β against T. These workers have since repeated their measurements using a sample of methyl chloride taken from the same cylinder as that used for the work reported here and obtained $\beta = 2{\cdot}0 \times 10^{-7}$ sec at 25°C in confirmation of the present result. Mass spectrometer measurements have shown that this sample was purer than the first (Lambert, private communication).

For the case of 1, 3-butadiene the calculations of β were carried out under the assumption that internal rotation does not contribute effectively to the specific heat ($C_V = 3R$), since only the *trans* form is found at room temperature (Aston *et al.* 1946). The value of β for this gas corresponds to the upper limiting value of Griffith (1950).

The value of β obtained for ethylene is low in comparison with other results and it is presumed that the measured sample was impure.

The results for boron trifluoride, acetylene and dichlorotetrafluoroethane provide new information since these gases have not previously been studied. It is probable that the sample of boron trifluoride was contaminated with water vapour since some attack on the ground glass joints of the apparatus was observed after several hours.

Limiting values have been calculated for the relaxation time of dichlorotetrafluoroethane because of the uncertain extent of the hindrance to internal rotation of this molecule about the C-C bond. Extreme values of $R/2$ and zero were taken for the specific heat associated with internal rotation.

It is customary to evaluate the number of collisions Z_{10} required for the deactivation of the lowest vibrational mode of the molecule from its first excited state to the ground state (Corran *et al.* 1958):

$$Z_{10} = Z\beta_1[1 - \exp(-hc\nu_1/kT)]$$

where ν_1 is the lowest vibrational wave number in cm^{-1}, $\beta_1 = C_1/C_{\mathrm{vib}}$ and Z is the number of bimolecular collisions per second. C_1 is the specific heat associated with the lowest vibrational mode and C_{vib} is the total vibrational specific heat. $Z = 4n\sigma^2(\pi RT/M)^{1/2}$ where n is the numerical density and σ is the collision diameter appropriate to a molecular model consisting of rigid spheres with an inverse-power attractive force acting between them. Values of σ were obtained from the viscosity data:

$$\sigma^2 = \frac{266{\cdot}93 \times 10^{-7}(MT^3)^{1/2}}{\eta(T+C)},$$

where η is the coefficient of viscosity and C is Sutherland's constant (Hirschfelder, Curtiss and Bird 1954).

If $\log_{10} Z_{10}$ is plotted against ν_1 a qualitative comparison can be made with figure 10 of the paper by Fogg and Lambert (1955). These authors consider results at 100°c for a larger number of gases which have been separated into two classes according to the extent of the infra-red activity of the lowest vibrational mode. The present results refer to 25°c and hence a direct comparison is not possible owing to the difference in temperature. Transposition according to the equations of Cottrell and Ream (1955) requires knowledge of results extending over a range of temperatures.

The point for boron trifluoride, the fundamental of which ($\nu_4 = 480{\cdot}4\,\mathrm{cm}^{-1}$) is infra-red active (Herzberg 1945, p. 299) lies midway between the two classes of Fogg and Lambert. Transposition to 100°c would tend to reduce $\log Z_{10}$ bringing the point for BF_3 nearer to the 'active' class. The point for acetylene lies closer to the 'active' class which is contrary to the general pattern since the fundamental ($\nu = 611{\cdot}8\,\mathrm{cm}^{-1}$) is infra-red inactive (Herzberg 1945, p. 288). However, this is a linear molecule for which category anomalous behaviour has previously been noted (Fogg and Lambert 1955).

The measurements for methane reported here and by Cottrell and Martin (1957) locate the corresponding point slightly closer to the 'active' line than do the results of Eucken and Aybar (1940) which have been used previously.

Measurements have also been made on fluoroform, chlorotrifluoromethane, methyl acetylene and methyl vinyl ether but final evaluation of these results is prevented by lack of data on the thermal conductivity of these substances at 25°c and 1 atm pressure. The authors would be grateful to learn of the existence of any such measurements.

ACKNOWLEDGMENTS

The authors wish to thank Dr. J. C. McCoubrey and Dr. W. D. McGrath for valuable discussion, and Dr. J. D. Lambert and Dr. A. Maccoll for kindly communicating results prior to publication. The work was supported by a grant from the Department of Scientific and Industrial Research to whom the authors are indebted. The logarithmic pen recorder used in the measurements was provided by the Scientific Investigations Grant-in-aid administered by the Royal Society and this assistance is gratefully acknowledged. P.D.E. is indebted to the Department of Scientific and Industrial Research for the provision of a maintenance grant and to the Worshipful Company of Clothworkers for further support.

REFERENCES

Amer. Inst. Phys. Hdbk., 1957 (New York: McGraw-Hill).

Andreae, J. H., 1957, *Proc. Phys. Soc.* B, **70**, 71.

Arnett, R. L., and Crawford, B. L., 1950, *J. Chem. Phys.*, **18**, 118.

Aston, J. G., Moessen, G. W., Hardy, H. C., and Szasz, G. J., 1944, *J. Chem. Phys.*, **12**, 458.

Aston, J. G., Szasz, G. J., Woolley, H. W., and Brickwedde, F. G., 1946, *J. Chem. Phys.*, **14**, 67.

Bass, R., and Lamb, J., 1957, *Proc. Roy. Soc.* A, **243**, 94; 1958, *Ibid.*, **247**, 168.

Benning, A. F., and McHarness, R. C., 1944, *Bull. Kin. Chem. Inc.*, Wilmington, Delaware, U.S.A.

Booth, H. S., and Carter, J. M., 1932, *J. Phys. Chem.*, **36**, 1359.

Burcik, E. J., Eyster, E. H., and Yost, D. M., 1941, *J. Chem. Phys.*, **9**, 118.

Byers, W. H., 1943, *J. Chem. Phys.*, **11**, 348.

Cooke, B. A., and Mackenzie, H. A. E., 1951, *J. S. Afr. Chem. Inst.* (New Series), **4**, 123.

Corran, P. G., Lambert, J. D., Salter, R., and Warburton, B., 1958, *Proc. Roy. Soc.* A, **224**, 212.

Cottrell, T. L., and Martin, P. E., 1957, *Trans. Faraday Soc.*, **53**, 1157.

Cottrell, T. L., and Ream, N., 1955, *Trans. Faraday Soc.*, **51**, 1453.

Davies, R. O., and Lamb, J., 1956, *Proc. Phys. Soc.* B, **69**, 293; 1957, *Quart. Rev. Chem. Soc., Lond.*, **11**, 134.

Dickens, P. G., and Linnett, J. W., 1957, *Proc. Roy. Soc.* A, **243**, 84.

Doss, M. P., 1943, *Physical Constants of the Principle Hydrocarbons* (N. York: Texas Co.).

Edmonds, P. D., and Lamb, J., 1958, *Proc. Phys. Soc.*, **71**, 17.

Eucken, A., and Aybar, S., 1940, *Z. phys. Chem.* B, **46**, 195.

Farkas, A., 1953, *Physical Chemistry of Hydrocarbons*, Vol. **2** (New York: Academic Press).

Fogg, P. G., and Lambert, J. D., 1955, *Proc. Roy. Soc.* A, **232**, 537.

Gelles, E., and Pitzer, K. S., 1953, *J. Amer. Chem. Soc.*, **75**, 5259.

Griffith, W., 1950, *J. Appl. Phys.*, **21**, 1319.

Herzberg, G., 1945, *Infra-red and Raman Spectra of Polyatomic Molecules* (New York: van Nostrand).

Hirschfelder, J. D., Curtiss, C. F., and Bird, R. B., 1954, *Molecular Theory of Gases and Liquids* (New York: Wiley).

Keyes, F. G., 1954, *Trans. Amer. Soc. Mech. Engrs*, **76**, 809.

Kneser, H. O., 1931, *Ann. Phys., Lpz.*, **11**, 761.

Lambert, J. D., Cotton, K. J., Pailthorpe, M. W., Robinson, A. M., Scrivens, J., Vale, W. R. F., and Young, R. M., 1955, *Proc. Roy. Soc.* A, **231**, 280.

Lambert, J. D., and Salter, R., 1957, *Proc. Roy. Soc.* A, **243**, 78.

Mackenzie, H. A. E., and Raw, C. J. G., 1953, *J. S. Afr. Chem. Inst.* (New Series), **6**, 8.

McCoubrey, J. C., and Singh, N. M., 1957, *Trans. Faraday Soc.*, **53**, 877.

Nomoto, O., Ikeda, T., and Kishimoto, T., 1952, *J. Phys. Soc. Japan*, **7**, 117.

Partington, J. R. 1949, *An Advanced Treatise on Physical Chemistry*, Vol. **I**, (London: Longmans).

Rossing, T. D., and Legvold, S., 1955, *J. Chem. Phys.*, **23**, 1118.

Ruff, O., and Keim, R., 1930, *Z. anorg. Chem.*, **192**, 249.

Sette, D., Busala, A., and Hubbard, J. C., 1955, *J. Chem. Phys.*, **23**, 787.

Stull, D. R., 1943, *Industr. Engng Chem.*, **36**, 1303.

Timmermans, J., 1950, *Physico-Chemical Constants of Pure Organic Compounds* (Amsterdam: Elsevier).

Vines, R. G., and Bennett, L. A., 1954, *J. Amer. Chem. Soc.*, **22**, 360.

Ziebland, H., and Burton, J. T. A., 1958, *Brit. J. Appl. Phys.*, **9**, 52.

A Prolate Spheroidal Field Magnetic Spectrometer with Source near the Equatorial Plane

By P. R. EVANS, N. J. FREEMAN, G. K. McGINTY,
B. H. ARMITAGE and H. O. W. RICHARDSON
Bedford College, University of London

MS. received 5*th May* 1958, *and in revised form* 14*th August* 1958

Abstract. A prolate spheroidal field β-spectrometer is described in which the source and detector are located on the same side of the focal ring slit. The trajectories reach distances of up to 38 cm from the axis and the ring slit has a radius of 33 cm. The relation between the resolution and transmission has been measured for four source diameters. Using a scintillation detector of 1·85 cm diameter and 1 cm length, a resolution W of 1·28% at a transmission T of 1% of 4π has been found for a source of 1 cm diameter. For a 1 mm source the measured values range from $W=0{\cdot}4\%$ at $T=0{\cdot}8\%$ to $W=1{\cdot}52\%$ at $T=5{\cdot}2\%$.

---

§ 1. The Focusing Principle

The design of the spectrometer to be described was based on experience with a smaller spheroidal field instrument at the University of Edinburgh (Braid and Richardson 1951, Richardson 1952 a). That spectrometer, in common with those described by Slätis and Siegbahn (1950), Daniel and Bothe (1954) and Alburger (1956), has the advantages possessed by all lens-type instruments in which a focal ring is formed in the equatorial or mid-plane of the field halfway between the source and the detector. The chief advantage is that the spherical aberration at the axis is so small that a small detector with a low background count can be used even when the rays are collected over a large solid angle. This reduction in aberration is connected with a tendency to form a second focal ring near the detector. In the uniform field lens spectrometer, for example, this tendency is absent and rays emitted at neighbouring angles diverge perpetually after passing the first focal ring and cross the axis along an extended focal line. It has been noted by Verster (1952) that in this case the maximum transmission is nearly proportional to the diameter of the detector.

The present instrument departs from earlier designs in two main respects. Firstly, it abandons the symmetry of the source and detector with respect to the field, and secondly, it seeks for the advantages which accrue from a larger size, the trajectories reaching a radius of 38 cm from the axis while the first focal ring, sometimes called the ring focus or the intermediate image, has a radius of 33 cm.

The asymmetry is so large that the source and final image both lie on the same side of the plane containing the first focal ring and its associated ring slit. The field near this ring turns back the rays in the meridional plane so sharply that for motion in that plane it acts rather like a concave mirror, giving a real inverted image. Photographs indicate that the reflected rays, if not stopped by the detector, would intersect in the meridional plane soon after they cross the axis. Thus the second focal ring no longer girdles the detector as it did in the Edinburgh spectrometer. However, the width of the beam at the axis is of the order of 1 cm so that the advantage of a small detector has not been lost. The instrument may be looked on as a wide-angle lens spectrometer with a large diameter ring-slit in which the spherical aberration at the axis is reduced to a low value by using a strong field gradient near the detector.

An advantage of the unsymmetrical arrangement is that it reduces the angle of emission of the focused rays from about 75° to about 45°, thus decreasing the effective thickness of disc sources by a factor of 1/2·73. Another gain is that the construction is simplified because one end of the vacuum chamber may be closed by a plane iron disc (marked 3 in figures 1 and 3) which does not require a magnetizing winding. The equipotential surface of this disc is now the mid-plane of the approximately spheroidal field. The source is placed in an axial hole in the disc and is appreciably shielded from the main field as can be seen from figure 4 in which the field strength is plotted along the axis. The shielding of the source causes a distortion of the field from the spheroidal form, which has little effect on the focusing but is convenient if one wishes to join on a second spectrometer for coincidence studies between electrons emitted in opposite directions. A smaller iron-clad spectrometer has been built for this purpose and is arranged to fit on the cylindrical source chamber 42 in figure 3 in place of the γ-ray counter 43.

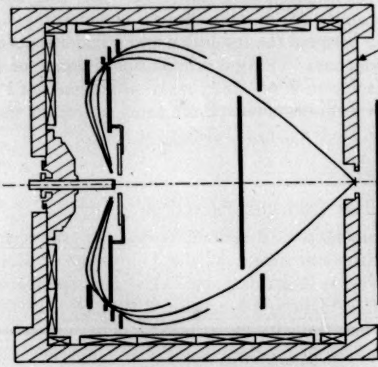

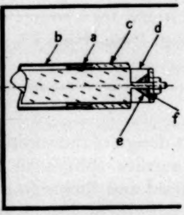

Figure 2.

Figure 1. Schematic diagram showing three monoenergetic rays projected on a meridional plane.

Figure 2. 1 cm phosphor and light pipe: a, centring screw ; b, brass tube ; c, brass shield ; d, phosphor ; e, MgO reflector ; f, Al disc.

Measured values of the resolution W are plotted against the transmission T in figure 8. $W = 1{\cdot}28\%$ at $T = 1\%$ of 4π can be obtained for a disc source of 1 cm diameter, giving an unusually large luminosity, defined as the product of T and the source area.

The trend of the curves for different values of source diameter is in fair agreement with the theory of Verster (1952), which predicts that the best resolution W obtainable with a given diameter d is equal to d divided by a dispersion parameter of approximate value 3·5 times the maximum radial coordinate of the focused rays. The numerical agreement implies that it is essential to use a spectrometer of large diameter if large disc sources are to be used for measurements of high resolution in any axially symmetric instrument and that the diameter required should be nearly independent of the type of spectrometer.

In common with all lens spectrometers a good resolution can only be expected, even with a point source, if the axial symmetry is perfect. The curves of figure 8 suggest that there is still some lack of axial symmetry in the instrument and also that the slit and detector system hitherto used does not achieve efficient collection at large values of d and T. Thus improvements in the performance are still possible.

§ 2. THE MAGNET

The magnet frame is made of soft annealed steel containing 0·05% carbon and has the shape of a hollow cylinder whose sides are formed by 56 bars, 1 in figure 3, of 1·5 in. × 2 in. cross section and whose ends are the two iron discs 2 and 3, each 36 in. diameter and 1·75 in. thick. The magnetic continuity between the end discs and the side bars is maintained by the 112 machined corner blocks 4.

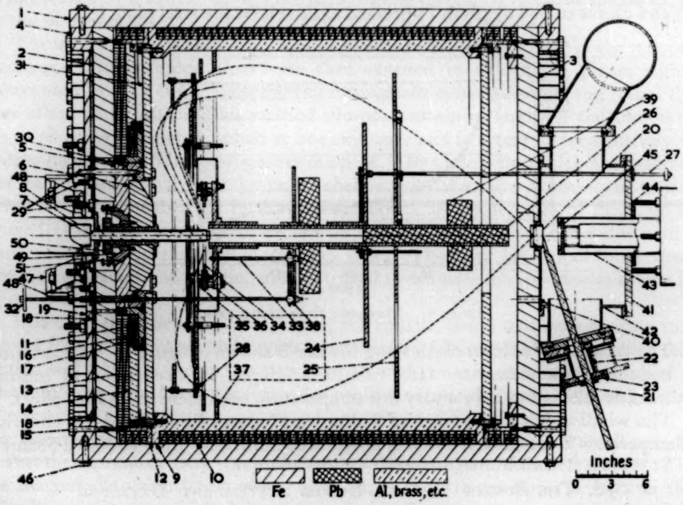

Figure 3. Axial section of spectrometer, viewed from above. Items 47 and 48 are peripheral attachments to the supporting chassis.

The left end disc 2 has a 6 in. axial hole which centralizes the pole ring 5. The latter carries the bevelled pole-piece 6 which is bored axially to take the Perspex light pipe 7 connecting the plastic scintillator to the photomultiplier 8.

The magnet frame encloses the aluminium vacuum tank 9 which also serves as a bobbin to carry a part of the magnetizing winding 10. This winding consists of a cylindrical portion of mean radius 17·5 in. and some pancake coils which line the inner surface of the left end disc 2.

Explicit expressions have been given and plotted elsewhere (Richardson 1952 b) for the current distributions which generate a prolate spheroidal field inside an iron-clad enclosure. It turns out in the present case that a uniform and nearly equal current density in both cylindrical and pancake windings is fairly satisfactory, but provision has been made for increasing the current density near the left pole piece by passing current through the small coils 11 which are of 0·25 in. × 0·07 in. copper strip with Lewmex plastic film insulation. The remainder of the winding consists of 0·5 in. × 0·035 in. bare copper strip interleaved with fibre-glass insulating tape.

The cylindrical part of the winding is cooled by circulation of air in the $\frac{1}{16}$ in. spaces between the 46 flat coils 10 wound on the vacuum tank and between the eight coils on the aluminium rings 12. These air spaces also provide passages for conducting strips to reach the base of each coil.

The two large pancake coils 13 are pressed by the aluminium plate 14 against the iron end disc 2 and are cooled by water pipes which enter through holes bored in two of the screws 15. Heat is conducted from the small coils 11 by the copper plate 16 and by another cooling pipe lying in a groove in the coil bobbin 17. The left end disc is cooled by pipes 18 pressed against it by the steel plate 19.

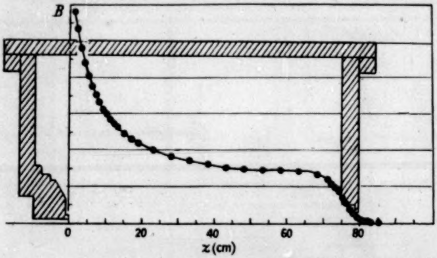

Figure 4. Magnetic field along axis.

The variation of field strength along the axis is shown in figure 4. It was found by measuring the transverse Hall voltage developed in a specimen of indium antimonide selected to have a very low temperature coefficient in its Hall effect.

The winding has a resistance of 9 ohms and focuses $B\rho = 1388$ gauss cm with 2·1 amperes. Thus about 2·06 kw of power are required for $B\rho = 10\,000$ (2·53 Mev).

§ 3. The Source Holder, Baffle System and Detector

The sources are mounted in the ring-shaped holder 20 (figure 3) which can be withdrawn by the rod 21 into the vacuum gate chamber 22. On sliding the chamber to the right and removing the cover 23 the source can be taken out.

The baffles 24 and 25 define the angular limits of the beam. The focal ring slit 28 is supplemented by three ring baffles such as 37 which should be placed so that they lie on a caustic formed by monoenergetic rays from a point source in the manner recommended by Hubert (1953). The width of the ring slit can be varied *in vacuo* by turning three screws coupled by a chain drive. The outer ring of the slit and its supplementary ring baffles are normally kept in a fixed position when the width is varied. The mechanism for the various adjustments is described in the Appendix.

The rays, after passing the ring slit, fall on the outer surface of the ring-shaped cylindrical scintillator d of 1·85 cm diameter and 1 cm length, shown in figure 2. The reflecting cone e is packed with magnesium oxide held in place by the Al foil f pressed by a Perspex washer. With silicone fluid to make optical contact with the plastic phosphor (type N.E.101) satisfactory pulses were found at energies of about 16 kev, using an E.M.I. 13-stage photomultiplier. Shorter phosphors of the same diameter, of length 2½ or 3 mm, were also used.

§ 4. PROCEDURE FOR LOCATING THE CAUSTIC CURVE

It was necessary to use an experimental method to locate the first focal ring because the only ray path computations available for the spheroidal field (Richardson 1949) were for a symmetrical arrangement of source and image and, in addition, the shape of the present field is not truly spheroidal.

An exploring baffle was made which could be moved along the axial tube 26 (figure 3). It consisted of a disc of 28 in. diameter in which were milled four concentric curved slits ¼ in. wide, having radii of 8, 10, 12 and 13 in., each extending over 30° of arc in the same 30° sector of the disc. Any one of the four slits could be uncovered by a shutter so that the rays coming through it could be investigated by the phosphor.

The tests showed that the ring focus lay close to the left hand end of the vacuum chamber. Photographic films were then exposed in meridional planes which intercepted 148 kev electrons spiralling through the concentric slits and round the edge of the 28 in. disc. This method allows an extensive family of trajectories in the rz plane to be photographed at one exposure and is a very convenient way of finding the electron optical properties of a field. By finding the position of shadows cast on the meridional plane by radial obstructions of known azimuth the trajectories can be reconstructed in three dimensions. A photograph of this kind in figure 5 (Plate) shows two sheaves of rays coming from the two outer slits with a third coming round the edge of the 28 in. disc. The three sheaves all touch their common envelope, the caustic, and were used to estimate the trajectories drawn in figure 3.

It is clear that the rays, after leaving the caustic, begin to converge again to a second focal ring on a second caustic near the axis. It seems likely that the intersection will take place after the rays have crossed the axis, at negative values of r. The focal ring is probably not formed at positive values of r, except at larger angles of emission.

The rays in figure 5 were obtained with no current flowing in the small coils 11 so that the current density was uniform over the plane part of the left end disc 2 of the magnet, its value being about 11% larger than the uniform density in the cylindrical coils 10. This difference is due to the $\frac{1}{16}$ in. air spaces between each coil in 10.

A greater field gradient may be obtained near the left pole face by bringing the coils 11 into the circuit. The photographs in this case show the rays to be turned back more sharply at the caustic, to reach the axis at a point nearer the centre of the chamber.

§ 5. TESTS OF THE INTENSITY DISTRIBUTION NEAR THE DETECTOR

The four ring baffles associated with the ring slit 28 were set up along a suitable caustic curve deduced from the photographs. The narrowness at the axis of the beam transmitted through this slit was confirmed by tests made with short cylindrical phosphors of lengths 2½ and 3 mm. Four different widths of ring slit were used, equivalent approximately to transmissions of 1·2, 2·5, 3 and 4% of 4π when received on a phosphor of length 1 cm from a point source (see § 6).

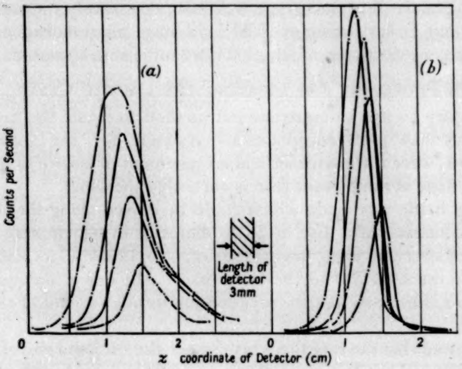

Figure 6. Curves (*a*) axial distributions of intensity near the detector due to a continuous β-spectrum for 4 different widths of ring slit ; curves (*b*) axial distributions of 148 kev electrons.

In the first type of test the counting rate at constant current was found for different values of *z*, the axial coordinate of the phosphor. The results, in the case of a source of 1 mm diameter, are shown in figure 6. The family of curves (*a*) was obtained with a flat region of the continuous spectrum of Th (B + C + C″) falling on the slit. With increasing transmission the width at half-height increased from 5·4 to 9 mm and a phosphor 2 cm long would be needed to collect the widest beam. The narrower set of curves (*b*) was obtained with predominantly monoenergetic electrons arranged to fall on the slit by setting the current on the peak of the strong F conversion line, with the phosphor in that position *z* which gave a maximum count for the continuous spectrum. Keeping the current at this value, the counting rate was then found at other positions *z*.

The half-widths of the four axial distributions of monoenergetic rays are smaller and range from 3·4 to 4·2 mm. The width is such that a phosphor of 1 cm length can collect 95% of the beam at the widest slit opening.

The greater spread with the continuous spectrum indicates that there is enough momentum dispersion along the axis to spread the small 'window' of momentum accepted by the ring slit over a range of *z* of order 1 cm.

Similar curves were taken with a source of 1 cm diameter. The half-widths now range from 11·5 to 12 mm for the continuous spectrum and from 7 to 8 mm for the F electrons and the length of scintillator needed to collect the whole beam is about 50% larger than for a 1 mm source.

In a second type of test β-ray line shapes were recorded at different positions *z* of the detector. Not only did the transmission vary with *z* but also the current at the peak of the line. This is another aspect of the momentum dispersion noted in the first type of test and is shown by the curves in figure 7 (*a*) taken with the ring slit in the widest of its four positions. The curves are profiles of the F line with a phosphor 3 mm long in seven positions 2 mm apart. The current at each peak varies nearly linearly with z with a mean dispersion of 0·56 cm for a 1% change in current.

The relation between the z coordinate of the centre of the beam at the image and the z coordinate of the source was investigated. It was found that an axial motion of the source of 1·2 cm caused the image to move 4 mm in the opposite direction. Such a contracurrent relation between source and image was reported for the Edinburgh spectrometer (Braid and Richardson 1951) in which the displacements were equal and opposite.

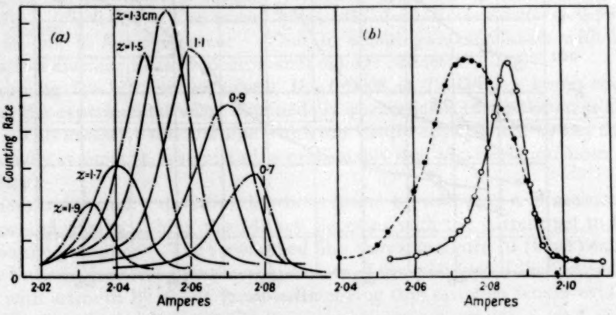

Figure 7. Curves (a) F line shapes at different axial positions z of a short detector with a wide ring slit ; curves (b) F line shapes with a long (1 cm) detector for sources of 1 mm and 1 cm diameter using a narrow ring slit.

Photographic tests at the detector which revealed a lack of axial symmetry are described in the next section. Better symmetry would undoubtedly make the curves narrower in figures 6 and 7 and allow shorter phosphors to be used.

§ 6. TESTS OF RESOLVING POWER AND TRANSMISSION

Measured values of the resolution W and transmission T are plotted in figure 8 for disc sources of four diameters d. W is the width at half-height of the 148 kev F line expressed as a fraction of the magnetizing current, and T is the fraction of the F electrons counted at the peak of the line. T was found by measuring the strength of the source by counting the α-rays from the daughter elements ThC and ThC′, using a masked thallium-activated potassium iodide scintillator which subtended a known solid angle. The F electrons were assumed to amount to 0·30 per disintegration and a correction was made for the life of ThC.

The sources were brass discs activated by exposure to thoron. The uniformity of the active deposit was fairly good, as can be seen from figure 9 which shows counting rates for α-rays coming through a pin-hole of diameter 0·5 mm in a brass plate which was moved parallel to the surface of the discs.

The points marked with crosses were obtained using a short phosphor of length 2½ mm as detector. The remainder were taken using a detector 1 cm long.

It is interesting to compare the curves for a given source diameter d with the formula of Verster (1952) $W = S_2T^2 + d/D$. This is expected to hold for mono-energetic rays in lens-type spectrometers in which the resolution is due to the selecting action of a focal ring slit. It is accurate only for small angles of emission, a condition not well satisfied in our case. It predicts a family of similar parabolae with their vertices at a distance d/D above the origin, whose slopes depend on the spherical aberration coefficient S_2. The parameter D represents the radial dispersion in the plane of the ring slit and has the approximate value $3{\cdot}5\, r_{\max}$, where $r_{\max}$ is the maximum radial coordinate of the focused rays.

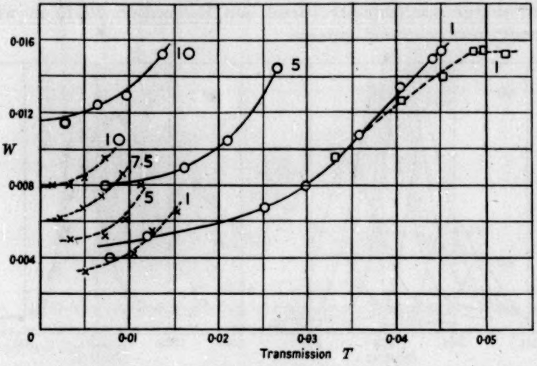

Figure 8. Resolution W plotted against transmission T (fraction of 4π). The diameter in mm of the source is written against each curve. Points marked with a cross were obtained with detectors of $2\frac{1}{2}$ mm length.

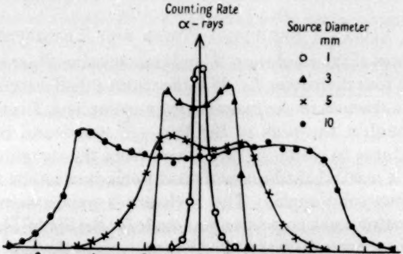

Figure 9. α-particle test of the uniformity of active deposit on the disc sources.

The curves obtained with the short phosphor show more curvature than is predicted by Verster's formula, which is only valid if all rays passed by the ring slit and the angle defining baffles are detected. The curves taken with the longer detector should follow the formula more closely because, with a single exception at $W=0{\cdot}004$, the points were found with the detector placed to receive as much as possible of the beam from the ring slit. As already noted, the beam is wider than 1 cm except with the 1 mm source, so that a fraction of the beam is missed, which increases both with *d* and with slit width. This readily explains the increase in curvature of the parabolae with *d*. A second factor having a similar effect arose from a non-optimum setting of the angle-defining baffles whose chief use is to reduce scattered radiation. The points marked with squares were found with these baffles opened to the limit permitted by the Pb shields.

Verster's formula predicts that the parabolae should cut the axis $T=0$ at $W=d/D$. Although this prediction is not fulfilled, it is clear that the vertical spacing of the parabolae is roughly proportional to *d*. An average value of $(\partial W/\partial d)_{T\,\text{const}}$ is 0·009. The theory gives $\partial W/\partial d=1/D=0{\cdot}008$ if $D=3{\cdot}5\,r_{\text{max}}$, $r_{\text{max}}=36$ cm, in fair agreement. Thus to obtain good resolution with large sources, it is essential to use a spectrometer of large diameter.

Assuming $D=126$ cm, we expect $W=0{\cdot}0008$ at $T=0$ for a 1 mm source, whereas the experimental value obtained by a reasonable extrapolation is about 0·003. This excessive residual line width can hardly be explained by any theory of an axially symmetric system and is presumably due to a deviation from axial symmetry.

Evidence for such a deviation has been found by wrapping a film round the detector and photographing the 148 kev electrons with the current set to focus them on the phosphor. The unwrapped film shown in figure 10 (Plate) exhibits a wavy line which proves that the *z* coordinate of the intercept of the focused rays varies with azimuth by about 4 mm. Removing this variation would evidently much improve the resolution at $T=0$.

The agreement with Verster's formula suggests that, for a given diameter of source, the best resolution of all lens spectrometers of the ring focus type will be nearly the same for the same maximum radius of path. Details of field shape will only influence the spherical aberration constant S_2.

ACKNOWLEDGMENTS

The construction of the spectrometer was made possible by a generous grant from the Department of Scientific and Industrial Research. We wish to thank Professor N. Feather for his support in the initial stages at Edinburgh. Gifts of a centrifugal bronze casting by the David Brown Foundries Co. and of special crystals of indium antimonide by Dr. G. K. Eaton of the Mullard Co., are gratefully acknowledged, and also the assistance of Messrs. P. J. Walland, R. Steed and F. Grimes.

One of us (G. K. McG.) received a grant from the University of Exeter, which also awarded Postgraduate Scholarships to B. H. A., N. J. F. and P. R. E.; N. J. F. and P. R. E. are indebted to Bedford College for the award of Research Studentships.

REFERENCES

ALBURGER, D. E., 1956, *Rev. Sci. Instrum.*, **27**, 991.
BRAID, T. H., and RICHARDSON, H. O. W., 1951, *Proc. Phys. Soc.* A, **64**, 163.
DANIEL, H., and BOTHE, W., 1954, *Z. Naturf.*, **9 a**, 402.
HUBERT, P., 1953, *Ann. Phys.*, **8**, 662.
RICHARDSON, H. O. W., 1949, *Phil. Mag.*, **40**, 233; 1952 a, *J. Sci. Instrum.*, **29**, 93; 1952 b, *Proc. Phys. Soc.* B, **65**, 5.
SLÄTIS, H., and SIEGBAHN, K., 1950, *Ark. Fys.*, **1**, 339.
VERSTER, N., 1952, *Progr. Nucl. Phys.*, **2**, 1.

APPENDIX

Constructional Details

The angle-defining baffles 24, 25 (figure 3) can be moved bodily along the axial guide tube 26 by the push rod 27. By rotating this rod the width of the angle defining slit can be varied because the rotation turns three parallel screws each carrying a sprocket wheel. The three wheels are coupled together by a brass ladder chain.

The width of the focal ring slit 28 can be varied in a similar way. The chain which couples the three screws is driven by a fourth sprocket (not visible in figure 3) turned by a $\frac{3}{16}$ in. shaft which enters the vacuum tank through an axial hole drilled in one of the non-magnetic stainless steel tension studs 29. The shaft passes through an O-ring seal in the bronze ring 30 into which the twelve tension studs are screwed.

An axial motion of the focal ring baffles 28 can be obtained by turning a second $\frac{3}{16}$ in. control rod 32, which turns the lead screw 33 by sprocket and chain. Two more control rods provide a centring motion to the slit assembly, which is mounted on four flanged wheels running on the top and bottom edges of the rectangular guide plate 34. An eccentric driven by one control rod gives a sideways motion, while the other turns a screw which raises the guide plate vertically between four flanged wheels mounted on the base 36. The tank is pumped out through twenty-four $\frac{1}{2}$ in. holes 40 in the end disc 3.

In order to obtain access to the interior a four-wheeled trolley (shown in figure 11, Plate) can be arranged to move the left end disc 2 with its corner blocks, coils, pole-piece and counter, as a unit. The chassis of the trolley is formed by two longer side bars 48, joined to the end discs by the large triangular blocks 47. For minor adjustments a simpler access route is opened by removing the screws holding the breech-block 49, the nut 50 and the light pipe 7.

The Narrowing of Nuclear Magnetic Resonance Spectra by Molecular Rotation in Solids

By E. R. ANDREW and R. A. NEWING
University College of North Wales, Bangor, Wales

MS. received 5th May 1958, and in final form 14th August 1958

Abstract. Molecular rotation in a solid causes a narrowing of the spectrum and a consequent reduction of its second moment. It is shown that the rotation also produces weak side-spectra, which are usually unobservable. If these side-spectra are included the second moment of the entire spectrum is the same as that for the rigid solid, thus preserving the invariance of the second moment. The cases of rotating and randomly reorienting pairs of nuclei are discussed in detail. The fourth moment of the entire spectrum is found to be increased by the motion, though that of the observable central portion is diminished.

---

§ 1. Introduction

The width of the magnetic resonance spectrum of light nuclei of spin number $\frac{1}{2}$ in a non-metallic crystal usually originates from nuclear magnetic dipolar interaction. The width may be regarded as a measure of the distribution of local magnetic fields over the nuclear sites in the crystal. If the nuclei at resonance are caused to move within the crystal by the hindered rotation of molecules, ions or groups containing them, the spectrum is found to become narrower. Gutowsky and Pake (1950), who examined such situations both theoretically and experimentally, showed that when the frequency of molecular reorientation is greater than the spectral width the mean local field determines the width of the spectrum, and this is usually smaller than the static local field in the absence of motion. They further showed how the formula of Van Vleck (1948) for the second moment of a dipolar-broadened spectrum is modified by hindered rotation. There are now many examples of narrowed spectra which have been quantitatively explained in terms of hindered motion within a crystal using Gutowsky and Pake's modification of Van Vleck's formula for the second moment of the spectrum.

Recently however Pake (1956) has drawn attention to an argument due to Anderson which leads to the conclusion that hindered rotation in a solid should not after all cause a reduction in the second moment of the nuclear magnetic resonance spectrum. Briefly summarized the argument is as follows. Van Vleck (1948) expresses the second moment in terms of the commutator of the nuclear Hamiltonian with the x-component of the spin angular momentum of the nuclei. Any term in the Hamiltonian which expresses the motion of the nuclei in the crystal will commute with the spin operator and will therefore not affect the commutator or the second moment. The second moment should therefore remain constant. This does not necessarily mean that the shape of the spectrum should remain the same. Indeed Pake shows that the fourth moment of the spectrum is increased by nuclear motion. Taken with the invariance of the second moment, the increase of fourth moment implies a narrowing of the central portion of the spectrum and strengthening of its skirts.

The purpose of this paper is to show how these apparently conflicting conclusions concerning the effect of hindered motion on the second moment can be reconciled. It is found that the motion does cause the spectrum to develop wide skirts of weak intensity, and that when these skirts are taken into account the second moment of the spectrum does remain invariant. In practice however these skirts become too weak to be detected when the rate of reorientation greatly exceeds the spectral width, and the second moment of the spectrum actually observed is reduced to just the value Gutowsky and Pake (1950) had earlier indicated. This earlier work is therefore not invalidated by the requirement of invariance of second moment, though the theoretical basis on which it rests needs qualification.

In the next section, § 2, the spectrum for nuclear pairs rotating with uniform angular velocity is first considered. This simple case gives good insight to the problem before treating in § 3 the more usual case of random reorientation of nuclear pairs.

§ 2. SPECTRUM FOR ROTATING PAIR

2.1. *Axis Normal to Pair*

Consider a crystal containing a static array of similarly-oriented well-separated identical pairs of nuclei having spin number $\frac{1}{2}$. Pake (1948) has shown that the nuclear magnetic resonance spectrum consists of two lines of equal intensity at angular frequencies given by

$$\omega = \gamma_a \left[H_0 \pm \epsilon\mu_b r^{-3} (3\cos^2\theta - 1)\right], \qquad \ldots\ldots (1)$$

where γ_a is the magnetogyric ratio of the nuclei at resonance, $\mathbf{H}_0$ is the constant applied magnetic field, μ_b is the magnetic moment of the nuclear neighbour in each pair, $\mathbf{r}$ is the internuclear vector, θ is the angle between $\mathbf{H}_0$ and $\mathbf{r}$, and ϵ is $\frac{3}{2}$ if the two nuclei in each pair are identical, and is unity if they are not identical. The second moment of this simple spectrum about its central frequency $\omega_0(=\gamma_a H_0)$, in terms of angular frequency, is therefore

$$S_2 = C^2 (3\cos^2\theta - 1)^2, \qquad \ldots\ldots (2)$$

where

$$C = \epsilon\gamma_a\mu_b r^{-3}. \qquad \ldots\ldots (2a)$$

Van Vleck's formula for second moment also gives this result.

Thus the spectrum for this static array can be regarded as arising from the presence, at the sites of the nuclei at resonance, of an effective local field whose component along $\mathbf{H}_0$ is given by

$$H_{\text{loc}} = \pm C\gamma_a^{-1} (3\cos^2\theta - 1), \qquad \ldots\ldots (3)$$

the plus and minus signs having equal probability. The description of dipolar interactions by means of a local field is not generally satisfactory when calculating the spectrum for a grouping more complicated than a pair, but even in such cases the use of (3) leads to the correct second moment. We shall extend the use of an effective local field to the case of a rotating pair.

Suppose now that each nuclear pair has an axis about which it can rotate (figure 1). The axes for all nuclear pairs are parallel to each other, and make an angle α with $\mathbf{H}_0$. We suppose that the axes are perpendicular to the nuclear

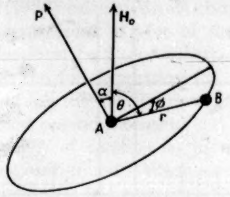

Figure 1. Diagram illustrating the rotation of a pair of nuclei A and B about an axis AP normal to the line AB joining them. The applied magnetic field **H₀** makes an angle α with the axis of rotation.

pairs; in § 2.2 a more general case is treated. First of all, however, we suppose that there is no rotation about these axes, but that the nuclear pairs are distributed with random, but fixed, azimuth angles ϕ about the axis. The spectrum from pairs with a given ϕ consists of two lines given by (1) in which we can put

$$\cos\theta = \sin\alpha\cos\phi. \qquad \ldots\ldots(4)$$

The second moment of this spectrum will be, from (2) and (4)

$$S_2(\phi) = C^2(9\sin^4\alpha\cos^4\phi - 6\sin^2\alpha\cos^2\phi + 1). \qquad \ldots\ldots(5)$$

The spectrum for all pairs, taking all ϕ with equal probability, has second moment

$$S_2 = \frac{1}{2\pi}\int_0^{2\pi} S_2(\phi)\,d\phi = C^2\left(\frac{27}{8}\sin^4\alpha - 3\sin^2\alpha + 1\right). \qquad \ldots\ldots(6)$$

Now let all the pairs rotate about their axes with the same uniform angular velocity ω_r. The sense of rotation is unimportant. We now have

$$\phi = \omega_r t \qquad \ldots\ldots(7)$$

in (4), where t is time, and the local field given by (3) is

$$\begin{aligned} H_{\mathrm{loc}} &= \pm C\gamma_a^{-1}(3\sin^2\alpha\cos^2\omega_r t - 1) \\ &= \mp C\gamma_a^{-1}[\tfrac{1}{2}(3\cos^2\alpha - 1) - \tfrac{3}{2}\sin^2\alpha\cos 2\omega_r t]. \end{aligned} \qquad \ldots\ldots(8)$$

Thus the local field consists of a static part and a fluctuating part; the mean local field is

$$\bar{H}_{\mathrm{loc}} = \mp C\gamma_a^{-1}[\tfrac{1}{2}(3\cos^2\alpha - 1)]. \qquad \ldots\ldots(9)$$

The Larmor frequency of precession of the nuclei is

$$\begin{aligned} \omega &= \gamma_a(H_0 + H_{\mathrm{loc}}) \\ &= \omega_0 \mp C[\tfrac{1}{2}(3\cos^2\alpha - 1) - \tfrac{3}{2}\sin^2\alpha\cos 2\omega_r t], \end{aligned} \qquad \ldots\ldots(10)$$

which is, of course, the same result as that given by (1) with (4) and (7). We notice that the Larmor frequency ω is frequency modulated at a frequency $2\omega_r$. It is convenient to write

$$\omega = \omega_0 \mp \omega_1 \pm \omega_2\cos 2\omega_r t, \qquad \ldots\ldots(11)$$

where

$$\left.\begin{aligned} \omega_0 &= \gamma_a H_0, \\ \omega_1 &= \tfrac{1}{2}C(3\cos^2\alpha - 1), \\ \omega_2 &= \tfrac{3}{2}C\sin^2\alpha. \end{aligned}\right\} \qquad \ldots\ldots(12)$$

The spectrum of angular frequencies of this frequency-modulated precession is illustrated in figure 2, and consists of two carrier components at frequencies

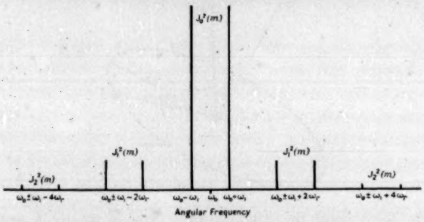

Figure 2. The spectrum from identical pairs of nuclei rotating uniformly with angular velocity ω_r about axes normal to the lines joining them. Broadening of the spectral lines by interaction between the pairs is omitted.

$\omega_0 \pm \omega_1$, each of which has an infinite set of side-frequencies set at separations $2n\omega_r$ on either side, where $n = 1, 2, 3 \ldots$. As is well known from the theory of frequency modulation the relative intensity of the carrier frequency is $J_0^2(m)$, and of the nth side-frequency is $J_n^2(m)$ where $J_n(m)$ is the Bessel function of order n, and m is the dimensionless modulation index defined as the ratio of the amplitude of modulation to the frequency of modulation, and is therefore given here by

$$m = \omega_2/2\omega_r. \qquad \ldots\ldots(13)$$

If all the energy in a frequency-modulated wave is to be accounted for, it is clear that we must have

$$J_0^2(m) + 2 \sum_{n=1}^{\infty} J_n^2(m) = \sum_{n=-\infty}^{\infty} J_n^2(m) = 1. \qquad \ldots\ldots(14)$$

This is in fact a well-known theorem (Watson 1922, p. 31).

Thus the nuclear magnetic resonance spectrum should be that illustrated in figure 2, and we now enquire its second moment about the central frequency ω_0. This is given by

$$\begin{aligned} S_2 &= \tfrac{1}{2} \sum_{n=-\infty}^{\infty} (\omega_1 + 2n\omega_r)^2 J_n^2(m) + \tfrac{1}{2} \sum_{n=-\infty}^{\infty} (-\omega_1 + 2n\omega_r)^2 J_n^2(m) \\ &= \omega_1^2 \sum_{n=-\infty}^{\infty} J_n^2(m) + 4\omega_r^2 \sum_{n=-\infty}^{\infty} n^2 J_n^2(m). \qquad \ldots\ldots(15) \end{aligned}$$

The first sum in (15) is unity, as indicated in (14); the second sum, using Neumann's expansion (Watson 1922, p. 36), is found to be $m^2/2$. Hence

$$\begin{aligned} S_2 &= \omega_1^2 + \tfrac{1}{2}\omega_2^2 \qquad \ldots\ldots(16) \\ &= C^2\left[\frac{27}{8}\sin^4\alpha - 3\sin^2\alpha + 1\right], \qquad \ldots\ldots(17) \end{aligned}$$

using (12). This value of the second moment for the uniformly rotating pairs is seen to be exactly equal to that found in (6) for the static array of pairs. Thus, provided the side-frequencies are included in the spectrum, the second moment is indeed invariant with respect to the rotation.

If, however, the side-frequencies are neglected, the spectrum just consists of the two carrier frequencies $(\omega_0 \pm \omega_1)$; its second moment is therefore ω_1^2, which, as a comparison with (16) shows, is less than that for the rigid array. This central portion of the spectrum, with its reduced second moment, is the part which Gutowsky and Pake (1950) calculated. It corresponds to the use of the mean local field given by expression (9) (or of the mean magnetic dipolar interaction energy which this local field represents), with the exclusion of the fluctuating part contained in the full expression (8). This fluctuating part of the interaction is responsible for the side-frequencies of the spectrum, whose inclusion provides an invariant second moment.

When the angular frequency of rotation ω_r increases the side-frequencies move further out and become less intense. When $\omega_r \gg \omega_2$, the modulation index $m \ll 1$, and the intensity of the first side-frequencies becomes

$$J_1^2(m) \simeq m^2/4 = \omega_2^2/16\omega_r^2 \ll 1, \qquad \ldots\ldots(18)$$

while the intensity of the remoter side-frequencies becomes negligible by comparison since $J_n^2(m)$ is of order m^{2n}. Thus the separation of the first side-frequencies increases proportionately with ω_r while their intensity falls as ω_r^{-2}, thus maintaining constant their contribution of $\omega_2^2/2$ to the second moment.

2.2. *General Axis*

Suppose now that the axes of rotation are not normal to the nuclear pairs (figure 3). The axes for all nuclear pairs are parallel to each other and make an angle α with $\mathbf{H}_0$ and an angle γ with $\mathbf{r}$. As in the previous section we first treat the case in which the pairs do not rotate about these axes, but instead are distributed with random, but fixed, azimuth angles ϕ about the axes. The spectrum from pairs with a given ϕ consists of two lines given by (1) in which

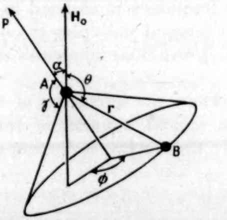

Figure 3. Diagram illustrating the rotation of a pair of nuclei A and B about an axis AP making an angle γ with the internuclear vector $\mathbf{r}$. The applied magnetic field $\mathbf{H}_0$ makes an angle α with the axis of rotation.

$$\cos\theta = \cos\alpha\cos\gamma + \sin\alpha\sin\gamma\cos\phi. \qquad \ldots\ldots(19)$$

The second moment $S_2(\phi)$ of this spectrum is given by (2) taken with (19). The spectrum for all pairs, taking all ϕ with equal probability, has second moment

$$\begin{aligned} S_2 &= \frac{1}{2\pi}\int_0^{2\pi} S_2(\phi)\,d\phi = (C^2/2\pi)\int_0^{2\pi}(9\cos^4\theta - 6\cos^2\theta + 1)\,d\phi \\ &= C^2[9\cos^4\alpha\cos^4\gamma + 27\sin^2\alpha\cos^2\alpha\sin^2\gamma\cos^2\gamma \\ &\qquad + \frac{27}{8}\sin^4\alpha\sin^4\gamma - 6\cos^2\alpha\cos^2\gamma - 3\sin^2\alpha\sin^2\gamma + 1], \end{aligned} \qquad \ldots\ldots(20)$$

using (19).

Now let all pairs rotate about their axes with the same uniform angular velocity ω_r. Substituting (7) in (3), and using (19), the local field is found to be

$$\begin{aligned}H_{\rm loc} = \pm C\gamma_a^{-1}[\tfrac{1}{2}(3\cos^2\alpha-1)(3\cos^2\gamma-1)+\tfrac{3}{2}\sin 2\alpha\sin 2\gamma\cos\omega_r t \\ +\tfrac{3}{2}\sin^2\alpha\sin^2\gamma\cos 2\omega_r t]. \qquad \ldots\ldots(21)\end{aligned}$$

Here again the local field consists of a static part and a fluctuating part; the mean local field is

$$\bar{H}_{\rm loc} = \pm C\gamma_a^{-1}[\tfrac{1}{2}(3\cos^2\alpha-1)(3\cos^2\gamma-1)]. \qquad \ldots\ldots(22)$$

The Larmor frequency of precession is therefore

$$\begin{aligned}\omega &= \gamma_a(H_0+H_{\rm loc}) \\ &= \omega_0 \pm (\omega_1+\omega_2\cos\omega_r t+\omega_3\cos 2\omega_r t), \qquad \ldots\ldots(23)\end{aligned}$$

where

$$\left.\begin{aligned}\omega_0 &= \gamma_a H_0, \\ \omega_1 &= \tfrac{1}{2}C(3\cos^2\alpha-1)(3\cos^2\gamma-1), \\ \omega_2 &= \tfrac{3}{2}C\sin 2\alpha\sin 2\gamma, \\ \omega_3 &= \tfrac{3}{2}C\sin^2\alpha\sin^2\gamma.\end{aligned}\right\} \qquad \ldots\ldots(24)$$

This case is more complicated than that treated in the previous section since the Larmor frequency is frequency-modulated at two frequencies ω_r and $2\omega_r$. Side-frequencies occur at integral multiples of ω_r on either side of the central carrier frequencies $(\omega_0 \pm \omega_1)$, and their intensities are given by binary products of Bessel functions.

It is not necessary to know the intensities of the side-frequencies explicitly in order to calculate the second moment of the spectrum. If the Larmor frequency is given by (23), the nuclear induction signal is proportional to

$$f(t) \equiv \sin\left[\int_0^t \omega\,dt\right] = \sin[(\omega_0+\omega_1)t+m_1\sin\omega_r t+m_2\sin 2\omega_r t] \qquad \ldots\ldots(25)$$

where $m_1=\omega_2/\omega_r$ and $m_2=\omega_3/2\omega_r$. For simplicity only the plus sign in (23) has been taken; there are obvious changes for the minus sign. This can be re-written as

$$\begin{aligned}f(t) &= \mathscr{I}\exp[i(\omega_0+\omega_1)t]\exp[im_1\sin\omega_r t]\exp[im_2\sin 2\omega_r t] \qquad \ldots\ldots(26) \\ &= \mathscr{I}\exp[i(\omega_0+\omega_1)t]\exp[\tfrac{1}{2}m_1(\xi-\xi^{-1})]\exp[\tfrac{1}{2}m_2(\xi^2-\xi^{-2})], \qquad \ldots\ldots(27)\end{aligned}$$

where $\xi=\exp(i\omega_r t)$. Now write

$$E(\xi) \equiv \exp[\tfrac{1}{2}m_1(\xi-\xi^{-1})]\exp[\tfrac{1}{2}m_2(\xi^2-\xi^{-2})] = \sum_{n=-\infty}^{\infty} A_n\xi^n, \qquad \ldots\ldots(28)$$

where the A_n may be expressed, if required, in terms of products of Bessel functions. Thus from (28)

$$E(\xi)E(\xi^{-1})=1, \qquad \ldots\ldots(29)$$

and also

$$\sum_{n=-\infty}^{\infty} A_n^2 = 1, \qquad \ldots\ldots(30)$$

since ΣA_n^2 is the coefficient of ξ^0 in (29) by virtue of the definition of $E(\xi)$ in (28). Also we find that

$$F(\xi) \equiv \xi\frac{d}{d\xi}E(\xi) = \tfrac{1}{2}[m_1(\xi+\xi^{-1})+2m_2(\xi^2+\xi^{-2})]E(\xi) = \sum_{n=-\infty}^{\infty} nA_n\xi^n. \qquad \ldots\ldots(31)$$

Hence, using (29)

$$F(\xi)F(\xi^{-1})=\tfrac{1}{4}[m_1(\xi+\xi^{-1})+2m_2(\xi^2+\xi^{-2})]^2=\sum_{n=-\infty}^{\infty}\sum_{m=-\infty}^{\infty} nmA_nA_m\xi^{n-m}. \qquad \ldots\ldots(32)$$

Thus the coefficient of ξ^0 in the first expression for $F(\xi)F(\xi^{-1})$ is equal to $\Sigma n^2A_n{}^2$, giving

$$\sum_{n=-\infty}^{\infty} n^2A_n{}^2=\tfrac{1}{2}(m_1{}^2+4m_2{}^2). \qquad \ldots\ldots(33)$$

The second moment of the spectrum of $f(t)$ about ω_0 is

$$\begin{aligned}S_2&=\sum_{n=-\infty}^{\infty}(\omega_1+n\omega_{\rm r})^2A_n{}^2\\ &=\omega_1{}^2\sum_{n=-\infty}^{\infty}A_n{}^2+2\omega_1\omega_{\rm r}\sum_{n=-\infty}^{\infty}nA_n{}^2+\omega_{\rm r}{}^2\sum_{n=-\infty}^{\infty}n^2A_n{}^2, \qquad \ldots\ldots(34)\\ &=\omega_1{}^2+\tfrac{1}{2}(\omega_2{}^2+\omega_3{}^2), \qquad \ldots\ldots(35)\end{aligned}$$

using (30) and (33), and using the fact that $\Sigma nA_n{}^2$ is zero, as can be proved by considering the coefficient of ξ^0 in $E(\xi^{-1})F(\xi)$. The second moment of the carrier and side-band system obtained by taking the minus sign in (23) is clearly the same as (35). The second moment of the entire spectrum is therefore given by (35). Using (24) in (35) we get

$$\begin{aligned}S_2&=\tfrac{1}{8}C^2[2(3\cos^2\alpha-1)^2(3\cos^2\gamma-1)^2+9\sin^2 2\alpha\sin^2 2\gamma+9\sin^4\alpha\sin^4\gamma]\\ &=C^2[9\cos^4\alpha\cos^4\gamma+27\sin^2\alpha\cos^2\alpha\sin^2\gamma\cos^2\gamma+\frac{27}{8}\sin^4\alpha\sin^4\gamma\\ &\qquad -6\cos^2\alpha\cos^2\gamma-3\sin^2\alpha\sin^2\gamma+1]. \qquad \ldots\ldots(36)\end{aligned}$$

This expression for the second moment of the uniformly rotating pairs is seen to be exactly equal to that found in (20) for the static array of pairs. Thus, again, provided we include the side-frequencies, the second moment of the spectrum is indeed invariant with respect to the rotation.

However, if the side-frequencies are neglected, the spectrum just consists of the two carrier frequencies $(\omega_0\pm\omega_1)$; its second moment is therefore $\omega_1{}^2$, which, as comparison with (35) shows, is less than that for the rigid array. Using (24), this second moment is

$$C^2[\tfrac{1}{4}(3\cos^2\alpha-1)^2(3\cos^2\gamma-1)^2], \qquad \ldots\ldots(37)$$

and this is just the diminished second moment calculated by Gutowsky and Pake (1950).

§ 3. SPECTRUM FOR RANDOMLY REORIENTING PAIR

While the case of uniformly rotating pairs, discussed in the previous section, is instructive, the actual movement of a nuclear pair about an axis in a crystal is usually by rapid random reorientation. This reorientational motion may be regarded as the superimposition of a large number of rotational frequencies whose spectrum extends to frequencies of order ω_τ, where $\tau\equiv1/\omega_\tau$ is the correlation time of the random motion. The frequency of Larmor precession is therefore frequency-modulated at all these frequencies, and the spectrum of the precessional motion has sidebands extending to frequencies of order ω_τ on either side of the carrier. In this section it is shown that in this case also the second moment remains invariant provided the sidebands are taken into account. The shape of the spectrum is also discussed.

For simplicity consider the axes of reorientation to be perpendicular to the nuclear pairs as in figure 1. The nuclear induction signal is proportional to

$$f(t) \equiv \sin\left[\int_0^t \omega dt\right] = \sin\left[(\omega_0 \pm \omega_1)t + \omega_2 \int_0^t \cos 2\phi(t) dt\right], \qquad \ldots\ldots (38)$$

where ω_0, ω_1 and ω_2 are defined in (12), and ϕ is no longer simply periodic. Suppose the random motion can be decomposed into an infinite set of frequencies p_s of amplitude a_s and phase ψ_s, so that

$$\cos 2\phi(t) = \sum_{s=1}^{\infty} a_s \cos(p_s t + \psi_s). \qquad \ldots\ldots (39)$$

If the axis of reorientation has 3-fold, 6-fold or higher symmetry the mean value of $\cos^2 2\phi(t)$ is $\frac{1}{2}$ and therefore

$$\sum_{s=1}^{\infty} a_s^2 = 1. \qquad \ldots\ldots (40)$$

Substituting (39) in (38) we get

$$f(t) = \sin\left[(\omega_0 \pm \omega_1)t + \sum_{s=1}^{\infty} m_s \sin(p_s t + \psi_s)\right], \qquad \ldots\ldots (41)$$

where $m_s = a_s \omega_2 / p_s$. ......(42)

Now remembering that

$$\exp(im \sin \chi) = \sum_{n=-\infty}^{\infty} \exp(in\chi) \mathrm{J}_n(m), \qquad \ldots\ldots (43)$$

we see that equation (41) can be re-written as

$$f(t) = \sum_{n_1=-\infty}^{\infty} \sum_{n_2=-\infty}^{\infty} \cdots \left[\prod_{q=1}^{\infty} \mathrm{J}_{n_q}(m_q)\right] \sin\left[\left(\omega_0 \pm \omega_1 + \sum_{s=1}^{\infty} n_s p_s\right) t + \sum_{s=1}^{\infty} n_s \psi_s\right]. \qquad \ldots\ldots (44)$$

The spectrum of $f(t)$ thus consists of two carrier frequencies $(\omega_0 \pm \omega_1)$, each with a set of side-frequencies at integral multiples of p_s on either side. The intensity of each side-frequency is $\prod_{q=1}^{\infty} \mathrm{J}_{n_q}{}^2(m_q)$. The second moment of the spectrum about ω_0 is therefore

$$\begin{aligned} S_2 &= \sum_{n_1=-\infty}^{\infty} \sum_{n_2=-\infty}^{\infty} \cdots (\omega_1 + n_1 p_1 + n_2 p_2 + \ldots)^2 \mathrm{J}_{n_1}{}^2(m_1) \mathrm{J}_{n_2}{}^2(m_2) \ldots \\ &= \sum_{n_1} \sum_{n_2} \cdots (\omega_1{}^2 + n_1{}^2 p_1{}^2 + n_2{}^2 p_2{}^2 + \ldots) \mathrm{J}_{n_1}{}^2(m_1) \mathrm{J}_{n_2}{}^2(m_2) \ldots \\ &\quad + 2 \sum_{n_1} \sum_{n_2} \cdots (n_1 \omega_1 p_1 + n_1 n_2 p_1 p_2 + \ldots) \mathrm{J}_{n_1}{}^2(m_1) \mathrm{J}_{n_2}{}^2(m_2) \ldots . \end{aligned} \qquad \ldots\ldots (45)$$

The first term in the first multiple summation in (45) is clearly just $\omega_1{}^2$. The second term, which is typical of the remainder in this summation, is

$$\begin{aligned} \sum_{n_1} \sum_{n_2} \cdots n_1{}^2 p_1{}^2 \mathrm{J}_{n_1}{}^2(m_1) \mathrm{J}_{n_2}{}^2(m_2) \ldots &= p_1{}^2 \sum_{n_1} n_1{}^2 \mathrm{J}_{n_1}{}^2(m_1) \sum_{n_2} \mathrm{J}_{n_2}{}^2(m_2) \sum_{n_3} \mathrm{J}_{n_3}{}^2(m_3) \ldots \\ &= \tfrac{1}{2} p_1{}^2 m_1{}^2. \end{aligned}$$

Hence the whole first summation is

$$\omega_1^2 + \tfrac{1}{2}\sum_{q=1}^{\infty} p_q^2 m_q^2. \qquad \ldots\ldots(46)$$

The second multiple summation in (45) is zero, since each term contains a factor of the form

$$\sum_{n=-\infty}^{\infty} n\mathrm{J}_n^2(m)$$

which is zero. Hence the second moment is given by (46), namely

$$S_2 = \omega_1^2 + \tfrac{1}{2}\sum_{q=1}^{\infty} p_q^2 m_q^2 = \omega_1^2 + \tfrac{1}{2}\omega_2^2, \qquad \ldots\ldots(47)$$

using (42) and (40). But this is just the result obtained in (16) for uniformly rotating systems. The same conclusion therefore follows that the second moment is equal to that for a static array of pairs, provided the side-band system is taken into account.†

We now consider the shape of the side-bands. There are side-frequencies at $(\omega_0 \pm \omega_1) \pm \sum_{s=1}^{\infty} n_s p_s$, having intensities $\prod_{s=1}^{\infty} \mathrm{J}_{n_s}^2(m_s)$. However, if $\omega_r \gg \omega_2$, then $m_s \ll 1$ for all p_s except the small proportion of frequencies less than ω_2. If $m_s \ll 1$ we may write $\mathrm{J}_0^2(m) \simeq 1$, $\mathrm{J}_1^2(m) \simeq m^2/4$, and we may neglect Bessel functions of higher order than the first, and products containing more than one Bessel function of the first order. We are then left only with side-frequencies at $(\omega_0 \pm \omega_1) \pm n_s p_s$, having intensity

$$\tfrac{1}{4}m_s^2 = \omega_2^2 a_s^2 / 4p_s^2. \qquad \ldots\ldots(48)$$

In equation (39) the random variation of $\cos 2\phi$ was represented by the superimposition of periodic motions at discrete frequencies p_s. These frequencies are closely spaced and may be described by a normalized spectral distribution function $\mathscr{J}(p)$. Hence, using (48), the intensity of the side-bands when $\omega_r \gg \omega_1, \omega_2$ is given to good approximation by

$$K(p) = \frac{\omega_2^2}{4p^2}\mathscr{J}(p). \qquad \ldots\ldots(49)$$

This expression is not of course satisfactory for $p \ll \omega_2$, for there the approximation $m \ll 1$ breaks down. It should, however, be satisfactory from frequencies of order ω_2 to ω_r and beyond.

The form of the function $\mathscr{J}(p)$ depends upon the correlation function for the random motion. Bloembergen, Purcell and Pound (1948) have shown that if the correlation function is exponential,‡ then

$$\mathscr{J}(p) = \frac{2\tau}{\pi(1+p^2\tau^2)}. \qquad \ldots\ldots(50)$$

With this reasonable assumption, the intensity of the side-bands is given by

$$K(p) = \frac{\omega_2^2\tau}{2\pi p^2(1+p^2\tau^2)}. \qquad \ldots\ldots(51)$$

---

† The argument may be readily extended to an axis of reorientation having 4-fold symmetry. This case is however slightly more complicated since equation (40) is no longer true.

‡ This assumption is not essential to the argument ; any reasonable correlation function leads to the same general conclusions.

The spectrum is illustrated in figure 4; there is the central part of the spectrum, consisting of the two carrier frequencies $(\omega_0 \pm \omega_1)$, which is broadened by the interactions of neighbouring nuclear pairs, and there is also the side-band spectrum given by (51). The normalized maximum intensity of the central spectrum is of order $1/\omega_1$. At $p \sim \omega_1$, where the side-band spectrum falls clear of the central spectrum, the side-band spectrum has intensity of order $\omega_2{}^2\tau/2\pi\omega_1{}^2$, from (51). Thus the ratio of side-band intensity here to maximum central intensity is of order $\omega_2{}^2/2\pi\omega_1\omega_\tau$, which is of order $\omega_1/2\pi\omega_\tau$ since ω_1 and ω_2 are of the same order. Thus if for example $\omega_\tau/\omega_1 = 10$ the side-band intensity here is only a few per cent of the peak intensity and the side-bands will be difficult to observe. Usually ω_τ increases rapidly with temperature and once temperatures have been reached at which the spectrum and second moment have become constant it can be assumed that the side-bands have become too weak to be measured. From (51) we see that the intensity of the side-band spectrum decreases as p^{-2} at first, and then in the neighbourhood of ω_τ it decreases more rapidly as p^{-4}. When $\omega_\tau/\omega_1 = 10$ the side-band intensity for $p \sim \omega_\tau$ is only of the order of 10^{-4} of the central peak intensity.

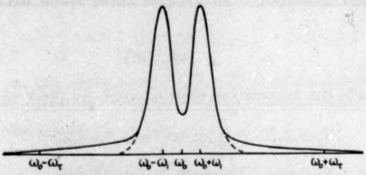

Figure 4. Schematic indication of the spectrum from identical pairs of nuclei reorienting randomly. The two central lines are shown broadened by interactions with other nuclear pairs. The intensity of the side-band spectrum is exaggerated and if drawn to scale would be much weaker.

§ 4. FOURTH MOMENT FOR REORIENTING PAIR

Consider the case of nuclear pairs capable of reorientation about axes normal to the internuclear vectors, (the case discussed in § 2.1). First let us calculate the fourth moment of the spectrum for a static array of pairs distributed about these axes with random, but fixed, azimuth angles ϕ. The spectrum from pairs with a given ϕ consists of two lines given by (1), and its fourth moment about ω_0, using (4) is

$$S_4(\phi) = C^4(3\sin^2\alpha\cos^2\phi - 1)^4. \qquad \ldots\ldots(52)$$

The spectrum for all pairs, taking all ϕ with equal probability, is

$$S_{4\text{stat}} = \frac{1}{2\pi}\int_0^{2\pi} S_4(\phi)\,d\phi = C^4\left[\frac{2835}{128}\sin^8\alpha - \frac{135}{4}\sin^6\alpha + \frac{81}{4}\sin^4\alpha - 6\sin^2\alpha + 1\right]. \qquad \ldots\ldots(53)$$

The expression (53) is readily shown to reduce to

$$S_{4\text{stat}} = \omega_1{}^4 + 3\omega_1{}^2\omega_2{}^2 + \tfrac{3}{8}\omega_2{}^4, \qquad \ldots\ldots(54)$$

where ω_1 and ω_2 are defined in (12).

Now let the pairs rotate about their axes with the same uniform angular velocity ω_{r}. As calculated in § 2.1 the spectrum now consists of two carrier and side-band systems at frequencies $(\omega_0 \pm \omega_1) \pm 2n\omega_{\mathrm{r}}$, each frequency component having intensity $\mathrm{J}_n^{\,2}(m)$, where $m = \omega_2/2\omega_{\mathrm{r}}$. The fourth moment of the spectrum about ω_0 is therefore

$$\begin{aligned} S_{4\mathrm{rot}} &= \sum_{n=-\infty}^{\infty} (\omega_1 + 2n\omega_{\mathrm{r}})^4 \mathrm{J}_n^{\,2}(m) \\ &= \omega_1^{\,4} \sum_{n=-\infty}^{\infty} \mathrm{J}_n^{\,2}(m) + 24\omega_1^{\,2}\omega_{\mathrm{r}}^{\,2} \sum_{n=-\infty}^{\infty} n^2\mathrm{J}_n^{\,2}(m) + 16\omega_{\mathrm{r}}^{\,4} \sum_{n=-\infty}^{\infty} n^4\mathrm{J}_n^{\,2}(m). \end{aligned} \qquad \ldots\ldots(55)$$

The terms involving odd powers of n have been omitted in (55) since the sums for these terms are zero. The first and second sums in (55) we have already encountered; they are given by unity and $\frac{1}{2}m^2$ respectively. The third sum is

$$\sum_{n=-\infty}^{\infty} n^4\mathrm{J}_n^{\,2}(m) = \frac{m^2}{2} + \frac{3m^4}{8}, \qquad \ldots\ldots(56)$$

as may be shown by manipulating Neumann's expansion (Watson 1922, p. 36). Inserting the values of the sums in (55) and using (13), we get

$$S_{4\mathrm{rot}} = \omega_1^{\,4} + 3\omega_1^{\,2}\omega_2^{\,2} + \tfrac{3}{8}\omega_2^{\,4} + 2\omega_2^{\,2}\omega_{\mathrm{r}}^{\,2}. \qquad \ldots\ldots(57)$$

The first three terms in (57) are seen to be the static fourth moment given by (54). Hence

$$S_{4\mathrm{rot}} = S_{4\mathrm{stat}} + 2\omega_2^{\,2}\omega_{\mathrm{r}}^{\,2}. \qquad \ldots\ldots(58)$$

Thus the fourth moment of the spectrum is increased by the motion. The increase comes from the side-bands; the fourth moment of the two central carrier lines is $\omega_1^{\,4}$ which is less than $S_{4\mathrm{stat}}$. Moreover, when $\omega_{\mathrm{r}} \gg \omega_1, \omega_2$ the second term in (58) is dominant, and determines the fourth moment.

The approximate quantum-mechanical estimate of the fourth moment given by Pake (1956) is

$$S_{4\mathrm{rot}} = \hbar^{-4}[E_{\mathrm{d}}^{\,4} + E_{\mathrm{d}}^{\,2}E_{\mathrm{m}}^{\,2}], \qquad \ldots\ldots(59)$$

where E_{d} is the energy of dipole–dipole interaction, which is of the order

$$E_{\mathrm{d}} \simeq \frac{\mu_a\mu_b}{r^3} \simeq C\hbar$$

and E_{m} is the motional energy of a nucleus, which here is of order $\hbar\omega_{\mathrm{r}}$. It is seen, therefore, that the fourth moment (58) calculated from our model is consistent with the quantum-mechanical estimate given in (59).

If the nuclear motion is not uniform, but has the nature of random reorientation, it becomes necessary to find the fourth moment of the side-band spectrum whose shape is given by $K(p)$ in equation (49). The result depends upon the functional form assumed for $\mathscr{J}(p)$; the use of (50) is unsatisfactory since it does not converge fast enough and leads to an infinite fourth moment. However, if we assume that $\mathscr{J}(p)$ is given by (50) for frequencies up to about ω_τ and then cuts off, the fourth moment of the side-band spectrum is of order $\omega_2^{\,2}\omega_\tau^{\,2}$. The two central carrier lines have a fourth moment $\omega_1^{\,4}$. The total fourth moment is therefore

$$S_4 \simeq \omega_1^{\,4} + \omega_2^{\,2}\omega_\tau^{\,2}, \qquad \ldots\ldots(60)$$

which is again consistent with (59). When $\omega_\tau \gg \omega_1, \omega_2$ the second term is dominant, the fourth moment being of order $\omega_2^2\omega_r^2$. However, this fourth moment comes from the side-band structure which in practice is unobservable. The fourth moment of the observable central part of the spectrum ω_1^4, is in fact less than the static fourth moment, given in (54).

§ 5. POLYCRYSTALLINE SPECIMENS

The preceding sections have been concerned with the spectra of single crystals. The spectrum for a powder is the sum of the spectra of the individual crystallites of which it is composed.

Pake (1948) has shown how the spectrum may be calculated for an isotropically distributed powder consisting of crystallites each containing identical pairs of nuclei rigidly arranged in static array. The spectrum from one crystallite consists of two lines at frequencies given by (1) and (2 a)

$$\omega = \omega_0 \pm C(3\cos^2\theta - 1). \qquad \ldots\ldots (61)$$

If the crystallites are distributed isotropically the proportion of nuclear pairs having polar angle in the range θ, $\theta + d\theta$ is $d(\cos\theta)$. Hence the intensity of the line for the powder at angular frequency ω is proportional to

$$\frac{d(\cos\theta)}{d\omega} \propto \left(1 \pm \frac{\Delta\omega}{C}\right)^{-1/2}, \qquad \ldots\ldots (62)$$

where $\Delta\omega$ is written for $(\omega - \omega_0)$; the positive sign applies in the range $-1 < \Delta\omega/C < 2$, and the negative sign in the range $-2 < \Delta\omega/C < 1$. This spectrum is shown by the broken line in figure 5(*a*). It is broadened by the interactions of the nuclear pairs, and a typically broadened spectrum is shown by the full line.

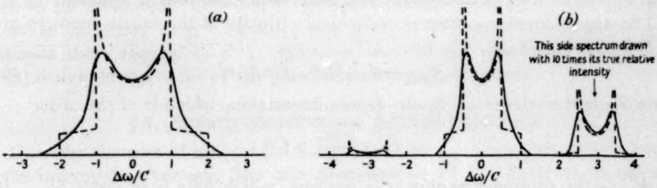

Figure 5. (*a*) Diagram showing the spectrum for polycrystalline material containing static pairs of nuclei. The broken line shows the calculated spectrum neglecting the interaction between different pairs. The full line shows the effect of this interaction in a typical case. (*b*) Diagram showing the spectrum for the same material in which the nuclear pairs are rotating uniformly with angular velocity (3/2)*C*. In order to show clearly the shape of the side-spectra the right-hand side-spectrum is magnified ten times. The broken lines show the calculated spectrum neglecting inter-pair broadening, while the full lines show the effect of this broadening in a typical case.

If now the nuclear pairs are rotating about axes normal to the internuclear vectors, as considered in § 2.1, the central part of the spectrum from one crystallite consists of the two carrier frequencies given by

$$\omega = \omega_0 \pm \omega_1 = \omega_0 \pm \tfrac{1}{2}C(3\cos^2\alpha - 1). \qquad \ldots\ldots (63)$$

If the crystallites are distributed isotropically the intensity of the line is therefore proportional to

$$\frac{d(\cos\alpha)}{d\omega} \propto \left(1 \pm \frac{2\Delta\omega}{C}\right)^{-1/2}, \qquad \ldots\ldots(64)$$

where the positive sign applies in the range $-\frac{1}{2} < \Delta\omega/C < 1$, and the negative sign in the range $-1 < \Delta\omega/C < \frac{1}{2}$. This spectrum is shown in figure 5(*b*); it has clearly the same geometrical shape as that in figure 5(*a*) for the rigid array of nuclei, but has just half the width.

The first upper side-frequencies are given by

$$\omega = \omega_0 \pm \omega_1 + 2\omega_\mathrm{r}. \qquad \ldots\ldots(65)$$

The intensity of these side-frequencies is proportional to

$$\mathrm{J}_1{}^2(m) \sim \omega_2{}^2/16\omega_\mathrm{r}{}^2 \propto \sin^4\alpha \qquad \ldots\ldots(66)$$

when $m \ll 1$. The intensity of the first side-frequency spectrum for the polycrystal is therefore proportional to

$$\mathrm{J}_1{}^2(m)\frac{d(\cos\alpha)}{d\omega} \propto \left(1 \mp \frac{\Delta\omega'}{C}\right)^2 \left(1 \pm \frac{2\Delta\omega'}{C}\right)^{-1/2}, \qquad \ldots\ldots(67)$$

where $\Delta\omega'$ is written for $(\omega - \omega_0 - 2\omega_\mathrm{r})$. This spectrum is also shown in figure 5 (*b*) for $\omega_\mathrm{r} = \frac{3}{2}C$. The side-frequency spectrum is roughly similar in shape and width to the central part of the spectrum. This is true also of the weaker higher-order side-frequencies. The spectrum for the *n*th side-frequency has intensity proportional to

$$J_n{}^2(m)\frac{d(\cos\alpha)}{d\omega} \propto \left(1 \mp \frac{\Delta\omega^{(n)}}{C}\right)^{2n} \left(1 \pm \frac{2\Delta\omega^{(n)}}{C}\right)^{-1/2}, \qquad \ldots\ldots(68)$$

when $m \ll 1$, where $\Delta\omega^{(n)}$ is written for $(\omega - \omega_0 - 2n\omega_\mathrm{r})$.

If the axis of rotation is not perpendicular to the nuclear pair direction, the spectrum is much the same. The main difference is that ω_1 is now given by (24) instead of (12), so that the central part of the spectrum is no longer reduced to exactly half the width of the spectrum for a static array, but is instead reduced by a factor $|\frac{1}{2}(3\cos^2\gamma - 1)|$.

If the motion consists of a random reorientation of the nuclear pairs the central part of the spectrum will be the same as for uniform rotation, while the side-band spectrum will spread over frequencies from $\omega_0 - \omega_\tau$ to $\omega_0 + \omega_\tau$ as in figure 4. The intensity of these side-bands will be too weak to observe when $\omega_\tau \gg \omega_1$.

§ 6. MORE GENERAL CASES

In the preceding sections nuclear pairs have been considered in some detail because they can be treated semi-classically. More complex groupings of nuclei would be more difficult to treat, but it is nevertheless possible to see the form the spectrum must take. A rapid uniform rotation of similar groupings of nuclei yields a spectrum consisting of a central part together with side-spectra centred on frequencies $\omega_0 \pm n\omega_\mathrm{r}$. These side-spectra have rapidly diminishing intensity as the order of side-band *n* increases. The central part of the spectrum has a second moment smaller than that for a rigid array, and calculable using Gutowsky and Pake's modification of Van Vleck's formula. The side-spectra have roughly similar width to the central part. The overall second moment, including the side-spectra, equals that for the rigid array. A rapid random reorientation produces a spectrum with the same narrowed central part, but with continuous weak side-bands running out to frequencies $\pm\omega_\tau$ on either side of ω_0. Again the second moment remains the same as that for a rigid array provided the weak side-bands are taken into account, but the second moment of the observable central part is reduced.

§ 7. CONCLUSIONS

The magnetic dipolar interactions between nuclei in a crystal in which there is rapid hindered rotation can be divided into two parts; a constant part representing the mean interaction, and a time-dependent part whose time-average is zero. The first part gives rise to a spectrum which is narrower than that for the same crystal in which the nuclei are static; the second part gives a weak wide spectrum which is normally unobservable. The second moment of the whole spectrum arising from both parts remains the same as that for the rigid array of nuclei. The second moment for the observable central part is reduced in the manner calculated earlier by Gutowsky and Pake (1950). The fourth moment of the entire spectrum is increased by the motion on account of the increased contribution from the time-dependent part of the interaction.

It is concluded that it is still safe to use Gutowsky and Pake's second-moment formulae for spectra narrowed by motion, provided one is satisfied that the side-band spectra are too weak to be observed. This condition can usually be satisfied by measuring the spectra over a range of increasing temperatures until a constant narrowed spectrum and second moment are obtained.

ACKNOWLEDGMENTS

This work was begun during a visit of one of us (E. R. A.) to the Physics Department of Stanford University in August 1957. He wishes to thank Dr. H. E. Weaver for posing the problem from which this paper developed, and to express his thanks also for helpful discussions, particularly with Dr. R. M. Cotts and Professor G. E. Pake.

REFERENCES

BLOEMBERGEN, N., PURCELL, E. M., and POUND, R. V., 1948, *Phys. Rev.*, **73**, 679.
GUTOWSKY, H. S., and PAKE, G. E., 1950, *J. Chem. Phys.*, **18**, 162.
PAKE, G. E., 1948, *J. Chem. Phys.*, **16**, 327; 1956, *Solid State Physics*, **2**, 1.
VAN VLECK, J. H., 1948, *Phys. Rev.*, **74**, 1168.
WATSON, G. N., 1922, *A Treatise on the Theory of Bessel Functions* (Cambridge : University Press).

Measurement of Electron Beam Energy using a Gas Čerenkov Detector[†]

By M. R. BHIDAY, R. E. JENNINGS and P. I. P. KALMUS
Department of Physics, University College London

MS. received 21st May 1958, and in final form 1st August 1958

Abstract. It is shown that the energy of a monoenergetic beam of fast electrons can be accurately determined by using a variable pressure gas Čerenkov detector. A description of a simple detector of this type, and results taken with a 4½ MEV electron beam, are given.

§ 1. Introduction

A SERIES of electron scattering experiments is being performed at University College London using the extracted beam of a 4½ MEV microtron. Phase stability conditions (Henderson, Heymann and Jennings 1953) have shown that the energy spread of this machine is about ± 50 kev, and by using a double focusing magnetic spectrometer a 'monoenergetic' beam with a spread of only ± 4 kev is obtained. However, while the energy spread of the beam can be reduced in this way and is known quite accurately, the energy of the beam itself is more difficult to determine. For many experiments it is desirable, and for some essential, to know the electron energy, absolutely, with an accuracy to better than 1%. An experiment to determine the radiative correction to elastic scattering which is being planned requires an absolute measurement of the electron energy to better than ± ½%. Since it cannot be assumed that the beam energy will remain constant during an experiment, energy determinations should be made at regular intervals during each run. This paper considers a number of possible methods and describes in detail the Čerenkov detector method which was tried.

§ 2. Methods Considered

The energy of the electrons in the beam can be determined to within a few per cent by measuring the radius of curvature r of the last orbit in the microtron; in this orbit the electrons pass from the resonator to the extractor along a semicircular orbit in a steady magnetic field H. The accuracy of obtaining the momentum and hence the energy of the electrons by measuring H and r is limited by the accuracy to which these quantities can be found. The field is not completely uniform along the orbit as the resonator is in a region of radially decreasing field, and the presence of the iron extractor tube also causes field variations in its vicinity. In addition there is an uncertainty in the value of r due to the finite size of the resonator hole (0·8 cm diameter) and of the hole at the entrance to the extractor tube (0·2 cm diameter) which in an orbit of diameter about 30 cm causes an uncertainty of ± 1·5%.

It would be possible to increase the accuracy of the measurements of r by confining the last orbit by a series of collimating slits, but in practice these slits would have to be extremely narrow. Detailed measurement of the magnetic field along the orbit would also be necessary if an overall accuracy of better than 1% was required.

[†] Presented at the Cambridge Nuclear Physics Conference, 10th April, 1958.

Two magnetic spectrometers with steel pole pieces are available for use in the experiments but as these were of the double focusing sector type having appreciable stray fields, a measurement of the field and the effective radius of curvature using beta particles of lower energy from a radioactive source could not be extrapolated up to the higher values required for 4½ MEV electrons without allowing for possible variation in the field shapes due to saturation effects. The construction of a more suitable magnetic spectrometer or electrostatic analyser would have involved considerable delay, and neither of these instruments could easily be incorporated into the experimental arrangement.

The ' hot wire' method whereby the behaviour of a charged particle is simulated by means of a current along a wire (Symonds 1955) although possibly capable of giving the required accuracy, could not be carried out at regular intervals during the scattering experiments but would require partial dismantling of the apparatus. Another method which was investigated depended on the kinematics of relativistic electron–electron collisions (Scott, Hanson and Lyman 1951). In the non-relativistic case a collision between a moving and a free stationary electron (in the laboratory frame of reference) would result in two outgoing electrons moving at right angles to each other, i.e. in the symmetrical case each would make an angle of 45° to the incident direction. At higher energies, for a symmetrical collision, the value of the angles falls below 45° and is energy dependent. Thus, by means of an electron–electron scattering experiment employing fast coincidences between two counters whose angular separation could be slowly varied until a maximum counting rate was obtained, it would be possible to measure the primary electron energy. A study of this method, however, revealed various difficulties, the main one again being the small width of the collimating slits which would be necessary.

The energy of particles whose velocity approaches the velocity of light may be measured by means of a Čerenkov detector. In such a detector light is emitted whenever the particle velocity in a transparent medium exceeds the phase velocity of light in that medium. To determine the particle velocity it is necessary to measure either the angle which the Čerenkov radiation makes with the electron beam or else to increase the refractive index of the medium gradually until the Čerenkov light is just emitted. For fast electrons whose velocity approaches $\mathbf{c}$ the threshold method is more convenient, using a gaseous medium and varying the pressure. In this way what is effectively measured is the difference of the particle velocity from that of light *in vacuo*, this difference being found in terms of the pressure and hence the refractive index of the gas.

Electrons of kinetic energy 4½ MEV have a velocity of about $0{\cdot}995\mathbf{c}$ and hence require a threshold refractive index of about 1·005 which can be obtained by using gases at pressures of 10 to 20 atmospheres. As these quantities can readily be measured and a Čerenkov ' probe ' can easily be built into the experimental system, this was the method finally adopted.

§ 3. THEORY AND GENERAL CONSIDERATIONS

If a charged particle with velocity v is moving through a medium having a refractive index n (for a given wavelength), Čerenkov radiation of that wavelength will be emitted if $v > \mathbf{c}/n$, i.e. if $\beta n > 1$ where $\mathbf{c}$ is the velocity of light *in vacuo* and $\beta = v/\mathbf{c}$. For gases the Gladstone and Dale approximation of the Lorentz–Lorenz law is sufficiently accurate for our purpose (better than 0·1%), so we take $n-1$ as being proportional to the density of the gas. If the behaviour of the gas is assumed to be that of an ideal gas we can write $n-1=kp$ where p is the pressure and k is a constant. The threshold pressure p_1 for Čerenkov radiation is then given by $\beta(1+kp_1)=1$. As the corresponding value for the total energy of the particle is very nearly proportional to $p_1^{-1/2}$ when $\beta \sim 1$, and as p_1 is of the order of 10 atmospheres in our case, the kinetic energy can be found very accurately.

The energy dW per length dl of path radiated per second is given by (Jelley 1953)

$$\frac{dW}{dl} = \frac{Ne^2}{\mathbf{c}^2}\int_{\beta n > 1}\left(1-\frac{1}{\beta^2 n^2}\right)\omega\, d\omega$$

where N is the number of electrons passing per second and ω is the angular frequency of the radiation. As βn varies from unity by $\pm 0{\cdot}0002$ in the range of interest, we can write with sufficient accuracy

$$\frac{dW}{dl} = \frac{2Ne^2}{\mathbf{c}^2}\int_{\beta n > 1}(\beta n - 1)\,\omega\, d\omega \qquad \ldots\ldots (1)$$

i.e.

$$\frac{dW}{dl} = \frac{2Ne^2}{\mathbf{c}^2}\int_{\beta(1+kp)>1}[\beta(1+kp)-1]\,\omega\, d\omega.$$

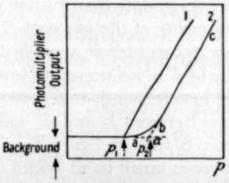

Figure 1.

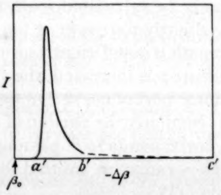

Figure 2.

Figure 1. The expected variation of Čerenkov intensity as a function of gas pressure. Curve 1, monoenergetic beam; curve 2, beam having velocity distribution as shown in figure 2. In both curves it is assumed that only a very narrow band of frequencies is being detected and the effect of dispersion is negligibly small.

If a very small band of frequencies emitted in the visible spectrum is measured using a photomultiplier, the output above the background should increase linearly with pressure for a monoenergetic beam of electrons, as shown in figure 1, curve 1, and the velocity β of the electrons is known from a value of the refractive index at the pressure p_1 and the corresponding temperature (velocity measured in terms of velocity of light $\mathbf{c}$).

In practice the transition will not be so sharp and will be rather similar to that shown by curve 2 in figure 1. This more gradual transition is due to a number of causes, including dispersion and energy loss of the input beam in the entrance window to the detector and also as it passes through the comparatively dense gas of the detector. However, the gas path can be made short because, unlike the use of a Čerenkov counter for the detection of single particles (e.g. Ascoli Balzanelli and Ascoli 1957), we are dealing here with a beam of particles ($N_{\text{average}} \sim 10^8$ electrons sec^{-1} pulsed at 50 p.p.s.) and the Čerenkov radiation is therefore far more intense per unit path length. Similarly the dispersion difficulty can be overcome by the use of a narrow band pass filter matched to the photomultiplier. These requirements will reduce the radiation received by the photomultiplier but this can easily be tolerated. The entrance window cannot be made too thin as it has to withstand a pressure of the order of 10 atmospheres but as the beam size is only of the order of a few millimetres the hole can be made small and a 0·003 inch foil of ' Melinex ' is suitable.

The electron beam intensity was monitored by placing an ionization chamber immediately behind the Čerenkov detector. Although the average output of the machine remained fairly constant, small fluctuations from pulse to pulse were smoothed out by using a detecting system with a time constant of the order of one second. It was also important to allow time after each change of pressure for the gas to reach the temperature of the surroundings.

Although in practice a sharp transition as in figure 1, curve 1, is not obtained, the output is found above the threshold to increase linearly with pressure, and it is of interest to consider the intersection at α obtained by extrapolating the line cb to meet the line which represents the constant background. This point can be found far more accurately than the beginning of the gradual rise at a.

The monoenergetic beam of electrons having velocity β_0 will, after passing through the entrance foil and gas of the detector, have a distribution of velocities as shown in figure 2, where electron flux I is plotted against velocity change $-\Delta\beta$ (which can easily be calculated from the energy-loss distribution). The distribution will be slightly narrower at the beginning of the gas path than at the end, but for a short path it is sufficiently accurate to consider an average distribution.

As the pressure p is increased, the value of $\beta' = 1/n$ moves to lower values of β, and the non-linear part of curve 2 of figure 1 corresponds to β' passing from a′ to b′ on figure 2. Similarly the portion of curve between b and c, which is approximately linear, corresponds to β' passing from b′ to c′ on figure 2.

The Čerenkov radiation emitted for a given small band-width is proportional to (see equation (1))

$$\int_{\beta n>1}(\beta n-1)I\,d\beta \text{ which is equal to } \int_{\beta>\beta'}\left(\frac{\beta}{\beta'}-1\right)I\,d\beta,\text{ i.e. } \int_{\beta>\beta'}(\beta-\beta')I\,d\beta \qquad \ldots\ldots(2)$$

with sufficient accuracy. It is now convenient to assume a sharp cut off at b′ to the distribution shown in figure 2. This approximation in our case only introduces an error in the final result of about 0·1% if b′ is taken at twice the peak value of $-\Delta\beta$, and the portion of curve 2 of figure 1 between b and c can then be taken as being linear. It follows from equation (2) that for β' between b′ and c′ the radiation emitted is proportional to $\bar{I}\,(\bar{\beta}-\beta')$ where

$$\bar{I} = \int_{\beta_0}^{\beta \text{ at b}'} I\,d\beta$$

and $\bar{\beta}$ is the value of β corresponding to electrons which lose the average value of $\Delta\beta$. At the point of intersection at α (figure 1) $\beta' = \bar{\beta}$. Hence the velocity β_0 (and the kinetic energy) of the electrons in the primary beam before it enters the detector can easily be deduced from calculations of the velocity loss distribution in the foil and gas.

The effect of dispersion will be to make the increase in signal at the threshold more gradual since Čerenkov light at the higher frequency end of the photomultiplier response curve will be emitted first as the pressure is increased. Thus at the point α on figure 1 the corresponding refractive index of the medium is for some average frequency of the Čerenkov radiation in the range corresponding to the band pass of the whole detector. To reduce dispersion, a filter is used, and in our apparatus this limits the range of wavelengths detected to a band from 4450 Å to 5000 Å. Although the value of $n-1$ for carbon dioxide varies by the order of one per cent for a pass band of this size in the visible region, it can be shown that if an ideal band pass filter of 550 Å and a photomultiplier having a constant energy response over this range were used the mean frequency can be taken as the effective frequency to better than 0·1%. In practice the easiest solution to the problem is to use a very narrow filter.

A number of other effects should be considered including the scattering of the input beam. It is however only the change in scattering with pressure for a comparatively small range in pressure above the threshold which is important, and this can be neglected, as can the slight increase in energy loss over the same range. It is important that the path of the beam through the detector should remain constant during the measurements and be known.

This method is capable of an accuracy of a few tenths of one per cent for the determination of the energy of a monoenergetic beam of particles. In the present experiment, however, an accuracy of this order is not claimed as the arrangement was not ideal and no attempt was made to find the corresponding refractive index of the gas to the required accuracy. The purpose of the experiment was to confirm the possibilities of the method and to help in the design of the final apparatus.

§ 4. DESIGN OF EXPERIMENTAL DETECTOR

In order to test the method, a detector of very simple design was constructed. This is shown in figure 3.

The electron beam coming from the machine enters the chamber through a ¼ inch diameter 0·003 inch 'Melinex' foil which has a thin aluminium film

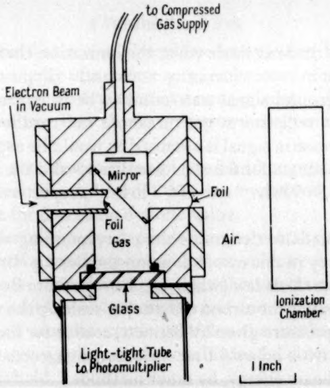

Figure 3. Čerenkov detector.

vacuum-deposited on its inside surface to prevent Čerenkov radiation produced in the foil from reaching the photomultiplier. The beam then passes through the chamber which contains gas at any desired pressure up to about 15 atmospheres. Čerenkov radiation is emitted if the gas pressure is above the threshold value and this radiation which is on a narrow cone in the forward direction is reflected into a photomultiplier by means of a mirror at 45°. This mirror consists of a tightly stretched aluminium-coated 0·003 inch 'Melinex' foil, the reflecting aluminium surface facing the beam. The mirror was made thin in order to prevent appreciable electron scattering into the output glass window. The electron beam then passes out of the chamber through another 'Melinex' foil, which is slightly thinner than the entrance foil and acts as a safety valve in case the pressure is accidentally raised to too high a value. A ¼ inch thick slab of glass separated the pressure system from a light-tight tube which contained a convex lens and a filter. In this way the Čerenkov radiation was made incident on the photomultiplier without the use of a solid light pipe and the photomultiplier was in a position where it could be screened from stray high energy radiations. It was found experimentally that very little Čerenkov radiation due to scattered electrons in the glass reached the photomultiplier. The electrons passing out of the detector were monitored by the ionization chamber.

The output from the photomultiplier was passed through a cathode follower to a wide band amplifier. As the microtron is pulsed, the output consists of pulses of amplitude proportional to the Čerenkov radiation emitted. The pulses from the amplifier were made to give a steady reading on a microammeter, the time constant of the circuit used being about a second.

The Čerenkov detector was connected to a cylinder of compressed gas. The gas used was carbon dioxide which, although not the most suitable in many respects, has the highest refractive index of the commonly available gases (freon would be higher) and hence has the lowest pressure threshold for Čerenkov radiation. Gas was let in or out of the chamber slowly to prevent rapid temperature fluctuations and the microammeter readings were plotted against pressure as measured on an ordinary Bourdon gauge.

§ 5. RESULTS

Several runs were made at times when the ionization chamber showed that the beam from the machine was remaining constant. Typical runs are shown in figure 4. The background signal was found to be independent of pressure and the onset of Čerenkov radiation at the threshold can readily be seen. At higher pressures a linear increase in signal is obtained as would be expected.

Both runs were made under the same conditions and the intercepts to find the pressure p_2 occur at 156·9 lb in^{-2} and 156·7 lb in^{-2} respectively above atmospheric pressure.

No attempt was made to determine the corresponding value of the refractive index to a high accuracy in this case, but using the Beattie–Bridgeman equation of state and the Gladstone–Dale law (which can be seen from Bennett's results (1956) to hold only approximately for carbon dioxide) to scale up the value of the refractive index at atmospheric pressure given by Bennett, a value for the kinetic energy of the beam is found to be a little below 4·6 MEV which is in agreement with approximate measurements of the beam energy, by other methods.

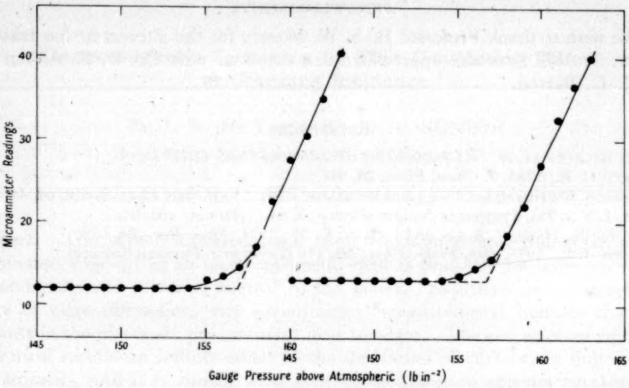

Figure 4. Experimental curve showing variation of Čerenkov intensity with gas pressure. The ordinate represents amplified photomultiplier output and the abscissa represents gas pressure above atmospheric. The two curves are displaced sideways for clarity.

§ 6. Future Developments

The Čerenkov detector shown in figure 3 is not suitable for use in the electron scattering experiments in its present form. A modified detector is being designed which can be withdrawn from the beam during the experiment and an improved monitor system is to be incorporated to measure the primary beam.

In the preliminary experiments no attempt was made to find the refractive index of the gas to the required accuracy.

In the final arrangement it will probably be necessary to include an interferometer in the pressure system to measure the refractive index directly.

§ 7. Conclusions

It has been shown that a gas Čerenkov detector can be used to obtain an absolute value for the energy of a monoenergetic beam of electrons at energies of a few MEV which is accurate to a few tenths of one per cent. At higher energies the method has the advantage that thinner windows can be used as the threshold pressure will be lower.

It is interesting to note that in principle it should be possible to make capsules containing a gas whose refractive index had been adjusted, before sealing off, to give a threshold value for β at some definite value.

As this type of detector only depends on the velocity of the particles it is suitable for any charged particles provided their velocity is such that β does not differ from unity by more than about 1%. With heavier particles the energy loss in the window and gas would be relatively less and the threshold therefore sharper. If used with a beam of monoenergetic particles, the method is simple to apply, but with longer gas paths single particles could also be detected at pressures only a little above the threshold.

ACKNOWLEDGMENTS

We wish to thank Professor H. S. W. Massey for the interest he has taken in this work. We have also appreciated conversations with Dr. D. K. Aitken and Dr. J. C. Barton.

REFERENCES

ASCOLI BALZANELLI, A., and ASCOLI, R., 1957, *Nuovo Cim.*, **6**, 1392.
BENNETT, C. E., 1956, *J. Chem. Phys.*, **24**, 98.
HENDERSON, C., HEYMANN, F. F., and JENNINGS, R. E., 1953, *Proc. Phys. Soc.* B, **66**, 41, 654.
JELLEY, J. V., 1953, *Progress in Nuclear Physics*, **3**, 84. (Review article).
SCOTT, M. B., HANSON, A. O., and LYMAN, E. M., 1951, *Phys. Rev.*, **84**, 638.
SYMONDS, J. L., 1955, *Rep. Progr. Phys.*, **18**, 116 (London : Physical Society).

Electromagnetic Scattering by Thin Conducting Plates at Glancing Incidence

By J. S. HEY and T. B. A. SENIOR
Royal Radar Establishment, Great Malvern, Worcs.

MS. received 20*th March* 1958, *and in revised form* 23*rd May* 1958

Abstract. The signal scattered back from rectangular and triangular plates illuminated edge-on in an electromagnetic field is found to be large when the incident magnetic vector is normal to the plates. Explanations are sought in terms of edge diffraction, and experimental measurements indicate that the currents in the plates are predominant near to edges. The extension of rigorous theoretical results on infinite edges to the derivation of currents in finite edges is discussed; and it is shown what type of modification appears necessary to account for the experimental observations. A method of testing a hypothetical current distribution for the boundary conditions is propounded.

§ 1. Introduction

The rigorous determination of the scattered radiation from perfectly conducting objects exposed to an incident electromagnetic field has only been achieved for a very limited number of special shapes of which the best known is the sphere. In certain circumstances approximations can be made. For instance, for conducting surfaces such that all radii of curvature are large compared with the wavelength Huygens' principle can be applied to evaluate with reasonable accuracy the scattered field near those directions where geometrical optics indicates a strong reflection would be expected. In an extension of this treatment, which also introduces the polarization, it is assumed that the current density at every point of the surface has the same value as if there were an infinite tangent plane at that point.

Such methods provide a useful guide to the magnitude and polarization of the scattered field in directions near those of specular reflection. The postulated current distributions do not however in general satisfy the boundary conditions specified by Maxwell's equations, and the methods do not predict the scattered field reliably in other directions. The failure is particularly marked if attempts are made to apply these methods to surfaces having edges and discontinuities.

An example of this failure occurs in the evaluation of the radiation returned from a disc edge-on with incident magnetic vector normal to the disc. If an infinite plane were illuminated at glancing incidence with the incident magnetic vector normal to the plane it is easily shown that the current vanishes as the glancing angle approaches zero. Hence an approximate method in which the disc is regarded as part of an infinite plane would predict that the radiation scattered back would be zero. In actual fact, as Hey *et al.* (1956) have shown experimentally, a strong signal may be returned. As the disc size is increased in comparison with the wavelength a series of maxima and minima occur in the echoed signal. Recent measurements with discs of diameters up to 10 λ have shown that the magnitude of the maxima increases as disc size is increased.

Whilst it is possible to derive a rigorous solution of the boundary conditions in order to determine the scattered field from a thin disc, the necessary computations are formidable. Experience has also shown that rigorous mathematical solutions of the scattering from finite objects of dimensions comparable with the wavelength are often disappointing in the sense that they appear as a long series of terms which do not reveal a physical picture which might lead to the approximate solution of similar problems. Since, as shown in this paper, experimental measurements indicate that the occurrence of strong back-scattering at glancing incidence from thin plates of finite dimensions occurs more generally than is commonly supposed, an attempt is here made to elucidate the phenomena involved, and to derive a valid approximate treatment.

§ 2. MEASUREMENTS OF ELECTROMAGNETIC SCATTERING

The measurements here described are of the returned signal from objects illuminated by an incident plane wave. The intensity of the scattered radiation in this direction is expressed in terms of the equivalent echoing area σ, defined by

$$\sigma = 4\pi \frac{\text{Returned power per unit solid angle}}{\text{Incident power flux density}}.$$

The experimental method has been described by Hey *et al.* (1956).† This is a laboratory method at a wavelength of $\lambda = 3{\cdot}2$ cm in which the Doppler effect is used to distinguish between the scattered signal from the surroundings and that from the object which is moved at a constant speed on a specially designed support.

The objects to be considered here are thin flat plates illuminated edge-on with the incident magnetic field vector normal to the plates. The plates are thus in the plane containing the direction of incidence and the electric vector of the incident field. The results of measurements on rectangular and triangular plates will now be described.

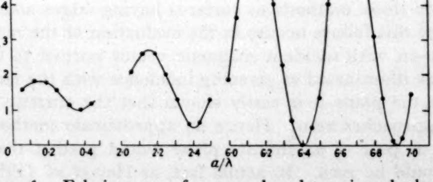

Figure 1. Echoing area of rectangular plates viewed edge-on.

---

† In the formulae of Appendix I of this reference, *f* should be replaced by 2*f* so as to conform with the tabulated values.

The measurements of the echoing areas of rectangular plates of width 2 λ for various lengths in the direction of incidence are illustrated in figure 1. These show that the echoing area varies periodically with each $\lambda/2$ increase of length. The measurements up to wavelengths of 7 λ indicate that the amplitudes of the maxima and the depth of the minima increase with length.

Measurements on isosceles triangular plates of semi-angle 15°, are shown in figure 2. The plates were orientated with the apex pointing in the opposite direction to that of the incident radiation. For these plates, the echoing area rises with increasing length, and there is only a very slight oscillatory component.

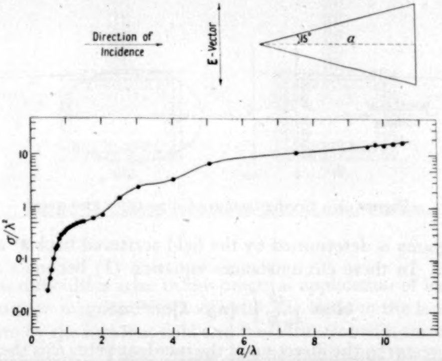

Figure 2. Echoing area of triangular plates viewed edge-on.

§ 3. RELATION BETWEEN ECHOING AREA AND CURRENT DISTRIBUTION

Although showing differing characteristics, the echoing area of the rectangular and triangular shapes attain high values. As the latter have no front edge normal to the direction of incidence it might have been anticipated without a deeper insight into the problem that the echoing area would have been very low. In order to attempt an explanation of the observed results it is necessary to consider the basic relationships connecting the echoing area and boundary conditions at the surface.

When a perfectly conducting object is placed in an electromagnetic field, the fundamental condition which must be satisfied is that the tangential component of the electric field vector at the surface must be zero. A current must flow in the surface of the conductor and produce a field which cancels the incident tangential electric field at all points of the surface. The boundary condition also implies that the normal component of the magnetic vector must also be zero at the surface.

In the following equations, the time factor $e^{i\omega t}$ is tacitly understood, where $i=\sqrt{(-1)}$, ω is the angular frequency and t is the time. The wave number is denoted by $k=2\pi/\lambda=\omega/c$ where c is the phase velocity in free space. Then from Maxwell's equations in m.k.s. units, the scattered magnetic and electric field vectors, $\mathbf{H}^s$ and $\mathbf{E}^s$, can be expressed in terms of the current density J at an element of surface of area dS by the equations

$$\mathbf{H}^{\mathrm{s}} = \operatorname{curl} \int \mathbf{J}\phi \, dS \qquad \ldots\ldots (1)$$

$$i\omega\epsilon \mathbf{E}^{\mathrm{s}} = k^2 \int \mathbf{J}\phi \, dS + \operatorname{grad} \operatorname{div} \int \mathbf{J}\phi \, dS \qquad \ldots\ldots (2)$$

where $\phi = \mathrm{e}^{-ikr}/4\pi r$, and r is the distance of the element dS from the field point. Consider now a flat plate in the x, z plane and an incident plane wave with the incident direction parallel to the x axis and the electric vector parallel to the z axis as shown in figure 3. It is clear from the above equations that to satisfy the boundary conditions involves the current distribution in both the x and z directions.

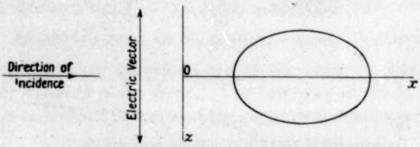

Figure 3. Configuration of directions and axes.

The echoing area is determined by the field scattered back at a large distance from the object. In these circumstances equation (1) becomes

$$\mathbf{H}^{\mathrm{s}} = \frac{-ik}{4\pi R} \int_{\mathrm{s}} [\mathbf{n}_0 \times \mathbf{J}] \mathrm{e}^{-ikr} \, dS \qquad \ldots\ldots (3)$$

where $\mathbf{n}_0$ is unit vector in the direction of the incident field, R is the mean distance of the scattering object and r the distance of the element dS from a suitably chosen reference plane normal to the direction of incidence in the vicinity of the body. Since, by definition, the echoing area σ is given by

$$\sigma = 4\pi R^2 \left| \frac{E^{\mathrm{s}}}{E^{\mathrm{i}}} \right|^2 = 4\pi R^2 \left| \frac{H^{\mathrm{s}}}{H^{\mathrm{i}}} \right|^2 \qquad \ldots\ldots (4)$$

it follows that

$$\sigma = \frac{\pi}{\lambda^2} \left| \int_{\mathrm{s}} [\mathbf{n}_0 \times \mathbf{J}] \mathrm{e}^{-ikr} \, dS \right|^2 \qquad \ldots\ldots (5)$$

if the incident magnetic field has unit amplitude. If the plates are in the x, z plane and the direction of incidence is parallel to the x axis, then

$$\sigma = \frac{\pi}{\lambda^2} \left| \int_{\mathrm{s}} J_z \mathrm{e}^{-ikx} \, dx \, dz \right|^2 \qquad \ldots\ldots (6)$$

and the echoing area is determined only by the z component of current.

The above discussion demonstrates firstly how the boundary conditions determine the current distribution on the plate, and secondly, that the echoing area is determined by one component only of the current flow. As the current distribution controls the scattering properties, attention was directed to methods of assessing and measuring the current.

§ 4. MEASUREMENTS OF SURFACE CURRENT

The surface current density at any point is related to the tangential magnetic field at that point by the equation

$$\mathbf{J} = [\mathbf{n} \times \mathbf{H}] \qquad \ldots\ldots (7)$$

where **n** is unit vector normal to the surface. Hence measurement of the tangential magnetic field determines the surface current distribution. A familiar technique for measuring a magnetic field is by the current induced in a wire loop, and the use of a loop to deduce currents in aerials and transmission lines is well known. The loop is usually screened as shown in figure 4 (*a*); the magnetic field induces a potential difference at the gap, which in turn induces a corresponding e.m.f. in the loop.

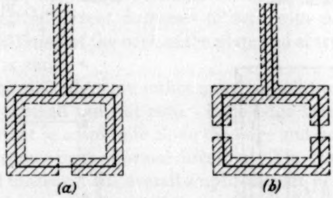

Figure 4. Loops for surface current measurement.

Two serious difficulties arise in the practical application of loops to measurements of the surface magnetic field. Firstly, the leads to the loop have currents induced on them by the incident field and these interact with the currents existing on the scattering plate. These effects can be minimized by making the cable thin and maintaining it perpendicular to the electric vector of the incident field. The second disadvantage is that if the split arm of the screen is parallel to the electric vector, an e.m.f. is induced across the gap and a corresponding e.m.f. in the loop even when the loop is placed with zero magnetic field normal to it. This difficulty remains with an unscreened loop. An arrangement which greatly reduces this type of excitation is shown in figure 4 (*b*) in which the split at the base is replaced by two splits one at each side.

With cautious use of loops arranged to minimize unwanted responses, it proved possible to obtain approximate amplitudes for the surface current distribution. Measurements were first made of the currents parallel to the direction of incidence. The results indicated that the current flow is concentrated near the edges of the plate and falls to zero at the centre. The amplitude of the edge current shown in figure 5 (*a*), increases towards the back of the plate, and also has an oscillatory component suggesting a stationary wave associated with a reflection of the current from the back of the plate.

Measurements were then made of the current flow normal to the direction of incidence. Results shown in figure 5 (*b*) indicate that a large current occurs at the front edge which falls with increasing distance from the front edge to a comparatively low value with some oscillatory variation, but as the back edge is approached there is an increase in magnitude.

The results for the currents in both directions reveal the predominating strength of the edge currents and suggest that the right approach in developing an approximate theory is to start by examining the edge effects more thoroughly.

The theoretical equations determining the currents have been solved exactly for infinite half planes. The extent to which current densities for infinite half planes can be adapted to derive the solutions for finite edges will now be studied.

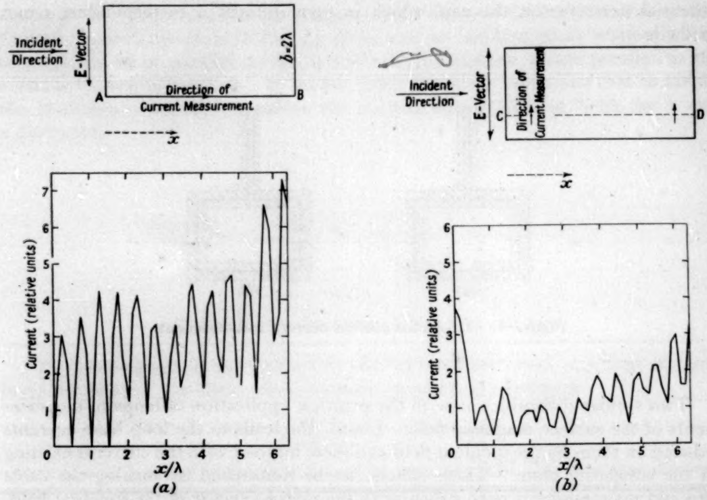

Figure 5. Current measurement on rectangular plates ; (*a*) currents parallel to the direction of incidence, (*b*) currents normal to the direction of incidence.

§ 5. THE EDGE CURRENTS

When a plate is viewed normally it seems reasonable to suppose that to a first approximation the current distribution over most of the surface will be the same as if the plate had been of infinite dimensions and these currents will determine the bulk of the scattered signal. The experimental results of Hey *et al.* (1956) indicated that this was valid for discs of diameter greater than about 2 λ.

When plates are viewed edge-on, however, the above approximations can no longer apply and it is the edges themselves which are likely to be of paramount importance. This leads us to seek an approximate theory in which the current distribution is determined by the edges. It is an edge of finite length which is of practical interest but no rigorous method is available for tackling this problem. An infinite edge, on the other hand, can be solved and the results are of relatively simple form.

In the Appendix expressions are obtained for the current density induced in a semi-infinite sheet of perfect conductivity by a plane wave at an arbitrary angle of incidence. This is done for each of two fundamental polarizations, and though the direction of current flow is, in general, inclined at an angle to the diffracting edge the normal component vanishes if the incident field has its electric vector along the edge. Moreover, the component of current parallel to the edge becomes infinite as $x^{-1/2}$; the component of current which is normal to the edge, however, has the form $x^{1/2}$ and therefore tends to zero.

In applying these results to a rectangular plate let us first assume that the currents contributed by each edge are the same as if the edges had been infinite. From equation (24) it is seen that the front edge produces a current parallel to itself which is constant in amplitude in the transverse z direction and which decays in the normal direction at a rate proportional to the inverse square root of the distance from the edge. A similar result, equation (25), holds for the rear edge but the amplitude is proportional to $\sin\phi/2$ where ϕ is the angle of incidence, and hence the current decreases to zero with ϕ. For small ϕ there will be little direct excitation of the back of the plate and at true glancing incidence the induced current is zero.

The results for the side edges are rather more complicated and we shall begin by assuming that ϕ is small but not zero. Each edge then produces a current parallel to itself constant in amplitude along the edge and decaying as the inverse square root of the distance in the normal direction. The current at the two edges are in anti-phase and moreover the overall amplitudes are proportional to $\sin^{-1/2}\phi$ which becomes infinite at glancing incidence. This clearly could not occur in practice and might be attributable to the impossibility of having a true plane wave of the postulated type propagating itself along the infinite edge. For a finite edge it is more reasonable, theoretically, to suppose that the current would build up with length the amplitude becoming greater as the distance from the front edge is increased. For this reason it will be assumed that the true side edge currents for a finite plate differ from equations (26) and (28) by having an amplitude factor which remains finite as ϕ tends to zero and which is an increasing function of distance along the plate. The postulated currents are therefore

$$J_x = \pm \exp(-i\pi/4 - ikx)\,\frac{f(x)}{\{\pi k(\tfrac{1}{2}b \pm z)\}^{1/2}} \qquad \ldots\ldots(8)$$

with the upper or lower sign for the left or right edge respectively. The function $f(x)$ is finite in the limit as ϕ tends to zero and is an increasing function of x.

If these formulae are compared with the experimental results a large measure of agreement is found. The front of the plate does support a large current which decays away from the edge. The measured rear-edge current is larger than theory would suggest; this could be accounted for by secondary excitation—by the very large longitudinal currents flowing along the side edges continuing their flow round the back.

The longitudinal currents are mainly confined to the side edges and decay, as expected, away from the edges. Along the edges themselves the current amplitudes build up from front to back. Superimposed upon this increase of amplitude is an oscillation which could be explained by partial reflection of the current at the discontinuity provided by the back edge.

Although no experimental measurements of the currents on a triangular plate have been carried out, an attempt can be made to derive the currents theoretically by a similar treatment. Since the direction of the incident field does not now lie along the side edges the currents here do not become infinite in the limit of glancing incidence and for this reason attention will be confined to the case $\phi = 0$. As a result the back edge is not directly excited by the incident field and any current here must be due to the side edges. Each of these generates a current parallel to itself which can be split into the components given in equations (30), (31). If the edges were infinite they would be infinitely excited and the amplitude would decay away from each edge as the square root of the normal distance.

§ 6. Echoing Areas

Having determined a theoretical distribution for the induced currents the corresponding echoing areas can be evaluated for comparison with experimental measurements.

In the case of a rectangular plate and a field at glancing incidence only the front edge provides a component J_z on both upper and lower surfaces and hence, from equations (24) and (6)

$$\sigma = \left| \frac{2b}{\pi} \int_0^{\sqrt{(2ka)}} \exp(-is^2)\, ds \right|^2. \qquad \ldots\ldots(9)$$

This can be evaluated with the aid of Fresnel integrals, and it is thus possible to arrive at the plot of echoing areas given in figure 6.

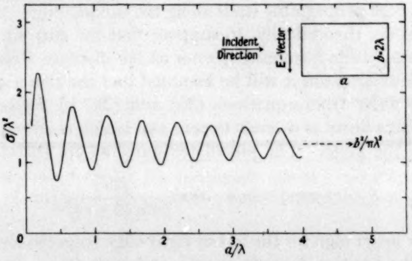

Figure 6. Echoing area of rectangular plates from infinite edge theory.

It will be observed that the fluctuations with length are relatively small and as ka increases σ oscillates about the constant value b^2/π. When ka is small its behaviour is in reasonable agreement with the experimental measurements given in figure 1. For larger ka, however, the measurements reveal an echoing area which has increased markedly above its value for smaller ka and the modulation has become almost 100%. This is no longer in accord with the approximate theory and the explanation is probably as follows.

Due to the large side currents there is an appreciable secondary excitation of the back edge and as we have seen there are reasons for supposing that the amplitude of the current here will increase with length of plate. A more complete expression for the current component J_z would therefore include a contribution from the back edge in the form of a term similar to that in equation (25) and having an increasing effect as the length of the plate is increased. Such an addition to J_z would appreciably affect the theoretical value of σ and bring it more into line with experiment.

The echoing area of a triangular plate will now be considered. If the total component J_z is obtained by adding the contribution indicated by equation (31) to the corresponding one for the right-hand edge, and doubling these to take into account the current on both upper and lower surfaces, an expression for σ is obtained in the form

$$\sigma = \frac{4}{\pi\lambda}\sin\gamma\left|\int_0^a\int_{-x\tan\gamma}^{x\tan\gamma}\left\{\frac{1}{(x\sin\gamma - z\cos\gamma)^{1/2}} + \frac{1}{(x\sin\gamma + z\cos\gamma)^{1/2}}\right\}e^{-2ikx}\,dx\,dz\right|^2 \quad \ldots\ldots(10)$$

where γ is the semi-angle of the plate and a is the overall length. Hence

$$\sigma = \frac{8a\lambda}{\pi}\left(\frac{\tan\gamma}{\pi}\right)^2\left|1 - \frac{e^{2ika}}{\sqrt{(2ka)}}\int_0^{\sqrt{(2ka)}}\exp(-is^2)\,ds\right|^2 \quad \ldots\ldots(11)$$

and the right-hand side is an increasing function of a. This expression can be evaluated with the aid of tables of the Fresnel integral to give the curve shown in figure 7.

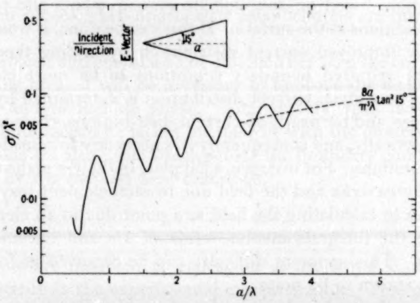

Figure 7. Echoing area of triangular plates derived from infinite edge theory.

For very small ka, σ increases as $(ka)^2$, but thereafter the mean curve is approximately a linear function of ka, as indicated by the dashed line in figure 7, apart from a small superimposed modulation whose relative magnitude decreases with increasing size of plate. If this curve is compared with the experimental results shown in figure 2 the magnitude of the experimental results is greater by a large factor.

A possible explanation of this discrepancy is suggested by comparison with the results obtained for rectangular plates in terms of a back-edge current excited by the side edges and becoming increasingly important as the length of the plate was increased. In the rectangular plate, marked interference effects due to front and back edges were produced. In the triangular plates the echoing area could be predominantly controlled by the current excited in the back edge. This would explain not only the large echoing areas found experimentally for the triangular plates, which were of fairly small semi-angle, but also the absence of any marked oscillatory modulation in the relation between echoing area and length. Alternatively, reflection of current in the side edges due to partial reflection at the discontinuities at the back edge could be important, since in triangular plates these currents have components in the z direction.

To refine the results it would be necessary to estimate the interaction between the edge currents and assign values to reflection coefficients at discontinuities. The accuracy of the postulated distribution could only be determined by examining the degree to which the resulting scattered field satisfied the boundary conditions at the surface of the plate, and in the next section a numerical method is developed for enabling this to be done.

§ 7. VERIFICATION OF CURRENT DISTRIBUTIONS

The current densities obtained experimentally as described in § 4 were only approximate. Moreover, they did not include the measurement of phase. In further work there would be much scope for refinements of technique in the determination of current amplitude and to include phase. Even so, there are likely to be uncertainties in measuring currents close to edges, where there may be a rapid spatial variation of field in the vicinity.

It is consequently desirable to be able to verify how closely a postulated current distribution, based on approximate measurements and theory, satisfies the boundary conditions at the surface. If this can be done, it would then appear feasible to derive improved current distribution by finding those adjustments which enable the required boundary conditions to be more closely satisfied.

The field due to a given current distribution is determined by equation (2). With most surfaces, and for nearly all current distributions, these integrals cannot be evaluated analytically, and consequently it is necessary to consider approximate numerical computations. For instance, a flat plate in the x, z plane may be divided into elements of area $\delta x \, \delta z$ and the field due to each element may be calculated. A difficulty arises in calculating the field at a point due to an element of area at the point, since the integrals involve terms in $1/r$ and become infinite as r approaches zero. This apparent difficulty can be removed as follows, and the resulting field is shown to be finite.

Consider a small circular element of surface of radius δa and centre at the point where the field is to be determined. If the element is small enough, the current variation over it may be ignored. The required integrals then include a term of the form

$$\int_0^{\delta a} \frac{e^{-ikr}}{r} \, dS,$$

which can be evaluated exactly for the circular element and is equal to $2\pi \, \delta a$. Without sensible error, the circular element may now be replaced by a square element of equal area. Hence for a square element centred on the field point and having side length δl it is found that

$$\int \frac{e^{-ikr}}{r} \, dS = 2\sqrt{\pi} \, \delta l. \qquad \ldots\ldots (12)$$

The required numerical computation for the whole surface may now proceed in Cartesian coordinates by dividing the surface into elements $\delta x \, \delta z$ where $\delta x = \delta z = \delta l$.

Such a method can very easily be tested on a thin strip where the current is essentially one-dimensional. For instance, when the computation is made for a narrow strip of length $\lambda/2$ in which the current has the form $I = I_0 \cos \beta z$ within the limits $z = \pm \lambda/4$, it is at once found that the field agrees very closely with that which can be derived by exact analysis for the particular case of a thin conductor.

To carry out the evaluation of the field over a surface by the above method of computation would in three dimensions be a somewhat formidable programme, but would be more practicable in two dimensions, as for flat plates. In view of the difficulty of deducing exact solutions analytically, the method of computation appears potentially to be very useful, particularly for the verification of currents deduced from approximate measurements or where attempts are made to postulate current distribution by the application of general principles.

§ 8. CONCLUSIONS

The characteristics of the echoing areas of rectangular and triangular plates at glancing incidence when the magnetic vector is normal to the plates have been shown to be explicable in terms of edge scattering. The strong edge currents demonstrated experimentally also conform to the currents derived theoretically for infinite half-planes when appropriate modifications are introduced for finite lengths.

If a more precise agreement is to be obtained between the current distributions and the echoing areas it will be necessary to improve the techniques of current measurement and to include phase. Alternatively, trial modifications in the current distributions can be tested for their fit with the observed echoing areas; correct solutions are also those which satisfy the boundary conditions which may be examined by the method here described.

ACKNOWLEDGMENTS

The authors are indebted to colleagues at the Royal Radar Establishment for their assistance in the experimental measurements. This paper is published by permission of the Controller, H.M. Stationery Office.

REFERENCES

CLEMMOW, P. C., 1951, *Proc. Roy. Soc.* A, **205**, 286.

HEY, J. S., STEWART, G. S., PINSON, J. T., and PRINCE, P. E. V., 1956, *Proc. Phys. Soc.* B, **69**, 1038.

APPENDIX

THE DERIVATION OF THE EDGE CURRENTS

It is convenient to obtain first a general expression for the currents induced in a perfectly conducting semi-infinite sheet by a three-dimensional plane wave incident upon it.

A Cartesian coordinate system (ξ, η, ζ) is chosen in terms of which the conducting sheet occupies the half-plane $\xi > 0$, $\eta = 0$, with the ζ axis lying along the diffracting edge.

In the first instance the incident field is taken to be an '**E**-polarized' plane wave whose electric vector reduces to one having only a component $\mathbf{E}_\zeta$ in the particular case of incidence in the plane normal to the edge. More generally, however, it is characterized by the absence of any magnetic component in the ζ direction and is defined by

$$\left.\begin{aligned} \mathbf{E}^{\mathrm{i}} &= ZA\cos\beta(\sin\beta\cos\alpha,\ \sin\beta\sin\alpha,\ -\cos\beta) \\ &\qquad \times\exp\{ik(\xi\cos\alpha\cos\beta+\eta\sin\alpha\cos\beta+\zeta\sin\beta)\}, \\ \mathbf{H}^{\mathrm{i}} &= A\cos\beta(\sin\alpha,\ -\cos\alpha,\ 0) \\ &\qquad \times\exp\{ik(\xi\cos\alpha\cos\beta+\eta\sin\alpha\cos\beta+\zeta\sin\beta)\}, \end{aligned}\right\} \quad \ldots\ldots(13)$$

where α, β are angles of incidence as shown in figure 8. The symbol A represents an arbitrary amplitude factor and Z is the intrinsic impedance of free space.

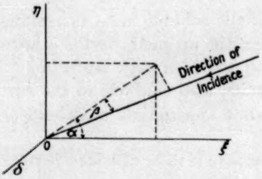

Figure 8. Configuration of directions used in Appendix.

The total (incident plus scattered) field can be found from the classical Sommerfeld solution using the method described by Clemmow (1951). If the solution for a field incident normally to the edge (see, for example, Clemmow 1951) is multiplied by $\exp(ik\zeta\sin\beta)$ and k is elsewhere replaced by $k\cos\beta$, it becomes

$$\begin{aligned} U = A\frac{e^{i\pi/4}}{\sqrt{\pi}}\exp(ik\zeta\sin\beta)\{&\exp[ikr\cos\beta\cos(\theta-\alpha)]F[-(2kr\cos\beta)^{1/2}\cos\tfrac{1}{2}(\theta-\alpha)] \\ &-\exp[ikr\cos\beta\cos(\theta+\alpha)]F[-(2kr\cos\beta)^{1/2}\cos\tfrac{1}{2}(\theta+\alpha)]\}, \end{aligned} \quad \ldots\ldots(14)$$

where r, θ are cylindrical coordinates, defined by $\xi=r\cos\theta$, $\eta=r\sin\theta$, and $F(\tau)$ is the Fresnel integral defined by

$$F(\tau)=\int_{\tau}^{\infty}\exp(-is^2\,ds). \quad \ldots\ldots(15)$$

The total field produced by the above incident field is then

$$\left.\begin{aligned} \mathbf{E} &= Z\left(-\frac{i\sin\beta}{k}\frac{\partial U}{\partial\xi},\ -\frac{i\sin\beta}{k}\frac{\partial U}{\partial\eta},\quad -\cos^2\beta U\right), \\ \mathbf{H} &= \frac{i}{k}\left(-\frac{\partial U}{\partial\eta},\ \frac{\partial U}{\partial\xi},\ 0\right). \end{aligned}\right\} \quad \ldots\ldots(16)$$

The current distribution is determined entirely by the magnetic field and since

$$\mathbf{J}=\mathbf{n}\times\mathbf{H},$$

where $\mathbf{n}$ is a unit vector normal to the surface, the currents excited on the upper surface ($\theta=0$) of the sheet are entirely in the ζ direction and are given by

$$J_{\zeta}=\frac{i}{kr}\left(\frac{\partial U}{\partial\theta}\right)_{\theta=0}. \quad \ldots\ldots(17)$$

The currents are therefore parallel to the edge and by inserting the expression for U into equation (17) we have

$$J_\zeta = -2A\frac{\exp(i\pi/4)}{\sqrt{\pi}}\cos\beta\sin\alpha\exp(ik\zeta\sin\beta)$$
$$\times\left\{\exp(ik\xi\cos\beta\cos\alpha)F[-(2k\xi\cos\beta)^{1/2}\cos\tfrac{1}{2}\alpha] - i\frac{\exp(-ik\xi\cos\beta)}{2(2k\xi\cos\beta)^{1/2}\cos\frac{1}{2}\alpha}\right\}. \quad \ldots\ldots(18)$$

The second fundamental type of incident field is an H-polarized plane wave defined by

$$\left.\begin{aligned}\mathbf{E}^{\mathrm{i}} &= BZ\cos\beta(\sin\alpha, -\cos\alpha, 0)\exp[ik(\xi\cos\alpha\cos\beta+\eta\sin\alpha\cos\beta+\zeta\sin\beta)],\\ \mathbf{H}^{\mathrm{i}} &= B\cos\beta(-\sin\beta\cos\alpha, -\sin\beta\sin\alpha, \cos\beta)\\ &\quad\times\exp[ik(\xi\cos\alpha\cos\beta+\eta\sin\alpha\cos\beta+\zeta\sin\beta)],\end{aligned}\right\} \quad \ldots\ldots(19)$$

where B is a further arbitrary amplitude factor. By taking the Sommerfeld solution for an H-polarized field and carrying out the modifications described above, an expression for U is obtained which differs from (14) only in the sign of the second term. The total field then follows by substituting into

$$\left.\begin{aligned}\mathbf{E} &= \frac{iZ}{k}\left(-\frac{\partial U}{\partial\eta}, \quad \frac{\partial U}{\partial\xi}, \quad 0\right),\\ \mathbf{H} &= \left(\frac{i\sin\beta}{k}\frac{\partial U}{\partial\xi}, \quad \frac{i\sin\beta}{k}\frac{\partial U}{\partial\eta}, \quad \cos^2\beta U,\right.\end{aligned}\right\} \quad \ldots\ldots(20)$$

and the corresponding current distribution on the upper surface of the sheet is

$$J_\xi = 2B\frac{\mathrm{e}^{i\pi/4}}{\sqrt{\pi}}\cos^2\beta\exp(ik\zeta\sin\beta+ik\xi\cos\beta\cos\alpha)F[-(2k\xi\cos\beta)^{1/2}\cos\tfrac{1}{2}\alpha], \quad \ldots\ldots(21)$$

$$J_\zeta = 2B\frac{\mathrm{e}^{i\pi/4}}{\sqrt{\pi}}\sin\beta\cos\beta\cos\alpha\exp(ik\zeta\sin\beta)\left\{\exp(ik\xi\cos\beta\cos\alpha)\right.$$
$$\left.\times F[-(2k\xi\cos\beta)^{1/2}\cos\tfrac{1}{2}\alpha] - i\frac{\cos\frac{1}{2}\alpha}{\cos\alpha}\frac{\exp(-ik\xi\cos\beta)}{(2k\xi\cos\beta)^{1/2}}\right\}. \quad \ldots\ldots(22)$$

Since any plane wave can be expressed as a combination of the above incident fields, equations (18), (21) and (22) represent the most general current distribution which can be set up on a semi-infinite sheet by an incident plane wave.

In order to employ these results to give the currents which would be excited on a rectangular or triangular plate by a field at glancing incidence, it will be assumed that each edge provides a contribution which is the same as if that edge had been infinite. If all interaction effects are then ignored, the currents produced by the individual edges can be found from equations (18), (21) and (22) by specifying A, B, α and β in a suitable manner.

Let us take first the case of a rectangular plate of length a and width b. A new coordinate system (x, y, z) is introduced having origin at the mid-point of the leading edge and such that the plate occupies the region $0 \leqslant x \leqslant a$, $-b/2 \leqslant z \leqslant b/2$ of the plane $y = 0$. In terms of these coordinates the incident field can be defined by the electric vector alone which lies in the z direction and is given by

$$E_z^{\,\mathrm{i}}=Z\exp\,[ik(x\cos\phi-y\sin\phi)], \qquad \ldots\ldots(23)$$

where ϕ is the (small) angle of incidence measured relative to the negative x axis. At glancing incidence, $\phi=0$.

Each of the four edges gives rise to one or more components of current whose expressions can be deduced from the above equations by appropriate transformations of coordinates and by assigning to α and β such values as will reduce either the incident field (13) or (19) to the form (23).

The transformations for the front and rear edges are relatively simple and are applied to the incident field (13). For the front edge ξ is replaced by x, ζ by z, α by $\pi-\phi$, β by 0 and A by -1 and equation (18) then becomes

$$J_z=2\frac{\mathrm{e}^{i\pi/4}}{\sqrt{\pi}}\,\sin\phi\left\{\exp\,(-ikx\cos\phi)F[-(2kx)^{1/2}\sin\tfrac{1}{2}\phi]-i\frac{\mathrm{e}^{-ikx}}{2(2kx)^{1/2}\sin\frac{1}{2}\phi}\right\},$$

which reduces to

$$J_z=\exp\,(-i\pi/4-ikx)(2/\pi kx)^{1/2} \qquad \ldots\ldots(24)$$

when ϕ is very small. For the rear edge the transformation is to replace ξ by $a-x$, ζ by $-z$, α by ϕ, β by 0 and A by $\exp\,(ika\cos\phi)$ and this gives

$$J_z=2\frac{\mathrm{e}^{i\pi/4}}{\sqrt{\pi}}\,\sin\phi\left\{\exp\,(-ikx\cos\phi)F[-\{2k(a-x)\}^{1/2}\cos\tfrac{1}{2}\phi]\right.$$
$$\left.-i\frac{\exp\,[+ikx-ika(1+\cos\phi)]}{2\{2k(a-x)\}^{1/2}\cos\frac{1}{2}\phi}\right\},$$

which reduces to

$$J_z=\exp\,[-i\pi/4-ik(2a-x)]\{2/\pi k(a-x)\}^{1/2}\sin\tfrac{1}{2}\phi \qquad \ldots\ldots(25)$$

for small ϕ. Both edges, therefore, generate currents parallel to themselves, the current density becoming infinite at the corresponding edge. In the case of the rear edge, however, the overall amplitude is proportional to ϕ and decreases to zero with ϕ.

To determine the currents attributable to the side edges it is necessary to employ the incident field (19) and to refer to the equations (21) and (22). For the left-hand side ($z=-b/2$, $y=0$) replace ξ by $z+b/2$, ζ by $-x$, α by $\pi/2$, β by $\pi/2-\phi$ and B by $\operatorname{cosec}\phi$ to give

$$J_x=-\exp\,[-i\pi/4-ikx\cos\phi-ik(z+\tfrac{1}{2}b)\sin\phi]\,\frac{\cos\phi}{\{\pi k(z+\frac{1}{2}b)\sin\phi\}^{1/2}}$$

and

$$J_z=2\frac{\mathrm{e}^{i\pi/4}}{\sqrt{\pi}}\sin\phi\exp\,(-ikx\cos\phi)F[-\{k(z+\tfrac{1}{2}b)\sin\phi\}^{1/2}],$$

and these reduce to

$$J_x=-\exp\,(-i\pi/4-ikx)\,\frac{\sin^{-1/2}\phi}{\{\pi k(z+\frac{1}{2}b)\}^{1/2}} \qquad \ldots\ldots(26)$$

and

$$J_z=\exp\,(i\pi/4-ikx)\sin\phi \qquad \ldots\ldots(27)$$

when ϕ is small. For the right-hand side the relevant transformation replaces ξ by $z-b/2$, ζ by x, α by $\pi/2$, β by $-\pi/2+\phi$ and B by $-\operatorname{cosec}\phi$ and gives

$$J_x=\exp\,[-i\pi/4-ikx\cos\phi-ik(\tfrac{1}{2}b-z)\sin\phi]\,\frac{\cos\phi}{\{\pi k(\frac{1}{2}b-z)\sin\phi\}^{1/2}},$$

$$J_z=2\frac{\mathrm{e}^{i\pi/4}}{\sqrt{\pi}}\sin\phi\exp\,(-ikx\cos\phi)F[-\{k(\tfrac{1}{2}b-z)\sin\phi\}^{1/2}],$$

reducing to

$$J_x = \exp(-i\pi/4 - ikx)\frac{\sin^{-1/2}\phi}{\{\pi k(\tfrac{1}{2}b - z)\}^{1/2}}, \qquad \ldots\ldots(28)$$

$$J_z = \exp(i\pi/4 - ikx)\sin\phi \qquad \ldots\ldots(29)$$

for small ϕ. Here again the induced currents are, in the main, parallel to the edges and become infinite at those edges which generate them. In addition, however, the overall amplitude of J_x becomes infinite when $\phi 0 =$ and this suggests that the propagation of a plane wave along an infinite edge would not be realizable in practice.

Let us now turn our attention to the case of a triangular sheet whose leading edges have the equation $z = \pm x\tan\gamma$, $0 \leqslant x \leqslant a$, where γ is the semi-vertical angle of the triangle. Since the rear edge is parallel to the z axis, it produces a current the expression for which is given by equation (25) and which tends to zero with ϕ. For simplicity we shall consider only glancing incidence ($\phi = 0$) and this enables the presence of the back edge to be ignored.

The transformations for the edge $z = -x\tan\gamma$ are $\xi = x\sin\gamma + z\cos\gamma$, $\zeta = -x\cos\gamma + z\sin\gamma$, $\alpha = \pi$, $\beta = \pi/2 - \gamma$ and $A = -\operatorname{cosec}\gamma$, and by applying these to equation (18) the induced currents are found to be

$$J_x = -\exp(-i\pi/4 - ikx)\frac{\sqrt{2}\cos\gamma}{\{\pi k(x\sin\gamma + z\cos\gamma)\sin\gamma\}^{1/2}} \qquad \ldots\ldots(30)$$

and

$$J_z = \exp(-i\pi/4 - ikx)\frac{\sqrt{2}\sin\gamma}{\{\pi k(x\sin\gamma + z\cos\gamma)\sin\gamma\}^{1/2}}. \qquad \ldots\ldots(31)$$

The currents attributable to the right-hand edge can be deduced from these by replacing γ by $\pi - \gamma$.

Magnetoresistance and Fermi Surface of Alkali Metals

By F. GARCÍA-MOLINER

Cavendish Laboratory, University of Cambridge†

Communicated by J. M. Ziman; *MS. received* 31*st July* 1958

Abstract. The observed magnetoresistance effects in low fields are used for an approximate estimate of the anisotropy of the Fermi surfaces of alkali metals. The elements appear to be arranged in order of increasing anisotropy as follows: sodium, rubidium, potassium, caesium, lithium. The Fermi surface in sodium is almost spherical. In lithium it is considerably anisotropic and it might even contact the Brillouin zone boundary.

---

§ 1. Introduction

The aim of this paper is to suggest plausible values of the anisotropy of the Fermi surface of alkali metals which might account for the observed magnetoresistance in low fields.

Considerable efforts to calculate from first principles the electronic structure of such supposedly simple metals have not been very fruitful. The discrepancies between various calculations are magnified if the results are used to estimate the magnetoresistance effect, as this is very sensitive to small details of the geometry of the Fermi surface.

Unfortunately, it is at present impossible to carry out accurate calculations based on magnetoresistance data of alkali metals because of the paucity of experimental information. First, no measurements suitable for the present purposes are available on single crystals. Secondly, the data on polycrystals are admittedly very inaccurate, sometimes only representing the order of magnitude. Thirdly, no systematic series of measurements has been carried out with the same specimen over a temperature range sufficiently wide to assess the possible influence of anisotropic scattering on magnetoresistance. Fourthly, the longitudinal effect has been largely neglected and we only possess scant information about its magnitude.

However discouraging the situation may seem, something can be done if one realizes the magnitude of the theoretical discrepancies mentioned above. To take the case of lithium, we find Fermi surfaces which predict effects differing by at least two orders of magnitude. Thus even a rough calculation can at least indicate what is definitely wrong.

It is in this spirit that the calculations reported in this paper have been done. No accuracy is claimed and the present conclusions only aim at suggesting plausible values.

§ 2. Assumptions involved in the Present Calculations

We shall now make the following approximations:

(*a*) we assume that the scattering at low temperatures can be described by an isotropic relaxation time; (*b*) we assume for the Fermi surface an expansion in Kubic harmonics:

$$k = K_0(E_k) + K_1(E_k)\, Y_4^{(c)}(\theta_1 \phi). \qquad \ldots\ldots (2.1)$$

---

† Now at Institute de Física " A. Santa Cruz ", Serrano, Madrid.

Here k is the modulus of the wave vector $\mathbf{k}$ and $E_{\mathbf{k}}$ is the energy associated to the state $\mathbf{k}$. In the absence of theoretical guidance about the shape of the Fermi surface, we simply assume that the real surface deviates from the free-electron sphere in such a direction as would make it tend to acquire the shape given by the strict 'tight-binding' model, that is a cube whose radius vectors are ordered $k_{100} < k_{110} < k_{111}$. This shape corresponds to the fourth Kubic harmonic $Y_4^{(c)}(\theta, \phi)$.

(*c*) We assume that an approximate model for a polycrystal is obtained by averaging the resistivity for all possible orientations in the single crystal. Actually, averaging the resistivity ρ or the conductivity σ gives the same answer to second order in the magnetic field strength H.

For a Fermi surface of the type (2.1), Davis (1936) has calculated the longitudinal and transverse magnetoresistance for low fields assuming $\mathbf{J}$ to be along a [100] axis and using the iterative solution of Jones and Zener (1934).

However (García-Moliner 1959) this is not sufficient to account for the observed ratio of longitudinal to transverse effect in polycrystals. Symmetry arguments (Seitz 1950) show that in a cubic single crystal at low fields the relative change in resistivity is $\Delta\rho/\rho = BH^2$, where B is of the form

$$B = b + c\,(\mathbf{h}\,.\,\mathbf{j})^2 + d \sum_{x,y,z} h_i^2 j_i^2. \qquad \ldots\ldots(2.2)$$

Here $\mathbf{h}$ and $\mathbf{j}$ are the unit vectors of $\mathbf{H}$ and of the electric current $\mathbf{J}$. For the cases $\mathbf{H} \parallel \mathbf{J}$ (longitudinal) and $\mathbf{H} \perp \mathbf{J}$ (transverse) we have, from (2.2),

$$(B_l)_{100} = b + c + d; \quad (B_t)_{100} = b. \qquad \ldots\ldots(2.3)$$

All the coefficients in (2.2) can, in principle, be expressed in terms of just two parameters measuring the anisotropy in the shape of the Fermi surface ($E_{\mathbf{k}} = \zeta$) and in the reciprocal Fermi velocity. These parameters are defined from (2.1) and from its derivative with respect to $E_{\mathbf{k}}$ (denoted by a prime) as follows:

$$A \equiv (K_1/K_0)_\zeta; \quad A' \equiv (K_1'/K_0')_\zeta. \qquad \ldots\ldots(2.4)$$

Davis' calculations give only the combinations b and $c + d$.

However, for a polycrystal we have, denoting by a bar the angle average†:

$$\bar{B}_l = b + c + \frac{3}{5}\,d; \quad \bar{B}_t = b + \frac{32}{105}\,d. \qquad \ldots\ldots(2.5)$$

To find $\bar{B}_l$ and $\bar{B}_t$ uniquely in terms of A and A' would require the evaluation of a further integral of considerable difficulty which is needed to calculate either c or d. For the reasons stated in the introduction, we shall instead take a semi-empirical approach which consists in using, as a third condition, the result of equating $\bar{B}_l/\bar{B}_t$ to the experimental value of B_l/B_t. This ratio is not known very accurately, but in lithium and sodium (e.g. Justi 1948) tends to be close to 1/3 (in fact, small changes in this number do not affect appreciably the results). We shall assume the value 1/3 for lithium and sodium. Potassium (see next section) will be treated in a different way.

For $\bar{B}_l/\bar{B}_t = 1/3$ we obtain

$$\bar{B}_t = (R/\rho_T)^2(26{\cdot}615A^2 - 3{\cdot}175AA' + 1{\cdot}744A'^2), \qquad \ldots\ldots(2.6)$$

where R is the Hall coefficient and ρ_T is the zero-field resistivity at the temperature T of experiment.

---

† These formulae can be checked in the case of copper. Experiments by Kapitza (1929) on polycrystals give $B_l/B_t0 = {\cdot}51$. Single crystal data by Olson and Rodríguez (1957) give, using the formulae of (2·5), $\bar{B}_l/\bar{B}_t = 0{\cdot}53 \pm 0{\cdot}21$.

We are interested in the value of the anisotropy parameter A. Unfortunately with only equation (2.6) to compare with experiment, this still depends on the ratio A'/A which is now undetermined and *has to be assumed.* It can be argued (García-Moliner 1959) that this value should be in the neighbourhood of 3 to 4 for not very anisotropic surfaces, although the spherical harmonics model might underestimate this ratio. We shall see presently that the most acceptable calculation that we find for lithium is that by Jones and Zener (1934), which suggests $A'/A \simeq 7 \cdot 5$. *We shall assume* $A'/A = 6$, as a compromise between 7·5 and our suggested value.

§ 3. APPLICATION TO PARTICULAR METALS

All quantities in this section, when not dimensionless, are expressed in Gaussian units.

We take 0°C as a reference temperature and call ρ_0 the resistivity and $s \equiv \rho_0/\rho_T$. We then have:

$$\Delta\rho/\rho_T = BH^2 = s^2 B\,(H/s)^2. \qquad \ldots\ldots (3.1)$$

We write

$$s^2 B = B^0; \quad H/s = H_0; \quad \Delta\rho/\rho_T = B^0 H_0^{\,2}, \qquad \ldots\ldots (3.2)$$

and reduce all data to these standard conditions.

Values of R and ρ_0 have been taken from Kittel (1956, p. 240).

Reduction of B to B^0 has been performed using the values of s given by the experimenters in each case. Sometimes the ratio s is given relative to a temperature different from 0°C (e.g. room temperature). In such cases the (slight) correction to 0°C has been made using values of the resistivity coefficient for the range $273\,°\mathrm{K} \leqslant T \leqslant 373\,°\mathrm{K}$ given by Grüneisen (1945).

In table 1 are given the various observed values which have been used in the theory and our estimates of the anisotropy parameters which fit the experimental data and describe plausible pictures of the Fermi surface of different metals. We describe the Fermi surface by its radius vectors in the three principal directions, compared with the mean radius k_m of the sphere containing the same volume. In the [110] and [111] directions we also compare with the distance k^B from the origin to the boundary of the first Brillouin zone.

We now make some comments on each particular case.

Lithium. Experiments by Kapitza (1929) at 77·8°K give B_t and hence $B_\mathrm{t}^0 = 5 \cdot 1 \times 10^{-14}$. Measurements by Justi (1948) at 20·4°K are insufficient to estimate B_t, but suggest a slightly higher value for B_t^0. Experiments by MacDonald (1957) at 4·2°K are very difficult to interpret because of possible size effects; in any case they tend to suggest a slightly lower value than Kapitza's. We have taken Kapitza's measurements for the experimental value.

Lithium has been the subject of several band-structure calculations. The anisotropy parameters for three such calculations giving the same shape for the Fermi surface are listed in table 2 together with the values of $\overline{B}_\mathrm{t}^0$ calculated from them.

It is clear that only Jones and Zener's calculation gives a plausible surface. Even allowing for errors in our approximations, which make the present estimates very crude, it is clearly impossible that the Fermi surface could be as nearly spherical as is predicted by Kohn and Rostoker (1954). Parmenter's (1952) calculation not only gives a worse estimate for $\overline{B}_\mathrm{t}^0$ but also gives $A'/A = 22$, which is very difficult to interpret.

Table 1. Observed Magnetoresistance and Suggested Anisotropy Parameters of the Fermi Surface of Alkali Metals (Gaussian units for B_t^0)

	$B_t^0 \times 10^{14}$	B_l/B_t	A'/A	$A \times 10^2$
Lithium	5·1	1/3	6·0	12·7
Sodium	0·9	1/3	6·0	1·7
Potassium	6·0	1·5	6·0	8·8
Rubidium	~10?	~1/3?	6·0?	$\lesssim$ 8??
Caesium	~ 1?	~1/3?	6·0	$\gtrsim$ 9??

	k_{100}	k_{110}	k_{111}
Lithium	$0{\cdot}866k_m$	$1{\cdot}034k_m = 0{\cdot}904k_{110}^B$	$1{\cdot}089k_m = 0{\cdot}777k_{111}^B$
Sodium	$0{\cdot}981k_m$	$1{\cdot}005k_m = 0{\cdot}876k_{110}^B$	$1{\cdot}013k_m = 0{\cdot}722k_{111}^B$
Potassium	$0{\cdot}944k_m$	$1{\cdot}014k_m = 0{\cdot}885k_{110}^B$	$1{\cdot}019k_m = 0{\cdot}726k_{111}^B$

Table 2. Calculated and Observed Values of the B_t^0 Coefficient in Lithium (Gaussian units)

	A'/A	$A \times 10^2$	$B_t^0 \times 10^{14}$
Kohn and Rostoker (1954)	2·9	0·8	$7{\cdot}8 \times 10^{-3}$
Parmenter (1952)	22·0	1·3	$5{\cdot}0 \times 10^{-1}$
Jones and Zener (1934)	7·5	5·1	1·1
Experimental (Kapitza 1929)	—	—	5·1

Sodium. Justi's measurements (1948) at 20·4°K and 14°K both suggest $B_t^0 = 0{\cdot}9 \times 10^{-14}$. The ratio $B_l/B_t \simeq 1/3$ appears fairly well defined. This leads to an almost spherical surface, in agreement with the general assumption that sodium is the nearest to a free-electron metal.

Potassium. This metal offers an interesting feature. Justi's measurements (1948) though not very accurate, would indicate $B_t^0 = 6 \times 10^{-14}$. Owing to the large value of $(R/\rho_0)^2$ in potassium ($4{\cdot}7 \times 10^{-14}$) it might appear, taking the same ratio $\overline{B}_l/\overline{B}_t = 1/3$, that the Fermi surface should be almost as isotropic as that of sodium, which seems inacceptable on the basis of low temperature measurements of electrical resistivity (MacDonald 1950, MacDonald and Mendelssohn 1948, 1950). However, the only available measurements on the same specimen of potassium (Justi 1948) give a longitudinal effect larger than the transverse. Unfortunately, Justi's measurements are insufficient for an accurate estimate of the B_l coefficient. With a certain amount of guesswork one obtains $B_l/B_t \simeq 1{\cdot}5$. This is the value quoted in table 1 and leads to a surface a little less anisotropic than that of lithium.

Rubidium and caesium. It is impossible to make even a crude calculation on these metals owing to the lack of experimental information. Only a rough guess, based on the sparse data, can be made and this suggests surfaces similar to that of potassium. However, the experimental data are simply insufficient to give a reliable estimate.

§ 4. CONCLUSIONS

Within the accuracy of the present analysis, the suggested order of increasing anisotropy of the Fermi surface of the alkali metals is: sodium, rubidium, potassium caesium and lithium. The relative order of any pair in the middle of the scale should not be taken too seriously. However, the extremes appear quite definite. Sodium has a very nearly spherical surface and lithium is considerably ansisotropic.

The shape of the Fermi surface of alkali metals has been recently studied by Cohen and Heine (1958) who have found essential agreement with the conclusion of the present paper. Their work suggests that in lithium the Fermi surface even contacts the zone boundary. This is not inconsistent with the present analysis if only small changes are allowed in the value used for R, which represents measurements of the 1880's.

ACKNOWLEDGMENTS

This work was done during the tenure of an exchange British Council Scholarship. Thanks are due to this and to the Spanish Research Council for financial support.

I am greatly indebted to Dr. J. M. Ziman for invaluable help and advice, especially in the preparation of the manuscript. I am also indebted to Drs. M. H. Cohen and V. Heine for letting me know about their work prior to publication.

REFERENCES

Cohen, M. H., and Heine, V., 1958, *Advanc. Phys.* (*Phil. Mag.* Suppl.), **7**, 395.
Davis, L., Jr., 1936, *Phys. Rev.*, **53**, 93.
García-Moliner, F., 1959, *Proc. Roy. Soc.*, A, **249**, in the press.
Grüneisen, E., 1945, *Ergebn. exakt Naturw.*, **21**, 50.
Jones, H., and Zener, C., 1934, *Proc. Roy. Soc.* A, **145**, 268.
Justi, E., 1948, *Ann. Phys., Lpz.*, (6), **3**, 148.
Kapitza, P., 1929, *Proc. Roy. Soc.* A, **123**, 292.
Kittel, C., 1956, *Introduction to Solid State Physics* (New York: Wiley).
Kohn, W., and Rostoker, N., 1954, *Phys. Rev.*, **108**, 590.
MacDonald, D. K. C., 1950, *Proc. Phys. Soc.* A, **63**, 290; 1957, *Phil. Mag.*, (8), **2**, 17.
MacDonald, D. K. C., and Mendelssohn, K., 1948, *Nature, Lond.*, **161**, 972; 1950, *Proc. Roy. Soc.* A, **202**, 103.
Olson, R., and Rodríguez, S., 1957, *Phys. Rev.*, **108**, 1212.
Parmenter, R. H., 1952, *Phys. Rev.*, **86**, 552.
Seitz, F., 1950, *Phys. Rev.*, **79**, 372.

Some Properties of Magnesium Fluoride crystallized from the Melt

By A. DUNCANSON AND R. W. H. STEVENSON

Department of Natural Philosophy, Aberdeen University

Communicated by R. V. Jones; MS. received 12th *May* 1958

Abstract. Magnesium fluoride crystals can be grown *in vacuo* using the Stockbarger technique. The melting point is 1255 ± 3°C. The crystal structure is of the tetragonal SnO_2 type, with lattice constant $a = 4{\cdot}621 \pm 0{\cdot}001$ Å and axial ratio 1 : 0·6601 ± 0·0001 giving $c = 3{\cdot}050$ Å at 18°C. The density is 3·1766 ± 0·0002 g cm^{-3} at 18°C.

MgF_2 is a uniaxial positive crystal, and the refractive indices are given for the ordinary and extraordinary rays at various wavelengths in the visible spectrum. The transparent region extends from 1100 Å to 1360 cm^{-1}. Infra-red reflectivity begins to rise at about 620 cm^{-1}, and peaks around 500 cm^{-1}.

The mean dielectric constant is $\epsilon_m = 5{\cdot}26$.

---

§ 1. INTRODUCTION

MANY single crystals of magnesium fluoride (MgF_2) have been grown in this department during the past four years. The largest specimens weigh over 2 kg, and have a diameter of 95 mm. The material is birefringent and may possibly be of use for polarizers in the ultra-violet and infrared regions. It has been employed as a window material in photon-counter tubes and also for reststrahlen plates.

§ 2. CRYSTAL GROWTH

Although MgF_2 occurs in nature as the mineral sellaite (Palache, Berman and Frondel 1951), this was not available as a raw material, and powder of the quality employed for the surface treatment of lenses was used. Several preliminary crystallizations by the Stockbarger process were needed to separate clear crystal, from which a good specimen could be grown.

Graphite was found to be a suitable crucible material for MgF_2, as for many other fluorides. Between 24 and 48 hours were spent in thoroughly vacuum drying the charge before the furnace temperature was raised. It was also found advisable to keep the maximum temperature only slightly above the melting point (1255°C). When these precautions were not observed, the material hydrolysed quite extensively and yielded a marble-white product.

The vapour pressure at the melting point was low and evaporation losses were negligible. Pressure was held as low as possible (1–2 μ) throughout growth. The growth rate was 1 mm h^{-1}.

§ 3. VARIOUS PROPERTIES

3.1. *Melting Point*

The melting point was determined by observation of the plateau in the cooling curve. A platinum/platinum–13% rhodium 'Thermopure' couple and a potentiometer were used. The bare loop of wire hung through the upper aperture of the furnace heater and was directly immersed in the molten salt. The crucible lid had a clearance slot, and the furnace aperture was closed with semicircular lids which could be adjusted after centring the thermocouple. Refractory beads were only used outside the heater, where they would not be attacked by the fumes.

The value derived from seven successive observations of the plateau was 1255 ± 3°c. The values in the literature are discordant. Simons (1950) quotes 1225°c, and the Handbook of Chemistry and Physics (Hodgman, Weast and Selby 1955) gives 1396°c.

3.2. *Density*

The density was determined by Archimedes' method, using distilled water, and polished specimens ranging from 15 g to 120 g in weight. The value corrected to 18°c was

$$\rho = 3{\cdot}1766 \pm 0{\cdot}0002\,\mathrm{g\,cm^{-3}}.$$

Magnesium fluoride is slightly soluble in water ($0{\cdot}076\,\mathrm{g\,l^{-1}}$ at 18°c), but the loss from a polished specimen immersed for a limited period was found to be negligible.

3.3. *Crystal Structure*

MgF_2 has the tetragonal SnO_2 type structure. Among the more recent determinations of the lattice constants are those by Buckley and Vernon (1925), Van Arkel (1925) and Goldschmidt (1926):

(*a*)	$a = 4{\cdot}66$ Å,	$c/a = 0{\cdot}66$,	$c = 3{\cdot}078$ Å,	$\rho_x = 3{\cdot}099\,\mathrm{g\,cm^{-3}}$
(*b*)	$a = 4{\cdot}69$ Å,	$c/a = 0{\cdot}659$,	$c = 3{\cdot}08$ Å,	$\rho_x = 3{\cdot}045\,\mathrm{g\,cm^{-3}}$
(*c*)	$a = 4{\cdot}62$ Å,	$c/a = 0{\cdot}663$,	$c = 3{\cdot}06$ Å,	$\rho_x = 3{\cdot}165\,\mathrm{g\,cm^{-3}}$.

Here the lattice constants were measured from photographs obtained with both Fe and Cu targets, giving $a = 4{\cdot}621 \pm 0{\cdot}001$ Å and an axial ratio $c/a = 0{\cdot}6601 \pm 0{\cdot}0001$ whence $c = 3{\cdot}050$ Å.

The computed density at 18°c is then $\rho_x = 3{\cdot}1772\,\mathrm{g\,cm^{-3}}$ which is in close agreement with the value derived from Archimedes' method.

3.4. *Cleavage and Polishing*

Good cleavage surfaces parallel to both *a* and *c* axes have occasionally been obtained, but conchoidal fracture was more common. Ground surfaces have been polished on pitch laps with rouge, but beeswax with putty powder appears to give a higher polish more rapidly.

3.5. *Refractive Indices*

The refractive indices were measured with a Hilger-Watts research spectrometer. The prism was oriented with the optic axis parallel to the base and bisecting the refracting angle. The faces were 25 mm × 27 mm in area.

The variation of prism angle with temperature was determined in the range 19° to 37°c by raising the temperature of the room and maintaining a steady value with a thermostat control. The rate of variation was $-0{\cdot}72''\,\mathrm{deg^{-1}}$ and the prism angle at 21°c was $60°\,13'\,10''$.

The rate of variation of deviation with temperature for the ordinary and extraordinary ray was measured over the same temperature range and at both ends of the visible spectrum.

Å	Ordinary	Extraordinary
4047	$+0{\cdot}18'' \text{ deg}^{-1}$	$0{\cdot}0'' \text{ deg}^{-1}$
7065	$+0{\cdot}075'' \text{ deg}^{-1}$	$-0{\cdot}2'' \text{ deg}^{-1}$

The rate at intermediate wavelengths was obtained by interpolation. With a MgF_2 prism oriented in this manner, the fall in prism angle with rising temperature is compensated by the rise in refractive index, and there is very little residual change in deviation.

The temperature coefficients of refractive index are:

Å	Ordinary	Extraordinary
4047	$+0{\cdot}23 \times 10^{-5} \text{ deg}^{-1}$	$+0{\cdot}17 \times 10^{-5} \text{ deg}^{-1}$
7065	$+0{\cdot}19 \times 10^{-5} \text{ deg}^{-1}$	$+0{\cdot}10 \times 10^{-5} \text{ deg}^{-1}$

The refractive indices were calculated from deviations corrected to a uniform temperature of 21°c and standard atmospheric pressure. The values at 4046, 5460 and 7065 Å were used to obtain the constants in the Hartmann interpolation formula $n = n_0 + c/(\lambda - \lambda_0)$. The formula for the ordinary ray at 21°c is $n = 1{\cdot}36957 + 35{\cdot}821/[\lambda - 1492{\cdot}5]$ and for the extraordinary ray $n = 1{\cdot}38100 + 37{\cdot}415/[\lambda - 1494{\cdot}7]$.

		Ordinary Ray		Extraordinary Ray	
	Å	Observed	Computed	Observed	Computed
Hg	4046·56	1·38359	—	1·39566	—
H	4340·465	1·38215	1·38214	1·39415	1·39415
Hg	4358·35	1·38207	1·38207	1·39407	1·39406
He	4471·48	1·38160	1·38159	1·39357	1·39357
Cd	4678·16	1·38082	1·38081	1·39275	1·39275
Cd	4799·92	1·38039	1·38040	1·39231	1·39232
He	4921·93	1·37001	1·38001	1·39192	1·39191
He	5015·68	1·37972	1·37973	1·39163	1·39162
Cd	5085·82	1·37953	1·37953	1·39142	1·39142
Hg	5460·74	1·37859	—	1·39043	—
He	5875·62	1·37774	1·37774	1·38954	1·38954
Na	5893·7	1·37770	1·37771	1·38950	1·38950
Hg	6234·37	1·37713	1·37712	1·38889	1·38889
Cd	6438·47	1·37681	1·37681	1·38858	1·38857
H_2	6562·79	1·37662	1·37663	1·38838	1·38838
He	6678·15	1·37647	1·37647	1·38822	1·38822
Hg	6907·16	1·37618	1·37618	1·38790	1·38791
He	7065·25	1·37599	—	1·38771	—

In the above table the 'computed' values have been obtained from the above formulae, and show that average discrepancy between the interpolation formula and the observed values is less than 1×10^{-5}, so that the formulae can be differentiated to give the dispersion $dn/d\lambda$

Å	Ordinary	Extraordinary
4000	$0{\cdot}56969 \times 10^{-5}$ Å^{-1}	$0{\cdot}59611 \times 10^{-5}$ Å^{-1}
5000	$0{\cdot}29116 \times 10^{-5}$ Å^{-1}	$0{\cdot}30451 \times 10^{-5}$ Å^{-1}
6000	$0{\cdot}17630 \times 10^{-5}$ Å^{-1}	$0{\cdot}18433 \times 10^{-5}$ Å^{-1}
7000	$0{\cdot}11809 \times 10^{-5}$ Å^{-1}	$0{\cdot}12345 \times 10^{-5}$ Å^{-1}

The reciprocal dispersive power ν_{CDF} is 105·4 for the ordinary ray, and 104·4 for the extraordinary ray.

3.6. *Dielectric Constant*

The dielectric constant was measured using a Marconi Q meter type T.F.329G. Crystal discs, approximately 1 in. in diameter, were tested in the dielectric loss jig T.J.155, which is an adjustable parallel plate condenser in which the crystal disc may be inserted.

Measurements were made over the frequency range 95 kc/s to 42 Mc/s on four discs, two of which were cast in a graphite mould, the other two being sawn from a crystal block. The moulded discs were oriented by chance with the optic axis at 40° to the disc normal, and the other two had the optic axis respectively perpendicular and parallel to the disc surface.

All specimen faces were finely ground and on each specimen measurements were made for thicknesses ranging from 5 to 2 mm.

In this frequency range there was no significant variation of the dielectric constant. The phase defect of the samples was too small for reliable measurement. The average values obtained were:

Angle between plate normal and optic axis (°)	0	40	90
Dielectric constant	4·87(ϵ_3)	5·08	5·45(ϵ_1)

For a disc cut with the optic axis at an angle θ to the plate normal the capacitance corresponds to an effective dielectric constant $\epsilon(\theta) = \epsilon_1 \sin^2\theta + \epsilon_3 \cos^2\theta$. With the above values for ϵ_1 and ϵ_3, the value for $\theta = 40°$ should be 5·11 which agrees reasonably well with the experimental value.

The mean dielectric constant $\epsilon_m = \frac{1}{3}(\epsilon_3 + 2\epsilon_1) = 5{\cdot}26$.

3.7. *Expansion of MgF_2*

The rate of variation of prism angle with temperature corresponds to a difference in the expansion coefficients α_1 and α_3, respectively perpendicular and parallel to the optic axis of amount $\alpha_3 - \alpha_1 = 0{\cdot}4 \times 10^{-5}\,\mathrm{deg}^{-1}$.

The cubic coefficient of expansion was measured by Klemm (1928) using a dilatometer method with mercury as the displaced fluid. The value of $2\alpha_3 + \alpha_1$ was $3{\cdot}2 \times 10^{-5}\,\mathrm{deg}^{-1}$. It should follow that $\alpha_1 = 0{\cdot}93 \times 10^{-5}$ and $\alpha_3 = 1{\cdot}33 \times 10^{-5}\,\mathrm{deg}^{-1}$.

Direct measurements of expansion were made on rectangular bars sawn from single crystals, with the optic axis respectively parallel and perpendicular to the bar axis, and also on cast cylindrical single crystal rods with the optic axis orientated by chance at angles of 23° and 63° with respect to the cylindrical axis. The lengths of the specimens ranged from 2·5 to 4 cm.

A Leitz dilatometer with Bollenrath head was used, with a vacuum tube to protect the specimen from atmospheric attack. Temperatures were determined with a 'Thermopure' platinum/platinum–13% rhodium thermocouple, and measurements extended over the range 0–500°c. The data were reduced by fitting a parabolic arc to the points so that $\alpha_t = \alpha + \beta t$, with higher terms in the expansion ignored.

Angle to optic axis (°)	0	23	63	90
$\alpha \times 10^5$	1·32(α_3)	1·24	0·99	0·86(α_1)

The data from the inclined rods, using $\alpha(\theta) = \alpha_1 \sin^2\theta + \alpha_3 \cos^2\theta$, give $\alpha_1 = 0{\cdot}90$ and $\alpha_3 = 1{\cdot}30 \times 10^{-5}\,\mathrm{deg}^{-1}$. Thus the mean values from the direct measurement are

$\alpha_1 = 0{\cdot}88$ and $\alpha_3 = 1{\cdot}31 \times 10^{-5}$ deg^{-1} giving $\alpha_3 - \alpha_1 = 0{\cdot}43 \times 10^{-5}$ in reasonable agreement with the prism angle data, and a cubic coefficient $3{\cdot}07 \times 10^{-5}$ deg^{-1} somewhat lower than the dilatometer value (3.2).

3.8. *Transmission.*

The transmission in the vacuum ultra-violet extends almost as far as that of lithium fluoride. There is some indication of an absorption band at about 1320 Å, but the marked fall in transmission does not occur until about 1150 Å. A specimen 1·9 mm thick transmitted 7% at 1100 Å. Specimens have been supplied for use as photon-counter windows.

In the infra-red MgF_2 is transparent to about 7·5 μ, the absorption coefficient rising to 1 cm^{-1} at a wave number of 1370 cm^{-1}.

3.9. *Reflectivity*

The reflectivity of MgF_2 has been measured in the KBr range (figure 1). It rises steeply in the region of 620 cm^{-1}; MgF_2 has an application as a reststrahlen plate, with properties intermediate between those of LiF and NaF. The reflectivity peaks near 500 cm^{-1} and falls off beyond 400 cm^{-1}. The reflectivity for unpolarized radiation incident at 20° to the normal did not vary appreciably with the orientation of the axis and was obtained by comparison with an aluminized optical flat

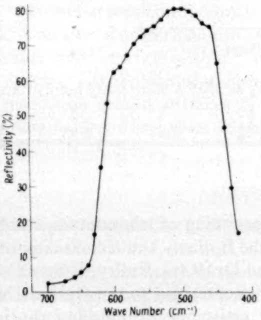

Figure 1. Infra-red reflectivity of MgF_2.

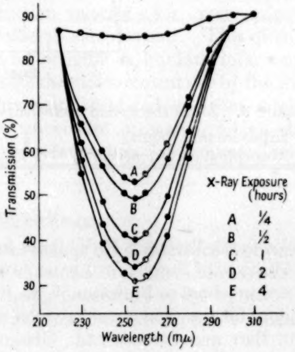

Figure 2. Ultra-violet transmission of MgF_2 after X-ray bombardment.

Wave number (cm^{-1})	650	640	630	620	610	600	550	500	450
Reflectivity (%)	5·8	7·9	16·7	35·7	53·6	62·5	74	80	65

3.10. *Ultra-violet Absorption in MgF_2 after X-ray Bombardment*

A polished disc was exposed in an X-ray beam at 6 cm from a molybdenum target (filament current 10 mA, tube voltage 48 kv) for times ranging from 15 minutes to 48 hours, and the ultra-violet transmission was measured with a

Hilger ' Uvispek '. Between each exposure the specimen was bleached in the radiation from an ultra-violet lamp, for the recovery even in strong daylight was very slow. The curves in figure 2 show that the absorption band at 2550 Å appears readily on short exposure.

In figure 3 the mean absorption coefficient (based on a disc thickness 3·43 mm) is shown as a function of exposure time, and there appears to be an approach to saturation at four hours.

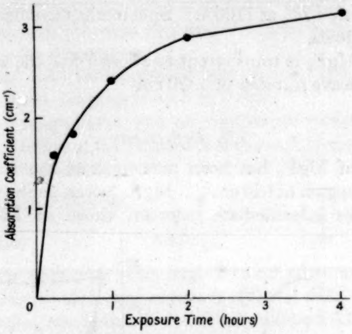

Figure 3. Mean absorption coefficient of MgF_2 at 2550 Å after x-ray bombardment.

Exposure time (hours)	¼	½	1	2	4
Absorption coefficient (cm^{-1})	1·59	1·82	2·41	2·88	3·16

ACKNOWLEDGMENTS

We thank Professor R. V. Jones for the provision of laboratory facilities and the Ministry of Supply for a grant covering the furnaces and technical assistance. We are indebted to Professor W. C. Price and Dr. R. G. Ridley, King's College, London, for the vacuum ultra-violet measurements, and to the Optical Department, Barr and Stroud, Ltd., Glasgow, for assistance in polishing the prism. We thank Mr. W. Mitchell for his skill and persistence in the construction and operation of the furnaces.

REFERENCES

VAN ARKEL, A. E., 1925, *Physica*, **5**, 162.
BUCKLEY, H. E., and VERNON, W. S., 1925, *Phil. Mag.*, **49**, 945.
GOLDSCHMIDT, V. M., 1926, *Geochemische Verteilungsgesetze*, VI (Oslo).
HODGMAN, C. D., WEAST, R. C., and SELBY, S. M., 1955, *Handbook of Chemistry and Physics* (Cleveland: Chemical Rubber Publishing Co.), 37th Edition, page 540.
KLEMM, W., 1928, *Z. Elektrochem.*, **34,** 525.
PALACHE, C., BERMAN, H., and FRONDEL, C., 1951, *Dana's System of Mineralogy* (London : Chapman and Hall), Vol. II, page 38.
SIMONS, J. H., 1950, *Fluorine Chemistry* (New York: Academic Press), Vol. I, page 35.

The Measurement of Surface Recombination Velocity on Silicon

BY A. H. BENNY AND F. D. MORTEN
Mullard Southampton Works, Millbrook, Southampton

MS. received 3rd July 1958, *and in final form* 16*th August* 1958

Abstract. The determination of the surface recombination velocity on a silicon filament by measurement of the spectral distribution of the photoconductivity is described. Results are presented indicating surface recombination velocities on etched surfaces of less than 75 cm sec^{-1} in dry oxygen, and greater than 7500 cm sec^{-1} in wet nitrogen. The measurements indicate that the surface recombination velocity may be a function of the carrier concentration at the surface.

§ 1. INTRODUCTION

A KNOWLEDGE of the surface recombination velocity s for excess minority carriers in semiconductors is of considerable importance. This quantity is measured on germanium by a number of methods, but little information on its value for silicon is available. In this note the measurement of s by the study of the spectral distribution of photoconductivity is considered, and some preliminary results on etched surfaces of n-type silicon are presented, which show values ranging from less than 75 cm sec^{-1} to greater than 7500 cm sec^{-1} under certain gaseous ambients.

§ 2. METHOD OF MEASUREMENT

When a photoconductor is illuminated, the change in conductance is governed by, amongst other factors, the bulk lifetime τ, the surface recombination velocity s, and the distribution in depth of the rate of carrier generation by the light. This may be altered by changing the wavelength, and hence the absorption coefficient, of the incident light.

The spectral response of a filamentary photoconductor, for constant photon intensity at all wavelengths, may be analysed qualitatively as follows. In the absence of surface recombination, the probability of recombination is the same throughout the filament, and the total excess carrier concentration and hence the photoconductivity is independent of where the carriers are generated. At short wavelengths, where the absorption coefficient is high, all the photons entering the specimen are absorbed. As the wavelength is increased the photoconductivity will remain constant until near the absorption edge when photons will begin to be transmitted and the photoconductivity will decrease.

In the presence of surface recombination the photoconductivity will in general be decreased. At short wavelengths the reciprocal absorption coefficient is less than the diffusion length for reasonable values of lifetime and the decrease will be greatest. As the wavelength is increased until the penetration depth is of the order of a diffusion length the number of carriers diffusing to and recombining at the surface will decrease. This will occur before an appreciable number of photons are transmitted if the specimen is thick compared with a diffusion length. The photoconductivity will rise with increasing wavelength until, as the absorption edge is approached, the photoconductivity will fall again.

By comparison of the observed spectral response of a silicon filament with theory the value of *s* may in principle be determined.

A somewhat similar method has been described by Harten and Schultz (1955) for measurements on germanium, and extended to silicon (Harten 1958). In this a diode with a thin base layer and a ring base contact is used. The free surface of the base region parallel to the junction is illuminated and the junction photo signal measured. This signal is related to the excess carrier concentration at the junction and varies qualitatively in the same manner as the bulk photoconductivity of a filament described above.

Bath and Cutler (1958) have recently described surface recombination measurements on silicon from the photoconductivity at two discrete wavelengths for one of which the penetration depth of the light is small and for the other large.

§ 3. THEORETICAL EXPRESSION

The change in conductance of a photoconductor upon illumination has been shown to be directly proportional to the total increase in carrier concentration N for small injection levels (Shockley 1950).

The quantity P proportional to N has been calculated by de Vore (1956), who obtained the expression

$$P=\frac{1}{\lambda^2-Z^2}\left\{\lambda^2(1-e^{-Z})-\frac{\xi\lambda Z(1+e^{-Z})+Z^2(1-e^{-Z})}{1+\xi\coth(Z/2)}\right\} \quad \ldots\ldots(1)$$

where

$$P=N/IA\tau$$

I = light flux entering the photoconductor (in photons $\mathrm{cm}^{-2}\,\mathrm{sec}^{-1}$), A = Area of illumination, τ = bulk lifetime of minority carriers, α = absorption coefficient of photoconductor at any wavelength, t = thickness of slab of photoconductor, D = diffusion constant of minority carriers, $L=\sqrt{(D\tau)}$ = diffusion length for minority carriers, $\lambda=t/L$, $\xi=sL/D$, $Z=\alpha t$.

The derivation of (1) assumes (i) illumination normal to the photoconductor surface, (ii) the photoconductor is large so that edge and end effects may be neglected, (iii) D, τ and s are constant, (iv) unit quantum efficiency, and (v) internal reflections are neglected. In the present measurements, only relative values of P are of importance, and (iv) may be replaced by the assumption of a constant quantum efficiency.

Expression (1) has been evaluated for several values of ξ, taking $\lambda=20$, and these are plotted in figure 1. These curves differ from those presented by de Vore in that they are not normalized at their peak value.

§ 4. EXPERIMENTAL ARRANGEMENTS

Measurements of photoconductivity were made on filaments cut from single-crystal silicon. The filaments were about 1 cm long, 3 mm wide and 2 mm thick. They were illuminated perpendicular to one of the largest faces, which were [111] crystal planes. The ends of the filaments were ground, nickel plated, soldered, masked with a lacquer to protect them during etching, and the device mounted in a small transparent-walled container in order to use various gaseous ambients. A steady electric field of a few volts per cm was maintained in the filament. The optical system used consisted of a Leiss double monochromator (Roberts 1952) with lithium fluoride prisms and an incandescent lamp as a source of light. In order to detect and amplify very small conductivity changes, the light was chopped at 800 c/s and the filament response fed through a matching transformer to an 800 c/s amplifier.

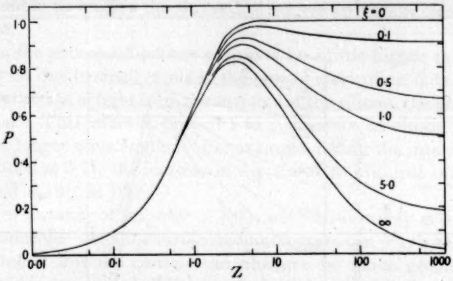

Figure 1. Relation between P and Z for various values of ξ.

§ 5. Results of Measurements

A number of silicon filaments have been examined. The general nature of results was similar for all. The results presented refer to an n-type bar, having resistivity of 5 Ωcm and minority carrier lifetime 20 μsec. For this material $\xi = s/750$ approximately. The relation between photon flux and signal from the filament was examined at three wavelengths. The linearity was excellent for light of wavelengths of 1·00 and 1·10 μ, the response being proportional to light intensity over ranges of 50 : 1 and greater. However, in some ambient conditions, the response was not linear at 0·85 μ. In view of this non-linearity, a constant photon intensity was used for obtaining spectral response curves. Photon intensities used were of the order of 4×10^{14} photons cm^{-2} sec^{-1}. Where non-linearity occurs, change in any background illumination will lead to a change in the response of the filament to a constant amplitude of chopped light. To avoid such effects, care was taken to minimize background illumination.

In order to compare figure 1 with experiment it is necessary to use optical absorption data. Further, the monochromator has a finite bandwidth, and this also affects the comparison of theoretical and experimental curves. A bandwidth varying from 40 to 60 mμ over the wavelength range used was the most useful compromise between light intensity and loss of resolution. A triangular band intensity distribution was assumed (Forsythe 1937).

Figure 2 (full lines) shows the functions of figure 1, with the ordinate plotted logarithmically, abscissa replotted against wavelength and with bandwidth correction applied. The photoresponse of a recently etched silicon filament was measured under three different ambient conditions: dry oxygen, wet oxygen and wet nitrogen. The response for dry oxygen was found to be constant within the limit of experimental error for wavelengths less than 1·02 μ, indicating that surface recombination had a negligible effect. The results for the three ambients (which were obtained consecutively under otherwise identical conditions) were all multiplied by the same numerical factor so that the curve for dry oxygen below $1{\cdot}02\,\mu$ fell on the theoretical curve for $s=0$. These normalized results are plotted in figure 2.

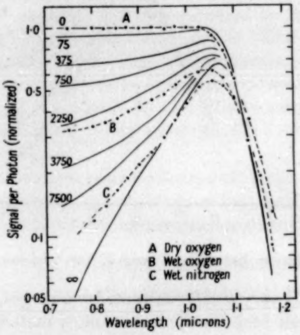

Figure 2. Observed spectral variation of photoconductivity (broken curves) compared with corrected theoretical curves for various values of s, marked in cm sec^{-1} (full lines).

The value $\lambda=20$ was used in calculating the curves of figures 1 and 2. These curves are only slowly dependent on changes in λ. As a result the theoretical curves of figure 2 may be used with but little error for cases where λ departs appreciably from 20. For the particular filament considered here, the value of λ was 18 ± 2.

The photoresponse at short wavelengths is dependent on the surface recombination velocity, and the magnitude of the response may be used to give a numerical value for s. Silicon filaments have been illuminated with light of a suitable short wavelength, such as $0{\cdot}75\,\mu$, and the photoresponse fed to a pen-recorder. The change of s with time, and the effect of various gaseous ambients may be studied by this means.

§ 6. DISCUSSION OF RESULTS

Considering figure 2, it is seen that there is good agreement between theoretical and experimental curves for wavelengths of less than $1{\cdot}0\,\mu$. The values of the surface recombination velocity may be determined from this region. It may be noted that values of $\xi = sL/D$ outside the limits of 10^{-1} and 10 are not obtainable with great accuracy by this method. The above limits for ξ correspond to $s=75$ cm sec^{-1} and $s=7500$ cm sec^{-1} for the filament considered. The form of the curve for dry oxygen has been taken as indicating that $\xi < 10^{-1}$, or $s < 75$ cm sec^{-1}. From figure 2, in wet oxygen $s=2500$–3000 cm sec^{-1}, and in wet nitrogen $s > 7500$ cm sec^{-1}.

Between 1·0 and $1{\cdot}1\mu$ the agreement between theoretical and experimental curves is not quite so good. However, there are considerable differences between the various sets of absorption data in the literature (Dash and Newman 1955, Fan, Shepherd and Spitzer 1956, Macfarlane and Roberts 1955), and in this wavelength range small differences in α have a marked effect on the shape of the calculated curves of figure 2. The measurements of Newman and Dash were used, as they cover the largest range of absorption coefficients. However, by taking values for the absorption between those of Newman and Dash, and Fan, Shepherd and Spitzer it is possible to modify the theoretical curves to obtain close agreement with experiment.

Beyond $1 \cdot 1\ \mu$ the photoconductivity is seen to be a little higher than expected. This may partly be due to small errors in the optical absorption data. However, due to internal reflection of light from the surfaces of the silicon, the photoresponse will be increased. This effect is expected to commence at about $1 \cdot 1\ \mu$ and to become larger at longer wavelengths. For example, taking the internal reflection coefficient of silicon as $0 \cdot 31$, the increase in signal due to multiple internal reflections is calculated as 38% at $1 \cdot 15\ \mu$.

Occurrence of linearity of response at $1 \cdot 0\ \mu$ and non-linearity at $0 \cdot 85\ \mu$ may be shown to be reasonable. At $1 \cdot 0\ \mu$ surface recombination can play a negligible role. The concentration of injected carriers can nowhere be much greater than $I\tau/t$, the value expected for zero s and all light uniformly absorbed. For the maximum light intensity used in the linearity investigations an injected carrier concentration of 10^{12} cm^{-3} is given, which is much less than the equilibrium majority carrier concentration of 10^{15} cm^{-3}. No non-linearity would therefore be expected under these conditions.

At $0 \cdot 85\ \mu$ the maximum injected carrier concentration will not be greater than $I\tau/L$† which is approximately 10^{13} cm^{-3}. This is still much less than the equilibrium carrier concentration, and it is therefore not expected that the bulk lifetime will change with light intensity. This leads one to the conclusion that the surface recombination can be affected by changes in light intensity at much lower levels than the bulk lifetime. The non-linearity indicates that s increases with increasing injection. This is in qualitative agreement with the results of Bath and Cutler (1958), who observed, above a certain injection level, that s is proportional to the excess carrier concentration at the surface.

§ 7. CONCLUSION

It is shown that the measurement of spectral distribution of photoconductivity may, under certain conditions, enable an estimate to be made of the surface recombination velocity of a silicon filament. The most sensitive conditions are when sL/D is of the order of unity, when this quantity may be determined to better than ±20%. Close agreement between theory and experiment is dependent on accurate values for the absorption coefficient of silicon at various wavelengths, but this does not seriously affect the values of s obtained. The surface recombination appears to be a function of injection level at concentrations small compared with the majority carrier concentration. It is found that the surface recombination may be varied over a wide range, from less than 75 cm sec^{-1} to greater than 7500 cm sec^{-1}, by change of the gaseous ambient.

ACKNOWLEDGMENTS

The authors wish to thank the Directors of Mullard Ltd. for permission to publish this article. We also wish to thank Dr. M. Smollett and Dr. G. K. Eaton for helpful discussions, and Miss B. E. Marcham who made some preliminary measurements.

---

† This is found by putting s equal to zero and absorption coefficient large and evaluating de Vore's expression for excess carrier concentration at the surface.

REFERENCES

BATH, H. M., and **CUTLER**, M., 1958, *J. Phys. Chem. Solids*, **5**, 171.

DASH, W. C., and **NEWMAN**, R., 1955, *Phys. Rev.*, **99**, 1151.

FAN, H. Y., **SHEPHERD**, M. L., and **SPITZER**, W., 1956, *Photoconductivity Conference, Atlantic City* (New York : Wiley), p. 184.

FORSYTHE, W. E., 1937, *The Measurement of Radiant Energy* (London : McGraw-Hill Book Co.).

HARTEN, H. U., 1958, *Philips Res. Rep.*, in the press.

HARTEN, H. U., and **SCHULTZ**, W., 1955, *Z. Phys.*, **141**, 319.

MACFARLANE, G. G., and **ROBERTS**, V., 1955, *Phys Rev.*, **98**, 1865.

ROBERTS, V., 1952, *J. Sci. Instrum.*, **29**, 134.

SHOCKLEY, W., 1950, *Electrons and Holes in Semiconductors* (New York: van Nostrand), p. 76.

DE VORE, H. B., 1956, *Phys. Rev.*, **102**, 86.

The Change of Spontaneous Magnetization with Hydrostatic Pressure

By D. GUGAN†
Department of Physics, Queen Mary College, University of London

Communicated by G. O. Jones; MS. received 7th May 1958 *and in revised form 29th July* 1958

Abstract. Measurements have been made of the effect of pressure on the spontaneous magnetization of nickel, cobalt, and a series of nickel alloys. The measurements were made using a thin-disc permeameter designed to produce high magnetic fields for only a very small power consumption. The results are in good general agreement with the results of other hydrostatic pressure experiments and with the results of experiments on the thermodynamically related 'forced' volume magnetostriction. An adequate verification of the important thermodynamic relation $(\partial V/\partial H)_{p,T} = -(\partial M/\partial p)_{H,T}$ has been obtained for the nickel–iron alloy system. The results do not agree with the anomalous results reported by Stacey who used Bridgman's thin-disc technique of generating high pressures. Under some conditions nickel shows an anomalously large, linear, decrease of spontaneous magnetization with pressure; possible reasons for this are discussed.

---

§ 1. INTRODUCTION

THE effect of pressure on the spontaneous magnetization of ferromagnetics is of great interest because two of the quantities defining the spontaneous magnetization at a given temperature (the saturation moment M_0 and the Curie temperature θ) are, in principle at least, particularly revealing functions of volume. The change of M_0 with pressure gives very direct information on the change of energy-band structure with pressure, information which should be of great assistance in understanding many of the magnetic and electrical properties of metals, and the change of θ with pressure gives direct information on the behaviour of the Heisenberg exchange energy as a function of interatomic distance. For given M_0 and θ the shape of the spontaneous magnetization curve is defined by a parameter which depends on the particular model of ferromagnetism which is being considered. This parameter also must be considered as a function of pressure. Several theoretical treatments have been given of the pressure effects; the most general of them are based on the thermodynamic relation relating the change of magnetic moment with pressure to the volume magnetostriction,

$$\left(\frac{\partial V}{\partial H}\right)_{p,T} = -\left(\frac{\partial M}{\partial p}\right)_{H,T} \qquad \ldots\ldots(1)$$

or, in terms of the intensity of magnetization I and the compressibility β,

$$\frac{1}{V}\left(\frac{\partial V}{\partial H}\right)_{p,T} = I\left[-\frac{1}{I}\left(\frac{\partial I}{\partial p}\right)_{H,T} + \beta\right]. \qquad \ldots\ldots(2)$$

This formula applies to isothermal, reversible changes at any magnetization, but, from the nature of magnetization curves, it is clear that it is most useful in the region of technical saturation. In this region we compare the pressure dependence of the spontaneous magnetization and the 'forced' volume magnetostriction †. For detailed theories of the pressure effects, more specific models of ferromagnetics must be considered; such theories are reviewed by Lee (1955) and by Gugan (1956).

---

† Now a Postdoctorate Fellow, National Research Laboratories, Ottawa, Canada.

At room temperatures all the possible magnetic changes make their contribution and it is difficult to discover the fundamental processes occurring; for this reason the most revealing experiments are those made either at the Curie temperature (Byelov 1949, Patrick 1954), or near to the absolute zero (Galperin, Larin and Shishkov 1953). These temperature regions are not convenient to work in experimentally however, and most of the existing experimental work is at room temperature. Low-field measurements of (B, H) curves under hydrostatic pressures have been made by Yeh (1925) and Steinberger (1933). Their results give little information on the change of spontaneous magnetization with pressure because for this it is necessary to work in the region of technical saturation and to use sensitive magnetic techniques to detect the very small changes which occur. Measurements in the saturation region have been made by Ebert and Kussmann (1937, 1938), and by von Klitzing and Gielessen (1956). Recent work by Jones and Stacey (1953) and Stacey (1956) using Bridgman's thin-disc method of generating high, quasi-hydrostatic pressures allows a future extension of the pressure range to about 100 000 atmospheres; unfortunately their results in the 10 000 atmosphere region are quite different from the results of experiments using true hydrostatic pressures.

Despite the difficulty in fundamental interpretation that has already been mentioned, the present work was performed at room temperature because there are still a number of discrepancies between the earlier experiments in the 10 000 atmosphere region. First, the results of Stacey are completely different from those of the other authors cited and it is important to discover the reason for this; second, the basic thermodynamic relation (1) can be given a thorough test for the diverse system of nickel–iron alloys (see, for instance, Bozorth 1951) and there are at present quite large discrepancies between the two sets of measurements.

§ 2. Experimental Methods

Some preliminary measurements were made on ring-shaped specimens with the objects of testing the apparatus and of obtaining more information on the behaviour of ferromagnetics in low fields. From these measurements it proved possible in certain cases to obtain information on the effect of pressure on the spontaneous magnetization; for a more thorough study of the pressure coefficients of spontaneous magnetization a permeameter was built which enabled measurements to be made in the regions of technical saturation of several substances.

2.1. *Apparatus*

The high-pressure apparatus was of a conventional design such as is adequately described by Newitt (1940) and by Bridgman (1949 a). The maximum pressure used in the experiments was about 5000 atm and the calculated values of the high pressure are accurate to about ± 2%. The all-steel construction of the high-pressure apparatus made it important to allow for possible magnetic interactions with the specimens in the working space. The design of the apparatus rendered these always small and reproducible, and tests were made to ensure that in no case was the final result of an experiment dependent on an interaction of this sort, or on any direct electrical coupling between the circuits.

---

† The 'forced' volume magnetostriction is the linear change of volume with field which is always found in ferromagnetics in high enough fields; see Lee (1955) for further details.

The magnetic measurements were all essentially of normal (B, H) curves obtained by a modification of the familiar ring-ballistic method of magnetic testing. The modification was to reverse simultaneously *two* accurately monitored primary currents, one to the specimen and the other to the primary of a Campbell variable mutual inductor; the resulting e.m.f's in the two secondary windings were fed in series-opposition to a sensitive, long-period, low resistance galvanometer (Tinsley type 4789) which thus acted as a fluxmeter. The method is ideally a null one with balance quickly obtained by adjustment of the mutual inductor. The lag of the e.m.f. from the specimen behind that from the inductor causes the galvanometer to give a small 'double kick', the sudden initial movement due to the inductor e.m.f. being followed by a more leisurely movement in the opposite direction caused by the specimen e.m.f. The balance is indicated when the *net* deflection of the galvanometer is zero and with practice it was possible in some cases to obtain balance settings reproducible to 2 parts in 10^5. This was as high as the short term stability of the apparatus (the stability over a period of a few hours). The absolute accuracy of measurements is of course much less than the short term stability of the apparatus and is probably only about 1 in 10^3, but by designing the experiments so that only the short term stability of the apparatus was involved in the pressure measurements, these were made with the full sensitivity of the apparatus. Provision was made for demagnetizing the specimens by using an alternating current which could be slowly reduced to values much smaller than the lowest magnetizing current.

2.2. *Low-Field Measurements*

The low-field measurements were made on small, ring-shaped specimens. These were wound with a single-layer, low-resistance secondary winding next to the insulated specimen surface, and with a multilayer primary winding wound as evenly as possible on top of this. The small size of the rings† enabled magnetizing fields of about 100 Oe to be obtained before the heat dissipation in the primary winding became excessive. The correction to the measured values of magnetization to allow for heating was quite small and was estimated from calibration experiments. The values of H, B and I were calculated in the usual way, see for instance Astbury (1952).

2.3. *High-Field Measurements*

Measurements at high magnetic fields are not possible on ring-shaped specimens, and an adaptation of the thin-disc permeameter described by Stacey (1956) was used for measurements in the technical saturation region of most of the specimens studied. Equivalent magnetic and electrical circuits of this permeameter are shown in figure 1. In this magnetic circuit nearly all the flux

† The largest ring used had dimensions o.d. 13 mm, i.d. 10 mm, length 5 mm.

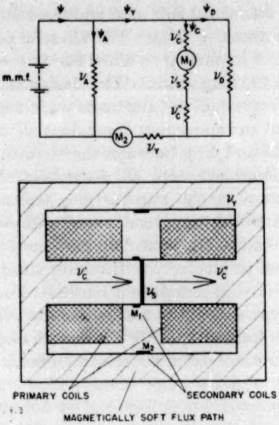

Figure 1. Equivalent magnetic and electrical circuits of the thin-disc permeameter.

through the permeameter yoke ψ_Y is forced through the thin-disc specimen of reluctance ν_S; when the permeameter reluctance is low, and when the specimen has an appreciably lower saturation magnetization than the material of the permeameter, most of the available magnetomotive force is concentrated across the specimen and quite high fields may be effective on it. An analysis of the equivalent electrical circuit (see the Appendix) shows that it is possible to construct (I, H) curves for the specimen from measurements of the flux linked with the two secondary coils, M_1 and M_2. Specimen permeabilities, μ, are given in terms of the specimen thickness, t, the measured quantity T ($T = R - R_0$; R and R_0 are the values of M_2/M_1 with and without the specimen in the magnetic circuit) and two constants A and θ which are determined from calibration experiments:

$$\frac{t}{\mu} = \frac{AT}{1-\theta T}. \qquad \ldots\ldots (3)$$

Corresponding values of the field H and the intensity of magnetization I can thus be directly calculated from the known values of μ and the induction B:

$$B = \frac{M_1 i_M}{A' N_2} \times 10^8 \text{ gauss}. \qquad \ldots\ldots (4)$$

The chief errors in (3) arise first, from uncertainty in the measured value of t, and second, from the possible occurrence of a very thin air gap between the specimen and the permeameter poles. A consideration of the quantity $(dI/dB)_{\text{obs}}$ shows that these errors have the effect of giving this quantity a finite limiting value (positive or negative) instead of the zero value expected at this order of accuracy. It was shown by Stacey (1956) that the departure from zero of the coefficient $(dI/dB)_{\text{obs}}$ gives a method of correcting any errors in the value of t inserted in equation (3). Applying this correction proves to have negligible effect on values of the pressure coefficient of magnetization.

The construction of the permeameter is shown in figure 2. The body of the permeameter was made of magnetically soft mild steel and it fitted closely inside the high pressure vessel. The permeameter was mounted rigidly on a multi-lead electrode head so that the whole device could easily be removed for changing specimens. The primary coils were wound with a total of 1634 turns of 30 s.w.g. 'Lewmex' coated copper wire which enabled a maximum induction of about 15 000 gauss to be established through the specimen at a current of 0·36 A and a dissipation of about 1·5 W. The specimens were punched exactly to size from thin foils of the material to be studied and were measured either in that condition or after annealing at 1100°C in hydrogen followed by slow cooling. The specimens were inserted through the windows shown in figure 2 and were clamped in position by the movable pole-piece. Careful alignment of the specimen between the

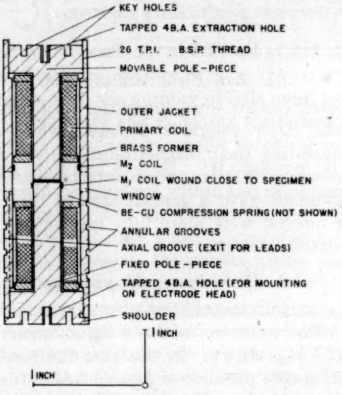
KEY HOLES
TAPPED 4B.A. EXTRACTION HOLE
26 T.P.I. B.S.P. THREAD
MOVABLE POLE-PIECE
OUTER JACKET
PRIMARY COIL
BRASS FORMER
M_2 COIL
M_1 COIL WOUND CLOSE TO SPECIMEN
WINDOW
BE-CU COMPRESSION SPRING (NOT SHOWN)
ANNULAR GROOVES
AXIAL GROOVE (EXIT FOR LEADS)
FIXED POLE-PIECE
TAPPED 4B.A. HOLE (FOR MOUNTING ON ELECTRODE HEAD)
SHOULDER
1 INCH
1 INCH

Figure 2. Constructional diagram of the thin-disc permeameter.

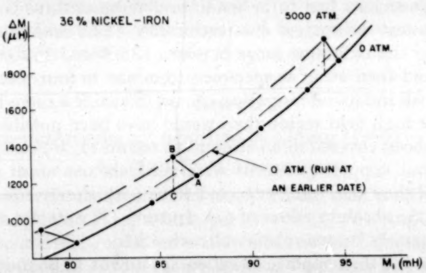

Figure 3. Typical example of the form of the permeameter results. The 0 atm curve is obtained from a constant pressure run and the 5000 atm curve is constructed from the results of several constant current runs between 0 and 5000 atm (A, B etc.). A 0 atm curve obtained from a different assembly of the apparatus is also shown.

lapped pole faces and careful cleaning of the specimen and the poles reduced the possible variations in the clamping conditions. These variations are very serious in principle because different clamping pressures can alter the magnetic reluctance of the circuit and thus T in equation (3). Experiment showed, however, that the variations were quite small (see figure 3 for example) and of such a sort that, although the calculated (I, H) curves might vary by several per cent, the pressure coefficients were not significantly affected.

§ 3. EXPERIMENTAL PROCEDURE

3.1. *Low-Field Measurements*

The low-field measurements were straightforward measurements of normal magnetization curves. After complete demagnetization the specimens were first examined by measuring their magnetization curves at constant pressures, usually 0 and approximately 5000 atm and in some cases at intermediate pressures also. These measurements gave a general idea of the changes taking place; regions of particular interest were more fully investigated by measurements at constant field and variable pressure.

3.2. *Permeameter Measurements*

The permeameter measurements were also of normal magnetization curves except that for each primary current used two inductometer balances were made, for M_1 and for $\Delta M(=M_2-M_1)$.† In this case the results were obtained by making measurements at zero pressure of M_1 and ΔM as functions of the primary current, and then, at a series of constant values of the primary current, by measuring both M_1 and ΔM as functions of pressure up to 5000 atm. In this way ΔM was obtained as a function of M_1 at fixed pressure, see figure 3 for examples. Only the two isobars at 0 and 5000 atm were calculated from the measured results because in no case was there any suggestion that the change of ΔM at constant M_1 (which is the important thing here) was not linear with pressure.

Knowing corresponding values of M_1 and ΔM, it is only necessary to know the constants A and θ in (3) in order to be able to calculate (I, H) curves as functions of pressure. A and θ vary with M_1 and with pressure so that very full calibration experiments had to be made to determine these constants and also, incidentally, to test the aptness of equation (3). The calibration measurements were made over the induction range between 12 500 and 15 200 gauss, first using no specimen and then using as specimen from one to four pieces of copper foil. This rather small induction range was chosen to enable a more intensive study to be made in the high field region than would have been possible had a wider induction range been covered in an attempt to record (I, H) curves starting at low fields. The four copper specimens were cut from one small piece of 0·001 in. copper foil and they were thus expected to be very closely equal in thickness so that, although the absolute values of t in equation (3) were not accurately known, they were accurately known relative to each other.

Assuming μ for the copper calibration specimens to be unity and unaffected by pressure within the sensitivity of this experiment (see Jones and Stacey 1953) we see how, after allowing for the changes of specimen dimensions with pressure, the results of the calibration experiments enable us to calculate at a series of fixed values of M_1 (or B) the constants A and θ at both 0 and 5000 atm. If n_a and n_b are the number of pieces of foil of thickness t used as calibration specimens, and if T_a and T_b are the corresponding values of T at fixed M_1, A and θ at this value of M_1 are given by

---

† The two secondary coils had an equal number of turns and could be connected in series-opposition into the galvanometer circuit; ΔM was thus directly measurable.

$$A = t\left(\frac{n_a n_b}{n_b - n_a}\right)\left(\frac{1}{T_a} - \frac{1}{T_b}\right); \quad \theta = \frac{1}{n_b - n_a}\left(\frac{n_b}{T_b} - \frac{n_a}{T_a}\right). \quad \ldots\ldots(5)$$

The use of four calibration specimens enables six values of each constant to be calculated at each fixed value of M_1, but because the error in the determination of the constants increases with the number of foils used, values of A and θ were calculated using n_a always unity and n_b taking the values two, three and four. The three pairs of values of n_a and n_b enable three values to be found for the functional dependence of A and θ on M_1. If equation (3) were exactly obeyed the three functions would be identical within the experimental error. In fact the functions differed slightly, but the differences were less than the absolute error in the measurements and these small discrepancies do not affect the conclusion that equation (3) represents the results within the experimental error. The values of A_0 and θ_0 at zero pressure were the smoothed, averaged values of the constants directly determined; the values at 5000 atm, A_{5000} and θ_{5000}, were found by adding to A_0 and θ_0 the smoothed, averaged differences between corresponding values of the constants at the two pressures. This process is necessary in order to obtain as accurately as possible the change of the constants with pressure; this change is known considerably more accurately than the absolute values of the constants and would be obscured by averaging separately the constants at the two pressures, e.g. at $B = 14\,200$ gauss, $A_0 = 149{\cdot}5 \pm 0{\cdot}5 \times 10^{-3}$ cm, while $A_{5000} - A_0 = 1{\cdot}8 \pm 0{\cdot}1 \times 10^{-3}$ cm.

Having calculated the constants one can easily calculate the (I, H) curves for each specimen at both 0 and 5000 atm and thus deduce the change of I with pressure from the magnetization curves in the region of technical saturation. Where adequately high fields were achieved the limiting slope of the (I, B) curves enabled the corrections for errors in the specimen thickness to be applied. This proved possible only in the case of nickel and the copper–nickel alloy where it appeared that the measured value of t was a few per cent in error.

The specimen thicknesses were measured by producing wedge fringes in mercury green light between two partly silvered optical flats.

§ 4. RESULTS

Detailed numerical results are tabulated by Gugan (1956).

4.1. *Low-Field Measurements*

Measurements were made on solid rings of both cold worked and annealed commerical nickel (Henry Wiggin Ltd., purity ~98%), on a ring spiral of H.C.R. alloy, a grain-oriented 48% nickel–iron alloy made by the Telegraph Construction and Maintenance Co. Ltd., and on a ring spiral of Permalloy F, a domain-oriented 64% nickel–iron alloy made by Standard Telephones and Cables Ltd. Only the results that give information about the change of spontaneous magnetization with pressure are presented here. Some of the specifically low field results are described by Gugan and Rowlands (1958). The pressure coefficients in high fields tended to the values, +0·05%/1000 atm for nickel; −0·13 ± 0·02%/1000 atm for H.C.R. alloy; +0·01 ± 0·02%/1000 atm for Permalloy F. These values must be quite close to the values of $(1/I_s)dI_s/dp$.

4.2. *High-Field Measurements in the Permeameter*

(*a*) *Rolled nickel* (Johnson, Matthey and Co. Ltd., spectrographically pure nickel, ~0·001% metallic impurity). These specimens were punched from foil supplied by the manufacturers and were not further treated. Two specimens, of thicknesses 0·005 and 0·003 in., were studied and both gave the same result, $(1/I_s)dI_s/dp = -0{\cdot}31 \pm 0{\cdot}04\%/1000$ atm (see figure 4 (*a*)). The absolute values of the saturation magnetization of the two specimens differ somewhat but this is to be expected in this method of measurement and it is much less significant than the similarity of the two pressure coefficients. This change is a factor of *ten* larger than has been found in either the direct high pressure measurements already cited or in the somewhat divergent experimental results for the volume magnetostriction in nickel (see Snoek (1937), Azumi and Goldman (1954)); it is of opposite sign to the anomalous result reported by Stacey (1956) and is, moreover, of quite different character.

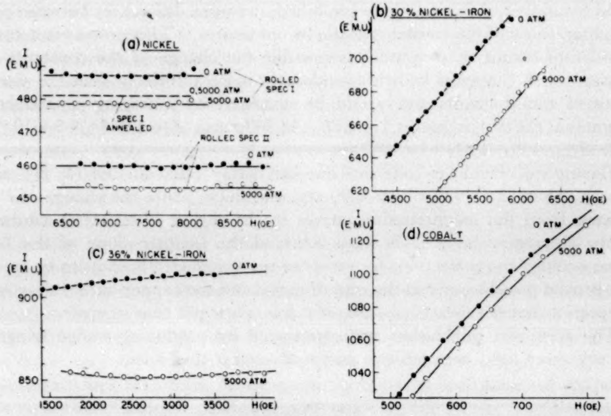

Figure 4. Typical magnetization curves calculated from the permeameter measurements. (*a*) Nickel. Specimen I, $t = 0{\cdot}005$ in.; specimen II, $t = 0{\cdot}003$ in. Note the change in behaviour after annealing specimen I. (*b*) 30% nickel–iron. (*c*) 36% nickel–iron. (*d*) Cobalt.

(*b*) *Annealed nickel*. This was the 0·005 in. specimen used above but remeasured after prolonged annealing in hydrogen at 1100°c followed by slow cooling. The two magnetization curves now coincide to give a pressure coefficient of spontaneous magnetization of 0·00 ± 0·04%/1000 atm, in good agreement with other hydrostatic pressure measurements and also with the volume magnetostriction measurements.

(*c*) 11·2 *atomic % copper–nickel.* Between 8000 and 10 400 Oe the value of I_s at zero pressure was 355 ± 1 e.m.u. and the pressure coefficient of spontaneous magnetization was −0·04 ± 0·03%/1000 atm. This, again, is quite different from Stacey's result but is consistent with the measurements of Ebert and Kussmann (1937) on alloys of higher copper concentration.

(*d*) 30% *nickel–iron* (R. 2799 alloy, Telegraph Construction and Maintenance Co. Ltd.). The specimen was very hard magnetically and the maximum magnetization obtained was only about 60% of the saturation magnetization, see figure 4 (*b*). The pressure coefficient of spontaneous magnetization cannot be found accurately from these results but, because the two isobars are closely parallel, the quantity $dI/dp = -11$ e.m.u./1000 atm may plausibly be identified with the change of spontaneous magnetization with pressure.

(*e*) 36% *nickel–iron* (commercial alloy, Nilo 36). This specimen shows a high degree of saturation, see figure 4 (*c*), and the pressure coefficient of spontaneous magnetization, −1·30 ± 0·05%/1000 atm, agrees excellently with other work.

(*f*) 48% *nickel–iron* (H.C.R. alloy, Telegraph Construction and Maintenance Co. Ltd.). The magnetization curves for this alloy extended close to technical saturation, and the value of the pressure coefficient, −0·14 ± 0·03%/1000 atm, is in excellent agreement with the result of the low-field measurements on this alloy.

(*g*) 50% *nickel–iron* (commercial alloy, Nilo 50). This alloy behaved like the preceding one and had a pressure coefficient of spontaneous magnetization of −0·08 ± 0·03%/1000 atm.

(*h*) *Cobalt* (Johnson, Matthey and Co. Ltd., spectrographically pure cobalt, ~0·001% metallic impurity). Cobalt is not a very suitable material for study in this apparatus because it has too high a spontaneous magnetization to enable very high fields to be effective across it. Nevertheless, the magnetization attained some 80% of its saturation value, see figure 4 (*d*), and these high pressure experiments extend considerably nearer saturation than any others previously reported. The pressure coefficient of magnetization was not constant even at the highest fields; it was about −0·08%/1000 atm at the highest field and appears to be tending to a smaller negative value or even to a small positive one. The only other indication of the size of the effect is from Kornetzki's volume magnetostriction measurements (1934) which indicate a value of about +0·02%/1000 atm.

§ 5. Discussion

Because of the difficulties in separating the processes occurring, no attempt has been made here to give a fundamental interpretation of the phenomena in terms of pressure induced changes in the quantities defined in the introduction. Instead, the present measurements are correlated, using equation (2), with measurements of the forced volume magnetostriction.

Apart from the result for rolled nickel which is discussed later, all the results agree fairly well with other work. For the nickel–iron alloys in particular, a detailed comparison of these results with those of other workers is possible and in figure 5 the measured values of the pressure coefficient have been compared with values of the forced volume magnetostriction. The previous measurements of the two effects are in fair agreement but have two regions of discrepancy, between 25 and 30% nickel, and between 40 and 80% nickel. The first of these

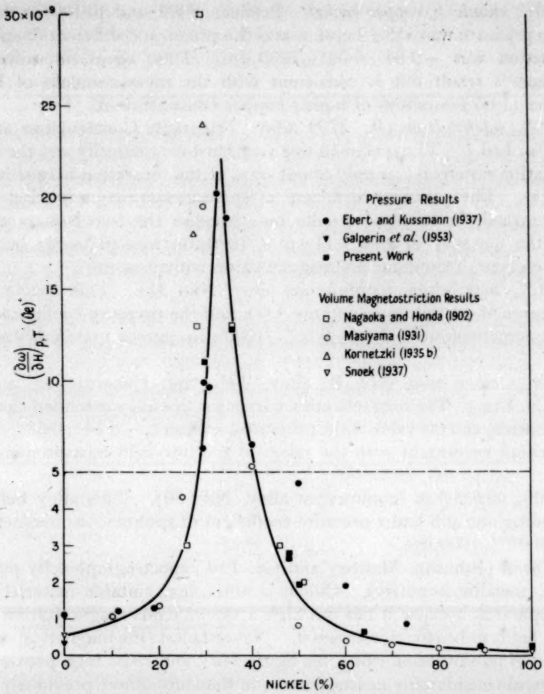

Figure 5. Nickel–iron alloys. Verification of the thermodynamic relation $(\partial V/\partial H)_{p,T} = -(\partial M/\partial p)_{H,T}$ for changes of spontaneous magnetization with pressure and the 'forced' volume magnetostriction. The heavy line is the most reliable line through these results (see text).

appears to be due to the rather low fields used in the volume magnetostriction work. These alloys are so hard magnetically that fields of the order 10 000 Oe are needed to reach technical saturation, and Ebert and Kussmann (1937) have shown that for these alloys fields of this order are needed in order to find the pressure coefficient of *spontaneous* magnetization. Also, Byelov (1950) has shown that there is quite a strong field dependence of the apparent 'forced' volume magnetostriction for alloys in this composition range. The present measurement on the 30% nickel alloy was at fields intermediate between those used in the existing magnetostriction and high pressure experiments, and the present result lies between the results found from these two sorts of experiments; it is, however, considerably nearer the previous pressure measurements and would probably coincide with them if higher fields had been available. The second region of discrepancy cannot be explained in this way and we must look for possible errors in previous experimental work. The present measurements again lie between the extremes of the previous work, but nearer to the results of the volume magnetostriction experiments in this case. The results are in excellent agreement with the results of Nagaoka and Honda (1902) although these do not agree very well with the later measurements of Masiyama (1931). The high-pressure experiments of Ebert and Kussmann seem for some reason to have given unduly large results in this region; if we ignore their results the discrepancy between the pressure and the volume magnetostriction measurements is reduced to about the size of the experimental errors. A possible source of error in Ebert and Kussmann's results is that their pressure coefficients were found by comparing the magnetizations of nominally similar specimens one of which was subjected to about 3000 atm pressure while the other was at atmospheric pressure. In the alloy region under discussion there is a well known order–disorder transition and it may be that the large effects found by Ebert and Kussmann arose because their specimens were not truly representative.

The present results for the 48% and 50% nickel–iron alloys are consistent with the assumption that we have been able to measure their pressure coefficient of spontaneous magnetization. There is certainly the possibility that the coefficients are slightly too *large* (because of inadequate saturation of the specimens) but it is doubtful whether this could reduce the corresponding values of the volume magnetostriction by more than about $0{\cdot}5 \times 10^{-9}\,\mathrm{Oe}^{-1}$. The good agreement of the results obtained by the two methods for the 48% nickel–iron alloy justifies the inclusion in figure 5 of the low field results for the two nickel–iron alloys.

The heavy line drawn in figure 5 is considered to be the line which best gives the volume magnetostriction corresponding to the variation of the spontaneous magnetization with pressure. The agreement with it of both the present pressure measurements and the existing volume magnetostriction measurements (apart from those in the 30% nickel region) provides a very satisfactory test of the thermodynamic relation (1).

The agreement between this research and existing work suggests very strongly that the thin-disc permeameter is a reliable device for measuring these pressure coefficients; thus the anomalous result for rolled nickel cannot be ascribed to the inadequacy of the apparatus. Similar results were obtained from two different specimens of spectrographically pure rolled nickel (which had, however, been subjected to the same manufacturing process) and the results are definite enough to rule out the possibility of experimental error. These results were amongst the first taken when it had not been expected that the mechanical condition could affect the high-field results. Usually this is true (cf. the other results of this research, and also the volume magnetostriction results of Snoek (1937) and of Kornetzki (1934, 1935 a)), but because the result became quite normal when one of the rolled nickel specimens was annealed and remeasured, it is evident that the mechanical condition of the specimens is *directly* responsible for this anomalous result. Rolling, apparently, is not in itself responsible for this behaviour because the 11·2 atomic % copper–nickel alloy which was rolled in the laboratory and which was used as a check on the results for nickel, proved to be quite normal. The result could be explained by an enormous increase in magnetocrystalline anisotropy of the material at high pressures but this seems unlikely because the two magnetization curves are closely parallel. It is possible that under the particular stress patterns in these specimens there is a tendency, augmented by pressure, to transform to a less magnetic form of nickel (body-centred cubic and hexagonal forms are known to exist under certain conditions, see LeClerc and Michel (1939), Finch *et al.* (1955)) but this does not seem likely in the bulk material. No other reason is known for this strange behaviour of rolled nickel but it is interesting to note that nickel behaves unexpectedly in several other ways at high pressures. Bridgman (1949 b, 1951) has found unexplained anomalies at about 10 000 atm in the electrical resistance and in the compressibility of nickel, the anomalies being similar to those associated with phase or electronic transitions.

The results of this research are in good general agreement with other related measurements and they are therefore quite in disagreement with the thin-disc measurements of Stacey (1956). It appears that the magnetic method he used is not fundamentally at fault, but that the method of generating high pressures, suitable where the compression far exceeds the yield point of the specimen (as in the experiments of Bridgman (1952), Chester and Jones (1953)), is not suitable when the yield point lies in the middle of the pressure range being examined; it is a notable feature of Stacey's results that there is an abrupt change in the character of the pressure effect in the region of the yield point of his specimens, about 2500 atm for nickel and the nickel alloys he investigated. According to von Klitzing and Gielessen (1956) there is no evidence that (apart from the volume effect) the spontaneous magnetization of nickel is changed by uniaxial compression. We cannot, therefore, ascribe Stacey's results to this but we must suppose either that the particular stress distribution in his specimens was responsible for the large increases of magnetization with compression that he found for all his saturated specimens† or that there was some undetected source of systematic error in his apparatus.

§ 6. CONCLUSIONS

The measurements of the change of spontaneous magnetization with hydrostatic pressure agree well with earlier work and so justify the theory of the thin-disc permeameter. The results remove an anomaly in the pressure measurements in the nickel–iron alloy system and the thermodynamic relation (1) has now been adequately tested for a series of alloys showing an extreme range of magnetic properties.

The results obtained by Stacey using the thin-disc technique of producing high pressures have not been confirmed and some possible reasons for this have been examined although no firm conclusion is possible. The anomalous results obtained on rolled nickel specimens, as well as the results of other authors on nickel, suggest that further work may reveal a high-pressure transition in nickel.

ACKNOWLEDGMENTS

I wish to thank Professor G. O. Jones for help and encouragement during this work which was originally suggested by him. I wish to thank Drs. J. S. Dugdale and J. W. Leech for their comments on this paper, and Dr. N. Kurti for his criticisms of an early version of this paper. I wish also to thank the

---

† Stacey's 36% nickel–iron alloy did not show this increase directly but the decrease he found was much less than is given by the results of figure 5, i.e. in this case also he obtained, *relatively*, an increase of magnetization with compression.

Department of Scientific and Industrial Research for the award of a maintenance allowance, the Central Research Fund of the University of London for the loan of apparatus, and Mr. W. A. G. Baldock of the Departmental workshop for skilful constructional work.

REFERENCES

ASTBURY, N. F., 1952, *Industrial Magnetic Testing* (London : Institute of Physics).
AZUMI, K., and GOLDMAN, J. E., 1954, *Phys. Rev.*, **93,** 630.
BOZORTH, R. M., 1951, *Ferromagnetism* (New York : van Nostrand).
BRIDGMAN, P. W., 1949 a, *The Physics of High Pressure*, 2nd Edn (London : Bell); 1949 b, *Proc. Amer. Acad. Arts Sci.*, **77,** 189; 1951, *Ibid.*, **79,** 149; 1952, *Large Plastic Flow and Fracture* (New York : McGraw-Hill).
BYELOV, K. P., 1949, *Zhurn. Eksp. Teor. Fiz.*, **19,** 346; 1950, *Ibid.*, **20,** 54.
CHESTER, P. F., and JONES, G. O., 1953, *Phil. Mag.*, **44,** 1281.
EBERT, H. and KUSSMANN, A., 1937, *Phys. Zeit.*, **38,** 437; 1938, *Ibid.*, **39,** 598.
FINCH, G. I., SINHA, K. P., and GOSWAMI, A., 1955, *J. Appl. Phys.*, **26,** 250.
GALPERIN, F. M., LARIN, S., and SHISHKOV, A., 1953, *Dok. Akad. Nauk S.S.S.R.*, **89,** 419.
GUGAN, D., 1956, *Ph.D. Thesis*, University of London.
GUGAN, D., and ROWLANDS, G., 1958, *Proc. Phys. Soc.*, **72,** 207.
JONES, G. O., and STACEY, F. D., 1953, *Proc. Phys. Soc. B.*, **66,** 255.
VON KLITZING, K. H., and GIELESSEN, J., 1956, *Z. Phys.*, **146,** 59.
KORNETZKI, M., 1934, *Z. Phys.*, **87,** 560; 1935 a, *Ibid.*, **97,** 662; 1935 b. *Ibid.*, **98,** 289.
LECLERC, W., and MICHEL, A., 1939, *C.R. Acad. Sci., Paris*, **208,** 1583.
LEE, E. W., 1955, *Rep. Progr. Phys.*, **18,** 184 (London : Physical Society).
MASIYAMA, Y., 1931, *Sci. Rep. Tôhoku Univ.*, **20,** 574.
NAGAOKA, H., and HONDA, K., 1902, *Phil. Mag.*, **4,** 45.
NEWITT, D. M., 1940, *Design of High Pressure Plant* (Oxford: University Press).
PATRICK, L., 1954, *Phys. Rev.*, **93,** 384.
SNOEK, J. L., 1937, *Physica*, **4,** 853.
STACEY, F. D., 1953, *Ph.D. Thesis*, University of London; 1956, *Canad. J. Phys.*, **34,** 304.
STEINBERGER, R. L., 1933, *Physics*, **4,** 153.
YEH, C. S., 1925, *Proc. Amer. Acad. Arts Sci.*, **60,** 503.

APPENDIX

Following closely Stacey's original argument (1953) we give here an analysis of the thin-disc permeameter.

In the equivalent electrical circuit of figure 1 the ψ values are the flux linkages with the various parts of the magnetic circuit, the linkages with the two secondary coils being conveniently given in terms of the balancing mutual inductances M_1 and M_2; the ν values are the magnetic reluctances in the various flux paths, ν_S is the reluctance of the specimen, ν_C ($\nu_C = \nu_C' + \nu_C''$) is the reluctance of the core of the permeameter, ν_Y is the reluctance of the yoke of the permeameter, ν_D is the reluctance to the flux linked with M_2 and not with M_1, and ν_A is the reluctance to the flux linked with neither M_1 nor M_2. Several assumptions are made in this analysis which are either refined at a later stage or are justified by the experimental test of the results of the analysis.

For a specimen of reluctance ν_S we have, writing $M_2/M_1 = R$,

$$\nu_S = \nu_D R - (\nu_D + \nu_C), \qquad \ldots\ldots (A1)$$

and with no specimen, i.e. ν_S zero,

$$0 = \nu'_D R_0 - (\nu_D' + \nu_C'). \qquad \ldots\ldots (A2)$$

Making the reasonable first assumption that ν_C and ν_D are functions of the core flux ψ_C only and *not* of ν_S, at fixed ψ_C (or what is in effect the same thing, at fixed M_1) we have $\nu_C = \nu_C'$ etc. and, therefore,

$$\nu_S = \nu_D (R - R_0). \qquad \ldots\ldots(A3)$$

Now there is inevitably a small contribution to M_1 from the leakage flux ψ_D; assuming this to be a linear function of the total leakage flux, i.e.

$$M_1 = (M_1)_{\mathrm{obs}} - \phi(\Delta M) \qquad \ldots\ldots(A4)$$

where ϕ is a small constant and $\Delta M = M_2 - M_1$, we insert (A4) into (A1) and (A2) and obtain an expression equivalent to (A3),

$$\begin{aligned} \nu_S &= \left\{\frac{\nu_D}{(1+\phi)\{1 - R_0\phi/(1+\phi)\}^2}\right\}\left[\frac{R - R_0}{1 - (R - R_0)\phi/(1+\phi)\{1 - R_0\phi/(1+\phi)\}}\right] \\ &\equiv C'\left[\frac{R - R_0}{1 - E(R - R_0)}\right]. \qquad \ldots\ldots(A5) \end{aligned}$$

the term C' contains ν_D which we have so far assumed to be indpendent of ν_S; we allow for a slight dependence by writing

$$\begin{aligned} C' &= C[1 + \delta\nu_S] \\ &\equiv C[1 + \alpha(R - R_0)] \qquad \ldots\ldots(A6) \end{aligned}$$

from (A3). On inserting (A6) into (A5) we obtain finally,

$$\nu_S = \frac{C(R - R_0)}{1 - \theta(R - R_0)} \equiv \frac{CT}{1 - \theta T} \qquad \ldots\ldots(A7)$$

θ is here compounded of the small constants ϕ and α.†

For a thin disc of uniform thickness t, cross-sectional area A' (A' is in practice made equal to the cross-sectional area of the permeameter core), and permeability μ, we have

$$\nu_S = t/\mu A'. \qquad \ldots\ldots(A8)$$

so that, writing $A'C = A$, we finally obtain an equation for specimen permeabilities

$$\frac{t}{\mu} = \frac{AT}{1 - \theta T}. \qquad \ldots\ldots(A9)$$

With values of A and θ known from calibration experiments, direct measurements of T and t enable values of the specimen permeabilities to be found.

---

† In order to justify using the constancy of M_1 as equivalent to the constancy of ψ_C (see above), it is necessary that ϕ in equation (A4) be small. Approximate evaluation of the constant showed that this was indeed the case so that in the experimental procedure adopted it is valid to make the necessary calculations at fixed values of $(M_1)_{\mathrm{obs}}$.

The Wave Mechanical Damped Harmonic Oscillator

By K. W. H. STEVENS
Department of Physics, University of Nottingham

MS. received 8th July 1958, and in final form 26th August 1958

Abstract. The classical problem of a damped harmonic motion is formulated wave mechanically, with particular reference to the charge in a tuned circuit, and the electromagnetic field in a resonant cavity. Results in close agreement with the classical problem are obtained, without using perturbation theory. The classical frequency appears in the time dependence of the eigenfunctions and the classical damping appears as a decay in the eigenvalues. Zero point energy and thermal noise are discussed. The formulation is expected to break down, at very high frequencies, for tuned circuits and it is suggested that the same may be true for cavity oscillations and travelling electromagnetic waves.

§ 1. INTRODUCTION

We have recently been interested in examining the properties of masers and parametric amplifiers from a wave mechanical point of view. Classically they operate because a negative resistance is introduced into a circuit tuned to the signal to be amplified. If this is so large that it more than cancels the resistance naturally in the circuit, oscillations occur. Below this oscillation threshold, amplification occurs. A problem which immediately arises is whether or not it is possible to describe a tuned circuit wave mechanically. If the tuned circuit is undamped, this seems to be possible (Weber 1954, 1956), a conclusion which is not too surprising in the limiting case in which the tuned circuit is taken as a cavity resonator, where radiation theory may be expected to apply. At the same time, for a lumped circuit, the result that the charge can be taken as a dynamical variable, even though we know that it is made up of very many electrons, is rather surprising, and in some ways similar to the Brownian motion ideas of Bohm (1957). For our threshold problem it is also necessary for the tuned circuit to be damped. Two ways are available for treating this case. The first begins with the undamped case and adds a suitable damping term, which is then handled by perturbation theory. The second, which we wish to describe, is one in which the attempt is made to set up a wave mechanical formulation of the tuned circuit problem as a whole, without adding the damping as a perturbation. From a very brief report of Kerner (1957) it seems that he has been thinking along the same lines. A recent paper (Kerner 1958) confirms this, but does not overlap seriously with the theory to be given below.

§ 2. CLASSICAL HAMILTONIAN

We suppose that the circuit is of the usual type, being composed of inductance L, capacitance C and resistance R. In the absence of an applied signal, which is the case we wish to consider first, the charge Q is governed by the well-known equation

$$L\frac{d^2Q}{dt^2}+R\frac{dQ}{dt}+\frac{Q}{C}=0. \qquad \ldots\ldots(1)$$

The first step in setting up the Hamiltonian is to find a Lagrangian $\mathscr{L}$ such that Lagrange's equation

$$\frac{d}{dt}\left(\frac{\partial\mathscr{L}}{\partial\dot{X}}\right)-\frac{\partial\mathscr{L}}{\partial X}=0 \qquad \ldots\ldots(2)$$

where X is a suitable dynamical variable, leads to equation (1), or its equivalent. For conservative systems $\mathscr{L}$ is the difference between the kinetic and potential energies. For non-conservative systems, such as the one we are considering, a suitable $\mathscr{L}$ may or may not exist. The important feature in our problem is that a Lagrangian function can be found. The Hamiltonian then follows formally. Suppose then we take the charge Q as variable, and set

$$\mathscr{L}\equiv A\mathrm{e}^{Rt/L}(\tfrac{1}{2}L\dot{Q}^2-Q^2/2C) \qquad \ldots\ldots(3)$$

where A is an arbitrary constant.

Substitution in (2), with $X=Q$, leads immediately to (1), as required. The momentum P, conjugate to Q, is now defined as

$$P=\frac{\partial\mathscr{L}}{\partial\dot{Q}}=AL\mathrm{e}^{Rt/L}\dot{Q}.$$

It will be noticed that the current, $-\dot{Q}$, is not conjugate to the charge, except when $R=0$. The Hamiltonian $\mathscr{H}$ is defined as $\mathscr{H}\equiv P\dot{Q}-\mathscr{L}$, expressed in terms of P and Q. Thus

$$\mathscr{H}\equiv\mathrm{e}^{-Rt/L}\frac{P^2}{2AL}+\mathrm{e}^{Rt/L}\frac{AQ^2}{2C}. \qquad \ldots\ldots(4)$$

The internal consistency can be tested by using Hamilton's equations

$$\dot{Q}=\frac{\partial\mathscr{H}}{\partial P} \quad\text{and}\quad \dot{P}=-\frac{\partial\mathscr{H}}{\partial Q}$$

which again lead to (1).

Before examining the possibility of quantizing this Hamiltonian it is instructive to consider what happens if, instead of using the charge Q as dynamical variable in the Lagrangian, we use $q=\mathrm{e}^{Rt/2L}\,Q$. This choice is suggested because the charge is known to decay exponentially with time. q should not decay but should oscillate with angular frequency $\Omega=(1/LC-R^2/4L^2)^{1/2}$. Then $\mathscr{L}$ becomes

$$A\left\{\tfrac{1}{2}L\left(\dot{q}-\frac{R}{2L}q\right)^2-\frac{q^2}{2C}\right\} \qquad \ldots\ldots(5)$$

and the Lagrange equation gives

$$\ddot{q}+\Omega^2q=0$$

as expected.

The momentum conjugate to q is $p=\partial\mathscr{L}/\partial\dot{q}=AL(\dot{q}-Rq/2L)$ so that $\mathscr{H}\equiv p\dot{q}-\mathscr{L}$ gives

$$\mathscr{H}\equiv\frac{p^2}{2AL}+\frac{Aq^2}{2C}+\frac{R}{2L}pq. \qquad \ldots\ldots(6)$$

This has the interesting property that the time does not appear explicitly.

§ 3. WAVE MECHANICAL HAMILTONIAN

The wave mechanical Hamiltonian is the differential operator which, through Schrödinger's equation, $i\hbar d/dt|\rangle = \mathscr{H}|\rangle$, describes the way in which any given state develops with time. The test of whether a particular Hamiltonian is the correct one for a given problem is a test of whether it leads to conclusions in agreement with experiment. In the case of atoms the wave mechanical Hamiltonian is obtained by first setting up the classical Hamiltonian in Cartesian coordinates and then replacing the classical conjugate variables by operators satisfying the commutation rule $qp-pq=i\hbar$. Difficulties are experienced if Cartesian coordinates are not used. In our problem we do not have anything corresponding to Cartesian coordinates and we therefore cannot say, *a priori*, whether the Hamiltonian which should be quantized should be (4) or (6), or possibly neither. It is however readily seen that (4) and (6) do not lead to the same Schrödinger equation. We shall, in fact, consider only the quantization of (4), for the equation from (6) turns out to be related to this, in a way which will be clear later, and (4) gives the required results.

We therefore suppose that the states of our system develop with time according to

$$i\hbar\frac{d}{dt}|\rangle = \left\{e^{-Rt/L}\frac{P^2}{2AL} + e^{Rt/L}\frac{AQ^2}{2C}\right\}|\rangle$$

with $QP-PQ=i\hbar$. To be specific we assume that at time t_0 we have a state $|t_0\rangle$ and wish to know what it becomes at some later time. We denote this latter state by $|t\rangle$. Suppose now that $|t\rangle = e^{iS}|T\rangle$, where S is an operator which vanishes when $t=t_0$. The equation for $|T\rangle$ is

$$i\hbar\frac{d}{dt}|T\rangle = \left[e^{-iS}\left\{e^{-Rt/L}\frac{P^2}{2AL} + e^{Rt/L}\frac{AQ^2}{2C}\right\}e^{iS} + \hbar\frac{\partial S}{\partial t}\right]|T\rangle.$$

We try to choose S so that the operator part of this does not contain t explicitly. By using the commutation rule it can be shown that

$$(PQ+QP)P^2 = P^2(PQ+QP+4i\hbar)$$

and a simple generalization shows that

$$f(PQ+QP)P^2 = P^2 f(PQ+QP+4i\hbar).$$

Similarly

$$f(PQ+QP)Q^2 = Q^2 f(PQ+QP-4i\hbar).$$

If S is chosen to be

$$\{R(t-t_0)/4\hbar L\}(PQ+QP)$$

it follows that

$$e^{-iS}P^2 e^{iS} = P^2\exp\{R(t-t_0)/L\}$$

and

$$e^{-iS}Q^2 e^{iS} = Q^2\exp\{-R(t-t_0)/L\}$$

and the equation for $|T\rangle$ becomes

$$i\hbar\frac{d}{dt}|T\rangle = \left[\exp(-Rt_0/L)\frac{P^2}{2AL} + \exp(Rt_0/L)\frac{AQ^2}{2C} + \frac{R}{4L}(PQ+QP)\right]|T\rangle.$$

If t_0 is set equal to zero, which implies no loss in generality, this equation is the same as that which would be obtained by quantizing (6), taking a symmetrized form for pq. Thus (6) would make $|T\rangle$ a state of the system, whereas (4) makes $e^{iS}|T\rangle$ a state.

It is now convenient to introduce two transformations. In the first we set

$$2P=(2AL\hbar\omega\exp(Rt_0/L))^{1/2}(Q_++Q_-)$$

$$2iQ=\left(\frac{2C}{A}\hbar\omega\exp(-Rt_0/L)\right)^{1/2}(Q_+-Q_-)$$

where $\omega^2=1/LC$.

Then $Q_-Q_+-Q_+Q_-=1$, so that Q_+ and Q_- can be regarded as creation and annihilation operators. We then define two new creation and annihilation operators, q_+ and q_- by

$$Q_+=i\cosh\theta\, q_++\sinh\theta\, q_- \text{ and } Q_-=\sinh\theta\, q_+-i\cosh\theta\, q_-$$

where $\tanh 2\theta=-R/2L\omega$. If R is taken as zero, $Q_+=iq_+$, $Q_-=-iq_-$ and the equation for $|T\rangle$ takes the undamped harmonic oscillator form

$$i\hbar\frac{d}{dt}|T\rangle=\tfrac{1}{2}\hbar\omega(Q_+Q_-+Q_-Q_+)|T\rangle.$$

If R is not zero it is only in terms of q_+ and q_- that this happens, the equation being

$$i\hbar\frac{d}{dt}|T\rangle=\frac{\hbar\Omega}{2}(q_+q_-+q_-q_+)|T\rangle$$

where $\Omega=(1/LC-R^2/4L^2)^{1/2}$. A particularly encouraging feature of this is that the classical angular frequency Ω is occurring in a natural way, whereas in the perturbation approach this does not seem to happen.

The general solution is built from particular solutions of this equation, which take the form $\exp\{-i(n+\frac{1}{2})\Omega(t-t_0)\}|n\rangle$, where $|n\rangle$ is a time-independent state, n is an integer giving the number of quanta,

$$q_+|n\rangle=(n+1)^{1/2}|n+1\rangle \text{ and } q_-|n\rangle=n^{1/2}|n-1\rangle.$$

The general expression for $|t\rangle$ is thus

$$|t\rangle=e^{iS}\sum_n\exp\{-i(n+\tfrac{1}{2})\Omega(t-t_0)\}|n\rangle\langle n|t_0\rangle.$$

§ 4. EQUIVALENT OPERATORS

Suppose now that at time t we require the matrix elements of an operator, such as Q, taken between two states $|t,1\rangle$ and $|t,2\rangle$. We shall show that this is equal to the matrix element of an equivalent operator $\tilde{Q}$ taken between the states $|t_0,1\rangle$ and $|t_0,2\rangle$ at time t_0 from which the states at t have developed. To see this we write

$$|t,1\rangle=e^{iS}\sum_n\exp\{-i(n+\tfrac{1}{2})\Omega(t-t_0)\}|n\rangle\langle n|t_0,1\rangle$$

and

$$|t,2\rangle=e^{iS}\sum_m\exp\{-i(m+\tfrac{1}{2})\Omega(t-t_0)\}|m\rangle\langle m|t_0,2\rangle$$

so that

$$\langle t,1|Q|t,2\rangle=\sum_{n,m}\exp\{i\Omega(n-m)(t-t_0)\}\langle t_0,1|n\rangle\langle n|e^{-iS}Q\,e^{iS}|m\rangle\langle m|t_0,2\rangle$$

$$=\exp\{-R(t-t_0)/2L\}\sum\exp\{i\Omega(n-m)(t-t_0)\}\langle t_0,1|n\rangle\langle n|Q|m\rangle\langle m|t_0,2\rangle$$

using

$$e^{-iS}Q\,e^{iS}=Q\exp\{-R(t-t_0)/2L\}.$$

Q can then be expressed in terms of q_+ and q_-, when simplification occurs because

$$\begin{aligned}\sum \exp\{i\Omega(n-m)(t-t_0)\}\langle t_0, 1|n\rangle\langle n|q_+|m\rangle\langle m|t_0, 2\rangle\\ = \sum \exp\{i\Omega(t-t_0)\}\langle t_0, 1|n\rangle\langle n|q_+|m\rangle\langle m|t_0, 2\rangle\\ = \exp\{i\Omega(t-t_0)\}\langle t_0, 1|q_+|t_0, 2\rangle\end{aligned}$$

and similarly for q_-. The net result is that

$$\langle t, 1|Q|t, 2\rangle = \langle t_0, 1|\tilde{Q}|t_0, 2\rangle$$

where

$$\tilde{Q} = -ie^{-Rt/2L}\left(\frac{C}{2A}\hbar\omega\right)^{1/2}[q_+(i\cosh\theta-\sinh\theta)\exp\{i\Omega(t-t_0)\}\\ + q_-(\sinh\theta+i\cosh\theta)\exp\{-i\Omega(t-t_0)\}].$$

$\tilde{Q}$ is thus an operator which, taken between the states from which $|t, 1\rangle$ and $|t, 2\rangle$ have developed, has the same elements as Q. Similar equivalents can be found for all operators of interest. Thus

$$\tilde{P} = e^{Rt/2L}\left(\frac{AL}{2}\hbar\omega\right)^{1/2}[q_+(i\cosh\theta+\sinh\theta)\exp\{i\Omega(t-t_0)\}\\ + q_-(\sinh\theta-i\cosh\theta)\exp\{-i\Omega(t-t_0)\}],$$

$$\tilde{P}^2 = (\tilde{P})^2 \text{ and } \tilde{Q}^2 = (\tilde{Q})^2.$$

The form of these operators shows that if at some time t the system is in an eigenstate of Q it returns to this eigenstate at intervals of $\pi/\Omega(=\tau_0)$. The eigenvalue is different at each return, being reduced by a factor $-\exp(-R\tau_0/2L)$. This is in complete agreement with the classical result for the charge, corresponding to a damped oscillation with period $2\tau_0$. The same is true for P. During each half-period the system first moves away from its initial eigenstate and then returns to it. Thus a second measurement within a halfperiod of a first measurement will disturb the system and will not give a definite value for the observable.

In considering the behaviour of the energy it is first necessary to decide which operator to use. For a conservative system the Hamiltonian must be used, but for our system, which is not conservative, it seems logical to use the quantum analogue of $\frac{1}{2}L\dot{Q}^2+\frac{1}{2}Q^2/C$. This is $(1/2A^2L)e^{-2Rt/L}P^2+Q^2/2C$, or $(e^{-Rt/L}/A)\mathscr{H}$. The above argument then shows that the energy eigenstate returns with period τ_0, the eigenvalue being reduced each time by $\exp(-R\tau_0/L)$, as required classically. There is, however, a slight difficulty which must be discussed. Consider the energy operator at some instant. Because t_0 is arbitrary we can conveniently take this time as t_0. In terms of Q_+ and Q_- the energy operator has the typical simple harmonic oscillator form, with eigenvalues $(n+\frac{1}{2})\hbar\omega\exp(-Rt_0/L)/A$. The occurrence of t_0 in this is at first sight disturbing. The reason becomes clearer if two observers are considered, whose origins of time do not coincide. If they both use the same formal Hamiltonian (4) they will predict, at any given instant, differing eigenvalues for the energy, which is unacceptable. The way round this difficulty is to allow each observer to have a different value for A, to be determined by the following procedure. Each observer must prepare a number of identical systems and at some convenient time t_0 must measure their energies. The theory predicts that these energies will only have the discrete values $(n+\frac{1}{2})\epsilon$, where ϵ is found from the measurement and n is an integer. He must then choose A so that $\hbar\omega \exp(-Rt_0/L)/A=\epsilon$, which fixes his Hamiltonian. The theory then shows that the energy eigenvalues after an interval τ are $(n+\frac{1}{2})\epsilon\, e^{-R\tau/L}$. The question of what happens about zero point energy in the damped harmonic oscillator can now be answered, because the quanta can be regarded as decaying with time and all become zero eventually. The zero point energy also decays exponentially.

The thermal behaviour of the system can be considered if we suppose that contact with a thermal bath at temperature T represents a situation in which the motion of the system is continually being interrupted by ' collisions ' which restore thermal equilibrium. We suppose that these collisions do not change the A in the Hamiltonian. After a sufficiently long time the energy quanta will have decayed so that they are less than $\boldsymbol{k}T$. Thermal equilibrium at a given instant then implies that the mean energy is $\boldsymbol{k}T$, for the mean energy of a simple harmonic oscillator of quantum ϵ is

$$\frac{\epsilon\sum(n+\frac{1}{2})\exp\{-(n+\frac{1}{2})\epsilon/\boldsymbol{k}T\}}{\sum\exp\{-(n+\frac{1}{2})\epsilon/\boldsymbol{k}T\}}=\tfrac{1}{2}\epsilon\coth\frac{\epsilon}{2\boldsymbol{k}T}$$

which is $\boldsymbol{k}T$ for $\epsilon \ll \boldsymbol{k}T$. Between collisions the quanta decay as $e^{-Rt/L}$, so that after an interval τ the mean energy is $\boldsymbol{k}T\, e^{-R\tau/L}$, and the rate of loss of energy is $R\boldsymbol{k}T\, e^{-R\tau/L}/L$. The probability that the system has not made a collision in this time is of the form $e^{-\tau/\lambda}$, where we assume that λ is much less than L/R. The average rate at which energy is lost is then

$$\frac{R}{L}\boldsymbol{k}T\frac{\int_0^\infty \exp\{-\tau(R/L+1/\lambda)\}d\tau}{\int_0^\infty \exp(-\tau/\lambda)d\tau}=\frac{R}{L}\boldsymbol{k}T\frac{1/\lambda}{(R/L+1/\lambda)}$$

$$\simeq\frac{R}{L}\boldsymbol{k}T.$$

This is the same as the classical result for the rate of energy dissipation in a resistance due to thermal fluctuations (McCombie 1953).

§ 5. EFFECT OF AN APPLIED VOLTAGE

So far it has been assumed that the tuned circuit is undergoing free oscillations. It is clearly of interest to consider what happens if a voltage is applied, and it is this problem which we now wish to consider. The classical charge equation is

$$L\frac{d^2Q}{dt^2}+R\frac{dQ}{dt}+\frac{Q}{C}=V$$

where V is the applied voltage, and proceeding as before the first step is to find a Lagrangian to give this. It is

$$\mathscr{L}\equiv Ae^{Rt/L}(\tfrac{1}{2}L\dot{Q}^2-Q^2/2C+QV).$$

Then

$$P=\frac{\partial L}{\partial\dot{Q}}=Ae^{Rt/L}L\dot{Q}$$

as before, and the Hamiltonian is

$$\mathscr{H}\equiv e^{-Rt/L}\frac{P^2}{2AL}+e^{Rt/L}\frac{AQ^2}{2C}-Ae^{Rt/L}VQ.$$

The quantization of this then leads to the Schrödinger equation

$$i\hbar\frac{d}{dt}|t\rangle=\left\{\mathrm{e}^{-Rt/L}\frac{P^2}{2AL}+\mathrm{e}^{Rt/L}\frac{AQ^2}{2C}-A\,\mathrm{e}^{Rt/L}VQ\right\}|t\rangle \qquad \ldots\ldots(7)$$

which becomes

$$i\hbar\frac{d}{dt}|T\rangle=\left\{\exp(-Rt_0/L)\frac{P^2}{2AL}+\exp(Rt_0/L)\frac{AQ^2}{2C}+\frac{R}{4L}(PQ+QP)\right.$$
$$\left.-A\exp\{R(t+t_0)/2L\}QV\right\}|T\rangle$$

on setting $|t\rangle=\mathrm{e}^{iS}|T\rangle$, where S is as previously defined. The term in V can be eliminated by setting $|T\rangle=\exp(i\lambda Q/\hbar)\exp(-i\mu P/\hbar)|\tau\rangle$, where λ and μ are functions of time which are to be chosen subsequently. Using the results

$$\exp(-i\lambda Q/\hbar)P\exp(i\lambda Q/\hbar)=P+\lambda \text{ and } \exp(i\mu P/\hbar)Q\exp(-i\mu P/\hbar)=Q+\mu$$

our equation becomes

$$i\hbar\frac{d}{dt}|\tau\rangle=\left[\exp\left(\frac{-Rt_0}{L}\right)\frac{(P+\lambda)^2}{2AL}\right.$$
$$+\exp\left(\frac{Rt_0}{L}\right)\frac{A(Q+\mu)^2}{2C}+\frac{R}{4L}\{(P+\lambda)(Q+\mu)+(Q+\mu)(P+\lambda)\}$$
$$\left.-AV\exp[R(t+t_0)/2L](Q+\mu)+(Q+\mu)\frac{d\lambda}{dt}-P\frac{d\mu}{dt}\right]|\tau\rangle. \qquad \ldots\ldots(8)$$

λ and μ are now to be chosen so that the coefficients of P and Q vanish and $\lambda=\mu=0$ when $t=t_0$. They must satisfy

$$\frac{\lambda}{AL}\exp\left(-\frac{Rt_0}{L}\right)+\frac{R}{2L}\mu-\frac{d\mu}{dt}=0 \qquad \ldots\ldots(9)$$

and

$$\frac{\mu A}{C}\exp\left(\frac{Rt_0}{L}\right)+\frac{R}{2L}\lambda-AV\exp\left\{\frac{R(t+t_0)}{2L}\right\}+\frac{d\lambda}{dt}=0. \qquad \ldots\ldots(10)$$

Then $|\tau\rangle$ satisfies

$$i\hbar\frac{d}{dt}|\tau\rangle=\{\tfrac{1}{2}\hbar\Omega(q_+q_-+q_-q_+)+g(t)\}|\tau\rangle$$

where $g(t)$ is the term independent of P and Q in (8), and does not need to be further specified. A possible solution of this is

$$|\tau\rangle=\exp\{-i(n+\tfrac{1}{2})\Omega(t-t_0)-iK(t)\}|n\rangle.$$

where

$$K(t)=\frac{1}{\hbar}\int_{t_0}^{t}g(t)dt.$$

The general solution of (7) is thus

$$|t\rangle=\mathrm{e}^{iS}\exp(i\lambda Q/\hbar)\exp(-i\mu P/\hbar)\exp(-iK(t))\sum_n\exp\{-i(n+\tfrac{1}{2})\Omega(t-t_0)\}$$
$$\times|n\rangle\langle n|t_0\rangle.$$

In the same way that equivalent operators were found when V was zero, we can now find equivalent operators with V non-zero. For Q we have

$$\langle t,1|Q|t,2\rangle=\sum\exp\{i\Omega(n-m)(t-t_0)\}\langle t_0,1|n\rangle\langle n|\exp(i\mu P/\hbar)\exp(-i\lambda Q/\hbar)\mathrm{e}^{-iS}Q\mathrm{e}$$
$$\times\exp(i\lambda Q/\hbar)\exp(i\mu P/\hbar)|m\rangle\langle m|t_0,2\rangle$$
$$=\exp\{-\mathrm{R}(t-t_0)/2L\}\sum\exp\{i\Omega(n-m)(t-t_0)\}$$
$$\times\langle t_0,1|n\rangle\langle n|Q+\mu|m\rangle\langle m|t_0,2\rangle.$$

Thus the operator equivalent to Q is $\tilde{Q}+\exp\{-R(t-t_0)/2L\}\mu$. Similarly, that for P is $\tilde{P}+\exp\{R(t-t_0)/2L\}\lambda$. We now solve the equations for λ and μ, by setting $\lambda=\exp\{R(t+t_0)/2L\}x$ and $\mu=\exp\{R(t-t_0)/2L\}y$, with $x=y=0$ when $t=t_0$. Then (9) becomes

$$\frac{dy}{dt}-\frac{x}{AL}=0$$

and (10) becomes

$$\frac{dx}{dt}+\frac{R}{L}x+y\frac{A}{C}-AV=0$$

so that

$$L\frac{d^2y}{dt^2}+R\frac{dy}{dt}+\frac{y}{C}=V.$$

This shows that y satisfies the same differential equation as the classical charge, and $\tilde{Q}+\exp\{-R(t-t_0)/2L\}\mu$ becomes $\tilde{Q}+y$. From our previous analysis we know that $\tilde{Q}$ is an operator which has an exponential decay part $\exp(-Rt/2L)$ and an oscillatory part of angular frequency Ω. Thus we see that if at time t_0 the system is in an eigenstate of charge, the state moves away from this eigenstate, returning with angular frequency Ω. At each return the charge is different, for $\tilde{Q}$ has decayed, while y has its classical value. As time goes on the excursions of the state away from the initial state get less, because of the decay of $\tilde{Q}$, and eventually the system stays in its initial eigenstate of charge, the eigenvalue being y, which has the classical value.

This analysis thus shows that the classical treatment of a tuned circuit with damping in terms of a forced oscillation and a natural decay has an exact counterpart in the wave mechanical treatment.

§ 6. The Cavity Resonator

In many cases the circuit element which has to be considered is a cavity resonator, rather than a tuned circuit, and we wish now to show how the above analysis can then be applied. A very elegant account of the properties of cavity modes has been given by Slater (1950) and our discussion will follow his general reasoning.

As is well known, a cavity resonator can be excited in an infinity of modes, but it is convenient to fix our attention on one of these. Then it can be shown that this has the general features of a standing wave, with the **E** and **H** vectors at any given point in the resonator varying in a sinusoidal way with time. There will also be a spatial variation in the amplitudes and directions of **E** and **H**, but not in the phase. Thus E will have the form $B\cos(\omega t+\phi)f(x,y,z)$ and H will be similar. The factor B could be absorbed into $f(x,y,z)$, but it is convenient not to do this, but to let B be proportional to the amplitude of excitation of E. $f(x,y,z)$ is then fixed by requiring that the integral of its square, taken over the volume of the resonator, equals some definite constant. It can then be shown that $B\cos(\omega t+\phi)$, where B may be a function of time, satisfies a differential equation which is of the same form as that satisfied by Q, the charge in a tuned circuit. With this established (and for the details we refer the reader to Professor Slater's book) the above wave mechanical discussion is immediately applicable to the cavity mode, with charge replaced by $B\cos(\omega t+\phi)$, which can conveniently be regarded as the ratio of the strength of E at any point to the value of $f(x, y, z)$ at that point. The fact that the cavity will support an infinity of modes presents no difficulty for they can be regarded as being quite independent of one another. A slight complication arises when two or more modes have the same frequency, for then the losses are not directly additive. This can be allowed for without difficulty. It should perhaps be remarked that although our analysis leads, for the free oscillation of a damped system, to the concept of energy quanta which decay with time, the system is still only resonant to its classical frequency and there is no suggestion that energy can be fed from one mode to another of a lower classical frequency.

§ 7. DISCUSSION

We have been able to show that it is possible to give a wave mechanical formulation of damped harmonic motion, whether the variable is the charge in a tuned circuit or the electric field in a cavity mode. The classical angular frequency plays an important role, for it is found that if at some instant the system is in an eigenstate of charge it returns to this eigenstate with the classical frequency. At each return, though, the eigenvalue is altered, in precisely the way required classically. This seems to be a very satisfactory description of the classical oscillator in wave mechanical terms.

There is, however, one aspect which certainly merits further examination. If we consider the tuned circuit we seem to have shown that the charge can be treated as a dynamical variable, and yet we know that it is actually the resultant of the motion of many electrons. If the circuit is undamped it is possible to assume that these electrons are in some sort of streamline flow, but this seems most unlikely when there is resistive damping, since this arises from scattering of the electrons. We are therefore led to suppose that the treatment we have been giving is only approximately correct. The error involved is apparently small: if it were not it would seem possible to detect the existence of the electron from tuned circuit measurements, and as far as we can see this has not been done. If, however, we could work with a circuit tuned to so high a frequency that its period is comparable with the collision time of the electrons, then discrepancies between our theory and experiment should certainly be revealed. We must therefore suppose that the treatment we have been giving, while adequate for explaining the ordinary properties of tuned circuits, is nevertheless an approximate theory, and that we cannot assume that it is even approximately in agreement with the facts at much higher frequencies. Let us now turn to the cavity resonator problem. We regarded the E of a cavity mode as being similar to the charge in a circuit, and we know they satisfy similar differential equations. Having quantized the cavity mode are we justified in assuming that the description is valid independently of the frequency? Or should we suppose that just as our description of the circuit is wrong at high frequencies, so should our description of the cavity mode also be wrong at high enough frequencies? We can see no reason why the description of the cavity mode can be extrapolated to frequencies at which observations have not been made, and we would like to suggest that, again, our treatment of this problem is only approximately correct. A point which then arises is that of how radiation in a vacuum differs from radiation in a cavity mode. In a cavity one deals with standing waves rather than travelling waves, and there is always damping. Whether these differences are enough to change the descriptions in a significant way seems doubtful. Nevertheless the whole of radiation theory seems to be based on the idea of quantizing the electromagnetic field for all frequencies, as we have done for our cavity mode. We know that in the equivalent tuned circuit problem we are making an error. How then do we know that there is no similar error in radiation theory?

REFERENCES

BOHM, D., 1957, *Proceedings of the Ninth Symposium of the Colston Research Society* (London : Butterworths Scientific Publications), p. 33.
KERNER, E. H., 1957, *Bull. Amer. Phys. Soc.*, **2,** 353 ; 1958, *Canad. J. Phys.*, **36,** 371.
MCCOMBIE, C. W., 1953, *Rep. Progr. Phys.*, **16,** 266 (London : Physical Society).
SLATER, J. C., 1950, *Microwave Electronics* (New York : van Nostrand).
WEBER, J., 1954, *Phys. Rev.*, **94,** 211 ; 1956, *Ibid.*, **101,** 1619.

Fluctuations of Photon Beams and their Correlations

By L. MANDEL

Department of Physics, Instrument Technology, Imperial College, London

MS. received 3rd *March* 1958, *and in revised form* 28th *April* 1958

Abstract. The distribution of counts from a photoelectric detector illuminated by light of bandwidth $\Delta\nu_0$ is analysed by associating the photons with Gaussian random waves. This is shown to lead to a full statistical description of the counts. It is shown that the number n_T in a time interval $T \ll 1/\Delta\nu_0$ obeys pure Bose–Einstein statistics, and that the fluctuations in longer intervals $T \gg 1/\Delta\nu_0$ are simply the density fluctuations of a boson assembly in a phase space of $\sim \Delta\nu_0 T$ cells. The correlation coefficient ρ of the fluctuations of counts from two detectors illuminated by partially coherent beams is found to be proportional to the local time average of the square of the coherence function $\langle \gamma_{12}^2 \rangle$. The correlation is shown to depend on the degeneracy of the beams in such a way that $\rho \to 2\langle \gamma_{12}^2 \rangle$ for highly degenerate beams. The results are all consistent with those obtained by Hanbury Brown and Twiss in 1957.

§ 1. INTRODUCTION

HANBURY Brown and Twiss (1956, 1958) and Twiss, Little and Hanbury Brown (1957) have described experiments in which they detected correlation between the arrival times of photons in two coherent light beams, but not in incoherent beams. It was first shown by Purcell (1956) that such correlation could be understood in terms of the non-classical fluctuations of photons.

The fluctuations in light beams and the resulting correlations have since been discussed by several authors. Jánossy (1957) and Wolf (1957) have examined the problem classically in terms of waves, while Hanbury Brown and Twiss (1957) have shown that identical results follow both from a classical analysis and a quantum analysis in terms of photons.

Here it is proposed to discuss the problem from the point of view of Purcell, in terms of the number of photons arriving in a certain time interval and to show that expressions for the variances and correlations are simply derivable by considering a photon beam as statistically associated with Gaussian random waves. This assumption, which is also implicit in Purcell's discussion and supported by the results of Hanbury Brown and Twiss (1957), is sufficient for a full statistical description of the fluctuations. It will be shown that it is consistent with the uncertainty principle, that it leads to the Bose–Einstein statistics in the appropriate case and that the fluctuations in short and long time intervals are the density fluctuations of an assembly of bosons in one and several cells of phase space respectively (Fürth 1928 a, b). The correlation between fluctuations in partially coherent beams will be seen to depend on the degeneracy of the beams, so that the effect should basically be regarded as a 'wave effect', as has already been suggested by Hanbury Brown and Twiss (1957).

The results obtained are consistent with those of Purcell (1956) and Hanbury Brown and Twiss (1957) but not with those of Fellgett (1949) and Clark Jones (1953).

§ 2. Fluctuations in an Homogeneous Beam

Consider a beam of light falling on some photoelectric detector, where n_T photoelectrons are ejected in a certain time interval T. Only the photoelectrons and not the photons are, of course, observable and our discussion must therefore be confined to the statistical behaviour of the photoelectrons. Although it is tempting to associate the ejection of a photoelectron with the arrival of a photon, this picture becomes inadmissible by the uncertainty principle for time intervals shorter than the reciprocal frequency spread of the light. We shall suppose that the light comes from a Gaussian random source (Jánossy 1957) emitting a narrow spectral line centred on the frequency ν_0, and that the line shape is describable by the normalized spectral density $\phi(\nu)$ with

$$\int_{-\infty}^{\infty} \phi(\nu)\, d\nu = 1 \text{ and } \phi(\nu) = \phi(-\nu).$$

While the shape of $\phi(\nu)$ is arbitrary we shall assume that its effective width $\Delta\nu_0$ defined by

$$\Delta{\nu_0}^2 = 2\int_0^{\infty} (\nu - \nu_0)^2 \phi(\nu)\, d\nu$$

is small compared with ν_0. We shall suppose for the moment that the light is plane polarized, and denote the instantaneous amplitude by $y(t)$ and the corresponding intensity, i.e. the square of $y(t)$ averaged over a few cycles, by $P(t)$. Thus

$$P(t) = \frac{\nu_0}{r}\int_{t-r/2\nu_0}^{t+r/2\nu_0} Q(t')\, dt', \qquad \ldots\ldots(1)$$

where $Q(t) = y^2(t)$ and where r is a small integer. We shall denote this form of average as a 'local' average and write

$$\frac{\nu_0}{r}\int_{t-r/2\nu_0}^{t+r/2\nu_0} Q(t')\, dt' = \langle Q(t) \rangle.$$

Thus, from (1), $P(t) = \langle Q(t) \rangle$.

The restriction to a 'homogeneous' beam ensures that there are no large phase differences between different elements of the beam. More specifically, it is assumed that the phase difference between any two elements is much less than $2\pi\nu_0/\Delta\nu_0$, so that their intensity cross-correlation function decreases with increasing delay.

We shall now associate photons with the Gaussian random wave $y(t)$, by defining a probability that a photoelectron is ejected in a short time interval between t and $t + dt$. If we consider first order transitions only significant, in which one photon gives rise to one photoelectron, then this probability will be given by $\alpha P(t)\, dt$, where α is the quantum sensitivity of the photoelectric detector, assumed constant over the narrow frequency range $\Delta\nu_0$. The observable $P(t)$ provides the only link between the wave and the particle descriptions of the beam.

The fluctuations of the number of particles n_T therefore have two causes. There are first of all the fluctuations of the wave intensity $P(t)$, determined by the spectral line shape and there is the stochastic association of particles with the wave intensity. This two-fold source of the fluctuations results in the departure from classical statistics, as we shall show.

Let $p_n(t, T)$ denote the probability that n photoelectrons are ejected in the interval between t and $t+T$. This probability is therefore itself a stochastic function of time. In particular, from the definition,

$$p_1(t, dt) = \alpha P(t)\, dt \qquad \ldots\ldots (2)$$

and the expectation value of n in the interval t to $t+T$ will be

$$\alpha \int_t^{t+T} P(t')\, dt'.$$

The condition (2) leads from first principles in the usual way to the Poisson distribution in n:

$$p_n(t, T) = \frac{1}{n!}\left[\alpha \int_t^{t+T} P(t')\, dt'\right]^n \exp\left[-\alpha \int_t^{t+T} P(t')\, dt'\right]. \qquad \ldots\ldots (3)$$

$p_n(t, T)$ is not, however, a distribution that can be found experimentally. For, when $P(t)$ fluctuates at random, the given interval t to $t+T$ is unique and only the ensemble averages, which are equal to the time averages for a stationary process, are observable. But the operation of averaging $p_n(t, T)$ over time when $P(t)$ is fluctuating will not, in general, result in another Poisson distribution. This departure of the observed distribution from the classical form can therefore be seen to be a general consequence of the association of particles with fluctuating waves. We may say that the fluctuations of the waves lead to the non-classical fluctuations of the quanta.

The limiting case $T \to \infty$ is exceptional, for, in that case,

$$\int_t^{t+T} P(t')\, dt'$$

is practically independent of t. The operation of averaging over time does not therefore substantially alter $p_n(t, T)$, which remains Poissonian.

In order to determine the mean number of counts in a fixed interval T we have to use equation (3) and average over n and t. If the time average is denoted by a bar we find:

$$\overline{n_T} = \sum_{n=0}^{\infty} \overline{n p_n(t, T)}$$

and, from the properties of the Poisson distribution,

$$= \alpha \overline{\int_t^{t+T} P(t')\, dt'}$$

$$= \alpha \bar{P} T. \qquad \ldots\ldots (4)$$

Also

$$\overline{n_T{}^2} = \sum_{n=0}^{\infty} \overline{n^2 p_n(t, T)}$$

and, again using the well-known properties of the Poisson distribution,

$$= \alpha \overline{\int_t^{t+T} P(t')\, dt'} + \overline{\left[\alpha \int_t^{t+T} P(t')\, dt'\right]^2}$$

$$= \overline{n_T} + \alpha^2 \int_0^T \int_0^T R_p(y-x)\, dy\, dx,$$

where $R_P(\tau)$ is the autocorrelation function of $P(t)$.

Instead of integrating over the xy plane we can convert the double integral into a single integral by putting $\tau = y - x$ (e.g. see Rice 1945). Thus:

$$\overline{n_T^2} = \overline{n_T} + 2\alpha^2 \int_0^T (T-\tau)\, R_P(\tau)\, d\tau, \qquad \ldots\ldots(5)$$

where we have made use of the symmetry of $R_P(\tau)$. Before proceeding further we shall examine the relation between $R_P(\tau)$ and the normalized spectral density $\phi(\nu)$ of the light.

If $R_y(\tau)$ is the autocorrelation function of $y(t)$ and $R_y(\tau)/\overline{y^2} = \gamma(\tau)$, then it is well known (e.g. Rice 1944) that $\gamma(\tau)$, the normalized autocorrelation function, and $\phi(\nu)$, the normalized spectral density, are related by a Fourier transformation. Thus

$$\gamma(\tau) = \int_{-\infty}^{\infty} \phi(\nu) \exp(2\pi i \nu \tau)\, d\nu \qquad \ldots\ldots(6)$$

in which $\phi(\nu) = \phi(-\nu)$.

We also have the result (Lawson and Uhlenbeck 1950) that, for a Gaussian random process,

$$R_Q(\tau) = \bar{Q}^2[1 + 2\gamma^2(\tau)], \qquad \ldots\ldots(7)$$

where $R_Q(\tau)$ is the autocorrelation function of $Q(\tau)$. Now, from the definition of $P(t)$,

$$\begin{aligned} R_P(\tau) &= \overline{\langle Q(t+\tau)\rangle \langle Q(t)\rangle} \\ &= \left(\frac{\nu_0}{r}\right)^2 \int_{-r/2\nu_0}^{r/2\nu_0} \int_{-r/2\nu_0}^{r/2\nu_0} \overline{Q(t+\tau+x)\, Q(t+y)}\, dx\, dy \\ &= \langle R_Q(\tau)\rangle, \qquad \ldots\ldots(8) \end{aligned}$$

whence $$R_P(\tau) = \bar{P}^2[1 + 2\langle \gamma^2(\tau)\rangle], \quad \text{since} \quad \bar{Q} = \bar{P}. \qquad \ldots\ldots(9)$$

It is shown in the Appendix that $\langle\gamma^2(\tau)\rangle$ is a slowly varying function of τ, which does not change much in an interval short compared with $1/\Delta\nu_0$, i.e. short compared with the characteristic coherence time of the light (e.g. Forrester 1956). In particular, $\langle\gamma^2(0)\rangle = \frac{1}{2}$. $R_P(\tau)$ is therefore also a slowly varying function and, like $\langle\gamma^2(\tau)\rangle$, it is appreciably different from zero only in a range of a few times $1/\Delta\nu_0$. We shall make use of these properties of $\langle\gamma^2(\tau)\rangle$ in evaluating the mean square fluctuations of n_T.

§ 3. THE MEAN SQUARED VARIATION OF n_T

On introducing (9) into (5) we obtain

$$\begin{aligned} \overline{\Delta n_T^2} &= \overline{n_T^2} - \overline{n_T}^2 \\ &= \overline{n_T} + 4\alpha^2 \bar{P}^2 \int_0^T (T-\tau)\langle\gamma^2(\tau)\rangle\, d\tau. \qquad \ldots\ldots(10) \end{aligned}$$

Since the integrand $(T-\tau)\langle\gamma^2(\tau)\rangle$ is never negative, it follows at once that the fluctuations of n_T are greater than predicted by the classical particle statistics. This result, which is of course characteristic of the so-called bunching of bosons, is here seen to follow directly from associating photons with Gaussian random waves.

If we denote the integral in (10) by $\frac{1}{4}T\xi$, where ξ has the dimension of time, we can write

$$\overline{\Delta n_T^2} = \overline{n_T}\{1 + \overline{n_T}(\xi/T)\}. \qquad \ldots\ldots(11)$$

Since $\langle\gamma^2(\tau)\rangle \leqslant \frac{1}{2}$ as shown in the Appendix, it follows from the definition of ξ that $\xi \leqslant T$ and

$$\overline{\Delta n_T^2} \leqslant \overline{n_T}\{1 + \overline{n_T}\}.$$

The relation (11) holds generally but, by making use of the properties of $\langle\gamma^2(\tau)\rangle$ derived in the Appendix, we can immediately evaluate ξ in two limiting cases.

Case (*a*): $\Delta\nu_0 T \ll 1$.

This condition would be extremely difficult to satisfy experimentally. Thus, the narrowest line width obtainable from a ^{198}Hg discharge corresponds to a $\Delta\nu_0$ of the order of 6×10^8 c/s (von Klüber 1958), so that, even with this source, we should be dealing with time intervals T less than about 10^{-9} sec. Nevertheless, the result for this case is interesting.

Since $\langle\gamma^2(\tau)\rangle$ does not depart much from $\frac{1}{2}$ in an interval $T \ll 1/\Delta\nu_0$,

$$\tfrac{1}{4}T\xi \simeq \int_0^T \tfrac{1}{2}(T-\tau)\,d\tau = \tfrac{1}{4}T^2,$$

so that $\xi = T$ and

$$\overline{\Delta n_T{}^2} = \overline{n_T}\{1+\overline{n_T}\}. \qquad \ldots\ldots(12)$$

This is the well-known formula for the fluctuations of the occupation numbers of a single cell in phase space for an assembly of bosons. The photoelectrons in the interval T therefore obey 'pure' Bose–Einstein statistics. The reason for this can be seen at once if we examine the size of the elementary cell in phase space. In the direction of the beam this extends over a distance $\mathbf{c}\Delta t$, where $\Delta t \sim 1/\Delta\nu_0$. Thus, the photons in an interval $T \ll 1/\Delta\nu_0$ as above, i.e. much shorter than the so-called coherence time of the light (e.g. Forrester 1956), occupy the same cell in phase space. By the uncertainty principle they are therefore intrinsically indistinguishable and n_T obeys pure Bose–Einstein statistics. We shall see in the next section that, when $\Delta\nu_0 T \ll 1$, the complete probability distribution follows very simply from equation (3).

The departure from the classical particle statistics is expressible by the 'degeneracy' factor $1+\overline{n_T}$ which is a measure of the extent to which photons share the same cell in phase space. The excess fluctuations correspond to what Hanbury Brown and Twiss (1957) called the wave interaction noise, although these authors did not consider the case $\Delta\nu_0 T \ll 1$. The degeneracy is also indicative of whether the wave or the particle properties of the beam predominate. In the visible region of the spectrum $\overline{n_T}$, and therefore the degeneracy, are normally small and the non-classical behaviour of a single photon beam is difficult to observe. Finally we note from (12) that the percentage fluctuation defined by

$$(\overline{\Delta n_T{}^2})^{1/2}/\overline{n_T} = (1+1/\overline{n_T})^{1/2}$$

is always greater than one, even at high intensities. This feature is again characteristic of a boson assembly and quite different from the behaviour of classical particles, for which the percentage fluctuation tends to zero at high intensities.

Case (*b*): $\Delta\nu_0 T \gg 1$.

This is the condition assumed to hold in the analyses of both Purcell (1956) and Hanbury Brown and Twiss (1957). It is of course almost invariably satisfied in experiments as shown above, but corresponds to a slightly more complicated situation.

Since $\langle\gamma^2(\tau)\rangle$ extends appreciably only over an interval of the order a few times $1/\Delta\nu_0$, the integral in (10) can be written

$$\tfrac{1}{4}T\xi \simeq \int_0^\infty T\langle\gamma^2(\tau)\rangle\,d\tau = \tfrac{1}{4}T\int_{-\infty}^{\infty} 2\langle\gamma^2(\tau)\rangle\,d\tau.$$

Although the exact value of ξ therefore depends on the shape of the spectral line, we can see that it will be of the order $1/\Delta\nu_0$, since $\langle\gamma^2(\tau)\rangle$ changes only slowly and $\langle\gamma^2(0)\rangle = \frac{1}{2}$. We can therefore write

$$\xi = \kappa/\Delta\nu_0$$

where κ is a number depending on the spectral density $\phi(\nu)$ but of the order 1. Equation (11) therefore becomes

$$\overline{\Delta n_T{}^2} = \overline{n_T}\{1 + \kappa\,\overline{n_T}/\Delta\nu_0 T\}. \qquad \ldots\ldots(13)$$

This is the relation first obtained by Purcell (1956). It can also be seen to be equivalent to that of Hanbury Brown and Twiss (1957), when the integral over time defining ξ is converted to one over frequency.

Since $\gamma(\tau)$ and $\phi(\nu)$ are a Fourier transform pair, we have from Parseval's theorem

$$\int_{-\infty}^{\infty} \gamma^2(\tau)\,d\tau = \int_{-\infty}^{\infty} \phi^2(\nu)\,d\nu,$$

so that

$$\xi = 4\int_{0}^{\infty} \phi^2(\nu)\,d\nu = \kappa/\Delta\nu_0.$$

From (13) we note that the degeneracy factor is smaller than before for the same $\overline{n_T}$. The reason for this can again be seen if we remember that we are now dealing with a volume of phase space containing roughly $\Delta\nu_0 T = s$ cells.† The mean number of photons per cell is therefore $\overline{n_T}/s = \overline{m}$ and (13) can be written

$$\overline{\Delta n_T{}^2} = \overline{n_T}(1 + \kappa\,\overline{m}) = \overline{n_T}(1 + \kappa s\,\overline{m}^2/\overline{n_T}).$$

This is the expression in the conventional form for the density fluctuations in a larger volume of phase space (Fürth, 1928 a, b). The degeneracy is less because we are dealing with a time interval in which not all the photons are intrinsically indistinguishable. The departure from the classical statistics is again due to those photons which share one cell and therefore would become important only at very great intensities.

The excess fluctuations given by (13) correspond to the wave interaction noise of Hanbury Brown and Twiss (1957). The results do not agree with those of Fellgett (1949, 1957) and Clark Jones (1953) obtained from thermodynamic arguments, who quote larger values. A likely reason for the discrepancy has already been given by Hanbury Brown and Twiss, namely that these authors equate the fluctuations of the detector output to the energy fluctuations of the light, whereas the two are stochastically connected. In any case, the formula of Fellgett is not consistent with that of a boson assembly in a phase space of $\Delta\nu_0 T$ cells.

It is interesting to note that the percentage fluctuation

$$(\overline{\Delta n_T{}^2})^{1/2}/\overline{n_T} = (1/\overline{n_T} + \kappa/\Delta\nu_0 T)^{1/2}$$

could be either greater or less than one, depending on $\overline{n_T}$, since n_T no longer obeys the pure Bose–Einstein statistics.

---

† By restricting the discussion to what we have called homogeneous beams, we ensure that the spacial extent of the beam over the photo-detector does not include more than one cell.

§ 4. THE DISTRIBUTION FUNCTION OF n_T WHEN $\Delta\nu_0 T \ll 1$

So far we have been concerned only with the variance of n_T, but, when $\Delta\nu_0 T \ll 1$, it is not difficult to derive the full distribution. This will be given by the time or ensemble average of $p_n(t, T)$ in equation (3). Now, since $P(t)$ does not vary much in an interval $T \ll 1/\Delta\nu_0$, it follows that

$$\alpha \int_t^{t+T} P(t')\,dt' \simeq \alpha P(t) T.$$

We therefore find from (3),

$$\overline{p_n(t, T)} = \frac{1}{n\,!}\,\overline{(\alpha PT)^n \exp(-\alpha PT)}. \qquad \ldots\ldots(14)$$

If the probability distribution of P is known, we can evaluate $\overline{p_n(t, T)}$ by averaging over the ensemble. Since $y(t)$ is a narrow band Gaussian random variable, the local average

$$\langle y^2(t) \rangle = P(t) = \tfrac{1}{2} W^2(t),$$

where $W(t)$ is the envelope of $y(t)$. Now the probability density of $W(t)$ has been shown by Rice (1944) to be of the form:

$$(W/\bar{P}) \exp(-W^2/2\bar{P}).$$

Hence, by transforming from W to P, we arrive at the probability density $p'(P)$ of P. Thus:

$$p'(P)\,dP = (1/\bar{P}) \exp(-P/\bar{P})\,dP.$$

We can now evaluate (14) by averaging over the ensemble and we obtain

$$\overline{p_n(t, T)} = \frac{1}{\bar{P} n\,!} \int_0^\infty (\alpha PT) \exp(-\alpha PT - P/\bar{P})\,dP.$$

The integral is the well-known factorial function integral and leads to

$$\overline{p_n(t, T)} = \{(1 + \alpha\bar{P}T)(1 + 1/\alpha\bar{P}T)^n\}^{-1}.$$

Since $\alpha\bar{P}T = \overline{n_T}$ from (4), we can write this as

$$\overline{p_n(t, T)} = (1 - w) w^n, \qquad \ldots\ldots(15)$$

where $w = \{1 + 1/\overline{n_T}\}^{-1}$. This is the Bose–Einstein distribution function in standard form for the numbers in a single cell of phase space. The distribution can be seen to arise naturally from the association of photons with Gaussian random waves, when $\Delta\nu_0 T \ll 1$.

§ 5. CORRELATION BETWEEN FLUCTUATIONS IN TWO BEAMS

Following the experimental work of Hanbury Brown and Twiss (1956, 1958) and Twiss, Little and Hanbury Brown (1957), the correlation between the fluctuations of two at least partially coherent beams has been studied theoretically by Purcell (1956), Wolf (1957), Jánossy (1957) and Hanbury Brown and Twiss (1957, 1958). The latter authors, in particular, have examined the problem in some detail and shown that the correlation between two beams and the 'excess' photon fluctuations of a single beam are very closely related.

Here it is proposed to show that similar relations are derivable very simply from equation (3) and that the correlation coefficient is very small unless the beams are substantially degenerate. We shall also find that, in sufficiently short time intervals, the correlation is independent of the spectral distribution.

We shall suppose that the two beams have the same spectral density, but not necessarily equal intensities $\overline{P_1}$ and $\overline{P_2}$ and that the degree of coherence is describable by the cross-correlation function $J_{12}(\tau)=\overline{y_1(t+\tau)y_2(t)}$ used by Wolf (1955). The normalized function $J_{12}(\tau)/(\overline{P_1}\,\overline{P_2})^{1/2}$ will be denoted by $\gamma_{12}(\tau)$. Wolf (1955) has shown that $\gamma_{12}(\tau)$ is an observable which is related to the visibility of the fringe system obtained from the superposition of the two beams. In the limit as the beams tend to complete coherence, $\gamma_{12}(\tau)\rightarrow\gamma(\tau)$.

From equation (3) we find

$$\overline{n_1 n_2} = \sum_{n_1=0}^{\infty}\sum_{n_2=0}^{\infty} \overline{n_1 n_2 p_{n_1}(t,T)p_{n_2}(t,T)} \qquad \ldots\ldots(16)$$

which reduces to

$$\alpha^2 \int_0^T \int_0^T R_{P_1P_2}(y-x)\,dy\,dx, \qquad \ldots\ldots(17)$$

where $R_{P_1P_2}(\tau)$ is the cross-correlation function of the two intensities.

By using the result of Wolf (1957) that

$$R_{Q_1Q_2}=\overline{Q_1}\,\overline{Q_2}\,[1+2\gamma_{12}^2(\tau)] \qquad \ldots\ldots(18)$$

and taking local averages as before we arrive at

$$R_{P_1P_2}=\overline{P_1}\,\overline{P_2}\,[1+2\langle\gamma_{12}^2(\tau)\rangle], \qquad \ldots\ldots(19)$$

where $\langle\gamma_{12}^2(\tau)\rangle$ is a slowly varying function of τ, as shown in the Appendix.

By substituting in (17) and transforming to a single integral over $\tau=y-x$ as before, we obtain for the cross-correlation function of the fluctuations

$$\overline{\Delta n_1\,\Delta n_2}=4\alpha^2\,\overline{P_1}\,\overline{P_2}\int_0^T (T-\tau)\,\langle\gamma_{12}^2(\tau)\rangle\,d\tau. \qquad \ldots\ldots(20)$$

The value of the integral appears to depend on the detailed form of $\langle\gamma_{12}^2(\tau)\rangle$. We can, however, simplify it appreciably if any path difference between the two partially coherent beams at the two photoelectric detectors is rather less than the coherence length $\mathbf{c}\Delta\nu_0$; in other words, if $\langle\gamma_{12}^2(\tau)\rangle$ is a decreasing function of τ.

Under these conditions P_1 and P_2 will be related by an expression of the form:

$$P_2(t)=aP_2'(t)+bP_1(t),$$

where a and b are positive numbers and $P_2'(t)$ is a function with the same spectral density as $P_1(t)$ but uncorrelated with it. This leads to

$$R_{P_1P_2}(\tau)=\overline{P_1}\,\overline{P_2}+b[R_{P_1}(\tau)-\overline{P_1}^2],$$

so that

$$\langle\gamma_{12}^2(\tau)\rangle=\tfrac{1}{2}\,\frac{R_{P_1P_2}(\tau)-\overline{P_1}\,\overline{P_2}}{\overline{P_1P_2}-\overline{P_1}\,\overline{P_2}}\;\frac{\overline{P_1P_2}-\overline{P_1}\,\overline{P_2}}{\overline{P_1}\,\overline{P_2}}$$
$$=2\langle\gamma^2(\tau)\rangle\langle\gamma_{12}^2(0)\rangle. \qquad \ldots\ldots(21)$$

It follows that, for beams with small path difference, only the zero-time cross-correlation enters into the equations, as has already been pointed out by Wolf (1955). An expression similar to (21) has also been derived by Hanbury Brown and Twiss (1957) from more detailed considerations.

Under these conditions also the integral in equation (20) has the same form as that encountered earlier in equation (10) and we can immediately write down the two limiting solutions.

For $\Delta\nu_0 T \ll 1$,

$$\overline{\Delta n_1 \Delta n_2} = 2\bar{n}_1 \bar{n}_2 \langle \gamma_{12}{}^2(0) \rangle \qquad \ldots\ldots (22)$$

and for $\Delta\nu_0 T \gg 1$,

$$\overline{\Delta n_1 \Delta n_2} = 2\bar{n}_1 \bar{n}_2 \, (\kappa / \Delta\nu_0 T) \langle \gamma_{12}{}^2(0) \rangle. \qquad \ldots\ldots (23)$$

Finally, when the two beams are unpolarized, these correlations are halved. Since the fluctuations in two normal planes of polarization are independent, we may associate uncorrelated numbers of photons $n_1{}'$ and $n_1{}''$ with each polarization, such that $\overline{n_1{}'} = \overline{n_1{}''} = \frac{1}{2}\bar{n}_1$ and $\overline{\Delta n_1 \Delta n_2} = 2\overline{\Delta n_1{}' \Delta n_2{}'}$.

The result for $\Delta\nu_0 T \gg 1$ is again equivalent to that obtained by Hanbury Brown and Twiss (1957), although expressed in a slightly different form. The case $\Delta\nu_0 T \ll 1$ was not considered by these authors and is unlikely to be of practical importance. But it is significant that the correlation in this case is independent of the spectral line shape. From (22) and (23) it is clear that $\overline{\Delta n_1 \Delta n_2}$ is directly proportional to the degeneracy of the beams, i.e. to the number of photons occupying the same cell in phase space.

§ 6. SUPERPOSITION OF COUNTS

When the counts n_1 and n_2 of two detectors illuminated by two similar partially coherent plane polarized beams are superposed, we obtained another variate whose degeneracy is in general intermediate between the plane polarized and the unpolarized case.

Thus if

$$n = n_1 + n_2,$$

$$\overline{\Delta n^2} = \overline{\Delta n_1{}^2} + \overline{\Delta n_2{}^2} + 2\overline{\Delta n_1 \Delta n_2}$$

and, by using the results of (12), (13), (22) and (23), we obtain

$$\overline{\Delta n^2} = \bar{n} \left\{ 1 + \bar{n} - \frac{2\bar{n}_1 \bar{n}_2}{\bar{n}} [1 - 2\langle \gamma_{12}{}^2(0) \rangle] \right\} \qquad \ldots\ldots (24)$$

for $\Delta\nu_0 T \ll 1$, or

$$\overline{\Delta n^2} = \bar{n} \left\{ 1 + \bar{n}\left(\frac{\kappa}{\Delta\nu_0 T} \right) - \frac{2\bar{n}_1 \bar{n}_2}{\bar{n}} \left(\frac{\kappa}{\Delta\nu_0 T} \right) [1 - 2\langle \gamma_{12}{}^2(0) \rangle] \right\} \text{ for } \Delta\nu_0 T \gg 1. \qquad \ldots\ldots (25)$$

Since $\langle \gamma_{12}{}^2(0) \rangle \leqslant \frac{1}{2}$, we see that the degeneracy of the distribution of n is generally less than that of n_1 and n_2. The difference depends on the normalized coherence factor $\langle \gamma_{12}{}^2(0) \rangle$. It follows at once that this factor also measures the extent to which the two beams share cells in phase space. In particular, for completely coherent beams, the statistical behaviour of n is identical with that of n_1 and n_2, since all the cells are shared. This has already been pointed out by Hanbury Brown and Twiss (1957).

§ 7. DISCUSSION

It has been shown that a full statistical description of the fluctuations in photon beams is possible by associating the photons with Gaussian random waves, which are describable by their spectral density $\phi(\nu)$. The validity of this approach has been questioned by Fellgett (1957), but it is seen to lead to completely consistent results. While the results are all concerned with the number of counts in a definite time interval T, they can immediately be applied to continuous fluctuation and correlation measurements. For all such measurements are limited by a certain resolving time T, which takes the place of the standard interval.

As shown by equation (15), the number n_T in an interval $T \ll 1/\Delta\nu_0$ obeys the pure Bose–Einstein distribution, as we should expect for a boson assembly in a single cell of phase space. In longer intervals the fluctuations of n_T correspond to the boson density fluctuations in a phase space containing $\sim\Delta\nu_0 T$ cells. From the equations (12), (13), (22) and (23) it is clear that the correlation between fluctuations depends essentially on the non-classical fluctuations of the photons, as has already been shown by Purcell (1956) and Hanbury Brown and Twiss (1957) and on the degree of coherence between the beams. These, in turn, depend on the extent of the cells in phase space in real space and time.

The degree of coherence is therefore derivable from correlation measurements (Hanbury Brown and Twiss 1956) as well as from interference experiments (Wolf 1955), although the former always yield the local average $\langle\gamma_{12}{}^2(\tau)\rangle$. This is of course to be expected, since $\gamma_{12}(\tau)$ contains phase information about the beams which is incompatible with the detection of single photons. Even with a perfect detector having $\alpha = 100\%$ the counts must not be too closely identified with the wave intensity.

There is another important difference between the time dependent correlation effect and the interference effect. Since the correlation depends essentially on two or more photons sharing cells in phase space, it depends on the degeneracy and therefore, unlike the interference effect, varies with the intensity of the beams. This becomes most obvious if we examine the normalized correlation coefficient

$$\rho = \overline{\Delta n_1 \Delta n_2}/(\overline{\Delta n_1{}^2}\,\overline{\Delta n_2{}^2})^{1/2}.$$

We then find

$$\rho = \frac{2\overline{n}_1\overline{n}_2(\kappa/\Delta\nu_0 T)\langle\gamma_{12}{}^2(0)\rangle}{\{\overline{n}_1\overline{n}_2(1+\overline{n}_1\,\kappa/\Delta\nu_0 T)(1+n_2\,\kappa/\Delta\nu_0 T)\}^{1/2}}$$

if $\Delta\nu_0 T \gg 1$, or

$$\rho = \frac{2\overline{n}_1\overline{n}_2\langle\gamma_{12}{}^2(0)\rangle}{\{\overline{n}_1\overline{n}_2(1+\overline{n}_1)(1+\overline{n}_2)\}^{1/2}}$$

if $\Delta\nu_0 T \ll 1$.

It can be seen that, although $\rho \propto \langle\gamma_{12}{}^2(0)\rangle$, it is very much less than $\langle\gamma_{12}{}^2(0)\rangle$ under conditions of low degeneracy, but tends to $2\langle\gamma_{12}{}^2(0)\rangle$ at high degeneracy. In particular, for highly degenerate completely coherent beams $\rho = 1$. The correlation is therefore appreciable only when the wave properties, as distinct from the particle properties, of the beam become evident. This confirms the view of Hanbury Brown and Twiss (1957) that the effect should be regarded basically as a wave effect and shows that it will be more difficult to detect in an experiment with light than with radio waves (Hanbury Brown and Twiss 1954). It is a considerable credit to these authors that they were able to detect the effect while working with a degeneracy of the order of a few times 10^{-3}.

ACKNOWLEDGMENT

The author is grateful to Dr. R. Fürth for some valuable discussions.

References

Clark-Jones, R., 1953, *Advances in Electronics* 5 (New York : Academic Press).
Fellgett, P. B., 1949, *J. Opt. Soc. Amer.*, **39,** 970; 1957, *Nature, Lond.*, **179,** 956.
Forrester, A. T., 1956, *Amer. J. Phys.*, **24,** 192.
Fürth, R., 1928 a, *Z. Phys.*, **48,** 323; 1928 b, *Ibid.*, **50,** 310.
Hanbury Brown, R., and Twiss, R. Q., 1954, *Phil. Mag.*, **45,** 663; 1956, *Nature, Lond.*, **177,** 27; 1957, *Proc. Roy. Soc.* A, **242,** 300; 1958, *Ibid.*, **243,** 291.
Jánossy, L., 1957, *Nuovo Cim.*, **6,** 111.
von Klüber, H., 1958, *Nature, Lond.*, **181,** 1007.
Lawson, J. L., and Uhlenbeck, G. E., 1950, *Threshold Signals* (New York: McGraw-Hill).
Purcell, E. M., 1956, *Nature, Lond.*, **178,** 1449.
Rice, S. O., 1944, *Bell Syst. Tech. J.*, **23,** 282; 1945, *Ibid.*, **24,** 46.
Twiss, R. Q., Little, A. G., and Hanbury Brown, R., 1957, *Nature, Lond.*, **180,** 324.
Wolf, E., 1955, *Proc. Roy. Soc.* A, **230,** 246; 1957, *Phil. Mag.*, **2,** 351.

APPENDIX

The Behaviour of $\langle \gamma_{12}^2(\tau) \rangle$

If $\phi_{12}(\nu)$ is the normalized cross power spectrum of the two beams, then

$$\gamma_{12}(\tau) = \int_{-\infty}^{\infty} \phi_{12}(\nu) \exp(2\pi i \nu \tau)\, d\nu.$$

Since $\phi_{12}(-\nu) = \phi_{12}^*(\nu)$, this can be written in the form

$$\gamma_{12}(\tau) = \int_0^{\infty} [\phi_{12}(\nu) \exp(2\pi i \nu \tau) + \phi_{12}^*(\nu) \exp(-2\pi i \nu \tau)]\, d\nu.$$

If we now introduce the substitution $\nu = \nu' + \nu_0$ and denote

$$\int_{-\nu_0}^{\infty} \phi_{12}(\nu_0 + \nu') \exp(2\pi i \nu' \tau)\ d\nu'$$

by $V(\tau)$, the equation becomes

$$\gamma_{12}(\tau) = V(\tau) \exp(2\pi i \nu_0 \tau) + V^*(\tau) \exp(-2\pi i \nu_0 \tau). \quad \ldots\ldots (\text{A}\,1)$$

Now by hypothesis, $\phi_{12}(\nu_0 + \nu')$ will be appreciably different from zero only for small ν' i.e. for $|\nu'| \lesssim \Delta\nu_0$. It follows from the integral defining $V(\tau)$ that this function will not change significantly in an interval $\Delta\tau \ll 1/\Delta\nu_0$. Thus $V(\tau)$ is a slowly varying function (i.e. compared with $y(t)$). From (A1)

$$\gamma_{12}^2(\tau) = V^2(\tau) \exp(4\pi i \nu_0 \tau) + V^{*2}(\tau) \exp(-4\pi i \nu_0 \tau) + 2\,|V(\tau)|^2. \quad \ldots\ldots (\text{A}\,2)$$

If we now calculate the local average, it follows at once from the properties of $V(\tau)$ that

$$\langle \gamma_{12}^2(\tau) \rangle = 2\,|V(\tau)|^2, \quad \ldots\ldots (\text{A}\,3)$$

so that $\langle \gamma_{12}^2(\tau) \rangle$ is also a slowly varying function of τ. In particular, for $\tau \ll 1/\Delta\nu_0$,

$$\langle \gamma_{12}^2(\tau) \rangle = \langle \gamma_{12}^2(0) \rangle.$$

If the two beams are completely coherent so that $\phi_{12}(\nu) = \phi(\nu)$,

$$V(0) = \int_0^{\infty} \phi(\nu)\, d\nu = \tfrac{1}{2}.$$

Hence

$$\langle \gamma^2(0) \rangle = \tfrac{1}{2}. \quad \ldots\ldots (\text{A}\,4)$$

Further, from the integral defining $V(\tau)$, we see that, for $\tau \gg 1/\Delta\nu_0$, the integrand contains a rapidly oscillating factor $\exp(2\pi i \nu' \tau)$. It follows that $V(\tau)$—and therefore $\langle \gamma_{12}^2(\tau) \rangle$—is small for $\tau \gg 1/\Delta\nu_0$.

Finally from

$$V(\tau)=\exp(-2\pi i\nu_0\tau)\int_0^\infty \phi_{12}(\nu)\exp(2\pi i\nu\tau)\,d\nu$$

we have,

$$|V(\tau)|=\left|\int_0^\infty \phi_{12}(\nu)\exp(2\pi i\nu\tau)\,d\nu\right|\leqslant\int_0^\infty|\phi_{12}(\nu)|\,d\nu. \quad \ldots\ldots(\text{A }5)$$

Hence, using (A 3) and (A 5) we see that, for a single coherent beam,

$$\langle\gamma^2(\tau)\rangle\leqslant\langle\gamma^2(0)\rangle=\tfrac{1}{2}.$$

The Saturation Magnetostriction of Nickel Crystals at Low Temperatures

By W. D. CORNER and F. HUTCHINSON
Department of Physics, Durham Colleges in the University of Durham

Communicated by G. D. Rochester; *MS. received 25th August* 1958

Abstract. The saturation magnetostriction λ of two single crystals of nickel has been measured over the temperature range 20°K to 500°K by a capacitance bridge method. The (λ, T) curves allow a reasonable extrapolation to absolute zero to be made, giving $\lambda_{111} = -28 \times 10^{-6}$, $\lambda_{100} = -57 \times 10^{-6}$, values which are of the same order as those calculated by Fletcher (1955), $\lambda_{111} = -44 \times 10^{-6}$, $\lambda_{100} = -187 \times 10^{-6}$.

An explanation is given for the discrepancy between the results obtained by Corner and Hunt (1955) and the present values.

---

§ 1. INTRODUCTION

THE variation of saturation magnetostriction with temperature in nickel crystals was measured by Corner and Hunt over the temperature range 90°K–630°K. The results showed, for the [100] direction, an anomalous maximum in the strain at about 125°K, the effect decreasing in magnitude below that temperature. Corner and Hunt were unable to achieve complete saturation and the values of λ_{100} below 150°K were obtained by extrapolation. It is desirable that the results in this region should be checked by bringing the specimen to complete saturation, and by making measurements at still lower temperatures to enable a reasonable extrapolation to absolute zero to be made. Values of λ_{100} and λ_{111} at absolute zero can then be compared with those calculated by Fletcher on a collective electron basis using a tight binding wave function approximation with spin orbit coupling as a perturbation. These measurements have therefore been made on the original specimens.

§ 2. APPARATUS

The apparatus for the measurement of magnetostriction was the same as used by Corner and Hunt, a differential condenser, the movement of the central plate producing a proportional voltage in a capacitance bridge. Magnetic fields of up to 10 500 oersteds were produced in a 44 kw water cooled solenoid, similar to that described by Daniels (1950). With this solenoid, a field uniformity of 0·30% was achieved over a length of 2 cm at its centre.

The general arrangement of the apparatus is shown in figure 1. The specimen A rests in an aluminium thimble (not shown) to compensate for thermal expansion and is held in a quartz tube B, the flanged top of which is held firm in the central brass tube C by two brass collars and fibre washers. The differential condenser is separated from the brass plate D by three quartz rods E, and the change of length of the specimen is coupled to the condenser by a twin bore quartz rod F. This rod is also used to take out the thermocouple leads, the thermocouple junction being in contact with the specimen. In order to stop ice forming round the displacement rod and restricting its movement at the point where it leaves the cold chamber, a small bellows G is soldered into plate D. A brass collar soldered to the top of the bellows holds a rubber 'O' ring against the displacement rod, the bellows being slightly extended so as to hold the rod firmly against the specimen. Above 80°K this is found to be unnecessary. The inlet tube for the liquid hydrogen, and outlet tube for the hydrogen gas are of Pyrex and sealed in position with Araldite.

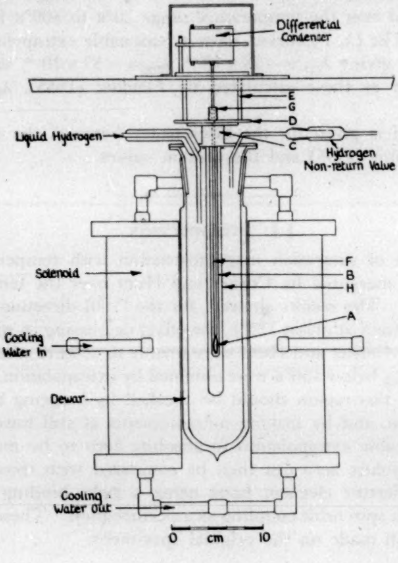

Figure 1. General arrangement of apparatus for the measurement of magnetostriction.

Temperatures from 80°K to 300°K were produced by filling the Dewar with liquid nitrogen and allowing this to boil away, measurements being made as the apparatus warmed up to room temperature. It was found necessary to fix a Pyrex tube H round the central quartz tube to stop the vibrations caused by the boiling of the liquid nitrogen from being transmitted to the displacement rod. The lowest temperatures were produced by filling the Dewar, previously cooled to 80°K, with liquid hydrogen. Temperatures above 300°K were obtained by filling the Dewar with silicone liquid MS550 at 550°K, and allowing the apparatus to cool down. A copper–constantan thermocouple was used over the whole range of temperature, the e.m.f. being measured by a bridge arrangement to an accuracy corresponding to $\pm \frac{1}{2}$°K.

The moving plate of the differential condenser used by Corner and Hunt was of Invar to reduce drift due to changes in the ambient temperature to a minimum. With the stronger fields used in this experiment it was found impracticable to reduce the stray field sufficiently to avoid errors due to magnetostrictive strain of the plate, so a brass plate was substituted and measures taken to reduce the changes in ambient temperature.

§ 3. RESULTS

Values of λ_{100} over the temperature range 20°K to 500°K, and of λ_{111} over the range 80°K to 500°K are shown in figure 2, the overall accuracy of these readings being ±5%. The field required to produce technical saturation in the [100] specimen is 5500 oersteds at 80°K, and 7500 oersteds at 20°K.

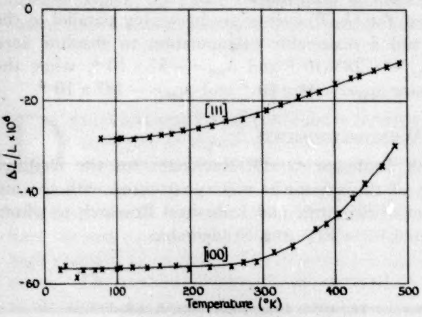

Figure 2. Variation of saturation magnetostriction with temperature in the [111] and [100] directions.

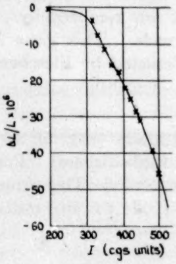

Figure 3. Variation of magnetostriction with intensity of magnetization in the [100] direction at 112°K.

§ 4. DISCUSSION

Above 150°K values of λ_{100} agree within experimental error with those of Corner and Hunt, and there is little difference in the general trend of the (λ_{100}, T) curves, but below 150°K the value of λ_{100} is constant. It is over this region that Corner and Hunt had to use extrapolated values. Figure 3 is a plot of their values of intensity of magnetization I against magnetostriction at 112°K, the lowest temperature at which results are available. It is possible to draw a curve through these points, assuming $I_s = 523$ c.g.s. units from the [111] specimen, giving $\lambda_{100} = -55 \times 10^{-6}$, a value consistent with the present results.

The general trend of the (λ_{111}, T) curve follows that of Corner and Hunt, but the absolute values of λ_{111} are 20% higher. This is most probably due to the effect of stress on the specimen. When the differential condenser is dismantled and reassembled, a different setting of the central plate will result in a change in the value of the stress applied to the specimen. This effect should be more pronounced when applied to a specimen in an easy direction of magnetization, an increase in compression causing a decrease in the value of the magnetostriction.

Forces applied to the top of the moving plate of the condenser give the values of λ_{111} and λ_{100} shown in the table. These results take into account the fact

Variation of Saturation Magnetostriction with Force
in the [111] and [100] Directions

Force (g wt)	250	350	450	750	950
$-\lambda_{111} \times 10^6$	23·1	22·5	21·6	19·1	17·5
$-\lambda_{100} \times 10^6$	55·2	55·2	55·2	52·7	52·0

that it requires a force of 250 g wt to move the central plate from one fixed plate to the other. They show that an increase of 200 g wt in the force applied to the [111] specimen from the differential condenser will bring both sets of results to within experimental error of each other.

From figure 2 it is seen that the (λ, T) curves are becoming parallel to the T axis at low temperatures, and a reasonable extrapolation to absolute zero may be made. This gives $\lambda_{111} = -28 \times 10^{-6}$ and $\lambda_{100} = -57 \times 10^{-6}$, while the values calculated by Fletcher are $\lambda_{111} = -44 \times 10^{-6}$ and $\lambda_{100} = -187 \times 10^{-6}$.

ACKNOWLEDGMENTS

The authors wish to thank Professor G. D. Rochester for the facilities placed at their disposal. Part of the apparatus was constructed with the aid of a grant from the Department of Scientific and Industrial Research to whom one of us (F. H.) is also indebted for a Research Studentship.

REFERENCES

CORNER, W. D., and HUNT, G. H., 1955, *Proc. Phys. Soc.* A, **68**, 133.
DANIELS, J. M., 1950, *Proc. Phys. Soc.* B, **63**, 1028.
FLETCHER, G. C., 1955, *Proc. Phys. Soc.* A, **68**, 1066.

Properties of the Metastable Helium Atoms

BY A. DALGARNO AND A. E. KINGSTON
Department of Applied Mathematics, The Queen's University of Belfast

Communicated by D. R. Bates; MS. received 30th June 1958

Abstract. The available theoretical values of the oscillator strengths of dipole transitions from each of the metastable states of helium are modified so that each set satisfies four different sum rules. They are then employed to evaluate the polarizabilities, the diamagnetic susceptibilities, the average energy losses for fast particle impact, the Lamb shift average excitation energies and the van der Waals interactions between normal and metastable helium atoms.

§ 1. INTRODUCTION

DALGARNO and LYNN (1957) have recently modified the theoretical oscillator strengths of dipole transitions from the ground state of helium so that they satisfy four different sum rules (Vinti 1932) and using them, have computed various properties of the helium atom, the results being in harmony with the available experimental data.† Subsequently Kabir and Salpeter (1957) have derived an expression for the continuum oscillator strengths in the limit of high energies of ejection, thus providing an additional control over the possible error. The method can be applied to other cases, particular interest being attached to the metastable states of helium.

§ 2. SUM RULES

If $\mathbf{r}_1$ and $\mathbf{r}_2$ are the position vectors of the two electrons of a metastable helium atom with wave function $\psi_0(\mathbf{r}_1, \mathbf{r}_2)$, then the oscillator strength of a dipole transition to the nth excited state with wave function $\psi_n(\mathbf{r}_1, \mathbf{r}_2)$ is defined as

$$f_n = \tfrac{1}{3}(E_0 - E_n)\ |(\psi_0, [\mathbf{r}_1 + \mathbf{r}_2]\,\psi_n)|^2 \qquad \ldots\ldots(1)$$

where E_0 and E_n are the binding energies of the metastable and the nth excited state respectively, measured in rydbergs, length being measured in units of a_0 ($a_0 = 5{\cdot}292 \times 10^{-9}$ cm).

The oscillator strengths satisfy the following sum rules (cf. Dalgarno and Lynn 1957):

(i) $\sum f_n/(E_0 - E_n)^2 = \alpha/4$ where α is the polarizability in units of $a_0{}^3$

(ii) $\sum f_n/(E_0 - E_n) = (\psi_0, [\mathbf{r}_1 + \mathbf{r}_2]^2\,\psi_0)/3$

(iii) $\sum f_n \qquad = 2$

(iv) $\sum f_n\,(E_0 - E_n) = 4\{E_0 + (\psi_0, \mathbf{p}_1 \cdot \mathbf{p}_2\psi_0)\}/3$ where $\mathbf{p}_i$ is the momentum of the ith electron

(v) $\sum f_n\,(E_0 - E_n)^2 = \dfrac{32\pi}{3}\,\{\psi_0, [\delta^{(3)}(\mathbf{r}_1) + \delta^{(3)}(\mathbf{r}_2)]\psi_0\}$

---

†Similar calculations have been carried out by W. F. Miller and R. L. Platzmann (private communication).

where $\delta^{(3)}(\mathbf{r})$ is the three-dimensional Dirac δ-function. In (i)–(v), the summation includes integrations over the continua but excludes the $n=0$ term.

Values of the polarizabilities α have been obtained by Buckingham and Dalgarno (1952) using a variational method (Buckingham 1937 a) but their accuracy may not be high and we shall not make use of (i) to derive f_n but shall instead evaluate (i) using our f_n.

No values of $(\psi_0, [\mathbf{r}_1+\mathbf{r}_2]^2\psi_0)$ were available and we have calculated them using the six-parameter Huang (1948) wave function

$$\psi_0(\mathbf{r}_1, \mathbf{r}_2) = (1 \pm P)\{c_1 + \alpha c_2(r_1+r_2) + \alpha c_3(r_2-r_1) + \alpha c_4 r_{12} + \alpha^2 c_5 r_{12}(r_1+r_2) + \alpha^2 c_6 r_{12}(r_2-r_1)\} \exp(-ar_1 - br_2), \qquad \ldots\ldots(2)$$

P denoting interchange of $\mathbf{r}_1$ and $\mathbf{r}_2$. A measure of the possible error for the 2^1S state is provided by comparing the value 15·9 of $(\psi_0, r_1{}^2\,\psi_0)$ with the value $16{\cdot}5_5$ obtained by Marriott and Seaton (1957) using an 11-parameter wave function depending upon r_1 and r_2 only, derived by Coolidge and James (1936). The error for the 2^3S state should be still smaller since no orthogonality difficulties arise in the variational determination of its wave function.

In determining (iv) the experimental binding energies were used together with the calculations of $(\psi_0, \mathbf{p}_1 \cdot \mathbf{p}_2\psi_0)$ by Stone (1955) who employed a modified form of (2). The error is negligible since $(\psi_0, \mathbf{p}_1 \cdot \mathbf{p}_2\psi_0)$ are very small compared with the binding energies.

For the 2^3S state, $(\psi_0, \delta^{(3)}(\mathbf{r}_1)\psi_0)$ has been evaluated by Teutsch and Hughes (1954) using (2). We have verified the result of this calculation and have similarly used (2) to evaluate the matrix element for the 2^1S state. The error should not be large for a simple 3-parameter wave function (Morse, Young and Haurwitz 1935) yields for both the 2^1S and 2^3S states a value 88·3 which is only slightly different from the values corresponding to (2).

The values of the summations (ii)–(v) are collected in table 1 which includes also the corresponding results for the ground state of helium (cf. Kinoshita 1957, Dalgarno and Lynn 1957, Dalgarno and Stewart 1958). The only matrix element with a ground state value markedly different from the metastable state values is that corresponding to the summation (ii). This difference merely reflects the fact that, in contrast to the metastable states, the ground state has no neighbouring levels with which it can combine by dipole transitions.

Table 1. Summations for Normal and Metastable Helium

Summation	1^1S	2^1S	2^3S
(ii)	0·753	10·55	7·54
(iii)	2	2	2
(iv)	8·17	5·74	5·81
(v)	121·3	87·1	88·4

§ 3. AUXILIARY CONDITIONS

There are two auxiliary conditions which provide useful additional controls over the accuracy of the derived oscillator strengths:

(i) For highly excited states it is to be expected that the oscillator strengths f_n will vary as C/n^3 where n is the principle quantum number of the active electron

(Hartree 1928) and the constant C equals twice the spectral head value of $df/d\epsilon$, ϵ rydbergs being the energy of the ejected electron (Hargreaves 1929).

(ii) The limiting form of the continuum oscillator strengths for infinite energies of ejection is given in the case of initial S states by

$$\frac{df}{d\epsilon} \sim \frac{512}{3\epsilon^{7/2}} \left| \int \psi_0(\mathbf{r}_1, 0)\, u(\mathbf{r}_1)\, d\mathbf{r}_1 \right|^2 \quad \ldots\ldots(3)$$

where $u(\mathbf{r}_1)$ is the final orbital of the passive electron (Kabir and Salpeter 1957).

§ 4. OSCILLATOR STRENGTHS

There have been several calculations of the oscillator strengths of dipole transitions in which the 2s electron of the metastable atom is excited to a higher *n*p orbital, various approximations being used for the initial and final wave functions. Hylleraas (1937) used linear combinations of Laguerre functions; Goldberg (1939) used a nine-parameter representation (Coolidge and James 1936) for the 2^1S state, hydrogenic orbitals for the n^1P states and screened hydrogenic orbitals (Morse, Young and Haurwitz 1935, Goldberg and Clogston 1939) for the 2^3S and n^3P states; Bates and Damgaard (1949) used the Coulomb approximation; Trefftz, Schluter, Dettmar and Jörgens (1957) and Bates and Dalgarno (1957, unpublished) used Hartree–Fock wave functions in both the dipole length and dipole velocity formulations (Chandrasekhar 1945), in contrast to previous work which was based upon the dipole length formulation only; for the 2^1S and 2^3S states, Trefftz *et al.* also used Hartree–Fock wave functions modified by the inclusion of a scale factor β and multiplication by $1+\alpha\beta r_{12}$, α and β being determined variationally. The results are collected in tables 2 and 3.

Table 2. Calculated Oscillator Strengths of Transitions: 2^1S–(1s *n*p)^{1}P

n		2	3	4	5	6
Hylleraas (1937)		0·392	0·150	0·062	0·025	0·012
Goldberg (1939)		0·389	0·157	0·057	0·025	0·014
		0·376	0·117	—	—	—
Bates and Damgaard (1949)		0·370	0·152	0·048	0·023	—
Hartree–Fock‡	Length	0·370	0·156	0·050	0·022†	0·012
	Velocity	0·358	0·158	0·051	0·023†	0·013
Modified Hartree–Fock	Length	—	0·206	—	—	—
	Velocity	—	0·165	—	—	—

†These values are obtained by interpolation in $n^3 f_n$.
‡Trefftz *et al.* (1957)

Table 3. Calculated Oscillator Strengths of Transitions: 2^3S–(1s *n*p)^{3}P

n		2	3	4	5	6
Hylleraas (1937)		0·559	0·052	0·031	0·013	0·007
Goldberg (1939)		0·542	0·083	0·027	0·012	0·007
		0·542	0·073	—	—	—
Bates and Damgaard (1949)		0·539	0·063	0·026	0·012	—
Hartree–Fock†‡	Length	0·568	0·057	0·023	0·011	—
	Velocity	0·600	0·050	0·021	0·010	—
Modified Hartree Fock†	Length	—	0·080	—	—	—
	Velocity	—	0·057	—	—	—

†Trefftz *et al.* (1957). ‡Bates and Dalgarno (unpublished).

It is not easy to select the best values. Trefftz *et al.* recommend their dipole velocity calculations using the modified Hartree–Fock wave functions, but the method of wave function modification is open to criticism (Hylleraas and Undheim 1930, Coolidge and James 1936) and the arguments of Dalgarno and Lewis (1956) suggest that the dipole length formulation is likely to be superior to the dipole velocity formulation at least for the $2^1S–2^1P$ and $2^3S–2^3P$ transitions. As a working model we adopt the Hartree–Fock dipole length values, which cannot be greatly in error.

Oscillator strengths of transitions in which the electron is excited to a continuum ϵp orbital have been computed by Huang (1948) who used the representation (2) for the initial state and the hydrogenic approximation for the continuum state in both the length and velocity formulations. Despite the reasonable harmony of the results obtained with the length and with the velocity formulations at low energies of ejection, it seems that the values for the photo-ionization of the 2^3S state must be seriously in error, for the spectral head value fails by more than a factor of two to satisfy the continuity condition (cf. § 3) if the Hartree–Fock length values are assumed to be nearly correct for the discrete transitions. The inaccuracy is confirmed by Burgess and Seaton (1958) who, using a generalization of the Coulomb approximation (Bates and Damgaard 1949), obtain values which do satisfy the continuity condition.

It is interesting to note that the results of Burgess and Seaton indicate that at the spectral head Huang's dipole length values are slightly more accurate than the velocity values. The arguments of Dalgarno and Lewis (1956) suggest that as the energy increases, the velocity formulation should become more accurate than the length formulation and this is found to be the case. The correct asymptotic forms for $df/d\epsilon$, obtained by substituting (2) into (3), are respectively $8{\cdot}90/\epsilon^{7/2}$ and $7{\cdot}75/\epsilon^{7/2}$ for the singlet and triplet metastables whereas the corresponding limits given by Huang's choice of wave functions are $13{\cdot}5/\epsilon^{7/2}$ and $11{\cdot}3/\epsilon^{7/2}$ in the length formulation compared to $8{\cdot}12/\epsilon^{7/2}$ and $8{\cdot}09/\epsilon^{7/2}$ in the velocity formulation.

No information appears to be available on transitions in which the 1s electron is excited to a higher *n*p orbital. Using the simple variational wave functions of Vinti (1932) for the final states and of Morse, Young and Haurwitz (1935) for the initial metastable states, we obtain the *f*-values listed in table 4. The length and velocity values agree only for the (1s 2s)–(2p 2s) transition but even this case is suspect since a further length calculation using the Hartree self-consistent field wave functions of Wilson and Lindsay (1935) yielded a value of about 0·29. This lack of agreement is to be expected since the simple wave functions used do not take proper account of correlation, which must be important for doubly-excited states of the type considered.

Table 4. Calculated Oscillator Strengths of Transitions: $2^{1,3}S–(np\,2s)^{1,3}P$

	Singlet		Triplet	
n	Length	Velocity	Length	Velocity
2	0·214	0·204	0·205	0·195
3	0·0201	0·0130	0·0204	0·0132
4	0·0084	0·0054	0·0086	0·0055

We have also calculated values of $df/d\epsilon$ for the transition (1s 2s)–(ϵp 2s) using the same initial wave functions and the hydrogenic approximation for the final states, the necessary analysis having been given by Bates (1946). The length and velocity values differ by a factor of about two and we shall not reproduce them here. The discrepancy must be due primarily to the inadequacy of the approximation for the ejected electron but its improvement presents a problem of considerable difficulty. We can, however, obtain the asymptotic forms with high accuracy by substituting (1) into (2), $u(\mathbf{r}_1)$ now being the final 2s orbital. There results $115/\epsilon^{7/2}$ for the 2^1S state and $176/\epsilon^{7/2}$ for the 2^3S state.

Transitions may also occur in which both electrons are excited to higher orbitals. No information is available about such transitions but presumably their oscillator strengths are small compared to those for single-electron jumps. We assume them to be negligible.

§ 5. MODIFIED OSCILLATOR STRENGTHS

Since the major uncertainty in the computed oscillator strengths resides in the values for transitions of the type (1s 2s)–(np 2s) and (1s 2s)–(ϵp 2s), we adopt the following procedure for deriving oscillator strengths consistent with the sum rules (ii)–(v): We assume initially that the Hartree–Fock dipole length values for (1s 2s)–(1s np) are correct, the value for 2^1S–5^1P being obtained by interpolation in $n^3 f_n$ and that the values of Burgess and Seaton (1958) for (1s 2s)–(1s ϵp) are correct for energies up to 1 rydberg above the spectral head. For the discrete transitions with $n > 6$ we assume $f_n = C/n^3$ and obtain C from the computations of Burgess and Seaton. In the case of the 2^3S state, we assume that Huang's dipole velocity calculations are correct for energies of ejection between 2 and 50 rydbergs and that the asymptotic form is applicable for energies greater than 100 rydbergs, the gaps remaining being filled by graphical interpolation. This is less arbitrary than it appears for Huang's dipole velocity results are in reasonable harmony with the Burgess–Seaton results at $\epsilon = 2$ rydbergs and with the asymptotic form at high energies. A similar method was used for the 2^1S state but the interpolated values are here rather more uncertain. The adopted continuum values are illustrated in the figure.

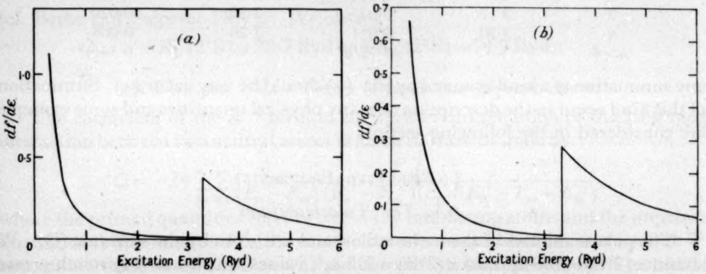

Modified oscillator strengths $df/d\epsilon$ for continuum transitions from the (*a*) 2^1S and (*b*) 2^3S states of helium.

The contributions to the sum rules (ii)–(v) were then evaluated numerically and subtracted from the totals listed in table 1, thus providing sum rules for the (1s 2s)–(*n*p 2s) and (1s 2s)–(ϵp 2s) transitions. These were dealt with by writing

$$\frac{df}{d\epsilon} = \frac{A}{\epsilon^4}\exp(-\alpha/\epsilon) + \frac{B}{\epsilon^{7/2}}\exp(-\beta/\epsilon^{1/2}) \qquad \ldots\ldots(4)$$

and proceeding in a manner similar to that of Dalgarno and Lynn (1957) except that the spectral head condition used by them was replaced by the asymptotic requirement.

In practice it was not possible to satisfy all the four sum values by manipulation of the constants A, B, α and β and the discrete values f_n. However, they were satisfied as nearly as possible, exact agreement with the sum rules then being obtained by slightly modifying the f-values of the (1s 2s)–(1s 2p) and (1s 2s)–(1s 3p) transitions considered earlier.

Although the accuracy of any individual oscillator strength cannot be high and indeed may be less than that of the Hartree–Fock length value, we reproduce our derived values in table 5 and the figure, for the overall pattern must be correct and any summation of a kind spanned by (ii)–(v) should be very accurate. Summations of this kind occur in the description of many physical quantities and some examples are considered in the following section.

Table 5 *a*. Modified Oscillator Strengths of Transitions: $2^{1,3}$S–(1s *n*p)^{1,3}P

	Singlet		Triplet	
n	Energy	f_n	Energy	f_n
2	0·04429	0·370	0·08416	0·535
3	0·1817	0·156	0·2344	0·0768
4	0·2299	0·0503	0·2859	0·0232
5	0·2522	0·0221	0·3095	0·0114
6	0·2644	0·0124	0·3222	0·0061
7	0·2717	0·0066	0·3298	0·0038
8	0·2765	0·0044	0·3347	0·0026
9	$0{\cdot}2797_5$	0·0031	0·3381	0·0018
10	0·2821	0·0023	0·3405	0·0013
$n > 10$	—	$2{\cdot}25/n^3$	—	$1{\cdot}32/n^3$

Table 5 *b*. Modified Oscillator Strengths of Transitions: $2^{1,3}$S–(*n*p 2s)^{1,3}P

	Singlet		Triplet	
n	Energy	f_n	Energy	f_n
2	2·99	0·320	2·86	0·435
3	3·17	0·027	3·22	0·020
4	3·20	0·011	3·26	$0{\cdot}008_5$
$n > 4$	—	$0{\cdot}72/n^3$	—	$0{\cdot}54/n^3$

§ 6. RELATED PROPERTIES

6.1. *The Polarizabilities*

The polarizabilities of the metastable states are given by the sum rule (i). We obtain $\alpha(2^1\text{S}) = 788\, a_0^3$ and $\alpha(2^3\text{S}) = 313\, a_0^3$, values which are very much greater than the polarizability $1{\cdot}39\, a_0^3$ of the ground state. Buckingham and Dalgarno (1952) have calculated $\alpha(2^3\text{S})$ variationally and obtain values of $202\, a_0^3$ and $310\, a_0^3$, the first corresponding to a representation of ψ_0 by the variational wave functions of Morse, Young and Haurwitz (1935) and the second to a representation by self-consistent field wave functions (Wilson and Lindsay 1935). It seems that with careful choice of unperturbed wave function, the Buckingham variational method (Buckingham 1937 a) is very suitable for excited atoms.

6.2. *The Magnetic Susceptibilities*

The diamagnetic susceptibility per g mol is given by

$$\chi = -7\cdot926 \times 10^{-7} (\psi_0, [\mathbf{r}_1{}^2 + \mathbf{r}_2{}^2] \psi_0).$$

This is best evaluated using the calculated values of the matrix elements rather than employing a sum of oscillator strengths. Using (2) we obtain

$$\chi (2^1\mathrm{S}) = -2\cdot52 \times 10^{-5}, \quad \chi (2^3\mathrm{S}) = -1\cdot80 \times 10^{-5}.$$

The 2^3S state is of course paramagnetic and its magnetic susceptiblity is given at temperature T by

$$\chi = \frac{0\cdot993}{T} - 1\cdot80 \times 10^{-5}.$$

6.3. *The Average Energy Losses for Fast Impacts*

The average energy loss for fast impacts is given in terms of a mean excitation energy I (cf. Mott and Massey 1949) and by using the Born approximation with some additional assumptions valid at high velocities of impact, Bethe (1930) has shown that

$$\ln I = \sum f_n \ln (E_0 - E_n) / \sum f_n.$$

We obtain $I(2^1\mathrm{S}) = 12\cdot2$ ev and $I(2^3\mathrm{S}) = 13\cdot3$ ev. The resulting energy losses for proton impacts are given in table 6.

Table 6. Average Energy Loss for Proton Impacts in Metastable Helium ($\mathrm{ev} \times 10^{-15}\,\mathrm{cm}^2$)

Impact energy (kev)	100	150	200	250	300	350	400	450	500	550	600
2^1S	13·7	10·4	8·51	7·23	6·32	5·62	5·08	4·64	4·28	4·04	3·71
2^3S	13·3	10·2	8·30	7·06	6·18	5·50	4·97	4·55	4·19	3·97	3·64

6.4. *The Lamb Shift Excitation Energy*

The Lamb shift excitation energy K_0 is given by

$$\ln K_0 = \frac{\sum f_n (E_0 - E_n)^2 \ln (E_0 - E_n)}{\sum f_n (E_0 - E_n)^2}$$

(cf. Bethe and Salpeter 1957). We obtain

$$K_0 (2^1\mathrm{S}) = 78\cdot7 \text{ Ryd and } K_0 (2^3\mathrm{S}) = 74\cdot9 \text{ Ryd}.$$

6.5. *Van der Waals Forces between two Helium Atoms*

The coefficient of the R^{-6} term in the series representation of the long range interaction between two neutral atoms is given in Hartree units by

$$C = -24 \sum_m \sum_n \frac{f_m f_n{}'}{(E_0 - E_m)(E_0{}' - E_n{}')(E_0 + E_0{}' - E_m - E_n{}')}$$

where the primed quantities refer to one of the interacting atoms and the unprimed quantities to the other. For the interaction of a normal helium atom with a 2^1S metastable atom we obtain $C = -83$ and for the interaction with a 2^3S metastable atom, we obtain $C = -58$, values much larger than the value -3 for two normal helium atoms (Dalgarno and Lynn 1957). Some comparison data are available for the $1^1\mathrm{S}$–$2^3\mathrm{S}$ coefficient which has been calculated by Buckingham and Dalgarno (1952) using a variational method due to Buckingham (1937 b). With the variational wave functions of Morse, Young and Haurwitz (1935) they obtain $C = -44$ and with self-consistent field wave functions they obtain $C = -65$, the latter value being in good agreement with the value obtained here. A similar situation occurred in connection with the polarizability.

The values of C for a pair of interacting metastable atoms are of interest in demonstrating the great magnitude of the forces between excited atoms. Thus for the 2^3S–2^3S interaction $C = -6{\cdot}5 \times 10^3$, for the 2^3S–2^1S interaction $C = -1{\cdot}1 \times 10^4$ and for the 2^1S–2^1S interaction $C = -2{\cdot}2 \times 10^4$.

Despite the fact that the summations describing the polarizabilities and van der Waals forces are outside the span of the known summations, the error in any one of the quantities discussed in this section will usually be much less than 5% except in the case of the Lamb shift where it may be as much as 20%.

ACKNOWLEDGMENTS

We are grateful to Professor D. R. Bates, Dr. M. J. Seaton and Dr. A. Burgess for communicating to us the results of their calculations and for allowing us to make use of them before their publication. One of us (A. E. K.) wishes to thank the Ministry of Education, Northern Ireland, for a research grant.

REFERENCES

BATES, D. R., 1946, *Mon. Not. R. Astr. Soc.*, **106**, 423.
BATES, D. R., and DAMGAARD, A., 1949, *Phil. Trans.* A, **242**, 101.
BETHE, H. A., 1930, *Ann. Phys., Lpz.*, **5**, 325.
BETHE, H. A., and SALPETER, E. E., 1957, *Handbuch der Physik*, **35** (Berlin : Springer).
BRANSDEN, B. H., and DALGARNO, A., 1953, *Proc. Phys. Soc.* A, **66**, 911.
BUCKINGHAM, R. A., 1937 a, *Proc. Roy. Soc.* A, **160**, 94 ; 1937 b, *Ibid.*, **160**, 113.
BUCKINGHAM, R. A., and DALGARNO, A., 1952, *Proc. Roy. Soc.* A, **213**, 506.
BURGESS, A., and SEATON, M. J., 1958, *Rev. Mod. Phys.*, **30**, 992, *Mon. Not. R. Astr. Soc.*, in the press.
CHANDRASEKHAR, S., 1945, *Astrophys. J.*, **102**, 223.
COOLIDGE, A. S., and JAMES, H. M., 1936, *Phys. Rev.*, **49**, 676.
DALGARNO, A., and LEWIS, J. T., 1956, *Proc. Phys. Soc.* A, **69**, 285.
DALGARNO, A., and LYNN, N., 1957, *Proc. Phys. Soc.* A, **70**, 802.
DALGARNO, A., and STEWART, A. L., 1958, *Proc. Roy. Soc.* **A**, **247**, 245.
GOLDBERG, L., 1939, *Astrophys. J.*, **90**, 414.
GOLDBERG, L., and CLOGSTON, A. M., 1939, *Phys. Rev.*, **56**, 696.
HARGREAVES, J., 1929, *Proc. Camb. Phil. Soc.*, **25**, 75.
HARTREE, D. R., 1928, *Proc. Camb. Phil. Soc.*, **24**, 426.
HUANG, S., 1948, *Astrophys. J.*, **108**, 354.
HYLLERAAS, E. A., 1937, *Z. Phys.*, **106**, 395.
HYLLERAAS, E. A., and UNDHEIM, B., 1930, *Z. Phys.*, **65**, 759.
KABIR, P. K., and SALPETER, E. E., 1957, *Phys. Rev.*, **108**, 1256.
KINOSHITA, T., 1957, *Phys. Rev.*, **105**, 1490.
MARRIOTT, R., and SEATON, M. J., 1957, *Proc. Phys. Soc.* A, **70**, 296.
MORSE, P. M., YOUNG, L. A., and HAURWITZ, E. S., 1935, *Phys. Rev.*, **48**, 948.
MOTT, N. F., and MASSEY, H. S. W., 1949, *The Theory of Atomic Collisions*, 2nd edn (Oxford : Clarendon Press).
STONE, A. P., 1955, *Proc. Phys. Soc.* A, **68**, 1152.
TEUTSCH, W. B., and HUGHES, V. W., 1954, *Phys. Rev.*, **95**, 1461.
TREFFTZ, E., SCHLUTER, A., DETTMAR, K. H., and JÖRGENS, K., 1957, *Z. Astrophys.*, **44**, 1.
VINTI, J. P., 1932, *Phys. Rev.*, **41**, 432.
WILSON, W. S., and LINDSAY, R. B., 1935, *Phys. Rev.*, **47**, 682.

Secondary Ionization Processes in Hydrogen at High Gas Pressures

By D. K. DAVIES, J. DUTTON and F. LLEWELLYN JONES
Department of Physics, University College of Swansea

MS. received 18*th July* 1958, *and in final form* 19*th August* 1958

Abstract. This paper describes accurate experimental measurements of the spatial growth of ionization in steady state conditions in hydrogen at high pressures (100 to 450 mm Hg) using an apparatus and procedure previously described (Crompton, Dutton and Haydon 1956). The values of the secondary ionization coefficient ω/α obtained from these measurements by means of the method of analysis developed in that paper show that, at a constant value of E/p (E the field, p the gas pressure), the value of ω/α is dependent both on the nature of the cathode and on the pressure of the gas. The variation in the value of ω/α with the material of the cathode shows that the predominant secondary ionization processes in hydrogen at high pressures are cathode dependent processes, thus confirming the previous work.

A theoretical investigation of the possible cathode-dependent processes in hydrogen shows that the variation in the value of ω/α with gas pressure may be satisfactorily explained on the assumption that the photo-electric process is predominant and that excited molecules undergo collisions of the second kind with neutral gas molecules, so that the molecular collision frequency affects the rate of production of photons. Theoretical computations of the value of ω/α based on the assumption that the photo-electric process at the cathode is the predominant secondary ionization process, and using previously measured values of the atomic constants involved, give good agreement with experiment.

Measurements of sparking potentials to within 1% show, in agreement with theory, that such measurements are not sufficiently precise to detect the departures from Paschen's law consequent on the observed dependence of the value of ω/α on gas pressure.

---

§ 1. INTRODUCTION

It is now well established (see Llewellyn Jones 1957) that for values of the parameter pd (p the gas pressure, d the gap distance) from low values up to those ~1000 cm mm Hg, the spatial growth of ionization in a parallel plate gap to which voltages V, less than the voltage V_S necessary to cause breakdown, are applied, is given by the Townsend relationship

$$I = I_0 e^{\alpha d} / \{1 - (\omega/\alpha)(e^{\alpha d} - 1)\} \qquad \ldots\ldots (1)$$

provided E/p (E is the field strength) is constant.

It follows that the criterion which predicts the value of the static breakdown voltage $V_S (= E d_S)$ at which the ionization current becomes self-maintained and independent of I_0 is

$$1 - (\omega/\alpha) \exp(\alpha d_S - 1) = 0. \qquad \ldots\ldots (2)$$

In these equations I_0 is the externally maintained initial current, liberated from the cathode by ultra-violet irradiation, α is the primary coefficient of ionization by electrons and ω/α is a generalized secondary coefficient which is approximately the linear sum of coefficients which represent the action of the secondary processes of ionization by photons (δ) and positive ions ($\alpha\gamma$) at the cathode, and by photons (η) and positive ions (β) in the gas.

The general mechanism of breakdown having been established, an important problem remaining is the identification of the secondary ionization processes operative in any given conditions. There are at least two complementary approaches to this problem; first, measurement of the temporal growth of ionization when a voltage greater than the sparking potential is applied to a gap may be used to derive important information concerning the particular ionization processes operative (Dutton, Haydon, Llewellyn Jones and Davidson 1953 a, Morgan 1956), second, very accurate measurement of the spatial growth of ionization at voltages below breakdown can also assist in the solution of this problem by enabling some of the possible secondary processes to be distinguished from the others. It is with this latter aspect that the present paper is concerned.

The first stages of an investigation leading to accurate determination of primary and secondary ionization coefficients at high values of the parameter *pd* in hydrogen were reported in a recent paper (Crompton, Dutton and Haydon 1956, hereinafter referred to as I). In that paper the conditions necessary for the accurate measurement of the spatial growth of ionization currents in the steady state were established, and the experimental apparatus and procedure developed to obtain these conditions were described in detail; the present paper reports the results of work using the same techniques.

In I an analysis of the errors involved in the computation of the coefficients α and ω/α from the observational data showed that in order to measure the coefficient α with an error of less than 1% it was necessary to measure the ionization currents themselves to the same order of accuracy. Such accuracy is difficult to achieve in practice in this region of high values of *pd*, largely because it entails the use of high voltage ($\sim$20 kv) supplies of very great stability (variations <1 in 10^5). Nevertheless, this degree of accuracy in the determination of α must be obtained, because, even when achieved, the generalized secondary coefficient ω/α is then determined only to within 10%, and this is considered to be the largest permissible error if any reliable deductions as to the processes which give rise to the coefficient are to be made. For this reason an apparatus in which it is possible to measure ionization currents to the required degree of accuracy was constructed as described in I.

It is the purpose of this paper to report and discuss further measurements made with this apparatus, in which the emphasis has been laid on the effect of changes in the gas pressure and cathode surface on the secondary ionization coefficient.

§ 2. EXPERIMENTAL RESULTS

2.1. *The Effect of Changes in the Material of the Cathode on the Secondary Ionization Coefficient*

The determination of the role of the cathode in the growth of pre-breakdown ionization is clearly the first step in the elucidation of which particular secondary ionization processes are predominant. It was shown in I that when the state of the cathode surface was altered by treatment in a spark or glow discharge there was an appreciable change in the secondary coefficient; this effect has also been observed in recent work (Wilkes, Hopwood and Peacock 1956, De Bitetto and Fisher 1956). Investigations have now been extended by us to measure the effects of a change in the cathode base metal as well as the surface state, and the results are shown in the table, where values of α and ω/α are given for four different electrodes in hydrogen at a value of E/p of 20 v cm^{-1} (mm Hg)$^{-1}$.

Values of α and ω/α in Hydrogen at $E/p = 20$ v cm^{-1} (mm Hg)$^{-1}$ and for $p = 360$ mm Hg for several Cathode Materials

Cathode	Aluminium	Nickel	Silver	Copper
α	2·66	2·66	2·64	2·68
$\omega/\alpha \times 10^3$	1·21	0·95	0·96	0·70

It can be seen that the variation in ω/α caused by the changes in the electrode material lie well outside the experimental error of 10%. It is also interesting to note that if published values of the work functions for the various untreated metal surfaces (see Weissler 1957) are used, then the values of ω/α given in the table are approximately inversely proportional to the work function. Although it was not possible to measure the work function in these experiments, the initial photoelectric current gave a good indication of the variation in the photo-electric sensitivity of a surface. The value of I_0 decreased from $1{\cdot}2 \times 10^{-12}$ A for the aluminium cathode to 2×10^{-13} A for the copper cathode, indicating that ω/α decreases as the photoelectric sensitivity decreases. Thus all the evidence indicates that the cathode plays an important role in the growth of ionization through the influence of changes in work function on the processes of secondary emission from the cathode, for example by positive ions or photons.

2.2. *The Effect of Gas Pressure on the Secondary Ionization Coefficient*

There were indications from the results given in I (see table 4) that the values of ω/α might be more dependent on gas pressure than on the values of E/p. A similar effect has also been noted by Wilkes, Hopwood and Peacock (1956). If such a pressure dependence of the coefficient ω/α does in fact exist, then it might well throw light on the nature of the secondary processes operative; such a result would also be important since it would mean that the sparking potential was not accurately a function of the parameter pd only, in these conditions. For these reasons a more extensive investigation of this effect was made in the present case.

The results are given in figure 1 in which the values ω/α obtained for the same value of E/p and for the same cathode surface but different gas pressures are plotted as a function of the gas pressure. It will be seen that there is an approximately linear dependence of ω/α on gas pressure. If a significant comparison of values of ω/α for various gas samples is to be made it is, of course, necessary that the gas samples should be of consistent purity throughout the experiments. In view of the high order of accuracy now attainable in determining the primary coefficient α, the criterion for consistent purity adopted in the present experiments was that each sample should give the same value of α to within the experimental error of 1%. Experience has shown that this is an extremely sensitive test, and slight variations in purity from sample to sample made it necessary to take a large number of results over a considerable period of time to obtain a set of results such as that given in figure 1. It should be emphasized that the results of figure 1 were obtained from a set of experiments which were carried out in random order; this procedure would make evident any permanent changes in the cathode surface which might be produced by, say, an increase in gas pressure. Sparking was carefully avoided throughout the experiments, and the values of ω/α at any given pressure were repeatable. Thus the observed variation of ω/α must definitely be attributed to the change in pressure and not to any change in the cathode surface.

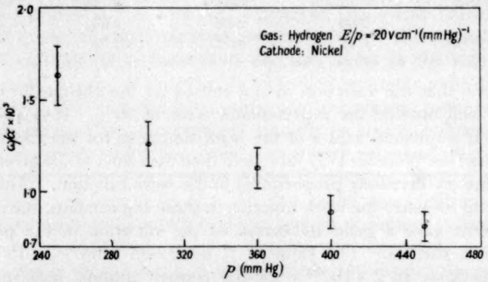

Figure 1. Experimental values of ω/α as a function of gas pressure in hydrogen at $E/p = 20$ v cm^{-1} (mm Hg)$^{-1}$. (Constant $\alpha/p = 7{\cdot}5 \times 10^{-3}$.)

2.3. *Measurement of Sparking Potential*

Since it is established that ω/α depends on the gas pressure, it follows that departures from Paschen's law must occur. It is therefore of interest to ascertain whether these departures are sufficiently large to be revealed in the conventional test of the law, which is carried out by measuring the sparking potential for various values of the parameter pd.

In the experiments so far discussed sparking was carefully avoided, because of its known effect on the secondary coefficient (see I) but now a further series of experiments was conducted in which a silver cathode was first 'conditioned' by a glow discharge and a series of low-energy sparks until a constant value of the sparking potential at any given pressure and value of pd was obtained. The sparking potentials for a number of pressures and gap separations were then measured by setting the gap distances and increasing the voltage on the irradiated gap slowly in steps until a spark was observed; the procedure was repeated several times at each gap separation and all gave values of the sparking potential with an error of less than 1%. The results are shown in figure 2 in which V_s is plotted against pd_s for the same pressure range used in the determinations of ω/α, the same value of pd_s being obtained at different pressures. It is seen that within the experimental error, the same value of V_s is obtained at the same value of pd_s for all pressures, thus indicating that there appears to be no departure from Paschen's law. It can be shown from simple considerations that there is in fact no inconsistency in these two apparently inconsistent experimental results—that there is a definite dependence of the coefficient ω/α (measured to within 10%) on pressure, while the breakdown potential (which depends on ω/α) is within the experimental error of 1% a function of pd and not of p alone. The explanation follows from the form of the breakdown criterion (2) which, as has been shown by Llewellyn Jones (1939), makes the sparking potential relatively insensitive to changes in ω/α at high gas pressures.

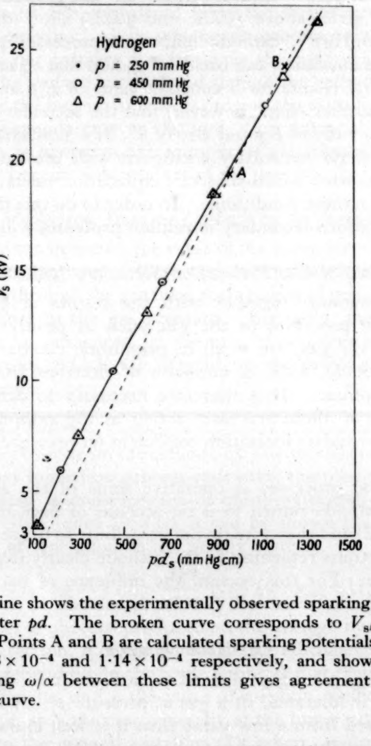

Figure 2. The full line shows the experimentally observed sparking potential as a function of the parameter pd. The broken curve corresponds to $V_s/pd_s = E/p = 20$ v cm^{-1} (mm Hg)$^{-1}$. Points A and B are calculated sparking potentials using $\alpha/p = 7{\cdot}5 \times 10^{-3}$ and $\omega/\alpha = 6{\cdot}93 \times 10^{-4}$ and $1{\cdot}14 \times 10^{-4}$ respectively, and show that the value of V_s calculated using ω/α between these limits gives agreement within 1% with the experimental curve.

The fact that measurements of the sparking distance at constant values of E/p are more sensitive to changes in the secondary coefficient (and thus more suited to the detection of departures from Paschen's law) may readily be seen from the graph. At a constant value of E/p, values of pd_s calculated using the measured value of α/p for that E/p must lie somewhere along a line drawn such that $V_s/pd_s = E/p =$ const. The line representing $V_s/pd_s = E/p = 20$ v cm^{-1} (mm Hg)$^{-1}$ is shown in figure 2; it is seen that points on this line lying between A and B are within 1% of the measured (V_s, pd) curve. Thus any values of ω/α lying between those necessary to give values corresponding to the points

A and B will give calculated values of pd_s (and thus of V_s) in agreement with experiment. The values of ω/α at A and B are $1{\cdot}14\times10^{-4}$ and $6{\cdot}93\times10^{-4}$ respectively; thus with the observed values of α, the secondary coefficient can actually vary by a factor of six and still give agreement with the observed (V_s, pd_s) curve within the experimental error of 1%.

§ 3. Theoretical Discussion of Results

The results of accurate measurements on the growth of pre-breakdown ionization currents given above (§ 2.1. and § 2.2.) show that in hydrogen at $E/p=20$ v cm^{-1} (mm Hg)$^{-1}$, cathode ionization processes play an important role in the growth of ionization and breakdown, and that equation (1) agrees well with the experimental results for a constant value of E/p and a constant value of p. The results further show, however, that the secondary coefficient ω/α is, in fact, a function not only of E/p but also of p. It is now interesting to consider how this variation of the secondary coefficient with pressure at constant E/p may be explained, and what information this explanation yields about the secondary processes operative in these conditions. In order to do this the effect of changes in pressure on the various secondary ionization processes will now be discussed.

3.1. *The Effects of Gas Pressure on Secondary Ionization Processes*

General considerations, together with the results of § 2.1, indicate that secondary ionization processes in the gas, such as positive ion ionization or photo-ionization of the gas, are small in magnitude compared with secondary processes at the cathode, such as emission of electrons from the cathode by positive ions or photons. It is therefore necessary to consider whether the operation of either of these processes acting at the cathode would lead to a dependence of the secondary ionization coefficient on pressure at a constant value of E/p.

If either of these processes is operative some of the secondary electrons emitted from the cathode return to it on account of back diffusion (Thomson 1928, Bradbury 1932) and therefore do not contribute to the secondary ionization. The number of electrons returning to the cathode clearly depends in some way on the gas pressure. For this reason, the influence of back diffusion on the secondary ionization coefficient will first be discussed.

3.2. *Back Diffusion*

Consider a parallel plate gap of fixed separation, from the cathode of which an electron current is liberated, in a gas at pressure p. If the voltage applied to the gap is increased from a low value then it is well known that the current increases from an initially low value to a value which is nearly independent of the voltage applied (over a certain limited range of voltage); the shape of this current–voltage curve is accounted for by back diffusion of the electrons and is dependent on the pressure. The question of interest to the present investigation is whether the loss of electrons to the current stream is dependent on pressure or on the ratio E/p. Both experiment (Theobald 1953) and theory (Thomson 1928, Bradbury 1932) have shown that the number of electrons lost due to back diffusion is a function of E/p only. Measurements of current–voltage characteristics during the present investigations have again confirmed this result. It would therefore appear that the process of back diffusion cannot account for the observed dependence of the secondary ionization coefficient on gas pressure. A detailed investigation of the ionization processes themselves must therefore be made.

3.3. *Emission of Electrons from the Cathode by Positive Ions*

The emission of electrons from the cathode by positive ions may be brought about by processes involving either the kinetic or the potential energy of the ions. In the region of E/p considered here, the mechanism is most probably one of 'potential emission', but whichever process occurs the number of secondary electrons per primary ionization in the gas $\alpha\gamma/\alpha$ will be a function only of E/p and of the surface material and state of the cathode. This is because the kinetic energy of the ions is dependent only on the ratio E/p, and the potential energy of the ions depends only on the ionization potential; so that whichever process of emission is operative the number of electrons emitted per incident positive ion, γ, is a constant independent of the pressure for a given value of E/p.

3.4. *Emission of Electrons from the Cathode by the Incidence of Photons*

The gas pressure can influence the value of the secondary ionization coefficient for the process δ/α in two ways. First, the absorption of photons as they travel towards the cathode through the gas from their points of generation in the current stream is proportional to the gas pressure. Secondly, the rate of generation of the photons can be influenced by the rate of collision of excited molecules with the gas molecules, which can depend on the pressure. These processes will now be considered.

3.4.1. *Absorption of Photons.*

If emission of electrons from the cathode by photons liberated in the avalanche is the only secondary ionization process operative, then, by reasoning analogous to that used previously in consideration of photo-ionization in the gas (Dutton, Haydon, and Llewellyn Jones 1953 b), it can be shown that the equation† for the spatial growth of ionization in the steady state is

$$I=I_0 \exp \alpha x \bigg/ \left\{1-\frac{kg\theta}{\alpha-\mu}(\exp(\alpha-\mu)x-1)\right\}, \qquad \ldots\ldots(3)$$

where θ is the number of photons produced on the average by one electron moving 1 cm in the field direction, k is the photoelectric efficiency of the photons, g a geometrical factor depending on the angle subtended at the cathode by the head of the electron avalanche, and μ the mean absorption coefficient of the photons in the gas. If $\mu \ll \alpha$, as is the case generally at the lower gas pressures, then this equation reduces to the general equation (1), when $\omega=\delta=kg\theta$, and negligible absorption of photons is tacitly assumed in the calculation of the values of ω/α given in § 2.2.

---

† The influence of resonance fluorescence, which causes the transit of photons across the gap to become analogous to a diffusion process, and degeneracy, which gives rise to a net loss of high energy photons, is not taken into account in this equation, as in the steady state these processes will not greatly influence the growth of ionization. In the non-steady state, on the other hand, these processes can be of vital significance and a full analysis of their influence on the growth of ionization will be given in a forthcoming paper in *Proc. Roy. Soc.* by P. M. Davidson of this Department.

At the high pressures used in the experiments described here, however, the absorption of photons in the gas may be appreciable, and it is now necessary to consider the more detailed relationship (3) which takes absorption into account in order to ascertain whether the value of ω/α calculated from equation (1) should depend on the pressure or not. Comparing relationships (1) and (3), it follows that the coefficient ω/α obtained can be expressed as

$$\omega/\alpha = \frac{kg\theta}{p} \frac{1}{(\alpha-\mu)/p} \frac{\{\exp[pd(\alpha-\mu)/p]-1\}}{\{\exp[pd\alpha/p]-1\}}. \qquad \ldots\ldots(4)$$

This expression shows that at constant value of E/p, ω/α is not a constant, but is a function of the product pd rather than of p alone. This result can also be seen on general similarity grounds by considering the excitation produced in two gaps of separation d_1 and d_2 in a gas at pressures p_1 and p_2 respectively, such that $p_1d_1 = p_2d_2$.

Before proceeding further it is necessary to ascertain whether the magnitude of the variation of ω/α with the parameter pd, indicated by expression (4), is such as to be observable in the present experiments. This is important, because the parameter pd varies along the $(I/I_0, d)$ growth curve. Using equation (4) with the experimentally observed values of the absorption coefficient, calculation of the variation of ω/α with the parameter pd shows that, for the conditions under which the above experiments were carried out, this variation is only about 4%. This is well within the experimental error ($\sim 10\%$) in obtaining values of ω/α and would therefore not be observable experimentally.

In order to demonstrate this small variation of ω/α with the parameter pd, it would be necessary to measure ionization currents with an error not greater than 0·1%, an order of accuracy which would be extremely difficult to achieve in practice in view of the difficulties outlined in § 1 (see I).

It is concluded that absorption of photons in the gas cannot account for the experimentally observed dependence of the calculated coefficient ω/α on the pressure alone.

3.4.2. *Destruction of Excited Molecules.*

At the high pressures used in these experiments it may readily be shown that the collision frequency of the gas molecules with each other lies between 0·3 and $0{\cdot}6 \times 10^{10}$ per second. Evidence on the lifetimes of excited states (see § 4) of the hydrogen molecule is scanty, but that which exists indicates lifetimes of about $3{\cdot}5 \times 10^{-8}$ sec (Slack 1926). If this is the case an excited molecule undergoes on the average from one to two hundred collisions (depending on the pressure) with neutral gas molecules during its lifetime. It is possible that in such collisions the excited molecule may be destroyed by, for example, giving up its energy to dissociate a neutral molecule either directly or indirectly. The destruction of excited states in this way would lead to an effective loss of high energy photons, and a consequent reduction in the secondary ionization produced by photons at the cathode. The number of excited molecules created in an electron avalanche is dependent only on the value of E/p, but the number destroyed by the above process is dependent only on the pressure. Hence if this process of destruction occurs the secondary ionization is a function of both E/p and p; furthermore, the secondary ionization decreases with increasing pressure at a constant value of E/p.

This process of the destruction of excited molecules by collision with neutral molecules thus predicts a decrease of ω/α with increasing pressure at constant value of E/p just as is observed experimentally, and is, in fact, the only one of the processes considered above which does. It remains to ascertain whether quantitative calculation, using known atomic data and reasonable values for the probability of the process of destruction, leads to values of ω/α in agreement with experiment.

§ 4. THEORETICAL CALCULATION OF THE SECONDARY IONIZATION COEFFICIENT

From the considerations of the previous section and other experimental evidence (Morgan 1956), it is concluded that the predominant secondary ionization process in hydrogen at high gas pressures is the photoelectric action at the cathode. It is therefore of interest to calculate values for the secondary ionization coefficient ω/α, assuming that it is entirely due to this process, and using previously observed values for the atomic constants.

It was seen in § 3.4.1. that if photoelectric emission at the cathode is the only secondary ionization process operative, and if absorption of the photoelectric radiation in the gas is taken into account, then the expression obtained for ω/α is

$$\omega/\alpha = \frac{kg\theta}{\alpha-\mu}\frac{\{\exp[pd(\alpha-\mu)/p]-1\}}{(\exp[pd\alpha/p]-1)}.$$

This expression now has to be corrected to take into account back diffusion (§ 3.2.) and the destruction of excited states by collisions of the second kind (§ 3.4.2.).

It has been shown by Thomson (1928) on the basis of kinetic theory that if n_0 electrons per second are liberated from the cathode then the number escaping completely into the gap is reduced by back diffusion to

$$n = n_0/\{1+u/(6\pi)^{1/2}W_-\},$$

where u is the most probable velocity with which electrons leave the cathode (Theobald 1953) and W_- is the drift velocity of the electrons. Applying this correction the expression for ω/α becomes

$$\omega/\alpha = \frac{1}{1+u/(6\pi)^{1/2}W_-}\frac{kg\theta}{\alpha-\mu}\frac{\{\exp[pd(\alpha-\mu)/p]-1\}}{(\exp[pd\alpha/p]-1)}.$$

Consider now the destruction of excited states. If the lifetime of an excited state of the molecule giving rise to the emission of photons is τ and its collision frequency with neutral molecules ν, then the number of collisions of such a molecule during its lifetime is $\nu\tau$. It follows that, if the probability of destruction of the excited state in collisions of the second kind is $P(d)$, the fraction of excited molecules destroyed is $\nu\tau P(d)$; this results in a reduction of the number of photons emitted from θ to $\theta(1-\nu\tau P(d))$. Thus ω/α is given by

$$\omega/\alpha = \frac{1}{1+u/(6\pi)^{1/2}W_-}\frac{kg\theta}{\alpha-\mu}\frac{\{\exp[pd(\alpha-\mu)/p]-1\}}{(\exp[pd\alpha/p]-1)}\{1-\nu\tau P(d\}. \quad \ldots\ldots(5)$$

The collision frequency ν may be written as $\nu=\kappa p$, and at constant values of E/p and of pd the expression

$$\frac{1}{1+u/(6\pi)^{1/2}W_-}\frac{kg\theta}{\alpha-\mu}\frac{\{\exp[pd(\alpha-\mu)/p]-1\}}{(\exp[pd\alpha/p]-1)}$$

is a constant ($= (\omega/\alpha)_0$, say), so that equation (5) may be written as

$$\omega/\alpha = (\omega/\alpha)_0(1 - \tau P(d)\kappa p). \qquad \ldots\ldots(6)$$

It is seen that a linear dependence of ω/α on pressure is to be expected. This is just what was found experimentally and shown in figure 3.

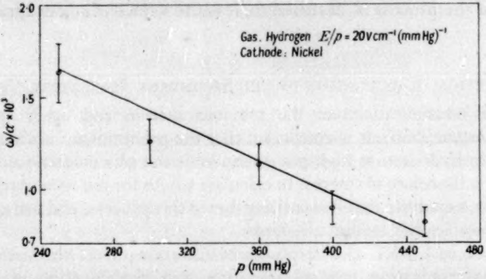

Figure 3. Calculated curve and experimental values of ω/α as a function of gas pressure in hydrogen at a value of $E/p = 20$ v cm^{-1} (mm Hg)$^{-1}$. The calculated curve was obtained using equation (5) and the values of the atomic constants given in the text.

Using equation (5) it is possible to calculate a value for ω/α provided the other quantities are known.. For the conditions corresponding to those in the present experiments all the quantities involved in the equation have, in fact, been determined experimentally or can be calculated, with the exception of the function $P(d)$. The procedure adopted here will therefore be to calculate values for $P(d)$ using the measured values of ω/α, in order to ascertain whether the value so calculated is of an order of magnitude which is reasonable and comparable with values obtained for other gases in which it has been measured.

There are no published experimental values for θ, so that in order to proceed with the calculation of ω/α it is necessary to calculate a value for θ theoretically†. In order to do this the possible states to which the hydrogen molecule can be excited, together with their cross sections, must be considered. The excited states with energies below the ionization potential 15·9 ev of the hydrogen molecule are the $1^3\Sigma_u$, $2^1\Sigma_u$, $2^1\Pi_u$ and $2^2\Sigma_g$ (see Massey and Burhop 1952). It is required to calculate the number of photons of sufficient energy to release electrons from the cathode, produced as a result of these excitations. Excitation to the $1^3\Sigma_u$ state results in the direct dissociation of the molecule without the emission of radiation, while excitation to the other levels gives rise to two groups of photons, those with energies within the range 10–13 ev (Lyman and Werner bands) resulting from excitation to the $2^1\Sigma_u$ and $2^1\Pi_u$ states which must return to the ground state ($1^1\Sigma_g$), and those with energies between 3 and 6 ev resulting from transitions from the $2^3\Sigma_g$ state to the $1^3\Sigma_u$ state which are followed by dissociation. There appears to exist no process whereby degradation of the energy of the high energy group can occur during its passage through the gas so that both groups reach the cathode; the number of photons emitted in each group is equal to the number of excitations to the $2^1\Sigma_u$ and $2^1\Pi_u$ states and to the $2^3\Sigma_g$ state respectively. Not all these photons will reach the cathode on account of the redistribution in direction brought about by resonance fluorescence, but this is allowed for in the calculation of ω/α by the inclusion of the absorption coefficient μ. Values of $F=\eta V$ (η the number of excitations produced on the average by one electron moving 1 cm in the field direction per unit field, V the excitation potential) for the $2^1\Pi_u$ and $2^3\Sigma_g$ states have been calculated assuming a Maxwellian energy distribution for the electrons and approximate, estimated values for the cross section (Lunt and Meek 1936); no values for the cross section of the $2^1\Sigma_u$ state seem to be available, but the cross section for excitation to this state is expected to be much less than for the excitation to the $2^1\Pi_u$ state, because of the nature of the transitions. If this is the case no significant error will be introduced by considering only the photons produced by the excitation to the $2^1\Pi_u$ and $2^3\Sigma_g$ states. The values of θ/α obtained for each of these states from the above values of F are 7 and 1·1 respectively, so that there are about six times as many high energy as low energy photons generated.

---

† *Note added in proof.* A recent paper by Corrigan and von Engel (1958) gives measured values of θ/α in agreement with those calculated above in the range of E/p here considered.

Curves for the photo-electric efficiency k of radiation falling on a nickel surface (Weissler 1957) show that the value of k for the group of high-energy photons is about ten times the value for the low-energy group of photons considered above. It would therefore appear that the greater part of the secondary ionization due to the photoelectric effect results from excitation to the $^1\Pi_u$ state which, on return to the ground state, gives photons of energy about 10 to 13 ev. The value of k for photons in this energy range falling on a nickel surface (Weissler 1957) has a mean value about 4×10^{-2} for an untreated surface, falling to about one tenth of this value for a very clean outgassed surface. It was not possible to measure k in the present experiments, but it seems likely that k for a cleaned surface subjected to ion bombardment by small ionization currents in hydrogen, as was the case here, will lie in the lower part of this range and a maximum value of 2×10^{-2} is therefore taken in these calculations. If the value for the photoelectric threshold of about 3250 Å for a nickel surface is used, then irradiation with ultra-violet light of wavelength in the range considered above will cause emission of electrons with a most probable velocity $u\simeq10^8$ cm sec^{-1}. This value of u, together with the measured value of $W_-=7\times10^6$ cm sec^{-1} (Townsend and Bailey 1921), is required to obtain the back diffusion.

The collision frequency ν at any pressure is readily obtained from standard tables assuming that the mean free path of the excited molecule is approximately the same as that for the neutral molecule.

The only other quantity required for the calculation of $P(d)$ is the absorption coefficient μ of the photons giving rise to the secondary emission from the cathode, that is photons with energies between 10 and 13 ev. There is a great need for reliable experimental data on absorption coefficients of photons with energies in this range. The most extensive investigations reported in this field are those of Weissler and his collaborators (1957), but these investigations were confined to higher energies from about 13·5 to 25 ev, and are thus not applicable in the present computations. Other published data are those of Raether (1938) and Jaffe, Craggs and Balakrishnan (1949). In Raether's experiments, radiation from a discharge in hydrogen was passed through a very thin celluloid window, and its absorption coefficient measured by the decrease in ionizations produced at various distances from the source in a cloud chamber containing hydrogen. The absorption coefficient of this high energy radiation of unspecified wavelength was 0·5 cm^{-1} at a gas pressure of 450 mm Hg. Jaffe *et al.*, from measurements of the discharge spread in Geiger counters, obtained a similar value for unfiltered high energy radiation. In the absence of more precise data for given wavelengths the above value of μ is used for the following computations.

It is thus possible to insert in equation (5) values for all the quantities required except $P(d)$. The values used are collected here for convenience: $\theta/\alpha=7$; $k=2\times10^{-2}$ electron photon^{-1}; g is calculated from the geometry of the systems to be about 1/6; $\mu/p=0{\cdot}11\times10^{-2}$ cm^{-1} (mm Hg)$^{-1}$; $\nu=0{\cdot}58\times10^{10}$ sec^{-1} at $p=450$ mm Hg; $\tau=3{\cdot}5\times10^{-8}$ sec. These values give

$$\omega/\alpha=2{\cdot}2\times10^{-3}(1-2{\cdot}03\times10^{2}P(d)). \qquad \ldots\ldots(7)$$

Recent results for lower gas pressures (Schmidt-Tiedemann 1958, Morgan 1956) indicate that in the region of E/p considered, probably about 80% of the secondary ionization in hydrogen is due to photo-electric action at the cathode. If this is also the case in the present experiments at high pressures then insertion of the experimental values of ω/α in equation (7) gives a value of about $3{\cdot}6\times10^{-3}$ for the probability that a collision between an excited hydrogen molecule and a neutral hydrogen molecule will be of the second kind. There are no published values for this probability in hydrogen, but for mercury measurements (Zemansky 1927) have shown that the probability is about 10^{-3}; measurements (Zemansky 1930) on quenching cross sections of helium and argon in mercury also indicate that the probability of a collision being of the second kind is of the same order in that case. Although the conditions are very different in these atomic systems from those in hydrogen the results are taken to indicate that the value obtained above is of a reasonable order of magnitude.

The values of ω/α calculated using the value $3{\cdot}6\times10^{-3}$ for $P(d)$ are shown in figure 3, and it is seen that there is good agreement with the experimental values which are also shown.

It may be concluded that the variation of ω/α with pressure, observed in the experiments at the higher pressures (of the order of half atmospheric), is satisfactorily accounted for on the assumption that the secondary ionization is predominantly of photoelectric origin, and that destruction of excited molecules in the avalanche by collisions of the second kind occur and so diminish the production of photons in the gas.

§ 5. CONCLUSIONS

Very accurate measurements of pre-breakdown ionization currents in uniform fields in hydrogen at high gas pressures have been made. These measurements show that in these conditions the secondary ionization coefficient ω/α depends on the nature and material of the cathode surface and also on the gas pressure.

The conclusions drawn from these observations may be summarized as follows:

1. Accurate measurements of pre-breakdown ionization currents in gases can yield important information concerning the nature of the secondary ionization occurring.

2. In hydrogen at a value of $E/p=20$ v cm^{-1} (mm Hg)$^{-1}$ the secondary ionization mechanism is cathode dependent, and thus the liberation of secondary electrons from the cathode by either photons or positive ions must play an important role.

3. The observed variation of ω/α with pressure may be satisfactorily explained on the assumptions that the predominant secondary ionization is the emission of electrons by photoelectric action at the cathode and that excited molecules undergo collisions of the second kind with neutral gas molecules.

4. Theoretical calculation of the secondary ionization coefficient using measured values of the atomic constants gives values in good agreement with experiment for reasonable values of the cross section for collisions of the second kind in which excited molecules are destroyed.

5. The departures from Paschen's law consequent on the dependence of the value of ω/α on pressure would not be experimentally significant in the measurement of (V_s, pd) curves.

ACKNOWLEDGMENTS

One of us (D.K.D.) wishes to express thanks to the University College of Swansea for a scholarship (1954–57) during the early stages of this investigation and to the Electricity Supply Research Council for a Research Fellowship during the period 1957–58. A grant for apparatus from the Research Council is also gratefully acknowledged. Thanks are due to R. W. Palmer who assisted in the measurements during the later stages of this work.

REFERENCES

BRADBURY, N. E., 1932, *Phys. Rev.*, **40**, 980.
CORRIGAN, S. J. B. and VON ENGEL, A., 1958, *Proc. Roy. Soc.* A, **245**, 335.
CROMPTON, R. W., DUTTON, J., and HAYDON, S. C., 1956, *Proc. Phys. Soc.* B, **69**, 2.
DE BITETTO, D. J., and FISHER, L. H., 1956, *Phys. Rev.*, **104**, 1213.
DUTTON, J., HAYDON, S. C., LLEWELLYN JONES, F., and DAVIDSON, P. M., 1953 a, *Brit. J. Appl. Phys.*, **4**, 170 ; 1953 b, *Proc. Roy. Soc.* A, **218**, 206.
JAFFE, A. A., CRAGGS, J. D., and BALAKRISHMAN, C., 1949, *Proc. Phys. Soc.* B, **62**, 39.
LLEWELLYN JONES, F., 1939, *Phil. Mag.*, **28**, 192 ; 1957, *Ionization and Breakdown in Gases* (London : Methuen and Co.).
LUNT, R. W., and MEEK, C. A., 1936, *Proc. Roy. Soc.* A, **157**, 146.
MASSEY, H. S. W., and BURHOP, E. H., 1952, *Electronic and Ionic Impact Phenomena* (Oxford : Clarendon Press).
MORGAN, C. G., 1956, *Phys. Rev.*, **104**, 566.
RAETHER, H., 1938, *Z. Phys.*, **110**, 611.
SCHMIDT-TIEDEMANN, K. J., 1958, *Z. Phys.*, **150**, 299.
SLACK, F. G., 1926, *Phys. Rev.*, **28**, 1.
THEOBALD, J. K., 1953, *J. Appl. Phys.*, **24**, 123.
THOMSON, J. J., 1928, *Conduction of Electricity through Gases*: I (Cambridge: University Press).
TOWNSEND, J. S., and BAILEY, V. A., 1921, *Phil. Mag.*, **42**, 873.
WEISSLER, 1957, *Handbuch der Physik*, **21**, 304 (Heidelberg : Springer).
WILKES, A., HOPWOOD, W., and PEACOCK, N. J., 1956, *Proc. Roy. Soc.* A, **235**, 334.
ZEMANSKY, M. W., 1927, *Phys. Rev.*, **29**, 513 ; 1930, *Ibid.*, **36**, 919.

The Fluorescence of Diamonds Excited by X-Rays

By I. G. MATTHEWS†
Department of Physics, University of Reading

Communicated by T. B. Rymer; MS. received 3rd April 1958, *and in revised form 7th August* 1958

Abstract. X-ray excited fluorescence spectra of type I and type II diamonds have been recorded photographically. The spectra so obtained are broadly similar for all specimens but they differ from those found with ultra-violet (3650 Å) excitation of the same specimens. The differences are described and a possible explanation is discussed.

V.
19

§ 1. Introduction

The work to be described has been carried out as part of a programme of research on the absorption and fluorescence of diamonds. The absorption results have been given by Clark, Ditchburn and Dyer (1956 a, b) and the ultra-violet excited fluorescence results by Dyer and Matthews (1957).

Ramachandran (1946) and Bishui (1951) each examined the x-ray excited fluorescence of diamonds at room temperature. Ramachandran investigated the variation in fluorescence intensity with the operating conditions of the x-ray tube, and recorded the fluorescence spectra of two specimens. The fluorescence was said to contain maxima at similar wavelengths to those found in the ultra-violet excited spectrum. Bishui did not find these maxima in the specimens which he examined. He also stated that type II diamonds do not fluoresce with x-ray excitation, whereas Ramachandran observed fluorescence from a specimen said to be type II. In a later paper Sen and Bishui (1956) have reported continuous emission between about 4000 and 5000 Å from seven type I and one type II specimens. Bull and Garlick (1950) have also reported that most diamonds exhibit a blue luminescence when excited by energetic particles or by x-rays.

§ 2. Experimental

The source of x-rays was a tube of demountable type used with a copper target. Throughout the experiments it was operated at 35 kv with a beam current at 15 mA. The x-rays left the tube via two beryllium windows, one on each side of the apparatus. Two experiments could therefore be performed simultaneously.

For room temperature experiments the specimen was held in contact with the beryllium window. Liquid nitrogen temperature experiments were carried out using an evacuated glass cell similar to that described by Clark, Ditchburn and Dyer (1956 a) for optical transmission measurements. A beryllium window was used to allow the x-rays to enter the tube, and the fluorescence left through a quartz window. The usual type of pumping and desiccating arrangements were employed.

---

† Now at Atomic Weapons Research Establishment, Aldermaston, Berks.

The fluorescence was reflected by a 45° surface silvered mirror to a convex quartz lens, which focused it on to the slit of a spectrograph. An *f*/12 quartz spectrograph and an *f*/3 Littrow mounting glass spectrograph were used both of which adequately resolved the structure in the ultra-violet excited emission (Dyer and Matthews 1957). Ilford F.P. Special, H.P.3, and Long Range Spectrum plates were available for each instrument, so that the spectral range from 2300 Å to 8800 Å could be covered. Exposure times varied between 1 and 20 hours. The diagrams shown in the paper have been obtained directly from microphotometer traces of the spectra and have not been corrected for the characteristics of the plates used. The rapid change of plate sensitivity for photon energies below 2·0 ev (6200 Å) means that straight-forward microphotometer traces in this region do not give the form of the spectra of the emitted light. Results are therefore not presented for spectra below 2·0 ev.

§ 3. Results

Eight specimens were selected for examination and emission spectra were obtained for each of them. They were chosen on the basis of their absorption and ultra-violet excited fluorescence spectra to cover the widest possible range of diamonds available. Two irradiated specimens were included. One of these, D.18.E, is of particular interest as it was originally cut from the same large diamond as D.78. Before irradiation these two specimens showed similar and homogeneous ultra-violet excited spectra, so that the X-ray fluorescence of D.18.E was, before treatment, similar to that of D.78.

Table 1. Diamonds used in the Examination of X-ray excited Fluorescence

Specimen	Type	3650Å excited Fluorescence	Notes
D.55	I	Strong blue	
D.78	I	Weak blue	
D.56	I	Mainly green	u.v. fluorescence shows one blue region
D.18.E	I	Green	electron irradiated and heated
D.27.A	I	Weak blue	neutron irradiated
D.43	II a or intermed.	Blue	
D.16	II a	Weak blue	
D.1	II b	None	weak blue phosphorescence with 2537 Å excitation

The specimens used, together with a brief description of them, are listed in table 1.

3.1. *Unirradiated Type I Diamonds*

D.78 and D.55 showed a continuous emission spectrum in the visible. This spectrum had its maximum in the blue region and decreased with decreasing wavelength. Some trace of fluorescence was recorded as far into the ultra-violet as about 3200 Å (3·9 ev) below which wavelength it would be lost by absorption in the specimen. The emission below about 4000 Å is weak compared with that in the visible region. Nothing has been detected in the region between 7000 Å and 9000 Å (1·8 and 1·4 ev).

The general shape of the visible emission spectrum is the same for D.55 and D.78. It consists of two broad bands, the positions of which bear some resemblance to the broad components, as opposed to the line components, of the 4150 Å and 5032 Å systems found with ultra-violet excited spectra (Dyer and Matthews 1957). Figure 1 shows a copy of a microphotometer trace of the spectrum of D.55 obtained on an H.P.3. plate.

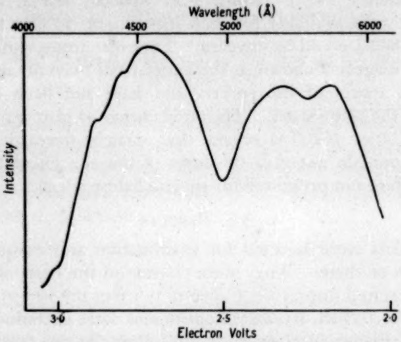

Figure 1. The x-ray excited fluorescence of D.55 at 80°K.

Both D.55 and D.78 show a minimum at 4150 Å. The maxima shown in figure 1 for D.55 between 2·7 ev and 2·9 ev correspond in position to the first two ancillary peaks of the ordinary 4150 Å emission found with ultra-violet excitation. They were not observed in the spectrum of D.78. Figure 1 was obtained with the specimen at 80°K; the room temperature spectrum is similar, except that the structure is less well defined. It was estimated that the 80°K spectrum was about twice the strength of that obtained at 290°K. A comparison of the strengths of the emission from D.78 and D.55 shows the latter to be the stronger, but the ratio between them is much less than the ratio of their ultra-violet excited emissions.

The third unirradiated type I specimen which was examined was D.56. The fluorescence excited by ultra-violet light in this specimen is mainly green, with the exception of one small region which is blue. The x-ray excited emission was found to be blue and no difference in intensity could be observed by eye between the two regions. The room temperature spectrum was very similar to that obtained for D.55 and D.78, except that with D.56 no minimum could be detected at 4150 Å and the band between about 5000 Å and 6000 Å was slightly higher relative to the emission between about 4000 Å and 5000 Å. At liquid nitrogen temperature the ratio of the heights of the two bands in D.56 is approximately the same as found at room temperature. Three lines now appear on the side of the higher wavelength band, corresponding to the first three ancillary lines in the 5032 Å emission system. They are relatively weak compared with the band upon which they are superimposed. In addition, weak minima appear at 5032 Å and on the high energy side of this line. These mimina correspond in position to the maxima in the 5032 Å absorption system. As in the case of the other two specimens so far described, there is a small amount of fluorescence in the near ultra-violet but none in the near infra-red. In each of the specimens examined an afterglow can be observed for a few seconds after switching off the x-ray tube, but no measurements have been made concerning this.

3.2. *Irradiated Type I Diamonds*

D.27.A is a specimen which has been neutron irradiated but not subsequently heated. The dose was sufficient to make the specimen a fairly deep green in colour. The absorption spectrum contained the 7410 Å system which is characteristic of irradiated diamonds (Clark, Ditchburn and Dyer 1956 a). The particular interest in the specimen was to see if any effect could be detected which could be associated with this system. The x-ray excited emission spectrum is similar to that obtained for other type I specimens except that the second broad band is slightly enhanced between about 5000 Å and 5500 Å. A spectrum obtained using a Long Range Spectrum plate shows no fluorescence in the 7000 Å to 9000 Å region. It would be here that any emission associated with the 7410 Å absorption system would probably occur.

D.18.E has been electron irradiated and heated at 900°C. After irradiation and heat treatment the colour of the x-ray excited fluorescence was green, as opposed to the blue in all unirradiated type I specimens examined. The spectrum obtained at 80°K in the 5000 Å to 6000 Å (2·48 ev to 2·07 ev) region is shown in figure 2. The broad band between 4000 Å and 5000 Å (3·10 ev to 2·48 ev) which was found in the other specimens was present, but its strength was small compared with the 5000 Å to 6000 Å band shown in the figure. (A comparison of exposure times required for D.18.E and D.78 suggests that the 5000 Å to 6000 Å band has been enhanced rather than the 4000 Å to 5000 Å one diminished.) The shape and position of the 5000 Å to 6000 Å band is similar to the background of the 5032 Å emission system which is excited by ultra-violet or visible light. This system will be strong in D.18.E, since it is caused by irradiation and heat

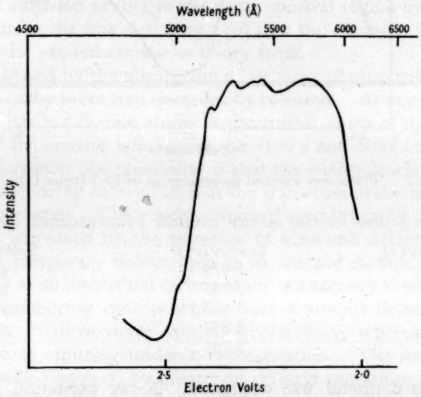

Figure 2. The x-ray excited fluorescence of D.18.E at 80°K.

treatment. The weak maxima shown in figure 2 correspond in position to the lines in the 5032 Å emission system.

3.3. *Type II Diamonds*

D.43, the specimen which was classified as being intermediate between type I and type IIa by Clark *et al.*, showed an emission spectrum with the same general features as the unirradiated type I specimens. D.16, which can be classified without doubt as a type IIa diamond, showed a similar spectrum. No evidence of weak subsidiary maxima or minima such as those found for D.55 was recorded. The strength of the fluorescence was less than that found in type I diamonds, but it was much stronger than would be predicted on the basis of a comparison of the strengths of the ultra-violet excited spectra.

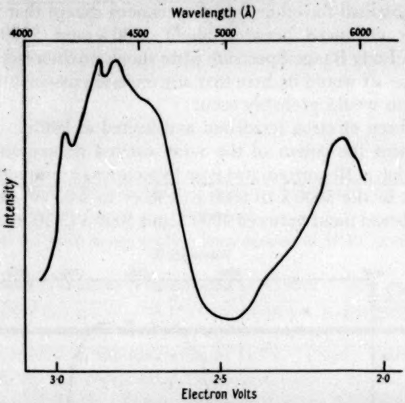

Figure 3. The X-ray excited fluorescence of D.1 (type IIb) at 80°K.

Table 2. Lines found in the X-ray excited Fluorescence of D.1 at 80°K

Wavelength (Å)	Energy (ev)	Relative strength
4175	2·970	medium
about 4275	2·900	very weak
4326	2·867	medium
4378	2·832	weak
4585	2·704	very weak

One type IIb diamond was examined. X-ray excitation produced a blue emission but its spectrum, particularly at 80°K was different from those previously described. At room temperature the spectrum shows the two broad bands which have been the chief feature of the other spectra. At 80°K the colour of the emission remains blue, but the shape of the spectrum is different, there being lines present. A copy of a microphotometer trace of the spectrum, obtained on an H.P.3 plate, is shown in figure 3. The photon energies corresponding to the lines found in this spectrum are given in table 2. The observation of such lines is most unexpected, since no line has ever been reported in phosphorescence or visible absorption spectra of type IIb diamonds.

§ 4. DISCUSSION

The spectrum shown by the majority of the specimens consists of two broad bands whose positions are similar to the positions of the 4150 Å and 5032 Å systems found using ultra-violet excitation. The enhancement of the x-ray excited emission in the region between 5000 Å and 6000 Å caused by electron irradiation and heat treatment is very similar to the enhancement of the ultra-violet excited 5032 Å emission system which is found after similar treatment. It seems that the x-ray excited fluorescence involves the same centres as those which give the ultra-violet excited fluorescence. Dyer and Matthews (1957) have shown that the centre which gives the 5032 Å emission when excited by ultra-violet or visible light is formed by the migration of interstitials or vacancies, which are induced by irradiation, to anchoring centres. Elliott, Matthews and Mitchell (1958) concluded from their experiments on the polarization of the luminescence that the axis of the anchored pair was probably ⟨110⟩, as would be the case for an interstitial carbon atom anchored to an interstitial impurity.

The weak maxima and minima which sometimes appear on the broad bands obtained with x-ray excitation at wavelengths corresponding to the lines usually found in the ultra-violet excited systems are probably caused by the re-absorption and re-emission of fluorescent radiation. This is indicated by the appearance of these features in specimens having strong absorption systems, and their absence in other specimens.

In the case of the x-ray excited emission we have to account for two main facts: (i) that the emission occurs in the same spectral region as for ultra-violet excitation but without the fine structure; (ii) that the emission is obtained even when the ultra-violet excited emission is very weak.

An electron released by the absorption of an x-ray photon will have sufficient energy to produce many more free electrons by collision. At any moment, therefore, there will be ionized carbon atoms in the crystal, some of them being in the neighbourhood of the centres which give the 4150 Å and 5032 Å systems. Concerning the 5032 Å system one possibility is that the energy levels are determined primarily by the anchoring centre but that the transition probability is low in an isolated anchoring centre. The results obtained could then be accounted for if the probability is increased by the presence of a second defect in an adjacent position—either a temporary defect such as an ionized carbon atom, or a permanent defect such as an interstitial carbon atom or a vacancy as mentioned above. Thus only those anchoring centres which have a second defect attached permanently give rise to ultra-violet excited fluorescence, whereas all anchoring centres are capable of emitting under x-ray excitation. The intensity of x-ray excited emission will, however, be greater in crystals containing some anchored pairs. This follows because in order to obtain emission from such a pair only the anchoring centre would need to be ionised, whereas if there were no anchored pairs both the anchoring centre and a neighbouring carbon atom would have to be ionized.

The presence of ionized carbon atoms near the anchoring centres will distort the field around the centres, and the distortion will be different for different positions of the ionized atom with respect to the centre. The nett effect will be to spread the levels into a broad band. Since the normal ultra-violet excited emission contains a high percentage of continuous background, only a few different positions of the ionized atom will be required to mask completely any structure.

A similar discussion can be given to account for the features of the x-ray excited blue emission.

This kind of mechanism provides an explanation for instance of the differences in emission characteristics of D.18.E and D.56. Under ultra-violet excitation both these crystals emit green light, there being more ‘ complete green ’ centres present than ‘ complete blue ’ centres. D.56 fluoresces blue under excitation with x-rays and this could arise from a large concentration of ‘ blue anchoring ’ centres whose presence is only revealed when neighbouring carbon atoms are ionized. Presumably in D.18.E there are fewer ‘ blue anchoring ’ centres.

At the present time it is not possible to give any more specific discussion of the nature of the emitting centres.

ACKNOWLEDGMENTS

The author wishes to thank Dr. E. W. J. Mitchell for help received in the preparation of this paper. Thanks are also due to Professor R. W. Ditchburn, Dr. J. F. H. Custers and Dr. H. B. Dyer for the interest they have taken in the work, and to Messrs Industrial Distributors (1946) Ltd for financial assistance.

REFERENCES

BISHUI, B. M., 1951, *Indian J. Phys.*, **25**, 575.
BULL, C., and GARLICK, G. F. J., 1950, *Proc. Phys. Soc.* A, **63**, 1283.
CLARK, C. D., DITCHBURN, R. W., and DYER, H. B., 1956 a, *Proc. Roy. Soc.* A, **234**, 363; 1956 b, *ibid*, **237**, 75.
DYER, H. B., and MATTHEWS, I. G., 1957, *Proc. Roy. Soc.* A, **243**, 320.
ELLIOTT, R. J., MATTHEWS, I. G., and MITCHELL, E. W. J., 1958, *Phil. Mag.*, **3**, 360.
RAMACHANDRAN, G. N., 1946, *Proc. Indian Acad. Sci.* A, **24**, 81.
SEN, S. N., and BISHUI, B. M., 1956, *Indian J. Phys.*, **30**, 620.

The Attachment of Slow Electrons in Air and Oxygen

By B. A. TOZER†, R. THORBURN‡ and J. D. CRAGGS
Department of Electrical Engineering, The University of Liverpool

MS. received 2nd May 1958, *and in revised form* 19*th August* 1958

Abstract. Calculations are presented to show that a satisfactory explanation of electron attachment coefficients, under low current discharge conditions, and for values of X/p greater than 10 v cm^{-1} (mm Hg)$^{-1}$ in both air and oxygen can be obtained if it is assumed that attachment takes place only in the form of resonant dissociative attachment to oxygen, and that a Maxwellian distribution of electron velocities exists in the electron swarm in discharges where the X/p values lie in the range $10 < X/p < 60$. Use of the electron drift and agitation velocity data of Crompton, Huxley and Sutton and of Townsend and Tizard shows better agreement with our calculations in the case of the latter workers' results.

§ 1. INTRODUCTION

In an earlier paper (Craggs, Thorburn and Tozer 1957) measurements, with an apparatus similar to that of Lozier (1934), of the cross section for electron attachment in oxygen have been reported and the values obtained used to show how the apparent discrepancy between the results of Harrison and Geballe (1953) and earlier workers, can be reconciled. It is our purpose here to show that if the calculations are carried out for the cases of both the Maxwellian and the Druyvesteyn distribution, for both oxygen and air, and using (in the case of air) different available sets of electron drift and agitation velocities, then a consistent picture is obtained only if attachment is assumed to be due to the dissociative attachment in oxygen and a Maxwellian distribution exists in the gas over the relevant range of values of X/p.

§ 2. CORRELATION OF LOW PRESSURE RESULTS WITH SWARM AND DISCHARGE EXPERIMENTS

The basis of the method has been described in our earlier paper (Craggs, Thorburn and Tozer 1957). Assuming a particular electron energy distribution, it is possible to calculate the effective cross section for a particular mean energy by use of the equation

$$\sigma_{\bar{E}}^{-} = \int {}_p\sigma \, n_p \, dp \Big/ \int n_p \, dp$$

where $\sigma_{\bar{E}}^{-}$ is the attachment cross section for the swarm of mean energy $\bar{E}$. σ_p is the cross section for, and n_p the number of, electrons of energy p. The quantity measured by Bradbury (1933), Kuffel (1958) and Herreng (1952) was

† Now at Queen Mary College, University of London.

‡ Now at Birkenhead Technical College.

not, in fact, $\sigma_{\bar{E}}^-$ but the quantity $\sigma_{\bar{E}}^- - \sigma_{\bar{E}}^+$ where $\sigma_{\bar{E}}^+$ is the effective cross section for ionization of the gas by electrons whose mean swarm energy is $\bar{E}$.

It is necessary when carrying out these calculations to allow for the relative mean free paths (i.e. the relative collision frequencies) of electrons of different energies, and, in the case of a gas mixture such as air, to allow for the difference between the mean free paths of the electrons for the two types of gas molecules. The result of these calculations is shown in figures 1 to 6. The curves for σ^- show the attachment which should occur in the gases under the conditions assumed to prevail, while the $\sigma^- - \sigma^+$ curves indicate the values to be expected from the work of Bradbury, Kuffel and Herreng and the other earlier workers. σ^+ is the effective ionization cross section.

§ 3. DISCUSSION

Figures 1 to 6 show the experimental curves and our curves obtained for air and oxygen, using different sets of data and the Maxwellian and Druyvesteyn energy distributions. In the case of oxygen the curves are not critically affected by choice of drift and agitation velocity data, and we have only drawn curves using the data of Crompton and Sutton (1957, private communication). The experimental attachment measurements we have employed are those of Harrison and Geballe (1953) and of Herreng (1952) whose results agree most nearly with the intermediate work of Burch and Geballe (1957). In the case of air, the choice of data has a far more important effect on the result of the calculation. The curves have been drawn for two sets of data, those of Townsend and Tizard (1913), and of Crompton, Huxley and Sutton (1953). Our σ^- and $\sigma^- - \sigma^+$ curves have been calculated as described above. The experimental attachment measurements employed here are those of Bradbury (1933) and of Kuffel (1958) who employed a Bradbury apparatus for his measurements, and of Harrison and Geballe. It will be seen that the recent results of Kuffel differ appreciably from the older values of Bradbury, and that the peak cross section value obtained in this later work is comparable with the peak value of our $\sigma^- - \sigma^+$ curve.

3.1. *Oxygen*

It will be noticed that in the case of a Maxwellian distribution a high degree of agreement has been reached between our curves and those obtained by direct experiment. In the case of a Druyvesteyn distribution it will be noticed that, although the agreement between the Harrison and Geballe curve and the rising part of the Herreng curve, on the one hand, and our σ^- curve on the other hand, is not so good as in the case of the Maxwellian distribution, the two sets of data are by no means incompatible. However, it should be noticed that for a Druyvesteyn distribution the ionization occurring in the gas is not sufficient to account for the discrepancy between the earlier swarm work (Bradbury, Herreng, Healey and Kirkpatrick 1941 and others) and the recent work of Harrison and Geballe (see curve $\sigma^- - \sigma^+$). Moreover, the results of Burch and Geballe indicate that the upward sweep of the Herreng curve should be continued, to join the Harrison and Geballe curve, when measurements independent of ionization effects are made. Thus, unless some experimental error, other than ionization effects, occurs in all the swarm experiments, and does not occur in the experiments of Harrison and Geballe, and of Burch and Geballe, it would appear that a Druyvesteyn distribution does not occur in oxygen in these conditions at values of X/p up to 60. It is unlikely that the contribution to attachment from the dissociative process can be much lower than our calculations suggest. Consideration of the processes described above shows that the only process capable of attaining any degree of importance in depressing the negative ion current is the detachment of electrons from O^- by collision with neutral oxygen molecules. However, this requires a combined energy (ion + molecule) at least equal to the electron affinity of oxygen ($\not< 1{\cdot}4$ ev). The ion kinetic energies, under the conditions of these experiments, are certainly very much lower than the electron energies, and there is experimental evidence that the energy does not differ appreciably from that of the molecules (Loeb 1955, p. 40) for values of X/p up to 40. As appreciable detachment could not occur due to this process unless the ion temperature exceeded the gas temperature by at least an order of magnitude, it does not appear possible to reconcile the results in this way.

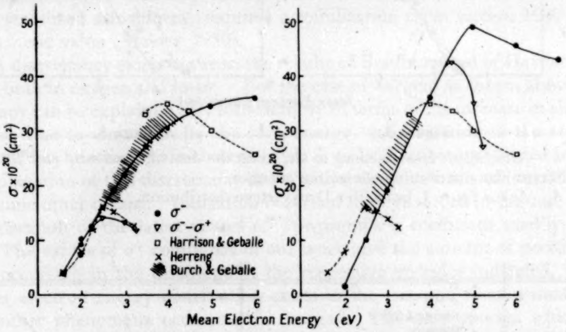

Figure 1. Figure 2.

Figure 1. Attachment cross sections in oxygen, using the data of Sutton and Crompton, for a Maxwellian distribution of electron energies.

Figure 2. As for figure 1, but with a Druyvesteyn distribution.

The closeness of the agreement between our calculated curves (figure 1) and the experimental curves, combined with the difficulty involved in explaining the attachment effects occurring in oxygen by any other means, must both be taken as strong evidence in favour of our contention that attachment in this gas is mainly due to dissociative attachment, and that a Maxwellian distribution of electron energies exists in the gas for mean electron energies in the range 0–6 ev.

3.2. *Air*

In assessing figures 3 to 6 it is necessary to appreciate the probable degree of accuracy of the experimental results of Harrison and Geballe and of Bradbury. It seems likely that the results reported by Kuffel (1958) are considerably more accurate than those of Bradbury (1933). The η/p (η = attachment coefficient) values obtained by Harrison and Geballe are obtained from analysis of the degree of curvature occurring in a curve of log i against d, and some idea of the probable accuracy of these curves can be gained from inspection of the curves obtained by Harrison and Geballe (1953) at $X/p = 50$ and $X/p = 60$. Values of η/p computed from these curves provide the two highest energy points on our Harrison and Geballe curve of cross section against mean electron energy (figures 3 to 6).

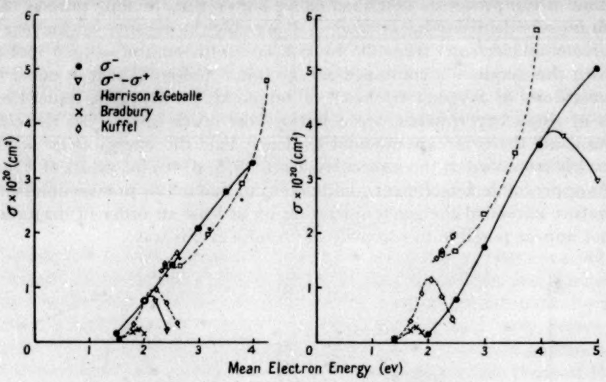

Figure 3. Figure 4.

Figure 3. Attachment cross sections in air, using the data of Townsend and Tizard, for a Maxwellian distribution of electron energies.
Figure 4. As for figure 3, but with a Druyvesteyn distribution.

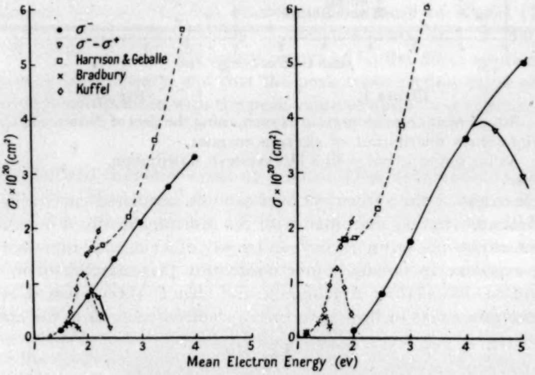

Figure 5. Figure 6.

Figure 5. Attachment cross sections in air, using the data of Crompton, Huxley and Sutton, for a Maxwellian distribution of electron energies.
Figure 6. As for figure 5, but with a Druyvesteyn distribution.

The accuracy of the drift and agitation velocity data on which interpretation of the experimental curves is based must also be considered. For drift velocities the measurements made by each of the two sets of workers we have considered agree well. The modern techniques evolved by Huxley and his co-workers make it likely that their results are the most accurate, but the difference is not in any case appreciable. On the other hand, the agitation velocity measurements differ widely between the different experimenters, and this has an important effect upon the conclusions reached. It is the different values of this quantity which are principally responsible for the widely differing results obtained in figures 3 and 5 and figures 4 and 6.

Finally, the experimental facts must be recalled:

(i) Bradbury carried out his attachment measurements over the pressure range 2–8 mm Hg, Harrison and Geballe worked in the range 30–80 mm Hg, while Prasad, at Liverpool, has worked in the range 60–700 mm Hg. None of these workers has observed any pressure effects. Thus, if any pressure-dependent effects occur, they must occur in the range 8–30 mm Hg, which is highly improbable, or else at pressures below 2 mm Hg, which, in the case of collision stabilized attachment, requires a stabilization cross section 1000 times the gas kinetic value (Massey 1950).

(ii) A discrepancy exists between the results of Bradbury and of Harrison and Geballe, both in oxygen and in air. For the case of oxygen, as shown above, this discrepancy can be explained very satisfactorily in terms of the increase in electron population due to ionization by the high energy ' tail ' existing in the electron swarm. If any picture of attachment in air is to be satisfactory it must include some explanation of this discrepancy in air, either again in terms of ionization, or else by some other means. Ionization is certain to be involved in the case of air, as consideration of the latest values of Townsend's α coefficient readily show.

(iii) The values of σ^+ computed in our work give the amount of positive ion current occurring in the discharge at the respective energies indicated, if that particular electron energy distribution exists in the gas, and remain unaffected by any other phenomena occurring in the gas. The only process which can reduce the actual positive ion current is recombination of the positive ions with electrons or negative ions, but as the experiments discussed here are carried out under low current conditions this effect must be entirely negligible.

Examination of figures 3 to 6 reveals that only figures 3 and 5 give reasonable agreement between our σ^- and $\sigma^- - \sigma^+$ curves on the one hand, and the experimental curves on the other hand.

The situations presented by figures 4 and 6 differ in detail, but are similar in their general implication. Each of these figures shows attachment occurring below the lower limit at which such effects can be expected due to dissociative attachment, each shows at higher energies an appreciably greater attachment cross section than that to be expected from dissociative attachment and each shows far too little positive ion current to account for the discrepancy between the Bradbury and the Harrison and Geballe results. While it is possible that either one or two collision stabilization processes, with stabilization cross sections several orders of magnitude greater than the gas kinetic value, occur in air to account for this discrepancy, and while it may be that something other than the ionization effect is the explanation of the discrepancy between the results of Harrison and Geballe and of Bradbury, we would submit that there is no experimental evidence to support such contentions, and that the explanation presented by figure 3 is not only the simplest, but also the most satisfactory.

§ 4. CONCLUSION

It is impossible, by arguments such as those presented above, to prove the existence of any particular electron energy distribution in air or oxygen, or to prove the existence of any particular attachment processes. We nevertheless feel that the greater simplicity of the explanation of attachment phenomena in these gases obtained by the adoption of a Maxwellian electron energy distribution, and by the assumption that in effect only dissociative attachment occurs, constitute strong evidence in favour of this interpretation.

ACKNOWLEDGMENTS

We are grateful to Professor Huxley and Dr. Crompton, both of Adelaide University, for helpful discussions and advice. One of us (B.A.T.) also wishes to express his gratitude to the Department of Scientific and Industrial Research for financial support.

REFERENCES

BRADBURY, N. E., 1933, *Phys. Rev.*, **44,** 885.

BURCH, D. S., and GEBALLE, R., 1957, *Phys. Rev.*, **106,** 183.

CRAGGS, J. D., THORBURN, R., and TOZER, B. A., 1957, *Proc. Roy. Soc.* A, **240,** 473.

CROMPTON, R. W., HUXLEY, L. G. H., and SUTTON, D. J., 1953, *Proc. Roy. Soc.* A, **218,** 507.

HARRISON, M. A., and GEBALLE, R., 1953, *Phys. Rev.*, **91,** 1.

HEALEY, R. H., and KIRKPATRICK, C. B., 1941, quoted by Healey and Reed (1941).

HEALEY, R. H., and REED, J. W., 1941, *The Behaviour of Slow Electrons in Gases* (Sydney: Amalgamated Radio (Australia) Ltd.).

HERRENG, P., 1952, *Cahiers de Phys.*, **38,** 7.

KUFFEL, E., 1958, *Proc. Phys. Soc.*, **71,** 516.

LOEB, L. B., 1955, *Basic Processes of Gaseous Electronics* (Berkeley and Los Angeles: University of California Press).

LOZIER, W. W., 1934, *Phys. Rev.*, **46,** 268.

MASSEY, H. S. W., 1950, *Negative Ions* (Cambridge: University Press).

TOWNSEND, J. S., and TIZARD, H. T., 1913, *Proc. Roy. Soc.* A, **88,** 336.

Elastic Scattering of Slow Ions in their Parent Gases

By M. R. C. McDOWELL
Department of Mathematics, Royal Holloway College

MS. received 13th May 1958, and in revised form 8th September 1958

Abstract. Total elastic scattering cross sections for H^+, H^-, He^+, Ne^+ and A^+ in their parent gases are calculated for energies between 0·1 ev and 10 kev, by an impact parameter method. The Massey–Mohr approximation is used for the phase shifts. The cross sections vary as the square of the logarithm of the energy above 100 ev, but at some energy between this and 0·1 ev change to an inverse one-third power dependence. Approximate interaction energies for $Ne_2{}^+$ and $A_2{}^+$ at large R are obtained from charge transfer data.

§ 1. INTRODUCTION

LITTLE information is available on the elastic scattering of heavy charged particles at low energies. Measurements of the cross section as a function of the impact energy have been reported, for a few simple cases, by Simons and his colleagues (Simons *et al.* 1943, Muschlitz and Simons 1952, Muschlitz, Bailey and Simons 1956, Cramer and Simons 1957). Differential cross sections over a restricted angular range, at energies above 25 kev are given by Everhart and by Fedorenko (Fedorenko 1954, Everhart, Stone and Carbone 1955, Carbone, Fuls and Everhart 1956).

There have been few theoretical studies. Massey and Smith (1933) discuss the elastic scattering of slow protons in helium and argon, while a brief discussion of argon atoms in argon is given by Massey and Mohr (1934). More recently Myers (1955, 1956) and Mason and Vanderslice (1957 a, b, and private communication) have attempted to account for Simons' results.

The available measurements of the total elastic scattering cross section refer to scattering through angles θ greater than some θ_0. Massey and Smith (1933) have pointed out that, since the scattered intensity per unit scattering angle increases very rapidly with decreasing scattering angle, the measured cross section will be but a small fraction of the true total cross section.

Classical mechanics yields an infinite cross section at all energies, whatever the form of the interaction. The quantum theory of atomic collisions leads, however, to a finite result in all cases for which the interaction potential vanishes at infinity more strongly than a Coulomb potential. The application of this theory requires a knowledge of the interaction of the atom and the scattered ion, over a wide range of nuclear separations. This information is available in only a few cases. However, it is possible, in principle, to obtain sufficient information on these interactions from measurements of charge transfer cross sections and mobilities.

In this paper we investigate the magnitude and energy variation of the total elastic scattering cross section of some simple singly charged ions in their parent gases.

§ 2. THEORY

Consider a single charged ion (say X^+) moving in its parent gas at low energies i.e. under semi-adiabatic conditions, such that the velocity of relative motion is small compared with the orbital electronic velocities (cf. Mott and Massey 1949). Under these conditions we may suppose that, at any instant during the collision, the colliding particles form a molecular ion X_2^+ with well defined interaction energies $V^{+,-}(R)$ at internuclear separation R, corresponding to states symmetric or antisymmetric with respect to interchange of the nuclei. In the cases we shall consider, since the states $V^{+,-}(R)$ tend to the same limit at large R and have the same multiplicity, the probabilities of the particles approaching along either are equal. We may therefore represent the total elastic scattering cross section (at relative momentum k) $Q_0(k^2)$ as the mean of the scattering by the two potentials $V^+(R)$ and $V^-(R)$.

$$Q_0(k^2)=\tfrac{1}{2}\{Q_0{}^+(k^2)+Q_0{}^-(k^2)\} \qquad \ldots\ldots(1)$$

where

$$Q_0{}^{+,-}(k^2)=\frac{4\pi}{k^2}\sum_{s=0}^{\infty}(2s+1)\sin^2\eta_s{}^{+,-} \qquad \ldots\ldots(2)$$

in which $\eta_s{}^{+,-}$ are the sth order phase shifts corresponding to the potentials $V^{+,-}(R)$. In the simple case of elastic scattering of protons by the hydrogen atoms a more rigorous theory may be developed (Bates, Massey and Stewart 1953). The total elastic scattering cross section $Q_0(k^2)$ is often regarded, for both theoretical and experimental purposes, as the sum of the direct elastic scattering cross section $Q_{\mathrm{el}}(k^2)$ and the cross section for charge transfer $Q_{\mathrm{T}}(k^2)$. These may be expressed in terms of the phase shifts $\eta_s{}^{+,-}$ as

$$Q_{\mathrm{el}}(k^2)=\frac{\pi}{k^2}\sum_{s=0}^{\infty}(2s+1)\{\cos^2(\eta_s{}^+-\eta_s{}^-)+1-\cos 2\eta_s{}^+-\cos 2\eta_s{}^-\} \qquad \ldots\ldots(3)$$

and

$$Q_{\mathrm{T}}(k^2)=\frac{\pi}{k^2}\sum_{s=0}^{\infty}(2s+1)\sin^2(\eta_s{}^+-\eta_s{}^-). \qquad \ldots\ldots(4)$$

At energies above some thousandths of an electron volt a large number of phase shifts enter the summations, which may then be replaced by integrations. Introducing the impact parameter $p=(s+\frac{1}{2})/k$ (all quantities being in atomic units) we have

$$Q_0{}^{+,-}(k^2)=8\int_0^{\infty}p\sin^2\{\eta^{+,-}(p)\}\,dp. \qquad \ldots\ldots(5)$$

Making the usual assumptions, that we can choose some $p=\bar{p}$ so that $\bar{p}$ is the largest value of p for which $|\eta^{+,-}(p)|$ attains the value $\pi/2$, and that for $p<\bar{p}$, $\sin\{\eta^{+,-}(p)\}$ oscillates rapidly, so that we may replace $\sin^2\{\eta^{+,-}(p)\}$ by its average value of $\frac{1}{2}$, we obtain

$$Q_0{}^{+,-}(k^2)=2\bar{p}^2{}_{+,-}+8\int_{\bar{p}_{+,-}}^{\infty}p\sin^2\{\eta^{+,-}(p)\}\,dp. \qquad \ldots\ldots(6)$$

The choice of $\bar{p}$ is of course arbitrary, and $Q_0{}^{+,-}(k^2)$ will oscillate as a function of $\bar{p}$. However, provided $\bar{p}\gg 1$, these oscillations of $Q_0(k^2,\bar{p})$ about the true value of $Q_0(k^2)$ are small (cf. § 6 (ii), and Dalgarno, McDowell and Williams 1958).

For slow heavy particle collisions we may employ the Langer–Jeffreys approximation to the phase shifts (Mott and Massey 1949) in the form

$$\eta_s=\int_{R_0}^{\infty}\{k^2-2\mu V(R)-s(s+1)/R^2\}^{1/2}dR-\int_{R_0'}^{\infty}\{k^2-s(s+1)/R^2\}^{1/2}dR \quad \ldots\ldots(7)$$

where R_0 and R_0' are the outermost zeros of their respective integrands and μ is the reduced mass of the system. For large s this becomes (Massey and Mohr 1934)

$$\eta_s\simeq\int_{R_0}^{\infty}\frac{\mu V(R)}{\{k^2-s(s+1)/R^2\}^{1/2}}dR \qquad \ldots\ldots(8)$$

which may be written in terms of the impact parameter p, as

$$\eta(p)\simeq\frac{\mu}{k}\int_{p}^{\infty}RV(R)/\{R^2-p^2\}^{1/2}dR. \qquad \ldots\ldots(9)$$

We shall assume, for simplicity, that the interaction energies may be expressed as

$$V^{+,-}(R)=\pm A^{+,-}\exp(-\alpha^{+,-}R)-\frac{c}{R^4}\left(\frac{e^2}{a_0}\right) \qquad \ldots\ldots(10)$$

in which $c=\frac{1}{2}\alpha e^2$, where α is the atomic polarizability. For this potential, the Massey–Mohr approximation to the phase shifts (9), becomes (Dalgarno and McDowell 1956)

$$\eta^{+,-}(p)\simeq-\frac{\mu}{k}\left\{\pm A^{+,-}pK_1(\alpha p)-\frac{\pi c}{4p^3}\right\} \qquad \ldots\ldots(11)$$

in which $K_1(\alpha p)$ is a first order modified Bessel Function of the second kind. The cross sections may then be obtained from (6) and (11).

§ 3. JUSTIFICATION OF THE IMPACT PARAMETER TREATMENT

The classical expression for $Q_0(k^2)$ is of course

$$Q_0(k^2)=2\pi\int_0^{\infty}p\,dp \qquad \ldots\ldots(12)$$

which diverges for all interactions (unless we introduce a cut-off) at all energies. That is according to classical mechanics the contribution to the elastic scattering from collisions having impact parameters between p and $p+dp$ is $2\pi p dp$. Our result (6) is equivalent (apart from a constant factor due to diffraction effects) to assuming that this is true for all $p<\bar{p}$, but avoids the divergence by adopting the correct quantal form for $p>\bar{p}$. This approximation requires justification.

The conditions for the validity of the classical description of a collision process have been investigated by Williams (1945). If over a range a, the scattering field has a strength V, in order that the orbit be well defined the de Broglie wavelength λ must be much less than a. Further, in order that the scattering angle should be well defined we must have

$$Va/\hbar v\gg 1 \qquad \ldots\ldots(13)$$

where v is the velocity of relative motion. The first of these conditions is satisfied in the energy range considered for all heavy particles. Taking for simplicity the potential $V=Ae^{-\alpha R}$, (13) shows that the classical approximation holds at impact parameters less than p provided

$$\frac{Ape^{-\alpha p}}{v}\gg 1. \qquad \ldots\ldots(14)$$

The phase shift for this potential, to the Massey–Mohr approximation, is

$$\eta(p) = -(\mu/k)\,ApK_1(\alpha p) \qquad \ldots\ldots(15)$$

and for $\alpha p \gg 1$ we can replace $K_1(\alpha p)$ by its asymptotic form, so that

$$\eta(p) \simeq -\left(\frac{\pi}{2\alpha}\right)^{1/2} \frac{Ap^{1/2}\mathrm{e}^{-\alpha p}}{v}. \qquad \ldots\ldots(16)$$

The condition (14) may then be written

$$\left(\frac{2\alpha p}{\pi}\right)^{1/2} \eta(p) \gg 1. \qquad \ldots\ldots(17)$$

We shall apply this approximation only when $|\eta(p)| > \frac{1}{4}\pi$, so (17) is equivalent to $(\frac{1}{2}\alpha p)^{1/2} \gg 1$. This condition is satisfied for all cases considered, except H^- in H at energies above 1 kev.

§ 4. FURTHER APPROXIMATIONS TO THE ELASTIC CROSS SECTION

It is of considerable interest to develop approximations which allow the energy dependence of the elastic scattering cross section to be displayed explicitly for various forms of interaction potential. These approximations also allow a rapid assessment of the magnitude of the cross section at any energy (in the adiabatic range) once the interaction energy is known. At large R we may assume that to a good approximation

$$A^+ = A^- = \tfrac{1}{2}A; \quad \alpha^+ = \alpha^-. \qquad \ldots\ldots(18)$$

So using (11), (6) becomes

$$Q_0^{+,-}(k^2) \simeq 2\bar{p}^2_{+,-} + 8\int_{\bar{p}_{+,-}}^{\infty} p\sin^2\left\{\frac{\mu}{k}\left[\pm\tfrac{1}{2}ApK_1(\alpha p) - \frac{\pi c}{4p^3}\right]\right\} dp. \qquad \ldots\ldots(19)$$

Choosing $\bar{p}_{+,-}$ such that $|\eta^{+,-}(\bar{p}_{+,-})| = \frac{1}{4}\pi$, and replacing $\sin\{\eta^{+,-}(p)\}$ by $\eta^{+,-}(p)$ for $p > \bar{p}$, (19) may be written as

$$Q_0^{+,-}(k^2) \simeq 2\bar{p}^2_{+,-} + \frac{8\mu^2}{k^2}\int_{\bar{p}_{+,-}}^{\infty} \left[\pm\tfrac{1}{2}Ap^{3/2}K_1(\alpha p) - \frac{\pi c}{4p^{5/2}}\right]^2 dp. \qquad \ldots\ldots(20)$$

This approximation may introduce errors of up to 10% in the contribution to $Q_0(k^2)$ from $p > \bar{p}$. However unless $\bar{p}$ is small, this contribution will be but a small part of $Q_0(k^2)$, so the total error will be much less than 10%. Provided that $\alpha\bar{p} \gg 1$ we may replace $K_1(\alpha p)$ by its asymptotic form (Dalgarno and McDowell 1956). Thus,

$$Q_0^{+,-}(k^2) \simeq 2\bar{p}^2_{+,-} + \frac{8\mu^2}{k^2}\int_{\bar{p}_{+,-}}^{\infty} \left[\pm\left(\frac{\pi A^2}{8\alpha}\right)^{1/2} p\mathrm{e}^{-\alpha p} - \frac{\pi c}{4p^{5/2}}\right]^2 dp. \qquad \ldots\ldots(21)$$

This approximation is adequate in all cases considered except H$^-$ in H, for which $\alpha^+ \simeq 0{\cdot}36$ and $\alpha^- \simeq 0{\cdot}20$. While (21) can be evaluated in closed form in terms of erfc $(\alpha\bar{p})$, it is convenient, provided c is small, to neglect terms in c except in determining $\bar{p}_{+,-}$. This gives

$$Q_0^{+,-}(k^2) \simeq 2\bar{p}^2_{+,-} + \frac{\pi\bar{p}_{+,-}}{4\alpha} \qquad \ldots\ldots(22)$$

where

$$\bar{p}_{+,-}\exp(-2\alpha\bar{p}_{+,-}) = \frac{\pi\alpha}{2A^2}\left|\frac{k}{\mu} \pm \frac{c}{p^3}\right|^2. \qquad \ldots\ldots(23)$$

Since $pK_1(\alpha p)$ decreases faster than p^{-3}, the terms in c must eventually dominate at sufficiently large p. In that case (21) becomes

$$Q_0(k^2) \simeq 2p^{*2} + \frac{\pi^2 \mu c^2}{16 E p^{*4}} \qquad \ldots\ldots(24)$$

with

$$p^* = \left(\frac{ck}{E}\right)^{1/3}. \qquad \ldots\ldots(25)$$

In intermediate cases recourse must be had to numerical integration of (6) using (11).

At low energies (22) and (23) indicate that $Q_0(k^2)$ is of the form

$$Q_0(k^2) = (\mathscr{A} \log E + \mathscr{B})^2 \qquad \ldots\ldots(26)$$

where $\mathscr{A}$ and $\mathscr{B}$ are constants. This gives a good fit to the calculated cross sections at energies above 1 ev in most cases. At lower energies the attractive forces dominate and (24) and (25) show that

$$Q_0(k^2) \propto E^{-1/3}. \qquad \ldots\ldots(27)$$

This may not hold down to zero energy, for eventually only a few phases will enter the summation (2) and its replacement by the integration (5) will be invalid.

Result (27) can be established directly from (5) using (11). For an interaction of the form $V(R) = -c/R^4$ we have

$$Q_0(k^2) = 8\pi \int_0^\infty p \sin^2 \left\{\frac{\pi \mu c}{4kp^3}\right\} dp \qquad \ldots\ldots(28)$$

so making the substitutions

$$\tfrac{1}{4}\pi\mu c = \beta, \quad y = p^{-3}, \qquad \ldots\ldots(29)$$

the integral in (28) is the Fourier sine transform of $y^{-5/3} \sin(\beta y/k)$. Thus (28) becomes (Erdelyi *et al.* 1954, p. 78)

$$Q_0(k^2) = \frac{2\pi^{8/3}}{3^{3/2}\Gamma(5/3)} \left(\frac{c^2 \mu}{E}\right)^{1/3}. \qquad \ldots\ldots(30)$$

Equations (26) and (27) or (30) suggest that a change in slope of the $(Q_0(E), E)$ curve is to be expected at some low energy. For all but two of the cases considered this occurs close to 1 ev. However, if both the reduced mass and the polarizability are large, the R^{-4} term may dominate to much higher energies. Alternatively, if the polarizability is small, and the repulsive forces fall off relatively slowly, they may mask the contribution from the attractive forces throughout our energy range.

§ 5. APPROXIMATIONS TO THE INTERACTION ENERGIES

Interaction energies $V^{+,-}(R)$, over a wide range of internuclear separations, are available only for the simplest homonuclear diatomic molecular ions such as H_2^+, H_2^- and He_2^+. However, in many other cases, considerable information on the charge transfer cross sections, and on the mobility as a function of temperature, is available (Dalgarno 1958).

Similar approximations to those used in § 4 show that the charge transfer cross section (4) may be represented by (Dalgarno and McDowell 1956)

$$Q_T(k^2) \simeq \tfrac{1}{2} p^{*2} + \frac{\pi^2 p^*}{16\alpha} \qquad \ldots\ldots(31)$$

where p^*, the largest impact parameter for which $|\eta^+(p)-\eta^-(p)|$ reaches $\pi/4$, is given by

$$p^* \exp(-2\alpha p^*) = \pi\alpha E/4\mu A^2 \qquad \ldots\ldots(32)$$

the difference in the interaction energies being

$$\Delta E(R) = V^+(R) - V^-(R) = A\mathrm{e}^{-\alpha R}. \qquad \ldots\ldots(33)$$

Neglecting p^* compared with p^{*2}, and denoting by $Q_{\mathrm{T}}(1)$ and $Q_{\mathrm{T}}(2)$ the charge transfer cross sections at impact energies E_1 and E_2, first approximations to A and α are given by A_0 and α_0 where

$$A_0{}^2 = \frac{\pi\alpha_0}{4\mu}\frac{E_1}{(2Q_{\mathrm{T}}(1))^{1/2}}\exp\{2\alpha(2Q_{\mathrm{T}}(1))^{1/2}\} \qquad \ldots\ldots(34)$$

and

$$\alpha_0 = \frac{1}{\sqrt{8}}\left|\frac{\log(E_1/E_2)}{\{Q_{\mathrm{T}}(1)\}^{1/2}-\{Q_{\mathrm{T}}(2)\}^{1/2}}\right|. \qquad \ldots\ldots(35)$$

These approximations A_0 and α_0 are then used to determine $Q_{\mathrm{T}}(k^2)$, and suitable second approximations are chosen by comparison with the experimental data. Two iterations usually suffice.

The interaction energies may then be written as

$$V^{+,-}(R) = \pm\frac{A}{2}\exp(-\alpha R) - \frac{c}{R^4} \qquad \ldots\ldots(36)$$

and $Q_0(k^2)$ determined. A further test of the derived A and α is available. They may be used to determine the mobility of the ion in its parent gas. The cross section effective in mobilities is $Q_{\mathrm{D}}(k^2)$,

$$Q_{\mathrm{D}}(k^2) \simeq 2\,[Q_{\mathrm{T}}(k^2) + Q_{\mathrm{p}}(k^2)] \qquad \ldots\ldots(37)$$

$Q_{\mathrm{p}}(k^2)$ being a small polarization correction (Dalgarno and McDowell 1956). At low energies, the computed $Q_{\mathrm{D}}(k^2)$ may be fitted by an expression of the form $(a\log E + b)^2$ where a and b are constants. The mobility κ is then given by

$$\kappa = \frac{3\sqrt{\pi}}{2^{7/2}}\frac{\boldsymbol{e}}{n_1 P_{12}{}'}\frac{1}{(\mu\boldsymbol{k}T)^{1/2}} \qquad \ldots\ldots(38)$$

in which $\boldsymbol{k}$ is Boltzmann's constant, T the absolute temperature, $\boldsymbol{e}$ the electronic charge, n_1 the gas number density and

$$P_{12}{}' = \{b^2 + ab(3 - 2\log\beta\gamma) + a^2(1 + \pi^2/16 - 3\log\beta\gamma + \log^2\beta\gamma)\} \qquad \ldots\ldots(39)$$

where γ is Euler's constant and $\beta = (\boldsymbol{k}T)^{-1}$.

§ 6. RESULTS AND DISCUSSION

Elastic scattering cross sections have been obtained for the positive ions of H, He, Ne and A in their parent gases, and for the negative ion of H in H, for centre of mass energies between 0·1 ev and 10 kev.

The accuracy of the cross sections will be determined primarily by the accuracy of the available interaction energies, and this varies considerably from case to case. It is discussed in more detail below. Further uncertainties arise from the use of approximations to the phase shift. It is difficult to assess the accuracy of the Massey–Mohr approximation. At those values of p for which we employ a phase shift analysis, the Massey–Mohr and Jeffreys' approximations are equivalent (since $s \gg 1$) and, further, tend in the limit of large s to the Born approximation (Massey and Mohr 1934, Dalgarno, McDowell and Williams 1958). Exact phase shifts for heavy particle scattering are not yet available. The further approximations developed in § 4 are in good agreement with (6) except in those cases for which $\bar{p}$ is small, or if the contribution to $Q_0(k)$ from $p > \bar{p}$ is a major part of the total. The first of these cases occurs only for H^- in H at energies above 1 kev, while the second occurs only for A^+ in A at energies below 100 ev.

(i) *He^+ in He.* The helium molecular ion $He_2{}^+$ has received considerable study. The most detailed results are those of Moiseiwitsch (1956). He used his calculated interactions to derive charge transfer cross sections (1956) and mobilities (Lynn and Moiseiwitsch 1957) in good agreement with experimental data. We have used these interactions to obtain $Q_0(k^2)$ and the results are presented in table 1.

Table 1. Charge transfer and elastic scattering cross sections (in units of $\pi a_0{}^2$) for He^+ in He, $Q_0(1)$ being calculated from Moiseiwitsch's energies and $Q_0(2)$ from the extrapolated charge transfer cross sections. Q_{Simons} is due to Cramer and Simons 1957

$\log_{10}E$ (ev)	-1	0	1	2	3
Q_T	41	33	25	19	13
$Q_0(1)$	244	89	64	43	26
$Q_0(2)$	208	118	84	56	35
Q_{Simons}	—	—	22	14	—

The observed charge transfer cross sections were extrapolated to low energies (cf. Dalgarno 1958) and used to determine an approximate $\Delta E(R)$. While A was given with considerable accuracy, α differed from Moiseiwitsch's value by 10%. Unfortunately $Q_0(k^2)$ is rather sensitive to α, and the approximate results, also shown in table 1, exceed those calculated from Moiseiwitsch's data by 30% at energies down to 1 ev. Below this energy the polarization term (which is the same for both interactions) dominates, and both sets of cross sections tend to the same value at very low energies. The error of 30% in the cross section calculated from the charge transfer data is not excessive, and could be considerably reduced if experimental charge transfer cross sections accurate to $0{\cdot}1\ \pi a_0{}^2$ were available. The approximate $\Delta E(R)$ would then be of considerable value.

Observed values of $Q_0(k^2)$ at 10 ev and 100 ev interpolated from the results of Cramer and Simons (1957) are also given in table 1. Their apparatus was such that, even at the entrance to the scattering chamber, collisions through angles $\theta < \theta_0 \simeq \tan^{-1} 0{\cdot}0731$ (i.e. $\theta_0 \simeq 4°$) were not recorded. It is clear from the table that their results are but a small fraction of the total cross section. Mason and Vanderslice (1957 a) have been able to reproduce Cramer and Simons' results, using Moiseiwitsch's interaction energies and a classical approximation to the scattering, but including only angles $\theta > \theta_0$. The effect of the rapid increase of scattered intensity with decreasing scattering angle becomes more significant as the impact energy increases, so that the fraction of the total cross section measured ($\theta > \theta_0$) should decrease rapidly with increasing impact energy. The available data do not cover a wide enough energy range to allow confirmation of this point.

(ii) *H^+ and H^- in H.* Very accurate interaction energies are available for $H_2{}^+$ (Bates, Ledsham and Stewart 1953) and fairly reliable results for $H_2{}^-$ were obtained by Dalgarno and McDowell (1956). These have been used to calculate $Q_0(k^2)$ using (6) and (11). The results are shown in table 2. While no experimental information is available, it has been suggested by Bates and Dalgarno

(1952) that at energies much greater than the binding energy of H_2 the cross sections for collisions with the molecule should be about twice those for collisions with atomic Hydrogen. Little can be said about the H^+ in H cross sections, except that they should be fairly reliable, being based on very accurate interaction energies. Polarization is relatively unimportant in the energy range considered, but begins to affect the cross sections at energies below 1 ev.

Table 2. Cross sections for H^+ and H^- in H in units of πa_0^2. (*a*) Dalgarno and Yadav (1953); (*b*) Dalgarno and McDowell (1956); (*c*) Simons *et al.* (1943); (*d*) Muschlitz, Bailey and Simons (1956); (*c*) and (*d*) are adjusted to refer to atomic hydrogen

	$\log_{10}E$ (ev)	0	1	2	3	4	
H^+	Q_T	54	41	29	19	10	(*a*)
	Q_0	165	118	80	50	27	
	Q_{Simons}	—	10	1·4	—	—	(*c*)
H^-	Q_T	240	158	90	39	6·2	(*b*)
	Q_0	1027	634	284	74	10	
	Q_{Simons}	—	4·6	3·1	—	—	(*d*)

The H^- in H case was of considerable interest. Owing to the low reduced mass and polarizability and the comparatively slow fall-off of the repulsive forces, the contribution from polarizability is negligible above 0·1 ev. The approximations of § 4 are unreliable in this case, chiefly because $\alpha\bar{p}$ is small and we cannot replace $K_1(\alpha\bar{p})$ by its asymptotic form. We have investigated the oscillations of $Q_0(k^2)$ as a function of $\bar{p}$, for $k^2 = 10^4$ and 10^6, since $\bar{p}$ is small only when k^2 is large. The amplitude of the oscillations increases with increasing energy, but the value of $Q_0(\bar{p})$, with $\bar{p}$ chosen such that $|\sin\eta(\bar{p})| = \pi/2$, lies within 1% of the mean in both cases, while the $\pi/4$ approximation differs from the mean by less than 5%. When $\alpha\bar{p} \gg 1$, i.e. at energies below 1 kev, the further approximations of § 4 give results within 10% of those obtained from (6). The quoted results for H^- in H cannot claim high accuracy for $E < 10$ ev, since at these energies the range of the potential important in determining $Q_0(k^2)$ extends out to R of the order of $\bar{p} \simeq (\frac{1}{2}Q_0)^{1/2}$, (i.e. $R > 15\,a_0$), while the interactions are extrapolations beyond $10\,a_0$. In both cases the total elastic scattering cross section is much larger than the charge transfer cross section at low energies, but the difference is not marked at high energies. This indicates a great preponderance of forward over backward scattering at low energies, the scattering becoming more nearly symmetrical about $\theta = \pi/2$ at the highest energies considered. However, the method used is unreliable at energies above 1 kev for hydrogen (Dalgarno and Yadav 1953) since it tends to overestimate the cross section at these energies in comparison with the Born approximation. The considerable difference in magnitude of both negative ion cross sections from the corresponding positive ion cross sections must be attributed to the very diffuse structure of the negative ion.

Some experimental data are available for elastic scattering of H^+ in H_2 (Simons *et al.* 1943, Muschlitz and Simons 1952) and of H^- in H_2 (Muschlitz, Bailey and Simons 1956). Representative values are shown in table 2. While part of the discrepancy may be due to the structure of H_2, most will arise, as in the He^+ case, from the poor angular resolution employed. Myers (1955, 1956) and Mason and Vanderslice (1957 b, and private communication) have shown that the observational data may be interpreted by a combination of attractive and repulsive inverse

R^n potentials, and that the H^- results are consistent with electron detachment data for H^- in H_2.

(iii) *Ne^+ in Ne and A^+ in A.* In these cases we may use extrapolated charge transfer cross sections (Dalgarno 1958) to obtain approximate interaction energies. For $Ne_2{}^+$ we find that the scattering potential may be represented by

$$\Delta E(R) = 11{\cdot}47 \exp\{-1{\cdot}180R\}, R \geqslant 7{\cdot}0\ a_0.$$

The resulting values of $Q_0(k^2)$ are shown in table 3 and compared with Dalgarno's values of $Q_T(k^2)$. At low energies almost all the scattering is in the forward direction, but as the energy increases charge transfer becomes somewhat more important, being about one third of the total at 1 kev. Polarization forces do not make a large contribution above 1 ev, but below that energy they rapidly dominate.

Table 3. Total elastic and charge transfer cross sections for Ne^+ and A^+ in their parent gases in units of $\pi a_0{}^2$

	$\log_{10}E$ (ev)	-1	0	1	2	3	4
Ne^+	Q_T†	47	38	30	23	17	—
	Q_0	285	154	115	86	60	36
A^+	Q_T†	84	73	62	52	43	—
	Q_0	1661	763	276	188	154	118

†Dalgarno (1958).

The interaction energies found for $A_2{}^+$ may be represented by

$$\Delta E(R) = 4{\cdot}29 \times 10^2 \exp\{-1{\cdot}215R\} \qquad \ldots\ldots (40)$$

where R is greater than $10\ a_0$. The reduced mass and polarizability are comparatively large and we cannot use (22) and (24) to evaluate $Q_0(k^2)$, except at very low energies where (24) becomes quite accurate. The change in slope of the ($Q_0(k^2)$, E) curve sets in near 50 ev, primarily because the position of the zero of $\eta^+(p)$ at energies below 50 ev lies inside the last value of $\bar{p}_+$ for which $|\eta^+(p)|$ reaches $\pi/4$. The effect of uncertainties in the available $E(R)$ was investigated by repeating the A^+ calculations with $\Delta E'(R) = 1{\cdot}66\Delta E(R)$. The resulting cross sections were the same below 10 ev, and the error at higher energies did not exceed 10%. Uncertainties in α would be more serious, but the resulting cross sections are unlikely to be in error by more than a factor of two at energies below 10 kev.

The only experimental data available are measurements of differential cross sections at energies above 25 kev and angles greater than 4° (Fedorenko 1954, Carbone, Fuls and Everhart 1956). Our method is very suspect at energies as high as 25 kev, since the internuclear distance is changing very rapidly, but it is of interest to examine the ratio of the scattered intensity at $\theta = 0°$ to that at $\theta = 4°$, using Massey and Smith's (1933) result,

$$I(0) = \mu E Q_0{}^2/16\pi^2 \ (a_0{}^2) \qquad \ldots\ldots (41)$$

and the Carbone *et al.* (1956) value of $I(4°) \simeq 2 \times 10^{-15}\ \text{cm}^2$. This leads to $I(0)/I(4°) \sim O(10^8)$. Classical theory predicts an infinite ratio. The only other quantal calculation is for protons in argon at a few ev (Massey and Smith 1933) where the ratio is of the order of (10^5). Allowing for the much lower energy the agreement is satisfactory. Further experimental work at small angles and low energies would be valuable, as would quantal calculations of the differential cross section at small angles.

ACKNOWLEDGMENTS

I should like to thank Dr. A. Dalgarno and a referee for helpful comments on an earlier version of this paper.

REFERENCES

BATES, D. R., and DALGARNO, A., 1952, *Proc. Phys. Soc.* A, **65**, 919.
BATES, D. R., LEDSHAM, K., and STEWART, A. L., 1953, *Phil. Trans. Roy. Soc.* A, **246**, 215.
BATES, D. R., MASSEY, H. S. W., and STEWART, A. L., 1953, *Proc. Roy. Soc.* A, **216**, 437.
CARBONE, R. J., FULS, E. N., and EVERHART, E., 1956, *Phys. Rev.*, **102**, 1524.
CRAMER, W. H., and SIMONS, J. H., 1957, *J. Chem. Phys.*, **26**, 1272.
DALGARNO, A., 1958, *Phil. Trans. Roy. Soc.* A, **250**, 426.
DALGARNO, A., and MCDOWELL, M. R. C., 1956, *Proc. Phys. Soc.* A, **69**, 615.
DALGARNO, A., MCDOWELL, M. R. C., and WILLIAMS, E. J. A., 1958, *Phil. Trans. Roy. Soc.* A, **250**, 411.
DALGARNO, A., and YADAV, H. N., 1953, *Proc. Phys. Soc.* A, **66**, 173.
ERDELYI, A., MAGNUS, W., OBERHETTINGER, F., and TRICOMI, F. G., 1954, *Tables of Integral Transforms,* Vol. **I** (London: McGraw-Hill).
EVERHART, E., STONE, A. N., and CARBONE, R. J., 1955, *Phys. Rev.*, **99**, 1287.
FEDORENKO, N. V., 1954, *J. Tech. Phys., Moscow*, **24**, 784.
LYNN, N., and MOISEIWITSCH, B. L., 1957, *Proc. Phys. Soc.* A, **70**, 474.
MASON, E. A., and VANDERSLICE, J. T., 1957 a, *Phys. Rev.*, **108**, 293; 1957 b, *J. Chem. Phys.*, **27**, 917.
MASSEY, H. S. W., and MOHR, C. B. O., 1934, *Proc. Roy. Soc.* A, **144**, 188.
MASSEY, H. S. W., and SMITH, R. A., 1933, *Proc. Roy. Soc.* A, **142**, 142.
MOISEIWITSCH, B. L., 1956, *Proc. Phys. Soc.* A, **69**, 653.
MOTT, N. F., and MASSEY, H. S. W., 1949, *Theory of Atomic Collisions*, 2nd edn (Oxford: Clarendon Press).
MUSCHLITZ, E. E., and SIMONS, J. H., 1952, *J. Phys. Chem.*, **56**, 837.
MUSCHLITZ, E. E., BAILEY, T. L., and SIMONS, J. H., 1956, *J. Chem. Phys.*, **24**, 1202.
MYERS, V. W., 1955, *J. Chem. Phys.*, **23**, 755; 1956, *Ibid.*, **25**, 1284.
SIMONS, J. H., FONTANA, C. M., MUSCHLITZ, E. E., and JACKSON, S. R., 1943, *J. Chem. Phys.*, **11**, 307.
WILLIAMS, E. J., 1945, *Rev. Mod. Phys.*, **17**, 217.

The Energy Levels of ^{31}P
I: γ-ray Spectra and Decay Schemes

By C. BROUDE, L. L. GREEN AND J. C. WILLMOTT
Nuclear Physics Research Laboratory, University of Liverpool

Communicated by H. W. B. Skinner; MS. received 23*rd June* 1958 *and in revised form* 18*th August* 1958

Abstract. Gamma-ray spectra have been studied at ten resonances in the reaction $^{30}Si(p,\gamma)^{31}P$ and decay schemes found by analysis of the spectra and coincidence experiments.

§ 1. INTRODUCTION

UNTIL recently it has been generally thought that the collective model of Bohr and Mottelson applied only to the heavier nuclei. The work of Litherland *et al.* (1956, 1957) has however shown that the Nilsson (1955) model can be used with qualitative success in the $A=25$ nuclei and Paul (1957) has been able to reproduce the levels of ^{19}F and some of their properties using this model as modified by Kerman (1956). It is clearly of interest to look for evidence of collective motion in other nuclei in this region in order to establish the range of validity of this model.

^{31}P is one of those spin $\frac{1}{2}$ nuclei whose magnetic moment deviates strongly from the Schmidt value and preliminary studies have indicated strong E2 transitions in this nucleus (Broude *et al.* 1956, Paul *et al.* 1956). Using the wave functions published by Nilsson one can estimate the distortion to be expected for any particular nucleus and for nuclei in the region of ^{25}Al the predicted shape is prolate in agreement with the experimental evidence. For ^{31}P and ^{29}Si the distortion is expected to be oblate and Bromley *et al.* (1957 a, b) have recently presented some evidence that collective motion is important in ^{29}Si and that the distortion is oblate. A detailed study of the levels of ^{31}P and their modes of decay is clearly of interest in deciding whether the Nilsson model is applicable in this region and if so whether the oblate trend has become established or whether vibrational instability is more important. In parts I and II we present the results of a study of the γ-rays emitted at ten resonances in the reaction $^{30}Si(p,\gamma)^{31}P$ and in part III we present a detailed comparison of the experimental data with the predictions of the Nilsson model.

§ 2. EXPERIMENTAL PROCEDURE

A beam of protons of energies up to 1100 kev was used to bombard a thin ^{30}Si target deposited on 0·01 in. gold backing. The γ-rays were detected in sodium iodide counters. The bulk of the work on the γ-ray spectra was done using a crystal $4\frac{1}{2}$ in. in diameter and $4\frac{1}{2}$ in. long optically coupled to a 5 in. diameter EMI photomultiplier. Some spectra were also taken using a somewhat larger crystal, 5 in. in diameter by 6 in. long. The output pulses were amplified, shaped, and then analysed by a Hutchinson–Scarrott pulse height analyser.

The analysis of complex spectra requires a knowledge of the γ-ray line shapes at all energies relevant to the reaction being studied. It is much easier to analyse the spectra if most of the pulses belonging to a particular γ-ray fall in the total capture peak; the position of a γ-ray is more easily recognized and the errors caused by subtraction are much reduced. From this point of view the line shapes are much improved if only the central region of the crystal is irradiated and so a 4 in. thick lead collimator shielded all but the central two inches of the front face of the crystal. The line shapes of well-isolated γ-rays were obtained with this arrangement and interpolated to any other required energy. Typical line shapes are shown in figure 1. The other faces of the crystal were surrounded by two inches of lead to reduce the stray background, and spurious γ-rays from the target backing were eliminated by bombarding the target a few kilovolts off resonance in a separate experiment.

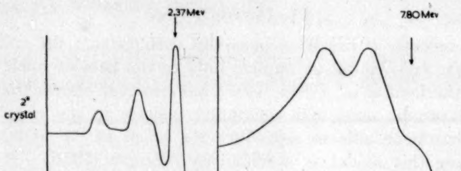

Figure 1. Gamma ray shapes at 2·37 and 7·80 MEV.

The intensity of a particular γ-ray is proportional to the total number of pulses it produces, i.e. to the area under the pulse height distribution curve for this γ-ray. To compare the intensities of γ-rays of different energies we evaluated the function A/eP for γ-rays of various energies, where A is the total area under the pulse height distribution curve, e the detection efficiency of the crystal and P the height of the total capture peak. By interpolation of this function the relative intensities of γ-rays can be obtained from the number of counts recorded at the maxima of the total capture peaks.

The effect of angular distributions on the measured relative intensities were minimized by taking the spectra with the detector set at the angle where $P_2(\cos\theta)$ is zero. Higher terms cannot be eliminated simultaneously but these do not occur as frequently or as strongly as the $P_2(\cos\theta)$ term in this reaction.

At each resonance the energies and intensities of the γ-rays were used to construct a preliminary decay scheme, which was then checked as far as possible by coincidence measurements. For these measurements a second sodium iodide crystal 2 in. diameter and 2 in. long was used to detect one γ-ray and the larger crystal the other γ-ray. To obtain a reasonable coincidence counting rate collimation of the larger crystal was dispensed with. The coincidence spectra were obtained as follows. The pulses from one crystal were fed to the pulse height analyser which, however, only recorded a pulse if another pulse occurred at the same time in the other crystal and fell within a particular region of the γ-ray spectrum defined by a single channel analyser. The coincidence unit had a resolving time of 1 microsecond and the ratio of chance to genuine counts varied between 5 and 10%.

§ 3. RESULTS

The early published work on the excited states of ^{31}P is of little value. The neutron groups from deuteron bombardment of natural silicon have been investigated but an unambiguous assignment of these groups to the various isotopes of silicon could not be made.

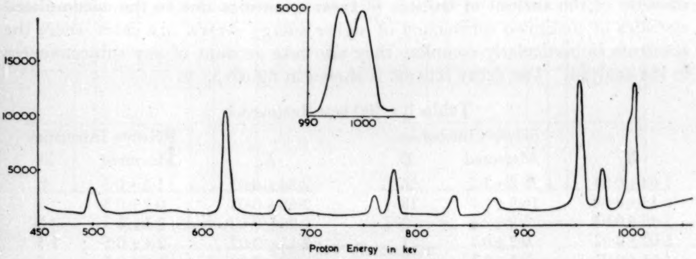

Figure 2. Excitation function of the reaction ^{30}Si(p,γ)^{31}P.

During the course of this work results on the inelastic scattering of 6 MeV protons from ^{31}P became available and we are indebted to Professor P. M. Endt for sending us these results prior to publication. Inelastic proton groups corresponding to levels in ^{31}P at 1·267, 2·235, 3·131, 3·292, 3·414, 3·508, 4·12, 4·19, 4·26, 4·44, 4·59, 4·64 and 4·78 MeV were observed with other possible levels at 5·03 MeV and 5·12 MeV (Endt and Paris 1957). The energy resolution of γ-ray spectrometry is such that this technique cannot approach the precision of the measurements just quoted. The knowledge of the exact position of the quartet of levels between 3·1 and 3·5 MeV has been of great value in interpreting the spectra at those resonances at which several of these levels are excited. The energies of the levels in the region from 4·0 to 5·0 Mev have not been used in this way because information on these levels was not available until after the level schemes for the (p, γ) work had been established. Comparison of the two sets of levels in this energy range shows that not all of the levels have been excited by the (p, γ) reaction but that those which have been observed by proton capture agree quite well with levels that occur in the inelastic scattering experiments.

Previous work on this reaction by Tangen (1946) showed two resonances, one at 367 kev, the other at 499 kev. The former was not observed by us. The excitation function in the region from 450 kev to 1080 kev is shown in figure 2. There are ten resonances due to ^{30}Si(p, γ) and an additional one at 873 kev due to the ^{19}F(p, γ)^{16}O reaction. The energies of the resonances have not been determined absolutely and we refer to them respectively as 500, 625, 675, 760, 775, 840, 955, 980, 995 and 1000 kev resonances. The observed widths of the resonances shown in the diagram are experimental and arise mainly from the target thickness.

The resonances are described in an order which most clearly elucidates the properties of the levels. Transitions which are obvious from energy and intensity considerations are not usually referred to in the text.

500 *keV Resonance*

The γ-rays observed at this resonance are shown in table 1. The relative intensities are normalized to give a total intensity of 100. The final column shows the intensity of each γ-ray accounted for in the decay scheme. The tolerance allocated to the energy and intensity measurements has been assessed from the clarity with which each γ-ray appears in the spectrum. They are a measure of the amount of latitude in these quantities due to the accumulated statistics of continued subtraction of higher energy γ-rays. In cases where the spectrum is particularly complex, they also take account of any subjectiveness in the analysis. The decay scheme is shown in figure 3.

Table 1. 500 kev Resonance

	Relative Intensities			Relative Intensities	
E_γ	Measured	D	E_γ	Measured	D
7·69 ± 0·04	35·6 ± 1·5	36	2·84 ± 0·03	1·3 ± 0·5	†
6·43 ± 0·04	16·9 ± 1·0	18	2·68 ± 0·03	0·9 ± 0·5	1
5·49 ± 0·03	2·9 ± 0·4	3	2·23 ± 0·02	3·5 ± 0·5	4·5
5·02 ± 0·02	0·7 ± 0·4	1	2·15 ± 0·02	2·4 ± 0·5	1·5
4·63 ± 0·02	7·1 ± 0·5	7	1·99 ± 0·02	1·1 ± 0·5	1·5
3·13 ± 0·02	7·1 ± 0·5	7	1·27 ± 0·01	18·9 ± 1·0	19·5

D, decay scheme. † Not accounted for.

All the γ-rays fit in with known levels in a simple way except the 2·84 Mev γ-ray and the cascade via the 6·43 Mev, 4·26 Mev and 2·23 Mev levels. This cascade occurs more strongly at other resonances and will not be discussed in detail here.

The only γ-ray left unexplained is the 2·84 Mev. As this lies quite close to the 2·68 Mev γ-ray and both have bad statistics due to continuous subtraction processes in the analysis, it is possible that there exists only one γ-ray of energy about 2·75 Mev, which is a more correct energy for the transition to the 5·00 Mev level.

Both the 2·23 and 3·13 MeV levels are shown (figure 3) as decaying only to the ground state, and it is of interest to estimate the upper limits on other possible decay modes which are not observed.

If the 2·23 MeV level decayed partially to the 1·27 MeV state, a 0·96 MeV γ-ray would result. An upper limit for the intensity of a γ-ray of this energy would be about 2% of the intensity of the strong 1·27 MeV γ-ray. Thus it can be concluded that if the 2·23 MeV level decays to the 1·27 MeV state, this decay cannot be more than 5% of the intensity of the ground state transition. In a similar way transitions from the 3·13 MeV state to the 2·23 and 1·27 MeV levels each cannot be more than 5% of the decay to the ground state.

From the decay scheme 63·5% of the total radiation observed is emitted from the resonance level. Using this value and the number of emitted γ-rays per incident proton a value of 0·24 ev is obtained for $(2J+1)\Gamma_\gamma$ at this resonance, assuming that the proton width is considerably larger than the radiation width.

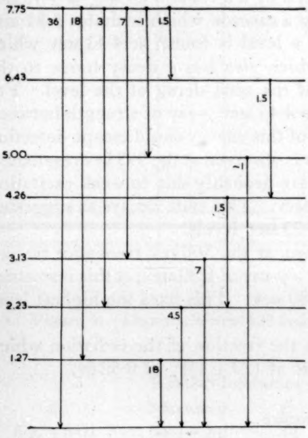

Figure 3. Decay schemes 500 kev.

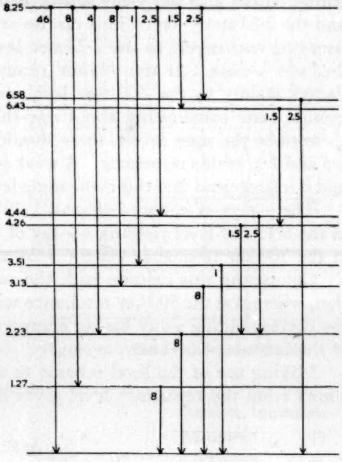

Figure 4. Decay schemes 1000 kev.

1000 *keV Resonance*

This is the stronger resonance of the doublet which occurs at approximately 1 MeV. The intensity measurements were made using a thin ($\sim$1 kev) target and the proton energy was adjusted so as to keep on the high side of the resonance. In this way, it was ensured that the lower resonance at 995 kev was not excited. The energies and intensities of the γ-rays observed at this resonance are shown in table 2 and the decay scheme in figure 4.

A coincidence experiment showed that only the 6·95 MeV γ-ray was in coincidence with the 1·27 MeV γ-ray and consequently there is no other source of 1·27 MeV radiation.

The observed intensity discrepancy can only be explained in terms of the bad statistics of the 6·95 MeV γ-ray which occurs just below the single quantum escape region of the strong ground state transition.

Table 2

E_γ	Relative Intensities Measured	D	E_γ	Relative Intensities Measured	D
8·22 ± 0·02	46·3 ± 2·0	46	3·13 ± 0·02	8·9 ± 0·8	8
6·95 ± 0·04	3·0 ± 1·5	8	2·24 ± 0·01	11·1 ± 0·5	12
6·55 ± 0·05	2·6 ± 1·0	2·5	2·00 ± 0·02	2·4 ± 0·5	1·5
6·04 ± 0·03	3·9 ± 0·5	4	1·79 ± 0·02	1·8 ± 0·5	1·5
5·07 ± 0·02	7·0 ± 0·5	8	1·63 ± 0·02	2·5 ± 0·5	2·5
4·77 ± 0·03	1·0 ± 0·5	1	1·28 ± 0·01	8·4 ± 0·5	8
3·81 ± 0·03	2·7 ± 0·4	2·5	1·10 ± 0·02	0·5 ± 0·3	†
3·47 ± 0·04	0·6 ± 0·4	1			

D, decay scheme. † Not accounted for.

The strength of the 6·04 Mev γ-ray to the 2·23 Mev level is 4% while the 2·23 Mev γ-ray itself has strength 11%. The coincidence spectrum obtained by gating on the 2·23 Mev γ-ray shows the 6·04 Mev γ-ray and also the 3·81 Mev γ-ray and the 2·23 Mev γ-ray. This can be explained by a level at 6·00 Mev or 4·43 Mev decaying exclusively to the 2·23 Mev level by a cascade which includes 3·81 and 2·23 Mev γ-rays. At the 995 kev resonance a level is found at 4·43 Mev which decays mainly to the 2·23 Mev level, but which also has a decay mode to the ground state constituting about one-third of the total decay of the level. For these to be the same levels, there should be a 4·43 Mev γ-ray of strength between 0·5 and 1% at this resonance. A weak γ-ray of this energy could escape detection and it is suggested that this is the same level as is observed at the 995 kev resonance.

The γ-rays of energy 2·00 and 1·79 Mev are probably due to weak excitation of the 6·43 Mev level yielding a γ-ray of 1·80 Mev. This state decays as suggested at the 500 kev resonance via the 4·26 and 2·23 Mev levels.

Comparing this cascade with the same one at the 500 kev resonance we see that, whereas at the 500 kev resonance we had a γ-ray of 1·30 Mev, at this resonance the corresponding γ-ray has an energy of 1·80 Mev. This fixes the highest level of the cascade at 6·43 Mev.

Making use of the level scheme to assess the fraction of the radiation which comes from the resonance level gives a value of $(2J+1)\Gamma_\gamma$ of 0·52 ev.

625 *kev Resonance*

Except for the 2·56 Mev γ-ray, the γ-rays not shown on the diagram can all be explained by a level at 4·17 Mev which decays to the 1·27 and 2·23 Mev states in the ratio of two to one. The system is so weak here that it is not shown on the decay scheme and will be discussed elsewhere. The level scheme is shown in figure 5. The value of $(2J+1)\Gamma_\gamma$ is 1·43 ev.

Table 3

E_γ	Relative Intensities Measured	D	E_γ	Relative Intensities Measured	D
7·84 ± 0·02	89·7 ± 2·0	90	2·56 ± 0·03	0·2 ± 0·1	†
6·61 ± 0·05		2	2·19 ± 0·03	0·2 ± 0·1	‡
5·03 ± 0·03	1·8 ± 0·3	2	1·87 ± 0·03	0·3 ± 0·1	‡
3·75 ± 0·02	0·8 ± 0·3	‡	1·24 ± 0·02	2·4 ± 0·1	2
2·89 ± 0·02	2·5 ± 0·2	2			

D, decay scheme. † Not accounted for. ‡ Not shown.

955 *kev Resonance*

The γ-ray intensities at this resonance are shown in table 4 and the proposed decay scheme in figure 6.

The only new level is at 3·29 Mev, fed by the 4·94 Mev γ-ray. The position of the level is taken from the accurate results of the inelastic scattering data. According to the intensities at this resonance the 3·29 Mev level decays equally to 1·27 and 2·23 Mev levels, emitting γ-rays of 2·02 and 1·06 Mev. As the level is weakly excited, it is not possible to decide its mode of decay with certainty. In particular, the third mode of decay available, a direct transition to the ground state, could easily constitute one-quarter of the level width and escape observation here.

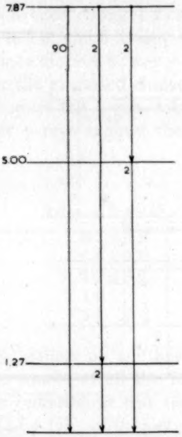

Figure 5. Decay schemes 625 kev.

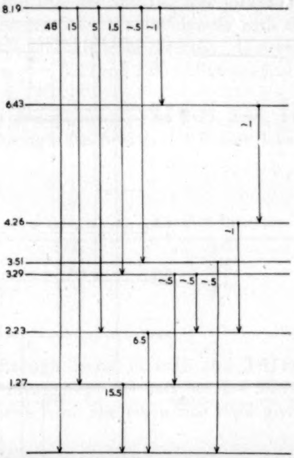

Figure 6. Decay schemes 955 kev.

Table 4

E_γ	Relative Intensities Measured	D	E_γ	Relative Intensities Measured	D
8·22 ± 0·03	48·3 ± 2·0	48	2·97 ± 0·02	0·6 ± 0·2	†
6·92 ± 0·03	13·9 ± 1·0	15	2·25 ± 0·02	6·7 ± 0·5	6·5
5·98 ± 0·03	5·5 ± 0·5	5	2·00 ± 0·02	0·8 ± 0·3	1·5
4·94 ± 0·02	1·8 ± 0·5	1·0	1·82 ± 0·02	0·8 ± 0·3	1·0
4·68 ± 0·03	0·7 ± 0·5	0·5	1·28 ± 0·01	17·7 ± 1·0	15·5
3·48 ± 0·02	0·6 ± 0·3	0·5	1·06 ± 0·02	0·5 ± 0·3	0·5

D, decay scheme. † Not accounted for.

This is the best resonance for estimating the intensity of a possible transition from the 2·23 Mev state to the 1·27 Mev state as the direct transition from the resonance to the 2·23 Mev state is strongest here. An upper limit of 5% of the normal decay mode to the ground state can be set on the cross-over transition. The value of $(2J+1)\Gamma_\gamma$ for this resonance is 0·63 ev.

840 *keV Resonance*

Table 5 shows the γ-ray intensities at this resonance. The decay scheme is shown in figure 7. The presence of γ-rays of 3·86, 2·94 and 1·95 Mev suggests that the level at 4·17 Mev which was weakly excited at the 625 kev resonance occurs with some strength at this resonance.

The 2 in. crystal was used to detect the 3·86 Mev γ-rays and the spectrum in coincidence was taken with the 4½ in. crystal. The experiment showed that γ-rays of energies 1·27, 1·95, 2·23 and 2·94 Mev were in coincidence with the 3·86 Mev γ-ray.

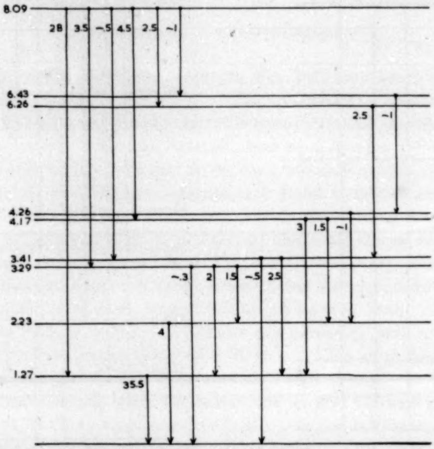

Figure 7. Decay schemes 840 kev.

The measured relative intensities of the γ-rays are

E_γ	1·27	1·95	2·23	2·94
Relative intensity	28 ± 7	13 ± 4	16 ± 4	42 ± 9

The results are consistent with the proposed decay scheme for the 4·17 Mev level. They show that the level decays via the 1·27 Mev level emitting a 2·94 Mev γ-ray and via the 2·23 Mev emitting a 1·95 Mev γ-ray. Within the errors, the former decay is twice as probable as the latter. The absence of a 4·17 Mev γ-ray

Table 5

	Relative Intensities			Relative Intensities	
E_γ	Measured	D	E_γ	Measured	D
6·81 ± 0·02	29·7 ± 1·7	28	2·25 ± 0·02	4·5 ± 0·5	4
4·82 ± 0·03	2·9 ± 0·5	3·5	2·13 ± 0·02	4·2 ± 0·5	3·5
4·56 ± 0·04	0·7 ± 0·5	0·5	1·95 ± 0·02	4·5 ± 0·5	4·5
3·87 ± 0·02	4·2 ± 0·5	4·5	1·83 ± 0·02	2·6 ± 0·5	2·5
3·43 ± 0·03	0·8 ± 0·5	0·8	1·64 ± 0·02	1·0 ± 0·5	1
2·94 ± 0·02	3·5 ± 0·5	3	1·26 ± 0·01	31·2 ± 2·0	35·5
2·81 ± 0·02	1·9 ± 0·5	2·5	1·06 ± 0·02	2·2 ± 0·5	1·5

D, decay scheme.

indicates that the decay of the 4·17 Mev level to the ground state is less than 5% of the radiation from this level.

The above cascade accounts for all of the 2·94 Mev γ-ray, but only one-third of the 1·95 and 2·23 Mev γ-rays. A further third can be accounted for if the 3·29 Mev level decays equally to the 2·23 and 1·27 Mev levels, as suggested at the 955 kev resonance. The transition to the latter level is indistinguishable from the 1·95 Mev transition in such a complex spectrum. To check this the single channel analyser was set across the peak of the 4·82 Mev γ-ray feeding the 3·29 Mev level; γ-rays of 2·00 Mev and 2·23 Mev of approximately equal intensity were observed. Nothing can be said about the 1·06 Mev and 1·27 Mev γ-rays also expected as a very strong 1·27 Mev γ-ray occurred from coincidences with the low energy tail of the 6·81 Mev γ-ray which feeds this level directly. However the coincidence of the 4·82 Mev γ-ray with γ-rays of 2·23 and 2·00 Mev is conclusive evidence for the proposed cascades.

Table 6 gives the γ-rays which are still unexplained. The 2·23, 2·15, 2·02 and 1·64 Mev γ-rays suggest the cascade through the 6·43 and 4·26 Mev levels.

Table 6

E_γ	Relative Intensity	E_γ	Relative Intensity
4·56	0·7 ± 0·5	2·02	1·0
3·43	0·8 ± 0·5	1·83	2·6
2·82	1·9 ± 0·5	1·64	1·0
2·25	1·0	1·26	
2·15	3·5		

The postulation of another cascade through levels at 6·26 and 3·41 Mev explains the source of all the remaining γ-rays except the very weak 4·56 Mev. 39% of the radiation at this resonance comes from the resonance level giving a value of $(2J+1)\Gamma_\gamma$ of 0·15 ev.

760 *keV Resonance*

The measured energies and intensities of the γ-rays observed at this resonance are given in table 7. The decay scheme is illustrated in figure 8.

The level at 4·17 Mev is prominent at this resonance and it offers another opportunity of confirming its mode of decay by coincidence experiments.

Table 7

	Relative Intensities			Relative Intensities	
E_γ	Measured	D	E_γ	Measured	D
7·89 ± 0·03	1·1 ± 0·5	1	2·93 ± 0·02	7·2 ± 0·5	7
6·75 ± 0·03	7·6 ± 0·5	8	2·50 ± 0·03	1·7 ± 0·5	†
5·76 ± 0·03	2·1 ± 0·5	2	2·23 ± 0·02	8·8 ± 0·5	7
4·69 ± 0·03	3·5 ± 0·5	3·5	2·15 ± 0·02	6·7 ± 0·5	5
4·57 ± 0·03	6·1 ± 0·5	6	1·96 ± 0·02	5·0 ± 0·5	5·2
4·47 ± 0·03	5·7 ± 0·5	6	1·73 ± 0·3	1·0 ± 0·5	†
3·81 ± 0·02	10·6 ± 0·5	11	1·26 ± 0·1	24·3 ± 1·0	21
3·51 ± 0·02	6·3 ± 0·5	6	1·04 ± 0·04	0·9 ± 0·5	1·2
3·34 ± 0·02	2·5 ± 0·5	2			

D, decay scheme. † Not accounted for.

A spectrum was obtained by gating the multichannel analyser with pulses due to the 3·84 MeV γ-ray and, on analysis, this gave γ-rays of the following energies and intensities

E_γ (MeV)	1·27	1·95	2·23	2·93
Relative intensity	31 ± 3	15 ± 4	17 ± 4	37 ± 3

These results agree excellently with those obtained earlier. Other corroborative experiments have been performed by gating on the 2·92 and 1·95 MeV γ-rays and give the expected results.

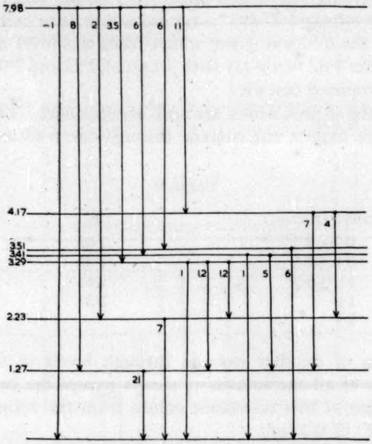

Figure 8. Decay schemes 760 kev.

A broad peak in the spectrum at 4·6 MeV has been assumed to be three γ-rays of energy 4·69, 4·57 and 4·47 MeV, the energies of transitions to the levels at 3·29, 3·41 and 3·51 MeV. Justification for this analysis can be found in the energies and intensities of the other γ-rays found at the resonance. We have attempted to confirm this analysis by coincidence experiments. Of the three levels, only the 3·41 MeV level feeds the 1·27 MeV state strongly. A spectrum in coincidence with the 1·27 MeV γ-ray should thus emphasize the feeder of the 3·41 MeV level as compared with the two close γ-rays on either side. This coincidence experiment confirms that by far the largest contribution to the 1·27 MeV γ-ray is from the 3·41 MeV level and the same experiment incidentally excludes any appreciable decay of the 3·51 MeV level to either the first or second excited state. This resonance is shown later to be of spin $\frac{5}{2}$, but distributions of the 4·47 and 3·51 MeV γ-rays do not show significant $P_4(\cos\theta)$ terms. Consequently the 3·51 MeV γ-ray accounts for all the intensity of the 4·47 MeV transition to the 3·51 MeV level. It thus appears that the 3·51 MeV level decays almost exclusively to the ground state.

Work on other resonances has shown that the 3·29 MeV level decays to the first two excited states, and has not so far established whether there is a direct transition to the ground state. Consideration of the relative intensities of the γ-rays involved, together with the existence of a 3·34 MeV γ-ray suggests that this level decays to the ground state with about the same intensity as its decay to the first and second excited states. Some of the 3·34 MeV γ-ray we think is also due to decay of the 3·41 MeV level to the ground, thus accounting for the energy discrepancy.

The value of $(2J+1)\Gamma_\gamma$ for this resonance is calculated, using the decay scheme, to be 0·10 ev.

980 *keV Resonance*

The γ-ray intensities are listed in table 8 together with intensities from the level scheme of figure 9. Angular distribution measurements at this resonance show $P_4(\cos\theta)$ terms and so the relative intensities may not be as precise as the errors in the table imply. Coincidence measurements on the low energy γ-rays proved the existence of the cascade through the 6·43 MeV level mentioned at previous resonances. If we subtract from the measured intensities the

Table 8

	Relative Intensities			Relative Intensities	
E_γ	Measured	D	E_γ	Measured	D
4·93 ± 0·03	13·6 ± 1	11	1·99 ± 0·01	18·2 ± 0·5	17
4·80 ± 0·03	6·0 ± 1	7	1·80 ± 0·01	7·5 ± 0·5	9
3·40 ± 0·03	3·0 ± 0·5	1	1·26 ± 0·01	21·4 ± 1·0	19
2·23 ± 0·01	8·3 ± 0·5	11	1·00 ± 0·02	6·7 ± 1·0	7
2·15 ± 0·01	9·8 ± 0·5	10			

D, decay scheme.

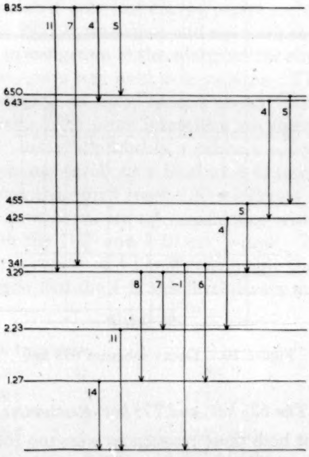

Figure 9. Decay schemes 980 kev.

contributions due to the cascades following the 4·93 and 4·80 MeV γ-rays and also the cascade via the 6·43 MeV level we are left with the following γ-rays with their residual relative intensities

E_γ	2·23	2·15	1·99	1·80	1·26	1·06
Residual intensity	—	—	7	3·5	7	2

Coincidence experiments on the 1·26 MeV level showed that, in addition to the expected γ-rays, the 1·26 MeV γ-ray was in coincidence with itself and there must therefore be a transition of this energy between higher energy levels. The 1·06 MeV γ-ray is known to arise from the transition between the 3·29 MeV and 2·23 MeV levels. The 3·29 MeV level also decays with about the same strength to the 1·27 MeV level and, taking these into account, we are left with three γ-rays of about the same strength and whose energies add up to slightly more than the difference between the excitation energy and the 3·29 MeV level. These results are shown in the level scheme where new levels are shown at 4·55 MeV and 6·50 MeV. Alternative level schemes are possible corresponding to different orders of the γ-rays in this triple cascade to the 3·29 MeV level. The value of $(2J+1)\Gamma_\gamma$ for this resonance is 0·07 ev.

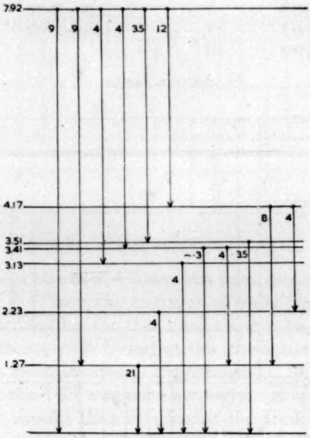

Figure 10. Decay schemes 675 kev.

The 675 *keV and* 775 *keV Resonances*

The γ-ray spectra at both these resonances were too complex for coincidence experiments to be done. The γ-ray intensities are shown in tables 9 and 10. It was found that all the γ-rays could be accounted for in terms of levels whose properties are already known and thus provided confirmatory evidence for the decay of some of the levels. The decay schemes are shown in figures 10 and 11. The calculated values of $(2J+1)\Gamma_\gamma$ are respectively 0·13 ev and 0·4 ev.

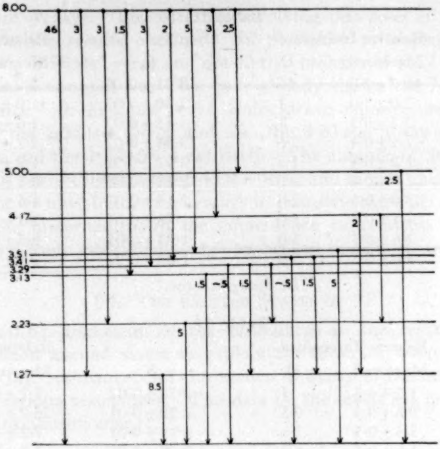

Figure 11. Decay schemes 775 kev.

995 *keV Resonance*

This resonance consists largely of low energy γ-rays and is easily separated from the 1000 kev resonance if only low energy γ-rays are counted. To ensure that only γ-rays from the 995 kev resonance and not from the 1000 kev resonance are counted, during the investigation of the spectrum the single channel analyser set to record low energy γ-rays was used as a monitor. The complete absence of a ground state transition from these spectra shows that the two resonances were successfully resolved. The γ-ray intensities are shown in table 11.

The intense 3·83 MeV γ-ray is probably a primary γ-ray and so is due to a transition from the resonance level, to a level at 4·42 MeV. A level is known to exist at 4·43 MeV from the (pp′) work. Coincidence experiments on the 3·83 MeV γ-ray showed it to be in strong coincidence with the 2·20 MeV γ-ray and to a less extent with the 1·27 and 1·10 MeV γ-rays. There was also some evidence for a γ-ray in the region of 4·5 MeV presumably the direct decay of the 4·42 MeV level. We suggest that the 4·42 MeV level decays mainly to the 2·23 MeV

Table 9

	Relative Intensities			Relative Intensities	
E_γ	Measured	D	E_γ	Measured	D
7·87 ± 0·03	9·0 ± 0·5	9	3·15 ± 0·02	4·1 ± 0·5	4
6·60 ± 0·03	8·7 ± 0·5	9	2·94 ± 0·02	8·0 ± 1·0	8
6·19 ± 0·03	1·4 ± 0·5	†	2·60 ± 0·02	1·9 ± 1·0	†
4·76 ± 0·03	3·6 ± 0·5	4	2·25 ± 0·02	4·0 ± 0·5	4
4·51 ± 0·03	4·1 ± 0·5	4	2·15 ± 0·02	4·5 ± 0·5	4
4·39 ± 0·03	4·1 ± 0·5	3·5	1·98 ± 0·02	5·2 ± 0·5	4
3·75 ± 0·02	10·1 ± 0·5	12	1·75 ± 0·02	0·9 ± 0·5	†
3·48 ± 0·02	3·8 ± 0·5	3·5	1·26 ± 0·01	22·6 ± 1·0	21
3·41 ± 0·02	0·3	0·3	1·06 ± 0·02	1·0 ± 0·5	†

D, decay scheme. † Not accounted for.

Table 10

E_γ	Relative Intensities Measured	D	E_γ	Relative Intensities Measured	D
7·98 ± 0·04	46·3 ± 2·0	46	3·41 ± 0·03	1·0 ± 0·5	0·5
6·71 ± 0·04	2·0 ± 1·0	3	3·30 ± 0·03	1·0 ± 0·5	0·5
5·80 ± 0·04	2·3 ± 0·5	3	3·15 ± 0·02	1·6 ± 0·5	1·5
4·98 ± 0·03	2·1 ± 0·4	2·5	3·04 ± 0·02	2·7 ± 0·5	2·5
4·84 ± 0·03	1·2 ± 0·4	1·5	2·92 ± 0·02	1·9 ± 0·5	2·0
4·68 ± 0·03	2·9 ± 0·4	3·0	2·24 ± 0·01	6·5 ± 0·5	5
4·56 ± 0·03	2·0 ± 0·4	2·0	2·15 ± 0·02	1·5 ± 0·5	1·5
4·40 ± 0·03	4·1 ± 0·4	5·0	1·98 ± 0·01	2·7 ± 0·5	2·5
3·82 ± 0·03	2·6 ± 0·3	3·0	1·27 ± 0·01	9·5 ± 0·5	8·5
3·51 ± 0·03	5·0 ± 0·5	5·0	1·03 ± 0·02	1·1 ± 0·5	1

D, decay scheme.

Table 11

E_γ	Relative Intensities Measured	D	E_γ	Relative Intensities Measured	D
6·94 ± 0·03	1·1 ± 0·3	1	2·58 ± 0·02	7·2 ± 0·5	7
6·03 ± 0·03	0·6 ± 0·3	0·5	2·20 ± 0·01	26·2 ± 1·0	26
4·85 ± 0·02	3·5 ± 0·5	2·5	2·14 ± 0·01	7·2 ± 0·5	8
4·70 ± 0·02	1·0 ± 0·5	1·5	2·00 ± 0·01	4·7 ± 0·5	8
4·42 ± 0·02	5·0 ± 0·5	4	1·27 ± 0·01	18·7 ± 1·0	18
3·83 ± 0·02	17·6 ± 1·0	19	1·10 ± 0·01	5·0 ± 1·0	3
3·48 ± 0·02	2·0 ± 0·5	1·5			

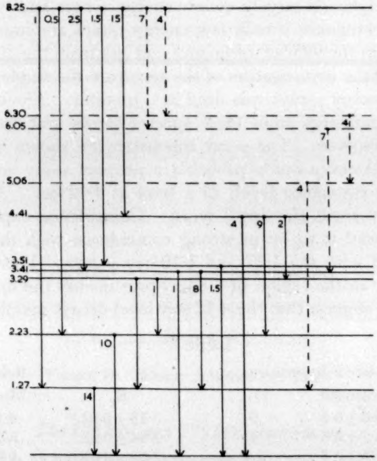

Figure 12. Decay schemes 995 kev.

level giving γ-rays of 2·23 and 2·19 MeV, which we have not resolved, and also partially to the ground state and 3·29 MeV level. Coincidence experiments on the combined group of γ-rays around 2 MeV showed the 2·20 MeV and 3·83 MeV in strong coincidence. The 2·58, 1·27 and 1·10 MeV γ-rays also showed up, but much more weakly. The cascades involving this level at 4·42 Mev do not entirely explain the results obtained. In particular no explanation has been suggested for the 2·58 Mev γ-ray and not all the intensity of the 1·27 and 2·20 Mev γ-rays has been accounted for. We have already shown the 2·58 Mev γ-ray to be in coincidence with the 2 Mev peak. Coincidence experiments on the 1·27 Mev γ-ray showed the 2·58 Mev γ-ray and also the 3·83 Mev γ-ray as expected, the 2·20 Mev γ-ray and the 1·27 Mev γ-ray itself. The absence of the 1·80 Mev γ-ray means that this cannot involve the 6·43 Mev level and to give an adequate account of these results we have found it necessary to postulate three new levels. In view of this and the uncertainties in the coincidence experiments we have shown these levels and their associated γ-rays by broken lines in figure 12.

§ 4. THE EXCITED STATES OF ^{31}P

The preceding discussion of the resonances in the reaction ^{30}Si(p, γ)^{31}P required eighteen excited states to explain the observed γ-rays. Seven levels occur at only one resonance, but the modes of decay of the other states can be compared at various resonances. The data on the levels are presented in order of increasing excitation energy.

1·27 *Mev Level*

This is the first excited state and occurs at all resonances.

2·23 *Mev Level*

The second excited state appears at every resonance but the direct transition to it only occurs with reasonable strength at the 955 kev resonance.

The level is found to decay to the ground state; the only other possible transition is to the 1·27 Mev level and has not been observed at any resonance. The upper limit of this transition has been estimated to be 5% of the decay to the ground state.

3·13 *Mev Level*

The level at 3·13 Mev occurs at four resonances, namely the 500, 1000, 675 and 775 kev resonances. At the first two of these it is not obscured by transitions to other close levels. The 3·13 Mev level decays only to the ground state. This mode of decay is derived from the 500 and 1000 kev resonances where the upper limit is estimated as 5% on possible transitions to the first and second excited states.

3·29 *Mev Level*

This level is found at six resonances, but is never sufficiently isolated from the adjacent levels for its decay mode to be established with complete certainty. The decay modes found at each resonance are shown in table 12. The values

Table 12. Decay Modes (%) for 3·29 Mev Level

	Resonance Energy (kev)					
	760	775	840	955	980	995
3·29→Ground state	30	0	8	0	0	0
3·29→1·27 Mev level	35	25	52	50	53	50
3·29→2·23 Mev level	35	75	40	50	47	50

obtained at the individual resonances are subject to large errors as they are based entirely on intensity measurements which are not very well determined. The uncertainty in the intensity measurements is due both to the weakness of the γ-rays and to the possible presence of $P_4(\cos\theta)$ terms at some of the resonances. This is probably the reason for the apparent discrepancy of the branching ratios at the 760 kev resonance. It appears that the most reliable values that can be allotted to the decay of the level would be that the decay via the 1·27 and 2·23 Mev levels occur with equal intensities, with the transition to the gound state accounting for some 5 or 10% of the total radiation.

3·41 *Mev Level*

Information on this level is obtained at six resonances but the same limitations apply to it as to the previously discussed 3·29 Mev level. The data on the mode of decay are given in table 13. The results are quite consistent and suggest that the transition from the 3·41 Mev level to the 1·27 Mev level constitutes about 85% of the radiation from this level, the other 15% being due to the transition to the ground state.

Table 13. Decay Modes (%) for 3·41 Mev Level

	Resonance Energy					
	675	760	775	840	980	995
3·41→ Ground state	7	17	25	17	14	11
3·41→ 1·27 Mev level	93	83	75	83	86	89

The possible transition to the 2·23 Mev level has an energy of 1·18 Mev and with an energy resolution of 9% in this region one would observe this γ-ray if it was a reasonable proportion of the decay of the 3·41 Mev level. In addition, there are no intensity discrepancies to suggest that the level decays in this additional mode. The most favourable resonance for setting an upper limit on this transition is at 980 kev. As at all resonances, the 1·27 Mev γ-ray is comparatively strong and would obscure a weak γ-ray of 1·18 Mev, but as all the intensity of the feeder transition for the 3·41 Mev level is accounted for, the decay to the 2·23 Mev level cannot be more than 7 or 8% of the radiation from the level.

3·51 *Mev Level*

This level has been found at five of the ten resonances which have been investigated. These are the resonances at proton energies 675, 760, 775, 955 and 995 kev, and at all of these the level has been shown to decay entirely to the ground state. The energies of transitions to the 1·27 and 2·23 Mev levels are 2·24 and 1·28 Mev with the consequence that only intensity measurements can rule out these transitions as possible modes of decay. The γ-rays which feed the level are never sufficiently strong or sufficiently well isolated to permit coincidence experiments on the mode of decay.

The level is most strongly fed at the 760 kev resonance where 6% of the total radiation comes from the transition to this level. The 3·51 Mev γ-ray itself is of equal intensity. The 760 kev resonance is later shown to have spin $\frac{5}{2}$ but the angular distribution of the γ-rays associated with the 3·51 Mev level do not have any significant $P_4(\cos\theta)$ terms to modify the intensity measurements. The equality of the intensities of γ-rays feeding the 3·51 Mev level and the γ-ray transition to the ground state is good at all resonances where the level occurs. Thus the decay of the 3·51 Mev level to ground state is at least 90% of the total mode of de-excitation.

4·17 *Mev Level*

This level is important in the decay schemes for the resonances at 675, 760 and 840 kev and occurs weakly at the 625 and 775 kev resonances. At the 760 and 840 kev resonances, coincidence experiments have shown that the 4·17 Mev level decays to the 1·27 and 2·23 Mev levels with relative probabilities of two to one. The relative intensities of the two decay modes agree well at all the resonances where this level is excited and there is no evidence for a 4·17 Mev γ-ray which would be the ground state transition. After the decay schemes were evolved, the results of the inelastic scattering of protons from ^{31}P showed that in this energy region, there are levels at 4·12, 4·19 and 4·26 Mev. A level at 4·26 Mev will be discussed in the next section but no level of energy 4·12 Mev has been observed. The following facts suggest that the level observed in the γ-ray measurements is one level and not a mixture of 4·12 and 4·19 Mev levels.

(*a*) The γ-ray which feeds the 4·17 Mev level has never been found to be significantly wider than a lone γ-ray of this energy.

(*b*) A γ-ray in the energy range 4·10 to 4·20 Mev has not been in evidence at any resonance, consequently if the 4·12 Mev level is excited its decay mode must be similar to that of the 4·17 Mev level to the extent that no ground state transitions occur.

(*c*) The mode of decay of the 4·17 Mev level as found experimentally is so consistent that it would be necessary to assume that the 4·12 and 4·17 Mev levels are excited in the same ratio at all resonances or that they decay in exactly the same way. In addition the level energy at all resonances is almost exactly that expected from the (pp′) experiment which is 4·19 ± 0·01 Mev. It seems therefore that only one level is excited which is the 4·19 Mev level found in the inelastic scattering experiments.

4·26 *Mev Level*

This is a member of the cascade from the resonance levels through the level at 6·42 Mev. It decays to the 2·23 Mev state. The energy of the 6·43 Mev level is fixed by the observed shifts at the five resonances at which the cascade is found. The order of the next two γ-rays in the cascade is not fixed and so the immediate energy level could be 4·26 and 4·42 Mev. Both these energies are observed in the (pp′) experiment. A 4·43 Mev γ-ray occurs at the 995 kev resonance indicating a level of this energy, but its decay properties are quite different from those which would be required for this cascade.

4·43 *Mev Level*

The 4·13 Mev level is required to explain the γ-rays in coincidence with the 3·83 Mev γ-ray at the 995 kev resonance. It also occurs weakly at the 1000 kev resonance. A level is also observed at this excitation in the (pp′) experiments.

The intensities at the 995 kev resonance show that this level decays 27% to the ground state, 60% to the 2·23 Mev state and 13% to the 3·29 Mev state, though these may be in error due to the fact that $P_4(\cos\theta)$ terms were observed in the angular correlations at 995 kev.

5·00 *Mev Level*

At the 500, 625 and 775 kev resonances, there is good evidence for a 5·00 Mev level which decays only to the ground state. At the 625 kev resonance it has been possible to verify this level by a coincidence experiment. The energy agrees with a possible level in the (pp′) work at 5·01 Mev.

6·25 *Mev Level*

This level is found only at the 840 kev resonance and consequently the γ-rays could be interpreted in terms of a level at 5·26 Mev by altering the order in the cascade. This level, either at 5·26 or 6·26 Mev decays to the 3·41 Mev level.

6·43 *Mev Level*

This is the level which decays entirely to the 4·26 Mev level. The shifts in γ-ray energy that occur as the proton energy changes over the five resonances at which it occurs show conclusively that the 6·43 Mev level is the first in the cascade.

6·55 *Mev Level*

At the 1000 kev resonance, two weak γ-rays occur whose energies add up to the full excitation energy which can be explained if an energy level at 6·55 Mev is accepted.

Levels at 4·55 and 6·50, and 5·06, 6·06 and 6·30 Mev have also been postulated. The first two levels occur only at the 980 kev resonance, and the last three only at the 995 kev resonance. In both cases the uncertainty as to the order in which cascading γ-rays occur means that the positions of these levels are not uniquely determined.

ACKNOWLEDGMENTS

One of us (C. B.) is indebted to the Department of Scientific and Industrial Research for a maintenance grant. We wish to thank Professor H. W. B. Skinner for much helpful discussion of this paper. The ^{30}Si targets were supplied by the Atomic Energy Research Establishment, Harwell.

REFERENCES

BROMLEY, D. A., GOVE, H. E., and LITHERLAND, A. E., 1957 b, *Canad. J. Phys.*, **35**, 1057.

BROMLEY, D. A., GOVE, H. E., PAUL, E. B., LITHERLAND, A. E., and ALMQUIST, E., 1957 a, *Canad. J. Phys.*, **35**, 1042.

BROUDE, C., GREEN, L. L., SINGH, J. J. and WILLMOTT, J. C., 1956, *Physica*, **22**, 1139.

ENDT, P. M., and PARIS, C. H., 1957, *Phys. Rev.*, **106**, 764.

KERMAN, A. K., 1956, *K. Danske Vidensk. Selsk., Mat-fys. Medd.*, **30**, 15.

LITHERLAND, A. E., MCMANUS, H., PAUL, E. B., BROMLEY, D. A., and GOVE, H. E., 1958, *Canad. J. Phys.*, **36**, 378.

LITHERLAND, A. E., PAUL, E. B., BARTHOLOMEW, G. A., and GOVE, H. E., 1956, *Phys. Rev.*, **102**, 208.

NILSSON, S. G., 1955, *K. Danske Vidensk. Selsk. Mat-fys. Medd.*, **29**, No. 16.

PAUL, E. B., 1957, *Phil. Mag.*, **2**, 311.

PAUL, E. B., BARTHOLOMEW, G. A., GOVE, H. E. and LITHERLAND, A. E., 1956, *Bull. Amer. Phys. Soc.*, **1**, 39.

TANGEN, R., 1946, *K. Norske Vidensk. Selsk. Skrifter*, **1**.

The Energy Levels of ^{31}P
II: Angular Distributions and Correlations

By C. BROUDE, L. L. GREEN and J. C. WILLMOTT
Nuclear Physics Research Laboratory, University of Liverpool

Communicated by H. W. B. Skinner; *MS. received 23rd June* 1958, *and in revised form 18th August* 1958

Abstract. Angular distributions and triple correlations have been measured at the resonances in the reaction $^{30}Si(p,\gamma)^{31}P$ discussed in Part I and spin and parity assignments made for levels in ^{31}P.

---

§ 1. INTRODUCTION

In order to determine the spins and parities of the levels of ^{31}P whose decay properties are discussed in Part I (Broude, Green and Willmott 1958) we have carried out angular correlation experiments at the various resonances. Four types of correlations were measured.

(1) The angular distribution of primary γ-rays with respect to the direction of the proton beam.

(2) The angular distribution of secondary γ-rays with respect to the proton beam direction.

(3) The angular distribution with respect to the proton beam direction of secondary γ-rays in coincidence with primary γ-rays detected in a crystal at 90° to the beam direction.

(4) As in (3) but with the secondary γ-ray detected in the fixed detector and the primary γ-ray in the moving detector.

The theoretical expression for the four types of distributions were calculated from the tables prepared by Ferguson and Rutledge (1957).

For the first two types of measurements the 2 in. crystal was used as a monitor and one of the large crystals, collimated as described earlier, was used as the moving detector. The angle subtended at the target by the latter crystal was 16°. Rose (1953) has discussed the effect of solid angle on measured angular distributions and has shown that there is a reduction of the coefficients of the Legendre polynomials with increasing solid angle. The correction to be applied to the experimental $P_2(\cos\theta)$ coefficients under the above conditions is 1%, which is considerably smaller than the probable errors on the coefficient.

For triple correlations the two large crystals were used. In this case a compromise must be made between the small solid angle which makes the attenuation correction small and the large solid angle required to give a reasonable coincidence counting rate. The attenuation corrections in this case are the products of the attenuation corrections for each crystal separately and can become very large especially for the $P_4(\cos\theta)$ terms. In the geometry used the angles subtended by the crystals at the target were both made equal to 33°. Numerical integration was used to estimate the attenuation factors, which amounted to 0·85 for the $P_2(\cos\theta)$ term and 0·62 for the $P_4(\cos\theta)$ term.

§ 2. THE SPINS AND PARITIES OF THE RESONANCE LEVELS

As ^{30}Si is a spin zero nucleus a resonance level of any given spin and parity can thus be formed only one way. The ground state of ^{31}P has spin and parity $\frac{1}{2}^+$ and in most cases the resonance level spin has been fixed by the angular distribution of the ground state transition.

500 *keV Resonance*

The ground state transition has a distribution $P_0 - (0{\cdot}41 \pm 0{\cdot}02)P_2(\cos\theta)$. This is consistent only with resonance spin $\frac{3}{2}^+$.

625 *keV Resonance*

All the radiation from this level was found to be isotropic and the spin must be either $\frac{1}{2}^\pm$.

760 *keV Resonance*

The weak ground state transition has a distribution $P_0 + (0{\cdot}41 \pm 0{\cdot}10)P_2(\cos\theta) - (0{\cdot}59 + 0{\cdot}10)P_4(\cos\theta)$ which can be compared with the theoretical expression for a $\frac{5}{2}^+$ to $\frac{1}{2}^+$ transition of $P_0 + 0{\cdot}57\, P_2(\cos\theta) - 0{\cdot}57\, P_4(\cos\theta)$.

Figure 1 shows graphically the agreement between the experimental points and the theoretical curve. This resonance is therefore $\frac{5}{2}^+$.

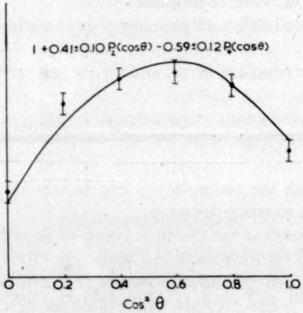

Figure 1. Angular distribution of the 760 kev resonance ground state transition. First term of expression given on graph should read P_0 not 1.

775 *keV Resonance*

The ground state transition has a distribution $P_0 - (0{\cdot}31 \pm 0{\cdot}01)P_2(\cos\theta)$ and the resonance is therefore $\frac{3}{2}^+$.

840 *keV Resonance*

No ground state transition occurs at this resonance but transitions to the levels at 1·27 and 4·17 MeV occur strongly and the angular distribution of both of these have been measured. Experiments at other resonances show that the 1·27 MeV level is $\frac{3}{2}^+$ and the 4·17 MeV level is $\frac{5}{2}^+$.

The observed distribution of the transition to the 1·27 MeV level is $P_0 - (0{\cdot}23 \pm 0{\cdot}01)P_2(\cos\theta)$ and is consistent with the resonance being either $\frac{3}{2}^+$ or $\frac{5}{2}^+$.

The distribution of the transition to the 4·17 Mev level is $P_0+(0\cdot43\pm0\cdot05)P_2(\cos\theta)$. If the resonance level were $\frac{3}{2}^+$ the maximum possible positive distribution obtained by mixing M1 and E2 radiation is $P_0+0\cdot377\,P_2(\cos\theta)$ which does not fit very well. On the other hand, a resonance spin of $\frac{5}{2}^+$ gives the observed distribution with M1/E2 amplitude ratio of $-0\cdot06$. The poor agreement with the theoretical distribution for $\frac{3}{2}^+$ resonance and the absence of the ground state transition which is strong at all other $\frac{3}{2}^+$ resonances thus indicate that the 840 kev resonance is almost certainly $\frac{5}{2}^+$.

955 *keV Resonance*

The ground state transition has an observed distribution of

$$P_0-(0\cdot72\pm0\cdot02)P_2(\cos\theta)$$

which is consistent only with a resonance spin of $\frac{3}{2}^+$.

980 *and* 995 *keV Resonances*

At these resonances the highest energy transitions are to levels of unknown spin but in both cases it was observed that $P_4(\cos\theta)$ terms appeared in the distributions so that the spins must be equal to or greater than $\frac{5}{2}$.

1000 *keV Resonance*

The ground state transition has a distribution of $P_0-(0\cdot55\pm0\cdot03)P_2(\cos\theta)$; this can be fitted if the resonance is $\frac{3}{2}^+$ with M1/E2 amplitude ratios of $-0\cdot03$ or $-1\cdot6$. Alternatively, the resonance might be $\frac{3}{2}^-$ when the theoretical distribution for a pure E1 transition is $P_0-0\cdot50P_2(\cos\theta)$. However, a transition also occurs to the 3·13 Mev level and gives an angular distribution of the form $P_0-(0\cdot27\pm0\cdot01)P_2(\cos\theta)$. This level is shown at the 500 kev resonance to be either $\frac{1}{2}^+$ or $\frac{3}{2}^+$. If the resonance were $\frac{3}{2}^-$ the distribution for these two possible spins of the 3·13 Mev level would be $P_0-0\cdot50P_2(\cos\theta)$ or $P_0+0\cdot4P_2(\cos\theta)$, thus ruling out the $\frac{3}{2}^-$ assignment. This level is therefore also $\frac{3}{2}^+$.

Summarizing, our results on the resonance levels (in kev) the spins and parities are as follows:

500	625	760	775	840	955	980	995	1000
$\frac{3}{2}^+$	$\frac{1}{2}^\pm$	$\frac{5}{2}^+$	$\frac{3}{2}^+$	$\frac{5}{2}^+$	$\frac{3}{2}^+$	$\geqslant\frac{5}{2}$	$\geqslant\frac{5}{2}$	$\frac{3}{2}^+$

§ 3. THE SPINS AND PARITIES OF THE LOWER STATES

1·27 *MeV Level*

At the 500 kev resonance the angular distribution of the direct transition to the 1·27 Mev level was measured with the result $W(\theta)=P_0+(0\cdot44\pm0\cdot02)P_2(\cos\theta)$. This result is consistent only with the 1·27 Mev level being $\frac{3}{2}^+$. It is of interest to determine the multipole mixing ratio of the decay of this level. To this end the distribution of the 1·27 Mev transition was measured with the result $W(\theta)=P_0-(0\cdot16\pm0\cdot02)P_2(\cos\theta)$. The amplitude mixing ratios $E2/M1=X$ required to fit the primary radiation are $+0\cdot027\pm0\cdot014$ or $+3\cdot5\pm0\cdot2$. Using these values one obtains the mixing ratio Y of secondary radiation as follows:

$$\text{for } X=+0\cdot027\quad Y=-1\cdot18\pm0\cdot24 \text{ or } -0\cdot20\pm0\cdot06$$
$$\text{for } X=+3\cdot5\quad Y=+0\cdot43\pm0\cdot04 \text{ or } -8\cdot7\pm1\cdot4.$$

The same set of experiments was carried out at the 955 kev resonance. The results were essentially similar and did not allow one to choose between the four possible values of Y. In order to decide between the four values, triple correlation experiments were carried out. In what follows geometry A refers to the experiment in which the distribution of the primary radiation is measured with respect to the secondary radiation which is detected in a crystal at 90° to the beam direction, while geometry B refers to the opposite case in which the primary radiation is detected at 90°.

After correction for solid angle effects the results were:

$$\text{Geometry A: } P_0 + (0{\cdot}79 \pm 0{\cdot}04)P_2\,;$$
$$\text{Geometry B: } P_0 + (0{\cdot}32 \pm 0{\cdot}04)P_2.$$

A large value of X for the primary radiation, which implies the transition is largely E2, leads to large $P_4(\cos\theta)$ terms in the theoretical expressions and the two corresponding values of Y may be discarded. The remaining values lead to the following results:

	Geometry A	Geometry B
(*a*) $X = +0{\cdot}02$ $Y = -1{\cdot}2$	$P_0 + 0{\cdot}83P_2$	$P_0 + 0{\cdot}27P_2$
(*b*) $X = +0{\cdot}02$ $Y = -0{\cdot}2$	$P_0 + 0{\cdot}94P_2$	$P_0 + 0{\cdot}28P_2$

It will be seen that while the first case gives good agreement for both geometries, only geometry B agrees well in the second case.

These experiments thus prove that the 1·27 Mev level is $\frac{3}{2}^+$ and its decay to the ground state proceeds by mixed multipole radiation in which the E2/M1 amplitude ratio is most probably −1·20.

The 2·23 Mev Level

The direct transition to the 2·23 Mev level at the 955 kev resonance is sufficiently strong for its angular distribution to be measured and also for the distribution of the transition from the 2·23 Mev level to the ground state. The results are

$$\text{Resonance} \rightarrow 2{\cdot}23\text{ Mev level } W_1(\theta) = P_0 - (0{\cdot}13 \pm 0{\cdot}02)P_2(\cos\theta)$$
$$2{\cdot}23\text{ Mev level} \rightarrow \text{ground state } W_2(\theta) = P_0 + (0{\cdot}39 \pm 0{\cdot}02)P_2(\cos\theta).$$

These two distributions limit the spin of the 2·23 Mev level to $\frac{3}{2}^+$ or $\frac{5}{2}^+$ but do not distinguish between them; to do this the two triple correlations have been measured. After corrections for solid angle the results are

$$\text{Geometry A: } P_0 + (0{\cdot}44 \pm 0{\cdot}07)P_2(\cos\theta)$$
$$\text{Geometry B: } P_0 + (0{\cdot}78 \pm 0{\cdot}08)P_2(\cos\theta) - (0{\cdot}33 \pm 0{\cdot}08)P_4(\cos\theta).$$

The presence of the $P_4(\cos\theta)$ term in geometry B proves that the spin of the 2·23 Mev level is $\frac{5}{2}^+$ or greater and it remains to show quantitative agreement with a spin and parity assignment of $\frac{5}{2}^+$.

If the 2·23 Mev level is $\frac{5}{2}^+$ the primary distribution is fitted by two multiple mixing ratios, each of which gives a unique distribution $W_2(\theta)$ for the ground state. These are:

$$(a)\ X = -5{\cdot}23 \pm 0{\cdot}06, \quad W_2(\theta) = P_0 - (0{\cdot}372 \pm 0{\cdot}005)P_2(\cos\theta)$$
$$(b)\ X = +0{\cdot}028 \pm 0{\cdot}018, \quad W_2(\theta) = P_0 + (0{\cdot}398 \pm 0{\cdot}004)P_2(\cos\theta).$$

The second distribution is in excellent agreement with the experimental results. Inserting the value $X = +0\cdot 028$ in the expressions for triple correlations we obtain the results:

$$\text{Geometry A: } P_0 + 0\cdot 52 P_2(\cos\theta)$$

$$\text{Geometry B: } P_0 + 0\cdot 81 P_2(\cos\theta) - 0\cdot 37 P_4(\cos\theta).$$

Again there is good agreement with the experimental results, showing that this level has spin and parity $\frac{5}{2}^+$.

The 3·13 *Mev Level*

The angular distributions of the primary and secondary radiations involving the level at 3·13 Mev have been measured at the 500 kev resonance and at the 1000 kev resonance. The results are

500 kev resonance	→	3·13 Mev level	$W(\theta) = P_0 - (0\cdot 55 \pm 0\cdot 06) P_2 (\cos\theta)$
3·13 Mev level	→	ground state	$W(\theta) =$ isotropic
1000 kev resonance	→	3·13 Mev level	$W(\theta) = P_0 - (0\cdot 27 \pm 0\cdot 02) P_2 (\cos\theta)$
3·13 Mev level	→	ground state	$W(\theta) = P_0 + (0\cdot 17 \pm 0\cdot 04) P_2 (\cos\theta)$.

Both resonances have a spin and parity of $\frac{3}{2}^+$. The observed distribution of the 3·13 Mev γ-ray at the 1000 kev resonance rules out $\frac{1}{2}^+$ as a possible spin of this state, while the isotropy of the same γ-ray at the 500 kev resonance excludes $\frac{5}{2}^+$ as an assignment, as in this case the distribution of the primary radiations would have to be $P_0 - 0\cdot 04 P_2 (\cos\theta)$ or $P_0 - 0\cdot 83 P_2 (\cos\theta)$ for the secondary radiation to be isotropic. If the level is $\frac{3}{2}^+$ the primary radiation at the 500 kev resonance is fitted by mixing ratios of $-0\cdot 9$ and $-1\cdot 93$, but as the experimental result is close to the maximum possible distribution with negative P_2 coefficient (i.e. $1 - 0\cdot 60 P_2$) a small variation in the coefficient of P_2 covers a large range of mixing parameters, and any ratio between $-0\cdot 8$ and $-2\cdot 2$ could fit the results within the errors.

The secondary radiation can be isotropic if the mixing ratio of the primary radiation has values of $\pm 0\cdot 58$. This possibility is excluded by the experimental values of the primary mixing ratio. Alternatively the isotropy of the secondary radiation can be obtained by mixing ratios of $+0\cdot 27$ or $-3\cdot 7$ for the secondary radiation. Because the lower limit on the mixing ratio of the primary radiation required by the experiment is close to $-0\cdot 58$, quite a large variation on the secondary mixing ratio is required to produce an observable anisotropy of the secondary radiation.

The experiments at the 1000 kev resonance lead to secondary mixing ratios of $-2\cdot 3 \pm 0\cdot 3$ or $0\cdot 12 \pm 0\cdot 04$. These are reasonably consistent with those obtained at the 500 kev resonance and lead to best estimates of $-3\cdot 0$ or $+0\cdot 16$. To choose between these, triple correlation experiments were carried out at the 500 kev resonance with the following results

$$\text{Geometry A: } W(\theta) = P_0 - (0\cdot 43 \pm 0\cdot 06) P_2$$

$$\text{Geometry B: } W(\theta) = P_0 + (0\cdot 11 \pm 0\cdot 07) P_2.$$

The table shows the calculated results for various values of primary and secondary mixing ratios X and Y.

X	Y	Geometry A	Geometry B
-1	-3	$P_0+1\cdot12P_2-0\cdot18P_4$	$P_0+0\cdot16P_2$
-2	-3	$P_0+0\cdot28P_2-0\cdot15P_4$	$P_0+0\cdot14P_2$
-1	$+0\cdot20$	$P_0-0\cdot51P_2-0\cdot05P_4$	$P_0+0\cdot13P_2$
-2	$+0\cdot20$	$P_0-0\cdot47P_2-0\cdot08P_4$	$P_0+0\cdot12P_2$
-1	$+0\cdot16$	$P_0-0\cdot44P_2-0\cdot09P_4$	$P_0+0\cdot22P_2$
-2	$+0\cdot16$	$P_0-0\cdot41P_2-0\cdot13P_4$	$P_0+0\cdot22P_2$

The results clearly exclude the high value of Y.

The 3·29 MeV Level

The distribution of the transition to this level occurring at the 840 kev resonance is given by $W(\theta)=P_0+(0\cdot46\pm0\cdot04)P_2(\cos\theta)$. If the 840 kev resonance is $\frac{5}{2}^+$ level, then this distribution is only consistent with the 3·29 Mev level also being $\frac{5}{2}^+$. If the resonance level were $\frac{3}{2}^+$ which does not seem likely the 3·29 Mev level could be $\frac{1}{2}^+$ or $\frac{3}{2}^+$.

The 3·51 *MeV Level*

The transition from the 760 kev resonance to this level has the distribution $W(\theta)=P_0-(0\cdot33\pm0\cdot08)P_2(\cos\theta)$. As the resonance level is $\frac{5}{2}^+$ this means that the 3·51 Mev level could be $\frac{3}{2}^-$, $\frac{3}{2}^+$ or possibly $\frac{5}{2}^+$. The best fit to the experimental curve in the last case requires a mixing ratio of $-0\cdot7$ and has a $P_4(\cos\theta)$ term with a coefficient of $-0\cdot12$, which is rather large. Putting this value of mixing ratio into the expression for the distribution from the 3·51 Mev level to the ground state one obtains $W(\theta)=P_0+0\cdot27P_2(\cos\theta)+0\cdot15P_4(\cos\theta)$ compared with the experimental value $W(\theta)=P_0+(0\cdot12\pm0\cdot03)P_2$. This eliminates $\frac{5}{2}^+$ as a possibility.

The same result eliminates $\frac{3}{2}^-$ as this gives $W(\theta)=P_0-0\cdot40P_2(\cos\theta)$ for the 3·51 Mev transition. Hence we are left with $\frac{3}{2}^+$ for this level, where the primary distribution is fitted with a mixing ratio of $-0\cdot033$, leading to a negligible $P_4(\cos\theta)$ term, and the secondary radiation is fitted with mixing ratios of $+0\cdot30$ or $-5\cdot3$.

The 4·17 MeV Level

The angular distribution of the 3·84 Mev and 2·93 Mev γ-rays associated with this level have been measured at the 760 kev resonance. The results are:

760 kev resonance → 4·17 Mev level $W(\theta)=P_0+(0\cdot45\pm0\cdot04)P_2$
4·17 Mev level → 1·27 Mev level $W(\theta)=P_0-(0\cdot55\pm0\cdot02)P_2$.

Both of these distributions could have small negative amounts of $P_4(\cos\theta)$, but the reduction of the residual mean squares is not sufficient to justify their inclusion.

Four spin and parity assignments are consistent with the primary distribution. These are $\frac{3}{2}^+$, $\frac{5}{2}^+$, $\frac{3}{2}^-$, $\frac{7}{2}^+$. The last two lead to unique distributions for the secondary radiation. These are:

(*a*) If the 4·17 Mev level is $\frac{5}{2}^-$, $W(\theta)=P_0-0\cdot26P_2$

(*b*) If the 4·17 Mev level is $\frac{7}{2}^+$ primary mixing ratios of $X=+0\cdot14$ and $-8\cdot3$ wiil fit the observed primary distribution, and lead to secondary distribution as follows:

For $X=+0\cdot14$ $W(\theta)=P_0+0\cdot43P_2-0\cdot19P_4$.
For $X=-8\cdot3$ $W(\theta)=P_0+0\cdot21P_2-0\cdot15P_4$.

None of these distributions fits the observed result.

If the 4·17 Mev level is $\frac{3}{2}^+$ the primary mixing ratios required are $+0{\cdot}45 \pm 0{\cdot}03$, but for this value there is no real value of the secondary mixing ratio which will give the observed result for the secondary distribution.

This leaves $\frac{5}{2}^+$ as a possible assignment, for which the observed primary distribution is fitted with $X=0$. Two secondary mixing ratios are possible, namely $-0{\cdot}25 \pm 0{\cdot}03$ or $-1{\cdot}7 \pm 0{\cdot}4$.

Thus the spin and parity of the 4·17 Mev level is determined as $\frac{5}{2}^+$.

The results of these experiments are summarized in figure 2 where the levels up to 5 Mev are shown with their decay modes and the spins and parities which have been determined here.

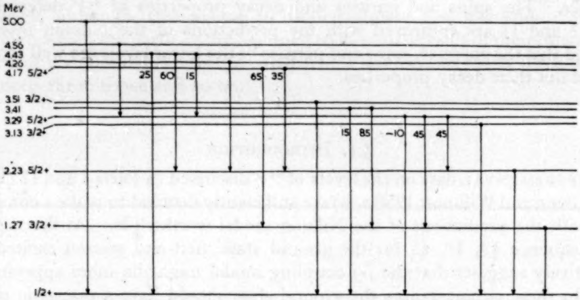

Figure 2. Energy levels of ^{31}P to an excitation of 5·00 Mev.

§ 4. Phasing of the Radiations

The theoretical correlations used have been calculated with the aid of tables prepared by Ferguson and Rutledge (1957). The phases of the mixed radiations however, are not the same as given in these tables. The phases used here differ from them in the following manner. In angular distributions the signs of the interference terms are opposite; in angular distributions with an intermediate radiation unobserved there is no change, while in triple correlations the sign of the interference term in the first radiation of a double cascade is changed. In this convention the phases obtained for mixed radiations are such that a direct comparison may be made with any calculation based on the convention used by Blatt and Weisskopf (1952).

Acknowledgments

We wish to thank Dr. R. Huby for his comments on the phasing of radiations in the report of Ferguson and Rutledge.

References

Blatt, J. M., and Weisskopf, V. F., 1952, *Theoretical Nuclear Physics* (New York: Wiley and Sons).

Broude, C., Green, L. L., and Willmott, J. C., 1958, *Proc. Phys. Soc.*, **72,** 1097.

Ferguson, A. J., and Rutledge, A. R., 1957, *Chalk River Report* C.R.P. 615.

Rose, M. E., 1953, *Phys. Rev.*, **91,** 610.

The Energy Levels of ^{31}P
III: Comparison with the Nilsson Model

By C. BROUDE, L. L. GREEN and J. C. WILLMOTT
Nuclear Physics Research Laboratory, University of Liverpool

Communicated by H. W. B. Skinner; MS. received 23rd June 1958 *and in revised form* 18*th August* 1958

Abstract. The spins and parities and decay properties of ^{31}P determined in Parts I and II are compared with the predictions of the Nilsson model. It is found that the energies, spins and parities of the lower levels are well accounted for but not their decay properties.

---

§ 1. Introduction

EXPERIMENTAL data on the levels of ^{31}P discussed in Parts I and II (Broude, Green and Willmott 1958 a, b) are sufficiently detailed to make a comparison with the predictions of the Nilsson model worthwhile. At first sight the level sequence $\frac{1}{2}^+$, $\frac{3}{2}^+$, $\frac{5}{2}^+$ for the ground state, first and second excited states respectively suggests that the *j–j* coupling model might be more appropriate to ^{31}P. In these circumstances the ground state should have a magnetic moment closely in agreement with the Schmidt value whereas it has one of the largest known deviations for a spin $\frac{1}{2}$ nucleus. This implies that there is a very considerable mixing of the s and d orbitals and simple predictions of level properties are not possible. The Weisskopf transition factors would give an E2/M1 amplitude ratio of 0·01 for the first excited state and predict that the E2 decay of the second excited state to the ground state should be less than 1% of the possible M1 decay to the 1·27 Mev state. In both cases however, the E2 transition is considerably stronger than this.

Calculations of ground state configurations on the Nilsson model by the Chalk River group suggest that the equilibrium distortion may change sign in the region of ^{28}Si and it is possible that collective vibrational motion may be important in this region of nuclei. Such motion has been studied for even–even nuclei by Wilets and Jean (1956), but to effect a comparison with the levels of ^{31}P one must also know the eigenvalues and eigenfunctions for a single particle coupled to such a core, and the necessary calculations have not yet been performed. However, it is of interest to make a detailed comparison with the Nilsson model to see if rotational properties are apparent and if so to see what sign of deformation is required. A similar analysis carried out by Bromley for the levels of ^{29}Si suggests that a rotational model with negative (oblate) deformation may be applicable.

§ 2. Comparison with the Nilsson Model

The first step in comparing the experimental results with the Nilsson model is to estimate the distortion and to determine which of the single particle intrinsic states given by Nilsson (1955) are relevant to this nucleus. We may do this by using the formula C2 given in the appendix to Nilsson's paper, but it is not to be expected that this will do anything but show the general trend. In practice it is found that, using the value of the ratio of spin-orbit coupling to well depth χ of 0·05 suggested by Nilsson, the possible intrinsic states of ^{31}P do not show minima at any distortion within the range of published calculations, the minima all being outside the range in the direction of oblate distortion. Increasing the value of χ produces equilibrium deformations critically dependent on the value of χ, although the nucleus always appears oblate.

This effect has been observed by Bromley *et al.* (1957) in ^{29}Si and Litherland *et al.* (1958) in ^{25}Al and it has been suggested that a better estimate of the single particle excitation can be obtained by a direct summation of the single particle eigenvalues, although this seems to underestimate the distortion. As the potential in which the particles are assumed to move is a result of their interaction, the effect of this method is to count two-particle interactions twice, three-particle interactions three times and so on.

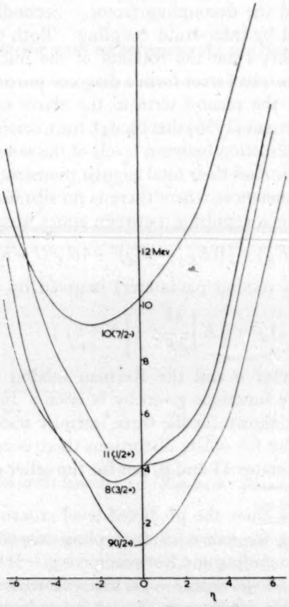

Figure 1. Intrinsic particle excitations in ^{31}P.

The results of this latter calculation are shown in figure 1 where the energy is plotted against a parameter η, equal to δ/χ, where δ is the nuclear deformation. The equilibrium deformations again show an oblate trend and the lowest intrinsic states have projections of their intrinsic angular momenta along the symmetry axis of $\Omega=\frac{1}{2}$, $\frac{3}{2}$ and $\frac{1}{2}$ respectively; they all have even parity. The next highest state has $\Omega=\frac{7}{2}$ and is of odd parity. No experimental evidence has been found for any odd parity states in ^{31}P up to the level of excitation studied. From these calculations we may conclude that the deformation is very probably oblate and that the relevant intrinsic states correspond to those labelled 8, 9 and 11 in Nilsson's paper.

If we can determine which of these states corresponds to the ground state it should be possible to determine the value of the equilibrium deformation from the ground state properties of the nucleus. States 9 and 11 are both possibilities as they both have $\Omega=\frac{1}{2}$.

The relative positions of the rotational energy levels based on these two states are affected by two factors. First the level ordering that occurs when the intrinsic state has $\Omega=\frac{1}{2}$ is anomalous and is of the form

$$E_{\text{rot}}=\frac{\hbar^2}{2\mathscr{I}}\left[I(I+1)+a(-1)^{I+1/2}(I+\tfrac{1}{2})\right].$$

The constant a is called the decoupling factor. Secondly, the positions of the various levels is affected by inter-band coupling. Both these effects are due to the Coriolis forces arising from the rotation of the nucleus as a whole. For a state with $\Omega=\frac{1}{2}$ the Coriolis forces form a diagonal portion of the energy matrix and are responsible for the second term in the above equation. When $\Omega\neq\frac{1}{2}$ it has been shown by Kerman (1956) that though the Coriolis forces are off diagonal terms they lead to an interaction between levels of the same spin, but which differ by unity in the projection K of their total angular momentum along the symmetry axis. (In normal circumstances where there is no vibrational excitation $K=\Omega$.) This interaction leads to a repulsion between states according to the equation

$$E(I)=\tfrac{1}{2}(E_{K+1}+E_K)\pm\tfrac{1}{2}\left[(E_{K+1}-E_K)^2+4A_K{}^2(I-K)(I+K+1)\right]^{1/2}$$

where A_K (the Kerman mixing parameter) is given by

$$A_K=\left\langle K\left|\frac{\hbar^2}{2\mathscr{I}}j_-\right|K+1\right\rangle;$$

both the decoupling factor a and the Kerman mixing parameter A_K can be calculated from the wave functions given by Nilsson. In figure 2 the values of A_K in units of $\hbar^2/2\mathscr{I}$ are shown for the three intrinsic states 8, 9 and 11 taken in pairs. It will be seen that for oblate distortions there is considerable interaction between levels based on states 11 and 8, but for the other combinations it is very weak.

In figures 3 and 4 we show the predicted level ordering for the levels based on states 9 and 11, using the values of decoupling constant calculated from the wave functions, but not including any Kerman mixing. It will be seen that for the band based on state 9 the level with $I=\frac{1}{2}$ is always lowest and, as this band does not mix to any appreciable extent with the other bands, this state of affairs will not be affected by Kerman mixing. On the other hand for the band based on state 11 we see that for most of the region of oblate distortion the $\frac{3}{2}$ level is lowest and the interaction of this level with the $\frac{3}{2}$ level from band 8 will depress this level still further (the $\frac{1}{2}$ level is not affected as it has no partner in band 8). Hence if the Nilsson model is to be applied then the state 9 of the Nilsson scheme must be taken as the ground state.

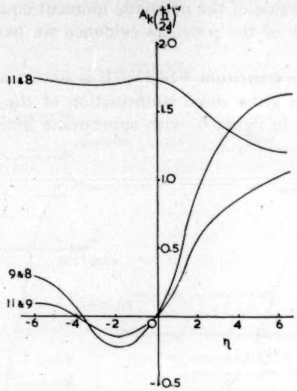

Figure 2. Rotation–particle coupling parameter A_K as a function of deformation.

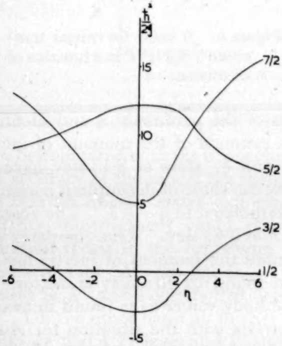

Figure 3. Rotational level order based on state 11.

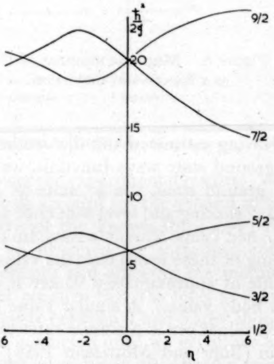

Figure 4. Rotational level order based on state 9.

As the Kerman mixing parameter for band 9 is small we have taken this band as being pure and it is now a straightforward matter to calculate the magnetic moment of ^{31}P as a function of η and to compare the results with experiment. The formula for the magnetic moment (Nilsson 1955, p. 29) contains, apart from details of the wave function, the spin and orbital gyromagnetic ratios of the odd particle and the gyromagnetic ratio of the surface g_R. For the curve plotted in figure 5 the hydrodynamic value of $g_R \simeq Z/A$ is used, but in practice it was found that a 25% variation in the value of g_R produced only a few per cent variation in the value of the magnetic moment at $\eta = -3$. The main factor affecting the result is the mixing of the s and d orbitals in the wave function.

The experimental value of the magnetic moment equals the theoretical value at $\eta = \pm 3$ and in view of the previous evidence we have taken $\eta = -3$ as our distortion parameter.

The *ft* value of the transition $^{31}S(\beta^+)^{31}P$ is not as accurately known as the magnetic moment, but gives some confirmation of the equilibrium distortion. The results are shown in figure 6, with appropriate limits.

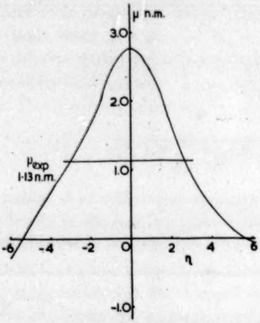

Figure 5. Magnetic moment of ^{31}P as a function of distortion.

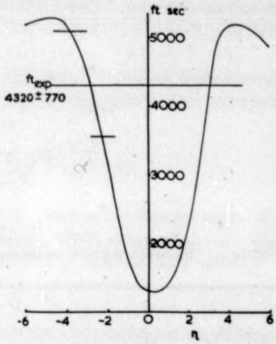

Figure 6. *ft* value for mirror transition $^{31}S(\beta^+)^{31}P$ as a function of distortion.

Having estimated the distortion in terms of the parameter η and identified the ground state wave function, we need an estimate of the moment of inertia. The ground state, the $\frac{5}{2}^+$ state at 2·23 Mev and $\frac{3}{2}^+$ state at 3·13 Mev have the relative spacing and level sequence as given by the value of decoupling parameter calculated using Nilsson's wave functions interpolated to $\eta = -3$. The absolute spacing of these levels fixes the value of $\hbar^2/2\mathscr{J}$ at 0·43 Mev. This compares with a value of approximately 95 kev if one assumes the moment of inertia has the rigid body value. A similar value has been found by Bromley *et al.* for ^{29}Si. These values are in a similar ratio to the rigid body values as is found in heavier nuclei (Bohr and Mottelson 1955) and contrasts with the situation for $A = 25$ where the values are much closer to the rigid body values.

Inserting $\hbar^2/2\mathscr{J} = 0{\cdot}43$ Mev into the expression for A_K we find a value of 0·73 Mev for this parameter as between states 8 and 11.

We now have all the information that is required to effect a comparison between the Nilsson model and the experimental level scheme, apart from relative position of the base states 8, 9 and 11.

State 9, of course, corresponds to the ground state of the nucleus and the result of suitably positioning the basic states 8 and 11 is shown in figure 7. The first three columns show the unmixed bands based on states 9, 11 and 8 respectively, using the calculated values of decoupling constant and the same moment of inertia throughout. The fourth column shows the effect of mixing the levels of bands 8 and 11, using the calculated value of the Kerman mixing parameter A_K. The fifth column gives all the energy levels generated in this way up to 5 Mev and

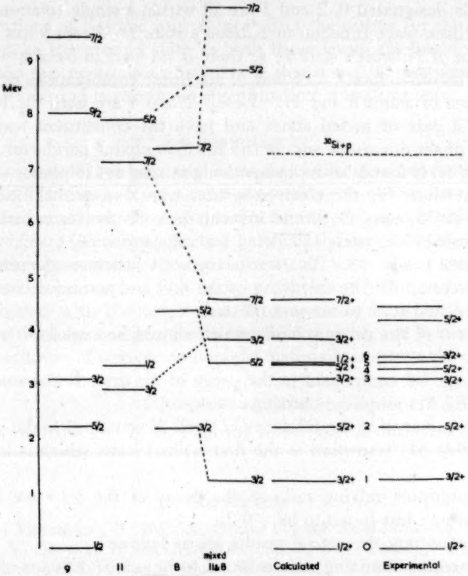

Figure 7. Spheroidal nucleus level scheme for ^{31}P.

is to be compared with the final column showing the experimental results. Within the accuracy of the model the theoretical levels account for the ground state and the first six excited states and give correctly all the known spins and parities. Further improvement could presumably be obtained by including rotation vibration terms in the expression for the energy and allowing the moment of inertia to vary between bands. The model predicts that the level at 3·41 Mev should be $\frac{1}{2}^+$ and suggests that one of the levels between 4 and 5 Mev should be $\frac{7}{2}^+$. On the other hand no further levels are predicted until we get above 8 Mev, while we find a $\frac{5}{2}^+$ level at 4·17 Mev and many more levels of unknown spin and parity above this level. Hence other mechanisms for producing new levels must be looked for. These exist in terms of core excitation and two particle excitation. Rough calculations show that it may only take a few Mev to excite a particle from one of the lower shells and thereby to produce fresh sets of rotational bands.

§ 3. ELECTROMAGNETIC TRANSITIONS

The agreement between the observed and predicted level sequence means that a definite wave function, based on the Nilsson model, can be assigned to each of the seven lowest levels, and these may be used to calculate transition probabilities. This is of interest as in general transition probabilities are far more sensitive to the details of the wave functions than are the relative positions of energy levels.

The levels designated 0, 2 and 3 are all within a single rotational band and have the intrinsic wave function of Nilsson's state 9. Level 5 has the intrinsic wave function of Nilsson's state 11 as there is no level in band 8 with which it can mix. The other levels, 2, 4 and 6, are linear combinations of the particle wave functions of states 8 and 11. Levels 2 and 4 are both the lower energy members of a pair of mixed states and have the constituent wave functions combined in phase due to the sign of the Kerman mixing parameter. Level 6 is the partner of level 2 and has its components mixing out of phase.

The expressions for the electromagnetic transition probabilities are taken from Nilsson (1955, eqns. 29, 35 and 36) with the collective terms included. The transitions probabilities were calculated for values of η of 0, -2, -4 and -6 and interpolated to $\eta = -3$. As a test of the wave functions the results of these calculations were applied to the decay of the first and second excited states and of the third excited state to the ground state.

The features of the decay scheme which should be explained by the model are as follows:

(*a*) The large E2 component in the decay of the first excited state. Experimentally the E2/M1 amplitude mixing ratio $= -1{\cdot}2$.

(*b*) The dominance of the E2 decay of the 2·23 MeV level to the ground state over the possible M1 transition to the first excited state, which is less than 5% of the former.

(*c*) The multipole mixing ratio of the decay of the 3·13 MeV level to the ground state which was found to be $+0{\cdot}2$.

The corresponding theoretical results are as follows:

(*a*) The theoretical mixing ratio is found to be $-0{\cdot}07$, a factor of sixteen too small.

(*b*) The result for the decay of the 2·23 MeV level depends on the assumed size of ratio χ of the spin-orbit coupling to well depth. Nilsson takes $\chi = 0{\cdot}05$ but there is some evidence (Bromley, private communication) that for these lighter nuclei a higher value should be used. If we take $\chi = 0{\cdot}1$ we get 40% to the ground state and 60% to the first excited state. The M1 transition is again too large.

(*c*) The mixing ratio for the decay of the 3·13 MeV level is found to be $+0{\cdot}4$ for $\chi = 0{\cdot}05$ and $+0{\cdot}7$ for $\chi = 0{\cdot}1$, both of which are at least right as far as sign and order of magnitude.

The first two results suggest that the wave functions used are not very realistic. However the strengths of the M1 transitions are very sensitive to what one assumes for the nature of the excited particle. There is some evidence in ^{30}P that isotopic spin is a good quantum number (Broude *et al.* 1956, Endt and Paris 1958) and so presumably the low-lying states of ^{31}P will also have isotopic spin as a good quantum number. In this case the excited particle cannot be purely a proton and the Nilsson states are not isotopic spin eigenfunctions. Calculations using wave functions constructed to be eigenstates of isotopic spin show that it is perfectly possible to obtain simultaneous agreement with the experimental results for the decay of the first two excited states. It is also possible that the small amount of coupling between band 9 and the other two bands might affect the results and in particular it might enhance the E2 strength of the decay of the first excited state. Clearly one very much needs an absolute measure of the decay properties of these states, such as could be provided by Coulomb excitation.

Considerations of isotopic spin do not affect the results for the decay of the 3·13 MeV level to the ground state as both these levels are based on Nilsson's state 9 and the two neutrons are likewise in this state. Consequently the wave function is unique and is already an eigenfunction of isotopic spin.

§ 4. CONCLUSION

The Nilsson model has been applied to the results obtained from the analysis of the ^{30}Si(p, γ)^{31}P data. It is found that by taking an oblate distortion to agree with the experimental value of the magnetic moment it is possible to obtain excellent agreement in energy, spin and parity of the first six excited states using only three other parameters, viz. the moment of inertia of the nucleus and the position of two base states. The decay properties of the first few levels have been investigated with the result that for transitions between bands the M1 strengths are too large compared with the E2 strengths, but it is suggested that the proper inclusion of isotopic spin might materially improve the situation.

ACKNOWLEDGMENT

We wish to thank Dr. E. B. Paul for some helpful discussions of Nilsson's paper.

REFERENCES

BOHR, A., and MOTTELSON, B., 1955, *K. Danske Vidensk. Selsk., Mat-fys. Medd.*, **30,** 1.
BROMLEY, D. A., GOVE, H. E. and LITHERLAND, A. E., 1957, *Canad. J. of Phys.*, **35,** 1057.
BROUDE, C., GREEN, L. L., SINGH, J. J., and WILLMOTT, J. C., 1956, *Phys. Rev.*, **101,** 1052.
BROUDE, C., GREEN, L. L., and WILLMOTT, J. C., 1958 a, *Proc. Phys. Soc.*, **72,** 1097; 1958 b, *Ibid.*, **72,** 1115.
ENDT, P. M., and PARIS, C. H., 1958, *Phys. Rev.*, **110,** 89.
KERMAN, A. K., 1956, *Dan. Mat. Fys. Med.*, **30,** No. 15.
LITHERLAND, A. E., MCMANUS, H., PAUL, E. B., BROMLEY, D. H., and GOVE, H. E., 1958, *Canad. J. Phys.*, **36,** 378.
NILSSON, S. G., 1955, *K. Danske Vidensk. Selsk., Mat-fys. Medd.*, **29,** 16.
WILETS, L., and JEAN, M. J., 1956, *Phys. Rev.*, **102,** 788.

Double Scattering Experiments with 970 Mev Protons

By C. J. BATTY and S. J. GOLDSACK
Physics Department, University of Birmingham

Communicated by P. B. Moon; *MS. received* 1st *September* 1958

Abstract. Nuclear emulsions have been used as detectors to measure the asymmetries produced in a double scattering experiment using 970 Mev protons. Targets of beryllium and carbon have been used and angles between 3° and 8° investigated. Small but significant asymmetries have been found and the experiments are compared with others in this energy region.

§ 1. Introduction

In an earlier communication (Batty and Goldsack 1957) the authors gave the results of a preliminary experiment to determine the polarization of protons scattered from carbon at 970 Mev. These experiments have now been repeated using a similar method, but with much improved beam conditions. In the present paper, the original experiments are described more fully, and compared with the newer experimental arrangement. The results of both experiments are summarized in §9.

§ 2. The Original Experiment

In the experiment referred to in the earlier article, protons scattered to the right through 4° (5½° in a few experiments) from a carbon target (the polarizer) in the vacuum chamber of the Birmingham synchrotron were scattered a second time in a carbon or beryllium block (the analyser). The particles were then examined using photographic plates as detectors. The experimental arrangement is shown in figure 1. The construction of the vacuum system of the synchrotron was such that the experiments had to be performed in the limited region between the thin stainless steel window A and the vacuum manifold B. The magnetic field in this region, together with the limited available space, made a counter experiment

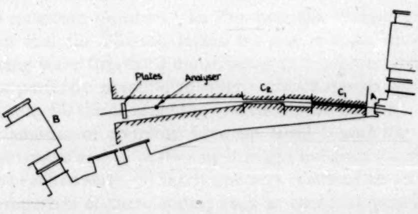

Figure 1. Apparatus used in experiments close to the synchrotron.

unfeasible, and the use of emulsions as detectors of the scattered particles was the only available technique. It suffers from the disadvantage of a poor energy threshold ($\sim$ 300 MeV), but collects particles at all angles at once, and measurements of the angle and position of a given particle in space are possible.

The beam was defined by two channels C_1 and C_2 (figure 1) built of a heavy alloy of tungsten, producing at the second target a well-defined beam of dimensions 1 cm high × 2 cm wide. The analysing target was usually a carbon block 2 in. × 2 in. × 2 in. thick but a beryllium block $1\frac{1}{2}$ in. × $1\frac{1}{2}$ in. × $1\frac{1}{2}$ in, and a carbon block 4 in. thick were occasionally used. The plates which were Ilford G5 5 in. × 1 in. × 200 μ thick, were exposed horizontally at a distance of 25 cm from the centre of the analyser. The plates were processed, and scanned using exactly the same technique as described in § 6 for the later experiments.

§ 3. THE LATER EXPERIMENTS

Shortly after the completion of the earlier experiments it became possible to modify the vacuum system of the synchrotron in such a way as to remove the obstruction presented by the vacuum manifold, so that the beam of interest now emerges from the machine and passes through a hole in the concrete shielding wall (see figure 2). By introducing a set of shims A to modify the fringing magnetic field of the synchrotron magnet (van der Raay 1957) it was possible to focus the particles passing through the window into a beam 4 cm high × 2 cm wide at a point 1 metre beyond the concrete wall. In this region conditions for experiments are vastly improved. The background is reduced and there is no appreciable magnetic field. The experiments previously reported were therefore repeated in this new beam, and the results obtained are likely to be more reliable than the earlier ones. The new beam is also suitable for counter experiments and recently these have been performed by Huq, Hutchinson, Law, Segar and White, to be published.

§ 4. EXPERIMENTAL ARRANGEMENT

The target position was adjusted to give a first scattering angle of $5\frac{1}{2}°$, particles passing through the thin window being focused by the magnetic shims. They then passed through two channels C_1 and C_2 in figure 2. The first of these was 3 in. wide and $\frac{3}{4}$ in. high and limited the height of the beam; the width of the beam produced at the analyser position by the magnetic focusing alone was satisfactory. The second channel was made large enough to pass the whole of the beam focused by the magnetic field, but removed background. This avoided the walls of the channel becoming a strong source of background particles. On leaving the iron channel the particles travelled $1\frac{1}{2}$ metres through the concrete shielding wall to the point where the analyser (a carbon or beryllium block as before) was placed.

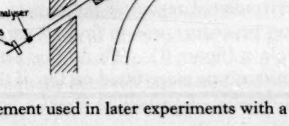

Figure 2. Arrangement used in later experiments with a focused beam.

Plates of Ilford G5 emulsion 5 in. × 1 in. × 200 μ were situated 25 cm from the centre of the carbon block, lying horizontally and with their length perpendicular to the beam direction.

The exposures varied according to the beam intensity, but were usually about 800 synchrotron pulses giving a total flux on the target of approximately 10^7 protons.

§ 5. THE BEAM ENERGY

In both experiments the energy of the circulating beam in the synchrotron was 980 ± 10 MEV; the protons may lose up to 10 MEV in the first target and continue to circulate, so that the mean energy of the beam hitting the first target was 975 ± 12 MEV. At angles of 4° and $5\frac{1}{2}°$ it is probable that elastic scattering is dominant, though there may well be an admixture of particles scattered with some loss of energy. In any case particles losing more than about 50 MEV in the first experiment and 30 MEV in the second could not have reached the analyser.

In contrast to this, the second scattering may be highly inelastic since, in the emulsion, a particle would not be recognized as different from a 970 MEV proton unless its energy was below 300 MEV. It follows that except at small angles, where elastic processes would be expected to dominate, the asymmetries obtained should be expected to be lower limits to those for elastically scattered particles.

§ 6. THE SCANNING PROCEDURE

Figure 3 is a schematic plan of the target and plate arrangement. The unscattered beam passed through the central part of the plate and the position and angle of the beam could be found by measurements carried out in this region. It is thus possible to define a point A which is the geometrical beam centre, and an angle which can be taken as zero for the scattering.

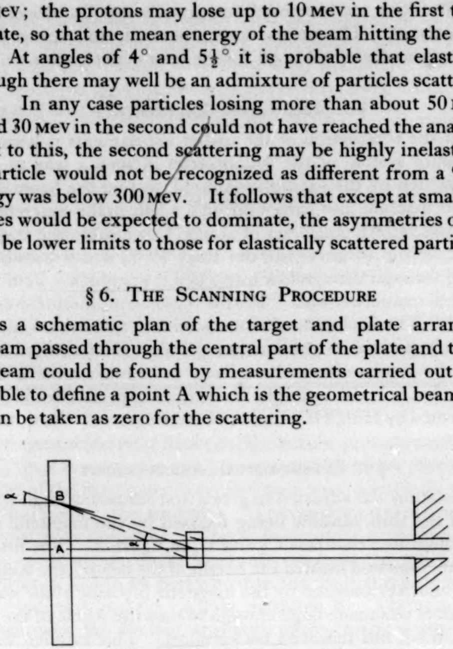

Figure 3. Geometry of scattering experiment.

Because some particles were scattered by the walls of the collimators, at a point such as B we can expect to find two groups of particles. Those from the collimators reached B at an angle distinct from those scattered by the analyser. The latter could only reach the plate within an angular range defined by the angle subtended at B by the irradiated region of the target. This was approximately 4°. Thus the scanning procedure was to find all particles at points such as B within ±2° of the angle α (figure 3). To do this conveniently, the plate was mounted on a special microscope stage fitted on top of the normal x and y motion of the microscope and capable of swivelling about a point 25 cm from the optic axis, coincident, relative to the plate, with the target position at the time of exposure. The long edge of the plate was parallel to the *y* axis of the microscope. As the stage was rotated the central angle was thus constant in the microscope.

In addition to this, an eyepiece protractor graticule was used to measure the angles. To avoid the delicate setting of the tracks on the protractor origin, the protractor was set in a slide which made it possible to set it on any track in the field of view without moving the microscope stage. The scanning procedure was as follows. First the beam centre A was located by counting tracks in the plate. The *y* coordinate of the stage was then adjusted so that the microscope axis passed through A when the swivelling stage was set at zero. The zero of the eyepiece protractor was adjusted to coincide with the mean angle of the tracks at the point A, by measuring the error and correcting it using the eyepiece goniometer. This could be done correct to $\pm\frac{1}{8}°$. During actual scanning, the swivelling stage was set-off from its zero a whole number of degrees, and the scanning was done by using the *y* motion of the main stage, so that the plate moved without rotation. A region 5 mm each side of the centre was scanned in this way, and all tracks noted within ±3° of the protractor zero. The procedure was then repeated with two degrees greater displacement of the swivelling stage. The great advantage of this method was that all scanning was done with the same angle region in the field of view, so that no scanner-preference for left or right could affect the measurements.

To avoid errors due to scanning efficiency, some exposures were performed with plates alternately emulsion up and emulsion down, and care was taken that the scanner did not know which type of plate he was examining. In addition, some of the plates were scanned twice and a detailed check made between the two sets of results. These checks showed that bias by the scanner could not account for the observed asymmetries.

§ 7. ANGULAR ACCURACY

Measurements were made with the protractor eyepiece to $\pm\frac{1}{8}°$, but the results were finally grouped in degree intervals. Thus the experimental accuracy of the angular measurement was $\pm\frac{1}{2}°$ rectangular distribution. In addition to this, there are the following sources of error: (*a*) the spread of the beam, (*b*) the divergence (or convergence) of the beam and (*c*) multiple scattering. The first and third of these can be measured together by examining the actual spread of the beam observed in the plates themsleves, and similarly the second can also be measured by measuring the change in the mean beam angle over the centre region of the plate. These three sources of error, folded together with the classifying interval, correspond to an angular spread in the points of ±0·7°.

In addition to these errors, there may be an error in the mean beam angle which could lead to spurious apparent asymmetries, because of the rapid change of cross section with angle. The zero angle could be determined to about ±0·125° on each plate. Since each experiment involved about eight plates, the mean error would be ±0·05° which could lead to asymmetries of the order of 0·02.

Lastly, mention should be made of the magnetic field present in the first series of experiments. This field should not affect the results in so far as a constant field would deviate all particles equally between target and the plates. However, there is a field gradient of 100 gauss cm^{-1} in the experimental region. This is easily shown to be equivalent to a displacement of the mean angle of the beam relative to the scattered particles of 0·03°, in such a direction as to reduce the apparent asymmetries by about 0·01.

§ 8. BACKGROUND RUNS

To determine what proportion of the measured tracks could originate in sources other than the scattering block, control runs in which the scattering block was removed were performed in all experiments. Since the experimental method was such that a particle was counted only if it reached the plates at an angle and position consistent with its origin in the scatterer, this background was always small. The only exception to this was the very small angles in the first series of experiments, when a rather large number of particles was observed coming from the target position at small anlges on the left of the beam. These were attributed to low-energy particles swept round by the magnetic field so as to reach the target position appearing to be scattered to the left. This effect was absent in the latter experiments. Where the background was appreciable, corrections were applied to the results.

§ 9. RESULTS

In all, six experiments were performed using the earlier arrangement described in § 2 and two using that described in § 4. The asymmetries observed are given in tables 1 and 2 and in figures 4 and 5. The errors shown are purely statistical.

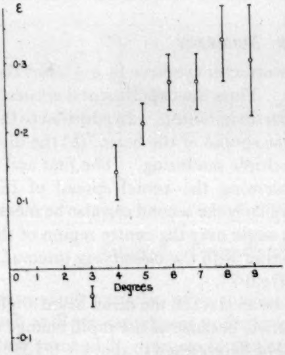

Figure 4. Asymmetries observed with a first scattering angle of 4° and reported in an earlier publication.

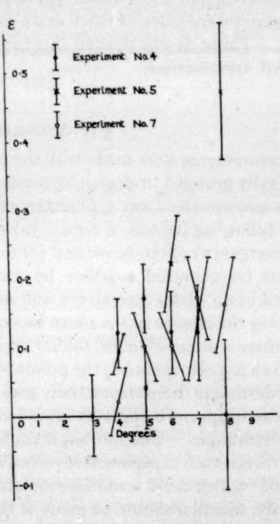

Figure 5. Asymmetries observed with a first scattering angle of $5\frac{1}{2}$°.

Table 1. Asymmetries observed using Arrangement described in §2

Experiment no.	Angle of 1st scatter (°)	Targets	Angle of scatter (degrees)					
			3°	4°	5°	6°	7°	8°
1	4	C–C[‡]	0·04 ± 0·09	0·36 ± 0·08	0·34 ± 0·08	0·55 ± 0·08	0·40 ± 0·14	0·28 ± 0·10
2	4	C–C[‡]	−0·06 ± 0·04	0·05 ± 0·04	0·19 ± 0·03	0·22 ± 0·04	0·25 ± 0·05	0·36 ± 0·08
3	4	C–C[†]	−0·05 ± 0·06	0·05 ± 0·06	0·19 ± 0·08	0·09 ± 0·13	0·11 ± 0·09	—
4	5½	C–C[†]	0·00 ± 0·06	0·12 ± 0·05	0·17 ± 0·05	0·12 ± 0·06	0·12 ± 0·07	0·00 ± 0·11
5	5½	C–C	−0·21 ± 0·10	0·09 ± 0·03	0·04 ± 0·06	0·22 ± 0·07	0·14 ± 0·09	0·47 ± 0·10
6	5½	C–Be	0·20 ± 0·10	0·23 ± 0·07	0·11 ± 0·08	0·15 ± 0·08	0·13 ± 0·10	−0·08 ± 0·13

[†] A 10 cm thick target was used in these experiments.

[‡] Previously reported by Batty and Goldsack (1957).

Table 2. Asymmetries observed using Arrangement described in §4

Experiment no.	Angle of 1st scatter (°)	Targets	Angle of scatter (degrees)					
			3°	4°	5°	6°	7°	8°
7	5½	C–C	—	0·02 ± 0·05	0·10 ± 0·05	0·10 ± 0·05	0·17 ± 0·06	0·16 ± 0·07
8	5½	Be–Be	0·07 ± 0·07	0·20 ± 0·08	0·23 ± 0·05	0·13 ± 0·06	0·01 ± 0·06	0·05 ± 0·08

§ 10. DISCUSSION

These results show fairly small but significant asymmetries both at angles of 4° and 5½° of first scatter. In the earlier publication (Batty and Goldsack 1957) the results were converted to give the polarization as a function of angle by dividing through by the square root of the asymmetry at 4°. It is now felt that this procedure is not correct in view of the possibly large amount of inelastic contamination at the second scattering (see § 5). We have therefore plotted in figures 4 and 5 the observed asymmetry as a function of angle.

The asymmetries observed in the various experiments are in reasonable agreement with each other with the exception of the earliest experiments at 4° and especially the first of these. The reason for the large asymmetries found there has never been fully understood, but may be due in some way to the proximity of the experiment to the machine giving spurious background which has not been correctly allowed for. It is felt that the later experiments are much more reliable due to the lower background.

The present results are in reasonable agreement with those obtained in this laboratory by Huq *et al.* using a counter system with alternative energy thresholds of 50 and 910 MEV. Most of our points fall between their curves for the two thresholds. Our results also agree with a reasonable extrapolation of lower energy results using a poor energy threshold (e.g. Mescheryakov, Nurushev and Stoletov 1957) and with a recent experiment similar to the present one but limited to angles less than 5° (Batty, Lock and March 1959).

ACKNOWLEDGMENTS

Our thanks are due to Professor P. B. Moon who initiated the work on this problem and to the synchrotron staff for their efficient operation of the machine. One of us (C. J. B.) wishes to acknowledge the receipt of a maintenance grant from the Department of Scientific and Industrial Research.

REFERENCES

BATTY, C. J., and GOLDSACK, S. J., 1957, *Proc. Phys. Soc.* A, **70,** 165.
BATTY, C. J., LOCK, W. O., and MARCH, P. V., 1959, *Proc. Phys. Soc.*, **73,** in the press.
MESCHERYAKOV, M. G., NURUSHEV, S. B., and STOLETOV, G. D., 1957, *J. Exp. Theor. Phys.*, **31,** 361 (translated in *Soviet Physics* (*J.E.T.P.*), **4,** 337).
VAN DER RAAY, H. B., 1957, *Nucl. Instrum.*, **1,** 351.

RESEARCH NOTES

Polarization of μ-Mesons Scattered by Mercury

By G. E. BROWN,† L. R. B. ELTON‡ and F. MANDL§

† Department of Mathematical Physics, University of Birmingham
‡ Physics Department, Battersea College of Technology
§ Atomic Energy Research Establishment, Harwell, Berks.

Communicated by R. E. Peierls; *MS. received* 20*th August* 1958

§ 1. Introduction

Recent developments relating to non-conservation of parity indicate that μ-mesons resulting from π-decays are polarized along the line of their flight. If this polarization can be turned so that a component perpendicular to the direction of motion results, it could conceivably be measured by observing the asymmetry in a further scattering by complex nuclei. If the component of initial polarization perpendicular to the direction of motion is P_i, and the polarization produced in scattering an unpolarized beam off the complex nucleus is $P(\theta)$, then the resulting asymmetry in the scattering of the unpolarized beam is $\epsilon = P_i P(\theta)$.

The scattering of μ-mesons by a complex nucleus is analogous to the Mott scattering of electrons, if we consider only scattering resulting from the static charge distribution. However, the wavelength of the meson is short compared with the nuclear radius, so it is essential to take into account the extension of the charge distribution in calculating the scattering of mesons.

We report here on a numerical calculation of the scattering by mercury of both μ^+ and μ^- mesons of velocity 0·8*c*. While this work was in progress, calculations by Franklin and Margolis (1958) for μ^--mesons of velocity 0·2*c* scattered by mercury were published, and we received extensive results for the scattering of both μ^--mesons and μ^+-mesons of various velocities by several nuclei from Dr. G. Rawitscher (private communication) and results for the scattering of μ^--mesons of velocities 0·2*c* and 0·4*c* by nuclei of $Z=48$ and 80 from Franklin, Margolis and Oberthal (1958). Since calculations have been carried out by these other groups, we shall present our numerical results concisely, but shall discuss here some general points not contained in the other work.

§ 2. Development

The charge distribution of Hg was assumed to be

$$\rho(r) = \rho_0 \{1 + \exp[(r^2 - R^2)/\beta^2]\}^{-1} \qquad \ldots\ldots (1)$$

with $R = 6{\cdot}34$ fermis and $\beta = R/2$. This charge distribution was found by Brown and Elton (1955) to give results in reasonable agreement with high energy electron scattering, although later Stanford calculations (Hahn, Ravenhall and Hofstadter 1956) indicate that the surface thickness given by our parameters may be somewhat large. A small change in surface thickness would not change our results appreciably, except at very large angles.

The calculations were carried out in the same way as those described by Brown and Elton (1955) and Brenner, Brown and Elton (1954). Calculation of the point charge Coulomb functions, which are necessary in order to obtain the phase shifts, was, however, more complicated in detail, since certain terms which vanish for the electron problem (when $v/c=1$) are important in this case.

In the case considered here, $kR=4{\cdot}53$, where k is the wave number of the μ-meson, so that the structure of the nucleus affected the large angle scattering markedly. We give results below for the cross section and polarization for both a point charge nucleus (Mott scattering) and for the extended charge of equation (1).

We define the polarization and other quantities in the same way as Franklin and Margolis (1958).

Table 1. Mott Scattering of μ^+-Mesons

Angle (°)	20	25	30	35	40	45	50	
$k^2\,d\sigma/d\Omega$	134	53·6	25·4	13·6	7·92	4·91	3·21	
Polarization	0·0038	0·0053	0·0073	0·0100	0·0132	0·0165	0·0208	
Angle (°)	55	60	65	70	75	80	85	90
$k^2\,d\sigma/d\Omega$	2·19	1·55	1·12	0·84	0·65	0·50	0·40	0·33
Polarization	0·0240	0·0277	0·0315	0·0358	0·0399	0·0438	0·0478	0·0512

Table 2. Scattering of μ^+-Mesons by the Extended Distribution

Angle (°)	20	25	30	35	40	45	50	
$k^2\,d\sigma/d\Omega$	115	38·1	14·4	5·86	2·49	1·09	0·49	
Polarization	−0·0001	−0·0017	−0·0043	−0·0076	−0·0114			
Angle (°)	55	60	65	70	75	80	85	90
$k^2\,d\sigma/d\Omega$	0·22	0·10	0·048	0·023	0·011	0·0057	0·0030	0·0016
Polarization	−0·0302	−0·0391	−0·0476	−0·0519	−0·0533	−0·0579	−0·0521	−0·0469

Table 3. Mott Scattering of μ^--Mesons

Angle (°)	20	25	30	35	40	45	50	
$k^2\,d\sigma/d\Omega$	163	70·5	36·3	21·0	13·3	8·97	6·37	
Polarization	0·0055	0·0072	0·0062	0·0020	−0·0058	−0·0173	−0·0323	
Angle (°)	55	60	65	70	75	80	85	90
$k^2\,d\sigma/d\Omega$	4·69	3·56	2·77	2·19	1·77	1·44	1·19	0·99
Polarization	−0·0506	−0·0717	−0·0955	−0·1215	−0·1495	−0·1791	−0·2102	−0·2423

Table 4. Scattering of μ^--Mesons by the Extended Distribution

Angle (°)	20	25	30	35	40	45	50	
$k^2\,d\sigma/d\Omega$	112	30·5	9·09	2·79	0·901	0·329	0·142	
Polarization	0·0035	0·0044	0·0064	0·0095	0·0139	0·0187	0·0219	
Angle (°)	55	60	65	70	75	80	85	90
$k^2\,d\sigma/d\Omega$	0·0691	0·0348	0·0169	0·0077	0·0032	0·0014	0·0006	0·0004
Polarization	0·0230	0·0224	0·0207	0·0183	0·0175	0·0202	0·0447	0·0641

The accuracy of the polarization in the μ^+ case is not very high at small angles, because calculating it involved taking the small difference of large numbers. However, we believe that it is sufficiently accurate to show the general trend.

The results for the Mott scattering of μ^--mesons agree with those of Sherman (1956) and for both the Mott scattering and scattering by the extended distribution of μ^+-mesons, with those of Rawitscher.

The predicted polarization from the extended charge distribution is, as can be seen, small. Although it is appreciable at large angles, the cross section for the extended charge distribution becomes very small here.

§ 3. SEMI-CLASSICAL CONSIDERATIONS

Some qualitative features of the results can be understood by semi-classical arguments, which we shall now sketch. The Dirac wave equation is†

$$(E-V+\boldsymbol{\alpha}\mathbf{p}+\beta m)\psi=0 \qquad \ldots\ldots(2)$$

where $\boldsymbol{\alpha}$ and β are the usual Dirac matrices and V is the potential. Expressing ψ as

$$\psi=\begin{pmatrix}\Phi\\ \Psi\end{pmatrix} \qquad \ldots\ldots(3)$$

where Φ and Ψ are two-component functions, we eliminate Φ, obtaining

$$\left\{(E-V)^2-m^2-p^2-\frac{1}{r}\frac{dV}{dr}\frac{1}{E-V+m}\left[\boldsymbol{\sigma}\,.\,\mathbf{L}+\frac{1}{i}\mathbf{r}\,.\,\mathbf{p}\right]\right\}\Psi=0 \qquad \ldots\ldots(4)$$

which is analogous to the Klein–Gordon equation with additional terms. For the case of the extended nucleus, the last term in equation (4) is everywhere small compared with the others. We neglect the term in $\mathbf{r}\,.\,\mathbf{p}$, but will keep the $(\boldsymbol{\sigma}\,.\,\mathbf{L})$ term to first order since we wish to describe spin-dependent effects. We also neglect V^2 compared with $2EV$ and the V in the denominator of the final term. These are all reasonable approximations for the case we consider above. We then solve the approximate equation

$$\left\{E^2-2EV-m^2-p^2-\frac{1}{E+m}\frac{1}{r}\frac{dV}{dr}\boldsymbol{\sigma}\,.\,\mathbf{L}\right\}\Psi=0. \qquad \ldots\ldots(5)$$

At small angles, the scattering amplitude $F(\theta,\phi)$ can be obtained fairly accurately from the semi-classical approximation‡ (Malenka 1954, Shapiro 1955, Schiff 1956). Conditions for the validity of this approximation are discussed in the papers referred to; we note here only that this approximation is more suitable than Born approximation for the problem in hand, since its validity does not depend on the phase shifts produced by V being small, whereas this is a necessary condition for Born approximation.

From the semi-classical approximation we obtain the following expression, valid at small angles, for the scattering amplitude

$$F(\theta,\phi)=f(\theta)-ig(\theta)\boldsymbol{\sigma}\,.\,\mathbf{n} \qquad \ldots\ldots(6)$$

with

$$\mathbf{n}=\frac{\mathbf{k}_i\times\mathbf{k}_f}{|\mathbf{k}_i\times\mathbf{k}_f|} \qquad \ldots\ldots(6.1)$$

---

† We use relativistic units $\hbar=c=1$ throughout.

‡ Calculations for the scattering of 125 MEV electrons by mercury have been carried out by one of the authors (G. E. B.) and show excellent agreement with phase shift calculations at angles $\lesssim 30°$. Electrons of such an energy have a value of kR similar to that of the mesons here.

where $\mathbf{k}_i$ and $\mathbf{k}_f$ are the initial and final momenta, and the other quantities are defined by§

$$f(\theta) = \frac{k}{i}\int_0^\infty bdb\mathrm{J}_0(kb\sin\theta)[\exp(i\chi_1)\cos\chi_2 - 1] \qquad \ldots\ldots(6.2)$$

$$g(\theta) = -k\int_0^\infty bdb\mathrm{J}_1(kb\sin\theta)\exp(i\chi_1)\sin\chi_2 \qquad \ldots\ldots(6.3)$$

$$\chi_1 = -\frac{E}{k}\int_{-\infty}^\infty Vdz,\quad \chi_2 = -\frac{1}{2k(E+m)}kb\int_{-\infty}^\infty \frac{1}{r}\frac{dV}{dr}dz \qquad \ldots\ldots(6.4)$$

where $f(\theta)$ and $g(\theta)$ are semi-classical approximations to the f and g occurring in the exact solutions (Mott and Massey 1949, p. 76).

The phase change χ_2 coming from the spin-dependent term is small; if we set $\cos\chi_2 = 1$ and $\sin\chi_2 = \chi_2$, we find (Köhler 1956, Levintov 1956)

$$g \simeq \frac{(E^2 - m^2)\sin\theta}{2E(E+m)}f. \qquad \ldots\ldots(7)$$

In the following table, we plot the ratios $|f|/|g|$ predicted by equation (7) and those found in the numerical calculations.

Table 5. Values of $|f|/|g|$

Angle (°)	20	25	30
Value predicted by eqn. (7)	0·069	0·087	0·104
Mott scattering of μ^--mesons	0·078	0·104	0·129
Scattering of μ^--mesons by extended charge	0·076	0·096	0·117
Mott scattering of μ^+-mesons	0·063	0·076	0·089
Scattering of μ^+-mesons by extended charge	0·062	0·076	0·088

The agreement between values from equation (7) and those actually found is fairly rough, but good enough to show that our approximations describe the situation well at small angles. Equation (7) predicts g and f to be in phase and, therefore, zero polarization. The fact that the polarizations found numerically go so rapidly to zero with decreasing angle is thus understandable, because at small angles our semi-classical arguments describe the situation well, and any polarization found in the accurate calculations must result from terms neglected in the preceding approximations.

The above development raises an interesting question: Do the polarizations from the point and extended charge distributions tend toward each other at very small angles? One knows, of course, that the cross sections do. But this is because the contributions from large impact parameters are the same in both cases, and these predominate over those from small impact parameters. However, just the contributions from large impact parameters are handled most accurately in our semi-classical approximations and, within the accuracy of these, no polarization results. Thus, since any polarization would be expected to come from small impact parameters, it need not be similar for the point and extended charge cases. We are unable to answer this question with our numerical calculations, because they do not give accurate results at small angles.

The main use of the semi-classical calculation has been to understand why the polarization goes rapidly to zero with decreasing angle and to give us a rough check on the ratios f/g. This approximate calculation would not apply to much lower energies, where V/E is not small.

---

§ In order to define χ_1 one must cut off the Coulomb field at a large distance, i.e. take $V = (Ze^2/r)\exp(-\lambda r)$, where λ is negligible compared with the inverse nuclear dimension.

ACKNOWLEDGMENTS

We would like to thank Dr. L. Castillejo for several helpful suggestions and criticisms, and Dr. B. Margolis and Dr. G. R. Rawitscher for useful discussions and for sending results before publication. We are grateful to Mr. J. L. Beeby for carrying out the numerical integration of the Dirac equation for the nuclear charge distribution and Mr. J. Stuttard, at the University of Birmingham, for performing most of the hand calculations. We are indebted to the Atomic Weapons Research Establishment, Aldermaston, for the use of the Mark I Ferranti Computer. One of the authors (G. E. B.) would like to thank the Institute for Theoretical Physics, University of Copenhagen, for hospitality and support during his stay there.

REFERENCES

BRENNER, S., BROWN, G. E., and ELTON, L. R. B., 1954, *Phil. Mag.*, **45**, 524
BROWN, G. E., and ELTON, L. R. B., 1955, *Phil. Mag.*, **46**, 164.
FRANKLIN, J., and MARGOLIS, B., 1958, *Phys. Rev.*, **109**, 525.
FRANKLIN, J., MARGOLIS, B., and OVERTHAL, H., 1958, *Phys. Rev* , **111**, 296.
HAHN, B., RAVENHALL, D. G., and HOFSTADTER, R., 1956, *Phys. Rev.*, **101**, 1131.
KÖHLER, H. S., 1956, *Nucl. Phys.*, **1**, 433.
LEVINTOV, I. I., 1956, *Dokl. Obsch. Sobr. Ak. Nauk S.S.S.R.*, **107**, 240.
MALENKA, B. J., 1954, *Phys. Rev.*, **95**, 522.
MASSEY, H. S. W., 1942, *Proc. Roy. Soc.* A, **181**, 14.
MOTT, N. F., and MASSEY, H. S. W., 1949, *The Theory of Atomic Collisions*, 2nd edn (Oxford: Clarendon Press).
SCHIFF, L. I., 1956, *Phys. Rev.*, **103**, 443.
SHAPIRO, I. I., 1955, *Thesis*, Harvard University.
SHERMAN, N., 1956, *Phys. Rev.*, **103**, 1601.

On the Enumeration of Mayer Cluster Integrals

BY H. N. V. TEMPERLEY
Atomic Weapons Research Establishment, Aldermaston, Berks.

MS. received 2nd *June* 1958, *and in final form* 15th *August* 1958

§ 1. INTRODUCTION

VARIOUS writers have called attention to the lack of asymptotic results for the numbers of cluster integrals b_l and β_k occurring in Mayer and Mayer's (1940) work. One would like estimates of the numbers of such integrals as functions of the number of molecules involved (l or $k+1$) and the number of lines m that the diagram contains. A few results are given by Riddell and Uhlenbeck (1953). It is elementary that m must lie between $l-1$ and $\frac{1}{2}l(l-1)$ and, on physical grounds, we are most interested in diagrams for which m is only slightly greater than l. For $m \geqslant l \log l$, it can be shown that 'almost all' diagrams are connected and irreducible, and the derivation of asymptotic formulae is fairly simple (Riddell and Uhlenbeck 1953), but this case is not very interesting physically.

The present investigation arose from a need for some fairly precise results for m in the region of l (Temperley 1958).

§ 2. THE GENERATING FUNCTION FOR b_l

In this note, we shall work with a hypothetical assembly whose cluster integrals b_l are a function of a single variable x, such that the coefficient of x^m in $b_l l\,!$ represents the number of diagrams for which l (distinguishable) molecules are connected by m lines, while $\beta_k\, k\,!$ is related to irreducible diagrams, in which $k+1$ molecules are connected by m lines in an analogous way. References to the b's or β's in this note are to be understood in this sense. The hypothetical assembly considered is one in which every molecule is interacting with every other with an interaction that is independent of the distance between any pair of molecules. The corresponding Boltzmann factor for each of the $N(N-1)/2$ interactions between two molecules is then represented by $1+x$, the configuration partition function for N molecules is $(1+x)^{N(N-1)/2}$, and by applying Mayer and Mayer's (1940) expression for the relation between cluster integrals and the grand partition function, we find

$$\exp g(x,z)=\exp\left(\sum_{l=1}^{\infty} b_l z^l\right)=\sum_{N=0}^{\infty}\left(\frac{z^N(1+x)^{N(N-1)/2}}{N!}\right) \qquad \ldots\ldots(1)$$

the volume of the hypothetical assembly being taken as unity. Equation (1) was derived by Riddell and Uhlenbeck (1953) by a practically equivalent argument. Any desired b_l can be obtained exactly by expanding the logarithm of the right-hand side of (1), but it does not seem to be possible to obtain any worth-while results for large l by this means, so we use an indirect attack.

We make use of the fact that the right-hand side of (1) satisfies a linear partial differential equation of 'heat-conduction' type in z and x.

$$z^2\frac{\partial^2 e^g}{\partial z^2}=2(1+x)\frac{\partial e^g}{\partial x}. \qquad \ldots\ldots(2)$$

We can transform this equation in various ways, at the expense of making it non-linear. Nevertheless, the transformed equation can be solved in series in certain limiting cases. We express (2) as a differential equation for g and try to solve it in series. We know that the lowest term in $b_l l\,!$ is $l^{l-2}x^{l-1}$ since it takes at least $l-1$ lines to join up l points, and such a diagram can contain no loops and therefore must be a Cayley tree, the number of which is known to be l^{l-2}. Since we are especially interested in enumerating diagrams for which l is large, but the number of 'extra' lines may be small, we are led to make the substitution $z=v/x$. The index of v then corresponds to the number of points while that of x corresponds to the excess of the number of lines over the number of points. We therefore look for a solution, starting with x^{-1}, in ascending powers of x. The known form of the coefficient of x^{-1},

$$\sum_l \frac{l^{l-2}v^l}{l!},$$

suggests a further change of variable from v to y, where $v=y\mathrm{e}^{-y}$. Carrying out this change of variable, and again solving as an ascending series in x, we find that the coefficients of successive powers of x are expressible as simple functions of y, although the expressions as functions of v involve infinite series. In fact we find

$$\sum_l b_l v^l=\frac{1}{x}\left(y-\frac{y^2}{2}\right)-\tfrac{1}{2}\log(1-y)-\frac{y}{2}-\frac{y^2}{4}+x\left(\frac{5}{24(1-y)^3}+\ldots.\right) \qquad \ldots\ldots(3)$$

and we can derive a simple recurrence relation if we retain only highest powers of $(1-y)^{-1}$. Our estimate for the leading term in the coefficient of x^t is

$$O(1)\left(\frac{3}{2}\right)^{t-1}\frac{t!}{3t}(1-y)^{-3t}, \qquad \ldots\ldots(4)$$

We can estimate the number of Mayer diagrams involving N points and t 'extra' lines as $N\,!$ times the coefficient of v^N in (4), which is easily evaluated if we express it as a contour integral, change back the variable from v to y, and use steepest descents. We estimate the number of diagrams as

$$O(1)\left(\frac{3}{2}\right)^{t-1}\frac{t!}{3t\,!}N\,!\,e^N(N)^{3t-1}. \qquad \ldots\ldots(5)$$

§ 3. IRREDUCIBLE DIAGRAMS

We introduce a new variable, defined by

$$q=z\frac{\partial g}{\partial z}=\sum_l l\,b_l z^l. \qquad \ldots\ldots(6)$$

By Mayer and Mayer's (1940) inversion formula, this is known to be equivalent to

$$z=q\exp\left(-\sum_k \beta_k q^k\right) \qquad \ldots\ldots(7)$$

which, by differentiation and the use of (6) followed by an integration with respect to q, leads to

$$g=q-\sum_k\frac{k}{k+1}\beta_k q^{k+1}. \qquad \ldots\ldots(8)$$

We now use (6) and (7) to change the independent variables in (2) from (z, x) to (q, x) and obtain

$$q^2-q+\frac{q}{(\partial g/\partial q)_x}=2(1+x)\sum_k\frac{1}{k+1}\frac{d\beta_k}{dx}q^{k+1}. \qquad \ldots\ldots(9)$$

Introducing the new function

$$S(x,q)=\sum_k\frac{\beta_k}{k+1}q^{k+1},$$

we find that equation (2) becomes

$$\tfrac{1}{2}q^2+\frac{\tfrac{1}{2}q^2\partial^2S/\partial q^2}{1-q\partial^2S/\partial q^2}=(1+x)\left(\frac{\partial S}{\partial x}\right)_q. \qquad \ldots\ldots(10)$$

As before, we are mainly interested in cases where the number of 'extra' lines may be small, so we change to a new independent variable $w=qx$. First, solving as an ascending series for w, we can verify the exact results of Riddell and Uhlenbeck (1953) for the numbers of irreducible clusters with one and two 'extra' lines, obtained by a quite different method:

$$\left.\begin{array}{l}\text{Rings with } N \text{ points, } N \text{ lines, } (N-1)\,!/2\\ \text{Clusters with } N \text{ points, } N+1 \text{ lines, } \dfrac{(N-3)(N+2)N!}{24} \text{ (a sign has been corrected)}\\ \text{Clusters with } N \text{ points, } N+2 \text{ lines, } \dfrac{(N^4+4N^3-15N^2-46N-40)(N-3N\,!}{1152}\end{array}\right\} \qquad \ldots\ldots(11)$$

Secondly, solving as an ascending series in x, we obtain a result very similar in form to (3), and, proceeding as before by retaining only the highest inverse powers of $1-w$, we obtain an estimate for the number of irreducible diagrams involving N points and t 'extra' lines of exactly the same form as (5) except that the factor e^N is omitted. In other words, the main difference between b_N and β_{N-1} is that N^N is replaced by $N!$, when N becomes large, the number of 'extra' lines being held fixed.

Actually we have, instead of (3),

$$S \simeq \frac{w^2}{2x} - \frac{w^2}{4} - \frac{w}{2} - \tfrac{1}{2}\log(1-w) + \frac{x}{12(1-w)^2} + \ldots . + \frac{5x^2}{48(1-w)^6} + \ldots . . \qquad \ldots\ldots (12)$$

We can pick out the main contribution to the coefficient of $w^N x^t$ and the results quoted without proof by Temperley (1958) can easily be derived from the expression corresponding to (5). These results were compared with Ford's (1954) data for $N=6$, in the above paper, agreement being already fairly good for this low value of N.

REFERENCES

FORD, G. W., 1954, *Thesis*, University of Michigan.
MAYER, J. E., and MAYER, M. G., 1940, *Statistical Mechanics* (New York : Wiley).
RIDDELL, R. J., and UHLENBECK, G. E., 1953, *J. Chem. Phys.*, **21**, 2056.
TEMPERLEY, H. N. V., 1958, *Proc. Phys. Soc.*, **71**, 238.

Polarization Changes during the Process of Ageing in Ferroelectrics of the $BaTiO_3$-Type

BY Z. PAJĄK AND J. STANKOWSKI
Polish Academy of Sciences, Institute of Physics, Dielectric Laboratory, Poznań

Communicated by A. Piekara; *MS. received* 29*th July* 1958

SOME properties of ferroelectrics of the perovskite type change their values with time, beginning from the production or from heating above the Curie point. This effect was first observed in the case of the dielectric permittivity (Kazarnovsky 1952, Piekara and Pająk 1952) and power factor (Novosiltsev, Khodakov and Shulman 1952, Bogoroditsky and Verbitskaya 1953), and subsequently for the electromechanical coupling factor and piezoelectric constant d_{31} (Mason 1955). Recently an effect consisting in a displacement of the Curie point (temperature of paraelectric–ferroelectric transition) was also observed (Pająk 1957). Such effects are termed ageing processes.

It seems reasonable to expect that the cause of all these phenomena resides in a change of the spontaneous polarization of the ferroelectrics. With this interpretation in view the dielectric hysteresis loops of barium metatitanate ceramics were investigated in samples immediately after production as well as in aged samples using the Sawyer–Tower method. Measurements showed that the high values of the spontaneous polarization P_s, the total polarization P, the coercive force E_c and hysteresis losses A observed in 'young' samples decrease with time and after a sufficiently long period the P_s, E_c and A vanish. Thus, the aged ferroelectrics show a behaviour similar to that of usual dielectrics, revealing nearly linear P/E dependence. Figure 1 (Plate) shows the changes mentioned above in the hysteresis loop. It will be seen that on production of the sample (figure 1 (*a*)) the hysteresis loop gives the usually observed values of $P=4{\cdot}6\ \mu\mathrm{c\ cm}^{-2}$, $P_s=2{\cdot}0\ \mu\mathrm{c\ cm}^{-2}$, $E_c=1\ \mathrm{kv\ cm}^{-1}$ and $A=1{\cdot}10^{-2}\ \mathrm{J\ cm}^{-3}$. After 2 days the ageing reduces P to about 90% of the original value, and after about six months one can see the loop shown in figure 1 (*b*), when $P_s=0$, $E_c=0$, $A=0$ and $P=2{\cdot}3\ \mu\mathrm{c\ cm}^{-2}$.

The above results are to be expected if one admits the domain mechanism of ageing, the idea of which was proposed by Bogoroditsky and Verbitskaya (1953). After the sintering process of the ceramic is accomplished the 'young' sample cools to room temperature passing through the Curie point. During the transition the structure composed of different randomly orientated domains appears in every grain of the ceramic. Mechanical stresses involved by the great number of 90° domain walls accompany this initial state which is also characterized by the fact that a considerable part of the domains are able to participate in a process of reorientation under the influence of the external applied field. Thus it follows that the 'young' sample shows large values of P, P_s, E_c and A. In this initial state, however, the free sample does not possess minimum domain interaction energy. This minimum is not attained immediately. It is necessary to release the existing stresses, and this is a process that proceeds spontaneously with time.

The aged sample is defined as one in which the interaction energy has attained its minimum. This state can be realized by forming 180° domains or other domain aggregates with $P_s=0$. Thus, the number of the 90° domain walls and the mechanical stresses involved are reduced to minimum, since the 180° domain wall energy is insignificant as compared to that of the 90° domain wall (Shirane, Jona and Pepinsky 1955). This ageing process leaves no more domains subject to reorientation. In weak external fields the aged sample behaves as a linear dielectric because the associated domains do not participate in the polarization.

The ageing sample passes through intermediate states, two of which are shown in figure 2 (Plate) for the same sample as in figure 1. Ageing during two days is sufficient for the constricted loops to appear, and after some months one can observe further changes leading up to double hysteresis loops. Some observations of such shapes of loops were made earlier (Kambe 1953, Heywang and Schoefer 1956) and interpreted as transient effects. However, it seems sure that these shapes are *the natural consequence of ageing* since such loops are not observed in the 'young' samples. Appearance of the double hysteresis loops at room temperature seems to be easily comprehensible if one takes into account the orientation of the domains in the sample undergoing ageing. Here, the number of movable domains is small (A vanishes), and the weak applied field does not cause reorientation of the domains, since the activation energy is too great. Applying a sufficiently strong field, it is possible to change the orientation of the movable domains. At this stage, the sample behaves similarly to a true antiferroelectric, and thus may be termed a *domain antiferroelectric*.

The ageing effects may be reversed by applying strong electric a.c. fields (Novosiltsev, Khodakov and Shulman 1952, Allsopp 1957), or still better, by heating the aged sample above the Curie point. Such reversion of the ageing process should be properly termed *rejuvenation*. Therefore the transient character of the hysteresis loops of aged samples seems explicable as a result of rejuvenation brought about by the electric field and leading to the usual shape of the loop. The effect previously observed and known as thermal hysteresis of the permittivity ϵ now appears to be a particular case of rejuvenation of the sample (Piekara and Pająk 1952). Thermal hysteresis consists in a displacement of the Curie point towards lower temperatures when ϵ is measured in process of cooling as compared with the Curie point measured in process of heating. Thus, hysteresis may be considered as a process of rejuvenation of the sample, and the difference between the $\epsilon(T)$ observed in cooling and the $\epsilon(T)$ as observed when reheating the sample is a measure of the first stage of ageing. Further ageing in turn involves similar displacement of the Curie point towards higher temperatures (Pająk 1957).

The ageing effects are more distinctly observed in various solid solutions of the perovskite type, e.g. in figure 3 (Plate) is shown a typical hysteresis loop for 0·05 $MgSnO_3 + 0{\cdot}95\ BaTiO_3$ solid solution after ageing. Further, it seems reasonable to assume that the increase of the number of defects and lattice distortions introduced into the $BaTiO_3$ structure by forming the solid solution may have some influence on the ageing process, since for these, the rejuvenation, when using the electrical field, proceeds more slowly than in pure $BaTiO_3$ ceramics. If the height of the potential barrier of the ferroelectric ion is increased in the presence of defects, it seems probable that the potential barrier of the domain wall should increase with the number of defects in the lattice. A similar part is played by defects in Rochelle salt, which also shows double hysteresis loops on introducing defects by contamination with foreign ions during crystal growth, or by irradiation with gamma and X-rays (Yureen 1957, Eysler 1957).

The results of a more detailed investigation of ferroelectric ageing will be published in *Acta Physica Polonica*.

The authors wish to thank Professor Dr. A. Piekara for directing the present investigation and for his valuable discussions.

References

Allsopp, H. L., 1957, *Phil. Mag.*, **2,** 1100.

Bogoroditsky, N. P., and Verbitskaya, T. N., 1953, *Dokl. Akad. Nauk SSSR*, **89,** 447.

Eysler, Y. I., 1957, *Izv. Akad. Nauk SSSR*, **21,** 334.

Heywang, W., and Schoefer, R., 1956, *Z. angew. Phys.*, **8,** 209.

Kambe, K., 1953, *J. Phys. Soc. Japan*, **8,** 15.

Kazarnovsky, D. M., 1952, *J. Tech. Phys., Moscow*, **22,** 553.

Mason, W. P., 1955, *J. Acoust. Soc. Amer.*, **27,** 73.

Novosiltsev, N. S., Khodakov, A. L., and Shulman, M. S., 1952, *Dokl. Akad. Nauk SSSR*, **83,** 829.

Pająk, Z., 1957, Arbeitstagung *Festkoerperphysik und Physik der Leuchtstoffe* in Erfurt.

Piekara, A., and Pająk Z.,, 1952, *Acta Phys. Polon.*, **11,** 256.

Shirane, G., Jonà, F., and Pepinsky, R., 1955, *Proc. Inst. Radio Engrs, N.Y.*, **43,** 1738.

Yureen, V. A., 1957, *Izv. Akad. Nauk SSSR*, **21,** 329.

Theory of Bloch Electrons in a Magnetic Field

By W. KOHN[†]

Imperial College of Science and Technology, London

Communicated by H. Jones; *MS. received 28th July* 1958

§ 1. INTRODUCTION

SINCE the study of this problem was begun by Landau (1930) and Peierls (1933) almost thirty years ago, a great many theoretical papers dealing with this subject have appeared. Unfortunately, many of these contain either some uncontrolled approximations or logical errors, so that the literature on this problem leaves the reader with a variety of uncertain and often mutually contradictory conclusions. The present work was undertaken in the hope of clarifying this situation. In this note we summarize our chief results. A detailed account is in preparation.

§ 2. GENERAL THEORY

We are concerned with the solution of the Schrödinger equation (Atomic Units will be used $(e=\hbar=m=1)$)

$$H\psi\equiv(\tfrac{1}{2}\mathbf{P}^2+V)=E\psi, \qquad \ldots\ldots(1)$$

where

$$\mathbf{P}=\mathbf{p}+\mathbf{A}/c, \qquad \ldots\ldots(2)$$

V is the periodic potential and $\mathbf{A}$ is the vector potential giving rise to the magnetic field $\mathfrak{H}$.

For $\mathbf{A}=0$, the eigenfunctions of (1) are the Bloch waves,

$$\phi_{n,\mathbf{k}}=u_{n,\mathbf{k}}\exp(i\mathbf{k}.\mathbf{r}),$$

and the corresponding eigenvalues the energy bands $\epsilon_n(\mathbf{k})$. We shall fix our attention on solutions of (1) associated with a non-degenerate band $\epsilon_m(\mathbf{k})$.

When the magnetic field does not vanish, the Hamiltonian H in (1) has non-vanishing matrix elements between Bloch waves associated with the band m and those belonging to other bands. As a first step it is desirable to contruct a new set of functions $\tilde{\phi}_{m,\mathbf{k}}$ such that $H\tilde{\phi}_{m,\mathbf{k}}$ can be expressed as a linear combination of the $\tilde{\phi}_{m,\mathbf{k}'}$ with the *same m*. This can be done, at least in an asymptotic sense[‡]. We have constructed such functions, which have furthermore the property that if $\mathbf{K}_\nu$ is a reciprocal lattice vector

$$\tilde{\phi}_{m,\mathbf{k}+\mathbf{K}_\nu}=\pm\tilde{\phi}_{m,\mathbf{k}}. \qquad \ldots\ldots(3)$$

For the subsequent development it is very convenient not to restrict $\mathbf{k}$ to the fundamental Brillouin zone, but to allow it to run over a large volume $\bar{\tau}_{\mathbf{k}}$ in

---

[†] On leave of absence from Carnegie Institute of Technology, Pittsburgh, U.S.A.

[‡] Our construction is a step by step process and we do not know if, for small enough magnetic fields, it converges strictly or only asymptotically. In the latter case all we can say is that $H\tilde{\phi}_{m,\mathbf{k}}$ can be expanded in terms of the $\tilde{\phi}_{m,\mathbf{k}}$, apart from a remainder which vanishes with the magnetic field $\mathscr{H}$ more rapidly than $\mathscr{H}^n$ where n is an arbitrarily large integer. For clarity of presentation we shall, in what follows, quote results which hold if our procedure converges strictly. Because of the possibility of only asymptotic convergence, these results may have errors vanishing with $\mathscr{H}$ more rapidly than $\mathscr{H}^n$, where n is arbitrary.

k space. Because of equation (3), the $\tilde{\phi}_{m,\mathbf{k}}$ are then of course *not* linearly independent.

The solutions of (1) corresponding to the band m can be written as

$$\psi = \int \tilde{A}(\mathbf{k})\tilde{\phi}_{m,\mathbf{k}} d\mathbf{k}, \qquad \ldots\ldots(4)$$

where the expansion coefficients $\tilde{A}(\mathbf{k})$ satisfy a Schrödinger equation of the form

$$\int (\mathbf{k}|\tilde{H}(\mathbf{P})|\mathbf{k}')\tilde{A}(\mathbf{k}')d\mathbf{k}' = E\tilde{A}(\mathbf{k}). \qquad \ldots\ldots(5)$$

The effective Hamiltonian $\tilde{H}(\mathbf{P})$ has a Fourier series expansion

$$\tilde{H}(\mathbf{P}) = \Sigma_l a_l \exp(i\mathbf{R}_l \cdot \mathbf{P}), \qquad \ldots\ldots(6)$$

where the $\mathbf{R}_l$ are the lattice vectors of the crystal. It has the important periodicity property

$$\tilde{H}(\mathbf{P} + \mathbf{K}_\nu) = \tilde{H}(\mathbf{P}). \qquad \ldots\ldots(7)$$

If we call†

$$s \equiv \mathscr{H}/c, \qquad \ldots\ldots(8)$$

the coefficients a_l can be expanded in a power series,

$$a_l = a_l^{(0)} + s a_l^{(1)} + s^2 a_l^{(2)} + \ldots\ldots \qquad \ldots\ldots(9)$$

When the crystal has a centre of inversion the odd terms in this expansion vanish. The $a_l^{(0)}$ are simply the coefficients of the Fourier expansion of the band in question

$$\epsilon_m(\mathbf{k}) = \Sigma_l a_l^{(0)} \exp(i\mathbf{k}\cdot\mathbf{R}_l). \qquad \ldots\ldots(10)$$

The $a_l^{(i)}$ for $i > 0$ are determined by an explicit construction.

Because of the linear dependence of the $\tilde{\phi}_{m,\mathbf{k}}$ it is found that most solutions $\tilde{A}(\mathbf{k})$ of (5) give rise to wave functions ψ, equation (4), which vanish identically. The corresponding eigenvalues are therefore physically meaningless. This fact enables one to resolve some apparent paradoxes in the literature.

§ 3. ENERGY LEVELS CORRESPONDING TO CLOSED CLASSICAL ORBITS

When one considers the motion of a Bloch wave packet under the influence of a magnetic field in the z direction, one finds that it follows a trajectory C in **k** space which is defined by the following equations:

$$C: \begin{cases} \epsilon_m(\mathbf{k}) = E \\ k_z \quad = \text{constant} \end{cases} \qquad \ldots\ldots(11)$$

By means of an elegant semi-classical argument, Onsager (1952) made it plausible that, for a given k_z, the allowed eigenvalues E are determined approximately by the implicit equation

$$\mathscr{A}(E, k_z)/2\pi = (n + \gamma)s \qquad \ldots\ldots(12)$$

where $\mathscr{A}$ is the area enclosed by C, n is an integer and γ is an unknown constant. This relationship is meaningful only when C is a closed curve, which is the case in most practical applications. Working with the Hamiltonian (6) we have obtained slightly sharper results.

---

† s is the magnetic energy of the electron expressed in atomic units of energy. Our entire development is based on the assumption that s is small compared with the relevant electronic energy in the absence of $\mathscr{H}$, but not necessarily small compared with kT.

If the crystal has a centre of symmetry, the allowed eigenvalues are implicitly determined by a power series in s,

$$\mathscr{A}(E,k_z)/2\pi = (n+\tfrac{1}{2})s + s^2/W(E,k_z) + \dots \qquad \dots\dots(13)$$

where $W(E,k_z)$ is an energy independent of $\mathscr{H}$. This result holds regardless of whether the trajectory is re-entrant or extends over more than one Brillouin zone.† The de Haas–van Alphen period P (Shoenberg 1957) is defined as $(\mathscr{H}_{n+1})^{-1} - (\mathscr{H}_n)^{-1}$ where $\mathscr{H}_n(=cs_n)$ is the field satisfying (13) for given E, k_z, and n. From (13) and (8) we find directly

$$P = (2\pi/c\mathscr{A})(1 - s^2\,2\pi/\mathscr{A}W + \dots\dots). \qquad \dots\dots(14)$$

The $\frac{1}{2}$ in equation (13) is, in principle, observable through the phase of the de Haas–van Alphen oscillations.

If the crystal does not have a centre of inversion, (13) must be replaced by

$$\mathscr{A}(E,k_z)/2\pi = (n+\gamma(E,k_z))s + s^2/W(E,k_z) + \dots\dots \qquad \dots\dots(15)$$

where γ has the following properties: $\gamma - \frac{1}{2}$ is an odd function of k_z and near the bottom and top of the band $\gamma \to \frac{1}{2}$. In general the deviation of γ from $\frac{1}{2}$ is of the order of unity. However, the de Haas–van Alphen period is still given by (14).

Broadening.

It is well known that, for free electrons, the energy levels corresponding to a given $\mathscr{H}$ and k_z are highly degenerate. For Bloch electrons the energy levels are also degenerate up to any power of s and given by equations (13) and (15). But, in addition, there is an exponentially small spreading of each degenerate eigenvalue into a band which is not contained in these equations. Let us consider a sequence of fields for which the centres of successive bands fall at a given energy E; and let us denote the widths of these bands by $\delta(E,k_z,s)$ and the difference between the centres of successive bands by $\Delta(E,k_z,s)$. Then for sufficiently small fields, and a crystal with a centre of symmetry, the Hamiltonian (6) gives

$$\frac{\delta(E,k_z,s)}{\Delta(E,k_z,s)} \simeq \frac{2}{\pi}\exp\left(-\frac{W_1(E,k_z)}{s}\right) \qquad \dots\dots(15)$$

where $W_1(E,k_z)$ is a characteristic energy independent of s‡. When E and k_z are such that a sequence of classical trajectories C, equation (11), nearly touch each other, W_1 approaches zero and the spreading becomes appreciable. However, only in very exceptional circumstances can this spreading become experimentally significant.

§ 4. ENERGY LEVELS CORRESPONDING TO OPEN CLASSICAL TRAJECTORIES

If $\mathscr{H}$ lies in some special crystallographic direction and E is near the middle of the band, the classical trajectories may extend indefinitely through the crystal, without closing. In this case, the energy spectrum, for given k_z, is almost continuous, broken only by small gaps. If we denote the magnitude of the gaps by δ' and the widths of the allowed regions by Δ', then, for small s, and a crystal with a centre of symmetry, the Hamiltonian (6) gives

---

† When this work was completed a paper by Zil'berman (1957 a) was brought to my attention, in which a similar though somewhat weaker result is given.

‡ In addition there may be a broadening smaller than any power of s due to the fact that our formalism may have only asymptotic validity (see footnote on p. 1148). The statement (Zil'berman 1957 a), that the broadening is in general of order s^2, appears to us incorrect. For a discussion of the broadening, see also Brailsford (1957).

$$\frac{\delta'}{\Delta'} \simeq \frac{2}{\pi}\exp\left(-\frac{W'_1(E,k_z)}{s}\right). \qquad \ldots\ldots(16)$$

The energy W_1' approaches zero when E approaches a value for which the open trajectories change to a sequence of closed ones §.

§ 5. DIAMAGNETISM

When the crystal has cubic symmetry, the diamagnetic susceptibility of a Fermi gas at low temperature is given by the following expression

$$\chi = -\frac{1}{48\pi^3c^2}\int\left[\frac{\partial^2\epsilon_m(\mathbf{k})}{\partial k_x^{\,2}}\frac{\partial^2\epsilon_m(\mathbf{k})}{\partial k_y^{\,2}} - \left(\frac{\partial^2\epsilon_m(\mathbf{k})}{\partial k_x\partial k_y}\right)^2\right]\frac{1}{\nabla_{\mathbf{k}}\epsilon_m(\mathbf{k})}dS$$
$$-\frac{1}{2\pi^3c^2}\int R(\mathbf{k})d\mathbf{k}; \qquad \ldots\ldots(17)$$

here the surface integral extends over the Fermi surface in the fundamental Brillouin zone; the volume integral extends over the occupied region of the fundamental Brillouin zone; and

$$R(\mathbf{k}) \equiv \Sigma_l a_l^{(2)} \exp(i\,\mathbf{k},\mathbf{R}_l) \qquad \ldots\ldots(18)$$

(see equations (6), (8), (9)). In general the two terms in equation (17) are of comparable magnitude.

ACKNOWLEDGMENTS

This work was supported in its early stages by the United States Office of Naval Research. The greater part of it was carried out while the author held a Senior Post Doctoral Fellowship of the National Science Foundation of the U.S.A. The author wishes to thank these Organizations for their support. He also takes great pleasure in expressing his appreciation to the staff of the Department of Mathematics of the Imperial College of Science and Technology, London, for their hospitality during his stay there.

REFERENCES

BRAILSFORD, A. D., 1957, *Proc. Phys. Soc.* A, **70,** 275.
LANDAU, L., 1930, *Z. Phys.*, **64,** 629.
ONSAGER, L., 1952, *Phil. Mag.*, **43,** 1006.
PEIERLS, R., 1933, *Z. Phys.*, **80,** 763.
SHOENBERG, D., 1957, *Progress in Low Temperature Physics,* Vol. 2 (Amsterdam: North Holland Publishing Company), p. 226.
Zil'berman, G. E., 1957 a, *J. Exp. Theor. Phys.*, **32,** 296; 1957 b, *Ibid.*, **33,** 387.

---

§ See however footnote on p. 1148. These gaps are also discussed by Zil'berman (1957 b).

V.
19

LETTERS TO THE EDITOR

International Union of Pure and Applied Physics

The International Union of Pure and Applied Physics has decided to sponsor the following meetings:

Place	Probable date	Subject	Organization
Cambridge, U.K.	29 June–3 July, 1959	Colloquium ' Superconductivity '	Prof. D. Shoenberg, Mond Lab., Cambridge
Paris	End of June 1959	Colloquium ' Theory of Gravitation'	Institut H. Poincaré, 11 rue P. Curie, Paris, 5^e^.
Moscow	July 1959	Commission and Colloquium ' High Energy Nuclear Physics'	Acad. Sci. U.S.S.R. & Prof. B. Rossi, M.I.T. Cambridge, Mass.
Moscow	End of July 1959	Colloquium and Commission ' Cosmic Rays '	Acad. Sci. U.S.S.R. & Prof. R. E. Marshak, University, Rochester
Stockholm	24–29 August 1959	International Commission on Optics and Colloquium ' Modern Systems for detecting and evaluating Optical Radiation '	Prof. E. Ingelstam Instituttionen for Fysik, Kungl. Tekniska Hogskolon, Valhallavägen, Stockholm
Stuttgart, Germany	2–3 September	Commission and Colloquium ' Acoustics '	Prof. C. W. Kosten, Mijnbouwplein 11, Delft. Dr. Meyer, Bürgerstrasse, Göttingen
Geneva, Switzerland	September 1959	Colloquium ' Particle Accelerators '	CERN, Geneva
Utrecht	12–16 June 1960	Commission and Colloquium ' Thermodynamics '	Prof. Van Hove, University, Utrecht
Kingston, Ont.	29 August–3 September 1960	Colloquium ' Nuclear Structures '	Dr. L. G. Elliott, Atomic Energy, Chalk River, Ont.
Toronto, Ont.	29 August–3 September 1960	Commission and Colloquium ' Very Low Temperatures '	Prof. A. C. G. Hallett, University, Toronto
Hamilton, Ont.	August or September, 1960	Colloquium ' Nuclidic Masses '	Mr. H. E. Duckworth, McMaster University, Hamilton
Praha	Not yet known	Commission and Colloquium ' Semiconductors '	Academy of Sciences Czechoslovakia
Brussels	Not yet known	Colloquium ' Thin Metallic Films '	Academy of Sciences Belgium

Place	Probable date	Subject	Organization
Basel	Not yet known	Colloquium ' Neutron Physics '	Prof. P. Huber, Klingelbergstrasse 82, Basel
Rochester, N.Y.	Not yet known	Colloquium ' High Energy Physics '	

The next general Assembly of the Union of Physics will meet in Ottawa, from 7 to 9 September 1960. The S.U.N. and Publications Commission will meet at the same time.

A working Committee has been formed, under the presidence of Professor Mattauch (Max Planck Institut für Chemie, Saarstrasse 23, Mainz), for proposing at this General Assembly resolutions on the precise evaluation of nuclidic masses.

3 Boulevard Pasteur,
Paris XV^{e}.

REVIEWS OF BOOKS

Eigenfunction Expansions associated with second order Differential Equations, Part II, by E. C. Titchmarsh. Pp. xi + 404. (Oxford: Clarendon Press, 1958.) 70*s*.

Part I of this work, published in 1946 and devoted to eigenfunction expansions associated with ordinary differential equations, is already well known to mathematicians and mathematical physicists as a beautiful treatment of an interesting branch of analysis. Part II, which now appears, deals with the corresponding problems relevant to second order partial differential equations, a subject in which there have been great advances in the last twenty years—many of them due to Professor Titchmarsh and his pupils. The numbers of the chapters of Part II follow on from those of Part I, and the list of references at the end of the present volume contain papers on ordinary differential equations as well as on partial differential equations and supersedes the bibliography at the end of Part I.

The bulk of the present volume (Chapters XI–XVIII) is concerned with eigenvalues, eigenfunctions, expansion theorems, and formulae of Parseval type for the Schrödinger equation

$$\Delta\psi + \{\lambda - q(\mathbf{x})\}\psi = 0,$$

in which $\mathbf{x}$ denotes the k-dimensional vector $(x, y, z, \ldots)$ and Δ denotes the corresponding Laplacian operator $\partial^2/\partial x^2 + \partial^2/\partial y^2 + \ldots$ The author's aim is to develop a general theory applicable to a wide class of cases—i.e. one which is not limited to the few cases in which the equation is separable. The main type of problem is that in which the equation holds throughout the whole of space, but this is approached by considering the equation to be valid over a rectangular region and then proceeding to the limit of infinite sides.

Chapter XI considers expansions in a rectangle in the two-dimensional case by a systematic use of the concept of the Green's function. The theory corresponding to the whole plane is given in Chapter XII. In Chapter XIII the theory is extended to the general case of k dimensions. In Chapter XIV two topics are discussed—problems with discrete eigenvalues and how these eigenvalues vary as $q(\mathbf{x})$ varies; the eigenfunction problem for a general *finite* region. The important special case in which the equation is separable is discussed in Chapter XV with the equations for the hydrogen atom and the hydrogen atom in an electric field being discussed as special problems.

To mathematical physicists probably the most interesting chapter is XVI dealing with theorems on the characterization of the spectrum and the dependence of the spectrum on the form of $q(\mathbf{x})$. There is no simple classification as in the one-dimensional case but there are some striking results, notably Titchmarsh's proof of Kato's theorem on the existence of discrete eigenvalues for the helium atom. Chapter XVII is concerned with the related topic of the distribution of eigenvalues, i.e. of the asymptotic behaviour as $\lambda \to \infty$ of $N(\lambda)$, the number of eigenvalues not exceeding λ. Another chapter of interest to theoretical physicists is XIX which deals with perturbation theory and places on a rigorous basis results which are familiar in unrigorous form and which as

Professor Titchmarsh remarks are " regarded with suspicion by analysts ". Chapter XX is concerned with continuous spectra treating a number of particular problems as well as the general theory. In Chapter XXI the author considers the case (of special interest in solid state physics) in which $q(\mathbf{x})$ is periodic; not much is known in the three-dimensional case but a few sections are devoted to it here.

Chapters XVIII and XXII are devoted to more theoretical matters—the former concerning itself with the establishment of theorems on the convergence and summability of the eigenfunction expansion of a function under wide conditions, and the latter with the proof of a number of theorems quoted in the text but which have no specific connexion with eigenfunction theory (integrals involving functions with singularities; Green's theorem; compact sequences of functions; boundary values of analytic functions; iterative methods; Langer's method; Laguerre polynomials; Tauberian theorems).

The whole book possesses that very special elegance associated with a work written by Professor Titchmarsh and published by the Oxford Press. Not only is the book attractively written; the printed page is itself a thing of beauty achieved by a happy collaboration between author and typographer. The author's attitude to the mathematics of physics is well known—it is the stimulus to the classical analyst. In this connection part of the preface is worth quoting: " It seems that physicists do not object to rigorous proofs provided that they are rather short and simple. I have much sympathy with this point of view. Unfortunately, it has not always been possible to provide proofs of this kind." May we venture to suggest to the author that we do not mind long proofs provided they are characterized by such elegance, and remind him that many a happy amateur can revel in the beauties of a Beethoven score without himself being able to write one note in the same vein. I. N. SNEDDON.

Physical Chemistry, by E. A. MOELWYN-HUGHES. Pp. vii + 1295. (London, New York: Pergamon Press, 1957.) 70*s*.

This is a monumental text-book of theoretical or mathematical physical chemistry presented with admirable clarity, uniformity and carefully chosen simple mathematics by a leading teacher of the subject. Each main subdivision is introduced by a phenomenological and historical account and followed by a theoretical and mathematical treatment. The subdivisions treated in order are: Maxwell–Boltzmann distribution and Brownian motion; elementary quantum mechanics and atomic structure; thermodynamics and chemical potentials; inter-molecular energy, virial coefficients and equations of state; partition functions for atoms, molecules, crystals and liquids; viscosity of gases and liquids; Fermi statistics and the metallic state; solutions and electrolytes; interfacial phenomena; chemical equilibria and reaction rates. Each chapter concludes with a carefully chosen set of examination questions and the book closes with appendices completing the elementary mathematical derivations used in the text.

Although one would have liked to have seen, in a book not specifically labelled theoretical physical chemistry, more details of experimental methods, this book is of outstanding pedagogic value. The inclusion of a great deal of tabulated experimental material makes it also a valuable tool to the research worker.

Its value in the latter respect could have been enhanced by omission of some of the early history and replacement by account of more recent research. A comprehensive account of current research in mathematical physical chemistry would require however a whole series of monographs and it might be hoped that the author would crown his work as Editor in Chief of such a series presented with the same clarity and uniformity, analogous to the famous Bourbaki series in pure mathematics. H. A. JAHN.

A Class-room Method for the Derivation of the 230 *Space Groups*, by N. V. BELOV. Translated by V. BALASHOV. Pp. 46. Published in the Proceedings of the Leeds Philosophical and Literary Society, Scientific Section, Vol. 8, Part 1, 1957. 7*s*. 6*d*.

In recent years Academicians Shubnikov and Belov and their students have developed a lively interest in the space groups, revivifying the topic of symmetry and making various extensions to the usual 230 space groups. Belov is properly insistent that students should become familiar with all the space groups and should not simply turn to the International Tables at the slightest excuse. This paper expounds a discursive rather than a strict system of derivation where each crystal class is taken and expanded to give the corresponding space groups. It is disappointing that no formula leading to a solution $x=230$ as the number of the space groups has yet been produced (although Weyl has produced one for the 32 point groups) and any method of deriving the space groups amounts to forming all possible combinations of the symmetry elements and eliminating the duplicated groups. The presentation is meant for students.

The translation, though adequate, is excessively literal and inelegant. Complex sentences, which are intelligible in the original because of the case endings, have become obscure. Misprints are few but there is a sign missing in the expression for B on p. 19. A. L. MACKAY.

Proceedings of the International Symposium on Isotope Separation (Amsterdam, 23rd–27th April, 1957), edited by J. KISTEMAKER, J. BIGELEISEN and A. O. C. NIER. Pp. xx + 704. (Amsterdam: North-Holland Publishing Company, 1958.) £5 12*s*. 0*d*.

Isotopes have become of great fundamental and technological importance during the last two decades because of the phenomenal growth of the atomic energy industry. Consequently many methods of isotope separation have been studied, and some brought to large scale application in order to obtain production quantities of particular isotopes of technological importance such as ^{235}U, D, and in lesser amounts, Li, ^{10}B, ^{13}C, ^{15}N and ^{18}O. Much of the technological information on the processes used, together with the background development experience, has been restricted to the research establishments concerned directly with the atomic energy and so the occasion of the first international symposium on isotope separation aroused general interest and was notable for the release of a great deal of hitherto restricted information.

Thus the proceedings of the conference provide an excellent review of the present state of the subject and deal thoroughly both with the fundamental principles and the practical application of a wide range of physical and chemical methods of isotope separation. There is also demonstrated the close collaboration necessary in this borderline field between chemists and physicists in the development of processes involving both chemical and physical principles.

For the purposes of the written record the papers have been grouped into 9 main parts dealing respectively with chemical engineering, molecular interactions (essentially isotope effects of fundamental importance to separation processes), chemical exchange, electromigration, distillation, thermal diffusion, diffusion, electromagnetic separation and ultracentrifuges. The papers are notable for their breadth and comprehensiveness since they mostly cover work which has been in progress over many years and with large teams of scientists. There is also much detailed discussion of the criteria for the selection of processes to suit particular requirements.

Besides the accounts of the main separation methods listed above, several of which are already used on a large scale, there are accounts also of what may be called minor methods which may have important specialist applications such as gas chromotography, ion exchange, and jet diffusion. Such methods together with the relatively new electromigration method can be applied to a number of elements including Mg, S, Cl, Br and various common metals as well as those listed above.

The main interest of those who attended the symposion was in the techniques of separation, but most scientists not directly concerned in this specialization will be more interested in the availability of particular isotopes and their applications in many fields of work. These readers will learn from this book that now any naturally occurring isotope of almost all the elements can be obtained in an enriched state. Thus the nuclear physicist has the possibility of studying almost any nuclide though the quantity available will depend on whether there is some technological interest in the isotope or whether the interest is purely academic when normally only the rather limited quantities obtained by electromagnetic separation are available.

The book, considered as a work of reference, has the defect of lacking a general subject index, while some of the papers, due to the strict time-table set by the editors in their entirely creditable and successful effort to achieve early publication of the conference proceedings, are only printed in abstract form. As some compensation there is a very detailed contents list. Most of the 63 papers are in English, 14 being in the other official conference languages, French and German.

The book is well illustrated and produced and constitutes not only an essential work of reference but also a worthy record of a memorable conference.

M. L. SMITH.

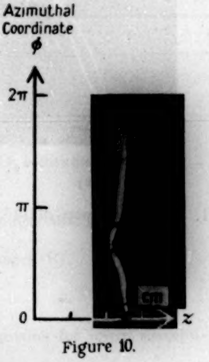

Figure 10.

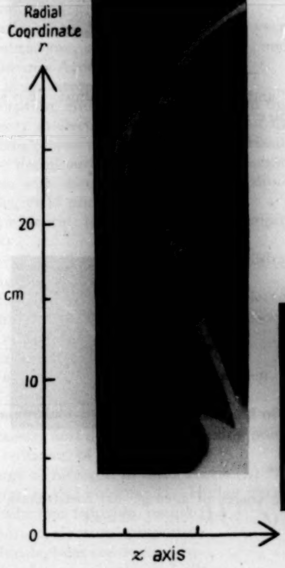

Figure 11.

Figure 5.

Figure 5. Composite photograph of 148 kev F electrons falling on a meridional plane. Caustic formation at the first focal ring, followed by a convergence towards a second focal ring near the axis, can be seen.

Figure 10. Unwrapped photograph of the locus of incidence of a focused sheaf of F line electrons upon the cylindrical surface of the detector The locus is crossed by shadows cast by radial obstructions and its curvature indicates a deviation from axial symmetry.

Figure 11. View of the magnet frame partially dismantled showing the left end disc and its magnetizing coils mounted on the trolley.

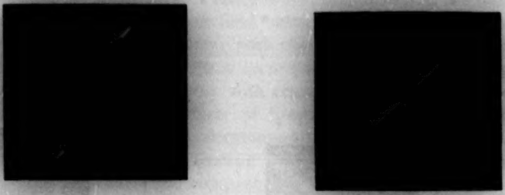

(*a*) (*b*)

Figure 1. Hysteresis loops of (*a*) 'young' and (*b*) aged $BaTiO_3$ ceramic. ($E = 5{\cdot}8$ kv cm^{-1}, 50 c/s.)

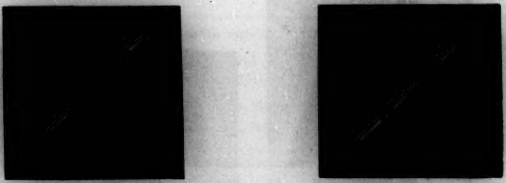

(*a*) (*b*)

Figure 2. Hysteresis loops at intermediate stages of ageing: (*a*) constricted, (*b*) double hysteresis loops. ($E = 7{\cdot}7$ kv cm^{-1}, 50 c/s.)

Figure 3. Double hysteresis loop of $MgSnO_3$–$BaTiO_3$ ceramic at room temperature. ($E = 32{\cdot}4$ kv cm^{-1}, 50 c/s.)

PROCEEDINGS OF THE PHYSICAL SOCIETY

1958—VOL. 72

SUBJECT INDEX

PAGE
Absorption, effect on mean wavelength of X-ray emission lines (L) 924
Absorption, resonant, of γ-rays in ^{14}N 337
Absorption spectra, infra-red, of α-quartz between 4 and 15μ 9
Absorption, ultrasonic, comparison in $MnSO_4$ and $MgSO_4$ solutions 81
Absorption, *see also* Acoustic, Sound
Absorptivity of anisotropic metals (R) 277
Acoustic absorption, and vibrational relaxation times of polyatomic gases . . . 940
Adiabatic theory in electron–atom collision calculations 701
Ageing of ferroelectrics of type $BaTiO_3$, polarization changes (R) 1144
Alkali metals, Fermi surface and magnetoresistance 996
Alloys, cerium with thorium, magnetic susceptibility 345
Alloys, Cu–As, yield phenomena in 33
Alloys, ferromagnetic, homogeneous, semi-empirical equation for initial susceptibility (R) 130
Alloys, gold–manganese, studies by neutron diffraction (R) 470
Alloys, uranium, gamma phase 425
Alloys, uranium, magnetic susceptibility and electrical resistance properties . . 757
Angular distributions of absorption and emission processes, and time reversal . 97
Assemblies, regular, dilution effects in 649
Atoms, helium-like, polarization (R) 889
Attachment of slow electrons in air and oxygen 1081

Barrier height, surface, in transistors, method of studying changes (R) . . . 910
Benzene, viscosity and density near freezing point (R) 454
Beta decay, radiative, of pion (R) 144
Binding energy of nitrogen in dislocations (L) 673
Binding energy of ^{16}O nucleus: II—Higher clusters 499
Binding in cadmium telluride, nature (L) 927
Bismuth telluride, electrical properties 733
Bismuth telluride, heat conduction in 17
Bismuth telluride, magnetothermal effects 401
Bismuth telluride, optical properties 545
Bismuth telluride, p-type, galvanomagnetic effects 380
Bloch electrons in magnetic field, theory (R) 1147
Branching ratio of thorium C (R) 300
Branching ratios of ^{86}Rb and ^{42}K . . . . corr. 675
Breakdown, electrical, of gases in uniform high frequency fields at low pressure . . 823
Breakdown, gas, ultra-high-frequency, between Rogowski electrodes . . . 625

Cadmium telluride, nature of binding in (L) 927
Calcium fluoride, elastic constants 566
Capture, radiative, cross sections for 14·5 MEV neutrons 505
Capture ratio, L/K, in ^{126}I 437
Carrier lifetime measurements, sweep-out effects in phase shift method (R) . . 267
Čerenkov detector, gas, measurement of electron beam energy by . . . 973
Coercive field of tri-glycine sulphate, dependence on temperature and frequency (L) . 306
Collective treatment of Fermi gas: I 685
Collision calculations, electron–atom, adiabatic theory in 701
Collisions, inelastic atomic, mass dependence (R) 293
Conducting plates, thin, electromagnetic scattering at glancing incidence . . 981

PAGE

Conductivity, electrical, *see* Electrical conductivity
Copper nuclear magnetic resonance in Cu–Ni and Cu–Mn alloys 797
Cross section, 1s–2s electron excitation, of hydrogen, calculation 121
Cross sections, electron collision, for nitrogen and oxygen (R) 287
Cross sections, radiative capture, for 14·5 MeV neutrons 505
Crystal surface and atom, molecular orbital theory of interaction 103
Crystals, magnesium fluoride crystallized from the melt 1001
Crystals, nickel, saturation magnetostriction at low temperatures 1049
Crystals, single, ferroelectric, polarization reversal process in (L) 307
Crystals, single, growth of orientated monolayer of lead on silver single-crystal substrate (R) 459
Crystals, single, uniaxial, demagnetizing energy and domain structure . . . 765
Crystals, tri-glycine sulphate, dependence of coercive field on temperature and frequency (L) 306
Cyclotron resonance observation of effect of strain on Ge and Si 514

Density matrix, variational methods based on 182
Diamonds, fluorescence excited by X-rays 1074
Dielectric constant of conducting liquids, measurement at low frequencies . . 441
Dielectric dispersion, application of Onsager's theory 532
Diffraction by an opaque strip (R) 901
Diffraction patterns, 'virtual' Fresnel (R) 303
Diffraction theory, scalar, for restricted aperture . . . . . . corr. 309
Diffusion across semiconductor–vapour interface 369
Diffusion, thermal, *see* Thermal diffusion
Discharge, high current, amplification of magnetic field by 618
Dislocations, binding energy of nitrogen in (L) 673
Dispersion theory and the optical model at low energies of neutron scattering . 70
Domain processes and interpretation of magnetic susceptibility and ΔE effect . . 604
Domain structure and demagnetizing energy of uniaxial single crystal 765

Elastic constants of calcium fluoride 566
Elastic scattering, *see* Scattering
Electrical conductivity and Hall effect of silicon 193
Electrical properties of bismuth telluride 733
Electron beam energy, measurement with gas Cerenkov detector 973
Electron lens, unconventional (R) 135
Electron temperatures in high electric fields, in germanium, experimental determination (R) 921
Electrons, Bloch, in magnetic field, theory (R) 1147
Electrons, free, direct measurement of *g*-factor (R) 891
Electrons, secondary, *see* Secondary electrons
Electrons, slow, attachment in air and oxygen 1081
Electrons, transmission through metallic foils 727
Energy bands in solids, cellular method (R) 281
Energy levels of ^{31}P: I—γ-ray spectra and decay schemes 1097
Energy levels of ^{31}P: II—Angular distributions and correlations 1115
Energy levels of ^{31}P: III—Comparison with Nilsson model 1122
Energy levels of polyatomic molecules 635
Energy transfer in organic systems: I—Photofluorescence of terphenyl-toluene solutions 53
Excitation of atomic hydrogen in 2s state 523
Excitation of atomic levels, compound ion model 326
Extension, model polycrystalline material in, X-ray intensities for (R) 137

Fermi gas, collective treatment: I 685
Fermi surface of alkali metals, and magnetoresistance 996
Ferroelectrics of type BaTiO$_3$, polarization changes during ageing (R) 1144

PAGE
Ferromagnetic anisotropy energy, pressure dependence 207
Ferromagnetics, polycrystalline, magnetostriction curves 249
Films, non-uniform, refractive index (R) 906
Films, thin oxide, on metals, colour 742
Flow anisotropy in theory of liquids 711
Fluid molecular order, determination (R) 887
Fluorescence, decay of CsI(Tl) in particles of different ionization density 1
Fluorescence of diamonds excited by x-rays 1074
Foils, metallic, transmission of electrons through 727
Fourier spectra of photographic images, determination 661
Fractures produced by stress pulses in glass-like solids 447
Freezing point, benzene, viscosity and density near (R) 454
Frequency response and apodization with incoherent light 749

Galvanomagnetic effects in p-type bismuth telluride 380
Gamma phase in uranium alloys 425
Gamma-ray lines from ^{152}Eu and ^{154}Eu, re-measurement (L) 148
Gamma rays, resonant absorption in ^{14}N 337
Gases, electrical breakdown in uniform high frequency fields at low pressures 823
Gases, ions in, mobilities, second approximation (R) 274
Germanium, experimental determination of electron temperatures in high electric fields (R) 921
Germanium, point contact injection ratio, temperature dependence (R) 264
Germanium, vibrational spectrum and specific heat (R) 914
g-factor of free electrons, direct measurement (R) 891

Hall effect and electrical conductivity of silicon 193
Harmonic oscillator, damped, wave mechanical 1027
Heat conduction in bismuth telluride 17
Heat treatment of polycrystalline cadmium oxide 65
Helium atoms, metastable, properties 1053
Helium atoms, two, energy of interaction between 201
Helium, excitation by electrons of low energy 786
Helium, non-relativistic Schrödinger equation, $(2p)^2\ {}^1S$ state solution (R) 141
Hydrogen, atomic, excited, charge transfer of protons in 694
Hydrogen, atomic, in 2s state, electron excitation 523
Hydrogen, calculation of 1s–2s electron excitation cross section 121
Hydrogen, secondary ionization processes at high gas pressures 1061
Hydrostatic pressure, change of spontaneous magnetization with 1013
Hysteresis loops associated with simple domain structure 244

Impurity carriers in silicon, temperature variation of concentration (R) 917
Inelastic atomic collisions, mass dependence (R) 293
Infra-red absorption, *see* Absorption
Infra-red emissivities of indium antimonide and germanium (R) 270
Insulators, temperature waves in, transport theory 391
Interaction, energy of, between two normal helium atoms, second order calculation 201
International Union of Pure and Applied Physics (L) 1151
Ion beams, carbon and nitrogen, ionization produced by (R) 462
Ion bombardment, and positive ion emission from metal surfaces (R) 467
Ionization coefficients, primary, at low gas pressures, experimental determination 363
Ionization produced by beams of carbon and nitrogen ions (R) 462
Ionization, secondary processes in hydrogen at high gas pressures 1061
Ionized gases, thermal diffusion in 353, corr. 675
Ions in gases, mobilities, second approximation (R) 274
Ions, slow, elastic scattering in parent gases 1087

Kerr effect, for study of magnetization of reflecting surface 233

PAGE

Lattice parameters, measurement with powder cameras, effect of Lorentz factor and dispersion (R) 908
Lead, growth of orientated monolayer on silver single-crystal substrate (R) . . . 459
Light, incoherent, apodization and frequency response with 749
Liquids, absorption of sound in sediments of small particles in liquids 933
Liquids, conducting, dielectric constant measurement at low frequencies. . . . 441
Liquids, theory, flow anisotropy in 711

Magnesium fluoride crystallized from the melt, properties 1001
Magnetic field, amplification by high current discharge 618
Magnetic materials, solid solution in $A^{III} B^{V}$ compounds 214
Magnetic properties, interpretation in terms of domain processes. 604
Magnetic properties of Perminvar 596
Magnetic susceptibilities of alloys of cerium with thorium 345
Magnetic susceptibility and electrical resistance properties of uranium alloys . . 757
Magnetism, *see* Domain structure, Hysteresis
Magnetization of reflecting surface, use of Kerr effect for study 233
Magnetization processes in polycrystalline manganese zinc ferrite. 224
Magnetization, spontaneous, change with hydrostatic pressure 1013
Magnetoresistance and Fermi surface of alkali metals. 996
Magnetostriction curves of polycrystalline ferromagnetics 249
Magnetostriction, saturation, of nickel crystals at low temperatures 1049
Magnetothermal resistance and magnetothermoelectric effects in bismuth telluride . 401
Mass dependence of inelastic atomic collisions (R) 293
Mayer cluster integrals, enumeration (R) 1141
Meson theory, cut-off, nucleon magnetic moment 49
Mesons, K, produced in high energy nuclear interactions, distribution 169
Mesons, μ, scattered by mercury, polarization (R) 1137
Mesons, π^-, photoproduction from boron 259
Mesons, π^0, photoproduction at helium 880
Metal surfaces, positive ion emission from, caused by ion bombardment (R) . . . 467
Metals, alkali, theory of phase transformations in 810
Metals, alkali, *see* Alkali metals
Metals, anisotropic, absorptivity (R) 277
Metals, colour of thin oxide films on 742
Metals, *see also* Foils, metallic
Microwave cavity spectrometer, source-modulated, design and performance . . 537
Microwave resonance, observation of effect of strain on Ge and Si 514
Mobilities of ions in gases, second approximation (R). 274
Molecular orbital theory of interaction between atom and crystal surface . . 103
Molecular theory, dilution effects in regular assemblies 649
Molecules, polyatomic, energy levels 635
Muon decay, polarized, energy dependence of spatial asymmetry. 781
Muons, negative, capture rates in various elements 494

Neutron diffraction studies of gold-manganese alloys (R) 470
Neutron scattering, optical model at low energies and dispersion theory . . . 70
Neutrons emitted from nuclei by protons, polarization 433
Noise, semiconductor, *see* Semiconductor
Nuclear interaction at 350 MEV, conservation of parity 429
Nuclear interactions, high energy, distribution on K-mesons in 169
Nuclear magnetic resonance, copper, in Cu–Ni and Cu–Mn alloys 797
Nuclear magnetic resonance in solid *cyclo*pentene 791
Nuclear magnetic resonance spectra, narrowing by molecular rotation in solids. . 959
Nuclear reaction theory, Wigner, eigenphaseshifts 874
Nucleon magnetic moment in cut-off meson theory 49

PAGE
Onsager's theory, application to dielectric dispersion . . . 532
Order, fluid molecular, determination (R) . . . 887
Organic systems, energy transfer: I—Photofluorescence of terphenyltoluene solutions 53
Oscillator, wave mechanical damped harmonic . . . 1027
Oxygen nucleus, ^{16}O, binding energy: II—Higher clusters . . . 499

Parity, conservation in nuclear interaction at 350 Mev . . . 429
Particles, of different ionization density, fluorescent decay of CsI(Tl) in . . . 1
Perminvar, magnetically annealed, reversible permeability and losses 596
Phase transformations in alkali metals, theory . . . 810
Photodisintegration of potassium by ^{7}Li(p,γ) radiation . . . 321
Photofluorescence of terphenyltoluene solutions . . . 53
Photographic images, Fourier spectra, determination . . . 661
Photon beams, fluctuations, and their correlations . . . 1037
Photoproduction of charged pions from deuterium (R) . . . 895
Photoproduction of π^0 mesons at helium . . . 880
Pinch, stabilized, scaling laws . . . 116
Pion, radiative beta decay (R) . . . 144
Pions, charged, photoproduction from deuterium (R) . . . 895
Point contact injection ratio in Ge, temperature dependence (R) . . . 264
Polarization of helium-like atoms (R) . . . 889
Polarization of μ-mesons scattered by mercury (R) . . . 1137
Polarization of neutrons emitted from nuclei by protons . . . 433
Polarization of protons from ^{12}C(d,p)^{13}C reaction . . . 88
Polarization reversal process in ferroelectric single crystals (L) . . . 307
Polarization, *see also* Stripping reactions
Polycrystalline cadmium oxide, heat treatment . . . 65
Positrons, slow, elastic scattering by hydrogen atoms (R) . . . 139
Pressure dependence of ferromagnetic anisotropy energy . . . 207
Protons, charge transfer in excited atomic hydrogen . . . 694
Protons, 970 Mev, double scattering experiments with . . . 1130
Protons, *see also* Scattering

Radiation, ^{7}Li(p,γ), photodisintegration of potassium by . . . 321
Reaction, ^{9}Be(α,n)^{12}C, stripping mechanism in (R) . . . 457
Reaction, ^{12}C(d,p)^{13}C, polarization of protons from . . . 88
Reflecting surface, magnetization, use of Kerr effect for study . . . 233
Refractive index of non-uniform films (R) . . . 906
Relativity, general, anisotropic cosmological solution (R) . . . 263
Relaxation times of solutions, theoretical and experimental (R) . . . 283
Relaxation times, vibrational, of polyatomic gases derived from measurements of acoustic absorption . . . 940
Resonance line of calcium, pressure shift and broadening (R) . . . 279
Response function of optical system, influence of spherical aberration . . . 411
Rubber containing colloidal carbon black, electron microscopic study . . . 42
Rupture propagation in inhomogeneous solids: rubber containing carbon black . 42

Scattering, double, experiments with 970 Mev protons . . . 1130
Scattering, elastic, of protons by tritons and ^{3}He . . . 770
Scattering, elastic, of slow ions in their parent gases . . . 1087
Scattering, elastic, of slow positrons by hydrogen atoms (R) . . . 139
Scattering, electromagnetic, by thin conducting plates at glancing incidence . . 981
Scattering, *see also* Neutron scattering
Schrödinger helium equation, non-relativistic, (2p)^2 ^{1}S state solution (R) . . 141
Secondary electrons, probability of multiple emissions . . . 717
Semiconductor noise as queuing problem . . . 27
Semiconductor–vapour interface, diffusion across . . . 369
Semiconductors, effect of magnetic field on absorption edge, theory . . . 553

PAGE

Semiconductors, effect of strain on Ge and Si observed by cyclotron resonance 514
Semiconductors, *see also* Bismuth telluride, Carrier, Germanium, Infra-red, Point contact, Silicon
Silicon, electrical conductivity and Hall effect 193
Silicon, impurity carriers in, temperature variation of concentration (R) 917
Silicon, measurement of surface recombination velocity 1007
Solid solution in zinc blende type $A_2^{III}B_3^{VI}$ compounds 867
Solids, bounded, propagation of ultrasonic waves, generation of secondary signals 841
Solids, energy bands in, cellular method (R) 281
Solids, glass-like, fractures produced by stress pulses in 447
Solids, inhomogeneous, rupture propagation in: rubber containing carbon black 42
Solids, molecular rotation, and narrowing of nuclear magnetic resonance spectra 959
Solutions, relaxation times of, theoretical and experimental (R) 283
Sound, absorption in sediments of small particles in liquids 933
Spectra, absorption, *see* Absorption
Spectra, line, pressure shift and broadening in resonance line of calcium (R) 279
Spectra, nuclear magnetic resonance, narrowing by molecular rotation in solids 959
Spectrometer, magnetic, prolate spheroidal field, with source near equatorial plane 949
Spectrometer, source-modulated microwave cavity spectrometer, design and performance 537
Spherical aberration, influence on response function of optical system 411
Spin correlation coefficient in p–p scattering at 382 MeV, 90° c.m. scattering angle (R) 289
Stripping reactions, measurement of polarizations in 489
Stripping, *see also under* Reaction
Sublimation nuclei (R) 296
Surface recombination velocity, measurement on silicon 1007
Surface tensions of liquid argon and nitrogen 854
Susceptibility, initial, of homogeneous ferromagnetic alloys, semi-empirical equation (R) 130
Susceptibility, *see also* Magnetic susceptibility
Suspensions of liquid globules in another liquid, ultrasonic propagation in 833

Temperature waves in insulators, transport theory 391
Thermal diffusion in ionized gases 353, corr. 675
Thermoelectric power at high temperature, absolute scale (R) 898
Thorium C, branching ratio (R) 300
Time reversal and relation between angular distributions of absorption and emission processes 97
Transistors, surface barrier height changes, method of study (R) 910
Transport theory of temperature waves in insulators 391

Ultra-high-frequency gas breakdown between Rogowski electrodes 625
Ultrasonic absorption, comparison in $MnSO_4$ and $MgSO_4$ solutions 81
Ultrasonic waves, propagation in bounded solids, generation of secondary signals 841
Ultrasonics, propagation in suspensions of liquid globules in another liquid 833
Uranium alloys, magnetic susceptibility and electrical resistance properties 757

Variational methods based on density matrix 182
Viscosity determination by oscillating vessel method: I—Theory 576
Viscosity determination by oscillating vessel method: II—Viscosity of water at 20°C 585

Wannier functions, properties (R) 301
Water, viscosity at 20°C 585

X-ray emission lines, effect of absorption on mean wavelength (L) 924
X-ray intensities for model polycrystalline material in simple extension (R) 137
X-rays, exciting fluorescence of diamonds 1074

Yield phenomena in Cu–As alloys 33

INDEX OF AUTHORS (WITH TITLES)

PAGE

Agu, B. N. C., Burdett, T. A., and Matsukawa, E.: The transmission of electrons through metallic foils 727

Allinson, P. A., and Richardson, E. G.: The propagation of ultrasonics in suspensions of liquid globules in another liquid 833

Alves, M. A. F., with Burcham, W. E.: The ionization produced by beams of carbon and nitrogen ions (R) 462

Anderson, J. M., with Barrington, R. E.: The probability of multiple emissions of secondary electrons 717

Andersson, B.: A re-measurement of two gamma-ray lines from ^{152}Eu and ^{154}Eu (L) 148

Andrew, E. R., and Newing, R. A.: The narrowing of nuclear magnetic resonance spectra by molecular rotation in solids 959

Andrews, E. H., and Walsh, A.: Rupture propagation in inhomogeneous solids: An electron microscopic study of rubber containing colloidal carbon black . 42

Archard, G. D.: An unconventional electron lens (R) 135

Armitage, B. H., with Evans, P. R., Freeman, N. J., McGinty, G. K., and Richardson, H. O. W.: A prolate spheroidal field magnetic spectrometer with source near the equatorial plane 949

Ashmore, A., Diddens, A. N., Huxtable, G. B., and Skarsvåg, K.: A measurement of the spin correlation coefficient C_{nn} in p–p scattering at 382 Mev, for 90° centre of mass scattering angle (R) 289

Astbury, A., Kemp, M. A. R., Lipman, N. H., Muirhead, H., Voss, R. G. P., Zangger, C., and Kirk, A.: Capture rates for negative muons in various elements 494

Austin, I. G.: The optical properties of bismuth telluride 545

Bacon, G. E., and Street, R.: Gold–manganese alloys; some preliminary studies by neutron diffraction (R) 470

Bainbridge, W., with Roscoe, R.: Viscosity determination by the oscillating vessel method: II—The viscosity of water at 20°c 585

Baranger, E., and Gerjuoy, E.: Some consequences of the compound ion model . 326

Barrington, R. E., and Anderson, J. M.: The probability of multiple emissions of secondary electrons 717

Barron, K., and Lawley, L. E.: Absorption of sound in sediments of small particles in liquids 933

Bastin, J. A., and Wright, R. W.: Heat treatment of polycrystalline cadmium oxide 65

Bates, L. F., Clow, H., Craik, D. J., and Griffiths, P. M.: Magnetization processes in a polycrystalline manganese zinc ferrite 224

Bates, L. F., and Loasby, R. G.: Magnetic susceptibility and electrical resistance properties of some uranium alloys 757

Bates, L. F., and Newmann, M. M.: The magnetic susceptibilities of alloys of cerium with thorium 345

Batty, C. J., and Goldsack, S. J.: Double scattering experiments with 970 Mev protons 1130

Beale, J. R. A., Thomas, D. E., and Watkins, T. B.: A method of studying surface barrier height changes on transistors (R) 910

Bell, D. A.: Semiconductor noise as a queuing problem 27

Bell, G. M.: Dilution effects in regular assemblies 649

Bellamy, E. H., with Hogg, W. R.: The photoproduction of charged pions from deuterium (R) 895

Bellamy, E. H., with Palit, P.: The photoproduction of π^0 mesons at helium . 880

Benny, A. H., and Morten, F. D.: The measurement of surface recombination velocity on silicon 1007

Bhiday, M. R., Jennings, R. E., and Kalmus, P. I. P.: Measurement of electron beam energy using a gas Čerenkov detector 973

PAGE

Bickerton, R. J.: The amplification of a magnetic field by a high current discharge 618

Bickerton, R. J., and London, H.: The scaling laws for the stabilized pinch . . 116

Biedenharn, L. C., and Willard, H. B.: Eigenphaseshifts in terms of Wigner's nuclear reaction theory 874

Birks, J. B., and Cameron, A. J. W.: Energy transfer in organic systems.: I—Photofluorescence of terphenyl-toluene solutions 53

Biswas, S. N.: Distribution of K-mesons produced in high energy nuclear interactions 169

Bokhari, M. S., Cookson, J. A., Hird, B., and Weesakul, B.: The polarization of protons from the ^{12}C(d, p)^{13}C reaction 88

Bokhari, M. S., with Hird, B., and Cookson, J. A.: Measurement of polarizations in stripping reactions 489

Bowley, A. E., Delves, R., and Goldsmid, H. J.: Magnetothermal resistance and magnetothermoelectric effects in bismuth telluride 401

Boyd, T. J. M.: Electron excitation of atomic hydrogen in the 2s state . . 523

Boyd, T. J. M., and Dalgarno, A.: Charge transfer of protons in excited atomic hydrogen 694

Bransden, B. H., and Robertson, H. H.: The elastic scattering of protons by tritons and ^{3}He 770

Broude, C., Green, L. L., and Willmott, J. C.: The energy levels of ^{31}P: I—γ-ray spectra and decay schemes 1097

Broude, C., Green, L. L., and Willmott, J. C.: The energy levels of ^{31}P: II—Angular distributions and correlations 1115

Broude, C., Green, L. L., and Willmott, J. C.: The energy levels of ^{31}P: III—Comparison with the Nilsson model 1122

Brown, G. E., and De Dominicis, C. T.: The optical model at low energies and dispersion theory 70

Brown, G. E., Elton, L. R. B., and Mandl, F.: Polarization of μ-mesons scattered by mercury (R) 1137

Bullough, R., Newman, R. C., and Wakefield, J.: Diffusion across a semiconductor–vapour interface 369

Burcham, W. E., and Alves, M. A. F.: The ionization produced by beams of carbon and nitrogen ions (R) 462

Burdett, T. A., with Agu, B. N. C., and Matsukawa, E.: The transmission of electrons through metallic foils 727

Burkhardt, G. H., Cassels, J. M., Rigby, M., Wetherell, A. M., and Wormald, J. R.: Radiative beta decay of the pion (R) 144

Callaby, D. R., with Lee, E. W., and Lynch, A. C.: The use of the Kerr effect for studying the magnetization of a reflecting surface 233

Cameron, A. J. W., with Birks, J. B.: Energy transfer in organic systems: I—Photofluorescence of terphenyl-toluene solutions 53

Cassels, J. M., with Burkhardt, G. H., Rigby, M., Wetherell, A. M., and Wormald, J. R.: Radiative beta decay of the pion (R) 144

Cassels, J. M., O'Keeffe, T. W., Rigby, M., and Wormald, J. R.: Energy dependence of the spatial asymmetry in polarized muon decay 781

Champion, J. V.: Flow anisotropy in the theory of liquids 711

Chapman, A. C., and Seymour, E. F. W.: Copper nuclear magnetic resonance in Cu–Ni and Cu–Mn alloys 797

Chapman, Sydney: Thermal diffusion in ionized gases . . . . 353, corr. 675

Clark, J. L., with Prowse, W. A.: Ultra-high-frequency gas breakdown between Rogowski electrodes 625

Clow, H., with Bates, L. F., Craik, D. J., and Griffiths, P. M.: Magnetization processes in a polycrystalline manganese zinc ferrite 224

Cole, G. H. A.: Determination of fluid molecular order (R) 887

Coleman, R. F., with Perkin, J. L., and O'Connor, L. P.: Radiative capture cross sections for 14·5 MeV neutrons 505

PAGE

Cookson, J. A., with Bokhari, M. S., Hird, B., and Weesakul, B.: The polarization of protons from the ^{12}C(d, p)^{13}C reaction 88
Cookson, J. A., with Hird, B., and Bokhari, M. S.: Measurement of polarizations in stripping reactions 489
Corner, W. D., and Hutchinson, F.: The saturation magnetostriction of nickel crystals at low temperatures 1049
Corrigan, S. J. B., and von Engel, A.: The excitation of helium by electrons of low energy 786
Cowley, J. M., and Moodie, A. F.: A new formulation of scalar diffraction theory for restricted aperture . . . . corr. 309
Craggs, J. D., with Tozer, B. A., and Thorburn, R.: The attachment of slow electrons in air and oxygen 1081
Craik, D. J., with Bates, L. F., Clow, H., and Griffiths, P. M.: Magnetization processes in a polycrystalline manganese zinc ferrite 224
Culpin, M. F., and Kemp, K. W.: Calculations of x-ray intensities for a model polycrystalline material in simple extension (R). 137
Cusack, N., and Kendall, P.: The absolute scale of thermoelectric power at high temperature (R) 898

Dabrowski, J.: On the binding energy of the ^{16}O nucleus: II—Higher clusters . 499
Dalgarno, A.: The polarization of helium-like atoms (R) 889
Dalgarno, A., with Boyd, T. J. M.: Charge transfer of protons in excited atomic hydrogen 694
Dalgarno, A., and Kingston, A. E.: Properties of the metastable helium atoms . 1053
Dalgarno, A., and Williams, A.: The second approximation to the mobilities of ions in gases (R) 274
Davies, D. K., Dutton, J., and Jones, F. Llewellyn: Secondary ionization processes in hydrogen at high gas pressures 1061
Day, G. A.: Sublimation nuclei (R) 296
De Dominicis, C. T., with Brown, G. E.: The optical model at low energies and dispersion theory 70
Delves, R., with Bowley, A. E., and Goldsmid, H. J.: Magnetothermal resistance and magnetothermoelectric effects in bismuth telluride. 401
Diddens, A. N., with Ashmore, A., Huxtable, G. B., and Skarsvåg, K.: A measurement of the spin correlation coefficient C_{nn} in p–p scattering at 382 MEV, for 90° centre of mass scattering angle (R) 289
Domanski, S.: The dependence of the coercive field of tri-glycine sulphate on temperature and frequency (L). 306
Drabble, J. R.: Galvanomagnetic effects in p-type bismuth telluride 380
Duncanson, A., and Stevenson, R. W. H.: Some properties of magnesium fluoride crystallized from the melt 1001
Dutton, J., with Davies, D. K., and Jones, F. Llewellyn: Secondary ionization processes in hydrogen at high gas pressures 1061

Edmonds, P. D., and Lamb, J.: Vibrational relaxation times of a number of polyatomic gases derived from measurements of acoustic absorption 940
Edwards, S. F.: The collective treatment of a Fermi gas: I 685
Elliott, R. J., McLean, T. P., and Macfarlane, G. G.: Theory of the effect of a magnetic field on the absorption edge in semiconductors 553
Elton, L. R. B., with Brown, G. E., and Mandl, F.: Polarization of μ-mesons scattered bu mercury (R) 1137
Emery, E. W., and Veall, N.: The branching ratios of ^{86}Rb and ^{42}K . . . corr. 675
von Engel, A., with Corrigan, S. J. B.: The excitation of helium by electrons of low energy 786
Englman, R.: The absorptivity of anisotropic metals (R) 277
Englman, R.: The transport theory of temperature waves in insulators . . 391
Evans, P. Rice, and Freeman, N. J.: The branching ratio of thorium C (R) . . 300

PAGE

Evans, P. R., Freeman, N. J., McGinty, G. K., Armitage, B. H., and Richardson, H. O. W.: A prolate spheroidal field magnetic spectrometer with source near the equatorial plane 949

Farago, P. S.: Proposed method for direct measurement of the g-factor of free electrons (R) 891
Fatehally, R. A., with Garlick, G. F. J., and Hough, J. M.: The nature of binding in cadmium telluride (L) 925
Fox, M., and Tebble, R. S.: The demagnetizing energy and domain structure of a uniaxial single crystal 765
Freeman, N. J., with Evans, P. Rice: The branching ratio of thorium C (R) . 300
Freeman, N. J., with Evans, P. R., McGinty, G. K., Armitage, B. H., and Richardson, H. O. W.: A prolate spheroidal field magnetic spectrometer with source near the equatorial plane 949

Gabathuler, E., with Scobie, J.: The L/K-capture ratio in ^{126}I 437
Gabathuler, E., with Stewart, D. T.: Some electron collision cross sections for nitrogen and oxygen (R) 287
García-Moliner, F.: Magnetoresistance and Fermi surface of alkali metals . . 996
Garlick, G. F. J., Hough, J. M., and Fatehally, R. A.: The nature of binding in cadmium telluride (L) 925
Gerjuoy, E., with Baranger, E.: Some consequences of the compound ion model . 326
Gerlich, D.: Temperature dependence of point contact injection ratio in germanium (R) 264
Gilbody, H. B., and Hasted, J. B.: Mass dependence of inelastic atomic collisions (R) 293
Goldsack, S. J., with Batty, C. J.: Double scattering experiments with 970 MeV protons 1130
Goldsmid, H. J.: Heat conduction in bismuth telluride 17
Goldsmid, H. J., with Bowley, A. E., and Delves, R.: Magnetothermal resistance and magnetothermoelectric effects in bismuth telluride 401
Goodbody, A. M.: The influence of spherical aberration on the response function of an optical system 411
Green, L. L., with Broude, C., and Willmott, J. C.: The energy levels of ^{31}P: I—γ-ray spectra and decay schemes 1097
Green, L. L., with Broude, C., and Willmott, J. C.: The energy levels of ^{31}P: II—Angular distributions and correlations 1115
Green, L. L., with Broude, C., and Willmott, J. C.: The energy levels of ^{31}P: III—Comparison with the Nilsson model 1122
Griffiths, G. M.: The resonant absorption of γ-rays in ^{14}N 337
Griffiths, P. M., with Bates, L. F., Clow, H., and Craik, D. J.: Magnetization processes in a polycrystalline manganese zinc ferrite 224
Grimley, T. B.: The molecular orbital theory of the interaction between an atom and a crystal surface 103
Grover, N. B., and Harnik, E.: Sweep-out effects in the phase shift method of carrier lifetime measurements (R) 267
Grünbaum, E.: The growth of an orientated monolayer of lead on a silver single-crystal substrate (R) 459
Gugan, D.: The change of spontaneous magnetization with hydrostatic pressure . 1013
Gugan, D., and Rowlands, G.: The pressure dependence of the ferromagnetic anisotropy energy 207

Harnik, E., with Grover, N. B.: Sweep-out effects in the phase shift method of carrier lifetime measurements (R) 267
Hart, A.: Hysteresis loops associated with a simple domain structure 244
Hasted, J. B., with Gilbody, H. B.: Mass dependence of inelastic atomic collisions (R) 293
Hawkins, T. D. H., with Moss, T. S.: The infra-red emissivities of indium antimonide and germanium (R) 270

PAGE
Heavens, O. S., and Kelly, J. C.: Refractive index of non-uniform films (R) . 906
Hey, J. S., and Senior, T. B. A.: Electromagnetic scattering by thin conducting plates at glancing incidence 981
Hill, N. E.: The application of Onsager's theory to dielectric dispersion . . 532
Hindmarsh, W. R.: Pressure shift and broadening in the resonance line in calcium (R) 279
Hird, B., with Bokhari, M. S., Cookson, J. A., and Weesakul, B.: The polarization of protons from the $^{12}C(d, p)^{13}C$ reaction 88
Hird, B., Cookson, J. A., and Bokhari, M. S.: Measurement of polarizations in stripping reactions 489
Hogg, W. R., and Bellamy, E. H.: The photoproduction of charged pions from deuterium (R) 895
Hoisington, R. W. R., Kellner, L., and Pentz, M. J.: Criteria determining the design and performance of a source-modulated microwave cavity spectrometer 537
Holøien, E.: On the $(2p)^2$ ^1S state solution of the non-relativistic Schrödinger helium equation (R) 141
Hough, J. M., with Garlick, G. F. J., and Fatehally, R. A.: The nature of binding in cadmium telluride (L) 925
Hu, P. M., and Parsons, R. W.: The viscosity and density of benzene near its freezing point (R) 454
Huby, R.: Time reversal and the relation between angular distributions of absorption and emission processes 97
Hughes, I. S., and March, P. V.: Photoproduction of π^- mesons from boron . 259
Hutchinson, F., with Corner, W. D.: The saturation magnetostriction of nickel crystals at low temperatures 1049
Huxtable, G. B., with Ashmore, A., Diddens, A. N., and Skarsvåg, K.: A measurement of the spin correlation coefficient C_{nn} in p–p scattering at 382 MeV, for 90° centre of mass scattering angle (R) 289

Jack, W., with Storey, R. S., and Ward, A.: The fluorescent decay of CsI(Tl) for particles of different ionization density 1
Jackson, R. C., with Lee, E. W.: A semi-empirical equation for the initial susceptibility of homogeneous ferromagnetic alloys (R) 130
Jennings, R. E., with Bhiday, M. R., and Kalmus, P. I. P.: Measurement of electron beam energy using a gas Čerenkov detector 973
Johnson, F. A., and Lock, J. M.: The vibrational spectrum and specific heat of germanium (R) 914
Jones, D. P., Murphy, P. G., and O'Neill, P. L.: Conservation of parity in a nuclear interaction at 350 MeV 429
Jones, Eifionydd, and Jones, F. Llewellyn: The experimental determination of the primary ionization coefficients at low gas pressures 363
Jones, F. Llewellyn, with Davies, D. K., and Dutton, J.: Secondary ionization processes in hydrogen at high gas pressures 1061
Jones, F. Llewellyn, with Jones, Eifionydd: The experimental determination of the primary ionization coefficients at low gas pressures 363

Kalmus, P. I. P., with Bhiday, M. R., and Jennings, R. E.: Measurement of electron beam energy using a gas Čerenkov detector 973
Kellner, L., with Hoisington, R. W. R., and Pentz, M. J.: Criteria determining the design and performance of a source-modulated microwave cavity spectrometer 537
Kelly, J. C., with Heavens, O. S.: Refractive index of non-uniform films (R) . 906
Kemp, K. W., with Culpin, M. F.: Calculations of x-ray intensities for a model polycrystalline material in simple extension (R) 137
Kemp, M. A. R., with Astbury, A., Lipman, N. H., Muirhead, H., Voss, R. G. P., Zangger, C., and Kirk, A.: Capture rates for negative muons in various elements 494

PAGE

Kendall, P., with Cusack, N.: The absolute scale of thermoelectric power at high temperature (R) . . . 898
Kingston, A. E., with Dalgarno, A.: Properties of the metastable helium atoms . 1053
Kirk, A., with Astbury, A., Kemp, M. A. R., Lipman, N. H., Muirhead, H., Voss, R. G. P., and Zangger, C.: Capture rates for negative muons in various elements . . . 494
Kohn, W.: Theory of Bloch electrons in a magnetic field (R) . . . 1147
Kohn, W., and Michaelson, S.: Properties of Wannier functions (R) . . . 301
Kolsky, H., and Shi, Y. Y.: Fractures produced by stress pulses in glass-like solids 447
Kor, S. K., with Verma, G. S.: A comparative study of ultrasonic absorption in $MnSO_4$ with $MgSO_4$ solutions . . . 81
Kundu, S. K.: Nucleon magnetic moment in cut-off meson theory . . . 49

Lamb, J., with Edmonds, P. D.: Vibrational relaxation times of a number of polyatomic gases derived from measurements of acoustic absorption . . . 940
Lawley, L. E., with Barron, K.: Absorption of sound in sediments of small particles in liquids . . . 933
Lawrenson, I. J., and Rushworth, F. A.: Nuclear magnetic resonance in solid *cyclo*pentene . . . 791
Leak, G. M., with Thomas, W. R.: The binding energy of nitrogen in a dislocation (L) . . . 673
Leck, J. H., with Riddoch, A.: Positive ion emission from metal surfaces caused by ion bombardment (R) . . . 467
Lee, E. W.: Magnetostriction curves of polycrystalline ferromagnetics . . . 249
Lee, E. W., Callaby, D. R., and Lynch, A. C.: The use of the Kerr effect for studying the magnetization of a reflecting surface . . . 233
Lee, E. W., and Jackson, R. C.: A semi-empirical equation for the initial susceptibility of homogeneous ferromagnetic alloys (R) . . . 130
Lee, E. W., and Troughton, A. G. H.: Reversible permeability and losses in magnetically annealed Perminvar . . . 596
Lewis, B., and Street, R.: The interpretation of magnetic susceptibility and the ΔE effect in terms of domain processes . . . 604
Lipman, N. H., with Astbury, A., Kemp, M. A. R., Muirhead, H., Voss, R. G. P., Zangger, C., and Kirk, A.: Capture rates for negative muons in various elements . . . 494
Little, V. I.: The measurement at low frequencies of the dielectric constant of conducting liquids . . . 441
Loasby, R. G.: The γ-phase in uranium alloys . . . 425
Loasby, R. G., with Bates, L. F.: Magnetic susceptibility and electrical resistance properties of some uranium alloys . . . 757
Lock, J. M., with Johnson, F. A.: The vibrational spectrum and specific heat of germanium (R) . . . 914
London, H., with Bickerton, R. J.: The scaling laws for the stabilized pinch . 116
Longhurst, R. S.: Diffraction by an opaque strip (R) . . . 901
Lynch, A. C., with Lee, E. W., and Callaby, D. R.: The use of the Kerr effect for studying the magnetization of a reflecting surface . . . 233
Lynn, N.: A second order calculation of the energy of interaction between two normal helium atoms . . . 201

Macdonald, J. A.: Apodization and frequency response with incoherent light . 749
McDowell, M. R. C.: Elastic scattering of slow ions in the parent gases . . 1087
Macfarlane, G. G., with Elliott, R. J., and McLean, T. P.: Theory of the effect of a magnetic field on the absorption edge in semiconductors . . . 553
McGinty, G. K., with Evans, P. R., Freeman, N. J., Armitage, B. H. and Richardson, H. O. W.: A prolate spheroidal field magnetic spectrometer with source near the equatorial plane . . . 949
McLean, T. P., with Elliott, R. J., and Macfarlane, G. G.: Theory of the effect of a magnetic field on the absorption edge in semiconductors . . . 553

PAGE
MacSwan, A. M.: The colour of thin oxide films on metals 742
Majumdar, S. Datta: Energy levels of polyatomic molecules 635
Mandel, L.: Fluctuations of photon beams and their correlations 1037
Mandl, F., with Brown, G. E., and Elton, L. R. B.: Polarization of μ-mesons scattered by mereury (R) 1137
Mansfield, R., and Williams, W.: The electrical properties of bismuth telluride . 733
March, N. H., and Young, W. H.: Variational methods based on the density matrix 182
March, P. V., with Hughes, I. S.: Photoproduction of π^- mesons from boron . 259
Marriott, R.: Calculation of the 1s–2s electron excitation cross section of hydrogen 121
Martin, V. M., Seaton, M. J., and Wallace, J. B. G.: On the use of the adiabatic theory in electron–atom collision calculations 701
Matsukawa, E., with Agu, B. N. C., and Burdett, T. A.: The transmission of electrons through metallic foils 727
Matthews, I. G.: The fluorescence of diamonds excited by X-rays 1074
Meakins, R. J.: Theoretical and experimental relaxation times of solutions (R) . 283
Michaelson, S., with Kohn, W.: Properties of Wannier functions (R) . . 301
Mitchell, W. H., with Putley, E. H.: The electrical conductivity and Hall effect of silicon 193
Moiseiwitsch, B. L.: Elastic scattering of slow positrons by hydrogen atoms (R) . 139
Moodie, A. F., with Cowley, J. M.: A new formulation of scalar diffraction theory for restricted aperture . . . . corr. 309
Morten, F. D., with Benny, A. H.: The measurement of surface recombination velocity on silicon 1007
Moss, T. S., and Hawkins, T. D. H.: The infra-red emissivities of indium antimonide and germanium (R) 270
Muirhead, H., with Astbury, A., Kemp, M. A. R., Lipman, N. H., Voss, R. G. P., Zangger, C., and Kirk, A.: Capture rates for negative muons in various elements 494
Murphy, P. G., with Jones, D. P., and O'Neil, P. L.: Conservation of parity in a nuclear interaction at 350 Mev 429

Newing, R. A., with Andrew, E. R.: The narrowing of nuclear magnetic resonance spectra by molecular rotation in solids 959
Newman, R. C., with Bullough, R., and Wakefield, J.: Diffusion across a semiconductor–vapour interface 369
Newmann, M. M., with Bates, L. F.: The magnetic susceptibilities of alloys of cerium with thorium 345
Nutkins, M. A. E.: Theory of phase transformations in alkali metals . . . 810

O'Connor, L. P., with Perkin, J. L., and Coleman, R. F.: Radiative capture cross sections for 14·5 Mev neutrons 505
O'Keeffe, T. W., with Cassels, J. M. Rigby,, M., and Wormald, J. R.: Energy dependence of the spatial asymmetry in polarized muon decay . . . 781
O'Neill, P. L., with Jones, D. P., and Murphy, P. G.: Conservation of parity in a nuclear interaction at 350 Mev 429
Ophel, T. R.: The photodisintegration of potassium by ^{7}Li(p, γ) radiation . . 321

Paige, E. G. S.: Experimental determination of electron temperature in high electric fields applied to germanium (R) 921
Pająk, Z., and Stankowski, J.: Polarization changes during the process of ageing in ferroelectrics of the BaTiO$_3$-type (R) 1144
Palit, P., and Bellamy, E. H.: The photoproduction of π^0 mesons at helium . . 880
Parsons, R. W., with Hu, P. M.: The viscosity and density of benzene near its freezing point (R) 454
Pentz, M. J., with Hoisington, R. W. R. and Kellner, L.: Criteria determining the design and performance of a source-modulated microwave cavity spectrometer 537

PAGE

Perkin, J. L., O'Connor, L. P., and Coleman, R. F.: Radiative capture cross sections for 14·5 MEV neutrons 505

Pike, E. R., and Wilson, A. J. C.: Effect of Lorentz factor and dispersion on measurement of lattice parameters with powder cameras (R). 908

Pincherle, L.: A note on the cellular method for energy bands in solids (R) . . 281

Prowse, W. A., and Clark, J. L.: Ultra-high-frequency gas breakdown between Rogowski electrodes 625

Prutton, M.: The polarization reversal process in ferroelectric single crystals (L) . 307

Putley, E. H.: The temperature variation of the concentration of impurity carriers in silicon (R) 917

Putley, E. H., and Mitchell, W. H.: The electrical conductivity and Hall effect of silicon 193

Raychaudhuri, A.: An anisotropic cosmological solution in general relativity (R) . 263

Redwood, M.: The generation of secondary signals in the propagation of ultrasonic waves in bounded solids 841

Richardson, E. G., with Allinson, P. A.: The propagation of ultrasonics in suspensions of liquid globules in another liquid 833

Richardson, H. O. W., with Evans, P. R., Freeman, N. J., McGinty, G. K. and Armitage, B. H.: A prolate spheroidal field magnetic spectrometer with source near the equatorial plane 949

Riddoch, A., and Leck, J. H.: Positive ion emission from metal surfaces caused by ion bombardment (R) 467

Rigby, M., with Burkhardt, G. H., Cassels, J. M., Wetherell, A. M., and Wormald, J. R.: Radiative beta decay of the pion (R) 144

Rigby, M., with Cassels, J. M., O'Keeffe, T. W., and Wormald, J. R.: Energy dependence of the spatial asymmetry in polarized muon decay 781

Robertson, H. H., with Bransden, B. H.: The elastic scattering of protons by tritons and ^{3}He 770

Roscoe, R.: Viscosity determination by the oscillating vessel method: I—Theoretical consideration 576

Roscoe, R., and Bainbridge, W.: Viscosity determination by the oscillating vessel method: II—The viscosity of water at 20°c 585

Rose-Innes, A. C.: Observation by cyclotron resonance of the effect of strain on germanium and silicon 514

Rowlands, G., with Gugan, D.: The pressure dependence of the ferromagnetic anisotropy energy 207

Rushworth, F. A., with Lawrenson, I. J.: Nuclear magnetic resonance in solid *cyclo*pentene 791

Saksena, B. D.: The infra-red absorption spectra of α-quartz between 4 and 15 microns 9

Schröder, K.: Yield phenomena in copper–arsenic alloys 33

Scobie, J., and Gabathuler, E.: The L/K-capture ratio in ^{126}I 437

Seaton, M. J., with Martin, V. M., and Wallace, J. B. G.: On the use of the adiabatic theory in electron–atom collision calculations. 701

Senior, T. B. A., with Hey, J. S.: Electromagnetic scattering by thin conducting plates at glancing incidence 981

Seymour, E. F. W., with Chapman, A. C.: Copper nuclear magnetic resonance in Cu–Ni and Cu–Mn alloys 797

Shi, Y. Y., with Kolsky, H.: Fractures produced by stress pulses in glass-like solids 447

Sillitto, R. M., and Wilson, M. D.: 'Virtual' Fresnel diffraction patterns (R) . 303

Skarsvåg, K., with Ashmore, A., Diddens, A. N., and Huxtable, G. B.: A measurement of the spin correlation coefficient C_{nn} in p–p scattering at 382 MEV, for 90° centre of mass scattering angle (R) 289

PAGE

Smith, B. A., with Woolley, J. C.: Solid solution in $A^{III}B^{V}$ compounds . . 214

Smith, B. A., with Woolley, J. C.: Solid solution in zinc blende type $A_2^{III}B_3^{VI}$ compounds 867

Squires, E. J.: The polarization of neutrons emitted from nuclei by protons . 433

Srinivasan, R.: Elastic constants of calcium fluoride 566

Stankowski, J., with Pająk, Z.: Polarization changes during the process of ageing in ferroelectrics of the $BaTiO_3$-type (R) 1144

Stansfield, D. : The surface tensions of liquid argon and nitrogen 854

Stevens, K. W. H. : The wave mechanical damped harmonic oscillator . . 1027

Stevenson, R. W. H., with Duncanson, A. : Some properties of magnesium fluoride crystallized from the melt 1001

Stewart, D. T., and Gabathuler, E. : Some electron collision cross sections for nitrogen and oxygen (R) 287

Storey, R. S., Jack, W., and Ward, A. : The fluorescent decay of CsI(Tl) for particles of different ionization density 1

Street, R., with Bacon, G. E. : Gold–manganese alloys ; some preliminary studies by neutron diffraction (R) 470

Street, R., with Lewis, B. : The interpretation of magnetic susceptibility and the ΔE effect in terms of domain processes 604

Swartz, J. C., with Wriedt, H. A. : The binding energy of nitrogen in a dislocation (L) 673

Tanner, N. W. : The stripping mechanism in the reaction $^{9}Be(\alpha, n)^{12}C$ (R). . 457

Tebble, R. S., with Fox, M. : The demagnetizing energy and domain structure of a uniaxial single crystal 765

Temperley, H. N. V. : On the enumeration of Mayer cluster integrals (R) . 1141

Thomas, D. E., with Beale, J. R. A., and Watkins, T. B. : A method of studying surface barrier height changes on transistors (R) 910

Thomas, W. R., and Leak, G. M. : The binding energy of nitrogen in a dislocation (L) 673

Thorburn, R., with Tozer, B. A., and Craggs, J. D. : The attachment of slow electrons in air and oxygen 1081

Townsend, W. G., and Williams, G. C. : The electrical breakdown of gases in uniform high frequency fields at low pressure 823

Tozer, B. A., Thorburn, R., and Craggs, J. D. : The attachment of slow electrons in air and oxygen 1081

Troughton, A. G. H., with Lee, E. W. : Reversible permeability and losses in magnetically annealed Perminvar 596

Veall, N., with Emery, E. W. : The branching ratios of ^{86}Rb and ^{42}K. . corr. 675

Verma, G. S., and Kor, S. K. : A comparative study of ultrasonic absorption in $MnSO_4$ with $MgSO_4$ solutions 81

Viénot, J. Ch. : Determination of the Fourier spectra of photographic images . 661

Voss, R. G. P., with Astbury, A., Kemp, M. A. R., Lipman, N. H., Muirhead, H., Zangger, C., and Kirk, A. : Capture rates for negative muons in various elements 494

Wakefield, J., with Bullough, R., and Newman, R. C. : Diffusion across a semiconductor–vapour interface 369

Wallace, J. B. G., with Martin, V. M., and Seaton, M. J. : On the use of the adiabatic theory in electron–atom collision calculations 701

Walsh, A., with Andrews, E. H. : Rupture propagation in inhomogeneous solids : An electron microscopic study of rubber containing colloidal carbon black . 42

PAGE

Ward, A., with Storey, R. S., and Jack, W. : The fluorescent decay of CsI(Tl) for particles of different ionization density 1
Watkins, T. B., with Beale, J. R. A., and Thomas, D. E. : A method of studying surface barrier height changes on transistors (R) 910
Weesakul, B., with Bokhari, M. S., Cookson, J. A., and Hird, B. : The polarization of protons from the $^{12}\mathrm{C}(d, p)^{13}\mathrm{C}$ reaction 88
Wetherell, A. M., with Burkhardt, G. H., Cassels, J. M., Rigby, M., and Wormald, J. R. : Radiative beta decay of the pion (R) 144
Willard, H. B., with Biedenharn, L. C. : Eigenphaseshifts in terms of Wigner's nuclear reaction theory 874
Williams, A., with Dalgarno, A. : The second approximation to the mobilities of ions in gases (R) 274
Williams, G. C., with Townsend, W. G. : The electrical breakdown of gases in uniform high frequency fields at low pressure 823
Williams, W., with Mansfield, R. : The electrical properties of bismuth telluride . 733
Willmott, J. C., with Broude, C., and Green, L. L. : The energy levels of $^{31}\mathrm{P}$: I—γ-ray spectra and decay schemes 1097
Willmott, J. C., with Broude, C., and Green, L. L. : The energy levels of $^{31}\mathrm{P}$: II—Angular distributions and correlations 1115
Willmott, J. C., with Broude, C., and Green, L. L. : The energy levels of $^{31}\mathrm{P}$: III—Comparison with the Nilsson model 1122
Wilson, A. J. C. : Effect of absorption on mean wavelength of x-ray emission lines (L) 924
Wilson, A. J. C., with Pike, E. R. : Effect of Lorentz factor and dispersion on measurement of lattice parameters with powder cameras (R) 908
Wilson, M. D., with Sillitto, R. M. : ' Virtual ' Fresnel diffraction patterns (R) . 303
Woolley, J. C., and Smith, B. A. : Solid solution in $\mathrm{A^{III}B^{V}}$ compounds 214
Woolley, J. C., and Smith, B. A. : Solid solution in zinc blende type $\mathrm{A_2{}^{III}B_3{}^{VI}}$ compounds 867
Wormald, J. R., with Burkhardt, G. H., Cassels, J. M., Rigby, M., and Wetherell, A. M. : Radiative beta decay of the pion (R) 144
Wormald, J. R., with Cassels, J. M., O'Keeffe, T. W., and Rigby, M. : Energy dependence of the spatial asymmetry in polarized muon decay 781
Wriedt, H. A., and Swartz, J. C. : The binding energy of nitrogen in a dislocation (L) 673
Wright, R. W., with Bastin, J. A. : Heat treatment of polycrystalline cadmium oxide 65

Young, W. H., with March, N. H. : Variational methods based on the density matrix 182

Zangger, C., with Astbury, A., Kemp, M. A. R., Lipman, N. H., Muirhead, H., Vos, R. G. P., and Kirk, A. : Capture rates for negative muons in various elements 494

V.
19

INDEX TO REVIEWS OF BOOKS

PAGE

Bayet, M. : *Physique electronique des gaz et des solides* 482
Beckerley, J. G. : *Annual review of nuclear science.* Vol. 7. 315
Belov, N. V. : *A class-room method for the derivation of the* 230 *space groups* 1155
Bikerman, J. J. : *Surface chemistry—Theory and applications* (2nd Edn) 927
Bitter, Francis : *Currents, fields and particles* 486
Bleaney, B. I., and Bleaney, B. : *Electricity and magnetism* 314
Bonamy, M. : *Servomécanismes, théorie et technologie* 478
Booth, A. D., Brandwood, L., and Cleave, J. P. : *Mechanical resolution of linguistic problems* 482
Booth, K. H. V. : *Programming for an automatic digital computer* 476
Born, Max : *Atomic physics* (6th Edn) 679
Born, Max : *Physik im Wandel meiner Zeit* 676
Bradley, J. E. S. : *Physics of nuclear fission* 931
Buckingham, R. A. : *Numerical methods* 150

Caldin, E. F. : *An introduction to chemical thermodynamics* 475
Champeix, R. : *Physique et technique des tubes electroniques, Tome* 1*—Eléments de technique du vide* 929
Constant, F. Woodbridge : *Theoretical physics—Thermodynamics, electromagnetism, waves and particles* 679
Creutz, E. : *Handbuch der Physik.* Vol. 45. *Nuclear instrumentation* II 931
Cullwick, E. G. : *Electromagnetism and relativity* 161

Diels, K., and Jaeckel, R. : *Leybold Vakuum-Taschenbuch* 929
Dirac, P. A. M. : *The principles of quantum mechanics* (4th Edn) 677
Dunning, J. R., and Prentice, B. R. : *Advances in nuclear engineering.* Vols. I and II (Proceedings of the Second Nuclear Engineering and Science Congress held at Philadelphia, 1957) 480

Edmonds, A. R. : *Angular momentum in quantum mechanics* 928
Eirlich, F. R. : *Rheology* : *Theory and applications* 676
Evans, J. : *The fundamental principles of transistors* 161

Farley, F. J. M. : *Elements of pulse circuits* 320
Field, F. H., and Franklin, J. L. : *Electron impact phenomena and the properties of gaseous ions* 476
Fisher, J. C., Johnston, W. G., Thomson, R., and Vreeland, T. : *Dislocations and mechanical properties of crystals* 678
Flügge, S. : *Handbuch der Physik.* Vol. 5, Part I : *Principles of quantum mechanics* I 479
Flügge, S. : *Handbuch der Physik.* Vol. 15. *Low temperature physics* II 162
Flügge, S. : *Handbuch der Physik.* Vol. 27. *Spectroscopy* II 156
Flügge, S. : *Handbuch der Physik.* Vol. 42. *Nuclear reactions* III 149
Flügge, S. : *Handbuch der Physik.* Vol. 50. *Astrophysics* I 319
Fox, L. : *Two-point boundary problems (in ordinary differential equations)* 165
Frisch, O. R. : *Progress in nuclear physics.* Vol. 6 680

Gintzon, E. L. : *Microwave measurements* 312
Guderley, K. G. : *Theorie schallnaher Strömungen* (Theory of transonic flow) 475
Guggenheim, E. A. : *Thermodynamics* (3rd Edn) 310

Hanbury Brown, R., and Lovell, A. C. B. : *The exploration of space by radio* 484
Hintenberger, H. : *Nuclear masses and their determination* 318

PAGE
H.M. Nautical Almanac Office : *Interpolation and allied tables* 311
Hooper, J. E., and Scharff, M. : *The cosmic radiation* 482
Hughes, D. J. : *Neutron cross sections* 309
Hughes, D. J. : *On nuclear energy : Its potential for peacetime uses* 317
Hughes, D. J., McLain, S., and Williams, C. : *Problems in nuclear engineering.* Vols I and II. 152

Van De Hulst, H. C. : *Light scattering by small particles* 154

Ioffe, A. F. : *Semiconductor thermoelements and thermoelectric cooling* 683

Jenkins, F. A., and White, H. E. : *Fundamentals of optics* (3rd Edn) 313

Karmazina, L. N., and Kurochkina, L. V. : *Tablitsy interpoljatsionnykh koèffitsientov* 152
Kistemaker, J., Bigeleisen, J., and Nier, A. C. C. : *Proceedings of the International Symposium on Isotope Separation* 1155

Lacey, William N., and Sage, Bruce H. : *Thermodynamics of one-component systems* 680
Landshoff, Rolf K. : *Review of magneto-hydrodynamics* (*A symposium*) 487
Leck, J. H. : *Pressure measurement in vacuum systems* 477
Lipkin, H. J. : *Proceedings of the Rehovoth conference on nuclear structure* 930
Loeb, Leonard B. : *Static electrification* 927
Longhurst, R. S. : *Geometrical and physical optics* 310
Longuet-Higgins, H. C. : *Molecular physics.* Vol. 1, No. 1 317

McLachlan, Jr., Dan : *X-ray crystal structure* 487
Martin, L. : *Advances in electronics and electron physics.* Vol. 9 488
Mason, B. J. : *The physics of clouds* 153
Massignon, D. : *Mécanique statistique des fluides—Fluctuations et propriétés locales* 677
Meetham, A. R. : *Basic physics* 312
Megaw, H. D. : *Ferroelectricity in crystals* 162
Miller, G. L. : *Zirconium* (*metallurgy of the rarer metals,* 2) (2nd Edn) 316
Moelwyn-Hughes, E. A. : *Physical chemistry* 1154

Noakes, G. R. : *New intermediate physics* 163

Payne-Gaposchkin, C. : *The galactic novae* 160
Penning, F. M. : *Electrical discharges in gases* 483
Pippard, A. B. : *The elements of classical thermodynamics* 485
Powell, L. S. : *Physics.* Volume II.—*Electricity and magnetism* 928
Post Office Research Station : Selected engineering reports : *Piezoelectricity* 156

Raymond, F. H. : *L'Automatique des informations* (*Evolution des Sciences No.* 9) 166
Rawer, Karl : *The ionosphere* 682
Rose, M. E. : *Elementary theory of angular momentum* 928
Rossi, B. : *Optics* 155

Schatzman, E. : *White Dwarfs* 319
Scott, J. F. : *A history of mathematics from antiquity to the beginning of the nineteenth century* 481
Seitz, F., and Turnbull, D. : *Solid state physics.* Vol. 4 478
Smart, W. M. : *Combination of observations* 484
Smith, C. J. : *Intermediate physics* 158

PAGE

Smith, R. A., Jones, F. E., and Chasmar, R. P. : *The detection and measurement of infra-red radiation* 157
Storer, E. James : *Passive network synthesis* 164

Titchmarsh, E. C. : *Eigenfunction expansions associated with second order differential equations* 1153
Van Tongeren, W., and Freese, F. : *Proceedings of the sixth international conference on spectroscopy* 682

Vagramyan, A. T., and Solovieva, Z. A. : *Le dépôt électrolytique des métaux* . . 681

von Weizsäcker, C. F. : *Zum Weltbild der Physik* (7th Edn) 318

Wilson, A. J. C. (Ed.) : *Structure reports*, Vol. 15 681
Wooster, W. A. : *Experimental crystal physics* 311

Printed in England
TAYLOR & FRANCIS, LTD., Red Lion Court, Fleet Street, London, E.C.4